HANDBOOK OF NANOMATERIALS FOR WASTEWATER TREATMENT

Fundamentals and Scale up Issues

Edited by
Bharat A. Bhanvase
Shirish H. Sonawane
Vijay B. Pawade
Aniruddha B. Pandit

ELSEVIER

Micro & Nano Technologies Series

Handbook of Nanomaterials for Wastewater Treatment

This book belongs to Badji Mokhtar Annaba University
Central Library

Copyright Elsevier 2025

This page intentionally left blank

This book belongs to Badji Mokhtar Annaba University Central Library

Copyright Elsevier 2025

Handbook of Nanomaterials for Wastewater Treatment

Fundamentals and Scale up Issues

Edited by

Bharat Bhanvase
Shirish Sonawane
Vijay Pawade
Aniruddha Pandit

ELSEVIER

This book belongs to Badji Mokhtar Annaba University Central Library

Copyright Elsevier 2025

Elsevier
Radarweg 29, PO Box 211, 1000 AE Amsterdam, Netherlands
The Boulevard, Langford Lane, Kidlington, Oxford OX5 1GB, United Kingdom
50 Hampshire Street, 5th Floor, Cambridge, MA 02139, United States

Copyright © 2021 Elsevier Inc. All rights reserved.

No part of this publication may be reproduced or transmitted in any form or by any means, electronic or mechanical, including photocopying, recording, or any information storage and retrieval system, without permission in writing from the publisher. Details on how to seek permission, further information about the Publisher's permissions policies and our arrangements with organizations such as the Copyright Clearance Center and the Copyright Licensing Agency, can be found at our website: www.elsevier.com/permissions.

This book and the individual contributions contained in it are protected under copyright by the Publisher (other than as may be noted herein).

Notices

Knowledge and best practice in this field are constantly changing. As new research and experience broaden our understanding, changes in research methods, professional practices, or medical treatment may become necessary.

Practitioners and researchers must always rely on their own experience and knowledge in evaluating and using any information, methods, compounds, or experiments described herein. In using such information or methods they should be mindful of their own safety and the safety of others, including parties for whom they have a professional responsibility.

To the fullest extent of the law, neither the Publisher nor the authors, contributors, or editors, assume any liability for any injury and/or damage to persons or property as a matter of products liability, negligence or otherwise, or from any use or operation of any methods, products, instructions, or ideas contained in the material herein.

Library of Congress Cataloging-in-Publication Data
A catalog record for this book is available from the Library of Congress

British Library Cataloguing-in-Publication Data
A catalogue record for this book is available from the British Library

ISBN: 978-0-12-821496-1

For information on all Elsevier publications
visit our website at https://www.elsevier.com/books-and-journals

Publisher: Matthew Deans
Acquisitions Editor: Simon Holt
Editorial Project Manager: Joshua Mearns
Production Project Manager: Kamesh Ramajogi
Cover Designer: Greg Harris

Typeset by SPi Global, India

ELSEVIER Book Aid International Working together to grow libraries in developing countries
www.elsevier.com • www.bookaid.org

This book belongs to Badji Mokhtar Annaba University Central Library Copyright Elsevier 2025

Contents

Contributors ..... *xxv*
Preface ..... *xxxi*

SECTION I: Introduction to nanomaterials for wastewater treatment: Fundamentals

Chapter 1: Introduction to nanomaterials for wastewater treatment *3*
Bhaskar Bethi, Shirish H. Sonawane, Bharat A. Bhanvase, and Jaykumar B. Bhasarkar
1.1 Introduction 3
1.1.1 Catalyst for organic component degradation: Nanocatalyst 4
1.1.2 Photocatalytic effect due to nanoscale: Bandgap 4
1.1.3 Disinfection using nanomaterials 5
1.1.4 Nanomaterials for sensing 6
1.2 Nanomaterials as adsorbents for wastewater treatment 6
1.2.1 Carbon nanotubes (CNTs) 6
1.2.2 Graphene nanomaterials 7
1.2.3 Metal and metal oxides 8
1.2.4 Magnetic nanoparticles 9
1.3 Metal oxide nanoparticles as photocatalyst 9
1.4 Nanocomposites for wastewater treatment 11
1.4.1 Bionanocomposites 11
1.4.2 Nanocomposites based on inorganic support 12
1.4.3 Nanocomposite hydrogels 14
1.5 Membrane-based technology 15
1.5.1 Nanocomposite membranes 17
1.6 Challenges and future direction 19
References 20

Chapter 2: Low-dimensional nanomaterials: Syntheses, physicochemical properties, and their role in wastewater treatment *27*
Dragana J. Jovanović
2.1 Introduction 27
2.2 Classification of nanomaterials 28
2.2.1 Semiconducting nanomaterials 28

This book belongs to Badji Mokhtar Annaba University Central Library
Copyright Elsevier 2025

2.2.2 Metal oxide nanomaterials ... 30
2.2.3 Carbon-based nanomaterials ... 31
2.3 Synthesis of low-dimensional nanomaterials ... 32
2.3.1 Synthesis of 0D nanomaterials (II–VI and III–V quantum dots) ... 33
2.3.2 Synthesis of 1D and 2D nanomaterials ... 37
2.3.3 Synthesis of carbon-based nanomaterials ... 39
2.3.4 Structure and morphology of II–VI and III–V semiconductor nanomaterials ... 40
2.4 Physicochemical properties ... 42
2.4.1 Optical properties of 0D of II–VI and III–V nanomaterials ... 42
2.4.2 Optical properties of 1D and 2D nanomaterials ... 46
2.5 Low-dimensional nanomaterials in wastewater treatment ... 48
2.6 Conclusion ... 49
Acknowledgments ... 50
References ... 50

Chapter 3: Potential risk and safety concern of nanomaterials used for wastewater treatment ... 59

Tariq Aziz, Shabnam Azad, Sidharth P. Nair, Jitendra Singh Verma, Ashish P. Unnarkat, Sharadwata Pan, and Ashutosh Namdeo

3.1 Introduction ... 59
3.2 Synthesis of nanoparticles, chemicals involved and their potential safety concern ... 63
3.2.1 Synthesis of zinc oxide nanoparticles ... 63
3.2.2 Synthesis of silver nanoparticles ... 65
3.2.3 Carbon nanotube synthesis ... 66
3.2.4 Iron oxide nanoparticle synthesis ... 68
3.2.5 Synthesis of TiO_2 nanoparticles ... 68
3.2.6 Other materials and metal oxides ... 68
3.3 Potential safety concerns of nanomaterials to flora and fauna ... 72
3.3.1 Zinc oxide (ZnO) nanoparticles ... 72
3.3.2 Silver nanoparticles ... 73
3.3.3 Carbon nanotubes and carbon-based nanomaterials/nanoparticles ... 74
3.3.4 Iron oxide and magnetic nanoparticles ... 74
3.3.5 Titanium dioxide (TiO_2) nanoparticles ... 75
3.4 Conclusion ... 76
References ... 76

Chapter 4: Advanced technologies for wastewater treatment: New trends ... 85

Jyoti Katiyar, Swapnil Bargole, Suja George, Rohidas Bhoi, and Virendra Kumar Saharan

4.1 Introduction ... 85
4.2 Advanced oxidation processes ... 87
4.2.1 Hydrodynamic cavitation ... 87
4.2.2 Sonolysis/acoustic cavitation ... 88
4.2.3 Photocatalysis ... 93
4.2.4 Fenton process ... 99

This book belongs to Badji Mokhtar Annaba University Central Library
Copyright Elsevier 2025

4.3 Hybrid AOP's involving nanocatalyst 101
4.3.1 Heterogeneous Fenton process 103
4.3.2 Heterogeneous photo-Fenton process 104
4.3.3 Sono photocatalytic process 111
4.3.4 Sono-Fenton process 116
4.3.5 Sono-photo-Fenton process 119
4.3.6 Photocatalytic oxidation with hydrodynamic cavitation 123
4.4 Conclusions 123
References 126

SECTION II: Photocatalytic nanocomposite materials: Preparation and applications

Chapter 5: Introduction, basic principles, mechanism, and challenges of photocatalysis 137

Prasad Mandade

5.1 Introduction 137
5.2 Basic principles and mechanism of photocatalysis 138
5.3 Source of water pollution, water treatment methods, and role of nanomaterials in wastewater treatment 141
5.3.1 Sources of water pollution 141
5.3.2 Water treatment methods 142
5.3.3 Role of nanomaterials in water treatment by photocatalysis 142
5.4 Overview on photocatalytic materials and factors affecting photocatalysis 144
5.4.1 Photocatalytic materials 144
5.4.2 Factor affecting photocatalysis 145
5.5 Challenges of photocatalysis in wastewater treatment 147
5.6 Summary 150
References 150

Chapter 6: Doped-TiO_2 and doped-mixed metal oxide-based nanocomposite for photocatalysis 155

Akash P. Bhat, Ananda J. Jadhav, Chandrakant R. Holkar, and Dipak V. Pinjari

6.1 Introduction 156
6.2 Mechanism of TiO_2 photocatalysis 157
6.2.1 Generation of charge carrier species and their recombination 157
6.2.2 Adsorption of chemicals to TiO_2 followed by their redox pathways 159
6.2.3 Radical attack on organics 161
6.3 Photoactivity of TiO_2 polymorphs 162
6.4 Advancements in TiO_2 photocatalysis for advanced oxidation technology 162
6.4.1 Surface modifications of TiO_2 162
6.4.2 Photocatalyst modification and doping 165

This book belongs to Badji Mokhtar Annaba University Central Library
Copyright Elsevier 2025

6.4.3 Photocatalytic membranes 166
6.4.4 Application of membranes 167
6.5 Photochemical reactors 168
6.5.1 Immersion well 170
6.5.2 Thin film 170
6.5.3 Annular 171
6.5.4 Multilamp 171
6.6 Combination/coupling with other (hybrid) treatment technologies 171
6.7 Challenges and issues for TiO_2 photo-catalysis for water treatment 172
6.8 Conclusion and future prospectus 174
References 175

Chapter 7: New graphene-based nanocomposite for photocatalysis 181

Gunvant H. Sonawane, Prakash K. Labhane, and Shirish H. Sonawane

7.1 Introduction 181
7.2 Graphene and its derivatives 182
7.2.1 Properties of graphene and its derivatives 182
7.2.2 Preparation methods of graphene and its derivatives 182
7.3 Graphene and its derivative-based photocatalyst 184
7.3.1 Synthesis of graphene and its derivatives based binary nanocomposites 184
7.3.2 Synthesis of graphene and its derivative-based ternary nanocomposites 186
7.4 Characterization of graphene and its derivatives 188
7.5 Photocatalytic applications 190
7.5.1 Photocatalytic study of graphene and its derivatives-based binary nanocomposites 192
7.5.2 Photocatalytic study of graphene and its derivatives-based ternary nanocomposites 193
7.6 Mechanism of photocatalytic degradation 194
7.7 Conclusion and future prospects 197
References 200

Chapter 8: Luminescence nanomaterials for photocatalysis 209

Amol Nande, Ashish Tiwari, Swati Raut, Renu Nayar, and S.J. Dhoble

8.1 Introduction—Basic principal of phosphor for photocatalysis 209
8.2 Mechanism and challenges of luminescence materials in photocatalysis 211
8.3 Rare-earth-doped inorganic phosphor materials for photocatalysis 213
8.3.1 Downconversion phosphors 213
8.3.2 Upconversion phosphors 216
8.3.3 Long-lasting phosphors 219
8.4 Nanophosphor for photocatalysis 221
8.4.1 Oxide-based nanophosphors 222
8.4.2 Sulfide-based phosphors 225
8.4.3 Plasmonic-metal nanoparticles 226
8.5 Synthesis of nanophosphors 227
8.5.1 Solid-sate reaction methods 227
8.5.2 Combustion method 230

This book belongs to Badji Mokhtar Annaba University Central Library
Copyright Elsevier 2025

8.5.3 Hydrothermal method ... 230
8.5.4 Sol-gel method ... 230
8.5.5 Co-precipitation method ... 231
8.5.6 Ball milling method ... 231
8.6 Application of photocatalysis in water purification ... 231
8.7 Conclusion and future perspectives of luminescence phosphor-based photocatalyst ... 233
8.8 Challenges and issues ... 233
References ... 234

Chapter 9: Magnetic nanomaterials-based photocatalyst for wastewater treatment ... 241

Prachi Upadhyay, Vijayanand S. Moholkar, and Sankar Chakma

9.1 Introduction ... 241
9.2 Source of water pollution and type of pollutants ... 242
9.2.1 Agricultural waste ... 243
9.2.2 Pharmaceutical waste ... 244
9.2.3 Industrial waste ... 244
9.2.4 Plastic waste ... 245
9.3 Types of water treatment techniques ... 246
9.3.1 Primary treatment ... 246
9.3.2 Secondary treatment ... 248
9.3.3 Tertiary treatment techniques ... 249
9.4 Case study of wastewater treatment using magnetic nanoparticles ... 261
9.4.1 Magnetic nanoparticles as adsorbents ... 261
9.4.2 Photocatalysis decontamination of water using magnetic nanoparticles ... 263
9.5 Limitations of magnetic nanomaterials ... 267
9.6 Future prospects and overview ... 267
References ... 268

Chapter 10: Nanomaterials for water splitting and hydrogen generation ... 277

Sagar D. Balgude and Satish P. Mardikar

10.1 Introduction ... 277
10.2 Developing photocatalysts for water splitting—Mechanistic aspects ... 280
10.3 Nanomaterials for water splitting ... 280
10.3.1 Metal oxides for water splitting ... 282
10.3.2 Metal sulfides for water splitting ... 291
10.3.3 Metal organic frameworks for water splitting ... 293
10.3.4 Carbon-based nanomaterials for water splitting ... 295
10.4 Sn_3O_4-ZnO nanoflowers for hydrogen generation under visible light—Case study ... 296
10.4.1 Preparation, characterization, and photoactivity of Sn_3O_4-ZnO nanoflowers ... 297
10.4.2 Results and discussion ... 298
10.5 Conclusions ... 302
References ... 303

This book belongs to Badji Mokhtar Annaba University Central Library
Copyright Elsevier 2025

Chapter 11: Nanomaterials for treatment of air pollutants *313*
Nikhil D. Bhavsar, Divya P. Barai, Bharat A. Bhanvase, and Shirish H. Sonawane
11.1 Introduction 313
11.2 Role of nanotechnology in various pollution treatment methods 314
11.3 Air pollutants 315
11.4 Nanotechnology in the treatment of air pollution 315
11.4.1 Treatment methods 315
11.4.2 Treatment of air pollutants 318
11.5 Pilot-scale studies 331
11.6 Challenges for the usage of nanomaterials for air pollution treatment 333
11.7 Summary and conclusion 334
References 335

SECTION III: Adsorbent nanomaterials: Preparation and applications

Chapter 12: Nanomaterials for adsorption of pollutants and heavy metals: Introduction, mechanism, and challenges *343*
Shailesh A. Ghodke, Utkarsh Maheshwari, Suresh Gupta, Shirish H. Sonawane, and Bharat A. Bhanvase
12.1 Introduction 343
12.2 Major industry effluents 344
12.3 Parameters affecting adsorption 345
12.3.1 Contact time 346
12.3.2 Adsorbent dosage 346
12.3.3 Initial concentration 347
12.3.4 pH 347
12.3.5 Temperature 348
12.3.6 Ionic strength 348
12.3.7 Dissolved organic matters 349
12.4 Adsorbent characterization 349
12.4.1 Scanning electron microscopy (SEM) 350
12.4.2 Energy dispersive X-ray spectroscopy (EDS) 351
12.4.3 Transmission electron microscopy image 351
12.4.4 Fourier-transform infrared spectroscopy 352
12.4.5 Brunauer-Emmett-Teller (BET) surface area 352
12.4.6 X-ray powder diffraction 353
12.4.7 Thermogravimetric analysis 353
12.5 Adsorption mechanism 354
12.5.1 π-π interaction 355
12.5.2 Electrostatic interaction 355
12.5.3 Hydrophobic interaction 356
12.5.4 Hydrogen bonding 356
12.6 Challenges in adsorption 357
12.7 Conclusion and future prospective 357
References 358

This book belongs to Badji Mokhtar Annaba University Central Library
Copyright Elsevier 2025

Chapter 13: New graphene nanocomposites-based adsorbents *367*
Marzieh Badiei, Nilofar Asim, Masita Mohammad, Mohammad Alghoul, Nurul Asma Samsudin, M. Akhtaruzzaman, Nowshad Amin, and Kamaruzzaman Sopian
13.1 Introduction 367
13.2 Graphene 368
13.3 Graphene oxide 371
13.4 Reduced graphene oxide 373
13.5 Functionalization 374
13.5.1 Covalent interaction 375
13.5.2 Noncovalent interaction 376
13.6 Kinetic of adsorption 377
13.7 Graphene-based inorganic nanocomposites 378
13.7.1 Metal and metal-oxides graphene-based nanocomposites 378
13.7.2 Magnetic graphene-based nanocomposites 382
13.8 Graphene-based organic nanocomposites 389
13.8.1 Graphene-based organic polymer nanocomposites 389
13.8.2 Graphene-based nanocomposites with multidentate organic chelating ligands and complexion agents 395
13.9 Challenges and future prospective 397
References 398

Chapter 14: Role of zeolite adsorbent in water treatment *417*
Vesna Krstić
14.1 Introduction 417
14.2 The nature of the zeolite 419
14.2.1 Composition and structure 419
14.2.2 Characterization of zeolites 422
14.3 Sorption of metal cations on zeolites and ion exchange 425
14.3.1 Possible sorption and ion-exchange mechanisms 425
14.3.2 Factors affecting the sorption process 431
14.3.3 Principles of ion exchange on zeolites 432
14.3.4 Organic cation sorption on zeolites 433
14.4 Essential characteristics of zeolites and modification processes 434
14.4.1 Physicochemical properties of zeolites 434
14.4.2 Procedures for the modification of zeolites 436
14.5 Application of zeolites in water treatment 448
14.5.1 Removal of metal ions from different wastewaters 448
14.5.2 Removal of the ammonium ion from water 448
14.5.3 Removal of radioactive elements from wastewater from nuclear power plants 450
14.6 Regulation of water hardness 451
14.7 Zeolite regeneration 454
14.8 Discussion 457
14.8.1 Sorption of metal cations on natural and synthetic zeolites 457
14.8.2 Sorption of metal cations on natural and modified zeolites 463

This book belongs to Badji Mokhtar Annaba University Central Library
Copyright Elsevier 2025

14.8.3 Sorption of ammonium and other ions on natural and modified zeolites 466
14.9 Conclusions and future perspectives 468
Acknowledgments 470
References 470

Chapter 15: Metal-organic framework nanocomposite-based adsorbents 483

Sachin R. Shirsath and Bharat A. Bhanvase

15.1 Introduction 483
15.2 Properties of MOF 484
15.3 Types of MOF 485
15.4 Synthesis methods 486
15.5 Nanocomposite-based MOFs 488
15.6 Applications of nanocomposite-based MOFs 489
15.6.1 Application of nanocomposite-based MOFs in adsorption 489
15.6.2 Applications of nanocomposite-based MOFs in industry 505
15.7 Challenges for MOFs 505
15.7.1 Challenges and issues for MOF as adsorbent for treatment of wastewater 506
15.8 Conclusion 507
References 508

Chapter 16: Advanced nanocomposite ion exchange materials for water purification 513

Manishkumar D. Yadav

16.1 Introduction 513
16.2 Types of nanocomposite IEX material 514
16.3 Preparation of nanocomposite IEX material 515
16.3.1 Background 515
16.3.2 Nanomaterials used in IEX materials 515
16.3.3 Processing methods 517
16.4 Characterization 520
16.4.1 Fourier transform infrared spectroscopy 520
16.4.2 X-ray diffraction 521
16.4.3 Thermogravimetric analysis 522
16.4.4 Scanning electron microscope 522
16.5 Application of nanocomposite IEX materials for water purification 524
16.6 Scale-up conundrum 530
16.7 Conclusions 530
References 531

This book belongs to Badji Mokhtar Annaba University Central Library
Copyright Elsevier 2025

SECTION IV: Nanomaterials for membrane synthesis: Preparation and applications

Chapter 17: Nanomaterials for membrane synthesis: Introduction, mechanism, and challenges for wastewater treatment *537*

Shriram Sonawane, Parag Thakur, Shirish H. Sonawane, and Bharat A. Bhanvase

17.1 Introduction 538
17.2 Conventional membranes 538
17.2.1 Ceramic membranes 539
17.2.2 Polymeric membranes 539
17.3 Nanomaterial-based membranes 540
17.3.1 Inorganic nanoparticle-based membranes 540
17.3.2 Nanofiber-based membranes 541
17.3.3 Carbon-based membranes 541
17.4 Nanomaterial-based membrane synthesis techniques 541
17.4.1 Phase inversion method 542
17.4.2 Interfacial polymerization (IP) 543
17.4.3 Layer-by-layer (LBL) assembly 545
17.4.4 Stretching and sintering 545
17.4.5 Track etching and electrospinning 545
17.4.6 Three-dimensional printing (3D printing) 546
17.5 Challenges for wastewater treatment 546
17.5.1 Antifouling challenges 546
17.5.2 Antibacterial challenges 546
17.5.3 Toxicity potential 548
17.6 Conclusions 549
References 549

Chapter 18: Carbon-based nanocomposite membranes for water purification *555*

Swapnil L. Sonawane, Prakash K. Labhane, and Gunvant H. Sonawane

18.1 Introduction to nanomaterials 555
18.2 Carbon-based nanocomposite materials (CNCMs) (polymer/hybrid) 557
18.3 Development and synthesis of carbon-based nanocomposite material 558
18.3.1 Solution mixing 558
18.3.2 Chemical vapor deposition 559
18.3.3 In situ colloidal precipitation 560
18.3.4 Polymer grafting 560
18.3.5 In situ polymerization 561
18.3.6 Phase inversion 562
18.3.7 Spray-assisted layer-by-layer 563

This book belongs to Badji Mokhtar Annaba University Central Library

Copyright Elsevier 2025

18.4 Fabrications techniques and types of carbon-based nanocomposite membrane 563
18.4.1 Carbon nanotube (CNT) membranes 564
18.4.2 CNT-polymer composite (CNT mixed-matrix membranes) 564
18.5 Applications of carbon-based nanocomposite membrane for water purification 565
18.5.1 Removal of organic/inorganic pollutants 565
18.6 Conclusion 569
References 570

Chapter 19: Nanocomposite membranes for heavy metal removal 575
Saurabh P. Tembhare, Divya P. Barai, Bharat A. Bhanvase, and M.Y. Salunkhe
19.1 Introduction 575
19.2 Need of heavy metals removal 577
19.3 Role of nanomaterials in wastewater treatment 578
19.4 Role of nanomaterials in nanocomposite membranes 579
19.5 Nanomaterials used for heavy metals removal 583
19.6 Synthesis of nanocomposite membranes 585
19.6.1 Phase inversion method 586
19.6.2 Interfacial polymerization method 588
19.7 Membranes for removal of different heavy metals from wastewater 588
19.7.1 Lead 588
19.7.2 Cadmium 589
19.7.3 Chromium 591
19.7.4 Copper 591
19.7.5 Nickel 593
19.7.6 Arsenic 593
19.8 Comparison of nanocomposite membranes with conventional processes for heavy metal removal 593
19.9 Challenges in industries 594
19.10 Summary 596
References 596

Chapter 20: Polymer nanocomposite membranes for wastewater treatment 605
Rahul Sudhakar Zambare and Parag Ramesh Nemade
20.1 Introduction 608
20.1.1 Water scarcity 608
20.1.2 Wastewater and its contaminants 608
20.1.3 Membranes in wastewater treatment 612
20.2 Polymeric membranes 613
20.2.1 Polymers for membrane synthesis 613
20.2.2 Issue with polymeric membranes 615
20.2.3 Use of nanocomposite membranes as a solution 617
20.3 Mixed-matrix membranes 619
20.3.1 Hydrophilic and amphiphilic polymer (HP)-incorporated in mixed-matrix membrane 619

This book belongs to Badji Mokhtar Annaba University Central Library
Copyright Elsevier 2025

20.3.2 Inorganic nanomaterials (iNPs)-incorporated in mixed-matrix membrane ... 631
20.3.3 Metal-organic frameworks-incorporated mixed-matrix membrane ... 632
20.3.4 Carbon nanomaterials (CNs)-incorporated in mixed-matrix membrane ... 632
20.4 Thin-film nanocomposite membrane ... 640
20.4.1 Inorganic nanomaterials (iNPs)-incorporated thin-film composite membrane ... 641
20.4.2 Bioinspired materials-incorporated thin film composite membrane ... 642
20.4.3 Metal-organic frameworks-incorporated thin-film composite membrane ... 643
20.4.4 Carbon nanomaterials-incorporated thin-film composite membrane ... 644
20.4.5 Thin-film nanocomposite membrane with nanoparticles in substrate ... 647
20.4.6 Chlorine stability of polyamide thin-film nanocomposite membrane ... 648
20.5 Surface-located nanoparticle membranes ... 649
20.5.1 Nanoporous graphene sheets ... 650
20.5.2 Graphene oxide surface-located membrane ... 650
20.5.3 Inorganic nanomaterials (iNPs) surface-located membranes ... 652
20.5.4 Metal-organic frameworks/covalent organic frameworks surface-located membrane ... 653
20.6 Perspective ... 654
20.7 Conclusion ... 655
References ... 655

Chapter 21: Responsive membranes for wastewater treatment ... 673
Ramesh P. Birmod, Vikesh G. Lade, and Rakesh D. Shambharkar
21.1 Introduction ... 673
21.2 Types of membranes ... 675
21.2.1 Isotropic (symmetric) membranes ... 676
21.2.2 Asymmetric (anisotropic) membranes ... 676
21.3 Membrane materials ... 677
21.4 Design and fabrication of responsive membrane ... 678
21.4.1 Preparation and processing of responsive materials ... 678
21.4.2 Functionalization by incubation in liquid ... 679
21.4.3 Functionalization by incorporation of responsive groups in base membrane ... 679
21.4.4 Functionalization by surface modification ... 681
21.5 Classification of stimulation approach and application in water treatment ... 683
21.5.1 Thermoresponsive membrane ... 684
21.5.2 pH/chemical-responsive membranes ... 685
21.5.3 Ionic strength/electrolyte/salt responsiveness ... 688
21.5.4 Electroresponsive membranes ... 689
21.5.5 Magnetoresponsive membranes ... 691
21.5.6 Photoresponsive membranes ... 692

This book belongs to Badji Mokhtar Annaba University Central Library
Copyright Elsevier 2025

21.6 Characteristics of stimuli-responsive membrane 692
21.6.1 Flexibility 692
21.6.2 Surface modification 693
21.7 Industrial applications 693
21.8 Conclusion 694
References 694

Chapter 22: Nanomaterial-based photocatalytic membrane for organic pollutants removal 699
Gauri A. Kallawar and Bharat A. Bhanvase
22.1 Introduction 699
22.2 Photocatalytic membrane materials 700
22.2.1 Hybrid photocatalytic membrane 701
22.2.2 Porous photocatalytic membranes 702
22.2.3 Polymer-based photocatalytic membrane 702
22.2.4 Graphene-based photocatalytic membrane 703
22.2.5 Graphitic carbon nitride-based photocatalytic membrane 704
22.2.6 CNT-based photocatalytic membrane 705
22.3 Photocatalytic membrane fabrication 706
22.3.1 Sol-gel dip-coating 706
22.3.2 Vacuum filtration 708
22.3.3 Ultrasonication 709
22.3.4 Chemical vapor deposition and plasma-enhanced chemical vapor deposition 710
22.3.5 Phase inversion method 710
22.3.6 Immersion method 711
22.3.7 Spinning/electrospinning method 712
22.3.8 Solvent casting method 714
22.4 Applications of photocatalytic membrane for removal of organic pollutant 715
22.5 Types of photocatalytic membrane reactors and their configurations 717
22.6 Treatment of organic pollutants by photocatalytic membrane 722
22.7 Challenges of photocatalytic membrane-based processes 725
22.8 Scale-up of photocatalytic membrane-based processes 726
22.9 Conclusions and future perspectives 727
References 729

SECTION V: Industrial water remediation processes: Current trends and scale-up challenges

Chapter 23: Introduction of water remediation processes 741
Vikesh G. Lade
23.1 Introduction 741
23.2 Physical methods of wastewater remediation 743
23.2.1 Screens 744

This book belongs to Badji Mokhtar Annaba University Central Library
Copyright Elsevier 2025

23.2.2 Grit chambers ... 745
23.2.3 Aeration ... 745
23.2.4 Sedimentation (clarification) ... 746
23.2.5 Filtration ... 746
23.2.6 Distillation ... 747
23.3 Physicochemical water treatment processes ... 749
23.3.1 Precipitation and coagulation ... 749
23.3.2 Adsorption ... 750
23.4 Chemical remediation ... 751
23.4.1 Chemical disinfection ... 751
23.4.2 Neutralization ... 752
23.4.3 Ion exchange ... 753
23.5 Biological remediation/treatment ... 753
23.5.1 Suspended growth process ... 754
23.5.2 Attached growth (biofilm) processes ... 756
23.5.3 Combined processes ... 757
23.6 Advanced/novel water remediation processes ... 757
23.6.1 Membrane technology ... 758
23.6.2 Electrodialysis ... 762
23.6.3 Electrocoagulation ... 762
23.7 Advanced oxidation processes ... 762
23.7.1 Chemical AOPs ... 763
23.7.2 Photochemical advanced oxidation processes ... 764
23.7.3 Sonochemical advanced oxidation processes ... 767
23.7.4 Electrochemical advanced oxidation processes ... 768
23.8 Nanomaterial for wastewater remediation ... 769
23.8.1 Biogenic metal nanoparticles ... 769
23.9 Path forward ... 770
23.10 Conclusion ... 771
References ... 772

Chapter 24: Nanocomposite photocatalysts-based wastewater treatment ... 779

Ananya Dey and Parag R. Gogate

24.1 Introduction ... 779
24.2 Types of nanocomposites and their synthesis ... 780
24.3 Advanced oxidation processes for wastewater treatment ... 780
24.4 Governing mechanism of photocatalysis ... 781
24.5 Different nanocomposites used as photocatalysts for wastewater treatment ... 782
24.5.1 Metal-doped nanocomposites ... 783
24.5.2 Nonmetal-doped nanocomposites ... 783
24.5.3 Binary metal oxides ... 785
24.5.4 Metal sulfides ... 785
24.5.5 Polymer-based nanocomposites ... 787

This book belongs to Badji Mokhtar Annaba University Central Library
Copyright Elsevier 2025

24.5.6 Graphene-based nanocomposites 787
24.5.7 Clay-based nanocomposites 789
24.6 Factors affecting the wastewater treatment using photocatalysis 789
24.6.1 Synthesis of photocatalysts 789
24.6.2 Catalyst loading 790
24.6.3 pH of the solution 793
24.6.4 Characteristics of the nanocomposite photocatalysts 794
24.6.5 Reaction temperature 795
24.6.6 Concentration of pollutants 795
24.6.7 Effect of type of light and intensity 797
24.6.8 Irradiation time 798
24.7 Recent trends in types of photocatalytic reactors 798
24.7.1 Photocatalytic membrane reactors 798
24.7.2 Microreactors and microfluidic reactors 802
24.7.3 Hybrid photoreactors 803
24.8 Challenges 804
24.9 Conclusions 805
References 805

Chapter 25: Nanomaterial-based advanced oxidation processes for degradation of waste pollutants 811

Jaykumar B. Bhasarkar and Dharmendra Kumar Bal

25.1 Introduction 811
25.2 Advanced oxidation processes 812
25.2.1 Supercritical water oxidation 813
25.2.2 Photocatalysis 814
25.2.3 Metal oxide-containing nanoparticles 816
25.2.4 Carbon-based nanoparticles 817
25.2.5 Ceramics-based nanoparticles 818
25.2.6 Polymer nanoparticles 818
25.3 Individual AOPs involving nanomaterials 819
25.3.1 Degradation of organic pollutants using different nanomaterials as photocatalysts 819
25.4 Hybrid AOPs 821
25.4.1 Ultrasound-assisted photocatalytic degradation of organic pollutants 821
25.5 Nonphotochemical AOPs 824
25.5.1 Sonolysis 824
25.5.2 Ozonation 824
25.5.3 Fenton process 825
25.5.4 Persulfate oxidation process 825
25.6 Factors affecting on AOP performance 826
25.7 Conclusions, challenges, and future directions 828
References 829

This book belongs to Badji Mokhtar Annaba University Central Library
Copyright Elsevier 2025

Chapter 26: Electro-photocatalytic degradation processes for dye/colored wastewater treatment 833

Siddharth D. Parashar, Anjali A. Meshram, and Sharad M. Sontakke

26.1 Introduction 833
26.2 Mechanisms of electro-photocatalysis 835
26.3 Experimental assembly in electro-photocatalysis 836
26.4 Effect of reaction conditions 840
26.4.1 Effect of applied cell voltage 841
26.4.2 Effect of photoanodic materials 842
26.4.3 Effect of photon source and light intensity 842
26.5 Scope for future work 844
References 844

Chapter 27: Fenton with zero-valent iron nanoparticles (nZVI) processes: Role of nanomaterials 847

Prashant L. Suryawanshi, Prachi Upadhyay, Bhaskar Bethi, Vijayanand S. Moholkar, and Sankar Chakma

27.1 Introduction 847
27.2 Synthesis methods for zero-valent iron nanoparticles 850
27.2.1 Synthesis of nZVI using chemical methods 850
27.2.2 Sonochemical synthesis of nZVI 851
27.2.3 Biological synthesis of nZVI 852
27.3 Influences of process parameters on synthesis of nZVI 854
27.3.1 Effect of initial Fe^{3+} concentration for the ZVI particle size 854
27.3.2 Effect of chemical reducing agent on the ZVI particle size 855
27.3.3 Effect of stabilizer concentration on the ZVI particle size 856
27.3.4 Effect of temperature for controlling the particle size of nZVI 857
27.3.5 Influence of reaction pH on formation of nZVI and particle size 857
27.4 Reaction mechanism and catalytic activity of nZVI for treatment of wastewater 858
27.5 Catalytic activity of nZVI for wastewater treatment 861
27.6 Future perspective and new directions 862
References 862

Chapter 28: Nanocomposite adsorbent-based wastewater treatment processes: Special emphasis on surface-engineered iron oxide nanohybrids 867

Satish P. Mardikar, V.R. Doss, P.D. Jolhe, R.W. Gaikwad, and S.S. Barkade

28.1 Introduction 867
28.2 Different strategies for synthesis of iron oxide hybrid adsorbents 868
28.3 Surface-engineered magnetic nanohybrids 870
28.3.1 Iron oxide functional groups for heavy metal removal 870
28.3.2 Iron-bimetal oxide NPs for heavy metal removal 872

This book belongs to Badji Mokhtar Annaba University Central Library

Copyright Elsevier 2025

28.3.3 Iron oxide-metal oxide nanoparticles for heavy metal removal ... 877
28.3.4 Iron oxide-polymer for heavy metal removal ... 879
28.3.5 Iron oxide-carbon nanotubes for heavy metal removal ... 882
28.3.6 Iron oxide-graphene for heavy metal removal ... 882
28.3.7 Iron oxide-biomaterial-based nanoparticles for heavy metal removal ... 884
28.4 Current trends and scale-up challenges ... 889
28.5 Conclusions ... 890
References ... 890

Chapter 29: Preparation of novel adsorbent (marble hydroxyapatite) from waste marble slurry for ground water treatment to remove fluoride ... 899
Suja George, Dhiraj Mehta, and Virendra Kumar Saharan
29.1 Introduction ... 899
29.2 Materials and methods ... 901
29.2.1 Materials ... 901
29.2.2 Preparation of calcium nitrate using MWP ... 902
29.2.3 Synthesis of MA-Hap ... 902
29.2.4 Reaction scheme ... 904
29.2.5 Characterization of MA-Hap ... 904
29.2.6 Adsorption experiments ... 905
29.3 Results and discussion ... 906
29.3.1 Synthesis reaction and yield ... 906
29.3.2 Characterization of MA-Hap ... 906
29.3.3 Batch defluoridation studies ... 916
29.3.4 Adsorption equilibrium isotherms ... 919
29.3.5 Kinetics of adsorption ... 919
29.3.6 Water quality parameters and regeneration ... 920
29.3.7 Energy efficacy of the MA-Hap synthesis methods ... 922
29.3.8 Column studies using MA-Hap pellets ... 923
29.4 Conclusions ... 924
Appendix ... 925
References ... 926

Chapter 30: Nanocomposite/nanoparticle in membrane-based separation for water remediation: Case study ... 929
Fatemeh Bagri, Sedigheh Bazgir, and Yagoub Mansourpanah
30.1 Introduction ... 929
30.2 Nanostructures ... 930
30.2.1 Carbon nanomaterials ... 930
30.2.2 Metal organic frameworks ... 938
30.2.3 Zeolites ... 944
30.2.4 Metal oxides nanoparticles ... 946
30.3 Challenges and future prospects ... 948
References ... 949

This book belongs to Badji Mokhtar Annaba University Central Library
Copyright Elsevier 2025

Chapter 31: The process for the removal of micropollutants using nanomaterials *957*
M.V. Bagal and S. Raut-Jadhav
31.1 Introduction 957
31.2 Types of MPs 959
31.3 Various methods applied for the treatment of MPs 960
31.3.1 Conventional methods 960
31.3.2 Advanced methods using nanomaterials 961
31.4 Photocatalytic process using nanomaterials 962
31.4.1 Nanomaterials applied as a photocatalyst 962
31.4.2 Factors influencing the photocatalysis process 968
31.5 Adsorption process using nanomaterials 972
31.5.1 Nanomaterials applied as an adsorbent 972
31.5.2 Factors affecting on adsorption 975
31.5.3 Adsorption kinetics 978
31.5.4 Adsorption isotherm or adsorption equilibrium 979
31.6 Membrane separation process using nanomaterials 981
31.6.1 Nanofibrous membranes 981
31.6.2 Nanocomposite membranes 983
31.7 Reactors applied for the treatment of MP using nanomaterials 988
31.7.1 The annular reactor 988
31.7.2 Spinning disc reactor 988
31.7.3 Optical fiber photo reactor 989
31.7.4 Ultraviolet light emitting diode–based reactor 990
31.7.5 Membrane photoreactor/photocatalytic membrane reactors 990
31.7.6 Microreactors 992
31.8 Nanomaterials applied at large-scale operation and associated challenges 993
31.9 Conclusion and a way forward 995
References 996

Chapter 32: Antimicrobial activities of nanomaterials in wastewater treatment: A case study of graphene-based nanomaterials *1009*
Svetlana Jovanović
32.1 The structure and properties of graphene-based nanomaterials 1009
32.2 Mechanisms of antibacterial action of graphene nanomaterials 1012
32.2.1 Physical/mechanical destruction 1014
32.2.2 Oxidative stress 1016
32.2.3 Photothermal effect 1018
32.2.4 Other antibacterial effects 1018
32.3 Water treatment with graphene-based nanomaterials 1020
32.3.1 Filtration 1021
32.3.2 Adsorption 1022
32.3.3 Photocatalysis and electrode deposition/degradation 1022

This book belongs to Badji Mokhtar Annaba University Central Library
Copyright Elsevier 2025

32.4 Antimicrobial action of graphene-based nanomaterials in wastewater treatment, synthesis, efficiency, and perspective in an industrial application ... 1024
32.4.1 Cost analysis ... 1027
32.5 Conclusions ... 1028
Acknowledgment ... 1029
Dedication ... 1029
References ... 1029

Chapter 33: Potential of nano biosurfactants as an ecofriendly green technology for bioremediation ... 1039
Mousumi Debnath, Neha Chauhan, Priyanka Sharma, and Indu Tomar
33.1 Introduction ... 1039
33.2 Use of biosurfactants as potential bioremediators ... 1040
33.2.1 Biosurfactants as the molecule for present and future applications ... 1040
33.2.2 Microorganisms producing biosurfactants ... 1040
33.2.3 Diverse habitats of biosurfactants ... 1042
33.2.4 Mechanism of action of the biosurfactant ... 1043
33.3 Recent trends for using nanoscale material as agents for bioremediation ... 1046
33.4 Nano biosurfactants as source of bioremediation ... 1048
33.5 Conclusions and future perspective ... 1050
References ... 1051

Chapter 34: Potential risk and safety concerns of industrial nanomaterials in environmental management ... 1057
Saurabh Joglekar and Renuka Gajaralwar
34.1 Introduction ... 1057
34.2 Health risk ... 1059
34.2.1 Ingestion ... 1059
34.2.2 Dermal ... 1059
34.2.3 Inhalation ... 1060
34.3 Toxicological impact ... 1061
34.3.1 Chemical composition ... 1061
34.3.2 Particle size ... 1062
34.3.3 Surface area and reactivity ... 1062
34.3.4 Surface treatments on particles, particularly for engineered nanoparticulates ... 1063
34.3.5 Degree of agglomeration ... 1063
34.3.6 Particle shape and/or electrostatic attraction potential ... 1063
34.4 Environmental impact ... 1064
34.4.1 Release during manufacturing ... 1064
34.4.2 Release in use ... 1065
34.4.3 Release in disposal ... 1065
34.5 Risk and safety associated for using INMs ... 1066
34.5.1 Associated risks ... 1067

This book belongs to Badji Mokhtar Annaba University Central Library
Copyright Elsevier 2025

34.5.2 Food industry 1070
34.5.3 Agri-food industry 1071
34.5.4 Automobile industry 1071
34.5.5 Aerospace industry 1071
34.6 Design of an ideal nanomaterial 1072
34.7 Conclusion 1073
References 1073

Chapter 35: A novel SnO_2/polypyrrole/SnO_2 nanocomposite modified anode with improved performance in benthic microbial fuel cell 1081

Mohammad Imran, Alka Mungray, Suresh Kumar Kailasa, and Arvind Kumar Mungray

35.1 Introduction 1081
35.2 Experimental work 1083
35.2.1 Acid-treatment of the electrode surface 1083
35.2.2 SnO_2 nanoparticles synthesis 1083
35.2.3 Preparation of nanocomposites of SnO_2/PPy 1084
35.2.4 Preparation of modified anodes 1084
35.2.5 Construction of BMFC reactors 1085
35.2.6 Physical and electrochemical characterization 1085
35.3 Results and discussion 1086
35.3.1 Surface characterization of modified anode 1086
35.3.2 Electrochemical analyses of the composite anode 1089
35.3.3 Working of reactors containing different anodes 1092
35.4 Conclusion 1096
Acknowledgments 1096
Declarations of interest 1096
References 1096

Chapter 36: Visible light photocatalysis: Case study (process) 1101

Sandeep Kumar Lakhera and Bernaurdshaw Neppolian

36.1 Introduction 1101
36.2 Visible light photocatalytic processes for wastewater treatment 1102
36.2.1 Heterogeneous photocatalysis 1103
36.2.2 Homogenous photocatalysis 1106
36.2.3 Hybrid processes 1107
36.3 Current trends and scale-up challenges 1114
36.4 Conclusions 1119
Acknowledgments 1120
References 1120

Chapter 37: Nanomaterials for wastewater treatment: Concluding remarks 1125

Bharat A. Bhanvase, V.B. Pawade, Shirish H. Sonawane, and A.B. Pandit

37.1 Introduction 1125
37.2 Nanomaterials and their properties for wastewater treatment 1127
37.2.1 Zero-valent nanomaterials 1127
37.2.2 Metal oxide nanomaterials 1128

This book belongs to Badji Mokhtar Annaba University Central Library
Copyright Elsevier 2025

37.2.3 Luminescent and Ln^{3+}-doped oxide nanomaterials 1129
37.2.4 Nanozeolites 1130
37.2.5 Carbon/graphene-supported nanocomposites 1131
37.2.6 Metal organic frameworks nanocomposites 1132
37.2.7 Nanocomposite membranes/nanocomposite photocatalytic membranes 1133
37.3 Current status and challenges of use of nanomaterial-based processes 1134
37.3.1 Photocatalytic nanomaterials-based processes 1134
37.3.2 Adsorbent nanomaterials-based processes 1136
37.3.3 Nanocomposite membranes-based processes 1138
37.3.4 Nanomaterial-based photocatalytic membrane-based processes 1140
37.3.5 Nanomaterials-based advanced oxidation processes 1140
37.3.6 Nanomaterial-based electro-oxidation processes 1143
37.3.7 Nanomaterials-based processes for removal for micropollutants 1144
37.4 Challenges for nanomaterial-based processes, potential risk, and safety concerns 1146
37.5 Concluding remarks 1146
References 1147

Index 1159

This book belongs to Badji Mokhtar Annaba University Central Library
Copyright Elsevier 2025

Contributors

M. Akhtaruzzaman Solar Energy Research Institute, Universiti Kebangsaan Malaysia, Bangi, Selangor, Malaysia

Mohammad Alghoul Center of Research Excellences in Renewable Energy Research Institute, King Fahd University of Petroleum & Minerals, Dhahran, Saudi Arabia

Nowshad Amin Institutes of Sustainable Energy, Universiti Tenaga Nasional (@The National Energy University), Kajang, Selangor, Malaysia

Nilofar Asim Solar Energy Research Institute, Universiti Kebangsaan Malaysia, Bangi, Selangor, Malaysia

Shabnam Azad Chemical Engineering, Engineering Sciences and Technology Division, CSIR-NEIST, Jorhat, Assam, India

Tariq Aziz Chemical Engineering, Engineering Sciences and Technology Division, CSIR-NEIST, Jorhat, Assam, India

Marzieh Badiei Independent Researcher, Mashhad, Iran

M.V. Bagal Department of Chemical Engineering, Bharati Vidyapeeth College of Engineering, Navi Mumbai, India

Fatemeh Bagri Membrane Research Laboratory, Lorestan University, Khorramabad, Iran

Dharmendra Kumar Bal School of Chemical Engineering, Vellore Institute of Technology, Vellore, India

Sagar D. Balgude Department of Engineering Science, D. Y. Patil College of Engineering, Savitribai Phule Pune University, Pune, India

Divya P. Barai Chemical Engineering Department, Laxminarayan Institute of Technology, Rashtrasant Tukadoji Maharaj Nagpur University, Nagpur, Maharashtra, India

Swapnil Bargole Department of Chemical Engineering, Malaviya National Institute of Technology, Jaipur, India

S.S. Barkade Department of Chemical Engineering, Sinhgad College of Engineering, Pune, India

Sedigheh Bazgir Membrane Research Laboratory, Lorestan University, Khorramabad, Iran

Bhaskar Bethi Department of Chemical Engineering, B.V. Raju Institute of Technology, Narsapur, Medak, Telangana, India

Bharat A. Bhanvase Chemical Engineering Department, Laxminarayan Institute of Technology, Rashtrasant Tukadoji Maharaj Nagpur University, Nagpur, Maharashtra, India

Jaykumar B. Bhasarkar Department of Pulp and Paper Technology, Laxminarayan Institute of Technology, R.T.M. Nagpur University, Nagpur, Maharashtra, India

Akash P. Bhat Department of Civil and Environmental Engineering, University of Illinois at Urbana-Champaign, Urbana, IL, United States

This book belongs to Badji Mokhtar Annaba University Central Library

Copyright Elsevier 2025

Nikhil D. Bhavsar Chemical Engineering Department, Laxminarayan Institute of Technology, Rashtrasant Tukadoji Maharaj Nagpur University, Nagpur, Maharashtra, India

Rohidas Bhoi Department of Chemical Engineering, Malaviya National Institute of Technology, Jaipur, India

Ramesh P. Birmod Chemical Engineering Department, Laxminarayan Institute of Technology, Rashtrasant Tukadoji Maharaj Nagpur University, Nagpur, Maharashtra, India

Sankar Chakma Department of Chemical Engineering, Indian Institute of Science Education and Research Bhopal, Bhopal, Madhya Pradesh, India

Neha Chauhan Department of Biosciences and Biotechnology, Banasthali Vidyapith, Vanasthali, Rajasthan, India

Mousumi Debnath Department of Biosciences, Manipal University Jaipur, Jaipur, Rajasthan, India

Ananya Dey Chemical Engineering Department, Institute of Chemical Technology; NMIMS Mukesh Patel School of Technology Management & Engineering, Mumbai, India

S.J. Dhoble Department of Physics, R. T. M., Nagpur University, Nagpur, India

V.R. Doss Department of Engineering Sciences, Sinhgad College of Engineering, Pune, India

R.W. Gaikwad Department of Chemical Engineering, Pravara Rural Engineering College, Loni, India

Renuka Gajaralwar Chemical Engineering Department, Laxminarayan Institute of Technology, Rashtrasant Tukadoji Maharaj Nagpur University, Nagpur, Maharashtra, India

Suja George Department of Chemical Engineering, Malaviya National Institute of Technology, Jaipur, India

Shailesh A. Ghodke Department of Chemical Engineering, Dr. D. Y. Patil Institute of Engineering, Management and Research, Pune, Maharashtra, India

Parag R. Gogate Chemical Engineering Department, Institute of Chemical Technology, Mumbai, India

Suresh Gupta Department of Chemical Engineering, Birla Institute of Technology and Science, Pilani, Rajasthan, India

Chandrakant R. Holkar Chemical Engineering Department, Institute of Chemical Technology, Mumbai, India

Mohammad Imran Department of Chemical Engineering, Sardar Vallabhbhai National Institute of Technology, Surat, India

Ananda J. Jadhav Chemical Engineering Department, Institute of Chemical Technology, Mumbai, India

Saurabh Joglekar Chemical Engineering Department, Laxminarayan Institute of Technology, Rashtrasant Tukadoji Maharaj Nagpur University, Nagpur, Maharashtra, India

P.D. Jolhe Department of Biotechnology, Sinhgad College of Engineering, Pune, India

Dragana J. Jovanović Vinča Institute of Nuclear Sciences, National Institute of the Republic of Serbia, University of Belgrade, Belgrade, Serbia

Svetlana Jovanović "Vinča" Institute of Nuclear Sciences – National Institute of the Republic of Serbia, University of Belgrade, Belgrade, Serbia

Suresh Kumar Kailasa Department of Applied Chemistry, Sardar Vallabhbhai National Institute of Technology, Surat, India

This book belongs to Badji Mokhtar Annaba University Central Library

Copyright Elsevier 2025

Gauri A. Kallawar Chemical Engineering Department, Laxminarayan Institute of Technology, Rashtrasant Tukadoji Maharaj Nagpur University, Nagpur; University Department of Chemical Technology, Dr. Babasaheb Ambedkar Marathwada University, Aurangabad, Maharashtra, India

Jyoti Katiyar Department of Chemical Engineering, Malaviya National Institute of Technology, Jaipur, India

Vesna Krstić Mining and Metallurgy Institute Bor, Bor, Serbia; University of Belgrade, Technical Faculty Bor, Bor, Serbia

Prakash K. Labhane Department of Chemistry, MGSM's Arts, Science and Commerce College, Chopda, Maharashtra, India

Vikesh G. Lade Chemical Engineering Department, Laxminarayan Institute of Technology, Rashtrasant Tukadoji Maharaj Nagpur University, Nagpur, Maharashtra, India

Sandeep Kumar Lakhera Department of Physics and Nanotechnology, SRM Institute of Science and Technology, Kattankulathur, Chennai, Tamil Nadu, India

Utkarsh Maheshwari Department of Chemical Engineering, Dr. D. Y. Patil Institute of Engineering, Management and Research, Pune, Maharashtra, India

Prasad Mandade Bioenergy and Energy Planning Research Group, EPFL, Lausanne, Switzerland

Yagoub Mansourpanah Membrane Research Laboratory, Lorestan University, Khorramabad, Iran

Satish P. Mardikar Department of Chemistry, Smt. R S College, SGB Amravati University, Amravati, India

Dhiraj Mehta Department of Chemical Engineering, Malaviya National Institute of Technology, Jaipur, India

Anjali A. Meshram Department of Chemical Engineering, Birla Institute of Technology and Science, K. K. Birla Goa Campus, Goa, India

Masita Mohammad Solar Energy Research Institute, Universiti Kebangsaan Malaysia, Bangi, Selangor, Malaysia

Vijayanand S. Moholkar Department of Chemical Engineering, Indian Institute of Technology Guwahati, Guwahati, Assam, India

Alka Mungray Department of Chemical Engineering, Sardar Vallabhbhai National Institute of Technology, Surat, India

Arvind Kumar Mungray Department of Chemical Engineering, Sardar Vallabhbhai National Institute of Technology, Surat, India

Sidharth P. Nair Department of Materials Science, Central University of Tamil Nadu, Thiruvarur, India

Ashutosh Namdeo Chemical Engineering, Engineering Sciences and Technology Division, CSIR-NEIST, Jorhat, Assam, India

Amol Nande Guru Nanak College of Science, Ballarpur, Chandrapur, India

Renu Nayar D. P. Vipra College, Bilaspur, India

Parag Ramesh Nemade Department of Chemical Engineering; Department of Oleochemicals and Surfactants Technology, Institute of Chemical Technology, Mumbai; Institute of Chemical Technology, Marathwada Campus, Jalna, India

Bernaurdshaw Neppolian SRM Research Institute, SRM Institute of Science and Technology, Kattankulathur, Chennai, Tamil Nadu, India

This book belongs to Badji Mokhtar Annaba University Central Library

Copyright Elsevier 2025

Sharadwata Pan School of Life Sciences Weihenstephan, Technical University of Munich, Freising, Germany

A.B. Pandit Department of Chemical Engineering, Institute of Chemical Technology, Mumbai, India

Siddharth D. Parashar Department of Chemical Engineering, Birla Institute of Technology and Science, K. K. Birla Goa Campus, Goa, India

V.B. Pawade Department of Applied Physics, Laxminarayan Institute of Technology, Rashtrasant Tukadoji Maharaj Nagpur University, Nagpur, MS, India

Dipak V. Pinjari National Centre for Nanosciences and Nanotechnology, University of Mumbai, Kalina Campus, Mumbai, India

Swati Raut Department of Physics, R. T. M., Nagpur University, Nagpur, India

S. Raut-Jadhav Department of Chemical Engineering, Bharati Vidyapeeth (Deemed to be University) College of Engineering, Pune, India

Virendra Kumar Saharan Department of Chemical Engineering, Malaviya National Institute of Technology, Jaipur, India

M.Y. Salunkhe Department of Physics, Institute of Science, Nagpur, Maharashtra, India

Nurul Asma Samsudin Institutes of Sustainable Energy, Universiti Tenaga Nasional (@The National Energy University), Kajang, Selangor, Malaysia

Rakesh D. Shambharkar Department of Civil Engineering, Dr. Babasaheb Ambedkar College of Engineering and Research, Rashtrasant Tukadoji Maharaj Nagpur University, Nagpur, Maharashtra, India

Priyanka Sharma Department of Biosciences, Manipal University Jaipur, Jaipur, Rajasthan, India

Sachin R. Shirsath Department of Chemical Engineering, Sinhgad College of Engineering, Pune, Maharashtra, India

Gunvant H. Sonawane Chemistry Research Laboratory, Kisan Arts Commerce and Science College, Parola, Maharashtra, India

Shirish H. Sonawane Department of Chemical Engineering, National Institute of Technology, Warangal, Telangana, India

Shriram Sonawane Department of Chemical Engineering, Visvesvaraya National Institute of Technology, Nagpur, Maharashtra, India

Swapnil L. Sonawane Department of Chemistry, JET's Zulal Bhilajirao Patil College, Dhule, Maharashtra, India

Sharad M. Sontakke Department of Chemical Engineering, Birla Institute of Technology and Science, K. K. Birla Goa Campus, Goa, India

Kamaruzzaman Sopian Solar Energy Research Institute, Universiti Kebangsaan Malaysia, Bangi, Selangor, Malaysia

Prashant L. Suryawanshi Department of Chemical Engineering, Indian Institute of Science Education and Research Bhopal, Bhopal, Madhya Pradesh, India

Saurabh P. Tembhare Chemical Engineering Department, Laxminarayan Institute of Technology, Rashtrasant Tukadoji Maharaj Nagpur University, Nagpur, Maharashtra, India

Parag Thakur Department of Chemical Engineering, Visvesvaraya National Institute of Technology, Nagpur, Maharashtra, India

This book belongs to Badji Mokhtar Annaba University Central Library

Copyright Elsevier 2025

Ashish Tiwari Dr. Bhimrao Ambedkar Government College, Pamgarh, India

Indu Tomar Department of Biosciences, Manipal University Jaipur, Jaipur, Rajasthan, India

Ashish P. Unnarkat Chemical Engineering Department, School of Technology, Pandit Deendayal Petroleum University, Raisan, Gandhinagar, Gujarat, India

Prachi Upadhyay Department of Chemical Engineering, Indian Institute of Science Education and Research Bhopal, Bhopal, Madhya Pradesh, India

Jitendra Singh Verma Chemical Engineering, Engineering Sciences and Technology Division, CSIR-NEIST, Jorhat, Assam, India

Manishkumar D. Yadav Department of Chemical Engineering, Institute of Chemical Technology, Mumbai, India

Rahul Sudhakar Zambare National University of Singapore, Singapore, Singapore

This book belongs to Badji Mokhtar Annaba University Central Library

Copyright Elsevier 2025

This page intentionally left blank

This book belongs to Badji Mokhtar Annaba University Central Library

Copyright Elsevier 2025

Preface

The deterioration of water quality and scarcity of potable water are persistent challenges faced globally. To respond to the issue of water scarcity, the removal of toxic organic and inorganic pollutants from water bodies and using wastewater as a secondary water source are essential to have clean water for all people and society. Furthermore, enhancing the water quality elicits social and economic support, both in developed and developing countries. Suitable water purification methodologies should be cost-effective and environmental friendly, with benefits both for industrial development and human progress.

Nanotechnology exhibits great potential to improve current water and wastewater treatment processes. Environmental nanotechnology has attracted increased attention in the past two decades. In the field of wastewater treatment, the use of nanomaterial has great potential in improving these processes. The synthesis methods and resulting physiochemical properties of various free nanomaterials, including carbon (CNT/graphene)-based nanomaterial, metal and metal oxide nanoparticles and nanocomposites, as well as noble metal nanoparticles and their performance mechanisms for the removal of various pollutants need to be collated, summarized, and presented in a comprehensive manner for the benefit of research scholars, faculties, and industries. Furthermore, for large-scale applications of wastewater treatment, nanomaterials face some inherent technical bottlenecks, such as aggregation, difficulty in subsequent separation, leakage into contact water, as well as its potential adverse effects on the ecosystem and human health. Hence, in "Handbook of Nanomaterials for Wastewater Treatment: Fundamentals and Scale-up Issues," chapters on the use of nanomaterials, their photocatalytic nanocomposites, their use as adsorbents for wastewater remediation processes, and their current status and challenges for large-scale usage have been incorporated, which provide a wide opportunity for readers working in the area of wastewater treatment to acquaint themselves.

This book will provide fundamental insights on the synthesis and use of nanomaterials for wastewater treatment, application of nanomaterials as effective catalysts and adsorbents, and their current status in the water treatment processes, along with challenges to be overcome are discussed. This book provides in-depth knowledge about the properties and applications of new advanced nanomaterials for wastewater treatment processes. The content will be useful for students, researchers, academicians, industrialists, etc. to solve some basic and complex

This book belongs to Badji Mokhtar Annaba University Central Library Copyright Elsevier 2025

problems related to the use of nanomaterials for the development of wastewater treatment processes and technologies. This book also:

- Explains the properties of the most commonly used nanomaterials in wastewater treatment.
- Describes the major nanoscale materials, their synthesis, and their application techniques for wastewater treatment.
- Assesses the major technological challenges of using such nanomaterials on an industrial scale in wastewater treatment.

This book includes five sections, namely (I) Introduction to Nanomaterials for Wastewater Treatment: Fundamentals; (II) Photocatalytic Nanocomposite Materials: Preparation and Applications; (III) Adsorbent Nanomaterials: Preparation and Applications; (IV) Nanomaterials for Membrane Synthesis: Preparation and Applications; and (V) Industrial Water Remediation Processes: Current Trends and Scale-up Challenges. This book has been categorized into 37 chapters in these sections. In Section I (Chapters 1–4), we have added fundamentals of the nanomaterials suitable for wastewater treatment with somewhat less emphasis as some of the topics are covered in previously published monographs. However, Section II (Chapters 5–11) gives very elaborate insights into novel and advanced nanocomposite materials like mixed metal oxides, doped metal oxides, graphene-based nanocomposites, and magnetic nanocomposite materials in photocatalysis and water splitting. In Section III (Chapters 12–16), we have included some insights on the new adsorbent nanomaterials for wastewater treatment applications. Furthermore, in Section IV (Chapters 17–22), details about nanomaterials used in composite membrane synthesis are included. In this section, various novel nanocomposite materials are considered for various membrane applications like nanofiltration, ultrafiltration, microfiltration, etc. along with their specific roles. Finally, in Section V (Chapters 23–37), details about water remediation processes are discussed. In this section, the role of nanomaterials is discussed and elaborated for various water remediation applications like photocatalyst-based wastewater treatment processes, nanomaterial-based advanced oxidation processes, electro-oxidation processes, nanocomposite adsorbent-based wastewater treatment processes, nanocomposite/nanoparticle in membrane-based separation, and purification processes for the removal of micropollutants using nanomaterials. In this section, current trends in these processes and challenges faced by researchers and industries for their commercialization and industrial implementation are described.

Furthermore, this book is also useful for students working in interdisciplinary areas like Renewable Energy Sources, Chemical Engineering & Technology, Environmental Engineering, Physics, Chemistry, Materials Science, Renewable and Sustainable Resources, and Environmental Science and Technology. This book will be also useful for the faculty and researchers of academic and research institutes working in these areas.

This book belongs to Badji Mokhtar Annaba University Central Library

Copyright Elsevier 2025

Bharat A. Bhanvase, Editor
Department of Chemical Engineering, Laxminarayan Institute of Technology,
Rashtrasant Tukadoji Maharaj Nagpur University, Nagpur, Maharashtra, India

Shirish H. Sonawane, Editor
Chemical Engineering Department, National Institute of Technology,
Warangal, Telangana, India

Vijay B. Pawade, Editor
Department of Applied-Physics, Laxminarayan Institute of Technology,
Rashtrasant Tukadoji Maharaj Nagpur University, Nagpur, Maharashtra, India

Aniruddha B. Pandit, Editor
Chemical Engineering Department, Institute of Chemical Technology,
Mumbai, Maharashtra, India

This book belongs to Badji Mokhtar Annaba University Central Library
Copyright Elsevier 2025

This page intentionally left blank

This book belongs to Badji Mokhtar Annaba University Central Library

Copyright Elsevier 2025

SECTION I

Introduction to nanomaterials for wastewater treatment: Fundamentals

This book belongs to Badji Mokhtar Annaba University Central Library

Copyright Elsevier 2025

This page intentionally left blank

This book belongs to Badji Mokhtar Annaba University Central Library

Copyright Elsevier 2025

CHAPTER 1

Introduction to nanomaterials for wastewater treatment

Bhaskar Bethi[a], Shirish H. Sonawane[b], Bharat A. Bhanvase[c], and Jaykumar B. Bhasarkar[d]

[a]Department of Chemical Engineering, B.V. Raju Institute of Technology, Narsapur, Medak, Telangana, India, [b]Department of Chemical Engineering, National Institute of Technology, Warangal, Telangana, India, [c]Chemical Engineering Department, Laxminarayan Institute of Technology, Rashtrasant Tukadoji Maharaj Nagpur University, Nagpur, Maharashtra, India, [d]Department of Pulp and Paper Technology, Laxminarayan Institute of Technology, R.T.M. Nagpur University, Nagpur, Maharashtra, India

1.1 Introduction

Production of clean water is crucial not only for human use but also for various purposes such as industrial, medical, etc. Water is one of the critical resources for various industries such as medical, pharmaceutical, food processing units, and various chemical industries. Due to urbanization and industrialization, a large quantity of wastewater has been released. Wastewater has many toxic and recalcitrant pollutants that may lead to environmental damage. Wastewater contaminants may include organic, inorganic, and biological pollutants. Some contaminants are toxic and hazardous in nature. Some heavy metals with high toxicity are also observed in wastewater effluent. Among these heavy metals, arsenic is one of the extreme elements, well known for a long time. Other heavy metals present in wastewater effluent with high toxicity are cadmium, chromium, mercury, lead, zinc, nickel, copper, and so on; they each have serious toxicities. Wastewater treatment techniques can be broadly divided into two categories, namely physical and chemical methods. The physical method is comprised of screening, sedimentation, gravity separation, desalination, distillation, evaporation, membrane, irradiation with UV and ultrasound, boiling, and condensation, etc. However, chemical methods include oxidation, chlorination, coagulation, and flocculation, etc. All of these methods can be combined on the basis of wastewater characteristics. However, these methods have some limitation on wastewater treatment such as not 100% efficient to remove all recalcitrant pollutants, higher operating costs, and reuse of costly chemicals. To overcome these issues, nanomaterial-embedded methods play a vital role in the treatment of wastewater.

Handbook of Nanomaterials for Wastewater Treatment. https://doi.org/10.1016/B978-0-12-821496-1.00012-X
Copyright © 2021 Elsevier Inc. All rights reserved.

This book belongs to Badji Mokhtar Annaba University Central Library Copyright Elsevier 2025

Nanomaterial-embedded methods have the capability to remove all types of recalcitrant pollutants in an efficient way with a high performance. Also, it is modular and multifunctional in nature for wastewater treatment. Various types of nanomaterials could be efficiently utilized for proper remediation of wastewater. A detailed discussion of these nanomaterial-embedded processes is given in subsequent sections. Several different nanotechnology-embedded mechanisms for wastewater treatment have been established in recent years. The most commonly and commercially used techniques are as follows [1–4]:

(1) Adsorption-based processes
(2) Photocatalytic-based processes
(3) Sensing and monitoring technology
(4) Membrane-based process
(5) Antimicrobial nanomaterials-based technology

In subsequent sections of the chapter, we have demonstrated the various features of these processes of wastewater treatment. In this chapter, we have also introduced a brief symposium on the current and future challenges in the way of practical usages of these processes.

1.1.1 Catalyst for organic component degradation: Nanocatalyst

Catalytic oxidation or photocatalysis is an innovative method for removing trace pollutants and microbial waterborne pathogens from contaminated water. This is an effective approach of pretreatment to increase the biodegradability of dangerous and nonbiodegradable pollutants [5]. Photocatalysis may also be used as a polishing step for treating organic recalcitrant compounds [6]. High ratio of surface area-to-volume of nanocatalysts displayed substantially improved catalysis efficiency over their voluminous counterparts. In addition, the nanosized semiconductor bandgap and crystalline structure demonstrated size-dependent behavior. Their capacity for redox electron-hole and distribution of photogenerated charges varied with different sizes [7].

1.1.2 Photocatalytic effect due to nanoscale: Bandgap

The sufficient bandgap energy of TiO_2 (3.2 eV) needs ultraviolet excitation to promote separation of charges within the catalyst. As presented in Fig. 1.1, TiO_2 could generate reactive species after UV irradiation, which may degrade pollutants entirely in a short time of reaction. Bandgap increases with the decrease of particle size due to nanoscale electron confinement, the so-called "quantum size effect." There are some drawbacks to nanoparticles too. As previously mentioned, due to the wide bandgap energy of TiO_2, UV irradiation is required, and the photocatalytic properties of nanoparticles are almost unremarkable under visible light. Therefore, experiments to boost the photocatalytic properties of nanoparticles under visible light and UV have been performed. Metal doping has been identified to lead the visible light

This book belongs to Badji Mokhtar Annaba University Central Library Copyright Elsevier 2025

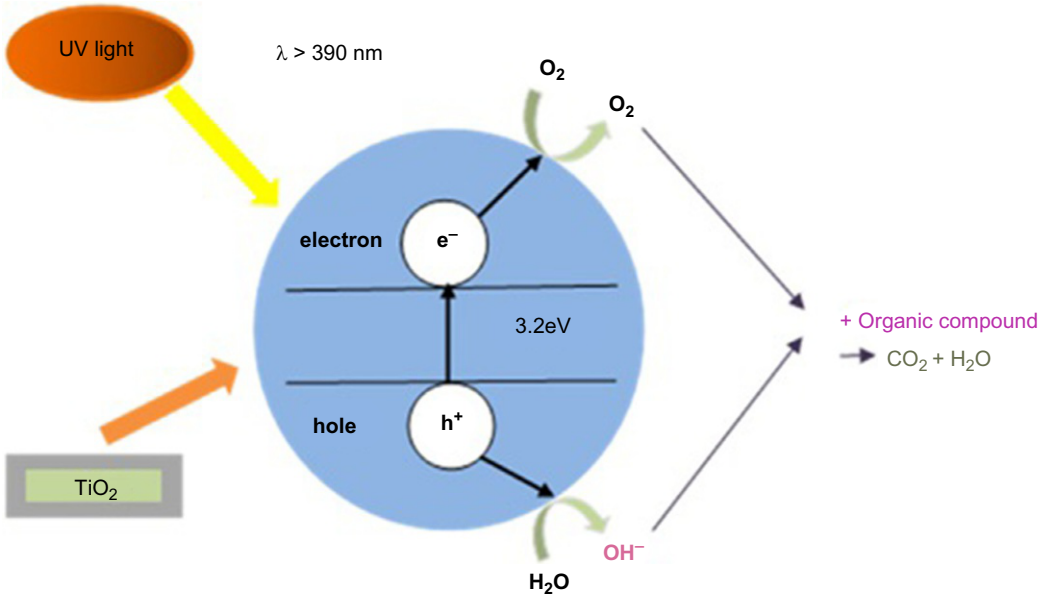

Fig. 1.1
Schematic visualization of the photocatalytic cycle mechanism on TiO_2. *Reprinted from with permission from B. Bethi, S.H. Sonawane, B.A. Bhanvase, S. Gumfekar, Nanomaterials based advanced oxidation processes for waste water treatment—a review, Chem. Eng. Process. 109 (2016) 178–189, Copyright © 2020.*

absorbance of TiO_2 nanoparticles and therefore enhance their photocatalytic activity in the presence of UV irradiation [8].

1.1.3 Disinfection using nanomaterials

Disinfection could be the final step but a crucial stage in treatment of water to prevent the spread of waterborne disease. The perfect disinfectant must possess the following assets:

(i) Wide spectra of antimicrobial in a limited period.
(ii) No noxious by-product generation.
(iii) Nontoxic to the habitats and health.
(iv) Small energy costs and ease of use.
(v) Simple to retain and also not corrosive in nature.
(vi) Safe disposal.

A variety of nanomaterials containing potent antimicrobial properties have been recently demonstrated, including chitosan nanoparticles [9], nanosilver (nAg) [10], photocatalytic TiO_2 [11], and carbon-based nanomaterials [12]. These nanomaterials kill microorganisms by producing toxins (e.g., Ag+). By close contact, it may break down the cell membrane or by

This book belongs to Badji Mokhtar Annaba University Central Library Copyright Elsevier 2025

generation of highly reactive oxygen species, respectively. Such antimicrobial nanomaterials, unlike traditional chemical disinfectants, have inactivated microorganisms through more natural methods intended to reduce the production of harmful by-products of disinfection [13].

1.1.4 Nanomaterials for sensing

Nowadays, conventional methods of sensing and monitoring are unable to detect extremely low micropollutant concentrations in complex water bodies. In urgent cases (e.g., accidents involving water), the immediate and on-site identification of contaminants and highly toxic substances is extremely essential. Nanomaterials like quantum dots, nanotubes of carbon, graphene, and rare metals such as Au or Ag exhibit some special properties such as electrochemical, electrical, or magnetic. These nanomaterials could be inserted into the detector or electrode materials to deliberately preconcentrate trace contaminants for identification. Any nanomaterials can increase the spectroscopic reaction by several magnitudes (e.g., Raman change or surface plasmon resonances) [14, 15]. A new generation of sensors based on nanocomposites has also been extensively researched for ecosystem tracking and detecting their ability toward pollutants [16].

1.2 Nanomaterials as adsorbents for wastewater treatment

1.2.1 Carbon nanotubes (CNTs)

Carbon nanotubes (CNTs) have been identified as one of the allotropes of carbon compound, and these might be chosen as structures of several carbon products. The shape of CNTs are essentially made of a cylindrical-like structure. Generally, CNTs are categorized in two main types: (1) single-walled CNTs (SWCNTs) and (2) multiwalled CNTs (MWCNTs); however, CNTs exist in the form of a circular shape crumpled in a tubular-like construction. The SWCNTs come in the form of single-walled with rolled graphene sheets. MWCNTs consist of multiple rolled graphene sheets. Schematic of the SWCNT and MWCNT structures is depicted in Fig. 1.2.

Due to the high ratio of surface-to-volume and regulated spread of the pore size, CNTs offer excellent adsorption ability and high sorption efficiency relative to traditional finer grained powder such as activated carbon (AC) with inherent constraints such as active surface area locations and sorption-activating capability. Numerous researches have shown that CNT's capability for adsorption relies on either functional group surface or adsorbent structure.

Joseph et al. [17] produced SWCNTs for the degradation of bisphenol A (BPA) and 17α-ethinyl estradiol (EE2) compounds from aqueous media. SWCNTs display the EE2 (95%–98%) and BPA (75%–80%) removal levels. Hu et al. [18] established the modification of MWCNTs adhering to the bar as a composite-coated stir bar to prepare polyaniline/hydroxyl MWCNTs

This book belongs to Badji Mokhtar Annaba University Central Library Copyright Elsevier 2025

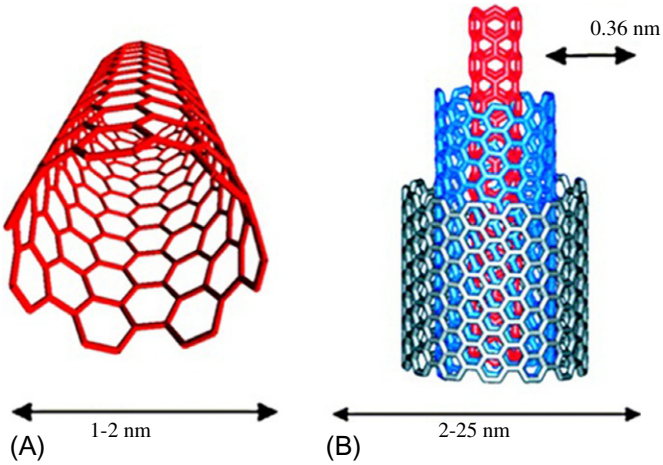

Fig. 1.2
Schematic diagram of SWCNTs (A) and MWCNTs (B). *Reprinted with permission from K. Zare, V.K. Gupta, O. Moradi, A.S.H. Makhlouf, M. Sillanpää, M.N. Nadagouda, H. Sadegh, R. Shahryari-ghoshekandi, A. Pal, Z.-J. Wang, A comparative study on the basis of adsorption capacity between CNTs and activated carbon as adsorbents for removal of noxious synthetic dyes: a review, J. Nanostruct. Chem. 5 (2015) 227–236, Copyright © 2020.*

(PANi/MWCNTs-OH) for the adsorption of phenols, antisteroidal no-inflammatory drug compounds, and polychlorinated biphenyls. These updated MWCNTs showed the ability to eliminate target components approximately 80%–99%. For two pharmaceutical products (diclofenac sodium and carbamazepine), Wei et al. [19] produced a new fine grain CNTs/Al_2O_3 composite with strong mechanical stability, hydrophilicity, heat tolerance property, and efficient sorbent. In the process of regeneration, the adsorbed pharmaceuticals may be decomposed. This process of hybridization influenced the creation of granular composites based on the CNTs.

1.2.2 Graphene nanomaterials

Another allotropy form of carbon is graphene. Graphene is a single graphite structure carbon layer (IUPAC) that presents an organized network structure of the honeycomb. It also exhibits excellent properties such as electrical and thermal conductivity. The use of graphene and graphene-based nanomaterials (Fig. 1.3) for rehabilitating the environment has been increasing exponentially since the last decade due to their unique properties. There seems to be an option to decide on whether graphene would be utilized as a carbon-based nanocomposite considering the quality, process capacity, and environmental implications of the material. Graphene is a CNT alternative and a suitable water treatment tool. Graphene oxide (GO) and reduced graphene oxide (RGO)-adjusted products have been thoroughly investigated for their own fitness to eliminate toxic compounds, such as Hg (II), As (III/V), etc. Wang et al. [20] have

This book belongs to Badji Mokhtar Annaba University Central Library Copyright Elsevier 2025

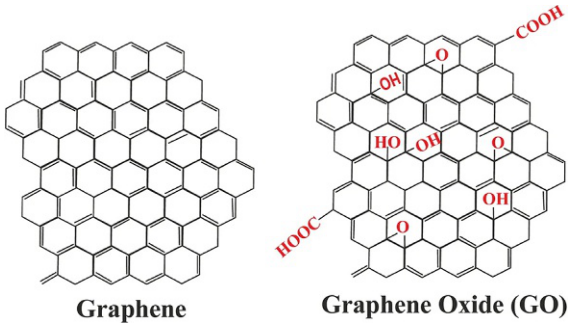

Fig. 1.3
Schematics diagram of graphene (A) and graphene oxide (B). *Reprinted with permission from S. Priyadarsini, S. Mohanty, S. Mukherjee, S. Basu, M. Mishra, Graphene and graphene oxide as nanomaterials for medicine and biology application, J. Nanostruct. Chem. 8 (2018) 123–137, Copyright 2018.*

studied the effect of various parameters such as pH, adsorbent dosage, and contact time on GO sorption capacity. The obtained results showed that Zn (II) tended to adsorb onto GO of about 246 mg/g with minimal equilibrium time and optimal pH 7. The effectively removal of As (V), As (III), and Pb (II) from polluted water may be achieved by unilayer GO compositions of manganese ferrite magnetic nanoparticles. The maximum adsorption capacity was obtained as 207, 673, and 146 mg/g for As (V), Pb (II), and As (III), respectively [21].

1.2.3 Metal and metal oxides

Sorption of contaminates from wastewater using nanoparticles has gained attention as an attractive separation media. Generally, the two important properties that resulted from nanoscale size, such as large ratio of surface area-to-volume than the bulk particles and chemical functionality of nanoparticles, improved the adsorption capacity as well as having higher affinity toward pollutant removal. Various studies on wastewater treatment have shown that the application of nanosorbents significantly affects the separation of different pollutants from aqueous medium. Nano-zero-valent iron (nZVI) and CNTs, a nanoscale adsorbent synthesized through chemical vapor deposition technique, is an effective sorbent material for elimination of nitrate from aqueous solution. Besides this, due to the unique magnetic property of nZVI and CNTs, the recalcitrant pollutant present in the wastewater may be removed by means of a magnet after completion of the treatment process [22].

In recent days, the oxides of aluminum, iron, and titanium nanoparticles have shown keen interest in the adsorption studies of metal ions. Among all metal oxides, iron oxide nanoparticles have been affirmed for effective adsorption of metal ions due to its high surface areas and ease of synthesis [23]. The various forms of metal oxides (goethite, amorphous and crystalline form of ferric oxide) have been studied for the effective degradation of metal ions [23, 24]. Iron oxides have been mainly utilized for the adsorption of copper [23], arsenic [25], etc. Zero-valent iron nanoparticles have also appeared to be more effective for the adsorption of

This book belongs to Badji Mokhtar Annaba University Central Library Copyright Elsevier 2025

other metal ions such as arsenic, silver, cadmium, chromium, etc. [26, 27]. Alumina is effective for adsorption of different metal ions such as cadmium, copper, chromium, lead, and mercury metal ions, owing to its low cost and design approach. [28].

The metal-containing nanoparticles are primarily comprised of zero-valent iron and oxides of ferric, Al, Mn, Mg, and cerium among the available adsorbents [29]. Because of the greater surface area and high activity induced by the influence of distance quantization, several reports revealed that nanosized-based metals and metal oxides show desirable adsorption toward heavy metal pollutants. Li et al. [30] have identified that nZVI shows a higher adsorption capacity of 343 mg/g for removal of Cu (II). It was also concluded that Cu (II) is converted into copper or cuprite (Cu_2O) upon adsorption. The adsorption of various metal ions such as Pb (II), Cu (II), or Zn (II) on nanosized hematite metal oxide have been studied. The various parameters (initial concentration, pH, contact, and temperature) have also been optimized for the maximum adsorption of these ions [31]. The results of this study indicated that the 100% Pb and Zn adsorption was achieved at 0.5 g/L of hematite nanoparticles. Nanosized TiO_2 has also been widely used in removing micropollutants, like compounds that destroy endocrines, cyanotoxins, and antibiotics [32]. However, the maximum adsorption capacity of 387 and 714 mg/g was obtained for Cd (II) and Hg (II) ions, respectively [33]. Zhang et al. [34] suggested that nanosized Al_2O_3 is an efficient material for complete removal of Tl (III) from aqueous media at acidic pH of 4.5.

1.2.4 Magnetic nanoparticles

Nanosized magnetite is another significant magnetic adsorbent offering relatively cheap, easy processing, and eco-friendly materials. Magnetite nanomaterials were applied to extract numerous pollutants from aqueous solutions, namely hexavalent chromium Cr (VI) [35], and other metal ions such as As (III/V), Zn (II), Cu(II), and Se (IV) b [36], methylene blue (MB) [37], and dichlorophenol [38]. The sol-gel method is one of the effective methods for preparation of nanoparticles. Hu et al. [35] prepared a 10-nm size of magnetic nanoparticles with a surface area of 198 m^2/g using sol-gel process. Another study was carried out by Wei and co-workers [36] for degradation of Selenium (Se). The concentration of Se was reduced from 100 to <5 μg/L in the presence of magnetite nanoparticles. In the presence of specific anions, nanosized magnetite exhibited strong selectivity against Se and high separation efficiency at lower solution pH [36].

1.3 Metal oxide nanoparticles as photocatalyst

By replacing the microscale catalysts with nanosized photocatalysts, the efficiency of the photocatalysis processes was improved. Due to its high surface area and good crystalline mesoporous layer, the nanoscale mesostructured titanium oxide (m-TiO_2) exhibits better photocatalytic efficiency than the commercial photocatalyst P25 (Degusa). To extend the

This book belongs to Badji Mokhtar Annaba University Central Library Copyright Elsevier 2025

efficiency of TiO_2 nanoparticles, TiO_2 nanoparticles could be doped with sufficient metallic or nonmetallic transition compounds [39]. Such TiO_2 modification has significantly enhanced TiO_2 photocatalytic activity within solar spectrum and decreases the integration of photoinduced electron-hole pairs as well.

Nanoparticles of metal oxides, namely TiO_2, CeO_2, and ZnO, were commonly studied for organic pollutant removal from water and wastewater. Nanoparticles of metal oxide were identified as good photocatalysts for the treatment of water due to their higher specific surface area and stronger photolytic activities [40]. Nanoparticles of MgO and magnesium (Mg) may be utilized as gram-positive (*Escherichia coli*) and gram-negative bacteria (Bacillus subtillus) to destroy/adsorb biocides [41]. The usage of nanostructured electrodes based on TiO_2 and Cu_2O in the electrocatalytic oxidation process exhibited an effective degradation of pollutants and larger COD removal level was reported [42]. Good biocidal activity against the *E. coli* and *Staphylococcus aureus* was observed under silver-SiO_2 nanocomposite as an upper layer with cross-linked chitosan [43]. Minerals of ferrites and iron like acaganeite, hematite, feroxyhyte, goethite, maghemite, lepidocrocite, ferrihydrite, and magnetite were used for adsorption in wastewater treatment [44]. Iron (Fe) and TiO_2 seem to be strong adsorbents to extract metal contaminants from the source. Nanocomposite catalyst Pd/Fe_3O_4 was used as a dehalogenation medium in treating specific wastewater [45]. Nanocrystalline TiO_2 and ZnO have been usually employed as a active photocatalyst for the removal of recalcitrant pollutants from wastewater in the last two decades [46–52]. Generally, the TiO_2 photocatalyst consists of a broad bandgap (3.2 eV) and can be considered a semiconductor; it was one of the benefits relative to many other semiconductor photocatalysts, which corresponds to near-UV exposure. The TiO_2 surface becomes excited in the presence of UV irradiation, and therefore the electrons of TiO_2 become excited and produce sets of electrons and holes. The water molecules are trapped by positive holes and become oxidized to produce free OH radicals. Hydroxyl radical's development tends to be cyclic in nature and commences the sequence of reactions over the TiO_2 surface. The photocatalytic process requires both a catalyst and a light source to start the oxidation reaction between free radicals and pollutants. The possible use of sunlight to initiate the photocatalytic oxidation process has brought more attention to the creation of these catalysts where it is appropriate to cover the entire solar spectrum. The activation of TiO_2 catalyst under irradiation of visible light source for degradation of acid red 44 is described by Moon et al. [53]. They have recorded the behavior of pH on dye adsorption onto 30-nm TiO_2 powder. This confirms the important factor in dye-photosensitization for the dye's adsorption onto the surface of TiO_2. Under visible irradiated conditions, the variations in the photocatalytic activation process are proposed with that of UV-irradiated environment. The dye-sensitized catalyst was used for the degradation of phenol in the presence of UV irradiation. Parra et al. [54] have studied the photodegradation under white light illumination of a standard textile dye (blue azo dye) on TiO_2-CdO-ZnO nanoporous combined thin films. The results of this study indicated that a faster rate of degradation of dye solutions was observed at optimum condition of $pH = 3$, initial concentrations of 100 mg/L, $T = 85°C$, and $H_2O_2 = 400$ mg/L. The activity of photodegradation

This book belongs to Badji Mokhtar Annaba University Central Library Copyright Elsevier 2025

was also observed for nanoporous TiO_2 films, but the rate of the dye degradation was slightly lower compared with nanoporous films coupled with TiO_2/CdO-ZnO. The novel mechanism of sulfur-doped TiO_2 as a photocatalyst was proposed by Yu et al. [55]. This study clearly identified that the activity of this catalyst was more effective for the killing of bacteria. Hydroxyl radical's generation under visible light illumination contributes to the successful degradation of gram-positive bacterium (micrococcus lylae). Min et al. [56] reported high activity by in situ oxidation and easy separation of the nanoscale polyaniline/titanium dioxide photocatalyst (PAn/TiO_2). The photocatalytic behavior of PAn/TiO_2 nanocomposites for the removal of MB dye in aqueous media under artificial light illumination was investigated. MB on PAn/TiO_2 could be degraded more effectively than on pure TiO_2. Venkatachalam et al. [57] stated that pure TiO_2 nanoparticles consist of anatase and rutile forms together but Zr^{4+}-coupled TiO_2 only supported the anatase form. Zr^{4+}-doped TiO_2 bandgap value was found to be larger than nano-TiO_2. The photocatalytic activity of the Zr^{4+}-coupled TiO_2 for 4-chlorophenol degradation were determined as more than either nano-TiO_2 and commercial TiO_2 (Degussa P25). For the degradation experiments, variables including initial concentration of 4-chlorophenol, catalyst dosage, solution pH, and intensity of light illumination have been optimized for utmost efficiency. Joshi et al. [58] have demonstrated the removal of Cr (VI) from wastewater using the TiO_2, ZnO, and CdS photocatalytic nanomaterials. The chromium quantity was extracted using a UV light photocatalyst and at a specific pH range. Among those photocatalysts, TiO_2 exhibited the maximum potential for elimination of Cr (VI) at pH = 2.

1.4 Nanocomposites for wastewater treatment

1.4.1 Bionanocomposites

Polymers are specialized aids for nanomaterials, because they typically have flexible elastic shapes, an outstanding property for mechanical and functional groups that are chemically connected. Nanocomposites dependent on the polymer are potential items for their sound efficiency in the water purification application. Many polymeric host forms are mainly biopolymeric agents including chitosan and cellulose. These were abundant in natural world and fairly environmentally friendly. Biopolymers can experience a major long-term application issue because they are biodegradable [59]. Cellulose did show strong chemical stability and mechanical efficiency. Khan et al. [60] have embedded ZrO_2 into the cellulose matrix and acquired nanohybrid cellulose/ZrO_2 particles, about 50 nm in thickness. The nanohybrid displayed strong Ni^{2+} selectivity with the adsorption efficiency being 79 mg/g. The method of adsorption was largely monolayer on homogeneous adsorbent surfaces. Varaprasad et al. [61] synthesized a nanocomposite fiber by attaching ZnO nanoparticles through sodium alginate matrix to a solution containing cellulose fibers. It has been confirmed as a successful antibacterial product.

This book belongs to Badji Mokhtar Annaba University Central Library Copyright Elsevier 2025

Chitosan could be the second polysaccharide highly prevalent to all after cellulose [62]. Chitosan has excellent features like strong reactivity, outstanding conduct of chelation, and stability [62]. The amino and hydroxyl groups function as active sites for toxins from water prepared as robust CS-Ag NPs by dissolving the Ag NPs in a chitosan solution. This solution was further used to produce a cast film with strong storage stability and good mechanical handling capability. This shows that various metal ions were effectively isolated and removed from wastewater. Approximately 95% and 16% removal efficiency was observed for foremost and Mn (II), respectively [62, 63]. Ouyang et al. [64] synthesized spherical structure of chitosan-CNT composite by a freeze-casting method. In this method, the nanocomposite was immersed into a mixed solution with liquid nitrogen. The composite beads displayed open-porous hierarchical structure, and mesopores from the exposed CNTs demonstrated strong adsorption capacity to bilirubin (43.6 mg/g) within 2 h of contact time. Copper-coated chitosan nanocomposite (CuCH) was used by Jaiswal et al. [65] to extract malathion, an organophosphorous pesticide, from agricultural runoff. Theme full efficiency at an optimal pH of 2.0 exceeded 322.6 ± 3.5 mg/g. In addition, in another study, ZnS quantum dots/chitosan nanocomposite were synthesized, and these acted as a heterogeneous, high-performance photocatalyst [66]. The nanocomposite was synthesized by colloidal chemical method at room temperature. The results showed that MB and methyl orange (MO) dyes were effectively destroyed in 2 h of contact time. The schematics of the polymer nanocomposite is represented in Fig. 1.4.

1.4.2 Nanocomposites based on inorganic support

Nanocomposite inorganic supports are predominantly comprised of AC, CNTs, and natural minerals. The AC is a traditional adsorbent commonly used in sewage and wastewater treatment. AC is an extremely soluble adsorbent with ample micropores (specific surface area 100–2000 m^2/g) and hydrophobic surface that could act as an outstanding nanoparticular help [67]. Arcibar-Orozco et al. [68] immobilized iron oxyhydroxide nanoparticles through $FeCl_3$ hydrolysis with the addition of phosphate. The addition of phosphate could significantly reduce the size of loaded iron nanoparticles. The resulting nanocomposites of AC-iron displayed a 40% increase in the efficiency of As (V) adsorption.

The loading of nano-ZnO onto a granular AC helps to improve the ability to remove Pb (II) with an adsorption capacity of 76.7 mg/g [69]. The maximum adsorption of Pb (II) was obtained due to the development of hydroxyl groups on the surface of the oxide. AC magnetite-embedded nanocomposites (Fe_3O_4) demonstrated exceptional efficiency in the elimination of aromatic contaminants. The saturated adsorbent could be processed as a backwash agent utilizing ethanol [70]. In addition, a bimetallic nanoparticle impregnated with Fe/Pb AC was formed using $NaBH_4$ by reductive deposition technique. Immobilized nanoalloy of Fe/Pb was well distributed on the surface. Ninety percent of 2-chlorobiphenyl as-synthesized AC

This book belongs to Badji Mokhtar Annaba University Central Library Copyright Elsevier 2025

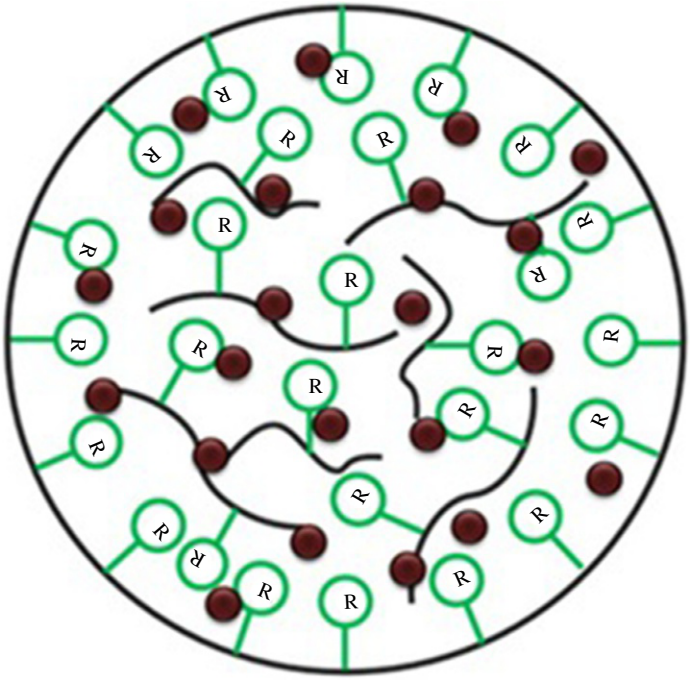

Fig. 1.4
Schematic presentation of polymer nanocomposite. *Reprinted with permission from Y. Zhang, B. Wu, H. Xu, H. Liu, M. Wang, Y. He, B. Pan. Nanomaterials-enabled water and wastewater treatment, Nano Impact 3–4 (2016) 22–39, Copyright © 2020.*

nanocomposite was reduced in 48 h, and 2-chlorobiphenyl residuals and dechlorination items were adsorbed simultaneously [71]. Shao et al. [72] investigated 4,4′-DCB adsorption utilizing methyl methacrylate-grafted MWCNTs (MMA). M-MWCNT–Fe3C nanocomposite (M-MWCNT-ICN) was used by Konicki et al. (2012) to extract red 23 from aqueous solution with a maximum capacity of 85.5 mg/g. Khatamian et al. [73] prepared nanocomposites ZnO/HZSM-5 for 4-nitrophenol (4-NPh) adsorption. They found that approximately 91% of 4-NPh (initially 20 mg/L) was extracted at pH = 5 within 90 min. Chong et al. [74] synthesized nanocomposites of TiO_2-zeolite for advanced industrial dyes application. The results indicated that the nanocomposite was pursuing an adsorption-oriented photocatalytic degradation, which is especially effective in extracting trace dye compounds.

Clay-based polymeric nanocomposites (CPNs) are a mixture of polymer and inorganic clay minerals that support organic as well as inorganic hosts. CPNs demonstrated dramatically improved mechanical and chemical resilience, heat resistance, high surface area, and decreased permeability to gas. The reduction of inorganic and organic micropollutants such as Co (II), Zn (II), Se (IV) and atrazine was commonly studied using numerous CPNs [75, 76]. Sepiolite-

This book belongs to Badji Mokhtar Annaba University Central Library Copyright Elsevier 2025

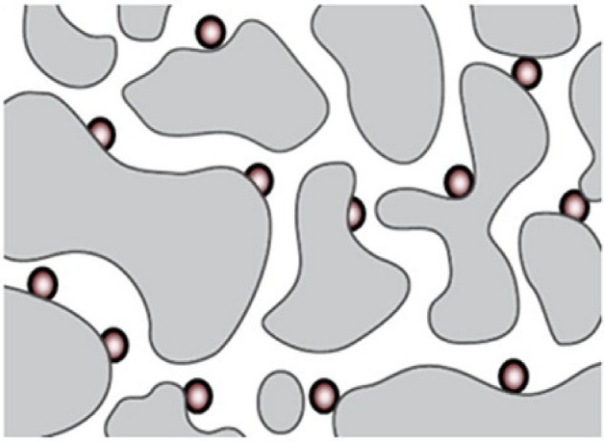

Fig. 1.5
Schematic presentation of activated carbon nanocomposite. *Reprinted with permission from Y. Zhang, B. Wu, H. Xu, H. Liu, M. Wang, Y. He, B. Pan. Nanomaterials-enabled water and wastewater treatment, Nano Impact 3–4 (2016) 22–39, Copyright © 2020.*

PDADMAC (polydialdiamethylammonium) CPNs were used for pretreatment of wastewater, resulting in a successful treatment of a 1610 mg/L TSS winery effluent by coagulflocculation in <2 min [77]. In fact, CPNs are safe resources for the elimination of toxins.

Schematic presentation of AC nanocomposite, which is an example of nanocomposites based on inorganic support, is given in Fig. 1.5.

1.4.3 Nanocomposite hydrogels

Apart from nanosorbents, nanoparticles-loaded polymer hydrogels have been shown as promising nanocomposite materials for the effective degradation of recalcitrant pollutants from wastewater. In the past decade, hydrogels have been successfully used for the removal of various dye molecules [78–80], as well as other inorganic and organic pollutants such as phenolic compounds [81], heavy metals [82], ammonia [83], and boron [84, 85] present in wastewater.

In recent years, researchers have meticulously modified polymer hydrogels with different nanoclays as fillers for improving the adsorption efficiency and mechanical stability of the hydrogels [86]. Over a decade, many polymers were modified with different nanoclays for enhancing the adsorption efficiency of various forms of nanocomposite hydrogels such as polyacrylamide (PAAm) with bentonite [86], montmorillonites [87], polyacrylic acid [88], and poly(N-isopropyl AAm) [89] with montmorillonites. The inexpensive and abundant availability of nanoclays are extensively used as a filler for the synthetization of various polymer nanocomposite hydrogels. The excellent physical, chemical, and mechanical

This book belongs to Badji Mokhtar Annaba University Central Library Copyright Elsevier 2025

properties of nanoclays made the nanocomposite hydrogels more effective than pure hydrogels [86].

Mittal et al. [90] have synthesized gum karaya and silica-grafted poly acrylic acid-*co*-acrylamide hybrid nanocomposite hydrogel. The synthesized nanocomposite hydrogel was studied for the adsorption of MB dye from an aqueous solution. The maximum adsorption capacity for nano-SiO_2-loaded hydrogel was found to be 1408.67 mg/g and therefore the extent of adsorption rate for MB dye solution. Li et al. [91] studied the adsorption of various dyes using laponite nanoclay-loaded polyacrylamide (PAAm) hydrogels. The synthesized nanocomposite hydrogel shows the adsorption of dyes in the order of BB 9 > BB 12 > BV 1. Rashidzadeh et al. [92] have employed the free radical polymerization method for the preparation of acrylic acid-*co*-acryl amide/clinoptilolite nanocomposite hydrogel. Those nanocomposites hydrogels showed about 99.47% of decolorization of MB dye. Mahdavinia et al. [93] have synthesized the magnetic clay/laponite-impregnated PVA nanocomposite hydrogel by using the freezing-thawing method. Clay/laponite-impregnated PVA nanocomposite was further used as an adsorbent for the degradation of MB dye from an aqueous solution. The results of this study claimed that the synthesized nanocomposite hydrogels exhibited the maximum absorption capacity of 251 mg/g. Further reuse of adsorbents after four regeneration cycles shows the maximum adsorption efficiency of 93% at the same adsorption capacity.

Shirsath et al. [94] studied the adsorption of Brilliant Green dye from aqueous solution using a poly (acrylic acid) hydrogel composite (Fig. 1.6). The kaoline clay was further incorporated on the prepared poly(acrylic acid) hydrogel composite. Convectional as well as ultrasound-assisted process was studied for the preparation of the nanocomposite. The maximum adsorption of dye molecules was observed at optimum reaction condition such as pH = 7, temperature = 35°C, initial dye concentration = 30 mg/L, and hydrogel loading = 1 g. The results of this study revealed that increasing contact time and concentration of dye molecules may increase adsorption efficiency.

1.5 Membrane-based technology

The main principal of the membrane is to allow a selective material through a semipermeable sheet, but it also restricts bacteria, viruses, salts, heavy metals, and some contaminants. The membrane can be operated using pressure-driven force or electrical techniques. Nowadays, membrane-based technology is found to be a more effective method for various applications such as wastewater treatment, etc. Generally, the basic mechanism of the membrane technology for wastewater treatment is to block the contaminants present in the wastewater (its size is larger than the pores of the membrane). Membrane technology can be divided into several types based on their performance, composition, and applications. The efficiency of the membrane greatly depends on the membrane material used for its fabrication. The nanomaterial-based

This book belongs to Badji Mokhtar Annaba University Central Library Copyright Elsevier 2025

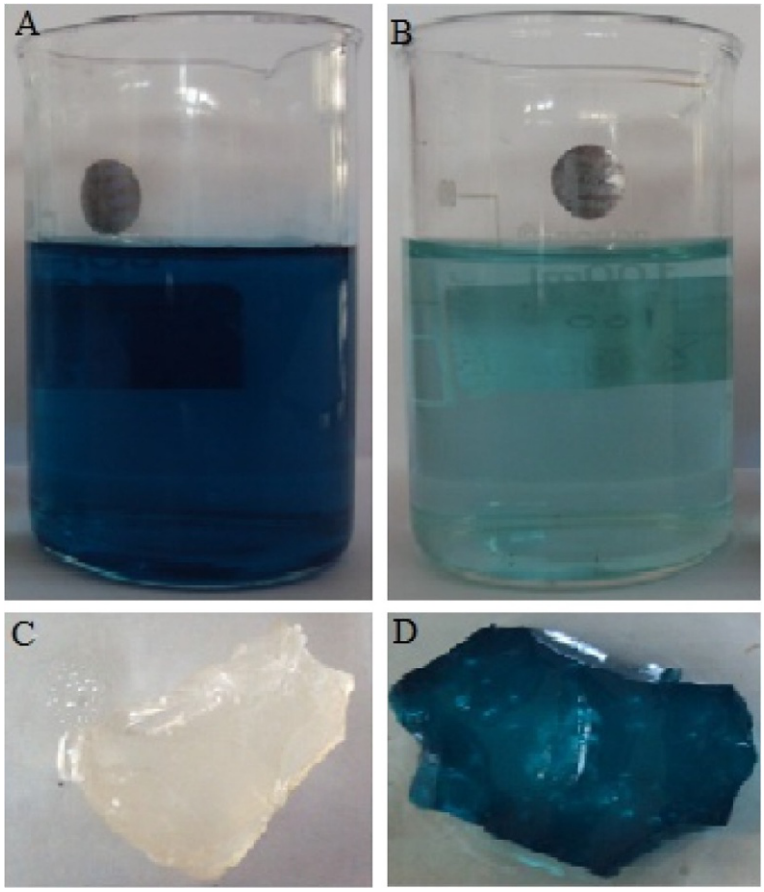

Fig. 1.6
Color (gray color in print version) changes of BG dye and hydrogel before (A, C) and after adsorption (B, D), respectively. *Reprinted with permissions from S.R. Shirsath, A.P. Patil, R. Patil, J.B. Naik, P.R. Gogate, S.H. Sonawane, Removal of brilliant green from wastewater using conventional and ultrasonically prepared poly(acrylic acid) hydrogel loaded with kaolin clay: a comparative study, Ultrason. Sonochem. 20 (2013) 914–923, Copyright © 2020.*

membranes show a beneficial effect in the improvement of membrane life, permeability, and thermal stability. Polymeric nanofibers and ceramics are another class of the membrane-based process. Electroplating method is the more efficient and effective method to fabricate a nanofiber due to its simplicity and cost effectiveness. The main advantages of these nanofibers are high surface area and porosity. The application of nanofibers can be easily manipulated based on the various applications. Several literatures have been published on the various applications of nanofiber-based technology [95–97]. This method is extremely useful for removal of small ions and molecules such as sodium, potassium, and chloride. These small ions can also be removed with the help of a reverse osmosis (RO)-based process. An electrospun

This book belongs to Badji Mokhtar Annaba University Central Library Copyright Elsevier 2025

nanofiber-based membrane can remove bacteria or viruses by means of size rejection. However, proper application of these methods for the removal of such bacteria or viruses is difficult due to small pore size. These small pore sizes are unable to remove the appropriate viral agents present in wastewater. However, a novel composite cellulose and poly(acrylonitrile-*co*-glycidyl methacrylate)-based membrane has the capability to remove 99.99% of these microorganisms (e-coli) [98]. Various researchers have studied the removal of toxic compounds from wastewater by means of thin-film composite membranes. These membranes can be fabricated by interfacial polymerization technique. The nanomaterial or nanocomposites are fused into the thin layer of the polymeric sheet to improve the interfacial property. Various nanomaterials have been employed such as nanozeolates, nanosilver, nano-TiO_2, and CNTs via interfacial polymerization technique. Another class of membrane is aquaporin or biological-based membrane. The selectivity of these permeables is higher toward water molecules and therefore rejects most molecules. Recent studies have shown that the aquaporin-based membranes have great potential to remove biological as well as ionic contaminants in an efficient way.

1.5.1 Nanocomposite membranes

As discussed in the previous section, membrane techniques involving ultrafiltration (UF), nanofiltration (NF), and RO processes are the developed technologies in water purification and desalination field. Many of the studies have reviewed the application of NF in various sections such as separation of cations, degradation of organic pollutants and biological matter, and removal of metal ions from groundwater as well as surface water.

Although many research studies have been attempted on the chemical modification of membrane surfaces by grafting hydrophilic monomers, satisfactory results were not observed toward the reduction of fouling on the membrane surface. Recent studies in wastewater treatment using nanotechnology have justified the advantages of nanomaterials in membrane technologies. Many studies [99–101] have reported the marked effect of nanoparticles used in membrane processes. Nanoparticles-embedded membranes have not only shown mitigation of membrane fouling, apart from this, it also improves the synergistic effect, desired structure, and functionalities of the membrane [102, 103].

Over the past decades, scientists have used different nanoparticles and mixtures of nanoparticles in the preparation of nanocomposite membranes, namely ZnO, GO, SiO_2, Fe, Alumina (Al_2O_3), TiO_2, Copper (Cu), Zirconium (ZrO_2), and Iron Oxide (Fe_2O_3). The addition of these nanomaterials have exhibited increased flux, salt rejection capacity, antifouling, and antibacterial properties [104–106].

Alkindy et al. [107] have synthesized the poly (ether sulfone) (PES)-based GO-SiO_2 matrix membrane by phase inversion method. The synthesized membrane was employed for the

This book belongs to Badji Mokhtar Annaba University Central Library Copyright Elsevier 2025

recovery of oil from oil refinery wastewater. This study claimed that addition of nanoparticles such as GO and silica (SiO_2) in PES matrix imparts extraordinary properties to the membrane. The nanocomposite membrane (PES/GO-SiO_2) showed 38% more oil recovery with maximum water flux compared with the individual PES membrane. Peyravi et al. [108] prepared the thin-film nanocomposite (TFN) NF membranes via in situ incorporation of TiO_2 nanoparticles in *co*-polyamide matrix. In this study, the authors improved the good agreement of TiO_2 nanoparticles in the polymer matrix by amine and chloride compounds. This study shows that the addition of TiO_2 nanoparticles in the polymer membrane matrix revealed a crucial effect on the performance of the NF membrane toward the improvement of methanol flux and rejection of dye. Aoudjit et al. [109] studied the immobilized TiO_2 nanoparticles on poly-vinylidene fluoride-trifluoro ethylene TiO_2/PVDF-TrFE nanocomposite membranes for the degradation of tartrazine.

As discussed in the previous section, photocatalytic nanomaterials have extraordinary physicochemical properties, and due to their nature, these could be potential candidates for a photocatalytic membrane for the degradation of tartrazine. This membrane exhibited sunlight photocatalytic activity of about 78% within 5 h. The obtained results revealed the secret about the suitability of TiO_2 nanoparticles-based PVDF-TrFE membrane for photocatalytic degradation of organic pollutants.

Huang et al. [110] synthesized the polyamide-based UF membranes with surface coating of GO nanosheets for enhancing the antifouling property. In this research, the authors adopted the vacuum filtration methodology for coating GO nanosheets, and it was employed for the recovery of oil from wastewater. Gao et al. [111] synthesized ultrathin and super-hydrophilic SW CNT membranes via sol-gel coating of titania (TiO_2) nanoparticles. In this work, the authors developed the sole shape and structure with nanoscale pore size of 20–60 nm and 60 nm for ultrathin SWCNT film. The synthesized nanocomposite possessed self-cleaning and antifouling properties after a number of oil water filtration tests owing to the photocatalytic activity of TiO_2 nanoparticles. Peng et al. [112] developed a polyvinylidene fluoride (PVDF)/RGO@SiO_2/PDA (polydopamine) nanocomposite hybrid membrane using surface deposition and vacuum filtration techniques. The synthesized nanocomposite membranes showed oil rejection of about 99% at room temperature.

A CNT-embedded membrane was described by Chen et al. [113]. The CNT-embedded membrane was fabricated by means of depositing CNT onto a ceramic surface of membrane through the chemical vapor method. It combined the function of ceramic pore channels and grown CNTs in the pores. The optimized condition of the CNT-ceramic membrane showed a rejection rate of 100% and flux rate of 36 L/hm^2/bar. These types of membranes also exhibit certain resistance to organic fouling of the membrane. The mechanism of flux enhancement by CNTs in nanocomposite membranes is depicted in Fig. 1.7.

This book belongs to Badji Mokhtar Annaba University Central Library Copyright Elsevier 2025

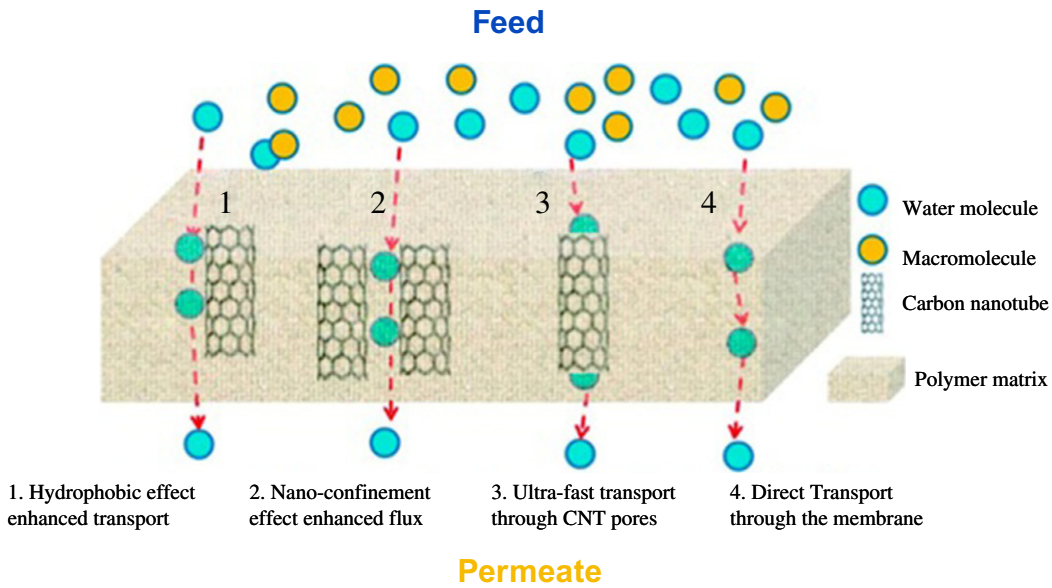

Fig. 1.7
The mechanism of flux enhancement by CNTs in nanocomposite membranes. *Reprinted with permission from S. Li, G. Liao, Z. Liu, Y. Pan, Q. Wu, Y. Weng, X. Zhang, Z. Yang, O.K.C. Tsui, Enhanced water flux in vertically aligned carbon nanotube arrays and polyethersulfone composite membranes, J. Mater. Chem. A 2 (2014) 12171–12176, Copyright © 2020.*

1.6 Challenges and future direction

A variety of different nanomaterials were intensively investigated as high-performance catalysts and adsorbent materials for eliminating inorganic and/or biological contaminants. Those nanomaterials usually showed diverse benefits, such as exceptional ability, high reaction kinetics, particular responsiveness to selective pollutants, improved photocatalytic responsiveness over a wide wavelength of light, and good antibacterial activity. Nanomaterials have become key elements of commercial and community water treatment plants as many changes happen toward its production of cost efficient and environmentally friendly nanomaterials. Several barriers remain to be resolved for the deployment of nanomaterials in engineering usage. Initially, due to the influence of Van der Waals forces as well as other effects, nanomaterials were typically unstable and appear to aggregate. Furthermore, extracting nanomaterials out of treated water is still a difficult task. Therefore, nanocomposites will improve existing water purification technologies significantly in this context. In summary, this chapter mainly deals with various aspects of nanotechnology-based wastewater treatment processes.

The main aim of this book is to explore the various physicochemical, structural, and surface properties of different nanoparticles and nanocomposites used for effective treatment of

This book belongs to Badji Mokhtar Annaba University Central Library Copyright Elsevier 2025

wastewater. This book also highlights several advantages and mechanistic aspects for scale of the processes in various engineering applications. The applications of nanomaterials and nanocomposites covered include the production of portable water through removal of toxic and recalcitrant pollutants from wastewater by using effective and efficient methods. Each chapter in this book covers a different nanomaterial-based technology and assesses the fundamental laws and principles. This book also explores the practical application of these processes, latest findings, recent and future scope of the processes, and some limitations associated with these processes. In general, this book helps to provide the basic fundamental idea to researchers, academicians, and professionals working in the area of nanotechnology, nanocomposites, wastewater treatment, and desalination process.

References

[1] V. Parmon, Nano-materials in catalysis, Mater. Res. Innov. 12 (2008) 60–61.
[2] X.J. Liang, A. Kumar, D. Shi, D. Cui, Nanostructures for medicine and pharmaceuticals, J. Nanomater. (2012) 1–2.
[3] A. Kusior, J. Klich-Kafel, A. Trenczek-Zajac, K. Swierczek, M. Radecka, K. Zakrzewska, TiO_2-SnO_2 nanomaterials for gas sensing and photocatalysis, J. Eur. Ceram. Soc. 33 (2013) 2285–2290.
[4] B. Bujoli, H. Roussiere, G. Montavon, L. Samia, J. Pascal, A. Bruno, F. Franck, P. Marc, M. Dominique, B. J. Michel, G. Jerome, O. Gauthier, L. Sarah, N. Guillaume, P. Muriel, L. Jean, T. Daniel, T. Charles, Novel phosphate-phosphonate hybrid nano-materials applied to biology, Prog. Solid State Chem. 34 (2006) 257–266.
[5] P.A.K. Reddy, P.V.L. Reddy, E. Kwon, K.H. Kim, T. Akter, S. Kalagara, Recent advances in photocatalytic treatment of pollutants in aqueous media, Environ. Int. 91 (2016) 94–103.
[6] X. Qu, P.J. Alvarez, Q. Li, Applications of nanotechnology in water and wastewater treatment, Water Res. 47 (2013) 3931–3946.
[7] A. Turki, C. Guillard, F. Dappozze, Z. Ksibi, G. Berhault, H. Kochkar, Phenol photocatalytic degradation over anisotropic TiO_2 nanomaterials: kinetic study, adsorption isotherms and formal mechanisms, Appl. Catal. B Environ. 163 (2015) 404–414.
[8] M.K. Seery, R. George, P. Floris, S.C. Pillai, Silver doped titanium dioxide nanomaterials for enhanced visible light photocatalysis, J. Photochem. Photobiol. A Chem. 189 (2007) 258–263.
[9] A. Higazy, M. Hashem, A. ElShafei, N. Shaker, M.A. Hady, Development of antimicrobial jute packaging using chitosan and chitosan-metal complex, Carbohydr. Polym. 79 (2010) 867–874.
[10] M. Rai, A. Yadav, A. Gade, Silver nanoparticles as a new generation of antimicrobials, Biotechnol. Adv. 27 (2009) 76–83.
[11] A.A. Hebeish, M.M. Abdelhady, A.M. Youssef, TiO_2 nanowire and TiO_2 nanowire doped Ag-PVP nanocomposite for antimicrobial and self-cleaning cotton textile, Carbohydr. Polym. 91 (2013) 549–559.
[12] G.S. Martynkova, M. Valaskova, Antimicrobial nanocomposites based on natural modified materials: areview of carbons and clays, J. Nanosci. Nanotechnol. 14 (2014) 673–693.
[13] Q.L. Li, S. Mahendra, D.Y. Lyon, L. Brunet, M.V. Liga, D. Li, P.J.J. Alvarez, Antimicrobial nanomaterials for water disinfection and microbial control: potential applications and implications, Water Res. 42 (2008) 4591–4602.
[14] S. Das, B. Sen, N. Debnath, Recent trends in nanomaterials applications in environmental monitoring and remediation, Environ. Sci. Pollut. Res. 22 (2015) 18333–18344.
[15] T. Pradeep, Noble metal nanoparticles for water purification: a critical review, Thin Solid Films 517 (2009) 6441–6478.

This book belongs to Badji Mokhtar Annaba University Central Library Copyright Elsevier 2025

[16] S. Shrivastava, N. Jadon, R. Jain, Next-generation polymer nanocomposite-based electrochemical sensors and biosensors: a review, TrAC Trends Anal. Chem. 82 (2016) 55–67.
[17] L. Joseph, J. Heo, Y.G. Park, J.R.V. Flora, Y. Yoon, Adsorption of bisphenol A and 17 alpha-ethinyl estradiol on single walled carbon nanotubes from seawater and brackish water, Desalination 281 (2011) 68–74.
[18] C. Hu, M. He, B. Chen, B. Hu, Simultaneous determination of polar and apolar compounds in environmental samples by a polyaniline/hydroxyl multi-walled carbon nanotubes composite-coated stir bar sorptive extraction coupled with high performance liquid chromatography, J. Chromatogr. A 1394 (2015) 36–45.
[19] H. Wei, S. Deng, Q. Huang, Y. Nie, B. Wang, J. Huang, G. Yu, Regenerable granular carbon nanotubes/alumina hybrid adsorbents for diclofenac sodium and carbamazepine removal from aqueous solution, Water Res. 47 (2013) 4139–4147.
[20] H. Wang, X.Z. Yuan, Y. Wu, H.J. Huang, G.M. Zeng, Y. Liu, X.L. Wang, N.B. Lin, Y. Qi, Adsorption characteristics and behaviors of graphene oxide for Zn(II) removal from aqueous solution, Appl. Surf. Sci. 279 (2013) 432–440.
[21] S. Kumar, R.R. Nair, P.B. Pillai, S.N. Gupta, M.A.R. Iyengar, A.K. Sood, Graphene oxide-$MnFe_2O_4$ magnetic nanohybrids for efficient removal of lead and arsenic from water, ACS Appl. Mater. Interfaces 6 (2014) 17426–17436.
[22] A. Azari, A.A. Babaei, R.R. Kalantary, A. Esrafili, M. Moazzen, B. Kakavandi, Nitrate removal from aqueous solution using carbon nanotubes magnetized by nano zero-valent iron, J. Mazandaran Univ. Med. Sci. 23 (2014) 14–27.
[23] Y.H. Huang, C.I. Hsueh, H.P. Cheng, L.C. Su, C.Y. Chen, Thermodynamics and kinetics of adsorption of Cu(II) onto waste iron oxide, J. Hazard. Mater. 144 (2007) 406–411.
[24] D. Pokhrel, T. Viraraghavan, Arsenic removal in an iron oxide-coated fungal biomass column: analysis of breakthrough curves, Bioresour. Technol. 99 (2008) 2067–2071.
[25] S. Dixit, J.G. Hering, Comparison of arsenic (V) and arsenic (III) sorption onto iron oxide minerals: implications for arsenic mobility, Environ. Sci. Technol. 37 (2003) 4182–4189.
[26] S.R. Kanel, L. Charlet, B. Manning, H. Choi, Removal of arsenic (III) from ground water by nanoscale zero-valent iron, Environ. Sci. Technol. 39 (2005) 1291–1298.
[27] S.M. Ponder, J.G. Darab, T.E. Mallouk, Remediation of chromium (VI) and Pb (II) aqueous solutions using supported nanoscale zero-valent iron, Environ. Sci. Technol. 34 (2000) 2564–2569.
[28] S. Pacheco, R. Rodriguez, Adsorption properties of metal ions using alumina nano-particles in aqueous and alcoholic solutions, J. Sol-Gel Sci. Technol. 20 (2001) 263–273.
[29] M. Hua, S. Zhang, B. Pan, W. Zhang, L. Lv, Q. Zhang, Heavy metal removal from water/wastewater by nanosized metal oxides: a review, J. Hazard. Mater. 211 (2012) 317–331.
[30] S.L. Li, W. Wang, W.L. Yan, W.X. Zhang, Nanoscale zero-valent iron (nZVI) for the treatment of concentrated Cu(II) wastewater: a field demonstration, Environ. Sci. Process Impacts 16 (2014) 524–533.
[31] H.J. Shipley, K.E. Engates, V.A. Grover, Removal of Pb(II), Cd(II), Cu(II), and Zn(II) by hematite nanoparticles: effect of sorbent concentration, pH, temperature, and exhaustion, Environ. Sci. Pollut. Res. Int. 20 (2013) 1727–1736.
[32] R. Fagan, D.E. McCormack, D.D. Dionysiou, S.C. Pillai, A review of solar and visible light active TiO_2 photocatalysis for treating bacteria, cyanotoxins and contaminants of emerging concern, Mater. Sci. Semicond. Process. 42 (2016) 2–14.
[33] T. Sheela, Y.A. Nayaka, R. Viswanatha, S. Basavanna, T.G. Venkatesha, Kinetics and thermodynamics studies on the adsorption of Zn(II), Cd(II) and Hg(II) from aqueous solution using zinc oxide nanoparticles, Powder Technol. 217 (2012) 163–170.
[34] L. Zhang, T. Huang, M. Zhang, X. Guo, Z. Yuan, Studies on the capability and behavior of adsorption of thallium on nano-Al_2O_3, J. Hazard. Mater. 157 (2008) 352–357.
[35] J. Hu, I. Lo, G. Chen, Removal of Cr(VI) by magnetite, Water Sci. Technol. 50 (2004) 139–146.
[36] X. Wei, S. Bhojappa, L.S. Lin, R.C. Viadero, Performance of nano-magnetite for removal of selenium from aqueous solutions, Environ. Eng. Sci. 29 (2012) 526–532.

This book belongs to Badji Mokhtar Annaba University Central Library Copyright Elsevier 2025

[37] S.-Y. Mak, D.H. Chen, Fast adsorption of methylene blue on polyacrylic acid-bound iron oxide magnetic nanoparticles, Dyes Pigments 61 (2004) 93–98.
[38] L.H. Cumbal, A.K. SenGupta, Preparation and characterization of magnetically active dual-zone sorbent, Ind. Eng. Chem. Res. 44 (2005) 600–605.
[39] T.Y. Peng, D. Zhao, H.B. Song, C.H. Yan, Preparation of lanthana-doped titania nanoparticles with anatase mesoporous walls and high photocatalytic activity, J. Mol. Catal. A Chem. 238 (2005) 119–126.
[40] S.J. Klaine, P.J.J. Alvarez, G.E. Batley, T.E. Fernandes, R.D. Handy, D.Y. Lyon, S. Mahendra, M. J. McLaughlin, J.R. Lead, Nanoparticles in the environment: behavior, fate, bioavailability and effects, Environ. Toxicol. Chem. 27 (2008) 1825–1851.
[41] P.K. Stoimenov, R.L. Klinger, G.L. Marchin, K.J. Klabunde, Metal oxide nanoparticles as bactericidal agents, Langmuir 18 (2002) 6679–6686.
[42] J.H. Chang, T.J. Yang, C.H. Tung, Performance of nano- and nonnano-catalytic electrodes for decontaminating municipal wastewater, J. Hazard. Mater. 163 (2009) 152–157.
[43] N. Mei, L. Xuguang, D. Jinming, J. Husheng, W. Liqiao, X. Bingshe, Antibacterial activity of chitosan coated Ag-loaded nano-SiO_2 composites, Carbohydr. Polym. 78 (2009) 54–59.
[44] L. Brittany, V. Carino, J. Kuo, L. Leong, R. Ganesh, Adsorption of organic compounds to metal oxide nanoparticles, in: Conference Presentation is Part of: General Environmental 2006, 2006.
[45] H. Hildebrand, K. Mackenzie, F.D. Kopinke, Pd/Fe_3O_4 nanocatalysts for selective dehalogenation in wastewater treatment processes—influence of water constituents, Appl. Catal. B Environ. 91 (2009) 389–396.
[46] R.S. Parra, I.H. Perez, M.E. Rincon, S.L. Ayala, M.C.R. Ahumada, Visible light-induced degradation of blue textile azo dye on TiO_2-CdO-ZnO coupled nanoporous films, Sol. Energy Mater. Sol. Cells 76 (2003) 189–199.
[47] J.C. Yu, W. Ho, J. Yu, H. Yip, P. Wong, J. Zhao, Efficient visible-light-induced photocatalytic disinfection on sulfur-doped nanocrystalline titania, Environ. Sci. Technol. 39 (2005) 1175–1179.
[48] F. Peng, H. Wang, H. Yu, S. Chen, Preparation of aluminum foil-supported nano-sized ZnO thin films and its photocatalytic degradation to phenol under visible light irradiation, Mater. Res. Bull. 41 (2006) 2123–2129.
[49] S. Min, F. Wang, Y. Han, An investigation on synthesis and photocatalytic activity of polyaniline sensitized nanocrystalline TiO_2 composites, J. Mater. Sci. 42 (2007) 9966–9972.
[50] N. Venkatachalam, M. Palanichamy, B. Arabindoo, V. Murugesan, Enhanced photocatalytic degradation of 4-chlorophenol by Zr^{4+} doped nano TiO_2, J. Mol. Catal. A Chem. 266 (2007) 158–165.
[51] H. Wang, C. Xie, W. Zhang, S. Cai, Z. Yang, Y. Gui, Comparison of dye degradation efficiency using ZnO powders with various size scales, J. Hazard. Mater. 141 (2007) 645–652.
[52] H.R. Pouretedal, A. Norozi, M.H. Keshavarz, A. Semnani, Nanoparticles of zinc sulfide doped with manganese, nickel and copper as nanophotocatalyst in the degradation of organic dyes, J. Hazard. Mater. 162 (2009) 674–681.
[53] J. Moon, C. Yeon Yun, K.-W. Chung, M.-S. Kang, J. Yi, Photocatalytic activation of TiO_2 under visible light using acid red 44, Catal. Today 87 (2003) 77–86.
[54] R. Suarez-Parra, I. Hernandez-Perez, M.E. Rinon, S. Lopez-Ayala, M.C. Roldan-Ahumada, Visible light-induced degradation of blue textile azo dye on TiO_2/CdO-ZnO coupled nanoporous films, Sol. Energy Mater. Sol. Cells 76 (2003) 189–199.
[55] J.C. Yu, W. Ho, J. Yu, H. Yip, P.K. Wong, J. Zhao, Efficient visible-light-induced photocatalytic disinfection on sulfur-doped nanocrystalline titania, Environ. Sci. Technol. 39 (2005) 1175–1179.
[56] S. Min, F. Wang, Y. Han, An investigation on synthesis and photocatalytic activity of polyaniline sensitized nanocrystalline TiO_2 composites, J. Mater. Sci. 42 (2007) 9966–9972.
[57] N. Venkatachalam, M. Palanichamy, B. Arabindoo, V. Murugesan, Enhanced photocatalytic degradation of 4-chlorophenol by Zr^{4+} doped nano TiO_2, J. Mol. Catal. A Chem. 266 (2007) 158–165.
[58] K.M. Joshi, V.S. Shrivastava, Photocatalytic degradation of chromium (VI) from wastewater using nano-materials like TiO_2, ZnO, and CdS, Appl. Nanosci. 1 (2011) 147–155.
[59] E. Guibal, Interactions of metal ions with chitosan-based sorbents: a review, Sep. Purif. Technol. 38 (2004) 43–74.

This book belongs to Badji Mokhtar Annaba University Central Library Copyright Elsevier 2025

[60] S.B. Khan, K.A. Alamry, H.M. Marwani, A.M. Asiri, M.M. Rahman, Synthesis and environmental applications of cellulose/ZrO_2 nanohybrid as a selective adsorbent for nickel ion, Compos. Part B 50 (2013) 253–258.
[61] K. Varaprasad, G.M. Raghavendra, T. Jayaramudu, J. Seo, Nano zinc oxide-sodium alginate antibacterial cellulose fibres, Carbohydr. Polym. 135 (2016) 349–355.
[62] E. Vunain, A.K. Mishra, B.B. Mamba, Dendrimers, mesoporous silicas and chitosanbasednanosorbents for the removal of heavy-metal ions: a review, Int. J. Biol. Macromol. 86 (2016) 570–586.
[63] L. Djerahov, P. Vasileva, I. Karadjova, R.M. Kurakalva, K.K. Aradhi, Chitosan film loaded with silver nanoparticles-sorbent for solid phase extraction of Al(III), Cd(II), Cu(II), Co(II), Fe(III), Ni(II), Pb(II) and Zn(II), Carbohydr. Polym. 147 (2016) 45–52.
[64] A. Ouyang, Q.M. Gong, J. Liang, Carbon nanotube-chitosan composite beads with radially aligned channels and nanotube-exposed walls for bilirubin adsorption, Adv. Eng. Mater. 17 (2015) 460–466.
[65] M. Jaiswal, D. Chauhan, N. Sankararamakrishnan, Copper chitosan nanocomposite: synthesis, characterization, and application in removal of organophosphorous pesticide from agricultural runoff, Environ. Sci. Pollut. Res. 19 (2012) 2055–2062.
[66] A.A.P. Mansur, H.S. Mansur, F.P. Ramanery, L.C. Oliveira, P.P. Souza, "Green" colloidal ZnS quantum dots/chitosan nano-photocatalysts for advanced oxidation processes: study of the photodegradation of organic dye pollutants, Appl. Catal. B Environ. 158 (2014) 269–279.
[67] K.Y. Foo, B.H. Hameed, Decontamination of textile wastewater via TiO_2/activated carbon composite materials, Adv. Colloid Interf. Sci. 159 (2010) 130–143.
[68] J.A. Arcibar-Orozco, M. Avalos-Borja, J.R. Rangel-Mendez, Effect of phosphate on the particle size of ferric oxyhydroxides anchored onto activated carbon: As(V) removal from water, Environ. Sci. Technol. 46 (2012) 9577–9583.
[69] Y. Kikuchi, Q. Qian, M. Machida, H. Tatsumoto, Effect of ZnO loading to activated carbon on Pb(II) adsorption from aqueous solution, Carbon 44 (2006) 195–202.
[70] P.Y. Furlan, M.E. Melcer, Removal of aromatic pollutant surrogate from water by recyclable magnetite-activated carbon nanocomposite: an experiment for general chemistry, J. Chem. Educ. 91 (2014) 1966–1970.
[71] H. Choi, S.R. Al-Abed, S. Agarwal, D.D. Dionysiou, Synthesis of reactive nano-Fe/Pd bimetallic system-impregnated activated carbon for the simultaneous adsorption and dechlorination of PCBs, Chem. Mater. 20 (2008) 3649–3655.
[72] D.D. Shao, J. Hu, Z.Q. Jiang, X.K. Wang, Removal of 4,4′-dichlorinated biphenyl from aqueous solution using methyl methacrylate grafted multiwalled carbon nanotubes, Chemosphere 82 (2011) 751–758.
[73] M. Khatamian, Z. Alaji, Efficient adsorption-photodegradation of 4-nitrophenol in aqueous solution by using ZnO/HZSM-5 nanocomposites, Desalination 286 (2012) 248–253.
[74] M.N. Chong, Z.Y. Tneu, P.E. Poh, B. Jin, R. Aryal, Synthesis, characterisation and application of TiO_2-zeolite nanocomposites for the advanced treatment of industrial dye wastewater, J. Taiwan Inst. Chem. Eng. 50 (2015) 288–296.
[75] G. Scocchi, P. Posocco, M. Fermeglia, S. Pricl, Polymer-clay nanocomposites: a multiscale molecular modeling approach, J. Phys. Chem. B 111 (2007) 2143–2151.
[76] E.I. Unuabonah, A. Taubert, Clay-polymer nanocomposites (CPNs): adsorbents of the future for water treatment, Appl. Clay Sci. 99 (2014) 83–92.
[77] G. Rytwo, The use of clay-polymer nanocomposites in wastewater pretreatment, Sci. World J. (2012) 1–7.
[78] A.T. Paulino, M.R. Guilherme, A.V. Reis, G.M. Campese, E.C. Muniz, J. Nozaki, Removal of methylene blue dye from an aqueous media using superabsorbent hydrogel supported on modified polysaccharide, J. Colloid Interface Sci. 301 (2006) 55–62.
[79] S. Li, Removal of crystal violet from aqueous solution by sorption into semi interpenetrated networks hydrogels constituted of poly(acrylic acid acrylamide-methacrylate) and amylase, Bioresour. Technol. 101 (2010) 2197–2202.
[80] P. Li, S. Siddaramaiah, N.H. Kim, S. Heo, J. Lee, Novel PAAm/Laponite clay nano-composite hydrogels with improved cationic dye adsorption behavior, Compos. Part B 39 (2008) 756–763.

This book belongs to Badji Mokhtar Annaba University Central Library Copyright Elsevier 2025

[81] H.E. Hamshary, S.E. Sigeny, M.F. Taleb, N.A.E. Kelesh, Removal of phenolic compounds using (2-hydroxyethyl ethacrylate/acrylamidopyridine) hydrogel prepared by gamma radiation, Sep. Purif. Technol. 57 (2007) 329–337.
[82] Y.H. Gad, Preparation and characterization of poly(2-acrylamido-2-methyl propane sulfonic acid)/chitosan hydrogel using gamma irradiation and its application in wastewater treatment, Radiat. Phys. Chem. 77 (2008) 1101–1107.
[83] Y. Zheng, A. Wang, Evaluation of ammonium removal using a chitosan-g-poly(acrylic acid)/rectorite hydrogel composite, J. Hazard. Mater. 171 (2009) 671–677.
[84] H. Liu, X. Ye, Q. Li, T. Kim, B. Qing, M. Guo, F. Ge, Z. Wu, K. Lee, Boron adsorption using a new boron-selective hybrid gel and the commercial resin D564, Colloids Surf. A Physicochem. Eng. Asp. 341 (2009) 118–126.
[85] H. Liu, B. Qing, X. Ye, Q. Li, K. Lee, Z. Wu, Boron adsorption by composite magnetic particles, Chem. Eng. J. 151 (2009) 235–240.
[86] K. Kabiri, M.J. Zohuriaan-Mehr, Superabsorbent hydrogel composites, Polym. Adv. Technol. 14 (2003) 438–444.
[87] D. Gao, R.B. Heimann, J. Lerchner, J. Seidel, G. Wolf, Development of a novel moisture sensor based on superabsorbent poly(acrylamide)-montmorillonite composite hydrogels, J. Mater. Sci. 36 (2001) 4567–4571.
[88] J. Wu, J. Lin, G. Li, C. Wei, Influence of the COOH and COONa groups and crosslink density of poly(acrylic acid)/montmorillonite superabsorbent composite on water absorbency, Polym. Int. 50 (2001) 1050–1053.
[89] X. Xia, J. Yih, N.A.D. Souza, Z. Hu, Swelling and mechanical behavior of poly (N-isopropylacrylamide)/Na-montmorillonite layered silicates composite gels, Polymer 44 (2003) 3389–3393.
[90] H. Mittal, A. Maity, S.S. Ray, Synthesis of co-polymer-grafted gum karaya and silica hybrid organic-inorganic hydrogel nano-composite for the highly effective removal of methylene blue, Chem. Eng. J. 279 (2015) 166–179.
[91] P. Li, Siddaramaiah, N.H. Kim, G.H. Yoo, J.H. Lee, Poly(acrylamide/laponite) nano-composite hydrogels: swelling and cationic dye adsorption properties, J. Appl. Polym. Sci. 111 (2009) 1786–1798.
[92] A. Rashidzadeh, A. Olad, D. Salari, The effective removal of methylene blue dye from aqueous solutions by NaAlg-g-poly(acrylic acid-co-acryl amide)/clinoptilolite hydrogel, Fibers Polym. 16 (2015) 354–362.
[93] G.R. Mahdavinia, M. Soleymani, M. Sabzi, H. Azimi, Z. Atlasi, Novel magnetic polyvinyl alcohol/laponite RD nano-composite hydrogels for efficient removal of methylene blue nano-composite, J. Environ. Chem. Eng. 5 (2017) 2617–2630.
[94] S.R. Shirsath, A.P. Patil, R. Patil, J.B. Naik, P.R. Gogate, S.H. Sonawane, Removal of brilliant green from wastewater using conventional and ultrasonically prepared poly(acrylic acid) hydrogel loaded with kaolin clay: a comparative study, Ultrason. Sonochem. 20 (2013) 914–923.
[95] F.E. Ahmed, B.S. Lalia, R. Hashaikeh, A review on electrospinning for membrane fabrication: challenges and applications, Desalination 356 (2015) 15–30.
[96] R. Balamurugan, S. Sundarrajan, S. Ramakrishna, Recent trends in nanofibrous membranes and their suitability for air and water filtrations, Membranes 1 (2011) 232–248.
[97] Q.L. Feng, J. Wu, G.Q. Chen, F.Z. Cui, T.N. Kim, J.O. Kim, A mechanistic study of the antibacterial effect of silver ions on *Escherichia coli* and *Staphylococcus aureus*, J. Biomed. Mater. Res. 52 (2000) 662–668.
[98] A. Sato, R. Wang, H. Ma, B.S. Hsiao, B. Chu, Novel nanofibrous scaffolds for water filtration with bacteria and virus removal capability, J. Electron. Microsc. 60 (2011) 201–209.
[99] AWWA Membrane Technology Research Committee, Recent advances and research need in membrane fouling, J. AWWA 97 (2005) 79–89.
[100] J.B. Li, J.W. Zhu, M.S. Zheng, Morphologies and properties of poly(phthala- zinone ether sulfone ketone) matrix ultrafiltration membranes with entrapped TiO_2 nanoparticles, J. Appl. Polym. Sci. 103 (2007) 3623–3629.
[101] J.F. Li, Z.L. Xu, H. Yang, L.Y. Yu, M. Liu, Effect of TiO_2 nanoparticles on the surface morphology and performance of microporous PES membrane, Appl. Surf. Sci. 255 (2009) 4725–4732.

This book belongs to Badji Mokhtar Annaba University Central Library
Copyright Elsevier 2025

[102] J.H. Li, Y.Y. Xu, L.P. Zhu, J.H. Wang, C.H. Du, Fabrication and characterization of a novel TiO_2 nanoparticle self-assembly membrane with improved fouling resistance, J. Membr. Sci. 326 (2009) 659–666.
[103] M.M. Cortalezzi, J. Rose, A.R. Barron, M.R. Wiesner, Characteristics of ultrafiltration ceramic membranes derived from alumoxane nanoparticles, J. Membr. Sci. 205 (2002) 33–43.
[104] A. Alpatova, M. Meshref, K.N. McPhedran, M.G. El-Din, Composite polyvinylidene fluoride (PVDF) membrane impregnated with Fe_2O_3 nanoparticles and multiwalled carbon nanotubes for catalytic degradation of organic contaminants, J. Membr. Sci. 490 (2015) 227–235.
[105] J.M. Arsuaga, A.R.G. Sotto, A. Martínez, S. Molina, B.T. Shivanand, D.A. Javier, Influence of the type, size, and distribution of metal oxide particles on the properties of nano-composite ultrafiltration membranes, J. Membr. Sci. 42 (2013) 131–141.
[106] Y.L. Wu, X.L. Liu, J.Y. Cui, M.J. Meng, J.D. Dai, C.X. Li, Y.S. Yan, Bioinspired synthesis of high-performance nano-composite imprinted membrane by a polydopamine-assisted metal-organic method, J. Hazard. Mater. 323 (2017) 663–673.
[107] M.B. Alkindy, V. Naddeo, F. Banat, S.W. Hasan, Synthesis of polyethersulfone (PES)/GO-SiO_2 mixed matrix membranes for oily wastewater treatment, Water Sci. Technol. (2019) 1–11.
[108] M. Peyravi, M. Jahanshahi, A. Rahimpour, A. Javadi, S. Hajavi, Novel thin film nano-composite membranes incorporated with functionalized TiO_2 nanoparticles for organic solvent nanofiltration, Chem. Eng. J. 241 (2014) 155–166.
[109] L. Aoudjit, P.M. Martins, F. Madjene, D.Y. Petrovykh, M.S. Lanceros, Photocatalytic reusable membranes for the effective degradation of tartrazine with a solar photoreactor, J. Hazard. Mater. 344 (2018) 408–416.
[110] Y. Huang, H. Li, L. Wang, Y. Qiao, C. Tang, C. Jung, Y. Yoon, S. Li, M. Yu, Ultrafiltration membranes with structure-optimized grapheneoxide coatings for antifouling oil/water separation, Adv. Mater. Interfaces 2 (2015) 1–8.
[111] S.J. Gao, Z. Shi, W.Z. Bin, F. Zhang, J. Jin, Photoinduced superwetting single-walled carbon nanotube/TiO_2 ultrathin network films for ultrafast separation of oil-in-water emulsions, ACS Nano 8 (2014) 6344–6352.
[112] Y. Peng, Z. Yu, L. Fei, Q. Chen, D. Yin, X. Min, A novel reduced graphene oxide-based composite membrane prepared via a facile deposition method for multifunctional applications: oil/water separation and cationic dyes removal, Sep. Purif. Technol. 200 (2018) 130–140.
[113] X.W. Chen, L. Hong, Y.F. Xu, Z.W. Ong, Ceramic pore channels with inducted carbon nanotubes for removing oil from water, ACS Appl. Mater. Interfaces 4 (2012) 1909–1918.

This book belongs to Badji Mokhtar Annaba University Central Library Copyright Elsevier 2025

This page intentionally left blank

This book belongs to Badji Mokhtar Annaba University Central Library

Copyright Elsevier 2025

CHAPTER 2

Low-dimensional nanomaterials: Syntheses, physicochemical properties, and their role in wastewater treatment

Dragana J. Jovanović

Vinča Institute of Nuclear Sciences, National Institute of the Republic of Serbia, University of Belgrade, Belgrade, Serbia

2.1 Introduction

During the past few decades, low-dimensional materials have gained the attention of intensive scientific research. The structure, size, shape, controlled preparation, and design of nanostructured materials are key factors in their development and applications. These materials are expected to show novel, unusual, physicochemical properties not shown by the corresponding bulk materials of the same composition. Due to very high ratio between surface area and volume, the nanoscaled materials have more atoms on their surface compared with their respective bulk counterparts, i.e., these materials possess a larger number of active sites, which has a significant effect on their activity and tends to interact with other materials and various functional groups [1, 2].

Due to superior physicochemical properties, these nanomaterials are suitable candidates for a wide variety of applications in everyday life: next-generation computer chips; ductile, machinable ceramics; insulation materials; on flat-panel displays with high-definition of resolution; electrochromic display devices; batteries with high energy density; magnets and sensors with high power and high sensitivity; automobiles with high fuel efficiency; aerospace components; longer-lasting satellites; and so on [3–6].

Nanomaterials have been widely used for numerous biomedical applications: in longer-lasting medical implants, as novel tissue engineering scaffolds, in photothermal and photodynamic cancer therapy, in targeted drug delivery systems, biosensing, bioimaging, antimicrobial effect, and so on [7–9]. Also, nanomaterials can be used as nanoadsorbents, nanocatalysts, nanofibers,

Handbook of Nanomaterials for Wastewater Treatment. https://doi.org/10.1016/B978-0-12-821496-1.00028-3
Copyright © 2021 Elsevier Inc. All rights reserved.

This book belongs to Badji Mokhtar Annaba University Central Library Copyright Elsevier 2025

and nanobiocides for the separation of organic pollutants, heavy metals, inorganic anions, bacteria, oil spills, and waste disposal from contaminated water [10–15].

The development and use of novel, low-cost nanomaterials with high specific surface area and reactivity, as well as high adsorption capacity, has received extensive attention in recent years for water treatment and environmental protection [16, 17].

In this chapter, we would like to briefly introduce general definitions of classification, methods of syntheses, and physicochemical properties of low-dimensional, zero-dimensional (0D), one-dimensional (1D), two-dimensional (2D), and three-dimensional (3D) nanomaterials, as well as their applications in wastewater treatment, i.e., techniques and methods for removal of chemical compounds/pollutants from water (adsorption and separation, catalytic oxidation, disinfection, and sensing) using these nanomaterial [18, 19].

2.2 Classification of nanomaterials

The first classification of nanomaterials was given at the end of the 20th century by Gleiter and Skorokhod [20, 21]. However, in these classifications, 0D, 1D, 2D, and 3D structures and carbon-based materials were not taken into account, but several years later Pokropivny and Skorokhod reported a new classification for nanomaterials, in which these low-dimensional materials are included [22]. Low-dimensional materials contain at least one geometrical dimension on a nanoscale range (1–100 nm) and exhibiting size effects. Most current research showed that nanomaterials can be organized into several material-based categories: semiconductor nanomaterials, inorganic oxide nanomaterials, carbon-based nanomaterials, and organic-based and composite-based nanomaterials [23].

2.2.1 Semiconducting nanomaterials

Semiconductors are solid materials in which their specific conductivity increases with increasing temperature. Silicon is the most famous semiconductor, but semiconductors are also some other elements of groups IV, V, and VI (Ge, P, As, Sb, Se, Te) as well as a large number of compounds: I–VII semiconductors (CuCl, CuBr, AgBr), II–VI semiconductors (CdS, CdSe, CdTe, ZnSe, PbS), III–V semiconductors (GaAs, GaP, InP), IV–VI semiconductors (PbS), and V–VI semiconductors (Bi_2S_3, Sb_2S_3) [24–27]. According to the zone solid-state theory, at absolute zero (0 K), in an intrinsic chemically pure semiconductor, the valence band is completely filled by electrons, while there are no electrons in the conduction band, i.e., the conduction band is empty. The zone between the valence and conduction bands is the so-called forbidden zone-energy region, and electrons cannot have those energies at all. The difference in energies between the bottom of the conductive band and the top of the valence band is the physical characteristic of each semiconductor, and it is called the energy gap or band gap (also bandgap). For materials commonly considered as semiconductors, this energy gap is in the

This book belongs to Badji Mokhtar Annaba University Central Library Copyright Elsevier 2025

Table 2.1: Physical constants (E_g—energy gap, λ—wavelength, ε—dielectric constant, m_e*—effective mass of electrons, m_h*—effective mass of holes, a_B—Bohr radius) for II–VI and III–V semiconductors.

Semiconductor	E_g/eV (λ/nm)	ε	m_e*	m_h*	a_B (nm)
ZnS	3.6 (344)	8.76	0.34	0.23	2.5
CdS	2.42 (512)	5.7	0.165	0.8	4.72
CdSe	1.74 (713)	6.1	0.13	0.6	6.04
CdTe	1.44 (861)	7.2	0.14	0.35	7.62
AlSb	1.60 (775)	11.0	0.09	0.4	15.85
GaP	2.24 (554)	11.1	0.35	0.5	5.7
GaAs	1.35 (919)	13.2	0.068	0.5	23.34
GaSb	0.67 (1850)	15.7	0.05	0.23	40.46
InP	1.27 (976)	12.4	0.067	0.65	21.61
InAs	0.36 (3444)	14.6	0.022	0.41	74.0
InSb	0.165 (7516)	17.7	0.014	0.4	138.49

region from 0.3 to 3.8 eV. At any temperature above 0 K, a number of electrons in a semiconductor have energy sufficient to pass into the conductive band. The number of electrons in the conductive band depends on the temperature (the conductivity of the material increases with temperature) and from energy gap width. In the transition from valence to conduction band, the electrons leave a empty place that acts as a moving positive particle, which is called a hole. The electron and its hole are delocalized, moving chaotically, and is attracted by the Coulomb's force, thus forming a bonded system called the exciton. The exciton is reminiscent of a hydrogen atom (hydrogen is a bonded system of two heterogeneous charges of the same magnitude at an intermediate distance, called the Bohr radius). Because of this similarity, the mean distance between an electron and its hole is called Bohr's exciton radius [28–30].

Bohr's exciton radius (a_B) is an important characteristic of semiconductor material and has different values for different materials. The typical value of a_B, as well as other physical constants (energy band gap, dielectric constant, effective mass of electrons, and effective mass of holes) for II–VI and III–V semiconductors are given in Table 2.1.

The energy gap is size dependent: energy band gap increases with decreasing particle size, the melting temperature and kinetics of chemical processes on the surface, as well as some other properties, were changed due to importance of quantum phenomena at the nanoscale.

In semiconductor bulk material crystals with macroscopic dimensions, the size of the exciton a_B is smaller than any of the three dimensions of the crystal ($a_B < d$), and therefore the exciton can move freely throughout the crystal. On the other hand, in the case of one or more dimensions of crystals of order of magnitude smaller than a_B, an extremely significant physical phenomenon occurs, the so-called quantum confinement. The movement of the exciton is then

This book belongs to Badji Mokhtar Annaba University Central Library Copyright Elsevier 2025

limited by the physical boundaries of the crystal, and there can be recognized 1D, 2D, and 3D configurations according to whether this motion is restricted in one, two, or three dimensions, respectively. If the materials have three dimensions larger than 100 nm and there is no limit in motion of the exciton, we have a standard bulk material that can also be called as a 3D (bulk) material. If nanostructures have components smaller than 100 nm, they can be classified using their geometrical dimensions: (i) if one dimension is in range from 1 to 100 nm, i.e., two dimensions are larger than 100 nm, the motion is limited in this one dimension (so-called 2D semiconductors: nanocoatings and quantum well); (ii) if two dimensions are in range from 1 to 100 nm and one dimension is larger than 100 nm, the motion is limited in these two dimensions (so-called 1D semiconductor: nanofibers, nanowires, and nanorods); and (iii) if all three dimensions are in the range between 1 and 100 nm, the motion is limited in all three dimensions (0D semiconductor: quantum dots). These materials possess specific physicochemical properties due to their geometric dimensionality [31–33].

In modern science and technology, semiconductor materials (quantum wells, quantum wires, quantum rods, and quantum dots) with quantum confinement are extremely important. Focus of attention is based on the quantum dots (0D) that can be defined as semiconductor crystals whose volume is less than the volume defined by the Bohr radius of that semiconductor. In other words, as mentioned before, movement of exciton in quantum dots is restricted in all three dimensions. The result of the confinement is the large difference in the electronic, optical, and catalytic properties of the nanocrystalline over the properties of the corresponding bulk (macroscopic) material. It is extremely significant that the nanoparticle exhibits a size effect as its properties change with the particle size [34].

2.2.2 Metal oxide nanomaterials

Metal oxide nanoparticles are a very important class of nanomaterials with applications in different fields of everyday life, science, and technology as catalysts, different sensors, environmental decontamination, ceramics, biomedicine, and so on. These nanoparticles have an intrinsic charge separation capacity that differentiates them from metals.

Many kinds of metal oxides, such as titanium dioxide (titania, TiO_2) [35, 36], zinc oxide (ZnO) [37, 38], zirconium dioxide (zirconia, ZrO_2) [39, 40], and aluminum oxide (alumina, Al_2O_3) [41] were prepared from solutions of corresponding metal salt by sol-gel or hydrothermal methods. These materials have received tremendous attention due to their unique physicochemical properties and the potential for applications in water purification: removal of metal ions and nitrates, defluoridation, degradation of dyes [42].

TiO_2 is a simple inorganic, nontoxic, and inexpensive metal oxide compound, mostly used as a material in photocatalysis, with good optical properties and high chemical stability of reaction condition, which has received huge attention in environmental cleanup technologies. TiO_2

This book belongs to Badji Mokhtar Annaba University Central Library Copyright Elsevier 2025

exists in four different crystal forms: anatase with tetragonal structure and $I4_1/amd$ space group, rutile with tetragonal structure and $P4_2/mnm$ space group, brookite with rhombohedral structure and Pbca space group, and TiO_2(B) with monoclinic structure and C2/m space group [43–47]. Among them, in microdimensions, the rutile possesses more better properties (refractive index, specific gravity, thermal and chemical stability) than anatase, while anatase is more stable in nanomaterials. Brookite is the rarest structure of TiO_2 in nature, and it is difficult to synthesize in pure form, while TiO_2(B) was synthesized as a metastable compound for the first time in the 1980s [48].

Due to large band gap of TiO_2 (anatase ~3.2 eV and rutile ~3 eV), these materials absorb less than 5% of the available solar photons in the ultraviolet region. The most promising ways for increasing photoactivity of TiO_2 are to find the best methods, such as annealing of the material at high temperatures, preparation of hybrids with nanomaterials, metal deposition, heterogeneous composites, anion/cation doping, and implantation of dye-sensitization or additional surface adsorbents to modify its surface and electronic structure [49].

ZnO is a low-cost multifunctional semiconductor with an energy gap of 3.2 eV with unique physical and chemical properties with very low toxicity, as well as good thermal stability, biocompatibility, and biodegradability [50, 51]. ZnO as an excellent catalyst has been studied for the degradation of numerous organic pollutants [38, 52–54]. ZnO can occur in 1D (nanorods, needles, rings, ribbons, tubes, belts, wires), 2D (nanoplates/nanosheets and nanopellets), and 3D structures (flowers, dandelions, snowflakes, coniferous urchin-like) [55].

Al_2O_3 nanoparticles could be multilateral adsorbents in the processes used for purification of water due to their large surface area, high potentials, and availability of surface to bind functional groups over the pollutants. Al_2O_3 is the most applied material in ceramic membranes due to its ability to resist high transmembrane pressures [56].

2.2.3 Carbon-based nanomaterials

Carbon-based nanomaterials such as graphene and graphene-oxide, as well as carbon nanotubes, nanofibers, and dots, have occupied much of the attention due to their excellent chemical and physical properties. The graphene-oxide on the surface possesses a hydrophobic nature, in comparison to the hydrophilic oxidized state of graphene which possesses polarized functional groups on its surface. The carbon nanotubes are staggered in a 1D cylindrical nanostructure, and this material possesses excellent thermal properties. In recent years, carbon dots have become excellent material for biosensing, delivery of drug, and bioimaging due to easy preparation and design, high biocompatibility, low toxicity, and good optical properties [57]. In recent years, carbon-based nanomaterials appear as very important materials involved in the purification processes of drinking water [58].

This book belongs to Badji Mokhtar Annaba University Central Library Copyright Elsevier 2025

2.3 Synthesis of low-dimensional nanomaterials

As is known, nanosized materials possess contrasting properties in comparison to bulk materials of the same composition because of the large number of atoms on the surface. The nonlinear optical properties, the difference in melting point, adsorption and fast diffusion, ductility at elevated temperatures, superparamagnetic behavior, unique catalytic, sensitive, and activity make nanosized materials very unique [59]. The schematic presentation of synthetic methods and techniques used in preparation/synthesis of nanomaterials are given in Fig. 2.1.

Different kinds of synthetic methods for new multifunctional, inorganic, low-dimensional nanomaterials with different sizes, shapes, and morphologies were used for their preparation regarding different applications. Usually, there are two different types of methods for preparation of nanomaterials: (i) a bottom-up method assembles the nanoscale basic units into larger (bulk) structures using chemical or physical forces, and (ii) a top-down method controls the process of formation of nanomaterials from bulk structures. A bottom-up approach includes physical (spray pyrolysis or ion-implantation) and chemical methods (coprecipitation,

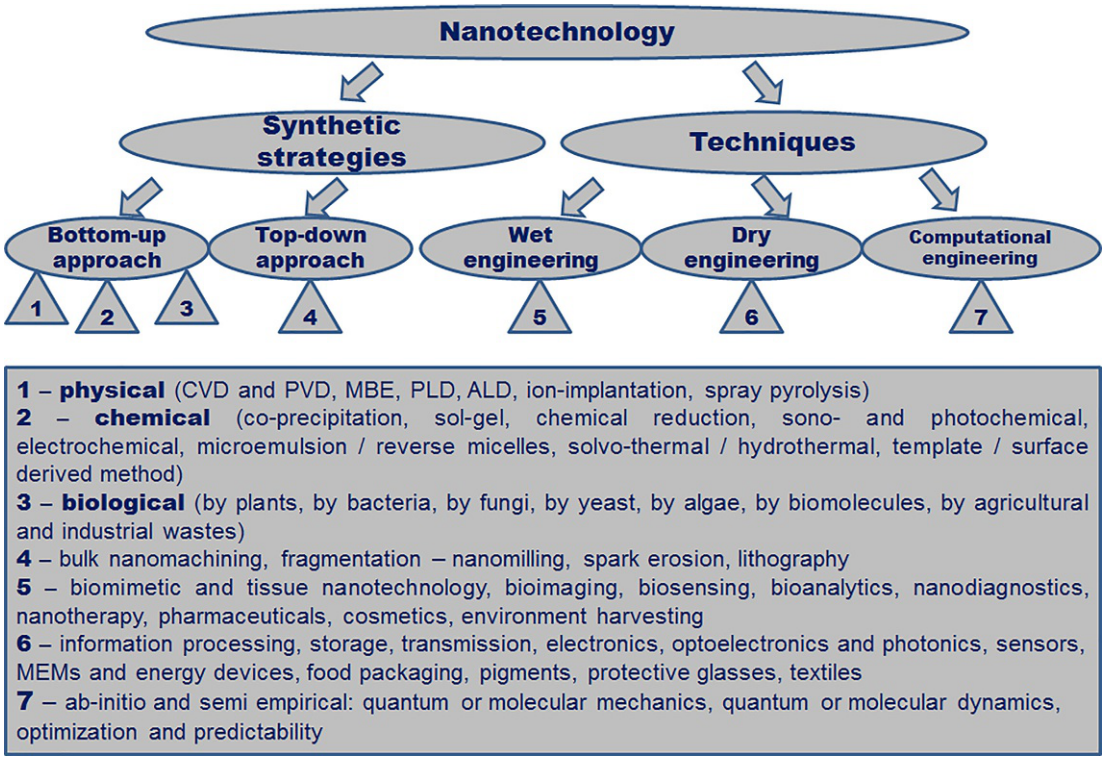

Fig. 2.1
Schematic representation of synthetic methods and techniques for preparation/synthesis of nanomaterials.

This book belongs to Badji Mokhtar Annaba University Central Library Copyright Elsevier 2025

colloidal, reverse micelles, sol-gel, hydrothermal/solvothermal method) and the biological synthesis and extraction of nanosized materials by plants, bacteria, fungi, algae, bacteria, or by agricultural and industrial wastes. A top-down approach includes bulk nanomachining, nanomilling, spark erosion, and so on. The usual technique for quantum and molecular design, modeling, and simulation of the properties of studied nanomaterials is computational engineering [59].

2.3.1 Synthesis of 0D nanomaterials (II–VI and III–V quantum dots)

In nanotechnology, the main aim is to obtain quantum dots with homogeneous distribution according to chemical composition, shape, size (monodispersion), and surface properties [60]. Wet synthesis for their preparation can be selected into two groups: a controlled precipitation and an organometallic method.

Before giving details about the synthesis, several terms encountered with colloidal nanoparticle synthesis should be introduced: colloidal stability, passivation, and monodispersity of particles.

After collision of colloidal particles in a dispersed medium, the repulsion or attraction forces come to be dominated in these nanoparticles. When force of attraction dominates between particles, they touch, aggregate, and form larger particles, which in the end lead to coagulation. To reach colloidal stability, it is necessary to keep balance between repulsion and attraction forces in a way similar to the stable mechanic equilibrium [61].

In colloidal chemistry, there are two ways to stabilize the colloidal solution: electrostatic and steric stabilization. Stabilization is reduced to: (a) enclosing a colloidal particle with a double electrical layer, so the connection of two particles is prevented by reflective electrostatic interactions between the layers; (b) surrounding the particle with a layer of adsorbed, or chemically bound, polymeric molecules, so that the layer is wide enough to physically prevent the convergence and therefore the coupling of the particles. Often, instead of stabilizing the colloid (colloidal solution), it is about passivation or (protective) overlap of colloidal particles. Stabilizers are used to stabilize colloids (also called coating agents or passivation agents) that prevent uncontrolled growth and aggregation of colloidal particles. Passivation stabilizes the colloidal nanoparticles, but it is also important in controlling the growth of nanoparticles and, very importantly, it allows the solubility of the particles in the appropriate solvent [62].

It was assumed that the particle size of the dispersed phase in the colloidal solution typically ranges from 1 to 1000 nm. When nearly all colloidal particles have the same size, the colloidal solution is monodisperse. Otherwise, there is polydispersed (heterodispersed) colloidal dispersion containing particles of different sizes; in this case, the distribution of sized particles should be discussed. The distribution is characterized by the mean (average) particle size and "width" of the distribution, i.e., mean square deviation. If the mean square deviation is less than 5%, the particles are monodisperse and a narrow particle size distribution gives them a very high surface area [63].

This book belongs to Badji Mokhtar Annaba University Central Library Copyright Elsevier 2025

LaMer and coworkers in the early of 1950s explained processes of colloidal formation including nucleation theory and transformation to nanoparticles [64, 65]. In his theory, it is necessary to have two stages in the formation of colloidal particles: rapid nucleation and slow crystal growth. In other words, it is necessary that crystallization occurs very quickly in the solvent while growth of crystals should be a very slow process. Namely, a short time of nucleation limits the distribution of particles by size, and if these conditions are satisfied, the colloidal particles grow uniformly and ultimately obtain particles that have, more or less, the same size, i.e., they are monodisperse. The size of the obtained particles increases with reaction time and rising of temperature. If nucleation and growth are successfully controlled, nanometer particles can be synthesized. In some colloids, there is another stage of the so-called Ostwald ripening; small crystals that are less stable dissolve and recrystallize on the surface of larger, more stable crystals. In this way, the particle size increases, but the number of particles decreases [66, 67]. It should be noted that there are few effective ways to narrow the distribution of particles after synthesis with postsynthetic techniques.

2.3.1.1 The method of controlled precipitation

The first synthesis of II–VI quantum dots of CdS and ZnS nanoparticles in the size of 3–6 nm originates from 1984 by Brus and coworkers [68–71]. Among the pioneers in the research of colloidal quantum dots is Mićić and coworkers [72, 73]. The method of controlled precipitation is based on the stopping of crystal growth and stabilization of colloids. For successful synthesis, the synthesized quantum dots should have a low solubility, be obtained at the corresponding value of pH and temperature, and their surface should be modified by a good choice of solvents and stabilizers. The monodisperse samples obtained in solvents have a small dielectric constant.

Synthesis of metal sulfide (MS; M is a metal II group of colloidal nanoparticles) consists of a chemical reaction between the corresponding solutions of cations and anions by mixing a diluted solution of the metals M^{2+} and S^{2-} ions. The solubility product of the obtained MS crystals is very small, and the MS will quantitatively precipitate [74]. The MS nanoparticles are usually synthesized in the reaction between an aqueous solution of metal salt (e.g., $Cd(ClO_4)$) and H_2S (or Na_2S) at room temperature involving slow injection of the Cd^{2+} ions into solution with S^{2-} ions, which are in a corresponding solvent (e.g., acetonitrile, methanol, or water). The precipitation of the final product will be based on the follow equation:

$$Cd(ClO_4) + Na_2S \rightarrow CdS + 2NaClO_4$$

To obtain colloidal particles in the size of a few nanometers, it is important to stop the growth of crystals after the formation of crystallization call (ending nucleation). Namely, tiny crystals (calls) must be protected from spontaneous dissolution and stabilized (protection against aggregation). The dynamics of nanoparticle formation are based on the equilibrium defined by the reaction, as well as from parameters such as the kind of solvent, dielectric constant of the solvent, temperature and concentration of the precursors, as well as the solubility of the

This book belongs to Badji Mokhtar Annaba University Central Library Copyright Elsevier 2025

obtained product. The solubility of synthesized CdS quantum dots in water at pH = 7 is about 7.9×10^{-5} mol L^{-1} [75].

The size of the prepared CdS quantum dots depends only on the kinetic parameters of the reaction and on stability of equilibrium, which depends on the size of crystals; for smaller crystals, it was moved to the right side because small crystals are more unstable than larger ones. In other words, "aging" or Oswald's ripening occurs [76]. As is known, the synthesis at lower temperature and solvents with lower dielectric constants reduce this Oswald's ripening; for examples in the solvents with lower dialectical constant, the stability of obtained small crystals is greater than in water. The short-chain alcohols and acetonitrile with higher dielectric constants are the most commonly used solvents in these syntheses [77].

The stable ZnS and CdS quantum dots in aqueous solution and in methanol without using any stabilizer, using acetonitrile as a solvent or adding polymers to aqueous solution, were synthesized in region size between 3.4 and 4.3 nm by Brus and coworkers [68–71].

The Brus's synthesis later was expanded by Weller on different semiconductors, such as CdSe, CdTe, ZnTe, HgTe, Zn_3P_2, and Cd_3P_2, using different coating agents, and stabilizers such as phosphates, amines, and thioalcohols. Samples of Zn_3P_2 and Cd_3P_2 show remarkable quantum configurations. For example, the bulk Cd_3P_2 powder is black, but in nanosized form, the particles change color from black to brown, red, orange, yellow, or completely white [78, 79].

Later, Wang et al. explained a simple method of synthesis for pure quantum dots involving the reduction of S to S^{2-} ions and Se to Se^{2-} ions in the presence of KBH_4, furthering their reaction with metal salts in the appropriate ratio and solvent at room temperature. It is important to note that solvent significantly affects the properties and uniformity in size of final products [80].

2.3.1.2 Organometallic synthesis of II–VI and III–V semiconductor nanoparticles

Bawendi et al. [81] applied organometallic synthesis for the first time in 1993 and obtained almost monodisperse CdS, CdSe, and CdTe nanoparticles with high quality. This was a key discovery because, in the meantime, it has been shown that this approach can be applied to other semiconductors. Today we have a very powerful technique for obtaining II–VI and III–V semiconductors. The most important is that organometallic synthesis shows great potential for industrial application.

The synthesis is carried out at higher temperatures (up to 300°C) in the reaction vessel with organometallic precursors in the presence of coordination solvent as stabilizing agents. Usually, two different kinds of precursors are used, but recent research was focused on intensely searching for new reactions/synthesis with a single precursor. In this synthesis, it is important to separate the occurrence of nucleation of nanocrystals from further growth. Experimentally, this is obtained by rapid injection of precursors into the heated solvent. The particle size control could be provided by adjusting the reaction temperature, time of crystal growth, and selection of suitable stabilizers [82].

This book belongs to Badji Mokhtar Annaba University Central Library Copyright Elsevier 2025

In the synthesis, phosphine derivatives, trioctylphosphine (TOP), and trioctylphosphine oxide (TOPO) are very important. Some of their characteristics include: the molecular weight of is TOP 370.6 g mol^{-1} and the boiling point is 284–291°C (at a reduced pressure of 50 mmHg), while the molecular weight of TOPO is 386.62 g mol^{-1} and it is in solid form at room temperature (melts at 50–55°C and boiling point is about 201–202°C at 2 mmHg). Schematic representation of two different synthesis methods, organometallic and aqueous colloidal synthesis, for preparation of CdSe quantum dots is shown in Fig. 2.2. Additionally, another combination of organometallic synthesis for II–VI and III–V semiconductor nanoparticles is presented in Table 2.2.

In recent years, several green approaches for preparation of CdSe, CdTe, and CdS quantum dots were developed. This synthesis was based on plant/microorganism-mediated biosynthesis using many natural products. Also, microorganisms such as fungi or bacteria (*Escherichia coli*) have been used in synthesis of different kinds of quantum dots [99–103]. Also, the capping

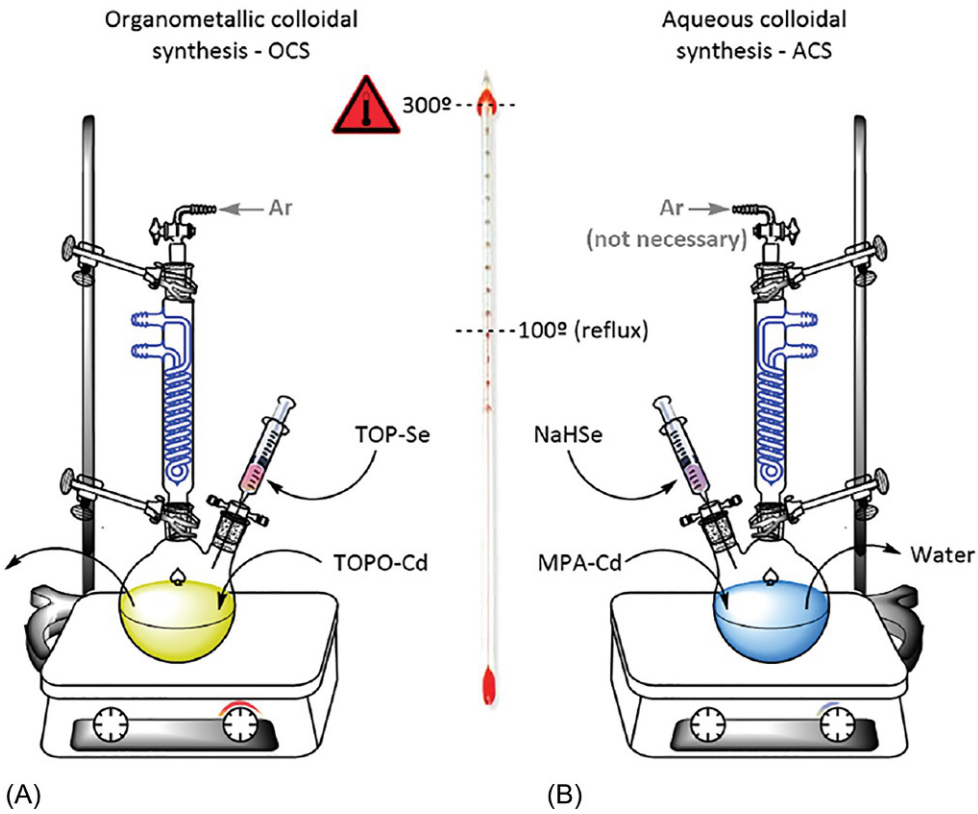

Fig. 2.2
Schematic representation for different methods of synthesis CdSe quantum dots: (A) organometallic colloidal synthesis and (B) aqueous colloidal synthesis.

This book belongs to Badji Mokhtar Annaba University Central Library
Copyright Elsevier 2025

Table 2.2: Organometallic synthesis of II–VI and III–V semiconductor nanoparticles.

	Precursors		Solvent	*T* (°C)	References
CdSe	Me_2Cd	TOPSe	TOPO, TOP	~300	[83, 84]
	Me_2Cd	TOPSe	HDA, TOP, TOPO	250–300	[85]
	Me_2Cd	$(TMS)_2Se$	TOPO, TOP	290–320	[83]
	CdO	TOPSe	HPA (TDPA), TOPO	~300	[85–87]
	CdO	TOPSe	SA, TOPO, HDA, TBP	320	[87]
	$CdCO_3$	TOPSe	SA, TOPO,TOP	300	[87, 88]
	Cd $(Ac)_2$	TOPSe	TOPO	270	[87, 88]
	Bis(metil-diselenocarbamate)Cd		TOPO	~200	[89]
CdS	Me_2Cd	$(TMS)_2S$	TOPO	290–320	[83]
	CdO	$(TMS)_2S$	TDPA(HDA), TOP, TOPO	~300	[86]
	Bis(metil-ditiocarbamate)Cd		TOPO	~200	[89]
CdTe	Me_2Cd	TOPTe	TOPO, TOP	~240	[83]
	Me_2Cd	$(BDMS)_2Te$	TOPO, TOP	290–320	[83]
	Me_2Cd	TOPTe	TOP, dodecylamine	150–220	[90]
	CdO	TOPTe	TDP, TOP	150–220	[90]
ZnSe	Me_2Zn,Et_2Zn	TOPSe	HDA, TOP	270–310	[91, 92]
	Bis(methyldiselenocarbamate)Zn		TOPO	~200	[89]
	Ethiyl(dimethyldiselenocarbamate)Zn		TOPO	~250	[93]
ZnS	Bis(methyl-dithiocarbamate)Zn		TOPO	~200	[89]
PbSe	Pb-oleate	TOPSe	Diphenyl ether, TOP	90–220	[94]
InP	$InCl_3$	$P(SiMe_3)_3$	TOPO	270	[95]
	$InCl_3$	$P(SiMe_3)_3$	TOPO, TOP	270	[96]
	$InCl_3$	$P(SiMe_3)_3$	DDA, TOP	~270	[97]
InAs	$InCl_3$	$As(SiMe_3)_3$	TOP	240–260	[98]
GaP	$GaCl_3$	$P(SiMe_3)_3$	TOPO, TOP	265	[98]
GaAs	$GaCl_3$	$As(SiMe_3)_3$	TOPO, TOP	150–450	[98]

agents are very important in determining the properties of quantum dots. Reducing the cytotoxicity, as well as the synthesis in aqueous solution, is very crucial. The starch-capped CdSe quantum dots with uniform size can be synthesized using photochemical synthesis in aqueous solution [104].

2.3.2 Synthesis of 1D and 2D nanomaterials

In recent years, a lot of various methods (spray pyrolysis, reverse micelles, coprecipitation, sol-gel, hydro (solvo) thermal) have been developed and used for synthesis of 1D and 2D nanomaterials with excellent optical properties.

This book belongs to Badji Mokhtar Annaba University Central Library Copyright Elsevier 2025

Here, the mentioned methods of synthesis will be briefly introduced and discussed. In the process of *ultrasonic spray pyrolysis*, aerosol generated from a precursor with aqueous colloidal solutions containing nanoparticles was introduced into a tubular flow reactor at corresponding temperature and using carrier gas. At the end of this reactor, after several processes of transformation and annealing of droplets, the desired powder material or film could be obtained [44].

A typical *reverse micelle method* is as follow. In two separate aqueous solutions of different precursors, oil (such as cyclohexane), surfactant (such as TRITON X-100), and cosurfactant (alcohols with short chains, such as *n*-pentanol) were added in corresponding volume ratio. After complete mixing of two separated reverse micelle systems, the mixture was allowed to stand at room temperature for many days. After centrifugation and washing, the obtained precipitate was dried and, in powder form, was used for other characterizations [105].

Using a simple *coprecipitation technique*, the nanosized materials were usually synthesized through hydrolysis of metal salt in the presence of any surfactants. In a typical procedure, the first precursor was dissolved in water including stirring and homogenization until a clear transparent solution was obtained. After that, the surfactant was added in corresponding molar ratio to precursor metal ions. Finally, in the previously obtained mixture, the solution of NaOH was added drop by drop to reach a value of pH until reaching the base medium. After that, the temperature is usually increased from room temperature up to 70°C or 80°C for many hours to complete the reaction. To obtain well-crystallized powder for characterizations, the obtained precipitate was centrifugated, washed, and annealed at corresponding temperature [106].

A typical *sol-gel* method is as follow. The precursors are usually separately dissolved in anhydrous ethanol and solutions are mixed dropwise with magnetic stirring for several hours at room temperature forming sol. The final powder was obtained by aging for several hours or a couple of days, drying at lower temperatures, and annealing calcinations of the prepared sol at higher temperatures.

The *hydrothermal technique* will be described during the procedure for TiO_2 preparation. Pure commercial (Degussa P25) TiO_2 powder was used as starting material that was mixed and stirred with aqueous solution of NaOH. This mixture was transferred in Teflon-lined stainless steel autoclave for hydrothermal treatment at corresponding temperature; the synthesis usually occurred at approximately 200°C for several hours or a couple of days in an oven. After synthesis and cooling to room temperature, the obtained precipitate was washed and centrifugated several times until all the Na^+ ions were removed. Finally, it was dried and then calcined at corresponding temperatures for several hours.

Pure structures of ZnO, TiO_2, CeO_2, as well as their hybrids, for example, TiO_2/SiO_2, obtained by spray pyrolysis, reverse micelles methods, or a simple coprecipitation technique at room temperature possess high photocatalytic activity, and these materials can be used as UV absorbers, in purification of water for decomposition of different organic pollutants, and to

This book belongs to Badji Mokhtar Annaba University Central Library Copyright Elsevier 2025

improve electrochemical performance in fuel cells [105–112]. Also, doped structures of TiO_2, as well as deposited films of TiO_2 onto an F-doped SnO_2 substrate with good photocatalytic properties for various applications, can be obtained by the spray pyrolysis method [113–116]. Also, N-F-co-doped TiO_2 powders with a very high photocatalytic activity can find potential application in air purification [117].

The metal-doped TiO_2 and W^{6+}-doped TiO_2 thin film prepared by a sol-gel method could find applications in photocatalysis [118–122]. The TiO_2-PbS hybrids and TiO_2-SiO_2, as well as Zr-doped VO_2 composites, were obtained by a sol-gel method giving strong photoconductance in the visible region, superhydrophilicity, and energy-saving material, respectively [123–125]. The TiO_2 nanorods and nanotubes were used as precursors in hydrothermal or microwave-hydrothermal method for preparation of mesoporous TiO_2 in anatase form and with high surface area, a promising material for energy and environmental application [126, 127].

The anatase TiO_2 particles in size approximately of 4 nm are usually synthesized by the colloidal chemistry method during hydrolysis of titanium tetrachloride ($TiCl_4$) in cold water (ice bath, $T = 0°C$) under vigorous stirring. Nanosized TiO_2 particles are very important as a material for various applications in everyday life due to their unique physiochemical properties [128, 129].

Also, other oxides such as MgO, WO_3, Fe_2O_3, and CuO/Cu_2O can be prepared by sol-gel methods that were used as photoelectrode coating materials [130–134].

2.3.3 Synthesis of carbon-based nanomaterials

Since the discovery of carbon dots in 2004 [135], considerable attention has been given in their preparation in very small (<10 nm) size and application for their excellent optical properties, nontoxicity effects, and low-cost synthetic methods. Among all techniques, laser ablation with high energy as well as at high temperature was used to produce quantum dots from a carbon target of a graphite powder/cement mixture. To enhance their photoluminescent properties, quantum yield, and brightness, the carbon dots synthesized by this method were additionally passivated with different molecular species, such as PEG and other polymers or with a layer of luminescent semiconductors, such as ZnS and ZnO [136, 137]. Also, different carbon-containing substrates such as various saccharides, amino acids, organic solvents, and proteins have been successfully used as targets using laser ablation for synthesis of carbon dots. Electrochemical technique used graphite rods as electrodes in an electrochemical cell in electrolyte solution in a mixture of NaOH and ethanol. The carbon dots prepared by this method were without uniform spherical morphologies but with distinct luminescence colors during different surface defects, morphology, and sizes of particle [138]. Many other synthetic "wet chemistry" methods have been used for preparation of carbon dots. Synthesis of the carbon dots is also possible from activated carbon or from acetone in NaOH solution acid treatment of

This book belongs to Badji Mokhtar Annaba University Central Library Copyright Elsevier 2025

carbon soot [139, 140]. In recent years, the hydrothermal treatment of different carbon precursors such as calamansi and pineapples wastes, lemon juice, and a lot of other carbon sources were used for synthesis of undoped or doped carbon quantum dots [141–143].

2.3.4 Structure and morphology of II–VI and III–V semiconductor nanomaterials

The conventional HRTEM and TEM images together with FFT of spherical CdS nanoparticles synthesized in oleylamine during the decomposition of precursors $Cd(OAc)_2 \times 2H_2O$, thiourea and salicylic acid, as well as from precursors $Cd(OAc)_2 \times 2H_2O$, thiosemicarbazide, and picolinic acid at $T = 120°C$ are presented in Fig. 2.3. The HRTEM images show polydisperse twins in the hexagonal phase in size range from 2 to 4 nm, while the SAED shows polycrystalline patterns with presence of orthorhombic and hexagonal phases. This orthorhombic phase is metastable, and it can be easily transformed to the hexagonal phase.

If different precursors are used during the synthesis, totally different morphologies are obtained, as presented in Fig. 2.4. For example, the nanorods and multipods were formed during decomposition of the salicylate precursors in a corresponding volume mixture of oleylamine

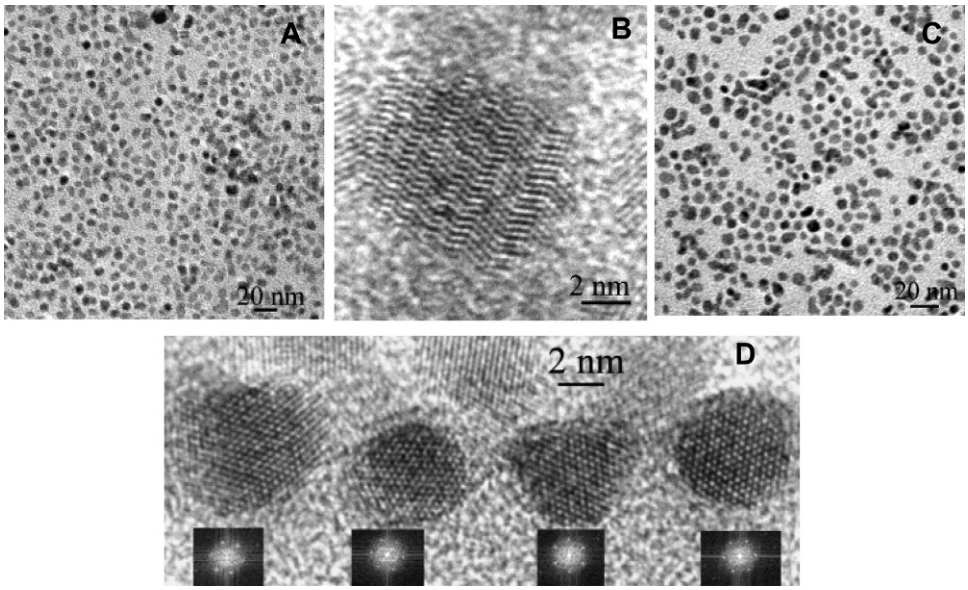

Fig. 2.3
Conventional TEM images of spherical CdS nanoparticles synthesized from precursors: oleylamine, $Cd(OAc)_2 \times 2H_2O$, thiourea and (A) salicylic acid or (C) picolinic acid, (B) HRTEM image of one of the particles shown in (A) reveals polysynthetic twins in the hexagonal phase and (D) HRTEM images and FFT for four nanoparticles with $[001]_{hex}$ zone axis orientation. *Adapted from T. Mandal, V. Stavila, I. Rusakova, S. Ghosh, K.H. Whitmire, Molecular precursors for CdS nanoparticles: synthesis and characterization of carboxylate–thiourea or –thiosemicarbazide cadmium complexes and their decomposition, Chem. Mater. 21 (2009) 5617–5626, with permission.*

This book belongs to Badji Mokhtar Annaba University Central Library Copyright Elsevier 2025

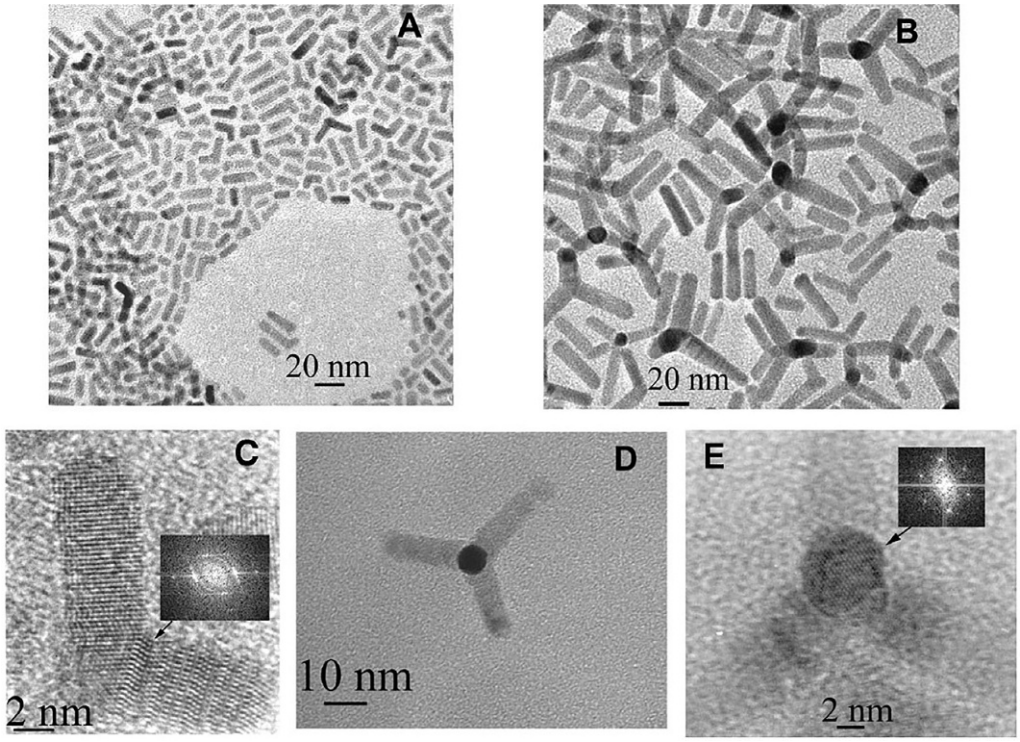

Fig. 2.4
Conventional HRTEM images of multibranched nanoparticles synthesized from precursor $Cd(OAc)_2 \times 2H_2O$, salicylic acid, thiosemicarbazide in oleyl amine in the presence of TOP and HCl. (A) Mixture of rods and bipods generated without using any dodecanethiol in the surfactant. (B) Mixture of rods, bipods, tripods, and tetrapods generated in the presence of a small amount of dodecanethiol. (C) HRTEM image one of the bipod structures shown in (A), FFT is obtained from the core of the particle. (D) Enlarged image of one of the tetrapod structures from (B). (E) HRTEM image of the tetrapod and FFT obtained from its central part. *Adapted from T. Mandal, V. Stavila, I. Rusakova, S. Ghosh, K.H. Whitmire, Molecular precursors for CdS nanoparticles: synthesis and characterization of carboxylate–thiourea or –thiosemicarbazide cadmium complexes and their decomposition, Chem. Mater. 21 (2009) 5617–5626, with permission.*

and TOP, while the rod-like nanoparticles were obtained with other precursors. On the other side, the tripods, tetrapods, and branches were obtained in the presence of a small amount of dodecanethiol in reaction mixture. The given SAED patterns of these CdS nanoparticles show the presence of face-centered cubic and hexagonal phases, while the hexagonal phase is most dominant [144].

The typical XRD pattern of CdSe quantum dots with cubic zinc blende structure is given in Fig. 2.5A, while Raman spectrum of the CdSe quantum dots with two characteristic peaks at 204 and 409 cm^{-1} is presented in Fig. 2.5B [107, 145].

This book belongs to Badji Mokhtar Annaba University Central Library Copyright Elsevier 2025

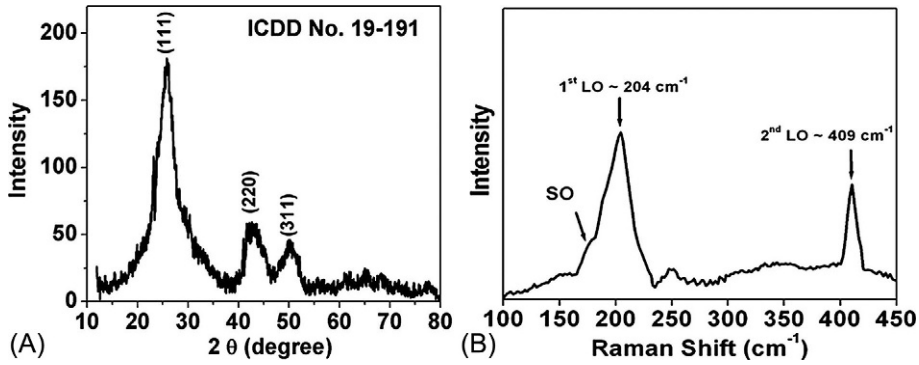

Fig. 2.5
(A) XRD pattern and (B) Raman spectra of CdSe quantum dots. *Adapted from B.N. Pawar, G. Cai, D. Ham, R.S. Mane, T. Ganesh, A. Ghule, R. Sharma, K.D. Jadhava, S.-H. Han, Preparation of transparent and conducting boron-doped ZnO electrode for its application in dye-sensitized solar cells, Sol. Energy Mater. Sol. Cells 93 (2009) 524–527, with permission.*

2.4 Physicochemical properties

2.4.1 Optical properties of 0D of II–VI and III–V nanomaterials

If one, two, or three dimensions of a semiconductor material are smaller than exciton Bohr radius of the same semiconductor, its properties change dramatically, and, very importantly, they exhibit a size effect and difference in comparison to corresponding bulk material/crystal. Here, the absorption and photoluminescence of semiconductor nanoparticles will be considered separately.

2.4.1.1 Absorption spectra

The observed changes in the absorption spectrum of the nanoparticles in comparation to bulk material such as blueshift, discretization of the spectrum, and increase in the absorption coefficient are extremely significant. For a given semiconductor, the energy gap (E_g) or band gap is an energy range where no electron states can exist, and it characterizes the electronic and optical properties of materials (see Table 2.3). For example, the $E_g = 1.74$ eV, at 300 K for bulk CdSe crystals larger than 6 nm. In other words, the bulk CdSe material can only absorb photons with an energy $E_g = 1.74$ eV, i.e., absorption exists only for wavelengths ≤ 713 nm, and this is the characteristic (limiting) wavelength of absorption for CdSe material. However, for CdSe nanocrystals smaller than 6 nm, the E_g increases with decreasing size, and it can be equivalent to moving λ_g to smaller wavelengths, i.e., toward the *blue region (from right to left side)* (*gray* in print version) of the spectrum, as it is known as "blueshift" of the wavelength. Fig. 2.6 presents absorption spectra of CdSe nanocrystals with several different sizes (left) and corresponding photoluminescence spectra under UV excitation at 380 nm (right) [146].

This book belongs to Badji Mokhtar Annaba University Central Library Copyright Elsevier 2025

Table 2.3: Examples for wastewater treatment using different nanomaterials.

Kind of nanoparticles	Target	Treatment mechanism
TiO_2, doped TiO_2	Organic pollutants	Photocatalysis, photocatalytic degradation
ZnO	Organic pollutants	Photocatalysis
CdS, CdSe	Organic pollutants	Photocatalysis
CdS, CdSe	Heavy metals, anions	Sensing, photoluminescence quenching
CdSe/ZnS	Organic pollutants	Disinfection, photocatalytic degradation
ZnS:Cu	Cationic dyes	Nanoadsorbent
ZnS/TiO_2	Dyes	Photocatalysis, photocatalytic degradation
S-graphene oxide/ZnS	Organic components	Photocatalysis, photocatalytic degradation
Carbon-based nanomaterials	Metal ions	Sensing, photoluminescence quenching
Graphene oxide	Dyes	Removal of dyes, adsorbent
Fe	Heavy metals, anions, organic pollutants	Reduction, adsorption
Ag, Au	Organic pollutants	Photocatalysis, photocatalytic degradation, adsorbent
Fe_3O_4	Heavy metals, organic compounds	Adsorption
Dendrimers	Heavy metals, organic pollutants	Encapsulation
Nanotubes	Heavy metals, anions, organic pollutants	Adsorption
Al_2O_3-based membranes	Organic components	Membrane for wastewater filtration

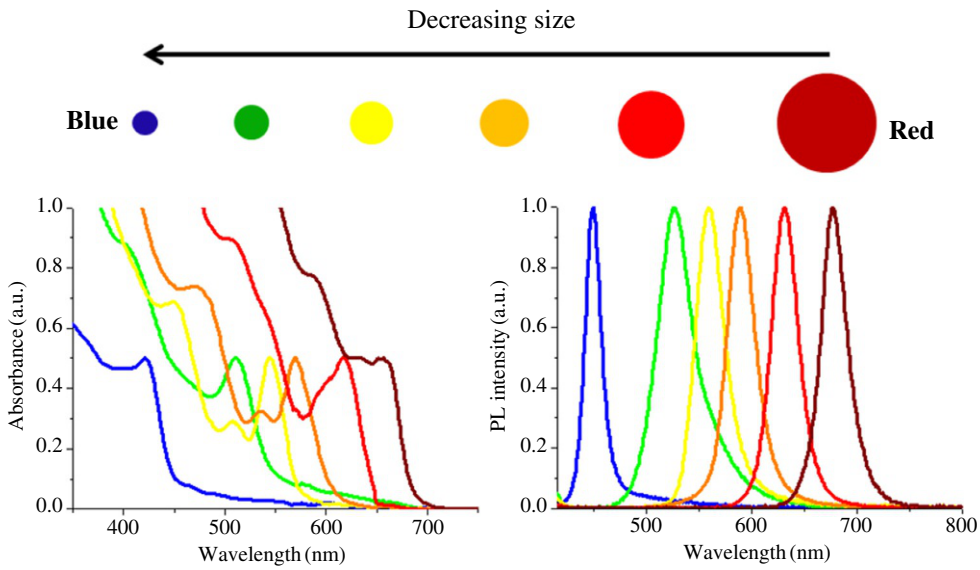

Fig. 2.6

Absorption spectra of differently sized CdSe nanocrystals (left) and corresponding photoluminescence spectra representing from deeper *red* to *blue (from right to left)* (*gray* in print version) emitting of CdSe nanocrystals under UV excitation at 380 nm. *Adapted from Y. Yuan, M. Krüger, M., Polymer-nanocrystal hybrid materials for light conversion applications, Polymers 4 (2012) 1–19, with permission.*

This book belongs to Badji Mokhtar Annaba University Central Library
Copyright Elsevier 2025

The phenomenon of pronounced peaks in the absorption spectra of nanoparticles is another important difference compared with the absorption spectra of bulk material. It should be emphasized that one or more peaks that occur also exhibit a quantum size effect: smaller particles have better defined and spaced peaks. The next difference in the absorption spectra of nanoparticles is based on absorption coefficient of the material, i.e., it could be explained that smaller particles absorb light better. It is interesting the bulk CdSe material has a brown color, whereas by reducing the particle size, this material changes color with maximum of absorption spectra at lower wavelengths with corresponding color. An increase in the peak height shows an increase in the absorption coefficient with a decreasing size of nanoparticles.

2.4.1.2 Photoluminescent spectra

If the semiconductor nanocrystals are illuminated by wavelengths lower than λ_g, emission occurs. The photoluminescent spectrum is a well-defined Gaussian peak that occurs near the excitation peak wavelength, and it should not depend on the excitation wavelength. In fact, there is a redshift of this peak in photoluminescent spectrum relative to the excitation peak, i.e., its wavelength of appearing in the luminescent peak is always at a higher wavelength than the excitation peak [147–150].

The particle's size affects the position of the peaks, and therefore a blueshift occurs in the luminescent spectra: for smaller particles, the maximum of the luminescent peak moves toward shorter wavelengths. Thus, luminescent quantum dots of CdSe can be created to change colors across the full region of visible spectrum. The peak width is typically 30 nm at room temperature, and it usually was measured at half-height of the luminescent peak. The peak width depends on several factors, but the particle size distribution is the most significant; the narrower distribution of particles has the smaller peak width. Another important parameter is so-called quantum yield, QY, which gives the probability of emission after absorption of an excitation photon. The maximum value of QY can be at 1 (or 100%) and for commercial fluorescent organic dyes is about 0.8 (or 80%). It has been shown that the passivation of the surface of the quantum dots has a great influence on the QY value. For example, when quantum dots are passivated by organic molecules, the QY is about 0.1 at room temperature, but its value can be increased by lowering the temperature. However, if the semiconductor particle is passivated by a layer of inorganic crystal or by another semiconductor, there is a remarkable improvement in the fluorescence properties.

2.4.1.3 3D quantum confinement

The size effect on absorption and photoluminescent properties of semiconductor nanoparticles remains to be explained. Classical Mie theory is known to describe how colloidal particles absorb and scatter light. However, for particles in size from 1 nm up to 10 nm, classical theory cannot explain the blueshift of the limit wavelength. This is the so-called quantum-mechanical phenomena. In colloidal semiconductor particles, the connection between size and optical

This book belongs to Badji Mokhtar Annaba University Central Library Copyright Elsevier 2025

spectra was developed in 1983 on the ZnS and CdS, and later was experimentally established on a large number of different nanometer-scale semiconductor materials [68–70].

The variation of E_g with particle size is described by a simple Brus's model. The optical properties of semiconductor nanoclusters, that is, the interaction of the electromagnetic field and the particle, are reduced in the first approximation to the interactions between electrons, holes, and their environments. Basically, this is a problem of two particles (positive and negative) of masses $m_e{}^*$ and $m_h{}^*$ that are attracted and moved by Coulomb's forces for spheres with radius R. This is the so-called approximation of effective masses, or the so-called effective mass of electron and effective mass of hole. The effective masses $m_e{}^*$ i $m_h{}^*$ are the characteristics of the material, and it varies for different semiconductors. The electron and hole make up the exciton moving as a whole, and the mean distance of the electrons and the hole is Bohr's exciton radius a_B. For a given material (determined by μ, $m_e{}^*$ i $m_h{}^*$), a_B is given by follow equation:

$$a_B = \frac{\hbar^2 \varepsilon}{e^2}\left[\frac{1}{m_e^*} + \frac{1}{m_h^*}\right] = \frac{\hbar^2 \varepsilon}{e^2 \mu^*}$$

where μ^* is reduced effective mass of exciton (as presented in Table 2.1). It is not difficult to solve the Schrödinger equation of motion exciton in the sphere with radius R, and to solve it we obtain the Brus equation:

$$E(R) = E_g + \frac{\hbar^2 \pi^2}{2R^2 \mu^*} - \frac{1.8e^2}{R\varepsilon}$$

where e is the elemental charge. The energy of the exciton ground state is given by Brus's formula, and in addition to constant for energy gap, E_g, there are two terms, term for kinetic energy of exciton and term for energy of the Coulomb interaction between particles. Thus, the width of the E_g in the semiconductor particle with spherical shape depends on the size of particle R. Using Brus's formula, we see the physical meaning of the width of the energy gap: this is the energy required to create a pair of electron-holes, while the second and third terms of Brus's formula are zero. The confinement energy in nanoparticles with limited exciton is always higher than E_g, and in the rough approximation it is proportional to $1/R^2$. Although the theory and experiment agree quite well, Brus's theory predictions deviate significantly for smaller particles. By using various semiempirical and exact methods, it is possible to achieve good agreement with experimental data.

It is extremely important to emphasize the difference between the energy states in the bulk material and in the quantum dots; for bulk materials, there are almost continuous bands of states, while quantum confinement results in a series of discrete states in nanoparticles, i.e., in quantum dots. The theory presented earlier is quite simple and explains the absorption spectra of quantum dots quite successfully. However, photoluminescence is far more difficult to explain and the field is far from a complete theory.

This book belongs to Badji Mokhtar Annaba University Central Library Copyright Elsevier 2025

2.4.2 Optical properties of 1D and 2D nanomaterials

Due to high excellent chemical and biological properties, photoreactivity and photostability, low-cost synthesis, and no toxicity, TiO_2 is one of the most studied materials used in basic research and practical applications.

The detailed mechanism of photocatalysis depends on the kind of pollutants. A step-by-step mechanism for photocatalysis for the TiO_2_based materials is as follows: (1) formation of charge carriers, (2) recombination of charge carriers, (3) trapping of a conduction-band electron, (4) trapping of a valence-band holes, (5) initiation of an oxidative pathway by holes, (6) initiation of a reductive pathway by electrons, and (7) hydrolysis or reactions with active oxygen species and photocatalytic reactions to yield mineralization products [151].

The valence and conduction band of anatase TiO_2 possess O 2p and Ti 3d orbitals, respectively, with band gap approximately at 3.2 eV. Photo-UV-irradiation results in charge separation of electrons into the conduction band and the holes in the valence band. These formed pairs of electrons and holes together present electron donors and acceptors [152].

To overcome the available limited solar light, there is a need to find TiO_2-based photocatalysts operating under visible light. Changing its band edge could be achieved by doping TiO_2 with*different cations such as S, N, Cr, V, In, Se, C, Pd, Cu, and Fe by plasmonic effects on*the*surface by metal Au or Ag nanoparticles, by formation of surface complex, by coupling*with visible-light-sensitive materials or quantum dots, by organic dye, or by vitamin C [153–158].

Photocatalytic degradation of dyes through semiconductor materials follows some complex pathways. If energy of irradiation for the material is higher than the band gap energy, TiO_2 surface is illuminated and active species are generated by oxidative degradation of the corresponding dye. The methyl orange (MO) as an organic dye was often used as a pollutant model for degradation. An example of degradation of MO using the photocatalyst TiO_2 under irradiation by solar simulator is given by following steps [159]:

$$TiO_2 + hv \rightarrow h_{vb}{}^{+} + e_{cb}{}^{-}$$

$$e_{cb}{}^{-} + O_2 \rightarrow O_2{}^{\bullet -}$$

$$h_{vb}{}^{+} + H_2O \rightarrow {}^{\bullet}OH + H^{+}$$

$$O_2{}^{\bullet -} + MO \rightarrow \text{degradation of product}$$

$${}^{\bullet}OH + MO \rightarrow \text{degradation of product}$$

Fig. 2.7 presents two examples of degradation rate for MO with time for TiO_2 photocatalysts doped with percentages (%) of Pd and N. From Fig. 2.7A, it can be concluded that degradation rate increased by increasing the doping of Pd, which indicates an increase of photocatalytic

This book belongs to Badji Mokhtar Annaba University Central Library Copyright Elsevier 2025

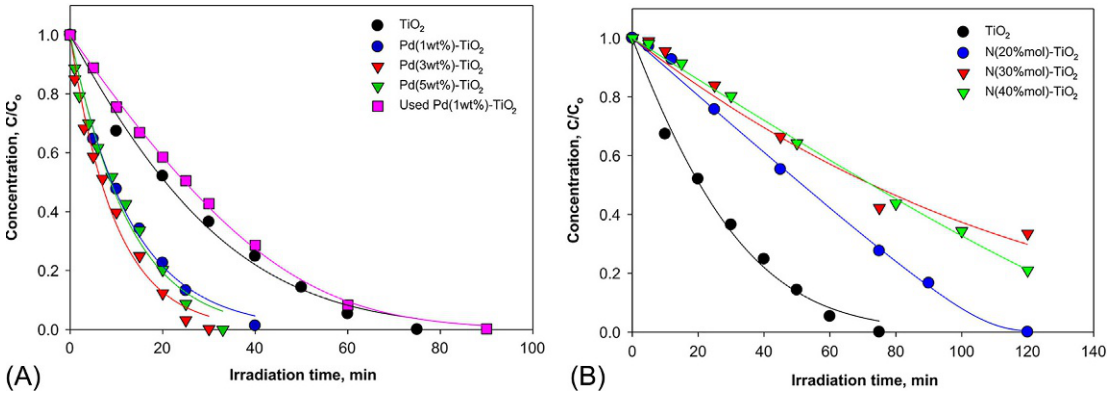

Fig. 2.7

(A) Degradation kinetics of MO by TiO_2, Pd (1 wt%)-, Pd (3 wt%)-, Pd (5 wt%)-doped TiO_2, and reused Pd (1 wt%)-TiO_2: 0.25 g/L photocatalyst, 40 ¼mol/L MO, no pH control, and AM1.5G irradiation and (b) degradation kinetics of MO by N (20 mol%)-, N (30 mol%)-, and N (40 mol%)-doped TiO_2: 0.25 g/L photocatalyst, 40 ¼mol/L MO, no pH control, and AM1.5G irradiation. *Adapted from M. Anas, D.S. Han, K. Mahmoud, H. Park, A. Abdel-Wahab, Photocatalytic degradation of organic dye using titanium dioxide modified with metal and non-metal deposition, Mat. Sci. Semicon. Proc. 41 (2016) 209–218, with permission.*

activity of the modified catalyst under sunlight. On other side, Fig. 2.7B presents dependence of the degradation rate by increasing percentages of doping TiO_2 by nitrogen under sunlight. From this figure, it can be concluded that the rate for degradation of undoped TiO_2 is faster than N-doped TiO_2. The reason for this may lead to a difference in particle size [159].

As discussed earlier, the size has a very large effect on absorption and photoluminescent properties of semiconductor nanoparticles. Here, several examples based on the difference in optical property between 0D and 1D nanomaterial will be described.

The properties can be changed by tuning the particle size during synthesis (changing temperature, time of synthesis, solvent, etc.) without any changes in the chemical composition. By reducing the size of CdSe quantum dots from 2 to 6 nm, it is possible to obtain nanoparticles emitting different colors, blue, green, yellow, orange, and red, under UV excitation [146].

In comparison to 0D quantum dots, the nanohybrids and anisotropic 1D and 2D nanocrystals (nanorods and nanoplatelets) exhibit larger absorption cross-section, higher quantum yields, and stronger quantum confinement [160]. Also, ZnO did not have any peaks in UV-Vis absorption spectrum, but after formation of 0D CdS quantum dots on 1D ZnO nanorods, there is a peak at about 380 nm due to electronic transitions in CdS, and optical band gap was changed [161].

This book belongs to Badji Mokhtar Annaba University Central Library Copyright Elsevier 2025

2.5 Low-dimensional nanomaterials in wastewater treatment

Low-dimensional nanomaterials have increasing presence in the environment and water/wastewater treatment technologies. Photocatalysis has been investigated as an effective wastewater treatment process in recent years, but there are still some challenges that need to be solved for industrial application, such as solar utilization efficiency, photocatalytic activities of membranes, testing under solar irradiation, and design of a photoreactor.

Abdel-Maksoud et al. studied and developed a TiO_2 photocatalytic reactor for scale-up and commercialization, and phenol was chosen as a model pollutant as its degradation depends on light intensity, exposure time, and pH of medium [162]. A coating of TiO_2 nanoparticles on the plastic sheet was used for wastewater treatment [163].

Modification of the current photocatalysts such as doping is a good pathway to enhance efficiency under solar irradiation. Photocatalytic degradation of organic dyes/pollutants depends on various factors such as the kind of oxidizing agent; pH of medium; initial concentration of dyes; kind, size, shape, and initial concentration of photocatalyst; reaction time and temperature; intensity and wavelength of light; and the presence of electron acceptors [164].

Kusic et al. studied the catalytic effect of CdSe/ZnS hybrid quantum dots in water treatment and disinfection for the degradation of different organic pollutants [165], while Mahmoodi et al. used CdSe quantum dots for degradation of dyes such as Violet 16, Blue 41, and Acid Blue 92 [166].

The fast recombination of electron-hole pairs in CdS irradiated by visible light is one limitation of the photocatalytic process. To slow down this process of recombination, there are different possibilities, for example, hybrids with different semiconductor materials or with materials with high surface areas, with noble metals, with conductive supports, and so on [167–171]. There are several examples based on the CdS nanoparticles used for significantly improved properties in photocatalysis, electrocatalysis, and wastewater treatment: nanocomposites composed of CdS and graphene, nanostructures with Au nanoparticles located at the outside most layer of CdS, composites of CdS and zeolitic imidazolate frameworks, as well as composites such as CdS/g-C_3N_4/MOF and CdS-TiO_2 [172–175]. The CdSe quantum dots functionalized by thiourea were used for sensing different kinds of metal ions. The selective quenching on the photoluminescence intensity of CdSe quantum dots in presence several metal ions with different concentration is presented in Fig. 2.8. The quenching was analyzed by Stern-Volmer equation, and it depends on the concentration of added ions.

All the previously mentioned carbon-based nanomaterials have shown great potential for wastewater treatment due to their low toxicity, high adsorption capacity and selectivity, excellent biocompatibility, and highly tunable photoluminescence properties [176–183]. Different kind of nanoparticles, targets, and main treatment mechanisms in water treatments are presented in Table 2.3.

This book belongs to Badji Mokhtar Annaba University Central Library Copyright Elsevier 2025

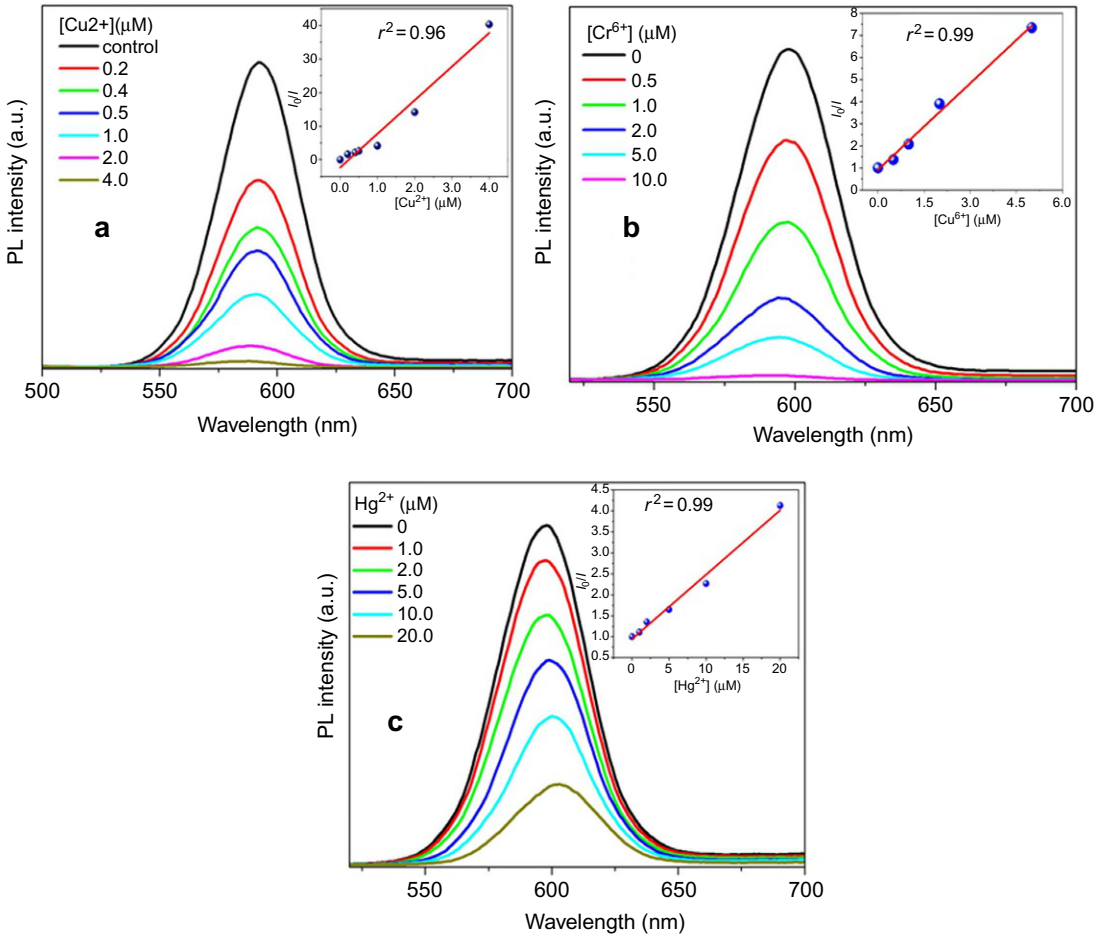

Fig. 2.8

Quenching of photoluminescence emission intensity in the CdSe QDs in presence of different metal ions: (A) Cu^{2+}, (B) Cr^{6+}, and (C) Hg^{2+}; insets on the all figures present Stern Volmer plots. *Adapted from B.N. Pawar, G. Cai, D. Ham, R.S. Mane, T. Ganesh, A. Ghule, R. Sharma, K.D. Jadhava, S.-H. Han, Preparation of transparent and conducting boron-doped ZnO electrode for its application in dye-sensitized solar cells, Sol. Energy Mater. Sol. Cells 93 (2009) 524–527, with permission.*

2.6 Conclusion

In recent years, research interest has increased for the development of new methods of synthesis and preparation of numerous different applications of low-dimensional nanomaterials. These materials are expected to show novel unusual physicochemical properties in comparation to corresponding bulk materials of the same composition. Due to a very high ratio between surface area and volume, the low-dimensional nanomaterials have more atoms on their surface

This book belongs to Badji Mokhtar Annaba University Central Library Copyright Elsevier 2025

compared with their respective bulk counterparts, thus these materials exhibit high visible-light photocatalytic activity. These excellent properties make them ideal for numerous new applications such as nanoadsorbents, nanocatalysts, nanofibers, and nanobiocides for separation of organic pollutants, heavy metals, inorganic anions, bacteria, oil spills, and waste disposal from contaminated water.

This chapter presented an all-encompassing review of developments, general definition of classification, methods of syntheses, trends and advances in research, as well as physicochemical properties of low-dimensional (0D, 1D, 2D, and 3D) nanomaterials. The main attention has been focused on syntheses of 0D, 1D, 2D, and 3D nanomaterials and the effects of size, shape, morphology, and crystal structures on their optical properties and further applications in wastewater treatment, i.e., removal of chemical compounds/pollutants from water (adsorption and separation, catalytic oxidation, disinfection, and sensing).

Acknowledgments

This work is supported by the Ministry of Education, Science, and Technological Development of the Republic of Serbia (451-03-68/2020-14/200017).

References

[1] P.V. Kamat, K. Murakoshi, Y. Wada, S. Yanagida, Semiconductor nanoparticles, in: H.S. Nalwa (Ed.), Handbook of Nanostructured Materials and Nanotechnology, Elsevier, New York, 2000, pp. 291–344.
[2] R. Khairutdinov, Chemistry of semiconductor nanoparticles, Russ. Chem. Rev. 67 (2) (1998) 109–122.
[3] K. Gajanana, S.N. Tijareb, Applications of nanomaterials, Mater. Today Proc. 5 (2018) 1093–1096.
[4] T.V. Gavrilović, D.J. Jovanović, K. Smits, M.D. Dramićanin, Multicolor upconversion luminescence of $GdVO_4$:Ln^{3+}/Yb^{3+} (Ln^{3+} = Ho^{3+}, Er^{3+}, Tm^{3+}, Ho^{3+}/Er^{3+}/Tm^{3+}) nanorods, Dyes Pigments 126 (2016) 1–7.
[5] M.A. Ebrahimzadeh, A. Tafazoli, J. Akhtari, P. Biparva, S. Eslami, Engineered silver nanoparticles, a new nanoweapon against cancer, Anti-Cancer Agents Med. Chem. 18 (2018) 1962–1969.
[6] Y. Zhong, B. Li, S. Li, S. Xu, Z. Pan, Q. Huang, L. Xing, W. Li, Bi nanoparticles anchored in N-doped porous carbon as anode of high energy density lithium ion battery, Nano-Micro Lett. 10 (2018) 56.
[7] V.S. Saji, H.-C. Choe, K. Yeung, Nanotechnology in biomedical applications – a review, Int. J. Nano Biomater. 3 (2) (2010) 119–139.
[8] L. Labrador-Páez, D.J. Jovanović, M.I. Marqués, K. Smits, S.D. Dolić, F. Jaque, H.E. Stanley, M. D. Dramićanin, J. García-Solé, P. Haro-González, D. Jaque, Unveiling molecular changes in water by small luminescent nanoparticles, Small 13 (2017) 1700968 (7 pp).
[9] B. del Rosal, A. Pérez-Delgado, E. Carrasco, D.J. Jovanović, M.D. Dramićanin, G. Dra∼ić, Á.J. de la Fuente, F. Sanz-Rodriguez, D. Jaque, Neodymium-based stoichiometric ultrasmall nanoparticles for multifunctional deep-tissue photothermal therapy, Adv. Opt. Mater. 4 (5) (2016) 782–789.
[10] F.D. Guerra, M.F. Attia, D.C. Whitehead, F. Alexis, Nanotechnology for environmental remediation: materials and applications, Molecules 23 (7) (2018) 1760.
[11] C.H. Lee, B. Tiwari, D. Zhang, Y.K. Yap, Water purification: oil–water separation by nanotechnology and environmental concerns, Environ. Sci. Nano 4 (2017) 514–525.
[12] W.-W. Tang, G.-M. Zeng, J.-L. Gong, J. Liang, P. Xu, C. Zhang, B.-B. Huanget, Impact of humic/fulvic acid on the removal of heavy metals from aqueous solutions using nanomaterials: a review, Sci. Total Environ. 468–469 (2014) 1014–1027.

This book belongs to Badji Mokhtar Annaba University Central Library Copyright Elsevier 2025

[13] J. Yan, L. Han, W. Gao, S. Xue, M. Chen, Biochar supported nanoscale zerovalent iron composite used as persulfate activator for removing trichloroethylene, Bioresour. Technol. 175 (2015) 269–274.
[14] F. Liu, J.H. Yang, J. Zuo, D. Ma, L. Gan, B. Xie, P. Wang, B. Yang, Graphene-supported nanoscale zero-valent iron: removal of phosphorus from aqueous solution and mechanistic study, J. Environ. Sci. 26 (8) (2014) 1751–1762.
[15] R.S. Kalhapure, S.J. Sonawane, D.R. Sikwal, M. Jadhav, S. Rambharose, C. Mocktar, T. Govender, Solid lipid nanoparticles of clotrimazole silver complex: an efficient antibacterial against Staphylococcus aureus and MRSA, Colloids Surf. B Biointerfaces 136 (2015) 651–658.
[16] T.C. Prathna, S.K. Sharma, M. Kennedy, Nanoparticles in household level water treatment: an overview, Sep. Purif. Technol. 199 (2018) 260–270.
[17] H. Lu, J. Wang, M. Stoller, T. Wang, Y. Bao, H. Hao, An overview of nanomaterials for water and wastewater treatment, Adv. Mater. Sci. Eng. 2016 (2016) 4964828 (10 pp).
[18] Y. Zhang, B. Wu, H. Xu, H. Liu, M. Wang, Y. He, B. Pan, Nanomaterials-enabled water and wastewater treatment, NanoImpact 3–4 (2016) 22–39.
[19] J. Jiang, Q. Zhang, X. Zhan, F. Chen, A multifunctional gelatin-based aerogel with superior pollutants adsorption, oil/water separation and photocatalytic properties, Chem. Eng. J. 358 (2019) 1539–1551.
[20] H. Gleiter, Nanostructured materials: basic concepts and microstructure, Acta Mater. 48 (2000) 1–29.
[21] V. Skorokhod, A. Ragulya, I. Uvarova, Physico-Chemical Kinetics in Nanostructured Systems, Academperiodica, Kyiv, 2001, 180.
[22] V.V. Pokropivny, V.V. Skorokhod, Classification of nanostructures by dimensionality and concept of surface forms engineering in nanomaterial science, Mater. Sci. Eng. C 27 (2007) 990–993.
[23] J. Jeevanandam, A. Barhoum, Y.S. Chan, A. Dufresne, K.D. Michael, Review on nanoparticles and nanostructured materials: history, sources, toxicity and regulations, Beilstein J. Nanotechnol. 9 (2018) 1050–1074.
[24] A.P. Alivisatos, Semiconductor clusters, nanocrystals, and quantum dots, Science 271 (1996) 933–937.
[25] P. Moriarty, Nanostructured materials, Rep. Prog. Phys. 64 (2001) 297–381.
[26] V.L. Colvin, D.M. Mittleman, Nanocrystals, in: Encyclopedia of Physical Chemisty and Chemical Physics, CRC Press, 2005 (online).
[27] A.L. Rogach, D.V. Talapin, H. Weller, Semiconductor nanocrystal, in: F. Caruso (Ed.), Colloids and Colloid Assemblies, Willey, 2004.
[28] S. Suresh, Semiconductor nanomaterials, methods and applications: a review, Nanosci. Nanotechnol. 3 (3) (2013) 62–74.
[29] K. Akiba, Electronic States of Narrow-Gap Semiconductors Under Multi-Extreme Conditions, Springer thesesSpringer, Singapore, 2019.
[30] S.M. Sze, K.K. Ng, Physics and Properties of Semiconductors—A Review, John Wiley and Sons, 2007.
[31] A.D. Yoffe, Low-dimensional systems: quantum size effects and electronic properties of semiconductor microcrystallites (zero-dimensional systems) and some quasi-two-dimensional systems, Adv. Phys. 51 (2002) 173–262.
[32] D. Bera, L. Qian, T.-K. Tseng, P.H. Holloway, Quantum dots and their multimodal applications: a review, Materials 3 (2010) 2260–2345.
[33] T. Edvinsson, Optical quantum confinement and photocatalytic properties in two-, one- and zero-dimensional nanostructures, R. Soc. Open Sci. 5 (2018) 180387.
[34] H.T. Grahn, Introduction to Semiconductor Physics, World Scientific Publishing Co Pte Ltd, Singapore, 1999.
[35] S.G. Ullattil, P. Periyat, Sol-gel synthesis of titanium dioxide, in: S.C. Pillai, S. Hehir (Eds.), Sol-Gel Materials for Energy, Environment and Electronic Applications, first ed., Springer International Publishing, 2017, pp. 271–283.
[36] M. Vranjes, J. Kuljanin-Jakovljevic, M. Milosevic, G. Ciric-Marjanovic, M. Stoiljkovic, Z. Konstantinovic, V. Pavlovic, D. Milivojevic, Z. Saponjic, Hydrothermal synthesis of Mn^{2+} doped titanate nanotubes: investigation of their structure and room temperature ferromagnetic behavior, Solid State Sci. 94 (2019) 155–161.

This book belongs to Badji Mokhtar Annaba University Central Library Copyright Elsevier 2025

[37] L. Znaidi, Sol–gel-deposited ZnO thin films: a review, Mater. Sci. Eng. B 174 (2010) 18–30.
[38] L.V. Trandafilović, D.J. Jovanović, X. Zhang, S. PtasiDska, M.D. Dramićanin, Enhanced photocatalytic degradation of methylene blue and methyl orange by ZnO:Eu nanoparticles, Appl. Catal. B Environ. 203 (2017) 740–752.
[39] M.V. Carević, N.D. Abazović, T.B. Novaković, V. Pavlović, M.I. Čomor, Zirconium dioxide nanopowders with incorporated Si^{4+} ions as efficient photocatalyst for degradation of trichlorophenol using simulated solar light, Appl. Catal. B Environ. 195 (2016) 112–120.
[40] B. Tyagi, K. Sidhpuria, B. Shaik, R.V. Jasra, Synthesis of nanocrystalline zirconia using sol-gel and precipitation techniques, Ind. Eng. Chem. Res. 45 (2006) 8643–8650.
[41] L. Yang, S. Yin, T. Sato, Synthesis of morphology controlled aluminum oxide by hydrothermal reaction, IOP Conf. Mater. Sci. Eng. 18 (2011) 032015.
[42] Z. Tian, X. Ge, Y. Wang, J. Xu, K. Song, Nanoparticles and nanocomposites with microfluidic technology, in: C. Liu, J.Z. Guo (Eds.), Polymer-Based Multifunctional Nanocomposites and Their Applications, Elsevier, Amsterdam, Oxford, Cambridge, 2019.
[43] N. Rahimi, R.A. Pax, M.N. Gray, Review of functional titanium oxides. I: TiO_2 and its modifications, Prog. Solid State Chem. 44 (2016) 86–105.
[44] I.M. Dugand∼ić, D.J. Jovanović, L.T. Mančić, N. Zheng, S.P. Ahrenkiel, O.B. Miloaević, Z. V. Šaponjić, J.M. Nedeljković, Surface modification of submicronic TiO_2 particles prepared by ultrasonic spray pyrolysis for visible light absorption, J. Nanopart. Res. 14 (2012) 1157.
[45] D.J. Jovanović, I.M. Dugand∼ić, G. Ćirić-Marjanović, T. Radetić, S.P. Ahrenkiel, O. B. Miloaević, J.M. Nedeljković, Z.V. Šaponjić, L.T. Mancic, Spherical assemblies of titania nanotubes generated through aerosol processing, Ceram. Int. 41 (2015) 14754–14759.
[46] I.M. Dugand∼ić, D.J. Jovanović, L.T. Mancić, O.B. Miloaević, S.P. Ahrenkiel, Z. V. Šaponjić, J.M. Nedeljković, Ultrasonic spray pyrolysis of surface modified TiO_2 nanoparticles with dopamine, Mater. Chem. Phys. 143 (2013) 233–239.
[47] L.T. Mancić, I.M. Dugand∼ić, O.B. Miloaević, D.J. Jovanović, Z.V. Šaponjić, M.E. Rabanal, L.S. G. Villalba, Aerosol-assisted processing of hierarchically organised TiO_2 nanoparticles, Int. J. Mater. Prod. Technol. 50 (3/4) (2015) 221–229.
[48] R. Marchand, L. Brohan, M. Tournoux, TiO_2(B) a new form of titanium dioxide and the potassium octatitanate $K_2Ti_8O_{17}$, Mater. Res. Bull. 15 (1980) 1129–1133.
[49] H. Park, Y. Park, W. Kim, W. Choi, Surface modification of TiO_2 photocatalyst for environmental applications, J. Photochem. Photobiol. C: Photochem. Rev. 15 (2013) 1–20.
[50] S. Kuriakose, B. Satpati, S. Mohapatra, Enhanced photocatalytic activity of codoped ZnO nanodisks and nanorods prepared by a facile wet chemical method, Phys. Chem. Chem. Phys. 16 (25) (2014) 12741–12749.
[51] S.J. Pearton, D.P. Norton, K. Ip, Y.W. Heo, T. Steiner, Recent progress inprocessing and properties of ZnO, Prog. Mater. Sci. 50 (3) (2005) 293–340.
[52] M. Miyauchi, A. Nakajima, T. Watanabe, K. Hashimoto, Photocatalysis and photoinduced hydrophilicity of various metal oxide thin films, Chem. Mater. 14 (6) (2002) 2812–2816.
[53] N.K. Singh, S. Saha, A. Pal, Methyl red degradation under UV illuminationand catalytic action of commercial ZnO: a parametric study, Desalin. Water Treat. 56 (2014) 1–11.
[54] J. Yu, X. Yu, Hydrothermal synthesis and photocatalytic activity of zinc oxide hollow spheres, Environ. Sci. Technol. 42 (13) (2008) 4902–4907.
[55] A. KoBodziejczak-Radzimska, T. Jesionowski, Zinc oxide—from synthesis to application: a review, Materials 7 (2014) 2833–2881.
[56] S.A. Younssi, M. Breida, B. Achiou, Alumina Membranes for Desalination and Water Treatment, Intechopen, London, UK, 2018.
[57] S. Noamani, S. Niroomand, M. Rastgar, M. Sadrzadeh, Carbon-based polymer nanocomposite membranes for oily wastewater treatment, NPJ Clean Water 2 (2019) 20.
[58] S.C. Smith, D.F. Rodrigues, Carbon-based nanomaterials for removal of chemical and biological contaminants from water: a review of mechanisms and applications, Carbon 91 (2015) 122–143.
[59] M.S. Chavali, M.P. Nikolova, Metal oxide nanoparticles and their applications in nanotechnology, SN Appl. Sci. 1 (2019) 607 (pp. 30).

This book belongs to Badji Mokhtar Annaba University Central Library Copyright Elsevier 2025

[60] A.V. Blaaderen, A. Vrij, Synthesis and characterization of monodisperse colloidal organo-silica spheres, J. Colloid Interface Sci. 156 (1993) 1–18.
[61] M. Akbulut, A.R.G. Alig, Y. Min, N. Belman, M. Reynolds, Y. Golan, J. Israelachvili, Forces between surfaces across nanoparticle solutions: role of size, shape, and concentration, Langmuir 23 (2007) 3961–3969.
[62] I. Capek, Modification and passivation of colloidal particles, in: I. Capek (Ed.), Nanocomposite Structures and Dispersions Science and Nanotechnology—Fundamental Principles and Colloidal Particles, vol. 23, Elsevier B.V., 2006, pp. 225–292 (Chapter 4).
[63] E. Matijević, Production of monodispersed colloidal particles, Ann. Rev. Mater. Sci. 15 (1985) 483–516.
[64] V.K. LaMer, Nucleation in phase transitions, Ind. Eng. Chem. 44 (1952) 1270–1277.
[65] V.K. LaMer, R.H. Dinegar, Theory, production and mechanism of formation of monodispersed hydrosols, J. Am. Chem. Soc. 72 (1950) 4847–4854.
[66] J. Polte, Fundamental growth principles of colloidal metal nanoparticles—a new perspective, CrystEngComm 17 (2015) 6809–6830.
[67] M. Seehra, A. Bristow, Noble and Precious Metals: Properties, Nanoscale Effects and Applications, InTechOpen, 2018.
[68] L.E. Brus, A simple model for the ionization potential, electron affinity, and aqueous redox potentials of small semiconductor crystallites, J. Chem. Phys. 79 (1983) 5566.
[69] L.E. Brus, Electron–electron and electron-hole interactions in small semiconductor crystallites: the size dependence of the lowest excited electronic state, J. Chem. Phys. 80 (1984) 4403.
[70] R. Rossetti, R. Hull, J.M. Gibson, L.E. Brus, Excited electronic states and optical spectra of ZnS and CdS crystallites in the J15 to 50 Å size range: evolution from molecular to bulk semiconducting properties, J. Chem. Phys. 82 (1984) 552.
[71] L.E. Brus, Electronic wave functions in semiconductor clusters: experiment and theory, J. Phys. Chem. 90 (1986) 2555–2560.
[72] J.M. Nedeljković, M.T. Nenadović, O.I. Mićić, A.J. Nozik, Enhanced photoredox chemistry in quantized semiconductor colloids, J. Phys. Chem. 90 (1986) 12–13.
[73] A.J. Nozik, F. Williams, M.T. Nenadović, T. Rajh, O.I. Mićić, Size quantization in small semiconductor particles, J. Phys. Chem. 89 (1985) 397–399.
[74] A.I. Gusev, A.A. Rempel, Nanocrystalline Materials, Cambridge International Science Publishing, 2004.
[75] S.W.F.M.V.H.T. Westerflier, J.J.M. Binsma, H.N. Stein, C. Vandecasteele, Solubility of particulate cadmium sulfide at pH = 1–14: a radiotracer study, J. Radioanal. Nucl. Chem. 111 (1987) 305–317.
[76] F. Arcudi, D.E. Westmoreland, E.A. Weiss, Colloidally stable CdS quantum dots in water with electrostatically stabilized weak-binding, sulfur-free ligands, Chem. Eur. J. 25 (2019) 14469–14474.
[77] A. Hassinen, I. Moreels, K.D. Nolf, P.F. Smet, J.C. Martins, Z. Hens, Short-chain alcohols strip X-type ligands and quench the luminescence of PbSe and CdSe quantum dots, acetonitrile does not, J. Am. Chem. Soc. 134 (51) (2012) 20705–20712.
[78] U. Resch, H. Weller, A. Henglein, Photochemistry and radiation chemistry of colloidal semiconductors. 33. Chemical changes and fluorescence in CdTe and ZnTe, Langmuir 5 (1989) 1015–1020.
[79] H. Weller, A. Fojtik, A. Henglein, Photochemistry of semiconductor colloids: properties of extremely small particles of Cd_3P_2 and Zn_3P_2, Chem. Phys. Lett. 117 (1985) 485–488.
[80] M. Henini (Ed.), Handbook of Self Assembled Semiconductor Nanostructures for Novel Devices in Photonics and Electronics, first ed., Elsevier Science, 2008.
[81] C.B. Murray, D.J. Norris, M.G. Bawendi, Synthesis and characterization of nearly monodisperse CdE (E = sulfur, selenium, tellurium) semiconductor nanocrystallites, J. Am. Chem. Soc. 115 (1993) 8706–8715.
[82] H. Zhong, T. Mirkovic, G.D. Scholes, Nanocrystal synthesis in reference module in materials science and materials engineering comprehensive, Nanosci. Technol. 5 (2011) 153–201.
[83] J.J. Li, Y.A. Wang, W. Guo, J.C. Keay, T.D. Mishima, M.B. Johnson, X. Peng, Large-scale synthesis of nearly monodisperse CdSe/CdS core/shell nanocrystals using air-stable reagents via successive ion layer adsorption and reaction, J. Am. Chem. Soc. 125 (2003) 12567–12575.
[84] C.B. Murray, C.R. Kagan, M.G. Bawendi, Synthesis and characterization of monodisperse nanocrystals and close-packed nanocrystal assemblies, Annu. Rev. Mater. Sci. 30 (2000) 545–610.

This book belongs to Badji Mokhtar Annaba University Central Library Copyright Elsevier 2025

[85] Z.A. Peng, X. Peng, Nearly monodisperse and shape-controlled CdSe nanocrystals via alternative routes: nucleation and growth, J. Am. Chem. Soc. 124 (2002) 3343–3353.
[86] Z.A. Peng, X. Peng, Formation of high-quality CdTe, CdSe, and CdS nanocrystals using CdO as precursor, J. Am. Chem. Soc. 123 (2001) 183–184.
[87] Z.A. Peng, X. Peng, Alternative routes toward high quality CdSe nanocrystals, Nano Lett. 1 (2001) 333–337.
[88] J. Aldana, Y.A. Wang, X. Peng, Photochemical instability of CdSe nanocrystals coated by hydrophilic thiols, J. Am. Chem. Soc. 123 (2001) 8844–8850.
[89] B. Ludolph, M.A. Malik, Novel single molecule precursor routes for the direct synthesis of highly monodispersed quantum dots of cadmium or zinc sulfide or selenide, Chem. Commun. 1998 (1998) 1849–1950.
[90] D.V. Talapin, S. Haubald, A.L. Rogach, A. Kornowski, M. Haase, H. Weller, A novel organometallic synthesis of highly luminescent CdTe nanocrystals, J. Phys. Chem. B 105 (2001) 2260–2263.
[91] M.A. Hines, P. Guyot-Sionnest, Bright UV-blue luminescent colloidal ZnSe nanocrystals, J. Phys. Chem. B 102 (1998) (1998) 3655–3657.
[92] D.J. Norris, N. Yao, F.T. Charnock, T.A. Kennedy, High-quality manganese-doped ZnSe nanocrystals, Nano Lett. 1 (2001) 3–7.
[93] N. Revaprasadu, M.A. Malik, P. O'Brien, M.M. Zulu, G. Wakefield, Single-source molecular precursors for the deposition of zinc selenide quantum dots, J. Mater. Chem. 8 (1998) 1885–1888.
[94] C.B. Murray, S. Sun, W. Gaschler, H. Doyle, T.A. Betley, C.R. Kagan, Colloidal synthesis of nanocrystals and nanocrystal superlattices, IBM J. Res. Develop. 45 (2001) 47–56.
[95] O.I. Micic, H.M. Cheong, H. Fu, A. Zunger, J.R. Spragre, A. Mascavenhis, A.J. Nozik, Size-dependent spectroscopy of InP quantum dots, J. Phys. Chem. B 101 (1997) 4904–4912.
[96] O. Micic, C.J. Curtis, K.M. Jones, J.R. Sprague, A.J. Nozik, Synthesis and characterization of InP quantum dots, J. Phys. Chem. 98 (1994) 4966–4969.
[97] D.V. Talapin, A.L. Rogach, I. Menis, S. Haubold, A. Kornowski, M. Haase, H. Weller, Synthesis and surface modification of amino-stabilized CdSe, CdTe and InP nanocrystals, Colloids Surf. A 202 (2002) 145–154.
[98] A.A. Guzelian, U. Banin, A.V. Kadavahich, X. Peng, A.P. Alivisatos, Colloidal chemical synthesis and characterization of InAs nanocrystal quantum dots, Appl. Phys. Lett. 69 (1996) 1432.
[99] M.N. Borovaya, A.P. Naumenko, N.A. Matvieieva, Y.B. Blume, A.I. Yemets, Biosynthesis of luminescent CdS quantum dots using plant hairy root culture, Nanoscale Res. Lett. 9 (1) (2014) 686.
[100] M. Rai, C. Posten (Eds.), Green Biosynthesis of Nanoparticles—Mechanisms and Applications, first ed., CAB International, Wallingford, UK, 2013.
[101] S.A. Kumar, A.A. Ansary, A. Ahmad, M.I. Khan, Extracellular biosynthesis of CdSe quantum dots by the fungus, Fusarium oxysporum, J. Biomed. Nanotechnol. 3 (2) (2007) 190–194.
[102] H. Bao, Z. Lu, X. Cui, Y. Qiao, J. Guo, J.M. Anderson, C.M. Li, Extracellular microbial synthesis of biocompatible CdTe quantum dots, Acta Biomater. 6 (9) (2010) 3534–3541.
[103] C. Mi, Y. Wang, J. Zhang, H. Huang, L. Xu, S. Wang, X. Fang, J. Fang, C. Mao, S. Xu, Biosynthesis and characterization of CdS quantum dots in genetically engineered *Escherichia coli*, J. Biotechnol. 153 (3–4) (2011) 125–132.
[104] A. Singh, A. Guleria, S. Neogy, M.C. Rath, UV induced synthesis of starch capped CdSe quantum dots: functionalization with thiourea and application in sensing heavy metals ions in aqueous solution, Arab. J. Chem. 13 (2020) 3149–3158.
[105] D. Zhang, L. Qi, J. Ma, H. Cheng, Formation of crystalline nanosized titania in reverse micelles at room temperature, J. Mater. Chem. 12 (2002) 3677–3680.
[106] N. Samaele, P. Amornpitoksuk, S. Suwanboon, Effect of pH on the morphology and optical properties of modified ZnO particles by SDS via a precipitation method, Powder Technol. 203 (2010) 243–247.
[107] B.N. Pawar, G. Cai, D. Ham, R.S. Mane, T. Ganesh, A. Ghule, R. Sharma, K.D. Jadhava, S.-H. Han, Preparation of transparent and conducting boron-doped ZnO electrode for its application in dye-sensitized solar cells, Sol. Energy Mater. Sol. Cells 93 (2009) 524–527.
[108] S.S. Hong, M.S. Lee, S.S. Park, G.D. Lee, Synthesis of nanosized TiO_2/SiO_2 particles in the microemulsion and their photocatalytic activity on the decomposition of p-nitrophenol, Catal. Today 87 (2003) 99–105.

This book belongs to Badji Mokhtar Annaba University Central Library Copyright Elsevier 2025

[109] Z.R. Khan, M.S. Khan, M. Zulfequar, M.S. Khan, Optical and structural properties of ZnO thin films fabricated by sol-gel method, Mater. Sci. Appl. 2 (2011) 340–345.
[110] P.H. Borse, L.S. Kankate, F. Dassenoy, W. Vogel, J. Urban, S.K. Kulkarni, Synthesis and investigations of rutile phase nanoparticles of TiO_2, J. Mater. Sci. Mater. Electron. 13 (2002) 553–559.
[111] Y. Bai, J. Wu, X. Qiu, J. Xi, J. Wang, J. Li, W. Zhu, L. Chen, Electrochemical characterization of Pt-CeO_2/C and Pt-$Ce_xZr_{1-x}O_2$/C catalysts for ethanol electro-oxidation, Appl. Catal. B Environ. 73 (2007) 144–149.
[112] F. Zhang, S.W. Chan, J.E. Spanier, E. Apak, Q. Jin, R.D. Robinson, I.P. Herman, Cerium oxide nanoparticles: size-selective formation and structural analysis, Appl. Phys. Lett. 80 (2002) 127–129.
[113] L. Castaneda, J.C. Alonso, A. Ortiz, E. Andrade, J.M. Saniger, J.G. Banuelos, Spray pyrolysis deposition and characterization of titanium oxide thin films, Mater. Chem. Phys. 77 (2002) 938–944.
[114] M. Okuya, N.A. Prokudina, K. Mushika, S. Kaneko, TiO_2 thin films synthesized by the spray pyrolysis deposition (SPD) technique, J. Eur. Ceram. Soc. 19 (1999) 903–906.
[115] M.O. Abou-Helal, W.T. Seeber, Preparation of TiO_2 thin films by spray pyrolysis to be used as a photocatalyst, Appl. Surf. Sci. 195 (2002) 53–62.
[116] N.J. Jeon, J.H. Noh, W.S. Yang, J.C. Kim, S. Ryu, J. Seo, S. Seok, Compositional engineering of perovskite materials for high-performance solar cells, Nature 517 (2015) 476–480.
[117] D. Li, H. Haneda, S. Hishita, N. Ohashi, Visible-light-driven N−F−codoped TiO_2 photocatalysts. 2. Optical characterization, photocatalysis, and potential application to air purification, Chem. Mater. 17 (2005) 2596–2602.
[118] C. Tao, S. Ruan, X. Zhang, G. Xie, L. Shen, X. Kong, W. Dong, C. Liu, W. Chen, Performance improvement of inverted polymer solar cells with different top electrodes by introducing a MoO_3, buffer layer, Appl. Phys. Lett. 93 (2008) 193307.
[119] X. Chen, S.S. Mao, Titanium dioxide nanomaterials: synthesis, properties, modifications, and applications, Chem. Rev. 107 (2007) 2891–2959.
[120] Y. Yang, H. Wang, X. Li, C. Wang, Electrospun mesoporous W^{6+}-doped TiO_2 thin films for efficient visible-light photocatalysis, Mater. Lett. 63 (2009) 331–333.
[121] N.N. Ilkhechi, F. Dousi, B.K. Kaleji, E. Salahi, Optical and structural properties of TiO_2 nanocomposite doped by Si and Cu at high temperature, Opt. Quant. Electron. 47 (2015) 1751–1763.
[122] J. Bahadur, S. Agrawal, V. Panwar, A. Parveen, K. Pal, Antibacterial properties of silver doped TiO_2 nanoparticles synthesized via sol-gel technique, Macromol. Res. 24 (2016) 488–493.
[123] P. Hoyer, R. Könenkamp, Photoconduction in porous TiO_2 sensitized by PbS quantum dots, Appl. Phys. Lett. 66 (1995) 349–351.
[124] M. Houmard, D. Riassetto, F. Roussel, A. Bourgeois, G. Berthomé, J.C. Joud, M. Langlet, Enhanced persistence of natural super-hydrophilicity in TiO_2-SiO_2 composite thin flms deposited via sol-gel route, Surf. Sci. 602 (2008) 3364–3374.
[125] W. Lu, G. Zhao, B. Song, J. Li, X. Zhang, G. Han, Preparation and thermochromic properties of sol-gel-derived Zr-doped VO_2 films, Surf. Coat. Technol. 320 (2017) 311–314.
[126] Z.V. Saponjić, N.M. Dimitrijević, D.M. Tiede, A.J. Goshe, X. Zuo, L.X. Chen, A. S. Barnard, P. Zapol, L. Curtiss, T. Rajh, Shaping nanometer-scale architecture through surface chemistry, Adv. Mater. 17 (2005) 965–971.
[127] J.N. Nian, H. Teng, Hydrothermal synthesis of single-crystalline anatase TiO_2 nanorods with nanotubes as the precursor, J. Phys. Chem. B 110 (2006) 4193–4198.
[128] T. Rajh, A.E. Ostafin, O.I. Mićić, D.M. Tiede, M.C. Thurnauer, Surface modification of small particle TiO_2 colloids with cysteine for enhanced photochemical reduction: an EPR study, J. Phys. Chem. 100 (1996) 4538–4545.
[129] N.D. Abazović, M.I. Čomor, M.D. Dramićanin, D.J. Jovanović, S.P. Ahrenkiel, J. M. Nedeljković, Photoluminescence of anatase and rutile TiO_2 particles, J. Phys. Chem. B 110 (2006) 25366–25370.
[130] J.W. Long, K.E. Swider-Lyons, R.M. Stroud, D.R. Rolison, Design of pore and matter architectures in manganese oxide charge-storage materials, Electrochem. Solid State Lett. 3 (2000) 453–456.
[131] P.G. Bruce, B. Scrosati, J.M. Tarascon, Nanomaterials for rechargeable lithium batteries, Angew. Chem. Int. Ed. 47 (2008) 2930–2946.

This book belongs to Badji Mokhtar Annaba University Central Library Copyright Elsevier 2025

[132] Y. Yang, D. Xu, Q. Wu, P. Diao, Cu_2O/CuO Bilayered composite as a high-efficiency photocathode for photoelectrochemical hydrogen evolution reaction, Sci. Rep. 6 (2016) 35158 (13 pp).
[133] X.Z. Yuan, W. Qu, J. Fahlman, Spinel $Ni_xCo_{2-x}O_4$ as a bifunctional air electrode for zinc air batteries, ECS Trans. 45 (2013) 105–112.
[134] C.-F. Chen, G. King, R.M. Dickerson, P.A. Papin, S. Gupta, W.R. Kellogg, G. Wu, Oxygen deficient $BaTiO_{3-x}$ perovskite as an efficient bifunctional oxygen electrocatalyst, Nano Energy 13 (2015) 423–432.
[135] M. Fu, F. Ehrat, Y. Wang, K.Z. Milowska, C. Reckmeier, A.L. Rogach, J.K. Stolarczyk, A. S. Urban, J. Feldmann, Carbon dots: a unique fluorescent cocktail of polycyclic aromatic hydrocarbons, Nano Lett. 15 (2015) 6030–6035.
[136] Y.-P. Sun, X. Wang, F. Lu, L. Cao, M.J. Meziani, P.G. Luo, L. Gu, L.M. Veca, Doped carbon nanoparticles as a new platform for highly photoluminescent dots, J. Phys. Chem. C 112 (2008) 18295–18298.
[137] H. Yu, X. Li, X. Zeng, Y. Lu, Preparation of carbon dots by non-focusing pulsed laser irradiation in toluene, Chem. Commun. 52 (2016) 819–822.
[138] H. Li, X. He, Z. Kang, H. Huang, Y. Liu, J. Liu, S. Lian, C.H.A. Tsang, X. Yang, S.-T. Lee, Water-soluble fluorescent carbon quantum dots and photocatalyst design, Angew. Chem. Int. Ed. 49 (2010) 4430–4434.
[139] S.C. Ray, A. Saha, N.R. Jana, R. Sarkar, Fluorescent carbon nanoparticles: synthesis, characterization, and bioimaging application, J. Phys. Chem. C 113 (2009) 18546–18551.
[140] L. Tian, D. Ghosh, W. Chen, S. Pradhan, X. Chang, S. Chen, Nanosized carbon particles from natural gas soot, Chem. Mater. 21 (2009) 2803–2809.
[141] B.T. Hoan, P.D. Tam, V.-H. Pham, Green synthesis of highly luminescent carbon quantum dots from lemon juice, J. Nanotechnol. 2019 (2019) 2852816 (9 pp).
[142] R.C. So, J.E. Sanggo, L. Jin, J.M.A. Diaz, R.A. Guerrero, J. He, Gram-scale synthesis and kinetic study of bright carbon dots from citric acid and citrus japonica via a microwave-assisted method, ACS Omega 2 (2017) 5196–5208.
[143] F. Lin, Y.W. Bao, F.-G. Wu, Carbon dots for sensing and killing microorganisms, C 5 (2019) 33 (21 pp).
[144] T. Mandal, V. Stavila, I. Rusakova, S. Ghosh, K.H. Whitmire, Molecular precursors for CdS nanoparticles: synthesis and characterization of carboxylate–thiourea or –thiosemicarbazide cadmium complexes and their decomposition, Chem. Mater. 21 (2009) 5617–5626.
[145] A.M. Kelley, Q. Dai, Z.-J. Jiang, J.A. Baker, D.F. Kelley, Resonance Raman spectra of wurtzite and zincblende CdSe nanocrystals, Chem. Phys. 422 (2013) 272–276.
[146] Y. Yuan, M. Krüger, Polymer-nanocrystal hybrid materials for light conversion applications, Polymers 4 (2012) 1–19.
[147] Q. Wang, A. Tang, Y. Liu, Z. Fang, S. Fu, A tunable photoluminescent composite of cellulose nanofibrils and CdS quantum dots, Nanomaterials 6 (2016) 164.
[148] E. Kuçur, J. Ziegler, T. Nann, Synthesis and spectroscopic characterization of fluorescent blue-emitting ultrastable CdSe clusters, Small 4 (2008) 883–887.
[149] A. Chakrabarty, S. Marre, R.F. Landis, V.M. Rotello, U. Maitra, A. Del Guerzob, C. Aymonier, Continuous synthesis of high quality CdSe quantum dots in supercritical fluids, J. Mater. Chem. C 3 (2015) 7561–7566.
[150] D. Thomas, H.O. Lee, C.K. Santiago, M. Pelzer, A. Kuti, E. Jenrette, M. Bahoura, Rapid microwave synthesis of tunable cadmium selenide (CdSe) quantum dots for optoelectronic applications, J. Nanomater. 2020 (2020) 5056875 8 pp.
[151] J. Schneider, M. Matsuoka, M. Takeuchi, J. Zhang, Y. Horiuchi, M. Anpo, D.W. Bahnemann, Understanding TiO_2 photocatalysis: mechanisms and materials, Chem. Rev. 114 (2014) 9919–9986.
[152] S. Higashimoto, Titanium-dioxide-based visible-light-sensitive photocatalysis: mechanistic insight and applications, Catalysts 9 (2) (2019) 201.
[153] S.G. Kumar, L.G. Devi, Review on modified TiO_2 photocatalysis under UV/visible light: selected results and related mechanisms on interfacial charge carrier transfer dynamics, J. Phys. Chem. A 115 (2011) 13211–13241.
[154] V. Kumaravel, S. Rhatigan, S. Mathew, J. Bartlett, M. Nolan, S.J. Hinder, P.K. Sharma, A. Singh, J. A. Byrne, J. Harrison, S.C. Pillai, J. Phys. Chem. C 123 (2019) 21083–21096.
[155] N. Turkten, Z. Cinar, A. Tomruk, M. Bekbolet, Copper-doped TiO_2 photocatalysts: application to drinking water by humic matter degradation, Environ. Sci. Pollut. Res. 26 (2019) 36096–36106.

This book belongs to Badji Mokhtar Annaba University Central Library Copyright Elsevier 2025

[156] W. Xie, R. Li, Q. Xu, Enhanced photocatalytic activity of Se-doped TiO_2 under visible light irradiation, Sci. Rep. 8 (2018) 8752.
[157] T. Ohno, Preparation of visible light active S-doped TiO_2 photocatalysts and their photocatalytic activities, Water Sci. Technol. 49 (2004) 159–163.
[158] T. Rajh, J.M. Nedeljkovic, L.X. Chen, O. Poluektov, M.C. Thurnauer, Improving optical and charge separation properties of nanocrystalline TiO_2 by surface modification with vitamin C, J. Phys. Chem. B 103 (1999) 3515–3519.
[159] M. Anas, D.S. Han, K. Mahmoud, H. Park, A. Abdel-Wahab, Photocatalytic degradation of organic dye using titanium dioxide modified with metal and non-metal deposition, Mater. Sci. Semicond. Process. 41 (2016) 209–218.
[160] T. Kodanek, H.M. Banbela, S. Naskar, P. Adel, N.C. Bigall, D. Dorfs, Phase transfer of 1- and 2-dimensional Cd-based nanocrystals, Nanoscale 7 (2015) 19300–19309.
[161] W. Lee, S.K. Min, V. Dhas, S.B. Ogale, S.-H. Han, Chemical bath deposition of CdS quantum dots on vertically aligned ZnO nanorods for quantum dots-sensitized solar cells, Electrochem. Commun. 11 (2009) 103–106.
[162] Y.K. Abdel-Maksouda, E. Imamb, A.R. Ramadan, TiO_2 water-bell photoreactor for wastewater treatment, Sol. Energy 170 (2018) 323–335.
[163] W.E. Sutisnaa, M. Rokhmata, D.Y. Rahmana, R. Murniatia, M. Khairurrijala Abdullaha, Batik wastewater treatment using TiO_2 nanoparticles coated on the surface of plastic sheet, Procedia Eng. 170 (2017) 78–83.
[164] K.M. Reza, A.S.W. Kurny, F. Gulshan, Parameters affecting the photocatalytic degradation of dyes using TiO_2: a review, Appl. Water Sci. 7 (2017) 1569–1578.
[165] H. Kusic, D. Leszczynska, N. Koprivanac, I. Peternel, Role of quantum dots nanoparticles in the chemical treatment of colored wastewater: catalysts or additional pollutants, J. Environ. Sci. 23 (2011) 1479–1485.
[166] N.M. Mahmoodi, M. Oveisi, A.M. Arabi, B. Karimi, Cadmium selenide quantum dots: synthesis, characterization, and dye removal ability with UV irradiation, Desalin. Water Treat. 2015 (2015) 1–7.
[167] Y. Bessekhouad, D. Robert, J.V. Weber, Bi_2S_3/TiO_2 and CdS/TiO_2 heterojunctions as an available configuration for photocatalytic degradation of organic pollutant, J. Photochem. Photobiol. A 63 (2004) 569–580.
[168] J.K. Jang, S.M. Ji, S.W. Bae, H.C. Son, J.S. Lee, Optimization of CdS/TiO_2 nanobulk composite photocatalysts for hydrogen production from Na_2S/Na_2SO_3 aqueous electrolyte solution under visible light ($\lambda \geq 420$ nm), J. Photochem. Photobiol. A 188 (2007) 112–119.
[169] T.T. Yang, W.T. Chen, Y.J. Hsu, K.H. Wei, T.Y. Lin, T.W. Lin, Interfacial charge carrier dynamics in core – shell Au-CdS nanocrystals, J. Phys. Chem. C 114 (2010) 11414–11420.
[170] S.Y. Ryu, W. Balcerski, T.K. Lee, M.R. Hoffmann, Photocatalytic production of hydrogen from water with visible light using hybrid catalysts of CdS attached to microporous and mesoporous silicas, J. Phys. Chem. C 111 (2007) 18195–18203.
[171] H. Zhang, Y.F. Zhu, Significant visible photoactivity and antiphotocorrosion performance of CdS photocatalysts after monolayer polyaniline hybridization, J. Phys. Chem. C 114 (2010) 5822–5826.
[172] X. Gao, X. Liu, Z. Zhu, Y. Gao, Q. Wang, F. Zhu, Z. Xie, Enhanced visible light photocatalytic performance of CdS sensitized TiO_2 nanorod arrays decorated with Au nanoparticles as electron sinks, Sci. Rep. 7 (2017) 973.
[173] Z. Yu, L. Qian, T. Zhong, Q. Ran, J. Huang, Y. Hou, F. Li, M. Li, Q. Sun, H. Zhang, Enhanced visible light photocatalytic activity of CdS through controllable self-assembly compositing with ZIF-67, Mol. Catal. 485 (2020) 110797.
[174] Y. Chen, B. Zhai, Y. Liang, Y. Li, J. Li, Preparation of $CdS/g\text{-}C_3N_4$/MOF composite with enhanced visible-light photocatalytic activity for dye degradation, J. Solid State Chem. 274 (2019) 32–39.
[175] Y. Huo, J. Zhang, X. Chen, H. Li, Synthesis of hollow $CdS\text{-}TiO_2$ microspheres with enhanced visible-light photocatalytic activity, Int. J. Photoenergy 2012 (2012) 907290 (5 pp).
[176] M. Nujić, M. Habuda-Stanić, Toxic Metal Ions in Drinking Water and Effective Removal Using Graphene Oxide, Nanocomposite, Springer International Publishing, Cham, Switzerland, 2019, pp. 373–395.
[177] A.A. Ihsanullah, A.M. Al-Amer, T. Laoui, M.J. Al-Marri, M.S. Nasser, M. Khraisheh, M.A. Atieh, Heavy metal removal from aqueous solution by advanced carbon nanotubes: critical review of adsorption applications, Sep. Purif. Technol. 157 (2016) 141–161.

This book belongs to Badji Mokhtar Annaba University Central Library Copyright Elsevier 2025

[178] X. Wang, Nanomaterials as sorbents to remove heavy metal ions in wastewater treatment, J. Environ. Anal. Toxicol. 02 (2012) 154 (7 pp).
[179] Z.L. Lee, M.A.A. Zaini, S.H. Tang, Porous Nanomaterials for Heavy Metal Removal, Springer International Publishing, Cham, Switzerland, 2019.
[180] S.P. Jovanović, Z. Syrgiannis, M.D. Budimir, D.D. Milivojević, D.J. Jovanovic, V.B. Pavlović, J. M. Papan, M. Bartenwerfer, M.M. Mojsin, M.J. Stevanović, B.M. Todorović Marković, Graphene quantum dots as singlet oxygen producer or radical quencher—the matter of functionalization with urea/thiourea, Mater. Sci. Eng. C 109 (2020) 110539.
[181] J. Prekodravac, B. Vasiljević, Z. Marković, D. Jovanović, D. Kleut, Z. Špitalský, M. Mičuaik, M. Danko, D. Bajuk-Bogdanović, B. Todorović-Marković, Green and facile microwave assisted synthesis of (metal-free) N-doped carbon quantum dots for catalytic applications, Ceram. Int. 45 (2019) 17006–17013.
[182] M. Budimir, Z. Marković, D. Jovanović, M. Vujisić, M. Mičuaík, M. Danko, A. Kleinová, H. Švajdlenková, Z. Špitalský, B. Todorović Marković, Gamma ray assisted modification of carbon quantum dot/polyurethane nanocomposites: structural, mechanical and photocatalytic study, RSC Adv. 9 (2019) 6278–6286.
[183] M. Kováčová, Z. M. Marković, P. Humpolíček, M. Mičuaík, H. Švajdlenková, A. Kleinová, M. Danko, P. Kubát, J. Vajďák, Z. Capáková, M. Lehocký, L. Münster, B.M. Todorović, Š.Z. Marković, Carbon quantum dots modified polyurethane nanocomposite as effective photocatalytic and antibacterial agents, ACS Biomater. Sci. Eng. 4 (2018) 3983–3993.

This book belongs to Badji Mokhtar Annaba University Central Library
Copyright Elsevier 2025

CHAPTER 3

Potential risk and safety concern of nanomaterials used for wastewater treatment

Tariq Aziz[a], Shabnam Azad[a], Sidharth P. Nair[b], Jitendra Singh Verma[a], Ashish P. Unnarkat[c], Sharadwata Pan[d], and Ashutosh Namdeo[a]

[a]Chemical Engineering, Engineering Sciences and Technology Division, CSIR-NEIST, Jorhat, Assam, India, [b]Department of Materials Science, Central University of Tamil Nadu, Thiruvarur, India, [c]Chemical Engineering Department, School of Technology, Pandit Deendayal Petroleum University, Raisan, Gandhinagar, Gujarat, India, [d]School of Life Sciences Weihenstephan, Technical University of Munich, Freising, Germany

3.1 Introduction

Water remains the prime reason for existence of life on Earth. Scarcity of water is alarming in a major part of the world including developed and developing nations. United Nations member states have set up 17 Sustainable Development Goals (SDG) for peace and prosperity of people and the planet. Amongst these goals, six are focused on *Clean Water and Sanitation* that, along with other goals, is key for inclusive economic growth and sustainable future [1]. Due to the fact that nearly 80% of all wastewater is discharged into the world's water bodies, this adds up to create an imbalance in ecological conditions and augment health and environmental hazards [2]. Looking at the current scenario of worldwide water scarcity, it is high time to address the issue related to wastewater with cost-effective and sustainable technologies, not only to meet the demand of the water supply for all, but also for a sustainable environment.

In the age of nanotechnology, most of the research directly or indirectly connects with nanosciences. The advent of nanotechnology has touched upon various applications such as food packaging, water treatment, paints and coating, surface modifications, drug delivery, compact electronics, and textiles. Looking at a broader perspective, the applications fall into four major areas: (a) nanomaterials, (b) nanomedicines, (c) nanofabrications, and (d) nanometrology [3]. Xia et al. [4] reported that the expected market capital is reported to reach $1 trillion per year by 2015, which comes from the sale of products employing

Handbook of Nanomaterials for Wastewater Treatment. https://doi.org/10.1016/B978-0-12-821496-1.00035-0
Copyright © 2021 Elsevier Inc. All rights reserved.

This book belongs to Badji Mokhtar Annaba University Central Library Copyright Elsevier 2025

nanotechnology. Furthermore, the global nanotechnology market is expected to rise by US $125 billion by 2024. Nanotechnology will make a mark on nearly all major sectors leading to applications in electronics, followed by biomedical, energy, automotive, defense, and agriculture. The effect of nanotechnology will be felt globally in all sectors [5]. Out of the four thrust areas, application in medicines and related products have a major share in the market. The research focus is expected to be in the fields of human health, defense, energy, agriculture, and environment [6].

Water and wastewater technologies include chemical precipitation, ion exchange, adsorption, membrane filtration, coagulation-flocculation, flotation, and electrochemical methods. All the available technologies are reaching their limits in improving water quality required by the current demand and stringent environmental regulations. The contaminants from pharmaceuticals and personal care products from the newly emerging household commodities have made us to look for novel solutions [7]. Qu et al. [8, 9] reviewed and compared the performances of traditional technologies and nanotechnology for water treatment. The author has categorized the pollutants into broad classes, and the most economical technique amongst the traditional nanotechnology in each category is reported. Nanotechnology has different perspective when it comes to developing nations. There are lot of opportunities for adopting these novel water treatment technologies. Developing nations look for a paradigm shift from the centralized treatment facilities to point-of-use waste treatment strategies. These technologies will be far more economical and will eliminate the need for skilled operators to handle centralized treatment facilities [10]. Nanomaterials are widely accepted for their effective performance in wastewater treatment, either as adsorbents or enhancers joining with a membrane, and other treatment processes of degradation and disinfection [10–13]. The trend of nanoparticles (NPs) is increasing as it can increase the efficiency of the overall process with added economic advantages, for example, a suitable adsorbate can reduce the size of the adsorption column thereby cutting down the cost associated with it. TiO_2, Ag, ZnO, carbon nanotubes (CNTs), and iron oxide NPs are widely used for water treatment as reported in the literature [11, 14, 15].

Nanotechnology provides us leapfrogging opportunities to improve water quality; however, the technology comes with a responsibility [10]. These small-size NPs have the capability to cross biological barriers in the body and can lead to unexpected toxicities [16]. The release of nanomaterials in the environment may occur during water treatment pre- and postprocessing operations. The long-term effects of exposure to nanomaterials and their implications to health and the environment are very less understood and documented. The life cycle of a nanomaterial is depicted in Fig. 3.1.

Release and/or exposure to nanomaterials may occur during the manufacturing stage, during handling consumer products, during waste disposal and treatment. With the widespread manufacture and use of nanomaterials, the concerns for occupational hazards in proper handling, disposal, storage, transport, and waste treatment are expected to rise [7].

This book belongs to Badji Mokhtar Annaba University Central Library Copyright Elsevier 2025

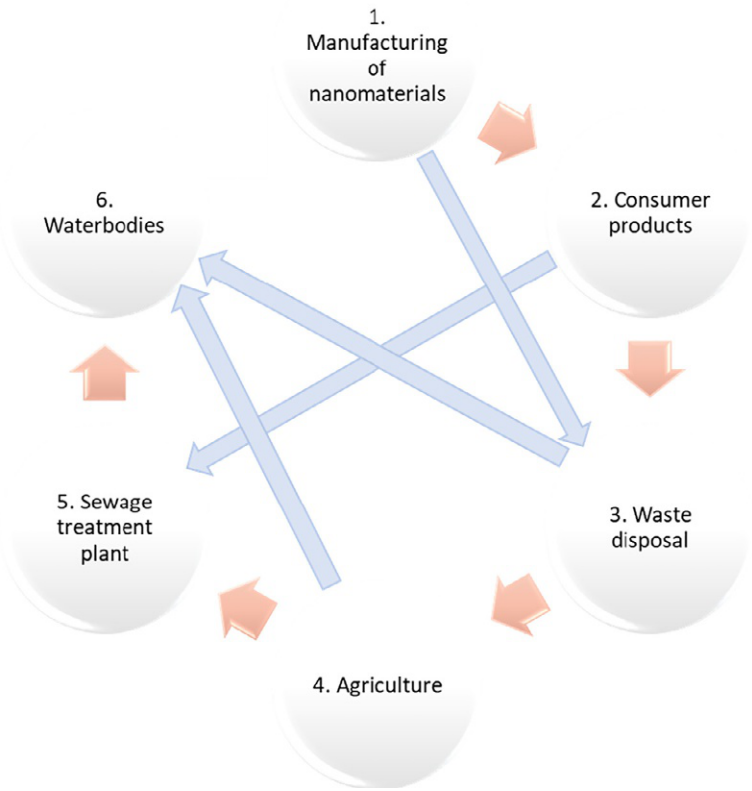

Fig. 3.1
Life cycle of nanomaterials (possibility of exposure scenario to farmers, consumers, aquatic and wild animals, and release scenario into landfills, water bodies, and farmland). *Adapted from Mirshafiee, V., Osborne, O.J., Sun, B., Xia, T., 2018. Handbook of Nanomaterials for Industrial Applications Safety Concerns of Industrial Engineered Nanomaterials. Elsevier Inc. https://doi.org/10.1016/B978-0-12-813351-4.00062-6.*

Aitken et al. [6] reported on exposure to NPs. All of these chemical manufacturing processes for the production of NPs may have exposure by inhalation, through the skin, or ingestion. Exposure to nanomaterials may also occur for workers who are working in product manufacturing units in the downstream processes and later to consumers using these products. According to the National Institute for Occupational Safety and Health (NIOSH), nanomaterial-enabled products such as nanocomposites, surface-coated materials, and materials comprising nanostructures, such as integrated circuits, are unlikely to pose a risk of exposure to consumers during their handling and usage, as these materials won't fall in the respirable range. It is also said that the production processes may lead to exposure to nanomaterials [17]. Schilling et al. [18] also revealed a similar conclusion from their review that the risk for humans from the use of nanostructured titanium dioxide (TiO_2) or zinc oxide (ZnO) used in cosmetic preparations or sunscreens is considered negligible [18]. The usage of

This book belongs to Badji Mokhtar Annaba University Central Library Copyright Elsevier 2025

nanotechnology for water treatment has further concerns. The primary concern is in the retention of nanomaterials and their sustained antimicrobial activity. The NPs, if escaped from the treatment system, will enter the product water and have a major effect by direct exposure to human health and ecosystems. Studies on the antimicrobial activities of nanomaterials are conducted in relatively clean solutions, and the performance of nanomaterials and antimicrobial activities in real wastewater system where there are multiple interferences may also differ to its sustained solution [19].

Nanomaterials have diverse shapes, sizes, and compositions that can affect the environment and human health differently. The fate of these nanomaterials depends on the process they undergo during interaction with the environment. The nanomaterials may form aggregations, interacting with particulate matter and organics to form colloids and affect aquatic life. It can accumulate in parts of the water bodies and/or lead to biological degradation. Aggregation will eventually subside the effect of NPs and reduce its effectiveness. The overall loss of surface area and thereby the reactivity of NPs reduce when forming agglomerates [20]. Toxic effect of nanomaterials on a part of planktons was reported by Zhu et al. [21]. The report was on Ag, TiO_2, CuO, and zero-valent iron NPs. Ag NPs are reported to inhibit the bacterial activity while TiO_2 is said to affect the plants and interfere in the growth cycle. Copper NPs are reported to have minor effect on the enzymatic activity of plankton. Similar was the case with zero-valent iron, which has a mild effect at low concentration while disturbing the growth cycle at higher concentrations. A detailed review on the aggregation phenomena at different levels and interaction with aquatic life in water bodies is given by Klaine et al. [22]. The fate of these NPs and toxic effects in marine environment are discussed in detail. Different nanomaterials in different capacities affect the water environment (plants, bacteria, and organisms) differently, although a higher concentration inhibits and has adverse effects.

Nyström and Fadeel [16] in their article proposed five grand challenges to the scientific community in which these must be cleared to achieve safe and sustainable usage of nanotechnologies. These five challenges are: (1) Develop instruments to monitor nanomaterial exposure in air and water; (2) Develop and validate methods to evaluate the toxicity of nanomaterials; (3) Develop models for predicting the effect of nanomaterials on the environment and human health; (4) Develop robust systems for evaluating health and environmental effect of nanomaterials over their entire life cycle; and (5) Develop strategic programs that enable relevant risk-focused research. These challenges were chosen to stimulate strategic research relevant to the safety of nanotechnology.

In this chapter, we are reviewing the potential risk and safety concerns of NPs that are widely used for wastewater treatment-related applications. Safety in handling of NPs is documented; however, safety of NPs' usage in water treatment and its implications on water quality is to be extensively reviewed here, which also includes synthesis protocols of NP preparation. We have carefully reviewed the synthesis protocols of NPs, and a detailed list of chemicals used in

This book belongs to Badji Mokhtar Annaba University Central Library Copyright Elsevier 2025

synthesis and their adverse effects has been compiled. This study is very important as any successful nanomaterials used for wastewater treatment has to be scaled up for commercial implication. Therefore, synthesis of nanomaterials with green synthesis is of prime importance to reduce the environmental effect. We have also tried to address the effect of nanomaterials on humans and animals. The application of nanotechnology in water treatment must have sustainability in every aspect and must address potential risk and safety concerns. Furthermore, this consolidation of scattered literature on the risk and safety of NPs will be useful for researchers working on NP-related applications in general and wastewater treatment in particular.

3.2 Synthesis of nanoparticles, chemicals involved and their potential safety concern

Nanoparticles/nanotechnology are widely used for water pollution remediation in various studies worldwide through adsorption, absorption, membrane filtration, and chemical reactions. NPs can enhance the effectiveness of these processes as they have high surface-to-volume ratio. For example, dispersing a nanomaterial onto an adsorbent or on the membrane can enhance the efficiency of the separation process. For the matter of degradation of pollutant through photocatalytic or advance oxidation process, a suitable nanocatalyst can really boost the overall process efficiency and thereby the economy of the overall process. Furthermore, the role, choice, and properties of these nanomaterials can be tuned depending on the applications such as disinfection/microbial control, heavy metal separation, pollution degradation, etc. [23–25]. Positive and negative effects of various nanomaterials, namely zero-valent iron, graphene, TiO_2, ZnO, Fe_3O_4, Ag NPs, and CNTs, in water environments were reported in detail by Zhu et al. [21]. The author discussed the behavior mechanism, remedial effect, and toxicity of these NPs in water environment.

Various techniques are reported in the literature concerning synthesis of nanomaterials. Some of the representative synthesis methods are listed in the tables in this chapter. The conventional methods used for the synthesis of NPs such as chemical and physical methods are creating toxic chemicals that are hazardous to our environment [26].

TiO_2, Ag, ZnO, CNTs, and iron oxide nanoparticles are widely used for water treatment as reported in the literature [11, 14, 15]. Herein, we discuss the detailed synthesis methods and chemicals involved and their potential hazards.

3.2.1 Synthesis of zinc oxide nanoparticles

In Table 3.1, a few techniques are listed for the synthesis of NPs using different techniques. Although these NPs are very effective in their respective fields, some chemicals used in these synthesis methods have serious effects on human health as well as the environment. For

This book belongs to Badji Mokhtar Annaba University Central Library Copyright Elsevier 2025

Table 3.1: Different synthesis methods for nanoparticles.

Synthesis method	Chemicals used	Structure	Size range (nm)	Remarks-health hazardous	Reference
Microwave-assisted hydrothermal	$Zn(NO_3)_2{\cdot}6H_2O$, $Zn(CH_3CO_2)_2{\cdot}2H_2O$, hydrazine hydrate, NH_3	Needle shape and flower shape	50–150	Hazardous, combustible, harmful if swallowed, irritating to eyes, respiratory system, and skin	[27]
Electrochemical	Zn electrode, $C_2H_2O_4{\cdot}2H_2O$, KCl, NaOH and HNO_3	Spherical and cylindrical	50–200	May cause kidney damage. Targets organs like kidney, heart, eye, skin, brain, etc.	[28]
Sonochemical	$Zn(NO_3)_2{\cdot}6H_2O$, KOH, cetyltrimethyl ammonium bromide ($C_{19}H_{42}BrN$)	Flake shaped	200–400	Harmful if swallowed, skin irritation, serious eye problem	[29]
Chemical vapor deposition	$Zn(CH_3CO_2)_2{\cdot}2H_2O$ and ethanol(CH_2CHOH)	Nanorod	Average diameter 90 and average length 596	Causes eye irritation, harmful if swallowed, very toxic to aquatic organisms	[30]
Solvothermal	Zinc acetylacetonate monohydrate, triethenolamine ($C_6H_{15}NO_3$), ethanol(CH_2CHOH) and 1-octanol ($CH_3(CH_2)_7OH$)	Spherical and rod shaped	Diameter—20 Length—100	Harmful if swallowed and causes eye irritation	[31]
Sol-gel	$Zn(CH_3CO_2)_2{\cdot}2H_2O$, $C_2H_2O_4.2H_2O$, NH_3, HCl, Absolute ethanol	Spherical shape	20	Very harmful for eyes, cause failure of internal organs	[30]
Microemulsion	Ethyl benzene acid sodium salt (EBS), dodecyl benzene sulfonic acid sodium salt (DBS), Xylene ($(CH_2)_2C_6H_4$), N_2H_4,	Nanorod	D_{EBS}—80 D_{DBS}—300	Harmful if inhaled, prolonged exposure may cause hearing damage	[32]

This book belongs to Badji Mokhtar Annaba University Central Library
Copyright Elsevier 2025

Table 3.1: Different synthesis methods for nanoparticles—cont'd

Synthesis method	Chemicals used	Structure	Size range (nm)	Remarks-health hazardous	Reference
Co-precipitation	$Zn(CH_3CO_2)_2{\cdot}2H_2O$ and ethanol (CH_2CHOH) Tetrahydrated zinc nitrate and NH_4OH	Crystal shaped	20–40	Can cause skin, eye, and respiratory irritations	[33]
Membrane-based	Different type of membrane (microporous, mesoporous, omniphobic, PAA/PVDF, etc.)				[34]

example, hydrazine hydrate used in microwave-assisted hydrothermal method of synthesis of ZnO NPs is carcinogenic as per MSDS data. Other harmful effects of chemicals involved in the synthesis protocols are irritation to eyes, respiratory system, and skin and kidney damage. These chemicals may also target organs like kidney, heart, eye, skin, and brain. Therefore, it is important to find green synthesis methods for production of large-scale nanomaterials to reduce their potential hazards and for sustainability. In these aspects, a few methods are listed in Table 3.2 for their perspective future scope. Table 3.2 shows different methods for synthesis of ZnO NPs, and these are generally green methods in which plants and other microorganisms are used for the synthesis process. These green/biological methods can be used as replacements for the dangerous chemical and physical methods [46].

3.2.2 Synthesis of silver nanoparticles

Synthesis of silver NPs is carried out using a technique according to the size, shape, and other properties required in different applications [47]. Conventional methods for silver NP synthesis with chemicals and their possible health hazardous is reported in Table 3.3. Health hazardous remarks were collected from the MSDS data sheet. Physical fabrication techniques such as evaporation/condensation, laser ablation, and thermal decomposition are mainly used for this purpose. Laser ablation is the latest and most efficient method for the synthesis of AgNPs with a spherical structure and size ranging from 2 to 50 nm. In the chemical method, reduction of silver salt using a reducing agent, stabilizer, and capping agent is widely applied [56]. Similarly, in the case of biological ways of production of silver NPs, reducing agent, stabilizer, and capping agents are used. The reducing agents used are plant extracts, fungus, and microorganisms. A wide varieties of plant extracts are used for the synthesis of silver NPs. Most of the plant parts

This book belongs to Badji Mokhtar Annaba University Central Library Copyright Elsevier 2025

Table 3.2: Sustainable method for synthesis of nanoparticles extracted from plants.

Plants	Zinc salt (source)	Remarks	Reference
Synthesis of nanoparticles extracted from plants			
***Aloe vera* leaves**	Zinc nitrate	25 nm average size	[35]
***Citrus aurantifolia* peel**	Zinc nitrate	8–12 nm, polyhedron shape	[36]
***Hibiscus subdariffa* leaves**	Zinc acetate	190–400 nm, dumbbell shape	[37]
Stevia leaves	Acetate	50 nm, rectangular	[38]
Algae	**Zinc salt (source)**	**Remarks**	**Reference**
Synthesis of nanoparticles extracted from algae			
Sargassum murticum	Zinc acetate	30–50 nm, spherical shape	[39]
C. peltata*, *H. valencia*, and *S. myriocystum	Zinc nitrate	Not defined	[40]
Fungi	**Zinc salt (source)**	**Remarks**	**Reference**
Synthesis of nanoparticles extracted from fungi			
Aspergillus fumigatus biomass	Zinc nitrate	3.8 mn, sphere	[41]
Aspergillus niger biomass	Zinc nitrate	61 nm, sphere	[42]
Bacteria	**Zinc salt (source)**	**Remarks**	**Reference**
Synthesis of nanoparticles extracted from bacteria			
Acinetobacter schindleri culture	Zinc nitrate	20–100 nm, sphere	[43]
Bacillus licheniformis biomass	Zinc acetate	620 nm, nanoflowers	[44]
***Lactobacillus plantarum* culture**	Zinc sulphate	13 nm, sphere	[45]

like leaves, seed, peel, stem, and even the whole plant are used in some cases (Table 3.4). While comparing with the chemical methods, these methods are more eco-friendly and less harmful to the environment as well as other organisms [63].

3.2.3 Carbon nanotube synthesis

CNTs have been widely known for a couple of decades. CNT was first produced in 1991 by Iijima using an arc discharge method [64]. CNTs are produced using techniques such as chemical vapor deposition (CVD), arc discharge, electrolysis, sonochemical or hydrothermal, laser ablation, etc. CNTs can be mainly divided into single-walled NT (SWNT) and multiwalled NT (MWNT). SWNT consist of a single-walled graphene, and MWNT is composed of many concentric tubes of graphene placed one inside the other. The structure and

This book belongs to Badji Mokhtar Annaba University Central Library
Copyright Elsevier 2025

This book belongs to Badji Mokhtar Annaba University Central Library

Table 3.3: Conventional methods for production of Ag nanoparticles.

Salts of Ag	Reducing agents	Capping agent/stabilizer	Nanoparticle size (nanometers)	Remarks-health hazardous	Reference
Silver nitrate	$C_6H_2(OH)_3COOH$	$C_6H_2(OH)_3COOH$ (gallic acid)	10–85	Skin and eye irritation	[48]
Silver nitrate	$(CH_2OH)_2$	Polyvidone	8–177	Effects on central nervous system and kidney	[49]
Silver nitrate	$NaBH_4$	$Na_3C_6H_5O_7$	4–6	Digestive and respiratory tract burns if swallowed or inhaled	[50]
Silver nitrate	$C_6H_{12}O_6$	Polyvidone	20–80	Not hazardous	[51]
Silver nitrate	Dextrose	Sodium hydroxide, carboxy methyl cellulose	5–15	Not hazardous	[52]
Silver nitrate	Sodium borohydride and sodium hydroxide	$C_{18}H_{34}O_2$ (Oleic acid) and $(C_3H_4O_2)_n$ polyacrylic acid	15–450	Digestive and respiratory tract burns if swallowed or inhaled	[53]
Silver nitrate	$C_6H_5NH_2$	Cetyltrimethlyammonium bromide	15–30	Causes allergic skin reactions and drowsiness or dizziness	[54]
Silver nitrate	Polyvidone and gelatin	Lactose, glucose, sucrose, and fructose	35	Not hazardous	[55]

Copyright Elsevier 2025

Table 3.4: Sustainable methods for synthesis of silver nanoparticles extracted from plants.

Plants	Plant part	Shape	Size (Nm)	Reference
Alternanthera dentate	Leaves	Spherical	50–100	[57]
Tribulus terrestris	Fruit	Spherical	16–28	[58]
Boerhaavia diffusa	Whole plant	Spherical	25	[59]
Pistacia atlantica	Seeds	Spherical	10–50	[60]
Thevetia peruviana	Latex	Spherical	10–30	[61]
Citrus sinensis	Peel	Spherical	10–35	[62]
Cocous nucifera	Inflorescence	Spherical	22	[58]

type of CNTs depend on the method of synthesis and the conditions provided [65]. Some of the synthesis methods and properties with health hazardous remarks are mentioned in Table 3.5.

3.2.4 Iron oxide nanoparticle synthesis

There are many methods of synthesis of iron oxide nanoparticles; commonly used methods are co-precipitation, microemulsion, sol-gel methods, and thermal decomposition [78]. Green synthesis is more relevant, which helps increase the biocompatibility and decrease the amount of environmental pollution. The contributions given by iron oxide NPs in the last decade is very promising. There is a wide variety of applications in which iron oxide NPs are used. Wastewater management, cosmetics, textiles, diagnosis of diseases, and health care are a few applications [79]. Some methods of synthesis of iron oxide NPs are listed in Table 3.6. By analyzing the chemicals used in the co-precipitation and hydrothermal methods (NH_4OH, $FeCl_3$), they have a hazardous effect on human beings and other organisms [80]. Continuous use of these chemicals on a large scale can create an imbalance in our ecosystem. Synthesis methods and properties of iron oxide NPs with health hazardous remarks are mentioned in Table 3.6.

3.2.5 Synthesis of TiO_2 nanoparticles

The preparation of titanium oxide NPs can be done in the form of powders, crystals, and thin films. TiO_2 NPs have a wide range of applications including water splitting. Some of the promising applications in the field of environment and energy are photovoltaics, photocatalysis, photochromic, and sensors [84]. The main methods of synthesis and properties are described in Table 3.7.

3.2.6 Other materials and metal oxides

In addition to the nanomaterials discussed, there are materials like graphene oxide (GO), SiO_2, mesoporous magnetic iron, carbon nanomaterials, and other metal oxides that were also used for the purpose of water treatment. Studies done in the case of GO say that it has a high-level

This book belongs to Badji Mokhtar Annaba University Central Library Copyright Elsevier 2025

Table 3.5: Synthesis of carbon nanotubes.

Method	Chemicals/Conditions	Type	Remarks-health hazardous	Reference
Arc discharge method for synthesis of carbon nanotubes				
Plasma rotating	Pure graphite electrodes, He	CNTs		[66]
Arc discharge	• Deionized water • NaCl solution • Liquid environments • Y/Ni and CaC_2/Ni catalyst, He • Ho/Ni catalyst	CNTs, SWNTs, MWNTs	Not hazardous	[64, 67, 68]
Arc discharge	• Mixture of nickel/cobalt/iron dash of sulfur, Ar:H_2 • KCl/iron sulfide catalyst, H_2 • FeS, CoS, NiS catalysts, H_2	DWNTs	Not hazardous	[69–71]
Pulsed arc	Pure graphite rods, deionized water	CNTs	Carcinogenic and cause serious injurt	[72]

Laser used	Chemicals/ Conditions	Type produced	Remarks	Reference
Laser ablation method for synthesis of carbon nanotubes				
CO_2 continuous and pulsed wave	• Power of laser: 400–900 W; C/Ni/Co, room Temp. Ar: 200–400 Torr • Gas nature Ar, He, N_2 50–500 Torr; C/Ni/Y • Catalyst composition, gas conditions: Ar, He, N_2 50–500 Torr, laser power density: 12–9-6 kW/cm^2 • Effect of furnace temperature	SWNT bundles SWNTs SWNTs CNTs	The carbon sources used are considered as hazardous but most of the catalysts do not fall under the hazardous category	[73]

Continued

This book belongs to Badji Mokhtar Annaba University Central Library

Copyright Elsevier 2025

Table 3.5: Synthesis of carbon nanotubes—cont'd

Laser used	Chemicals/ Conditions	Type produced	Remarks	Reference
Pulsed Nd:YAG	• Effect of the laser intensity • Target composition	SWNTs CNTs	–	[73]
Method	**Chemicals/ Conditions**	**Type**	**Remarks**	**Reference**
Chemical vapor deposition method for synthesis of carbon nanotubes				
Microwave plasma-enhanced	Co-Ti/Si substrate in absence of a buffer layer	Vertically aligned SWNTs	Mildly hazardous; can cause skin irritations	[74]
Simple CVD	Acetylene, titanate modified palygorskite	Filled CNTs	Palygorskite is carcinogenic	[75]
Alcohol CVD	Cu/MgO	CNTs	Slightly dangerous, causes irritation to eyes	[76]
Thermal CVD	Co/SiO_2, Ar/H_2 and NH_3/N_2	Aligned CNTs	Hazardous long-term exposure causes severe damage to human health as well as the environment	[77]

Table 3.6: Synthesis of Iron oxide nanoparticles.

Synthesis techniques	Chemicals/Conditions	Properties	Remarks-health hazardous	Reference
Co-precipitation	$FeCl_2$, $FeCl_3$, sodium hydroxide or ammonium hydroxide	Quick and low-cost	Harmful if swallowed, skin burns and eye damage	[80]
Microemulsion	Oil/water/surfactant	Controlled dimensions of particle		
Hydrothermal/ solvothermal	Fe salts, surfactants	Restricted control on dimensions	Harmful if swallowed, skin burns and eye damage	
Green synthesis	*Mentha pulegium* leaf extract, $FeCl_3$	Cubical shape and narrow band gap		[81]
Green synthesis	$(Fe(NO_3)_3 \cdot 9H_2O$, Stevia leaves extract	Size less than 25 nm		[82]
Green synthesis	Avecinnia marina flower, $FeCl_3$	Size between 10 and 40 nm		[83]

This book belongs to Badji Mokhtar Annaba University Central Library
Copyright Elsevier 2025

Table 3.7: Methods for synthesis of titanium oxide nanoparticles.

Process	Raw materials	Properties	Remarks-health hazardous	Reference
Sol-gel technique	• Titanium (IV) tetraisopropoxide and ethanol/ isopropanol • Titanium (isopropoxide) and sulphuric acid	Hybrid spheres 3–6 nm	Causes eye skin and respiratory tract irritation, harmful if inhaled	[85]
Microemulsion technique	$TiCl_4$ solution emulsified into the oil phase	Spheres		[86]
Precipitation	Aqueous $TiCl_4$ solution with ammonium hydroxide as precipitation agent		Causes severe skin, eye, and digestive tract burns; harmful if swallowed; mist or vapor extremely irritating to eyes and respiratory tract	[87]
Hydrothermal method	Hydrothermal H_2O_2 oxidation starting from metallic Ti	Nanofibers and nanotubes microspheres 200 nm	Harmful if inhaled; causes serious eye damage	[88]
Solvothermal method	Titanium (IV) *n*-butoxide	9–15 nm	Irritant to eyes, skin, mucous membranes, and respiratory system; may be harmful by ingestion, skin absorption, and inhalation	[89]
Electrochemical method	TiF_6, NH_4		May be corrosive to metals, toxic if swallowed, toxic in contact with skin, causes severe skin burns and eye damage, may cause respiratory irritation	[90]
Biological method	Lactobacilli	Tetragonal, 35 nm		[91]

capacity to absorb water contaminants in various ranges. GO use in wastewater treatment is restricted due to its toxicity and the difficulties of performing centrifugation after the adsorption process [92]. In the application of GO, ultrafiltration or nanofiltration method is mainly used in which GO is embedded with a polymeric membrane or used as a nanocomposite combined with the other nanomaterials. Poly-acrylonitrile (PAN), Edetate disodium (EDTA), Nanoscale Zero-Valent Iron (nZVI), poly(amideimide)-polyethyleneimine (PAI-PEI), GO/TiO_2-polyvinylidene fluoride (GO/TiO_2-PVDF), and some biopolymers are used with GO

This book belongs to Badji Mokhtar Annaba University Central Library Copyright Elsevier 2025

as a membrane for hybrid ultrafiltration [92–98]. Silicon dioxide on orange peel waste is another novel material used in water treatment applications. Orange peel waste is taken and SiO_2 nanospheres are chemically impaled to it. This will act as a very good adsorbent with very high capacity of heavy metal adsorption [99]. Mesoporous magnetic Fe_2O_3 in carbon is mainly used for the purpose of arsenic removal. This material shows excellent capacity of arsenic adsorption [100]. The NPs of metal oxides are widely used in the water treatment process. Antimicrobial and dye removal properties of these metal oxides are highly appreciated. Oxides of aluminum, silicon, iron, cobalt, and nickel are also used other than the metal oxide NPs mentioned earlier [101, 102]. Although these studied nanomaterials seem effective, they are prepared using variety of chemicals, which can be potentially hazardous to health and the environment.

3.3 Potential safety concerns of nanomaterials to flora and fauna

In the following section, we review the potential exposure hazards of TiO_2, Ag, ZnO, CNTs, and iron oxide nanoparticles to microorganisms, animals, and humans.

3.3.1 Zinc oxide (ZnO) nanoparticles

Various aquatic organisms, such as *Vibrio fisheri*, *Daphnia magna*, *Thamnocephalusplatyurus*, *Escherichia coli*, and *Bacillus subtilis*, are detrimentally influenced by nano-ZnO materials and ZnO NPs ([12, 13]; and references therein), which could be mediated by the proportions of soluble organic content in the aquatic ecosystem [103]. The risk quotient (RQ) of nano-ZnO, in fact, was reported to be noteworthy in sewage treatment plant discharges compared with the surface water [104]. As shown by Heinlaan et al. [105], the common size range of the ZnO NPs rendering such harmful effects was between 50 and 70 nm. One potent route of ZnO NP penetration in humans is through a wide-scale usage of personal care products, thereby highlighting the danger of skin permeation of such NPs. Infusion of ZnO NPs has been ultimately associated with gross disadvantages, including photocatalytic actions postexposure to sunlight, impairment of nucleic acid functionalities, triggering hypersensitivity, amongst others [106–108]. The harmful effects of ZnO NPs have also been demonstrated on human keratinocytes and mouse fibroblasts, with skin sensitizing and phototoxic implications [109]. These NPs can also induce potent neurological damages, including crossing the blood-brain barrier and causing inflammation and cellular toxicity ([110]; and references therein). In addition to TiOs NPs, the growth-inhibitory influences of zinc oxide NPs have also been highlighted in a number of marine phytoplankton species [111]. Acute, time-dependent toxicity, due to exposure to ZnO NPs, has been reported in some fishes, which caused a total morbid effect [112]. The authors further noted that this could be due to the generation of free radicals and enhanced lipid peroxidation in brain cells. In plants, especially, the ZnO NPs cause

This book belongs to Badji Mokhtar Annaba University Central Library Copyright Elsevier 2025

a myriad of damaging effects, including generation of free radicals and cellular toxicity, ultimately leading to diminished growth and expression of specific genes and underprivileged degree of photosynthesis, amongst others [96, 97].

3.3.2 Silver nanoparticles

The harmful influences of silver NPs toward a wide range of microscopic and thriving soil population, including earthworms, plants, and microbes, were recently reported by McKee and Filser [113]. The authors further noted that the effects of silver NPs were particularly more severe on the bacterial species compared with the fungal ones, and that the detrimental effects of such NPs could be traced even at low proportions. Furthermore, the shape of silver NPs also contributes to toxicity [114]. In spite of significant applications of silver NPs toward water treatment and recycling processes, concerns could be noted regarding their ill effects toward generating toxicity and affecting human well-being in general [115, 116]. A myriad of health issues has also been reported and highlighted in animals, i.e., chickens, mice, rats, amongst others, linked to silver NP-mediated toxicity, including compromised functionalities associated with mitochondria, ion outflow across cellular membranes, cellular contraction, amongst others ([117]; and references therein). The authors further note that proportions of silver NPs, ranging between 1 and 10 ppm, present a significant human health risk attributed to nanosilver noxiousness. The RQ of nanosilver was in fact shown to be extraordinarily high in both surface water as well as in the discharges from sewage handling facilities [104]. The heightened and obvious danger of silver NPs, compared with silver ions, was demonstrated by Bilberg et al. [118] based on their static renewal experiments on zebrafish. Wang et al. [119] have reported that silver NPs can affect the reproductive development in zebrafish by stimulating the generation of reactive oxygen species (ROS) and the death of follicles. Past studies have also confirmed the disadvantages of exposing silver NPs to human keratinocytes, in terms of cellular noxiousness mediated by enhanced penetration of membranes by the NPs causing protein and lipid peroxidation [120, 121]. Animal reproductive systems, especially in male species, could be severely compromised upon exposure to nanoranged silver NPs mainly due to the generation of ROS and associated genetic toxicity and oxidative stress [110, 122]. The nitrogen-fixing abilities of some bacterial species could be severely impaired upon exposure to silver NPs [123]. In addition, these NPs have also been reported to induce impairment of the constituents in the bacterial cell wall and general bacterial cell disruption [124]. Silver nanotubes are also known to be potent inducers of toxic influences in fishes and larvae, causing disruption of membranes, death of erythrocytes and embryos, amongst others [110]. It has been reported that, in plants, compared with soluble silver, engineered silver NPs present more risks of affected growth and evolution, as well as sprouting of seeds [121]. Additionally, the derogatory effects of the silver NPs have been highlighted depending on the dose, ultimately affecting crop productivity, also because of the ability to affect the whole plant, i.e., from leaf to the roots [110, 125].

This book belongs to Badji Mokhtar Annaba University Central Library Copyright Elsevier 2025

3.3.3 Carbon nanotubes and carbon-based nanomaterials/nanoparticles

Despite their applicability in water handling, CNTs have been implicated with potent challenges, including demonstrating toxicity and water insolubility [126]. In addition, CNT shapes have also been reported to be a potent contributor to toxicity manifestation [127]. Particularly, the challenge in laying out an exhaustive database concerning the toxicity of allotropic nanomaterials, such as CNTs as well as fullerenes, lies with the absence of bulk counterparts, which guarantee even more stringent risk assessment criteria [8, 9]. The harmful effects of fullerene NPs, as well as both double-walled and single-walled CNTs on aquatic organisms, including Rainbow trouts, the amphibian *Xenopus laevis*, and daphnia, were reported by past studies ([12, 13]; and references therein), which highlight a myriad of effects, such as enhanced respiratory toxicity, concentration-dependent noxious influences, and generation of ROS or free radicals. The derogatory effects of related NPs, including C60 suspensions, were highlighted in algae, bacteria, and daphnia, including cell and tissue death and bioaccumulation [128–130]. However, around a decade ago, Gottschalk et al. [104], reported that both fullerenes as well as CNTs show no noteworthy RQ in both surface water and effluents from sewage treatment plants. Moreover, carbon-based NPs can also cause potent damages to the animal reproductive system and evolution of the fetus, including gene expression of ovaries, generation of spermatozoa, and general organ growth and development [131]. Miranda et al. [132] reported that carbon-based NPs can cause necrosis in microbial species by raising the level of serum enzymes, such as lactate dehydrogenase and acid phosphatase. Very recently, Park et al. [133] collated extensive information on the toxicity of graphene nanomaterials on humans. The damaging influences of the carbon-based nanomaterials have also been shown in plants, including diminished growth of their roots and shoots, as well as negatively affecting the microbial population in their root environments [134].

3.3.4 Iron oxide and magnetic nanoparticles

Although iron oxide NPs have been traditionally inked with comparatively lower risks of toxicity to both human and other organisms due to the lower iron concentrations, which are being discharged to the water embodiments, higher doses of iron oxide NPs could seriously disturb this balance, while increasing the risks of toxicity manifold [135]. At the same time, the authors assert that the toxicity evaluation pertaining to iron oxide or magnetic NPs in general is still at a nascent stage, thereby requiring urgent attention. In general, a wide range of detrimental effects of metallic NPs on bacteria could be found [136], including free radical-mediated mutilation, diminished gene expression, respiration, and protein synthesis and growth. The pathway of exposure of iron oxide NPs, as well as the physiochemical features, also affect the toxicity as shown by Patil et al. [137]. In addition to several other metallic NPs, iron oxide NPs have been reported to decrease the total amino acid content in the grains of

This book belongs to Badji Mokhtar Annaba University Central Library Copyright Elsevier 2025

peanut plants [138]. Recently, the toxicity of magnetic iron oxide NPs has been investigated both at the cellular and molecular levels in both nonhuman and human cell lines [139]. The authors reported a wide range of harmful implications, including damage to cytoskeleton, mitochondria, and plasma membrane, apoptosis, and reduction in cell viability, while negatively affecting cellular integrity and movements. In higher vertebrates, such as chicken embryos, the detrimental influences of magnetic iron oxide NPs have been highlighted, mainly from the purview of neuronal degeneration or injury [140]. Toxic potential of iron oxide NPs was highlighted toward human osteoblasts, in the form of reduced cell viability, when co-cultured in high NP concentrations [141]. Mahmoudi et al. [142] demonstrated the generation of ROS in three different types of human cell lines, i.e., kidney, heart, and brain, upon exposure to superparamagnetic iron oxide NPs. Murray et al. [143] demonstrated the generation of oxidative stress and secretion of inflammatory intermediaries in vitro in both murine epidermal cells as well as human epidermal keratinocytes upon exposure to similar NPs. Additionally, both water- and land-based animal models have been shown at a greater risk from exposure to engineered NPs via cellular organ damage and membrane lipid peroxidation from metallic and other NPs, mainly because they are ecologically copious and omnipresent ([110]; and references therein).

3.3.5 Titanium dioxide (TiO_2) nanoparticles

Past studies have reported on the unfavorable implications of TiO_2 NPs in the form of their phototoxic influences, as well as the synthesis of ROS, when exposed to ultraviolet (UV) radiations [126]. Mansfield et al. [144] have reported on the normal sunlight stimulated toxic effects of TiO_2 NPs on aquatic species such as *D. magna*. In fact, upon excitation by UV, as noted by the authors, the toxicity could be amplified by almost more than an order of magnitude. The harmful influences of TiO_2 NPs on aquatic organisms, including invertebrates, algae, fish, bacteria, and plants, have been well documented by Gehrke et al. [12, 13], including diminished procreation, breathing anguish, pathological modifications in intestine and gills, as well as developmental and communication transformations. As reported by the authors, the kind and proportions of same NPs also affect algae. The time of exposure to these NPs is also critical in determining the extent of toxicity, as was demonstrated by Zhu et al. [145] based on their experiments on daphnia. The RQ of nano-TiO_2 was reported to be lowest in both surface water as well as sewage treatment plant effluents, in comparison to both nanosilver and nano-ZnO [104]. Additionally, chemistry plays a crucial role in toxicity induction, as evidenced by the discriminating rutile and anatase TiO_2, as well as the hydroxyl radical-mediated oxidative DNA impairment and toxicity within the cells [146, 147]. On the other hand, although Warheit et al. [148] reported that TiO_2 NPs could be associated with only lower degrees of toxicity in pulmonary tissues, with a diminished inflammation probability, the role of such NPs in cytotoxicity, DNA damage, and other irregularities postdermal penetration into human, rat, and rabbits has been highlighted ([146]; and references therein). The light-induced toxicity,

This book belongs to Badji Mokhtar Annaba University Central Library Copyright Elsevier 2025

synthesis of ROS, and related membrane impairment caused by TiO_2 NPs (10–100 nm size range) in four varied marine phytoplankton species has been reported [149]. In zebrafish, TiO_2 NPs can affect various stages of reproduction by damaging the production of eggs and increasing embryo deaths [119]. The exposure site is also an important factor, as the entrapment of TiO_2 NPs in the gills and intestine seemed to induce no noteworthy neurotoxic influences in goldfish [150].

3.4 Conclusion

Nanotechnology and nanosciences have touched each and every aspect of human life whether it's in the form of clothing, pharmaceuticals, cosmetics, coatings, and paints to nanodevices in the medical field. Water treatment technologies have been using these nanomaterials in various forms; some of the nanomaterials used were zinc oxide, iron oxide, titanium oxide, silver NPs, and CNTs. These nanomaterials come through a lot of processes via physical and chemical routes and have different properties to be applied in different water treatment applications. In its life cycle from manufacturing to its disposal in the form of product, nanomaterials touch upon various sectors and has interaction with humans, flora, and fauna. This chapter has compared conventional manufacturing through different chemical routes and its interference with people during synthesis. The implication of these chemicals on the health of people is addressed and tabulated. Green synthesis is the buzzword for the sustainable future. The chapter has also reviewed the green methods available for the synthesis of a variety of nanomaterials. The application of nanotechnology in water treatment must have sustainability in every aspect and must address potential risks and safety concerns. The effect of these NPs on flora and fauna is discussed widely in the last part of the chapter. Nanomaterials and nanotechnology provide us with boundless opportunities, but the implications and after effects must be considered. Novelty has come with a responsibility for the sustainable future. The size has given advantages for use to change the properties for applications but at the same time it is also breaking barriers and has the potential to enter the human body through injection, inhalation, and other interactions. The interactions leading to toxicity and mutation in the human biological systems has been discussed. Ensuring reliable, clean, and affordable water to all will remain a global challenge for the future. The technological advancement in the field of nanoscience is going to play a critical role for transforming water treatment systems into a different paradigm but of prime importance is taking care of the safety concerns for flora and fauna and presenting the world with a sustainable solution.

References

[1] Sustainable Development Goals, https://www.undp.org/content/undp/en/home/sustainable-development-goals.html (Accessed 5 March 2020), n.d.
[2] The Reuse Opportunity, Wastewater Report, The International Water Association, 2018, pp. 2–21.

This book belongs to Badji Mokhtar Annaba University Central Library Copyright Elsevier 2025

[3] Y. Teow, P.V. Asharani, M. Prakash Hande, S. Valiyaveettil, Health impact and safety of engineered nanomaterials, Chem. Commun. 47 (25) (2011) 7025–7038.
[4] T. Xia, N. Li, A.E. Nel, Potential health impact of nanoparticles, Annu. Rev. Public Health 30 (1) (2009) 137–150.
[5] Research and Markets, Global Nanotechnology Market (by Component and Applications), Funding & Investment, Patent Analysis and 27 Companies Profile & Recent Developments—Forecast to 2024, (2018).
[6] R.J. Aitken, M.Q. Chaudhry, A.B.A. Boxall, M. Hull, Manufacture and use of nanomaterials: current status in the UK and global trends, Occup. Med. 56 (5) (2006) 300–306.
[7] A.S. Adeleye, et al., Engineered nanomaterials for water treatment and remediation: costs, benefits, and applicability, Chem. Eng. J. 286 (2016) 640–662, https://doi.org/10.1016/j.cej.2015.10.105.
[8] X. Qu, J. Brame, Q. Li, P.J.J. Alvarez, Nanotechnology for a safe and sustainable water supply: enabling integrated water treatment and reuse, Acc. Chem. Res. 46 (3) (2013) 834–843, https://doi.org/10.1021/ar300029v.
[9] X. Qu, J. Brame, Q. Li, P.J.J. Alvarez, Nanotechnology for a safe and sustainable water supply: enabling integrated water treatment and reuse, Acc. Chem. Res. 46 (3) (2013) 834–843.
[10] J. Brame, Q. Li, P.J.J. Alvarez, Nanotechnology-enabled water treatment and reuse: emerging opportunities and challenges for developing countries, Trends Food Sci. Technol. 22 (11) (2011) 618–624, https://doi.org/10.1016/j.tifs.2011.01.004.
[11] M. Anjum, et al., Remediation of wastewater using various nano-materials, Arab. J. Chem. 12 (8) (2019) 4897–4919, https://doi.org/10.1016/j.arabjc.2016.10.004.
[12] I. Gehrke, A. Geiser, A. Somborn-Schulz, Innovations in nanotechnology for water treatment, Nanotechnol. Sci. Appl. 8 (2015), https://doi.org/10.2147/NSA.S43773. 17 pp.
[13] I. Gehrke, A. Geiser, A. Somborn-Schulz, Innovations in nanotechnology for water treatment, Nanotechnol. Sci. Appl. 8 (2015) 1–17.
[14] M.I. Fadlalla, P. Senthil Kumar, V. Selvam, S. Ganesh Babu, Recent Advances in Nanomaterials for Wastewater Treatment, Springer Nature, Switzerland, 2019.
[15] X. Qu, P.J.J. Alvarez, Q. Li, Applications of nanotechnology in water and wastewater treatment, Water Res. 47 (12) (2013) 3931–3946, https://doi.org/10.1016/j.watres.2012.09.058.
[16] A.M. Nyström, B. Fadeel, Safety assessment of nanomaterials: implications for nanomedicine, J. Control. Release 161 (2) (2012) 403–408, https://doi.org/10.1016/j.jconrel.2012.01.027.
[17] M. Methner, L. Hodson, C. Geraci, Nanoparticle emission assessment technique (NEAT) for the identification and measurement of potential inhalation exposure to engineered nanomaterials part A, J. Occup. Environ. Hyg. 7 (3) (2010) 127–132.
[18] K. Schilling, et al., Human safety review of 'nano' titanium dioxide and zinc oxide, Photochem. Photobiol. Sci. 9 (4) (2010) 495–509.
[19] Q. Li, et al., Antimicrobial nanomaterials for water disinfection and microbial control: potential applications and implications, Water Res. 42 (18) (2008) 4591–4602, https://doi.org/10.1016/j.watres.2008.08.015.
[20] E. Kabir, et al., Environmental impacts of nanomaterials, J. Environ. Manag. 225 (2018) 261–271, https://doi.org/10.1016/j.jenvman.2018.07.087.
[21] Y. Zhu, et al., Behavior, remediation effect and toxicity of nanomaterials in water environments, Environ. Res. 174 (2019) 54–60, https://doi.org/10.1016/j.envres.2019.04.014.
[22] S.J. Klaine, et al., Nanomaterials in the environment: behaviour, fate, bioavailability, and effects, Environ. Toxicol. Chem. 27 (9) (2008) 1825–1851.
[23] A. Buthiyappan, A.R.A. Aziz, W.M.A.W. Daud, Recent advances and prospects of catalytic advanced oxidation process in treating textile effluents, Rev. Chem. Eng. 32 (1) (2016) 1–47.
[24] F.D. Guerra, M.F. Attia, D.C. Whitehead, F. Alexis, Nanotechnology for environmental remediation: materials and applications, Molecules 23 (7) (2018) 1760.
[25] M. Jiang, Y. Qi, H. Liu, Y. Chen, The role of nanomaterials and nanotechnologies in wastewater treatment: a bibliometric analysis, Nanoscale Res. Lett. 13 (2018) 233.
[26] H. Agarwal, S. Venkat Kumar, S. Rajeshkumar, Resource-efficient technologies review article—a review on green synthesis of zinc oxide nanoparticles—an eco-friendly approach, Resour. Effic. Technol. 3 (4) (2017) 406–413.

This book belongs to Badji Mokhtar Annaba University Central Library Copyright Elsevier 2025

[27] M. Thamima, S. Karuppuchamy, Microwave assisted synthesis of zinc oxide nanoparticles, Int. J. ChemTech Res. 8 (11) (2015) 250–256.
[28] V. Anand, V.C. Srivastava, Zinc oxide nanoparticles synthesis by electrochemical method: optimization of parameters for maximization of productivity and characterization, J. Alloys Compd. 636 (2015) 288–292.
[29] S. Ghosh, D. Majumder, A. Sen, S. Roy, Facile sonochemical synthesis of zinc oxide nanoflakes at room temperature, Mater. Lett. 130 (2014) 215–217.
[30] C. Boon, L. Yong, A. Wahab, A review of ZnO nanoparticles as solar photocatalysts : synthesis, mechanisms and applications, Renew. Sust. Energ. Rev. 81 (July 2016) (2018) 536–551.
[31] A. Šarić, G. Štefanić, G. Dražić, M. Gotić, Solvothermal synthesis of zinc oxide microspheres, J. Alloys Compd. 652 (2015) 91–99.
[32] S.K. Lim, S.-H. Hwang, S. Kim, H. Park, Preparation of ZnO nanorods by microemulsion synthesis and their application as a CO gas sensor, Sens. Actuators B Chem. 160 (1) (2011) 94–98.
[33] V.R. Kumar, P.R.S. Wariar, V.S. Prasad, J. Koshy, A novel approach for the synthesis of nanocrystalline zinc oxide powders by room temperature co-precipitation method, Mater. Lett. 65 (13) (2011) 2059–2061.
[34] L.H. Chen, et al., Omniphobic membranes for direct contact membrane distillation: effective deposition of zinc oxide nanoparticles, Desalination 428 (2018) 255–263.
[35] S. Gunalan, R. Sivaraj, V. Rajendran, Green synthesized ZnO nanoparticles against bacterial and fungal pathogens, Prog. Nat. Sci.: Mater. Int. 22 (6) (2012) 693–700.
[36] O.J. Nava, et al., Fruit peel extract mediated green synthesis of zinc oxide nanoparticles, J. Mol. Struct. 1147 (2017) 1–6.
[37] N. Bala, et al., Green synthesis of zinc oxide nanoparticles using hibiscus subdariffa leaf extract: effect of temperature on synthesis, anti-bacterial activity and anti-diabetic activity, RSC Adv. 5 (7) (2015) 4993–5003.
[38] M. Khatami, H.Q. Alijani, H. Heli, I. Sharifi, Rectangular shaped zinc oxide nanoparticles: green synthesis by Stevia and its biomedical efficiency, Ceram. Int. 44 (13) (2018) 15596–15602.
[39] S. Azizi, M.B. Ahmad, F. Namvar, R. Mohamad, Green biosynthesis and characterization of zinc oxide nanoparticles using brown marine macroalga *Sargassum muticum* aqueous extract, Mater. Lett. 116 (2014) 275–277.
[40] S. Nagarajan, K.A. Kuppusamy, Extracellular synthesis of zinc oxide nanoparticle using seaweeds of Gulf of Mannar, India, J. Nanobiotechnol. 11 (1) (2013) 1–11.
[41] R. Raliya, J.C. Tarafdar, ZnO nanoparticle biosynthesis and its effect on phosphorous-mobilizing enzyme secretion and gum contents in clusterbean (*Cyamopsis tetragonoloba* L.), Agric. Res. 2 (1) (2013) 48–57.
[42] V.N. Kalpana, et al., Biosynthesis of zinc oxide nanoparticles using culture filtrates of *Aspergillus niger*: antimicrobial textiles and dye degradation studies, OpenNano 3 (March) (2018) 48–55.
[43] S. Busi, et al., Extracellular synthesis of zinc oxide nanoparticles using acinetobacter schindleri SIZ7 and its antimicrobial property against foodborne pathogens, J. Microbiol. Biotechnol. Food Sci. 05 (05) (2016) 407–411.
[44] R.M. Tripathi, et al., ZnO Nanoflowers: novel biogenic synthesis and enhanced photocatalytic activity, J. Photochem. Photobiol. B Biol. 141 (2014) 288–295.
[45] E. Selvarajan, V. Mohanasrinivasan, Biosynthesis and characterization of ZnO nanoparticles using *Lactobacillus plantarum* VITES07, Mater. Lett. 112 (2013) 180–182.
[46] M. Bandeira, et al., Green synthesis of zinc oxide nanoparticles: a review of the synthesis methodology and mechanism of formation, Sustain. Chem. Pharm. 15 (February) (2020) 100223.
[47] T.M. Tolaymat, et al., An evidence-based environmental perspective of manufactured silver nanoparticle in syntheses and applications: a systematic review and critical appraisal of peer-reviewed scientific papers, Sci. Total Environ. 408 (2010) 999–1006.
[48] G.A. Martínez-Castañón, et al., Synthesis and antibacterial activity of silver nanoparticles with different sizes, J. Nanopart. Res. 10 (8) (2008) 1343–1348.
[49] Y. Sun, B. Mayers, T. Herricks, Y. Xia, Polyol synthesis of uniform silver nanowires: a plausible growth mechanism and the supporting evidence, Nano Lett. 3 (7) (2003) 955–960.
[50] B. Mahltig, et al., Preparation of silver nanoparticles suitable for textile finishing processes to produce textiles with strong antibacterial properties against different bacteria types, Z. Naturforsch. B: Chem. Sci. 66 (9) (2011) 905–916.

This book belongs to Badji Mokhtar Annaba University Central Library Copyright Elsevier 2025

[51] H. Wang, X. Qiao, J. Chen, S. Ding, Preparation of silver nanoparticles by chemical reduction method, Colloids Surf. A Physicochem. Eng. Asp. 256 (2–3) (2005) 111–115.
[52] P. Prema, S. Thangapandiyan, G. Immanuel, CMC stabilized nano silver synthesis, characterization and its antibacterial and synergistic effect with broad spectrum antibiotics, Carbohydr. Polym. 158 (2017) 141–148.
[53] C.C. Li, et al., Effects of capping agents on the dispersion of silver nanoparticles, Colloids Surf. A Physicochem. Eng. Asp. 419 (2013) 209–215.
[54] Z. Khan, S.A. Al-Thabaiti, A.Y. Obaid, A.O. Al-Youbi, Preparation and characterization of silver nanoparticles by chemical reduction method, Colloids Surf. B: Biointerfaces 82 (2) (2011) 513–517.
[55] P.K. Sahoo, et al., Synthesis of silver nanoparticles using facile wet chemical route, Def. Sci. J. 59 (4) (2009) 447–455.
[56] J. Natsuki, T. Natsuki, Y. Hashimoto, A review of silver nanoparticles: synthesis methods, properties and applications, Int. J. Mater. Sci. Appl. 4 (5) (2015) 325–332.
[57] J.R. Nakkala, R. Mata, A.K. Gupta, S.R. Sadras, Biological activities of green silver nanoparticles synthesized with Acorous Calamus rhizome extract, Eur. J. Med. Chem. 85 (2014) 784–794.
[58] R. Mariselvam, et al., Green synthesis of silver nanoparticles from the extract of the inflorescence of *Cocos nucifera* (Family: Arecaceae) for enhanced antibacterial activity, Spectrochim. Acta A Mol. Biomol. Spectrosc. 129 (2014) 537–541.
[59] P. Yao, R. Tao, H.-y. Wu, J. Zhou, Green synthesis of silver nanoparticles using tea polyphenols and their catalytic activity in degradation of acid red B, in: International Conference on Energy, Power and Environmental Engineering (ICEPEE 2017), 2017, pp. 442–447.
[60] B. Sadeghi, A. Rostami, S.S. Momeni, Facile green synthesis of silver nanoparticles using seed aqueous extract of *Pistacia atlantica* and its antibacterial activity, Spectrochim. Acta A Mol. Biomol. Spectrosc. 134 (2015) 326–332.
[61] N. Nyoman Rupiasih, A. Aher, S. Gosavi, P.B. Vidyasagar, Green synthesis of silver nanoparticles using latex extract of *Thevetia peruviana*: a novel approach towards poisonous plant utilization, J. Phys. Conf. Ser. 423 (1) (2013) 012032.
[62] S. Kaviya, et al., Biosynthesis of silver nanoparticles using citrus Sinensis peel extract and its antibacterial activity, Spectrochim. Acta A Mol. Biomol. Spectrosc. 79 (3) (2011) 594–598.
[63] S. Ahmed, M. Ahmad, B.L. Swami, S. Ikram, A review on plants extract mediated synthesis of silver nanoparticles for antimicrobial applications: a green expertise, J. Adv. Res. 7 (1) (2016) 17–28.
[64] M. Jahanshahi, A. Dehghani, Fabrication, purification and characterization of carbon nanotubes: arc-discharge in liquid media (ADLM), in: Syntheses and Applications of Carbon Nanotubes and Their Composites, IntechOpen, 2013.
[65] J. Prasek, et al., Methods for carbon nanotubes synthesis—review, J. Mater. 21 (2011) 15872–15884.
[66] C. Somu, et al., Synthesis of various forms of carbon nanotubes by arc discharge methods-comprehensive review, Int. Res. J. Eng. Technol. 04 (2017) 344–354.
[67] Y.L. Hsin, K.C. Hwang, F.-R. Chen, J.-J. Kai, Production and in-situ metal filling of carbon nanotubes in water, Adv. Mater. 13 (11) (2001) 830–833.
[68] H. Lange, et al., Nanocarbon production by arc discharge in water, Carbon 41 (8) (2003) 1617–1623.
[69] Y. Saito, T. Nakahira, S. Uemura, Growth conditions of double-walled carbon nanotubes in arc discharge, J. Phys. Chem. B 107 (4) (2003) 931–934.
[70] E. Flahaut, Double-walled carbon nanotubes: synthesis and filling by 1-D nanocrystals BT, in: A. Vaseashta, D. Dimova-Malinovska, J.M. Marshall (Eds.), Nanostructured and Advanced Materials for Applications in Sensor, Optoelectronic and Photovoltaic Technology, Springer Netherlands, Dordrecht, 2005, pp. 281–286.
[71] H. Qiu, et al., High-efficient synthesis of double-walled carbon nanotubes by arc discharge method using chloride as a promoter, Carbon 44 (3) (2006) 516–521.
[72] K. Imasaka, et al., Production of carbon nanoonions and nanotubes using an intermittent arc discharge in water, Thin Solid Films 506–507 (2006) 250–254.
[73] A. Szabó, et al., Synthesis methods of carbon nanotubes and related materials, Materials 3 (5) (2010) 3092–3140.

This book belongs to Badji Mokhtar Annaba University Central Library Copyright Elsevier 2025

[74] J.L. Qi, et al., Syntheses of carbon nanomaterials by radio frequency plasma enhanced chemical vapor deposition, J. Alloys Compd. 486 (1–2) (2009) 265–272.
[75] M. Lu, W.-M. Liu, X.-Y. Guo, H.-L. Li, Coiled carbon nanotubes growth via reduced-pressure catalytic chemical vapor deposition, Carbon 42 (2004) 805–811.
[76] E. Terrado, et al., Carbon nanotube growth on cobalt-sprayed substrates by thermal CVD, Mater. Sci. Eng. C 26 (2006) 1185–1188.
[77] R. Engel-Herbert, H. Pforte, T. Hesjedal, CVD synthesis and purification of single-walled carbon nanotubes using silica-supported metal catalyst, Mater. Lett. 61 (2007) 2589–2593.
[78] E.A. Campos, et al., Synthesis, characterization and applications of iron oxide nanoparticles—a short review, J. Aerosp. Technol. Manag. 7 (2015) 267–276.
[79] M.O. Ansari, et al., Iron oxide nanoparticles-synthesis, surface modification, applications and toxicity: a review, Mater. Focus 6 (January 2018) (2017) 1–11.
[80] E. Matei, A. Predescu, E. Vasile, A. Predescu, Properties of magnetic iron oxides used as materials for wastewater treatment, J. Phys. Conf. Ser. 304 (1) (2011) 012022.
[81] A. Bouafia, S.E. Laouini, Green synthesis of Iron oxide nanoparticles by aqueous leaves extract of *Mentha pulegium* L.: effect of ferric chloride concentration on the type of product, Mater. Lett. 265 (2020) 127364.
[82] M. Khatami, et al., Super-paramagnetic iron oxide nanoparticles (SPIONs): greener synthesis using Stevia plant and evaluation of its antioxidant properties, J. Clean. Prod. 208 (2019) 1171–1177.
[83] P. Karpagavinayagam, C. Vedhi, Green synthesis of iron oxide nanoparticles using *Avicennia marina* flower extract, Vacuum 160 (2019) 286–292.
[84] P. Nyamukamaba, et al., Synthetic methods for titanium dioxide nanoparticles, in: Titanium Dioxide—Material for a Sustainable Environment, IntechOpen, 2018.
[85] G. Colón, M.C. Hidalgo, J.A. Navı´o, A novel preparation of high surface area TiO_2 nanoparticles from alkoxide precursor and using active carbon as additive, Catal. Today 76 (2–4) (2002) 91–101.
[86] V. Chhabra, et al., Synthesis, characterization, and properties of microemulsion-mediated nanophase TiO_2 particles, Langmuir 11 (9) (1995) 3307–3311.
[87] H. Namin, H.H. Eslami, M. Ranjbar, Effect of aging and calcination on morphology and properties of synthesized nanocrystalline TiO2, Int. J. Mod. Phys. B 22 (18–19) (2008) 3210–3215.
[88] D.-S. Seo, J.-K. Lee, H. Kim, Preparation of nanotube-shaped TiO_2 powder, J. Cryst. Growth 229 (1–4) (2001) 428–432.
[89] S.-H. Lee, et al., Synthesis of TiO_2 photocatalyst thin film by solvothermal method with a small amount of water and its photocatalytic performance, J. Photochem. Photobiol. A Chem. 146 (1–2) (2001) 121–128.
[90] J.M. Macák, H. Tsuchiya, P. Schmuki, High-aspect-ratio TiO_2 nanotubes by anodization of titanium, Angew. Chem. Int. Ed. 44 (14) (2005) 2100–2102.
[91] A.K. Jha, K. Prasad, Biosynthesis of metal and oxide nanoparticles using lactobacilli from yoghurt and probiotic spore tablets, Biotechnol. J. 5 (3) (2010) 285–291.
[92] C.S. Cheng, et al., Toward 3D graphene oxide gels based adsorbents for high-efficient water treatment via the promotion of biopolymers, J. Hazard. Mater. 263 (2013) 467–478.
[93] L. Cui, et al., EDTA functionalized magnetic graphene oxide for removal of Pb(II), Hg(II) and Cu(II) in water treatment: adsorption mechanism and separation property, Chem. Eng. J. 281 (2015) 1–10, https://doi.org/10.1016/j.cej.2015.06.043.
[94] K. Goh, et al., Graphene oxide as effective selective barriers on a hollow fiber membrane for water treatment process, J. Membr. Sci. 474 (2015) 244–253, https://doi.org/10.1016/j.memsci.2014.09.057.
[95] L. Ren, J. Dong, Z. Chi, H. Huang, Reduced graphene oxide-nano zero value iron (RGO-NZVI) micro-electrolysis accelerating Cr(VI) removal in aquifer, J. Environ. Sci. (China) 73 (Vi) (2018) 96–106, https://doi.org/10.1016/j.jes.2018.01.018.
[96] J. Wang, et al., Graphene oxide as an effective barrier on a porous nanofibrous membrane for water treatment, ACS Appl. Mater. Interfaces 8 (9) (2016) 6211–6218.
[97] X. Wang, X. Yang, S. Chen, Q. Li, W. Wang, C. Hou, X. Gao, L. Wang, S. Wang, Zinc oxide nanoparticles affect biomass accumulation and photosynthesis in Arabidopsis, Front. Plant Sci. 6 (Jan 2016) (2016) 1243, https://doi.org/10.3389/fpls.2015.01243.

This book belongs to Badji Mokhtar Annaba University Central Library Copyright Elsevier 2025

[98] Z. Xu, et al., Photocatalytic antifouling PVDF ultrafiltration membranes based on synergy of graphene oxide and TiO_2 for water treatment, J. Membr. Sci. 520 (2016) 281–293, https://doi.org/10.1016/j.memsci.2016.07.060.
[99] J. Saini, V.K. Garg, R.K. Gupta, Green synthesized SiO_2@OPW nanocomposites for enhanced lead (II) removal from water, Arab. J. Chem. 13 (1) (2020) 2496–2507, https://doi.org/10.1016/j.arabjc.2018.06.003.
[100] Z. Wu, W. Li, P.A. Webley, D. Zhao, General and controllable synthesis of novel mesoporous magnetic iron oxide@carbon encapsulates for efficient arsenic removal, Adv. Mater. 24 (4) (2012) 485–491.
[101] L.H. Li, J. Xiao, P. Liu, G.W. Yang, Super adsorption capability from amorphousization of metal oxide nanoparticles for dye removal, Sci. Rep. 5 (2015) 1–6.
[102] H. Mu, Y. Chen, N. Xiao, Effects of metal oxide nanoparticles (TiO_2, Al_2O_3, SiO_2 and ZnO) on waste activated sludge anaerobic digestion, Bioresour. Technol. 102 (22) (2011) 10305–10311.
[103] I. Blinova, A. Ivask, M. Heinlaan, M. Mortimer, A. Kahru, Ecotoxicity of nanoparticles of CuO and ZnO in natural water, Environ. Pollut. 158 (1) (2010) 41–47, https://doi.org/10.1016/j.envpol.2009.08.017.
[104] F. Gottschalk, T. Sonderer, R.W. Scholz, B. Nowack, Modeled environmental concentrations of engineered nanomaterials (TiO_2, ZnO, Ag, CNT, fullerenes) for different regions, Environ. Sci. Technol. 43 (24) (2009) 9216–9222, https://doi.org/10.1021/es9015553.
[105] M. Heinlaan, A. Ivask, I. Blinova, H.-C. Dubourguier, A. Kahru, Toxicity of nanosized and bulk ZnO, CuO and TiO_2 to bacteria *Vibrio fischeri* and crustaceans *Daphnia magna* and *Thamnocephalus platyurus*, Chemosphere 71 (7) (2008) 1308–1316, https://doi.org/10.1016/j.chemosphere.2007.11.047.
[106] Y. Liu, M. Tourbin, S. Lachaize, P. Guiraud, Nanoparticles in wastewaters: hazards, fate and remediation, Powder Technol. 255 (2014) 149–156, https://doi.org/10.1016/j.powtec.2013.08.025.
[107] F. Menzel, T. Reinert, J. Vogt, T. Butz, Investigations of percutaneous uptake of ultrafine TiO2 particles at the high-energy ion nanoprobe LIPSION, Nucl. Inst. Methods Phys. Res. B 219–220 (1–4) (2004) 82–86, https://doi.org/10.1016/j.nimb.2004.01.032.
[108] L. Reijnders, Cleaner nanotechnology and hazard reduction of manufactured nanoparticles, J. Clean. Prod. 14 (2) (2006) 124–133, https://doi.org/10.1016/j.jclepro.2005.03.018.
[109] Y.S. Jang, E.Y. Lee, Y.-H. Park, S.H. Jeong, S.G. Lee, Y.-R. Kim, M.-K. Kim, S.W. Son, The potential for skin irritation, phototoxicity, and sensitization of ZnO nanoparticles, Mol. Cell. Toxicol. 8 (2) (2012) 171–177, https://doi.org/10.1007/s13273-012-0021-9.
[110] N. Prajitha, S.S. Athira, P.V. Mohanan, Bio-interactions and risks of engineered nanoparticles, Environ. Res. 172 (2019) 98–108, https://doi.org/10.1016/j.envres.2019.02.003.
[111] R.J. Miller, H.S. Lenihan, E.B. Muller, N. Tseng, S.K. Hanna, A.A. Keller, Impacts of metal oxide nanoparticles on marine phytoplankton, Environ. Sci. Technol. 44 (19) (2010) 7329–7334, https://doi.org/10.1021/es100247x.
[112] S. Saddick, M. Afifi, O.A. Abu Zinada, Effect of Zinc nanoparticles on oxidative stress-related genes and antioxidant enzymes activity in the brain of *Oreochromis niloticus* and *Tilapia zillii*, Saudi J. Biol. Sci. 24 (7) (2017) 1672–1678, https://doi.org/10.1016/j.sjbs.2015.10.021.
[113] M.S. McKee, J. Filser, Impacts of metal-based engineered nanomaterials on soil communities, Environ. Sci.: Nano 3 (3) (2016) 506–533, https://doi.org/10.1039/c6en00007j.
[114] S. Pal, Y.K. Tak, J.M. Song, Does the antibacterial activity of silver nanoparticles depend on the shape of the nanoparticle? A study of the gram-negative bacterium *Escherichia coli*, Appl. Environ. Microbiol. 73 (6) (2007) 1712–1720, https://doi.org/10.1128/AEM.02218-06.
[115] C.A. Dos Santos, M.M. Seckler, A.P. Ingle, I. Gupta, S. Galdiero, M. Galdiero, A. Gade, M. Rai, Silver nanoparticles: therapeutical uses, toxicity, and safety issues, J. Pharm. Sci. 103 (7) (2014) 1931–1944, https://doi.org/10.1002/jps.24001.
[116] R.R. Miranda, A.G. Bezerra Jr., C.A. Oliveira Ribeiro, M.A.F. Randi, C.L. Voigt, L. Skytte, K. L. Rasmussen, F. Kjeldsen, F. FilipakNeto, Toxicological interactions of silver nanoparticles and non-essential metals in human hepatocarcinoma cell line, Toxicol. In Vitro 40 (2017) 134–143, https://doi.org/10.1016/j.tiv.2017.01.003.
[117] R.R. Khaydarov, R.A. Khaydarov, O. Gapurova, I. Garipov, F.M. Lutfi, Silver nanoparticles as a biocide for water treatment applications, in: R. Prasad, T. Karchiyappan (Eds.), Advanced Research in Nanosciences for Water Technology, Nanotechnology in the Life SciencesSpringer, Cham, 2019, pp. 407–419.

This book belongs to Badji Mokhtar Annaba University Central Library Copyright Elsevier 2025

[118] K. Bilberg, M.B. Hovgaard, F. Besenbacher, E. Baatrup, In vivo toxicity of silver nanoparticles and silver ions in zebrafish (*Danio rerio*), J. Toxicol. 2012 (2012) 293784, https://doi.org/10.1155/2012/293784.
[119] J. Wang, X. Zhu, X. Zhang, Z. Zhao, H. Liu, R. George, J. Wilson-Rawls, Y. Chang, Y. Chen, Disruption of zebrafish (*Danio rerio*) reproduction upon chronic exposure to TiO_2 nanoparticles, Chemosphere 83 (4) (2011) 461–467, https://doi.org/10.1016/j.chemosphere.2010.12.069.
[120] W. Lu, D. Senapati, S. Wang, O. Tovmachenko, A.K. Singh, H. Yu, P.C. Ray, Effect of surface coating on the toxicity of silver nanomaterials on human skin keratinocytes, Chem. Phys. Lett. 487 (1–3) (2010) 92–96, https://doi.org/10.1016/j.cplett.2010.01.027.
[121] L. Yin, B.P. Colman, B.M. McGill, J.P. Wright, E.S. Bernhardt, Effects of silver nanoparticle exposure on germination and early growth of eleven wetland plants, PLoS One 7 (10) (2012), https://doi.org/10.1371/journal.pone.0047674.
[122] X. Luo, S. Xu, Y. Yang, L. Li, S. Chen, A. Xu, L. Wu, Insights into the ecotoxicity of silver nanoparticles transferred from *Escherichia coli* to *Caenorhabditis elegans*, Sci. Rep. 6 (2016) 36465, https://doi.org/10.1038/srep36465.
[123] J. Beddow, B. Stolpe, P. Cole, J.R. Lead, M. Sapp, B.P. Lyons, I. Colbeck, C. Whitby, Effects of engineered silver nanoparticles on the growth and activity of ecologically important microbes, Environ. Microbiol. Rep. 6 (5) (2014) 448–458, https://doi.org/10.1111/1758-2229.12147.
[124] T.T. Duong, T.S. Le, T.T.H. Tran, T.K. Nguyen, C.T. Ho, T.H. Dao, T.P.Q. Le, H.C. Nguyen, D.K. Dang, T. T.H. Le, P.T. Ha, Inhibition effect of engineered silver nanoparticles to bloom forming cyanobacteria, Adv. Nat. Sci. Nanosci. Nanotechnol. 7 (3) (2016) 035018, https://doi.org/10.1088/2043-6262/7/3/035018.
[125] M. Rui, C. Ma, X. Tang, J. Yang, F. Jiang, Y. Pan, Z. Xiang, Y. Hao, Y. Rui, W. Cao, B. Xing, Phytotoxicity of silver nanoparticles to peanut (*Arachis hypogaea* L.): physiological responses and food safety, ACS Sustain. Chem. Eng. 5 (8) (2017) 6557–6567, https://doi.org/10.1021/acssuschemeng.7b00736.
[126] G. Ghasemzadeh, M. Momenpour, F. Omidi, M.R. Hosseini, M. Ahani, A. Barzegari, Applications of nanomaterials in water treatment and environmental remediation, Front. Environ. Sci. Eng. 8 (4) (2014) 471–482, https://doi.org/10.1007/s11783-014-0654-0.
[127] C.D. Vecitis, K.R. Zodrow, S. Kang, M. Elimelech, Electronic-structure-dependent bacterial cytotoxicity of single-walled carbon nanotubes, ACS Nano 4 (9) (2010) 5471–5479, https://doi.org/10.1021/nn101558x.
[128] A. Baun, S.N. Sørensen, R.F. Rasmussen, N.B. Hartmann, C.B. Koch, Toxicity and bioaccumulation of xenobiotic organic compounds in the presence of aqueous suspensions of aggregates of nano-C60, Aquat. Toxicol. 86 (3) (2008) 379–387, https://doi.org/10.1016/j.aquatox.2007.11.019.
[129] B.K. Gaiser, A. Biswas, P. Rosenkranz, M.A. Jepson, J.R. Lead, V. Stone, C.R. Tyler, T.F. Fernandes, Effects of silver and cerium dioxide micro- and nano-sized particles on *Daphnia magna*, J. Environ. Monit. 13 (5) (2011) 1227–1235, https://doi.org/10.1039/c1em10060b.
[130] X. Tao, J.D. Fortner, B. Zhang, Y. He, Y. Chen, J.B. Hughes, Effects of aqueous stable fullerene nanocrystals (nC60) on *Daphnia magna*: evaluation of sub-lethal reproductive responses and accumulation, Chemosphere 77 (11) (2009) 1482–1487, https://doi.org/10.1016/j.chemosphere.2009.10.027.
[131] R.D. Brohi, L. Wang, H.S. Talpur, D. Wu, F.A. Khan, D. Bhattarai, Z.-U. Rehman, F. Farmanullah, L.-J. Huo, Toxicity of nanoparticles on the reproductive system in animal models: a review, Front. Pharmacol. 8 (SEP) (2017) 606, https://doi.org/10.3389/fphar.2017.00606.
[132] A.A. Miranda, S.M. Shaikh, P.R. Sarode, P.V. Desai, Carbon nanoparticle toxicity to marine algae *Navicula longa* and *Isochrysis galbana*, Indian J. Mar. Sci. 41 (4) (2012) 331–337.
[133] M.V.D.Z. Park, E.A.J. Bleeker, W. Brand, F.R. Cassee, M. Van Elk, I. Gosens, W.H. De Jong, J.A. J. Meesters, W.J.G.M. Peijnenburg, J.T.K. Quik, R.J. Vandebriel, A.J.A.M. Sips, Considerations for safe innovation: the case of graphene, ACS Nano 11 (10) (2017) 9574–9593, https://doi.org/10.1021/acsnano.7b04120.
[134] Y. Hao, C. Ma, Z. Zhang, Y. Song, W. Cao, J. Guo, G. Zhou, Y. Rui, L. Liu, B. Xing, Carbon nanomaterials alter plant physiology and soil bacterial community composition in a rice-soil-bacterial ecosystem, Environ. Pollut. 232 (2018) 123–136, https://doi.org/10.1016/j.envpol.2017.09.024.

This book belongs to Badji Mokhtar Annaba University Central Library Copyright Elsevier 2025

[135] P.K. Boruah, P. Borthakur, M.R. Das, Magnetic metal/metal oxide nanoparticles and nanocomposite materials for water purification, in: Nanoscale Materials in Water Purification, Elsevier, 2019, pp. 473–503.
[136] M.A. Maurer-Jones, I.L. Gunsolus, C.J. Murphy, C.L. Haynes, Toxicity of engineered nanoparticles in the environment, Anal. Chem. 85 (6) (2013) 3036–3049, https://doi.org/10.1021/ac303636s.
[137] U.S. Patil, S. Adireddy, A. Jaiswal, S. Mandava, B.R. Lee, D.B. Chrisey, In vitro/in vivo toxicity evaluation and quantification of iron oxide nanoparticles, Int. J. Mol. Sci. 16 (10) (2015) 24417–24450, https://doi.org/10.3390/ijms161024417.
[138] M. Rui, C. Ma, J. C. White, Y. Hao, Y. Wang, X. Tang, J. Yang, F. Jiang, A. Ali, Y. Rui, W. Cao, G. Chen, B. Xing, Metal oxide nanoparticles alter peanut (*Arachis hypogaea* L.) physiological response and reduce nutritional quality: a life cycle study, Environ. Sci. Nano 5 (9) (2018) 2088–2102, https://doi.org/10.1039/c8en00436f.
[139] B. Laffon, N. Fernández-Bertólez, C. Costa, F. Brandão, J.P. Teixeira, E. Pásaro, V. Valdiglesias, Cellular and molecular toxicity of iron oxide nanoparticles, Adv. Exp. Med. Biol. 1048 (2018) 199–213, https://doi.org/10.1007/978-3-319-72041-8_12.
[140] S. Patel, S. Jana, R. Chetty, S. Thakore, M. Singh, R. Devkar, Toxicity evaluation of magnetic iron oxide nanoparticles reveals neuronal loss in chicken embryo, Drug Chem. Toxicol. 42 (1) (2019) 1–8, https://doi.org/10.1080/01480545.2017.1413110.
[141] S.-F. Shi, J.-F. Jia, X.-K. Guo, Y.-P. Zhao, B.-Y. Liu, D.-S. Chen, Y.-Y. Guo, X.-L. Zhang, Toxicity of iron oxide nanoparticles against osteoblasts, J. Nanopart. Res. 14 (9) (2012) 1091, https://doi.org/10.1007/s11051-012-1091-2.
[142] M. Mahmoudi, S. Laurent, M.A. Shokrgozar, M. Hosseinkhani, Toxicity evaluations of superparamagnetic iron oxide nanoparticles: cell "vision" versus physicochemical properties of nanoparticles, ACS Nano 5 (9) (2011) 7263–7276, https://doi.org/10.1021/nn2021088.
[143] A.R. Murray, E. Kisin, A. Inman, S.-H. Young, M. Muhammed, T. Burks, A. Uheida, A. Tkach, M. Waltz, V. Castranova, B. Fadeel, V. E. Kagan, J.E. Riviere, N. Monteiro-Riviere, A.A. Shvedova, Oxidative stress and dermal toxicity of iron oxide nanoparticles in vitro, Cell Biochem. Biophys. 67 (2) (2013) 461–476, https://doi.org/10.1007/s12013-012-9367-9.
[144] C.M. Mansfield, M.M. Alloy, J. Hamilton, G.F. Verbeck, K. Newton, S.J. Klaine, A.P. Roberts, Photo-induced toxicity of titanium dioxide nanoparticles to *Daphnia magna* under natural sunlight, Chemosphere 120 (2015) 206–210, https://doi.org/10.1016/j.chemosphere.2014.06.075.
[145] X. Zhu, Y. Chang, Y. Chen, Toxicity and bioaccumulation of TiO_2 nanoparticle aggregates in *Daphnia magna*, Chemosphere 78 (3) (2010) 209–215, https://doi.org/10.1016/j.chemosphere.2009.11.013.
[146] H. Jafarizadeh-Malmiri, Z. Sayyar, N. Anarjan, A. Berenjian, Potential hazards of nanoparticles, in: Nanobiotechnology in Food: Concepts, Applications and Perspectives, Springer, Cham, 2019, pp. 115–135.
[147] J.F. Reeves, S.J. Davies, N.J.F. Dodd, A.N. Jha, Hydroxyl radicals (OH) are associated with titanium dioxide (TiO_2) nanoparticle-induced cytotoxicity and oxidative DNA damage in fish cells, Mutat. Res. Fundam. Mol. Mech. Mutagen. 640 (1–2) (2008) 113–122, https://doi.org/10.1016/j.mrfmmm.2007.12.010.
[148] D.B. Warheit, R.A. Hoke, C. Finlay, E.M. Donner, K.L. Reed, C.M. Sayes, Development of a base set of toxicity tests using ultrafine TiO_2 particles as a component of nanoparticle risk management, Toxicol. Lett. 171 (3) (2007) 99–110, https://doi.org/10.1016/j.toxlet.2007.04.008.
[149] R.J. Miller, S. Bennett, A.A. Keller, S. Pease, H.S. Lenihan, TiO2 nanoparticles are phototoxic to marine phytoplankton, PLoS One 7 (1) (2012) e30321, https://doi.org/10.1371/journal.pone.0030321.
[150] M. Ates, V. Demir, R. Adiguzel, Z. Arslan, Bioaccumulation, subacute toxicity, and tissue distribution of engineered titanium dioxide nanoparticles in goldfish (*Carassius auratus*), J. Nanomater. 2013 (2013) 460518https://doi.org/10.1155/2013/460518.

This book belongs to Badji Mokhtar Annaba University Central Library Copyright Elsevier 2025

This page intentionally left blank

This book belongs to Badji Mokhtar Annaba University Central Library

Copyright Elsevier 2025

CHAPTER 4

Advanced technologies for wastewater treatment: New trends

Jyoti Katiyar, Swapnil Bargole, Suja George, Rohidas Bhoi, and Virendra Kumar Saharan

Department of Chemical Engineering, Malaviya National Institute of Technology, Jaipur, India

4.1 Introduction

Water is one of the essential components required in the growth and survival of human beings as well as all living species. Water is available in huge quantities all over the world, but only about 1% of it is easily available for utilization [1]. As per a new report published by World Health Organization (WHO) in 2015, more than 1.1 billion people are struggling worldwide in order to acquire access to pure drinking water [2]. Exponential population growth and rapidly growing industrialization are two major causes of water pollution. The main purpose to treat wastewater is to mineralize the various complex nondegradable pollutants that are present in various industrial/domestic effluents so that they can be safely discharged and do not contaminate the surface water and ground waters. The industrial effluents contain various types of organic and inorganic pollutants and are hence required to be treated by various physical, chemical, and biological treatment techniques to obtain water quality within permissible limits as prescribed by the various regulatory bodies.

Conventional biological treatment methods such as aerobic, anaerobic, and facultative processes are available, but they need to be intensified further because these individual processes are incapable of causing complete breakdown of the highly complex biorefractory pollutants present in wastewater [3]. Moreover, chemical methods including adsorption, ion exchange, membrane filtration, and chemical oxidation are also available, but these methods usually generate large amounts of waste sludge and, moreover, require large quantity of chemicals for treating the bulk of effluent [4]. Besides, the process time required by these

Handbook of Nanomaterials for Wastewater Treatment. https://doi.org/10.1016/B978-0-12-821496-1.00011-8
Copyright © 2021 Elsevier Inc. All rights reserved.

This book belongs to Badji Mokhtar Annaba University Central Library Copyright Elsevier 2025

techniques is really high, and complete mineralization of the pollutants in the effluent stream is not always possible. Many industries also face several challenges in the scale-up of these techniques. Therefore in the search of an alternative approach, many researchers have worked on the use of advanced oxidation processes (AOPs) for the wastewater treatment [5–7]. In the past few decades, a number of AOP-based techniques and hybrid approaches have been developed, which offer an enormous capacity in generating hydroxyl radicals ($^{\bullet}OH$) that are capable to degrade highly complex biorefractory pollutants into smaller intermediates that can be further degraded by the biological methods. AOPs generate various reactive oxygen species (ROS) and $^{\bullet}OH$ of higher oxidation potential, which oxidize organic/inorganic and nonbiodegradable compounds at standard temperature and pressure [8]. AOPs consist of different processes such as photocatalytic oxidation, Fenton process, acoustic cavitation (AC) or sonolysis, hydrodynamic cavitation (HC), and ozonation. Most of these techniques can be used as a single process or can be coupled with another technique to make hybrid processes that are more efficient.

In the past decade, nanomaterials were also successfully applied by researchers into various areas such as medical science, catalysis, and wastewater treatment. It has been established that using nanomaterials can be a superior option for wastewater treatment because of their distinctive properties such as nano size, large surface area, high chemical reactivity, strong solution mobility, lower cost, reusability, high efficiency [9], strong mechanical property, porosity, dispersibility, and hydrophobicity [10]. This chapter mainly presents different aspects of the nanomaterials-based AOPs, which had been applied for the degradation/mineralization of different complex organics and inorganic pollutants in wastewater treatment. Researchers had reported successful utilization of different varieties of nanomaterials such as carbonaceous nanomaterials, zeolites, dendrimers, nanosorbents, nanostructured catalytic membranes, nanorods, nanofiltration membranes, and carbon nanotubes (NTs) for application in the degradation of various organic/inorganic pollutants and toxic metal ions present in wastewater [8–11].

This chapter comprises a definite review of AOPs, such as photocatalytic oxidation [ultraviolet (UV) radiation/near UV light/sunlight in the presence of a semiconductor catalyst], Fenton chemistry [ferrous sulfate + hydrogen peroxide (H_2O_2), i.e., Fenton's reagent], and cavitation (ultrasonication or HC) and their combinations. It presents a detailed review on the mechanism of the various AOPs in degradation of water pollutants along with some recommendation toward optimization of parameters. Apart from that, the effects and significance of various hybrid combinations of AOPs such as heterogeneous Fenton process, heterogeneous photo-Fenton process, sono-photocatalysis process, sono-Fenton Process, photocatalytic oxidation coupled with HC, and sono-photo-Fenton process for application in wastewater treatment has been discussed along with some guidelines for process scale-up.

This book belongs to Badji Mokhtar Annaba University Central Library Copyright Elsevier 2025

4.2 Advanced oxidation processes

AOPs are defined as processes that involve the generation and use of the $^{\bullet}OH$ radicals as a strong oxidant to destroy (oxidize/mineralize) the organic compounds that cannot be oxidized by conventional oxidants such as gaseous oxygen, ozone, and chlorine. The $^{\bullet}OH$ reacts with the dissolved constituents, initiating a series of oxidation reactions until the constituents are completely mineralized to CO_2 and H_2O. The AOP processes include the different oxidation technologies such as cavitation, photocatalytic oxidation, sonolysis, and Fenton chemistry.

4.2.1 Hydrodynamic cavitation

Cavitation process comprises the sequential formation, growth, and subsequent collapse of microcavities within a very short duration, which thereafter causes prolonged physical and chemical effects within the aqueous medium so as to achieve the desired transformation [12]. As a consequence, these cavitational effects include generation of hot spots and high-intensity turbulence, and this resultant energy is subsequently diffused to the molecular level within the liquid, thereby causing the generation of $^{\bullet}OH$ that induce chemical changes in the form of oxidation of pollutants.

HC is simply generated by varying the flow conditions of a liquid by passing it through a constriction fitted in a conduit. The variation of pressure when flowing through these constrictions such as venturi and orifice with different geometries lead to the generation of hot spots or cavities [13, 14]. The geometrical configuration of a HC device is designed in such way that the kinetic energy of the liquid increases, and thus, as per the momentum conservation principle (Bernoulli's theorem), the local pressure falls below the vapor pressure of liquid at the vena contracta, leading to the generation of numerous vapor cavities. Consequently, as the liquid jet expands downstream, the velocity decreases, and as the pressure is recovered in the downstream section of the device, it results in the collapse of the cavities. These sudden pressure and velocity variations in HC cause the generation of hot spots, and as a result, numerous effects such as physical and chemical transformations are initiated within the liquid. The physical effects include generation of shockwaves, microjets, and interfacial turbulence that are mainly responsible for controlling the physical transformations [15]. However, the chemical effects, which are mainly the formation of hydroxyl free radicals in the liquid, are the main driving force to bring about the chemical changes in chemical processing applications. Particularly in the application of wastewater treatment, the chemical effects contribute to the generation of free radicals that diffuse into the bulk liquid and decompose or degrade the pollutants by means of their oxidation. During HC treatment, the water molecules get dissociated into $^{\bullet}OH$ and hydrogen radicals ($H^{\bullet}$) under extreme temperature and pressure conditions. These $^{\bullet}OH$ with high oxidation potential oxidize organic pollutant molecules present in the wastewater and thereby degrade the organic compounds.

This book belongs to Badji Mokhtar Annaba University Central Library
Copyright Elsevier 2025

The reaction mechanisms that take place during the generation of free radicals and the mineralization of organic particles in the effluent using HC are as given in Eqs. (4.1)–(4.3).

$$HC + H_2O \rightarrow {}^{\cdot}H + {}^{\cdot}OH \tag{4.1}$$

$${}^{\cdot}OH + {}^{\cdot}OH \rightarrow H_2O_2 \tag{4.2}$$

$${}^{\cdot}OH + \text{organic molecules1} \rightarrow CO_2 + H_2O + \text{some intermediates} \tag{4.3}$$

Various studies have proved that HC offers better degradation efficiency, consumes lower energy, requires less maintenance, and is easy to couple with other AOPs so as to produce the desired removal in wastewater treatment. HC can be effectively coupled with photocatalysis, Fenton, ozone, and many others AOPs, indicating a synergy so as to enhance the efficiency of the degradation of the organic pollutants. Also, this hybrid technique has been established as an effective pretreatment technique in reducing the high organic load of complex organics, thereby increasing the biodegradability of real industrial effluents. Some of the important research studies that have been reported in the past decade for the degradation of various organic dye molecules such as Acid red, Congo red, Orange, Rhodamine dye, and triazophos using HC alone and in hybrid combinations with ozone, Fenton, and TiO_2 photocatalyst in wastewater treatment are summarized in Table 4.1.

4.2.2 Sonolysis/acoustic cavitation

Sonication of water by ultrasonic sound waves having high frequencies ranging from 16 kHz to 2 MHz leads to the formation, growth, and collapse of microcavities through compression and rarefaction cycles, which is known as sonolysis or AC. When adequate negative pressure appears within the liquid, the average molecular distance between liquid molecules becomes higher than the critical molecular distance that bound liquid molecules together, and therefore the liquid molecules breakdown, and cavities are created [21]. These cavities grow in size until the maximum negative pressure has been reached. The growth and collapse of these cavities result in the generation of high pressure, temperature, and highly reactive $^{\bullet}OH$ by thermal decomposition of water and oxygen. The efficiency of the AC reactor depends on the intensity of the cavity collapse, which is directly proportional to the total number of cavitational events occurring inside the reactor and the final cavity collapse pressure. In order to obtain higher efficiency, several operational parameters such as intensity of sound waves, frequency of ultrasound, and calorimetric efficiency of ultrasonic equipment need to be optimized. The efficiency of the sonolysis process is also dependent on the solvent properties, for example, vapor pressure, viscosity, surface tension, and density. The solvent with low density and high vapor pressure is favorable for sonication. The implosion of cavitation bubbles leads to the oxidation of contaminant with the help of pyrolysis, which occurs at high pressure and temperature (2000 atm and 10,000 K, approximately) within the hot spots in the aqueous medium [22]. A schematic representation of the sonolysis process is shown in Fig. 4.1.

This book belongs to Badji Mokhtar Annaba University Central Library Copyright Elsevier 2025

Table 4.1: Studies in wastewater treatment applying hydrodynamic cavitation.

Organic pollutant	Equipment and techniques	Optimum operating conditions	Percentage degradation of organic pollutant	References
Acid Red-18	HC reactor: orifice plate, venturi (2 mm)	Initial conc. of AR-18 = 15 ppm, Inlet pressure = 6 bar, TiO_2 = 300 mg/L, pH 3.0, temp. = 35°C, H_2O_2 = 300 mg/L	Without TiO_2: HC—orifice = 80%, HC—venturi = 66% Ultrasonic cavitation = 50% With TiO_2: HC—orifice = 88.1%, HC—venturi = 70.4% Ultrasonic cavitation = 64.8% within 120 min	[16]
Rhodamine B	HC setup, square venturi tube (1.77 mm, 6 degrees)	Initial conc. of Rhodamine B = 10 mg/L, Fe^{3+}:TiO_2 = 0.05:1.00 M, Inlet pressure = 3.0 bar, pH 3.0, temp. = 40°C	HC + Fe^{3+} + doped TiO_2 = 91.11% within 150 min	[17]
Congo Red (CR) and sulfamethoxazole (SMX)	HC reactor: (15 L), centrifugal pump 1-HP, cavitating device: venturi	Initial conc. of Congo Red = 5 mg/L, Pressure = 10.3 kPa, Dosage of *N*,*N*-dimethyl-*p*-nitrosoaniline (pNDA) as scavenger = 10 μM, pH of pNDA = 5.2	Removal of Congo Red = 50% within 4 min Removal of SMX = 25% within 60 min	[18]
Triazophos	HC reactor: reciprocating pump 1.1 kW, orifice plate (25 mm pipe diameter and 2 mm orifice hole)	Initial conc. of triazophos = 20 mg/L, Inlet pressure = 5 bar, Solution pH 3, Ratio of	Degradation using HC = 50%, TOC removal using HC = 30%, HC + Fenton = 83%, TOC removal = 56%,	[7]

Continued

This book belongs to Badji Mokhtar Annaba University Central Library

Copyright Elsevier 2025

Table 4.1: Studies in wastewater treatment applying hydrodynamic cavitation—cont'd

Organic pollutant	Equipment and techniques	Optimum operating conditions	Percentage degradation of organic pollutant	References
		Triazophos:$FeSO_4$:H_2O_2 = 1:4:4 Ozone flow rate = 1.95 g/h	Synergetic index = 3.34, HC + ozonation = 100% TOC removal using HC + ozonation = 96% within 90 min	
Orange-G	HC reactor:(15 L), Cavitating devices: 1. Circular venturi of 2 mm throat diameter 2. Slit venturi (width 6 mm, height 1.9 mm and length 1.9 mm) 3. Orifice plate of 2 mm throat diameter	Initial conc. of Orange-G = 50 μM, Inlet pressure in orifice plate = 5 bar Inlet pressure in slit venturi = 3 bar, Inlet pressure in circular venturi Solution pH 2.0, Cavitation number: Orifice plate = 0.24 Slit venturi = 0.29 Circular venturi = 0.15	Degradation of Orange-G dye: Slit venturi = 92% Circular venturi = 76% Orifice plate = 45% Reduction in total organic carbon (TOC): Using slit venturi = 37% Using circular venturi = 28% Using orifice plate = 14% (within 120 min)	[19]
Acid Red 88	HC reactor: (15 L), cavitating device: venturi	Initial conc. of Acid Red 88 = 100 μM, Conc. of H_2O_2 = 4000 μM, Molar ratio of dye to H_2O_2 = 1:40 Inlet pressure = 5 bar, pH 2.0, Cavitation number = 0.30	Decolorization of Acid Red 88 dye using HC = 92% TOC removal = 35% HC + H_2O_2 = 100%, TOC removal = 72% within 120 min	[20]

This book belongs to Badji Mokhtar Annaba University Central Library

Copyright Elsevier 2025

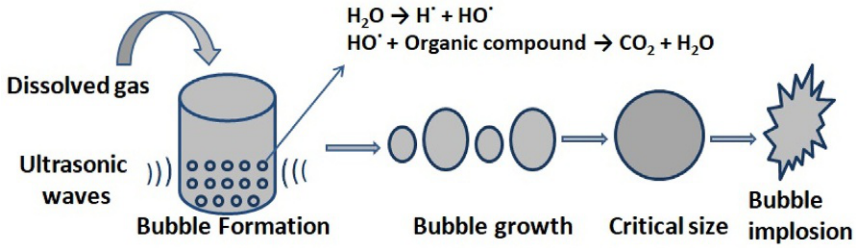

Fig. 4.1
Schematic representation of sonolysis process.

The generalized reaction mechanism for the production of $H^{\bullet}$ and $^{\bullet}OH$ radicals in the sonolysis process through cavitation is as given in Eq. (4.4), and H_2O_2 is also produced simultaneously as per Eq. (4.5) [23].

$$H_2O +)))) \rightarrow H^{\bullet} + {}^{\bullet}OH \tag{4.4}$$

$$H_2O +)))) \rightarrow 1/2H_2 + 1/2H_2O_2 \tag{4.5}$$

Table 4.2 presents a summary of some studies carried out in the area of wastewater treatment using sonication along with their experimental conditions and percentage degradation. Over the past few years, researchers had used the ultrasonication technique for the removal of various recalcitrant organic/inorganic compounds such as phenol [31], chloro-aromatic compounds [32], pesticides, herbicides, benzene-based compounds, polycyclic aromatic hydrocarbons, aqueous carbon tetrachloride, and organic dyes [33] present in wastewater.

Sonication alone may not be efficient for the complete degradation of organic pollutants because of their high polarity toward water, less amount of $^{\bullet}OH$ radicals generated, and lack of dissipated power as only about 3% of the delivered power is dissipated into the solution. To overcome such problems, many researchers developed hybrid AOPs such as ultrasonication + ozone/H_2O_2, sono-photocatalysis, sono-Fenton, photo Fenton, and many others to enhance the extent of degradation of organic pollutants [34]. This can be attributed to the fact that hybrid AOPs provide higher rate of $^{\bullet}OH$ radical generation and formation of secondary oxidation species. Yasman et al. [35] analyzed the performance of sono-electrochemical-Fenton process for the removal of 2,4-dichlorophenoxyacetic acid and 2,4-dichlorophenol from the aqueous solution. A higher degradation was obtained in sono-electro-Fenton process when compared with sono-electrochemical process, sono-Fenton process, and only Fenton process. The higher efficiency of sono-electro-Fenton process was because of the enhanced generation of $^{\bullet}OH$ radicals owing to oxidative and reductive electrochemical reactions within the process.

This book belongs to Badji Mokhtar Annaba University Central Library Copyright Elsevier 2025

Table 4.2: Wastewater treatment applying sonolysis process.

Organic pollutant	Equipment	Optimum operating conditions	Results	References
Acid Blue 7	Ultrasonic bath operating (36 kHz, 150 W)	Dosage of metal organic frame (MOF-2) catalyst = 0.6 g/L, Dosage of $S_2O_8^{2-}$ **= 6 mmol/L, Acid Blue 7 vol. = 100 mL Temp. = 25°C**	US + MOF-2 = 49.02%, US + MOF-2 + $S_2O_8^{2-}$ **= 63.43% within 60 min**	[24]
C.I. Reactive Orange 107	Ultrasound system (60 W, 850 kHz)	Initial conc. of C.I. Reactive Orange 107 = 50 mg/L, pH 11, Temp. = 30°C	80% within 4 h	[25]
Basic Red 29	Ultrasound system (300 kHz, 80 W)	Initial conc. of Basic Red 29 = 30 mg/L, Dosage of TiO_2 = 100 mg/L, Dosage of Fe^{2+} = 15 mg/L, Temp. = 25°C, pH 3	US = 5%, US + TiO_2 = 10% US + Fe^{2+} = 35% US + Fe^{2+} + TiO_2 = 64%	[26]
Benzophenone-3	Ultrasonic processor VCX-500 Sonics (20 kHz), cylindrical glass reactor	Initial conc. of benzophenone-3 = 3.9 mg/L, Ultrasonic power = 55.9 W, pH 2, 6.5	Benzophenone-3: pH (6.5) = 66.83% pH (2) = 80.91%. within 60 min COD reduction: 80%	[27]
Pyridine	Ultrasonic cleaner bath (360 W and 40 kHz)	Initial conc. of pyridine = 100 ppm, Air flow = 1.5 L/min, pH 9.1, Temp. = 40°C	Pyridine removal = 70% within 180 min	[28]
Dye wastewater	Sonication apparatus (500 W and 20 kHz)	COD = 13,000 mg/L pH 6 Ultrasonic power = 500 W	COD removal (without dipping) = 71.45% COD removal (with dipping) = 82.18% within 90 min	[29]

This book belongs to Badji Mokhtar Annaba University Central Library
Copyright Elsevier 2025

Table 4.2: Wastewater treatment applying sonolysis process—cont'd

Organic pollutant	Equipment	Optimum operating conditions	Results	References
Furfural	Ultrasonic processor = 750 W, 250 kHz (Model: VCX 750; Sonics Inc., USA)	Initial conc. of furfural = 25 mg/L, Power density = 3000 W/L, pH 2	Binary solution: Furfural = 83% within 120 min Mixed solution: Furfural = 80% Phenol = 93% COD = 93% within 180 min	[30]

4.2.3 Photocatalysis

The photocatalytic oxidation process is one of the most important techniques in the area of wastewater treatment. During this process, the solid semiconducting photocatalysts, such as TiO_2, WO_3, ZnO, Fe_2O_3, and SnO_2, oxidize the pollutant in the presence of light having energy higher than the bandgap energy of the catalyst [36, 37]. When photons of sufficient energy levels fall on the surface of a catalyst, electrons and holes are created, and this initiates oxidation and reduction reactions over the catalyst surface.

During the photocatalytic oxidation process, light gets absorbed on the surface of the photocatalyst, which is generally a semiconductor having wide band gap, and this leads to the formation of electrons and holes on its surface. Owing to the continuous irradiation, absorption of light by the semiconductor catalyst occurs, and therefore the electrons move from the valence band to the conduction band forming positively charged holes and negatively charged electrons in the valence and conduction bands, respectively. The presence of holes and electrons on the surface of photocatalyst gives rise to oxidation and reduction reactions. The negatively charged electrons react with any positively charged pollutant molecules or react with electron acceptors such as O_2 to generate the radical anion $O_2^{\bullet -}$. The positively charged holes generated by photocatalysis react with pollutant molecules and water molecules to produce $^{\bullet}OH$ radicals, which subsequently oxidize the organic pollutant molecules [38].

The mechanism of photocatalysis process is explained as follows in Eqs. (4.6)–(4.12), and a pictorial representation is shown in Fig. 4.2.

$$UV + MO \rightarrow MO\left(h^{+} + e^{-}\right) \tag{4.6}$$

Here MO is metal oxide, and UV represents UV light energy

$$h^{+} + H_2O \rightarrow H^{+} + {}^{\cdot}OH \tag{4.7}$$

This book belongs to Badji Mokhtar Annaba University Central Library Copyright Elsevier 2025

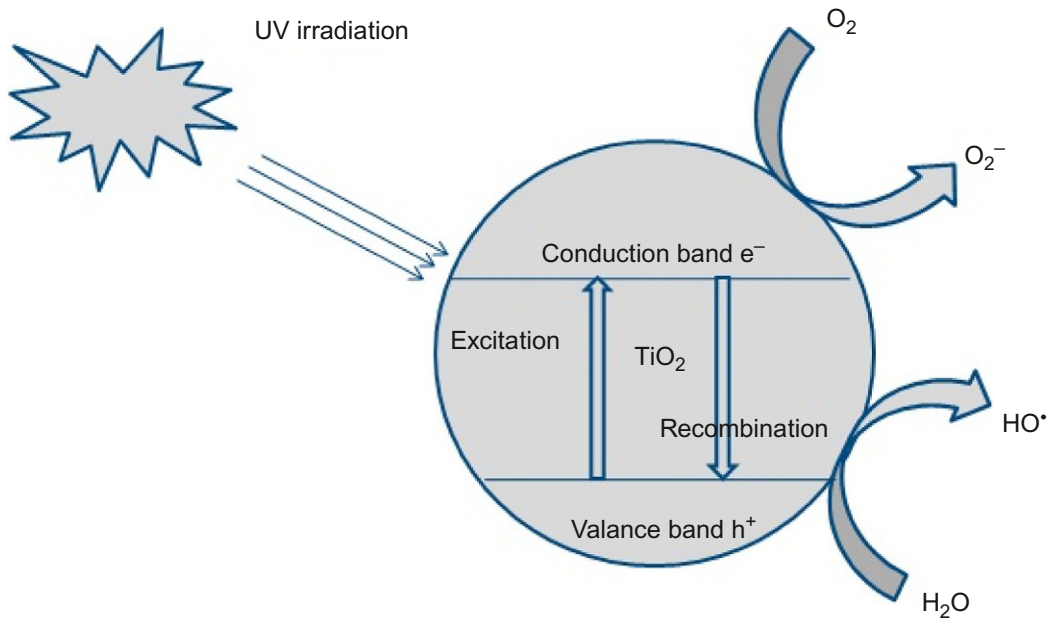

Fig. 4.2
Schematic representation of photocatalytic process.

$$2h^+ + 2H_2O \rightarrow 2H^+ + H_2O_2 \tag{4.8}$$

$$H_2O_2 \rightarrow HO^{\cdot} + {}^{\cdot}OH \tag{4.9}$$

$$e^- + O_2 \rightarrow {}^{\cdot}O_2^- \tag{4.10}$$

$${}^{\cdot}O_2^- + H^+ \rightarrow HO^{\cdot}{}_2 \tag{4.11}$$

$$HO^{\cdot}{}_2 + H^+ \rightarrow {}^{\cdot}O_2^- \rightarrow H_2O_2 + O_2 \tag{4.12}$$

Table 4.3 presents some of the work done in the area of photocatalysis oxidation for wastewater treatment. Many researchers have synthesized different photocatalysts using various techniques such as sol-gel processes, microwave-assisted synthesis, and electrochemical, hydrothermal, solvothermal, impregnation, and precipitation methods [5].

TiO_2 nanomaterials have unique structural, morphological, and optoelectronic properties that make them excellent applicants for light compelled applications in the environmental protection and energy conversion field [52]. TiO_2 photocatalyst in the form of slurries, thin films, and composites exhibit excellent photocatalytic activity so as to degrade pollutants present in wastewater. Moreover, TiO_2 is the most commonly used photocatalyst because of its cost-effectiveness, nontoxicity, ability of regeneration, photocatalytic efficiency, and high

This book belongs to Badji Mokhtar Annaba University Central Library Copyright Elsevier 2025

This book belongs to Badji Mokhtar Annaba University Central Library

Table 4.3: Wastewater treatment applying photocatalysis process.

Photocatalyst	Synthesis process	Equipment	Organic pollutant	Optimum operating conditions	Percentage degradation of organic pollutant	References
Ferrites MFe_2O_4: M = (Co, Ni, Cu, Zn) (NiF)	Co-precipitation-oxidation method	–	Methylene Blue, Methyl Orange, Bromo Green, Methyl Red	Initial conc. of dye = 10 mg/L, Catalyst dosage = 0.5 g/L, H_2O_2 = 5 mmol/L, pH 7, UV-C power = 16 W	Methylene Blue = 89%, Methyl Orange = 92%, Bromo Green = 93%, Methyl Red = 78% within 1 min TOC removal = 60% after 50 min	[39]
Reduced graphene oxide-BiOBr	Modified hummers method, facile synthesis procedure	Photocatalytic set up, Xenon lamp (300 W)	Rhodamine-B	Initial conc. = 10 ppm, Dosage of graphene-BiOBr = 0.5 mg/mL	Pristine BiOBr = 80% Graphene-BiOBr = 100% after 70 min	[40]
CdSe quantum dots/GO	Facile chemical precipitation method	Solar intensity (1250 × 100 Lu ± 100)	Brilliant Green dye	Initial conc. = 10 mg/L, Dosage of CdSe QDs = 30 mg	By using CdSeQDs = 81.9% By using CdSe/GO = 95.5% within 90 min	[41]

Continued

Copyright Elsevier 2025

This book belongs to Badji Mokhtar Annaba University Central Library

Table 4.3: Wastewater treatment applying photocatalysis process—cont'd

Photocatalyst	Synthesis process	Equipment	Organic pollutant	Optimum operating conditions	Percentage degradation of organic pollutant	References
Zinc oxide (ZnO)	Sol-gel method	UV lamp (1000 W, 365 nm)	Methyl Orange	Initial conc. = 30 mg/L, Dosage of ZnO = 0.2 g/L, pH 2, calcination temp. = 400°C	99.70% within 30 min	[42]
Polyaniline (PANI)/ZnO nanocomposite	Precipitation method	Photo reactor visible light irradiation, projection lamp (7748XHP 250 W, Philips)	Methyl Orange, Methylene Blue	Reaction temp. = 25°C, Initial conc. of solution = 1 mg/mL	Methyl Orange = 98.3, Methylene Blue = 99.2 within 180 min	[43]
Novel Bi_2S_3-sensitized BiOCl	Facile ion exchange methods	Photoreaction apparatus, UV Lamp Xe (500 W)	Rhodamine B	Initial conc. of dye = 10 mg/L, Catalyst dosage = 0.03 g, pH 8.5, $\lambda >$ 400 nm	98% within 2 h	[44]
Nanocrystalline—WO_3	Precipitate methods	Glass reactor	Safranin-O dye (Basic Red-2)	Initial conc. of dye = 5.7×10^{-4} M, Catalyst dosage = 1 g/L, pH 10, λ = 355 nm, Laser energy = 140 mJ	94% within 10 min	[36]

Copyright Elsevier 2025

This book belongs to Badji Mokhtar Annaba University Central Library

ZnO/CdO nanorod	Thermal decomposition method	Photoreactor, projection lamp (97748XHP 250 W Philips, 532 nm)	Methylene Blue	Initial conc. = 3×10^{-5} M, Catalyst dosage = 1 g/L, pH 10, λ = 355 nm	97.80% within 6 h	[45]
Nd-doped ZnO	Improved sol-gel method	–	Cl Reactive Blue 4	Initial conc. of dye = 20 mg/L, Catalyst dosage = 0.1 g/L, pH 11	91.25% within 90 min	[46]
Ag-doped TiO_2	–	Pyrex photo reactor, high-pressure mercury lamp (400 W)	Azo dye	Initial conc. of dye = 30 mg/L, Catalyst dosage = 0.03 g, pH 8–9	100% within 2.5 h	[47]
Fe-ZnO	Impregnation method	Batch photoreactor (250 mL), Xenon lamp (1500 W)	2,4-Dichlorophenol	Initial conc. = 5 mg/L, Dosage of Fe-ZnO = 1.5 g/L, pH 8.5	95% within 90 min	[48]
MoO_3/Zn nanorod	Hydrothermal method	–	2,4-Dichlorophenoxyacetic acid	Initial conc. = 20 mg/L, Catalyst dosage = 1.5 g/L, pH 7.04	99.20% within 120 min	[49]

Continued

Copyright Elsevier 2025

This book belongs to Badji Mokhtar Annaba University Central Library

Table 4.3: Wastewater treatment applying photocatalysis process—cont'd

Photocatalyst	Synthesis process	Equipment	Organic pollutant	Optimum operating conditions	Percentage degradation of organic pollutant	References
ZnO	Sol-gel method	Nonconcentrating type slurry reactor	2,4- Dichlorophenol	Initial conc. of dye = 0.05 g/L, Dosage of ZnO = 2 g/L, pH 5.5, λ = 285 nm, Intensity of UV sunlight = 5100 W/m^2	98% within 160 min	[50]
TiO_2	–	Annular photoreactor, OSRAM UV lamp HNS 6 W G5, 42 V, 6.00 W	Different organic pollutants (organic carbon content removal)	Initial conc. of total carbon = 32 mg/L, Catalyst dosage = 0.5 g/L, H_2O_2 = 66.6 mg/L, pH 6–7, λ = 254 nm	UV + TiO_2 = 58% UV + H_2O_2 = 53% UV + TiO_2 + H_2O_2 + Fe (III) = 84% within 120 min	[51]

Copyright Elsevier 2025

stability. In order to maximize the specific surface area of the catalyst, which enhances the catalytic reactions and results in maximum efficiency, nano forms of TiO_2 are widely used. TiO_2 NTs not only provide large surface-to-volume ratio but also have strong adsorption capacity and reactivity. Different techniques such as electrochemical anodic oxidation and alkaline hydrothermal treatment methods are used to prepare TiO_2 NTs, nanosheets, nanocrystals, and nanoparticles. But TiO_2 photocatalyst has also some disadvantages such as recombination of generated redox environment, infective use of solar light, low adsorption capacity for hydrophobic contaminants, difficulty in the recovery of the TiO_2 nanoparticles after wastewater treatment, and its selectivity [53].

To overcome these drawbacks, semiconductors such as ZnO, ZnS, WO_3, SnO_2, MoS_2, Fe_2O_3, and CdS have been developed for photocatalysis. Also, the structure, surface morphology, and photocatalytic activity of the catalyst has been improved by using doped semiconductors. Doping has been proved to be an effective way to increase the thermal instability of the semiconductors crystal structure [54]. The physicochemical properties such as crystalline nature, size of crystallites, and large surface area are being considered before choosing the dopants. Recently, researchers [55] had also investigated nanoscale heterojunctions by the deposition of nano-sized metal oxides on thin films. Heterojunctions are combination of two different semiconductor compounds having an unequal band gap, and that provides extended recombination time to electron-hole pairs.

Sakthivel et al. [56] evaluated the photocatalytic activity of TiO_2 and ZnO in the presence of sunlight for the degradation of acid brown 14. Complete mineralization of acid brown 14 was observed after 120 and 300 min using ZnO and TiO_2 catalysts, respectively. This is attributed to the fact that ZnO absorbs more solar light making it more efficient than TiO_2. The extent of degradation by ZnO was studied in the pH range of 3–11, and it was observed that the rate of degradation increased with an increase in pH till an optimum value at pH 10 because alkaline pH favors the formation of $^{\bullet}OH$. However, in the case of TiO_2, maximum degradation was observed at acidic pH 3 because acidic pH leads to the strong adsorption of dye molecules on to the catalyst surface because of the electrostatic interactions between the positively charged catalyst surface and dye anions. Guo et al. [57] synthesized hollow porous gold nanoparticles (HPGNPs) by one-step solution phase method, and those were utilized for the degradation of 4 nitro-phenol at ambient temperature.

4.2.4 Fenton process

The concept of Fenton reaction was first suggested by Fenton, when he observed the oxidation of tartaric acid by H_2O_2 in the presence of ferrous (Fe^{2+}) ions. This process (Fig. 4.3) is one of the prominent AOP that produces highly reactive $^{\bullet}OH$ for the degradation/mineralization of organic compounds. This process has been used as pretreatment or posttreatment for the

This book belongs to Badji Mokhtar Annaba University Central Library Copyright Elsevier 2025

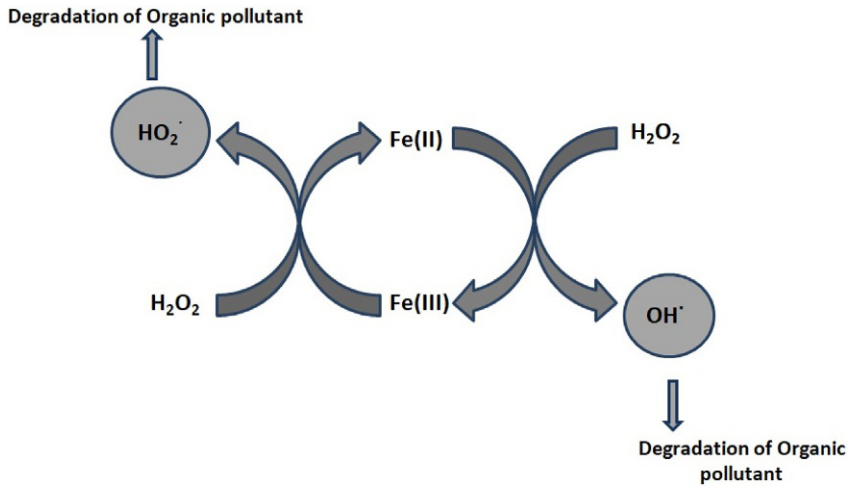

Fig. 4.3
Schematic representation of Fenton process.

degradation of pollutant from landfill leachate [6]. During Fenton process, H_2O_2 reacts with ferrous ion Fe(II) in acidic conditions to generate ferric ion, $^{\bullet}OH$, and hydroxyl anion. These reactive species can oxidize organic and inorganic contaminants present in the solution. The reaction mechanism of the Fenton process is described in Eqs. (4.13)–(4.23). The ferric ion further gets reduced to ferrous ion and a peroxide radical by H_2O_2. The rate of ferric ion formation reaction of (Eq. 4.13) is higher than the rate of its reduction reaction (Eqs. 4.19 and 4.20), which proves that the production rate of Fe^{2+} ions is slower than its consumption rate [58]. The $^{\bullet}OH$ degrade organic compounds into CO_2, H_2O, and various intermediate products. H_2O_2 also reacts with Fe^{3+} reducing to Fe^{2+}as mentioned in reaction Eq. (4.19).

$$Fe^{2+} + H_2O_2 \rightarrow Fe^{3+} + OH^- + HO^{\bullet} \tag{4.13}$$

$$HO^{\cdot} + H_2O_2 \rightarrow H_2O + HOO^{\cdot} \tag{4.14}$$

$$HOO^{\cdot} + H_2O_2 \rightarrow H_2O + HO^{\cdot} + O_2 \tag{4.15}$$

$$Fe^{2+} + HO^{\bullet} \rightarrow Fe^{3+} + OH^- \tag{4.16}$$

$$HO^{\cdot} + H_2O_2 \rightarrow H_2O + H^+ + O_2^- \cdot \tag{4.17}$$

$$Fe^{3+} + O_2^- \cdot \rightarrow Fe^{2+} + O_2 \tag{4.18}$$

$$Fe^{3+} + H_2O_2 \rightarrow Fe^{2+} + H^+ + HOO^{\cdot} \tag{4.19}$$

$$Fe^{3+} + HOO^{\cdot} \rightarrow Fe^{2+} + O_2 + H^+ \tag{4.20}$$

This book belongs to Badji Mokhtar Annaba University Central Library Copyright Elsevier 2025

$$H^+ + H_2O_2 + O_2^- \cdot \rightarrow H_2O + O_2 + HO^{\cdot} \quad (4.21)$$

$$Fe^{2+} + HO^{\cdot} + H^+ \rightarrow Fe^{3+} + H_2O \quad (4.22)$$

$$HO^{\cdot} + HO^{\cdot} \rightarrow H_2O_2 \quad (4.23)$$

Many researchers have studied Fenton chemistry for the oxidation of different organic pollutants such as organic dyes, aromatic and phenolic compounds, herbicides, and pesticides, which are summarized in Table 4.4. During Fenton oxidation of organic pollutants, some important parameters that need to be considered to increase the efficiency of the process are ratio of H_2O_2 to ferrous ion concentration, operating pH, and initial concentration of pollutants. Solution pH is the most affecting factor in the Fenton process, and optimum pH has been observed under acidic conditions around 3 pH in most of the cases [68]. At very low pH (pH $<$ 2.5), the formation of $(Fe(II)(H_2O))^{2+}$ complex takes place, which reacts with H_2O_2 and reduces the total amount of $^{\bullet}OH$. At higher pH (pH $>$ 4), the rate of decomposition get reduced because of lack of free ion species in the aqueous solution owing to the formation of Fe(II) complexes in buffer [69], while in the basic range of pH, precipitation of ferric oxyhydroxides takes place. Therefore iron acts as a catalyst with maximum catalytic activity around pH 3, and the precipitation of Fe ions is prevented at this pH. The presence of iron oxide can be replaced by transition metals, which may also increase the efficiency of process in terms of TOC removal.

As observed in Table 4.4, 90%–100% color/COD removal is achieved around 120 min in the Fenton process; however, the dosage of Fe^{2+} ions and H_2O_2 is a crucial factor, which will determine the overall efficiency and cost of the process [70]. The rate of degradation of organic pollutant increases with an increase in the concentration of Fe^{2+} ions until it reaches an optimum concentration, and beyond that, an increase in TDS is observed. Also, as the amount of H_2O_2 goes beyond an optimum value, scavenging of $^{\bullet}OH$ radicals take place, and the residual H_2O_2 increases the chemical oxygen demand (COD) content [71]. Excess amount of H_2O_2 can also kill the microorganisms, which may subsequently reduce the efficiency of downstream biological processes. Fenton process can become economical owing to the ease of magnetic separation of residual iron for reuse and is more feasible for scale-up. Moreover, many researchers have coupled Fenton process with other techniques such as photo-Fenton, sono-Fenton, and sono-photo-Fenton processes, thereby removing the pH barrier of Fenton process and enhancing the degradation rate of organic pollutants.

4.3 Hybrid AOP's involving nanocatalyst

The AOPs such as photocatalytic oxidation, cavitation, ozonation, and Fenton techniques when applied individually are found to be inefficient in causing the complete degradation of many organic and inorganic pollutants. Therefore various hybrid AOP combinations of Fenton and

This book belongs to Badji Mokhtar Annaba University Central Library Copyright Elsevier 2025

Table 4.4: Wastewater treatment applying Fenton process.

Organic pollutant	Optimum operating conditions	Results	References
Amoxicillin (AMX)	Conc. of AMX—10 mg/L, dosage of $FeSO_4$—30 mg/L, pH—3.0, H_2O_2 = 375 mg/L	100% within 12 min	[59]
Waste drilling mud (poly aluminum chloride)	PAC dose = 1000 mg/L, pH 3, H_2O_2 dosage = 500 mg/L, Fe(II) = 250 mg/L, molar ratio of Fe^{2+} H_2O_2 = 0.5, temp = 25°C	TOC removal = 90% within 150 min, BOD/TOC ratio = 0.83 within 120 min	[60]
Produced water	Molar ratio of $[H_2O_2]/[Fe^{2+}]$ = 2–75, $H_2O_2 = 0.12 \times 10^{-3}$ mol/L to 3 mol/L, pH 3.5	COD removal = 91% within 120 min	[61]
Cytostatic agent imatinib mesylate (IM)	H_2O_2 = 30 mmol/L, Fe^{2+} = 3 mmol/L, conc. of IM = 0.045 mmol/L	98.92%	[62]
Direct Blue 71	Conc. of DB 71 = 100 mg/L, pH 3.0, Fe^{2+} = 3 mg/L, H_2O_2 = 125 mg/L	Color removal = 94% COD removal = 50.7% within 20 min	[63]
Acid Orange 7	Initial conc. of Acid Orange 7 = 30 mg/L, H_2O_2 dosage = 2 mM, catalyst (recyclable DAWSON-type hetero polyanion) dosage = 0.01 g, pH 4, molar ratio of H_2O_2/AO7 = 0.02, temp = 25°C	100% within 60 min	[64]
3-Methylindol	Initial conc. of 3-methylindol = 20 mg/L, Fe-MABs = 0.8 g/L, H_2O_2 = 9.8 mmol/L, temp. = 25°C, pH 3	100% within 120 min	[65]
2,4-Dichlorophenol (2,4-DCP)	Initial conc. of 2,4-DCP = 200 mg/L, pH 2.5, treatment time = 2 h, H_2O_2 = 580 mg/L, conc. of Fe^{2+} = 20 mg/L	71% within 120 min	[66]
Catechol	Initial conc. of catechol = 110 mg/L, pH 3, $FeSO_4$ = 75–600 mg/L, H_2O_2 = 75–700 mg/L, treatment time = 30 min	COD removal = 83% within 30 min with $H_2O_2/FeSO_4$ ratio of 600/500 (w/w), aromaticity removal = 93%. within 30 min with $H_2O_2/FeSO_4$, ratio of 2000/500 (w/w)	[67]

ultrasonication/HC coupled with nanophotocatalysts and H_2O_2 such as the heterogeneous Fenton, photo-Fenton, sono-photo-Fenton, sono-photocatalysis, and HC combined with photocatalysis are being developed to improve the degradation efficiency [72]. Many studies demonstrate the enhanced efficiency of these hybrid AOPs for successful degradation of pollutants in aqueous solution [5, 73–75].

This book belongs to Badji Mokhtar Annaba University Central Library
Copyright Elsevier 2025

4.3.1 Heterogeneous Fenton process

The major drawbacks of the Fenton process include pH dependency, sludge formation and handling difficulty, and slow regeneration of Fe^{2+} and its recovery, which make this process less efficient for treating industrial effluents. However, heterogeneous Fenton processes comprising heterogeneous catalysts such as iron and iron minerals, waste iron, and iron oxides can overcome these challenges and could be feasible for industrial applications. The mechanism of homogeneous Fenton process is well established, but the mechanism of heterogeneous Fenton reactions is still unresolved and requires to be understood by visualizing and accounting for all the intermediates steps and generated radicals.

Heterogeneous Fenton process involves a series of steps such as the adsorption of reactant onto the catalyst surface, surface chemical reaction, and desorption of products [76]. Heterogeneous Fenton process mainly produces two types of ROS such as $^{\cdot}OH$ and hydroperoxyl radicals $HO_2^{\cdot}$ through a series of surface reactions over the catalyst surface.

The mechanism of heterogeneous Fenton process has been described as follows in Eqs. (4.24)–(4.26), and a pictorial process representation is also given in Fig. 4.4. H_2O_2 initially gets adsorbed over the surface of heterogeneous Fenton catalyst and reacts with iron surface transferring one electron to the metal and thus producing a transitional state for the surface site ($\equiv Fe^{II} \cdot O_2H$) according to Eq. (4.24). This surface site ($\equiv Fe^{II}$ surfaces) is further deactivated through the dissociation of the peroxide radical as per Eq. (4.25), which further reacts with H_2O_2 to produce $^{\bullet}OH$ radicals, and surface sites gets regenerated as given in Eq. (4.26). In the subsequent steps, free radicals may also get consumed by surface sites, H_2O_2, and also get scavenged by reacting with each other [76]. This mechanism has been proposed by many researchers but still further conclusive evidence is required in this direction.

$$\equiv Fe^{III} - OH + H_2O_2 \leftrightarrow \left(\equiv Fe^{II} \cdot O_2H\right) + H_2O \tag{4.24}$$

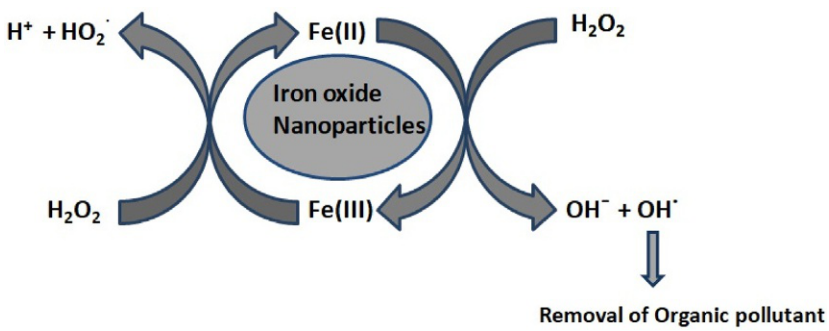

Fig. 4.4
Schematic representation of heterogeneous Fenton process.

This book belongs to Badji Mokhtar Annaba University Central Library Copyright Elsevier 2025

$$\left(\equiv Fe^{II} \cdot O_2H\right) \rightarrow \equiv Fe^{II} + HO_2^{\cdot} \tag{4.25}$$

$$\equiv Fe^{II} + H_2O_2 \rightarrow \equiv Fe^{III} - OH + {}^{\cdot}OH \tag{4.26}$$

Some of the work done on wastewater treatment using heterogeneous Fenton process is summarized in Table 4.5. Roy et al. [78] prepared the Fe_3O_4@hollow@$mSiO_2$ nanoparticles from yolk-shell by an ultrasound-assisted Fenton-persulfate system for application in the degradation of sulfadiazine (SDZ). It was observed that ultrasonication improves leaching rate of Fe^{2+}/Fe^{3+} ions from the metal core and their diffusion into the bulk medium through silica shell and thus enhances the degradation of SDZ several fold. Hassan et al. [85] evaluated the degradation of anthraquinone reactive blue 4 (RB4) using Fe-ball clay (FE-BC) as a heterogeneous catalyst. It was observed that with increase in the concentration of Fe^{2+} ions or higher catalyst loading, decolorization of RB4 increased. This may be attributed to the fact that more active catalyst surface sites were available with higher dosage of catalyst, which accelerates the decomposition of H_2O_2. A maximum of 99% degradation of reactive blue 4 was observed in 140 min at pH 3 for an initial concentration of 50 mg/L at the optimum dosages of 5 g/L of Fe-BC and H_2O_2. In addition to this, the heterogeneous catalyst (Fe-BC) demonstrated good stability without any formation of iron hydroxide sludge.

4.3.2 Heterogeneous photo-Fenton process

Heterogeneous photo-Fenton process is a hybrid method comprising UV radiation, photocatalyst, and Fenton oxidation. In this process, reaction occurs in the presence of Fenton reagent [hydrogen peroxide (H_2O_2) and ferrous ion (Fe(II))] and UV-Vis irradiation ($\lambda < 600$ nm) on the catalyst surfaces. The presence of UV light initiates the photolysis reaction over the catalyst surface and thus increases the rate of generation of $^{\bullet}OH$, thereby increasing pollutant degradation rate. The presence of UV radiation also enhances the regeneration rate of Fe^{2+} ions [86]. The efficiency of heterogeneous photo-Fenton process depends on the transparency of water that ensures the transmission of light. In the case of heterogeneous Fenton process, the working range of pH gets widened because it utilizes solid iron oxides as a catalyst instead of free ferrous/ferric ions. Moreover, the presence of a light source also elevates the overall degradation efficiency by enhancing the generation of $^{\bullet}OH$ and regeneration of Fe(II)/Fe(III) surfaces [87]. The mechanism of heterogeneous photo Fenton process is described in Eqs. (4.27)–(4.29), and a pictorial process representation is also given in Fig. 4.5.

The mechanism of the heterogeneous photo-Fenton reaction involves the generation of ROS such as $^{\bullet}OH$ and $HO^{\bullet}{}_2$, according to Eq. (4.27)–(4.29), and the degradation reaction of the organic pollutant molecules by these radicals. During the Fenton process, Fe^{2+} get oxidized to ferric ion (Fe^{3+}) and then reduced back to Fe^{2+}. The efficiency of Fenton oxidation is greatly affected by the regeneration rate of Fe^{2+} ions, but it has been reported that the reduction of Fe^{3+} to Fe^{2+} occurs much more slowly than the backward process. Thus there is need to accelerate

This book belongs to Badji Mokhtar Annaba University Central Library Copyright Elsevier 2025

This book belongs to Badji Mokhtar Annaba University Central Library

Table 4.5: Wastewater treatment applying heterogeneous Fenton process.

Fenton catalyst	Synthesis process	Equipment and techniques	Organic pollutant	Optimum operating conditions	Percentage degradation of organic pollutant	References
α-Fe_2O_3 and Fe_3O_4	Solvothermal method	Reactor vessel	Sulfadiazine (SDZ)	Conc. of dye = 20 ppm, pH 4, inlet pressure = 10 atm, $Na_2S_2O_8$ = 348.5 mg/L, H_2O_2 = 0.95 mL/L, catalyst dosage (α-Fe_2O_3) = 181.8 mg/L	81% within 90 min	[77]
Yolk-shell nanoparticles Fe_3O_4@hollow@$mSiO_2$	Microconvection by sonication	Microprocessor-controlled ultrasound probe (20 kHz, 500 W), Glass beaker (100 mL)	Sulfadiazine (SDZ)	Concentration of SDZ = 100 ppm, pK_a of sulfadiazine = 6.28, pH 5	93.14% within 1 h	[78]
Pyrite cinder (PC)	–	–	Mixture of Tectilon Yellow 3R, Tectilon Red 2B, Tectilon Blue 4R, Maxilon Yellow GL Maxilon Red 3GL N, Maxilon Blue TL, Tectilon Yellow 3R	Initial conc. of textile effluent = 702 mg/L, pH 3, dosage of PC = 40 g/L, H_2O_2 = 50 Mm	H_2O_2 + PC = 75%	[79]
Nanoscale zero-valent iron (nZVI)	–	COD Tester, UV spectrophotometer	Amoxicillin (AMX)	Initial conc. of AMX = 50 mg/L, pH 3.0, H_2O_2 = 6.6 mM, Dosage of nZVI = 500 mg/L, Rotary speed = 150 rpm, Temp. = 30°C	H_2O_2 + nZVI = 86.5% COD removal = 71.2% within 25 min	[80]

Continued

Copyright Elsevier 2025

This book belongs to Badji Mokhtar Annaba University Central Library

Table 4.5: Wastewater treatment applying heterogeneous Fenton process—cont'd

Fenton catalyst	Synthesis process	Equipment and techniques	Organic pollutant	Optimum operating conditions	Percentage degradation of organic pollutant	References
Nanoparticulate zero-valent iron (nZVI)	Solution method	Conical flask (25 mL), Rotary shaker	4-Chloro-3-methyl phenol (CMP)	Initial conc. of CMP = 0.7 mM, Dosage of nZVI =0.5 g/L, H_2O_2 = 3.0 mM, pH 6.1	nZVI + H_2O_2 = 100% within 15 min TOC removal = 63% after 60 min	[81]
$Co_xFe_{3-x}O_4$ magnetic nanoparticle	Hydrothermal method	250 mL closed batch reactor	Rhodamine B	Conc. of RhB = 0.014 mmol/L, pH 3.0, Dosage of $Co_xFe_{3-x}O_4$ = 0.05 g/L, Oxone = 1.0 mmol/L	$Co_xFe_{3-x}O_4$ + Oxone = 80% within 60 min	[82]
Nanoparticle Fe_3O_4	Co-precipitation method	Reaction vessel	Phenol	Conc. of phenol = 210 mg/L, pH 3–9, H_2O_2 = 1.0. g/L	Removal efficiency of phenol = 100% COD removal efficiency = 70% within 180 min	[83]

Copyright Elsevier 2025

Steel industry waste	–	–	Methyl Orange	Initial conc. of dye = 20 mg/L, Catalyst dosage = 200 mg/L, H_2O_2 = 34 Mm, pH 2	Catalyst + H_2O_2 = 98% within 30 min	[84]
Fe ball clay	Impregnation method	–	Anthraquinone dye Reactive Blue 4	Conc. of RB 4 = 50 mg/L, Fe-BC dosage = 5.0 g/L, pH 3.0, H_2O_2 = 20 mL, Temp. = 30°C	Fe-BC + H_2O_2 = 99% within 140 min	[85]

This book belongs to Badji Mokhtar Annaba University Central Library

Copyright Elsevier 2025

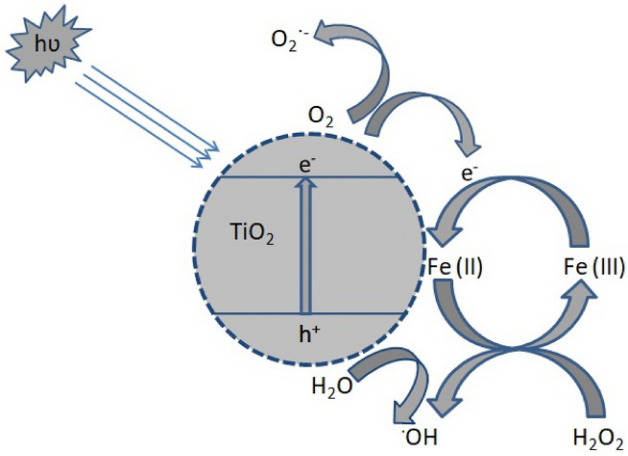

Fig. 4.5
Schematic representation of heterogeneous photo-Fenton process.

the Fe(II) regeneration in the Fenton-based reaction. In photo-Fenton process, H_2O_2 plays an important role for the production of $OOH^{\bullet}$ radicals, according to Eq. (4.28). The photon treatment of solid iron oxides accelerate the regeneration of Fe(II)/Fe(III) as shown in Eq. (4.29).

$$Fe^{3+} + H_2O + h\upsilon \rightarrow Fe^{2+} + H^+ + HO^{\cdot} \tag{4.27}$$

$$H_2O_2 + {}^{\cdot}OH \xrightarrow{h\upsilon} \cdot OOH + H_2 \tag{4.28}$$

$$Fe^{3+} + H_2O_2 \xrightarrow{h\upsilon} Fe^{2+} + HO_2^{\cdot} + H^+ \tag{4.29}$$

Some of the studies related to use of heterogeneous photo-Fenton process in the degradation of various dyes such as Rhodamine B, methylene blue, methyl violet, Evans blue, Black B azo dyes, and phenol are summarized in Table 4.6. The important parameters that affect the entire heterogeneous photo-Fenton process are the solution concentration, pH, catalyst dosage, hydrogen peroxide dosage, and UV power. Concentration of catalyst is also a very crucial factor in the photo-Fenton process because it affects the generation of highly reactive free radicals, but very high concentrations of Fe catalyst cause turbidity in the reaction mixture, which reduces the penetration of UV light and results in lower degradation rates.

Kalal et al. [91] synthesized heterogeneous photo-Fenton catalysts such as copper pyrovanadate ($Cu_2V_2O_7$) and chromium tetravanadate ($Cr_2V_4O_{13}$) for the degradation of Evans blue. They had reported the complete degradation of Evans blue dye into inorganic compounds such as CO_2, SO_2^-, and NO_3^- at conditions of pH 6–7. Heterogeneous photo-Fenton process is found to be more efficient than the homogeneous photo-Fenton process, offering several advantages

This book belongs to Badji Mokhtar Annaba University Central Library Copyright Elsevier 2025

This book belongs to Badji Mokhtar Annaba University Central Library

Table 4.6: Wastewater treatment applying heterogeneous photo-Fenton process.

Photocatalyst	Synthesis process	Equipment and techniques	Organic pollutant	Optimum operating conditions	Percentage degradation of organic pollutant	References
TiO_2/Schwertmannite	Solvent-free milling method	Cylindrical Pyrex vessel, Xenon arc lamp (500 W BL-GHX-CH500)	RhodamineB (RhB)	Conc. of RhB = 20 mg/L, Catalyst dosage = 0.3 g/L, H_2O_2 = 10 mmol/L, pH 4	100% within 60 min	[88]
Nano-sized zincated hydroxyapatite (Zn-HA)	Chemical precipitation method	Halogen lamp: HLX 64653; Osram, Germany (250 W) Thermostatic water bath	Methylene Blue (MB)	Conc. of MB = 30 mg/L, pH 10, H_2O_2 = 0.05 M	H_2O_2 + UV + Zn-HA = 100% within120 min	[89]
Zero-valent metallic iron powder (Fe^0), peroxymono sulfate (PMS), peroxy di sulfate (PDS)	–	Circular glass reactor (176.6 cm^2), UV lamp: MP mercury vapor lamp (125 W)	Methyl violet (MV)	Initial conc. of MV = 20 ppm, Fe^0 dosage = 20 mg, H_2O_2 = 10 ppm, PDS = 30 ppm, PMS = 30 ppm, pH 3	Fe^0 + UV + H_2O_2 = 100% Within 2 h. After four times of recycling: Fe^0 + UV + PMS = 98% Fe^0 + UV + PDS = 94%	[90]
Copper pyrovanadate ($Cu_2V_2O_7$) and chromium tetravanadate ($Cr_2V_4O_{13}$)	Wet chemical method, simple aqueous process	Tungsten lamp 200 W (Philips), reaction vessel, muffle furnace, water filter	Evans blue	For $Cu_2V_2O_7$ pH 6.0, conc. of Evans blue = 1.0×10^{-5} M, catalyst dosage = 0.06 g, H_2O_2 = 0.35 mL, Light intensity = 70 mW/cm^2 For $Cr_2V_4O_{13}$ pH 7.0, conc. of Evans blue = 0.8×10^{-5}, catalyst dosage = 0.05 g, H_2O_2 = 0.35 mL, light intensity = 70 mW/cm^2	UV + H_2O_2 + $Cu_2V_2O_7$ = 77.78% UV + H_2O_2 + $Cr_2V_4O_{13}$ = 79% within 120 min	[91]
Fe_3O_4-GO nanocomposite	Co-precipitation and	Quartz reactor xenon lamp 500 W	Phenol	Initial conc. of phenol = 20 mg/L, pH 5.0, H_2O_2 = 10.0 mmol/L, catalyst	Phenol removal = 98.8%	[92]

Continued

Copyright Elsevier 2025

This book belongs to Badji Mokhtar Annaba University Central Library

Table 4.6: Wastewater treatment applying heterogeneous photo-Fenton process—cont'd

Photocatalyst	Synthesis process	Equipment and techniques	Organic pollutant	Optimum operating conditions	Percentage degradation of organic pollutant	References
	hydrothermal method			dosage = 0.25 g/L, temp. = 30°C	TOC removal = 81.3% 120 min after five recycles	
Fe-exchanged zeolite of Y-type	Solution processing	Reaction vessel and magnetic stirrer, UV lamp	Black B azo dye	Initial conc. of dye = 1.00 × 10^{-3} M, H_2O = 2440 ppm, 1 λ_{max} = 590 nm	H_2O_2 + UV + Fe = 80% H_2O_2 + Fe + Solar = 98.7% within 5 h	[93]
Fe_2O_3-pillared rectorite (Fe-R) clay	Solvothermal method	Photo reactor UV Lamp 300 W, 420-nm cut of filter	Rhodamine B and 4-nitro phenol (4-NP)	Initial conc. of RhB = 100 mg/L, Initial conc. of 4-NP = 50 mg/L, pH =5.0, H_2O_2 = 15.0 mmol/L, catalyst dosage = 0.50 g/L	Catalyst + H_2O_2 = 99.3% COD removal = 87% within 100 min	[94]

Copyright Elsevier 2025

such as less sludge formation, lesser leaching of ferrous/ferric ions, catalyst reusability, wide working pH range, and long-term stability of the photocatalyst.

4.3.3 Sono photocatalytic process

As the name implies, sonophotocatalytic process is the combination of ultrasonication (sonolysis) and UV irradiation in the presence of photocatalyst. The advantages of using this hybrid approach are: higher degradation rates owing to the enhanced rate of generation of $^{\bullet}OH$ radicals, lower operating cost, and higher photocatalyst activity owing to the continuous cleaning of the catalyst surface under the ultrasonication.

The mechanism of sonophotocatalysis is described in Eqs. (4.30)–(4.36), and a pictorial representation is given in Fig. 4.6. In this combined oxidation process, sonolysis of water generates $H^{\bullet}$ and $^{\bullet}OH$ radicals through cavitation as per Eq. (4.30). These $H^{\bullet}$ radicals further react with H_2O_2 in the presence of UV irradiation to produce $^{\bullet}OH$ radicals, as per Eq. (4.32), and concurrently, H_2O_2 also break into $^{\bullet}OH$ radicals under UV light, as per Eq. (4.33) [23]. Simultaneously, under the photocatalysis process, dissolved oxygen reduces to superoxide, as per Eq. (4.34), which subsequently reacts with H_2O_2 to produce $^{\bullet}OH$ radicals, as per Eq. (4.35), and H_2O_2 itself gets reduced to $^{\bullet}OH$ radicals through the reaction with the surface-generated electrons through Eq. (4.36).

$$H_2O +)))) \rightarrow H^{\bullet} + {}^{\bullet}OH \tag{4.30}$$

$$H_2O +)))) \rightarrow 1/2H_2 + 1/2H_2O_2 \tag{4.31}$$

$$H_2O_2 + H^{\bullet} \rightarrow H_2O + {}^{\bullet}OH \tag{4.32}$$

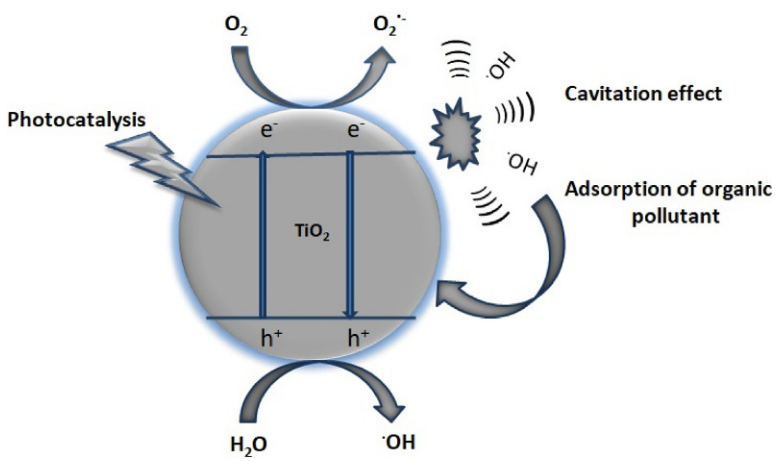

Fig. 4.6
Schematic representation of sono-photocatalytic process.

This book belongs to Badji Mokhtar Annaba University Central Library Copyright Elsevier 2025

$$H_2O_2 \xrightarrow{hv} 2^{\bullet}OH \tag{4.33}$$

$$e^- + O_2 \rightarrow O_2^{\cdot -} \tag{4.34}$$

$$H_2O_2 + O_2^{\cdot -} \rightarrow {}^{\bullet}OH + OH^- + O_2 \tag{4.35}$$

$$H_2O_2 + e^- \rightarrow {}^{\bullet}OH + OH^- \tag{4.36}$$

The efficiency of sono-photocatalytic process depends on the pollutant concentration, photocatalyst dosage, solution pH, dissolved oxygen level, ultrasonic power density (W/mL), UV irradiation intensity (W/m^2), and temperature.

The efficiency of any combined process (hybrid process) can be evaluated in terms of the synergetic coefficient, which is defined as the ratio of rate constants of the combined process to the sum of rate constants of all individual processes. If the synergistic coefficient for any hybrid process is found to be greater than one, then the combined process produces higher degradation efficiency and should be preferred over the individual processes. The synergistic coefficient of the sono-photocatalytic process is determined by Eq. (4.37).

$$\text{Synergistic coefficient} = \frac{K_{\text{sonophotocatalysis}}}{K_{\text{sonolysis}} + K_{\text{sonocatalysis}} + K_{\text{photocatalysis}}} \tag{4.37}$$

Molesh et al. [95] studied the degradation of trypan blue (TB) and vesuvine (VS) using a visible light photocatalyst Ag_3PO_4/Bi_2S_3-HKUST-1-MOF synthesized by the ultrasound-assisted solvothermal method and carried out in a continuous flow-loop photocatalytic reactor fitted with blue LED light. The process parameters were optimized using central composite design by response surface methodology, and they reported a maximum degradation of 98.44% and 99.36% of TB and VS, respectively, for an initial dye concentration of 25 mg/L, solution flow rate of 70 mL/min, 25 min of irradiation and sonication time, pH of 6.0, and 0.25 g/L of photocatalyst dosage. At these optimum operating conditions, the synergetic coefficient was found to be 2.53, which indicated that the combined process had greater efficiency when compared with the individual processes. Some of the other studies reported on sono-photocatalytic process are summarized in Table 4.7.

Sono-photocatalysis appears to be a promising process for the treatment of domestic and industrial effluents because it works without any extreme physical conditions. The combination of ultrasonication and photocatalysis increases the rate of formation of $^{\bullet}OH$ radicals, and ultrasonication eliminates the drawbacks of photocatalysis because it improves the opacity, surface area, and porosity of the catalyst, which ultimately results in enhanced photocatalytic efficiency. Recent development in sono-photocatalytic system is to replace the UV irradiation with natural sunlight, which could reduce the cost factor and make it a more efficient system.

This book belongs to Badji Mokhtar Annaba University Central Library
Copyright Elsevier 2025

This book belongs to Badji Mokhtar Annaba University Central Library

Table 4.7: Wastewater treatment applying sono-photocatalytic process.

Photocatalyst	Synthesis process	Equipment and technique	Organic pollutant	Optimum operating conditions	Percentage degradation of organic pollutant	References
Cu/ Fe_3O_4@SiO_2	Electrochemical method	Reactor vessel (50 mL), ultrasonic bath (25 kHz)	Mixture of Tartrazine (TR) and Methylene Blue (MB)	Conc. of dye = 50 mg/L, Catalyst dosage = 0.3 g/L Solution pH 3.0, H_2O_2 = 20 mL, Temp. = 30°C, Sonication time = 10 min, Ultrasound frequency = 25 kHz	TR = 99.98%, MB = 99.96%	[95]
ZnO/TiO_2	Sono loading treatment	Bench scale sonophotoreactor	Begazole Black B (BBB)	Conc. of BBB = 60 mg/L, catalyst dosage = 2 g/L, H_2O_2 = 160 mg/ L, pH 5, Ultrasound power = 76 W, Sonication time = 40 min, Ultrasound frequency = 20 kHz	100% within 40 min	[96]
CuO TiO_2	–	Sonochemical reactor (3 L) UV lamp 9 W	Rhodamine 6G	Initial conc. of dye = 10 ppm, CuO = 1.5 g/L, TiO_2 = 4 g/L, pH 12.5, Methanol (scavengers) = 4.5 mL/L, n. butanol (scavengers) = 1.5 mL/L, Ultrasound power = 170 W, Sonication time = 180 min, Ultrasound frequency = 50 kHz	CuO + US = 59.2%, CuO + US + UV = 60.8%, US + UV + TiO_2 = 63.3% within 180 min	[97]

Continued

Copyright Elsevier 2025

This book belongs to Badji Mokhtar Annaba University Central Library

Table 4.7: Wastewater treatment applying sono-photocatalytic process—cont'd

Photocatalyst	Synthesis process	Equipment and technique	Organic pollutant	Optimum operating conditions	Percentage degradation of organic pollutant	References
Iron doped TiO_2	Hydrothermal process	Conical flask (25 mL) Rotary Shaker	Diazinon	Initial conc. of dye = 30 mg/L, Solution pH 5.5, Catalyst dosage = 0.4 g/L, Dopant percentage = 1.5%, Ultrasound power = 100 W, Sonication time = 100 min, Ultrasound frequency = 37 kHz	85% within 100 min	[98]
ZnO	–	Glass reactor with UV lamp and cooling jacket, Ultrasonic processor 750 W, Ultrasonic frequency = 20 kHz	Direct Blue 71	Initial conc. of dye = 100 mg/L Conc. of catalyst = 1 g/L. pH 2.5 H_2O_2 = 75 mg/L. US Power = 95 W, US frequency = 20 kHz, Temp. = 20°C, Sonication time = 20 min	H_2O_2 + US + ZnO = 98% within 20 min	[99]
Heterogeneous TiO_2 catalyst	–	Photo reactor sono reactor, UV lamp (10 W) Sonicator (20 kHz, 500 W)	Rhodamine B	Initial conc. of dye = 10 mg/L, pH 2.5 acidic or 11 basis, TiO_2 = 0.5 mg/L, H_2O_2 = 5 and 10 mM, respectively, Temp. = 25°C, Ultrasound power = 500 W, Sonication time = 120 min, Ultrasound frequency = 20 kHz	68% within 120 min	[100]

Copyright Elsevier 2025

This book belongs to Badji Mokhtar Annaba University Central Library

Sulfur doped TiO_2 nanoparticle	Sol gel method	Photoreactor, digital ultrasonic bath	Reactive Blue 19	Conc. of dye = 20 mg/L, pH 3.0, US Power = 100 W, Temp. = 25°C, Ultrasound power = 300 W, Sonication time = 120 min, Ultrasound frequency = 35 kHz	90% within 120 min	[101]
TiO_2 P-25	–	Reactor volume (1000 mL) UV Chamber, Reaction Vessel. UV black fluorescent lamps (8 × 40 W)	Alizarin Reactive Red	Initial conc. of dye = 0.1 g/L, pH 4.8, TiO_2 = 0.3 g/L, H_2O_2 = 0.3 g/L, Sonication time = 180 min	UV + H_2O_2 = 85%, UV + US +TiO_2 = 94% within 180 min	[102]
Sensitized TiO_2	–	Photoreactor, Halogen lamp 50 W, Ultrasonic cleaning bath (47 kHz, 130 W)	Reactive Red (RR) 120	Initial conc. of dye = 50 mg/L, TiO_2 = 2.5 g/L, Solution pH 4, Quencher amount = 100 mg/L, Ultrasound power = 130 W, Sonication time = 25 min, Ultrasound frequency = 47 kHz	H_2O_2 + nZVI + UV = 86.5% COD removal = 71.2% within 25 min	[103]
(Fe^{3+}) and heterogeneous TiO_2	–	Jacketed glass reactor (250 mL), Xenon arc lamp (450 W)	Acid red 88	Initial conc. of dye = 0.09 mM, TiO_2 = 1 g/L, Fe^{3+} = 0.05 Mm, pH 2.7, Ultrasound power = 35 mW/mL, Sonication time = 4 h, Ultrasound frequency = 213 kHz	67% within 50 min TOC removal: 93% within 4 h	[104]+

Copyright Elsevier 2025

4.3.4 Sono-Fenton process

Sono-Fenton process can overcome the disadvantages of Fenton process such as narrow range of working pH and slow diffusion of Fe^{2+} ions. The mechanism of sono-Fenton process is given in Eqs. (4.38)–(4.41). In the Fenton reactions, Fe^{2+} reacts with H_2O_2 to produce $^{\bullet}OH$ radicals and Fe^{3+} ions, which subsequently react with H_2O_2 to produce an intermediate complex $FeOOH^{2+}$, according to Eqs. (4.38), (4.39). As discussed in the earlier section, the regeneration rate of Fe^{2+} ions is very slow. However, in the presence of ultrasonication, $FeOOH^{2+}$ dissociates to Fe^{2+} and $^{\bullet}OOH$, as per Eq. (4.40), which is a fast reaction, and the generated Fe^{2+} ions further react with H_2O_2 to produce more $^{\bullet}OH$ radicals, as per Eq. (4.41). Some fraction of H_2O_2 also directly decomposes into $^{\bullet}OH$ in the presence of ultrasonication. Thus the combination of ultrasonication and Fenton enhances the rate of generation of $^{\bullet}OH$ by increasing the regeneration rate of Fe^{2+} [105]. A pictorial representation of sono-Fenton process is shown in Fig. 4.7.

$$Fe^{2+} + H_2O_2 \rightarrow Fe^{3+} + {}^{\bullet}OH + OH^- \tag{4.38}$$

$$Fe^{3+} + H_2O_2 \rightarrow FeOOH^{2+} + H^+ \tag{4.39}$$

$$FeOOH^{2+} +))) \rightarrow Fe^{2+} + {}^{\bullet}OOH \text{ (fast)} \tag{4.40}$$

$$Fe^{2+} + H_2O_2 +))) \rightarrow Fe^{3+} + {}^{\bullet}OH + OH^- \tag{4.41}$$

The efficiency of the sono-Fenton process depends on the Fenton reagent concentration, pH, dissolved oxygen level, and temperature. A summary of some of the studies reported on sono-Fenton process is given in Table 4.8. It was observed from these studies that acidic conditions favor the degradation of the pollutant in this combined process. Moreover, it is desirable to optimize the dosage of H_2O_2 and Fe^{2+} so as to improve the overall efficacy of the degradation process. Akram et al. [108] investigated the combined effect of ultrasonication and Fenton process for the degradation of Rhodamine B dye and found that ultrasonication alone cannot degrade Rhodamine B, whereas Fenton process alone was effective only for

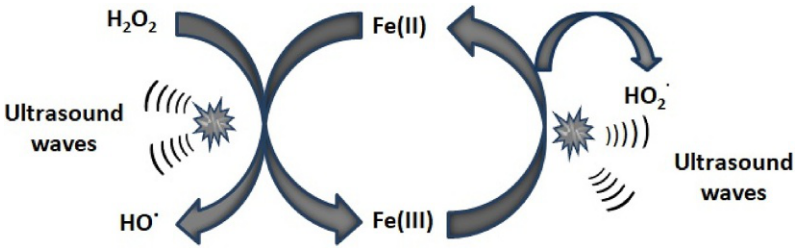

Fig. 4.7
Schematic representation of sono-Fenton process.

This book belongs to Badji Mokhtar Annaba University Central Library Copyright Elsevier 2025

Table 4.8: Wastewater treatment applying sono-Fenton process.

Organic pollutant	Equipment and techniques	Optimum operating conditions	Percentage degradation of organic pollutant	References
Textile effluent	Glass beaker with a programmable jar tester (600 mL), ultrasonic cleaner	Fenton process: pH 3, Fe^{2+} = 0.10 g/L, H_2O_2 = 2.20 g/L, Ultrasonic power = 35 kHz, Fenton + US process: pH 3, Fe^{2+} = 0.05 g/L, H_2O_2 = 1.65 g/L, Ultrasonic power = 35 kHz	Fenton + H_2O_2 = 95% within 90 min, Fenton + H_2O_2 + US = 99% within 60 min	[106]
Ibuprofen (IBP)	Jacketed glass reactor (1 L)	Initial conc. of IBP = 20 mg/L, pH (2.6–8.0), Ultrasound power density (25–100 W/L), Sonication frequency (12–862 kHz), H_2O_2 = 6.4 mM, Fe^{2+}(iron sulfate heptahydrate ($FeSO_4 \cdot 7H_2O$) = 0.134 mM	US + H_2O_2 + Fe^{2+} = 60% within 3 h, TOC removal = 50% within 3 h	[105]
Alachlor	Jacketed cylindrical reactor (1 L), sonicator (100 W)	Initial conc. of alachlor =50 mg/L, pH 3, H_2O_2 = 120 mg/L at the dosing rate of 2 mg/min $FeSO_4 \cdot 7H_2O$ (Fe^{2+}) = 30 mg/L, Ultrasonic power = 100 W	US + Fe^{2+} + H_2O_2 = 100% within 60 min US + H_2O_2 = 95% within 60 min	[107]
Rhodamine B	Ultrasonicator (30 kHz ± 3 kHz, 120 W)	Initial conc. of dye = 0.2 kg/m^3, H_2O_2 = 9.795 mM, $FeSO_4$ conc. = 1.79 × 10^{-2} mol/L, pH 3	Fenton + H_2O_2 = 73.68% after 15 min US + H_2O_2 = 92.39% after 15 min Fenton + US + H_2O_2 = 93.85% after 15 min	[108]
Reactive Blue 69	Plasma reactor, ball mill	Conc. of dye = 20 mg/L, pH 5, H_2O_2 = 1 mM, Ultrasonic power density = 300 W/L, Plasma modified pyrites = 0.6 g/L	US + H_2O_2 + PMP = 100 within 40 min	[109]

Continued

This book belongs to Badji Mokhtar Annaba University Central Library

Copyright Elsevier 2025

Table 4.8: Wastewater treatment applying sono-Fenton process—cont'd

Organic pollutant	Equipment and techniques	Optimum operating conditions	Percentage degradation of organic pollutant	References
Total petroleum hydrocarbons (TPH), Petroleum hydrocarbon (PHC)	Sonicator 3000 generator (20 kHz), Beaker (100 mL)	Initial mass of TPH = 431.5 ± 11.4 mg, $FeSO_4 \cdot 7H_2O$ = 0.63 g, H_2O_2 = 15 mL, Ultrasonic power = 60 W	TPH: US = 22.6% Fenton = 13.8% US + Fenton = 43.1% within 5 min PHC: US = 56.7% Fenton = 39.1% US + Fenton = 46.5% within 5 min	[110]
C.I. reactive yellow 145	Ultrasonic water bath (35 kHz, 80 W)	Initial conc. of dye = 50 mg/L, Fenton process: pH 3, Fe^{2+} = 20 mg/L, H_2O_2 = 20 mg/L, Ultrasonic power = 35 kHz Fenton + US process: pH 3, Fe^{2+} = 20 mg/L, H_2O_2 = 15 mg/L, Ultrasonic power = 80 W	Color removal: Fenton + H_2O_2 = 91% within 60 min, Fenton + H_2O_2 + US = 95% within 60 min COD removal: Fenton + H_2O_2 = 47% within 60 min, Fenton + H_2O_2 + US = 51% within 60 min	[111]
Rhodamine B	Ultrasonic horn (20 kHz)	pH 5, temp. = 55°C, conc. of dye = 0.02 mmol/L, Fe_3O_4 magnetic nanoparticles as peroxides mimetic (Co-precipitation method) = 0.5 g/L, H_2O_2 conc. = 40 mmol/L	Fenton + US + H_2O_2 = 95% within 15 min	[112]
C.I. Acid orange 7	Reactor (300 mL), ultrasonic generator (20 kHz, 250 W)	Conc. of dye = 79.5 mg/L, pH 3, H_2O_2 = 7.77 mmol/L, [FeOOH] goethite = 0.3 g/L. ultrasonic power density = 80 W/L	Dye decolorization: H_2O_2 + goethite + US = 99.5% after 30 min goethite + US = 99% after 30 min, Mineralization (TOC removal): H_2O_2 + goethite + US = 90%	[113]

decolorization of low concentrated dye solutions. But the combined effect of sono-Fenton process was found to be very effective for the decolorization of highly concentrated (i.e., 0.2 kg/m^3) dye solutions, and at the optimum process conditions, almost 94% decolorization of Rhodamine B was obtained using the combination of Fenton and ultrasonication process.

This book belongs to Badji Mokhtar Annaba University Central Library
Copyright Elsevier 2025

4.3.5 Sono-photo-Fenton process

As the name implies, Sono-photo-Fenton process is the combination of ultrasonication, UV irradiation, and Fenton reagent. This combined process can significantly enhance the production of $^{\bullet}OH$ radicals in an aqueous solution. Sonolysis of water produced $^{\bullet}OH$ radicals, but because of the faster recombination rate of $^{\bullet}OH$ radicals, significant amount of these generated radicals is not used for the oxidation of organic pollutant molecules in the solution. The $^{\bullet}OH$ radicals instantaneously recombine into H_2O_2, which has less oxidation potential than $^{\bullet}OH$; however, the application of UV light dissociates the hydrogen peroxide produced by the recombination of $^{\bullet}OH$ and in turn increases the amount of $^{\bullet}OH$ in the solution. In the Fenton process, hydrogen peroxide get activated by iron ions to produce the $^{\bullet}OH$ [114]. The generation of $^{\bullet}OH$ radicals in the Fenton reaction increases with UV light irradiation and sonolysis [115].

It has been reported that the dosage of Fe^{2+}ions required during sono-photo-Fenton is very less compared to Fenton alone, and this combined approach reduces the amount of Fe^{2+} ions present in the treated water or the residual COD, which is very important from a point of industrial application. The pictorial representation of sono-photo-Fenton process is shown in Fig. 4.8.

Some of the studies reported on sono-photo-Fenton process are given in Table 4.9. Torres-Palma et al. investigated on the degradation of bisphenol using sono-photo-Fenton process and observed 93% reduction in the dissolved organic carbon (DOC) after 4 h, whereas only 5%, 6%, and 22% of DOC removal was obtained using individual processes such as photocatalysis, sonolysis, and photo-Fenton process, respectively, for the same treatment time.

Segura et al. 2009 [124] investigated the degradation of phenol using sono-photo-Fenton process using Fe_2O_3/SBA-15 as a heterogeneous catalyst in an acidic medium at pH 3 and

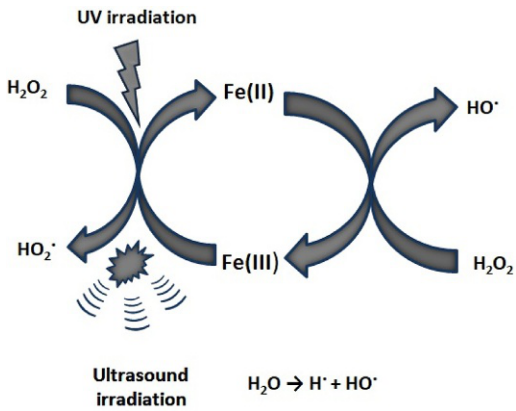

Fig. 4.8
Schematic representation of sono-photo-Fenton process.

This book belongs to Badji Mokhtar Annaba University Central Library Copyright Elsevier 2025

This book belongs to Badji Mokhtar Annaba University Central Library

Table 4.9: Wastewater treatment applying sono-photo-Fenton process.

Photocatalyst	Synthesis process	Equipment and techniques	Organic pollutant	Optimum operating conditions	Percentage degradation of organic pollutant	References
Metal oxychlorides of Fe(I), Cu (II), Zn (III), and Bi (IV)	–	Double jacket quartz reactor (120 mL), sonicator (750 W, 20 kHz), UV lamp (6 W)	Nitrobenzene	Initial conc. of NB = 20 ppm, pH 7, Conc. of FeOCl (I), CuOCl (II), ZnOCl (III) and BiOCl (IV) = 0.1 g/L, H_2O_2 = 5 mM	US + UV + Fenton = 46% (Fe), US + UV + Fenton = 41% (Cu), US + UV + Fenton = 35% (Zn) US + UV + Fenton = 33% (Bi) within 60 min	[116]
Fe_3O_4/ZnO/ graphene	Sol-gel method, hydrothermal method	Ultrasonic bath (40 kHz, 150 W) UV-C lamps (40 W), Xe lamp (40 W)	Methylene blue (MB) and Congo red	Initial conc. of dye = 40 mg/L, pH 3 H_2O_2 = 4 mL, F3Z-1G and F3Z-3G	Fenton + H_2O_2 = 85% (MB) and 88% (CR) within 60 min UV light + US + Fenton + H_2O_2 = 100% (MB, CR) UV-vis light + US + Fenton + H_2O_2 = 93% MB and 97% CR within 120 min	[117]
$LaFeO_3$ perovskite	Sol-gel method	Cylindrical reactor, high pressure Na lamps (150 W), ultrasonic probe (20 kHz, 40 W)	Bisphenol-A (BPA)	Initial conc. = 15 ppm, H_2O_2 = 2.38 mM, Amount of $LaFeO_3$ = 0.5 g/dm^3 pH 6.7	BPA removal: $LaFeO_3$ + H_2O_2 + US + visible light = 21.8% $LaFeO_3$ + US + visible light = 20.8%	[118]

Copyright Elsevier 2025

This book belongs to Badji Mokhtar Annaba University Central Library

					$LaFeO_3 + H_2O_2 +$ US = 19.9% $LaFeO_3 + H_2O_2 +$ visible light = 12.7% COD removal: 11.2% within 3 h	
Heterogeneous TiO_2 nanoparticles	–	UV reactor (100 W, 365 nm), ultrasonic probe (150 W)	Sodium alginate (NaAlg)	Initial conc. of NaAlg = 10 g/L, TiO_2 = 0.1 g/L, H_2O_2 = 0.35 g/L, Fe(II) = 0.5 mmol/L	NaAlg degradation (n) = 0.51	[119]
$FeSO_4 \cdot 7H_2O$	–	Ultrasonicator, photochemical reactor, medium pressure mercury lamp (125 W)	Reactive Black 5	Conc. of Dye = 0.1 g/L, pH 4, Fe^{2+} = 0.050 g/L, H_2O_2 = 0.150 g/L	Fenton = 69%, UV + Fenton = 93% UV + US + Fenton = 98%	[120]
Mesoporous silica iron-doped catalyst (CC)	Co-Condensation method	Water bath, peristaltic pump, ultrasonic transducers, mechanical stirrer, UV lamp, reactor, bath tank, snake tube	C.I. Acid Orange 7	Initial conc. of dye = 100 mg/L, H_2O_2 = 8 mmol/L, pH 2.0, Fe_2O_3/SBA-15 = 0.3 g/L, Ultrasonic power = 99 W	H_2O_2 + Catalyst + US = 84.9 H_2O_2 + Catalyst + US + UV = 76.6 within 60 min	[121]
TiO_2 and Fe^{3+}	–	Glass reactor (250 mL), Xenon arc lamp (450 W)	Monocrotophos (MCP)	Initial conc. of MCP = 0.12 mM, [Fe^{3+}] = 0.025 mM, pH 2.7	US + UV + Fe^{3+} = 91% within 15 min US + Fe^{3+} = 35% within 15 min UV + Fe^{3+} = 89% within 15 min	[122]
Fe^{2+} and TiO_2	–	Jacketed glass reactor (500 mL) Ultrasound (300 kHz/80 W)	Bisphenol	Initial conc. of bisphenol = 118 μmol/L, pH 3, Fe^{2+} = 10 mmol/L, TiO_2 = 50 mg/L	US + UV + TiO_2 + Fe^{2+} = 75% after 4 h	[123]

Continued

Copyright Elsevier 2025

This book belongs to Badji Mokhtar Annaba University Central Library

Table 4.9: Wastewater treatment applying sono-photo-Fenton process—cont'd

Photocatalyst	Synthesis process	Equipment and techniques	Organic pollutant	Optimum operating conditions	Percentage degradation of organic pollutant	References
Fe_2O_3-SBA-15	Co-condensation process	Ultrasonic sonicator 3000 (20 KHz), medium pressure mercury lamp (150 W Heraeus-TQ-150), Cylindrical glass vessel (400 mL)	Phenolic aqueous solution	Conc. of phenolic solution = 2.5 mM, H_2O_2 = 35 mM, catalyst was suspended into the aqueous solution (0.6 g/L), pH 3	TOC removal: US + Fenton = 27% UV + Fenton = 37% UV + US =52% UV + US + Fenton = 90% within 6 h Phenol removal: UV + US + Fenton = 100% within 3 h	[124]

Copyright Elsevier 2025

obtained 45% reduction in the TOC, whereas 30% and 40% TOC reduction was obtained with individual sono-Fenton and photo-Fenton processes, respectively.

4.3.6 Photocatalytic oxidation with hydrodynamic cavitation

In the past decade, the combination of HC with photocatalysis is widely studied for the degradation of recalcitrant pollutants. Photocatalysis involves the acceleration of a photo chemical reaction in the presence of catalyst, and its efficiency depends on the irradiating surface area, surface characteristics, concentration of the reactants, and the adsorption desorption phenomenon over the catalyst surface. The major problem associated with the photocatalysis process is the exhaustion of the catalyst surfaces by the pollutant molecules, which blocks the UV activation and reduces the efficiency. Recently photocatalysis coupled with HC is found to be a well-established technique in the area of wastewater treatment because most of the limitations of photocatalysis are overcome by HC effects. The extreme cavitational conditions created during cavity collapse and formation of microjets clean the surface of the photocatalyst and enhance its porosity. HC also enhances the mass transfer of the reactant and product species between the surface of the catalyst and bulk solution. The HC-induced effects increase the overall surface area of the catalyst because of the fragmentation or deagglomeration of catalyst particles forming finer solids, which enhances the rate of adsorption of pollutant molecules. HC also induces chemical effects such as increasing the concentration of $^{\bullet}OH$ radicals in combination with the photocatalytic process, thereby enhancing the rate of degradation of the pollutant. Some of the studies related to HC coupled with photocatalysis are reported in Table 4.10.

4.4 Conclusions

The various wastewater treatment methodologies discussed in this chapter have their own merits and demerits regarding their application for wastewater treatment. The hybrid processes are proved to enhance the degradation rate owing to the increased production of $^{\bullet}OH$ radicals. The demerits of photocatalysis and Fenton process such as noneffective distribution or scattering of UV light, nonuniform suspension of photo catalyst, settling of catalyst, regeneration, and lower production rate of $^{\bullet}OH$ radicals can be overcome by combining photocatalysis and Fenton with ultrasonication and HC. One of the challenges to be explored include the utilization of solar (visible) light instead of UV source for photoexcitation of the semiconductor materials, which is also another aspect to be developed to reduce the cost of the hybrid process of photocatalysis and cavitation. As most of the research work has been on nanoparticles/photocatalytic materials synthesized using raw materials/chemicals available in the market, more focus should be on waste valorization in the synthesis of nano-photocatalysts, which will definitely reduce the overall cost of the process.

This book belongs to Badji Mokhtar Annaba University Central Library Copyright Elsevier 2025

This book belongs to Badji Mokhtar Annaba University Central Library

Table 4.10: Wastewater treatment applying hydrodynamic cavitation coupled with photocatalysis process.

Photocatalyst	Synthesis process	Equipment and techniques	Organic pollutant	Optimum operating conditions	Percentage degradation of organic pollutant	References
Sm- and N-doped TiO_2	Convectional sol-gel method, ultrasound-assisted sol-gel process	Photocatalytic reactor, HC reactor, UV lamp (300 W) (wavelength >400 nm), cavitating device (slit venturi) HC + photocatalysis, US + photocatalysis	4-Acetamidophenol (AMP)	Initial conc. of AMP = 50 ppm, Irradiation intensity = 2.47 W/cm^2, TiO_2 dosage = 2 g/L, Inlet pressure = 5 bar, pH 6.8, US horn frequency = 20 kHz, input power = 750 W	Sm-doped TiO_2 = 60% N-doped TiO_2 = 63% US + UV = 87%, HC + UV = 91% within 180 min	[5]
TiO_2	–	HC set up, photocatalytic, mercury lamp (250 W) (wavelength 350–750 nm), cavitating device orifice (2 mm throat) HC, HC + H_2O_2, HC + Fenton, HC + photo Fenton, HC + photolytic	Mixture of ternary dye wastewater (Methylene blue, Methyl orange, and Rhodamine-B)	Initial conc. of dye = 30 ppm, Inlet pressure = 6 bar, pH 3, Reaction volume = 5 L, HC + H_2O_2 (Molar ratio of dye: H_2O_2 = 1:40), HC + Fenton ($FeSO_4 \cdot 7H_2O$: H_2O_2 = 1:30), TiO_2 dosage = 200 mg/L	TOC removal: HC = 8.53%, HC + H_2O_2 = 16.95% HC + Fenton = 38.42% HC + photo-Fenton = 41.28% HC + UV = 14.01% HC + UV + TiO_2 = 15.63% Color removal: HC = 8.28%	[125]

Copyright Elsevier 2025

This book belongs to Badji Mokhtar Annaba University Central Library

					HC + photo-Fenton = 98.86% HC + UV = 7 4.53% HC + UV + TiO_2 = 82.13% (within 120 min)	
TiO_2	–	HC reactor, UV254 lamp	Tetracycline	Initial conc. of dye = 30 mg/L, Reaction volume = 4 L, Time = 90 min, pH 4.2, TiO_2 dosage = 100 mg/L	HC + UV + TiO_2 = 78.2% within 90 min	[126]
Bismuth-doped TiO_2	–	HC set up, HC, HC + H_2O_2, HC + photocatalysis	Methylene Blue (MB)	Initial conc. of dye = 50 ppm, Inlet pressure = 5 bar, pH 2, HC + H_2O_2 (MB: H_2O_2 = 1:20), Bismuth doped TiO_2 dosage = 200 mg/L	HC = 32.32%, HC + UV + Bi-doped TiO_2 = 64.58%, HC + H_2O_2 = 100% within 120 min	[127]
Sensitized TiO_2	–	HC reactor, UV lamp (250 W), cavitating device slit venturi	Diclofenac sodium	Initial conc. of diclofenac sodium = 20 ppm, TiO_2 dosage = 0.2 g/L, pH 4, Inlet pressure = 3 bar, temp = 35°C	H_2O_2 + nZVI = 86.5% COD removal = 71.2% within 25 min	[128]

Copyright Elsevier 2025

Because most of the research work reported in this chapter was studied only on a laboratory scale with significantly low batch volumes, therefore, the feasibility studies and the scale-up of these hybrid processes on an industrial scale need to be explored further with detailed design, parameter optimization and development of feasible reactor configurations for the different hybrid processes. Therefore extensive research incorporating simulators needs to be developed and studied to see the effect of various operational parameters on the process mechanism in the degradation of the pollutant, which will also be helpful in the designing of AOP-based reactors for industrial applications.

Furthermore, the efficiency of these processes for real industrial effluents needs to be tested. These hybrid AOPs may also be advantageous if they are used as a pretreatment technique prior to the conventional biological treatment units. These studies would be helpful in designing the AOP-based reactors that will augment the conventional treatment techniques in the existing common effluent treatment plants.

References

[1] D. Grey, D. Garrick, D. Blackmore, J. Kelman, M. Muller, C. Sadoff, Water security in one blue planet: twenty-first century policy challenges for science. Philos. Trans. R. Soc. A: Math. Phys. Eng. Sci. 371 (2013) 2020, https://doi.org/10.1098/rsta.2012.0406.

[2] A.S. Adeleye, J.R. Conway, K. Garner, Y. Huang, Y. Su, A.A. Keller, Engineered nanomaterials for water treatment and remediation: costs, benefits, and applicability. Chem. Eng. J. 286 (2016) 640–662, https://doi.org/10.1016/j.cej.2015.10.105.

[3] F.C. Moreira, R.A.R. Boaventura, E. Brillas, V.J.P. Vilar, Remediation of a winery wastewater combining aerobic biological oxidation and electrochemical advanced oxidation processes. Water Res. 75 (2015) 95–108, https://doi.org/10.1016/j.watres.2015.02.029.

[4] G. Crini, E. Lichtfouse, Advantages and disadvantages of techniques used for wastewater treatment. Environ. Chem. Lett. 17 (2019) 145–155, https://doi.org/10.1007/s10311-018-0785-9.

[5] S. Rajoriya, S. Bargole, S. George, V.K. Saharan, P.R. Gogate, A.B. Pandit, Synthesis and characterization of samarium and nitrogen doped TiO_2 photocatalysts for photo-degradation of 4-acetamidophenol in combination with hydrodynamic and acoustic cavitation. Sep. Purif. Technol. 209 (2019) 254–269, https://doi.org/10.1016/j.seppur.2018.07.036.

[6] A.R. Dincer, N. Karakaya, E. Gunes, Y. Gunes, Removal of COD from oil recovery industry wastewater by the advanced oxidation processes (AOP) based on H_2O_2. Glob. Nest J. 10 (2008) 31–38, https://doi.org/10.30955/gnj.000479.

[7] P.R. Gogate, P.N. Patil, Combined treatment technology based on synergism between hydrodynamic cavitation and advanced oxidation processes. Ultrason. Sonochem. 25 (2015) 60–69, https://doi.org/10.1016/j.ultsonch.2014.08.016.

[8] J.L. Wang, L.J. Xu, Advanced oxidation processes for wastewater treatment: formation of hydroxyl radical and application. Crit. Rev. Environ. Sci. Technol. 42 (2012) 251–325, https://doi.org/10.1080/10643389.2010.507698.

[9] Y. Wu, H. Pang, Y. Liu, X. Wang, S. Yu, D. Fu, J. Chen, X. Wang, Environmental remediation of heavy metal ions by novel-nanomaterials: a review. Environ. Pollut. 246 (2019) 608–620, https://doi.org/10.1016/j.envpol.2018.12.076.

[10] A.A. Yaqoob, T. Parveen, K. Umar, M.N. Mohamad Ibrahim, Role of nanomaterials in the treatment of wastewater: a review. Water (2020), https://doi.org/10.3390/w12020495.

This book belongs to Badji Mokhtar Annaba University Central Library

Copyright Elsevier 2025

[11] G.Z. Kyzas, K.A. Matis, Nanoadsorbents for pollutants removal: a review. J. Mol. Liq. 203 (2015) 159–168, https://doi.org/10.1016/j.molliq.2015.01.004.
[12] S.S. Sawant, A.C. Anil, V. Krishnamurthy, C. Gaonkar, J. Kolwalkar, L. Khandeparker, D. Desai, A. V. Mahulkar, V.V. Ranade, A.B. Pandit, Effect of hydrodynamic cavitation on zooplankton: a tool for disinfection. Biochem. Eng. J. 42 (2008) 320–328, https://doi.org/10.1016/j.bej.2008.08.001.
[13] P.R. Gogate, A.B. Pandit, A review and assessment of hydrodynamic cavitation as a technology for the future. Ultrason. Sonochem. 12 (2005) 21–27, https://doi.org/10.1016/j.ultsonch.2004.03.007.
[14] S. Bargole, S. George, V. Kumar Saharan, Improved rate of transesterification reaction in biodiesel synthesis using hydrodynamic cavitating devices of high throat perimeter to flow area ratios. Chem. Eng. Process. Process Intensif. 139 (2019) 1–13, https://doi.org/10.1016/j.cep.2019.03.012.
[15] S. Bargole, J. Carpenter, S. George, V.K. Saharan, Process intensification of synthesis of biodiesel using a novel recirculating flow ultrasonication reactor. Chem. Eng. Process. Process Intensif. 122 (2017) 21–30, https://doi.org/10.1016/j.cep.2017.09.010.
[16] P.B. Dhanke, S.M. Wagh, Intensification of the degradation of Acid RED-18 using hydrodynamic cavitation. Emerg. Contam. 6 (2020) 20–32, https://doi.org/10.1016/j.emcon.2019.12.001.
[17] G. Li, L. Yi, J. Wang, Y. Song, Hydrodynamic cavitation degradation of Rhodamine B assisted by Fe^{3+}-doped TiO_2: mechanisms, geometric and operation parameters. Ultrason. Sonochem. 60 (2020) 104806https://doi.org/10.1016/j.ultsonch.2019.104806.
[18] E.R. Bandala, O.M. Rodriguez-Narvaez, On the nature of hydrodynamic cavitation process and its application for the removal of water pollutants, air. Soil Water Res. 12 (2019) 1–6, https://doi.org/10.1177/1178622119880488.
[19] V.K. Saharan, M.A. Rizwani, A.A. Malani, A.B. Pandit, Effect of geometry of hydrodynamically cavitating device on degradation of orange-G. Ultrason. Sonochem. 20 (2013) 345–353, https://doi.org/10.1016/j.ultsonch.2012.08.011.
[20] V.K. Saharan, A.B. Pandit, P.S. Satish Kumar, S. Anandan, Hydrodynamic cavitation as an advanced oxidation technique for the degradation of Acid Red 88 dye. Ind. Eng. Chem. Res. 51 (2012) 1981–1989, https://doi.org/10.1021/ie200249k.
[21] J. González-García, V. Sáez, I. Tudela, M.I. Díez-Garcia, M.D. Esclapez, O. Louisnard, Sonochemical treatment of water polluted by chlorinated organocompounds. A review. Water 2 (2010) 28–74, https://doi.org/10.3390/w2010028.
[22] D.V. Pinjari, A.B. Pandit, Cavitation milling of natural cellulose to nanofibrils. Ultrason. Sonochem. 17 (2010) 845–852, https://doi.org/10.1016/j.ultsonch.2010.03.005.
[23] C.G. Joseph, G. Li Puma, A. Bono, D. Krishnaiah, Sonophotocatalysis in advanced oxidation process: a short review. Ultrason. Sonochem. 16 (2009) 583–589, https://doi.org/10.1016/j.ultsonch.2009.02.002.
[24] A.J. Sisi, A. Khataee, M. Fathinia, B. Vahid, Ultrasonic-assisted degradation of a triarylmethane dye using combined peroxydisulfate and MOF-2 catalyst: synergistic effect and role of oxidative species. J. Mol. Liq. 297 (2020) 111838https://doi.org/10.1016/j.molliq.2019.111838.
[25] O. Tunc Dede, Z. Aksu, A. Rehorek, Sonochemical degradation of C.I. reactive Orange 107. Environ. Eng. Sci. 36 (2019) 158–171, https://doi.org/10.1089/ees.2018.0076.
[26] Z. Boutamine, O. Hamdaoui, S. Merouani, Enhanced sonolytic mineralization of basic red 29 in water by integrated ultrasound/Fe^{2+}/TiO_2 treatment. Res. Chem. Intermed. 43 (2017) 1709–1722, https://doi.org/10.1007/s11164-016-2724-3.
[27] H. Zúñiga-Benítez, J. Soltan, G.A. Peñuela, Application of ultrasound for degradation of benzophenone-3 in aqueous solutions. Int. J. Environ. Sci. Technol. 13 (2016) 77–86, https://doi.org/10.1007/s13762-015-0842-x.
[28] M.A. Elsayed, Ultrasonic removal of pyridine from wastewater: optimization of the operating conditions. Appl. Water Sci. 5 (2015) 221–227, https://doi.org/10.1007/s13201-014-0182-x.
[29] R.R. Nair, R.L. Patel, Treatment of dye wastewater by sonolysis process, international journal of research in modern engineering and emerging, Technology 2 (2014) 1–6.

This book belongs to Badji Mokhtar Annaba University Central Library Copyright Elsevier 2025

[30] Z.Z. Ismail, A.S. Jasim, Ultrasonic treatment of wastewater contaminated with furfural. IDA J. Desalin. Water Reuse 6 (2014) 103–111, https://doi.org/10.1179/2051645214y.0000000028.
[31] H. Nakui, K. Okitsu, Y. Maeda, R. Nishimura, Effect of coal ash on sonochemical degradation of phenol in water. Ultrason. Sonochem. 14 (2007) 191–196, https://doi.org/10.1016/j.ultsonch.2006.04.003.
[32] Y. Jiang, C. Pétrier, T. David Waite, Kinetics and mechanisms of ultrasonic degradation of volatile chlorinated aromatics in aqueous solutions. Ultrason. Sonochem. 9 (2002) 317–323, https://doi.org/10.1016/S1350-4177(02)00085-8.
[33] M.M. Tauber, G.M. Guebitz, A. Rehorek, Degradation of azo dyes by laccase and ultrasound treatment. Appl. Environ. Microbiol. 71 (2005) 2600–2607, https://doi.org/10.1128/AEM.71.5.2600-2607.2005.
[34] W.L. Wang, Q.Y. Wu, N. Huang, T. Wang, H.Y. Hu, Synergistic effect between UV and chlorine (UV/chlorine) on the degradation of carbamazepine: influence factors and radical species. Water Res. 98 (2016) 190–198, https://doi.org/10.1016/j.watres.2016.04.015.
[35] Y. Yasman, V. Bulatov, V. Gridin, S. Agur, N. Galil, R. Armon, I. Schechter, A new sono-electrochemical method for enhanced detoxification of hydrophilic chloroorganic pollutants in water. Ultrason. Sonochem. 11 (2004) 365–372, https://doi.org/10.1016/j.ultsonch.2003.10.004.
[36] K. Hayat, M.A. Gondal, M.M. Khaled, Z.H. Yamani, S. Ahmed, Laser induced photocatalytic degradation of hazardous dye (safranin-O) using self synthesized nanocrystalline WO_3. J. Hazard. Mater. 186 (2011) 1226–1233, https://doi.org/10.1016/j.jhazmat.2010.11.133.
[37] H. Tju, A. Taufik, R. Saleh, Enhanced UV photocatalytic performance of magnetic Fe_3O_4/CuO/ZnO/NGP nanocomposites. J. Phys. Conf. Ser. 710 (2016), https://doi.org/10.1088/1742-6596/710/1/012005.
[38] V.K. Saharan, D.V. Pinjari, P.R. Gogate, A.B. Pandit, Advanced Oxidation Technologies for Wastewater Treatment: An Overview. Elsevier Ltd., 2014https://doi.org/10.1016/B978-0-08-099968-5.00003-9
[39] N.K. Gupta, Y. Ghaffari, S. Kim, J. Bae, K.S. Kim, M. Saifuddin, Photocatalytic degradation of organic pollutants over MFe_2O_4 (M = Co, Ni, Cu, Zn) nanoparticles at neutral pH. Sci. Rep. 10 (2020) 1–11, https://doi.org/10.1038/s41598-020-61930-2.
[40] A.M. Alansi, M. Al-Qunaibit, I.O. Alade, T.F. Qahtan, T.A. Saleh, Visible-light responsive BiOBr nanoparticles loaded on reduced graphene oxide for photocatalytic degradation of dye. J. Mol. Liq. 253 (2018) 297–304, https://doi.org/10.1016/j.molliq.2018.01.034.
[41] N. Thirugnanam, H. Song, Y. Wu, Photocatalytic degradation of Brilliant Green dye using CdSe quantum dots hybridized with graphene oxide under sunlight irradiation. Cuihua Xuebao/Chin. J. Catal. 38 (2017) 2150–2159, https://doi.org/10.1016/S1872-2067(17)62964-4.
[42] X. Chen, Z. Wu, D. Liu, Z. Gao, Preparation of ZnO photocatalyst for the efficient and rapid photocatalytic degradation of azo dyes. Nanoscale Res. Lett. 12 (2017) 4–13, https://doi.org/10.1186/s11671-017-1904-4.
[43] R. Saravanan, E. Sacari, F. Gracia, M.M. Khan, E. Mosquera, V.K. Gupta, Conducting PANI stimulated ZnO system for visible light photocatalytic degradation of coloured dyes. J. Mol. Liq. 221 (2016) 1029–1033, https://doi.org/10.1016/j.molliq.2016.06.074.
[44] J. Cao, B. Xu, H. Lin, B. Luo, S. Chen, Novel Bi 2S 3-sensitized BiOCl with highly visible light photocatalytic activity for the removal of rhodamine B. Catal. Commun. 26 (2012) 204–208, https://doi.org/10.1016/j.catcom.2012.05.025.
[45] R. Saravanan, H. Shankar, T. Prakash, V. Narayanan, A. Stephen, ZnO/CdO composite nanorods for photocatalytic degradation of methylene blue under visible light. Mater. Chem. Phys. 125 (2011) 277–280, https://doi.org/10.1016/j.matchemphys.2010.09.030.
[46] Y. Zhou, S.X. Lu, W.G. Xu, Photocatalytic activity of Nd-doped ZnO for the degradation of C.I. Reactive Blue 4 in aqueous suspension, Environ. Prog. Sustain. Energy 28 (2009) 226–233. http://doi.wiley.com/10.1002/ep.10318.
[47] V. Mirkhani, S. Tangestaninejad, M. Moghadam, M.H. Habibi, Iranian chemical society photocatalytic degradation of azo dyes catalyzed by Ag doped TiO_2 photocatalyst, J. Iran. Chem. Soc. 6 (2009) 578–587. https://link.springer.com/content/pdf/10.1007/BF03246537.pdf.

This book belongs to Badji Mokhtar Annaba University Central Library Copyright Elsevier 2025

[48] P. Kiattisaksiri, P. Khamdahsag, P. Khemthong, N. Pimpha, N. Grisdanurak, Photocatalytic degradation of 2,4-dichlorophenol over Fe-ZnO catalyst under visible light. Korean J. Chem. Eng. 32 (2015) 1578–1585, https://doi.org/10.1007/s11814-014-0379-6.

[49] S.M. Lam, J.C. Sin, A.Z. Abdullah, A.R. Mohamed, Investigation on visible-light photocatalytic degradation of 2,4-dichlorophenoxyacetic acid in the presence of MoO_3/ZnO nanorod composites. J. Mol. Catal. A: Chem. 370 (2013) 123–131, https://doi.org/10.1016/j.molcata.2013.01.005.

[50] M. Ba-Abbad, A.A. Kadhum, A.B. Mohamad, M. Takriff, K. Sopian, Solar photocatalytic degradation of environmental pollutants using ZnO prepared by sol-gel: 2,4-dichlorophenol as case study. Int. J. Thermal Environ. Eng. 1 (2010) 37–42, https://doi.org/10.5383/ijtee.01.01.006.

[51] S.G. Poulopoulos, A. Yerkinova, G. Ulykbanova, V.J. Inglezakis, Photocatalytic treatment of organic pollutants in a synthetic wastewater using UV light and combinations of TiO_2, H_2O_2 and Fe(III). PLoS One 14 (2019) 1–20, https://doi.org/10.1371/journal.pone.0216745.

[52] X. Lü, B. Xia, C. Liu, Y. Yang, H. Tang, TiO_2-based nanomaterials for advanced environmental and energy-related applications. J. Nanomater. 2016 (2016), https://doi.org/10.1155/2016/8735620.

[53] P. Magalhães, L. Andrade, O.C. Nunes, A. Mendes, Titanium dioxide photocatalysis: fundamentals and application on photoinactivation, Rev. Adv. Mater. Sci. 51 (2017) 91–129.

[54] P.A.K. Reddy, P.V.L. Reddy, E. Kwon, K.H. Kim, T. Akter, S. Kalagara, Recent advances in photocatalytic treatment of pollutants in aqueous media. Environ. Int. 91 (2016) 94–103, https://doi.org/10.1016/j.envint.2016.02.012.

[55] S.Z. Tseng, C.R. Lin, H. Sen Wei, C.H. Chan, S.H. Chen, Nanopatterned silicon substrate use in heterojunction thin film solar cells made by magnetron sputtering. Int. J. Photoenergy 2014 (2014), https://doi.org/10.1155/2014/707543.

[56] S. Sakthivel, B. Neppolian, M.V. Shankar, B. Arabindoo, M. Palanichamy, V. Murugesan, Solar photocatalytic degradation of azo dye: comparison of photocatalytic efficiency of ZnO and TiO_2. Sol. Energy Mater. Sol. Cells 77 (2003) 65–82, https://doi.org/10.1016/S0927-0248(02)00255-6.

[57] M. Guo, J. He, Y. Li, S. Ma, X. Sun, One-step synthesis of hollow porous gold nanoparticles with tunable particle size for the reduction of 4-nitrophenol. J. Hazard. Mater. 310 (2016) 89–97, https://doi.org/10.1016/j.jhazmat.2016.02.016.

[58] S.M. Aramyan, Advances in Fenton and Fenton based oxidation processes for industrial effluent contaminants control—a review. Int. J. Environ. Sci. Nat. Resour. 2 (2017), https://doi.org/10.19080/ijesnr.2017.02.555594.

[59] M. Verma, A.K. Haritash, Degradation of amoxicillin by Fenton and Fenton-integrated hybrid oxidation processes. J. Environ. Chem. Eng. 7 (2019) 102886https://doi.org/10.1016/j.jece.2019.102886.

[60] R. Ding, Y. Wang, X. Chen, Y. Gao, M. Yang, Extended Fenton's process: toward improving biodegradability of drilling wastewater. Water Sci. Technol. 79 (2019) 1790–1797, https://doi.org/10.2166/wst.2019.179.

[61] T. Afzal, M.H. Isa, M. Raza Ul Mustafa, Removal of organic pollutants from produced water using Fenton oxidation. E3S Web Conf. 34 (2018) 1–7, https://doi.org/10.1051/e3sconf/20183402035.

[62] F. Ghrib, T. Saied, N. Bellakhal, Experimental design methodology applied to the degradation of a cytostatic agent the imatinib mesylate using Fenton process. Chem. Africa 2 (2019) 103–111, https://doi.org/10.1007/s42250-018-00033-y.

[63] N. Ertugay, F.N. Acar, Removal of COD and color from Direct Blue 71 azo dye wastewater by Fenton's oxidation: kinetic study. Arab. J. Chem. 10 (2017) S1158–S1163, https://doi.org/10.1016/j.arabjc.2013.02.009.

[64] A. Tabaï, O. Bechiri, M. Abbessi, Degradation of organic dye using a new homogeneous Fenton-like system based on hydrogen peroxide and a recyclable Dawson-type heteropolyanion. Int. J. Ind. Chem. 8 (2017) 83–89, https://doi.org/10.1007/s40090-016-0104-x.

[65] S. Ben Hammouda, N. Adhoum, L. Monser, Synthesis of magnetic alginate beads based on Fe_3O_4 nanoparticles for the removal of 3-methylindole from aqueous solution using Fenton process. J. Hazard. Mater. 294 (2015) 128–136, https://doi.org/10.1016/j.jhazmat.2015.03.068.

This book belongs to Badji Mokhtar Annaba University Central Library Copyright Elsevier 2025

[66] P.J.D. Ranjit, K. Palanivelu, C.S. Lee, Degradation of 2,4-dichlorophenol in aqueous solution by sono-Fenton method. Korean J. Chem. Eng. 25 (2008) 112–117, https://doi.org/10.1007/s11814-008-0020-7.
[67] G. Lofrano, L. Rizzo, M. Grassi, V. Belgiorno, Advanced oxidation of catechol: a comparison among photocatalysis, Fenton and photo-Fenton processes. Desalination 249 (2009) 878–883, https://doi.org/10.1016/j.desal.2009.02.068.
[68] F.J. Rivas, F.J. Beltrán, J. Frades, P. Buxeda, Oxidation of *p*-hydroxybenzoic acid by Fenton's reagent. Water Res. 35 (2001) 387–396, https://doi.org/10.1016/S0043-1354(00)00285-2.
[69] E.M. Cuerda-Correa, M.F. Alexandre-Franco, C. Fernández-González, Advanced oxidation processes for the removal of antibiotics from water. An overview. Water 12 (2020), https://doi.org/10.3390/w12010102.
[70] A. Babuponnusami, K. Muthukumar, A review on Fenton and improvements to the Fenton process for wastewater treatment. J. Environ. Chem. Eng. 2 (2014) 557–572, https://doi.org/10.1016/j.jece.2013.10.011.
[71] N. Pani, V. Tejani, T.S. Anantha-Singh, A. Kandya, Simultaneous removal of COD and ammoniacal nitrogen from dye intermediate manufacturing industrial wastewater using Fenton oxidation method. Appl. Water Sci. 10 (2020) 1–7, https://doi.org/10.1007/s13201-020-1151-1.
[72] J. Madhavan, J. Theerthagiri, D. Balaji, S. Sunitha, Ultrasound : an overview, Molecules 24 (2019) 1–18.
[73] S. Rajoriya, S. Bargole, V.K. Saharan, Degradation of a cationic dye (Rhodamine 6G) using hydrodynamic cavitation coupled with other oxidative agents: reaction mechanism and pathway. Ultrason. Sonochem. 34 (2016) 183–194, https://doi.org/10.1016/j.ultsonch.2016.05.028.
[74] S. Rajoriya, S. Bargole, V.K. Saharan, Ultrasonics sonochemistry degradation of reactive blue 13 using hydrodynamic cavitation : effect of geometrical parameters and different oxidizing additives. Ultrason. Sonochem. 37 (2017) 192–202, https://doi.org/10.1016/j.ultsonch.2017.01.005.
[75] S. Rajoriya, S. Bargole, S. George, V.K. Saharan, Treatment of textile dyeing industry effluent using hydrodynamic cavitation in combination with advanced oxidation reagents. J. Hazard. Mater. 344 (2018), https://doi.org/10.1016/j.jhazmat.2017.12.005.
[76] J. He, X. Yang, B. Men, D. Wang, Interfacial mechanisms of heterogeneous Fenton reactions catalyzed by iron-based materials: a review. J. Environ. Sci. (China) 39 (2016) 97–109, https://doi.org/10.1016/j.jes.2015.12.003.
[77] K. Roy, V.S. Moholkar, Sulfadiazine degradation using hybrid AOP of heterogeneous Fenton/persulfate system coupled with hydrodynamic cavitation. Chem. Eng. J. (2019) 121294, https://doi.org/10.1016/j.cej.2019.03.170.
[78] K. Roy, C. Agarkoti, R.S. Malani, B. Thokchom, V.S. Moholkar, Mechanistic study of sulfadiazine degradation by ultrasound-assisted Fenton-persulfate system using yolk-shell Fe_3O_4@hollow@$mSiO_2$ nanoparticles. Chem. Eng. Sci. 217 (2020) 115522https://doi.org/10.1016/j.ces.2020.115522.
[79] Đ. Kerkez, M. Bečelić-Tomin, A. Kulić, D. Tomašević Pilipović, A. Leovac Maćerak, B. Dalmacija, M. Prica, Treatment of Wastewater Containing Dye Mixture Using Pyrite Cinder in Heterogeneous Fenton Process. (2018) pp. 169–173, https://doi.org/10.24867/grid-2018-p20.
[80] S. Zha, Y. Cheng, Y. Gao, Z. Chen, M. Megharaj, R. Naidu, Nanoscale zero-valent iron as a catalyst for heterogeneous Fenton oxidation of amoxicillin. Chem. Eng. J. 255 (2014) 141–148, https://doi.org/10.1016/j.cej.2014.06.057.
[81] L. Xu, J. Wang, A heterogeneous Fenton-like system with nanoparticulate zero-valent iron for removal of 4-chloro-3-methyl phenol. J. Hazard. Mater. 186 (2011) 256–264, https://doi.org/10.1016/j.jhazmat.2010.10.116.
[82] S. Su, W. Guo, Y. Leng, C. Yi, Z. Ma, Heterogeneous activation of oxone by $CoxFe_{3-x}O_4$ nanocatalysts for degradation of Rhodamine B. J. Hazard. Mater. 244–245 (2013) 736–742, https://doi.org/10.1016/j.jhazmat.2012.11.005.
[83] W. Wang, Q. Mao, H. He, M. Zhou, Fe_3O_4 nanoparticles as an efficient heterogeneous Fenton catalyst for phenol removal at relatively wide pH values. Water Sci. Technol. 68 (2013) 2367–2373, https://doi.org/10.2166/wst.2013.497.
[84] M.E.M. Ali, T.A. Gad-Allah, M.I. Badawy, Heterogeneous Fenton process using steel industry wastes for methyl orange degradation. Appl. Water Sci. 3 (2013) 263–270, https://doi.org/10.1007/s13201-013-0078-1.

This book belongs to Badji Mokhtar Annaba University Central Library Copyright Elsevier 2025

[85] H. Hassan, B.H. Hameed, Fe-clay as effective heterogeneous Fenton catalyst for the decolorization of Reactive Blue 4. Chem. Eng. J. 171 (2011) 912–918, https://doi.org/10.1016/j.cej.2011.04.040.
[86] C. Wang, H. Liu, Z. Sun, Heterogeneous photo-Fenton reaction catalyzed by nanosized iron oxides for water treatment. Int. J. Photoenergy 2012 (2012), https://doi.org/10.1155/2012/801694.
[87] S. Rahim Pouran, A.R. Abdul Aziz, W.M.A. Wan Daud, Review on the main advances in photo-Fenton oxidation system for recalcitrant wastewaters. J. Ind. Eng. Chem. 21 (2015) 53–69, https://doi.org/10.1016/j.jiec.2014.05.005.
[88] Y. Zhu, C. Zeng, R. Zhu, Y. Xu, X. Wang, H. Zhou, J. Zhu, H. He, TiO_2/Schwertmannite nanocomposites as superior co-catalysts in heterogeneous photo-Fenton process. J. Environ. Sci. (China) 80 (2019) 208–217, https://doi.org/10.1016/j.jes.2018.12.014.
[89] V.D. Doan, V.T. Le, T.T.N. Le, H.T. Nguyen, Nanosized zincated hydroxyapatite as a promising heterogeneous photo-Fenton-like catalyst for methylene blue degradation. Adv. Mater. Sci. Eng. 2019 (2019), https://doi.org/10.1155/2019/5978149.
[90] L.G. Devi, M. Srinivas, M.L. Aruna Kumari, Heterogeneous advanced photo- Fenton process using peroxymonosulfate and peroxydisulfate in presence of zero valent metallic iron: a comparative study with hydrogen peroxide photo-Fenton process. J. Water Process Eng. 13 (2016) 117–126, https://doi.org/10.1016/j.jwpe.2016.08.004.
[91] S. Kalal, A. Pandey, R. Ameta, P.B. Punjabi, Heterogeneous photo-Fenton-like catalysts $Cu_2V_2O_7$ and $Cr_2V_4O_{13}$ for an efficient removal of azo dye in water. Cogent Chem. 2 (2016) 1–12, https://doi.org/10.1080/23312009.2016.1143344.
[92] L. Yu, J. Chen, Z. Liang, W. Xu, L. Chen, D. Ye, Degradation of phenol using Fe_3O_4-GO nanocomposite as a heterogeneous photo-Fenton catalyst. Sep. Purif. Technol. 171 (2016) 80–87, https://doi.org/10.1016/j.seppur.2016.07.020.
[93] M. Blanco, A. Martinez, A. Marcaide, E. Aranzabe, A. Aranzabe, Heterogeneous Fenton catalyst for the efficient removal of azo dyes in water. Am. J. Anal. Chem. 05 (2014) 490–499, https://doi.org/10.4236/ajac.2014.58058.
[94] G. Zhang, Y. Gao, Y. Zhang, Y. Guo, Fe_2O_3-pillared rectorite as an efficient and stable Fenton-like heterogeneous catalyst for photodegradation of organic contaminants. Environ. Sci. Technol. 44 (2010) 6384–6389, https://doi.org/10.1021/es1011093.
[95] S. Mosleh, M.R. Rahimi, M. Ghaedi, A. Asfaram, R. Jannesar, F. Sadeghfar, A rapid and efficient sonophotocatalytic process for degradation of pollutants: statistical modeling and kinetics study. J. Mol. Liq. 261 (2018) 291–302, https://doi.org/10.1016/j.molliq.2018.03.115.
[96] M. Ghasemi, S.M. Ghoreishian, M. Norouzi, K. Badii, K. Ozaee, C.H. Kwak, Y.S. Huh, Optimization of sonophotocatalytic decolorization of Begazol Black B by loaded, double-sided nanophotocatalysts on porous substrate: a central composite design approach. J. Taiwan Inst. Chem. Eng. 93 (2018) 166–175, https://doi.org/10.1016/j.jtice.2018.06.034.
[97] N.B. Bokhale, S.D. Bomble, R.R. Dalbhanjan, D.D. Mahale, S.P. Hinge, B.S. Banerjee, A.V. Mohod, P. R. Gogate, Sonocatalytic and sonophotocatalytic degradation of rhodamine 6G containing wastewaters. Ultrason. Sonochem. 21 (2014) 1797–1804, https://doi.org/10.1016/j.ultsonch.2014.03.022.
[98] S. Tabasideh, A. Maleki, B. Shahmoradi, E. Ghahremani, G. McKay, Sonophotocatalytic degradation of diazinon in aqueous solution using iron-doped TiO_2 nanoparticles. Sep. Purif. Technol. 189 (2017) 186–192, https://doi.org/10.1016/j.seppur.2017.07.065.
[99] N. Ertugay, F.N. Acar, The degradation of Direct Blue 71 by sono, photo and sonophotocatalytic oxidation in the presence of ZnO nanocatalyst. Appl. Surf. Sci. 318 (2014) 121–126, https://doi.org/10.1016/j.apsusc.2014.01.178.
[100] C. Camacho-Alvarado, C.O. Castillo-Araiza, R.S. Ruiz-Martinez, Degradation and mineralization of a cationic dye by a sequential photo-sono catalytic process. Int. J. Chem. React. Eng. 15 (2017) 1–11, https://doi.org/10.1515/ijcre-2017-0078.

This book belongs to Badji Mokhtar Annaba University Central Library Copyright Elsevier 2025

[101] M.A.N. Khan, M. Siddique, F. Wahid, R. Khan, Removal of reactive blue 19 dye by sono, photo and sonophotocatalytic oxidation using visible light. Ultrason. Sonochem. 26 (2015) 370–377, https://doi.org/10.1016/j.ultsonch.2015.04.012.

[102] A. Verma, P. Sangwan, D. Dixit, Sonophotocatalytic degradation studies of alizarin reactive red dye. Arab. J. Sci. Eng. 39 (2014) 7477–7482, https://doi.org/10.1007/s13369-014-1309-y.

[103] S.K. Kavitha, P.N. Palanisamy, Photocatalytic and sonophotocatalytic degradation of reactive red 120 using dye sensitized TiO_2 under visible light, World Acad. Sci. Eng. Technol. 73 (2011) 1–6.

[104] J. Madhavan, P.S. Sathish Kumar, S. Anandan, F. Grieser, M. Ashokkumar, Degradation of acid red 88 by the combination of sonolysis and photocatalysis. Sep. Purif. Technol. 74 (2010) 336–341, https://doi.org/10.1016/j.seppur.2010.07.001.

[105] S. Adityosulindro, L. Barthe, K. González-Labrada, U.J. Jáuregui Haza, H. Delmas, C. Julcour, Sonolysis and sono-Fenton oxidation for removal of ibuprofen in (waste)water. Ultrason. Sonochem. 39 (2017) 889–896, https://doi.org/10.1016/j.ultsonch.2017.06.008.

[106] S.G. Cetinkaya, M.H. Morcali, S. Akarsu, C.A. Ziba, M. Dolaz, Comparison of classic Fenton with ultrasound Fenton processes on industrial textile wastewater. Sustain. Environ. Res. 28 (2018) 165–170, https://doi.org/10.1016/j.serj.2018.02.001.

[107] C. Wang, C.-W. Hou, C. Liu, Decontamination of alachlor by continuously dosed sono-Fenton process: effects of system parameters and kinetics study. Mod. Environ. Sci. Eng. 2 (2016) 1–10, https://doi.org/10.15341/mese(2333-2581)/01.02.2016/001.

[108] M. Akram, C.S. Chowdhury, A. Chakrabarti, Removal of Rhodamine B dye from wastewater by ultrasound-assisted Fenton process: a comparison between bath and probe type sonicators, Environ. Sci. Ind. J. 12 (2016) 115.

[109] A. Khataee, P. Gholami, B. Vahid, S.W. Joo, Heterogeneous sono-Fenton process using pyrite nanorods prepared by non-thermal plasma for degradation of an anthraquinone dye. Ultrason. Sonochem. 32 (2016) 357–370, https://doi.org/10.1016/j.ultsonch.2016.04.002.

[110] J. Zhang, J. Li, R. Thring, L. Liu, Application of ultrasound and Fenton's reaction process for the treatment of oily sludge. Procedia Environ. Sci. 18 (2013) 686–693, https://doi.org/10.1016/j.proenv.2013.04.093.

[111] C. Özdemir, M.K. Öden, S. Şahinkaya, E. Kalipçi, Color removal from synthetic textile wastewater by sono-Fenton process. Clean: Soil Air Water 39 (2011) 60–67, https://doi.org/10.1002/clen.201000263.

[112] N. Wang, L. Zhu, M. Wang, D. Wang, H. Tang, Sono-enhanced degradation of dye pollutants with the use of H_2O_2 activated by Fe_3O_4 magnetic nanoparticles as peroxidase mimetic. Ultrason. Sonochem. 17 (2010) 78–83, https://doi.org/10.1016/j.ultsonch.2009.06.014.

[113] H. Zhang, H. Fu, D. Zhang, Degradation of C. I. Acid Orange 7 by ultrasound enhanced heterogeneous Fenton-like process. J. Hazard. Mater. 172 (2009) 654–660, https://doi.org/10.1016/j.jhazmat.2009.07.047.

[114] A. Shokri, Application of sono-photo-Fenton process for degradation of phenol derivatives in petrochemical wastewater using full factorial design of experiment. Int. J. Ind. Chem. 9 (2018) 295–303, https://doi.org/10.1007/s40090-018-0159-y.

[115] K.E. Barrera-Salgado, G. Ramírez-Robledo, A. Álvarez-Gallegos, C.A. Pineda-Arellano, F. Z. Sierra-Espinosa, J.A. Hernández-Pérez, S. Silva-Martínez, Fenton process coupled to ultrasound and UV light irradiation for the oxidation of a model pollutant. J. Chem. 2016 (2016) 16–18, https://doi.org/10.1155/2016/4262530.

[116] A.E. Elmetwally, G. Eshaq, A.M. Al-sabagh, F.Z. Yehia, C.A. Philip, N.A. Moussa, Separation and purification technology insight into heterogeneous Fenton-sonophotocatalytic degradation of nitrobenzene using metal oxychlorides. Sep. Purif. Technol. 210 (2019) 452–462, https://doi.org/10.1016/j.seppur.2018.08.029.

[117] R. Saleh, A. Taufik, Degradation of methylene blue and Congo-red dyes using Fenton, photo-Fenton, sono-Fenton, and sonophoto-Fenton methods in the presence of iron(II,III) oxide/zinc oxide/graphene (Fe_3O_4/ZnO/graphene) composites. Sep. Purif. Technol. 210 (2019) 563–573, https://doi.org/10.1016/j.seppur.2018.08.030.

This book belongs to Badji Mokhtar Annaba University Central Library

Copyright Elsevier 2025

[118] M. Dükkancı, Sono-photo-Fenton oxidation of bisphenol-A over a $LaFeO_3$ perovskite catalyst. Ultrason. Sonochem. 40 (2018) 110–116, https://doi.org/10.1016/j.ultsonch.2017.04.040.
[119] Q. Zhou, Y. Liu, G. Yu, F. He, K. Chen, D. Xiao, X. Zhao, Y. Feng, J. Li, Degradation kinetics of sodium alginate via sono-Fenton, photo-Fenton and sono-photo-Fenton methods in the presence of TiO_2 nanoparticles. Polym. Degrad. Stab. 135 (2017) 111–120, https://doi.org/10.1016/j.polymdegradstab.2016.11.012.
[120] A. Verma, A. Kaur Hura, D. Dixit, Sequential photo-Fenton and sono-photo-Fenton degradation studies of Reactive Black 5 (RB5). Desalin. Water Treat. 56 (2015) 677–683, https://doi.org/10.1080/19443994.2014.940390.
[121] X. Zhong, S. Royer, H. Zhang, Q. Huang, L. Xiang, S. Valange, J. Barrault, Mesoporous silica iron-doped as stable and efficient heterogeneous catalyst for the degradation of C.I. Acid Orange 7 using sono-photo-Fenton process. Sep. Purif. Technol. 80 (2011) 163–171, https://doi.org/10.1016/j.seppur.2011.04.024.
[122] J. Madhavan, P.S. Sathish Kumar, S. Anandan, F. Grieser, M. Ashokkumar, Sonophotocatalytic degradation of monocrotophos using TiO_2 and Fe^{3+}. J. Hazard. Mater. 177 (2010) 944–949, https://doi.org/10.1016/j.jhazmat.2010.01.009.
[123] R.A. Torres-Palma, J.I. Nieto, E. Combet, C. Pétrier, C. Pulgarin, An innovative ultrasound, Fe^{2+} and TiO_2 photoassisted process for bisphenol a mineralization. Water Res. 44 (2010) 2245–2252, https://doi.org/10.1016/j.watres.2009.12.050.
[124] Y. Segura, R. Molina, F. Martínez, J.A. Melero, Integrated heterogeneous sono-photo Fenton processes for the degradation of phenolic aqueous solutions. Ultrason. Sonochem. 16 (2009) 417–424, https://doi.org/10.1016/j.ultsonch.2008.10.004.
[125] M.S. Kumar, S.H. Sonawane, B.A. Bhanvase, B. Bethi, Treatment of ternary dye wastewater by hydrodynamic cavitation combined with other advanced oxidation processes (AOP's). J. Water Process Eng. 23 (2018) 250–256, https://doi.org/10.1016/j.jwpe.2018.04.004.
[126] X. Wang, J. Jia, Y. Wang, Combination of photocatalysis with hydrodynamic cavitation for degradation of tetracycline. Chem. Eng. J. 315 (2017) 274–282, https://doi.org/10.1016/j.cej.2017.01.011.
[127] M.S. Kumar, S.H. Sonawane, A.B. Pandit, Degradation of methylene blue dye in aqueous solution using hydrodynamic cavitation based hybrid advanced oxidation processes. Chem. Eng. Process. Process Intensif. 122 (2017) 288–295, https://doi.org/10.1016/j.cep.2017.09.009.
[128] M.V. Bagal, P.R. Gogate, Degradation of diclofenac sodium using combined processes based on hydrodynamic cavitation and heterogeneous photocatalysis. Ultrason. Sonochem. 21 (2014) 1035–1043, https://doi.org/10.1016/j.ultsonch.2013.10.020.

This book belongs to Badji Mokhtar Annaba University Central Library Copyright Elsevier 2025

This page intentionally left blank

This book belongs to Badji Mokhtar Annaba University Central Library

Copyright Elsevier 2025

SECTION II

Photocatalytic nanocomposite materials: Preparation and applications

This book belongs to Badji Mokhtar Annaba University Central Library

Copyright Elsevier 2025

This page intentionally left blank

This book belongs to Badji Mokhtar Annaba University Central Library

Copyright Elsevier 2025

CHAPTER 5

Introduction, basic principles, mechanism, and challenges of photocatalysis

Prasad Mandade

Bioenergy and Energy Planning Research Group, EPFL, Lausanne, Switzerland

5.1 Introduction

Production of any chemical products such as petroleum, plastics, textiles, and pharmaceutical products, involves catalytic reaction at some stage of the production process [1]. Fast pace of modernization with the most recent advancements in technologies make our lives comfortable, but it results in increased toxic chemicals and pollutants that pose severe dangers to living beings [2]. Biological catalysts, i.e., enzymes regulate all chemical reactions in living organisms, representing the importance of the catalytic processes. At the beginning of the 19th century, catalytic processes were coined by Berzelius. Photocatalysis remains a recent discipline compared with conventional catalysis and separated by the activation of photon absorption rather than by thermal activation. Photocatalysis finds multiple applications in different sectors addressing energy and environmental issues such as self-cleaning coatings of building materials and devices for decontamination of air and water. Extensive studies and research have been done in photocatalysis for wastewater treatment, which will continue to fulfill its practical applications. Metal oxides are largely used in such applications due to their versatility and varied physical properties [3, 4].

Photocatalysis represents a simple way of utilization of natural sunlight to develop a sustainable society by efficient harvesting. The photocatalytic process was discovered by scientist Edmond Becquerel in 1839 from natural photosynthesis. In natural photosynthesis, plants, microalgae, and a few microscopic organisms collect energy from sunlight that helps in transformation of CO_2 and H_2O to carbohydrate. Solar energy can be converted into the forms of heat and electricity directly and can further be utilized for different applications. In recent times, newer photocatalytic technologies were developed to meet our increasing energy demands due to challenges faced in terms of harvesting, storage, and utilization by the intermittent nature of sunlight as energy [1, 5].

Handbook of Nanomaterials for Wastewater Treatment. https://doi.org/10.1016/B978-0-12-821496-1.00016-7
Copyright © 2021 Elsevier Inc. All rights reserved.

This book belongs to Badji Mokhtar Annaba University Central Library

Copyright Elsevier 2025

Applications of photocatalysis have expanded rapidly especially in energy and the environment in the last four decades. The word "photocatalysis" is comprised of two parts: the prefix "photo," which means "light," and "catalysis," which is the process to decompose a reactant using a catalyst that modifies the rate of a chemical reaction [6, 7]. A catalyst does not directly take part in the reaction, but it accelerates the rate of transformation. The method of activation is the major difference between a conventional catalyst and a photocatalyst. A conventional catalyst is activated by heat, whereas a photocatalyst is activated by photons of suitable energy. The photocatalyst in the photocatalysis process plays the same role as chlorophyll in photosynthesis. This mimic of natural processes uses artificial materials with extensive research in chemistry, biology, and physics to achieve water splitting, CO_2 fixation, green organ synthesis, and environmental purification through sunlight [7–9].

Photocatalytic reactions can occur homogeneously or heterogeneously. Heterogeneous photocatalysis is more intensively studied due to its potential applications in different sectors. In heterogeneous photocatalysis, the reaction scheme implies the development of an interface between a strong metal photocatalyst and a liquid containing the reactants and products of the reaction [10]. In the case of homogeneous photocatalysis, reactants and the photocatalyst exist in the same phase. Most regularly used homogeneous photocatalysis processes involve the use of ozone, transition metal oxide, and photo-Fenton systems (Fe^+ and Fe^+/H_2O_2), which have •OH as the reactive species that is used to reduce the reaction time. However, homogeneous catalytic processes produce huge waste materials and pose significant challenges to separate the catalyst from the reaction mixture that causes environmental and ecological stability [11, 12]. Homogeneous catalysts tend to deposit on the reactor wall and also cause corrosion to various industrial materials [13]. Here, we will restrict application of nanomaterials to treat wastewater. Several novel nanomaterials are being used for treatment of groundwater, surface water, as well as wastewater contaminated with organic and inorganic solutes, toxic metal ions, and microorganisms [14].

Photocatalysis was first discovered by Honda-Fujishima, using titania that is based on photoelectrochemical water splitting [15]. Photocatalysis as a rapidly developing field of research has high potential for a wide range of applications in industries to provide a solution for clean energy and environment by developing pollution-free technologies [7]. Novel nanomaterials offer a large surface area, modified surface properties, unique electron conduction properties, etc., which help in contaminated wastewater treatment [16]. This chapter discusses the mechanism of photocatalysis including basic principles, limitations, and challenges to employ photocatalysis for wastewater treatment in detail.

5.2 Basic principles and mechanism of photocatalysis

Photocatalysis utilizes light to enact the substance that helps increase the rate of a chemical without participating in the reaction. Photocatalysis can be carried out either by direct irradiation or by the irradiation of a catalyst, which lowers the activation energy needed for

This book belongs to Badji Mokhtar Annaba University Central Library Copyright Elsevier 2025

primary reaction. Photocatalysis initiates reduction and oxidation (redox) reactions in the presence of the irradiated semiconductors [2]. Fig. 5.1 represents the similarities and differences between natural and artificial photocatalysis. In natural photocatalysis, chlorophyll arrests sunlight to convert water and carbon dioxide into oxygen and glucose, whereas artificial photocatalysis utilize photocatalysts to create strong oxidizing agents and electronic holes that break the organic matter into carbon dioxide and water [10, 18].

Photocatalytic reaction primarily depends on photon energy and properties of the catalyst. Absorption of light and the resultant photoexcitation of electron-hole pairs takes place as the energy of the incident photons matches or surpasses the band gap. Radiations prompt the progress of electrons from the valance band (VB) to the conduction band (CB), leaving an equivalent number of empty destinations (gaps) [19]. Fig. 5.2 shows schematic representation of photocatalytic mechanism using TiO_2 photocatalyst. When titanium dioxide (TiO_2) absorbs ultraviolet (UV) radiation from sunlight or another source, it produces electron-hole pairs. The electron of the VB of titanium dioxide becomes energized when lit by light. The excess energy of this electron helps to promote it to the CB of TiO_2 by creating a negative electron (e−) and positive hole (h+) pair. This stage is known as the semiconductor's "photoexcitation" stage, and the energy difference between the VBs and CBs is known as the band gap [21–23].

The positive hole of titanium dioxide breaks a water molecule to generate hydrogen gas and hydroxyl radical. Hydroxyl radicals are responsible for degradation of pollutants due to their strong oxidizing power. The negative electron reacts with an oxygen molecule to form a superoxide anion. These electrons actuate the redox reactions, and the holes and electrons undergo progressive oxidation and reduction reactions adsorbed on the surface of the

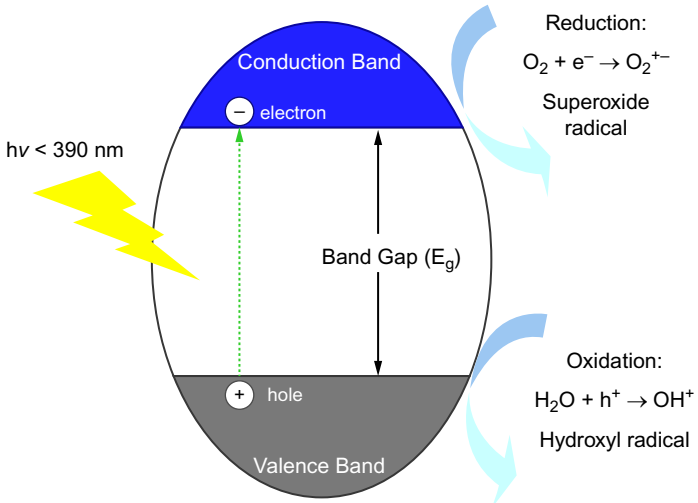

Fig. 5.1
Illustration of natural and artificial photosynthesis [17]. *Redrawn with permission from Y. Zheng, Z. Pan, X. Wang, Advances in photocatalysis in China, Chin. J. Catal. 34 (2013) 524–535. Copyright (2013) Elsevier.*

This book belongs to Badji Mokhtar Annaba University Central Library Copyright Elsevier 2025

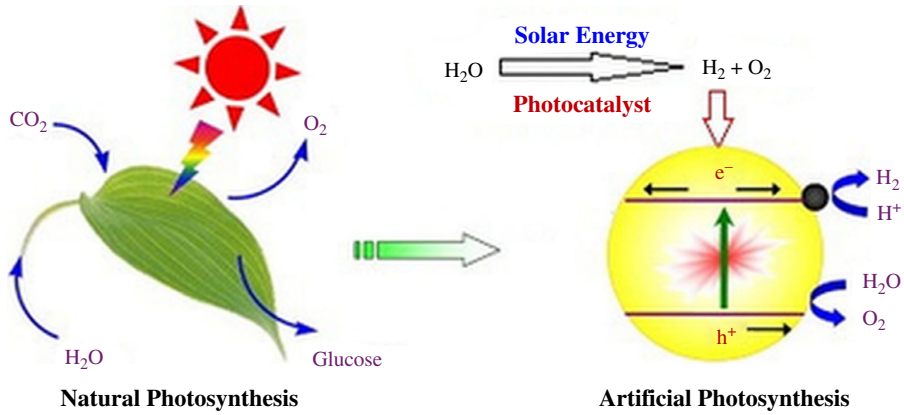

Fig. 5.2
Schematic diagram of photocatalytic mechanism of Ti^{3+} self-doped TiO_2 for the visible-light response [20]. *Reprinted with permission from M. Pelaez, N.T. Nolan, S.C. Pillai, M.K. Seery, P. Falaras, A.G. Kontos, P.S.M. Dunlop, J.W.J. Hamilton, J.A. Byrne, K. O'Shea, M.H. Entezari, D.D. Dionysiou, A review on the visible light active titanium dioxide photocatalysts for environmental applications, Appl. Catal. B: Environ. 125 (2012) 331–349. Copyright (2012) Elsevier.*

semiconductor to produce the desired products continuing until the availability of light. The mechanism of photocatalytic reaction of TiO_2 lies behind the strong oxidation strength of the hydroxyl radical. Photocatalytic oxidation can effectively disinfect, deodorize, and purify air, water, and any surface area. TiO_2 semiconductor is initiated by a system including radical receptive species through the accompanying series reactions. The active radical species formed were often found to be $\bullet O_2^-$, $\bullet HO_2$, and $\bullet OH$ [24].

The photocatalyst surface contains absorbed water that is oxidized by positive holes made in the VB because of the electrons shifting toward the CB due to light irradiation that forms hydroxyl (OH•) radicals [11, 25, 26]. These hydroxyl (OH•) radicals react with organic material present in the dye. In presence of oxygen, the intermediate radicals in the organic compounds give rise to radical chain reactions by consuming the oxygen leaving the organic matter to decompose to produce carbon dioxide and water [27]. The reduction of oxygen contained in the air occurs because of the pairing reaction that takes place as an alternative to hydrogen generation due to oxygen being an easily reducible substance [19]. Superoxide anions are formed by the reaction of CB electrons with dissolved oxygen species that become attached to the intermediate products in the oxidative reaction to hydrogen peroxide and then to water. The reduction is more favorable in organic matter than in water. In this manner, a high concentration of organic matter leads to the formation of a larger number of positive holes resulting in reduction of the carrier recombination, thus consequently enhancing the photocatalytic activity [27].

This book belongs to Badji Mokhtar Annaba University Central Library Copyright Elsevier 2025

5.3 Source of water pollution, water treatment methods, and role of nanomaterials in wastewater treatment

The importance of maintaining a clean environment has been expanding as of late because of the environmental contamination into water, land, and air that occurs due to disposal or discharge of material that causes an ecological imbalance or decreases the quality of life [12, 28]. Water is essentially required for life on Earth. An increase in consumption of underground water resources and improper wastewater management propels interest in the research community. Even small amounts of water effluents have the potential to adversely affect human health and other ecosystems. Thus, the discharged industrial wastewater requires proper sewage treatment to avoid adverse effects. Although different wastewater treatment technologies are available, there is a need for an efficient, less time-consuming, and comparatively cheaper method as a major tool for allowing access to safe water for all [11, 29].

5.3.1 Sources of water pollution

Water is a regenerative ecological asset; however, there could be an issue if the pollution load surpasses its normal regenerative limit. Release of contaminants from industries as well as farming activities have become major sources that influence a vast majority of water bodies in the environmental framework [26, 30]. Increasing number of industrial chemical products are producing a major portion of the contamination in industrial waste streams. The textile industry is one of the highest polluting wastewater industries among all industrial sectors [31]. Globally, more than 0.7 million tons of organic synthetic dyes are synthesized annually for use in different sectors such as textile, food, leather goods, plastics, industrial painting, cosmetics, and consumer electronics [21]. Colorants or additives and pigments are also contributing to significant wastewater generation [32, 33]. Various contaminants released from paper and pulp industries include sulfur compounds and nitrogen oxides emitted to the air and organic compounds, nutrients, and metals discharged in the effluent wastewater [34]. The fundamental driver of surface water and groundwater pollution are modern releases such as overabundance utilization of agrochemicals, for example, pesticides, fungicides, composts, and landfilling household wastes [28]. By and large, wastewater treatment is an intense issue because of a few reasons that are recorded as follows:

- High concentrations of total dissolved solids (TDS)
- Presence of toxic and heavy metals such as Cr, As, Cu, Cd, etc.
- Presence of nonbiodegradables
- Presence of dissolved silica and free chlorine
- Presence of complex aromatic molecular structures that make it difficult to degrade

This book belongs to Badji Mokhtar Annaba University Central Library Copyright Elsevier 2025

It was observed that effluents during the production processes of various industries can cause unfavorable environmental pollution and potentially damage the ecosystem health. Due to this, it necessitates efficient, economic wastewater treatment before discharging to water bodies [11, 32–34].

5.3.2 Water treatment methods

Several water treatment techniques have been developed for removal of contaminants from waste industrial effluents. Different treatments including physical, biological, and chemical have been employed to treat wastewater. Large numbers of conservative processes are also used for treatment of various types of industrial wastewater from pharmaceutical, chemical, pulp and paper, textile, and dyes industries. The characteristics of industrially generated wastewater varies not only with the type of industry but also with the type of processes within the same industry [26, 29]. These characteristics are massively diverse than domestic wastewater that usually possesses similar compositional quality and quantity. Oller et al. [35] summarized the combination of advanced oxidation processes (AOPs) and biological treatment methods for treatment of industrial wastewater coming from textile industries, paper mills, olive mills, wineries, distilleries, etc. Gupta et al. [29] discussed different types of primary, secondary, and tertiary water treatment and recycling techniques along with their basic principles, applications, costs, maintenance, and suitability. The selection of treatment technologies mainly depends on:

- Type of wastewater
- Treatment adaptability
- Mineralization of main and intermediate contaminants
- Wastewater treatment efficiency
- Recycling capacity and potential utilization of treated water
- Cost-effectiveness and eco-friendliness

AOPs are viewed as profoundly serious water treatment innovations when contrasted with traditional strategies due to high chemical stability and/or low biodegradability for removal of organic pollutants. AOPs are typically costly, and so their combination with a biological treatment process is reported to reduce operating costs. Gogate and Pandit [36] suggested the hybrid water treatment methods, a majority of which are in combination with AOPs. This is because of an inability of the individual wastewater treatment methods to exhibit good economics and a high degree of energy efficiency.

5.3.3 Role of nanomaterials in water treatment by photocatalysis

Diversity of water contamination, its magnitude, and intensity vary drastically for different industries due to a growing demand for different chemical products. This reduces the availability of clean water and intensifies the potential for a water-related crisis. Several studies

This book belongs to Badji Mokhtar Annaba University Central Library Copyright Elsevier 2025

focused on the environmental applications of photocatalysis, recent advances, and trends considering different fundamental parameters that focus on the various contaminants such as dyes, phenols, nitrogen, and sulfur containing compounds in wastewater [37–40]. Several researchers demonstrated the application of photocatalysis using different catalysts such as ZnS-CuS-CdS, ZnS-WS_2-CdS, C_3N_4-CdS, and carbon spheres/CdS, Pd-Cr_2O_3-CdS for wastewater treatment to remove contaminants from wastewater in different industries. These studies have also discussed the cost, benefits, and applicability of engineered nanomaterials (ENM) for different wastewater treatments to remove persistent organic pollutants (POPs), heavy metals, and other pollutants from wastewater and soil [41–45].

Saravanan et al. [2] manufactured ZnO/Ag/CdO ternary nanocomposite for degradation of textile effluents using thermal decomposition and showed degradation of more than 90% of effluent in 210 min under visible light irradiation indicating high photocatalytic activity due to the synergistic effect of different properties of the ternary nanocomposite. Petronella et al. [46] reviewed synthesis of nanocomposite materials and their applications focusing on degradation of pollutants from water or air using polymers such as fluorinated polymers or organosilane hybrids integrated in a photoreactor. Yamashita et al. [47] illustrated the use of TiO_2 photocatalysts for degradation of wastewater containing 2-propanol at 275 K under visible light ($\lambda > 450$ nm) irradiation showing effective photocatalytic reactivity. Qiu et al. [48] examined removal of methyl orange, phenol, and rhodamine B by ZnO/poly-(fluorene-*co*-thiophene) photocatalyst and found complete removal of rhodamine and 40% removal of other two compounds after 2 h irradiation with three 1 W LED (light-emitting diode) lights. Bahnemann [6] reviewed the application of photocatalysis for wastewater treatment using different solar reactors. Kositzi et al. [49] presented the reduction of organic content present in synthetic municipal wastewater by applying both heterogeneous and homogeneous photocatalytic methods and illustrated simple, economically reasonable, and practical solutions to the processing of this liquid waste.

Mills et al. [37] studied water purification by using TiO_2 as a photocatalyst for wastewater treatment containing high concentration of organic pollutant. Robert and Malato [50] demonstrated heterogeneous photocatalysis as a promising technology using detoxification of organic compounds in water with titanium dioxide. Ahmad et al. [51] studied applications of different nanoparticles to treat wastewater focusing on safe drinking water applications. With these numerous applications and new potential challenges in waste treatment, nanomaterials using photocatalysis will play a major role in the future. Rizzo et al. [52] investigated detoxification of an urban wastewater effluent polluted with pharmaceuticals using TiO_2 photocatalysis. Cai et al. [16] summarized the application of nanomaterials for removing dyes from wastewater using carbonaceous nanomaterials, nanosized TiO_2, and graphitic carbon nitride (g-C_3N_4) and also pointed out challenges including high cost and poor separation performance of nanomaterial-based process, which limits its engineering application at a commercial scale. Xu et al. [53] discussed iron oxide nanomaterials for wastewater treatment and difficulties associated in their in-vitro and in-vivo application studies due to initial

This book belongs to Badji Mokhtar Annaba University Central Library Copyright Elsevier 2025

development of these techniques still being at an experimental or pilot stage. Adeleye et al. [44] reviewed conventional technologies and emerging applications of nanotechnology in wastewater treatment and environmental remediation considering various aspects such as cost, benefit, and applicability based on the level of contamination of the ENM. Their study also pointed out the need for research to focus on developing methods with less energy intensive synthesis of nanoparticles that require cheap feedstock.

5.4 Overview on photocatalytic materials and factors affecting photocatalysis

Different types of materials are used in photocatalytic processes for different applications. Semiconductors are particularly useful as photocatalysts due to their electronic structure, light absorption properties, charge transport characteristics, and excited-state lifetimes [10]. In recent years, various inorganic materials have been investigated as photocatalysts with their applications expanded to reactions in photocatalysis due to their versatility. Various applications of these nanomaterials are demonstrated for the photocatalytic degradation of organic pollutants present in wastewater. Different factors affecting photocatalytic activity along with the photocatalytic material need to be thoroughly examined prior to their application [40].

5.4.1 Photocatalytic materials

The design of catalytic materials is traditionally a trial and error process, while development of such materials relies on experiments. A candidate catalyst synthesized, characterized, and tested under best conditions leads to a lengthy evolution of new materials with different characteristics such as activity, stability, selectivity, and regenerability [11, 54]. Since the discovery of water photolysis using TiO_2 electrodes, the focus of research has been on TiO_2 for removal of environmental pollutants. TiO_2 can utilize approximately 5% of the total incident solar energy because of its wide band gap (3–3.2 eV). In the last few decades, several efforts have been made to modify TiO_2, by doping with different elements along with the development of heterojunctions by combining TiO_2 with metals such as Pt or Pd, or other semiconductors such as NiO, WO_3, $SrTiO_3$, RuO_2, or CdS for better light sensitization [55]. A TiO_2 photocatalyst is photochemically stable to strong acids and bases, nontoxic, inexpensive, noncorrosive, and commercially available at various crystalline forms [54].

Lee et al. [56] reviewed the application of TiO_2 catalyst along with doping of other metallic particles for water treatment applications illustrating the removal of organic contaminants. Lu et al. [57] reviewed the application of zero-valent metal nanoparticles (Ag, Fe, and Zn), carbon

This book belongs to Badji Mokhtar Annaba University Central Library Copyright Elsevier 2025

nanotubes (CNTs), metal oxide nanoparticles (titania, zinc oxide, and iron oxides), and nanocomposites for wastewater treatment and discussed the challenges regarding widespread acceptability and commercialization along with potential environmental and health risk. Lee et al. [58] employed ZnO as a promising photocatalyst showing higher photocatalytic activity compared with others to remove organic contaminants from wastewater. Bhanvase et al. [59] reviewed the application of graphene-TiO_2 and doped graphene-TiO_2 nanocomposite photocatalysts for water and wastewater treatment and discussed the importance of doping of various metals, metal oxides, or nonmetals. Srikanth et al. [60] discussed recent advancements in supporting materials such as glass CNTs and graphine oxide, zeolites, and polymers for immobilized photocatalytic applications for degradation of organic pollutants in wastewater.

Notwithstanding metal oxides, a few chalcogenides have been researched with respect to their photocatalytic action. Various sulfides, nitrides, and oxynitrides are examined as alternative materials for solar photocatalysis. After the 1990s, with the rapid development of nanotechnology and advanced characterization methods, enthusiasm for photocatalysis research from a scientific and engineering point of view has grown exponentially. For example, TEM, EELS, and XPS gave extraordinary chances for photocatalysis to understand its foreseen potential [28, 61]. Santhosh et al. [41] reviewed the role of different nanomaterials such as carbon-based materials and metal oxide nanomaterials to remove toxic contaminants from wastewater using adsorption and photocatalysis. Preparation and application of photocatalytic nanocomposite materials for degradation of pollutants was reviewed by Petronella et al. [46]. Photocatalytic materials applied for various natural applications incorporated a wide scope of semiconductor materials, for example, parallel, ternary, and quaternary oxides. Alongside, a huge number of sulfides, nitrides, and oxynitrides have been additionally examined as elective materials to TiO_2 for visible light or solar photocatalysis.

5.4.2 Factor affecting photocatalysis

A few elements influence the photocatalytic procedure, for example, size, shape, and surface structure alongside the piece of reactant material that affects the activity and selectivity of catalysts. Other factors such as reaction pH and temperature, light intensity, quantity of catalyst, and concentration of wastewater affect the photocatalysis process. Importance of surface defects lies in the fact that they determine corrosion, adsorption, and catalytic behavior for many oxides [2]. The structure of the catalyst and its morphology plays a key role in accomplishing prevalent photocatalytic action. Nanomaterials with large surface areas and smaller sizes show higher proficiency in the photocatalytic response by expanding surface-to-volume proportion, which upgrades a number of active sites and interfacial charge carrier transfer rates accomplishing higher synergistic activities.

This book belongs to Badji Mokhtar Annaba University Central Library Copyright Elsevier 2025

Electrostatic interactions between charged particles and the contaminants influence the surface properties of the catalyst material and help in determining the effect of pH on the rate of reaction [62]. The degradation rate in a photocatalytic reaction relies upon the intensity of incident light. Quanta of light consumed by any photocatalyst or reactant are given by the quantum yield known as the ratio of the rate of reaction to the rate of assimilation of radiation. The amount of catalyst also influences the efficiency of photocatalytic degradation. If the amount of catalyst increases, it results in an increase in active sites on the semiconductor surface. However, an increase in catalyst loading beyond an optimum concentration reduces the degradation rate due to a decrement in the light penetration depth in the solution. The type of pollutant and their concentration are also important factors for the photocatalysis process [21].

Malato et al. [63] exhibited the reliance of photocatalytic action on response temperature that is fundamentally dependent on activation energy of the material in a photocatalytic reaction. Ahmed et al. [64] contemplated the effect of various working boundaries on the photocatalytic degradation of pesticides and phenols in wastewater. Results of the investigation detailed that the photocatalytic corruption of natural mixtures relies upon the sort and organization of the photocatalyst, light power, introductory substrate fixation, measure of impetus, pH of the response medium, ionic parts in water, dissolvable sorts, oxidizing specialists/electron acceptors, impetus application mode, and calcination temperature in the water condition. Optimization of the previously mentioned parameters is needed to ensure a sustainable operation. Reza et al. [65] conducted photocatalytic degradation of dyes utilizing TiO_2 and examined various boundaries, for example, pH, impetus fixation, substrate focus, and the nearness of oxidants. The study demonstrated how response temperature and power of light additionally influence dye degradation.

Akpan and Hameed [31] examined the parameters affecting the photocatalytic degradation of dyes utilizing TiO_2-based photocatalysts. Their findings revealed that parameters, for example, pH, oxidizing reagent, temperature at which the catalyst must be calcined, dopant(s) substance, and catalyst stacking have individual effects on the photocatalytic corruption of any dye in wastewaters. Ye et al. [66] carried out degradation of metoprolol using TiO_2 nanotube and analyzed the effect of catalyst and operational parameters on photocatalytic activity. Barka et al. [67] explored the factors affecting degradation of Rhodamine B using TiO_2-coated nonwoven paper as a catalyst and showed the temperature-dependency of photodegradation by finding an increase in degradation with temperature. Their study showed the presence of the Cl^-, CH_3COO^-, and HPO_4^{2-} ions reduce the photodegradation; however, the presence of SO_4^{2-} increased the rate of degradation.

A study on degradation of tetracycline (TC) in wastewater has been carried out using photocatalysis to evaluate the influence of different parameters by Saadati et al. [68]. The reported findings suggested operating parameters such as type of photocatalyst, initial

This book belongs to Badji Mokhtar Annaba University Central Library Copyright Elsevier 2025

concentration of TC, amount of catalyst, pH of medium, oxidizing agents/electron acceptors, and the presence of ionic components in solution significantly affects the photocatalytic degradation rate of TC. This provided an extensive understanding of the whole process and presented massive opportunities for its application in dyes degradation [68]. Ahmed et al. [69] reviewed the photocatalytic degradation of wastewater considering the different factors such as pH, temperature, concentration of the contaminant, reaction time, morphology and quantity of photocatalyst, dissolved oxygen, etc. using different nanomaterials. Merabet et al. [70] examined the photocatalytic degradation of indole on a recirculating reactor using UV/TiO_2 process. The effects of initial concentration, amount of catalyst, pH, agitation, and flow rate of the solution on the photodegradation were studied. Results demonstrated that for indole elimination, optimal pH is about 6–7 and optimal value of catalyst loading is 1 g/L. An increase in recirculating rate decreases the degradation rate due to the reduction in residence time. Also, agitation speed is found to have little influence on degradation due to improvement in the mass transfer step.

In summary, there are intrinsic and extrinsic factors related to the photocatalytic semiconductor affecting the mechanism and kinetics of photocatalytic reactions in aqueous media. Effectiveness of a photocatalyst relies upon the competition of different interface transfer processes involving electrons and holes and their deactivation by recombination. Crystallographic phase, exposed crystal face, crystallite size, and presence of dopants, vacancies, impurities, and different surface states are the intrinsic factors, while the photocatalytic conditions (pH, contamination and its underlying focus, the nearness of polluting influences in the framework, light force, impetus measurements, and stream rate) are the extrinsic parameters.

5.5 Challenges of photocatalysis in wastewater treatment

Application of nanomaterials has been increasing widely in different sectors along with wastewater treatment. Nanomaterials have emerged as exciting photocatalysts with important physicochemical properties beneficial for photocatalysis that can provide large surface areas, diverse morphologies, crystalline structure, etc. Alongside these different properties, for example, molecule size and degree of aggregation decide the adsorption ability of photocatalysts that has a huge effect to productively continue numerous photocatalytic responses. In spite of the fact that a number of advantages are related to photocatalysis, generally speaking, it faces a few problems that should be tended to such as relying on the application and type of waste [26].

One of the most important challenges of photocatalysis is to maximize the surface area with various geometries of nanostructures to achieve maximum overall efficiency. Another key challenge is that the photocatalytic capability is a function of nature of its surface/interface

This book belongs to Badji Mokhtar Annaba University Central Library Copyright Elsevier 2025

chemistry. The surface energy and chemisorption characteristics play important roles in governing the selectivity, rate, and potential of redox reactions on the photocatalyst surface. The most significant property relevant to the photocatalytic semiconductor is the energy band configuration that determines the absorption of incident photons. Photocatalysts function only in UV or near UV range of the electromagnetic spectrum with limited efficiency because of various factors including a mismatch between semiconductor band gap and the solar spectrum, inefficient charge separation, and transport. In this manner, energy band engineering is a crucial part of designing and fabricating semiconductor photocatalysts [11]. Systems consisting of dispersed nanocrystals bring new challenges associated with high surface area-to-volume ratios and the fact that at least two reactions are occurring on each particle to balance the charge. Progress in this area could be stimulated by closer examination of the parallels and differences between dispersions and mesoporous electrodes of the same material. Researchers recognized the importance of synergistic collaboration with different areas such as materials science, chemical biology, and drug discovery along with synthetic chemistry for the bright future of photochemical synthesis [9, 71].

Maeda et al. [72] explored recent progress and potential challenges in photocatalytic water reviewing the photocatalyst preparation, co-catalysts development, and related physical and material chemistry considering the economic viability aspects of the overall process. Several studies discussed the challenges regarding the design of new photocatalyst nanomaterials considering higher stability and efficiency as well as lower cost of production are needed [73–75]. Malto et al. [63] pointed out nanomaterial chemistry research challenges like slow kinetics, low photoefficiency, and unpredictable mechanisms as obstacles for producing efficient and sustainable nanomaterials.

Farouk et al. [76] highlighted deactivation of TiO_2 catalyst during textile wastewater treatment and pointed out need for more investigation in area of TiO_2 poisoning and inhibition activity by some ions present in textile wastewater to address the current challenges. Brame et al. [77] discussed the challenges and opportunities of ENMs for differential water treatment at point-of use as well as community for multiple applications to enhance the effectiveness in developing countries. Wang et al. [78] summarized nanostructured photocatalysts for water disinfection and discussed novel and green methods of synthesis and characterization, catalyst immobilization, recycling methods, and photocatalytic reactor design along with bacterial inactivation to accelerate the practical industrial applications of photocatalysis. Xue et al. [79] brought up the difficulties in regard to cost-viability and specialized obstructions of nanomaterials for their business applications in water and wastewater treatment. Their study additionally talked about possible dangers of nanomaterials on human and environmental health. Tugaoen et al. [80] demonstrated photocatalysis as a transformative technology for reduction of nitrate to innocuous nitrogen with considerable selectivity; however, several challenges related to pH, optimal particle size, aspect ratio, shape or morphology, and

This book belongs to Badji Mokhtar Annaba University Central Library Copyright Elsevier 2025

composition of composite nanoparticle photocatalysts along with photon flux, energy flux, and optimal wavelength range need to addressed for efficient removal of nitrate from wastewater. Future development and commercialization of photocatalysis is still challenging as far as cost-effectivity, technical hurdles, and potential environmental and human risk are concerned.

Several harmful effects of nanomaterials are found, and there remain huge gaps in knowledge about the nature and association of nanoparticles with the ecological framework. More examination is expected to assess the soundness of such networks in an assortment of test frameworks to completely decide the potential for human introduction to the nanoscale parts of financially accessible items and future items. The long-term efficacies of such nanotechnologies are largely unknown because lab studies are mostly conducted for a relatively short period of time. Research that will address the implication of nanotechnologies in long-term performance of wastewater treatment is very crucial [22]. Santosh et al. [41] called attention to disadvantages related to nanomaterials use that must be arranged identified with the large-scale manufacturing of nanomaterials and their handy use. Besides, the accessibility of gigantic amounts of nanomaterials at financially feasible costs for water treatment can be a severe issue for industrial applications. Another important challenge is the prevention of the release of nanomaterials into the environment and simultaneously their accumulation for long periods of time. Spasiano et al. [81] have critically analyzed the status of solar photocatalysis focusing on the different materials and their application in their current commercial status and pointed out the future opportunities and challenges regarding the efficiency, cost, and use of different materials for commercial viability of photocatalysis.

As the composition and pH of industrial wastewater varies from region to region, endeavors ought to be made for the improvement of photocatalytic materials that work in various types of conditions, for example, various temperatures, pH conditions, as well as contaminant concentrations. For this purpose, research related to doping and modifications of TiO_2 and other semiconductors must be in a wider range of operating conditions. Another challenge is optimizing catalyst immobilization strategies to obtain maximum surface area of the photocatalyst that can be irradiated and avoiding the problems associated with agglomeration and catalyst recovery, which is of great concern in slurry-based photoreactors [81, 82]. While much consideration has been centered on the turn of events and expected advantages of nanomaterials for water treatment forms, concerns have likewise been realized regarding possible human and ecological harm. Without a doubt, it has been demonstrated that properties of nanomaterials that make them appealing (e.g., size, structure, shape, reactivity) may likewise make them harmful. However, it is difficult to evaluate the magnitude at which these nanomaterials can affect health and environment because of underdeveloped methods and tools. Finally, elucidating and understanding the mechanisms for the application of nanomaterials for wastewater treatment in a sustainable manner is a need of our time to address several challenges [83].

This book belongs to Badji Mokhtar Annaba University Central Library Copyright Elsevier 2025

5.6 Summary

Motivation of photocatalysis can be followed back by comprehension of natural photosynthesis that is not quite the same as traditional catalysis. Photocatalytic technology offers several advantages such as: (i) substitution to energy-intensive conventional methods of treatment using pollution-free and renewable solar energy; (ii) production of harmless products, unlike conventional methods due to pollutants transferring from one phase to another; (iii) efficient utilization for destruction of hazardous contaminants such as herbicides, pesticides, and detergents and industrial contaminants like dyes, toxic metal ions, etc. in different wastewater streams; (iv) requires mild reaction conditions and reaction time is modest with lesser chemical input; (v) minimal secondary waste generation; and (vi) possible applications in hydrogen generation, gaseous phase, and aqueous treatments as well for solid (soil) phase treatments to some extent [70].

Despite the intense efforts over four decades' research in photocatalysis field, it's still in the early phase of its development, and several efforts are yet needed to make effects in the real world. Although many uncertainties are involved in the application of photocatalysis, in future it will surely lead to bright technological developments. It is an emerging technology that has a variety of applications in different fields including degradation of organics and dyes, antibacterial action, and fuel generation through water splitting and CO_2 reduction. Photocatalytic processes need to be developed in a way that offer cost-efficiency, sustainability, robustness, and ease for their implementation compared with other developed processes that lead to industry application. Photocatalysis guarantees an answer for difficulties related with the irregular idea of daylight, which is considered an inexhaustible and extreme vitality source to control exercises on Earth. In this way, the utilization of sun-oriented light as a reagent in oxidative catalysis utilizing a photocatalyst can possibly push toward a maintainable future that has a generally negligible natural effect. Photocatalysis is a simple yet complex phenomenon; simple because of working and utilization, and complex in terms of validating the results in a technically comprehensible form. Hence, solar photocatalysis is found to be a prospective yet challenging technology expected to address a wide scope of applications with profound understanding, more research, feasible engineering, and broad design considerations.

References

[1] J.C. Garcia, Catalysis and Photocatalysis Over TiO_2 Surfaces Detailed From First Principles, (Ph.D. Thesis) Worcester Polytechnic Institute, 2014, pp. 1–132.
[2] R. Saravanan, M.M. Khan, V.K. Gupta, E. Mosquera, F. Gracia, V. Narayanan, A. Stephen, ZnO/Ag/CdO nanocomposite for visible light-induced photocatalytic degradation of industrial textile effluents, J. Colloid Interface Sci. 452 (2015) 126–133.
[3] B. Ohtani, Great challenges in catalysis and photocatalysis, Front. Chem. 5 (79) (2017) 1–3.
[4] S. Lacombe, N. Keller, Photocatalysis: fundamentals and applications in JEP 2011, Environ. Sci. Pollut. Res. 19 (2012) 3651–3654.

This book belongs to Badji Mokhtar Annaba University Central Library Copyright Elsevier 2025

[5] S. Zhu, D. Wang, Photocatalysis: basic principles, diverse forms of implementations and emerging scientific opportunities, Adv. Energy Mater. 7 (1700841) (2017) 1–24.
[6] D. Bahnemann, Photocatalytic water treatment: solar energy applications, Sol. Energy 77 (2004) 445–459.
[7] A.O. Ibhadon, P. Fitzpatrick, Review: heterogeneous photocatalysis: recent advances and applications, Catalysts 3 (2013) 189–218.
[8] S. Weon, F. He, W. Choi, Status and challenges in photocatalytic nanotechnology for cleaning air polluted with volatile organic compounds: visible light utilization and catalyst deactivation, Environ. Sci. Nano 6 (2019) 3185–3214.
[9] L.M. Peter, Photo electrochemistry: from basic principles to photocatalysis, in: Fundamental Aspects of Photocatalysis, Royal Society of Chemistry, Publishing, 2016, pp. 1–28 (Chapter 1).
[10] D.I. Kondarides, Photocatalysis, in: Encyclopedia of Life Support System (EOLSS) Website: Http://Www.eolss.net/Sample-Chapters/c06/e6-190-16-00.pdf, Encyclopedia of Life Support Systems, 2010, pp. 1–11.
[11] M.M. Khan, D. Pradhan, Y. Sohn, Nanocomposites for Visible Light-Induced Photocatalysis, Springer Series on Polymer and Composite MaterialsSpringer, Cham, 2017.
[12] S. Rehman, R. Ullah, A.M. Butt, N.D. Gohar, Strategies of making TiO_2 and ZnO visible light active, J. Hazard. Mater. 170 (2–3) (2009) 560–569.
[13] M.E. Ali, M.M. Rahman, S.M. Sarkar, S.B.A. Hamid, Heterogeneous metal catalysts for oxidation reactions, J. Nanomater. (2014) 1–23.
[14] J. Theron, J.A. Walker, T.E. Cloete, Nanotechnology and water treatment: applications and emerging opportunities, Crit. Rev. Microbiol. 34 (1) (2008) 43–69.
[15] Y.M. Hunge, A.A. Yadav, Basics and advanced developments in photocatalysis—a review, Int. J. Hydrol. 2 (4) (2018) 539–540.
[16] Z. Cai, Y. Sun, W. Liu, F. Pan, P. Sun, J. Fu, An overview of nanomaterials applied for removing dyes from wastewater, Environ. Sci. Pollut. Res. 24 (2017) 15882–15904.
[17] Y. Zheng, Z. Pan, X. Wang, Advances in photocatalysis in China, Chin. J. Catal. 34 (2013) 524–535.
[18] D. Gust, T.A. Moore, A.L.M. Moore, Realizing artificial photosynthesis, Faraday Discuss. 155 (2012) 9–26.
[19] J. Hagen, Industrial Catalysis: A Practical Approach/Jens Hagen, second ed., Wiley, Weinheim, 2006.
[20] M. Pelaez, N.T. Nolan, S.C. Pillai, M.K. Seery, P. Falaras, A.G. Kontos, P.S.M. Dunlop, J.W.J. Hamilton, J. A. Byrne, K. O'Shea, M.H. Entezari, D.D. Dionysiou, A review on the visible light active titanium dioxide photocatalysts for environmental applications, Appl. Catal. B Environ. 125 (2012) 331–349.
[21] K. Rajeshwar, M.E. Osugi, W. Chanmanee, C. R. Chenthamarakshan, M. Zanoni, P. Kajitvichyanukul, R. Krishnan-Ayer, Heterogeneous photocatalytic treatment of organic dyes in air and aqueous media, J. Photochem. Photobiol. C 9 (4) (2008) 171–192.
[22] X. Qu, P.J.J. Alvarez, Q. Li, Applications of nanotechnology in water and wastewater treatment, Water Res. 47 (2013) 3931–3946.
[23] M.M. Khan, S.F. Adil, A. Al-Mayouf, Metal oxides as photocatalysts, J. Saudi Chem. Soc. 19 (5) (2015) 462–464.
[24] V. Augugliaro, M. Bellardita, V. Loddo, G. Palmisanoa, L. Palmisano, S. Yurdakal, Overview on oxidation mechanisms of organic compounds by TiO_2 in heterogeneous photocatalysis, J. Photochem. Photobiol. C: Photochem. Rev. 13 (2012) 224–245.
[25] F. Huang, A. Yan, H. Zhao, Influences of doping on photocatalytic properties of TiO_2 photocatalyst, in: Semiconductor Photocatalysis – Materials, Mechanisms and Applications, IntechOpen, 2016.
[26] A. Hernández-Ramírez, I. Medina-Ramirez, Photocatalytic Semiconductors: Synthesis, Characterization, and Environmental Applications, Springer, New York, 2014.
[27] A. Fujishima, K. Honda, Electrochemical photolysis of water at a semiconductor electrode, Nature 238 (5358) (1972) 37–38.
[28] M.N. Chong, B. Jin, C.W.K. Chow, C. Saint, Recent developments in photocatalytic water treatment technology: a review, Water Res. 44 (10) (2010) 2997–3027.
[29] V.K. Gupta, I. Ali, T.A. Saleh, A. Nayak, S. Agarwal, Chemical treatment technologies for waste-water recycling- an overview, RSC Adv. 2 (16) (2012) 6380–6388.

This book belongs to Badji Mokhtar Annaba University Central Library Copyright Elsevier 2025

[30] S. Navalon, A. Dhakshinamoorthy, M. Alvaro, H. Garcia, Photocatalytic CO_2 reduction using non-titanium metal oxides and sulfides, ChemSusChem 6 (2013) 562–577.
[31] U.G. Akpan, B.H. Hameed, Parameters affecting the photocatalytic degradation of dyes using TiO_2-based photocatalysts: a review, J. Hazard. Mater. 170 (2–3) (2009) 520–529.
[32] U. Pagga, D. Brown, The degradation of dyestuffs: part II behaviour of dyestuffs in aerobic biodegradation tests, Chemosphere 15 (4) (1986) 479–491.
[33] K.R. Jegannathan, P.H. Nielsen, Environmental assessment of enzyme use in industrial production—a literature review, J. Clean. Prod. 42 (2013) 228–240.
[34] H.K. Moo-Young, Pulp and paper effluent management, Water Environ. Res. 79 (10) (2007) 1733–1741.
[35] I. Oller, S. Malato, J.A. Sánchez-Pérez, Combination of advanced oxidation processes and biological treatments for wastewater decontamination—a review, Sci. Total Environ. 409 (2011) 4141–4166.
[36] P.R. Gogate, A.B. Pandit, A review of imperative technologies for wastewater treatment II: hybrid methods, Adv. Environ. Res. 8 (2004) 553–597.
[37] A. Mills, R.H. Davies, D. Worsley, Water purification by semiconductor photocatalysis, Chem. Soc. Rev. 22 (1993) 417–425.
[38] C. Byrne, G. Subramanian, S.C. Pillai, Recent advances in photocatalysis for environmental applications, J. Environ. Chem. Eng. 6 (2018) 3531–3555.
[39] N.M. Gupta, Factors affecting the efficiency of a water splitting photocatalyst: a perspective, Renew. Sust. Energ. Rev. 71 (2017) 585–601.
[40] R. Ameta, S.C. Ameta, Photocatalysis: Principles and Applications, CRC Press, 2016.
[41] C. Santhosh, V. Velmurugan, G. Jacob, S.K. Jeong, A.N. Grace, A. Bhatnagar, Role of nanomaterials in water treatment applications: a review, Chem. Eng. J. 306 (2016) 1116–1137.
[42] R. Kaplan, B. Erjavec, G. Drazic, J. Grdadolnik, A. Pintara, Simple synthesis of anatase/rutile/brookite TiO_2 nanocomposite with superior mineralization potential for photocatalytic degradation of water pollutants, Appl. Catal. B Environ. 181 (2016) 465–474.
[43] L.V. Bora, R.K. Mewada, Visible/solar light active photocatalysts for organic effluent treatment: fundamentals, mechanisms and parametric review, Renew. Sust. Energ. Rev. 76 (2017) 1393–1421.
[44] A.S. Adeleye, J.R. Conway, K. Garner, Y. Huang, Y. Su, A.A. Keller, Engineered nanomaterials for water treatment and remediation: costs, benefits, and applicability, Chem. Eng. J. 286 (2016) 640–662.
[45] L. Zhang, M. Fang, Nanomaterials in pollution trace detection and environmental improvement, Nano Today 5 (2010) 128–142.
[46] F. Petronella, A. Truppi, C. Ingrosso, T. Placido, M. Striccoli, M.L. Curri, A. Agostiano, R. Comparelli, Nanocomposite materials for photocatalytic degradation of pollutants, Catal. Today 281 (2017) 85–100.
[47] H. Yamashita, M. Harada, J. Misaka, M. Takeuchi, K. Ikeue, M. Anpo, Degradation of propanol diluted in water under visible light irradiation using metal ion-implanted titanium dioxide photocatalysts, J. Photochem. Photobiol. A Chem. 148 (2002) 257–261.
[48] R. Qiu, D. Zhang, Y. Mo, L. Song, E. Brewer, X. Huang, Y. Xiong, Photocatalytic activity of polymer-modified ZnO under visible light irradiation, J. Hazard. Mater. 156 (2008) 80–85.
[49] M. Kositzi, I. Poulios, S. Malato, J. Caceres, A. Campos, Solar photocatalytic treatment of synthetic municipal wastewater, Water Res. 38 (2004) 1147–1154.
[50] D. Roberta, S. Malato, Solar photocatalysis: a clean process for water detoxification, Sci. Total Environ. 291 (2002) 85–97.
[51] I.Z. Ahmad, A. Ahmad, H. Tabassum, M. Kuddus, Applications of nanoparticles in the treatment of wastewater, in: Handbook of Ecomaterials, Springer, 2017, pp. 1–25.
[52] L. Rizzo, S. Meric, M. Guida, D. Kassinos, V. Belgiorno, Heterogenous photocatalytic degradation kinetics and detoxification of an urban wastewater treatment plant effluent contaminated with pharmaceuticals, Water Res. 43 (2009) 4070–4078.
[53] P. Xu, G.M. Zeng, D.L. Huang, C.L. Feng, S. Hu, M.H. Zhao, C. Lai, Z. Wei, C. Huang, G.X. Xie, Z.F. Liu, Use of iron oxide nanomaterials in wastewater treatment: a review, Sci. Total Environ. 424 (2012) 1–10.
[54] Y.H. Peng, G.F. Huang, W.Q. Huang, Visible-light absorption and photocatalytic activity of Cr-doped TiO_2 nanocrystal films, Adv. Powder Technol. 23 (2012) 8–12.

This book belongs to Badji Mokhtar Annaba University Central Library Copyright Elsevier 2025

[55] A.L. Linsebigler, G. Lu, J.T. Yates Jr., Photocatalysis on TiO_2 surfaces: principles, mechanisms, and selected results, Chem. Rev. 95 (1995) 735–758.
[56] S.Y. Lee, S.J. Park, Review: TiO_2 photocatalyst for water treatment applications, J. Ind. Eng. Chem. 19 (2013) 1761–1769.
[57] H. Lu, J. Wang, M. Stoller, T. Wang, Y. Bao, H. Hao, An overview of nanomaterials for water and wastewater treatment, Adv. Mater. Sci. Eng. (2016) 1–10.
[58] K.M. Lee, C.W. Lai, K.S. Ngai, J.C. Juan, Recent developments of zinc oxide based photocatalyst in water treatment technology: a review, Water Res. 88 (2016) 428–448.
[59] B.A. Bhanvase, T.P. Shende, S.H. Sonawane, A review on graphene-TiO_2 and doped graphene-TiO_2 nanocomposite photocatalyst for water and wastewater treatment, Environ. Technol. Rev. 6 (1) (2017) 1–14.
[60] B. Srikanth, R. Goutham, R.B. Narayan, A. Ramprasath, K.P. Gopinath, A.R. Sankaranarayanan, Recent advancements in supporting materials for immobilised photocatalytic applications in waste water treatment, J. Environ. Manag. 200 (2017) 60–78.
[61] S. Shen, C. Kronawitter, G. Kiriakidis, An overview of photocatalytic materials, J. Materiomics 3 (2017) 1–2.
[62] D. Friedmann, C. Mendive, D. Bahnemann, TiO_2 for water treatment: parameters affecting the kinetics and mechanisms of photocatalysis, Appl. Catal. B Environ. 99 (2010) 398–406.
[63] S. Malato, P. Fernandez-Ibanez, M.I. Maldonado, J. Blanco, W. Gernjak, Decontamination and disinfection of water by solar photocatalysis: recent overview and trends, Catal. Today 147 (2009) 1–59.
[64] S. Ahmed, M.G. Rasul, R. Brown, M.A. Hashib, Influence of parameters on the heterogeneous photocatalytic degradationof pesticides and phenolic contaminants in wastewater: a short review, J. Environ. Manag. 92 (2011) 311–330.
[65] K.M. Reza, A.S.W. Kurny, F. Gulshan, Parameters affecting the photocatalytic degradation of dyes using TiO_2: a review, Appl. Water Sci. 7 (2017) 1569–1578.
[66] Y. Ye, Y. Feng, H. Bruninga, D. Yntema, H.H.M. Rijnaarts, Photocatalytic degradation of metoprolol by TiO_2 nanotube arrays and UVLED: effects of catalyst properties, operational parameters, commonly present water constituents, and photo-induced reactive species, Appl. Catal. B Environ. 220 (2018) 171–181.
[67] N. Barka, S. Qourzal, A. Assabbane, A. Nounah, Y.A. Ichou, Factors influencing the photocatalytic degradation of rhodamine B by TiO_2-coated non-woven paper, J. Photochem. Photobiol. A Chem. 195 (2008) 346–351.
[68] F. Saadati, N. Keramati, M.M. Ghazi, Influence of parameters on the photocatalytic degradation of tetracycline in wastewater: a review, Crit. Rev. Environ. Sci. Technol. 46 (8) (2016) 757–782.
[69] S.N. Ahmed, W. Haider, Heterogeneous photocatalysis and its potential applications in water and wastewater treatment: a review, Nanotechnology 29 (2018) 1–30.
[70] S. Merabet, A. Bouzaza, D. Wolbert, Photocatalytic degradation of indole in a circulating upflow reactor by UV/TiO_2 process-influence of some operating parameters, J. Hazard. Mater. 166 (2009) 1244–1249.
[71] P. Moroz, A. Boddy, M. Zamkov, Challenges and prospects of photocatalytic applications utilizing semiconductor nanocrystals, Front. Chem. 6 (353) (2018) 1–7.
[72] K. Maeda, K. Domen, Photocatalytic water splitting: recent progress and future challenges, J. Phys. Chem. Lett. 18 (1) (2010) 2655–2661.
[73] H. Tong, S. Ouyang, Y. Bi, N. Umezawa, M. Oshikiri, J. Ye, Nano-photocatalytic materials: possibilities and challenges, Adv. Mater. 24 (2012) 229–251.
[74] R. Saravanan, F. Gracia, A. Stephen, Basic principles, mechanism, and challenges of photocatalysis, in: Nanocomposites for Visible Light-Induced Photocatalysis, Springer, 2017, pp. 19–40.
[75] F. Fresno, R. Portela, S. Suarez, J.M. Coronado, Photocatalytic materials: recent achievements and near future trends, J. Mater. Chem. A 2 (2014) 2863–2884.
[76] H.U. Farouk, A.A.A. Raman, W.M.A. Daud, TiO_2 catalyst deactivation in textile wastewater treatment: current challenges and future advances, J. Ind. Eng. Chem. 33 (2016) 11–21.
[77] J. Brame, Q. Li, P.J.J. Alvarez, Nanotechnology enabled water treatment and reuse: emerging opportunities and challenges for developing countries, Trends Food Sci. Technol. 22 (2011) 618–624.
[78] W. Wang, G. Li, D. Xia, T. An, H. Zhao, P.K. Wong, Photocatalytic nanomaterials for solar-driven bacterial inactivation: recent progress and challenges, Environ. Sci.: Nano 4 (2017) 782–799.

This book belongs to Badji Mokhtar Annaba University Central Library Copyright Elsevier 2025

[79] X. Xue, R. Cheng, L. Shi, Z. Ma, X. Zheng, Nanomaterials for water pollution monitoring and remediation, Environ. Chem. Lett. 15 (2017) 23–27.
[80] H.O. Tugaoen, S.G. Segura, K. Hristovski, P. Westerhoff, Challenges in photocatalytic reduction of nitrate as a water treatment technology, Sci. Total Environ. 599–600 (2017) 1524–1551.
[81] D. Spasiano, R. Marotta, S. Malato, P.F. Ibanez, I.D. Somma, Solar photocatalysis: materials, reactors, some commercial, and pre-industrialized applications. A comprehensive approach, Appl. Catal. B Environ. 170–171 (2015) 90–123.
[82] M.R.D. Khaki, M.S. Shafeeyan, A.A.A. Raman, W.M.A. Daud, Application of doped photocatalysts for organic pollutant degradation—a review, J. Environ. Manag. 198 (2017) 78–94.
[83] P.C. Ray, H. Yu, P.P. Fu, Toxicity and environmental risks of nanomaterials: challenges and future needs, J. Environ. Sci. Health C 27 (1) (2009) 1–35.

This book belongs to Badji Mokhtar Annaba University Central Library

Copyright Elsevier 2025

CHAPTER 6

Doped-TiO_2 and doped-mixed metal oxide-based nanocomposite for photocatalysis

Akash P. Bhat[a], Ananda J. Jadhav[b], Chandrakant R. Holkar[b], and Dipak V. Pinjari[c]

[a]Department of Civil and Environmental Engineering, University of Illinois at Urbana-Champaign, Urbana, IL, United States, [b]Chemical Engineering Department, Institute of Chemical Technology, Mumbai, India, [c]National Centre for Nanosciences and Nanotechnology, University of Mumbai, Kalina Campus, Mumbai, India

Nomenclature

1D	one-dimensional
AOP	advanced oxidation processes
APR	annular photoreactor
APS	atmospheric plasma spraying
CB	conduction band
DCA	dichloroacetic acid
DMAC	dimethylacetamide
e^-	electron
ECB	conduction band energy level
e−CB	electrons in the conduction band
EDTA	ethylenediaminetetraacetic acid
eV	electron-volt
EVB	valence band energy level
Fs	femtoseconds
F-TiO_2	fluorine-doped titanium dioxide photocatalyst
H	Plank's constant
h^+	hole
h+VB	holes in the valence band
HOMO-LUMO	highest occupied molecular orbital-lowest unoccupied molecular orbital
Hn	photon's energy
LCA	life cycle assessment
LSPR	localized surface plasmonic resonance
Ns	nanoseconds
O_3	ozone
OH	hydroxyl radicals
PCD	photocatalytic degradation

Handbook of Nanomaterials for Wastewater Treatment. https://doi.org/10.1016/B978-0-12-821496-1.00018-0
Copyright © 2021 Elsevier Inc. All rights reserved.

This book belongs to Badji Mokhtar Annaba University Central Library

Copyright Elsevier 2025

PET	polyethylene terephthalate
PR	photoreactor
ps	picoseconds
Pt_0	zero-charge platinum
Pt_{ox}	oxidized platinum
PVDF	polyvinylidene fluoride
R_{ads}	organic pollutant (surface adsorbed)
SPES	sulfonated polyethersulfone
TCA	trichloroacetic acid
TEA	techno-economic analysis
TiO_2	titanium dioxide photocatalyst
μs	microseconds
UV	ultraviolet
VB	valence band
ζ	photonic efficiency
n	photonic frequency

6.1 Introduction

Photocatalytic research is based on process intensifications related to the use of chemical reactions coupled with solar energy. The development of solar energy technologies can be divided into solar batteries [1, 2], solar heat [3], and photocatalysis [4]. One of the most important technologies among them is the conversion of solar energy into chemical energy. This conversion is based on the subsequent use of this chemical energy for driving a favorable chemical reaction. In 1970s, the study of hydrogen production by water splitting driven by solar light photocatalysis was first reported by Formenti et al. [5] and Fujishima and Honda [6], and research on explosives began. Afterward, subsequent research and industrial applications of TiO_2 photocatalysis has been increasing in the fields of hydrogen production [7, 8], air cleaning [9], metal anticorrosion [10] and hydrophilic [11, 12], self-purification [13], and antibacterial activity [14, 15]. Various such technologies have been made available in the market [16].
A photocatalyst is a "compound or chemical that accelerates the solar or UV photo reaction," and the photocatalyst needs to fulfill the following criteria: (1) the photocatalyst cannot directly participate or be consumed during a chemical reaction and (2) provides additional mechanistic routes to the chemical reaction, in addition to the existing route with an accelerated rate. Semiconductor molecules, generally used as photocatalysts, contain a valence band (VB) with stable-energy electrons and an empty conduction bands (CBs) at a higher energy level. Incident photons are used to excite the electrons to a higher energy level subsequently to induce a reaction with the surface-absorbed chemical or the pollutant through a redox reaction. This is called the photocatalytic reaction [17]. Photocatalytic reactions refer to the solar or UV energy absorption within the bandgap of the semiconductor photocatalyst and thereby a photogenerated electron transfer. Because all semiconductors possess a sufficient bandgap and electrons in VB, all semiconductor materials can be theoretically used as photocatalysts.

This book belongs to Badji Mokhtar Annaba University Central Library Copyright Elsevier 2025

However, there are only few practically effective semiconductors that can be used as photocatalysts, and TiO_2 is the most widely used among them.

Advanced oxidation processes (AOPs) involve ozone, hydrogen peroxide, UV, sonolysis, and Fenton individually or in combination for rapid destruction and subsequent mineralization of pollutants from water. AOPs are based on the formation and involvement of oxidizing radicals and their consequent attack on the organic pollutants. Over the past few years, AOPs have received considerable attention because of the possibility of complete mineralization of pollutants without producing waste sludge and its application in treating nonbiodegradable and recalcitrant organic pollutants. Heterogeneous photocatalysis has been considered as an advanced oxidation technology for the treatment of contaminants from water and wastewater. Advanced oxidation technologies are a powerful tool in water and wastewater treatment and are currently being applied to a variety of scales all over the world.

TiO_2 photocatalysis generated interest in its effectiveness in generating oxidant hydroxyl radical species. Research has focused on photocatalytic oxidation because of its environmentally friendly nature. Like most other advanced oxidation processes, TiO_2 photocatalysis can lead to destruction and mineralization of organic contaminants with no harmful end products through adsorption of the reactant to the catalyst surface from the bulk electron transfer and attack of radical species on reactant reaction at the surface, including formation of radicals on the carbon chain, peroxyl radical formation on the carbon chain and breaking of the reactant carbon chain, desorption of the pollutants, and finally, removal of products from the interfacial region. Photocatalytic oxidation has also been termed as a green engineering process. This book chapter reports the photocatalysis by TiO_2, which is discussed with respect to understanding the fundamentals of photocatalysis, recent modifications in the photocatalysts, and combinations with other processes and scale-up.

6.2 Mechanism of TiO_2 photocatalysis

TiO_2 photocatalytic treatment process uses energy from UV or solar irradiation to breakdown and mineralize various organic and inorganic pollutants in the wastewater. The photocatalysis degradation process is an effective heterogeneous process and has the following three steps as explained in detail further.

6.2.1 Generation of charge carrier species and their recombination

The principle of photocatalytic reactions is the photogeneration of holes and electrons inside a semiconductor upon absorption of a photon with an energy that is equal to or higher than the semiconductor bandgap. These holes and electrons are subsequently involved in oxidation and reduction reactions with suitable species in the system. The photogenerated electrons may move to another electrode (e.g., platinum electrode) inducing reduction reaction, while holes

This book belongs to Badji Mokhtar Annaba University Central Library Copyright Elsevier 2025

remain in TiO_2, migrating to its surface, inducing oxidation. It is widely agreed that the primary reactions accountable for the photocatalytic activity of a material are these redox reactions of photogenerated electron-hole pairs. The efficiency of these reactions can be evaluated with photonic efficiency ζ or yield, the ratio of the rate of formation or yield of reaction products to the incident photon flow. Because the amount of absorbed light cannot be measured owing to scattering by the semiconductor, all the incident light is considered for calculation of yield, also sometimes called the apparent quantum yield. Photonic efficiency is found to be rather small. Most photogenerated electron-hole pairs recombine immediately and rapidly after excitation, which reduces the ζ values (<10%) for most semiconductor photocatalysis reactions. Without recombination mechanisms, the efficiency or yield would approach an ideal value if unity, that is, if it is assumed that the desired reaction happens so quickly before the reverse reaction of the electron to recombine with the holes. As compared to other semiconductor materials, titanium dioxide (TiO_2) has been demonstrated to be one of the most promising materials for photocatalytic applications because of its higher photonic efficiency ($\zeta = 10\%$). TiO_2 is also cheaper than other photocatalytic materials, nontoxic, photostable, and chemically inert.

$$TiO_2 + hv \rightarrow TiO_2\left(e^-_{cb} + h^+_{vb}\right) \tag{6.1}$$

Semiconductors possess a void region with no energy levels between the top of the VB to the bottom of the CB called the bandgap. Multiple electronic energy states may be formed at the solid surface in the bandgap. The semiconductor TiO_2 has a wide bandgap with 3.0–3.2 eV of energy. TiO_2 bandgap requires excitation by light wavelength range smaller than 400 nm. Once excited, valence band holes and CB electrons are trapped within these energy levels within femtosecond timescales. These species are trapped for 100 ps–10 ns and then recombine in the range of 10–100 ns. Initially, the oxidizing species, holes, are photogenerated in the VB ($h^+{}_{VB}$), and the reducing species, the electrons, are generated in the CB ($e^-{}_{CB}$). It is thermodynamically favorable for these carriers to move from the bulk to the surface. The holes move to the surface, where surface trapped-holes mediate the oxidation. At the surface, these sites correspond to five coordinated Ti^+ and O^- surface ions.

Electron-hole recombination is the reverse of reaction (6.2) resulting in dissipation of heat and no chemical change. Electron-hole recombination is one of the most important processes that contribute to efficiency and yield losses in photoelectrodes. The quantum efficiency of the photocatalytic reaction is dependent on the competition between the desired photocatalytic reaction and the loss owing to recombination. In any real photocatalytic system, recombination occurs, and the concentration of holes and electrons at the surface is not equal. Carrier traps may be used to trap electrons and holes on the surface, leading to a more efficient photocatalytic reaction. Charge carrier traps suppress recombination and increase the timescale the electrons and holes would have for the desired reaction. The timescale of recombination is about 1 μs, much larger than the timescale for the generation (in fs and ps) [18]. If the timescales can be

This book belongs to Badji Mokhtar Annaba University Central Library Copyright Elsevier 2025

understood and processes can be harnessed to trap charges and avoid the recombination, photocatalytic degradation (PCD) can be enhanced. Nonideal surface and bulk irregularities induced during the preparation of semiconductors are associated with energy starts differently from the energy bands of the bulk semiconductor. These energy states act as surface traps for trapping electrons and holes. Modification of semiconductor surface to enhance carrier trapping and thereby increase the efficiency includes the addition of metals, combination with other semiconductors, or addition of dopants. These processes are commonly studied to modify and enhance photocatalytic degradation processes.

$$e^-_{CB} + h^+_{VB} \rightarrow \text{Heat} \tag{6.2}$$

6.2.2 Adsorption of chemicals to TiO_2 followed by their redox pathways

The energy band positions in TiO_2 are suitable for reactions with most environmental pollutants. The conduction band energy level (E_{CB}) of TiO_2 lies at -0.51 V at neutral pH, slightly above the reduction potential for oxygen (-0.33 V), the most commonly used oxidant in environmental redox degradation reactions. Similarly, the VB potential for TiO_2 is +2.69 V at neutral pH, lower than most inorganic and organic electron donors (contaminants). The valence bond holes can be transferred to the surface water or surface-attached titanol groups (hydroxyl groups), inducing oxidation. Upon desorption from the surface, free hydroxyl radicals can be produced, a strong oxidizer. Oxidation of surface adsorbed organic compounds can be induced with the free hydroxyl radicals. Degradation and full mineralization of organics is a synergistic effect of generation and reaction of holes, electrons, and other surface phenomena such as the generation of radicals.

A sequence of reactions that take place in the mechanisms proposed in several studies is listed further. OH^- and H_2O groups are most abundant on the surface of TiO_2; it is likely that holes will react with abundant species. For the reaction to occur, the oxidation potential must be higher than the valence band energy (E_{VB}). Because the band positions and potentials are a function of pH, the oxidation potential for a reaction must be higher for the whole pH range.

$$\text{Ti(IV)} + e^-_{CB} \rightarrow \text{Ti(III)} \tag{6.3}$$

$$\text{Ti(III)}\left(e^-_{CB}\right) + O_2 \rightarrow TiO_2\text{(IV)} - O_2^{\bullet -} \text{ (Surface adsorbed)} \tag{6.4}$$

$$TiO_2\text{(IV)}\left(h^+_{vb}\right) + H_2O \rightarrow TiO_2\text{(IV)} + H^+ + OH^\bullet \tag{6.5}$$

$$R_{ads} + h^+_{vb} \rightarrow R^+_{ads} \tag{6.6}$$

$$TiO_2\left(h^+_{vb}\right) + OH^- \rightarrow TiO_2 - OH^\bullet \text{ (Surface adsorbed)} \tag{6.7}$$

$$O_2^{\bullet -} + H^+ \rightarrow HO_2^\bullet \tag{6.8}$$

This book belongs to Badji Mokhtar Annaba University Central Library
Copyright Elsevier 2025

$$HO_2^{\bullet} + HO_2^{\bullet} \rightarrow H_2O_2 + O_2 \tag{6.9}$$

$$TiO_2\left(e_{CB}^{-}\right) + H_2O_2 \rightarrow OH^{\bullet} + OH^{-} \tag{6.10}$$

$$H_2O_2 + O_2^{\bullet -} \rightarrow OH^{\bullet} + OH^{-} + O_2 \tag{6.11}$$

$$H_2O_2 + hv \rightarrow 2OH^{\bullet} \tag{6.12}$$

Photoexcited CB electrons react with oxygen to form $O_2^{\bullet -}$. CB electrons in acidic or neutral conditions reduce the surface of Ti^{4+} with adsorbed H_2O on the surface, reacting immediately with oxygen to form superoxo TiOO•. Superoxo radical is reduced to form peroxo (TiOO). Peroxo with protonation is equivalent to hydroperoxo (TiOOH), which then forms the surface hydroxyl groups on TiO_2. In alkaline medium, the adsorbed O_2 directly reacts with CB electron to produce $O_2^{\bullet -}$. This radical is converted to hydrogen peroxide or $HO_2^{\bullet}$ (pH < 4.8). The reaction mechanism is as shown in Fig. 6.1.

OH• radical has been reported as one of the most important species in oxidation, although recent studies have reported that the reaction of OH• radical may not be dominant in PCD processes. OH• radical is formed by photocatalytic reduction of H_2O_2. The formation of OH• radical is very sensitive to oxygen concentration, the reduction process for oxygen, which leads to the formation of $O_2^{\bullet -}$, and H_2O_2 is the key step in the formation of OH•.

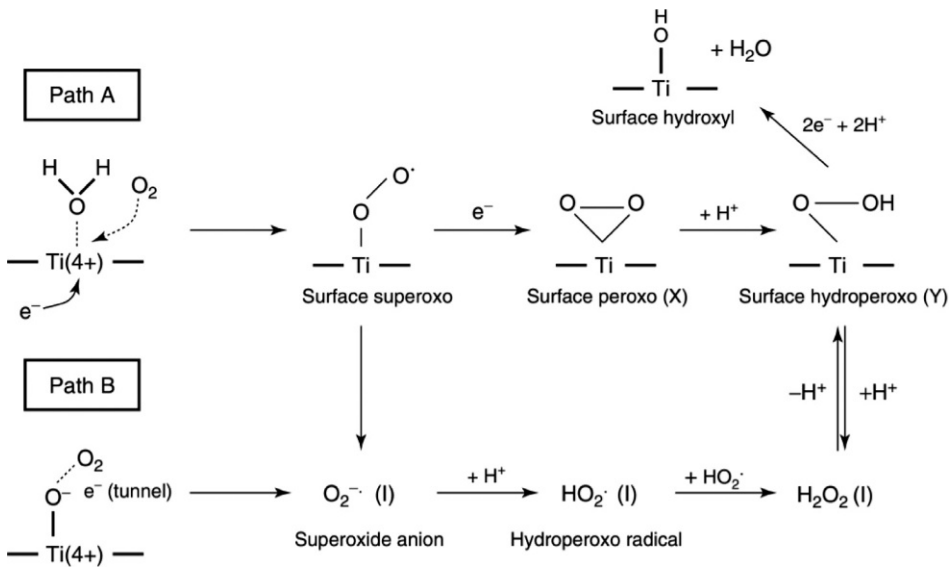

Fig. 6.1
Reaction paths for conduction band photoexcited electron-initiated oxygen reduction leading to the production of hydroperoxo radical, hydrogen peroxide, and surface hydroxyl radical on TiO_2 semiconductor. *Reprinted with permission from R. Nakamura, A. Imanishi, K. Murakoshi, Y. Nakato. In situ FTIR studies of primary intermediates of photocatalytic reactions on nanocrystalline TiO_2 films in contact with aqueous solutions, J. Am. Chem. Soc. 125 (2003) 7443–7450, https://doi.org/10.1021/ja029503q. American Chemical Society.*

This book belongs to Badji Mokhtar Annaba University Central Library Copyright Elsevier 2025

Singlet oxygen molecule $^1O_2$ is also an important species in PCD mechanisms. The disproportionation of $O_2^{\bullet -}$ through the formation of $HO_2^{\bullet}$ results in the formation of singlet oxygen. Alternatively, $O_2^{\bullet -}$ may be easily oxidized by an h^+ to form the singlet oxygen. Singlet oxygen is reactive with certain organic compounds such as amines and olefins.

$$2HO_2^{\bullet} \rightarrow (HOOOOH) \rightarrow 1O_2 + H_2O_2 \tag{6.13}$$

$$O_2^{\bullet -} + h^+ \rightarrow 1O_2 \tag{6.14}$$

6.2.3 Radical attack on organics

The hydroxyl radicals (the primary oxidizing species) along with other species mentioned earlier initiate reactions leading to subsequent oxidation of adsorbed organic pollutants [19].

$$Ti(IV) - OH^{\bullet} + R_{ads} \rightarrow Ti(IV) + R_{ads}{}' \tag{6.15}$$

$$OH^{\bullet} + R_{ads} \rightarrow R_{ads}{}' \tag{6.16}$$

Even though adsorbed sites help in the radical attack on organics, it is not necessary for the organics to be adsorbed (i.e., organics in free TiO_2 sites)

$$Ti\,(IV) - OH^{\bullet} + R \rightarrow Ti(IV) + R' \tag{6.17}$$

$$OH^{\bullet} + R \rightarrow R' \tag{6.18}$$

A series of reactions take place upon the attack of radicals on the adsorbed pollutants leading to oxidation, reduction and subsequent degradation and complete mineralization of the organics. In simpler terms, the reactions can be described as follows.

$$\text{Organic Substrate} + h^+_{vb} \rightarrow \text{Oxidation products} \tag{6.19}$$

$$\text{Organic Substrate} + e^-_{Cb} \rightarrow \text{Reduction Products} \tag{6.20}$$

$$\text{Organic Substrate} + OH^{\bullet} \rightarrow \text{Degradation Products} \tag{6.21}$$

The movement of the h^+_{VB} to the surface depends on how free and delocalized they are in the crystal lattice structure. h^+_{VB} is transferred to the chemical for oxidation. Here, direct or indirect oxidation can occur depending on the fate of the electrons and holes, which can follow several pathways. TiO_2 semiconductor can donate electrons for the reduction of an electron acceptor (mostly oxygen in a well-aerated solution). The rate and probability of charge transfer depends on the respective positions of the VB and CB in the semiconductor and the redox potential of the adsorbed molecule. Immediate oxidation of the pollutant may take place when holes are directly transferred to the adsorbed pollutant or direct photocatalysis. Holes may be transferred to adsorbed water molecules, where hydroxyl radicals are produced, which react with the pollutant resulting in oxidation products or indirect photocatalysis. Direct photolysis takes place where the pollutant molecules are strongly adsorbed onto the photocatalyst, while

This book belongs to Badji Mokhtar Annaba University Central Library Copyright Elsevier 2025

indirect photocatalysis takes place in systems with weak pollution adsorption with weak electronic contact. The indirect photolysis rate may be in principle as fast as direct photolysis but is most likely to be slower. The timescale for indirect photolysis and its oxidation rate will vary and depends on how long the surface hydroxyl radical groups take to migrate to meet the target molecule. The surface hydroxyl radical groups may also be desorbed into the solution, acting as free radicals for reacting with the pollutant. Hydroxyl radical reactions will dominate the photocatalytic systems with weak pollutant adsorption. Unlike systems with strong adsorption, blocking and poisoning of semiconductor surface in weakly adsorbed systems is unlikely.

6.3 Photoactivity of TiO_2 polymorphs

The two most commonly reported TiO_2 polymorphs for their photocatalytic activity are anatase and rutile, both tetragonal phases. The other phases, brookite and monoclinic TiO_2, are not widely studied for photocatalytic degradation. Rutile is considered to be the most stable phase of the two. While anatase can be synthesized easily at lower temperatures (<400°C), rutile generally starts predominantly appearing at higher temperatures (400–600°C). It is generally reported that anatase is more efficient in photocatalytic activities when compared to its counterpart, rutile. Rutile has been indicated to be rarely active in photocatalytic degradation of organic contaminants, although some studies demonstrate otherwise. There are a few disagreements on the effect of the polymorphic structure on the photoactivity. Various aromatics, phenols, organic acids, amines, dyes, surfactants, and alcohols have been studied for photocatalytic degradation, where anatase phase has been more efficient than their rutile counterparts. The differences in photocatalytic activities are attributed to variations in Fermi level, surface properties, and thermodynamic constrains for rutile. There have been multiple studies on anatase-rutile mixtures, the most common being Degussa P25, demonstrating a superior performance over individual phases. The contact of both phases leads to an improvement in efficiency of charge separation and formation of p-n junctions in the semiconductor. The aim of this research is to develop rutile-anatase interfaces and study their properties, their nanocrystalline structure, for more efficient photocatalytic degradation.

6.4 Advancements in TiO_2 photocatalysis for advanced oxidation technology

6.4.1 Surface modifications of TiO_2

6.4.1.1 Metal deposition

This is the most frequently studied modification for TiO_2 to affect the photochemical properties of its surface. Metal deposition involves the loading of metal nanoparticles at the TiO_2 surface by either photodeposition [20] or impregnation [21]. UV irradiation on metal-modified TiO_2 surfaces induces a Fermi level equilibration between the metal and TiO_2 through charge

This book belongs to Badji Mokhtar Annaba University Central Library Copyright Elsevier 2025

distribution, subsequently shifting the Fermi level leading to a more efficient electron transfer in the system. This promotes photocatalytic reactions on the TiO_2-metal interfacial surface. Metals that have been commonly studied and employed in TiO_2 photocatalysis are Au, Pt, Ag, Pd, Ru, and Rh.

The primary purpose of the addition of Pt nanoparticles to the TiO_2 surface is to act as a CB electron sink [22]. Pt has a lower Fermi level, which promotes interfacial charge separation at the metal-semiconductor interface [23]. Photocurrent, charge separation, and CB electron transfer are greatly enhanced by the presence of surface Pt on TiO_2, enhancing the potential of photocatalytic degradation of pollutants on the surface. The pathway for trichloroacetate degradation can be significantly altered by platinized TiO_2 surfaces. Unlike bare TiO_2, the reductive pathway generates dichloroacetate radical, which rapidly and completely degrades on reaction with dissolved oxygen forming no stable intermediates [24, 25]. While bare TiO_2 PCD always needs oxygen, platinized TiO_2 PCD can occur in anoxic conditions. However, studies have shown that the effect of addition of interfacial Pt may not be always positive for photocatalytic degradation [26]. Pt-enhanced photocatalytic degradation of Rhodamine-B and several phenolic compounds was not observed in several studies, leading to disagreeing effects of the platinization of the TiO_2 surface [27]. These inconsistent effects may be ascribed to various redox behaviors of substrate and Pt, charge transfer, oxidation states, defect states, and platinum morphology and size. Studies have shown that the oxidation state of Pt is detrimental to the initial degradation rate for chlorinated organic pollutants [28]. In comparison between Pt_{ox} and Pt_0 with TiO_2, Pt_{ox} has been studied and was shown to reduce the rate of degradation of TCE because of external charge recombination on the platinized surface, while Pt_0 reactivity has been similar to bare TiO_2, leading to inconsistent results for platinized TiO_2 [29].

Transition metals such as Pt and Pd have a stronger affinity toward ammonia than Au and Ag. Transition metals on the TiO_2 surface can be used to oxidize ammonium compounds selectively to dinitrogen. Pt interacts with the lone-pair electron on nitrogen atom, thereby catalyzing anoxic degradation of alkylamine pollutants. This mechanism only works on neutral alkylamines with electron lone-pair. Gold and silver nanoparticles have the property of localized surface plasmonic resonance (LSPR), which has been harnessed for photocatalysis. The oscillation of free electron charge in nanoparticles in the range of 20–100 nm upon incidence of visible light causes electron transfer from the photoexcited metal to the CB in TiO_2. This has been utilized for visible light photocatalysis [30].

6.4.1.2 Surface adsorbates

Inorganic adsorbates such as fluoride, carbonate, phosphate, and sulfate often change the photocatalytic activity of TiO_2 semiconductors. The influence of inorganic adsorbates is because of the modification of surface charge, surface functional groups, and surface acidity of the illuminated semiconductor. The most extensively studied surface adsorbate is fluoride, also called surface-fluorinated TiO_2 (F-TiO_2). The adsorption of fluoride on the surface of

This book belongs to Badji Mokhtar Annaba University Central Library Copyright Elsevier 2025

TiO_2 is a ligand exchange reaction between fluoride and surface hydroxyl radicals on TiO_2 (Titanol groups). Surface fluorination of metal oxides is restricted to acidic pH range (<5). While bulk crystal structures and optical properties are not influenced, photocatalytic activity is greatly influenced by surface fluorination of metal oxides. With surface fluorination, the hydrophilic nature of TiO_2 surface changes, photocatalytic oxidation rate increases, and photogeneration of hydroxyl radicals is enhanced. The enhanced photocatalytic activity is because of the generation of free hydroxyl radicals. Unlike in bare TiO_2, VB holes cannot react with surface hydroxyl groups and hence must react with free adsorbed water molecules to generate free hydroxyl radicals. Free hydroxyl radicals can travel to the bulk from the F-TiO_2 surface to mediate oxidation of contaminants remotely from the surface. The mechanism for PCD shifts from VB mediated oxidation to free hydroxyl-mediated oxidation [31, 32].

Studies have shown that F-TiO_2 has enhanced the photocatalytic degradation rate of phenol by three times [33], acetaldehyde and methylene blue slightly [34], acid red 1 by 2.5 times [35], and acid orange 7 [33], trimethylammonium [36], and acetaldehyde by 1.5–2.5 times [37]. Degradation of recalcitrant cyanuric acid was observed with F-TiO_2, which cannot be degraded by bare TiO_2 [38]. The generation of hydrogen peroxide was highly enhanced with F-TiO_2, and superoxo and peroxo species can be readily liberated [39, 40]. There also have been reports on the negative and neutral effects of surface fluorination. While phenol degradation enhanced in anatase suspension, it was retarded in rutile suspension [41]. In some cases, surface fluorination receded the photocatalytic degradation rate (DCA, TCA, benzene, xylene) [33], while in the case of toluene, there was no change in photocatalytic degradation [42]. The effects of surface-fluorinated TiO_2 are complex and not straightforward. While VB holes mediate the generation of free hydroxyl radicals, the high electronegativity of surface fluorine might trap CB electrons, further modifying interfacial charge transfer. The effects also depend upon the type of substrates and are difficult to be generalized.

6.4.1.3 Surface charge modification

Interactions of TiO_2 with charged compounds are pH-sensitive, and photocatalytic activity of TiO_2 in ionic substrates is affected by pH changes. The surface charge of TiO_2 can be modified to change the photocatalytic activity and reaction mechanisms. Silica, zeolites, alumina, and zircona are surface charge modifiers commonly used in research. Silica-coated TiO_2 modify the surface to carry negative charge in a wider pH range (>3) and have been studied frequently to enhance PCD rates for cationic substrates [36, 43]. Similarly, zeolites have also been studied to modify the surface to introduce negative charges owing to the substitution of Al^{+3} into the silica structure [44, 45]. Titania encapsulated in zeolite frameworks favors the degradation of cationic substrates because of the negative charges in the zeolite structure. Ionic polymers have also been used to modify surface charges. Nafion is a common resin used for surface charge

This book belongs to Badji Mokhtar Annaba University Central Library Copyright Elsevier 2025

modification. Cationic substrates can easily be ion-exchanged to the hybrid surface to change the reaction mechanism of PCD and enhancing the PCD rates [46–48].

6.4.1.4 Dye anchoring

Anchoring dyes on TiO_2 surface have been recently studied for degradation of pollutants under visible light-driven illumination and solar photochemical cells. The most commonly used dyes are ruthenium bipyridyl derivatives and complexes [49] or organic dyes and humic acids [50, 51]. The photoelectrochemical process is initiated when the preadsorbed dye molecules on TiO_2 surface are photoexcited by the HOMO-LUMO process. There is an electron transfer to the CB of TiO_2 from the excited dye, generating electrons used for photodegradation of adsorbed pollutants. The dye is oxidized and can be regenerated using appropriate electron donors. Alcohols, organic acids, and EDTA have been employed as sacrificial electron donors. In water treatment applications, water can be used as an electron donor to reduce and regenerate the oxidized ruthenium bipyridyl complexes.

Anchoring RuIIL3 complexes to metal-deposited TiO_2 showed enhancement of photoreductive degradation of contaminants such as CCl_4 and TCA [52]. Pt metal exhibited the highest enhancement in photocatalytic activity. Al_2O_3 thin layer could further improve the degradation by ca. 75% [53]. The presence of a barrier between the dye and the semiconductor retards the electron injection to the CB and the back recombination for adsorbate recovery. The former is much slower, making it the rate-limiting step. Modification of surface properties chances not only the photocatalytic properties but also the overall kinetics of the process. The selection of functional groups anchored on to TiO_2 is critically important for photocatalytic systems. A study showed that anchoring phosphonate (P) groups instead of the widely studied carboxylate groups on TiO_2 enhanced not only the adsorption of the dye on the surface of TiO_2 but also the photoreductive degradation for CCl_4 and TCA [54, 55].

6.4.2 Photocatalyst modification and doping

The purpose of doping semiconductors is to create defect states in the bandgap to enhance the interfacial charge transfer. These defect states trap the VB holes and CB electrons, thereby inhibiting and retarding the recombination of holes and electrons. The type of dopant used is critical in determining the overall activity of the photocatalysts. Dopants can be metallic or nonmetallic.

Enhanced degradation of carbon tetrachloride has been studied with doped-TiO_2 photocatalysis using Fe(III), Mo(V), Ru(III), Rh(III), Re(V), Os(III), and V(IV) as dopants under UV irradiation; While the same studies reported that doping with cobalt and aluminum retarded the photocatalytic activity. Degradation of 4-chlorophenol has been studied with photocatalysts doped with Ru, Rh, Pt, Co, Ir, Au, Pd, and Ni under visible light irradiation. Platinum ion-doped TiO_2 has been studied for degradation of methylene blue and phenol and oxidation of iodide.

This book belongs to Badji Mokhtar Annaba University Central Library Copyright Elsevier 2025

Noble metals have been studied extensively as surface modifications for TiO_2 when compared to dopants dispersed in the semiconductor lattice.

Studies have also shown doping TiO_2 with nonmetallic elements such as carbon, sulfur, boron and nitrogen could yield visible light photocatalytic activity. The results for the photocatalytic degradation of organics using nitrogen-doped TiO_2 have been controversial and have had contradicting effects [56]. Similarly, carbon-doped TiO_2 has also shown contradicting results. The state of carbon impurity has been interpreted differently in various studies depending on the type of preparation such as carbon mounting [57], sol-gel [58], carbon coating [57], and electron beam evaporation [59], yielding different states of carbon dopants: anions [60] and cations [61] leading to contradicting degradation performances.

6.4.3 Photocatalytic membranes

Photocatalytic membrane processes have become one of the most efficient technologies for water treatment because of low footprint, efficient performance, and ease of maintenance. Photocatalytic membrane processes or photocatalytic membrane reactors were developed by integrating the processes of photocatalytic oxidation and membrane separation. Photocatalytic membranes can be beneficial because they possess the property of physical separation during membrane filtration and catalytic oxidation owing to TiO_2 photocatalysis in a single reactor. Leong et al. classified photocatalytic membrane reactors into four major types: slurry photocatalytic reactor sequentially followed by membrane filtration, membrane itself submerged in a slurry photocatalytic reactor as a single unit, membrane placed inside a reactor with walls with a fixed photocatalyst coating, and photocatalytic membranes such as pure TiO_2 porous or composite membrane [62]. Photocatalytic membranes have gained much attention over the past years and generally outperform conventional membranes because of lower membrane fouling potential. In conventional membranes, cake formation leads to pore blocking and higher cost of operation, while in photocatalytic membranes, organics are degraded by oxygen reactive radicals under UV irradiation, reducing the cake formation and reducing the pollutant concentration in the concentrate.

TiO_2 membrane supports can be a variety of materials, including polymers, ceramic, or metallic. Polymer and ceramic membranes are most commonly and widely used for photocatalytic membranes [63, 64]. Pure TiO_2 membranes include fabrication using TiO_2 nanofibers and nanowires [63, 65].

6.4.3.1 TiO_2 polymer membranes

Polymer membranes are the most commonly used membrane for environmental applications. Polymers that are used as supports include polyamide, polyvinylidene fluoride (PVDF), polyester, PVDF/sulfonated polyether sulfone, polyethersulfone, polyacrylonitrile, and polyethylene terephthalate (PET). They can be further classified based on the method of

This book belongs to Badji Mokhtar Annaba University Central Library Copyright Elsevier 2025

fabrication (1) TiO_2 nanoparticle-coated polymers or (2) TiO_2 nanoparticles blended in the membrane solution before casting.

Coated polymer membranes are formed by the hydrogen bonding between Ti^{+4} atom and the two oxygen in the carboxylic group in the polymer. Examples of polymer support are polyamide thin film supported on polysulfone, polyethersulfone/polyimide blend, and polyethersulfone. Many studies have shown that this bond is not strong enough and leads to deterioration of performance over a long period of time [66]. The second method is to disperse the nanoparticles into the membrane matrix. Several studies have reported casting solutions consisting of polyethersulfone and dimethylacetamide (DMAC) or PVDF-sulfonated polyethersulfone (SPES). Blended membranes have been shown to have a more porous structure when compared to deposited membranes. In the comparison between blended and deposited membranes, blended membranes showed less photosensitivity because of shielding of UV waves from penetration, and pore blockage was less in cast/deposited membranes.

6.4.3.2 TiO_2 ceramic membranes

Al_2O_3 has been extensively studied as support for TiO_2 particles. Ceramic membranes support the immobilization of TiO_2, and they are more mechanically and thermally stable when compared to polymer membranes. Sol dip-coating has been widely used as a fabrication method for ceramic membranes to form a continuous and uniform coating for TiO_2 on the ceramic material. The addition of hydroxyapatite to control membrane biofouling and the addition of Fe_0 to the sol dip method to introduce Fenton reactions has also been studied. Atmospheric plasma spraying (APS) is a simple, low cost, and quick process for immobilizing TiO_2 on ceramic substrates. Chemical vapor deposition is used to fabricate silica-based membranes. In this method, the pore size and thickness can be easily controlled.

6.4.3.3 Pure TiO_2 membranes

There have been recent improvements in the fabrication of pure TiO_2 membranes. These include TiO_2 nanowires, nanofibers, and nanotubes in the form of 1D free-standing membranes. There are challenges in scaling up these membranes for water treatment applications.

6.4.4 Application of membranes

The performance of TiO_2 membrane processes is evaluated by its pollutant degradation efficiency and the membrane flux. A balance between pollutant degradation (photocatalytic activity) and membrane flux needs to be considered to achieve the required overall performance of the membranes. Applications of membrane photocatalytic reactors for water treatment have been significantly studied. Removal of recalcitrant and persistent organic chemicals such as methylene blue [67, 68], direct black [69], methyl orange [67, 70], rhodamine B [63, 65], humic acids [71, 72], indigo carmine [73], creatinine [74], 2,4-dichlorophenol [75], trimethoprim,

This book belongs to Badji Mokhtar Annaba University Central Library Copyright Elsevier 2025

4-chlorophenol [76], and total organic matter [68] has been studied with membrane photocatalytic reactors. Photocatalytic membranes have also been studied for disinfection applications. Most studies for disinfection and bacterial degradation have been done using *E. coli*. Reactive species such as O_2^-, H_2O_2, and OH• radical formed during the photocatalytic reactions are responsible for the antibacterial effect. Rejection of natural organic matter in water was shown to increase by 5% with membrane photocatalytic reactors leading to a potential decrease in membrane fouling. Nanostructures, nanotubes, and nanowires in membranes have shown promising results and deserve further investigation in laboratory and pilot-scale systems for water treatment applications (Fig. 6.2).

6.5 Photochemical reactors

Multiple factors affect the design of a photocatalytic reactor, and all such aspects should be taken into consideration, such as selection of radiation sources, output power, dimensions, use of mirrors and reflectors, use of coolant and cooling jackets, cleaning procedures, semiconductor concentrations, active surface area, particle aggregate sizes, film thicknesses, light intensity, pH, and competition with other adsorbates.

Photochemical reactors can be widely classified into two types based on the use of catalyst: immobilized catalyst photoreactors and suspension photoreactors. Immobilized catalyst reactors are also called fixed-bed or thin-film catalyst photoreactors, where the catalyst is fixed and immobilized as a thin film to a support surface, and water or air to be treated flows through the reactor on the illuminated thin film. Suspension bed consists of catalyst particles dispersed in the solution to be treated. The amount of contact between the catalyst and untreated water is crucial for the degradation of pollutants. The contact surface area of suspension bed reactors is higher because of smaller and distributed particle size when compared to a thin film reactor. Each of the suspended type or fixed-bed type has its own advantages and disadvantages. Advantages of suspended reactors include uniform catalyst distribution, high surface area, low catalyst fouling, and low-pressure drop, while those of immobilized reactors include the possibility of continuous operation and no need for a separate downstream separation unit. Disadvantages in suspended photoreactors include the requirement of a downstream separation unit, increasing system costs and reducing the feasibility for a scale-up, and difficulty in light scattering owing to suspension. In fixed-bed reactors, plates or walls coated with catalyst require a laminar flow of solution causing a mass transfer limitation, possibility of catalyst deactivation and washout, and restricted volume processing capabilities. Each of these reactor types (Fig. 6.3), immobilized or suspension, can be installed as an immersion well or a flat well reactor. For immobilized systems, the reactant can be liquid, gas, or vapor. Various reactor types have been studied for each reactant type and reactor type mentioned earlier: thin-film reactors include membrane reactor, corrugated plate reactor, rotating disc, Carberry photoreactor, optical fiber reactor for liquid reactants, annular wall and circulated system

This book belongs to Badji Mokhtar Annaba University Central Library Copyright Elsevier 2025

This book belongs to Badji Mokhtar Annaba University Central Library

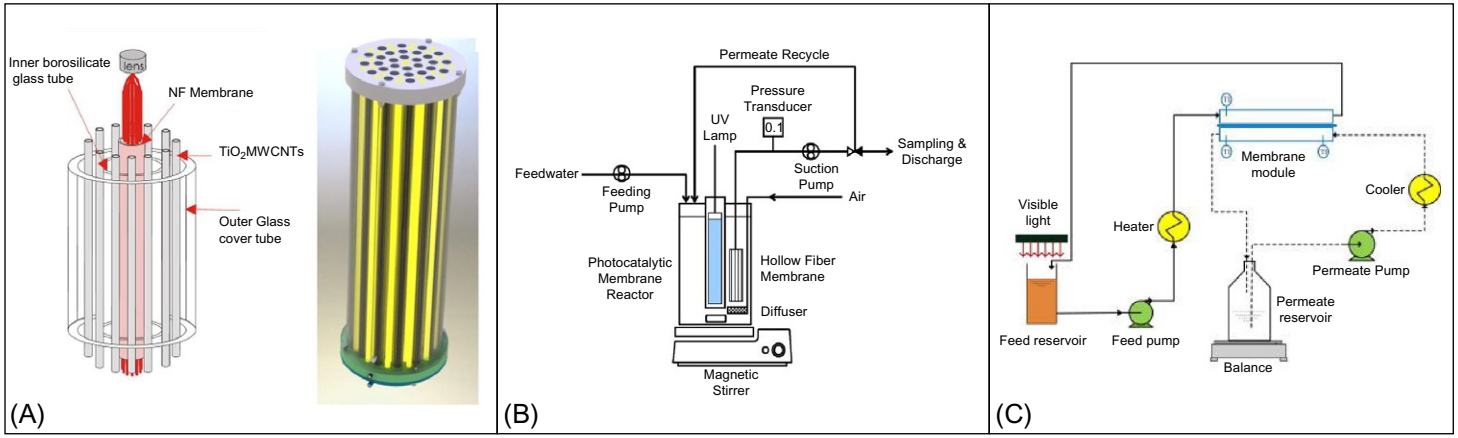

Fig. 6.2

Schematic of photocatalytic membrane reactors. (A) TiO_2 multiwalled carbon nanotube structure with nanofiltration membrane, (B) hybrid membrane-UV reactor for slurry type TiO_2 dispersion, and (C) sequential photoreactor and membrane separation process. *Reprinted with permission from K.-H. Choo, R. Tao, M.-J. Kim, Use of a photocatalytic membrane reactor for the removal of natural organic matter in water: effect of photoinduced desorption and ferrihydrite adsorption, J. Membr. Sci. 322 (2008) 368–374, https://doi.org/10.1016/j.memsci.2008.05.069; Y. Huo, Z. Xie, X. Wang, H. Li, M. Hoang, R.A. Caruso, Methyl orange removal by combined visible-light photocatalysis and membrane distillation, Dyes Pigments 98 (2013) 106–112, https://doi.org/10.1016/j.dyepig.2013.02.009; G.E. Romanos, C.P. Athanasekou, F.K. Katsaros, N.K. Kanellopoulos, D.D. Dionysiou, V. Likodimos, P. Falaras, Double-side active TiO_2-modified nanofiltration membranes in continuous flow photocatalytic reactors for effective water purification, J. Hazard. Mater. 211–212 (2012) 304–316, https://doi.org/10.1016/j.jhazmat.2011.09.081.*

Copyright Elsevier 2025

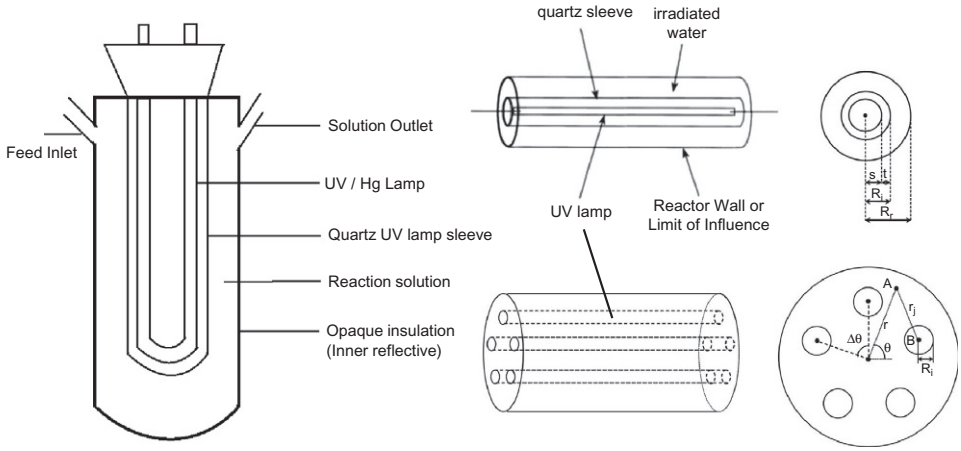

Fig. 6.3
Schematic representation of the most commonly used photoreactors: Immersion well laboratory-scale reactor *(left)*, annular continuous flow reactor *(top right)*, and multilamp photoreactor *(bottom right)*. *Part of the figure reprinted with permission from T. Coenen, W. Van de Moortel, F. Logist, J. Luyten, J.F.M. Van Impe, J. Degrève, Modeling and geometry optimization of photochemical reactors: single- and multi-lamp reactors for UV–H_2O_2 AOP systems, Chem. Eng. Sci. 96 (2013) 174–189, https://doi.org/10.1016/j.ces.2013.03.056.*

reactor for gaseous reactants, and carbon foam-based reactor for vapor reactants. The reactant is usually liquid in suspended photoreactors. The examples of suspended solution reactors are photocatalytic ultrafiltration reactor, rotating drum, Taylor vortex, falling film slurry, internally circulating slurry bubble column, and fluidized bed photoreactor.

6.5.1 Immersion well

Immersion well photoreactors are the most used photocatalytic reactor for laboratory-scale use, research, and evaluation purposes. Immersion well reactors can be batch or continuous. It consists of a vessel with multiple necks with a UV lamp immersed in it. Because it is a laboratory-scale reactor, the oxidant reactant flow and temperature can be easily monitored. The catalyst in immersion well photoreactor can be immobilized thin film on the reactor wall or in suspension form with a stirrer.

6.5.2 Thin film

Thin-film reactors are best suited for small volumes of water to be treated because of mass transfer limitation and the required laminar flow.

This book belongs to Badji Mokhtar Annaba University Central Library Copyright Elsevier 2025

6.5.3 Annular

Annular photoreactor (APR) was designed to provide for continuous operation in a photocatalytic reactor. Most photocatalytic reactors that were developed prior to annular PRs were unintentionally batch mode for optimized design. APR allows continuous mode of operation with a microfiltration membrane separation unit downstream for catalyst recovery and reuse. APR can be operated with or without recirculation. Catalyst in this reactor is in suspended form. APR is generally made of concentric pyrex glass tubes with UV/light source in the innermost section of the reactor, protected with a glass proctor, followed by the reaction section and then the cooling jacket. The outer part is covered with an opaque material.

6.5.4 Multilamp

One of the very first studies on the use of multiple lamps for photocatalytic degradation was done by Shon et al. [77]. The higher efficiency of degradation was because of an increased illuminated surface area of the catalyst. Further studies on monolithic and flat plate reactors showed that there exists an optimum number of lamps, their separation distance and location depending on the type of reactant and the reactor.

6.6 Combination/coupling with other (hybrid) treatment technologies

Coupling TiO_2 photocatalysis with other treatment methods has been studied in the past to increase the efficiency of pollutant degradation. Such methods include electrocatalysis, electrocoagulation, sonocatalysis, Fenton systems, and biological systems.

Application of electrocoagulation with iron anode and cathode, prior photocatalysis has been shown to increase the pollutant removal in terms of chemical oxygen demand (COD) of the treated water. Electrocoagulation removes the majority of colloidal and suspended organic substances, and sequencing it with photocatalytic oxidation assists in the removal of refractory chemical compounds by complete mineralization [78]. Electrocoagulation prior to PCD also assists in color and dye removal and decrease in turbidity of wastewater [79]. An improvement in optical characteristics of wastewater thereby increases the efficiency of following photocatalytic degradation. This hybrid process has been studied usually for wastewaters from paper and cellulose industries [80].

Sonochemistry or ultrasonic cavitation has not only been studied for hybrid photocatalytic treatment but also has been widely studied for synthesis of TiO_2 particles. In terms of application for water treatment, sonochemical irradiation can be applied simultaneously with UV/light irradiation on the semiconductor to increase the production of reactive radicals on the semiconductor surface by adding an extra source. While sometimes compete mineralization

This book belongs to Badji Mokhtar Annaba University Central Library Copyright Elsevier 2025

cannot be achieved in only sonochemical processes [81], simultaneous sono-photochemical degradation can achieve complete mineralization leading to a zero-waste process [82]. Hydrophobic compounds can be degraded by sonochemical irradiation, while hydrophilic materials adsorb onto the semiconductor surface, consequently leading to their photocatalytic degradation. Similarly, the benefits of the combined process include additional activation of the catalyst surface owing to cavitational fragmentation, enhancement of mass transport from the bulk to the surface, and a decrease in blocking of catalyst sites. The synergistic effect of sonochemistry and photochemistry in this process is dependent on the catalyst loading, where higher loading of catalyst can create a detrimental effect on the cavitation process. Degradation of multiple chemical compounds such as organic aromatics, carboxylic acids, hydrocarbons and alcohols [83], organic dyes [84–86], herbicides and pesticides [87,88], and chemical warfare agents [89] have been studied using sono-photocatalytic hybrid process.

Photo-Fenton and sonophoto-Fenton processes have also been studied to operate synergistically [90]. Substantial work has been reported for synergistic and additive effects using the combined process for phenol and phenolic compounds [91,92], organic dyes [93,94], and textile effluents [95]. The factors that govern the combined process are light intensity, Fe concentration, and pH.

The use of a combination of photocatalysis and ozonation is an attractive alternative to other combined processes because of the high efficiency of the formation of strongly oxidizing hydroxyl radicals. The treatment of various groups of compounds using this method has been widely reported, including organic acids, alcohols, nitrogen-containing compounds, textile effluents, and dyes [96,97]. Ozone doze, pH, and catalyst choice are important factors in the degradation efficiency.

Hydrodynamic cavitation, in combination with TiO_2 photocatalysis, provides an opportunity for a low-cost scale-up of the process. Generation of hydroxyl radicals during hydrodynamic cavitation is a well-studied phenomenon and is regarded as an economically attractive alternative to AOPs. Addition of TiO_2 photocatalysis synergistically supplements the formation of hydroxyl radicals for oxidizing the target pollutants [98,99]. Common pollutants investigated for photocatalytic and assisted-hybrid degradation processes are listed in Table 6.1.

6.7 Challenges and issues for TiO_2 photo-catalysis for water treatment

One of the challenges in the application of photocatalysis in water treatment systems is whether the process could be a stand-alone or a pretreatment process. While in some cases, photocatalytic degradation can be used as a pretreatment to reduce the residence time in the following bioreactor or reduce the cost of ozonation and advanced oxidation processes, some reports have demonstrated >90% degradation of certain compounds, advocating it for a stand-alone process.

This book belongs to Badji Mokhtar Annaba University Central Library Copyright Elsevier 2025

Table 6.1: List of common pollutants investigated (not exhaustive) for photocatalytic and assisted-hybrid degradation processes.

Process	Chemicals investigated
Photocatalysis	Aliphatic organic: bromomethane, butyric acid, chloroethane, chloroethene, chloroethylene, chloromethane, cyclohexane, cyclohexene, ethanoic acid, ethanol, formic acid, glucose, heptane, isobutene, malic acid, methanol, oxalic acid, paraffins, pentane, propanoic acid, and propanol. Aromatics and phenolics: Chlorobenzene, chloronitrobenzene, phenol, chlorophenol, fluorophenol, biphenyls, polychlorinated biphenyls, hydroquinone, catechol, methylcatechol, cresol, nitrophenol acid, yellow 23, direct yellow 12, benzoic acid, aminobenzoic acid, phthalic acid, salicylic acid, hydroxybenzoic acid, and chlorobenzoic acid. Dyes: Azo dyes, methylene blue, rhodamine B, textile dye effluent, acid red 14, indigo, indigo carmine, alirazin S, Congo red, methyl orange, methyl red, crocein orange, gentian violet, CI acid yellow 23, and direct yellow 12. Surfactants: Sodium dodecyl sulfate, polyethylene glycol, sodium dodecyl benzene sulfonate, trimethyl phosphate. Herbicides and pesticides: Atrazine, Acaricide, prometron, pyridaben, propetryne, bentazon, chlopyrifoes, cypermethrin, chlorothanil, monuron, organocholorine pesticides, DDT, aldrin, parathion, lindane, organophorsphorus, pyrimiphos methyl, paraquot, diuron, and triazole.
Electrocoagulation-photocatalysis	Acid Orange II, Aniline, antiinflammatory drugs, chlorophenols, pharmaceuticals, phenobarbital, phenolic compounds, picloram, rhodamine B, and several dyes.
Sonophotocatalysis	1,4-Dichlorobenzene (1,4-DCB), 4-chloro-2-nitro phenol (4C2NP), acid red 88, acid yellow 23 dye, alachlor, aldehydes, basic violet 1, and basic green 4.
Photo-Fenton	Aniline, azo-dyes, bisphenol, bleaching effluent, catechol, chlorophenols, CI reactive dye, explosives, imidacloprid, landfill leachate, nitrophenols, pesticides, pharmaceuticals, phenol, phenolic compounds, sulfamethaxazole, textile effluents, etc.
Cavitation-assisted photocatalysis	Diclofenac, tetracycline, CI reactive Red 2, brilliant red, abamectin, crystal violet, Rhodamine B, etc.

Some part reprinted with permission from H. Choi, S.R. Al-Abed, D.D. Dionysiou, E. Stathatos, P. Lianos, TiO_2-based advanced oxidation nanotechnologies for water purification and reuse, in: I.C. Escobar, A.I. Schäfer (Eds.), Sustainability Science and Engineering, Elsevier, 2010, pp. 229–254, https://doi.org/10.1016/S1871-2711(09)00208-6 (Chapter 8).

At the same time, a stand-alone photodegradation process will require a low flow rate, significantly deteriorating the kinetics of degradation and increasing the time of treatment.

Adsorption of solar spectra is a key challenge in current photocatalytic treatment. UV light may not be always available or feasible for the scale-up of the process. Catalyst development should focus on utilizing the solar spectrum to a greater extent. Immobilization of catalyst remains yet another challenge for photocatalysis. Immobilizing a catalyst onto the surface will provide more efficient solid-liquid separation.

This book belongs to Badji Mokhtar Annaba University Central Library Copyright Elsevier 2025

Effective designs for combined and hybrid photocatalytic systems must lead to studies on pilot-plant level, because combined processes can yield synergistic and additive effects on degradation. Setup of pilot plants, simulating and modeling pilot plants, performing a life cycle assessment (LCA) and techno-economic analysis (TEA) on such pilot plants remain as another challenge in photocatalytic systems.

There will be a lot of challenges when it comes to industrial-scale wastewater treatment using photocatalysis. The gap in scientific literature will make it challenging to design a pilot plant. Important factors such as reactions kinetics and mass transfer limitations will lead to nonideality in design. Furthermore, modeling complexities will add to the challenges. The most important factor in industrialization of PCD processes is cost optimization and reduction in energy consumption. There have been several wastewater treatment pilot plants that use PCD for textile and dye water treatment. Most studies conclude that with large capacities, the possibility of using UV light is infeasible. Similarly, contact and mass transfer idealities diminish as the reactor size increases. Multiple passes and recycling in pilot reactors have to be studied for an increase in efficiency.

6.8 Conclusion and future prospectus

Semiconductor photocatalysis has become more prominent because of its ability to use UV or solar light to bring about complete mineralization of a vast range of organic pollutants in water. One of the most important aspects of using TiO_2-based photocatalytic treatment is the complete mineralization of pollutants and generation of zero waste. Other advantages include low cost of semiconductor, no requirements of additional chemicals, applicability in a variety of concentration ranges, disinfection of water, antifouling properties, sustainable use of energy, decreased overall costs, removal of toxic anions, metals, and nonbiodegradable materials, and nonselective radical attack on all organics present.

The application of visible light-induced photocatalysis is limited because of the physiochemical properties of the materials. Modifications such as dye sensitization have been used to reduce the bandgap for improving the activity of the photocatalyst activation under visible light. A more careful understanding and design of such modifications and their effect on the physiochemical properties are required for applying visible-light photocatalysis for water and wastewater treatment.

Immobilized photocatalytic systems need to be better designed to deal with problems associated with running out of catalyst during the process, leakage, and deactivation of the photocatalyst. Immobilizing the photocatalyst can also reduce the size of the reactor.

Implementation of PCD processes on an industrial level requires proper design and construction of photoreactors to harvest energy. Solar light must be integrated into the process by widening the light absorption spectrum of the photocatalyst.

This book belongs to Badji Mokhtar Annaba University Central Library Copyright Elsevier 2025

Photocatalytic membrane offers promising applications in pollutant degradation and an opportunity for a scale-up of the process. Nanostructured, nanofiber membranes need more investigation and pilot plant studies. Economic analyses on membrane reactors and hybrid systems such as hydrodynamic cavitation need to be done to justify the applicability of such reactors on a wide-scale application.

References

[1] N.S. Lewis, Toward cost-effective solar energy use, Science 315 (2007) 798–801, https://doi.org/10.1126/science.1137014.

[2] A. Nottrott, J. Kleissl, B. Washom, Energy dispatch schedule optimization and cost benefit analysis for grid-connected, photovoltaic-battery storage systems, Renew. Energy 55 (2013) 230–240, https://doi.org/10.1016/j.renene.2012.12.036.

[3] S. Bouadila, S. Kooli, M. Lazaar, S. Skouri, A. Farhat, Performance of a new solar air heater with packed-bed latent storage energy for nocturnal use, Appl. Energy 110 (2013) 267–275, https://doi.org/10.1016/j.apenergy.2013.04.062.

[4] Y. Shavisi, S. Sharifnia, S.N. Hosseini, M.A. Khadivi, Application of TiO_2/perlite photocatalysis for degradation of ammonia in wastewater, J. Ind. Eng. Chem. 20 (2014) 278–283, https://doi.org/10.1016/j.jiec.2013.03.037.

[5] M. Formenti, F. Juillet, P. Meriaudeau, S.J. Teichner, P. Vergnon, Preparation in a hydrogen-oxygen flame of ultrafine metal oxide particles. Oxidative properties toward hydrocarbons in the presence of ultraviolet radiation, J. Colloid Interface Sci. 39 (1972) 79–89, https://doi.org/10.1016/0021-9797(72)90144-0.

[6] A. Fujishima, K. Honda, Electrochemical photolysis of water at a semiconductor electrode, Nature 238 (1972) 37–38, https://doi.org/10.1038/238037a0.

[7] S. Kim, M. Kang, Hydrogen production from methanol steam reforming over Cu–Ti–P oxide catalysts, J. Ind. Eng. Chem. 18 (2012) 969–978, https://doi.org/10.1016/j.jiec.2011.10.009.

[8] Y. Moriya, T. Takata, K. Domen, Recent progress in the development of (oxy)nitride photocatalysts for water splitting under visible-light irradiation, Coord. Chem. Rev. 257 (2013) 1957–1969, https://doi.org/10.1016/j.ccr.2013.01.021.

[9] J. Mo, Y. Zhang, Q. Xu, J.J. Lamson, R. Zhao, Photocatalytic purification of volatile organic compounds in indoor air: a literature review, Atmos. Environ. 43 (2009) 2229–2246, https://doi.org/10.1016/j.atmosenv.2009.01.034.

[10] M.R. Hoffmann, S.T. Martin, W. Choi, D.W. Bahnemann, Environmental applications of semiconductor photocatalysis, Chem. Rev. 95 (1995) 69–96, https://doi.org/10.1021/cr00033a004.

[11] B. Liu, K. Nakata, M. Sakai, H. Saito, T. Ochiai, T. Murakami, K. Takagi, A. Fujishima, Hierarchical TiO_2 spherical nanostructures with tunable pore size, pore volume, and specific surface area: facile preparation and high-photocatalytic performance, Catal. Sci. Technol. 2 (2012) 1933–1939, https://doi.org/10.1039/C2CY00509C.

[12] R. Wang, K. Hashimoto, A. Fujishima, M. Chikuni, E. Kojima, A. Kitamura, M. Shimohigoshi, T. Watanabe, Light-induced amphiphilic surfaces, Nature 388 (1997) 431–432, https://doi.org/10.1038/41233.

[13] K. Katsumata, C.E.J. Cordonier, T. Shichi, A. Fujishima, Photocatalytic activity of $NaNbO_3$ thin films, J. Am. Chem. Soc. 131 (2009) 3856–3857, https://doi.org/10.1021/ja900394x.

[14] J.-Y. Choi, K.-H. Kim, K.-C. Choy, K.-T. Oh, K.-N. Kim, Photocatalytic antibacterial effect of TiO_2 film formed on Ti and TiAg exposed to *Lactobacillus acidophilus*, J. Biomed. Mater. Res. B: Appl. Biomater. 80B (2007) 353–359, https://doi.org/10.1002/jbm.b.30604.

[15] H.R. Pant, H.J. Kim, M.K. Joshi, B. Pant, C.H. Park, J.I. Kim, K.S. Hui, C.S. Kim, One-step fabrication of multifunctional composite polyurethane spider-web-like nanofibrous membrane for water purification, J. Hazard. Mater. 264 (2014) 25–33, https://doi.org/10.1016/j.jhazmat.2013.10.066.

This book belongs to Badji Mokhtar Annaba University Central Library Copyright Elsevier 2025

[16] S.-Y. Lee, S.-J. Park, TiO_2 photocatalyst for water treatment applications, J. Ind. Eng. Chem. 19 (2013) 1761–1769, https://doi.org/10.1016/j.jiec.2013.07.012.
[17] A. Fujishima, X. Zhang, D. Tryk, TiO_2 photocatalysis and related surface phenomena, Surf. Sci. Rep. 63 (2008) 515–582, https://doi.org/10.1016/j.surfrep.2008.10.001.
[18] T. Yoshihara, R. Katoh, A. Furube, Y. Tamaki, M. Murai, K. Hara, S. Murata, H. Arakawa, M. Tachiya, Identification of reactive species in photoexcited nanocrystalline TiO_2 films by wide-wavelength-range (400 – 2500 nm) transient absorption spectroscopy, J. Phys. Chem. B 108 (2004) 3817–3823, https://doi.org/10.1021/jp031305d.
[19] H. Choi, S.R. Al-Abed, D.D. Dionysiou, E. Stathatos, P. Lianos, TiO_2-based advanced oxidation nanotechnologies for water purification and reuse, in: I.C. Escobar, A.I. Schäfer (Eds.), Sustainability Science and Engineering, Elsevier, 2010, pp. 229–254. (Chapter 8) https://doi.org/10.1016/S1871-2711(09)00208-6.
[20] A. Li, Z. Cui, W. Li, Preparation and photocatalytic activity for rhodamine B of Ag-TiO_2/SnO_2 thin films, Xiyou Jinshu Cailiao Yu Gongcheng/Rare Metal Mater. Eng. 38 (2009) 303–307.
[21] J.S. Jang, S.H. Choi, H.G. Kim, J.S. Lee, Location and state of Pt in platinized CdS/TiO_2 photocatalysts for hydrogen production from water under visible light, J. Phys. Chem. C 112 (2008) 17200–17205, https://doi.org/10.1021/jp804699c.
[22] M. Jakob, H. Levanon, P.V. Kamat, Charge distribution between UV-irradiated TiO_2 and gold nanoparticles: determination of shift in the Fermi level, Nano Lett. 3 (2003) 353–358, https://doi.org/10.1021/nl0340071.
[23] V. Subramanian, E. Wolf, P.V. Kamat, Semiconductor-metal composite nanostructures. To what extent do metal nanoparticles improve the photocatalytic activity of TiO_2 films?, J. Phys. Chem. B 105 (2001) 11439–11446, https://doi.org/10.1021/jp011118k.
[24] W. Choi, Nano Pt particles on TiOi and their effects on photocatalytic reactivity, J. Ind. Eng. Chem. 9 (2003) 96–101.
[25] S. Kim, W. Choi, Dual photocatalytic pathways of trichloroacetate degradation on TiO_2: effects of nanosized platinum deposits on kinetics and mechanism, J. Phys. Chem. B 106 (2002) 13311–13317, https://doi.org/10.1021/jp0262261.
[26] H. Einaga, M. Harada, S. Futamura, T. Ibusuki, Generation of active sites for CO photooxidation on TiO_2 by platinum deposition, J. Phys. Chem. B 107 (2003) 9290–9297.
[27] W. Zhao, C. Chen, X. Li, J. Zhao, H. Hidaka, N. Serpone, Photodegradation of sulforhodamine-B dye in platinized titania dispersions under visible light irradiation: influence of platinum as a functional co-catalyst, J. Phys. Chem. B 106 (2002) 5022–5028, https://doi.org/10.1021/jp020205p.
[28] J. Lee, W. Choi, Photocatalytic reactivity of surface platinized TiO_2: substrate specificity and the effect of Pt oxidation state, J. Phys. Chem. B 109 (2005) 7399–7406, https://doi.org/10.1021/jp044425+.
[29] J. Chen, D.F. Ollis, W.H. Rulkens, H. Bruning, Photocatalyzed oxidation of alcohols and organochlorides in the presence of native TiO_2 and metallized TiO2 suspensions. Part (I): photocatalytic activity and pH influence, Water Res. 33 (1999) 661–668, https://doi.org/10.1016/S0043-1354(98)00261-9.
[30] W. Hou, Z. Liu, P. Pavaskar, W.H. Hung, S.B. Cronin, Plasmonic enhancement of photocatalytic decomposition of methyl orange under visible light, J. Catal. 277 (2011) 149–153, https://doi.org/10.1016/j.jcat.2010.11.001.
[31] J.S. Park, W. Choi, Remote photocatalytic oxidation mediated by active oxygen species penetrating and diffusing through polymer membrane over surface fluorinated TiO_2, Chem. Lett. 34 (2005) 1630–1631, https://doi.org/10.1246/cl.2005.1630.
[32] J.S. Park, W. Choi, Enhanced remote photocatalytic oxidation on surface-fluorinated TiO_2, Langmuir 20 (2004) 11523–11527, https://doi.org/10.1021/la048051n.
[33] H. Park, W. Choi, Effects of TiO_2 surface fluorination on photocatalytic reactions and photoelectrochemical behaviors, J. Phys. Chem. B 108 (2004) 4086–4093.
[34] J. Tang, H. Quan, J. Ye, Photocatalytic properties and photoinduced hydrophilicity of surface-fluorinated TiO_2, Chem. Mater. 19 (2007) 116–122, https://doi.org/10.1021/cm061855z.
[35] M. Mrowetz, E. Selli, Enhanced photocatalytic formation of hydroxyl radicals on fluorinated TiO_2, Phys. Chem. Chem. Phys. 7 (2005) 1100–1102, https://doi.org/10.1039/b500194c.
[36] M.S. Vohra, K. Tanaka, Photocatalytic degradation of aqueous pollutants using silica-modified TiO_2, Water Res. 37 (2003) 3992–3996, https://doi.org/10.1016/S0043-1354(03)00333-6.

This book belongs to Badji Mokhtar Annaba University Central Library Copyright Elsevier 2025

[37] W.-S. Kim, D.-H. Kim, A study on the polishing machining of diamond for jewelry, J. Trans. Korean Soc. Mach. Tool Eng. 15 (2006) 127–132.
[38] A. Jańczyk, E. Krakowska, G. Stochel, W. Macyk, Singlet oxygen photogeneration at surface modified titanium dioxide, J. Am. Chem. Soc. 128 (2006) 15574–15575, https://doi.org/10.1021/ja065970m.
[39] V. Maurino, C. Minero, G. Mariella, E. Pelizzetti, Sustained production of H_2O_2 on irradiated TiO_2-fluoride systems, Chem. Commun. (2005) 2627–2629, https://doi.org/10.1039/b418789j.
[40] M. Mrowetz, E. Selli, H_2O_2 evolution during the photocatalytic degradation of organic molecules on fluorinated TiO_2, New J. Chem. 30 (2006) 108–114, https://doi.org/10.1039/b511320b.
[41] Y. Xu, K. Lv, Z. Xiong, W. Leng, W. Du, D. Liu, X. Xue, Rate enhancement and rate inhibition of phenol degradation over irradiated anatase and rutile TiO_2 on the addition of NaF: new insight into the mechanism, J. Phys. Chem. C 111 (2007) 19024–19032, https://doi.org/10.1021/jp076364w.
[42] M. Lewandowski, D.F. Ollis, Halide acid pretreatments of photocatalysts for oxidation of aromatic air contaminants: rate enhancement, rate inhibition, and a thermodynamic rationale, J. Catal. 217 (2003) 38–46, https://doi.org/10.1016/S0021-9517(03)00030-7.
[43] M.S. Vohra, J. Lee, W. Choi, Enhanced photocatalytic degradation of tetramethylammonium on silica-loaded titania, J. Appl. Electrochem. 35 (2005) 757–763, https://doi.org/10.1007/s10800-005-1365-9.
[44] S. Artkla, W. Kim, W. Choi, J. Wittayakun, Highly enhanced photocatalytic degradation of tetramethylammonium on the hybrid catalyst of titania and MCM-41 obtained from rice husk silica, Appl. Catal. B: Environ. 91 (2009) 157–164, https://doi.org/10.1016/j.apcatb.2009.05.019.
[45] G. Zhang, W. Choi, S.H. Kim, S.B. Hong, Selective photocatalytic degradation of aquatic pollutants by titania encapsulated into FAU-type zeolites, J. Hazard. Mater. 188 (2011) 198–205, https://doi.org/10.1016/j.jhazmat.2011.01.105.
[46] A. Kumar, N. Mathur, Photocatalytic degradation of aniline at the interface of TiO_2 suspensions containing carbonate ions, J. Colloid Interface Sci. 300 (2006) 244–252, https://doi.org/10.1016/j.jcis.2006.03.046.
[47] H. Park, W. Choi, Visible-light-sensitized production of hydrogen using perfluorosulfonate polymer-coated TiO_2 nanoparticles: an alternative approach to sensitizer anchoring, Langmuir 22 (2006) 2906–2911, https://doi.org/10.1021/la0526176.
[48] H. Park, W. Choi, Photocatalytic reactivities of Nafion-coated TiO_2 for the degradation of charged organic compounds under UV or visible light, J. Phys. Chem. B 109 (2005) 11667–11674, https://doi.org/10.1021/jp051222s.
[49] D. Wang, Y. Sun, Q. Shang, X. Wang, T. Guo, H. Guan, Q. Lu, Effects of the conjugated structure of Fe–bipyridyl complexes on photoinduced electron transfer in TiO_2 photocatalytic systems, J. Catal. 356 (2017) 32–42, https://doi.org/10.1016/j.jcat.2017.09.009.
[50] S.K. Choi, S. Kim, J. Ryu, S.K. Lim, H. Park, Titania nanofibers as a photo-antenna for dye-sensitized solar hydrogen, Photochem. Photobiol. Sci. 11 (2012) 1437–1444, https://doi.org/10.1039/c2pp25054c.
[51] S.K. Choi, H.S. Yang, J.H. Kim, H. Park, Organic dye-sensitized TiO_2 as a versatile photocatalyst for solar hydrogen and environmental remediation, Appl. Catal. B: Environ. 121–122 (2012) 206–213, https://doi.org/10.1016/j.apcatb.2012.04.011.
[52] E. Bae, W. Choi, Highly enhanced photoreductive degradation of perchlorinated compounds on dye-sensitized metal/TiO_2 under visible light, Environ. Sci. Technol. 37 (2003) 147–152, https://doi.org/10.1021/es025617q.
[53] W. Kim, T. Tachikawa, T. Majima, W. Choi, Photocatalysis of dye-sensitized TiO_2 nanoparticles with thin overcoat of Al_2O_3: enhanced activity for H_2 production and dechlorination of CCl_4, J. Phys. Chem. C 113 (2009) 10603–10609, https://doi.org/10.1021/jp9008114.
[54] E. Bae, W. Choi, Effect of the anchoring group (carboxylate vs phosphonate) in Ru-complex-sensitized TiO_2 on hydrogen production under visible light, J. Phys. Chem. B 110 (2006) 14792–14799, https://doi.org/10.1021/jp062540+.
[55] E. Bae, W. Choi, J. Park, H.S. Shin, S.B. Kim, J.S. Lee, Effects of surface anchoring groups (carboxylate vs phosphonate) in ruthenium-complex-sensitized TiO_2 on visible light reactivity in aqueous suspensions, J. Phys. Chem. B 108 (2004) 14093–14101, https://doi.org/10.1021/jp047777p.
[56] J.L. Gole, J.D. Stout, C. Burda, Y. Lou, X. Chen, Highly efficient formation of visible light tunable TiO_2-xNx photocatalysts and their transformation at the nanoscale, J. Phys. Chem. B 108 (2004) 1230–1240.

This book belongs to Badji Mokhtar Annaba University Central Library Copyright Elsevier 2025

[57] B. Tryba, T. Tsumura, M. Janus, A.W. Morawski, M. Inagaki, Carbon-coated anatase: adsorption and decomposition of phenol in water, Appl. Catal. B: Environ. 50 (2004) 177–183, https://doi.org/10.1016/j.apcatb.2004.01.003.

[58] Y.K. Kim, H. Park, How and to what extent do carbon materials catalyze solar hydrogen production from water?, Appl. Catal. B: Environ. 125 (2012) 530–537, https://doi.org/10.1016/j.apcatb.2012.06.018.

[59] Y. Choi, T. Umebayashi, M. Yoshikawa, Fabrication and characterization of C-doped anatase TiO_2 photocatalysts, J. Mater. Sci. 39 (2004) 1837–1839, https://doi.org/10.1023/B:JMSC.0000016198.73153.31.

[60] S.-W. Hsu, T.-S. Yang, T.-K. Chen, M.-S. Wong, Ion-assisted electron-beam evaporation of carbon-doped titanium oxide films as visible-light photocatalyst, Thin Solid Films 515 (2007) 3521–3526, https://doi.org/10.1016/j.tsf.2006.10.113.

[61] W. Ren, Z. Ai, F. Jia, L. Zhang, X. Fan, Z. Zou, Low temperature preparation and visible light photocatalytic activity of mesoporous carbon-doped crystalline TiO_2, Appl. Catal. B: Environ. 69 (2007) 138–144, https://doi.org/10.1016/j.apcatb.2006.06.015.

[62] S. Leong, A. Razmjou, K. Wang, K. Hapgood, X. Zhang, H. Wang, TiO_2 based photocatalytic membranes: a review, J. Membr. Sci. 472 (2014) 167–184, https://doi.org/10.1016/j.memsci.2014.08.016.

[63] P. Liu, H. Liu, G. Liu, K. Yao, W. Lv, Preparation of TiO_2 nanotubes coated on polyurethane and study of their photocatalytic activity, Appl. Surf. Sci. 258 (2012) 9593–9598, https://doi.org/10.1016/j.apsusc.2012.05.154.

[64] S.-J. You, G.U. Semblante, S.-C. Lu, R.A. Damodar, T.-C. Wei, Evaluation of the antifouling and photocatalytic properties of poly(vinylidene fluoride) plasma-grafted poly(acrylic acid) membrane with self-assembled TiO_2, J. Hazard. Mater. 237–238 (2012) 10–19, https://doi.org/10.1016/j.jhazmat.2012.07.071.

[65] J. Liao, S. Lin, N. Pan, S. Li, X. Cao, Y. Cao, Fabrication and photocatalytic properties of free-standing TiO_2 nanotube membranes with through-hole morphology, Mater. Charact. 66 (2012) 24–29, https://doi.org/10.1016/j.matchar.2012.02.005.

[66] Y. Mansourpanah, S.S. Madaeni, A. Rahimpour, A. Farhadian, A.H. Taheri, Formation of appropriate sites on nanofiltration membrane surface for binding TiO_2 photo-catalyst: performance, characterization and fouling-resistant capability, J. Membr. Sci. 330 (2009) 297–306, https://doi.org/10.1016/j.memsci.2009.01.001.

[67] H.-J. Hong, S.K. Sarkar, B.-T. Lee, Formation of TiO_2 nano fibers on a micro-channeled Al_2O_3-ZrO_2/TiO_2 porous composite membrane for photocatalytic filtration, J. Eur. Ceram. Soc. 32 (2012) 657–663, https://doi.org/10.1016/j.jeurceramsoc.2011.10.010.

[68] L. Liu, Z. Liu, H. Bai, D.D. Sun, Concurrent filtration and solar photocatalytic disinfection/degradation using high-performance Ag/TiO_2 nanofiber membrane, Water Res. 46 (2012) 1101–1112, https://doi.org/10.1016/j.watres.2011.12.009.

[69] H. Zhang, X. Quan, S. Chen, H. Zhao, Y. Zhao, Fabrication of photocatalytic membrane and evaluation its efficiency in removal of organic pollutants from water, Sep. Purif. Technol. 50 (2006) 147–155, https://doi.org/10.1016/j.seppur.2005.11.018.

[70] G.E. Romanos, C.P. Athanasekou, F.K. Katsaros, N.K. Kanellopoulos, D. D. Dionysiou, V. Likodimos, P. Falaras, Double-side active TiO_2-modified nanofiltration membranes in continuous flow photocatalytic reactors for effective water purification, J. Hazard. Mater. 211–212 (2012) 304–316, https://doi.org/10.1016/j.jhazmat.2011.09.081.

[71] Y.-F. Lin, K.-L. Tung, Y.-S. Tzeng, J.-H. Chen, K.-S. Chang, Rapid atmospheric plasma spray coating preparation and photocatalytic activity of macroporous titania nanocrystalline membranes, J. Membr. Sci. 389 (2012) 83–90, https://doi.org/10.1016/j.memsci.2011.10.018.

[72] H. Song, J. Shao, Y. He, B. Liu, X. Zhong, Natural organic matter removal and flux decline with PEG–TiO_2-doped PVDF membranes by integration of ultrafiltration with photocatalysis, J. Membr. Sci. 405–406 (2012) 48–56, https://doi.org/10.1016/j.memsci.2012.02.063.

[73] O. Tahiri Alaoui, Q.T. Nguyen, C. Mbareck, T. Rhlalou, Elaboration and study of poly (vinylidene fluoride)–anatase TiO_2 composite membranes in photocatalytic degradation of dyes, Appl. Catal. A: Gen. 358 (2009) 13–20, https://doi.org/10.1016/j.apcata.2009.01.032.

[74] B. Barni, A. Cavicchioli, E. Riva, L. Zanoni, F. Bignoli, I.R. Bellobono, F. Gianturco, A. De Giorgi, H. Muntau, L. Montanarella, S. Facchetti, L. Castellano, Pilot-plant-scale photodegradation of phenol in aqueous solution by photocatalytic membranes immobilizing titanium dioxide (PHOTOPERM® process), Chemosphere 30 (1995) 1861–1874, https://doi.org/10.1016/0045-6535(95)00067-I.

This book belongs to Badji Mokhtar Annaba University Central Library Copyright Elsevier 2025

[75] L. Liu, F. Chen, F. Yang, Stable photocatalytic activity of immobilized FeO/TiO_2/ACF on composite membrane in degradation of 2,4-dichlorophenol, Sep. Purif. Technol. 70 (2009) 173–178, https://doi.org/10.1016/j.seppur.2009.09.013.

[76] J. Kleine, K.-V. Peinemann, C. Schuster, H.-J. Warnecke, Multifunctional system for treatment of wastewaters from adhesive-producing industries: separation of solids and oxidation of dissolved pollutants using doted microfiltration membranes, Chem. Eng. Sci. 57 (2002) 1661–1664, https://doi.org/10.1016/S0009-2509(02)00043-X.

[77] H.K. Shon, S. Vigneswaran, H.H. Ngo, J.H. Kim, Chemical coupling of photocatalysis with flocculation and adsorption in the removal of organic matter, Water Res. 39 (2005) 2549–2558.

[78] M. Boroski, A.C. Rodrigues, J.C. Garcia, L.C. Sampaio, J. Nozaki, N. Hioka, Combined electrocoagulation and TiO_2 photoassisted treatment applied to wastewater effluents from pharmaceutical and cosmetic industries, J. Hazard. Mater. 162 (2009) 448–454, https://doi.org/10.1016/j.jhazmat.2008.05.062.

[79] A. Suárez-Escobar, A. Pataquiva-Mateus, A. López-Vasquez, Electrocoagulation—photocatalytic process for the treatment of lithographic wastewater. Optimization using response surface methodology (RSM) and kinetic study, Catal. Today 266 (2016) 120–125, https://doi.org/10.1016/j.cattod.2015.09.016.

[80] M. Boroski, A.C. Rodrigues, J.C. Garcia, A.P. Gerola, J. Nozaki, N. Hioka, The effect of operational parameters on electrocoagulation–flotation process followed by photocatalysis applied to the decontamination of water effluents from cellulose and paper factories, J. Hazard. Mater. 160 (2008) 135–141, https://doi.org/10.1016/j.jhazmat.2008.02.094.

[81] E.A. Serna-Galvis, J. Silva-Agredo, A.L. Giraldo, O.A. Flórez, R.A. Torres-Palma, Comparison of route, mechanism and extent of treatment for the degradation of a β-lactam antibiotic by TiO_2 photocatalysis, sonochemistry, electrochemistry and the photo-Fenton system, Chem. Eng. J. 284 (2016) 953–962, https://doi.org/10.1016/j.cej.2015.08.154.

[82] R.A. Torres, J.I. Nieto, E. Combet, C. Pétrier, C. Pulgarin, Influence of TiO_2 concentration on the synergistic effect between photocatalysis and high-frequency ultrasound for organic pollutant mineralization in water, Appl. Catal. B: Environ. 80 (2008) 168–175, https://doi.org/10.1016/j.apcatb.2007.11.013.

[83] I. Fatimah, Preparation of TiO_2-ZnO and its activity test in sonophotocatalytic degradation of phenol, in: Presented at the IOP Conference Series: Materials Science and Engineering, IOP Publishing, 2016, p. 012003.

[84] R. Kumar, G. Kumar, M.S. Akhtar, A. Umar, Sonophotocatalytic degradation of methyl orange using ZnO nano-aggregates, J. Alloys Compd. 629 (2015) 167–172, https://doi.org/10.1016/j.jallcom.2014.12.232.

[85] M. May-Lozano, V. Mendoza-Escamilla, E. Rojas-García, R. López-Medina, G. Rivadeneyra-Romero, S. A. Martinez-Delgadillo, Sonophotocatalytic degradation of Orange II dye using low cost photocatalyst, J. Clean. Prod. 148 (2017) 836–844, https://doi.org/10.1016/j.jclepro.2017.02.061.

[86] S. Mosleh, M.R. Rahimi, M. Ghaedi, K. Dashtian, Sonophotocatalytic degradation of trypan blue and vesuvine dyes in the presence of blue light active photocatalyst of Ag3PO4/Bi2S3-HKUST-1-MOF: central composite optimization and synergistic effect study, Ultrason. Sonochem. 32 (2016) 387–397, https://doi.org/10.1016/j.ultsonch.2016.04.007.

[87] S. Mosleh, M.R. Rahimi, Intensification of abamectin pesticide degradation using the combination of ultrasonic cavitation and visible-light driven photocatalytic process: synergistic effect and optimization study, Ultrason. Sonochem. 35 (2017) 449–457, https://doi.org/10.1016/j.ultsonch.2016.10.025.

[88] P. Sathishkumar, R.V. Mangalaraja, O. Rozas, C. Vergara, H.D. Mansilla, M. A. Gracia-Pinilla, S. Anandan, Sonophotocatalytic mineralization of norflurazon in aqueous environment, Chemosphere 146 (2016) 216–225, https://doi.org/10.1016/j.chemosphere.2015.12.011.

[89] Y.-C. Chen, A.V. Vorontsov, P.G. Smirniotis, Enhanced photocatalytic degradation of dimethyl methylphosphonate in the presence of low-frequency ultrasound, Photochem. Photobiol. Sci. 2 (2003) 694–698, https://doi.org/10.1039/B300444A.

[90] Q. Sun, Y. Hong, Q. Liu, L. Dong, Synergistic operation of photocatalytic degradation and Fenton process by magnetic Fe_3O_4 loaded TiO_2, Appl. Surf. Sci. 430 (2018) 399–406, https://doi.org/10.1016/j.apsusc.2017.08.085.

[91] A. Babuponnusami, K. Muthukumar, Degradation of phenol in aqueous solution by Fenton, sono-Fenton and sono-photo-Fenton methods, Clean: Soil Air Water 39 (2011) 142–147, https://doi.org/10.1002/clen.201000072.

This book belongs to Badji Mokhtar Annaba University Central Library Copyright Elsevier 2025

[92] Y. Segura, R. Molina, F. Martínez, J.A. Melero, Integrated heterogeneous sono–photo Fenton processes for the degradation of phenolic aqueous solutions, Ultrason. Sonochem. 16 (2009) 417–424, https://doi.org/10.1016/j.ultsonch.2008.10.004.
[93] M.S. Lucas, J.A. Peres, Decolorization of the azo dye reactive black 5 by Fenton and photo-Fenton oxidation, Dyes Pigments 71 (2006) 236–244, https://doi.org/10.1016/j.dyepig.2005.07.007.
[94] M. Muruganandham, M. Swaminathan, Decolourisation of reactive Orange 4 by Fenton and photo-Fenton oxidation technology, Dyes Pigments 63 (2004) 315–321, https://doi.org/10.1016/j.dyepig.2004.03.004.
[95] M. Pérez, F. Torrades, X. Domènech, J. Peral, Fenton and photo-Fenton oxidation of textile effluents, Water Res. 36 (2002) 2703–2710, https://doi.org/10.1016/S0043-1354(01)00506-1.
[96] M. Mehrjouei, S. Müller, D. Möller, A review on photocatalytic ozonation used for the treatment of water and wastewater, Chem. Eng. J. 263 (2015) 209–219, https://doi.org/10.1016/j.cej.2014.10.112.
[97] J. Xiao, Y. Xie, H. Cao, Organic pollutants removal in wastewater by heterogeneous photocatalytic ozonation, Chemosphere 121 (2015) 1–17, https://doi.org/10.1016/j.chemosphere.2014.10.072.
[98] M.V. Bagal, P.R. Gogate, Degradation of diclofenac sodium using combined processes based on hydrodynamic cavitation and heterogeneous photocatalysis, Ultrason. Sonochem. 21 (2014) 1035–1043, https://doi.org/10.1016/j.ultsonch.2013.10.020.
[99] X. Wang, J. Jia, Y. Wang, Combination of photocatalysis with hydrodynamic cavitation for degradation of tetracycline, Chem. Eng. J. 315 (2017) 274–282, https://doi.org/10.1016/j.cej.2017.01.011.

This book belongs to Badji Mokhtar Annaba University Central Library
Copyright Elsevier 2025

CHAPTER 7

New graphene-based nanocomposite for photocatalysis

Gunvant H. Sonawane[a], Prakash K. Labhane[b], and Shirish H. Sonawane[c]

[a]*Chemistry Research Laboratory, Kisan Arts Commerce and Science College, Parola, Maharashtra, India,*
[b]*Department of Chemistry, MGSM's Arts, Science and Commerce College, Chopda, Maharashtra, India,*
[c]*Department of Chemical Engineering, National Institute of Technology, Warangal, Telangana, India*

7.1 Introduction

Graphene (G) and its derivatives are finding use for various applications and have arisen as a high-flier on the prospect of materials science [1–10]. The first well-known example of G was introduced by British chemist Benjamin Collins Brodie in 1859. He prepared G by treating G flakes in an oxidative environment [11]. However, in 2004, Andre Geim and Kostya Novoselov of the University of Manchester won the Nobel Prize for their discovery of G [12]. G is a thin, two-dimensional (2D), polyaromatic, sp^2 carbon hexagonal network that is the lightest, strongest, most electrically and thermally conductive material, which has found many applications to captivate the attention of the scientific community [13]. Since the last decade, G has gained huge interest, steady progress in commercialization, and is widely used by different scientific communities for various applications. To date, the production of G increased from 14 tons to nearly 1200 tons [14]. The long-range, 2D sp^2 carbon hexagonal network system in G offers extraordinary physical properties, extremely large specific surface area (2630 $m^2\ g^{-1}$), high elasticity, thermal and electricity conductivity, captivating electronic properties, and most importantly charge carrier's behavior as massless relativistic particles [15]. Due to an exceptional mechanical property, G succeeds as an outstanding material for various potential applications such as solar cells, sensors, hydrogen generation via water-splitting, energy storage devices, and catalytic activities [16]. G is a zero-gap 2D semimetal with tiny overlap between valence band (VB) and conduction band (CB) plus high surface area, which makes it an appropriate nanoadsorbent and nanocatalyst [15, 17]. Despite the excellent features of pristine G sheets, low dispersion in water, agglomeration in solution due to Van der Waals interactions, and difficult bottom-up synthesis limits their

Handbook of Nanomaterials for Wastewater Treatment. https://doi.org/10.1016/B978-0-12-821496-1.00015-5
Copyright © 2021 Elsevier Inc. All rights reserved.

This book belongs to Badji Mokhtar Annaba University Central Library Copyright Elsevier 2025

photocatalytic applications [18–19]. However, the surface properties of G can be modified by chemical or thermal process, which offers great prospects for functionalized G-based materials.

7.2 Graphene and its derivatives

7.2.1 Properties of graphene and its derivatives

Unlike G, graphene oxide (GO) has different functional groups such as hydroxyl, carbonyl, epoxy, and carboxyl groups on the basal plane and at sheet edges [20]. These oxygen-containing functional groups permit an easy dispersion and high colloidal stability of GO in water and conferred exceptional mechanical, colloidal, and optical properties. The extended GO properties further can be modified and exploited for various kinds of applications including solar cells, sensors, supercapacitors, generation of neurons, cellular migration, drug delivery, membranes, multifunctional gels, water purification, and many more [21]. GO has a high theoretical surface area (2620 m^2 g^{-1}), and this lightly well-defined material has been commonly prepared by chemical methods [22]. GO is frequently fabricated by chemical exfoliation of graphite under strong acidic and oxidative environments. The content of oxygen in GO mostly depends on preparation conditions/methods and varies accordingly [23]. GO is a promising adsorptive material for the removal of organic dyes, metals, and pharmaceuticals from wastewater [24]. However, the use of strong oxidizing agent such as potassium permanganate reveals many defects in GO's crystalline network, which considerably lowers its conductive properties than that of pristine G [19, 21]. Nevertheless, these properties can be partly restored by chemical or thermal reduction of GO into reduced GO (referred as rGO or RGO). The reduction of GO substantially removes the oxygen functional groups (epoxy) and attains properties closer to both pristine G (i.e., high surface area and strength including relatively good conductivity) and GO (i.e., easy to disperse in water) [19, 25]. RGO acts as an intermediate between G and GO [13]. The structural conversion of G to rGO via GO can be envisaged in Fig. 7.1. The variable properties along with production cost of G, GO, and rGO have been reported by Perreault et al. [26] and is tabulated in Table 7.1.

7.2.2 Preparation methods of graphene and its derivatives

The common techniques used for the preparation of G are mechanical exfoliation, chemical synthesis, chemical vapor deposition (CVD), epitaxial growth on electrically insulating surfaces, and SiC pyrolysis [26–28]. Mechanical exfoliation techniques involved the cleavage of G layers from the bulk highly ordered pyrolytic graphite. High-quality and large-area G flakes can be prepared by these techniques. These techniques are extremely labor-intensive and time consuming; nevertheless, several outstanding properties of G have been revealed by mechanical exfoliation techniques [29]. In CVD methods, organic molecules in hydrocarbon gas or solid forms are used as a carbon source. The CVD method produces a low amount of G,

This book belongs to Badji Mokhtar Annaba University Central Library Copyright Elsevier 2025

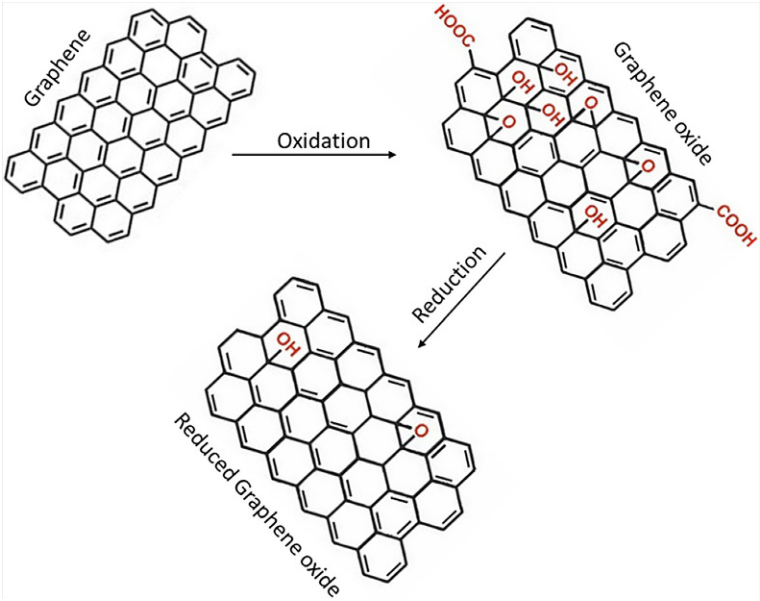

Fig. 7.1
Structures of G, GO, and rGO [26]. *Reproduced from F. Perreault, A.F. De Faria, M. Elimelech, Environmental applications of graphene-based nanomaterials, Chem. Soc. Rev. 44 (2015) 5861–5896. Copyright (2015) Royal Society of Chemistry.*

Table 7.1: Summary of structure and key properties of graphene-based materials relevant for photocatalysis [26].

Material	Synthesis methods	C:O ratio	Production cost
G	Chemical vapor deposition, thermal decomposition, graphite exfoliation	No oxygen	High
GO	Oxidation and exfoliation of graphite	2–4	Low
rGO	Reduction of graphite oxide	8–246	Low

Reproduced from F. Perreault, A.F. De Faria, M. Elimelech, Environmental applications of graphene-based nanomaterials, Chem. Soc. Rev. 44 (2015) 5861–5896. Copyright (2015) Royal Society of Chemistry.

as well as requiring high operating temperature and expensive substrate similar like the epitaxial method [30]. SiC pyrolysis has been reported as an effective method to prepare G with high quality [31]. The yield, cost, and other properties of G depend on the strategy applied for preparation [30].

For the synthesis of GO, oxidative-exfoliation chemical routes have been adopted over the years [32]. The renowned approaches for the synthesis of GO are Brodie method, Staudenmaier method, Hofmann method, and Hummers method with their modified forms. The pioneer of

This book belongs to Badji Mokhtar Annaba University Central Library Copyright Elsevier 2025

GO was Brodie, who in 1859 prepared GO by oxidation of graphite using potassium chlorate ($KClO_3$) and fuming nitric acid (HNO_3), a strong oxidizing mixture [33].

Later in 1898, L. Staudenmaier improved Brodie's preparation method by the reaction with an excess of the oxidizing agent ($KClO_3$-fuming HNO_3) and concentrated sulfuric acid. The excess of oxidizing agents with concentrated H_2SO_4 (to increase the acidity of the mixture) simplified the GO synthesis process [34]. However, this method is hazardous and time consuming [35].

Later, in 1937, Hofmann et al. reported the oxidation of graphite by concentrated sulfuric acid with concentrated nitric acid and $KClO_3$ for the preparation of graphite oxide [36]. A strong oxidizing agent, $KClO_3$ oxidizes the graphite powder in acids solution considered an in situ source of reactive dioxygen. Several researchers followed the Hofmann method to synthesize GO by captivating view of variety of applications [37].

In 1958, Hummers and Offeman reported the most popular method frequently used to oxidize powdered graphite into GO. In Hummers methods, potassium permanganate ($KMnO_4$) was used as the main oxidant together with some supporting agents like sodium nitrate ($NaNO_3$). Although, the yield of GO can be improved by this method, nevertheless, it was difficult to control its structure [38]. Several modifications to the Hummers approach were reported to improve and control the final properties of GO [39–41]. In most of the modifications, the use of $NaNO_3$ has been avoided by increasing the amount of $KMnO_4$. This suggests that the $NaNO_3$ may not be an essential supporting agent in Hummers preparative method of GO [42]. Despite low oxidation potential of $NaNO_3$, it acts as an intercalation agent and assists in the oxidation of graphite to GO [38].

7.3 Graphene and its derivative-based photocatalyst

It has been reported that coupling of commonly reported photocatalysts with exclusive sp^2 hybrid carbon network materials offers greater adsorption, effective photoinduced charge separation, and light-absorption range to visible light region. Accordingly, G-based material has an ability to offer an effective route for various photocatalytic applications.

7.3.1 Synthesis of graphene and its derivatives based binary nanocomposites

The inadequate exploitation of light energy and rapid recombination of photogenerated charge carriers limits the photocatalytic performance of commonly studied semiconductors. However, these limitations of semiconductors can be minimized by coupling or forming heterojunctions with G and its derivatives. G can act as a conductive mediator via its honeycomb 2D carbon skeleton [43]. The heterogeneous G-based semiconductor photocatalyst enables an effective

This book belongs to Badji Mokhtar Annaba University Central Library Copyright Elsevier 2025

charge separation by trapping photoinduced electrons via sp^2 hybridized carbon network, extended photoresponse, and high adsorption capacity [44].

Solution mixing, sol-gel, microwave, and hydrothermal methods were commonly adopted to prepare G-based binary nanocomposites. In the solution mixing method, the dispersed solutions of both metal oxides (semiconductors) and G were allowed to mix with continuous stirring. After mixing and stirring, the usual processes such as centrifugation, washing, and drying are carried out to get binary G-metal oxide composite [45]. Ishaq et al. [46] fabricated binary rGO/$MeFe_2O_4$ (Me = Mn, Ni) composite by simple, scalable, and environmentally sustainable methods. The precursors of Me and Fe in 1:2 ratio was added into dispersed solution of GO followed by vigorous stirring at appropriate temperature under N_2 protection and later in air. The pH of the solution was adjusted to 11–12 by NaOH solution. The solution was allowed to cool at room temperature followed by centrifugation, washing, and drying to get binary rGO/$MeFe_2O_4$ nanocomposite.

The sol-gel is the most popular method to prepare nanoparticles, which can be extended to fabricate G-based binary composite. It has been used in situ preparation of metal oxide nanostructures deposited on GO/rGO sheets [47]. Grace et al. [48] prepared TiO_2-G nanocomposite by situ sol-gel process method. The functional groups on GO/rGO offer a reactive and anchoring site for nucleation growth of nanoparticles, consequently, enabling chemical bonding between GO/rGO surfaces with resulting metal oxide nanostructures [47].

Chhabra et al. [49] prepared MnO_2-rGO binary nanocomposite by a facile hydrothermal method. In this report, the $KMnO_4$ was added to a dispersed rGO aqueous solution. After the addition of HCl in mixed dispersed solution, the hydrothermal treatment was placed in an oven at 160°C for 6 h. Hydrothermal method allows control of the morphology and distribution of nanoparticles on the GO or rGO sheets by varying the parameters like concentration of precursor's solution, reaction time, and temperature. Xue and Zou reported the uniform distribution of zinc oxide nanoparticles on rGO, which enables the interfacial charge transfer and lowers the recombination rate of photoinduced electron-hole pairs, a major aspect of an excellent photocatalyst [50].

Microwave treatment could be a convenient approach for the preparation of G-metal oxide nanocomposites. The benefits of microwave treatment are it is less time consuming, avoids the use of reducing agent for reduction GO, and allows simultaneous growth of nanoparticles on the rGO sheets [51].

He et al. [52] prepared $CoFe_2O_4$-rGO composites by ball-milling method with the reaction containing graphite oxide colloid (2.5 wt%), $Co(NO_3)_2 \cdot 6H_2O$, and $Fe(NO_3)_3 \cdot 9H_2O$. The $NH_3 \cdot H_2O$ solution was used to adjust pH of the reaction mixture. The mixed contents were milled using an Oscillating Mill MM400 to get final binary composite followed by washing with

This book belongs to Badji Mokhtar Annaba University Central Library Copyright Elsevier 2025

distilled water and freeze drying. The reaction was carried by using nontoxic chemical reagents at low temperature.

7.3.2 Synthesis of graphene and its derivative-based ternary nanocomposites

G and its derivative-based ternary nanocomposites can be synthesized by similar methods as reported for binary nanocomposites. Jiang et al. [53] have fabricated multifunctional crumpled G-based ternary nanocomposite via an aerosol route for advanced water treatment. The aerosol route exploits water evaporation-induced confinement forces to crumple GO efficiently. To overcome the restacking issues of G sheets, crumpled G-based ternary photocatalysts were developed through an aerosol route. Similarly, ternary mixed-dimensional TiO_2/MoS_2 hybrid embedded into the three-dimensional (3D) G aerogel was prepared by hydrothermal reduction process [54]. A facile single-step solvothermal route was reported for the synthesis of Mn-ZnO/G ternary nanocomposite photocatalyst [55]. Raja and coworkers followed the hydrothermal method to prepare highly effective rGO-$BiVO_4$-ZnO photocatalyst [56]. The ternary magnetite Fe_3O_4/CeO_2/GO, an active visible light-driven photocatalyst, were fabricated via a facile ultrasonic-assisted method [57]. Xin et al. [58] reported a facile, low-temperature, chemical reduction approach for the preparation of ternary aerogel composite by integration of AgBr nanoparticles with 3D reduced GO aerogel (RGA) and plasmonic Ag nanoparticles to investigate photocatalytic performance for bacteria inactivation.

Another approach for enhancing the photocatalytic activity of G-based ternary composite is the combination with semiconductor and polymer material. Ni et al. [59] reported facile two-step method for the preparation of a ternary nanocomposite, composed of polystyrene (PS) microsphere, rGO, and ceria nanoparticles. Conventional dispersion polymerization was followed to prepare PS microspheres, while modified Hummers method was used to prepare GO. Initially, PS and GO were mixed in water under ultrasonic treatment. Hydrazine hydrate was injected in the mixed solution, and later the reaction system was heated to get PS/rGO nanocomposite. Second, the aqueous dispersion of PS/rGO nanocomposites was added to aqueous solution of $Ce(NO_3)_3$ with constant stirring. Appropriate amount of hexamethylenetetramine solution was inserted in this solution, and thermal treatment was given at 40°C for 2 h to get PS/rGO@ceria (PS/rGO@CeO_2) nanocomposite.

Metal-free approach for the synthesis of 3D porous G-carbon quantum dots (CQDs)/ gC_3N_4(CNN) nanosheet aerogel ternary photocatalyst was reported recently [60]. In this report, first, CQDs were loaded on CNN sheets through hydrothermal process. The π-π stacking interactions facilitates the loading and allows conversion to binary CQDs/CNN. Afterward, binary CQDs/CNN was mixed with GO, and the hydrothermal treatment was given in an autoclave where the reduction of GO and simultaneous formation of a ternary CQDs/CNN composite occurs. Fig. 7.2 illustrates the fabrication scheme of a ternary CQDs/CNN composite.

This book belongs to Badji Mokhtar Annaba University Central Library Copyright Elsevier 2025

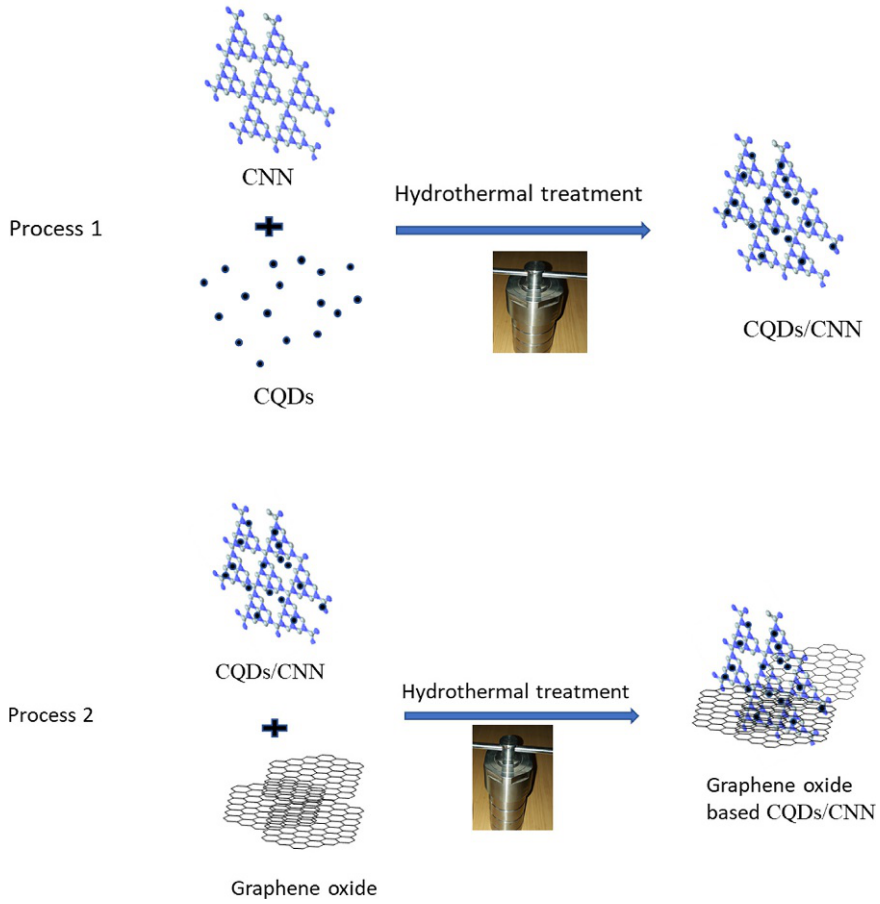

Fig. 7.2
Fabrication scheme of a ternary graphene-carbon quantum dots (CQDs)/gC_3N_4 (CNN) composite [60]. *Reproduced from H. He, L. Huang, Z, Zhong, S. Tan, Constructing three-dimensional porous graphene-carbon quantum dots/g-C_3N_4 nanosheet aerogel metal-free photocatalyst with enhanced photocatalytic activity, Appl. Surf. Sci. 441 (2018) 285–294. Copyright (2018) Elsevier.*

Our group followed the wet impregnation for the preparation of rGO-ZnO nanocomposite. The GO and appropriate amount of polyvinylpyrrolidone were mixed and ultrasonicated in deionized water to get dispersed solution of GO. ZnO nanoparticles (previously prepared by sol-gel method) were added into the dispersed solution of GO. The mixture was allowed to agitate at room temperature for an hour. Finally, precipitate of rGO-ZnO nanocomposite was separated by centrifugation followed by washing and drying [61]. Similar method was followed by our group for the preparation of ternary Mg-doped ZnO nanoparticles decorated on GO sheets [44]. However, the morphology and distribution of nanoparticles on the GO sheets by wet impregnation method was difficult to control. The agglomeration and nonuniform

This book belongs to Badji Mokhtar Annaba University Central Library Copyright Elsevier 2025

distribution of ZnO nanoparticles on GO sheets may restrict the exploitation of optimum surface area and electron mobility of G during the photocatalytic process. It was reported that the morphology and distribution of nanoparticles on GO sheets can be controlled by hydrothermal method. Recently, our group prepared highly efficient solar light-assisted Mn-doped ZnO nanoparticles uniformly grafted on rGO sheets by hydrothermal method [62].

Likewise, other inorganic metal oxides, metal sulfides, carbon compounds, etc. have been successfully used to fabricate another G-based binary and ternary nanocomposite photocatalysts via different synthetic methods [63–68].

7.4 Characterization of graphene and its derivatives

The instrument techniques explored in characterization of G and its derivatives are X-ray diffraction (XRD) spectroscopy, Fourier transform infrared (FTIR) spectroscopy, UV-visible spectroscopy, Raman spectroscopy, X-ray photoelectron spectroscopy (XPS), scanning electron microscopy (SEM), and transmission electron microscopy (TEM).

The XRD analysis is an important technique to reveal the conversion of G into GO and further into rGO. X-ray powder diffractometer with incident beam of 1.54 Å wavelength (Cu Kα radiations) are generally used to collect XRD data. XRD analysis may also be used to investigate the crystal phase and the interlayer spacing in solid form of material [69]. When the XRD pattern is recorded in a range of 2θ from 5 to 70 degrees, the pristine G structure exhibits one sharp and strong peak at $2\theta \approx 26$ degrees with an interplanar spacing of 0.334 nm. The conversion of G into GO can be confirmed by the disappearance of strong diffraction peak at $2\theta \approx 26$ degrees and the appearance of new diffraction peak at $2\theta \approx 9.98$ degrees, corresponding to interplanar spacing at 0.80–0.83 nm [70]. The variation of interplanar spacing is due to variation in degree of oxidation in G [71]. The strong oxidation of G completely removes the diffraction peak at $2\theta \approx 26$ degrees, while mild oxidation gives rise to weak diffraction peak at this 2θ value along with the strong diffraction peak at $2\theta \approx 9.98$ degrees [62]. The rGO exhibits the broader diffraction peak at $2\theta \approx 24$–27 degrees. During the chemical reduction of GO into rGO, oxygen-containing functional groups may be eliminated significantly to restore π-conjugated structure of G, which can be confirmed through the disappearance of peak at $2\theta \approx 9.98$ degrees and the appearance of broader diffraction peak at $2\theta \approx 24$–27 degrees for rGO [72].

FTIR spectra provides evidence in support of conversion of GO into rGO. The oxygen-containing functional groups in GO can be easily identified by IR spectra. The major IR peak approximately at 3410 cm^{-1} is due to stretching of hydroxyl group, and the other peak approximately at 1720 cm^{-1} may be due C═O carbonyl stretching of carboxylic moieties at the edges of GO, while the peak approximately at 1050 cm^{-1} is due to stretching vibration peaks of C—O (epoxy) and C—O (alkoxy) group stretching [73]. The peaks approximately at 1620 cm^{-1} may belong to stretching of C═C alkene groups. As reduction of GO into rGO

This book belongs to Badji Mokhtar Annaba University Central Library Copyright Elsevier 2025

eliminates some of the oxygen-containing functional groups, the GO peak intensities associated to alkoxy and hydroxyl groups decrease significantly in rGO [74].

The UV-visible spectroscopy, another tool, can be used to find the conversion of GO into rGO. For G, the absorption maximum peak is mainly due to $\pi \rightarrow \pi^*$ transitions of aromatic C—C bonds. For GO, $\pi \rightarrow \pi^*$ transitions peak is observed approximately at 230 nm along with another peak approximately at 310 nm attributed to the $n \rightarrow \pi^*$ transition of the C═O bonds [75]. The conversion of G into GO can be analyzed through the redshift of $\pi \rightarrow \pi^*$ transitions peak that occurs approximately at 269 nm for rGO. This redshift may be as a result of the restoration of sp^2 hybridized carbon atoms and increase in concentration of π-electrons [76].

Raman spectroscopy has proved to be an essential tool to analyze crystal structure and disorder of carbon-based materials. Raman scattering is strongly sensitive to the electronic structure and, therefore, is an efficient technique to characterize G-based materials [77]. For all carbon-based materials, there are two main bands, D band and G band. The D band is associated with disorders and defects in G and characterized by peaks at around 1324–1346 cm^{-1}, while the G band is related to the vibration of sp^2-bonded carbon of graphite and characterized by peaks at around 1490–1691 cm^{-1} [78]. For the highly regular structure of graphite, a prominent G peak is expected around at 1584.5 cm^{-1}. After oxidation of G into GO, the G band becomes broadened and shifts to lower side approximately at 1579.2 cm^{-1}. Furthermore, in GO, some carbon atoms transformed from sp^2 hybridized state to sp^3 hybridized state, and the D band around at 1332 cm^{-1} becomes prominent [79]. After reduction of GO, the G band of rGO may broaden and D/G intensity ratio may slightly increase. Besides, the intensity ratio of the D to G bands (I_D/I_G) indicates the conversion of GO to rGO. The decrease in the ratio I_D/I_G indicates the formation of some sp^2 hybridized carbon in rGO. Accordingly, smaller I_D/I_G demonstrates better reduction of GO to rGO [77].

The GO and rGO contains oxygen-containing functional groups attached to carbon such as carbonyl (C═O), carboxyl (COOH), hydroxyl (OH), epoxy (C—O—C), and a lot of water molecules. The evaluation of (C 1s and O 1s) such functional groups can be quantitatively and qualitatively analyzed by XPS [80]. Park et al. [81] reported that GO shows two large peaks resulted from C1s XPS spectra at 284.6 eV, corresponding to sp^2 carbons and the peak at 286.7 eV, corresponding to C—O single bond of hydroxyl and 1,2-epoxide functional groups. A broad small peak at occurs approximately at 288–289 eV, corresponding to C═O double bond of carboxyl and ketonic functional groups. However, the peaks associated to those oxygenated functional groups may significantly decrease after the reduction of GO, as the oxygen atoms are removed to a large extent.

To analyze the morphologies of materials, SEM is an essential tool. Our group prepared GO by modified Hummers method using graphite powder as a precursor. The SEM images of as-prepared samples are shown in Fig. 7.3. It is clear that GO has wrinkled aggregates as a result of oxidation of graphite agglomerates. Furthermore, the oxidation process generates

This book belongs to Badji Mokhtar Annaba University Central Library Copyright Elsevier 2025

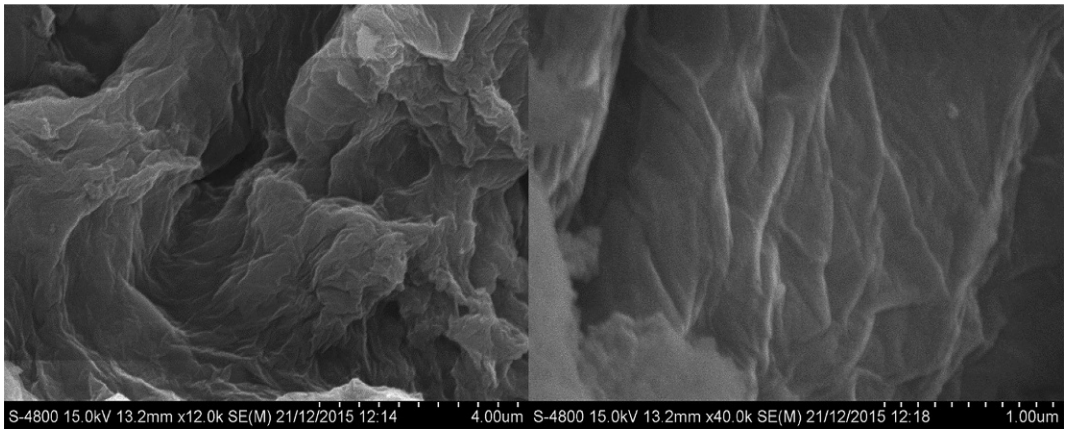

Fig. 7.3
SEM images of graphene oxide (GO) prepared by modified Hummers method.

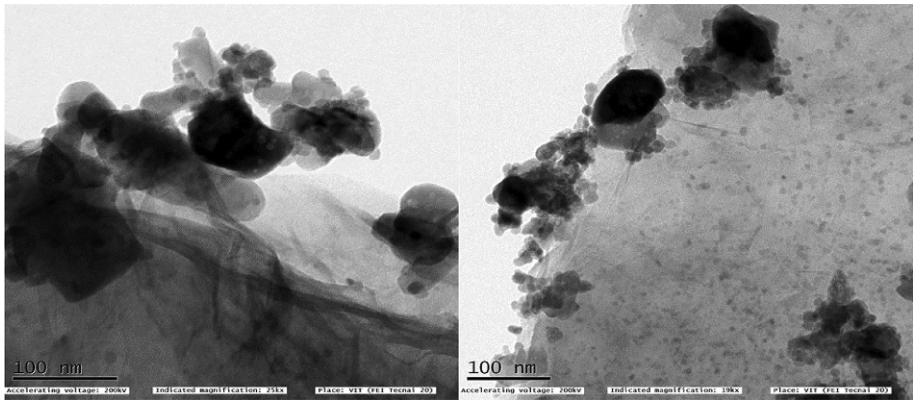

Fig. 7.4
TEM images of graphene oxide-based ternary composite prepared by wet-impregnation method.

oxygen-containing functional groups on the surfaces of graphite sheets, which increased the distance of GO sheets [82]. Additionally, nanostructural analysis of G-based material can be carried out by TEM. The TEM images of G oxide-based ternary nanocomposite prepared by our group are shown in Fig. 7.4. The TEM images confirmed that the nanoparticles with distinct grain boundaries are successfully deposited on the GO sheets.

7.5 Photocatalytic applications

The heterogeneous semiconductor photocatalytic oxidations have many features such as easy operation, complete degradation of organic pollutants without generating secondary pollution, and importantly green technology for environmental remediation [83–84]. However, most of

This book belongs to Badji Mokhtar Annaba University Central Library
Copyright Elsevier 2025

the commonly reported semiconductors suffer from fast recombination of photoinduced electron-hole pair and also requires UV radiation for promoting the charge separation [85–86]. G and its derivative-based semiconductor photocatalyst overcomes these limitations. G and its derivatives exhibit an ample surface area for adsorption and, therefore, can be an attractive alternative over conventional adsorbents, such as activated carbon and mesoporous carbons [87]. Highly acidic nature of the components present on the surface of GO permits the effective adsorption of organic pollutant molecules and cations and therefore greatly enhanced the adsorption efficiency [62]. Moreover, G sheets act as trapping sites for photoinduced electrons of a semiconductor, which utterly improved the photocatalytic efficiency of G-based semiconductor catalyst.

Since Honda and Fujishima discovered the splitting of water into H_2 and O_2 gas on TiO_2 electrodes, there has been a variety of semiconductors tested as potential catalysts for various photocatalytic applications [88]. However, the wide bandgap and the charge separation of photoinduced electron-hole pairs are the main concerns associated with commonly tested semiconductors to act as an efficient photocatalyst for the generation of hydrogen gas and oxygen gas via water-splitting process [89]. The heterojunction formation effectively lowers the charge recombination of semiconductors. Two-dimensional G sheets and its derivatives are reported as best co-catalysts to form composites with semiconductors for operative water-splitting [90]. G and its derivatives facilitate the migration of photogenerated charges to reaction sites and minimize the recombination rate of photoinduced electron-hole pairs. Besides, it provides high surface area, a more conductive surface, and lowers the bandgap of the semiconductor [91].

Another important photocatalytic application of G-based catalyst is CO_2 reduction. Reducing carbon dioxide (CO_2) into other useful hydrocarbons or CO with photocatalysts is the best way to resolve environmental pollution. G and its derivatives-based composite photocatalyst also offers a simple and effective route for recycling CO_2 into value-added chemicals. Various narrow bandgap semiconductors were used to prepare G and its derivatives-based photocatalysts, which were examined for CO_2 reduction [92]. The photoactive (mostly semiconductor) material is excited after irradiation to generate charge carriers. For excitation, the photon's energy should equal or be higher than bandgap energy to that of photoactive semiconductor. G sheets in the composites act as trapping sites for photogenerated electrons and thus minimizes the recombination of electron-hole pairs of semiconductors. The hole in the VB of a semiconductor oxidizes H_2O to O_2 and releases H^+, while electrons in the CB of a semiconductor as well migrated at G sheets reduces CO_2 to CO, CH_3OH, and CH_4 with the support of H^+ by sequence of chemical reactions [93]. G in the composites provides high surface area for adsorption of CO_2 molecule. Besides, it provides reactive surface for interaction with adsorbed CO_2 molecule and accordingly enhanced the photocatalytic performance [93].

This book belongs to Badji Mokhtar Annaba University Central Library Copyright Elsevier 2025

7.5.1 Photocatalytic study of graphene and its derivatives-based binary nanocomposites

Amongst several applications of G and its derivatives, the construction of heterogeneous G and its derivative-based photocatalyst is one of the most outstanding processes [94]. G and its derivatives (GO and rGO) behave as extremely weak catalysts. Besides, it can perform as a co-catalyst in a semiconductor/G-based composite to assist and improve the photocatalytic performance of semiconductors [95]. Until now, heterogeneous photocatalysts played a vital part in reaching highly efficient photocatalysis processes. Although a majority of photocatalysts suffer from low quantum yield, high rate of recombination of charge carriers, and low efficiency under solar/visible light irradiation. These are issues of concern that utterly limit the practical applications of heterogeneous photocatalysis at a large scale. The heterojunction of G with semiconductors provides a facile strategy to overwhelm these concerns [96]. The photogenerated electrons in semiconductors are rapidly transferred through the sp^2-hybridized network of G sheets and efficiently reduce electron-hole pair recombination and enhanced the photocatalytic efficiency of the semiconductor [97].

Recent studies have revealed the role of G and its derivatives in the enhancement of photocatalytic activity of commonly used semiconductors such as TiO_2, ZnO, CeO_2, SnO_2, CdS, ZrO_2, etc. [98–99]. The enhancement of the photocatalytic activity is mostly attributed to the formation of a novel electronic configuration system, which constrains the recombination of electron-hole pairs of semiconductors via withdrawing the excited electrons by π-π bond present in a G-based composite [61].

Our group has reported the photocatalytic potential of rGO-ZnO binary nanocomposite prepared by wet impregnation method for the degradation of methylene blue dye under UV light. It was observed that rGO-ZnO composite shows exceptional photocatalytic activity compared with ZnO alone. The strong interfacial charge transfer between ZnO and rGO enables efficient separation of the photoinduced electrons-hole pairs in the composite [61].

Nguyen and coworkers prepared ZnO/G nanocomposite photocatalyst with controlled morphology for the treatment of organic wastewater under solar light. ZnO/G nanocomposite exhibited excellent photocatalytic performance and can be a promising catalyst for the degradation of organic pollutants owing to its low cost, excellent recyclability, and stability [100]. Chen et al. [101] evaluated the photocatalytic efficiency of CdS/G composites prepared through solid-state chemical method at mild temperature. It has been reported that the composites exhibited excellent photocatalytic efficiency as a result of higher specific surface area, excellent light absorption ability, efficient charge carrier separation, and enhanced redox ability. Consequently, G has an important role in the composites during photocatalytic processes.

He and coworkers proposed a facile room-temperature hydrolysis method to prepare a composite of GO foam coated with bismuth oxoiodide. BiOI flake arrays were vertically and

This book belongs to Badji Mokhtar Annaba University Central Library Copyright Elsevier 2025

uniformly distributed on the surface of GO foam. It was further reported that GO foam coated with bismuth oxyiodide enables effective charge carrier separation, improves the contact between BiOI and the reactants, and subsequently exhibits excellent photocatalytic activity for the oxidization of phenol under visible light [102]. Yang et al. [103] developed recyclable 3D MoS_2 nanosheets/G aerogel heterostructure via a facile hydrothermal method for photodegradation of antibiotic residues in water. The prepared 3D MoS_2 nanosheets/G aerogel binary heterostructure exhibited decent photocatalytic activity toward the degradation of antibiotics residues under visible light.

Recently, Bellamkonda et al. [104] reported excellent H_2 production rate over TiO_2 hybridized G composites catalyst prepared by solution-based hydrolysis of titanium tetrachloride in the presence of G. G-based TiO_2 binary nanocomposites were tesed as active and highly efficient photocatalysts in comparison with bare TiO_2 for water-splitting under solar light irradiation. The improved photocatalytic efficiency of G-based TiO_2 nanocomposite was due to lowering in recombination rate of the photoinduced electron-hole pairs. Zinc oxide-rGO (ZnO/rGO) has been also widely reported as an effective photocatalyst for water-splitting. Ghorbani et al. [105] prepared 3D sphere-like ZnO/rGO nanocomposite by sol-gel route and reported it as an efficient catalyst for the production of H_2 gas via water-splitting.

7.5.2 Photocatalytic study of graphene and its derivatives-based ternary nanocomposites

Jiang et al. [53] have reported that multifunctional crumpled G-TiO_2-magnetite ternary core-shell nanostructures has many times greater aqueous-based photocatalytic efficiency compared with bare TiO_2. Sharma et al. [106] tested cobalt oxide-loaded TiO_2/rGO composite as an efficient visible light photocatalyst for the degradation of 2-chlorophenol. The better performance of ternary composite was due to more hydroxyl radical and superoxide radicals generated via redox reactions brought by the cobalt doping. In another report, Raja et al. [56] have examined needle with spherical shape ternary rGO-$HoVO_4$-TiO_2 photocatalyst prepared by simple hydrothermal method for degradation of ibuprofen under visible light. Photodecomposition efficiency of rGO-$HoVO_4$-TiO_2 ternary composite material was observed as high for the removal of ibuprofen as compared to $HoVO_4$, TiO_2, rGO-$HoVO_4$, and rGO-TiO_2 at pH 7. The synergetic effect, coupling of $HoVO_4$-TiO_2, and formation of heterojunction with rGO are the major factors for excellent photocatalytic efficiency. Abdel-Wahed et al. [107] evaluated the core double-shell $MnFe_2O_4$@rGO@TiO_2 superparamagnetic photocatalyst for wastewater treatment under solar light. In this ternary composite, $MnFe_2O_4$ acts as a recombination center while rGO withdraws the excited electrons from CB of TiO_2 and increases the lifetime of charge carriers, thereby, enhancing the photocatalytic activity.

New ternary g-C_3N_4/MoS_2/G (CN/MG) with a 2D heterojunction photocatalyst was constructed via an in situ adsorption method for the degradation of rhodamine B under visible light irradiation [108]. This ternary 2D-layered structural hybrid photocatalyst significantly

This book belongs to Badji Mokhtar Annaba University Central Library Copyright Elsevier 2025

facilitates the separation of photogenerated electron-hole pairs and therefore significantly enhanced the photocatalytic activity. Besides, ternary 2D-layered heterojunction provides abundant reactive sites for photodegradation.

Our group examined the photocatalytic performance of ZnO, binary ZnO-GO, and ternary Mg/ZnO-GO for the degradation of *p*-nitrophenol (PNP) and indigo carmine (IC) under sunlight [44]. The composites have excellent photodegradation rate for both PNP and IC. The extended solar light absorption, higher adsorptivity, and effective charge separation owing to 2D л conjugation structure of GO are the major influences for excellent photocatalytic performance of the composites. However, exceptional photocatalytic efficiency of ternary Mg/ZnO-GO compared with binary ZnO-GO may be attributed to the trapping of electrons from the CB via Mg^{2+} ions present in the lattice of ZnO.

7.6 Mechanism of photocatalytic degradation

The possible photocatalytic degradation mechanism of the G-based binary photocatalyst is shown in Fig. 7.5. The introduction of G or its derivatives to frequently used semiconductor photocatalysts significantly expand the photocatalytic efficiency. After light irradiation and receiving energy equal or greater than the bandgap energy of semiconductor, the electrons are promoted from VB to CB and produce electron-hole pairs. The holes in the VB generates hydroxyl radicals in aqueous solution, while the excited electrons in CB generates active oxygen species (superoxide radical anions) by activating adsorbed oxygen. It was confirmed

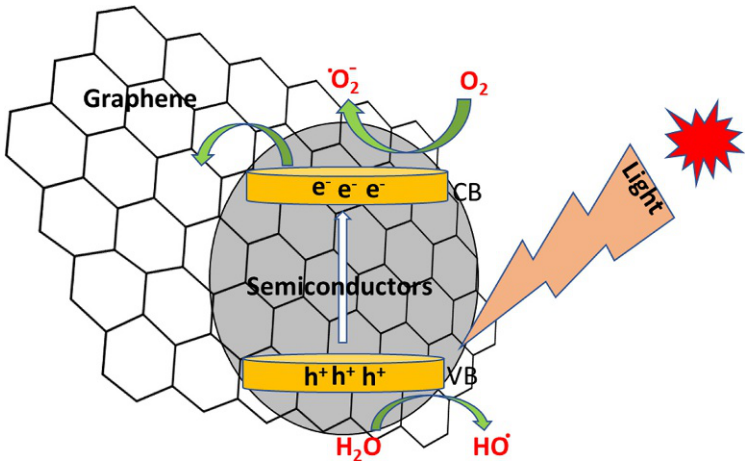

Fig. 7.5

The plausible photocatalytic mechanism of the graphene-based binary photocatalyst [61]. *Reproduced from P.K. Labhane, L.B. Patle, V.R. Huse, G.H. Sonawane, S.H. Sonawane, Synthesis of reduced graphene oxide sheets decorated by zinc oxide nanoparticles: crystallographic, optical, morphological and photocatalytic study, Chem. Phys. Lett. 661 (2016) 13–19. Copyright (2016) Elsevier.*

This book belongs to Badji Mokhtar Annaba University Central Library Copyright Elsevier 2025

that holes, superoxide radical anions, or hydroxyl radicals are the main species responsible for the degradation of organic pollutants. The scavengers' study has been widely used to find the active species during degradation process [61]. In the binary G-based composite, the excited electrons from the CB can be easily transferred to G sheets and lowers the recombination of electron-hole pairs.

G and its derivatives-based metal ion (Mn^{2+}, Mg^{2+}, $Ce^{3+,}$ etc.)-doped semiconductor ternary composite were tested as excellent photocatalysts compared with its respective binary composites. The metal ions, which occupy the interstitial sites in the lattice of semiconductors, further lower the recombination of electron-hole pairs by trapping photogenerated electrons and thereby can extend the photocatalytic performance [62]. The plausible mechanism of G and its derivatives-based metal ion-doped semiconductor ternary composite photodegradation is briefly described in Fig. 7.6.

Moreover, G-based cerium ion-doped semiconductor ternary composite has an extra advantage. The cerium ions exist in two oxidation states: Ce^{3+} and Ce^{4+} at the catalyst surface [96]. GO sheets prevent the recombination of e^-/h^+ pairs via capturing the photogenerated electrons, whereas Ce^{4+} ions can act as a scavenger in the composites by trapping the CB electrons and reduce to Ce^{3+}. The presence of extended sp^2 hybrid carbon framework in GO sheets enables effective charge transfer and Ce^{4+} ion acts as scavengers for photoinduced electrons in G-based cerium ion-doped semiconductor ternary composite, which jointly contributes to improved photocatalytic efficiency [109].

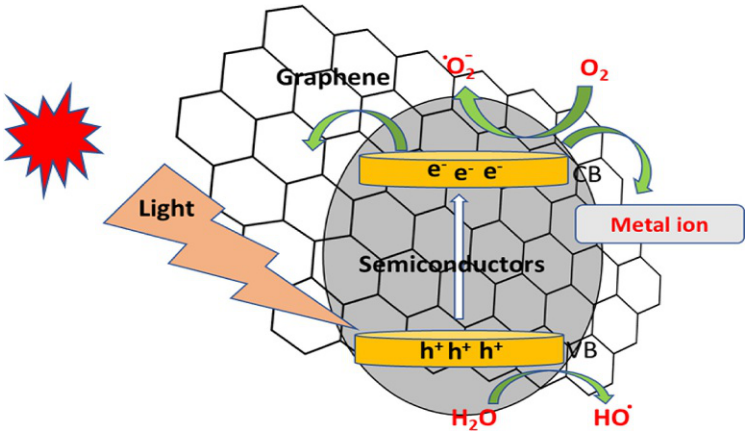

Fig. 7.6

The plausible photocatalytic mechanism of the graphene-based ternary photocatalyst [42].

Reproduced from P.K. Labhane, S.H. Sonawane, G.H. Sonawane, S.P. Patil, V.R. Huse, Influence of Mg doping on ZnO nanoparticles decorated on graphene oxide (GO) crumpled paper like sheet and its high photo catalytic performance under sunlight, J. Phys. Chem. Solids 114 (2018) 71–82. Copyright (2018) Elsevier.

This book belongs to Badji Mokhtar Annaba University Central Library Copyright Elsevier 2025

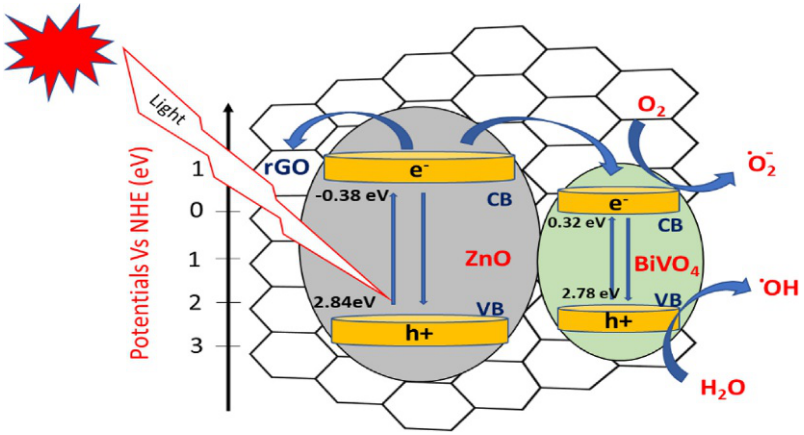

Fig. 7.7
The plausible photocatalytic mechanism of the graphene-based ternary heterojunction [56].
Reproduced from A. Raja, P. Rajasekaran, K. Selvakumar, M. Arunpandian, K. Kaviyarasu, S. Asath Bahadur, M. Swaminathan, Visible active reduced graphene oxide-$BiVO_4$-ZnO ternary photocatalyst for efficient removal of ciprofloxacin, Sep. Purif. Technol. 233 (2020) 115996. Copyright (2020) Elsevier.

Furthermore, ternary composites of two coupled semiconductor heterojunctions anchored onto GO sheets have been reported as efficient photocatalysts [110]. As reported earlier in Section 7.3.2, Raja and coworkers prepared rGO-$BiVO_4$-ZnO ternary photocatalyst by hydrothermal method. The $BiVO_4$ and ZnO have suitable band energy levels for the migration of photoinduced electrons from the CB of ZnO to $BiVO_4$. The lower value of CB of ZnO (−0.38 eV) than $BiVO_4$ (+0.32 eV) indicates vectorial flow of electrons from ZnO to $BiVO_4$, which enables effective photoinduced charge separation [56]. Furthermore, rGO contributes strongly to the separation of electron-hole pairs and extends the light absorption. These effects effectively increase the photocatalytic activity as shown in Fig. 7.7.

He et al. [60] reported on 3D porous G-CQDs/gC_3N_4 nanosheet aerogel metal-free ternary catalyst with high adsorption capacity and photocatalytic activity. The porous G increases the adsorption of dye, while the multifunctional CQDs provides effective absorbance of light in the ternary composite. The probable mechanism for the enhanced photocatalytic performance of G-CQDs/gC_3N_4 nanosheet for the removal of methyl orange under visible light is shown in Fig. 7.8. The photoinduced electrons of CNN produce $O_2^{\bullet-}$ by reduction of O_2, and the $O_2^{\bullet-}$ radicals slightly oxidize H_2O to generate •OH active species. The VB of CNN is more positive than the energy level of HO^- or H_2O, therefore the holes are directly involved in oxidation process without generating •OH radicals by reaction with water molecule.

Iwashina et al. [111] examined the Z-scheme photocatalyst for water-splitting under visible light irradiation. In Z-scheme systems containing rGO-TiO_2 (n-type semiconductor), binary composite behaves as an O_2-evolving photocatalyst, while various metal sulfides (p-type

This book belongs to Badji Mokhtar Annaba University Central Library Copyright Elsevier 2025

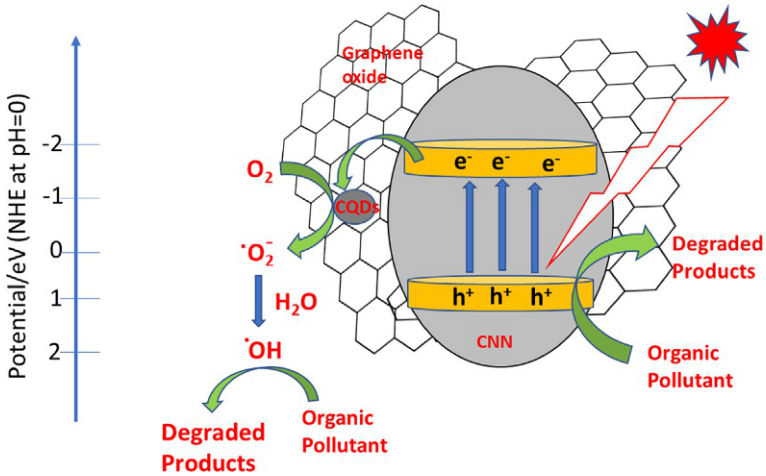

Fig. 7.8
The plausible photocatalytic mechanism of the graphene-based ternary carbon dots andcarbon nitride heterojunction [60]. *Reproduced from H. He, L. Huang, Z, Zhong, S. Tan, Constructing three-dimensional porous graphene-carbon quantum dots/g-C_3N_4 nanosheet aerogel metal-free photocatalyst with enhanced photocatalytic activity, Appl. Surf. Sci. 441 (2018) 285–294. Copyright (2018) Elsevier.*

semiconductor) act as H_2-evolving photocatalysts. RGO behaves as an electron transport mediator from O_2 to H_2 evolution, as shown in Fig. 7.9.

Chen et al. [112] prepared $BiVO_4$ quantum dots/rGO composites for the reduction of CO_2. This work pointed out that the rGO widened the bandgap of $BiVO_4$ (approximately to 2.7 eV from 2.4 eV) and facilitates the more energetic photogenerated electrons to reduce CO_2. Additionally, rGO prolonged the lifetime of photogenerated charge carriers by its electron capturing ability and consequently improved the photocatalytic activity. The plausible mechanism of reduction of CO_2 by $BiVO_4$ quantum dots/rGO composites is shown in Fig. 7.10. Furthermore, the reduction of CO_2 into CO, CH_4, or other hydrocarbons generally occurs at the potential of about −0.2 to −0.6 V verses NHE [113].

Some recent G and its derivatives-based photocatalysts with preparation methods and their various applications are summarized in Table 7.2.

7.7 Conclusion and future prospects

G and its derivatives-based photocatalyst offers many opportunities for various applications. The binary and ternary G-based photocatalyst provide a simple, stable, and low-cost alternative with excellent photocatalytic efficiency for organic pollutant degradations, hydrogen generation via water-splitting, and carbon dioxide reduction.

This book belongs to Badji Mokhtar Annaba University Central Library Copyright Elsevier 2025

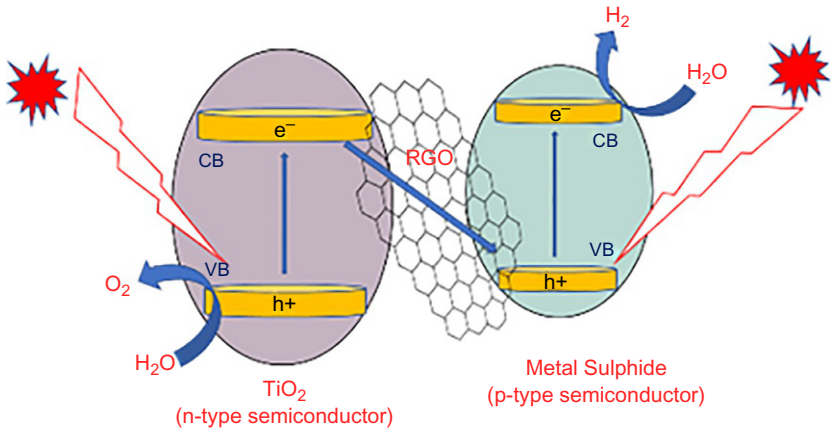

Fig. 7.9

The photocatalytic splitting of H_2O into H_2 and O_2 by graphene-based ternary nanocomposite [111]. *Reproduced from K. Iwashina, A. Iwase, Y.H. Ng, R. Amal, A. Kudo, Z-schematic water-splitting into H_2 and O_2 using metal sulfide as a hydrogen-evolving photocatalyst and reduced graphene oxide as a solid-state electron mediator, J. Am. Chem. Soc. 137 (2015) 604–607. Copyright (2015) American Chemical Society.*

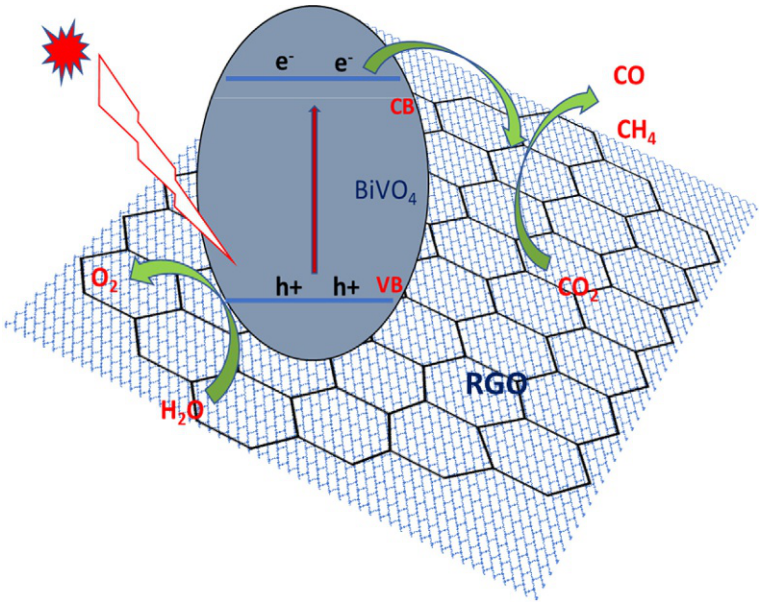

Fig. 7.10

The photocatalytic conversion of CO_2 by graphene-based ternary nanocomposite. *Reproduced from L. Chen, M. Zhang, J. Yang, Y. Li, Y. Sivalingam, Q. Shi, M. Xie, W. Han, Synthesis of $BiVO_4$ quantum dots/reduced graphene oxide composites for CO_2 reduction, Mater. Sci. Semicond. Process. 102 (2019) 104578. Copyright (2019) Elsevier.*

This book belongs to Badji Mokhtar Annaba University Central Library
Copyright Elsevier 2025

Table 7.2: Graphene-based composites: preparation methods and their photocatalytic applications.

Photocatalyst	Fabrication method	Photocatalytic applications	References
C_3N_4/rGO/C-TiO_2	An in situ synthesis method	Decomposition of NOx	[114]
Graphene@ZnO	Shear-assisted liquid exfoliation	Organic pollutant degradation	[115]
$Mn_{0.5}Cd_{0.5}S$/rGO-MoS_2 composite	Facile in situ growth process	H_2 evolution	[116]
$ZnIn_2S_4$/g-C_3N_4/graphene	Hydrothermal method	Hydrogen evolution	[117]
CdS-Bi_2MoO_6/rGO	Solvothermal method	Degradation of antibiotic ciprofloxacin	[118]
GO-Ag	Sonochemical method	Removal of dye from wastewater	[119]
rGO/TiO_2	Hydrothermal process	Hydrogen production	[120]
Bi_2S_3-$BiVO_4$-graphene aerogel	Facile hydrothermal method	Removal of Cr(VI) and bisphenol from water samples	[121]
$Bi_2O_2CO_3$/graphene quantum dots	Sonochemical method	Photocatalytic oxidation of NO	[122]
Lead Bismuth oxybromide/graphene oxide	Hydrothermal method	Removal of carbon dioxide, crystal violet dye, and 2-hydroxybenzoic acid	[123]
$BiVO_4$/$FeVO_4$@rGO	Hydrothermal method	Removal of tetracycline and hexavalent chromium ions from water	[124]
MoS_2/rGO	Hydrothermal method	Degradation of ranitidine and *N*-nitroso dimethylamine formation	[125]
TiO_2-rGO	Hydrothermal method	Degradation of formalin in aquaculture's waters	[126]
2D g-C_3N_4/Bi_2WO_6/rGO	Microwave-assisted method	Degradation of ibuprofen	[127]
TiO_2/g-C_3N_4/rGO	Electrospinning technique	Degradation of dye	[128]
Ag_2CrO_4/TiO_2/Au/r-GO nanostructures biofilm	Impregnation and in situ reduction method	Degradation of dye	[129]
rGO/$CuFe_2O_4$-TiO_2	Ultrasound assisted wet impregnation method	H_2 evolution by water-splitting	[130]
CuO-TiO_2/rGO	Wet impregnation method	Sonophotodegradation of organic pollutants	[131]

This book belongs to Badji Mokhtar Annaba University Central Library
Copyright Elsevier 2025

In this chapter, the history, preparation, and characterization of G and its derivatives-based photocatalyst have been discussed in details. Furthermore, this report highlights the latest and future directions for the development of advanced G-based photocatalysts. This chapter will help the scientific community to improve design strategies and optimize the performance of G-based photocatalysts in the field of material science. Recently another class of G derivative has emerged known as G quantum dots, which has gained huge interest worldwide. Researchers are working to develop functionalized G quantum dots toward the applications of various fields including medical, material, environmental, and many more.

Although G and its derivatives-based photocatalyst overcome challenges like utilization of visible/solar light, adsorption ability, photocorrosion, specific surface area, and active sites for photocatalytic reactions, there are still a few challenges to deal with before its implementation at an industrial level. Controlling the morphologies, structure, and electronic properties of G is one of the challenges, as it decides their hydrophily and capacity to produce active sites. Furthermore, the vast scale production of high-quality G and its derivatives-based photocatalyst is required in wastewater treatment at an industrial level. In the last few years, there has been huge growth in reports/works related to synthesis and different applications G-based photocatalyst. However, durability and continuous activity are the other challenges that need to be checked to find the practical application of G and its derivatives-based photocatalyst. Furthermore, the photocatalytic conversion of CO_2 has not been checked on a large scale. Therefore, there is a need to give more emphasis to solve the issues of new energy generation and removal of environmental pollution via a green approach.

References

[1] B. Qiu, M. Xing, J. Zhang, Recent advances in three-dimensional graphene-based materials for catalysis applications, Chem. Soc. Rev. 47 (2018) 2165–2216.
[2] X. Gong, G. Liu, Y. Li, D.Y.W. Yu, W.Y. Teoh, Functionalized-graphene composites: fabrication and applications in sustainable energy and environment, Chem. Mater. 28 (2016) 8082–8118.
[3] X. Li, L. Zhi, Graphene hybridization for energy storage applications, Chem. Soc. Rev. 47 (2018) 3189–3216.
[4] D. Morales-Acosta, J.D. Flores-Oyervides, J.A. Rodríguez-González, N. M. Sánchez-Padilla, R. Benavides, S. Fernández-Tavizón, J.A. Mercado-Silva, Comparative methods for reduction and sulfonation of graphene oxide for fuel cell electrode applications, Int. J. Hydrogen Energy 44 (2019) 12356–12364.
[5] M. Ghadiyali, S. Chacko, Hydrogenated-graphene-encapsulated graphene: a versatile material for device applications, ACS Omega 4 (2019) 17494–17503.
[6] S.P. Sasikala, J. Lim, I.H. Kim, H.J. Jung, T. Yun, T.H. Han, S.O. Kim, Graphene oxide liquid crystals: a frontier 2D soft material for graphene-based functional materials, Chem. Soc. Rev. 47 (2018) 6013–6045.
[7] R. Imani, F. Mohabatpour, F. Mostafavi, Graphene-based nano-carrier modifications for gene delivery applications, Carbon 140 (2018) 569–591.
[8] J. Xiao, W. Lv, Y. Song, Q. Zheng, Graphene/nanofiber aerogels: performance regulation towards multiple applications in dye adsorption and oil/water separation, Chem. Eng. J. 338 (2018) 202–210.
[9] P.C. Ooi, M.A.S.M. Haniff, M.F.M.R. Wee, C.F. Dee, B.T. Goh, M.A. Mohamed, B.Y. Majlis, Reduced graphene oxide preparation and its applications in solution-processed write-once-read-many-times graphene-based memory device, Carbon 124 (2017) 547–554.

This book belongs to Badji Mokhtar Annaba University Central Library Copyright Elsevier 2025

[10] Y. Hu, Á.I. López-Lorente, B. Mizaikoff, Graphene-based surface enhanced vibrational spectroscopy: recent developments, challenges, and applications, ACS Photonics 6 (2019) 2182–2197.
[11] A. Madni, S. Noreen, I. Maqbool, F. Rehman, A. Batool, P.M. Kashif, M. Rehman, N. Tahir, M. I. Khan, Graphene-based nanocomposites: synthesis and their theranostic applications, J. Drug Target. 26 (2018) 858–883.
[12] Y. Xue, H. Chen, D. Yu, S. Wang, M. Yardeni, Q. Dai, M. Guo, et al., Oxidizing metal ions with graphene oxide: the in-situ formation of magnetic nanoparticles on self-reduced graphene sheets for multifunctional applications, Chem. Commun. 47 (2011) 11689–11691.
[13] K. Thakur, B. Kandasubramanian, Graphene and graphene oxide-based composites for removal of organic pollutants: a review, J. Chem. Eng. Data 64 (2019) 833–867.
[14] W. Kong, H. Kum, S.-H. Bae, J. Shim, H. Kim, L. Kong, Y. Meng, K. Wang, C. Kim, J. Kim, Path towards graphene commercialization from lab to market, Nat. Nanotechnol. 14 (2019) 927–938.
[15] X. Huang, X. Qi, F. Boey, H. Zhang, Graphene-based composites, Chem. Soc. Rev. 41 (2012) 666–686.
[16] A. Jilani, M.H.D. Othman, M.O. Ansari, S.Z. Hussain, A.F. Ismail, I.U. Khan, Graphene and its derivatives: synthesis, modifications, and applications in wastewater treatment, Environ. Chem. Lett. 16 (2018) 1301–1323.
[17] A.M. Chávez, R.R. Solís, F.J. Beltrán, Magnetic graphene TiO_2-based photocatalyst for the removal of pollutants of emerging concern in water by simulated sunlight aided photocatalytic ozonation, Appl. Catal. Environ. 262 (2020) 118275.
[18] A.T. Smith, A.M. LaChance, S. Zeng, B. Liu, L. Sun, Synthesis, properties, and applications of graphene oxide/reduced graphene oxide and their nanocomposites, Nano Mater. Sci. 1 (2019) 31–47.
[19] A. Gholampour, M.V. Kiamahalleh, D.N.H. Tran, T. Ozbakkaloglu, D. Losic, From graphene oxide to reduced graphene oxide: impact on the physiochemical and mechanical properties of graphene–cement composites, ACS Appl. Mater. Interfaces 9 (2017) 43275–43286.
[20] A. Iqbal, S. Sajjad, S.A.K. Leghari, Low cost graphene oxide modified alumina nanocomposite as solar light induced photocatalyst, ACS Appl. Nano Mater. 1 (2018) 4612–4621.
[21] R. Tarcan, O. Todor-Boer, I. Petrovai, C. Leordean, S. Astilean, I. Botiz, Reduced graphene oxide today, J. Mater. Chem. C 8 (2020) 1198–1224.
[22] S.K. Sahoo, G. Hota, Amine-functionalized GO decorated with ZnO-$ZnFe_2O_4$ nanomaterials for remediation of Cr (VI) from water, ACS Appl. Nano Mater. 2 (2019) 983–996.
[23] C. Lu, P.-J.J. Huang, B. Liu, Y. Ying, J. Liu, Comparison of graphene oxide and reduced graphene oxide for DNA adsorption and sensing, Langmuir 32 (2016) 10776–10783.
[24] A. Filina, N. Yousefi, M. Okshevsky, N. Tufenkji, Antimicrobial hierarchically porous graphene oxide sponges for water treatment, ACS Appl. Bio Mater. 2 (2019) 1578–1590.
[25] H.Y. Hafeez, S.K. Lakhera, N. Narayanan, S. Harish, Y. Hayakawa, B.-K. Lee, B. Neppolian, Environmentally sustainable synthesis of a $CoFe_2O_4$–TiO_2/rGO ternary photocatalyst: a highly efficient and stable photocatalyst for high production of hydrogen (solar fuel), ACS Omega 4 (2019) 880–891.
[26] F. Perreault, A.F. De Faria, M. Elimelech, Environmental applications of graphene-based nanomaterials, Chem. Soc. Rev. 44 (2015) 5861–5896.
[27] H.C. Lee, W.-W. Liu, S.-P. Chai, A.R. Mohamed, A. Aziz, N. Cheng-Seong Khe, M. S. Hidayah, U. Hashim, Review of the synthesis, transfer, characterization and growth mechanisms of single and multilayer graphene, RSC Adv. 7 (2017) 15644–15693.
[28] W. Zhao, M. Fang, F. Wu, H. Wu, L. Wang, G. Chen, Preparation of graphene by exfoliation of graphite using wet ball milling, J. Mater. Chem. 20 (2010) 5817–5819.
[29] M. Yi, Z. Shen, A review on mechanical exfoliation for the scalable production of graphene, J. Mater. Chem. A 3 (2015) 11700–11715.
[30] N. Raghavan, S. Thangavel, G. Venugopal, A short review on preparation of graphene from waste and bioprecursors, Appl. Mater. Today 7 (2017) 246–254.
[31] H. Zhang, F. Ding, H. Li, Q. Fei, H. Meng, G. Hongwei, Controlled synthesis of monolayer graphene with a high quality by pyrolysis of silicon carbide, Mater. Lett. 244 (2019) 171–174.

This book belongs to Badji Mokhtar Annaba University Central Library Copyright Elsevier 2025

[32] P. Ranjan, S. Agrawal, S. Apurva, T. Rajagopala Rao, J. Balakrishnan, A.D. Thakur, A low-cost non-explosive synthesis of graphene oxide for scalable applications, Sci. Rep. 8 (2018) 1–13.
[33] R.K. Singh, R. Kumar, D.P. Singh, Graphene oxide: strategies for synthesis, reduction and frontier applications, RSC Adv. 6 (2016) 64993–65011.
[34] B.K. Ong, H.L. Poh, C.K. Chua, M. Pumera, Graphenes prepared by Hummers, Staudenmaier and Hofmann methods for analysis of TNT-based nitroaromatic explosives in seawater, Electroanalysis 24 (2012) 2085–2093.
[35] X. Liu, R. Ma, X. Wang, Y. Ma, Y. Yang, L. Zhuang, S. Zhang, J.C. Riffat Jehan, X. Wang, Graphene oxide-based materials for efficient removal of heavy metal ions from aqueous solution: a review, Environ. Pollut. 252 (2019) 62–73.
[36] P.P. Brisebois, M. Siaj, Harvesting graphene oxide—years 1859 to 2019: a review of its structure, synthesis, properties and exfoliation, J. Mater. Chem. C 8 (2020) 1517–1547.
[37] Q.A. Khan, A. Shaur, T.A. Khan, Y.F. Joya, M.S. Awan, Characterization of reduced graphene oxide produced through a modified Hoffman method, Cogent Chem. 3 (2017) 1298980.
[38] Y. Hou, S. Lv, L. Liu, X. Liu, High-quality preparation of graphene oxide via the Hummers' method: understanding the roles of the intercalator, oxidant, and graphite particle size, Ceram. Int. 46 (2020) 2392–2402.
[39] W.-T. Chang, Y.-H. Chao, C.-W. Li, K.-L. Lin, J.-J. Wang, S. Rajesh Kumar, S.J. Lue, Graphene oxide synthesis using microwave-assisted vs. modified Hummer's methods: efficient fillers for improved ionic conductivity and suppressed methanol permeability in alkaline methanol fuel cell electrolytes, J. Power Sources 414 (2019) 86–95.
[40] C. Botas, P. Álvarez, P. Blanco, M. Granda, C. Blanco, R. Santamaría, L.J. Romasanta, R. Verdejo, M. A. López-Manchado, R. Menéndez, Graphene materials with different structures prepared from the same graphite by the Hummers and Brodie methods, Carbon 65 (2013) 156–164.
[41] J.H. Kang, T. Kim, J. Choi, J. Park, Y.S. Kim, M.S. Chang, H. Jung, K.T. Park, S.J. Yang, C.R. Park, Hidden second oxidation step of Hummers method, Chem. Mater. 28 (2016) 756–764.
[42] J. Guerrero-Contreras, F. Caballero-Briones, Graphene oxide powders with different oxidation degree, prepared by synthesis variations of the Hummers method, Mater. Chem. Phys. 153 (2015) 209–220.
[43] M. Li, C. Song, Y. Wu, M. Wang, Z. Pan, S. Yang, M. Liang, S. Han, L. Xu, G. Lu, Novel Z-scheme visible-light photocatalyst based on $CoFe_2O_4$/BiOBr/graphene composites for organic dye degradation and Cr (VI) reduction, Appl. Surf. Sci. 478 (2019) 744–753.
[44] P.K. Labhane, S.H. Sonawane, G.H. Sonawane, S.P. Patil, V.R. Huse, Influence of Mg doping on ZnO nanoparticles decorated on graphene oxide (GO) crumpled paper like sheet and its high photo catalytic performance under sunlight, J. Phys. Chem. Solid 114 (2018) 71–82.
[45] E. Tao, Z. Ma, S. Yang, Y. Li, D. Ma, Z. Xing, Y. Li, Enhanced electrical conductivity of TiO_2/graphene: the role of introducing Ca^{2+}, J. Alloys Compd. 827 (2020) 154280.
[46] S. Ishaq, M. Moussa, F. Kanwal, M. Ehsan, M. Saleem, T.N. Van, DusanLosic, Facile synthesis of ternary graphene nanocomposites with doped metal oxide and conductive polymers as electrode materials for high performance supercapacitors, Sci. Rep. 9 (2019) 1–11.
[47] C. Hu, T. Lu, F. Chen, R. Zhang, A brief review of graphene–metal oxide composites synthesis and applications in photocatalysis, J. Chin. Adv. Mater. Soc. 1 (2013) 21–39.
[48] A.A. Grace, K.P. Divya, V. Dharuman, J.H. Hahn, Single step sol-gel synthesized Mn_2O_3-TiO_2 decorated graphene for the rapid and selective ultra-sensitive electrochemical sensing of dopamine, Electrochim. Acta 302 (2019) 291–300.
[49] T. Chhabra, A. Kumar, A. Bahuguna, V. Krishnan, Reduced graphene oxide supported MnO_2 nanorods as recyclable and efficient adsorptive photocatalysts for pollutants removal, Vacuum 160 (2019) 333–346.
[50] B. Xue, Y. Zou, Uniform distribution of ZnO nanoparticles on the surface of graphene and its enhanced photocatalytic performance, Appl. Surf. Sci. 440 (2018) 1123–1129.
[51] L. Tang, Y.R. Lee, J. Kim, J.-J. Shim, Photocatalytic activity of reduced graphene oxide/SnO_2 nanocomposites prepared in ionic liquid, Synth. Met. 201 (2015) 54–60.

This book belongs to Badji Mokhtar Annaba University Central Library Copyright Elsevier 2025

[52] G. He, J. Ding, J. Zhang, Q. Hao, H. Chen, One-step ball-milling preparation of highly photocatalytic active $CoFe_2O_4$-reduced graphene oxide heterojunctions for organic dye removal, Ind. Eng. Chem. Res. 54 (2015) 2862–2867.
[53] Y. Jiang, W.-N. Wang, P. Biswas, J.D. Fortner, Facile aerosol synthesis and characterization of ternary crumpled graphene–TiO_2–magnetite nanocomposites for advanced water treatment, ACS Appl. Mater. Interfaces 6 (2014) 11766–11774.
[54] H. Qiao, Z. Huang, S. Liu, Y. Tao, Z. Hu, M. Li, X. Qi, Novel mixed-dimensional photocatalysts based on 3D graphene aerogel embedded with TiO_2/MoS_2 hybrid, J. Phys. Chem. C 123 (2019) 10949–10955.
[55] M. Ahmad, E. Ahmed, W. Ahmed, A. Elhissi, Z.L. Hong, N.R. Khalid, Enhancing visible light responsive photocatalytic activity by decorating Mn-doped ZnO nanoparticles on graphene, Ceram. Int. 40 (2014) 10085–10097.
[56] A. Raja, P. Rajasekaran, K. Selvakumar, M. Arunpandian, K. Kaviyarasu, S. Asath Bahadur, M. Swaminathan, Visible active reduced graphene oxide-$BiVO_4$-ZnO ternary photocatalyst for efficient removal of ciprofloxacin, Sep. Purif. Technol. 233 (2020) 115996.
[57] R. Hassandoost, S.R. Pouran, A. Khataee, Y. Orooji, S.W. Joo, Hierarchically structured ternary heterojunctions based on Ce^{3+}/Ce^{4+} modified Fe_3O_4 nanoparticles anchored onto graphene oxide sheets as magnetic visible-light-active photocatalysts for decontamination of oxytetracycline, J. Hazard. Mater. 376 (2019) 200–211.
[58] X. Xin, S.-H. Li, N. Zhang, Z.-R. Tang, X. Yi-Jun, 3D graphene/AgBr/Ag cascade aerogel for efficient photocatalytic disinfection, Appl. Catal. Environ. 245 (2019) 343–350.
[59] X. Ni, J. Zhang, L. Hong, Y. Cheng, Y. Li, Reduced graphene oxide@ceria nanocomposite-coated polymer microspheres as a highly active photocatalyst, Colloids Surf. A: Physicochem. Eng. Asp. 567 (2019) 161–170.
[60] H. He, L. Huang, Z. Zhong, S. Tan, Constructing three-dimensional porous graphene-carbon quantum dots/g-C_3N_4 nanosheet aerogel metal-free photocatalyst with enhanced photocatalytic activity, Appl. Surf. Sci. 441 (2018) 285–294.
[61] P.K. Labhane, L.B. Patle, V.R. Huse, G.H. Sonawane, S.H. Sonawane, Synthesis of reduced graphene oxide sheets decorated by zinc oxide nanoparticles: crystallographic, optical, morphological and photocatalytic study, Chem. Phys. Lett. 661 (2016) 13–19.
[62] P.K. Labhane, L.B. Patle, G.H. Sonawane, S.H. Sonawane, Fabrication of ternary Mn doped ZnO nanoparticles grafted on reduced graphene oxide (RGO) sheet as an efficient solar light driven photocatalyst, Chem. Phys. Lett. 710 (2018) 70–77.
[63] A.Z. Saravani, M. Nadimi, M.A. Aroon, A.E. Pirbazari, Magnetic $TiO_2/NiFe_2O_4$/reduced graphene oxide nanocomposite as a recyclable photocatalyst for photocatalytic removal of methylene blue under visible light, J. Alloys Compd. 803 (2019) 291–306.
[64] G. Li, J. Hou, W. Zhang, P. Li, G. Liu, Y. Wang, K. Wang, Graphene-bridged WO_3/MoS_2 Z-scheme photocatalyst for enhanced photodegradation under visible light irradiation, Mater. Chem. Phys. 246 (2020) 122827.
[65] W. Zhang, F. Jie, Y. Wang, X. Zhang, J. Li, Enhanced visible-light photocatalytic activity of ZnS/BiOBr/graphene oxide ternary composite, J. Phys. Chem. Solid 127 (2019) 19–27.
[66] W. Zhang, S. Huo, S. Yang, Y. Zhong, S. Zhang, H. Wang, X. Zhong, Y. Fang, Ternary monolithic ZnS/CdS/rGO photomembrane with desirable charge separation/transfer routes for effective photocatalytic and photoelectrochemical hydrogen generation, Chem. Asian J. 14 (2019) 3431–3441.
[67] S. Zhang, B. Li, X. Wang, G. Zhao, B. Hu, Z. Lu, T. Wen, J. Chen, X. Wang, Recent developments of two-dimensional graphene-based composites in visible-light photocatalysis for eliminating persistent organic pollutants from wastewater, Chem. Eng. J. 390 (2020) 124642.
[68] M.M. Kandy, Carbon-based photocatalysts for enhanced photocatalytic reduction of CO_2 to solar fuels, Sustainable Energy Fuels 4 (2020) 469–484.
[69] N.M.S. Hidayah, W.-W. Liu, C.-W. Lai, N.Z. Noriman, C.-S. Khe, U. Hashim, H.C. Lee, Comparison on graphite, graphene oxide and reduced graphene oxide: synthesis and characterization, AIP Conf. Proc. 1892 (2017) 150002 1–5.

This book belongs to Badji Mokhtar Annaba University Central Library Copyright Elsevier 2025

[70] S.Y. Toh, K.S. Loh, S.K. Kamarudin, W.R.W. Daud, Graphene production via electrochemical reduction of graphene oxide: synthesis and characterisation, Chem. Eng. J. 251 (2014) 422–434.
[71] D.C. Marcano, D.V. Kosynkin, J.M. Berlin, A. Sinitskii, Z. Sun, A. Slesarev, L.B. Alemany, W. Lu, J. M. Tour, Improved synthesis of graphene oxide, ACS Nano 4 (2010) 4806–4814.
[72] H.Ö. Doğan, D. Ekinci, Ü. Demir, Atomic scale imaging and spectroscopic characterization of electrochemically reduced graphene oxide, Surf. Sci. 611 (2013) 54–59.
[73] N. Sharma, V. Sharma, Y. Jain, M. Kumari, R. Gupta, S.K. Sharma, K. Sachdev, Synthesis and characterization of graphene oxide (GO) and reduced graphene oxide (rGO) for gas sensing application, Macromol. Symp. 376 (2017) 1700006 1–5.
[74] S. Stankovich, R.D. Piner, S.B.T. Nguyen, R.S. Ruoff, Synthesis and exfoliation of isocyanate-treated graphene oxide nanoplatelets, Carbon 44 (2006) 3342–3347.
[75] C.K. Chua, M. Pumera, Chemical reduction of graphene oxide: a synthetic chemistry viewpoint, Chem. Soc. Rev. 43 (2014) 291–312.
[76] J. Phiri, L.-S. Johansson, P. Gane, T. Maloney, A comparative study of mechanical, thermal and electrical properties of graphene-, graphene oxide-and reduced graphene oxide-doped microfibrillated cellulose nanocomposites, Compos. Part B: Eng. 147 (2018) 104–113.
[77] X. Mei, X. Meng, W. Fengmin, Hydrothermal method for the production of reduced graphene oxide, Physica E 68 (2015) 81–86.
[78] D. Ickecan, R. Zan, S. Nezir, Eco-friendly synthesis and characterization of reduced graphene oxide, J. Phys. Conf. Ser. 902 (2017) 012027 1–5.
[79] J. Shen, Y. Hu, M. Shi, X. Lu, C. Qin, C. Li, M. Ye, Fast and facile preparation of graphene oxide and reduced graphene oxide nanoplatelets, Chem. Mater. 21 (2009) 3514–3520.
[80] L. Stobinski, B. Lesiak, A. Malolepszy, M. Mazurkiewicz, B. Mierzwa, J. Zemek, P. Jiricek, I. Bieloshapka, Graphene oxide and reduced graphene oxide studied by the XRD, TEM and electron spectroscopy methods, J. Electron Spectrosc. Relat. Phenom. 195 (2014) 145–154.
[81] S. Park, J. An, J.R. Potts, A. Velamakanni, S. Murali, R.S. Ruoff, Hydrazine-reduction of graphite-and graphene oxide, Carbon 49 (2011) 3019–3023.
[82] J. Long, S. Li, J. Liang, Z. Wang, B. Liang, Preparation and characterization of graphene oxide and it application as a reinforcement in polypropylene composites, Polym. Compos. 40 (2019) 723–729.
[83] K.S. Bhavsar, P.K. Labhane, R.B. Dhake, G.H. Sonawane, Solvothermal synthesis of activated carbon loaded CdS nanoflowers: boosted photodegradation of dye by adsorption and photocatalysis synergy, Chem. Phys. Lett. 744 (2020) 137202.
[84] Z. Zhang, L. Bai, Z. Li, Q. Yang, L. Jing, Review of strategies for the fabrication of heterojunctional nanocomposites as efficient visible-light catalysts by modulating excited electrons with appropriate thermodynamic energy, J. Mater. Chem. A 7 (2019) 10879–10897.
[85] K.S. Bhavsar, P.K. Labhane, R.B. Dhake, G.H. Sonawane, Crystal structures, morphological, optical, adsorption, kinetic and photocatalytic degradation studies of activated carbon loaded BiOBr nanoplates prepared by solvothermal method, Inorg. Chem. Commun. 104 (2019) 134–144.
[86] S. Dong, J. Feng, M. Fan, Y. Pi, L. Hu, X. Han, M. Liu, J. Sun, J. Sun, Recent developments in heterogeneous photocatalytic water treatment using visible light-responsive photocatalysts: a review, RSC Adv. 5 (2015) 14610–14630.
[87] M. Khan, M.N. Tahir, S.F. Adil, H.U. Khan, M. Rafiq, H. Siddiqui, A.A. Al-warthan, W. Tremel, Graphene based metal and metal oxide nanocomposites: synthesis, properties and their applications, J. Mater. Chem. A 3 (2015) 18753–18808.
[88] K. Maeda, Photocatalytic water splitting using semiconductor particles: history and recent developments, J. Photochem. Photobiol. C: Photochem. Rev. 12 (2011) 237–268.
[89] S. Chen, D. Huang, P. Xu, W. Xue, L. Lei, M. Cheng, R. Wang, X. Liu, R. Deng, Semiconductor-based photocatalysts for photocatalytic and photoelectrochemical water splitting: will we stop with photocorrosion? J. Mater. Chem. A 8 (2020) 2286–2322.
[90] D. Mateo, A. García-Mulero, J. Albero, H. García, N-doped defective graphene decorated by strontium titanate as efficient photocatalyst for overall water splitting, Appl. Catal. Environ. 252 (2019) 111–119.

This book belongs to Badji Mokhtar Annaba University Central Library Copyright Elsevier 2025

[91] P. Kumar, R. Boukherroub, K. Shankar, Sunlight-driven water-splitting using two-dimensional carbon-based semiconductors, J. Mater. Chem. A 6 (2018) 12876–12931.
[92] S. Matavos-Aramyan, S. Soukhakian, M.H. Jazebizadeh, M. Moussavi, M.R. Hojjati, On engineering strategies for photoselective CO_2 reduction—a thorough review, Appl. Mater. Today 18 (2019) 100499.
[93] M.-Q. Yang, X. Yi-Jun, Photocatalytic conversion of CO_2 over graphene-based composites: current status and future perspective, Nanoscale Horiz. 1 (2016) 185–200.
[94] X. Li, J. Yu, S. Wageh, A.A. Al-Ghamdi, J. Xie, Graphene in photocatalysis: a review, Small 12 (2016) 6640–6696.
[95] J. Albero, D. Mateo, H. García, Graphene-based materials as efficient photocatalysts for water splitting, Molecules 24 (2019) 906.
[96] P.K. Labhane, G.H. Sonawane, Fabrication of raspberry-shaped reduced graphene oxide labelled Fe/CeO_2 ternary heterojunction with an enhanced photocatalytic performance, Inorg. Chem. Commun. 113 (2020) 107809.
[97] L. Zhu, Z. Liu, P. Xia, H. Li, Y. Xie, Synthesis of hierarchical ZnO and graphene composites with enhanced photocatalytic activity, Ceram. Int. 44 (2018) 849–856.
[98] L. Cheng, Q. Xiang, Y. Liao, H. Zhang, CdS-based photocatalysts, Energ. Environ. Sci. 11 (2018) 1362–1391.
[99] R.K. Upadhyay, N. Soin, S.S. Roy, Role of graphene/metal oxide composites as photocatalysts, adsorbents and disinfectants in water treatment: a review, RSC Adv. 4 (2014) 3823–3851.
[100] M.L. Baynosa, D. Tuma, Y.R. Lee, J.-J. Shim, Solvent-driven morphology-controlled synthesis of highly efficient long-life ZnO/graphene nanocomposite photocatalysts for the practical degradation of organic wastewater under solar light, Appl. Surf. Sci. 486 (2019) 37–51.
[101] F. Chen, X. Jin, D. Jia, Y. Cao, H. Duan, M. Long, Efficient treament of organic pollutants over CdS/graphene composites photocatalysts, Appl. Surf. Sci. 504 (2020) 144422.
[102] R. He, Z. Lou, J. Gui, B. Tang, X. Difa, Room-temperature synthesis of BiOI/graphene oxide foam composite for phenol removal under visible light, Appl. Surf. Sci. 504 (2020) 144370.
[103] X. Yang, Z. Chen, J. Fang, Q. Yang, Z. Wan, X. Qian, D. Zhou, C. Liu, M. Chen, Freestanding 3D MoS_2 nanosheets/graphene aerogel heterostructure as a recyclable photocatalyst for efficiently degrading antibiotic residues, Mater. Lett. 252 (2019) 5–7.
[104] S. Bellamkonda, N. Thangavel, H.Y. Hafeez, B. Neppolian, G. Ranga Rao, Highly active and stable multi-walled carbon nanotubes-graphene-TiO_2 nanohybrid: an efficient non-noble metal photocatalyst for water splitting, Catal. Today 321 (2019) 120–127.
[105] M. Ghorbani, H. Abdizadeh, M. Taheri, M.R. Golobostanfard, Enhanced photoelectrochemical water splitting in hierarchical porous ZnO/reduced graphene oxide nanocomposite synthesized by sol-gel method, Int. J. Hydrogen Energy 43 (2018) 7754–7763.
[106] S. Ajit, B.-K. Lee, Rapid photo-degradation of 2-chlorophenol under visible light irradiation using cobalt oxide-loaded TiO_2/reduced graphene oxide nanocomposite from aqueous media, J. Environ. Manage. 165 (2016) 1–10.
[107] M.S. Abdel-Wahed, A.S. El-Kalliny, M.I. Badawy, M.S. Attia, T.A. Gad-Allah, Core double-shell $MnFe_2O_4$@rGO@TiO_2 superparamagnetic photocatalyst for wastewater treatment under solar light, Chem. Eng. J. 382 (2020) 122936.
[108] H. Tian, M. Liu, W. Zheng, Constructing 2D graphitic carbon nitride nanosheets/layered MoS_2/graphene ternary nanojunction with enhanced photocatalytic activity, Appl. Catal. Environ. 225 (2018) 468–476.
[109] P.K. Labhane, L.B. Patle, V.R. Huse, G.H. Sonawane, Synthesis of Ce doped ZnO nanoparticles coupled with graphene oxide as efficient photocatalyst for the degradation of dye under day light, AIP Conf. Proc. 1953 (2018) 030008 1–5.
[110] C. Prasad, Q. Liu, H. Tang, G. Yuvaraja, J. Long, A. Rammohan, G.V. Zyryanov, An overview of graphene oxide supported semiconductors based photocatalysts: properties, synthesis and photocatalytic applications, J. Mol. Liq. 297 (2019) 111826.
[111] K. Iwashina, A. Iwase, Y.H. Ng, R. Amal, A. Kudo, Z-schematic water splitting into H_2 and O_2 using metal sulfide as a hydrogen-evolving photocatalyst and reduced graphene oxide as a solid-state electron mediator, J. Am. Chem. Soc. 137 (2015) 604–607.

This book belongs to Badji Mokhtar Annaba University Central Library Copyright Elsevier 2025

[112] L. Chen, M. Zhang, J. Yang, Y. Li, Y. Sivalingam, Q. Shi, M. Xie, W. Han, Synthesis of $BiVO_4$ quantum dots/reduced graphene oxide composites for CO_2 reduction, Mater. Sci. Semicond. Process. 102 (2019) 104578.
[113] M. Han, S. Zhu, S. Lu, Y. Song, T. Feng, S. Tao, J. Liu, B. Yang, Recent progress on the photocatalysis of carbon dots: classification, mechanism and applications, Nano Today 19 (2018) 201–218.
[114] C. Noda, Y. Asakura, K. Shiraki, A. Yamakata, S. Yin, Synthesis of three-component C_3N_4/rGO/C-TiO_2 photocatalyst with enhanced visible-light responsive photocatalytic deNOx activity, Chem. Eng. J. 390 (2020) 124616.
[115] F. Rouzafzay, R. Shidpour, M.Z.M. Al-Abri, F. Qaderi, A. Ahmadi, M.T.Z. Myint, Graphene@ZnO nanocompound for short-time water treatment under sun-simulated irradiation: effect of shear exfoliation of graphene using kitchen blender, J. Alloys Compd. 829 (2020) 154614.
[116] Y. Liu, Z. Gong, Y. Xie, H. Lv, B. Zhang, Revealing the synergetic effects of graphene and MoS_2 on boosted photocatalytic H_2 production of $Mn_{0.5}Cd_{0.5}S$ photocatalyst, Appl. Surf. Sci. 505 (2020) 144637.
[117] S. Manchala, V.S.R.K. Tandava, L.R. Nagappagari, S.M. Venkatakrishnan, D. Jampaiah, Y.M. Sabri, S. K. Bhargava, V. Shanker, Fabrication of a novel $ZnIn_2S_4$/gC_3N_4/graphene ternary nanocomposite with enhanced charge separation for efficient photocatalytic H_2 evolution under solar light illumination, Photochem. Photobiol. Sci. 18 (2019) 2952–2964.
[118] Z. Chen, J. Liang, X. Xu, G. He, H. Chen, CdS–Bi_2MoO_6/RGO nanocomposites for efficient degradation of ciprofloxacin under visible light, J. Mater. Sci. 55 (2020) 6065–6077.
[119] S. Kumari, P. Sharma, S. Yadav, J. Kumar, A. Vij, P. Rawat, S. Kumar, et al., A novel synthesis of the graphene oxide-silver (GO-Ag) nanocomposite for unique physiochemical applications, ACS Omega 5 (2020) 5041–5047.
[120] H. Wang, G. Wang, Y. Zhang, Y. Ma, Q. Zhang, P. Hongqin, W. Xu, D. Gao, B. Wang, X. Qi, Preparation of RGO/TiO_2 photocatalyst and the mechanism of its hydrothermal process, J. Chin. Chem. Soc. 66 (2019) 734–739.
[121] Q. Liang, S. Ploychompoo, J. Chen, T. Zhou, H. Luo, Simultaneous Cr(VI) reduction and bisphenol A degradation by a 3D Z-scheme Bi_2S_3-$BiVO_4$ graphene aerogel under visible light, Chem. Eng. J. 384 (2020) 123256.
[122] Y. Liu, Y. Zhou, S. Yu, Z. Xie, Y. Chen, K. Zheng, S. Mossin, et al., Defect state assisted Z-scheme charge recombination in $Bi_2O_2CO_3$/graphene quantum dot composites for photocatalytic oxidation of NO, ACS Appl. Nano Mater. 3 (2020) 772–781.
[123] F.-Y. Liu, Y.-M. Dai, F.-H. Chen, C.-C. Chen, Lead bismuth oxybromide/graphene oxide: synthesis, characterization, and photocatalytic activity for removal of carbon dioxide, crystal violet dye, and 2-hydroxybenzoic acid, J. Colloid Interface Sci. 562 (2020) 112–124.
[124] R. Yang, Z. Zhu, C. Hu, S. Zhong, L. Zhang, B. Liu, W. Wang, One-step preparation (3D/2D/2D) $BiVO_4$/FeVO@rGO heterojunction composite photocatalyst for the removal of tetracycline and hexavalent chromium ions in water, Chem. Eng. J. 390 (2020) 124522.
[125] X. Zou, J. Zhang, X. Zhao, Z. Zhang, MoS_2/rGO composites for photocatalytic degradation of ranitidine and elimination of NDMA formation potential under visible light, Chem. Eng. J. 383 (2020) 123084.
[126] J.F. Leal, S.M.A. Cruz, B.T.A. Almeida, V.I. Esteves, P.A.A.P. Marques, E.B.H. Santos, TiO_2–rGO nanocomposite as an efficient catalyst to photodegrade formalin in aquaculture's waters, under solar light, Environ. Sci.: Water Res. Technol. 6 (2020) 1018–1027.
[127] S.-H. Liu, W.-T. Tang, P.-H. Chou, Microwave-assisted synthesis of triple 2D g-C_3N_4/Bi_2WO_6/rGO composites for ibuprofen photodegradation: kinetics, mechanism and toxicity evaluation of degradation products, Chem. Eng. J. 387 (2020) 124098.
[128] L. Hu, J. Yan, C. Wang, B. Chai, J. Li, Direct electrospinning method for the construction of Z-scheme TiO_2/g-C_3N_4/rGO ternary heterojunction photocatalysts with remarkably ameliorated photocatalytic performance, Chin. J. Catal. 40 (2019) 458–469.
[129] R. Biswas, S. Mete, M. Mandal, B. Banerjee, H. Singh, I. Ahmed, K. KantaHaldar, Novel green approach for fabrication of Ag_2CrO_4/TiO_2/Au/r-GO hybrid biofilm for visible light-driven photocatalytic performance, J. Phys. Chem. C 124 (2020) 3373–3388.

This book belongs to Badji Mokhtar Annaba University Central Library Copyright Elsevier 2025

[130] H.Y. Hafeez, S.K. Lakhera, P. Karthik, M. Anpo, BernaurdshawNeppolian, Facile construction of ternary $CuFe_2O_4$-TiO_2 nanocomposite supported reduced graphene oxide (rGO) photocatalysts for the efficient hydrogen production, Appl. Surf. Sci. 449 (2018) 772–779.

[131] S.G. Babu, P. Karthik, M.C. John, S.K. Lakhera, M. Ashokkumar, J. Khim, B. Neppolian, Synergistic effect of sono-photocatalytic process for the degradation of organic pollutants using CuO-TiO_2/rGO, Ultrason. Sonochem. 50 (2019) 218–223.

This book belongs to Badji Mokhtar Annaba University Central Library

Copyright Elsevier 2025

This page intentionally left blank

This book belongs to Badji Mokhtar Annaba University Central Library

Copyright Elsevier 2025

CHAPTER 8

Luminescence nanomaterials for photocatalysis

Amol Nande[a], Ashish Tiwari[b], Swati Raut[c], Renu Nayar[d], and S.J. Dhoble[c]

[a]Guru Nanak College of Science, Ballarpur, Chandrapur, India, [b]Dr. Bhimrao Ambedkar Government College, Pamgarh, India, [c]Department of Physics, R. T. M., Nagpur University, Nagpur, India, [d]D. P. Vipra College, Bilaspur, India

8.1 Introduction—Basic principal of phosphor for photocatalysis

As we have seen, evolution of technology in every field of science has exploded; for example, the telephone has changed to the mobile phone, and with it we can perform any possible work—making calls, transferring money, shopping, reading, entertainment, and much more. This suggests that we rely on constant development of technology and scientific knowledge, which supports and solves the necessities of our society. Therefore, researchers have been continuously trying to develop a better world around us by increasing the properties of materials that can be used in industries in more efficient and better ways. However, humans always relate development with industry, although industries provide us with job vacancies and development discussed before. But the mass production of anything leaves us with pollution such as air pollution and water pollution. Therefore, another problem is to purify air and water pollution due to industry. Photocatalysis could be one of the solutions for purifying air and water pollution.

Photocatalysis is a photoinduced catalytic process. Photocatalytic materials absorb electromagnetic radiation in which electrons absorb incident photons and jump from valance band (VB) to conduction band (CB), and therefore holes are produced in the VB, as shown in Fig. 8.1. During this process (called photocatalysis), energy and momentum is conserved, which depicts that photons have same energy as the bandgap. Moreover, in this process, photogenerated holes undergo oxidation process; at the same time, reduction happens due to photogenerated electrons. This process, first mentioned by Dr. Alexander Eibner in 1911, was the first explanation of photocatalysis phenomenon provided by Landau in 1913 [1, 2].

Handbook of Nanomaterials for Wastewater Treatment. https://doi.org/10.1016/B978-0-12-821496-1.00005-2
Copyright © 2021 Elsevier Inc. All rights reserved.

This book belongs to Badji Mokhtar Annaba University Central Library Copyright Elsevier 2025

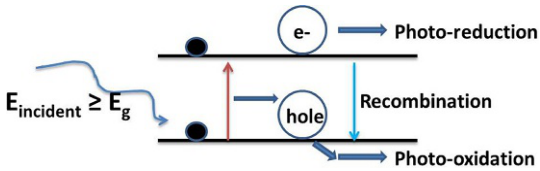

Fig. 8.1
Schematic diagram showing photocatalysis process.

Although the process was first explained in the early 19th century, there was not much work performed due to a lack of practical applications. For the last couple of decades, the photoinduced catalysis process was used to clean air pollution and water pollution. The photocatalytic materials sensitive to photons or light act as photosensitizer for bleaching dyes in the presence of oxygen, causing discoloration of organic chemicals by photo-oxidation, although the materials retain it after the process. The most groundbreaking work in this field was by Fujishima and Honda [3], who reported on the production of pure hydrogen using water and sunlight. The process involves a rutile electrode (which is photosensitive to ultraviolet light) and a platinum electrode (for electrical load) in which hydrogen is produced using water and sunlight. Another pioneer work to mention in field of photosensitizers is the photo-oxidation of isopropanol on rutile stannous oxide (TiO_2). Also in the presence of TiO_2 and oxygen and in alkaline conditions, cyanide degraded to cyanate [4, 5]. Current studies signify that photocatalysis and photocatalyst materials show various interesting real-life applications such as purifying industrial wastewater, isolating metal ions from polluted air as well as air pollution, producing hydrogen gas from water molecules, etc. [6–8]. This clearly suggests the photocatalysis field evolved to become an established technology that also holds the solution for many real-life problems for human society in an environment friendly manner. However, the bandgap of the materials determines their ability to work under visible light radiation [9, 10].

Luminescent phosphors that are capable of emitting high-energy photons by absorbing two or more low-energy photons (called upconverting luminescent phosphors) opens up new research opportunities in this field. These materials contain luminescent dopants or activators (such as Eu, Tb, Tm, Er, etc.) that contain an intermediate transition, which allows an electron to absorb a low-energy photon and jump to intermediate states and to a VB by absorbing another low-energy photon; the electron jumps back to CB by emitting combined energy, which is obviously greater than the incident of low-energy photons [11–15]. Luminescent materials have host and dopant materials. The host materials (like $BiWO_6$, $SrTiO_3$, CdS, etc.) cannot absorb low-energy photons due to wide bandgap. However, upconverting luminescent activators absorb low-energy photons and convert them to high-energy photons (by absorbing more than one photon). This enables band-to-band transition in host materials. In this process, the host materials maintain their photocatalytic activity like redox reaction of electrons in VB and holes in CB. In addition to upconverting phosphors, long persistent phosphors (LPP) are another more efficient candidate for photocatalytic activities. These materials have electrons with high

This book belongs to Badji Mokhtar Annaba University Central Library Copyright Elsevier 2025

mobility from the VB to trap levels, which can act as electron storage level. This favors photocatalytic properties [16, 17]. The trap levels in LPP generate oxygen vacancy defects when they are doped with rare-earth metal ions [17]. It is considered that electrons are in these trapped levels. Later, during recombination of electrons and holes, energy releases in the form of phosphorescence. In this process, electrons release slowly and allow more electrons and holes. This promotes the photocatalysis process [17–19]. However, there are many things to explore in this field.

In this chapter, we focused mainly on the detailed mechanism and challenges of luminescence materials in photocatalysis followed by the effect of rare-earth metal doping in inorganic phosphors, which are further utilized in the field of photocatalysis. Later, we will focus on what the effect of nanosized luminescent phosphors on photocatalysis will be. This follows the synthesis and characterization of inorganic nanophosphor materials and their properties used in photocatalysis. The chapter also contains discussion about nanophosphor material applications in water purification and hydrogen generation mechanisms. Last, we provide our conclusion with the future scope in this field.

8.2 Mechanism and challenges of luminescence materials in photocatalysis

As we discussed in the previous section, the main requirement is to improve the efficiency of a photocatalyst and make it work with solar irradiation so that it can be easily adaptable by industries to use for water and air purification of their waste materials. To do this, we have to understand the process of photocatalysis; the main requirement for a photocatalysis process is the presence of bandgap energy (a separation between CB and VB) and formation of an electron-hole pair. The electron and hole recombines and releases heat energy or initiates and promotes reduction and oxidation reactions by interactions. Moreover, as shown in Fig. 8.1, a photocatalyst must start oxidation and reduction process simultaneously. The most common photocatalyst materials are TiO_2 and ZnO, which are used to oxidize toxic materials in industrial wastes [20–24]. However, a semiconductor has very wide bandgap, so low photon energy would not be sufficient to initiate the photocatalysis process. In contrast, luminescence phosphors provide an extra intermediate level that ultimately causes the initiation of the oxidation and reduction processes for low photon energy radiations as well. There are inorganic and organic luminescence phosphors, but in this chapter we confined our writing toward different types of inorganic phosphors and their utilization in photocatalysis activities. Further luminescence effect is also categorized on the basis of excitation source (i.e., if light is an excitation source, then observed luminescence effect is photoluminescence) such as cathode-luminescence, photoluminescence, chemiluminescence, X-ray luminescence, bioluminescence, and thermoluminescence. Because we are interested in applications of luminescent materials in photocatalysis phenomenon, we discuss only photoluminescence in this chapter.

Generally, inorganic phosphors are lanthanide (rare-earth elements)-doped compounds (such as oxides, halides, aluminates, sulfates, phosphates, and silicates) that are capable of emitting light

This book belongs to Badji Mokhtar Annaba University Central Library Copyright Elsevier 2025

at a specified wavelength when exposed to or excited by electromagnetic radiation [25–27]. In these phosphors, rare-earth elements act as a luminescent center with precisely tuned color emission due to their 4f-5d transitions. Rare-earth luminescent dopant exists in phosphor as 2^+ or 3^+ ions. When these atoms lose two electrons in outer 6s electrons, they transform into divalent ions. And if another electron is lost from 5d-orbital or 4f-orbital, they produce a trivalent ion. One may wonder how the same metal ion shows similar properties in different host compounds (e.g., Eu shows close to red emission band). The reason for this is 4f orbitals of rare earth penetrate the xenon core appreciably and, because of this, they do not overlap significantly in bonding with ligands or host materials. This suggests their isolation from the influence of the host materials, and hence electronic properties are essentially unaffected by the environment. Also, these materials are incapable of π bonds, and thus there are no double- or triple-bond formations with transition metals. These properties make rare-earth materials interesting to use in inorganic phosphors as a luminescent center.

When a photon is incident on inorganic phosphor electron in VB or ground state jumps to CB or excited state, then the excited electron returns back to ground state either by radiative transition or by nonradiative transition, as shown in Fig. 8.2. The radiative transition is the luminescence that occurs by emission of a photon of definite energy, which is mostly smaller than the absorption photon energy. Nonradiative transition is when an excited electron decays to ground state by emitting phonons. No emission is observed in this transition, but the absorbed energy is emitted in the form of heat energy. Radiative and nonradiative transitions are happening simultaneously and competing with each other. However, for better luminescence process, radiative transition should be dominating compared with nonradiative transition and should convert absorbed excitation energy into photons.

Experimentally, photocatalysis was studied by monitoring degradation of dyes like methylene blue or methylene orange in an aqueous solution. These dyes show absorbance peak at a particular wavelength, for example, methylene blue has an absorbance band at 665 nm. One can measure the absorbance intensity as a function of time, and systematic decrease absorbance intensity suggests concentration of dye decreases in the solution. One can calculate degradation percentage as a function of time as:

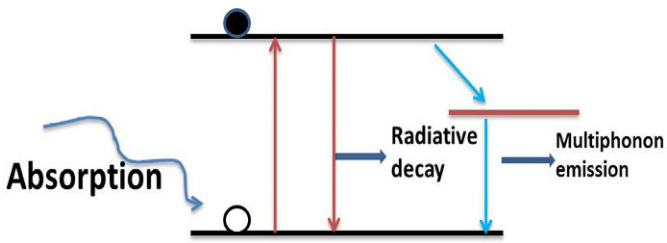

Fig. 8.2
A schematic showing radiative and nonradiative (multiphonon emission) decay.

This book belongs to Badji Mokhtar Annaba University Central Library Copyright Elsevier 2025

$$\text{Degradation}\,(\%) = (A_0 - A_t) \times 100 \Big/ A_0$$

Here, A_0 and A_t are the absorbance measured before and after light exposure, respectively. Researchers have observed both the increase and decrease in photocatalytic activity by using luminescence phosphors [17, 28–30]. The samples with lower luminescence produce more electrons and holes during the phosphorescence process compared with samples with higher luminescence, which use maximum electron-holes pairs to give off emissions. As a matter of fact, the photocatalytic process is increased for more free carriers. From this, we can say that luminescence material with poor luminescent properties can produce more electrons or holes, which ultimately enhanced the photocatalysis process. In the following section, we explained how rare-earth metal ion-doped inorganic phosphor helps increase the efficiency of traditional photocatalysts in detail.

8.3 Rare-earth-doped inorganic phosphor materials for photocatalysis

As discussed earlier, when inorganic materials (such as oxide, borate, phosphate, etc.) are doped with rare-earth materials, they emit colors as they become excited by electromagnetic radiations due to 4f-5d transitions of divalent and trivalent rare-earth metal ion.

The inorganic phosphors include downconverting phosphors, upconverting phosphors, and long-lasting phosphors. Downconverting phosphors convert high-energy photons into low-energy photons while upconverting phosphors convert low-energy photons to high-energy photons. In addition to these two phosphors, long-lasting phosphors are the phosphors that glow after turning off the external irradiation source [18, 31–36]. In this section of the chapter, downconverting phosphors, upconverting phosphors, long-lasting phosphors, and their applications in the field of photocatalysis will be discussed.

8.3.1 Downconversion phosphors

As mentioned previously, these phosphors are the most common phosphors that basically absorb high-energy photons (low-energy wavelength photons), and longer wavelength or low-energy photons are being emitted. Fig. 8.3A depicts that electrons in ground state or VB absorb high-energy photons and jump to excited state or CB later instead of coming back to ground state. Fig. 8.3B shows an example of downconversion and upconversion of mechanism for luminescence phosphors.

An example of downconversion mechanism for Tb^{3+} and Yb^{3+}-doped $KYb(WO_4)_2$ phosphor are shown in Fig. 8.3B [37, 38]. In $KYb(WO_4)_2$, the phosphor is excited to 308 nm to Tb^{3+} ions; they observe Tb^{3+} ($^5D_4 \rightarrow {}^2F_{5/2}$) as well as for Yb^{3+} ($^5F_{5/2} \rightarrow {}^2F_{7/2}$) emission. This results by considering the energy transfer from Tb^{3+} to Yb^{3+} as cross-relaxation is observed between $D_4 \rightarrow {}^7F_0$ and $^5F_{5/2} \rightarrow {}^2F_{7/2}$ transitions. This is a nonresonant energy transfer that can be

This book belongs to Badji Mokhtar Annaba University Central Library Copyright Elsevier 2025

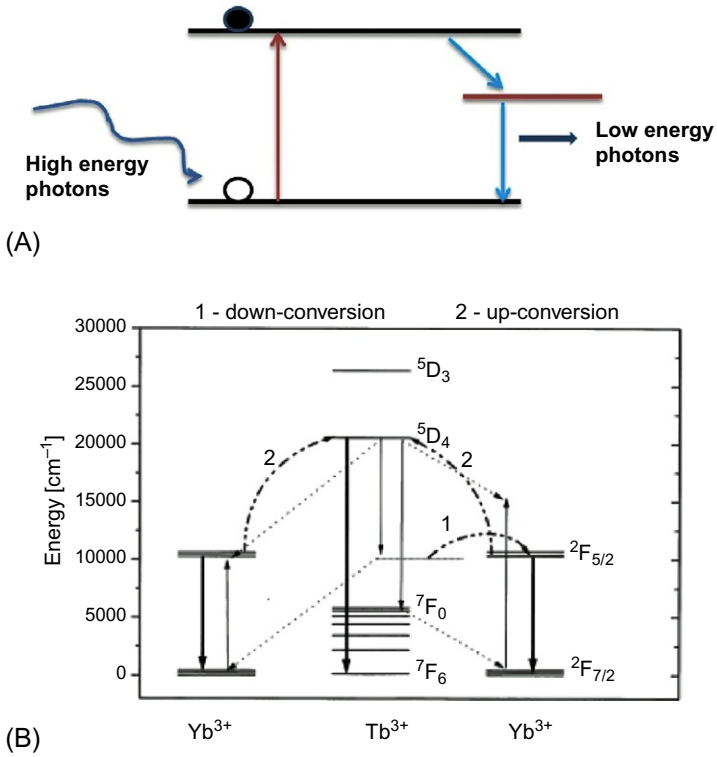

Fig. 8.3

(A) Schematic shows downconversion phenomenon in inorganic phosphors. (B) Typical example for schematic energy level diagram for downconversion mechanism and upconversion mechanism in Yb and Tb ions [37]. *Produced with Copyright @ 2001 Elsevier Science permission.*

explained using Miyakawa-Dexter model with the rate constant given by $k(\Delta E) = \begin{bmatrix} n+1 \\ n \end{bmatrix}^N k(0)\exp(-\gamma\Delta E)$, where, γ is the electron-phonon coupling parameter [39]. The presented results suggest that, along with the relaxation process of D_4 states of Tb^{3+} ions, downconversion process is happening in the system as shown in Fig. 8.3B [40]. $^5D_4 \rightarrow {}^2F_{5/2} + {}^2F_{5/2}$ transition is expected when Tb^{3+} excited energy is dispensed between two different Yb^{3+} ions. This process is nothing but a downconversion process. It is also proven that the downconversion process for Tb^{3+} and Yb^{3+}-doped $KYb(WO_4)_2$ phosphor is power- and temperature-dependent. It suggests that, with increasing temperature, downconversion process increased as there is a better matching of energy levels [37]. A similar Tb^{3+} and Yb^{3+} energy transfer is observed for $Yb_xY_{1-x}PO_4$: Tb^{3+}, Y_2O_3 and $GdBO_3$:Tb^{3+}, $Yb3^+$ [41, 42].

An illustration of typical photoluminescence spectrum is shown in Fig. 8.4A. The figure depicts photoluminescence emission for Y_2O_3S: Eu using 400 nm excitation wavelengths. The peaks are observed in red and orange emission peaks, which happened due to $5d^0 \rightarrow 7f^2$ and $5d^0 \rightarrow 7f^0$

This book belongs to Badji Mokhtar Annaba University Central Library Copyright Elsevier 2025

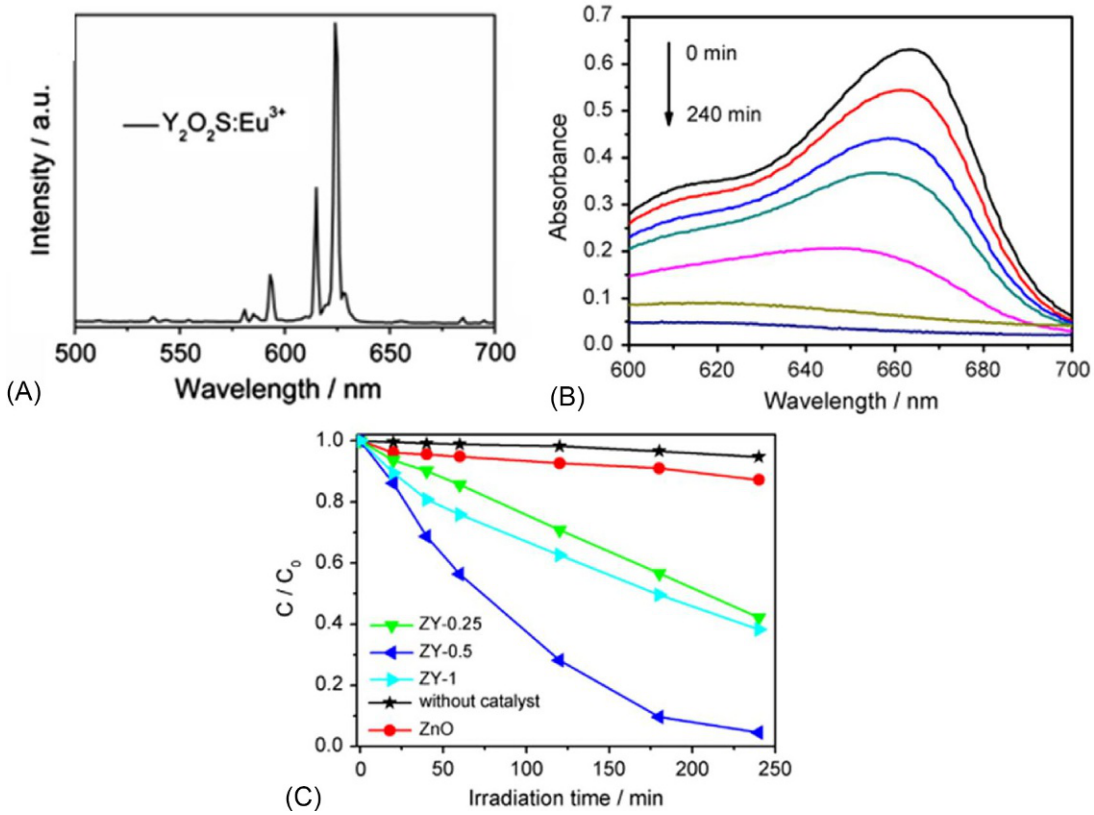

Fig. 8.4

(A) An example showing photoluminescence spectra for downconversion phosphor Y_2O_2S: Eu. (B) Absorption study of methylene blue as a function of time irradiation using photocatalysis ZnO-Y_2O_2S: Eu. (C) Time-dependent photodegradation of methylene blue using ZnO-Y_2O_2S: Eu photocatalyst [43]. *Figure used with permission Copyright @ 2013 Elsevier.*

or $5d^0 \rightarrow 7f^1$ transitions. The luminescence phosphor supports electron transfer process and reduces photogenerated charge carrier recombination in host photocatalysis ZnO. With increasing concentration of dopant, the photocatalytic activities increased until reaching a certain concentration. Afterward, the photocatalytic activities decreased with further increasing concentration of dopant. For a particular concentration of dopant (in this case 0.5), absorbance of methylene blue decreased with increase in exposure time of the mixture, as shown in Fig. 8.4B. Furthermore, the improvement in photocatalysis process with increasing concentration of luminescence phosphor was confirmed and is shown in Fig. 8.4C. From the figure, it is clear that the inorganic phosphor and ZnO do not have photocatalysis activity. However, ZnO-Y_2O_3S: Eu showed better photocatalysis process and maximum activity for 0.5%. It is also interesting to note that, without light irradiation, the degradation process is negligible [43].

This book belongs to Badji Mokhtar Annaba University Central Library Copyright Elsevier 2025

As explained previously, when phosphor absorbs a high-energy photon and converts it to a low-energy photon, the phosphor is termed as a downconversion process [44]. This property can be utilized to carry out a photocatalysis process in which the higher wavelength photon can be absorbed by a given dye so that the dye gets to its excited state and several electron-hole pairs are generated. Self-sensitized degradation of dye is increased [45, 46]. The reported works suggest that downconverting phosphors doped with rare-earth metal ion increases the photocatalytic activities as the doped phosphors help to match the energy of photons required to carry out the activities [6, 29, 38, 47]. Apart from the mentioned phosphors, photocatalytic activity using Ce^{3+}-, Sm^{3+}-, Dy^{3+}-, and Eu^{3+}-doped oxides, which are downconverting inorganic phosphors, used their inherent property for self-sensitized degradation of dyes [43, 48–50]. This inferred that the self-degradation of water pollution from industries can be enhanced when downconversion phosphors combine with photocatalysts. Thus it can be concluded that downconversion luminescence phosphors definitely increase the photocatalytic activity in UV-visible light and can be used for cleaning industrial wastewater.

8.3.2 Upconversion phosphors

As our discussion continues, it is clear that industrial applications are more intended to increase the photocatalyst absorption properties from ultraviolet radiation to visible radiation as well-known photocatalysts like TiO_2 or ZnO absorbed a lesser amount of solar energy [51, 52]. In this case, upconverting luminescence phosphors provide new insight. Upconverting phosphors are composed of a host lattice and luminescent activator. The host materials are inert materials whereas luminescence activators are optically active cations.

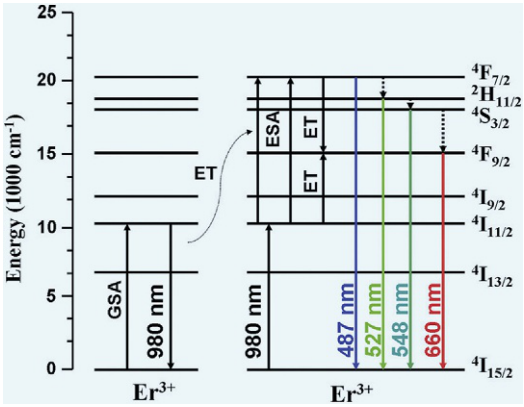

Fig. 8.5
Schematic showing energy level representing upconversion process in Er^{3+} [53, 54]. *Used with permission Copyright @ 2013 Elsevier.*

This book belongs to Badji Mokhtar Annaba University Central Library
Copyright Elsevier 2025

A typical example of energy transfer mechanism in upconverting luminescent phosphor is shown in Fig. 8.5. From the figure, it is clear that when photons incident on Er^{3+}-doped luminescent phosphors, the ion is excited from energy level $^4I_{15/2}$ to energy level $^4I_{9/2}$ by the absorption of light. During nonradiative transitions ($^4I_{9/2} \rightarrow {}^4I_{15/2}$), energy releases; this energy is absorbed by neighboring Er^{3+} ion of energy state $^4I_{11/2}$ ($^4I_{13/2}$). Later, neighboring Er^{3+} ion is excited to $^4F_{3/2}$ ($^2H_{11/2}$) state, which goes through a number of steps as ($^4I_{9/2}$, $^4I_{11/2}$) → ($^4I_{15/2}$, $^4F_{3/2}$) and ($^4I_{9/2}$, ^{4}I13/2) → ($^4I_{15/2}$, $^2H_{11/2}$). This suggests that a two-photon process is responsible for upconversion emission viz. green ($^2H_{11/2}$/$^4S_{3/2} \rightarrow {}^4I_{15/2}$) and red ($^4F_{9/2} \rightarrow {}^4I_{15/2}$) [53–56]. This mechanism is also observed for other Er^{3+}-doped upconverting phosphors such as $Y_3Al_5O_{12}$, $YAlO_3$, CaF_2, NYF_4, and $CaY(WO_4)_2$.

These phosphors show wide applications in the field of photocatalysis. Generally these phosphors combine with semiconductors like TiO_2 and ZnO to form hybrid components with superior photocatalytic active compounds [57–59]. These composites absorb solar light in the photocatalytic process, and it is observed that the degradation rate of color dyes increased up to 90% in 60 min as compared to pure semiconductor materials [58]. Researchers also have studied Yb, Tm, and co-doped upconverting luminescence phosphors and observed their effect on photocatalytic activities. They observed the enhancement of photocatalytic activities [60–63].

An example explaining energy transfer process in upconversion as a function of time is shown in Fig. 8.6A. From the figure, it is clear that excited state absorbance dominates closer to 410 nm, and afterward the energy transfer process is more prominent. At last, after a few microseconds, excited absorption process is denominated in the spectra. The analysis also supports two color excitation favors excited state absorption, hence leading to upconversion effect from $^2P_{3/2}$ state [64]. The application of upconversion process in photocatalysis is explained by studying degradation of organic dyes as a function of exposure time. Fig. 8.6B illustrates the analysis used for the degradation study. The figure showed that when photocatalysts like TiO_2 are coated with upconverting phosphor like YAG: Er, the significant absorption peak disappeared when it irradiates for more time. In this study, the photodegradation of congo red dye has been studied for TiO_2 /YAG: Er combination. The significant peaks at 500 nm disappeared eventually as irradiation time increased [65]. The mechanism is explained in the next section.

The previous discussion clearly suggests that the upconverting phosphors increase the formation of electron-hole pairs leading to significantly enhanced photocatalytic process in a pure semiconductor. The free electrons are utilized to decompose organics absorbed by the host or semiconductor, and hence water molecules oxidize to generate hydroxyl molecule and dissipated organic solutions [45, 66]. The photon-generated electrons at CB reduces O_2 and O_2^-, and H_2O_2 and OH are formed, which are highly reactive ions. Thus these ions can mineralize pollutants from organic pollution to CO_2 and H_2O.

This book belongs to Badji Mokhtar Annaba University Central Library Copyright Elsevier 2025

This book belongs to Badji Mokhtar Annaba University Central Library

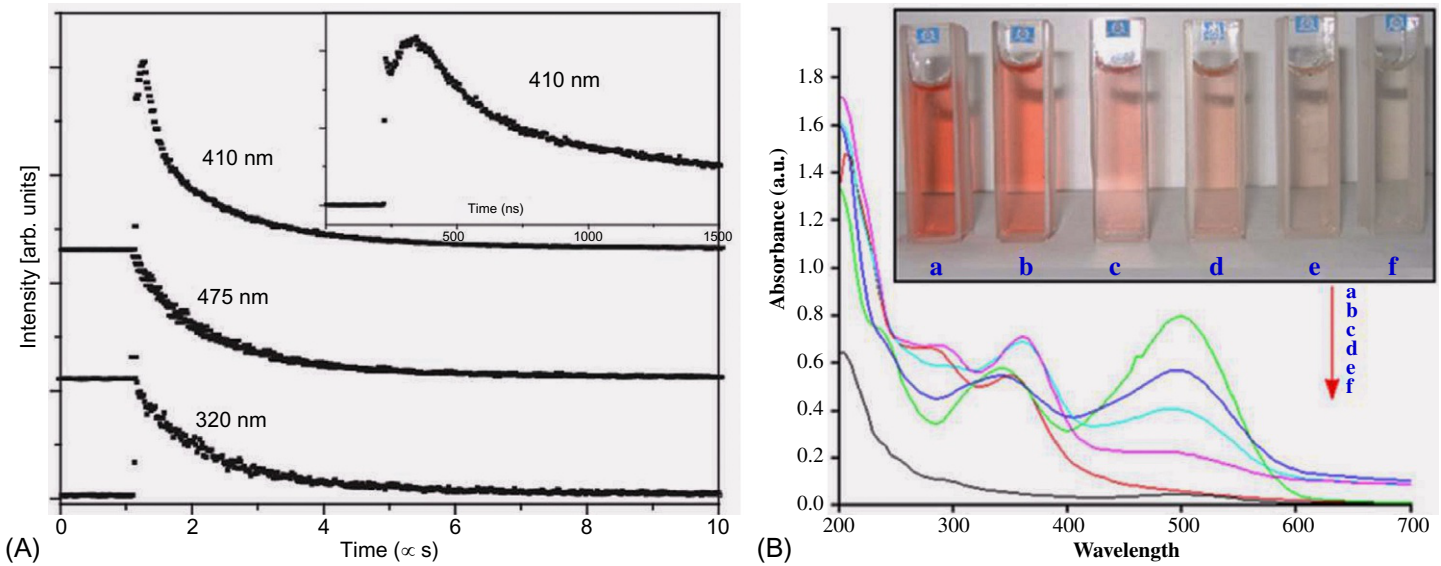

Fig. 8.6

(A) A typical example showing decay profile of upconversion luminescence of inorganic phosphor YAG: Er after using excitation wavelength of 618 nm with a higher time resolution shown in inset [64]. (Figure used with permission Copyright @ 2005 Elsevier.) (B) Ultraviolet-visible spectra of degradation of congo red dye using YAG: Er-coated TiO_2 sample as a function of irradiation time [65]. (Figure used with permission Copyright @ 2008 Elsevier.)

Copyright Elsevier 2025

8.3.3 Long-lasting phosphors

As discussed at the beginning of this section, along with downconverting and upconverting phosphors, long-lasting phosphors also play an important role to increase photocatalytic activities. The long-lasting phosphors like $SrAl_2O_4$:Eu/Dy [67], $CdSiO_3$:Gd/Bi [68], $CaAl_2O_4$:Eu/Nd [69], and $Sr_4Al_{14}O_{25}$:Eu/Dy [70] excite the photocatalyst and the process continues after switching off the light sources. This is due to long-lasting phosphors emitting energy slowly once they are excited by an external source (as these phosphors store energy) [31]. Long-lasting phosphor mechanism states that when incident photon excites one rare-earth metal ion to CB, a hole escapes VB creating a rare-earth metal ion. The generated hole is either absorbed by the other rare-earth-doped element or by the host material giving it one additional ionic state (e.g., Dy^{3+} change to Dy^{4+}). Furthermore, as energy is released in the form of heat energy, trapped hole returns to VB again. The created hole is again trapped by the first rare-earth metal ion to get back to its original ionic state with simultaneous emission of a photon [71].

The published work confirmed that the long-lasting phosphors are used with photocatalysts to enhance photocatalysis process and to carry out photocatalytic activity in the dark [68]. It is seen that long-lasting phosphors can be charged either by solar irradiation or artificial sources like mercury lamps and sodium lamps; later, these phosphors re-emit photons in dark, as shown in Fig. 8.7. This is an ideal condition required for activating photocatalyst for the photocatalysis process [72].

According to the literature, $CaAl_2O_4$:EuNd phosphor coated with TiO_2 initiated photocatalytic reaction in visible irradiations. The coupling of TiO_2 with the phosphor bends the junction region and allows TiO_2 crystals to be photoreactive under visible irradiations as well as in darkness by using photons emitted by the long-lasting phosphors [73].

A typical example of emission spectra for long-lasting phosphor is shown in Fig. 8.8A. The spectra are similar to other inorganic phosphors ($MgAl_2O_4$:Dy) where emission intensity increases with dopant concentration and reaching a maximum intensity for 3% Dy doping. Above 3% dopant concentration, intensity of emission spectra decreases with increasing dopant concentration. The phosphor has a long-lasting effect explained by finite transition time.

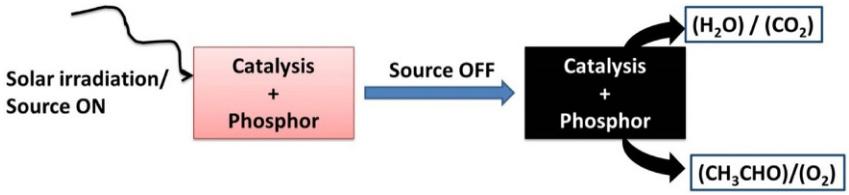

Fig. 8.7
Schematic illustrates the photocatalytic process for a long-lasting phosphor with photocatalyst.

This book belongs to Badji Mokhtar Annaba University Central Library Copyright Elsevier 2025

This book belongs to Badji Mokhtar Annaba University Central Library

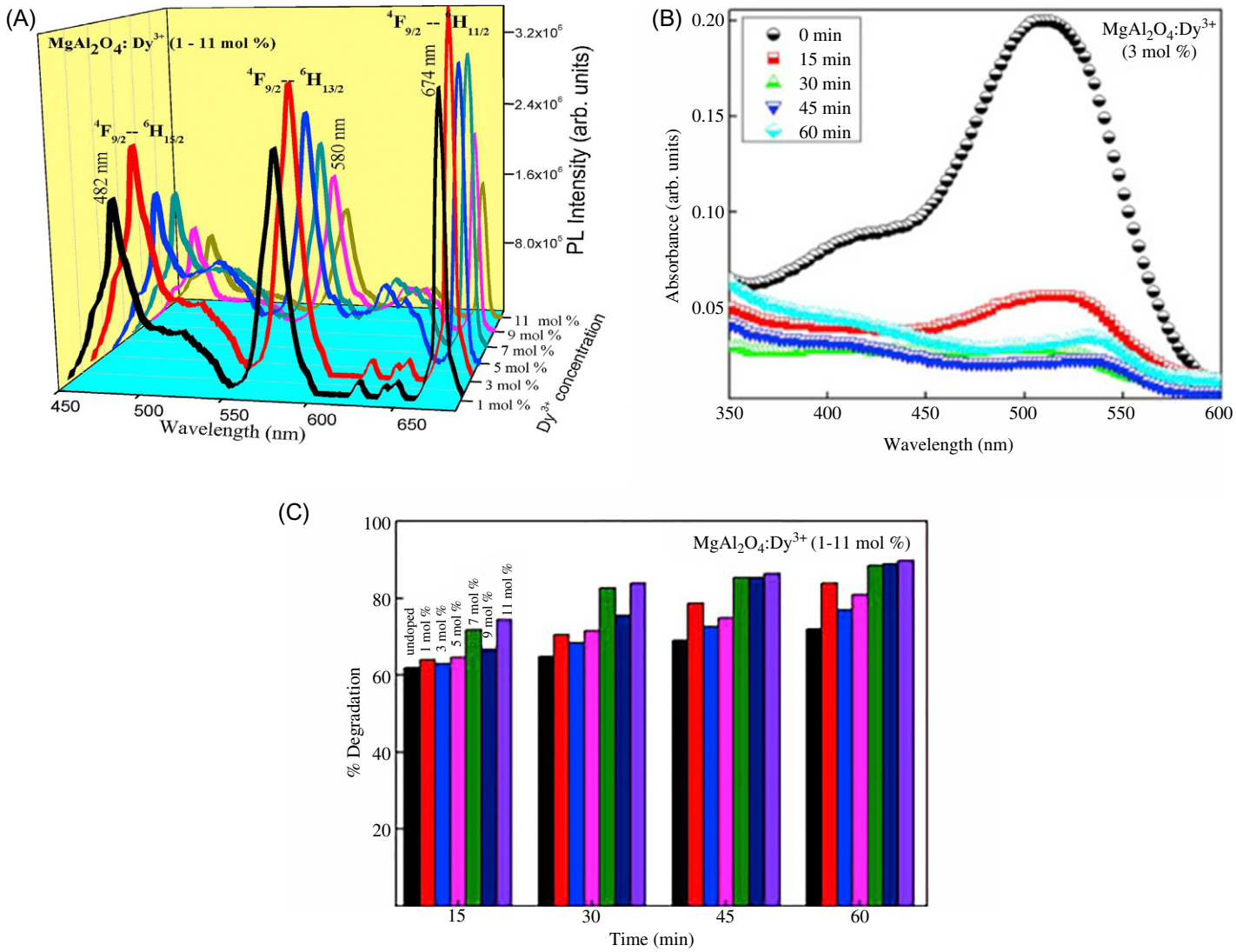

Fig. 8.8

(A) Typical example showing emission spectra for long-lasting phosphors ($MgAl_2O_4$:Dy). (B) An example showing degradation of acid red-88 dye with time using long-lasting phosphors ($MgAl_2O_4$:Dy). (C) Percentage decomposition acid red-88 dye as a function of time for different concentration of dopant Dy [74]. *These diagrams are used with permission Copyright @ 2017 Elsevier.*

Copyright Elsevier 2025

Also, the absorbance spectra showed that decomposition of the acid red-88 solution increases with time, as shown in Fig. 8.8B. The figure also confirmed that the absorbance decreases with increasing exposure time and obtained minimum absorbance for 60 min exposure of the system. Furthermore, the photocatalytic effect on acid red-88 solution showed that the photocatalytic effect enhanced with dopant concentration, as shown in Fig. 8.8C. The figure showed that degradation also increases with time and concentration. Maximum photocatalysis efficiency was observed for 11% Dy concentration in $MgAl_2O_4$:Dy phosphor [74].

On a similar track, ZnO:Co + Ag and $Sr_4Al_{14}O_{25}$:EuDy phosphor was studied for degradation of methyl orange dye in power-saving mode [70]. It is clearly explained that long-lasting phosphor is capable of carrying out photocatalysis process even after tuning of external light source, which can also allow a significant reduction of energy consumption.

8.4 Nanophosphor for photocatalysis

Nanophosphors increase surface area for photoinduced reactions as a nanometer size provides better surface to conduct a photoinduced reaction. This increases the absorption rate, photoreduction rate, photoinduced carrier density, and subsequently synergistically enhancing the surface photoactivity [75]. Semiconductor nanophosphors have served as ideal and efficient photocatalysts for three decades [72]. It meets several properties of an ideal photocatalyst, viz. stability, cost effective, and photoactive. Semiconductors that have high bandgap energies are competent enough for catalyzing chemical reactions. Some of the widely used semiconductor nanophosphors are α-Fe_2O_3, WO_3, ZnS, TiO_2, ZnO, and $SrTiO_3$ [76–78]. Size quantization in semiconductor particles induces radical changes in many important properties of the material. It not only affects the electronic properties of the semiconductor particle, like sustaining discrete Highest Occupied Molecular Orbitals (HOMO) and Lowest Unoccupied Molecular Orbitals (LUMO), but also influences the charge carrier dynamics. As we discussed earlier in the chapter, photocatalysts induced and enhanced chemical transformation and chemical reaction. Photocatalytic degradation of pollutants due to industrial uses, and production of harmful substances from heating and transportation requires an efficient photocatalyst. Furthermore, the process involves adsorption of electrons, and electron-holes are generated that accompanied reduction and oxidation reactions. Photoactivity of that material denies the rate of the reaction [79].

In this section, we have discussed many strategies that have been proposed for better performance of commonly used photocatalysts (especially semiconductors), like impurity, semiconductor coupling, high-energy facet exposing, and morphology tailoring. We have tried to bring forth correlations between these properties and the photocatalytic performance of various nanophosphors systems.

This book belongs to Badji Mokhtar Annaba University Central Library Copyright Elsevier 2025

8.4.1 Oxide-based nanophosphors

Several promising multifunctional oxide-based nanophosphors for photocatalysis and general lighting applications have been extensively researched. This section describes metal oxide–based nanophosphors with enhanced photocatalytic activities, especially outlining their chemical and physical properties. The complex interactions that occur during the photocatalyst preparation, taking into consideration synthesis methodology, composition, as well as functional properties, have been discussed.

8.4.1.1 TiO_2 nanophosphors

TiO_2 has been used extensively as a photocatalyst with a wide variety of applications from cleaning wastewater to production of pure hydrogen gas from water [80]. It has exhibited an ability to carry out redox reactions and formation of free radicals like hydroxyl molecule oxygen ions.

It is observed that adding dopants in TiO_2 enhances its photocatalytic activities. Recent studies are more focused on the morphology and shape of TiO_2 nanoparticle. Also exposed facets affect photocatalytic performance and its activity. Hence, to understand photocatalytic activities of a TiO_2 nanoparticle system, fundamental knowledge of TiO_2 is necessary. The structural morphology, particle size analysis, and quantum confinement of TiO_2 nanoparticle are understood by standard techniques like absorbance technique, TEM, SEM, and other advanced technology. This suggests that particle size of TiO_2 has outstanding effects on photoreaction as particle's size has a direct effect interface between solid and liquid as well as available surface for the reaction.

TiO_2 exists in two polymorphic forms. One has 3.2 eV energy bandgap that corresponds to 386 nm absorbance wavelength. However, the other form is comparatively smaller bandgap (3.02 eV) and absorbance wavelength observed at 416 nm, which is in visible range [81]. The existing polymorphic forms are actively involved in photocatalysis process. Under the effect of ultraviolet exposure of TiO_2, the incident photons are absorbed by TiO_2. Therefore, an electron is excited to the CB from the VB, creating holes at the VB. The photogenerated pairs are responsible for photovoltaic process and photocatalysis process [82].

Nevertheless, TiO_2 experiences some difficulties in practical utilization like (1) the aggregation of nanoparticles in the reaction system, hence significantly decreasing the effective surface area, and diminishing the photocatalytic activity. (2) Separate nanoparticles from pollutants is a difficult and complex process after the photocatalysis process. To enhance the immobility/separability of TiO_2 nanoparticles, TiO_2 nanoparticles are covered with SiO_2, which is cost-effective, stable against heat, and does not interact with others. This produces different crystal phases. After irradiation, photogenerated charge is channelized from one phase red color rutile to the other phase (anatase). This process separates the photogenerated charges,

This book belongs to Badji Mokhtar Annaba University Central Library Copyright Elsevier 2025

which helps enhance the photocatalysis process of TiO_2. Musaev et al. investigated photocatalytic performance of the SiO_2-TiO_2 nanoparticles on photo-oxidative degradation of the alkylphenol derivative aqueous solution [83]. Furthermore, photocatalytic process increases when SiO_2-TiO_2 nanoparticles are incorporated in a nanoporous network [83].

Due to wide bandgap, TiO_2 depicts poor performance in visible light, and this enhances the electron-hole recombination process. Therefore, efficiency of photocatalysis process decreases for pure TiO_2. Hence functionalization of TiO_2 with graphene and graphene oxide can be a good modification. TiO_2/rGO film catalyst significantly increases the photodegradation process. Also TiO_2/PSS sample increases photocatalysis activity nearly 13 times more than TiO_2 [84]. The enhancement in degradation process is due to formation of Ti–O–C bond, which forms porous multilayer structures. This cultivates photogenerated charges activities like separation of charges. It is observed that the photocatalysis process is stable for eight times of repeating the process.

The photocatalytic activity of TiO_2 also increases when TiO_2 is incorporated with nanofibrous membrane. Sundaran et al. showed that using polyurethane/rGO-TiO_2 (PU/rGO-TiO_2) composite membrane helps to separate TiO_2 nanoparticles after the process. The composites along with the membrane successfully enhanced wastewater treatment process [85].

On a similar track, the photocatalysis process is increased when TiN coated on TiO_2 or TiO_2 is doped by Nb. This increases the available surface area of reaction and hence enhanced the degradation process. Tsai et al. recently studied TiN coated on TiO_2 for degradation of methylene blue dye in water. Moreover, metal dopant like Nb decreases bandgap and hence increases the degradation process. Recently, properties of carbon dots-TiO_2 nanomaterials, g-C_3N_4/TiO_2, graphene/TiO_2 nanomaterials and various applications, such as photocatalytic degradation of organic pollutants, water-splitting, photoelectrochemical cell, photocatalytic CO_2 reduction, and disinfection of bacteria have been described by Dong et al. [86].

Bandgap of nitrogen atom is comparable to visible light photons. It is observed that TiO_2 nanotubes provide more area for absorption, which reduces the recombination process of photogenerated charges. This combination is used to purify wastewater as well as produce hydrogen and oxygen gas [87].

8.4.1.2 Bismuth molybdate (Bi_2MoO_6)

Employing traditional semiconductor photocatalysts has practical limitations due to wide bandgap, which reduces the creation of photogenerated charges in visible light. This negatively affects the photocatalysis process. It is therefore much needed to develop an efficient photocatalyst to overcome the previously mentioned difficulties. Oxides like bismuth molybdate (Bi_2MoO_6) are considered as good candidates for this process [88]. Bi_2MoO_6 has a narrow bandgap that allows to formation of photogenerated charge carriers in presence of visible light. However, this increases recombination of photogenerated electron-hole pairs.

This book belongs to Badji Mokhtar Annaba University Central Library Copyright Elsevier 2025

This fast recombination negatively affects the photocatalysis process. One of the solutions to increase the efficiency of a photocatalysis process is by making heterojunction nanocomposites of Bi_2MoO_6. CdS-Bi_2MoO_6/reduced graphene oxide are well-studied nanocomposites in which reduced graphene oxide increases the mobility of photogenerated charge carriers. Hence there are decreases in the recombination process and increases in the photocatalysis process. Cheng and group showed that CdS-Bi_2MoO_6/reduced graphene oxide nanocomposites degraded ciprofloxacin faster than Bi_2MoO_6 [88, 89].

Cheng et al. prepared and studied Bi_2MoO_6 and $Bi_{3.64}Mo_{0.36}O_{6.55}$; the former had MoO_6 octahedra while the latter was comprised of MoO_4 tetrahedra. Due to their different crystal structures, their chemical and physical properties are different. Therefore, optical properties (like photoluminescence and band edge position) and electrochemical properties (like binding energy) are different for both structures. In comparison with both samples, the first sample showed better photogenerated charge separation and migration behavior. These result in higher photocatalytic activities for the photoreduction of carbon dioxide compared with $Bi_{3.64}Mo_{0.36}O_{6.55}$ [89].

The photocatalytic processes also increased for hollow microspheres of Bi_2MoO_6 that are prepared using carbon microsphere templates. The observed bandgap of hollow microspheres of Bi_2MoO_6 is 2.45 eV. The laboratory study of methyl orange and methylene blue dye showed that the hollow microspheres of Bi_2MoO_6 enhanced the degradation process under ultraviolet and visible light irradiation [90].

Apart from water treatment and photodegradation of CO_2, Bi_2MoO_6 is used to remove heavy metal ions and degrade organic dye. Xu et al. reported synthesis and characterization of quantum dots of Bi_2MoO_6. The studied results confirmed that quantum dots Bi_2MoO_6 increases the photocatalytic performance to remove heavy metal (chromium) and degradation of orange dye under visible light exposure [91].

Thus, it is confirmed Bi_2MoO_6 and their nanocomposites and quantum dots enhanced photocatalytic activity for wastewater or polluted water and are able to remove heavy metal ions from polluted water under visible light irradiation. It also enhanced photodegradation of CO_2 under visible light irradiation.

8.4.1.3 Zinc oxide (ZnO)

Another most studied semiconductor for photocatalysis process is ZnO. It has distinguished catalytic, electrical, and optical properties. Due to its large energy bandgap (3.37 eV), it has large room temperature binding energy (60 meV). This makes it a stronger candidate for solar cell, optoelectronic, sensors, and photocatalyst applications [92, 93].

However, due to its wide bandgap, photogenerated electron-hole recombination rate is quite high. This hampered the photocatalysis process. To increase its photocatalysis process, one has

This book belongs to Badji Mokhtar Annaba University Central Library Copyright Elsevier 2025

to control the recombination process, separating electron-hole and improving light harvesting. These can be achieved by doping noble metals like silver and gold, which enhance charge migration and electron-hole separation. Recently, Thinh et al. employed plasma electrolytic oxidation (PEO) method to silver nanoparticle-doped ZnO thin film in which silver nanoparticles were dispersed on the surface of ZnO films [94]. This system increases the photoluminescence emission while silver-ZnO films are doped with gold nanoparticles. This suppressed photoluminescence emission, but photocatalysis process increased. The researchers studied photocatalysis activity for Rhodamine B and observed the activity enhanced for the gold nanoparticle–deposited silver-ZnO films [94].

8.4.2 Sulfide-based phosphors

Another photocatalyst used for water treatment under visible light irradiation is metal sulfide. However, metal sulfides undergo oxidation when they are used as photocatalysts for water treatment in visible light. Instead of photodegradation of water, sulfide ion is intended to oxidize. This causes photodegradation of the sulfur-based photocatalyst.

Hence appropriate strategies must be used to reduce the photodegradation of the catalyst. The use of suitable sacrificial reagents help reduce the photocorrosion of the sulfides under irradiation, and the photocorrosion can be oppressed using electron donor such as Na_2S/Na_2SO_3 mixture [95].

The heterogeneous photocatalysis involving sulfide-based semiconductor nanomaterials is studied extensively to understand and enhance photocatalytic degradation process for organic dyes, pesticides, and phenolic compounds in wastewater [96, 97].

The photocatalytic activity of sulfide-based semiconductor nanomaterials depends on its adsorption capability, energy bandgap, crystal structure, particle size, and their morphology. It is also affected by recombination rate of photogenerated charge carriers and surface utilized for the reaction. Recently, it is observed that tunable bandgap is possible for multicomponent sulfide compounds, like $Mn_xCd_{1-x}S$, and n-type semiconductor has been applied for practical applications. But due to photocorrosion and fast recombination of electron-hole pairs, this problem has to be addressed. It is observed that use of a co-catalyst with host photocatalyst helps to increase separation and transfer time of photogenerated carriers. This helps to reduce recombination process and hence increases the photocatalytic activities. Han et al. recently used NiS as a co-catalyst along with $Mn_{0.3}Cd_yS$ nanorods as host photocatalyst. This resulted in an increase in photocatalysis process and enhanced the production of H_2 gas; also it increased the quantum yield [98].

Copper sulfide nanocomposites and thin films show interesting photocatalytic process under visible light irradiation [99]. It is observed that two semiconductors deposited separately produced high charge mobility. These structures are referred to as tandem structures.

This book belongs to Badji Mokhtar Annaba University Central Library Copyright Elsevier 2025

The examples of these structures are Cu_xS/SnO_2, ZnO/Cu_xS-CuO/SnO_2, and TiO_2/Cu_xS-CuO/SnO_2. The high mobility of photogenerated charge carriers enhanced the photocatalysis process [99].

Optical properties of metal sulfide can be increased using d-block element as dopants. Recent studies showed that zirconium-doped ZnS enhanced optical properties of the host. They reported that Zr doping in ZnS lattice resulted in ~11% increase in photocatalytic performance of doped samples for degradation of methylene blue dye [100]. Ceramic ZnS nanocomposites also showed good performance for cleaning wastewater using photocatalysis process. It is observed that the nanocomposites were able to degrade methylene blue and methylene orange under solar irradiation, and the photodegradation is better than the ZnS nanoparticles [101]. One can also increase photocatalytic activity when ZnS materials are embedded in microporous structure like zeolite. Microporous structure reduces coalescence of ZnS structure, therefore producing its stability. The nanostructure size provides better surface for adsorption. This helps to reduce the photogenerated charge carriers recombination and enhanced the photocatalytic activity [102].

Other metal sulfides like CdS are able to absorb visible light but have a wider bandgap compared with other semiconductors that enhanced the recombination process. Therefore, these materials are poor photocatalysts. It is observed that CdS composites with inorganic phosphors like $CdS/SrAl_2O_4:Eu^{2+},Dy^{3+}$ composite (whose emission spectra of inorganic phosphor overlap with CdS absorption spectra) showed nice photocatalytic activities [103].

8.4.3 Plasmonic-metal nanoparticles

Plasmonic-metal nanoparticles (PNPs) are known for effectively harvesting light energy due to their wide range of energy bandgap, which falls under the visible spectrum [104]. Due to sensitive bandgap of PNPs, the incident light is absorbed by the electrons in VB. The optical properties are sensitive to PNP's particle size and their morphology. This optical behavior can be utilized as a photocatalyst for wastewater treatment and water-splitting.

The energy of the incident light can be acquired by the conduction electrons of the metal nanostructures. The optical properties of the PNPs strongly depend upon the size and morphology of the nanoparticle and have been employed for visible light photocatalysis to enhance the semiconductor photocatalytic activity on water-splitting or dye degradation. Plasmonic photocatalysis describes the synergetic association of plasmonic effects and catalytic effects in metallic nanoparticles. Recent developments have shown that advantageous catalytic behaviors, such as reduced activation barriers and enhanced product selectivity, originated from nonthermal behaviors and are produced by this synergy. Metal oxide core–shelled metal nanoparticles provide isolation to metal ions and also prevent them from coalescence. Further metal insulator junctions reduce the recombination process and enhance

This book belongs to Badji Mokhtar Annaba University Central Library Copyright Elsevier 2025

the photocatalytic activity [105, 106]. Verma et al. recently reviewed the synthesis of mesoporous silica–supported color- and morphology-controlled Ag nanoparticles and their surface decoration with active bimetallic species like palladium, platinum, ruthenium, nickel, and cobalt [107]. The plasmon-mediated photocatalytic reactions were extensively discussed for hydrogen production from ammonia borane, Suzuki-Miyaura coupling, and nitroaromatics reduction under visible light irradiation.

From the previous discussion, it is clear that metal nanoparticles, when coated with semiconductors or insulators, provide heterojunction and reduce coalescence of these nanoparticles. So, nanoparticles provide better surface-to-volume ratio for adsorption and hence better adsorption enhances adsorption reaction. Also heterojunction prevents recombination of photogenerated charge carriers, which ultimately cultivate and increase the photocatalysis process for wastewater treatment and splitting water molecules.

8.5 Synthesis of nanophosphors

This section discusses synthesis of nanophosphors and the characterizations required to study them. Before discussing synthesis and characterization techniques, we provide a list of selected papers published in last couple of years to provide insight, as shown in Table 8.1. The table contains synthesized phosphors, synthesis methods, and photocatalytic activities studied. The materials mentioned in the table suggest the current progress in the field of photocatalysis using luminescent materials, studied materials, and exposure to new researchers.

8.5.1 Solid-sate reaction methods

The solid-state reaction is one of the conventional methods for the synthesis of multielement inorganic phosphors. In this method, all the initial chemicals are weighted according to appropriate stoichiometric ratio. The samples are mixed, milled, and calcined or stirred in an agate mortar, then the reaction is sintered to high temperature (closer to melting point) in a furnace, which should be just enough to have adequate diffusion to complete the solid-state reaction without actually melting the constituents. Later the samples are cooled down to room temperature. Solid-state reaction is simple to perform, and the starting materials are anything right from low-cost oxides, and the reactions are clean as do not involve any precursor chemical or precipitation agent or fuel.

There are certain disadvantages with this method like requirement of very high temperature and possibility of inhomogeneity of the phosphor; this method is widely used to prepare silicate, aluminate, or tungsten oxide phosphors [118, 120]. It is difficult to make uniform particles using solid-state reaction method.

This book belongs to Badji Mokhtar Annaba University Central Library Copyright Elsevier 2025

This book belongs to Badji Mokhtar Annaba University Central Library

Table 8.1: Table depicts selected inorganic luminescent materials used for photocatalytic activities with their preparation methods and references for details study.

Luminescent material	Preparation of luminescent material	Studied photocatalytic activity and performance	References
$CaTiO_3$:Pr	Combustion	• Studied for degradation of methylene blue • Highest degradation rate was 93.6%	[108]
$Sr_2MgSi_2O_7$:Eu	Sintering	• Studied degradation in methyl orange • Reduced photocatalytic activity	[109]
$Eu_xTb_{1-x}L(DMF)_2(NO_3)$		• Degradation of rhodamine	[110]
TiO_2:Tm	Hydrothermal	• Photodegradation of phenol and 2-phenol • Tm-doped phosphor showed better results	[47]
$Ag@SiO_2@YF_3$:Ho@TiO_2 Luminescent phosphor YF_3:Ho		• Photodegradation of RhB • Photocatalytic effect greatly enhanced	[111]
ZnO-SnO [112]	Sol-gel	• Evaluated by blue dye • Photocatalytic activities increased	[112]
BiOBr:Yb/Er		• Photodegradation of RhB • Increases photocatalysis process	[113]
$Bi_4O_5I_2$:Yb/Er	Hydrothermal	• Photodegradation of RhB • Increases photocatalysis process	[114]
$ZnGa_2O_4$Cr/Bi	Ethylene glycol-assisted hydrothermal	• RhB is used to study photocatalytic performance • Doping improved photocatalytic degradation efficiency of RhB	[115]
Polyvinyl alcohol-ZnS (composite films)	Solvent casting process	• Studied degradation of methylene blue • The films exhibits superior photocatalytic performance	[116]

Copyright Elsevier 2025

This book belongs to Badji Mokhtar Annaba University Central Library

Zn_2SiO_4:Ga	Sol-gel	• Studied photodegradation of household insecticide • Improved photodegradation efficiency	[117]
$ZnWO_4$:Ti	Solid-state reaction	• Decomposition rate studied on RhB • High photocatalytic activity and better degradation rate is observed	[118]
MgO	Hydrothermal	• Studied against organic pollutants • Efficient under sunlight irradiation	[119]
AlN:Sm	Solid-state reaction	• Studied hydrogen evolution activity	[120]
ZnS:Mn/CNT	Co-precipitation method	• Studied electron-hole recombination process • CNT effectively increased the photocatalytic activity	[6]
YAG:ce/ZnO	Ball-milling method	• Photocatalytic activity studied for degradation of sulfathiazole • Nanosized shell showed higher photocatalytic activity	[121]

Copyright Elsevier 2025

8.5.2 Combustion method

The required nanophosphor can be prepared using combustion methods. Liquid combustion method is found to be more appropriate for synthesis of nanophosphor than solid combustion method. The method is either microwave-assisted or furnace-assisted. In this process, the solutions of stoichiometrically weighed metal salts (nitrate or halide or sulfate) are prepared in water or alcohol. The mixture is stirred (minimum 1 h) to get a clear solution. Once clear solution formed, then fuel like urea or citric acid is mixed with the solution; the solution is again stirred for minimum 1 h at constant temperature between 50°C and 100°C. The theoretical molar ration of fuel and the solution are calculated considering valences of the oxidizer and the fuel [122]. The final mixture (fuel + salt solution) is placed into a microwave oven or furnace at constant power or constant temperature. The solution underwent dehydration, and the salt solution and fuel decomposed to form various gasses that exploded to white flame. This method is an exothermic process that continues for 2–3 min to yield white powder [108, 123].

8.5.3 Hydrothermal method

All chemicals with appropriate weights are taken for this method. We take metal salts for the reaction like metal nitrate or metal halides or metal sulfate. These metals of proper weights are considered as starting materials. The starting materials are dissolved in water or ethanol solution at room temperature, and afterward the combined solution is stirred vigorously for nearly 1 h. After nearly 1 h, the precipitation agent like NaOH is added to the mixture and stirred for ~1 h. The hydrothermal reaction is generally carried out in a Teflon autoclave under normal pressure at 50–100°C. The precipitation is washed with distilled water a couple of times and dried in an oven for a minimum of 12–15 h [115, 124]. Using this method, 5 nm to a few micrometer particle synthesis is possible.

8.5.4 Sol-gel method

It is again a bottom-up method for nanoparticle synthesis. It is a wet-chemical technique that uses a chemical solution called sol (short form of solution) colloidal to produce integrated network called a gel. All starting materials (generally metal salts like nitrates, which are easily soluble in water) are weighed in stoichiometric amount and combined in a glass beaker. Then they dissolve in distilled water and the mixture stirred until a transparent solution is formed. Later, the mixture is kept in an oven at constant temperature (~100°C) forming a homogenous gel. The obtained gel is heated at higher temperature and ground using mortar and pestle. Using this method, one can synthesize nanoparticles from 1 nm to a few micrometers.

This book belongs to Badji Mokhtar Annaba University Central Library
Copyright Elsevier 2025

8.5.5 Co-precipitation method

Co-precipitation method is the simplest synthesis process among them all. It is considered that the molecular motion and hence the chemical reaction may proceed very comfortably in liquid state. In this method, all precursors are taken in nitrate or sulfate or halide form so that they are easily dissolved in water or ethanol. The precursors also contain precipitation or reducing agent to obtain precipitations. First of all, precursors are dissolved separately in distilled water in separate beakers. All the solutions are mixed in one beaker and stirred for ~30 min and afterward the beaker is kept in an oven at 100°C until water is evaporated [125, 126]. Using this method, it is possible to synthesize nanoparticles from ~5 nm to several 100 nm.

8.5.6 Ball milling method

It is top-down approach starting from presynthesized inorganic phosphors. It is an energy-efficient synthesis method to generate nanoparticles of different size and dimensionality. The milled materials (in this case, inorganic phosphors) receive kinetic energy from moving balls. This energy is utilized to reduce the size of milled materials by breaking the chemical bonds of the materials. The amount of energy transferred depends upon milling speed, milling media, ball-to-powder ratio, and duration of milling process. The only problem with this process is requirement of a cooling system as it involves very high local temperature and has to maintain high pressure.

When presynthesized phosphors are added into a vial along with balls, it leads to disintegration of the powder. This result is first refinement of crystalline size, and the crystalline size can be controlled by milling parameters. It is possible to synthesize nanoparticles from 10 nm to several hundreds of nanometer [121, 127].

8.6 Application of photocatalysis in water purification

It is well studied that photocatalysis is a useful technique to break down various inorganic and organic compounds in wastewater. If semiconductors (like TiO_2) have a bandgap closer to ultraviolet or visible reason, those semiconductors can purify or split water in solar irradiation. The photocatalysis degradation involves following process: (a) organic pollutant particles in waster transfer to surface of photocatalyst; (b) organic pollutant adsorbed on the photocatalysis surface; (c) photocatalysis reaction on its surface; (d) the absorb organic pollutant degrade from its surface; and (e) the degraded organic pollutant particles settles in bulk fluid [128, 129]. These steps are widely considered as photodegradation of organic materials using visible light-sensitive photocatalyst like TiO_2. When a photocatalyst is exposed to ultraviolet radiations, photogenerated holes are generated in the VB. The photogenerated holes react with OH^- or H_2O and produce OH^-. This radical degraded the organic compounds in the wastewater. The photogenerated electron is also produced in CB. This electron is trapped in O_2,

This book belongs to Badji Mokhtar Annaba University Central Library Copyright Elsevier 2025

which prevents photogenerated charge carriers produced in the photocatalyst process. The recombination of photogenerated electron-holes affects the efficiency of photocatalysis activity by the photocatalyst; more the recombination, less the efficiency of the photocatalyst. The OH reacts with organic products to produce degradation product. The combination of organic compound and photogenerated holes gives oxidation products, and when an organic compound reacts with photogenerated electron, it produces reduction product. In this process, oxidizing and reducing radicals on photocatalyst surface destroys toxic agents and unwanted organic compounds [80, 130–132]. However, if the oxygen molecule is not present, then the photogenerated electrons combine with holes and reduce the efficiency of photocatalysis process. Thus it is a challenge to develop efficient redox catalyst able to degrade organics in solar radiation and also work against the recombination process. This is considered useful to clean industrial polluted water, especially wastewater from textile industries [80].

One can enhance the photocatalytic activity by several methods like using nanosized semiconductor crystallites instead of bulk and modifying photocatalysts by using metal or nonmetal ions as dopant or preparing their nanocomposites with other oxides [133]. For these systems, the lifetime of photogenerated electrons or holes can be tuned using photoluminescence material or hybrid structure of photoluminescence and photocatalyst materials. It explained downconverting phosphors, upconverting phosphors, and long-lasting or persistence luminescence phosphors. Furthermore, it is mentioned that under ultraviolet radiations, the electrons located in a semiconductor jump to the CB. The electron is immediately trapped by the rare-earth metal ion, which tends to cease the recombination of photogenerated electron and holes. Later the electron is captured by molecular oxygen to make superoxide O_2^- anion and hydrogen peroxide. These new anions react to produce OH^- anion. Also the produced holes interact with a hydroxyl group or water molecule and hydroxyl radicals are formed. At last, these molecules oxidize the organic molecules in the wastewater to yield the final products [52, 59, 99, 134]. An example of the previously explained process is given here; the reaction depicts dye degradation using Tb^{3+}-doped ZrO_2 phosphor/semiconductor [135].

$$
\begin{aligned}
&ZrO_2 + h\gamma \rightarrow ZrO_2(\text{hole}) + ZrO_2(\text{electron})\\
&ZrO_2(\text{electron}) + Tb^{3+} \rightarrow ZrO_2 + Tb^{2+}\\
&Tb^{2+} + O_2 \rightarrow Tb^{3+} + O_2{}^-\\
&Tb^{2+} + O_2 + H^+ \rightarrow Tb^{3+} + H_2O_2\\
&ZrO_2(\text{hole}) + H_2O/OH^- \rightarrow ZrO_2 + OH^- + H^+\\
&\text{Dye} + OH^-/H^+/H_2O_2 \rightarrow \text{End}-\text{product}
\end{aligned}
$$

According to Vidhya et al. [135], ZrO_2 absorbs the photon from solar irradiation and generates an electron at CB and a hole at VB. The electron is trapped by the Tb^{3+} ion and immediately oxidized to produce reacted oxygen radical or hydrogen per-oxide molecule. Also the hole was trapped by the water molecule present in the wastewater and hydroxyl ions were formed.

This book belongs to Badji Mokhtar Annaba University Central Library
Copyright Elsevier 2025

Finally, all the free radicals reacted with organic dye to produce final product. This process ultimately degrades the dye and photocatalysis activity increases as the recombination process is controlled by absorbing electron by Tb^{3+} ion to Tb^{2+} ion. It is observed that by increasing Tb^{3+} ion in the phosphor, photocatalysis process increases up to a particular concentration of Tb^{3+} ion.

There are studies that explain about optimum rare-earth metal ion concentration. By adding an appropriate concentration of rare-earth metal ions, the high photocatalytic activity is observed for that luminesce phosphor. This is due to, with increasing dopant, the space charge layer increases as penetration depth of light into the materials increases. Thus it makes recombination electron-hole pairs easier than for other concentrations of dopant, which causes low photocatalytic decolorization efficiency. Moreover, the excess of dopant in the phosphors is responsible for a recombination process that decreases photocatalytic activity [133, 134].

8.7 Conclusion and future perspectives of luminescence phosphor-based photocatalyst

The evolution of photocatalysis technology and light-driven chemical reactions are growing more strikingly and have been revealed as a significant way of exploring environmentally benign, green synthetic, and sustainable processes so that it can be used in industries to purify wastewater more efficiently and at low energy consumption. This can be possible by combining luminescence phosphors with traditional photocatalysis. This will provide more opportunities to work photocatalysts more efficiently as the recombination photoelectron-holes are stopped by luminescence phosphors. Also the phosphors worked at ultraviolet to visible region; thus the redox reaction in a photocatalysis process can be tuned by solar irradiation itself. On top of that, long-lasting phosphors emit photons in the dark, which makes them a strong candidate to carry out photocatalysis reactions even in the dark. Therefore, we confined our discussion on application of inorganic luminescence phosphors in the field of photocatalysis.

In this chapter, the insight of luminescence phenomenon helping photocatalysis effect is explained in detail. The basic principal of phosphor for photocatalysis is explained with its proper mechanism. The literature also suggests that rare-earth-doped phosphor increases the efficiency of the photocatalysis process. However, it is still a growing field and much work can be performed to achieve better and more efficient photocatalysis combining with luminescence phosphor.

8.8 Challenges and issues

It is observed that photocatalysis activities change with dopant concentration of rare-earth materials. It is not as simple as saying the photocatalysis process increases with dopant concentration, as the photocatalysis process is high for a particular dopant concentration.

This book belongs to Badji Mokhtar Annaba University Central Library Copyright Elsevier 2025

Therefore, it is necessary to find the perfect dopant concentration to get an efficient photocatalysis process. The literature also supports that a good luminescent phosphor has better recombination process, which decreases the efficiency of photocatalysis process. However, if we find a right combination of inorganic phosphor and catalyst, the photocatalysis process enhanced and the degradation process is quite high. As discussed in the previous section, catalysts like ZnO are very inefficient photocatalysts, but when it combined with inorganic phosphor, photodegradation process enhanced drastically [43]. Thus, it is necessary to find a good combination to get an efficient photocatalysis process.

The main issue with using rare-earth dopant phosphors is to remove these heavy metal ions after the reaction. The easiest solution is to use such combination that retains their structures after photodegradation process. The studied organic dyes confirmed that, in the near future, these compounds will be used for wastewater treatments in industries as well. However, more study is required to use these samples for cleaning industrial wastes.

References

[1] M. Landau, Le phénomène de la photocatalyse, Compt. Rend. 156 (1913) 1894–1896.
[2] J.J. Rueda-Marquez, I. Levchuk, P.F. Ibañez, M. Sillanpää, A critical review on application of photocatalysis for toxicity reduction of real wastewaters, J. Clean. Prod. 258 (2020) 120694.
[3] A. Fujishima, K. Honda, Electrochemical photolysis of water at a semiconductor electrode, Nature 238 (1972) 37–38.
[4] R. Bickley, G. Munuera, F. Stone, Photoadsorption and photocatalysis at rutile surfaces: II. Photocatalytic oxidation of isopropanol, J. Catal. 31 (1973) 398–407.
[5] S.N. Frank, A.J. Bard, Heterogeneous photocatalytic oxidation of cyanide ion in aqueous solutions at titanium dioxide powder, J. Am. Chem. Soc. 99 (1977) 303–304.
[6] A. Sharifi, L. Montazerghaem, A. Naeimi, A.R. Abhari, M. Vafaee, G.A.M. Ali, H. Sadegh, Investigation of photocatalytic behavior of modified ZnS:Mn/MWCNTs nanocomposite for organic pollutants effective photodegradation, J. Environ. Manage. 247 (2019) 624–632.
[7] D. Robert, S. Malato, Solar photocatalysis: a clean process for water detoxification, Sci. Total Environ. 291 (2002) 85–97.
[8] A. Patsoura, D.I. Kondarides, X.E. Verykios, Photocatalytic degradation of organic pollutants with simultaneous production of hydrogen, Catal. Today 124 (2007) 94–102.
[9] A. Kudo, Y. Miseki, Heterogeneous photocatalyst materials for water splitting, Chem. Soc. Rev. 38 (2009) 253–278.
[10] A. Kudo, Photocatalyst materials for water splitting, Catal. Surv. Jpn. 7 (2003) 31–38.
[11] J. Silver, M. Martinez-Rubio, T. Ireland, G. Fern, R. Withnall, Yttrium oxide upconverting phosphors. 3. Upconversion luminescent emission from europium-doped yttrium oxide under 632.8 nm light excitation, J. Phys. Chem. B 105 (2001) 9107–9112.
[12] X. Zhang, E. Daran, C. Serrano, F. Lahoz, Up-conversion fluorescence in MBE-grown Nd^{3+}-doped LaF_3/CaF_2 waveguides, J. Lumin. 87 (2000) 1011–1013.
[13] J. Silver, E. Barrett, P. Marsh, R. Withnall, Yttrium oxide upconverting phosphors. 5. Upconversion luminescent emission from holmium-doped yttrium oxide under 632.8 nm light excitation, J. Phys. Chem. B 107 (2003) 9236–9242.
[14] H. Yang, Z. Dai, Z. Sun, Upconversion luminescence and kinetics in Er^{3+}: $YAlO_3$ under 652.2 nm excitation, J. Lumin. 124 (2007) 207–212.

This book belongs to Badji Mokhtar Annaba University Central Library
Copyright Elsevier 2025

[15] W. Qin, D. Zhang, D. Zhao, L. Wang, K. Zheng, Near-infrared photocatalysis based on YF3: Yb^{3+}, Tm^{3+}/TiO_2 core/shell nanoparticles, Chem. Commun. 46 (2010) 2304–2306.
[16] T. Peng, L. Huajun, H. Yang, C. Yan, Synthesis of $SrAl_2O_4$: Eu, Dy phosphor nanometer powders by sol–gel processes and its optical properties, Mater. Chem. Phys. 85 (2004) 68–72.
[17] C. García, L. Diaz-Torres, J. Oliva, M. Romero, P. Salas, Photocatalytic activity and optical properties of blue persistent phosphors under UV and solar irradiation, Int. J. Photoenergy 2016 (2016) 1–8.
[18] F. Clabau, X. Rocquefelte, S. Jobic, P. Deniard, M.-H. Whangbo, A. Garcia, T. Le Mercier, Mechanism of phosphorescence appropriate for the long-lasting phosphors Eu^{2+}-doped $SrAl_2O_4$ with codopants Dy^{3+} and B^{3+}, Chem. Mater. 17 (2005) 3904–3912.
[19] A.L. Linsebigler, G. Lu, J.T. Yates Jr., Photocatalysis on TiO_2 surfaces: principles, mechanisms, and selected results, Chem. Rev. 95 (1995) 735–758.
[20] U.G. Akpan, B.H. Hameed, Parameters affecting the photocatalytic degradation of dyes using TiO_2-based photocatalysts: a review, J. Hazard. Mater. 170 (2009) 520–529.
[21] L. Liu, Y. Li, Understanding the reaction mechanism of photocatalytic reduction of CO_2 with H_2O on TiO_2-based photocatalysts: a review, Aerosol Air Qual. Res. 14 (2014) 453–469.
[22] M. Ge, Q. Li, C. Cao, J. Huang, S. Li, S. Zhang, Z. Chen, K. Zhang, S.S. Al-Deyab, Y. Lai, One-dimensional TiO_2 nanotube photocatalysts for solar water splitting, Adv. Sci. 4 (2017) 1600152.
[23] M. Samadi, M. Zirak, A. Naseri, E. Khorashadizade, A.Z. Moshfegh, Recent progress on doped ZnO nanostructures for visible-light photocatalysis, Thin Solid Films 605 (2016) 2–19.
[24] I. Ani, U. Akpan, M. Olutoye, B. Hameed, Photocatalytic degradation of pollutants in petroleum refinery wastewater by TiO_2-and ZnO-based photocatalysts: recent development, J. Clean. Prod. 205 (2018) 930–954.
[25] C. Feldmann, T. Jüstel, C.R. Ronda, P.J. Schmidt, Inorganic luminescent materials: 100 years of research and application, Adv. Funct. Mater. 13 (2003) 511–516.
[26] G. Blasse, Luminescence of inorganic solids: from isolated centres to concentrated systems, Prog. Solid State Chem. 18 (1988) 79–171.
[27] B. Di Bartolo, V. Goldberg, D. Pacheco, Luminescence of Inorganic Solids, Springer, 1978.
[28] R. Borja-Urby, L. Díaz-Torres, P. Salas, E. Moctezuma, M. Vega, C. Ángeles-Chávez, Structural study, photoluminescence, and photocatalytic activity of semiconducting $BaZrO_3$: Bi nanocrystals, Mater. Sci. Eng. B 176 (2011) 1382–1387.
[29] D. Wojcieszak, D. Kaczmarek, J. Domaradzki, M. Mazur, Correlation of photocatalysis and photoluminescence effect in relation to the surface properties of TiO_2: Tb thin films, Int. J. Photoenergy 2013 (2013) 1–9.
[30] C. García, L. Diaz-Torres, P. Salas, M. Guzman, C. Angeles-Chavez, Photoluminescent and photocatalytic properties of bismuth doped strontium aluminates blended with titanium dioxide, Mater. Sci. Semicond. Process. 37 (2015) 105–111.
[31] Q. Fei, C. Chang, D. Mao, Luminescent properties of $Sr_2MgSi_2O_7$ and $Ca_2MgSi_2O_7$ long lasting phosphors activated by Eu^{2+}, Dy^{3+}, J. Alloys Compd. 390 (2005) 133–137.
[32] L. Lin, M. Yin, C. Shi, W. Zhang, Luminescence properties of a new red long-lasting phosphor: Mg_2SiO_4: Dy^{3+}, Mn^{2+}, J. Alloys Compd. 455 (2008) 327–330.
[33] C. Feldmann, T. Jüstel, C. Ronda, D. Wiechert, Quantum efficiency of down-conversion phosphor $LiGdF_4$: Eu, J. Lumin. 92 (2001) 245–254.
[34] J. McKittrick, L.E. Shea-Rohwer, Down conversion materials for solid-state lighting, J. Am. Ceram. Soc. 97 (2014) 1327–1352.
[35] A. Zhang, Z. Sun, G. Liu, Z. Fu, Z. Hao, J. Zhang, Y. Wei, Ln^{3+} (Er^{3+}, Tm^{3+} and Ho^{3+})-doped NaYb $(MoO_4)_2$ upconversion phosphors as wide range temperature sensors with high sensitivity, J. Alloys Compd. 728 (2017) 476–483.
[36] H. Guo, Two-and three-photon upconversion of LaOBr: Er^{3+}, Opt. Mater. 29 (2007) 1840–1843.
[37] W. Stręk, A. Bednarkiewicz, P. Dereń, Power dependence of luminescence of Tb^{3+}-doped KYb $(WO_4)_2$ crystal, J. Lumin. 92 (2001) 229–235.

This book belongs to Badji Mokhtar Annaba University Central Library Copyright Elsevier 2025

[38] J.-L. Yuan, X.-Y. Zeng, J.-T. Zhao, Z.-J. Zhang, H.-H. Chen, X.-X. Yang, Energy transfer mechanisms in Tb^{3+}, Yb^{3+} codoped Y_2O_3 downconversion phosphor, J. Phys. D. Appl. Phys. 41 (2008) 105406.
[39] T. Miyakawa, D.L. Dexter, Phonon sidebands, multiphonon relaxation of excited states, and phonon-assisted energy transfer between ions in solids, Phys. Rev. B 1 (1970) 2961–2969.
[40] R. Wegh, H. Donker, K. Oskam, A. Meijerink, Visible quantum cutting in Eu^{3+}-doped gadolinium fluorides via downconversion, J. Lumin. 82 (1999) 93–104.
[41] P. Vergeer, T. Vlugt, M. Kox, M. Den Hertog, J. Van der Eerden, A. Meijerink, Quantum cutting by cooperative energy transfer in $Yb_xY_{1-x}PO_4$: Tb^{3+}, Phys. Rev. B 71 (2005) 014119.
[42] Q. Zhang, C. Yang, Z. Jiang, X. Ji, Concentration-dependent near-infrared quantum cutting in $GdBO_3$: Tb^{3+}, Yb^{3+} nanophosphors, Appl. Phys. Lett. 90 (2007) 061914.
[43] X. Liu, L. Pan, J. Li, K. Yu, Z. Sun, C.Q. Sun, Light down-converting characteristics of ZnO–Y_2O_2S: Eu^{3+} for visible light photocatalysis, J. Colloid Interface Sci. 404 (2013) 150–154.
[44] A.M. Inamuddin, G.S. Inamuddin, A. Kumar, E. Lichtfouse, A.M. Asiri, Cheronet, Nanophotocatalysis and Environmental Applications, Springer International Publishing, 2019.
[45] X. Liu, H. Chu, J. Li, L. Niu, C. Li, H. Li, L. Pan, C.Q. Sun, Light converting phosphor-based photocatalytic composites, Cat. Sci. Technol. 5 (2015) 4727–4740.
[46] X. Liu, X. Wang, H. Li, J. Li, L. Pan, J. Zhang, G. Min, Z. Sun, C. Sun, Enhanced visible light photocatalytic activity of ZnO doped with down-conversion $NaSrBO_3$: Tb^{3+} phosphors, Dalton Trans. 44 (2015) 97–103.
[47] P. Mazierski, P.N.A. Caicedo, T. Grzyb, A. Mikolajczyk, J. K. Roy, E. Wyrzykowska, Z. Wei, E. Kowalska, T. Puzyn, A. Zaleska-Medynska, Experimental and computational study of Tm-doped TiO_2: the effect of Li^+ on Vis-response photocatalysis and luminescence, Appl. Catal. B Environ. 252 (2019) 138–151.
[48] X. Liu, X. Wang, H. Li, L. Pan, T. Lv, Z. Sun, C. Sun, Microwave-assisted synthesis of ZnO–$Y_3Al_5O_{12}$: Ce^{3+} composites with enhanced visible light photocatalysis, J. Mater. Chem. 22 (2012) 16293–16298.
[49] X. Jiang, Y. Wang, C. Pan, Micro-arc oxidation of TC4 substrates to fabricate TiO_2/YAG: Ce^{3+} compound films with enhanced photocatalytic activity, J. Alloys Compd. 509 (2011) L137–L141.
[50] Y. Zheng, J. Lin, Q. Wang, Emissions and photocatalytic selectivity of $SrWO_4$: Ln^{3+} (Eu^{3+}, Tb^{3+}, Sm^{3+} and Dy^{3+}) prepared by a supersonic microwave co-assistance method, Photochem. Photobiol. Sci. 11 (2012) 1567–1574.
[51] W. Mekprasart, W. Pecharapa, Synthesis and characterization of nitrogen-doped TiO_2 and its photocatalytic activity enhancement under visible light, Energy Procedia 9 (2011) 509–514.
[52] W. Mekprasart, R. Noonuruk, W. Jarernboon, W. Pecharapa, Quasi-solid-state dye-sensitized solar cells based on TiO_2/NiO core–shell nanocomposites, J. Nanosci. Nanotechnol. 11 (2011) 6483–6489.
[53] X. Wang, X. Kong, G. Shan, Y. Yu, Y. Sun, L. Feng, K. Chao, S. Lu, Y. Li, Luminescence spectroscopy and visible upconversion properties of Er^{3+} in ZnO nanocrystals, J. Phys. Chem. B 108 (2004) 18408–18413.
[54] X. Wu, K.W. Kwok, F. Li, Upconversion fluorescence studies of sol–gel-derived Er-doped KNN ceramics, J. Alloys Compd. 580 (2013) 88–92.
[55] M. Tsuda, K. Soga, H. Inoue, S. Inoue, A. Makishima, Upconversion mechanism in Er^{3+}-doped fluorozirconate glasses under 800 nm excitation, J. Appl. Phys. 85 (1999) 29–37.
[56] A. Kanoun, N. Jaba, H. Mejri, H. Maaref, A. Selmi, Effects of activator ion concentration on the upconversion processes in Er^{3+}-doped TeO_2–ZnO glass, Phys. Status Solidi A 188 (2001) 1145–1151.
[57] W. Tobler, W. Durisch, High-performance selective Er-doped YAG emitters for thermophotovoltaics, Appl. Energy 85 (2008) 483–493.
[58] L. Yin, J. Gao, J. Wang, X. Luan, P. Kang, Y. Li, K. Li, X. Zhang, Synthesis of Er^{3+}: $Y_3Al_5O_{12}$ and its effects on the solar light photocatalytic activity of TiO_2–ZrO_2 composite, Res. Chem. Intermed. 38 (2012) 523–536.
[59] J. Wang, J. Li, B. Liu, Y. Xie, G. Han, Y. Li, L. Zhang, X. Zhang, Preparation of nano-sized mixed crystal TiO_2-coated Er^{3+}: $YAlO_3$ by sol–gel method for photocatalytic degradation of organic dyes under visible light irradiation, Water Sci. Technol. 60 (2009) 917–926.
[60] J. de Wild, J. Rath, A. Meijerink, W. Van Sark, R. Schropp, Enhanced near-infrared response of a-Si: H solar cells with β-$NaYF_4$: Yb^{3+} (18%), Er^{3+} (2%) upconversion phosphors, Sol. Energy Mater. Sol. Cells 94 (2010) 2395–2398.

This book belongs to Badji Mokhtar Annaba University Central Library Copyright Elsevier 2025

[61] W. Wang, Y. Li, Z. Kang, F. Wang, C.Y. Jimmy, A NIR-driven photocatalyst based on α-NaYF4: Yb, Tm@ TiO_2 core–shell structure supported on reduced graphene oxide, Appl. Catal. B Environ. 182 (2016) 184–192.
[62] Y. Zhang, Z. Hong, Synthesis of lanthanide-doped NaYF 4@ TiO_2 core–shell composites with highly crystalline and tunable TiO_2 shells under mild conditions and their upconversion-based photocatalysis, Nanoscale 5 (2013) 8930–8933.
[63] G. Wang, Q. Peng, Y. Li, Upconversion luminescence of monodisperse CaF_2: Yb^{3+}/Er^{3+} nanocrystals, J. Am. Chem. Soc. 131 (2009) 14200–14201.
[64] H.L. Xu, S. Kröll, Upconversion dynamics in Er^{3+}-doped YAG, J. Lumin. 111 (2005) 191–198.
[65] J. Wang, R. Li, Z. Zhang, W. Sun, R. Xu, Y. Xie, Z. Xing, X. Zhang, Efficient photocatalytic degradation of organic dyes over titanium dioxide coating upconversion luminescence agent under visible and sunlight irradiation, Appl. Catal. A Gen. 334 (2008) 227–233.
[66] S. Huang, N. Zhu, Z. Lou, L. Gu, C. Miao, H. Yuan, A. Shan, Near-infrared photocatalysts of $BiVO_4$/CaF_2: Er^{3+}, Tm^{3+}, Yb^{3+} with enhanced upconversion properties, Nanoscale 6 (2014) 1362–1368.
[67] J. Botterman, P.F. Smet, Persistent phosphor $SrAl_2O_4$: Eu, Dy in outdoor conditions: saved by the trap distribution, Opt. Express 23 (2015) A868–A881.
[68] P. Feng, Y. Wei, Y. Wang, J. Zhang, H. Li, Z. Ci, Long persistent phosphor $CdSiO_3$: Gd^{3+}, Bi^{3+} and potential photocatalytic application of $CdSiO_3$: Gd^{3+}, Bi^{3+}@ TiO_2 in dark, J. Am. Ceram. Soc. 99 (2016) 2368–2375.
[69] J.-S. Kim, H.-J. Sung, B.-J. Kim, Photocatalytic characteristics for the nanocrystalline TiO_2 on the Ag-doped $CaAl_2O_4$:(Eu, Nd) phosphor, Appl. Surf. Sci. 334 (2015) 151–156.
[70] V. Havasi, B. Vödrédi, Á. Kukovecz, Photocatalytic performance of $Sr_4Al_{14}O_{25}$: Eu, Dy phosphor assisted ZnO: Co^+ Ag nanocomposite under continuous and pulsed illumination, Catal. Today 284 (2017) 107–113.
[71] T. Matsuzawa, Y. Aoki, N. Takeuchi, Y. Murayama, A new long phosphorescent phosphor with high brightness, $SrAl_2O_4$: Eu^{2+}, Dy^{3+}, J. Electrochem. Soc. 143 (1996) 2670.
[72] N. Waiskopf, Y. Ben-Shahar, U. Banin, Photocatalytic hybrid semiconductor–metal nanoparticles; from synergistic properties to emerging applications, Adv. Mater. 30 (2018) 1706697.
[73] J.-S. Kim, S.-W. Kim, S.-C. Jung, Photocatalytic reaction characteristics of the titanium dioxide supported on the long phosphorescent phosphor by a low pressure chemical vapor deposition, J. Nanosci. Nanotechnol. 14 (2014) 7751–7755.
[74] C. Pratapkumar, S.C. Prashantha, H. Nagabhushana, M.R. Anilkumar, C.R. Ravikumar, H. P. Nagaswarupa, D.M. Jnaneshwara, White light emitting magnesium aluminate nanophosphor: near ultra violet excited photoluminescence, photometric characteristics and its UV photocatalytic activity, J. Alloys Compd. 728 (2017) 1124–1138.
[75] N. Waiskopf, U. Banin, Colloidal quantum materials for photocatalytic applications, in: Curious 2018, Springer, 2019, pp. 105–117.
[76] J. Ke, Semiconductor nanocrystals for environmental catalysis, in: Advanced Nanomaterials for Pollutant Sensing and Environmental Catalysis, Elsevier, 2020, pp. 119–163.
[77] S. Weon, F. He, W. Choi, Status and challenges in photocatalytic nanotechnology for cleaning air polluted with volatile organic compounds: visible light utilization and catalyst deactivation, Environ. Sci. Nano 6 (2019) 3185–3214.
[78] T. Su, Z. Qin, H. Ji, Z. Wu, An overview of photocatalysis facilitated by 2D heterojunctions, Nanotechnology 30 (2019) 502002.
[79] W.S. Koe, J.W. Lee, W.C. Chong, Y.L. Pang, L.C. Sim, An overview of photocatalytic degradation: photocatalysts, mechanisms, and development of photocatalytic membrane, Environ. Sci. Pollut. Res. 27 (2019) 2522–2565.
[80] M. Al-Mamun, S. Kader, M. Islam, M. Khan, Photocatalytic activity improvement and application of UV-TiO_2 photocatalysis in textile wastewater treatment: a review, J. Environ. Chem. Eng. 7 (2019) 103248.
[81] Y.-F. Li, Z.-P. Liu, Particle size, shape and activity for photocatalysis on titania anatase nanoparticles in aqueous surroundings, J. Am. Chem. Soc. 133 (2011) 15743–15752.
[82] Y. Lan, Y. Lu, Z. Ren, Mini review on photocatalysis of titanium dioxide nanoparticles and their solar applications, Nano Energy 2 (2013) 1031–1045.

This book belongs to Badji Mokhtar Annaba University Central Library Copyright Elsevier 2025

[83] K. Musaev, D. Mirkhamitova, A. Yarbekov, S. Nurmanov, K. Akbarov, O. Ruzimuradov, Facile synthesis of SiO_2–TiO_2 photocatalyst nanoparticles for degradation of phenolic water pollutants, SN Appl. Sci. 1 (2019) 1164.
[84] D. Zhang, X. Zhang, Q. Sun, S. Zheng, J. Hao, Y. Wang, Continuous photocatalysis based on layer-by-layer assembly of separation-free TiO_2/reduced graphene oxide film catalysts with increased charge transfer and active site, Eur. J. Inorg. Chem. 2019 (2019) 721–729.
[85] S.P. Sundaran, C. Reshmi, P. Sagitha, A. Sujith, Polyurethane nanofibrous membranes decorated with reduced graphene oxide–TiO_2 for photocatalytic templates in water purification, J. Mater. Sci. 55 (2020) 5892–5907.
[86] C. Dong, M. Xing, J. Lei, J. Zhang, TiO_2/carbon composite nanomaterials for photocatalysis, in: Current Developments in Photocatalysis and Photocatalytic Materials, Elsevier, 2020, pp. 303–321.
[87] X. Hou, X. Liu, J. Han, H. Liu, J. Yao, D. Li, L. Wang, B. Liao, J. Li, R. Zhang, Enhanced photoelectrocatalytic degradation of organic pollutants using TiO_2 nanotubes implanted with nitrogen ions, J. Mater. Sci. 55 (2020) 5843–5860.
[88] Z. Chen, J. Liang, X. Xu, G. He, H. Chen, CdS–Bi_2MoO_6/RGO nanocomposites for efficient degradation of ciprofloxacin under visible light, J. Mater. Sci. 55 (2020) 6065–6077.
[89] L. Cheng, L. Liu, D. Wang, F. Yang, J. Ye, Synthesis of bismuth molybdate photocatalysts for CO_2 photo-reduction, J. CO_2 Util. 29 (2019) 196–204.
[90] R. Abazari, A.R. Mahjoub, J. Shariati, S. Noruzi, Photocatalytic wastewater purification under visible light irradiation using bismuth molybdate hollow microspheres with high surface area, J. Clean. Prod. 221 (2019) 582–586.
[91] J. Xu, J. Yue, J. Niu, M. Chen, Synergistic removal of Cr (VI) and dye contaminants by 0D/2D bismuth molybdate homojunction photocatalyst under visible light, Appl. Surf. Sci. 484 (2019) 1080–1088.
[92] K.M. Lee, C.W. Lai, K.S. Ngai, J.C. Juan, Recent developments of zinc oxide based photocatalyst in water treatment technology: a review, Water Res. 88 (2016) 428–448.
[93] C.B. Ong, L.Y. Ng, A.W. Mohammad, A review of ZnO nanoparticles as solar photocatalysts: synthesis, mechanisms and applications, Renew. Sust. Energy Rev. 81 (2018) 536–551.
[94] V. Thinh, V. Lam, T. Bach, N. Van, D. Manh, D. Tung, N. Lien, U. Thuy, T. Anh, N. Tung, Enhanced optical and photocatalytic properties of Au/Ag nanoparticle-decorated ZnO films, J. Electron. Mater. 49 (2020) 2625–2632.
[95] M. Curie, l, Hydrogen production from water splitting using photosemiconductor catalysts, in: Renewable Hydrogen Technologies: Production, Purification, Storage, Applications and Safety, 2013p. 43.
[96] L. Cheng, Q. Xiang, Y. Liao, H. Zhang, CdS-based photocatalysts, Energy Environ. Sci. 11 (2018) 1362–1391.
[97] T. Di, Q. Xu, W. Ho, H. Tang, Q. Xiang, J. Yu, Review on metal sulphide-based Z-scheme photocatalysts, ChemCatChem 11 (2019) 1394–1411.
[98] Y. Han, Q. Zhang, Z. Liang, J. Geng, X. Dong, $Mn_{0.3}Cd_{0.7}S$ nanorods modified with NiS clusters as photocatalysts for the H_2 evolution reaction, J. Mater. Sci. 55 (2020) 5390–5401.
[99] L. Isac, C. Cazan, E. Alexandru, L. Andronic, Copper sulfide based heterojunctions as photocatalysts for dyes photodegradation, Front. Chem. 7 (2019) 694.
[100] J. Sharma, A. Gupta, O. Pandey, Effect of Zr doping and aging on optical and photocatalytic properties of ZnS nanopowder, Ceram. Int. 45 (2019) 13671–13678.
[101] S.-D. Yoon, Y.-H. Yun, M. Huh, Preparation and photocatalytic properties of ceramic nanocomposites added zinc sulfide nanoparticles, J. Inorg. Organomet. Polym. Mater. 30 (2020) 3521–3530.
[102] K. Djebli, H. Tebani, A. Abdessemed, N. Keghouche, Structural, optical and photocatalytic properties of ZnS/zeolite Y nanoparticles synthesized by γ-ray irradiation, Mater. Sci. Semicond. Process. 103 (2019) 104599.
[103] Y. Xiao, B. Luo, B. Cheng, Q. Huang, Y. Ye, L. Fang, L. Zhou, S. Lei, Enhanced visible light catalysis activity of CdS-sheathed $SrAl_2O_4$: Eu^{2+}, Dy^{3+} nanocomposites, Dalton Trans. 47 (2018) 7941–7948.
[104] S. Peiris, J. McMurtrie, H.-Y. Zhu, Metal nanoparticle photocatalysts: emerging processes for green organic synthesis, Cat. Sci. Technol. 6 (2016) 320–338.

This book belongs to Badji Mokhtar Annaba University Central Library Copyright Elsevier 2025

[105] S. Talebzadeh, C. Queffélec, D.A. Knight, Surface modification of plasmonic noble metal–metal oxide core–shell nanoparticles, Nanoscale Adv. 1 (2019) 4578–4591.
[106] N. Jiang, D. Li, L. Liang, Q. Xu, L. Shao, S.-B. Wang, A. Chen, J. Wang, (Metal yolk)/(porous ceria shell) nanostructures for high-performance plasmonic photocatalysis under visible light, Nano Res. 13 (2019) 1354–1362.
[107] P. Verma, Y. Kuwahara, K. Mori, H. Yamashita, Mesoporous silica–supported Ag-based plasmonic photocatalysts, in: Current Developments in Photocatalysis and Photocatalytic Materials, Elsevier, 2020, pp. 353–368.
[108] Q. Yin, Z. Yang, K. Qiu, P. Zhang, Luminescence and photocatalytic performance of $Ca_{1-x}TiO_3:Pr^{3+}$ material, Integr. Ferroelectr. 200 (2019) 90–98.
[109] L. Zhang, H. Wu, Y. Jin, H. Sun, D. Liu, Y. Lv, G. Ju, L. Chen, Y. Hu, Competition of luminescence and photocatalysis in melilite: recombination and transportation of electrons, Phys. B Condens. Matter 573 (2019) 87–91.
[110] F. Wang, Y. Pu, X. Zhang, F. Zhang, H. Cheng, Y. Zhao, A series of multifunctional lanthanide metal-organic frameworks for luminescent sensing and photocatalytic applications, J. Lumin. 206 (2019) 192–198.
[111] X. Xu, Y. Sun, Q. Zhang, H. Cai, Q. Li, S. Zhou, Synthesis and photocatalytic activity of plasmon-enhanced core-shell upconversion luminescent photocatalytic Ag@ SiO_2@ YF_3: Ho^{3+}@ TiO_2 nanocomposites, Opt. Mater. 94 (2019) 444–453.
[112] A.M. Ali, N.A. Ghazwani, H. Algarni, A.A. Ismail, Synthesis of ZnO–SnO_2 nanocomposites: impact of polyethylene glycol on morphological, luminescence and photocatalytic properties, Res. Chem. Intermed. 45 (2019) 3089–3106.
[113] Y. Li, L. Yao, Z. Yin, Z. Cheng, S. Yang, Y. Zhang, Defect-induced abnormal enhanced upconversion luminescence in BiOBr: Yb^{3+}/Er^{3+} ultrathin nanosheets and its influence on visible-NIR light photocatalysis, Inorg. Chem. Front. 7 (2020) 519–528.
[114] Y. Li, Z. Cheng, Y. Peng, S. Yang, Y. Zhang, Modulation of single-band red upconversion luminescence in Er^{3+}/Yb^{3+} codoped bismuth oxyiodide nanoplates by bandgap engineering and their application in NIR photocatalysis, Ceram. Int. 46 (2020) 6351–6359.
[115] A. Tuerdi, A. Abdukayum, Dual-functional persistent luminescent nanoparticles with enhanced persistent luminescence and photocatalytic activity, RSC Adv. 9 (2019) 17653–17657.
[116] M.M. Rahman Khan, S. Pal, M.M. Hoque, M.R. Alam, M. Younus, H. Kobayashi, Simple fabrication of PVA–ZnS composite films with superior photocatalytic performance: enhanced luminescence property, morphology, and thermal stability, ACS Omega 4 (2019) 6144–6153.
[117] J. Zhou, J. Huang, Y. Xia, H. Ou, Z. Li, Two-in-one ultraviolet persistent luminescent catalyst suitable for high concentration photodegradation, Sci. Total Environ. 699 (2020) 134342.
[118] Y.-M. Pan, W. Zhang, Z.-F. Hu, Z.-Y. Feng, L. Ma, D.-P. Xiong, P.-J. Hu, Y.-H. Wang, H.-Y. Wu, L. Luo, Synthesis of Ti^{4+}-doped $ZnWO_4$ phosphors for enhancing photocatalytic activity, J. Lumin. 206 (2019) 267–272.
[119] K. Karthik, S. Dhanuskodi, C. Gobinath, S. Prabukumar, S. Sivaramakrishnan, Fabrication of MgO nanostructures and its efficient photocatalytic, antibacterial and anticancer performance, J. Photochem. Photobiol. B Biol. 190 (2019) 8–20.
[120] Z. Fan, Z. Ye, Y. Qie, Y. Liu, H. Yang, Photoluminescence and photocatalytic hydrogen evolution properties of orange-red emitting $AlN:Sm^{3+}$, J. Mater. Sci. Mater. Electron. 30 (2019) 20109–20118.
[121] L. Zammouri, A. Aboulaich, B. Capoen, M. Bouazaoui, M. Sarakha, M. Stitou, R. Mahiou, Synthesis of YAG: Ce/ZnO core/shell nanoparticles with enhanced UV-visible and visible light photocatalytic activity and application for the antibiotic removal from aqueous media, J. Mater. Res. 34 (2019) 1318–1330.
[122] S. Jain, K. Adiga, V.P. Verneker, A new approach to thermochemical calculations of condensed fuel-oxidizer mixtures, Combust. Flame 40 (1981) 71–79.
[123] N. Pradal, G. Chadeyron, S. Thérias, A. Potdevin, C.V. Santilli, R. Mahiou, Investigation on combustion derived $BaMgAl_{10}O_{17}$: Eu^{2+} phosphor powder and its corresponding PVP/$BaMgAl_{10}O_{17}$: Eu^{2+} nanocomposite, Dalton Trans. 43 (2014) 1072–1081.

This book belongs to Badji Mokhtar Annaba University Central Library Copyright Elsevier 2025

[124] L. Diaz-Torres, P. Salas, J. Perez-Huerta, C. Angeles-Chavez, E. De la Rosa, A new blue, green and red upconversion emission nanophosphor: $BaZrO_3$: Er, Yb, J. Nanosci. Nanotechnol. 8 (2008) 6425–6430.
[125] Y. Tian, W.-H. Cao, X.-X. Luo, Y. Fu, Preparation and luminescence property of Gd_2O_2S: Tb X-ray nanophosphors using the complex precipitation method, J. Alloys Compd. 433 (2007) 313–317.
[126] Q. Xiao, L. Xiao, Y. Liu, X. Chen, Y. Li, Synthesis and luminescence properties of needle-like $SrAl_2O_4$: Eu, Dy phosphor via a hydrothermal co-precipitation method, J. Phys. Chem. Solids 71 (2010) 1026–1030.
[127] H.K. Yang, J.H. Jeong, Synthesis, crystal growth, and photoluminescence properties of YAG:Eu^{3+} phosphors by high-energy ball milling and solid-state reaction, J. Phys. Chem. C 114 (2010) 226–230.
[128] D. Chen, M. Sivakumar, A.K. Ray, Heterogeneous photocatalysis in environmental remediation, Dev. Chem. Eng. Miner. Process. 8 (2000) 505–550.
[129] R. Ameta, S. Benjamin, A. Ameta, S.C. Ameta, Photocatalytic degradation of organic pollutants: a review, in: Materials Science Forum, Trans Tech Publ, 2013, pp. 247–272.
[130] Q. Xiang, J. Yu, P.K. Wong, Quantitative characterization of hydroxyl radicals produced by various photocatalysts, J. Colloid Interface Sci. 357 (2011) 163–167.
[131] E. Grabowska, J. Reszczynska, A. Zaleska, Mechanism of phenol photodegradation in the presence of pure and modified-TiO_2: a review, Water Res. 46 (2012) 5453–5471.
[132] I.K. Konstantinou, T.A. Albanis, TiO_2-assisted photocatalytic degradation of azo dyes in aqueous solution: kinetic and mechanistic investigations: a review, Appl. Catal. B Environ. 49 (2004) 1–14.
[133] J. Liqiang, Q. Yichun, W. Baiqi, L. Shudan, J. Baojiang, Y. Libin, F. Wei, F. Honggang, S. Jiazhong, Review of photoluminescence performance of nano-sized semiconductor materials and its relationships with photocatalytic activity, Sol. Energy Mater. Sol. Cells 90 (2006) 1773–1787.
[134] L. Gomathi Devi, S. Girish Kumar, K. Mohan Reddy, C. Munikrishnappa, Effect of various inorganic anions on the degradation of Congo Red, a di azo dye, by the photo-assisted Fenton process using zero-valent metallic iron as a catalyst, Desalin. Water Treat. 4 (2009) 294–305.
[135] Y. Vidya, K. Gurushantha, H. Nagabhushana, S. Sharma, K. Anantharaju, C. Shivakumara, D. Suresh, H. Nagaswarupa, S. Prashantha, M. Anilkumar, Phase transformation of ZrO_2: Tb^{3+} nanophosphor: color tunable photoluminescence and photocatalytic activities, J. Alloys Compd. 622 (2015) 86–96.

This book belongs to Badji Mokhtar Annaba University Central Library
Copyright Elsevier 2025

CHAPTER 9

Magnetic nanomaterials-based photocatalyst for wastewater treatment

Prachi Upadhyay[a], Vijayanand S. Moholkar[b], and Sankar Chakma[a]

[a]Department of Chemical Engineering, Indian Institute of Science Education and Research Bhopal, Bhopal, Madhya Pradesh, India, [b]Department of Chemical Engineering, Indian Institute of Technology Guwahati, Guwahati, Assam, India

9.1 Introduction

Water is one of the constituents required for sustainable development and crucial for food production, industrial development, energy production, and survival of all forms of life on this planet. Water is the link that connects the human with the environment and is greatly affected by the changing climatic conditions. The first emphasis that was laid on wastewater treatment was in the year 1900–1970 by the United States of the Federal Water Pollution Control Act Amendments of 1972 (Public Law 92–500) (also referred to as the Clean Water Act) with the aim to achieve fishable and swimmable water. At that time, the main objective was eradication of pathogens, remediation of biodegradable waste, and elimination of suspended, floatable, and colloidal materials. Presently, several global summits and seminars are being organized now to increase awareness in the society about the effect of global warming and pollution on water. According to the United Nations Water Development Report 2019, there has been an increase in consumption of water by 1% annually, and this continuous rise is because of the increasing population and other socioeconomic factors. The maximum water is used in agricultural activities (i.e., 69%), followed by industrial requirement (i.e., 19%), and finally, household demand of about 12% [1]. Therefore in order to sustain this increase of water demands, the country needs a regulatory body to regulate the use of water and also formulate strict laws on its pollution so that the future demand can be met easily without putting any pressure on the environment.

The waste that is usually discharged is either pure organic or inorganic waste, sometimes the combination of both. Wastewater can be classified on the basis of endocrine-disrupting chemicals (EDCs), biochemical oxygen demand (BOD), chemical oxygen demand (COD),

Handbook of Nanomaterials for Wastewater Treatment. https://doi.org/10.1016/B978-0-12-821496-1.00008-8
Copyright © 2021 Elsevier Inc. All rights reserved.

This book belongs to Badji Mokhtar Annaba University Central Library Copyright Elsevier 2025

active pharmaceutical ingredients (APIs), total suspended solids (TSS), toxic ions, total dissolved solids (TDS), water pH, organic loadings, etc. Depending upon the source of contamination such as pharmaceutical industry that contains high APIs, the values of these parameters vary from industry to agriculture or domestic wastewater [2]. The untreated wastewater that contains toxins may carry the unwanted materials and become the parts of our food chain or may seep back into the ground making the soils infertile and toxic [3]. Therefore the governments should make some parameters, and all industries should follow to regulate the serenity of the water sources.

Recently, many industries have emphasized on the zero liquid discharge (ZLD) management strategy so that most of the water that is being discharged is recycled within the industry. But the limitation of this technique is high cost and high energy consumption. Therefore to tackle this problem, a membrane-based technology (i.e., reverse osmosis) is being used as a part of ZLD method to minimize the energy consumption and overall cost for treatment. Few more techniques, other than reverse osmosis, which have been found in industries are forward osmosis, thermal evaporation, electrodialysis, and membrane distillation [4,5]. Apart from these, other techniques such as advanced oxidation, size exclusion, and sorption are also found to be effective for treatment of waste effluent. However, the experimental variables such as solution pH, catalyst concentration, temperature, and treatment time may vary from technique to technique for treating the effluent of various chemical and process industries, including textile industry [6]. In view of these, the water crisis needs a proper risk assessment and analysis of the present technologies for treatment of wastewater—which are not considered earlier and discharge the water back to the rivers without proper treatment. But the scenario at this moment has changed, and recycling of water is very much needed for conservation of it for agricultural practices and drinking purpose.

9.2 Source of water pollution and type of pollutants

Only 2.5% of the water is available on the earth's surface as freshwater and is suitable for drinking. There are three different sources of water (1) Groundwater—it is the water stored beneath the earth surface in soil, sand, and rocks, (2) Surface water—it is in the form of lakes and flowing rivers, and (3) Stormwater—it is in the form of rainfall, hail, snowmelt, etc. [7]. Even though it appears that there are several sources of water, but the reality is most of them are either polluted or depleted. Urbanization and industrialization are the two major factors behind the increase of water pollution. The wastewater effluents from industries are continuously being released into the rivers, creating serious health issues for all the living beings. According to the UN report, about 2 million tons of wastewater per day from sewage, industries, and agriculture pollutes the water bodies, and the estimated equivalent weight is to be 6.8 billion of human population. Furthermore, the annual wastewater generation is approx. 1500 km^3, which is six-folds higher while all rivers present in the world are combined [8]. The direct effect of all these

This book belongs to Badji Mokhtar Annaba University Central Library Copyright Elsevier 2025

can be observed on our ecosystem and deteriorating human health. The pollutants mainly consist of heavy metals, textile dyes, insecticides, pharmaceutical drugs, and bacteria. Owing to poor monitoring condition, many emerging pollutants have not been reported yet, and the impact of these pollutants to the society is still unknown [9].

UNESCO have divided major sources of water pollutants categories into (1) Agricultural waste mainly composed of insecticides and pesticides, (2) Pharmaceutical waste comprising drugs such as antibiotics, steroids, and hormones, (3) Personal hygiene products such as soaps, fragrances, insect repellents, and cosmetic creams, and (4) Industrial effluents from dye industries, industrial additives, plasticizers, etc. [10]. The period of degradation time of these pollutants varies from a few months to several years. It has been observed that some pollutants remain in the environment for more than 250 years, while in the human body for more than 10 years [11]. The by-products that are obtained after degradation are very toxic and harmful for the environment and human health. A rough estimation of pollutants that is being released in the environment every year has been done, and according to the sources, the pesticides that are being employed in agricultural activities are more than 4 million tons, and the release of heavy metals from the electronic waste is about 20–50 million tons and still increasing [12,13].

9.2.1 Agricultural waste

To meet the demands of the increasing population and to sustain this demand, the use of pesticides has been increased significantly. Insecticides and pesticides provide protection to the crops from different insects and pests, thus protecting the crops from diseases. But the physicochemical properties of the pesticides highly affect the environment. They are highly toxic and can disrupt many ecological processes in the water basin. Pesticides can be further categorized based on the target organism, such as insecticides, fumigants, fungicides, herbicides, and rodenticides; and on the basis of their chemical structure, such as organophosphates, organochlorines, carbamate esters, phosphine, ethylene bromide, hexachlorobenzene, and chlorophenoxy compounds [14]. Sometimes to increase the soil fertility, farmers use animal wastes after mixing with soils. But if applied in large quantity, it acts as a waste because it exceeds the limit that soil can hold and plants can utilize it. This manure reaches groundwater through infiltration and runoffs, affecting the quality of drinking water. Animal manure is a combination of inorganic and organic materials such as phosphorus, nitrogen, antimicrobial compounds, and some heavy metals. This will depend on the veterinary practices (pharmaceutical treatment) and the management of farm livestock. The antimicrobial agents help the animals against all sorts of diseases such as prophylaxis, improve fertility, and increase their growth. One of the main factors behind agriculture waste is lack of awareness toward unregulated checking because agriculture is the source of food for all [15,16].

This book belongs to Badji Mokhtar Annaba University Central Library Copyright Elsevier 2025

9.2.2 Pharmaceutical waste

There are different sources that are responsible for the increase in pharmaceutical waste in water bodies such as leaking sewer lines, accidental and permitted discharge in water, used chemicals in household and hospitals, and pet and livestock wastes. This waste includes hormones, antibiotics, disinfectants, drugs, surfactants, antioxidants, etc. For instance, adverse effects such as feminization of male fishes owing to the harmful effects of the hormones in freshwaters [17]. More than 80 different types of chemicals have been detected during the wastewater treatment, and the majority of chemicals are pharma grade. The pharmaceutical process industries can be categorized as: (1) plants-based extractions (vitamins/antibiotics/enzymes, etc.), (2) developed organic chemicals plants, (3) drug blending, formulation, and development plants (capsules/tablets/solutions, etc.), (4) fermentation, and (5) organic chemicals synthesis plants (usually medium to large plants) based on the production method [18]. Different types of production methods release different types of chemicals in the wastewater; and if left untreated, they start disrupting the aquatic life and act as a source of many waterborne diseases. The pharmaceutical products and their by-products pose an equal hazard, and sometimes, the by-products are even more toxic in nature and remain in water pharmacologically active for several years. The unused drugs or expiry drugs are usually discarded in landfills or in toilets, which can be considered as a potential source of contamination. Pharmaceutical drugs such as sulfamethoxazole, erythromycin, naproxen, sulfasalazine, cyclophosphamide, or metabolite can exist in the environment for more than a year [19]. The major contribution for the pharmaceutical contamination is because of the inefficient treatment of wastewater from the pharmaceutical industries followed by municipal wastewater treatment. Most of the waste released is nonbiodegradable, and hence a conventional treatment technology is usually not sufficient for effective treatment [20].

9.2.3 Industrial waste

Industries are responsible for producing three different categories of waste depending upon the process of production: (1) liquid wastes (wastewater from different processes), (2) solid wastes (left raw materials, by-products, defective items, and hazardous waste), and (3) air pollutants (toxic gases, CO_2, etc). Sometimes, the waste of one category can also act as the waste for another category, like if the solid wastes are dumped without any check, then they can contaminate the water bodies through rains, or the volatile organics discharged in water can also create air pollution. The wastewater from the industries is usually released at higher temperature when compared to agricultural wastewater or municipal wastewater and also very toxic in nature. The waste from each process before discharging needs to be separated and converted into less toxic matter; and further treatment is required to minimize or eliminate the toxic compounds completely from the water [21]. After pharmaceutical, it's the textile industry that discharges heavily numerous textile dyes in water bodies. Textile industries require more

This book belongs to Badji Mokhtar Annaba University Central Library Copyright Elsevier 2025

than 200–350 cubic meters of freshwater for production of 1 ton of dye products [22]. The chemicals released contain a combination of organic and inorganic substances such as dyes, softening agents, pigments, surfactants, oils, and other additives added to increase the luster and shelf life of the products. Owing to the release of these chemicals, the physical properties of water such as pH, alkalinity, conductivity, COD, suspended solids, and color changes. It becomes difficult to treat such type of wastewater using biological methods because of the presence of recalcitrant compounds [23]. The products such as automobiles, plastic wares, clothes, and furniture use different types of dyes and paints to give them aesthetic value or more better finishing. Once the product is discarded in the open environment, it again acts as the source of pollution for the water because these dyes and paints leach out with time and get mixed into the water. As a result, water is contaminated with high concentrations of dyes hazardous for the human health and for the aquatic life because the structure of these organic chemicals contains chromophores, and when sunlight falls on it, it absorbs light, disrupting the photosynthesis process of aquatic organisms [22]. To tackle this problem, different methodologies are being adopted such as adsorption, advanced oxidation processes, Fenton process, photochemical, electrochemical, sonochemical, biological, chemical, and physicochemical methods [24].

Cosmetic industries, which are the other most dominant sector, employ many chemicals, and their waste usually consists of surfactant, oil, suspended solids, and fats. A variety of cosmetic products is manufactured based on the market demands. Irrespective of the cosmetic industry and consumer, many products find their way back to the environment such as ultraviolet (UV) filters (1,7,7-trimethyl-3-(phenylmethylene) bicyclo[2.2.1]heptan-2-one-3-BC, 1,7,7-trimethyl-3-[(4-methoxyphenyl)methylene]-bicyclo[2.2.1]heptan-2-one-4-MBC) and polycyclic musk (Hexahydrohexamethyl cyclopentabenzopyran or HHCB), and 7-acethyl-1,1,3,4,4,6-hexamethyl-1,2,3,4 tetrahydronaphthalene-tonalide or AHTN). Their long-term exposure can lead to many serious diseases in humans such as hormonal imbalance, and skin irritation. Different techniques such as coagulation, electrocoagulation, advance oxidation process, and electro-Fenton processes are in use to eradicate them from the water bodies [25,26].

9.2.4 Plastic waste

Plastic pollution is one of the most serious pollutions that the whole world is currently facing. When plastics first came in the market, they bought a huge revolution. Heavy metal-based product was immediately replaced by plastic because it is easy to carry and cheap. Although the plastics have made life easy in many aspects, the major danger is their nonbiodegradability. Plastics take several years to degrade. The plastic menace has shown an increase with time; since 2015, more than 6.3 billion tons of plastic pollutant have been produced, of which 79% has entered the natural environment and landfills. It has greatly affected the freshwater, soil,

This book belongs to Badji Mokhtar Annaba University Central Library Copyright Elsevier 2025

and marine life. Many countries have even pledged to ban the single-use plastics [27]. Microplastics with size less than 5 mm are creating the most harmful debris on the planet. A new ecological niche "plastisphere" is being formed and is one of the sources for pathogenic bacteria such as Pseudomonas, Acinetobacter, Escherichia, and fungi such as Cryptococcus and Rhodotorula. This plastic debris enters into the food chain slowly through the potable water, soil, beverages, and aquatic animals. As the plastic debris sustains for prolonged time in the environment, it becomes susceptible to thermal degradation, oxidation, UV irradiation, and biodegradation. This changes the chemical structure, molecular weight, mechanical strength, and oxygen amount of the plastic. The degradation process is very slow and takes many years to degrade the plastic completely. Therefore it becomes very important to have a clear insight of the aging process of these microplastics so that they can be eliminated completely from the environment; advanced oxidation processes are being viewed as an important technique apart from other techniques such as biological processes for complete degradation of waste plastics from water [28,29].

9.3 Types of water treatment techniques

Wastewater treatment technologies can be classified broadly either as physicochemical processes or as biological processes. Methods such as chlorination, ultrafiltration, electrodialysis, sonochemical, Fenton reaction-based processes, advance oxidation processes, adsorption, coagulation, immobilization, photocatalysis, and photolysis come under the category of physicochemical methods; while the biological wastewater treatment methodologies mainly consist of activated sludge process, aerobic and anaerobic degradation, phytoremediation, membrane bioreactor, and biosorption [30]. A series of steps is followed for the treatment of wastewater from its source before releasing it back to the environment. The major treatment techniques are pretreatment or primary treatment, secondary treatment, followed by a tertiary process. The primary target behind this is to make water suitable for drinking and other purposes; further to reclaim important nutrients, minerals, metals, and other beneficial resources. Pretreatment process is mainly done to remove suspended solids from wastewater—which can interfere with the subsequent processes. Therefore this process maintains the pH and removes any debris or suspended solid particles. Secondary treatment mainly constitutes the biological processes and helps in the removal of soluble and insoluble pollutants using aerobic and anaerobic techniques. The final treatment is the tertiary treatment process that utilizes the advanced techniques for the water treatment and also makes the water fit for drinking [31,32]. A brief overview of all the methods is as follows:

9.3.1 Primary treatment

It is the initial treatment or the primary process that is used to treat the wastewater. The efficiency is low compared to secondary or tertiary treatment process, but it is very effective for removal of solid impurities in bulk. The primary treatment process can employ physical

This book belongs to Badji Mokhtar Annaba University Central Library Copyright Elsevier 2025

separation methods such as screening and filtration or chemical-based processes such as coagulation and flocculation [31]. The different methods of primary treatment technique are described further.

9.3.1.1 Screening, centrifugal separation, and filtration

The screening, centrifugal separation, and filtration techniques enable the removal of suspended solid particles. Screening is the initial process and consists of different mesh sizes so as to retain the higher size particles and let pass the lower size particles. The impurities mainly consist of wood, cloth, plastics, human and animal excreta, kitchen waste, etc. Approximately, 5%–25% of impurities are removed through this process [31–33]. In centrifugal separation technique, high-speed rotation is provided for separating noncolloidal solids of 1.0 μm size. The principle of centrifugation separation is based on the difference in densities. The counter flow, countercurrent flow, solid-bowl, and basket type are some of the centrifugal machines that are in use for the separation or removal of oil and greases [31,33]. Filtration technique involves passing wastewater through very small pores of a medium or membrane lying in the range of 0.1–0.5 μm. Bacteria, oil, suspended impurities, etc. can be removed with the help of filtration technique. The treated water can then be further treated by employing membrane-based separation process, adsorption, or ion-exchange [31].

9.3.1.2 Gravity separation and sedimentation

The wastewater in a tank is left unperturbed for different time intervals so that grits, suspended solids, and slits can be settled down by gravitational force. The interval depends on the weight and pollutants' density or the speed of moving fluid. The sedimentation process comprises two main operations: first is thickening in which the concentration of feed stream is increased, and the other is clarification in which the solids are removed from a relatively diluted solution. Approximately, 60% of the suspended solids are removed during the gravity settling process. The application of this process is mainly in refinery and paper industries because of its cost-effectiveness and efficiency [31].

9.3.1.3 Coagulation and flocculation

This is a chemical treatment process and helps to enhance the effectiveness of primary treatment and reduces the secondary treatment stages. It involves three stages or unit operations: first is fast mixing, followed by flocculation, and finally, settling. Initially, the chemical is added and is mixed thoroughly with the help of mixers. In the coagulation process, alum, activated silica, iron materials, aluminum salts, and starch are usually added. In some cases, synthetic polymers with cationic and anionic or nonionic charges are used. The controlling factors that highly impact on the coagulation process are temperature, pH, and contact duration. Owing to the addition of these chemicals as coagulating or flocculating agents, a perturbation or disturbance is created in the system owing to which sedimentation of suspended particles occur. For flocculation of coagulating particles, two types of mechanical flocculators and static hydraulic flocculators are used [31,34,35].

This book belongs to Badji Mokhtar Annaba University Central Library Copyright Elsevier 2025

9.3.2 Secondary treatment

Organic matter comprises 45%–50% of the dissolved solids in wastewater. Carbon, hydrogen, oxygen in combination with nitrogen, and some other elements such as iron, phosphorus, and sulfur constitute the organic waste. Secondary water treatment utilizes microbes for the treatment of wastewater. This method is very important because it converts waste into valuable fuel or resources such as water, ammonia gas, carbon dioxide, alcohol, nitrate, and glucose. Furthermore, these microbes in the form of bacteria or fungal strains reduce the toxicity of inorganic waste. Based on the treatment technique, secondary treatment can be either aerobic or anaerobic conditions [31,36].

9.3.2.1 Aerobic process

In aerobic treatment techniques, the dissolved oxygen (DO) present in the water is utilized by facultative bacteria for degrading organic pollutants through aerobic conditions. The reaction that is involved in this process is expressed by Eq. (9.1):

$$\text{Organic Matters} + \text{Bacteria} + O_2 \rightarrow \text{Bacteria} + H_2O + CO_2 + \text{By} - \text{products} \tag{9.1}$$

It is evident from the equation that the presence of oxygen is very important for the bacteria to carry out the desired conversion. Therefore continuous supply of air should be made by forcing it through a compressor or blower inside the tank, including proper circulation. Other parameters that influence the reaction are holding time, system temperature, nature of the bacteria, and water pH. Aerobic treatment is performed by using activated sludge process or oxidation or trickling filters. The technique is useful for the mitigation of volatile organics, phosphates, dissolved and suspended organics, biological oxygen demand (BOD), COD, nitrates, etc. This method provides 90% reduction in organic waste, but the only limitation is the excess bio-solids that also require posttreatment technologies that are not economical [31,35].

9.3.2.2 Anaerobic process

The anaerobic process occurs in the deficiency of oxygen and is known as putrefaction. This process involves facultative bacteria in anaerobic conditions to degrade the toxic organic waste into nontoxic compounds and the release of gases such as methane, ammonia, hydrogen sulfide, and nitrogen. Eq. (9.2) shows the reaction mechanism for anaerobic process:

$$\text{Organic Matter} + \text{Bacteria} \rightarrow \text{Bacteria} + CO_2 + CH_4 + \text{By} - \text{products} \tag{9.2}$$

Anaerobic systems can treat wastewater with COD values more than 4000 mg/L compared to aerobic processes that can treat only wastewater with COD of around 1000 mg/L. The main benefit of anaerobic treatment is that it is less energy consuming and beneficial nutrients can be extracted. The operating parameters that need to be monitored while working on anaerobic system are temperature and toxicity because both can disturb the system. The main limitation of anaerobic wastewater treatment is its relatively time-consuming process [31,35,37].

This book belongs to Badji Mokhtar Annaba University Central Library
Copyright Elsevier 2025

9.3.3 Tertiary treatment techniques

9.3.3.1 Evaporation, crystallization, and distillation

Evaporation is a very effective technique for removal of nonvolatile contaminants from the wastewater. This technique operates at temperature higher than the ambient conditions so that water evaporates, which is further collected by condensing it as pure water. The mechanical and vacuum evaporators are mainly utilized for this technique. Most of the time the water is also circulated back for other industrial purposes such as boilers and cooling towers. The industries that usually prefer evaporation techniques are food industries, fertilizer, and pharmaceutical and petroleum industries. Fouling, scaling, suspended solids, and foaming are the setbacks that this method suffers [31].

Crystallization is a useful technique when the concentration of total dissolved solids is high. This method is also used for the regulation of pH by breaking down sulfite, ammonia, and bicarbonate into different gases. In this process, the concentration of pollutants is increased up to a limit where they start crystallizing out and get separated to a pure solid form. This technique has the advantage of recovering valuable materials along with pure water. The advantages of crystallization method over other technologies are recovery rate is high, easy to operate, stable, energy-efficient, easy to scale-up, and almost no requirement of other supporting materials, such as catalyst, membrane, oxidant, or reducing agent. The crystallization process can be performed through different techniques such as cooling, evaporation, membrane distillation, reaction, and drowning-out crystallization. Wastewater from the paper and dye industries, gas and coal boilers, and cooling towers is treated using this method. To remove nitrogen, ammonia, and phosphorus from wastewater, Struvite crystallization is an efficient method [31,35,38].

Distillation, like evaporation, is a thermal treatment process for wastewater treatment and requires energy. The vapors of the water are condensed by passing it through the cooling towers. The water obtained through this method is 99% pure, but the only condition is that the wastewater should not contain any volatile impurities. Multistage boilers and double distillation units are used depending upon the process or type of industry from which wastewater is being released [31].

9.3.3.2 Membrane processing

Membrane filtration technique is an advanced wastewater treatment method used for separating heavy metals, removal of color, salinity, and oil from wastewater. It is a simple technology that requires no external thermal treatment, chemical additives, and easy to control and scale-up. The basic mechanism of membrane separation process involves size selection, Donnan exclusion, and solution diffusion. Membranes are made up of small pores and when wastewater is passed through it, the larger particles are retained on the membrane surface depending on the

This book belongs to Badji Mokhtar Annaba University Central Library Copyright Elsevier 2025

pore size, and the rest of the smaller particles pass through it. The larger particles retained on the membrane surface is known as filter cake; therefore the membrane should always be cleaned properly to avoid any fouling, which is a major problem in membrane technology. The membrane efficiency is evaluated on the basis of the permeate flux and the rejection. Depending on the pore size, membrane processing can be classified further as ultrafiltration, reverse osmosis, and nanofiltration [35].

***Ultrafiltration*:** The pore size of the ultrafiltration membrane lies between 10 and 100 nm and is effective for the elimination of biological contaminants, for example, viruses, bacteria, and chemical pollutants such as color pigments, heavy metal ions, and some natural organic colloids. It also requires less pressure in comparison to reverse osmosis and nanofiltration. Because of the large pore size, many metal ions and dye molecules can easily pass through it. To prevent this, various surfactants are used above their critical micelle concentration (CMC) value for "micellar-enhanced ultrafiltration (MEUF)," which leads to 99% rejection of heavy metals in the filter cake [35]. For instance, with sodium dodecyl sulfate (SDS) as a surfactant, it is possible to achieve 99.3% of methylene blue dye removal with polysulfone membrane at 300 KPa and 99.0% of methylene blue dye removal with polyvinylidene fluoride-titanium dioxide membrane at very less pressure of 50 KPa [39]. Similarly, Lin et al. have achieved separation of more than 90% for Co^{+2}, Ni^{+2}, and Cu^{+2} metal ions with SDS and cellulose membranes [40].

***Nanofilteration*:** The pore dimension of the membrane in nanofiltration is less than 10 nm and mainly used for separation of heavy metal ions from wastewater stream and water softening. The main benefits of nanofiltration technique over other membrane-based technology are lower osmotic pressure difference, high rate of permeate flux, high rate of retention of salts, and cost-effectiveness. The working principle of nanofiltration is based on Donnan and steric exclusion. Donnan exclusion theory states that if membranes with positive surface charges have high rejection rate and flux for cations (e.g., heavy metals). However, NF membranes usually have negative or neutral charge because of synthesis and fabrication procedures. Therefore the desired rejection and flux is not achieved. The main focus is now on the synthesis of positively charged membranes to enhance the effectiveness of heavy metal separation [35,41].

***Reverse osmosis*:** Reverse osmosis is the most popular technology for wastewater treatment, and it has been employed for elimination and concentration approach at micro- and macrolevels for elimination of ionic, nonionic, and highly soluble toxic impurities. This technique can effectively remove 99% of bacteria, soluble organic pollutants, and total dissolved solids. Sanitary waste, municipal waste, and different industrial (pulp and paper industries, galvanic, dairy, food, oil and gas, and power plants) pollutants can be effectively treated using reverse osmosis. This technique employs more pressure than the osmotic pressure to carry out the removal through a semipermeable membrane. The hydrophilic nature of the membrane allows easy passage of the water and retains any soluble impurities on its surface. Cellulose, polyamide, and polyether-based membranes are used to carry out the separation. Operating parameters that affect the separation process are pressure, pore size, solute's molecular weight,

This book belongs to Badji Mokhtar Annaba University Central Library Copyright Elsevier 2025

and operating time. The only limitations with reverse osmosis are it wastes lots of water; it is energy-intensive, and comparatively expensive. Because of its nonselective nature toward ions, it deprives the drinking water with all the required essential minerals [31,35]. The effectiveness of the reverse osmosis membrane can be evaluated using the following equation:

$$\text{Retention}\% = \frac{C_F - C_P}{C_F} \times 100$$

$$\text{Working Effeciency (WE)} = 1 - \frac{C_P}{C_F}$$

where C_F = molar concentration of the solute, C_P = molar concentration of solute in the permeate (filtrate), and WE = working efficiency of the membrane. In reverse osmosis, separation of pollutants is affected by the partition coefficients of solutes between membrane and water. It involves the free energy of interaction between active sites of the membrane surface and water [31].

9.3.3.3 Adsorption

As we are discussing further about the different technologies for wastewater treatment, it is difficult to conclude that one technology is sufficient for effective treatment of different pollutants. Most of the techniques suffer from toxic sludge as by-product, which requires further treatment, increasing the maintenance and operational cost. Additionally, the processes are sometimes very complicated and require a lot of precision for handling. Owing to this, adsorption-based technology is more popular, with advantages such as ease of processing and simplicity in operation. Adsorption process comes under tertiary treatment, and it means any pollutant left after the biological processes, and primary treatment will be taken care of by this process. Activated charcoal (AC) is the most popular adsorbent that has been in use for elimination of organic and inorganic pollutants, including textiles dyes and heavy metals. Adsorption too suffers from limitations such as regeneration of adsorbents, disposal issues when the adsorbent loses activity, and cost of the fresh adsorbent [42]. Adsorption is popular because it requires less chemicals, water, and energy, and therefore developing countries prefer adsorption as it requires less power and money. Numerous adsorbents are available commercially and depending upon the pollutant type, it can be selected. Flow or column method and batch methods are mainly in use for the adsorption process. In batch mode, adsorbate is added in the aqueous suspension, and the uniformity is maintained using continuous mixing or agitation. The column mode is mainly used in industries in which a fixed bed of adsorbate is made through which the wastewater flows at a fixed rate [43].

For the study of adsorption, different theories and models are used. Adsorption is a mass transfer phenomenon, and the complete adsorption phenomenon takes place in three major steps: (1) external diffusion or film diffusion (diffusion of the particles across the liquid envelope around the adsorbent particles); (2) internal dispersion or intraparticle diffusion (dispersion in the liquid that contained in intricacies or the pores); and (3) mass action or

This book belongs to Badji Mokhtar Annaba University Central Library Copyright Elsevier 2025

adsorption-desorption between the active sites of adsorbate [44]. For thorough understanding and measurement of adsorption process, isotherms are drawn, which are curves formed using computational expressions. These expressions are based on Gibbs adsorption isotherm, which is a relationship for the thermodynamic aspects at the interface. The isotherms provide information about the adsorption capacity of adsorbent, mechanism of the adsorption of solute on the surface of the adsorbent, effect of pressure, and the type of isotherms for categorizing the systems through the isotherms curve and its initial slope. The most common isotherm that is in use is Langmuir and Freundlich adsorption isotherm. In Langmuir adsorption isotherm, the curve generated the initial slope that is directly proportional to the loss active site upon increasing solute concentration, and with decreasing active sites, the curve forms a plateau. From Langmuir isotherm, the quantity of solute that is adsorbed on active site of the adsorbent can be estimated. Freundlich isotherm, on the other hand, explains the adsorption phenomenon at the solid-liquid interface [43,45]. Other controlling parameters for the adsorption process are temperature, pH, adsorbent's active sites, and concentration of the adsorbent and solute [43]. Adsorption process has been used for separation of many heavy metals such as arsenic and antimony, including several contaminants. One of the advantages of adsorption is that the adsorbents can be synthesized from cheap raw materials such as sawdust, vegetable waste, and fertilizer waste. These adsorbents can remove up to 90% of the various pollutants and are of low cost as well [46,47]. The large surface area of the nanoparticles provides more binding site for the adsorption of the pollutants. Some of the emerging nanoadsorbents are stannous oxide, akaganeite, cobalt ferrite, gold, copper, zirconia, maghemite, iron hydroxide, iron, iron oxide, titanium oxide, silica, nickel oxide, cadmium sulfide, anatase, zinc oxide, zinc sulfide, alumina, and some alloys. Zeolites and carbon nanotubes (CNTs) are very popular as adsorbents because of their high stability and surface area [48].

9.3.3.4 Advance oxidation method

For the portable drinking water treatment first time in the 1980s, advanced oxidation processes employing energetic hydroxyl or sulfate radicals as the primary oxidizing agent were tested. Advance oxidation methods are very popular for degradation of inorganic and organic recalcitrant pollutants. Earlier advance oxidation processes were confined only to the study of hydroxyl radicals (•OH) for treatment of wastewater, but with time, sulfate radicals also became a part. The in-situ generation of these powerful radicals helps in degrading the pollutants without generating any other waste stream [49,50]. •OH with oxidation potential E^0 ($\bullet OH/H_2O$) = 2.8 eV have always been looked forward for the mineralization of harmful pollutants in the water. With time, sulfate radicals also gained popularity mainly because of their high lifetime (i.e., 30–40 μs) compared to •OH that have an average lifetime of only 20 ns [51,52]. Combined effect of these radicals with other processes such as UV, Ozone, and Fenton has shown remarkable results because of the generation of many reactive radicals, but intermittently, it may also lead to decrease in degradation rate owing to the release of excessive reactive species that act as self-scavenger [53]. One of the advantages of advanced oxidation process is that the biodegradability of the wastewater intensifies during the mineralization

This book belongs to Badji Mokhtar Annaba University Central Library Copyright Elsevier 2025

process [54]. Contamination of water with arsenic is one of the major issues that are being dealt worldwide and the main focus for its removal is on separation methods such as sedimentation, filtration, chemical coagulation, ion-exchange process, and adsorption. But owing to their limitations, they can remove only <60% arsenate and <30% arsenite from the wastewater. Furthermore, the major arsenic concentration in water is in the form of arsenite that amounts to more than 50% of total arsenic concentration and is also very toxic in nature. In this regard, AOP-based methods have been found to be efficient in reducing the toxicity of water by reducing the arsenite form into arsenate form, which is also very less toxic [55,56].

AOPs constitute the following processes: Fenton, photo-Fenton, electro-Fenton, sono-Fenton, photocatalysis, persulfate/peroxymonosulfate, anodic oxidation, zero-valent metal/H^+/O_2, sonochemical methods, ozonation, catalytic ozonation, etc. These processes are discussed in the subsequent sections separately [57].

(A) **Homogeneous photocatalysis process**

Photolytic degradation of pollutants can take place through any of the three techniques: (1) direct degradation using a light source, that is, photolysis, (2) combination of photolysis and supplementary oxidant (e.g., O_3, O_2, H_2O_2, etc.), and (3) combination of photolysis and a catalyst that is active in UV-visible region [58]. It is a very clean and environmentally friendly technique that utilizes light energy for the degradation of pollutants. Photon energy of UV light is high enough to break the bonds in a chemical compounds. For this, high-pressure mercury lamps with 185 nm, 253.7 nm, and 365 nm are mainly used as the source of UV light. Other light sources include fluorescent lamps, xenon lamps, and sunlight, which provide energy in UV and visible region of the spectrum [59,60]. UV irradiation is a very popular method and is in use for advanced treatment processes for the efficient disinfection and sterilization of bacteria and other pharmacologically active compounds in wastewater, leaving very minimal by-products along with being noncorrosive to the treatment and water supply systems. The major limitation is that many times after the removal of the UV source, the bacteria or the molecules get reactivated and require very high intensity of UV radiations [61].

(i) *Sonochemical methods*

The application of ultrasound or sonolysis method involves the phenomenon of acoustic cavitation for degradation of pollutants. Acoustic cavitation is defined by the generation, growth, and implosive bursting of the microbubbles. During the transient collapse of microbubbles, heat is generated, leading to formation of hot spots and thus generation of highly reactive species such as •OH, •H, $HO_2^{\cdot -}$, and H_2O_2. This method is very efficient for the mineralization of contaminated water because there is generation of powerful oxidizing OH radicals during the collapse of the bubbles and formation of pyrolysis zone inside the bubbles owing to heat generation inside the bubbles [62]. The governing equations (9.3)–(9.7) for the sonochemical degradation are:

This book belongs to Badji Mokhtar Annaba University Central Library Copyright Elsevier 2025

$$H_2O + \text{Ultrasound Energy} \rightarrow {}^{\bullet}H + {}^{\bullet}OH \tag{9.3}$$

$$O_2 + \text{Ultrasound Energy} \rightarrow 2{}^{\bullet}O \tag{9.4}$$

$$H_2O + {}^{\bullet}O \rightarrow 2\,{}^{\bullet}OH \tag{9.5}$$

$$O_2 + {}^{\bullet}H \rightarrow {}^{\bullet}OH + {}^{\bullet}O \tag{9.6}$$

$${}^{\bullet}OH + {}^{\bullet}OH \rightarrow H_2O_2 \tag{9.7}$$

The highly reactive and short-lived •OH may recombine and produced H_2O_2 [63]—which can further be utilized for the generation of OH radicals under the UV irradiation. The operating parameters of this method that affect the degradation of contaminants are operating frequency, power, and temperature [64]. Even for the toxic wastewater, sonochemical method can be easily applied with other AOPs to enhance the efficiency and complete mineralization [65–67].

(ii) *Fenton reaction*

Fenton-based processes generate active •OH by reacting with hydrogen peroxide with iron. These in-situ generated active species immediately attack the recalcitrant pollutants molecules present in wastewater. In 1894, H. J. H. Fenton had identified that hydrogen peroxide (H_2O_2) in the presence of ferrous (Fe^{+2}) salts results in oxidation of tartaric acid through the following reaction mechanism [68].

$$Fe^{+2} + H_2O_2 \rightarrow Fe^{+3} + OH^- + {}^{\bullet}OH \tag{9.8}$$

$$Fe^{+3} + H_2O_2 \rightarrow Fe^{+2} + H^+ + HO_2^{\bullet} \tag{9.9}$$

$$Fe^{+3} + HO_2^{\bullet} \rightarrow Fe^{+2} + H^+ + O_2 \tag{9.10}$$

One of the main benefits of employing Fenton reaction is that it is environment friendly and easy to handle. The synergistic effect of Fenton with other processes such as sonochemical, photocatalytic, and electrocatalytic gives more effective results for degradation of several pharmaceuticals and industrial wastes [69,70]. The factors affecting the Fenton process are pH, concentration of ferrous ions, H_2O_2 and pollutant, operating temperature, and coagulation. The other modified and hybrid Fenton-based processes that are being used for degradation are [71]:

(a) Fenton-like [$H_2O_2 + Fe^{+3}/m^{+n}$]
(b) Sonolysis/Fenton [($H_2O_2 + Fe^{+2}$)/US]
(c) Photolysis/Fenton [($H_2O_2 + Fe^{+2}$)/UV]
(d) Electrochemical/Fenton
(e) Sonolysis/Electrochemical/Fenton
(f) Photolysis/Electrochemical/Fenton
(g) Sonolysis/Photolysis/Fenton

Sometimes, the limitation linked with homogeneous Fenton process is that it requires a large amount of Fe^{2+} ion in the reaction mixture, and it is more than the standard value, as well as the

This book belongs to Badji Mokhtar Annaba University Central Library Copyright Elsevier 2025

maintenance of pH. Additionally, it is difficult to scale-up the homogeneous AOPs for large water flow rate because it may create the problem of sludge formation at the final neutralization step [71].

(iii) *Ozonation and catalytic ozonation*

It was in 1906 in France that the ozone was first used as the disinfectant of drinking water, and later on, more than 1000 ozone-based facilities all over Europe have come up. At few places, ozone is in use as the main disinfectant, and at other places, it is only used for oxidation to control the odor, color, and to decrease the iron and magnesium content of the drinking water. Earlier, chlorine was the first choice for water disinfectant, but with time, ozone is replacing mainly because the ozone doesn't generate by-products such as trihalomethanes that are detrimental to human health. Ozone is also a good coagulating agent than chlorine, and finally, on decomposition, ozone produces more powerful oxidizing radicals than itself [72]. In aqueous state, ozone is highly unstable, and the pH of the water greatly affects its decomposition because hydroxide ions initiate its decomposition. The highlighting attribute of ozone lies in the production of nonselective strong oxidizing agents such as •OH radicals in water. Ozone is mainly responsible for the disinfection, while for oxidation process, ozone and •OH both are required [73]. Ozone is a highly unstable gas; therefore it should be generated at the place where it will be used. UV light and cold discharge plasma processes are the two methods for the production of O_3 gas [72]. The major limitation of ozonation process is that it generates by-products, such as aldehyde, *N*-nitrosodimethylamine (NDMA), and bromate, which coagulate in water and require further treatment. Therefore ozonation cannot be used alone, and it should be performed in combination with other treatment methods such as biological processes. In Switzerland, for elimination of emerging pollutants, there are plants operating efficiently employing biological filtration after ozonation process [74,75].

(B) **Heterogeneous photocatalytic technique**

Heterogeneous photocatalytic is another emerging technique under the advance oxidation process for mineralization of pollutants. The photocatalytic degradation is an easy and simple technique for in-situ generation of powerful radicals such as •OH, superoxide radicals ($O_2^{\bullet-}$), and hydroperoxy radicals ($HO_2^{\bullet}$). These highly reactive radicals attack the organic molecules and their intermediates generating CO_2 and H_2O as end products [76]. The photocatalysts are activated under UV or visible light irradiation. Because the earth receives less than 5% of UV energy emitted by the sun, the visible light energy active photocatalysts are in more demand. If a catalyst is active in the visible range of the sun, then the process also becomes cheap because the energy from the sun is free and also environment friendly. The benefits of heterogeneous photocatalysis are: (1) reaction takes place at normal room temperature conditions, (2) catalysts are recyclable, environment friendly, and cost-effective, (3) the primary requirement is the presence of wide bandgap and oxygen; therefore semiconductor nanoparticles are very popular for photocatalysis, and air can easily fulfill the requirement of oxygen, and (4) the by-products from photocatalysis are simpler molecules such as H_2O and CO_2 [77]. When the

This book belongs to Badji Mokhtar Annaba University Central Library Copyright Elsevier 2025

semiconductors are dispersed uniformly in the solution and irradiated with suitable light energy, the electrons jump from the highest occupied molecular orbital (HOMO) to the lowest unoccupied molecular orbital (LUMO), leaving a hole behind. The electron-hole (e^-–h^+) pair generated in the process is now capable to carry out the redox reaction. Langmuir-Hinshelwood rate equation is the equation that governs heterogeneous photocatalysis, where the catalyst activity is directly affected by the reactant numbers adsorbed on the catalyst surface [78]. To exploit the benefits of the created hole and electron pairs, it is important to prevent the recombination of these. Therefore suitable scavengers or surface defects should be introduced in the system. In this way, the electrons or the holes will be trapped, and the redox reaction can take place easily. The electrons in the CB are good reducing agents (+0.5 to −1.5 eV with respect to NHE) and the holes in the VB are good oxidizing agents (+1.0 to +3.5 eV with respect to NHE) [77].

TiO_2 semiconductor nanoparticles have been intensively explored as catalyst for photocatalytic degradation of numerous organic molecules, and more than 70% of the research paper for wastewater treatment is TiO_2-based. One of the prime focuses of TiO_2-based research is to bring its bandgap (3.2 eV) in visible light region [51]. To further improve its catalytic activity, doping of TiO_2 with metal nanoparticles or combining it with other semiconductor nanoparticles is under constant process [79]. Ferrite nanoparticles in combination with TiO_2 or with other nanoparticles provide a great alternative to achieve the photocatalytic degradation of different organic contaminants such as insecticides [80]. Several research studies are being done in this direction to further enhance the photocatalytic activity of magnetic nanoparticles because of their easy separation and high efficiency.

(i) *Advantage of magnetic materials in water treatment*

Magnetism is a property that provides information about the motion or the behavior of any material in the applied external magnetic field. The presence of unpaired electron in the electronic configuration in the structure of metal ions is the main factor for this partial magnetic activity. The reason for strong magnetic activity in iron-based materials is also because of the presence of several unbounded electrons in its shell [81]. Different materials show different behavior such as ferrimagnetism, diamagnetism, paramagnetism, ferromagnetism, antiferromagnetism, and super-paramagnetism, depending upon their reaction to the magnetic field applied. A few magnetic materials based on the metals, oxides, and alloys of Ni, Co, Fe, and their nanocomposites are highly active in external magnetic field because they have aligned synergy of the unpaired electron spins of atoms in the lattice plane [82]. Materials that are diamagnetic in nature have filled orbitals and show very weak magnetism in the presence of external magnetic field. Owing to this, they possess negative magnetic moments and negative value of magnetic susceptibility, that is, when an external magnetic field is applied, the dipoles are aligned in the opposite direction with respect to the magnetic field. Contrary to this, paramagnetic materials possess some unbounded electrons in their orbitals and show partial

This book belongs to Badji Mokhtar Annaba University Central Library Copyright Elsevier 2025

magnetic character. Furthermore, in the presence of external magnetic field, the value of magnetic moment and susceptibility is positive, and the net magnetic moment of the material is zero in the absence of external magnetic field because there is no interaction between the individual magnetic moments. Ferromagnetic materials, owing to the presence of large number of unbounded electrons, possess strong magnetic activity, and even in the absence of external magnetic field, their magnetism is preserved for a longer duration of time. Thus the value of net magnetic moment and susceptibility is positive. Antiferromagnetic materials show some similarity to ferromagnetic materials, but the difference exists in the magnetic domains that are aligned in the reverse direction of the external magnetic field. In the absence of external magnetic field, antiferromagnetic materials do not show any magnetic nature, while a very low net magnetic moment is present when there is external magnetic field. The main reason behind this behavior is because of the antiparallel coupling with adjacent atoms or ions, which cancels out the net magnetic moment in the materials. Ferrimagnetic materials also show similarity to ferromagnetic materials, but they differ in the net magnetic moments. Some ferromagnetic materials also show permanent magnetic nature, depending on their structure. Superparamagnetic materials also show ferromagnetic nature, that is, only when the particle size of ferromagnetic materials is less than 10 nm and show a much low magnetic property [81].

With the high aspect ratio and confinement, nanomaterials have shown many promising results in the field of catalytic conversion, environmental applications, energy storage devices, electronics, and optics. In this regard, nanostructure materials with magnetic properties have gained popularity because of their superparamagnetic properties that avoid agglomeration of particles once the field is removed, high recyclability, and high target selectivity by improving the functionality [83]. The other advantage of employing magnetic nanoparticles over nonmagnetic nanoparticles for wastewater treatment is that they are easily recoverable by applying external magnetic field. Thus they can be employed for several cycles without losing their activity [84].

The catalysts that are employed for the treatment of wastewater are comparatively expensive; therefore it becomes very important that they don't lose their activity for multiple cycles and are easily recoverable without any loss. Different separation approaches and technologies for the recovery of catalysts, such as nanofiltration, liquid-liquid phase separation employing ionic liquids, supercritical media, and perfluorinated solvents, and support materials are being used, which not only increase the cost but are also responsible for generating secondary sludge. Hence magnetic separation becomes an effective tool that requires less energy or other chemicals for the effective recovery of the catalyst, but the only requirement is that either the catalyst should possess magnetic activity or some magnetically active support materials should be used [85].

Magnetic nanoparticles can be synthesized using either top-down approach or bottom-up approach. Some of the key factors that are essential while synthesizing magnetic nanoparticles

This book belongs to Badji Mokhtar Annaba University Central Library Copyright Elsevier 2025

are: (1) achieving uniform size distribution of particles, (2) optimization and reproducibility of same size particles, (3) uniform morphology of the nanoparticles, (4) long shelf life of the particles and (5) materials should also possess good crystallinity with a definite crystal structure [86]. The size and morphology of the nanomaterials strongly affects the magnetic properties, in addition to their inherent magnetic aspect and magnetocrystalline anisotropy. In the case of nanorods with high aspect ratio, if morphology anisotropy is more than the crystalline anisotropy, then favored alignment of magnetization will be parallel to the long axis. But with nanoparticles having small aspect ratio like with disc morphology, the in-plane magnetization will be favored [87,88]. Organic molecule ligands such as polyethylene glycol (PEG) play a vital role for the surface modification of magnetic nanoparticles, enabling the easy immobilization of metal ions onto its surface. Furthermore, these coatings protect the magnetic core from agglomeration or oxidation and increase the stability of the as-synthesized magnetic nanoparticles [89].

Iron-based oxide and zero-valent iron (ZVI) nanoparticles have gained popularity for the removal of both organic and inorganic pollutants mainly because of their simple synthesis procedure using physicochemical methods, ease in reuse and regeneration, and strong affinity and selectivity toward the pollutant. The other advantage of iron-based magnetic nanoparticles is that they can also be synthesized using waste iron as done by Giri et al. for the adsorption of Congo red (CR) dye and methylene blue from wastewater. The Fe_3O_4 nanoparticles had been prepared using acid leaching and coprecipitation from waste iron of steel and iron industry. The absorption efficiency that was reached was around 85% and can be improved further [90]. These magnetic adsorbents are easily recoverable and therefore will not act as secondary pollutants. Carbon-based magnetic nanocomposites have also shown promising results in this regard. Zhan et al. have developed a highly efficient magnetic hybrid nanostructure of carboxylic multiwalled CNT-amino-functionalized Fe_3O_4 for the removal of copper ions. The Langmuir model result shows that adsorption of 30.49 mg/g of copper ions was observed and was easy to remove from the water [91]. Some other magnetically active nanocomposites are $CoFe_2O_4$-ZnS [92], Fe_3O_4/TiO_2 [93], Fe_3O_4/C [94], $CoFe_2O_4$-Cr_2O_3-SiO_2 [95], and Fe_3O_4-SiO_2-NH_2 [96]. Some photoactive ferrite nanoparticles for degradation of organic dyes, agricultural waste, and pharmaceutical wastes are titanium-based TiO_2/Fe_3O_4 and $TiO_2/SiO_2/Fe_3O_4$ [97], spinel-type ferrites MFe_2O_4 (M = Zn, Co, Mn, Ni, Mg, etc.), etc. [98].

(ii) *Different type of magnetic materials used for water treatment*

***Iron-based magnetic nanoparticles*:** Iron being a strong reducing agent degrades a wide range of recalcitrant pollutants [99]. Iron oxides consist of iron in different form of oxides, hydroxides, and oxy-hydroxides, containing Fe in +2 and/or +3 states, along with O_2^- and/or OH^- ions. As of now, 16 different pure phases of iron oxides have been discovered with different colors and lusters. These are five polymorphs of FeOOH and four of Fe_2O_3, followed by $Fe(OH)_3$, $Fe(OH)_2$, $Fe_5HO_8.4H_2O$, Fe_3O_4, and FeO. The primary advantages that nanoiron provides over other nanomaterials are biodegradability and comparatively less toxicity.

This book belongs to Badji Mokhtar Annaba University Central Library Copyright Elsevier 2025

Furthermore, being an abundant material, iron is inexpensive and easily available [84]. Fe-based nanoparticles such as magnetite (Fe_3O_4), ZVI, hematite (α-Fe_2O_3), and maghemite (γ-Fe_2O_3) have gained significant popularity in this regard and are being continuously modified to improve their functionality to enhance the catalytic properties for wastewater treatment. The modification is done by either incorporating inorganic or organic materials [100–102]. The main advantage lies in their high stability, along with other properties such as redox potential, high chemical affinity toward specific oxy-ions, and surface charges [103].

ZVI nanoparticles have been widely explored for the dechlorination of pesticides such as DDT, elimination of toxic heavy metal ions, and removal of recalcitrant pollutants. ZVI nanoparticles convert the oxidation state of heavy metals to lower oxidation states, thus reducing their toxicity and increasing their separation [104–106]. One major limitation encountered during the degradation of pollutants is self-oxidization of iron in the presence of dissolved air forming Fe^{+2} or Fe^{+3} ions because of high reactivity of the ZVI nanoparticles. This conversion is more favorable in the presence of oxygen and acidic conditions. Hydrogen is released when zero-valent nanoparticles come in contact with water, and the stability of the nanoparticles also gets reduced. One prominent solution of this type of problem is covering the surface of ZVI nanoparticles with thin layer of some suitable polymer or surfactant or grafting it into some other suitable support [107–110].

Magnetite (Fe_3O_4) is a magnetic nanomaterial, and recently, it attracted the interest of scientific community for utilizing it in contaminated groundwater treatment plant owing to its superparamagnetic properties, high surface area, and reductive capacity [111]. Fe in its +2 state present in Fe_3O_4 has been employed for the reduction of heavy metals such as Cr(VI) and Tc(VII) through a coupled reduction sorption process [105,112].

Maghemite (γ-Fe_2O_3) nanoparticles show ferromagnetism under external magnetic field and are comparatively much stable than Fe_3O_4 nanoparticles in aqueous solutions. In this study, mainly the elimination of divalent heavy metals has been explored because of its high selectivity toward maghemite [113]. Agglomeration of maghemite nanoparticles can be avoided by coating their surface with suitable surfactants such as SDS [114] and functional groups such as EDTA and glycine [115,116]. The hematite (α-Fe_2O_3) nanoparticles show photocatalytic activity below 500 nm and are more stable polymorphs of Fe_2O_3 in aqueous solution, and under the effect of external magnetic field, they show antiferromagnetism, superparamagnetism, or weak ferromagnetism behavior, depending upon the synthesis method and shape [117]. Hematite catalysts are quite popular because of their large surface area, cost-effectiveness, defined structure, and even when all activity is lost, they can still be employed for the production of pig iron and can degrade effectively 99% of dye within 120 min [118].

Spinel ferrites are MFe_2O_4 (where $M = Mg^{+2}$, Zn^{+2}, Co^{+2}, Ni^{+2}, Mn^{+2} etc.) type magnetic nanoparticles and have gained popularity because of active magnetic characteristics, high chemical oxidation resistance, and large surface area in comparison to Fe oxide nanoparticles. On the basis of crystal structure, spinel ferrites can either be regular or inverse spinels. Regular

This book belongs to Badji Mokhtar Annaba University Central Library Copyright Elsevier 2025

or normal spinels are MN_2X_4 type, where M and N in the spinel framework can be divalent and trivalent (or tetravalent) cations, respectively. For example, if M represents a divalent cation such as Ba(VI), Co(IV), Cu(II), Ca(VI), Cd(IV), Fe(IV), Ni(IV), Mn(IV), Mg(IV), and Zn(IV), then N represents a trivalent metal cation such as Al(VI), Cr(VI), Ga(VI), In(VI), Mn(VI), Sn(IV), and Zn(VI). The inverse spinel structure may be expressed as: $(N^{III})^{tet}(M^{II}N^{III})^{oct}O_4$, for instance, Fe_3O_4 (ferrite), $CoFe_2O_4$, or $NiFe_2O_4$. Also, the inverse spinel structures are denoted as: $CoFe_2O_4 = Fe^{III}(Co^{II}Fe^{III})O_4$, $Fe_3O_4 = Fe^{III}(Fe^{II}Fe^{III})O_4$, or $NiFe_2O_4 = Fe^{III}(Ni^{II}Fe^{III})O_4$ [98]. The characteristic features of the nanoparticles are greatly affected by the type of metal and its size, nature, and location in the crystal lattice. For instance, metal cations such as Al^{+3}, Mg^{+2}, and Zn^{+2} increase the stability of the ferrites. If transition metals such as Cu^{+2}, Mn^{+2}, and Ni^{+2} are in the crystal lattice, the redox properties of the ferrites change. Ferrites, owing to their crystal lattice structure, offer the benefits of having a narrow band gap that is active in visible light range, and the catalytic efficiency also improves. Visible light active catalysts are in demand for the catalytic degradation of dyes, drugs, and pesticides. Therefore spinel ferrites provide many benefits in terms of degradation under photocatalysis process [119].

***Carbon-based magnetic nanoparticles*:** The carbon-based nanomaterials can be classified in different allotropes of carbon that comprises diamond, graphene, fullerene, and CNTs. Generally, carbon-based nanoparticles have high aspect ratio, good adsorption efficiency, excellent mechanical stability, good optoelectrical property, and are environment friendly. Liu et al. have reported preparation of grapheme-supported ZVI nanoparticles for separation of phosphorus. Graphene prevents agglomeration and oxidation of ZVI nanoparticles and provides mechanical strength to these magnetic nanocomposites [110]. Zheng et al. have successfully prepared a novel Fe_3O_4-Urushiol-Graphene Fenton catalyst for the elimination of toxic rhodamine B (RB) and methylene blue dyes. Herein, Urushiol, an environmentally benign material, was used to provide stability to the Fe_3O_4 nanoparticles and to enhance the number of active sites on graphene oxide. This nanohybrid catalyst can degrade the two dyes completely within 60 min and can retain its activity for seven cycles [120]. Similarly, other carbon-based magnetic nanohybrids remove efficiently heavy metal ions such as chromium and other bio-recalcitrant pollutants [121,122].

***Zeolite based magnetic nanoparticles*:** Zeolites are microporous, crystalline, and possess three-dimensional structure of hydrated aluminosilicate. The high adsorption efficiency of zeolites is because of their open arrangement; while the presence of overall negative charge on their surface can easily attract positively charged cations. Several attempts are being made to modify some magnetic properties in the zeolite structures so that the adsorbed heavy metal can easily be removed from it [123]. In this regard, magnetic core-shell zeolite nanoparticles [124] and magnetic nanocomposites [123] are very effective for adsorptive removal of organic pollutants such as Cr(VI), including heavy metal ions [125], cephalexin (CEX) [126], and mercury (Hg^{2+}) [127].

This book belongs to Badji Mokhtar Annaba University Central Library Copyright Elsevier 2025

9.4 Case study of wastewater treatment using magnetic nanoparticles

9.4.1 Magnetic nanoparticles as adsorbents

Magnetic adsorbents are emerging class of adsorbents where oxides of metals Co, Ni, Cu, and Fe are used in combination with other support materials or are functionalized to improve the removal efficiency. On applying magnetic field, the nanoadsorbents can be recovered because of the presence of magnetically active structure of the molecule [128]. The magnetic adsorbents are utilized for mineralization of contaminated wastewater and the detailed investigations are discussed further.

***Treatment of inorganic contaminants in wastewater*:** Chromium, lead, mercury, arsenic, fluorides, copper, cadmium, and phosphorus are some of the inorganic pollutants that are continuously polluting the water sources causing many diseases such as cancer, skin irritation, and hormonal imbalance [128]. Chromium exists as hexavalent and trivalent chromium ions, but the most stable and toxic form of chromium is Cr(VI). On the other hand, Cr(III) forms hydroxides and oxides, resulting in precipitation out. Cr(III) is also considerably less toxic compared to Cr(VI), but its toxicity increases with the concentration. A two-step process is used for the efficient separation of Cr(VI) from aqueous phase. The first and primary step is to reduce Cr(VI) into Cr(III) because it is easy to separate, followed by its removal using the magnetic adsorbents [129]. The highest removal efficiency has been achieved by ZVI nanoparticles because they can easily reduce the hexavalent chromium ions into trivalent ions in acidic pH. Gong et al. have investigated the separation of Cr(VI) ions from wastewater using synthesized nanocomposites of ZVI coated with protective triple layer of carbon-polyaniline so that the H^+ ions from the solution does not hamper and reduce the ZVI core. This system can reduce 1.0 mg/mL of Cr(VI) ions from the solution at pH 2 and can absorb up to 508 mg/g [130]. Qiu et al. have employed carbon-iron-based nanocomposites for reduction and elimination of Cr(VI). Two different kinds of Fe sources have been used, viz., Fe_3O_4 and $Fe(NO_3)_3$. At neutral pH value, $Fe(NO_3)_3$-carbon nanocomposites showed 98.1% removal efficiency, while the efficiency decreased at acidic pH. Contrary to this, Fe_3O_4-carbon nanocomposites efficiency increased at acidic pH, and 327.5 mg/g Cr(VI) was separated from wastewater [129].

Arsenic has been categorized in Group-1 of carcinogenic compounds by the International Agency for Research on Cancer (IARC), and the WHO has set the permissible limit of arsenic in water up to 10 μg/L. Arsenic occurs in nature as arsenate As(V) ($HAsO_4^{-2}$) and as arsenite As(III) (H_3AsO_3). As(V) is the dominating form, which is present in oxidizing conditions, and As(III) is present under low reducing conditions. Arsenic finds its way in the environment through some natural processes, such as weathering away of minerals and microbial activities, and through human-induced activities such as mineral processing and use of arsenic-based chemicals in pesticides, herbicides, and dyes [131,132]. To separate arsenic completely from wastewater, it is desired to oxidize As(III) to As(V), followed by precipitation of As(V).

This book belongs to Badji Mokhtar Annaba University Central Library Copyright Elsevier 2025

Furthermore, for high affinity and efficiency toward arsenic removal, iron-based oxides are quite popular; for instance, iron oxy-hydroxides such as ferrihydrites ($Fe_{10}O_{14}(OH)_2$), akaganeite (b-FeOOH), lepidocrocite (g-FeOOH), and goethite (a-FeOOH), nanoscale zero-valent ion (nZVI), and iron-based composites [133]. Yu et al. have synthesized using green method cellulose-Fe oxide-based magnetic nanocomposites for the separation of arsenic. Cellulose acts as a matrix where Fe_2O_3 nanoparticles are uniformly distributed. It is highly sensitive to external magnetic field and shows superparamagnetic nature. The Langmuir adsorption result shows that these nanocomposites can remove 23.16 mg/g of arsenite and 32.11 mg/g of arsenate from water [134]. Graphene oxide is also a good adsorbent, but owing to its high dispersion in water, it becomes difficult to recover for reuse. Therefore to avoid such problems, excess iron oxide up to 51% was loaded to enhance the magnetic property (12.8 emu/g) of graphene oxide and enhanced adsorption for the removal of about 54.18 mg/g of As(III) and 26.76 mg/g of As(IV) with significantly enhanced adsorption [135].

Zhang et al. have developed magnetic cellulose-chitosan carbon foam for the separation of Cu(II) from industrial effluent. Chitosan is an alkaline polysaccharide bio-sorbent with amino and hydroxyl functional group and can form ligand with different metal ions, including zinc, copper, lead, and cadmium. Cellulose is a polymer with different functional groups and good adsorption properties. Because chitosan and cellulose both are nonmagnetic in nature and to impart magnetic properties, Fe_3O_4 as a magnetic core in carbon foam is blended with this composite. This core-shell nanocomposite not only preserves its high adsorption capacity but also increases its magnetic properties. A 115.65 mg/g of Cu(II) was adsorbed at pH 6.0 and temperature of 30°C. For the first 2 h, the adsorption of Cu(II) on the core-shell nanocomposite observed the pseudo first-order reaction kinetic, while the results of entire adsorption data were fitted well with pseudo second-order reaction kinetic model [136].

***Mineralization of organic pollutants conta*min*ated wastewater*:** Magnetic nanoparticles have also been successfully utilized for the treatment of organic waste such as dyes, drugs, surfactants, and volatile organic wastes. Madrakian et al. have combined an organic adsorbent with magnetite nanoparticles to study the adsorption of different dyes, viz., janus green, crystal violet, thionine, reactive blue 19, methylene blue, CR, and neutral red. The magnetite nanoparticles loaded onto the tea leaves help in improving the overall efficiency of the adsorbent and ease of separation of the catalyst using magnetic decantation. The adsorption study was performed at ambient conditions and under optimized parameters for the removal of cationic and anionic dyes, and the removal efficiency was up to 98%. The adsorption results were around 126.58 mg/g for neutral red, 129.87 mg/g for janus green, 128.21 mg/g for thionine, 113.64 mg/g for crystal violet, 82.64 mg/g for crystal red, 119.05 mg/g for methylene blue, and 87.72 mg/g for reactive blue. The pseudo second-order reaction kinetic model was found to be more suitable for the adsorption nature of cationic dyes; while pseudo first-order model was found to be best fitted for anionic dyes, RB, and CR [137]. D'Cruz and co-workers have studied the elimination of pharmaceutically active drug from wastewaters, Promazine, using

This book belongs to Badji Mokhtar Annaba University Central Library Copyright Elsevier 2025

synthesized AC-based magnetic nanocomposites. Activated carbon is widely used absorbent for the separation of several contaminants from industrial effluent because of its high porous nature and high loading uptake. However, the only limitation is in its recovery once the adsorption process is completed. Therefore the addition of magnetic Fe_3O_4 nanoparticles enhances its removal and recovery efficiency. This AC-Fe_3O_4 magnetic nanocomposite resulted in 99.97% removal, with maximum uptake capacity of 101.01 mg/g within 6 min and fits perfectly in pseudo second-order kinetic model and Langmuir isotherm model [138]. Guo et al. have prepared a bimetallic Mg-Fe-based magnetic nanoparticle incorporated in the matrix of AC. This MgO/Fe_3O_4-AC nanocomposite efficiently removes malachite green from wastewater. The adsorption capacity was 4031.96 mg/g, and the adsorption data fit perfectly with Freundlich isotherm and pseudo first-order model [139]. In another study, malachite green was removed using synthesized graphitic carbon nitride-based magnetic nanocomposite, that is, g-C_3N_4/Fe_3O_4/ZIF-8. The adsorption using this adsorbent was about 3412 mg/g, and the adsorption model confirms the pseudo second-order model [140].

9.4.2 Photocatalysis decontamination of water using magnetic nanoparticles

It is very important to understand why there has been a keen interest in finding a substitute for TiO_2-based photocatalysts knowing that they are still dominating a large research area in the field of photocatalysis. The major limitation that TiO_2 provides is that its bandgap is huge, that is, it is found to be mainly active in UVA (400–320 nm) region and UVB (320–290 nm) region. Thus utilizing a very less part of sun energy makes it less energy efficient. Additionally, it has been observed that TiO_2 loses its activity with time and is not very efficient for higher ppm concentration of pollutants, thus requiring high intensity of light energy [79]. Also, TiO_2 possesses low affinity for hydrophobic organic pollutants, decreasing the degradation rate and increasing mass transfer resistance, making it difficult for the organic pollutant to adsorb effectively on the catalyst surface [141]. For the efficient degradation of any type of pollutants, it is important that the photocatalyst is dispersed properly in the solution, it possesses good surface area, low mass transfer resistance for the easy adsorption of pollutants on the surface, and works efficiently under visible light or sunlight for sustainability [142]. To overcome the limitations, several photocatalysts have been developed with different type of support materials for the efficient degradation of the pollutants, but some of the benefits that magnetic nanomaterials provide are: (1) magnetic nanoparticles are easy to separate and recycle, (2) nontoxic in nature, (3) do not cause photocorrosion, (4) high chemical stability, (5) visible light active, (6) good magnetic properties, and (7) good biocompatibility [143]. For instance, Ferrite-based magnetic nanomaterials on interaction with light produce electron-hole pairs like other semiconductor nanoparticles, resulting in the generation of highly reactive species such as OH• and $O_2^{\cdot -}$, which help in faster degradation of the pollutants. But with the addition of H_2O_2, the system transits to Fenton-like process, where there is a reaction between Fe^{+2} and H_2O_2, which further enhances the degradation activity, and it is not possible if we are using TiO_2 as a catalyst

This book belongs to Badji Mokhtar Annaba University Central Library Copyright Elsevier 2025

or other semiconductor nanoparticles. The other added advantage of using Ferrite nanoparticles is that there is reduction or no formation of sludge, increase in number of cycles without losing any activity, and easy to work at neutral pH, which is usually difficult to achieve in a conventional Fenton-type process.

Zhao et al. have developed an environment friendly catalyst, utilizing yeast as carbon support for TiO_2-Fe_3O_4 core-shell nanoparticles. This photocatalyst was irradiated under 350 W Xenon lamps (200–800 nm) for degradation of tetracycline. The photocatalyst was stable for six cycles and showed degradation efficiency up to 86% [144]. The ferrites-based materials can be classified as spinel type (MFe_2O_4), garnet type ($M_3Fe_5O_{12}$), or hexagonal type ($MFe_{12}O_{19}$) based on their crystal morphology, where M signifies one or more divalent transition metals (Fe, Mn, Co, Cu, Ni, Cu, and Zn). Transition metal ferrites are very efficient in different applications, including catalysis [145]. For instance, Jahanara and Farhadi have developed a spinel-based magnetic nanocomposite of $CdTiO_3$-$CuFe_2O_4$. Here $CdTiO_3$ provides support to the spherical nanoparticles of $CuFe_2O_4$. The photocatalytic activity of this nanocomposite was studied on methylene blue dye, and it was observed that Methylene blue was 100% degraded by $CdTiO_3$-$CuFe_2O_4$ and H_2O_2 under visible light irradiation within 90 min of treatment. Furthermore, the catalyst has shown positive results for several cycles [146]. The organic pollutants that are generated from agricultural practices are very toxic for the environment. One such pollutant is imidacloprid that belongs to the class of neonicotinoid insecticides that are soluble in water. Naghizadeh et al. have successfully degraded this organic pollutant using ZnO semiconductor nanoparticles and cobalt-based ferrite nanoparticles in a single nanocomposite of $ZnO/CoFe_2O_4$ synthesized using co-precipitation method. The source of energy was provided using 50 W LED lamp, and the working pH range was 2–10. The optimized study showed that at pH 10, the highest degradation rate was achieved because the generation of •OH is high. The degradation efficiency was only about 56.24% with ZnO and 58.45% with $CoFe_2O_4$, and the highest degradation efficiency of 98.11% was seen with $ZnO/CoFe_2O_4$ nanocomposite [80]. TiO_2 semiconductor nanoparticles have dominated as photocatalyst for many years but showed low efficiency because of the electron-hole pair fast recombination rate. Hence synthesis of different nanocomposites to improve the efficiency of TiO_2 naomaterials has attracted the researchers. The combination of TiO_2 and magnetic nanoparticles is very efficient because it lowers the electron-hole pair recombination rate and improves the catalytic efficiency. Nguyen et al. have synthesized a heterostructured TiO_2-based magnetic nanocomposites by combining it with $ZnFe_2O_4$ using a facile solvothermal method. Under UV light (365 nm), visible light (465 nm), and solar simulator, $TiO_2/ZnFe_2O_4$ has been reported to be effective for degradation of Bisphenol-A (BPA). BPA has been seen as a recent threat for the environment and has been in extensive use for the production of packaging materials for the food and beverage industries. BPA finds a way easily into water sources through domestic and industrial waste and is very toxic and detrimental to human health. $TiO_2/ZnFe_2O_4$ heterogeneous photocatalyst can effectively degrade BPA under visible light for more than 10

This book belongs to Badji Mokhtar Annaba University Central Library Copyright Elsevier 2025

cycles with rate constant of 0.191–0.218 min^{-1}. The radical scavenger study showed that the photogenerated holes and oxygen-containing radicals are the main active species responsible for BPA degradation within 30 min [147]. In another study, degradation of monocrotophos, an organophosphorous insecticide and very toxic in nature, has been reported using core-shell nanocomposite of Fe_3O_4-mesoporous TiO_2 synthesized through sol-gel method, and the process showed complete degradation of monocrotophos within 45 min under UV light and 82% reduction of total organic carbon (TOC) [148]. Additionally, the catalyst also showed good recoverability and activity for four cycles. Fu and co-workers have developed Fe_3O_4-based nanocomposite, wherein Fe_3O_4 is in the core, and a thin layer of SiO_2 is followed by another layer of TiO_2 on it. Reduced graphene oxide (RGO) provides support to this core-shell nanocomposite. Thus Fe_3O_4@SiO_2@TiO_2-Co/rGO nanohybrid acts as an efficient photocatalyst in degrading methylene blue dye by 92.41% under visible light region and is able to retain its activity even after five cycles [149].

On the other hand, heterogeneous Fenton reaction, an advanced oxidation technique, using magnetic nanoparticles has been found to be a very efficient technique that produces powerful radicals that attack the organic pollutants without producing sludge or toxic compounds. The rate of Fenton reaction can be increased by coupling it with other techniques such as UV, microwave, ultrasound, and electrochemical method [71,150]. There are several benefits of employing Fe-based nanomaterials such as easy removal of catalyst because of magnetic nature, the stability of catalyst is good, the carbonates present in the reaction solution do not interfere in the system, and the pH of the effluent lies in the range of 5–9, which provides a good working range. But the only limitation is slower degradation rate of the organic pollutants, which can be avoided by incorporating chelating agents such as EDTA, malonate, oxalate, and citrate [54].

Wang et al. has synthesized a very efficient magnetic hybrid of Fe_3O_4-multiwalled carbon nanotube (MWCNT) that can work effectively under a wide pH range of 1.0–10.0, can degrade methylene blue from 88.13% to 98.68% within 2 h, and can achieve 35.6% of TOC reduction efficiency in 12 h. Herein, MWCNT acts as a support for the Fe_3O_4 nanoparticles, and because it possesses good electronic transfer property, it improves the working efficiency of Fe_3O_4 nanoparticles [151]. Zhou et al. has synthesized core-shell magnetic nanoparticles of Fe-C doped with boron and nitrogen for degradation of an antibiotic levofloxacin (LFX) drug that belongs to the class of fluoroquinolones (FQs), which are difficult to degrade using biological and chemical processes. However, Fenton reaction can degrade up to 85.5% of the drug in 120 min [152].

Recently, zero-valent iron nanoparticles (ZVIN) are found to be very efficient in inducing Fenton-like reactions as given by Eq. (9.11)

$$Fe^0 + O_2 + 2H^+ \rightarrow Fe^{+2} + H_2O_2 \tag{9.11}$$

This book belongs to Badji Mokhtar Annaba University Central Library Copyright Elsevier 2025

Xu and Wang achieved 100% degradation of p-chlorocresol, a potential chemical used as biocide and in cosmetic products, within 15 min. The NZVI has shown as an excellent heterogeneous catalyst with initial dose 0.5 g/L with 3.0 mM of H_2O_2 and 0.70 mM pollutant concentration at pH 6.1, and 63% of TOC was obtained within 60 min of reaction. The degradation followed a two-step first-order reaction kinetics, during which the first stage was a slow heterogeneous degradation, and the second stage was fast degradation through Fenton-like reaction at the NZVI surface. In this case, •OH played the major role in degradation process, and it has been experienced by using scavengers [153]. Similarly, Machado et al. degraded ibuprofen up to 66% in aqueous solution using only NZVI and more than 95% using NZVI Fenton-like reaction [154]. Babuponnusami and Muthukumar degraded phenol using a hybrid process of photoelectro-Fenton-like reaction with ZVIN at optimum current density of 12 mA/cm^2. The other optimum operating parameters were pH 6.2, concentration of phenol 200 mg/L, catalyst dosage of 0.5 g/L, and 500 mg/L H_2O_2. The degradation kinetics followed pseudo first-order kinetics. This technique offers faster degradation compared to individual techniques [71]. Faheem et al. for the degradation of phenol utilized an eco-friendly method of using the Fenton sludge as the iron source for the development of Cu_2O-$CuFe_2O_4$ microparticles. The high efficiency is because of the generation of Fe^{+2} and Fe^{+3} redox pair along with the presence of Cu^{+1} and Cu^{+2}, which react with H_2O_2 to release •OH radicals. The rate of reaction increases because of the increase in release of Fe^{+2} ions. Additionally, the as-synthesized Cu_2O-$CuFe_2O_4$ magnetic particles showed high reusability and stability. The degradation of phenol using Cu_2O-$CuFe_2O_4$ was around 85.5% within first 30 min and increased to around 97.2% in 60 min, and the TOC efficiency was about 85.6% [155]. Wang et al. have studied degradation of harmful orange II organic dye using prepared novel hybrid g-C_3N_4/α-Fe_2O_3/Fe_3O_4 catalyst. Herein, g-C_3N_4 is a metal-free polymeric semiconductor that can withstand high temperature and is also visible light active. Combining α-Fe_2O_3 and Fe_3O_4 with g-C_3N_4 enable to work in a wide pH range, visible light, and magnetically active catalyst. This magnetic nanocomposite showed high light-harvesting behavior, low electron-hole recombination rate, and high photo-Fenton efficiency. Eqs. (9.12)–(9.17) show the degradation mechanism of orange II dye through photo-Fenton reaction, and a high removal efficiency can be achieved in 60 min using this hybrid catalyst [156].

$$\mathrm{g-C_3N_4/\alpha-Fe_2O_3/Fe_3O_4} + h\upsilon \rightarrow e^- + h^+ \tag{9.12}$$

$$\mathrm{Fe^{+3} + e^- \rightarrow Fe^{+2}} \tag{9.13}$$

$$\mathrm{H_2O_2 + Fe^{+2} \rightarrow Fe^{+3} + {}^{\bullet}OH + OH^-} \tag{9.14}$$

$$\mathrm{O_2 + e^- \rightarrow O_2^{\bullet -}} \tag{9.15}$$

$$h^+ + \mathrm{H_2O \rightarrow O_2} \tag{9.16}$$

$$h^+/\mathrm{O_2^{\bullet -}}/{}^{\bullet}\mathrm{OH + Orange\ II \rightarrow Products} \tag{9.17}$$

This book belongs to Badji Mokhtar Annaba University Central Library
Copyright Elsevier 2025

9.5 Limitations of magnetic nanomaterials

Magnetic nanoparticles, even with advantages such as high recovery and high activity, also have some limitations that need to be taken care of for the effective wastewater treatment. For instance, ZVIN experience oxidation, aggregation, and separation issues. When moving from a natural environment toward industrial wastewater, there is a lot of variation in the pH values, which has a direct impact on the adsorption activity of the magnetic nanoparticles. Particle size also affects the recovery of magnetic nanoparticles, larger the size of the magnetic nanoparticles, lower is the recovery and reactivity. Therefore proper optimization of all the factors becomes essential before moving from laboratory scale to pilot plant scale and finally, to industrial level [99].

9.6 Future prospects and overview

With the growth of population and speedy development of industrialization and agricultural activities, the threat to the water reserves continues to grow at an alarming rate. Thus it is always a necessity to build up different and efficient water treatment techniques that can minimize pollutants in the water and eliminate them completely so that no trace of any contaminant is left. Magnetic nanomaterials with high surface to volume ratio, good adsorption efficiency, superparamagnetic nature, high selectivity, and ease of separation are very effective for the treatment of bio-recalcitrant pollutants in the wastewater [83,90]. Magnetic nanomaterials mainly consist of iron in the form of Fe_3O_4 [111], γ-Fe_2O_3 [113], ZVIN, and spinel type (e.g., $Co_2Fe_3O_4$) [98]. To prevent the oxidation of upper layer of iron-based magnetic nanomaterials, different hybrid nanocomposites and core-shell nanoparticles are also under development, which not only prevent the oxidation but also provide support to structure, augment the number of active sites, and increase the overall efficiency of the catalyst [129,134,135,148,149]. Magnetic nanoparticles for the wastewater treatment as adsorbent [128], photocatalysts [144], and the catalyst for Fenton-like process [156] have been explored extensively and require a lot of improvement so that unnecessary sludge generation can be reduced and complete mineralization can be achieved. Magnetic nanomaterials open the door for many novel materials that can be used for effective treatment of wastewater. Considering all the advantages associated with the magnetic nanoparticles, it is important to develop a mechanism for better understanding; hence the synthesis and surface changes are required for improving the properties. Surface modifications by grafting the magnetic nanoparticles with other nanomaterials or making a thin layer of another material helps to increase the stability and decrease the toxicity, but sometimes, it may lead to decrease in the active sites. Furthermore, it is very essential that the catalyst should not lose its efficiency and must possess catalytic activity for several cycles so that the operating cost can be minimized [99].

This book belongs to Badji Mokhtar Annaba University Central Library
Copyright Elsevier 2025

References

[1] The United Nations World Water Development Report, https://www.unwater.org/publications/world-water-development-report-2019/, 2019.

[2] G. Tchobanoglous, F. Burton, H.D. Stensel, Wastewater engineering: an overview. in: Wastewater Engineering Treatment Disposal Reuse, 1991, pp. 1–24, https://doi.org/10.1016/0309-1708(80)90067-6.

[3] K.M. Yenkie, Integrating the three E's in wastewater treatment: efficient design, economic viability, and environmental sustainability. Curr. Opin. Chem. Eng. 26 (2019) 131–138, https://doi.org/10.1016/j.coche.2019.09.002.

[4] T. Tong, M. Elimelech, The global rise of zero liquid discharge for wastewater management: drivers, technologies, and future directions. Environ. Sci. Technol. 50 (2016) 6846–6855, https://doi.org/10.1021/acs.est.6b01000.

[5] M. Elimelech, W.A. Phillip, The future of seawater desalination: energy, technology, and the environment. Science 333 (2011) 712–717, https://doi.org/10.1126/science.1200488.

[6] A.P.v.W. Fischer, J. Hollender, E. Cornelissen, R. Hofman, J.P. van der Hoek, Development and application of relevance and reliability criteria for water treatment removal efficiencies of chemicals of emerging concern. Water Res. 161 (2019) 274–287, https://doi.org/10.1016/j.watres.2019.05.088.

[7] J.H. Musser, Practical Treatment. (1918), https://doi.org/10.1097/00007611-191806000-00023.

[8] UN WWAP, United Nations World Water Assessment Programme, the World Water Development Report 1: Water for People, Water for Life, UNESCO, Paris, France, 2003.

[9] V. Geissen, H. Mol, E. Klumpp, G. Umlauf, M. Nadal, M. van der Ploeg, S.E.A.T.M. van de Zee, C. J. Ritsema, Emerging pollutants in the environment: a challenge for water resource management. Int. Soil Water Conserv. Res. 3 (2015) 57–65, https://doi.org/10.1016/j.iswcr.2015.03.002.

[10] United Nations Educational, Scientific and Cultural Organization (UNESCO), Emerging Pollutants in Water and Wastewater, https://en.unesco.org/emergingpollutants, 2017. Accessed 30 January 2020.

[11] S. Sinkkonen, J. Paasivirta, Degradation half-life times of PCDDs, PCDFs and PCBs for environmental fate modeling. Chemosphere 40 (2000) 943–949, https://doi.org/10.1016/S0045-6535(99)00337-9.

[12] D. Grube, T. Donaldson, L.W. Kiely, Pesticides Industry Sales and Usage, 2006 and 2007 Market Estimates, U.S, Environmental Protection Agency, 2011.

[13] C.S. Wong, S. Wu, N.S. Duzgoren-Aydin, A. Aydin, M.H. Wong, Trace metal contamination of sediments in an e-waste processing village in China. Environ. Pollut. 145 (2007) 434–442, https://doi.org/10.1016/j.envpol.2006.05.017.

[14] M. Gavrilescu, Fate of pesticides in the environment and its bioremediation. Eng. Life Sci. 5 (2005) 497–526, https://doi.org/10.1002/elsc.200520098.

[15] E.R. Campagnolo, K.R. Johnson, A. Karpati, C.S. Rubin, D.W. Kolpin, M. T. Meyer, M. McGeehin, Antimicrobial residues in animal waste and water resources proximal to large-scale swine and poultry feeding operations. Sci. Total Environ. 299 (2002) 89–95, https://doi.org/10.1016/S0048-9697(02)00233-4.

[16] J.L. Schnoor, Agriculture: the last unregulated source. Environ. Sci. Technol. 48 (2014) 4635–4636, https://doi.org/10.1021/es5015168.

[17] D.G.J. Larsson, C. de Pedro, N. Paxeus, Effluent from drug manufactures contains extremely high levels of pharmaceuticals. J. Hazard. Mater. 148 (2007) 751–755, https://doi.org/10.1016/j.jhazmat.2007.07.008.

[18] C. Gadipelly, A. Pérez-González, G.D. Yadav, I. Ortiz, R. Ibáñez, V.K. Rathod, K. V. Marathe, Pharmaceutical industry wastewater: review of the technologies for water treatment and reuse. Ind. Eng. Chem. 53 (2014) 11571–11592, https://doi.org/10.1021/ie501210j.

[19] E. Zuccato, D. Calamari, M. Natangelo, R. Fanelli, Presence of therapeutic drugs in the environment. Lancet 355 (2000) 1789–1790, https://doi.org/10.1016/S0140-6736(00)02270-4.

[20] S. Mompelat, B. Le Bot, O. Thomas, Occurrence and fate of pharmaceutical products and by-products, from resource to drinking water. Environ. Int. 35 (2009) 803–814, https://doi.org/10.1016/j.envint.2008.10.008.

[21] Y.I. Matatov-Meytal, M. Sheintuch, Catalytic abatement of water pollutants. Ind. Eng. Chem. 37 (1998) 309–326, https://doi.org/10.1021/ie9702439.

This book belongs to Badji Mokhtar Annaba University Central Library

Copyright Elsevier 2025

[22] J. Lin, W. Ye, J. Huang, B. Ricard, M.
C. Baltaru, B. Greydanus, S. Balta, J. Shen, M. Vlad, A. Sotto, P. Luis, B. Van Der Bruggen, Toward resource recovery from textile wastewater: dye extraction, water and base/acid regeneration using a hybrid NF-BMED process. ACS Sustain. Chem. Eng. 3 (2015) 1993–2001, https://doi.org/10.1021/acssuschemeng.5b00234.
[23] A. Yadav, S. Mukherji, A. Garg, Removal of chemical oxygen demand and color from simulated textile wastewater using a combination of chemical/physicochemical processes. Ind. Eng. Chem. 52 (2013) 10063–10071, https://doi.org/10.1021/ie400855b.
[24] R. Zou, I. Angelidaki, B. Jin, Y. Zhang, Feasibility and applicability of the scaling-up of bio-electro-Fenton system for textile wastewater treatment. Environ. Int. 134 (2020), https://doi.org/10.1016/j.envint.2019.105352.
[25] P.P. Marcinowski, J.P. Bogacki, J.H. Naumczyk, Cosmetic wastewater treatment using the Fenton, photo-Fenton and H_2O_2/UV processes. J. Environ. Sci. Health, Part A: Tox. Hazard. Subst. Environ. Eng. 49 (2014) 1531–1541, https://doi.org/10.1080/10934529.2014.938530.
[26] J. Bogacki, P. Marcinowski, E. Zapałowska, J. Maksymiec, J. Naumczyk, Cosmetic wastewater treatment by the ZVI/H_2O_2 process. Environ. Technol. 38 (2017) 2589–2600, https://doi.org/10.1080/09593330.2016.1271020.
[27] L. Jia, S. Evans, S. van der Linden, Motivating actions to mitigate plastic pollution. Nat. Commun. 10 (2009) 9–11, https://doi.org/10.1038/s41467-019-12666-9.
[28] A. Parthasarathy, A.C. Tyler, M.J. Hoffman, M.A. Savka, A.O. Hudson, Is plastic pollution in aquatic and terrestrial environments a driver for the transmission of pathogens and the evolution of antibiotic resistance? Environ. Sci. Technol. 53 (2019) 1744–1745, https://doi.org/10.1021/acs.est.8b07287.
[29] P. Liu, L. Qian, H. Wang, X. Zhan, K. Lu, C. Gu, S. Gao, New insights into the aging behavior of microplastics accelerated by advanced oxidation processes. Environ. Sci. Technol. 53 (2019) 3579–3588, https://doi.org/10.1021/acs.est.9b00493.
[30] S. Bhattacharya, A.B. Gupta, A. Gupta, A. Pandey, Water Remediation (Energy Environment and Sustainability). first ed., Springer, 2018, https://doi.org/10.1007/978-981-10-7551-3.
[31] V.K. Gupta, I. Ali, T.A. Saleh, A. Nayak, S. Agarwal, Chemical treatment technologies for waste-water recycling—an overview. RSC Adv. 2 (2012) 6380–6388, https://doi.org/10.1039/c2ra20340e.
[32] R.S. Ramalho, Introduction to Wastewater Treatment Processes, Academic Press. 2nd Edition, (2013)https://doi.org/10.1016/C2009-1-28564-9.
[33] P.N. Cheremisinoff, Handbook of Water and Wastewater Treatment Technology. Routledge, 2019https://doi.org/10.1201/9780203752494.
[34] I.M. Ismail, A.S. Fawzy, N.M. Abdel-Monem, M.H. Mahmoud, M.A. El-Halwany, Combined coagulation flocculation pre treatment unit for municipal wastewater. J. Adv. Res. 3 (2012) 331–336, https://doi.org/10.1016/j.jare.2011.10.004.
[35] S. Bolisetty, M. Peydayesh, R. Mezzenga, Sustainable technologies for water purification from heavy metals: review and analysis. Chem. Soc. Rev. 48 (2019) 463–487, https://doi.org/10.1039/c8cs00493e.
[36] M. Libhaber, A.O. Jaramillo, Sustainable Treatment and Reuse of Municipal Wastewater. IWA Publishing, 2016, https://doi.org/10.2166/9781780400631.
[37] Y.J. Chan, M.F. Chong, C.L. Law, D.G. Hassell, A review on anaerobic-aerobic treatment of industrial and municipal wastewater. Chem. Eng. J. 155 (2009) 1–18, https://doi.org/10.1016/j.cej.2009.06.041.
[38] H. Lu, J. Wang, T. Wang, N. Wang, Y. Bao, H. Hao, Crystallization techniques in wastewater treatment: an overview of applications. Chemosphere 173 (2017) 474–484, https://doi.org/10.1016/j.chemosphere.2017.01.070.
[39] H.P. Ngang, B.S. Ooi, A.L. Ahmad, S.O. Lai, Preparation of PVDF-TiO2 mixed-matrix membrane and its evaluation on dye adsorption and UV-cleaning properties. Chem. Eng. 197 (2012) 359–367, https://doi.org/10.1016/j.cej.2012.05.050.
[40] W. Lin, L. Jing, Z. Zhu, Q. Cai, B. Zhang, Removal of heavy metals from mining wastewater by micellar-enhanced ultrafiltration (MEUF): experimental investigation and monte carlo-based artificial neural network modeling. Water Air Soil Pollut. 228 (2017), https://doi.org/10.1007/s11270-017-3386-5.

This book belongs to Badji Mokhtar Annaba University Central Library Copyright Elsevier 2025

[41] S.H. Ahmad, C.S. Mohd-Setapar, A. Chuong, W.A. Khatoon, R. Wani, M.R. Kumar, Recent advances in new generation dye removal technologies: novel search for approaches to reprocess wastewater. RSC Adv. 5 (2015) 30801–30818, https://doi.org/10.1039/c4ra16959j.
[42] S. De Gisi, G. Lofrano, M. Grassi, M. Notarnicola, Characteristics and adsorption capacities of low-cost sorbents for wastewater treatment: a review. Sustain. Mater. Technol. 9 (2016) 10–40, https://doi.org/10.1016/j.susmat.2016.06.002.
[43] P.Z. Ray, H.J. Shipley, H. J, Inorganic nano-adsorbents for the removal of heavy metals and arsenic: a review. RSC Adv. 5 (2015) 29885–29907, https://doi.org/10.1039/c5ra02714d.
[44] H. Qiu, L. Lv, B.C. Pan, Q.J. Zhang, W.M. Zhang, Q.X. Zhang, Critical review in adsorption kinetic models. J. Zheijang Univ. Sci. A 10 (2009) 716–724, https://doi.org/10.1631/jzus.A0820524.
[45] C.H. Giles, T.H. MacEwan, S.N. Nakhwa, D. Smith, Studies in adsorption: part XI. A system of classification of solution adsorption isotherms, and its use in diagnosis of adsorption mechanisms and in measurement of specific surface areas of solids. J. Chem. Soc. (1960) 3973–3993, https://doi.org/10.1039/JR9600003973.
[46] G. Ungureanu, S. Santos, R. Boaventura, C. Botelho, Arsenic and antimony in water and wastewater: overview of removal techniques with special reference to latest advances in adsorption. J. Environ. Manage. 151 (2015) 326–342, https://doi.org/10.1016/j.jenvman.2014.12.051.
[47] I. Ali, M. Asim, T.A. Khan, Low cost adsorbents for the removal of organic pollutants from wastewater. J. Environ. Manage. 113 (2012) 170–183, https://doi.org/10.1016/j.jenvman.2012.08.028.
[48] A.A. Basheer, New generation nano-adsorbents for the removal of emerging contaminants in water. J. Mol. Liq. 261 (2018) 583–593, https://doi.org/10.1016/j.molliq.2018.04.021.
[49] Y. Deng, R. Zhao, Advanced oxidation processes (AOPs) in wastewater treatment. Curr. Pollut. Rep. 1 (2015) 167–176, https://doi.org/10.1007/s40726-015-0015-z.
[50] S.J. Mazivila, I.A. Ricardo, J.M.M. Leitão, J.C.G. Esteves da Silva, A review on advanced oxidation processes: from classical to new perspectives coupled to two- and multi-way calibration strategies to monitor degradation of contaminants in environmental samples. Trends Environ. Anal. Chem. 24 (2019) 1–10, https://doi.org/10.1016/j.teac.2019.e00072.
[51] B. Bethi, S.H. Sonawane, B.A. Bhanvase, S.P. Gumfekar, Nanomaterials-based advanced oxidation processes for wastewater treatment: a review. Chem. Eng. Process. Process Intensif. 109 (2016) 178–189, https://doi.org/10.1016/j.cep.2016.08.016.
[52] P.V. Nidheesh, R. Rajan, Removal of Rhodamine B from a water medium using hydroxyl and sulphate radicals generated by iron loaded activated carbon. RSC Adv. 6 (2016) 5330–5340, https://doi.org/10.1039/C5RA19987E.
[53] R. Dewil, D. Mantzavinos, I. Poulios, M.A. Rodrigo, New perspectives for advanced oxidation processes. J. Environ. Manage. 195 (2017) 93–99, https://doi.org/10.1016/j.jenvman.2017.04.010.
[54] P.V. Nidheesh, Heterogeneous Fenton catalysts for the abatement of organic pollutants from aqueous solution: a review. RSC Adv. 5 (2015) 40552–40577, https://doi.org/10.1039/C5RA02023A.
[55] L. Feenstra, J. van Erkel, Arsenic in Groundwater: Overview and Evaluation of Removal Methods, Int. Groundw. Resour. Assess. Cent, 2007, pp. 1–23.
[56] B.K. Mandal, K.T. Suzuki, Arsenic round the world: a review. Talanta 58 (2002) 201–235, https://doi.org/10.1016/S0039-9140(02)00268-0.
[57] D.S. Babu, V. Srivastava, P.V. Nidheesh, M.S. Kumar, Detoxification of water and wastewater by advanced oxidation processes. Sci. Total Environ. 696 (2019), https://doi.org/10.1016/j.scitotenv.2019.133961.
[58] D.F. Laine, I.F. Cheng, The destruction of organic pollutants under mild reaction conditions: a review. Microchem. J. 85 (2007) 183–193, https://doi.org/10.1016/j.microc.2006.07.002.
[59] J. Pina, O.L.C. Fournier, Photolysis and chromatographic analysis of biphenyl and diphenyl ether mixtures in soil by infrared lamp irradiation assessing the feasibility of using the district heat demand forecast. Energy Procedia 142 (2017) 3566–3571, https://doi.org/10.1016/j.egypro.2017.12.246.
[60] Z.L. Ye, C.Q. Cao, J.C. He, R.X. Zhang, H.Q. Hou, Photolysis of organic pollutants in wastewater with 206 nm UV irradiation. Chin. Chem. Lett. 20 (2009) 706–710, https://doi.org/10.1016/j.cclet.2008.12.033.

This book belongs to Badji Mokhtar Annaba University Central Library Copyright Elsevier 2025

[61] M. Pei, B. Zhang, Y. He, J. Su, K. Gin, O. Lev, G. Shen, S. Hu, State of the art of tertiary treatment technologies for controlling antibiotic resistance in wastewater treatment plants. Environ. Int. 131 (2019), https://doi.org/10.1016/j.envint.2019.105026.

[62] S. Suslick, J.R. BlakePerutz, Y. Didenko, M.M. Fang, T. Hyeon, K.J. Kolbeck, W.B. McNamara, M. M. Mdleleni, M. Wong, Acoustic cavitation and its chemical consequences. Philos. Trans. R. Soc. Lond. Ser. A 357 (1999) 335–353, https://doi.org/10.1098/rsta.1999.0330.

[63] E.A. Serna-Galvis, D. Montoya-Rodríguez, L. Isaza-Pineda, M. Ibáñez, F. Hernández, A. Moncayo-Lasso, R. A. Torres-Palma, Sonochemical degradation of antibiotics from representative classes-considerations on structural effects, initial transformation products, antimicrobial activity and matrix. Ultrason. Sonochem. 50 (2019) 157–165, https://doi.org/10.1016/j.ultsonch.2018.09.012.

[64] N. Tran, P. Drogui, S.K. Brar, Sonochemical techniques to degrade pharmaceutical organic pollutants. Environ. Chem. Lett. 13 (2015) 251–268, https://doi.org/10.1007/s10311-015-0512-8.

[65] G.K. Dinesh, S. Chakma, Degradation kinetic study of cholesterol lowering statin drug using sono-hybrid techniques initiated by metal-free polymeric catalyst. J. Taiwan Inst. Chem. Eng. 100 (2019) 95–104, https://doi.org/10.1016/j.jtice.2019.04.009.

[66] G.K. Dinesh, S. Chakma, Mechanistic investigation in degradation mechanism of 5-fluorouracil using graphitic carbon nitride. Ultrason. Sonochem. 50 (2019) 311–321, https://doi.org/10.1016/j.ultsonch.2018.09.032.

[67] S. Chakma, S. Praneeth, V.S. Moholkar, Mechanistic investigations in sono-hybrid (ultrasound/Fe^{2+}/UVC) techniques of persulfate activation for degradation of azorubine. Ultrason. Sonochem. 38 (2017) 652–663, https://doi.org/10.1016/j.ultsonch.2016.08.015.

[68] S. Chakma, V.S. Moholkar, Physical mechanism of sono-Fenton process. AICHE J. 59 (2013) 4303–4313, https://doi.org/10.1002/aic.14150.

[69] J. Liang, S. Komarov, N. Hayashi, E. Kasai, Improvement in sonochemical degradation of 4-chlorophenol by combined use of Fenton-like reagents. Ultrason. Sonochem. 14 (2007) 201–207, https://doi.org/10.1016/j.ultsonch.2006.05.002.

[70] S.O. Ganiyu, M. Zhou, C.A. Martínez-Huitle, Heterogeneous electro-Fenton and photoelectro-Fenton processes: a critical review of fundamental principles and application for water/wastewater treatment. Appl. Catal. Environ. 235 (2018) 103–129, https://doi.org/10.1016/j.apcatb.2018.04.044.

[71] B. Ponnusami, K. Muthukumar, Degradation of phenol in aqueous solution by Fenton, sono-Fenton and sono-photo-Fenton methods. Clean: Soil, Air, Water 39 (2011) 142–147, https://doi.org/10.1002/clen.201000072.

[72] W.H. Glaze, Drinking-water treatment with ozone. Environ. Sci. Technol. 21 (1987) 224–230, https://doi.org/10.1021/es00157a001.

[73] U. Von Gunten, Ozonation of drinking water: part I. oxidation kinetics and product formation. Water Res. 37 (2003) 1443–1467, https://doi.org/10.1016/S0043-1354(02)00457-8.

[74] Y. Lee, U. Von Gunten, Advances in predicting organic contaminant abatement during ozonation of municipal wastewater effluent: reaction kinetics, transformation products, and changes of biological effects. Environ. Sci.: Water Res. Technol. 2 (2016) 421–442, https://doi.org/10.1039/c6ew00025h.

[75] R.I.L. Eggen, J. Hollender, A. Joss, M. Schärer, C. Stamm, Reducing the discharge of micropollutants in the aquatic environment: the benefits of upgrading wastewater treatment plants. Environ. Sci. Technol. 48 (2014) 7683–7689, https://doi.org/10.1021/es500907n.

[76] D.I. Patsoura, X.E.V. Kondarides, Photocatalytic degradation of organic pollutants with simultaneous production of hydrogen. Catal. Today 124 (2007) 94–102, https://doi.org/10.1016/j.cattod.2007.03.028.

[77] S. Malato, P. Fernández-Ibáñez, M.I. Maldonado, J. Blanco, W. Gernjak, Decontamination and disinfection of water by solar photocatalysis: recent overview and trends. Catal. Today 147 (2009) 1–59, https://doi.org/10.1016/j.cattod.2009.06.018.

[78] J.M. Herrmann, Photocatalysis fundamentals revisited to avoid several misconceptions. Appl. Catal. Environ. 99 (2010) 461–468, https://doi.org/10.1016/j.apcatb.2010.05.012.

This book belongs to Badji Mokhtar Annaba University Central Library

Copyright Elsevier 2025

[79] M.D. Hernández-Alonso, F. Fresno, S. Suárez, J.M. Coronado, Development of alternative photocatalysts to TiO_2: challenges and opportunities. Energ. Environ. Sci. 2 (2009) 1231–1257, https://doi.org/10.1039/b907933e.

[80] M. Naghizadeh, M.A. Taher, A.M. Tamaddon, Facile synthesis and characterization of magnetic nanocomposite $ZnO/CoFe_2O_4$ hetero-structure for rapid photocatalytic degradation of imidacloprid. Heliyon 5 (2019) e02870, https://doi.org/10.1016/j.heliyon.2019.e02870.

[81] S. Nagappan, C.-S. Ha, Emerging trends in superhydrophobic surface based magnetic materials: fabrications and their potential applications. J. Mater. Chem. A 3 (2015) 3224–3251, https://doi.org/10.1039/c4ta05078a.

[82] J. Yuan, Y. Xu, A.H.E. Müller, One-dimensional magnetic inorganic-organic hybrid nanomaterials. Chem. Soc. Rev. 40 (2011) 640–655, https://doi.org/10.1039/c0cs00087f.

[83] C. Baresel, V. Schaller, C. Jonasson, C. Johansson, R. Bordes, V. Chauhan, A. Sugunan, J. Sommertune, S. Welling, Functionalized magnetic particles for water treatment. Heliyon 5 (2019) e02325, https://doi.org/10.1016/j.heliyon.2019.e02325.

[84] B.I. Kharisov, H.V.R. Dias, O.V. Kharissova, M. Jiménez-Pérez, B.O. Pérez, B.M. Flores, Iron-containing nanomaterials: synthesis, properties, and environmental applications. RSC Adv. 2 (2012) 9325–9358, https://doi.org/10.1039/c2ra20812a.

[85] L.M. Rossi, N.J.S. Costa, F.P. Silva, R. Wojcieszak, Magnetic nanomaterials in catalysis: advanced catalysts for magnetic separation and beyond. Green Chem. 16 (2014) 2906–2933, https://doi.org/10.1039/c4gc00164h.

[86] T. Hyeon, Chemical synthesis of magnetic nanoparticles. Chem. Commun. (2003) 927–934, https://doi.org/10.1039/b207789b.

[87] S. Singamaneni, V.N. Bliznyuk, C. Binek, E.Y. Tsymbal, Magnetic nanoparticles: recent advances in synthesis, self-assembly and applications. J. Mater. Chem. 21 (2011) 16819–16845, https://doi.org/10.1039/c1jm11845e.

[88] J.R. Choi, S.J. Oh, H. Ju, J. Cheon, Massive fabrication of free-standing one-dimensional Co/Pt nanostructures and modulation of ferromagnetism via a programmable barcode layer effect. Nano Lett. 5 (2005) 2179–2183, https://doi.org/10.1021/nl051190k.

[89] A. Mukhopadhyay, N. Joshi, K. Chattopadhyay, G. De, A facile synthesis of PEG-coated magnetite (Fe_3O_4) nanoparticles and their prevention of the reduction of cytochrome C. ACS Appl. Mater. Interfaces 4 (1) (2012) 142–149, https://doi.org/10.1021/am201166m.

[90] S.K. Giri, N.N. Das, G.C. Pradhan, Synthesis and characterization of magnetite nanoparticles using waste iron ore tailings for adsorptive removal of dyes from aqueous solution. Colloids Surf. A Physicochem. Eng. Asp. 389 (2011) 43–49, https://doi.org/10.1016/j.colsurfa.2011.08.052.

[91] Y. Zhan, H. Hu, Y. He, Z. Long, X. Wan, G. Zeng, Novel amino-functionalized Fe_3O_4/carboxylic multi-walled carbon nanotubes: one-pot synthesis, characterization and removal for Cu(II). Russ. J. Appl. Chem. 89 (2016) 1894–1902, https://doi.org/10.1134/S1070427216110227.

[92] K.K. Senapati, C. Borgohain, P. Phukan, $CoFe_2O_4$-ZnS nanocomposite: a magnetically recyclable photocatalyst. Cat. Sci. Technol. (11) (2012) 2361–2366, https://doi.org/10.1039/c2cy20400b.

[93] T. Xin, M. Ma, H. Zhang, J. Gu, S. Wang, M. Liu, Q. Zhang, A facile approach for the synthesis of magnetic separable Fe_3O_4@TiO_2, core shell nanocomposites as highly recyclable photocatalysts. Appl. Surf. Sci. 288 (2014) 51–59, https://doi.org/10.1002/ejic.201100707.

[94] L. Zhou, G. Zhang, J. Tian, D. Wang, D. Cai, Z. Wu, Functionalized Fe_3O_4@C nanospheres with adjustable structure for efficient hexavalent chromium removal. ACS Sustain. Chem. Eng. 5 (2017) 11042–11050, https://doi.org/10.1021/acssuschemeng.7b02983.

[95] K.K. Senapati, C. Borgohain, P. Phukan, Photocatalytic degradation of methylene blue in water using $CoFe_2O_4$-Cr_2O_3–SiO_2 fluorescent magnetic nanocomposite. J. Mol. Catal. A Chem. 346 (2011) 111–116, https://doi.org/10.1016/j.molcata.2011.07.001.

[96] S. Zhan, Y. Yang, Z. Shen, J. Shan, Y. Li, S. Yang, D. Zhu, Efficient removal of pathogenic bacteria and viruses by multifunctional amine-modified magnetic nanoparticles. J. Hazard. Mater. 274 (2014) 115–123, https://doi.org/10.1016/j.jhazmat.2014.03.067.

This book belongs to Badji Mokhtar Annaba University Central Library Copyright Elsevier 2025

[97] B. Prevot, D. Fabbri, E. Pramauro, C. Baiocchi, C. Medana, E. Montoneri, V. Boffa, Sensitizing effect og bio-based chemicals from urban wastes on the photodegradation of azo-dyes, J. Photochem. Photobiol. A Chem. 209 (2010) 224–231.

[98] S. Chandrasekaran, C. Bowen, P. Zhang, Z. Li, Q. Yuan, X. Ren, L. Deng, Spinel photocatalysts for environmental remediation, hydrogen generation, CO_2 reduction and photoelectrochemical water splitting. J. Mater. Chem. A 6 (2018) 11078–11104, https://doi.org/10.1039/c8ta03669a.

[99] S.C.N. Tang, I.M.C. Lo, Magnetic nanoparticles: essential factors for sustainable environmental applications. Water Res. 47 (2013) 2613–2632, https://doi.org/10.1016/j.watres.2013.02.039.

[100] D. Lopez-Tejedor, R. Benavente, J.M. Palomo, Iron nanostructured catalysts: design and applications. Cat. Sci. Technol. 8 (2018) 1754–1776, https://doi.org/10.1039/c7cy02259j.

[101] Y. Deng, D. Qi, C. Deng, X. Zhang, D. Zhao, Superparamagnetic high-magnetization microspheres with an Fe_3O_4@SiO_2 core and perpendicularly aligned mesoporous SiO_2 shell for removal of microcystins. J. Am. Chem. Soc. 130 (2008) 28–29, https://doi.org/10.1021/ja0777584.

[102] S.A. Elfeky, S.E. Mahmoud, A.F. Youssef, Applications of CTAB modified magnetic nanoparticles for removal of chromium (VI) from contaminated water. J. Adv. Res. 8 (2017) 435–443, https://doi.org/10.1016/j.jare.2017.06.002.

[103] K. Simeonidis, S. Mourdikoudis, E. Kaprara, M. Mitrakas, L. Polavarapu, Inorganic engineered nanoparticles in drinking water treatment: a critical review. Environ. Sci.: Water Res. Technol. 2 (2016) 43–70, https://doi.org/10.1039/c5ew00152h.

[104] G.D. Sayles, G. You, M. Wang, M.J. Kupferle, DDT, DDD, and DDE dechlorination by zero-valent iron. Environ. Sci. Technol. 31 (1997) 3448–3454, https://doi.org/10.1021/es9701669.

[105] Y.T. He, S.J. Traina, Cr(VI) reduction and immobilization by magnetite under alkaline pH conditions: the role of passivation. Environ. Sci. Technol. 39 (2005) 4499–4504, https://doi.org/10.1021/es0483692.

[106] S.H. Joo, A.J. Feitz, T.D. Waite, Oxidative degradation of the carbothioate herbicide, molinate, using nanoscale zero-valent iron. Environ. Sci. Technol. 38 (2004) 2242–2247, https://doi.org/10.1021/es035157g.

[107] Y. Liu, S.A. Majetich, R.D. Tilton, D.S. Sholl, G.V. Lowry, TCE dechlorination rates, pathways, and efficiency of nanoscale iron particles with different properties. Environ. Sci. Technol. 39 (5) (2005) 1338–1345, https://doi.org/10.1021/es049195r.

[108] J.L. Wilson, P. Poddar, N.A. Frey, H. Srikanth, K. Mohomed, J. P. Harmon, S. Kotha, J. Wachsmuth, Synthesis and magnetic properties of polymer nanocomposites with embedded iron nanoparticles. J. Appl. Phys. 95 (2004) 1439–1443, https://doi.org/10.1063/1.1637705.

[109] L. Alidokht, A.R. Khataee, A. Reyhanitabar, S. Oustan, Reductive removal of Cr(VI) by starch-stabilized Fe0 nanoparticles in aqueous solution. Desalination 270 (2011) 105–110, https://doi.org/10.1016/j.desal.2010.11.028.

[110] F. Liu, J.H. Yang, J. Zuo, D. Ma, L. Gan, B. Xie, P. Wang, B. Yang, Graphene-supported nanoscale zero-valent iron: removal of phosphorus from aqueous solution and mechanistic study. J. Environ. Sci. 26 (2014) 1751–1762, https://doi.org/10.1016/j.jes.2014.06.016.

[111] W. Yantasee, C.L. Warner, T. Sangvanich, R.S. Addleman, T.G. Carter, R.J. Wiacek, G. E. Fryxell, C. Timchalk, M.G. Warner, Removal of heavy metals from aqueous systems with thiol functionalized superparamagnetic nanoparticles. Environ. Sci. Technol. 41 (2007) 5114–5119, https://doi.org/10.1021/es0705238.

[112] J. Farrell, W.D. Bostick, R.J. Jarabek, J.N. Fiedor, Electrosorption and reduction of pertechnetate by anodically polarized magnetite. Environ. Sci. Technol. 33 (1999) 1244–1249, https://doi.org/10.1021/es980086k.

[113] V. Jawed, L.M.P. Saxena, Engineered nanomaterials and their surface functionalization for the removal of heavy metals: a review. J. Water Process Eng. 33 (2020) 101009https://doi.org/10.1016/j.jwpe.2019.101009.

[114] A. Afkhami, M. Saber-Tehrani, H. Bagheri, Modified maghemite nanoparticles as an efficient adsorbent for removing some cationic dyes from aqueous solution. Desalination 263 (2010) 240–248, https://doi.org/10.1016/j.desal.2010.06.065.

This book belongs to Badji Mokhtar Annaba University Central Library Copyright Elsevier 2025

[115] Y. Huang, A.A. Keller, EDTA functionalized magnetic nanoparticle sorbents for cadmium and lead contaminated water treatment. Water Res. 80 (2015) 159–168, https://doi.org/10.1016/j.watres.2015.05.011.
[116] N.C. Feitoza, T.D. Gonçalves, J.J. Mesquita, J.S. Menegucci, M.K.M.S. Santos, J.A. Chaker, R.B. Cunha, A. M.M. Medeiros, J.C. Rubim, M.H. Sousa, Fabrication of glycine-functionalized maghemite nanoparticles for magnetic removal of copper from wastewater. J. Hazard. Mater. 264 (2014) 153–160, https://doi.org/10.1016/j.jhazmat.2013.11.022.
[117] X. Zhang, H. Li, S. Wang, F.R.F. Fan, A.J. Bard, Improvement of hematite as photocatalyst by doping with tantalum. J. Phys. Chem. C 118 (2014) 16842–16850, https://doi.org/10.1021/jp500395a.
[118] Z. Cao, M. Qin, B. Jia, Y. Gu, P. Chen, A.A. Volinsky, X. Qu, One pot solution combustion synthesis of highly mesoporous hematite for photocatalysis. Ceram. Int. 41 (2015) 2806–2812, https://doi.org/10.1016/j.ceramint.2014.10.100.
[119] E. Casbeer, V.K. Sharma, X.Z. Li, Synthesis and photocatalytic activity of ferrites under visible light: a review. Sep. Purif. Technol. 87 (2012) 1–14, https://doi.org/10.1016/j.seppur.2011.11.034.
[120] X. Zheng, H. Cheng, J. Yang, D. Chen, R. Jian, L. Lin, One-pot solvothermal preparation of Fe_3O_4-urushiol-graphene hybrid nanocomposites for highly improved Fenton reactions. ACS Appl. Nano Mater. 1 (2018) 2754–2762, https://doi.org/10.1021/acsanm.8b00446.
[121] L. Guo, Q. Da An, Z.Y. Xiao, S.R. Zhai, L. Cui, Inherent N-doped honeycomb-like carbon/Fe_3O_4 composites with versatility for efficient microwave absorption and wastewater treatment. ACS Sustain. Chem. Eng. 7 (2019) 9237–9248, https://doi.org/10.1021/acssuschemeng.9b00067.
[122] S. Saber-Samandari, H. Joneidi-Yekta, M. Mohseni, Adsorption of anionic and cationic dyes from aqueous solution using gelatin-based magnetic nanocomposite beads comprising carboxylic acid functionalized carbon nanotube. Chem. Eng. J. 308 (2017) 1133–1144, https://doi.org/10.1016/j.cej.2016.10.017.
[123] M. Liu, B.D. Xi, L.A. Hou, S. Yu, Magnetic multi-functional nano-fly ash-derived zeolite composites for environmental applications. J. Mater. Chem. A 1 (2013) 12617–12626, https://doi.org/10.1039/c3ta13180g.
[124] X. Wang, Y. Cui, Y. Wang, X. Song, J. Yu, Fabrication and catalytic performance of highly stable multifunctional core-shell zeolite composites. Inorg. Chem. 52 (2013) 10708–10710, https://doi.org/10.1021/ic401357s.
[125] N.H. Mthombeni, M.S. Onyango, O. Aoyi, Adsorption of hexavalent chromium onto magnetic natural zeolite-polymer composite. J. Taiwan Inst. Chem. Eng. 50 (2015) 242–251, https://doi.org/10.1016/j.jtice.2014.12.037.
[126] T.J. Mohseni-Bandpi, E. Al-Musawi, M. Ghahramani, S. Zarrabi, S.A.V. Mohebi, Improvement of zeolite adsorption capacity for cephalexin by coating with magnetic Fe_3O_4 nanoparticles. J. Mol. Liq. 218 (2016) 615–624, https://doi.org/10.1016/j.molliq.2016.02.092.
[127] M. Yin, Z. Li, Z. Liu, X. Yang, J. Ren, Magnetic self-assembled zeolite clusters for sensitive detection and rapid removal of mercury(II). ACS Appl. Mater. Interfaces 4 (2012) 431–437, https://doi.org/10.1021/am201516q.
[128] D. Mehta, S. Mazumdar, S.K. Singh, Magnetic adsorbents for the treatment of water/wastewater—a review. J. Water Process Eng. 7 (2015) 244–265, https://doi.org/10.1016/j.jwpe.2015.07.001.
[129] H.G. Qiu, X. Yan, J. Guo, Y. Wang, D. Sun, Q. Wang, M. Khan, X. Zhang, B.L. Weeks, D. P. Young, Z. Guo, S. Wei, Cellulose derived magnetic mesoporous carbon nanocomposites with enhanced hexavalent chromium removal. J. Mater. Chem. A 2 (2014) 17454–17462, https://doi.org/10.1039/c4ta04040f.
[130] K. Gong, Q. Hu, Y. Xiao, X. Cheng, H. Liu, N. Wang, B. Qiu, Z. Guo, Triple layered core-shell ZVI@carbon@polyaniline composite enhanced electron utilization in Cr(VI) reduction. J. Mater. Chem. A 6 (2018) 11119–11128, https://doi.org/10.1039/c8ta03066a.
[131] J.G. Hering, I.A. Katsoyiannis, G.A. Theoduloz, M. Berg, S.J. Hug, Arsenic removal from drinking water: experiences with technologies and constraints in practice. J. Environ. Eng. 143 (2017) 1–9, https://doi.org/10.1061/(ASCE)EE.1943-7870.0001225.

This book belongs to Badji Mokhtar Annaba University Central Library Copyright Elsevier 2025

[132] L. Fang, X. Min, R. Kang, H. Yu, S.G. Pavlostathis, X. Luo, Development of an anion imprinted polymer for high and selective removal of arsenite from wastewater. Sci. Total Environ. 639 (2018) 110–117, https://doi.org/10.1016/j.scitotenv.2018.05.103.

[133] L. Hao, M. Liu, N. Wang, G. Li, A critical review on arsenic removal from water using iron-based adsorbents. RSC Adv. 8 (2018) 39545–39560, https://doi.org/10.1039/c8ra08512a.

[134] X. Yu, S. Tong, M. Ge, J. Zuo, C. Cao, W. Song, One-step synthesis of magnetic composites of cellulose@iron oxide nanoparticles for arsenic removal. J. Mater. Chem. A 1 (2013) 959–965, https://doi.org/10.1039/c2ta00315e.

[135] F. Yu, S. Sun, J. Ma, Enhanced removal performance of arsenate and arsenite by magnetic graphene oxide with high iron oxide loading. Phys. Chem. Chem. Phys. 17 (2015) 4388–4397, https://doi.org/10.1039/c4cp04835k.

[136] Z. Zhang, H. Li, J. Li, X. Li, Z. Wang, X. Liu, L. Zhang, A novel adsorbent of core-shell construction of chitosan-cellulose magnetic carbon foam: synthesis, characterization and application to remove copper in wastewater. Chem. Phys. Lett. 731 (2019) 136573https://doi.org/10.1016/j.cplett.2019.07.001.

[137] T. Madrakian, A. Afkhami, M. Ahmadi, Adsorption and kinetic studies of seven different organic dyes onto magnetite nanoparticles loaded tea waste and removal of them from wastewater samples. Spectrochim. Acta A Mol. Biomol. Spectrosc. 99 (2012) 102–109, https://doi.org/10.1016/j.saa.2012.09.025.

[138] M. D'Cruz, M.O. Madkour, E.A.-H. Amin, Efficient and recoverable magnetic AC-Fe_3O_4 nanocomposite for rapid removal of promazine from wastewater. Mater. Chem. Phys. 240 (2020) 122109https://doi.org/10.1016/j.matchemphys.2019.122109.

[139] F. Guo, X. Jiang, X. Li, X. Jia, S. Liang, L. Qian, Synthesis of MgO/Fe_3O_4 nanoparticles embedded activated carbon from biomass for high-efficient adsorption of malachite green. Mater. Chem. Phys. 240 (2020) 122240https://doi.org/10.1016/j.matchemphys.2019.122240.

[140] L. Zhao, W. Lv, J. Hou, Y. Li, J. Duan, S. Ai, Synthesis of magnetically recyclable g-C_3N_4/Fe_3O_4/ZIF-8 nanocomposites for excellent adsorption of malachite green. Microchem. J. 152 (2019) 104425, https://doi.org/10.1016/j.microc.2019.104425.

[141] H. Dong, G. Zeng, L. Tang, C. Fan, C. Zhang, X. He, Y. He, An overview on limitations of TiO_2-based particles for photocatalytic degradation of organic pollutants and the corresponding countermeasures. Water Res. 79 (2015) 128–146, https://doi.org/10.1016/j.watres.2015.04.038.

[142] S.Q. Liu, Magnetic semiconductor nano-photocatalysts for the degradation of organic pollutants. Environ. Chem. Lett. 10 (2012) 209–216, https://doi.org/10.1007/s10311-011-0348-9.

[143] P. Mishra, S. Patnaik, K. Parida, An overview of recent progress on noble metal pollutant degradation and H_2 evolution. Cat. Sci. Technol. 4 (2019) 916–941, https://doi.org/10.1039/c8cy02462f.

[144] X. Zhao, Z. Lu, J. Kan, C. Yi, N. Gao, Z. Zhu, Synthesis of stable core—shell structured TiO_2@Fe_3O_4 based on carbon derived from yeast with an enhanced photocatalytic ability. RSC Adv. 52 (2016) 46889–46899, https://doi.org/10.1039/c6ra04633a.

[145] B.I. Kharisov, H.V.R. Dias, O.V. Kharissova, Mini-review: ferrite nanoparticles in the catalysis. Arab. J. Chem. 12 (2019) 1234–1246, https://doi.org/10.1016/j.arabjc.2014.10.049.

[146] K. Jahanara, S. Farhadi, A magnetically separable plate-like cadmium titanate—copper ferrite nanocomposite with enhanced visible-light photocatalytic degradation. RSC Adv. 27 (2019) 15615–15628, https://doi.org/10.1039/c9ra01968e.

[147] T.B. Nguyen, R.A. Doong, Heterostructured $ZnFe_2O_4$/TiO_2 nanocomposites with a highly recyclable visible-light-response for bisphenol A degradation. RSC Adv. 7 (2017) 50006–50016, https://doi.org/10.1039/c7ra08271a.

[148] L. Zheng, H. Xu, F. Pi, X. Sun, Photocatalytic degradation of monocrotophos under UV illumination. RSC Adv. 90 (2016) 87273–87281, https://doi.org/10.1039/c6ra13423h.

[149] X.L. Fu, Y. Wang, L. Li, Z. Zhang, Preparation and characterization of Fe_3O_4@SiO_2@TiO_2-Co/rGO magnetic visible light photocatalyst for water treatment. RSC Adv. 35 (2019) 20256–20265, https://doi.org/10.1039/c9ra04002a.

This book belongs to Badji Mokhtar Annaba University Central Library

Copyright Elsevier 2025

[150] S. Qiu, D. He, J. Ma, T. Liu, T.D. Waite, Electrochimica acta kinetic modeling of the electro-Fenton process: quantification of reactive oxygen species generation. Electrochim. Acta 176 (2015) 51–58, https://doi.org/10.1016/j.electacta.2015.06.103.

[151] H. Wang, H. Jiang, S. Wang, W. Shi, J. He, H. Liu, Y. Huang, Fe_3O_4–MWCNT magnetic nanocomposites as efficient peroxidase mimic catalysts in a Fenton- like reaction for water purification without pH. RSC Adv. 86 (2014) 45809–45815, https://doi.org/10.1039/c4ra07327d.

[152] H. Zhou, S. Wu, Y. Zhou, Y. Yang, J. Zhang, L. Luo, X. Duand, S. Wangd, L. Wange, D.C.W. Tsang, Insights into the oxidation of organic contaminants by iron nanoparticles encapsulated within boron and nitrogen co-doped carbon nanoshell: catalyzed Fenton-like reaction at natural pH. Environ. Int. 128 (2019) 77–88, https://doi.org/10.1016/j.envint.2019.04.006.

[153] L. Xu, J. Wang, A heterogeneous Fenton-like system with nanoparticulate zero-valent iron for removal of 4-chloro-3-methyl phenol. J. Hazard. Mater. 186 (2011) 256–264, https://doi.org/10.1016/j.jhazmat.2010.10.116.

[154] S. Machado, W. Stawiński, P. Slonina, A.R. Pinto, J.P. Grosso, H.P.A. Nouws, J. T. Albergaria, C. Delerue-Matos, Application of green zero-valent iron nanoparticles to the remediation of soils contaminated with ibuprofen. Sci. Total Environ. 461–462 (2013) 323–329, https://doi.org/10.1016/j.scitotenv.2013.05.016.

[155] M. Faheem, X. Jiang, L. Wang, J. Shen, Synthesis of Cu_2O-$CuFe_2O_4$ microparticles from Fenton sludge and its application in the Fenton process: the key role of Cu_2O in the catalytic degradation of phenol. RSC Adv. 8 (2018) 5740–5748, https://doi.org/10.1039/c7ra13608k.

[156] Z. Wang, Y. Fan, R. Wu, Y. Huo, H. Wu, F. Wang, X. Xu, Novel magnetic g-C_3N_4/α-Fe_2O_3/Fe_3O_4 composite for the very effective visible-light-Fenton degradation of Orange II. RSC Adv. 8 (2018) 5180–5188, https://doi.org/10.1039/c7ra13291c.

This book belongs to Badji Mokhtar Annaba University Central Library

Copyright Elsevier 2025

CHAPTER 10

Nanomaterials for water splitting and hydrogen generation

Sagar D. Balgude[a] and Satish P. Mardikar[b]

[a]*Department of Engineering Science, D. Y. Patil College of Engineering, Savitribai Phule Pune University, Pune, India,* [b]*Department of Chemistry, Smt. R S College, SGB Amravati University, Amravati, India*

10.1 Introduction

The global anthropogenic demands are presently satisfied by fossil fuels that contribute to about ~86% of total energy. According to the present rate of energy consumption, the fossil fuels are expected to withstand for mere next 40 years [1]. Moreover, their use is also leading to severe climate changes because of evolution of large volumes of CO_2 during combustion. Thus energy crisis is one of the most crucial challenges in this century. The research in this area is mainly focused on development of renewable energy resources, which will effectively reduce CO_2 emissions. Energy substructure utilizing hydrogen (H_2) holds a great potential as clean, safe, and sustainable energy. Energy requirements can be fulfilled from H_2 either through combustion or in a H_2-fuel cell. Additionally, H_2 serves as major feedstock in many industrial processes, including Fischer-Tropsch synthesis and ammonia synthesis. Therefore water splitting for H_2 production is indubitably one of the utmost significant tactics to solar energy conversion. In this context, three different approaches can be manipulated for H_2 generation through water splitting, namely, (1) photoelectrochemical (PEC), (2) photochemical, and (3) thermochemical methods [2]. UV-visible light-driven semiconductor photocatalyst-mediated water splitting to produce H_2 and O_2 is a fairly promising method. Several researchers have attempted the development of photocatalyst material for photochemical reaction so far. However, a stable photocatalyst with good recycling ability for visible light-driven water splitting is still demanding. Consequently, enormous research efforts are still being devoted toward the development of stable photocatalyst with favorable band-edge potential for water splitting and bandgap value <3 [3].

Handbook of Nanomaterials for Wastewater Treatment. https://doi.org/10.1016/B978-0-12-821496-1.00026-X
Copyright © 2021 Elsevier Inc. All rights reserved.

This book belongs to Badji Mokhtar Annaba University Central Library Copyright Elsevier 2025

In general, semiconductors possess separate valence and conduction bands, leading to interlining bandgap to those of insulators and conductors. Application of adequate photochemical energy causes excitation of electrons from valence band to conduction band, leaving behind holes. The electron-hole pairs so generated bring about oxidation-reduction reactions, leading to water splitting [4]. Typically, electrons reduce protons to H_2 molecules, and holes oxidize the oxygen anions. The redox reactions are feasible only if the utmost echelon of the valence band is more positive than water oxidation level ($E_{O2/H2O}$, 1.23 V vs. normal hydrogen electrode; NHE), while the lowest level of the conduction band should be more negative than the H_2 evolution potential ($E_{H2/H2O}$, 0 V vs. NHE).

$$H_2O + 2h^+ \rightarrow 2H^+ + ½O_2 \quad \left(E^0{}_{\text{Oxidation}} = -1.23\,\text{eV}\right) \tag{10.1}$$

$$2H^+ + 2e^- \rightarrow H_2 \quad \left(E^0{}_{\text{reduction}} = 0.00\,\text{eV}\right) \tag{10.2}$$

$$H_2O \rightarrow H_2 + ½O_2 \tag{10.3}$$

Thus a semiconductor with minimal bandgap of 1.23 eV is suitable for water splitting. Consequently, titanium dioxide (TiO_2), zirconia (ZrO_2), potassium tantalum trioxide ($KTaO_3$), strontium titanate ($SrTiO_3$), and bismuth vanadate ($BiVO_4$) proved to be excellent water-splitting photocatalytic materials [5–7]. However, fulfilling just the water-splitting redox potential may not be the enough condition for individual photocatalyst with superior water splitting. These catalysts include SiC, ZnO, and CdS. The photoactivity of these semiconductors is limited by redundant photocorrosion during water splitting. Photocorrosion occurs because of self-oxidation of photocatalyst anion owing to photogenerated holes instead of water. Another confront for water-splitting photocatalysts is their operability. Majority of the semiconductor photocatalysts are operable under UV-light, which measures to be only c.4% of the total solar energy [5–7]. Visible light-active photocatalysts with improved solar energy competence are highly sought-after. Transition metal oxides having comparatively enough stability owing to the presence of electronegative oxygen atom represent the conventional water-splitting photocatalytic materials [7]. Typically, these can be classified depending upon their *d* orbital structure. Transition metals, including titanium (Ti), vanadium (V), niobium (Nb), and tungsten (W), owing to their vacant *d* orbitals possess low valence band energy, and consequently, large bandgaps exhibit low photocatalytic reaction rates. However, the visible light absorption competence of these materials can be well manipulated by defect engineering.

Fig. 10.1 depicts the schematic exemplification of photochemical water splitting. For photochemical or PEC water splitting, semiconductor photocatalyst and sacrificial intermediate as electron source are the essential components. The indispensable working principles of both systems are indistinguishable; they only differ in their setup.

This book belongs to Badji Mokhtar Annaba University Central Library Copyright Elsevier 2025

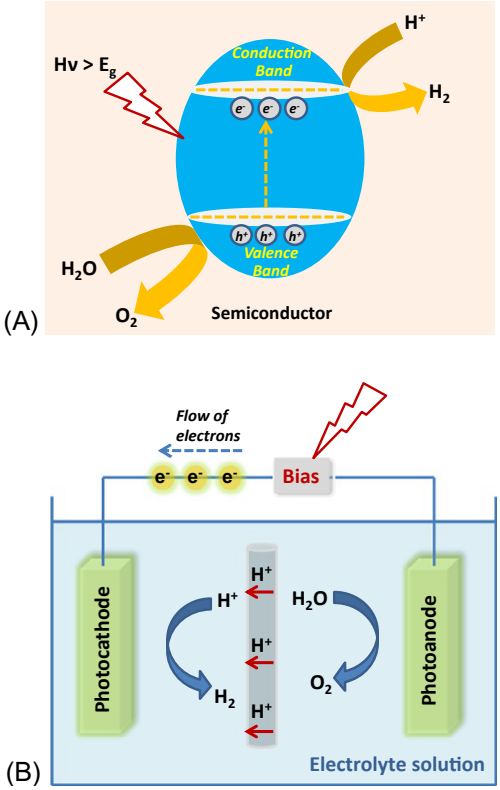

Fig. 10.1
Schematic exemplification of (A) photochemical water splitting (B) photoelectrochemical water splitting.

Because photochemical water-splitting reactions are driven by the potential engendered at semiconductor-electrolyte interface, the photocatalyst should be stable enough to resist photocorrosion in varied electrolyte solutions. Additionally, the rate of water splitting also depends upon the band-edge positions of the semiconductor photocatalyst. Schematic illustration of PEC water splitting is shown in Fig. 10.1B. The typical PEC water splitting initiates with the illumination of photocatalyst material with suitable light energy, the absorption of which leads to the generation of charge carriers (electrons and holes). Electrons and holes so produced then regulate various reactions such as obstruction of H^+ to H_2 gas and oxidation of water at conduction band. Depending upon the type of photochemical reaction, semiconductor material can be realized as either photo-cathode or photo-anode in the presence of electrolyte solution [8].

This book belongs to Badji Mokhtar Annaba University Central Library Copyright Elsevier 2025

10.2 Developing photocatalysts for water splitting—Mechanistic aspects

Considering the Gibbs free energy values, the projected energy required for water splitting into H_2 and O_2 accounts to be $\Delta G^0 = 237.13$ kJ mol^{-1}, which is thermodynamically unfavorable. The literature review reveals that various semiconductor metal oxide materials, either bare or coupled with other components, have been developed and tested for H_2 generation through water splitting. Usually, as far as water-splitting application is concerned, two types of photocatalyst systems can be designed—(1) metal oxide with single-step excitation and (2) *Z*-scheme photocatalyst system. As discussed earlier, while continuing with the water-splitting reactions, photons having suitable energy excite the semiconductor photocatalyst, which further expels electrons to conduction band from valence band wherein leaving behind holes. However, further progress of water splitting supported by reduction of H^+ and water oxidation caused because of electrons and holes is dependent on the band-edge positions of photocatalyst material. For smooth progress of water splitting, the conduction band should be having more negative potential than that required for H^+ reduction (0 V Vs. NHE at pH = 0), and the valence band should be more positive to that of water oxidation potential (1.23 V Vs. NHE at pH = 0), as exemplified in Fig. 10.2A. Thus it concludes that a semiconductor photocatalyst material having bandgap >1.23 eV would be an appropriate contender for water splitting photocatalyst through single-step excitation.

Development of *Z*-scheme photocatalyst system is motivated by the natural excitations in two different photosystems in green plants [9]. A *Z*-scheme photocatalyst for water splitting comprises two different semiconductors for independent H_2 and O_2 evolution in connection with redox moderator vehicle (Fig. 10.2B). At photosystem I, accountable for H_2 evolution, H^+ are reduced by conduction band electrons, and reductive mediators are oxidized by holes in valence band. Concurrently, at photosystem II, acting as O_2-evolution photocatalyst, electrons revert the oxidized mediator back to its reduced stage, and O_2 is generated by oxidation of water by the holes. Parenthetically, the water splitting is accomplished. Thus the rigorous bandgap necessities as such in single-component photocatalyst system are tranquiled in *Z*-scheme photocatalyst.

10.3 Nanomaterials for water splitting

In this chapter, we focused on recent advancements in nanosized photocatalyst materials for photochemical H_2 production through water splitting followed by discussion on a case study.

This book belongs to Badji Mokhtar Annaba University Central Library
Copyright Elsevier 2025

This book belongs to Badji Mokhtar Annaba University Central Library

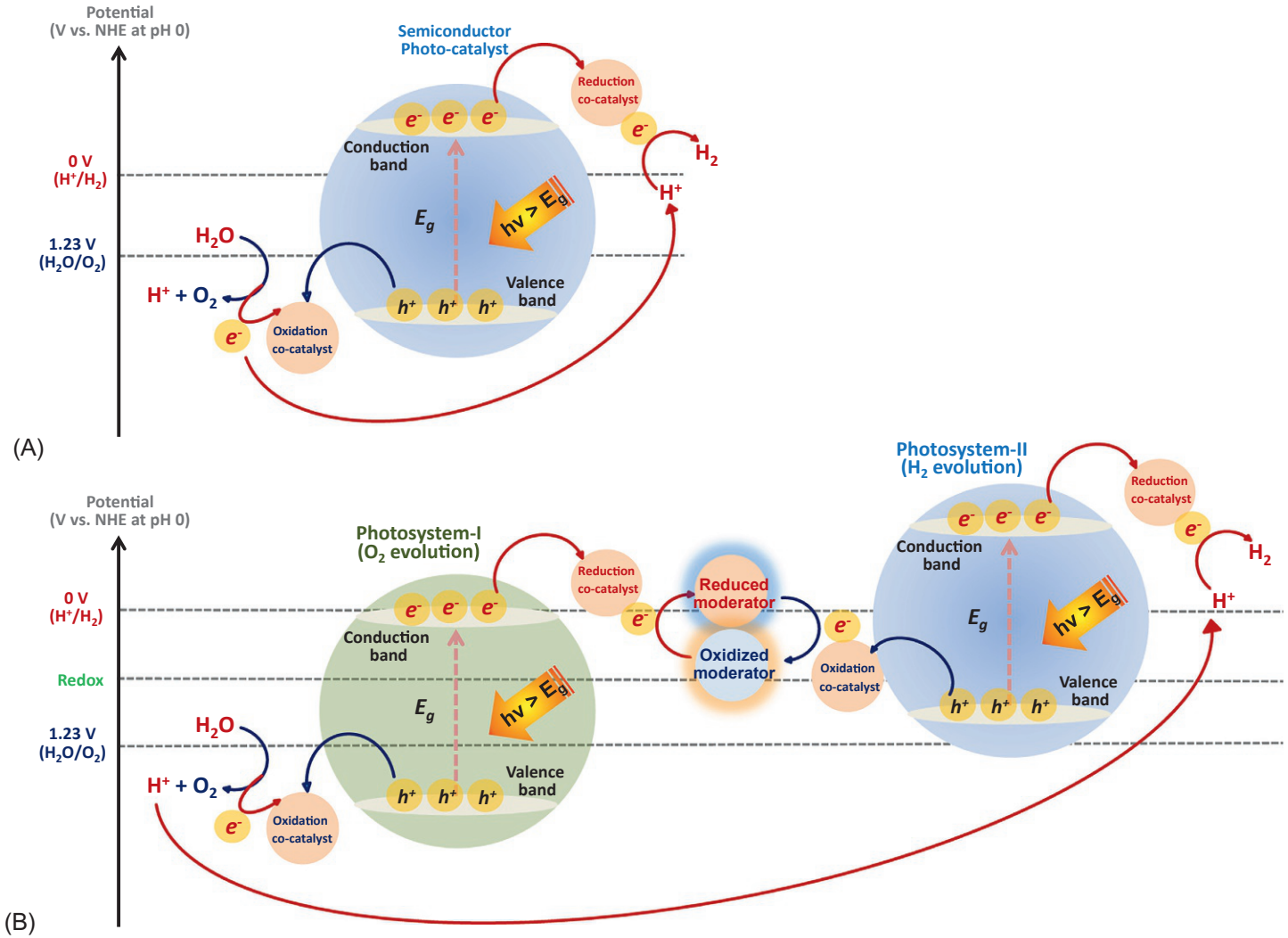

Fig. 10.2
Schematic energy diagrams pertaining to mechanistic aspects of photocatalyst-mediated water splitting through (A) single-step excitation and (B) *Z*-scheme overall splitting.

Copyright Elsevier 2025

10.3.1 Metal oxides for water splitting

10.3.1.1 Titanium oxide (TiO_2)-based nanomaterials for water splitting

The pioneering report by Fujishima and Honda on TiO_2-based photoanodes for water splitting has led to massive interest in further investigations for photocatalyst development [10]. However, even after a period of more than 40 years, the search for appropriate photocatalyst to be engaged for the water splitting is still an open contest. Accordingly, substantial number of photocatalysts has been developed for water splitting by several authors. Among these photocatalysts, TiO_2-based nanomaterials have proved to be the best contention. TiO_2 exists in three different crystal phases, *viz*., anatase, rutile, and brookite. Anatase is a metastable phase with broad bandgap of ~3.2 eV and regarded as favorable for photocatalysis. Rutile phase is thermodynamically stable with bandgap ~3.0 eV; however, it exhibits inferior photoactivities to that of anatase phase. The photoactivities of brookite phase are yet to be explored in detail. Recently, numerous research efforts have been devoted for development of various hierarchical nanomorphs of TiO_2 as high-efficiency photocatalysts for water splitting. These include nanorods, nanobelts, nanofibers, nanowires, etc. [11]. Compared to bulk, the nanomaterials with one-dimensional morphology are expected to provide incessant corridors for electron flow and enhance holes-electrolyte interactions, which ultimately improve energy harvesting efficiency. In this context, Su et al. [12] reported TiO_2 nanowire arrays by hydrothermal method. The nanowire arrays with 7.2 μm length demonstrated the best performance.

Rahman et al. [13] have reported catalyst-mediated pulsed laser deposition (PLD) method for synthesis of different morphologies of 1D TiO_2 nanostructures. Sunlight-driven PEC water-splitting experiments using these nanomaterials revealed maximum activity in visible region, representing 87% overall photocurrent for nanowires.

Simelys Hernandez et al. [14] reported comparative water-splitting activities of four different photocatalyst materials under AM1.5G-simulated sunlight: TiO_2 nanoparticles (NPs) and nanotubes (NTs), ZnO nanowires, and ZnO@TiO_2 core-shell structures with specific thickness of about 1.5 μm. PEC studies on these nanostructures revealed photocurrent saturation in case of both TiO_2 NPs and NTs attaining 0.02 and 0.12 mA/cm^2, respectively, for potential values of about 0.3 and 0.6 V vs. RHE, whereas ZnO nanowires and ZnO@TiO_2 core–shell structures demonstrated linearly rising photocurrent 0.45 and 0.63 mA/cm^2 at 1.7 V vs. RHE, respectively. However, under concentrated light conditions, the TiO_2 NTs displayed a boosted performance compared to the ZnO@TiO_2 core-shells. Under concentrated light, despite the identical thickness, the higher photocurrents observed in the case of TiO_2 NTs, ZnO nanowires, and ZnO@TiO_2 1D nanostructures compared to that of TiO_2 film was attributed to proficient electron inoculation at the semiconducto-electrolyte interface and a faster electron transport from the photoanode to the substrate.

This book belongs to Badji Mokhtar Annaba University Central Library Copyright Elsevier 2025

Introduction of either substitutional or interstitial impurities in the form of metal cations or anions in titania crystal may lead to familiarization of interband energy states associated with reduction of TiO_2 photothreshold energy. Despite several reports on doped titania photocatalyst materials, the inconsistent results on the effects of hosting impurities on the photocatalytic activity of TiO_2 have been obtained. Band structure of titania can be suitably altered by doping. Introduction of metal cation may lead to generation of donor and acceptor energy levels above VB and below CB of TiO_2, respectively. Additionally, crystallinity alterations and defect induction can be realized by cation doping in TiO_2.

Iodine (I), Nitrogen (N), Carbon (C), and fluorine (F) are the common nonmetal and anions employed for enhancing the visible light water splitting of TiO_2 nanomaterials [15–19]. In fact, nonmetal dopants are more beneficial than metal dopants [20].

N was utilized as the most common nonmetal dopant in recent studies for improving the water-splitting activity of TiO_2 [21–24].

Co-doped TiO_2 with metal-metal [25] or metal-nonmetal [26] has also proven to be promising approach for bandgap narrowing, which helps to uphold charge equilibrium by reducing recombination. In a report by Hsin-yu Lin et al. [27], microwave hydrothermal method was employed for synthesis of metal ion (M = Cr, Ni, Cu, Nb) and N co-doped TiO_2 for H_2 production by water splitting in presence of methanol as sacrificial intermediate. Copper along with N co-doped TiO_2 catalyst exhibited 27.4 mmol g^{-1} h^{-1} rate of H_2 evolution under UV light irradiation, which was the highest. The enhanced activity of Cu-$_{10}$-$TiO_{2-x}N_y$ was ascribed to increased visible light absorption owing to Cu-N codoping which resulted impurity positions, and mesoporous framework enabled efficient charge separation.

In an attempt to develop TiO_2-based photocatalyst able to absorb in visible region, several authors have attempted narrowing of TiO_2 bandgap by doping with S; however, the visible light response of S-doped TiO_2 remained uncertain [28–38]. Visible light response of the composite photocatalyst depends upon the nature (anionic S^{2-} or cationic S^{4+} and S^{6+}) and the operational doping type (substitutional/interstitial) of the S-doping species. Sun et al. [39] reported S_2^{2-}-doped TiO_2 material for photocatalytic H_2-production under visible light. The observed H_2 evolution performance of S_2^{2-}-doped TiO_2 was benefitted owing to the newly occupied strong localized electronic states located at 0.9–1.6 eV above the VB of TiO_2.

Although charge separation efficiency and light-harvesting ability of a photocatalyst pushes the rate of water-splitting reactions, the harmonization of both of these parameters in a single component is a challenging task. In this regard, Xu et al. [40] attempted fabrication of TiO_2 nanobelts-TiO_2(B)/anatase hetrojunctions through hydrothermal method. The fabricated hybrid structure played a dual role by means of enhanced light absorption by coarsened surface of nanobelt structure and effective separation of photogenerated charge carriers by TiO_2(B)/anatase heterophase junctions. As a result, enhanced H_2 evolution activity was obtained for

This book belongs to Badji Mokhtar Annaba University Central Library Copyright Elsevier 2025

TiO_2 nanobelts with Pt as cocatalyst. Wang et al. [41] reported a nanoring-nanotube dual TiO_2 anatase construction with an improved charge transfer rate. Nevertheless, achieving command over its surface-prevailing PEC properties remains a dilemma. Wang et al. [42] also demonstrated the prospect for improving the PEC performance by constructing hierarchical rutile TiO_2 nanobranched arrays having photocurrent density of 10.05 mA/cm^2. Liu et al. [43] reported for TiO_2 nanobranch decorated TiO_2 nanofibers as a multiphase composite for PEC water splitting. Anatase nanofiber as a support and rutile nanorod as a branch in a composite photocatalyst provided controlled interfaces of different phases, which provided a stable platform for enhanced charge separation efficiency. As a consequence, PEC water-splitting efficiency was improved. The observed photocurrent density of the composite TiO_2 electrode was 0.95 mA/cm^2, which was almost twofold excess compared to that of pristine TiO_2 nanorod.

In addition to the interfacial engineering, compositing TiO_2 with optically active conjugated polymers for effective light harvesting has also been investigated by some researchers. The coupling of TiO_2 with conjugated polymer proved to be fruitful for widening the light-harvesting province and overwhelming electron-hole recombination concurrently. In such efforts, Murat Rakap et al. [44] have reported polymer-immobilized palladium supported on TiO_2 catalyst for H_2 generation. Maximum H_2 generation rate of ~642 mL H_2 min^{-1} (g Pd)$^{-1}$ and ~4367 mL H_2 min^{-1} (g Pd)$^{-1}$ was measured by the hydrolysis of AB at 25°C and 55 ± 0.5°C, respectively. Yang et al. [45] reported a covalent organic polymer (i.e., COP-64) coupled TiO_2 nanosheet composite photocatalyst for H_2 generation. The COP-64 provided more reaction active sites by increasing the specific surface area and also improved light harvesting in visible light region. Additionally, the proper energy level of COP-64 provided charge transfer channels and favored the electron transfer. The synthesized COP-64-anchored TiO_2 composite demonstrated H_2 production rate of 15.02 mmol h^{-1} g^{-1}, which was 63% more than that of bare TiO_2 nanosheets (9.20 mmol h^{-1} g^{-1}). Zhang et al. [46] reported conjugated polymer (poly-benzothiadiazole flake)/black TiO_2 hybrid photocatalyst for H_2 generation. The BE-black TiO_2 demonstrated 30% enhancement compared to BE-TiO_2 catalyst for H_2 production under visible light ($\lambda > 420$ nm) irradiation. Recently, Yu et al. [47] reported a poly-2,6-diaminopyridine (PDAP) and TiO_2 microspheres based heterostructure as a photoanode for PEC water splitting. The photoanode attained a high applied bias photon-to-current efficiency at low bias demonstrating a photocurrent density of 1.56 mA cm^2 at 1.23 V vs. RHE under AM 1.5 G. The enhanced PEC performance of composite heterostructure was attributed to Type II heterojunction and coexistence of Ti^{3+} and Ti^{4+}.

Single-step synthesis methods for designing herojunctions or hierarchical architectures look as if to be lacking in to meet the need of substantial increase in photoactivities of the materials. In this background, the simultaneous design of heterostructures and hierarchical architectures to maximize the synergistic effects and thereby remarkably enhanced performance proved to be beneficial. Wang et al. [48] reported fabrication of $K_2Ti_6O_{13}/TiO_2$ heterojunction with remarkably improved charge separation efficiency.

This book belongs to Badji Mokhtar Annaba University Central Library Copyright Elsevier 2025

Dubey et al. [49] reported Cu_2O NPs modified TiO_2 NTs through wet chemical treatment for H_2 generation. According to report, crystalline structure of vertically aligned TiO_2 nanotube remains unaltered even after admixing with Cu_2O NPs. However, the H_2 generation rate of the composite was highly dependent on Cu_2O content. The optimum photocurrent density and H_2 generation rate have been found to be 3.4 mA cm^{-2} and 127.5 mmole cm^{-2} h^{-1} under 1.5 AM solar white light irradiance.

An et al. [50] reported two-step hydrothermal method for synthesis of hierarchical $TiO_2@In_2O_3$ heteroarchitecture photoanodes for PEC water splitting. The hierarchical nanorod morphology of TiO_2 in $TiO_2@In_2O_3$ photoelectrodes facilitated the electron transfer from In_2O_3 to the counter electrode through conducting substrate. The close interaction of large heterostructure boundary and facile electron transfer through $TiO_2@In_2O_3$ heterojuction photoelectrodes resulted in enhanced PEC H_2 evolution performance. Lu et al. [51] reported hierarchical CdS/m-TiO_2/G ternary photocatalyst through negative-positive-negative hierarchical electrostatic assembly synthesis for highly active visible light-induced H_2 production from water splitting with high stability.

Orbitals hybrid and bonding energy to atom-stress distortion were studied for investigating the nanojunction effect of ternary photocatalyst. The superior recital of the ternary composite was owing to three factors. First, tri-layer electric structure of m-TiO_2/Cd^{2+}/GO facilitated the dispersion of CdS in core-shell structure, which offered the structural stability and reduced CdS leaching. Second, CdS/m-TiO_2/G-based atomic-scaled heterojunctions facilitated effective transfer of charge carriers resulting in enhanced photoactivity of CdS. Third, Ti(IV) domain mediated quick transfer of photogenerated holes, thrusting the oxidation reaction. The representative structure of CdS/m-TiO_2/G ternary photocatalyst and separation and transfer of photogenerated charge carriers in it is schematically depicted in Fig. 10.3.

10.3.1.2 Zinc oxide (ZnO)-based nanomaterials for water splitting

Both the elements, *viz*., zinc (Zn^{2+}) and oxygen (O^{2-}) constituting ZnO occurs in high abundance in earth's crust [52]. ZnO exhibits three different crystal phases, *viz*., rock salt, zinc blende, and hexagonal wurtzite, among which the latter is considered as the most stable. The piezoelectricity and direct wide bandgap exhibited by ZnO has made its sustainability for variety of applications. However, the paramount demonstration of ZnO-based piezoelectric nanogenerator (PNG) has made enormous interests for its development in PEC and photocatalytic application [53]. Several research reports pertaining to sole utilization of ZnO for photocatalytic water splitting have been attempted; however, the integral wide bandgap along with fast recombination rate associated with it still demands further development. For example, Janet et al. [54] have demonstrated hierarchical ZnO architectures by two different methods, *viz*., wet heterogeneous etching and homogeneous chemical precipitation. Hexagonal ZnO plates with high defect concentration obtained by wet etching demonstrated maximum H_2 generation rate of 35 μmolh^{-1} 0.1 g^{-1}. In another report by Núñez and co-workers [55],

This book belongs to Badji Mokhtar Annaba University Central Library Copyright Elsevier 2025

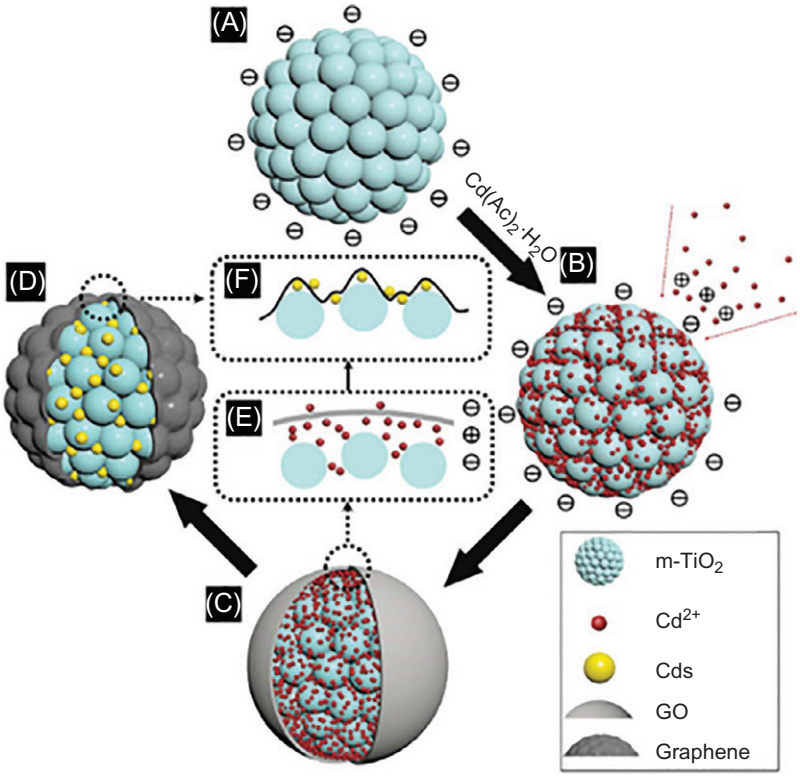

Fig. 10.3

Scheme illustrating the negative-positive-negative hierarchical electrostatic assembly synthesis of CdS/m-TiO_2/G. (A) m-TiO_2 bead with negatively charged surface in DMSO solution. (B) Formation of an electronic-bi-layer after absorption of Cd^{2+} ontoTiO$_2$. (C) Hierarchical m-TiO_2/GO core-shell structure filled Cd^{2+} after adding the graphene oxide nanosheets. (D) Hierarchical CdS/m-TiO_2/G after solvothermal treatment for the formation of CdS and chemical reduction of GO. (E) Ionic interactions proposed during the formation of the hierarchical m-TiO_2/GO filled with Cd^{2+}. (F) Formation and well-dispersion of CdS in the hierarchical CdS/m-TiO_2/G structure. *Reproduced from Y. Lu, X. Cheng, G. Tian, H. Zhao, L. He, J. Hu, S.-M. Wu, Y. Dong, G.-G. Chang, S. Lenaerts, S. Siffert, G. Van Tendeloo, Z.-F. Li, L.-L. Xu, X.-Y. Yang, B.-L. Su, Hierarchical CdS/m-TiO_2/G ternary photocatalyst for highly active visible light-induced hydrogen production from water splitting with high stability, Nano Energy 47 (2018) 8–17, https://doi.org/10.1016/j.nanoen.2018.02.021 with permission from Elsevier.*

hydrothermal fabrication of Ga-modified Pt/ZnO photocatalyst for H_2 production was reported. The authors investigated the formation of surplus $ZnGa_2O_4$ phase with spinel structure owing to higher Ga assimilation, which resulted in detrimental effect on H_2 production. Yet, in another report by Luévano-Hipólito and co-workers [56], facile sonochemical synthesis was attempted for ZnO NP-based photocatalyst for H_2 production. The H_2 production rate was monitored by analyzing the ration of intensity of (002) to (100) planes. The detrimental effect on H_2 evolution performance was attributed to ZnO photocorrosion owing to generous oxygen vacancies resulted by lesser percentage of (002) planes in the crystal structure.

This book belongs to Badji Mokhtar Annaba University Central Library Copyright Elsevier 2025

In an attempt to further increase the photocatalytic H_2 generation performance of ZnO-based materials, use of additional components have been reported by several authors. These include majorly use of TiO_2. For example, Al-Mayman and co-workers [57] reported sol-gel synthesized TiO_2-ZnO photocatalysts for H_2 production. The reported H_2 production rate accounts to be 1048 mmol h^{-1} by TiO_2-10 wt.% ZnO composite, which was too high than that of bare TiO_2 (151 mmol h^{-1}) and TiO_2 P25 (595 mmol h^{-1}) photocatalysts.

Besides TiO_2, Cu_2O, CuO, and SnO_{2-x} have also been used to fabricate ZnO-based heterostructures with enhanced solar light absorbance. Lou and co-workers [58] reported plasmonic Cu NPs-anchored Cu_2O/ZnO heterojunction nanostructure (Cu@Cu_2O/ZnO) for H_2 production. The Cu@Cu_2O/ZnO heterojunction nanocomposite (30wt% Cu@Cu_2O loading) exhibited the highest H_2 evolution rate of 1472.2 μmol h^{-1} g^{-1}. The remarkable uplift of photocatalytic H_2 generation performance was attributed to effective separation of photoexcited charge carriers caused by hierarchical construction of Cu@Cu_2O/ZnO nanostructured heterojunction nanostructure. The mechanism of water-splitting photoactivity of as-synthesized Cu@Cu_2O/ZnO nanocomposite was speculated on the basis of photoluminescence (PL) spectra. According to report, compared to bare ZnO, the PL intensities of Cu@Cu_2O-loaded ZnO composites exhibited decreasing trend and further continues a decreasing drift with increasing Cu@Cu_2O content, indicating the important role of Cu@Cu_2O for facilitating the charge transfer and dropping the charge recombination rate.

Li and co-workers [59] have demonstrated enhanced H_2 generation performance of ZnO/SnO_{2-x} NPs. The enhanced performance with maximum H_2 production rate of 182.6 mmol h^{-1} g^{-1} was ascribed to augmented oxygen vacancies and ZnO coupling. Similarly, Liang and co-workers [60] reported Ta_3N_5ZnO-based direct *Z*-scheme photocatalyst for enhanced H_2 generation by reducing the recombination rate of electrons and holes.

Alternate significant approaches for enhancing the photoactivities of ZnO include its decoration with metal sulfides. Accordingly, CdS, ZnS, and MoS_2 have been widely used by several authors. In this regard, Tso and co-workers [61] have reported CdS-ZnO core-shell nanowires as photocatalyst for H_2 production. The direct bandgap 2.43 eV and ample CB potential (for H^+ to H_2) reduction associated with CdS have led to enormous development as photocatalyst material. However, the rapid recombination of charge carriers and less stability restricted its bare use. ZnO have been used to inhibit photocorrosion of CdS in acid solution. During fabrication, initially, CdS NWs were grown by vapor phase transport and condensation deposition process on a silica substrate. Followed by this, an RF sputter deposition was conducted for deposition of ZnO shell. The TEM image and EDS line scan on as-synthesized CdS-ZnO core-shell nanowire are shown in Fig. 10.4. The figure clearly indicates the dominant distribution of Zn than those of Cd and S, predominantly on the shell area. According to report, the H_2 generation performance of CdS nanowires with 20 nm ZnO shell was 1200 μmol g^{-1} h^{-1}, which was too high compared to bare CdS (35 μmol g^{-1} h^{-1}) within 4 h. The enhanced H_2 generation performance was attributed to ZnO shell, which prevents CdS photocorrosion and

This book belongs to Badji Mokhtar Annaba University Central Library Copyright Elsevier 2025

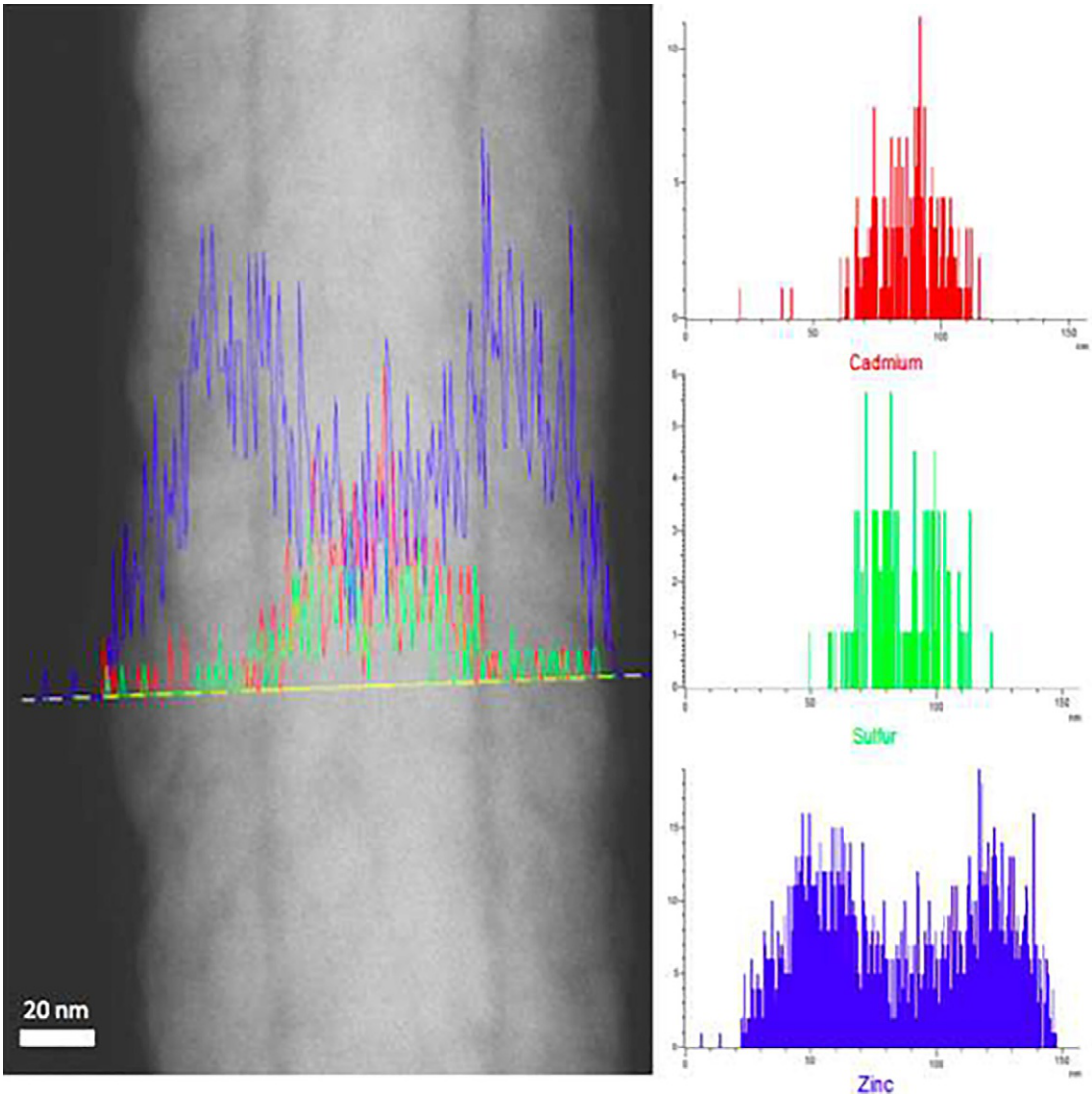

Fig. 10.4
EDS line scan on CdS-ZnO core-shell nanowire. Signals of Cd, S, and Zn are represented by red, green, and blue lines—(light gray, gray, and dark gray in print version), l, respectively. The range of Zn signal obviously extends beyond those of Cd and S signals. *Reproduced from S. Tso, W.-S. Li, B.-H. Wu, L.-J. Chen, Enhanced H_2 production in water splitting with CdS-ZnO core-shell nanowires, Nano Energy 43 (2018) 270–277, https://doi.org/10.1016/j.nanoen.2017.11.048 with permission from Elsevier.*

alleviates the photogenerated charge recombination. The SEM and TEM images of bare CdS and CdS-ZnO core–shell nanowires after 4-h exposure under 300 W Xe lamp irradiance in 0.05 M ascorbic acid are shown in Fig. 10.5. It is noticeable that the surface of bare CdS nanowires appears to be significantly putrefied compared to that of CdS-ZnO core-hell nanowires.

This book belongs to Badji Mokhtar Annaba University Central Library
Copyright Elsevier 2025

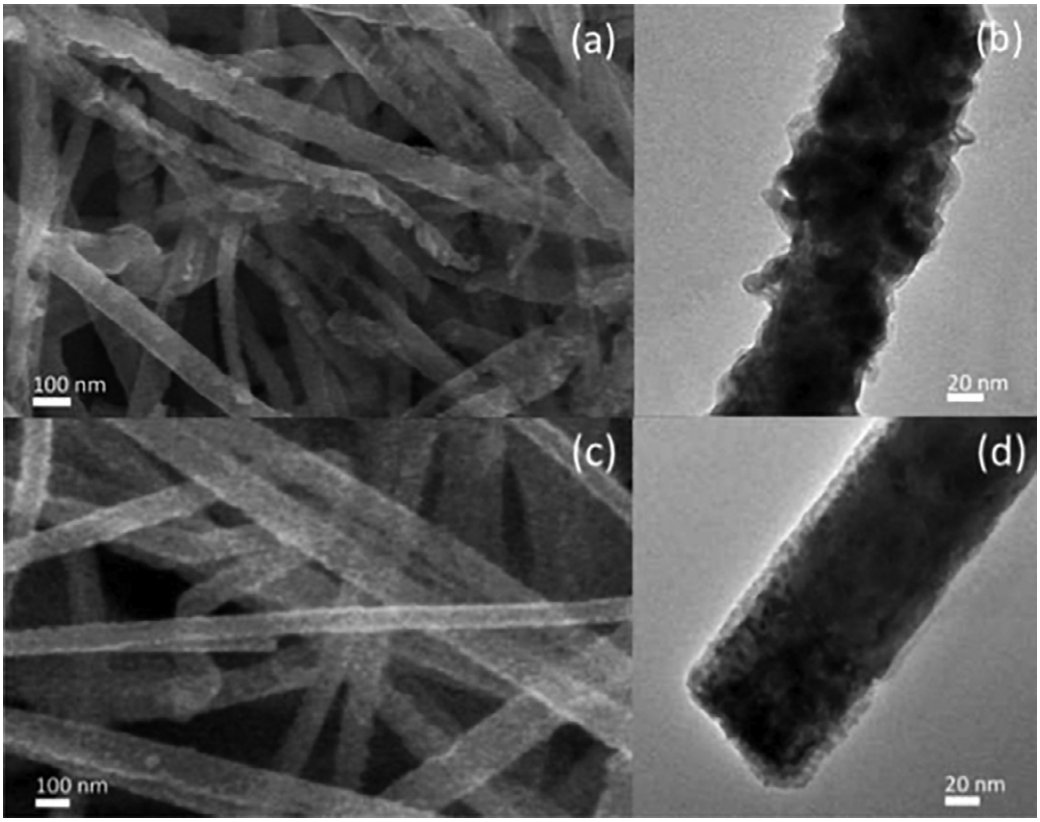

Fig. 10.5
(A) SEM image of CdS nanowires. (B) TEM image of a CdS nanowire with rugged surface after 4-h exposure under 300 W Xe lamp in 0.05 M ascorbic acid. (C) SEM image of CdS-ZnO core-shell nanowires, (D) TEM image of a CdS-ZnO core-shell nanowire after 4-h exposure under 300 W Xe lamp irradiance in 0.05 M ascorbic acid. *Reproduced from S. Tso, W.-S. Li, B.-H. Wu, L.-J. Chen, Enhanced H2 production in water splitting with CdS-ZnO core-shell nanowires, Nano Energy 43 (2018) 270–277, https://doi.org/10.1016/j.nanoen.2017.11.048 with permission from Elsevier.*

In another report by Zhao et al. [62], a simple photodeposition route has been explored for ZnO/CdS photocatalyst for H_2 generation. According to experimental investigations, during ZnO/CdS-mediated H_2 evolution process, ZnS is generated in situ in the presence of $Na_2S + Na_2SO_3$ solution. Consequently, ZnO-ZnS/CdS ternary composite so formed facilitates effective separation and transfer of photogenerated charge carriers, leading to improved photoactivity. Similarly, Wang and co-workers [63] reported higher photoactivity of ZnO-CdS@Cd (1.92 mmol h^{-1}) than that of corresponding ZnO-CdS@Pd (0.38 mmol h^{-1}).

Owing to the fact that ZnO possesses photoinduced holes with strong oxidation efficiency and ZnS holds photogenerated electrons with highly negative reduction potential, numerous efforts have been devoted toward development of ZnO-ZnS dual junction for enhancing photocatalytic

This book belongs to Badji Mokhtar Annaba University Central Library Copyright Elsevier 2025

efficiency. The fabrication of ZnO-ZnS composite is generally followed either by partial oxidation of ZnS [64,65] or by partial suulfidation of ZnO [66,67]. Recently, Bak et al. [64] reported hydrothermal fabrication of ZnS Core-ZnO shell photocatalyst under controlled oxygen atmosphere for H_2 generation. The observed maximum H_2 production rate was (1665 μmol g^{-1} h^{-1}) demonstrated by core-shell sample oxidized at 16.2 kPa oxygen contents. Thermal processing-induced crystal defect states were responsible for enhanced photocatalytic activity.

10.3.1.3 Layered Perovskite-based nanomaterials for water splitting

Perovskites exhibits cubic crystal structure with a formula ABO_3 in which cations are located at sites A and B. Cation at site A is generally larger in ionic radius compared to that of cation at site B. The two cations are linked by means of oxygen through ionic bond. Various crystal geometries of perovskite can be assembled simply by monitoring the lattice sites of cation and anion [68]. Liu et al. [69] have reported a summary of detailed structural characteristics of different perovskites in a review paper.

Various perovskite photocatalyst materials, including titanates [70], tantalates [71,72], niobates [73], and ferrites [74], have been synthesized by variety of preparation methods, including hydrothermal, solvothermal, sol-gel, and chemical vapor deposition (CVD).

Titanate-based perovskites ($MTiO_3$) with bandgap (>3.0 eV) exhibits good photostability and excellent photocorrosion and thus are widely employed for photocatalytic applications after supplementary adaptations. Generally, single/double element doping is adopted for altering the optical properties of photocatalyst to meet the visible light absorption criteria.

In single element, doping A or B cation sites are substituted by heteroatom having similar ionic radii. Replacing cation at site A relocates conduction band toward more negative potential to facilitate the photoactivity, while replacement of cation at site B generates new acceptor levels above valence band [75,76]. For the meantime, new acceptor levels below CB can be created by substituting O-atom in ABO_3 with anionic dopants [77].

For example, Zhang et al. [78] have recently stated ultrasonic assisted sol-gel method for preparation of copper-doped $CaTiO_3$ photocatalysts and reported their photocatalytic water-splitting activities. According to the report, 2 mol% Cu^{2+}-doped $CaTiO_3$ photocatalyst exhibited eight times increased photocatalytic H_2 evolution capacity compared to pure $CaTiO_3$ owing to the transition from the donor levels formed by Cu^{2+} to the conduction band of copper-doped $CaTiO_3$.

Likewise, several authors have also provoked to dope the host perovskite material with two elements simultaneously at either same site (B site) or at two different sites (A, B, or O sites). In this context, Kang and co-workers [79] have reported preparation of Cr- and Ta-doped $SrTiO_3$ by spray-pyrolysis, which demonstrated improved photocatalytic performance compared to

This book belongs to Badji Mokhtar Annaba University Central Library Copyright Elsevier 2025

single element-doped composites. In another report by Yu et al. [80], Cr- and B-doped $SrTiO_3$ photocatalysts demonstrated improved performance than that of Cr-doped $SrTiO_3$.

Besides single/double-element doping, the use of cocatalysts along with perovskite materials for uplifting the photocatalytic performance has also been implemented by several authors. In this regard, Zeng et al. [81] reported improved photocatalytic H_2 production performance of cocatalyst aided rod-like $NiTiO_3$-coupled g-C_3N_4 composite photocatalyst having strong visible light absorption than $NiTiO_3$-coupled g-C_3N_4 having bulk flocculent morphology. Furthermore, a recent research published by Yin et al. [82] reveals that H_2 evolution performance of $SrTiO_3$ co-catalyzed by CdS was considerably higher to those of single counterparts, *viz*., CdS and $SrTiO_3$.

Along with different modification strategies, including doping, employment of cocatalysts, etc., synthesis routes have also been found to affect the different characteristics and thereby H_2 evolution performance of perovskite. For example, Wang et al. [83] studied the comparative H_2 production efficiencies of electrospun $MgTiO_3$ nanofiber and NP synthesized by sol-gel method. The eightfold excess H_2 evolution performance of nanofibers over NPs was attributed to higher surface area of nanofibers.

10.3.2 Metal sulfides for water splitting

Metal sulfide-based nanomaterials with facile tunable properties have attracted scientific research interest for renewable energy applications. Metal sulfides are semiconducting compounds containing sulfur anion bonded with a metal cation, which may be in mono-, bi-, or multiform. The wide range of available metal sulfides provides potential materials with novel functional properties for diverse applications. The following section describes an overview of different metal sulfide-based nanomaterials that have been recently developed for photocatalytic H_2 production.

10.3.2.1 Zinc sulfide (ZnS) and cadmium sulfide (CdS)-based nanomaterials for water splitting

Depending upon the precursor source and synthetic route, ZnS and CdS can exhibit two different crystal forms, *viz*., cubic zinc blende and hexagonal wurtzite, which differ slightly in their crystal symmetries and bandgap values [84]. In particular, the bandgaps of zinc-blende (2.3 eV) and wurtzite (2.4 eV) crystal forms of CdS are smaller compared to those of zinc-blende (3.72 eV) and wurtzite (3.77 eV) of ZnS. As far as photocatalytic activities of these crystal forms are concerned, the wurtzite form exhibit superior H_2 evolution capacity compared to that of zinc-blende form owing to abundant amount of exposed (0001) facets [85]. Although the CdS constituent having comparatively smaller bandgap is expected to exhibit good photoactivity, intrinsically, it has greater chances of charge recombination. On the other hand, the ZnS constituent having large bandgap has lesser possibilities of visible light absorption.

This book belongs to Badji Mokhtar Annaba University Central Library Copyright Elsevier 2025

Therefore majority of the research reports are dedicated to modified ZnS or CdS composite materials for improved light-harvesting capacity.

Generally, doping or formation of new heterostructured composite is employed for designing photocatalyst with good photoactivities. Several dopants, including Ni^{2+}, Bi^{3+}, In, and Cd, have been employed for shifting the absorption edge of ZnS toward visible region [86–89]. Recently, Tie and co-workers [90] reported single-step synthesized N-doped ZnS microspheres for organic pollutant removal and H_2 production. The superior performance of ZnS was attributed to extended visible light absorption efficiencies favored owing to N doping.

Lee and co-worker's [91] reported sonochemical synthesis of hollow copper-doped ZnS nanostructures for water splitting. As per the experimental observations, copper could form new energy levels between the VB and the CB of ZnS. According to Ming Dong and co-workers' report, the bandgap of Cu-doped ZnS can be effectively narrowed by hybridization of substitutional Cu 3d and S 3p orbitals. Additionally, the separation and migration of the photogenerated charge carriers can be benefited by effective mass ratio of photogenerated holes and electrons (mh*/me*) in CuZn-ZnS [92].

Furthermore, Hong and co-workers [93] demonstrated a chronological method for fabricating three-component (ZnS, CuS, and CdS) photocatalyst for solar light-driven water splitting. The ZnS particles, as a base material prepared by colloidal precipitation method, were successively modified by adding CuS (cation exchange reaction) and CdS (ionic reaction) precursors. The superior photocatalytic activity was attributed to improved charge flow and light absorption facilitated because of heterostructured ZnS-CuS–CdS photocatalyst. Numerous other heterostructures, *viz*., ZnS/g-C_3N_4 [94], $SrTiO_3$-T/CdZnS [95], *Z*-Scheme Pt/ZnS-ZnO [96], ZnO/ZnS@$Cu(OH)_2$ [97], and ZnO-ZnS/graphene have been reported for photocatalytic H_2 production [98].

In case of CdS, Jian-Wen Shi and co-workers studied Se-doped CdS quantum dots with tunable trap levels for excellent H_2 evolution performance [99]. Se-doping elevated Fermi level position of CdS, leading to the capture of electrons. $CdS_{0.9}Se_{0.1}$ exhibited the best photocatalytic H_2 evolution rate of 29.12 mmol h^{-1} g^{-1}. In another report by Hengming Huang and co-workers, phosphorus-doped CdS (CdS-P) homojunction nanostructures for efficient H_2 evolution have been reported [100]. The elevated VBM of P-doped CdS territory owing to orbital hybridization of p 2p and S 2p and the oriented built-in electric field of CdS-P facilitated the efficient extraction of carriers from inside to surface of the photocatalyst.

Besides these, various other CdS-based photosystems, *viz*., $NiCo_2S_4$/CdS [101], CdSexTe1-x@CdS [102], NiO@Ni-ZnO/reduced graphene oxide/CdS [103], MoS_2/CdS clusters@rGO [104], NiSe/MnO_2-CdS [105], conjugated polymer/CdS *Z*-scheme hybrid [106], and1D/2D CdS/MoS_2 (CM) heterojunctions [107], were also reported for H_2 production.

This book belongs to Badji Mokhtar Annaba University Central Library Copyright Elsevier 2025

10.3.2.2 Molybdenum sulfide (MoS_2) and Tungsten sulfide (WS_2)-based nanomaterials for water splitting

Transition metal dichalcogenides (TMDCs) with indirect bandgap (1.3–1.8 eV), specifically MoS_2 and WS_2 have widespread use as a photocatalysts for H_2 production. Generally, TMDCs exhibit three different structural forms, *viz*., 1T (trigonal), 2H (hexagonal), and 3R (rhombohedral). As far as photocatalytic efficiencies of these structural forms are concerned, trigonal and hexagonal forms are more beneficial. Additionally, TMDCs exhibit 2D graphitelike structure that leads to strong anisotropy in electrical, thermal, and chemical properties [108]. These unique structural characteristics and tunable bandgap of TMDCs offer themselves as a potential candidate as cocatalyst to replace noble metals [109,110].

Zhongqin Lian and co-workers have recently reported hydrothermal/solvothermally synthesized CdS@1T-MoS_2 core-shell nanostructured photocatalysts for H_2 generation [111]. The study revealed that the close interfacial contact between CdS core and 1T-MoS_2 shell facilitated high charge transfer ability and abundant active sites of 1T-MoS_2, which resulted in improved photoactivity. Lin Yang et al. reported Au NPs@MoS_2 core-shell photocatalysts for water splitting [112]. The effect of MoS_2 coverage on the water-splitting efficiency of Au NPs@MoS_2 core-shell hybrid structures has been systematically studied. The experimental results reveal that the composite with moderate coverage exhibits the best water-splitting efficiency. Furthermore, Faze Wang and co-workers reported ammonium intercalated MoS_2/Ni_3S_2 core-shell nanofibers for water splitting operable over wide range of alkaline media [113]. The reasons of improved photocatalytic efficiency were attributed to the hierarchical nanostructures, which provided abundant active sites for H_2 evolution. Additionally, as evidenced by DFT calculations, intercalation of ammonium ions facilitated the chemisorption of protons to MoS_2. Table 10.1 summarizes H_2 generation properties of several metal sulfide photocatalysts.

10.3.3 Metal organic frameworks for water splitting

Exclusive semiconductor characteristics with tunable morphologies of MOF-based photocatalysts were first revealed for photocatalytic water reduction by Yusuke Kataoka et al. in 2009 [132]. Consequently, Cludia Gomes Silva et al. reported Zr-based two water-resistant MOF photocatalysts, *viz*., UiO-66 and UiO-66(NH_2), exhibiting photocatalytic activity for H_2 generation in methanol or water/methanol mixture [133].

Hereafter, a rapid development in MOFs-based photocatalysts for H_2 generation was perceived, which can be evidenced by several review articles in this area [134–137]. MOFs-based nanomaterials for water splitting can be generally classified on the basis of coordinating metal. Although noble metals exhibit good catalytic activity, there are very few reports on noble metal-based MOFs for H_2 generation because of high production cost. However, the first

This book belongs to Badji Mokhtar Annaba University Central Library Copyright Elsevier 2025

Table 10.1: Summary of different metal sulfide-based photocatalysts for H_2 production.

Sr. no.	Photocatalyst nanomaterial	Synthesis method	Sacrificial agent employed	Activity (μmol h^{-1} g^{-1})	References
01	Heterostructured CdS/ZnO	Sequential precipitation method	Sodium sulfide, sodium sulfite	1805	[114]
02	GO-CdS@TaON hybrid composites	Hydrothermal method	Sodium sulfide, sodium sulfite	633	[115]
03	Core-shell g-C3N4/CdS	Solvothermal method, followed by chemisorption	Sodium sulfide, sodium sulfite	4200	[116]
04	MoS_2-graphene/CdS NP/nanorods	Hydrothermal method	Lactic acid	2320	[117]
05	ZnS:Ag_2S porous nanosheets	Thermal decomposition	Sodium sulfide, sodium sulfite	104	[118]
06	CdSe/CdS-Au-graphene nanocrystals	SILAR method	Sodium sulfide, sodium sulfite	3113	[119]
07	Ni-doped Stainless steel@ZnS composite	Solvothermal	Sodium sulfide, sodium sulfite	14,600	[120]
08	NiS/ZnxCd$_{1-x}$S/RGO ternary nanocomposite	Coprecipitation, followed by hydrothermal method	Sodium sulfide, sodium sulfite	205	[121]
09	CuS/$Cd_{0.3}Zn_{0.7}S$ NPs	Two-step method	Sodium sulfide, sodium sulfite	3520	[122]
10	CuS/ZnS hexagonal plates	Solvothermal method	Sodium sulfide, sodium sulfite	1233	[123]
11	Core-shell $Ni(OH)_2$-CdS/g-C_3N	Mixed	Sodium sulfide, sodium sulfite	115.2	[124]
12	Ni_3N/CdS nanorods	In situ synthesis method	Sodium sulfide, sodium sulfite	~60	[125]
13	Ag_2S-ZnO@ZnS core-shell nanorods	Hydrothermal method	Sodium sulfide, sodium sulfite	6406	[126]
14	Ag_2S/ZnS/C nanofiber	Solid state cation exchange route	Sodium sulfide, sodium sulfite	224	[127]
15	CuS/g-C_3N_4 nanocomposites	In situ synthesis method	Triethanolamine	17	[128]
16	Bi_2S_3/ZnS hierarchical structures	Solvothermal method	Sodium sulfide, sodium sulfite	176	[129]
17	N-doped graphene/ZnS nanorods	Thermal annealing	Sodium sulfide, sodium sulfite	1755	[130]
18	CuS-ZnS/CNTF nanocomposites	Hydrothermal method	Sodium sulphide, sodium sulfite	1213	[131]
20	Graphene/ZnO-ZnS nanocomposite	Sequential heating method	Glycerol	1070	[98]

This book belongs to Badji Mokhtar Annaba University Central Library
Copyright Elsevier 2025

Ru-based MOF photocatalyst $[Ru_2(p\text{-}BDC)_2]_n$ was reported by Kataoka et al. [132]. During photocatalysis experiment, $Ru(bpy)_3^{2+}$ MV^{2+} (methyl viologen) and EDTA-2Na (ethylenediaminetetracetic acid were employed as photosensitizer, electron relay, and sacrificial agent, respectively. The photocatalyst demonstrated good photocatalytic activity with TON of 8.16. Consequently, a series of similar photocatalysts such as $[Rh_2(p\text{-}BDC)_2]_n$ [138], $[Ru_2(p\text{-}BDC)_2X]_n$ (X = Cl, Br and BF_4) [139], and $[Ru_2(MTCPP)BF_4]$ (M = H_2, Zn; TCPP = Tetrakis(4-carboxyphenyl)porphyrin) [140] were reported.

10.3.4 Carbon-based nanomaterials for water splitting

10.3.4.1 Graphene-based nanomaterials for water splitting

Graphene is a 2-D honeycomb-like structure tightly bounded by sp^2-hybridized C atoms [141]. Owing to different fascinating characteristics, *viz*., large surface area, abundant adsorption sites, and cost-effective nature, it has attracted foremost research attention, especially in photocatalysis. Moreover, it exhibits good interaction ability toward transition metals. Surface characteristics of graphene can be fine-tuned by facile chemical modifications, which can improve the catalytic performance.

Among the several synthetic methodologies such as CVD [142], graphite exfoliation [143], and substrate supported epitaxial growth [144], modified Hummer's method [145] is most popular and widely used for synthesis of graphene. In this method, powdered graphite is oxidized by strong chemical oxidants and then exfoliated. The single layer graphene sheets are then obtained by reduction of exfoliated graphene.

Initial studies highlighting the role of graphene in photocatalysis speculated that it assists as a cocatalyst and boosts the photoactivity of a semiconductor material. However, recently, it has been demonstrated that some graphene-based materials exhibit inherent photoactivity owing to defects generated during synthesis [146]. The presence of heteroatoms, *viz*., oxygen (O), N, boron (B), and phosphorus (P), substituting C atoms and holes endangered in lattice are the mainly recognized defects during graphene synthesis [147]. Ideally, presence of these defects in graphene induces the semiconductor behavior. Furthermore, it has been demonstrated that miniature amounts of metal/metal oxide NPs in vicinity of graphene sheets develop a heterojunction that can advance its photocatalytic activity [148]. Several studies demonstrate that modification of graphene with semiconductor materials improves the photocatalytic activity of graphene owing to efficient charge transfer. In this context, Jia and co-workers [149] have reported CdS NPs-anchored N-doped graphene composite photocatalyst for water splitting. According to the report, the composite photocatalyst also demonstrated the effective control to CdS photocorrosion. In another report by Zou and co-workers [150], a significant enhancement in the photocatalytic activity of N-doped graphene sheets has been reported by coupling it with g-C_3N_4.

This book belongs to Badji Mokhtar Annaba University Central Library Copyright Elsevier 2025

10.3.4.2 Graphitic carbon nitride (g-C_3N_4)-based nanomaterials for water splitting

Unlike graphene, the exceptional electron transfer ability and favorable band-edge positions (−1.1 eV CB and +1.6 eV VB vs. NHE), graphitic carbon nitride (g-C_3N_4) has also been employed and reported for photocatalytic H_2 production by several authors [148]. The extent of defects in 2-dimensional π-conjugated layered polymeric structure of g-C_3N_4 determines the electrical conductivity and photocatalytic activity [151]. Moreover, the ample specific surface area associated with exfoliated monolayered g-C3N4 favors the photocatalytic reactions. The first report on photocatalytic H_2 production by Pt NPs-anchored g-C_3N_4 was reported by Wang and co-workers in 2009 [152]. After this, several reports were published with improved photocatalytic activity of g-C_3N_4 by different modifications.

Among the various methods employed for improving the photoactivity of g-C3N4, external doping is considered as the most popular one. In this context, Antil and co-workers [153] reported facile thermal polymerization for synthesis of N-abundant g-C3N4 with good photocatalytic H_2 evolution ability. The improved photoactivity was attributed to facile electron transfer ability and plentiful existence of –NHx moieties. A thermal-assisted co-doping of sulfur (S), P, and oxygen (O) into exfoliated g-C_3N_4 nanosheets for ideal water splitting was reported by Liu and co-workers [154]. Along with doping, fabricating composite heterostructures with metal oxide/sulfide, including $Ni(OH)_2$ [155], CoOx [156], TiO_2 [157,158], CdS [159], and ZnS [160], were also reported to enhance charge separation and light absorption characteristics.

10.4 Sn_3O_4-ZnO nanoflowers for hydrogen generation under visible light—Case study

In recent decades, a lot of research has been carried out by the researchers on development of photocatalysts that can proficiently transform solar energy into H_2 [161,162]. The literature contains several reports describing nanomaterials used in generation of H_2, including binary composite structure based on ZnO, TiO_2, and g-C_3N_4 [163–165]. The efficiency of these binary composite, however, is still limited by the more recombination of photogenerated e^-/h+. It was observed that the noble metals accumulated on the semiconductor photocatalyst surface as cocatalysts could limit the recombination of charge carriers, thus improving the efficiency of the evolution of H_2. But considering the fact that noble metals are uncommon and high-priced, they are not likely for use in practical applications. The demand for energy continues with increasing population and economic growth all over the world. Nowadays, photocatalysis is one of the emerging technology for production H_2 from water to meet increasing global energy crisis. In literature, many researcher reports the efficient photocatalyst, including NiO/TiO_2 [166], $CdMoO_4$/g-C_3N_4 [167], Bi_2S/$BiVO_4$ [168], Pr_2NiO_4/SnO_2 [169], etc. These reports have enlightened the scope to study such materials in view of their photocatalytic ability.

This book belongs to Badji Mokhtar Annaba University Central Library Copyright Elsevier 2025

However, preparing an efficient photocatalyst for the evolution of H_2 from water under solar light is still desirable. In this context, very limited studies have been reported on Sn_3O_4-based nanomaterials as a photocatalyst. Herein, we are reporting simple hydrothermal method for synthesis of flower-like Sn_3O_4-ZnO nanostructures. The synthesized nanostructures were characterized by various physicochemical characterization techniques. Furthermore, the photocatalytic H_2 production through water splitting was explored at room temperature.

10.4.1 Preparation, characterization, and photoactivity of Sn_3O_4-ZnO nanoflowers

Sn_3O_4-ZnO nanostructures were synthesized by facile hydrothermal method using zinc nitrate ($Zn(NO_3)_2 \cdot 6H_2O$), stannous chloride ($SnCl_2 \cdot 2H_2O$) as a substrate, and oxalic acid as capping agent. Zinc nitrate ($Zn(NO_3)_2 \cdot 6H_2O$), oxalic acid, and sodium hydroxide were purchased from Merck. Stannous chloride ($SnCl_2 \cdot 2H_2O$) was purchased from Sigma Aldrich. In a typical synthesis, zinc nitrate (0.034 M) and oxalic acid (0.023 M) were admixed using a magnetic stirrer. Then to this solution, stannous chloride (0.004 M) was added. The above mixture was constantly stirred for another 10–15 min. The pH of the solution was then adjusted to 11 by slowly adding aq. NaOH solution (0.2 M). After complete addition, the mixture was poured into a teflon-lined autoclave reactor and hydrothermally treated at 180°C for 20 h. After treatment, the autoclave was cooled down naturally to room temperature. The obtained precipitate so formed was centrifuged and washed several times with deionized water and ethanol and dried at 50°C in oven for 12 h. Finally, these dried Sn_3O_4-ZnO nanostructures were then subjected to various physicochemical characterizations prior to test for H_2 generation.

The structural analysis and phase purity of Sn_3O_4-ZnO nanostructures was examined by Raman spectra (model Jobin Yvon T64000). The crystalline structure and impurity investigation of as-synthesized nanostructures was further confirmed by X-ray diffraction (XRD) analysis (model Rigaku Miniflex X-ray diffractometer) with Cu Kα irradiation at $\lambda = 1.5406$ Å. UV-visible absorption spectra of aqueous suspension were recorded on a JASCOV-570 spectrophotometer. The surface morphology of prepared samples was investigated by Field Emission Scanning Electron Microscope using JEOL-JSM 6700F.

The as-synthesized photocatalysts were tested for H_2 evaluation from water splitting. Typical experiments were performed in 250 mL round-bottom flask containing 100 mL of double distilled water and 25 mL of methanol as sacrificial reagent. The dissolved oxygen was removed from reaction mixture by purging argon. During experiments, 100 mg of catalyst was added to this solution. The photocatalytic H_2 evolution was studied under solar light irradiation. The reaction progress was monitored by gauging evolved gas with the help of eudiometer. The amount of gas evolved as a function of time was noted, and data were used for further calculations. The quantification of H_2 gas evolved was analyzed by using gas chromatography operated using a 5 Å capillary column and a thermal conductivity detector. (Model Shimadzu GC-2014, Porapak-Q packed column, TCD, N_2-UHP carrier).

This book belongs to Badji Mokhtar Annaba University Central Library Copyright Elsevier 2025

10.4.2 Results and discussion

The phase purity and crystallinity of the as-synthesized Sn_3O_4-ZnO nanostructures were studied by XRD. The diffractogram is as shown in Fig. 10.6. The X-ray diffractogram of Sn_3O_4-ZnO nanostructure shows that the material is composed of both hexagonal wurtzite phase of ZnO and triclinic structure of the Sn_3O_4. From the figure, the diffraction peaks appearing at 31.1, 34.2, 35.96, 47.4, 56.24, 61.17, 65.3, 66.25, and 68.2 (in degrees) correspond to the (100, 002, 101, 102, 110, 103, 200, 112, 201) planes of ZnO. Well-crystallized diffraction peaks are in agreement with the JCPDS card No. 89-0510. Additionally, the reflecting planes (101, 111, 122), (130, 132) correspond to the triclinic phase Sn_3O_4 (JCPDS card #16-0737) [170]. From the figure, it can be observed that the XRD diffractogram exhibits mixed phase of ZnO and Sn_3O_4, indicating the formation of Sn_3O_4-ZnO nanostructures. No residual impurity phases were observed in XRD, which clearly indicates good crystallinity of as-synthesized Sn_3O_4-ZnO nanostructure.

Furthermore, the crystalline composition and impurity investigation of Sn_3O_4-ZnO nanostructure was performed using Raman spectroscopy, and the results are shown in Fig. 10.7. The characteristics band appearing at 331, 442, and 702 cm^{-1} can be assigned to hexagonal wurtzite phase of ZnO [171]. The bands around 143, 174, and 249 cm^{-1} can be assigned to characteristic phonon modes of triclinic phase of Sn_3O_4 [172]. In the case of ZnO, the most intense band appearing at 442 cm^{-1} is characteristic of E2 mode of hexagonal wurtzite structure of ZnO. In the case of Sn_3O_4, the band appearing at 249 cm^{-1} may be because of oxidation of the sample and is in well accordance with the previous reports [173]. The characteristic band of Sn_3O_4 and ZnO exists simultaneously in Raman spectrum of Sn_3O_4-ZnO. These findings indicate that the Sn_3O_4-ZnO nanostructure has been formed, and no impurity bands other than

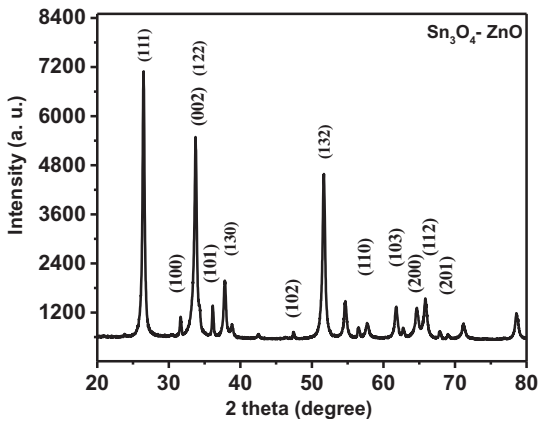

Fig. 10.6
XRD spectrum of as-synthesized Sn_3O_4-ZnO nanostructure.

This book belongs to Badji Mokhtar Annaba University Central Library
Copyright Elsevier 2025

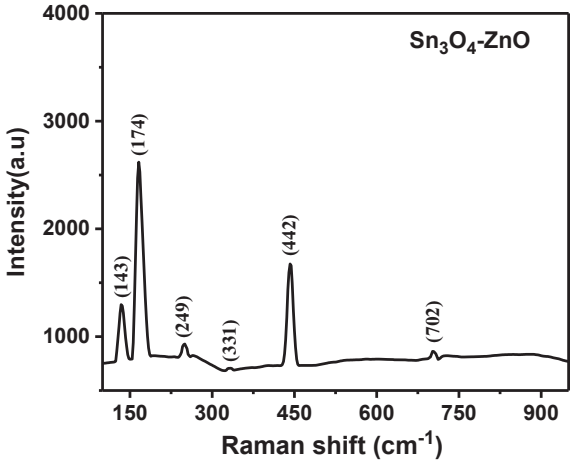

Fig. 10.7
Raman spectrum of as-synthesized Sn_3O_4-ZnO nanostructure.

ZnO and Sn_3O_4 were observed in the recorded spectra, which clearly indicate good crystallinity of Sn_3O_4-ZnO nanostructure.

The surface morphology of the as-synthesized Sn_3O_4-ZnO nanostructure was analyzed by the FESEM, and the results are shown in Fig. 10.8. The lower magnification FESEM image (Fig. 10.8A) indicates that the obtained Sn_3O_4-ZnO is composed of large quantity of well-dispersed flower-like structures. The diameter of the flower ranges from 500 nm to 3 μm, and these nanostructures have been uniformly grown. The higher magnification image presenting closer observation of Sn_3O_4-ZnO nanostructure is shown in Fig. 10.8B and C. From the figure, it can be seen that these flower-like nanostructures are formed by the assembly of numerous irregular nanosheets. These nanosheets have thickness ~5–30 nm and are grown vertically (Fig. 10.8D). For the synthesis of flower-like structure capping agent, oxalic acid played an important role in the growth of nanostructures.

The energy dispersive X-ray (EDX) spectroscopy elemental mapping images of Sn_3O_4-ZnO nanocomposite are shown in Fig. 10.9. Fig. 10.9A shows red, green, and yellow colors representing the distribution of zinc, oxygen, and tin elements, respectively, in a composite. The EDX spectra further demonstrated that Sn_3O_4-ZnO contained Zn, Sn, and O elements, and no other impurities were observed, which is shown in Fig. 10.9. Therefore based on the FESEM and EDX analyses, it could be concluded that a fascinating structure is formed in the Sn_3O_4-ZnO.

Fig. 10.10 shows the UV-visible diffuse reflectance spectra (UVDRS) of Sn_3O_4-ZnO nanostructures. The figure reveals that the intense absorption onset of Sn_3O_4 and ZnO observed at 385 and 465 nm, respectively, which clearly shows that as-synthesized Sn_3O_4-ZnO

This book belongs to Badji Mokhtar Annaba University Central Library Copyright Elsevier 2025

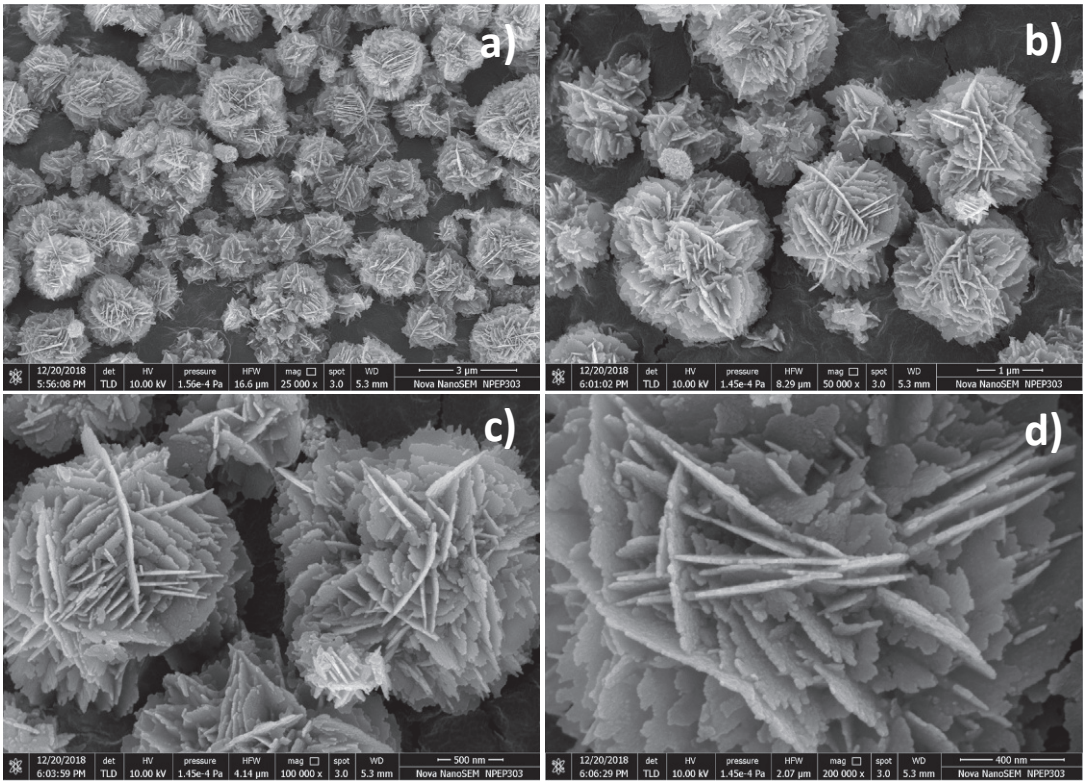

Fig. 10.8
FESEM images of as-synthesized Sn_3O_4-ZnO nanoflowers at different magnifications.

nanostructures can carry out the photocatalytic H_2 production reaction by absorbing UV and visible light, respectively. These results can be attributed to presence of both ZnO and Sn_3O_4 in the nanostructure [174,175]. The corresponding Tauc's plot of Sn_3O_4-ZnO nanostructures was plotted for clarity in bandgap (inset of Fig. 10.10). The estimated bandgap energy of Sn_3O_4-ZnO was found to be 2.59 eV. From the energy gap, it can be seen that the Sn_3O_4-ZnO absorb extremely wide range of light compared to Sn_3O_4 and ZnO.

Considering good spectral response of Sn_3O_4-ZnO nanostructures, the photocatalytic activity of as-synthesized nanostructures was investigated for the production of H_2 via water splitting. Additionally, the water-splitting activity was also compared to ZnO and Sn_3O_4.

Fig. 10.11 shows the time-dependent plot of amount of H_2 generated with respect to time under sunlight irradiation in presence of Sn_3O_4-ZnO catalyst. From the figure, it can be observed that the amount of H_2 generated is increasing with illumination of time. The hydrothermally synthesized Sn_3O_4-ZnO nanostructures showed utmost H_2 generation, that is, 101.2 μmol/0.1 g/h, which was considerably higher when compared to ZnO and Sn_3O_4. The rate of H_2

This book belongs to Badji Mokhtar Annaba University Central Library
Copyright Elsevier 2025

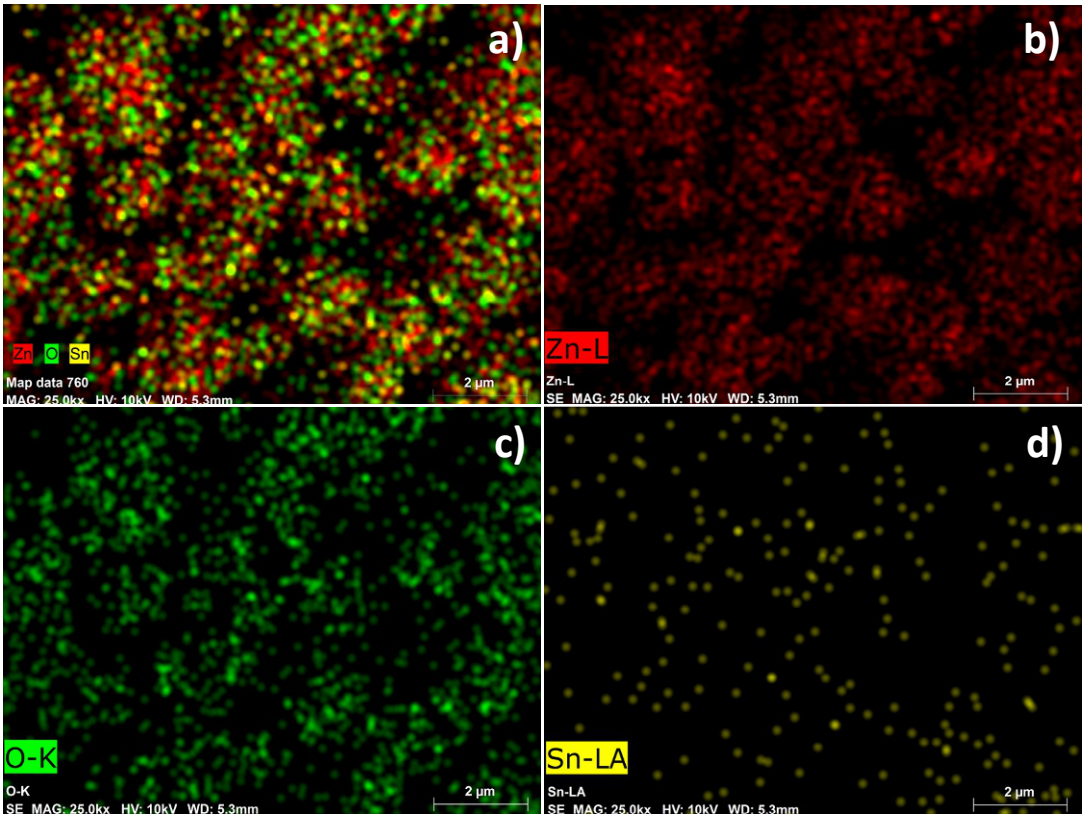

Fig. 10.9
The energy dispersive X-ray spectroscopy (EDX) elemental mapping images of Sn_3O_4-ZnO nanoflowers.

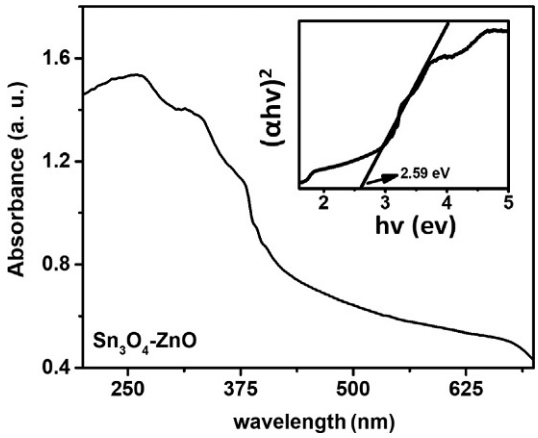

Fig. 10.10
UV-visible diffused reflectance spectra of as-synthesized Sn_3O_4-ZnO nanoflowers. Inset shows the corresponding Tauc's plot.

This book belongs to Badji Mokhtar Annaba University Central Library
Copyright Elsevier 2025

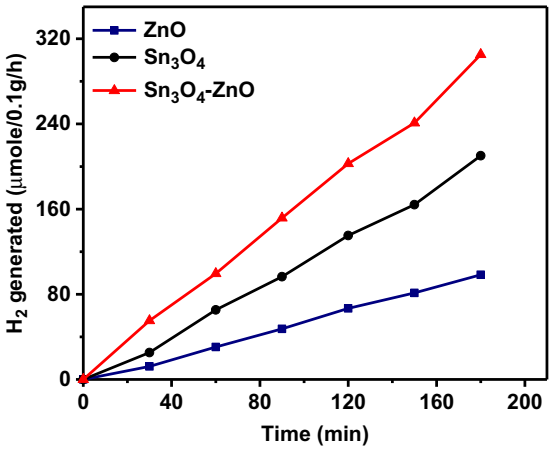

Fig. 10.11
Time-dependent plot of amount of hydrogen generated with respect to time under sunlight irradiation in the presence of Sn_3O_4-ZnO catalyst.

generation for ZnO and Sn_3O_4 were observed to be 32.64 μmol/0.1 g/h and 72.48 μmol/0.1g/h, respectively. These results show that the Sn_3O_4-ZnO could split water under sunlight irradiation. Overall, the Sn_3O_4-ZnO nanostructure shows superior photocatalytic activity owing to its morphology, band structure, and crystallinity.

10.5 Conclusions

This account summarizes the different nanomaterials, including metal oxides, sulfides, metal organic frameworks (MOFs), and C-based materials for water splitting and H_2 generation. Starting from the mechanistic aspects of photocatalytic water splitting, photocatalytic recitals of different nanomaterials have been demonstrated. Among various metal oxide photocatalysts, TiO_2-based nanomaterials have proved to be the best contention. Yet the substantial need for increasing photoactivities of TiO_2-based materials has led to research efforts for designing and development of hierarchical heterostructured architectures. Among the most widely studied metal sulfide nanomaterials, majority of the research reports are dedicated to modified ZnS or CdS composite materials for improved light-harvesting capacity. Besides, metal oxides and metal sulfide-based nanomaterials, exclusive semiconductor characteristics, and tunable morphologies of MOF-based photocatalysts have also been practiced for H_2 generation through water splitting. The unique structure facilitating the electron transfer and lattice-induced defects offers wide scope for employability of C-based materials, including graphene and graphitic C nitrides. Furthermore, a case study on facile hydrothermal synthesis of Sn_3O_4-ZnO flower-like nanostructures for water splitting has been described in detail. The flower-like Sn_3O_4-ZnO nanostructures possesses superior photocatalytic performance for generation of H_2 under sunlight irradiation. The excellent photocatalytic activity of the flower-like Sn_3O_4-ZnO

This book belongs to Badji Mokhtar Annaba University Central Library Copyright Elsevier 2025

was ascribed to its photoabsorption ability owing to the narrowing band structure, flower-like morphology, and good crystallinity. In conclusion, the amalgamation of two or three components (metal oxide/metal sulfide/MOFs grafted with C-based nanomaterials) jointly with finely tuned crystal facets possibly will give rise to a new-fangled photocatalyst with excellent photocatalytic activity for water splitting.

References

[1] M.G. Walter, E.L. Warren, J.R. McKone, S.W. Boettcher, Q. Mi, E.A. Santori, N.S. Lewis, Solar water splitting cells. Chem. Rev. 110 (2010) 6446–6473, https://doi.org/10.1021/cr1002326.

[2] A. Steinfeld, Solar thermochemical production of hydrogen—a review. Sol. Energy 78 (2005) 603–615, https://doi.org/10.1016/j.solener.2003.12.012.

[3] K. Maeda, K. Domen, Solid solution of GaN and ZnO as a stable photocatalyst for overall water splitting under visible light. Chem. Mater. 22 (2010) 612–623, https://doi.org/10.1021/cm901917a.

[4] N.S. Lewis, Light work with water. Nature 414 (2001) 589–590, https://doi.org/10.1038/414589a.

[5] M. Grätzel, Front matter. in: Energy Resources Through Photochemistry and Catalysis, Elsevier, 1983, p. iii, https://doi.org/10.1016/B978-0-12-295720-8.50001-6.

[6] N. Serpone, E. Pelizzetti, Photocatalysis: Fundamentals and Applications, Wiley, 1989.https://books.google.co.in/books?id=SigpAQAAMAAJ.

[7] Y.V. Pleskov, Y.Y. Gurevich, The fundamentals of semiconductor physics. in: Semiconductor Photoelectrochemistry, Springer US, Boston, MA, 1986, pp. 1–41, https://doi.org/10.1007/978-1-4684-9078-7_1.

[8] S. Ikeda, T. Itani, K. Nango, M. Matsumura, Overall water splitting on tungsten-based photocatalysts with defect pyrochlore structure. Catal. Lett. 98 (2004) 229–233, https://doi.org/10.1007/s10562-004-8685-y.

[9] Y. Wang, H. Suzuki, J. Xie, O. Tomita, D.J. Martin, M. Higashi, D. Kong, R. Abe, J. Tang, Mimicking natural photosynthesis: solar to renewable H_2 fuel synthesis by Z-scheme water splitting systems. Chem. Rev. 118 (2018) 5201–5241, https://doi.org/10.1021/acs.chemrev.7b00286.

[10] A. FUJISHIMA, K. HONDA, Electrochemical photolysis of water at a semiconductor electrode. Nature 238 (1972) 37–38, https://doi.org/10.1038/238037a0.

[11] H.S. Kim, S.H. Kang, Effect of hydrogen treatment on anatase TiO_2 nanotube arrays for photoelectrochemical water splitting. Bull. Korean Chem. Soc. 34 (2013) 2067–2072, https://doi.org/10.5012/bkcs.2013.34.7.2067.

[12] J. Su, L. Guo, High aspect ratio TiO_2 nanowires tailored in concentrated HCl hydrothermal condition for photoelectrochemical water splitting. RSC Adv. 5 (2015) 53012–53018, https://doi.org/10.1039/C5RA06149K.

[13] M.A. Rahman, S. Bazargan, S. Srivastava, X. Wang, M. Abd-Ellah, J.P. Thomas, N.F. Heinig, D. Pradhan, K.T. Leung, Defect-rich decorated TiO_2 nanowires for super-efficient photoelectrochemical water splitting driven by visible light. Energy Environ. Sci. 8 (2015) 3363–3373, https://doi.org/10.1039/C5EE01615K.

[14] S. Hernández, D. Hidalgo, A. Sacco, A. Chiodoni, A. Lamberti, V. Cauda, E. Tresso, G. Saracco, Comparison of photocatalytic and transport properties of TiO_2 and ZnO nanostructures for solar-driven water splitting. Phys. Chem. Chem. Phys. 17 (2015) 7775–7786, https://doi.org/10.1039/C4CP05857G.

[15] W.-C. Lin, W.-D. Yang, I.-L. Huang, T.-S. Wu, Z.-J. Chung, Hydrogen production from methanol/water photocatalytic decomposition using Pt/$TiO_{2-x}N_x$ catalyst. Energy Fuel 23 (2009) 2192–2196, https://doi.org/10.1021/ef801091p.

[16] G. Liu, C. Sun, X. Yan, L. Cheng, Z. Chen, X. Wang, L. Wang, S.C. Smith, G.Q. Max u, H.-M. Cheng, Iodine doped anatase TiO_2 photocatalyst with ultra-long visible light response: correlation between geometric/electronic structures and mechanisms. J. Mater. Chem. 19 (2009) 2822, https://doi.org/10.1039/b820816f.

[17] V.J. Babu, M.K. Kumar, A.S. Nair, T.L. Kheng, S.I. Allakhverdiev, S. Ramakrishna, Visible light photocatalytic water splitting for hydrogen production from N-TiO_2 rice grain shaped electrospun

This book belongs to Badji Mokhtar Annaba University Central Library Copyright Elsevier 2025

nanostructures. Int. J. Hydrogen Energy 37 (2012) 8897–8904, https://doi.org/10.1016/j.ijhydene.2011.12.015.
[18] J. Fang, F. Wang, K. Qian, H. Bao, Z. Jiang, W. Huang, Bifunctional N-doped mesoporous TiO_2 photocatalysts. J. Phys. Chem. C 112 (2008) 18150–18156, https://doi.org/10.1021/jp805926b.
[19] G. Zhang, X. Ding, Y. Hu, B. Huang, X. Zhang, X. Qin, J. Zhou, J. Xie, Photocatalytic degradation of 4BS dye by N,S-codoped TiO_2 pillared montmorillonite photocatalysts under visible-light irradiation. J. Phys. Chem. C 112 (2008) 17994–17997, https://doi.org/10.1021/jp803939z.
[20] S. Martha, P. Chandra Sahoo, K.M. Parida, An overview on visible light responsive metal oxide based photocatalysts for hydrogen energy production. RSC Adv. 5 (2015) 61535–61553, https://doi.org/10.1039/C5RA11682A.
[21] K.K. Mandari, A.K.R. Police, J.Y. Do, M. Kang, C. Byon, Rare earth metal Gd influenced defect sites in N doped TiO_2: defect mediated improved charge transfer for enhanced photocatalytic hydrogen production. Int. J. Hydrogen Energy 43 (2018) 2073–2082, https://doi.org/10.1016/j.ijhydene.2017.12.050.
[22] R. Shi, Z. Li, H. Yu, L. Shang, C. Zhou, G.I.N. Waterhouse, L.-Z. Wu, T. Zhang, Effect of nitrogen doping level on the performance of N-doped carbon quantum dot/TiO_2 composites for photocatalytic hydrogen evolution. ChemSusChem 10 (2017) 4650–4656, https://doi.org/10.1002/cssc.201700943.
[23] Y.-P. Peng, H. Chen, C.P. Huang, The synergistic effect of photoelectrochemical (PEC) reactions exemplified by concurrent perfluorooctanoic acid (PFOA) degradation and hydrogen generation over carbon and nitrogen codoped TiO_2 nanotube arrays (C-N-TNTAs) photoelectrode. Appl. Catal. B Environ. 209 (2017) 437–446, https://doi.org/10.1016/j.apcatb.2017.02.084.
[24] L.K. Preethi, R.P. Antony, T. Mathews, L. Walczak, C.S. Gopinath, A study on doped heterojunctions in TiO_2 nanotubes: an efficient photocatalyst for solar water splitting. Sci. Rep. 7 (2017) 14314, https://doi.org/10.1038/s41598-017-14463-0.
[25] J. Huang, G. Li, Z. Zhou, Y. Jiang, Q. Hu, C. Xue, W. Guo, Efficient photocatalytic hydrogen production over Rh and Nb codoped TiO_2 nanorods. Chem. Eng. J. 337 (2018) 282–289, https://doi.org/10.1016/j.cej.2017.12.088.
[26] X. Wang, R. Long, D. Liu, D. Yang, C. Wang, Y. Xiong, Enhanced full-spectrum water splitting by confining plasmonic Au nanoparticles in N-doped TiO_2 bowl nanoarrays. Nano Energy 24 (2016) 87–93, https://doi.org/10.1016/j.nanoen.2016.04.013.
[27] H. Lin, C. Shih, Efficient one-pot microwave-assisted hydrothermal synthesis of M (M=Cr, Ni, Cu, Nb) and nitrogen co-doped TiO_2 for hydrogen production by photocatalytic water splitting. J. Mol. Catal. A Chem. 411 (2016) 128–137, https://doi.org/10.1016/j.molcata.2015.10.026.
[28] R. Asahi, Visible-light photocatalysis in nitrogen-doped titanium oxides. Science 293 (2001) 269–271, https://doi.org/10.1126/science.1061051.
[29] S.U.M. Khan, Efficient photochemical water splitting by a chemically modified *n*-TiO_2. Science 297 (2002) 2243–2245, https://doi.org/10.1126/science.1075035.
[30] M. Zhu, C. Zhai, L. Qiu, C. Lu, A.S. Paton, Y. Du, M.C. Goh, New method to synthesize S-doped TiO_2 with stable and highly efficient photocatalytic performance under indoor sunlight irradiation. ACS Sustain. Chem. Eng. 3 (2015) 3123–3129, https://doi.org/10.1021/acssuschemeng.5b01137.
[31] S. Sakthivel, H. Kisch, Daylight photocatalysis by carbon-modified titanium dioxide. Angew. Chem. Int. Ed. 42 (2003) 4908–4911, https://doi.org/10.1002/anie.200351577.
[32] J.H. Park, S. Kim, A.J. Bard, Novel carbon-doped TiO_2 nanotube arrays with high aspect ratios for efficient solar water splitting. Nano Lett. 6 (2006) 24–28, https://doi.org/10.1021/nl051807y.
[33] M. Andersson, V. Alfredsson, P. Kjellin, A.E.C. Palmqvist, Macroscopic alignment of silver nanoparticles in reverse hexagonal liquid crystalline templates. Nano Lett. 2 (2002) 1403–1407, https://doi.org/10.1021/nl0256412.
[34] W. Zhao, W. Ma, C. Chen, J. Zhao, Z. Shuai, Efficient degradation of toxic organic pollutants with Ni_2O_3/$TiO_{2-x}B_x$ under visible irradiation. J. Am. Chem. Soc. 126 (2004) 4782–4783, https://doi.org/10.1021/ja0396753.
[35] T. Umebayashi, T. Yamaki, H. Itoh, K. Asai, Band gap narrowing of titanium dioxide by sulfur doping. Appl. Phys. Lett. (2002), https://doi.org/10.1063/1.1493647.

This book belongs to Badji Mokhtar Annaba University Central Library Copyright Elsevier 2025

[36] X. Chen, C. Burda, The electronic origin of the visible-light absorption properties of C-, N- and S-doped TiO_2 nanomaterials. J. Am. Chem. Soc. 130 (2008) 5018–5019, https://doi.org/10.1021/ja711023z.
[37] S.Y. Arman, H. Omidvar, S.H. Tabaian, M. Sajjadnejad, S. Fouladvand, S. Afshar, Evaluation of nanostructured S-doped TiO_2 thin films and their photoelectrochemical application as photoanode for corrosion protection of 304 stainless steel. Surf. Coat. Technol. (2014), https://doi.org/10.1016/j.surfcoat.2014.04.020.
[38] K. Iwaya, R. Shimizu, H. Aida, T. Hashizume, T. Hitosugi, Atomically resolved silicon donor states of β-Ga_2O_3. Appl. Phys. Lett. (2011), https://doi.org/10.1063/1.3578195.
[39] S. Sun, J. Zhang, P. Gao, Y. Wang, X. Li, T. Wu, Y. Wang, Y. Chen, P. Yang, Full visible-light absorption of TiO_2 nanotubes induced by anionic S_2^{2-}-doping and their greatly enhanced photocatalytic hydrogen production abilities. Appl. Catal. B Environ. (2017), https://doi.org/10.1016/j.apcatb.2017.01.027.
[40] X. Xu, Y. Guo, Z. Liang, H. Cui, J. Tian, Remarkable charge separation and photocatalytic efficiency enhancement through TiO_2(B)/anatase hetrophase junctions of TiO_2 nanobelts. Int. J. Hydrogen Energy 44 (2019) 27311–27318, https://doi.org/10.1016/j.ijhydene.2019.08.174.
[41] F. Wang, Y. Liu, W. Dong, M. Shen, Z. Kang, Tuning TiO_2 photoelectrochemical properties by nanoring/nanotube combined structure. J. Phys. Chem. C 115 (2011) 14635–14640, https://doi.org/10.1021/jp203665j.
[42] H. Wang, Y. Bai, Q. Wu, W. Zhou, H. Zhang, J. Li, L. Guo, Rutile TiO_2 nano-branched arrays on FTO for dye-sensitized solar cells. Phys. Chem. Chem. Phys. 13 (2011) 7008, https://doi.org/10.1039/c1cp20351g.
[43] X. Liu, X.E. Cao, Y. Liu, X. Li, M. Wang, M. Li, Branched multiphase TiO_2 with enhanced photoelectrochemical water splitting activity. Int. J. Hydrogen Energy 43 (2018) 21365–21373, https://doi.org/10.1016/j.ijhydene.2018.09.193.
[44] M. Rakap, E.E. Kalu, S. Özkar, Polymer-immobilized palladium supported on TiO_2 (Pd-PVB-TiO_2) as highly active and reusable catalyst for hydrogen generation from the hydrolysis of unstirred ammonia-borane solution. Int. J. Hydrogen Energy (2011), https://doi.org/10.1016/j.ijhydene.2010.10.097.
[45] Q. Yang, P. Peng, Z. Xiang, Covalent organic polymer modified TiO_2 nanosheets as highly efficient photocatalysts for hydrogen generation. Chem. Eng. Sci. 162 (2017) 33–40, https://doi.org/10.1016/j.ces.2016.12.071.
[46] X. Zhang, J. Xiao, C. Peng, Y. Xiang, H. Chen, Enhanced photocatalytic hydrogen production over conjugated polymer/black TiO_2 hybrid: the impact of constructing active defect states. Appl. Surf. Sci. 465 (2019) 288–296, https://doi.org/10.1016/j.apsusc.2018.09.105.
[47] Y. Yu, N. Zhong, J. Zheng, S. Tang, X. Ye, T. Zeng, W. Yu, Z. He, S. Song, A heterostructured catalyst composed of poly-2,6-diaminopyridine and TiO_2 microspheres used as a photoanode for efficient water splitting. Int. J. Hydrogen Energy 45 (2020) 216–229, https://doi.org/10.1016/j.ijhydene.2019.10.211.
[48] Q. Wang, H. Zhu, B. Li, Synergy of Ti-O-based heterojunction and hierarchical 1D nanobelt/3D microflower heteroarchitectures for enhanced photocatalytic tetracycline degradation and photoelectrochemical water splitting. Chem. Eng. J. (2019), https://doi.org/10.1016/j.cej.2019.122072.
[49] P.K. Dubey, R. Kumar, R.S. Tiwari, O.N. Srivastava, A.C. Pandey, P. Singh, Surface modification of aligned TiO_2 nanotubes by Cu_2O nanoparticles and their enhanced photo electrochemical properties and hydrogen generation application. Int. J. Hydrogen Energy (2018), https://doi.org/10.1016/j.ijhydene.2018.02.127.
[50] G.W. An, M.A. Mahadik, G. Piao, W.-S. Chae, H. Park, M. Cho, H.-S. Chung, J.S. Jang, Hierarchical TiO_2@In_2O_3 heteroarchitecture photoanodes: mechanistic study on interfacial charge carrier dynamics through water splitting and organic decomposition. Appl. Surf. Sci. 480 (2019) 1–12, https://doi.org/10.1016/j.apsusc.2019.02.196.
[51] Y. Lu, X. Cheng, G. Tian, H. Zhao, L. He, J. Hu, S.-M. Wu, Y. Dong, G.-G. Chang, S. Lenaerts, S. Siffert, G. Van Tendeloo, Z.-F. Li, L.-L. Xu, X.-Y. Yang, B.-L. Su, Hierarchical CdS/m-TiO_2/G ternary photocatalyst for highly active visible light-induced hydrogen production from water splitting with high stability. Nano Energy 47 (2018) 8–17, https://doi.org/10.1016/j.nanoen.2018.02.021.
[52] K. Barbalace, Periodic Table of Elements, EnvironmentalChemistry.com, 2015.
[53] Z.L. Wang, Piezoelectric nanogenerators based on zinc oxide nanowire arrays. Science 312 (2006) 242–246, https://doi.org/10.1126/science.1124005.

This book belongs to Badji Mokhtar Annaba University Central Library Copyright Elsevier 2025

[54] C.M. Janet, S. Navaladian, B. Viswanathan, T.K. Varadarajan, R.P. Viswanath, Heterogeneous wet chemical synthesis of superlattice-type hierarchical ZnO architectures for concurrent H_2 production and N_2 reduction. J. Phys. Chem. C 114 (2010) 2622–2632, https://doi.org/10.1021/jp908683x.
[55] J. Núñez, F. Fresno, A.E. Platero-Prats, P. Jana, J.L.G. Fierro, J.M. Coronado, D.P. Serrano, V.A. de la Peña O'Shea, Ga-promoted photocatalytic H_2 production over Pt/ZnO nanostructures. ACS Appl. Mater. Interfaces 8 (2016) 23729–23738, https://doi.org/10.1021/acsami.6b07599.
[56] E. Luévano-Hipólito, L.M. Torres-Martínez, Sonochemical synthesis of ZnO nanoparticles and its use as photocatalyst in H_2 generation. Mater. Sci. Eng. B 226 (2017) 223–233, https://doi.org/10.1016/j.mseb.2017.09.023.
[57] S.I. Al-Mayman, M.S. Al-Johani, M.M. Mohamed, Y.S. Al-Zeghayer, S.M. Ramay, A.S. Al-Awadi, M.A. Soliman, TiO_2ZnO photocatalysts synthesized by sol-gel auto-ignition technique for hydrogen production. Int. J. Hydrogen Energy 42 (2017) 5016–5025, https://doi.org/10.1016/j.ijhydene.2016.11.149.
[58] Y. Lou, Y. Zhang, L. Cheng, J. Chen, Y. Zhao, A stable plasmonic Cu@Cu_2O/ZnO heterojunction for enhanced photocatalytic hydrogen generation. ChemSusChem 11 (2018) 1505–1511, https://doi.org/10.1002/cssc.201800249.
[59] M. Li, Y. Hu, S. Xie, Y. Huang, Y. Tong, X. Lu, Heterostructured ZnO/SnO_{2-x} nanoparticles for efficient photocatalytic hydrogen production. Chem. Commun. 50 (2014) 4341–4343, https://doi.org/10.1039/C3CC49485C.
[60] Y.-H. Liang, M.-W. Liao, M. Mishra, T.-P. Perng, Fabrication of Ta_3N_5ZnO direct Z-scheme photocatalyst for hydrogen generation. Int. J. Hydrogen Energy 44 (2019) 19162–19167, https://doi.org/10.1016/j.ijhydene.2018.07.117.
[61] S. Tso, W.-S. Li, B.-H. Wu, L.-J. Chen, Enhanced H_2 production in water splitting with CdS-ZnO core-shell nanowires. Nano Energy 43 (2018) 270–277, https://doi.org/10.1016/j.nanoen.2017.11.048.
[62] H. Zhao, Y. Dong, P. Jiang, G. Wang, H. Miao, R. Wu, L. Kong, J. Zhang, C. Zhang, Light-assisted preparation of a ZnO/CdS nanocomposite for enhanced photocatalytic H_2 evolution: an insight into importance of in situ generated ZnS. ACS Sustain. Chem. Eng. 3 (2015) 969–977, https://doi.org/10.1021/acssuschemeng.5b00102.
[63] X. Wang, G. Liu, L. Wang, Z.-G. Chen, G.Q.M. Lu, H.-M. Cheng, ZnO-CdS@Cd heterostructure for effective photocatalytic hydrogen generation. Adv. Energy Mater. 2 (2012) 42–46, https://doi.org/10.1002/aenm.201100528.
[64] D. Bak, J.H. Kim, Oxidation driven ZnS core-ZnO shell photocatalysts under controlled oxygen atmosphere for improved photocatalytic solar water splitting. J. Power Sources (2018), https://doi.org/10.1016/j.jpowsour.2018.04.007.
[65] E. Hong, J.H. Kim, Oxide content optimized ZnS-ZnO heterostructures via facile thermal treatment process for enhanced photocatalytic hydrogen production. Int. J. Hydrogen Energy 39 (2014) 9985–9993, https://doi.org/10.1016/j.ijhydene.2014.04.137.
[66] Y. Hu, H. Qian, Y. Liu, G. Du, F. Zhang, L. Wang, X. Hu, A microwave-assisted rapid route to synthesize ZnO/ZnS core-shell nanostructures via controllable surface sulfidation of ZnO nanorods. CrystEngComm 13 (2011) 3438, https://doi.org/10.1039/c1ce05111c.
[67] Y. Piña-Pérez, O. Aguilar-Martínez, P. Acevedo-Peña, C. E. Santolalla-Vargas, S. Oros-Ruíz, F. Galindo-Hernández, R. Gómez, F. Tzompantzi, Novel ZnS-ZnO composite synthesized by the solvothermal method through the partial sulfidation of ZnO for H_2 production without sacrificial agent. Appl. Catal. B Environ. 230 (2018) 125–134, https://doi.org/10.1016/j.apcatb.2018.02.047.
[68] P. Kanhere, Z. Chen, A review on visible light active perovskite-based photocatalysts. Molecules 19 (2014) 19995–20022, https://doi.org/10.3390/molecules191219995.
[69] G. Zhang, G. Liu, L. Wang, J.T.S. Irvine, Inorganic perovskite photocatalysts for solar energy utilization. Chem. Soc. Rev. 45 (2016) 5951–5984, https://doi.org/10.1039/C5CS00769K.
[70] M.A. Bin Adnan, K. Arifin, L.J. Minggu, M.B. Kassim, Titanate-based perovskites for photochemical and photoelectrochemical water splitting applications: a review. Int. J. Hydrogen Energy 43 (2018) 23209–23220, https://doi.org/10.1016/j.ijhydene.2018.10.173.

This book belongs to Badji Mokhtar Annaba University Central Library Copyright Elsevier 2025

[71] Z. Zhao, R. Li, Z. Li, Z. Zou, Photocatalytic activity of La-N-codoped $NaTaO_3$ for H_2 evolution from water under visible-light irradiation. J. Phys. D Appl. Phys. 44 (2011) 165401, https://doi.org/10.1088/0022-3727/44/16/165401.

[72] M. Yang, X. Huang, S. Yan, Z. Li, T. Yu, Z. Zou, Improved hydrogen evolution activities under visible light irradiation over $NaTaO_3$ codoped with lanthanum and chromium. Mater. Chem. Phys. (2010), https://doi.org/10.1016/j.matchemphys.2010.02.015.

[73] D.Y. Wan, Y.L. Zhao, Y. Cai, T.C. Asmara, Z. Huang, J.Q. Chen, J. Hong, S.M. Yin, C.T. Nelson, M.R. Motapothula, B.X. Yan, D. Xiang, X. Chi, H. Zheng, W. Chen, R. Xu, A. Ariando, A.M. Rusydi, M.B.H. Minor, M. Breese, M. Sherburne, Q.-H.X. Asta, T. Venkatesan, Electron transport and visible light absorption in a plasmonic photocatalyst based on strontium niobate. Nat. Commun. 8 (2017) 15070, https://doi.org/10.1038/ncomms15070.

[74] K.M. Parida, K.H. Reddy, S. Martha, D.P. Das, N. Biswal, Fabrication of nanocrystalline $LaFeO_3$: an efficient sol-gel auto-combustion assisted visible light responsive photocatalyst for water decomposition. Int. J. Hydrogen Energy 35 (2010) 12161–12168, https://doi.org/10.1016/j.ijhydene.2010.08.029.

[75] A.Y. Fasasi, M. Maaza, E.G. Rohwer, D. Knoessen, C. Theron, A. Leitch, U. Buttner, Effect of Zn-doping on the structural and optical properties of $BaTiO_3$ thin films grown by pulsed laser deposition. Thin Solid Films 516 (2008) 6226–6232, https://doi.org/10.1016/j.tsf.2007.11.123.

[76] W.L. Gao, H.M. Deng, D.J. Huang, P.X. Yang, J.H. Chu, Microstructure and optical properties of Zn-doped $BaTiO_3$ thin films. J. Phys. Conf. Ser. 276 (2011) 012163, https://doi.org/10.1088/1742-6596/276/1/012163.

[77] J.-H. Yan, Y.-R. Zhu, Y.-G. Tang, S.-Q. Zheng, Nitrogen-doped $SrTiO_3/TiO_2$ composite photocatalysts for hydrogen production under visible light irradiation. J. Alloys Compd. 472 (2009) 429–433, https://doi.org/10.1016/j.jallcom.2008.04.078.

[78] H. Zhang, G. Chen, Y. Li, Y. Teng, Electronic structure and photocatalytic properties of copper-doped $CaTiO_3$. Int. J. Hydrogen Energy 35 (2010) 2713–2716, https://doi.org/10.1016/j.ijhydene.2009.04.050.

[79] H.W. Kang, S. Bin Park, H2 evolution under visible light irradiation from aqueous methanol solution on $SrTiO_3$:Cr/Ta prepared by spray pyrolysis from polymeric precursor. Int. J. Hydrogen Energy 36 (2011) 9496–9504, https://doi.org/10.1016/j.ijhydene.2011.05.094.

[80] H. Yu, J. Wang, S. Yan, T. Yu, Z. Zou, Elements doping to expand the light response of $SrTiO_3$. J. Photochem. Photobiol. A Chem. 275 (2014) 65–71, https://doi.org/10.1016/j.jphotochem.2013.10.014.

[81] Y. Zeng, Y. Wang, J. Chen, Y. Jiang, M. Kiani, B. Li, R. Wang, Fabrication of high-activity hybrid $NiTiO_3$/g-C3N4 heterostructured photocatalysts for water splitting to enhanced hydrogen production. Ceram. Int. 42 (2016) 12297–12305, https://doi.org/10.1016/j.ceramint.2016.04.177.

[82] X.-L. Yin, L.-L. Li, D.-C. Li, D.-H. Wei, C.-C. Hu, J.-M. Dou, Room temperature synthesis of CdS/$SrTiO_3$ nanodots-on-nanocubes for efficient photocatalytic H_2 evolution from water. J. Colloid Interface Sci. 536 (2019) 694–700, https://doi.org/10.1016/j.jcis.2018.10.097.

[83] L. Wang, G. Yang, S. Peng, J. Wang, D. Ji, W. Yan, S. Ramakrishna, Fabrication of $MgTiO_3$ nanofibers by electrospinning and their photocatalytic water splitting activity. Int. J. Hydrogen Energy 42 (2017) 25882–25890, https://doi.org/10.1016/j.ijhydene.2017.08.194.

[84] Y.J. Yuan, D. Chen, Z.T. Yu, Z.G. Zou, Cadmium sulfide-based nanomaterials for photocatalytic hydrogen production. J. Mater. Chem. A (2018), https://doi.org/10.1039/c8ta00671g.

[85] W. Zhu, D. Han, L. Niu, T. Wu, H. Guan, Z-scheme Si/$MgTiO_3$ porous heterostructures: noble metal and sacrificial agent free photocatalytic hydrogen evolution. Int. J. Hydrogen Energy 41 (2016) 14713–14720, https://doi.org/10.1016/j.ijhydene.2016.06.118.

[86] A. Kudo, M. Sekizawa, Photocatalytic H_2 evolution under visible light irradiation on Ni-doped ZnS photocatalyst. Chem. Commun. (2000) 1371–1372, https://doi.org/10.1039/b003297m.

[87] J.H. Bang, R.J. Helmich, K.S. Suslick, Nanostructured ZnS:Ni^{2+} photocatalysts prepared by ultrasonic spray pyrolysis. Adv. Mater. 20 (2008) 2599–2603, https://doi.org/10.1002/adma.200703188.

[88] J. Zhang, S. Liu, J. Yu, M. Jaroniec, A simple cation exchange approach to Bi-doped ZnS hollow spheres with enhanced UV and visible-light photocatalytic H_2-production activity. J. Mater. Chem. 21 (2011) 14655, https://doi.org/10.1039/c1jm12596f.

This book belongs to Badji Mokhtar Annaba University Central Library Copyright Elsevier 2025

[89] Y. Yu, G. Chen, Q. Wang, Y. Li, Hierarchical architectures of porous ZnS-based microspheres by assembly of heterostructure nanoflakes: lateral oriented attachment mechanism and enhanced photocatalytic activity. Energy Environ. Sci. (2011), https://doi.org/10.1039/c1ee01271a.

[90] L. Tie, R. Sun, H. Jiang, Y. Liu, Y. Xia, Y.-Y. Li, H. Chen, C. Yu, S. Dong, J. Sun, J. Sun, Facile fabrication of N-doped ZnS nanomaterials for efficient photocatalytic performance of organic pollutant removal and H_2 production. J. Alloys Compd. 807 (2019) 151670, https://doi.org/10.1016/j.jallcom.2019.151670.

[91] G.J. Lee, S. Anandan, S.J. Masten, J.J. Wu, Sonochemical synthesis of hollow copper doped zinc sulfide nanostructures: optical and catalytic properties for visible light assisted photosplitting of water. Ind. Eng. Chem. Res. (2014), https://doi.org/10.1021/ie500663n.

[92] M. Dong, P. Zhou, C. Jiang, B. Cheng, J. Yu, First-principles investigation of Cu-doped ZnS with enhanced photocatalytic hydrogen production activity. Chem. Phys. Lett. 668 (2017) 1–6, https://doi.org/10.1016/j.cplett.2016.12.008.

[93] E. Hong, D. Kim, J.H. Kim, Heterostructured metal sulfide (ZnS-CuS-CdS) photocatalyst for high electron utilization in hydrogen production from solar water splitting. J. Ind. Eng. Chem. 20 (2014) 3869–3874, https://doi.org/10.1016/j.jiec.2013.12.092.

[94] X. Hao, J. Zhou, Z. Cui, Y. Wang, Y. Wang, Z. Zou, Zn-vacancy mediated electron-hole separation in ZnS/g-C3N4 heterojunction for efficient visible-light photocatalytic hydrogen production. Appl. Catal. B Environ. (2018), https://doi.org/10.1016/j.apcatb.2018.02.006.

[95] T. Yu, Z. Lv, K. Wang, K. Sun, X. Liu, G. Wang, L. Jiang, G. Xie, Constructing $SrTiO_3$-T/CdZnS heterostructure with tunable oxygen vacancies for solar-light-driven photocatalytic hydrogen evolution. J. Power Sources (2019), https://doi.org/10.1016/j.jpowsour.2019.227014.

[96] X. Wang, Z. Cao, Y. Zhang, H. Xu, S. Cao, R. Zhang, All-solid-state Z-scheme Pt/ZnS-ZnO heterostructure sheets for photocatalytic simultaneous evolution of H_2 and O_2. Chem. Eng. J. (2020), https://doi.org/10.1016/j.cej.2019.123782.

[97] P. Madhusudan, Y. Wang, B.N. Chandrashekar, W. Wang, J. Wang, J. Miao, R. Shi, Y. Liang, G. Mi, C. Cheng, Nature inspired ZnO/ZnS nanobranch-like composites, decorated with $Cu(OH)_2$ clusters for enhanced visible-light photocatalytic hydrogen evolution. Appl. Catal. B Environ. 253 (2019) 379–390, https://doi.org/10.1016/j.apcatb.2019.04.008.

[98] C.J. Chang, Y.G. Lin, H.T. Weng, Y.H. Wei, Photocatalytic hydrogen production from glycerol solution at room temperature by ZnO-ZnS/graphene photocatalysts. Appl. Surf. Sci. (2018), https://doi.org/10.1016/j.apsusc.2018.05.004.

[99] J.-W. Shi, D. Sun, Y. Zou, D. Ma, C. He, X. Ji, C. Niu, Trap-level-tunable Se doped CdS quantum dots with excellent hydrogen evolution performance without co-catalyst. Chem. Eng. J. 364 (2019) 11–19, https://doi.org/10.1016/j.cej.2019.01.147.

[100] H. Huang, B. Dai, W. Wang, C. Lu, J. Kou, Y. Ni, L. Wang, Z. Xu, Oriented built-in electric field introduced by surface gradient diffusion doping for enhanced photocatalytic H_2 evolution in CdS nanorods. Nano Lett. 17 (2017) 3803–3808, https://doi.org/10.1021/acs.nanolett.7b01147.

[101] C. Li, S. Du, H. Wang, S.B. Naghadeh, A. Allen, X. Lin, G. Li, Y. Liu, H. Xu, C. He, J. Z. Zhang, P. Fang, Enhanced visible-light-driven photocatalytic hydrogen generation using $NiCo_2S_4$/CdS nanocomposites. Chem. Eng. J. 378 (2019) 122089, https://doi.org/10.1016/j.cej.2019.122089.

[102] G. Liu, Z. Ling, Y. Wang, H. Zhao, Near-infrared CdSexTe1-x@CdS "giant" quantum dots for efficient photoelectrochemical hydrogen generation. Int. J. Hydrogen Energy 43 (2018) 22064–22074, https://doi.org/10.1016/j.ijhydene.2018.10.076.

[103] F. Chen, L. Zhang, X. Wang, R. Zhang, Noble-metal-free NiO@Ni-ZnO/reduced graphene oxide/CdS heterostructure for efficient photocatalytic hydrogen generation. Appl. Surf. Sci. (2017), https://doi.org/10.1016/j.apsusc.2017.05.214.

[104] C. Xue, H. An, G. Yang, Facile construction of MoS_2/CdS eutectic clusters anchored on rGO edge with enhanced hydrogen generation performance. Catal. Today 317 (2018) 99–107, https://doi.org/10.1016/j.cattod.2018.01.023.

[105] W. Zhen, X. Ning, M. Wang, Y. Wu, G. Lu, Enhancing hydrogen generation via fabricating peroxide decomposition layer over NiSe/MnO_2-CdS catalyst. J. Catal. 367 (2018) 269–282, https://doi.org/10.1016/j.jcat.2018.09.019.

This book belongs to Badji Mokhtar Annaba University Central Library Copyright Elsevier 2025

[106] X. Zhang, J. Xiao, M. Hou, Y. Xiang, H. Chen, Robust visible/near-infrared light driven hydrogen generation over Z-scheme conjugated polymer/CdS hybrid. Appl. Catal. B Environ. 224 (2018) 871–876, https://doi.org/10.1016/j.apcatb.2017.11.038.

[107] W. Zhao, J. Liu, Z. Ding, J. Zhang, X. Wang, Optimal synthesis of platinum-free 1D/2D CdS/MoS_2 (CM) heterojunctions with improved photocatalytic hydrogen production performance. J. Alloys Compd. (2020), https://doi.org/10.1016/j.jallcom.2019.152234.

[108] K. Chang, X. Hai, J. Ye, Transition metal disulfides as noble-metal-alternative co-catalysts for solar hydrogen production. Adv. Energy Mater. 6 (2016) 1502555, https://doi.org/10.1002/aenm.201502555.

[109] X. Zong, J. Han, G. Ma, H. Yan, G. Wu, C. Li, Photocatalytic H_2 evolution on CdS loaded with WS2 as cocatalyst under visible light irradiation. J. Phys. Chem. C (2011), https://doi.org/10.1021/jp2006777.

[110] X. Zong, G. Wu, H. Yan, G. Ma, J. Shi, F. Wen, L. Wang, C. Li, Photocatalytic H_2 evolution on MoS_2/CdS catalysts under visible light irradiation. J. Phys. Chem. C (2010), https://doi.org/10.1021/jp904350e.

[111] Z. Lian, Y. Liu, H. Liu, H. Zhou, Z. Chang, W. Li, Fabrication of CdS@1T-MoS_2 core-shell nanostructure for enhanced visible-light-driven photocatalytic H_2 evolution from water splitting. J. Taiwan Inst. Chem. Eng. (2019), https://doi.org/10.1016/j.jtice.2019.10.002.

[112] L. Yang, S. Guo, X. Li, Au nanoparticles@MoS_2 core-shell structures with moderate MoS_2 coverage for efficient photocatalytic water splitting. J. Alloys Compd. (2017), https://doi.org/10.1016/j.jallcom.2017.02.240.

[113] F. Wang, H. Wu, H. Sun, L. Ma, W. Shen, Y. Li, M. Zheng, Hierarchical MoS_2/Ni_3S_2 core-shell nanofibers for highly efficient and stable overall-water-splitting in alkaline media. Mater. Today Energy (2018), https://doi.org/10.1016/j.mtener.2018.09.004.

[114] X. Wang, G. Liu, Z.G. Chen, F. Li, L. Wang, G.Q. Lu, H.M. Cheng, Enhanced photocatalytic hydrogen evolution by prolonging the lifetime of carriers in ZnO/CdS heterostructures. Chem. Commun. (2009), https://doi.org/10.1039/b904668b.

[115] J. Hou, Z. Wang, W. Kan, S. Jiao, H. Zhu, R.V. Kumar, Efficient visible-light-driven photocatalytic hydrogen production using CdS@TaON core-shell composites coupled with graphene oxide nanosheets. J. Mater. Chem. (2012), https://doi.org/10.1039/c2jm15791h.

[116] J. Zhang, Y. Wang, J. Jin, J. Zhang, Z. Lin, F. Huang, J. Yu, Efficient visible-light photocatalytic hydrogen evolution and enhanced photostability of core/shell CdS/g-C_3N_4 nanowires. ACS Appl. Mater. Interfaces (2013), https://doi.org/10.1021/am403327g.

[117] M. Liu, F. Li, Z. Sun, L. Ma, L. Xu, Y. Wang, Noble-metal-free photocatalysts MoS_2-graphene/CdS mixed nanoparticles/nanorods morphology with high visible light efficiency for H_2 evolution. Chem. Commun. 50 (2014) 11004, https://doi.org/10.1039/C4CC04653F.

[118] X. Yang, H. Xue, J. Xu, X. Huang, J. Zhang, Y.B. Tang, T.W. Ng, H.L. Kwong, X.M. Meng, C.S. Lee, Synthesis of porous ZnS:Ag_2S nanosheets by ion exchange for photocatalytic H_2 generation. ACS Appl. Mater. Interfaces (2014), https://doi.org/10.1021/am5020953.

[119] J. Zhang, P. Wang, J. Sun, Y. Jin, High-efficiency plasmon-enhanced and graphene-supported semiconductor/metal core-satellite hetero-nanocrystal photocatalysts for visible-light dye photodegradation and H_2 production from water. ACS Appl. Mater. Interfaces (2014), https://doi.org/10.1021/am505371g.

[120] C.J. Chang, Z. Lee, C.F. Wang, Photocatalytic hydrogen production by stainless steel@ZnS core-shell wire mesh photocatalyst from saltwater. Int. J. Hydrogen Energy (2014), https://doi.org/10.1016/j.ijhydene.2014.06.144.

[121] J. Zhang, L. Qi, J. Ran, J. Yu, S.Z. Qiao, Ternary NiS/Zn_xCd_{1-x} S/reduced graphene oxide nanocomposites for enhanced solar photocatalytic H_2-production activity. Adv. Energy Mater. 4 (2014) 1301925, https://doi.org/10.1002/aenm.201301925.

[122] D.V. Markovskaya, S.V. Cherepanova, A.A. Saraev, E.Y. Gerasimov, E.A. Kozlova, Photocatalytic hydrogen evolution from aqueous solutions of Na_2S/Na_2SO_3 under visible light irradiation on CuS/$Cd_{0.3}Zn_{0.7}S$ and Ni $Cd_{0.3}Zn_{0.7}S_{1+}$. Chem. Eng. J. 262 (2015) 146–155, https://doi.org/10.1016/j.cej.2014.09.090.

[123] L. Wang, H. Chen, L. Xiao, J. Huang, CuS/ZnS hexagonal plates with enhanced hydrogen evolution activity under visible light irradiation. Powder Technol. 288 (2016) 103–108, https://doi.org/10.1016/j.powtec.2015.10.042.

This book belongs to Badji Mokhtar Annaba University Central Library Copyright Elsevier 2025

[124] Z. Yan, Z. Sun, X. Liu, H. Jia, P. Du, Cadmium sulfide/graphitic carbon nitride heterostructure nanowire loading with a nickel hydroxide cocatalyst for highly efficient photocatalytic hydrogen production in water under visible light. Nanoscale (2016), https://doi.org/10.1039/c6nr00160b.
[125] Z. Sun, H. Chen, L. Zhang, D. Lu, P. Du, Enhanced photocatalytic H_2 production on cadmium sulfide photocatalysts using nickel nitride as a novel cocatalyst. J. Mater. Chem. A 4 (2016) 13289–13295, https://doi.org/10.1039/C6TA04696G.
[126] M.-H. Hsu, C.-J. Chang, H.-T. Weng, Efficient H_2 production using Ag_2 S-coupled ZnO@ZnS core-shell nanorods decorated metal wire mesh as an immobilized hierarchical photocatalyst. ACS Sustain. Chem. Eng. 4 (2016) 1381–1391, https://doi.org/10.1021/acssuschemeng.5b01387.
[127] S. Yue, B. Wei, X. Guo, S. Yang, L. Wang, J. He, Novel Ag2S/ZnS/carbon nanofiber ternary nanocomposite for highly efficient photocatalytic hydrogen production. Catal. Commun. (2016), https://doi.org/10.1016/j.catcom.2015.12.020.
[128] T. Chen, C. Song, M. Fan, Y. Hong, B. Hu, L. Yu, W. Shi, In-situ fabrication of CuS/g-C_3N_4 nanocomposites with enhanced photocatalytic H_2-production activity via photoinduced interfacial charge transfer. Int. J. Hydrogen Energy 42 (2017) 12210–12219, https://doi.org/10.1016/j.ijhydene.2017.03.188.
[129] M. Nawaz, Morphology-controlled preparation of Bi_2S_3-ZnS chloroplast-like structures, formation mechanism and photocatalytic activity for hydrogen production. J. Photochem. Photobiol. A Chem. 332 (2017) 326–330, https://doi.org/10.1016/j.jphotochem.2016.09.005.
[130] M. Azarang, M. Sookhakian, M. Aliahmad, M. Dorraj, W.J. Basirun, B.T. Goh, Y. Alias, Nitrogen-doped graphene-supported zinc sulfide nanorods as efficient Pt-free for visible-light photocatalytic hydrogen production. Int. J. Hydrogen Energy (2018), https://doi.org/10.1016/j.ijhydene.2018.06.082.
[131] C.-J. Chang, Y.-H. Wei, W.-S. Kuo, Free-standing CuS-ZnS decorated carbon nanotube films as immobilized photocatalysts for hydrogen production. Int. J. Hydrogen Energy 44 (2019) 30553–30562, https://doi.org/10.1016/j.ijhydene.2018.04.229.
[132] Y. Kataoka, K. Sato, Y. Miyazaki, K. Masuda, H. Tanaka, S. Naito, W. Mori, Photocatalytic hydrogen production from water using porous material $[Ru_2(p\text{-}BDC)_2]n$. Energy Environ. Sci. (2009), https://doi.org/10.1039/b814539c.
[133] C.G. Silva, I. Luz, F.X. Llabrés, I. Xamena, A. Corma, H. García, Water stable Zr-Benzenedicarboxylate metal-organic frameworks as photocatalysts for hydrogen generation. Chem. A Eur. J. (2010), https://doi.org/10.1002/chem.200903526.
[134] T. Zhang, W. Lin, Metal-organic frameworks for artificial photosynthesis and photocatalysis. Chem. Soc. Rev. (2014), https://doi.org/10.1039/c4cs00103f.
[135] S. Wang, X. Wang, Multifunctional metal-organic frameworks for photocatalysis. Small (2015), https://doi.org/10.1002/smll.201500084.
[136] J. Hao, X. Xu, H. Fei, L. Li, B. Yan, Functionalization of metal-organic frameworks for photoactive materials. Adv. Mater. 30 (2018) 1705634, https://doi.org/10.1002/adma.201705634.
[137] B. Zhu, R. Zou, Q. Xu, Metal-organic framework based catalysts for hydrogen evolution. Adv. Energy Mater. (2018), https://doi.org/10.1002/aenm.201801193.
[138] Y. Kataoka, Y. Miyazaki, K. Sato, T. Saito, Y. Nakanishi, Y. Kiatagwa, T. Kawakami, M. Okumura, K. Yamaguchi, W. Mori, Modification of MOF catalysts by manipulation of counter-ions: experimental and theoretical studies of photochemical hydrogen production from water over microporous diruthenium (II, III) coordination polymers. Supramol. Chem. (2011), https://doi.org/10.1080/10610278.2010.527976.
[139] K. Sato, Y. Kataoka, W. Mori, Photochemical production of hydrogen from water using microporous porphyrin coordination lattices. J. Nanosci. Nanotechnol. (2012), https://doi.org/10.1166/jnn.2012.5411.
[140] Q. Xiang, J. Yu, M. Jaroniec, Graphene-based semiconductor photocatalysts. Chem. Soc. Rev. (2012), https://doi.org/10.1039/c1cs15172j.
[141] A. Reina, X. Jia, J. Ho, D. Nezich, H. Son, V. Bulovic, M.S. Dresselhaus, K. Jing, Large area, few-layer graphene films on arbitrary substrates by chemical vapor deposition. Nano Lett. (2009), https://doi.org/10.1021/nl801827v.

This book belongs to Badji Mokhtar Annaba University Central Library Copyright Elsevier 2025

[142] J.H. Lee, D.W. Shin, V.G. Makotchenko, A.S. Nazarov, V.E. Fedorov, Y.H. Kim, J.-Y. Choi, J.M. Kim, J.-B. Yoo, One-step exfoliation synthesis of easily soluble graphite and transparent conducting graphene sheets. Adv. Mater. 21 (2009) 4383–4387, https://doi.org/10.1002/adma.200900726.

[143] S.Y. Zhou, G.-H. Gweon, A.V. Fedorov, P.N. First, W.A. de Heer, D.-H. Lee, F. Guinea, A.H. Castro Neto, A. Lanzara, Erratum: substrate-induced bandgap opening in epitaxial graphene. Nat. Mater. 6 (2007) 916, https://doi.org/10.1038/nmat2056.

[144] H. Bai, C. Li, G. Shi, Functional composite materials based on chemically converted graphene. Adv. Mater. (2011), https://doi.org/10.1002/adma.201003753.

[145] L. Jia, D.H. Wang, Y.X. Huang, A.W. Xu, H.Q. Yu, Highly durable N-doped graphene/CdS nanocomposites with enhanced photocatalytic hydrogen evolution from water under visible light irradiation. J. Phys. Chem. C (2011), https://doi.org/10.1021/jp2023617.

[146] P. Kumar, R. Boukherroub, K. Shankar, Sunlight-driven water-splitting using two-dimensional carbon based semiconductors. J. Mater. Chem. A (2018), https://doi.org/10.1039/c8ta02061b.

[147] F. Banhart, J. Kotakoski, A.V. Krasheninnikov, Structural defects in graphene. ACS Nano (2011), https://doi.org/10.1021/nn102598m.

[148] W. Zhang, Y. Li, X. Zeng, S. Peng, Synergetic effect of metal nickel and graphene as a cocatalyst for enhanced photocatalytic hydrogen evolution via dye sensitization. Sci. Rep. (2015), https://doi.org/10.1038/srep10589.

[149] J.-P. Zou, L.-C. Wang, J. Luo, Y.-C. Nie, Q.-J. Xing, X.-B. Luo, H.-M. Du, S.-L. Luo, S.L. Suib, Synthesis and efficient visible light photocatalytic H_2 evolution of a metal-free g-C_3N_4/graphene quantum dots hybrid photocatalyst. Appl. Catal. B Environ. 193 (2016) 103–109, https://doi.org/10.1016/j.apcatb.2016.04.017.

[150] J. Fu, J. Yu, C. Jiang, B. Cheng, g-C_3N_4-based heterostructured photocatalysts. Adv. Energy Mater. (2018), https://doi.org/10.1002/aenm.201701503.

[151] A. Mishra, A. Mehta, S. Basu, N.P. Shetti, K.R. Reddy, T.M. Aminabhavi, Graphitic carbon nitride (g–C3N4)–based metal-free photocatalysts for water splitting: a review. Carbon N. Y. (2019), https://doi.org/10.1016/j.carbon.2019.04.104.

[152] X. Wang, K. Maeda, A. Thomas, K. Takanabe, G. Xin, J.M. Carlsson, K. Domen, M. Antonietti, A metal-free polymeric photocatalyst for hydrogen production from water under visible light. Nat. Mater. 8 (2009) 76–80, https://doi.org/10.1038/nmat2317.

[153] B. Antil, L. Kumar, K.P. Reddy, C.S. Gopinath, S. Deka, Direct thermal polymerization approach to N-rich holey carbon nitride nanosheets and their promising photocatalytic H_2 evolution and charge-storage activities. ACS Sustain. Chem. Eng. (2019), https://doi.org/10.1021/acssuschemeng.9b00626.

[154] Q. Liu, J. Shen, X. Yu, X. Yang, W. Liu, J. Yang, H. Tang, H. Xu, H. Li, Y. Li, J. Xu, Unveiling the origin of boosted photocatalytic hydrogen evolution in simultaneously (S, P, O)-codoped and exfoliated ultrathin g-C_3N_4 nanosheets. Appl. Catal. B Environ. (2019), https://doi.org/10.1016/j.apcatb.2019.02.020.

[155] J. Yu, S. Wang, B. Cheng, Z. Lin, F. Huang, Noble metal-free $Ni(OH)_2$-g-C_3N_4 composite photocatalyst with enhanced visible-light photocatalytic H_2-production activity. Catal. Sci. Technol. (2013), https://doi.org/10.1039/c3cy20878h.

[156] Y. Zhu, T. Wan, X. Wen, D. Chu, Y. Jiang, Tunable Type I and II heterojunction of CoOx nanoparticles confined in g-C_3N_4 nanotubes for photocatalytic hydrogen production. Appl. Catal. B Environ. 244 (2019) 814–822, https://doi.org/10.1016/j.apcatb.2018.12.015.

[157] H. Hou, F. Gao, L. Wang, M. Shang, Z. Yang, J. Zheng, W. Yang, Superior thoroughly mesoporous ternary hybrid photocatalysts of TiO_2/WO_3/g-C_3N_4 nanofibers for visible-light-driven hydrogen evolution. J. Mater. Chem. A 4 (2016) 6276–6281, https://doi.org/10.1039/C6TA02307J.

[158] Y. Tan, Z. Shu, J. Zhou, T. Li, W. Wang, Z. Zhao, One-step synthesis of nanostructured g-C_3N_4/TiO_2 composite for highly enhanced visible-light photocatalytic H_2 evolution. Appl. Catal. B Environ. (2018), https://doi.org/10.1016/j.apcatb.2018.02.056.

[159] F. Cheng, H. Yin, Q. Xiang, Low-temperature solid-state preparation of ternary CdS/g-C_3N_4/CuS nanocomposites for enhanced visible-light photocatalytic H_2-production activity. Appl. Surf. Sci. 391 (2017) 432–439, https://doi.org/10.1016/j.apsusc.2016.06.169.

[160] R. Rameshbabu, P. Ravi, M. Sathish, Cauliflower-like CuS/ZnS nanocomposites decorated g-C_3N_4 nanosheets as noble metal-free photocatalyst for superior photocatalytic water splitting. Chem. Eng. J. (2019), https://doi.org/10.1016/j.cej.2018.10.180.

This book belongs to Badji Mokhtar Annaba University Central Library Copyright Elsevier 2025

[161] M.E. Demir, G. Chehade, I. Dincer, B. Yuzer, H. Selcuk, Synergistic effects of advanced oxidization reactions in a combination of TiO_2 photocatalysis for hydrogen production and wastewater treatment applications. Int. J. Hydrogen Energy 44 (2019) 23856–23867, https://doi.org/10.1016/j.ijhydene.2019.07.110.

[162] P. Fragiacomo, M. Genovese, Modeling and energy demand analysis of a scalable green hydrogen production system. Int. J. Hydrogen Energy 44 (2019) 30237–30255, https://doi.org/10.1016/j.ijhydene.2019.09.186.

[163] Y. Xiao, H. Yu, X.T. Dong, Ordered mesoporous CeO_2/ZnO composite with photodegradation concomitant photocatalytic hydrogen production performance. J. Solid State Chem. (2019), https://doi.org/10.1016/j.jssc.2019.120893.

[164] Y. Li, R. Fu, M. Gao, X. Wang, B-N co-doped black TiO_2 synthesized via magnesiothermic reduction for enhanced photocatalytic hydrogen production. Int. J. Hydrogen Energy 44 (2019) 28629–28637, https://doi.org/10.1016/j.ijhydene.2019.09.121.

[165] R. He, H. Liang, C. Li, J. Bai, Enhanced photocatalytic hydrogen production over Co_3O_4@g-C_3N_4 p-n junction adhering on one-dimensional carbon fiber. Colloids Surf. A Physicochem. Eng. Asp. (2020), https://doi.org/10.1016/j.colsurfa.2019.124200.

[166] X. Zhao, W. Xie, Z. Deng, G. Wang, A. Cao, H. Chen, B. Yang, Z. Wang, X. Su, C. Yang, Salt templated synthesis of NiO/TiO_2 supported carbon nanosheets for photocatalytic hydrogen production. Colloids Surf. A Physicochem. Eng. Asp. (2020), https://doi.org/10.1016/j.colsurfa.2019.124365.

[167] B. Chai, J. Yan, G. Fan, G. Song, C. Wang, In situ fabrication of $CdMoO_4$/g-C_3N_4 composites with improved charge separation and photocatalytic activity under visible light irradiation. Chinese J. Catal. (2020), https://doi.org/10.1016/S1872-2067(19)63383-8.

[168] F. Li, D.Y.C. Leung, Highly enhanced performance of heterojunction Bi_2S_3/$BiVO_4$ photoanode for photoelectrocatalytic hydrogen production under solar light irradiation. Chem. Eng. Sci. 211 (2020) 115266, https://doi.org/10.1016/j.ces.2019.115266.

[169] M. Benamira, H. Lahmar, L. Messaadia, G. Rekhila, F.Z. Akika, M. Himrane, M. Trari, Hydrogen production on the new hetero-system Pr_2NiO_4/SnO_2 under visible light irradiation. Int. J. Hydrogen Energy (2019), https://doi.org/10.1016/j.ijhydene.2019.11.064.

[170] A. Huda, P.H. Suman, L.D.M. Torquato, B.F. Silva, C.T. Handoko, F. Gulo, M.V.B. Zanoni, M. O. Orlandi, Visible light-driven photoelectrocatalytic degradation of acid yellow 17 using Sn_3O_4 flower-like thin films supported on Ti substrate (Sn_3O_4/TiO_2/Ti). J. Photochem. Photobiol. A Chem. 376 (2019) 196–205, https://doi.org/10.1016/j.jphotochem.2019.01.039.

[171] P.V. Adhyapak, S.P. Meshram, I.S. Mulla, S.K. Pardeshi, D.P. Amalnerkar, Controlled synthesis of zinc oxide nanoflowers by succinate-assisted hydrothermal route and their morphology-dependent photocatalytic performance. Mater. Sci. Semicond. Process 27 (2014) 197–206, https://doi.org/10.1016/j.mssp.2014.06.040.

[172] S. Balgude, Y. Sethi, B. Kale, D. Amalnerkar, P. Adhyapak, Sn_3O_4 microballs as highly efficient photocatalyst for hydrogen generation and degradation of phenol under solar light irradiation. Mater. Chem. Phys. 221 (2019) 493–500, https://doi.org/10.1016/j.matchemphys.2018.08.032.

[173] S.D. Balgude, Y.A. Sethi, B.B. Kale, D.P. Amalnerkar, P.V. Adhyapak, ZnO decorated Sn_3O_4 nanosheet nano-heterostructure: a stable photocatalyst for water splitting and dye degradation under natural sunlight. RSC Adv. 9 (2019) 10289–10296, https://doi.org/10.1039/C9RA00788A.

[174] H.M. Cao, Z. Liu, T. Liu, S. Duo, L. Huang, S. Yi, L. Cai, Well-organized assembly of ZnO hollow cages and their derived Ag/ZnO composites with enhanced photocatalytic property. Mater. Charact. (2020), https://doi.org/10.1016/j.matchar.2020.110125.

[175] L. Xu, W. Chen, S. Ke, S. Zhang, M. Zhu, Y. Zhang, W. Shi, S. Horike, L. Tang, Construction of heterojunction Bi/Bi_5O_7I/Sn_3O_4 for efficient noble-metal-free Z-scheme photocatalytic H_2 evolution. Chem. Eng. J. 382 (2020) 122810, https://doi.org/10.1016/j.cej.2019.122810.

This book belongs to Badji Mokhtar Annaba University Central Library Copyright Elsevier 2025

CHAPTER 11

Nanomaterials for treatment of air pollutants

Nikhil D. Bhavsar[a], Divya P. Barai[a], Bharat A. Bhanvase[a], and Shirish H. Sonawane[b]

[a]*Chemical Engineering Department, Laxminarayan Institute of Technology, Rashtrasant Tukadoji Maharaj Nagpur University, Nagpur, Maharashtra, India,* [b]*Department of Chemical Engineering, National Institute of Technology, Warangal, Telangana, India*

11.1 Introduction

Industrial revolution was a blessing to mankind, but it also fetched a curse called "Pollution" with it, which is harming the environment and all living species on earth. The increased demand for materials and technologies bring comfort to human life, improve living, and help in fighting diseases. On the other hand, along with increased production in industries, pollution is also increasing. Various human activities such as construction, manufacturing, irrigation, and farming result in various types of pollution. This has resulted in this situation where our environment is contaminated with various pollutants, causing degradation of the quality of the air that we breathe, water that we drink, and food that we eat, posing a serious threat. So we need to mitigate this problem by employing various techniques and develop technologies that can help reduce emission at source or can efficiently treat pollutants already present in the environment. Nanotechnology is considered as a promising technology that can help to mitigate these problems. There have been numerous studies on the treatment of wastewater through the use of nanotechnology. Researchers have developed membranes [1–5] and photoactive materials [6, 7]. These technologies exploit the properties of nanomaterials and provide outstanding solutions for sustainable wastewater treatment. Photoactive materials play a major role in such technologies.

Similarly, air pollution also is a major threat to the environment. Air pollution occurs when excessive, harmful toxic gases or particulates are released in the air. The main air pollutants include CO_2, NO_x, volatile organic compounds (VOCs), etc. Surprisingly, 91% of the global population is exposed to air that has pollutants in amounts exceeding the limits stated by WHO

Handbook of Nanomaterials for Wastewater Treatment. https://doi.org/10.1016/B978-0-12-821496-1.00023-4
Copyright © 2021 Elsevier Inc. All rights reserved.

This book belongs to Badji Mokhtar Annaba University Central Library Copyright Elsevier 2025

[8]. State of Global Air report 2019 [9] compared all mortality factors of 2017 and found that air pollution ranks fifth in the list of leading risk factors, causing 5 million deaths in the year globally. Of these, 1.6 million deaths were because of pollution of ambient air. Air pollution has become a major concern for India as most of its cities face huge air quality issues. Various essential steps and major policy reforms are undertaken by the government in order to decrease such high levels of pollution such as the implementation of new and more stringent emission norms for vehicles [10], National Action Plan on Climate Change [11], and adaption of renewable energy sources [12]. Currently, lots of efforts are put by various groups of researchers in developing various nanomaterials that can effectively and more efficiently treat these pollutants. Kong et al. [13] developed photocatalyst for the reduction of CO_2, whereas Ganesh et al. [14] used silica nanoparticle to treat CO_2. Singh et al. [15] investigated ZnO nanoparticles for NO_2 removal whereas Sun et al. [16] also developed photocatalyst to treat VOC. This is a result of the ability of this technology to offer control over various properties of the nanomaterials for specific functionality [17, 18]. This chapter focuses on nanomaterials that are used in the treatment of air pollutants.

11.2 Role of nanotechnology in various pollution treatment methods

The growing interest in nanotechnology is because of the ability to control and modify materials at nanoscale to obtain desired properties and functionalities [19]. The anisotropic growth of lanthanide orthophosphate nanomaterials was studied by Yan et al. [20], and it was found that these properties depend upon the structural and kinetic factors of the synthesis process. The size, shape, and composition of the nanomaterials can even be altered by altering the synthesis parameters [21]. Currently, nanotechnology is applied in the field of the environment in three different ways namely, pollution prevention, detection, and remediation [18, 22, 23].

Nanotechnology is being employed to improve the quality of water and obtain clean water. Remediation, separation, and filtration by use of reactive media are some of the methods by which nanotechnology is employed [22]. The remediation process is used to remove, rather minimize water contaminants. Various nanomaterials such as zeolites, carbon nanotubes (CNTs), and biopolymers are constantly engineered. Water remediation using iron, ferritin nanomaterial, amphiphilic polyurethane, and polyurethane acrylate anionomer is successfully done by researchers [24–26]. Nanofiltration, nanocrystalline zeolites, single-enzyme nanoparticle, self-assembled monolayers on mesoporous silica, tunable biopolymers, dendrimers, and dendritic polymers are various nanotechnologies used for water treatment [27–30]. Similarly, nanotechnology is also utilized for cleaning the air by removing or degrading the contaminants. Various methods and materials are continuously investigated by researchers. Adsorption, photocatalysis, and nanofiltration are the various methods by which

This book belongs to Badji Mokhtar Annaba University Central Library Copyright Elsevier 2025

nanotechnology is employed in the treatment of air pollutants. These are discussed in detail in this chapter.

11.3 Air pollutants

The Earth's climate and ecosystem are highly influenced and affected by the quality of air. Motor vehicles, power generation, heating systems used for building, waste incineration, and manufacturing industries are the major sources causing ambient air pollution, whereas household air pollution is a result of use of fossil fuels for cooking and lighting purposes. These various sources and activities emit air pollutants such as CO, SO_2, polyaromatic hydrocarbons, VOCs, and particulate matter (PM), which can be composed of NH_4, NaCl, sulfates, nitrates, black carbon, mineral dust, and water. WHO has reported that 9 out of 10 individuals breath air that is contaminated with a high levels of pollutants [8]. Air pollutants are divided into two categories, namely primary pollutants and secondary pollutants [31].

Pollutants that are emitted directly by sources such as industries, engines running on fossil fuels, burning of fuels, and volcano eruptions into the atmosphere are called as primary pollutants. These are mainly carbon monoxide, carbon dioxide, nitrogen oxide, sulfur oxide, hydrocarbons, PM, etc. On the other hand, secondary pollutants are those that are produced by the reaction of primary pollutants among themselves or with water vapor and sunlight. These include sulfuric acid, ozone, peroxyacyl nitrate, etc. Information regarding these pollutants is summarized in Table 11.1.

11.4 Nanotechnology in the treatment of air pollution

Various technologies are being extensively evaluated for mitigating the problem of air pollution, one of which is nanotechnology. Nanomaterials of different kinds are being extensively investigated for the treatment of air pollutants. This is a result of various advantageous properties of materials that can be exploited at nanoscale compared to their bulk counterparts.

11.4.1 Treatment methods

11.4.1.1 Adsorption

One of the well-known processes used for the removal of contaminants from a mixture is adsorption. In this process, the substance to be adsorbed, called as adsorbate, gets accumulated either on the surface or within the pores of the adsorbent. Physical (physisorption) or chemical (chemisorption) forces help in the process of adsorption. The van der Waal forces are dominant in physisorption, whereas chemical forces of interaction between adsorbent and adsorbate are dominant in chemisorption [36]. The efficiency of conventional adsorbents is

This book belongs to Badji Mokhtar Annaba University Central Library Copyright Elsevier 2025

Table 11.1: Summary about various air pollutants [31–35].

Pollutants	Sources	Adverse effects
CO	Petrol/diesel combustion, volcanic eruption, industries smoke	Affects central nervous system, heart attack, it combines with hemoglobin to form carboxyhemoglobin
CO_2	Petrol/diesel combustion, volcanic eruption, industries smoke	Global warming
NO_x	Petrol/diesel combustion, volcanic eruption, industries smoke	Eyes and nasal irritation, pulmonary discomfort, asthma, and bronchitis
NH_3	Agricultural waste, ammoniacal fertilizers, fuel combustion	Formation of particulate matter
Pb	Mining, smelting, pigments, paints, fuel combustion	Eyes and lungs irritation, visibility reduction, high blood pressure, and kidney damage
SO_2	Fossil fuel combustion, volcanic eruption	Eyes and lungs irritation, asthma, chronic bronchitis, visibility reduction, acid rain
H_2S	Sulfur springs and lakes, saline marshes	Irritates the eyes, nose, throat, and respiratory system and causes nausea, vomiting, staggering, headache, and dizziness
VOCs	Volcanic eruptions, industrial smoke, paints, plywood, cooking, cigarette smoke, deodorant, cosmetic products, petrochemical plants, petroleum reservoirs, etc.	Asthma, reduced pulmonary function, nasopharyngeal cancer, throat irritation, headache, dizziness, fatigue, and leukemia
Hydrocarbon	Petrol/diesel combustion, solvents, cleaning product, varnishes, and waxes	Eyes and lungs irritation
Particulate matter	Petrol/diesel combustion, building, mining, manufacture of cement, ceramic, and bricks, smelting, etc.	Asthma, lung cancer, cardiovascular diseases, vascular inflammation, atherosclerosis
Aerosol	Vegetation fire, fossil fuel/biofuel combustion, and volcanic eruptions	Changes the amount of heat that gets in or out of the atmosphere, affects the way clouds form, cardiopulmonary diseases, and lung cancers

highly dependent on their structures and is usually limited by various factors such as surface area or active sites, selectivity toward adsorbate, and adsorption kinetics. At the nanoscale, one can surely find significant improvement with larger availability of specific surface area along with associated sorption sites, short intraparticle diffusion distance, and tunable pore size and surface chemistry [37]. That is why these technologies seem to provide promising solutions. Fig. 11.1 shows the reactive adsorption of SO_2 on the surface of activated carbons (ACs) with iron nanoparticles deposited on it [38] as studied by Kennedy et al. [36].

This book belongs to Badji Mokhtar Annaba University Central Library
Copyright Elsevier 2025

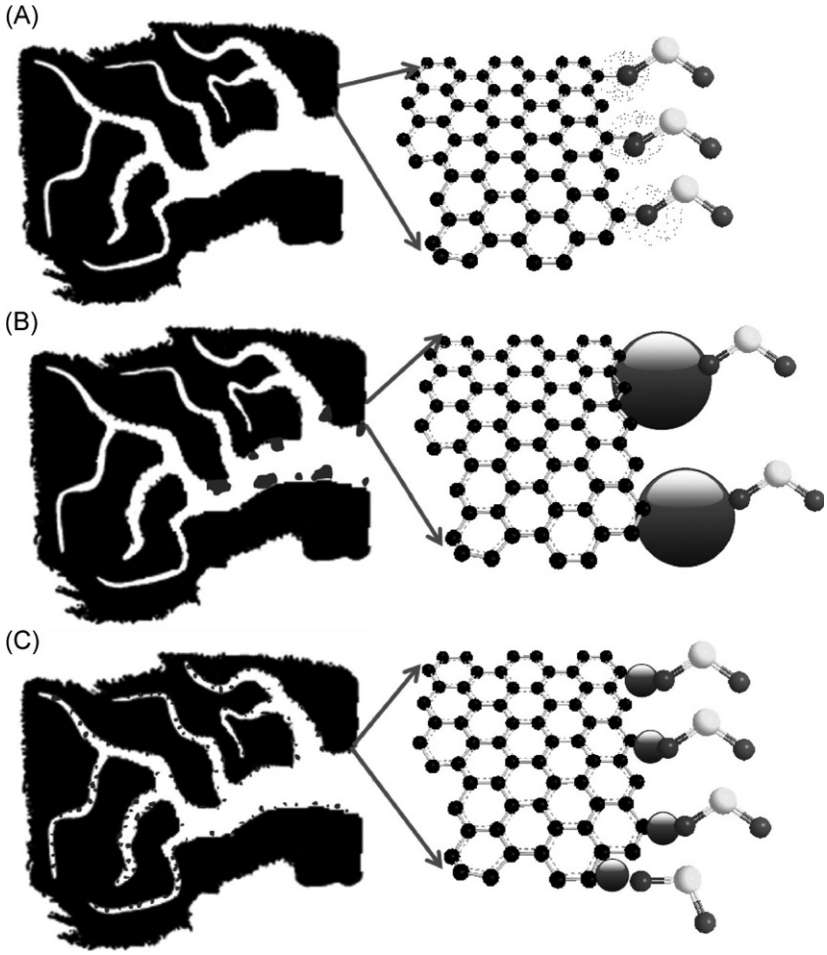

Fig. 11.1
Illustration of SO_2 adsorption on activated carbon decorated with iron nanoparticles. (A) Chemisorption of SO_2 on activated carbon. (B) Decrease in absorption due to presence of large iron nano-particles of activated carbon surface. (C) Increased in absorption sites resulting due to tiny size iron nano-particles. *Reproduced with permission from J.A. Arcibar-Orozco, J.R. Rangel-Mendez, T. J. Bandosz, Reactive adsorption of SO_2 on activated carbons with deposited iron nanoparticles, J. Hazard. Mater. 246–247 (2013) 300–309, https://doi.org/10.1016/j.jhazmat.2012.12.001. Copyright 2013, Elsevier.*

11.4.1.2 Photocatalysis

Photocatalysis is considered as a sustainable technology for the treatment and mitigating the problem of air pollution. Change in bandgap at the nanoscale is one of the properties being exploited for achieving photoactivity, thus making use of the material as a photocatalyst. Because of the change in the bandgap, these photocatalysts can generate reactive oxygen species (ROS) or charge-carrying species when illuminated by UV-vis radiation. These charged

This book belongs to Badji Mokhtar Annaba University Central Library Copyright Elsevier 2025

species or ROS can then be used to degrade or convert pollutants into harmless components [39–41]. The photocatalytic activity of materials strongly depends on the absorption efficiency of a photon from irradiation, the formation of charge carrier species, migration of charge, and recombination efficiency [42]. The surface oxygen vacancy plays a crucial role in the mediation of electron-hole separation and transfer of surface charge in the photocatalytic process [41, 43]. The graphical representation of photocatalytic degradation of VOC on Pt/N-TiO_2 photocatalyst is shown in Fig. 11.2, as done by Sun et al. [16]. As visible light is incident on photocatalyst, it results in formation of electron-hole pair, and the electron jumps to valence band and the hole in conduction band. The formed electron-hole pair produces reactive or charged oxygen that attacks on toluene and oxidizes it to produce less harmful products. Table 11.2 represents a summary of energy bandgap of some common nanoparticles.

11.4.1.3 Nanofiltration

Nanofiltration is an approach similar to conventional filtration to separate components from mixtures, except the fact that the components are targeted at the molecular level. In this method, nanostructured membranes are employed, which have pores small enough to be capable of separating one component molecule from a mixture. Various methods are used to synthesize ultrafine fibers from various materials such as ceramics and polymers. Nanofibers made with these methods form mats with complex pore structure, which results in high specific surface area and porosity. According to specific applications, various properties of nanofibers such as diameter, morphology, composition, secondary structure, and spatial alignment can be easily manipulated [47, 48].

11.4.2 Treatment of air pollutants

11.4.2.1 CO_2

CO_2 is one of the most common air pollutants and greenhouse gases emitted during burning of fossil fuels [34, 35]. According to Brown and Green report [49] published in 2019, CO_2 emissions increased by 1.8% in 2018. Exposure to CO_2 at high concentration may cause breathing problems, unconsciousness, and even death [34]. Various nanomaterials are continuously being studied for their ability to treat, reduce, or capture CO_2.

Kong et al. [13] developed a photocatalyst to reduce CO_2 in the presence of UV-vis-NIR radiation. The photocatalyst was synthesized by one-step solvothermal approach. This helped in inducing oxygen vacancies in Bi_2WO_6 (Bi_2WO_6-OV). This photocatalyst was reported to have a nanoplatelet structure with length ranging from 38 to 60 nm and an average thickness of 16 nm. The experiment to evaluate the ability of photocatalyst to reduce CO_2 was conducted at room temperature and atmospheric pressure with continuous exposure to UV, vis, and NIR irradiations. They reported that after 8 h of continuous exposure to UV, visible, and NIR light, the yield of CH_4 resulting from the reduction of CO_2 was 6.17, 4.28, and 0.39 μmol/g, respectively. The results indicated that Bi_2WO_6-OV is nearly inactive under the NIR region, and Bi_2WO_6-OV shows 2.1 and 3-fold increase in performance in UV-vis region over Bi_2WO_6.

This book belongs to Badji Mokhtar Annaba University Central Library Copyright Elsevier 2025

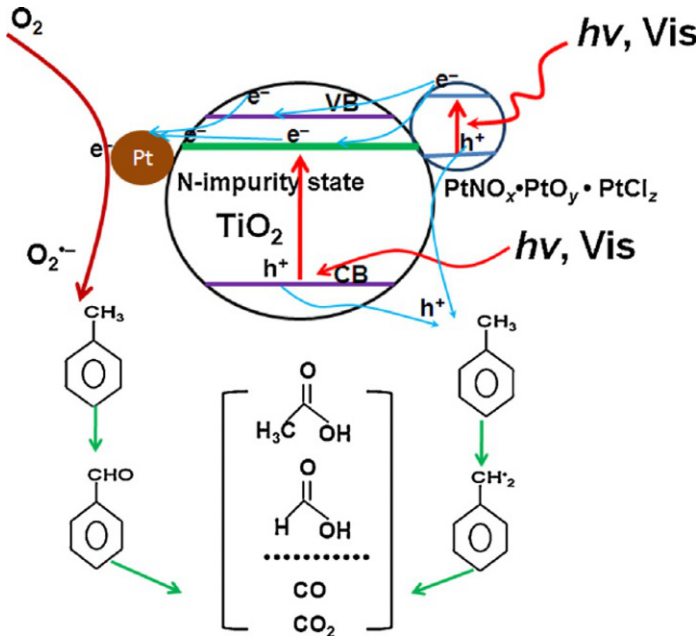

Fig. 11.2

Graphical depiction of photocatalytic degradation of VOC on Pt/N-TiO_2 photocatalyst. *Reproduced with permission from H. Sun, R. Ullah, S. Chong, H.M. Ang, M.O. Tadé, S. Wang, Room-light-induced indoor air purification using an efficient Pt/N-TiO_2 photocatalyst, Appl. Catal. B Environ. 108–109 (2011) 127–133, https://doi.org/10.1016/j.apcatb.2011.08.017. Copyright 2011, Elsevier.*

Table 11.2: Summary of some common nanoparticles energy band gap.

Nanoparticle	Bandgap (ev)	References
ZnS	3.7	[44]
CdS	2.5	[44]
TiO_2	3–3.2	[16, 36, 45]
La-TiO_2	2.8	[45]
Sr-TiO_3	3.2	[39]
La-FeO_3	2.6	[39]
$BiWO_6$	2.7	[13]
$BiPO_4$	4.1	[40]
H-Ga_2O_3	4.75	[46]

They further extended the experiment and checked the ability of Bi_2WO_6-OV to reduce CO_2 to CH_4 under simulated solar light irradiation and reported a yield of CH_4 as 13.94 μmol/g, indicating a 2.8-fold increase in photocatalytic activity owing to the presence of oxygen vacancies. Ganesh et al. [14] synthesized silica nanoparticles doped with lithium and zirconium by one-pot sol-gel method and used it as an adsorbent to capture CO_2. To evaluate the adsorption capacity of synthesized adsorbent, a thermogravimetric analyzer was used.

This book belongs to Badji Mokhtar Annaba University Central Library Copyright Elsevier 2025

High purity CO_2 at a flow rate of 30 mL/min was used to carry out adsorption at three different temperatures: 25°C, 50°C, and 75°C at atmospheric pressure. Initial activation of the sample was done in N_2 atmosphere at 200°C for 1 h. They reported 50 mg/g of CO_2 adsorption at 25°C and a decrease in adsorption with an increase in temperature owing to the rise in the mobility of the adsorbate.

Upendar et al. [50] synthesized alkali metal (Na, K) titanate nanotube and used it as adsorbent of CO_2. This adsorbate was synthesized by hydrothermal method. The adsorption experiment was carried out in a fixed-bed reactor of length 30 cm and an inner diameter of 10 mm. This reactor was filled with 1 g of adsorbent and glass beads. The adsorbent was activated by heating it at 200°C for 1 h. A mixture of 10% CO_2 and remaining helium was passed through a fixed bed of adsorbate. The experiment was conducted at three different temperatures: 50°C, 70°C, and 90°C. They reported the adsorption capacity for sodium titanate (Na-Ti-NT) with a surface area up to 92 m^2/g to be 4.415 mmol/g and for potassium titanate (K-Ti-NT) with surface area 263 m^2/g to be 2.334 mmol/g at 50°C. Also, a decrease in adsorption capacity with an increase in temperature was reported. Mishra and Ramaprabhu [51] synthesized nanocomposite comprising graphite nanoplatelets (GNPs) with deposition of Pd nanoparticles over it. On average, 25 wt% loading of Pd nanoparticles was done on GNPs. Having a surface area of 10.32 m^2/g and an average pore diameter of about 20 nm, this composite was investigated for CO_2 adsorption. The adsorption measurements were performed using high-pressure Seiverts' apparatus, with the incorporation of Van der Waals equations. They reported a 15%–20% enhancement in adsorption of CO_2 resulting because of Pd nanoparticle deposition compared with the performance of only GNPs. Investigations were carried out at three different temperatures and 11 bar pressure. Reported CO_2 adsorption capacities for Pd-GNP and functionalized GNP at 25°C were 0.0051 and 0.0043 mol/g, respectively. The adsorption capacity was found to be increasing with an increase in pressure (Fig. 11.3), whereas it decreased with an increase in temperature.

Pan et al. [46] photocatalytically reduced CO_2 to CO. For this reduction, they synthesized gallium oxide with platinum nanoparticles dispersed on it (Pt/Ga_2O_3). Gallium oxide was first prepared using gallium nitrate and urea and then dispersed into an aqueous solution containing a predefined amount of H_2PtCl_6, which led to the dispersion of 1 wt% Pt on Ga_2O_3. To evaluate the reduction capability of prepared Pt/Ga_2O_3, a closed gas circulation-evacuation reactor of capacity 300 mL was used to perform the photocatalytic reduction. This reactor is first filled with 100 mL of water with 200 mg of catalyst powder, that is, Pt/Ga_2O_3 dispersed in it. CO_2 gas was filled at a pressure of 1.01 bar in the reactor. This reactor was exposed to irradiation from Xenon lamp (300 W), and the temperature of the reactor was kept constant by circulation of water. Ga_2O_3 with 1 wt% Pt nanoparticles dispersed on it showed the highest CO evolution rate of 21 μmol/h. When Pt content was higher than 1 wt%, deterioration in photocatalytic performance was observed. The main factor that affects the performance of catalyst to reduce CO_2 was the presence of oxygen vacancies.

This book belongs to Badji Mokhtar Annaba University Central Library Copyright Elsevier 2025

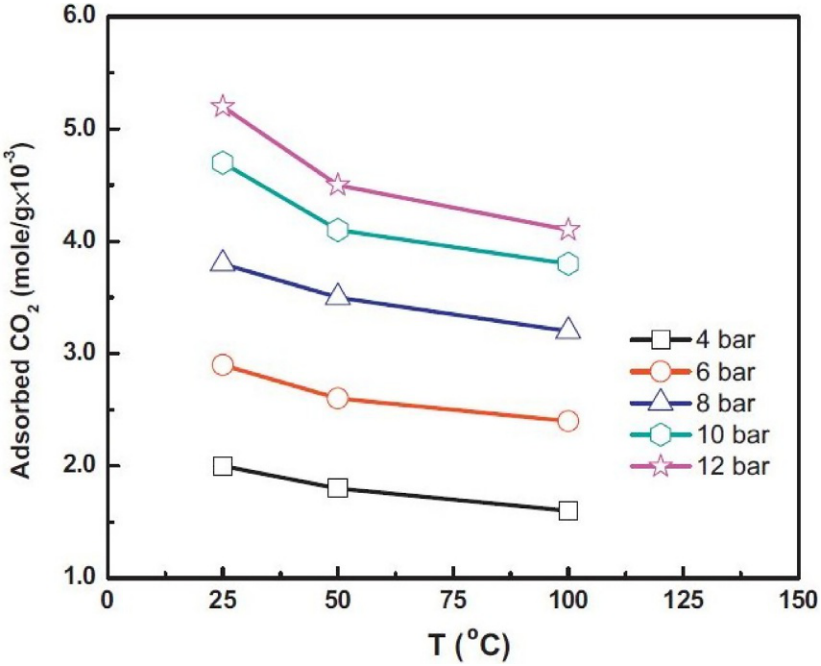

Fig. 11.3
Variation of adsorption capacity of Pd-GNP with temperature and pressure. *Reproduced with permission from A.K. Mishra, S. Ramaprabhu, Palladium nanoparticles decorated graphite nanoplatelets for room temperature carbon dioxide adsorption, Chem. Eng. J. 187 (2012) 10–15, https://doi.org/10.1016/j.cej.2011.01.024. Copyright 2012, Elsevier.*

Koci et al. [44] also photocatalytically reduced CO_2 over montmorillonite (MMT) deposited with CdS and ZnS nanoparticles. MMT deposited with CdS or ZnS was synthesized by the one-pot method. The performance of the prepared catalyst was evaluated in the photocatalytic reactor. A total of 12 mg of photocatalyst was dispersed in 120 mL of 0.2 M NaOH and fed to the reactor. This solution was saturated with fluid grade supercritical CO_2. This reaction mixture was then exposed to irradiation by Hg lamp (8 W). The reduction of CO_2 resulted in gaseous products such as CH_4, H_2, and CO. They reported that when the reaction mixture was irradiated at 254 nm wavelength UV radiation, the amount of H_2 produced was higher when compared to CH_4 and CO by one and two orders of magnitude, respectively. The yield by use of ZnS-MMT and CdS/ZnS-MMT was higher for all reaction products when compared to that exhibited by CdS-MMT. When the reaction mixture was exposed to irradiation at 365 nm, no CH_4 was found to be produced. The amount of H_2 produced was higher when compared to the amount of CO produced by one order of magnitude. Noticeably, ZnS-MMT and CdS-MMT showed nearly indifferent activities; for CdS/ZnS-MMT, eight times higher yield of H_2 resulted than that of ZnS-MMT and CdS-MMT photocatalysts. For CO, a decreasing trend in yield was observed as CdS-MMT > ZnS-MMT > CdS/ZnS-MMT.

This book belongs to Badji Mokhtar Annaba University Central Library Copyright Elsevier 2025

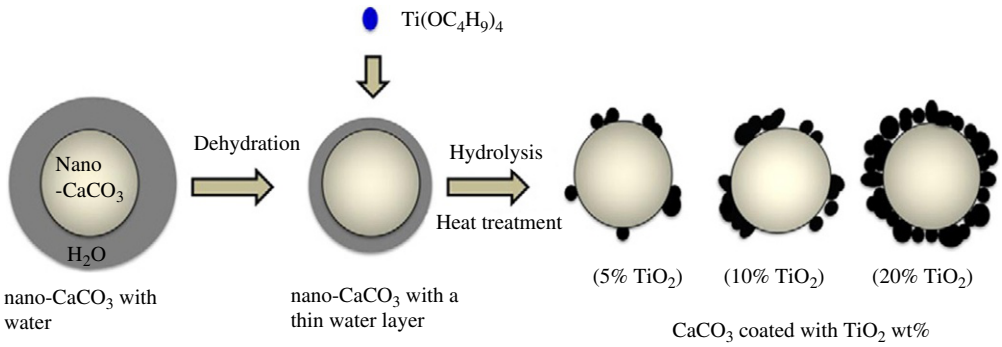

Fig. 11.4
Schematic representation of formation of TiO_2 coating on nano $CaCO_3$. *Reproduced with permission from Y. Wang, Y. Zhu, S. Wu, A new nano CaO-based CO_2 adsorbent prepared using an adsorption phase technique, Chem. Eng. J. 218 (2013) 39–45, https://doi.org/10.1016/j.cej.2012.11.095. Copyright 2013, Elsevier.*

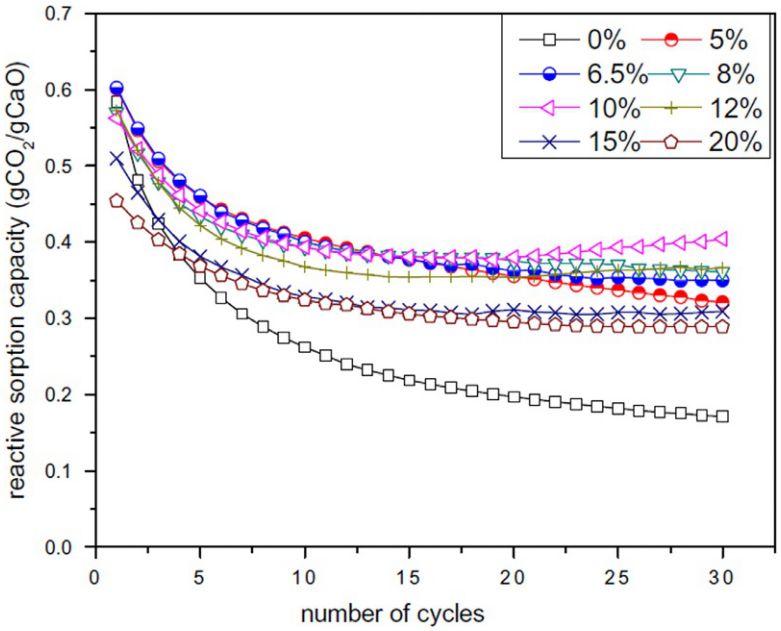

Fig. 11.5
Cyclic CO_2 sorption capability with variation in TiO_2 coating nano $CaCO_3$ sorbent. *Reproduced with permission from Y. Wang, Y. Zhu, S. Wu, A new nano CaO-based CO_2 adsorbent prepared using an adsorption phase technique, Chem. Eng. J. 218 (2013) 39–45, https://doi.org/10.1016/j.cej.2012.11.095. Copyright 2013, Elsevier.*

Wang et al. [52] synthesized nano CaO-based CO_2 adsorbent. The adsorption phase technique was employed to synthesize TiO_2-coated nano $CaCO_3$ (Fig. 11.4). A sample with different TiO_2 content ranging from 5% to 20% mass fraction was prepared for evaluating the effect of TiO_2 coating on the performance of adsorbent (Fig. 11.5). A 4.5–11.6 nm thick coating resulted in a

This book belongs to Badji Mokhtar Annaba University Central Library Copyright Elsevier 2025

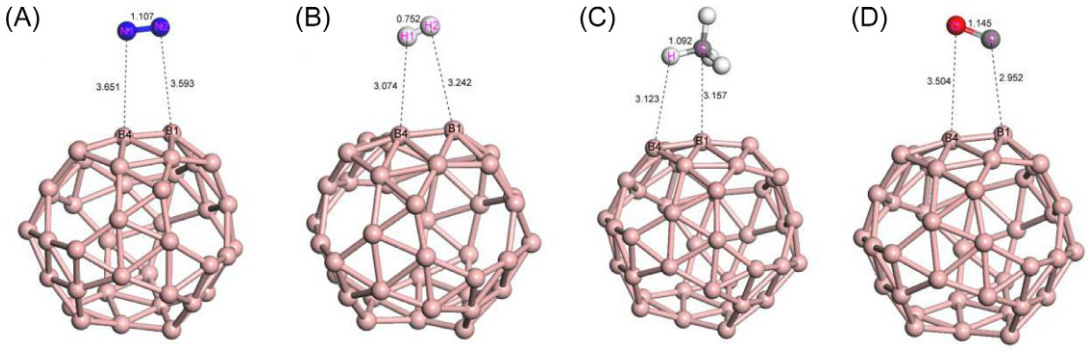

Fig. 11.6

Structures of (A) N_2, (B) H_2, (C) CH_4, and (D) CO adsorbed on B_{40} Fullerene. *Reproduced with permission from H. Dong, B. Lin, K. Gilmore, T. Hou, S.T. Lee, Y. Li, B40 fullerene: an efficient material for CO_2 capture, storage and separation, Curr. Appl. Phys. 15 (2015) 1084–1089, https://doi.org/10.1016/j.cap.2015.06.008. Copyright 2015, Elsevier.*

variation of TiO_2. The sorption capacity of the prepared adsorbent was conducted using a thermogravimetric analyzer and also in a fixed-bed reactor. The experiment was carried out repeatedly, and it was reported that the reactive sorption capacity of the prepared samples was initially higher and it decreased rapidly for the initial six cycles, but afterward, the decay rate was slow. After 30 cycles, a fairly constant reactive sorption capacity was observed. Smaller decay ratio was noted for a sample with TiO_2 content more than 8%, indicating improved durability owing to TiO_2 coating, and 8%–10% TiO_2 was found to be optimal. After 30 cycles of reactive adsorption-desorption, the highest sorption capacity and lowest decay ratio of 0.404 g of CO_2/g of CaO and 28.3%, respectively, were noted for the sample with 10% TiO_2 content. Ping et al. [53] synthesized MgO-coated nano CaO for CO_2 adsorption. The adsorption phase reaction method was employed for synthesis purpose. MgO was coated at different wt% varying from 6 to 25 wt% in the presence of alkaline liquids NaOH or NH_4OH, among which 12 wt% was found to be optimal. A thermogravimetric analyzer was used to measure the sorption performance of the prepared adsorbent. The experiment was conducted for 10 min under carbonation at a temperature of 600°C with 0.2 MPa partial pressure of CO_2 in N_2 and 10 min calcination in N_2 at 730°C temperature and atmospheric pressure. It was reported that alkaline liquid had an effect on the sorption capacity of the prepared samples, and adsorbent prepared using NaOH decays faster than that prepared with NH_4OH. Adsorbent prepared by the adsorption phase method shows better cyclic CO_2 sorption performance and no decay in the sorption capacity even after 30 cycles.

Dong et al. [54] numerically studied the capability of B_{40} fullerene to capture, store, and separate CO_2 by density functional calculation (Fig. 11.6). B_{40} showed good selectivity and high adsorption of CO_2 up to 13.87 mmol/g. Zhao et al. [55] theoretically evaluated the capability of peanut-shaped carbon nanotubes (PSNTs) and N-doped PSNTs to capture CO_2. It was concluded that PSNTs and N-doped PSNTs can adsorb CO_2 more effectively when

This book belongs to Badji Mokhtar Annaba University Central Library Copyright Elsevier 2025

compared to single-walled carbon nanotube (SWCNT). At 298 K and 5000 kPa and at 10,000 kPa, 4.15 mmol/g and 8.3 mmol/g of CO_2, respectively, was adsorbed by PSNT and N-doped PSNT.

11.4.2.2 NO_x

NO_x are a group of air pollutants that include NO, NO_2, and N_2O. NO_x can cause problems such as acid rain, photochemical smog, heavy haze, and various health-related issues. Conventionally, various methods are used to remove NO_x such as selective catalytic and noncatalytic reduction, storage and reduction, oxidation, and photocatalytic methods [35, 41, 56, 57]. Recently, a lot of attention is given to nanotechnology to tackle with these pollutants. Efforts of the various research groups and their findings are discussed further.

Long and Yang [58] investigated CNTs as adsorbent of NO. They synthesized CNTs by catalytic decomposition of acetylene. The synthesized CNTs had an outer and inner diameter in the range of 5–10 nm and 2–4 nm, respectively. The adsorption experiment was conducted in a quartz tube holding 10 mg of sample. This sample prior to adsorption was treated at 500°C for 30 min in the presence of helium. The gas fed to the experimental apparatus had a composition of 1000 ppm NO, 500 ppm SO_2, 10% CO_2, 5% O_2, and remaining helium. The total flow rate was maintained at 250 mL/min. They reported that when CNT is exposed to the mixture of 1000 ppm NO + 5% O_2, 78 mg/g of NO was adsorbed after 120 min, indicating good adsorption capacity of CNT toward NO. Singh et al. [15] investigated ZnO nanoparticles as an adsorbent for NO_2. The experimental setup included a U-shaped tube with glass beads placed in it. Approximately, 1 g of ZnO nanoparticle with an average size of 20 nm was placed in this tube. The reactive gas was fed at a rate of 30 mL/min, and ZnO nanoparticles were exposed to this stream for 20 min. Exposure of the ZnO nanoparticles to NO_2 resulted in NO_3 chemisorption. An enhancement was reported in adsorption capacity when ZnO was exposed to water-saturated air before exposure to reactive gas. Sato et al. [59] synthesized nanoparticles of Pd, Ru, Rh, and Pd_x-Ru_{1-x} (x ranging from 0.1 to 0.9) and deposited them on γ-Al_2O_3 supports. These supported catalysts were then placed in a fixed-bed flow reactor, and their ability to reduce NO_x was investigated. Rh and Pd_x-Ru_{1-x} (x ranging from 0.1 to 0.9) were able to reduce up to 100% NO_x between temperatures 200°C and 250°C, whereas Pd and Ru exhibited the same at around 350°C. N_2 was found to be a major product of the reaction, whereas N_2O was also reported being formed in temperature range 200–250°C. Above 350°C, all NO_x was found to be reduced to N_2.

Ho et al. [45] synthesized lanthanum-doped TiO_2 (La-TiO_2) for photocatalytic degradation of acetone. Lanthanum used for doping was recycled from waste fluorescent powder. The sol-gel method was used for synthesizing La-TiO_2. This prepared photocatalyst was immobilized on a commercial porous ceramic filter and was investigated for degradation of simulated gas NO at a concentration of 500 ppb in a continuous flow reactor. The experiment was conducted at room temperature under visible light. Xenon lamp of 300 W was used as a source of visible light. The relative humidity (RH) of the fed stream was varied from 0% to 100% by the use of

This book belongs to Badji Mokhtar Annaba University Central Library Copyright Elsevier 2025

humidification chamber. From the experiment, it was reported that up to 98% of photocatalytic removal efficiency can be obtained by 0.5 wt% La-TiO_2 under visible light. Zhang et al. [60] synthesized bismuth subcarbonate $(BiO)_2CO_3$/graphene or graphene oxide nanocomposite by using the one-pot method. These self-assembled nanoflakes of $(BiO)_2CO_3$ on nanosheets of graphene or graphene oxide were then applied in the treatment of NO. These nanoflakes were reported to be in the size range of 25–120 nm. These prepared nanocomposites, that is, $(BiO)_2CO_3$, $(BiO)_2CO_3$ on graphene, and $(BiO)_2CO_3$ on graphene oxide, in the presence of NO gas when exposed to simulated solar irradiation reported to effectively degrade 54.8%, 63.5% and 61.6% of NO, respectively, within 30 min.

Zhang et al. [61] synthesized perovskite $LaFeO_3/SrTiO_3$ nanocomposite through solution-based method. The performance of this prepared photocatalyst was investigated in a photoreactor, holding 0.1 g of photocatalyst. This reactor was introduced with a mixture of NO/air having a concentration of 400 ppb at the flow rate of 3 L/min. Photocatalyst was allowed to attain adsorption-desorption equilibrium for 30 min. After that, it was exposed to irradiation by a xenon lamp (300 W). The experiment was carried out at ambient conditions. It was reported that prepared $LaFeO_3$-$SrTiO_3$ nanocomposite was able to remove 40% of NO, indicating good performance of photocatalyst in the treatment of NO. Zhang et al. [62] synthesized silver-doped $SrTiO_3$ (Ag-$SrTiO_3$) photocatalyst through the one-pot solvothermal method. The prepared photocatalyst had nanocube morphology with an average size of 40 nm. Continuous gas flow reactor having 4.5-L volume was used to evaluate the performance of this photocatalyst. About 0.1 g of photocatalyst was placed inside the reactor. A gas stream with 400 ppb NO concentration was introduced to the reactor at a constant flow rate of 3 L/min. They reported that 30% of NO was removed by 0.5% Ag-doped $SrTiO_3$. It was also noted that increasing doping does not improve NO removal substantially, and hence 0.5% Ag doping was considered to be optimum.

Hu et al. [63] synthesized nanocomposite photocatalyst $Bi_2O_2CO_3$-MoS_2 on carbon nanofibers ($Bi_2O_2CO_3$-MoS_2-CNFs) for removal of NO (Fig. 11.7). The photocatalytic activity of the prepared photocatalyst was evaluated using a continuous flow reactor, with 0.15 g of catalyst placed inside the reactor. NO/air stream with NO concentration of 600 ppb was introduced to the reactor at a flow rate of 2.4 L/min. The whole experiment was carried out at ambient conditions. It was reported that the prepared nanocomposite photocatalyst at the end of the experiment was able to attain NO removal ratio of 68%, indicating good performance of the prepared photocatalyst at low NO concentrations.

Ai et al. [64] synthesized bismuth oxybromide (BiOBr) nanoplate microspheres photocatalyst by using the sol-gel method. Nanoplates were interwoven to form microspheres of size ranging from 2 to 5 μm. This prepared photocatalyst was used for the degradation of NO under visible light. Degradation performance of the prepared photocatalyst was evaluated by the use of a continuous flow reactor of volume 4.5 L containing 0.2 g of catalyst placed inside. About 400 ppb concentration of NO/air mixed stream was introduced to the reactor at the constant flow rate of 4 L/min. After reaching the adsorption-desorption equilibrium, the reactor was

This book belongs to Badji Mokhtar Annaba University Central Library Copyright Elsevier 2025

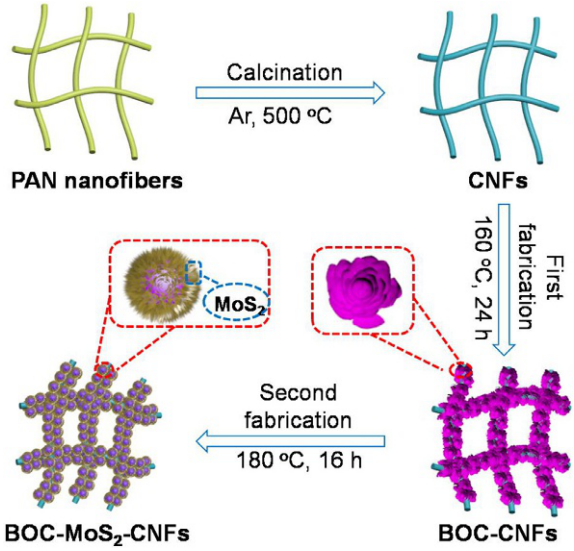

Fig. 11.7
Schematic illustration of the fabrication of BOC-MoS_2-CNFs. *Reproduced with permission from J. Hu, D. Chen, N. Li, Q. Xu, H. Li, J. He, J. Lu, In situ fabrication of $Bi_2O_2CO_3/MoS_2$ on carbon nanofibers for efficient photocatalytic removal of NO under visible-light irradiation, Appl. Catal. B Environ. 217 (2017) 224–231, https://doi.org/10.1016/j.apcatb.2017.05.088. Copyright 2017, Elsevier.*

illuminated with irradiation from a tungsten halogen lamp (300 W). A 45% NO removal was observed within 10 min under UV-visible light.

11.4.2.3 SO_x

SO*x* (sulfur monoxide) are a group of air pollutants that include gaseous and particulate chemical species such as SO, SO_2, SO_3, and S_2O. Sulfur oxide and sulfate particles can cause severe health problems related to the respiratory and cardiovascular system and also environmental problems, including acid rain, damaging foliage, and hampering growth [32, 34, 35, 57].

Arcibar-Orozco et al. [38] performed reactive adsorption on iron nanoparticle-deposited AC. For this, a commercial AC, Filtrasorb 400 was treated in order to deposit two differently sized iron nanoparticles (Fe-NP). One sample that was prepared with iron nanoparticle size ranging from 15 to 30 nm, with iron content in sample 1.39%, was named as AC-M, and the other sample that was prepared to deposit iron nanoparticle size ranging from 3 to 4 nm, with iron content in the sample 1.12%, was named as AC-MP. Evaluation of effectiveness to remove SO_2 from air was carried out in a column made up of glass with an internal diameter of 0.9 cm and 370 mm in length. About 2 cm^3 of carbon was packed in the column. The inlet stream flow rate was kept constant at 450 mL/min, with a constant SO_2 concentration of 1000 ppmv. The experiment was performed at ambient conditions and in dry and moist air. Appropriate

This book belongs to Badji Mokhtar Annaba University Central Library Copyright Elsevier 2025

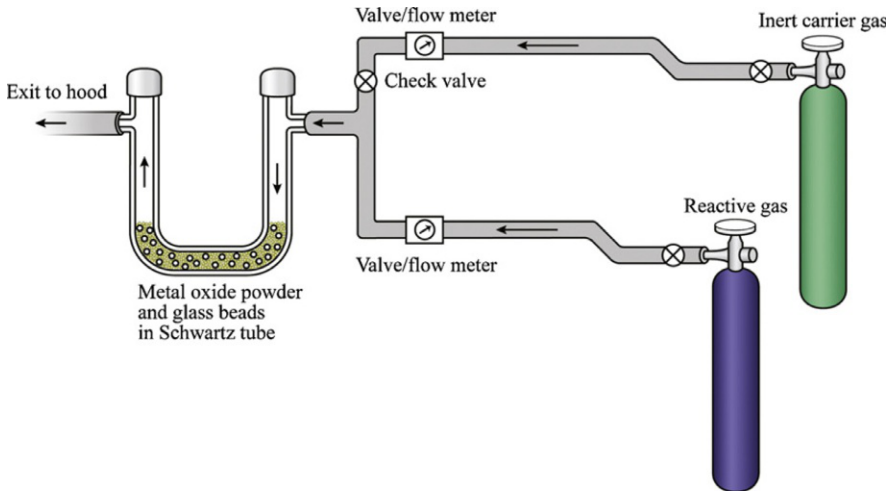

Fig. 11.8
Schematic illustration of experimental setup used for adsorption of SO_2 and NO_2 by metal oxide and metal hydroxide powders. *Reproduced with permission from J. Singh, A. Mukherjee, S.K. Sengupta, J. Im, G. W. Peterson, J.E. Whitten, Sulfur dioxide and nitrogen dioxide adsorption on zinc oxide and zirconium hydroxide nanoparticles and the effect on photoluminescence, Appl. Surf. Sci. 258 (2012) 5778–5785, https://doi.org/10.1016/j.apsusc.2012.02.093. Copyright 2012, Elsevier.*

pretreatment was carried out for performing the experiment at two different conditions. AC with the surface area of 1051 m^2/g showed 32 mg/g adsorption capacity of SO_2 at a breakthrough point in moist condition, whereas in the dry condition, it was 18 mg/g. The sample AC-M with the surface area of 980 m^2/g showed 26 mg/g adsorption capacity of SO_2 at a breakthrough point in moist condition, whereas in the dry condition, it was 18 mg/g. The sample AC-MP with the surface area of 879 m^2/g showed 60 mg/g adsorption capacity of SO_2 at a breakthrough point in moist condition, whereas in the dry condition, it was 19 mg/g. The presence of Fe-NP of size 3–4 nm helped in capturing SO_2, and also, adsorption in wet conditions was much more effective than that in dry conditions.

Long and Yang [58] also investigated CNT as an adsorbent of SO_2. When the CNT sample was exposed to the mixture of 500 ppm SO_2 + 5% O_2, 29 mg/g of SO_2 was adsorbed after 120 min of exposure. When subsequently the same sample was exposed to helium, 8.6 mg/g of SO_2 was desorbed in 60 min. Singh et al. [15] investigated ZnO nanoparticles as an adsorbent for SO_2. The experimental setup included a U-shaped tube with glass beads placed in it (Fig. 11.8). Approximately, 1 g of ZnO nanoparticle with an average size of 20 nm was placed in this tube. The reactive gas was fed at the rate of 30 mL/min, and the ZnO nanoparticles were exposed to this stream for 20 min. They noted that the exposure of ZnO nanoparticles to SO_2 results in SO_3 chemisorption. An enhancement was reported in adsorption capacity when ZnO was exposed to water-saturated air before exposure to reactive gas. This increase in uptake was attributed to the changes in the morphology and surface area. A 10-fold increase was reported in the adsorption of SO_2 resulting because of hydration.

This book belongs to Badji Mokhtar Annaba University Central Library Copyright Elsevier 2025

11.4.2.4 Volatile organic compounds

VOCs are organic chemicals that can readily emit vapors from their solid or liquid forms at ambient temperature. Many VOCs are toxic and may cause cancer or other severe effects on health [35]. And hence, their presence in ambient air must be kept low, i.e., below the levels prescribed by WHO. Nanotechnology is continuously employed by various research groups for the treatment of VOCs, which are discussed in this section.

Ho et al. [45] synthesized and investigated lanthanum-doped TiO_2 (La-TiO_2) for photocatalytic degradation of acetone. Recycled lanthanum was used in the sol-gel method for synthesizing La-TiO_2. This photocatalyst was immobilized on a commercial porous ceramic filter. It was further used to degrade acetone at a concentration of 1000 ppb at ambient temperature under visible light. From the experiment, it was reported that up to 38% of photocatalytic removal efficiency can be obtained by 0.5 wt% La-TiO_2 under visible light. Sun et al. [16] developed Pt/N-TiO_2 photocatalyst and used it for the degradation of phenol, acetone, toluene, ethanol, 2-propanol, *n*-hexane, and trichloroethylene. Pt/N-TiO_2 was synthesized using the sol-gel method. The prepared Pt/N-TiO_2 was reported to have a particle size of 10 nm. Experiment to investigate the performance of the prepared photocatalyst in the degradation of VOC was carried out in batch and continuous reactors. The batch system was irradiated with Xenon arc lamp (300 W) and employed 0.1 g of photocatalyst. On the other hand, the continuous system was irradiated with a fluorescent lamp and employed 0.2 g of photocatalyst. They reported that Pt/N-TiO_2 can degrade the above chemicals in the presence of light at varying efficiencies (Fig. 11.9). When

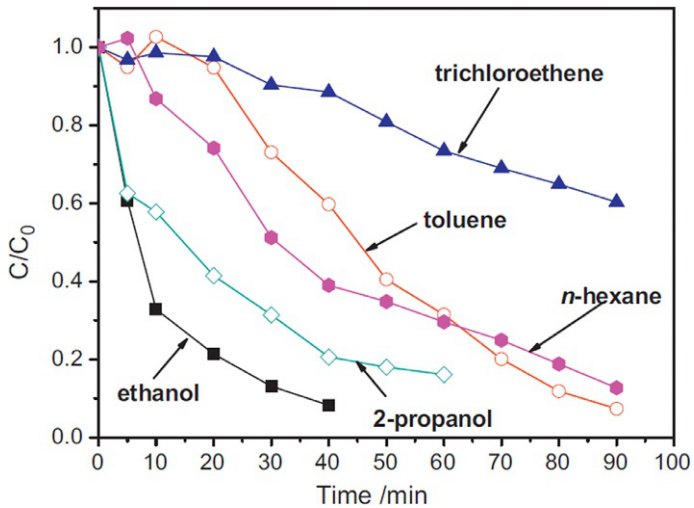

Fig. 11.9
Degradation of VOCs on Pt/N-TiO_2 photocatalyst. *Reproduced with permission from H. Sun, R. Ullah, S. Chong, H.M. Ang, M.O. Tadé, S. Wang, Room-light-induced indoor air purification using an efficient Pt/N-TiO_2 photocatalyst, Appl. Catal. B Environ. 108–109 (2011) 127–133, https://doi.org/10.1016/j.apcatb.2011.08.017. Copyright 2011, Elsevier.*

This book belongs to Badji Mokhtar Annaba University Central Library Copyright Elsevier 2025

exposed to wavelengths longer than 387 nm, Pt/N-TiO_2 photocatalyst was able to completely degrade phenol and acetone in 60 min. Almost 80% of *n*-hexane and toluene got degraded in 90 min, 2-propanol in 60 min, and 90% of ethanol got degraded in 40 min. These results show that Pt/N-TiO_2 has good photocatalytic activity and can degrade VOCs efficiently.

Rengaa et al. [65] synthesized AC from bamboo and deposited nanoparticles of silver on it. This silver-decorated AC (Ag-AC) was used to remove VOC, more specifically formaldehyde, from the air by adsorption. The AC was prepared by carbonizing bamboo and activated by 25 vol% KOH solution. The deposition of Ag-NP was achieved by mixing the Ag-NP solution with AC and stirred for 24 h, which resulted in approximately 4 wt% deposition of Ag-NP. The prepared Ag-AC and AC were used for adsorption of formaldehyde. The experiment was carried out in a fixed-height continuous packed bed column for evaluating the effect of initial concentration in influent and influent flow rates. For this, gas was fed at a constant flow rate of 500 mL/min and with variation in inlet concentration of formaldehyde from 100 to 1000 ppm. They observed that exhaustion time, which was defined as the time when $C_{out}/C_{in} = 0.95$ for Ag-AC, was higher when compared to AC fixed-bed. Higher inlet concentration caused earlier exhaustion. To evaluate the effect of influent flow rate, formaldehyde concentration in the influent stream was kept constant at 300 ppm, and the influent flow rate was varied from 350 to 500 mL/min. They observed that exhaustion occurred earlier for higher flow rate (500 mL/min) compared to lower flow rate (350 mL/min). At the same flow rates, the Ag-AC bed took longer breakthrough time than that taken by AC bed alone. Overall, it was observed that formaldehyde was 2.36 times better adsorbed by the Ag-AC column than that by the neat AC column. Kannangara et al. [66] synthesized nitrogen-doped TiO_2 (N-TiO_2) nanoparticles and used them to photocatalytically degrade toluene (Fig. 11.10). The sol-gel method was used to prepare N-TiO_2 photocatalyst. By using the doctor-blade method, a 0.213 g thin film of the photocatalyst was coated on a glass plate of 1 cm^2 area. To evaluate the photocatalytic activity of N-TiO_2, the prepared thin-film glass plate was placed in a quartz cell with an initial toluene concentration of 2 μL. This cell was then placed under a solar simulator (US-900). Degradation of 45% of toluene was observed in 110 min of exposure to irradiation. Additionally, it was also observed that degradation efficiency was improved with an increase in N-TiO_2 amount in thin film from 0.71 to 5 mg. Degradation efficiency was found to be increasing with an increase in the thickness of the film up to some optimal thickness after which efficiency started decreasing. It was reported that degradation efficiency was the highest (82.39%) for 9.26 μm thick photocatalytic film having 1 mg content of N-TiO_2. Hsu and Lu [67] used SWCNTs oxidized by HCl, HNO_3, and NaClO solutions for adsorption of isopropyl alcohol vapor. They calculated the adsorption capacity by Langmuir model to be 63.48 mg/g for SWCNT, 54.43 mg/g for HCl treated SWCNT, 72.99 mg/g for HNO_3 treated SWCNT, and, the highest, 103.56 mg/g for NaClO treated SWCNT.

Chuang at el. [68] employed carbonized bamboo (CB) with TiO_2 nanoparticles for the removal of benzene and toluene by adsorption. They synthesized CB–TiO_2 composite (CBC) by depositing the TiO_2 nanoparticles separately made by the sol-gel method on carbonized

This book belongs to Badji Mokhtar Annaba University Central Library Copyright Elsevier 2025

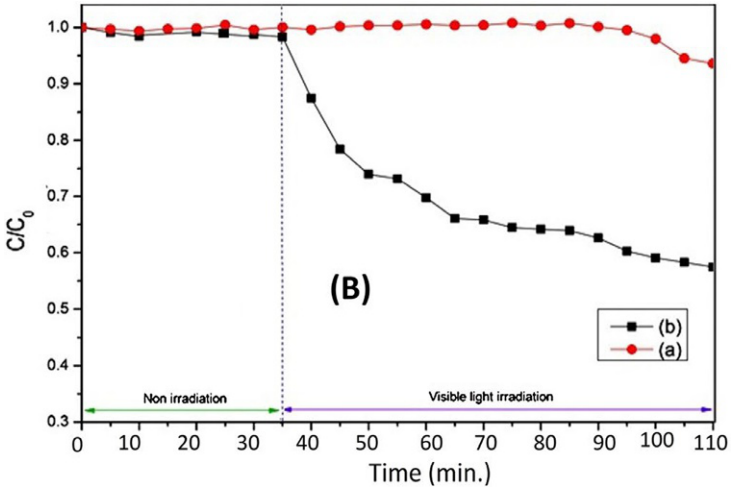

Fig. 11.10
Degradation of toluene by N-TiO_2 (A) in the absence of and (B) under visible light irradiation.
Reproduced with permission from Y.Y. Kannangara, R. Wijesena, R.M.G. Rajapakse, K.M.N. de Silva, Heterogeneous photocatalytic degradation of toluene in static environment employing thin films of nitrogen-doped nano-titanium dioxide, Int. Nano Lett. 8 (2018) 31–39, https://doi.org/10.1007/s40089-018-0230-x. Copyright 2018, Springer Nature [The source of this image is an open access article distributed under the Creative Commons Attribution (CC-BY) License (http://creativecommons.org/licenses/by/4.0/)].

Moso bamboo. The average deposited TiO_2 particle size was 28 nm. Two samples with different TiO_2 deposition were made and named as CBC1 and CBC2. In addition, a mixture of CB and TiO_2 (CBM) was prepared with 1:1 (CBM1) and 2:1 (CBM2) mass ratio of CB:TiO_2 to investigate synergetic effects. Experiment to investigate the photocatalytic activity of prepared material and synergistic effect of sorption were carried out in a closed chamber of volume 0.03 m^3, which was exposed to UV irradiation, with UV source having a light intensity of 0.5 mW/cm at wavelength of 365 nm. About 5 g of sorption sample was coated on a glass plate having an area of 100 cm^2 and placed inside the closed chamber. At an internal circulation rate of 1.5 L/min, both benzene and toluene were injected at a concentration of 45 ppmv. The experimental run was carried out for a total of 180 min for each sample. From the experiment, it was reported that CBC1 and CBC2 were able to remove 54% and 72% of benzene, respectively, which was greater than the removal efficiency of CBM1 of 45% and CBM2 of 55%. For toluene, reported removal efficiency for CBC1 and CBC2 was 48% and 71%, respectively, which was higher than that reported for CBM1 (41%) and CBM2 (51%). These results clearly demonstrate that the deposition of the TiO_2 nanoparticles improves the sorption capacity of material, and that CBM and CBC were more efficient in removing benzene than toluene.

Lee et al. [69] investigated activated carbon nanofiber (ACNF) as an adsorbent of formaldehyde. They synthesized ACNF by carbonizing and steam-activating electrospun polyacrylonitrile (PAN) nanofiber. The carbonization of PAN was carried out at 600°C for 1 h

This book belongs to Badji Mokhtar Annaba University Central Library Copyright Elsevier 2025

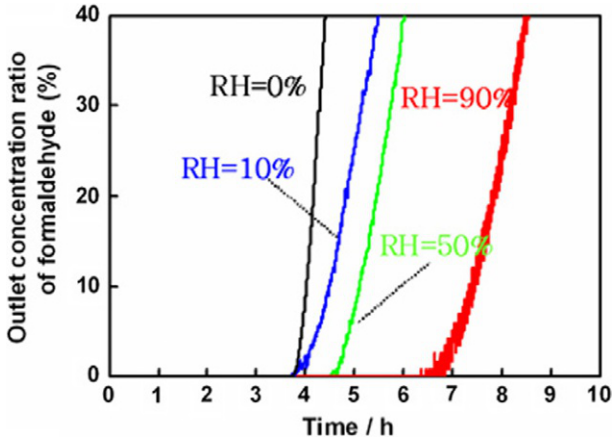

Fig. 11.11
Breakthrough curves of formaldehyde (22 ppm) in dry condition with respect to RH during steam activation of PAN nanofiber. *Reproduced with permission from K.J. Lee, N. Shiratori, G. H. Lee, J. Miyawaki, I. Mochida, S.H. Yoon, J. Jang, Activated carbon nanofiber produced from electrospun polyacrylonitrile nanofiber as a highly efficient formaldehyde adsorbent, Carbon N. Y. 48 (2010) 4248–4255, https://doi.org/10.1016/j.carbon.2010.07.034. Copyright 2010, Elsevier.*

in flowing helium gas. Steam was added in helium gas flow to carry out steam-activation with humidity ranging from 0% to 90%. Adsorption experiment was performed in a fixed-bed column with a length of 40 and 8 mm of diameter. About 0.05 g of prepared adsorbent was filled in a column. The experiment was carried out for dry and wet conditions. In the case of dry condition, formaldehyde gas at a concentration of 22 ppm was fed to the column at a constant flow rate of 100 mL/min (Fig. 11.11). For the case of wet condition, the inlet stream had formaldehyde concentration at 11 ppm and a RH of 50%. From the experiment, it was reported that ACNF activated under 90% humidity performed better than the sample prepared at lower humidity. The breakthrough time for this ACNF for inlet gas concentration of 11 ppm was reported to be 10.5 h under the dry conditions and 5 h at 50% RH conditions. The breakthrough time is the time at which the output concentration of formaldehyde reaches 1% of the inlet. The ACNF was able to adsorb 0.05 and 0.023 mmol/g of formaldehyde in dry and humid experimental conditions, respectively. These results demonstrated that ACNF was capable of adsorbing formaldehyde, and that this capability was owing to the presence of nitrogen and shallow microporosity.

11.5 Pilot-scale studies

As discussed in the previous section, a lot of research has been conducted in laboratory to study about the treatment of air pollutants with the use of nanomaterials. Researchers are now extending their investigation to evaluate applicability and performance of the nanomaterials on a large scale by various means.

This book belongs to Badji Mokhtar Annaba University Central Library Copyright Elsevier 2025

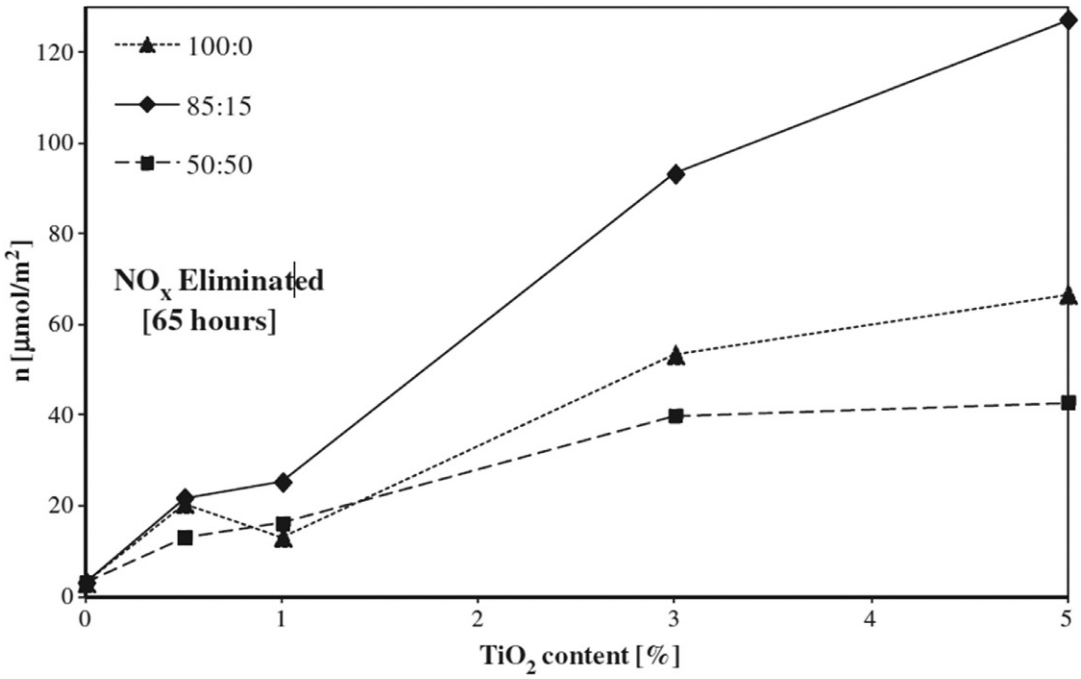

Fig. 11.12

NO_x removal by various prepared samples in 65 h. *Reproduced with permission from C. Cárdenas, J. I. Tobón, C. García, J. Vila, Functionalized building materials: photocatalytic abatement of NO_x by cement pastes blended with TiO_2 nanoparticles, Constr. Build. Mater. 36 (2012) 820–825, https://doi.org/10.1016/j.conbuildmat.2012.06.017. Copyright 2012, Elsevier.*

Cárdenas et al. [63] prepared bricks of cement paste containing nanoparticles of TiO_2. Commercial TiO_2 nanopowder of anatase and rutile phases were blended in different proportions in Type I Colombian Portland white cement to prepare samples with TiO_2 content from 0 to 5 wt%, each sample containing different anatase: rutile ratio. The experiment was conducted under UV irradiation and 1 ppmv NO concentration. Sample containing 5 wt% TiO_2 exhibited higher removal of NO_x, and the sample with anatase: rutile ratio of 85:15 was more photocatalytically active in early age in contradiction to the sample with 100:0, which was more photocatalytically active in late age. Figs. 11.12 and 11.13 show the trend of NO_x removal by various prepared samples in 65 h and 28 days, respectively [70].

Huang et al. [64] developed air purifier incorporating nanoparticles on the filter medium. The filter was coated with TiO_2 hydrosol, with ions of metal and nonmetal dispersed on it. This filter was exposed to UV light irradiation. Air was flown over coated filter by using fan, and pollutants were decomposed there. This research group also developed a street lamp for mitigating the problem of ozone in Xi'an, China. This street lamp had a module fitted inside by the use of which the filter clears PM and a photocleaning module consisting of ceramics coated with TiO_2 decomposing pollutants. The air surrounding the lamp is pumped inside from bottom of street lamp, where it first passes through filter and then through photocatalytic module to the outlet from top.

This book belongs to Badji Mokhtar Annaba University Central Library Copyright Elsevier 2025

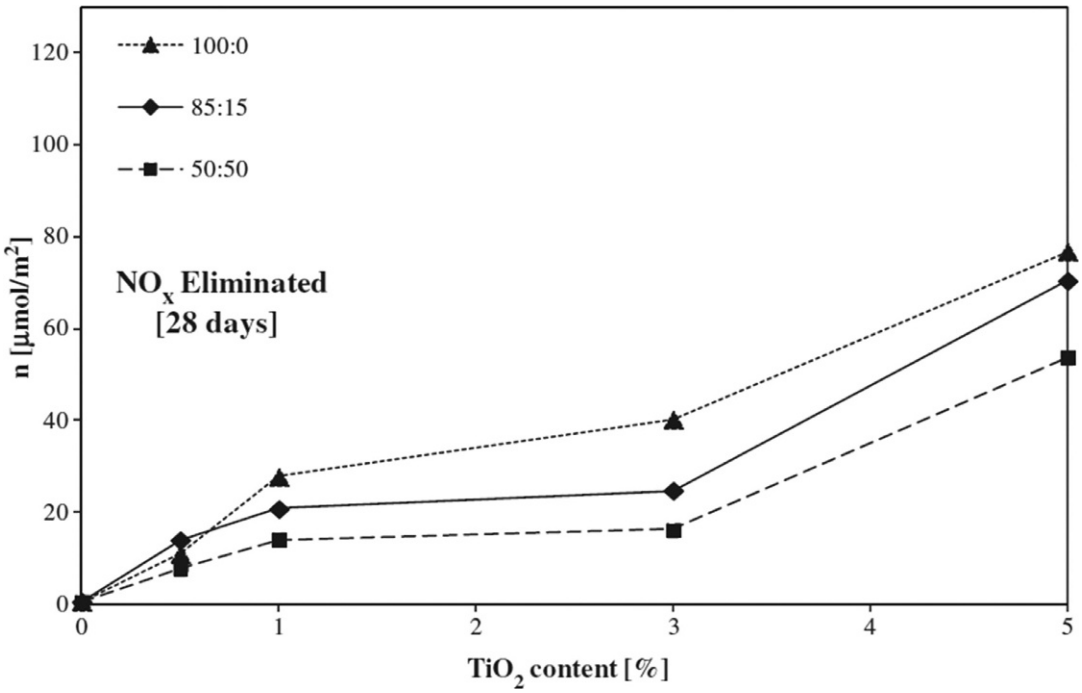

Fig. 11.13
NO_x removal by various prepared samples in 28 days. *Reproduced with permission from C. Cárdenas, J. I. Tobón, C. García, J. Vila, Functionalized building materials: photocatalytic abatement of NO_x by cement pastes blended with TiO_2 nanoparticles, Constr. Build. Mater. 36 (2012) 820–825, https://doi.org/10.1016/j.conbuildmat.2012.06.017. Copyright 2012, Elsevier.*

11.6 Challenges for the usage of nanomaterials for air pollution treatment

Even though nanotechnology exhibits remarkable material properties that can be exploited for air pollution treatment, there are also some challenges faced by this technology that limits its application on a large scale. One big challenge is manufacturing of nanomaterials. Most of the methods used to synthesize nanomaterials are energy-intensive and not scalable for a higher rate of production. Another problem is associated with the physical properties of prepared nanomaterial, i.e., particle size, shape, and agglomeration of particles that can affect the performance of these materials [66]. As discussed by Li et al. [71], activity of TiO_2 nanoparticle depends on shape. This activity dependence can be attributed to the variation in surface charge density of nanoparticles. Pan et al. [46] reported a decrease in performance of photocatalyst with an increase in platinum content because of aggregation at a higher platinum concentration. Similarly, agglomeration was reported by Kannangara [66] with an increase in nanoflim thickness and hence a decrease in performance. The performance of these nanomaterials can also get affected by the surrounding conditions such as temperature, pressure, and humidity. [23]. Mishra et al. [51] reported a decrease in adsorption capacity with

This book belongs to Badji Mokhtar Annaba University Central Library Copyright Elsevier 2025

an increase in temperature. This is because higher temperature of the adsorbed molecules imparts enough energy to break the bond formed with substrate during adsorption. Humidity, as discussed by researchers, need to be at optimum level for satisfactory performance. At lower humidity level, water vapor can get condensed into capillaries and can block adsorption or reactive site of substrate. Higher humidity level also might result in surface coverage on nanomaterial by formation of water layer that can consequently block the interaction between substrate and gaseous pollutants [15, 45, 69]. Hence, it is important to maintain constant and optimum operating conditions for consistent results. Once these hurdles are overcome, a robust technology handy for air pollution control can be developed.

11.7 Summary and conclusion

Air is an eternal need of each and every living being on the planet for the survival. Continuous and unsupervised release of unwanted harmful and toxic gases or particulates causes such degradation in the quality of air that only 1 out of 10 lives gains access to air that complies with the WHO guidelines. It has become imperative to tackle this problem for the survival and well-being of living creatures and the environment. Various strategies and policies are being adopted and implemented by the government to discourage the use of technologies that can adversely affect the environment. Various methods and technologies are continuously explored and developed for the treatment of air pollutants. As discussed in this chapter, nanotechnology possesses immense potential in the treatment of air pollutants because of its incomparable properties. Although nanomaterials offer such great advantages, their use for the treatment of air pollutants is very limited because of high costs. Hence an efficient, eco-friendly, and cheap technique is required to manufacture nanomaterials on a large scale and utilize them for the treatment of air pollutants.

Even if the technology of using nanomaterials for removal of air pollutants seems to have emerged as an effective method from the point of view of researchers, it still lags in a few aspects as far as industrial applicability is concerned. Some nanomaterials and their synthesis processes promote “clean” and “green” concepts complying with the environmental norms, which must be feasible enough for scaling-up. A lot of literature available report improvement in nanomaterial properties when some other nanomaterial is associated with it. The technologies that aid in enhancing the qualities of nanomaterials involve doping, functionalization, and other modification techniques. But these technologies also tend to deteriorate the environmental friendliness of the nanomaterials. For example, TiO_2 is a safe and comparatively nontoxic material. However, addition of some metal-based nanomaterials may increase its toxicity apart from property enhancement.

Industrial applications are obviously large-scale applications that require large amounts of materials. In contradiction to laboratory scale, the synthesis, application, and disposal of nanomaterials may possess loads of expenditure. The various methods for the development of efficient nanomaterials for air pollution control involve laboratory-based methods that possess

This book belongs to Badji Mokhtar Annaba University Central Library Copyright Elsevier 2025

some uncertainties for scaling-up in view of their large-scale applications. Thus eco-friendly, green, and cost-effective synthesis methods for nanomaterials need to be developed. Research in the field of development of nanomaterials for air pollution reduction also must provide guidelines for optimal use of nanomaterials for maximum pollutant removal in order to make the system feasible for large-scale industrial applications. Application of nanomaterials for any purpose increases the risks of exposure to the harmful elements that may have potential health hazards. Along with all the aspects of application of nanomaterials for air pollution treatment, guided frameworks or algorithms for risk assessment of the technology can give an insight about the possible health issues that prove to be of major concern. In addition to all of the above, conversion of the targeted pollutant into useful products can prove to be one of the greatest discoveries that can profit industries thereby increasing their willingness to use such technologies. In view of the outstanding flexibility of nanomaterials to be molded in accordance with the application, the best possible design of an air pollution control system incorporating nanomaterials must be developed to extend this laboratory scale science to an industry-oriented technology.

References

[1] M.M. Cortalezzi, V. Colvin, M.R. Wiesner, Controlling submicron-particle template morphology: effect of solvent chemistry. J. Colloid Interface Sci. 283 (2005) 366–372, https://doi.org/10.1016/j.jcis.2004.08.171.

[2] A. Rether, M. Schuster, Selective separation and recovery of heavy metal ions using water-soluble N-benzoylthiourea modified PAMAM polymers. React. Funct. Polym. 57 (2003) 13–21, https://doi.org/10.1016/j.reactfunctpolym.2003.06.002.

[3] M.S. Diallo, L. Balogh, A. Shafagati, J.H. Johnson, Poly (amidoamine) dendrimers: a new class of high capacity chelating agents for Cu (II) ions, Environ. Sci. Technol. 33 (1999) 0–4.

[4] M.N. Subramaniam, P.-S. Goh, W.-J. Lau, B.-C. Ng, A.F. Ismail, Development of nanomaterial-based photocatalytic membrane for organic pollutants removal. in: Advanced Nanomaterials for Membrane Synthesis and Its Applications, Elsevier, 2019, pp. 45–67, https://doi.org/10.1016/B978-0-12-814503-6.00003-3.

[5] M. Amini, M. Arami, N.M. Mahmoodi, A. Akbari, Dye removal from colored textile wastewater using acrylic grafted nanomembrane. Desalination 267 (2011) 107–113, https://doi.org/10.1016/j.desal.2010.09.014.

[6] K.M. Joshi, V.S. Shrivastava, Photocatalytic degradation of chromium (VI) from wastewater using nanomaterials like TiO_2, ZnO, and CdS. Appl. Nanosci. 1 (2011) 147–155, https://doi.org/10.1007/s13204-011-0023-2.

[7] Y. Liu, C. Hou, T. Jiao, J. Song, X. Zhang, R. Xing, J. Zhou, L. Zhang, Q. Peng, Self-assembled AgNP-containing nanocomposites constructed by electrospinning as efficient dye photocatalyst materials for wastewater treatment. Nanomaterials 8 (2018) 35, https://doi.org/10.3390/nano8010035.

[8] M. López Portillo, Air pollution, Salud Publica Mex. 24 (1982) 523–531.

[9] Health Effects Institute, State of Global Air 2019, Health Effects Institute, 2019, 24. https://www.stateofglobalair.org/sites/default/files/soga_2019_report.pdf.

[10] The Hindu, (n.d.) SC bans sale of BS-IV vehicles from 2020.

[11] Bureau of Energy Efficiency, (n.d.) Climate Change.

[12] G.O.I, Resolution | Ministry of New and Renewable Energy | Government of India, https://mnre.gov.in/resolution, 2010.

[13] X.Y. Kong, Y.Y. Choo, S.P. Chai, A.K. Soh, A.R. Mohamed, Oxygen vacancy induced Bi_2WO_6 for the realization of photocatalytic CO_2 reduction over the full solar spectrum: from the UV to the NIR region. Chem. Commun. 52 (2016) 14242–14245, https://doi.org/10.1039/c6cc07750a.

This book belongs to Badji Mokhtar Annaba University Central Library Copyright Elsevier 2025

[14] M. Ganesh, P. Hemalatha, M.M. Peng, H.T. Jang, One pot synthesized Li, Zr doped porous silica nanoparticle for low temperature CO_2 adsorption. Arab. J. Chem. 10 (2017) S1501–S1505, https://doi.org/10.1016/j.arabjc.2013.04.031.

[15] J. Singh, A. Mukherjee, S.K. Sengupta, J. Im, G.W. Peterson, J.E. Whitten, Sulfur dioxide and nitrogen dioxide adsorption on zinc oxide and zirconium hydroxide nanoparticles and the effect on photoluminescence. Appl. Surf. Sci. 258 (2012) 5778–5785, https://doi.org/10.1016/j.apsusc.2012.02.093.

[16] H. Sun, R. Ullah, S. Chong, H.M. Ang, M.O. Tadé, S. Wang, Room-light-induced indoor air purification using an efficient Pt/N-TiO_2 photocatalyst. Appl. Catal. B Environ. 108–109 (2011) 127–133, https://doi.org/10.1016/j.apcatb.2011.08.017.

[17] I. Khan, K. Saeed, I. Khan, Nanoparticles: properties, applications and toxicities. Arab. J. Chem. 12 (2019) 908–931, https://doi.org/10.1016/j.arabjc.2017.05.011.

[18] E.F. Mohamed, Nanotechnology: future of environmental air pollution control. Environ. Manage. Sustain. Dev. 6 (2017) 429, https://doi.org/10.5296/emsd.v6i2.12047.

[19] J. Jeevanandam, A. Barhoum, Y.S. Chan, A. Dufresne, M.K. Danquah, Review on nanoparticles and nanostructured materials: history, sources, toxicity and regulations. Beilstein J. Nanotechnol. 9 (2018) 1050–1074, https://doi.org/10.3762/bjnano.9.98.

[20] R. Yan, X. Son, X. Wang, Q. Peng, Y. Li, Crystal structures, anisotropic growth, and optical properties: controlled synthesis of lanthanide orthophosphate one-dimensional nanomaterials. Chem. A Eur. J. 11 (2005) 2183–2195, https://doi.org/10.1002/chem.200400649.

[21] R.S. Geonmonond, A.G.M. Da Silva, P.H.C. Camargo, Controlled synthesis of noble metal nanomaterials: motivation, principles, and opportunities in nanocatalysis. An. Acad. Bras. Cienc. 90 (2018) 719–744, https://doi.org/10.1590/0001-3765201820170561.

[22] S. Das, B. Sen, N. Debnath, Recent trends in nanomaterials applications in environmental monitoring and remediation. Environ. Sci. Pollut. Res. 22 (2015) 18333–18344, https://doi.org/10.1007/s11356-015-5491-6.

[23] R.K. Ibrahim, M. Hayyan, M.A. AlSaadi, A. Hayyan, S. Ibrahim, Environmental application of nanotechnology: air, soil, and water. Environ. Sci. Pollut. Res. 23 (2016) 13754–13788, https://doi.org/10.1007/s11356-016-6457-z.

[24] Y. Wu, Q. Yue, Y. Gao, Z. Ren, B. Gao, Performance of bimetallic nanoscale zero-valent iron particles for removal of oxytetracycline. J. Environ. Sci. (China) 69 (2018) 173–182, https://doi.org/10.1016/j.jes.2017.10.006.

[25] W. Tungittiplakorn, L.W. Lion, C. Cohen, J.Y. Kim, Engineered polymeric nanoparticles for soil remediation. Environ. Sci. Technol. 38 (2004) 1605–1610, https://doi.org/10.1021/es0348997.

[26] Q. Li, S. Mahendra, D.Y. Lyon, L. Brunet, M.V. Liga, D. Li, P.J.J. Alvarez, Antimicrobial nanomaterials for water disinfection and microbial control: potential applications and implications. Water Res. 42 (2008) 4591–4602, https://doi.org/10.1016/j.watres.2008.08.015.

[27] I.S. Yunus, A. Harwin, D. Kurniawan, A.I. Adityawarman, Nanotechnologies in water and air pollution treatment. Environ. Technol. Rev. 1 (2012) 136–148, https://doi.org/10.1080/21622515.2012.733966.

[28] B. Van Der Bruggen, C. Vandecasteele, T. Van Gestel, W. Doyen, R. Leysen, A review of pressure-driven membrane processes in wastewater treatment and drinking water production. Environ. Prog. 22 (2003) 46–56, https://doi.org/10.1002/ep.670220116.

[29] B. Van der Bruggen, M. Mänttäri, M. Nyström, Drawbacks of applying nanofiltration and how to avoid them: a review. Sep. Purif. Technol. 63 (2008) 251–263, https://doi.org/10.1016/j.seppur.2008.05.010.

[30] N. Hilal, H. Al-Zoubi, N.A. Darwish, A.W. Mohammad, M. Abu Arabi, A comprehensive review of nanofiltration membranes: treatment, pretreatment, modelling, and atomic force microscopy. Desalination 170 (2004) 281–308, https://doi.org/10.1016/j.desal.2004.01.007.

[31] W.G. Tucker, Air pollution, indoor air pollution and control. in: Kirk-Othmer Encyclopedia of Chemical Technology, John Wiley & Sons, Inc., Hoboken, NJ, USA, 2003, https://doi.org/10.1002/0471238961.0109181620210311.a01

[32] X. Pan, Sulfur oxides. in: Encyclopedia of Environmental Health, Elsevier, 2019, pp. 823–829, https://doi.org/10.1016/B978-0-12-409548-9.11333-8.

This book belongs to Badji Mokhtar Annaba University Central Library

Copyright Elsevier 2025

[33] M. Shiraiwa, K. Ueda, A. Pozzer, G. Lammel, C.J. Kampf, A. Fushimi, S. Enami, A.M. Arangio, J. Fröhlich-Nowoisky, Y. Fujitani, A. Furuyama, P.S.J. Lakey, J. Lelieveld, K. Lucas, Y. Morino, U. Pöschl, S. Takahama, A. Takami, H. Tong, B. Weber, A. Yoshino, K. Sato, Aerosol health effects from molecular to global scales. Environ. Sci. Technol. 51 (2017) 13545–13567, https://doi.org/10.1021/acs.est.7b04417.

[34] US EPA, (n.d.) Air Topics | Environmental Topics.

[35] G.D. Thurston, Outdoor air pollution: sources, atmospheric transport, and human health effects, in: International Encyclopedia of Public Health, Elsevier Inc, 2016, pp. 367–377.

[36] K.K. Kennedy, K.J. Maseka, M. Mbulo, Selected adsorbents for removal of contaminants from wastewater: towards engineering clay minerals. Open J. Appl. Sci. 08 (2018) 355–369, https://doi.org/10.4236/ojapps.2018.88027.

[37] X. Qu, P.J.J. Alvarez, Q. Li, Applications of nanotechnology in water and wastewater treatment. Water Res. 47 (2013) 3931–3946, https://doi.org/10.1016/j.watres.2012.09.058.

[38] J.A. Arcibar-Orozco, J.R. Rangel-Mendez, T.J. Bandosz, Reactive adsorption of SO_2 on activated carbons with deposited iron nanoparticles. J. Hazard. Mater. 246–247 (2013) 300–309, https://doi.org/10.1016/j.jhazmat.2012.12.001.

[39] Y. Huang, W. Wang, Y. Zhang, J. Cao, R. Huang, X. Wang, Synthesis and Applications of Nanomaterials With High Photocatalytic Activity on Air Purification. Elsevier Inc., 2019, https://doi.org/10.1016/b978-0-12-814497-8.00010-2

[40] Y. Lv, Y. Zhu, Y. Zhu, Enhanced photocatalytic performance for the $BiPO_4$-x nanorod induced by surface oxygen vacancy. J. Phys. Chem. C 117 (2013) 18520–18528, https://doi.org/10.1021/jp405596e.

[41] J. Lasek, Y.H. Yu, J.C.S. Wu, Removal of NOx by photocatalytic processes. J. Photochem. Photobiol. C Photochem. Rev. 14 (2013) 29–52, https://doi.org/10.1016/j.jphotochemrev.2012.08.002.

[42] Y. Huang, Y. Gao, Q. Zhang, J.J. Cao, R.J. Huang, W. Ho, S.C. Lee, Hierarchical porous $ZnWO_4$ microspheres synthesized by ultrasonic spray pyrolysis: characterization, mechanistic and photocatalytic NO_x removal studies. Appl. Catal. A Gen. 515 (2016) 170–178, https://doi.org/10.1016/j.apcata.2016.02.007.

[43] M. Kong, Y. Li, X. Chen, T. Tian, P. Fang, F. Zheng, X. Zhao, Tuning the relative concentration ratio of bulk defects to surface defects in TiO_2 nanocrystals leads to high photocatalytic efficiency. J. Am. Chem. Soc. 133 (2011) 16414–16417, https://doi.org/10.1021/ja207826q.

[44] K. Kočí, P. Praus, M. Edelmannová, N. Ambrožová, I. Troppová, D. Fridrichová, G. Słowik, J. Ryczkowski, Photocatalytic reduction of CO_2 over CdS, ZnS and core/shell CdS/ZnS nanoparticles deposited on montmorillonite. J. Nanosci. Nanotechnol. 17 (2017) 4041–4047, https://doi.org/10.1166/jnn.2017.13093.

[45] C.C. Ho, F. Kang, G.M. Chang, S.J. You, Y.F. Wang, Application of recycled lanthanum-doped TiO_2 immobilized on commercial air filter for visible-light photocatalytic degradation of acetone and NO. Appl. Surf. Sci. 465 (2019) 31–40, https://doi.org/10.1016/j.apsusc.2018.09.136.

[46] Y.X. Pan, Z.Q. Sun, H.P. Cong, Y.L. Men, S. Xin, J. Song, S.H. Yu, Photocatalytic CO_2 reduction highly enhanced by oxygen vacancies on Pt-nanoparticle-dispersed gallium oxide. Nano Res. 9 (2016) 1689–1700, https://doi.org/10.1007/s12274-016-1063-4.

[47] D. Li, Y. Xia, Electrospinning of nanofibers: reinventing the wheel?. Adv. Mater. 16 (2004) 1151–1170, https://doi.org/10.1002/adma.200400719.

[48] Y. Xia, Y. Peidong, One-dimensional nanostructure: synthesis, characterization and application. Adv. Mater. (2003) 353–389, https://doi.org/10.1002/chin.200820223.

[49] Climate Transparency, Brown to Green Report, http://www.climate-transparency.org/g20-climate-performance/g20report2018, 2019.

[50] K. Upendar, A. Sri Hari Kumar, N. Lingaiah, K.S. Rama Rao, P.S. Sai Prasad, Low-temperature CO_2 adsorption on alkali metal titanate nanotubes. Int. J. Greenhouse Gas Control 10 (2012) 191–198, https://doi.org/10.1016/j.ijggc.2012.06.008.

[51] A.K. Mishra, S. Ramaprabhu, Palladium nanoparticles decorated graphite nanoplatelets for room temperature carbon dioxide adsorption. Chem. Eng. J. 187 (2012) 10–15, https://doi.org/10.1016/j.cej.2011.01.024.

This book belongs to Badji Mokhtar Annaba University Central Library

Copyright Elsevier 2025

[52] Y. Wang, Y. Zhu, S. Wu, A new nano CaO-based CO_2 adsorbent prepared using an adsorption phase technique. Chem. Eng. J. 218 (2013) 39–45, https://doi.org/10.1016/j.cej.2012.11.095.
[53] H. Ping, Y. Wang, S. Wu, RSC advances preparation of MgO-coated nano CaO using adsorption phase reaction technique for CO_2 sorption. RSC Adv. 6 (2016) 41239–41246, https://doi.org/10.1039/C6RA05452H.
[54] H. Dong, B. Lin, K. Gilmore, T. Hou, S.T. Lee, Y. Li, B40 fullerene: an efficient material for CO_2 capture, storage and separation. Curr. Appl. Phys. 15 (2015) 1084–1089, https://doi.org/10.1016/j.cap.2015.06.008.
[55] T. Zhao, Q. Wang, Y. Kawazoe, P. Jena, A metallic peanut-shaped carbon nanotube and its potential for CO_2 capture. Carbon N. Y. 132 (2018) 249–256, https://doi.org/10.1016/j.carbon.2018.02.061.
[56] P. Granger, V.I. Parvulescu, Catalytic NOx abatement systems for mobile sources: from three-way to lean burn after-treatment technologies. Chem. Rev. 111 (2011) 3155–3207, https://doi.org/10.1021/cr100168g.
[57] T.M. Chen, J. Gokhale, S. Shofer, W.G. Kuschner, Outdoor air pollution: nitrogen dioxide, sulfur dioxide, and carbon monoxide health effects. Am. J. Med. Sci. 333 (2007) 249–256, https://doi.org/10.1097/MAJ.0b013e31803b900f.
[58] R.Q. Long, R.T. Yang, Carbon nanotubes as a superior sorbent for nitrogen oxides. Ind. Eng. Chem. Res. 40 (2001) 4288–4291, https://doi.org/10.1021/ie000976k.
[59] K. Sato, H. Tomonaga, T. Yamamoto, S. Matsumura, N.D. B. Zulkifli, T. Ishimoto, M. Koyama, K. Kusada, H. Kobayashi, H. Kitagawa, K. Nagaoka, A synthetic pseudo-Rh: NO x reduction activity and electronic structure of Pd-Ru solid-solution alloy nanoparticles. Sci. Rep. 6 (2016) 1–7, https://doi.org/10.1038/srep28265.
[60] W. Zhang, F. Dong, W. Zhang, Capture of atmospheric CO_2 into $(BiO)_2$ CO_3/graphene or graphene oxide nanocomposites with enhanced photocatalytic performance. Appl. Surf. Sci. 358 (2015) 75–83, https://doi.org/10.1016/j.apsusc.2015.08.172.
[61] Q. Zhang, Y. Huang, S. Peng, Y. Zhang, Z. Shen, J. ji Cao, W. Ho, S.C. Lee, D.Y.H. Pui, Perovskite $LaFeO_3$-$SrTiO_3$ composite for synergistically enhanced NO removal under visible light excitation. Appl. Catal. B Environ. 204 (2017) 346–357, https://doi.org/10.1016/j.apcatb.2016.11.052.
[62] Q. Zhang, Y. Huang, L. Xu, J.J. Cao, W. Ho, S.C. Lee, Visible-light-active plasmonic Ag-$SrTiO_3$ nanocomposites for the degradation of NO in air with high selectivity. ACS Appl. Mater. Interfaces 8 (2016) 4165–4174, https://doi.org/10.1021/acsami.5b11887.
[63] J. Hu, D. Chen, N. Li, Q. Xu, H. Li, J. He, J. Lu, In situ fabrication of $Bi_2O_2CO_3$/MoS_2 on carbon nanofibers for efficient photocatalytic removal of NO under visible-light irradiation. Appl. Catal. B Environ. 217 (2017) 224–231, https://doi.org/10.1016/j.apcatb.2017.05.088.
[64] Z. Ai, W. Ho, S. Lee, L. Zhang, Efficient photocatalytic removal of NO in indoor air with hierarchical bismuth oxybromide nanoplate microspheres under visible light. Environ. Sci. Technol. 43 (2009) 4143–4150, https://doi.org/10.1021/es9004366.
[65] W.D.P. Rengga, A. Chafidz, M. Sudibandriyo, M. Nasikin, A.E. Abasaeed, Silver nano-particles deposited on bamboo-based activated carbon for removal of formaldehyde. J. Environ. Chem. Eng. 5 (2017) 1657–1665, https://doi.org/10.1016/j.jece.2017.02.033.
[66] Y.Y. Kannangara, R. Wijesena, R.M.G. Rajapakse, K.M.N. de Silva, Heterogeneous photocatalytic degradation of toluene in static environment employing thin films of nitrogen-doped nano-titanium dioxide. Int. Nano Lett. 8 (2018) 31–39, https://doi.org/10.1007/s40089-018-0230-x.
[67] S. Hsu, C. Lu, Modification of single-walled carbon nanotubes for enhancing isopropyl alcohol vapor adsorption from air streams. Sep. Sci. Technol. 42 (2007) 2751–2766, https://doi.org/10.1080/01496390701515060.
[68] C.S. Chuang, M.K. Wang, C.H. Ko, C.C. Ou, C.H. Wu, Removal of benzene and toluene by carbonized bamboo materials modified with TiO_2. Bioresour. Technol. 99 (2008) 954–958, https://doi.org/10.1016/j.biortech.2007.03.003.
[69] K.J. Lee, N. Shiratori, G.H. Lee, J. Miyawaki, I. Mochida, S.H. Yoon, J. Jang, Activated carbon nanofiber produced from electrospun polyacrylonitrile nanofiber as a highly efficient formaldehyde adsorbent. Carbon N. Y. 48 (2010) 4248–4255, https://doi.org/10.1016/j.carbon.2010.07.034.

This book belongs to Badji Mokhtar Annaba University Central Library Copyright Elsevier 2025

[70] C. Cárdenas, J.I. Tobón, C. García, J. Vila, Functionalized building materials: photocatalytic abatement of NO_x by cement pastes blended with TiO_2 nanoparticles. Constr. Build. Mater. 36 (2012) 820–825, https://doi.org/10.1016/j.conbuildmat.2012.06.017.

[71] Y.F. Li, Z.P. Liu, Particle size, shape and activity for photocatalysis on titania anatase nanoparticles in aqueous surroundings. J. Am. Chem. Soc. 133 (2011) 15743–15752, https://doi.org/10.1021/ja206153v.

This book belongs to Badji Mokhtar Annaba University Central Library

Copyright Elsevier 2025

This page intentionally left blank

This book belongs to Badji Mokhtar Annaba University Central Library

Copyright Elsevier 2025

SECTION III

Adsorbent nanomaterials: Preparation and applications

This book belongs to Badji Mokhtar Annaba University Central Library

Copyright Elsevier 2025

This page intentionally left blank

This book belongs to Badji Mokhtar Annaba University Central Library

Copyright Elsevier 2025

CHAPTER 12

Nanomaterials for adsorption of pollutants and heavy metals: Introduction, mechanism, and challenges

Shailesh A. Ghodke[a], Utkarsh Maheshwari[a], Suresh Gupta[b], Shirish H. Sonawane[c], and Bharat A. Bhanvase[d]

[a]Department of Chemical Engineering, Dr. D. Y. Patil Institute of Engineering, Management and Research, Pune, Maharashtra, India [b]Department of Chemical Engineering, Birla Institute of Technology and Science, Pilani, Rajasthan, India [c]Department of Chemical Engineering, National Institute of Technology, Warangal, Telangana, India [d]Chemical Engineering Department, Laxminarayan Institute of Technology, Rashtrasant Tukadoji Maharaj Nagpur University, Nagpur, Maharashtra, India

12.1 Introduction

The past decade witnessed enormous technical developments in the field of process industries producing a variety of pollutants. Typical industries producing these pollutants are nuclear power plants, process plants, pharmaceuticals, metallurgical, dyes and pigment manufacturing, etc. [1–3]. Some of the typical organic pollutants present in the wastewater are surfactants, pesticides, detergents, pharmaceuticals, etc. The major share of the inorganic pollutants is heavy metals and petroleum products [4–6]. This resulted in the production of a large amount of effluent water that needs to be treated before use. Therefore the provision of clean and fresh water has become important. Living organisms require water, and a huge amount of water is required for humans for domestic use [7]. This poses a need related to water remediation and treatment technologies to be feasible concerning their initial and running cost, recyclability, sustainability, and so on.

Various conventional processes such as ion exchange [8], chemical precipitation [9], membrane filtration [10, 11], adsorption [12–14], coagulation [15, 16], electrodialysis [17], and photocatalysis [18, 19] have been used in the removal of pollutants. However, use of such technologies has proved to have some disadvantages such as high initial investment, higher operating costs, lower removal efficiencies, and production of by-products and sludge [20–25]. Among the available methods, adsorption has become one of the preferred methods because of

Handbook of Nanomaterials for Wastewater Treatment. https://doi.org/10.1016/B978-0-12-821496-1.00032-5
Copyright © 2021 Elsevier Inc. All rights reserved.

This book belongs to Badji Mokhtar Annaba University Central Library Copyright Elsevier 2025

its advantages such as simplicity, low investments, high surface area, wide-range of adsorbents, and regeneration [26–28]. Considering the volume of effluent from process industries, it is necessary to find the low-cost adsorbent with higher removal efficiency and the one that is environmental friendly.

Past few years have witnessed significant applications of nanotechnology, which resulted in the application of nanotechnology in almost all industrial sectors. These developments have been possible because of characteristic features such as ease of handling/processing, microbial disinfection, fast dissolution, sufficient reactive sites, and thermal and electric properties [29].

In addition, some nanomaterials represent better removal efficiency when compared to their bulk counterpart [30]. The higher ratio of surface area to particle size at the nanoscale results in alteration of physical properties such as higher surface area and number of active sites [31]. Also, the reduction in size of particles leads to a higher surface area, which in turn increases the density of active sites per unit mass. Subsequently, greater surface free energy results in high surface reactivity. Nanomaterials often come in various forms such as wires, films, colloids, particles, quantum dots, and tubes. Each of the nanomaterial necessarily has at least one physical dimension, less than 100 nm [32]. With the advantage of flexibility in fine-tuning of synthesized nanomaterials, they can be used in variety of water treatment processes.

This study focuses on recent studies reported for adsorption of pollutant and heavy metals using nanomaterials. The factors influencing adsorption process such as contact time, adsorbent dosage, initial concentration, pH, ionic strength, dissolved organic matters, and temperature are discussed in detail. Detailed analysis related to adsorption mechanisms for various types of effluents are discussed thoroughly. Finally, future prospects in use of nanoparticles-based adsorption are discussed in brief.

12.2 Major industry effluents

Considering the abundance and toxicity levels, all the organic and inorganic materials are to be removed from the industrial effluents before their release into the atmosphere directly or indirectly. Effluents from mining, fertilizer, battery, tanneries, paper, and coating industries are one of the major sources of heavy metals [33]. Heavy metals are stable and persistent, forming stable complexes during chemical treatments.

The presence of heavy metals in trace amounts can prove to be toxic and carcinogenic to humans. Also, they are nonbiodegradable and tend to accumulate in living organisms [34]. Studies related to health hazards of heavy metals such as copper, zinc, chromium, nickel, and lead have indicated their direct impact on human physiology [35]. Cadmium was found to provide higher bioaccumulation tendency, and it has a very long half-life period in human bodies [36]. Traces of lead in parts per million (ppm) level can be detrimental because it causes cancer, kidney diseases, anemia, or, in some cases, damages the central nervous system [37].

This book belongs to Badji Mokhtar Annaba University Central Library Copyright Elsevier 2025

Furthermore, children are prone to have lower IQ when they are exposed to lead [38]. Excessive intake of essential element zinc through drinking water may also lead to various symptoms such as stomach cramps, vomiting, skin irritation, and anemia.

Many industries such as textiles, pulp and paper, gasoline, and pharmaceuticals use synthetic dyestuff as coloring agents [39, 40]. Typically, a dye molecule is synthesized from chemicals possessing toluene, xylene, benzene, anthracene, etc. [41–43]. These basic structures make the synthesized molecules toxic with high solubility. At the same time, dye molecules are resistant to biodegradation, heat, and oxidizing agents [44]. If dye molecules are discharged in aqueous bodies, their recalcitrance nature makes the aqueous bodies colored, resulting in the lack of sunlight penetration. This further results in higher biological oxygen demand and chemical oxygen demand values [42, 45, 46]. As discussed by Yagub et al., dye molecules, even in small concentrations, may affect the reproductive system, liver, kidney, central nervous system, etc. [47].

Phenolic compounds comprise phenol, mono, and polyphenols, including substituted phenols. Phenolic compounds have weak acidic properties and are used as intermediates for various chemical processes. Effluents from chemical process industries such as dyes and pigments, rubber, gasoline, pharmaceuticals, and agrochemicals contain traces of phenol and phenolic compounds.

Considering the characteristics of these compounds to produce teratogenic effect, toxicity, and carcinogenic effect, the maximum discharge concentration is 0.5 ppm [48]. Phenol produces unpleasant odor and taste and also generates negative effects in biological processes. Phenolic products, in higher concentrations, can remain stable for a longer period in the atmosphere [49–52].

Because the removal of major industrial effluents is to be removed according to the norms of environmental agencies, there is an urgent need for treatment methodology for an efficient removal. The treatment technologies should also be flexible enough to consider the various effluent parameters such as pH, ionic strength, temperature, and bulk concentration [53].

In view of these, nanomaterials can provide a larger surface area, higher porosity, smaller particle size, selective adsorption, the surface to volume ratio, and desirable hydrophobicity. Furthermore, their considerable binding capacity (number of active sites) and regeneration cycles make them potential candidates in effluent treatment.

12.3 Parameters affecting adsorption

When it comes to adsorption, a number of parameters are responsible for the process of various pollutants on the different types of the adsorbents and especially, the carbonaceous materials. The following sections discuss the individual parameters in detail. The nanomaterials are

This book belongs to Badji Mokhtar Annaba University Central Library Copyright Elsevier 2025

required to be validated by utilizing a variety of characterization systems that are discussed in further sections.

12.3.1 Contact time

Contact time is among the significant parameters during the adsorption phenomenon. The kinetic parametric information can be acquired from the data registered from the experiments performed to evaluate the consequence of the contact time. These data help during the adsorption process for proposing the rate kinetics for metal removal.

Contact time variation is evaluated and assessed by conducting the kinetic experiments for various metal ions removal, keeping the other parameters at optimized parametric values. These experimental data provide the optimum time required by the adsorbent for the maximum adsorption of the pollutant [39, 54–56]. The kinetic study is often represented by utilizing the removal of the pollutant on percentage basis and the solid phase concentration of the adsorbent, often termed as the adsorption capacity [57]. It is normally observed that in the initial phases, amid the boost in contact time, the percentage removal quickly improves, and afterward, it augments slowly with the added extension of the contact time. Once the equilibrium is achieved with the total adsorption of the pollutant or total saturation of the adsorbent, the percentage removal reaches a stable value. On the same front, the concentration on adsorbent phase also amplifies with the boost in the contact time, which is basically because of the increasing time provided to the pollutant to get attached onto the surface of the adsorbent working as the live site for the adsorption.

During the primary process, the pollutant adsorption pace is faster owing to the hefty concentration gradient among the adsorbate concentration and the adsorbent solid phase metal concentration. This may have resulted because of the presence of accessible live sites for adsorption in the preliminary process. In the subsequent phases, the pace of metal removal onto the adsorption declines, which may be owing to the diffusion among the intraparticle components, which turns out to be more prevailing [58, 59].

This directs toward enhancement in resistances of mass transfer, leading to solute transmission to the inner adsorption spots from the adsorbent surface. Furthermore, the live adsorption locations get flooded with period leading to the reduction in the adsorption rate.

12.3.2 Adsorbent dosage

The adsorbent dosage is among other significant parameters considered on the effective and economic front. The consequence of dose of the adsorbent on the heavy metal elimination is also evaluated for obtaining the most favorable quantity of the adsorbent dosage utilized for the efficient pollutant elimination. Lesser than the optimum value will lead to a lesser removal of the pollutant, whereas higher amount of the adsorbent dosage will not be required for the

This book belongs to Badji Mokhtar Annaba University Central Library Copyright Elsevier 2025

removal system because it will be expensive. Normally, the trend obtained is that, with an increasing amount of the adsorbent, there is a boost in the pollutant elimination. With amplification in the dosage of the adsorbent, there will be availability of greater quantity of live sites for the adsorption that further leads to reduction in the adsorption capacity evaluated, keeping the amount of adsorbent utilized. During the experimentation, researchers have tried adsorbent dosage ranging from 4 to 80 g/L of the effluents. With the availability of more active sites in comparison to the limited number of metal ions available for the removal, a higher percentage removal of the pollutants is obtained. Thus for the experimental studies, there is a trade-off required to be identified among the removal and the solid concentration, leading to the optimum consumption of the adsorbent for optimum pollutant elimination [6, 60–64].

12.3.3 Initial concentration

The pollutants in the industry vary from industry to industry not only in terms of quality but even in terms of quantity. On the similar front, the behavior of the adsorbent also changes with the change in the pollutant amount. Thus the pollutant concentration effect on the performance of adsorbent for pollutant removal is a must to be evaluated [60, 65, 66].

Researchers have utilized different range of heavy metal pollutants concentration ranging from 10 to 200 mg/L. The research shows that, with a rise in the pollutant amount, the removal percentage declines. Whereas the solid phase concentration rises. The lower the initial concentration of the pollutants, the higher will be the removal efficiency of the adsorbents. This rise in concentration is because of the exploitation of the added active spots accessible for adsorption at elevated preliminary metal concentration. The reduction in the amputation results because of the accessibility of inadequate active spots for adsorption. The active spots available convert into saturated spots past an evident threshold of the adsorbate. On adding the pollutant concentration, there will be a restriction in the adsorption process and therefore will be present in the outlet solution. The trade-off amid the adsorbent phase concentration and percentage removal suggests the optimum initial concentration [41, 67–69].

12.3.4 pH

The effluents from different industries will be having different acidic or basic nature. The behavior of the adsorbent may vary as a result of the nature of the pollutant. The adsorption route may be preferable in one condition, whereas it may be reluctant in another condition. Thus the further substantial parameter that must be considered is the outcome of the variation in pH on the pollutants removal [44, 70–74].

Normally, the results show that solid phase concentration varies with a surge in the pH value of the adsorbate, thus supporting the adsorption of pollutants, particularly metal ions at lesser pH.

This book belongs to Badji Mokhtar Annaba University Central Library Copyright Elsevier 2025

It is reported that, at higher pH, that is, above 6, the metal ions precipitate over the adsorbent surface, thus reducing the removal [75, 76].

The research shows that, during the removal of Cr(VI) ions, lower pH is preferred during the process. The research shows that the pH of the effluent after the treatment increases, which may be because of the addition of OH^- ions. These OH^- ions may be available from the degradation of the hydroxyl groups during adsorption process; whereas it is detected that the elimination of Zn(II) metal ions leads to decline in the pH of the solution while supporting the adsorption phenomenon at lesser pH. The ionic adsorption prevails till the adsorption site is neutralized utilizing the opposite charged ions [77, 78].

A lower pH is preferred for adsorption when the adsorbent is activated, and the surfaces are positively charged through activation. The metal ions form negative ion complexes that can be easily adhered on to the positive plane of the activated adsorbent. Thus ions with the negative charge can be effectively removed from the activated adsorbent at a lower pH. At a higher pH, the adsorption decreases, which may be shifting of the negative ion complexes to the positive or less charged ions. Sometimes, it is also considered that the lower pollutant removal at higher pH, that is, basic medium is because of the competition among the OH^- and negative ion complexes [26, 79, 80].

12.3.5 Temperature

The temperature as a parameter of the effluent plays a different purpose in pollutant removal. The effluents from industries will be at different temperatures as per the processes and their origin. The consequence of temperature on the removal of pollutants can be evaluated by performing equilibrium batch experiments at different temperatures. These experimental data also supports the explanation of the thermodynamic behavior of the process. This also can suggest the impulsive character of the adsorption phenomenon [70, 81, 82].

The research shows that the pollutant removal is preferred at lower temperature, preferably at room temperature. However, the adsorption reduces at a higher temperature. It is also observed that passing the hot water through the saturated adsorbent promotes desorption because it will promote the delinking of the bonding of the ions [83–85].

12.3.6 Ionic strength

The ionic strength of the pollutants and the adsorbents also acts as a vital role in pollutant removal. The interaction of various ions at the interface of the adsorbent and adsorbate are responsible for the low or higher adsorption of the pollutants. Here, pH also plays a significant task because it shifts the system to acidic or basic nature. The potential required for adsorption lessens with the rise in pH, reducing the adsorption at a higher pH

This book belongs to Badji Mokhtar Annaba University Central Library Copyright Elsevier 2025

[86]. The consequence of the ionic strength on anion partitioning has been studied to recognize and discriminate between the specific and nonspecific adsorptions [87]. It was pragmatic that the change in the ionic strength doesn't affect the specific adsorption but positively influenced the nonspecific adsorption, which may be because of the aggressive adsorption with contradict actions. The presence of other metal ions will definitely reduce the adsorption of the specified pollutant because of the utilization of the active sites by the other available ions. The pH above which ionic strength increases the adsorption behavior is called as the characteristic pH. Below this pH, the ionic strength does not participate as a chief patron in adsorption process. [88–91].

12.3.7 Dissolved organic matters

The presence of dissolved organic matters in the adsorbate gives a mixed effect on the adsorption of metal ions and other pollutants. One of the researchers performed laboratory experiments that showcased the adsorption of cadmium as a chemical phenomenon and where the dissolved organic matters within the soils are strengthening the mixture of cadmium to soil facade, which inhibited the desorption process [92]. It is observed that the dissolved organic matters promoted the mercury desorption from the soils. The pace of mercury adsorption was constantly lowered down by the presence of dissolved organic matters [93]. The effect of dissolved organic matters on the heavy metal pollutant removal varies with the change in the pH of the solution. Here the dissolved organic matters comprise a mixture that is heterogeneous in nature owing to its combination of humic substances, amino acids, enzymes, and organic acids that are an obstacle to the adsorption of heavy metal ions. Few researchers have suggested the utilization of dissolved organic matters as the catalyst and give the catalytic upshot on the adsorption of metal pollutants. The dissolved organic matters work as the mediator for the pollutant removal [92, 94]. Some of the polyvinylpyrolidone-coated magnetite nanoparticles illustrated better adsorption routine for the removal of bisphenol and ketoprofen. The adsorbents demonstrated high-quality performance for the pollutants removal, even as their elimination through other activated carbon that drastically repressed by the aggressive inhibition of dissolved organic matter with micropollutants [29, 95–97].

12.4 Adsorbent characterization

Adsorption process is a surface phenomenon. The surface of the adsorbent must be available for the adsorption process as per the requirement for the removal of the specific pollutant. Different pollutants require different surface properties. The surface can be evaluated using different techniques of characterization such as SEM, EDS, TEM, FTIR, BET surface area, and XRD.

This book belongs to Badji Mokhtar Annaba University Central Library Copyright Elsevier 2025

12.4.1 Scanning electron microscopy (SEM)

Scanning electron microscopy (SEM) is regarded as one of the preferred practices for the study of the surface morphology and especially, the dimensional property [98]. Field emission spectrometers are available for the SEM analysis, which can be utilized nowadays and give mere specific images. These images can be scaled from a range of 1 μm to 1 nm. As the process of SEM analysis is utilizing the electron technique, there is always a requirement of the electron conducting agent available on the surface of the testing material. If the testing material is nonconducting, there is a requirement of coating the material with the electron conducting Energy dispersive X-ray spectroscopy agents, preferably some soft metal agents, which are not affecting the surface morphology of the testing materials. An SEM image of an activated neem bark is shown in Fig. 12.1.

The SEM shown in Fig. 12.1 confirms the presence of nanopores, which makes it a nano-sized adsorbent for the adsorption process. Similar adsorbents with nano-sized pores are preferred because they will provide higher surface area for adsorption. The availability of more surface area will help in obtaining a higher adsorption capacity, finally leading to a higher pollutant removal.

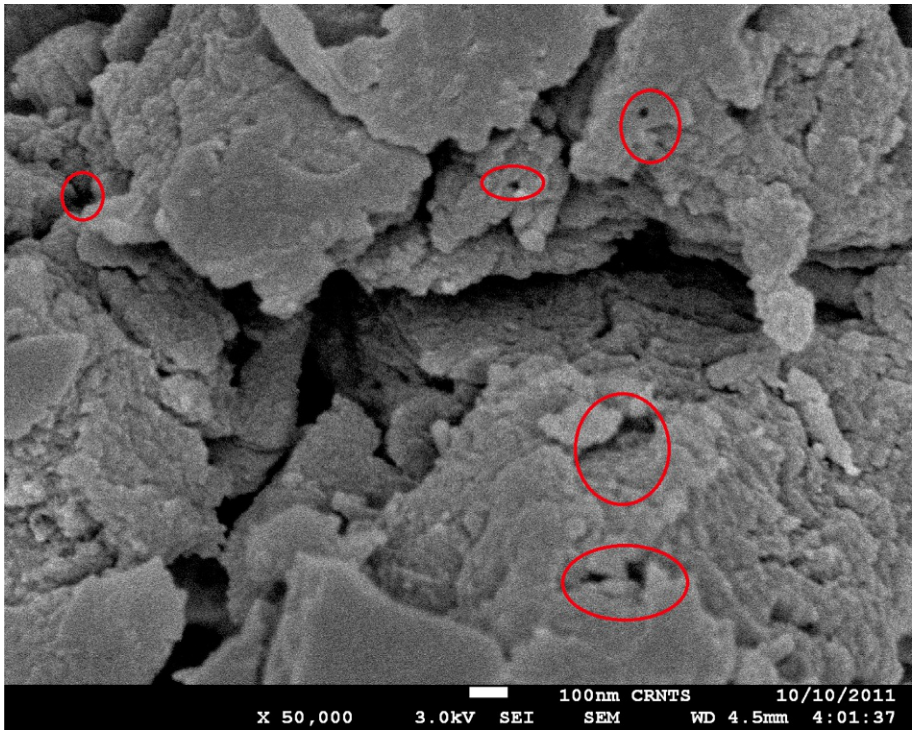

Fig. 12.1
SEM of fresh activated neem bark ready for adsorption [6].

This book belongs to Badji Mokhtar Annaba University Central Library
Copyright Elsevier 2025

12.4.2 Energy dispersive X-ray spectroscopy (EDS)

The energy dispersive X-ray spectroscopy (EDS), or sometimes also known as EDX, is also considered as a characterization technique for developed adsorbents. The equipment required for the EDS analysis is an X-ray associated with the SEM equipment only [99]. The EDS analysis will provide the elemental content available on the surface of the testing material. Fig. 12.2 shows a sample EDS analysis of the activated neem bark utilized on pure Cr(VI) solution for the removal of Chromium(VI).

The EDS shown in Fig. 12.2 shows the elemental analysis on the surface of the activated neem bark. The peaks of the graphs are being tracked. It is shown that Cr, C, and O are available on the surface of the adsorbent, which confirms the adsorption of Cr on the carbonaceous adsorbent. It also shows the availability of Pt and St on the surface of the adsorbent, which was because of the coating of the electron-conducting agent on the surface of the nonconducting testing material.

12.4.3 Transmission electron microscopy image

The transmission electron microscopy (TEM) images are obtained from the electron transactions with resources when an electron beam is passed on throughout the testing material sample [100]. The TEM images provide more specific images of the surface because of its 3-D effect. Thus the images obtained from the TEM analysis give a more magnified view of the sample in comparison to the SEM images. Owing to the magnification and the 3-D analysis techniques, TEM provides a more detailed surface morphology to understand the behavior of the interactions before and after the interactions. The TEM images can also help in understanding the thickness of the outer surface of the testing material [101].

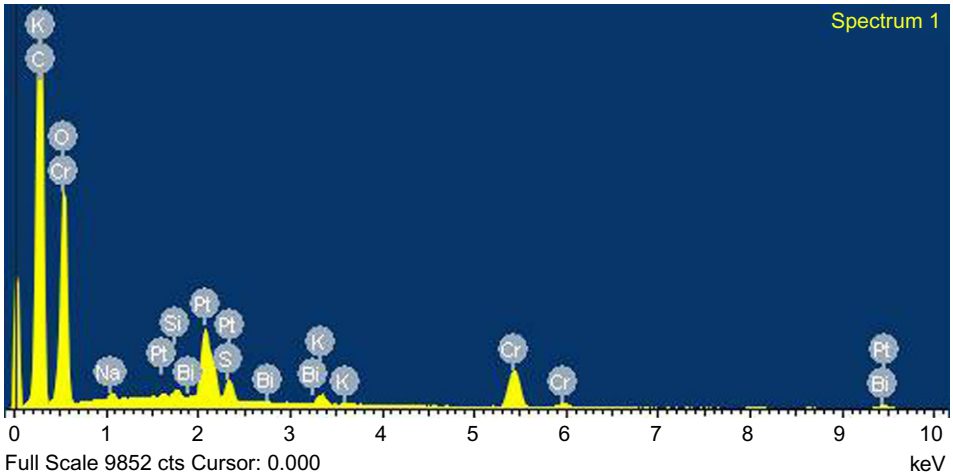

Fig. 12.2
EDS for used activated neem bark on pure Cr(VI) solution [6].

This book belongs to Badji Mokhtar Annaba University Central Library
Copyright Elsevier 2025

12.4.4 Fourier-transform infrared spectroscopy

Fourier-transform infrared spectroscopy (FTIR) is utilized for identifying the functional groups available on the adsorbent. This analysis of the functional group helps in understanding the mechanism of the adsorption that promotes the adsorption process [102]. The output of the FTIR analysis is shown in the form of graphical analysis, where the y-axis represents the transmittance or absorbance, and the x-axis represents the wavelength. A sample FTIR analysis is shown in Fig. 12.3.

The peaks of the graphical representation are identified and correlated to the prescribed reference literature to understand the functional groups available on the surface of the testing materials. These functional groups may be responsible for the adsorption and thus can be utilized for proposing the mechanism of the adsorption process.

12.4.5 Brunauer-Emmett-Teller (BET) surface area

Brunauer-Emmett-Teller (BET) surface area analyzer uses the N_2 adsorption isotherm as reference for the analysis of the surface area of the testing material [103]. This analysis process straightly provides the amount of the surface area and pore size available in the testing material for the process. The testing material is first purged with the ideal gas, and later, it allows the nitrogen to be passed, which on comparison provides the available surface area. The adsorption is preferred to be occurring at a colder temperature; thus the adsorption phenomenon during analysis is conducted at sublower temperature with the utilization of the liquid nitrogen, that is, the cryogenic environment. Desorption of the gas follows the process that is preferred to occur at room temperature, that is, approximately 25°C.

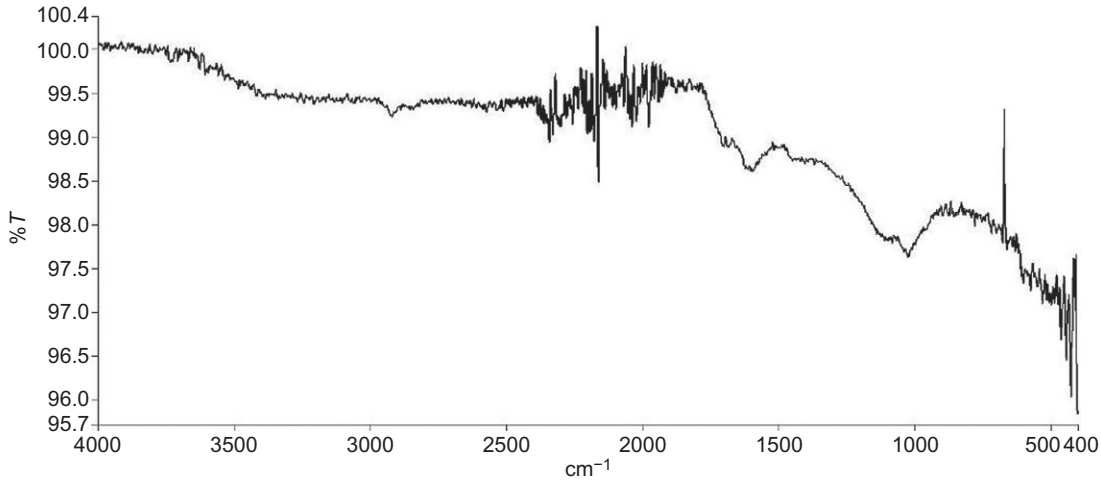

Fig. 12.3
FTIR spectra of for fresh activated adsorbent for 4000–400 cm^{-1} wavelength [6].

This book belongs to Badji Mokhtar Annaba University Central Library
Copyright Elsevier 2025

BET analyzer works on the basic principle of considering the homogeneous surface. It is an extension of the Langmuir model, considering the monolayer adsorption during the adsorption process. This is because of the consideration of all the exterior spots to have the equivalent adsorption energy for the adsorbate.

12.4.6 X-ray powder diffraction

X-ray powder diffraction (XRD) is also utilized to study the surface property. This analysis will enlighten about the crystallanity or the amorphous nature of the testing materials. For the XRD analysis, very small amount of material is utilized of an order of 0.2 g, which is finely powdered and consistently dispersed on the testing plate. One of the most used XRD analyzer is Rigaku Miniflex II [104]**.** For the analysis, diffractometers utilize different radiations such as Cu-Kα radiation with a wavelength of 1.54 Å. The angle 2θ in the setup of the XRD fluctuate in a range of 10–90 degrees at a measurable step of 0.01 degrees. The analysis of the XRD is on the basis of the peak observed. If a sharp peak is observed, it infers a crystalline nature; otherwise, an amorphous nature of the surface is inferred. Among the crystalline structure, Scherrer's formula can be utilized to estimate the particle size using the peak data [6]. A sample XRD plot is shown in Fig. 12.4, which shows the amorphous nature of the developed activated carbon.

12.4.7 Thermogravimetric analysis

Thermogravimetric analysis or thermal gravimetric analysis (TGA) is a method of thermal analysis to determine the mass degradation with the variation in temperature. In this process of analysis, the mass of a sample is measured over time with a uniform change in temperature. This

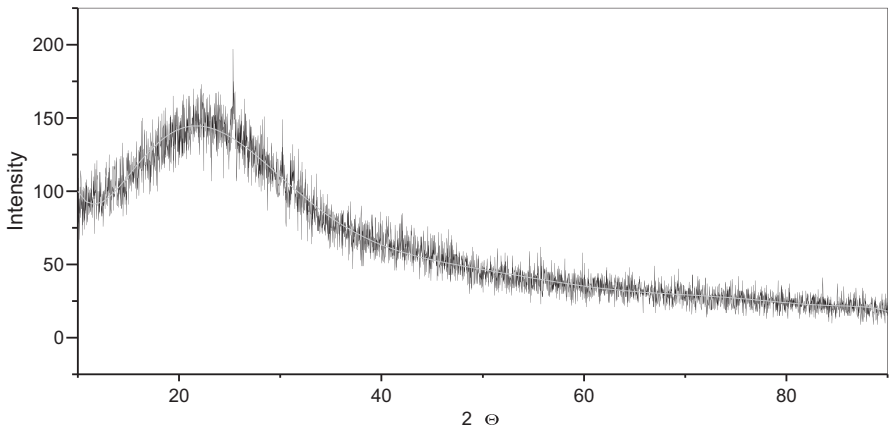

Fig. 12.4
Powder X-ray diffraction pattern for developed activated carbon [6].

This book belongs to Badji Mokhtar Annaba University Central Library Copyright Elsevier 2025

gives the degradation of the mass because of the increase in the temperature; along with the TGA, a number of times represents the derivative thermogravimetric analysis (DTA) too. A uniform heating rate is provided to the testing material to understand the mass degradation with an increase in the temperature [105].

A sample TGA analysis plot is shown in Fig. 12.5. The initial variation in slope comes whenever there is a reduction of mass because of the loss of moisture. Furthermore, the next variation in the slope provides the mass variation owing to the combustion of the testing material. This slope may provide an inference of the material, which is available as per the combustion temperature observed.

12.5 Adsorption mechanism

Mechanism of the adsorption is required to be studied because it is significant for the selection of the appropriate adsorbent as per the pollutant to be removed. Mechanisms vary from adsorbent to adsorbent, as well as pollutant to pollutant and even condition to condition. The polarity, pH, π-π interactions, electrostatic interactions, hydrogen bonding, covalent bonding, etc. lead to the attractions and interactions of the adsorbents and the various pollutants, especially among the carbonaceous adsorbents and polar adsorbate [29, 106]. An adsorbent

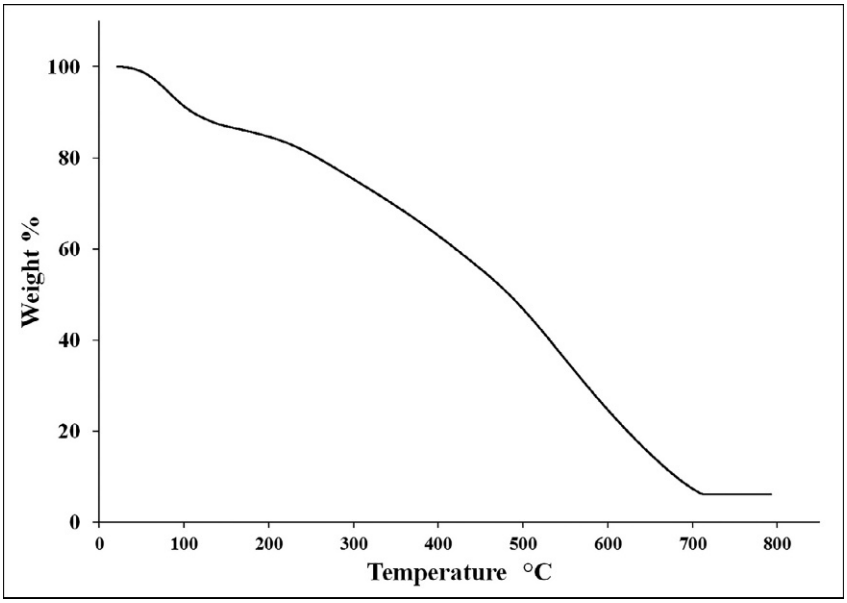

Fig. 12.5
TGA thermograph of the developed activated carbon [6].

This book belongs to Badji Mokhtar Annaba University Central Library
Copyright Elsevier 2025

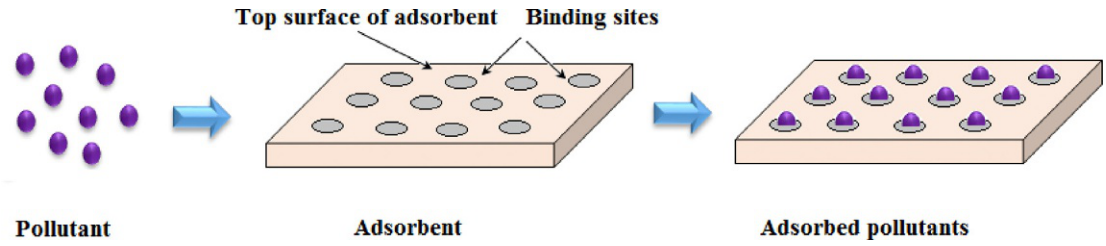

Fig. 12.6
Adsorption mechanism for Cu(II) or Pb(II) removal on nanoporous adsorption.

when utilized for Cu(II) or Pb(II) removal can give the mechanism as shown [107] in Fig. 12.6. Here the adsorption mechanism shown is more of the physiosorption type where the surface plays an important role to get the pollutant adhere to the surface of the adsorbent for performing the adsorption.

12.5.1 π-π interaction

The π-π interactions are also popularly recognized as the π-π electron donor-acceptor interactions among the adsorbent and the adsorbate, especially the aromatic rings. The aromatic groups work as the electron retreating groups on the aromatic ring, while the N_2 groups often work as the electron acceptors [108, 109]. These interactions are much observed on the exterior of the carbon nanotubes and graphites that are graphine-dominated and π electron-rich regions along with the compounds accepting the π electrons. This is inferred from the triclosan adsorption [110, 111]. Researchers have reported the similar π-π interactions during the adsorption of tyrosine, tetracycline, and sulfamethoxazole on activated carbonaceous nanotubes. The other pollutants that are aromatic in nature were removed using adsorption on carbonaceous materials through π-π interactions. More the aromatic rings, the more they will be dominating with the π-π interactions [109, 112–115].

12.5.2 Electrostatic interaction

The electrostatic interactions may be contributing significantly to the adsorption affinity of the pollutant. These electrostatic interactions occur because of the charges available on the surface of the adsorbate and adsorbent. The solution pH is supposed to be at the isoelectric point, that is, pH_{zpc}. In the solution with a pH different than the pH_{zpc}, the carbonaceous adsorbents are supposed to have a variable charge that can either be negative or positive. The other pollutants can also be charged and discharged at diverse pH using the electrostatic exchanges, which will influence the adsorption of the pollutants on the adsorbents [115–117].

The electrostatic interaction of the solution is affected may be because of the occurrence of the oxygenated functional groups on the carbon nanotubes and pharmaceutical and personal care

This book belongs to Badji Mokhtar Annaba University Central Library Copyright Elsevier 2025

products, where the pH will be responsible for the propanating and depropanating of the functional groups [118].

The research also prevails that the adsorption of fewer metal ions such as Cd(II) on hydrous phyllosilicate mineral, vermiculite reduces the negative charge of the exterior surface. Thus the interaction among the cadmium cation and the negative zeta potential on the adsorbent surface displays a significant part on the solid phase concentration of the pollutant, that is, adsorption capacity. This shows the dependency of the ion exchange and electrostatic interaction for the cadmium cation utilizing the adsorbent [116, 119–122].

12.5.3 Hydrophobic interaction

Hydrophobic interactions are also known as the hydrophobic partitioning. Hydrophobic interactions are another means for carbonaceous materials to remove hydrophobic pollutants through the adsorption process. The hydrophobic interactions will unite with the entropic forces that will motivate the hydrophobic organic compounds extracted from the aqueous solution, which is owing to the feeble surface interactions consequential from Vander wall forces. All of these initiate with the breaking of the component in the hydrophobic domains [123, 124]. The researchers have observed that maximum adsorption capacity is observed when carbonaceous adsorbents are having zero-charged density and the molecular states for the emerging contaminants, thus having a well-built hydrophobic interaction. Because the charge is negligible, the bonding enthalpies are negligible in the process [108, 125]. These hydrophobic interactions are also responsible as the principal mechanism for the pH-dependent adsorption of the sulfonamides [126–128].

12.5.4 Hydrogen bonding

Hydrogen bonding is among the opportunities for the adsorption of the removal of the pollutants. These hydrogen bonds are developed between the aromatic rings and carbonaceous materials, which is because of the presence of the electron supplier and the compounds enclosing the O_2-containing functional groups [114].

The research also shows that hydrogen bonding plays a major role in the adsorption of diols on the carboxylated multiwalled carbon nanotubes and graphene oxides. Adsorption of these diols on the carbonaceous nanomaterials was to a great extent effective in comparison to the sediments, resulting from π-π interactions and hydrogen bonding [129].

There will be two-step interactions of the hydrogen bonding that takes place in the activated carbon-methylene green 5 dye system. The first one is owing to the presence of the surface hydrogen of the hydroxyl group on the carbonaceous activated adsorbents, in addition to the suitable atom of the methylene green 5 dyes. This behavior is identified as the dipole-dipole hydrogen bonding. The other interaction of the molecules may be because of the presence of

This book belongs to Badji Mokhtar Annaba University Central Library Copyright Elsevier 2025

hydroxyl groups above the activated carbons along with the aromatic rings on the methylene green 5 dye molecules [127, 130–132].

12.6 Challenges in adsorption

It has been reported that numerous adsorbents are used for the pollutant elimination in the adsorption process. These materials include biological waste, biomaterials, low-cost materials, nanoparticles, carbon nanotubes, etc., which are utilized as active adsorbents for wastewater treatment. Although thorough research is conducted for different pollutant removals using various adsorbents, still there are a number of limitations that are restricting the use of adsorption as an effective removal technique in the industry.

The primary limitations are the effectiveness on the basis of cost and efficiency of the proposed materials. In developing countries such as Russia and India, the researchers are still struggling with the cost-effective wastewater treatment technology, which can be effective and simultaneously efficient for pollutant removal too. In most of the cases, most of the cost-effective adsorbents are not efficient for pollutant removal or vice versa. Thus there is a scope of identifying a suitable low-cost material that can be nanoscaled, providing sufficient pollutant removal at a low operating cost [38, 127, 133, 134]. It is also observed that the adsorbents are having capacity to remove one or two metal ions, where as per the requirement of the industry, there is dire need to have an adsorbent that can remove multiple metal ions simultaneously. There is need of the hour to work on the ways to identify the technique to be utilized to activate the surface of the adsorbent, which can be utilized for the removal of multiple metal ions [6, 135].

Another challenge in the adsorption process is that the adsorbents with good removal capacity are costly in nature; therefore the regeneration of the saturated adsorbent after the process is the need of the hour. The regeneration of the used adsorbent will lead to shifting the process to an economic mode. There are hardly any research works that reported the regeneration of the adsorbent with hot water. Few more studies have reported the regeneration with chemicals. The important challenge that persists is the storage or the recovery of the metal/pollutant from the used adsorbent so that the pollutant is isolated or used again [6, 22, 136–138].

12.7 Conclusion and future prospective

Many studies have depicted the effective utilization of nanomaterials for pollutant removal. The use of nanoadsorbents was found to have a higher effluent removal efficiency when compared to the conventional adsorbents. The nanomaterials developed have shown specific physicochemical properties responsible for adsorption behavior, even at low initial concentrations. The adsorption capacity of any adsorbent depends on the number of available binding sites, which limits the effect of adsorbent dose during the pollutant adsorption process

This book belongs to Badji Mokhtar Annaba University Central Library Copyright Elsevier 2025

[139]. Because of the particle size being in the nanometric range, it is difficult to obtain dispersion stability and separation from suspension. This issue may be addressed by the surface functionalization of nanoadsorbents. Also, the provision of magnetic characteristics can provide the possibilities to easily separate the nanoadsorbents from the suspension medium. To determine the rate of adsorption and adsorption mechanism, data estimation related to kinetics, thermodynamics, and adsorption isotherms is important. From the studies reported herein, it is difficult to enlist the best nanoadsorbents because the experimental conditions such as effluent concentration, adsorbent size, feed temperature, and pH are different.

Furthermore, it is required to perform experimental analysis at pilot scale with operating conditions similar to the industrial scale. Such studies should be pertaining to economics, regeneration, and stability in order to achieve robust process parameters with least environmental impact [136]. Studies related to cost analysis are to be performed so as to evaluate the use of nanoadsorbents at the industrial scale. The detailed cost analysis is required from the initial investment to the entire life cycle of adsorbent (adsorption and desorption) until the regeneration of the adsorbent. Studies related to the use of nanoadsorbent even after utilization is to be made. These studies will be useful in guiding feasibility analysis of their use as fillers, brick manufacturing, land filling, and landscaping [140]. Nevertheless, further experimental analysis is required to find the best possible alternatives to find economic and environmental friendly nanoadsorbent for pollutant removal in process industries.

References

[1] B.V. Babu, S. Gupta, Removal of Cr(VI) from wastewater using activated tamarind seeds as an adsorbent. J. Environ. Eng. Sci. 7 (2008) 553–557, https://doi.org/10.1139/s08-025.

[2] U. Maheshwari, S. Gupta, Removal of Cr(VI) from wastewater using activated neem bark in a fixed-bed column: interference of other ions and kinetic modelling studies. Desalin. Water Treat. 57 (2016) 8514–8525, https://doi.org/10.1080/19443994.2015.1030709.

[3] H.S. Rai, M.S. Bhattacharya, J. Singh, T.K. Bansal, P. Vats, U.C. Banerjee, Removal of dyes from the effluent of textile and dyestuff manufacturing industry: a review of emerging techniques with reference to biological treatment. Crit. Rev. Environ. Sci. Technol. 35 (2005) 219–238, https://doi.org/10.1080/10643380590917932.

[4] G. Gangadhar, U. Maheshwari, S. Gupta, Application of nanomaterials for the removal of pollutants from effluent streams. Nanosci. Nanotechnol. Asia 2 (2012) 140–150, https://doi.org/10.2174/2210681211202020140.

[5] A. Jawed, V. Saxena, L.M. Pandey, Engineered nanomaterials and their surface functionalization for the removal of heavy metals: a review. J. Water Process. Eng. 33 (2020) 101009, https://doi.org/10.1016/j.jwpe.2019.101009.

[6] U. Maheshwari, Removal of Metal Ions from Wastewater Using Adsorption : Experimental and Theoretical Studies Removal of Metal Ions From Wastewater Using Adsorption : Experimental and Theoretical Studies, Birla Institute of Technology and Science, Pilani (BITS Pilani), 2015.

[7] M.M. Khin, A.S. Nair, V.J. Babu, R. Murugan, S. Ramakrishna, A review on nanomaterials for environmental remediation. Energy Environ. Sci. 5 (2012) 8075–8109, https://doi.org/10.1039/c2ee21818f.

[8] L.-L. Li, X.-Q. Feng, R.-P. Han, S.-Q. Zang, G. Yang, Cr(VI) removal via anion exchange on a silver-triazolate MOF. J. Hazard. Mater. 321 (2017) 622–628, https://doi.org/10.1016/j.jhazmat.2016.09.029.

This book belongs to Badji Mokhtar Annaba University Central Library Copyright Elsevier 2025

[9] L.K. Wang, D.A. Vaccari, Y. Li, N.K. Shammas, L.K. Wang, Y.-T. Hung, N.K. Shammas (Eds.), Chemical precipitation BT—physicochemical treatment processes, Humana Press, Totowa, NJ, 2005, pp. 141–197, https://doi.org/10.1385/1-59259-820-x:141.

[10] B.A.M. Al-Rashdi, D.J. Johnson, N. Hilal, Removal of heavy metal ions by nanofiltration. Desalination 315 (2013) 2–17, https://doi.org/10.1016/j.desal.2012.05.022.

[11] M. Chen, K. Shafer-Peltier, S.J. Randtke, E. Peltier, Competitive association of cations with poly(sodium 4-styrenesulfonate) (PSS) and heavy metal removal from water by PSS-assisted ultrafiltration. Chem. Eng. J. 344 (2018) 155–164, https://doi.org/10.1016/j.cej.2018.03.054.

[12] B. Belhamdi, Z. Merzougui, M. Trari, A. Addoun, A kinetic, equilibrium and thermodynamic study of l-phenylalanine adsorption using activated carbon based on agricultural waste (date stones). J. Appl. Res. Technol. 14 (2016) 354–366, https://doi.org/10.1016/j.jart.2016.08.004.

[13] U. Maheshwari, S. Gupta, Kinetic and equilibrium studies of Cr(VI) removal from aqueous solutions using activated neem bark, Res. J. Chem. Environ. 15 (2011) 939–943.

[14] F.-M. Pellera, A. Giannis, D. Kalderis, K. Anastasiadou, R. Stegmann, J.-Y. Wang, E. Gidarakos, Adsorption of Cu(II) ions from aqueous solutions on biochars prepared from agricultural by-products. J. Environ. Manag. 96 (2012) 35–42, https://doi.org/10.1016/j.jenvman.2011.10.010.

[15] Y.-Y. Lau, Y.-S. Wong, T.-T. Teng, N. Morad, M. Rafatullah, S.-A. Ong, Coagulation-flocculation of azo dye acid Orange 7 with green refined laterite soil. Chem. Eng. J. 246 (2014) 383–390, https://doi.org/10.1016/j.cej.2014.02.100.

[16] S. Zhao, B. Gao, Q. Yue, Y. Wang, Effect of Enteromorpha polysaccharides on coagulation performance and kinetics for dye removal. Colloids Surf. A Physicochem. Eng. Asp. 456 (2014) 253–260, https://doi.org/10.1016/j.colsurfa.2014.05.035.

[17] D. Babilas, P. Dydo, Selective zinc recovery from electroplating wastewaters by electrodialysis enhanced with complex formation. Sep. Purif. Technol. 192 (2018) 419–428, https://doi.org/10.1016/j.seppur.2017.10.013.

[18] G. Naudin, T. Entradas, B. Barrocas, O.C. Monteiro, Titanate nanorods modified with nanocrystalline ZnS particles and their photocatalytic activity on pollutant removal. J. Mater. Sci. Technol. 32 (2016) 1122–1128, https://doi.org/10.1016/j.jmst.2016.09.001.

[19] C.H. Nguyen, R.-S. Juang, Efficient removal of cationic dyes from water by a combined adsorption-photocatalysis process using platinum-doped titanate nanomaterials. J. Taiwan Inst. Chem. Eng. 99 (2019) 166–179, https://doi.org/10.1016/j.jtice.2019.03.017.

[20] N. Ferroudj, J. Nzimoto, A. Davidson, D. Talbot, E. Briot, V. Dupuis, A. Bée, M. S. Medjram, S. Abramson, Maghemite nanoparticles and maghemite/silica nanocomposite microspheres as magnetic Fenton catalysts for the removal of water pollutants. Appl. Catal. B Environ. 136–137 (2013) 9–18, https://doi.org/10.1016/j.apcatb.2013.01.046.

[21] S.A. Ghodke, S.H. Sonawane, B.A. Bhanvase, I. Potoroko, Advanced engineered nanomaterials for the treatment of wastewater. C.B.T.-H. of N. for I.A. Mustansar Hussain in: Micro and Nano Technologies, Elsevier, 2018, pp. 959–970, https://doi.org/10.1016/B978-0-12-813351-4.00055-9 (Chapter 53).

[22] S. Gupta, B.V. Babu, Experimental, kinetic, equilibrium and regeneration studies for adsorption of Cr(VI) from aqueous solutions using low cost adsorbent (activated flyash). Desalin. Water Treat. 20 (2010) 168–178, https://doi.org/10.5004/dwt.2010.1546.

[23] S. Gupta, B.V. Babu, Modeling, simulation, and experimental validation for continuous Cr(VI) removal from aqueous solutions using sawdust as an adsorbent. Bioresour. Technol. 100 (2009) 5633–5640, https://doi.org/10.1016/j.biortech.2009.06.025.

[24] S. Gupta, P.B.V. Babu, Theoretical & experimental investigations for removal of pollutants using adsorption, in: Department of Chemical Engineering, Birla Institute of Technology & Science (BITS)-Pilani, Pilani Campus, Pilani, 2008.

[25] J. Rivera-Utrilla, M. Sánchez-Polo, M.Á. Ferro-García, G. Prados-Joya, R. Ocampo-Pérez, Pharmaceuticals as emerging contaminants and their removal from water. A review. Chemosphere 93 (2013) 1268–1287, https://doi.org/10.1016/j.chemosphere.2013.07.059.

This book belongs to Badji Mokhtar Annaba University Central Library Copyright Elsevier 2025

[26] B.V. Babu, S. Gupta, Adsorption of Cr(VI) using activated neem leaves: kinetic studies. Adsorption 14 (2008) 85–92, https://doi.org/10.1007/s10450-007-9057-x.
[27] Y. Wu, H. Pang, Y. Liu, X. Wang, S. Yu, D. Fu, J. Chen, X. Wang, Environmental remediation of heavy metal ions by novel-nanomaterials: a review. Environ. Pollut. 246 (2019) 608–620, https://doi.org/10.1016/j.envpol.2018.12.076.
[28] G. Zhao, X. Huang, Z. Tang, Q. Huang, F. Niu, X. Wang, Polymer-based nanocomposites for heavy metal ions removal from aqueous solution: a review. Polym. Chem. 9 (2018) 3562–3582, https://doi.org/10.1039/C8PY00484F.
[29] L. Zhao, J. Deng, P. Sun, J. Liu, Y. Ji, N. Nakada, Z. Qiao, H. Tanaka, Y. Yang, Nanomaterials for treating emerging contaminants in water by adsorption and photocatalysis: systematic review and bibliometric analysis. Sci. Total Environ. 627 (2018) 1253–1263, https://doi.org/10.1016/j.scitotenv.2018.02.006.
[30] X. Qu, P.J.J. Alvarez, Q. Li, Applications of nanotechnology in water and wastewater treatment. Water Res. 47 (2013) 3931–3946, https://doi.org/10.1016/j.watres.2012.09.058.
[31] G.Z. Kyzas, K.A. Matis, Nanoadsorbents for pollutants removal: a review. J. Mol. Liq. 203 (2015) 159–168, https://doi.org/10.1016/j.molliq.2015.01.004.
[32] A.S. Edelstein, R. C, Nanomaterials: Synthesis, Properties and Applications, 2nd ed., CRC Press, 1998.
[33] V.K. Gupta, P.J.M. Carrott, M.M.L. Ribeiro Carrott, Suhas, Low-cost adsorbents: growing approach to wastewater treatment—a review. Crit. Rev. Environ. Sci. Technol. 39 (2009) 783–842, https://doi.org/10.1080/10643380801977610.
[34] M.K. Uddin, A review on the adsorption of heavy metals by clay minerals, with special focus on the past decade. Chem. Eng. J. 308 (2017) 438–462, https://doi.org/10.1016/j.cej.2016.09.029.
[35] National Health and Medical Research Council, Australian Drinking Water Guidelines Paper 6: National Water Quality Management Strategy, (2011)version 3.4 Updated October 2017.
[36] T. Shahryari, A. Mostafavi, D. Afzali, M. Rahmati, Enhancing cadmium removal by low-cost nanocomposite adsorbents from aqueous solutions; a continuous system. Compos. Part B Eng. 173 (2019) 106963, https://doi.org/10.1016/j.compositesb.2019.106963.
[37] R. Naseem, S.S. Tahir, Removal of Pb(II) from aqueous/acidic solutions by using bentonite as an adsorbent. Water Res. 35 (2001) 3982–3986, https://doi.org/10.1016/S0043-1354(01)00130-0.
[38] M. Ghorbani, O. Seyedin, M. Aghamohammadhassan, Adsorptive removal of lead (II) ion from water and wastewater media using carbon-based nanomaterials as unique sorbents: a review. J. Environ. Manag. 254 (2020) 109814, https://doi.org/10.1016/j.jenvman.2019.109814.
[39] R. Bhargavi, U. Maheshwari, S. Gupta, Synthesis and use of alumina nanoparticles as an adsorbent for the removal of Zn(II) and CBG dye from wastewater. Int. J. Ind. Chem. 6 (2015) 31–41, https://doi.org/10.1007/s40090-014-0029-1.
[40] U. Maheshwari, A review on adsorption process for the removal of dyes from textile industry effluent, in: AIChE (Ed.), 2013 AIChE Annual Meeting, San Francisco, CA, USA, 2013p. 276.
[41] A.M. Aljeboree, A.N. Alshirifi, A.F. Alkaim, Kinetics and equilibrium study for the adsorption of textile dyes on coconut shell activated carbon. Arab. J. Chem. (2014), https://doi.org/10.1016/j.arabjc.2014.01.020.
[42] G. Crini, Non-conventional low-cost adsorbents for dye removal: a review. Bioresour. Technol. 97 (2006) 1061–1085, https://doi.org/10.1016/j.biortech.2005.05.001.
[43] R. Gong, Y. Sun, J. Chen, H. Liu, C. Yang, Effect of chemical modification on dye adsorption capacity of peanut hull. Dyes Pigments 67 (2005) 175–181, https://doi.org/10.1016/j.dyepig.2004.12.003.
[44] V.K. Gupta, R. Kumar, A. Nayak, T.A. Saleh, M.A. Barakat, Adsorptive removal of dyes from aqueous solution onto carbon nanotubes: a review. Adv. Colloid Interf. Sci. 193–194 (2013) 24–34, https://doi.org/10.1016/j.cis.2013.03.003.
[45] S.A.S. Chatha, M. Asgher, S. Ali, A.I. Hussain, Biological color stripping: a novel technology for removal of dye from cellulose fibers. Carbohydr. Polym. 87 (2012) 1476–1481, https://doi.org/10.1016/j.carbpol.2011.09.041.
[46] L.W. Man, P. Kumar, T.T. Teng, K.L. Wasewar, Design of experiments for malachite green dye removal from wastewater using thermolysis—coagulation-flocculation. Desalin. Water Treat. 40 (2012) 260–271, https://doi.org/10.1080/19443994.2012.671257.

This book belongs to Badji Mokhtar Annaba University Central Library Copyright Elsevier 2025

[47] M.T. Yagub, T.K. Sen, S. Afroze, H.M. Ang, Dye and its removal from aqueous solution by adsorption: a review. Adv. Colloid Interf. Sci. 209 (2014) 172–184, https://doi.org/10.1016/j.cis.2014.04.002.

[48] L. Zhou, H. Cao, C. Descorme, Y. Xie, Phenolic compounds removal by wet air oxidation based processes. Front. Environ. Sci. Eng. 12 (2017) 1, https://doi.org/10.1007/s11783-017-0970-2.

[49] M.N. Amin, A.I. Mustafa, M.I. Khalil, M. Rahman, I. Nahid, Adsorption of phenol onto rice straw biowaste for water purification. Clean Technol. Environ. Policy 14 (2012) 837–844, https://doi.org/10.1007/s10098-012-0449-6.

[50] G.L. Dotto, J.A.V. Costa, L.A.A. Pinto, Kinetic studies on the biosorption of phenol by nanoparticles from *Spirulina* sp. LEB 18. J. Environ. Chem. Eng. 1 (2013) 1137–1143, https://doi.org/10.1016/j.jece.2013.08.029.

[51] S. Kumar, M. Zafar, J.K. Prajapati, S. Kumar, S. Kannepalli, Modeling studies on simultaneous adsorption of phenol and resorcinol onto granular activated carbon from simulated aqueous solution. J. Hazard. Mater. 185 (2011) 287–294, https://doi.org/10.1016/j.jhazmat.2010.09.032.

[52] G. Vázquez, R. Alonso, S. Freire, J. González-Álvarez, G. Antorrena, Uptake of phenol from aqueous solutions by adsorption in a *Pinus pinaster* bark packed bed. J. Hazard. Mater. 133 (2006) 61–67, https://doi.org/10.1016/j.jhazmat.2004.12.041.

[53] K. Yang, B. Xing, Adsorption of organic compounds by carbon nanomaterials in aqueous phase: Polanyi theory and its application. Chem. Rev. 110 (2010) 5989–6008, https://doi.org/10.1021/cr100059s.

[54] U. Maheshwari, S. Gupta, Performance evaluation of activated neem bark for the removal of Zn(II) and Cu(II) along with other metal ions from aqueous solution and synthetic pulp & paper industry effluent using fixed-bed reactor. Process. Saf. Environ. Prot. 102 (2016) 547–557, https://doi.org/10.1016/j.psep.2016.05.009.

[55] U. Maheshwari, S. Gupta, A novel method to identify optimized parametric values for adsorption of heavy metals from waste water. J. Water Process. Eng. 9 (2016) e21–e26, https://doi.org/10.1016/j.jwpe.2014.12.007.

[56] U. Maheshwari, B. Mathesan, S. Gupta, Efficient adsorbent for simultaneous removal of cu(II), Zn(II) and Cr(VI): kinetic, thermodynamics and mass transfer mechanism. Process. Saf. Environ. Prot. 98 (2015) 198–210, https://doi.org/10.1016/j.psep.2015.07.010.

[57] U. Maheshwari, S. Gupta, Removal of Cr(VI) from wastewater using a natural nanoporous adsorbent: experimental, kinetic and optimization studies. Adsorpt. Sci. Technol. 33 (2015) 71–88, https://doi.org/10.1260/0263-6174.33.1.71.

[58] M. Doğan, M. Alkan, A. Türkyilmaz, Y. Özdemir, Kinetics and mechanism of removal of methylene blue by adsorption onto perlite. J. Hazard. Mater. 109 (2004) 141–148, https://doi.org/10.1016/j.jhazmat.2004.03.003.

[59] L. Zheng, Z. Dang, X. Yi, H. Zhang, Equilibrium and kinetic studies of adsorption of Cd(II) from aqueous solution using modified corn stalk. J. Hazard. Mater. 176 (2010) 650–656, https://doi.org/10.1016/j.jhazmat.2009.11.081.

[60] G. Huang, J.X. Shi, T.A.G. Langrish, Removal of Cr(VI) from aqueous solution using activated carbon modified with nitric acid. Chem. Eng. J. 152 (2009) 434–439, https://doi.org/10.1016/j.cej.2009.05.003.

[61] P.C. Mishra, R.K. Patel, Removal of lead and zinc ions from water by low cost adsorbents. J. Hazard. Mater. 168 (2009) 319–325, https://doi.org/10.1016/j.jhazmat.2009.02.026.

[62] S. Nethaji, A. Sivasamy, G. Thennarasu, S. Saravanan, Adsorption of malachite green dye onto activated carbon derived from *Borassus aethiopum* flower biomass. J. Hazard. Mater. 181 (2010) 271–280, https://doi.org/10.1016/j.jhazmat.2010.05.008.

[63] P. Venkateswarlu, M.V. Ratnam, D.S. Rao, M.V. Rao, Removal of chromium from an aqueous solution using *Azadirachta indica* (neem) leaf powder as an adsorbent, Int. J. Phys. Sci. 2 (2007) 188–195.

[64] K.L. Wasewar, B. Prasad, S. Gulipalli, Removal of selenium by adsorption onto granular activated carbon (GAC) and powdered activated carbon (PAC). Clean Soil Air Water 37 (2009) 872–883, https://doi.org/10.1002/clen.200900188.

[65] S. Ghorai, K.K. Pant, Investigations on the column performance of fluoride adsorption by activated alumina in a fixed-bed. Chem. Eng. J. 98 (2004) 165–173, https://doi.org/10.1016/j.cej.2003.07.003.

This book belongs to Badji Mokhtar Annaba University Central Library Copyright Elsevier 2025

[66] Y. Kalmykova, A.-M. Strömvall, B.-M. Steenari, Adsorption of Cd, Cu, Ni, Pb and Zn on Sphagnum peat from solutions with low metal concentrations. J. Hazard. Mater. 152 (2008) 885–891, https://doi.org/10.1016/j.jhazmat.2007.07.062.
[67] P.S. Kumar, K. Kirthika, Equilibrium and kinetic study of adsorption of nickel from aqueous solution onto bael tree leaf powder, J. Eng. Sci. Technol. 4 (2009) 351–363.
[68] N. Öztürk, D. Kavak, Adsorption of boron from aqueous solutions using fly ash: batch and column studies. J. Hazard. Mater. 127 (2005) 81–88, https://doi.org/10.1016/j.jhazmat.2005.06.026.
[69] H. Singh, V.K. Rattan, Comparison of hexavalent chromium adsorption from aqueous solutions by various biowastes and granulated activated carbon. Indian Chem. Eng. 56 (2014) 12–28, https://doi.org/10.1080/00194506.2014.881002.
[70] M. Eloussaief, I. Jarraya, M. Benzina, Adsorption of copper ions on two clays from Tunisia: pH and temperature effects. Appl. Clay Sci. 46 (2009) 409–413, https://doi.org/10.1016/j.clay.2009.10.008.
[71] M. Kapur, M.K. Mondal, Mass transfer and related phenomena for Cr(VI) adsorption from aqueous solutions onto *Mangifera indica* sawdust. Chem. Eng. J. 218 (2013) 138–146, https://doi.org/10.1016/j.cej.2012.12.054.
[72] T. Liu, Z.-L. Wang, X. Yan, B. Zhang, Removal of mercury (II) and chromium (VI) from wastewater using a new and effective composite: pumice-supported nanoscale zero-valent iron. Chem. Eng. J. 245 (2014) 34–40, https://doi.org/10.1016/j.cej.2014.02.011.
[73] F.A. Pavan, E.S. Camacho, E.C. Lima, G.L. Dotto, V.T.A. Branco, S.L.P. Dias, Formosa papaya seed powder (FPSP): preparation, characterization and application as an alternative adsorbent for the removal of crystal violet from aqueous phase. J. Environ. Chem. Eng. 2 (2014) 230–238, https://doi.org/10.1016/j.jece.2013.12.017.
[74] X. Wang, R. Sun, C. Wang, pH dependence and thermodynamics of Hg(II) adsorption onto chitosan-poly(vinyl alcohol) hydrogel adsorbent. Colloids Surf. A Physicochem. Eng. Asp. 441 (2014) 51–58, https://doi.org/10.1016/j.colsurfa.2013.08.068.
[75] M.R. Awual, I.M.M. Rahman, T. Yaita, M.A. Khaleque, M. Ferdows, pH dependent Cu(II) and Pd(II) ions detection and removal from aqueous media by an efficient mesoporous adsorbent. Chem. Eng. J. 236 (2014) 100–109, https://doi.org/10.1016/j.cej.2013.09.083.
[76] R.A.K. Rao, F. Rehman, Adsorption studies on fruits of gular (Ficus glomerata): removal of Cr(VI) from synthetic wastewater. J. Hazard. Mater. 181 (2010) 405–412, https://doi.org/10.1016/j.jhazmat.2010.05.025.
[77] C. Gabaldón, P. Marzal, J. Ferrer, A. Seco, Single and competitive adsorption of Cd and Zn onto a granular activated carbon. Water Res. 30 (1996) 3050–3060, https://doi.org/10.1016/S0043-1354(96)00165-0.
[78] K.L. Wasewar, Adsorption of metals onto tea factory waste: a review, Int. J. Res. Rev. Appl. Sci. 3 (2010).
[79] S. Gupta, B.V. Babu, Removal of toxic metal Cr(VI) from aqueous solutions using sawdust as adsorbent: equilibrium, kinetics and regeneration studies. Chem. Eng. J. 150 (2009) 352–365, https://doi.org/10.1016/j.cej.2009.01.013.
[80] K. Muthukumaran, S. Beulah, Removal of chromium (VI) from wastewater using chemically activated *Syzygium jambolanum* nut carbon by batch studies. Procedia Environ. Sci. 4 (2011) 266–280, https://doi.org/10.1016/j.proenv.2011.03.032.
[81] E. Errais, J. Duplay, F. Darragi, I. M'Rabet, A. Aubert, F. Huber, G. Morvan, Efficient anionic dye adsorption on natural untreated clay: kinetic study and thermodynamic parameters. Desalination 275 (2011) 74–81, https://doi.org/10.1016/j.desal.2011.02.031.
[82] T. Wang, P. Zhang, D. Wu, M. Sun, Y. Deng, R.L. Frost, Effective removal of zinc (II) from aqueous solutions by tricalcium aluminate (C3A). J. Colloid Interface Sci. 443 (2015) 65–71, https://doi.org/10.1016/j.jcis.2014.11.046.
[83] F.-B. Liang, Y.-L. Song, C.-P. Huang, J. Zhang, B.-H. Chen, Adsorption of hexavalent chromium on a lignin-based resin: equilibrium, thermodynamics, and kinetics. J. Environ. Chem. Eng. 1 (2013) 1301–1308, https://doi.org/10.1016/j.jece.2013.09.025.
[84] N. Rajamohan, M. Rajasimman, R. Rajeshkannan, V. Saravanan, Equilibrium, kinetic and thermodynamic studies on the removal of aluminum by modified *Eucalyptus camaldulensis* barks. Alex. Eng. J. 53 (2014) 409–415, https://doi.org/10.1016/j.aej.2014.01.007.

This book belongs to Badji Mokhtar Annaba University Central Library Copyright Elsevier 2025

[85] J. Wang, L. Ding, J. Wei, F. Liu, Adsorption of copper ions by ion-imprinted simultaneous interpenetrating network hydrogel: thermodynamics, morphology and mechanism. Appl. Surf. Sci. 305 (2014) 412–418, https://doi.org/10.1016/j.apsusc.2014.03.102.

[86] T. Xu, J.G. Catalano, Effects of ionic strength on arsenate adsorption at aluminum hydroxide-water interfaces. Soil Syst. 2 (1) (2018), https://doi.org/10.3390/soils2010001.

[87] K.F. Hayes, C. Papelis, J.O. Leckie, Modeling ionic strength effects on anion adsorption at hydrous oxide/solution interfaces. J. Colloid Interface Sci. 125 (1988) 717–726, https://doi.org/10.1016/0021-9797(88)90039-2.

[88] J. Antelo, M. Avena, S. Fiol, R. López, F. Arce, Effects of pH and ionic strength on the adsorption of phosphate and arsenate at the goethite-water interface. J. Colloid Interface Sci. 285 (2005) 476–486, https://doi.org/10.1016/j.jcis.2004.12.032.

[89] T. Mitani, C. Nakajima, I.E. Sungkono, H. Ishii, Effects of ionic strength on the adsorption of heavy metals by swollen chitosan beads. J. Environ. Sci. Health., Part A Environ. Sci. Eng.Toxicol 30 (1995) 669–674, https://doi.org/10.1080/10934529509376224.

[90] R. Xu, J. Jiang, C. Cheng, Effect of ionic strength on specific adsorption of ions by variable charge soils: experimental testification on the adsorption model of Bowden et al. BT—molecular environmental soil science at the interfaces in the Earth's critical zone, in: J. Xu, P.M. Huang (Eds.), Springer, Berlin Heidelberg, Berlin, Heidelberg, 2010, pp. 78–80.

[91] R. Xu, Y. Wang, D. Tiwari, H. Wang, Effect of ionic strength on adsorption of As(III) and As(V) on variable charge soils. J. Environ. Sci. 21 (2009) 927–932, https://doi.org/10.1016/S1001-0742(08)62363-3.

[92] Y. Huang, C. Fu, Z. Li, F. Fang, W. Ouyang, J. Guo, Effect of dissolved organic matters on adsorption and desorption behavior of heavy metals in a water-level-fluctuation zone of the three gorges reservoir, China. Ecotoxicol. Environ. Saf. 185 (2019) 109695. https://doi.org/10.1016/j.ecoenv.2019.109695.

[93] Y. Yang, L. Liang, D. Wang, Effect of dissolved organic matter on adsorption and desorption of mercury by soils. J. Environ. Sci. 20 (2008) 1097–1102, https://doi.org/10.1016/S1001-0742(08)62155-5.

[94] P. He, Q. Yu, H. Zhang, L. Shao, F. Lü, Removal of copper (II) by biochar mediated by dissolved organic matter. Sci. Rep. 7 (2017) 1–10, https://doi.org/10.1038/s41598-017-07507-y.

[95] M. Alizadeh Fard, A. Vosoogh, B. Barkdoll, B. Aminzadeh, Using polymer coated nanoparticles for adsorption of micropollutants from water. Colloids Surf. A Physicochem. Eng. Asp. 531 (2017) 189–197, https://doi.org/10.1016/j.colsurfa.2017.08.008.

[96] T. Gao, L. Yang, H. Pang, Effect of dissolved organic matter on migration of heavy metals in soils. in: 2010 International Conference on Multimedia Technology, 2010 ICMT, 2010, https://doi.org/10.1109/ICMULT.2010.5631015 3.

[97] S. Shen, S. Yang, Q. Jiang, M. Luo, Y. Li, C. Yang, D. Zhang, Effect of dissolved organic matter on adsorption of sediments to oxytetracycline: an insight from zeta potential and DLVO theory. Environ. Sci. Pollut. Res. 27 (2020) 1697–1709, https://doi.org/10.1007/s11356-019-06787-3.

[98] L. Crouzier, A. Delvallée, S. Ducourtieux, L. Devoille, C. Tromas, N. Feltin, A new method for measuring nanoparticle diameter from a set of SEM images using a remarkable point. Ultramicroscopy 207 (2019) 112847, https://doi.org/10.1016/j.ultramic.2019.112847.

[99] H. Guo, S. Zhang, Z. Kou, S. Zhai, W. Ma, Y. Yang, Removal of cadmium(II) from aqueous solutions by chemically modified maize straw. Carbohydr. Polym. 115 (2015) 177–185, https://doi.org/10.1016/j.carbpol.2014.08.041.

[100] Y. Seekaew, O. Arayawut, K. Timsorn, C. Wongchoosuk, S. Yaragalla, R. Mishra, S. Thomas, N. Kalarikkal, T.R.N. Maria (Eds.), Synthesis, characterization, and applications of graphene and derivatives, Elsevier, 2019, pp. 259–283, https://doi.org/10.1016/B978-0-12-813248-7.00009-2 H.J.B.T.-C.-B.N. (Chapter 9).

[101] D. Tobołа, J. Morgiel, Ł. Maj, TEM analysis of surface layer of Ti-6Al-4V ELI alloy after slide burnishing and low-temperature gas nitriding. Appl. Surf. Sci. 515 (2020) 145942, https://doi.org/10.1016/j.apsusc.2020.145942.

[102] H.B. Asberry, C.-Y. Kuo, C.-H. Gung, E.D. Conte, S.-Y. Suen, Characterization of water bamboo husk biosorbents and their application in heavy metal ion trapping. Microchem. J. 113 (2014) 59–63, https://doi.org/10.1016/j.microc.2013.11.011.

This book belongs to Badji Mokhtar Annaba University Central Library Copyright Elsevier 2025

[103] Z. Wang, G. Liu, H. Zheng, F. Li, H.H. Ngo, W. Guo, C. Liu, L. Chen, B. Xing, Investigating the mechanisms of biochar's removal of lead from solution. Bioresour. Technol. 177 (2015) 308–317, https://doi.org/10.1016/j.biortech.2014.11.077.
[104] D. Seetha, G. Velraj, FT-IR, XRD, SEM-EDS, EDXRF and chemometric analyses of archaeological artifacts recently excavated from Chandravalli in Karnataka state, South India. Radiat. Phys. Chem. 162 (2019) 114–120, https://doi.org/10.1016/j.radphyschem.2019.03.017.
[105] M. Almazrouei, S. Elagroudy, I. Janajreh, Transesterification of waste cooking oil: quality assessment via thermogravimetric analysis. Energy Procedia 158 (2019) 2070–2076, https://doi.org/10.1016/j.egypro.2019.01.478.
[106] G. Ersan, O.G. Apul, F. Perreault, T. Karanfil, Adsorption of organic contaminants by graphene nanosheets: a review. Water Res. 126 (2017) 385–398, https://doi.org/10.1016/j.watres.2017.08.010.
[107] Y. Xie, X. Yuan, Z. Wu, G. Zeng, L. Jiang, X. Peng, H. Li, Adsorption behavior and mechanism of mg/Fe layered double hydroxide with Fe_3O_4-carbon spheres on the removal of Pb(II) and cu(II). J. Colloid Interface Sci. 536 (2019) 440–455, https://doi.org/10.1016/j.jcis.2018.10.066.
[108] M. Keiluweit, M. Kleber, Molecular-level interactions in soils and sediments: the role of aromatic π-systems. Environ. Sci. Technol. 43 (2009) 3421–3429, https://doi.org/10.1021/es8033044.
[109] H.N. Tran, Y.F. Wang, S.J. You, H.P. Chao, Insights into the mechanism of cationic dye adsorption on activated charcoal: the importance of Π-Π interactions. Process. Saf. Environ. Prot. 107 (2017) 168–180, https://doi.org/10.1016/j.psep.2017.02.010.
[110] L. Ji, Y. Shao, Z. Xu, S. Zheng, D. Zhu, Adsorption of monoaromatic compounds and pharmaceutical antibiotics on carbon nanotubes activated by KOH etching. Environ. Sci. Technol. 44 (2010) 6429–6436, https://doi.org/10.1021/es1014828.
[111] H. Liu, J. Zhang, N. Bao, C. Cheng, L. Ren, C. Zhang, Textural properties and surface chemistry of lotus stalk-derived activated carbons prepared using different phosphorus oxyacids: adsorption of trimethoprim. J. Hazard. Mater. 235–236 (2012) 367–375, https://doi.org/10.1016/j.jhazmat.2012.08.015.
[112] J. Chen, W. Chen, D. Zhu, Adsorption of nonionic aromatic compounds to single-walled carbon nanotubes: effects of aqueous solution chemistry. Environ. Sci. Technol. 42 (2008) 7225–7230, https://doi.org/10.1021/es801412j.
[113] W. Chen, L. Duan, D. Zhu, Adsorption of polar and nonpolar organic chemicals to carbon nanotubes. Environ. Sci. Technol. 41 (2007) 8295–8300, https://doi.org/10.1021/es071230h.
[114] B. Pan, B. Xing, Adsorption mechanisms of organic chemicals on carbon nanotubes. Environ. Sci. Technol. 42 (2008) 9005–9013, https://doi.org/10.1021/es801777n.
[115] Y. Wang, J. Zhu, H. Huang, H.-H. Cho, Carbon nanotube composite membranes for microfiltration of pharmaceuticals and personal care products: capabilities and potential mechanisms. J. Membr. Sci. 479 (2015) 165–174, https://doi.org/10.1016/j.memsci.2015.01.034.
[116] E. Padilla-Ortega, R. Leyva-Ramos, J. Mendoza-Barron, Role of electrostatic interactions in the adsorption of cadmium(II) from aqueous solution onto vermiculite. Appl. Clay Sci. 88–89 (2014) 10–17, https://doi.org/10.1016/j.clay.2013.12.012.
[117] F.W. Sousa, M.J. Sousa, I.R.N. Oliveira, A.G. Oliveira, R.M. Cavalcante, P.B.A. Fechine, V.O.S. Neto, D. de Keukeleire, R.F. Nascimento, Evaluation of a low-cost adsorbent for removal of toxic metal ions from wastewater of an electroplating factory. J. Environ. Manag. 90 (2009) 3340–3344, https://doi.org/10.1016/j.jenvman.2009.05.016.
[118] H.-H. Cho, H. Huang, K. Schwab, Effects of solution chemistry on the adsorption of ibuprofen and Triclosan onto carbon nanotubes. Langmuir 27 (2011) 12960–12967, https://doi.org/10.1021/la202459g.
[119] J.-L. Gong, X.-Y. Wang, G.-M. Zeng, L. Chen, J.-H. Deng, X.-R. Zhang, Q.-Y. Niu, Copper (II) removal by pectin-iron oxide magnetic nanocomposite adsorbent. Chem. Eng. J. 185–186 (2012) 100–107, https://doi.org/10.1016/j.cej.2012.01.050.
[120] J. Saikia, Y. Sikdar, B. Saha, G. Das, Malachite nanoparticle: a potent surface for the adsorption of xanthene dyes. J. Environ. Chem. Eng. 1 (2013) 1166–1173, https://doi.org/10.1016/j.jece.2013.09.002.

This book belongs to Badji Mokhtar Annaba University Central Library Copyright Elsevier 2025

[121] C. Souza, D. Majuste, V.S.T. Ciminelli, Effects of surface properties of activated carbon on the adsorption mechanism of copper cyanocomplexes. Hydrometallurgy 142 (2014) 1–11, https://doi.org/10.1016/j.hydromet.2013.11.003.

[122] Q.-Q. Zhong, Q.-Y. Yue, Q. Li, B.-Y. Gao, X. Xu, Removal of Cu(II) and Cr(VI) from wastewater by an amphoteric sorbent based on cellulose-rich biomass. Carbohydr. Polym. 111 (2014) 788–796, https://doi.org/10.1016/j.carbpol.2014.05.043.

[123] S.W. Nam, D.J. Choi, S.K. Kim, N. Her, K.D. Zoh, Adsorption characteristics of selected hydrophilic and hydrophobic micropollutants in water using activated carbon. J. Hazard. Mater. 270 (2014) 144–152, https://doi.org/10.1016/j.jhazmat.2014.01.037.

[124] K. Pyrzynska, A. Stafiej, M. Biesaga, Sorption behavior of acidic herbicides on carbon nanotubes. Microchim. Acta 159 (2007) 293–298, https://doi.org/10.1007/s00604-007-0739-6.

[125] C. Lu, Y.-L. Chung, K.-F. Chang, Adsorption thermodynamic and kinetic studies of trihalomethanes on multiwalled carbon nanotubes. J. Hazard. Mater. 138 (2006) 304–310, https://doi.org/10.1016/j.jhazmat.2006.05.076.

[126] C.A. Cooper, Y.S. Lin, M. Gonzalez, Separation properties of surface modified silica supported liquid membranes for divalent metal removal/recovery. J. Membr. Sci. 229 (2004) 11–25, https://doi.org/10.1016/j.memsci.2003.09.023.

[127] R. Gusain, N. Kumar, S.S. Ray, Recent advances in carbon nanomaterial-based adsorbents for water purification. Coord. Chem. Rev. 405 (2020) 213111, https://doi.org/10.1016/j.ccr.2019.213111.

[128] X. Yu, L. Zhang, M. Liang, W. Sun, pH-dependent sulfonamides adsorption by carbon nanotubes with different surface oxygen contents. Chem. Eng. J. 279 (2015) 363–371, https://doi.org/10.1016/j.cej.2015.05.044.

[129] W. Sun, M. Li, W. Zhang, J. Wei, B. Chen, C. Wang, Sediments inhibit adsorption of 17β-estradiol and 17α-ethinylestradiol to carbon nanotubes and graphene oxide. Environ. Sci. Nano 4 (2017) 1900–1910, https://doi.org/10.1039/C7EN00416H.

[130] M.A. Al-Ghouti, J. Li, Y. Salamh, N. Al-Laqtah, G. Walker, M.N.M. Ahmad, Adsorption mechanisms of removing heavy metals and dyes from aqueous solution using date pits solid adsorbent. J. Hazard. Mater. 176 (2010) 510–520, https://doi.org/10.1016/j.jhazmat.2009.11.059.

[131] M. Goyal, R. Dhawan, M. Bhagat, Adsorption of dimethyl sulfide vapors by activated carbons. Colloids Surf. A Physicochem. Eng. Asp. 322 (2008) 164–169, https://doi.org/10.1016/j.colsurfa.2008.02.047.

[132] H.N. Tran, S.-J. You, H.-P. Chao, Fast and efficient adsorption of methylene green 5 on activated carbon prepared from new chemical activation method. J. Environ. Manag. 188 (2017) 322–336, https://doi.org/10.1016/j.jenvman.2016.12.003.

[133] A.E. Burakov, E.V. Galunin, I.V. Burakova, A.E. Kucherova, S. Agarwal, A.G. Tkachev, V. K. Gupta, Adsorption of heavy metals on conventional and nanostructured materials for wastewater treatment purposes: a review. Ecotoxicol. Environ. Saf. 148 (2018) 702–712, https://doi.org/10.1016/j.ecoenv.2017.11.034.

[134] R.K. Thines, N.M. Mubarak, S. Nizamuddin, J.N. Sahu, E.C. Abdullah, P. Ganesan, Application potential of carbon nanomaterials in water and wastewater treatment: a review. J. Taiwan Inst. Chem. Eng. 72 (2017) 116–133, https://doi.org/10.1016/j.jtice.2017.01.018.

[135] S. Khandgave, A. Kothavade, S. Gupta, U. Maheshwari, Scope of utilization of mix-bed adsorbent for effective multi-pollutant removal, in: Proceedings of International Conference on Advances in Chemical and Petrochemical Engineering (ACAPE-2020), Department of Chemical Engineering and Petroleum Studies, Zakir Husain College of Engineering and Technology, Aligarh Muslim University, Aligarh, 2020, p. 9.

[136] A.M. Awad, R. Jalab, A. Benamor, M.S. Nasser, M.M. Ba-Abbad, M. El-Naas, A.W. Mohammad, Adsorption of organic pollutants by nanomaterial-based adsorbents: an overview. J. Mol. Liq. 301 (2020) 112335, https://doi.org/10.1016/j.molliq.2019.112335.

[137] K.S. Hwang, C. Dae Ki, G. Sung Yong, C. Sung Yong, Adsorption and thermal regeneration of methylene chloride vapor on an activated carbon bed. Chem. Eng. Sci. 52 (1997) 1111–1123, https://doi.org/10.1016/S0009-2509(96)00470-8.

This book belongs to Badji Mokhtar Annaba University Central Library Copyright Elsevier 2025

[138] S. Wadhawan, A. Jain, J. Nayyar, S.K. Mehta, Role of nanomaterials as adsorbents in heavy metal ion removal from waste water: a review. J. Water Process Eng. 33 (2020) 101038, https://doi.org/10.1016/j.jwpe.2019.101038.

[139] S.A. Jadhav, H.B. Garud, A.H. Patil, G.D. Patil, C.R. Patil, T.D. Dongale, P.S. Patil, Recent advancements in silica nanoparticles based technologies for removal of dyes from water. Colloid Interface Sci. Commun. 30 (2019) 100181, https://doi.org/10.1016/j.colcom.2019.100181.

[140] Y.Y. Zhou, J. Lu, Y.Y. Zhou, Y. Liu, Recent advances for dyes removal using novel adsorbents: a review. Environ. Pollut. 252 (2019) 352–365, https://doi.org/10.1016/j.envpol.2019.05.072.

This book belongs to Badji Mokhtar Annaba University Central Library

Copyright Elsevier 2025

CHAPTER 13

New graphene nanocomposites-based adsorbents

Marzieh Badiei[a], Nilofar Asim[b], Masita Mohammad[b], Mohammad Alghoul[c], Nurul Asma Samsudin[d], M. Akhtaruzzaman[b], Nowshad Amin[d], and Kamaruzzaman Sopian[b]

[a]Independent Researcher, Mashhad, Iran, [b]Solar Energy Research Institute, Universiti Kebangsaan Malaysia, Bangi, Selangor, Malaysia, [c]Center of Research Excellences in Renewable Energy Research Institute, King Fahd University of Petroleum & Minerals, Dhahran, Saudi Arabia, [d]Institutes of Sustainable Energy, Universiti Tenaga Nasional (@The National Energy University), Kajang, Selangor, Malaysia

13.1 Introduction

Among the several physical and chemical processes offered for the removal of contaminants and toxic materials, adsorption is considered the most suitable method [1]. This is due to its simplicity, high efficiency, and low cost compared with other techniques such as ion exchange, chemical precipitation, coagulation, membrane filtration, etc. [2].

New carbon-based materials, mainly graphene-based materials, have been widely studied [3, 4]. Graphite, which is a 3D allotrope of carbon, constitutes of graphene sheets with 3.37 Å distance between planes [5]. The intrinsic characteristics of graphite, mainly electrical conductivity and chemical resistance, make it the main source of graphene [6]. In 2004, single-layer graphene was separated from graphite utilizing a mechanical cleavage technique that was revolutionary in the field of material science [7]. Subsequently, Andre Geim and Konstantin Novoselov were awarded the Nobel Prize for the discovery of 2D graphene sheets. To date, varieties of fabrication methods for graphene sheets and graphene-based composites have been developed to exploit their fascinating features in practical applications.

Graphene-based materials mainly graphene, graphene oxide (GO), and reduced graphene oxide (rGO) have been introduced as efficient and low-cost adsorbents [8]. They have a large specific surface area with high porosity; therefore, these groups of carbon-based materials have exhibited adsorption toward organic and inorganic materials [9]. In addition, functional groups

Handbook of Nanomaterials for Wastewater Treatment. https://doi.org/10.1016/B978-0-12-821496-1.00006-4
Copyright © 2021 Elsevier Inc. All rights reserved.

This book belongs to Badji Mokhtar Annaba University Central Library Copyright Elsevier 2025

distributed on the planar and edges of graphene sheets support varieties of interactions between the adsorbent and pollutant structure. Therefore, determining the types of interactions involved in adsorption is essential to improve the selective performance of the adsorbent. According to reports, the most reported interactions are π-π stacking, electrostatic, Van der Waals forces, and H-bonds [10, 11].

Graphene-based adsorbents have reactive groups on the edges and surface that are essential for their adsorption characteristics. Chemical and physical surface modification of these materials are possible as they allow for the introduction of desired heteroatoms and groups on the carbon surface while also enhancing the surface's chemistry for selective adsorption of target molecules [12]. Surface chemistry of a material, defined by the surface area, pore volume, and pore-size distribution, improve the structural stability of molecules under the influence of functional groups and their modifications [13]. A variety of organic and inorganic nanomaterials were applied to modify graphene and its derivatives for desired applications [14]. Depending on the functional groups, graphene nanocomposites have revealed potential adsorption capability for varieties of applications including energy and gas storage [15] as well as detection and elimination of heavy metals [2], organic dyes [16], cationic and anionic dyes [17], polycyclic aromatic hydrocarbons [18], pharmaceuticals [19, 20], pesticides [21], herbicides [22], and volatile organic compounds (VOCs) [23]. In fact, surface modifications of these adsorbents provide certain characteristics required for certain applications. Although some studies have described graphene as a nontoxic material [24], the toxicity and danger of functionalized graphene-based composites to human's health have not yet been entirely reported, thus disposal of their by-products to the environment should still be considered a liability.

In this chapter, the authors review the latest research completed on graphene nanocomposites, their functionalization, and their applications, most notably for adsorption. Finally, a conclusion and perspectives on the preparation and functionalization methods for stimulating development for wider applications are given to conclude this chapter.

13.2 Graphene

Three-dimensional (3D) graphite has a structure consisting of monolayers of graphene sheets stacking over via Van der Waals forces and π-π interactions (Fig. 13.1). The carbon atoms are strongly bound in a hexagonal honeycomb lattice with a molecular bond length of 0.142 nm to form a planar 2D structure that is commonly called graphene. Thus, the most utilized and common resource for preparation of graphene is graphite.

Therefore, graphene is the stable 2D single layer of carbon structure that consist of 2D aromatic macromolecules because of the π-conjugated structure of six-atom rings [25]. The molecular bond length is 0.142 nm and thickness of each layer is about 0.33 nm [26] as shown in Fig. 13.2.

This book belongs to Badji Mokhtar Annaba University Central Library Copyright Elsevier 2025

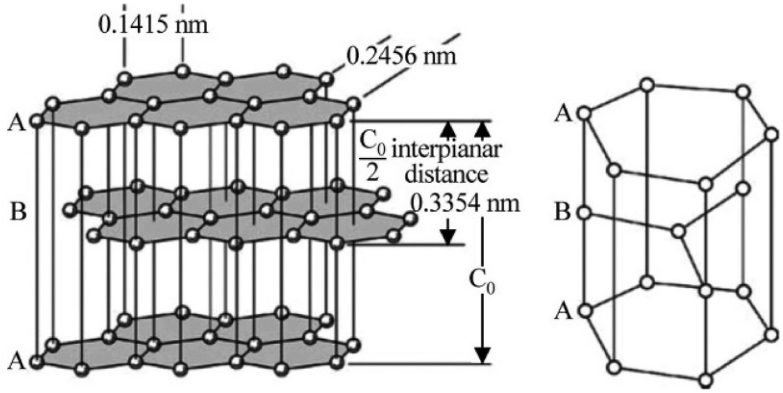

Fig. 13.1
The crystal structure (hexagonal) of flake graphite. *Reproduced from A.D. Jara, A. Betemariam, G. Woldetinsae, J.Y. Kim, Purification, application and current market trend of natural graphite: a review, Int. J. Min. Sci. Technol. (2019). with permission.*

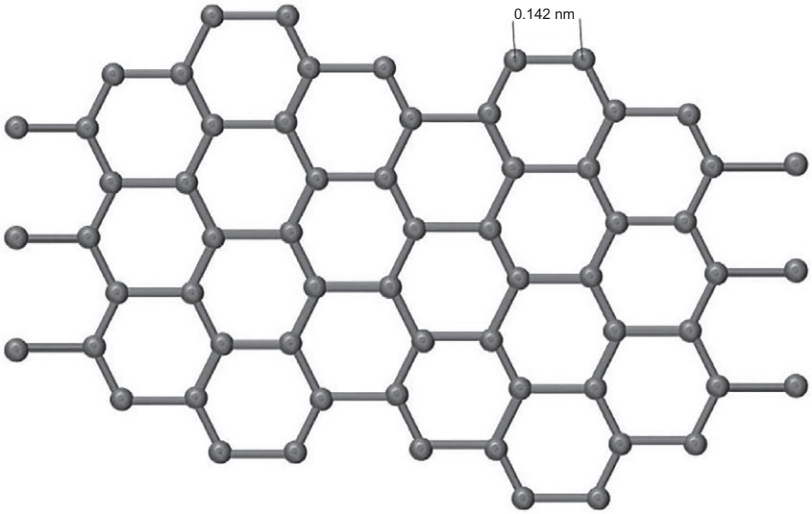

Fig. 13.2
Honeycomb lattice of graphene structure with c-c bonds length of 0.142 nm. *Reproduced from J. Phiri, P. Gane, T.C. Maloney, General overview of graphene: production, properties and application in polymer composites, Mater. Sci. Eng. B 215 (2017) 9–28. with permission from ACS.*

Novoselov and his co-workers [7] developed the first physical method for the preparation of high purity graphene sheets though mechanical exfoliation of graphite crystals that brought him the Nobel Prize in 2010. Mechanical exfoliation, however, was not recognized to be suitable for mass production. The most common and latest methods developed for the fabrication or extraction of graphene are chemical exfoliation [27, 28], chemical vapor deposition (CVD) [29], thermal CVD [30, 31], microwave synthesis [32], and colloidal suspension from graphite

This book belongs to Badji Mokhtar Annaba University Central Library Copyright Elsevier 2025

oxide [33]. All methods, however, suffer from some drawbacks. The selection of preparation method is dependent on the preferred size and purity of the target product.

The chemical structure and morphology of graphene layers well explains its distinctive properties [34], mainly high surface area, excellent mechanical strength, high electrical and thermal conductivity, as well as high optical transmittance. Due to its unique structure, varieties of substances, mainly metal particles, polymers and biomolecules, drugs, and cells, can be immobilized on the graphene surface to prepare nanocomposites for extensive applications [34,35]. The chemical morphology of graphene makes available unlimited possibilities for its functionalization.

There are monolayer, bilayer, and trilayer graphene made of one, two, and three graphitic layers, respectively. The notable physical and chemical properties of graphene are superior due to its availability as a single layer. In aqueous solutions, the π-π interactions between layers of graphene resulted in agglomeration of layers [36]. Moreover, graphene is the building block of other graphitic materials including spherical structures, 1D structures, or 3D layered structures as shown in Fig. 13.3.

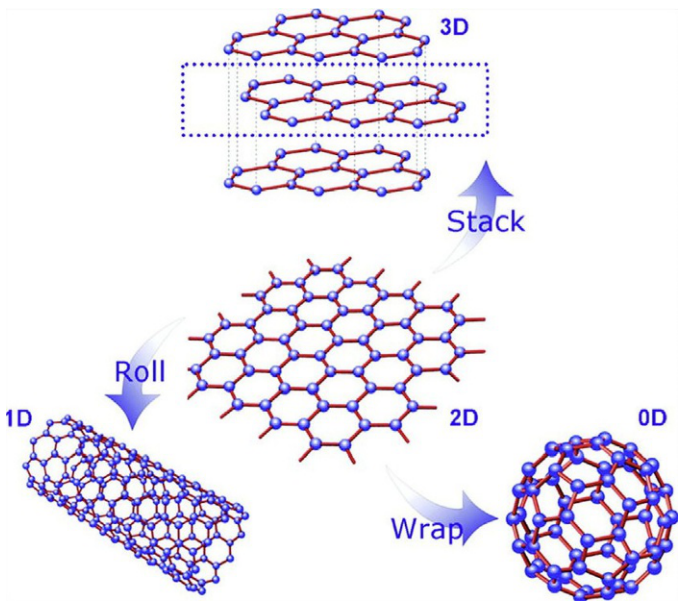

Fig. 13.3
Graphene as a building block of allotropes of carbon with different topologies and dimensionalities.
Reproduced from L.P. Lingamdinne, J.R. Koduru, R.R. Karri, A comprehensive review of applications of magnetic graphene oxide based nanocomposites for sustainable water purification, J. Environ. Manag. 231 (2019) 622–634. with permission.

This book belongs to Badji Mokhtar Annaba University Central Library Copyright Elsevier 2025

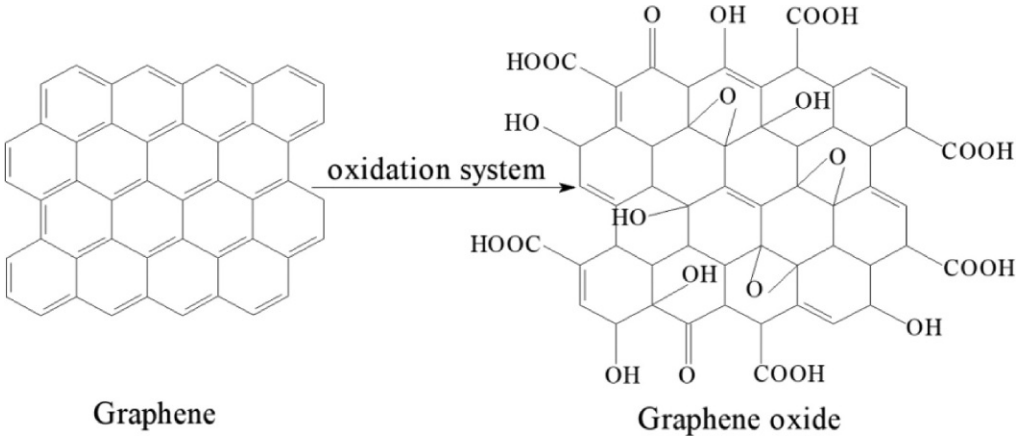

Fig. 13.4
Structure of graphene and graphene oxide (GO). *Reproduced from B. Li, J. Yao, J. Niu, J. Liu, L. Wang, M. Feng, Y. Sun, Effects of graphene oxide on the structure and properties of regenerated wool keratin films, Polymers 10 (2018) 1318.*

13.3 Graphene oxide

GO is a 2D carbonaceous layered material that consists of a carbon sheet with many interesting chemical, mechanical, and electrochemical properties [13,37]. GO is the oxidized derivative of graphene synthesized through chemical or thermal reduction processes with oxygen containing polar functional groups including hydroxyl (—OH), epoxide (C—O—C), and carboxyl (—COOH) groups [38] as shown in Fig. 13.4. Carboxylate groups with negative charge are situated at the edges while epoxide and hydroxyl groups are situated at the basal plane of GO.

A few chemical synthesis methods for oxidizing graphite to GO were developed by Staudenmaier [39], Hummers and Offeman [40], and Brodie [41]. The Hummers method is the most popular method performed through oxidative attack on the sp^2 carbons of the graphene structure using sulfuric acid (H_2SO_4) and potassium permanganate ($KMnO_4$) continued by the addition of hydrogen peroxide and completed through exfoliation of graphite oxide for preparation of GO. This is accomplished by a sonication process [42–44] or new methods, such as thermal exfoliation [45] or innovative directional freezing [46,47]. The Hummers method was gradually optimized by altering variables like reaction duration, temperature, type, and dosage of reactants [48,49]. Currently, most GO are manufactured via the chemical oxidation process that utilize chemicals including $KClO_4$ and HNO_3 [6]. In these reports, the thickness of layers in GO has been measured about ~1 nm compared with 0.3–0.6 nm thickness for pristine graphene [50–52]. This difference might be due to the oxygen-containing groups attached to the basal plane and edges of GO.

This book belongs to Badji Mokhtar Annaba University Central Library Copyright Elsevier 2025

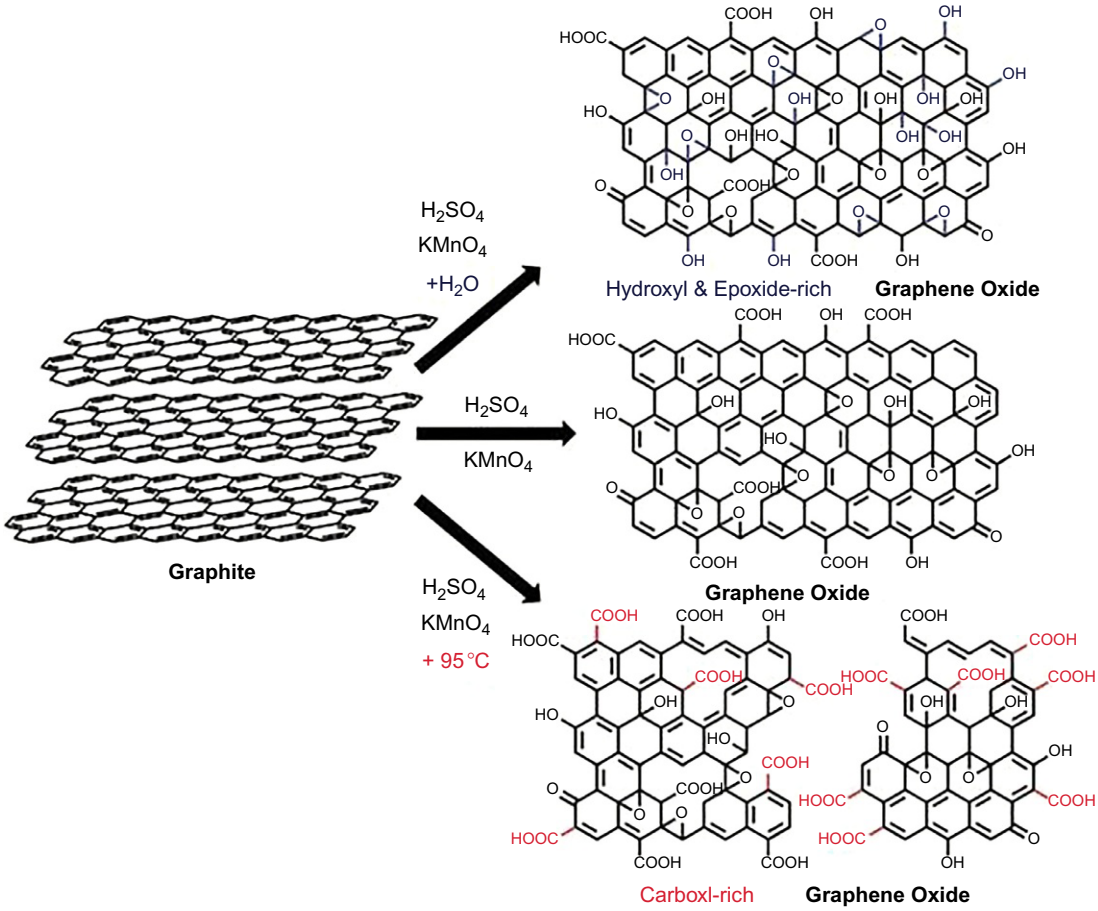

Fig. 13.5

The synthesis of GOs with controlled species of oxygenated groups. *Reproduced from J. Chen, Y. Zhang, M. Zhang, B. Yao, Y. Li, L. Huang, C. Li, G. Shi, Water-enhanced oxidation of graphite to graphene oxide with controlled species of oxygenated groups, Chem. Sci. 7 (2016) 1874–1881.*

In an interesting study [53], Hummers method was modified to prepare oxidized GO sheets with controlled contents of carboxyl, epoxide, as well as hydroxyl groups via control of water in the reaction system (Fig. 13.5).

The well-known structure of GO is represented by carboxylic acid at the edges and hydroxyl and epoxide groups depicted at the basal plane [42]. In fact, GO has the same structure as graphene but is covalently modified with oxygen-containing groups located at basal planes and edges. It is concluded that GO still holds its original 2D structure and the benefits involved with this structure. Carboxylate functional groups at the edges represent negative charge, thus GO is considered pH dependent [54–56]. The existing hydroxyl and epoxide functional groups impart

This book belongs to Badji Mokhtar Annaba University Central Library
Copyright Elsevier 2025

the hydrophobic nature and contribute to π-π interactions [57]. The carboxylate and hydroxyl groups on GO surface can develop hydrogen bonding and Van der Waals interactions to enhance its adsorption capacity toward pesticides and pharmaceuticals. The whole sheet is strongly hydrophilic because of polar oxygen-containing groups and therefore is soluble in several solvents particularly in water, while insoluble in organic solvents such as toluene and chloroform [58].

13.4 Reduced graphene oxide

Reduction of GO via chemical or electrochemical as well as thermal procedures [45,59,60] produces rGO with the structure shown in Fig. 13.6. The rGO obtains improved properties through the reduction of GO materials. For example, GO has high dispersion in aqueous media compared with graphite. It is, however, insoluble in a majority of organic solvents. Therefore, subsequent to the exfoliation process, GO can be modified to rGO to obtain the sufficient conjugated structure of graphene that is vital for adsorption of molecules with aromatic structures, e.g., organic dyes [61–63].

Reducing agents that are generally used for the synthesis of rGO include hydrazine hydrate [64], dimethylhydrazine [65], ascorbic acid [66], amino acids [67], proteins [68], and microorganisms [69]. Reducing GO via the thermal process can be performed through heating GO materials to a range of temperatures between 250°C and 800°C [70,71]. The method of preparation would definitely affect the morphology, chemistry, and properties of the resulting rGO.

In some respects, rGO is not as perfect as graphene or GO. For example, rGO has shown lower conductivity compared with pristine graphene [72]. There are also some defects on the surface of rGO; however, these defects promote covalent or noncovalent interactions with inorganic and organic materials [73]. Compared with pristine graphite, GO and rGO have high dispersion

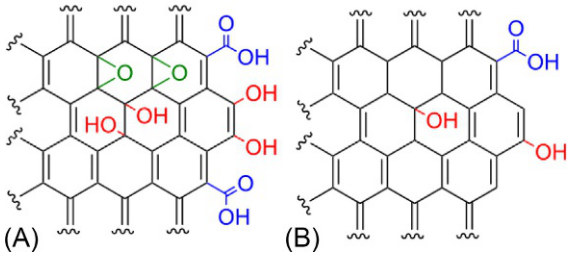

Fig. 13.6
Partial structure of the (A) graphene oxide (GO) and (B) reduced graphene oxide (rGO). *Reproduced from A. Kasprzak, A. Zuchowska, M. Poplawska, Functionalization of graphene: does the organic chemistry matter? Beilstein J. Org. Chem. 14 (2018) 2018–2026.*

This book belongs to Badji Mokhtar Annaba University Central Library Copyright Elsevier 2025

in aquatic media due to their higher interplanar distance and/or decreased interplanar π-π interactions. Despite all these defects, the properties of nanomaterial with rGO can be improved by modifying the rGO using chemicals and 2D materials. In comparison to GO, rGO was reported as a more suitable adsorbent for a variety of dye molecules because its structure allows for electrostatic interaction, π-π interaction, hydrophobic interactions, as well as structural conjugation [16,62,74].

13.5 Functionalization

Graphene-based materials have huge potential in endless applications because of the vast functionalization options offered by their surfaces. Chemical modification of GO through covalent or noncovalent functionalization can be conducted to fabricate nanocomposites for multiple applications. Functionalization can improve specific properties of composites including mechanical and thermal stability, electronic conductivity, chemical selectivity, and solubility [75,76]. Consequently, functionalization improves their specific applications such as adsorption of pollutants, dispersion in solvent media, as well as attainment affinity for polymeric matrix. For example, GO generally has higher adsorption capacity on cationic metals. Removal of anions could be possible when GO is modified with organic materials or metal oxides [77]. It can, therefore, be said that functionalized graphene-based nanocomposites exhibit great potential in various areas, mainly in catalysis [78–80], energy storage [81], electronics [82–84], biomedicine such as drug delivery [85,86], and environmental treatment [87–91]. Research on modification of graphene-based materials is an ongoing work in carbonaceous-based material science.

The basis of functionalization of GO is its high specific surface area and existence of active groups that are responsible for interaction with other molecules [92]. This chapter discusses the commonly used chemicals for functionalization of GO as well as different applications of the modified nanocomposite.

Graphene-based materials, mainly GO, can form new hybrid composites by combining with different inorganic and organic compounds. The new nanocomposite benefits from the synergistic effects of the combined material's properties. Regarding any designed application, the existing active groups and sites of the graphene-based material should be considered. Utilization of organic modifiers denotes a cost-effective and eco-friendly approach in the functionalization of GO for treatments of dyes, heavy metals, and pharmaceuticals in the environment. There is more attention to the synthesis of multifunctional nanomaterials such as nanocomposites with antimicrobial capacity along with adsorption of metal ions for wastewater decontamination applications [93,94]. The multifunctionality of functionalized GO offers a variety of applications in several fields such as adsorption, sensing, and catalysis [83,95–97].

This book belongs to Badji Mokhtar Annaba University Central Library Copyright Elsevier 2025

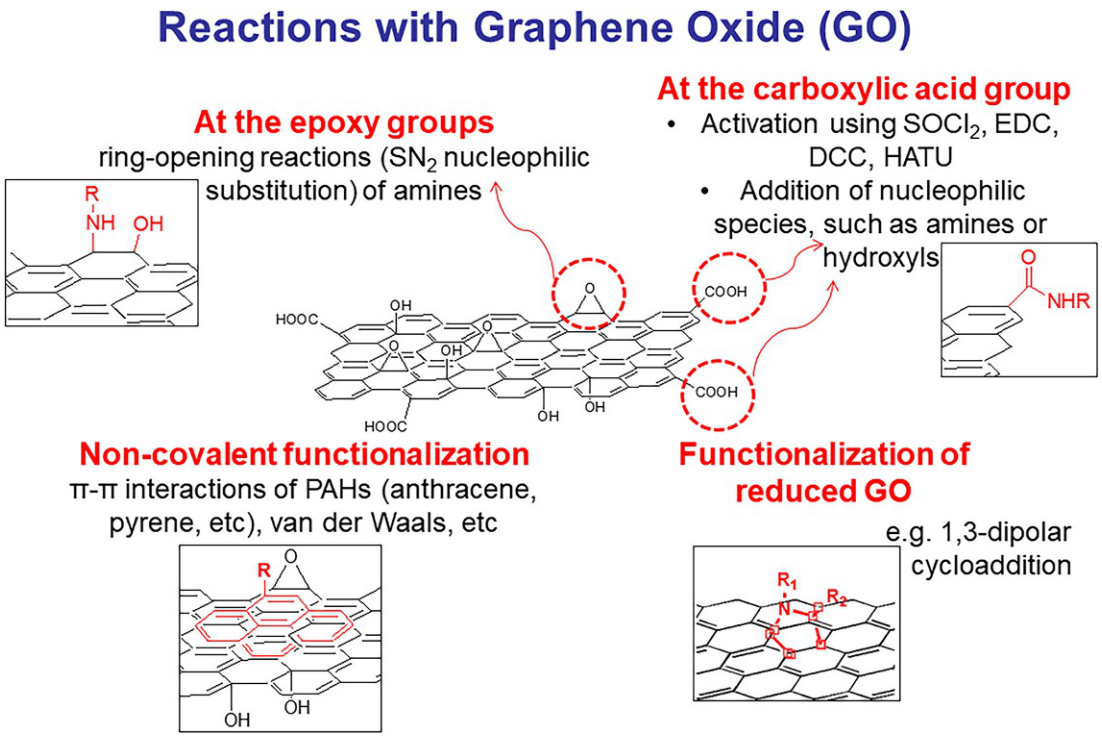

Fig. 13.7

Different approaches for the functionalization of GO. *Reproduced from I.V. Pavlidis, M. Patila, U.T. Bornscheuer, D. Gournis, H. Stamatis, Graphene-based nanobiocatalytic systems: recent advances and future prospects, Trends Biotechnol. 32 (2014) 312–320, with permission.*

The interactions that lead to chemical functionalization of graphene-based materials are either covalent or noncovalent mainly through hydrogen bonding, hydrophobic, and π-π interactions. Covalent functionalization results in covalent bonds by converting sp^2 into sp^3 orbitals. However, the weak noncovalent intermolecular forces like Van der Waals forces exist between the graphene and the desired ligand. In a majority of reports about functionalization of GO, the carboxylic ending groups are employed to bind with long alkyl chains through esterification or amidation. Fig. 13.7 schematically represents different interactions for chemical modifications of GO.

13.5.1 Covalent interaction

Covalent functionalization typically is amide or ester bond formation through amidation or esterification reactions of the carboxyl groups. In this process, small molecules or polymers [98,99] containing amine or hydroxyl groups react with the carboxyl groups present on the edges. Accordingly, covalent interactions will be the cause of change in the chemical nature of

This book belongs to Badji Mokhtar Annaba University Central Library Copyright Elsevier 2025

graphene-based materials or the molecule that is bound to it, therefore leading to a change in properties of the products. The covalent interaction between graphene and organic molecules alters the sp^2 hybrid state to a sp^3 state [100]. In other words, the covalent interaction between organic molecules with sp^2 carbons strongly disturbs the extended π-conjunction and changes the electronic properties [101]. Furthermore, functionalization of the graphene surface through covalent interactions is employed to prepare graphene-based polymer materials. In 2019, Cui and his co-workers [102] functionalized GO through amidation for chemotherapy-based synergistic tumor therapy. In 2017, researchers combined GO with benzene-1,4-diboronic acid to prepare boronic esters through the esterification of GO for gas adsorption [103]. In another study [104], surface esterification of GO was performed via reaction of meta toluic acid with oxygen atoms on the surface. The functionalized material showed excellent dispersion in water and was suggested for gas and humidity sensors. Guo and his co-workers [105] developed a flexible method for the covalent double functionalization of GO via opening of the epoxide ring and then by covalent amidation. The advantage of this approach is that the structure and properties of GO are preserved for a variety of applications. Covalent modification through epoxy groups was studied by Zahirifar and his co-workers [106]. The epoxy groups were functionalized via nucleophilic substitution reactions on α-carbon of the epoxide ring. They used octadecylamine as the nucleophile to prepare octadecylamine-functionalized, GO/PVDF dual-layer, flat sheet membrane for desalination via air gap membrane distillation.
Recently, the covalent amide linkage has been used to bind biocompatible molecules to graphene sheets. Basu et al. [107] prepared a rGO-multiwalled carbon nanotube (CNT) nanocomposite material via functionalization with poly-L-lysinesuitable with improved sensitivity to detect biomolecules in aqueous systems. The amide linkage improved the solubility of graphene sheets, hence the rGO sheets acted as a connector between biomolecule and graphene sheet.

13.5.2 Noncovalent interaction

Noncovalent interactions happen between materials with functional groups and graphene via electrostatic interactions or π-π interactions. These kinds of interactions cannot modify the chemical features of the individual molecules. Noncovalent interactions are more versatile than covalent interactions since the conjugated sheets are relatively preserved [100,108,109]. These kinds of interactions are generally applied for biomolecules as well as biomedicines with optical or electronic properties. Indeed, noncovalent interactions offer strong binding with organic molecule without affecting the extended π-conjunction of graphene. Noncovalent interactions are divided into electrostatic, π-π, as well as hydrophobic interactions. Schematic of noncovalent interactions of GO has been depicted in Fig. 13.7. The GO sheets carry a net negative charge because of carboxylate groups on the surface. Accordingly, the surface charge density follows the pH of the aqueous solution. The carboxyl functional groups provide efficient sites for functionalization using cationic molecules, hence they have been used for

This book belongs to Badji Mokhtar Annaba University Central Library Copyright Elsevier 2025

elimination of organic cationic contaminants [110] including organic dyes [16] and toxic cations like Cu(II) [111], Cd(II), and Pb(II) [112] from aquatic systems. The separation process is the result of different interactions, mainly electrostatic interaction between cations and GO at the supramolecular level. According to a report, GO-chitosan templates were prepared through the electrostatic interaction between negatively charged groups, e.g., —COOH and phenolic —OH groups in GO with $—NH^{3+}$ groups in chitosan [113]. This happens during the ultrasonication step in the synthesis process of Polypyrrole/Chitosan/GO (PPy/CS/GO), which efficiently removes the P4R dye.

Furthermore, graphene-based materials are made up aromatic rings with a delocalized π orbital that helps the π-π interaction. These types of interactions lead to drug delivery potential through development of bonds between water-insoluble aromatic drugs and graphene materials [95,114,115]. Furthermore, hydrophobic domains suitable for the modification of GO through hydrophobic interactions are available on the unoxidized domains of GO's basal planes [111]. Gao [116] utilized GO for adsorption of tetracycline and concluded that tetracycline was strongly deposited on the GO surface via π-π interaction and cation-π bonding. Recently, π-π interactions were reported to be the main interactions between dyes and rGO-Cys when cysteine-modified rGO (rGO-Cys) effectively adsorbed different anionic and cationic dyes [117]. Moreover, according to Peng [118], grafted GO was utilized as hydrophobic interaction-binding sites for extraction of ellagic acid. These researchers prepared GO-grafted cotton fiber and applied it as the stationary adsorbent for the extraction of ellagic acid from pomegranate peel.

13.6 Kinetic of adsorption

The adsorption capacity is a parameter of great importance that is defined by the amount of contaminant that is eliminated from the solution by means of unit mass of developed adsorbent. The adsorption capacity of an adsorbent, mainly GO and rGO as well as their derivatives, is highly influenced by its physical properties, i.e., specific surface area and porosity of its structure as well as chemical properties including functional groups located on the surface of adsorbent [1,119–121]. However, rapid and fast adsorption of materials onto the surface of an adsorbent for elimination of contaminants is the second key feature that influence efficiency of an adsorbent [122,123]. The change in the amount of either reactants or products (or both of them) per unit of time is usually the basic parameter to calculate the kinetic of adsorption. The kinetic of adsorption directly affect time of contact between adsorbent and adsorbate, and longer removal time is not favorable [124,125]. Accordingly, kinetic aspect of an adsorption reaction is important because it presents critical parameters that control the mechanism of reaction including rate of adsorption as well as maximum adsorption capacity (qe). Several kinetic models, mainly pseudo-first order equation [126], pseudo-second order model [88,127], and intraparticle diffusion model [128,129], are commonly applied to test the experimental

This book belongs to Badji Mokhtar Annaba University Central Library Copyright Elsevier 2025

data. According to diffusion model in a solution [88], the first stage of adsorption is migration of adsorbate from bulk phase to liquid film boundary around the adsorbent. Then, adsorbate migrates into the pores on the surface of adsorbent (film diffusion). Next, adsorbate migrates within the pore, which is referred to as intraparticle diffusion. Finally, adsorption inside the adsorbent is completed.

Also, equilibrium study of adsorption is necessary since this is qualitative information about adsorbate-adsorbent surface interactions [130]. Accordingly, isotherm models are developed to support understanding of an adsorption mechanism [131]. The adsorption behavior of contaminants are usually evaluated using equilibrium isotherm models, mainly Langmuir [132], Freundlich [133], Redlich-Peterson [134], and Dubinin-Radushkevich [135]. These isotherm models illustrate how the molecules of contaminants are distributed between solid phase of adsorbent and the liquid phase when the reaction is in an equilibrium state [136]. Moreover, the higher value of correlation coefficient (R^2) of one model determines its better fitness with experimental data compared with other isotherm models. The Langmuir adsorption describes a homogenous adsorption of monolayer of adsorbate on active sites of a surface with uniform energy of adsorption. The Freundlich isotherm model, however, refers to a multilayer adsorption that happens on a surface of heterogeneous distribution of active sites while the energy of adsorption of adsorbate molecules is not uniform.

Overall, these studies provide information necessary for optimization of new adsorbent for selective and effective removal of contaminants from the aqueous solutions and environment.

The adsorption capacity of different types of graphene-based adsorbents as well as proposed adsorption mechanisms has been discussed in the present chapter.

13.7 Graphene-based inorganic nanocomposites

13.7.1 Metal and metal-oxides graphene-based nanocomposites

Hybrid graphene-based composite materials of inorganic nanoparticles (NPs) have shown significant and useful performance in diverse applications such as heterogeneous catalysis [137–139], electrocatalysis [140] and photocatalysis [104,141], energy storage [142], CO_2 adsorption [143], and dye removal [132].

Graphene materials have excellent properties, mainly large surface area, excellent electrical and mechanical features, and chemical inertness, and are thus widely applied as supportive frameworks for metal/metal oxide NPs [144]. This is evidenced by a work by Chandra and his co-workers [145] who reported a higher binding capacity of GO- and rGO-supported materials compared with that of free metal NPs. Moreover, some of mixed metal oxides adsorbents including MgAl-, CuAl-, and CoAl-MMOs materials that were supported or unsupported on

This book belongs to Badji Mokhtar Annaba University Central Library Copyright Elsevier 2025

GO were synthesized [146]. The hybrid nanomaterials showed excellent adsorption capacity for the removal of heavy thiophenic compounds from liquid hydrocarbons. Moreover, selectivity in adsorption performance and thermal stability of mixed metal oxides was enhanced when supported on GO. The experimental data adequately described by the Freundlich isotherms and adsorption equilibrium isotherms clearly demonstrated marked enhancement of DBT uptake upon incorporation of GO into MMO adsorbent.

In general, GO can strongly interact with inorganic NPs and toxic metal ions in aquatic and soil environments. Sheng et al. [147] investigated the adsorption and co-adsorption of GO and Ni on goethite (a-FeOOH) and hematite (a-Fe_2O_3) over a particular range of pH. The presence of GO improved co-adsorption of Ni on both minerals due to strong interaction of Ni with oxygen functional groups on GO.

In another study [148], manganese dioxide-GO nanocomposite was synthesized through the fixation of crystallographic MnO_2 (α, γ) on the surface of GO. The product was utilized for the simultaneous removal of thorium Th (IV) and uranium U (VI) radionuclides ions. The simultaneous adsorption capacities of Th(IV) (408.8 mg/g) and U(VI) (66.8 mg/g) on α-GOM2 were higher than those on GO or MnO_2, which suggests a competitive interaction between Th(IV) and U(VI) may exist in solution. Presumably, the metal ions with higher valence and smaller radius may be easier to be adsorbed onto the adsorbent. Moreover, α-GOM2 as a hybrid material keeps a higher surface area (2001 m^2/g) with more adsorption sites available for metal ions compared with GO (1711 m^2/g). The functionalization of GO surface with metal oxides limits the accumulation of GO's sheets.

Zheng et al. [132] studied the adsorption of GO-NiFe LDH composite and NiFe LDH on the anionic contaminants including Cr(VI), methyl orange (MO), and Congo red (CR). The GONiFeLDH composite exhibited a highly porous structure leading to larger equilibrium adsorption capacity for anionic contaminants including 239.2 mg/g for CR, 177.3 mg/g for MO, and 43.0 mg/g for Cr(VI). The adsorption of three contaminants was better interpreted by pseudo-second order kinetic model and followed Liu isotherm model. The main adsorption mechanism of CR, MO, and Cr(VI) were involved in electrostatic attraction and ions exchange. Moreover, surface complexation contributed to the Cr(VI) adsorption, and π-π interactions contributed to MO and CR adsorption.

Another investigation showed that increasing hydrogen binding of hydroxyl groups in bimetal oxide nanocomposite (Cd_2O_3/Bi_2O_3@GO) as adsorbent and N-containing group in MO (MO) increased the adsorption capacity of adsorbent [149]. The adsorption capacity of nanocomposite for MO was measured to be 544 mg/g equals to 95% removal efficiency. The adsorption followed the Langmuir isotherms and pseudo-second order kinetic model.

Table 13.1 shows latest reports on removal of heavy metal ions using graphene-based nanocomposites.

This book belongs to Badji Mokhtar Annaba University Central Library Copyright Elsevier 2025

Table 13.1: Graphene-based nanocomposites for adsorption of heavy metal contaminants.

Nanocomposite	Target contaminant	Max adsorption capacity (mg/g)	Ref.
Graphene/GO/rGO nanocomposites			
Exfoliated graphite (EG)	Pb(II)	106	[150]
GO	Cu(II)	94.33	[151]
GO	U(VI)	935	[152]
GO	Cu(II)	277.77	[153]
GO	Pb(II)	937.65	[154]
rGO	Pb(II)	92.99	[154]
rGO	Pb(II)	82	[155]
rGO	Cu (II)	93	[155]
Metal/metal oxides/MOF/magnetic graphene-based nanocomposites			
MGOCS	Ni(II)	12.24	[156]
MGOCS	Ni(II)	80.48	[157]
MGO/2-MBT	Cr(VI)	94.02	[158]
MGO/polyDADMAC	Cr(VI)	95.2	[159]
GO-montmorillonite (GMN)	Pb(II)	19.39	[160]
Al-GO	F(I)	38.31	[161]
GO@SiO_2	Hg(II)	40.7	[162]
GO-LaF	As(V)	18.52	[163]
NiF-rGO	Pb(II)	99% removal	[164]
MGL	Pb(II)	192.3	[165]
MGL	Cd(II)	23.04	[165]
MGL	Cu(II)	45.05	[165]
SiO_2@GO-NH2	Cu(II)	102.8	[166]
γ-PGA-Fe_3O_4-GO-(o-MWCNTs)	Ni(II)	384	[167]
γ-PGA-Fe_3O_4-GO-(o-MWCNTs)	Cu(II)	574	[167]
γ-PGA-Fe_3O_4-GO-(o-MWCNTs)	Cd(II)	625	[167]
rGO-PDTC/Fe_3O_4	Cu(II)	113	[168]
rGO-PDTC/Fe_3O_4	Pb(II)	147	[168]
Fe_3O_4@GO/MnOx	Cu(II)	62.65	[169]
MEG	Pb(II)	68	[150]
$ZrO(OH)_{1.33}Cl_{0.66}$-rGO	F(I)	44.14	[170]
MGO	Cd(II)	234	[171]
MGO	As(V)	14	[171]
MGO	Pb(II)	200	[172]
MGO	Cr(III)	24.330	[172]
MGO	Cu(II)	62.893	[172]
MGO	Zn(II)	51.020	[172]

This book belongs to Badji Mokhtar Annaba University Central Library
Copyright Elsevier 2025

Table 13.1: Graphene-based nanocomposites for adsorption of heavy metal contaminants—cont'd

Nanocomposite	Target contaminant	Max adsorption capacity (mg/g)	Ref.
Organic polymers/graphene-based nanocomposites			
CSMGO	As(III)	45	[77]
***n*-GO@HTCS**	Cr(VI)	42.64	[173]
GO/CMCS	Ag(I)	151.30	[174]
GO/CMCS	Cu(II)	95.37	[174]
GO/CMCS	Pb(II)	249.38	[174]
CS/GO	Co(II)	224.8	[175]
CS/GO	Ni(II)	423.7	[175]
CS-GO	Cr(VI)	104.16	[176]
CS/EDTA-silane/mGO	Pb(II)	2.33 mmoL/g	[177]
CS/EDTA-silane/mGO	Cd(II)	1.05 mmoL/g	[177]
CGC	Ce(III)	109.1	[178]
PVA/GO/SA hydrogel	Pb(II)	279.43	[179]
3D-GO/Ca-Alg2-PAN	Cu(II)	5.99 mmoL/g	[180]
Go-CaAlg hydrogel	Au	81.87	[181]
Y-GO-SA hydrogel	As(V)	273.39	[182]
GO-TETA-DAC	Cu(II)	65.1	[183]
GO-TETA-DAC	Pb(II)	80.9	[183]
GO-HBP-NH_2-CMC	Pb(II)	152.86	[184]
GO-HBP-NH_2-CMC	Cu(II)	137.48	[184]
EDTA-2Na/(Ppy)/rGO (EPGA)	Cr(VI)	361	[185]
EDTA-MCS/GO	Pb(II)	206.52	[186]
EDTA-MCS/GO	Cu(II)	207.26	[186]
EDTA-MCS/GO	As(III)	42.75	[186]
3D CD@RGO	Hg (II)	96.6%	[187]
PANI@GO-MWNT	Cr(VI)	66.67	[188]
RGO-BC	Pb(II)	26.10	[189]
GO-CC	Hg(II)	68.8	[190]
GO@AS	Ni(II)	69.93	[191]
GO@AS	Cd(II)	121.95	[191]
GO-PEG (200)	Pb(II)	204.50	[192]
GO-PEG (200)	Cu(II)	48.04	[192]
GO-PEG (200)	Cd(II)	80.48	[192]
GO-PEG (200)	Mn(II)	36.1	[192]
GO-PEG (200)	Er(III)	23.1	[192]
GO-PEG (200)	Y(III)	12.2	[192]
GOCOOH	Cu(II)	357.14	[153]
GO-MTO	Hg(II)	Up to 99%	[193]
βCD-GO	Cd(II)	117.07	[194]
Fe3O4-C3N3S3/rGO	Pb(II)	270.3	[168]

Continued

This book belongs to Badji Mokhtar Annaba University Central Library

Copyright Elsevier 2025

Table 13.1: Graphene-based nanocomposites for adsorption of heavy metal contaminants—cont'd

Nanocomposite	Target contaminant	Max adsorption capacity (mg/g)	Ref.
Fe3O4-C3N3S3/rGO	Hg(II)	400.0	[168]
GO PEDOT:PSS	U(VI)	384.51	[195]
4-Aminoantipyrine-GO	Cu(II)	4.950 mmol/g	[196]
4-Aminoantipyrine-GO	Pb(II)	4.502 mmol/g	[196]
4-Aminoantipyrine-GO	Ni(II)	4.699 mmol/g	[196]

Porous inorganic graphene-based nanocomposites have been also studied for elimination of gaseous pollutants. Theoretical and experimental investigations revealed that adsorption of gas molecules on GO is normally stronger than that of pristine graphene because active defect sites like carbonyl and hydroxyl groups exist on GO [197]. Main toxic and gaseous pollutants include CO_2, CO, NH_3, NOx, SOx, H_2S, and VOCs. For example, GO with its layered structure and strong acidity has been introduced as a suitable adsorptive material for basic gases. In one study [198], NH_3 ammonia adsorption using GO was investigated while another group [199] had prepared GO-polyoxometalate nanocomposites that showed higher ammonia retention compared with pure GO. Metal oxides that are decorated on GO layers improve its total porosity as well as acidic groups. They [198] also prepared zirconium-hydroxide/graphene nanocomposites for the removal of toxic SO_2 gas. A nanocomposite made up of GO/Cu oxides for adsorption of toxic H_2S was prepared by Mabayoje et al. [200]. In addition, GO was functionalized with NPs of Al and Li [201]. The prepared nanocomposites were employed for the adsorption of gases with acidic property including CO_2, NO_2, and SO_2. The researchers explained that the interaction of Li and Al with the hydroxyl and epoxy groups on GO provided robust adsorption sites for these acidic gases. Moreover, the aforementioned supported material MgAl-MMO/GO was prepared [146] with improved thermal cycling stability and the product showed high adsorption capacity for CO_2.

Metal-organic frameworks (MOFs) are high porous adsorbents with large surface area utilized for environmental purification. Modification of these compounds with GO has provided hybrid nanocomposites with promising features and promising capacity toward small molecules adsorption and water and air purification [2,202–206]. Various graphene-based nanocomposites for adsorption of noxious gases have been listed in Table 13.2.

13.7.2 Magnetic graphene-based nanocomposites

Magnetic nanocomposites are chemical compounds that can be recovered easily from the solution; they have been commonly used in wastewater treatment industry [222]. Magnetic-functionalized GO nanocomposites have been introduced as a class of adsorbents that mainly

This book belongs to Badji Mokhtar Annaba University Central Library Copyright Elsevier 2025

Table 13.2: Graphene-based nanocomposites for adsorptive removal of gas pollutants.

Nanocomposite	Target contaminant	Max adsorption capacity (mmol/g)	Ref.
Graphene/GO/rGO nanocomposites			
GO	CO_2	0.3	[120]
GO	SO_2	325 mg/g	[207]
GO fiber	SO_2	320 mg/g	[208]
Metal oxides/MOF/magnetic graphene-based nanocomposites			
(MOF) (UiO-66-NH_2/GO)	CO_2	6.41	[209]
MOF-200	CO_2	1.17	[210]
MOF-200/GO	CO_2	1.34	[210]
MOF-200	CH_4	0.15	[210]
MOF-200/GO	CH_4	0.20	[210]
MOF/GO (Ni-AGO5)	CO_2	6.8	[211]
GO-Fe_3O_4	CO_2	2.3	[212]
NSGO-Fe_3O_4	CO_2	2.0	[212]
GO/TiO_2	CO_2	0.987	[213]
Organic polymers/graphene-based nanocomposites			
TEPA/GO	CO_2	1.2	[120]
GO fiber/PVA	SO_2	380 mg/g	[208]
Aminated GO	CO_2	1.2	[120]
NH_2-rGO/(MDEA) nanofluid	CO_2	16.2% increase	[214]
NH_2-rGO/(MDEA) nanofluid	H_2S	17.7% increase	[214]
PANI/GO5	CO_2	7.11	[215]
Polypyrrole/GO5	CO_2	7.20	[215]
Cu-BTC/GO2	CO_2	9.59	[215]
Polypyrrole/GO	CO_2	4.3	[216]
PANI-GO	CO_2	3.2	[212]
PANI-NSGO	CO_2	2.5	[215]
GO/MDEA nanofluid	CO_2	Up to 10.4%	[214]
(PEI)/GO/MDEA nanofluid	CO_2	10.4% improvement	[217]
TEPA-GO	CO_2	1.2	[120]
GO-benzylamine (GOF-1)	CO_2	24.7 mL/g	[218]
GO-benzylamine (GOF-1)	N_2	58.5 mL/g	[218]
GO-p-xylylenediamine (GOF-2)	CO_2	34.1 mL/g	[218]
GO-p-xylylenediamine (GOF-2)	N_2	77.1 mL/g	[218]
GO-APTES	N_2	179	[219]
GO/activated carbon	SO_2	896 mg/g	[220]
UiO-66/GO	CO_2	6.10	[209]
N-GOs	CO_2	1.36	[221]

This book belongs to Badji Mokhtar Annaba University Central Library
Copyright Elsevier 2025

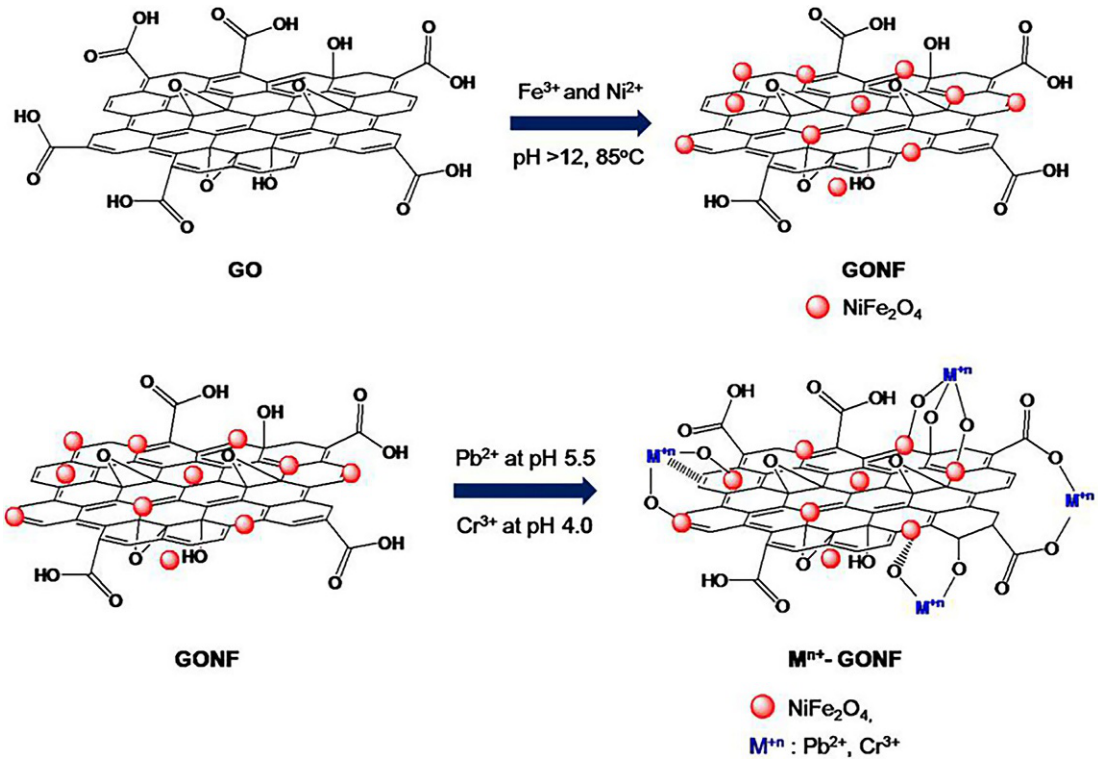

Fig. 13.8
Schematic of preparation of magnetic GONF composite (MGONF), followed by adsorption of Pb(II) and Cr(III) onto MGONF. *Reproduced from L.P. Lingamdinne, J.R. Koduru, Y.-L. Choi, Y.Y. Chang, J.-K. Yang, Studies on removal of Pb(II) and Cr(III) using graphene oxide based inverse spinel nickel ferrite nano-composite as sorbent, Hydrometallurgy 165 (2016) 64–72, with permission.*

follow the magnetic solid-phase extraction (MSPE) method [223,224] with significant advantages for separation processes. Separation of graphene materials from aqueous solution is difficult because of good dispersion in water. The magnetic separation process is time-consuming, although it does not include difficult steps such as filtration [117] or centrifugation [225]. Fig. 13.8 depicts the preparation process of magnetic GO (MGO) and adsorption of metals onto the nanocomposite.

According to previous studies, a variety of metal oxides have been incorporated in GO-based nanocomposites to synthesize magnetic nanomaterials, mainly graphene ferrite-based composites including Fe_3O_4/GO [145,226] and Fe_3O_4/reduced MGO [227,228]. The presence of carboxylic, epoxy, and hydroxyl functional groups on GO significantly enhanced its capability for the adsorption of metal contaminants. Meanwhile, the synergistic effect of graphene with magnetic NPs such as ferrite NPs improves its potential for the elimination of contaminants [229]. Consequently, employing the external magnetic field allows magnetized

This book belongs to Badji Mokhtar Annaba University Central Library Copyright Elsevier 2025

GO (MGO) to show high adsorption capability toward toxic contaminants in wastewater treatment and effortlessly helps separate them from aqueous solutions [230]. Numerous studies have been completed on magnetite (Fe_3O_4)-based materials for environmental application via the MSPE process because of its eco-friendly nature, ease of separation, and high surface area [231,232].

There are many studies about MGO nanocomposites and their ability in elimination of heavy metals such as arsenic [124,145,233], chromium [234], lead [124,163,164], copper and zinc [235], cadmium [236], and cobalt [234]. Heavy metals have been determined as toxic contaminants of aquatic wastewaters.

Liu and his co-workers [237] successfully removed Co(II) using MGO. In their next study [234], they prepared porous Fe_3O_4 hollow microspheres/GO composite to eliminate Cr(VI). The prepared MGO showed improved sorption capacity for adsorption of Cr(VI) in comparison to GO. The sorption isotherms indicated that adsorption is more efficient at higher temperature. The parameters of Langmuir model calculated from the sorption isotherms fitted well with experimental data. The intraparticle diffusion model indicated that adsorption is a two-step process including instantaneous adsorption as well as gradual adsorption step that is the rate-limiting stage of this adsorption process. Employing a magnetic field facilitates separation of adsorbent from aqueous system.

In another study by Deng et al. [238], Cd(II) and ionic dyes, i.e., orange Gelb (OG) and methylene blue (MB) were simultaneously removed using MGO. The fabricated MGO showed better adsorption capacity toward OG (20.85 mg/g) and MB (64.23 mg/g) than that of exfoliated GO for OG (5.98 mg/g) and MB (17.3 mg/g). The higher adsorption capacity of MGO contributed to π-π interactions as well as electrostatic interactions between aromatic and positively charged adsorbates with negatively charged groups on the MGO. The kinetic data were well followed with pseudo-second order model, and isotherm data fitted well with Langmuir model.

Synthesis of MGO impregnated with α-Fe_2O_3 for the elimination of Eriochrome Black T (EBT) from textile wastewater was studied by Khurana et al. [88]. The maximum adsorption capacity of toxic azo dye was 210.53 mg/g that followed Langmuir model, while the rate of adsorption of EBT followed pseudo-second order kinetics.

Gupta et al. [239] prepared a MGO through co-precipitation to examine the adsorption of methadone from the water supplies. Methadone was successfully removed at a range of 87.2 mg/g under optimal temperature and pH, as well as adsorbent dose conditions of 295.7 K, 6.2, and 0.0098 g, respectively. The results revealed a monolayer adsorption process that best fitted with the Langmuir isotherm model.

Other studies, however, revealed that reduced MGO (MrGO) has bigger capacity for adsorption of all metal ions. For example, Fe_3O_4-rGO (M-rGO) composites were synthesized for the

This book belongs to Badji Mokhtar Annaba University Central Library Copyright Elsevier 2025

removal of As(III) and As(V) ions. The product showed excellent adsorption capacity of over 99.9% for both cations [145]. Moreover, Lingamdinne et al. [124] study revealed that removal efficiency of rMGO in the removal of As(III) and As(V) was 106.40 and 65.78 mg/g, respectively, and both rates were higher than that for MGO. According to results, adsorption of As on rMGO surface can be explained by electrostatic interaction or complexation mechanism at pH 6.5 and suggested that intraparticle diffusion was not incorporated in adsorption mechanism. At this pH, As(V) is negatively charged and As(III) is a neutral species, hence, it could be adsorbed onto a positively charged surface of nanocomposite.

Boruah and his co-workers [240] studied the adsorption capacity of Fe_3O_4-supported rGO nanocomposites for the elimination of pesticides, i.e., ametryn, simazine, prometryn, atrazine, and simeton. The magnetic rGO nanocomposites revealed higher adsorption performance compared with rGO sheets. Adsorption equilibrium was obtained at pH 5.0, 25°C, and 70 min with adsorption efficiencies of 93.61%, 91.34%, 88.55%, 81.22%, and 75.24% for ametryn, prometryn simazine, simeton, and atrazine, respectively. The higher adsorption efficiency of ametryn and prometryn that follow the pseudo-second order kinetic model may be attributed to their higher electrostatic interactions with adsorbent. It indicated that a rate-limiting step of reaction is chemisorption between the active sites of Fe_3O_4-rGO nanocomposites and metal ions.

Despite all these advantages, nano-metal ferrites have poor stability as an important drawback. Therefore, hybrid magnetic materials were synthesized. A variety of hybrid magnetic oxides such as Fe_3O_4 [241], $CoFe_2O_4$ [242], $NiFe_2O_4$ [243], MnO_2 [244,245], Mn_3O_4 [246], and other hybrid nanocomposites have also been prepared.

For example, Lingamdinne et al. [124,164] studied fabrication of a hybrid nanocomposite composed of nickel ferrite incorporated in GO/rGO for the elimination of Pb(II), Co(II), Cr(III), As(III) and As(V), U(VI), and Th (IV) from aqueous solution. The removal performance of hybrid nanocomposites was excellent with an ease of separation from the aqueous system and can be regenerated for up to five cycles with minimum loss of adsorption capability. In another study [247], Fe_3O_4-reduced graphite oxide-MnO_2 composites were synthesized for the elimination of As(III) and As(V) from water. The adsorbent was utilized for treatment of real samples of groundwater containing 1 mg/L of As(III) and As(V), and the low residual of contaminants confirmed the efficiency of nanocomposite for treatment of drinking water. Yang et al. [248] studied elimination potential of rGO zero-valent nickel and NiAl-mixed metal oxide (rGO/Ni/MMO) for MO from aqueous solution. The magnetic hybrid nanocomposite was an excellent adsorbent for MO (84.2 mg/g). Moreover, the Redlich-Peterson isotherm proved that adsorption process was not an ideal monolayer adsorption.

Different types of magnetic graphene-based nanocomposites that have been investigated for removal of a variety of contaminants are listed in Tables 13.1–13.3.

This book belongs to Badji Mokhtar Annaba University Central Library Copyright Elsevier 2025

Table 13.3: Graphene-based nanocomposites for adsorption of organic contaminants.

Nanocomposite	Target contaminant	Max adsorption capacity (mg/g)	Ref.
Graphene/GO/rGO nanocomposites			
GO	Diesel	1335	[249]
GO	Phenol	74%	[250]
GO	Phenol	135.6	[251]
GO	2-Chlorophenol (2-CP)	191.3	[251]
GO	4-Chlorophenol (4-CP)	237.7	[251]
GO	2,4-Dichlorophenol (DCP)	398.6	[251]
GO	Bisphenol A (BPA)	420.9	[251]
GO	2,4,6-Trichlorophenol (TCP)	585.8	[251]
GO	Methylene Blue (MB)	379.89	[252]
GO	Bisphenol A (BPA)	17.27	[253]
sGO	Cresyl Violet (CV)	125.0	[254]
sGO	Methylene Blue (MB)	123.3	[254]
sGO	Acridine Orange (AO)	94.6	[43]
3D-rGA	Tetrabromobisphenol A (TBBPA)	128.37	[255]
Metal oxides/MOF/magnetic graphene-based nanocomposites			
MGOCS	Active Blue 19 (RB19)	102.06	[157]
Gd_2O_3/Bi_2O_3@GO	Methyl Orange	544	[149]
MOF/GO	Methylene Blue (MB)	97%	[256]
Cu-BDC@GO	Bisphenol A (BPA)	182.2	[119]
rGO-Fe_3O_4	Phenazopyridine (medicinal)	14.064	[257]
MGO	Malachite Green MG	322.6	[17]
MGO	Methylene Blue (MB)	243.9	[17]
MGO	Methyl Violet MV	212.8	[17]
Pt-Co@GO	Methylene Blue (MB)	273.6	[258]
PAA-rGO	Congo red	166.7	[259]
Gd_2O_3/Bi_2O_3@GO	Methyl Orange	544	[149]
Bi_2O_3@GO	Methyl Orange	308	[149]
Gd_2O_3@GO	Methyl Orange	392	[149]
Fe_3O_4-GO	Tetracycline (TC)	252	[171]
MGO-Si	Sulfamethoxazole	15.46	[260]
MIL-101(Cr)@GO	Sulfadiazine (SDZ)	135.14	[261]
MIL-101(Cr)@GO	Sulfamethoxazole (SMX)	101.01	[261]
MIL-101(Cr)@GO	Sulfadoxine (SDX)	119.05	[261]
Graphene/Fe_3O_4	Tebuconazole	85.2%–96.0%	[262]
GO-GMN	p-Nitrophenol (PNP)	14.90	[160]
ZnO/Ag/GO	Naphthalene	500	[263]
GO@SiO_2	Methyl mercury (MeHg)	91.4	[162]
GO@SiO_2	Ethyl mercury (EtHg)	103.8	[162]

Continued

This book belongs to Badji Mokhtar Annaba University Central Library

Copyright Elsevier 2025

Table 13.3: Graphene-based nanocomposites for adsorption of organic contaminants—cont'd

Nanocomposite	Target contaminant	Max adsorption capacity (mg/g)	Ref.
rGO/Fe_3O_4	Arsanilic acid	313.7	[264]
Zr-GO/Alg	Organophosphate	189.06	[265]
MGO	Organophosphate	93.28	[266]
MGO/PS	Bisphenol A (BPA)	50.25	[253]
MGO/CS	Bisphenol A (BPA)	86.2	[253]
MGO-PANI	Bisphenol A (BPA)	31.8	[253]
CNF-GnP	Methylene Blue (MB)	1178.5	[267]
CNF-GnP	Congo red (CR)	585.3	[267]
G/TEMPO-CNF	Methylene Blue (MB)	227.27	[268]
MGCI-Cu	Hemoglobin (Hb)	769	[269]
Organic polymers/graphene-based nanocomposites			
CS-EDTA-MGO	Rhodamine B	1085	[270]
MGO @ melamine formaldehyde resin	Congo Red (CR)	257.07	[271]
EDTA-GO/corncob	Crystal Violet (CV)	203.9	[272]
PAN/β-cyclodextrin/GO	Crystal Violet (CV)	15.84	[273]
PDA-rGO-kaolin	Methylene Blue (MB)	39.663	[274]
MCS/GO	Chrysoidine Y	~700	[275]
MGO @ melamine formaldehyde	Methyl Blue (MB)	418.41	[271]
Polyamine-MGO	Methyl Violet (MV)	243	[276]
Polyamine-MGO	Acid Red 88 (AR88)	303	[276]
GO-TA	Malachite Green	500	[277]
PQ/G	Alizarin Red S (ARS)	3290	[278]
PAM/GO/n-Hap	Malachite Green	297	[279]
PMMA-GO	Crystal Violet (CV)	0.574	[128]
PMMA-GO-ZnO	Crystal Violet (CV)	1.912	[128]
PMMA/GO	Malachite Green	6.561	[280]
PMMA/GO-Fe_3O_4	Malachite Green	11.01	[280]
βCD-GO	Methylene Blue (MB)	23.98	[194]
GONH/PAA/salep	Methyl Violet (MV)	99.83%	[281]
CNF/GO	Methylene Blue (MB)	265.6	[282]
CNF/GO	Congo Red (CR)	21.5	[282]
CNF/GO	Oil	25.6	[282]
Fe_3O_4@SiO_2-NH_2/GOx/MIP	Cephalosporins (cefoperazone, cephalexin, cefazolin)	80.2%–111.7%	[283]
GO-Psf	Ciprofloxacin	82.781	[284]
rGO-Psf	Ciprofloxacin	21.486	[284]
Y-GO-SA	Tetracycline (TC)	477.9	[182]

This book belongs to Badji Mokhtar Annaba University Central Library
Copyright Elsevier 2025

Table 13.3: Graphene-based nanocomposites for adsorption of organic contaminants—cont'd

Nanocomposite	Target contaminant	Max adsorption capacity (mg/g)	Ref.
(PVAm)-GO-(o-MWCNTs)-Fe_3O_4	Phenol	224.21	[285]
(PVAm)-GO-(o-MWCNTs)-Fe_3O_4	Hydroquinone	293.25	[285]
PDA-GO	Paraquat (PQ)	101.01	[286]
PDA-GO	Nile Blue (NB)	131.58	[286]
rGO-BC	Atrazine	67.55	[189]
GO/Alg	2,4-Dichlorophenoxyacetic acid	150.4	[287]
NrGO	Organophosphate	169.7	[288]
NrGO/Fe_3O_4	Organophosphate	135.3	[288]
3D-HND-GO	Congo Red	23.8	[289]
3D (TKF-rGO)	Oil	54.13 g/g	[290]
rGO/CS	Oil	18–45 g/g	[291]
CS/GO	Benzene	147	[292]
CS/GO	Toluene	60	[292]
CS/GO	Naphthalene	8	[292]

13.8 Graphene-based organic nanocomposites

13.8.1 Graphene-based organic polymer nanocomposites

Many carbonaceous materials like CNTs and graphene are extensively studied as nanofillers to develop polymers with significant gas barrier properties and better mechanical, thermal, and electrical properties [293]. Development of properties in nanocomposite depends upon quality of interactions between filler and matrix. Desirable properties for nanofillers include purity and quality as well as dispersion potential within the matrix, nonagglomeration into the matrix, and their alignment within the polymer matrix directly affect the functionality and quality of polymer nanocomposites [294,295]. The amount of filler loading is a critical factor that controls the stability, flexibility, and chemical functionality of the nanocomposite.

According to reports [296], graphene is the favorable nanofiller for polymer matrices and has been introduced as a potential replacement of CNTs because of its higher surface-to-volume ratio than CNTs [297]. Graphene with special mechanical properties is a noble candidate for reinforcement in nanocomposites. Numerous studies investigated the incorporation of graphene-based derivatives into polymers, including epoxy [298], polystyrene (PS) [299], polypropylene (PP) [300], polyethylene terephthalate [301], polyaniline (PANI) [302], polymethylmethacrylate (PMMA) [280], and cellulose [303] for diverse applications. The electrical conductivity of these types of nanocomposites is improved, thus, these

This book belongs to Badji Mokhtar Annaba University Central Library Copyright Elsevier 2025

nanocomposites have been generally applied to supercapacitors [304] and supercapacitor electrodes [305]. Other different organic conductive polymers such as polythionine [235,306], polypyrrole [307–309], and polyaniline have been used to modify GO-based adsorbents to enhance the adsorptive capacity of resulting composites since these are harmless with economic cost [310].

Karandish and his co-workers [311] synthesized rGO-polyaniline (rGO-PANI) nanocomposites for the removal of Co(II) from water resources as well as food samples. The synergistic effects of polyaniline and GO resulted in improvements in its adsorption performance. GO/polyaniline/manganese oxide ternary nanocomposites (GO/PANI/Mn_2O_3) had also been synthesized for the removal of Indigo Carmine (IC), which is an organic dye pollutant [136]. Since the pseudo-second order kinetic model best fitted this experiment, the adsorption process may be controlled by chemisorption. Moreover, the Langmuir isotherms suggest homogenous distribution of active sites on a nanocomposite. Zhang et al. [312] prepared GO/polyamidoamine dendrimers (GO/PAMAMs), and its adsorption behavior toward Pb(II), Cd(II), Cu(II), and Mn(II) was investigated. According to results, the adsorption of aforementioned metals onto GO/PAMAMs was a chemical adsorption while following second order-type reaction kinetics. The adsorption capacities reported for Pb(II) was 568.18 mg/g, Cd(II) was 253.81 mg/g, Cu(II) was 68.68 mg/g, and Mn(II) was 18.29 mg/g.

Polyaniline itself was used to remove heavy metals and dyes. Many studies have been published on the incorporation of GO and polyaniline in the preparation of hybrid materials for various applications, mainly the elimination of heavy metals and organic dyes [188,313,314]. Up to this date, many methods have been used to prepare GO-PANI nanocomposites with various functional groups to enhance the properties that need to be developed [315,316].

Since GO has oxygen-containing functional groups, it generally owns a negative charge density with hydrophilic nature. It thus has great potential in ultrafiltration applications because of its great features that facilitate gas adsorption. For example, the interlayer spacing of 0.6–1.2 nm between GO sheets has been reported to make it a good candidate as a gas barrier material for gas molecules. Besides that, the 1-nm nanochannels that exist between GO sheets act as nanopores for the molecular sieving mechanism. The nanopores selectively pass water molecules because of the hydrophilic nature of GO while not permitting bigger molecules than the spacing to pass. In general, CO_2 adsorption ability is principally related to the nanoporous structure of the adsorbent including the presence of open metal sites. In addition, the functionalization of graphene has been reported as a good approach to increase adsorption of carbon dioxide (CO_2) gas [221,317,318]. In one study [212], hybrid nanocomposites of GO with polyaniline and Fe_3O_4 NPs were synthesized for the adsorption of CO_2. A combination of polyaniline with GOs sheets further increased the CO_2 adsorption capacity of up to 3.2 mmol/g for PANI-GO. Fe_3O_4 NPs increased the adsorption of CO_2 up to 2.3 mmol/g for MG-GO. Increasing the micropore volume in the prepared nanocomposites seemed to be the key factor

This book belongs to Badji Mokhtar Annaba University Central Library Copyright Elsevier 2025

for the higher adsorption capacity of CO_2. Nevertheless, utilizing GO instead of graphene leads to higher CO_2 retention capacity, better CO_2 selectivity, and easier recyclability, which thus enhances its potential applications in industrial gas adsorption, ultrafiltration, and storage. According to adsorption kinetic data and isotherms, the process is described as a reversible physisorption process. Some of latest studies on CO_2 removal using these composites have been listed in Table 13.2.

However, the efficiency of graphene materials as adsorbents substantially increases when different types of natural organic polymers [319] are directly attached to the surface of graphene sheets. The resulting nanocomposites possess stronger bonding capacity with target molecules and higher selectivity for desired contaminants [4,320]. In this way, the integrated advantages of both filler and matrix as active materials are practical for development of adsorption performance. A number of researchers have successfully used graphene or hybrid nanofiller-based polymer nanocomposites for wastewater purification [321] where these nanocomposites acted as absorbing agents.

Herein are a few examples of the most common graphene-natural organic polymer nanocomposites.

13.8.1.1 Graphene/alginate nanocomposites

Alginate is a natural polysaccharide that is obtained mainly from seaweed and algae. The molecule is composed of (1–4)-linked b-D-mannuronic acid (M) and a-L-guluronic acid (G) units. Alginate is biodegradable and harmless. These characteristics have made it suitable as a stabilizer and emulsifier in the food industry and for biomedical applications [322]. Alginates have been combined with graphene as fillers to prepare aerogels [323] and nanocomposites with enhanced functionality as an adsorbent [265,324–326].

Wu and his co-workers [327] compared the adsorption capability of graphene

oxide/calcium alginate (GO/CA) nanocomposite to that of calcium alginate for the removal of ciprofloxacin (CPX) from wastewater. The experimental data fitted well with pseudo-second order kinetic model, and the Langmuir isotherm represented higher determination coefficients. They found that the nanocomposite successfully removed CPX through a chemical-controlling process to levels as high as 78.9% compared with only 30% using calcium alginate. The intraparticle diffusion model also confirmed that adsorption was a multistep process. In another study, GO was encapsulated in calcium alginate to form macroporous alginic beads for elimination of acridine orange dye [328]. The integration of GO with CA matrix enhanced the overall adsorption kinetics and improved the practical pH range in comparison to using CA alone. The nonlinear Langmuir isotherm model suggested the monolayer adsorption of AO over homogenous sites within the CA.

This book belongs to Badji Mokhtar Annaba University Central Library Copyright Elsevier 2025

Tasmia and his co-workers [329] prepared iron crosslinked alginate encapsulated in MGO (Fe-alg-MGO) beads to remove ECH and BPA through adsorption from water samples. The maximum adsorption capacity for ECH and BPA was recorded as 6.73 and 7.01 mg/g, respectively. The adsorption capacities better fitted with the pseudo-second order kinetic model while the equilibrium data were in good agreement with the Langmuir model. The prepared magnetic nanocomposite has shown potential as an eco-friendly adsorbent. Klongklaew [330] synthesized a more complex and efficient microcomposite PANI/GOx/G18-SiO_2-Fe_3O_4 alginate hydrogel for adsorption of fluoroquinolones in food samples. The composite has a double porous structure with increased surface area and more adsorption sites for contaminant. The important feature of this composite is its ability to modify with high-affinity chemicals for extraction of different contaminants.

In one study, a GO/calcium alginate nanocomposite successfully removed 181 mg/g for a dose of 0.05 g per 100 mL MB solution in the wide range of 4.5–10.2 of pH [331]. According to kinetic pseudo-second order model, the adsorption possibly proceeds through sharing electrons between adsorbent and MB as adsorbate. In another study [332], the diversities of multivalent cations, i.e., Na, Ca, Ba, and Fe were used to synthesize GO/alginate nanocomposite.

13.8.1.2 Graphene/chitosan nanocomposites

The functionalization of graphene-based materials with chitosan has really been a successful step in improvement of hydrophilicity and biocompatibility of graphene-based nanocomposites leading to expanding their applications as an adsorbent.

Chitosan (CS) is a natural biopolymer prepared through the deacetylation of chitin. It has hydrophilic functional groups, mainly amino as well as carboxyl groups. The adsorptive ability of chitosan in the removal of pollutants is highly contributed by the abundant presence of these groups, which are easily protonated, making the molecule susceptible to chemical modifications [333,334]. It is obvious that CS will bring about considerable economic and social benefits [335]. Combining the advantages of graphene-based materials and CS, different types of promising materials including aerogels [336,337], hydrogels [338], and nanocomposites can be obtained [339].

For example, a 3D chitosan-graphene nanocomposite with structural features such as large surface area and high porosity was fabricated [340]. The adsorbent successfully removed reactive black 5 with 97.5% efficiency of 1 mg/L dye. Indeed, the anionic functional groups on GO interacted with CS matrix through electrostatic interactions and hydrogen bonding, which simplified its good dispersion in the matrix [341]. The resulting new nanomaterial consisted of a combination of advantages of both reactants. The suggested interaction between GO and CS has been depicted in Fig. 13.9. Furthermore, Fig. 13.10 represents the comparative FTIR spectra of GO functionalized with chitosan.

This book belongs to Badji Mokhtar Annaba University Central Library Copyright Elsevier 2025

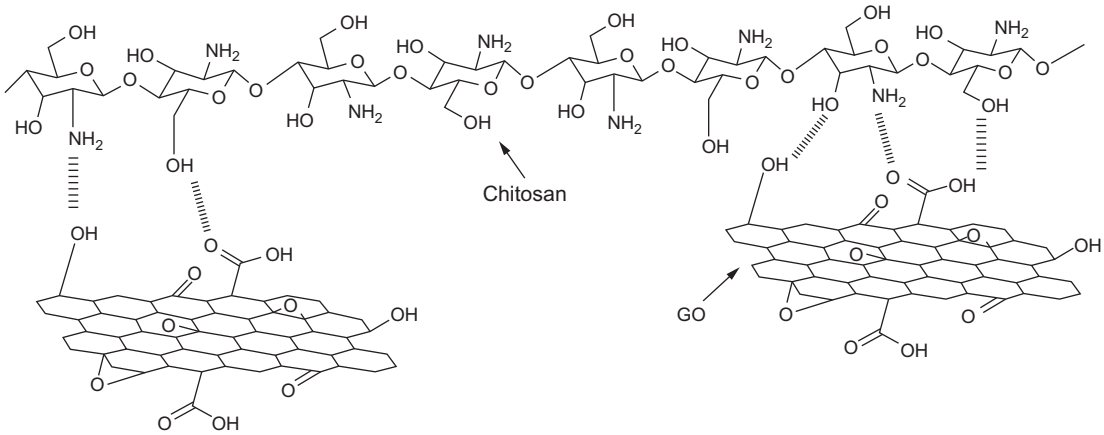

Fig. 13.9

Scheme for the interaction between graphene oxide (GO) and chitosan (CS). *Reproduced from P.R. Sivashankari, M. Prabaharan, Chitosan/carbon-based nanomaterials as scaffolds for tissue engineering, in: S. Jana, S. Maiti, S. Jana (Eds.), Biopolymer-Based Composites, Woodhead Publishing, 2017 (Chapter 12).*

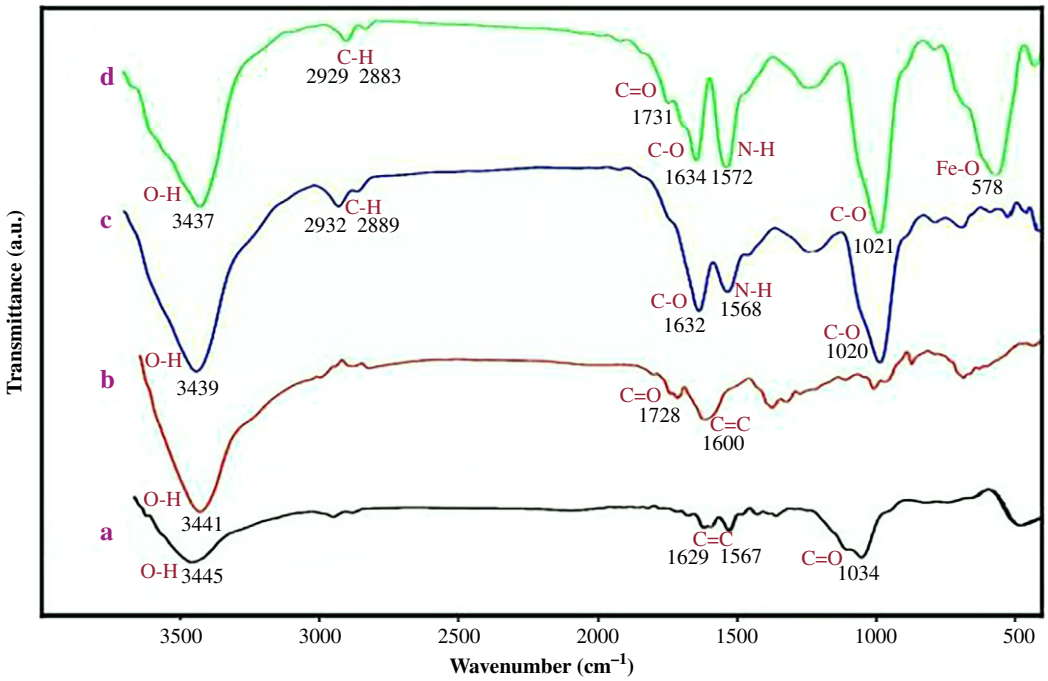

Fig. 13.10

FTIR spectra of (A) graphite, (B) GO, (C) chitosan, and (D) chitosan functionalized 3D graphene nanocomposite. *Reproduced from R. Nasiri, N. Arsalani, Y. Panahian, One-pot synthesis of novel magnetic three-dimensional graphene/chitosan/nickel ferrite nanocomposite for lead ions removal from aqueous solution: RSM modelling design, J. Clean. Prod. 201 (2018) 507–515, with permission.*

This book belongs to Badji Mokhtar Annaba University Central Library Copyright Elsevier 2025

Recently, magnetic chitosan has been developed as novel materials for environmental treatment [342,343]. For example, Subedi [127] fabricated a magnetic chitosan (Chi@Fe_3O_4) nanocomposite that was then reacted with GO to obtain Chi@Fe_3O_4GO. The adsorption capacity of both materials for the adsorption of chromium (Cr(VI)) from water was evaluated. The maximum adsorption levels were 142.32 and 100.51 mg/g for Chi@Fe_3O_4 and Chi@Fe_3O_4GO, respectively. The Freundlich isotherms predicted that monolayer adsorption of Cr(VI) may be performed on heterogeneous surface of Chi@Fe_3O_4GO. Furthermore, the intraparticle diffusion data suggested a two-phase adsorption process involving diffusion of Cr(VI) onto the surface of nanocomposite followed by a slow adsorption step that was considered as the rate-limiting step of the adsorption process.

Similary, Zhang and his co-workers [344] employed the synergistic effect of GO, Fe_3O_4, and chitosan to fabricate a series of chitosan-magnetic GO (CS/MGO) nanocomposites with high capability of removal of Cr(VI) from aqueous solution. The magnetic nanocomposite was introduced as a regenerative bioadsorbent for the cleanup of Cr(VI). The kinetic data proved significant progress in the adsorptive ability of the new nanocomposite.

Besides, Travlou et al. [345] prepared a nanocomposite material from GO with magnetic chitosan for adsorption of Reactive Black 5. The XRD characterization revealed that a major fraction of chitosan's amine groups were inserted between the GO layers to interact with epoxy and carboxyl groups of matrixes to reduce and ruin the layered structure of GO. In fact, GO has the ability to insert small molecules or polymers between its layers. The synthesis of GO-CS composite usually comprises the GO reduction step. The pseudo-second order model best fitted with the experimental data and kinetic analysis predicted a relatively fast adsorption process. The kinetic data indicated at the equilibrium time of adsorption, and surface adsorption changed to intraparticle diffusion.

In addition, the increased adsorption capacity of GO-magnetic chitosan composites toward dyes can relatively be attributed to the strong π-π interactions formed between the aromatic ring of the dye molecule and the carboxylate groups on the basal planes of GO.

13.8.1.3 Graphene/cellulose nanocomposites

Nanocellulose, nanocellulose fibrils, and nanocellulose derivatives have attracted great attention as carbonaceous materials due to their economic cost and high biodegradability [346,347]. Cellulose is the most abundant available renewable biopolymer resource worldwide. The cellulose molecule is generally made up of linear chains of glucose molecules linked together by β-(1 → 4)-glycosidic bonds whereby one molecule can be comprised of up to 20,000 units or less. Nanocellulose and its derivatives encompass reactive carboxyl moieties ($COONa^+$) and have excellent mechanical strength that make them suitable candidates in the fabrication of mechanically robust composites such as aerogels and hydrogels [348]. Cellulose nanocomposites composed of graphene-based materials have exhibited higher

This book belongs to Badji Mokhtar Annaba University Central Library Copyright Elsevier 2025

adsorption capability since graphene provides a variety of electrostatic interactions and hydrogen bonding with cellulose nanofibrils (CNF). Therefore, many attempts have been done to modify cellulose with additional functional groups [349] and fabricating nanocomposites with improved properties. Those studies inspired by the intrinsic properties of GO and nanocellulose fibers and the combination of these nanomaterials was done through promising methods to optimize the properties and functionalities of the prepared nanocomposite for industrial applications.

For example, Hussain et al. [268] fabricated hybrid graphene/cellulose nanofibers (GO/CNFs) monoliths for the adsorption of MB. The nanocomposite adsorbent showed highest adsorption capacity at 227.27 mg/g for MB, which is more than that reported for graphene-based monoliths. According to experimental data, monolayer adsorption of dye followed the Langmuir isotherm model. The electrostatic interactions along with high surface area of adsorbent are the mechanism suggested for adsorption of dye.

Moreover, Mi and his co-workers [350] prepared a fluorinated hybrid aerogel (FHA) composed of GO, CNF, and silica NPs. The prepared adsorbent nanocomposite was considered as a 3D superhydrophobe material for adsorption of oils.

The nanocomposites of bacterial cellulose (BC) with GO exhibited significant adsorption capacity of metal ions [351]. The adsorption efficiency was dependent on the GO content, metal ion concentration, and pH of aqueous solution. The adsorption data of metal ions that followed the pseudo-second order kinetics was fitted well with Freundlich isotherm model suggesting adsorption through electrostatic interactions, while a difference in heterogenous adsorption sites on GO surface was also predicted.

Some of the latest reports on adsorptive application of cellulose nanocomposites using graphene-based materials are listed in Tables 13.1–13.3.

13.8.2 Graphene-based nanocomposites with multidentate organic chelating ligands and complexion agents

The oxidation of graphite to GO can provide many active groups on the surface of the GO that become suitable sites for the attachment of metal ions. These groups, mainly —COOH, —C═O, and —OH, make GO a highly potential superadsorbent [42]. They are the important chemical functional groups for an effective adsorbent [54,320,352]. Moreover, the large specific surface area of GO provides many anchoring positions for the functionalization of chitosan (CS), ethylenediaminetetraacetic acid (EDTA), and other organic polymers [270]. All these features eventually increase the level of heavy metal adsorption.

Ethylenediaminetetraacetic acid (EDTA) is widely recognized for developing suitable chelates with metal ions, so EDTA is a suitable material for adsorption of toxic metals [353, 354].

This book belongs to Badji Mokhtar Annaba University Central Library Copyright Elsevier 2025

Chelating groups are well connected to the surface of GO between N-(trimethoxysilylpropyl) ethylenediamine triacetic acid (EDTA-silane) and —OH groups on the surface of GO through a salinization reaction. There are many reports about graphene-based nanomaterials modified with EDTA with excellent adsorption affinity toward heavy metal pollutants [177,270,272,355,356]. Upon linking to the surface of GO, EDTA acts as a chelating agent to prepare a stable chelate with toxic metal ions.

Research was performed to study the adsorption and desorption of Pb(II) on EDTA-GO nanocomposite [357]. GO modified with EDTA through the salinization process revealed improved adsorption behavior due to the chelating ability of EDTA. The adsorption capability of the nanocomposite varied according to the pH of the solution, accordingly surface complexation and formation of a complex between Pb(II) and EDTA is suggested. A maximum adsorption of 479 mg/g at pH 6.8 for Pb (II) was reported using the new nanocomposite. The researchers had also previously examined the chemical modification of graphene sheets with N-(trimethoxysilylpropyl) ethylenediamine triacetic acid via a salinization reaction [358]. The new nanocomposite revealed increased dispersion in water with high conductivity.

In a study by Shahzad et al. [186], EDTA-functionalized magnetic chitosan GO (EDTA-MCS/GO) nanocomposites were fabricated and evaluated for elimination of Pb(II), Cu(II), and As(III) from aqueous solutions. Actually, the effective removal of both divalent (Pb(II) and Cu(II)) and trivalent As(III) metal ions was evaluated using the EDTA-MCS/GO nanocomposites. The nanocomposite recorded highest adsorption levels of 206.52, 207.26, and 42.75 mg/g for Pb(II), Cu(II), and As(III), respectively. According to pseudo-second order kinetic model that better fitted with experimental data, adsorption process was illustrated as chemisorption including chemical interactions between functional groups of nanocomposites and metal ions.

As another organic chelating agent, GO was modified using 3-aminophenol for the adsorption of triazole fungicides from natural water as well as juice. The new composite was prepared from poly 3-aminophenol and GO in alkalie media [359]. Moreover, GO was modified with 4-aminothiophenol and with 3-aminopropyltriethoxysilane through introduction of —SH moieties and —NH_2 moieties to GO, respectively [360]. The adsorption isotherms and sorption kinetics of both functionalized GOs showed increased adsorption capacity than that of pristine GO for elimination of Cu(II) and MB from the aqueous solutions. It is suggested that —SH and —NH2 groups that are grafted to the GO structure provide chelation with metal ions.

Meanwhile, various robust complexing agents such as 2,2′-dipyridylamine (DPA) [361], 2-pyridinecarboxaldehyde thiosemicarbazone (2-PTSC) [362], diaminocyclohexanetetraacetic acid (DCTA) [363, 364], and cyclodextrin [365, 366] have also been used to functionalize the surface of GO and increase the adsorption potential of GO through developing specific binding and providing complexes with heavy metal ions. In fact, these ligands change the positive and

This book belongs to Badji Mokhtar Annaba University Central Library Copyright Elsevier 2025

negative charges of the adsorbent surface and affect the distribution of metal ions on the surface of adsorbent.

Some of the latest studies on common organic chelating ligands and complexion agents used for the modification of GO are listed in Tables 13.1–13.3.

13.9 Challenges and future prospective

Graphene and its derivative materials as carbonaceous materials have demonstrated their effectiveness as new adsorbents for the removal of inorganic and organic contaminants of any kind. Because of the wide range of applications for nanocomposites, it is not possible to discuss in brief review all the aspects of these graphene-based adsorbents. In a laboratory scale, the adsorption of pollutants using graphene has been proven to be remarkable because of its physiochemical properties such as large surface area and considerable unsaturated and delocalized electrons, etc. There are numerous graphene-based materials with multifold adsorption capacity varying by oxidized graphene nanocomposites such as GO and rGO to magnetic graphene composites and inorganic-based materials such as N-doped graphene. Synthesis of oxidized derivatives of graphene, mainly GO and rGO, enhances its hydrophilic properties multifold, thus increasing its potential to react with organic and inorganic contaminants for enhancing physical or chemical adsorption on its surface. Even nanocomposites prepared with biopolymers like chitosan, alginate, and cellulose were successfully applied for treatment of effluents.

However, there are multiple challenges for industrial-scale employment of graphene-based adsorbents in wastewater treatment. The important issues are about minimizing the cost for production of large quantities of nanocomposites with low environmental effects. Wastewater treatment procedure needs large quantities of highly efficient adsorbents at low cost. Deploying the full potential of adsorbent nanocomposites in practical applications needs to consider and solve the challenging problems that are divided to economic and environmental implications.

The first economic challenge is that high quality adsorbent should be fabricated through environmental friendly methods at low cost. If the performance of an adsorbent is low because of inefficient design of the molecule, modification of the material might be lead to better performance that could be completed by a simple, efficient, and cost-effective process. Despite the considerable adsorption capacity of these composites for organic and inorganic pollutants, their production is not still economical in comparison to conventional adsorbents, mainly zeolites and carbon active materials. The more complex functionalized graphene-based nanocomposites with higher cost of preparation usually show higher adsorption performance that reveals the necessity of developing lower cost but novel and more efficient functionalization techniques.

This book belongs to Badji Mokhtar Annaba University Central Library Copyright Elsevier 2025

Moreover, the feasibility of industrial graphene-based adsorbents depends on the ability of simultaneous removal of different types of contaminants and pollutants in wastewater applications. A majority of adsorption studies investigate one-component aqueous solutions, which is not a realistic situation.

Besides, environmental considerations are another important issue in the development of graphene-based adsorbents. The life cycle assessment of graphene-based composites should be investigated to reveal their fate and their transformation in the environment. There is lack of information about the long-term physical and chemical transformation of graphene derivatives in the environment. Increasing the manufacture and application of graphene-based materials will increase the release of graphene and its derivatives in industrial effluents, hence, its toxicity as a threat for human beings and environment should be investigated. Furthermore, reusability potential and stability of these materials in real wastewater systems must be addressed to design simple, efficient, and low-cost regeneration methods that release minimum secondary toxicity to the environment. Since the effect of graphene-based materials on human health and the environment has yet to be determined, it is evident that there still remains a need for effective techniques for separation of graphene nanocomposites from solutions even after the adsorption process.

The evolution of synthesis for a variety of graphene-based nanocomposites ensure that graphene-based polymer composites are widely studied, and these type of carbonaceous adsorbents would be efficient materials for a wide range of applications, mainly water treatment and removal of contaminants. However, there are still many problems that must be considered and studied for these composites to reach their full potential compared with other well-known adsorbents. This chapter associates the recent literature published for adsorption of toxic and contaminants using graphene-based materials and their mechanisms.

References

[1] S. Li, P. Yang, X. Liu, J. Zhang, W. Xie, C. Wang, C. Liu, Z. Guo, Graphene oxide based dopamine mussel-like cross-linked polyethylene imine nanocomposite coating with enhanced hexavalent uranium adsorption, J. Mater. Chem. A 7 (2019) 16902–16911.
[2] X. Liu, R. Ma, X. Wang, Y. Ma, Y. Yang, L. Zhuang, S. Zhang, R. Jehan, J. Chen, X. Wang, Graphene oxide-based materials for efficient removal of heavy metal ions from aqueous solution: a review, Environ. Pollut. 252 (2019) 62–73.
[3] I. Ali, X. Mbianda, A. Burakov, E. Galunin, I. Burakova, E. Mkrtchyan, A. Tkachev, V. Grachev, Graphene based adsorbents for remediation of noxious pollutants from wastewater, Environ. Int. 127 (2019) 160–180.
[4] V. Singh, D. Joung, L. Zhai, S. Das, S.I. Khondaker, S. Seal, Graphene based materials: past, present and future, Prog. Mater. Sci. 56 (2011) 1178–1271.
[5] D. Chung, Review graphite, J. Mater. Sci. 37 (2002) 1475–1489.
[6] A. Adetayo, D. Runsewe, Synthesis and fabrication of graphene and graphene oxide: a review, J. Compos. Mater. 9 (2019) 207.
[7] K.S. Novoselov, A.K. Geim, S.V. Morozov, D. Jiang, Y. Zhang, S.V. Dubonos, I.V. Grigorieva, A. A. Firsov, Electric field effect in atomically thin carbon films, Science 306 (2004) 666–669.

This book belongs to Badji Mokhtar Annaba University Central Library Copyright Elsevier 2025

[8] N. Baig, M. Sajid, T.A. Saleh, Graphene-based adsorbents for the removal of toxic organic pollutants: a review, J. Environ. Manag. 244 (2019) 370–382.
[9] P. Jayakaran, G. Nirmala, L. Govindarajan, Qualitative and quantitative analysis of graphene-based adsorbents in wastewater treatment, Int. J. Chem. Eng. 2019 (2019) 1–17.
[10] Z. Hasanzade, H. Raissi, Investigation of graphene-based nanomaterial as nanocarrier for adsorption of paclitaxel anticancer drug: a molecular dynamics simulation study, J. Mol. Model. 23 (2017) 36.
[11] G.-H. Yang, D.-D. Bao, H. Liu, D.-Q. Zhang, N. Wang, H.-T. Li, Functionalization of graphene and applications of the derivatives, J. Inorg. Organomet. Polym. Mater. 27 (2017) 1129–1141.
[12] X. Wang, Y. Liu, H. Pang, S. Yu, Y. Ai, X. Ma, G. Song, T. Hayat, A. Alsaedi, X. Wang, Effect of graphene oxide surface modification on the elimination of Co(II) from aqueous solutions, Chem. Eng. J. 344 (2018) 380–390.
[13] H. Ahmad, M. Fan, D. Hui, Graphene oxide incorporated functional materials: a review, Compos. Part B 145 (2018) 270–280.
[14] F.V. Ferreira, L.D.S. Cividanes, F.S. Brito, B.R.C. De Menezes, W. Franceschi, E.A.N. Simonetti, G. P. Thim, Functionalization of graphene and applications, in: Functionalizing Graphene and Carbon Nanotubes, Springer, 2016.
[15] C. Tang, H.-F. Wang, J.-Q. Huang, W. Qian, F. Wei, S.-Z. Qiao, Q. Zhang, 3D hierarchical porous graphene-based energy materials: synthesis, functionalization, and application in energy storage and conversion, Electrochem. Energy Rev. 2 (2019) 332–371.
[16] A. Molla, Y. Li, B. Mandal, S.G. Kang, S.H. Hur, J.S. Chung, Selective adsorption of organic dyes on graphene oxide: theoretical and experimental analysis, Appl. Surf. Sci. 464 (2019) 170–177.
[17] M. Akrami, S. Danesh, M. Eftekhari, Comparative study on the removal of cationic dyes using different graphene oxide forms, J. Inorg. Organomet. Polym. Mater. 29 (2019) 1785–1797.
[18] I. Hussain, A. Hussain, A. Ahmad, H. Rahman, M.F. Alajmi, F. Ahmed, S. Amir, New generation graphene oxide for removal of polycyclic aromatic hydrocarbons, in: Graphene-Based Nanotechnologies for Energy and Environment, Elsevier, 2019.
[19] K. Balasubramani, N. Sivarajasekar, M. Naushad, Effective adsorption of antidiabetic pharmaceutical (metformin) from aqueous medium using graphene oxide nanoparticles: equilibrium and statistical modelling, J. Mol. Liq. 112426 (2020).
[20] M.-F. Li, Y.-G. Liu, G.-M. Zeng, N. Liu, S.-B. Liu, Graphene and graphene-based nanocomposites used for antibiotics removal in water treatment: a review, Chemosphere (2019).
[21] V.H. Braga, M.B. Leão, P.C. Da Rosa, C.F.D.M. Jauris, Graphene-based nanomaterials for adsorption and removal of pesticides: a review, in: Anais do Salão Internacional de Ensino, Pesquisa e Extensão, 2019p. 10.
[22] T.G. Chatzimitakos, K.K. Karali, C.D. Stalikas, Magnetic graphene oxide as a convenient nanosorbent to streamline matrix solid-phase dispersion towards the extraction of pesticides from vegetables and their determination by GC-MS, Microchem. J. 151 (2019) 104247.
[23] V. Kumar, Y.-S. Lee, J.-W. Shin, K.-H. Kim, D. Kukkar, Y.F. Tsang, Potential applications of graphene-based nanomaterials as adsorbent for removal of volatile organic compounds, Environ. Int. 135 (2020) 105356.
[24] T. Lazarević-Pašti, V. Anićijević, M. Baljozović, D.V. Anićijević, S. Gutić, V. Vasić, N.V. Skorodumova, I. A. Pašti, The impact of the structure of graphene-based materials on the removal of organophosphorus pesticides from water, Environ. Sci. Nano 5 (2018) 1482–1494.
[25] A.K. Geim, K.S. Novoselov, The rise of graphene, in: Nanoscience and Technology: A Collection of Reviews From Nature Journals, World Scientific, 2010.
[26] S. Eigler, Graphene. An introduction to the fundamentals and industrial applications edited by Madhuri Sharon and Maheshwar Sharon, Angew. Chem. Int. Ed. 55 (2016) 5122.
[27] M.S.A. Bhuyan, M.N. Uddin, M.M. Islam, F.A. Bipasha, S.S. Hossain, Synthesis of graphene, Int. Nano Lett. 6 (2016) 65–83.
[28] P. Kamedulski, A. Ilnicka, J.P. Lukaszewicz, M. Skorupska, Highly effective three-dimensional functionalization of graphite to graphene by wet chemical exfoliation methods, Adsorption 25 (2019) 631–638.

This book belongs to Badji Mokhtar Annaba University Central Library Copyright Elsevier 2025

[29] S. Das, J. Drucker, Nucleation and growth of single layer graphene on electrodeposited Cu by cold wall chemical vapor deposition, Nanotechnology 28 (2017) 105601.
[30] S. Lee, W.K. Park, Y. Yoon, B. Baek, J.S. Yoo, S.B. Kwon, D.H. Kim, Y.J. Hong, B.K. Kang, D. H. Yoon, Quality improvement of fast-synthesized graphene films by rapid thermal chemical vapor deposition for mass production, Mater. Sci. Eng. B 242 (2019) 63–68.
[31] T. Seyller, A. Bostwick, K. Emtsev, K. Horn, L. Ley, J. Mcchesney, T. Ohta, J. D. Riley, E. Rotenberg, F. Speck, Epitaxial graphene: a new material, Phys. Status Solidi B 245 (2008) 1436–1446.
[32] G. Xin, W. Hwang, N. Kim, S.M. Cho, H. Chae, A graphene sheet exfoliated with microwave irradiation and interlinked by carbon nanotubes for high-performance transparent flexible electrodes, Nanotechnology 21 (2010) 405201.
[33] J.I. Paredes, S. Villar-Rodil, P. Solís-Fernández, A. Martínez-Alonso, J. Tascon, Atomic force and scanning tunneling microscopy imaging of graphene nanosheets derived from graphite oxide, Langmuir 25 (2009) 5957–5968.
[34] W. Choi, J.-W. Lee, Graphene: Synthesis and Applications, CRC Press, 2016.
[35] V. Dhinakaran, M. Lavanya, K. Vigneswari, M. Ravichandran, M. Vijayakumar, Review on exploration of graphene in diverse applications and its future horizon, Mater. Today Proc. 27 (2020) 824–828.
[36] S. Ryu, C. Mudry, C.-Y. Hou, C. Chamon, Masses in graphenelike two-dimensional electronic systems: topological defects in order parameters and their fractional exchange statistics, Phys. Rev. B 80 (2009) 205319.
[37] D. Chen, H. Feng, J. Li, Graphene oxide: preparation, functionalization, and electrochemical applications, Chem. Rev. 112 (2012) 6027–6053.
[38] P. Brisebois, M. Siaj, Harvesting graphene oxide—years 1859 to 2019: a review of its structure, synthesis, properties and exfoliation, J. Mater. Chem. C 8 (2020) 1517–1547.
[39] L. Staudenmaier, Verfahren zur darstellung der graphitsäure, Ber. Dtsch. Chem. Ges. 31 (1898) 1481–1487.
[40] W.S. Hummers Jr., R.E. Offeman, Preparation of graphitic oxide, J. Am. Chem. Soc. 80 (1958) 1339.
[41] B. Brodie, Sur le poids atomique du graphite, Ann. Chim. Phys. 59 (1860) e472.
[42] D.R. Dreyer, S. Park, C.W. Bielawski, R.S. Ruoff, The chemistry of graphene oxide, Chem. Soc. Rev. 39 (2010) 228–240.
[43] S. Pan, I.A. Aksay, Factors controlling the size of graphene oxide sheets produced via the graphite oxide route, ACS Nano 5 (2011) 4073–4083.
[44] R. Yuan, J. Yuan, Y. Wu, L. Chen, H. Zhou, J. Chen, Efficient synthesis of graphene oxide and the mechanisms of oxidation and exfoliation, Appl. Surf. Sci. 416 (2017) 868–877.
[45] S.N. Alam, N. Sharma, L. Kumar, Synthesis of graphene oxide (GO) by modified hummers method and its thermal reduction to obtain reduced graphene oxide (rGO), Graphene 6 (2017) 1–18.
[46] I. Ogino, Y. Yokoyama, S. Iwamura, S.R. Mukai, Exfoliation of graphite oxide in water without sonication: bridging length scales from nanosheets to macroscopic materials, Chem. Mater. 26 (2014) 3334–3339.
[47] X. Xu, L. Liu, H. Geng, J. Wang, J. Zhou, Y. Jiang, M. Doi, Directional freezing of binary colloidal suspensions: a model for size fractionation of graphene oxide, Soft Matter 15 (2019) 243–251.
[48] R. Muzyka, M. Kwoka, Ł. Smędowski, N. Díez, G. Gryglewicz, Oxidation of graphite by different modified Hummers methods, New Carbon Mater. 32 (2017) 15–20.
[49] N. Zaaba, K. Foo, U. Hashim, S. Tan, W.-W. Liu, C. Voon, Synthesis of graphene oxide using modified hummers method: solvent influence, Procedia Eng. 184 (2017) 469–477.
[50] L.J. Cote, F. Kim, J. Huang, Langmuir-Blodgett assembly of graphite oxide single layers, J. Am. Chem. Soc. 131 (2008) 1043–1049.
[51] S. Gilje, S. Han, M. Wang, K.L. Wang, R.B. Kaner, A chemical route to graphene for device applications, Nano Lett. 7 (2007) 3394–3398.
[52] S. Stankovich, D.A. Dikin, R.D. Piner, K.A. Kohlhaas, A. Kleinhammes, Y. Jia, Y. Wu, S.T. Nguyen, R. S. Ruoff, Synthesis of graphene-based nanosheets via chemical reduction of exfoliated graphite oxide, Carbon 45 (2007) 1558–1565.

This book belongs to Badji Mokhtar Annaba University Central Library Copyright Elsevier 2025

[53] J. Chen, Y. Zhang, M. Zhang, B. Yao, Y. Li, L. Huang, C. Li, G. Shi, Water-enhanced oxidation of graphite to graphene oxide with controlled species of oxygenated groups, Chem. Sci. 7 (2016) 1874–1881.
[54] A.M. Dimiev, S. Eigler, Graphene Oxide: Fundamentals and Applications, John Wiley & Sons, 2016.
[55] A.M. Dimiev, S. Eigler, Mechanism of formation and chemical structure of graphene oxide, in: Graphene Oxide: Fundamentals and Applications, John Wiley & Sons, Ltd., Hoboken, NJ, 2016, pp. 36–84
[56] M. Mathesh, J. Liu, N.D. Nam, S.K. Lam, R. Zheng, C.J. Barrow, W. Yang, Facile synthesis of graphene oxide hybrids bridged by copper ions for increased conductivity, J. Mater. Chem. C 1 (2013) 3084–3090.
[57] V.C. Sanchez, A. Jachak, R.H. Hurt, A.B. Kane, Biological interactions of graphene-family nanomaterials: an interdisciplinary review, Chem. Res. Toxicol. 25 (2011) 15–34.
[58] F. Pendolino, N. Armata, Graphene Oxide in Environmental Remediation Process, Springer, 2017.
[59] B. Gadgil, P. Damlin, C. Kvarnström, Graphene vs. reduced graphene oxide: a comparative study of graphene-based nanoplatforms on electrochromic switching kinetics, Carbon 96 (2016) 377–381.
[60] A. Kaushal, S. Dhawan, V. Singh, Determination of crystallite size, number of graphene layers and defect density of graphene oxide (GO) and reduced graphene oxide (RGO), in: AIP Conference Proceedings, AIP Publishing LLC, 2019 030106.
[61] A. Bazgir, A. Khorshidi, H. Kamani, S.D. Ashrafi, D. Naghipour, Modeling of azo dyes adsorption on magnetic $NiFe_2O_4$/RGO nanocomposite using response surface methodology, J. Environ. Health Sci. Eng. (2019) 1–17.
[62] L. Gan, B. Li, Y. Chen, B. Yu, Z. Chen, Green synthesis of reduced graphene oxide using bagasse and its application in dye removal: a waste-to-resource supply chain, Chemosphere 219 (2019) 148–154.
[63] A.C. Pradhan, M.K. Sahoo, K. Parida, G.R. Rao, Construction of surfactant/polymer/copolymer-templated mesoporous reduced graphene oxide nanoparticles for adsorption applications, Graphene Technol. 4 (2019) 53–59.
[64] S. Stankovich, D.A. Dikin, G.H. Dommett, K.M. Kohlhaas, E.J. Zimney, E.A. Stach, R.D. Piner, S. T. Nguyen, R.S. Ruoff, Graphene-based composite materials, Nature 442 (2006) 282–286.
[65] N.I. Kovtyukhova, P.J. Ollivier, B.R. Martin, T.E. Mallouk, S.A. Chizhik, E.V. Buzaneva, A. D. Gorchinskiy, Layer-by-layer assembly of ultrathin composite films from micron-sized graphite oxide sheets and polycations, Chem. Mater. 11 (1999) 771–778.
[66] M. Cobos, M.J. Fernández, M.D. Fernández, Graphene based poly(vinyl alcohol) nanocomposites prepared by in situ green reduction of graphene oxide by ascorbic acid: influence of graphene content and glycerol plasticizer on properties, Nano 8 (2018) 1013.
[67] J. Wang, E.C. Salihi, L. Šiller, Green reduction of graphene oxide using alanine, Mater. Sci. Eng. C 72 (2017) 1–6.
[68] K. De Silva, H.-H. Huang, R. Joshi, M. Yoshimura, Chemical reduction of graphene oxide using green reductants, Carbon 119 (2017) 190–199.
[69] Y. Chen, Y. Niu, T. Tian, J. Zhang, Y. Wang, Y. Li, L.-C. Qin, Microbial reduction of graphene oxide by *Azotobacter chroococcum*, Chem. Phys. Lett. 677 (2017) 143–147.
[70] H. Saleem, M. Haneef, H.Y. Abbasi, Synthesis route of reduced graphene oxide via thermal reduction of chemically exfoliated graphene oxide, Mater. Chem. Phys. 204 (2018) 1–7.
[71] I. Sengupta, S. Chakraborty, M. Talukdar, S.K. Pal, S. Chakraborty, Thermal reduction of graphene oxide: how temperature influences purity, J. Mater. Res. 33 (2018) 4113–4122.
[72] S. Sadhukhan, T. K. Ghosh, D. Rana, I. Roy, A. Bhattacharyya, G. Sarkar, M. Chakraborty, D. Chattopadhyay, Studies on synthesis of reduced graphene oxide (RGO) via green route and its electrical property, Mater. Res. Bull. 79 (2016) 41–51.
[73] P. Feicht, S. Eigler, Defects in graphene oxide as structural motifs, ChemNanoMat 4 (2018) 244–252.
[74] D. Robati, M. Rajabi, O. Moradi, F. Najafi, I. Tyagi, S. Agarwal, V.K. Gupta, Kinetics and thermodynamics of malachite green dye adsorption from aqueous solutions on graphene oxide and reduced graphene oxide, J. Mol. Liq. 214 (2016) 259–263.
[75] R.A. Bueno, J.I. Martínez, R.F. Luccas, N.R. Del Árbol, C. Munuera, I. Palacio, F. J. Palomares, K. Lauwaet, S. Thakur, J.M. Baranowski, Highly selective covalent organic functionalization of epitaxial graphene, Nat. Commun. 8 (2017) 15306.

This book belongs to Badji Mokhtar Annaba University Central Library Copyright Elsevier 2025

[76] Z. Xiang, Q. Dai, J.F. Chen, L. Dai, Edge functionalization of graphene and two-dimensional covalent organic polymers for energy conversion and storage, Adv. Mater. 28 (2016) 6253–6261.
[77] A. Sherlala, A. Raman, M. Bello, A. Buthiyappan, Adsorption of arsenic using chitosan magnetic graphene oxide nanocomposite, J. Environ. Manag. 246 (2019) 547–556.
[78] R. Eivazzadeh-Keihan, R. Taheri-Ledari, N. Khosropour, S. Dalvand, A. Maleki, S. M. Mousavi-Khoshdel, H. Sohrabi, Fe_3O_4/GO@ melamine-ZnO nanocomposite: a promising versatile tool for organic catalysis and electrical capacitance, Colloids Surf. A Physicochem. Eng. Asp. 587 (2020) 124335.
[79] S. Rana, S.B. Jonnalagadda, Synthesis and characterization of amine functionalized graphene oxide and scope as catalyst for Knoevenagel condensation reaction, Catal. Commun. 92 (2017) 31–34.
[80] R. Ye, J. Dong, L. Wang, R. Mendoza-Cruz, Y. Li, P.-F. An, M.J. Yacamán, B.I. Yakobson, D. Chen, J. M. Tour, Manganese deception on graphene and implications in catalysis, Carbon 132 (2018) 623–631.
[81] A. Adán-Más, T. Silva, L. Guerlou-Demourgues, L. Bourgeois, C. Labrugere-Sarroste, M. Montemor, Nickel-cobalt oxide modified with reduced graphene oxide: performance and degradation for energy storage applications, J. Power Sources 419 (2019) 12–26.
[82] Y. Dong, L. Chen, W. Chen, X. Zheng, X. Wang, E. Wang, rGO functionalized with a highly electronegative Keplerate-type polyoxometalate for high-energy-density aqueous asymmetric supercapacitors, Chem. Asian J. 13 (2018) 3304–3313.
[83] A. Gevaerd, S.F. Blaskievicz, A.J. Zarbin, E.S. Orth, M.F. Bergamini, L.H. Marcolino-Junior, Nonenzymatic electrochemical sensor based on imidazole-functionalized graphene oxide for progesterone detection, Biosens. Bioelectron. 112 (2018) 108–113.
[84] P. Zhao, X. Ye, Y. Zhu, H. Jiang, J. Pan, Z. Wan, C. Jia, C. Yang, Iodine-steam functionalized reduced graphene oxide/oxidized carbon yarn electrodes for knittable fibriform supercapacitor, J. Power Sources 442 (2019) 227188.
[85] S. Ma, Y. Si, F. Wang, L. Su, C. Xia, J. Yao, H. Chen, X. Liu, Interaction processes of ciprofloxacin with graphene oxide and reduced graphene oxide in the presence of montmorillonite in simulated gastrointestinal fluids, Sci. Rep. 7 (2017) 1–11.
[86] X.T. Zheng, X.Q. Ma, C.M. Li, Highly efficient nuclear delivery of anti-cancer drugs using a bio-functionalized reduced graphene oxide, J. Colloid Interface Sci. 467 (2016) 35–42.
[87] H. Guo, X. Ma, C. Wang, J. Zhou, J. Huang, Z. Wang, Sulfhydryl-functionalized reduced graphene oxide and adsorption of methylene blue, Environ. Eng. Sci. 36 (2019) 81–89.
[88] I. Khurana, A.K. Shaw, J.M. Khurana, P.K. Rai, Batch and dynamic adsorption of Eriochrome Black T from water on magnetic graphene oxide: experimental and theoretical studies, J. Environ. Chem. Eng. 6 (2018) 468–477.
[89] K.C. Lai, L.Y. Lee, B.Y.Z. Hiew, S. Thangalazhy-Gopakumar, S. Gan, Environmental application of three-dimensional graphene materials as adsorbents for dyes and heavy metals: review on ice-templating method and adsorption mechanisms, J. Environ. Sci. 79 (2019) 174–199.
[90] N.H. Othman, N.H. Alias, M.Z. Shahruddin, N.F.A. Bakar, N.R.N. Him, W.J. Lau, Adsorption kinetics of methylene blue dyes onto magnetic graphene oxide, J. Environ. Chem. Eng. 6 (2018) 2803–2811.
[91] N. Yao, C. Li, J. Yu, Q. Xu, S. Wei, Z. Tian, Z. Yang, W. Yang, J. Shen, Insight into adsorption of combined antibiotic-heavy metal contaminants on graphene oxide in water, Sep. Purif. Technol. 236 (2020) 116278.
[92] A. Kasprzak, A. Zuchowska, M. Poplawska, Functionalization of graphene: does the organic chemistry matter? Beilstein J. Org. Chem. 14 (2018) 2018–2026.
[93] H.H. Mohamed, I. Hammami, H.A. Baghdadi, S.S. Al-Jameel, Multifunctional TiO_2 microspheres-rGO as highly active visible light photocatalyst and antimicrobial agent, Mater. Express 8 (2018) 345–352.
[94] Q. Zhang, Q. Hou, G. Huang, Q. Fan, Removal of heavy metals in aquatic environment by graphene oxide composites: a review, Environ. Sci. Pollut. Res. 27 (2020) 190–209.
[95] V. Georgakilas, J.N. Tiwari, K.C. Kemp, J.A. Perman, A.B. Bourlinos, K.S. Kim, R. Zboril, Noncovalent functionalization of graphene and graphene oxide for energy materials, biosensing, catalytic, and biomedical applications, Chem. Rev. 116 (2016) 5464–5519.

This book belongs to Badji Mokhtar Annaba University Central Library Copyright Elsevier 2025

[96] A. Mirmohseni, M. Azizi, M.S.S. Dorraji, Cationic graphene oxide nanosheets intercalated with polyaniline nanofibers: a promising candidate for simultaneous anticorrosion, antistatic, and antibacterial applications, Prog. Org. Coat. 139 (2020) 105419.
[97] P. Xu, W. Yang, D. Niu, M. Yu, M. Du, W. Dong, M. Chen, P.J. Lemstra, P. Ma, Multifunctional and robust polyhydroxyalkanoate nanocomposites with superior gas barrier, heat resistant and inherent antibacterial performances, Chem. Eng. J. 382 (2020) 122864.
[98] J. Shen, M. Shi, B. Yan, H. Ma, N. Li, Y. Hu, M. Ye, Covalent attaching protein to graphene oxide via diimide-activated amidation, Colloids Surf. B: Biointerfaces 81 (2010) 434–438.
[99] J. Zhu, Y. Li, Y. Chen, J. Wang, B. Zhang, J. Zhang, W.J. Blau, Graphene oxide covalently functionalized with zinc phthalocyanine for broadband optical limiting, Carbon 49 (2011) 1900–1905.
[100] V. Georgakilas, M. Otyepka, A.B. Bourlinos, V. Chandra, N. Kim, K.C. Kemp, P. Hobza, R. Zboril, K. S. Kim, Functionalization of graphene: covalent and non-covalent approaches, derivatives and applications, Chem. Rev. 112 (2012) 6156–6214.
[101] S. Niyogi, E. Bekyarova, M.E. Itkis, H. Zhang, K. Shepperd, J. Hicks, M. Sprinkle, C. Berger, C.N. Lau, W. A. Deheer, Spectroscopy of covalently functionalized graphene, Nano Lett. 10 (2010) 4061–4066.
[102] X. Cui, W. Cheng, W. Xu, W. Mu, X. Han, Functional graphene derivatives for chemotherapy-based synergistic tumor therapy, Nano 14 (2019) 1930006.
[103] E. Haque, M.M. Islam, E. Pourazadi, S. Sarkar, A.T. Harris, A.I. Minett, E. Yanmaz, S.M. Alshehri, Y. Ide, K. C.W. Wu, Boron-functionalized graphene oxide-organic frameworks for highly efficient CO_2 capture, Chem. Asian J. 12 (2017) 283–288.
[104] R. Kumar, M. Kumar, A. Kumar, R. Singh, R. Kashyap, S. Rani, D. Kumar, Surface modification of graphene oxide using esterification, Mater. Today Proc. 18 (2019) 1556–1561.
[105] S. Guo, Y. Nishina, A. Bianco, C. Menard-Moyon, A flexible method for covalent double functionalization of graphene oxide, Angew. Chem. Int. Ed. (2019).
[106] J. Zahirifar, J. Karimi-Sabet, S.M.A. Moosavian, A. Hadi, P. Khadiv-Parsi, Fabrication of a novel octadecylamine functionalized graphene oxide/PVDF dual-layer flat sheet membrane for desalination via air gap membrane distillation, Desalination 428 (2018) 227–239.
[107] A.K. Basu, A.N. Sah, A. Pradhan, S. Bhattacharya, Poly-L-lysine functionalised MWCNT-rGO nanosheets based 3-d hybrid structure for femtomolar level cholesterol detection using cantilever based sensing platform, Sci. Rep. 9 (2019) 1–13.
[108] J. Liu, J. Tang, J.J. Gooding, Strategies for chemical modification of graphene and applications of chemically modified graphene, J. Mater. Chem. 22 (2012) 12435–12452.
[109] D. Wu, F. Zhang, H. Liang, X. Feng, Nanocomposites and macroscopic materials: assembly of chemically modified graphene sheets, Chem. Soc. Rev. 41 (2012) 6160–6177.
[110] W. Czepa, D. Pakulski, S. Witomska, V. Patroniak, A. Ciesielski, P. Samorì, Graphene oxide-mesoporous SiO_2 hybrid composite for fast and efficient removal of organic cationic contaminants, Carbon 158 (2020) 193–201.
[111] C. Minitha, M. Lalitha, Y. Jeyachandran, L. Senthilkumar, Adsorption behaviour of reduced graphene oxide towards cationic and anionic dyes: co-action of electrostatic and π-π interactions, Mater. Chem. Phys. 194 (2017) 243–252.
[112] D. Pakulski, W. Czepa, S. Witomska, A. Aliprandi, P. Pawluć, V. Patroniak, A. Ciesielski, P. Samorì, Graphene oxide-branched polyethylenimine foams for efficient removal of toxic cations from water, J. Mater. Chem. A 6 (2018) 9384–9390.
[113] N. Salahuddin, H. El-Daly, R.G. El Sharkawy, B.T. Nasr, Synthesis and efficacy of PPy/CS/GO nanocomposites for adsorption of ponceau 4R dye, Polymer 146 (2018) 291–303.
[114] S.M. Mousavi, S.A. Hashemi, Y. Ghasemi, A.M. Amani, A. Babapoor, O. Arjmand, Applications of graphene oxide in case of nanomedicines and nanocarriers for biomolecules: review study, Drug Metab. Rev. 51 (2019) 12–41.
[115] H. Tang, Y. Zhao, S. Shan, X. Yang, D. Liu, F. Cui, B. Xing, Theoretical insight into the adsorption of aromatic compounds on graphene oxide, Environ. Sci. Nano 5 (2018) 2357–2367.

This book belongs to Badji Mokhtar Annaba University Central Library Copyright Elsevier 2025

[116] Y. Gao, Y. Li, L. Zhang, H. Huang, J. Hu, S.M. Shah, X. Su, Adsorption and removal of tetracycline antibiotics from aqueous solution by graphene oxide, J. Colloid Interface Sci. 368 (2012) 540–546.
[117] J. Xiao, J. Wang, H. Fan, Q. Zhou, X. Liu, Recent advances of adsorbents in solid phase extraction for environmental samples, Int. J. Environ. Anal. Chem. 96 (2016) 407–435.
[118] R. Peng, Q. Wu, J. Chen, R. Ghosh, X. Chen, Isolation of ellagic acid from pomegranate peel extract by hydrophobic interaction chromatography using graphene oxide grafted cotton fiber adsorbent, J. Sep. Sci. 41 (2018) 747–755.
[119] M.A. Ahsan, V. Jabbari, M.T. Islam, R.S. Turley, N. Dominguez, H. Kim, E. Castro, J. A. Hernandez-Viezcas, M.L. Curry, J. Lopez, Sustainable synthesis and remarkable adsorption capacity of MOF/graphene oxide and MOF/CNT based hybrid nanocomposites for the removal of bisphenol a from water, Sci. Total Environ. 673 (2019) 306–317.
[120] Y. Liu, B. Sajjadi, W.-Y. Chen, R. Chatterjee, Ultrasound-assisted amine functionalized graphene oxide for enhanced CO_2 adsorption, Fuel 247 (2019) 10–18.
[121] M. Lv, L. Yan, C. Liu, C. Su, Q. Zhou, X. Zhang, Y. Lan, Y. Zheng, L. Lai, X. Liu, Non-covalent functionalized graphene oxide (GO) adsorbent with an organic gelator for co-adsorption of dye, endocrine-disruptor, pharmaceutical and metal ion, Chem. Eng. J. 349 (2018) 791–799.
[122] Y. Dong, C. Yi, S. Yang, J. Wang, P. Chen, X. Liu, W. Du, S. Wang, B.-F. Liu, A substrate-free graphene oxide-based micromotor for rapid adsorption of antibiotics, Nanoscale 11 (2019) 4562–4570.
[123] Y. Yang, W. Yu, S. He, S. Yu, Y. Chen, L. Lu, Z. Shu, H. Cui, Y. Zhang, H. Jin, Rapid adsorption of cationic dye-methylene blue on the modified montmorillonite/graphene oxide composites, Appl. Clay Sci. 168 (2019) 304–311.
[124] L.P. Lingamdinne, J.R. Koduru, Y.-L. Choi, Y.-Y. Chang, J.-K. Yang, Studies on removal of Pb(II) and Cr(III) using graphene oxide based inverse spinel nickel ferrite nano-composite as sorbent, Hydrometallurgy 165 (2016) 64–72.
[125] N.A. Travlou, G.Z. Kyzas, N.K. Lazaridis, E.A. Deliyanni, Functionalization of graphite oxide with magnetic chitosan for the preparation of a nanocomposite dye adsorbent, Langmuir 29 (2013) 1657–1668.
[126] S. Şahin, Z. Ciğeroğlu, O.K. Özdemir, M. Bilgin, E. Elhussein, Ö. Gulmez, Recovery of hydroxytyrosol onto graphene oxide nanosheets: equilibrium and kinetic models, J. Mol. Liq. 285 (2019) 213–222.
[127] N. Subedi, A. Lähde, E. Abu-Danso, J. Iqbal, A. Bhatnagar, A comparative study of magnetic chitosan (Chi@ Fe_3O_4) and graphene oxide modified magnetic chitosan (Chi@ Fe_3O_4GO) nanocomposites for efficient removal of Cr(VI) from water, Int. J. Biol. Macromol. 137 (2019) 948–959.
[128] M. Rajabi, K. Mahanpoor, O. Moradi, Thermodynamic and kinetic studies of crystal violet dye adsorption with poly(methyl methacrylate)-graphene oxide and poly(methyl methacrylate)-graphene oxide-zinc oxide nanocomposites, J. Appl. Polym. Sci. 136 (2019) 47495.
[129] C. Sun, Z. Wang, L. Chen, F. Li, Fabrication of robust and compressive chitin and graphene oxide sponges for removal of microplastics with different functional groups, Chem. Eng. J. 393 (2020) 124796.
[130] T.J.M. Fraga, L.E.M. De Lima, Z.S.B. De Souza, M.N. Carvalho, E.M.P.D.L. Freire, M.G. Ghislandi, M. A. Da Motta, Amino-Fe_3O_4-functionalized graphene oxide as a novel adsorbent of methylene blue: kinetics, equilibrium, and recyclability aspects, Environ. Sci. Pollut. Res. 26 (2019) 28593–28602.
[131] B.Y.Z. Hiew, L.Y. Lee, X.J. Lee, S. Gan, S. Thangalazhy-Gopakumar, S.S. Lim, G.-T. Pan, T.C.-K. Yang, Adsorptive removal of diclofenac by graphene oxide: optimization, equilibrium, kinetic and thermodynamic studies, J. Taiwan Inst. Chem. Eng. 98 (2019) 150–162.
[132] Y. Zheng, B. Cheng, W. You, J. Yu, W. Ho, 3D hierarchical graphene oxide-NiFe LDH composite with enhanced adsorption affinity to Congo red, methyl orange and Cr(VI) ions, J. Hazard. Mater. 369 (2019) 214–225.
[133] T. Huang, M. Yan, K. He, Z. Huang, G. Zeng, A. Chen, M. Peng, H. Li, L. Yuan, G. Chen, Efficient removal of methylene blue from aqueous solutions using magnetic graphene oxide modified zeolite, J. Colloid Interface Sci. 543 (2019) 43–51.
[134] R. Soni, D.P. Shukla, Synthesis of fly ash based zeolite-reduced graphene oxide composite and its evaluation as an adsorbent for arsenic removal, Chemosphere 219 (2019) 504–509.
[135] Z. Ciğeroğlu, O.K. Özdemir, S. Şahin, A. Haşimoğlu, Naproxen adsorption onto graphene oxide nanopowders: equilibrium, kinetic, and thermodynamic studies, Water Air Soil Pollut. 231 (2020) 101.

This book belongs to Badji Mokhtar Annaba University Central Library Copyright Elsevier 2025

[136] A.H. Gemeay, R.G. Elsharkawy, E.F. Aboelfetoh, Graphene oxide/polyaniline/manganese oxide ternary nanocomposites, facile synthesis, characterization, and application for indigo carmine removal, J. Polym. Environ. 26 (2018) 655–669.
[137] M. Gopiraman, S. Saravanamoorthy, D. Deng, A. Ilangovan, I.S. Kim, I.M. Chung, Facile mechanochemical synthesis of nickel/graphene oxide nanocomposites with unique and tunable morphology: applications in heterogeneous catalysis and supercapacitors, Catalysts 9 (2019) 486.
[138] B. Ye, M. Lee, B. Jeong, J. Kim, D.H. Lee, J.M. Baik, H.-D. Kim, Partially reduced graphene oxide as a support of Mn-Ce/TiO_2 catalyst for selective catalytic reduction of NOx with NH3, Catal. Today 328 (2019) 300–306.
[139] K. Zhang, J.M. Suh, T.H. Lee, J.H. Cha, J.-W. Choi, H.W. Jang, R.S. Varma, M. Shokouhimehr, Copper oxide-graphene oxide nanocomposite: efficient catalyst for hydrogenation of nitroaromatics in water, Nano Converg. 6 (2019) 6.
[140] E. Urbanczyk, A. Maciej, A. Stolarczyk, M. Basiaga, W. Simka, The electrocatalytic oxidation of urea on nickel-graphene and nickel-graphene oxide composite electrodes, Electrochim. Acta 305 (2019) 256–263.
[141] R. Hassandoost, S.R. Pouran, A. Khataee, Y. Orooji, S.W. Joo, Hierarchically structured ternary heterojunctions based on Ce^{3+}/Ce^{4+} modified Fe_3O_4 nanoparticles anchored onto graphene oxide sheets as magnetic visible-light-active photocatalysts for decontamination of oxytetracycline, J. Hazard. Mater. 376 (2019) 200–211.
[142] M. Serrapede, M. Fontana, A. Gigot, M. Armandi, G. Biasotto, E. Tresso, P. Rivolo, A facile and green synthesis of a MoO_2-reduced graphene oxide aerogel for energy storage devices, Materials 13 (2020) 594.
[143] R. Vinodh, C.M. Babu, A. Abidov, M. Palanichamy, H.T. Jang, Facile synthesis of amine modified silica/reduced graphene oxide composite sorbent for CO_2 adsorption, Mater. Lett. 247 (2019) 44–47.
[144] R.J.H. Navasingh, R. Kumar, K. Marimuthu, S. Planichamy, A. Khan, A.M. Asiri, M. Asad, Graphene-based nano metal matrix composites: a review, in: Nanocarbon and its Composites, Elsevier, 2019.
[145] V. Chandra, J. Park, Y. Chun, J.W. Lee, I.-C. Hwang, K.S. Kim, Water-dispersible magnetite-reduced graphene oxide composites for arsenic removal, ACS Nano 4 (2010) 3979–3986.
[146] R. Menzel, D. Iruretagoyena, Y. Wang, S.M. Bawaked, M. Mokhtar, S.A. Al-Thabaiti, S.N. Basahel, M. S. Shaffer, Graphene oxide/mixed metal oxide hybrid materials for enhanced adsorption desulfurization of liquid hydrocarbon fuels, Fuel 181 (2016) 531–536.
[147] G. Sheng, C. Huang, G. Chen, J. Sheng, X. Ren, B. Hu, J. Ma, X. Wang, Y. Huang, A. Alsaedi, Adsorption and co-adsorption of graphene oxide and Ni(II) on iron oxides: a spectroscopic and microscopic investigation, Environ. Pollut. 233 (2018) 125–131.
[148] N. Pan, L. Li, J. Ding, S. Li, R. Wang, Y. Jin, X. Wang, C. Xia, Preparation of graphene oxide-manganese dioxide for highly efficient adsorption and separation of Th(IV)/U(VI), J. Hazard. Mater. 309 (2016) 107–115.
[149] T.R. Das, P.K. Sharma, Bimetal oxide decorated graphene oxide (Gd_2O_3/Bi_2O_3@GO) nanocomposite as an excellent adsorbent in the removal of methyl orange dye, Mater. Sci. Semicond. Process. 105 (2020) 104721.
[150] T.T. Nguyen, T.N.T. Nguyen, L.G. Bach, D.T. Nguyen, T.P.Q. Bui, Adsorptive removal of Pb(II) using exfoliated graphite adsorbent: influence of experimental conditions and magnetic $CoFe_2O_4$ decoration, IIUM Eng. J. 20 (2019) 202–215.
[151] M. Fathy, R. Hosny, M. Keshawy, A. Gaffer, Green synthesis of graphene oxide from oil palm leaves as novel adsorbent for removal of Cu(II) ions from synthetic wastewater, Graphene Technol. 4 (2019) 33–40.
[152] P. Yang, H. Zhang, Q. Liu, J. Liu, R. Chen, J. Yu, J. Hou, X. Bai, J. Wang, Nano-sized architectural design of multi-activity graphene oxide (GO) by chemical post-decoration for efficient uranium(VI) extraction, J. Hazard. Mater. 375 (2019) 320–329.
[153] R.L. White, C.M. White, H. Turgut, A. Massoud, Z.R. Tian, Comparative studies on copper adsorption by graphene oxide and functionalized graphene oxide nanoparticles, J. Taiwan Inst. Chem. Eng. 85 (2018) 18–28.
[154] J. Zhang, X. Xie, C. Liang, W. Zhu, X. Meng, Characteristics and mechanism of Pb(II) adsorption/desorption on GO/r-GO under sulfide-reducing conditions, J. Ind. Eng. Chem. 73 (2019) 233–240.

This book belongs to Badji Mokhtar Annaba University Central Library Copyright Elsevier 2025

[155] S. Ahmad, A. Ahmad, S. Khan, S. Ahmad, I. Khan, S. Zada, P. Fu, Algal extracts based biogenic synthesis of reduced graphene oxides (rGO) with enhanced heavy metals adsorption capability, J. Ind. Eng. Chem. 72 (2019) 117–124.
[156] L.T. Tran, H.V. Tran, T.D. Le, G.L. Bach, L.D. Tran, Studying Ni(II) adsorption of magnetite/graphene oxide/chitosan nanocomposite, Adv. Polym. Technol. 2019 (2019).
[157] T.T.N. Le, V.T. Le, M.U. Dao, Q.V. Nguyen, T.T. Vu, M.H. Nguyen, D.L. Tran, H.S. Le, Preparation of magnetic graphene oxide/chitosan composite beads for effective removal of heavy metals and dyes from aqueous solutions, Chem. Eng. Commun. 206 (2019) 1337–1352.
[158] A. Sheikhmohammadi, S.M. Mohseni, B. Hashemzadeh, E. Asgari, R. Sharafkhani, M. Sardar, M. Sarkhosh, M. Almasiane, Fabrication of magnetic graphene oxide nanocomposites functionalized with a novel chelating ligand for the removal of Cr(VI): modeling, optimization, and adsorption studies, Desalin. Water Treat. 160 (2019) 297–307.
[159] N. Li, Q. Yue, B. Gao, X. Xu, Y. Kan, P. Zhao, Magnetic graphene oxide functionalized by poly dimethyl diallyl ammonium chloride for efficient removal of Cr(VI), J. Taiwan Inst. Chem. Eng. 91 (2018) 499–506.
[160] C. Zhang, J. Luan, W. Chen, X. Ke, H. Zhang, Preparation of graphene oxide-montmorillonite nanocomposite and its application in multiple-pollutants removal from aqueous solutions, Water Sci. Technol. 79 (2019) 323–333.
[161] A. Rajput, S.K. Raj, P.P. Sharma, V. Yadav, H. Sarvaia, H. Gupta, V. Kulshrestha, Synthesis and characterization of aluminium modified graphene oxide: an approach towards defluoridation of potable water, J. Dispers. Sci. Technol. 40 (2019) 1101–1109.
[162] S. Yang, D. Zhang, H. Cheng, Y. Wang, J. Liu, Graphene oxide as an efficient adsorbent of solid-phase extraction for online preconcentration of inorganic and organic mercurials in freshwater followed by HPLC-ICP-MS determination, Anal. Chim. Acta 1074 (2019) 54–61.
[163] L.P. Lingamdinne, J.R. Koduru, Y.-Y. Chang, S.-H. Kang, J.-K. Yang, Facile synthesis of flowered mesoporous graphene oxide-lanthanum fluoride nanocomposite for adsorptive removal of arsenic, J. Mol. Liq. 279 (2019) 32–42.
[164] L.P. Lingamdinne, J.R. Koduru, Y.-Y. Chang, R.R. Karri, Process optimization and adsorption modeling of Pb(II) on nickel ferrite-reduced graphene oxide nano-composite, J. Mol. Liq. 250 (2018) 202–211.
[165] Q. Huang, Y. Chen, H. Yu, L. Yan, J. Zhang, B. Wang, B. Du, L. Xing, Magnetic graphene oxide/MgAl-layered double hydroxide nanocomposite: one-pot solvothermal synthesis, adsorption performance and mechanisms for Pb^{2+}, Cd^{2+}, and Cu^{2+}, Chem. Eng. J. 341 (2018) 1–9.
[166] M. Li, J. Feng, K. Huang, S. Tang, R. Liu, H. Li, F. Ma, X. Meng, Amino group functionalized SiO_2@ graphene oxide for efficient removal of Cu(II) from aqueous solutions, Chem. Eng. Res. Des. 145 (2019) 235–244.
[167] L. Wang, D. Hu, X. Kong, J. Liu, X. Li, K. Zhou, H. Zhao, C. Zhou, Anionic polypeptide poly(γ-glutamic acid)-functionalized magnetic Fe_3O_4-GO-(o-MWCNTs) hybrid nanocomposite for high-efficiency removal of Cd(II), Cu(II) and Ni(II) heavy metal ions, Chem. Eng. J. 346 (2018) 38–49.
[168] W. Fu, Z. Huang, Magnetic dithiocarbamate functionalized reduced graphene oxide for the removal of Cu(II), Cd(II), Pb(II), and Hg(II) ions from aqueous solution: synthesis, adsorption, and regeneration, Chemosphere 209 (2018) 449–456.
[169] H. Zhang, Q. Chang, Y. Jiang, H. Li, Y. Yang, Synthesis of KMnO4-treated magnetic graphene oxide nanocomposite (Fe_3O_4@GO/MnOx) and its application for removing of Cu^{2+} ions from aqueous solution, Nanotechnology 29 (2018) 135706.
[170] J. Zhang, Y. Kong, Y. Yang, N. Chen, C. Feng, X. Huang, C. Yu, Fast capture of fluoride by anion-exchange zirconium-graphene hybrid adsorbent, Langmuir 35 (2019) 6861–6869.
[171] D. Huang, J. Wu, L. Wang, X. Liu, J. Meng, X. Tang, C. Tang, J. Xu, Novel insight into adsorption and co-adsorption of heavy metal ions and an organic pollutant by magnetic graphene nanomaterials in water, Chem. Eng. J. 358 (2019) 1399–1409.
[172] Q.-U. Ain, M.U. Farooq, M.I. Jalees, Application of magnetic graphene oxide for water purification: heavy metals removal and disinfection, J. Water Process Eng. 33 (2020) 101044.

This book belongs to Badji Mokhtar Annaba University Central Library Copyright Elsevier 2025

[173] S. Periyasamy, P. Manivasakan, C. Jeyaprabha, S. Meenakshi, N. Viswanathan, Fabrication of nano-graphene oxide assisted hydrotalcite/chitosan biocomposite: an efficient adsorbent for chromium removal from water, Int. J. Biol. Macromol. 132 (2019) 1068–1078.
[174] J. Luo, C. Fan, Z. Xiao, T. Sun, X. Zhou, Novel graphene oxide/carboxymethyl chitosan aerogels via vacuum-assisted self-assembly for heavy metal adsorption capacity, Colloids Surf. A Physicochem. Eng. Asp. 578 (2019) 123584.
[175] D. Zhang, N. Li, S. Cao, X. Liu, M. Qiao, P. Zhang, Q. Zhao, L. Song, X. Huang, A layered chitosan/graphene oxide sponge as reusable adsorbent for removal of heavy metal ions, Chem. Res. Chin. Univ. 35 (2019) 463–470.
[176] M.S. Samuel, J. Bhattacharya, S. Raj, N. Santhanam, H. Singh, N.P. Singh, Efficient removal of chromium (VI) from aqueous solution using chitosan grafted graphene oxide (CS-GO) nanocomposite, Int. J. Biol. Macromol. 121 (2019) 285–292.
[177] A. Shahbazi, N.N. Marnani, Z. Salahshoor, Synergistic and antagonistic effects in simultaneous adsorption of Pb(II) and Cd(II) from aqueous solutions onto chitosan functionalized EDTA-silane/mGO, Biocatal. Agric. Biotechnol. 22 (2019) 101398.
[178] Y. Hao, Y. Cui, J. Peng, N. Zhao, S. Li, M. Zhai, Preparation of graphene oxide/cellulose composites in ionic liquid for Ce(III) removal, Carbohydr. Polym. 208 (2019) 269–275.
[179] Y. Yu, G. Zhang, L. Ye, Preparation and adsorption mechanism of polyvinyl alcohol/graphene oxide-sodium alginate nanocomposite hydrogel with high Pb(II) adsorption capacity, J. Appl. Polym. Sci. 136 (2019) 47318.
[180] J.-W. Choi, H.J. Kim, H. Ryu, S. Oh, S.-J. Choi, Three-dimensional double-network hydrogels of graphene oxide, alginate, and polyacrylonitrile for copper removal from aqueous solution, Environ. Eng. Res. 25 (6) (2019) 924–929.
[181] S. Saha, M. Venkatesh, H. Basu, M.V. Pimple, R.K. Singhal, Recovery of gold using graphene oxide/calcium alginate hydrogel beads from a scrap solid state detector, J. Environ. Chem. Eng. 7 (2019) 103134.
[182] J. He, F. Ni, A. Cui, X. Chen, S. Deng, F. Shen, C. Huang, G. Yang, C. Song, J. Zhang, D. Tian, L. Long, Y. Zhu, L. Luo, New insight into adsorption and co-adsorption of arsenic and tetracycline using a Y-immobilized graphene oxide-alginate hydrogel: adsorption behaviours and mechanisms, Sci. Total Environ. 701 (2020) 134363.
[183] M. Yao, Z. Wang, Y. Liu, G. Yang, J. Chen, Preparation of dialdehyde cellulose graftead graphene oxide composite and its adsorption behavior for heavy metals from aqueous solution, Carbohydr. Polym. 212 (2019) 345–351.
[184] Q. Kong, S. Preis, L. Li, P. Luo, Y. Hu, C. Wei, Graphene oxide-terminated hyperbranched amino polymer-carboxymethyl cellulose ternary nanocomposite for efficient removal of heavy metals from aqueous solutions, Int. J. Biol. Macromol. 149 (2020) 581–592.
[185] J. Chen, Q. Liang, S. Ploychompoo, H. Luo, Functional rGO aerogel as a potential adsorbent for removing hazardous hexavalent chromium: adsorption performance and mechanism, Environ. Sci. Pollut. Res. (2020).
[186] A. Shahzad, W. Miran, K. Rasool, M. Nawaz, J. Jang, S.-R. Lim, D.S. Lee, Heavy metals removal by EDTA-functionalized chitosan graphene oxide nanocomposites, RSC Adv. 7 (2017) 9764–9771.
[187] P. Qiu, S. Wang, C. Tian, Z. Lin, Adsorption of low-concentration mercury in water by 3D cyclodextrin/graphene composites: synergistic effect and enhancement mechanism, Environ. Pollut. 252 (2019) 1133–1141.
[188] M.O. Ansari, R. Kumar, S.A. Ansari, S.P. Ansari, M.A. Barakat, A. Alshahrie, M.H. Cho, Anion selective pTSA doped polyaniline@graphene oxide-multiwalled carbon nanotube composite for Cr(VI) and Congo red adsorption, J. Colloid Interface Sci. 496 (2017) 407–415.
[189] Y. Zhang, B. Cao, L. Zhao, L. Sun, Y. Gao, J. Li, F. Yang, Biochar-supported reduced graphene oxide composite for adsorption and coadsorption of atrazine and lead ions, Appl. Surf. Sci. 427 (2018) 147–155.
[190] T. Esfandiyari, N. Nasirizadeh, M. Dehghani, M.H. Ehrampoosh, Graphene oxide based carbon composite as adsorbent for Hg removal: preparation, characterization, kinetics and isotherm studies, Chin. J. Chem. Eng. 25 (2017) 1170–1175.
[191] N. Yari Moghaddam, B. Lorestani, M. Cheraghi, S. Jamehbozorgi, Adsorption of Cd and Ni from water by graphene oxide and graphene oxide-almond shell composite, Water Environ. Res. 91 (2019) 475–482.

This book belongs to Badji Mokhtar Annaba University Central Library Copyright Elsevier 2025

[192] J.-Y. Yang, B.-Y. Yue, J. Teng, X. Xu, X.-R. Zhao, X.-Y. Jiang, J.-G. Yu, F.-L. Zhou, Aqueous metal ions adsorption by poly (ethylene glycol)-modified graphene oxide: surface area and surface chemistry effects, Desalin. Water Treat. 138 (2019) 147–158.
[193] B. Khodavirdilo, N. Samadi, R. Ansari, Synthesis of graphene oxide-melamine-TioOxalic acid nanocomposite and its application in the elimination of mercury (II) ions, Iran. Chem. Commun. 7 (2019) 71–78.
[194] R.K.S. Rathour, J. Bhattacharya, A. Mukherjee, β-Cyclodextrin conjugated graphene oxide: a regenerative adsorbent for cadmium and methylene blue, J. Mol. Liq. 282 (2019) 606–616.
[195] S. Song, K. Wang, Y. Zhang, Y. Wang, C. Zhang, X. Wang, R. Zhang, J. Chen, T. Wen, X. Wang, Self-assembly of graphene oxide/PEDOT: PSS nanocomposite as a novel adsorbent for uranium immobilization from wastewater, Environ. Pollut. 250 (2019) 196–205.
[196] A.E.-F.F. Shaaban, A.A.E.-S. Khalil, B.S. Elewa, M. Ismail, U.M. Eldemerdash, A new modified exfoliated graphene oxide for removal of copper (II), lead (II) and nickel (II) ions from aqueous solutions, Egypt. J. Chem. 62 (2019) 1823–1849.
[197] S. Tang, Z. Cao, Adsorption of nitrogen oxides on graphene and graphene oxides: insights from density functional calculations, J. Chem. Phys. 134 (2011) 044710.
[198] M. Seredych, T.J. Bandosz, Effects of surface features on adsorption of SO_2 on graphite oxide/$Zr(OH)_4$ composites, J. Phys. Chem. C 114 (2010) 14552–14560.
[199] C. Petit, T.J. Bandosz, Graphite oxide/polyoxometalate nanocomposites as adsorbents of ammonia, J. Phys. Chem. C 113 (2009) 3800–3809.
[200] O. Mabayoje, M. Seredych, T.J. Bandosz, Enhanced reactive adsorption of hydrogen sulfide on the composites of graphene/graphite oxide with copper (hydr) oxychlorides, ACS Appl. Mater. Interfaces 4 (2012) 3316–3324.
[201] C. Chen, K. Xu, X. Ji, L. Miao, J. Jiang, Enhanced adsorption of acidic gases (CO_2, NO_2 and SO_2) on light metal decorated graphene oxide, Phys. Chem. Chem. Phys. 16 (2014) 11031–11036.
[202] Z. Goharibajestani, A. Yurum, Y. Yurum, Effect of transition metal oxide nanoparticles on gas adsorption properties of graphene nanocomposites, Appl. Surf. Sci. 475 (2019) 1070–1076.
[203] A. Khan, J.E. Szulejko, P. Samaddar, K.-H. Kim, W. Eom, S.B. Ambade, T.H. Han, The effect of diverse metal oxides in graphene composites on the adsorption isotherm of gaseous benzene, Environ. Res. 172 (2019) 367–374.
[204] N.M. Mahmoodi, M. Oveisi, E. Asadi, Synthesis of NENU metal-organic framework-graphene oxide nanocomposites and their pollutant removal ability from water using ultrasound, J. Clean. Prod. 211 (2019) 198–212.
[205] N.M. Mahmoodi, M. Oveisi, M. Bakhtiari, B. Hayati, A. A. Shekarchi, A. Bagheri, S. Rahimi, Environmentally friendly ultrasound-assisted synthesis of magnetic zeolitic imidazolate framework-graphene oxide nanocomposites and pollutant removal from water, J. Mol. Liq. 282 (2019) 115–130.
[206] M. Muschi, C. Serre, Progress and challenges of graphene oxide/metal-organic composites, Coord. Chem. Rev. 387 (2019) 262–272.
[207] D.J. Babu, F.G. Kuhl, S. Yadav, D. Markert, M. Bruns, M.J. Hampe, J.J. Schneider, Adsorption of pure SO_2 on nanoscaled graphene oxide, RSC Adv. 6 (2016) 36834–36839.
[208] İ.Ö. Yuksek, Ö. Alptoğa, P. Altay, N. Karatepe, A. Önen, N. Ucar, Effect of PVA addition on SO_2 adsorption properties of GO fibers, in: IOP Conference Series: Materials Science and Engineering, IOP Publishing, 2018 012050.
[209] Y. Cao, H. Zhang, F. Song, T. Huang, J. Ji, Q. Zhong, W. Chu, Q. Xu, UiO-66-NH_2/GO composite: synthesis, characterization and CO_2 adsorption performance, Materials 11 (2018) 589.
[210] S. Ullah, M.A. Bustam, A.G. Al-Sehemi, M.A. Assiri, F.A. Abdul Kareem, A. Mukhtar, M. Ayoub, G. Gonfa, Influence of post-synthetic graphene oxide (GO) functionalization on the selective CO_2/CH_4 adsorption behavior of MOF-200 at different temperatures; an experimental and adsorption isotherms study, Microporous Mesoporous Mater. 296 (2020) 110002.
[211] L. Asgharnejad, A. Abbasi, A. Shakeri, Ni-based metal-organic framework/GO nanocomposites as selective adsorbent for CO_2 over N_2, Microporous Mesoporous Mater. 262 (2018) 227–234.

This book belongs to Badji Mokhtar Annaba University Central Library Copyright Elsevier 2025

[212] S. Rodríguez-García, R. Santiago, D. López-Díaz, M.D. Merchan, M.M. Velázquez, J.L. G. Fierro, J. Palomar, Role of the structure of graphene oxide sheets on the CO_2 adsorption properties of nanocomposites based on graphene oxide and polyaniline or Fe_3O_4-nanoparticles, ACS Sustain. Chem. Eng. 7 (2019) 12464–12473.
[213] K.S. Nazari, A. Noorpoor, N.M. Mahmoodi, Adsorption performance indicator for power plant CO_2 capture on graphene oxide/TiO_2 nanocomposite, Iran. J. Chem. Chem. Eng. 38 (3) (2019) 293–307.
[214] V. Irani, A. Tavasoli, M. Vahidi, Preparation of amine functionalized reduced graphene oxide/methyl diethanolamine nanofluid and its application for improving the CO_2 and H_2S absorption, J. Colloid Interface Sci. 527 (2018) 57–67.
[215] B. Szczęśniak, J. Choma, Graphene-containing microporous composites for selective CO2 adsorption, Microporous Mesoporous Mater. 292 (2020) 109761.
[216] V. Chandra, S.U. Yu, S.H. Kim, Y.S. Yoon, D.Y. Kim, A.H. Kwon, M. Meyyappan, K.S. Kim, Highly selective CO_2 capture on N-doped carbon produced by chemical activation of polypyrrole functionalized graphene sheets, Chem. Commun. 48 (5) (2012) 735–737.
[217] R. Aghehrochaboki, Y.A. Chaboki, S.A. Maleknia, V. Irani, Polyethyleneimine functionalized graphene oxide/methyldiethanolamine nanofluid: preparation, characterization, and investigation of CO_2 absorption, J. Environ. Chem. Eng. 7 (2019) 103285.
[218] L. Chen, X. Jiang, J. Qiu, D. Ma, Y. Sun, H. Yang, Q. Liu, Y. Cao, W. Li, Selective CO_2 adsorption and H_2 storage in two porous amine-pillared graphene oxide frameworks, J. Solid State Chem. 279 (2019) 120980.
[219] N.F.T. Arifin, N.A.N. Zulkipli, N. Yusof, A.F. Ismail, F. Aziz, W.N.W. Salleh, J. Jaafar, N.A.H. M. Nordin, N. Sazali, Preparation and characterization of APTES-functionalized graphene oxide for CO_2 adsorption, System 61 (2019) 297–305.
[220] N. Ucar, Ö. Alptoğa, A. Önen, N. Karatepe, P. Altay, Improvement of SO_2 adsorption capacity of fiber web surface produced from continous graphene oxide fiber, J. Text. Inst. 110 (3) (2019) 358–367.
[221] A.A. Alghamdi, A.F. Alshahrani, N.H. Khdary, F.A. Alharthi, H.A. Alattas, S.F. Adil, Enhanced graphene CO oxide 2 adsorption sheets (N-GOs) by nitrogen-doped prepared by employing polymeric precursors, Materials (2020) 103 (Element-Doped Functional Carbon-Based Materials).
[222] S. Yu, X. Wang, X. Tan, X. Wang, Sorption of radionuclides from aqueous systems onto graphene oxide-based materials: a review, Inorg. Chem. Front. 2 (2015) 593–612.
[223] P. Shi, N. Ye, Magnetite–graphene oxide composites as a magnetic solid-phase extraction adsorbent for the determination of trace sulfonamides in water samples, Anal. Methods 6 (2014) 9725–9730.
[224] X. Zhang, J. Niu, Y. Yang, P. Qin, S. Tian, J. Zhu, M. Lu, Fe_3O_4 nanoparticles as the adsorbent of magnetic solid-phase extraction for clean and preconcentration of maltol and ethyl maltol in food samples followed by HPLC analysis, J. Liq. Chromatogr. Relat. Technol. 40 (2017) 832–838.
[225] X. Zang, Q. Chang, M. Hou, C. Wang, Z. Wang, Graphene grafted magnetic microspheres for solid phase extraction of bisphenol A and triclosan from water samples followed by gas chromatography-mass spectrometric analysis, Anal. Methods 7 (2015) 8793–8800.
[226] Y. Yao, S. Miao, S. Liu, L.P. Ma, H. Sun, S. Wang, Synthesis, characterization, and adsorption properties of magnetic Fe_3O_4@ graphene nanocomposite, Chem. Eng. J. 184 (2012) 326–332.
[227] S. Bai, X. Shen, X. Zhong, Y. Liu, G. Zhu, X. Xu, K. Chen, One-pot solvothermal preparation of magnetic reduced graphene oxide-ferrite hybrids for organic dye removal, Carbon 50 (2012) 2337–2346.
[228] P. Bhunia, G. Kim, C. Baik, H. Lee, A strategically designed porous iron-iron oxide matrix on graphene for heavy metal adsorption, Chem. Commun. 48 (2012) 9888–9890.
[229] T.V. Tran, P.V. Thinh, T.D. Nguyen, L. Bach, Preparation of graphene oxide-XFe_2O_4 (X = Co, Mn, Ni) nanocomposites and their application in adsorption organic dye from aqueous solution, J. Mater. Sci. Surf. Eng. 5 (2017) 619–621.
[230] H.Y. Koo, H.J. Lee, H.A. Go, Y.B. Lee, T.S. Bae, J.K. Kim, W.S. Choi, Graphene-based multifunctional iron oxide nanosheets with tunable properties, Chem. Eur. J. 17 (2011) 1214–1219.
[231] J. Wang, B. Tang, T. Tsuzuki, Q. Liu, X. Hou, L. Sun, Synthesis, characterization and adsorption properties of superparamagnetic polystyrene/Fe_3O_4/graphene oxide, Chem. Eng. J. 204 (2012) 258–263.
[232] Q. Zhou, Y. Wang, J. Xiao, H. Fan, Adsorption and removal of bisphenol A, α-naphthol and β-naphthol from aqueous solution by Fe_3O_4@ polyaniline core-shell nanomaterials, Synth. Met. 212 (2016) 113–122.

This book belongs to Badji Mokhtar Annaba University Central Library Copyright Elsevier 2025

[233] F. Yu, S. Sun, J. Ma, S. Han, Enhanced removal performance of arsenate and arsenite by magnetic graphene oxide with high iron oxide loading, Phys. Chem. Chem. Phys. 17 (2015) 4388–4397.
[234] M. Liu, T. Wen, X. Wu, C. Chen, J. Hu, J. Li, X. Wang, Synthesis of porous Fe_3O_4 hollow microspheres/graphene oxide composite for Cr(VI) removal, Dalton Trans. 42 (2013) 14710–14717.
[235] K. Molaei, H. Bagheri, A.A. Asgharinezhad, H. Ebrahimzadeh, M. Shamsipur, SiO_2-coated magnetic graphene oxide modified with polypyrrole-polythiophene: a novel and efficient nanocomposite for solid phase extraction of trace amounts of heavy metals, Talanta 167 (2017) 607–616.
[236] A. Sa'Adi, Z. Es'haghi, Azo-phenol ligand surface-active magnetic graphene oxide nanosheets as solid-phase adsorbents for extraction of cadmium in food samples, J. Food Meas. Charact. 13 (2019) 579–591.
[237] M. Liu, C. Chen, J. Hu, X. Wu, X. Wang, Synthesis of magnetite/graphene oxide composite and application for cobalt (II) removal, J. Phys. Chem. C 115 (2011) 25234–25240.
[238] J.-H. Deng, X.-R. Zhang, G.-M. Zeng, J.-L. Gong, Q.-Y. Niu, J. Liang, Simultaneous removal of Cd(II) and ionic dyes from aqueous solution using magnetic graphene oxide nanocomposite as an adsorbent, Chem. Eng. J. 226 (2013) 189–200.
[239] V.K. Gupta, S. Agarwal, M. Asif, A. Fakhri, N. Sadeghi, Application of response surface methodology to optimize the adsorption performance of a magnetic graphene oxide nanocomposite adsorbent for removal of methadone from the environment, J. Colloid Interface Sci. 497 (2017) 193–200.
[240] P.K. Boruah, B. Sharma, N. Hussain, M.R. Das, Magnetically recoverable Fe_3O_4/graphene nanocomposite towards efficient removal of triazine pesticides from aqueous solution: investigation of the adsorption phenomenon and specific ion effect, Chemosphere 168 (2017) 1058–1067.
[241] C. Lv, J. Zhang, G. Li, H. Xi, M. Ge, T. Goto, Facile fabrication of self-assembled lamellar PANI-GO-Fe_3O_4 hybrid nanocomposites with enhanced adsorption capacities and easy recyclicity towards ionic dyes, Colloids Surf. A Physicochem. Eng. Asp. 585 (2020) 124147.
[242] S. Chang, Q. Zhang, Y. Lu, S. Wu, W. Wang, High-efficiency and selective adsorption of organic pollutants by magnetic $CoFe_2O_4$/graphene oxide adsorbents: experimental and molecular dynamics simulation study, Sep. Purif. Technol. 238 (2020) 116400.
[243] S. Zhao, C. Ge, Z. Yan, J. Zhang, S. Ren, H. Liang, F. Chen, X. Li, One-pot microwave-assisted combustion synthesis of $NiFe_2O_4$-reduced graphene oxide composite for adsorptive desulfurization of diesel fuel, Mater. Chem. Phys. 229 (2019) 294–302.
[244] S. Ploychompoo, J. Chen, H. Luo, Q. Liang, Fast and efficient aqueous arsenic removal by functionalized MIL-100 (Fe)/rGO/δ-MnO_2 ternary composites: adsorption performance and mechanism, J. Environ. Sci. 91 (2020) 22–34.
[245] T.S. Sreeprasad, S.M. Maliyekkal, K.P. Lisha, T. Pradeep, Reduced graphene oxide-metal/metal oxide composites: facile synthesis and application in water purification, J. Hazard. Mater. 186 (2011) 921–931.
[246] J.-P. Zou, H.-L. Liu, J. Luo, Q.-J. Xing, H.-M. Du, X.-H. Jiang, X.-B. Luo, S.-L. Luo, S.L. Suib, Three-dimensional reduced graphene oxide coupled with Mn_3O_4 for highly efficient removal of Sb(III) and Sb(V) from water, ACS Appl. Mater. Interfaces 8 (2016) 18140–18149.
[247] X. Luo, C. Wang, S. Luo, R. Dong, X. Tu, G. Zeng, Adsorption of As(III) and As(V) from water using magnetite Fe_3O_4-reduced graphite oxide-MnO_2 nanocomposites, Chem. Eng. J. 187 (2012) 45–52.
[248] Z. Yang, S. Ji, W. Gao, C. Zhang, L. Ren, W.W. Tjiu, Z. Zhang, J. Pan, T. Liu, Magnetic nanomaterial derived from graphene oxide/layered double hydroxide hybrid for efficient removal of methyl orange from aqueous solution, J. Colloid Interface Sci. 408 (2013) 25–32.
[249] A. Diraki, H.R. Mackey, G. McKay, A. Abdala, Removal of emulsified and dissolved diesel oil from high salinity wastewater by adsorption onto graphene oxide, J. Environ. Chem. Eng. 7 (2019) 103106.
[250] M. Mukherjee, S. Goswami, P. Banerjee, S. Sengupta, P. Das, P.K. Banerjee, S. Datta, Ultrasonic assisted graphene oxide nanosheet for the removal of phenol containing solution, Environ. Technol. Innov. 13 (2019) 398–407.
[251] W. Wang, Q. Gong, Z. Chen, W.D. Wang, Q. Huang, S. Song, J. Chen, X. Wang, Adsorption and competition investigation of phenolic compounds on the solid-liquid interface of three-dimensional foam-like graphene oxide, Chem. Eng. J. 378 (2019) 122085.

This book belongs to Badji Mokhtar Annaba University Central Library Copyright Elsevier 2025

[252] S. Ding, S. Sun, H. Xu, B. Yang, Y. Liu, H. Wang, D. Chen, R. Zhang, Preparation and adsorption property of graphene oxide by using waste graphite from diamond synthesis industry, Mater. Chem. Phys. 221 (2019) 47–57.
[253] K. Rekos, Z.-C. Kampouraki, C. Sarafidis, V. Samanidou, E. Deliyanni, Graphene oxide based magnetic nanocomposites with polymers as effective bisphenol—a nanoadsorbents, Materials 12 (2019) 1987.
[254] D. Coello-Fiallos, E. Cazzanelli, A. Tavolaro, P. Tavolaro, M. Arias, L. Caputi, Cresyl violet adsorption on sonicated graphite oxide, J. Nanosci. Nanotechnol. 18 (2018) 3006–3011.
[255] W. Zhang, J. Chen, Y. Hu, Z. Fang, J. Cheng, Y. Chen, Adsorption characteristics of tetrabromobisphenol A onto sodium bisulfite reduced graphene oxide aerogels, Colloids Surf. A Physicochem. Eng. Asp. 538 (2018) 781–788.
[256] M. Tanhaei, A.R. Mahjoub, V. Safarifard, Sonochemical synthesis of amide-functionalized metal-organic framework/graphene oxide nanocomposite for the adsorption of methylene blue from aqueous solution, Ultrason. Sonochem. 41 (2018) 189–195.
[257] H. Karimi-Maleh, M. Shafieizadeh, M.A. Taher, F. Opoku, E.M. Kiarii, P. P. Govender, S. Ranjbari, M. Rezapour, Y. Orooji, The role of magnetite/graphene oxide nano-composite as a high-efficiency adsorbent for removal of phenazopyridine residues from water samples, an experimental/theoretical investigation, J. Mol. Liq. 298 (2020) 112040.
[258] M.S. Nas, M.H. Calimli, H. Burhan, M. Yılmaz, S.D. Mustafov, F. Sen, Synthesis, characterization, kinetics and adsorption properties of Pt-Co@GO nano-adsorbent for methylene blue removal in the aquatic mediums using ultrasonic process systems, J. Mol. Liq. 296 (2019) 112100.
[259] A. Pourjavadi, M. Nazari, M. Kohestanian, S.H. Hosseini, Polyacrylamide-grafted magnetic reduced graphene oxide nanocomposite: preparation and adsorption properties, Colloid Polym. Sci. 297 (2019) 917–926.
[260] N. Ninwiwek, P. Hongsawat, P. Punyapalakul, P. Prarat, Removal of the antibiotic sulfamethoxazole from environmental water by mesoporous silica-magnetic graphene oxide nanocomposite technology: adsorption characteristics, coadsorption and uptake mechanism, Colloids Surf. A Physicochem. Eng. Asp. 580 (2019) 123716.
[261] X. Jia, S. Li, Y. Wang, T. Wang, X. Hou, Adsorption behavior and mechanism of sulfonamide antibiotics in aqueous solution on a novel MIL-101(Cr)@GO composite, J. Chem. Eng. Data 64 (2019) 1265–1274.
[262] Z. Wang, J. Zhang, B. Hu, J. Yu, J. Wang, X. Guo, Graphene/Fe_3O_4 nanocomposite for effective removal of ten triazole fungicides from water solution: Tebuconazole as an example for investigation of the adsorption mechanism by experimental and molecular docking study, J. Taiwan Inst. Chem. Eng. 95 (2019) 635–642.
[263] N. Mukwevho, R. Gusain, E. Fosso-Kankeu, N. Kumar, F. Waanders, S.S. Ray, Removal of naphthalene from simulated wastewater through adsorption-photodegradation by ZnO/Ag/GO nanocomposite, J. Ind. Eng. Chem. 81 (2020) 393–404.
[264] N. You, X.-F. Wang, J.-Y. Li, H.-T. Fan, H. Shen, Q. Zhang, Synergistic removal of arsanilic acid using adsorption and magnetic separation technique based on Fe_3O_4@ graphene nanocomposite, J. Ind. Eng. Chem. 70 (2019) 346–354.
[265] S. Shan, H. Tang, Y. Zhao, W. Wang, F. Cui, Highly porous zirconium-crosslinked graphene oxide/alginate aerogel beads for enhanced phosphate removal, Chem. Eng. J. 359 (2019) 779–789.
[266] L. Bai, L. Yuan, Y. Ji, H. Yan, Effective removal of phosphate from aqueous by graphene oxide decorated with α-Fe_2O_3: kinetic, isotherm, thermodynamic and mechanism study, Arab. J. Sci. Eng. 43 (2018) 3611–3620.
[267] Z. Yu, C. Hu, A.B. Dichiara, W. Jiang, J. Gu, Cellulose nanofibril/carbon nanomaterial hybrid aerogels for adsorption removal of cationic and anionic organic dyes, Nano 10 (2020) 169.
[268] A. Hussain, J. Li, J. Wang, F. Xue, Y. Chen, T. Bin Aftab, D. Li, Hybrid monolith of graphene/TEMPO-oxidized cellulose nanofiber as mechanically robust, highly functional, and recyclable adsorbent of methylene blue dye, J. Nanomater. 2018 (2018) 1–12.
[269] Y. Liang, J. Liu, L. Wang, Y. Wan, J. Shen, Q. Bai, Metal affinity-carboxymethyl cellulose functionalized magnetic graphene composite for highly selective isolation of histidine-rich proteins, Talanta 195 (2019) 381–389.

This book belongs to Badji Mokhtar Annaba University Central Library Copyright Elsevier 2025

[270] N.N. Marnani, A. Shahbazi, A novel environmental-friendly nanobiocomposite synthesis by EDTA and chitosan functionalized magnetic graphene oxide for high removal of rhodamine B: adsorption mechanism and separation property, Chemosphere 218 (2019) 715–725.
[271] J. Chen, M. Jiang, J. Han, K. Liu, M. Liu, Q. Wu, Syntheses of magnetic GO @ melamine formaldehyde resin for dyes adsorption, Mater. Res. Express 6 (2019) 086103.
[272] H. Wang, X. Lai, W. Zhao, Y. Chen, X. Yang, X. Meng, Y. Li, Efficient removal of crystal violet dye using EDTA/graphene oxide functionalized corncob: a novel low cost adsorbent, RSC Adv. 9 (2019) 21996–22003.
[273] A.I. Abd-Elhamid, M.R. El-Aassar, G.F. El Fawal, H.M.A. Soliman, Fabrication of polyacrylonitrile/β-cyclodextrin/graphene oxide nanofibers composite as an efficient adsorbent for cationic dye, Environ. Nanotechnol. Monit. Manag. 11 (2019) 100207.
[274] K. He, G. Zeng, A. Chen, Z. Huang, M. Peng, T. Huang, G. Chen, Graphene hybridized polydopamine-kaolin composite as effective adsorbent for methylene blue removal, Compos. Part B 161 (2019) 141–149.
[275] F.A. Shammala, B. Chiswell, Removal of Chrysoidine Y from water by graphene-based nanocomposite derivatives with magnetic chitosan nanocomposite, Int. J. Appl. Pharm. Sci. Res. 4 (2019) 17–33.
[276] G. Abdi, A. Alizadeh, J. Amirian, S. Rezaei, G. Sharma, Polyamine-modified magnetic graphene oxide surface: feasible adsorbent for removal of dyes, J. Mol. Liq. 289 (2019) 111118.
[277] A. Al-Kinani, M. Gheibi, M. Eftekhari, Graphene oxide-tannic acid nanocomposite as an efficient adsorbent for the removal of malachite green from water samples, Model. Earth Syst. Environ. 5 (2019) 1627–1633.
[278] A. Burakov, E. Neskoromnaya, A. Babkin, Removal of the alizarin red S anionic dye using graphene nanocomposites: a study on kinetics under dynamic conditions, Mater. Today Proc. 11 (2019) 392–397.
[279] H. Hosseinzadeh, S. Ramin, Fabrication of starch-graft-poly (acrylamide)/graphene oxide/hydroxyapatite nanocomposite hydrogel adsorbent for removal of malachite green dye from aqueous solution, Int. J. Biol. Macromol. 106 (2018) 101–115.
[280] M. Rajabi, K. Mahanpoor, O. Moradi, Preparation of PMMA/GO and PMMA/GO-Fe3O4 nanocomposites for malachite green dye adsorption: kinetic and thermodynamic studies, Compos. Part B 167 (2019) 544–555.
[281] G.R. Bardajee, S.S. Hosseini, C. Vancaeyzeele, Graphene oxide nanocomposite hydrogel based on poly (acrylic acid) grafted onto salep: an adsorbent for the removal of noxious dyes from water, New J. Chem. 43 (2019) 3572–3582.
[282] J. Wei, S.-H. Gui, J.-H. Wu, D.-D. Xu, Y. Sun, X.-Y. Dong, Y.-Y. Dai, Y.-F. Li, Nanocellulose-graphene oxide hybrid aerogel to water purification, Appl. Environ. Biotechnol. 4 (2019) 11–17.
[283] M. Nurrokhimah, P. Nurerk, P. Kanatharana, O. Bunkoed, A nanosorbent consisting of a magnetic molecularly imprinted polymer and graphene oxide for multi-residue analysis of cephalosporins, Microchim. Acta 186 (2019) 822.
[284] S. Indherjith, S. Karthikeyan, J.H.R. Monica, K. Krishna Kumar, Graphene oxide & reduced graphene oxide polysulfone nanocomposite pellets: an alternative adsorbent of antibiotic pollutant-ciprofloxacin, Sep. Sci. Technol. 54 (2019) 667–674.
[285] K. Zhou, J. Zhang, Y. Xiao, Z. Zhao, M. Zhang, L. Wang, X. Zhang, C. Zhou, High-efficiency adsorption of and competition between phenol and hydroquinone in aqueous solution on highly cationic amino-poly (vinylamine)-functionalized GO-(o-MWCNTs) magnetic nanohybrids, Chem. Eng. J. (2020) 124223.
[286] N. Alipour, H. Namazi, Removing Paraquat and Nile blue from aqueous solution using double-oxidized graphene oxide coated by polydopamine nanocomposite, Int. J. Environ. Sci. Technol. 16 (2019) 3203–3210.
[287] A.F. Hassan, Enhanced adsorption of 2,4-dichlorophenoxyacetic acid from aqueous medium by graphene oxide/alginate composites, Desalin. Water Treat. 141 (2019) 187–196.
[288] M.Y. Akram, S. Ahmed, L. Li, N. Akhtar, S. Ali, G. Muhyodin, X.-Q. Zhu, J. Nie, N-doped reduced graphene oxide decorated with Fe_3O_4 composite: stable and magnetically separable adsorbent solution for high performance phosphate removal, J. Environ. Chem. Eng. 7 (2019) 103137.
[289] A. Zeraatkar Moghaddam, E. Ghiamati, R. Pakar, M.R. Sabouri, M.R. Ganjali, A novel and an efficient 3-D high nitrogen doped graphene oxide adsorbent for the removal of Congo red from aqueous solutions, Pollution 5 (2019) 501–514.
[290] Z. Luo, D. Li, S. Tan, L. Huang, Preparation and oil-water separation of 3D kapok fiber-reduced graphene oxide aerogel, J. Chem. Technol. Biotechnol. 95 (2020) 639–648.

This book belongs to Badji Mokhtar Annaba University Central Library Copyright Elsevier 2025

[291] J. Hu, J. Zhu, S. Ge, C. Jiang, T. Guo, T. Peng, T. Huang, L. Xie, Biocompatible, hydrophobic and resilience graphene/chitosan composite aerogel for efficient oil-water separation, Surf. Coat. Technol. 385 (2020) 125361.
[292] C.E. Flores-Chaparro, C.J. Castilho, I. Kulaots, R.H. Hurt, J.R. Rangel-Mendez, Pillared graphene oxide composite as an adsorbent of soluble hydrocarbons in water: pH and organic matter effects, J. Environ. Manag. 259 (2020) 110044.
[293] L.-Z. Guan, L. Zhao, Y.-J. Wan, L.-C. Tang, Three-dimensional graphene-based polymer nanocomposites: preparation, properties and applications, Nanoscale 10 (2018) 14788–14811.
[294] P. Mukhopadhyay, R.K. Gupta, Trends and frontiers in graphene-based polymer nanocomposites, Plast. Eng. 67 (2011) 32–42.
[295] X. Yang, Y. Tu, L. Li, S. Shang, X.-M. Tao, Well-dispersed chitosan/graphene oxide nanocomposites, ACS Appl. Mater. Interfaces 2 (2010) 1707–1713.
[296] S. Park, D.A. Dikin, S.T. Nguyen, R.S. Ruoff, Graphene oxide sheets chemically cross-linked by polyallylamine, J. Phys. Chem. C 113 (2009) 15801–15804.
[297] G. Mittal, V. Dhand, K.Y. Rhee, S.-J. Park, W.R. Lee, A review on carbon nanotubes and graphene as fillers in reinforced polymer nanocomposites, J. Ind. Eng. Chem. 21 (2015) 11–25.
[298] F. Marra, J. Lecini, A. Tamburrano, L. Pisu, M.S. Sarto, Broadband electromagnetic absorbing structures made of graphene/glass-fiber/epoxy composite, IEEE Trans. Microwave Theory Tech. (2019).
[299] K. Rekos, Z.C. Kampouraki, V. Samanidou, E. Deliyanni, Magnetic graphene oxide-polystyrene and magnetic activated carbon-polystyrene nanocomposites as sorbents for bisphenol A, in: EGU General Assembly Conference Abstracts, 2016.
[300] S. Sánchez-Valdes, A. Zapata-Domínguez, J. Martinez-Colunga, J. Mendez-Nonell, L. Ramos De Valle, A. Espinoza-Martinez, A. Morales-Cepeda, T. Lozano-Ramirez, P. Lafleur, E. Ramirez-Vargas, Influence of functionalized polypropylene on polypropylene/graphene oxide nanocomposite properties, Polym. Compos. 39 (2018) 1361–1369.
[301] P. Mikhaylov, M. Vinogradov, I. Levin, G. Shandryuk, A. Lubenchenko, V. Kulichikhin, Synthesis characterization of polyethylene terephthalate-reduced graphene oxide composites, in: IOP Conference Series: Materials Science and Engineering, IOP Publishing, 2019 012036.
[302] N. Almasi, S. Hosseinzadeh, S. Hatamie, G. Taheri Sangsari, Stable conductive and biocompatible scaffold development using graphene oxide (GO) doped polyaniline (PANi), Int. J. Polym. Mater. Polym. Biomater. 69 (2019) 1–11.
[303] C. Wan, J. Li, Graphene oxide/cellulose aerogels nanocomposite: preparation, pyrolysis, and application for electromagnetic interference shielding, Carbohydr. Polym. 150 (2016) 172–179.
[304] G. Sahoo, N. Sarkar, D. Sahu, S.K. Swain, Nano gold decorated reduced graphene oxide wrapped polymethylmethacrylate for supercapacitor applications, RSC Adv. 7 (2017) 2137–2150.
[305] S. Ramesh, S. Khandelwal, K.Y. Rhee, D. Hui, Synergistic effect of reduced graphene oxide, CNT and metal oxides on cellulose matrix for supercapacitor applications, Compos. Part B 138 (2018) 45–54.
[306] M. Zeeb, H. Farahani, Graphene oxide/Fe_3O_4@polythionine nanocomposite as an efficient sorbent for magnetic solid-phase extraction followed by high-performance liquid chromatography for the determination of duloxetine in human plasma, Chem. Pap. 72 (2018) 15–27.
[307] S. Ebrahimpoor, V. Kiarostami, M. Khosravi, M. Davallo, A. Ghaedi, Bees metaheuristic algorithm with the aid of artificial neural networks for optimization of acid red 27 dye adsorption onto novel polypyrrole/SrFe 12 O 19/graphene oxide nanocomposite, Polym. Bull. 76 (2019) 6529–6553.
[308] S. Li, X. Lu, Y. Xue, J. Lei, T. Zheng, C. Wang, Fabrication of polypyrrole/graphene oxide composite nanosheets and their applications for Cr(VI) removal in aqueous solution, PLoS One 7 (2012).
[309] C. Zhou, H. Zhu, Q. Wang, J. Wang, J. Cheng, Y. Guo, X. Zhou, R. Bai, Adsorption of mercury (II) with an Fe_3O_4 magnetic polypyrrole-graphene oxide nanocomposite, RSC Adv. 7 (2017) 18466–18479.
[310] A. Mehdinia, Z. Shoormeij, A. Jabbari, Trace determination of lead (II) ions by using a magnetic nanocomposite of the type Fe_3O_4/TiO_2/PPy as a sorbent, and FAAS for quantitation, Microchim. Acta 184 (2017) 1529–1537.

This book belongs to Badji Mokhtar Annaba University Central Library Copyright Elsevier 2025

[311] S. Karandish, M. Chamsaz, M.H. Arbab Zavar, M. Gheibi, Reduced graphene oxide-polyaniline nanocomposite as an efficient adsorbent for solid phase extraction of Co^{2+} followed by electrothermal atomic absorption spectrometry, Int. J. Environ. Anal. Chem. 98 (2018) 1135–1148.
[312] F. Zhang, B. Wang, S. He, R. Man, Preparation of graphene-oxide/polyamidoamine dendrimers and their adsorption properties toward some heavy metal ions, J. Chem. Eng. Data 59 (2014) 1719–1726.
[313] E. El-Sharkaway, R.M. Kamel, I.M. El-Sherbiny, S.S. Gharib, Removal of methylene blue from aqueous solutions using polyaniline/graphene oxide or polyaniline/reduced graphene oxide composites, Environ. Technol. 41 (22) (2019) 2854–2862.
[314] A. Ghahramani, M. Gheibi, M. Eftekhari, Polyaniline-coated reduced graphene oxide as an efficient adsorbent for the removal of malachite green from water samples, Polym. Bull. 76 (2019) 5269–5283.
[315] A. Deb, M. Kanmani, A. Debnath, K.L. Bhowmik, B. Saha, Ultrasonic assisted enhanced adsorption of methyl orange dye onto polyaniline impregnated zinc oxide nanoparticles: kinetic, isotherm and optimization of process parameters, Ultrason. Sonochem. 54 (2019) 290–301.
[316] H. Qiu, X. Luo, J. Wang, X. Zhong, S. Qi, Synthesis and characterization of ternary polyaniline/barium ferrite/reduced graphene oxide composite as microwave-absorbing material, J. Electron. Mater. 48 (2019) 4400–4408.
[317] A.K. Mishra, S. Ramaprabhu, Nanostructured polyaniline decorated graphene sheets for reversible CO_2 capture, J. Mater. Chem. 22 (2012) 3708–3712.
[318] A.K. Mishra, S. Ramaprabhu, Enhanced CO_2 capture in Fe_3O_4-graphene nanocomposite by physicochemical adsorption, J. Appl. Phys. 116 (2014) 064306.
[319] X. Huang, X. Qi, F. Boey, H. Zhang, Graphene-based composites, Chem. Soc. Rev. 41 (2012) 666–686.
[320] R.K. Singh, R. Kumar, D.P. Singh, Graphene oxide: strategies for synthesis, reduction and frontier applications, RSC Adv. 6 (2016) 64993–65011.
[321] P.P. Singh, Environmental remediation by nanoadsorbents-based polymer nanocomposite, in: New Polymer Nanocomposites for Environmental Remediation, Elsevier, 2018.
[322] P.S.P. Batista, A.M.M.B. De Morais, M.M.E. Pintado, R.M.S.C. De Morais, Alginate: pharmaceutical and medical applications, in: Extracellular Sugar-Based Biopolymers Matrices, Springer, 2019.
[323] D. Xiao, M. He, Y. Liu, L. Xiong, Q. Zhang, L. Wei, L. Li, X. Yu, Strong alginate/reduced graphene oxide composite hydrogels with enhanced dye adsorption performance, Polym. Bull. 77 (2020) 6609–6623.
[324] W.M. Algothmi, N.M. Bandaru, Y. Yu, J.G. Shapter, A.V. Ellis, Alginate-graphene oxide hybrid gel beads: an efficient copper adsorbent material, J. Colloid Interface Sci. 397 (2013) 32–38.
[325] J. Li, J. Ma, S. Chen, Y. Huang, J. He, Adsorption of lysozyme by alginate/graphene oxide composite beads with enhanced stability and mechanical property, Mater. Sci. Eng. C 89 (2018) 25–32.
[326] E. Platero, M.E. Fernandez, P.R. Bonelli, A.L. Cukierman, Graphene oxide/alginate beads as adsorbents: influence of the load and the drying method on their physicochemical-mechanical properties and adsorptive performance, J. Colloid Interface Sci. 491 (2017) 1–12.
[327] S. Wu, X. Zhao, Y. Li, C. Zhao, Q. Du, J. Sun, Y. Wang, X. Peng, Y. Xia, Z. Wang, Adsorption of ciprofloxacin onto biocomposite fibers of graphene oxide/calcium alginate, Chem. Eng. J. 230 (2013) 389–395.
[328] L. Sun, B. Fugetsu, Graphene oxide captured for green use: influence on the structures of calcium alginate and macroporous alginic beads and their application to aqueous removal of acridine orange, Chem. Eng. J. 240 (2014) 565–573.
[329] Tasmia, J. Shah, M.R. Jan, Eco-friendly alginate encapsulated magnetic graphene oxide beads for solid phase microextraction of endocrine disrupting compounds from water samples, Ecotoxicol. Environ. Saf. 190 (2020) 110099.
[330] P. Klongklaew, P. Kanatharana, O. Bunkoed, Development of doubly porous composite adsorbent for the extraction of fluoroquinolones from food samples, Food Chem. 309 (2020) 125685.
[331] Y. Li, Q. Du, T. Liu, J. Sun, Y. Wang, S. Wu, Z. Wang, Y. Xia, L. Xia, Methylene blue adsorption on graphene oxide/calcium alginate composites, Carbohydr. Polym. 95 (2013) 501–507.
[332] H. Zheng, J. Yang, S. Han, The synthesis and characteristics of sodium alginate/graphene oxide composite films crosslinked with multivalent cations, J. Appl. Polym. Sci. (2016) 133.

This book belongs to Badji Mokhtar Annaba University Central Library Copyright Elsevier 2025

[333] W.W. Ngah, L. Teong, M. Hanafiah, Adsorption of dyes and heavy metal ions by chitosan composites: a review, Carbohydr. Polym. 83 (2011) 1446–1456.
[334] L. Zhang, Y. Zeng, Z. Cheng, Removal of heavy metal ions using chitosan and modified chitosan: a review, J. Mol. Liq. 214 (2016) 175–191.
[335] Q. Zia, M. Tabassum, H. Gong, J. Li, A review on chitosan for the removal of heavy metals ions, J. Fiber Bioeng. Inform. 12 (2019) 103–128.
[336] K. Wu, X. Liu, Z. Li, Y. Jiao, C. Zhou, Fabrication of chitosan/graphene oxide composite aerogel microspheres with high bilirubin removal performance, Mater. Sci. Eng. C 106 (2020) 110162.
[337] Z. Xie, J. Zhu, Y. Bi, H. Ren, X. Chen, H. Yu, Nitrogen-doped porous graphene-based aerogels toward efficient heavy metal ion adsorption and supercapacitor applications, Phys. Status Solidi Rapid Res. Lett. 14 (2020) 1900534.
[338] T.S. Vo, T.T.B.C. Vo, J.W. Suk, K. Kim, Recycling performance of graphene oxide-chitosan hybrid hydrogels for removal of cationic and anionic dyes, Nano Convergence 7 (2020) 4.
[339] H. Yuan, L.-Y. Meng, S.-J. Park, A review: synthesis and applications of graphene/chitosan nanocomposites, Carbon Lett. 17 (2016) 11–17.
[340] J.-S. Cheng, J. Du, W. Zhu, Facile synthesis of three-dimensional chitosan-graphene mesostructures for reactive black 5 removal, Carbohydr. Polym. 88 (2012) 61–67.
[341] M. Sabzevari, D.E. Cree, L.D. Wilson, Graphene oxide-chitosan composite material for treatment of a model dye effluent, ACS Omega 3 (2018) 13045–13054.
[342] S. Debnath, A. Maity, K. Pillay, Magnetic chitosan-GO nanocomposite: synthesis, characterization and batch adsorber design for Cr(VI) removal, J. Environ. Chem. Eng. 2 (2014) 963–973.
[343] J. Sun, W. Guo, J. Ji, Z. Li, X. Yuan, F. Pi, Y. Zhang, X. Sun, Removal of patulin in apple juice based on novel magnetic molecularly imprinted adsorbent Fe_3O_4@SiO_2@CS-GO@MIP, LWT Food Sci. Technol. 118 (2020) 108854.
[344] B. Zhang, R. Hu, D. Sun, T. Wu, Y. Li, Fabrication of chitosan/magnetite-graphene oxide composites as a novel bioadsorbent for adsorption and detoxification of Cr(VI) from aqueous solution, Sci. Rep. 8 (2018) 15397.
[345] N.A. Travlou, G.Z. Kyzas, N.K. Lazaridis, E.A. Deliyanni, Functionalization of graphite oxide with magnetic chitosan for the preparation of a nanocomposite dye adsorbent, Langmuir 29 (2013) 1657–1668.
[346] R. Kabiri, H. Namazi, Nanocrystalline cellulose acetate (NCCA)/graphene oxide (GO) nanocomposites with enhanced mechanical properties and barrier against water vapor, Cellulose 21 (2014) 3527–3539.
[347] O. Shoseyov, D. Kam, T.B. Shalom, Z. Shtein, S. Vinkler, Y. Posen, Nanocellulose composite biomaterials in industry and medicine, in: Extracellular Sugar-Based Biopolymers Matrices, Springer, 2019.
[348] J. Huang, A. Dufresne, N. Lin, Nanocellulose: From Fundamentals to Advanced Materials, John Wiley & Sons, 2019.
[349] N.M. Aboamera, A. Mohamed, A. Salama, T. Osman, A. Khattab, An effective removal of organic dyes using surface functionalized cellulose acetate/graphene oxide composite nanofibers, Cellulose 25 (2018) 4155–4166.
[350] H.-Y. Mi, X. Jing, H.-X. Huang, X.-F. Peng, L.-S. Turng, Superhydrophobic graphene/cellulose/silica aerogel with hierarchical structure as Superabsorbers for high efficiency selective oil absorption and recovery, Ind. Eng. Chem. Res. 57 (2018) 1745–1755.
[351] H. Luo, F. Feng, F. Yao, Y. Zhu, Z. Yang, Y. Wan, Improved removal of toxic metal ions by incorporating graphene oxide into bacterial cellulose, J. Nanosci. Nanotechnol. 20 (2020) 719–730.
[352] S.H. Dave, C. Gong, A.W. Robertson, J.H. Warner, J.C. Grossman, Chemistry and structure of graphene oxide via direct imaging, ACS Nano 10 (2016) 7515–7522.
[353] Y.-Y. Deng, X.-F. Xiao, D. Wang, B. Han, Y. Gao, J.-L. Xue, Adsorption of Cr(VI) from aqueous solution by ethylenediaminetetraacetic acid-chitosan-modified metal-organic framework, J. Nanosci. Nanotechnol. 20 (2020) 1660–1669.
[354] J. Mahmud, M. Hasanuzzaman, K. Nahar, A. Rahman, M. Fujita, EDTA reduces cadmium toxicity in mustard (*Brassica juncea* L.) by enhancing metal chelation, antioxidant defense and glyoxalase systems, Acta Agrobot. 72 (2019) 1722.

This book belongs to Badji Mokhtar Annaba University Central Library Copyright Elsevier 2025

[355] S. Khadivi, L. Edjlali, A. Akbarzadeh, K. Seyyedi, Enhanced adsorption behavior of amended EDTA-graphene oxide for methylene blue and heavy metal ions, Int. J. Environ. Sci. Technol. 16 (2019) 8151–8160.
[356] C. Zhao, L. Ma, J. You, F. Qu, R.D. Priestley, Edta-and amine-functionalized graphene oxide as sorbents for Ni(II) removal, Desalin. Water Treat. 57 (2016) 8942–8951.
[357] C.J. Madadrang, H.Y. Kim, G. Gao, N. Wang, J. Zhu, H. Feng, M. Gorring, M.L. Kasner, S. Hou, Adsorption behavior of EDTA-graphene oxide for Pb(II) removal, ACS Appl. Mater. Interfaces 4 (2012) 1186–1193.
[358] S. Hou, S. Su, M.L. Kasner, P. Shah, K. Patel, C.J. Madarang, Formation of highly stable dispersions of silane-functionalized reduced graphene oxide, Chem. Phys. Lett. 501 (2010) 68–74.
[359] M. Kadivar, A. Aliakbar, A new composite based on graphene oxide-poly 3-aminophenol for solid-phase microextraction of four triazole fungicides in water and fruit juices prior to high-performance liquid chromatography analysis, Food Chem. 299 (2019) 125127.
[360] D. Chen, H. Zhang, K. Yang, H. Wang, Functionalization of 4-aminothiophenol and 3-aminopropyltriethoxysilane with graphene oxide for potential dye and copper removal, J. Hazard. Mater. 310 (2016) 179–187.
[361] R. Zare-Dorabei, S.M. Ferdowsi, A. Barzin, A. Tadjarodi, Highly efficient simultaneous ultrasonic-assisted adsorption of Pb(II), Cd(II), Ni(II) and Cu(II) ions from aqueous solutions by graphene oxide modified with 2,2′-dipyridylamine: central composite design optimization, Ultrason. Sonochem. 32 (2016) 265–276.
[362] A. Tadjarodi, S. Moazen Ferdowsi, R. Zare-Dorabei, A. Barzin, Highly efficient ultrasonic-assisted removal of Hg(II) ions on graphene oxide modified with 2-pyridinecarboxaldehyde thiosemicarbazone: adsorption isotherms and kinetics studies, Ultrason. Sonochem. 33 (2016) 118–128.
[363] I. Duru, D. Ege, A.R. Kamali, Graphene oxides for removal of heavy and precious metals from wastewater, J. Mater. Sci. 51 (2016) 6097–6116.
[364] S. Liu, H. Wang, L. Chai, M. Li, Effects of single- and multi-organic acid ligands on adsorption of copper by Fe_3O_4/graphene oxide-supported DCTA, J. Colloid Interface Sci. 478 (2016) 288–295.
[365] M.U. Tahir, X. Su, M. Zhao, Y. Liao, R. Wu, D. Chen, Preparation of hydroxypropyl-cyclodextrin-graphene/Fe_3O_4 and its adsorption properties for heavy metals, Surf. Interfaces 16 (2019) 43–49.
[366] J. Wang, W. Zhang, J. Wei, Fabrication of poly(β-cyclodextrin)-conjugated magnetic graphene oxide by surface-initiated RAFT polymerization for synergetic adsorption of heavy metal ions and organic pollutants, J. Mater. Chem. A 7 (2019) 2055–2065.

This book belongs to Badji Mokhtar Annaba University Central Library
Copyright Elsevier 2025

CHAPTER 14

Role of zeolite adsorbent in water treatment

Vesna Krstić

Mining and Metallurgy Institute Bor, Bor, Serbia; University of Belgrade, Technical Faculty Bor, Bor, Serbia

14.1 Introduction

Water is a precious resource necessary for life on the Earth. The rapid development of industry and infrastructure requires the additional exploitation of water resources for human consumption [1]. Due to the fact that a large percentage of the world's population uses groundwater for drinking, monitoring groundwater quality is of great importance [2, 3]. A major problem with water pollution is caused by toxic metals from the mining industry and metal processing, since they accumulate in living organisms, unlike organic pollutants that are biodegradable. Both pollutants affect the human health and environmental pollution [4, 5].

To remove toxic metal ions from water, various methods such as sorption, chemical and electrochemical deposition, ion exchange, filtration, flotation, extraction, electrocoagulation, reverse osmosis, electrodialysis, etc. are used [4, 6, 7]. Chemical precipitation is the most widely used method, but it is not effective when the concentration of metal ions is low in water, which is a very common occurrence. Moreover, the result of chemical deposition is sludge as additional waste, the formation of which is the main problem for the application of this procedure, and which requires additional problem-solving [8].

The cost-effectiveness of treating water from toxic ions, primarily from the toxic metal ions, has led to the development of sorption processes as a method for achieving satisfactory levels of treated wastewater. Sorption is one of the simplest and cheapest techniques for effectively removing metal ions from water [4, 9]. Prasad et al. [10] point out that the sorbent must be environmentally friendly, inexpensive, and efficient for a wide range of different concentrations of pollutants.

One of the possible solutions for water treatment is zeolites, since zeolites have all the essential characteristics of an environmentally friendly material. According to Flanigen [11]: "The history of zeolites and molecular sieves is reviewed from the discovery of the first zeolite

Handbook of Nanomaterials for Wastewater Treatment. https://doi.org/10.1016/B978-0-12-821496-1.00024-6
Copyright © 2021 Elsevier Inc. All rights reserved.

This book belongs to Badji Mokhtar Annaba University Central Library Copyright Elsevier 2025

mineral in 1756 through the explosion in new molecular sieve structures and compositions in the 1980's. R. M. Barrer's early pioneering work in adsorption and synthesis began the era of synthetic zeolites. The discovery of the commercially significant synthetic zeolites A, X and Y by R. M. Milton and D. W. Breck in the late 1940's to early 1950's led to their introduction by Union Carbide Corporation as a new class of industrial adsorbents in 1954, and in 1959 as hydrocarbon conversion catalysts …". Based on these data, it is obvious that zeolite has attracted the attention of researchers for more than 250 years, and it has been studied for a variety of applications (in catalysis, medicine, veterinary medicine, agriculture, then in food, textile, and other industries), and it has been especially used in recent decades and has proven to be very effective in treating water, as many studies suggest. The world's annual production of natural zeolite is estimated to be around 4 million tons, of which about 2.25 million tons is used in China alone [12]. There are a large number of papers in academic literature in which zeolites have been shown to remove pollutants very successfully from wastewater and are frequently used in water treatment.

Ion-exchange properties of zeolites are used in various industries [13, 14], and in recent years have increasingly been used to remove anions and cations from water [15, 16], due to their unique properties such as controlled water treatment, high ion removal efficiency, process speed, etc. The sorption and ion-exchange properties of zeolites are used to selectively separate cations from aqueous solutions. Oter and Akcay [17] used natural clinoptilolites from deposits in Turkey to selectively isolate lead(II), copper(II), zinc(II), and nickel(II). Sprynskyy et al. [18] have studied the removal of Ni^{2+}, Cu^{2+}, Pb^{2+}, and Cd^{2+} ions from a solution with natural and HCl-treated clinoptilolite from deposits in Ukraine. Their explanation was that there is no significant difference in the binding capacity of Cu^{2+}, Pb^{2+}, and Cd^{2+} between the mono- and multiionic systems. Based on this result, they concluded that for different cations there are certain centers on the zeolite. Unlike them, Oter and Akcay [17] have concluded that there occurs significantly less removal of Pb^{2+}, Ni^{2+}, Cu^{2+}, and Zn^{2+} ions on clinoptilolite from the deposits in Turkey when it comes to the multiion compared to the one-ion system, but that clinoptilolite still removes these cations very efficiently.

Panayotova and Velikov [19] have studied about the kinetics of the removal of Cd^{2+}, Pb^{2+}, Cu^{2+}, Ni^{2+}, and Zn^{2+} ions from mono-cation solutions or from their mixtures on natural zeolite from deposits in Bulgaria. They have shown that lead ions bind most to the zeolite and that by treating the starting zeolite with NaCl, better removal of heavy metals as well as a higher value of the distribution coefficients is achieved. The study of the removal of Pb^{2+} and Cd^{2+} on Na-modified zeolite from a deposit in Turkey was researched by Çulfaz and Yağız [20], and they showed that the removal of lead ions is energetically more favorable than the removal of cadmium ions. Perić et al. [21] have analyzed the removal of Pb^{2+}, Zn^{2+}, and Cu^{2+} on natural zeolite from deposits in Croatia. In doing so, they showed that this zeolite binds most of the Pb^{2+} ions, followed by Cu^{2+} and at least Zn^{2+}. The authors showed that processes such as ion exchange and adsorption are responsible for the removal of cations on the zeolite, and that at higher concentrations precipitation on the zeolite

This book belongs to Badji Mokhtar Annaba University Central Library Copyright Elsevier 2025

surface occurs. The maximum amounts of Pb^{2+}, Cu^{2+}, and Zn^{2+} ions were removed at 86, 78, and 41 mEq/100 g, respectively.

Llanes-Monter et al. [22] have examined the removal of Pb^{2+} using a natural clinoptilolite from a deposit in Mexico. In their work, they showed that the maximum bound amount of lead ions on this clinoptilolite is 140 mEq/100 g at pH 3. The removal of ions such as Cu^{2+}, Zn^{2+}, Cd^{2+}, Pb^{2+}, and NH_4^+ on natural zeolite and with 0.5 M NaCl-treated zeolite from a deposit in Italy was studied by Langella et al. [23] and from their study they concluded that zeolite selectivity for cations is represented by the following order $NH_4^+ > Pb^{2+} > Cd^{2+} > Cu^{2+} \approx Zn^{2+}$.

Zeolite exhibits high affinity and high selectivity for the ammonium ion in water. A number of papers have been published in the field of the removal of NH_4^+ ions from water [24–26]. Mumpton [26] states that during biological treatment with activated sludge, the nitrification process is accelerated by the use of clinoptilolite, which selectively exchanges NH_4^+ ions from wastewater and provides an ideal medium for the growth of nitrifying bacteria, which then oxidize NH_4^+ ions to nitrates. Bare et al. [24] have shown the pathway of ion exchange of NH_4^+ ions using zeolite Y and the processing of the parent zeolite leading to the other zeolite sample. Li et al. [27] examined the removal of NH_4^+ ions from drinking water by zeolites. Based on the results obtained, they concluded that this zeolite could also be effectively used to remove the NH_4^+ ions from drinking water.

The problem of economically viable and efficient wastewater treatment exists worldwide. This paper outlines the main characteristics of zeolites as ion exchangers and adsorbers in water treatment services. Knowledge of the structure and capabilities of zeolites, whether natural or synthetic, as well as the origin and composition of wastewater, allows us to more quickly and efficiently address the problems of water treatment instantaneously. The mechanisms of the adsorption properties of zeolites, both natural and modified, with respect to the affinity of the removal of pollutants from water, are presented in this chapter. Zeolite regrowth has been carefully considered as one of the important factors in the water treatment chain. In order to avoid the accumulation of liquid waste, the possibility of using electrolysis with a dimensionally stable anode (DSA) and returning useful components to the production process is suggested.

14.2 The nature of the zeolite

14.2.1 Composition and structure

Zeolites form a group of minerals of a regular and well-defined crystalline structures. These are usually hydrated aluminosilicates of alkali and alkaline-earth cations. Zeolites can be represented by the general formula, as shown by Diego Gatta and Lotti [28]:

$$M^{+}{}_{x} \cdot M^{2+}{}_{y} \left[Al_{(x+2y)} Si_{n-(x+2y)} O_{2n} \right] \cdot mH_2O$$

This book belongs to Badji Mokhtar Annaba University Central Library
Copyright Elsevier 2025

where M^+ represents the metal cation of the elements of the IA group (Li^+, Na^+, K^+, …), and M^{2+} elements of the IIA group (Ca^{2+}, Sr^{2+}, Ba^{2+}, …), where the number of molecules and atoms usually are $m < n$. The crystalline structure of the zeolite is based on the TO_4 tetrahedron where T represent an atom that can be trivalent (Al, B, Ga), tetravalent (Si, Ge), or pentavalent (P). Tetrahedra, which are connected to each other via a common oxygen atom, represent the primary building block of the zeolite. Tetrahedra TO_4 (SiO_4 or AlO_4), linked by oxygen atoms, have an O/(Al + Si) ratio of 2 [29, 30]. The bonding via the forks prevents the dense packing of the anion layers, which is why the crystalline structures of the aluminosilicates have the so-called open structures with properly spaced cavities connected by channels in all the three directions. Primary structural units, tetraders, create two- and three-dimensional secondary structural units, and a three-dimensional spatial mesh structure is created with pores and cavities characteristic of zeolites, as Baerlocher et al. [31] systematically show in the Atlas of the Zeolite.

The difference in the size of the $[SiO_4]^{4-}$ and $[AlO_4]^{5-}$ tetrahedral charges leads to an imbalance in the charge, that is, an excess of a negative charge occurs in the zeolite structure. The excess of this negative charge is balanced by cations of monovalent and divalent elements, mostly alkaline and alkaline earth metals (Na^+, K^+, Ca^{2+}, Mg^{2+}), which are located in channels and cavities of zeolites, together with water molecules. These cations are bound by the weak attractive forces and can be easily removed and replaced by other cations, and that is why they are called interchangeable cations [32, 33]. Cation exchange ability is quantitatively expressed as the cation exchange capacity (CEC), mmol M^+/g zeolite. Natural zeolites, depending on the degree of substitution of silicon by aluminium, have the capacity cation exchange from 1 to 4 mmol M+/g of zeolite. These are higher values of CEC most of the other sorbents.

The structure of zeolites can be represented in many ways, each starting from TO_4 tetrahedron as primary building units. The tetrahedra are further connected to form 4-, 5-, 6-, 8-, 10-, and 12-membered rings or secondary building units (SBUs) [33, 34]. By connecting the SBUs, cages are formed, which are further interconnected, forming channels in the structure. The diversity of the arrangement of cages in space conditions the formation of different zeolite structures, as shown in Fig. 14.1, as presented by Weitkamp [35] in his paper, summarizes the literature data.

For example, the Linde type A structure belonging to the zeolite group 3, shown in Fig. 14.2, is composed of the so-called sodalite or β-cages and double four-membered rings (D4P), which form a characteristic channel and cavity system. There are eight β-cages arranged on the horns of the cube, while in the center of the cube there is the largest cavity in the lattice, called the α-cage, Fig. 14.2. Variable cations M, as shown in the general zeolite formula, occupy positions located at the interface of the α- and β-cage contact [36]. Of all zeolites, the most produced is zeolite A.

This book belongs to Badji Mokhtar Annaba University Central Library Copyright Elsevier 2025

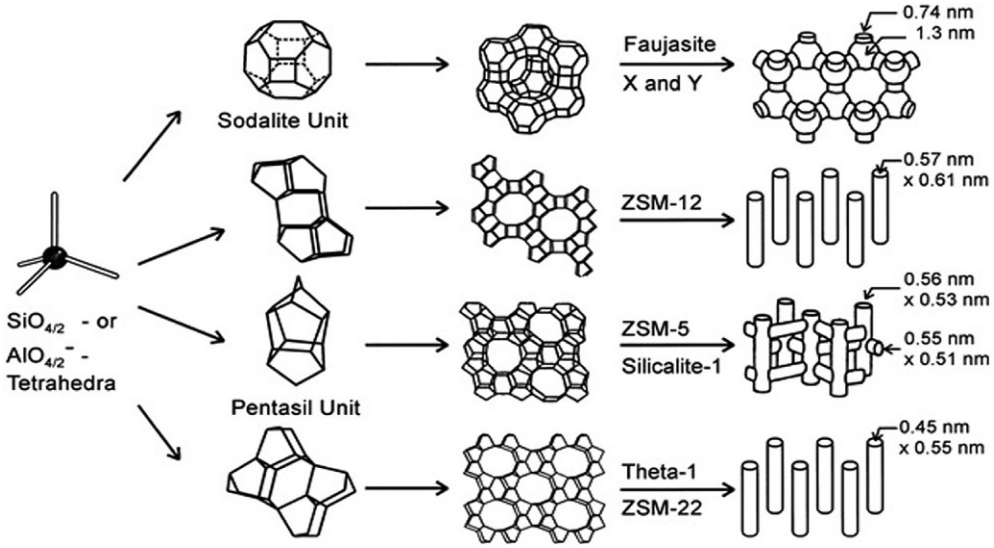

Fig. 14.1

Structures of some zeolites and their micropore systems and dimensions. *Reprinted with permission from J. Weitkamp, Zeolites and catalysis, Solid State Ionics 131 (2000) 175–188, https://doi.org/10.1016/S0167-2738(00)00632-9.*

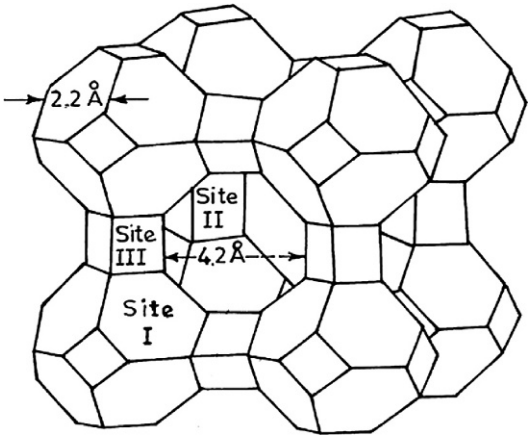

Fig. 14.2

Structure of zeolite molecular sieve-A showing site locations of cations. *Reprinted with permission from V.K. Kaushik, R.P. Vijayalakshmi, N.V. Choudary, S.G.T. Bhat, XPS studies on cation exchanged zeolite A, Microporous Mesoporous Mater. 51 (2002) 139–144, https://doi.org/10.1016/S1387-1811(01)00473-5.*

Zeolites crystallize so that extremely regular pores and channels appear in them, allowing only certain types of ions and water molecules to pass through such a structure [24, 37]. The microporous and mesoporous structures of zeolites make them suitable for use as sorbents [38].

This book belongs to Badji Mokhtar Annaba University Central Library Copyright Elsevier 2025

Zeolites form a group of about 200 different types of minerals. Zeolites can be natural and synthetic. Although more than 40 known accessory zeolites have been isolated, only seven (mordenite, clinoptilolite, cabazite, erionite, fererite, ifilipsite, and analcime) are present in sufficient quantity and adequate purity in nature because they are economically viable for exploitation [39]. The number of synthetic zeolites is much higher and amounts to about 160, of which a smaller number is produced and has practical applications [31, 40]. Natural zeolites are divided into seven major groups: group 1 (analcime—ANA; laumontite—LAU; phillipsite—PHI), group 2 (erionite—ERI), group 3 (zeolite A), group 4 (chabazite—CHA), group 5 (natrolite—NTA), group 6 (mordenite—MOR), and group 7 (heulandite—HEU; clinoptilolite—CLI). For group 1, the exchangeable cations are Na, K, Ca, Rb, Cs, for group 2 are K, Na, Ca, Mg, for group 4, 5, and 6 exchangeable cations are Na, Ca, K, and for group 7 are Na, K, Ca, Sr, Ba. The groups are defined according to their crystal structure, morphology, physical characteristics, pathways of formation of secondary units in the three-dimensional structure, free pore volume, and type of exchangeable cations in the zeolite structure. Each time a new zeolite structure is reported, it is reviewed by the structure committee of the International Zeolite Association (IZA-SC) and, if found to be unique, is assigned a three-letter structure code, such as CLI, MOR, ANA, etc. This code is part of the official IUPAC nomenclature of microporous materials [31]. Useful information about the structure of the zeolite can be found on the website of "Database of Zeolite Structures" (http://www.iza-structure.org/databases/) and the website of "IZA International Zeolite Association" (http://www.iza-online.org/). The chemical formulas of some natural and some synthetic zeolites are given in Table 14.1.

Bare et al. [24], Fig. 14.3, have presented a synthetic route for the US-Y zeolite, starting from the Na-Y over NH_4,H-deAl-Y, with a multiple Na^+ ion exchange and with a regime by appropriate calcination. Thus, the zeolites NaY, NH_4 H-deAl-Y, and US-Y showed Si/Al ratios of 3.0, 2.0, and 1.3, respectively. The authors then presented the results from the synthesized zeolites in their detailed study using X-ray diffraction (XRD) and X-ray photoelectron spectroscopy (XPS) analysis, variable kinetic energy XPS analysis, and a low-energy ion-scattering study. The results of such studies provide a detailed monitoring of the structure of the synthesized zeolites, which makes it easier to understand the application of zeolites themselves in water treatment.

Shamsudin et al. [41] listed in Table 14.2 the prices per kilogram of commonly used materials as sorbents, thus confirming that zeolites are among the cheapest materials.

14.2.2 Characterization of zeolites

For the complete characterization of zeolites, a large number of analytical and instrumental techniques are generally used, due to the very complex mineralogical composition of natural zeolites and the consequence of the uneven distribution of the various phases and elements in the zeolite material.

This book belongs to Badji Mokhtar Annaba University Central Library Copyright Elsevier 2025

Table 14.1 Chemical oxide formula of some natural and synthetic zeolites.

Natural zeolites		Synthetic zeolites	
Name	**Typical unit-cell formula**	**Name**	**Typical unit-cell formula**
Analcime	$Na_{16}(Al_{16}Si_{32}O_{96})\cdot 16H_2O$	**Zeolites A**	$Na_2O\cdot Al_2O_3\cdot 2SiO_2\cdot 4.5H_2O$
Chabazite	$Ca_2(Al_4Si_8O_{24})\cdot 12H_2O$	**Zeolites N-A**	$(Na, TMA)_2O\cdot Al_2O_3\cdot 4.8SiO_2\cdot 7H_2O$
Clinoptilolite	$(Na,K)_6(Al_6Si_{30}O_{72})\cdot 20H_2O$	**Zeolites H**	$K_2O\cdot Al_2O_3\cdot 2SiO_2\cdot 4H_2O$
Erionite	$NaK_2MgCa_{1.5}(Al_8Si_{28}O_{72})\cdot 28H_2O$	**Zeolites L**	$(K_2Na_2)O\cdot Al_2O_3\cdot 6SiO_2\cdot 5H_2O$
Faujasite	$Na_{20}Ca_{12}Mg_8(Al_{60}Si_{132}O_{384})\cdot 235H_2O$	**Zeolites X**	$Na_2O\cdot Al_2O_3\cdot 2.5SiO_2\cdot 6H_2O$
Ferrierite	$(Na,K)Mg_2Ca_{0.5}(Al_6Si_{30}O_{72})\cdot 20H_2O$	**Zeolites Y**	$Na_2O\cdot Al_2O_3\cdot 4.8SiO_2\cdot 8.9H_2O$
Heulandite	$(Na,K)Ca_4(Al_9Si_{27}O_{72})\cdot 24H_2O$	**Zeolites W**	$K_5Ca_2(H_2O)_{24}[Al_9Si_{23}O_{64}]$
Laumontite	$Ca_4(Al_8Si_{16}O_{48})\cdot 16H_2O$	**Zeolites O**	$(Na_2, K_2, TMA_2{}^{a})O\cdot Al_2O_3\cdot 7SiO_2\cdot 3.5H_2O$
Mordenite	$Na_3KCa_2(Al_8Si_{40}O_{96})\cdot 28H_2O$	**Zeolites P**	$Na_2O\cdot Al_2O_3\cdot 2–5SiO_2\cdot 5H_2O$
Natrolite	$Na_{16}(Al_{16}Si_{24}O_{80})\cdot 16H_2O$	**Zeolites Ω**	$(Na, TMA^{a})_2O\cdot Al_2O_3\cdot 7SiO_2\cdot 5H_2O$
Phillipsite	$K_2(Ca_{0.5},Na)_4(Al_6Si_{10}O_{32})\cdot 12H_2O$	**Zeolites ZK-4**	$0.85Na_2O\cdot 0.15(TMA^{a})2O\cdot Al_2O_3\cdot 3.3SiO_2\cdot 6H_2O$
Wairakite	$Ca_8(Al_{16}Si_{32}O_{96})\cdot 16H_2O$	**ZSM-5**	$Na_nAl_nSi_{96-n}O_{192}\cdot 16H_2O$ $(0 < n < 27)$

[a]$TMA–(CH_3)_4N^+$.

Modified from J. Wen, H.R. Dong, G.M. Zeng, Application of zeolite in removing salinity/sodicity from wastewater: a review of mechanisms, challenges and opportunities, J. Clean. Product. 197 (2018) 1435–1446, https://doi.org/10.1016/j.jclepro.2018.06.270; D. Georgiev, B. Bogdanov, K. Angelova, I. Markovska, Y. Hristov, Synthetic zeolites – structure, classification, current trends in zeolite synthesis – review, in: Paper Presented at the Economics and Society Development on the Base of Knowledge International Science Conference, Stara Zagora, Bulgaria, 2009. https://www.semanticscholar.org/paper/SYNTHETIC-ZEOLITES-STRUCTURE-%2C-CLASIFICATION-%2C-IN-Georgiev-Bogdanov/75641030be4773302a3002971eee6d17bce5c356.

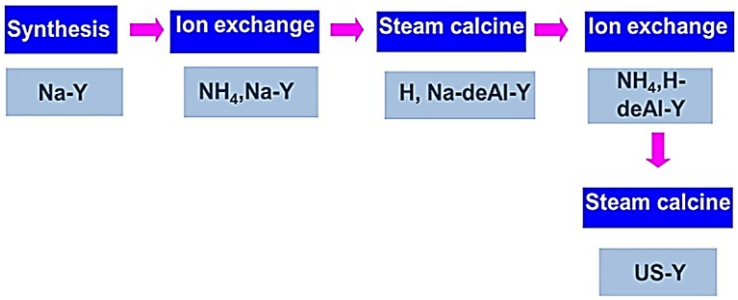

Fig. 14.3

Schematic illustrating the processing of the parent zeolite leading to the other zeolite samples studied. *Reprinted with permission from S.R. Bare, A. Knop-Gericke, D. Teschner, M. Hävacker, R. Blume, T. Rocha, R. Schlögl, A.S.Y. Chan, N. Blackwell, M.E. Charochak, R. ter Veen, H.H. Brongersma, Surface analysis of zeolites: an XPS, variable kinetic energy XPS, and low energy ion scattering study, Surf. Sci. 648 (2016) 376–382, https://doi.org/10.1016/j.susc.2015.10.048.*

This book belongs to Badji Mokhtar Annaba University Central Library Copyright Elsevier 2025

Table 14.2 Cost of different sorbents.

Adsorbent	Price (US$/kg)
Bentonite	0.005–0.46
Zeolite	0.03–0.07
Titanium dioxide	0.2
Zinc oxide	0.23–0.28
Calcium carbonate	145
Chitin	5–20
Chitosan	15.43
Activated carbon	20–22

Reprinted with permission from M.S. Shamsudin, S.F. Azha, M. Shahadat, S. Ismail, Cellulose/bentonite-zeolite composite adsorbent material coating for treatment of N-based antiseptic cationic dye from water, J. Water Process Eng. 29 (2019) 100764, https://doi.org/10.1016/j.jwpe.2019.02.004.

The chemical composition of natural and modified zeolites is determined by atomic absorption spectroscopy (AAS). Samples were previously subjected to alkaline melting and evaporation. The CEC of natural and modified zeolites is determined by the standard ammonium acetate method. The amount of exchangeable cations (K^+, Na^+, Mg^{2+}, Ca^{2+}, and Fe^{3+}) is determined by AAS.

XRD enables the quantitative determination of the mineralogical composition (phase composition) of zeolite materials, including the type of zeolite, and is crucial for further applications of natural zeolite. Some methods for using XRD are standardized, such as ASRM D 3906:2019 [42] and ASTM D3942:2019 [43]. The size and morphology of crystals in zeolite samples have been commonly studied by scanning electron microscope (SEM) and transmission electron microscopy [44], followed by an analysis system, whose work is based on an energy dispersive X-ray spectroscopy (EDXS) analysis system, which is linked to an electron microscope, which captures the sample. An obvious advantage of the EDXS basic analysis over conventional chemical analysis is that we can obtain the basic composition of the selected phase in the material and not just in the sample mass. The average basic composition of the sample, using EDXS, was usually obtained from the surface data of the sample with three or more different photographs.

Basic information, on the accessibility of pores for ions and molecules, can be obtained by Brunauer-Emmett-Teller (BET) assays based on nitrogen physisorption. This determines the textural characteristics of natural and modified zeolites as determined by adsorption/desorption of gaseous nitrogen at liquid nitrogen temperature (−196°C). The samples are placed in a vacuum in order to release the gas in a certain time interval. Specific surface area of the samples was calculated based on BET equations (S_{BET}). The total pore volume (TPV) was determined from the desorption isotherm. BET values are usually in the range of 15–40 $m^2\ g^{-1}$ [45–47].

This book belongs to Badji Mokhtar Annaba University Central Library
Copyright Elsevier 2025

The concentration of acid centers in the zeolite lattice is usually determined by Fourier-transform infrared spectroscopy (FTIR) by treating the zeolite sample with a strong base, most commonly pyridine. Pyridine binds to the Lewis and Brønsted acid centers, resulting in the appearance of characteristic vibrational bands; the vibrational band at 1455 cm^{-1} corresponds to the interaction of the pyridine with the Lewis acid center, while the band at about 1540 cm^{-1} originates from the bond that the pyridine attains with the Brønsted proton [35, 48–50].

Thermal analysis, thermogravimetric-differential thermal analysis (TG-DTG) makes it easy to determine whether a monolayer or bilayer has formed on the zeolite surface. For zeolites with a bilayer, two peaks are observed on the DTG curve, with peaks at about 200°C and 400°C, corresponding to the breaking of the bonds between the surfactant layers and the breaking of the bond between the surfactant and the zeolite surface, respectively. When the surfactant formed a monolayer on the surface of the zeolite, only one peak at 400°C was observed on the DTG curve corresponding to the disconnection between the surfactant and the zeolite [44, 51].

XPS uses low-energy X-ray photons (usually Kα aluminum or magnesium) to ionize surface atoms, and the energy of the ejected electrons is measured. This method provides information on the bonding of chemical elements in materials. Also, this method can be used to monitor the oxidation process of chemical elements on the zeolite surface [24, 36, 52–54].

14.3 Sorption of metal cations on zeolites and ion exchange

At the contact of the solution and the solid phase, the zeolite, various physicochemical processes take place, which include the interactions of both the solvent and the solute with the zeolite. The most common types of interactions between aqueous solutions of cations and inorganic sorbents, zeolites, are protonization/deprotonization of surface functional groups of sorbents, ion exchange, complex formation with surface functional groups of sorbents, and dissolution/precipitation. These processes often take place simultaneously, so it is difficult to determine which ion removal process is dominant or to determine the proportion of individual mechanisms.

14.3.1 Possible sorption and ion-exchange mechanisms

To describe the sorption of ionic species on the solid phase, a model of surface complexation is most commonly used, whereby during the interaction of ions and the surface, bonds of different strengths are formed, weak physical bonds and the formation of electrostatic outer sphere complexes, chemical interactions involving the construction of inner sphere complexes. Construction of the inner sphere complex involves mechanisms of ligand alteration, the establishment of a covalent bond, a hydrogen bond, steric or orientation effects. The construction of the outer sphere complex is usually referred to as nonspecific sorption, while the construction of the inner sphere complex represents specific sorption [55].

This book belongs to Badji Mokhtar Annaba University Central Library Copyright Elsevier 2025

External sphere complexes occur if at least one solvent molecule (water) is located between the charged surface functional group (Si/Al—OH_2^+ or Si/Al—O^-) and the bound ion. Internal sphere complexes are formed when the sorbed ions form a direct coordinate-covalent bond with the Si/Al—OH surface functional groups, regardless of the nature of the surface charge. Inner sphere complexes can be formed with 1:1 stoichiometry, forming mono-complexes, or with 1:2 stoichiometry, forming bi-complexes [55].

During the process of sorption of M^{z+} metal ions on the zeolite, complexes are first formed that capture ion-exchange reactions (nonspecific sorption) between M^{z+} from the solution and alternating ions from the zeolite structure (mainly Na^+ and Ca^{2+}) that pass into the solution [56]. The process of ion exchange depends on the size of the hydrated ions, concentration, and the charge of the ions. Ions with a smaller hydrated radius penetrate more easily into the pores of zeolites that house exchangeable cations, so that the power of exchange is greater, the lower the degree of hydration. Also, with higher charge ions, the degree of ion exchange is higher [57, 58]. As the sorption process progresses, metal ions also bind to the inner active sites of the zeolite, forming complexes of the inner sphere. The complexes thus formed are more stable due to the formation of a stronger covalent bond. The formation of these complexes can be represented by reactions from Eqs. (14.1) to (14.3), in which Si/Al denotes Si or Al from the zeolite structure and CE is a cation exchangeable [59]:

Inner sphere complexes, reactions (14.1) and (14.2):

$$\equiv \mathrm{Si/Al\text{-}OH} + \mathrm{M}^{z+} \rightleftarrows \equiv \mathrm{Si/Al\text{-}OM}^{(z-1)+} + \mathrm{H}^+ \tag{14.1}$$

$$\equiv 2\mathrm{Si/Al\text{-}OH} + \mathrm{M}^{z+} \rightleftarrows \equiv (\mathrm{Si/Al\text{-}O})_2\mathrm{M}^{(z-2)+} + 2\mathrm{H}^+ \tag{14.2}$$

Complexes of the outer sphere, reaction (14.3):

$$\equiv (\mathrm{Si/Al\text{-}O}^-)_z \cdots z/n\,\mathrm{C}^{n+} + \mathrm{M}^{z+} \rightleftarrows \equiv (\mathrm{Si/Al\text{-}O}^-)_z \cdots \mathrm{M}^{z+} + z/n\,\mathrm{CE}^{n+} \tag{14.3}$$

Complexation of the outer sphere is generally a stoichiometric, fast, and reversible process, whereas the complexation of the inner sphere is slower and can be considered as a nonreversible reaction. Generally, when metal ions are sorbed on the zeolite, complexes of both the outer and inner spheres are formed. Most M^{z+} metal ions can form complexes with anionic ligands that are possibly present in the solution.

The mechanisms of sorption of metal ions from a solution are dependent on the pH of the solution, because during the H^+ process, ions participate in many reactions both in solution and in the solid phase. An explanation for the movement of H^+ ions could be given if it is accepted that H^+ ions from all sources (released from the solid phase, sorbed, and added to the solution from external sources) are components of equilibrium [59], Eq. (14.4):

$$\mathrm{H}^+(\mathrm{s}) \rightleftarrows \mathrm{H}^+(\mathrm{aq}) \tag{14.4}$$

This book belongs to Badji Mokhtar Annaba University Central Library
Copyright Elsevier 2025

H^+ (aq) ions sorbed by zeolites cause protonation of surface functional groups (Si/Al is either Si or Al), Eqs. (14.5)–(14.7):

$$\equiv S\text{—}OH + H^+ \rightleftarrows \equiv S\text{—}OH_2^+ \tag{14.5}$$

$$\equiv S\text{—}O^- + H^+ \rightleftarrows \equiv S\text{—}OH \tag{14.6}$$

$$\equiv Si\text{—}O^-\text{—}Al\equiv \overset{H^+}{\leftrightarrow} \equiv Si\text{—}OH\text{—}Al\equiv \overset{H^+}{\leftrightarrow} \equiv S\text{—}OH_2^+\text{—}Al\equiv \tag{14.7}$$

On the other hand, the released H^+ ions are formed as a result of the formation of the inner sphere complex (Eqs. 14.1 and 14.2), ion exchange (Eq. 14.3), or deprotonation of surface functional groups at pH > pH_{tnn}.

In general, lowering the pH of the solution decreases the sorption of the metal cation due to increased protonization (increase of positive charge of the sorbent), decrease of the possibility of formation of the inner sphere complex, and "competition" of H^+ ions for a variable place in the zeolite structure [18]. On the other hand, the increase in pH increases sorption mainly due to the decrease in the positive charge, that is, the increase of the negative charge of the surface and the deposition of metal hydroxide on the sorbent surface. In addition to its effect on sorption, the pH value of the solution also affects the stability of zeolites in the aqueous medium, especially in the case of zeolites with low Si content, which are unstable in the acidic environment due to the leaching of aluminum. When balancing the zeolite with solutions of the acidic and near-neutral medium, the aluminum leaches by reaction (14.8):

$$\equiv Al\text{—}OH + H^+ \rightleftarrows \equiv Al\text{—}OH_2^+ \leftrightarrow Al^{3+} + H_2O \tag{14.8}$$

The result of reaction (14.8) is an increase in the pH of the solution. When Al^{3+} ion crosses into solution, hydrolysis reaction, reactions (14.9) and (14.10) occur:

$$Al^{3+} + H_2O \rightleftarrows Al(OH)_2^+ + H^+ \tag{14.9}$$

$$Al(OH)_2^+ + H_2O \rightleftarrows Al(OH)_2^+ + H^+ \tag{14.10}$$

Reactions (14.9) and (14.10) produce an H^+ ion, which lowers the pH of the solution. It is evident that the final concentration of H^+ ions, measured at equilibrium, represents the mean of the concentration of H^+ ions sorbed according to reaction (14.8) and the concentration of H^+ ions released according to reactions (14.9) and (14.10).

Under alkaline experimental conditions, the lack of H^+ ions in solution leads to the inhibition of Al dissolution. However, under neutral or bases conditions [60], the presence of OH^- initiates the leaching of Al, and a final product is a precipitate of $Al(OH)_3$ where express with the reactions from (14.11) to (14.13):

$$Al^{3+} + OH^- \rightleftarrows Al(OH)_2^+ \tag{14.11}$$

This book belongs to Badji Mokhtar Annaba University Central Library

Copyright Elsevier 2025

$$Al(OH)_2^+ + OH^- \rightleftarrows Al(OH)_2^+ \tag{14.12}$$

$$Al(OH)_2^+ + OH^- \rightleftarrows Al(OH)_3 \downarrow \tag{14.13}$$

Generally, silicon dissolution takes place under conditions of both acidic and basic environments, with the minimum dissolution at pH equal to pHtnn. The dissolution of Si is higher at basic pH values because the Si—O bonds are polarized and weakened by the presence of the charged ≡Si—O$^-$ surface group, which eventually leads to the leaching of silicon atoms [60].

Wibowo et al. [61] have explained the mechanism of adsorption on the clinoptilolite surface using the electrical double layer theory. According to this theory, there is an electric double layer around the zeolite dispersed in solution. The first layer of the zeolite attracts positive ions bound by Van der Waals forces and repels negative ions by electrostatic repulsion, Fig. 14.4. The second layer is a diffuse layer with a poorer electrical potential than the first layer, which still attracts negatively charged particles; nevertheless, the formed entities are stable. Outside the diffuse layer, the ions move freely. The zeta potential occurs when the total electrical potential is reduced to zero and then the adsorption process ceases, Fig. 14.3 [3, 61].

14.3.1.1 Types of adsorption isotherms

The adsorption isotherm is essential to describe the phenomenon of retention or release, that is, the mobility of a substance from a liquid or gaseous environment to a solid phase at a constant temperature and pH [62, 63]. The adsorption equilibrium or the ratio of adsorbed to the residual amount of adsorbate in solution is established when the phase containing the adsorbate has been in contact with the adsorbent for a certain period of time, has been in equilibrium with the concentration of adsorbate in solution and represents a dynamic equilibrium at the phase boundary [64]. Table 14.3 lists the most commonly used adsorption isotherm models with formulas, descriptions, determining factors, and operating conditions.

In general terms, the mathematical correlation that plays an important role with respect to the modeling steps, the operational design, and the practical applicability of adsorption systems is described graphically, by expressing the solid phase concentration against the remaining concentration in solution [65]. The physicochemical parameters of the adsorbents, together with the associated thermodynamic assumptions, provide insight into the adsorption mechanism, surface properties as well as the degree of affinity of the adsorbents [41, 66].

Based on the adsorption isotherms, it is relatively easy to determine whether it is possible to apply a particular adsorbent for adsorption. In the case of liquid phase adsorption, the equilibrium adsorption isotherms represent the dependence of the adsorbed amount of matter on the equilibrium concentration of adsorbates in solution.

This book belongs to Badji Mokhtar Annaba University Central Library Copyright Elsevier 2025

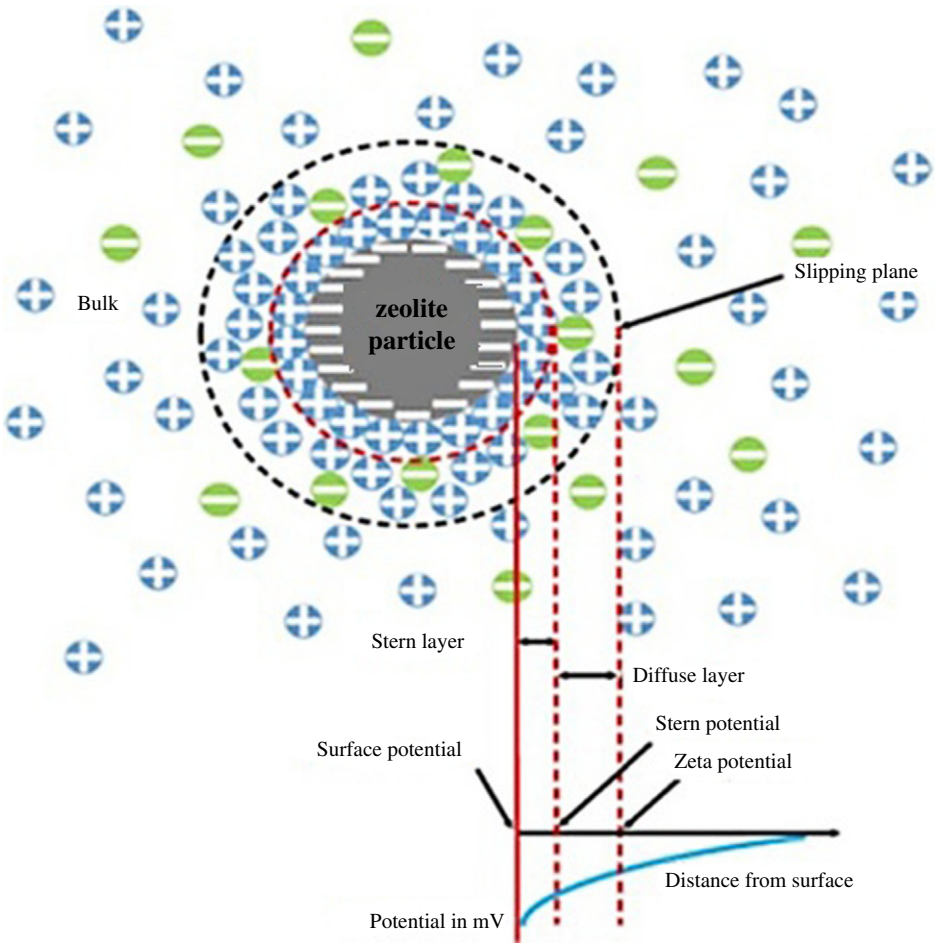

Fig. 14.4
Illustration of the adsorption mechanism of ions onto the zeolite surface. *Reprinted with permission from E. Wibowo, M. Rokhmat, K. Sutisna, M. Abdullah, Reduction of seawater salinity by natural zeolite (Clinoptilolite): adsorption isotherms, thermodynamics and kinetics, Desalination 409 (2017) 146–156, https://doi.org/10.1016/j.desal.2017.01.026.*

14.3.1.2 Adsorption kinetics

Adsorption kinetics provides insight into the reaction rate and the sorption mechanism involving mass transfer, diffusion, and reaction on the adsorbent surface during adsorption. The process of adsorption of adsorbates from aqueous solutions to the adsorbent consists of several phases such as: external mass transfer over the boundary layer or diffusion film between the liquid phase and the outer surface of the adsorbent; diffusion that takes place in the adsorbent particles whereby the adsorbate solution enters the adsorbent pores; the formation of physical or chemical bonds of the adsorbate at the active centers in the pores of the adsorbent [67, 68].

This book belongs to Badji Mokhtar Annaba University Central Library Copyright Elsevier 2025

Table 14.3: Determining factors of adsorption isotherms.

Adsorption model[a]	Description	Deter. factor	Condition
Langmuir isotherm $q_e = k_L C_e q_{max}/1 + k_L C_e$	Based on the assumption, adsorption occurs on a homogeneous surface which each molecule own constant enthalpies and sorption activation energy without interaction between adsorbed molecules; monolayer adsorption	Separation factor R_L: $R_L = 1/1 + k_L C_i$	$R_L > 1$, unfavorable adsorption $R_L = 1$, linear adsorption $R_L = 0$, irreversible adsorption $0 < R_L < 1$, favorable adsorption
Freundlich isotherm $q_f = k_f C_e^{1/n}$	Based on the assumption that the adsorption occurs on a heterogeneous surface with interaction between adsorbed molecules	N	$n = 1$, linear adsorption $n < 1$, favorable adsorption $n > 1$, unfavorable adsorption The smaller of $1/n$, the greater of expected heterogeneity
Temkin isotherm $q_e = B_T \ln(A_T C_e)$	Based on the assumption that the decrease in the heat of adsorption of all molecules in the surface layer is linear; uniform distribution of binding energies	B_T	$B_T < 8$ kJ mol^{-1}, physical adsorption
Dubinin-Radushkevich isotherm $q_e = q_s \exp(-\beta\varepsilon^2)$	Based on Gaussian energy distribution onto a heterogeneous surface	Energy E: $E = \frac{1}{\sqrt{2\beta}}$	$E < 8$ kJ mol^{-1}, physical adsorption $8 < E < 16$ kJ mol^{-1}, chemical adsorption

[a]Where q_e (mg g^{-1}) refers to the adsorption capacity at equilibrium; k_L refers to the equilibrium constant of Langmuir model; q_{max} (mg g^{-1}) refers to the maximum adsorption capacity; k_f (mg g^{-1}) refers to Freundlich isotherm constant, which is an approximation indicator of adsorption capacity; n refers to adsorption intensity; A_T is an equilibrium binding constant; B_T refers to a Temkin isotherm constant; T(K) is the absolute temperature; R is the gas constant (8.314×10^{-3} kJ/K mol); q_s refers to theoretical isotherm saturation capacity; b refers to Dubinin-Radushkevich isotherm constant; and ε refers to the Polanyi potential (J/mol).

Reprinted with permission from J. Wen, H.R. Dong, G.M. Zeng, Application of zeolite in removing salinity/sodicity from wastewater: a review of mechanisms, challenges and opportunities, J. Clean. Product. 197 (2018) 1435–1446, https://doi.org/10.1016/j.jclepro.2018.06.270.

The most common kinetic models used to monitor the kinetics of adsorption processes are Lagergren's pseudo-first-order model and Ho's pseudo-second-order model, while interfacial and particle diffusion models are most commonly used to determine the mechanism of adsorption [69, 70].

14.3.1.3 Thermodynamics of adsorption processes

Thermodynamic analysis of adsorption processes is performed at different temperatures, primarily by calculating the standard Gibbs free energy [71]. The enthalpy and adsorption entropy are calculated using the thermodynamic relation for Gibbs free energy. The spontaneity of the adsorption process can be seen from the value of Gibbs free energy [72]. A negative value

This book belongs to Badji Mokhtar Annaba University Central Library Copyright Elsevier 2025

of this size suggests that the adsorption process is spontaneous, that is, the system uses its own energy for the process of adsorption [41, 73].

14.3.2 Factors affecting the sorption process

In the solid-liquid system, the nature of the sorption (surface development, pore size distribution, functional group content, impurity content, regeneration ability) and the nature of the sorbate (size, structure, and shape of molecules/ions, polarity, dissociation ability) have an impact on the sorption process, pH of solution, and presence of other ions in solution, temperature, etc.

The most important properties of the solid sorbent are chemical and phase composition, structure, specific surface area, and porosity. Porosity is one of the most important characteristics of zeolites. The TPV in the zeolite structure is about 35%, which indicates the openness of the lattice itself and the adsorption capacity of the zeolite. The specific surface area of porous materials is determined by a method that measures the volume of adsorbed gas at different pressures to produce adsorption isotherms. The analysis of the obtained data is done by calculating by specific surface area, volume, and surface area of the micropore and mesopores, and the pore size distribution. The specific surface area of the zeolite can also be 700 $m^2\ g^{-1}$, while the TPV of the zeolite ranges from 0.1 to 0.35 $cm^3\ g^{-1}$ [74].

An essential characteristic of solid sorbents for sorption from an electrolyte solution is the zero charge point. The zero charge point represents that pH value at which the solid phase surface charge density is zero ($pH = pH_{tnn}$). This characteristic of the solid phase is a function of the number of positively and negatively charged surface groups. If the pH value of the electrolyte solution is equal to pH_{tnn}, then the number of charged surface centers is equal to zero or there is a certain number of charged centers, but the number of positively charged centers is equal to the number of negatively charged centers. In case the pH of the electrolyte solution is lower than pH_{tnn}, the solid phase surface is positively charged as a result of the association of H^+ ions from the solution with the surface functional groups of the sorbate [49, 75]. If the pH of the solution is higher than pH_{tnn}, the surface is negatively charged due to the dissociation of surface hydroxyl groups. In either case, the resulting positive or negative charge is offset by the excess of the collected counter ions in the double electric layer region, Fig. 14.4 [3, 61]. The point of zero charge is determined by the surface properties of natural and modified zeolites. The zero charge point is determined by the balancing method. The process consists in balancing a certain volume of a solution of an indifferent electrolyte of a certain ionic strength and pH and a certain amount of powder of the test sample [76].

Specific sorption, which involves the formation of ion pairs and the construction of surface complexes between sorbates and active sites on the surface of a solid sorbent, shifts the zero charge point toward lower pH values in the case of specific cation sorption, or higher pH values in the case of specific anion sorption. Specific sorption of cations reduces the number of

This book belongs to Badji Mokhtar Annaba University Central Library Copyright Elsevier 2025

available sites on the surface of the sorbent for sorption of H^+ ions, leaving an excess of H^+ ions in the aqueous solution, which leads to a decrease in the pH value and, consequently, the pH_{tnn}. The specific sorption of anions reduces the number of available sites on the surface of the sorbent for sorption of OH-ions, leaving an excess of OH-ions in the aqueous solution, which leads to an increase in pH and, consequently, pH_{tnn} [77].

The solubility of adsorbates is of paramount importance for sorption. The degree of sorption is inversely proportional to the solubility of the sorbate in the liquid phase from which the sorption takes place. This dependence can be explained by the need to disconnect the sorbate-liquid phase, as a prerequisite for sorption to occur. The ion will be better sorbed if the surface has the opposite charge or if it builds a heavy soluble compound on the surface of the sorbent. The sorption of metal ions on the solid phase surface is also affected by the electronegativity of the metal. The greater the electronegativity of the metal, the stronger the connection that is established between a metal ion and an oxygen atom in surface groups [78–80].

The pH value of the aqueous solution is an important parameter for controlling the sorption process. Knowledge of the effect of pH is essential for the removal of certain pollutants from water, and especially metal ions [81], because the pH of the solution affects both the degree of ionization and surface charge of the sorbent and the ionic species found in solution. Depending on the pH, metal ions are present in various chemical forms in water. For all metals there is an optimum pH value at which the maximum efficiency of removal occurs [82]. Most metal ions (M^{z+}) can form complexes with inorganic ligands such as the OH^- ion, and the degree of complex formation depends on the pH of the solution. The fact that both hydrogen and hydroxyl ions are easily sorbed indicates that the pH of the solution greatly influences the sorption process [79,83].

14.3.3 Principles of ion exchange on zeolites

Ion exchange means reversible ion exchange between a solid and a solution. During ion exchange, the ions from the solution bind to a zeolite, which releases a stoichiometrically equivalent amount of ions of the same charge. The ion exchanger, the zeolite, is built as a three-dimensional skeleton on which positive or negative electrical charges are fixed. The skeleton creates a semipermeable system into which ions diffuse. The exchanger, the zeolite, is electrically neutral because the fixed ions bound to the skeleton of the exchanger are offset by the moving ions of the opposite electric charge [14,84,85].

When the zeolite, as a natural ion exchanger, comes into contact with a solution of ions other than moving ions bound to the exchanger, the ions will penetrate the ion exchanger grain until equilibrium is reached. This equilibrium is known as the Donnan equilibrium. The exchange of ions between the exchanger and the electrolyte solution can only occur between the ions of the same charge and is reversible. This means that cations are exchanged

This book belongs to Badji Mokhtar Annaba University Central Library Copyright Elsevier 2025

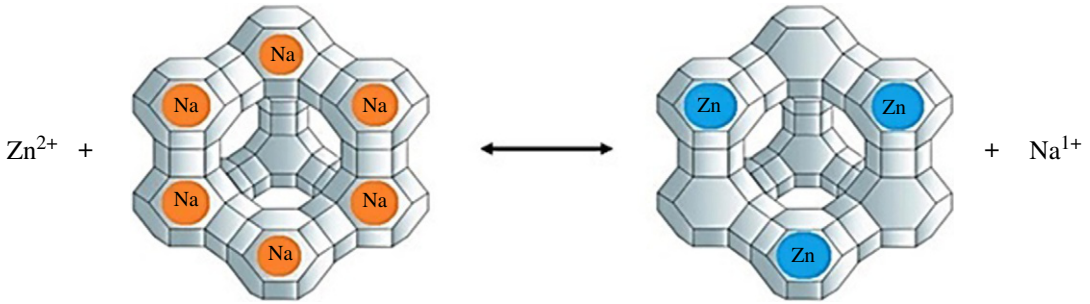

Fig. 14.5
Ion-exchange mechanism of zeolite Y. *Reprinted with permission from R. Tekin, N. Bac, Antimicrobial behavior of ion-exchanged zeolite X containing fragrance, Microporous Mesoporous Mater. 234 (2016) 55–60, https://doi.org/10.1016/j.micromeso.2016.07.006.*

with cations and anions are exchanged with anions. Depending on whether the cations or anions are exchanged, the exchangers can be divided into cationic and anionic [14,85]. Tekin and Bac [86] have shown in Fig. 14.5, in a simple way, the mechanism of ion exchange of Cu^{2+} and Na^{+} on the zeolite.

The ion exchange can take place in a column filled with an ion exchanger, and after saturation of the active groups of the exchanger with ions from the solution, the ion exchanger is regenerated with a solution of the dissolved ion dissolving agent for the exchanger, thereby retranslating the exchanger to its initial ionic form [13,14,21,87].

14.3.4 Organic cation sorption on zeolites

As zeolites contain hydrated inorganic cations, their surface is hydrophilic and shows no affinity for hydrophobic weakly polar organic molecules. In order for the zeolite to be used for the sorption of polar and weakly polar organic pollutants, it is necessary to modify the zeolite with surfactants. Namely, the exchangeable cations on the surface of the zeolite can be replaced by long-chain organic cations, whereby an organo-mineral complex whose surface is hydrophobic is formed, allowing the sorption of chemical species that could not be sorbed on the natural zeolite. The dimensions of long-chain organic cations are almost always several times larger than the dimensions of clinoptilolite channels so that their sorption occurs only on the outer surface of the mineral [34,88]. At concentrations of less than the outer capacity of the cation, an organic cation to the surface of the zeolite binds by electrostatic interactions with the negatively charged surface, while in a higher concentration of organic cations on the external capacity cation, leads to the formation of the bilayer, such that the second layer is bound by hydrophobic interaction to the first [49,89].

This book belongs to Badji Mokhtar Annaba University Central Library Copyright Elsevier 2025

The sorption of pollutants on the corresponding mineral depends both on the sorbent properties, such as crystal structure, total charge and charge distribution, sorbent pore size, surface availability and the like, and on the properties of the pollutant itself [90]. Thus, for example, it is known that the pH of the medium plays an important role in the sorption of the cation due to its effect on the metal ions in the solution and also on the ionization of the chemically active sites on the sorbent. Fiol and Villaescusa [91] showed that the total charge of the sorbent surface can play a very important role in sorption processes, so determining the protonization and deprotonization behavior of sorbent in aqueous solutions may be useful to explain the mechanism of sorption of a specific pollutant; the pH at which the concentration of negative and positive charges on the sorbent surface is equal, i.e., the total amount of surface charge equals zero, represents the zero charge point, pH_{pzc}, Fig. 14.4 [49, 75].

14.4 Essential characteristics of zeolites and modification processes

Zeolites are inactive in nature. Their adsorption capacity and CEC are activated by mechanical processing, crushing, and grinding. Zeolites are characterized by a structure with cavities and channels that house active centers that can sorb harmful or useful components. Active centers in zeolites can serve as binding sites for some new compounds, giving these minerals new characteristics, which greatly expands their application. Activated zeolite is used as an ecological preparation for a variety of purposes, as mentioned in the Introduction to this paper. In the chemical industry, synthetic zeolites are most commonly applied, with well-defined properties that are in accordance with the requirements of a given process. The use of zeolites involves a wide variety of human activities, and has lately been the most widely used in the field of environmental protection. The cation exchange property has been used to apply zeolites as a sorbent for water treatment. Zeolites can be used as a cation exchanger to remove heavy metals from wastewater, to remove ammonia from drinking water, to remove radioactive cations from radioactive waste liquids, to regulate water hardness, etc.

14.4.1 Physicochemical properties of zeolites

Zeolites from different deposits have different characteristics and specificities. In natural sites where zeolites occur, impurities such as calcium or magnesium carbonates, quartz, feldspar, etc., are also present [92]. This significantly determines the properties of zeolites. Differences in zeolite properties are also the result of different crystallinity, specific surface area, thermal characteristics, etc. Natural zeolites are generally colorless, but when alkali and alkaline earth metal cations are replaced by transition metal cations, zeolites can appear colored.

The most important property of zeolites is their porous structure. As a rule, the aluminosilicate grid is made up of channels and cavities of size 2–20 Å [32,93]. The specific structure of the

This book belongs to Badji Mokhtar Annaba University Central Library Copyright Elsevier 2025

channels and cavities in the lattice results in a large internal surface, available for various reactions and sorption. Opened the inlets of the cavities and the channels have a regular shape its size corresponding to the size of the molecule, which provides the characteristics of zeolites as the molecular sieve. Depending on the size of the openings and channels, zeolites selectively retain or leak certain molecules. Sorption takes place both on the external crystallographic planes and in pores and channels, if the dimensions of the molecule to be sorbed are smaller than the dimensions of pores and channels. Because of this, zeolites are not only used in case of need for high sorption, but have also proven to be outstanding selective sorbents for the separation or purification of substances.

Cations located in channels and cavities are highly mobile, giving zeolites the properties of ion exchangers, while water molecules from channels and cavities can be easily desorbed and resorbed without disrupting the crystal lattice. The ability to exchange constituent cations and release water without noticeably altering the structure of the natural zeolite is possible up to 400°C when the zeolite still temperature-stable [32, 94]. At temperatures above 400°C, the crystal lattice is destroyed. The destruction of the crystal lattice of the zeolite occurs in a highly acidic environment, while at pH > 6 the natural zeolites are stable [93].

Another feature of zeolites, which is of great importance for their application, is the possession of acidic centers (Brønsted and Lewis) that arise as a result of a negative charge. Brønsted acid centers originate from protons that are associated with an oxygen atom from the alumina network, which are linked to aluminum, Fig. 14.7. Brønsted acid centers are proton donors, and Lewis acid centers are electron acceptors, Fig. 14.8 [32].

Most of the physical and chemical properties of zeolites depend on the aluminum content of the zeolite. Al—O—Al bonding is not possible in the crystalline structure of zeolites, so the $SiO_2/Al_2O_3 < 1$ ratio is not possible [95, 96]. The content of Al in the zeolite can vary over a wide range, so the Si/Al ratio is from 1 to ∞ [32]. Zeolites rich in Al have a hydrophilic character, so they adsorb strongly polar molecules, e.g., water, and are therefore used in considerable quantities as drying agents. The increasing content of Si in the zeolite increases their hydrophobic character, so zeolites of this type are used for sorption of fewer polar molecules. The transition from the hydrophilic to the hydrophobic mode is about 20 for SiO_2/Al_2O_3 ratio [97].

The effect of the polarity of the molecule sorbed on the sorption process itself is based on the general rule that polar substances are more strongly sorbed on the polar sorbent. Zeolites are polar sorbents, so they are used for sorption of polar substances. Thus water, ammonia, sulfur dioxide, and carbon dioxide can be removed from the gas or liquids in which they are present using the appropriate zeolite and under certain conditions. Materials which are poorly polar and nonpolar have little or no sorption. Sorption of weakly polar molecules requires a change in the surface charge of zeolites and hydrophobicity of the surface, Fig. 14.14, which can be achieved by modifying the surface with long-chain organic cations [32].

This book belongs to Badji Mokhtar Annaba University Central Library Copyright Elsevier 2025

14.4.2 Procedures for the modification of zeolites

Although zeolites have proven to be effective sorbents for the removal of toxic metal cations from the aquatic environment, in recent decades increasing attention has been paid to modifying zeolites to improve the general physicochemical properties of zeolites. In this way, the specific surface area of the zeolite is increased, thereby increasing the capacity of cation exchange and determining the selectivity to a particular cation or group of cations [98]. By modifying the zeolite, it is possible to improve the sorption properties of the zeolite. For changes in the surface properties of zeolites, the most commonly used methods are the activation of zeolites by chemical means, thermal activation, modification of surfactants, and modification by metal oxides. However, in the case of selecting a practical application, the economic cost-effectiveness of the modified zeolites should also be taken into account, i.e., the material and financial costs of synthesis, as well as during the exploitation of the zeolite.

14.4.2.1 Activation by chemical means

Activation by chemical means involves the use of a suitable activating agent such as acids, bases, or salts. Chemical modification with inorganic salts ($NaCl$, $CaCl_2$, $BaCl_2$, NH_4Cl, $FeCl_3$) or cationic surfactant (hexadecyl methylammonium bromide, i.e., HDTMA) enhances the properties of the zeolite and increases its efficiency in water treatment [45, 99–101]. For the successful modification of natural zeolites, the presence of a highly concentrated solution of inorganic salts on its surface is significant. Under normal conditions, large cavities and entrances to channels within the zeolite structure are filled with water molecules, forming hydration spheres around alternating cations. After contact of the zeolite and a solution of inorganic salts (e.g., NaCl), there is an exchange of cations (H^+, or Na^+) from a solution with alternating ions (Na^+, K^+, Ca^{2+}, Mg^{2+}) from the zeolite network. Chemical agents disrupt the crystalline structure, change the pore size, or remove some of the impurities from the zeolite, thereby improving the sorption capacity of the zeolite [102].

The chemical modification of zeolites by $FeCl_3$ solution is defined by system parameters, such as the pH value, ionic strength of the solution, oxidation-reduction conditions, iron concentration, and type of salt used (chlorides, sulfates, nitrates, perchlorates, etc.).

Acid treatment of natural zeolites, using HCl or H_2SO_4, removes impurities that block pores and gradually replaces the exchangeable cations with H^+ ions, thereby translating the zeolites into the H-form [103]. The structural changes brought about by acid treatment include an increase in the specific surface area and an increase in microporosity and mesoporosity [103]. The effect of acid on zeolites depends on the SiO_2/Al_2O_3 ratio. As this ratio increases, zeolites become less sensitive to the action of acids. In zeolites with a high Si content, the crystal structure remains stable even after exposure to acid. Clinoptilolite, as a natural zeolite mineral with high silicon content ($Si/Al \geq 4$), is characterized by high acid stability [104]. Zeolites with a very high Si content dissolve in a very alkaline environment.

This book belongs to Badji Mokhtar Annaba University Central Library Copyright Elsevier 2025

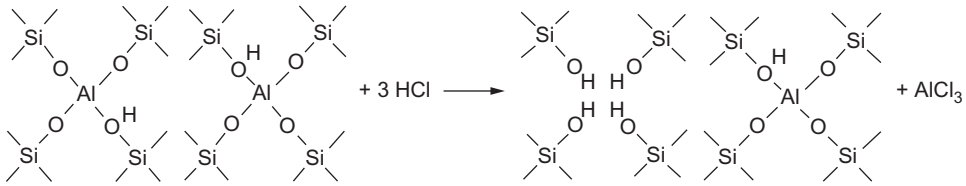

Fig. 14.6

Activation of a natural zeolite by acid, the H-shaped zeolites. *Reprinted with permission from H. Valdés, R.F. Tardón, C.A. Zaror, Role of surface hydroxyl groups of acid-treated natural zeolite on the heterogeneous catalytic ozonation of methylene blue contaminated waters, Chem. Eng. J. 211–212 (2012) 388–395, https://doi.org/10.1016/j.cej.2012.09.069.*

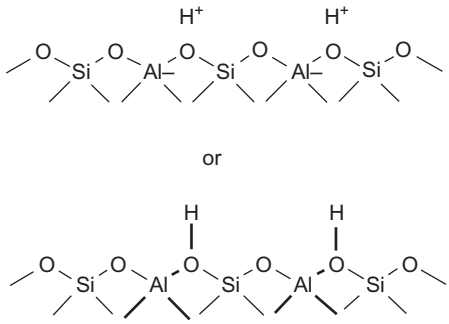

Fig. 14.7

Brønsted acid sites ("bridging hydroxyl groups") in zeolites. *Reprinted with permission from M. Stöcker, Gas phase catalysis by zeolites, Microporous Mesoporous Mater. 82 (2005) 257–292, https://doi.org/10.1016/j.micromeso.2005.01.039.*

The H-shaped zeolites, which are acid-activated relative to untreated zeolites, have improved sorption properties, which is explained by the size of the hydronium ions. Due to their small size, H^+ ions cause significantly less interference with the diffusion of sorbates through channels than hydrated metal cations [105]. The H-form of the zeolite is most commonly obtained by treatment with acids, Fig. 14.6, or ion exchange, and then annealing the zeolite at 400°C [106].

Dapaah et al. [107] achieved high Brönsted acidity by treating zeolites with a solution of ammonium salts [NH_4Cl and $(NH_4)_2SO_4$], which is the most important factor in many sorption properties of zeolites, which is explained by the higher polarization power of hydronium ions relative to naturally occurring cations. The authors noted that annealing releases ammonia and the H^+ ion remains on the surface of the zeolite, causing Brönsted acid centers to be generated in zeolite pores [107]. In this way, they developed a possible mechanism for the generation of Brönsted and Lewis active centres on the zeolite surface, Fig. 14.7 [108].

This book belongs to Badji Mokhtar Annaba University Central Library Copyright Elsevier 2025

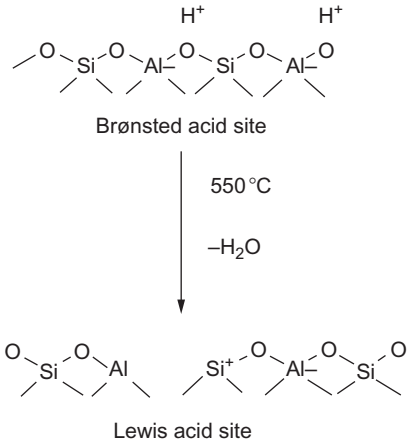

Fig. 14.8
Formation of Lewis acid sites in zeolites (simplified version—not taking into account the model of "true Lewis acid sites"). *Reprinted with permission from M. Stöcker, Gas phase catalysis by zeolites, Microporous Mesoporous Mater. 82 (2005) 257–292, https://doi.org/10.1016/j.micromeso.2005.01.039.*

By calcining zeolites at 550°C, when water is released from the zeolite pore, as explained by Stöcker [108], Brønsted acid sites move to Lewis acid sites in zeolites, Fig. 14.8.

The concentration of acidic centers in the zeolite lattice is usually determined by infrared (IR) spectroscopy by treating the zeolite sample with a strong base, most commonly pyridine. Pyridine binds to Lewis and Brønsted acid centers, resulting in the appearance of characteristic vibrational bands, Fig. 14.9. The vibrational band at 1455 cm^{-1} corresponds to the interaction of pyridine with the Lewis acid center, while the band at about 1540 cm^{-1} originates from the bond that pyridine makes with the Brønsted proton [35,49,108].

On the IR spectrum of the non-pyridine-treated H-Y zeolite, Fig. 14.8, a band at 3550 cm^{-1} is attributed to vibrations of the OH group in sodalite cages, Fig. 14.1. As well as a band at 3640 cm^{-1} corresponding to the OH groups located in super-coils of aluminosilicate lattice, Fig. 14.2 (Site I). Pyridine molecules (0.58 nm) cannot enter the sodalite cages (0.28 nm) because of the small size of the openings, so that the vibrational band at 3550 cm^{-1} remains visible after adsorption. Large openings at the entrance to the supercages (0.8 nm) allow passage of pyridine molecules and attachment to acidic sites, resulting in the disappearance of the vibrational band at 3640 cm^{-1} [35]. In Fig. 14.10, Shariatinia and Bagherpour [50] showed the full FTIR spectrum as a function of transmittance (%) of synthetic zeolite Y, while Wahono et al. [53] in Fig. 14.13 presented the entire FTIR spectrum as a function of adsorbance (%), indicating structural bonds in the zeolite.

Christidis et al. [109] found that treatment with KOH did not significantly affect the structure of the zeolite, but there was a moderate increase in mesoporosity and microporosity, as well as the

This book belongs to Badji Mokhtar Annaba University Central Library Copyright Elsevier 2025

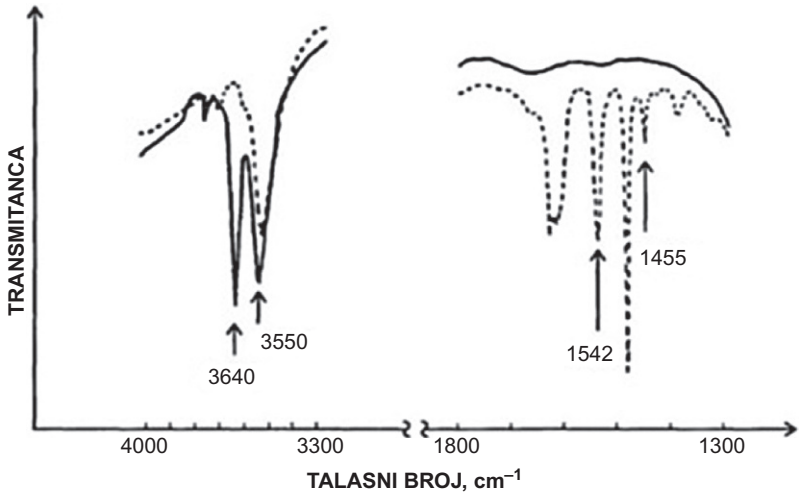

Fig. 14.9

IR spectra of H-Y zeolites before *(solid line)* and after *(dashed line)* adsorption of pyridine. *Reprinted with permission from J. Weitkamp, Zeolites and catalysis, Solid State Ionics 131 (2000) 175–188, https://doi.org/10.1016/S0167-2738(00)00632-9.*

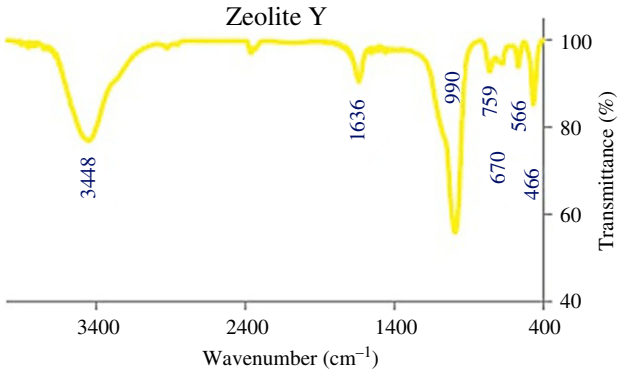

Fig. 14.10

FTIR analysis of synthetic zeolite Y. *Reprinted with permission from Z. Shariatinia, A. Bagherpour, Synthesis of zeolite NaY and its nanocomposites with chitosan as adsorbents for lead(II) removal from aqueous solution, Powder Technol. 338 (2018) 744–763, https://doi.org/10.1016/j.powtec.2018.07.082.*

surface area and volume of the micropores, and it was necessary to take into account the process temperature due to the possible sintering of zeolite crystals. It was concluded that during the alkaline activation process of the zeolite, there is a slow layered dissolution of the zeolite structure, partial replacement of exchangeable cations with K^+ ion from KOH, dissolution of amorphous and poorly crystallized material in the natural zeolite.

This book belongs to Badji Mokhtar Annaba University Central Library Copyright Elsevier 2025

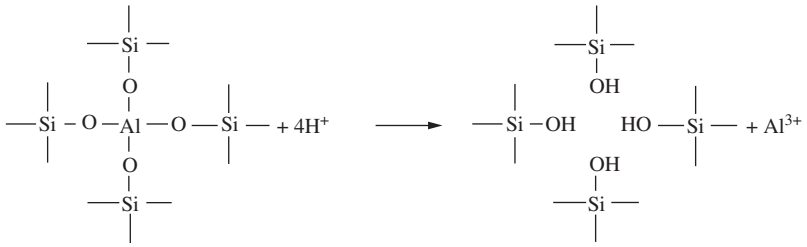

Fig. 14.11
Dealumination process of zeolites. *Reprinted with permission from N. Al-Jammal, T. Juzsakova, B. Zsirka, V. Sebestyén, J. Németh, I. Cretescu, T. Halmágyi, E. Domokos, Á. Rédey, Modified Jordanian zeolitic tuff in hydrocarbon removal from surface water, J. Environ. Manage. 239 (2019) 333–341, https://doi.org/10.1016/j.jenvman.2019.03.079.*

Matijašević et al. [105] treated zeolite clinoptilolite (Ca-clino) with acids of different basicity, single-base hydrochloric acid, two-base oxalic, and triple-base citric acid to test the effect of acid type on the stability of the zeolite structures. It was found that treatment with these acids led to a decrease in the aluminum content of clinoptilolite, that is, to a partial dealumination, Fig. 14.11. The authors found that the highest SiO_2/Al_2O_3 ratio was achieved with hydrochloric acid treatment and the lowest when treated with citric acid. It was found that the content of CaO, MgO, Na_2O, and K_2O was reduced during the treatment of zeolites with acids, on the basis of which the authors assumed that there was an ionic exchange of calcium with the hydronium ion, as well as the dissolution of the calcite mineral present in the starting sample. The content of Ca^{2+} and Mg^{2+} ions in the filtrate after treatment with oxalic and citric acid, and the content of Na^+ ions in the filtrate after treatment with all three test acids was less than the content in the Ca-clino. The content of Ca^{2+} and Mg^{2+} ions in the filtrate after treatment with HCl was higher than the content of these ions in the Ca-clino, which confirmed that these cations were present except in alternating positions and in the structure of the starting sample. The low content of Al^{3+} ions in the filtrate after Ca-clino citric acid treatment indicates that ion exchange of inorganic cations with the hydronium ion is predominant during treatment with tribasic acid [105]. The process of zeolite delineation is shown in Fig. 14.11 [110, 111].

Chamnankid et al. [112] treated the zeolite with a solution of NaOH of different concentrations. Treatment of the zeolite with an alkaline solution caused the breakdown of the Si—O—Al bond and the formation of Si—OH and Al—OH bonds. The results showed that the specific surface area and TPV of the zeolite treated with 0.05 M NaOH gradually decreased relative to the starting zeolite, whereas due to complete disruption of the crystal structure, after treatment with 0.25 M NaOH solution, the specific surface area and TPV were significantly reduced. Interestingly, during treatment with 0.25 M NaOH, new strong acidic centers were formed, while the Si/Al ratio was not significantly changed due to the presence of aluminum species on the outer surface of the zeolite.

By comparing the characteristics of natural zeolite and zeolite treated with 2 M NaCl solution, Bektas and Kara [113] found that treatment with NaCl solution increased the sorption

This book belongs to Badji Mokhtar Annaba University Central Library Copyright Elsevier 2025

capacity of zeolite. Treatment of natural zeolite with 2 M NaCl solution led to a decrease in the SiO_2/Al_2O_3 ratio, an increase in the specific surface area, and a decrease in the volume of micropores. The selectivity of zeolites toward exchangeable cations is $K^+ > Ca^{2+} > Na^+$. Compared to Na^+ ions, K^+ and Ca^{2+} ions were strongly bound to clinoptilolite and longer exposure to high sodium concentration was required to alter these ions in the zeolite. It was also found that part of the K^+ and Ca^{2+} ions was not interchangeable, which explained that these ions are bound to impurities in the zeolite [114]. Çoruh [115] reached similar conclusions. In this case too, treatment with 2 M NaCl solution increased the sorption capacity of the zeolite, which was also explained by the increase in the content of Na^+ ions while reducing the concentration of Ca^{2+} and K^+ ions in the zeolite.

Exposure of clinoptilolites to the NaCl solution led to sodium-rich zeolites (Na-zeolites), known as good ion exchangers. It is also observed that during the milling process of clinoptilolite, the fine dust fraction partially covers the clinoptilolite surface and pore openings, resulting in pore clogging leading to a lesser ion exchange capacity and a lower ion-exchange rate. Pore clogging can affect the ion-exchange capacity. Treatment with the NaCl solution can remove dust particles from the surface of zeolite crystals, making the channels more passable in the zeolite, thus facilitating the diffusion of cations through channels in the zeolite and increasing the sorption capacity of the zeolite. The facilitated diffusion in the case of treated zeolite is perhaps the main reason for the different sorption rates on natural and treated zeolites.

To remove anions from water, the zeolite surface must be modified by a solution of inorganic salts such as $FeCl_3$, whose adsorption on the zeolite surface leads to the formation of oxy-hydroxide, which then forms stable complexes with anions in solution. This modification may result in the formation, to a lesser or greater extent, of an adsorption layer on the zeolite surface and a modification of the zeolite surface charge, from negative to positive [116].

14.4.2.2 Thermal activation

Zeolites have remarkably good thermal stability that varies from structure to structure of zeolites, but is most dependent on the SiO_2/Al_2O_3 ratio and the type of exchangeable cation. The thermal stability of zeolites increases with increasing Si/Al ratio as more energy is needed to break the Si—O bond compared to the Al—O bond. This is due to the different bond lengths, d(Al—O) is 1.75 Å and d(Si—O) is 1.62 Å. When the zeolite is heated, water leaves the channels in the zeolite structure, that is, the zeolite is dehydrated. Lower dehydration temperatures are expected for zeolites with a higher Si/Al ratio, due to the increased hydrophobicity of their surface. After complete dehydration by the annealing process, the cavities and channels in the zeolite can be refilled with water molecules or other liquids and gases with diameters smaller than the diameters of the cavities and channels. Fully or partially dehydrated zeolite is thermally activated and can quickly rehydrate, i.e., absorb water from the atmosphere. During the thermal activation process, the organic components are completely removed [117–119].

This book belongs to Badji Mokhtar Annaba University Central Library Copyright Elsevier 2025

Vasylechko et al. [120] found that thermal treatment affects natural and acid-activated zeolites in different ways. For natural zeolite (clinoptilolite), there is virtually no structural change up to 300°C. The destruction of the crystalline structure of the zeolite occurs in the temperature range between 350°C and 550°C. Only at 900°C was the crystal structure completely destroyed. For acid-activated clinoptilolite, destruction of the crystal structure was observed after 150°C. Significant structural changes were observed in the temperature range between 350°C and 450°C, while in this case, the crystal structure was completely destroyed at 900°C. In both cases, annealing of the zeolite was followed by loss of water.

Tomazović et al. [121, 122] presented the mechanism of thermal treatment of H-clinoptilolite in three stages, Fig. 14.12.

Step 1 (Fig. 14.12) shows that annealing at 300°C results in a partial transformation of H-clinoptilolite, with an increase in the number of surface OH groups. Considering the active sorption centers of zeolites toward metal ions, which are most commonly associated with surface OH groups, it is evident that a smaller increase in the sorption efficiency of H-clinoptilolites at 300°C is directly related to the increase in the number of surface OH groups. At 400°C, stage 2 (Fig. 14.12), the process of formation of the zeolite amorphous structure is accelerated. The increase in the sorption capacity of H-clinoptilolite annealed at a temperature of about 600°C, step 3 Fig. 14.12, can be attributed to the newly formed silanol bonds (Si—O—Si) at the free tetrahedral sites formed during step 2 of the zeolite process.

Thermal treatment at high temperatures, depending on the modification of the sample and the temperature, can increase the pore volume by removing the water molecules and the organic

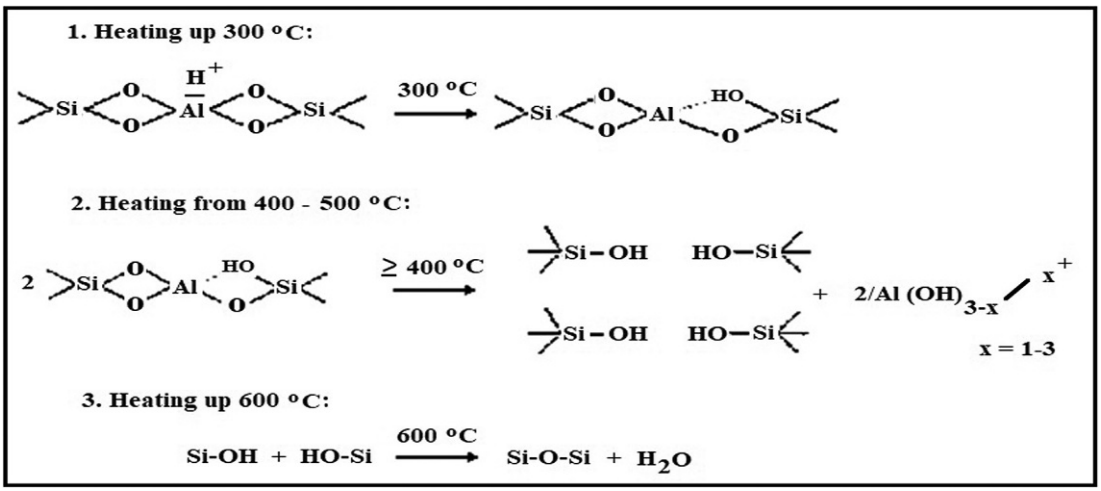

Fig. 14.12
Mechanism of thermal treatment of H-clinoptilolite in three stages. *Modified after B. Tomazović, T. Ćeranić, G. Sijarić, The properties of the NH_4-clinoptilolite. Part 1, Zeolites 16 (1996) 301–308, https://doi.org/10.1016/0144-2449(95)00118-2.*

This book belongs to Badji Mokhtar Annaba University Central Library
Copyright Elsevier 2025

matter contained therein. The water present in the structure of the zeolite constitutes approximately 10%–25% of the total mass of the zeolite. For the effective use of zeolites in water treatment, it is necessary to know the properties of zeolites during the process, as well as their structural stability with respect to treatment at elevated temperatures. For example, clinoptilolite (CLI) and erionite (ERI) are structurally stable up to 750°C, while for mordenite (MOR) it is 800°C and analcime (ANA) is 700°C. Laumontite (LAU) has a stable structure up to 500°C, while heulandite (HEU) retains a crystalline structure up to 300°C [123].

Plasma-activated natural mordenite-clinoptilolites have been activated by Wahono et al. [53]. Researchers have shown that plasma activation caused a significant transformation of the chemical and physical properties of zeolites and improved the porous characteristics of zeolites. Part of the results of the plasma-activated zeolite are shown in Fig. 14.13, using different techniques. The FTIR spectrum shows that there are no significant differences between the natural and the plasma-activated zeolites, thus confirming that there was no destruction of the structure of the zeolite. Method-activated zeolite plasma is one of the activation methods for zeolites to which attention should be paid in future.

14.4.2.3 Modification of surface-active substances

Due to the excess of a negative charge in the structure of zeolites, natural zeolites usually have a very low affinity for anions and exhibit a low sorption capacity for organic molecules in an aqueous solution. To change the surface properties of zeolite, a method of modification is the modification of surface-active substances [103, 124]. Exchangeable cations in the zeolite structure enable the modification of the zeolite surface by active cationic substances [125, 126]. By modifying the surface-modified zeolite (SMZ), zeolites are coated with organic polar molecules, which can alter the essential properties of zeolites, for example, from a hydrophilic surface, to a hydrophobic one. Thus, SMZs do not have the ability to absorb water, but they have the ability to attract anions (e.g., CrO_4^{2-}, AsO_4^-, PO_4^-), then different radicals and complex organic compounds instead of cations. At the crystal lattice level, SMZs still have the cationic sorbent property, and they have the anionic sorbent capability only on the surface. The CEC of SMZs is significantly reduced relative to the natural zeolite, and the decrease is as pronounced as the zeolite particles become smaller.

The most commonly used zeolite modification agents for surfactants are: HDTMA (hexadecyltrimethylammonium), TMA (tetramethylammonium), TEA (tetraethylammonium bromide), CTMA (cetyltrimethylammonium), ODMBA (octadecylmethylbenzylammonium) bromide), BDTDA (benzyltetradecylammonium), HMNA (*N*, *N*, *N*, *N′*, *N′*, *N′*-hexamethyl-1,9-nonandiammonium dibromide), EHDDMA (ethylhexadecyldimethyl ammonium), etc. [103].

This book belongs to Badji Mokhtar Annaba University Central Library Copyright Elsevier 2025

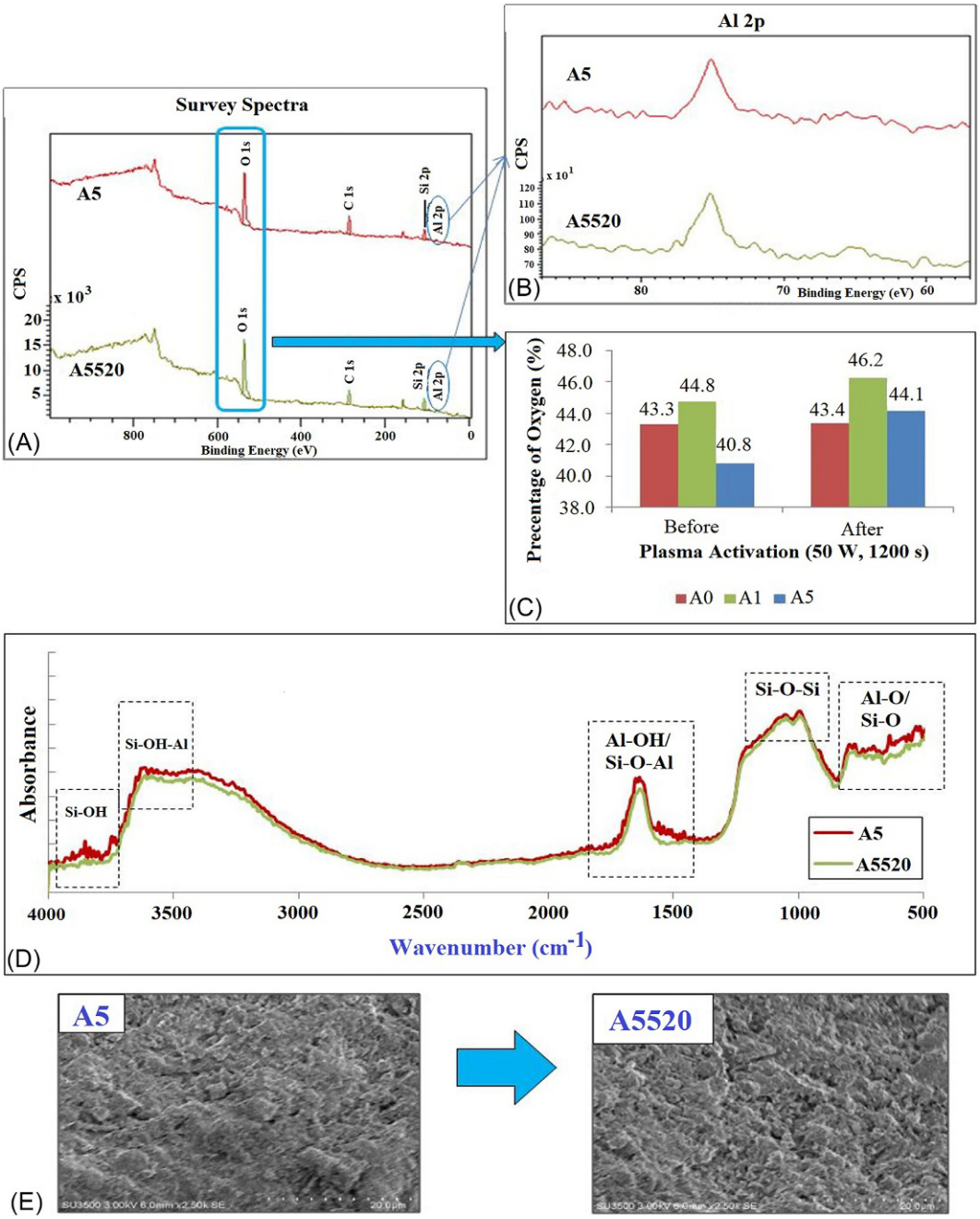

Fig. 14.13

(A) XPS Survey spectra of A5 zeolite before and after plasma treatment; (B) Al 2p region zoom; (C) oxygen percentage of zeolites as determined by XPS before and after plasma treatment; (D) FTIR spectra of A5 zeolite; and (E) SEM images of the zeolite before and after plasma treatment. *Reprinted with permission from S.K. Wahono, A. Suwanto, D.J. Prasetyo, Hernawan, T.H. Jatmiko, K. Vasilev, Plasma activation on natural mordenite-clinoptilolite zeolite for water vapor adsorption enhancement, Appl. Surf. Sci. 483 (2019) 940–946, https://doi.org/10.1016/j.apsusc.2019.04.033.*

This book belongs to Badji Mokhtar Annaba University Central Library
Copyright Elsevier 2025

A general model of zeolite modification by SMZ is the formation of a solid-liquid phase boundary monolayer by the Cullon electrostatic attraction forces between the negatively charged zeolite surface and the positively charged SMZ, which occur at SMZ concentrations at or below the critical micelle concentration (CMC). If the concentration of SMZ in solution exceeds the CMC, the formation of a double layer begins with hydrophobic bonding where Van der Waals forces are formed [103, 125], as shown in Fig. 14.14. In this way, the zeolite surface contains positively charged sites where anions can be sorbed.

Lin et al. [127], in order to remove Cu^{2+} ions, surface-modified the natural zeolite cetylpyridinium bromide (CPB) and thus immobilized humic acid on SMZ (HA-SMZ). XRD analysis of the untreated clinoptilolite showed that the crystalline structure remained intact after SMZ and immobilization of HA molecules on SMZ [128].

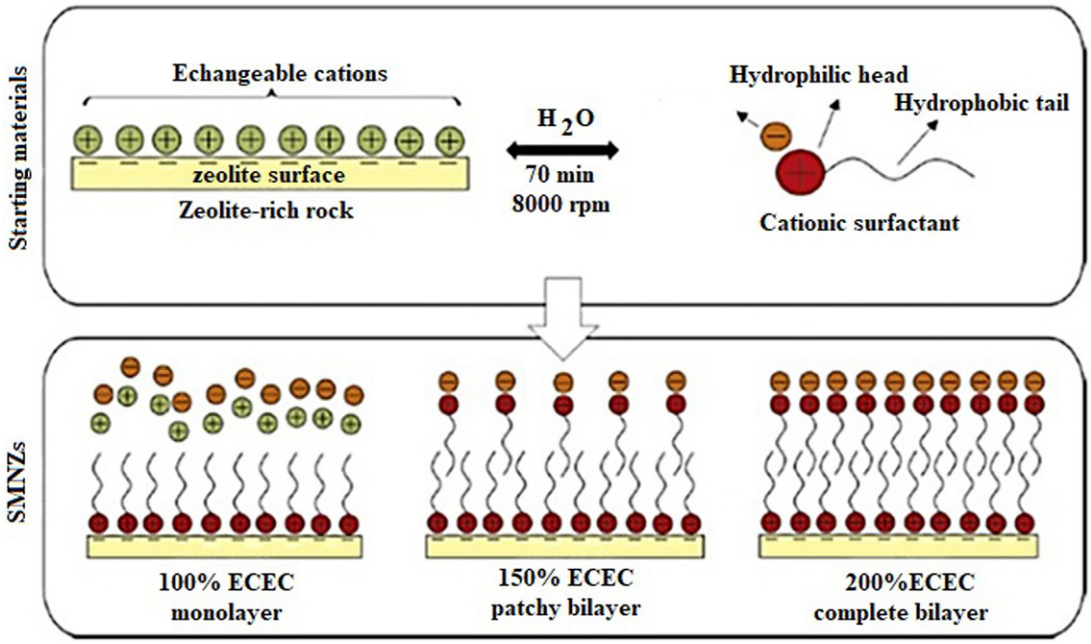

Fig. 14.14
Schematic representation of the surface modification of the zeolite by interaction with different amounts of cation surfactant. *Reprinted with permission from F. Izzo, M. Mercurio, B. de Gennaro, P. Aprea, P. Cappelletti, A. Daković, C. Germinario, C. Grifa, D. Smiljanic, A. Langella, Surface modified natural zeolites (SMNZs) as nanocomposite versatile materials for health and environment, Colloids Surf. B Biointerfaces 182 (2019) 110380, https://doi.org/10.1016/j.colsurfb.2019.110380.*

This book belongs to Badji Mokhtar Annaba University Central Library Copyright Elsevier 2025

14.4.2.4 Modification by iron oxides

Oxides or hydroxides of iron(III) are also active sorbents of toxic metal ions, so increasingly zeolites are modified precisely with iron(III) compounds. The improved properties of such modified zeolites are explained by the formation of new active sites for the sorption of toxic metal cations [129].

Many authors have examined the form in which iron(III) is present in iron(III)-modified zeolite, in order to explain the mechanism of sorption of toxic metal ions onto iron (III)-zeolite [8, 58, 130–133]. However, due to significant variation in the chemistry of iron in the environment of oxygen-containing ligands and the simultaneous presence of different types of Fe species, the abundance of which depends on the procedure for the preparation and treatment of Fe-zeolites, the links between iron forms and zeolites are not clearly established. However, the method commonly used in catalysis and material testing, which can help in solving the problem of determining the form of Fe in the modified zeolite is XPS. One useful example of XPS analysis for determining the oxidation state of Fe on a material surface is shown in Fig. 14.15 [36, 52]. In most cases, individual ions of divalent and trivalent iron, oxy hydroxy complexes, polymeric oxide species, and other types of iron oxide are simultaneously present in the zeolite. However, an important conclusion drawn from the study of mixed Fe-zeolite systems is that these materials have physicochemical properties that allow their application in various fields of research.

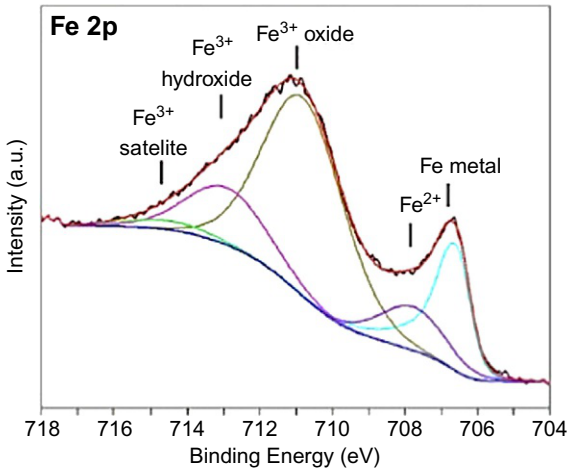

Fig. 14.15

High-resolution XPS of Fe 2p with background subtraction and curve fitting. *Reprinted with permission from J. Peng, F. Moszner, J. Rechmann, D. Vogel, M. Palm, M. Rohwerder, Influence of Al content and pre-oxidation on the aqueous corrosion resistance of binary Fe-Al alloys in sulphuric acid, Corros. Sci. 149 (2019) 123–132, https://doi.org/10.1016/j.corsci.2018.12.040.*

This book belongs to Badji Mokhtar Annaba University Central Library
Copyright Elsevier 2025

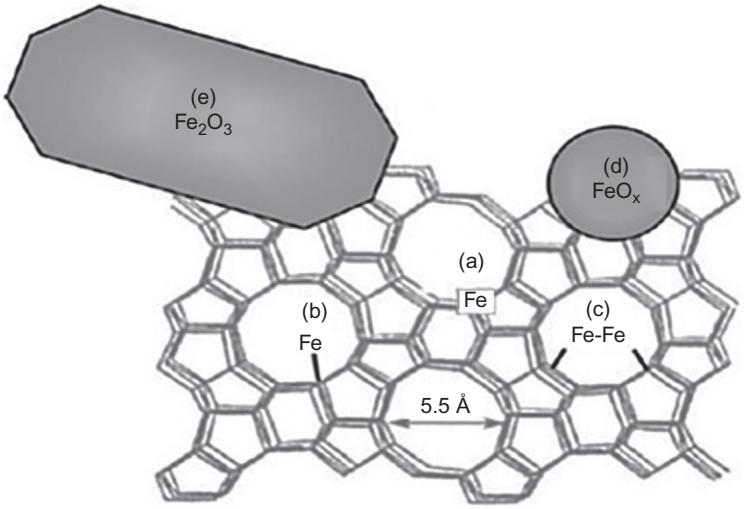

Fig. 14.16
Schematic representation of the different Fe species identified in FeZSM-5. *Reprinted with permission from J. Pérez-Ramírez, G. Mul, F. Kapteijn, J.A. Moulijn, A.R. Overweg, A. Doménech, A. Ribera, I.W.C.E. Arends, Physicochemical characterization of isomorphously substituted FeZSM-5 during activation, J. Catal. 207 (2002) 113–126, https://doi.org/10.1006/jcat.2002.3511.*

Different forms of iron have been identified in zeolite ZSM-5-modified iron, FeZSM-5, Fig. 14.16: (a) isolated ions or ions in the lattice (isomorphic substitution), (b) in cationic positions in channels in the zeolite, (c) binuclear and (d) FeOx iron oxide nanoparticles of $\leq$2 nm, and (e) large iron oxide particles (Fe_2O_3), about 25 nm in size, distributed on the surface of zeolite crystals [134, 135].

Dimirkou and Doula [8] modified clinoptilolite with a solution of iron Fe (III)-nitrate under very basic conditions, at a temperature of 70°C for a period of 60 h in order to obtain a mixed sorbent of Fe(III)-Clin. Elemental analysis of Fe(III)-Clin showed that the Si/Al ratio was almost the same as the Si/Al ratio in clinoptilolite, with a total Fe content of 14.1%. The Fe/Al ratio was 1.23, indicating that the amount of Fe introduced during the synthesis exceeds the ion exchange capacity of the starting material. On this basis, it was concluded that Fe(III)-Clin also contains an additional fraction of iron ions that does not participate in the charge balancing due to isostructural replacement. The specific surface area of the modified zeolite (151 $m^2\ g^{-1}$) is much larger than that of untreated clinoptilolite (31 $m^2\ g^{-1}$). XRD analysis of Fe (III)-Clin showed that crystallinity was decreased, but no new phase presence was detected. The FTIR spectrum of the modified zeolite also showed vibrations characteristic of the untreated zeolite, while vibrations characteristic of Fe oxides were not observed [129]. Similar conclusions were reached by Kragović et al. [58].

The above-mentioned authors, during the modification of the natural zeolite of clinoptilolite by the addition of $FeCl_3 \times 6H_2O$ under very basic conditions, found that, although the

This book belongs to Badji Mokhtar Annaba University Central Library Copyright Elsevier 2025

modification of the natural zeolite with Fe (III) ions was carried out, there was no significant change in the content of Si or Al in the Fe (III)-modified sample zeolite. The content of Na^+ ions in iron(III)-modified zeolite was observed to be lower than that in the natural one, while the content of K^+ ions was increased due to the modification procedure. The zero charge point (pH_{tnn}) of natural zeolite was 6.8, while the zero charge point of iron(III)-modified zeolite (pH_{tnn}) increased to 7.5.

Sun et al. [133] also modified the natural zeolite using $FeCl_3$. The modification was performed at a temperature of 70–80°C for a period of 2 h. XRD diffractogram of natural and modified zeolites before and after sorption showed that the modified samples retain high crystallinity. The number and position of diffraction peaks did not change, indicating that no phase transformation occurred during treatment. The FTIR spectrum of the modified zeolite showed vibrations characteristic of the natural zeolite, while XRD, XPS, and EDX analyses of the natural and modified zeolites showed that Fe(III) was impregnated on the surface of the natural zeolite.

14.5 Application of zeolites in water treatment

14.5.1 Removal of metal ions from different wastewaters

Although there are many sources of metal ion pollution, the metal-processing industry is one of the potentially largest environmental pollutants of toxic metals. The wastewater from mines poses a serious threat to human health and the environment, because it contains toxic metals in the living world, of which the following are particularly relevant: Cu^{2+}, Pb^{2+}, Cd^{2+}, Ni^{2+}, $Cr^{3+/6+}$, $As^{3+/5+}$, Zn^{2+}, and Hg^{2+} [82]. Álvarez-Ayuso et al. [78] have demonstrated the successful application of zeolites for the treatment of wastewater from the electroplating process. In addition to the effluent from the electroplating process, a group of researchers came to the conclusion that the preliminary treatment of the effluent from the mine could successfully be carried out using zeolite [136].

Zeolites have proven to be effective sorbents for the removal of these aforementioned metal ions from atmospheric waters generated from highways and urban environments [137–139]. Taffarel and Rubio [140] reviewed and collected the sorption data of clinoptilolite natural and modified zeolite reported in Table 14.4. They also stated the way the zeolite was treated. The modified zeolites show a significant increase in the adsorbed ions—toxic metals.

14.5.2 Removal of the ammonium ion from water

Ammonia in the environment is part of the global nitrogen cycle. In surface waters, ammonium salts can come into contact with the microbial nitrification that produces hydrogen, which consumes oxygen; in certain acidification and oxygen depletion systems they can pose major

This book belongs to Badji Mokhtar Annaba University Central Library Copyright Elsevier 2025

Table 14.4: Influence of zeolite pretreatment on metal ion uptake.

Metal ions	Treatment	Zeolite	q_{max} (mg g^{-1})	
			Natural	Modified
Pb^{2+}	NaCl	Clinoptilolite	80.93	122.40
	NaCl	Clinoptilolite (50%)	78.70	85.00
	NaCl	Clinoptilolite (50%)	32.65	64.52
	HCl and NH_4Cl	Clinoptilolite (75%)	–	27.70
	$NaNO_3$	Clinoptilolite	93.24	103.60
Cu^{2+}	NaCl	Clinoptilolite (50%)	4.78	12.11
	HCl and NH_4Cl	Clinoptilolite (75%)	–	25.76
Zn^{2+}	NaCl	Clinoptilolite (50%)	4.54	8.14
	NaCl	Clinoptilolite	4.40	8.00
Ni^{2+}	HCl and NH_4Cl	Clinoptilolite (75%)	–	13.03
	$NaNO_3$	Clinoptilolite	3.67	10.21
Ba^{2+}	$NaNO_3$	Clinoptilolite	20.60	54.94
Cd^{2+}	NaCl	Clinoptilolite (50%)	9.50	14.30
	HCl and NH_4Cl	Clinoptilolite (75%)	–	4.22
	$NaNO_3$	Clinoptilolite	25.29	38.21
Mn^{2+}	KOH and $Fe(NO_3)_3$	Clinoptilolite (90%)	7.69	27.12

A part reprinted with permission from S.R. Taffarel, J. Rubio, J., On the removal of Mn^{2+} ions by adsorption onto natural and activated Chilean zeolites, Miner. Eng. 22 (2009) 336–343, https://doi.org/10.1016/j.mineng.2008.09.007.

environmental problems, and as much as a third of acid rain can be attributed to the emission of ammonia into the environment [141].

Nitrogen occurs in water in the form of ammonia, nitrite, nitrate, and organic nitrogen. Organic nitrogen decomposes in water to ammonia, which is readily assimilated into the bacterial cells, leading to their net growth and high oxygen consumption during this process, which has a negative impact on the aquatic ecosystems. The presence of ammonia in water also makes it harmful for human consumption, and it is necessary to remove ammonia from the water before can be used for drinking. The term ammonia refers to both the nonionized, NH_3, and the ionized forms, NH_4^+ (aq). Ammonia, present in low concentrations in drinking water, is generally not considered to be a direct cause of health problems in humans, since it is readily metabolized by the liver and kidneys, and is excreted as such. However, the presence of ammonia in water can cause a wide range of problems during the treatment and distribution of drinking water. Eq. (14.14) shows the binding of NH_4^+ in the zeolite structure, as shown by Belchinskaya et al. [111].

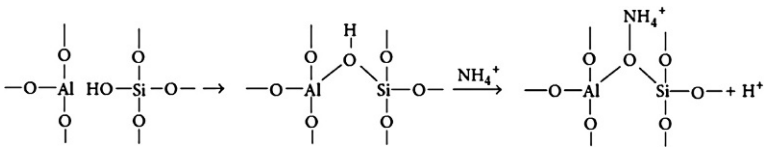

(14.14)

This book belongs to Badji Mokhtar Annaba University Central Library
Copyright Elsevier 2025

Table 14.5: Influence of zeolite pretreatment on NH_4^+ ion uptake.

Zeolite	Treatment	q_{max} (mg g^{-1})		References
		Natural	Modified	
Clinoptilolite (50%)	NaCl	8.15	12.26	[143]
Clinoptilolite (48%)	NaCl	13.40	18.30	[144]
Clinoptilolite	NaOH	31.50	75.20	[145]
Clinoptilolite	NaCl and NaOH	10.49	19.29	[146]

The presence of ammonia in water leads to the development of microorganisms and the appearance of odor and taste in water. Therefore, the maximum permitted concentration of ammonia in water is 0.5 mg L^{-1}, according to the Council Directive 98/83/EC of November 3, 1998 on the quality of water intended for human consumption. The natural level of ammonia in groundwater and surface water is below 0.2 mg L^{-1} while anaerobic groundwater can contain up to 3 mg L^{-1}. Ammonia in water is an indicator of possible bacterial activity, sewage and animal waste [141, 142]. Belchinskaya et al. [111] have shown that the NH_4^+ ions were exchanged with certain cations from zeolite in the next row the $Ca^{2+} > Mg^{2+} > Na^+ > K^+$. Table 14.5 summarizes some of the sorption data of NH_4^+ ions from water using zeolite.

The major sources of ammonia pollution are fertilizers applied on agricultural land, ammonia from the air, sewage, septic tanks, atmospheric precipitation, dead animals, debris from aquatic organisms, eroded soil and sediments, natural fertilizers, organic matter in water, and many others. The sources of pollution vary depending on the specificities and characteristics of the natural and urbanized environment. Due to its many unique properties, such as high treatment capacity, high removal efficiency, low cost, and fast kinetics, adsorption has been recognized as an effective and economical method for ammonia removal, in accordance with the data available today [25, 142].

The search for cheaper and readily available adsorbents for the removal of ammonium ions has become the main objective of research today, and to date, a number of papers have been published on the use of cheap adsorbents. One of the most commonly used ion exchangers for ammonium ion removal is zeolite [24, 25, 114]. The negative charge, which is balanced with cations by zeolites, is easily replaceable by certain cationic species such as NH_4^+.

14.5.3 Removal of radioactive elements from wastewater from nuclear power plants

Application of zeolite in solving the problem of radioactive waste usually comes down to the removal of ^{137}Cs and ^{90}Sr from radioactive waste streams, because zeolites are stronger and more resistant than organic ion exchangers and are not sensitive to radiation, Table 14.6, [140, 147–149]. Organic resins are less commonly used because of their higher ion-exchange

This book belongs to Badji Mokhtar Annaba University Central Library Copyright Elsevier 2025

Table 14.6: Influence of zeolite pretreatment on ion uptake.

Ion	Treatment	Zeolite	q_{max} (mg g^{-1}) Natural	Modified	References
Sr^{2+}	$NaNO_3$	Clinoptilolite	10.51	23.65	[147]
	–	Zeolite-A	96.15	107.50	[148]
Cs^{+}	$NaNO_3$	Clinoptilolite	15.28	21.26	[147]
	–	Zeolite-A	102.00	113.60	[148]

capacity, higher reaction rates, and better chemical resistance. In contrast, zeolites exhibit higher ion-exchange selectivity, good resistance to temperature and radiation.

According to Misaelides [150], zeolite shows increased selectivity toward monovalent ions, such as Cs^{+}. This property indicates the possibility of significant application of zeolites for nuclear waste management, by immobilization of radioactive cesium isotopes. Removal of radioactive isotopes of cesium by zeolite from radioactive liquid waste has been investigated by Borai et al. [149]. Based on the research results obtained, the authors mentioned concluded that zeolite can be used for purification of radioactive liquid waste at a low cost. Awual et al. [151] also examined the removal of radioactive isotopes of cesium by zeolite and concluded that it can be successfully applied for wastewater treatment at the Fukushima Nuclear Power Plant in Japan.

14.6 Regulation of water hardness

The ability to change cations is one of the most important properties of zeolites used in water softening. Hard water has high concentrations of Ca^{2+} and Mg^{2+} ions, which can be a serious problem in industrial processes, in households, and for human health [152]. For example, hard water causes scale to build up on the walls of boilers, leading to an increase in energy consumption for heating water [153].

In the water softening process, Ca^{2+} and Mg^{2+} ions are replaced by exchangeable cations from the zeolite structure, primarily Na^{+} ions. The exchangeable cations in the aluminosilicate lattice of the zeolite are bound by weak electrostatic bonds, so they can be easily modified by certain cations from a solution [153]. Zeolite gradually loses its efficiency and must regenerate. Regeneration is usually performed by passing a concentrated solution of NaCl through the zeolite. Various natural zeolites can be used to soften water by ion exchange, but they are often used synthetically with special characteristics specialized for the purpose.

Xue et al. [152] examined water softening with the synthetic zeolite NaA. Based on the results obtained, they determined that the NaA zeolite is very effective for removing Ca^{2+} ions from the solution by the ion-exchange process and that the contact time is only a few minutes. However, in addition to Ca^{2+} ions, it is necessary to simultaneously remove the Mg^{2+} ions,

This book belongs to Badji Mokhtar Annaba University Central Library Copyright Elsevier 2025

which, in most cases, are found together with Ca^{2+} ions. The removal of Mg^{2+} ions by a zeolite at room temperature is not efficient enough, due to the limited diffusion of Mg^{2+} ions in the zeolite pores and competition with Ca^{2+} ions for alternating sites in the zeolite [154, 155]. The removal of Mg^{2+} ions is a major limitation for the indicated zeolite application.

Systems with a packed sorbent particle layer consist of a simple structure made up of a column into which fluid is injected, usually in a downward direction. In this way, laminar flow through the layer is achieved with fluid/particle contact at low shear stresses. These systems have been examined in wastewater treatment, using natural and modified natural zeolites [156, 157], as well as in drinking water softening treatment. Liu et al. [2] have practically applied knowledge in the field of adsorption to natural activated clinoptilolite, to solve the specific problem of supplying the population with quality drinking water, using a semiindustrial plant. Researchers examined the sorption capacity of seven clinoptilolite deposits located in drinking water use. The idea of the study was to experimentally investigate the static sorption of clinoptilolites and the dynamic sorption of a fixed-bed [158–162] associated with the degassing column. In this way, they determined the factors affecting water treatment, to determine the use of natural zeolite to soften drinking water, up to the level prescribed for water hardness according to local standards, Fig. 14.17. It extends the lifetime of the zeolite column to the time of regeneration and the final use of the zeolite.

Liu et al. [2] have thoroughly discussed and calculated the operating conditions of production and technological combinations of softening drinking water, Fig. 14.17. This possibility was confirmed by a pilot test, Fig. 14.18, which provides a new solution for the groundwater softening process for use by the population. Comparative analysis, cost, and performance indicate that NaCl is the most appropriate agent for the regeneration of clinoptilolite in a fixed-bed column. The results show that the water quality meets the standard of drinking water when combined with a degasser. The degasser is used to remove a portion of Ca^{2+} ions in water, forming $CaCO_3$. Two fixed-bed columns are connected in the system, Fig. 14.18, for the reason that when one is saturated and needs time to regenerate, groundwater softening can proceed via another ready-to-use fixed-bed column, which would provide a continuous process of water treatment.

The sorption efficiency of clinoptilolite was high when the retention time was 20–25 min in the pilot experiments. The reaction mechanism was mainly a substitution reaction according to the ion balance, and the treatment capacity of the degasser in combination with fixed-bed was 20% higher than that of the layer [2, 82]. Despite the advantages of packaged layer systems, primarily due to their simple construction and handling, these systems also have disadvantages due to the appearance of ducts and dead zones, and thus concentration and temperature gradients. In addition, layer congestion is relatively common.

Fluidized bed systems differ from packaged bed systems in that the surface velocities of fluid are large enough to initiate particles in the bed, leading to a fluidization state. This type of

This book belongs to Badji Mokhtar Annaba University Central Library Copyright Elsevier 2025

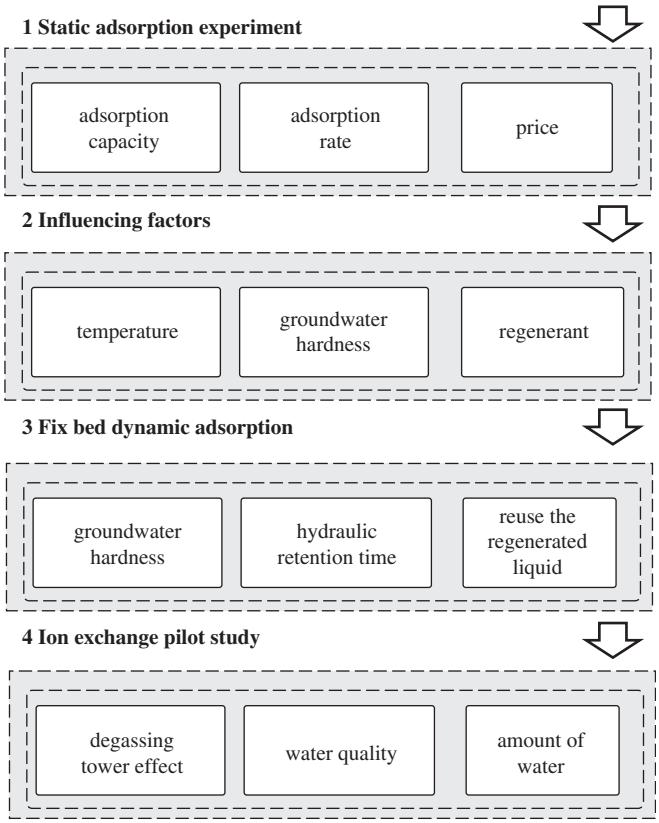

Fig. 14.17
Schematic representation of the principles of monitored parameters and operating conditions of the water hardening system. *Modified from W. Liu, R.P. Singh, S. Jothivel, D. Fu, Evaluation of groundwater hardness removal using activated clinoptilolite, Environ. Sci. Pollut. Res. (2019) 1–9, https://doi.org/10.1007/s11356-019-06193-9.*

particle layer is called a fluidized bed because it acquires certain fluid characteristics. Fluidized bed systems offer solution to most problems that occur with packaged bed systems [163–166]. The advantages of using a fluidized bed are simple control, good mixing of fluidized particles floating in the fluid, providing uniform fluid distribution, low shear stress values, high mass and heat transfer rates thanks to efficient mixing, generally slow response to changes in operating conditions, and thus a simple process control, as well as its applicability on a small and large scale.

Some disadvantages of using a fluidized bed are the possible fragmentation and abrasion of particles, as well as the erosion of pipe and column walls due to collisions with particles. Fluidized bed columns are used for drying operations, heat exchange, sorption, desorption, and many other operations where good contact between fluid and solid particles is required.

This book belongs to Badji Mokhtar Annaba University Central Library Copyright Elsevier 2025

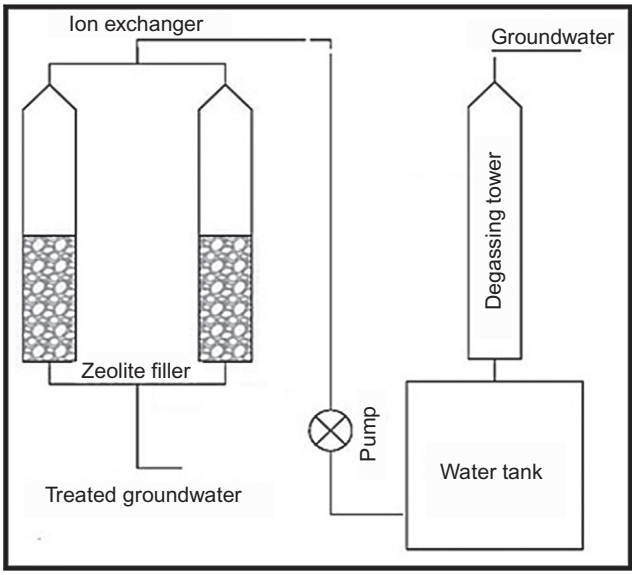

Fig. 14.18
Schematic illustration of a degasser in combination with a fixed-bed system for the treatment of softening of drinking water. *Modified from W. Liu, R.P. Singh, S. Jothivel, D. Fu, Evaluation of groundwater hardness removal using activated clinoptilolite, Environ. Sci. Pollut. Res. (2019) 1–9, https://doi.org/10.1007/s11356-019-06193-9.*

14.7 Zeolite regeneration

The regeneration of saturated zeolites is a very important phase in the operating cycle of ion exchangers or sorbent. Revitalization of pores filled with pollutant zeolites is performed by the action of specific regeneration chemicals [167, 168]. Regeneration chemicals restore the active sites and specific surface area of the zeolite based on the principle of ion exchange [169], oxidation [170], or dissolution. Braschi et al. [171] have schematically illustrated the sorption and regeneration of zeolite Y in Fig. 14.19 by combining solvent extraction and thermal treatment of the zeolite used in the water purification process from sulfonamide antibiotics.

Huang et al. [169] presented the mechanism of ion exchange of ammonia on the zeolite and the process of hypochlorite regeneration with formulas (14.15)–(14.17):

$$\text{Zeolite} - NH_4^+ + Na^+ \leftrightarrow \text{Zeolite} - Na^+ + NH_4^+ \tag{14.15}$$

$$H^+ + ClO^- \rightarrow HClO \tag{14.16}$$

$$2NH_4^+ + 3HClO \rightarrow N_2 + 3H_2O + 5H^+ + 3Cl^- \tag{14.17}$$

This book belongs to Badji Mokhtar Annaba University Central Library
Copyright Elsevier 2025

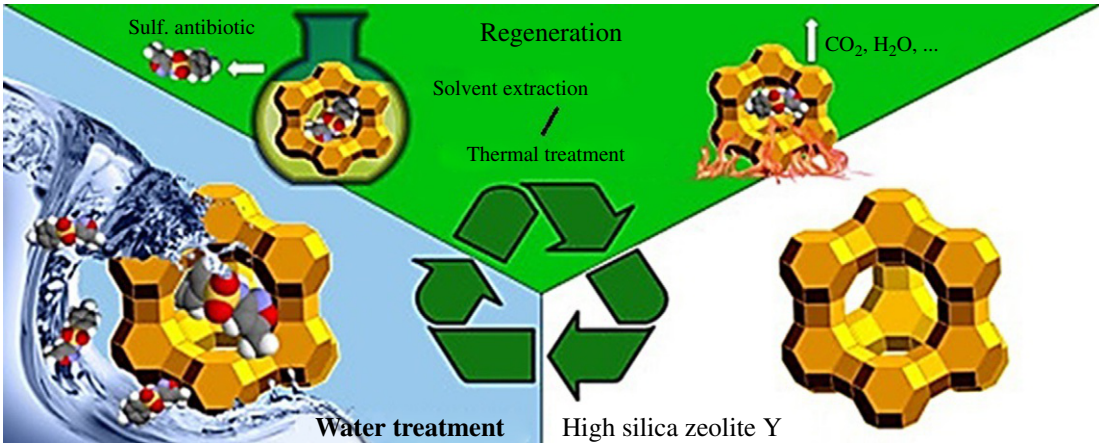

Fig. 14.19
Schematic representation of water purification by zeolite Y and zeolite regeneration. *Reprinted with permission I. Braschi, S. Blasioli, E. Buscaroli, D. Montecchio, A. Martucci, Physicochemical regeneration of high silica zeolite Y used to clean-up water polluted with sulfonamide antibiotics, J. Environ. Sci. 43 (2016) 302–312, https://doi.org/10.1016/j.jes.2015.07.017.*

Du et al. [172] found that a concentration of 0.5 mol L^{-1} NaCl at elevated pH values was sufficient for complete regeneration of native Chinese clinoplilolite from ammonium ions. Li et al. [173] tested a new concept for the removal of ammonia from aqueous solutions by zeolites, followed by electrochemical oxidation, Fig. 14.20, for the regeneration of zeolites. In the first mode, the $(NH_4)_2SO_4$ solution was passed through an ion-exchange column, where ammonia was concentrated in the zeolite. In addition to the electrochemical oxidation/regeneration, the amount of conversion of adsorbed ammonia to nitrogen over the zeolite is greater than 98%. The amount of nitrite conversion was less than 2%, wherein not detect ammonia or nitrites in the regenerated solution. The regeneration solution can be used multiple times over a long period of time with the addition of 2.0 g L^{-1} NaCl solution in the regeneration solution, saving the chemical reagent [174]. Simultaneous regeneration of zeolites and removal of ammonia using electrolysis in the presence of chloride, using an anode based on Ti/IrO_2-Pt and a cathode of Fe in an undivided electrolytic cell, as studied by Li et al. [173], are presented in Fig. 14.20.

Zeolites can be fully regenerated using the method of Li et al. [173], since after zeolite regeneration, NH_4^+ (aq) or nitrites were not detected in solution. More than 97% of NH_4^+ (aq) was converted to nitrogen and less than 3% was converted to nitrates. Li et al. [173] have shown that the regeneration solution is effective after use in five cycles. In this way, both water resources and chemical reagents are stored. The electrochemical method has proven to be a good possibility for complete zeolite regeneration and simultaneous removal of ammonia from the system [173]. The application of electrocatalysts based on platinum metals at the surface of

This book belongs to Badji Mokhtar Annaba University Central Library Copyright Elsevier 2025

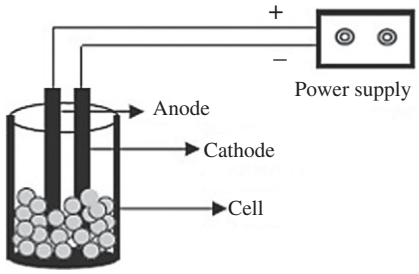

Fig. 14.20
Diagram of the electrochemical apparatus. *Reprinted with permission from M. Li, C. Feng, Z. Zhang, X. Lei, N. Chen, N. Sugiura, Simultaneous regeneration of zeolites and removal of ammonia using an electrochemical method, Microporous Mesoporous Mater. 127(3) (2010) 161–166, https://doi.org/10.1016/j.micromeso.2009.07.009.*

Ti anode and a possible mechanism of the reaction of alloying at low temperatures on the surface of a DSA were explained by Krstić and Pešovski [175, 176]. Krstić and Pešovski [175, 176] outlined the possibilities of using DSA in electrolysis for various industrial uses, as well as the possibility of treating wastewater from organic and inorganic pollutants [82]. On the other hand, Trumić et al. [177–182] have examined in detail the behavior of platinum metal alloys as catalysts at high temperatures for the catalytic oxidation of ammonia, as well as the possibility of reducing the loss of platinum metals in the industrial process, since their cost is very high.

Lahav et al. [183] tested a process for the removal of ammonia from anaerobic-lagoon swine waste based on ion exchange and electrochemical regeneration. The process, consisting of daily sequential operations of adsorption, chemical regeneration, and electro-oxidation of ammonia in the regeneration solution, proved to be feasible to reduce the ammonia concentration in the wastewater from about 1.000 to about 60 mg L^{-1}. Desorption studies of ammonium ions from zeolites show that ion exchange is reversible when a 1% NaCl solution was used for desorption. However, Leyva-Ramos et al. [184] showed that more ammonium ions were desorbed when a 1% KCl solution was used and that the results showed that the ammonium ion altered on the zeolite reached a new equilibrium that was reached below the equilibrium reached during adsorption. The selectivity of clinoptilolites declined in the following order $K^+ > NH_4^+ > Na^+$. Synthetic zeolites bind ammonium ions effectively, unlike natural zeolites that have a quarter of the capacity of synthetic zeolites. The regeneration of natural zeolites is less effective than the regeneration of synthetic zeolites. Synthetic zeolites can generally be regenerated with saturated NaCl and Na-hypochlorite solution [185].

The results of the removal of ammonia from aqueous solutions, using zeolite synthesized from ash by the fusion method, which combines alkaline fusion followed by hydrothermal treatment, were published by Zhang et al. [186]. The CEC increased from 0.03 to 2.79 mEq/g during the synthesis process. The effects of contact time, pH, ammonium inlet

This book belongs to Badji Mokhtar Annaba University Central Library Copyright Elsevier 2025

concentration, adsorbent dosing, and the presence of other cations and anions were investigated. The study results show that these parameters have significant effects on the removal of ammonium from synthesized zeolites. The maximum ammonium ion adsorption capacity obtained was 24.3 mg g^{-1}. The regenerated zeolite had almost the same adsorption capacity of ammonium ions as the synthesized zeolite. For this reason, the results obtained indicate that the synthesized zeolite is a promising material for the removal of ammonium ions from water [187–189].

Testing the removal of Fe^{2+} and Co^{2+} from an aqueous solution was performed using a packed layer of zeolite NaY, wherein it is shown that the zeolite is more selective with respect to Co^{2+} in relation to Fe^{2+} [190]. Regeneration was performed using a solution of 2 mol dm^{-3} $NaNO_3$, where about 80% was desorbed in the case of both ions. The capacity of regenerated zeolite reported was to decreased about 10%–15% [190]. Margeta et al. [123] presented the results of the desorption efficiency of Pb^{2+}, Zn^{2+}, Cd^{2+}, Cu^{2+}, and Ni^{2+} ions for the regeneration of natural zeolite-clinoptilolite using different concentrations of a desorbing solution such as 3 M KCl, 0.5 M NaCl, 1 M KNO_3, 0.1 M HCl, etc., depending on the metal desorbed from the zeolite. The desorption efficiency of zeolite had a value of over 95% for the release of individual metal ions.

14.8 Discussion

14.8.1 Sorption of metal cations on natural and synthetic zeolites

Natural and synthetic zeolites, in addition to their multiple uses, are also used to remove toxic metal ions from synthetic solutions and different wastewater solutions. To this end, many authors have examined sorption of cations under different conditions, from single-component and multicomponent solutions, at different pH, at different temperatures, at different contact times of sorbent and sorbate [136, 191, 192]. The selectivity of zeolites to metal ions depends on the purity of the natural zeolites, the experimental conditions of the synthetic zeolites, as well as the experimental conditions when testing sorption, and therefore there are differences in published results.

Egashira et al. [191] examined the removal of Cu^{2+}, Zn^{2+}, and Mn^{2+} ions from one-component synthetic solutions on a natural zeolite. The sorption was tested in an acidic medium at pH values of 2.5–5 to avoid the precipitation of metal hydroxide at higher pH values. The reported results showed that the sorption capacity increased with an increase in the initial pH value and then remained almost unchanged for pH range of 3 –5. The amount of Cu^{2+}, Zn^{2+}, and Mn^{2+} ions that sorbed on zeolite were 0.16, 0.14, and 0.13 mmol g^{-1} and 2.5, 0.20, 0.15, and 0.14 mmol g^{-1}, respectively, for pH value 3 and 5. The sorption range obtained is consistent with the values of the hydration radii.

This book belongs to Badji Mokhtar Annaba University Central Library Copyright Elsevier 2025

The authors conclude that an increase in the sorption capacity occurs with the increase of the pH value of the solution, with the mechanism of precipitation. The authors showed that, in addition to the commonly used neutralization method, the sorption method can be successfully used to treat wastewater from mines.

Similar conclusions were reached by Merrikhpour and Jalali [192]. In order to treat industrial wastewater, they examined the removal of Cd^{2+}, Cu^{2+}, Ni^{2+}, and Pb^{2+} ions from one-component synthetic solutions by sorption on natural zeolite, at a pH of 5.5. Sorption has also been investigated with different masses of sorbent, at different pH values, at different contact times of sorbent and sorbate, etc. The results obtained during the different equilibration periods show that the sorption of Pb^{2+} ion is very fast and that virtually the whole quantity of this ion is absorbed in the first 40 min, while in the case of Cd^{2+}, Cu^{2+}, and Ni^{2+} ions a gradual increase in sorption was observed according to the time and that the optimal contact time is 24 h. The results of the pH test showed that the sorption of the cations investigated increased with increasing the initial pH from 2 to 4, and then remained almost unchanged in the initial pH range of 4–7. With the increasing pH, the concentration of OH ions in the solution increases, causing the metal to precipitate. The zeolite selectivity toward metal ions, explained on the basis of ionic radius values, dissociation constants [193], and metal electronegativity [194], should decrease in the $Pb^{2+} > Ni^{2+} > Cu^{2+} > Cd^{2+}$ series. A different sorption sequence obtained experimentally has been explained by these authors as the deposition of metal hydroxide, which can have a significant effect on the removal process of the ions studied on the natural zeolite.

Motsi et al. [136] also examined the removal of Fe^{3+}, Cu^{2+}, Mn^{2+}, and Zn^{2+} ions in addition to single-component and multicomponent synthetic solutions at an initial pH of 3.5 to investigate the effect of cation competition. The results obtained showed that in the case of Fe^{3+} ions only, the amount of absorbed Fe^{3+} ions from the multicomponent solution was approximately similar to the amount sorbed from the single-component solution, which the authors explained by the deposition mechanism as the main mechanism for the removal of Fe^{3+} ions. The sorption of the other three test cations was significantly reduced in multicomponent solutions compared to single-component ones, more so in the case of a higher concentration solution, indicating that different sorption mechanisms are involved in the sorption of test cations from the solution.

In order to treat industrial wastewater, Sayed and Khater [195] examined the removal of Cd^{2+} and Pb^{2+} ions by sorption on natural zeolite. The sorption was tested from one-component solutions, at a pH of 5.5 and a constant temperature of 30°C. The results obtained showed that the sorption of Cd^{2+} and Pb^{2+} ions decreased with increasing concentration of metal ions in aqueous solutions. These results indicate that with an increasing concentration of metal ions in an aqueous solution, less favorable sites are involved in the sorption process. Using the sorption isotherms, it was observed that the Langmuir model describes the sorption process more effectively than the Freundlich model. Pb^{2+} ions have better sorption, and in this case, the

This book belongs to Badji Mokhtar Annaba University Central Library Copyright Elsevier 2025

authors explained with a smaller hydration radius and higher electronegativity of Pb^{2+} ions relative to Cd^{2+} ions.

Erdem et al. [56] examined the removal of Co^{2+}, Cu^{2+}, Zn^{2+}, and Mn^{2+} ions from one-component solutions by sorption on natural zeolite (clinoptilolite) at a pH of about 6–7. An experiment was carried out to test the suitability of three different adsorption isotherm models: the Langmuir model, the Freundlich model, and the Dubinin-Radushkevich (DR) model. The results obtained showed the most approximate correlation between the experimental results and the Langmuir model. The sorption sequence obtained of $Co^{2+} > Cu^{2+} > Zn^{2+} > Mn^{2+}$ was explained by the fact that the ions of the tested metals in aqueous solutions are surrounded by six water molecules and pass through channels in the zeolite in this form. Since the charge of the studied cations is the same (+2), the authors concluded that the charge does not affect the sorption efficiency, but the cation hydration radius is very significant and the cation of the largest hydration radius is the least absorbed. Based on the results of the sorption energy E (kJ mol^{-1}), the authors concluded that the tested ions are sorbed by the ion-exchange mechanism.

Alvarez-Ayuso et al. [78] examined the sorption of Cr^{3+}, Ni^{2+}, Zn^{2+}, Cu^{2+}, and Cd^{2+} ions on clinoptilolite, a natural zeolite, and a synthetic zeolite NaP1, for the purpose of the purification of sewage by the electroplating process. Sorption was investigated from one-component solutions at pH values of 4 (for Cr ion), 5 (for Cu ion), and 6 (for Ni, Zn and Cd ions). The results of testing the influence of contact time on the amount of sorbed ions showed that for Ni, Zn, and Cd ions, the equilibrium was reached after 1 h of equilibration, but in this case also the highest amount was sorbed at the beginning of the process. The sorption on the synthetic zeolite was significantly faster. Based on the sorption isotherms, the sorption capacities of the synthetic zeolite reported to be about ten times higher than the natural zeolite, which were expressed in mmol g^{-1} for Cr (0.838), Cu (0.795), Zn (0.499), Cd (0.452), and Ni (0.342) determined on the synthetic zeolite NaP1 and Cr (0.079), Cu (0.093), Zn (0.053), Cd (0.041), and Ni (0.034) determined on the natural zeolite. This is consistent with the higher H^+ ion-exchange capacity and higher CEC of the synthetic zeolite, which is due to the low Si:Al ratio (Si/Al clinoptilolite 4.8 and Si/Al NaP1 1.7). In general, zeolites with a lower Si/Al ratio have higher sorption capacities of metal ions [196, 197].

Pitcher et al. [137] examined and compared the ability of synthetic zeolite and natural zeolite (mordenite) to reduce the concentration of Pb^{2+}, Cu^{2+}, Zn^{2+}, and Cd^{2+} ions in synthetic solutions. The pH of the starting solutions was not adjusted and was 3.2 in the case of synthetic solutions and 7.1 in the case of highway atmospheric water. These authors have found that synthetic zeolite is significantly more efficient than natural zeolite, for sorption of metal cations from both real and synthetic solutions. The pH of the solution after contact with the synthetic zeolite was increased to 8.5 in the case of synthetic solutions and to pH 9.0 in the case of true highway atmospheric water, which is typical of synthetic zeolites because ion exchange of H^+ ions with zeolite ions decreases the concentration of H^+ ions in solution. The change in pH in

This book belongs to Badji Mokhtar Annaba University Central Library Copyright Elsevier 2025

the case of natural zeolite application was much lower (slightly increased to 3.6 in synthetic solutions, and decreased to 5.3 in highway atmospheric waters). The released sodium ions in the case of both zeolite tests showed that an ion-exchange process had taken place. The higher amount of released sodium ions from the synthetic zeolite explains the higher sorption capacity of the synthetic zeolite. However, in alkaline environments, after contact with the synthetic zeolite, the metal cations investigated tend to precipitate on the zeolite surface. On this basis, the authors concluded that the mechanism of removal by the natural zeolite of the metals investigated is probably the mechanism of ion exchange. Therefore the synthetic zeolite is presumably both the mechanism of ion exchange and the mechanism of deposition.

Günay et al. [70] examined the removal of Pb^{2+} ions by sorption on natural zeolite (clinoptilolite). The maximum sorption capacity, at an initial pH of 4.5, was 80.9 mg g^{-1}. The results obtained, using Langmuir, Freundlich, DR, and Temkin models, showed that the sorption process can best be described by the Temkin model. The value of the sorption energy ($E = 9.157$ kJ mol^{-1}) indicated that the removal of Pb^{2+} ions was carried out by an ion-exchange mechanism. The results of the study of the effect of contact time of sorbent and sorbate showed that the removal of Pb^{2+} ions by sorption on clinoptilolite increased with time, reaching the maximum sorption value in the first 60–120 min, and then remained constant. The results obtained of the sorption kinetics were analyzed using the pseudo-first and pseudo-second-order models and the Elovich model, on the basis of which it was determined that the sorption of Pb^{2+} ions can best be described using the pseudo-first-order model. A negative change in Gibbs energy, ΔG of -8.86 kJ mol^{-1}, indicates that the sorption process of Pb^{2+} ions on clinoptilolite is a spontaneous process at room temperature.

Wang et al. [198] examined the removal of Pb^{2+} and Cu^{2+} ions from single-component solutions on natural zeolite. The results obtained by determining the sorption isotherms, at a pH of 5, showed that the amount of Pb^{2+} and Cu^{2+} ions adsorbed on the natural zeolite was 68 and 23 mg g^{-1}, respectively. The sorption isotherms showed that Langmuir's model best describes the sorption process. Examination of the influence of pH in the interval from 3 to 8 confirmed that with increasing pH of the solution, the sorption of Pb^{2+} and Cu^{2+} ions increased. The authors observed significant changes in the sorption of Pb^{2+} and Cu^{2+} ions at pH >6, which occur probably due to the deposition of Pb^{2+} and Cu^{2+} ions on the zeolite surface. The results obtained are explained by these authors by the fact that the sorption of metal ions on the zeolite takes place by ion-exchange mechanism and deposition mechanism.

El-Kamash et al. [199] examined the sorption of Zn^{2+} and Cd^{2+} ions on synthetic zeolite A at temperatures of 298, 313, and 333 K. The results obtained showed an increase in the amount of sorption of Zn^{2+} and Cd^{2+} ions with increasing temperature, which the authors explained by increasing the number of active sites on the surface available for sorption on synthetic zeolite A. Another reason may be a change in pore size and a decrease in the thickness of the boundary layer with increasing temperature, which leads to a decrease in the resistance to mass transfer of the sorbate in the boundary layer. The sorption kinetics showed that, in this case, the largest

This book belongs to Badji Mokhtar Annaba University Central Library Copyright Elsevier 2025

amount was also sorbed at the beginning of the process, within the first 20 min and completed after 45 min of equilibration. Testing of the experimental data for sorption kinetics with theoretical models showed that the sorption process best describes by a pseudo-second-order model. That led the authors to conclude that the degree sorption is chemical, chemisorption. Good agreement with Freundlich and DR is shown. Based on the values of sorption energies, the authors concluded that Cd^{2+} and Zn^{2+} ions are sorbed on synthetic zeolite A by an ion-exchange mechanism. The positive value of Gibbs free energy (ΔG^{Θ}) indicated that there is an energy barrier and that the sorption process is not a spontaneous process. The positive value of enthalpy change, $\Delta H\Theta$, indicated that the sorption process is an endothermic process.

Castaldi et al. [16] examined the sorption of Pb^{2+}, Cd^{2+}, and Zn^{2+} ions from single-component and multicomponent solutions on natural zeolite at a constant pH of 5.5. The test results show a different trend of sorption of the mentioned ions depending on whether the sorption takes place from single-component or multicomponent solutions. When tested from single-component solutions, the sorption decreases in the series $Zn^{2+} > Pb^{2+} > Cd^{2+}$, while for multicomponent solutions the sorption decreases in the next series, $Pb^{2+} > Cd^{2+} > Zn^{2+}$. Such a different sorption trend is explained by the competition between these three ions. It is assumed that in a multielement solution, the zeolite is less selective for Zn^{2+} ion because its hydration radius and hydration energy are higher than the hydration radii and hydration energy of Pb^{2+} and Cd^{2+} ions. The interaction between the sorbent and Pb^{2+}, Cd^{2+}, and Zn^{2+} ions was assumed to be of a physical nature, that is, electrostatic attraction occurs between the negatively charged zeolite surface and the positively charged metal ions (ion exchange).

Oter and Akcay [17] investigated the removal of Pb^{2+}, Cu^{2+}, Zn^{2+}, and Ni^{2+} ions from one-component and multicomponent solutions on natural zeolite, at a pH of 5.0. The test results showed the same sorption trend of the mentioned ions, whether sorption occurs from single-component or multicomponent solutions. However, the amounts of metal ions sorbed on the zeolite differed significantly in the case of sorption from single-component solutions from sorption from multicomponent solutions. The best sorption of Pb^{2+} ion is explained in this case by the lowest hydration radius and the lowest value of the hydration energy of Pb^{2+} ion. The sorption from the multicomponent solution is probably weaker due to the strong interactions of Pb^{2+} ions with the zeolite, which interfere less with the sorption of Zn^{2+} ions compared with the sorption of Cu^{2+} and Ni^{2+} ions, thus explaining the much lower sorption of Cu^{2+} and Ni^{2+} ions from multicomponent solutions.

To investigate the effect of cation competition, Merrikhpour and Jalali [192] examined the removal of Cd^{2+}, Cu^{2+}, Ni^{2+}, and Pb^{2+} ions from single-component and multicomponent synthetic solutions, at an initial pH of 5.5. The results obtained showed that the sorption of the tested ions from multicomponent solutions was significantly lower than the sorption from the single-component solutions, which the authors explained in this case also by the competition between these four cations. Experiments with multicomponent solutions have shown that sorption decreases in the series $Cu^{2+} > Ni^{2+} > Pb^{2+} > Cd^{2+}$. That is why the authors assumed

This book belongs to Badji Mokhtar Annaba University Central Library Copyright Elsevier 2025

that zeolite is more selective for Cu^{2+} ion in a multicomponent solution, as opposed to Pb^{2+} ions. The difference in zeolite selectivity indicates that the zeolite is more selective for Pb^{2+} ion in the absence of competition with Cd^{2+}, Cu^{2+}, and Ni^{2+} ions.

A number of scientists have examined and compared the sorption of metal ions on zeolites from single-component and multicomponent systems. Table 14.7 shows useful information on the influence of some types of zeolite for different pH values when metal ion uptake occurs. The general conclusion is that the sorption of divalent metal ions from multicomponent systems is lower than the sorption from single-component systems, which is most often the result of competition between ions [16, 18, 200–202]. It is also noted that the mechanism of sorption in a multicomponent system is complicated. The behavior of each metal ion in a system containing multiple metal ions depends mainly on the concentration and properties of the other ions present, the pH of the solution, the physical and chemical properties of both the sorbent and the sorbate [200].

Table 14.7 Influence of type of zeolite and pH on metal ion uptake.

Ions	Zeolite	BET (m^2 g^{-1})	pH	Favorable isotherms	q_{max} (mg g^{-1})		References
					Natural	Synthetic	
Cu^{2+}	CLP	31	2.5	Langmuir	10.17	–	[191]
	CLP	31	3–5	Langmuir	12.71	–	[191]
	CLP	–	5	Langmuir	5.91	50.52	[78]
	CHA	159	2.5	Langmuir	8.26	–	[191]
	CHA	159	3–5	Langmuir	11.44	–	[191]
	tuff	16	5	Langmuir	23.00	–	[198]
Pb^{2+}	CLP	–	4.5	Temkin	80.90	122.40	[70]
	tuff	16	5	Langmuir	68.00	–	[198]
Zn^{2+}	CLP	31	2.5	Langmuir	8.90	–	[191]
	CLP	31	3–5	Langmuir	9.53	–	[191]
	CHA	159	2.5	Langmuir	4.45	–	[191]
	CHA	159	3–5	Langmuir	6.99	–	[191]
	MOR	26	2.5	Langmuir	52.74	–	[191]
	MOR	26	3–5	Langmuir	53.38	–	[191]
	CLP	–	6	Langmuir	3.36	31.71	[78]
Mn^{2+}	CLP	31	2.5	Langmuir	8.26	–	[191]
	CLP	31	3–5	Langmuir	9.53	–	[191]
	CHA	159	2.5	Langmuir	6.99	–	[191]
	CHA	159	3–5	Langmuir	7.63	–	[191]
	MOR	26	2.5	Langmuir	10.80	–	[191]
	MOR	26	3–5	Langmuir	10.80	–	[191]
Cr^{3+}	CLP	–	4	Langmuir	5.02	53.25	[78]
Cd^{2+}	CLP	–	6	Langmuir	2.61	28.73	[78]
Ni^{2+}	CLP	–	6	Langmuir	2.16	21.73	[78]

BET, surface area; *CLP*, clinoptilolite; *MOR*, mordenite; *CHA*, chabazite; *tuff*, natural zeolite tuff.

This book belongs to Badji Mokhtar Annaba University Central Library
Copyright Elsevier 2025

14.8.2 Sorption of metal cations on natural and modified zeolites

Motsi et al. [136] examined the effect of thermal activation of natural zeolite on the sorption efficiency of Fe^{3+}, Cu^{2+}, Mn^{2+}, and Zn^{2+} ions. The thermal treatment was performed in two ways, by annealing the samples for 30 min at 200°C, 400°C, and 800°C and exposing the natural zeolite to microwave energy of 2.45 GHz at 950 W for 15 and 30 min. The thermally activated zeolite samples were then equilibrated with one-component synthetic solutions. The results obtained showed that in the case of zeolite exposed to microwave radiation, the rate of sorption initially increased and then began to decrease after 30 min. Sorption on annealed zeolite compared to untreated zeolite was faster and more efficient in the case of applied temperatures of 200°C and 400°C, while annealing at high temperature of 800°C led to a decrease in sorption efficiency. The increase in sorption rate and sorption capacity, as a result of thermal treatment, was explained by the authors by removing water from natural zeolite channels. In this way, the channels became empty, which enabled faster and higher sorption of the tested ions and thus improved the sorption capacity of the zeolite. In zeolite samples subjected to extreme thermal conditions (800°C), removal of water caused changes to the surface of the samples, porosity was reduced, which caused a decrease in the sorption capacity of the zeolite.

Çoruh [115] examined the removal of Zn^{2+} ions by natural and activated zeolites. For this purpose, samples of natural clinoptilolite, clinoptilolite treated with 2 M NaCl for 24 h, and clinoptilolite treated with 0.1 M HCl for 5 h were used. Also, tests were performed at different pH values of the solution and at different temperatures ranging from 10°C to 90°C. The results of the pH influence test showed that the efficiency of Zn^{2+} ion removal by the sorbents tested remained almost unchanged when the initial pH of the solution increased from 4 to 7. The efficiency of the zeolite to remove Zn^{2+} ions was increased and reached the highest value at pH 8. The efficiency of the removal of metal ions increases with increasing pH of the solution, which is explained by the "competition" of H^+ ions with metal ions for sorption sites on the zeolite. The results of testing the effect of temperature on the sorption of Zn^{2+} ions by the sorbents tested have shown that sorption capacities increase with increasing temperature. By comparing the sorption properties of natural and activated zeolites, it was found that activation achieved more efficient removal of Zn^{2+} ions. The most efficient removal was achieved by activation with NaCl, which was explained by the increased concentration of Na^+ ions and, consequently, greater ionic exchange.

Vasylechko et al. [120] examined the sorption of Cd^{2+} ions on natural zeolite and zeolite activated by various acids (1 M HCl, 1 M HNO_3, and 0.5 M H_2SO_4) at a temperature of 20°C, at a pH of 5.6 for 24 h. After 24 h of zeolite activation, the aluminum (III) content of the solutions was also determined. The results obtained showed a significant increase in the sorption capacity of H-clinoptilolite toward Cd^{2+} ion compared to natural clinoptilolite, which was explained by the fact that the most variable positions are occupied by H^+ ions, which are small in size, which greatly simplifies access to cadmium ions by active sorption centers, and thus the sorption of Cd^{2+}

This book belongs to Badji Mokhtar Annaba University Central Library Copyright Elsevier 2025

ions increases. The highest sorption capacity was achieved by treatment with 1 M HCl, which was explained by the aforementioned authors by the solubility of Al^{3+} ions. Namely, the results obtained of testing the content of Al^{3+} ions showed that after treatment of zeolites with acids, there was a partial elimination of Al^{3+} ions from the zeolite structure and that even a slight loss of Al^{3+} ions led to a decrease in the sorption capacity of clinoptilolite toward Cd^{2+} ion. The amount of dissolved aluminium depended on the nature of the acid. It was highest in the case of H_2SO_4, followed by HNO_3 and smallest in the case of HCl. Thus explaining the highest sorption capacity of the zeolite activated with 1 M HCl for Cd^{2+} ion.

Lin et al. [127] examined the sorption of Cu^{2+} ions on surface-activated natural zeolite (SMZ) and on SMZ with immobilized humic acid (HA-SMZ). The surface modification of the zeolite was carried out with CPB at an initial pH of 6 for 24 h. The results obtained showed that HA-SMZ had a higher sorption efficiency for Cu^{2+} ion compared to SMZ. The CPB and HA molecules are too large to enter the inner zeolite channels and their concentration on the natural zeolite is restricted only to the outer cation exchangeable sites, indicating that the exchange of Cu^{2+} ions with exchangeable cations from the zeolite structure is an important mechanism affecting the sorption of Cu^{2+} ions at SMZ and HA-SMZ. Examination of the effect of the pH of the solution showed that the sorption of Cu^{2+} ions on HA-SMZ is highly dependent on the pH of the solution and that the sorption efficiency increases with increasing the initial pH of the solution from 3 to 7. The low sorption capacity of Cu^{2+} ions in a strongly acidic solution is explained in this case by the "competition" of H^+ ions with metal ions for zeolite sorption sites. In addition, with the increasing pH of the solution, more carboxyl and phenolic groups are formed in HA-SMZ and this increases the negative charge on the sorbent surface, thus facilitating the sorption of Cu^{2+} ions on the sorbent by electrostatic interactions and surface complexation. The amount of metal hydroxide increases with increasing pH of the solution, which also enhances the sorption of Cu^{2+} ions by the precipitation mechanism [203, 204]. The results obtained of sorption kinetics, analyzed using pseudo-first- and pseudo-second-order kinetic models and intraparticle diffusion models, showed that the process of sorption of Cu^{2+} ions to HA-SMZ can be well described by the pseudo-second-order kinetic model. The agreement of the obtained experimental data with different models of adsorption isotherms was also investigated and the best agreement with the Langmuir model was determined. The obtained sorption energy values of E indicate that the sorption of Cu^{2+} ions onto HA-SMZ occurs by chemical sorption. The thermodynamic parameters (Gibbs free energy change, enthalpy change, and entropy change) showed that the sorption of Cu^{2+} ions to HA-SMZ is spontaneous and the process is endothermic. The Gibbs free energy change values suggest that the sorption of Cu^{2+} ions onto HA-SMZ takes place through an ion-exchange process. Based on the values of E and ΔG, the authors concluded that the sorption of Cu^{2+} ions onto HA-SMZ involves both the ion-exchange process and the chemical sorption process and that the predominant mechanisms of Cu^{2+} ion sorption to HA-SMZ are surface complexation (with

This book belongs to Badji Mokhtar Annaba University Central Library Copyright Elsevier 2025

carboxyl and phenolic groups of immobilized HA molecules) and ion changes (with exchangeable cations in the inner channels of the zeolite).

Ali et al. [15] examined the sorption of Pb^{2+} ions on the naturally occurring and surface-modified synthetic zeolite ZSM-5. Modifications of the zeolite were performed with tetrapropylammonium bromide (TPABr), *n*-propyl amine (*n*-PA), tetrabutylammonium bromide (TBABr), and cetyltrimethylammonium bromide (CTAB). The results obtained showed that the sorption capacity of the sorbents against Pb^{2+} ion investigated decreased in the series TPABr-SMZ > TBABr-SMZ > CTAB-SMZ > Na-ZSM-5 > *n*-PA-SMZ, which was explained by the channel size in ZSM-5 and the size of the modifier molecule. The highest sorption capacity of TPABr-SMZ may be related to easier introduction of TBABr within channels in the zeolite structure and complexation with lead ions. The authors explained the lower sorption of Pb^{2+} ions of TBABr and CTAB-modified zeolite compared to the sorption on TPABr-SMZ by the fact that TBABr and CTAB molecules are slightly larger than the channel openings in clinoptilolite and thus block openings and interfere with the sorption of other cations (metal ions). Bhattacharyya and Gupta [205] found that TBABr and CTAB reduce the diffusion of Pb^{2+} ions in the zeolite, which they also explained by channel blocking. On the other hand, the *n*-PA molecule has smaller dimensions than the channel dimensions in the ZSM-5 and when introduced into the channels to balance the negative charge, it may be that the *n*-PA molecules cannot balance the different charges located close to each other, so that only one part of the cation can be altered with *n*-PA. The size of *n*-PA molecules may be responsible for slow diffusion in the inner channels of zeolites.

Leyva-Ramos et al. [126] examined the sorption of Cr^{6+} on natural zeolite and hexadecyltrimethylammonium (HDTMA)-modified zeolite at a pH 6. Significantly, the sorption of Cr^{6+} on the modified zeolite is about 22 times higher than that on the natural zeolite. The authors have explained this by the fact that the natural zeolite has removable places of mainly cationic nature, thereby enabling a cation exchange. While Cr^{6+} in an aqueous solution was present as the anion ($HCrO_4^-$ or CrO_4^{2-}), the sorption of Cr^{6+} on the natural zeolite was insignificant. Testing the effect of the pH of the solution, they showed that the sorption capacity of the modified zeolite is highly dependent on the pH of the solution and decreases with an increasing pH, which the authors explained by the different types of Cr present in the solutions at different pH values.

Kragović et al. [206] examined the effect of temperature on the rate and amount of Pb^{2+} ions sorbed on natural and iron(III)-modified zeolite. The results obtained of the sorption kinetics test are best described by the pseudo-second-order equation. The results of the thermodynamic parameter determination showed that for low initial concentrations of Pb^{2+}, the sorption on both sorbents is a spontaneous process. With increasing concentration, the sorption process is no longer spontaneous. For iron(III)-modified zeolite, the ΔG^{Θ} value was lower than that for

This book belongs to Badji Mokhtar Annaba University Central Library Copyright Elsevier 2025

natural zeolite, and more negative in a wider concentration range, indicating, according to these authors, the greater number of active sites available for spontaneous sorption of Pb^{2+} ions. In addition, the value of ΔG^{Θ}, which becomes negative with increasing temperature, suggests that an increase in temperature leads to an intensification of sorption. Positive values of enthalpy change (ΔH^{Θ}) indicated that sorption of Pb^{2+} ions on both sorbents is an endothermic process. Positive values of entropy (ΔS^{Θ}) indicate a spontaneous sorption process of lead ions on both sorbents. On the basis of the comprehensive results obtained, these authors concluded that the mechanism for the sorption of Pb^{2+} ion on natural and iron(III)-modified zeolite is complex and includes ion exchange, a mechanism internal to the complexing and the deposition of lead on the surface of the zeolite [58, 206].

Feng et al. [57], in order to remove the Pb^{2+}, Cu^{2+}, and Cd^{2+} ions, modified clinoptilolite with magnetite and $Fe(OH)_3$. At a pH of 6.8, initial concentrations of test cations of 100 mg dm^{-3} each and a balancing time of 1 h, the sorption of Pb^{2+}, Cu^{2+}, and Cd^{2+} ions on untreated clinoptilolite was 58, 14, and 11 mg g^{-1}, respectively. It was also shown in this case that the efficiency of sorption of toxin metal ions increases with increasing pH of the solution. At higher pH values, the formation of metal hydroxides on the surface of clinoptilolite contributes to the increase in the amount of sorbed ions. In addition to the sorption of toxic metal cations, iron(III)-zeolite was also used to test the removal of individual anions from water.

Stanić et al. [207] examined the sorption of As^{5+} ions on natural and iron(III)-chloride-modified zeolite. The tests were performed at room temperature for 24 h. The authors proved that the modified zeolite sorbs gave significantly higher amounts of As^{5+} ions compared to the natural zeolite. Similar conclusions were reached by Jeon et al. [208], who also examined the sorption of As^{5+} ions on natural and iron(III)-modified zeolites. In this case, the modification of the natural zeolite was carried out with an aqueous solution of iron(III)-chloride. The maximum absorbed amount of As^{5+} ion on iron(III)-modified zeolite was 0.68 mg g^{-1}, which is a very small capacity. The groups of authors such as Zeng et al. and Li et al. have also examined the removal of arsenic with the use of native zeolite and iron-modified zeolite [132, 209]. Based on the results obtained, it was shown that for the removal of arsenic, iron (III)-modified zeolite is more effective than natural zeolite [130, 132, 209]. The results show that more effort is needed to modify the zeolite in order to improve the results of the sorption of arsenic and the sorption results of other metal ions that pollute the water.

14.8.3 Sorption of ammonium and other ions on natural and modified zeolites

Demir et al. [210] studied the removal of ammonium ions from an aqueous solution by ion exchange, using columns filled with natural zeolite. The results show that conditioning (mechanical activation by shredding) of zeolites increases the ion-exchange capacity, but also that the smaller particle size leads to a greater ion-exchange capacity due to the larger available surface area. The actual ion-exchange capacity of conditioned fine (1.00 mm) and coarse

This book belongs to Badji Mokhtar Annaba University Central Library Copyright Elsevier 2025

fractions (2.00 mm) of clinoptiolite was found to be 0.57 and 0.38 mEq g^{-1} zeolite, respectively.

Malekian et al. [211] used a natural zeolite, which is suitable as an ion exchanger for NH_4^+ (aq) ammonium. They determined the ability to remove ammonium ions from aqueous solutions with different concentrations of Na^+ (0.03, 0.1, and 0.3 mol L^{-1}) using the native Iranian zeolite *meso* and nanoparticles. The results obtained show that the input concentrations of NH_4^+ (aq) and Na^+ (aq) have a significant influence on the amount of NH_4^+ (aq) exchanged.

Malovanyy et al. [212] studied the application of four types of ion-exchange materials in filled columns, namely strongly and weakly acidic ion-exchange resins, as well as natural and synthetic zeolites. The removal efficiency of ammonium ions was shown to be greater than 95%. Alshameri et al. [213] published the results of the potential use of natural zeolite and its effect on the efficiency of ammonium ion removal (NH_4^+ (aq)), and this study shows that modified Yemeni zeolite has significant potential as an economically viable and effective adsorbing material, for the removal of ammonium ions from aqueous solution. Zhao et al. [214] reported that magnetic zeolite can be used to remove ammonium ions, thanks to its good adsorption performance and easy separation process from an aqueous solution. Rahmani et al. [215], Thornton et al. [216, 217], Yao et al. [188], Bai et al. [187], Zhang et al. [189] also addressed the use of natural and activated zeolites for sorption of ammonium ions from water and showed that zeolites are a potential adsorber for this use.

The exchange capacity of ammonium ions from natural CHA was examined by Leyva-Ramos et al. [218]. The effects of temperature and pH on the ammonium ion-exchange capacity of CHA were examined, with the capacity increased by increasing the temperature from 15°C to 35°Cand at pH values from 3 to 6. The natural CHA was modified by hydrothermal treatment using NaCl and KCl solutions. The modification was found to affect the exchange capacity of ammonium ions on CHA. The capacity of natural CHA is compared with the capacity of natural clinoptilolite, and the results obtained show that the capacity of CHA is 1.43 times higher than that of clinoptilolite.

Moussavi et al. [219] examined the applicability of natural zeolite for the simultaneous removal of ammonia and humic acids at different pH values, at initial concentrations of ammonia and humic acids, and obtained maximum experimental values of the adsorption capacity of ammonia and humic acids, as binary components of 49.7 and 10.5 mg g^{-1}, respectively.

Sun et al. [133] examined the removal of fluoride ions from drinking water on a zeolite-modified solution of $FeCl_3$ at a concentration of 0.1 mol dm^{-3}. An examination of the rate of removal of fluoride ions from drinking water at pH 6.7 showed that balancing occurred after 2 h. Investigation of the influence of pH on the sorption capacity showed that the capacity increased to pH 7 and then decreased, which was explained by the competition between the hydroxyl ions and fluoride ions for the iron (III)-zeolite active sites. Generally, the sorption capacities at all

This book belongs to Badji Mokhtar Annaba University Central Library Copyright Elsevier 2025

the pH values tested were small, not greater than 1 mg g^{-1}, but higher than the natural zeolite capacity, as confirmed by Hortigüela et al. [220].

14.9 Conclusions and future perspectives

Zeolites occupy a significant place among the most commonly used sorbents, due to their availability in large quantities in many parts of the world, and because of the substantial number of synthetic forms. Low price, low product solubility, high specific surface area, good mechanical and thermal properties are essential features that allow zeolites to be ideal candidates for the sorption of pollutants from the liquid phase and for water treatment. In terms of environmental protection, the large sorption capacity of zeolites for toxic ions is of great importance. In order to improve the sorption capacity of natural zeolites, to increase their selectivity for a particular ion or group of ions, and to improve their general physicochemical properties, zeolites can be modified in various ways, depending on the application desired.

Efficiency in water treatment depends on the type and quantity of zeolites used, zeolite porosity, particle size of pollutants, initial concentration of contaminants (cation/anion), solution pH, ionic strength of the solution, temperature, pressure, contact time between zeolite and solution, and presence of other organic and inorganic contaminants. High ion-exchange capacity and relatively high specific surface area and low prices make zeolites attractive sorbents in the removal of pollutants from wastewater. Due to an excess negative charge on the surface of the zeolite, which is the result of the isomorphic replacement of silicon by aluminum in primary structural units, natural zeolites belong to the group of cationic exchangers.

Natural zeolites' unique three-dimensional porous structure, with their remarkable ion-exchange and sorption capabilities, creates the possibility of developing numerous applications which prove acceptable for environmental use. Their effectiveness, in different fields of application, depends on certain physicochemical properties, which are closely related to their geological deposits. Zeolites can lose or bind water reversibly and alter constitutional cations without changing their structure.

The need to modify zeolites in order to obtain appropriate characteristics is always possible, given the large number of different processes in which they are used. Natural zeolites can be modified by a single or combined treatment, such as chemical modification and heating. The chemical and thermal treatment of zeolites can result in cationic migration, which affects the location of cations in zeolite pores. The methods used to modify the zeolite pore are crucial because on these depend the properties of the zeolite as a sorbent. The ion exchange and sorption processes in the zeolite solution system are competitive.

The ratio of oxide components in natural zeolite material depends on the geological deposit. The chemical composition of zeolites is very important for the efficiency of the water treatment process and gives an insight into the main ratio of the composition of the basic oxide

This book belongs to Badji Mokhtar Annaba University Central Library Copyright Elsevier 2025

components of zeolites (SiO_2 and Al_2O_3), exchangeable ions, and other elements that are present at lower concentrations. According to the exchangeable ion ratio, the type of zeolite can sometimes be predetermined. Natural zeolites have an advantage over other ion-exchange materials because they are inexpensive and exhibit excellent selectivity for different cations at normal temperatures. Mostly cations such as K^+, Na^+, Ca^{2+}, and Mg^{2+} are exchanged, which are nontoxic to the environment.

Like all other processes for water purification, sorption processes have advantages and disadvantages. The advantages are economical, high efficiency of removal of pollutants, possibility of regeneration of sorbed matter, and availability of sorbents in nature. The disadvantages are reflected in the necessity of regeneration of the sorbent, which leads to the formation of liquid waste, or the disposal of nonregenerated sorbent, i.e., the generation of solid waste. Also, in the case of sorbent regeneration, the sorption capacity decreases with the increasing number of regeneration cycles.

A fixed particle layer is often used in industrial processes in sorption systems, and the potential role of zeolites in the fluidized system has recently been investigated. The advantages of a fixed-bed system are its simple construction and handling, as well as laminar fluid flow. The disadvantages are the appearance of channels and dead zones that lead to concentration and temperature gradients. Fluidization makes it possible to overcome these problems due to the efficient mixing of the liquid and solid phases, which also provides higher rates of mass and heat transfer. Zeolites allow a simple and low-cost implementation and maintenance of industrial-scale water treatment facilities.

In the case of the application of zeolites in the function of wastewater treatment, there is no unique solution, since wastewater is generated in accordance with its use and application. It has been shown that the use of natural and modified zeolites has a number of advantages and that the zeolite selected can be adjusted to the pH of the soil; thus, natural and regenerated zeolites do not cause extra pollution in the environment. Future perspectives for the application of zeolites in the process of water treatment, reflected in further research possibilities, should be economically viable modifications of zeolites to solve the problem. Since zeolite regeneration generates liquid waste rich in different toxic ions, they can be separated from zeolites and concentrated by solvent extraction. The next step in solving the problem of such waste generation could be electrolysis using DSA. The use of DSA in given operating conditions also varies on a case-by-case basis. For this reason, the attention of researchers should also be directed at the synthesis of DSA for a specific use. One result suggested would be the oxidation of organic pollutants and another result would be the purification of water by metal ions. In this way, the extraction and return of certain metal ions from the zeolite selected would occur and these ions could be incorporated into the production process and production of the pure cathode metals (copper, zinc, chromium, etc.), as useful components that would reduce the cost of wastewater treatment. Combining the method of adsorption and ion exchange of zeolites with

This book belongs to Badji Mokhtar Annaba University Central Library Copyright Elsevier 2025

electrolysis could well be one of the most promising possible solutions for wastewater treatment, which is in the service of the protection of water resources and the environment.

Acknowledgments

This review was supported by the Ministry of Education and Science of the Republic of Serbia. The author wishes to express her gratitude to the Ministry for Agreement No. 451-03-9/2021-14/200052. The author is also thankful to Prof. Dr. C. Blanco and especially to Prof. N. Bolton, M. Gorišek, and J. Fleming for their overall support and selfless assistance. In addition, the author is thankful to her loved ones for their patience and understanding while she was engaged on the research in preparation for this chapter, which deals with a matter of such importance to mankind today.

References

[1] M.J. Ibarrola-Rivas, S. Nonhebel, Assessing changes in availability of land and water for food (1960–2050): an analysis linking food demand and available resources. Outlook Agric. 45 (2) (2016) 124–131, https://doi.org/10.1177/0030727016650767.
[2] W. Liu, R.P. Singh, S. Jothivel, D. Fu, Evaluation of groundwater hardness removal using activated clinoptilolite. Environ. Sci. Pollut. Res. (2019) 1–9, https://doi.org/10.1007/s11356-019-06193-9.
[3] J. Wen, H.R. Dong, G.M. Zeng, Application of zeolite in removing salinity/sodicity from wastewater: a review of mechanisms, challenges and opportunities. J. Clean. Prod. 197 (2018) 1435–1446, https://doi.org/10.1016/j.jclepro.2018.06.270.
[4] V. Krstić, T. Urošević, B. Pešovski, A review on adsorbents for treatment of water and wastewaters containing copper ions. Chem. Eng. Sci. 192 (2018) 273–287, https://doi.org/10.1016/j.ces.2018.07.022.
[5] D. Lončar, J. Paunković, V. Jovanović, V. Krstić, Environmental and social responsibility of companies across European Union countries—panel data analysis. Sci. Total Environ. 657 (2019) 287–296, https://doi.org/10.1016/j.scitotenv.2018.11.482.
[6] F. Fu, Q. Wang, Removal of heavy metal ions from wastewaters: a review. J. Environ. Manage. 92 (2011) 407–418, https://doi.org/10.1016/j.jenvman.2010.11.011.
[7] T. Sahan, D. Ozturk, Investigation of Pb(II) adsorption onto pumice samples: application of optimization method based on fractional factorial design and response surface methodology. Clean Techn. Environ. Policy 16 (2014) 819–831, https://doi.org/10.1007/s10098-013-0673-8.
[8] A. Dimirkou, M.K. Doula, Use of clinoptilolite and an Fe-overexchanged clinoptilolite in Zn^{2+} and Mn^{2+} removal from drinking water. Desalination 224 (2008) 280–292, https://doi.org/10.1016/j.desal.2007.06.010.
[9] G. Venkatesan, U. Senthilnathan, S. Rajam, Cadmium removal from aqueous solutions using hybrid eucalyptus wood based activated carbon: adsorption batch studies. Clean Techn. Environ. Policy 16 (2014) 195–200, https://doi.org/10.1007/s10098-013-0628-0.
[10] M. Prasad, H.Y. Xu, S. Saxena, Multi-component sorption of Pb(II), Cu(II) and Zn(II) onto low-cost mineral adsorbent. J. Hazard. Mater. 154 (2008) 221–229, https://doi.org/10.1016/j.jhazmat.2007.10.019.
[11] E.M. Flanigen, Chapter 2: Zeolites and molecular sieves an historical perspective. Stud. Surf. Sci. Catal. 58 (1991) 13–34, https://doi.org/10.1016/S0167-2991(08)63599-5.
[12] R.L. Virta, Geological Survey Minerals Yearbook, Zeolites, (2009)83.1–83.3.
[13] G. Afreen, D. Mittal, S. Upadhyayula, Biomass-derived phenolics conversion to C10–C13 range fuel precursors over metal ion-exchanged zeolites: physicochemical characterization of catalysts and process parameter optimization. Renew. Energy 149 (2020) 489–507, https://doi.org/10.1016/j.renene.2019.12.064.
[14] R. Sharma, T. Segato, M.-P. Delplancke, H. Terryn, G.V. Baron, J.F.M. Denayer, J. Cousin-Saint-Remi, Hydrogen chloride removal from hydrogen gas by adsorption on hydrated ion-exchanged zeolites. Chem. Eng. J. 381 (2020) 122512, https://doi.org/10.1016/j.cej.2019.122512.

This book belongs to Badji Mokhtar Annaba University Central Library Copyright Elsevier 2025

[15] I.O. Ali, A.M. Hassan, S.M. Shaaban, K.S. Soliman, Synthesis and characterization of ZSM-5 zeolite from rice husk ash and their adsorption of Pb^{2+} onto unmodified and surfactant-modified zeolite. Sep. Purif. Technol. 83 (2011) 38–44, https://doi.org/10.1016/j.seppur.2011.08.034.

[16] P. Castaldi, L. Santona, S. Enzo, P. Melis, Sorption processes and XRD analysis of a natural zeolite exchanged with Pb^{2+}, Cd^{2+} and Zn^{2+} cations. J. Hazard. Mater. 156 (2008) 428–434, https://doi.org/10.1016/j.jhazmat.2007.12.040.

[17] O. Oter, H. Akcay, Use of natural clinoptilolite to improve water quality: sorption and selectivity studies of lead(II), copper(II), zinc(II), and nickel(II). Water Environ. Res. 79 (3) (2007) 329–335, https://doi.org/10.2175/106143006X111880.

[18] M. Sprynskyy, B. Buszewski, A.P. Terzyk, J. Namieśnik, Study of the selection mechanism of heavy metal (Pb^{2+}, Cu^{2+}, Ni^{2+} and Cd^{2+}) adsorption on clinoptilolite. J. Colloid Interface Sci. 304 (2006) 21–28, https://doi.org/10.1016/j.jcis.2006.07.068.

[19] M. Panayotova, B. Velikov, Kinetics of heavy metal ions removal by use of natural zeolite. J. Environ. Sci. Health A 37 (2002) 139–147, https://doi.org/10.1081/ESE-120002578.

[20] M. Çulfaz, M. Yağız, Ion exchange properties of natural clinoptilolite: lead-sodium and cadmium-sodium equilibria. Sep. Purif. Technol. 37 (2004) 93–105, https://doi.org/10.1016/j.seppur.2003.08.006.

[21] J. Perić, M. Trgo, N.V. Medvidović, Removal of zinc, copper and lead by natural zeolite—a comparison of adsorption isotherms. Water Res. 38 (2004) 1893–1899, https://doi.org/10.1016/j.watres.2003.12.035.

[22] M.M. Llanes-Monter, M.T. Olguin, M.J. Solache-Rios, Lead sorption by a Mexican, clinoptilolite-rich tuff. Environ. Sci. Pollut. Res. 14 (2007) 397–403, https://doi.org/10.1065/espr2006.10.357.

[23] A. Langella, M. Pansini, P. Cappelletti, B. Gennaro, M. Gennaro, C. Colella, NH_4^+, Cu^{2+}, Zn^{2+}, Cd^{2+} and Pb^{2+} exchange for Na^+ in a sedimentary clinoptilolite, North Sardinia, Italy. Microporous Mesoporous Mater. 37 (2000) 337–343, https://doi.org/10.1016/S1387-1811(99)00276-0.

[24] S.R. Bare, A. Knop-Gericke, D. Teschner, M. Hävacker, R. Blume, T. Rocha, R. Schlögl, A.S.Y. Chan, N. Blackwell, M.E. Charochak, R. ter Veen, H.H. Brongersma, Surface analysis of zeolites: an XPS, variable kinetic energy XPS, and low energy ion scattering study. Surf. Sci. 648 (2016) 376–382, https://doi.org/10.1016/j.susc.2015.10.048.

[25] I. Graça, D. Chadwick, NH_4-exchanged zeolites: unexpected catalysts for cyclohexane selective oxidation. Microporous Mesoporous Mater. 294 (2020) 109873, https://doi.org/10.1016/j.micromeso.2019.109873.

[26] F.A. Mumpton, La roca magica: uses of natural zeolites in agriculture and industry. Proc. Natl. Acad. Sci. U. S. A. 96 (1999) 3463–3470, https://doi.org/10.1073/pnas.96.7.3463.

[27] M. Li, X. Zhu, F. Zhu, G. Ren, G. Cao, L. Song, Application of modified zeolite for ammonium removal from drinking water. Desalination 271 (2011) 295–300, https://doi.org/10.1016/j.desal.2010.12.047.

[28] G. Diego Gatta, P. Lotti, Chapter 1: Systematics, crystal structures, and occurrences of zeolites, in: M. Mercurio, B. Sarkar, A. Langella (Eds.), Modified Clay and Zeolite Nanocomposite Materials, Elsevier Inc., 2019, pp. 1–25

[29] R. Millini, Application of modeling in zeolite science. Catal. Today 41 (1998) 41–51, https://doi.org/10.1016/S0920-5861(98)00037-6.

[30] R. Millini, C. Perego, The role of molecular mechanics and dynamics methods in the development of zeolite catalytic processes. Top. Catal. 52 (2009) 42–66, https://doi.org/10.1007/s11244-008-9133-9.

[31] C. Baerlocher, L.B. McCusker, D.H. Olson, Atlas of Zeolite Framework, sixth revised ed., Elsevier, The Netherlands, 2007.

[32] V.J. Inglezakis, A.A. Zorpas (Eds.), Handbook of Natural Zeolites, Bentham Science Publishers, 2012, https://doi.org/10.2174/97816080526151120101.

[33] R.A. Le Febre, High-silica zeolites and their use as catalyst in organic chemistry, repository, (1989)tudelft.nl/assets/…541f-463e.../as_lefebre_20070323.pdf.

[34] N. Jiang, R. Shang, S.G.J. Heijman, L.C. Rietveld, High-silica zeolites for adsorption of organic micro-pollutants in water treatment: a review. Water Res. 144 (2018) 145–161, https://doi.org/10.1016/j.watres.2018.07.017.

This book belongs to Badji Mokhtar Annaba University Central Library

Copyright Elsevier 2025

[35] J. Weitkamp, Zeolites and catalysis. Solid State Ion. 131 (2000) 175–188, https://doi.org/10.1016/S0167-2738(00)00632-9.
[36] V.K. Kaushik, R.P. Vijayalakshmi, N.V. Choudary, S.G.T. Bhat, XPS studies on cation exchanged zeolite A. Microporous Mesoporous Mater. 51 (2002) 139–144, https://doi.org/10.1016/S1387-1811(01)00473-5.
[37] A.M. Fonseca, I.C. Neves, Study of silver species stabilized in different microporous zeolites. Microporous Mesoporous Mater. 181 (2013) 83–87, https://doi.org/10.1016/j.micromeso.2013.07.018.
[38] C. Blanco, V. Krstić, C. Pesquera, A. Perdigon, F. González, Mesoporous materials as supports of Rh catalysts. Synthesis, characterization and catalytic application, zeolites and related materials—trends, targets and challenges. Stud. Surf. Sci. Catal. 174B (2008) 1343–1346, https://doi.org/10.1016/S0167-2991(08)80138-3.
[39] R.T. Yang, Adsorbents: Fundamentals and Applications. Copyright © 2003 John Wiley & Sons, Inc, 2003, https://doi.org/10.1002/047144409X.
[40] D.S. Coombs, A. Alberti, T. Armbruster, G. Artioli, C. Colella, E. Galli, et al., Recommended nomenclature for zeolite minerals: report of the Subcommittee on Zeolites of International Mineralogical Association, Commission on new minerals and minerals names, Can. Mineral. 35 (1997) 1571–1606.
[41] M.S. Shamsudin, S.F. Azha, M. Shahadat, S. Ismail, Cellulose/bentonite-zeolite composite adsorbent material coating for treatment of N-based antiseptic cationic dye from water. J. Water Process Eng. 29 (2019) 100764, https://doi.org/10.1016/j.jwpe.2019.02.004.
[42] ASTM D3906, Standard Test Method for Determination of Relative X-Ray Diffraction Intensities of Faujasite-Type Zeolite-Containing Materials, (2019).
[43] ASTM D3942, Standard Test Method for Determination of the Unit Cell Dimension of a Faujasite-Type Zeolite, (2019).
[44] A. Bolshakov, R. van de Poll, T. van Bergen-Brenkman, S.C.C. Wiedemann, N. Kosinov, E.J.M. Hensen, Hierarchically porous FER zeolite obtained via FAU transformation for fatty acid isomerization. Appl. Catal. Environ. 263 (2020) 118356, https://doi.org/10.1016/j.apcatb.2019.118356.
[45] Š. Cerjan-Stefanović, N. Zabukovec Logar, K. Margeta, N. Novak Tušar, I. Arčon, K. Maver, J. Kovač, V. Kaučič, Structural investigation of Zn^{2+} sorption on clinoptilolite tuff from the Vranjska Banja deposit in Serbia. Microporous Mesoporous Mater. 105 (3) (2007) 251–259, https://doi.org/10.1016/j.micromeso.2007.04.033.
[46] D. Lončarević, Ž. Ćupić, Chapter 4: The perspective of using nanocatalysts in the environmental requirements and energy needs of industry, in: S. Thomas, Y. Grohens, Y.B. Pottathara (Eds.), Industrial Applications of Nanomaterials, Micro and Nano Technologies, Elsevier Inc., 2019, pp. 91–122
[47] M.R. Ruiz, V. Krstić, A. Chiriac, F. González, C. Pesquera, C. Blanco, Síntesis y caracterización de arcillas modificadas: PILC's y de productos zeolíticos. Estudio de distintas variables de trabajo, Ed. Universidad de Vest de Timisoara-Rumanía, Serie de Monografii de Chimie, II deo; ISSN 1584-1277 – Edvol. 52, Universidad Vests, Timisoara, Romania, 2004, pp. 1–45 (in Spanish).
[48] C. Blanco, M.R. Ruiz, V. Krsic, C. Pesquera, F. Gonzalez, A. Chiriac, Materiales de Bentonita, Sílice y Alúmina. Métodos de purificación, caracterización de los materiales de partida, arcillas modificadas sintetizadas, y catalizadores metálicos soportados. Análisis de los productos de una reacción catalítica, Ed. Universidad de Vest de Timisoara-Rumanía, Serie de Monografii de Chimie, I deo; ISSN 1584-1277 – Edvol. 51, Universidad Vests, Timisoara, Romania, 2004, pp. 1–45 (in Spanish).
[49] M.S.H. Hashemi, F. Eslami, R. Karimzadeh, Organic contaminants removal from industrial wastewater by CTAB treated synthetic zeolite Y. J. Environ. Manage. 233 (2019) 785–792, https://doi.org/10.1016/j.jenvman.2018.10.003.
[50] Z. Shariatinia, A. Bagherpour, Synthesis of zeolite NaY and its nanocomposites with chitosan as adsorbents for lead(II) removal from aqueous solution. Powder Technol. 338 (2018) 744–763, https://doi.org/10.1016/j.powtec.2018.07.082.
[51] H. Guan, E. Bestland, C. Zhu, H. Zhu, D. Albertsdottir, J. Hutson, C.T. Simmons, M. Ginic-Markovic, X. Tao, A.V. Ellis, Variation in performance of surfactant loading and resulting nitrate removal among four selected natural zeolites. J. Hazard. Mater. 183 (2010) 616–621, https://doi.org/10.1016/j.jhazmat.2010.07.069.

This book belongs to Badji Mokhtar Annaba University Central Library Copyright Elsevier 2025

[52] J. Peng, F. Moszner, J. Rechmann, D. Vogel, M. Palm, M. Rohwerder, Influence of Al content and pre-oxidation on the aqueous corrosion resistance of binary Fe-Al alloys in sulphuric acid. Corros. Sci. 149 (2019) 123–132, https://doi.org/10.1016/j.corsci.2018.12.040.
[53] S.K. Wahono, A. Suwanto, D.J. Prasetyo, Hernawan, T.H. Jatmiko, K. Vasilev, Plasma activation on natural mordenite-clinoptilolite zeolite for water vapor adsorption enhancement. Appl. Surf. Sci. 483 (2019) 940–946, https://doi.org/10.1016/j.apsusc.2019.04.033.
[54] X. Wang, C.A. Plackowski, A.V. Nguyen, X-ray photoelectron spectroscopic investigation into the surface effects of sulphuric acid treated natural zeolite. Powder Technol. 295 (2016) 27–34, https://doi.org/10.1016/j.powtec.2016.03.025.
[55] Y.F. Zhou, R.J. Haynes, Sorption of heavy metals by inorganic and organic components of solid wastes: significance to use of wastes as low-cost adsorbents and immobilizing agents. Crit. Rev. Environ. Sci. Technol. 40 (2010) 909–977, https://doi.org/10.1080/10643380802586857.
[56] E. Erdem, N. Karapinar, R. Donat, The removal of heavy metal cations by natural zeolites. J. Colloid Interface Sci. 280 (2004) 309–314, https://doi.org/10.1016/j.jcis.2004.08.028.
[57] D. Feng, C. Aldrich, H. Tan, Removal of heavy metal ions by carrier magnetic separation of adsorptive particulates. Hydrometallurgy 56 (2000) 359–368, https://doi.org/10.1016/S0304-386X(00)00085-2.
[58] M. Kragović, A. Daković, Ž. Sekulić, M. Trgo, M. Ugrina, J. Perić, G.D. Gatta, Removal of lead from aqueous solutions by using the natural and Fe(III)-modified zeolite. Appl. Surf. Sci. 258 (2012) 3667–3673, https://doi.org/10.1016/j.apsusc.2011.12.002.
[59] M.K. Doula, Simultaneous removal of Cu, Mn and Zn from drinking water with the use of clinoptilolite and its Fe-modified form. Water Res. 43 (2009) 3659–3672, https://doi.org/10.1016/j.watres.2009.05.037.
[60] M. Doula, A. Ioannou, A. Dimirkou, Copper adsorption and Si, Al, Ca, Mg, and Na release from clinoptilolite. J. Colloid Interface Sci. 245 (2002) 237–250, https://doi.org/10.1006/jcis.2001.7961.
[61] E. Wibowo, M. Rokhmat, K. Sutisna, M. Abdullah, Reduction of seawater salinity by natural zeolite (Clinoptilolite): adsorption isotherms, thermodynamics and kinetics. Desalination 409 (2017) 146–156, https://doi.org/10.1016/j.desal.2017.01.026.
[62] S.J. Allen, G. McKay, J.F. Porter, Adsorption isotherm models for basic dye adsorption by peat in single and binary component systems. J. Colloid Interface Sci. 280 (2) (2004) 322–333, https://doi.org/10.1016/j.jcis.2004.08.078.
[63] G. Limousin, J.P. Gaudet, L. Charlet, S. Szenknect, V. Barthès, M. Krimissa, Sorption isotherms: a review on physical bases, modeling and measurement. Appl. Geochem. 22 (2) (2007) 249–275, https://doi.org/10.1016/j.apgeochem.2006.09.010.
[64] M. Ghiaci, A. Abbaspur, R. Kia, F. Seyedeyn-Azad, Equilibrium isotherm studies for the sorption of benzene, toluene, and phenol onto organo-zeolites and as-synthesized MCM-41. Sep. Purif. Technol. 40 (3) (2004) 217–229, https://doi.org/10.1016/j.seppur.2004.03.001.
[65] M.C. Ncibi, Applicability of some statistical tools to predict optimum adsorption isotherm after linear and non-linear regression analysis. J. Hazard. Mater. 153 (2008) 207–212, https://doi.org/10.1016/j.jhazmat.2007.08.038.
[66] E. Bulut, M. Özacar, İ.A. Şengil, Adsorption of malachite green onto bentonite: equilibrium and kinetic studies and process design. Microporous Mesoporous Mater. 115 (3) (2008) 234–246, https://doi.org/10.1016/j.micromeso.2008.01.039.
[67] L. Abramian, H. El-Rassy, Adsorption kinetics and thermodynamics of azo-dye Orange II onto highly porous titania aerogel. Chem. Eng. J. 150 (2–3) (2009) 403–410, https://doi.org/10.1016/j.cej.2009.01.019.
[68] Z. Cheng, X. Liu, M. Han, W. Ma, Adsorption kinetic character of copper ions onto a modified chitosan transparent thin membrane from aqueous solution. J. Hazard. Mater. 182 (1–3) (2010) 408–415, https://doi.org/10.1016/j.jhazmat.2010.06.048.
[69] A. Dąbrowski, Adsorption—from theory to practice. Adv. Colloid Interface Sci. 93 (1–3) (2001) 135–224, https://doi.org/10.1016/S0001-8686(00)00082-8.
[70] A. Günay, E. Arslankaya, İ. Tosun, Lead removal from aqueous solution by natural and pretreated clinoptilolite: adsorption equilibrium and kinetics. J. Hazard. Mater. 146 (1–2) (2007) 362–371, https://doi.org/10.1016/j.jhazmat.2006.12.034.

This book belongs to Badji Mokhtar Annaba University Central Library Copyright Elsevier 2025

[71] Z.A. Al-Anber, M.A.S. Al-Anber, Thermodynamics and kinetic studies of iron (III) adsorption by olive cake in a batch system, J. Mex. Chem. Soc. 52 (2008) 108–115.
[72] G. Hamscher, S. Sczesny, H. Hoper, H. Nau, Determination of persistent tetracycline residues in soil fertilized with liquid manure by high-performance liquid chromatography with electrospray ionization tandem mass spectrometry. Anal. Chem. 74 (2002) 1509–1518, https://doi.org/10.1021/ac015588m.
[73] S. Wongcharee, V. Aravinthan, L. Erdei, Mesoporous activated carbon-zeolite composite prepared from waste macadamia nut shell and synthetic faujasite. Chin. J. Chem. Eng. 27 (2019) 226–236, https://doi.org/10.1016/j.cjche.2018.06.024.
[74] P. Payra, P.K. Dutta, Zeolites: a primer. in: S.M. Auerbach, K. Carrado, P.K. Dutta (Eds.), Handbook of Zeolite Science and Technology, vol. 1, Marcel Dekker Inc, New York, 2003, pp. 1–19, https://doi.org/10.1201/9780203911167.pt1.
[75] M.M. Kragović, A.S. Daković, S.Z. Milićević, Ž.T. Sekulić, S.K. Milonjić, Influence of organic cations sorption on the point of zero charge of natural zeolite, Chem. Ind. (2009) 325–330. (in Serbian), https://doi.org/10.2298/HEMIND0904325K.
[76] L. Čerović, S. Milonjić, D. Bahloul-Hourlier, B. Doucey, Surface properties of silicon nitride powders. Colloids Surf. A Physicochem. Eng. Asp. 197 (2002) 147–156, https://doi.org/10.1016/S0927-7757(01)00863-9.
[77] B.M. Babić, S.K. Milonjić, M.J. Polovina, B.V. Kaludierović, Point of zero charge and intrinsic equilibrium constants of activated carbon cloth. Carbon 37 (1999) 477–481, https://doi.org/10.1016/S0008-6223(98)00216-4.
[78] E. Álvarez-Ayuso, A.G. Sancheza, X. Querol, Purification of metal electroplating waste waters using zeolites. Water Res. 37 (2003) 4855–4862, https://doi.org/10.1016/j.watres.2003.08.009.
[79] L.M. Cozmuta, A.M. Cozmuta, A. Peter, C. Nicula, H. Tutu, D. Silipas, E. Indrea, Adsorption of heavy metal cations by Na-clinoptilolite: equilibrium and selectivity studies. J. Environ. Manage. 137 (2014) 69–80, https://doi.org/10.1016/j.jenvman.2014.02.007.
[80] L.I. Vico, Acid-base behaviour and Cu^{2+} and Zn^{2+} complexation properties of the sepiolite/water interface. Chem. Geol. 198 (2003) 213–222, https://doi.org/10.1016/S0009-2541(03)00002-0.
[81] M.V. Dinu, E.S. Dragan, Evaluation of Cu^{2+}, Co^{2+} and Ni^{2+} ions removal from aqueous solution using a novel chitosan/clinoptilolite composite: kinetics and isotherms. Chem. Eng. J. 160 (2010) 157–163, https://doi.org/10.1016/j.cej.2010.03.029.
[82] V. Krstić, Some effective methods for treatment of wastewater from Cu production, in: Inamuddin, M. I. Ahamed, E. Lichtfouse (Eds.), Water Pollution and Remediation: Heavy Metals. Environmental Chemistry for a Sustainable World, 53 Springer, Cham, 2021, pp. 313–440. https://doi.org/10.1007/978-3-030-52421-0_12.
[83] A. Dimirkou, Uptake of Zn^{2+} ions by a fully iron-exchanged clinoptilolite. Case study of heavily contaminated drinking water samples. Water Res. 41 (2007) 2763–2773, https://doi.org/10.1016/j.watres.2007.02.045.
[84] S.M. Al-Jubouri, S.M. Holmes, Immobilization of cobalt ions using hierarchically porous 4A zeolite-based carbon composites: ion-exchange and solidification. J. Water Process Eng. 33 (2020) 101059, https://doi.org/10.1016/j.jwpe.2019.101059.
[85] S. Beisl, S. Monteiro, R. Santos, A.S. Figueiredo, M.G. Sánchez-Loredo, M.A. Lemos, F. Lemos, M. Minhalma, M. Norbertade Pinho, Synthesis and bactericide activity of nanofiltration composite membranes – cellulose acetate/silver nanoparticles and cellulose acetate/silver ion exchanged zeolites. Water Res. 149 (2019) 225–231, https://doi.org/10.1016/j.watres.2018.10.096.
[86] R. Tekin, N. Bac, Antimicrobial behavior of ion-exchanged zeolite X containing fragrance. Microporous Mesoporous Mater. 234 (2016) 55–60, https://doi.org/10.1016/j.micromeso.2016.07.006.
[87] A. Weiss, About sealing of waste disposals by clays with special consideration of organic compounds in percolating water. Appl. Clay Sci. 4 (1989) 193–209, https://doi.org/10.1016/0169-1317(89)90008-2.
[88] E.J. Sulliven, D.B. Hunter, R.S. Bowman, Topological and thermal properties of surfactant-modified clinoptilolite studied by Tapping-Mode® atomic force microscopy and high-resolution thermogravimetric analysis. Clays Clay Miner. 45 (1997) 42–53, https://doi.org/10.1346/CCMN.1997.0450105.

This book belongs to Badji Mokhtar Annaba University Central Library Copyright Elsevier 2025

[89] Z. Li, R.S. Bowman, Sorption of perchloroethylene by surfactant-modified zeolite as controlled by surfactant loading. Environ. Sci. Technol. 32 (1998) 2278–2282, https://doi.org/10.1021/es971118r.
[90] A. Huwiga, S. Freimund, O. Käppelib, H. Dutlerb, Mycotoxin detoxication of animal feed by different adsorbents. Toxicol. Lett. 122 (2001) 179–188, https://doi.org/10.1016/S0378-4274(01)00360-5.
[91] N. Fiol, I. Villaescusa, Determination of sorbent point zero charge: usefulness in sorption studies. Environ. Chem. Lett. 7 (2009) 79–84, https://doi.org/10.1007/s10311-008-0139-0.
[92] V.J. Inglezakis, The concept of capacity in zeolite ion-exchange systems. J. Colloid Interface Sci. 281 (2005) 68–79, https://doi.org/10.1016/j.jcis.2004.08.082.
[93] H. Ghobarkar, O. Schiif, U. Guth, Zeolites-from kitchen to space. Prog. Solid State Chem. 27 (1999) 29–73, https://doi.org/10.1016/S0079-6786(00)00002-9.
[94] C. Colella, W.S. Wise, The IZA handbook of natural zeolites: a tool of knowledge on the most important family of porous minerals. Microporous Mesoporous Mater. 189 (2014) 4–10, https://doi.org/10.1016/j.micromeso.2013.08.028.
[95] E.C. Hass, P.G. Mezey, P.J. Plath, A non-empirical molecular orbital study on loewenstein's rule and zeolite composition. J. Mol. Struct. THEOCHEM 76 (1981) 389–399, https://doi.org/10.1016/0166-1280(81)85092-0.
[96] W. Loewenstein, The distribution of aluminum in the tetrahedra of silicates and aluminates, Am. Mineral. 39 (1–2) (1954) 92–96.
[97] Ullmann's Encyclopedia of Industrial Chemistry, fifth edition, VCH, Weinheim, Germany, 1996/1997 Section A, 28 vols, Section B, 8 vol. DM 19 400.
[98] M.K. Doula, Removal of Mn^{2+} ions from drinking water by using clinoptilolite and a clinoptilolite-Fe oxide system. Water Res. 40 (2006) 3167–3176, https://doi.org/10.1016/j.watres.2006.07.013.
[99] J.V. Kumar, S. Hayashi, Modification on natural clinoptilolite zeolite for its NH_4^+ retention capacity. J. Hazard. Mater. 169 (1) (2009) 29–35, https://doi.org/10.1016/j.jhazmat.2009.03.052.
[100] P. Chutia, S. Kato, T. Kojima, S. Satokawa, Adsorption of As(V) on surfactant modified natural zeolites. J. Hazard. Mater. 162 (1) (2009) 204–211, https://doi.org/10.1016/j.jhazmat.2008.05.024.
[101] C.R. Oliveira, J. Rubio, New basis for adsorption of ionic pollutants onto modified zeolites. Miner. Eng. 20 (6) (2007) 552–558, https://doi.org/10.1016/j.mineng.2006.11.002.
[102] H.K. Beyer, Dealumination Techniques for Zeolites, Molecular Sieves, vol. 3, Springer-Verlag, Berlin, Heidelberg, 2002.
[103] S. Wang, Y. Peng, Natural zeolites as effective adsorbents in water and wastewater treatment. Chem. Eng. J. 156 (2010) 11–24, https://doi.org/10.1016/j.cej.2009.10.029.
[104] Y.G. Basabe, I.R. Iznaga, L.-C. de Menorval, P. Llewellyn, G. Maurin, D.W. Lewis, R. Binions, M. Autie, A.R.R. Salvador, Step-wise dealumination of natural clinoptilolite: structural and physicochemical characterization. Microporous Mesoporous Mater. 135 (2010) 187–196, https://doi.org/10.1016/j.micromeso.2010.07.008.
[105] S.D. Matijašević, A.S. Daković, D.A. Ileš, A.Z. Milićević, Adsorpcija uranil-jona na modifikovanim klinoptilolitima. Chem. Ind. 63 (2009) 407–414, https://doi.org/10.2298/HEMIND0905407M.
[106] H. Valdés, R.F. Tardón, C.A. Zaror, Role of surface hydroxyl groups of acid-treated natural zeolite on the heterogeneous catalytic ozonation of methylene blue contaminated waters. Chem. Eng. J. 211–212 (2012) 388–395, https://doi.org/10.1016/j.cej.2012.09.069.
[107] J.K.A. Dapaah, L. Andalaluna, T. Kobayashi, Enhancement of catalytic activity of natural zeolites by surface modification for 1-buten izomerization, Mem. Muroran Inst. Technol. 47 (1997) 89–95.
[108] M. Stöcker, Gas phase catalysis by zeolites. Microporous Mesoporous Mater. 82 (2005) 257–292, https://doi.org/10.1016/j.micromeso.2005.01.039.
[109] G.E. Christidis, D. Moraetis, E. Keheyan, L. Akhalbedashvili, N. Kekelidzec, R. Gevorkyand, H. Yeritsyane, H. Sargsyan, Chemical and thermal modification of natural HEU-type zeolitic materials from Armenia, Georgia and Greece. Appl. Clay Sci. 24 (2003) 79–91, https://doi.org/10.1016/S0169-1317(03)00150-9.
[110] N. Al-Jammal, T. Juzsakova, B. Zsirka, V. Sebestyén, J. Németh, I. Cretescu, T. Halmágyi, E. Domokos, Á. Rédey, Modified Jordanian zeolitic tuff in hydrocarbon removal from surface water. J. Environ. Manage. 239 (2019) 333–341, https://doi.org/10.1016/j.jenvman.2019.03.079.

This book belongs to Badji Mokhtar Annaba University Central Library Copyright Elsevier 2025

[111] L. Belchinskaya, L. Novikova, V. Khokhlov, J. Tkhi Ly, Contribution of ion-exchange and non-ion-exchange reactions to sorption of ammonium ions by natural and activated aluminosilicate sorbent. J. Appl. Chem. 2013 (2013) 1–9, https://doi.org/10.1155/2013/789410.
[112] B. Chamnankid, C. Ratanatawanate, K. Faungnawakij, Conversion of xylose to levulinic acid over modified acid functions of alkaline-treated zeolite Y in hot-compressed water. Chem. Eng. J. 258 (2014) 341–347, https://doi.org/10.1016/j.cej.2014.07.036.
[113] N. Bektas, S. Kara, Removal of lead from aqueous solutions by natural clinoptilolite: equilibrium and kinetic studies. Sep. Purif. Technol. 39 (2004) 189–200, https://doi.org/10.1016/j.seppur.2003.12.001.
[114] L. Ćurković, Š. Cerjan-Stefanović, T. Filipan, Metal ion exchange by natural and modified zeolites. Water Res. 31 (6) (1997) 1379–1382, https://doi.org/10.1016/S0043-1354(96)00411-3.
[115] S. Çoruh, The removal of zinc ions by natural and conditioned clinoptilolites. Desalination 225 (2008) 41–57, https://doi.org/10.1016/j.desal.2007.06.015.
[116] A.I. Stefanakis, C.S. Akratos, G.D. Gikas, V.A. Tsihrintzis, Effluent quality improvement of two pilot-scale, horizontal subsurface flow constructed wetlands using natural zeolite (clinoptilolite). Microporous Mesoporous Mater. 124 (1–3) (2009) 131–143, https://doi.org/10.1016/j.micromeso.2009.05.005.
[117] C. Blanco Delgado, V.R. Krstić, C. Pesquera González, F. González Martinez, Modified clays, PILC's, applied in catalysis. Chem. Ind. 65 (1) (2011) 37–41, https://doi.org/10.2298/HEMIND100906066D.
[118] H. Liu, T. Shen, T. Li, P. Yuan, G. Shi, X. Bao, Green synthesis of zeolites from a natural aluminosilicate mineral rectorite: effects of thermal treatment temperature. Appl. Clay Sci. 90 (2014) 53–60, https://doi.org/10.1016/j.clay.2014.01.006.
[119] X. Zeng, Q.H. Fang, Y.W. Liu, Effect of thermal activation energy on dislocation emission from an elliptically blunted crack tip. Physica B 447 (2014) 15–18, https://doi.org/10.1016/j.physb.2014.04.037.
[120] V.O. Vasylechko, G.V. Gryshchouk, Y.B. Kuzma, V.P. Zakordonskiy, L.O. Vasylechko, L.O. Lebedynets, M.B. Kalytovsk, Adsorption of cadmium on acid modified Transcarpathian clinoptilolite. Microporous Mesoporous Mater. 60 (2003) 183–196, https://doi.org/10.1016/S1387-1811(03)00376-7.
[121] B. Tomazović, T. Ćeranić, G. Sijarić, The properties of the NH_4-clinoptilolite. Part 1. Zeolites 16 (1996) 301–308, https://doi.org/10.1016/0144-2449(95)00118-2.
[122] B. Tomazović, T. Ćeranić, G. Sijarić, The properties of the NH_4-clinoptilolite. Part 2. Zeolites 16 (1996) 309–312, https://doi.org/10.1016/0144-2449(95)00117-4.
[123] K. Margeta, N. Zabukovec Logar, M. Siljeg, A. Farkas, Natural zeolites in water treatment—how effective is their use. in: W. Elshorbagy (Ed.), Water Treatment, InTech, 2013, https://doi.org/10.5772/50738.
[124] H. Kazemian, M.H. Mallah, Removal of chromate ion from contaminated synthetic water using MCM-41/ZSM-5 composite, Iran. J. Environ. Health Sci. Eng. 5 (2008) 73–77.
[125] F. Izzo, M. Mercurio, B. de Gennaro, P. Aprea, P. Cappelletti, A. Daković, C. Germinario, C. Grifa, D. Smiljanic, A. Langella, Surface modified natural zeolites (SMNZs) as nanocomposite versatile materials for health and environment. Colloids Surf. B Biointerfaces 182 (2019) 110380, https://doi.org/10.1016/j.colsurfb.2019.110380.
[126] R. Leyva-Ramos, A. Jacobo-Azuara, P.E. Diaz-Flores, R.M. Guerrero-Coronado, J. Mendoza-Barron, M. S. Berber-Mendoza, Adsorption of chromium(VI) from an aqueous solution on a surfactant-modified zeolite. Colloids Surf. A Physicochem. Eng. Asp. 330 (2008) 35–41, https://doi.org/10.1016/j.colsurfa.2008.07.025.
[127] J. Lin, Y. Zhan, Z. Zhu, Adsorption characteristics of copper (II) ions from aqueous solution onto humic acid-immobilized surfactant-modified zeolite. Colloids Surf. A Physicochem. Eng. Asp. 384 (2011) 9–16, https://doi.org/10.1016/j.colsurfa.2011.02.044.
[128] Y.H. Zhan, Z.L. Zhu, J.W. Lin, Y.L. Qiu, J.F. Zhao, Removal of humic acid from aqueous solution by cetylpyridinium bromide modified zeolite. J. Environ. Sci. 22 (2010) 1327–1334, https://doi.org/10.1016/S1001-0742(09)60258-8.
[129] M.K. Doula, Synthesis of a clinoptilolite-Fe system with high Cu sorption capacity. Chemosphere 67 (4) (2007) 731–740, https://doi.org/10.1016/j.chemosphere.2006.10.072.
[130] M.B. Baskan, A. Pala, Removal of arsenic from drinking water using modified natural zeolite. Desalination 281 (2011) 396–403, https://doi.org/10.1016/j.desal.2011.08.015.

This book belongs to Badji Mokhtar Annaba University Central Library Copyright Elsevier 2025

[131] S. Jevtić, I. Arčon, A. Rečnik, B. Babić, M. Mazaj, J. Pavlović, D. Matijašević, M. Nikšić, N. Rajić, The iron(III)-modified natural zeolitic tuff as an adsorbent and carrier for selenium oxyanions. Microporous Mesoporous Mater. 197 (2014) 92–100, https://doi.org/10.1016/j.micromeso.2014.06.008.
[132] Z. Li, J.S. Jean, W.T. Jiang, P.H. Chang, C.J. Chen, L. Liao, Removal of arsenic from water using Fe-exchanged natural zeolite. J. Hazard. Mater. 187 (2011) 318–323, https://doi.org/10.1016/j.jhazmat.2011.01.030.
[133] Y. Sun, Q. Fang, J. Dong, X. Cheng, J. Xu, Removal of fluoride from drinking water by natural stilbite zeolite modified with Fe (III). Desalination 277 (2011) 121–127, https://doi.org/10.1016/j.desal.2011.04.013.
[134] R. Bosinceanu, N. Sulitanu, Synthesis and characterization of FeO(OH)/Fe_3O_4 nanoparticles encapsulated in zeolite matrix, J. Optoelectron. Adv. Mater. 10 (2008) 3482–3486.
[135] J. Pérez-Ramírez, G. Mul, F. Kapteijn, J.A. Moulijn, A.R. Overweg, A. Doménech, A. Ribera, I.W.C. E. Arends, Physicochemical characterization of isomorphously substituted FeZSM-5 during activation. J. Catal. 207 (2002) 113–126, https://doi.org/10.1006/jcat.2002.3511.
[136] T. Motsi, N.A. Rowson, M.J.H. Simmons, Adsorption of heavy metals from acid mine drainage by natural zeolite. Int. J. Miner. Process. 92 (2009) 42–48, https://doi.org/10.1016/j.minpro.2009.02.005.
[137] S.K. Pitcher, R.C.T. Slade, N.I. Ward, Heavy metal removal from motorway stormwater using zeolites. Sci. Total Environ. 334–335 (2004) 161–166, https://doi.org/10.1016/j.scitotenv.2004.04.035.
[138] K.R. Reddy, T. Xie, S. Dastgheibi, Removal of heavy metals from urban stormwater runoff using different filter materials. J. Environ. Chem. Eng. 2 (2014) 282–292, https://doi.org/10.1016/j.jece.2013.12.020.
[139] P. Wu, Y.S. Zhou, Simultaneous removal of coexistent heavy metals from simulated urban stormwater using four sorbents: a porous iron sorbent and its mixtures with zeolite and crystal gravel. J. Hazard. Mater. 168 (2009) 674–680, https://doi.org/10.1016/j.jhazmat.2009.02.093.
[140] S.R. Taffarel, J. Rubio, On the removal of Mn^{2+} ions by adsorption onto natural and activated Chilean zeolites. Miner. Eng. 22 (2009) 336–343, https://doi.org/10.1016/j.mineng.2008.09.007.
[141] H. Zhu, Y. Li, L. Wu, S. Yu, C. Xin, P. Sun, Q. Xiao, H. Zhao, Y. Zhang, T. Qin, Impact of the atmospheric deposition of major acid rain components, especially NH_4, on carbonate weathering during recharge in typical karst areas of the Lijiang River basin, southwest China. Appl. Geochem. 114 (2020) 104518, https://doi.org/10.1016/j.apgeochem.2019.104518.
[142] Y. Cai, D. Li, Y. Liang, H. Zeng, J. Zhang, Autotrophic nitrogen removal process in a potable water treatment biofilter that simultaneously removes Mn and NH_4^+-N. Bioresour. Technol. 172 (2014) 226–231, https://doi.org/10.1016/j.biortech.2014.09.027.
[143] A. Cincotti, N. Lai, R. Orrù, G. Cao, Sardinian natural clinoptilolites for heavy metals and ammonium removal: experimental and modeling. Chem. Eng. J. 84 (3) (2001) 275–282, https://doi.org/10.1016/S1385-8947(00)00286-2.
[144] A.H. Englert, J. Rubio, Characterization and environmental application of a Chilean natural zeolite. Int. J. Miner. Process. 75 (1–2) (2005) 21–29, https://doi.org/10.1016/j.minpro.2004.01.003.
[145] S.-J. Kang, K. Egashira, Modification of different grades of Korean natural zeolites for increasing cation exchange capacity. Appl. Clay Sci. 12 (1–2) (1997) 131–144, https://doi.org/10.1016/S0169-1317(97)00002-1.
[146] Y.F. Wang, F. Lin, W.Q. Pang, Ammonium exchange in aqueous solution using Chinese natural clinoptilolite and modified zeolite. J. Hazard. Mater. 142 (1–2) (2007) 160–164, https://doi.org/10.1016/j.jhazmat.2006.07.074.
[147] H. Faghihian, M. Ghannadi Marageh, H. Kazemian, The use of clinoptilolite and its sodium form for removal of radioactive cesium, and strontium from nuclear wastewater and Pb^{2+}, Ni^{2+}, Cd^{2+}, Ba^{2+} from municipal wastewater. Appl. Radiat. Isot. 50 (4) (1999) 655–660, https://doi.org/10.1016/S0969-8043(98)00134-1.
[148] A. Kiliyankil Vipin, S. Ling, B. Fugetsu, Removal of Cs^+ and Sr^{2+} from water using MWCNT reinforced zeolite-A beads. Microporous Mesoporous Mater. 224 (2016) 84–88, https://doi.org/10.1016/j.micromeso.2015.11.024.
[149] E.H. Borai, R. Harjula, L. Malinen, A. Paajanen, Efficient removal of cesium from low-level radioactive liquid waste using natural and impregnated zeolite minerals. J. Hazard. Mater. 172 (2009) 416–422, https://doi.org/10.1016/j.jhazmat.2009.07.033.

This book belongs to Badji Mokhtar Annaba University Central Library Copyright Elsevier 2025

[150] P. Misaelides, Application of natural zeolites in environmental remediation: a short review. Microporous Mesoporous Mater. 144 (2011) 15–18, https://doi.org/10.1016/j.micromeso.2011.03.024.
[151] M.R. Awual, T. Yaita, T. Taguchi, H. Shiwaku, S. Suzuki, Y. Okamoto, Selective cesium removal from radioactive liquid waste by crownether immobilized new class conjugate adsorbent. J. Hazard. Mater. 278 (2014) 227–235, https://doi.org/10.1016/j.jhazmat.2014.06.011.
[152] Z. Xue, Z. Li, J. Ma, X. Bai, Y. Kang, W. Hao, R. Li, Effective removal of Mg^{2+} and Ca^{2+} ions by mesoporous LTA zeolite. Desalination 341 (2014) 10–18, https://doi.org/10.1016/j.desal.2014.02.025.
[153] V. Sivasankar, T. Ramachandramoorthy, Water softening behaviour of sand materials—mimicking natural zeolites in some locations of Rameswaram Island, India. Chem. Eng. J. 171 (2011) 24–32, https://doi.org/10.1016/j.cej.2011.03.032.
[154] L. Aljerf, High-efficiency extraction of bromocresol purple dye and heavy metals as chromium from industrial effluent by adsorption onto a modified surface of zeolite: kinetics and equilibrium study. J. Environ. Manage. 225 (2018) 120–132, https://doi.org/10.1016/j.jenvman.2018.07.048.
[155] A.R. Loiola, J.C.R.A. Andrade, J.M. Sasaki, L.R.D. da Silva, Structural analysis of zeolite NaA synthesized by a cost-effective hydrothermal method using kaolin and its use as water softener. J. Colloid Interface Sci. 367 (2012) 34–39, https://doi.org/10.1016/j.jcis.2010.11.026.
[156] R. Han, L. Zou, X. Zhao, Y. Xu, F. Xu, Y. Li, Y. Wang, Characterization and properties of iron oxide-coated zeolite as adsorbent for removal of copper(II) from solution in fixed bed column. Chem. Eng. J. 149 (2009) 123–131, https://doi.org/10.1016/j.cej.2008.10.015.
[157] M.A. Stylianou, M.P. Hadjiconstantinou, V.J. Inglezakis, K.G. Moustakas, M.D. Loizidou, Use of natural clinoptilolite for the removal of lead, copper and zinc in fixed bed column. J. Hazard. Mater. 143 (2007) 575–581, https://doi.org/10.1016/j.jhazmat.2006.09.096.
[158] M.B. Baskan, A. Pala, Batch and fixed-bed column studies of arsenic adsorption on the natural and modified clinoptilolite. Water Air Soil Pollut. 225 (2014) 1798, https://doi.org/10.1007/s11270-013-1798-4.
[159] C.E. Borba, E.A. Silva, S. Spohr, G.H.F. Santos, R. Guirardello, Application of the mass action law to describe ion exchange equilibrium in a fixed-bed column. Chem. Eng. J. 172 (1) (2011) 312–320, https://doi.org/10.1016/j.cej.2011.06.002.
[160] J. Qu, T. Song, J. Liang, X. Bai, Y. Li, Y. Wei, S. Huang, L. Dong, Y. Jin, Adsorption of lead (II) from aqueous solution by modified Auricularia matrix waste: a fixed-bed column study. Ecotoxicol. Environ. Saf. 169 (2019) 722–729, https://doi.org/10.1016/j.ecoenv.2018.11.085.
[161] M. Sulaiman, E. Climent, A. Hammouti, A. Wachs, Mass transfer towards a reactive particle in a fluid flow: numerical simulations and modeling. Chem. Eng. Sci. 199 (2019) 496–507, https://doi.org/10.1016/j.ces.2018.12.051.
[162] M.A. Thombare, P.V. Chavan, S.B. Bankar, D.V. Kalaga, Solid-liquid circulating fluidized bed: a way forward. Rev. Chem. Eng. 35 (1) (2019) 1–44, https://doi.org/10.1515/revce-2017-0017.
[163] X. Cheng, X.T. Bi, Modeling and simulation of nitrogen oxides adsorption in fluidized bed reactors. Chem. Eng. Sci. 96 (2013) 42–54, https://doi.org/10.1016/j.ces.2013.03.052.
[164] M. Jovanovic, Ž. Grbavcic, N. Rajic, B. Obradovic, Removal of Cu(II) from aqueous solutions by using fluidized zeolite A beads: hydrodynamic and sorption studies. Chem. Eng. Sci. 117 (2014) 85–92, https://doi.org/10.1016/j.ces.2014.06.017.
[165] M. Jovanovic, I. Arcon, J. Kovac, N.N. Tusar, B. Obradovic, N. Rajic, Removal of manganese in batch and fluidized bed systems using beads of zeolite A as adsorbent. Microporous Mesoporous Mater. 226 (2016) 378–385, https://doi.org/10.1016/j.micromeso.2016.02.026.
[166] M.A. Stylianou, V.J. Inglezakis, M. Loizidou, Comparison of Mn, Zn, and Cr removal in fluidized- and fixed-bed reactors by using clinoptilolite. Desalin. Water Treat. 53 (12) (2015) 3355–3362, https://doi.org/10.1080/19443994.2014.934103.
[167] C. Kassargy, S. Awad, G. Burnens, G. Upreti, K. Kahine, M. Tazerout, Study of the effects of regeneration of USY zeolite on the catalytic cracking of polyethylene. Appl. Catal. Environ. 244 (2019) 704–708, https://doi.org/10.1016/j.apcatb.2018.11.093.
[168] E. Katsou, S. Malamis, M. Tzanoudaki, K.J. Haralambous, M. Loizidou, Regeneration of natural zeolite polluted by lead and zinc in wastewater treatment systems. J. Hazard. Mater. 189 (3) (2011) 773–786, https://doi.org/10.1016/j.jhazmat.2010.12.061.

This book belongs to Badji Mokhtar Annaba University Central Library Copyright Elsevier 2025

[169] H. Huang, L. Yang, Q. Xue, J. Liu, L. Hou, L. Ding, Removal of ammonium from swine wastewater by zeolite combined with chlorination for regeneration. J. Environ. Manage. 160 (2015) 333–341, https://doi.org/10.1016/j.jenvman.2015.06.039.

[170] Y. Nakasaka, T. Tago, H. Konno, A. Okabe, T. Masuda, Kinetic study for burning regeneration of coked MFI-type zeolite and numerical modeling for regeneration process in a fixed-bed reactor. Chem. Eng. J. 207–208 (2012) 368–376, https://doi.org/10.1016/j.cej.2012.06.138.

[171] I. Braschi, S. Blasioli, E. Buscaroli, D. Montecchio, A. Martucci, Physicochemical regeneration of high silica zeolite Y used to clean-up water polluted with sulfonamide antibiotics. J. Environ. Sci. 43 (2016) 302–312, https://doi.org/10.1016/j.jes.2015.07.017.

[172] Q. Du, S. Liu, Z. Cao, Y. Wang, Ammonia removal from aqueous solution using natural Chinese clinoptilolite. Sep. Purif. Technol. 44 (3) (2005) 229–234, https://doi.org/10.1016/j.seppur.2004.04.011.

[173] M. Li, C. Feng, Z. Zhang, X. Lei, N. Chen, N. Sugiura, Simultaneous regeneration of zeolites and removal of ammonia using an electrochemical method. Microporous Mesoporous Mater. 127 (3) (2010) 161–166, https://doi.org/10.1016/j.micromeso.2009.07.009.

[174] M. Li, C. Feng, Z. Zhang, R. Zhao, X. Lei, R. Chen, N. Sugiura, Application of an electrochemical-ion exchange reactor for ammonia removal. Electrochim. Acta 55 (2009) 159–164, https://doi.org/10.1016/j.electacta.2009.08.027.

[175] V. Krstić, B. Pešovski, Novel multifunctional two layer catalytic activated titanium electrodes for various technological and environmental processes. Arab. J. Chem. 2017 (2017), https://doi.org/10.1016/j.arabjc.2017.05.023 (in press).

[176] V. Krstić, B. Pešovski, Reviews the research on some dimensionally stable anodes (DSA) based on titanium. Hydrometallurgy 185 (2019) 71–75, https://doi.org/10.1016/j.hydromet.2019.01.018.

[177] B. Trumić, L. Gomidželović, V. Trujić, V. Krstić, D. Stanković, Comparative analysis of high temperature strength of platinum and its binary alloys with low content of alloying element, Chem. Ind. 66 (3) (2012) 395–401. (in Serbian)https://doi.org/10.2298/HEMIND110718106T.

[178] B. Trumić, L. Gomidželović, S. Marjanović, V. Krstić, A. Ivanović, S. Dimitrijević, Pt-Rh alloys: investigation of creep rate and rupture time at high temperatures. Mater. Test. 55 (1) (2013) 38–42, https://doi.org/10.3139/120.110406.

[179] B. Trumić, L. Gomidželović, S. Marjanović, V. Krstić, A. Ivanović, S. Dimitrijević, Pt-Rh alloys: investigation of tensile strength and elongation at high temperatures. Arch. Metall. Mater. 2 (60) (2015) 643–647, https://doi.org/10.1515/amm-2015-0186.

[180] B. Trumić, L. Gomidželović, A. Ivanović, S. Dimitrijević, S. Marjanović, V. Krstić, D. Stanković, Platinum alloys with metals from I_B group of the periodic table of elements, Copper 40 (1) (2015) 17–24 (in Serbian).

[181] B. Trumić, L. Gomidželović, S. Marjanović, A. Ivanović, V. Krstić, S. Dimitrijević, Pt-Pd system: investigation of mechanical properties. Kovove Mater. 54 (2016) 139–145, https://doi.org/10.4149/km_2016_2_139.

[182] B. Trumić, L. Gomidželović, S. Marjanović, A. Ivanović, V. Krstić, Platinum-based alloys: investigation of the effect of impurities content on creep rate, rupture time and relative elongation at high temperatures. Mater. Res. 20 (1) (2017) 191–199, https://doi.org/10.1590/1980-5373-mr-2016-0240.

[183] O. Lahav, Y. Schwartz, P. Nativ, Y. Gendel, Sustainable removal of ammonia from anaerobic-lagoon swine waste effluents using an electrochemically-regenerated ion exchange process. Chem. Eng. J. 218 (2013) 214–222, https://doi.org/10.1016/j.cej.2012.12.043.

[184] R. Leyva-Ramos, G. Aguilar-Armenta, L.V. Gonzalez-Gutierrez, R.M. Guerrero-Coronado, J. Mendoza-Barron, Ammonia exchange on clinoptilolite from mineral deposits located in Mexico. J. Chem. Technol. Biotechnol. 79 (2004) 651–657, https://doi.org/10.1002/jctb.1035.

[185] G. Gruett, Contaminant Removal Made Easy, Water Quality Products, 2007.https://www.wqpmag.com/contaminant-removal-made-easy.

[186] M. Zhang, H. Zhang, D. Xu, L. Han, D. Niu, B. Tian, J. Zhang, L. Zhang, W. Wu, Removal of ammonium from aqueous solutions using zeolite synthesized from fly ash by a fusion method. Desalination 271 (1–3) (2011) 111–121, https://doi.org/10.1016/j.desal.2010.12.021.

This book belongs to Badji Mokhtar Annaba University Central Library

Copyright Elsevier 2025

[187] S.-X. Bai, L.-M. Zhou, Z.-B. Chang, C. Zhang, M. Chu, Synthesis of Na-X zeolite from Longkou oil shale ash by alkaline fusion hydrothermal method. Carbon Resour. Convers. 1 (3) (2018) 245–250, https://doi.org/10.1016/j.crcon.2018.08.005.
[188] Z.T. Yao, M.S. Xia, Y. Ye, L. Zhang, Synthesis of zeolite Li-ABW from fly ash by fusion method. J. Hazard. Mater. 170 (2–3) (2009) 639–644, https://doi.org/10.1016/j.jhazmat.2009.05.018.
[189] W. Zhang, Z. Zhou, Y. An, S.L. Du, D.N. Ruan, C.Y. Zhao, N. Ren, X.C. Tian, Optimization for zeolite regeneration and nitrogen removal performance of a hypochlorite-chloride regenerant. Chemosphere 178 (2017) 565–572, https://doi.org/10.1016/j.chemosphere.2017.03.091.
[190] J.S. Kim, M.A. Keane, The removal of iron and cobalt from aqueous solutions by ion exchange with Na-Y zeolite: batch, semi-batch and continuous operation. J. Chem. Technol. Biotechnol. 77 (2002) 633–640, https://doi.org/10.1002/jctb.618.
[191] R. Egashira, S. Tanabe, H. Habak, Adsorption of heavy metals in mine wastewater by Mongolian natural zeolite. Procedia Eng. 42 (2012) 49–57, https://doi.org/10.1016/j.proeng.2012.07.394.
[192] H. Merrikhpour, M. Jalali, Comparative and competitive adsorption of cadmium, copper, nickel, and lead ions by Iranian natural zeolite. Clean Techn. Environ. Policy 15 (2013) 303–316, https://doi.org/10.1007/s10098-012-0522-1.
[193] S.K. Ouki, M. Kavannagh, Treatment of metal-contaminated waste waters by use of natural zeolites. Water Sci. Technol. 39 (1999) 115–122, https://doi.org/10.2166/wst.1999.0638.
[194] M. Vidal, M.J. Santos, T. Abrao, J. Rodriguez, A. Rigol, Modeling competitive metal sorption in a mineral soil. Geoderma 149 (2009) 189–198, https://doi.org/10.1016/j.geoderma.2008.11.040.
[195] M.A.A. Sayed, M.S. Khater, Removing cadmium and lead from wastewater using natural zeolite isotherm models, Middle East J. Appl. Sci. 3 (2013) 98–104.
[196] H. Leinonen, J. Lehto, Purification of metal finishing waste waters with zeolites and activated carbons. Waste Manage. Res. 19 (2001) 45–57, https://doi.org/10.1177/0734242X0101900106.
[197] S.K. Ouki, M. Kavannagh, Performance of natural zeolites for the treatment of mixed metal-contaminated effluents. Waste Manage. Res. 15 (1997) 383–394, https://doi.org/10.1006/wmre.1996.0094.
[198] S. Wang, T. Terdkiatburana, M.O. Tad'e, Adsorption of Cu(II), Pb(II) and humic acid on natural zeolite tuff in single and binary systems. Sep. Purif. Technol. 62 (1) (2008) 64–70, https://doi.org/10.1016/j.seppur.2008.01.004.
[199] A.M. El-Kamash, A.A. Zaki, M.A. El Geleel, Modeling batch kinetics and thermodynamics of zinc and cadmium ions removal from waste solutions using synthetic zeolite A. J. Hazard. Mater. B127 (2005) 211–220, https://doi.org/10.1016/j.jhazmat.2005.07.021.
[200] K.S. Hui, C.Y.H. Chao, S.C. Kot, Removal of mixed heavy metal ions in wastewater by zeolite 4A and residual products from recycled coal fly ash. J. Hazard. Mater. B127 (2005) 89–101, https://doi.org/10.1016/j.jhazmat.2005.06.027.
[201] V.J. Inglezakis, M.D. Loizidou, H.P. Grigoropoulou, Ion exchange of Pb^{2+}, Cu^{2+}, Fe^{3+}, and Cr^{3+} on natural clinoptilolite: selectivity determination and influence of acidity on metal uptake. J. Colloid Interface Sci. 261 (2003) 49–54, https://doi.org/10.1016/S0021-9797(02)00244-8.
[202] R. Petrus, J. Warchol, Heavy metal removal by clinoptilolite. An equilibrium study in multi-component systems. Water Res. 39 (2005) 819–830, https://doi.org/10.1016/j.watres.2004.12.003.
[203] O. Gok, A. Ozcan, B. Erdem, A.S. Ozcan, Prediction of the kinetics, equilibrium and thermodynamic parameters of adsorption of copper(II) ions onto 8-hydroxy quinolone immobilized bentonite. Colloids Surf. A Physicochem. Eng. Asp. 317 (2008) 174–185, https://doi.org/10.1016/j.colsurfa.2007.10.009.
[204] Y. Li, Q.Y. Yue, B.Y. Gao, Adsorption kinetics and desorption of Cu(II) and Zn(II) from aqueous solution onto humic acid. J. Hazard. Mater. 178 (2010) 455–461, https://doi.org/10.1016/j.jhazmat.2010.01.103.
[205] K.G. Bhattacharyya, S.S. Gupta, Adsorption of a few heavy metals on natural and modified kaolinite and montmorillonite. Adv. Colloid Interface Sci. 140 (2008) 114–131, https://doi.org/10.1016/j.cis.2007.12.008.
[206] M. Kragović, A. Daković, M. Marković, J. Krstić, G.D. Gatta, N. Rotiroti, Characterization of lead sorption by the natural and Fe(III)-modified zeolite. Appl. Surf. Sci. 283 (2013) 764–774, https://doi.org/10.1016/j.apsusc.2013.07.016.

This book belongs to Badji Mokhtar Annaba University Central Library Copyright Elsevier 2025

[207] T. Stanić, A. Daković, A. Živanović, M. Tomašević-Čanović, V. Dondur, S. Milićević, Adsorption of arsenic (V) by iron (III)-modified natural zeolitic tuff. Environ. Chem. Lett. 7 (2009) 161–166, https://doi.org/10.1007/s10311-008-0152-3.

[208] C.S. Jeon, K. Baek, J.K. Park, Y.K. Ohc, S.D. Lee, Adsorption characteristics of As(V) on iron-coated zeolite. J. Hazard. Mater. 163 (2009) 804–808, https://doi.org/10.1016/j.jhazmat.2008.07.052.

[209] Z. Li, W.T. Jiang, J.S. Jean, H. Hong, L. Liao, G. Lv, Combination of hydrous iron oxide precipitation with zeolite filtration to remove arsenic from contaminated water. Desalination 280 (2011) 203–207, https://doi.org/10.1016/j.desal.2011.07.009.

[210] A. Demir, A. Gunay, E. Debik, Ammonium removal from aqueous solution by ion-exchange using packed bed natural zeolite. Water SA 28 (3) (2002) 329–336, https://doi.org/10.4314/wsa.v28i3.4903.

[211] R. Malekian, J. Abedi-Koupai, S.S. Eslamian, S.F. Mousavi, K.C. Abbaspour, M. Afyuni, Ion exchange process for ammonium removal and release using natural Iranian zeolite. Appl. Clay Sci. 51 (3) (2011) 323–329, https://doi.org/10.1016/j.clay.2010.12.020.

[212] A. Malovanyy, H. Sakalova, Y. Yatchyshyn, E. Plaza, M. Malovanyy, Concentration of ammonium from municipal wastewater using ion exchange process. Desalination 329 (2013) 93–102, https://doi.org/10.1016/j.desal.2013.09.009.

[213] A. Alshameri, A. Ibrahim, A.M. Assabri, X. Lei, H. Wang, C. Yan, The investigation into the ammonium removal performance of Yemeni natural zeolite: modification, ion exchange mechanism, and thermodynamics. Powder Technol. 258 (2014) 20–31, https://doi.org/10.1016/j.powtec.2014.02.063.

[214] Y. Zhao, B. Zhang, X. Zhang, J. Wang, J. Liu, R. Chen, Preparation of highly ordered cubic NaA zeolite from halloysite mineral for adsorption of ammonium ions. J. Hazard. Mater. 178 (2010) 658–664, https://doi.org/10.1016/j.jhazmat.2010.01.136.

[215] A.R. Rahmani, A.H. Mahvi, A.R. Mesdaghinia, S. Nasseri, Investigation of ammonia removal from polluted waters by clinoptilolite zeolite. Int. J. Environ. Sci. Technol. 1 (2) (2004) 125–133, https://doi.org/10.1007/BF03325825.

[216] A. Thornton, P. Pearce, S.A. Parsons, Ammonium removal from solution using ion exchange on to MesoLite, anequilibrium study. J. Hazard. Mater. 147 (3) (2007) 883–889, https://doi.org/10.1016/j.jhazmat.2007.01.111.

[217] A. Thornton, P. Pearce, S.A. Parsons, Ammonium removal from digested sludge liquors using ion exchange. Water Res. 41 (2) (2007) 433–439, https://doi.org/10.1016/j.watres.2006.10.021.

[218] R. Leyva-Ramos, J.E. Monsivais-Rocha, A. Aragon-Piña, M.S. Berber-Mendoza, R.M. Guerrero-Coronado, P. Alonso-Davila, J. Mendoza-Barron, Removal of ammonium from aqueous solution by ion exchange on natural and modified chabazite. J. Environ. Manage. 91 (12) (2010) 2662–2668, https://doi.org/10.1016/j.jenvman.2010.07.035.

[219] G. Moussavi, S. Talebi, M. Farrokhi, R.M. Sabouti, The investigation of mechanism, kinetic and isotherm of ammonia and humic acid co-adsorption onto natural zeolite. Chem. Eng. J. 171 (3) (2011) 1159–1169, https://doi.org/10.1016/j.cej.2011.05.016.

[220] L.G. Hortigüela, J.P. Pariente, R. García, Y. Chebude, I. Díaz, Natural zeolites from Ethiopia for elimination of fluoride from drinking water. Sep. Purif. Technol. 120 (2013) 224–229, https://doi.org/10.1016/j.seppur.2013.10.006.

This book belongs to Badji Mokhtar Annaba University Central Library Copyright Elsevier 2025

This page intentionally left blank

This book belongs to Badji Mokhtar Annaba University Central Library

Copyright Elsevier 2025

CHAPTER 15

Metal-organic framework nanocomposite based adsorbents

Sachin R. Shirsath[a] and Bharat A. Bhanvase[b]

[a]*Department of Chemical Engineering, Sinhgad College of Engineering, Pune, Maharashtra, India,* [b]*Chemical Engineering Department, Laxminarayan Institute of Technology, Rashtrasant Tukadoji Maharaj Nagpur University, Nagpur, Maharashtra, India*

15.1 Introduction

A class of solids has been developed over the past few decades, which contain metal ions linked by molecular species that are known as metal-organic frameworks (MOFs). MOFs are also known as porous coordination polymers. These are hybrid organic–inorganic materials rising as beneficial crystalline microporous materials [1, 2]. These materials were proposed by Yaghi and coworkers [3] for the first time. MOFs possess exceptional properties among different types of mesoporous and microporous materials toward varied applications [4]. MOFs offer high thermal stability that ensures their utility for a broad temperature window [5].

Metal oxide units connected by organic linkers through strong covalent bonds form the structure of MOFs. MOFs possess one-, two-, or three-dimensional structures. The structure is a combination of coordination bonds connecting metal cations such as Zn^{2+} and electron donors such as amines or carboxylates. The flexibility with which these components can be substituted has resulted in a wide-ranging class of MOF structures. The self-assembly of these components results in robust pores, the structure of which does not collapse even if the solvent or other "guest" molecules occupying them are removed [4]. For a solid to be categorized as an MOF, it should offer certain properties such as strong bonding that provides robustness, modifiable linking units through organic synthesis, and a geometrically precise structure. A vastly used adsorbent such as activated carbon possesses large open porosity and huge specific surface area. However, it has a disordered structure.

MOFs are a distinctive group of crystalline materials with vast network structures. MOFs act as molecular sieves for the preferential adsorption of dyes and other pollutants owing to their pore size, shape, and dimensionality. The structure of MOFs can be easily tailored by

Handbook of Nanomaterials for Wastewater Treatment. https://doi.org/10.1016/B978-0-12-821496-1.00027-1
Copyright © 2021 Elsevier Inc. All rights reserved.

This book belongs to Badji Mokhtar Annaba University Central Library Copyright Elsevier 2025

appropriately choosing their building blocks (i.e., metal and organic linker) [6]. Alteration in the connection of the inorganic moiety and the nature of the organic linker can be the reason for easy tuning of MOFs pore size and shape from a microporous to a mesoporous scale. Owing to the simple alteration of MOFs, the range of their potential applications is increasing continuously [7].

The formulation of desired MOFs is dictated by several factors and the choice of organic ligand is a prime factor in the assembly of desired MOFs. Owing to interactions with guest molecules, MOFs offer a high framework flexibility and shrinkage/expansion unlike other solid matters, such as carbons and oxides or zeolites.

Prominent structural attributes of MOFs are exceptionally high porosity (up to 90% free volume) and internal surface areas that are larger than Langmuir surface area of 10,000 m^2/g [1]. Although high surface areas are known to be offered by activated carbons and zeolites, MOFs have no dead volume, which results in the highest porosities and tremendous surface areas [8]. Porous compounds actually contain nanometer-sized spaces, which has resulted in attracting the chemists, physicists, and material scientists to study the novel phenomena in them [9]. The large surface area and porosity enhance mass transfer process in MOFs, whereas the unsaturated metal atoms, metal-hydroxyl, and other functional groups in the structure offer valuable adsorption sites for inorganic oxyanions [10]. Extraordinary network flexibility of MOFs, which is closely related with the coordination bonds, noncovalent bonds, and weak interactions, gives the MOFs an edge over the conventional porous materials such as zeolites, activated carbons, and metal oxides. As a result, some of the MOFs demonstrate the strange (or stepwise/sigmoid/multistep) adsorption isotherm patterns [11]. Additional important features of MOFs are simple functionalization and modification of the inner pore surface [12].

15.2 Properties of MOF

As discussed earlier, MOFs have very large surface areas, adjustable surface chemistries, and structural properties such as stability, porosity, crystallinity, flexibility, and topology. Highly developed porosity, organic-inorganic nature with a homogeneous dispersion of components, and controlled pore size are some of the important features of MOFs as against conventional inorganic materials. Additionally, they are highly suitable for modifications and pairing with different classes of materials [13]. Nevertheless, poor chemical stability of MOFs puts a limit on their potential usefulness. To make these MOFs more versatile and improve their applicability to realistic applications, it is imperative to improve their properties and bring in novel functionalities. Hence a combination of MOFs with wide range of functional materials to merge the merits and alleviate the shortcomings of individual components has been proposed. Substitution of organic functional groups into MOFs structure is projected to augment the host-guest chemistry (where host is MOF and guests are other

This book belongs to Badji Mokhtar Annaba University Central Library Copyright Elsevier 2025

small molecules). For improving the efficacy of MOFs for different applications, tuning and optimizing this host-guest chemistry by functionalizing with organic functional groups is the best way [14].

Among the various applications of MOFs, adsorption has attracted major interests of the researchers because of simple operation, highly efficient treatment, lower cost, absence of toxic by-products, and environment friendliness [10]. The adjustable porous structures and surface charge, versatile functionalization methods (e.g., de nova and postsynthetic methods), and large surface areas of MOFs render them superior over other conventional porous materials for molecular sorption and separation [15, 16]. As the surface area and porosity rise, adsorption increases because of accessibility to a large number of exchange sites and a larger diffusion rate through the framework. High porosity facilitates mass transfer process [10]. Alteration in the linkers used in the synthesis process can lead to tuning of crystalline structure, pore structure, order, size, and shape of MOFs for improved adsorption. Large surface area and highly porous structure are beneficial for their application in separation of ions, drug delivery, gas storage, catalysis, and removal of heavy metals from industrial wastewater [17, 18]. To check the porosity, adsorption measurements are performed and neutron scattering is used to determine sorption sites. Equivalent surface area is calculated according to the Langmuir equation by using nitrogen sorption at 77 K or argon uptake at 87 K [8].

15.3 Types of MOF

Tailored nanoporous host materials with high mechanical and thermal stability are formed because of the self-assembly and linking of metal ions acting as coordination centers through a range of polyatomic organic bridging ligands. Transition metal ions are frequently used as connectors for the construction of coordination polymers. MOFs with diverse structural and practical properties can be formulated by varying metal ion/clusters. For this, a range of combinations of inorganic building blocks and vast types of organic linkers having different geometries, lengths, and functionalities are used [14]. Organic functional groups can be classified according to their chemical and structural characteristics.

Organic functional groups are carbonyl-based functions (amide, squaramide, urea, imide, ketone, oxalamide, carboxyl) and few other groups such as hydrazone, oxygen-based functions (hydroxyl, ether), sulfur-based functions (thiol and sulfide, sulfonate), nitrogen-based functions (ionic N-based functions, heterocyclic azine N-based functions, heterocyclic azole N-based, and noncyclic N-based functions), and other functions such as halogen-based functional groups, phosphonate, and fluorine [14]. Most of the times, the use of functional groups improves the performance of MOFs, but occasionally, it has been found that functional groups have these positive effects at the cost of negative effects as well. So the knowledge of structural and chemical properties of functional groups is essential for a researcher.

This book belongs to Badji Mokhtar Annaba University Central Library Copyright Elsevier 2025

15.4 Synthesis methods

Different methods adopted for the synthesis of MOFs end up in the synthesis of compounds that are typical results of a particular method. Different synthesis methods lead to different crystallization rates, particle sizes, size distributions, adsorption properties, and morphologies that affect the resultant material properties. Diffusion of guest molecules inside MOFs can be affected by different particle sizes in porous materials which can have an impact on catalytic reactions or the adsorption and separation of molecules.

In conventional synthesis, electric heating without any parallelization of reactions is used for carrying out reactions. For the synthesis reactions, two temperature ranges, such as solvothermal and nonsolvothermal, are defined. Reactions taking place under autogenous pressure above the boiling point of the solvent in closed vessels are termed as solvothermal reactions, whereas nonsolvothermal reactions take place at or below boiling point under ambient pressure. As the nonsolvothermal reactions take place under ambient pressure, the setup requirements are also minimal. In the case of low-temperature reactions, simple molecular or ionic crystals are formed.

Synthesis of MOFs is normally done using well-soluble salts as metal component sources. They include metal nitrates, metal sulfates, metal acetates, etc. The organic constituents are generally mono-, di-, tri- and tetracarboxylic acids that are delivered in polar organic solvents such as amine (triethylamine) or amide (dimethylformamide, diethylformamide) [8]. The syntheses of MOFs are done under moderate conditions and choosing a particular combination of molecular units results in desired extended network, which is known as bottom-up method. Two vital components of MOFs, the starting reagents, with which the primary framework of the coordination polymer is constructed, are connectors and linkers. Additionally, blocking ligands, counteranions, and nonbonding guests or template molecules are the auxiliary components [9]. For precise control over pore size and spatial cavity arrangement, suitable metal centers, ligands, and synthesis conditions are selected [19]. During the synthesis of MOFs, compositional parameters, such as molar ratios of starting materials, solvent, pH, etc., along with process parameters such as reaction time, temperature, and pressure are changed [20]. Changes in concentration, temperature, solvent polarity, and pH can lead to low-quality crystals, lower yields, or may form totally new phases [2]. Reaction temperature strongly affects product formation. For example, morphology of the produced crystals is highly dependent on the reaction temperature. At higher temperatures, it has been observed that more condensed/dense structures are formed. Sometimes it becomes necessary to have higher temperature to achieve suitable crystallinity and higher reaction rates, but extended reaction times at higher temperatures can result in degradation of the MOF. However, during early years, the emphasis was on low temperature operations that are known to produce simple molecular or ionic crystals.

This book belongs to Badji Mokhtar Annaba University Central Library
Copyright Elsevier 2025

The prime objective of MOF synthesis is to maintain and control the synthesis conditions that result in definite inorganic building blocks without decomposition of the organic linker. One important thing that needs to be ensured is the kinetics of crystallization, which must allow nucleation and growth of the desired phase [20]. Various groups around the world have employed diverse synthetic methods for MOFs synthesis, with particular reference to reaction temperatures and reactors.

The main aim in practicing different MOF synthesis methods is to scale-up so as to increase production and to lessen time of synthesis process. In a typical method, a mixture of ligand and metal salt is heated in a solvent for 12–48 h. Although these methods produce high-quality crystals, most of the methods are time-consuming and difficult to scale above 1 g. Hence the methods requiring minimum reaction time and the quantity of solvent are preferred on a laboratory scale and commercialization of MOF materials [4].

There are numerous papers published on the synthesis of MOFs using various techniques. To name a few, solvothermal and hydrothermal at room temperature [21–24], microwave radiation [25], ultrasonic irradiation method [26], and electrochemical process [27] are some of them.

All the abovementioned synthesis methods have certain advantages and disadvantages. Microwave and sonochemical methods are normally used for speeding up the rates of reactions and producing smaller crystals as against conventional electric heating. In the case of microwave heating, acceleration in the reaction rates is because of high temperatures that are rapidly achieved in solvents absorbing microwaves. Sonochemical method produces nanocrystalline particles that are quite useful in adsorptive applications. Thus shorter reaction times, typically between 10 and 60 min, result in quantitative yields and small particles. Although microwave and sonochemical methods reduce the reaction times, both these methods use solvents. Hence mechanochemical synthesis is preferred sometimes from the environmental point of view where one can avoid the use of organic solvents as it is a solvent-free method. In mechanochemical synthesis, reaction is carried out at room temperature where the linker molecules and metal salts mixture is ground together in a ball mill to form the MOF [4, 20].

Sometimes, the activation of MOFs is required to exploit their full potential. Activated MOFs are critical in postsynthetic modification reactions for reduction of the number of side reactions that may take place [20]. After synthesis, it becomes necessary to get insight into the properties of MOFs; hence a thorough characterization of MOFs is carried out. These materials are highly porous materials and crystalline as well. Most often, crystallinity and phase purity are studied by X-ray diffraction (XRD), whereas the adsorption measurements are done to confirm the porosity. When these materials are used in catalysis, the mass transfer becomes an influential parameter, which makes it necessary to have first hand information

This book belongs to Badji Mokhtar Annaba University Central Library Copyright Elsevier 2025

about the crystal size and size distribution. This information is normally collected by using scanning electron microscopy.

15.5 Nanocomposite-based MOFs

Although MOFs have been found to have diverse applications, they still possess certain disadvantages that limit their use. For example, poor water stability of MOFs is a prime concern, which results in the collapse of its materials owing to loss of crystallinity, which is attributed to the fragility of the metal/ligand junctions. Also, MOFs have comparatively less thermostability than their structural cousins, that is, zeolites. In comparison to porous materials such as activated carbon, MOFs do not possess atomically dense pores, which results in limiting their capacity to retain small molecules because of the weak dispersive forces. Moreover, the mesopores-micropores combination is favored for the adsorption of tiny molecules. Mesopores assist in diffusion and augment the kinetics during the separation applications, whereas micropores are responsible for superior adsorption capacity. To address these issues, structural changes in MOFs are needed for the improvement in their performance. Two different approaches are proposed to deal with these issues such as modification in MOF by functionalization of the ligands, tuning of the metal/ligand interactions or selection of different metals and/or ligands, and building MOF-based composites [28]. Combining MOFs with appropriate materials such as porous carbon, metals, carbon nanotubes (CNTs), graphene-based materials, and silica are used for the formation of composites [29, 30]. One MOF with one or more distinct constituent materials, including other MOFs form the MOF composites materials. A composite is a multicomponent material having multiple phases with minimum one continuous phase. According to the formation of MOF composite, there are two basic types—discontinuous phase and continuous phase. Discontinuous MOFs are not frequently utilized in adsorption applications, rather these are mainly prepared for applications where composites require different sizes/shapes and demand easy handling. The second type of MOF composites are those with continuous MOFs used for adsorption applications. These composites find applications in industrial processes because they can merge the properties of the phases and have capability to tune the properties [20, 31]. The properties are distinctive of the individual components. Various advantages of MOFs (high porosity, structural adaptivity, and flexibility) and different types of functional materials (electrical, magnetic, optical, and catalytic properties) are combined together for exploring new physical and chemical properties for the composite materials [1].

Thus by combining MOFs and suitable materials, physical and chemical properties, morphology, kinetics of synthesis, and stability of MOFs can be appreciably improved [32, 33]. Several methods such as pre/in situ synthesis or postsynthesis modifications are employed for synthesis of MOF composites. Of late, researchers have preferred the latter method owing to its simplicity [34]. Amalgamation of functional species in MOFs is done through postimpregnation of metal nanospecies by chemical vapor deposition and one-pot synthesis

This book belongs to Badji Mokhtar Annaba University Central Library Copyright Elsevier 2025

that includes addition of either the functional species or its precursors straight into the medium growing the MOF [35].

15.6 Applications of nanocomposite-based MOFs

Owing to the specific properties MOFs possess, they find use in various applications. Ricco et al. [19] have reviewed the applications of MOFs. MOFs are principally used for storage of gas and separation [13, 36], heterogeneous catalysis [37–39], photocatalysis [38, 40], sensing [41, 42], drug delivery, biosensing and other medical applications [43, 44], and removal/separation of hazardous chemicals [45, 46]. MOF composites can be utilized for all applications where MOFs are used. Furthermore, new possibilities can open out where individual MOFs have limitations [7].

15.6.1 Application of nanocomposite-based MOFs in adsorption

In most applications of MOFs, adsorption is observed to be the main phenomenon; so MOF composites applications in different areas by adsorption processes are discussed in this section. The pore surface properties are important from the adsorption point of view. So a lot of work is being done for decoration and consequently the modification or change of the pore surface properties in MOFs. Two categories in the case of adsorption techniques are (1) gas-phase adsorption and (2) liquid-phase adsorption. Moreover, one of the significant properties of MOFs is that they possess special and specific chemical functionalities that are useful for selective adsorption of some species [7]. This is quite useful for selective separation of constituents from the mixtures. In addition to this, the other advantages of adsorption are that it can be performed at low temperatures, energy requirements are low, it is cost-effective, and there is less generation of harmful secondary products. Of the numerous papers available on the applications of MOFs, some of them are discussed here.

15.6.1.1 Adsorption of gases

With growing requirement of efficient, energy-saving, and environmentally friendly processes for the gas separation, different adsorbents with tunable surface properties and customized structures are designed. Adsorptive processes find wide applications in industries with use of porous solid adsorbents. Owing to large surface area, adjustable pore size, and controllable properties, as well as good thermal stability, MOF is a potential candidate for gas separations as adsorbent. Li et al. [47] has written a review on selective gas adsorption and separation in MOFs. In this review, authors have discussed about the possible mechanisms of adsorption observed in MOFs and attempted to establish key relationships between adsorption properties and features of the framework. Also, theoretical background from adsorption equilibrium to diffusion dynamics through molecular simulations is reviewed. Another review is presented by Rowsell and Yaghi [2] on the use of MOFs as materials for hydrogen storage. Lot of challenges have been observed in the production of hydrogen, followed by distribution, storage,

This book belongs to Badji Mokhtar Annaba University Central Library Copyright Elsevier 2025

and usage, and improvements are sought for the efficient and safe storage of the volatile fuel. Authors have systematically discussed hydrogen storage requirements, storage technologies, and MOFs for hydrogen storage through adsorption. Several strategies for enhancing hydrogen uptake in these materials are presented in this review.

Graphene nanosheets and MOFs as hybrid porous materials are found to be an attractive option for adsorption of gases. Graphene oxide possesses unique properties such as extraordinary atomic density and a large amount of surface functional groups which renders it as the best additive with other materials. Integration of graphene oxide into MOFs improves the water resistance and thermal stability of the composites along with better surface area and adsorption properties. It also has pronounced effect on the morphology and structure of the material with which it forms a composite. A vast range of graphene-MOF adsorbents has been used for the separation of gases. Petit and Bandosz [28] reviewed metal-organic framework/graphite oxide composites as separation media for small molecule gases at ambient conditions. This study was done from surface engineering standpoint. In this paper, authors elaborated the idea of the metal-organic framework (MOF)/graphite oxide composites that have emerged for separation of small molecule gases at atmospheric conditions. Substantial enhancement in porosity of the composites is attributed to the pores formation at the interface of graphite oxide and MOF crystals. It has also been reported by the authors that upon exposure to toxic gases, the MOF structure collapsed; however, it was preserved after adsorption of CO_2. In another review, Szczęśniak et al. [13] have discussed gas adsorption properties of hybrid graphene-MOF materials. The main focus of this review was toward the graphene-MOF hybrids for gas capture and storage of gases such as CO_2, hydrogen, volatile organic compounds (VOCs), and methane.

Asgharnejad et al. [29] synthesized Ni-based metal-organic framework (MOF)/graphene oxide nanocomposite as preferential adsorbent for CO_2 over N_2 at ambient pressure, proposed schematic of which is shown in Fig. 15.1. Composites with different graphene oxide contents (5, 9, and 15 wt% of the initial material weight) were synthesized, and their CO_2/N_2 adsorption selectivity was investigated. Among them, the composite with 5% graphene oxide exhibited maximum CO_2/N_2 selectivity, which was three times better than the parent MOF selectivity at the same conditions, as shown in Fig. 15.2; whereas the gas uptake of the composite was found to be similar to that of parent MOF.

Chen et al. [30] synthesized copper-based MOF and graphite oxide by solvothermal method for separation of CO_2/CH_4 and CO_2/N_2, and its schematic is shown in Fig. 15.3. The wt% of graphite oxide content of the synthesized composites was varied as 2%, 5%, 8%, and 10% of parent MOF precursors total weight. Individual adsorption isotherm measurements at different temperatures for CO_2, CH_4, and N_2 were obtained. Ideal adsorbed solution theory was used to estimate selectivities of CO_2/CH_4 and CO_2/N_2. MOF with 5% graphite oxide content revealed the highest CO_2 uptake at 298 K and 100 kPa, as shown in Fig. 15.4. For the same composite, CO_2/CH_4 and CO_2/N_2 adsorption selectivities were 37.2 and 8.6,

This book belongs to Badji Mokhtar Annaba University Central Library Copyright Elsevier 2025

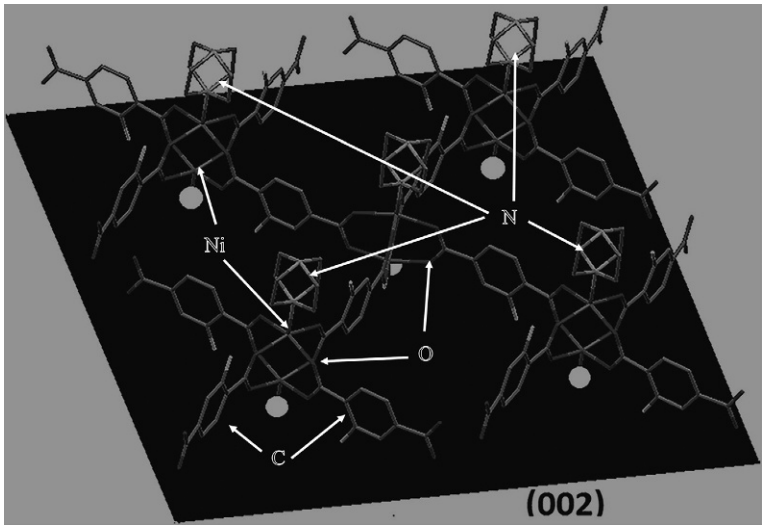

Fig. 15.1
Schematic of proposed bonding between graphene oxide and MOF along [002] direction of the MOF. Here, hydrogen and guest molecules are not shown. Different functional groups on the surface of graphene oxide are indicated in figure [29]. *Reprinted with permission from L. Asgharnejad, A. Abbasi, A. Shakeri, Ni-based metal-organic framework/GO nanocomposites as selective adsorbent for CO_2 over N_2, Microporous Mesoporous Mater. 262 (2018) 227–234. Copyright (2018) Elsevier.*

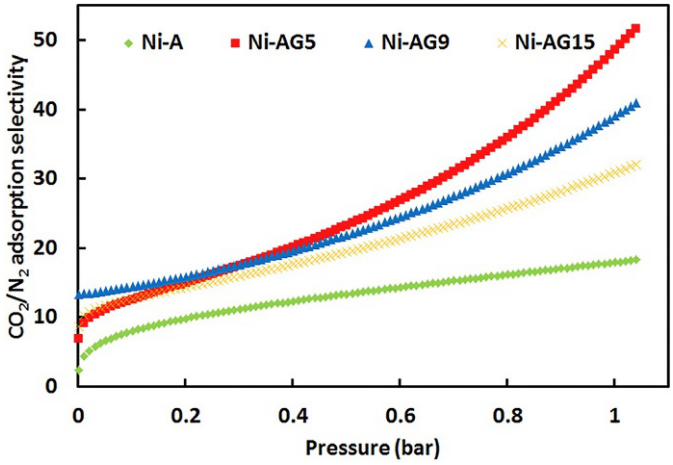

Fig. 15.2
Selectivities of CO_2/N_2 adsorption calculated of Ni-A and its composite for CO_2 (15%) and N_2 (85%) at 298 K by IAST [29]. *Reprinted with permission from L. Asgharnejad, A. Abbasi, A. Shakeri, Ni-based metal-organic framework/GO nanocomposites as selective adsorbent for CO_2 over N_2, Microporous Mesoporous Mater. 262 (2018) 227–234. Copyright (2018) Elsevier.*

This book belongs to Badji Mokhtar Annaba University Central Library Copyright Elsevier 2025

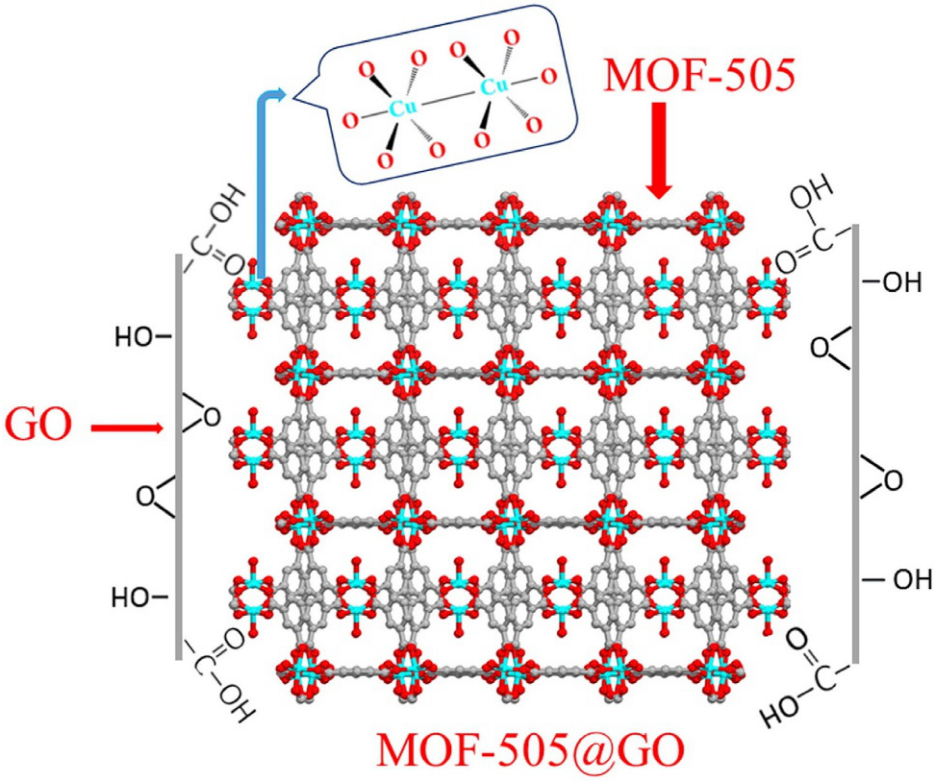

Fig. 15.3
Schematic view of copper-based MOF-505-graphite oxide composite formation [30]. *Reprinted with permission from Y. Chen, D. Lv, J. Wu, J. Xiao, H. Xi, Q. Xia, Z. Li, A new MOF-505@GO composite with high selectivity for CO_2/CH_4 and CO_2N_2 separation, Chem. Eng. J. 308 (2017) 1065–1072. Copyright (2017) Elsevier.*

respectively, which shows an increment of 33.8% and 13.2%, respectively, when compared to parent MOF.

In another work, MOF composites with different ratios of graphite oxide were prepared and used for ammonia removal at dry conditions [48]. Synergetic effects of MOF and graphite oxide showed higher ammonia uptake when compared with parent materials. However, it was also observed that when large quantity of ammonia was retained, it ultimately resulted in the collapse of the MOF-5 structure in the composites.

A hybrid composite of acid-treated multiwalled carbon nanotubes (MWCNTs) and MOF-5 was synthesized [49]. The hybrid composite showed similar morphology and crystal structure similar to the virgin MOF-5, but it had high Langmuir specific surface area ranging from 2160 to 3550 m^2/g. Also, the hydrogen storage capacity of the composite was increased by 50% and the stability was also improved in the presence of ambient moisture. The variation in hydrogen storage for MWCNTs, MOFMC, and MOF-5 at different temperatures is shown in Fig. 15.5.

This book belongs to Badji Mokhtar Annaba University Central Library Copyright Elsevier 2025

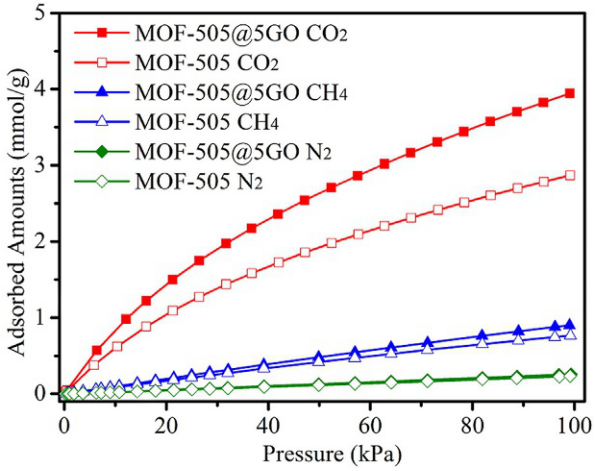

Fig. 15.4
Amounts of CO_2, CH_4, and N_2 adsorbed on copper-based MOF and copper-based MOF-graphite oxide (5%) at 298 K [30]. *Reprinted with permission from Y. Chen, D. Lv, J. Wu, J. Xiao, H. Xi, Q. Xia, Z. Li, A new MOF-505@GO composite with high selectivity for CO_2/CH_4 and CO_2/N_2 separation, Chem. Eng. J. 308 (2017) 1065–1072. Copyright (2017) Elsevier.*

Pazoki et al. [23] synthesized microporous copper carboxylate MOF by solvothermal method for adsorption of methane. Experiments were performed at pressure and temperature of 1–20 bar and 298 K, respectively. The experimental set up used is shown in Fig. 15.6. The results revealed high sorption capacity of the composite (11.78 mmol/g) for CH_4, which can be ascribed to the appropriate framework pore diameter. The variation of methane adsorption with pressure is depicted in Fig. 15.7.

Two MOFs were synthesized from polycarboxylate and bis(imidazole) ligands by hydrothermal method [24]. The sorption behavior of first MOF for different gases N_2, H_2, CH_4, and CO_2 showed higher selectivity for CO_2 over CH_4. The second MOF was used for dye adsorption. Two porous lanthanide MOFs synthesized by using 3,5-bis(2-carboxy-phenoxy)-benzoic acid (H_3BCPB) were prepared under solvothermal conditions [50]. N_2, CH_4, and CO_2 gas adsorption properties of these two MOFs were evaluated at various temperatures. Results indicated that the adsorption amounts of both MOFs for CO_2 were substantially higher than those of CH_4 under similar conditions indicating possible application of MOFs in natural gas purification. Ti-incorporated MOF structure (MIL-125) and its amine-functionalized (NH_2-MIL-125) form were synthesized by a solvothermal method [37]. Basic MOF structure was found to be unstable in aqueous solution, whereas NH_2-MIL-125 was stable in water and in heptanes. At 298 K, NH_2-MIL-125 showed low CO_2 adsorption quantity (136 mg/g) but exceptional selectivity over N_2 (>27:1). Furthermore, the composite was tested for reusability, and completely reversible adsorbent regeneration was observed for NH_2-MIL-125 at 298 K for four adsorption-desorption cycles for CO_2.

This book belongs to Badji Mokhtar Annaba University Central Library Copyright Elsevier 2025

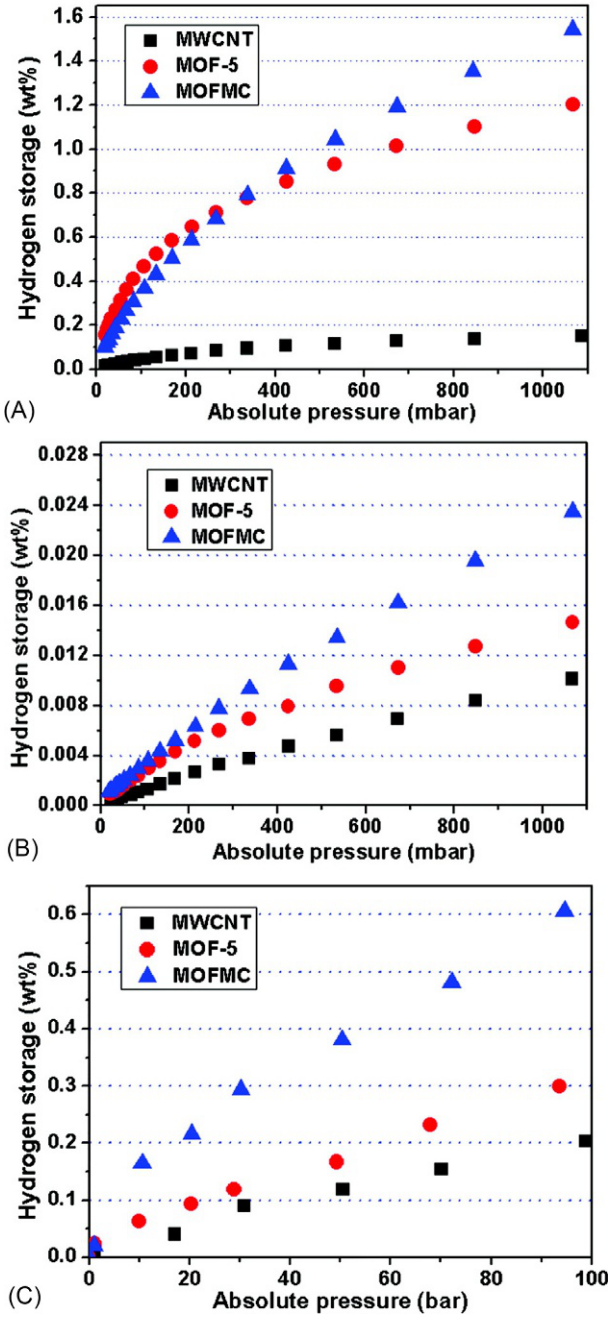

Fig. 15.5

H_2 adsorption capacity measured in volumetric at low pressure of MOFMC, MOF-5, and MWCNTs at temperatures (A) 77 K and (B) 298 K and (C) measured in gravimetrically at high pressure H_2 Adsorption at 298 K [49]. *Reprinted with permission from S.J. Yang, J.Y. Choi, H.K. Chae, J.H. Cho, K.S. Nahm, C.R. Park, Preparation and enhanced hydrostability and hydrogen storage capacity of CNT@MOF-5 hybrid composite, Chem. Mater. 21 (2009) 1893–1897. Copyright (2009) American Chemical Society.*

This book belongs to Badji Mokhtar Annaba University Central Library Copyright Elsevier 2025

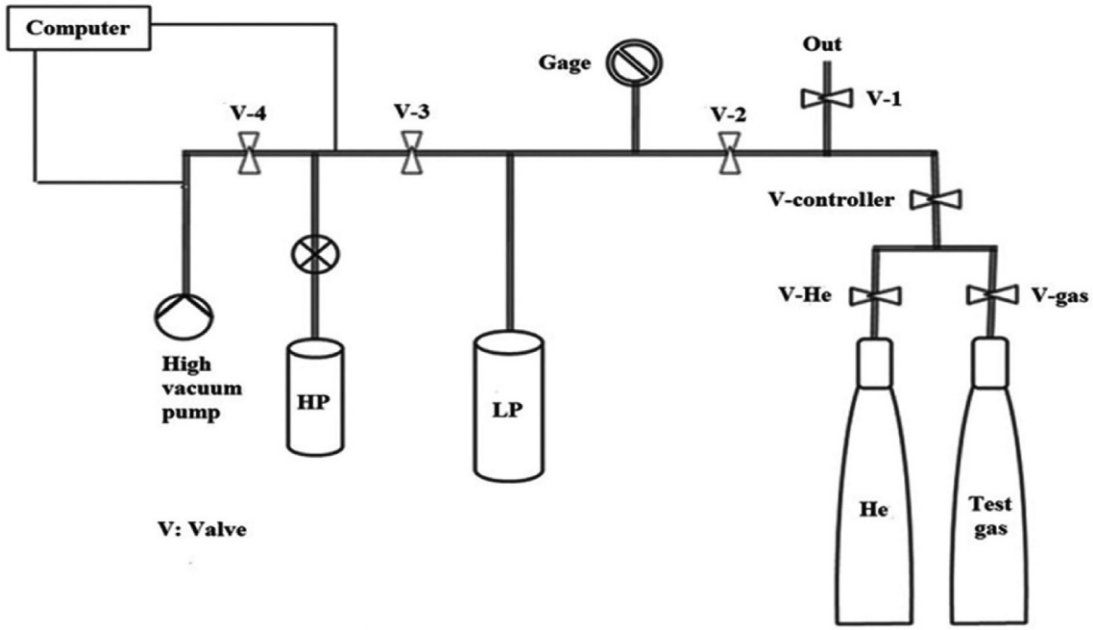

Fig. 15.6

Experimental setup used for the adsorption of methane [23]. *Reprinted with permission from H. Pazoki, M. Anbia, Synthesis of a microporous copper carboxylate metal organic framework as a new high capacity methane adsorbent, Polyhedron 171 (2019) 108–111. Copyright (2019) Elsevier.*

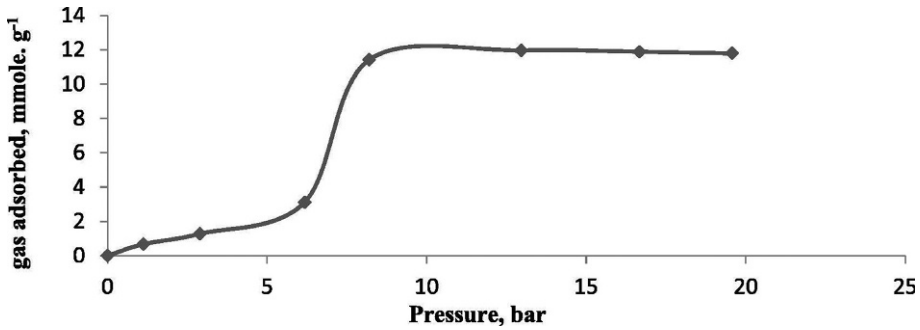

Fig. 15.7

The variation of CH_4 adsorption with pressure by Cu-BDC at 298 K [23]. *Reprinted with permission from H. Pazoki, M. Anbia, Synthesis of a microporous copper carboxylate metal organic framework as a new high capacity methane adsorbent, Polyhedron 171 (2019) 108–111. Copyright (2019) Elsevier.*

This book belongs to Badji Mokhtar Annaba University Central Library Copyright Elsevier 2025

15.6.1.2 Adsorption of dyes

The dyes are obnoxious materials that do not degrade easily because of their stability to light and oxidation reactions. Therefore it is important to work out strategies for their treatment and removal from polluted water. Search for the suitable adsorbents for removal of dyes from contaminated water has been taken up by numerous researchers. Recently, MOFs and MOF composites are regularly used for dye bearing wastewater remediation. MOFs offer high adsorption capacity, rapid uptake, and easy regeneration. Adeyemo et al. [51] discussed MOFs as adsorbents for dye adsorption. The adsorption of dyes is dependent upon important parameters, which includes the surface functionalization, hydrophilic/hydrophobic nature, surface charges, and textural properties of the MOFs.

Crystalline ZnO nanoparticles embedded in carbon matrix have been synthesized by carbonization of porous metal-organic framework MOF-5. The ZnO/C nanocomposite showed cubic particle morphology and high surface area of the precursor MOF-5. The ZnO/C nanocomposite showed excellent methylene blue (MB) adsorption because of the presence of oxygen-containing hydrophilic functional groups on its surface. The degradation mechanism on the ZnO/C-MOF-5 nanocomposite is shown in Fig. 15.8 [52].

Zeolitic imidazolate framework (ZIF-8) as an MOF and its hybrid nanocomposite based on graphene oxide (GO) and CNTs were prepared at an ambient temperature [32]. The prepared nanomaterials were utilized as adsorbents for removing cationic dye, Malachite Green (MG) from colored wastewater. Removal of dye using hybrid nanocomposites was

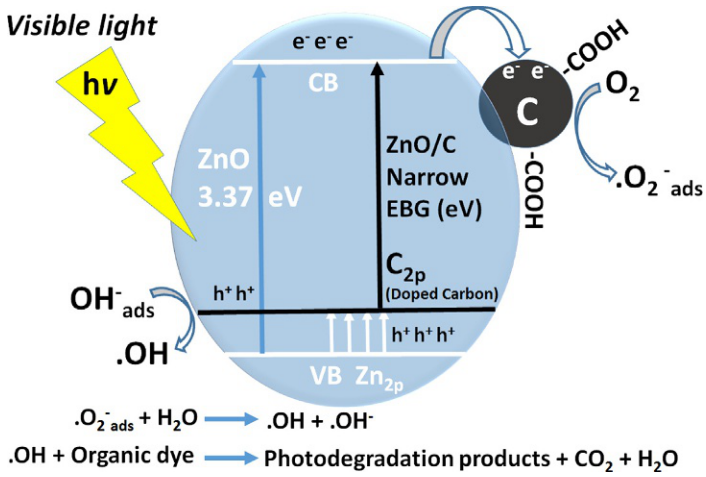

Fig. 15.8
Mechanism of dye degradation in MOF-derived ZnO/C nanocomposite and shift in energy band gap under visible light [52]. *Reprinted with permission from M.Z. Hussain, A. Schneemann, R.A. Fischer, Y. Zhu, Y. Xia, MOF derived porous ZnO/C nanocomposites for efficient dye photodegradation, ACS Appl. Energy Mater. 1 (2018) 4695–4707. Copyright (2018) American Chemical Society.*

This book belongs to Badji Mokhtar Annaba University Central Library Copyright Elsevier 2025

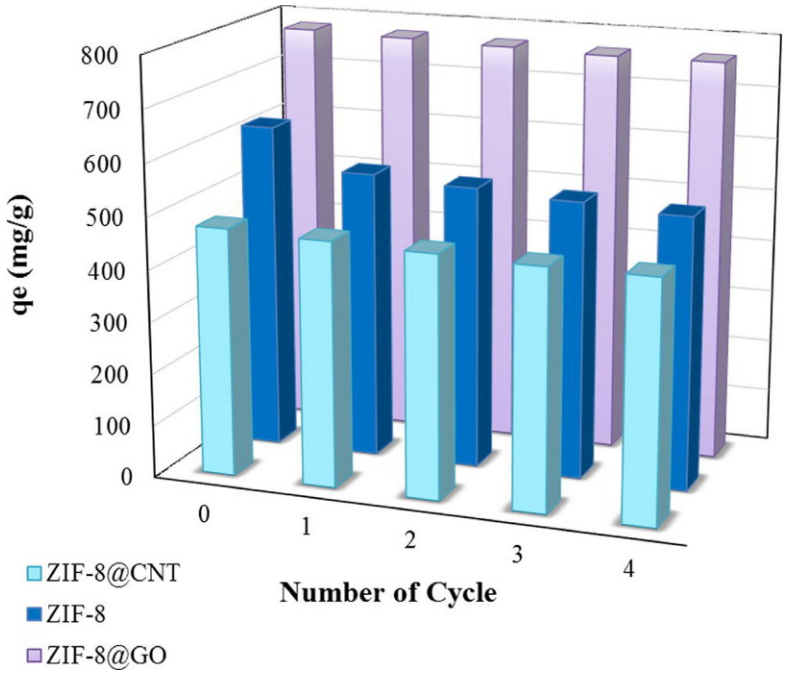

Fig. 15.9
Recyclability of GO-CNTs/ZIF-8 nanocomposite for adsorption of malachite green at condition $C_o = 50$ mg L^{-1}, mass of adsorbent = 0.01 g and volume = 150 mL [32]. *Reprinted with permission from J. Abdi, M. Vossoughi, N.M. Mahmoodi, I. Alemzadeh, Synthesis of metal-organic framework hybrid nanocomposites based on GO and CNT with high adsorption capacity for dye removal, Chem. Eng. J. 326 (2017) 1145–1158. Copyright (2017) Elsevier.*

higher than that using pristine MOF. Effect of different operational parameters such as MOF loading dosage, adsorbent dosage, dye concentration, solution pH, and temperature was evaluated for batch adsorption study. The hybrid nanocomposites were regenerated and reused for more than four cycles as shown in Fig. 15.9.

Of late, various magnetic MOFs are fabricated by researchers because of their ease for separation from aqueous solutions by magnets facilitating the easy recycle [53]. MOF-based magnetic nanostructures are extensively used for removal of dyes from wastewater because of their exceptional physicochemical performance. The coprecipitation method was used for modification of MIL-88A with magnetic nanoparticles for preparing a magnetic Fe_3O_4/MIL-88A composite for adsorption of bromophenol blue. The results indicated that the composite has hexagonal rod-like structure and excellent magnetic property for magnetic separation. Maximum adsorption capacity of Fe_3O_4/MIL-88A composite for bromophenol blue was 167.2 mg/g. The nanocomposite was regenerated and reused, and it was observed that after five cycles, it adsorbed almost 94% of the initial adsorption amount. Moreover, to test the

This book belongs to Badji Mokhtar Annaba University Central Library Copyright Elsevier 2025

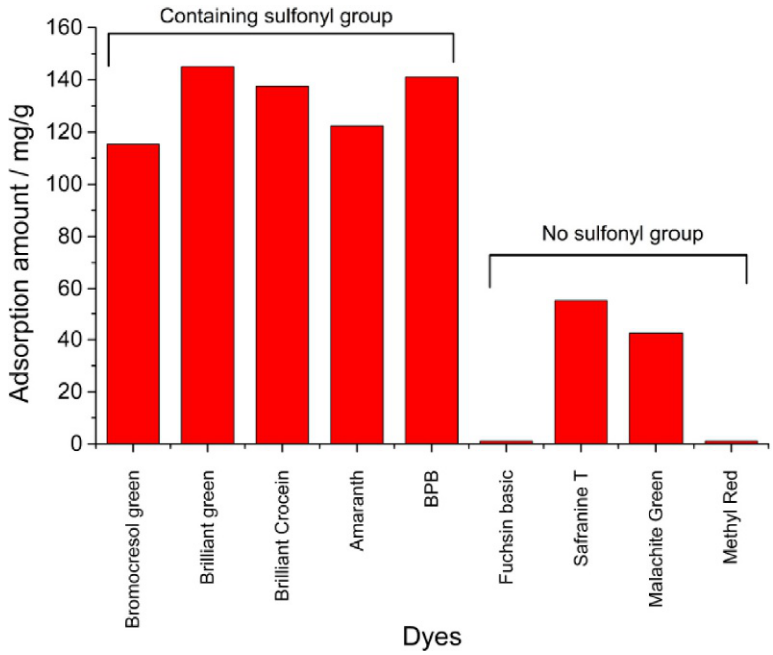

Fig. 15.10

Comparison of various dyes adsorption amount on magnetic Fe_3O_4/MIL-88A composite [54].
Reprinted with permission from Y. Liu, Y. Huang, A. Xiao, H. Qiu, L. Liu, Preparation of magnetic Fe_3O_4/MIL-88A nanocomposite and its adsorption properties for bromophenol blue dye in aqueous solution, Nanomaterials 9 (2019) 51. Copyright (2019) MDPI, Open access Creative Common CC BY license.

applicability of the same nanocomposite for multiple uses, it was used for adsorbing eight other dyes viz., Bromocresol Green, Brilliant Crocein, Brilliant Green, MG, Amaranth, Safranine T, Fuchsin Basic, and Methyl Red. The magnetic composite showed good adsorption and affinity toward dyes containing sulfonyl groups as shown in Fig. 15.10 [54].

Similarly, a magnetic MOF Fe_3O_4@AMCA-MIL-53 (Al) nanocomposite was used for the removal of MB and MG dyes from aqueous environment. The composite showed maximum adsorption capacity of 1.02 and 0.90 mmol/g for MB and MG dyes, respectively. Effect of initial pH on adsorption of MB and MG was studied as shown in Fig. 15.11. The attachment of MB and MG dyes was through carboxylate and amide groups owing to electrostatic interaction, π-π interaction, and hydrogen bonding as shown in Fig. 15.12. The desorption studies for two dyes from the nanocomposite were also done with satisfactory results [55].

In another work, a magnetic nanocomposite with Fe_3O_4 and activated charcoal (AC) designated as MIL-100(Fe)@Fe_3O_4@AC was prepared by hydrothermal method and utilized for adsorbing Rhodamine B (RB) dye. Surface areas of activated charcoal, Fe_3O_4@AC, and MIL-100(Fe)@Fe_3O_4@AC were measured as 121, 351, and 620 m^2/g, respectively. In about

This book belongs to Badji Mokhtar Annaba University Central Library
Copyright Elsevier 2025

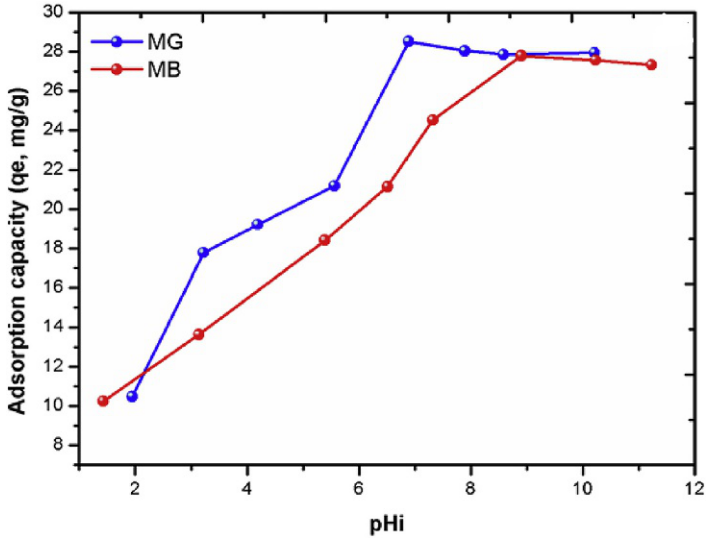

Fig. 15.11
The effect of pH on MB and MG adsorption by Fe_3O_4@AMCA-MIL53(Al) nanocomposite [55].
Reprinted with permission from A.A. Alqadami, M. Naushad, Z.A. Alothman, T. Ahamad, Adsorptive performance of MOF nanocomposite for methylene blue and malachite green dyes: kinetics, isotherm and mechanism, J. Environ. Manage. 223 (2018) 29–36. Copyright (2018) Elsevier.

40 min of contact time, 769.23 mg/g of RB dye was adsorbed, which is a very high capacity when compared with other adsorbents. Even after several cycles, the nanocomposite exhibited good reusability [56]. Wang et al. [57] prepared Fe_3O_4/MIL-101(Cr) by a simple reduction-precipitation method for application as an adsorbent for removal of acid red and orange G from water. The nanocomposite characterization showed that it has large surface area, strong magnetism, and excellent dispersion effect. The reusability of Fe_3O_4/MIL-101(Cr) was also studied by regenerating the composite. It was observed that without any loss of activity, the nanocomposite was reused minimum six times. $MgFe_2O_4$/MOF composite synthesized by solvothermal method was applied for adsorbing RB and Rhodamine 6G (Rh6G) from water by Tian et al. [58]. Rapid removal of both the dyes was observed in a very short time of less than 5 min with adsorption capacities of 219.78 and 306.75 mg/g for RB and Rh6G, respectively. Adsorption data were fitted with the pseudo-second-order kinetic model. Prepared material was reused at least 10 times by washing with acetonitrile solution.

One of the ways of modifying the structure of MOFs is by incorporation of functional groups into the building component ligand, which is useful for forming highly porous MOFs for adsorption of dye. A metal-organic framework (Zn-MOF) with carbonyl group based on fluorenone-2,7-dicarboxylate ligand was prepared and utilized for selective adsorption of cationic dyes such as MB, Crystal violet, and RB from aqueous solution [59]. Structural characterization of the Zn-MOF revealed that the carbonyl groups arising from the ligand

This book belongs to Badji Mokhtar Annaba University Central Library Copyright Elsevier 2025

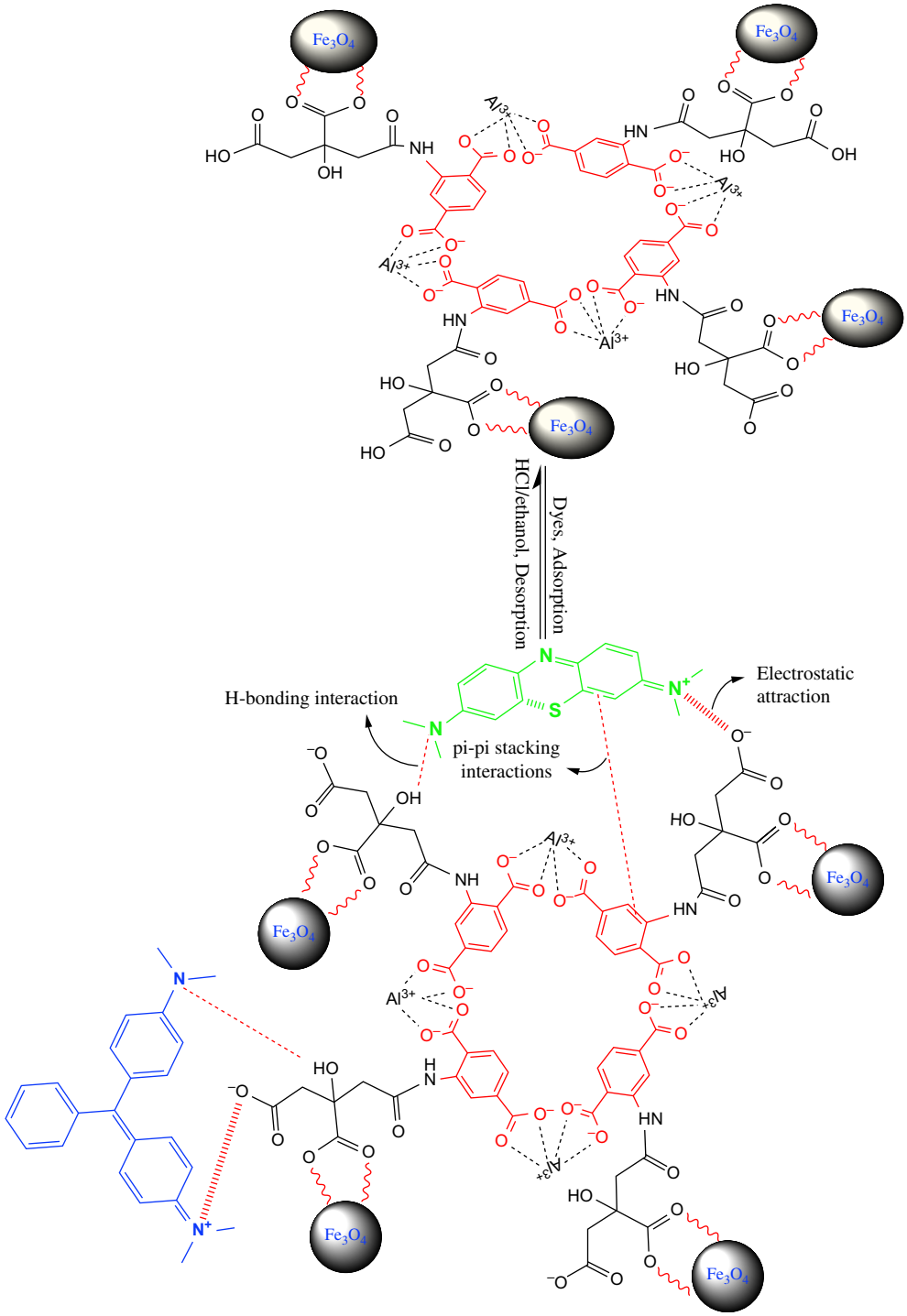

Fig. 15.12

The mechanism of adsorption-desorption on Fe_3O_4@AMCA-MIL53(Al) nanocomposite on MG and MB dyes [55]. *Reprinted with permission from A.A. Alqadami, M. Naushad, Z.A. Alothman, T. Ahamad, Adsorptive performance of MOF nanocomposite for methylene blue and malachite green dyes: kinetics, isotherm and mechanism, J. Environ. Manage. 223 (2018) 29–36. Copyright (2018) Elsevier.*

This book belongs to Badji Mokhtar Annaba University Central Library
Copyright Elsevier 2025

furnished the pore surface. They are beneficial for adsorption of cationic dyes. For MB, the highest adsorption capacity was found to be 326 mg/g. MOF based on manganous (II) ions and a paddle wheel ligand (Mn-BTB) was synthesized with 47.1% porosity for the adsorption of large dye molecules [6]. The MOF was utilized for selective dye adsorption of an anionic dye, methyl orange (MO) and cationic dyes such as MB and RB. The experimental results indicated that Mn-BTB with an anionic framework was favorable for the selective adsorption of cationic dyes. Hossein et al. [60] synthesized zirconium-based MOF with improved water stability. Structural characterization techniques such as XRD, field-emission scanning electron microscopy, and N_2 adsorption/desorption were used for monitoring the alteration of MOF by water aging. Water stability was tested for a period of 12 months. This MOF was used for selective adsorption of an anionic dye (MO) and a cationic dye (MB) from aqueous solution. Results indicated that the structure of MOF was principally retained and its adsorption capacity was reduced by a small margin after extended water aging. The adsorption capacity of MOF for MO was higher than that for MB, especially under acidic and neutral conditions.

15.6.1.3 General adsorption

Apart from the regular use of MOF composites for adsorption of gases and dyes, these composites are used quite frequently for adsorbing other chemical constituents as well. MOFs are used for the refinement of petroleum by aiding in removal of nitrogenous compounds and sulfur-containing compounds. Some of the applications of this type are discussed here.

Fuels such as diesel and gasoline contain sulfur-containing compounds such as thiophene (Th), benzothiophene (BT), and dimethyl dibenzothiophene (DMDBT). The contents of these fuels must be removed so as to reduce air pollution and prevent deactivation of catalysts. Ullah et al. [61] studied the adsorption of BT from model fuel on MOF modified with bicomponent zirconium (IV) benzene-tricarboxylate Zr(BTC) and its postsynthetic modified hybrid form with dodeca-tungstophosphoric acid (HPW/Zr(BTC)). It formed a ball and stick structure as shown in Fig. 15.13. Adsorption capacity of Zr(BTC) was improved by incorporation of dodeca-tungstophosphoric acid, which was attributed to the availability of additional acid sites for adsorption of BT. Adsorption kinetics followed a pseudo-second-order model. The adsorbent was reused after regeneration and it was observed that the adsorption sites were retained because of regeneration.

Polyoxometallate (POM)-loaded porous HKUST-1was used by Khan et al. [62] for adsorption of BT. A 26% increase in maximum adsorption capacity was found because of loading of POM, whereas the porosity of the composite was found to be decreased. A similar work was done by the same group where Cu^+-loaded MOF (MIL-100-Fe) was tested as adsorbent for BT [63]. The effect of Cu^+ content and maximum adsorption capacity was also calculated. By increasing the copper content up to a Cu/Fe (wt/wt) ratio of 0.07, the maximum adsorption capacity increased by 14% as against the virgin MIL-100-Fe without Cu^+ loading as shown in Fig. 15.14.

This book belongs to Badji Mokhtar Annaba University Central Library Copyright Elsevier 2025

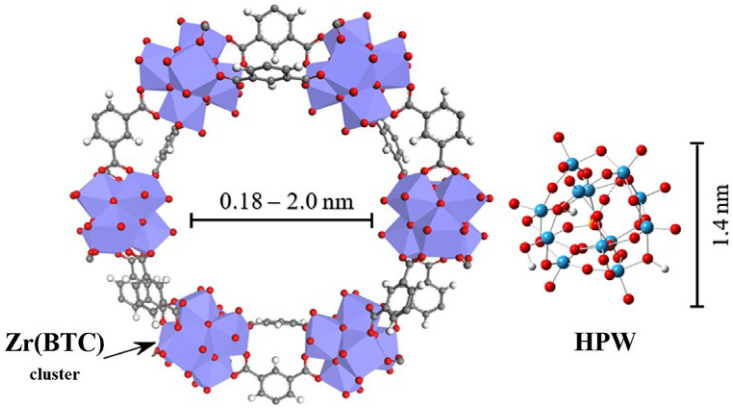

Fig. 15.13
Representation of ball and stick structure of Zr(BTC) MOF model and dedeca-tungstophosphoric acid (HPW) [61]. *Reprinted with permission from L. Ullah, G. Zhao, N. Hedin, X. Ding, S. Zhang, X. Yao, Y. Nie, Y. Zhang, Highly efficient adsorption of benzothiophene from model fuel on a metal-organic framework modified with dodeca-tungstophosphoric acid, Chem. Eng. J. 362 (2019) 30–40. Copyright (2019) Elsevier.*

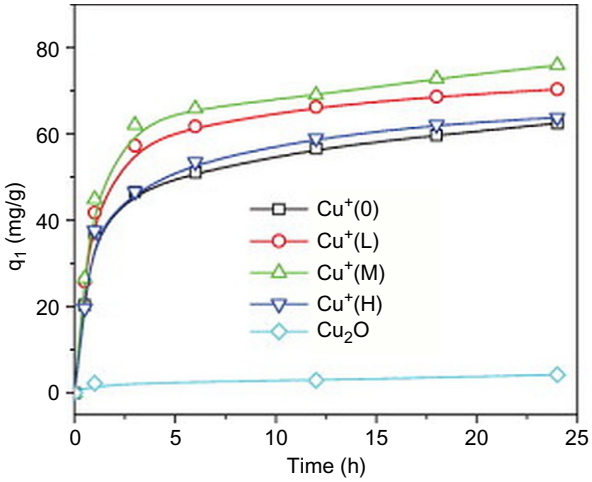

Fig. 15.14
Effect of Cu^+ and contact time on benzothiophene adsorption at condition of initial concentration of benzothiophene 1000 μg/g and temperature 25°C, respectively, where $L = 0.05$(wt/wt), $M = 0.07$(wt/wt), and $H = 0.1$ (wt/wt) [63]. *Reprinted with permission from N.A. Khan, S.H. Jhung, Low-temperature loading of Cu+ species over porous metal-organic frameworks (MOFs) and adsorptive desulfurization with Cu+-loaded MOFs, J. Hazard. Mater. 237 (2012) 180–185. Copyright (2012) Elsevier.*

This book belongs to Badji Mokhtar Annaba University Central Library
Copyright Elsevier 2025

In another work, Khan et al. [64] studied the ionic-liquids supported on MOFs for adsorptive desulfurization. The adsorptive capacity of ionic liquids supported on MIL-101 was 71% higher than virgin MIL-101. The acid-base interactions between the acidic ionic liquid and basic BT was the reason for improvement in the adsorption capacity. A composite of ionic liquid/MOFs has been found to be very effective for removing sulfur-containing compounds when compared to pristine MOFs [65]. MIL-101 was impregnated with phosphotungstic acid (PWA) and tested as an adsorbent for the liquid-phase adsorption of nitrogen-containing compounds from a model fuel [31]. The model fuel contained a mixture of compounds such as BT, quinoline, and indole. The adsorption selectivity of both MOFs MIL-101 and PWA-impregnated MIL-101s for quinoline was enormous when compared to BT. A 1% PWA impregnation in MIL-101 enhanced the adsorption capacity for quinolone by 20%, whereas for indole, it marginally reduced with PWA impregnation. Moreover, the adsorbent was found to be reusable for many cycles.

VOCs such as toluene, benzene, acetone, or ethanol are the most important air pollutants responsible for photochemical reactions leading to photochemical smog and damage of the ozone layer. VOCs are highly toxic, mutagenic, and carcinogenic, causing lot of health concerns to the population. For the removal of benzene, adsorbents with specific properties such as high surface area, micro-mesoporous structure, and large micropore volume are desired. Barbara et al. [13] fabricated graphene-MOF composite through facile crystallization of MOF in mesopores of a 3D graphene. The composite consisting of a weight ratio of 1:2 of graphene and MOF showed approximately twice-larger benzene adsorption capacity (24.5 mmol/g at 20°C) and relative pressure close to unity as against that of pure MOF. Interestingly, at the same conditions, pure graphene showed higher quantity of benzene adsorption (33.6 mmol/g), but at low and moderate relative pressures, the benzene adsorption was quite lesser than that of pure MOF. Furthermore, the composite exhibited improved thermal stability than the pristine MOF.

Lin et al. [66] investigated selective adsorption of ions from aqueous solutions with MOFs. Selective separation of precious metals can be a new sustainable development concept of "urban mining." Zr(IV)-cluster-based MOFs were synthesized for adsorption of Pd(II) from acidic aqueous solutions that contained Ni(II), Co(II), Pd (II), and Pt(IV). Different Zr-MOFs composites were synthesized, and UiO-66-NH_2 showed the highest Pd(II) selectivity, which was almost 181 times higher than that of Pt(IV) as shown in Fig. 15.15.

In situ modification of Fe-MOF with Al^{3+} was done by Wang et al. [10] for preparing Al@Fe-MOF composite for adsorption of selenite (Se(IV)). When compared with Fe-MOF, the adsorption capacity of Al@Fe-MOF was higher by 77%, whereas the specific surface area was increased by 112%. For Fe-MOF, at a pH higher than 5.0, hydrolysis occurred, but it did not occur in the pH range of 3.0–7.0 for Al@Fe-MOF.

This book belongs to Badji Mokhtar Annaba University Central Library Copyright Elsevier 2025

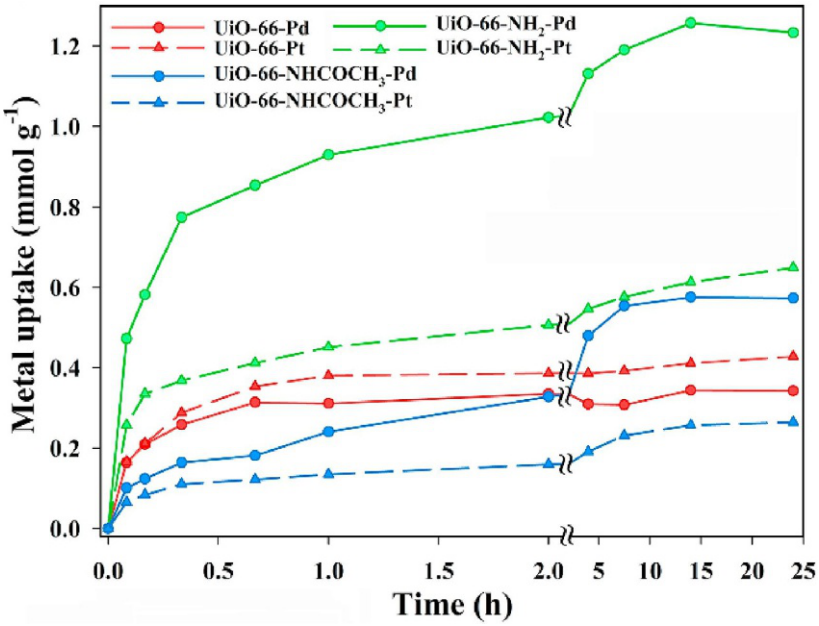

Fig. 15.15

Uptake of Pd(II) and Pt(IV) in UiO-66, UiO-66-NH_2, and UiO-66-$NHCOCH_3$ from the solution of 1.0 mmol $L^{-1}$of single Pd(II) and Pt(IV) [66]. *Reprinted with permission from S. Lin, J.K. Bediako, C.W. Cho, M.H. Song, Y. Zhao, J.A. Kim, J.W. Choi, Y.S. Yun, Selective adsorption of Pd(II) over interfering metal ions (Co(II), Ni(II), Pt(IV)) from acidic aqueous phase by metal-organic frameworks, Chem. Eng. J. 345 (2018) 337–344. Copyright (2018) Elsevier.*

In earlier section, the utility of magnetic MOFs for adsorptive removal of dyes is discussed. Magnetic MOFs can also be used for separation of antibiotics from water. The presence of residual antibiotics in water can be responsible for the evolution and development of drug-resistant bacteria. Minocycline (MC) is one of those antibiotics that are found in wastewater. Fe_3O_4@MIL-68 (Al), a magnetic aluminum-based MOF, was prepared and used as an adsorbent for removing MC from aqueous solutions [53]. Thorough characterization of MOFs indicated that the basic structure of MIL-68(Al) remained unaltered because of addition of Fe_3O_4 nanoparticles. The experiments indicated that 248.05 mg/g of MC was adsorbed onto Fe_3O_4@MIL-68 (Al), and the adsorption kinetics followed a pseudo-second-order model. Hasan et al. [67] investigated liquid-phase adsorption naproxen and clofibric acid, which are pharmaceuticals and personal care products, using MOFs MIL-101 and MIL-100-Fe. Adsorptive capacity of these two MOFs was compared with activated carbon, and it was found that both MOFs offered higher adsorption than activated carbon.

This book belongs to Badji Mokhtar Annaba University Central Library
Copyright Elsevier 2025

15.6.2 Applications of nanocomposite-based MOFs in industry

Very high-level surface areas, porosities, pore size, and broad range of chemical inorganic-organic compositions of MOFs have attracted interests of many researchers from academia and industry and several hundred MOFs have been identified. The high porosity and nonexistence of hidden volumes in MOFs make them useful for volume specific applications such as separation, adsorption, purification, and catalytic reactions. There are few reports of industrial applications of MOFs, mainly in catalysis and gas purification, storage, and separation. Mueller et al. [68] have given the details about the prospective industrial applications of MOFs in catalysis and gas processing. In this paper, catalytic activation of alkynes, removal of impurities form natural gas, pressure swing separation of rare gases such as krypton and xenon, and finally, hydrogen storage on Cu-based MOF have been discussed. The Cu-based MOF was synthesized using an electrochemical route. Czaja et al. [8] reviewed the synthesis, characterization, and applications of MOFs from an industrial perspective. Potential applications of MOFs in chemical industry have been reviewed in this article, where applications of MOFs for catalysis, gas purification, gas separation, and gas storage are discussed [8]. They had attempted hydrogen storage on large-scale prototype. The experiments were done at 77 K and up to 40 bar. At these experimental conditions, different materials such as Cu-EMOF, IRMOF-8, Zn-EZIF, MOF-177, and MOF-5 were tried. It was observed that MOF-177 gave the best results.

15.7 Challenges for MOFs

Although MOFs offer many advantages, many of the them possess major limitations such as low light and water resistance, poor mechanical strength and electrical conductivity, and susceptibility to degrade even at ambient conditions. Their weak stability and low water resistance leads to the steady deterioration of their crystalline structures [13]. Strength and reactivity of any MOF framework mainly depends on its metal-ligand interactions in which the metal-containing clusters are often susceptible to ligand substitution by water or other nucleophiles. This means that the frameworks can get collapsed when exposed to moist air. Some types of MOFs may collapse because of high temperature exposure or vacuum treatment or may be over a period of time. To improve the stability of the framework, different methods such as utilization of high-valence metal ions or nitrogen-donor ligands are tried [69].

MOFs have been regularly used for adsorption of toxic gases/vapors. However, all the adsorption capacity data measurements are done under unrealistic high-pressure conditions (e.g., >1000 Pa), limiting the practical utility of MOFs at around ambient conditions. In a comparative study, the adsorption properties of MOF-199 [M199] and UiO-66 [U6]) for benzene adsorption were compared with activated carbon across 0.01–5 Pa benzene.

This book belongs to Badji Mokhtar Annaba University Central Library Copyright Elsevier 2025

The maximum adsorption capacity of M199 was estimated to be 94.8 mg/g, which was marginally greater than activated carbon (93.5 mg/g), whereas for U6, it was 27.1 mg/g, which is very less when compared with the other two. Furthermore, with the decrease in initial loading partial pressure, the adsorption capacity of M199 drastically dropped [70].

Some of the limitations for MOFs are related to the synthesis processes. One of the key hurdles in the utility of MOFs is the lack of high-throughput synthesis processes, where larger quantities can be synthesized in short time at ambient pressure. Many MOFs are prepared in water or through slow diffusion methods that are effective but possess some drawbacks. Nonaqueous synthesis methods require days or weeks for completion, eliminating the possibility of those methods for industrial utility [51]. Some methods require the use of an autoclave but from an industrial point of view it is not a preferred option [71]. Also, the production of MOFs in the mesoporous range is preferred because if the pore diameters are in micropore range, it reduces the quantity of dyes adsorbed [51]. Additionally, some of the points that must be given considerations are the availability and cost of the raw materials, synthesis procedures, method of activation, requirements of achieving high yields, reducing the amount of impurities, and use of minor quantities of solvents [20]. From the cost point of view, the reuse of MOFs is expected. So the methods for the regeneration are very important, and a lot of improvements can be done in regeneration methods; however, they will require extensive research work [51].

15.7.1 Challenges and issues for MOF as adsorbent for treatment of wastewater

As discussed earlier, MOFs are promising materials as adsorbents or photocatalytic materials for purification of wastewater. By changing the metal ions or organic linkers, development of a variety of morphologies and structures of novel MOFs is possible. As a result, they find wide usage in wastewater treatment, but still a lot of issues are involved in full-fledged use of MOFs in wastewater treatment. Some limitations of MOFs, which limit their usage in wastewater treatment, are lower structural stability, dispersibility, and solubility. The concurrent effect of extremely small particle sizes and inadequate mechanical strength are also causing some limitations for their use in wastewater treatment [69, 72]. Reusability of the adsorbent materials is also an important issue because it requires additional treatments to be given to the used adsorbents. So the processes of regeneration and reuse of the MOFs are of prime importance. Extensive work is essential to find improved physical methods for regenerating exhausted adsorbents so that those can become economically viable. Thus the adsorbent material is termed to be effective if it offers strong adsorption capacity, high selectivity for specific compounds, mechanical/chemical strength, and regenerability. To improve the MOF stability, different functionalization methods are used for a range of MOFs with varying sorption properties in water. The production of water-stable MOFs requires understanding the breakdown mechanisms in existing MOFs. Another major drawback of MOFs is the pore size having diameters in micropore range, which limits the quantity of dyes

This book belongs to Badji Mokhtar Annaba University Central Library Copyright Elsevier 2025

that can get adsorbed in the MOF framework. Hence synthesis of MOFs with pores in the mesoporous size range is required [51]. The competitive performance of MOFs in presence of multiple pollutants is also a major issue. Furthermore, the removal of metalloids with different valences simultaneously is one of the major challenges that needs to be taken care of [17].

A whole lot of work is still to be done to alter the structure of MOFs or convert them into a useful form for adsorbing a wide range of organic contaminants in waste water. To overcome the limitations of MOFs, some of the remedial measures are discussed by Kumar et al. [73], which are (1) high selectivity for targeted toxic ions and fast sorption kinetics (2) suitable particle sizes that will allow continuous flow of waste through the MOF-based membrane/column/thin film and (3) higher mechanical strength to survive high water pressures.

Moreover, MOF materials are also used in combination with water treatment units such as membrane filtration, magnetic nanoparticles, and graphene for enhancing water treatment efficiency [18]. Although MOFs have shown a lot of enhancements in performance for adsorptive applications, most of these results are at laboratory scale, and limited applications are found at commercial scale, which points out a gap between the conversion of MOFs research at laboratory scale to commercialization. Some of the major hurdles in this transformation are reported as production capacity (space-time yield), cost, properties, purity, and stability. As a result, only few MOFs are translated from laboratory to large-scale real-world applications [17].

15.8 Conclusion

In conclusion, it can be said that MOFs are a class of crystalline materials having infinite network structures, offering ultrahigh porosity and substantially high internal surface areas. The exceptional characteristic of MOFs is their amazing network flexibility, which is closely associated with the coordination bonds, noncovalent bonds, and weak interactions. However, MOFs demonstrate some disadvantages such as poor chemical stability that limits exploitation of their full potential. In order to make these MOFs more versatile and improve their applicability to realistic applications, it is imperative to improve their properties and introduce new functionalities. Hence a combination of MOFs with wide range of functional materials to merge the merits and alleviate the shortcomings of individual components has been proposed. Numerous MOFs having diverse structural and practical properties can be formulated by altering metal ion/clusters, employing a range of combinations of inorganic building blocks and a wide range of organic linkers having variable geometries, lengths, and functionalities.

The maximum use of MOFs is based on adsorption, which forms the basis for different applications. MOFs are principally used for gas storage and separation, removal/separation of hazardous chemicals, heterogeneous catalysis, photocatalysis, sensing, drug delivery, biosensing, and other medical applications.

This book belongs to Badji Mokhtar Annaba University Central Library Copyright Elsevier 2025

Although MOFs offer many advantages, still many of the MOFs possess major limitations such as low light and water resistance, poor mechanical strength and electrical conductivity, and susceptibility to degradation even at ambient conditions. Future efforts can be directed toward overcoming these shortcomings of MOFs. Cost effectiveness of the synthesis methods is another major area that can have a huge impact on use of MOFs as alternatives to the expensive activated carbon. Long-term use and reuse of MOFs is expected from the cost point of view. So the methods for regeneration are very important, and a lot of improvements can be done in regeneration methods but will require extensive research work.

References

[1] Q.-L. Zhu, Q. Xu, Metal–organic framework composites. Chem. Soc. Rev. 43 (2014) 5468–5512, https://doi.org/10.1039/C3CS60472A.
[2] J.L.C. Rowsell, O.M. Yaghi, Metal–organic frameworks: a new class of porous materials. Microporous Mesoporous Mater. 73 (2004) 3–14, https://doi.org/10.1016/j.micromeso.2004.03.034.
[3] H. Li, M. Eddaoudi, M. O'Keeffe, O.M. Yaghi, Design and synthesis of an exceptionally stable and highly porous metal-organic framework. Nature 402 (1999) 276–279, https://doi.org/10.1038/46248.
[4] S.T. Meek, J.A. Greathouse, M.D. Allendorf, Metal-organic frameworks: a rapidly growing class of versatile nanoporous materials. Adv. Mater. 23 (2011) 249–267, https://doi.org/10.1002/adma.201002854.
[5] D. Britt, D. Tranchemontagne, O.M. Yaghi, Metal-organic frameworks with high capacity and selectivity for harmful gases. Proc. Natl. Acad. Sci. U. S. A. 105 (2008) 11623–11627, https://doi.org/10.1073/pnas.0804900105.
[6] J. He, J. Li, W. Du, Q. Han, Z. Wang, M. Li, A mesoporous metal-organic framework: potential advances in selective dye adsorption. J. Alloys Compd. 750 (2018) 360–367, https://doi.org/10.1016/j.jallcom.2018.03.393.
[7] I. Ahmed, S.H. Jhung, Composites of metal-organic frameworks: preparation and application in adsorption. Mater. Today 17 (2014) 136–146, https://doi.org/10.1016/j.mattod.2014.03.002.
[8] A.U. Czaja, N. Trukhan, U. Müller, Industrial applications of metal-organic frameworks. Chem. Soc. Rev. 38 (2009) 1284–1293, https://doi.org/10.1039/b804680h.
[9] S. Kitagawa, R. Kitaura, S.I. Noro, Functional porous coordination polymers. Angew. Chem. Int. Ed. 43 (2004) 2334–2375, https://doi.org/10.1002/anie.200300610.
[10] R. Wang, H. Xu, K. Zhang, S. Wei, W. Deyong, High-quality Al@Fe-MOF prepared using Fe-MOF as a micro-reactor to improve adsorption performance for selenite. J. Hazard. Mater. 364 (2019) 272–280, https://doi.org/10.1016/j.jhazmat.2018.10.030.
[11] W.G. Shim, K.J. Hwang, J.T. Chung, Y.S. Baek, S.J. Yoo, S.C. Kim, H. Moon, J.W. Lee, Adsorption and thermodesorption characteristics of benzene in nanoporous metal organic framework MOF-5. Adv. Powder Technol. 23 (2012) 615–619, https://doi.org/10.1016/j.apt.2011.07.002.
[12] H.R. Moon, D.W. Lim, M.P. Suh, Fabrication of metal nanoparticles in metal-organic frameworks. Chem. Soc. Rev. 42 (2013) 1807–1824, https://doi.org/10.1039/c2cs35320b.
[13] B. Szczęśniak, J. Choma, M. Jaroniec, Gas adsorption properties of hybrid graphene-MOF materials. J. Colloid Interface Sci. 514 (2018) 801–813, https://doi.org/10.1016/j.jcis.2017.11.049.
[14] S. Ali Akbar Razavi, A. Morsali, Linker functionalized metal-organic frameworks. Coord. Chem. Rev. 399 (2019) 213023, https://doi.org/10.1016/j.ccr.2019.213023.
[15] M. Ding, X. Cai, H.-L. Jiang, Improving MOF stability: approaches and applications. Chem. Sci. 10 (2019) 10209–10230, https://doi.org/10.1039/C9SC03916C.
[16] S. Zhuang, R. Cheng, J. Wang, Adsorption of diclofenac from aqueous solution using UiO-66-type metal-organic frameworks. Chem. Eng. J. 359 (2019) 354–362, https://doi.org/10.1016/j.cej.2018.11.150.

This book belongs to Badji Mokhtar Annaba University Central Library Copyright Elsevier 2025

[17] S. Ramanayaka, M. Vithanage, A. Sarmah, T. An, K.-H. Kim, Y.S. Ok, Performance of metal–organic frameworks for the adsorptive removal of potentially toxic elements in a water system: a critical review. RSC Adv. 9 (2019) 34359–34376, https://doi.org/10.1039/C9RA06879A.

[18] A. Ansari, V.U. Siddiqui, I. Khan, M.K. Akram, W. Ahmad, A.K. Siddiqi, A.M. Asiri, Metal-organic-frameworks (MOFs) for industrial wastewater treatment, in: A. Khan, B.M. Abu-Zaid, M.A. Hussein, A. M. Asiri, M. Azam (Eds.), Metal-Organic Framework Composites: Volume I, 53 Materials Research Forum, 2019, pp. 1–28.

[19] R. Ricco, L. Malfatti, M. Takahashi, A.J. Hill, P. Falcaro, Applications of magnetic metal-organic framework composites. J. Mater. Chem. A 1 (2013) 13033–13045, https://doi.org/10.1039/c3ta13140h.

[20] N. Stock, S. Biswas, Synthesis of metal-organic frameworks (MOFs): routes to various MOF topologies, morphologies, and composites. Chem. Rev. 112 (2012) 933–969, https://doi.org/10.1021/cr200304e.

[21] M. Anbia, V. Hoseini, Enhancement of CO_2 adsorption on nanoporous chromium terephthalate (MIL-101) by amine modification. J. Nat. Gas Chem. 21 (2012) 339–343, https://doi.org/10.1016/S1003-9953(11)60374-5.

[22] D.J. Tranchemontagne, J.R. Hunt, O.M. Yaghi, Room temperature synthesis of metal-organic frameworks: MOF-5, MOF-74, MOF-177, MOF-199, and IRMOF-0. Tetrahedron 64 (2008) 8553–8557, https://doi.org/10.1016/j.tet.2008.06.036.

[23] H. Pazoki, M. Anbia, Synthesis of a microporous copper carboxylate metal organic framework as a new high capacity methane adsorbent. Polyhedron 171 (2019) 108–111, https://doi.org/10.1016/j.poly.2019.07.013.

[24] J. Zhang, L. Gao, Y. Wang, L. Zhai, X. Wang, L. Fan, T. Hu, Two trinuclear cluster-based 3D interpenetrated metal-organic frameworks with selective adsorption and antiferromagnetic properties. J. Solid State Chem. 271 (2019) 303–308, https://doi.org/10.1016/j.jssc.2019.01.003.

[25] S.H. Jhung, J.H. Lee, J.W. Yoon, C. Serre, G. Férey, J.S. Chang, Microwave synthesis of chromium terephthalate MIL-101 and its benzene sorption ability. Adv. Mater. 19 (2007) 121–124, https://doi.org/10.1002/adma.200601604.

[26] W.J. Son, J. Kim, J. Kim, W.S. Ahn, Sonochemical synthesis of MOF-5. Chem. Commun. (2008) 6336–6338, https://doi.org/10.1039/b814740j.

[27] M. Schlesinger, S. Schulze, M. Hietschold, M. Mehring, Evaluation of synthetic methods for microporous metal-organic frameworks exemplified by the competitive formation of $[Cu_2(btc)_3(H_2O)_3]$ and $[Cu_2(btc)(OH)(H_2O)]$. Microporous Mesoporous Mater. 132 (2010) 121–127, https://doi.org/10.1016/j.micromeso.2010.02.008.

[28] C. Petit, T.J. Bandosz, Engineering the surface of a new class of adsorbents: metal-organic framework/graphite oxide composites. J. Colloid Interface Sci. 447 (2015) 139–151, https://doi.org/10.1016/j.jcis.2014.08.026.

[29] L. Asgharnejad, A. Abbasi, A. Shakeri, Ni-based metal-organic framework/GO nanocomposites as selective adsorbent for CO_2 over N_2. Microporous Mesoporous Mater. 262 (2018) 227–234, https://doi.org/10.1016/j.micromeso.2017.11.038.

[30] Y. Chen, D. Lv, J. Wu, J. Xiao, H. Xi, Q. Xia, Z. Li, A new MOF-505@GO composite with high selectivity for CO_2/CH_4 and CO_2/N_2 separation. Chem. Eng. J. 308 (2017) 1065–1072, https://doi.org/10.1016/j.cej.2016.09.138.

[31] I. Ahmed, N.A. Khan, Z. Hasan, S.H. Jhung, Adsorptive denitrogenation of model fuels with porous metal-organic framework (MOF) MIL-101 impregnated with phosphotungstic acid: effect of acid site inclusion. J. Hazard. Mater. 250–251 (2013) 37–44, https://doi.org/10.1016/j.jhazmat.2013.01.024.

[32] J. Abdi, M. Vossoughi, N.M. Mahmoodi, I. Alemzadeh, Synthesis of metal-organic framework hybrid nanocomposites based on GO and CNT with high adsorption capacity for dye removal. Chem. Eng. J. 326 (2017) 1145–1158, https://doi.org/10.1016/j.cej.2017.06.054.

[33] B. Szczęśniak, J. Choma, M. Jaroniec, Ultrahigh benzene adsorption capacity of graphene-MOF composite fabricated via MOF crystallization in 3D mesoporous graphene. Microporous Mesoporous Mater. 279 (2019) 387–394, https://doi.org/10.1016/j.micromeso.2019.01.022.

[34] M. Oveisi, M. Alinia Asli, N.M. Mahmoodi, Carbon nanotube based metal-organic framework nanocomposites: synthesis and their photocatalytic activity for decolorization of colored wastewater. Inorg. Chim. Acta 487 (2019) 169–176, https://doi.org/10.1016/j.ica.2018.12.021.

[35] P. Falcaro, A.J. Hill, K.M. Nairn, J. Jasieniak, J.I. Mardel, T.J. Bastow, S.C. Mayo, M. Gimona, D. Gomez, H. J. Whitfield, R. Riccò, A. Patelli, B. Marmiroli, H. Amenitsch, T. Colson, L. Villanova, D. Buso, A new method

This book belongs to Badji Mokhtar Annaba University Central Library Copyright Elsevier 2025

to position and functionalize metal-organic framework crystals. Nat. Commun. 2 (2011) 237, https://doi.org/10.1038/ncomms1234.
[36] L.J. Murray, M. Dinc, J.R. Long, Hydrogen storage in metal-organic frameworks. Chem. Soc. Rev. 38 (2009) 1294–1314, https://doi.org/10.1039/b802256a.
[37] S.N. Kim, J. Kim, H.Y. Kim, H.Y. Cho, W.S. Ahn, Adsorption/catalytic properties of MIL-125 and NH2-MIL-125. Catal. Today 204 (2013) 85–93, https://doi.org/10.1016/j.cattod.2012.08.014.
[38] A. Corma, H. García, F.X. Llabrés i Xamena, Engineering metal organic frameworks for heterogeneous catalysis. Chem. Rev. 110 (2010) 4606–4655, https://doi.org/10.1021/cr9003924.
[39] J. Liu, L. Chen, H. Cui, J. Zhang, L. Zhang, C.-Y. Su, Applications of metal-organic frameworks in heterogeneous supramolecular catalysis. Chem. Soc. Rev. 43 (2014) 6011–6061, https://doi.org/10.1039/c4cs00094c.
[40] Y. Li, H. Xu, S. Ouyang, J. Ye, Metal–organic frameworks for photocatalysis. Phys. Chem. Chem. Phys. 18 (2016) 7563–7572, https://doi.org/10.1039/C5CP05885F.
[41] I. Stassen, N. Burtch, A. Talin, P. Falcaro, M. Allendorf, R. Ameloot, An updated roadmap for the integration of metal–organic frameworks with electronic devices and chemical sensors. Chem. Soc. Rev. 46 (2017) 3185–3241, https://doi.org/10.1039/C7CS00122C.
[42] L.E. Kreno, K. Leong, O.K. Farha, M. Allendorf, R.P. Van Duyne, J.T. Hupp, Metal–organic framework materials as chemical sensors. Chem. Rev. 112 (2012) 1105–1125, https://doi.org/10.1021/cr200324t.
[43] I. Imaz, M. Rubio-Martínez, J. An, I. Solé-Font, N.L. Rosi, D. Maspoch, Metal-biomolecule frameworks (MBioFs). Chem. Commun. 47 (2011) 7287–7302, https://doi.org/10.1039/c1cc11202c.
[44] A.C. McKinlay, R.E. Morris, P. Horcajada, G. Férey, R. Gref, P. Couvreur, C. Serre, BioMOFs: metal-organic frameworks for biological and medical applications. Angew. Chem. Int. Ed. 49 (2010) 6260–6266, https://doi.org/10.1002/anie.201000048.
[45] J. Li, X. Wang, G. Zhao, C. Chen, Z. Chai, A. Alsaedi, T. Hayat, X. Wang, Metal-organic framework-based materials: superior adsorbents for the capture of toxic and radioactive metal ions. Chem. Soc. Rev. 47 (2018) 2322–2356, https://doi.org/10.1039/c7cs00543a.
[46] J.-R. Li, J. Sculley, H.-C. Zhou, Metal–organic frameworks for separations. Chem. Rev. 112 (2012) 869–932, https://doi.org/10.1021/cr200190s.
[47] J.R. Li, R.J. Kuppler, H.C. Zhou, Selective gas adsorption and separation in metal-organic frameworks. Chem. Soc. Rev. 38 (2009) 1477–1504, https://doi.org/10.1039/b802426j.
[48] C. Petit, T.J. Bandosz, Enhanced adsorption of ammonia on metal-organic framework/graphite oxide composites: analysis of surface interactions. Adv. Funct. Mater. 20 (2010) 111–118, https://doi.org/10.1002/adfm.200900880.
[49] S.J. Yang, J.Y. Choi, H.K. Chae, J.H. Cho, K.S. Nahm, C.R. Park, Preparation and enhanced hydrostability and hydrogen storage capacity of CNT@MOF-5 hybrid composite. Chem. Mater. 21 (2009) 1893–1897, https://doi.org/10.1021/cm803502y.
[50] L. Gao, J. Zhang, L. Zhai, X. Wang, L. Fan, T. Hu, Gas adsorption and fluorescent sensing properties of two porous lanthanide metal–organic frameworks based on 3,5-bis(2-carboxy-phenoxy)-benzoic acid. Polyhedron 165 (2019) 171–176, https://doi.org/10.1016/j.poly.2018.12.015.
[51] A.A. Adeyemo, I.O. Adeoye, O.S. Bello, Metal organic frameworks as adsorbents for dye adsorption: overview, prospects and future challenges. Toxicol. Environ. Chem. 94 (2012) 1846–1863, https://doi.org/10.1080/02772248.2012.744023.
[52] M.Z. Hussain, A. Schneemann, R.A. Fischer, Y. Zhu, Y. Xia, MOF derived porous ZnO/C nanocomposites for efficient dye Photodegradation. ACS Appl. Energy Mater. 1 (2018) 4695–4707, https://doi.org/10.1021/acsaem.8b00822.
[53] Y.Y. Zhang, Q. Liu, C. Yang, S.C. Wu, J.H. Cheng, Magnetic aluminum-based metal organic framework as a novel magnetic adsorbent for the effective removal of minocycline from aqueous solutions. Environ. Pollut. 255 (2019) 113226, https://doi.org/10.1016/j.envpol.2019.113226.

This book belongs to Badji Mokhtar Annaba University Central Library Copyright Elsevier 2025

[54] Y. Liu, Y. Huang, A. Xiao, H. Qiu, L. Liu, Preparation of magnetic Fe_3O_4/MIL-88A nanocomposite and its adsorption properties for bromophenol blue dye in aqueous solution. Nanomaterials 9 (2019) 51, https://doi.org/10.3390/nano9010051.

[55] A.A. Alqadami, M. Naushad, Z.A. Alothman, T. Ahamad, Adsorptive performance of MOF nanocomposite for methylene blue and malachite green dyes: kinetics, isotherm and mechanism. J. Environ. Manage. 223 (2018) 29–36, https://doi.org/10.1016/j.jenvman.2018.05.090.

[56] A. Hamedi, F. Trotta, M. Borhani Zarandi, M. Zanetti, F. Caldera, A. Anceschi, M.R. Nateghi, In situ synthesis of MIL-100(Fe) at the surface of Fe_3O_4@AC as highly efficient dye adsorbing nanocomposite. Int. J. Mol. Sci. 20 (2019) 5612, https://doi.org/10.3390/ijms20225612.

[57] T. Wang, P. Zhao, N. Lu, H. Chen, C. Zhang, X. Hou, Facile fabrication of Fe_3O_4/MIL-101(Cr) for effective removal of acid red 1 and orange G from aqueous solution. Chem. Eng. J. 295 (2016) 403–413, https://doi.org/10.1016/j.cej.2016.03.016.

[58] H. Tian, J. Peng, T. Lv, C. Sun, H. He, Preparation and performance study of $MgFe_2O_4$/metal–organic framework composite for rapid removal of organic dyes from water. J. Solid State Chem. 257 (2018) 40–48, https://doi.org/10.1016/j.jssc.2017.09.017.

[59] J. Zhang, F. Li, Q. Sun, Rapid and selective adsorption of cationic dyes by a unique metal-organic framework with decorated pore surface. Appl. Surf. Sci. 440 (2018) 1219–1226, https://doi.org/10.1016/j.apsusc.2018.01.258.

[60] H. Molavi, A. Hakimian, A. Shojaei, M. Raeiszadeh, Selective dye adsorption by highly water stable metal-organic framework: long term stability analysis in aqueous media. Appl. Surf. Sci. 445 (2018) 424–436, https://doi.org/10.1016/j.apsusc.2018.03.189.

[61] L. Ullah, G. Zhao, N. Hedin, X. Ding, S. Zhang, X. Yao, Y. Nie, Y. Zhang, Highly efficient adsorption of benzothiophene from model fuel on a metal-organic framework modified with dodeca-tungstophosphoric acid. Chem. Eng. J. 362 (2019) 30–40, https://doi.org/10.1016/j.cej.2018.12.141.

[62] N.A. Khan, S.H. Jhung, Adsorptive removal of benzothiophene using porous copper-benzenetricarboxylate loaded with phosphotungstic acid. Fuel Process. Technol. 100 (2012) 49–54, https://doi.org/10.1016/j.fuproc.2012.03.006.

[63] N.A. Khan, S.H. Jhung, Low-temperature loading of Cu^+ species over porous metal-organic frameworks (MOFs) and adsorptive desulfurization with Cu^+-loaded MOFs. J. Hazard. Mater. 237–238 (2012) 180–185, https://doi.org/10.1016/j.jhazmat.2012.08.025.

[64] N.A. Khan, Z. Hasan, S.H. Jhung, Ionic liquids supported on metal-organic frameworks: remarkable adsorbents for adsorptive desulfurization. Chem. A Eur. J. 20 (2014) 376–380, https://doi.org/10.1002/chem.201304291.

[65] S.H. Jhung, N.A. Khan, Z. Hasan, Analogous porous metal-organic frameworks: synthesis, stability and application in adsorption. CrystEngComm 14 (2012) 7099–7109, https://doi.org/10.1039/c2ce25760b.

[66] S. Lin, J.K. Bediako, C.-W. Cho, M.-H. Song, Y. Zhao, J.-A. Kim, J.-W. Choi, Y.-S. Yun, Selective adsorption of Pd(II) over interfering metal ions (Co(II), Ni(II), Pt(IV)) from acidic aqueous phase by metal-organic frameworks. Chem. Eng. J. 345 (2018) 337–344, https://doi.org/10.1016/j.cej.2018.03.173.

[67] Z. Hasan, J. Jeon, S.H. Jhung, Adsorptive removal of naproxen and clofibric acid from water using metal-organic frameworks. J. Hazard. Mater. 209–210 (2012) 151–157, https://doi.org/10.1016/j.jhazmat.2012.01.005.

[68] U. Mueller, M. Schubert, F. Teich, H. Puetter, K. Schierle-Arndt, J. Pastré, Metal-organic frameworks – prospective industrial applications. J. Mater. Chem. 16 (2006) 626–636, https://doi.org/10.1039/b511962f.

[69] M. Bosch, M. Zhang, H.-C. Zhou, Increasing the stability of metal-organic frameworks. Adv. Chem. 2014 (2014) 1–8, https://doi.org/10.1155/2014/182327.

[70] K. Vikrant, C.J. Na, S.A. Younis, K.H. Kim, S. Kumar, Evidence for superiority of conventional adsorbents in the sorptive removal of gaseous benzene under real-world conditions: test of activated carbon against novel metal-organic frameworks. J. Clean. Prod. 235 (2019) 1090–1102, https://doi.org/10.1016/j.jclepro.2019.07.038.

This book belongs to Badji Mokhtar Annaba University Central Library Copyright Elsevier 2025

[71] C.G. Carson, K. Hardcastle, J. Schwartz, X. Liu, C. Hoffmann, R.A. Gerhardt, R. Tannenbaum, Synthesis and structure characterization of copper terephthalate metal-organic frameworks. Eur. J. Inorg. Chem. 2009 (2009) 2338–2343, https://doi.org/10.1002/ejic.200801224.
[72] C. Wang, X. Liu, N. Keser Demir, J.P. Chen, K. Li, Applications of water stable metal–organic frameworks. Chem. Soc. Rev. 45 (2016) 5107–5134, https://doi.org/10.1039/C6CS00362A.
[73] P. Kumar, V. Bansal, K.-H. Kim, E.E. Kwon, Metal-organic frameworks (MOFs) as futuristic options for wastewater treatment. J. Ind. Eng. Chem. 62 (2018) 130–145, https://doi.org/10.1016/j.jiec.2017.12.051.

This book belongs to Badji Mokhtar Annaba University Central Library
Copyright Elsevier 2025

CHAPTER 16

Advanced nanocomposite ion exchange materials for water purification

Manishkumar D. Yadav

Department of Chemical Engineering, Institute of Chemical Technology, Mumbai, India

Abbreviations

CNT	carbon nanotube
CDI	capacitive deionization
FT-IR	Fourier transform infrared spectroscopy
IEX	ion exchange
IEC	ion exchange capacity
MWCNT	multiwalled carbon nanotube
SEM	scanning electron microscope
TGA	thermogravimetric analysis

16.1 Introduction

The top 10 problems that humanity will be facing in the next 50 years include lack of portable water to millions of the people. The essential component on the Earth for all the vital activities of human beings is water. Owing to aggressive industrialization, civilization, agricultural activities, domestic activities, and growth of population, the quality of water of our water resources is continuously deteriorating [1]. Purification of water requires efficient removal of salts, organics, pathogens, fertilizers, heavy metals, pharmaceuticals, and various other carcinogenic compounds [2, 3]. Potential water sources include seawater, river water, produced water, and ground water [4]. One of the major roadblocks in establishing an economical technology for water purification from such water sources is variation in ion concentrations in such water sources. Various researchers across the globe are concentrating their efforts in developing various methodologies, technology, etc. for water treatment [5].

Ion exchange (IEX) materials have received enormous attention by researchers because of their wide application in a variety of areas such as wastewater treatment, portable water production, and chemical industry [6, 7]. Incorporation of nanomaterials into IEX materials have been reported in literature to a large extent, that is, nanocomposite IEX materials [7, 8]. The primary

Handbook of Nanomaterials for Wastewater Treatment. https://doi.org/10.1016/B978-0-12-821496-1.00014-3
Copyright © 2021 Elsevier Inc. All rights reserved.

This book belongs to Badji Mokhtar Annaba University Central Library Copyright Elsevier 2025

purpose of inclusion of nanomaterials is to improve the properties of IEX materials. A thorough understanding of nanocomposite IEX materials in terms of material synthesis and synergy between the reinforcement/filler material with the matrix is of utmost importance for the rational development of IEX materials for desired application. Key recent advancements in IEX nanocomposite research utilizing nanomaterials such as carbon nanotubes (CNTs), graphene, silica, and silver nanoparticles in enhancing properties such as mechanical strength, IEX capacity, and thermal stability are discussed. In addition, application of nanocomposite IEX materials in latest techniques such as capacitive desalination, electromembrane desalination has also been discussed. In this chapter, a comprehensive overview of IEX nanocomposite materials comprising the fundamentals, recent developments, and their applications in water treatment is provided.

16.2 Types of nanocomposite IEX material

In general, the word composite implies a combination of two or more different materials to obtain exotic properties of both the materials. Most of the composite materials consist of one continuous phase and one or more discontinuous phase. The continuous phase is known as matrix, while the discontinuous phase is known as reinforcement or filler material.
A nanocomposite is a composite consisting of one component in which at least one component has at least one dimension in nanometer range. Nanocomposite IEX materials consist of nanoparticles with IEX properties. Nanocomposites can be classified depending upon the type of filler, that is, the nanoscale materials such as metal, ceramic, clay, and polymers with continuous phase, either polymer-based or nonpolymer-based. Fig. 16.1 depicts the classification of nanocomposites. In case of nanocomposite IEX material, the reinforcement or

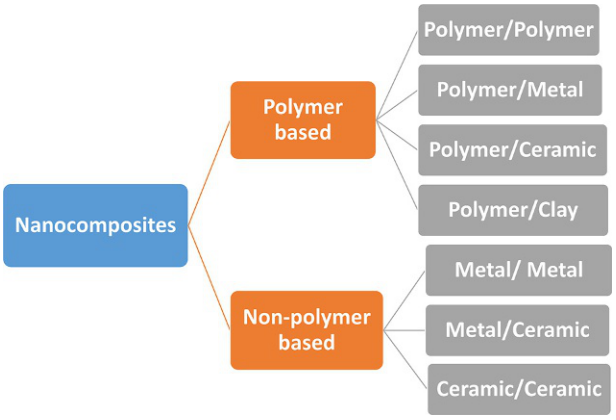

Fig. 16.1
The classification of nanocomposites.

This book belongs to Badji Mokhtar Annaba University Central Library
Copyright Elsevier 2025

filler material is in nano dimension, while the matrix can be in various forms such as resin beads, porous membranes, foams, fibers, and hollow fibers. In this chapter, we will restrict the details related to resin beads and porous membranes IEX matrices for the sake of brevity.

A plethora of nanomaterials, polymers, and techniques to synthesize nanocomposite IEX materials have been developed by the researchers across the globe. Depending upon the type of material, the blending ratio of nanoparticle and polymer, and optimum content of nanomaterial, the functionalization of polymer matrix is decided. Depending upon the properties of nanomaterials and synergistic effect between the matrix and filler, the type of nanomaterial, functionalization of matrix, along with suitable method to incorporate the filler into the matrix is chosen. In addition, the ease of mass production of nanomaterials, along with economic factors and toxicity, is the important factor considered while choosing suitable nanomaterial as filler for IEX nanocomposite. Details of nanomaterials along with methodologies for the synthesis of nanocomposites have been discussed in subsequent sections.

16.3 Preparation of nanocomposite IEX material

16.3.1 Background

Various methodologies are reported for the synthesis of nanocomposite IEX materials. The choice of methodology to be selected for the synthesis of such materials depends upon various factors such as cost, efficiency, end use, and life cycle. Although one of the basic requirements for a nanocomposite IEX materials is an excellent interaction between the matrix and filler materials, providing maximum mechanical and thermal stability without compromising over the presence of functional groups for IEX. Some of the widely used methodologies for the preparation of nanocomposite IEX materials are discussed further. Readers are suggested to refer recent reviews published over this topic for more details [2, 7, 9–11].

16.3.2 Nanomaterials used in IEX materials

Literature is awash with reports of various nanomaterials utilized as fillers in nanocomposite IEX materials and subsequently used for water purification. Direct comparison of such nanocomposites for water purification is deceptive because the methodologies, test conditions, and presence of various kinds of impurities reported by various researchers vary significantly. To compare various IEX materials (either resin beads or membranes), a common basis needs to be defined. Ion exchange capacity (IEC) is defined as the total functional groups or active sites liable for IEX [12]. IEC is quantified through acid-base titration, and it is an intrinsic property of any IEX material. Various nanomaterials used in nanocomposites are discussed briefly in the subsequent sections.

This book belongs to Badji Mokhtar Annaba University Central Library Copyright Elsevier 2025

16.3.2.1 Low-dimension carbon

CNTs: CNTs are hollow seamless cylinders, made up of honeycomb lattice carbon structure, possessing diameter in nanometer range [13]. Since the discovery of CNTs, this carbon allotrope has drawn considerable attention of researchers because of their extraordinary mechanical, electrical, and thermal properties [14]. CNTs have been utilized in various applications such as batteries [15], hydrogen storage [16], and composites [17]. Owing to high aspect ratio of CNTs, it is one of the most favorable candidates as a filler in polymer nanocomposites. CNTs are classified on the basis of number of honeycomb lattice carbon structure, that is, graphene layers rolled to form a seamless cylinder. Single-walled carbon nanotubes consist of single graphene sheet, with diameters ranging from 0.4 to 2.5 nm [18], while multiwalled carbon nanotubes (MWCNTs) comprise concentric graphene sheets varying from 2 to 10 in numbers and diameter of the tube in the range of 3–20 nm [19]. CNTs have been incorporated as reinforcement in both IEX resin beads [20] and membrane [21]. CNTs offer mechanical strength along with ion-conducting paths. Homogeneous dispersion of CNTs in polymer matrix is the key to the performance of nanocomposite IEX materials. Functionalization of CNTs is also explored by various researchers to increase the interfacial bonding between CNTs and the polymer matrix [22]. In addition, functionalization of CNTs also aids in dispersion of CNTs into the polymer matrix along, while the functional groups also acts as IEX site, enhancing the IEC of the nanocomposite [7].

Graphene: Graphene is a 2D nanomaterial consisting of honeycomb lattice carbon structure, which is a basic unit structure of graphite [23]. In addition to pristine graphene, derivatives of graphene such as graphene oxide (GO) and reduced graphene oxide (RGO) are also utilized as reinforcement material. The exceptional properties such as high electrical conductivity, high mechanical strength, and large specific surface area of graphene and its derivatives make it one of the most researched carbon allotropes for various applications [24]. Graphene and its derivatives have been used as reinforcement in high-strength composites [24], Li-ion batteries [25], biomedical applications [26], supercapacitors [27], energy storage [28], etc. Various reports have been published over the synthesis of graphene-based nanomaterials-modified IEX materials [10, 29]. To make the processing or incorporation of graphene into the polymer matrix, it is necessary to attach functional groups at the edges and/or onto the surface to facilitate better interaction between reinforcement and polymer matrix [30]. Similar to CNTs, graphene-based nanomaterials such as GO, functionalized GO, and RGO have been synthesized by various routes and reported in literature [31]. Nanocomposite IEX materials based on graphene as reinforcement material have been reported to perform better in terms of high ionic conductivity and mechanical strength.

16.3.2.2 Metal oxide

Metal oxides are primarily synthesized through bottom-up approaches, viz., sol-gel, hydrothermal, precipitation, etc. Size, shape, surface chemistry, and biocompatibility are the characteristics of the metal oxides assessed before utilized as reinforcement material. Zinc oxide (ZnO), titanium (IV) oxide, iron oxide, aluminum oxide (Al_2O_3), manganese oxide

This book belongs to Badji Mokhtar Annaba University Central Library Copyright Elsevier 2025

(MnO_2), zirconium oxide (ZrO_2) are examples of a few metal oxides reported in literature as reinforcement nanomaterials for IEX nanocomposites. ZnO nanoparticles are widely used in sensors, photocatalysis, solar cells, etc. Parvizian et al. [32] reported synthesis of cation exchange nanocomposite membrane consisting of polyvinyl chloride as matrix and ZnO nanoparticles as filler materials. The authors reported that with the increase in content of ZnO nanoparticles (10 wt%) in the matrix, the water content of the membrane increased. Diffusion of water through the membrane increased with the increase in hydrophilicity of the nanocomposite IEX membrane owing to the presence of ZnO nanoparticles that possess high affinity toward water. However, when the ZnO nanoparticles concentration in the matrix was increased beyond 10 wt%, it led to decrease in the water content because of the filling of pores by ZnO nanoparticles. Inorganic nanoparticles such as Al_2O_3 have been explored as filler in IEX nanocomposite material. Hosseini et al. [33] synthesized cation exchange nanocomposite membranes using Al_2O_3 as filler and polyvinyl chloride as matrix. Similar to the case of ZnO nanoparticles, Al_2O_3 nanoparticles also enhance the water content in the synthesized nanocomposite membrane because of its hydrophilic nature. On the other hand, addition of Al_2O_3 led to a minute decrease in IEC from 2.75 to 2.25 meq g^{-1}. The major concern about the usage of metal oxide nanoparticles in IEX nanocomposite is toxicity. The level of toxicity of nanomaterials must be taken into account before their usage in water treatment.

16.3.2.3 Silica

Oxide nanoparticle based on silica is a widely researched material among various other nanoparticle oxides. Ease of synthesis, better control over size, size distribution, and morphology are a few reasons for the same. Incorporation of SiO_2 into polymer matrix has been found to have a profound effect on thermal and mechanical properties. Various reports exist over the usage of silica into polymer matrix and utilization as IEX material [34, 35]. The presence of silica improved IEC substantially along with improvement in thermal and mechanical stabilities of IEX material. Zuo et al. [36] reported anion exchange membranes based on poly(vinylidene fluoride) as matrix and SiO_2 nanoparticles as filler. It was found that as the amount of filler, that is, SiO_2 nanoparticles increased in matrix from 0 to 2 wt%, the IEC of the membrane increased from 0.786 to 1.226 meq g^{-1}. Increase in IEC can be attributed to the hydrophilic property of SiO_2 nanoparticles embedded into the polymer matrix. SiO_2 being chemically inert in nature and easy to synthesize is the widely used inorganic filler material.

16.3.3 Processing methods

16.3.3.1 Graft copolymerization/crosslinking

Graft copolymerization technique can be classified into two subsections, viz., free radical polymerization and controlled radical polymerization. Here, cross-linking agents are blended with monomers that are either ionic or neutral in the presence of a suitable solvent. The polymerization

This book belongs to Badji Mokhtar Annaba University Central Library Copyright Elsevier 2025

reaction is initiated by a redox initiator, while solvent aids in reducing the risk of high temperature rise by acting as heat sink. Unreacted initiator, monomers, and cross-linking agents are removed by successive washing with a suitable solvent. Now the filler material as per the requirement can be grafted over the cross-linked polymer by precipitation or any other suitable methodology. Graft polymerization method can be used to synthesize both nanocomposite IEX resins as well as membranes. Ni et al. [37] reported removal of phosphate from contaminated water using nanocomposite of titanium dioxide and polystyrene beads (Ti-NS). The polystyrene beads were synthesized using cross-linking polymerization methodology, followed by incorporation of titanium into the pores of polystyrene beads through precipitation method.

16.3.3.2 Suspension polymerization

In this methodology, monomer and initiator, both are insoluble in the polymerization medium, but initiator is soluble in the monomer. Here, the polymerization takes place in the monomer droplets. With the help of a suspension agent, the monomer is suspended in a medium in the form of small droplet with help of mixer and stabilizing agent. Polymerization reaction is catalyzed thermally, and temperature ranges usually between 200°C and 1000°C. Monomer droplets get transformed into beads in the micron range. Suspension polymerization method is commonly employed to synthesize nanocomposite IEX resins. Fath et al. [20] reported synthesis of nanocomposite IEX resin based on polystyrene divinylbenzene copolymer as continuous phase and MWCNTs as filler material. The authors synthesized the nanocomposite using styrene and divinylbenzene as monomers, benzyl peroxide (BPO) as initiator, and sodium dodecyl sulfate as suspension agent into toluene solution. BPO led to the formation of free radicals on both copolymer (styrene and divinylbenzene) and MWCNTs, which aids in the grafting of MWCNTs over the polymer network uniformly.

16.3.3.3 In situ polymerization

In situ polymerization involves mixing of monomers and filler nanomaterial in the presence of a solvent followed by polymerization. Polymerization is initiated by any initiator, by heating externally, or UV light irradiation. In situ polymerization technique is avoided when filler material, that is, nanomaterial interferes in the process of polymerization. In this technique, compatibility of filler material with the polymer is of utmost importance. Compatibility can also be improved by surface modification of the filler material.

16.3.3.4 Blending

Blending is one of the widely used techniques for the synthesis of nanocomposites based on polymer matrix. Here, instead of starting with monomers, the nanocomposite is prepared using polymer and filler as starting material. Polymer is dissolved in a suitable solvent along with filler material (nanomaterial) and mixed using homogenizer or sonicator (bath or probe). The major advantages of this method include reproducibility, simplicity, and amenability for large-scale synthesis. Blending or solution blending method is primarily used for the preparation of nanocomposite IEX membranes. A schematic of blending method is shown in Fig. 16.2.

This book belongs to Badji Mokhtar Annaba University Central Library Copyright Elsevier 2025

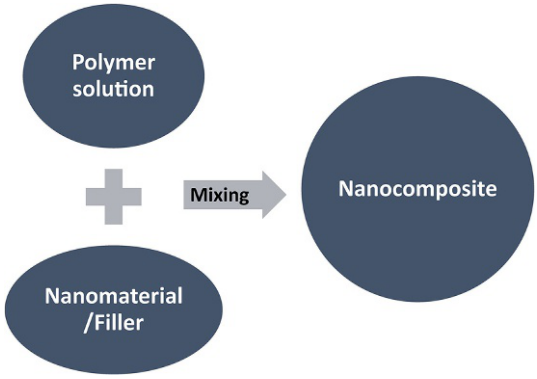

Fig. 16.2
Schematic of most commonly used preparation methods for nanocomposites: blending.

16.3.3.5 Sol-gel

In sol-gel technique, instead of filler or nanomaterial, precursor of filler is mixed with polymer in a suitable solvent, followed by hydrolysis and precipitation of nanomaterial. Precipitation is carried out either by pH change or by hydrothermal method. This method is limited to the nanomaterials existing in chloride form, or a similar method can be utilized to prepare nanocomposites. In addition, sol-gel technique involves multisteps, which increase the cost of the process in comparison to blending methodology. In contrast to the blending approach, sol-gel technique offers better interconnections of nanomaterial and the matrix. A schematic of sol-gel method is shown in Fig. 16.3.

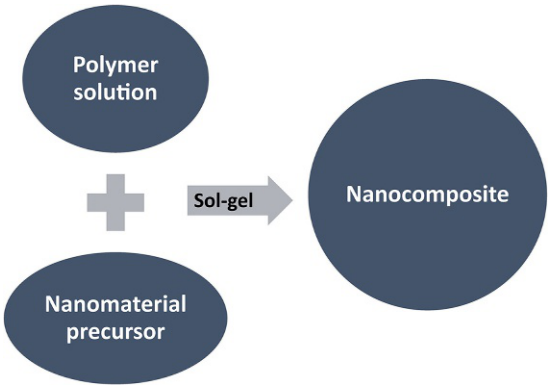

Fig. 16.3
Schematic of most commonly used preparation methods for nanocomposites: sol-gel.

This book belongs to Badji Mokhtar Annaba University Central Library Copyright Elsevier 2025

16.4 Characterization

To compare the performance of various IEX nanocomposite materials, a standard protocol for characterization of such materials is essential. Structure-property relationship can be established by using various spectroscopic techniques. The following section discusses the various characterization techniques that are commonly used to characterize IEX nanocomposite materials.

16.4.1 Fourier transform infrared spectroscopy

One of the preferred methods to carry out infrared (IR) spectroscopy is FT-IR, that is, Fourier transform infrared spectroscopy. Here, when sample is irradiated with IR radiation, the sample absorbs some radiation while rest is transmitted. The signal resulting out of the sample is unique or fingerprint of the sample. FT-IR is widely used to characterize IEX resins because the amount of sample required for characterization is minimal. In addition, both cation and anion can be characterized in mixture also, which is one of the major advantages of FT-IR technique. Fathy et al. [20] synthesized cation exchange resin based on MWCNTs. The authors synthesized cation exchange nanocomposite using polystyrene divinyl benzene copolymer (PS-DVB) and pristine MWCNTs. Fig. 16.4 depicts the FT-IR spectra of the sulfonate nanocomposite based on PS-DVB and MWCNTs. A peak around 1170 cm^{-1} depicts the presence of $S = 0$ group. Because the nanocomposite is hygroscopic in nature, a broad peak at 1695 cm^{-1} represents the presence of moisture present in the sample.

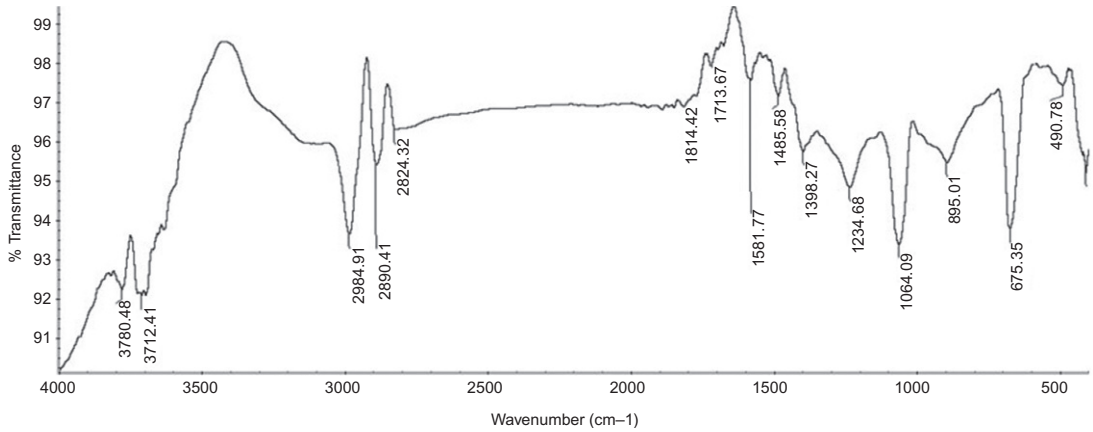

Fig. 16.4
FT-IR of sulfonate polystyrene divinyl benzene with 1 wt% MWCNT resin. *Reproduced with permission from M. Fathy, T. Abdel Moghny, A.E. Awad Allah, A.E. Alblehy, Cation exchange resin nanocomposites based on multi-walled carbon nanotubes, Appl. Nanosci. 4 (2014) 103–112, https://doi.org/10.1007/s13204-012-0178-5.*

This book belongs to Badji Mokhtar Annaba University Central Library
Copyright Elsevier 2025

16.4.2 X-ray diffraction

X-ray diffraction (XRD) is a primary technique for characterization of compounds based on diffraction pattern. Crystalline materials possess long-range ordering, which is observed as sharp peaks in XRD and well-defined using Bragg's equation. Braag's equation relates the wavelength of X-ray, interplanar spacing in the crystal, and glancing angle of incidence. El-Latif et al. [38] synthesized nano-zirconium vanadate inorganic IEX resin for sorption of cesium, cobalt, and nickel from an aqueous solution. Zirconium vanadate ion exchangers were synthesized using three distinct methods: homogeneous precipitation, sol-gel precipitation, and hydrothermal. In addition, samples were given alkaline treatment while synthesizing using sol-gel precipitation and hydrothermal techniques. Fig. 16.5 represents the XRD pattern of nano-zirconium vanadate ion exchanger. It can be observed that nanocomposite synthesized using sol-gel technique represents amorphous nature of the resin along with minor crystalline peaks. Sol-gel technique along with alkali treatment depicts a similar XRD pattern, with sharp peaks of higher intensity, indicating an increase in crystallinity owing to alkali treatment. The XRD pattern for nanocomposite synthesized using homogeneous precipitation technique indicates the presence of some sharp peaks (around 32 degrees) of higher intensity in comparison to the resins synthesized using sol-gel technique. Thus the resin synthesized using homogeneous precipitation method can be termed as polycrystalline material. In the case of hydrothermal

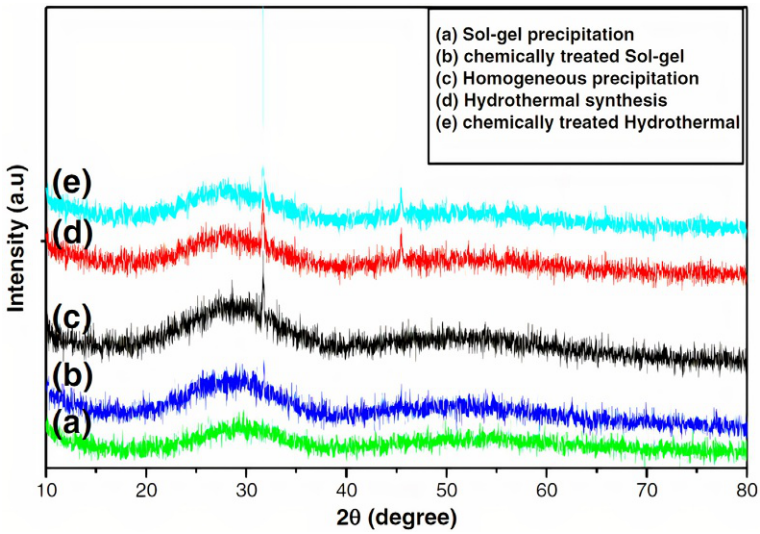

Fig. 16.5
X-ray diffraction pattern of nano-zirconium vanadate prepared using the three different techniques and their alkaline-treated ion exchangers. *Reproduced with permission from M.M. Abd El-Latif, M.F. Elkady, Kinetics study and thermodynamic behavior for removing cesium, cobalt and nickel ions from aqueous solution using nano-zirconium vanadate ion exchanger, Desalination 271 (2011) 41–54, https://doi.org/10.1016/j.desal.2010.12.004.*

This book belongs to Badji Mokhtar Annaba University Central Library
Copyright Elsevier 2025

technique, the synthesized nanocomposite possesses a higher degree of crystallinity in comparison to the other two methods, with additional peaks at 47 and 63 degrees, respectively, observed in the XRD pattern. As observed in the case of sol-gel technique, in the case of hydrothermal method of synthesis, crystallinity increased with the treatment of alkali, which is confirmed by increased intensity of the peaks in XRD pattern.

16.4.3 Thermogravimetric analysis

Thermogravimetric analysis (TGA) is a technique whereby the weight of the substance in an environment heated or cooled at a controlled rate is recorded as a function of time or temperature. Using TGA, various information is obtained such as thermal stability of materials, oxidative stability of materials, composition in case of multicomponent system, decomposition kinetics of the materials, moisture, and volatile component of the materials. Gahlot et al. [39] synthesized a nanocomposite IEX membrane consisting of GO and sulfonated polyethersulfone (SPES). The synthesized anion exchange nanocomposite membrane is utilized for desalination purpose. TGA was reported for various compositions of SPES and GO (designated as SG-*n* where *n* is wt% of GO in membrane). It can be observed from Fig. 16.6 that as wt% of GO increases in the membrane, the thermal stability of the nanocomposite decreases. The decrease in thermal stability can be accounted for the hydroxyl and carboxyl groups present on the GO surface.

16.4.4 Scanning electron microscope

Scanning electron microscope (SEM) is one of the most versatile instruments used to understand the morphology and chemical compositions of the object. SEM produces images by scanning the object/sample with a high energy beam of electrons. During interaction of

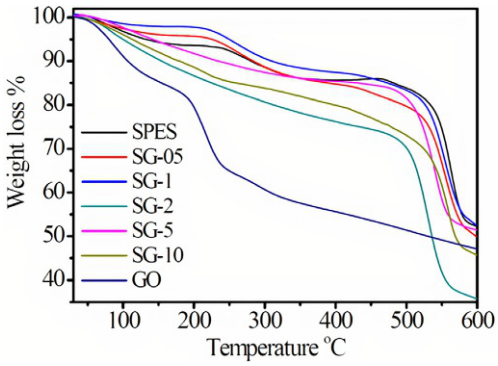

Fig. 16.6
TGA thermograms for different SPES/GO composite membranes. *Reproduced with permission from S. Gahlot, P.P. Sharma, H. Gupta, V. Kulshrestha, P.K. Jha, Preparation of graphene oxide nano-composite ion-exchange membranes for desalination application, RSC Adv. 4 (2014) 24662–24670, https://doi.org/10.1039/C4RA02216E.*

This book belongs to Badji Mokhtar Annaba University Central Library
Copyright Elsevier 2025

electrons with the sample surface, electrons produce secondary electrons (SE), backscattered electrons (BSE), and X-rays. The signals are collected by the detectors, and the image of the object/sample is displayed on a computer screen. SE and BSE detectors help in imaging the sample, while X-rays help in understanding the composition of the sample. Nie et al. [37] synthesized a composite of titanium oxide (Ti) embedded in polystyrene beads (NS) modified with quaternary ammonium ions. The aim of the nanocomposite anion exchange resin was to utilize it for removal of phosphate. It can be observed from Fig. 16.7 the Ti-NS nanocomposite possesses spherical shape with porous structure. Fig. 16.7 depicts the uniform distribution of Ti (representing TiO_2 particles) and Cl (representing quaternary ammonium ions group) over the cross-section of Ti-NS nanocomposite.

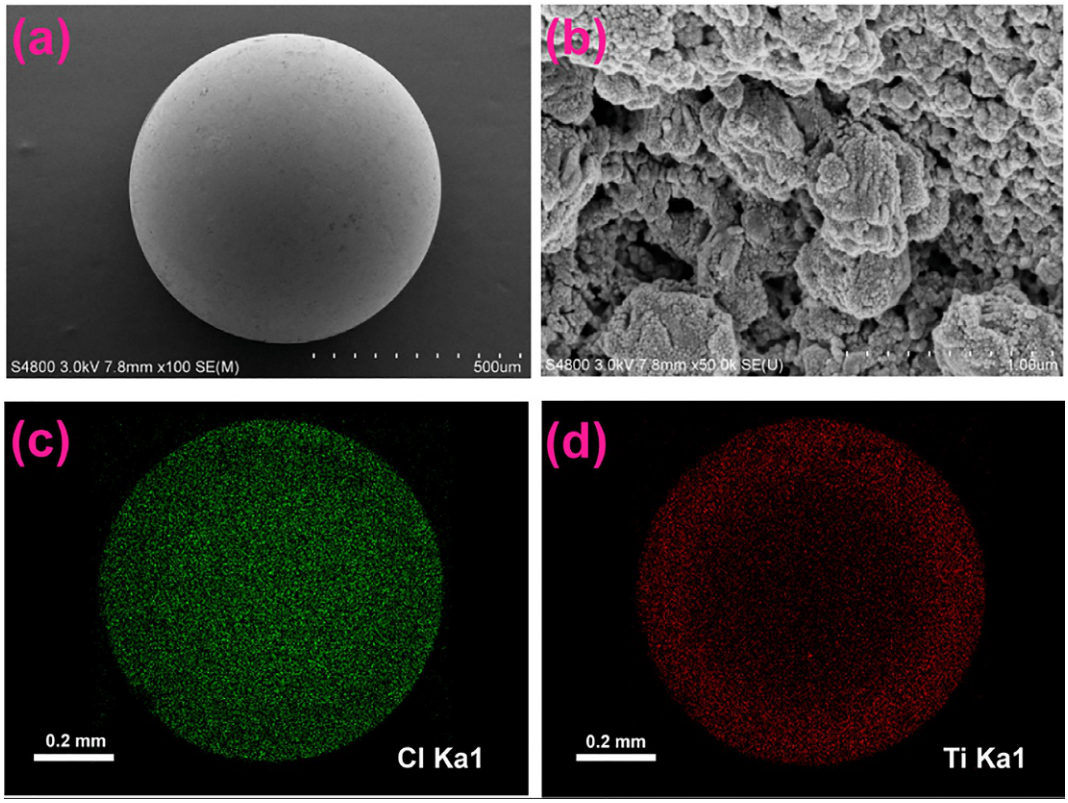

Fig. 16.7

Characterization of Ti-NS: (A) SEM image of the spherical profile bead; (B) SEM image of inner surface of Ti-NS; (C) cross-section of Cl distribution of Ti-NS by SEM-EDS; (D) cross-section of Ti distribution of Ti-NS by SEM-EDS. *Reproduced with permission from G. Nie, L. Wu, Y. Du, H. Wang, Y. Xu, Z. Ding, Z. Liu, Efficient removal of phosphate by a millimeter-sized nanocomposite of titanium oxides encapsulated in positively charged polymer, Chem. Eng. J. 360 (2019) 1128–1136, https://doi.org/10.1016/j.cej.2018.10.184.*

This book belongs to Badji Mokhtar Annaba University Central Library
Copyright Elsevier 2025

16.5 Application of nanocomposite IEX materials for water purification

IEX material usually comprises two main components: (1) substrate (mostly hydrophobic in nature and (2) immobilized functionalized group with mobile counter ions. Depending upon the ionic group present, IEX materials are classified into two groups: cation exchange and anion exchange materials. Carboxylic, sulfonic, and phosphoric are some common functional groups present on a cation exchange material. While imidazole cations and quarternary ammonium cations are a few examples of functional groups present on an anion exchange material. In this chapter, recent reports published on nanocomposite IEX materials in the form of resin beads and membranes will be discussed. Table 16.1 illustrates the list of nanocomposite IEX resins reported in literature.

Urbano et al. [40] reported the synthesis and application of polymer-clay nanocomposite IEX resin for arsenic adsorption. Polymer was synthesized through in situ radical polymerization with *N*-methyl-D-glucamine as monomer. Reinforcement, that is, clay (montmorillonite) utilized in the study was organically modified to enhance the interaction between the polymer and clay. Batch adsorption studies revealed that arsenate adsorption capacity with the synthesized IEX resins were approximately 55 mg, as per the gram of resin, and followed Langmuir isotherm. In adsorption process, pH is one of the major factors that decides the efficacy of the process. Because hydronium concentrations can influence the resin-ligand structure along with the speciation of metal ions in aqueous solution, the maximum sorption capacity of arsenic was reported in the pH range of 3.5–6.0. Effect of counter ions or interfering ions such as phosphate and sulfate anions over the sorption of arsenate was also studied. It was found that sulfate anions caused greatest interference because of similarity in structure with the arsenate anion. Efficacy of the nanocomposite IEX resin for the removal of arsenate anions were also tested for real waste, that is, water sample from Camarones River. It was reported by the authors that the sorption capacity of nanocomposite IEX resin decreased to 70% when utilized for real waste arsenic sorption, depicting the importance of matrix solution on the nanocomposite IEX performance. Aqueous radioactive waste is one of the hazardous wastes that needs to be handled carefully. Dissolved metals in radioactive waste need to be concentrated, followed by recovery and subsequent disposal. Abd El-Latif and Elkady [38] reported the usage of inorganic nanocomposite IEX resins for the removal of radionuclides such as cesium, cobalt, and nickel from aqueous nuclear waste effluent. Nano-zirconium vanadate was prepared by three methods: sol-gel, homogeneous precipitation, and hydrothermal synthesis, with IEC of 0.4, 1.24, and 1.8 meq g^{-1}, respectively. To have more insight on solute uptake rate, a detailed kinetics study has been reported for this study. The authors reported that cesium sorption followed second-order and Elovich kinetic model, while sorption kinetics of cobalt and nickel followed first-order, second-order, and Elovich kinetic models. Activation energy for the sorption process was found to be 42 kJ/mol, indicating diffusion controlled process.

This book belongs to Badji Mokhtar Annaba University Central Library Copyright Elsevier 2025

This book belongs to Badji Mokhtar Annaba University Central Library

Table 16.1: List of nanocomposite IEX resins reported in prior art.

IEX type	Continuous phase	Reinforcement	IEC ($meqg^{-1}$)	Adsorption isotherm	Application	References
Anion exchange	PVbNMDG	Montmorillonite	–	Langmuir	Arsenate adsorption from aqueous solution	[40]
Cation exchange	PSDVB	MWCNTs	0.46	–	–	[20]
Anion exchange	Sodium vanadate	Zirconium	1.80	Elovich	Cesium, cobalt, and nickel adsorption from aqueous solution	[38]
Anion exchange	PSDVB	Titanium dioxide	–	–	Phosphate removal from aqueous solution	[37]
Cation exchange	Sodium tungstate and sodium molybdate	Titanium (IV) chloride	2.41	–	Lead and chromium removal from aqueous solution	[41]
Cation exchange	Polyaniline	Zirconium (IV) sulfosalicylate	1.80	–	Lead, mercury, and zirconium removal from lead storage battery waste and natural water	[42]
Cation exchange	Rescorcinol-formaldehyde resin	Silver nanoparticles	–	Langmuir	Mercury (II) removal from aqueous solution	[43]
Anion exchange	Ammonia modified corn straw	Zirconium (IV) oxide nanoparticles	–	Langmuir	Phosphate removal from aqueous solution	[44]

PVbNMDG, poly (*N*-(4-vinyl benzyl)-*N*-methyl-D-glucamine); *PSDVB*, polystyrene-divinylbenzene.

Copyright Elsevier 2025

Phosphate sequestration is a must to avoid eutrophication. Nie et al. [37] reported the synthesis of novel nanocomposite IEX resin consisting of reinforcement as titanium dioxide impregnated inside a millimeter-sized polymer with ammonium groups bounded to the surface of the polymer, that is, polystyrene divinylbenzene. The authors reported that the sorption of phosphates from aqueous solution occurs through two different interactions, that is, ligand exchange reactions with hydroxyl groups on titanium dioxide and IEX with quaternary ammonium ions grafted on polymeric backbone. The pH range of 6.5–7.5 was reported to be favorable for the adsorption of phosphate. Authors had also reported the effect of coexisting anions such as $(SO_4)^{-2}$, $(NO_3)^{-1}$, and Cl^{-1} on the sorption capacity of the nanocomposite IEX resin. It was found that at very molar concentration of counter anions as high as 50 times of initial phosphate concentration in aqueous solution, the sorption capacity remains unaffected. The reason for this was attributed to the functional groups and reinforcement present in the nanocomposite. Ammonium function groups present over the polymer backbone resulted in electrostatic interactions between the phosphate and competing anions. On the other hands, the titanium dioxide particles present as filler preferentially adsorb phosphate through inner sphere complexation. Fixed-bed column study was also reported by the authors; the breakthrough point was approximately 400 bed volumes for synthetic aqueous solution, comprising phosphates and other competing anions. In addition to synthetic waste, real bioeffluents were also tested for phosphate sorption, which also yielded in positive results. Exhausted column could be easily regenerated using binary solution comprising NaCl and NaOH. Recently, Hu et al. [44], on a similar concept, reported usage of nanocomposite consisting of amino-modified corn straw and zirconium oxide nanoparticles for selective removal of phosphate from an aqueous solution.

Heavy metals being nonbiodegradable tend to accumulate in living organisms and possess carcinogenic effects. Numerous heavy metals from industrial waste water end up in water bodies and contribute toward water and soil pollution. IEX materials are widely employed for sorption of heavy metals from waste water because of its simple, economical, and effective application. Kelta et al. [41] reported sorption of heavy metals from aqueous solution using nano-titanium(IV) tungstomolybdate synthesized through homogeneous precipitation using urea. Synthesized nanocomposite IEX resin acted as a bifunctional ion exchanger verified through pH titration curves. The authors reported selective sorption of heavy metals such as lead and chromium cations from aqueous solutions, with distribution coefficient as high as 10,767 and 11,800 mL g^{-1}, respectively. Nabi et al. [42] reported synthesis of organic-inorganic cation exchanger through sol-gel process for heavy metal ions uptake from aqueous solution. Polyaniline Zr(IV) sulfosalicylate IEX resin was tested for sorption of heavy metals such as lead, mercury, and zirconium, both in synthetic waste and real waste from industries based on lead storage battery manufacturing. The authors demonstrated usage of synthesized nanocomposite IEX resin at elevated temperature (up to 300°C) retaining 98% IEC. Siva et al. [43] reported effective removal of toxic metal mercury from aqueous solution using IEX resin

This book belongs to Badji Mokhtar Annaba University Central Library Copyright Elsevier 2025

consisting of silver nanoparticles as filler and polymer backbone structure. The polymer backbone used in the study was synthesized using resorcinol-formaldehyde resin modified with sulfonated *Euphorbia hirta* charcoal, while the silver nanoparticles were synthesized through biological reduction method using *Cyperus rotundus* grass extract, which acts as both a capping and reducing agent. It was found that the synthesized IEX resin nanocomposite possessed a high selectivity toward sorption of mercury ions (Hg^{2+}) from aqueous solution. The sorption mechanism involved potential Donnan membrane effect owing to the sulfonic present in the polymer backbone, which resulted in enhanced concentration and penetration of Hg^{2+}, ions followed by segregation owing to reinforced silver nanoparticles. In addition to batch adsorption studies, column studies were also carried out, and efficient bed volumes were reported in the range of 4000–5000.

Electromembrane processes are widely used in (1) the chlor-alkali process, (2) energy storage, (3) fuel cells and (4) water purification through desalination by electrodialysis, diffusion dialysis, and membrane capacitive deionization (CDI). IEX membranes are widely used in such electromembrane processes, and hence various scientists across the globe have intensified the research efforts toward the synthesis and application of such membranes. Electrochemical properties of IEX membranes dictate the efficacy. In addition, chemical, mechanical, and thermal stabilities determine the life of such membranes. IEX membranes blended with nanomaterials have been proven to be effective in improving the physicochemical properties of such membranes. In addition to IEC of nanocomposite IEX membranes, other parameters such as membrane water content, membrane potential, transport number, selectivity, and flux are also quantified to compare with pristine membranes. Table 16.2 illustrates the list of literature published over the usage of nanocomposite IEX membranes for water treatment.

Moghadassi et al. [45] reported that surface characteristics play a pivotal role in determining the separation efficiency of membranes. The authors modified PVC-based cation IEX membrane with PAA/MWCNTs. It was found that the IEC of unmodified PVC membrane and modified PVC membrane is 1.26 and 1.46 meq g^{-1}, respectively. Addition of a modifier into the PVC resulted in enhancement of cationic functional group and hence an increase in IEC. Ionic permeability and flux were also measured for the modified membrane. It was found that sodium permeability and flux increase in modified membranes, possessing MWCNTs in the range of 0.1–0.3 wt%. The reason attributed toward such increase is the synergy between the carboxylic and sulfonate functional groups present in the modified membrane. Similar to MWCNTs, other carbon allotropes such as GO have also been exploited by researchers as filler for nanocomposite IEX membranes. Gahlot et al. [39] reported the synthesis of nanocomposite IEX membrane consisting of GO as reinforcement and sulfonate polyethersulfone (SPES) as continuous phase. The water uptake capacity of synthesized nanocomposite IEX membrane decreased in comparison to unmodified SPES membrane because of reduction of pore size of membrane owing to the presence of GO. The suitability of synthesized nanocomposite IEX membrane was

This book belongs to Badji Mokhtar Annaba University Central Library Copyright Elsevier 2025

Table 16.2: List of nanocomposite IEX membranes reported in prior art.

IEX type	Continuous phase	Reinforcement	IEC (meq g^{-1})	Application	References
Cation exchange membrane	PVC/PAA	MWCNTs	1.46	Electrodialysis process for water recovery and waste water treatment	[45]
Cation exchange membrane	PVC	Iron oxide	1.72	Electrodialysis process for lead removal	[46]
Cation exchange membrane	PVDF	Silica	1.98	Electrodialysis process	[47]
Anion exchange membrane	PVDF	Silica	1.19		
Anion exchange membrane	PVDF/PANI	Reduced graphene oxide	1.28	Membrane capacitive deionization process for salt removal	[48]
Cation exchange membrane	SPES	Graphene oxide	1.27	Electrodialysis for water desalination	[39]
Cation exchange membrane	PC/SBR	MWCNTs	1.54		[21]
Cation exchange membrane	SPES	f-Silica	2.15	Donnan dialysis process for lead and cadmium removal from aqueous solution	[34]
Cation exchange membrane	PVC	Graphene oxide nanoplates	1.4	–	[49]

PVC, polyvinyl chloride; *PAA*, polyacrylic acid; *SPES*, sulfonated polyethersulfone; *PVDF*, polyvinylidene fluoride; *PANI*, polyaniline.

checked for water desalination through electrodialysis experiments. Current efficiency and energy consumption for salt removal from water were 97.4% and 4.3 k W h kg^{-1}, respectively.

CDI is an electrosorptive water purification process. CDI involves usage of IEX membrane with high IEC and high electrical conductivity. Zhang et al. [48] reported synthesis of highly conductive anion nanocomposite IEX membrane using RGO and polyaniline (PANI) as filler materials, while polyvinylidene fluoride (PVDF) as polymer matrix or back bone. It was found that addition of RGO/PANI in the PVDF membrane had substantial effects on increasing the electrical conductivity, and hence the modified IEX membranes possessed high sorption capacity and salt removal efficiency. Zuo et al. [47] also reported nanocomposite IEX membrane with

This book belongs to Badji Mokhtar Annaba University Central Library
Copyright Elsevier 2025

PVDF polymer matrix with SiO_2 nanoparticles as fillers and subsequently applied for electrodialysis process. The effects of various parameters on electrodialysis process such as current density and feed flow rate were studied in detail. It was found that PVDF-SiO_2 membranes performed better in comparison of pristine PVDF membranes in terms of desalination.

In addition to desalination, IEX membranes have also been researched for removal of heavy metals dissolved in water. Hosseini et al. [46] reported the synthesis of heterogeneous cation nanocomposite IEX membrane for electrodialysis process with polyvinyl chloride as polymer matrix and iron oxide as inorganic fillers. The synthesized nanocomposite IEX membrane was characterized using monovalent and bivalent ionic solutions, that is, NaCl and $BaCl_2$. Electrodialysis for lead removal was also carried out in test cell as shown in Fig. 16.8. The authors reported that the dialytic rate of lead (Pb^{2+}) ions sorption increases with the increase in concentration of filler material in the nanocomposite IEX membrane. Berbar et al. [34] exploited the concept of surface functionalization and reported the synthesis of sulfonated polyethersulfone as polymer matrix along with functionalized silica nanoparticles as reinforcement for nanocomposite IEX membrane. The authors were able to adsorb and separate lead (Pb^{2+}) and cadmium (Cd^{2+}) successfully using the modified cation exchange membrane.

Tremendous efforts of researchers are dedicated toward reduction in energy consumption of water treatment through IEX materials. In addition to the design of such novel nanocomposite IEX materials, new process design and scale-up studies need to be undertaken to make this technology viable and effective for large-scale application.

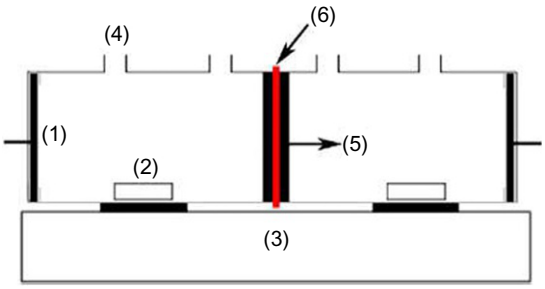

Fig. 16.8

Schematic diagram of test cell: (1) Pt electrode, (2) magnetic bar, (3) stirrer, (4) orifice, (5) rubber ring, and (6) membrane. *Reproduced with permission from S.M. Hosseini, E. Jashni, M. Habibi, M. Nemati, B. Van der Bruggen, Evaluating the ion transport characteristics of novel graphene oxide nanoplates entrapped mixed matrix cation exchange membranes in water deionization, J. Membr. Sci. 541 (2017) 641–652, https://doi.org/10.1016/j.memsci.2017.07.022.*

This book belongs to Badji Mokhtar Annaba University Central Library Copyright Elsevier 2025

16.6 Scale-up conundrum

Scale-up can be defined as a pathway in which a physical or chemical process is transferred from the laboratory scale or pilot scale to the plant scale [50]. IEX process essentially takes place in isothermal conditions, and it is mainly governed by mass transfer phenomenon. Hydrodynamic characteristics such as liquid distribution, liquid holdup, and maldistribution are the parameters to be considered while designing fixed beds consisting of IEX resins or membrane separation units consisting of IEX membranes. Design of industrial scale fixed bed is usually based on laboratory scale unit for the evaluation of the large-scale fixed-bed performance. The critical parameters in fixed bed design are resin or particle size and the contact time. The rate of IEX is a strong function of size of IEX resin particle size. In addition, the size of the resin particle governs the pressure drop across the column. Hence it is recommended to utilize narrow particle size range of resin particles because larger sized particles control the rate of IEX, while smaller sized particles control the pressure drop. In the case of membrane process, the preliminary step in the design of industrial scale membrane module is the evaluation of performance of membrane experimentally. The objective of any membrane system is to process a fixed quantity of feed in specified time with reproducibility. Pilot-scale experiments must be carried out with major focus on the concentration dependence of flux, flux profile over time, and reproducibility.

Majority of the studies reported in the literature is based on laboratory data. The major obstacle in the scale-up of IEX system based on nanocomposites is the availability of filler material in bulk scale at economical cost. Various methodologies to synthesize nanocomposites have also been studied in depth, but engineering aspects that are extremely helpful in scale-up is still missing. More efforts are required to understand the engineering aspects and scale-up data for design of industrial scale IEX systems based on nanocomposites.

16.7 Conclusions

The present overview on the recent developments in nanocomposite IEX materials for water treatment indicates that nanomaterials incorporated IEX materials can be suitable candidates for enhancing the efficacy of such materials. Important recent achievements in the field of nanocomposite IEX materials have shown usage of low-dimensional carbon such as CNTs, graphene and its derivatives, metal oxide, silica as potential candidates in improving the properties of IEX materials at laboratory scale. Apart from the intrinsic characteristics of the material, the selection of appropriate methodology for the incorporation of nanomaterials into the matrix decides the required properties of IEX materials. Further work needs to be done in the area of optimization of processing parameters to have precise control in the composition and structure of modified IEX materials. Typical applications of nanocomposite IEX membranes include electrodialysis, CDI, etc. Technical difficulties involved in industrial scale usage of

This book belongs to Badji Mokhtar Annaba University Central Library Copyright Elsevier 2025

such applications must be resolved with engineering expertise. More efforts must be concentrated into percolation studies related to nanocomposite IEX materials, structure-property relationship between the nanomaterials and matrix, while surface modification of nanomaterials must be studied in depth to understand and achieve properties such as fouling resistance, high electrical conductivity, and IEC.

References

[1] M.R. Landsman, R. Sujanani, S.H. Brodfuehrer, C.M. Cooper, A.G. Darr, R.J. Davis, K. Kim, S. Kum, L. K. Nalley, S.M. Nomaan, C.P. Oden, A. Paspureddi, K.K. Reimund, L.S. Rowles III, S. Yeo, D.F. Lawler, B. D. Freeman, L.E. Katz, Water treatment: are membranes the panacea? Annu. Rev. Chem. Biomol. Eng. 11 (2019) 1–27, https://doi.org/10.1017/CBO9781107415324.004.

[2] I. Ali, New generation adsorbents for water treatment, Chem. Rev. 112 (2012) 5073–5091, https://doi.org/10.1021/cr300133d.

[3] I. Levchuk, J.J. Rueda Márquez, M. Sillanpää, Removal of natural organic matter (NOM) from water by ion exchange – a review, Chemosphere 192 (2018) 90–104, https://doi.org/10.1016/j.chemosphere.2017.10.101.

[4] A.B. Pandit, J.K. Kumar, Clean water for developing countries, Annu. Rev. Chem. Biomol. Eng. 6 (2015) 217–246, https://doi.org/10.1146/annurev-chembioeng-061114-123432.

[5] P. Rajasulochana, V. Preethy, Comparison on efficiency of various techniques in treatment of waste and sewage water – a comprehensive review, Resour. Technol. 2 (2016) 175–184, https://doi.org/10.1016/j.reffit.2016.09.004.

[6] H.L. Beohner, A.B. Mindler, Ion exchange in waste treatment, Ind. Eng. Chem. 41 (1949) 448–452, https://doi.org/10.1021/ie50471a004.

[7] A. Alabi, A. AlHajaj, L. Cseri, G. Szekely, P. Budd, L. Zou, Review of nanomaterials-assisted ion exchange membranes for electromembrane desalination, Npj Clean Water 1 (2018) 10, https://doi.org/10.1038/s41545-018-0009-7.

[8] S.M. Hosseini, M.M.B. Usefi, M. Habibi, F. Parvizian, B. Van der Bruggen, A. Ahmadi, M. Nemati, Fabrication of mixed matrix anion exchange membrane decorated with polyaniline nanoparticles to chloride and sulfate ions removal from water, Ionics (Kiel) 25 (2019) 6135–6145, https://doi.org/10.1007/s11581-019-03151-w.

[9] J. Ran, L. Wu, Y. He, Z. Yang, Y. Wang, C. Jiang, L. Ge, E. Bakangura, T. Xu, Ion exchange membranes: new developments and applications, J. Membr. Sci. 522 (2017) 267–291, https://doi.org/10.1016/j.memsci.2016.09.033.

[10] M.N. Subramaniam, P.S. Goh, W.J. Lau, A.F. Ismail, The roles of nanomaterials in conventional and emerging technologies for heavy metal removal: a state-of-the-art review, Nanomaterials 9 (2019), https://doi.org/10.3390/nano9040625.

[11] S.K. Kumar, R. Krishnamoorti, Nanocomposites: structure, phase behavior, and properties, Annu. Rev. Chem. Biomol. Eng. 1 (2010) 37–58, https://doi.org/10.1146/annurev-chembioeng-073009-100856.

[12] S. Khodami, S. Mehdipour-Ataei, S. Babanzadeh, Preparation, characterization, and performance evaluation of sepiolite-based nanocomposite membrane for desalination, J. Ind. Eng. Chem. 82 (2020) 164–172, https://doi.org/10.1016/j.jiec.2019.10.009.

[13] M.D. Yadav, A.W. Patwardhan, J.B. Joshi, K. Dasgupta, Selective synthesis of metallic and semi-conducting single-walled carbon nanotube by floating catalyst chemical vapour deposition, Diam. Relat. Mater. 97 (2019) 107432, https://doi.org/10.1016/j.diamond.2019.05.017.

[14] V.N. Popov, Carbon nanotubes: properties and application, Mater. Sci. Eng. R Rep. 43 (2004) 61–102, https://doi.org/10.1016/j.mser.2003.10.001.

[15] B.J. Landi, M.J. Ganter, C.D. Cress, R.A. DiLeo, R.P. Raffaelle, Carbon nanotubes for lithium ion batteries, Energy Environ. Sci. 2 (2009) 638–654, https://doi.org/10.1039/b904116h.

This book belongs to Badji Mokhtar Annaba University Central Library

Copyright Elsevier 2025

[16] S.V. Sawant, S. Banerjee, A.W. Patwardhan, J.B. Joshi, K. Dasgupta, Synthesis of boron and nitrogen co-doped carbon nanotubes and their application in hydrogen storage, Int. J. Hydrogen Energy 45 (2020) 13406–13413, https://doi.org/10.1016/j.ijhydene.2020.03.019.
[17] M. Monthioux, Carbon Meta-Nanotubes: Synthesis, Properties and Applications, (2011) pp. 1–426, https://doi.org/10.1002/9781119954743.
[18] M.D. Yadav, K. Dasgupta, A.W. Patwardhan, A. Kaushal, J.B. Joshi, Kinetic study of single-walled carbon nanotube synthesis by thermocatalytic decomposition of methane using floating catalyst chemical vapour deposition, Chem. Eng. Sci. (2019) 91–103, https://doi.org/10.1016/j.ces.2018.10.050.
[19] M.D. Yadav, A.W. Patwardhan, J.B. Joshi, K. Dasgupta, Kinetic study of multi-walled carbon nanotube synthesis by thermocatalytic decomposition of methane using floating catalyst chemical vapour deposition, Chem. Eng. J. 377 (2019) 119895, https://doi.org/10.1016/j.cej.2018.09.056.
[20] M. Fathy, T. Abdel Moghny, A.E. Awad Allah, A.E. Alblehy, Cation exchange resin nanocomposites based on multi-walled carbon nanotubes, Appl. Nanosci. 4 (2014) 103–112, https://doi.org/10.1007/s13204-012-0178-5.
[21] S.M. Hosseini, S.S. Madaeni, A.R. Khodabakhshi, Preparation and characterization of PC/SBR heterogeneous cation exchange membrane filled with carbon nano-tubes, J. Membr. Sci. 362 (2010) 550–559, https://doi.org/10.1016/j.memsci.2010.07.015.
[22] S. Mallakpour, S. Soltanian, Surface functionalization of carbon nanotubes: fabrication and applications, RSC Adv. 6 (2016) 109916–109935, https://doi.org/10.1039/c6ra24522f.
[23] M.D. Yadav, K. Dasgupta, A. Kushwaha, A.P. Srivastava, A.W. Patwardhan, D. Srivastava, J.B. Joshi, Few layered graphene by floating catalyst chemical vapour deposition and its extraordinary H_2O_2 sensing property, Mater. Lett. 199 (2017) 180–183, https://doi.org/10.1016/j.matlet.2017.04.085.
[24] X.J. Lee, B.Y.Z. Hiew, K.C. Lai, L.Y. Lee, S. Gan, S. Thangalazhy-Gopakumar, S. Rigby, Review on graphene and its derivatives: synthesis methods and potential industrial implementation, J. Taiwan Inst. Chem. Eng. 98 (2019) 163–180, https://doi.org/10.1016/j.jtice.2018.10.028.
[25] X. Cai, L. Lai, Z. Shen, J. Lin, Graphene and graphene-based composites as Li-ion battery electrode materials and their application in full cells, J. Mater. Chem. A 5 (2017) 15423–15446, https://doi.org/10.1039/c7ta04354f.
[26] Y. Yang, A.M. Asiri, Z. Tang, D. Du, Y. Lin, Graphene based materials for biomedical applications, Mater. Today 16 (2013) 365–373, https://doi.org/10.1016/j.mattod.2013.09.004.
[27] M.F. El-Kady, Y. Shao, R.B. Kaner, Graphene for batteries, supercapacitors and beyond, Nat. Rev. Mater. 1 (2016) 1–14, https://doi.org/10.1038/natrevmats.2016.33.
[28] L. Bai, Y. Zhang, W. Tong, L. Sun, H. Huang, Q. An, N. Tian, P.K. Chu, Graphene for energy storage and conversion: synthesis and interdisciplinary applications, Electrochem. Energy Rev. 3 (2020) 395–430, https://doi.org/10.1007/s41918-019-00042-6.
[29] P.P. Sharma, S. Gahlot, B.M. Bhil, H. Gupta, V. Kulshrestha, An environmentally friendly process for the synthesis of an fGO modified anion exchange membrane for electro-membrane applications, RSC Adv. 5 (2015) 38712–38721, https://doi.org/10.1039/c5ra04564a.
[30] Y. Wen, J. Yuan, X. Ma, S. Wang, Y. Liu, Polymeric nanocomposite membranes for water treatment: a review, Environ. Chem. Lett. 17 (2019) 1539–1551, https://doi.org/10.1007/s10311-019-00895-9.
[31] A. Jilani, M.H.D. Othman, M.O. Ansari, S.Z. Hussain, A.F. Ismail, I.U. Khan, Inamuddin, Graphene and its derivatives: synthesis, modifications, and applications in wastewater treatment, Environ. Chem. Lett. 16 (2018) 1301–1323, https://doi.org/10.1007/s10311-018-0755-2.
[32] F. Parvizian, S.M. Hosseini, A.R. Hamidi, S.S. Madaeni, A.R. Moghadassi, Electrochemical characterization of mixed matrix nanocomposite ion exchange membrane modified by ZnO nanoparticles at different electrolyte conditions "pH/concentration" J. Taiwan Inst. Chem. Eng. 45 (2014) 2878–2887, https://doi.org/10.1016/j.jtice.2014.08.017.
[33] S.M. Hosseini, A. Gholami, P. Koranian, M. Nemati, S.S. Madaeni, A.R. Moghadassi, Electrochemical characterization of mixed matrix heterogeneous cation exchange membrane modified by aluminum oxide

This book belongs to Badji Mokhtar Annaba University Central Library Copyright Elsevier 2025

nanoparticles: mono/bivalent ionic transportation, J. Taiwan Inst. Chem. Eng. 45 (2014) 1241–1248, https://doi.org/10.1016/j.jtice.2014.01.011.

[34] Y. Berbar, Z.E. Hammache, S. Bensaadi, R. Soukeur, M. Amara, B. Van der Bruggen, Effect of functionalized silica nanoparticles on sulfonated polyethersulfone ion exchange membrane for removal of lead and cadmium ions from aqueous solutions, J. Water Process Eng. 32 (2019) 100953, https://doi.org/10.1016/j.jwpe.2019.100953.

[35] X. Tong, B. Zhang, Y. Fan, Y. Chen, Mechanism exploration of ion transport in nanocomposite cation exchange membranes, ACS Appl. Mater. Interfaces 9 (2017) 13491–13499, https://doi.org/10.1021/acsami.7b01541.

[36] X. Zuo, S. Yu, X. Xu, J. Xu, R. Bao, X. Yan, New PVDF organic-inorganic membranes: the effect of SiO_2 nanoparticles content on the transport performance of anion-exchange membranes, J. Membr. Sci. 340 (2009) 206–213, https://doi.org/10.1016/j.memsci.2009.05.032.

[37] G. Nie, L. Wu, Y. Du, H. Wang, Y. Xu, Z. Ding, Z. Liu, Efficient removal of phosphate by a millimeter-sized nanocomposite of titanium oxides encapsulated in positively charged polymer, Chem. Eng. J. 360 (2019) 1128–1136, https://doi.org/10.1016/j.cej.2018.10.184.

[38] M.M. Abd El-Latif, M.F. Elkady, Kinetics study and thermodynamic behavior for removing cesium, cobalt and nickel ions from aqueous solution using nano-zirconium vanadate ion exchanger, Desalination 271 (2011) 41–54, https://doi.org/10.1016/j.desal.2010.12.004.

[39] S. Gahlot, P.P. Sharma, H. Gupta, V. Kulshrestha, P.K. Jha, Preparation of graphene oxide nano-composite ion-exchange membranes for desalination application, RSC Adv. 4 (2014) 24662–24670, https://doi.org/10.1039/C4RA02216E.

[40] B.F. Urbano, B.L. Rivas, F. Martinez, S.D. Alexandratos, Water-insoluble polymer-clay nanocomposite ion exchange resin based on N-methyl-d-glucamine ligand groups for arsenic removal, React. Funct. Polym. 72 (2012) 642–649, https://doi.org/10.1016/j.reactfunctpolym.2012.06.008.

[41] B. Kelta, A.M. Taddesse, O.P. Yadav, I. Diaz, Á. Mayoral, Nano-crystalline titanium(IV) tungstomolybdate cation exchanger: synthesis, characterization and ion exchange properties, J. Environ. Chem. Eng. 5 (2017) 1004–1014, https://doi.org/10.1016/j.jece.2017.01.018.

[42] S.A. Nabi, M. Shahadat, R. Bushra, A.H. Shalla, A. Azam, Synthesis and characterization of nano-composite ion-exchanger; its adsorption behavior, Colloids Surf. B Biointerfaces 87 (2011) 122–128, https://doi.org/10.1016/j.colsurfb.2011.05.011.

[43] S. Siva, S. Sudharsan, R. Sayee Kannan, Synthesis, characterization and ion-exchange properties of novel hybrid polymer nanocomposites for selective and effective mercury(II) removal, RSC Adv. 5 (2015) 79665–79678, https://doi.org/10.1039/c5ra13004b.

[44] Y. Hu, Y. Du, G. Nie, T. Zhu, Z. Ding, H. Wang, L. Zhang, Y. Xu, Selective and efficient sequestration of phosphate from waters using reusable nano-Zr(IV) oxide impregnated agricultural residue anion exchanger, Sci. Total Environ. 700 (2020) 1–11, https://doi.org/10.1016/j.scitotenv.2019.134999.

[45] A.R. Moghadassi, P. Koranian, S.M. Hosseini, M. Askari, S.S. Madaeni, Surface modification of heterogeneous cation exchange membrane through simultaneous using polymerization of PAA and multi walled carbon nano tubes, J. Ind. Eng. Chem. 20 (2014) 2710–2718, https://doi.org/10.1016/j.jiec.2013.10.059.

[46] S.M. Hosseini, M. Askari, P. Koranian, S.S. Madaeni, A.R. Moghadassi, Fabrication and electrochemical characterization of PVC based electrodialysis heterogeneous ion exchange membranes filled with Fe_3O_4 nanoparticles, J. Ind. Eng. Chem. 20 (2014) 2510–2520, https://doi.org/10.1016/j.jiec.2013.10.034.

[47] X. Zuo, S. Yu, W. Shi, Effect of some parameters on the performance of eletrodialysis using new type of PVDF-SiO_2 ion-exchange membranes with single salt solution, Desalination 290 (2012) 83–88, https://doi.org/10.1016/j.desal.2012.01.009.

[48] Y. Zhang, L. Zou, Y. Wimalasiri, J.Y. Lee, Y. Chun, Reduced graphene oxide/polyaniline conductive anion exchange membranes in capacitive deionisation process, Electrochim. Acta 182 (2015) 383–390, https://doi.org/10.1016/j.electacta.2015.09.128.

This book belongs to Badji Mokhtar Annaba University Central Library

Copyright Elsevier 2025

[49] S.M. Hosseini, E. Jashni, M. Habibi, M. Nemati, B. Van der Bruggen, Evaluating the ion transport characteristics of novel graphene oxide nanoplates entrapped mixed matrix cation exchange membranes in water deionization, J. Membr. Sci. 541 (2017) 641–652, https://doi.org/10.1016/j.memsci.2017.07.022.
[50] V. Inglezakis, S. Poulopoulos, Adsorption, Ion Exchange and Catalysis, Elsevier, 2006.

This book belongs to Badji Mokhtar Annaba University Central Library

Copyright Elsevier 2025

SECTION IV

Nanomaterials for membrane synthesis: Preparation and applications

This book belongs to Badji Mokhtar Annaba University Central Library

Copyright Elsevier 2025

This page intentionally left blank

This book belongs to Badji Mokhtar Annaba University Central Library

Copyright Elsevier 2025

CHAPTER 17

Nanomaterials for membrane synthesis: Introduction, mechanism, and challenges for wastewater treatment

Shriram Sonawane[a], Parag Thakur[a], Shirish H. Sonawane[b], and Bharat A. Bhanvase[c]

[a]Department of Chemical Engineering, Visvesvaraya National Institute of Technology, Nagpur, Maharashtra, India, [b]Department of Chemical Engineering, National Institute of Technology, Warangal, Telangana, India, [c]Chemical Engineering Department, Laxminarayan Institute of Technology, Rashtrasant Tukadoji Maharaj Nagpur University, Nagpur, Maharashtra, India

Nomenclature

CA	cellulose acetate
CN	nitrocellulose
CE	cellulose esters
PS	polysulfone
PES	polyether sulfone
GO	graphene oxide
SEM	scanning electron microscopy
XRD	X-ray diffraction
FT-IR	Fourier transform infrared
TGA	thermo gravity analysis
EDX	energy dispersive X-ray spectroscopy
mMSN	modified mesoporous silica nanoparticles
PA	polyamide
LbL	layer by layer
IP	interfacial polymerization
TFN	thin film nanocomposites
TFC	thin film composites
SRNF	solvent-resistant nanofiltration
FESEM	scanning electron microscopy
AFM	atomic force microscopy
TEM	transmission electron microscopy
CNT	carbon nanotube
SWCNT	single-walled carbon nanotubes
NIPS	nonsolvent-induced phase separation
TIPS	thermally induced phase separation
SNIPS	self-assembled and nonsolvent-induced phase separation

Handbook of Nanomaterials for Wastewater Treatment. https://doi.org/10.1016/B978-0-12-821496-1.00009-X
Copyright © 2021 Elsevier Inc. All rights reserved.

This book belongs to Badji Mokhtar Annaba University Central Library

Copyright Elsevier 2025

17.1 Introduction

Membrane technology is one of the promising separation technologies of the 21st century. Permeable membranes are used to selectively transfer materials through these membranes. Generally, the main use of membrane technology can be seen in gaseous or liquid separation processes. Heat is not required in these processes, thus membrane separation processes have the advantage of having less energy consumption than thermal separation processes like distillation and crystallization. The next decade is very crucial for mankind, as many countries are facing a serious water crisis. Thus, highly efficient water treatment methods are urgently required to face these issues.

The ability to process a large amount of feed is the basic requirement for good membranes. Selectivity toward a particular component is also a desirable characteristic. Antifouling capacity and mechanical strength are also important characteristics [1]. Ceramic membranes and polymer membranes are common types of membranes generally used. Ceramic membranes are synthesized by using metal hydroxides to attach to the surface of porous supporting materials. Ceramic membranes are more widely used than polymeric membranes. But due to comparatively less mechanical strength than polymeric membranes, these membranes are prohibited from high-pressure applications [2, 3]. Polymeric membranes are comparatively stronger than ceramic membranes. Polymeric membranes are also known as organic membranes, and ceramic membranes are called inorganic membranes.

Nanotechnology is a branch of technology that deals with the synthesis and application of materials with dimensions less than 100 nm [4]. Nanotechnology is considered to have high potential to solve problems in membrane technology [5]. In the last few years, many researchers have tried to develop new membranes based on nanotechnology and also described the mechanism for the separation process. Graphene and carbon nanotubes (CNTs) are mainly used to develop these membranes [6–9]. In recent years, film-based membranes are also good in separation performance, but they are not suitable for high-pressure operation, and after some time these membranes have less porosity [10]. In this chapter, we have reviewed the recent trends and breakthroughs in membrane synthesis and challenges like fouling, bacterial growth, and toxicity due to nanomaterials. Challenges are discussed with some of the prominent nanomaterials used in industrial application of membranes.

17.2 Conventional membranes

Membranes are a barrier layer to prohibit the passage of selective materials through it. Conventional membranes are divided into polymeric and ceramic membranes. Fig. 17.1 represents the details of the classifications. The following two are important classifications of conventional membranes.

This book belongs to Badji Mokhtar Annaba University Central Library
Copyright Elsevier 2025

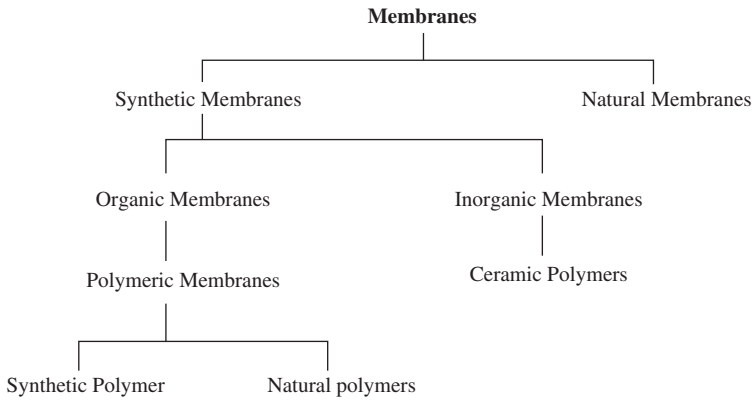

Fig. 17.1
Classification of conventional membranes.

17.2.1 Ceramic membranes

Ceramic membranes are synthesized by using an inorganic material such as alumina, titanium, zirconium oxides, silicon carbide, or some glassy materials. Ceramic membranes have more thermal stability than polymeric membranes. Ceramic membranes generally have a sandwich-like structure of three layers. The first layer is the support layer, the second or middle layer is the transition layer, and the last is the function layer. As the name indicates, the support layer is useful to provide support and mechanical strength to the membrane system. The transition layer is useful to prevent particles from passing through the membrane. The function layer is an important part of the system for the identification of the membrane. According to this layer, the membrane system is classified into different categories like microfiltration, ultrafiltration, and nanofiltration [11, 12]. Sol-gel method and surface modification methods are used to synthesize ceramic membranes.

17.2.2 Polymeric membranes

Polymeric membranes are the first choice of the membrane separation industry, because they are very economic and good in applications. Affinity toward a particular component is the most important characteristic required in polymeric membranes.

In polymeric membranes, it is also easy to control the pore size of the membrane during formation. High flexibility and smaller space is required for the installation. We need to choose a polymer each time according to the task. Cellulose acetate (CA), polyacrylonitrile (PAN), polyimide, polycarbonate (PC), polyethylene (PE), and polypropylene (PP), and polytetrafluoroethylene (PTFE) are common examples of polymeric membranes. Generally,

This book belongs to Badji Mokhtar Annaba University Central Library Copyright Elsevier 2025

polymers like polyvinylidene fluoride (PVDF) ultrafiltration membranes are embedded with nanomaterials like metal/metal oxide or CNTs to improve the performance of the polymeric membrane [13, 14].

17.3 Nanomaterial-based membranes

Generally, conventional membranes are used in water purification purposes, but fouling is the main problem in conventional membranes. Many attempts are made to improve the performance of the membranes by chemical methods [15]. Nanotechnological applications in membrane technology have made impressive results [1, 6–9, 15–19]. Generally, metals/metal oxide, nanofiber, or carbon-based materials like graphene and CNTs are used with polymeric or ceramic materials to increase the efficiency of the membrane. Fig. 17.2 represents the composite membrane.

17.3.1 Inorganic nanoparticle-based membranes

There are two methods to use nanoparticles in membrane technology. Nanoparticles can be used separately as a layer in the membrane, or nanoparticles can be used as a filler in the membrane material during synthesis [21]. Metal/metal oxide-based nanomaterials, nanosized

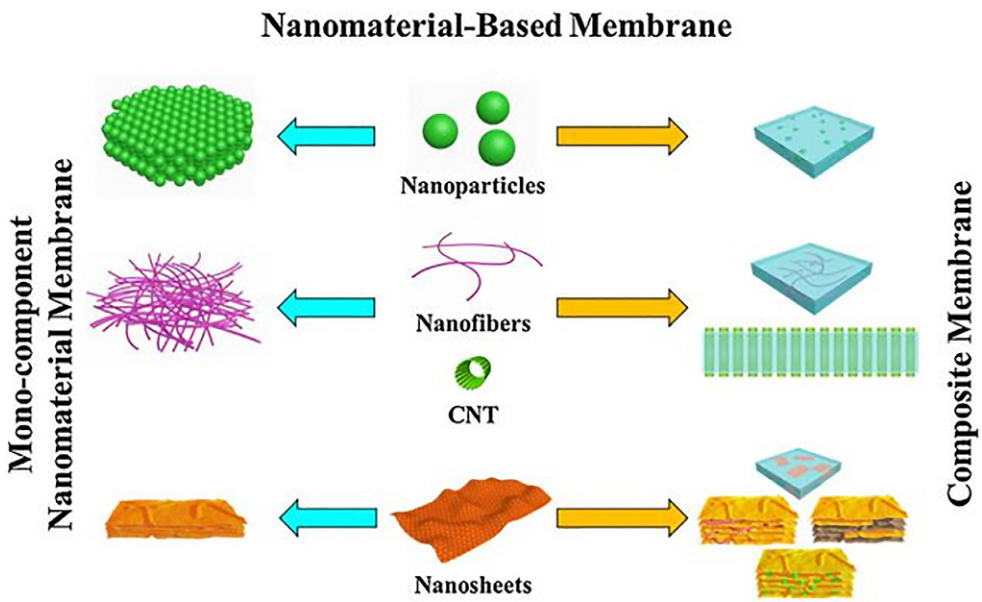

Fig. 17.2
Nanomaterial-based membranes [20]. *Reprinted with permission from Y. Ying, W. Ying, Q. Li, D. Meng, G. Ren, R. Yan, X. Peng, Recent advances of nanomaterial-based membrane for water purification, Appl. Mater. Today 7 (2017) 144–158. Copyright (2017) Elsevier.*

This book belongs to Badji Mokhtar Annaba University Central Library Copyright Elsevier 2025

polymers, and carbon-based nanomaterials can be used as a nanomaterial for this purpose. Metals and metal oxides are generally used as filler in membranes. SiO_2 and modified SiO_2 are used to reject the sodium sulfate, and aminosilanized TiO_2 rejects NaCl more efficiently. Similarly, alumina and zinc oxide TiO_2 [22, 23] are successfully attached to the polymeric membrane.

Hilal et al. published a very good review article on the metal/metal oxide nanoparticle-based polymeric membranes [24]. In this paper, the emphasis is more on the various nanoparticles and their role in the synthetic membrane. Silver, iron, zirconium, silica, aluminum, titanium, and magnesium-based membranes are discussed. Proton exchange membranes are used in fuel cells, and iron nanoparticle-based membranes are useful in such applications. Silica nanoparticle-based membranes are useful to produce pure gases with less impurity content. This nanocomposite has a property to trap impurities. Thus, this nanoparticle is useful in various applications like drinking water purposes because it is inert.

Novel membrane preparation methods like molecular layer deposition method are also used to prepare the TiO_2 nanoparticle-based membrane. These types of membranes are used to prepare nanofiltration membranes [25].

17.3.2 Nanofiber-based membranes

Nanofibers are fibers having a diameter of less than 100 nm. Nanofibers are good for interlocking and porous membrane formation. Electrospinning is mainly used to synthesize nanofibers. Cellulose is one of the oldest known fiber materials [26]. The use of nanofiber-based membranes in oil-water separation is a less time-consuming and more energy-efficient method [27].

17.3.3 Carbon-based membranes

Carbon nanomaterials are gaining increased attention due to high mechanical, thermal, and chemical applications. Graphene, CNTs, and fullerenes are examples of carbon-based materials. These nanomaterials increase chemical, thermal, and physical stability. Carbon-based materials are also useful to increase the antibacterial and catalytic properties [28–30].

Graphene oxide (GO) has various functional groups in its structure, thus this structure provides compatibility with more composites. Polymeric membranes have shown good compatibility with GO [31].

17.4 Nanomaterial-based membrane synthesis techniques

Nanomaterials are fabricated into the matrix of a membrane by different conventional approaches like sol-gel method, graft polymerization, layer-by-layer method, stretching, phase

This book belongs to Badji Mokhtar Annaba University Central Library Copyright Elsevier 2025

inversion technique, interfacial polymerization, sintering, track etching, coating, and electrospinning. The sol-gel method is not used generally due to poor dispersion of nanomaterials and thermal stresses in the membrane. Some attempts are made to use the sol-gel method for synthesizing organic-inorganic membranes [32]. The following important synthesis methods are discussed in detail.

17.4.1 Phase inversion method

Phase inversion technique is also known as a phase separation technique. In this method, controlled phase transformation is done from the liquid phase of a polymer to the solid phase. An antisolvent is used to separate the polymer from the solvent. Water is mainly used as an antisolvent. Immersion precipitation is a widely used method among the phase inversion techniques. Generally, four mechanisms are used in this method as follows [33]:

- Solution temperature reduction method
- Immersion of the polymer solution into antisolvent
- Exposure of the polymer solution to a vapor of antisolvent
- Evaporation of the solvent in atmospheric air or at high temperature

Phase inversion rate and membrane characteristics can be influenced by solvent solubility in the antisolvent, polymer insolubility in the antisolvent, and antisolvent temperature [34]. Phase inversion method is represented in Fig. 17.3.

Phase inversion technique is an industrially reliable technique due to its cost-effectiveness. The phase separation method is further classified into the following two methods.

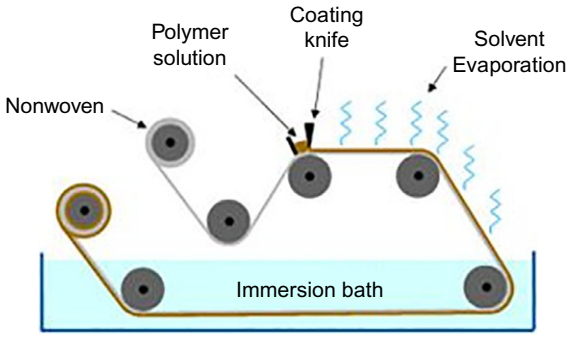

Fig. 17.3
Schematic representation of the phase inversion technique [35]. *Reprinted with permission from S. Rangou, K. Buhr, V. Filiz, J.I. Clodt, B. Lademann, J. Hahn, A. Jung, V. Abetz, Self-organized isoporous membranes with tailored pore sizes, J. Membr. Sci. 451 (2014) 266–275. Copyright (2014) Elsevier.*

This book belongs to Badji Mokhtar Annaba University Central Library
Copyright Elsevier 2025

17.4.1.1 Nonsolvent-induced phase separation technique (NIPS)

This method is performed by adding antisolvent into a solution of solvent and polymer. Generally, water is an antisolvent or nonsolvent. Loeb and Souriranjan used this method initially for membrane synthesis. They synthesized the polymeric reverse osmosis membrane using this technique. CA is taken as a polymer and acetone as a solvent. The solution of both components is allowed to pass through water. Magnesium perchlorate is used as a pore-forming agent. These membranes showed better results than commercial membranes available [36].

NIPS can be modified for the copolymer-based membranes. This method is called a self-assembled and nonsolvent-induced phase separation technique.

17.4.1.2 Self-assembled and nonsolvent-induced phase separation (SNIPS)

The different arrangements of the chain of the polymer can be useful for the selective application of the polymeric membrane. The copolymer arrangement is possible in membrane synthesis. The extruder is used to mix the polymer, then the mixture is compressed by mold and etching. During extrusion, nanoparticles can be added. Selective localization of the nanoparticles can be useful to selective chain formation, and thus we can prepare nanomaterial-based polymeric membranes [37].

17.4.1.3 Thermally induced phase separation (TIPS)

In this method, a polymer solution with a high boiling point and comparatively lower molecular weight is used as a solvent. This liquid is cooled after the casting of dope. Two separate phases are formed after cooling. The absence of antisolvent and thermal energy dissipation are the distinguishing parameters of the method. Studies suggested that many polymeric membranes are hard to synthesize by NIPS but easy to synthesize by TIPS [38].

17.4.2 Interfacial polymerization (IP)

Interfacial polymerization mostly is used to fabricate membranes than other fabrication techniques. Fig. 17.4 represents the schematic representation of the interfacial polymerization. Interfacial polymerization is done due to advantages like higher loading capacity and uniform dispersion of nanoparticles like zeolite in the polyamide layer. Nanoparticles increase surface roughness, but surface hydrophilicity remains the same [40]. Modified mesoporous silica nanoparticles/polyamide is prepared by interfacial polymerization. Trimesoyl chloride (TMC) and piperazine (PIP) are the main components of the synthesis process. Silica nanoparticles are modified by using amino groups and added into the piperazine phase. After the interaction between aqueous modified mesoporous silica nanoparticles/piperazine phase and TMC, the covalent bond is developed between both phases. The concentration of nanoparticles is important to manipulate the pure water flux [41]. Hydrophilized ordered mesoporous carbon (H-OMC) is also used for the fabrication of polyamide thin film nanocomposite (PA-TFN)

This book belongs to Badji Mokhtar Annaba University Central Library Copyright Elsevier 2025

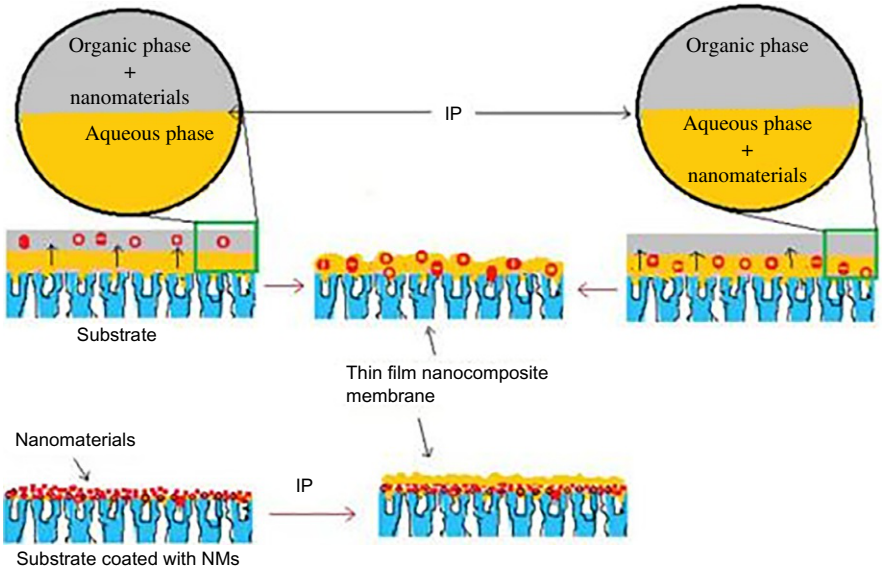

Fig. 17.4
Interfacial polymerization (IP) technique for membrane synthesis [39]. *Reprinted with permission from J.M. Gohil, R.R. Choudhury, Introduction to nanostructured and nano-enhanced polymeric membranes: preparation, function, and application for water purification, in: Nanoscale Materials in Water Purification, Elsevier, 2019, pp. 25–57. Copyright (2019) Elsevier.*

membranes. This interaction improved the performance of the membrane. Membrane with 5 wt % loading shows higher water permeability than other loading values [42]. Even metal alkoxide like titanium tetraisopropoxide, bis(triethoxysilyl)ethane, and phenyltriethoxysilane are used to prepare the membrane of polyamide [43]. Aminosilanized TiO_2 nanoparticles are functionalized into TMC and *m*-phenylenediamine (*m*-PDA). The functionalization of nanoparticles is characterized by XRD and FT-IR. Morphological and surface study is done by SEM and EDX. Heat resistivity is studied by TGA. This membrane improved salt rejection rate by 54% [44]. Nanoparticles of silver and acid-treated multiwalled CNTs are jointly added into the thin film nanocomposite membrane. Silver nanoparticles are loaded with 10 wt% in the thin film layer, and CNT is loaded with 5 wt% in the support layer. Pure water permeability is increased by 20% and 23%, respectively [45]. Even silica nanoparticles are added to the fluoropolyamide membrane. This membrane showed a 94% salt rejection rate [46]. There were several attempts made to increase the CNT-based membrane fabrication methods. The attempts aim to develop the membranes with a higher solvent rejection rate [47]. Poly(vinyl alcohol) (PVA) matrix is poured on the support of a 20% volume fraction of PSf with and without a well-dispersed synthesized aluminosilicate single-walled CNTs (SWCNT). Due to the presence of hydrophilic nanotubes, the water flux was increased [48].

This book belongs to Badji Mokhtar Annaba University Central Library Copyright Elsevier 2025

17.4.3 Layer-by-layer (LBL) assembly

This method deposits an alternate layer of oppositely charged materials, and these layers are separated by wash steps. Immersion technique, spin technique, spray technique, and electromagnetic techniques are used for this purpose [49]. The presence of opposite charges allows us to use the multilayer membranes. Based on the size and charge, the particle carrying GO nanosheets is used to separate the water. There is a scope of development of GO-based nanomembranes [50].

We can easily represent these systems of layer-by-layer assembly. If + and − are oppositely charged poly ions, then two bilayers can be represented as W + W − W + W − W where W is the wash layer. Electrostatic attraction is not the only interaction between the layers. The hydrophobic attraction is also an important force [51]. Multilayer systems encourage other forces to play a vital role. Thus, layer-by-layer can be used to synthesize hydrogen-bonded films [52], hydrophobic solvents [53], nanoparticles [54], and other nontraditional systems [55].

Nanofiltration, forward and reverse membrane, desalination, and pervaporation membranes are synthesized by the layer-by-layer membrane synthesis technique [56].

17.4.4 Stretching and sintering

Mechanical stretching is an important parameter for polymer alignment and arrangement of the chain. Thus, it is useful for semicrystalline materials like PTFE. The polymer is extruded, stretched, and made in the form of sheets. Stretching is done according to the application. Temperature drawn polymer thickness and speed of extrusion are the operational parameters for the process [57].

In the sintering technique, powdered materials are compressed and then sintered at a predefined temperature. Microfiltration membranes are made by the sintering technique [58].

17.4.5 Track etching and electrospinning

Materials are directly exposed to high radiation. Thus, tracks are formed due to this exposure. Exposure time and energy are important parameters of membrane synthesis [59].

In the electrospinning method, fibers are spun by an electrostatic force. This electrospun fiber has pores of the submicron range. The high electrical field is applied at the capillary nozzle, and the polymer remains there for a while. Change is developed in the liquid polymer. The hemispherical shape is generated after an increase in electric power. Then, after a certain point, electrical force is considerably more than the surface tension. Thus, the path of the jet can be controlled by the electrical force [60].

This book belongs to Badji Mokhtar Annaba University Central Library
Copyright Elsevier 2025

17.4.6 Three-dimensional printing (3D printing)

In this method, the material is printed on the matrix. Three-dimensional printing is classified into three categories: solid printing, liquid printing, and powder-based printing. These classifications are based on the feed material used. Before processing the material, we must ensure that the material is melt processable. The resolution of the printer and material type are a major concern. The current instrumentation available is best fitted for the microscale level. Thus, there is scope for further development for nanoscale-level instruments [61].

17.5 Challenges for wastewater treatment

17.5.1 Antifouling challenges

Because of the deposition of the fouling agents, ultrafiltration and microfiltration membranes need frequent cleaning. Nanoparticles can play a vital role in the prohibition of the deposition of fouling agents. Membrane fouling is an important challenge that needs to be tackled. Researchers have found materials like zwitterionic materials to tackle fouling of membranes [62]. Bioinspired adhesion chemistry, supramolecular chemistry, mineralization chemistry, click chemistry, and coupling chemistry are promising fields of chemistry that play an important role in the fouling process [63].

To increase the permeation rate of water is the main aim of the development of various membranes. Permeability is the most important ability to be considered during the selection of nanocomposite membranes. Increased permeability increases the efficiency of the membrane. Various kinds of cross-linkers are used to increase permeation efficiency. Organoclay/chitosan nanocomposite is coated on PVDF/chitosan nanocomposite and performance of the membrane is good despite no addition of a cross-linker [64]. Some researchers also tried to improve the interfacial polymerization method to increase permeability and selectivity of the process. The author also suggests that improvements can be done in this regard [65]. *O*-(carboxymethyl)-chitosan nanofiltration membrane is functionalized by GO nanosheets to enhance the permeation and salt rejection rate, showing promising results [66]. Due to its better efficiency, three-stage antifouling mechanism is receiving greater attention. Fig. 17.5 represents the schematic of the three-stage antifouling mechanism. In this mechanism, fouling agents are separated in the first stage by steric hindrance and hydration layer effect. Here, hydraulic pressure is an important parameter for performance efficiency. Then, in the second stage, low surface energy will play a role, and due to hydrophobicity, the electrostatic mechanism will separate the fouling agents. Finally, foulant will accumulate to form the cake [67].

17.5.2 Antibacterial challenges

Microbial growth on the membrane is one of the main reasons to decrease the performance of the membrane. Copper, titanium dioxide, silver nanoparticles, and GOs also have antibacterial activity.

This book belongs to Badji Mokhtar Annaba University Central Library Copyright Elsevier 2025

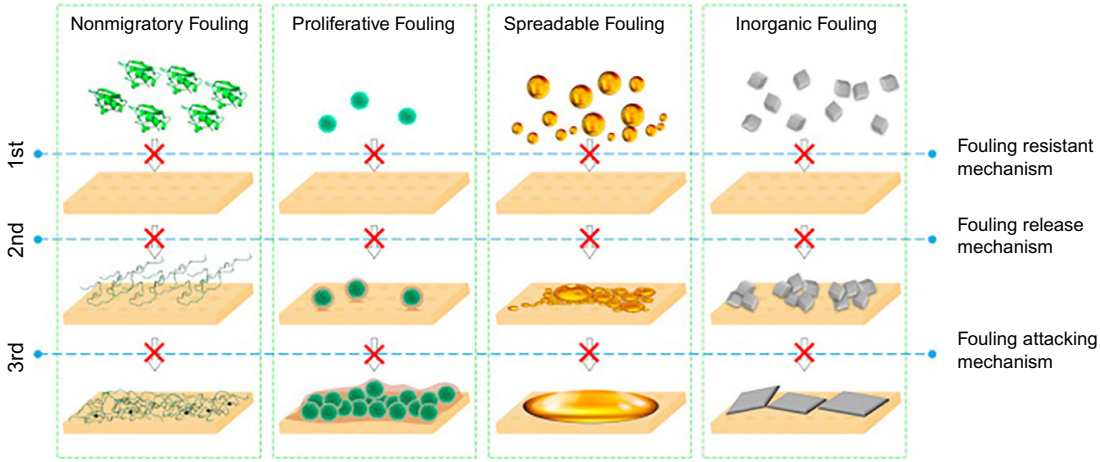

Fig. 17.5
Schematic representation of three-stage antifouling mechanism [67]. *Reprinted with permission from X. Zhao, R. Zhang, Y. Liu, M. He, Y. Su, C. Gao, Z. Jiang, Antifouling membrane surface construction: chemistry plays a critical role, J. Membr. Sci. 551 (2018) 145–171. Copyright (2018) Elsevier.*

17.5.2.1 Silver nanoparticles

Silver has been used as an antibacterial agent for a long time [68]. Growth of *Balantidium coli* (*B. coli*) bacteria is affected by the silver nanoparticle [69]. Silver nanoparticles are one of the most studied nanoparticles. The exact killing mechanism of the silver nanoparticle is not fully explained in the literature, but it is suggested that the silver ion can manipulate the DNA of bacteria [70]. Silver and titanium nanoparticle-based membranes are useful to reduce the biological fouling of the membrane. All the pseudomonas are found dead on a silver nanoparticle-based polyamide membrane [71].

17.5.2.2 Titanium dioxide nanoparticles

Titanium dioxide is cheaper than silver nanoparticles, thus it can be used instead of silver nanoparticles. Titanium oxide can instantly deactivate the cells of bacteria. It can break the synthesis process of bacteria. This leads to reduction in growth of bacteria. It is observed that lower concentration of nanoparticles is better in efficiency than a higher concentration. High concentration does not form a thin film of membrane and may tend to agglomerate [72]. Researchers have conducted good reviews using titanium dioxide nanoparticles [73].

17.5.2.3 Copper nanoparticles

Copper nanoparticle is also a good antifungal and antibacterial element. The concern is that the copper nanoparticle can also be toxic. Thus, it is necessary to control the release of the copper nanoparticle in the flow [74].

This book belongs to Badji Mokhtar Annaba University Central Library Copyright Elsevier 2025

17.5.2.4 Metal oxide-based nanoparticles

Metal oxides are also a star performer in antibacterial activity. Metal oxides are less harmful compared with other nanoparticles [75]. Alkaline earth metal-based oxides like MgO and CaO are mainly used. ZnO is also a good alternative. ZnO is a better modification agent to remove *E. coli* bacteria [76].

17.5.2.5 Carbon-based nanoparticles

GO is better in the killing of *E. coli* bacteria. The sharp molecular structure of GO is a main reason of the destruction of the bacteria. Larger length have comparatively better performance in antibacterial activity [77]. Deposition of the bacteria is an important reason behind the decrease in the permeate flux.

SWCNTs are also useful for the antimicrobial property of the polyamide membranes. SWCNTs are first purified, and then ozonolysis is done. Then these functionalized SWCNTs are attached to the polymer matrix by a covalent bond. This improved surface has inactivated 60% of the bacteria attached to the membrane [67].

17.5.3 Toxicity potential

Nanoparticles used in membrane synthesis are diverse, and their application is increasing day by day. Many biological processes are being disturbed by nanotechnological applications. However, no monitoring of the production of nanoparticles is available. No health or safety analysis is done in many industrial processes. Thus, the use of nanoparticles in membrane synthesis is dangerous without strict manufacturing policies and monitoring. Thus, nanotoxicity has become a major subject of concern [78].

Researchers found that the nanomaterials are highly dangerous for human cells. Nanomaterials like silver, silica, and carbon-based materials like CNTs and GOs are some examples. Agglomeration of the nanomaterial in human cells may lead to serious health issues. Thus, it is important to control the nanoparticle concentration in membrane synthesis.

17.5.3.1 Silver and silica nanoparticles

Silver is most cytotoxic element. It is advised that silver nanocoating should not be done for dressings and other coating applications [79]. Even for noncytotoxic doses, silver is harmful. The lung is an easy target for the element, and through the nasopharyngeal system, the drug can reach to the brain as well [80]. Thus, it is wise to restrict the silver nanoparticles in membrane synthesis considering the adverse effect on human health.

Silica nanoparticles are less cytotoxic than silver nanoparticles. But agglomerated silica can be harmful to the protein [81]. Cytotoxicity is mainly dependent on the size of the nanoparticles, and silica nanoparticles lead to oxidative stress in the human body [82].

This book belongs to Badji Mokhtar Annaba University Central Library
Copyright Elsevier 2025

17.5.3.2 Carbon-based nanomaterials

CNT is considered a nontoxic element. But some studies are indicating that chronic toxicity can be seen after use of CNT-based nanomaterials. But these can be overcome by functionalization of the CNT with a suitable element [83]. Acute pulmonary inflammation is seen after consumption of the SWCNT [84].

Fullerence is an important carbon-based nanomaterial. Suspended fullerence can kill bacteria, fish, and even cause harm to human health [85, 86]. Preparation method of fullerence is the main parameter for its toxicity [87].

17.5.3.3 Copper nanoparticles

Copper nanoparticles are one of the good choices for membrane synthesis. But there is a lack of information of its effect on the human body. Copper become toxic when it is consumed in excess quantity by living things [88]. The liver and kidney are easy targets of copper nanoparticles if they are orally consumed. Gastrointestinal tract is also affected due to copper nanoparticles [89]. But copper is used in industry on a large scale, thus it is important to conduct toxicological research on this topic.

17.6 Conclusions

In this chapter, we have reviewed the types of conventional and nanomaterial-based membranes, mechanisms, and challenges in nanomaterial-based membranes. Interfacial polymerization is an important and most used method to synthesize nanomaterial-based membranes. The sol-gel method is avoided due to the poor dispersion quality of nanomaterials. Graphene and carbon nanoparticles are promising nanomaterials for nanofiltration applications. There are many challenges ahead in membrane applications like less durability due to fouling and bacterial growth on the membrane. This leads to less permeability and ultimately less membrane efficiency. We also emphasized the toxicity potential of materials used for membrane synthesis, which needs to be improved.

References

[1] M.M. Pendergast, E.M. Hoek, A review of water treatment membrane nanotechnologies, Energ. Environ. Sci. 4 (6) (2011) 1946–1971.
[2] P. Wu, Y. Xu, Z. Huang, J. Zhang, A review of preparation techniques of porous ceramic membranes, J. Ceram. Process. Res. 16 (1) (2015) 102–106.
[3] T. Tsuru, Nano/subnano-tuning of porous ceramic membranes for molecular separation, J. Sol-Gel Sci. Technol. 46 (3) (2008) 349–361.
[4] S. Sonawane, P. Thakur, R. Paul, Study on thermal property enhancement of MWCNT based polypropylene (PP) nanocomposites, Mater. Today Proc. 27 (Part 1) (2020) 550–555.

This book belongs to Badji Mokhtar Annaba University Central Library Copyright Elsevier 2025

[5] K.P. Ramaiah, K. Mishra, A. Atkar, S. Sridhar, Pervaporation separation of chlorinated environmental pollutants from aqueous solutions by castor oil based composite interpenetrating network membranes, Chem. Eng. J. 387 (2020) 124050.
[6] L. Huang, M. Zhang, C. Li, G. Shi, Graphene-based membranes for molecular separation, J. Phys. Chem. Lett. 6 (14) (2015) 2806–2815.
[7] G. Liu, W. Jin, N. Xu, Two-dimensional-material membranes: a new family of high-performance separation membranes, Angew. Chem. Int. Ed. 55 (43) (2016) 13384–13397.
[8] X. Wang, B.S. Hsiao, Electrospun nanofiber membranes, Curr. Opin. Chem. Eng. 12 (2016) 62–81.
[9] G. Liu, W. Jin, N. Xu, Graphene-based membranes, Chem. Soc. Rev. 44 (15) (2015) 5016–5030.
[10] M.S. Oak, T. Kobayashi, H.Y. Wang, T. Fukaya, N. Fujii, pH effect on molecular size exclusion of polyacrylonitrile ultrafiltration membranes having carboxylic acid groups, J. Membr. Sci. 123 (2) (1997) 185–195.
[11] T.Y. Chiu, A.E. James, Effects of axial baffles in non-circular multi-channel ceramic membranes using the organic feed, Sep. Purif. Technol. 51 (3) (2006) 233–239.
[12] T. Tsuru, Inorganic porous membranes for liquid phase separation, Sep. Purif. Methods 30 (2) (2001) 191–220.
[13] Z. Song, M. Fathizadeh, Y. Huang, K.H. Chu, Y. Yoon, L. Wang, M. Yu, TiO_2 nanofiltration membranes prepared by molecular layer deposition for water purification, J. Membr. Sci. 510 (2016) 72–78.
[14] M. He, K. Gao, L. Zhou, Z. Jiao, M. Wu, J. Cao, Z. Jiang, Zwitterionic materials for antifouling membrane surface construction, Acta Biomater. 40 (2016) 142–152.
[15] J. Kim, B. Van der Bruggen, The use of nanoparticles in polymeric and ceramic membrane structures: review of manufacturing procedures and performance improvement for water treatment, Environ. Pollut. 158 (7) (2010) 2335–2349.
[16] Y. Ying, Y. Yang, W. Ying, X. Peng, Two-dimensional materials for novel liquid separation membranes, Nanotechnology 27 (33) (2016) 332001.
[17] H. Huang, Y. Ying, X. Peng, Graphene oxide nanosheet: an emerging star material for novel separation membranes, J. Mater. Chem. A 2 (34) (2014) 13772–13782.
[18] J. Narr, T. Viraraghavan, Y. Jin, Applications of nanotechnology in water/wastewater treatment: a review, Fresen. Environ. Bull. 16 (4) (2007) 320–329.
[19] M. Baghbanzadeh, D. Rana, C.Q. Lan, T. Matsuura, Effects of inorganic nano-additives on properties and performance of polymeric membranes in water treatment, Sep. Purif. Rev. 45 (2) (2016) 141–167.
[20] Y. Ying, W. Ying, Q. Li, D. Meng, G. Ren, R. Yan, X. Peng, Recent advances of nanomaterial-based membrane for water purification, Appl. Mater. Today 7 (2017) 144–158.
[21] J. He, X.M. Lin, H. Chan, L. Vukovic, P. Král, H.M. Jaeger, Diffusion and filtration properties of self-assembled gold nanocrystal membranes, Nano Lett. 11 (6) (2011) 2430–2435.
[22] S.Y. Lee, H.J. Kim, R. Patel, S.J. Im, J.H. Kim, B.R. Min, Silver nanoparticles immobilized on thin-film composite polyamide membrane: characterization, nanofiltration, antifouling properties, Polym. Adv. Technol. 18 (7) (2007) 562–568.
[23] E.S. Kim, B. Deng, Fabrication of polyamide thin-film nanocomposite (PA-TFN) membrane with hydrophilized ordered mesoporous carbon (H-OMC) for water purifications, J. Membr. Sci. 375 (1–2) (2011) 46–54.
[24] C. Kong, T. Kamada, T. Shintani, M. Kanezashi, T. Yoshioka, T. Tsuru, Enhanced performance of inorganic-polyamide nanocomposite membranes prepared by metal-alkoxide-assisted interfacial polymerization, J. Membr. Sci. 366 (1–2) (2011) 382–388.
[25] F.Y. Zhao, Q.F. An, Y.L. Ji, C.J. Gao, A novel type of polyelectrolyte complex/MWCNT hybrid nanofiltration membranes for water softening, J. Membr. Sci. 492 (2015) 412–421.
[26] N. Wang, S. Ji, G. Zhang, J. Li, L. Wang, Self-assembly of graphene oxide and polyelectrolyte complex nanohybrid membranes for nanofiltration and pervaporation, Chem. Eng. J. 213 (2012) 318–329.
[27] P. Daraei, S.S. Madaeni, E. Salehi, N. Ghaemi, H.S. Ghari, M.A. Khadivi, E. Rostami, Novel thin-film composite membrane fabricated by mixed matrix nanoclay/chitosan on PVDF microfiltration support: preparation, characterization and performance in dye removal, J. Membr. Sci. 436 (2013) 97–108.

This book belongs to Badji Mokhtar Annaba University Central Library Copyright Elsevier 2025

[28] L.X. Dong, X.C. Huang, Z. Wang, Z. Yang, X.M. Wang, C.Y. Tang, A thin-film nanocomposite nanofiltration membrane prepared on support with in situ embedded zeolite nanoparticles, Sep. Purif. Technol. 166 (2016) 230–239.
[29] N. Cini, T. Tulun, G. Decher, V. Ball, Step-by-step assembly of self-patterning polyelectrolyte films violating (almost) all rules of layer-by-layer deposition, J. Am. Chem. Soc. 132 (24) (2010) 8264–8265.
[30] P.S. Goh, B.C. Ng, W.J. Lau, A.F. Ismail, Inorganic nanomaterials in polymeric ultrafiltration membranes for water treatment, Sep. Purif. Rev. 44 (3) (2015) 216–249.
[31] M. Hu, B. Mi, Enabling graphene oxide nanosheets as water separation membranes, Environ. Sci. Technol. 47 (8) (2013) 3715–3723.
[32] G.N.B. Baroña, M. Choi, B. Jung, High permeate flux of PVA/PSf thin film composite nanofiltration membrane with aluminosilicate single-walled nanotubes, J. Colloid Interface Sci. 386 (1) (2012) 189–197.
[33] M.L. Luo, J.Q. Zhao, W. Tang, C.S. Pu, Hydrophilic modification of poly (ether sulfone) ultrafiltration membrane surface by self-assembly of TiO_2 nanoparticles, Appl. Surf. Sci. 249 (1–4) (2005) 76–84.
[34] S. Roy, S.A. Ntim, S. Mitra, K.K. Sirkar, Facile fabrication of superior nanofiltration membranes from interfacially polymerized CNT-polymer composites, J. Membr. Sci. 375 (1–2) (2011) 81–87.
[35] S. Rangou, K. Buhr, V. Filiz, J.I. Clodt, B. Lademann, J. Hahn, A. Jung, V. Abetz, Self-organized isoporous membranes with tailored pore sizes, J. Membr. Sci. 451 (2014) 266–275.
[36] S. Loeb, S. Sourirajan, Sea water demineralization by means of an osmotic membrane, in: Saline Water Conversion—II, vol. 38, 1963, pp. 117–132.
[37] S.P. Nunes, R. Sougrat, B. Hooghan, D.H. Anjum, A.R. Behzad, L. Zhao, K.V. Peinemann, Ultraporous films with uniform nanochannels by block copolymer micelles assembly, Macromolecules 43 (19) (2010) 8079–8085.
[38] G.T. Caneba, D.S. Soong, Polymer membrane formation through the thermal-inversion process. 1. Experimental study of membrane structure formation, Macromolecules 18 (12) (1985) 2538–2545.
[39] J.M. Gohil, R.R. Choudhury, Introduction to nanostructured and nano-enhanced polymeric membranes: preparation, function, and application for water purification, in: Nanoscale Materials in Water Purification, Elsevier, 2019, pp. 25–57.
[40] H. Wu, B. Tang, P. Wu, MWNTs/polyester thin film nanocomposite membrane: an approach to overcome the trade-off effect between permeability and selectivity, J. Phys. Chem. C 114 (39) (2010) 16395–16400.
[41] A. Tiraferri, C.D. Vecitis, M. Elimelech, Covalent binding of single-walled carbon nanotubes to polyamide membranes for antimicrobial surface properties, ACS Appl. Mater. Interfaces 3 (8) (2011) 2869–2877.
[42] L. Yan, Y.S. Li, C.B. Xiang, S. Xianda, Effect of nano-sized Al_2O_3-particle addition on PVDF ultrafiltration membrane performance, J. Membr. Sci. 276 (1–2) (2006) 162–167.
[43] Y. Shimazaki, M. Mitsuishi, S. Ito, M. Yamamoto, Preparation of the layer-by-layer deposited ultrathin film based on the charge-transfer interaction, Langmuir 13 (6) (1997) 1385–1387.
[44] T.H. Bae, I.C. Kim, T.M. Tak, Preparation and characterization of fouling-resistant TiO_2 self-assembled nanocomposite membranes, J. Membr. Sci. 275 (1–2) (2006) 1–5.
[45] A. Isogai, T. Saito, H. Fukuzumi, TEMPO-oxidized cellulose nanofibers, Nanoscale 3 (1) (2011) 71–85.
[46] Q. Zhang, X. Fan, H. Wang, S. Chen, X. Quan, Fabrication of Au/CNT hollow fiber membrane for 4-nitrophenol reduction, RSC Adv. 6 (2016) 41114–41121.
[47] N.L. Le, P.H.H. Duong, S.P. Nunes, Advanced polymeric and organic-inorganic membranes for pressure driven processes, in: Reference Module in Chemistry, Molecular Sciences and Chemical Engineering, Elsevier, Amsterdam, Netherlands, 2017.
[48] H. Wu, B. Tang, P. Wu, Optimizing polyamide thin film composite membrane covalently bonded with modified mesoporous silica nanoparticles, J. Membr. Sci. 428 (2013) 341–348.
[49] E.S. Kim, G. Hwang, M.G. El-Din, Y. Liu, Development of nanosilver and multi-walled carbon nanotubes thin-film nanocomposite membrane for enhanced water treatment, J. Membr. Sci. 394 (2012) 37–48.
[50] K. Goh, H.E. Karahan, L. Wei, T.-H. Bae, A.G. Fane, R. Wang, et al., Carbon nanomaterials for advancing separation membranes: a strategic perspective, Carbon 109 (2016) 694–710.
[51] S. Liu, T.H. Zeng, M. Hofmann, E. Burcombe, J. Wei, R. Jiang, et al., Antibacterial the activity of graphite, graphite oxide, graphene oxide, and reduced graphene oxide: membrane and oxidative stress, ACS Nano 5 (9) (2011) 6971–6980.

This book belongs to Badji Mokhtar Annaba University Central Library Copyright Elsevier 2025

[52] D. Hu, Z.L. Xu, Y.M. Wei, High-performance silica–fluoropolyamide nanofiltration membrane prepared by interfacial polymerization, Sep. Purif. Technol. 110 (2013) 31–38.
[53] B. Rajaeian, A. Rahimpour, M.O. Tade, S. Liu, Fabrication and characterization of polyamide thin-film nanocomposite (TFN) nanofiltration membrane impregnated with TiO_2 nanoparticles, Desalination 313 (2013) 176–188.
[54] G. Arthanareeswaran, T.S. Devi, M. Raajenthiren, Effect of silica particles on cellulose acetate blend ultrafiltration membranes: part I, Sep. Purif. Technol. 64 (1) (2008) 38–47.
[55] F. Liu, M.M. Abed, K. Li, Preparation and characterization of poly (vinylidene fluoride) (PVDF) based ultrafiltration membranes using nano γ-Al_2O_3, J. Membr. Sci. 366 (1–2) (2011) 97–103.
[56] M. Wasim, A. Sabir, M. Shafiq, A. Islam, T. Jamil, Preparation and characterization of composite membrane via layer by layer assembly for desalination, Appl. Surf. Sci. 396 (2017) 259–268.
[57] S.H. Tabatabaei, P.J. Carreau, A. Ajji, Microporous membranes obtained from polypropylene blend films by stretching, J. Membr. Sci. 325 (2) (2008) 772–782.
[58] P. Wang, P. Huang, N. Xu, J. Shi, Y.S. Lin, Effects of sintering on properties of alumina microfiltration membranes, J. Membr. Sci. 155 (2) (1999) 309–314.
[59] Y. Komaki, Growth of fine holes by the chemical etching of fission tracks in polyvinylidene fluoride, Nucl. Tracks 3 (1–2) (1979) 33–44.
[60] J. Doshi, D.H. Reneker, Electrospinning process and applications of electrospun fibers, in: Conference Record of the 1993 IEEE Industry Applications Conference Twenty-Eighth IAS Annual Meeting, IEEE, 1993, pp. 1698–1703.
[61] W.S. Tan, C.K. Chua, T.H. Chong, A.G. Fane, A. Jia, 3D printing by selective laser sintering of polypropylene feed channel spacers for spiral wound membrane modules for the water industry, Virtual Phys. Prototyp. 11 (3) (2016) 151–158.
[62] N.A. Kotov, Layer-by-layer self-assembly: the contribution of hydrophobic interactions, Nanostruct. Mater. 12 (5–8) (1999) 789–796.
[63] J.A. Prince, S. Bhuvana, V. Anbharasi, N. Ayyanar, K.V.K. Boodhoo, G. Singh, Ultrawetting graphene-based PES ultrafiltration membrane-a novel approach for successful oil-water separation, Water Res. 103 (2016) 311–318.
[64] I.M. Wienk, R.M. Boom, M.A.M. Beerlage, A.M.W. Bulte, C.A. Smolders, H. Strathmann, Recent advances in the formation of phase inversion membranes made from amorphous or semi-crystalline polymers, J. Membr. Sci. 113 (2) (1996) 361–371.
[65] J.J. Richardson, M. Björnmalm, F. Caruso, Technology-driven layer-by-layer assembly of nanofilms, Science 348 (6233) (2015) aaa2491.
[66] H. Strathmann, K. Kock, The formation mechanism of phase inversion membranes, Desalination 21 (3) (1977) 241–255.
[67] X. Zhao, R. Zhang, Y. Liu, M. He, Y. Su, C. Gao, Z. Jiang, Antifouling membrane surface construction: chemistry plays a critical role, J. Membr. Sci. 551 (2018) 145–171.
[68] J. Gibbard, Public health aspects of the treatment of water and beverages with silver, Am. J. Public Health Nations Health 27 (2) (1937) 112–119.
[69] P. Thakur, S.S. Sonawane, S.H. Sonawane, B.A. Bhanvase, Nanofluids-based delivery system, encapsulation of nanoparticles for stability to make stable nanofluids, in: Encapsulation of Active Molecules and Their Delivery System, Elsevier, 2020, p. 141.
[70] D.Y. Zhang, J. Liu, Y.S. Shi, Y. Wang, H.F. Liu, Q.L. Hu, J. Zhu, Antifouling polyimide membrane with surface-bound silver particles, J. Membr. Sci. 516 (2016) 83–93.
[71] Y. Li, H. Mao, H. Zhang, G. Yang, R. Ding, J. Wang, Tuning the microstructure and permeation property of thin-film nanocomposite membrane by functionalized inorganic nanospheres for solvent resistant nanofiltration, Sep. Purif. Technol. 165 (2016) 60–70.
[72] A. Kubacka, M.S. Diez, D. Rojo, R. Bargiela, S. Ciordia, I. Zapico, M. Ferrer, Understanding the antimicrobial mechanism of TiO_2-based nanocomposite films in a pathogenic bacterium, Sci. Rep. 4 (2014) 4134.

This book belongs to Badji Mokhtar Annaba University Central Library Copyright Elsevier 2025

[73] S. Remanan, M. Sharma, S. Bose, N.C. Das, Recent advances in preparation of porous polymeric membranes by unique techniques and mitigation of fouling through surface modification, ChemistrySelect 3 (2) (2018) 609–633.
[74] A. Razmjou, J. Mansouri, V. Chen, The effects of mechanical and chemical modification of TiO_2 nanoparticles on the surface chemistry, structure and fouling performance of PES ultrafiltration membranes, J. Membr. Sci. 378 (1–2) (2011) 73–84.
[75] M. Ben-Sasson, X. Lu, S. Nejati, H. Jaramillo, M. Elimelech, In situ surface functionalization of reverse osmosis membranes with biocidal copper nanoparticles, Desalination 388 (2016) 1–8.
[76] Y.J. Jo, E.Y. Choi, N.W. Choi, C.K. Kim, Antibacterial and hydrophilic characteristics of poly (ether sulfone) composite membranes containing zinc oxide nanoparticles grafted with hydrophilic polymers, Ind. Eng. Chem. Res. 55 (28) (2016) 7801–7809.
[77] Y. Tu, M. Lv, P. Xiu, T. Huynh, M. Zhang, M. Castelli, R. Zhou, Destructive extraction of phospholipids from *Escherichia coli* membranes by graphene nanosheets, Nat. Nanotechnol. 8 (8) (2013) 594.
[78] L.Y. Ng, A.W. Mohammad, C.P. Leo, N. Hilal, Polymeric membranes incorporated with metal/metal oxide nanoparticles: a comprehensive review, Desalination 308 (2013) 15–33.
[79] V.K. Poon, A. Burd, In vitro cytotoxity of silver: implication for clinical wound care, Burns 30 (2) (2004) 140–147.
[80] G. Oberdörster, Z. Sharp, V. Atudorei, A. Elder, R. Gelein, W. Kreyling, C. Cox, Translocation of inhaled ultrafine particles to the brain, Inhal. Toxicol. 16 (6–7) (2004) 437–445.
[81] T.K. Barik, B. Sahu, V. Swain, Nanosilica—from medicine to pest control, Parasitol. Res. 103 (2) (2008) 253.
[82] F. Wang, F. Gao, M. Lan, H. Yuan, Y. Huang, J. Liu, Oxidative stress contributes to silica nanoparticle-induced cytotoxicity in human embryonic kidney cells, Toxicol. In Vitro 23 (5) (2009) 808–815.
[83] M.L. Schipper, N. Nakayama-Ratchford, C.R. Davis, N.W.S. Kam, P. Chu, Z. Liu, S.S. Gambhir, A pilot toxicology study of single-walled carbon nanotubes in a small sample of mice, Nat. Nanotechnol. 3 (4) (2008) 216.
[84] D.B. Warheit, B.R. Laurence, K.L. Reed, D.H. Roach, G.A. Reynolds, T.R. Webb, Comparative pulmonary toxicity assessment of single-wall carbon nanotubes in rats, Toxicol. Sci. 77 (1) (2004) 117–125.
[85] D.Y. Lyon, P.J. Alvarez, Fullerene water suspension (nC60) exerts antibacterial effects via ROS-independent protein oxidation, Environ. Sci. Technol. 42 (21) (2008) 8127–8132.
[86] A. Dhawan, J.S. Taurozzi, A.K. Pandey, W. Shan, S.M. Miller, S.A. Hashsham, V.V. Tarabara, Stable colloidal dispersions of C60 fullerenes in water: evidence for genotoxicity, Environ. Sci. Technol. 40 (23) (2006) 7394–7401.
[87] K.T. Kim, M.H. Jang, J.Y. Kim, S.D. Kim, Effect of preparation methods on toxicity of fullerene water suspensions to Japanese medaka embryos, Sci. Total Environ. 408 (22) (2010) 5606–5612.
[88] I. Bremner, Manifestations of copper excess, Am. J. Clin. Nutr. 67 (5) (1998) 1069S–1073S.
[89] D.R. Winge, R.K. Mehra, Host defenses against copper toxicity, in: International Review of Experimental Pathology, vol. 31, Academic Press, 1990, pp. 47–83.

This book belongs to Badji Mokhtar Annaba University Central Library Copyright Elsevier 2025

This page intentionally left blank

This book belongs to Badji Mokhtar Annaba University Central Library

Copyright Elsevier 2025

CHAPTER 18

Carbon-based nanocomposite membranes for water purification

Swapnil L. Sonawane[a], Prakash K. Labhane[b], and Gunvant H. Sonawane[c]

[a]Department of Chemistry, JET's Zulal Bhilajirao Patil College, Dhule, Maharashtra, India, [b]Department of Chemistry, MGSM's Arts, Science and Commerce College, Chopda, Maharashtra, India, [c]Chemistry Research Laboratory, Kisan Arts Commerce and Science College, Parola, Maharashtra, India

18.1 Introduction to nanomaterials

Clean and safe water plays a vital role in human health and the ecosystem; however, the 785 million people around the world are having difficulties accessing basic drinking water service, as reported by the World Health Organization (WHO) (https://www.who.int/news-room/fact-sheets/detail/drinking-water). Though natural water sources are available, the scarcity and poor water quality is an issue in many parts of the world. The sudden increase in population and industrial growth is responsible for the world's water pollution. Basically, there are different types of impurities present in water, which include hybrid pollutants (organic-inorganic) and microorganisms [1, 2]. Since contaminated water introduces harmful disease that can cause illness or even death, it is an alarming concern worldwide. Therefore new development in advanced technology for water purification (treatment of wastewater/desalination/recycle/reuse/recovery) is in high demand [3, 4]. This would help to overcome the 21st century challenge for obtaining fresh and safe water (for beneficial use) and to save the natural resources of water on the earth.

A suitable material with high durability, inexpensive, high porosity, high separation capacity, and reusability are the basic requirements for obtaining fresh/safe water [5, 6]. With respect to this, nanotechnology offers an excellent platform where an advanced nanomaterial having required properties (flexibility, high mechanical/thermal strength, stability, high adsorption capacity, etc.) can be developed [7, 8]. Nanomaterials (nanoparticles such as metal oxide, graphene, CNTs, TiO_2, zeolites, etc.) in the form of various shapes/size (1–100 nm) and morphology are available for sustainable development (Fig. 18.1). With applications in the fields of medicine, antibacterial properties, redox and photocatalytic properties, energy storage, adsorption, sensing/detection of pollutant, filler in membrane, etc., nanomaterials can also address environmental problems such as purification of water and wastewater treatment [9–11].

Handbook of Nanomaterials for Wastewater Treatment. https://doi.org/10.1016/B978-0-12-821496-1.00036-2
Copyright © 2021 Elsevier Inc. All rights reserved.

This book belongs to Badji Mokhtar Annaba University Central Library Copyright Elsevier 2025

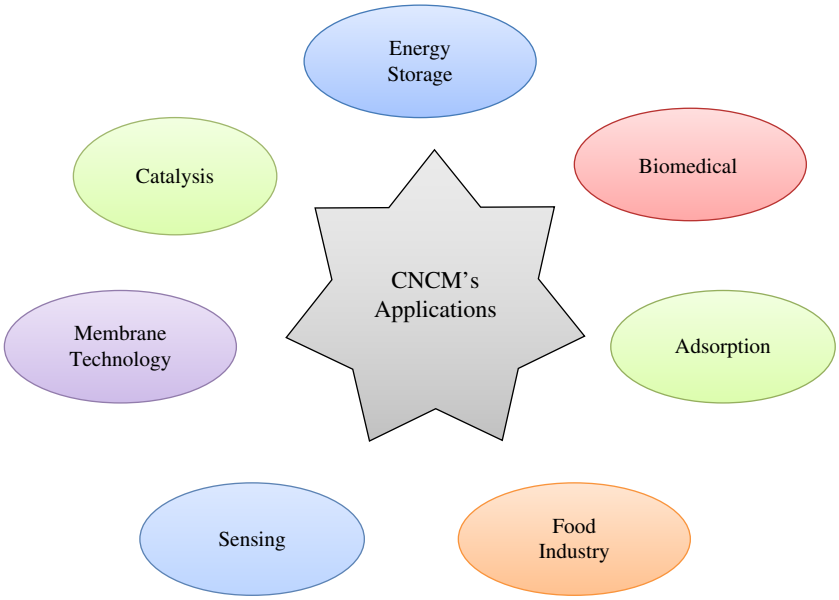

Fig. 18.1
Applications of carbon-based nanocomposite materials (CNCMs).

Membrane technology (using polymer or ceramic material) is one of the most structured fields and has potential applications in pressure-driven water separation and purification [12–14], for example, reverse osmosis (RO) that uses desalination of saline water to get freshwater, ultrafiltration (UF), microfiltration (MF), nanofiltration (NF), and membrane distillation (MD) that allows certain-size (micropollutants) particles. However, the cost, stability, and operational issues remain challenging [14]. On the other hand, forward osmosis (FO) and pressure-retarded osmosis (PRO) are nonpressure-driven membranes that show low fouling capacity, whereas low permeation limits its utility [15]. However, in the last few years, the field for utilization of composite material (incorporating/mixing/combining two different materials) for technology development has grown, where attention is being given to carbon-based materials [16].

Carbon-based nanomaterial, because of its one-dimensional tubular or two-dimensional graphene sheet, has outstanding properties that draw attention in several fields such as carbon material or in the form of composite material [17, 18]. As depicted in Fig. 18.2, carbon-based material such as carbon nanotubes (CNTs); for example, single-walled carbon NTs (SWCNT), multiwalled carbon NTs (MWCNT), and carbon nanofibers (CNF)) is the allotropes of tetravalent carbon having sp^2-hybridized two-dimensional arrangements (graphite) [19, 20].

The individual stacking of CNTs on each other is due to the pi-pi stacking and Van der Waals forces among them. Carbon-based material is stable (biologically, chemically, physically,

This book belongs to Badji Mokhtar Annaba University Central Library Copyright Elsevier 2025

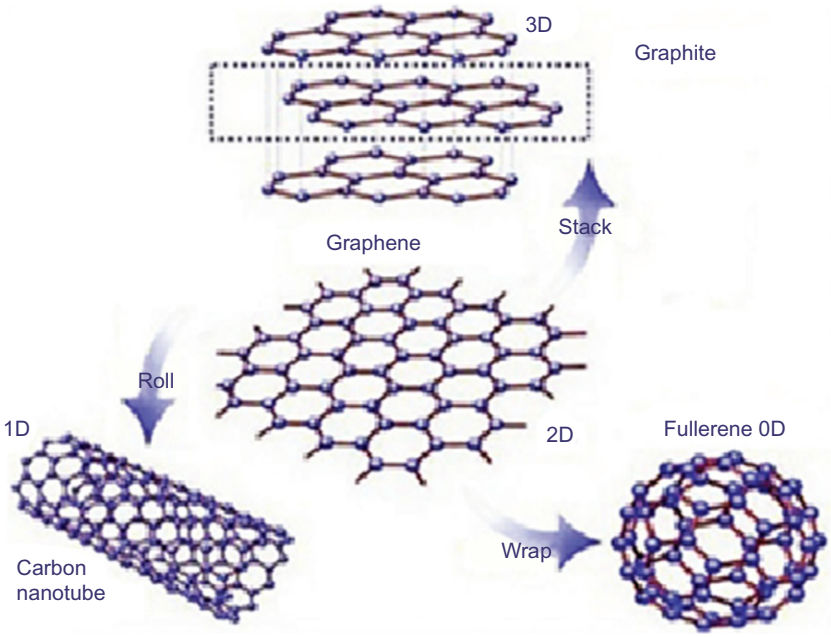

Fig. 18.2
Graphene at different stages: roll, stack, wrap [20]. *Reprinted with permission from X. Wan, Y. Huang, Y. Chen, Focusing on energy and optoelectronic applications: a journey for graphene and graphene oxide at large scale, Acc. Chem. Res. 45 (2012) 598–607. Copyright (2012) American Chemical Society.*

thermally, and mechanically) and has excellent water permeability; therefore, it is being extensively used in fabrication of membranes (directly or as a filler for improving the performance of material) for water treatment (purification/filtration/desalination/etc.) [21–24]. Labhane et al. developed the reduced graphene oxide (rGO)-decorated ZnO nanoparticles composite as a photocatalytic material for dye degradation under UV light [25]. In fact, as an antibacterial agent, carbon-based materials [CNT, graphene, graphene oxide (GO)] have great potential to inhibit the growth of bacteria by direct contact using nanosheets as reported by Liu et al. [26]. In this chapter, we present the exploitation of carbon-based nanocomposite material in the field of membrane technology for water treatment, water purification, desalination, removal of (organic/hybrid) impurities, etc.

18.2 Carbon-based nanocomposite materials (CNCMs) (polymer/hybrid)

CNTs, due to their low density, ease of functionalization, large surface area, good adsorption property, and mechanical strength, prompt the use of this material for many applications in advancing science and technology [21, 25]. However, the hydrophobic nature limits the utility

This book belongs to Badji Mokhtar Annaba University Central Library Copyright Elsevier 2025

of CNTs, particularly in membrane science. For example, the uniform distribution of CNTs in the membrane/matrix is quite challenging, as CNTs stack with each other and form agglomerated assembly [27, 28]. To overcome this problem, tuning the properties of CNTs by functionalization or cross-linking approach is the best method [29]. The functionalization of CNT offers a suitable interaction between matrixes, which ultimately improves not only the properties but also the performance of the resulting membrane, which is applicable in water purification and wastewater treatment [30]. Generally when the nanomaterial/nanoparticle is introduced/mixed with macroscopic or matrix material, the resulting clay/film/material is called a nanocomposite material [31]. High performance polymer membranes could be developed by combining polymers with carbon-based material. Polymer nanocomposite membrane was developed via layer-by-layer GO coating on aromatic polymer surface where the chemically inert nature of the GO layer played the role of chlorine barrier, and membrane degradation in salt was rejected [32]. Recently, it has been shown that the field of 3D printing technology (additive manufacturing) is driving innovation in the separation science. However, the fabrication cost and scalability issue are challenging tasks [33].

18.3 Development and synthesis of carbon-based nanocomposite material

The next section deals with the development of carbon-based nanocomposite material and their synthesis methods.

18.3.1 Solution mixing

The solution mixing is a simple method, frequently used for the preparation of carbon-based polymer nanocomposites. This method involves the sonication, shear mixing, or stirring of carbon material and a polymeric matrix in a suitable solvent. After proper mixing in a suitable solvent, the resulting solution can be evaporated or precipitated [34]. Faraguna et al. [35] have recently reported a solution mixing method for the preparation of polystyrene nanocomposites with functionalized CNTs. In this report, two-step procedures were adopted for solution mixing. In the first step, separately functionalized CNTs and masterbatch powder (DPS) both were added into previously prepared 30 g of a 0.1 wt% polystyrene solution in toluene. The dispersion was obtained by ultrasonic fingers (60% amplitude, 400 W, 2 min, Hielscher). The second step was completed by mixing the dispersed solution of CNTs with 30 g of 35 wt% solution of polystyrene with a Turax homogenizer (9500 rpm, 2 min). After the complete homogenization of samples, it was transferred into a Petri dish followed by vacuum drying at 130°C for 1 h and then at 80°C for overnight, respectively. Furthermore, Sun et al. [36] prepared polystyrene (PS)/MWNTs nanocomposite in an organic solvent (toluene) aided by the Gemini surfactant via solution mixing method.

This book belongs to Badji Mokhtar Annaba University Central Library Copyright Elsevier 2025

18.3.2 Chemical vapor deposition

Chemical vapor deposition (CVD) is one of the most versatile and popular thin film deposition methods. Long-time CVD method has been used for CNT production; it is a medium-temperature (500–1100°C) process, different from electric arc discharge and laser vaporization. These other common methods are usually classified as short-time and high-temperature processes (>3000°C) [21].

In the CVD method, the precursors are decomposed or heated on the preselected substrate at high temperature and allowed to grow on the surface of the substrate. Furthermore, CVD has another form, viz., atomic layer deposition (ALD), which is commonly used to produce layered thin films of a material [37]. Fig. 18.3 illustrates a typical CVD on the substrate.

The CVD offers a low-cost and controlled scalable way for growing high-quality, large-area 2D materials;, therefore, it is explored for fundamental research and applications of 2D materials [40]. Likewise, CVD is frequently explored to synthesize CNTs. The advantages of CVD for the preparation of CNTs are the high yield of nanotubes, inexpensive, and required low temperature; therefore, it is more accessible for lab applications [41]. Tang et al. [42] reported

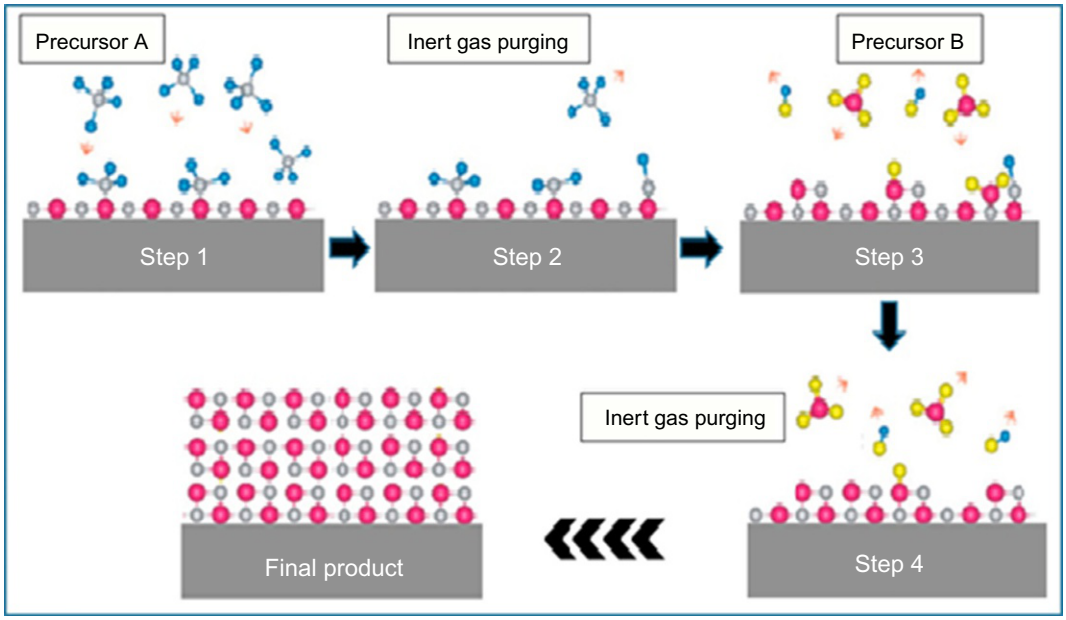

Fig. 18.3
Chemical vapor deposition process [38, 39]. *Reprinted with permission from M. Benelmekki, A. Erbe, Nanostructured thin films—background, preparation and relation to the technological revolution of the 21st century, in: Frontiers of Nanoscience, Elsevier, 2019, pp. 1–34. Copyright (2019) Elsevier; H. Kim, H.-B.-R. Lee, Applications of atomic layer deposition to nanofabrication and emerging nanodevices, Thin Solid Films 517 (2009) 2563–2580. Copyright (2009) Elsevier.*

This book belongs to Badji Mokhtar Annaba University Central Library Copyright Elsevier 2025

the preparation of MWNTs by the CVD method. The polypropylene was subjected to catalytic combustion in the presence of organically modified clay and Ni catalyst to yield MWNTs at a higher extent.

18.3.3 In situ colloidal precipitation

Ho et al. [43] presented the synthesis of polyvinylidene fluoride (PVDF) membrane by in situ colloidal precipitation method. The coagulation bath and nanoadditives, such as GO and oxidized MWCNTs (OMWCNTs), played a vital role for obtaining the PVDF membrane. In this process, a PVDF powder was dissolved in *N*,*N*-dimethylacetamide (DMAc) at 65°C with continuous mechanical stirring for 4 h using an overhead stirrer to prepare a membrane polymer solution. The complete dissolution of the polymer was ensured by additional stirring of the membrane polymer solution at 40°C for another 4 h. Furthermore, to remove trapped air bubbles, the membrane polymer solution was left overnight at room temperature. The resulting membrane polymer solution was spread on a flat nonwoven polyester membrane attached to a glass plate. To remove the residual solvent, the glass plate with the membrane film was immersed into a coagulation bath for a day. Finally, the obtained membranes were kept in ultrapure water and used for further characterization. FTIR measurement of membrane confirmed the presence of GO and OMWCNTs in the membrane matrix.

18.3.4 Polymer grafting

The cross-linked polyethylenimine (PEI)-grafted carboxylated CNT intermediate layer was reported by Soyekwo and coworkers [44]. It began with the preparation of PEI aqueous solutions with different amounts of glutaraldehyde (GA). For the fabrication of membranes, the homogeneous aqueous solution of MWCNT was filtered using a vacuum-assisted assembly technique. Then, cross-linked PEI solution (20%) was exposed to an ultrasonic bath agitation for about 15 min. Afterward, agitated cross-linked PEI solution was submersed with the MWCNT layer by flirtation with vacuum down to 0.20 bar for uniform distribution of MWCNT to obtain the cross-linked PEI-grafted MWCNT membrane.

Roy et al. [45] reported polymer grafting method for the preparation of MWCNTs matrix by ultraviolet/ozone treatment. The active surface of the material is good for promoting the polymerization; for that, the MWCNTs were exposed to UVO (UV/O_3) radiation. The UVO-treated CNTs were taken with the 2-acrylamido-2-methylpropane sulfonic acid (AMPS) monomer solution (10 wt% in water) in three-neck round-bottom flasks. To remove the moisture, the mixture was stirred followed by continuous degassing of nitrogen bubbling. The graft polymerization was carried out for 6 h with constant stirring at 70°C. To remove the homopolymer and unreacted residuals, the grafted MWCNTs were continuously washed with hot DI water, methanol, and acetone mixture, respectively. The purified poly-AMPS (PAG), grafted MWCNTs were vacuum dried overnight to remove all traces of the solvents. This

This book belongs to Badji Mokhtar Annaba University Central Library Copyright Elsevier 2025

polymer matrix was specially designed to improve the filler efficiency, strong interactions between filler–matrix, and throughout the distribution of single nanotubes in the membrane matrix.

18.3.5 In situ polymerization

In situ polymerization is a commonly used method for the synthesis of carbon-based polymer nanocomposites. In this method, the monomer and carbon precursors are initially dissolved in a common solvent. To obtain the uniform dispersion, the solution was subjected to ultrasonic treatments. An initiator was then added to the dispersed solution to induce polymerization or to obtain the desired composites having ordered layer structure [46].

In another example, MWCNTs/polyaniline (PANI)/polyethersulfone (PES) composite membranes were developed by Lee et al. [27] using in situ polymerization method. The natural organic matter present in water can be removed by this composite membrane. The preparation process involved two steps: initially, the complex between MWCNTs/PANI was formed by in situ polymerization, and then MWCNTs/PANI/PES membrane was constructed by phase inversion method. The synthesis details of nanocomposite and the fabrication process of MWCNTs/PANI/PES composite membrane are presented in Fig. 18.4a and b.

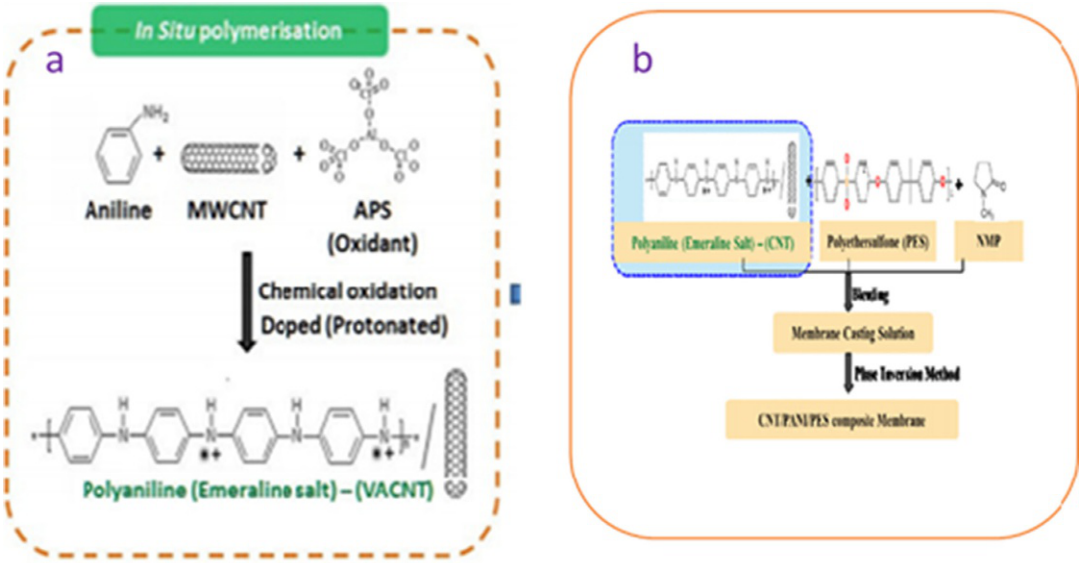

Fig. 18.4
Synthesis of (a) MWCNTs/PANI nanocomposite; (b) fabrication procedure of MWCNTs/PANI/PES composite membrane [27]. *Reprinted with permission from J. Lee, Y. Ye, A.J. Ward, C. Zhou, V. Chen, A.I. Minett, S. Lee, Z. Liu, S.-R. Chae, J. Shi, High flux and high selectivity carbon nanotube composite membranes for natural organic matter removal, Sep. Purif. Technol. 163 (2016) 109–119. Copyright (2016) Elsevier.*

This book belongs to Badji Mokhtar Annaba University Central Library Copyright Elsevier 2025

18.3.6 Phase inversion

It is a commonly used method for the multiwalled nanomembrane (MNMs) fabrication. The membrane fabrication is carried out by immersion of a homogeneous polymer/nanofiller material in a nonsolvent bath for converting a single phase into a two-phase system. Majeed et al. [47] fabricated hydroxyl-functionalized MWCNTs blended with polyacrylonitrile (PAN) for the preparation of ultrafiltration membranes via phase inversion process. The membranes casting solution consist of 14 wt% PAN, 86 wt% *N*,*N*-dimethylformamide (DMF), while the MWCNTs, used in PAN nanocomposite membranes, had 0.77 mmol/g hydroxyl-functional groups. However, the solution for nanocomposite membranes has the composition of 14 wt% PAN/MWCNTs and 86 wt% of DMF, respectively. To obtain dispersed solution, MWCNTs were taken into DMF and the resultant mixture was sonicated (sonication bath operated at 55 W) for 5 min. Furthermore, the PAN was taken into the dispersed solution and the mixture was stirred for 48 h at 70°C, which eventually converted the solution into the homogeneous phase. The resulting homogeneous solution was allowed to cool at room temperature and degassed to confirm complete removal of air bubbles before membrane casting. The polymer solution was cast with a doctor blade on the nonwoven polyester attached to a glass plate and immersed immediately into the coagulation bath containing water at 20°C. After the precipitation, the remaining solvent on the membranes was removed by keeping in water at room temperature for 24 h. Fig. 18.5a shows surface morphology and Fig. 18.5b shows cross-sectional morphology of the PAN, respectively.

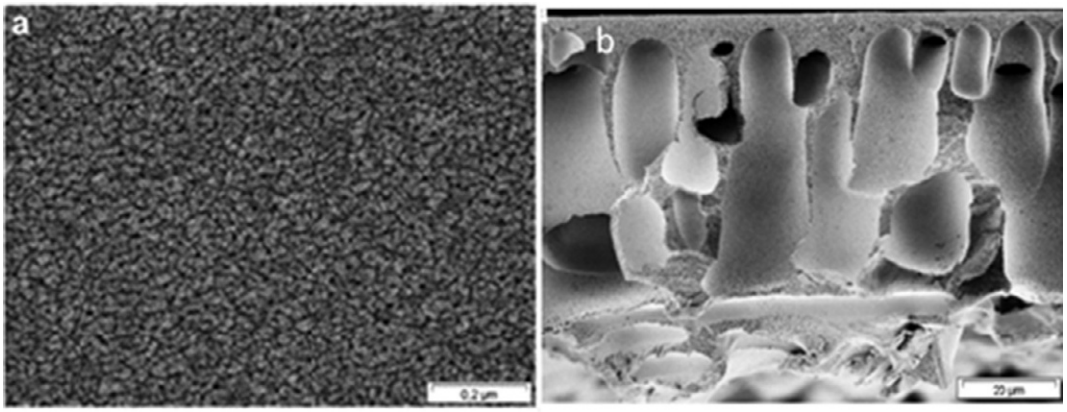

Fig. 18.5
Scanning electron microscopy (a) surface image of PAN membrane; (b) cross-section images of PAN membranes [47]. *Reprinted with permission from S. Majeed, D. Fierro, K. Buhr, J. Wind, B. Du, A. Boschetti-de-Fierro, V. Abetz, Multi-walled carbon nanotubes (MWCNTs) mixed polyacrylonitrile (PAN) ultrafiltration membranes, J. Membr. Sci. 403–404 (2012) 101–109. Copyright (2012) Elsevier.*

This book belongs to Badji Mokhtar Annaba University Central Library
Copyright Elsevier 2025

El Badawi et al. [48] discussed the phase inversion method for the preparation of MWCNT/cellulose acetate (CNT/CA) nanocomposite membranes where acetone is used as a solvent and 20 wt% deionized water as a nonsolvent, respectively. The thicknesses and morphology of membranes were determined by field emission scanning electron microscope (FESEM), while Brauner, Emett, and Teller (BET) surface area of the composites were determined by N_2 adsorption (at 77 K). It was observed that the existence of small amounts of CNTs (0.0005 and 0.005 wt%) extensively improved water permeation rates. Furthermore, at higher content (0.01 wt%) of CNT, membrane porosity and surface area were found to decrease as a result of a decrease in permeation.

Recently, Saba and coworkers [19] prepared asymmetric microporous polyether sulfone (PES)/polyvinyl alcohol-GO-sodium alginate (PVAGO-NaAlg) nanocomposite hydrogel (HG)-blended nanofiltration membranes for water purification. The nonsolvent-induced phase inversion (NIPS) method was used for the development of membranes. The obtained results significantly revealed that the presence of HG increases the hydrophilicity of the membrane, which resulted in better permeability and antifouling ability.

18.3.7 Spray-assisted layer-by-layer

Liu and coworkers [49] fabricated functionalized multiwalled CNTs (f-MWCNTs)-blended polyelectrolyte multilayers (PEMs) deposited on commercial PES membrane by spray-assisted layer-by-layer technique for water purification. Initially, the MWCNTs were functionalized in a mixture of acid (Conc HNO_3:Conc H_2SO_4). The f-MWCNTs solution was washed with DI water and filtered with 0.45-mm nylon filter to attain neutral pH of the solution followed by vacuum oven drying. Furthermore, 1 mg/mL polycation spray solution (PSS) was obtained by adding poly diallyl-dimethylammonium chloride (PDDA) into DI water, which was spiked into the f-MWCNTs solution having different weight ratio of f-MWCNTs/PSS. The spray solution was deposited by spray-assisted layer-by-layer techniques on pretreated polyether sulfone substrate (PES) mounted on a holder vertically. The number of cycles for the deposition of polyanion spray was carried out, with occasional rinse with DI water followed by drying using filtered air. Finally, the polycation spray was applied from an air pistol under 20 psi of compressed air, which resulted in the desired membrane [49].

18.4 Fabrications techniques and types of carbon-based nanocomposite membrane

Because of their unique properties, CNM have been widely used in membrane fabrication technology. However, it is important to have homogeneity, close contact, and uniform dispersion of CNC into the matrix/support used for the membrane fabrication [50, 51]. Whereas, depending on the structure, substrate, and composite involved in the membrane, the

This book belongs to Badji Mokhtar Annaba University Central Library Copyright Elsevier 2025

resulting membranes are mainly either organic (polymer) and/or inorganic composite-based membranes [47]. Also, the fabricated membrane can be classified into (a) free-standing or self-supported CNC-based membrane and (b) surface-modified composite membrane (either CNC embedded in a polymer matrix). The important and regular methods for the CNMs-based membrane fabrication involves blending methods (blending of CNM with polymer material followed by stirring or sonication), CVD/CVD-template method, in situ polymerization method, layer-by-layer self-assembly method, or direct coating method and bucky paper-based approach. In fact, the alignment of CNT (alone or with the matrix) in the membrane either vertically or horizontally is also important [2, 52].

18.4.1 Carbon nanotube (CNT) membranes

Generally, spray/spin coating, vacuum filtration, and drop casting are also common methods used for the development of free-standing or self-supporting GO membranes. Self-supporting membranes of GO have more interest compared to other CNC and CNT materials. This is because the GO assembly forms a stacked layer structure due to the presence of carbonyl, hydroxyl, and epoxy functionality, which produce stable dispersion and allows for keeping a suitable distance between two GO sheets (network of nanocapillaries) and results in high permeability of water molecules. The obtained GO-based membrane has good mechanical and flexible properties [53]. For example, using the vacuum filtration techniques, GO-TiO_2 membrane was fabricated and characterized well by XRD, FE-SEM, TEM, and HR-TEM. It was found that, due to the presence of TiO_2 nanoparticles, the distance between GO sheets increased and resulted in the formation of channels for passing water [54]. Similarly, drop-casting method (2 mg/mL GO suspension) has been utilized for the fabrication of GO free-standing membrane. The GO membrane was well characterized by SEM and AFM, and it showed selective ion penetration properties. The resulting membrane is used for the nanofiltration of sodium ions, barrier separation, and water purification [51].

The well-defined free-standing composite membrane of CNT was fabricated using vacuum filtration method in which polycarbonate support was used. The films were then peeled off from the polycarbonate support by simply immersing in ethanol. According to the authors, the obtained membrane could have applications in separation science [55]. Kar et al. fabricated self-supported CNF membrane using electrospinning of polyacrylonitrile fibers. The good hydrophilicity, smooth surface, flexibility, and large surface area of the membrane resulted in high salt absorption in the desalination experiment [56].

18.4.2 CNT-polymer composite (CNT mixed-matrix membranes)

Polymers are important and effective building blocks in development of membrane technology because of their flexibility, processability, film forming ability, mechanical stability, and durability [14, 57]. For example, addition of CNM into a polymer matrix affects the structure

This book belongs to Badji Mokhtar Annaba University Central Library Copyright Elsevier 2025

and membrane properties such as flux, hydrophilicity, mechanical strength, rejection, and antimicrobial behavior [58]. The composition, having various types of CNM-based nanoparticle and polymers, showed potential applications in developing hybrid membranes for water purification [15, 59]. For example, melt mix/blending method and solvent mixing technique can be used for the development of CNT-embedded thermoplastic composite or by separate mixing of CNT and polymer in a suitable solvent. The long-time high power ultrasonication, high temperature, or shear mixing is used for better dispersion of CNT into the polymer matrix [60]. However, as compared to previous methods, in situ polymerization is one of the convenient methods for debundled or dispersion of CNTs into polymer matrix [61]. In this method, the CNT is dispersed into the monomer solution (having initiator and catalyst) before polymerization, which results in high loading of CNT into the obtained CNT/polymer matrix. The stronger interaction between polymer and CNT material is a good characteristic of this method; however, the requirement of large quantities of solvent limits its applications [60, 62]. For example, Yin et al. reported the fabrication of thin film nanocomposite of GO and polyimide by in situ interfacial polymerization process. The higher incorporation and dispersion of GO into the polymer matrix showed enhancement in membrane performance for water purification [4]. Finally, the performance of the membrane highly depends on the amount of filler material used, functionality present in the matrix or CNM material, thickness, roughness, and surface area of the formed composite material in the membrane processing for sustainable growth [12, 58].

18.5 Applications of carbon-based nanocomposite membrane for water purification

Carbon-based nanocomposite membrane technologies have been practically developed for desalination, treatment of industrial contaminates, oily wastewater, and removal of heavy metals from aqueous solution. In the next section, we will discuss the important applications of carbon-based nanocomposite membrane for water purification.

18.5.1 Removal of organic/inorganic pollutants

Removal of hybrid (organic and inorganic) pollutants from water is very important and has attracted attention worldwide [58–61]. Among the various physical and chemical methods for water treatment, membrane technologies come out as remarkable and advanced technologies [63]. The CNT's membrane is the most widely recognized next generation membrane as it offers high flux, high selectivity, and low fouling. The inner hollow cores with molecularly smooth hydrophobic graphitic walls and nanoscale pore diameters of CNTs allows for ultraefficient transport of water molecules [56].

This book belongs to Badji Mokhtar Annaba University Central Library Copyright Elsevier 2025

The major types of functional CNT membranes used are: vertically aligned CNT membranes (VACNT), horizontally aligned CNT membranes (HACNT), and mixed matrix membranes (MMMs). These membranes (VCNT, HACNT, and MMMs) are reported for the removal of heavy metals, arsenic, natural organic matters, pharmaceutical, personal care products, and inactivation of bacteria and virus. Water transport and rejection mechanisms of these membranes are demonstrated in Fig. 18.6a–c [2].

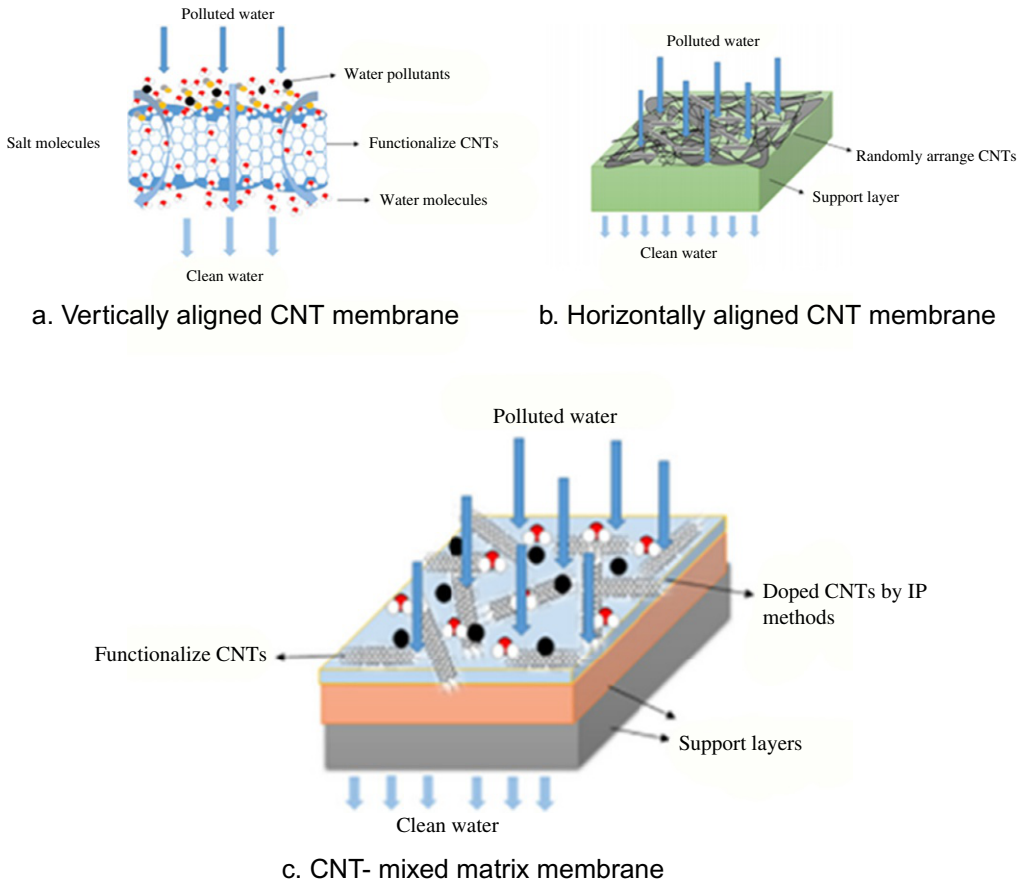

Fig. 18.6

Water transport and rejection mechanism of three major CNTs membranes with detailed depictions [2, 64]. *Reprinted with permission from R. Das, Md.E. Ali, S.B.A. Hamid, S. Ramakrishna, Z.Z. Chowdhury, Carbon nanotube membranes for water purification: A bright future in water desalination, Desalination 336 (2014) 97–109. Copyright (2014) Elsevier; S. Ali, S.A.U. Rehman, H.-Y. Luan, M.U. Farid, H. Huang, Challenges and opportunities in functional carbon nanotubes for membrane-based water treatment and desalination, Sci. Total Environ. 646 (2019) 1126–1139. Copyright (2019) Elsevier.*

This book belongs to Badji Mokhtar Annaba University Central Library
Copyright Elsevier 2025

Luan et al. [65] examined the performance of nanocomposite (Cu/CNT-polymer) materials for arsenic present in water. The top conventional polymeric membrane was deposited by Cu nanoparticles intercalating into carboxylated/hydroxylated CNTs. The Cu/CNT polymer composite membrane showed excellent ability toward the removal of arsenite from aqueous solutions at varying pH.

Further study conducted by Lee et al. [66] evaluated the various forms of CNTs for water treatment applications. Their results demonstrate that CNT's membrane effectively obstruct bacterial adhesion and resist biofilm formation.

Recently, Si and coauthors [67] reported the mechanically strong, flexible superhydrophobic with high-strength electroconductive stainless steel CNT (SS-CNT) membrane for electrochemical water treatment. The membranes showed greater robustness and high stability for long-term water filtration process. The authors further claimed that electrochemically conducting SS-CNT membrane could be extended to other possible applications such as membrane evaporation and adsorption for the effective treatment of various organic pollutants including pharmaceutical and personal care products, antibiotics, endocrine disrupting compounds in water, etc.

Liu et al. [68] fabricated the robust, antifouling polyethyleneimine (PEI)-trimesoyl chloride (TMC)-CNTs nanohybrid membranes. It showed super-strong mechanical strength, high water permeation, and underwater superoleophobicity for oil/water separation. The amino groups present in PEI along with carboxyl groups resulting from hydrolysis of acyl chloride in TMC have the ability to bind large amounts of water molecules. The precise stacking of CNTs resulted in the formation of a robust hydration layer with the hierarchical nanostructure. The underwater adhesion force of oil on the membrane surface was very low.

Recently, Tofighy and Mohammadi [69] synthesized a new positively charged membrane carbon nanomaterial (CNN) from charcoal and hyperbranched polyethyleneimine (HPEI), a cross-linking agent. The performance of the cross-linked membrane was evaluated for the removal of divalent heavy metal ions present in contaminated water. The report showed that the CNM-HPEI cross-linked membrane with positively charged surface has excellent potential for the removal of divalent heavy metal ions (Zn^{2+}, Cd^{2+}, Cu^{2+}, Ni^{2+}, and Pb^{2+}) from aqueous solutions with a rejection greater than 90%. The synergy of steric hindrance and Donnan electrostatic exclusion could have a major effect on the high rejection rate of divalent heavy metal ions.

Peydayesh et al. [70] prepared the positively charged hybrid PES membranes with incorporation of triethylenetetramine (TETA)-functionalized MWCNT (TETA-MWCNT). The resulting membranes were evaluated for the separation of cationic (Crystal violet and Rhodamine B) and anionic dye (Orange G and Indigo carmine) by filtration of aqueous solutions. Eq. (18.1) was used to calculate the capacity of membrane in the rejection of solutes.

This book belongs to Badji Mokhtar Annaba University Central Library Copyright Elsevier 2025

$$R = \left(1 - \frac{C_p}{C_f}\right) \times 100 \tag{18.1}$$

where C_p and C_f are permeate and feed concentrations. To evaluate the dye separation performance of the membranes, feed aqueous solutions of NaCl, Na_2SO_4, $MgSO_4$, and $MgCl_2$ salts were used. This report confirms excellent ability of the membranes for the removal of both cationic and anionic dye with high rejection rate and could be useful in the textile industry for dye treatment [70].

In another study, poly (vinylidene fluoride)/polyaniline/MWCNT nanocomposite ultrafiltration membranes were prepared for the removal of natural organic matter [71]. The obtained membrane showed good electrostatic interaction and exhibited high rejection of humic acid (a model organic matter used for the study).

Furthermore, many reports have been published on functionalized graphene-polymer composite membranes [72, 73]. The work revealed that the functionalized graphene-polymer membrane has great potential for water treatment with enhanced water for permeability, antifouling, solute rejection ability, chlorine resistance, and mechanical stability [74]. Recently, Kang et al. [75] prepared GO/polyamide (GO-PA) composite nanofiltration membrane for the rejection of salts via spin-assisted interfacial polymerization strategy. The pure water permeation of GO-PA membrane was reported to be high with more than 90% rejection rate for Na_2SO_4. In addition, the GO-PA membrane displayed a high selectivity between divalent and monovalent ions with excellent stability.

Wang and coworkers [76] developed a high permeable CNT-rGO composite membrane for purification of contaminated water. The structure of CNT-rGO composite membranes vary with preparation conditions. For example, the ultrasonic treatment that is generally used for mixing and dispersion greatly affects the structure of CNT/rGO membrane. For example, the mixed and separate sonication of CNT and rGO produce different structures of membrane. Fig. 18.7 shows that membrane 1 is for mixed sonication and membrane 2 is for separate sonication, respectively.

The formation of packed and flat layered structure of rGO on the substrate membrane may be due to uneven dispersion (membrane 1). The resultant structure (membrane 1) has smaller porosity with a longer permeation channel for water molecules. On the other hand, the even intercalation of CNTs in the rGO layer prevented layer-by-layer deposition of rGO flakes on the substrate membrane and leads to the formation of bent rGO layer. The resultant structure (membrane 2) has increased interflake space, enabling passing of water molecules through the composite layer. Therefore, the permeability of membrane 2 is higher than membrane 1. Even dispersion of CNTs into rGO flakes resulted in higher membrane permeability, good antifouling property, and removal efficiency for pharmaceuticals and personal care products.

This book belongs to Badji Mokhtar Annaba University Central Library Copyright Elsevier 2025

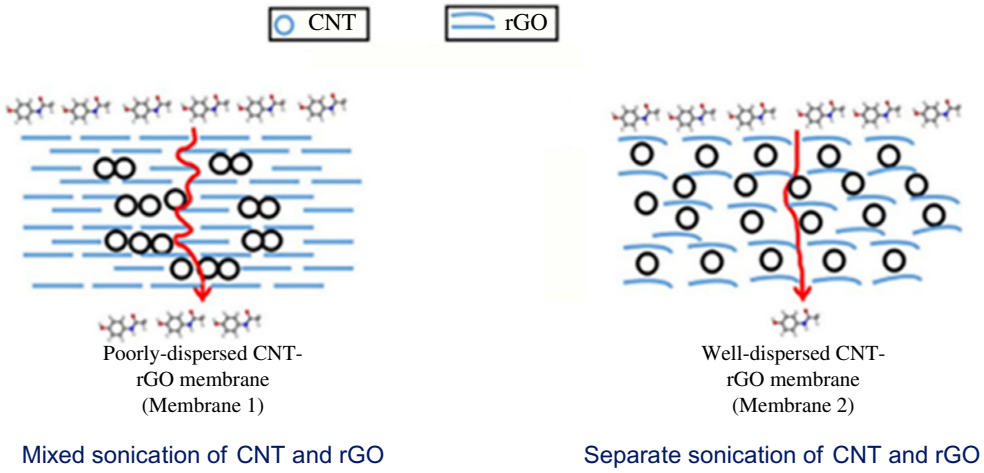

Fig. 18.7
Theoretical diagrams of the rGO-CNT composite membranes for water permeation and filtration of pharmaceuticals and personal care products [76]. *Reprinted with permission from Y. Wang, Y. Liu, Y. Yu, H. Huang, Influence of CNT-rGO composite structures on their permeability and selectivity for membrane water treatment, J. Membr. Sci. 551 (2018) 326–332. Copyright (2018) Elsevier.*

18.6 Conclusion

No doubt that carbon-based nanomaterials are potential candidates for advanced development in membrane technology. This chapter is aimed to summarize and highlight the recent development in carbon-based nanocomposite membranes for water purification. These membranes have an excellent potential for the removal of heavy metals, arsenic, natural organic matters, pharmaceuticals, personal care products, and inactivation of bacteria and virus from wastewater. Additionally, these membranes have the ability to treat oily wastewater. The various methods were reported for the modification, commercial, and economical production of carbon-based nanocomposite membranes. Even though the outstanding properties of carbon-based material alone shows their potential application in the field of water purification, the problem of uniform dispersion, complete contact, alignment of carbon-based material, fabrication of membrane on a large scale, high cost, and durability with suitable stability are challenging tasks, and to address these issues fundamental as well and applied work is needed in this field.

Among various carbon-based composite membranes, the functionalized/cross-linked CNT-based polymer composites membrane has unique advantages for water treatment. However, the high mechanical stabilities, superior water permeability, antifouling, solute rejection ability, and good ion resistance are worthwhile for further improvement of these membranes. Also, the

This book belongs to Badji Mokhtar Annaba University Central Library Copyright Elsevier 2025

functionalization of carbon-based material is limited to specific matrix/polymers; therefore, more focus should be given in the development of such material. Furthermore, for electrochemical water treatment, carbon-based stainless-steel membranes have greater robustness and stability for long-term water filtration processes. Recent progress in 3D printing technology for membrane fabrication is a good initiative for new development in membrane science, and more research should be conducted.

Membrane technology is an emerging field; however, the current problems and challenges regarding the membrane stability, high permeation flux, separation performance, industrial scale development, commercial approach of membrane fabrication, reusability, long-term stability, and practical applications of membrane should be considered, and further research should be investigated.

References

[1] Y. Wang, J. Zhu, H. Huang, H.-H. Cho, Carbon nanotube composite membranes for microfiltration of pharmaceuticals and personal care products: capabilities and potential mechanisms, J. Membr. Sci. 479 (2015) 165–174, https://doi.org/10.1016/j.memsci.2015.01.034.

[2] S. Ali, S.A.U. Rehman, H.-Y. Luan, M.U. Farid, H. Huang, Challenges and opportunities in functional carbon nanotubes for membrane-based water treatment and desalination, Sci. Total Environ. 646 (2019) 1126–1139, https://doi.org/10.1016/j.scitotenv.2018.07.348.

[3] M. Elimelech, W.A. Phillip, The future of seawater desalination: energy, technology, and the environment, Science 333 (2011) 712–717, https://doi.org/10.1126/science.1200488.

[4] J. Yin, B. Deng, Polymer-matrix nanocomposite membranes for water treatment, J. Membr. Sci. 479 (2015) 256–275, https://doi.org/10.1016/j.memsci.2014.11.019.

[5] S. Qiu, L. Wu, X. Pan, L. Zhang, H. Chen, C. Gao, Preparation and properties of functionalized carbon nanotube/PSF blend ultrafiltration membranes, J. Membr. Sci. 342 (2009) 165–172, https://doi.org/10.1016/j.memsci.2009.06.041.

[6] J. Lee, S. Jeong, Z. Liu, Progress and challenges of carbon nanotube membrane in water treatment, Crit. Rev. Environ. Sci. Technol. 46 (2016) 999–1046, https://doi.org/10.1080/10643389.2016.1191894.

[7] P.H.C. Camargo, K.G. Satyanarayana, F. Wypych, Nanocomposites: synthesis, structure, properties and new application opportunities, Mater. Res. 12 (2009) 1–39, https://doi.org/10.1590/S1516-14392009000100002.

[8] A. Nagar, T. Pradeep, Clean water through nanotechnology: needs, gaps, and fulfillment, ACS Nano 14 (2020) 6420–6435, https://doi.org/10.1021/acsnano.9b01730.

[9] B. Bethi, S.H. Sonawane, B.A. Bhanvase, S.P. Gumfekar, Nanomaterials-based advanced oxidation processes for wastewater treatment: a review, Chem. Eng. Process. Process Intensif. 109 (2016) 178–189, https://doi.org/10.1016/j.cep.2016.08.016.

[10] B.A. Bhanvase, T.P. Shende, S.H. Sonawane, A review on graphene–TiO_2 and doped graphene–TiO_2 nanocomposite photocatalyst for water and wastewater treatment, Environ. Technol. Rev. 6 (2017) 1–14, https://doi.org/10.1080/21622515.2016.1264489.

[11] M. Ates, A.A. Eker, B. Eker, Carbon nanotube-based nanocomposites and their applications, J. Adhes. Sci. Technol. 31 (2017) 1977–1997, https://doi.org/10.1080/01694243.2017.1295625.

[12] M.G. Buonomenna, Membrane processes for a sustainable industrial growth, RSC Adv. 3 (2013) 5694, https://doi.org/10.1039/c2ra22580h.

[13] M. Padaki, R. Surya Murali, M.S. Abdullah, N. Misdan, A. Moslehyani, M.A. Kassim, N. Hilal, A. F. Ismail, Membrane technology enhancement in oil–water separation. A review, Desalination 357 (2015) 197–207, https://doi.org/10.1016/j.desal.2014.11.023.

This book belongs to Badji Mokhtar Annaba University Central Library Copyright Elsevier 2025

[14] S.P. Nunes, P.Z. Culfaz-Emecen, G.Z. Ramon, T. Visser, G.H. Koops, W. Jin, M. Ulbricht, Thinking the future of membranes: perspectives for advanced and new membrane materials and manufacturing processes, J. Membr. Sci. 598 (2020) 117761, https://doi.org/10.1016/j.memsci.2019.117761.
[15] A. Lee, J.W. Elam, S.B. Darling, Membrane materials for water purification: design, development, and application, Environ. Sci.: Water Res. Technol. 2 (2016) 17–42, https://doi.org/10.1039/C5EW00159E.
[16] A.M. Díez-Pascual, Carbon-based polymer nanocomposites for high-performance applications, Polymers 12 (2020) 872, https://doi.org/10.3390/polym12040872.
[17] S. Hong, C. Constans, M.V. Surmani Martins, Y.C. Seow, J.A. Guevara Carrió, S. Garaj, Scalable graphene-based membranes for ionic sieving with ultrahigh charge selectivity, Nano Lett. 17 (2017) 728–732, https://doi.org/10.1021/acs.nanolett.6b03837.
[18] S. Noamani, S. Niroomand, M. Rastgar, M. Sadrzadeh, Carbon-based polymer nanocomposite membranes for oily wastewater treatment, Npj Clean Water 2 (2019) 20, https://doi.org/10.1038/s41545-019-0044-z.
[19] N. Saba, M. Jawaid, H. Fouad, O.Y. Alothman, Nanocarbon: preparation, properties, and applications, in: Nanocarbon and its Composites, Elsevier, 2019, pp. 327–354, https://doi.org/10.1016/B978-0-08-102509-3.00009-2.
[20] X. Wan, Y. Huang, Y. Chen, Focusing on energy and optoelectronic applications: a journey for graphene and graphene oxide at large scale, Acc. Chem. Res. 45 (2012) 598–607, https://doi.org/10.1021/ar200229q.
[21] C.N.R. Rao, A. Govindaraj, Carbon nanotubes, in: Nanoscience and Nanotechnology Series, second ed., Royal Society of Chemistry, Cambridge, 2011, pp. 1–242, https://doi.org/10.1039/9781849732840-00001 (Chapter 1).
[22] M.H.-O. Rashid, S.F. Ralph, Carbon nanotube membranes: synthesis, properties, and future filtration applications, Nanomaterials 7 (2017) 99, https://doi.org/10.3390/nano7050099.
[23] B. Sarkar, S. Mandal, Y.F. Tsang, P. Kumar, K.-H. Kim, Y.S. Ok, Designer carbon nanotubes for contaminant removal in water and wastewater: a critical review, Sci. Total Environ. 612 (2018) 561–581, https://doi.org/10.1016/j.scitotenv.2017.08.132.
[24] A. Kommu, J.K. Singh, A review on graphene-based materials for removal of toxic pollutants from wastewater, Soft Mater. (2020) 1–26, https://doi.org/10.1080/1539445X.2020.1739710.
[25] P.K. Labhane, L.B. Patle, V.R. Huse, G.H. Sonawane, S.H. Sonawane, Synthesis of reduced graphene oxide sheets decorated by zinc oxide nanoparticles: crystallographic, optical, morphological and photocatalytic study, Chem. Phys. Lett. 661 (2016) 13–19, https://doi.org/10.1016/j.cplett.2016.08.041.
[26] S. Liu, T.H. Zeng, M. Hofmann, E. Burcombe, J. Wei, R. Jiang, J. Kong, Y. Chen, Antibacterial activity of graphite, graphite oxide, graphene oxide, and reduced graphene oxide: membrane and oxidative stress, ACS Nano 5 (2011) 6971–6980, https://doi.org/10.1021/nn202451x.
[27] J. Lee, Y. Ye, A.J. Ward, C. Zhou, V. Chen, A.I. Minett, S. Lee, Z. Liu, S.-R. Chae, J. Shi, High flux and high selectivity carbon nanotube composite membranes for natural organic matter removal, Sep. Purif. Technol. 163 (2016) 109–119, https://doi.org/10.1016/j.seppur.2016.02.032.
[28] Z. Wang, F. He, J. Guo, S. Peng, X.Q. Cheng, Y. Zhang, E. Drioli, A. Figoli, Y. Li, L. Shao, The stability of a graphene oxide (GO) nanofiltration (NF) membrane in an aqueous environment: progress and challenges, Mater. Adv. 1 (2020) 554–568, https://doi.org/10.1039/D0MA00191K.
[29] S.F. Anis, R. Hashaikeh, N. Hilal, Functional materials in desalination: a review, Desalination 468 (2019) 114077, https://doi.org/10.1016/j.desal.2019.114077.
[30] M. Sianipar, S.H. Kim, K. Khoiruddin, F. Iskandar, I.G. Wenten, Functionalized carbon nanotube (CNT) membrane: progress and challenges, RSC Adv. 7 (2017) 51175–51198, https://doi.org/10.1039/C7RA08570B.
[31] H.D. Beyene, T.G. Ambaye, Application of sustainable nanocomposites for water purification process, in: Inamuddin, S. Thomas, R.K. Mishra, A.M. Asiri (Eds.), Sustainable Polymer Composites and Nanocomposites, Springer International Publishing, Cham, 2019, pp. 387–412, https://doi.org/10.1007/978-3-030-05399-4_14.
[32] W. Choi, J. Choi, J. Bang, J.-H. Lee, Layer-by-layer assembly of graphene oxide nanosheets on polyamide membranes for durable reverse-osmosis applications, ACS Appl. Mater. Interfaces 5 (2013) 12510–12519, https://doi.org/10.1021/am403790s.

This book belongs to Badji Mokhtar Annaba University Central Library Copyright Elsevier 2025

[33] L.D. Tijing, J.R.C. Dizon, I. Ibrahim, A.R.N. Nisay, H.K. Shon, R.C. Advincula, 3D printing for membrane separation, desalination and water treatment, Appl. Mater. Today 18 (2020) 100486, https://doi.org/10.1016/j.apmt.2019.100486.
[34] P.-C. Ma, N.A. Siddiqui, G. Marom, J.-K. Kim, Dispersion and functionalization of carbon nanotubes for polymer-based nanocomposites: a review, Compos. A: Appl. Sci. Manuf. 41 (2010) 1345–1367, https://doi.org/10.1016/j.compositesa.2010.07.003.
[35] F. Faraguna, P. Pötschke, J. Pionteck, Preparation of polystyrene nanocomposites with functionalized carbon nanotubes by melt and solution mixing: investigation of dispersion, melt rheology, electrical and thermal properties, Polymer 132 (2017) 325–341, https://doi.org/10.1016/j.polymer.2017.11.014.
[36] X.-Y. Sun, F.-J. Zhang, C. Kong, Porous g-C_3N_4/WO_3 photocatalyst prepared by simple calcination for efficient hydrogen generation under visible light, Colloids Surf. A: Physicochem. Eng. Asp. 594 (2020) 124653, https://doi.org/10.1016/j.colsurfa.2020.124653.
[37] A.A. Iqbal, N. Sakib, A.K.M.P. Iqbal, D.M. Nuruzzaman, Graphene-based nanocomposites and their fabrication, mechanical properties and applications, Materialia 12 (2020) 100815, https://doi.org/10.1016/j.mtla.2020.100815.
[38] M. Benelmekki, A. Erbe, Nanostructured thin films—background, preparation and relation to the technological revolution of the 21st century, in: Frontiers of Nanoscience, Elsevier, 2019, pp. 1–34, https://doi.org/10.1016/B978-0-08-102572-7.00001-5.
[39] H. Kim, H.-B.-R. Lee, Applications of atomic layer deposition to nanofabrication and emerging nanodevices, Thin Solid Films 517 (2009) 2563–2580.
[40] Z. Cai, B. Liu, X. Zou, H.-M. Cheng, Chemical vapor deposition growth and applications of two-dimensional materials and their heterostructures, Chem. Rev. 118 (2018) 6091–6133, https://doi.org/10.1021/acs.chemrev.7b00536.
[41] Y. Manawi, Ihsanullah, A. Samara, T. Al-Ansari, M. Atieh, A review of carbon nanomaterials' synthesis via the chemical vapor deposition (CVD) method, Materials 11 (2018) 822, https://doi.org/10.3390/ma11050822.
[42] T. Tang, X. Chen, X. Meng, H. Chen, Y. Ding, Synthesis of multiwalled carbon nanotubes by catalytic combustion of polypropylene, Angew. Chem. Int. Ed. 44 (2005) 1517–1520, https://doi.org/10.1002/anie.200461506.
[43] K.C. Ho, Y.H. Teow, W.L. Ang, A.W. Mohammad, Novel GO/OMWCNTs mixed-matrix membrane with enhanced antifouling property for palm oil mill effluent treatment, Sep. Purif. Technol. 177 (2017) 337–349, https://doi.org/10.1016/j.seppur.2017.01.014.
[44] F. Soyekwo, Q. Zhang, R. Gao, Y. Qu, R. Lv, M. Chen, A. Zhu, Q. Liu, Metal in situ surface functionalization of polymer-grafted-carbon nanotube composite membranes for fast efficient nanofiltration, J. Mater. Chem. A 5 (2017) 583–592, https://doi.org/10.1039/C6TA07567C.
[45] S. Roy, T. Das, Y. Ming, X. Chen, C.Y. Yue, X. Hu, Specific functionalization and polymer grafting on multiwalled carbon nanotubes to fabricate advanced nylon 12 composites, J. Mater. Chem. A 2 (2014) 3961, https://doi.org/10.1039/c3ta14528j.
[46] W.K. Chee, H.N. Lim, N.M. Huang, I. Harrison, Nanocomposites of graphene/polymers: a review, RSC Adv. 5 (2015) 68014–68051, https://doi.org/10.1039/C5RA07989F.
[47] S. Majeed, D. Fierro, K. Buhr, J. Wind, B. Du, A. Boschetti-de-Fierro, V. Abetz, Multi-walled carbon nanotubes (MWCNTs) mixed polyacrylonitrile (PAN) ultrafiltration membranes, J. Membr. Sci. 403–404 (2012) 101–109, https://doi.org/10.1016/j.memsci.2012.02.029.
[48] N. El Badawi, A.R. Ramadan, A.M.K. Esawi, M. El-Morsi, Novel carbon nanotube–cellulose acetate nanocomposite membranes for water filtration applications, Desalination 344 (2014) 79–85, https://doi.org/10.1016/j.desal.2014.03.005.
[49] W. Liu, C. Li, Y. Ren, X. Sun, W. Pan, Y. Li, J. Wang, W. Wang, Carbon dots: surface engineering and applications, J. Mater. Chem. B 4 (2016) 5772–5788, https://doi.org/10.1039/C6TB00976J.
[50] Z.A. Karim, A. Hafeez, A.F. Ismail, The fabrication of carbon-based polymer nanocomposite, in: Carbon-Based Polymer Nanocomposites for Environmental and Energy Applications, Elsevier, 2018, pp. 3–25, https://doi.org/10.1016/B978-0-12-813574-7.00001-0.

This book belongs to Badji Mokhtar Annaba University Central Library Copyright Elsevier 2025

[51] S. Gao, D. Wang, W. Fang, J. Jin, Ultrathin membranes: a new opportunity for ultrafast and efficient separation, Adv. Mater. Technol. 5 (2020) 1901069, https://doi.org/10.1002/admt.201901069.
[52] J. Lee, Carbon nanotube-based membranes for water purification, in: Nanoscale Materials in Water Purification, Elsevier, 2019, pp. 309–331, https://doi.org/10.1016/B978-0-12-813926-4.00017-3.
[53] R.R. Nair, H.A. Wu, P.N. Jayaram, I.V. Grigorieva, A.K. Geim, Unimpeded permeation of water through helium-leak-tight graphene-based membranes, Science 335 (2012) 442–444, https://doi.org/10.1126/science.1211694.
[54] C. Xu, A. Cui, Y. Xu, X. Fu, Graphene oxide–TiO_2 composite filtration membranes and their potential application for water purification, Carbon 62 (2013) 465–471, https://doi.org/10.1016/j.carbon.2013.06.035.
[55] X. Peng, J. Jin, E.M. Ericsson, I. Ichinose, General method for ultrathin free-standing films of nanofibrous composite materials, J. Am. Chem. Soc. 129 (2007) 8625–8633, https://doi.org/10.1021/ja0718974.
[56] S. Kar, R.C. Bindal, P.K. Tewari, Carbon nanotube membranes for desalination and water purification: challenges and opportunities, Nano Today 7 (2012) 385–389, https://doi.org/10.1016/j.nantod.2012.09.002.
[57] Y. Wen, J. Yuan, X. Ma, S. Wang, Y. Liu, Polymeric nanocomposite membranes for water treatment: a review, Environ. Chem. Lett. 17 (2019) 1539–1551, https://doi.org/10.1007/s10311-019-00895-9.
[58] M.A. Silva, H.P. Felgueiras, M.T.P. de Amorim, Carbon based membranes with modified properties: thermal, morphological, mechanical and antimicrobial, Cellulose 27 (2020) 1497–1516, https://doi.org/10.1007/s10570-019-02861-8.
[59] Y. Manawi, V. Kochkodan, M.A. Hussein, M.A. Khaleel, M. Khraisheh, N. Hilal, Can carbon-based nanomaterials revolutionize membrane fabrication for water treatment and desalination?, Desalination 391 (2016) 69–88, https://doi.org/10.1016/j.desal.2016.02.015.
[60] T.K. Gupta, S. Kumar, Fabrication of carbon nanotube/polymer nanocomposites, in: Carbon Nanotube-Reinforced Polymers, Elsevier, 2018, pp. 61–81, https://doi.org/10.1016/B978-0-323-48221-9.00004-2.
[61] B.A. Bhanvase, S.H. Sonawane, Ultrasound assisted in situ emulsion polymerization for polymer nanocomposite: a review, Chem. Eng. Process. Process Intensif. 85 (2014) 86–107, https://doi.org/10.1016/j.cep.2014.08.007.
[62] J.N. Coleman, U. Khan, W.J. Blau, Y.K. Gun'ko, Small but strong: a review of the mechanical properties of carbon nanotube–polymer composites, Carbon 44 (2006) 1624–1652, https://doi.org/10.1016/j.carbon.2006.02.038.
[63] S. Yadav, H. Saleem, I. Ibrar, O. Naji, A.A. Hawari, A.A. Alanezi, S.J. Zaidi, A. Altaee, J. Zhou, Recent developments in forward osmosis membranes using carbon-based nanomaterials, Desalination 482 (2020) 114375, https://doi.org/10.1016/j.desal.2020.114375.
[64] R. Das, M.E. Ali, S.B.A. Hamid, S. Ramakrishna, Z.Z. Chowdhury, Carbon nanotube membranes for water purification: a bright future in water desalination, Desalination 336 (2014) 97–109, https://doi.org/10.1016/j.desal.2013.12.026.
[65] H. Luan, B. Teychene, H. Huang, Efficient removal of As(III) by Cu nanoparticles intercalated in carbon nanotube membranes for drinking water treatment, Chem. Eng. J. 355 (2019) 341–350, https://doi.org/10.1016/j.cej.2018.08.104.
[66] B. Lee, Y. Baek, M. Lee, D.H. Jeong, H.H. Lee, J. Yoon, Y.H. Kim, A carbon nanotube wall membrane for water treatment, Nat. Commun. 6 (2015) 7109, https://doi.org/10.1038/ncomms8109.
[67] Y. Si, C. Sun, D. Li, F. Yang, C.Y. Tang, X. Quan, Y. Dong, M.D. Guiver, Flexible superhydrophobic metal-based carbon nanotube membrane for electrochemically enhanced water treatment, Environ. Sci. Technol. 54 (2020) 9074–9082, https://doi.org/10.1021/acs.est.0c01084.
[68] Y. Liu, Y. Su, J. Cao, J. Guan, L. Xu, R. Zhang, M. He, Q. Zhang, L. Fan, Z. Jiang, Synergy of the mechanical, antifouling and permeation properties of a carbon nanotube nanohybrid membrane for efficient oil/water separation, Nanoscale 9 (2017) 7508–7518, https://doi.org/10.1039/C7NR00818J.
[69] M.A. Tofighy, T. Mohammadi, Divalent heavy metal ions removal from contaminated water using positively charged membrane prepared from a new carbon nanomaterial and HPEI, Chem. Eng. J. 388 (2020) 124192, https://doi.org/10.1016/j.cej.2020.124192.

This book belongs to Badji Mokhtar Annaba University Central Library Copyright Elsevier 2025

[70] M. Peydayesh, T. Mohammadi, O. Bakhtiari, Effective treatment of dye wastewater via positively charged TETA-MWCNT/PES hybrid nanofiltration membranes, Sep. Purif. Technol. 194 (2018) 488–502, https://doi.org/10.1016/j.seppur.2017.11.070.

[71] B. Hudaib, V. Gomes, J. Shi, C. Zhou, Z. Liu, Poly (vinylidene fluoride)/polyaniline/MWCNT nanocomposite ultrafiltration membrane for natural organic matter removal, Sep. Purif. Technol. 190 (2018) 143–155, https://doi.org/10.1016/j.seppur.2017.08.026.

[72] I. Akin, E. Zor, H. Bingol, M. Ersoz, Green synthesis of reduced graphene oxide/polyaniline composite and its application for salt rejection by polysulfone-based composite membranes, J. Phys. Chem. B 118 (2014) 5707–5716, https://doi.org/10.1021/jp5025894.

[73] W.-S. Hung, S.-M. Chang, R.L.G. Lecaros, Y.-L. Ji, Q.-F. An, C.-C. Hu, K.-R. Lee, J.-Y. Lai, Fabrication of hydrothermally reduced graphene oxide/chitosan composite membranes with a lamellar structure on methanol dehydration, Carbon 117 (2017) 112–119, https://doi.org/10.1016/j.carbon.2017.02.088.

[74] X. Wang, Y. Zhao, E. Tian, J. Li, Y. Ren, Graphene oxide-based polymeric membranes for water treatment, Adv. Mater. Interfaces 5 (2018) 1701427, https://doi.org/10.1002/admi.201701427.

[75] X. Kang, X. Liu, J. Liu, Y. Wen, J. Qi, X. Li, Spin-assisted interfacial polymerization strategy for graphene oxide-polyamide composite nanofiltration membrane with high performance, Appl. Surf. Sci. 508 (2020) 145198, https://doi.org/10.1016/j.apsusc.2019.145198.

[76] Y. Wang, Y. Liu, Y. Yu, H. Huang, Influence of CNT-rGO composite structures on their permeability and selectivity for membrane water treatment, J. Membr. Sci. 551 (2018) 326–332, https://doi.org/10.1016/j.memsci.2018.01.031.

This book belongs to Badji Mokhtar Annaba University Central Library

Copyright Elsevier 2025

CHAPTER 19

Nanocomposite membranes for heavy metal removal

Saurabh P. Tembhare[a], Divya P. Barai[a], Bharat A. Bhanvase[a], and M.Y. Salunkhe[b]

[a]Chemical Engineering Department, Laxminarayan Institute of Technology, Rashtrasant Tukadoji Maharaj Nagpur University, Nagpur, Maharashtra, India, [b]Department of Physics, Institute of Science, Nagpur, Maharashtra, India

19.1 Introduction

The public health and environment are apparently in great danger because of industrial wastewater release that contains toxic heavy and transition metals and other leachate [1]. Hence there is an urgent need of sustainable and innovative wastewater treatment technologies, which are efficient, environmental friendly, and cheap. In view of this, the government regulations about the environment, especially for heavy metal concentration in water, have become stricter in various countries over the past two decades [2]. Thus there is a worldwide concern about the development of an effective wastewater treatment technique. Industrialization processes are main contributors for the release of heavy metals in the environment, resulting in the decline of quality of health [3]. Processes such as chemical precipitation [4], adsorption [5], coagulation-flocculation [6], biosorption [7], and ion exchange [8] have been used to treat wastewater containing heavy metals, but these processes have some drawbacks such as high operational costs because of the chemicals used, more time requirement, nonreusability, high pressure, and cost of handling of sludge and its disposal [7,9–12]. The membrane technology/membrane separation processes offer several advantages such as cost effectiveness, no phase change, easy fabrication, eco-friendliness, energy efficiency, high removal efficiency, and significant performance in the removal of heavy metals ions. Hence this technology has been in use since the past recent years in commercial applications [10,13,14]. Previously, polymeric membranes were widely used in membrane separation processes. But these membranes possessed disadvantages that can be overcome by incorporation of nanomaterials into them while conserving their inherent advantages [15].

Handbook of Nanomaterials for Wastewater Treatment. https://doi.org/10.1016/B978-0-12-821496-1.00017-9
Copyright © 2021 Elsevier Inc. All rights reserved.

This book belongs to Badji Mokhtar Annaba University Central Library Copyright Elsevier 2025

The incorporation of both organic and inorganic nanomaterials in membranes leads to new class of membranes, that is, nanocomposite membranes that are claimed to have enhanced the performance of the membrane in terms of hydrophilicity, thermal and chemical stability, permeability, mechanical strength, and porosity in comparison with conventional membranes as studied by many researchers [15,16]. Mixed matrix membrane is an emerging material used for various applications such as gas separation, water purification, heavy metals removals, and desalination [17–19]. Nanocomposite materials are highly specific and selective in nature, and because of their unique properties, they have diverse applications in various fields [20,21]. This is mainly because of the technological developments in the field of nanoscience that allows one to achieve controlled synthesis and fabrication of such materials. Nanocomposite materials, as the name suggests, are made up of two or more materials, either of which is in nanoscale. The nanocomposite membranes offer excellent durability, mechanical strength, and good hydraulic properties with its reusability over many cycles of operation [22]. This technique utilizes polyamide, polysulfone, polyvinyl alcohol, chitosan, polymethyl methacrylate, polyetherimide, and cellulose acetate (CA) membrane and comprise micro to nanofiltration [3,23–30]. Membranes are generally made up of polymeric materials because of their unique mechanical properties, chemistry, and tunable surface pore size [31]. Chitosan polymer has high removal capacity of proteins, dyes, and heavy metal ions because it has binding/chelating capability through hydroxyl and amino groups [32]. Polyetherimide membrane has outstanding acidic and alkaline resistance, superior film-forming ability, strong mechanical and chemical stability, and low cost [33]. Blending of polymer with additives polymer also enhances the pure water flux, hydrophilicity, and rejection of heavy metals. Gholami et al. [34] blended CA with polyvinyl chloride and reported that an increase in the concentration of CA in the membrane leads to increased pure water flux and hydrophilicity, while heavy metal ions rejection increases after a certain concentration (10% of CA). The materials used in the preparation of a membrane and the morphology of surface membrane are the two factors on which the physiochemical properties of a membrane surface depends [30]. The selection of an effective and inexpensive wastewater treatment method also depends upon the factors such as initial concentration of heavy metal, reliability/flexibility of plant, the impact on environment, and the performance of overall treatment compared with other technologies [2]. This is because of the selective nature of the membrane toward specific pollutants. Membrane technologies are also used in combination with other techniques conventionally used for heavy metals removal. Combination of adsorption and membrane filtration are mainly employed for heavy metal removal from wastewater [3,35,36]. Nanocomposite membrane acquires properties of both inorganic and organic materials, resulting in better separation characteristics such as selectivity, chemical resistance, thermal stability, permeability, and mechanical strength [37]. The performance of nanocomposite membranes depends on mainly skin layer of asymmetric membrane, while supporting layer has a little influence. The dense top skin layer carries out separation, and the porous sublayer/support layer provides mechanical strength [3]. The schematic representation of nanocomposite

This book belongs to Badji Mokhtar Annaba University Central Library Copyright Elsevier 2025

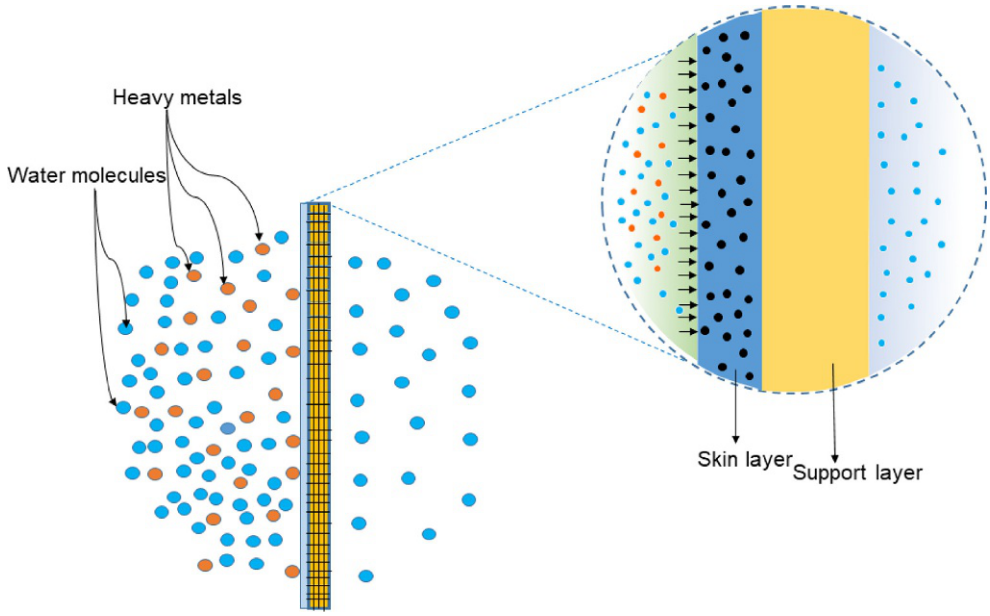

Fig. 19.1
Schematic representation of nanocomposite membrane for heavy metals removal.

membrane for heavy metals removal is shown in Fig. 19.1. In this, wastewater containing heavy metals are passed through the nanocomposite membrane having a skin layer of nanomaterials and support layer of suitable polymers. The water molecules are able to pass through the membrane, retaining the heavy metals on the membrane. Membrane separation technologies do not require additional chemicals, which is the main advantage of such processes [38]. Since the past decade, researchers have put much effort on fabricating the nanocomposite membrane possessing desired characteristics such as physical and chemical properties, permeability, and selectivity for particular applications [15].

19.2 Need of heavy metals removal

Lack of potable water is a global challenge that needs to be addressed at the earliest. The main attention is toward wastewater containing toxic heavy metals because it possesses a serious risk to human beings and environment. This is because most of them are carcinogenic in nature [31]. One of the major sources of heavy metals in the surroundings is industrial effluents that are discharged in large volumetric quantities, which can be mainly due to absence, failure, or inadequacy of conventional wastewater treatment methods to treat such wastes. Also, it is because these processes do not meet the discharge limits proposed by environmental and health organizations [39]. The retention of even trace amounts of heavy metals into natural water leads to prime health problems for humans and animals [20,40]. With the rapid development in

This book belongs to Badji Mokhtar Annaba University Central Library Copyright Elsevier 2025

commercial ventures such as paper industries, tanneries, metal plating facilities, batteries and pesticides, printing and photography, mining operations, pigment manufacturing, iron and steel production, and nonferrous metal industries, especially in developing countries, wastewater containing heavy metals indirectly or directly get released into environment. Heavy metals are not biodegradable unlike organic pollutants. Also, they are not environmentally persistent and can accumulate in living organisms, leading to various diseases. Heavy metal ions are toxic or carcinogenic in nature. Lead, zinc, arsenic (As), nickel, copper, chromium, and cadmium are heavy metals that possess harmful properties and attract immense concern in municipal and industrial wastewater treatment processes [3,9,35,41]. Microcorrosion of copper piping or fitting in the water plumbing systems are also the reasons of copper pollution in domestic drinking water [42,43].

19.3 Role of nanomaterials in wastewater treatment

Nanomaterials are specific in nature, and hence they have gained a lot of attention in water remediation in the past few decades. There are limitations offered by the existing processes for water remediation, while the use of nanomaterials-based technologies are claimed to have suppressed them, giving rise to high-performance systems. In the past few years, there is an increase in research based on nanomaterials-based adsorbents, antibacterial agents, photocatalysts, and membrane technologies as shown in Fig. 19.2 [44]. Nanoadsorbents possess small size, active surface area, and high porosity, which make them capable of removing contaminants of varying speciation behavior, hydrophobicity, and molecular size and have ample capacities to bind pollutants [45,46]. Nanoadsorbents can be also regenerated by

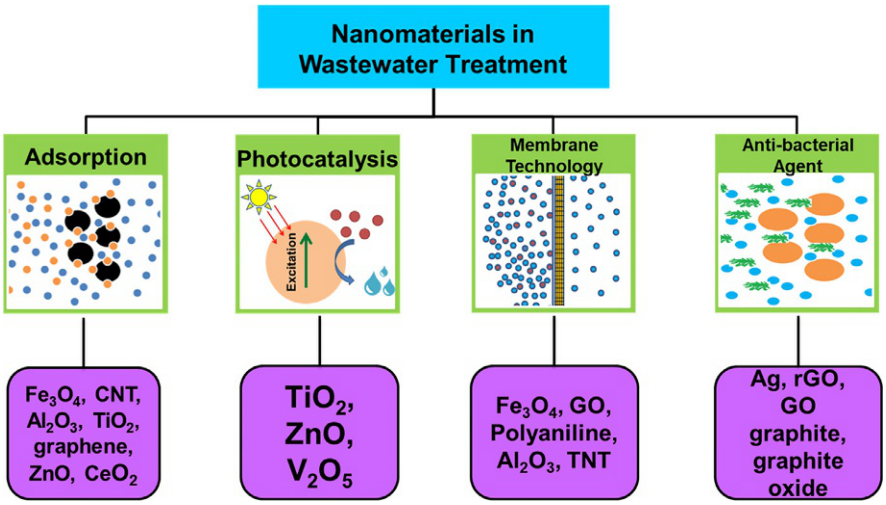

Fig. 19.2
Application of nanomaterials in wastewater treatment.

This book belongs to Badji Mokhtar Annaba University Central Library
Copyright Elsevier 2025

chemical methods after their adsorption capacity is exhausted. Because of their tiny size, they exhibit large surface to volume ratio, which enhances their adsorption capacity and imparts unique characteristics such as high reactivity and catalytic potential. These characteristics make them better adsorbing materials than traditionally used materials [47,48].

The world is facing the problem of infectious diseases caused by the microorganisms present in water. Owing to evolutionary changes, there is an increase in resistance of such microorganisms toward the existing antibiotics, and hence the use of nano-antimicrobials that can resist the activity of bacterial growth is proved to be effective [49,50]. Carbon-based nanomaterials (graphite and graphene) and silver nanocomposites showed antibacterial activity against *Escherichia coli* [44].

Various toxic organic compounds and trace contaminants are removed from wastewater using photocatalytic degradation, which works on the principle of formation and recombination of electron-hole pairs generating hydroxyl radicals (•OH), after getting exposed to ultraviolet or visible light radiation, which are responsible for degradation of organic pollutants. Such processes that involve oxidation of pollutants by reactions with generated •OH are called as advanced oxidation processes. Preferably, the semiconductor materials are used because they have good photocatalytic activity owing to lesser band gap energy [44]. The nanosized photocatalysts improve performance of photocatalysis process owing to their high specific surface area. Nanosized photocatalysts possess narrow band gap [iron oxide nanomaterials (2.2 eV) and conventional TiO_2 (3.2 eV)], which attributes to the efficient formation of electron-hole pairs [51].

Since the past decade, membrane technology has evolved as the new process for heavy metals removal from wastewater [52–55]. Usually, the membrane is made up of polymer materials, which has specific pore size responsible for separation of heavy metals ions. This is possible because heavy metals ions such as Pb^{2+} and Cd^{2+} possess a particular ionic radius. The conventional membranes are hydrophobic in nature and subject to fouling, which results in less water flux through the membrane. In addition, they also have low mechanical strength. By the incorporation of nanomaterials in such membranes, their hydrophilicity, fouling resistance, mechanical strength, porosity, membrane morphology, and swelling are enhanced. The nanomaterials responsible for enhancing these properties of membranes along with their preparation methods and role in nanocomposite membranes in removal of different heavy metals are discussed in this chapter.

19.4 Role of nanomaterials in nanocomposite membranes

Selective removal of a wide range of targeted compounds from contaminated water is possible with some nanoparticles [56]. The incorporation of nanoparticles into membrane is likely to enhance the desired properties of membrane. Fig. 19.3 shows the properties enhanced by

This book belongs to Badji Mokhtar Annaba University Central Library Copyright Elsevier 2025

Fig. 19.3
Properties enhanced by nanomaterials in nanocomposite membranes.

addition of nanomaterials in a nanocomposite membrane. The addition of nanoparticles to the membrane enhances pure water permeation when compared with pristine membrane [57]. With an increase in concentration of polyaniline from 5 to 10 wt% in membrane, pure water flux increased by 3.2%. Swelling of membrane also enhances with the increase in the concentration of nanoparticle [1]. Swelling properties are directly connected with the water content of the membrane. The swelling of pristine chitosan membrane increased from 33.91% to 37.70% by the addition of 1.25 wt% zeolite nanoparticle in it [30]. The hydrophilicity and membrane morphology in water increased with the addition of nanoparticles. Owing to this, nanoparticles obstruction diminishes the interaction between polymer and solvent molecules, and hence solvent molecules can easily diffuse from polymer matrix into coagulation bath [58,59]. The membrane hydrophilicity increased by the relocation of nanoparticles on the top surface of membrane in contrast to pristine membrane, which results in enhanced permeate flux. The membrane hydrophilicity is dependent on water contact angle. The lesser the angle of water contact, more is its hydrophilicity, which results in better water flux and separation properties [57]. The nature of membrane shifts toward hydrophilic with the addition of nanoparticles/nanocomposite materials owing to decrease in water contact angle. About 13 wt% Fe_3O_4-talc nanocomposite particles added to polysulfone membrane reduced water contact angle to

This book belongs to Badji Mokhtar Annaba University Central Library Copyright Elsevier 2025

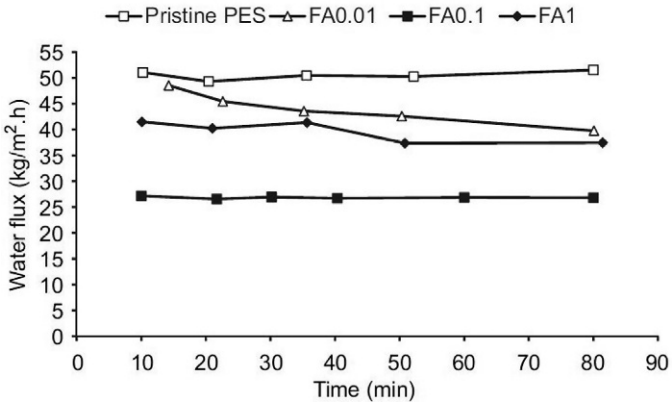

Fig. 19.4

The variation of pure water flux of membrane with time [62]. *Reprinted with permission from P. Daraei, S.S. Madaeni, N. Ghaemi, E. Salehi, M.A. Khadivi, R. Moradian, B. Astinchap, Novel polyethersulfone nanocomposite membrane prepared by PANI/Fe_3O_4 nanoparticles with enhanced performance for Cu(II) removal from water, J. Membr. Sci. 415–416 (2012) 250–259. Copyright (2012) Elsevier.*

30 degrees from 75 degrees (for pristine polysulfone membrane) [35]. About 1.25 wt% addition of zeolite nanoparticles on chitosan membrane decreased the water contact angle to 59.2 degrees when compared to pristine chitosan membrane having water contact angle 74.2 degrees [30].

The surface modification of membrane with nanomaterials results in enhanced hydrophilicity, antifouling, water uptake, and pure water flux. The surface area (BET surface area) also enhances by addition of nanoparticles on membrane [16]. The fouling in membrane is promoted by the hydrophobicity and membrane roughness. The addition of nanoparticles on membrane shows hydrophilic nature and smooth surface, which does not promote fouling, in contradiction to the conventional hydrophobic and rougher membrane [30].

The addition or incorporation of nanoparticles in membrane also improved antifouling properties [16,60]. The flux through the membrane is decided by two key factors—the porosity and hydrophilicity of membrane [61]. Fig. 19.4 shows the variation of pure water flux (PWF) with respect to time for polyether sulfone nanocomposite membrane embedded with different concentration of polyaniline/Fe_3O_4 nanoparticles [62]. The hydraulic resistance of membrane decreases with an increase in flux [3].

With an increase in concentration of polyaniline from 5 to 10 wt% in membrane, the pure water flux increased by 3.2% [1]. It has been found in a study that the permeate enhanced with an increase in transmembrane pressure for nanocomposite membrane, as shown in Fig. 19.5 [30]. The variation of flux with the concentration of nanoparticles is as shown in Fig. 19.6 [29].

The problem associated with Fe_3O_4 nanoparticles is that they oxidize and dissolve easily and also create a problem during recycling process because of their small size. Their co-aggregation

This book belongs to Badji Mokhtar Annaba University Central Library Copyright Elsevier 2025

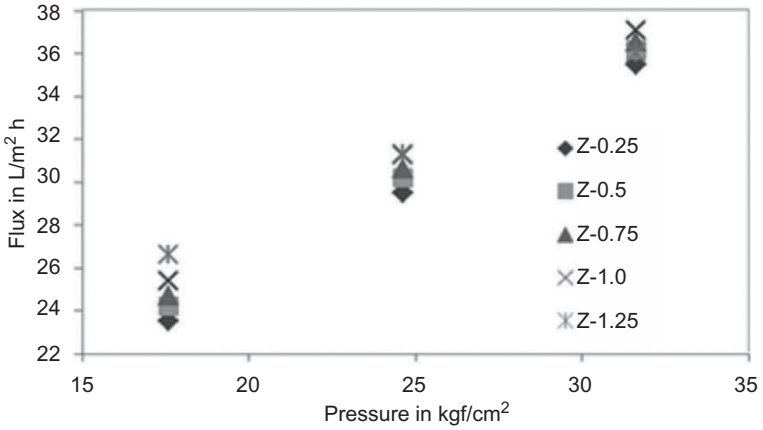

Fig. 19.5
The variation of flux with transmembrane pressure in zeolite/chitosan nanocomposite membrane [30]. *Reprinted with permission from M. Mukhopadhyay, S.R. Lakhotia, A.K. Ghosh, R.C. Bindal, Removal of arsenic from aqueous media using zeolite/chitosan nanocomposite membrane, Sep. Sci. Technol. 54 (2019) 282–288. Copyright (2019) Taylor & Francis.*

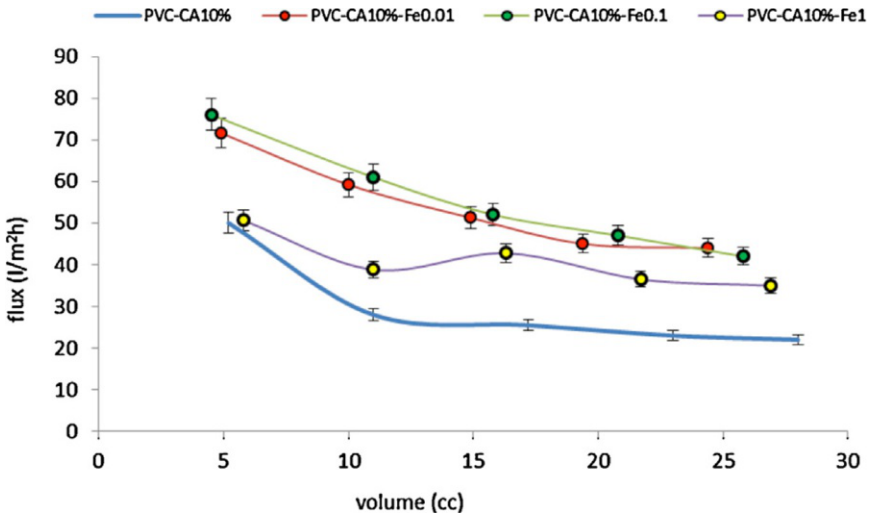

Fig. 19.6
The variation of flux with nanoparticles concentration in the PVC membrane [34]. *Reprinted with permission from A. Gholami, A.R. Moghadassi, S.M. Hosseini, S. Shabani, F. Gholami, Preparation and characterization of polyvinyl chloride based nanocomposite nanofiltration-membrane modified by iron oxide nanoparticles for lead removal from water, J. Ind. Eng. Chem. 20 (2014) 1517–1522. Copyright (2014) Elsevier.*

This book belongs to Badji Mokhtar Annaba University Central Library Copyright Elsevier 2025

also tends to reduce the effective surface area and hence the reaction reactivity [35]. Addition of nanoparticles to casting solution enhances the membrane permeability. With the addition of 13 wt% Fe_3O_4-talc to the casting solution (18 wt% polysulfone and 69 wt% *N*-methyl-2-pyrrolidone), the maximum membrane permeability was recorded to be 25 L/m^2 h for Pb solution and 29.5 L/m^2 h for Ni solution at feed pressure of 3 bar [35].

The membrane with higher porosity can be produced by the addition of nanoparticles in casting solution. In the case of Fe_3O_4 nanoparticle addition, higher porosity membranes were produced [35]. The chitosan membrane has 20.38% porosity, which increased to 45.81% owing to addition of 1.25 wt% zeolite nanoparticles in it [30]. Similar results were obtained by Hebbar et al. [3] according to which they reported an increase in porosity from 39.2% to 61.4% by addition of 4 wt% bentonite clay nanoparticles.

Accumulation of nanoparticles on the surface of membrane results in decrease of water flux of nanocomposite membrane because of pore blockage [36]. Also, due to cation hydration capacity of different metals, bigger size ions diffuse slowly and even could not pass through small size of membrane, resulting in decrease of flux. For example, copper has maximum extent of hydration than that of nickel and cadmium [3]. The porosity and skin layer thickness of prepared membrane depend on the exchange rate of solvent and nonsolvent during phase inversion method in the case of nanocomposite membrane. Hence there is less porosity in nanocomposite membrane as result of decreasing the exchange rate of nonsolvent and solvent [36]. The addition of nanoparticles also increases the thickness of skin layer [36].

The effective area of particles is reduced by the block created due to accumulation and agglomeration of nanoparticles, especially at high concentrations [34,62,63]. Gholami et al. [34] observed that water content of the membrane also increases with increase in concentration of nanoparticles up to 0.1 wt% as shown in Fig. 19.7 [29]. The mechanical strength of membrane is also affected by addition of nanoparticles as shown in Fig. 19.8.

19.5 Nanomaterials used for heavy metals removal

Various types of nanomaterials are employed to remove heavy metals from wastewater. Fe_3O_4 nanoparticles [34,35,62], graphene oxide (GO) [16,36], zeolite [30], and activated bentonite clay [3] are commonly used. The incorporation of nanomaterials in nanocomposite membrane improves the performance of membrane. A new kind of nanomaterials namely, titanate nanotubes, is used to remove As(V) from aqueous solutions impregnated in polyethersulfone/titanate nanotube nanocomposite membrane. Because of low point of zero charge, large amount of hydroxyl groups are present on the surface owing to which it has high surface area [64]. Multifunctional nanomaterials homogenized with mixed matrix membrane have been fabricated, which results in enhanced water permeability and antifouling properties [65,66]. The affinity between the polymers and the nanomaterial still exists as a problem in developing

This book belongs to Badji Mokhtar Annaba University Central Library Copyright Elsevier 2025

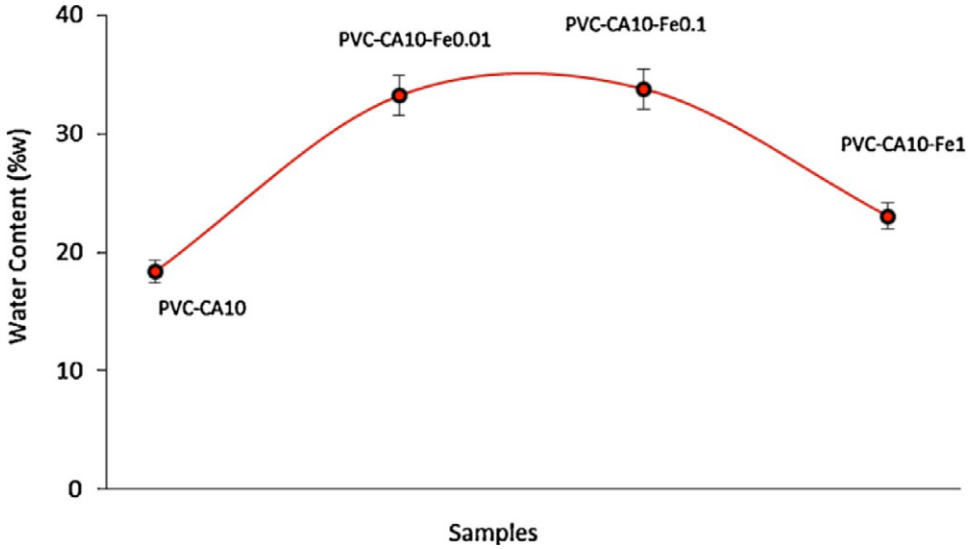

Fig. 19.7

The variation of concentration of nanoparticle in water content [34]. *Reprinted with permission from A. Gholami, A.R. Moghadassi, S. M. Hosseini, S. Shabani, F. Gholami, Preparation and characterization of polyvinyl chloride-based nanocomposite nanofiltration-membrane modified by iron oxide nanoparticles for lead removal from water, J. Ind. Eng. Chem. 20 (2014) 1517–1522. Copyright (2014) Elsevier.*

high-performance thin-film nanocomposite membranes [67]. ZnO, SiO_2, TiO_2, iron oxides, GO, and carbon nanotubes are incorporated in the fabrication of nanocomposite membranes [36]. The uniform distribution of nanoparticles in the membrane matrix is rendered by low dispersion ability and high aggregating properties of the Al_2O_3, zeolite, TiO_2, and carbon nanotubes, which otherwise enhances the performance of membrane. Microdefects are caused by the agglomeration and nonuniform distribution of nanoparticles, which inhibits membrane property enhancement [68–70].

Because of high surface area and superior properties of GO, it has gained great attention as a nanofiller. Functionalized sheets of carbon known as GO possessing epoxy, hydroxyl, and carboxyl groups can be used as membrane modifiers and membrane material [71,72]. Zeolite is an inorganic microporous crystalline nanomaterial with well-defined pore structure and unique sorption and ion exchange properties. It is extensively used in water treatment processes such as adsorption, water softening, and radioactive and heavy metals removal [73]. Owing to intrinsic adsorptive properties, versatile nature, and chemical structure because of the presence of various oxygenated functional groups, including carbonyl and carboxylic acid, epoxy, and hydroxyl on basel plane of GO nanoparticles, there is an increasing use of GO for heavy metals removal [74–77]. The surface modification of GO nanoparticles with polymerization of specific monomers such as polyaniline results in superior properties, mainly adsorption [36]. Bentonite clay nanoparticles offer great advantages in terms of physical isolation of heavy

This book belongs to Badji Mokhtar Annaba University Central Library Copyright Elsevier 2025

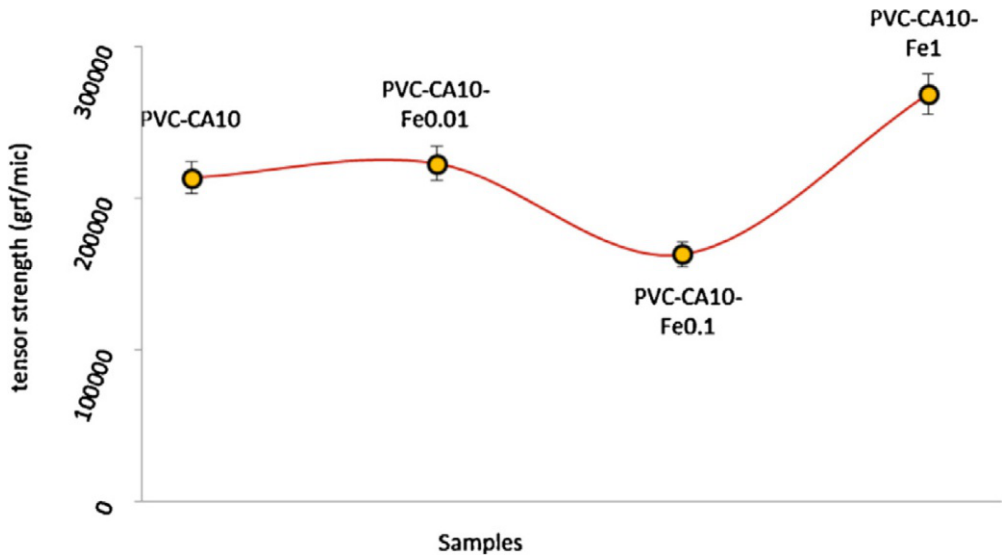

Fig. 19.8

The variation of mechanical strength with nanoparticle concentration [34]. *Reprinted with permission from A. Gholami, A. R. Moghadassi, S. M. Hosseini, S. Shabani, F. Gholami, Preparation and characterization of polyvinyl chloride-based nanocomposite nanofiltration-membrane modified by iron oxide nanoparticles for lead removal from water, J. Ind. Eng. Chem. 20 (2014) 1517–1522. Copyright (2014) Elsevier.*

metals from contaminated water. Being negatively charged, they increase the hydrophilicity and ion exchange capacity and thus heavy metals adsorption [3]. Ferric oxide nanoparticles possess features such as biocompatibility, good biodegradation, excellent chemical and thermal stability, and magnetic properties and are used to remove selective metals from aqueous systems [34].

19.6 Synthesis of nanocomposite membranes

In separation technology, the use of polymeric membranes is increasing owing to their effective, energy saving, and environmental friendly characteristics. The variety of membrane structure and properties, selectivity, pore formation control, ease of preparation, and low cost of polymer make them eligible for industrial applications [15]. Polysulfone, an amorphous material, is most popularly used in membrane fabrication because of its chemical inertness, high thermal stability, great membrane-forming properties, and high mechanical strength. But due to its hydrophobic nature, it shows major problems during treatment of wastewater and other pollutants, thus resulting into low water flux [78–80]. The incorporation of hydrophilic nanomaterials on polysulfone membrane results in higher water flux than pristine polysulfone membrane. The polysulfone membrane also results in fouling phenomenon because of

This book belongs to Badji Mokhtar Annaba University Central Library Copyright Elsevier 2025

hydrophobic property [81]. Pore size distribution is affected by the amount (%) of polysulfone in the membrane. As the polymer concentration in the membrane formulation increases, the pore size of membrane decreases [16].

19.6.1 Phase inversion method

Porous membrane with macrovoids, thin surface layer, and finger-like pores in the structure can be achieved by the instantaneous phase inversion between nonsolvent and solvent in coagulation bath, which results in large amount of heavy metal ions passing through the membrane. There is an increase in the number and size of pores with an increase in nonsolvent diffusion speed [35,82,83]. Gohil and Choudhary [84] proposed the schematic for the incorporation of nanomaterials into membrane by the phase inversion method and blending as shown in Fig. 19.9. Daraei et al. [62] used phase inversion method to prepare the nanocomposite membrane of polyethersulfone and polyaniline (PANI)/Fe_3O_4 nanoparticles in which definite quantities of polyethersufone and polyvinylpyrrolidine are allowed to dissolve in *N*,*N*-dimethylacetamide (400 rpm for 24 h). Because of magnetic nature of polyaniline (PANI)/Fe_3O_4 nanoparticles, it was first dispersed in *N*,*N*-dimethylacetamide with the assist of ultrasonication and was then put into polyethersulfone solution. The homogeneous solution obtained after the ultrasonication of this mixture containing nanoparticles diffusing into

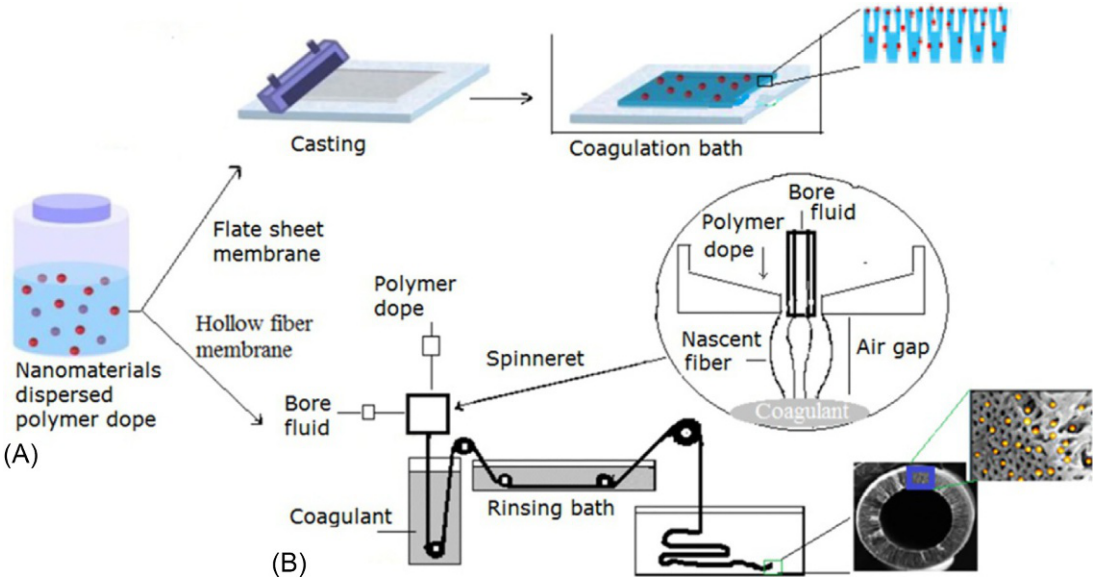

Fig. 19.9

Schematic representation of phase inversion method and blending [84]. *Reprinted with permission from J.M. Gohil, R.R. Choudhury, Introduction to Nanostructured and Nano-enhanced Polymeric Membranes: Preparation, Function, and Application for Water Purification, Elsevier Inc., 2019. Copyright (2019) Elsevier.*

This book belongs to Badji Mokhtar Annaba University Central Library Copyright Elsevier 2025

polyethersulfone solution was then casted as a film using applicator at room temperature. The incorporation of alumina nanoparticles on the polyethersulfone/polyvinylpyrrolidone matrix has been done through phase inversion method in which definite amount of alumina nanoparticles (<100 nm) were added into DMAc and were then allowed to sonicate for 15 min. The polyethersulfone and polyvinylpyrrolidone solution added to the mixture was then stirred and sonicated for 30 min. The casting of solution was done with homemade knife, and it was then dipped into distilled water at room temperature. After 24 h in distilled water, the membrane was placed between spacing of two filter papers for 24 h for drying [85]. A dry-wet phase inversion method has been used by Gohari et al. [64] to fabricate the polyethersulfone / titanate nanotubes (TNTs) nanocomposite adsorptive membranes in which the weight ratio of TNT:polyethersulfone is varied. Initially, the pore-forming agent polyvinylpyrrolidone was dissolved in *N*-methylpyrrolidinone, and then predetermined amount of TNT was added to the mixture under continuous stirring and allowed to sonicate for 12 h to prevent agglomeration of TNTs. The dried polyethersulfone pellets were added to the suspension under continuous stirring at temperature of 60°C and were then sonicated for 30 min to eliminate air bubbles. A flat sheet membrane was fabricated by casting homogeneous doped solution on to smooth, clean flat glass plate using a self-made casting knife. This was then allowed to stand for evaporation of solvent for 30 s in air of relative humidity of 70%. To induce phase inversion, a cast film was immersed in deionized water, after which the membrane was peeled off from glass plate, moved to deionized water bath, and then stored at room temperature for 3–4 days to evaporate any

Table 19.1: Summary on nanocomposite membranes prepared by phase inversion method and their applications.

S. no.	Nanocomposite membrane prepared by phase inversion method	Application/use	Removal efficiency	Reference
1	Mixed matrix membrane of polysulfone/Fe_3O_4 nanoparticle-talc	Ni^{2+} and Pb^{2+} heavy metal ion removal	96.2% for Ni^{2+} 99.4% for Pb^{2+}	[35]
2	GO nanoparticle modified with polyaniline (by in situ polymerization) embedded on polyethersulfone membrane	Pb^{2+} removal	98% for Pb^{2+}	[36]
3	Zeolite nanoparticle cross-linked with chitosan polymer	As(III)	>94% for As(III)	[30]
4	Activated bentonite clay deposited on polyetherimide membrane	Ni^{2+}, Cu^{2+}, and Cd^{2+}	76.2% for Ni^{2+} 82.5% for Cu^{2+} 69.3% for Cd^{2+}	[3]
5	Ferric oxide nanoparticle impregnated on polyvinyl chloride membrane blended with cellulose acetate	Pb^{2+}	–	[34]

This book belongs to Badji Mokhtar Annaba University Central Library
Copyright Elsevier 2025

residual solvent. Nanocomposite membranes prepared by phase inversion method along with their applications by researchers are summarized in Table 19.1.

19.6.2 Interfacial polymerization method

A thin-film nanocomposite membrane formed by interfacial polymerization (IP) showed enhanced permeance and selectivity when compared to membrane formed by phase inversion method [73,86,87]. Zhu et al. [88] used IP technique to prepare thin-film nanocomposite-modified ZIF-8 polyamide nanofilms supported on hydrolyzed polyacrylonitrile (HPAN) membrane. In brief, different amounts (0.05% w/v, 0.10% w/v, and 0.20% w/v) of modified ZIF-8 (mZIF-8) nanoparticle by poly-sodium 4-styrenesulfonate (PSS) were uniformly dispersed in piperazine monomer through sonication for 1 h. Aqueous solutions were first poured into the membrane holder supported by HPAN membrane and were allowed to contact for particle deposition, while excess solution was removed using bibulous paper and superficial drying. The HPAN membrane saturated with solution was further dipped into organic solution containing 0.2% w/v trimesoyl chloride in *n*-hexane for 1 min. After the reaction was accomplished, the organic solution was removed and further polymerized for 10 min at 70°C. The final prepared membrane was rinsed prior to use and then stored in deionized water [88].

19.7 Membranes for removal of different heavy metals from wastewater

Generally, the dead-end UF systems are used for removal of heavy metal ions in experiments using some effective membrane filtration area. The schematic of dead-end test cell is shown in Fig. 19.10 [16]. Moradihamedani et al. [35] used dead-end UF system as an experimental set up having effective surface area of 13.8 cm^2.

19.7.1 Lead

Lead (Pb) is one of the toxic heavy metals usually found in Pb^{2+} and Pb^{4+} forms in aquatic medium and is harmful even at low concentrations [89]. In ancient times, Pb was widely used because of its superior physical and chemical properties such as softness, ductility, poor conductivity, resistance to corrosion, and malleability. It is one of the nonessential metals and is mainly found naturally in environment. The presence of Pb in severe amounts in human beings can damage the kidney, reproductive system, liver, hematological and cardiovascular systems, brain capacities, central nervous system, and essential cellular procedures [31,90,91]. For treatment of lead concentrations of 100 ppm, the NaX nanoparticles incorporated in polysulfone composite membrane under the transmembrane pressure of 1 bar have been reported [39]. A 99.4% Pb rejected from 50 mg/L Pb^{2+}solution by the polysulfone membrane impregnated with 9 wt% Fe_3O_4-talc nanocomposite at feed pressure of 3 bar has been found

This book belongs to Badji Mokhtar Annaba University Central Library Copyright Elsevier 2025

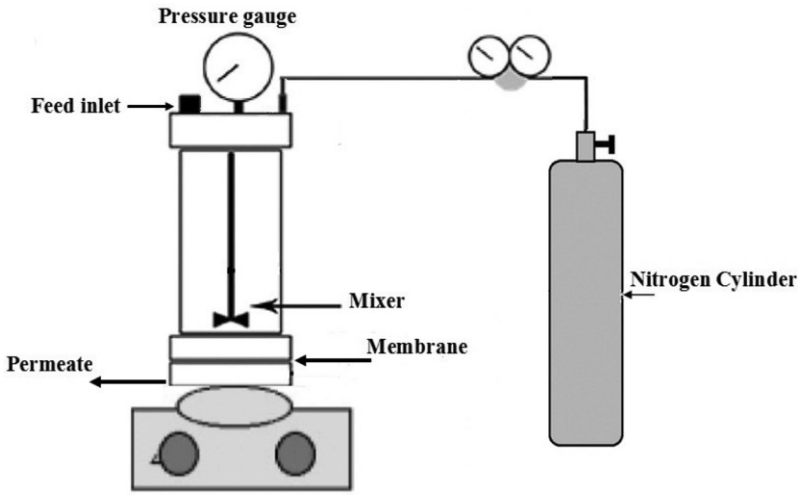

Fig. 19.10
Schematic of dead-end test cell for treatment of wastewater [16]. *Reprinted with permission from M.G. Kochameshki, A. Marjani, M. Mahmoudian, K. Farhadi, Grafting of diallyldimethylammonium chloride on graphene oxide by RAFT polymerization for modification of nanocomposite polysulfone membranes using in water treatment, Chem. Eng. J. 309 (2017) 206–221. Copyright (2017) Elsevier.*

[35]. In addition, 0.25 wt% GO nanoparticle modified with polyaniline (in situ polymerization) incorporated on polyethersulfone membrane has exhibited 98% Pb ions rejection from feed concentration of 5 mg/L at pH of 6 [36]. Gholami et al. [34] fabricated polyvinyl chloride nanocomposite membrane modified with 10 wt% CA and 0.1 wt% iron oxide nanoparticles, which showed better Pb removal, as shown in Fig. 19.11.

19.7.2 Cadmium

Cadmium is a potential carcinogenic agent categorized by US Environmental Protection Agency (EPA) and possesses severe health risk to humans if exposed. Kidney dysfunction can occur due to prolonged exposure to cadmium or even death if exposed at high levels [92,93]. Incorporation of gold nanoparticles into polydopamine/polyethylenimine matrix through co-deposition followed by cross-linking to form nanocomposite membrane with positive charge results in 86.8%, 90.4%, and 88.3% rejection of cadmium chloride, nickel chloride, and zinc chloride, respectively [94]. Modification of GO with poly-diallyldimethylammonium chloride (5 wt% GO-PDADMAC) by control radical polymerization of reversible addition-fragmentation chain transfer incorporated on polysulfone (23%) membrane resulted in high percentage (88.68%) separation of Cd^{2+}, as shown in Fig. 19.12 [16]. Impregnated

This book belongs to Badji Mokhtar Annaba University Central Library Copyright Elsevier 2025

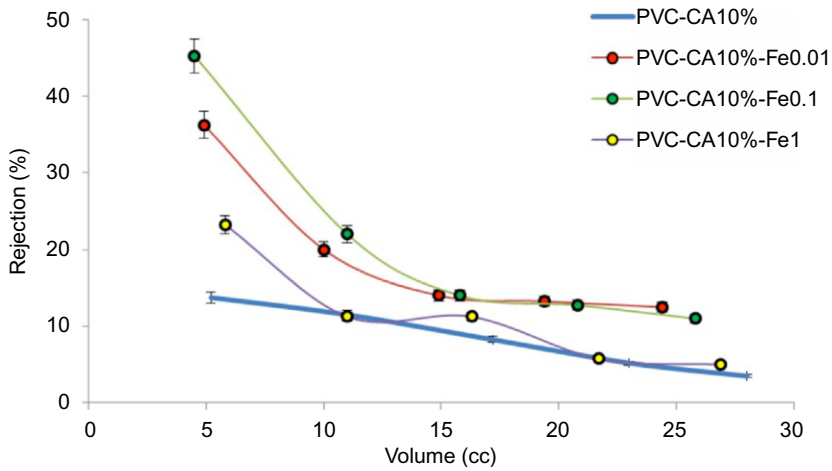

Fig. 19.11

The variation of lead removal with nanoparticles concentration [34]. *Reprinted with permission from A. Gholami, A.R. Moghadassi, S.M. Hosseini, S. Shabani, F. Gholami, Preparation and characterization of polyvinyl chloride based nanocomposite nanofiltration-membrane modified by iron oxide nanoparticles for lead removal from water, J. Ind. Eng. Chem. 20 (2014) 1517–1522. Copyright (2014) Elsevier.*

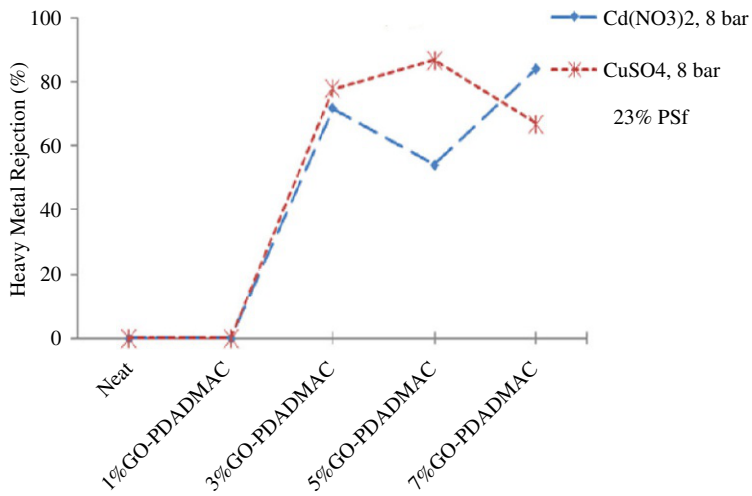

Fig. 19.12

Rejection of heavy metals by modified graphene oxide embedded on polysulfone nanocomposite membrane [16]. *Reprinted with permission from M.G. Kochameshki, A. Marjani, M. Mahmoudian, K. Farhadi, Grafting of diallyldimethylammonium chloride on graphene oxide by RAFT polymerization for modification of nanocomposite polysulfone membranes using in water treatment, Chem. Eng. J. 309 (2017) 206–221. Copyright (2017) Elsevier.*

This book belongs to Badji Mokhtar Annaba University Central Library Copyright Elsevier 2025

activated bentonite clay nanoparticles on polyetherimide rejected 69.3% Cd^{2+} ions from 250 ppm feed solution, while 56.8% from 1000 ppm feed solution [3].

19.7.3 Chromium

Chromium (Cr) exists in two oxidation states, that is, Cr(III) and Cr(VI) and is considered as nonbiodegradable, toxic, and carcinogenic pollutant. Cr(III) is less toxic and an essential nutrient in mammals for glucose metabolism while, Cr(VI) is hazardous to human health and a strictly regulated pollutant. The World Health Organization (WHO) recommends maximum concentration of Cr(VI) in drinking water to be 0.5 ppm. Cr is mainly eluted by the industries such as paint, paper, dye, electroplating, and metal finishing [95–98]. The existing removal techniques for Cr generate sludge in large amounts with Cr in high concentrations, which creates a problem of toxic sludge disposal [5]. The nanocomposite membrane prepared by the poly(acrylonitrile)-*co*-poly(methylacrylate) copolymer and polyaniline results in higher flow rate and rejection of Cr(VI) ions, which depends on concentration of polyaniline, pH, and initial concentration of solution. A 5 wt% polyaniline in membrane was able to remove Cr(VI) from 50 and 100 ppm Cr(VI), solution but it failed in the treatment of 250 ppm Cr(VI) solution, resulting in no Cr(VI) ion rejection. For the treatment of 250 ppm Cr(VI) solution, an increase in concentration of polyaniline from 5 to 10 wt% in membrane resulted in successful removal of Cr(VI). pH plays a dominant role in Cr(VI) rejection. In acidic condition, that is, pH of 2, maximum rejection of Cr(VI) was 99.3% for 50 ppm Cr(VI) solution, while at pH of 7, it decreased to 82%. Similarly, with 100 ppm Cr(VI) solution, the rejection dropped from 98% to 47% as pH was increased from 2 to 7, and with 250 ppm Cr(VI) solution, the drop in rejection for rise in pH from 2 to 7 was 97%–61%. The fluxes are in the range of 1000–17,000 l/m^2 h for the poly(acrylonitrile)-*co*-poly(methylacrylate) copolymer-polyaniline nanocomposite membrane [1].

19.7.4 Copper

The taste, color, or smell of water does not get altered by the presence of copper in it; hence copper-contaminated water is always unnoticeable. Although copper is a vital micronutrient for humans, but its excess quantities lead to abdominal diseases such as diarrhea, convulsion, nausea, cramps, and vomiting [43,99]. Copper(II) solution having concentration of 5 and 10 mg/L when treated by polyethersulfone nanocomposite membrane containing 0.1 wt% polyaniline (PANI)/Fe_3O_4 nanoparticles resulted in the removal of 75% and 80% copper ions after 2 h of processing time. It showed the highest ion rejection and lowest water flux as shown in Fig. 19.13 [62]. The rejection of Cu^{2+} is maximum when compared to Ni^{2+} and Cd^{2+} in activated bentonite clay/polyetherimide nanocomposite membrane because of its small ion size with the highest positive charged density, which extends to maximum hydration in copper when compared to other two metals. Rejection of these metals increases with the increase in pH of

This book belongs to Badji Mokhtar Annaba University Central Library Copyright Elsevier 2025

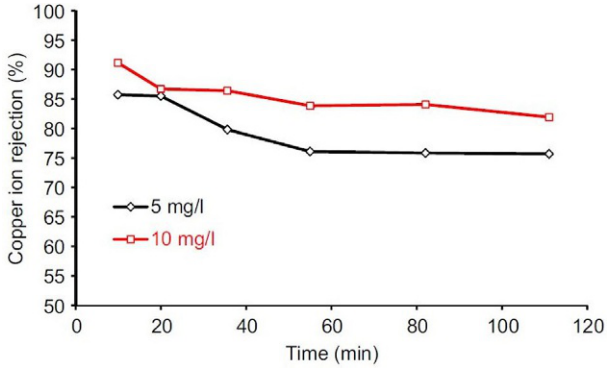

Fig. 19.13
Copper ion rejection using 0.1 wt% PANI/Fe_3O_4 embedded on polyethersulfone membrane with respect to time for two different initial concentrations [62]. *Reprinted with permission from P. Daraei, S.S. Madaeni, N. Ghaemi, E. Salehi, M.A. Khadivi, R. Moradian, B. Astinchap, Novel polyethersulfone nanocomposite membrane prepared by PANI/Fe_3O_4 nanoparticles with enhanced performance for Cu(II) removal from water, J. Membr. Sci. 415–416 (2012) 250–259. Copyright (2012) Elsevier.*

Table 19.2: Summary on copper rejection by different nanocomposite membranes.

S. no.	Nanocomposite membrane	% Removal	Feed concentration	Reference
1	5 wt% GO modified with poly-diallyldimethylammonium chloride incorporated on 20% polysulfone membrane	88.68	–	[16]
2	Activated bentonite clay nanoparticle imparted on polyetherimide membrane	82.5	250 ppm	[3]
3	Polypyrrole coated on Al_2O_3 (1.0 wt%) incorporated on polyethersulfone membrane	81	–	[101]
4	Alumina nanoparticles (1 wt%) impregnated on polyethersulfone membrane	67	20 mg/L (pH 5.0)	[85]
5	Metformine-modified silica-coated Fe_3O_4 nanoparticles (0.1 wt%) embedded on polyethersulfone membrane	92	20 mg/L (pH 5.0)	[57]

feed solution because the negative charge on the membrane surface is enhanced [3,100]. Table 19.2 provides a summary on copper rejection by different nanocomposite membranes found from literature available.

This book belongs to Badji Mokhtar Annaba University Central Library
Copyright Elsevier 2025

19.7.5 Nickel

A critical amount of nickel can lead to gastrointestinal distress, serious kidney and lung sickness, besides pulmonary fibrosis and skin dermatitis, and it is most commonly recognized as a human cancer-causing agent [102]. About 9 wt% Fe_3O_4-talc nanocomposite incorporated in polysulfone membrane resulted in 96.2% nickel rejection from 50 mg/L Ni^{2+} aqueous solution [35]. Activated bentonite clay nanoparticles embedded on polyetherimide membrane was able to reject 76.2% and 64.8% Ni^{2+} from 250 and 1000 ppm feed solutions, respectively.

19.7.6 Arsenic

Arsenic (As) is one of the major contaminants of drinking water across various countries, and millions of people possess a high risk of As-contaminated water. The occurrence of As is in several oxidation states (−3, 0, +3, +5). It is colorless, odorless, and is found predominantly in aqueous media as oxyanions of arsenite [As(III)] and arsenate [As(V)] in inorganic forms, mainly in ground and surface water, respectively. In water, As(III) is 10–60 times more harmful or toxic than As(V). A long-term exposure of As-contaminated water results in various kinds of cancers in the kidney, skin, lungs, and bladder, as shown in a previous study [64,103–107]. The US-EPA had set the permissible As concentration to 10 μg/L for drinking water by 2006 [108]. The primary and secondary treatment processes are unable to remove As, and hence new technologies such as membrane processes are on demand for heavy metal removal [109]. An asymmetric flat sheet of polyethersulfone /titanate nanotubes (TNTs) nanocomposite adsorptive membrane has been used to remove As(V). The membrane results in high-quality permeate, which has As concentration below 10 μg/L, which is lesser than that permitted for drinking water. This was possible with a ratio of 1.5:1 for polyethersulfone:TNT by weight, which has high regeneration feasibility [by desorbing As(V) using 0.1 M NaOH solution] under continuous ultrafiltration experiment, resulting in Langmuir adsorption model [64]. The chitosan membrane embedded with 1.25 wt% zeolite nanoparticle rejected 94.9% As(III) from 1000 μg/L arsenic trioxide solution at the transmembrane pressure of 31.64 kgf/cm^2 [30].

19.8 Comparison of nanocomposite membranes with conventional processes for heavy metal removal

The conventional process such as chemical precipitation, coagulation-flocculation, adsorption, and ion exchange are used for the removal of heavy metals from wastewater streams. These processes possess some limitations when applied in practice. Chemical precipitation involves the chemical reaction of precipitating agent and dissolved metal ions, resulting in insoluble solid phase occurring at a particular pH, mainly at basic conditions (pH of 11). Mostly, calcium hydroxide and lime are employed as precipitating agents. However, they result in excessive

This book belongs to Badji Mokhtar Annaba University Central Library Copyright Elsevier 2025

sludge formation, which increases the cost of sludge disposal and impact on environment owing to sludge disposal. Also, it requires large amount of chemicals and has poor settling, slow, and aggregated metal precipitation [11,110,111]. Coagulation-flocculation involves the addition of coagulant to destabilize the colloidal particles, which results in sedimentation followed by flocculation of unstable particles into bulky floccules to increase their particle size. The basic pH condition is effective for heavy metal removal in this process. It consumes a large amount of chemicals, hence high operational cost. A toxic sludge in large volume is also generated, which creates disposal problem [11,112]. Ion exchange involves the reversible exchange of ions between the liquid and solid phase. Ions from an electrolyte solution are removed by using resin, while other ions of similar charge in chemically equivalent amount are released without the change in structure of the resin. Unlike coagulation-flocculation and chemical precipitation, ion exchange does not create any sludge disposal problem, but it requires relevant pretreatment systems to remove suspended solid from wastewater. Along with it, ion exchange resins are suitable for all heavy metals removal but are not available and possess high operational and capital cost [11,113–115]. Adsorption is also a well-known technique for heavy metallic ions removal from water, which is effective and budget-saving [9]. Adsorption involves transfer of a substance from liquid phase to solid surface where it gets bound by physical and/or chemical interactions. Adsorbents require high surface area and surface reactivity. In the adsorption process, the extra posttreatment is required to remove adsorbents from the water source, which automatically increases the overall costs of process. The cost effectiveness and technical applicability are the two major factors associated with selection of adsorbent for heavy metal removal [11,116]. The limitations offered by the conventional processes are overcome by nanocomposite membrane techniques. The nanocomposite membranes do not generate sludge, thus reducing the operational cost. Nanocomposite membranes involve single-step processes, which reduce the cost of posttreatment. The pretreatment and/or adjustment of pH are not required in nanocomposite membrane processes. The regeneration of membrane can be successfully done so as to reduce the heavy metals concentration to permissible levels as required by US-EPA and WHO standards. The conventional techniques such as coagulation and flocculation, ion exchange, membrane filtration, and chemical precipitation experience some drawbacks and are subjected to some restrictions and practicability applications. The membrane systems offer supremacy over the conventional separation techniques such as high separation efficiency, small footprint, eco-friendliness, and low energy consumption [117]. While selecting any treatment for heavy metals removal, cost-effectiveness, plant simplicity, and technical applicability must be taken into consideration.

19.9 Challenges in industries

A new evolved technology related to wastewater treatment not only possesses many advantages over the conventional processes but also has to face numerous challenges during fabrication, application, and disposal. Whenever any technology is scaled-up to industries level, it has to

This book belongs to Badji Mokhtar Annaba University Central Library Copyright Elsevier 2025

face many challenges during implementation, mainly owing to conditions of bench-scale studies that differ significantly and affect the performance. Nanocomposite membrane proves to be a promising technology for wastewater treatment on bench-scale studies; however, the industrialization of this technology has rarely been reported mainly because of the above reasons. It includes bulk production of nanocomposite membrane, agglomeration of nanoparticles on the membrane, and fouling and regeneration of membrane. One must check the toxicity of nanomaterials used in the membrane if it is exposed to the environment [118]. Toxicity is also a major concern that must be addressed when it comes to disposal of a membrane. Owing to the poor interaction or stability of nanomaterials, it may get leached out during long-run filtration process, which affects its effective surface area and consequently, the adsorption of heavy metals on the membrane. The study related to the potential hazardous effects of nanomaterials used in the nanocomposite membrane must be taken into consideration to understand nanomaterials interaction, migration, and behavior with living organisms and abiotic components of the environments. Owing to the high cost of nanomaterials, the use of nanomaterials in wastewater treatment still snags, mainly in developing countries [119].

Nanocomposite membrane technologies are pressure-driven processes, which require energy for external pressure during separation operation [118]. Laboratory-scale studies are conducted in controlled environment and known, rather prepared samples of wastewater. But, along with heavy metals, various inorganic and organic pollutants are present in actual industrial wastewater, which resist the high selective adsorption of heavy metal ions. They also tend to block the pores of membrane, and the membrane is subjected to fouling due to timely accumulation of these pollutants [118]. Agglomeration prevents uniform dispersion of nanomaterials in polymer matrices [120]. Compatibility and interaction of nanomaterials with polymer matrices persuade their performance when inside the polymer matrix [121,122]. All these are some of the major challenges that must be addressed during the fabrication of nanocomposite membranes [123]. The dispersion of nanoparticles is limited in casting solution of polymeric membrane for nanomaterials having diameter <100 nm, which results in agglomeration and nonuniform distribution of nanoparticles in polymer matrix. Agglomeration also results in alteration of nanocomposite membrane characteristics such as antifouling properties, hydrophilicity, pore size, and roughness [124,125]. Leaching of nanoparticles is caused by the poor adhesion/interaction between the nanoparticles and polymer membrane, which causes stagnation in nanocomposite membrane, along with many environmental issues due to potential toxicity of some nanoparticles [126]. Membrane fouling is one of the primary issues, which needs to be tackled at large-scale applications. It occurs due to accumulation of various impurities, which block the pores and create a barrier for permeation of water. This reduces the life span of membrane and requires high maintenance cost. Large amounts of cleaning agents are used for regeneration, which makes this technology more expensive. This also increases the transmembrane pressure requirement for the same output [15]. The main challenge that has to be addressed during commercialization of nanocomposite membrane is the

This book belongs to Badji Mokhtar Annaba University Central Library Copyright Elsevier 2025

durability of nanomaterials under various operating conditions and degradability of nanomaterials at the end of useful service life [127,128]. Researchers need to develop simple, cost-effective, and reliable techniques for the synthesis of nanocomposite membrane that must endure and be resistant toward all types of pollutants and fouling in actual waste condition [118].

19.10 Summary

Nanocomposite membranes have evolved as a new technology for the treatment of wastewater. The presence of heavy metals in wastewater possesses serious toxicity to plants, animals, and human beings, even at low concentrations. Nanomaterials have great potential for wastewater treatment as an adsorbent, photocatalyst, antimicrobial agent, and in membrane separation. In the membrane separation, the incorporation of nanomaterials enhances the desired properties of membrane such as mechanical strength, swelling, hydrophilicity, water flux, porosity and fouling resistance, and hence the performance of the membrane, eventually converting it into nanocomposite membranes. Phase inversion method and IP are used to fabricate the nanocomposite membranes. The nanocomposite membranes are successfully used to remove the heavy metals ions such as Cd^{2+}, Ni^{2+}, Pb^{2+}, Cu^{2+}, Cr^{2+}, and As(III) from wastewater. They exhibit excellent properties and produce great results for removal or at least reduction in concentration of these pollutants from water. The bench-scale study showed an excellent performance for removal of heavy metals from wastewater. But this technology also possesses some challenges for scaling up to the industrial level because the conditions are very different from bench-scale studies. Various nanocomposite membranes are used for the removal of heavy metals, which are discussed in this chapter. In addition, the comparison of nanocomposite membranes with various other technologies is also discussed.

References

[1] M. Sankir, S. Bozkir, B. Aran, Preparation and performance analysis of novel nanocomposite copolymer membranes for Cr(VI) removal from aqueous solutions. Desalination 251 (2010) 131–136, https://doi.org/10.1016/j.desal.2009.09.134.

[2] Z. Karim, A.P. Mathew, V. Kokol, J. Wei, M. Grahn, High-flux affinity membranes based on cellulose nanocomposites for removal of heavy metal ions from industrial effluents. RSC Adv. 6 (2016) 20644–20653, https://doi.org/10.1039/c5ra27059f.

[3] R.S. Hebbar, A.M. Isloor, A.F. Ismail, Preparation and evaluation of heavy metal rejection properties of polyetherimide/porous activated bentonite clay nanocomposite membrane. RSC Adv. 4 (2014) 47240–47248, https://doi.org/10.1039/c4ra09018g.

[4] O. Tünay, N.I. Kabdaşli, Hydroxide precipitation of complexed metals. Water Res. 28 (1994) 2117–2124, https://doi.org/10.1016/0043-1354(94)90022-1.

[5] K. Kadirvelu, K. Thamaraiselvi, C. Namasivayam, Removal of heavy metals from industrial wastewaters by adsorption onto activated carbon prepared from an agricultural solid waste. Bioresour. Technol. 76 (2001) 63–65, https://doi.org/10.1016/S0960-8524(00)00072-9.

This book belongs to Badji Mokhtar Annaba University Central Library

Copyright Elsevier 2025

[6] F.M. Pang, P. Kumar, T.T. Teng, A.K. Mohd Omar, K.L. Wasewar, Removal of lead, zinc and iron by coagulation-flocculation. J. Taiwan Inst. Chem. Eng. 42 (2011) 809–815, https://doi.org/10.1016/j.jtice.2011.01.009.

[7] B. Mattuschka, G. Straube, Biosorption of metals by a waste biomass. J. Chem. Technol. Biotechnol. 58 (1993) 57–63, https://doi.org/10.1002/jctb.280580108.

[8] S.Y. Kang, J.U. Lee, S.H. Moon, K.W. Kim, Competitive adsorption characteristics of Co^{2+}, Ni^{2+}, and Cr^{3+} by IRN-77 cation exchange resin in synthesized wastewater. Chemosphere 56 (2004) 141–147, https://doi.org/10.1016/j.chemosphere.2004.02.004.

[9] F. Fu, Q. Wang, Removal of heavy metal ions from wastewaters: a review. J. Environ. Manage. 92 (2011) 407–418, https://doi.org/10.1016/j.jenvman.2010.11.011.

[10] A. Bera, J.S. Trivedi, S.B. Kumar, A.K.S. Chandel, S. Haldar, S.K. Jewrajka, Anti-organic fouling and anti-biofouling poly(piperazineamide) thin film nanocomposite membranes for low pressure removal of heavy metal ions. J. Hazard. Mater. 343 (2018) 86–97, https://doi.org/10.1016/j.jhazmat.2017.09.016.

[11] T.A. Kurniawan, G.Y.S. Chan, W.H. Lo, S. Babel, Physico-chemical treatment techniques for wastewater laden with heavy metals. Chem. Eng. J. 118 (2006) 83–98, https://doi.org/10.1016/j.cej.2006.01.015.

[12] R.K. Rattan, S.P. Datta, P.K. Chhonkar, K. Suribabu, A.K. Singh, Long-term impact of irrigation with sewage effluents on heavy metal content in soils, crops and groundwater—a case study. Agric. Ecosyst. Environ. 109 (2005) 310–322, https://doi.org/10.1016/j.agee.2005.02.025.

[13] C.F. Lin, C.H. Wu, H.T. Lai, Dissolved organic matter and arsenic removal with coupled chitosan/UF operation. Sep. Purif. Technol. 60 (2008) 292–298, https://doi.org/10.1016/j.seppur.2007.09.002.

[14] X. Wei, X. Kong, S. Wang, H. Xiang, J. Wang, J. Chen, Removal of heavy metals from electroplating wastewater by thin-film composite nanofiltration hollow-fiber membranes. Ind. Eng. Chem. Res. 52 (2013) 17583–17590, https://doi.org/10.1021/ie402387u.

[15] S. Al Aani, C.J. Wright, M.A. Atieh, N. Hilal, Engineering nanocomposite membranes: addressing current challenges and future opportunities. Desalination 401 (2017) 1–15, https://doi.org/10.1016/j.desal.2016.08.001.

[16] M.G. Kochameshki, A. Marjani, M. Mahmoudian, K. Farhadi, Grafting of diallyldimethylammonium chloride on graphene oxide by RAFT polymerization for modification of nanocomposite polysulfone membranes using in water treatment. Chem. Eng. J. 309 (2017) 206–221, https://doi.org/10.1016/j.cej.2016.10.008.

[17] N. Savage, M.S. Diallo, Nanomaterials and water purification: opportunities and challenges. J. Nanopart. Res. (2005) 331–342, https://doi.org/10.1007/s11051-005-7523-5.

[18] W. Salim, W.W. Ho, Recent developments on nanostructured polymer-based membranes. Curr. Opin. Chem. Eng. 8 (2015) 76–82, https://doi.org/10.1016/j.coche.2015.03.003.

[19] T. Humplik, J. Lee, S.C. O'Hern, B.A. Fellman, M.A. Baig, S.F. Hassan, M.A. Atieh, F. Rahman, T. Laoui, R. Karnik, E.N. Wang, Nanostructured materials for water desalination. Nanotechnology 22 (2011) 19, https://doi.org/10.1088/0957-4484/22/29/292001.

[20] G. Sharma, D. Pathania, M. Naushad, N.C. Kothiyal, Fabrication, characterization and antimicrobial activity of polyaniline Th(IV) tungstomolybdophosphate nanocomposite material: efficient removal of toxic metal ions from water. Chem. Eng. J. 251 (2014) 413–421, https://doi.org/10.1016/j.cej.2014.04.074.

[21] O.M. Vatutsina, V.S. Soldatov, V.I. Sokolova, J. Johann, M. Bissen, A. Weissenbacher, A new hybrid (polymer/inorganic) fibrous sorbent for arsenic removal from drinking water. React. Funct. Polym. 67 (2007) 184–201, https://doi.org/10.1016/j.reactfunctpolym.2006.10.009.

[22] Y.-M. Zheng, S.-W. Zou, K.G.N. Nanayakkara, T. Matsuura, J.P. Chen, Adsorptive removal of arsenic from aqueous solution by a PVDF/zirconia blend flat sheet membrane. J. Membr. Sci. 374 (2011) 1–11, https://doi.org/10.1016/j.memsci.2011.02.034.

[23] L. Gzara, M. Dhahbi, Removal of chromate anions by micellar-enhanced ultrafiltration using cationic surfactants. Desalination 137 (2001) 241–250, https://doi.org/10.1016/S0011-9164(01)00225-9.

[24] A. Hafiane, D. Lemordant, M. Dhahbi, Removal of hexavalent chromium by nanofiltration. Desalination 130 (2000) 305–312, https://doi.org/10.1016/S0011-9164(00)00094-1.

This book belongs to Badji Mokhtar Annaba University Central Library

Copyright Elsevier 2025

[25] S.S. Chen, B.C. Hsu, C.H. Ko, P.C. Chuang, Recovery of chromate from spent plating solutions by two-stage nanofiltration processes. Desalination 229 (2008) 147–155, https://doi.org/10.1016/j.desal.2007.08.015.
[26] U. Danis, C. Aydiner, Investigation of process performance and fouling mechanisms in micellar-enhanced ultrafiltration of nickel-contaminated waters. J. Hazard. Mater. 162 (2009) 577–587, https://doi.org/10.1016/j.jhazmat.2008.05.098.
[27] C. Neelakandan, G. Pugazhenthi, A. Kumar, Preparation of NOx modified PMMA–EGDM composite membrane for the recovery of chromium(VI). Eur. Polym. J. 39 (2003) 2383–2391, https://doi.org/10.1016/S0014-3057(03)00183-6.
[28] S. Sachdeva, A. Kumar, Synthesis and modeling of composite poly(styrene-*co*-acrylonitrile) membrane for the separation of chromic acid. J. Membr. Sci. 307 (2008) 37–52, https://doi.org/10.1016/j.memsci.2007.09.013.
[29] H.F. Shaalan, M.H. Sorour, S.R. Tewfik, Simulation and optimization of a membrane system for chromium recovery from tanning wastes. Desalination 141 (2001) 315–324, https://doi.org/10.1016/S0011-9164(01)85008-6.
[30] M. Mukhopadhyay, S.R. Lakhotia, A.K. Ghosh, R.C. Bindal, Removal of arsenic from aqueous media using zeolite/chitosan nanocomposite membrane. Sep. Sci. Technol. 54 (2019) 282–288, https://doi.org/10.1080/01496395.2018.1459704.
[31] M. Hua, S. Zhang, B. Pan, W. Zhang, L. Lv, Q. Zhang, Heavy metal removal from water/wastewater by nanosized metal oxides: a review. J. Hazard. Mater. 211–212 (2012) 317–331, https://doi.org/10.1016/j.jhazmat.2011.10.016.
[32] J. Floch, M. Hideg, Application of ZW-1000 membranes for arsenic removal from water sources. Desalination 162 (2004) 75–83, https://doi.org/10.1016/S0011-9164(04)00029-3.
[33] Z.K. Xu, L.Q. Shen, Q. Yang, F. Liu, S.Y. Wang, Y.Y. Xu, Ultrafiltration hollow fiber membranes from poly(ether imide): preparation, morphologies and properties. J. Membr. Sci. 223 (2003) 105–118, https://doi.org/10.1016/S0376-7388(03)00312-0.
[34] A. Gholami, A.R. Moghadassi, S.M. Hosseini, S. Shabani, F. Gholami, Preparation and characterization of polyvinyl chloride based nanocomposite nanofiltration-membrane modified by iron oxide nanoparticles for lead removal from water. J. Ind. Eng. Chem. 20 (2014) 1517–1522, https://doi.org/10.1016/j.jiec.2013.07.041.
[35] P. Moradihamedani, K. Kalantari, A.H. Abdullah, N.A. Morad, High efficient removal of lead(II) and nickel(II) from aqueous solution by novel polysulfone/Fe_3O_4–talc nanocomposite mixed matrix membrane. Desalin. Water Treat. 57 (2016) 28900–28909, https://doi.org/10.1080/19443994.2016.1193449.
[36] N. Ghaemi, S. Zereshki, S. Heidari, Removal of lead ions from water using PES-based nanocomposite membrane incorporated with polyaniline modified GO nanoparticles: performance optimization by central composite design. Process. Saf. Environ. Prot. 111 (2017) 475–490, https://doi.org/10.1016/j.psep.2017.08.011.
[37] M. Zanetti, S. Lomakin, G. Camino, Polymer layered silicate nanocomposites. Macromol. Mater. Eng. 279 (2000) 1–9, https://doi.org/10.1002/1439-2054(20000601)279:1<1::AID-MAME1>3.0.CO;2-Q.
[38] M. Amini, M. Arami, N.M. Mahmoodi, A. Akbari, Dye removal from colored textile wastewater using acrylic grafted nanomembrane. Desalination 267 (2011) 107–113, https://doi.org/10.1016/j.desal.2010.09.014.
[39] Y. Yurekli, Removal of heavy metals in wastewater by using zeolite nano-particles impregnated polysulfone membranes. J. Hazard. Mater. 309 (2016) 53–64, https://doi.org/10.1016/j.jhazmat.2016.01.064.
[40] M. Sekar, V. Sakthi, S. Rengaraj, Kinetics and equilibrium adsorption study of lead (II) onto activated carbon prepared from coconut shell. J. Colloid Interface Sci. 279 (2004) 307–313, https://doi.org/10.1016/j.jcis.2004.06.042.
[41] K. Lizama Allende, T.D. Fletcher, G. Sun, The effect of substrate media on the removal of arsenic, boron and iron from an acidic wastewater in planted column reactors. Chem. Eng. J. 179 (2012) 119–130, https://doi.org/10.1016/j.cej.2011.10.069.

This book belongs to Badji Mokhtar Annaba University Central Library Copyright Elsevier 2025

[42] N.G. Turan, O. Ozgonenel, Optimizing copper ions removal from industrial leachate by explored vermiculite—a comparative analysis. J. Taiwan Inst. Chem. Eng. 44 (2013) 895–903, https://doi.org/10.1016/j.jtice.2013.03.004.

[43] R. Camarillo, J. Llanos, L. García-Fernández, Á. Pérez, P. Cañizares, Treatment of copper (II)-loaded aqueous nitrate solutions by polymer enhanced ultrafiltration and electrodeposition. Sep. Purif. Technol. 70 (2010) 320–328, https://doi.org/10.1016/j.seppur.2009.10.014.

[44] C. Santhosh, V. Velmurugan, G. Jacob, S.K. Jeong, A.N. Grace, A. Bhatnagar, Role of nanomaterials in water treatment applications: a review. Chem. Eng. J. 306 (2016) 1116–1137, https://doi.org/10.1016/j.cej.2016.08.053.

[45] S. Pacheco, M. Medina, F. Valencia, J. Tapia, Removal of inorganic mercury from polluted water using structured nanoparticles. J. Environ. Eng. 132 (2006) 342–349, https://doi.org/10.1061/(ASCE)0733-9372(2006)132:3(342).

[46] K. Yang, B. Xing, Desorption of polycyclic aromatic hydrocarbons from carbon nanomaterials in water. Environ. Pollut. 145 (2007) 529–537, https://doi.org/10.1016/j.envpol.2006.04.020.

[47] K. Hristovski, A. Baumgardner, P. Westerhoff, Selecting metal oxide nanomaterials for arsenic removal in fixed bed columns: from nanopowders to aggregated nanoparticle media. J. Hazard. Mater. 147 (2007) 265–274, https://doi.org/10.1016/j.jhazmat.2007.01.017.

[48] L. Li, M. Fan, R. Brown, J. Leeuwen, J. Wang, W. Wang, Y. Song, P. Zhang, Synthesis, properties and environmental applications of nanoscale iron-based materials: a review. Comments Inorg. Chem. 27 (2006) 1–32, https://doi.org/10.1080/02603590500496721.

[49] WHO, Global Report for Research on Infectious Diseases of Poverty, (2012) ISBN: 9789241564489.

[50] N. Cioffi, N. Ditaranto, L. Torsi, L. Sabbatini, Approaches to synthesis and characterization of spherical and anisotropic copper nanomaterials. in: Nanotechnologies Life Sci, 2010https://doi.org/10.1002/9783527610419.ntls0123.

[51] P. Xu, G.M. Zeng, D.L. Huang, C.L. Feng, S. Hu, M.H. Zhao, C. Lai, Z. Wei, C. Huang, G.X. Xie, Z. F. Liu, Use of iron oxide nanomaterials in wastewater treatment: a review. Sci. Total Environ. 424 (2012) 1–10, https://doi.org/10.1016/j.scitotenv.2012.02.023.

[52] F. Ferella, M. Prisciandaro, I. De Michelis, F. Veglio', Removal of heavy metals by surfactant-enhanced ultrafiltration from wastewaters. Desalination 207 (2007) 125–133, https://doi.org/10.1016/j.desal.2006.07.007.

[53] M. Mohsen-Nia, P. Montazeri, H. Modarress, Removal of Cu^{2+} and Ni^{2+} from wastewater with a chelating agent and reverse osmosis processes. Desalination 217 (2007) 276–281, https://doi.org/10.1016/j.desal.2006.01.043.

[54] Z.V.P. Murthy, L.B. Chaudhari, Separation of binary heavy metals from aqueous solutions by nanofiltration and characterization of the membrane using Spiegler-Kedem model. Chem. Eng. J. 150 (2009) 181–187, https://doi.org/10.1016/j.cej.2008.12.023.

[55] T. Mohammadi, A. Razmi, M. Sadrzadeh, Effect of operating parameters on Pb^{2+} separation from wastewater using electrodialysis. Desalination 167 (2004) 379–385, https://doi.org/10.1016/j.desal.2004.06.150.

[56] V. Vatanpour, S.S. Madaeni, R. Moradian, S. Zinadini, B. Astinchap, Novel antibifouling nanofiltration polyethersulfone membrane fabricated from embedding TiO_2 coated multiwalled carbon nanotubes. Sep. Purif. Technol. 90 (2012) 69–82, https://doi.org/10.1016/j.seppur.2012.02.014.

[57] N. Ghaemi, S.S. Madaeni, P. Daraei, H. Rajabi, S. Zinadini, A. Alizadeh, R. Heydari, M. Beygzadeh, S. Ghouzivand, Polyethersulfone membrane enhanced with iron oxide nanoparticles for copper removal from water: application of new functionalized Fe_3O_4 nanoparticles. Chem. Eng. J. 263 (2015) 101–112, https://doi.org/10.1016/j.cej.2014.10.103.

[58] T.H. Bae, T.M. Tak, Effect of TiO_2 nanoparticles on fouling mitigation of ultrafiltration membranes for activated sludge filtration. J. Membr. Sci. 249 (2005) 1–8, https://doi.org/10.1016/j.memsci.2004.09.008.

[59] V. Vatanpour, S.S. Madaeni, A.R. Khataee, E. Salehi, S. Zinadini, H.A. Monfared, TiO_2 embedded mixed matrix PES nanocomposite membranes: influence of different sizes and types of nanoparticles on antifouling and performance. Desalination 292 (2012) 19–29, https://doi.org/10.1016/j.desal.2012.02.006.

This book belongs to Badji Mokhtar Annaba University Central Library Copyright Elsevier 2025

[60] A. Rezvani-Boroujeni, M. Javanbakht, M. Karimi, C. Shahrjerdi, B. Akbari-adergani, Immoblization of thiol-functionalized nanosilica on the surface of poly(ether sulfone) membranes for the removal of heavy-metal ions from industrial wastewater samples. Ind. Eng. Chem. Res. 54 (2015) 502–513, https://doi.org/10.1021/ie504106y.
[61] R. Kumar, A.F. Ismail, M.A. Kassim, A.M. Isloor, Modification of PSf/PIAM membrane for improved desalination applications using Chitosan coagulation media. Desalination 317 (2013) 108–115, https://doi.org/10.1016/j.desal.2013.03.008.
[62] P. Daraei, S.S. Madaeni, N. Ghaemi, E. Salehi, M.A. Khadivi, R. Moradian, B. Astinchap, Novel polyethersulfone nanocomposite membrane prepared by PANI/Fe_3O_4 nanoparticles with enhanced performance for Cu(II) removal from water. J. Membr. Sci. 415–416 (2012) 250–259, https://doi.org/10.1016/j.memsci.2012.05.007.
[63] Z.H. Zhang, Q.F. An, T. Liu, Y. Zhou, J.W. Qian, C.J. Gao, Fabrication and characterization of novel SiO_2-PAMPS/PSF hybrid ultrafiltration membrane with high water flux. Desalination 297 (2012) 59–71, https://doi.org/10.1016/j.desal.2012.04.017.
[64] R.J. Gohari, W.J. Lau, E. Halakoo, A.F. Ismail, F. Korminouri, T. Matsuura, M.S. Jamshidi Gohari, M.N. K. Chowdhury, Arsenate removal from contaminated water by a highly adsorptive nanocomposite ultrafiltration membrane. New J. Chem. 39 (2015) 8263–8272, https://doi.org/10.1039/c5nj00690b.
[65] S. Zinadini, A.A. Zinatizadeh, M. Rahimi, V. Vatanpour, H. Zangeneh, Preparation of a novel antifouling mixed matrix PES membrane by embedding graphene oxide nanoplates. J. Membr. Sci. 453 (2014) 292–301, https://doi.org/10.1016/j.memsci.2013.10.070.
[66] J. Zhu, M. Tian, Y. Zhang, H. Zhang, J. Liu, Fabrication of a novel "loose" nanofiltration membrane by facile blending with chitosan-montmorillonite nanosheets for dyes purification. Chem. Eng. J. 265 (2015) 184–193, https://doi.org/10.1016/j.cej.2014.12.054.
[67] C. Wang, Z. Li, J. Chen, Z. Li, Y. Yin, L. Cao, Y. Zhong, H. Wu, Covalent organic framework modified polyamide nanofiltration membrane with enhanced performance for desalination. J. Membr. Sci. 523 (2017) 273–281, https://doi.org/10.1016/j.memsci.2016.09.055.
[68] F. Liu, M.R.M. Abed, K. Li, Preparation and characterization of poly(vinylidene fluoride) (PVDF) based ultrafiltration membranes using nano γ-Al_2O_3. J. Membr. Sci. 366 (2011) 97–103, https://doi.org/10.1016/j.memsci.2010.09.044.
[69] S.M. Doke, G.D. Yadav, Process efficacy and novelty of titania membrane prepared by polymeric sol-gel method in removal of chromium(VI) by surfactant enhanced microfiltration. Chem. Eng. J. 255 (2014) 483–491, https://doi.org/10.1016/j.cej.2014.05.098.
[70] A. Venault, Y. Chang, J.R. Wu, D.M. Wang, Influence of solvent composition and non-solvent activity on the crystalline morphology of PVDF membranes prepared by VIPS process and on their arising mechanical properties. J. Taiwan Inst. Chem. Eng. 45 (2014) 1087–1097, https://doi.org/10.1016/j.jtice.2013.08.014.
[71] R. Mukherjee, P. Bhunia, S. De, Impact of graphene oxide on removal of heavy metals using mixed matrix membrane. Chem. Eng. J. 292 (2016) 284–297, https://doi.org/10.1016/j.cej.2016.02.015.
[72] Z.B. Zhang, J.J. Wu, Y. Su, J. Zhou, Y. Gao, H.Y. Yu, J.S. Gu, Layer-by-layer assembly of graphene oxide on polypropylene macroporous membranes via click chemistry to improve antibacterial and antifouling performance. Appl. Surf. Sci. 332 (2015) 300–307, https://doi.org/10.1016/j.apsusc.2015.01.193.
[73] Z. Li, J.S. Jean, W.T. Jiang, P.H. Chang, C.J. Chen, L. Liao, Removal of arsenic from water using Fe-exchanged natural zeolite. J. Hazard. Mater. 187 (2011) 318–323, https://doi.org/10.1016/j.jhazmat.2011.01.030.
[74] L. Cui, Y. Wang, L. Gao, L. Hu, L. Yan, Q. Wei, B. Du, EDTA functionalized magnetic graphene oxide for removal of Pb(II), Hg(II) and Cu(II) in water treatment: adsorption mechanism and separation property. Chem. Eng. J. 281 (2015) 1–10, https://doi.org/10.1016/j.cej.2015.06.043.
[75] A.A.P. Khan, A. Khan, M.M. Rahman, A.M. Asiri, Conventional surfactant-doped poly(o-anisidine)/GO nanocomposites for benzaldehyde chemical sensor development. J. Sol-Gel Sci. Technol. 77 (2016) 361–370, https://doi.org/10.1007/s10971-015-3862-6.

This book belongs to Badji Mokhtar Annaba University Central Library Copyright Elsevier 2025

[76] A.A.P. Khan, A. Khan, M.M. Rahman, A.M. Asiri, M. Oves, Lead sensors development and antimicrobial activities based on graphene oxide/carbon nanotube/poly(O-toluidine) nanocomposite. Int. J. Biol. Macromol. 89 (2016) 198–205, https://doi.org/10.1016/j.ijbiomac.2016.04.064.

[77] P. Tan, J. Sun, Y. Hu, Z. Fang, Q. Bi, Y. Chen, J. Cheng, Adsorption of Cu^{2+}, Cd^{2+} and Ni^{2+} from aqueous single metal solutions on graphene oxide membranes. J. Hazard. Mater. 297 (2015) 251–260, https://doi.org/10.1016/j.jhazmat.2015.04.068.

[78] E. Bet-moushoul, Y. Mansourpanah, K. Farhadi, M. Tabatabaei, TiO_2 nanocomposite based polymeric membranes: a review on performance improvement for various applications in chemical engineering processes. Chem. Eng. J. 283 (2016) 29–46, https://doi.org/10.1016/j.cej.2015.06.124.

[79] E. Mahmoudi, L.Y. Ng, M.M. Ba-Abbad, A.W. Mohammad, Novel nanohybrid polysulfone membrane embedded with silver nanoparticles on graphene oxide nanoplates. Chem. Eng. J. 277 (2015) 1–10, https://doi.org/10.1016/j.cej.2015.04.107.

[80] C.P. Leo, W.P. Cathie Lee, A.L. Ahmad, A.W. Mohammad, Polysulfone membranes blended with ZnO nanoparticles for reducing fouling by oleic acid. Sep. Purif. Technol. 89 (2012) 51–56, https://doi.org/10.1016/j.seppur.2012.01.002.

[81] F. Ran, S. Nie, W. Zhao, J. Li, B. Su, S. Sun, C. Zhao, Biocompatibility of modified polyethersulfone membranes by blending an amphiphilic triblock co-polymer of poly(vinyl pyrrolidone)-*b*-poly(methyl methacrylate)-*b*-poly(vinyl pyrrolidone). Acta Biomater. 7 (2011) 3370–3381, https://doi.org/10.1016/j.actbio.2011.05.026.

[82] P. Moradihamedani, N.A. Ibrahim, W.M.Z.W. Yunus, N.A. Yusof, Separation of CO_2 from CH_4 by pure PSF and PSF/PVP blend membranes: effects of type of nonsolvent, solvent, and PVP concentration. J. Appl. Polym. Sci. 130 (2013) 1139–1147, https://doi.org/10.1002/app.39288.

[83] J. Diani, K. Gall, Finite strain 3D thermoviscoelastic constitutive model. Society (2006) 1–8, https://doi.org/10.1002/pen.

[84] J.M. Gohil, R.R. Choudhury, Introduction to Nanostructured and Nano-Enhanced Polymeric Membranes: Preparation, Function, and Application for Water Purification. Elsevier Inc., 2019https://doi.org/10.1016/b978-0-12-813926-4.00038-0

[85] N. Ghaemi, A new approach to copper ion removal from water by polymeric nanocomposite membrane embedded with γ-alumina nanoparticles. Appl. Surf. Sci. 364 (2016) 221–228, https://doi.org/10.1016/j.apsusc.2015.12.109.

[86] Y.L. Ji, Q.F. An, Y.S. Guo, W.S. Hung, K.R. Lee, C.J. Gao, Bio-inspired fabrication of high perm-selectivity and anti-fouling membranes based on zwitterionic polyelectrolyte nanoparticles. J. Mater. Chem. A 4 (2016) 4224–4231, https://doi.org/10.1039/c6ta00005c.

[87] Y. Pan, R. Xu, Z. Lü, S. Yu, M. Liu, C. Gao, Enhanced both perm-selectivity and fouling resistance of poly(piperazine-amide) nanofiltration membrane by incorporating sericin as a co-reactant of aqueous phase. J. Membr. Sci. 523 (2017) 282–290, https://doi.org/10.1016/j.memsci.2016.10.011.

[88] J. Zhu, L. Qin, A. Uliana, J. Hou, J. Wang, Y. Zhang, X. Li, S. Yuan, J. Li, M. Tian, J. Lin, B. Van der Bruggen, Elevated performance of thin film nanocomposite membranes enabled by modified hydrophilic MOFs for nanofiltration. ACS Appl. Mater. Interfaces 9 (2017) 1975–1986, https://doi.org/10.1021/acsami.6b14412.

[89] N. Abdullah, R.J. Gohari, N. Yusof, A.F. Ismail, J. Juhana, W.J. Lau, T. Matsuura, Polysulfone/hydrous ferric oxide ultrafiltration mixed matrix membrane: preparation, characterization and its adsorptive removal of lead (II) from aqueous solution. Chem. Eng. J. 289 (2016) 28–37, https://doi.org/10.1016/j.cej.2015.12.081.

[90] R. Naseem, S.S. Tahir, Removal of Pb(II) from aqueous/acidic solutions by using bentonite as an adsorbent. Water Res. 35 (2001) 3982–3986, https://doi.org/10.1016/S0043-1354(01)00130-0.

[91] J. García-Lestón Julia, J. Méndez, E. Pásaro, B. Laffon, Genotoxic effects of lead: an updated review. Environ. Int. 36 (2010) 623–636, https://doi.org/10.1016/j.envint.2010.04.011.

[92] E. Katsou, S. Malamis, K.J. Haralambous, Industrial wastewater pre-treatment for heavy metal reduction by employing a sorbent-assisted ultrafiltration system. Chemosphere 82 (2011) 557–564, https://doi.org/10.1016/j.chemosphere.2010.10.022.

This book belongs to Badji Mokhtar Annaba University Central Library Copyright Elsevier 2025

[93] R.K. Gautam, A. Mudhoo, G. Lofrano, M.C. Chattopadhyaya, Biomass-derived biosorbents for metal ions sequestration: adsorbent modification and activation methods and adsorbent regeneration. J. Environ. Chem. Eng. 2 (2014) 239–259, https://doi.org/10.1016/j.jece.2013.12.019.
[94] Y. Lv, Y. Du, Z.X. Chen, W.Z. Qiu, Z.K. Xu, Nanocomposite membranes of polydopamine/electropositive nanoparticles/polyethyleneimine for nanofiltration. J. Membr. Sci. 545 (2018) 99–106, https://doi.org/10.1016/j.memsci.2017.09.066.
[95] S.A. Katz, H. Salem, The toxicology of chromium with respect to its chemical speciation: a review. J. Appl. Toxicol. 13 (1993) 217–224, https://doi.org/10.1002/jat.2550130314.
[96] A.M. Yusof, N.A.N.N. Malek, Removal of Cr(VI) and As(V) from aqueous solutions by HDTMA-modified zeolite Y. J. Hazard. Mater. 162 (2009) 1019–1024, https://doi.org/10.1016/j.jhazmat.2008.05.134.
[97] F.N. Acar, E. Malkoc, The removal of chromium(VI) from aqueous solutions by *Fagus orientalis* L. Bioresour. Technol. 94 (2004) 13–15, https://doi.org/10.1016/j.biortech.2003.10.032.
[98] G. Arslan, E. Pehlivan, Batch removal of chromium(VI) from aqueous solution by Turkish brown coals. Bioresour. Technol. 98 (2007) 2836–2845, https://doi.org/10.1016/j.biortech.2006.09.041.
[99] Y.H. Wang, S.H. Lin, R.S. Juang, Removal of heavy metal ions from aqueous solutions using various low-cost adsorbents. J. Hazard. Mater. 102 (2003) 291–302, https://doi.org/10.1016/S0304-3894(03)00218-8.
[100] B. Tansel, J. Sager, T. Rector, J. Garland, R.F. Strayer, L. Levine, M. Roberts, M. Hummerick, J. Bauer, Significance of hydrated radius and hydration shells on ionic permeability during nanofiltration in dead end and cross flow modes. Sep. Purif. Technol. 51 (2006) 40–47, https://doi.org/10.1016/j.seppur.2005.12.020.
[101] N. Ghaemi, P. Daraei, Enhancement in copper ion removal by PPy@Al_2O_3 polymeric nanocomposite membrane. J. Ind. Eng. Chem. 40 (2016) 26–33, https://doi.org/10.1016/j.jiec.2016.05.027.
[102] C.E. Borba, R. Guirardello, E.A. Silva, M.T. Veit, C.R.G. Tavares, Removal of nickel(II) ions from aqueous solution by biosorption in a fixed bed column: experimental and theoretical breakthrough curves. Biochem. Eng. J. 30 (2006) 184–191, https://doi.org/10.1016/j.bej.2006.04.001.
[103] S. Atkinson, Filtration technology verified to remove arsenic from drinking water. Membr. Technol. 2006 (2006) 8–9, https://doi.org/10.1016/S0958-2118(06)70658-9.
[104] W. Tang, Y. Su, Q. Li, S. Gao, J.K. Shang, Mg-doping: a facile approach to impart enhanced arsenic adsorption performance and easy magnetic separation capability to α-Fe_2O_3 nanoadsorbents. J. Mater. Chem. A 1 (2013) 830–836, https://doi.org/10.1039/c2ta00271j.
[105] J.C. Ng, J. Wang, A. Shraim, A global health problem caused by arsenic from natural sources. Chemosphere 52 (2003) 1353–1359, https://doi.org/10.1016/S0045-6535(03)00470-3.
[106] P.L. Smedley, D.G. Kinniburgh, A review of the source, behaviour and distribution of arsenic in natural waters. Appl. Geochem. 17 (2002) 517–568, https://doi.org/10.1016/S0883-2927(02)00018-5.
[107] B. Liu, D. Wang, H. Li, L. Wang, L. Zhang, As(III) removal from aqueous solution using α-Fe_2O_3-impregnated chitosan beads. in: Proceedings—2010 International Conference on Digital Manufacturing and Automation (ICDMA 2010), 2010, pp. 289–292, https://doi.org/10.1109/ICDMA.2010.320.
[108] R.Y. Ning, Arsenic removal by reverse osmosis. Desalination 143 (2002) 237–241, https://doi.org/10.1016/S0011-9164(02)00262-X.
[109] A. Oehmen, R. Valerio, J. Llanos, J. Fradinho, S. Serra, M.A.M. Reis, J.G. Crespo, S. Velizarov, Arsenic removal from drinking water through a hybrid ion exchange membrane—coagulation process. Sep. Purif. Technol. 83 (2011) 137–143, https://doi.org/10.1016/j.seppur.2011.09.027.
[110] X.J. Yang, A.G. Fane, S. MacNaughton, Removal and recovery of heavy metals from wastewaters by supported liquid membranes. Water Sci. Technol. (2001) 341–348, https://doi.org/10.2166/wst.2001.0109.
[111] M. Türkmen, Removal of Heavy Metals from Wastewaters by Use of Natural Zeolites, İzmir Institute of Technology İzmir, Turkey, 2001.
[112] L. Semerjian, G.M. Ayoub, High-pH—magnesium coagulation—flocculation in wastewater treatment, Adv. Environ. Res. 7 (2003) 389–403.

This book belongs to Badji Mokhtar Annaba University Central Library Copyright Elsevier 2025

[113] B.L. Loeb, Water reuse. Ozone Sci. Eng. 38 (2016) 243–244, https://doi.org/10.1080/01919512.2016.1189292.
[114] S. Rengaraj, K.H. Yeon, S.H. Moon, Removal of chromium from water and wastewater by ion exchange resins. J. Hazard. Mater. 87 (2001) 273–287, https://doi.org/10.1016/S0304-3894(01)00291-6.
[115] S. Ahmed, S. Chughtai, M.A. Keane, The removal of cadmium and lead from aqueous solution by ion exchange with Na-Y zeolite. Sep. Purif. Technol. 13 (1998) 57–64, https://doi.org/10.1016/S1383-5866(97)00063-4.
[116] S. Babel, T.A. Kurniawan, A research study on Cr(VI) removal from contaminated wastewater using natural zeolite. J. Ion Exch. 14 (2003) 289–292, https://doi.org/10.5182/jaie.14.Supplement_289.
[117] R. Zhang, Y. Liu, M. He, Y. Su, X. Zhao, M. Elimelech, Z. Jiang, Antifouling membranes for sustainable water purification: strategies and mechanisms. Chem. Soc. Rev. 45 (2016) 5888–5924, https://doi.org/10.1039/c5cs00579e.
[118] A.M. Nasir, P.S. Goh, M.S. Abdullah, B.C. Ng, A.F. Ismail, Adsorptive nanocomposite membranes for heavy metal remediation: recent progresses and challenges. Chemosphere 232 (2019) 96–112, https://doi.org/10.1016/j.chemosphere.2019.05.174.
[119] J. Brame, Q. Li, P.J.J. Alvarez, Nanotechnology-enabled water treatment and reuse: emerging opportunities and challenges for developing countries. Trends Food Sci. Technol. 22 (2011) 618–624, https://doi.org/10.1016/j.tifs.2011.01.004.
[120] Y. Li, G. He, S. Wang, S. Yu, F. Pan, H. Wu, Z. Jiang, Recent advances in the fabrication of advanced composite membranes. J. Mater. Chem. A 1 (2013) 10058–10077, https://doi.org/10.1039/c3ta01652h.
[121] S. Kar, R.C. Bindal, P.K. Tewari, Carbon nanotube membranes for desalination and water purification: challenges and opportunities. Nano Today 7 (2012) 385–389, https://doi.org/10.1016/j.nantod.2012.09.002.
[122] F. Paquin, J. Rivnay, A. Salleo, N. Stingelin, C. Silva, Multi-phase semicrystalline microstructures drive exciton dissociation in neat plastic semiconductors. J. Mater. Chem. C 3 (2015) 10715–10722, https://doi.org/10.1039/b000000x.
[123] F.Y. Zhao, Y.L. Ji, X.D. Weng, Y.F. Mi, C.C. Ye, Q.F. An, C.J. Gao, High-flux positively charged nanocomposite nanofiltration membranes filled with poly(dopamine) modified multiwall carbon nanotubes. ACS Appl. Mater. Interfaces 8 (2016) 6693–6700, https://doi.org/10.1021/acsami.6b00394.
[124] L.Y. Ng, A.W. Mohammad, C.P. Leo, N. Hilal, Polymeric membranes incorporated with metal/metal oxide nanoparticles: a comprehensive review. Desalination 308 (2013) 15–33, https://doi.org/10.1016/j.desal.2010.11.033.
[125] A. Razmjou, J. Mansouri, V. Chen, The effects of mechanical and chemical modification of TiO_2 nanoparticles on the surface chemistry, structure and fouling performance of PES ultrafiltration membranes. J. Membr. Sci. 378 (2011) 73–84, https://doi.org/10.1016/j.memsci.2010.10.019.
[126] C. Dong, G. He, H. Li, R. Zhao, Y. Han, Y. Deng, Antifouling enhancement of poly(vinylidene fluoride) microfiltration membrane by adding $Mg(OH)_2$ nanoparticles. J. Membr. Sci. 387–388 (2012) 40–47, https://doi.org/10.1016/j.memsci.2011.10.007.
[127] J. Kim, B. Van der Bruggen, The use of nanoparticles in polymeric and ceramic membrane structures: review of manufacturing procedures and performance improvement for water treatment. Environ. Pollut. 158 (2010) 2335–2349, https://doi.org/10.1016/j.envpol.2010.03.024.
[128] A.P. Kumar, D. Depan, N. Singh Tomer, R.P. Singh, Nanoscale particles for polymer degradation and stabilization-trends and future perspectives. Prog. Polym. Sci. 34 (2009) 479–515, https://doi.org/10.1016/j.progpolymsci.2009.01.002.

This book belongs to Badji Mokhtar Annaba University Central Library Copyright Elsevier 2025

This page intentionally left blank

This book belongs to Badji Mokhtar Annaba University Central Library

Copyright Elsevier 2025

CHAPTER 20

Polymer nanocomposite membranes for wastewater treatment

Rahul Sudhakar Zambare[a] **and Parag Ramesh Nemade**[b,c,d]

[a]*National University of Singapore Singapore, Singapore,* [b]*Department of Chemical Engineering, Institute of Chemical Technology, Mumbai, India,* [c]*Department of Oleochemicals and Surfactants Technology, Institute of Chemical Technology, Mumbai, India,* [d]*Institute of Chemical Technology, Marathwada Campus, Jalna, India*

Abbreviations

P_s	solute permeability coefficient
P_w	water permeability coefficient
A100	aluminum terephthalate
AAO	anodic aluminum oxide
Ads	adsorption
AgNP	Ag nanoparticles
AgNPs	silver nanoparticles
Ago	amine GO
AL-DS	active layer facing draw solution
AL-FS	active layer facing feed solution
aPES	poly(arylene ether sulfone)
APTS	3-aminopropyltriethoxysilane
AQP	aquaporins
AQP Z	aquaporin Z
ATRP	atom transfer radical polymerization
BIM	bio-inspired materials
BOD	biological oxygen demand
BSA	bovine serum albumin
C300	copper benzene-1,3,5-tricarboxylate
CAP	cellulose acetate phthalate
CBB	Coomassie Brilliant Blue
CCG	chemically converted graphene
CN	carbon nanomaterials
CNT	carbon nanotubes
COD	chemical oxygen demand
COF	covalent organic frameworks
Cov	covalent linkage
CP	concentration polarization
CS	candle soot

Handbook of Nanomaterials for Wastewater Treatment. https://doi.org/10.1016/B978-0-12-821496-1.00021-0
Copyright © 2021 Elsevier Inc. All rights reserved.

This book belongs to Badji Mokhtar Annaba University Central Library

Copyright Elsevier 2025

CS	chitosan
Cyto C	cytochrome c
DMAEMA	*N*,*N*-dimethylamino-2-ethyl methacrylate
DMF	dimethylformamide
DMSO	dimethyl sulfoxide
DOC	dissolved organic carbon
DY	Direct Yellow
EB	3,8-diamino-5-ethyl-6-phenylphenanthridinium bromide (ethidium bromide)
ED	electrodialysis
F300	iron benzene-1,3,5-tricarboxylate
FEEMs	fluorescence excitation emission matrices
fGO	functionalized GO
F-MWCNTs	functionalized multiwalled carbon nanotubes
FO	forward osmosis
FRR	flux rejection ratio
GO	graphene oxide
GOT	GO-tannic acid
GQDs	graphene quantum dots
HA	humic acid
HP	hydrophilic polymer
HPEI	hyperbranched polyethylenimine
ICIC	5-isocyanato-isophthaloyl chloride
iGO	isocyanate-functionalized GO
iGO	isocyanate-treated graphene oxide
iNPs	inorganic nanomaterials
IRMOF	isoreticular metal-organic framework
LBL	layer by layer
LDH	layered double hydroxides
LMH	flux unit, L m^{-2} h^{-1}
MB	methylene blue
MBR	membrane bioreactor
MCE	mixed cellulose ester
MD	membrane distillation
MF	microfiltration
MMMs	mixed-matrix membranes
MO	methyl orange
MOF	metal-organic framework
MOx	metal oxide
MPD	m-phenylenediamine
MWCNT	multiwalled carbon nanotubes
MWD	molecular weight distribution
NF	nanofiltration
N-GOQD	nitrogen doped GO quantum dots
NIPAAm	N-isopropyl acrylamino
NLDH	nanolayerd double hydroxide
NMP	N-methyl-2-pyrrolidone
NP	nanoparticles
NPPCS	N-propylphosphonyl chitosan
NSCS	N-succinyl chitosan
ODA	octadecylamine
OMWCNTs	oxidized carbon nanotubes

This book belongs to Badji Mokhtar Annaba University Central Library
Copyright Elsevier 2025

OMWCNTs	one-dimensional oxidized carbon nanotubes
OSN	organic solvent nanofiltration
OVA	ovalbumin
P(AN-AA)	poly(acrylonitrile-*co*-acrylic acid)
P(AN-MAA)	poly(acrylonitrile-*co*-methyl acrylic acid)
PA	polyamide
PAA	polyacrylamide
PAN	polyacrylamide
PC	photocatalysis
PEBAX	polyether block amide
PEG	polyethylene glycol
PEI	polyethylenimine
PES	polyethersulfone
PI	polyimide
PIP	piperazine
PLA	polylactic acide
PPA	polypiperazinamide
PSF	polysulfone
PSS	poly(sodium 4-styrenesulfonate)
PTFE	polytetrafluoroethylene
PV	pervaporation
PVDF	polyvinylidene fluoride
PVP	polyvinylpyrrolidone
QDs	quantum dots
RhB	rhodamine B
RO	reverse osmosis
SA	sodium alginate
SDG	sustainable development goals
SEM	scanning electron microscope
sGO	sulfonated GO
SLN	surface-located nanoparticles
SPE	solid polymer electrolyte
SWCNTs	single-walled carbon nanotubes
TFC	thin-film composite
TFN	thin-film nanocomposite
TFN-i	thin-film nanocomposite—nanoparticles in the top layer
TFN-ii	thin-film nanocomposite—nanoparticles in the substrate
TMC	trimesoyl chloride/1,3,5-benzenetricarbonyl chloride
TMPyP	tetrakis(1-methyl-pyridinium-4-yl)porphyrin
Tp	1,3,5-triformylphloroglucinol
UF	ultrafiltration
UiO	Universitetet i Oslo
UN	United Nations
UV	ultraviolet
VA-CNT	vertically aligned carbon nanotube
xGnPs	exfoliated graphite nanoplatelets
XRD	X-ray diffraction
ZIF	zeolitic imidazolate framework
ZPNPs	zwitterionic polyelectrolyte nanoparticles
β	constant
λ	constant

This book belongs to Badji Mokhtar Annaba University Central Library
Copyright Elsevier 2025

20.1 Introduction

Rapid growth in population and industrialization has generated tremendous demand for water. Water resources are limited, and increasingly, water is being sourced from reservoirs at unsustainable rates. In such a world, neglecting opportunities for treatment and reuse of wastewater to fulfill a few of the water demands is unthinkable. Wastewater is long been seen as a burden for disposal or as a cost center when treatment is demanded by regulations. Neglect in wastewater treatment has seen significant deterioration in the quality of water in river, ponds, lakes, and oceans. UN estimates indicate that approximately 80% of the wastewater generated is released into the environment without treatment. However, with increasing scarcity, the outlook toward wastewater is changing. Increasingly, wastewater is being collected, treated, and reused.

20.1.1 Water scarcity

Water is a valuable resource necessary for all living things to survive. Fresh water demand originates mainly from four sources—agriculture, industry, energy production, and human consumption. Population growth and industrialization contribute toward the high demand for fresh water, resulting in a strain on the water resources. Over 2.7 billion people live in the water-stressed areas that experience the drought-like conditions for at least 1 month every year. Around 1.1 billion people do not have regular access to fresh drinking water [1]. Fig. 20.1 shows the projected water scarcity by 2025, and about two-thirds of the world will be facing shortage of drinking water, while approximately, 1.8 billion people may find difficulty in finding water to drink [2].

The lack of clean and safe drinking water is big a challenge because of rapid population growth, severe shortage of clean water resources, and environmental pollution. In 2015, UN General Assembly has released the 17 sustainable development goals (SDGs) to be achieved by 2030. SDGs focus on reducing environmental pollution, management of wastewater and treatment, and impact on surrounding water quality for sustainable development [3].

20.1.2 Wastewater and its contaminants

Any human activity involving water generates wastewater. Commonly cited, only 1% of the wastewater is contaminants. The composition of contaminants constitution (1%) varies depending on the source and the activity. The contaminants include suspended, colloidal, and dissolved solids. Wastewater is generated from domestic and industrial establishments and is mixed with surface water and groundwater [3]. The significant contaminants in untreated wastewater and treatment concerns are summarized in Table 20.1 [4]. Wastewater generated from domestic sources includes human excreta, organic matter, microorganisms, and may also

This book belongs to Badji Mokhtar Annaba University Central Library
Copyright Elsevier 2025

This book belongs to Badji Mokhtar Annaba University Central Library

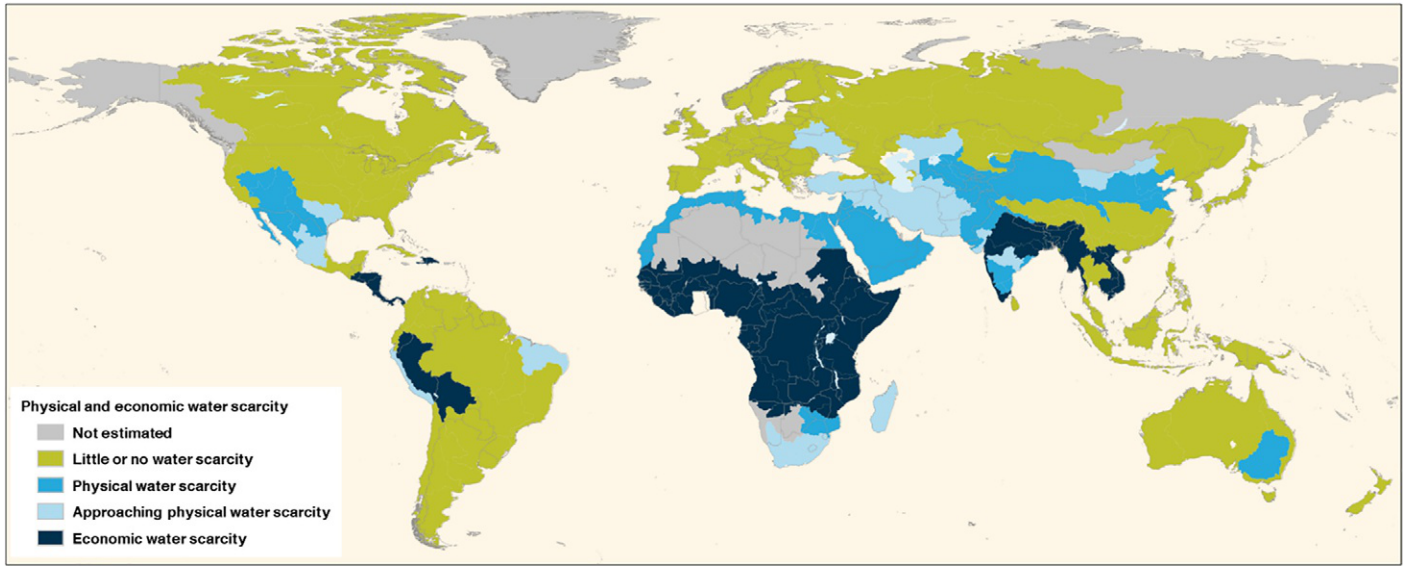

Fig. 20.1
Projected world's water scarcity in 2025. *From U. N. Environment, Global Environment Outlook 6—GEO 6: Healthy Planet, Healthy People, Nairobi. U. N. Environment, 2019.*

Copyright Elsevier 2025

Table 20.1: Important contaminants present in wastewater.

Contaminants	Reason for importance
Suspended solids	Leads to development of sludge deposits and anaerobic conditions to the aquatic environment
Pathogenic organisms	Cause infectious diseases
Priority pollutants	Content of inorganic and organic compounds that may be toxic, carcinogenic, mutagenic, or teratogenic
Refractory organics	Resist conventional wastewater treatment, require advanced oxidation processes for treatment, and may include pesticides, surfactants, etc.
Biodegradable organics	Carbohydrates, fats, and proteins. Can deplete dissolved oxygen in the water and cause algal bloom, eutrophication, and dead ecosystem
Dyes and heavy metals	Generated by commercial and industrial activities
Dissolved inorganic	Constituents such as calcium, sodium, and sulfate
Emerging pollutants	Effects of individual contaminants are only studied marginally, and cumulative impacts are unknown. Recognized impact of individual pollutants includes endocrine disruption, birth defects, developmental disorders, cancers, and growing resistance to antibiotics in bacteria

include emerging pollutants. Emerging pollutants are defined as "any synthetic or naturally occurring chemical or any microorganism that is not commonly monitored in the environment but has the potential to enter the environment and cause adverse ecological and (or) human health effects." The emerging pollutants include pharmaceuticals, steroids and hormones, personal care products, pesticides and herbicide, microplastics, industrial additives, plasticizers, etc.

Urban water runoff may contain a wide range of contaminants, including products of incomplete combustion, soot, motor oils, heavy oils, and organic/nondegradable trash. Agricultural runoff may contain nutrients from fertilizers, pesticides, pathogenic microorganisms, etc. Industrial wastewater may contain chemicals depending on the industry. For example, paper and pulp industry wastes include chlorinated lignosulfonic acids, chlorinated organic compounds, and colored compounds; also, waters contain high chemical oxygen demand (COD), biological oxygen demand (BOD), suspended solids, etc. Wastewater from metallurgical and mining industries contains ammonia, cyanides, hydraulic oils, tailings, heavy metals, fine particulates, acids, etc. High BOD is a characteristic of dairy and food industry wastes. Coloring agents, sugars, proteins, fats, acids, alkalies, particulates, and emerging pollutants such as hormones and antibiotics are also commonly found in food industry effluents. Surfactants, biocides, stabilizers, suspended solids, acids, alkali, and salts are usually seen in textile waters. Organic chemical industry effluents contain pesticides,

This book belongs to Badji Mokhtar Annaba University Central Library Copyright Elsevier 2025

pharmaceuticals, dyes, petrochemicals, intermediates, surfactants, plasticizers, and additives. The composition may greatly vary depending upon the industry and process.

A significant amount of wastewater is released into the environment directly without adequate treatment. Contamination of wastewater has significant detrimental impact on human health, quality of water resources, and economic productivity. The impact of pollutants on health, environmental, and economic output is presented in Fig. 20.2. The contaminants in wastewater get diluted as the wastewater mixes with rivers and lakes and

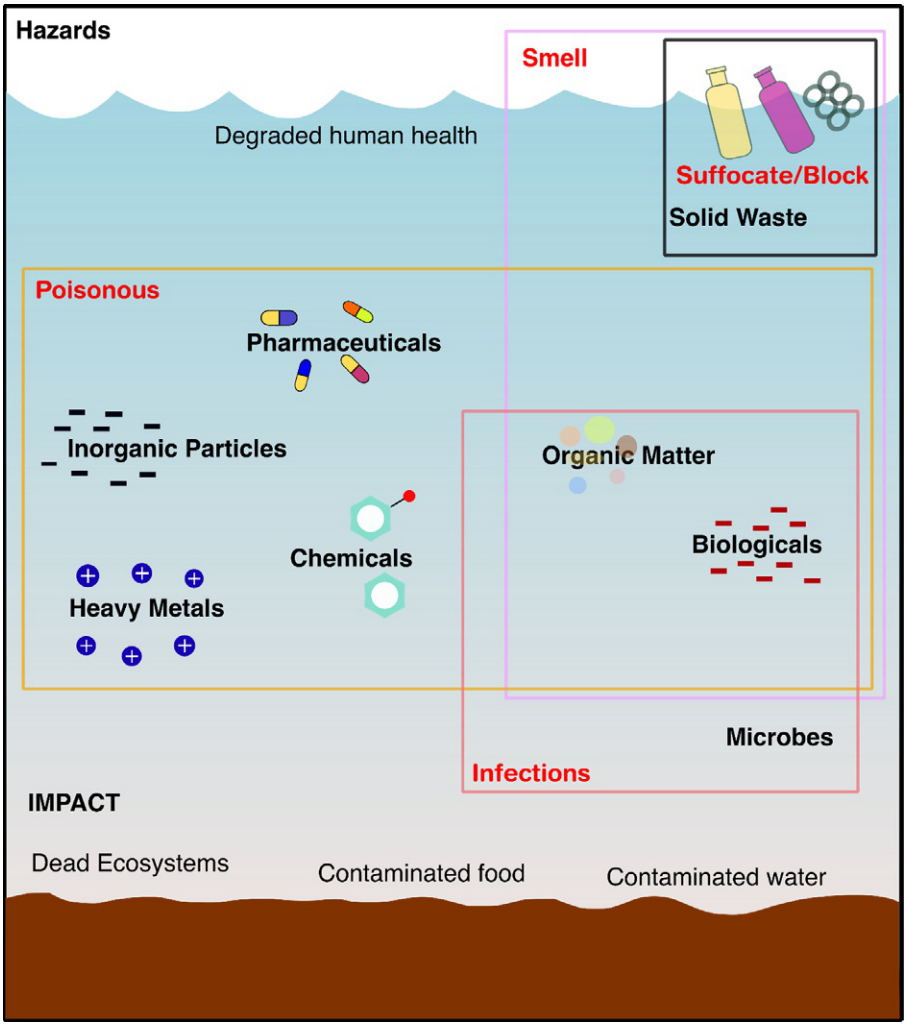

Fig. 20.2
Impact of untreated components on ecology. *From WWAP (United Nations World Water Assessment Programme), The United Nations World Water Development Report 2017. Wastewater: The Untapped Resource, UNESCO, Paris, 2017.*

This book belongs to Badji Mokhtar Annaba University Central Library
Copyright Elsevier 2025

eventually end up in the seas and oceans. The toxicity owing to heavy metals, inorganic suspended solids, and corrosive chemicals cause adverse effects on aquatic life. Solid wastes such as plastics can choke organisms. Heavy dose of organic chemicals and biological wastes can lead to dead ecosystems, algal blooms, microbial growth, and infectious diseases. Contaminated water leads to decreased productivity of agriculture and diseases in population, in addition to other issues [5, 6].

20.1.3 Membranes in wastewater treatment

With the demand of fresh water and handling of wastewater, many wastewater treatment technologies are being developed to produce portable and nonportable water. Wastewater treatment includes physical, chemical, and biological processes that are classified as primary, secondary, and tertiary wastewater treatment. Wastewater once collected is subjected to settling and skimming to remove large suspended impurities. Flocculants may be added to enhance the rate of settling. This process of physical removal of pollutants is known as primary treatment. The wastewater is then subjected to secondary treatment through aerobic or anaerobic microbial treatment. The microbial treatment through activated sludge process is the workhorse technology of wastewater treatment, but this process requires large volume reactors and large amount of sludge production [7].

Membrane separation is a well-known and competent technique used for wastewater treatment at large volume because of their ease in implementation and operation, high efficiency, durability, and declining cost. Membrane-based processes are undergoing a rapid rate of change in the performance capabilities to substitute or serve as an alternative approach for existing technologies. Membrane is an interface or barrier that allows only specific molecules to pass through it and rejecting others depending upon the pore size and selectivity under the influence of driving force. In membrane filtration process, the feed stream is separated into two different streams; permeate contains those molecules that are passed through the membrane, and retentate contains solute and other particles that are rejected by the membrane. Membrane technology has several advantages on conventional separation processes such as selective separation, compact modular construction, stationary parts, and stable filtration characteristics [8, 9]. Selectivity and permeability are important parameters for the membrane application. The driving forces in membrane filtration processes could be differences in pressure, concentration, temperature, electric potential, or a combination of these variables. The membrane processes are classified based on driving force, separation mechanism, and the rejection properties of the membrane.

Membranes can be made from inorganic films or polymeric materials. Inorganic membranes find use in high temperature and corrosive applications. However, brittleness, relative difficulty in manufacture, and higher costs have limited the applications of inorganic membranes. Polymeric membranes are most common because of versatility, tunability, and robustness.

This book belongs to Badji Mokhtar Annaba University Central Library Copyright Elsevier 2025

Nanocomposite inorganic membranes form a minority of wastewater treatment applications and are not the focus of this chapter.

20.2 Polymeric membranes

Polymeric membranes are easy to synthesize and have excellent thermal, chemical, mechanical, and hydrolytic stability [9, 10]. Polymeric membranes have many advantages such as easy operation, energy-efficiency, low cost, and inherent simplicity. Selective permeation of desired species can be produced by developing physico-chemical characteristics of the membrane material [10]. A variety of polymeric membranes have been developed based on applications such as microfiltration (MF), ultrafiltration (UF), nanofiltration (NF), reverse osmosis (RO), pervaporation (PV), electrodialysis (ED), and gas separations. Membranes used in MF and UF are porous, while RO membranes are nonporous or dense. NF filtration membranes are loose RO membranes or could be porous membranes with ionic character. Fig. 20.3 shows the different pressure-driven membrane filtration processes and their characteristics, including type of solute rejection, pore size range, separation mechanism, operating pressure range, and tentative flux range.

20.2.1 Polymers for membrane synthesis

Different polymers are used to develop the desired membrane. Polysulfone (PSF), polyethersulfone (PES), polyvinylidene fluoride (PVDF), cellulose acetate (CA), polyacrylonitrile (PAN), polyimide, polyvinyl alcohol, polytetrafluoroethylene (PTFE), polypropylene (PP), polyvinyl chloride, and cellulose nitrate are being used in the preparation of polymeric membranes [9–18]. The chemical structures of commonly used polymeric membrane materials are shown in Fig. 20.4. Of these, PP and PVDF are frequently used for MF applications. PSF and PES are most commonly used in UF and as substrate for NF and RO membrane applications. PSF has excellent chemical and thermal stability, high glass transition temperature, excellent strength and flexibility, and good film-forming properties [19]. PSF-based membranes are widely used in a range of applications in liquid separation [20–22] and gas separation processes [23, 24].

The important characteristics of membranes are average pore size, pore size distribution, pore density, water contact angle of the surface of the membrane, hydrophilicity of the pores, crystallinity of the polymer, tensile strength, surface zeta potential, surface charge, membrane structure, thickness of the top layer, the underlying substructure, method of membrane synthesis, etc., in addition to the hydraulic properties such as membrane permeability and solute rejection [25–30]. The membranes can be tuned depending upon the applications. The membranes can be modified by modifying the properties of the polymers, changing polymers, blending polymers, the additives used, the pore size, pore density, and pore size distribution, or

This book belongs to Badji Mokhtar Annaba University Central Library Copyright Elsevier 2025

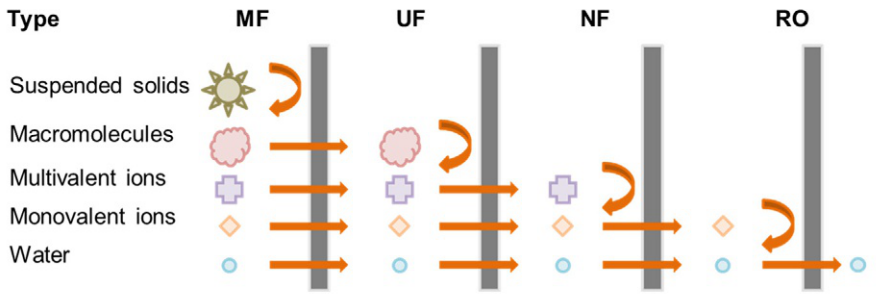

	MF	UF	NF	RO
Pore size (nm)	50 – 5000	1 – 100	0.5 – 2	< 0.5
Separation mechanism	Size exclusion	Size exclusion	Size exclusion, Donnan exclusion	Solution diffusion, size exclusion
Pressure (bar)	< 2	1 – 5	5 – 20	10 – 100
Flux range (LMH/bar)	> 50	10 – 50	1.4 – 12	0.05 – 1.4

Fig. 20.3
Different pressure-driven membrane filtration processes and their characteristics.

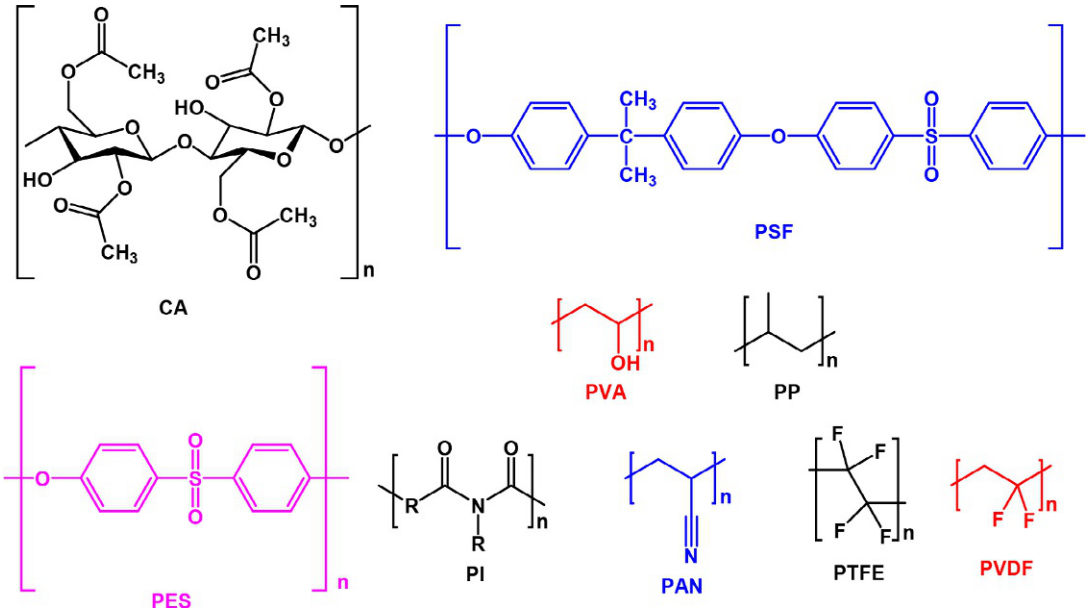

Fig. 20.4
Chemical structures of polymeric membrane materials.

This book belongs to Badji Mokhtar Annaba University Central Library
Copyright Elsevier 2025

by surface functionalization to change the surface characteristics of the membranes based on the application requirements.

20.2.2 Issue with polymeric membranes

20.2.2.1 Flux rejection trade-off

Membrane flux and rejection are the most important performance parameters for membrane separations. The membrane permeability and the rejection are usually correlated inversely [31]. The origin of the relationship is intuitive; if permeability of the membrane is higher, then it is less likely for the membrane to separate the water from solutes, suspended solids, etc. The trade-off is equally valid for porous and nonporous membranes. A higher flux in MF and UF membranes indicates large pore size and large pore density, and with large pore size, the molecular weight cutoff or particle rejection is likely to be lower. For nonporous membranes, the mechanism of permeation is better explained by solution and diffusion phenomena [32, 33]. The solute and solvent both dissolve in the dense layer and diffuse across the membrane and elute out. The rejection is a combination of solubility coefficient of solute or solvent in polymer and the diffusion coefficient. An investigation in permeability-rejection upper bound like that theorized for gas separations proposed an empirical equation (20.1). The terms P_s and P_w are

$$\frac{P_w}{P_s} = \frac{\lambda}{(P_w)^{\beta}} \tag{20.1}$$

permeability of coefficients of solute and water through the membrane, respectively, while λ and β are constants whose values are 1.4×10^{-7} and 2, respectively [34]. While the parameters λ and β are backed by fundamental theory in case of gas separations, similar theoretical backing for these parameters in the case of liquid filtration does not exist.

20.2.2.2 Fouling

Membrane fouling is significant reduction in the membrane performance because of deposition of particles and solution on the surface and inside the pores of the membranes. Membrane fouling reduces the performance necessitating significant overdesign in terms of membrane area. As the cake and fouling build up on the membrane, the resistance of membrane increases, resulting in an increase in energy consumption. The fouling of membrane depends upon the fluid characteristics, membrane characteristics, and operating conditions. Strategies applied to improve membrane performance are change in operating conditions such as mechanical or gas scouring, backflushing, liquor modification, or membrane modification. Membrane modification through incorporation of nanomaterials on the surface and inside the matrix of the membranes is reported to increase the throughput.

The physical and chemical properties of membrane material play an important role during filtration. Polymeric membranes are inherently hydrophobic and are susceptible to fouling

This book belongs to Badji Mokhtar Annaba University Central Library Copyright Elsevier 2025

because of organic molecules. Fouling is primarily caused by adsorption of solutes and suspended particles on the membrane surface and inside the pores. The concentration of rejected solutes and particles naturally is higher near the membrane surface than in the bulk. This phenomenon is known as concentration polarization (CP). The flux loss due to CP is reversible if the layer owing to CP is removed. If the concentration of solutes is higher than the solubility, the solute will precipitate on the membrane surface causing pore blocking and narrowing. The rejected particles also create a cake layer that increases the resistance to permeation of fluid causing drop in flux. A few particles that are finer than the membrane pores may be transmitted or get deposited inside the pores causing pore narrowing. This pore narrowing, blockage, and deposition of solutes on the surface of the membrane causing degraded performance is termed as fouling. The fouling may be reversible or irreversible. Cleaning will restore the performance of the membranes to certain extent; however, the performance loss owing to irreversible fouling is permanent [35]. It results in higher operational cost, shorter lifespan, and irreproducible separation performance. The fouling in aqueous applications is because of inorganic and organic salts, neutral organic molecules, proteins, and macromolecules, and suspended solids. The membrane materials play an important role in the susceptibility to fouling [36]. In aqueous applications, membrane hydrophilicity plays an important role in the reduction of membrane fouling. Water strongly binds to hydrophilic surface making it less likely for foulants to adhere to the membrane surface. The modification of the membrane materials can improve the performance of the membrane for suitable application. Membrane hydrophilicity, smoothness, surface charge on membrane, hydrogen bonding, electrostatic forces, and Van der Waals forces between solute and surface are the significant factors that affect the fouling in membranes [13, 37, 38].

Fouling resistance can be improved by increasing the hydrophilicity of membrane surface and pores. Water forms a protective layer on the hydrophilic membrane surface, thereby preventing adhesion of foulants [39]. In hydrophilic membranes, the water molecules can easily move to the interior of the membranes, which results in enhancement in permeability. Polymers are inherently hydrophobic because of organic backbone. Surface modifications to increase hydrophilicity and reduce fouling of the membranes are reported. Deposition of hydrophilic polymers such as methyl cellulose, poly(vinyl methyl) ethers [40], polyethylene glycol (PEG) [41], and polyethyleneimine [42] are reported. Modifying the surface of membranes using acids such as sulfuric acid, hydrofluoric, hydrochloric, and nitric acids have increased the hydrophilicity of the membrane surface, improved flux, and reduced fouling [43]. Use of low-temperature plasma for increasing the surface hydrophilicity of UF membranes showed an increase in oxygen functional groups [44]. Various other modification methods include homogeneous blending [12, 45–48], cross-linking [16], surface grafting [49, 50], gamma radiation [51], UV irradiation [52, 53], addition of amphiphilic block copolymers [54–56]. The surface modifications for fouling resistance like deposition of polymers also tend to reduce permeate flux, while others like plasma treatment or treatment by oxidizing acids also tend to increase the molecular weight cutoff.

This book belongs to Badji Mokhtar Annaba University Central Library Copyright Elsevier 2025

20.2.3 Use of nanocomposite membranes as a solution

Inclusion of nanomaterials in the polymer matrix can change the properties of the membranes, overcoming the flux-rejection trade-off. The nanomaterials were dispersed in the polymer matrix and used for gas separations to overcome the Robeson upper bound [57, 58] and now have been extended for use in liquid separations as well. Addition of nanomaterials within the membranes for water treatment has primarily been driven by the need to improve fouling-resistant and permeate flux. Several different approaches have been reported to include nanomaterials (Fig. 20.5) within the membranes to improve the properties, namely, (1) mixed-matrix membranes (MMMs); (2) thin-film nanocomposite (TFN) membranes; (3) surface-located nanocomposite (SLN) membranes [26].

In the MMMs, nanoparticles are dispersed in the polymer matrix during synthesis of the membrane. The particles are distributed uniformly in the matrix. These type of membranes are commonly synthesized for UF applications [59, 60]. The MMMs are synthesized commonly by phase inversion techniques. In the modification of regular phase inversion, the polymer solution is doped with nanoparticles, and then a thin film is cast and subsequently subjected to phase inversion to give a nanocomposite membrane. In membranes synthesized by electrospinning, the nanoparticles are dispersed in the polymer solution to be electrospun into the membrane [61]. The nanomaterials are included in the membranes to improve antifouling properties, increase hydrophilicity, decrease roughness, and change pore size, pore size distribution, and pore density. Additionally, the nanomaterials have also reported to impart antimicrobial and photocatalytic properties to the membrane.

In the TFN membranes, the membranes themselves are composite membranes with top layer and substrate being made of different materials. The TFN membranes are further subdivided into two categories: (1) nanoparticles dispersed in the substrate and (2) nanoparticles dispersed in the thin top layer. The TFN membranes are commonly used for RO or NF. The TFN membranes with nanoparticles dispersed in the substrate are synthesized by first synthesizing a MMM with nanomaterial and polymer, followed by subsequent modification to include a top layer to generate TFN membrane with nanocomposite substrate. Improving hydrophilicity, decreasing roughness, and increasing resistance to compaction are some of the applications reported for these types of membranes. Polyamide thin-film composite (TFC) membranes with nanoparticles in the top layer are used for NF and RO. The top layer is synthesized by interfacial polymerization of polyamine dissolved in aqueous phase and polyacid chloride dissolved in organic phase. The nanomaterials can be dispersed in either the aqueous phase or the organic phase. Improving hydrophilicity and increasing permeability to the water in RO and NF is of utmost importance; thus hydrophilic fillers are used. The hydrophilic fillers disperse in aqueous solution, and therefore, nanomaterials dispersed in aqueous phase are most commonly reported.

This book belongs to Badji Mokhtar Annaba University Central Library Copyright Elsevier 2025

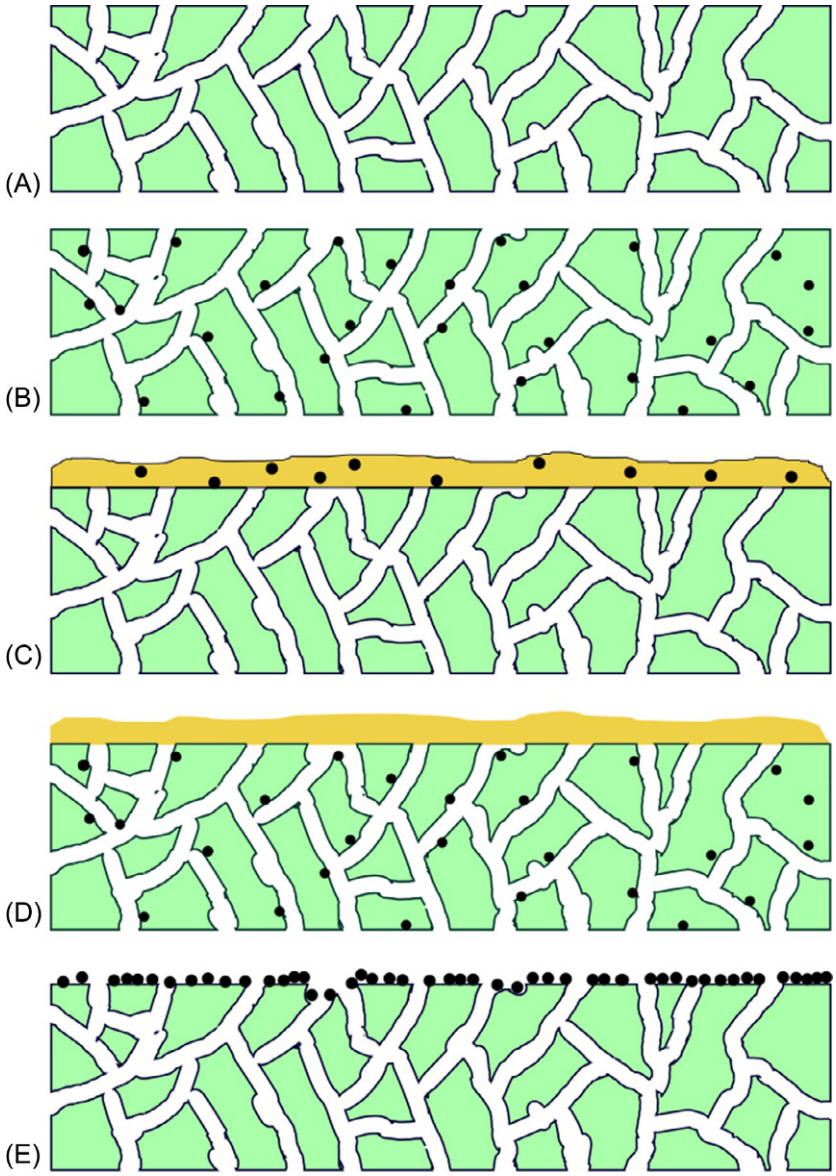

Fig. 20.5
Schematic of nanocomposite membranes. (A) Regular membrane; (B) mixed-matrix membrane; (C) thin-film nanocomposite membrane with nanoparticles in the top layer; (D) thin-film nanocomposite membrane with nanoparticles in the substrate layer; and (E) surface-located nanocomposite membrane.

This book belongs to Badji Mokhtar Annaba University Central Library
Copyright Elsevier 2025

The SLN membranes are those in which nanomaterials are deposited on the surface of an existing membrane through surface modification. These types of membranes are reported for a wide range of applications from UF, RO, and NF. SLN is synthesized by surface modification of existing asymmetric or TFC membrane. The nanoparticles are then deposited on the surface by self-assembly, coating, electrodeposition, grafting, adsorption, and precipitation, among other techniques. Increasing hydrophilicity of the surface, imparting antimicrobial or photocatalytic properties, and increasing fouling resistance are the primary drivers for synthesis of SLN membranes. A list of different nanocomposite membranes for various applications is presented in Table 20.2.

20.3 Mixed-matrix membranes

Blending of hydrophilic materials in polymer matrix is a common and widely used method to fabricate polymeric MMM. Blending is a physical mixing of additives in the polymer solution without any chemical reaction. Typically, the phase inversion method was used for the preparation of MMM. The incorporation of additives in the polymer matrix improves the membrane structural features, permeability, and surface properties. A significant amount of literature on the blending techniques is available [9, 62]. Polymer blends are classified as either homogeneous or heterogeneous depending upon the nature of the additive and solvents.

Different types of additives—hydrophilic, hydrophobic, amphiphilic, and inorganic material blending in polymer matrix showed an improvement in the hydrophilicity and antifouling properties of MMM [39]. The type of nonsolvent and additive properties make the polymer solution thermodynamically unstable, and the solvent located between the polymers chains diffuse out in the nonsolvent bath during phase inversion process. The hydrophilic additives increase the phase inversion kinetics rate, which results in the formation of microvoids and more interconnected pores [89].

20.3.1 Hydrophilic and amphiphilic polymer (HP)-incorporated in mixed-matrix membrane

The hydrophilic additives have good compatibility with polymers used to prepare the membrane, resulting in higher performance. The commonly used hydrophilic additives are PEG [62, 63], polyvinylpyrrolidone (PVP) [12, 64, 65], polyethylene oxide (PEO) [66, 67], and cellulose acetate phthalate (CAP) [68–70]. These improve the membrane microstructure, permeability, and protein adsorption resistance. A hydrophilic water-soluble chitosan and its derivatives, N-propylphosphonyl chitosan (NPPCS) and N-succinyl chitosan (NSCS), were blended with PSF to fabricate mixed-matrix UF membrane for heavy metal rejection [71]. The membrane showed good transition metal ion rejection of 92%–98% for Cu, Ni, and Cd. Sulfonated, PEGylated

This book belongs to Badji Mokhtar Annaba University Central Library Copyright Elsevier 2025

This book belongs to Badji Mokhtar Annaba University Central Library

Table 20.2: Nanocomposite membranes reported for various applications.

Process	Filler type	Application	Filler	Polymer	membrane type	Loading (%w/v)	Remark	Reference
				HP in MMM				
UF	HP	UF/protein rejection	PEG-400	PS	MMM	0–10	Increased hydrophilicity, porosity and water flux, UF membrane 70 kDa	[62, 63]
UF	HP	UF/protein rejection	PVP-15 k	CA	MMM	0–6	Effects of PVP loading and coagulation bath temperature on morphology and performance studied	[12]
NF	HP	Vapor separation	PVP	Polyetherimide	MMM	5	Toluene/methane separation, increased selectivity factor, but the stability decreased in the long run	[64]
UF	HP	Membrane bioreactors	PVP	PVDF	MMM	Blend	Leaching of PVP enlarged pores and hydrophobic membrane	[65]
SPE	HP	Lithium-ion batteries	PEO-PPO-PEO	PVDF	MMM	Blend	Higher ionic conductivity and electrochemical stability	[66]
SPE	HP	Solid-state ion cell	PEO-$Mg(NO_3)_2$	PVP	MMM	Blend	Good solid-state Mg ion cells, higher ionic conductivity	[67]
UF	HP	Antimicrobial	CAP/PVP	PES	MMM	2	High flux, better mechanical strength, and antifouling surface	[68]
UF	HP	Morphology study	CAP	PAN	MMM	Blend	DMSO solvent creates porous structure, the highest permeability, and MWCO but poor tensile strength. NMP and DMF yield denser structure with better mechanical property	[69]
UF	HP	Antimicrobial	PEG/CAP	PAN	MMM	2	Best fouling resistance against BSA.	[70]
UF	HP	Heavy metal separation	CS/NSCS/NPPCS	PS	MMM	5	Maximum rejection of 98%, 95%, and 92% for Cu, Ni, and Cd, respectively, with flux of 117 LMH	[71]
UF	HP	Antimicrobial	Poly(methyl methacrylate-acrylic acid-vinyl pyrrolidone)	PES	MMM	Blend	pH responsive and improved antifouling property	[72]
UF	HP	pH sensitivity	P(AN-AA) and P(AN-MAA)	PES	MMM	Blend	Both polymers showed evident pH sensitivity	[73]
UF	HP	Aqueous filtration	NIPAAm and DMAEMA	PES	MMM	Blend	Improved hydrophilicity and the filtration performance	[74]

Copyright Elsevier 2025

This book belongs to Badji Mokhtar Annaba University Central Library

Table 20.2: Nanocomposite membranes reported for various applications—cont'd

Process	Filler type	Application	Filler	Polymer	membrane type	Loading (%w/v)	Remark	Reference
iNPs in MMM								
PC	MOx	Photocatalysis	Ag/TiO_2	PVDF	MMM		Antimicrobial and photocatalytic degradation of norfloxacin	[75]
PC	MOx	Photocatalysis	L-Histidine-doped TiO_2-CdS	PES	MMM	0.1–1	98% FRR under visible light	[76]
UF	MOx	Oil water separation	$AlSi_2O_6$	PS	MMM	0.1–7.5	>97% flux recovery ratio	[77]
UF	MOx	Antimicrobial	Ag_3PO_4/ZnAlCu-NLDH	PES	MMM	0.5	Long life of nanofillers, higher flux	[78]
UF	MOx	Heavy metal removal	$Mg(OH)_2$	PES	MMM		High flux, high rejection	[79]
PC, UF	Metal	Self-cleaning	Citrate-stabilized gold	PES	MMM	0.5–2	>95% FRR, visible light degradation of humic acid compounds	[80]
UF	LDH	Dye filtration	Layered double hydroxides	PEI	MMM		Conducive to the transport of ions and water molecules, rejection of macromolecules	[81]
UF	LDH	Oil-water separation	NiCo-LDH	PVDF	MMM		Superhydrophilicity/underwater superoleophobicity	[82]
MOF in MMM								
UF	MOF	Dye removal	F300, A100, and C300	PAN	MMM	0.1	40% flux increase, no change in rejection of dextran	[83]
UF	MOF	Dye filtration	ZIF-8	PES	MMM	0.02–0.1	Removal of Malachite green	[84]
UF	MOF	Oil-water separation	ZIF-8	PLA	MMM		Electrospun, efficient oil-water separation of unstabilized emulsion	[85]
UF	MOF	Protein filtration	UiO-66@GO	PES	MMM	0.5–3.0	350% flux increase and 44% increase in % rejection to 85%	[86]
CN in MMM								
UF	CN	Protein filtration	Amine-GO	PS	MMM	1%	300% flux increase, no change in rejection, 15% tensile strength increase Low fouling	[87]
UF	CN	Antimicrobial	MWCNT	PES	MMM	2	Improved fouling resistance caused by natural water	[45]
UF	CN	Antimicrobial	ICIC/MWCNT	PS	MMM	0.19	Increased porosity, less adsorption of protein on membrane	[46]
UF	CN	Conductive polymer	GO	Polymer	MMM	Blend	Additional chemical treatment to GO required to increase electrical conductivity	[88]

Continued

Copyright Elsevier 2025

This book belongs to Badji Mokhtar Annaba University Central Library

Table 20.2: Nanocomposite membranes reported for various applications—cont'd

Process	Filler type	Application	Filler	Polymer	membrane type	Loading (%*w*/*v*)	Remark	Reference
UF	CN	Antimicrobial	iGO	PS	MMM	1	Negatively charged membrane, smooth surface, improved hydrophilicity, and antifouling property	[11]
UF	CN	Membrane bioreactor	GO	PS	MMM	1	Enhanced antifouling capability for MBR	[89]
UF	CN	Antimicrobial/dye filtration	GO	PES	MMM	0.5	Improved antibiofouling property, mean pore radius, porosity, and water flux	[90]
UF	CN	Salt filtration	GO	PS	MMM	2000 ppm	Enhanced hydrophilicity, 72% Na_2SO_4 rejection	[91]
UF	CN	Morphology study	GO	PS	MMM	2	Improved thermal and mechanical properties	[92]
UF	CN	Antimicrobial/ permeability	GO	PVDF	MMM	2	Higher hydrophilicity, higher flux recovery ratio (FRR)	[93]
UF	CN	Aqueous filtration	Hydrophilic polyurethane	PVDF	MMM	Blend	Hydrophilic membrane, controlled MWCO	[13]
UF	CN	Protein filtration	GO-x/PEG-400	PS	MMM	1	Microporous membrane, enhanced hydrophilicity and antifouling property with GO oxidation degree	[94]
UF	CN	Antimicrobial/ permeability	Sulfonated-GO	PVDF	MMM	0.4–1.2	Enhanced hydrophilicity, water flux, antifouling, and mechanical performance	[95]
UF	CN	Antimicrobial/ permeability	HPEI-GO	PES	MMM	Blend	Good antibacterial against *E. coli* and mechanical performance	[96]
UF	CN	Antimicrobial	PE-g-GO, GO-NH_2	Polyolefin	MMM	Blend	Cost effective antimicrobial membranes for water purification	[97]
UF	CN	Membrane distillation	*n*-Butylamine-GO	PVDF	MMM	0.5	Flux of 61.9 kg m^{-2} h^{-1} and a salt rejection of 99.9% using seawater as the feed at 80 °C.	[98]
UF	CN	Antimicrobial/ permeability	APTS-GO	PVDF	MMM	Blend	Enhanced mechanical strength, superior hydrophilicity, water flux, and BSA rejection rate	[99]
UF	CN	Antimicrobial	Ag-decorated GO	PS	MMM	Blend	Greater antibacterial properties, improved permeability and solute rejection	[100]
UF	CN	Antimicrobial	Ag-amine-GO-MOF	PES	MMM	Blend	excellent antibiofouling activity, self-cleaning membrane surface	[101]

Copyright Elsevier 2025

This book belongs to Badji Mokhtar Annaba University Central Library

Table 20.2: Nanocomposite membranes reported for various applications—cont'd

Process	Filler type	Application	Filler	Polymer	membrane type	Loading (%w/v)	Remark	Reference
UF	CN	Antimicrobial	Au/xGnPs	PS	MMM	Blend	Catalytically active, resistant to compaction, higher permeable membrane	[102]
UF	CN	Antimicrobial	TiO_2-GO	PS	MMM	Blend	Improved surface roughness, reduced irreversible HA fouling	[103]
UF	CN	Antimicrobial	Oxidized MWCNTs/GO	PVDF	MMM	Blend	Antiirreversible fouling performance for BSA	[104]
UF	CN	Antimicrobial	CNT	PES	MMM	Blend	Less protein adsorption	[105]
UF	CN	Antimicrobial	Carboxyl MWNTs	PS	MMM	1.5	Highly porous membrane structure and hydrophilic surface	[106]
UF	CN	Physical morphology	Oxidized MWCNT	PVDF	MMM	Blend	Enhanced hydrophilicity, porosity, pore size and surface roughness	[107]
UF	CN	Heavy metal removal	fMWCNT	PS	MMM	Blend	Enhanced chromium and cadmium removal from water in acidic condition	[108]
UF	CN	Antimicrobial/ permeability	Phenylenediamine-MWCNT	PES	MMM	1	Higher antifouling properties against BSA	[109]
UF	CN	Antimicrobial/ permeability	fMWCNT	PS	MMM	Blend	Influenced morphology and permeation of membrane	[46]
UF	CN	Antimicrobial/ permeability	GO/OMWCNTs	PVDF	MMM	Blend	Improved permeation and antifouling properties	[110]
UF	CN	Antimicrobial	VA-CNT	Epoxy resin	MMM	Blend	Higher BSA rejection and lower irreversible fouling	[111]
UF	CN	Estrogenic pollutants removal	Fullerene C60	Polyphenylene oxide	MMM	Blend	>95% Estrone rejection and higher flux	[112]
UF	CN	Antimicrobial/ permeability	Oxidized nanocarbon black	PS	MMM	1	Excellent antifouling properties and mechanical strength at lower filler content	[113]
UF	CN	Aqueous filtration	CS/PEG	CA	MMM	Blend	Promising substrate for water desalination, high salt rejection	[114]
UF	CN	Antimicrobial/ permeability	Fullerene, astralene, or graphite soot	Polyamide	MMM	Blend	Good water flux recovery after protein contact, Fullerene and astralene increased hydrophobicity	[115].
iNPs in TFN-i								
RO	Metal	Salt filtration/ antimicrobial	Ag	PA	TFN-i		Improved antibacterial activity, water flux 2.1 LMH/bar, NaCl rejection 98.64%	[116]
RO	Metal	Salt filtration/ antimicrobial	Ag	PA	TFN-i		Higher rejection of salt, boron, and small molecular organic compounds, water flux 2.5 LMH/bar, NaCl rejection 99.1%	[117]
RO	MOx	Salt filtration	TiO_2	PA	TFN-i		Water flux 2.6 LMH/bar, NaCl rejection 99.7%	[118]

Continued

Copyright Elsevier 2025

This book belongs to Badji Mokhtar Annaba University Central Library

Table 20.2: Nanocomposite membranes reported for various applications—cont'd

Process	Filler type	Application	Filler	Polymer	membrane type	Loading (%w/v)	Remark	Reference
RO	MOx	Salt filtration	TiO_2	PA	TFN-i		Water flux 1.6 LMH/bar, NaCl rejection 97.7%	[119]
RO	MOx	Salt filtration	SiO_2	PA	TFN-i		Water flux 1.2 LMH/bar, NaCl rejection 91.1%	[120]
RO	MOx	Salt filtration	SiO_2	PA	TFN-i		Water flux 1.1 LMH/bar, NaCl rejection 92.0%	[121]
RO	MOx	Salt filtration	Fluorinated SiO_2	PA	TFN-i		Water flux 2.5 LMH/bar, NaCl rejection 98.6%	[122]
RO	MOx	Salt filtration	CeO_2	PA	TFN-i		Water flux 2.8 LMH/bar, NaCl rejection 98.0%	[123]
RO	MOx	Salt filtration	Polymer-modified silica	PA	TFN-i		Water flux 0.6 LMH/bar, NaCl rejection 97.7%	[124]
NF	MOx	Salt filtration	NaA Zeolite	PA	TFN-i		200% flux increase, same rejection, one of the earliest TFN papers, water flux 12.4 LMH/bar, NaCl rejection 94.0%	[125]
NF	MOx	Salt filtration	Zeolites	PA	TFN-i		Better flux	[126]
NF	MOx	Salt filtration	Alumina	PA	TFN-i		Better flux	[127]
NF	MOx	Salt filtration	Aluminosilicate nanotubes	PA	TFN-i		Better flux	[128]
NF	MOx	Salt filtration	Mesoporous silica	PA	TFN-i		Better flux	[129]
NF	MOx	Salt filtration, antimicrobial	Ag	PA	TFN-i		Antimicrobial, increased flux	[130]
NF	MOx	Salt filtration	TiO_2	PA	TFN-i			[131]
NF	MOx	Salt filtration	Aminosilanized TiO_2	PES coated porous α-Al_2O_3 hollow fiber	TFN-I	0.005–0.1	Flux improved twofold, but rejection reduced by 50%, water flux 1.6 LMH/bar, NaCl rejection 54%	[131]
NF	MOx	Dioxane removal	Silica	PA	TFN-i	5–28	300% flux improvement but significantly lower rejection	[132]
FO	MOx	Pharmaceutical/ antimicrobial	TiO_2/AgNPs	PS	TFN-i	0.3	Removal of antibiotic-resistant genes and bacteria during dewatering by FO	[133]
PC	MOx	Photocatalysis	Bi-plasmonic nanocomposite (Au-Ag)/poly acrylic acid	PA	TFN-i		Ofloxacin, MB degradation, gram negative bacteria deactivation	[134]
NF	MOx	Salt separation, water softening	Isophthalic acid/ aluminum nitrate	PA	TFN-i	0.5–2	Improvement in flux and rejection	[135]
NF	MOx	Salt separation	TiO_2	PA	TFN-i	0.05–0.1	Sulfur rejection of sulfur recovery unit (SRU) wastewater 99.9% rejection, higher flux, and higher rejection	[136]

Copyright Elsevier 2025

This book belongs to Badji Mokhtar Annaba University Central Library

Table 20.2: Nanocomposite membranes reported for various applications—cont'd

Process	Filler type	Application	Filler	Polymer	membrane type	Loading (%w/v)	Remark	Reference
PC	MOx	Antimicrobial	Palygorskite/TiO_2	PA	TFN-i	0.1–0.5	25 LMH/bar water flux, 1.6 fold higher than control, antimicrobial under UV	[137]
RO	Metal	Antimicrobial	Ag	PA	TFN-i		Ultrasmall Ag nanoclusters ($d < 2$ nm)	[138]
RO	Metal	Antimicrobial	Ag	PA	TFN-i		Ag nanoparticles	[139, 140]
RO	Metal	Antimicrobial	Ag	PA	TFN-i		In situ AgNP generation	[141]
FO	Metal	Antimicrobial	Ag/TiO_2	PA	TFN-i		Combination of photocatalytic and antimicrobial action	[133]
RO	Metal	Antimicrobial	Ag/Palygorskite	PA	TFN-i		Sustained antimicrobial activity, low fouling	[142]
RO	Metal	Antimicrobial	Ag/zeolite	PA	TFN-i		Sustained antimicrobial activity, low fouling	[143, 144]
RO	Metal	Antimicrobial	Ag/MOF	PA	TFN-i		Sustained antimicrobial activity, low fouling	**MOF** [145, 146]
RO	Metal	Antimicrobial	Ag/ZnO	PA	TFN-i		Ag@ZnO core-shell nanoparticle with enhanced antimicrobial activity, low fouling	[147]
RO	Metal	Antimicrobial	Ag	PA	TFN-i		Sustained antimicrobial activity, lower surface roughness	[148]
RO	Metal	Antimicrobial	Cu	PA	TFN-i		Enhanced antimicrobial activity, 100% flux increase	[149]
RO	Metal	Antimicrobial	Cu/Fe-Fe_2O_3	PA	TFN-i	0.25	98% decrease in CFU concentration	[150]
BIM-TFN-i								
RO	BIM	Salt filtration	AQP-Z	PA on PSF	TFN-i	10 mM	40% higher water permeability than brackish water RO membrane, water permeability 4.0 LMH/bar, NaCl rejection 97%	[151]
NF	BIM	Salt filtration	PDA coated proteoliposomes	Poly(amide-imide)	TFN-i	4 mM	AQP-Z maintained high activity under thermal treatment at 343 K for 2 h, water flux 36.6 LMH/bar, NaCl rejection 95%	[152]
NF	BIM	Salt filtration/ antimicrobial	Zwitterionic polyelectrolyte nanoparticles	PA on PS	TFN-i	0.1	High water permeability of 10.1 LMH/bar and improved NaCl/ Na_2SO_4 selectivity, fouling resistance against BSA	[153]
FO	BIM	Salt filtration	AQP-Z	PA on PES hollow fiber	TFN-i	0.5 mM	200% times high flux than commercial BW30 membrane, super-high water flux in FO with lowest salt back diffusion, water flux 8.0 LMH/bar, NaCl rejection 97.0%	[154]

Continued

Copyright Elsevier 2025

This book belongs to Badji Mokhtar Annaba University Central Library

Table 20.2: Nanocomposite membranes reported for various applications—cont'd

Process	Filler type	Application	Filler	Polymer	membrane type	Loading (%*w*/*v*)	Remark	Reference
RO	BIM	Salt filtration	AQPs	PA on PS	TFN-i	10 mM	Require half the applied pressure to achieve the same water flux as a commercial membrane, less energy consumption, water flux 4.1 LMH/bar, NaCl rejection 97.2%	[155]
CN in TFN-i								
RO	CN	Salt filtration/ chemical stable	GO	PA on PS	TFN-i	100 ppm	Higher water flux, salt rejection, chlorine stability, and mechanical strength, stable in acidic and alkaline conditions, water flux 2 LMH/bar, NaCl rejection 97.0%	[156]
RO	CN	Salt filtration/ antimicrobial	GO	PA	TFN-i	0.12	High flux without significant reduction in salt rejection, superior antimicrobial activity, water flux 0.2 LMH/bar, NaCl rejection 87.0%	[157]
RO	CN	Salt filtration/ antimicrobial	Exfoliated, size-controlled GO	PA	TFN-i		Water permeability and antibiofouling property enhanced by 80% and 98%, respectively, rejection is retained at 48,000 ppm h chlorination, water flux 1.1 LMH/bar, NaCl rejection 99.4%, chemical stability	[158]
NF	CN	Natural organic removal	GO	PA on PS	TFN-i	0–0.012	Thin and dense membrane, tested real river water, water flux 20.1 LMH/bar, UV_{254} rejection 62.0%, dissolved organic carbon rejection 41.1%	[159]
NF	CN	Natural organic removal	PA	PA	TFN-i	–	Pristine polyamide membrane, water flux 18.7 LMH/bar, UV_{254} rejection 32.8%, dissolved organic carbon rejection 17.4%	[159]
NF	CN	Salt and dye filtration	Starch-GO	PA on PS	TFN-i		Increased hydrophilicity because of starch and GO, water flux increased by 80%, higher Na_2SO_4 rejection >96.0%, reactive green 19 and reactive violet-1 rejection >99.9%	[160]
NF	CN	Salt filtration/ antimicrobial	PEG-GO	PA on PS	TFN-i		Higher rejection, lowering of contact angle with better antifouling properties	[161]

Copyright Elsevier 2025

This book belongs to Badji Mokhtar Annaba University Central Library

Table 20.2: Nanocomposite membranes reported for various applications—cont'd

Process	Filler type	Application	Filler	Polymer	membrane type	Loading (%w/v)	Remark	Reference
NF	CN	Salt filtration	TiO_2-GO	PA on PS	TFN-i	1.25% w/w polymer	High water permeability of 6.1 LMH/bar	[162]
RO	CN	Salt filtration	GO	PA	TFN-i	0.015	Enhanced permeability due to multilayer structure of GO, interlayer spacing acts as water channels, water flux 2.9 LMH/bar, NaCl rejection 93.8%, Na_2SO_4 rejection 97.3%	[163]
RO	CN	Salt filtration/ antimicrobial	GO	PA on PS	TFN-i	53, 107, and 160 ppm	A trade-off was observed between enhanced permeability and reduced fouling resistance, GO in TFC membrane more effective as fouling controlled filler and restricted as membrane performance enhancer	[164]
NF	CN	Salt filtration	Hydrotalcite/GO	PA on PES	TFN	Top layer	Improved flux and salt rejection	[165]
NF	CN	Salt filtration/ antimicrobial	GQDs	PA	TFN-i		High water flux and excellent antifouling against BSA, humic acid and emulsified oil solutions, water flux 51.0 LMH/bar, NaCl rejection 80.0%	[166]
RO	CN	Salt filtration	Carbon dots	PA	TFN-i		Hydrophilic carbon dots improved RO performance, water flux 5.7 LMH/bar, NaCl rejection 99.0%	[167]
RO	CN	Salt filtration	Na^+-CQDs	PA	TFN-i		Brackish water desalination, water flux 4.3 LMH/bar, NaCl rejection 98.6%	[168]
RO	CN	Salt filtration/ antimicrobial/ chemical resistance	GOQDs	PA	TFN-i		Improved antifouling and chlorine resistance, water flux 2.3 LMH/bar, NaCl rejection 98.8%	[169]
RO	QDs	Salt filtration	N-GOQDs	PA	TFN-i		High water flux desalination, water flux 1.7 LMH/bar, NaCl rejection 93.0%	[170]
MOF in TFN-i								
NF	MOF	Dye removal	Poly(sodium 4-styrene sulfonate) modified ZIF	PA	TFN-i	0.05–0.2	200% flux increase, no change in Na_2SO_4 rejection Dye rejection	[171]
Ads	MOF	Heavy metal removal	UiO-66	PA	TFN-i	0.05–0.2	Removal of thorium, enrichment factor of 250	
Ads	MOF	Metal rejection, Pb	Amine-functionalized MOF	Ceramic	TFN-i	Top layer	61% rejection of Pb^{2+} ions	[172]
FO	MOF	Salt rejection/ dewatering	UiO-66	PA	TFN-i	0.1	52% flux increase	[173]

Continued

Copyright Elsevier 2025

This book belongs to Badji Mokhtar Annaba University Central Library

Table 20.2: Nanocomposite membranes reported for various applications—cont'd

Process	Filler type	Application	Filler	Polymer	membrane type	Loading (%w/v)	Remark	Reference
FO	MOF	Salt rejection/ dewatering	Ag-MOF	PA	TFN-i	0.04	29% flux increase, lower flux decline than control	[146]
NF	MOF	Antimicrobial	MOF/GO	PA	TFN-i		MIC of 128 mg/L, 4.1 LMH/bar	[174]
NF	MOF	Metal rejection, copper	IRMOF-3/GO	PS	TFN-i	Top layer	> 90% rejection and 31 LMH flux at 7 bar	[175]
RO	MOF	Desalination	ZIF-8	PA	TFN-i	0.05–0.4	162% higher flux no change in rejection	[176]
RO	MOF	Desalination	ZIF-8	PA	TFN-i	0.2–0.4	High water permeability	[177]
RO	MOF	Dye filtration	ZIF-8/Chitosan	PVDF	TFN-i		350% higher flux Higher NaCl rejection	[178]
UF	MOF	Dye filtration	ZIF-8/Gelatin	PVDF	TFN-i	2 μm top layer	Flux decreased by 80% Rhodamine rejection increased from 0% to 90%	[179]
NF	COF	Dye filtration	Tp-MPD	PA	TFN-i	Top layer	50 LMH/bar PWF and 99.5% congo red rejection	[180]
NF	COF	Dye filtration	EB-COF:Br		TFN-i	Top layer	48 LMH/bar water flux, 99.9% methyl orange rejection	[181]
NF	COF	OSN	Ag^+@COF/PEBAX	PS	TFN-i	Top layer	High rejection of thiophene, desulfurization of diesel	[182]
Fillers in TFN-ii								
RO	CN	Salt filtration	PA	GO-mixed PS	TFN-ii	0.5–1.8 wt% to PS	High mechanical strength, highly porous support when compared to that of support layer of conventional RO membrane, water flux 5.4 LMH/bar, NaCl rejection 98.2%	[183]
RO	CN	Salt filtration/ chemical stable	PA	aPES/GO/aGO	TFN-ii		Much higher chlorine resistance than pristine polyamide membrane, water flux 28.4 LMH/ bar, NaCl rejection 98.4%	[184]
RO	CN	Salt filtration/ chemical stable	aPES	aPES	TFN-ii		Water flux 32.5 LMH/bar, NaCl rejection 94.3%	[184]
UF	CN	Oil-water separation	Oxidized MWNTs	PEBAX	TFN-i	0–20	535% flux increase, no change in rejection	[185]
FO	CN	Dewatering	MWCNT	PS	TFN-ii		High flux, finger-like morphology	[186]
FO	CN	Dewatering	$g\text{-}C_3N_4$	PS	TFN-ii	0.05	270% higher flux	[187]
FO	MOx	Dewatering	TiO_2	PS	TFN-ii	0.5–0.6	>100% flux improvement in FO	[188–190]
FO	MOx	Dewatering	Hydroapatite	CA	TFN-ii		High flux, low internal CP	[191]
FO	Zeolite	Dewatering	Zeolite	PS	TFN-ii	0.5	>High flux	[192]
FO	Clay	Dewatering	Bentonite	PVDF	TFN-ii	0–2.0	High flux, 40 LMH/bar	[193]
FO	Cov	Antibiotic wastewater treatment	Polyacrylamide	PVDF	TFN-ii	Laminate on substrate	High rejection and high flux for TC, FO-MD hybrid process	[194]
FO	LDH	Dewater	Layered double hydroxide nanoparticles	PS	TFN-ii		High flux, low internal CP	[195]

Copyright Elsevier 2025

This book belongs to Badji Mokhtar Annaba University Central Library

Table 20.2: Nanocomposite membranes reported for various applications—cont'd

Process	Filler type	Application	Filler	Polymer	membrane type	Loading (%w/v)	Remark	Reference
Commercial membrane								
NF	NF270	Salt filtration	Dow-filmtec	PA	TFN	–	Water flux 15.1 LMH/bar, NaCl rejection 55.0%	[196]
RO	BW30	Salt filtration	Dow-filmtec	PA	TFN	–	Water flux 3.9 LMH/bar, NaCl rejection 97.9%	[197]
RO	SW30HR	Salt filtration	Dow-filmtec	PA	TFC	–	Water flux 1.9 LMH/bar, NaCl rejection 99.0%	[183]
RO	LFC-1	Salt filtration	Hydranautics	PA	TFC	–	Water flux 2.7 LMH/bar, NaCl rejection 98.4%	[183]
RO	SWC5	Salt filtration	Hydranautics	PA	TFC	–	Water flux 1.6 LMH/bar, NaCl rejection 97.9%	[183]
RO	SW400ES	Salt filtration	Nano H_2O	PA	TFC	–	Water flux 2.7 LMH/bar, NaCl rejection 99.0%	[183]
RO	FE	Salt filtration	Woongjin	PA	TFC	–	Water flux 2.9 LMH/bar, NaCl rejection 98.9%	[183]
Free standing								
NF	COF	OSN	COM	–	Free standing		High rejection of dyes, pharmaceuticals in organic solution	[198]
PC	MOx	Disinfection	Ag/BiOI/TiO_2		Free standing		7.5 log inactivation of *E. coli* in 1 h under visible light. Ag-decorated BiOI embedded on TiO_2 nanofibers	[199]
CN in SLN								
NF	CN	Salt/dyes filtration	CCG	MCE, PVDF, or AAO	SLN	≈22–53 nm	An ultrathin coating, water flux 21.8 LMH/bar, >99% retention for organic dyes, 20%–60% retention for salts	[200]
NF	CN	Dyes separation/ antimicrobial	SWCNT/GO	Polymer	SLN	40 nm	An ultrathin membrane, 97.4%–98.7% retention of BSA, cyto c, CBB and RhB dyes, water fluxes 660–720 LMH/bar	[201]
RO	CN	Salt separation	TMPyP/GO	Polymer	SLN	Top layer	GO swelling controlled by cross-linking TMPyP, created 1 nm channel size for water permeation, and salt ion retention.	[202]
NF	CN	Salt/dye filtration/ antimicrobial	MWCNT/GO	Polymer	SLN	Top layer	More than twofold water flux that graphene NF membrane (GNm), high dye rejection, and moderate salt rejection, excellent antifouling performance for SA and HA but low for BSA	[203]

Continued

Copyright Elsevier 2025

This book belongs to Badji Mokhtar Annaba University Central Library

Table 20.2: Nanocomposite membranes reported for various applications—cont'd

Process	Filler type	Application	Filler	Polymer	membrane type	Loading (%*w*/*v*)	Remark	Reference
NF	CN	Salt separation	PEI/GO	Polymer	LBL	Top layer	Positively charged membrane, water flux of 4.2 LMH/bar, and rejections of 93.9% and 38.1%, respectively, for Mg^{2+} and Na^{+}	[204]
NF	CN	Water softening	PAI-PEI/GO	Polymer	LBL	Dip coat	86% higher in water permeability, improved mechanical strength, good stability against cross-flow rate	[205]
NF	CN	Heavy metal removal	Polyamine/GO	Torlon composite	LBL	Top layer	Long-term stability, low surface defects and narrow pore size membrane, water permeability of 4.7 LMH/bar, rejection >95% toward Ni^{2+}, Pb^{2+} and Zn^{2+}	[206]
NF	CN	Salt/dye filtration	Polyelectrolyte/GO	Polycarbonate	LBL	Top layer	Charge-gated ion transport, high rejection rate along with high water permeability	[207]
iNPs in SLN								
RO	Metal	Antimicrobial	Ag	PA	SLN		Zwitterionic surface, strong binding between Ag and surface	[208]
RO	Metal	Antimicrobial	Cu-GO	PA	SLN		Covalently attached Ag through cysteamine/GO	[209]
RO	Metal	Antimicrobial	Cu	PA	SLN		Spray and spin assisted LBL assembly	[210]
RO	Metal	Antimicrobial	Ag attached to cysteamine	PA	SLN		Covalently attached Ag through cysteamine	[211]
MOF/COF in SLN								
Ads	MOF	Emerging pollutants	ZIF-8	PTFE	SLN	20	200% flux increase, 40% increase of progesterone adsorption removal by adsorption	[212]
UF	MOF	Dye filtration	ZIF-8	PVDF	SLN	Top layer	200% flux increase, better rejection	[213]
UF	MOF	Dye filtration	ZIF-8	PAN	SLN	150 nm top layer	96% flux increase, 8% higher rejection of methylene blue	[214]
UF	MOF	Dye filtration	ZIF-8	PEI	SLN	Top layer by IP	High flux and high rejection of methylene blue	[215]
NF	MOF	Emerging pollutants	ZIF-8	PA	SLN, TFN-i	0.02–0.1	Pharmaceuticals	[216]
NF	COF	Salt filtration	Hexaazatrinaphthalene and pyrene tetraone	PES	SLN	Stacking	2260 LMH/bar water flux and >99% rejection of Oct_4N	[217]

Copyright Elsevier 2025

hydrophilic groups-modified polymers exhibit excellent miscibility with polymers, which results in highly hydrophilic membranes with protein fouling resistance [19, 22].

Amphiphilic polymers, also called as self-organizing materials, as additives in polymer matrix have demonstrated enhancement in hydrophilicity and antifouling properties of the membranes [39, 218]. Amphiphilic polymers are generally prepared by free radical solution polymerization [72], reversible addition-fragmentation chain transfer polymerization (RAFT) [74], or atom transfer radical polymerization (ATRP) [73].

20.3.2 Inorganic nanomaterials (iNPs)-incorporated in mixed-matrix membrane

Various inorganic additives are also used to increase the membrane mechanical strength, hydrophilicity, and permeability, creating new generation membranes for specific applications. The commonly used inorganic additives incorporated in polymer membrane are lithium chloride [219], potassium perchlorate ($KClO_4$) [220], nanoparticles of silver (Ag) [221, 222], titanium dioxide (TiO_2) [223, 224], zinc oxide (ZnO) [225], zirconium dioxide (ZrO_2) [226], silicon dioxide (SiO_2) [227], and aluminum oxide (Al_2O_3) [228]. One of the earliest reports of use of nanomaterials in the improvement of MBR was through self-assembled TiO_2 nanocomposite membranes. Commercial PES membranes were modified by addition of sulfonic acid groups and then dipped in TiO_2 nanoparticle solution. Over 88% decrease in cake resistance was observed on coating with TiO_2 [229–231]. Nano TiO_2 containing PVDF hollow fiber membranes showed 50% decrease in fouling resistance, while the MBR operating efficiency improved showing 34% and 78% removal of N and P, respectively, from simulated wastewater in algal MBR [232]. About 75% reduction in the membrane resistance was observed for MBR application on dispersing 0.03% Al_2O_3 nanoparticles in PSF during membrane synthesis [233]. Approximately, 2- to 3.2-fold improvement in permeate flux was observed, with marginal degradation in MBR performance [234, 235]. Reduction of membrane resistance and improving biofouling resistance is the aim of including nanofillers in or on the surface of the membrane in MBR. The PES surface modified with ZnO and Ag nanoparticles improved the filterability of fruit juice in MBR [236]. In order to reduce biofouling because of adherence of bacteria, heparin, quaternary ammonium, and silver nanoparticles were blended in chitosan-cellulose acetate membranes. The study showed that antiadhesion approach to reduce biofouling was more effective than killing bacteria on the surface [237]. Polyethylene-silica membrane reduced biofouling by 27%, with increase in surface hydrophilicity [238].

The improvements in the performance were attributed to the increase in hydrophilicity, lowering of surface zeta potential, decrease in average roughness, and increase in the pore diameter. However, it must be noted that although significant improvement was observed in the membrane permeability, the performance did not degrade in terms of COD/BOD reduction or in terms of suspended solids in the permeate.

This book belongs to Badji Mokhtar Annaba University Central Library Copyright Elsevier 2025

Rich literature exists on the use of metal oxide nanoparticles in MMMs. Over 200 publications are reported on these materials. The most commonly reported metal oxides are TiO_2, ZnO, Al_2O_3, SiO_2, MnO_2, Fe_2O_3, etc. These particles are dispersed in polymers such as PVDF, PES, and PS. Several reviews are available on these applications [26, 239]. Electrospun photocatalytic and antimicrobial membranes were made by dispersing Ag/TiO_2 in PVDF-hexafluoropropylene. About >65% degradation of norfloxacin and deactivation of gram-positive and gram-negative bacteria was obtained [75]. UF membrane containing L-histidine-doped TiO_2-CdS nanoparticles in PES were used for stabilization of water pond from milk powder processing industry. The membranes displayed excellent antifouling properties, especially under visible light, giving a recovery of over 98%. Citrate-stabilized gold nanoparticles dispersed in PS UF membranes were utilized for visible light degradation of humic acid compounds deposited on the membrane during filtration. Over 95% recovery of flux was obtained after irradiation [80].

20.3.3 Metal-organic frameworks-incorporated mixed-matrix membrane

Metal-organic frameworks (MOFs) are made up of clusters of metals connected by organic linkers, which form a flexible framework with porous structure. MOFs were used as promising additives in membrane because of their high surface area, porous structure, controllable pore size, and functionality. Lee and co-workers incorporated F300, aluminum terephthalate (A100), and C300 MOFs in PAN membrane and observed up to 40% increase in the flux over the control membrane [83]. No change in rejection of dextran indicated that the molecular weight cutoff was unchanged. ZIF-8 stabilized in gelatin was dispersed in PES, which increased the rejection of malachite green from 20%–70% to almost 95%–100% [84]. ZIF-8 nanoparticles were incorporated in polylactic acid and electrospun for efficient separation of unstabilized oil-water emulsions [85], although the flux was not reported. UiO-66 MOF containing Zr-carboxylate bonds dispersed in PES showed over 350% flux when compared to control for separation of proteins, in addition to almost 44% increase in protein rejection over control.

20.3.4 Carbon nanomaterials (CNs)-incorporated in mixed-matrix membrane

Carbon nanomaterials (CNs), in specific graphite, graphene, graphene oxide (GO), carbon nanotubes (CNTs), fullerenes, and amorphous carbon have comprehensively reviewed for exceptional water transport and sieving properties [240]. CNs have large surface area, high thermal stability, and various functional groups on surface. CNTs [45, 46] and GO [11, 88–91] were used as additives in the polymeric membranes. Blending of CNs in polymer matrix showed decrease in CP and fouling of the MMMs. Graphene is a two-dimensional allotropic form of carbon, formed by single layers of carbon atoms arranged in a honeycomb structure [241]. The structure consists of sp^2 hybridized carbon atoms arranged at the lattice of hexagonal crystal held

This book belongs to Badji Mokhtar Annaba University Central Library Copyright Elsevier 2025

by σ- and π-bonds. The material is blessed with unique physical properties of high surface area, and high mechanical and thermal stability. It is unique as it is harder than diamond yet more elastic than rubber; tougher than steel yet lighter than aluminum.

20.3.4.1 Graphene oxide-based membranes

GO with abundant oxygen-containing functional groups has very good hydrophilicity and has been getting much attention in membrane technology [242–246]. GO-based membranes are generally developed with different functionalities by blending with polymer matrix [11, 89–91], layer-by-layer (LBL) [247–249], vacuum or pressure-assisted functional coating [200, 243, 244, 250–257], TFC by interfacial polymerization [156–158, 163, 258–264], and freestanding filter [265–268] to bring in certain properties to the membranes. Research and development on GO-based membrane has been developing rapidly in the past decade. Although many challenges remain, GO-based membranes are still considered as the next generation of advanced membranes. The strategic area of focus to research for promising applications of GO-based membranes has been drawn by Goh et al. [240], as shown in Fig. 20.6.

Some of the important areas being considered for the development of GO-based membranes include the development of GO nanosheets with desired functionality, highly hydrophilic GO-based membrane for antifouling properties, and stability of GO laminate membrane in

Fig. 20.6
Strategic areas of focus for GO-based membranes.

This book belongs to Badji Mokhtar Annaba University Central Library Copyright Elsevier 2025

aqueous environment. Commercial viability, materials requirement, and processing needed for different GO-based membranes are presented in Fig. 20.7.

20.3.4.2 GO-incorporated mixed-matrix membrane

GO-incorporated MMMs are exhaustively studied for UF and MF applications. The phase inversion method is commonly used to fabricate MMMs. Generally, GO is dispersed in solvent by sonication to get homogeneous dispersion. Then the dried polymer is dissolved into the GO/solvent dispersion. After getting homogeneous dope solution, it is degassed and cast on a clean glass plate using film applicator. The wet film on glass plate is immersed in nonsolvent (water) bath for phase separation. Nonsolvent-induced phase inversion method creates an asymmetric structure. GO has been studied as an additive to different polymers to form MMM with higher hydrophilicity and antifouling properties. To improve the

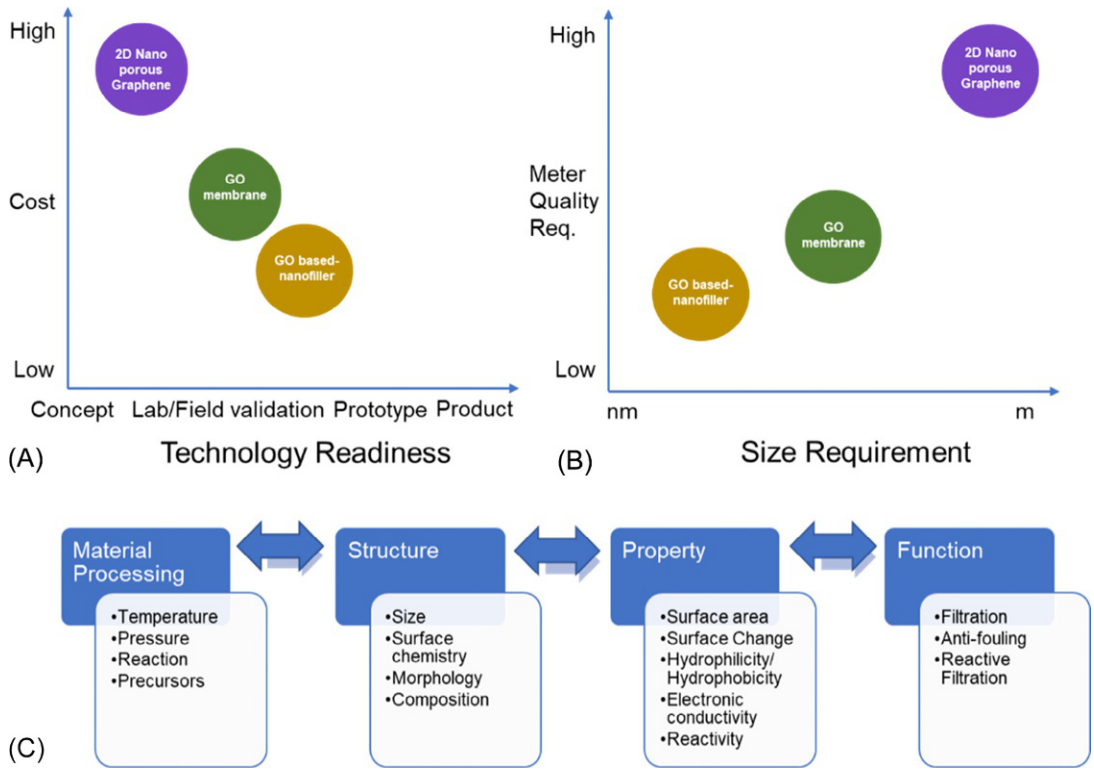

Fig. 20.7

(A) Commercial viabilities levels of GO-based membranes for water treatment. (B) Size and quality requirement of GO-based materials for the different membranes. (C) Stages requirement on GO-based material processing to membrane applications. *Adapted from Y. Jiang, P. Biswas, J.D. Fortner, A review of recent developments in graphene-enabled membranes for water treatment, Environ. Sci.: Water Res. Technol. 2 (2016) 915–922, https://doi.org/10.1039/C6EW00187D.*

This book belongs to Badji Mokhtar Annaba University Central Library
Copyright Elsevier 2025

performance of GO-based MMMs, various chemical functionalities and inorganic nanoparticles have been hybridized with GO.

The blending of GO in polymer matrix affects the membrane surface properties and pore configuration [89]. GO has abundant oxygen-containing functional groups that help to disperse uniformly in dope solution. Uniformly distributed hydrophilic GO particles enhance the phase inversion kinetics during the phase separation [92]. The precipitation of polymer and GO nanosheets results in membranes having smooth surface, interconnected porous structure with higher permeability and higher mechanical strength. Blending of GO results in the negatively charged surface of membrane generated from oxygen-containing functional groups (acid groups) of GO, which lowers water contact angle and enhances hydrophilicity [91]. GO attracts the water molecules and forms a protecting water layer by hydrogen bonding on the membrane surface. This protecting water layer is quite strong and does not allow solute/protein molecules to pass through the membrane, resulting higher fouling resistance [39]. GO blended in PVDF displayed significantly lower membrane and pore resistance for MBR applications [269]. In addition, the negatively charged surface repeals the protein molecules by electrostatic repulsion, which gives higher antifouling properties [13, 93, 270].

The permeability of GO-blended membrane with an increase in GO concentration up to a certain level decreases thereafter. The decline in membrane permeability is attributed to the formation of dense skin layer and reduction in pore size. A higher loading of GO shows an increase in the viscosity of casting solution that slows phase inversion and leads to the development of dense top layer and wider finger-like structures in the bottom layer. The overview of MMMs containing GO concentration below and above of critical level was reviewed by Hegab et al. [271].

The effect of different concentrations of GO in MMM can be explained based on GO hydrophilicity and viscosity of casting solution as follows: during the phase inversion process, polymer solidification starts at interface of the wet film and nonsolvent, which leads to forming a dense skin layer. Furthermore, a dense skin layer hinders the solvent and nonsolvent exchange, and crystallization occurs at a weak point in the sublayer than through the top layer, which leads to forming a wider finger-like structure in the bottom layer [89, 90, 94, 272]. At lower concentration, the hydrophilicity of GO is dominant, and it enhances the diffusion rate between solvent and nonsolvent, resulting in densely porous structure and higher permeability. At higher GO concentration, the viscosity of casting solution increases; it depresses the diffusion rate between the solvent and nonsolvent, which leads to taking a longer de-mixing time to complete the phase inversion process that results in the formation of a dense skin layer and less porous membrane.

Blending of functionalized GO (fGO) with hydrophilic functional group enhances the dispersion in organic solvent and shows excellent compatibility with polymer, resulting in the increase in hydrophilicity, porosity, permeability, and antifouling properties of MMMs [11, 95–98, 273, 274].

This book belongs to Badji Mokhtar Annaba University Central Library Copyright Elsevier 2025

The blending of highly hydrophilic fGO showed a good dispersion in casting solution and increased the thermodynamic instability of the mixture in nonsolvent bath. This resulted in the de-mixing of solvent and nonsolvent during phase separation and formation of a large number of smaller pores in the membrane surface, even with small quantities of fGO. At higher loading of fGO, a decrease in pore size and porosity of the membrane is obtained, perhaps owing to the increase in viscosity of casting solution. Nevertheless, for the same viscosity of polymer casting solution, fGO can be used at higher loading when compared to that of unfunctionalized GO, which results in more hydrophilic membrane. This is attributed to the reduction of π-π stacking in fGO. At the same time, blending of low amounts of fGO is enough to increase the hydrophilicity and performance of the polymeric MMMs. Hegab and Zou [271] showed an overview of fGO/polymer MMMs at higher and lower concentrations of critical level. The functionalization of GO with hydrophilic groups attract more water molecules than GO, which enable them to be diffused at a higher rate through the membrane during phase inversion, improving the permeability. Some of the fGO-blended polymer membranes are discussed further.

Three different polyamine (ethylenediamine, diethylenetriamine, and triethylenetetramine) fGO-embedded PSF MMMs were synthesized using phase inversion method by Zambare et al. [273]. The effect of chain length of polyamine in fGO on the performance of PSF MMM was analyzed. Addition of polyamine to GO increased spacing between GO nanosheets and improved dispersion in polymer dope solution. The presence of polar groups on fGO induced the phase separation zone, which created membranes with higher porosity and finer pores. As a result, the fGO/PSF membrane showed enhanced surface hydrophilicity, water permeability, and fouling resistance against bovine serum albumin (BSA). The fGO/PSF membrane showed a remarkably high water flux of 170.5 LMH/bar, a threefold increase over corresponding control membrane, BSA rejection of 90.5%, and higher normalized recovered water flux after fouling. The contact angle was lowered due to the presence of amino groups on GO in the membranes, which lowered the affinity of BSA toward the membrane. Lower affinity generated higher recovered flux, and thus fouling potential was low. The fGO/PSF membrane showed potential for the progress of high-throughput UF membranes for use in protein and colloid separation. Next, highly hydrophilic sulfonated GO (sGO) was blended in PVDF membrane, which resulted in improvement in hydrophilicity, permeability, and antifouling of hybrid UF membrane [95]. sGO bared a stronger hydrogen-bonding group, such as —SO_3H, compared to that of GO, which resulted in a strong electrostatic repulsion with BSA molecules and showed excellent antifouling and a high water flux recovery ratio. Isocyanate functionalized graphene oxide (iGO) was well-dispersed in organic solvent and showed better compatibility with PSF. The MMMs prepared by blending of iGO in PSF have exhibited excellent antifouling properties because of enhancement in hydrophilicity, negative zeta potential, and improved smoothness of surface [11]. The PES membrane blending with hyper-branched polyethylenimine (HPEI) fGO has good mechanical strength and antifouling performance. However, the permeability of these membranes decreased marginally when compared to that of unmodified PES membrane [96].

This book belongs to Badji Mokhtar Annaba University Central Library Copyright Elsevier 2025

Furthermore, GO was functionalized with 3-aminopropyltriethoxysilane (APTS) and blended in PVDF matrix at different ratio to make MMM through phase inversion technique [99]. The fGO showed properties suggesting higher stability in organic solvent. Significantly more negative zeta potential demonstrated that APTS functionalization of GO had homogeneous dispersion in organic solvents. fGO-blended PVDF membranes presented good mechanical strength, superior hydrophilicity, water flux, BSA flux, and rejection rate than unmodified PVDF membranes and GO-blended PVDF membranes.

Various inorganic nanoparticles, such as Ag [100, 101], Au [102], TiO_2 [103], CNT [104], and conjugated GO hybrid composite have been synthesized and blended as *co*-functional additive into polymeric matrix. Conjugation of NPs on GO nanosheets resulted in increased stability, and layer spacing between GO nanosheets proved to be helpful for water treatment application. The resulting MMMs exhibited synergistic properties generated from the combination of two types of materials. Ag nanoparticles (AgNPs)-decorated GO nanosheets were blended in PSF MMM [100]. Uniform distribution of Ag in membrane revealed greater antibacterial properties. The membrane also showed improved hydrophilicity, permeability, and solute rejection with the presence of Ag-GO nanosheets. A study on Ag-amine-GO containing MOF-based UF membrane was studied in literature [101]. It showed excellent antibiofouling activity by developing a killing and self-cleaning membrane surface.

The presence of Ag-amine fGO changed the surface chemistry of membrane that reduced contact angle and increased the water flux when compared to the control PES membrane. Moreover, Ag-amine fGO content membrane showed long-term inhibition to microbes during protein filtration that opened a viable solution for wastewater purification. Furthermore, gold (Au) nanoparticles-decorated exfoliated graphite nanoplatelets (xGnPs) were used as hierarchical nanofillers in PSF MMM [102]. The resulted porous asymmetric UF membrane was catalytically active, resistant to compaction, and showed higher permeability than control membrane. Results demonstrated that the catalytic activity was largely dependent on the loading of Au nanoparticles on xGnPs. A TiO_2-GO nanocomposite was synthesized by sol-gel method, and it was explored as a nanofiller to fabricate PSF mixed-matrix UF membrane [103]. The resultant hybrid membranes showed hydrophilic asymmetric structure with improved surface roughness that reduced irreversible humic acid fouling during removal from aqueous solution.

Generally, noble metals are toxic to microorganisms and show great fouling resistance properties to the membrane. However, the usages of inorganic particles in MMM have limitations owing to leaching of these particles at harsh operating conditions. Leached inorganic particles may exhibit toxicity in drinking water and are, thus, problematic to be used in drinking water applications. On the other hand, carbon-based nanomaterials have shown good compatibility with polymer MMM and negligible leaching problem during operation. Therefore, carbon-based nanomaterials are the best nanofillers in polymer matrix, which improved the performance of MMM [104]. The developed GO/MWCNTs-blend PVDF

This book belongs to Badji Mokhtar Annaba University Central Library Copyright Elsevier 2025

membrane revealed a remarkable antiirreversible fouling performance for BSA filtration experiments.

20.3.4.3 Carbon nanotubes, fullerenes, and amorphous carbon-incorporated mixed-matrix membranes

The structure consists of rolled-up sheets of single-layer carbon atoms (graphene) arranged in a cylindrical fashion. Structural features play an important role in deciding the property of the CNTs [275]. The unique rolled structure of CNTs exhibit considerably high aspect ratios, giving high mechanical strength, while chirality and hexagonal orientation of atoms in single-walled CNTs (SWCNTs) manipulate the electrical conductivity. CNTs have a wide range of applications in water treatment [276].

CNT/PES MMMs were prepared by phase inversion method that showed good antifouling properties against BSA and ovalbumin (OVA) protein [105]. The CNT/PES membrane results showed less protein adsorption when compared to the bare PES membrane at neutral pH in static conditions. Moreover, high flux recovery ratio and less irreversible fouling ratio of CNT/PES membrane compared to bare PES membrane and commercial UF membrane (PES; Radel H2000, Solvay) are shown to have the potential to alleviate the effects of protein fouling, thereby enabling membranes to be used for longer protein filtration after simple water washing. Furthermore, functionalized MWCTs were used as binders in MMM to increase their dispersion in polymer dope solution and to make high permeable membranes [46, 106–109].

Highly dispersed carboxyl-functionalized MWNTs were prepared by treating with strong and blended with PSF membranes [106]. The prepared MWNTs/PSF membranes were characterized thoroughly, which showed a highly porous membrane structure and hydrophilic surface. The porosity of membranes increased along with the contents of MWNTs up to 1.5 wt %, then decreased, and at 4 wt% of MWNTs, it became even smaller than bare PSF membrane. The MWNTs/PSF membranes showed higher flux and good rejection of PEG (10 kDa) and polyvinylpyrrolidone (PVP 55 kDa) than bare PSF membrane. The effect of oxygen-containing groups of MWCNTs (oxidized MWCN) on PVDF mixed matrix was investigated [107]. The oxidized MWCNT/PVDF exhibited an enhanced hydrophilicity, porosity, pore size, and surface roughness. The oxygen-containing groups of inorganic fillers determined the structure, morphology, and performance of UF membranes.

The effect of three different functionalized (F-) (oxidized, amide, azide) MCNTs on morphology, and permeation properties of PSF composite membranes (MWCNT/PSF) were studied for application in hexavalent chromium and divalent cadmium removal from aqueous solutions [108]. MWCNT/PSF composite membranes made through the phase inversion of polymer-DMF with water-isopropanol antisolvent showed higher hydrophilicity but reduced flux and reduced pore size based on the functional groups on nanotubes than the pure PSF membrane. Furthermore, the MWCNT/PSF composite membranes showed enhanced thermal stability and

This book belongs to Badji Mokhtar Annaba University Central Library Copyright Elsevier 2025

enhanced heavy metal rejection. Hexavalent chromium and divalent cadmium metal separation from water in acidic condition was found to be increased with an increasing amount of MWCNTs. A study on phenylenediamine functionalized multiwalled carbon nanotubes (F-MWCNTs) and polyvinylpyrrolidone-blended PES membranes increased hydrophilicity, porosity, pore size, surface roughness, and BSA rejection and showed better antifouling properties with a concentration of F-MWCNT of up to 1% [109]. In isocyanate and isophthaloyl chloride-modified MWCNT-PSF membrane, the presence of MWCNT in membrane matrix suppressed the adsorption of protein on membrane and thus alleviated membrane fouling [46].

The mixing of long and tortuous one-dimensional oxidized carbon nanotubes (OMWCNTs) inhibited the stacking of GO by bridging with adjacent GO sheet and inhibiting their aggregation [110]. The GO/OMWCNTs/PVDF membrane demonstrated impressive antifouling prospects. Because membrane fouling is one of the most critical issues in aqueous filtration, a focused study on understanding of membrane fouling of vertically aligned carbon nanotube (VA-CNT) membranes was investigated [111]. The VA-CNTs membrane was made by thermal chemical vapor deposition, and the deposited VA-CNTs were filled by epoxy resin to increase mechanical strength to withstand high-pressure filtration. These VA-CNT membranes were further surface-modified by graft polymerization of methacrylic acid to improve the performance. The VA-CNT membranes were tested for fouling and rejection of BSA and were compared with commercial UF membrane (UE4040). The membrane results showed that higher BSA rejection and lower irreversible fouling was attributed to an increase in hydrophilicity and surface charge.

Fullerene is the third allotropic form of carbon having structure consists of five- and six-member carbon rings (or sometimes heptagonal) attached through single or double bonds to give a spherical arrangement of sp^2 hybridized carbons [277]. Fullerene can occur in numerous carbon cluster (C_n) ($n > 20$) sizes consisting of 30–3000 carbon atoms. The most stable C_{60} fullerene molecule composed of 12 pentagons and 20 hexagons of sp^2 hybridized carbon atoms, each linked to three other carbon atoms. Asymmetric UF membrane based on composition of fullerene C_{60} and hydrophobic polymer, polyphenylene oxide was studied on removing estrogenic pollutants from water. Membrane containing fullerene C_{60} showed good estrone rejection (more than 95%) and exhibited higher flux than pure polyphenylene oxide membranes [112].

Amorphous carbon is one of the primitive forms of carbon known to mankind under various denominations such as coal, soot, and carbide-derived carbon. Various forms of amorphous carbon can be obtained through incomplete combustion of plant and animal matters [278]. Carbon atoms are randomly distributed without any ideal bonding where, they are free, reactive, and do not have any crystal lattice confinements. The amorphous carbon is commonly categorized in three classes namely diamond-like-carbon (sp^3), graphite-based carbon, and carbyne (sp), depending upon the close resemblance to either of the allotropic crystal arrangement and hybridization [279].

This book belongs to Badji Mokhtar Annaba University Central Library Copyright Elsevier 2025

PSF/oxidized nanocarbon black mixed-matrix UF membrane prepared through phase inversion method improved hydrophilicity and water permeate flux while lowering fouling tendencies [113]. The inclusion of 1.0 wt% oxidized nanocarbon black in PSF matrix enhanced water permeate flux from 188.5 to 307 LMH, BSA rejection up to 97.6%, with a flux recovery ratio of 89.4% after three cycle of permeation. Nanocomposite membranes of CA, PEG, and candle soot (CS) nanoparticles prepared using phase inversion technique showed as a promising substrate for water desalination [114]. CS nanoparticles contributed in improving the salt rejection with relatively low flux properties. Furthermore, polyamide (polyphenyleneisophthalamide) UF asymmetric membranes modified with nanocarbon additive (fullerene, astralene, or graphite soot) and the effect of carbon additives on the performance of these membranes was studied [115]. The membranes modified with fullerene and astralene demonstrate good water flux recovery after being in contact with a protein mixture (FRR 0.8–0.9), in contrast to straight polyamide membranes and those modified with carbon black (FRR < 0.45). This is because addition of fullerene and astralene increases the hydrophobicity of the membrane matrix and decreases its sorption capacity for proteins. Modification of the polyamide with fullerene and astralene improves the UF performance of the membranes.

20.4 Thin-film nanocomposite membrane

The TFC membranes are dominantly used in NF and RO processes for water purification. The three-layers configuration of TFC membrane are composed of a dense ultrathin selective polyamide-based top layer on microporous UF or MF membrane sublayer, followed by nonwoven fabric support. The highly cross-linked dense polyamide top layer defines selectivity of membrane, the middle layer is microporous substrate to provide support for thin film, and the bottom layer is the reinforcing fabric support for additional mechanical strength.

Thin polyamide top layer is produced by interfacial polymerization of amine in aqueous solution and carbonyl chloride in organic solution. Amines used in the TFC membranes include m-phenylene diamine, p-phenylene diamine, piperazine, N-N′-diaminopiperazine, N-(2-aminoethyl)-piperazine, ethylene diamine, oligomers of ethylene diamine, polyethylene imine, etc. Trimesoyl chloride is the most commonly used carbonyl chloride. The trade-off between permeability and selectivity and low fouling resistance of polymeric membranes are limitations of the TFC membrane.

The top layer of the TFC membranes is dense-driven by necessity to reject ions. Consequently, permeate flux is lower. The research in TFC membranes has focused on increasing permeate flux while maintaining or enhancing ionic selectivity and reducing fouling. The largest application of TFC membranes is RO of water and NF of aqueous solutions. The feed to the TFC membranes is pretreated with one or more stages of MF, UF, softening, etc. Therefore fouling is not a significant concern. However, attachment of biofilm because of growth of algae or other microorganisms owing to continuous contact with water is a significant area of concern, and energies have been directed toward increasing hydrophilicity to prevent adhesion

This book belongs to Badji Mokhtar Annaba University Central Library Copyright Elsevier 2025

or formation of biofilm. Most approaches can broadly classified as: (1) chemical modifications of monomers and polymer, (2) surface modification of polyamide film, and (3) inclusion of nanomaterials within the membranes [280–282].

Various techniques have been implemented on both the active surface layer and bottom sublayer to improve the TFC membrane permeability, fouling resistance, and chlorination stability. Nanomaterials are included in the active layer to improve the selectivity and permeability of the membranes. The active layer is less than 0.5 μm in thickness; therefore the amount of nanomaterials that is required is very small. Nanomaterials dispersed in the active layer have to be lower than the top layer thickness; otherwise, the selectivity is significantly affected [283]. Nanomaterials that have been critically studied in wastewater treatment are inorganic nanofillers, bioinspired materials (BIMs), and carbon-based nanomaterials such as graphene and graphene-based derivatives. The performance of TFC membrane depends upon the type, size, surface charge, and amount of fillers added.

20.4.1 Inorganic nanomaterials (iNPs)-incorporated thin-film composite membrane

Inorganic engineered nanoparticles (iNPs) are highly stable, nontoxic, hydrophilic, and biocompatible nanomaterials that showed excellent water treatment ability with different methods. A wide variety of inorganic nanomaterials showed improvement in performance of TFC membrane for water treatment application. Inorganic nanomaterials, such as AgNPs [116, 117], titanium dioxide (TiO_2) [118, 119], silicon dioxide (SiO_2) [120–122], cerium oxide (CeO_2) [123], and polymer modified silica [124], were integrated in polyamide layer. The incorporation of iNPs in TFC membrane increased the surface hydrophilicity and free volume in polyamide layer; however, some studies showed declined selectivity. Addition of iNPs in polyamide layer displayed enhanced membrane permeability because of increased hydrophilicity and defect formation, which may compromise membrane selectivity because of weakened integrity of selective layers.

Ag and copper nanoparticles are added in the top layer of the membrane to provide robust antibacterial and antibiofouling protection to the membranes [138, 149, 150]. These nanoparticles may be synthesized ex situ and mixed with either amine or TMC [139] or may be generated in situ through reduction [140, 141]. One of the concerns is the discharge of too high concentration of Ag^+ ions, which may be detrimental, expensive, or cause the membrane to lose biofouling capacity quickly. Covalent functionalization of Ag nanoparticle for inclusion in the TFN top layer is reported through amine functionalities. The amine-terminated AgNPs are distributed within the amine during IF, and subsequently, amine AgNPs became a part of the polyamide matrix [148]. There are several reports of use of AgNPs in conjunction with TiO_2 [133], ZnO, or other photocatalytic nanoparticles such as perovskites [142], MOF [145, 146], GO [284], and zeolites [143, 144]. Rich literature exists on TiO_2, ZnO, and SiO_2 [285] decorated with AgNP. Recently, few reports have appeared, including core-shell nanoparticles to improve biofouling capability [147].

This book belongs to Badji Mokhtar Annaba University Central Library Copyright Elsevier 2025

Improvement in fouling resistance of the TFC membrane is of great interest in water treatment applications. A facile method for in situ loading of AgNPs on the TFC membrane showed strong antibacterial activity for three model bacteria (*Escherichia coli*, *Pseudomonas aeruginosa*, and *Staphylococcus aureus*) [116]. AgNPs showed significantly suppressed biofilm formation on the functionalized polyamide membranes, leading to reduction of more than 75% in the number of live bacteria attached to the membrane, without impacting salt selectivity, surface roughness, hydrophilicity, or zeta potential, although 17% reduction in water permeability was observed. Furthermore, a study on hydrophilic AgNPs-induced selective nanochannels in TFN polyamide membrane was reported [117]. In another study, approximately 2.5 nm-sized nanochannels were induced in active layer through the use of AgNP owing to the hydrolysis of trimesoyl chloride monomers at the surface of AgNP by water film surrounding the particle. The optimized membrane showed threefold increase in membrane water permeability, with a pure water flux of 50 LMH at 20 bar and NaCl rejection of 99.1%. The membrane also showed improved rejection of Boron and low molecular weight emerging pollutants solutions. The enhancement was attributed to size exclusion, enhanced Donnan exclusion, and suppressed hydrophobic interactions.

Similarly, over twofold increase in permeability of the TFC NF membranes with similar or marginally lower salt rejections are reported through the use of iNPs, such as zeolites [126], mesoporous silica [129], alumina nanoparticles [127], aluminosilicate nanotubes [128], Ag NPs [130], and TiO_2 [131]. A study on aminosilanized TiO_2 NPs-embedded TFC NF membrane on PES-coated porous α-Al_2O_3 ceramic hollow fiber membrane was reported [131]. Silane functionality on TiO_2 NPs helped to improve their dispersion in polyamide layer owing to reduction in surface energy and improved thermal stability of membrane. At 0.005 wt%, loading of aminosilanized TiO_2 NPs in TCF membrane improved the NaCl (2000 ppm) rejection to 54% and water flux to 12.3 LMH at 7.6 bar. The membrane flux was further improved up to twofold when compared to the pure TFC membrane by the incorporation of higher percentage of the aminosilanized TiO_2 nanoparticles but the cost of 50% decrease in NaCl rejection.

20.4.2 Bioinspired materials-incorporated thin film composite membrane

BIMs-based membranes offered great potential as a disruptive water treatment technology because of their potential of improving membrane permeability without conceding solute rejection. Aquaporins (AQPs) are one of the popular family of proteins, which can serve as channels in the transfer of water through the membrane. AQPs have hourglass-shape water channel with a narrow canal of 0.28 nm that can transport a single water molecule only. An earlier study showed that the water permeability of AQP-based RO membranes may achieve water permeance up to 600 $L\,m^{-2}\,h^{-1}\,bar^{-1}$, which is over 100-fold higher than the permeance of commercially available seawater RO membranes [286]. A robust and high-performance AQP-based biomimetic membranes was fabricated by interfacial polymerization method,

This book belongs to Badji Mokhtar Annaba University Central Library Copyright Elsevier 2025

where AQP Z-containing proteoliposomes were added to the aqueous solution of m-phenylenediamine (MPD) [151]. Addition of AQP enhanced membrane properties such as surface hydrophilicity, fouling resistance, and smoothness. The membranes achieved water permeability of 4 L m^{-2} h^{-1} bar^{-1}, with NaCl rejection of 97% at 5 bar operating pressure. A similar study on AQP-based biomimetic membrane showed good stability and long-term performance in RO application [155]. The polydopamine-modified proteoliposome, incorporated with AQP Z, was embedded into the top layer by crosslinking of polyethylenimine with the membrane [152]. The optimum membrane showed 36.6 LMH/bar water permeability and 95% $MgCl_2$ rejection. Inspired by "water channel" of biological membranes, antifouling TFC membrane with high permselectivity based on zwitterionic polyelectrolyte nanoparticles (ZPNPs) was synthesized [153]. Optimized TFC-ZPNPs membrane exhibited high water permeability of 10.1 LMH/bar and improved NaCl/Na_2SO_4 selectivity (28.4). The ZPNPs act as building blocks to improve water pathway and increased membrane surface hydrophilicity and electronegativity, and reduced the surface roughness, leading to an enhanced fouling resistance against the BSA. AQP Z-based TFC hollow fiber membrane showed 8 LMH/bar permeability, almost 200% as much as the permeability of commercial RO membrane (BW30), and above 97.5% NaCl (500 ppm) rejection [154]. Moreover, it showed good flux during forward osmosis (FO) experiments with low salt back diffusion.

20.4.3 Metal-organic frameworks-incorporated thin-film composite membrane

MOFs in TFC membrane can be an emerging nanomaterial with much potential to improve performance. MOFs consist of both an organic and an inorganic fragment. The organic part can be made compatible with polyamide to give a high-performance membrane. Incorporation of highly porous MOFs in TFC membrane showed enhanced permeability. High-flux TFC membranes consisting of different MOFs [ZIF-8, MIL-53(Al), NH_2-MIL-53(Al) and MIL-101 (Cr)] were fabricated for organic solvent NF application [287]. MOFs were included in polyamide top layer by homogeneously dispersing them in TMC solution. Fabricated membrane's performance was evaluated based on methanol (MeOH) and tetrahydrofuran (THF) permeances and rejection of styrene oligomers (PS).

MIL-101(Cr)-embedded TFC membrane showed excellent increase in permeance, from 1.5 to 3.9 and from 1.7 to 11.1 LMH/bar for MeOH/PS and THF/PS, respectively. Improvement in methanol and tetrahydrofuran rejection indicated a MWCO of less than 232. Poly(sodium 4-styrenesulfonate) (PSS)-modified ZIF-8 (mZIF) increased hydrophilicity of the MOF, which when included in PA layer in NF membranes increased the hydrophilicity of the layer. mZIF-PA membrane flux was over 200% higher than control for no change in rejection of Na_2SO_4 [171]. The improvements in the properties were attributed to enhanced hydrophilicity and additional negative charge on the surface. GO/MOF composite in PA TFN membrane was shown to be antimicrobial [174]. IRMOF/GO composite PA TFN membrane showed high flux

This book belongs to Badji Mokhtar Annaba University Central Library Copyright Elsevier 2025

and high rejection. ZIF-8/chitosan layer on PVDF displayed 350% water flux increase [178]. Silica-dispersed PA TFN membrane was used for dioxane removal, which showed 300% improvement in flux; however, significantly lower rejection was observed [132]. COF based on Tp and MPD membrane exhibited excellent flux of 50 LMH/bar, with over 99.5% rejection of Congo red dye. The membrane performance was better than previously reported GO- or MOF-containing membranes [180]. Excellent rejection of thiophene from octane was obtained using Ag^{+}@COF embedded in PEBAX coated on PS membrane. Enrichment factor of 6.8 was obtained even though the molecular difference was only 1 Å [182].

20.4.4 Carbon nanomaterials-incorporated thin-film composite membrane

Polyamide TFC membranes have been widely used for water treatment in NF and RO processes because of their high selectivity and stable structure. However, membrane fouling, high energy consumption, and degradation of polyamide structure by chlorination are the main catches of TFC membrane. Meanwhile, GO has been demonstrated as a versatile nanomaterial because of its unique properties, such as super hydrophilicity, high mechanical strength, biocompatibility, and fast water transport through nanochannels. The use of GO in membrane modification strategies have resulted in higher hydrophilicity, increase in stability, and higher strength to the TFC membranes. GO is extensively used as functional nanomaterial when compared to other inorganic nanomaterials with similar functionalities because of better dispersion in different solvents owing to abundant oxygen functional groups. The incorporation of GO in TFC membrane has created an alternative opportunity to improve membrane permeability and antifouling properties in water treatment processes. The modification of TFC membrane using GO nanosheets as a functional filler can be done through two routes—incorporation in polyamide active thin layer and use in microporous polymer sublayer.

TFC membrane fabricated by incorporation of GO nanosheets in active top layer has attracted attention because of the synergistic effect of both polyamide and GO nanosheets. GO gives superior properties to the TFC membrane membranes because of its unique nanostructure and physical, chemical, and mechanical properties. The oxygen functionalities on GO help to disperse well in solvent during interfacial polymerization [163]. The hydrophilicity of active layer is increased by embedding GO into the polyamide layer that results in the enhanced permeability and antifouling properties [159]. Also, an intermolecular hydrogen bonding between oxygen functional groups of GO and the amide groups of polyamide could protect the amide bond from being attacked by chlorine [184]. Furthermore, incorporation of GO nanosheets in polyamide have increased the mechanical properties of TFC membrane [283]. GO nanosheets can be embedded in polyamide active layer of TFC membrane during interfacial polymerization by dispersing in either aqueous phase of diamine [156–159] or organic phase of acid chloride [163, 164, 283].

This book belongs to Badji Mokhtar Annaba University Central Library Copyright Elsevier 2025

The literature on GO incorporated in aqueous phase of diamine is reported. The TFC membrane was prepared from GO nanosheets incorporated in aqueous phase containing MPD followed by interfacial polymerization of MPD-TMC on PSF substrate [156]. At 100 ppm of GO content in polyamide layer of TFC membrane, water flux of 29.6 LMH at 15 bar and an NaCl (2000 ppm) rejection of $\geq$97% was observed. Moreover, the membrane observed to be stable in both acidic and alkaline conditions. He et al. reported the water transport through the membrane was enhanced by selective diffusion at the interface of polymer matrix and embedded GO nanosheets [157]. Compared to pristine polyamide membrane, the water flux of hybrid TFC membrane with 0.12 wt% of GO was found to increase by up to 80% from 0.12 to 0.23 LMH/bar, without significant reduction in salt rejection. GO-embedded hybrid TFC membrane showed superior antimicrobial activity. Size-controlled GO nanosheets dispersed in aqueous solution of MPD solution improved water permeability and antibiofouling property of the TFC membrane by approximately 80% and 98%, respectively [158]. The salt rejection of membrane was retained under chlorine exposure of 48,000 ppm/h. The enhanced performance of membrane was ascribed to both size and loading of GO, which resulted in higher hydrophilicity, surface charge, and smooth surface. The GO-modified TFC membrane was prepared on commercial PSF UF membrane using interfacial polymerization process and used for natural organic removal form real river water [159]. Different concentrations of GO, from 0 to 0.012 wt %, were dispersed in aqueous solution of 2% (*w*/*v*) MPD and further used with 0.1% (w/v) TMC solution to coat a thin layer of polyamide. Addition of GO in the TFC membrane showed increased hydrophilicity (lower contact angle) and thinner and denser polyamide layer, which contributed to the enhanced water permeability when compared to pristine polyamide TFC membrane. At 0.004 wt% of GO in TFC membrane, the highest water flux of 23.3 LMH at 8 bar was demonstrated when compared to flux 18.7 LMH of pristine PA-TFC membrane. Then, GO-TFC membrane was tested for the removal of natural organic matter from water and antifouling performance. Real river water sample before and after filtration were analyzed with ultraviolet (UV) absorbance, dissolved organic carbon (DOC), fluorescence excitation emission matrices (FEEMs), and molecular weight distribution (MWD). At 0.012 wt% of GO in TFC membrane, the removal rates of UV_{254} (62.0%) and DOC (41.1%) were shown, which nearly doubled than that of the pristine PA-TFC membrane. Also, after 5 h of continuous filtration of real river water, the flux decline using GO-TFC membrane was much less when compared to pristine PA-TFC membrane, which showed better antifouling performance. Addition of appropriate amount of GO in TFC membrane provided not only higher water permeation and natural organic matter removal but also resulted in better fouling resistance properties, which shows the great potential of such membranes in water treatment. Starch-GO included in PA layer through ester linkages increased water flux by over 80% while increasing the rejection of Na_2SO_4 and greater than 99.9% rejection of reactive green 19 and reactive violet-1. The increase was attributed to higher hydrophilicity of the layer because of the presence of hydrophilic starch and GO [160].

This book belongs to Badji Mokhtar Annaba University Central Library Copyright Elsevier 2025

GO nanosheets with an interlayer spacing of approximately 0.83 nm were dispersed in organic phase of TMC at different concentrations, from 0 to 0.02 wt% [163]. Later, GO-embedded TFC membrane was fabricated using aqueous phase of MPD solution and organic phase of TMC-GO by in situ interfacial polymerization process. Results showed that GO nanosheets were dispersed well in polyamide layer and their incorporation enhanced TFC membrane permeability and salt rejection. At 0.015 wt% of GO in organic TMC solution during interfacial polymerization, GO-TFC membrane showed an increase in permeate flux to 59.4 LMH at 20.7 bar, when compared to 39.0 LMH of pristine TFC membrane with marginal reduction in the rejections of NaCl and Na_2SO_4. This study showed that water channels were formed in the interlayer spacing of GO, which enhanced permeability. Furthermore, a work on the limitations of TFC membrane permeability-selectivity trade-off, the susceptibility of polyamide layer, and fouling propensity was carried out by Inurria et al. [164]. The study showed that TFC membrane embedding GO in polyamide layer had the potential to address these limitations by providing fouling resistance properties and solute selectivity. Different amounts, 53 ppm (TFC-low), 107 ppm (TFC-medium), and 160 ppm (TFC-high), of GO were dispersed in organic phase of 0.15 wt% TMC solution, and 3.5 wt% aqueous MPD solution was used to fabricate GO-embedded polyamide layer on PSF substrate by interfacial polymerization. Antifouling properties and antimicrobial capacity of GO-TFC membrane increased with the loading of GO, but membrane permeability decreased with higher loading. Hence a trade-off was observed between enhanced permeability and reduced fouling resistance, and only one positive effect of GO could be obtained at a time. Incorporation of GO in the TFC membrane appeared to be more effective as fouling controlled filler and restricted as membrane performance enhancer.

Further studies showed that GO can be used to make loose RO or NF membrane for water treatment. Cross-linking with functional groups on edges of GO sheets increased stiffness of the polyamide chains of TFN membranes. Increased rejection and higher hydrophilicity along with improvement in antifouling properties was obtained in PEG-modified GO dispersed in polyamide TFC membrane, although the permeate flux of the resultant membrane declined [161]. Use of reduced GO with TiO_2 (about 1.25% *w*/w polymer) [162] and exfoliated hydrotalcite/GO nanosheets in polyamide layer using interfacial polymerization of polyethyleneimine and trimesoyl chloride showed improved water flux and salt rejection [165].

Graphene quantum dots (GQDs) with a smaller size (~2 nm) and higher crystallinity share most of the excellent features of GO and could be synthesized in small sizes by a facile and controllable "bottom-up" method [288]. The synthetic GQDs can be used in fabricating TFN membranes to improve water permeability and fouling resistance ability. [166] studied fabrication of GQDs-incorporated TFN membrane with enhanced water permeability and fouling resistance properties. GQDs were incorporated into polyamide layer during interfacial polymerization of piperazine (PIP) and TMC, which resulted in a smooth surface and

This book belongs to Badji Mokhtar Annaba University Central Library Copyright Elsevier 2025

hydrophilic TFN membrane. In NF experiments, GQDs-embedded TFN membrane showed a high water flux of 102 LMH at operation pressure of 2 bar, and excellent antifouling performance was tested using 1 g/L BSA, humic acid, and emulsified oil solutions [167]. Incorporation of hydrophilic carbon dots smoothen the polyamide layer and enhance water permeability and rejection properties. Next, Na^+-functionalized carbon quantum dots were used in TFN hollow fiber membranes to improve the performance for brackish water desalination [168]. GO quantum dot-incorporated RO membrane prepared using pressure-assisted method showed enhanced antifouling and chlorine resistance properties [169]. The nitrogen-doped GO quantum dots (N-GOQD)-incorporated polyamide TFN RO membrane also showed a high flux for the desalination process [170].

20.4.5 Thin-film nanocomposite membrane with nanoparticles in substrate

GO as functional materials in sublayers of TFC membrane are important to increase permeability and reduce fouling with the pores of the membrane. In TFC membrane, it is considered that the performance of the membrane depends upon the selective polyamide top layer, and microporous sublayer usually provides surface for interfacial polymerization and mechanical strength. Nevertheless, the structure of sublayer, roughness, pore size, pore structure, and porosity have influenced the microstructure and performance of the TFC membrane [289, 290]. The required sublayer should possess desirable macrovoid-free and fully sponge-like morphology, which provides excellent membrane strength and helps to reduce internal CP, thus leading to the water flux enhancement. Because interfacial polymerization is based on diffusion-controlled kinetics [291], the adsorption of diamine monomer on the sublayer plays an important role to make uniform TFC membrane. The incorporation of thickness-controlled GO in PSF sublayer has improved membrane hydrophilicity, increased water flux, and enhanced mechanical strength of TFC RO membrane [183]. Single-layer GO platelets having an average thickness of about 1.5 nm were desired to make the PSF sublayer with high mechanical strength and porous structure. Highly porous PSF support layer reinforced by thickness-controlled GO (0.5, 0.9, and 1.8 wt% to PSF) was prepared by phase inversion method. The mechanical strength of the GO-embedded highly porous support layer was comparable to that of support layer of conventional RO membrane. Polyamide membrane coated on GO/PSF support layer showed 1.6–4 times higher water permeability at 15.5 bars (5.42 LMH/bar) with comparable salt rejection (98.2%, 2000 ppm NaCl) when compared to RO membrane prepared by the modification of active layer and some commercial RO membrane, Dow-filmtec SW30HR (1.93 LMH/bar, 99.0%), Hydranautics LFC-1 (2.72 LMH/bar, 98.4%), Hydranautics SWC5 (1.56 LMH/bar, 97.9%), Nano H_2O SW400ES (2.67 LMH/bar, 99.0%), and Woongjin FE (2.94 LMH/bar, 98.9%). Next, polyamide active layer coated on GO-induced PSF microporous sublayer displayed high chlorine resistance and stable RO performance [184]. Hydrophilic sulfonated poly(arylene ether sulfone), GO and amine GO-modified PSF (aPES/GO/aGO) membrane showed water flux of 28.4 LMH at 55 bar, which was higher than that of 23.2 LMH of

This book belongs to Badji Mokhtar Annaba University Central Library Copyright Elsevier 2025

the PA membrane. The chlorine resistance of membrane was performed by immersing membrane in aqueous sodium hypochlorite solution (300 ppm). The aPES/GO/aGO membrane showed a much higher chlorine resistance than the pristine polyamide membrane. The aPES/GO/aGO RO membrane showed promising use in the seawater desalination process, without significant decrease in performance in the presence of chlorine.

Substrate properties essay an important role in the performance of the membrane, particularly so in FO. The internal CP is lower in membranes with substrate having finger-like pores rather than the spongy structure [292]. Nanocomposite substrates have finger-like pore structures accompanied by finely porous top layer. About 0.6% TiO_2 in PS substrate showed over 100% increase in flux in FO in both AL-FS and AL-DS modes. Zeolite-infused PS substrate displayed significantly higher flux; similarly, flux improvement was obtained with MWCNT dispersed in PES substrate with finger-like pores [186, 192]. TNF-ii membranes containing zeolite in PS substrate showed less flux decrease due to lower compaction. The presence of nanoparticles increased compressive strength of the substrate, which improved the performance of the RO membrane [293]. Shah et al. synthesized FO membrane with electrospun PVDF substrate containing bentonite, which showed exceptionally high FO flux [193]. Self-supported electrospun PAA-laminated PVDF substrate exhibited higher hydrophilicity along with high flux, giving approximately 99.3% rejection of tetracycline and up to 22% water recovery in hybrid FO-MD process [194].

20.4.6 Chlorine stability of polyamide thin-film nanocomposite membrane

TFN membranes primarily comprise polyamide thin active layer and microporous UF/MF sublayer. TFN membranes are widely used in RO, NF, and FO applications. The polyamide top layer dominates the performance of membrane, that is, mainly depends upon its hydrophilicity, fouling resistance properties, and chemical stability, particularly chlorine resistivity. Chlorine is commonly used in water purification and sea water desalination processes to kill microorganisms and minimize biofouling [294]. Chlorine and other strong oxidizing agents attach polyamide backbone through interaction with lone electron pairs on N or O atoms in amide, resulting in the formation of N-chloramines [295]. Therefore the development of chlorine-resistant polyamide membranes is crucial in water treatment to enhance membrane lifespan, reduce the membrane process complexity, and the cost of water processing.

The existing RO membrane chlorine stability and antifouling properties was improved by thin coating of unimpeded and stable GO on polyamide layer [296]. Small size (~200 nm) GO flakes were used for thin coating of 50 nm and thick coating of 200 nm, which was achieved by a "removing-transferring" method. The GO coating was highly permeable to water, with a high level of salt rejection. Additionally, it significantly improved the chlorine stability of polyamide membrane by obstructing the diffusion of reactive chlorine. Next, the octadecylamine-grafted GO and fluorinated monomer incorporated in polyamide layer of TFN

This book belongs to Badji Mokhtar Annaba University Central Library Copyright Elsevier 2025

membrane (TFNMA-GO-ODA) demonstrated excellent chlorine resistant properties and improved NF performance [297]. The TFNMA-GO-ODA showed water permeability of 8.3 LMH/bar, which was around 2.5-fold than that of pristine piperazine TFC membrane, and a high rejection of 98.4% against Na_2SO_4. The existence of fluorine-containing groups and protective effect of stable GO nanosheets benefitted the excellent chlorine resistance to TFN membrane. Then, self-polymerized tannic acid on the surface of GO (GOT) was incorporated in polyamide RO TFN membrane (PA-GOT) by interfacial polymerization method [298]. Enhanced hydrophilicity, oxidative stress capability, barrier property, and compatibility with polyamide matrix of tannic acid-coated GO improved the water flux, fouling, and chlorine resistance properties of PA-GOT TFN membrane.

A different approach was used to integrate GO nanoplatelets in polyamide layer by an LBL technique, such as alternating layers of GO nanoplatelets and polyamide, and GO nanoplatelets on top of the polyamide layer [299]. GO nanoplatelets-embedded polyamide membrane retained its salt rejection when compared to that of pristine polyamide membrane upon chlorine exposure. Furthermore, highly hydrophilic, chemical robust, and ultrafast water permeable GO multilayers were coated on the polyamide TFC membrane by LBL deposition of oppositely charged GO nanosheets [300]. GO multilayers on the TFC membrane achieved a dual-action barrier coating, which increased the antifouling performance and reduced chlorine-induced degradation of polyamide layer, preserving their salt separation performance. Increased surface hydrophilicity and lower roughness of GO nanosheets principally enhanced the fouling resistance, whereas robust nature of GO nanosheets formed a chlorine barrier for the underlying PA membrane. Also, GO nanosheets (d-spacing 0.48 nm) cross-linked poly (N-isopropylacrylamide-*co*-*N*,*N*′-methylene-bisacrylamide) polymer thin film (40 nm) was coated on a porous nylon substrate using spin coater [301]. Fabricated GO-TFN membrane showed FO water flux of 25.8 LMH and NaCl rejection of 99.9% along with excellent chlorine stability, in addition to the improved mechanical stability.

20.5 Surface-located nanoparticle membranes

In wastewater treatment, remarkable progress in research has been done in the design and development of graphene-based membranes. SLN membranes are composite membranes with nanoparticles situated on the surface of underlying membrane. Surface properties of the base membrane are modified due to the presence of nanomaterials. Among graphene and its derivatives, nanoporous graphene sheets [302–304] and GO laminates [200, 243, 244, 305] were commonly employed [306]. The desalination performance of these membranes is critically dependent on the pore size and chemical functionalization of nanosheets. Nanoporous graphene membrane consists of a single layer graphene sheet having nanopores of defined size. The selectivity is achieved through size and Donnan exclusion between charged moieties and graphene/GO pores. In the GO laminates, the interlayer distance primarily determines the pore size and ionic selectivity.

This book belongs to Badji Mokhtar Annaba University Central Library Copyright Elsevier 2025

20.5.1 Nanoporous graphene sheets

After the isolation of graphene in 2004 [307], significant research has been carried out on its applications in a variety of fields such as membrane, catalysis, composites, electronics, sensors, and energy. Graphene is a flat monolayer of carbon atoms closely packed into a two-dimensional intact sheet. The creation of nanosize pores in the graphene sheets has opened applications in water treatment. Surwade et al. used oxygen plasma to etch nanoscale pores in the graphene sheets to achieve almost 100% salt rejection and fast water transport [304]. These properties were attributed to the monoatomic thickness of top layer, its chemical and mechanical stability, and its flexibility. A molecular dynamics study was done by Cohen-Tanugi and Grossman to investigate the desalination performance by single-layer graphene nanosheets with nanometer scale pores [302]. Results proposed that it could effectively separate the NaCl ions from water with several orders of magnitude higher flux than conventional RO membrane.

Hydrophilic functionalization (hydroxyl groups) of graphene pores roughly doubled the water flux of the membrane. However, an increase in water flux gave inconsistency in salt rejection because of the ability of hydroxyl groups to substitute the water molecules that are part of hydration shell of the ions. The finding emphasizes the role of hydration sphere of ions on the performance of the membranes. Hydroxyl groups substituting for water molecules effectively decreases hydration radius and aids leakage of ions through hydrophilic channels. In practical application, nanoporous graphene sheets showed defects that caused leakage through membrane during molecular separation. To overcome the leakage through defects in graphene sheet, a multiscale leakage sealing method was invented by O'Hern et al. [303]. The impermeable and nonpolar nature graphene pores were selectively blocked to reduce defects, which resulted in centimeter scale membrane for molecular separation. The leakage-free membrane exhibited filtration performance consistent with earlier molecular dynamics simulations study by Cohen-Tanugi and Grossman [302]. However, it is very difficult to make defect-free, single-layer nano porous graphene membrane for selective separation.

20.5.2 Graphene oxide surface-located membrane

Various techniques have been used to fabricate GO coating membrane for water purification. Nair et al. [242] showed micrometer thick freestanding GO lamellar membrane fabricated through vacuum filtration of GO suspensions showed a negligible resistance to water transport through membrane, while liquids, vapors, and gases, even helium can't permeate through. The results were attributed to low friction to the flow of water molecules through two-dimensional capillaries made by subnanometer-spaced GO laminates. The water molecules have several orders of magnitude higher permeability than small organic molecules such as methanol, acetone, and hexane. In the following study by Joshi et al. [243], it was observed that GO laminates in dry state can hold vacuum. In wet state, GO laminates act as molecular sieves with a cutoff of ~0.9 nm. Ions with diameter smaller than the cutoff such as K^+, Mg^{2+}, and AsO_4^{3-}

This book belongs to Badji Mokhtar Annaba University Central Library Copyright Elsevier 2025

ions showed higher permeation through the membrane, with all almost the same rate, independent of ion charge. The fast permeation was ascribed to the capillary-like high pressure acting on the ions inside the graphene laminates.

The abovementioned studies [242, 243] revealed that nanochannels between GO nanosheets have great potential for water purification. Mechanistic studies to elucidate water and ion transport in GO membranes showed that water molecules flow across the defects, pores, through the interedge area, through the interconnected nanochannels between GO nanosheets, and with a tortuous path over the hydrophobic nonoxidized region instead of flow over the hydrophilic oxidized region [244, 305]. Flow of water molecules on the nonoxidized GO is almost frictionless, extremely fast, and favorable energetically. Any ion or molecule with hydration diameter of 0.9 nm or less was able to pass through the nanochannels created by GO laminate, whereas all the larger size diameter molecules were blocked. The studies revealed that size exclusion was appeared to be the dominant sieving mechanism in GO laminate membrane.

The cutoff size of GO laminate membrane can be controlled by adjusting the GO spacing through sandwiching the appropriately sized molecule or species between GO nanosheets. Based on the targeted ions or molecules, membrane cutoff has been adjusted for selective separation. Different size species, such as small functional groups, polyelectrolyte, and nanoparticle or nanofibers were intercalated into the laminates to adjust GO spacing for selective separation. Moreover, precisely controlled nanoscale channels distributed GO laminate membranes have advantages when compared to traditionally used polymeric membranes. GO-coated membranes were typically fabricated by vacuum filtration of GO suspensions or LBL deposition configuration.

Water flux of 21.8 LMH/bar, >99% retention for organic dyes, and ca. 20%–60% retention for ion salts was observed from ultrathin (22–53 nm thick) chemically converted graphene-based NF membranes fabricated on microporous substrates using vacuum filtration [200]. Two-dimensional nanomaterials, SWCNT-intercalated GO ultrathin laminar film fabricated using vacuum filtration method exhibited separation of molecules with sizes greater than 1.8 nm [201]. The film with a thickness of 40 nm effectively separated Coomassie Brilliant Blue, BSA, cytochrome C, and Rhodamine B, with permeability in the range of 660–720 LMH/bar. SWCNT-intercalated GO membrane showed high separation efficiencies of 97.4%–98.7% and exhibited excellent pH stabilities.

GO-coated membrane synthesized by vacuum filtration showed lack of sufficient bonding between GO nanosheets because of swelling, instability in aqueous environment, or disorder of GO coating during membrane filtration, especially in cross-flow configuration. The swelling of GO nanosheets in membrane was controlled by cross-linking GO nanosheets with cationic tetrakis(1-methyl-pyridinium-4-yl)porphyrin (TMPyP) by a vacuum-assisted approach [202]. Nonoxide regions of GO were used as cross-linking sites to create 1 nm-sized channels for permeation. A twofold increase in water flux was obtained by including CNT in expanded GO nanosheets in

This book belongs to Badji Mokhtar Annaba University Central Library Copyright Elsevier 2025

SLN-NF membrane over membrane (G-CNTm) with only GO, while the rejection performance was unchanged. [203]. The fouling resistance of G-CNTm was good for SA and HA but suffered protein fouling, which was attributed to strong interactions between graphene sheets and BSA.

LBL method showed the stabilized GO layers through electrostatic interaction between GO nanosheets or through covalent bonding. A new type of water separation GO membrane was made through LBL deposition of GO nanosheets cross-linked with TMC on a polydopamine-coated PSF membrane [247]. In such membranes, water can flow through the nanochannels between GO layers, while unwanted solutes are rejected by size exclusion and charge effects. The membrane exhibited an MWCO of 500 Da for dye, with a water flux fourfold higher than commercial NF membranes. The overall thickness of stack of GO laminates deposited on the substrate can be controlled by varying the concentration of GO in the feed solution that is subjected to vacuum filtration. The number of LBL cycles can also be used to control the amount of GO deposited. Increasing the number of layers deposited, the rejection of solute increases, while overall permeability of membrane decreases. A positively charged polyethylenimine (PEI)/GO membrane made using LBL technique displayed excellent rejection as the surface acquired greater positive charge [204]. The GO surface-deposited poly(amide-imide)-polyethyleneimine (PAI-PEI) hollow fiber NF membrane presented 86% higher in water permeability and improved mechanical property [205]. The GO deposition using LBL showed good stability, even when subjected to a backwashing pressure of 100,000 Pa and fluid velocity of 14 cm/s, which showed the potential of using this GO-modified hollow fiber membrane for large-scale water softening applications. Furthermore, the GO/Torlon composite hollow fiber membrane fabricated by LBL approach showed high stability and heavy metal recovery [206]. GO nanosheets efficiently covered the surface defects and made narrow pore size membrane. Highly charged nanochannels were created in polyelectrolyte (PE) intercalated amine reduced GO membrane (PE@ArGO and mPE@ArGO) using vacuum-assisted LBL methodology [207]. High water permeability and salt rejection was attained due to distinct surface charge of the PE@ArGO (+4.37 mC/m^2) and mPE@ArGO (−4.28 mC/m^2) membrane. It was the first report on GO membranes with high density positive/negative charge gated ion transport behavior. Among the UF applications of SLN membranes, inclusion of oxidized MWCT in PEBAX increased flux fivefold, at no change in oil rejection because of increase in hydrophilicity of the layer [185]. ZIF-8/Gelatin on PVDF membranes showed 80% decrease in water flux but 90% increase in rhodamine rejection [179].

20.5.3 Inorganic nanomaterials (iNPs) surface-located membranes

The adhesion of Ag to the film was improved by functionalizing the surface of the AgNP or the membrane. Thiol functionalities are commonly employed because strong binding exists between Ag and thiol groups [211]. PA surface-grafted with zwitterionic polymer followed by

This book belongs to Badji Mokhtar Annaba University Central Library Copyright Elsevier 2025

deposition of AGNP showed antimicrobial and antiadhesive activities [308]. Zwiterionic surface treatment strongly binding Ag^+ ions was reported with excellent antimicrobial activity [208]. Copper nanoparticles were deposited on the surface of RO membranes by spray and spin technique. Only a minor degradation of flux and rejection was obtained; however, significant bacterial inactivation in static and cross-flow filtration was observed [210]. Surface modification using hydrophilic nanoparticles described above is also reported with a high degree of success in improving the membrane throughput. Photoinduced super wetting CNT-TiO_2 network separated oil-water emulsion, with a flux of 30,000 LMH/bar. The flux was over to orders of magnitude higher than that reported for commercial membranes, with a high separation efficiency [309]. The primary objective is to increase the hydrophilicity to prevent oil from depositing on the membrane surface and thereby avoiding the formation of oily layer on the membrane.

20.5.4 Metal-organic frameworks/covalent organic frameworks surface-located membrane

ZIF-8 layer was immobilized on PTFE and used as adsorptive membrane for the removal of emerging pollutants such as progesterone; up to 20% by weight of ZIF-8 was used in these membranes. Over 95% rejection was obtained over three cycles [212]. The inclusion of ZIF-8 resulted in an increase in the water flux of the membrane as well. ZIF-8 grown on PVDF membrane increased the flux of the membrane by over 200% without change in rejection. Studies with ZIF-8 top layer on PAN and PEI membranes showed an increase in flux up to 96%, coupled with higher rejection of methylene blue [214, 215].

COF nanosheets made from 3,8-diamino-5-ethyl-6-phenylphenanthridinium bromide with 1,3,5-triformylphloroglucinol (TFP) deposited bottom-up showed excellent permeation properties, with pure water flux as high as 48 LMH/bar and 99.9% rejection of methyl orange. The high flux was attributed to electrostatic attraction between positively charged COF and anionic dye [181]. Stacked COF made from brominated hexaazatrinaphthalene and pyrene tetraone deposited on 200 nm pore size membrane showed greater than 2250 LMH/bar flux, with almost complete rejection of Oct_4N. The high rejection is attributed to uniform pore size with highly hydrophilic channels [217]. Free standing COF showed a high degree of stacking and uniform pore size with excellent stability in organic solvents. Tunable pore size of 2–3 nm was obtained, with high rejection for vitamin B-12, curcumin, rose Bengal, tetracycline, etc. [198]. Nanofibrous electrospun membranes made from Ag-decorated BiOI nanosheets embedded on TiO_2 gave 7.5 log inactivation of *E. coli* within 1 h [199].

This book belongs to Badji Mokhtar Annaba University Central Library Copyright Elsevier 2025

20.6 Perspective

Nanomaterials are added to membranes to improve their performance. Polymers with carbon backbone are robust, manipulated easily into membranes, and do not swell in water. Polymers are hydrophobic, which makes them susceptible to fouling due to natural organic matter, proteins, suspended solids, biofilm formation, etc. Inclusion of nanomaterials in the membranes increases hydrophilicity and thus decreases the fouling potential. Membrane formation is also affected by the inclusion of nanomaterials. In asymmetric membranes made using phase inversion, hydrophilic nanomaterials act as nuclei for phase separation, giving rise to an elongated finger-like pore structure. This structure gives higher porosity, both in the top layer and in the bulk. At the surface, the top layer pore density increases with large number of small-sized pores, while in the bulk, large finger-like pores are formed. The result is that the membranes have higher permeability and higher rejection. Thus the flux-rejection trade-off is overcome. TFC polyamide layer added on top of these MMMs have found application in FO. There is significant decrease in the internal CP in the TFC FO membranes with nanocomposite substrates. This effect is observed in both cases when the substrate is facing the feed solution or is in contact with draw solution.

Nanomaterials are also added in TFC membranes. The TFC membranes are used for RO or NF. In these use cases, the aim of addition of nanomaterials is to decrease contact angle to make the PA layer hydrophilic, enhance flux, and most importantly, prevent the growth of biofilm. Several approaches with inclusion of inorganic, organic, and CNs have been reported. Ag and copper-based biocidal TFN membranes have been demonstrated to decrease the biofouling. However, the life of the antimicrobial agents in the membranes is not explored widely; only a few reports have discussed regeneration of these coatings. Surface treatment and deposition of hydrophilic, biocidal nanoparticles on the surface forms the SLN category of nanocomposite membranes. The crux of the studies in this type of membranes is the decrease in the water contact angle to increase hydrophilicity, decrease fouling potential, and importantly, stability of the coating. Frequently, the surface is modified, and nanomaterials are bonded by van der Waals forces, electrostatic attractive forces, or by covalent modifications.

In the approaches sum up in the chapter have been that empirical, fundamental studies on structure-property relationship of the nanoparticle and membranes are needed. Another concern has been in creating a uniform dispersion of nanoparticles within the matrix. Aggregation of nanoparticles in TFN severely affects the performance. Aggregation can generate defects that will cause nonspecific solute and solvent transport, drastically degrading the rejection. The inclusion of photocatalytic nanoparticles in the matrix imparts self-cleaning properties; however, the mechanism of self-cleaning is through the generation of oxygen-based free radicals that degrade the rejected materials deposited on the surface. These radicals are nonspecific and have tendency to damage membrane and the rejected cake layer. Finally, the

This book belongs to Badji Mokhtar Annaba University Central Library Copyright Elsevier 2025

addition of nanoparticles tends to make the membranes more expensive; therefore a process for synthesis of nanomaterials at low cost is also an important challenge to be overcome.

20.7 Conclusion

Membrane separations have become an indispensable method of treatment for the recovery of wastewater. The challenges faced in the use of membrane separations for wastewater treatment are still control of fouling and low permeate flux. The nanomaterials included in MMMs are used to decrease water contact angle, which improves antifouling resistance and increases long-term flux. Hydrophilic nanomaterials have also shown to affect the membrane pore structure to increase the number of pores with lower average pore size to increase rejection and flux at the same time. Similarly, nanomaterials in the top layer increase hydrophilicity and water flux in NF and RO operations, with no adverse effect on the rejection. The nanomaterials in the substrate in TFC membranes have led to increase in permeate flux in FO owing to lower internal CP. SLNs are installed on the surface of membranes through a variety of methods such as self-assembly and grafting. The driver for SLN membranes is tuning membrane surface to increase hydrophilicity, impart antifouling, and photocatalytic properties. These membranes can oxidize fouling layer to give a self-cleaning surface. Thus the use of nanomaterials in membranes have shown the potential to minimize fouling and improve permeate flux without affecting rejection or molecular weight cutoff, thus overcoming the flux-rejection tradeoff. A few nanocomposite membranes are being commercialized, while additional research is needed to translate the gains obtained in the membrane performance with the additional environmental and commercial costs of manufacturing.

References

[1] Water Scarcity Issues: We're Running Out of Water, FEW Resources.Org. (2020). http://www.FEWResources.org/water-scarcity-issues-were-running-out-of-water.html (Accessed 11 July 2020).
[2] U. N. Environment, Global Environment Outlook 6—GEO 6: Healthy Planet, Healthy People, Nairobi, Cambridge University Press, 2019 doi:10.1017/9781108627146.
[3] WWAP (United Nations World Water Assessment Programme), The United Nations World Water Development Report 2017. Wastewater: The Untapped Resource, UNESCO, Paris, 2017 2017.
[4] Waste-Water Treatment Technologies: A General Review, United Nations, Economic and Social Commission for Western Asia, 2003.
[5] R.P. Schwarzenbach, T. Egli, T.B. Hofstetter, U. von Gunten, B. Wehrli, Global water pollution and human health. Annu. Rev. Environ. Resour. 35 (2010) 109–136, https://doi.org/10.1146/annurev-environ-100809-125342.
[6] G. Hutton, M. Varughese, The Costs of Meeting the 2030 Sustainable Development Goal Targets on Drinking Water, Sanitation, and Hygiene. The World Bank, 2016, https://doi.org/10.1596/K8543.
[7] M. Gander, B. Jefferson, S. Judd, Aerobic MBRs for domestic wastewater treatment: a review with cost considerations. Sep. Purif. Technol. 18 (2000) 119–130, https://doi.org/10.1016/S1383-5866(99)00056-8.
[8] K.C. Khulbe, C. Feng, T. Matsuura, The art of surface modification of synthetic polymeric membranes. J. Appl. Polym. Sci. 115 (2010) 855–895, https://doi.org/10.1002/app.31108.

This book belongs to Badji Mokhtar Annaba University Central Library Copyright Elsevier 2025

[9] A.L. Ahmad, A.A. Abdulkarim, B.S. Ooi, S. Ismail, Recent development in additives modifications of polyethersulfone membrane for flux enhancement. Chem. Eng. J. 223 (2013) 246–267, https://doi.org/10.1016/j.cej.2013.02.130.
[10] D. Rana, T. Matsuura, Surface modifications for antifouling membranes. Chem. Rev. 110 (2010) 2448–2471, https://doi.org/10.1021/cr800208y.
[11] H. Zhao, L. Wu, Z. Zhou, L. Zhang, H. Chen, Improving the antifouling property of polysulfone ultrafiltration membrane by incorporation of isocyanate-treated graphene oxide, Phys. Chem. Chem. Phys. 15 (2013) 9084–9092.
[12] E. Saljoughi, T. Mohammadi, Cellulose acetate (CA)/polyvinylpyrrolidone (PVP) blend asymmetric membranes: preparation, morphology and performance. Desalination 249 (2009) 850–854, https://doi.org/10.1016/j.desal.2008.12.066.
[13] N. Pezeshk, D. Rana, R.M. Narbaitz, T. Matsuura, Novel modified PVDF ultrafiltration flat-sheet membranes. J. Membr. Sci. 389 (2012) 280–286, https://doi.org/10.1016/j.memsci.2011.10.039.
[14] J. Hu, C. Zhang, J. Cong, H. Toyoda, M. Nagatsu, Y. Meng, Plasma-grafted alkaline anion-exchange membranes based on polyvinyl chloride for potential application in direct alcohol fuel cell. J. Power Sources 196 (2011) 4483–4490, https://doi.org/10.1016/j.jpowsour.2011.01.034.
[15] H. Sun, S. Liu, B. Ge, L. Xing, H. Chen, Cellulose nitrate membrane formation via phase separation induced by penetration of nonsolvent from vapor phase. J. Membr. Sci. 295 (2007) 2–10, https://doi.org/10.1016/j.memsci.2007.02.019.
[16] B. Bolto, T. Tran, M. Hoang, Z. Xie, Crosslinked poly(vinyl alcohol) membranes. Prog. Polym. Sci. 34 (2009) 969–981, https://doi.org/10.1016/j.progpolymsci.2009.05.003.
[17] T. Kitamura, S. Okabe, M. Tanigaki, K.-I. Kurumada, M. Ohshima, S.-I. Kanazawa, Morphology change in polytetrafluoroethylene (PTFE), porous membrane caused by heat treatment. Polym. Eng. Sci. 40 (2000) 809–817, https://doi.org/10.1002/pen.11210.
[18] B. Yuan, C. Bao, L. Song, N. Hong, K.M. Liew, Y. Hu, Preparation of functionalized graphene oxide/polypropylene nanocomposite with significantly improved thermal stability and studies on the crystallization behavior and mechanical properties. Chem. Eng. J. 237 (2014) 411–420, https://doi.org/10.1016/j.cej.2013.10.030.
[19] M. Ulbricht, Advanced functional polymer membranes. Polymer 47 (2006) 2217–2262, https://doi.org/10.1016/j.polymer.2006.01.084.
[20] K. Majewska-Nowak, Synthesis and properties of polysulfone membranes. Desalination 71 (1989) 83–95, https://doi.org/10.1016/0011-9164(89)80001-3.
[21] T. Xiang, Y. Xie, R. Wang, M.-B. Wu, S.-D. Sun, C.-S. Zhao, Facile chemical modification of polysulfone membrane with improved hydrophilicity and blood compatibility. Mater. Lett. 137 (2014) 192–195, https://doi.org/10.1016/j.matlet.2014.09.037.
[22] C. Dizman, M.A. Tasdelen, Y. Yagci, Recent advances in the preparation of functionalized polysulfones. Polym. Int. 62 (2013) 991–1007, https://doi.org/10.1002/pi.4525.
[23] N. Jusoh, L.K. Keong, A. Mohd Shariff, Preparation and characterization of polysulfone membrane for gas separation. Adv. Mater. Res. 917 (2014) 307–316, https://doi.org/10.4028/www.scientific.net/AMR.917.307.
[24] T.A. Barbari, S.S. Datwani, Gas separation properties of polysulfone membranes treated with molecular bromine. J. Membr. Sci. 107 (1995) 263–266, https://doi.org/10.1016/0376-7388(95)00122-0.
[25] C. Bellona, J.E. Drewes, P. Xu, G. Amy, Factors affecting the rejection of organic solutes during NF/RO treatment—a literature review. Water Res. 38 (2004) 2795–2809, https://doi.org/10.1016/j.watres.2004.03.034.
[26] J. Yin, B. Deng, Polymer-matrix nanocomposite membranes for water treatment. J. Membr. Sci. 479 (2015) 256–275, https://doi.org/10.1016/j.memsci.2014.11.019.
[27] K.A. Mauritz, R.B. Moore, State of understanding of nafion. Chem. Rev. 104 (2004) 4535–4586, https://doi.org/10.1021/cr0207123.
[28] G.R. Guillen, Y. Pan, M. Li, E.M.V. Hoek, Preparation and characterization of membranes formed by nonsolvent induced phase separation: a review. Ind. Eng. Chem. Res. 50 (2011) 3798–3817, https://doi.org/10.1021/ie101928r.

This book belongs to Badji Mokhtar Annaba University Central Library Copyright Elsevier 2025

[29] E.V. Ballou, T. Wydeven, Solute rejection by porous glass membranes. II. Pore size distributions and membrane permeabilities. J. Colloid Interface Sci. 41 (1972) 198–207, https://doi.org/10.1016/0021-9797(72)90109-9.
[30] S. Singh, K.C. Khulbe, T. Matsuura, P. Ramamurthy, Membrane characterization by solute transport and atomic force microscopy. J. Membr. Sci. 142 (1998) 111–127, https://doi.org/10.1016/S0376-7388(97)00329-3.
[31] A. Elrasheedy, N. Nady, M. Bassyouni, A. El-Shazly, Metal organic framework based polymer mixed matrix membranes: review on applications in water purification. Membranes 9 (2019) 88, https://doi.org/10.3390/membranes9070088.
[32] A. Katchalsky, R. Spangler, Dynamics of membrane processes. Q. Rev. Biophys. 1 (1968) 127–175, https://doi.org/10.1017/S0033583500000524.
[33] J.G. Wijmans, R.W. Baker, The solution-diffusion model: a review. J. Membr. Sci. 107 (1995) 1–21, https://doi.org/10.1016/0376-7388(95)00102-I.
[34] G.M. Geise, H.B. Park, A.C. Sagle, B.D. Freeman, J.E. McGrath, Water permeability and water/salt selectivity tradeoff in polymers for desalination. J. Membr. Sci. 369 (2011) 130–138, https://doi.org/10.1016/j.memsci.2010.11.054.
[35] G. Belfort, R.H. Davis, A.L. Zydney, The behavior of suspensions and macromolecular solutions in crossflow microfiltration. J. Membr. Sci. 96 (1994) 1–58, https://doi.org/10.1016/0376-7388(94)00119-7.
[36] G.M. Geise, H.-S. Lee, D.J. Miller, B.D. Freeman, J.E. McGrath, D.R. Paul, Water purification by membranes: the role of polymer science. J. Polym. Sci. B Polym. Phys. 48 (2010) 1685–1718, https://doi.org/10.1002/polb.22037.
[37] S. Boributh, A. Chanachai, R. Jiraratananon, Modification of PVDF membrane by chitosan solution for reducing protein fouling. J. Membr. Sci. 342 (2009) 97–104, https://doi.org/10.1016/j.memsci.2009.06.022.
[38] D. Rana, T. Matsuura, Surface modifications for antifouling membranes. Chem. Rev. 110 (2010) 2448–2471, https://doi.org/10.1021/cr800208y.
[39] A.L. Ahmad, A.A. Abdulkarim, B.S. Ooi, S. Ismail, Recent development in additives modifications of polyethersulfone membrane for flux enhancement. Chem. Eng. J. 223 (2013) 246–267, https://doi.org/10.1016/j.cej.2013.02.130.
[40] L.E.S. Brink, S.J.G. Elbers, T. Robbertsen, P. Both, The anti-fouling action of polymers preadsorbed on ultrafiltration and microfiltration membranes. J. Membr. Sci. 76 (1993) 281–291, https://doi.org/10.1016/0376-7388(93)85225-L.
[41] A. Naz, R. Sattar, M. Siddiq, Polymer membranes for biofouling mitigation: a review. Polym-Plast. Tech. Mat. 58 (2019) 1829–1854, https://doi.org/10.1080/25740881.2019.1576200.
[42] H.-C. Yang, K.-J. Liao, H. Huang, Q.-Y. Wu, L.-S. Wan, Z.-K. Xu, Mussel-inspired modification of a polymer membrane for ultra-high water permeability and oil-in-water emulsion separation. J. Mater. Chem. A 2 (2014) 10225–10230, https://doi.org/10.1039/C4TA00143E.
[43] A. Kulkarni, D. Mukherjee, W.N. Gill, Flux enhancement by hydrophilization of thin film composite reverse osmosis membranes. J. Membr. Sci. 114 (1996) 39–50, https://doi.org/10.1016/0376-7388(95)00271-5.
[44] M. Ulbricht, G. Belfort, Surface modification of ultrafiltration membranes by low temperature plasma. I. Treatment of polyacrylonitrile. J. Appl. Polym. Sci. 56 (1995) 325–343, https://doi.org/10.1002/app.1995.070560304.
[45] E. Celik, H. Park, H. Choi, H. Choi, Carbon nanotube blended polyethersulfone membranes for fouling control in water treatment. Water Res. 45 (2011) 274–282, https://doi.org/10.1016/j.watres.2010.07.060.
[46] S. Qiu, L. Wu, X. Pan, L. Zhang, H. Chen, C. Gao, Preparation and properties of functionalized carbon nanotube/PSF blend ultrafiltration membranes. J. Membr. Sci. 342 (2009) 165–172, https://doi.org/10.1016/j.memsci.2009.06.041.
[47] R. Kumar, A.M. Isloor, A.F. Ismail, S.A. Rashid, A.A. Ahmed, Permeation, antifouling and desalination performance of TiO_2 nanotube incorporated PSf/CS blend membranes. Desalination 316 (2013) 76–84, https://doi.org/10.1016/j.desal.2013.01.032.
[48] F. Sadeghi, A. Ajji, P.J. Carreau, Microporous membranes obtained from polypropylene blends with superior permeability properties. J. Polym. Sci. B Polym. Phys. 46 (2008) 148–157, https://doi.org/10.1002/polb.21350.

This book belongs to Badji Mokhtar Annaba University Central Library Copyright Elsevier 2025

[49] T.T. Nguyen, P. Bandyopadhyay, X. Li, N.H. Kim, J.H. Lee, Effects of grafting methods for functionalization of graphene oxide by dodecylamine on the physical properties of its polyurethane nanocomposites. J. Membr. Sci. 540 (2017) 108–119, https://doi.org/10.1016/j.memsci.2017.06.040.
[50] J.-S. Gu, H.-Y. Yu, L. Huang, Z.-Q. Tang, W. Li, J. Zhou, M.-G. Yan, X.-W. Wei, Chain-length dependence of the antifouling characteristics of the glycopolymer-modified polypropylene membrane in an SMBR. J. Membr. Sci. 326 (2009) 145–152, https://doi.org/10.1016/j.memsci.2008.09.043.
[51] M.I. Vázquez, R. de Lara, P. Galán, J. Benavente, Modification of cellulosic membranes by γ-radiation: effect on electrochemical parameters and protein adsorption. Colloids Surf. A Physicochem. Eng. Asp. 270–271 (2005) 245–251, https://doi.org/10.1016/j.colsurfa.2005.06.008.
[52] L.Y. Ng, A. Ahmad, A.W. Mohammad, Alteration of polyethersulphone membranes through UV-induced modification using various materials: a brief review. Arab. J. Chem. 10 (2017) S1821–S1834, https://doi.org/10.1016/j.arabjc.2013.07.009.
[53] J.M. Yang, C.Y. Chiang, H.Z. Wang, C.C. Yang, Two step modification of poly(vinyl alcohol) by UV radiation with 2-hydroxy ethyl methacrylate and sol-gel process for the application of polymer electrolyte membrane. J. Membr. Sci. 341 (2009) 186–194, https://doi.org/10.1016/j.memsci.2009.06.004.
[54] C. Nardin, W. Meier, Hybrid materials from amphiphilic block copolymers and membrane proteins. Rev. Mol. Biotechnol. 90 (2002) 17–26, https://doi.org/10.1016/S1389-0352(01)00052-6.
[55] J. Kowal, X. Zhang, I.A. Dinu, C.G. Palivan, W. Meier, Planar biomimetic membranes based on amphiphilic block copolymers. ACS Macro Lett. 3 (2014) 59–63, https://doi.org/10.1021/mz400590c.
[56] H. Endo, J. Allgaier, G. Gompper, B. Jakobs, M. Monkenbusch, D. Richter, T. Sottmann, R. Strey, Membrane decoration by amphiphilic block copolymers in bicontinuous microemulsions. Phys. Rev. Lett. 85 (2000) 102–105, https://doi.org/10.1103/PhysRevLett.85.102.
[57] L.M. Robeson, Correlation of separation factor versus permeability for polymeric membranes. J. Membr. Sci. 62 (1991) 165–185, https://doi.org/10.1016/0376-7388(91)80060-J.
[58] T.-S. Chung, L.Y. Jiang, Y. Li, S. Kulprathipanja, Mixed matrix membranes (MMMs) comprising organic polymers with dispersed inorganic fillers for gas separation. Prog. Polym. Sci. 32 (2007) 483–507, https://doi.org/10.1016/j.progpolymsci.2007.01.008.
[59] A. Bottino, G. Capannelli, V. D'Asti, P. Piaggio, Preparation and properties of novel organic-inorganic porous membranes. Sep. Purif. Technol. 22–23 (2001) 269–275, https://doi.org/10.1016/S1383-5866(00)00127-1.
[60] I. Genné, W. Doyen, W. Adriansens, R. Leysen, Organo-mineral ultrafiltration membranes. Filtr. Sep. 34 (1997) 964–966, https://doi.org/10.1016/S0015-1882(97)86673-6.
[61] M. Wasim, A. Sabir, M. Shafiq, A. Islam, M. Azam, T. Jamil, Mixed matrix membranes: two step process modified with electrospun (carboxy methylcellulose sodium salt/sepiolite) fibers for nanofiltration. J. Ind. Eng. Chem. 50 (2017) 172–182, https://doi.org/10.1016/j.jiec.2017.02.011.
[62] Y. Ma, F. Shi, J. Ma, M. Wu, J. Zhang, C. Gao, Effect of PEG additive on the morphology and performance of polysulfone ultrafiltration membranes. Desalination 272 (2011) 51–58, https://doi.org/10.1016/j.desal.2010.12.054.
[63] J.-H. Kim, K.-H. Lee, Effect of PEG additive on membrane formation by phase inversion. J. Membr. Sci. 138 (1998) 153–163, https://doi.org/10.1016/S0376-7388(97)00224-X.
[64] C. Hying, E. Staude, The influence of polyvinylpyrrolidone (PVP) in polyetherimid/PVP blend membranes upon vapor separation. J. Membr. Sci. 144 (1998) 251–257, https://doi.org/10.1016/S0376-7388(98)00059-3.
[65] M.O. Mavukkandy, M.R. Bilad, A. Giwa, S.W. Hasan, H.A. Arafat, Leaching of PVP from PVDF/PVP blend membranes: impacts on membrane structure and fouling in membrane bioreactors. J. Mater. Sci. 51 (2016) 4328–4341, https://doi.org/10.1007/s10853-016-9744-7.
[66] Z.-Y. Cui, Y.-Y. Xu, L.-P. Zhu, J.-Y. Wang, Z.-Y. Xi, B.-K. Zhu, Preparation of PVDF/PEO-PPO-PEO blend microporous membranes for lithium ion batteries via thermally induced phase separation process. J. Membr. Sci. 325 (2008) 957–963, https://doi.org/10.1016/j.memsci.2008.09.022.
[67] K.M. Anilkumar, B. Jinisha, M. Manoj, S. Jayalekshmi, Poly(ethylene oxide) (PEO)—poly(vinyl pyrrolidone) (PVP) blend polymer based solid electrolyte membranes for developing solid state magnesium ion cells. Eur. Polym. J. 89 (2017) 249–262, https://doi.org/10.1016/j.eurpolymj.2017.02.004.

This book belongs to Badji Mokhtar Annaba University Central Library Copyright Elsevier 2025

[68] A. Rahimpour, S.S. Madaeni, Polyethersulfone (PES)/cellulose acetate phthalate (CAP) blend ultrafiltration membranes: preparation, morphology, performance and antifouling properties. J. Membr. Sci. 305 (2007) 299–312, https://doi.org/10.1016/j.memsci.2007.08.030.

[69] A. Roy, P. Bhunia, S. De, Solvent effect and macrovoid formation in cellulose acetate phthalate (CAP)—polyacrylonitrile (PAN) blend hollow fiber membranes. J. Appl. Polym. Sci. 134 (2017), https://doi.org/10.1002/app.44366.

[70] M. Mondal, S. De, Characterization and antifouling properties of polyethylene glycol doped PAN-CAP blend membrane. RSC Adv. 5 (2015) 38948–38963, https://doi.org/10.1039/C5RA02889B.

[71] R. Kumar, A.M. Isloor, A.F. Ismail, Preparation and evaluation of heavy metal rejection properties of polysulfone/chitosan, polysulfone/N-succinyl chitosan and polysulfone/N-propylphosphonyl chitosan blend ultrafiltration membranes. Desalination 350 (2014) 102–108, https://doi.org/10.1016/j.desal.2014.07.010.

[72] W. Zou, Y. Huang, J. Luo, J. Liu, C. Zhao, Poly(methyl methacrylate-acrylic acid-vinyl pyrrolidone) terpolymer modified polyethersulfone hollow fiber membrane with pH sensitivity and protein antifouling property. J. Membr. Sci. 358 (2010) 76–84, https://doi.org/10.1016/j.memsci.2010.04.028.

[73] J. Ren, W. Zhao, C. Cheng, M. Zhou, C. Zhao, Comparison of pH-sensitivity between two copolymer modified polyethersulfone hollow fiber membranes. Desalination 280 (2011) 152–159, https://doi.org/10.1016/j.desal.2011.06.069.

[74] Z. Yi, L. Zhu, L. Cheng, B. Zhu, Y. Xu, A readily modified polyethersulfone with amino-substituted groups: its amphiphilic copolymer synthesis and membrane application. Polymer 53 (2012) 350–358, https://doi.org/10.1016/j.polymer.2011.11.053.

[75] H. Salazar, P.M. Martins, B. Santos, M.M. Fernandes, A. Reizabal, V. Sebastián, G. Botelho, C.J. Tavares, J. L. Vilas-Vilela, S. Lanceros-Mendez, Photocatalytic and antimicrobial multifunctional nanocomposite membranes for emerging pollutants water treatment applications. Chemosphere 250 (2020) 126299, https://doi.org/10.1016/j.chemosphere.2020.126299.

[76] H. Zangeneh, Z. Rahimi, A.A. Zinatizadeh, S.H. Razavizadeh, S. Zinadini, l-Histidine doped-TiO_2-CdS nanocomposite blended UF membranes with photocatalytic and self-cleaning properties for remediation of effluent from a local waste stabilization pond (WSP) under visible light. Process. Saf. Environ. Prot. 136 (2020) 92–104, https://doi.org/10.1016/j.psep.2020.01.022.

[77] N.S. Naik, M. Padaki, S. Déon, G. Karunakaran, N. Dizge, M. Saxena, The efficient mixed matrix antifouling membrane for surfactant stabilized oil-in-water nanoemulsion separation. J. Water Process. Eng. 32 (2019) 100959, https://doi.org/10.1016/j.jwpe.2019.100959.

[78] L. Ghalamchi, S. Aber, V. Vatanpour, M. Kian, Development of an antibacterial and visible photocatalytic nanocomposite microfiltration membrane incorporated by Ag_3PO_4/CuZnAl NLDH. Sep. Purif. Technol. 226 (2019) 218–231, https://doi.org/10.1016/j.seppur.2019.05.104.

[79] R. Jamshidi Gohari, W.J. Lau, T. Matsuura, E. Halakoo, A.F. Ismail, Adsorptive removal of Pb(II) from aqueous solution by novel PES/HMO ultrafiltration mixed matrix membrane. Sep. Purif. Technol. 120 (2013) 59–68, https://doi.org/10.1016/j.seppur.2013.09.024.

[80] M.R. Esfahani, N. Koutahzadeh, A.R. Esfahani, M.D. Firouzjaei, B. Anderson, L. Peck, A novel gold nanocomposite membrane with enhanced permeation, rejection and self-cleaning ability. J. Membr. Sci. 573 (2019) 309–319, https://doi.org/10.1016/j.memsci.2018.11.061.

[81] S. Zhao, H. Zhu, Z. Wang, P. Song, M. Ban, X. Song, A loose hybrid nanofiltration membrane fabricated via chelating-assisted in-situ growth of Co/Ni LDHs for dye wastewater treatment. Chem. Eng. J. 353 (2018) 460–471, https://doi.org/10.1016/j.cej.2018.07.081.

[82] J. Cui, Z. Zhou, A. Xie, Q. Wang, S. Liu, J. Lang, C. Li, Y. Yan, J. Dai, Facile preparation of grass-like structured NiCo-LDH/PVDF composite membrane for efficient oil-water emulsion separation. J. Membr. Sci. 573 (2019) 226–233, https://doi.org/10.1016/j.memsci.2018.11.064.

[83] J.-Y. Lee, C.Y. Tang, F. Huo, Fabrication of porous matrix membrane (PMM) using metal-organic framework as green template for water treatment. Sci. Rep. 4 (2014) 1–5, https://doi.org/10.1038/srep03740.

[84] S.M. Maroofi, N.M. Mahmoodi, Zeolitic imidazolate framework-polyvinylpyrrolidone-polyethersulfone composites membranes: from synthesis to the detailed pollutant removal from wastewater using cross flow

This book belongs to Badji Mokhtar Annaba University Central Library Copyright Elsevier 2025

system. Colloids Surf. A Physicochem. Eng. Asp. 572 (2019) 211–220, https://doi.org/10.1016/j.colsurfa.2019.03.093.

[85] X. Dai, Y. Cao, X. Shi, X. Wang, The PLA/ZIF-8 nanocomposite membranes: the diameter and surface roughness adjustment by ZIF-8 nanoparticles, high wettability, improved mechanical property, and efficient oil/water separation. Adv. Mater. Interfaces 3 (2016) 1600725, https://doi.org/10.1002/admi.201600725.

[86] J. Ma, X. Guo, Y. Ying, D. Liu, C. Zhong, Composite ultrafiltration membrane tailored by MOF@GO with highly improved water purification performance. Chem. Eng. J. 313 (2017) 890–898, https://doi.org/10.1016/j.cej.2016.10.127.

[87] R.S. Zambare, K.B. Dhopte, A.V. Patwardhan, P.R. Nemade, Polyamine functionalized graphene oxide polysulfone mixed matrix membranes with improved hydrophilicity and anti-fouling properties. Desalination 403 (2017) 24–35, https://doi.org/10.1016/j.desal.2016.02.003.

[88] A. Ammar, A.M. Al-Enizi, M.A. AlMaadeed, A. Karim, Influence of graphene oxide on mechanical, morphological, barrier, and electrical properties of polymer membranes. Arab. J. Chem. 9 (2016) 274–286, https://doi.org/10.1016/j.arabjc.2015.07.006.

[89] J. Lee, H.-R. Chae, Y.J. Won, K. Lee, C.-H. Lee, H.H. Lee, I.-C. Kim, J.-M. Lee, Graphene oxide nanoplatelets composite membrane with hydrophilic and antifouling properties for wastewater treatment, J. Membr. Sci. 448 (2013) 223–230.

[90] S. Zinadini, A.A. Zinatizadeh, M. Rahimi, V. Vatanpour, H. Zangeneh, Preparation of a novel antifouling mixed matrix PES membrane by embedding graphene oxide nanoplates. J. Membr. Sci. 453 (2014) 292–301, https://doi.org/10.1016/j.memsci.2013.10.070.

[91] B.M. Ganesh, A.M. Isloor, A.F. Ismail, Enhanced hydrophilicity and salt rejection study of graphene oxide-polysulfone mixed matrix membrane. Desalination 313 (2013) 199–207, https://doi.org/10.1016/j.desal.2012.11.037.

[92] M. Ionita, A.M. Pandele, L. Crica, L. Pilan, Improving the thermal and mechanical properties of polysulfone by incorporation of graphene oxide. Compos. Part B 59 (2014) 133–139, https://doi.org/10.1016/j.compositesb.2013.11.018.

[93] C. Zhao, X. Xu, J. Chen, F. Yang, Effect of graphene oxide concentration on the morphologies and antifouling properties of PVDF ultrafiltration membranes. J. Environ. Chem. Eng. 1 (2013) 349–354, https://doi.org/10.1016/j.jece.2013.05.014.

[94] R.S. Zambare, K.B. Dhopte, P.R. Nemade, C.Y. Tang, Effect of oxidation degree of GO nanosheets on microstructure and performance of polysulfone-GO mixed matrix membranes. Sep. Purif. Technol. 244 (2020) 116865, https://doi.org/10.1016/j.seppur.2020.116865.

[95] S. Ayyaru, Y.-H. Ahn, Application of sulfonic acid group functionalized graphene oxide to improve hydrophilicity, permeability, and antifouling of PVDF nanocomposite ultrafiltration membranes. J. Membr. Sci. 525 (2017) 210–219, https://doi.org/10.1016/j.memsci.2016.10.048.

[96] L. Yu, Y. Zhang, B. Zhang, J. Liu, H. Zhang, C. Song, Preparation and characterization of HPEI-GO/PES ultrafiltration membrane with antifouling and antibacterial properties. J. Membr. Sci. 447 (2013) 452–462, https://doi.org/10.1016/j.memsci.2013.07.042.

[97] P.K.S. Mural, A. Banerjee, M.
S. Rana, A. Shukla, B. Padmanabhan, S. Bhadra, G. Madras, S. Bose, Polyolefin based antibacterial membranes derived from PE/PEO blends compatibilized with amine terminated graphene oxide and maleated PE. J. Mater. Chem. A 2 (2014) 17635–17648, https://doi.org/10.1039/C4TA03997A.

[98] K.-J. Lu, J. Zuo, T.-S. Chung, Novel PVDF membranes comprising n-butylamine functionalized graphene oxide for direct contact membrane distillation. J. Membr. Sci. 539 (2017) 34–42, https://doi.org/10.1016/j.memsci.2017.05.064.

[99] Z. Xu, J. Zhang, M. Shan, Y. Li, B. Li, J. Niu, B. Zhou, X. Qian, Organosilane-functionalized graphene oxide for enhanced antifouling and mechanical properties of polyvinylidene fluoride ultrafiltration membranes. J. Membr. Sci. 458 (2014) 1–13, https://doi.org/10.1016/j.memsci.2014.01.050.

[100] E. Mahmoudi, L.Y. Ng, M.M. Ba-Abbad, A.W. Mohammad, Novel nanohybrid polysulfone membrane embedded with silver nanoparticles on graphene oxide nanoplates. Chem. Eng. J. 277 (2015) 1–10, https://doi.org/10.1016/j.cej.2015.04.107.

This book belongs to Badji Mokhtar Annaba University Central Library Copyright Elsevier 2025

[101] J.A. Prince, S. Bhuvana, V. Anbharasi, N. Ayyanar, K.V.K. Boodhoo, G. Singh, Self-cleaning metal organic framework (MOF) based ultra filtration membranes—a solution to bio-fouling in membrane separation processes. Sci. Rep. 4 (2014) 6555, https://doi.org/10.1038/srep06555.

[102] C.A. Crock, A.R. Rogensues, W. Shan, V.V. Tarabara, Polymer nanocomposites with graphene-based hierarchical fillers as materials for multifunctional water treatment membranes. Water Res. 47 (2013) 3984–3996, https://doi.org/10.1016/j.watres.2012.10.057.

[103] M. Kumar, Z. Gholamvand, A. Morrissey, K. Nolan, M. Ulbricht, J. Lawler, Preparation and characterization of low fouling novel hybrid ultrafiltration membranes based on the blends of GO-TiO_2 nanocomposite and polysulfone for humic acid removal. J. Membr. Sci. 506 (2016) 38–49, https://doi.org/10.1016/j.memsci.2016.02.005.

[104] J. Zhang, Z. Xu, M. Shan, B. Zhou, Y. Li, B. Li, J. Niu, X. Qian, Synergetic effects of oxidized carbon nanotubes and graphene oxide on fouling control and anti-fouling mechanism of polyvinylidene fluoride ultrafiltration membranes. J. Membr. Sci. 448 (2013) 81–92, https://doi.org/10.1016/j.memsci.2013.07.064.

[105] E. Celik, L. Liu, H. Choi, Protein fouling behavior of carbon nanotube/polyethersulfone composite membranes during water filtration. Water Res. 45 (2011) 5287–5294, https://doi.org/10.1016/j.watres.2011.07.036.

[106] J.-H. Choi, J. Jegal, W.-N. Kim, Fabrication and characterization of multi-walled carbon nanotubes/polymer blend membranes. J. Membr. Sci. 284 (2006) 406–415, https://doi.org/10.1016/j.memsci.2006.08.013.

[107] J. Ma, Y. Zhao, Z. Xu, C. Min, B. Zhou, Y. Li, B. Li, J. Niu, Role of oxygen-containing groups on MWCNTs in enhanced separation and permeability performance for PVDF hybrid ultrafiltration membranes. Desalination 320 (2013) 1–9, https://doi.org/10.1016/j.desal.2013.04.012.

[108] P. Shah, C.N. Murthy, Studies on the porosity control of MWCNT/polysulfone composite membrane and its effect on metal removal. J. Membr. Sci. 437 (2013) 90–98, https://doi.org/10.1016/j.memsci.2013.02.042.

[109] A. Rahimpour, M. Jahanshahi, S. Khalili, A. Mollahosseini, A. Zirepour, B. Rajaeian, Novel functionalized carbon nanotubes for improving the surface properties and performance of polyethersulfone (PES) membrane. Desalination 286 (2012) 99–107, https://doi.org/10.1016/j.desal.2011.10.039.

[110] J. Zhang, Z. Xu, M. Shan, B. Zhou, Y. Li, B. Li, J. Niu, X. Qian, Synergetic effects of oxidized carbon nanotubes and graphene oxide on fouling control and anti-fouling mechanism of polyvinylidene fluoride ultrafiltration membranes. J. Membr. Sci. 448 (2013) 81–92, https://doi.org/10.1016/j.memsci.2013.07.064.

[111] S.-M. Park, J. Jung, S. Lee, Y. Baek, J. Yoon, D.K. Seo, Y.H. Kim, Fouling and rejection behavior of carbon nanotube membranes. Desalination 343 (2014) 180–186, https://doi.org/10.1016/j.desal.2013.10.005.

[112] S.L. Ong, J.Y. Hu, Y.F. Biryulin, G.A. Polotskaya, Fullerene-containing polymer membranes for rejection of estrogenic compounds in water. Fullerenes Nanotubes Carbon Nanostruct. 14 (2006) 463–466, https://doi.org/10.1080/15363830600666159.

[113] A. Khan, T.A. Sherazi, Y. Khan, S. Li, S.A.R. Naqvi, Z. Cui, Fabrication and characterization of polysulfone/modified nanocarbon black composite antifouling ultrafiltration membranes. J. Membr. Sci. 554 (2018) 71–82, https://doi.org/10.1016/j.memsci.2018.02.063.

[114] A.E. Abdelhamid, A.M. Khalil, Polymeric membranes based on cellulose acetate loaded with candle soot nanoparticles for water desalination. J. Macromol. Sci. A 56 (2019) 153–161, https://doi.org/10.1080/10601325.2018.1559698.

[115] G.A. Polotskaya, A.V. Pen'kova, N.N. Sudareva, A.E. Polotskii, A.M. Toikka, Polyamide ultrafiltration membranes modified with nanocarbon additives. Russ. J. Appl. Chem. 81 (2008) 236–240, https://doi.org/10.1134/S1070427208020146.

[116] M. Ben-Sasson, X. Lu, E. Bar-Zeev, K.R. Zodrow, S. Nejati, G. Qi, E.P. Giannelis, M. Elimelech, In situ formation of silver nanoparticles on thin-film composite reverse osmosis membranes for biofouling mitigation. Water Res. 62 (2014) 260–270, https://doi.org/10.1016/j.watres.2014.05.049.

[117] Z. Yang, H. Guo, Z. Yao, Y. Mei, C.Y. Tang, Hydrophilic silver nanoparticles induce selective nanochannels in thin film nanocomposite polyamide membranes. Environ. Sci. Technol. 53 (2019) 5301–5308, https://doi.org/10.1021/acs.est.9b00473.

[118] A.M.A. El-Aassar, Improvement of reverse osmosis performance of polyamide thin-film composite membranes using TiO_2 nanoparticles. Desalin. Water Treat. 55 (2015) 2939–2950, https://doi.org/10.1080/19443994.2014.940206.

This book belongs to Badji Mokhtar Annaba University Central Library Copyright Elsevier 2025

[119] B. Khorshidi, I. Biswas, T. Ghosh, T. Thundat, M. Sadrzadeh, Robust fabrication of thin film polyamide-TiO_2 nanocomposite membranes with enhanced thermal stability and anti-biofouling propensity. Sci. Rep. 8 (2018) 1–10, https://doi.org/10.1038/s41598-017-18724-w.
[120] G.L. Jadav, P.S. Singh, Synthesis of novel silica-polyamide nanocomposite membrane with enhanced properties. J. Membr. Sci. 328 (2009) 257–267, https://doi.org/10.1016/j.memsci.2008.12.014.
[121] A. Peyki, A. Rahimpour, M. Jahanshahi, Preparation and characterization of thin film composite reverse osmosis membranes incorporated with hydrophilic SiO_2 nanoparticles. Desalination 368 (2015) 152–158, https://doi.org/10.1016/j.desal.2014.05.025.
[122] R. Pang, K. Zhang, Fabrication of hydrophobic fluorinated silica-polyamide thin film nanocomposite reverse osmosis membranes with dramatically improved salt rejection. J. Colloid Interface Sci. 510 (2018) 127–132, https://doi.org/10.1016/j.jcis.2017.09.062.
[123] Y. Wang, B. Gao, S. Li, B. Jin, Q. Yue, Z. Wang, Cerium oxide doped nanocomposite membranes for reverse osmosis desalination. Chemosphere 218 (2019) 974–983, https://doi.org/10.1016/j.chemosphere.2018.11.207.
[124] S.G. Kim, J.H. Chun, B.-H. Chun, S.H. Kim, Preparation, characterization and performance of poly(aylene ether sulfone)/modified silica nanocomposite reverse osmosis membrane for seawater desalination. Desalination 325 (2013) 76–83, https://doi.org/10.1016/j.desal.2013.06.017.
[125] B.-H. Jeong, E.M.V. Hoek, Y. Yan, A. Subramani, X. Huang, G. Hurwitz, A.K. Ghosh, A. Jawor, Interfacial polymerization of thin film nanocomposites: a new concept for reverse osmosis membranes. J. Membr. Sci. 294 (2007) 1–7, https://doi.org/10.1016/j.memsci.2007.02.025.
[126] H. Dong, X.-Y. Qu, L. Zhang, L.-H. Cheng, H.-L. Chen, C.-J. Gao, Preparation and characterization of surface-modified zeolite-polyamide thin film nanocomposite membranes for desalination. Desalin. Water Treat. 34 (2011) 6–12, https://doi.org/10.5004/dwt.2011.2789.
[127] T.A. Saleh, V.K. Gupta, Synthesis and characterization of alumina nano-particles polyamide membrane with enhanced flux rejection performance. Sep. Purif. Technol. 89 (2012) 245–251, https://doi.org/10.1016/j.seppur.2012.01.039.
[128] G.N.B. Baroña, M. Choi, B. Jung, High permeate flux of PVA/PSf thin film composite nanofiltration membrane with aluminosilicate single-walled nanotubes. J. Colloid Interface Sci. 386 (2012) 189–197, https://doi.org/10.1016/j.jcis.2012.07.049.
[129] H. Wu, B. Tang, P. Wu, Optimizing polyamide thin film composite membrane covalently bonded with modified mesoporous silica nanoparticles. J. Membr. Sci. 428 (2013) 341–348, https://doi.org/10.1016/j.memsci.2012.10.053.
[130] S.Y. Lee, H.J. Kim, R. Patel, S.J. Im, J.H. Kim, B.R. Min, Silver nanoparticles immobilized on thin film composite polyamide membrane: characterization, nanofiltration, antifouling properties. Polym. Adv. Technol. 18 (2007) 562–568, https://doi.org/10.1002/pat.918.
[131] B. Rajaeian, A. Rahimpour, M.O. Tade, S. Liu, Fabrication and characterization of polyamide thin film nanocomposite (TFN) nanofiltration membrane impregnated with TiO_2 nanoparticles. Desalination 313 (2013) 176–188, https://doi.org/10.1016/j.desal.2012.12.012.
[132] P.S. Singh, V.K. Aswal, Characterization of physical structure of silica nanoparticles encapsulated in polymeric structure of polyamide films. J. Colloid Interface Sci. 326 (2008) 176–185, https://doi.org/10.1016/j.jcis.2008.07.025.
[133] H. Chen, S. Zheng, L. Meng, G. Chen, X. Luo, M. Huang, Comparison of novel functionalized nanofiber forward osmosis membranes for application in antibacterial activity and TRGs rejection. J. Hazard. Mater. 392 (2020) 122250, https://doi.org/10.1016/j.jhazmat.2020.122250.
[134] M. Amoli-Diva, E. Irani, K. Pourghazi, Photocatalytic filtration reactors equipped with bi-plasmonic nanocomposite/poly acrylic acid-modified polyamide membranes for industrial wastewater treatment. Sep. Purif. Technol. 236 (2020) 116257, https://doi.org/10.1016/j.seppur.2019.116257.
[135] F. Kianfar, E. Kianfar, Synthesis of isophthalic acid/aluminum nitrate thin film nanocomposite membrane for hard water softening. J. Inorg. Organomet. Polym. 29 (2019) 2176–2185, https://doi.org/10.1007/s10904-019-01177-1.

This book belongs to Badji Mokhtar Annaba University Central Library Copyright Elsevier 2025

[136] H. Azizi Namaghi, M. Pourafshari Chenar, A. Haghighi Asl, M. Esmaeili, A. Pihlajamäki, M. Kallioinen, M. Mänttäri, Ultra-desulfurization of sulfur recovery unit wastewater using thin film nanocomposite membrane. Sep. Purif. Technol. 221 (2019) 211–225, https://doi.org/10.1016/j.seppur.2019.03.096.

[137] T. Zhang, Z. Li, W. Wang, Y. Wang, B. Gao, Z. Wang, Enhanced antifouling and antimicrobial thin film nanocomposite membranes with incorporation of Palygorskite/titanium dioxide hybrid material. J. Colloid Interface Sci. 537 (2019) 1–10, https://doi.org/10.1016/j.jcis.2018.10.092.

[138] Q. Guo, J. Li, T. Chen, Q. Yao, J. Xie, Antimicrobial thin-film composite membranes with chemically decorated ultrasmall silver nanoclusters. ACS Sustain. Chem. Eng. 7 (2019) 14848–14855, https://doi.org/10.1021/acssuschemeng.9b02929.

[139] A. Mollahosseini, A. Rahimpour, A new concept in polymeric thin-film composite nanofiltration membranes with antibacterial properties. Biofouling 29 (2013) 537–548, https://doi.org/10.1080/08927014.2013.777953.

[140] S.Y. Lee, H.J. Kim, R. Patel, S.J. Im, J.H. Kim, B.R. Min, Silver nanoparticles immobilized on thin film composite polyamide membrane: characterization, nanofiltration, antifouling properties. Polym. Adv. Technol. 18 (2007) 562–568, https://doi.org/10.1002/pat.918.

[141] M. Ben-Sasson, X. Lu, E. Bar-Zeev, K.R. Zodrow, S. Nejati, G. Qi, E.P. Giannelis, M. Elimelech, In situ formation of silver nanoparticles on thin-film composite reverse osmosis membranes for biofouling mitigation. Water Res. 62 (2014) 260–270, https://doi.org/10.1016/j.watres.2014.05.049.

[142] W. Wang, Y. Li, W. Wang, B. Gao, Z. Wang, Palygorskite/silver nanoparticles incorporated polyamide thin film nanocomposite membranes with enhanced water permeating, antifouling and antimicrobial performance. Chemosphere 236 (2019) 124396, https://doi.org/10.1016/j.chemosphere.2019.124396.

[143] M.L. Lind, B.-H. Jeong, A. Subramani, X. Huang, E.M.V. Hoek, Effect of mobile cation on zeolite-polyamide thin film nanocomposite membranes. J. Mater. Res. 24 (2009) 1624–1631, https://doi.org/10.1557/jmr.2009.0189.

[144] J. Wu, C. Yu, Q. Li, Regenerable antimicrobial activity in polyamide thin film nanocomposite membranes. J. Membr. Sci. 476 (2015) 119–127, https://doi.org/10.1016/j.memsci.2014.11.030.

[145] S.F. Seyedpour, A. Rahimpour, G. Najafpour, Facile in-situ assembly of silver-based MOFs to surface functionalization of TFC membrane: a novel approach toward long-lasting biofouling mitigation. J. Membr. Sci. 573 (2019) 257–269, https://doi.org/10.1016/j.memsci.2018.12.016.

[146] A. Zirehpour, A. Rahimpour, M. Ulbricht, Nano-sized metal organic framework to improve the structural properties and desalination performance of thin film composite forward osmosis membrane. J. Membr. Sci. 531 (2017) 59–67, https://doi.org/10.1016/j.memsci.2017.02.049.

[147] X. Huang, Y. Chen, X. Feng, X. Hu, Y. Zhang, L. Liu, Incorporation of oleic acid-modified Ag@ZnO core-shell nanoparticles into thin film composite membranes for enhanced antifouling and antibacterial properties. J. Membr. Sci. 602 (2020) 117956, https://doi.org/10.1016/j.memsci.2020.117956.

[148] R. Reis, L.F. Dumée, L. He, F. She, J.D. Orbell, B. Winther-Jensen, M.C. Duke, Amine enrichment of thin-film composite membranes via low pressure plasma polymerization for antimicrobial adhesion. ACS Appl. Mater. Interfaces 7 (2015) 14644–14653, https://doi.org/10.1021/acsami.5b01603.

[149] A.Y. Cherif, O. Arous, N. Mameri, J. Zhu, A.A. Said, I. Vankelecom, K. Simoens, K. Bernaerts, B.V. der Bruggen, Fabrication and characterization of novel antimicrobial thin film nano-composite membranes based on copper nanoparticles. J. Chem. Technol. Biotechnol. 93 (2018) 2737–2747, https://doi.org/10.1002/jctb.5631.

[150] M. Armendariz Ontiveros, Y. Quintero, A. Llanquilef, M. Morel, L. Argentel Martínez, A. García García, A. Garcia, Anti-biofouling and desalination properties of thin film composite reverse osmosis membranes modified with copper and iron nanoparticles. Materials 12 (2019) 2081, https://doi.org/10.3390/ma12132081.

[151] Y. Zhao, C. Qiu, X. Li, A. Vararattanavech, W. Shen, J. Torres, C. Hélix-Nielsen, R. Wang, X. Hu, A. G. Fane, C.Y. Tang, Synthesis of robust and high-performance aquaporin-based biomimetic membranes by interfacial polymerization-membrane preparation and RO performance characterization. J. Membr. Sci. 423–424 (2012) 422–428, https://doi.org/10.1016/j.memsci.2012.08.039.

[152] X. Li, R. Wang, F. Wicaksana, C. Tang, J. Torres, A.G. Fane, Preparation of high performance nanofiltration (NF) membranes incorporated with aquaporin Z. J. Membr. Sci. 450 (2014) 181–188, https://doi.org/10.1016/j.memsci.2013.09.007.

This book belongs to Badji Mokhtar Annaba University Central Library Copyright Elsevier 2025

[153] Y.-L. Ji, Q.-F. An, Y.-S. Guo, W.-S. Hung, K.-R. Lee, C.-J. Gao, Bio-inspired fabrication of high perm-selectivity and anti-fouling membranes based on zwitterionic polyelectrolyte nanoparticles. J. Mater. Chem. A 4 (2016) 4224–4231, https://doi.org/10.1039/C6TA00005C.
[154] X. Li, S. Chou, R. Wang, L. Shi, W. Fang, G. Chaitra, C.Y. Tang, J. Torres, X. Hu, A.G. Fane, Nature gives the best solution for desalination: aquaporin-based hollow fiber composite membrane with superior performance. J. Membr. Sci. 494 (2015) 68–77, https://doi.org/10.1016/j.memsci.2015.07.040.
[155] S. Qi, R. Wang, G.K.M. Chaitra, J. Torres, X. Hu, A.G. Fane, Aquaporin-based biomimetic reverse osmosis membranes: stability and long term performance. J. Membr. Sci. 508 (2016) 94–103, https://doi.org/10.1016/j.memsci.2016.02.013.
[156] M.E.A. Ali, L. Wang, X. Wang, X. Feng, Thin film composite membranes embedded with graphene oxide for water desalination. Desalination 386 (2016) 67–76, https://doi.org/10.1016/j.desal.2016.02.034.
[157] L. He, L.F. Dumée, C. Feng, L. Velleman, R. Reis, F. She, W. Gao, L. Kong, Promoted water transport across graphene oxide-poly(amide) thin film composite membranes and their antibacterial activity. Desalination 365 (2015) 126–135, https://doi.org/10.1016/j.desal.2015.02.032.
[158] H.-R. Chae, J. Lee, C.-H. Lee, I.-C. Kim, P.-K. Park, Graphene oxide-embedded thin-film composite reverse osmosis membrane with high flux, anti-biofouling, and chlorine resistance. J. Membr. Sci. 483 (2015) 128–135, https://doi.org/10.1016/j.memsci.2015.02.045.
[159] S. Xia, L. Yao, Y. Zhao, N. Li, Y. Zheng, Preparation of graphene oxide modified polyamide thin film composite membranes with improved hydrophilicity for natural organic matter removal. Chem. Eng. J. 280 (2015) 720–727, https://doi.org/10.1016/j.cej.2015.06.063.
[160] J.P. Ambre, K.B. Dhopte, P.R. Nemade, V.H. Dalvi, High flux hyperbranched starch-graphene oxide piperazinamide composite nanofiltration membrane. J. Environ. Chem. Eng. 7 (2019) 103300, https://doi.org/10.1016/j.jece.2019.103300.
[161] Y. Mansourpanah, H. Shahebrahimi, E. Kolvari, PEG-modified GO nanosheets, a desired additive to increase the rejection and antifouling characteristics of polyamide thin layer membranes. Chem. Eng. Res. Des. 104 (2015) 530–540, https://doi.org/10.1016/j.cherd.2015.09.002.
[162] M. Safarpour, V. Vatanpour, A. Khataee, M. Esmaeili, Development of a novel high flux and fouling-resistant thin film composite nanofiltration membrane by embedding reduced graphene oxide/TiO_2. Sep. Purif. Technol. 154 (2015) 96–107, https://doi.org/10.1016/j.seppur.2015.09.039.
[163] J. Yin, G. Zhu, B. Deng, Graphene oxide (GO) enhanced polyamide (PA) thin-film nanocomposite (TFN) membrane for water purification. Desalination 379 (2016) 93–101, https://doi.org/10.1016/j.desal.2015.11.001.
[164] A. Inurria, P. Cay-Durgun, D. Rice, H. Zhang, D.-K. Seo, M.L. Lind, F. Perreault, Polyamide thin-film nanocomposite membranes with graphene oxide nanosheets: balancing membrane performance and fouling propensity. Desalination 451 (2019) 139–147, https://doi.org/10.1016/j.desal.2018.07.004.
[165] X. Wang, H. Wang, Y. Wang, J. Gao, J. Liu, Y. Zhang, Hydrotalcite/graphene oxide hybrid nanosheets functionalized nanofiltration membrane for desalination. Desalination 451 (2019) 209–218, https://doi.org/10.1016/j.desal.2017.05.012.
[166] R. Bi, Q. Zhang, R. Zhang, Y. Su, Z. Jiang, Thin film nanocomposite membranes incorporated with graphene quantum dots for high flux and antifouling property. J. Membr. Sci. 553 (2018) 17–24, https://doi.org/10.1016/j.memsci.2018.02.010.
[167] Y. Li, S. Li, K. Zhang, Influence of hydrophilic carbon dots on polyamide thin film nanocomposite reverse osmosis membranes. J. Membr. Sci. 537 (2017) 42–53, https://doi.org/10.1016/j.memsci.2017.05.026.
[168] W. Gai, D.L. Zhao, T.-S. Chung, Thin film nanocomposite hollow fiber membranes comprising Na^+-functionalized carbon quantum dots for brackish water desalination. Water Res. 154 (2019) 54–61, https://doi.org/10.1016/j.watres.2019.01.043.
[169] X. Song, Q. Zhou, T. Zhang, H. Xu, Z. Wang, Pressure-assisted preparation of graphene oxide quantum dot-incorporated reverse osmosis membranes: antifouling and chlorine resistance potentials. J. Mater. Chem. A 4 (2016) 16896–16905, https://doi.org/10.1039/C6TA06636D.

This book belongs to Badji Mokhtar Annaba University Central Library Copyright Elsevier 2025

[170] M. Fathizadeh, H.N. Tien, K. Khivantsev, Z. Song, F. Zhou, M. Yu, Polyamide/nitrogen-doped graphene oxide quantum dots (N-GOQD) thin film nanocomposite reverse osmosis membranes for high flux desalination. Desalination 451 (2019) 125–132, https://doi.org/10.1016/j.desal.2017.07.014.

[171] J. Zhu, L. Qin, A. Uliana, J. Hou, J. Wang, Y. Zhang, X. Li, S. Yuan, J. Li, M. Tian, J. Lin, B. Van der Bruggen, Elevated performance of thin film nanocomposite membranes enabled by modified hydrophilic MOFs for nanofiltration. ACS Appl. Mater. Interfaces 9 (2017) 1975–1986, https://doi.org/10.1021/acsami.6b14412.

[172] J.-X. Hou, J.-P. Gao, J. Liu, X. Jing, L.-J. Li, J.-L. Du, Highly selective and sensitive detection of Pb^{2+} and UO^{22+} ions based on a carboxyl-functionalized Zn(II)-MOF platform. Dyes Pigments 160 (2019) 159–164, https://doi.org/10.1016/j.dyepig.2018.08.012.

[173] D. Ma, S.B. Peh, G. Han, S.B. Chen, Thin-film nanocomposite (TFN) membranes incorporated with super-hydrophilic metal-organic framework (MOF) UiO-66: toward enhancement of water flux and salt rejection. ACS Appl. Mater. Interfaces 9 (2017) 7523–7534, https://doi.org/10.1021/acsami.6b14223.

[174] J. Wang, Y. Wang, Y. Zhang, A. Uliana, J. Zhu, J. Liu, B. Van der Bruggen, Zeolitic imidazolate framework/graphene oxide hybrid nanosheets functionalized thin film nanocomposite membrane for enhanced antimicrobial performance. ACS Appl. Mater. Interfaces 8 (2016) 25508–25519, https://doi.org/10.1021/acsami.6b06992.

[175] Z. Rao, K. Feng, B. Tang, P. Wu, Surface decoration of amino-functionalized metal-organic framework/graphene oxide composite onto polydopamine-coated membrane substrate for highly efficient heavy metal removal. ACS Appl. Mater. Interfaces 9 (2017) 2594–2605, https://doi.org/10.1021/acsami.6b15873.

[176] J. Duan, Y. Pan, F. Pacheco, E. Litwiller, Z. Lai, I. Pinnau, High-performance polyamide thin-film-nanocomposite reverse osmosis membranes containing hydrophobic zeolitic imidazolate framework-8. J. Membr. Sci. 476 (2015) 303–310, https://doi.org/10.1016/j.memsci.2014.11.038.

[177] T.H. Lee, J.Y. Oh, S.P. Hong, J.M. Lee, S.M. Roh, S.H. Kim, H.B. Park, ZIF-8 particle size effects on reverse osmosis performance of polyamide thin-film nanocomposite membranes: importance of particle deposition. J. Membr. Sci. 570–571 (2019) 23–33, https://doi.org/10.1016/j.memsci.2018.10.015.

[178] M.R.S. Kebria, A. Rahimpour, G. Bakeri, R. Abedini, Experimental and theoretical investigation of thin ZIF-8/chitosan coated layer on air gap membrane distillation performance of PVDF membrane. Desalination 450 (2019) 21–32, https://doi.org/10.1016/j.desal.2018.10.023.

[179] Y. Guo, X. Wang, P. Hu, X. Peng, ZIF-8 coated polyvinylidenefluoride (PVDF) hollow fiber for highly efficient separation of small dye molecules. Appl. Mater. Today 5 (2016) 103–110, https://doi.org/10.1016/j.apmt.2016.07.007.

[180] R. Wang, X. Shi, A. Xiao, W. Zhou, Y. Wang, Interfacial polymerization of covalent organic frameworks (COFs) on polymeric substrates for molecular separations. J. Membr. Sci. 566 (2018) 197–204, https://doi.org/10.1016/j.memsci.2018.08.044.

[181] W. Zhang, L. Zhang, H. Zhao, B. Li, H. Ma, A two-dimensional cationic covalent organic framework membrane for selective molecular sieving. J. Mater. Chem. A 6 (2018) 13331–13339, https://doi.org/10.1039/C8TA04178D.

[182] F. Pan, M. Wang, H. Ding, Y. Song, W. Li, H. Wu, Z. Jiang, B. Wang, X. Cao, Embedding Ag+@COFs within Pebax membrane to confer mass transport channels and facilitated transport sites for elevated desulfurization performance. J. Membr. Sci. 552 (2018) 1–12, https://doi.org/10.1016/j.memsci.2018.01.038.

[183] J. Lee, J.H. Jang, H.-R. Chae, S.H. Lee, C.-H. Lee, P.-K. Park, Y.-J. Won, I.-C. Kim, A facile route to enhance the water flux of a thin-film composite reverse osmosis membrane: incorporating thickness-controlled graphene oxide into a highly porous support layer. J. Mater. Chem. A 3 (2015) 22053–22060, https://doi.org/10.1039/C5TA04042F.

[184] S.G. Kim, D.H. Hyeon, J.H. Chun, B.-H. Chun, S.H. Kim, Novel thin nanocomposite RO membranes for chlorine resistance. Desalin. Water Treat. 51 (2013) 6338–6345, https://doi.org/10.1080/19443994.2013.780994.

[185] X. Wang, X. Chen, K. Yoon, D. Fang, B.S. Hsiao, B. Chu, High flux filtration medium based on nanofibrous substrate with hydrophilic nanocomposite coating. Environ. Sci. Technol. 39 (2005) 7684–7691, https://doi.org/10.1021/es050512j.

This book belongs to Badji Mokhtar Annaba University Central Library Copyright Elsevier 2025

[186] Y. Wang, R. Ou, Q. Ge, H. Wang, T. Xu, Preparation of polyethersulfone/carbon nanotube substrate for high-performance forward osmosis membrane. Desalination 330 (2013) 70–78, https://doi.org/10.1016/j.desal.2013.09.028.

[187] M. Rezaei-Dasht Arzhandi, M.H. Sarrafzadeh, P.S. Goh, W.J. Lau, A.F. Ismail, M.A. Mohamed, Development of novel thin film nanocomposite forward osmosis membranes containing halloysite/graphitic carbon nitride nanoparticles towards enhanced desalination performance. Desalination 447 (2018) 18–28, https://doi.org/10.1016/j.desal.2018.08.003.

[188] D. Emadzadeh, W.J. Lau, T. Matsuura, M. Rahbari-Sisakht, A.F. Ismail, A novel thin film composite forward osmosis membrane prepared from PSf-TiO_2 nanocomposite substrate for water desalination. Chem. Eng. J. 237 (2014) 70–80, https://doi.org/10.1016/j.cej.2013.09.081.

[189] D. Emadzadeh, W.J. Lau, T. Matsuura, A.F. Ismail, M. Rahbari-Sisakht, Synthesis and characterization of thin film nanocomposite forward osmosis membrane with hydrophilic nanocomposite support to reduce internal concentration polarization. J. Membr. Sci. 449 (2014) 74–85, https://doi.org/10.1016/j.memsci.2013.08.014.

[190] D. Emadzadeh, W.J. Lau, A.F. Ismail, Synthesis of thin film nanocomposite forward osmosis membrane with enhancement in water flux without sacrificing salt rejection. Desalination 330 (2013) 90–99, https://doi.org/10.1016/j.desal.2013.10.003.

[191] A.L. Ohland, V.M.M. Salim, C.P. Borges, Nanocomposite membranes for osmotic processes: incorporation of functionalized hydroxyapatite in porous substrate and in selective layer. Desalination 463 (2019) 23–31, https://doi.org/10.1016/j.desal.2019.04.010.

[192] N. Ma, J. Wei, S. Qi, Y. Zhao, Y. Gao, C.Y. Tang, Nanocomposite substrates for controlling internal concentration polarization in forward osmosis membranes. J. Membr. Sci. 441 (2013) 54–62, https://doi.org/10.1016/j.memsci.2013.04.004.

[193] A.A. Shah, Y.H. Cho, S.-E. Nam, A. Park, Y.-I. Park, H. Park, High performance thin-film nanocomposite forward osmosis membrane based on PVDF/bentonite nanofiber support. J. Ind. Eng. Chem. 86 (2020) 90–99, https://doi.org/10.1016/j.jiec.2020.02.016.

[194] S.-F. Pan, Y. Dong, Y.-M. Zheng, L.-B. Zhong, Z.-H. Yuan, Self-sustained hydrophilic nanofiber thin film composite forward osmosis membranes: preparation, characterization and application for simulated antibiotic wastewater treatment. J. Membr. Sci. 523 (2017) 205–215, https://doi.org/10.1016/j.memsci.2016.09.045.

[195] P. Lu, S. Liang, L. Qiu, Y. Gao, Q. Wang, Thin film nanocomposite forward osmosis membranes based on layered double hydroxide nanoparticles blended substrates. J. Membr. Sci. 504 (2016) 196–205, https://doi.org/10.1016/j.memsci.2015.12.066.

[196] C.Y. Tang, Y.-N. Kwon, J.O. Leckie, Effect of membrane chemistry and coating layer on physiochemical properties of thin film composite polyamide RO and NF membranes. I. FTIR and XPS characterization of polyamide and coating layer chemistry. Desalination 242 (2009) 149–167, https://doi.org/10.1016/j.desal.2008.04.003.

[197] C.Y. Tang, Q.S. Fu, A.P. Robertson, C.S. Criddle, J.O. Leckie, Use of reverse osmosis membranes to remove perfluorooctane sulfonate (PFOS) from semiconductor wastewater. Environ. Sci. Technol. 40 (2006) 7343–7349, https://doi.org/10.1021/es060831q.

[198] S. Kandambeth, B.P. Biswal, H.D. Chaudhari, K.C. Rout, H. Shebeeb Kunjattu, S. Mitra, S. Karak, A. Das, R. Mukherjee, U.K. Kharul, R. Banerjee, Selective molecular sieving in self-standing porous covalent-organic-framework membranes. Adv. Mater. 29 (2017) 1603945, https://doi.org/10.1002/adma.201603945.

[199] J. Song, J. Yu, G. Sun, Y. Si, B. Ding, Visible-light-driven, hierarchically heterostructured, and flexible silver/bismuth oxyiodide/titania nanofibrous membranes for highly efficient water disinfection. J. Colloid Interface Sci. 555 (2019) 636–646, https://doi.org/10.1016/j.jcis.2019.08.017.

[200] Y. Han, Z. Xu, C. Gao, Ultrathin graphene nanofiltration membrane for water purification. Adv. Funct. Mater. 23 (2013) 3693–3700, https://doi.org/10.1002/adfm.201202601.

[201] S.J. Gao, H. Qin, P. Liu, J. Jin, SWCNT-intercalated GO ultrathin films for ultrafast separation of molecules. J. Mater. Chem. A 3 (2015) 6649–6654, https://doi.org/10.1039/C5TA00366K.

This book belongs to Badji Mokhtar Annaba University Central Library Copyright Elsevier 2025

[202] X.-L. Xu, F.-W. Lin, Y. Du, X. Zhang, J. Wu, Z.-K. Xu, Graphene oxide nanofiltration membranes stabilized by cationic porphyrin for high salt rejection. ACS Appl. Mater. Interfaces 8 (2016) 12588–12593, https://doi.org/10.1021/acsami.6b03693.

[203] Y. Han, Y. Jiang, C. Gao, High-flux graphene oxide nanofiltration membrane intercalated by carbon nanotubes. ACS Appl. Mater. Interfaces 7 (2015) 8147–8155, https://doi.org/10.1021/acsami.5b00986.

[204] Q. Nan, P. Li, B. Cao, Fabrication of positively charged nanofiltration membrane via the layer-by-layer assembly of graphene oxide and polyethylenimine for desalination. Appl. Surf. Sci. 387 (2016) 521–528, https://doi.org/10.1016/j.apsusc.2016.06.150.

[205] K. Goh, L. Setiawan, L. Wei, R. Si, A.G. Fane, R. Wang, Y. Chen, Graphene oxide as effective selective barriers on a hollow fiber membrane for water treatment process. J. Membr. Sci. 474 (2015) 244–253, https://doi.org/10.1016/j.memsci.2014.09.057.

[206] Y. Zhang, S. Zhang, J. Gao, T.-S. Chung, Layer-by-layer construction of graphene oxide (GO) framework composite membranes for highly efficient heavy metal removal. J. Membr. Sci. 515 (2016) 230–237, https://doi.org/10.1016/j.memsci.2016.05.035.

[207] X. Song, R.S. Zambare, S. Qi, B.N. Sowrirajalu, A.P. James Selvaraj, C.Y. Tang, C. Gao, Charge-gated ion transport through polyelectrolyte intercalated amine reduced graphene oxide membranes. ACS Appl. Mater. Interfaces 9 (2017) 41482–41495, https://doi.org/10.1021/acsami.7b13724.

[208] M. Yi, C.H. Lau, S. Xiong, W. Wei, R. Liao, L. Shen, A. Lu, Y. Wang, Zwitterion-Ag complexes that simultaneously enhance biofouling resistance and silver binding capability of thin film composite membranes. ACS Appl. Mater. Interfaces 11 (2019) 15698–15708, https://doi.org/10.1021/acsami.9b02983.

[209] W. Ma, A. Soroush, T.V.A. Luong, M.S. Rahaman, Cysteamine- and graphene oxide-mediated copper nanoparticle decoration on reverse osmosis membrane for enhanced anti-microbial performance. J. Colloid Interface Sci. 501 (2017) 330–340, https://doi.org/10.1016/j.jcis.2017.04.069.

[210] W. Ma, A. Soroush, T. Van Anh Luong, G. Brennan, M.S. Rahaman, B. Asadishad, N. Tufenkji, Spray- and spin-assisted layer-by-layer assembly of copper nanoparticles on thin-film composite reverse osmosis membrane for biofouling mitigation. Water Res. 99 (2016) 188–199, https://doi.org/10.1016/j.watres.2016.04.042.

[211] J. Yin, Y. Yang, Z. Hu, B. Deng, Attachment of silver nanoparticles (AgNPs) onto thin-film composite (TFC) membranes through covalent bonding to reduce membrane biofouling. J. Membr. Sci. 441 (2013) 73–82, https://doi.org/10.1016/j.memsci.2013.03.060.

[212] D. Ragab, H.G. Gomaa, R. Sabouni, M. Salem, M. Ren, J. Zhu, Micropollutants removal from water using microfiltration membrane modified with ZIF-8 metal organic frameworks (MOFs). Chem. Eng. J. 300 (2016) 273–279, https://doi.org/10.1016/j.cej.2016.04.033.

[213] A. Karimi, V. Vatanpour, A. Khataee, M. Safarpour, Contra-diffusion synthesis of ZIF-8 layer on polyvinylidene fluoride ultrafiltration membranes for improved water purification. J. Ind. Eng. Chem. 73 (2019) 95–105, https://doi.org/10.1016/j.jiec.2019.01.010.

[214] R. Zhang, S. Ji, N. Wang, L. Wang, G. Zhang, J.-R. Li, Coordination-driven in situ self-assembly strategy for the preparation of metal-organic framework hybrid membranes. Angew. Chem. Int. Ed. 53 (2014) 9775–9779, https://doi.org/10.1002/anie.201403978.

[215] L. Yang, Z. Wang, J. Zhang, Zeolite imidazolate framework hybrid nanofiltration (NF) membranes with enhanced permselectivity for dye removal. J. Membr. Sci. 532 (2017) 76–86, https://doi.org/10.1016/j.memsci.2017.03.014.

[216] S. Basu, M. Balakrishnan, Polyamide thin film composite membranes containing ZIF-8 for the separation of pharmaceutical compounds from aqueous streams. Sep. Purif. Technol. 179 (2017) 118–125, https://doi.org/10.1016/j.seppur.2017.01.061.

[217] V.A. Kuehl, J. Yin, P.H.H. Duong, B. Mastorovich, B. Newell, K.D. Li-Oakey, B.A. Parkinson, J. O. Hoberg, A highly ordered nanoporous, two-dimensional covalent organic framework with modifiable pores, and its application in water purification and ion sieving. J. Am. Chem. Soc. 140 (2018) 18200–18207, https://doi.org/10.1021/jacs.8b11482.

This book belongs to Badji Mokhtar Annaba University Central Library

Copyright Elsevier 2025

[218] F. Liu, N.A. Hashim, Y. Liu, M.R.M. Abed, K. Li, Progress in the production and modification of PVDF membranes. J. Membr. Sci. 375 (2011) 1–27, https://doi.org/10.1016/j.memsci.2011.03.014.
[219] L.-Z. Zhang, Y.-Y. Wang, C.-L. Wang, H. Xiang, Synthesis and characterization of a PVA/LiCl blend membrane for air dehumidification. J. Membr. Sci. 308 (2008) 198–206, https://doi.org/10.1016/j.memsci.2007.09.056.
[220] S.M. Hosseini, S.S. Madaeni, A.R. Heidari, A.R. Moghadassi, Preparation and characterization of polyvinyl chloride/styrene butadiene rubber blend heterogeneous cation exchange membrane modified by potassium perchlorate. Desalination 279 (2011) 306–314, https://doi.org/10.1016/j.desal.2011.06.022.
[221] X. Cao, M. Tang, F. Liu, Y. Nie, C. Zhao, Immobilization of silver nanoparticles onto sulfonated polyethersulfone membranes as antibacterial materials. Colloids Surf. B: Biointerfaces 81 (2010) 555–562, https://doi.org/10.1016/j.colsurfb.2010.07.057.
[222] D.Y. Koseoglu-Imer, B. Kose, M. Altinbas, I. Koyuncu, The production of polysulfone (PS) membrane with silver nanoparticles (AgNP): physical properties, filtration performances, and biofouling resistances of membranes. J. Membr. Sci. 428 (2013) 620–628, https://doi.org/10.1016/j.memsci.2012.10.046.
[223] Y. Yang, P. Wang, Q. Zheng, Preparation and properties of polysulfone/TiO_2 composite ultrafiltration membranes. J. Polym. Sci. B Polym. Phys. 44 (2006) 879–887, https://doi.org/10.1002/polb.20715.
[224] V. Vatanpour, S.S. Madaeni, A.R. Khataee, E. Salehi, S. Zinadini, H.A. Monfared, TiO_2 embedded mixed matrix PES nanocomposite membranes: influence of different sizes and types of nanoparticles on antifouling and performance. Desalination 292 (2012) 19–29, https://doi.org/10.1016/j.desal.2012.02.006.
[225] C.P. Leo, W.P. Cathie Lee, A.L. Ahmad, A.W. Mohammad, Polysulfone membranes blended with ZnO nanoparticles for reducing fouling by oleic acid. Sep. Purif. Technol. 89 (2012) 51–56, https://doi.org/10.1016/j.seppur.2012.01.002.
[226] X. Shen, T. Xie, J. Wang, P. Liu, F. Wang, An anti-fouling poly(vinylidene fluoride) hybrid membrane blended with functionalized ZrO_2 nanoparticles for efficient oil/water separation. RSC Adv. 7 (2017) 5262–5271, https://doi.org/10.1039/C6RA26651G.
[227] A. Cui, Z. Liu, C. Xiao, Y. Zhang, Effect of micro-sized SiO_2-particle on the performance of PVDF blend membranes via TIPS. J. Membr. Sci. 360 (2010) 259–264, https://doi.org/10.1016/j.memsci.2010.05.023.
[228] Y.M. Mojtahedi, M.R. Mehrnia, M. Homayoonfal, Fabrication of Al_2O_3/PSf nanocomposite membranes: efficiency comparison of coating and blending methods in modification of filtration performance. Desalin. Water Treat. 51 (2013) 6736–6742, https://doi.org/10.1080/19443994.2013.769918.
[229] T.-H. Bae, T.-M. Tak, Preparation of TiO_2 self-assembled polymeric nanocomposite membranes and examination of their fouling mitigation effects in a membrane bioreactor system. J. Membr. Sci. 266 (2005) 1–5, https://doi.org/10.1016/j.memsci.2005.08.014.
[230] T.-H. Bae, I.-C. Kim, T.-M. Tak, Preparation and characterization of fouling-resistant TiO_2 self-assembled nanocomposite membranes. J. Membr. Sci. 275 (2006) 1–5, https://doi.org/10.1016/j.memsci.2006.01.023.
[231] T.-H. Bae, T.-M. Tak, Effect of TiO_2 nanoparticles on fouling mitigation of ultrafiltration membranes for activated sludge filtration. J. Membr. Sci. 249 (2005) 1–8, https://doi.org/10.1016/j.memsci.2004.09.008.
[232] W. Hu, J. Yin, B. Deng, Z. Hu, Application of nano TiO_2 modified hollow fiber membranes in algal membrane bioreactors for high-density algae cultivation and wastewater polishing. Bioresour. Technol. 193 (2015) 135–141, https://doi.org/10.1016/j.biortech.2015.06.070.
[233] M.R. Mehrnia, Y.M. Mojtahedi, M. Homayoonfal, What is the concentration threshold of nanoparticles within the membrane structure? A case study of Al_2O_3/PSf nanocomposite membrane. Desalination 372 (2015) 75–88, https://doi.org/10.1016/j.desal.2015.06.022.
[234] S. Yu-Chun, H. Chihpin, P.J. Ruhsing, H. Wen-Pin, C. Min-Chia, Fouling mitigation by TiO_2 composite membrane in membrane bioreactors. J. Environ. Eng. 138 (2012) 344–350, https://doi.org/10.1061/(ASCE)EE.1943-7870.0000419.
[235] M. Tavakolmoghadam, T. Mohammadi, M. Hemmati, F. Naeimpour, Surface modification of PVDF membranes by sputtered TiO_2: fouling reduction potential in membrane bioreactors. Desalin. Water Treat. 57 (2016) 3328–3338, https://doi.org/10.1080/19443994.2014.984635.

This book belongs to Badji Mokhtar Annaba University Central Library
Copyright Elsevier 2025

[236] G.T. Demirkol, N. Dizge, T.O. Acar, O.M. Salmanli, N. Tufekci, Influence of nanoparticles on filterability of fruit-juice industry wastewater using submerged membrane bioreactor. Water Sci. Technol. 76 (2017) 705–711, https://doi.org/10.2166/wst.2017.255.
[237] C.X. Liu, D.R. Zhang, Y. He, X.S. Zhao, R. Bai, Modification of membrane surface for anti-biofouling performance: effect of anti-adhesion and anti-bacteria approaches. J. Membr. Sci. 346 (2010) 121–130, https://doi.org/10.1016/j.memsci.2009.09.028.
[238] M. Amini, H. Etemadi, A. Akbarzadeh, R. Yegani, Preparation and performance evaluation of high-density polyethylene/silica nanocomposite membranes in membrane bioreactor system. Biochem. Eng. J. 127 (2017) 196–205, https://doi.org/10.1016/j.bej.2017.08.015.
[239] H. Saleem, S.J. Zaidi, Nanoparticles in reverse osmosis membranes for desalination: a state of the art review. Desalination 475 (2020) 114171, https://doi.org/10.1016/j.desal.2019.114171.
[240] K. Goh, H.E. Karahan, L. Wei, T.-H. Bae, A.G. Fane, R. Wang, Y. Chen, Carbon nanomaterials for advancing separation membranes: a strategic perspective. Carbon 109 (2016) 694–710, https://doi.org/10.1016/j.carbon.2016.08.077.
[241] W. Choi, I. Lahiri, R. Seelaboyina, Y.S. Kang, Synthesis of graphene and its applications: a review. Crit. Rev. Solid State Mater. Sci. 35 (2010) 52–71, https://doi.org/10.1080/10408430903505036.
[242] R.R. Nair, H.A. Wu, P.N. Jayaram, I.V. Grigorieva, A.K. Geim, Unimpeded permeation of water through helium-leak-tight graphene-based membranes. Science 335 (2012) 442–444, https://doi.org/10.1126/science.1211694.
[243] R.K. Joshi, P. Carbone, F.C. Wang, V.G. Kravets, Y. Su, I.V. Grigorieva, H.A. Wu, A.K. Geim, R. R. Nair, Precise and ultrafast molecular sieving through graphene oxide membranes. Science 343 (2014) 752–754, https://doi.org/10.1126/science.1245711.
[244] B. Mi, Graphene oxide membranes for ionic and molecular sieving. Science 343 (2014) 740–742, https://doi.org/10.1126/science.1250247.
[245] J. Abraham, K.S. Vasu, C.D. Williams, K. Gopinadhan, Y. Su, C.T. Cherian, J. Dix, E. Prestat, S.J. Haigh, I. V. Grigorieva, P. Carbone, A.K. Geim, R.R. Nair, Tunable sieving of ions using graphene oxide membranes. Nat. Nanotechnol. 12 (2017) 546–550, https://doi.org/10.1038/nnano.2017.21.
[246] R.K. Joshi, S. Alwarappan, M. Yoshimura, V. Sahajwalla, Y. Nishina, Graphene oxide: the new membrane material. Appl. Mater. Today 1 (2015) 1–12, https://doi.org/10.1016/j.apmt.2015.06.002.
[247] M. Hu, B. Mi, Layer-by-layer assembly of graphene oxide membranes via electrostatic interaction. J. Membr. Sci. 469 (2014) 80–87, https://doi.org/10.1016/j.memsci.2014.06.036.
[248] S. Qi, W. Li, Y. Zhao, N. Ma, J. Wei, T.W. Chin, C.Y. Tang, Influence of the properties of layer-by-layer active layers on forward osmosis performance. J. Membr. Sci. 423 (2012) 536–542, https://doi.org/10.1016/j.memsci.2012.09.009.
[249] J.S. Park, S.M. Cho, W.-J. Kim, J. Park, P.J. Yoo, Fabrication of graphene thin films based on layer-by-layer self-assembly of functionalized graphene nanosheets. ACS Appl. Mater. Interfaces 3 (2011) 360–368, https://doi.org/10.1021/am100977p.
[250] B. Lian, J. Deng, G. Leslie, H. Bustamante, V. Sahajwalla, Y. Nishina, R.K. Joshi, Surfactant modified graphene oxide laminates for filtration. Carbon 116 (2017) 240–245, https://doi.org/10.1016/j.carbon.2017.01.102.
[251] Y.T. Nam, J. Choi, K.M. Kang, D.W. Kim, H.-T. Jung, Enhanced stability of laminated graphene oxide membranes for nanofiltration via interstitial amide bonding. ACS Appl. Mater. Interfaces 8 (2016) 27376–27382, https://doi.org/10.1021/acsami.6b09912.
[252] Y. Zhang, S. Zhang, T.-S. Chung, Nanometric graphene oxide framework membranes with enhanced heavy metal removal via nanofiltration. Environ. Sci. Technol. 49 (2015) 10235–10242, https://doi.org/10.1021/acs.est.5b02086.
[253] B. Lee, K. Li, H.S. Yoon, J. Yoon, Y. Mok, Y. Lee, H.H. Lee, Y.H. Kim, Membrane of functionalized reduced graphene oxide nanoplates with angstrom-level channels, Sci. Rep. 6 (2016) srep28052 https://doi.org/10.1038/srep28052.
[254] G. Eda, G. Fanchini, M. Chhowalla, Large-Area Ultrathin Films of Reduced Graphene Oxide as a Transparent and Flexible Electronic Material, https://www.scienceopen.com/document?vid=32906c9c-52ec-4325-88ba-895837d0d548, 2008. Accessed 8 December 2017.

This book belongs to Badji Mokhtar Annaba University Central Library Copyright Elsevier 2025

[255] C.-N. Yeh, K. Raidongia, J. Shao, Q.-H. Yang, J. Huang, On the origin of the stability of graphene oxide membranes in water. Nat. Chem. 7 (2015) 166–170, https://doi.org/10.1038/nchem.2145.
[256] H. Li, Z. Song, X. Zhang, Y. Huang, S. Li, Y. Mao, H.J. Ploehn, Y. Bao, M. Yu, Ultrathin, molecular-sieving graphene oxide membranes for selective hydrogen separation. Science 342 (2013) 95–98, https://doi.org/10.1126/science.1236686.
[257] Nature Communications, Ultrafast Viscous Water Flow Through Nanostrand-Channelled Graphene Oxide Membranes, https://www.nature.com/articles/ncomms3979, 2013. Accessed 8 December 2017.
[258] H.-R. Chae, C.-H. Lee, P.-K. Park, I.-C. Kim, J.-H. Kim, Synergetic effect of graphene oxide nanosheets embedded in the active and support layers on the performance of thin-film composite membranes. J. Membr. Sci. 525 (2017) 99–106, https://doi.org/10.1016/j.memsci.2016.10.034.
[259] J. Wang, C. Zhao, T. Wang, Z. Wu, X. Li, J. Li, Graphene oxide polypiperazine-amide nanofiltration membrane for improving flux and anti-fouling in water purification. RSC Adv. 6 (2016) 82174–82185, https://doi.org/10.1039/C6RA17284A.
[260] S. Bano, A. Mahmood, S.-J. Kim, K.-H. Lee, Graphene oxide modified polyamide nanofiltration membrane with improved flux and antifouling properties. J. Mater. Chem. A 3 (2015) 2065–2071, https://doi.org/10.1039/C4TA03607G.
[261] Q. Liu, G.-R. Xu, Graphene oxide (GO) as functional material in tailoring polyamide thin film composite (PA-TFC) reverse osmosis (RO) membranes. Desalination 394 (2016) 162–175, https://doi.org/10.1016/j.desal.2016.05.017.
[262] S. Hermans, H. Mariën, C. Van Goethem, I.F. Vankelecom, Recent developments in thin film (nano) composite membranes for solvent resistant nanofiltration. Curr. Opin. Chem. Eng. 8 (2015) 45–54, https://doi.org/10.1016/j.coche.2015.01.009.
[263] N. Misdan, A.F. Ismail, N. Hilal, Recent advances in the development of (bio)fouling resistant thin film composite membranes for desalination. Desalination 380 (2016) 105–111, https://doi.org/10.1016/j.desal.2015.06.001.
[264] L. Shen, S. Xiong, Y. Wang, Graphene oxide incorporated thin-film composite membranes for forward osmosis applications. Chem. Eng. Sci. 143 (2016) 194–205, https://doi.org/10.1016/j.ces.2015.12.029.
[265] L. Chen, G. Shi, J. Shen, B. Peng, B. Zhang, Y. Wang, F. Bian, J. Wang, D. Li, Z. Qian, G. Xu, G. Liu, J. Zeng, L. Zhang, Y. Yang, G. Zhou, M. Wu, W. Jin, J. Li, H. Fang, Ion sieving in graphene oxide membranes via cationic control of interlayer spacing. Nature 550 (2017) 380, https://doi.org/10.1038/nature24044.
[266] H. Liu, H. Wang, X. Zhang, Facile fabrication of freestanding ultrathin reduced graphene oxide membranes for water purification. Adv. Mater. 27 (2015) 249–254, https://doi.org/10.1002/adma.201404054.
[267] Y.P. Tang, D.R. Paul, T.S. Chung, Free-standing graphene oxide thin films assembled by a pressurized ultrafiltration method for dehydration of ethanol. J. Membr. Sci. 458 (2014) 199–208, https://doi.org/10.1016/j.memsci.2014.01.062.
[268] D.A. Dikin, S. Stankovich, E.J. Zimney, R.D. Piner, G.H.B. Dommett, G. Evmenenko, S.T. Nguyen, R. S. Ruoff, Preparation and characterization of graphene oxide paper. Nature 448 (2007) 457, https://doi.org/10.1038/nature06016.
[269] C. Zhao, X. Xu, J. Chen, G. Wang, F. Yang, Highly effective antifouling performance of PVDF/graphene oxide composite membrane in membrane bioreactor (MBR) system. Desalination 340 (2014) 59–66, https://doi.org/10.1016/j.desal.2014.02.022.
[270] A.M. Dimiev, L.B. Alemany, J.M. Tour, Graphene oxide. Origin of acidity, its instability in water, and a new dynamic structural model. ACS Nano 7 (2013) 576–588, https://doi.org/10.1021/nn3047378.
[271] H.M. Hegab, L. Zou, Graphene oxide-assisted membranes: fabrication and potential applications in desalination and water purification. J. Membr. Sci. 484 (2015) 95–106, https://doi.org/10.1016/j.memsci.2015.03.011.
[272] P. Anadão, R.R. Montes, H.S. de Santis, H. Wiebeck, Rheology assessment of PSf/NMP solution and its influence on membrane structure. Defect Diffus. Forum 326–328 (2012) 422–427, https://doi.org/10.4028/www.scientific.net/DDF.326-328.422.
[273] R.S. Zambare, K.B. Dhopte, A.V. Patwardhan, P.R. Nemade, Polyamine functionalized graphene oxide polysulfone mixed matrix membranes with improved hydrophilicity and anti-fouling properties. Desalination 403 (2017) 24–35, https://doi.org/10.1016/j.desal.2016.02.003.

This book belongs to Badji Mokhtar Annaba University Central Library Copyright Elsevier 2025

[274] J. Safari, S. Gandomi-Ravandi, S. Ashiri, Organosilane sulfonated graphene oxide in the Biginelli and Biginelli-like reactions. New J. Chem. 40 (2016) 512–520, https://doi.org/10.1039/C5NJ01741F.
[275] D. Tasis, N. Tagmatarchis, A. Bianco, M. Prato, Chemistry of carbon nanotubes. Chem. Rev. 106 (2006) 1105–1136, https://doi.org/10.1021/cr050569o.
[276] Ihsanullah, Carbon nanotube membranes for water purification: developments, challenges, and prospects for the future. Sep. Purif. Technol. 209 (2019) 307–337, https://doi.org/10.1016/j.seppur.2018.07.043.
[277] C. Thilgen, F. Diederich, Structural aspects of fullerene chemistrya journey through fullerene chirality. Chem. Rev. 106 (2006) 5049–5135, https://doi.org/10.1021/cr0505371.
[278] X. Deng, L. Mammen, H.-J. Butt, D. Vollmer, Candle soot as a template for a transparent robust superamphiphobic coating. Science 335 (2012) 67–70, https://doi.org/10.1126/science.1207115.
[279] J. Robertson, Amorphous carbon. Curr. Opin. Solid State Mater. Sci. 1 (1996) 557–561, https://doi.org/10.1016/S1359-0286(96)80072-6.
[280] M. Paul, S.D. Jons, Chemistry and fabrication of polymeric nanofiltration membranes: a review. Polymer 103 (2016) 417–456, https://doi.org/10.1016/j.polymer.2016.07.085.
[281] Preparation and Characterization of Novel Triple Layer Hydrophilic-Hydrophobic Composite Membrane for Desalination Using Air Gap Membrane Distillation, ScienceDirect, (n.d.). https://www.sciencedirect.com/science/article/pii/S1383586613004796 (Accessed 18 January 2019).
[282] J.A. Prince, G. Singh, D. Rana, T. Matsuura, V. Anbharasi, T.S. Shanmugasundaram, Preparation and characterization of highly hydrophobic poly(vinylidene fluoride)—clay nanocomposite nanofiber membranes (PVDF-clay NNMs) for desalination using direct contact membrane distillation. J. Membr. Sci. 397–398 (2012) 80–86, https://doi.org/10.1016/j.memsci.2012.01.012.
[283] J. Yin, B. Deng, Polymer-matrix nanocomposite membranes for water treatment. J. Membr. Sci. 479 (2015) 256–275, https://doi.org/10.1016/j.memsci.2014.11.019.
[284] A.F. Faria, C. Liu, M. Xie, F. Perreault, L.D. Nghiem, J. Ma, M. Elimelech, Thin-film composite forward osmosis membranes functionalized with graphene oxide-silver nanocomposites for biofouling control. J. Membr. Sci. 525 (2017) 146–156, https://doi.org/10.1016/j.memsci.2016.10.040.
[285] S.-H. Park, Y.-S. Ko, S.-J. Park, J.S. Lee, J. Cho, K.-Y. Baek, I.T. Kim, K. Woo, J.-H. Lee, Immobilization of silver nanoparticle-decorated silica particles on polyamide thin film composite membranes for antibacterial properties. J. Membr. Sci. 499 (2016) 80–91, https://doi.org/10.1016/j.memsci.2015.09.060.
[286] A. Taubert, Controlling water transport through artificial polymer/protein hybrid membranes. PNAS 104 (2007) 20643–20644, https://doi.org/10.1073/pnas.0710864105.
[287] S. Sorribas, P. Gorgojo, C. Téllez, J. Coronas, A.G. Livingston, High flux thin film nanocomposite membranes based on metal-organic frameworks for organic solvent nanofiltration. J. Am. Chem. Soc. 135 (2013) 15201–15208, https://doi.org/10.1021/ja407665w.
[288] Y. Dong, J. Shao, C. Chen, H. Li, R. Wang, Y. Chi, X. Lin, G. Chen, Blue luminescent graphene quantum dots and graphene oxide prepared by tuning the carbonization degree of citric acid. Carbon 50 (2012) 4738–4743, https://doi.org/10.1016/j.carbon.2012.06.002.
[289] A.K. Ghosh, E.M.V. Hoek, Impacts of support membrane structure and chemistry on polyamide-polysulfone interfacial composite membranes. J. Membr. Sci. 336 (2009) 140–148, https://doi.org/10.1016/j.memsci.2009.03.024.
[290] P. Sukitpaneenit, T.-S. Chung, High performance thin-film composite forward osmosis hollow fiber membranes with macrovoid-free and highly porous structure for sustainable water production. Environ. Sci. Technol. 46 (2012) 7358–7365, https://doi.org/10.1021/es301559z.
[291] S.S. Dhumal, S.J. Wagh, A.K. Suresh, Interfacial polycondensation—modeling of kinetics and film properties. J. Membr. Sci. 325 (2008) 758–771, https://doi.org/10.1016/j.memsci.2008.09.002.
[292] J. Wei, C. Qiu, C.Y. Tang, R. Wang, A.G. Fane, Synthesis and characterization of flat-sheet thin film composite forward osmosis membranes. J. Membr. Sci. 372 (2011) 292–302, https://doi.org/10.1016/j.memsci.2011.02.013.
[293] M.M. Pendergast, A.K. Ghosh, E.M.V. Hoek, Separation performance and interfacial properties of nanocomposite reverse osmosis membranes. Desalination 308 (2013) 180–185, https://doi.org/10.1016/j.desal.2011.05.005.

This book belongs to Badji Mokhtar Annaba University Central Library Copyright Elsevier 2025

[294] M. Al-Abri, B. Al-Ghafri, T. Bora, S. Dobretsov, J. Dutta, S. Castelletto, L. Rosa, A. Boretti, Chlorination disadvantages and alternative routes for biofouling control in reverse osmosis desalination. Npj Clean Water 2 (2019) 1–16, https://doi.org/10.1038/s41545-018-0024-8.
[295] V.T. Do, C.Y. Tang, M. Reinhard, J.O. Leckie, Degradation of polyamide nanofiltration and reverse osmosis membranes by hypochlorite. Environ. Sci. Technol. 46 (2012) 852–859, https://doi.org/10.1021/es203090y.
[296] R. Hu, C. Wang, X. Liu, Y. He, G. Zhao, H. Zhu, Facile fabrication of unimpeded and stable graphene oxide coating on reverse osmosis membrane for dual-functional protection. ChemistrySelect 3 (2018) 12122–12130, https://doi.org/10.1002/slct.201802801.
[297] S.-M. Xue, C.-H. Ji, Z.-L. Xu, Y.-J. Tang, R.-H. Li, Chlorine resistant TFN nanofiltration membrane incorporated with octadecylamine-grafted GO and fluorine-containing monomer. J. Membr. Sci. 545 (2018) 185–195, https://doi.org/10.1016/j.memsci.2017.09.075.
[298] H.J. Kim, Y.-S. Choi, M.-Y. Lim, K.H. Jung, D.-G. Kim, J.-J. Kim, H. Kang, J.-C. Lee, Reverse osmosis nanocomposite membranes containing graphene oxides coated by tannic acid with chlorine-tolerant and antimicrobial properties. J. Membr. Sci. 514 (2016) 25–34, https://doi.org/10.1016/j.memsci.2016.04.026.
[299] M. Abbaszadeh, D. Krizak, S. Kundu, Layer-by-layer assembly of graphene oxide nanoplatelets embedded desalination membranes with improved chlorine resistance. Desalination 470 (2019) 114116, https://doi.org/10.1016/j.desal.2019.114116.
[300] W. Choi, J. Choi, J. Bang, J.-H. Lee, Layer-by-layer assembly of graphene oxide nanosheets on polyamide membranes for durable reverse-osmosis applications. ACS Appl. Mater. Interfaces 5 (2013) 12510–12519, https://doi.org/10.1021/am403790s.
[301] S. Kim, X. Lin, R. Ou, H. Liu, X. Zhang, G.P. Simon, C.D. Easton, H. Wang, Highly crosslinked, chlorine tolerant polymer network entwined graphene oxide membrane for water desalination. J. Mater. Chem. A 5 (2017) 1533–1540, https://doi.org/10.1039/C6TA07350F.
[302] D. Cohen-Tanugi, J.C. Grossman, Water desalination across nanoporous graphene. Nano Lett. 12 (2012) 3602–3608, https://doi.org/10.1021/nl3012853.
[303] S.C. O'Hern, D. Jang, S. Bose, J.-C. Idrobo, Y. Song, T. Laoui, J. Kong, R. Karnik, Nanofiltration across defect-sealed nanoporous monolayer graphene. Nano Lett. 15 (2015) 3254–3260, https://doi.org/10.1021/acs.nanolett.5b00456.
[304] S.P. Surwade, S.N. Smirnov, I.V. Vlassiouk, R.R. Unocic, G.M. Veith, S. Dai, S.M. Mahurin, Water desalination using nanoporous single-layer graphene. Nat. Nanotechnol. 10 (2015) 459–464, https://doi.org/10.1038/nnano.2015.37.
[305] J. Deng, Y. You, H. Bustamante, V. Sahajwalla, R.K. Joshi, Mechanism of water transport in graphene oxide laminates. Chem. Sci. 8 (2017) 1701–1704, https://doi.org/10.1039/C6SC03909J.
[306] F. Perreault, A.F. de Faria, M. Elimelech, Environmental applications of graphene-based nanomaterials. Chem. Soc. Rev. 44 (2015) 5861–5896, https://doi.org/10.1039/C5CS00021A.
[307] K.S. Novoselov, A.K. Geim, S.V. Morozov, D. Jiang, Y. Zhang, S.V. Dubonos, I.V. Grigorieva, A. A. Firsov, Electric field effect in atomically thin carbon films. Science 306 (2004) 666–669, https://doi.org/10.1126/science.1102896.
[308] C. Liu, A.F. Faria, J. Ma, M. Elimelech, Mitigation of biofilm development on thin-film composite membranes functionalized with zwitterionic polymers and silver nanoparticles. Environ. Sci. Technol. 51 (2017) 182–191, https://doi.org/10.1021/acs.est.6b03795.
[309] S.J. Gao, Z. Shi, W.B. Zhang, F. Zhang, J. Jin, Photoinduced superwetting single-walled carbon nanotube/TiO_2 ultrathin network films for ultrafast separation of oil-in-water emulsions. ACS Nano 8 (2014) 6344–6352, https://doi.org/10.1021/nn501851a.

This book belongs to Badji Mokhtar Annaba University Central Library Copyright Elsevier 2025

CHAPTER 21

Responsive membranes for wastewater treatment

Ramesh P. Birmod[a], Vikesh G. Lade[a], and Rakesh D. Shambharkar[b]

[a]Chemical Engineering Department, Laxminarayan Institute of Technology, Rashtrasant Tukadoji Maharaj Nagpur University, Nagpur, Maharashtra, India, [b]Department of Civil Engineering, Dr. Babasaheb Ambedkar College of Engineering and Research, Rashtrasant Tukadoji Maharaj Nagpur University, Nagpur, Maharashtra, India

21.1 Introduction

With the growing population, water pollution is becoming a major concern for mankind and the ecosystem. Two of the greatest challenges threatening the sustainable developments of human society are crises of water supply and pollution control [1]. Thousands of people die daily because of diseases caused by water pollution. In 2015, the United Nations (UN) recommended "clean water and sanitation" as one of the 17 sustainable development goals (SDGs) [2]. Therefore, it is necessary to treat the wastewater rejected from various sources like industrial, domestic, agricultural, and many other sources.

There are several methods available to treat wastewater in wastewater treatment plants such as oxidation ditch (OD), anaerobic-anoxic-oxic (A2/O), anaerobic-oxic (A/O), sequencing batch reactor (SBR), conventional activated sludge (CAS), biological film (BF), and advanced techniques. Out of these processes, use of membrane technology for wastewater treatment has rapidly grown so far. There are various reasons for this, and one of the best reasons among them is that it utilizes zero additives and chemicals with relatively low energy consumption. Thus, it minimizes the chances of problems related to human health [3–5]. Many technologies are being developed for the advancement in the synthesis and application of membranes. Some pioneers also tried to gain acceptance earlier in 1980s for the utilization of membranes in water and wastewater treatment [6]. Membranes made up of new materials are being used rapidly for treatment of wastewater. In terms of cost effectiveness, membrane technology utilizes smaller land area, but on the other hand, ultrafiltration (UF) membrane system equipment and construction cost is 5.6% greater compared with a traditional system [7].

Handbook of Nanomaterials for Wastewater Treatment. https://doi.org/10.1016/B978-0-12-821496-1.00037-4
Copyright © 2021 Elsevier Inc. All rights reserved.

This book belongs to Badji Mokhtar Annaba University Central Library Copyright Elsevier 2025

Membrane technology is a generalized term assigned to a number of characteristic separation processes involving membranes. Purification of water or wastewater is carried out more often using membranes. Nowadays, membranes are on the competitive edge over conventional purification technologies. A membrane has unique characteristics and action similar to a filter where water flows through the barrier and catches suspended solids and other substances. Membrane's action is more profound in a manner like a selective separation wall. This selective separation can be elaborated as a membrane allows certain substances to pass through, while other substances are caught. One of the promising methods of separation and purification is membrane filtration, which is seen and used as an alternative for purification technologies (e.g., sand filtration, extraction, distillation, etc.). One factor that restricts the use of membrane technology in wider practice is membrane fouling, which can be termed as the deposition of solute impurity particles resulting in rapid reduction of flux. When the deposition takes place onto the membrane surface, it is termed as external fouling, and if it takes place into the pores of membrane, it is called internal fouling [8, 9]. Fouling can be removed in the case of reverse fouling by applying strong physical cleaning methods (for example, application of hydrodynamic forward or reverse flushing with strong shear-force). But this will not be possible in the case of irreversible fouling that occurs when a strong matrix of solute particles is formed above the membrane surface. It will then be very difficult to remove the solute particles by any physical technique [10]. Conventional cleaning technique is also an effective method, but use of chemical cleaning reagents have their own negative effects because the surface chemistry of the membrane may alter and hence change the permeate quality [11]. Fouling may also be inhibited by changing the properties of the feed solution, changing membrane surface properties, thereby changing the chemistry and flow pattern, etc.

Advancements have been made to overcome these negative effects on membranes for wastewater treatment. Smart materials are being created whose surface technology can be regulated by external stimuli. The reversible alteration of properties of smart polymers in response to a change in the stimuli (viz., temperature, pH/chemical, ionic strength/electrolyte/salt concentration, electric, magnetic fields, and light) that can result in the manipulation of responsive polymer remotely via "on-demand" can also act as an "on-off" switch control. Smart membranes are thus adaptive to external stimuli and can form self-assembled monolayers (surface modifications) or polymer thin films [12]. The responsive membranes are gaining importance in many fields such as controlled drug delivery, smart bioseparation, environmental remediation, water and wastewater treatment by mitigation of membrane fouling, and oxygen enrichment, etc. This chapter focuses on stimuli-responsive membrane (SRM) having reversibly switchable physiochemical properties, which is a very interesting topic of research and development concerning wastewater treatment.

This book belongs to Badji Mokhtar Annaba University Central Library Copyright Elsevier 2025

21.2 Types of membranes

In recent years, with regard to progress in material science and manufacturing technology, membrane technology has opened up new avenues for research, development, and application. This has led to development and synthesis of a number of membrane materials having different and unique properties. There are various ways the membranes can be classified. The major factors on which membranes can be classified are: (i) the nature of the membrane material, (ii) the membrane structure and surface morphology, (iii) geometrical shapes and fabrication types, and (iv) transport mechanism and separation process.

On the basis of the nature of membrane materials, they can be classified as synthetic and biological. Synthetic membranes can be classified into organic membranes, inorganic membranes (ceramic, metallic, carbon, zeolite, glass, etc.), and hybrid (inorganic-organic) membranes (Fig. 21.1). With the aim to serve various engineering applications, classification depending on membrane geometry can be deemed as flat sheet, tubular, capillary, and hollow fiber membranes. Again, membranes are classified as dense and porous, whereas transport mechanism can be defined as Knudsen diffusion, molecular sieving, and selective surface flow, etc.

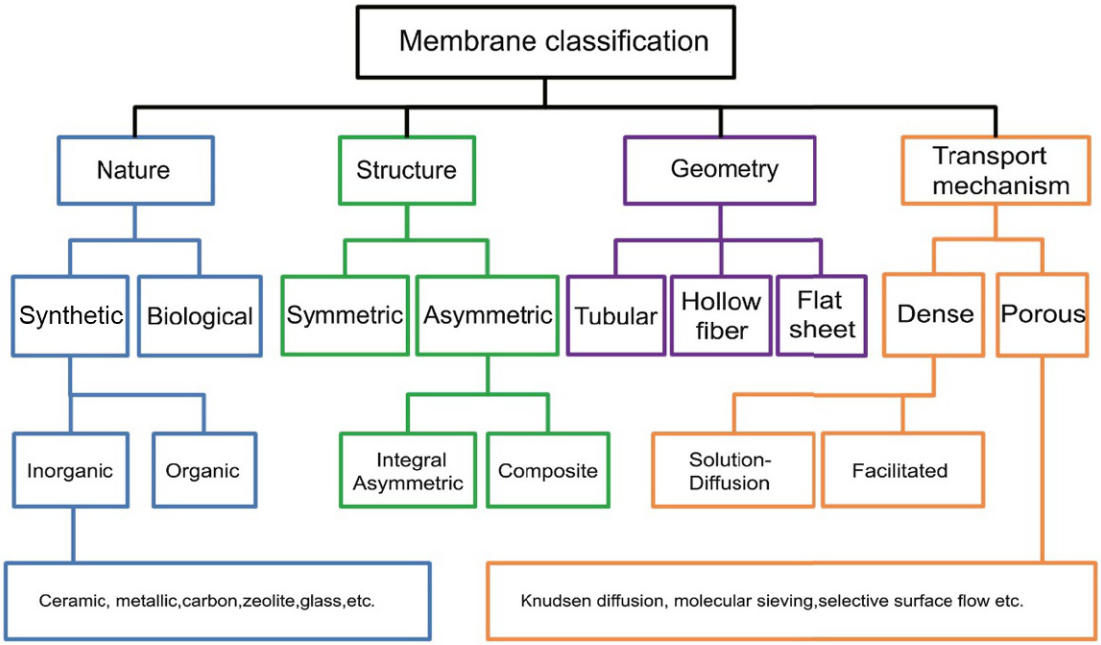

Fig. 21.1
The classification of membranes. *Adapted from Z. Dai, L. Ansaloni, L. Deng, Recent advances in multi-layer composite polymeric membranes for CO_2 separation: a review, Green Energy Environ. 1 (2016) 102–128, https://doi.org/10.1016/j.gee.2016.08.001.*

This book belongs to Badji Mokhtar Annaba University Central Library Copyright Elsevier 2025

Depending upon the stimulus, responsive polymer gels can change two-dimensional bending/actuation motion or volumetric swelling or collapse, and thereby change their shapes in a controlled and reversible manner [13]. Since the polymer accountable for stimuli-response is enclosed by pores or encapsulated in a support, the change in the shape (response) is different in SRMs as compared to polymer gels. Membranes that can adjust their physiochemical properties in reaction to external environmental conditions/stimuli are classified as SRMs. External stimuli can modify the interfacial and mass transfer properties of the responsive membrane [14]. The classification based on the structure and morphology of SRMs is done in isotropic and anisotropic membranes. The following section describe details related to isotropic and anisotropic membranes.

21.2.1 Isotropic (symmetric) membranes

Symmetric (isotropic) membranes have an even structure all over the membrane thickness. The entire structure determines the separation properties of isotropic membranes (Fig. 21.2). The classification of the symmetric membranes is based on the separation regime into microporous, nonporous, dense, and electrically charged membrane. The structure and function of the microporous membranes is similar to any conventional filter. Molecular size of the solute and pore size distribution are major factors that decide the separation of feed solution in porous membranes. A porous membrane is a highly voided configuration (micro and/or macro) with arbitrarily dispersed interconnected pores. These voided pores are very small, and their diameters are in the range of 10–100 nm. The major application of these membranes is in microfiltration processes [15].

The composition of nonporous dense membranes consists of a dense polymeric film through which permeate transfers via diffusion because of the driving force of concentration, pressure, or electrical potential gradient. Dense membrane for separation is preferred in most of the processes like pervaporation, gas separation, and reverse osmosis as it enhances permeate flux due to anisotropic structure.

21.2.2 Asymmetric (anisotropic) membranes

Asymmetric (anisotropic) membranes have comparatively dense, very thin surface layer reinforced on an open, much thicker porous support. The surface layer and its substructure is fabricated in a single operation or distinctly. The membrane performance is determined entirely by the thin, dense, porous surface layer. The thickness of the membrane is reciprocally proportional to the permeate flux. All commercial processes use anisotropic membranes because of the benefits of an increase in membrane thickness, thereby higher permeate fluxes, and reduced resistance to pressure.

This book belongs to Badji Mokhtar Annaba University Central Library Copyright Elsevier 2025

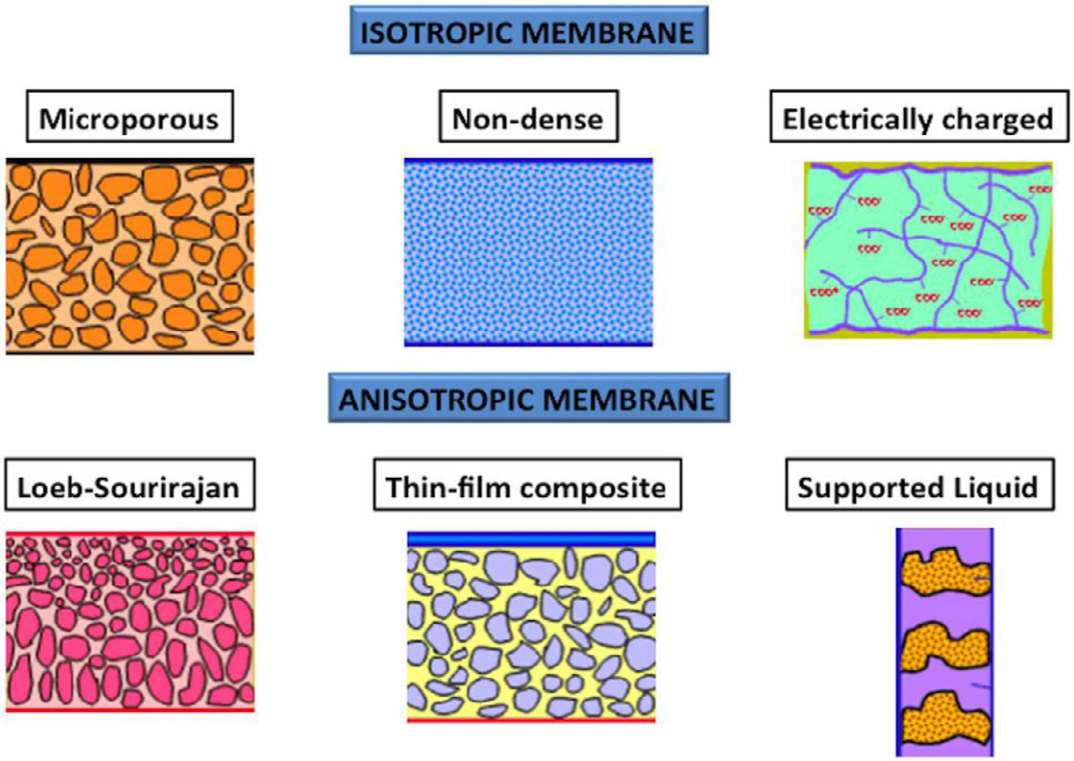

Fig. 21.2
The schematic top view of isotropic and anisotropic membranes. *Reprinted with permission from J. Martín, E.J. Díaz-Montaña, A.G. Asuero, Recovery of anthocyanins using membrane technologies: a review, Crit. Rev. Anal. Chem. 48 (2018) 143–175.*

Asymmetric membranes are classified into three basic categories: (i) Loeb-Sourirajan membranes, (ii) thin film composites, and (iii) supported liquid membranes. Loeb-Sourirajan membrane is the membrane where the variation in pore size of a subsurface layer from top/skin layer is quite significant (10–15 times). A thin film composite membrane consists of a thin dense polymer surface layer over a thick microporous film, which is responsible for separation of molecules.

21.3 Membrane materials

There are different materials to fabricate membranes such as organic (e.g., polymers) or inorganic types (e.g., metal oxides, zeolites, carbons, etc.) membranes. Different polymers that are hydrophilic in nature, such as poly(sulfone) (PS), poly(ether sulfone) (PES) family,

This book belongs to Badji Mokhtar Annaba University Central Library Copyright Elsevier 2025

poly(acrylonitrile) (PAN), cellulose acetate (CA), and poly(carbonate) are used for membrane synthesis. The selective layer for the membrane can also be synthesized using polymers that are hydrophobic in nature, viz., poly(vinylidene fluoride) (PVDF) and poly(amide).

The membrane material plays a major role in the performance; it directly interacts with the feed solution during the operation. Therefore, the selection of the membrane material is a major task before considering any operation involving the membrane. The properties of membrane such as contact angle (hydrophilic or hydrophobic), surface modification, liquid entry pressure, and porosity and pore size are of importance while designing the membrane separation process.

21.4 Design and fabrication of responsive membrane

The major advantage and design criteria of the SRMs is a controlled and predictable response of these membranes to external stimuli. There are many design and production protocols, and these can be classified by four ways: (i) preparation of responsive materials (polymers or copolymers) and their processing into membranes, (ii) functionalization by incubation in liquid, (iii) functionalization by incorporating responsive groups/molecules in base membrane, and (iv) surface modification of existing membranes using various chemical/physical methods for incorporation of stimuli-responsive polymers.

Design approach of SRMs involves their synthesis from polymers, copolymers, and polymer-additive mixtures. The designed membrane will have the anticipated layer thickness, mechanical properties, pore structure, and barrier structure. This design approach is not sufficient to get the optimal membrane surface characteristics, and therefore surface modification is a vital characteristic of the design of responsive membranes. In the surface modification approach, the responsive properties are introduced on the surface maintaining base membrane, thereby imparting functionality, which enhances membrane performance.

21.4.1 Preparation and processing of responsive materials

The stimuli-responsive polymer can be synthesized by blending pure polymer and copolymers. The various processes used for the synthesis and processing of SRMs are radiation-based process, solvent casting, and phase inversion.

Radiation-based processes are based on an approach where a blend of stimuli-responsive and cross-linking monomers (and/or prepolymers) are coated onto a porous film surface, and this coated layer is then cured by UV irradiation. Formulation used for the layer coating can have chemical additives for various applications including controlled release applications. There are a number of monomers that can be used for the synthesis of composite membranes

This book belongs to Badji Mokhtar Annaba University Central Library Copyright Elsevier 2025

with permeation/release profiles that respond to changes in external environmental stimuli such as pH, temperature, ionic strength, etc.

Development of a composite membrane can be done using solvent casting. In this method, the responsive membrane is synthesized by casting a solution of mixtures containing stimuli-responsive polymers or copolymers onto flat surfaces. The process of membrane synthesis involves the dissolution of responsive polymers or copolymers in a suitable solvent, casting the solutions obtained on flat glass plates, thereby allowing evaporation of the solvent. The free-standing membranes so formed are dried and cross-linked by annealing them.

The fabrication of SRM can be done using traditional techniques like wet phase-inversion process. After casting of responsive polymers or copolymer-containing solutions on flat surfaces, it is then immersed in a suitable solvent like water to enable formation of membrane.

21.4.2 Functionalization by incubation in liquid

The hydrolysis of polyacrylonitrile (PAN) microporous membranes is accomplished by immersion in aqueous NaOH solution at about 50°C for a specified time and then washed thoroughly using deionized water until neutral. One of the actions of this hydrolysis is production of thin poly(acrylic acid) (PAA) layer on the external surface of membrane. Swelling of the PAN membrane incubated in amine and hydroxide solutions at pH values above pK_a of PAA enhances deprotonation of carboxylic groups [16].

21.4.3 Functionalization by incorporation of responsive groups in base membrane

There are two methods by which responsive groups can be incorporated in base membrane in situ and postsynthesis. The basic criteria in in situ method is that the responsive group is an integral part of one of the monomers used for the synthesis of the membrane, whereas postsynthesis method is based on the incorporation of the reactive group prior to membrane casting after the membrane polymer is synthesized.

The in situ method yields interpenetrating polymer networks (IPNs) where high level of cross-linking is attributed because of the incorporation of responsive groups giving good mechanical strength. This can be elaborated by the example of polystyrene-*block*-poly(*N*,*N*-dimethylaminoethyl methacrylate) (PS-*b*-PDMAEMA) copolymer. The membranes were synthesized from this copolymer via nonsolvent-induced phase separation (NIPS) process. The responsive membranes were used in UF application [17]. To form the stimuli-responsive IPN membrane, a stimuli-responsive monomer is polymerized within a physically entrapped copolymer in presence of an initiator and a cross-linker.

At pH of 2 and room temperature, low water flux was found, and as temperature was increased to 65°C, marginal decrease in flux was observed. This was attributed to an increase in

This book belongs to Badji Mokhtar Annaba University Central Library Copyright Elsevier 2025

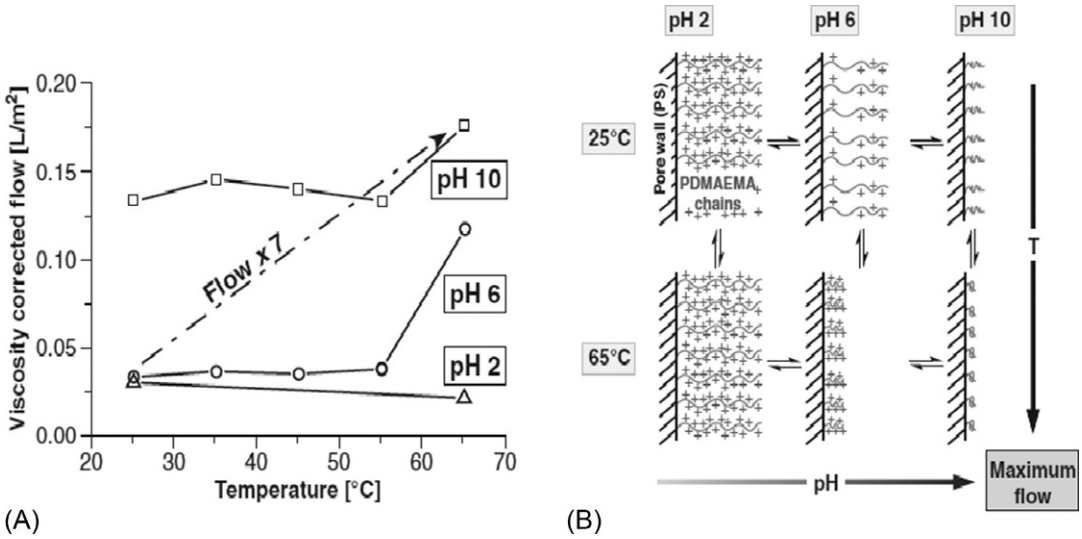

Fig. 21.3

The application of PS-*b*-PDMAEMA membrane in ultrafiltration with water flux studied as function of (A) schematic illustration of effect of temperature along the inner part of the membrane pores and (B) at different pH values and temperatures. *Reprinted under the terms of the STM agreement from F. Schacher, M. Ulbricht, A.H.E. Müller, Self-supporting, double stimuli-responsive porous membranes from polystyrene-block-poly(N,N-dimethylaminoethyl methacrylate) diblock copolymers, Adv. Funct. Mater. 19 (2009) 1040–1045, https://doi.org/10.1002/adfm.200801457.*

temperature of the PDMAEMA segments, making it protonated and resulting in a more prolonged and extended conformation (see Fig. 21.3A). At pH 6, low water flux is observed because of partial protonation of the chains (Fig. 21.3B, upper middle). Increase of temperature to 55°C has no significant effect on flux. However, fourfold increase in flux at 65°C is observed. This is because there is low charge density on PDMAEMA segments above 55°C, which allows breakdown of chains at temperatures greater than the lower critical solution temperature (LCST). With an increase in pH to 10, higher water flux observed. The increase in flux is due to full deprotonation of the PDMAEMA chains (Fig. 21.3B, right). At high pH and temperature, sevenfold increase in water flux is observed in comparison to low pH and temperature.

An example of postsynthesis strategy is membrane made of poly(methacrylic acid) (PMAA) grafted on polyethersulfone (PES) where benzoyl peroxide (BPO) is used as an initiator [18]. Asymmetric UF membranes (PES-*g*-PMAA) are fabricated with the help of a phase inversion process by casting copolymer. The pH-responsive property to the membrane is offered by the PMAA component. The water flux is independent on pH for PES membrane as can be seen in Fig. 21.4. However, the water flux is dependent on the pH for membrane cast of PES-*g*-PMAA. The substantial decrease in aqueous solution flux between pH 4.0 and

This book belongs to Badji Mokhtar Annaba University Central Library
Copyright Elsevier 2025

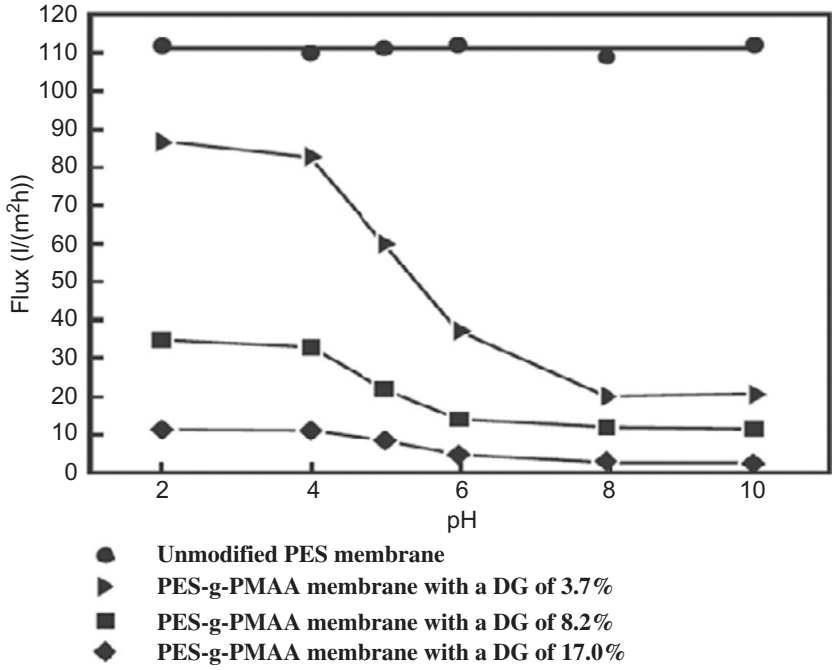

Fig. 21.4
Effect of pH on water flux using different membranes. *Reprinted with permission from Q. Shi, Y. Su, X. Ning, W. Chen, J. Peng, Z. Jiang, Graft polymerization of methacrylic acid onto polyethersulfone for potential pH-responsive membrane materials, J. Membr. Sci. 347 (2010) 62–68, https://doi.org/10.1016/j.memsci.2009.10.006. Copyright (2010) Elsevier.*

6.0 is observed. However, as degree of grafting (DG) increases, the decrease in flux is less. The PMAA coverage on the membrane surface rises as DG is increased resulting in decreased membrane pore size. The solvent/nonsolvent exchange rate during membrane casting is reduced because of relatively high hydrophilic nature of PMAA. Although the PES-*g*-PMAA membrane has high surface coverage of pH-sensitive PMAA, the membrane with low DG was evidently highly sensitive to pH change.

21.4.4 Functionalization by surface modification

Surface modification of membranes using responsive materials is a promising method that can provide attractive properties and convert the membranes into valuable products. This technique has a higher degree of control above surface properties and bids flexibility of grafting material onto the external surface of the membrane, thereby overcoming limitations of the existing membrane [19, 20]. The standards for the successful membrane modification are: (i) maintenance of membrane bulk properties such as pore structure and porosity and

This book belongs to Badji Mokhtar Annaba University Central Library Copyright Elsevier 2025

(ii) incorporation of functional (responsive) responsive materials that retains sensitivity toward external surrounding cues [14].

There are basically two distinct approaches by which the membrane surface modifications can be brought about: (i) chemical binding (covalent attachment) using a process like "grafting-to" and "grafting-from" and (ii) physical bonding using physical mass transfer operations like adsorption, interfacial cross-linking, and pore-filling.

21.4.4.1 Grafting-to

The "grafting-to" methodology introduces a preformed polymer chain with end-functionalized small molecules or large macromolecules covalently attached to the membrane surface. Since the preformed responsive group can be purified prior to grafting, the control is easier. However, the chain molecular weight of the responsive group defines the functionality and response of the membrane surface layer.

The CA UF membrane grafted with a thermoresponsive hydroxypropyl cellulose (HPC) film layer was prepared by Gorey and coworkers [21]. This membrane was fouling-resistant, and the film could be collapsed or expanded. The film collapses upon increase in temperature and expands upon decrease in temperature; this immediate response of the membrane generates an extensive motion at the molecular level (nanometer scale) alongside the surface. The responsive property was determined by atomic force microscopy with the analysis of roughness of the membrane in the solution of different temperature. The study showed that the change in roughness is primarily responsible for the extension and collapse of the surface attached below and above LCST (46°C).

21.4.4.2 Grafting-from: Surface-initiated modification

The "grafting-from" method is a heterogeneous, two-step, surface-initiated polymerization process. The two steps are: (i) an initiator precursor is immobilized on the membrane surface, and (ii) the polymer growth is instigated by monomer addition to immobilized initiator sites. The advantage of grafting-from technique is that the monomer can be added over time thereby the thickness of grafting layer is regulated, and much higher polymer surface densities are possible. However, the technique makes it comparatively harder to regulate the final length of responsive membrane and to attain reproducible surface arrangements. The kinetically control grafting density and graft chain length can be selectively controlled during progress of reaction. Highly defined polymer brushes with controlled chain density and length can be achieved by controlled polymerization methods. Surface-initiated grafting-from polymerization methods are photoinitiated grafting (UV and non-UV), anionic and cationic polymerization, redox-initiated grafting, ring-opening metathesis polymerization (ROMP), nitroxide mediated polymerization (NMP), plasma-initiated grafting, reversible addition-fragmentation chain-transfer polymerization (RAFT), and atom transfer radical polymerization (ATRP) [14,20]. Due to mild polymerization conditions and tolerance to impurities, ATRP is most

This book belongs to Badji Mokhtar Annaba University Central Library Copyright Elsevier 2025

preferred among these controlled polymerization methods. As well as UV-induced graft, polymerization is also preferred for the reason of low cost of operation, mild reaction conditions, and ease of operation.

Polymer chain density is one of significant distinction in considering membrane modification by grafted polymers. For the "grafting-to" method, it depends on the chain's molecular weight, whereas for the "grafting-from" method, it is an independent design parameter. Grafting density is a significant parameter, as it prominently affects the final performance of the membranes. High grafting density can be important as it shields the underlying membrane support from fouling agents. However, high grafting density limits the response to external stimuli since the chains are bounded in an extended configuration. Flexibility in membrane design can be provided by the tailor grafting densities independently of polymer chain molecular weight.

21.5 Classification of stimulation approach and application in water treatment

The problem that arises with membranes as discussed earlier is fouling of membranes. It is very obvious that fouling will not take place if the resistance of the membrane remains unaffected in the operation. Fouling can be minimized by disturbing the concentration polarization on the membrane surface. The fixed mass transfer area and driving force are there when we consider the membranes for water treatment for filtration process. In the case of environmental responsive membranes, the transmembrane resistance (TMR) and mass-transfer properties can be tuned as per external responsive conformational modification of the membrane [22].

Self-regulated and controlled response to the various external stimuli with reversible surface properties is one of the most important factors responsible for the improved interest in SRM. Separation process, biosensing materials, drug delivery, and many more are some of the applications of these materials [23]. Membrane scientists also have great opportunities in the synthesis of artificial smart membranes with self-regulated resistance that can prove to be of great use in the field of science and technology.

Husson [24] explained the responsive mechanism of functional materials as a two-step process. Functional materials such as nanogel, polymer, and nanoparticle have their conformational transitions that are triggered by the external environment, which can be observed by a change in membrane separation performance. Change in structural configuration of the responsive material in response to external stimuli is the main design criteria for the synthesis of SRM. The mechanism by which typical external or environmental stimuli have an effect on the responsive membrane is discussed in the following section.

This book belongs to Badji Mokhtar Annaba University Central Library Copyright Elsevier 2025

21.5.1 Thermoresponsive membrane

Thermoresponsive membranes or temperature-responsive membranes are polymers that, when subjected to environmental temperature change, go through reversible phase transition [25]. Thermoresponsive membranes actuate and react to the addition and elimination of heat stimuli through an amalgamation of conduction and convection that alters the surrounding solvent quality as a characteristic critical temperature threshold is attained. Fig. 21.5 shows reversible and "on-off" switchable properties in response to temperature changes in a thermoresponsive smart polymeric material.

The most extensively utilized smart polymers are thermoresponsive polymers, one of the distinctive properties of which is a reversibly alterable phase (or volume) transition that occurs due to temperature variation. The temperature-responsive membranes are normally synthesized by solution casting of copolymers and polymer mixtures as IPNs, nanocomposites, and microcapsules.

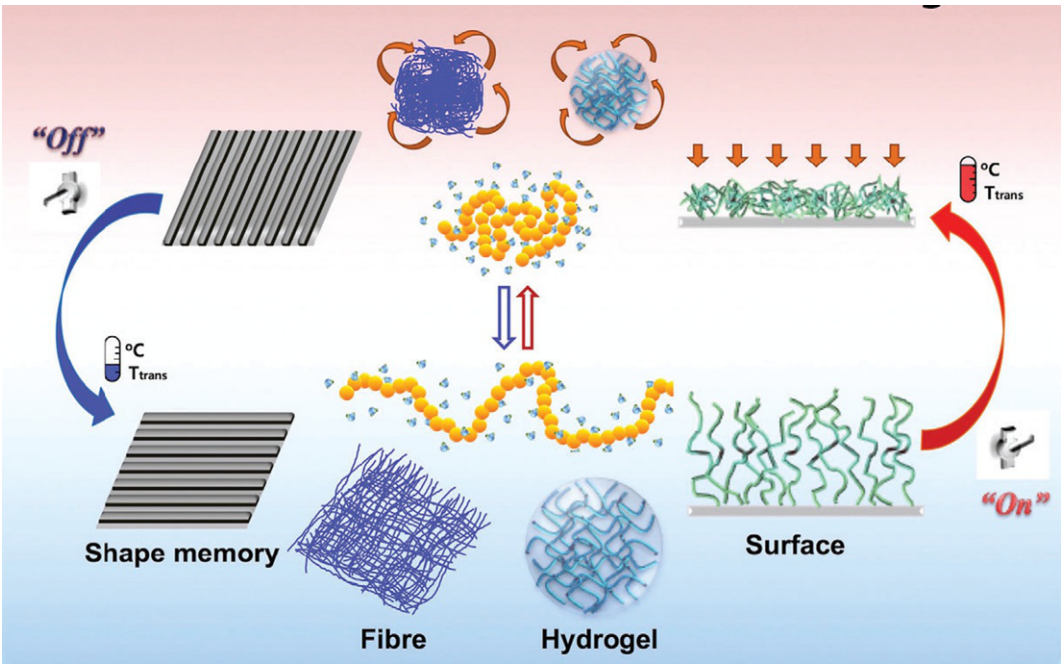

Fig. 21.5
The mechanistic representation of reversible and "on-off" switchable response to change in temperature for thermoresponsive membrane. *Reprinted with permission Y.-J. Kim, Y.T. Matsunaga, Thermo-responsive polymers and their application as smart biomaterials, J. Mater. Chem. B 5 (2017) 4307–4321, https://doi.org/10.1039/C7TB00157F.*

This book belongs to Badji Mokhtar Annaba University Central Library
Copyright Elsevier 2025

Poly(*N*-isopropylacrylamide) (PNIPAAm), its monomer *N*-isopropylacrylamide (NIPAAm), and related copolymers are some of the oldest membrane materials having thermoresponsive behaviors [26]. The polymer PNIPAAm is soluble in water at room temperature; however, it is subjected to partition of phase at temperatures greater than 32°C (LCST). Due to hydrophobic and hydrophilic (i.e., hydrogen bonding), the hydrated polymer chains are preferentially bonded together and dissociated by thermal energy and precipitated in aqueous solution, thereby phase transition occurs and alters the membrane structure and properties [14].

The substantial reduction in the water flux through a PNIPAAm-functionalized membrane temperature below its LCST was observed. The membrane cleaning can be performed using a temperature-change (between 25°C and 35°C) cleaning method. Fouling bovine serum albumin (BSA) was easily washed out by water from the responsive membrane surface, demonstrating a high flux recovery rate of about 97.6% as compared to the initial flux [27].

There are other notable thermoresponsive polymers such as poly(*N*-vinylcaprolacam) (PVCL), polyacrylamide (PAAm), poly(acrylic acid) (PAAc), poly(*N*,*N*-dimethylaminoethyl methacrylate) (PDMAEMA), poly(*N*,*N*-diethylacrylamide) (PDEAAm), hydroxyethyl cellulose (HEC), hydroxypropyl cellulose (HPC), poly(methyl vinyl ether) (PMVE), polyvinyl chloride (PVC), *N*-vinylcaprolactam (NVCl), poly(2-ethyl-2-oxazoline) (PEtOx), poly(ethylene glycol)/poly(ethylene oxide) (PEG/PEO), etc. [11, 28].

Additional stimuli-responsive moieties can be augmented with copolymer, and double or multisensitivity can be established. The thermoresponsive monomer and other ionizable monomers like acrylic acid (AA) can be combined to obtain pH-sensitive thermoresponsive polymers.

21.5.2 pH/chemical-responsive membranes

Source of triggering a response in pH-responsive membrane can be free ions/molecules that, once externally introduced, can diffuse in and out by convection through polymer to counterbalance the oppositely charged ions at polymer bulk or side chain [29]. Similarly, chemical-responsive membranes respond to the chemical species by transforming the change in membrane pore size by chemical stimulus [30]. The viscoelastic response can be provided by the ionic aggregation of polymer cross-lining at the nanometer scale, which has an effect on mechanical properties, and the compatibility among different polymers in the blend is increased. Some of the examples of the pH-responsive polymers are ions-doped polymers (polyelectrolytes, ionic polymers, conjugated polymers) and uncharged polymers gelled using ionic molecule such as ionic liquid or solvent-bearing ionic group. The reversible alteration in shape and/or volume can be observed when these polymers are subjected to external fields including thermal, electrical, and pH [29, 31]. The speed of the stimuli change is a function of: (i) external mass transport (depends on the surrounding reservoir), (ii) internal mass transport

This book belongs to Badji Mokhtar Annaba University Central Library Copyright Elsevier 2025

(depends on the properties of membrane matrix), and (iii) chemical reaction with the responsible chemical groups/moieties hanging or terminally attached to the polymers. Bulk pH-responsive membranes are synthesized by solution forming of copolymers and polymer mixtures as IPNs and micro/nanocomposites.

The charged polymers like polyelectrolytes (PELs) or ionic polymers can swell or collapse in response to a variation in the quality of the surrounding solvent as stimulus. Depending on ionic dissociation or association of weak PELs in aqueous solution, negative or positive charges are secured as a result of release or capture of H^+ or OH^-. Most of these PELs act as pH-responsive precursors due to collective ionization behaviors. pH, salt concentration, and intrinsic proton affinity (i.e., dissociation constant, pK_a, or pK_b) are the major operating parameters responsible for the dissociation of the ionizable groups [32].

The negatively charged ions (i.e., polyanion) such as poly(acrylic acid) (PAA) and positively charged ions (i.e., polycation) such as poly(2-vinylpyridine) (P2VP) and poly(4-vinylpyridine) (P4VP) are some of the examples of weak PELs that respond to changes in surrounding pH. In the negatively charged PELs, as pH is increased, the carboxyl acid groups of PAA (—COOH) release HC. The schematic representation of pH-responsive (poly(4-vinyl pyridine) (P4VP)) microgel-assembled membrane is depicted in Fig. 21.6.

The representative example of pH-responsive UF membranes can be taken from a study by Latulippe and coworkers [33] who synthesized a membrane by filling the openings of other microfiltration membranes. The studies related to the effect of pH and salt concentration for the change in transmembrane pressure (TMP) at constant flux revealed the abnormal salt concentration dependence on permeability. With an increase in pH, TMP is increased due to deprotonation of carboxyl acid groups that swell the structure of the pore-filling gel. The profound increase in the pH-responsive property was observed as a result of addition of NaCl. At higher pH, with a rise in salt concentration, the TMP decreased. This behavior is attributed to the fact that the hydraulic resistance is reduced as a result of a rearrangement of the gel network to heterogeneous structure and salt charge repulsion effects between polymer chains, whereas the effect of increasing salt concentration gives rise to an increase in TMP. The increase in polymer ionization of acrylamide-acrylic acid copolymers was observed as a result of increasing ionic strength [34].

High hydrophobicity at low pH, which is a result of the switchable wettability characteristics, is an important property for water purification and management applications, especially for oil/water separation [35–37]. Electrospun polyimide (PI) nanofiber was used as the membrane matrix dip-coated in decanoic acid (DA)-TiO_2 and silica nanoparticles (SNPs), i.e., SNP/DA-TiO_2/PI membrane. The solution pH and ammonia vapor can trigger the pH response in the membrane with the wettability transition of the membrane. At pH 12 or greater, the responsive membrane becomes hydrophilic and superoleophobic, and due to repulsive forces, only water can pass through the membrane and oil is retained on the upper

This book belongs to Badji Mokhtar Annaba University Central Library Copyright Elsevier 2025

This book belongs to Badji Mokhtar Annaba University Central Library

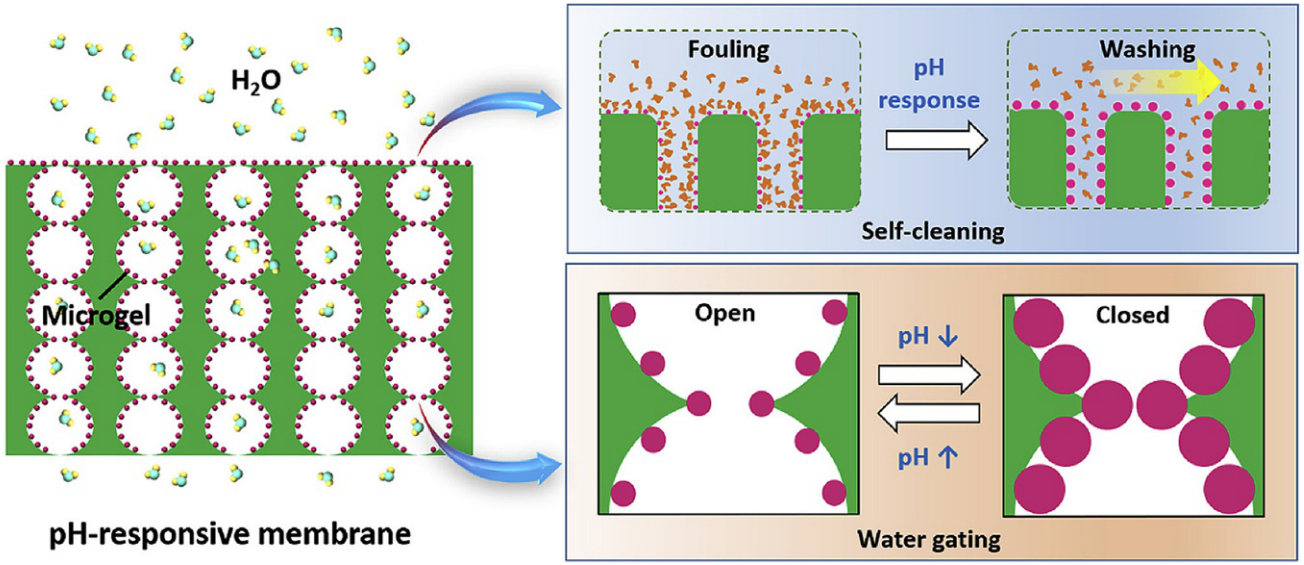

Fig. 21.6

The schematic representation of pH-responsive (poly(4-vinyl pyridine) (P4VP)) microgel-assembled membrane. *Reprinted with permission from H. Liu, S. Yang, Y. Liu, M. Miao, Y. Zhao, A. Sotto, C. Gao, J. Shen, Fabricating a pH-responsive membrane through interfacial in-situ assembly of microgels for water gating and self-cleaning, J. Membr. Sci. 579 (2019) 230–239, https://doi.org/10.1016/j.memsci.2019.03.010. Copyright (2010) Elsevier.*

Copyright Elsevier 2025

membrane boundary. Hydrophobicity of the membrane could be improved by ammonia vapor treatment, thereby only water can pass through the membrane. The pH-responsive SNP/DA-TiO_2/PI membrane exhibited exceptionally high flux and >99% efficiency of separation [37].

21.5.3 Ionic strength/electrolyte/salt responsiveness

The ionic strength or salinity is the adaptive response of the chain conformation and secondary structures of PELs. The ions and counterions, viz., Na^+ and Cl^- in aqueous NaCl solution, which is fully dissociated, are major factors responsible for the ionic strength [28]. The inverse proportional relationship exists between the electrostatic screening length to the square root of ionic strength imposed on electrostatic field from the pendant group. Freely diffusing ions are a profound function of a number of densities and valences along the polymer backbone of the fixed charged groups. It adopted an expanded, rod-like structure when PELs are fully ionized. As the ionic strength increased, electrostatic screening became stronger with rise in salt concentration, which reduced electrostatic screening length. Due to this, the PELs shrank or collapsed further as the intermolecular repulsion along the PEL chains were slowly screened out. In the case of high ionic strength, PELs may subside and act as neutral polymers without any chain enlargement. The sensitive behavior of ionic strength is called the "polyelectrolyte effect."

An additional fascinating and practical ionic-strength dependency is termed as antipolyelectrolyte effect [38, 39]. It is a depiction of polyzwitterion at monochain level and, compared with organic inner salt and inorganic salts, such as amphoteric hydrogels [40] or polyzwitterions [41], which carry a uniform number of both positively and negatively charged groups making the polymers electrically neutral. A polymer of sulfobetaine was prepared in which cationic quaternary ammonium and anionic sulfonate are co-located on the same monomeric entity belonging to a member of zwitterionic PELs, and they assume a collapsed, microspherical structure because of the electrostatic magnetism between neighboring or opposite charges. Fig. 21.7 shows composite membranes of zwitterionic copolymers of sulfobetaine methacrylamide (SBMI) and sulfobetaine methacrylate (SBMA) [42] representing ionic strength and thermo-responsive polyethersulfone, respectively. Investigation of diffusion phenomenon and chain size of polyzwitterion single chain in extremely dilute aqueous solution over a wide range of added salt was performed using fluorescence correlation spectroscopy. The single chains of polyzwitterions undergo expansion with an increase of salt concentration due to introduction of inorganic salts and organic inner salts. With increased salt concentration, presence of electrolytes (i.e., co-ions and counterions) was gradually screened out or it disrupted the intra- and/or interchain associations of these opposite charges, thereby releasing previously associated chain segments from the collapsed state [43]. This observation specifies that the breakup of the dipole-dipole attraction between the zwitterion

This book belongs to Badji Mokhtar Annaba University Central Library Copyright Elsevier 2025

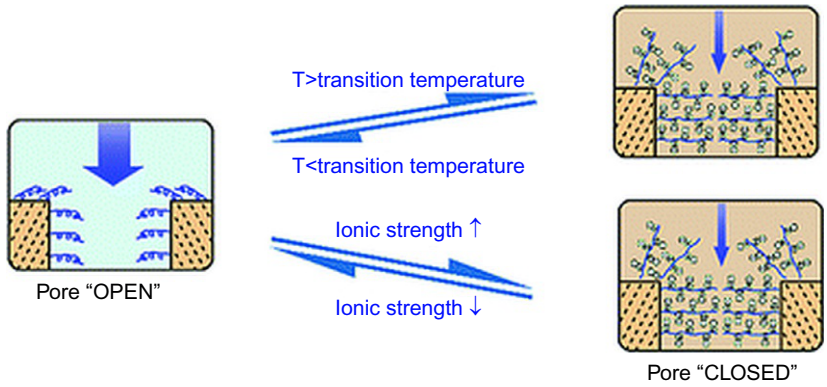

Fig. 21.7
The representation of ionic strength- and thermoresponsive polyethersulfone composite membranes using zwitterionic copolymers. *Reprinted with permission from T. Xiang, T. Lu, W.-F. Zhao, C.-S. Zhao, Ionic strength- and thermo-responsive polyethersulfone composite membranes with enhanced antifouling properties, New J. Chem. 42 (2018) 5323–5333, https://doi.org/10.1039/C8NJ00039E.*

units is the mechanism of the antipolyelectrolyte effect of polyzwitterions. This unique salt dependency is therefore useful for incorporating ionic strength responsiveness within the membranes.

21.5.4 Electroresponsive membranes

Electroresponsive membranes are those membranes in which surface properties, especially its potential and charge, are altered using an external electric field or potential signal [44]. But this technology suffers due to the poor properties of the prevailing conductive membranes [45]. The main concern during water treatment is the sustainability of the electroresponsive membrane subjected to aqueous solutions with high electrical conductivity and extreme conditions like exposure to radical temperatures or destructive chemicals. In designing electric/magnetic field responsive membranes, two general approaches are considered. The first approach makes use of surface coatings or bulk materials that undergo reversible molecular transitions when exposed to an electric field as an external field, whereas the second method exploits the fact that there is a change in surface properties of anisotropic nanoparticles if oriented at an interface in a controlled way due to an electric field, as shown in Fig. 21.8. Response can be induced with the change in the electrical field and electromagnetic radiation. The response is not limited by mass transport of the change agent and is similar to photoirradiation.

Yamauchi and coworkers [46] used PVA/PAA composite membranes and studied the electrically controlled protein permeation. The diffusion of high molecular weight ionic solute

This book belongs to Badji Mokhtar Annaba University Central Library Copyright Elsevier 2025

This book belongs to Badji Mokhtar Annaba University Central Library

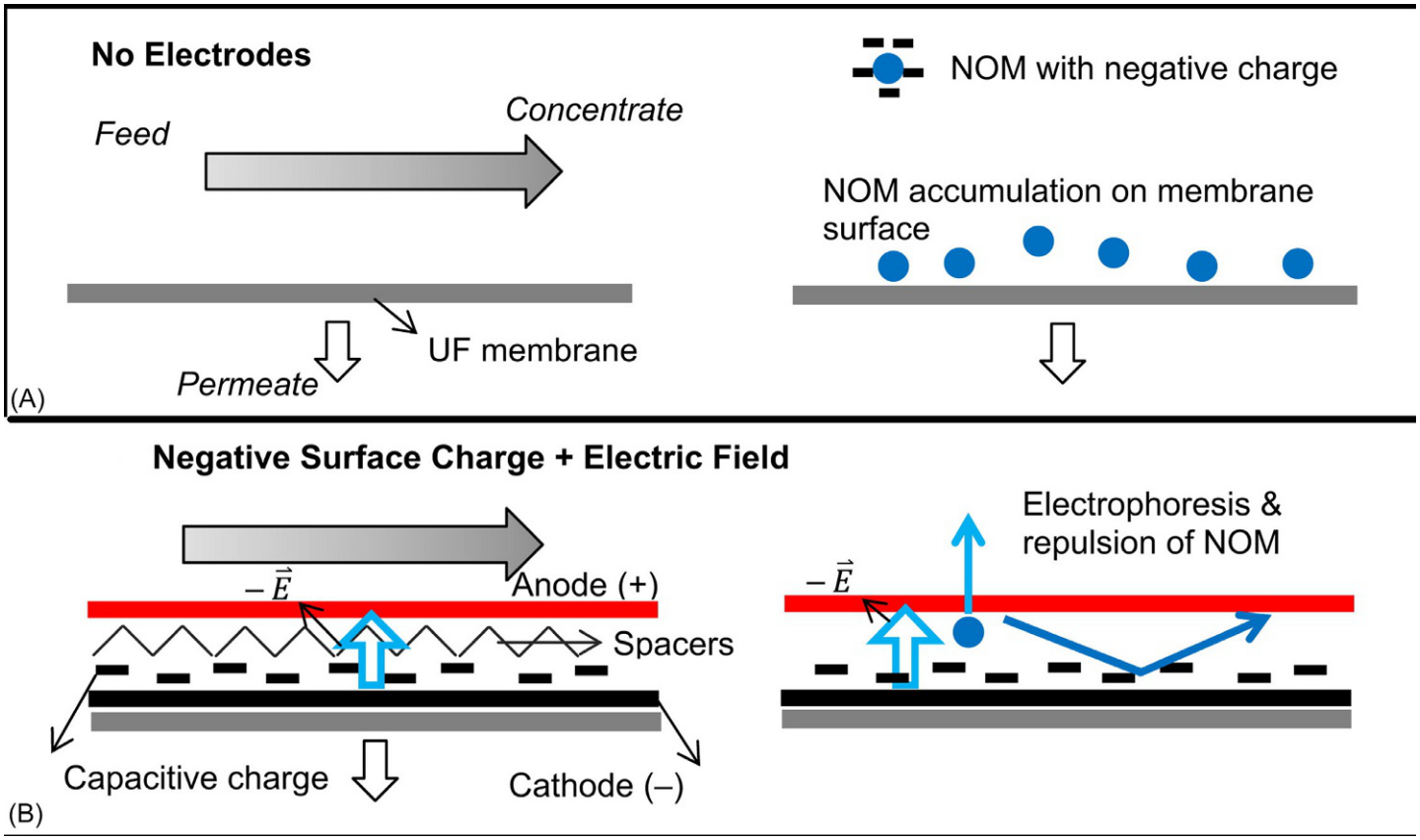

Fig. 21.8

Assembly of basic and electroresponsive cross-flow system. (A) The high fouling propensity basic cross-flow cell and (B) the electroresponsive membrane with negative surface charge and electric field. *Reprinted with permission from Q. Zhang, C.D. Vecitis, Conductive CNT-PVDF membrane for capacitive organic fouling reduction, J. Membr. Sci. 459 (2014) 143–156, https://doi.org/10.1016/j.memsci.2014.02.017.*

Copyright Elsevier 2025

proteins were activated by the PEL gel membrane. The appreciable reversible contraction and expansion in PEL hydrogels were observed due to an electric field. Therefore, membranes prepared from PEL hydrogels are applicable in an electric field for size-controlled solute permeation.

21.5.5 Magnetoresponsive membranes

The magnetic nanoparticles are applied because of high magnetic properties, excessive surface area-to-volume ratio, and good chemical and thermal stability [47]. Such properties justify the use of magnetic nanoparticles in drugs and biosensing, etc. [48]. The application of magnetic nanoparticles is not limited to sorbent but also the environmental application, as in removal of organic dyes [49] and heavy metals [50] from wastewater. On these distinctive features of magnetic nanoparticles, different nanocomposite polymeric membranes were suggested in the modern era [47, 51]. The pictorial representation of magnetoresponsive membrane system of anisotropic nanoparticles is depicted in Fig. 21.9.

PES with PANI/Fe_3O_4 nanoparticles are combined to form nanocomposite membrane [51]. This membrane were used for removal of copper ions from a dead-end filtration system. The output of this control membrane in comparison with the nanocomposite membrane included 0.1 wt% nanoparticles, which showed that nanocomposite could remove copper ion, but flux of pure water was reduced. Enhanced rejection is credited to an increased affinity of the magnetic nanoparticles for heavy metals [7, 52]. Even a lesser amount of water flux was resulted by the modified membrane, and constant water flux was obtained by synthesized

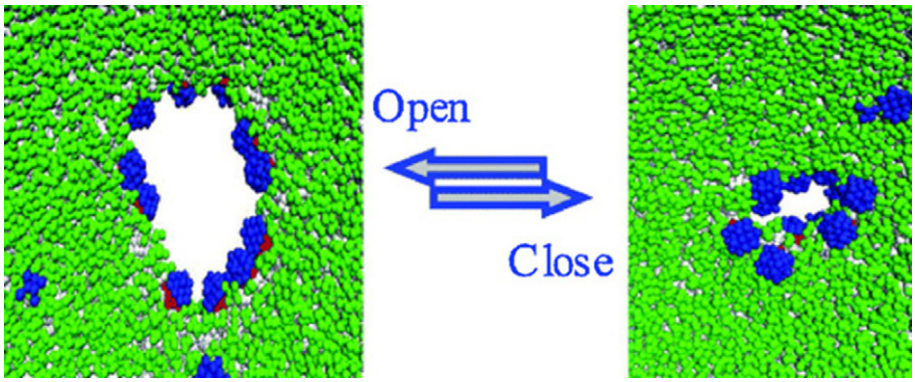

Fig. 21.9
The pictorial representation of magnetoresponsive membrane system of anisotropic nanoparticles.
Reproduced with permission from A. Alexeev, W.E. Uspal, A.C. Balazs, Harnessing Janus nanoparticles to create controllable pores in membranes, ACS Nano 2 (2008) 1117–1122. Copyright (2008) American Chemical Society.

This book belongs to Badji Mokhtar Annaba University Central Library Copyright Elsevier 2025

nanocomposite membrane throughout the test of four-cycle filtration. It clarified the outstanding reusability and durability of the modified membrane in filtration operations [51].

21.5.6 Photoresponsive membranes

Highly selective and accelerated photoresponsiveness can be imparted to a membrane without changing the chemical potential of the system in the membrane housing, which is optically transparent [53]. The nature of the membrane barrier decides the effect of the photosensitized reactions on the characteristics of the membrane. The photochromic molecules/units (e.g., azobenzene, spiropyran, diarylethene, viologen) are incorporated in the membrane polymer for the synthesis of the photoresponsive membrane. These photochromic molecules absorb light and undergo reversible photoisomerization (photochromism) reactions as result of molecular changes in color, size, polarity, and charge. The molecular changes are responsible for switching the chromophoric moiety among two or more states.

21.6 Characteristics of stimuli-responsive membrane

The chemical charge transfer [14], ultrasonic irradiation [54, 55], and redox reactions [56] can be used to fabricate SRMs. These responsive membranes have novel characteristics that make these membranes specialized in applications. The following sections describe the properties of these membranes.

21.6.1 Flexibility

An important property of SRM that has increased its value is reversible microphase segregation. SRMs respond to external stimuli by altering their conformation along end groups, backbone, or side chains. They can also be combined with porous or nonporous membranes [14]. By varying the length of polymer chain of the membrane or molecular arrangement or chemical composition, properties of sophisticated responsive membranes can be changed such as surface hydrophilicity and pore dimension in accordance with their stimuli [56, 57].

The responsive polymer can be attached to the membrane surface in a controlled manner to create a thin film of polymer, also identified as polymer brushes [58–60]. There are numerous polymer deposition techniques that can be used to modify top surfaces or pores of the membrane such as chemical vapor deposition, layer-by-layer (LBL) assembly, plasma-induced grafting, coating, spin-coating, etc. [11]. Responsive polymers that are attached to the surface and have freely moveable ends swiftly interact with environmental stimuli. During the filtration process, intrinsic properties of porous substrates remain unaltered, and it provides mechanical strength [23].

This book belongs to Badji Mokhtar Annaba University Central Library
Copyright Elsevier 2025

The size of the membrane can be varied by controlling the external cues and phase transition behavior of the matrix polymer grafted on the pore wall of the membrane. When a contrasting external field is applied, an expanded configuration of polymer is formed, which is then followed by conformational change. This facilitates the switching property to either hold or release the aimed compound. Another interesting feature to note is that the functional polymer can vary the hydrophobic or hydrophilic nature of the surface of the membrane, when subjected to external stimuli [11].

A nonporous membrane can be made responsive when a stimuli-responsive material is blended with bulk of a membrane material [14]. The conformational change in the functional polymer will occur by affecting the swelling degree of the membrane. This improves the selectivity and permeability of the membrane. Hydrogel membranes are formed by blending responsive nanogels in the whole membrane network [11].

Because of the previously mentioned flexibilities, smart membranes have found wider application in various fields. Formation of responsive membranes by "blending" has a major advantage in that it is a simple process. On the contrary, it has a relatively slower response. The reason behind it is that the functional materials are enclosed within the membrane network where the conformational change is smaller than the exposed linear polymer [61].

21.6.2 Surface modification

To enhance the properties and for overcoming limitations of existing membranes, modifications are needed to incorporate a higher amount of control over density and flexibility [14, 19, 20]. The chain molecular weight is the major factor that decides the functionality of the responsive layer. Two groups of scientists [20, 62] have studied the effect of grafted chain length and density by altering initiator concentration in solution, also the polymerization time using surface-initiated atom transfer radical polymerization (ATRP). ATRP provides feasibility to control the chain growth of polymerization and stops it after a specific time. One of the governing factors for deciding the performance of SRM is the grafted chain density. For modification of membranes with responsive polymers, there are two distinct surface modification techniques: grafting-to and grafting-from, which are discussed in detail in Section 21.4.4.

21.7 Industrial applications

SRMs have found wider industrial applications with ever-evolving technologies. The responsive membranes have also found exclusive and impactful applications in the water treatment process. Newer avenues of application are provided to responsive membranes in view of their numerous properties such as reversible and switchable properties, surface energy, and wettability. These properties also include self-cleaning ability that helps mitigate

This book belongs to Badji Mokhtar Annaba University Central Library Copyright Elsevier 2025

membrane fouling, which is considered as one of its major problems. In the case of magnetoresponsive membranes, there is an improved antifouling property due to the decreased effect of concentration polarization. This occurs as a result of the flexible movement of magnetoresponsive nanobrushes leading to mixing at low Reynolds number on the membrane surface. The technology can be commercialized to the industrial level, if we could the design a membrane profile in combination with the magnetic field apparatus for large-scale manufacturing [11].

Due to lack of spatial deviation of magnetic field strength inside the solenoid, nanoparticles are unable to accomplish actuation. Actuation motion is a motion in which rotational motion and lateral motion occur. The magnetic force acting on a nanoparticle reduces it to zero due to absence of spatial derivation of magnetic field strength. This eventually prevents sideways motion of the nanoparticle, and thus lateral motion becomes zero. Therefore, alteration of a magnetic field direction only rotates the nanoparticles at a static location with magnetic dipole moment pointing toward a specific direction. Due to the incomplete actuation motion, the complete detachment of the attached organic foulant is not possible as it does not possess enough shear strength. This can be resolved by having separate small sections of solenoids in which the arrangement is then divided alternately into two sections, X and Y. This kind of membrane design can be used for treating drinking water or wastewater at an industrial level [11].

21.8 Conclusion

In this chapter, we discussed SRMs and how they are becoming a growing topic of research and finding wider industrial applications. The concept of various types of membranes including symmetric, asymmetric, and their preparation methods were discussed. The materials used for the synthesis and fabrication of the SRM is studied. Various methods of the design and fabrication of the responsive membrane is discussed at length. The conformational changes occurring within membranes in response to external stimuli, namely ionic, electric, and magnetic fields, temperature, pH, and photo, have been discussed. The properties of the responsive membrane with an emphasis on the concept of flexibility of SRM was also explained. Along with these concepts, a review of the development of SRMs with their applications in water treatment was accomplished.

References

[1] C.J. Vörösmarty, P.B. McIntyre, M.O. Gessner, D. Dudgeon, A. Prusevich, P. Green, S. Glidden, S.E. Bunn, C. A. Sullivan, C.R. Liermann, P.M. Davies, Global threats to human water security and river biodiversity, Nature 467 (2010) 555–561, https://doi.org/10.1038/nature09440.

[2] S. Jāhāna, Human Development Report 2015: Work for Human Development, United Nations Development Programme, 2015.

This book belongs to Badji Mokhtar Annaba University Central Library

Copyright Elsevier 2025

[3] C.M. Chew, M.K. Aroua, M.A. Hussain, W.M.Z.W. Ismail, Evaluation of ultrafiltration and conventional water treatment systems for sustainable development: an industrial scale case study, J. Clean. Prod. 112 (2016) 3152–3163, https://doi.org/10.1016/j.jclepro.2015.10.037.
[4] E.N. Laboy-Nieves, F.C. Schaffner, A. Abdelhadi, M.F.A. Goosen, Environmental Management, Sustainable Development and Human Health, CRC Press, 2008.
[5] A. Schafer, Natural Organics Removal Using Membranes: Principles, Performance, and Cost, CRC Press, 2001.
[6] L.F. Greenlee, D.F. Lawler, B.D. Freeman, B. Marrot, P. Moulin, Reverse osmosis desalination: water sources, technology, and today's challenges, Water Res. 43 (2009) 2317–2348, https://doi.org/10.1016/j.watres.2009.03.010.
[7] P. Sabbatini, F. Rossi, G. Thern, A. Marajofsky, M.M.F. de Cortalezzi, Iron oxide adsorbers for arsenic removal: a low cost treatment for rural areas and mobile applications, Desalination 248 (2009) 184–192, https://doi.org/10.1016/j.desal.2008.05.104.
[8] R.W. Baker, Membrane Technology and Applications, John Wiley & Sons, 2012.
[9] Y. Wang, J.-H. Kim, K.-H. Choo, Y.-S. Lee, C.-H. Lee, Hydrophilic modification of polypropylene microfiltration membranes by ozone-induced graft polymerization, J. Membr. Sci. 169 (2000) 269–276, https://doi.org/10.1016/S0376-7388(99)00345-2.
[10] H. Yamamura, K. Kimura, Y. Watanabe, Mechanism involved in the evolution of physically irreversible fouling in microfiltration and ultrafiltration membranes used for drinking water treatment, Environ. Sci. Technol. 41 (2007) 6789–6794, https://doi.org/10.1021/es0629054.
[11] S.-C. Low, Q.-H. Ng, Progress of stimuli responsive membranes in water treatment, in: W.-J. Lau, A.F. Ismail, A. Isloor, A. Al-Ahmed (Eds.), Advanced Nanomaterials for Membrane Synthesis and Its Applications Micro and Nano Technologies, Elsevier, 2019, pp. 69–99, https://doi.org/10.1016/B978-0-12-814503-6.00004-5 (Chapter 4).
[12] S. Hernandez, A. Saad, L. Ormsbee, D. Bhattacharyya, Nanocomposite and responsive membranes for water treatment, in: N.P. Hankins, R. Singh (Eds.), Emerging Membrane Technology for Sustainable Water Treatment, Elsevier, 2016, pp. 389–431.
[13] S.K. Ahn, R.M. Kasi, S.C. Kim, N. Sharma, Y. Zhou, Stimuli-responsive polymer gels, Soft Matter 4 (2008) 1151–1157, https://doi.org/10.1039/b714376a.
[14] D. Wandera, S.R. Wickramasinghe, S.M. Husson, Stimuli-responsive membranes, J. Membr. Sci. 357 (2010) 6–35, https://doi.org/10.1016/j.memsci.2010.03.046.
[15] J. Martín, E.J. Díaz-Montaña, A.G. Asuero, Recovery of anthocyanins using membrane technologies: a review, Crit. Rev. Anal. Chem. 48 (2018) 143–175.
[16] H.R. Lohokare, S.C. Kumbharkar, Y.S. Bhole, U.K. Kharul, Surface modification of polyacrylonitrile based ultrafiltration membrane, J. Appl. Polym. Sci. 101 (2006) 4378–4385.
[17] F. Schacher, M. Ulbricht, A.H.E. Müller, Self-supporting, double stimuli-responsive porous membranes from polystyrene-block-poly(*N*,*N*-dimethylaminoethyl methacrylate) diblock copolymers, Adv. Funct. Mater. 19 (2009) 1040–1045, https://doi.org/10.1002/adfm.200801457.
[18] Q. Shi, Y. Su, X. Ning, W. Chen, J. Peng, Z. Jiang, Graft polymerization of methacrylic acid onto polyethersulfone for potential pH-responsive membrane materials, J. Membr. Sci. 347 (2010) 62–68, https://doi.org/10.1016/j.memsci.2009.10.006.
[19] K. Dutta, S. De, Smart responsive materials for water purification: an overview, J. Mater. Chem. A 5 (2017) 22095–22112, https://doi.org/10.1039/C7TA07054C.
[20] Q. Yang, S.R. Wickramasinghe, Responsive membranes for water treatment, in: Responsive Membranes and Materials, Wiley Online Books, 2012, https://doi.org/10.1002/9781118389553.ch6.
[21] C. Gorey, I.C. Escobar, C. Gruden, M. Coleman, O. Mileyeva-Biebesheimer, Development of smart membrane filters for microbial sensing, Sep. Sci. Technol. 43 (2008) 4056–4074, https://doi.org/10.1080/01496390802414502.

This book belongs to Badji Mokhtar Annaba University Central Library Copyright Elsevier 2025

[22] Q. Yang, H.H. Himstedt, M. Ulbricht, X. Qian, S. Ranil Wickramasinghe, Designing magnetic field responsive nanofiltration membranes, J. Membr. Sci. 430 (2013) 70–78, https://doi.org/10.1016/j.memsci.2012.11.068.
[23] L. Chu, R. Xie, X. Ju, Stimuli-responsive membranes: smart tools for controllable mass-transfer and separation processes, Chin. J. Chem. Eng. 19 (2011) 891–903, https://doi.org/10.1016/S1004-9541(11)60070-0.
[24] S.M. Husson, Synthesis aspects in the design of responsive membranes, in: D. Bhattacharyya, T. Schäfer, S.R. Wickramasinghe, S. Daunert (Eds.), Responsive Membranes and Materials, John Wiley & Sons, 2013, pp. 73–96.
[25] Q. Zhang, C. Weber, U.S. Schubert, R. Hoogenboom, Thermoresponsive polymers with lower critical solution temperature: from fundamental aspects and measuring techniques to recommended turbidimetry conditions, Mater. Horiz. 4 (2017) 109–116, https://doi.org/10.1039/C7MH00016B.
[26] H.G. Schild, Poly(N-isopropylacrylamide): experiment, theory and application, Prog. Polym. Sci. 17 (1992) 163–249, https://doi.org/10.1016/0079-6700(92)90023-R.
[27] H. Guo, J. Huang, X. Wang, The alternate temperature-change cleaning behaviors of PNIPAAm grafted porous polyethylene membrane fouled by proteins, Desalination 234 (2008) 42–50, https://doi.org/10.1016/j.desal.2007.09.068.
[28] K. Wee, R. Bai, Stimuli-responsive membranes, in: E.M. Hoek, V.V. Tarabara (Eds.), Encyclopedia of Membrane Science and Technology, Wiley Online Library, 2013, pp. 1–55.
[29] P. Antony, S.K. De, Ionic thermoplastic elastomers: a review, J. Macromol. Sci. C: Polym. Rev. 41 (2001) 41–77.
[30] S. Darvishmanesh, X. Qian, S.R. Wickramasinghe, Responsive membranes for advanced separations, Curr. Opin. Chem. Eng. 8 (2015) 98–104, https://doi.org/10.1016/j.coche.2015.04.002.
[31] M. Shahinpoor, Y. Bar-Cohen, J.O. Simpson, J. Smith, Ionic polymer-metal composites (IPMCs) as biomimetic sensors, actuators and artificial muscles—a review, Smart Mater. Struct. 7 (1998) R15–R30, https://doi.org/10.1088/0964-1726/7/6/001.
[32] L. Brannon-Peppas, N.A. Peppas, Equilibrium swelling behavior of pH-sensitive hydrogels, Chem. Eng. Sci. 46 (1991) 715–722, https://doi.org/10.1016/0009-2509(91)80177-Z.
[33] D.R. Latulippe, A.M. Mika, R.F. Childs, R. Ghosh, C.D.M. Filipe, Flux performance and macrosolute sieving behavior of environment responsive formed-in-place ultrafiltration membranes, J. Membr. Sci. 342 (2009) 227–235.
[34] K. El Brahmi, M. Rawiso, J. François, Potentiometric titration of acrylamide-acrylic acid copolymers: influence of the concentration, Eur. Polym. J. 29 (1993) 1531–1537.
[35] Y. Xiang, J. Shen, Y. Wang, F. Liu, L. Xue, A pH-responsive PVDF membrane with superwetting properties for the separation of oil and water, RSC Adv. 5 (2015) 23530–23539, https://doi.org/10.1039/C5RA00739A.
[36] S. Zhang, J. Guo, X. Ma, X. Peng, Z. Qiu, J. Ying, J. Wang, Smart PDMS sponge with switchable pH-responsive wetting surface for oil/water separation, New J. Chem. 41 (2017) 8940–8946, https://doi.org/10.1039/C7NJ01067B.
[37] W. Ma, S.K. Samal, Z. Liu, R. Xiong, S.C. De Smedt, B. Bhushan, Q. Zhang, C. Huang, Dual pH- and ammonia-vapor-responsive electrospun nanofibrous membranes for oil-water separations, J. Membr. Sci. 537 (2017) 128–139, https://doi.org/10.1016/j.memsci.2017.04.063.
[38] A.E. English, S. Mafé, J.A. Manzanares, X. Yu, A.Y. Grosberg, T. Tanaka, Equilibrium swelling properties of polyampholytic hydrogels, J. Chem. Phys. 104 (1996) 8713–8720.
[39] S.E. Kudaibergenov, V.B. Sigitov, Swelling, shrinking, deformation, and oscillation of polyampholyte gels based on vinyl 2-aminoethyl ether and sodium acrylate, Langmuir 15 (1999) 4230–4235.
[40] J.P. Baker, H.W. Blanch, J.M. Prausnitz, Swelling properties of acrylamide-based ampholytic hydrogels: comparison of experiment with theory, Polymer (Guildf.) 36 (1995) 1061–1069.
[41] D.B. Thomas, Y.A. Vasilieva, R.S. Armentrout, C.L. McCormick, Synthesis, characterization, and aqueous solution behavior of electrolyte-and pH-responsive carboxybetaine-containing cyclocopolymers, Macromolecules 36 (2003) 9710–9715.
[42] T. Xiang, T. Lu, W.-F. Zhao, C.-S. Zhao, Ionic strength- and thermo-responsive polyethersulfone composite membranes with enhanced antifouling properties, New J. Chem. 42 (2018) 5323–5333, https://doi.org/10.1039/C8NJ00039E.

This book belongs to Badji Mokhtar Annaba University Central Library Copyright Elsevier 2025

[43] P. Mary, D.D. Bendejacq, M.-P. Labeau, P. Dupuis, Reconciling low-and high-salt solution behavior of sulfobetaine polyzwitterions, J. Phys. Chem. B 111 (2007) 7767–7777.
[44] A. Ronen, S.L. Walker, D. Jassby, Electroconductive and electroresponsive membranes for water treatment, Rev. Chem. Eng. 32 (2016) 533–550, https://doi.org/10.1515/revce-2015-0060.
[45] S. Wang, S. Liang, P. Liang, X. Zhang, J. Sun, S. Wu, X. Huang, In-situ combined dual-layer CNT/PVDF membrane for electrically-enhanced fouling resistance, J. Membr. Sci. 491 (2015) 37–44, https://doi.org/10.1016/j.memsci.2015.05.014.
[46] T. Yamauchi, E. Kokufuta, Y. Osada, Electrically controlled protein permeation through a poly (vinyl alcohol)/poly (acrylic acid) composite membrane, Polym. Gels Networks 1 (1993) 247–255.
[47] A. Gholami, A.R. Moghadassi, S.M. Hosseini, S. Shabani, F. Gholami, Preparation and characterization of polyvinyl chloride based nanocomposite nanofiltration-membrane modified by iron oxide nanoparticles for lead removal from water, J. Ind. Eng. Chem. 20 (2014) 1517–1522, https://doi.org/10.1016/j.jiec.2013.07.041.
[48] S. Laurent, D. Forge, M. Port, A. Roch, C. Robic, L. Vander Elst, R.N. Muller, Magnetic iron oxide nanoparticles: synthesis, stabilization, vectorization, physicochemical characterizations, and biological applications, Chem. Rev. 108 (2008) 2064–2110, https://doi.org/10.1021/cr068445e.
[49] Z. Zhang, J. Kong, Novel magnetic Fe_3O_4@C nanoparticles as adsorbents for removal of organic dyes from aqueous solution, J. Hazard. Mater. 193 (2011) 325–329, https://doi.org/10.1016/j.jhazmat.2011.07.033.
[50] J. Liu, Z. Zhao, G. Jiang, Coating Fe_3O_4 magnetic nanoparticles with humic acid for high efficient removal of heavy metals in water, Environ. Sci. Technol. 42 (2008) 6949–6954, https://doi.org/10.1021/es800924c.
[51] P. Daraei, S.S. Madaeni, N. Ghaemi, E. Salehi, M.A. Khadivi, R. Moradian, B. Astinchap, Novel polyethersulfone nanocomposite membrane prepared by PANI/Fe_3O_4 nanoparticles with enhanced performance for Cu(II) removal from water, J. Membr. Sci. 415–416 (2012) 250–259, https://doi.org/10.1016/j.memsci.2012.05.007.
[52] H. Park, H. Choi, As(III) removal by hybrid reactive membrane process combined with ozonation, Water Res. 45 (2011) 1933–1940, https://doi.org/10.1016/j.watres.2010.12.024.
[53] D. He, H. Susanto, M. Ulbricht, Photo-irradiation for preparation, modification and stimulation of polymeric membranes, Prog. Polym. Sci. 34 (2009) 62–98.
[54] M.H. Casimiro, J.P. Leal, M.H. Gil, Characterisation of gamma irradiated chitosan/pHEMA membranes for biomedical purposes, Nucl. Instrum. Methods Phys. Res. Sect. B 236 (2005) 482–487, https://doi.org/10.1016/j.nimb.2005.04.023.
[55] J. Kost, Ultrasound induced delivery of peptides, J. Control. Release 24 (1993) 247–255, https://doi.org/10.1016/0168-3659(93)90183-6.
[56] M.K. Sinha, M.K. Purkait, Preparation and characterization of stimuli-responsive hydrophilic polysulfone membrane modified with poly (N-vinylcaprolactam-co-acrylic acid), Desalination 348 (2014) 16–25, https://doi.org/10.1016/j.desal.2014.06.007.
[57] X. Qiu, X. Ren, S. Hu, Fabrication of dual-responsive cellulose-based membrane via simplified surface-initiated ATRP, Carbohydr. Polym. 92 (2013) 1887–1895, https://doi.org/10.1016/j.carbpol.2012.11.080.
[58] O. Azzaroni, A.A. Brown, W.T.S. Huck, Tunable wettability by clicking counterions into polyelectrolyte brushes, Adv. Mater. 19 (2007) 151–154, https://doi.org/10.1002/adma.200601257.
[59] J.J. Keating, J. Imbrogno, G. Belfort, Polymer brushes for membrane separations: a review, ACS Appl. Mater. Interfaces 8 (2016) 28383–28399, https://doi.org/10.1021/acsami.6b09068.
[60] R. Malaisamy, D. Berry, D. Holder, L. Raskin, L. Lepak, K.L. Jones, Development of reactive thin film polymer brush membranes to prevent biofouling, J. Membr. Sci. 350 (2010) 361–370, https://doi.org/10.1016/j.memsci.2010.01.011.
[61] M.A.C. Stuart, W.T.S. Huck, J. Genzer, M. Müller, C. Ober, M. Stamm, G.B. Sukhorukov, I. Szleifer, V.V. Tsukruk, M. Urban, F. Winnik, S. Zauscher, I. Luzinov, S. Minko, Emerging applications of stimuli-responsive polymer materials, Nat. Mater. 9 (2010) 101–113, https://doi.org/10.1038/nmat2614.
[62] D. Wandera, H.H. Himstedt, M. Marroquin, S.R. Wickramasinghe, S.M. Husson, Modification of ultrafiltration membranes with block copolymer nanolayers for produced water treatment: the roles of polymer chain density and polymerization time on performance, J. Membr. Sci. 403–404 (2012) 250–260, https://doi.org/10.1016/j.memsci.2012.02.061.

This book belongs to Badji Mokhtar Annaba University Central Library Copyright Elsevier 2025

This page intentionally left blank

This book belongs to Badji Mokhtar Annaba University Central Library

Copyright Elsevier 2025

CHAPTER 22

Nanomaterial-based photocatalytic membrane for organic pollutants removal

Gauri A. Kallawar[a,b] and Bharat A. Bhanvase[a]

[a]*Chemical Engineering Department, Laxminarayan Institute of Technology, Rashtrasant Tukadoji Maharaj Nagpur University, Nagpur, Maharashtra, India,* [b]*University Department of Chemical Technology, Dr. Babasaheb Ambedkar Marathwada University, Aurangabad, Maharashtra, India*

22.1 Introduction

In the past few decades, photocatalysis has been established as an excellent process for wastewater treatment. Photocatalysis has been applied in various fields like air purification, wastewater remediation, hydrogen production by water-splitting, etc. [1, 2]. Also, with increased industrial and human activities, several contaminants are frequently released into the environment. Organic pollutant is one of the types of contaminants, and it requires a lot of attention for its removal due to its low biodegradability. These pollutants remain in the environment for a longer duration, therefore they are called persistent organic pollutants (POPs) [3]. There pollutants originate from chemicals that now or at some point were used as insecticides, pharmaceutical chemicals, industrial solvents, personal care products, etc.

Various water treatment techniques like photo-Fenton, ozonation, electrocoagulation [4], membrane technology, photocatalytic oxidation, and advanced oxidation process (AOP) are being investigated for removal of such pollutants [4–8]. The photocatalytic process is effective, nonselective, robust, and reuses catalysts in which the formation of an electron and hole pair takes place due to incident photons. Furthermore, nanomaterial-based photocatalysts have several advantages like high efficiency, flexibility for multiple applications, and suitability for reactions [9]. These electron-hole pairs participate in a reaction by producing reactive organic species like hydroxyl radicals or superoxide radicals [10, 11]. Various vital steps involved in a photocatalytic degradation mechanism are selection of suitable light irradiation, electron-hole pair separation, effective trapping of holes and electrons, and excellent electron mobility [12–14]. The number of photocatalysts active in UV, Vis, or NIR light are being fabricated and investigated for degradation of various pollutants as well as for hydrogen generation [15, 16].

Handbook of Nanomaterials for Wastewater Treatment. https://doi.org/10.1016/B978-0-12-821496-1.00007-6
Copyright © 2021 Elsevier Inc. All rights reserved.

This book belongs to Badji Mokhtar Annaba University Central Library Copyright Elsevier 2025

Titanium dioxide has been applied extensively for photocatalytic degradation of various organic contaminants [12]. Photoinduced production of reactive species like hydroxyl and other oxygen-containing radicals is essential in semiconductor photocatalysis for degradation of organic pollutants [17, 18]. The main challenge of this process is the recovery of the photocatalyst from slurry effluent, which is reported to be very difficult. This issue can be addressed very well with immobilization of a photocatalyst on the membrane or into the membrane matrix, which is considered a promising approach. This immobilization of the photocatalyst in the membrane matrix imparts photocatalytic properties to polymeric membranes. Also, the membranes have very good filtration properties with the incorporation of photocatalyst materials in the matrix. This gives a synergetic effect, which improves pollutant removal and degradation from effluents.

In a conventional membrane, the separation of the pollutants depends on the various properties of the membranes like permeability, stability, and selectivity [19]; however, these membranes suffer from fouling, which is a major problem [20]. This can be overcome with the incorporation of photocatalytic nanomaterials in the membrane matrix, which helps in the reduction of fouling by degradation effect [21]. Further advantages of incorporation of photocatalyst nanomaterials in membrane matrix are (1) formation of less harmful product [22], (2) helps in the prevention of fouling, (3) can be used in organic synthesis, (4) energy generation, (5) has antimicrobial activity, (6) provides strength, permselectivity, and enhanced membrane properties [23–27]. Furthermore, coupling of membrane separation and photocatalysis has the potential to improve the efficiency of organic wastewater treatment [28]. Molinari et al. [29] studied diverse configurations of the combination of membrane separation and photocatalysis and reported various cases wherein the catalyst is deposited on a membrane, catalyst in suspension, and entrapment of photocatalyst on a membrane, and each were discussed by the authors. In some cases, a membrane is used for pretreatment where its job is to perform the separation only, and photocatalysis is carried out in another unit [30].

In view of this, the present chapter discusses various aspects of nanomaterial-based photocatalytic membrane for effective removal of organic pollutants present in wastewater.

22.2 Photocatalytic membrane materials

Nanostructured materials being utilized for environmental remediation applications include metal oxide, zeolite, photocatalytic nanomaterial, modified nanoparticle, aerogels, etc. These engineered nanomaterials can be used for incorporation in the membrane matrix. Furthermore, membranes are classified as polymeric, organomineral, ceramic, or metallic [19]. The photocatalytic membranes, after incorporation of the nanomaterials in the membrane matrix, similarly could be categorized as organic, polymeric, metallic, ceramic, or hybrid. The hybrid membrane may involve a combination of organic, polymeric, metallic, or ceramic materials. Also, several studies have shown that carbonaceous nanomaterial-based membranes have

This book belongs to Badji Mokhtar Annaba University Central Library Copyright Elsevier 2025

several merits like flux, permeability, and stability as compared to polymer-based membranes [9]. Nanofibers also have been incorporated in membranes because of their high surface area, porosity, and flexibility [31]. Metal organic frameworks and graphitic carbon nitride have also been utilized for photocatalytic membrane materials [32]. Other than these nanomaterials, to prepare photocatalytic membranes, various materials like polyvinylidene fluoride (PVDF), polysulfone, polyethersulfone, cellulose acetate, alumina, titania, stainless steel, carbon nanotubes (CNTs), and graphene oxide (GO) have been used [23]. These selected nanomaterials have diverse properties like permselectivity and strength, support properties, mechanical properties, etc., and have a synergetic effect that substantially contribute in the properties of photocatalytic membranes for the degradation of organic pollutants [24, 26, 33]. Various types of membranes are discussed in the following sections.

22.2.1 Hybrid photocatalytic membrane

Hybrid ceramic-metallic composite membrane is one class of photocatalytic membranes. The ceramic-metallic composite membranes combine the advantages of ceramic layer and metallic supports. However, several ceramic-metallic composite membranes face cracking due to sintering, and this is a major problem. Lin et al. [34] investigated the membrane cracking problem of Ag-doped TiO_2/Ti ceramic-metallic membrane structure and have worked on resolving this problem. It is believed that the ductile properties of doped Ag nanoparticles enhance the strength of the formed membrane, which avoids the cracking of membrane [34].

Furthermore, several researchers have investigated the hybrid photocatalytic membrane for the degradation of various pollutants. In a study by Xu et al. [35], enhancement in photocatalysis and antifouling properties was observed with an incorporation of N-doped graphene and TiO_2 in the membrane. This shows that the addition of nanomaterials monitors the properties of the resulting photocatalytic membrane. Titanium dioxide as a photocatalyst has been extensively used for the degradation of various organic pollutants, and therefore titanium dioxide-based nanocomposite photocatalytic membranes are being fabricated by incorporating TiO_2 nanomaterials of various shapes and sizes in different polymers [36–38]. This helps in the immobilization of nanoparticles and can be effectively used for the degradation of organic contaminants present in water [39]. Furthermore, doping of Ag on TiO_2 photocatalytic membrane was fabricated with multiple layers on alumina support, and doping of Ag on TiO_2 provides excellent photocatalytic activity and antibacterial action in a photocatalytic reactor system [40]. Incorporation of nanorods in the membrane matrix greatly enhances the membrane performance. In view of this, Ahmad and coworkers [41] prepared a photocatalytic membrane comprised of titanium dioxide nanorods, diethylene glycol, and alumina in a hybrid membrane. TiO_2 nanorods played an important role in preventing the fouling of alumina support, whereas diethylene glycol played an important role in controlling morphological nanostructure of titanium dioxide [41]. The support used in the hybrid photocatalytic membrane in the

This book belongs to Badji Mokhtar Annaba University Central Library Copyright Elsevier 2025

fabrication of a photocatalytic membrane plays a major role. Zhang et al. [42] synthesized composite membranes with improved photocatalytic properties due to presence of silica and titanium dioxide nanotubes. In this case, alumina was reported to be a better support for the membrane. Furthermore, ceramic membranes are UV light-resistant and can prove to be a suitable membrane material when a UV-based photocatalytic membrane is applied for the wastewater treatment. In the preparation of hybrid photocatalytic membranes, dispersion of nanomaterials in the membrane matrix is an utmost parameter, and compatibility of these materials is also essential, which enhances the performance of the wastewater treatment process.

Hybrid photocatalytic membranes were prepared with the incorporation of various nanomaterials like titanium dioxide nanowires, CNTs, and zinc oxide nanorods in membrane matrix, due to which these membranes showed improved mechanical strength and photocatalytic activity. Furthermore, the presence of multichannel pores due to incorporation of these nanomaterials in the membrane matrix provides the architecture of a photocatalytic membrane that favors the mass transfer with higher membrane flux and low fouling. These nanomaterials present in the membrane matrix help in effective separation of electron and holes generated in the photocatalytic degradation process.

22.2.2 Porous photocatalytic membranes

The architecture of the membrane also plays an important role in deciding the performance of the membrane. Porous and layered photocatalytic membranes are also being fabricated with suitable material that forms the layer architecture. Mesoporous structured and layered photocatalytic membranes can be prepared by coating. For the same, the alumina membranes were coated with titanium dioxide nanoparticles, which enhances the porosity of the membranes and, in turn, the performance. From such investigations, it is clear that alumina can prove to be good support [43]. A porous material is found to be useful for the fabrication of photocatalytic membrane. In a study, three-dimensional membranes from porous anodic aluminum oxide as substrate were prepared. Layered double hydroxide membranes have shown enhanced photocatalytic activity [44].

22.2.3 Polymer-based photocatalytic membrane

To fabricate the polymer-based photocatalytic membrane, polymeric material is coated, embedded, or blended with selected photocatalytic material, which results in a photocatalytic membrane. Zakeritabar et al. [45] synthesized polysulfone membrane modified with ZrO_2 and SnO_2 nanocomposite photocatalyst. The prepared membrane was evaluated for the degradation of pollutants present in the effluent collected from antibiotic manufacturers. It was observed that ZrO_2 and SnO_2 nanocomposites reduce the interaction between the residual particle and membrane surface. Li et al. [46] compared the performance of various PVDF membranes modified with TiO_2, nitrogen-doped TiO_2, TiO_2/GO, and nitrogen-doped TiO_2/GO for degradation of methylene blue (MB) dye under UV and sunlight irradiations. The presence of

This book belongs to Badji Mokhtar Annaba University Central Library Copyright Elsevier 2025

GO significantly improved the performance of the membrane. The nitrogen doping affected the bandwidth of photocatalyst and, in turn, led to enhanced activity in sunlight. Incorporation of these nanomaterials also resolved the problem of membranes fouling [46]. Polydopamine-modified RGO/Ag_3PO_4 nanocomposites were prepared by Zhang et al. [47], and prepared nanocomposites were coated on PVDF membrane. Functionalization of RGO/Ag_3PO_4 nanocomposites with polydopamine found enhanced adhesion properties. The resulting membrane showed enhanced hydrophilicity, which was further applied for the degradation of MB dye and showed its successful degradation. The modifier used, i.e., polydopamine has several advantages like good UV and visible light absorption ability, photoconductivity, enhanced generation of electron and hole pairs, etc. Incorporation of GO improves permeability and antifouling characteristics of the membrane and also provides strength to the membrane [47].

Furthermore, porous SiO_2 shell void/NO_2 core particles were prepared and embedded on a polycarbonate membrane [48]. These membranes showed good performance for the degradation of pollutants. The diffusion velocity of oil droplets and methyl orange in channels of the membrane and presence of strong oxidizing radicals on TiO_2 greatly affects photocatalytic degradation.

22.2.4 Graphene-based photocatalytic membrane

Graphene-based nanomaterials are appropriate for wastewater treatment due to their various excellent properties [12, 13, 49–52]. Graphene derivatives like GO have found application in environmental remediation and is considered a popular nanomaterial. The GO could be used in pristine form, a mixture of GO and inert material, functionalized form, and hybrid form [53]. The various properties like hydrophilicity of GO can be controlled with the presence of the functional groups like epoxide, carboxyl, and hydroxide [54]. Due to the excellent properties of GO, it is used in the fabrication of various membranes, which has the potential to perform better than pristine membranes [55].

Safarpour et al. [56] prepared a membrane with the use of reduced GO (rGO), TiO_2, and PVDF. The PVDF photocatalytic membrane loaded with rGO and TiO_2 nanomaterials enhanced its hydrophobic and antifouling properties, and these are considered to be excellent additives for the preparation of antifouling membranes. Zhu et al. [57] studied the one-step preparation and application of GO/TiO_2 photocatalytic membranes in a crossflow mode. In this work, the loading of GO affects the flux through the membrane, which is reported to be decreased with an increase in the loading of GO on the membrane. However, incorporation of GO and TiO_2 in the membrane, i.e., GO/TiO_2 membranes, the flux is found to be enhanced. The presence of GO and GO/TiO_2 in the membrane showed good strength pressurized under 0.3 MPa for 1 h. Furthermore, Wei et al. [58] developed nanoscale water transport channels with rGO and graphitic carbon nitride in the membrane, and these types of membranes have self-cleaning properties.

This book belongs to Badji Mokhtar Annaba University Central Library Copyright Elsevier 2025

Yu et al. [59] prepared a novel rGO/poly(dopamine)/$Bi_{12}O_{17}Cl_2$-cellulose acetate membrane with the modification of a commercial cellulose acetate membrane. This formed membrane showed antifouling behavior, photocatalytic behavior under visible light, and better stability. The use of dopamine during the fabrication of the membrane enhances the adherence between $Bi_{12}O_{17}Cl_2$ with graphene matrix and cellulose acetate membrane. The important properties gained by photocatalytic membrane with the incorporation of $Bi_{12}O_{17}Cl_2$ is flexibility, which is due to the flexible nature of GO and better compatibility between GO and $Bi_{12}O_{17}Cl_2$. Furthermore, the presence of rGO helps in the reduction of recombination rate of electron and holes. The presence of an amino group, hydroxyl group, and π-π conjugation in the formed composite enhances adsorption of a MB dye. Membranes prepared with Fe_2O_3/TiO_2 and GO show a synergistic effect between GO and TiO_2, which supports the separation of electrons and holes during photocatalysis. Incorporation of Fe_2O_3 nanoparticles played a significant role in the removal of humic acid by adsorption [60].

Overall, graphene or graphene derivatives like GO remain in flattened layered structure, which results in the formation of a tight stacked structure, and these can have great separation capabilities by introducing nanopores or rebuilding 2D nanochannels among graphene sheets [61]. Consequently, graphene derivatives like GO are beneficial to filter membranes due to several promising properties of GO. The presence of oxygen functionalities present in the GO creates a negative charge on the GO membrane surface and therefore can be applied in nanofiltration for the separation of dyes, salt ions, and small molecules with higher separation efficiency. Incorporation of photocatalytic materials in the membrane along with graphene or graphene derivatives degrades the pollutants present in the wastewater that avoids the fouling of the membrane, which generally occurs due to deposition of pollutants on the membrane. This problem can be efficiently handled with graphene or graphene derivatives incorporated in the photocatalytic membrane.

22.2.5 Graphitic carbon nitride-based photocatalytic membrane

Out of the various AOPs, photocatalysis is considered cost effective, which shows further flexibility in process design. During the degradation process, photocatalysts applied in the process tend to agglomerate due to its fine nature that lowers the efficacy of the photocatalysis. The recovery of these fine nanophotocatalysts is very critical at large-scale wastewater treatment applications. The incorporation of these nanomaterials in the membrane matrix or coating on the membrane resolves these problems.

Several researchers have worked on graphitic carbon nitride (C_3N_4) with mesoporous structure due to their various outstanding properties like photocatalytic properties, nontoxicity, metal-free nature, and narrow bandgap (~2.7 eV) [62, 63]. Ultrathin mesoporous C_3N_4 nanosheet generally provides more narrow bandgap, which has adequate light absorption compared to that of bulk g-C_3N_4 [64]. These types of materials suffer from problems like higher recombination

This book belongs to Badji Mokhtar Annaba University Central Library Copyright Elsevier 2025

rate of the formed electron-hole pairs, which in turn reduces the photocatalytic performance. These problems can be overcome with a combination of mesoporous C_3N_4 with excellent semiconductors like TiO_2, CuS, ZnO, etc. [63, 65]. Also this combination shifts the UV light range application of TiO_2 to a broader visible light range, which provides a synergistic effect [65]. This type of combination, i.e., mesoporous C_3N_4 and TiO_2 are generally incorporated in the membrane matrix, which forms photocatalytic membrane reactor systems [66] that have applications in wastewater treatment for organic degradation, physical filtration, and antibacterial properties in a single unit [67–69]. Graphitic carbon nitride/TiO_2 nanocomposite is successfully incorporated into the polysulfone matrix to fabricate a photocatalytic membrane. The membrane was useful for the degradation of sulfamethoxazole [70]. The photocatalytic membrane was prepared by incorporating oxygenated graphitic carbon nitride with hydrophilic surface modifying macromolecules, i.e., modified polyether sulfones, and the presence of oxygenated graphitic carbon nitride in PES/LSMM-OGCN membrane leads to the sponge-like structure, which was used for the degradation of pollutants and efficient separation [71].

22.2.6 CNT-based photocatalytic membrane

CNT-based technologies are favorable for water treatment due to large surface area, high aspect ratio, high chemical reactivity, low cost, and eco-friendly nature of CNTs. CNTs are applied widely for adsorption, sensing, catalysis, photocatalysis, desalination, etc. Chemical functionalization of CNTs alters π-π carbon network, and hence CNT functionalization protects and provides the hydrophobic nature to the CNT structure. CNTs in the membrane could be vertically aligned or in mixed matrix form [72]. Conventional membrane materials limit the performance of membranes for water treatment. CNTs have the potential for performance as nanochannels for water purification [73]. Liu et al. [74] prepared photocatalytic membranes consisting of Ag-doped GO and titanate nanotubes, and the prepared membranes were applied in photocatalysis and filtration in a single unit for the treatment of wastewater. Compared with GO/titanate nanotubes, Ag/GO/P25-based membrane showed enhanced photocatalytic degradation of MB dye. Furthermore, the presence of GO in the membrane matrix enhances properties like transparency and compressive strength. Zhang et al. [42] synthesized composite membranes with photocatalytic properties with incorporation of silica and TiO_2 nanotubes in membrane matrix with alumina support for the membrane. This photocatalytic membrane showed almost 85% degradation of direct black 168, which was substantially higher compared with that of photocatalysis alone and membrane alone.

The choice of material for fabrication of photocatalytic membrane depends upon various factors such as application, ease of preparation of nanomaterials, cost, and synergistic effect of membrane separation and photolysis. The photocatalyst is either coated on the membrane or can be blended/incorporated in the membrane matrix. Materials such as alumina and polymers

This book belongs to Badji Mokhtar Annaba University Central Library Copyright Elsevier 2025

are being used as supports for the membrane, which decides the life of the membrane. The optical properties of a selected photocatalyst and its reusability govern the membrane operation. The fouling tendency, hydrophilicity, and many other properties of the membrane are influenced by the photocatalytic membrane material. Hence, while deciding the material of construction for a photocatalytic membrane, it is important to keep in mind all these aspects.

22.3 Photocatalytic membrane fabrication

For the fabrication of photocatalytic membrane, various methods have been employed in the practice including vacuum filtration, phase inversion, electrospraying, spinning, and deposition techniques. Furthermore, a combination of various techniques is preferred to achieve the specific properties of the photocatalytic membrane. Sonication is also regarded as an important technique for uniform deposition/dispersion of a photocatalyst on the membrane surface or in membrane matrix, respectively. If the fibers are to be prepared and used in different modules, then spinning process is selected for uniform dispersion or uniform deposition in or on the membrane matrix, which achieves the targeted morphology of formed photocatalytic membrane. In some cases, nanoparticles are prepared and then coated on the membrane and sometimes nanomaterials are incorporated into the membrane matrix, which is per the application of photocatalytic membrane for targeted treatment of pollutants present in wastewater. Fig. 22.1 summarizes major photocatalytic membrane fabrication techniques, which are discussed in the following sections.

22.3.1 Sol-gel dip-coating

Sol-gel method is considered to be the simplest method for the preparation of nanostructures. Typically, sol is prepared from a precursor solution and is kept from aging, and then drying is accomplished, which results in the formation of a network. Sol-gel technique has emerged as one of the promising methods for the preparation of a photocatalytic membrane. In this method, careful selection of solvents and temperature are the key parameters. However, it suffers from the disadvantage like higher time for aging and poor control on the morphology of the nanostructures formed during hydrolysis and gel formation.

Sol-gel dip-coating process is used for the fabrication of photocatalytic membranes. In this process, initially, titania sols are prepared, which is done by hydrolysis of metal oxide precursors and dip-coated on a suitable porous supports like alumina. Multilayered mesoporous membrane can also be prepared by dip-coating process. After this step, they are heated at high temperature to obtain a metal oxide-coated membrane. Fig. 22.2 illustrates the preparation of photocatalytic membrane with sol-gel dip-coating method. Initial concentration of metal oxide in sol has a significant effect on the final properties of prepared membrane. The addition of pore-directing agents as reported by Choi and coworkers [76–78] can also affect the final porosity and size of pores in the membrane. Incorporation of a suitable photocatalyst with a

This book belongs to Badji Mokhtar Annaba University Central Library Copyright Elsevier 2025

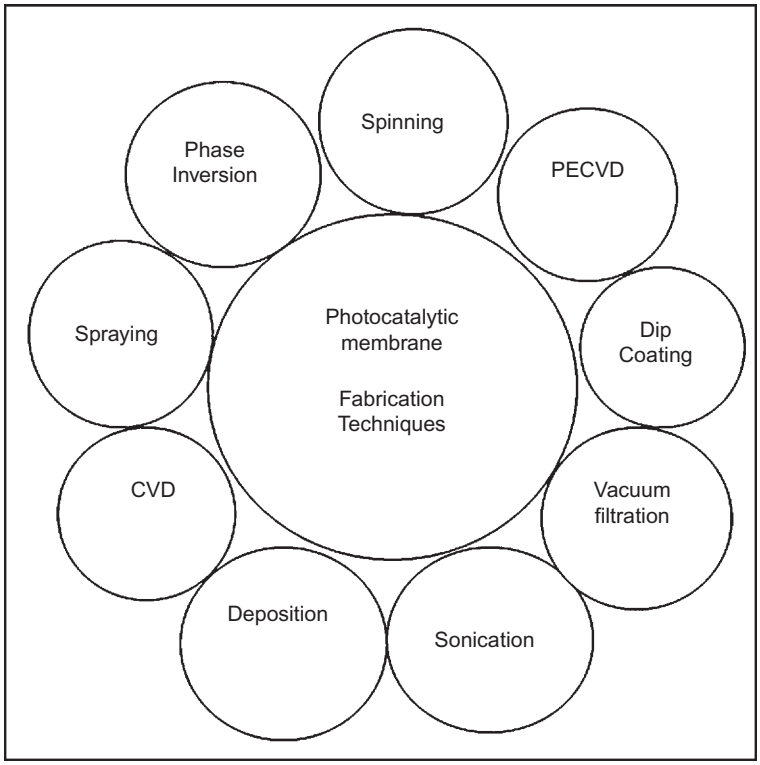

Fig. 22.1
Major photocatalytic membrane synthesis techniques.

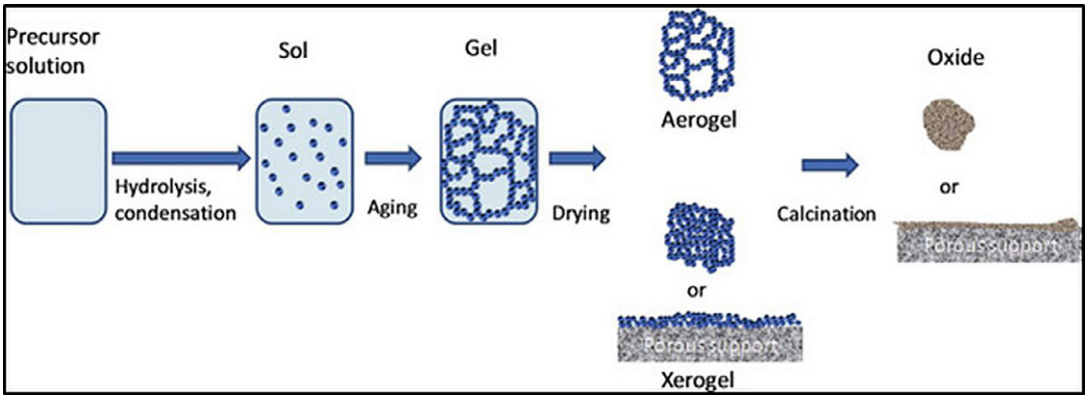

Fig. 22.2
Schematic illustration of preparation of membrane by sol-gel method [75]. *Reprinted with permission from A. Comite, Preparation of silica membranes by sol-gel method, in: Curr. Trends Future Dev. Membr. Silica Membr. Prep. Model. Appl. Commer., Elsevier Inc., 2017, pp. 3–23. Copyright (2017) Elsevier.*

This book belongs to Badji Mokhtar Annaba University Central Library Copyright Elsevier 2025

support layer also plays a significant role in the fabrication of multilayer membranes [78]. In their research work, Choi et al. [76] prepared TiO_2/Al_2O_3 photocatalytic and antibiofouling membranes by sol-gel method. Sol-gel method seems to be promising in the preparation of a highly porous photocatalytic membrane with high pore size distribution, which offers more separation ability and is free from cracks or pinholes.

Furthermore, it is possible to prepare a photocatalytic membrane by dip-coating on the single side of the substrate like alumina. Here, the number of layers of coating offered on the substrate play a significant role in the photocatalytic activity of the membrane [77]. The dip-coating method offers a possibility in the preparation of multicoated membranes. In comparison to vacuum and spray method, sol-gel dip-coating method offers stable formation of coating on the substrate. This multilayered membrane, prepared by dip-coating, has robust structure with good mechanical strength, which makes it suitable for water treatment and can be reused. Charaborty et al. [79] immobilized TiO_2 on a hollow fiber ultrafiltration membrane by spray coating, vacuum coating, and sol-gel dip-coating. For spray coating, the TiO_2 suspension was passed through an apparatus consisting of a frame, rotor, sprayer, and variable speed motor. The membrane was continuously sprayed with dispersion and dried. In a vacuum coating method, the membrane is fixed inside a glass chamber. A feed solution of TiO_2 powder was recirculated in the shell side of the membrane. The lumen side was subjected to a vacuum environment. The permeate thus flows through the lumen causing attachment of nanoparticles on the membrane. However, the TiO_2 nanoparticles became detached by both these methods due to poor immobilization. The immobilization of TiO_2 on the membrane was very well achieved through sol-gel dip-coating. The important steps involved in the sol-gel method like hydrolysis, condensation, aging, drying, and calcination during the preparation of photocatalytic membrane is well described in Fig. 22.2.

This process offers a simple fabrication route for the photocatalytic membrane. However, the major drawback is the selection of solvent and temperature. Template-based sol-gel methods can be employed to a variety of chemicals, which cannot be considered as an eco-friendly approach. Furthermore, this coating process involves calcinations at a suitable ramp rate; therefore, careful selection of temperature is important. Homogeneous structure of the formed membrane is highly dependent on the heating and cooling steps in dip-coated film.

22.3.2 Vacuum filtration

Vacuum filtration is a simple technique used for the preparation of a photocatalytic membrane. In this process, generally, a cellulose membrane is taken and a suspension containing photocatalyst nanomaterials is vacuum filtered through the selected membrane, which provides the deposition of photocatalyst nanomaterials on the membrane leading to the formation of a photocatalytic membrane [80]. A typical process is described in Fig. 22.3 for preparation of a photocatalytic membrane by intercalating RGO, PDA, and $Bi_{12}O_{17}Cl_2$ and then vacuum filtration. This method also provides a simple route to assemble the nanomaterials on the surface of a mixed cellulose ester membrane [59].

This book belongs to Badji Mokhtar Annaba University Central Library Copyright Elsevier 2025

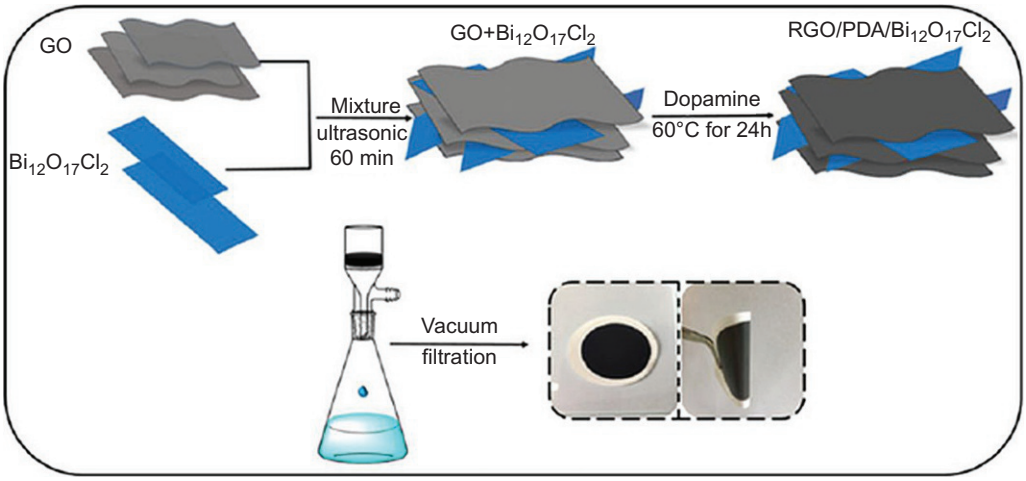

Fig. 22.3
Vacuum filtration process for the fabrication of photocatalytic membrane [59]. *Reprinted with permission from Z. Yu, X. Min, F. Li, D. Yin, Y. Peng, G. Zeng, A mussel-inspired method to fabricate a novel reduced graphene oxide/$Bi_{12}O_{17}Cl_2$ composites membrane for catalytic degradation and oil/water separation, Polym. Adv. Technol. 30 (2019) 101–109. Copyright (2019) John Wiley and Sons.*

In a simple process, well-dispersed GO, Cu_2O nanowires, and TiO_2 nanowires were mixed, and mixed cellulose ester was added on via vacuum filtration. Later, a free-standing heterojunction photocatalytic membrane was prepared by air drying and peeling. The vacuum filtration enables creating a simple route for the fabrication of the membranes. The preparation of a photocatalytic membrane can be accomplished with the selection of appropriate components that are active in visible light [81]. A photocatalytic membrane was reported to be prepared with various process steps like hydrothermal, colloidal blending, and vacuum filtration method. In the same, membranes were prepared with the deposition/incorporation of Fe_2O_3/TiO_2 and GO nanomaterials. This provides the synergistic effect between GO and Fe_2O_3, and TiO_2 aids the separation of electron and hole during photocatalysis [60].

This process offers easy deposition of nanomaterials on the cellulose membrane making it possible to assemble various components, which are the major advantages of this technique. However, the number of cycles of operation of membrane and its ability to function in extreme operation need to be tested.

22.3.3 Ultrasonication

Ultrasound-assisted processes are very useful for the uniform dispersion of the nanomaterials in the membrane matrix [82, 83]. This is attributed to the intense environment generated by cavitation effects due to the collapse of cavities in the suspension. This intense environment provides microstreaming, intense turbulence, and shearing action that facilitate the uniform

This book belongs to Badji Mokhtar Annaba University Central Library Copyright Elsevier 2025

dispersion of photocatalytic nanomaterials in the membrane matrix. Therefore, ultrasonication is useful for the effective distribution of a photocatalyst on the membrane [84, 85].

The use of ultrasonication in the preparation of a photocatalytic membrane is found effective in the dispersion of the reactants and can achieve a desired degree of dispersion in a short time at room temperature. However, it cannot be considered as a standalone method for membrane fabrication. Ultrasound is generally used in combination with other techniques, which offers several advantages as mentioned earlier over other methods when used alone. The capacity of the sonicator makes the method effective for a small batch; however, the scale-up issues need to be addressed.

22.3.4 Chemical vapor deposition and plasma-enhanced chemical vapor deposition

In a chemical vapor deposition (CVD) process, solid material is deposited from a precursor vapor due to chemical reactions arising on or in the locality of a substrate surface [86]. The deposition can be in the form of coatings, powders, or single crystals on the substrates. With the help of CVD process, uniform film thickness with a high level of purity and performance can be achieved on the substrates. CVD process has various merits over conventional processes like formation of 3D coating with complete coverage, higher deposition rates, CVD reactor is reasonably simple to scale-up, etc. Furthermore, plasma-enhanced CVD (PECVD) process has been also applied in the production of nanomaterials, which deposit inorganic films. It has been executed for the fabrication of nanomaterials like TiO_2 films for photocatalytic applications. PE CVD process works on the low temperature deposition. The CVD and PECVD processes have been applied for the fabrication of photocatalytic membranes, which show better performance in wastewater treatment [87–89].

The selection of substrate and precursor has great influences on the formation of nanosheets in the CVD technique, which could lead to the formation of membranes with improved properties [87]. CVD and PECVD techniques have the potential to prepare nanomaterial-based thin films with desired thickness. The high temperatures to which the material is subjected is a limitation of this method. Furthermore, this process requires an oxygen plasma generator, high temperature regions, and an inert atmosphere. The preparation of crack-free thin films with a uniform morphology with the use of vapor deposition techniques is still a challenge. The technique has a possibility of scale-up but has major limitations like cost, maintenance, and operation of vapor deposition device.

22.3.5 Phase inversion method

Phase inversion method for membrane preparation was developed in 1960, and it is still a widely used method for fabrication of membrane. In this method, polymer solution of base material is converted to solid phase from liquid phase in a controlled environment. This step is then followed by a de-mixing step, which results in a polymer-rich and polymer-lean

This book belongs to Badji Mokhtar Annaba University Central Library Copyright Elsevier 2025

phase. The polymer-rich phase gradually gets converted to solid, and the polymer-lean phase leads to the formation of pores in the solid material [90]. The phase inversion method has been employed for the fabrication of photocatalytic membrane, which was accomplished by adding boron-doped TiO_2/SiO_2 and cobalt ferrite nanoparticles into a polymeric solution. In this technique, it is important to see interaction of nanoparticles with the casting solution [21].

In phase inversion, several solvents are used in the preparation of the membrane. Also, phase inversion method has been found successful in the preparation of conventional membranes, which leads to the possibility of its application in the preparation of photocatalytic membrane with polymeric material as one of the constituents. However, a major problem could be caused due to residual solvent.

22.3.6 Immersion method

This is the simplest method to incorporate nanoparticles in a membrane. In this method, the solution of nanoparticles is prepared. Then, the membrane is immersed in this solution of nanoparticles and nanoparticles are allowed to be deposited on and into the porous surface of the membrane. This involves two basic steps; one is coating and another is evaporation of the solvent. This technique offers a way to modify membrane properties by incorporating nanomaterials [92]. Fig. 22.4 depicts the schematic illustration of immersion method for fabrication of a photocatalytic membrane. Studies reported in the literature have showed that

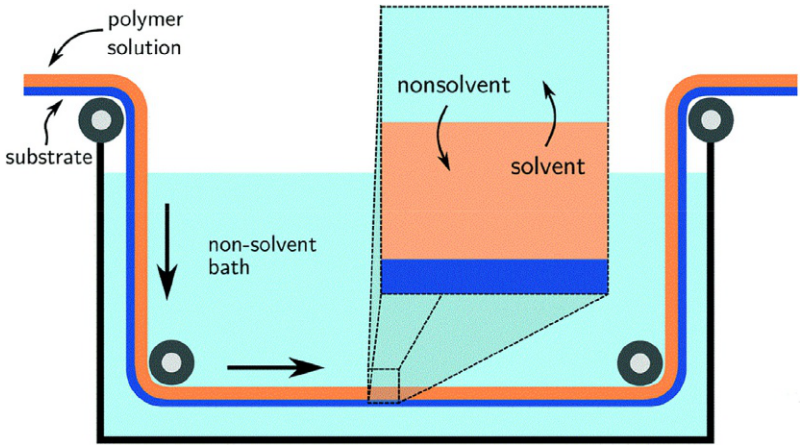

Fig. 22.4
Schematic illustration of Immersion method for membrane preparation [91]. *Reprinted with permission from D.R. Tree, K.T. Delaney, H.D. Ceniceros, T. Iwama, G.H. Fredrickson, A multi-fluid model for microstructure formation in polymer membranes, Soft Matter. 13 (2017) 3013–3030. Copyright (2017) Royal Society of Chemistry.*

This book belongs to Badji Mokhtar Annaba University Central Library Copyright Elsevier 2025

the membrane structure and polymer solution profile, dispersion, and phase separation are closely related [91].

In this technique, the transfer of nanoparticles on and inside the membrane is a big challenge during the preparation of photocatalytic membrane. The solubility, transfer of solvent, movement of nanoparticles, and interaction of nanoparticles with the polymer also play important roles in the preparation of a photocatalytic membrane. The trapping of nanoparticles is a major advantage, and there is no need to worry about the recovery of the photocatalyst. Furthermore, the polymeric membrane preparation process is well known, which offers the selection of an appropriate nanoparticle for its blending within the polymeric matrix leading to formation of a highly functionalized photocatalytic membrane.

22.3.7 Spinning/electrospinning method

Methods like electrospinning, spinning, or coextrusion have been well explored for preparation of fibers. In the field of membrane technology, the techniques have been applied for the preparation of fibrous membranes. The major advantage of these techniques is the ability to prepare fibers in a short duration. There is possibility of a scale-up option for these techniques. From the literature, it has been suggested that the membrane with fibers, as its basic structural element, is prepared easily with this method. This has been observed for photocatalytic membranes also.

A coextrusion method is used for the preparation of dual-layer, hollow-fiber photocatalytic membranes. A dual-layer, hollow-fiber membrane has several merits such as cost effectiveness, high performance, and ability to incorporate nanomaterial in the membrane matrix. A dual-layer spinneret has been used for the synthesis. The photocatalytic membrane is fabricated using the dry/wet cospinning technique. The coextrusion technique acts as a powerful tool in managing the thickness of layers and distribution of photocatalyst [93]. Furthermore, electrospinning technique is widely applied for fabrication of polymer-based membrane. In this, polymer melt solution is sprayed through nozzles and simultaneously high-voltage electricity is applied. This causes evaporation of solute from the sprayed solution, and a solidified matrix is obtained on the collection disk. Thus, the electrospinning technique can be effectively used for the preparation of ultrafine polymeric fibers. Electrospinning process has several merits compared with various membrane fabrication techniques, like high surface-to-volume ratio, ability to handle a variety of polymers, ability to form core-shell structures, and fiber functionalization [94]. Fig. 22.5 depicts the electrospinning process for membrane fabrication.

Electrospinning is one of the important membrane fabrication techniques being used for the fabrication of photocatalytic membranes by the deposition of photocatalysts on support [31]. Three-dimensional nanofibers can be created by trapping nanoparticles in the fiber network

This book belongs to Badji Mokhtar Annaba University Central Library Copyright Elsevier 2025

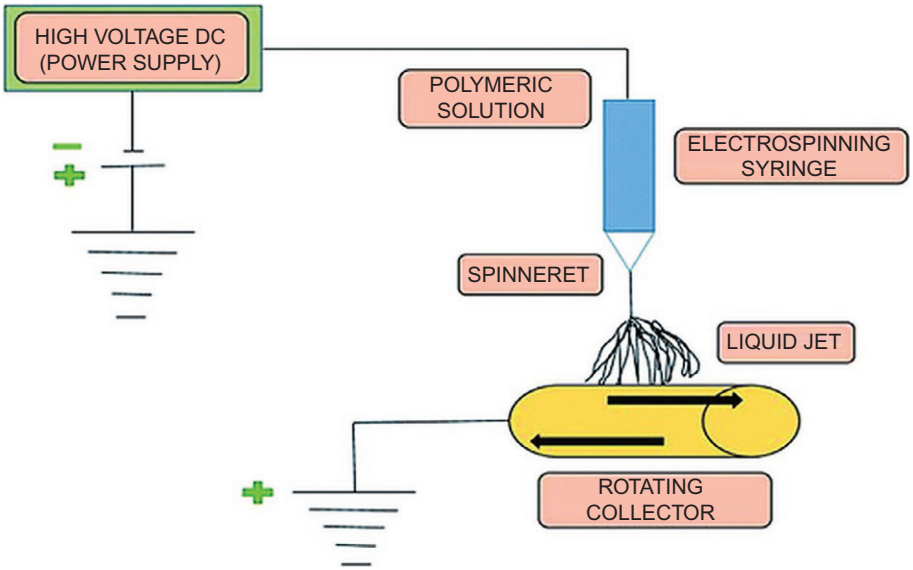

Fig. 22.5
Schematic illustration of electrospinning method for membrane preparation [94]. *Reprinted with permission from S.S. Ray, S.S. Chen, C.W. Li, N.C. Nguyen, H.T. Nguyen, A comprehensive review: electrospinning technique for fabrication and surface modification of membranes for water treatment application, RSC Adv. 6 (2016) 85495–85514. Copyright (2016) Royal Society of Chemistry.*

using the process of electrospinning. In an experiment, a photocatalytic membrane was prepared using nylon fibers as support and shield. In one process, titania nanoparticles were placed on a substrate and nanofibers were electrospun on top of this layer to shield the nanoparticles. In another process, Nylon-6 solution was electrospun and TiO_2 nanoparticles were electrosprayed on it continuously. Electrospinning process can generate fibers with desired morphology with proper control of the spinning condition and solution properties. Furthermore, the electrospinning could be applied in batch and continuous mode [95].

A hollow-fiber membrane was fabricated by phase inversion and using a spinneret in which dope solution and bore liquid were concurrently passed, and thereby the fibers formed were collected and washed. These types of membranes showed higher antifouling activity, which is attributed to photocatalytic properties in visible light. The photocatalytic membrane can be fabricated with a combination of phase inversion and spinning. The spinning conditions such as spinneret diameter, spinneret temperature, dope solution, bore liquid, coagulation bath, casting solution, etc. are considered to be some important parameters in the process [96]. The schematic representation of fabrication of fiber membrane and its modification process is depicted in Fig. 22.6. The parameters affecting electrospinning process are applied voltage, feed rate, nature of solution, voltage of base plate or collector, tip-collector distance, etc. The major limitation of this process is cost of the device.

This book belongs to Badji Mokhtar Annaba University Central Library Copyright Elsevier 2025

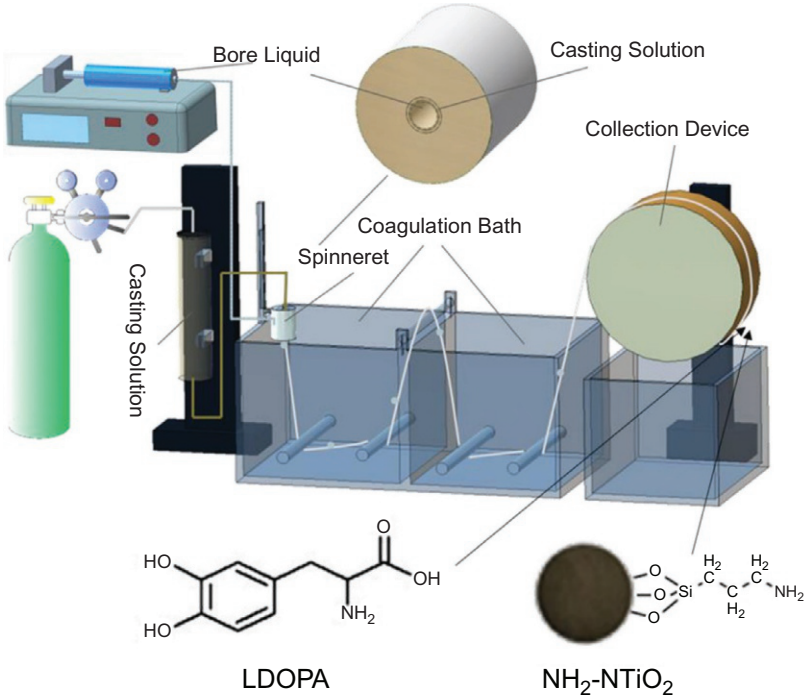

Fig. 22.6
Schematic representation of hollow-fiber membrane fabrication and modification process [96].
Reprinted with permission from P. Wan, Z. Zhang, B. Deng, Photocatalytic polysulfone hollow fiber membrane with self-cleaning and antifouling property for water treatment, Ind. Eng. Chem. Res. 58 (2019) 3339–3348. Copyright (2019) American Chemical Society.

22.3.8 Solvent casting method

This is another simple method of membrane preparation. In this method for preparation of composite membrane, nanoparticles are added in solvent. For better dispersion, the solution is sonicated. After this, a *co*-polymer is added to the solution and mixed thoroughly, then it is poured into a mold and the solvent is allowed to evaporate. Once the solvent evaporates, a composite membrane is obtained. This is a simple approach to immobilize nanomaterial in the membrane matrix. While selecting the polymer, its inert nature, stability, and behavior in the presence of UV or visible light radiation is considered [97, 98]. Fig. 22.7 depicts the stepwise schematic representation of solvent casting method for the fabrication of photocatalytic membranes.

Solvent casting offers a simple approach to prepare membranes with different combinations of nanomaterials. The cast solution determines the properties of the formed membranes. The

This book belongs to Badji Mokhtar Annaba University Central Library Copyright Elsevier 2025

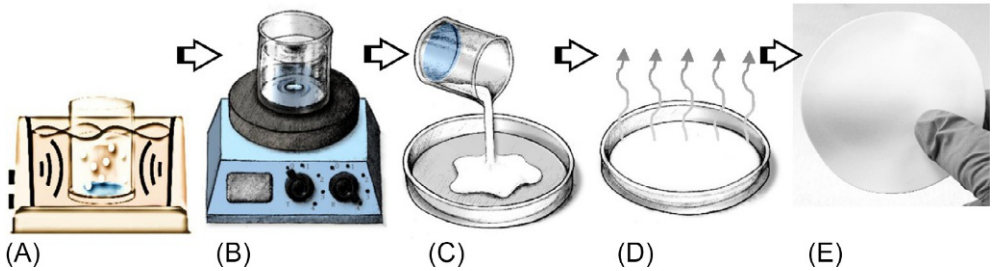

Fig. 22.7
Schematic illustration of solvent casting method for 8% TiO_2/PVDF-TrFE nanocomposite membrane preparation. (A) Ultrasonic bath of DMF and TiO_2 nanoparticles; (B) magnetic stirring of DMF, TiO_2 nanoparticles, and the added PVDF-TrFE; (C) pouring the solution onto a glass support; (D) solvent evaporation at room temperature; (E) membrane after complete evaporation of the solvent [97].
Reprinted with permission from L. Aoudjit, P.M. Martins, F. Madjene, D.Y. Petrovykh, S. Lanceros-Mendez, Photocatalytic reusable membranes for the effective degradation of tartrazine with a solar photoreactor, J. Hazard. Mater. 344 (2018) 408–416. Copyright (2018) Elsevier.

process requires solvent and support in the preparation of the membrane. Furthermore, large scale production of membrane option can be considered. The major limitation of this process is aggregation of nanoparticles during formation of the membrane. Table 22.1 represents a summary of various methods applied for the preparation of photocatalytic membranes used for the wastewater treatment processes.

22.4 Applications of photocatalytic membrane for removal of organic pollutant

Pollutants are any substance that, when released into the environment, can cause harm to life and the environment. These are generated due to various human activities like construction, energy generation, agricultural activities, or maybe as the result of some natural processes like the eruption of a volcano. Organic pollutants are also called POPs because, once created, they remain in the environment forever. Many of these POPs are the result of human activities. The source of organic pollutants are chemicals such as insecticides, pharmaceutical chemicals, industrial solvents, personal care products, etc. [3]. It has been estimated that, for humans, if there was no incidence of direct contact with a POP, then 90% of the exposure to a POP happens through the diet [112]. Hence it becomes important to prevent POP from going into the ecosystem and food chain. Various conventional chemical and physical treatment methods like oxidation, adsorption, and photocatalytic degradation are usually employed for removal and treatment of organic pollutants [113].

This book belongs to Badji Mokhtar Annaba University Central Library Copyright Elsevier 2025

Table 22.1: Summary of various methods used for photocatalytic membrane.

Membrane type	Photocatalyst	Preparation method	References
PVDF, PES, PSF	TiO_2	Phase inversion	[99–102]
PES	ZnO/MWCNT	Phase inversion	[103]
PVDF, PES	TiO_2	Dip-coating	[104]
Al_2O_3	TiO_2	Dip-coating	[105]
Ceramic hollow fiber	TiO_2	Dip-coating	[106]
Al_2O_3	SiO_2/ZnO	Dip-coating	[107]
Nylon-6	TiO_2	Electrospinning	[95, 108]
PVDF, PTFE	BiOBr/Ag	Electrospinning	[109]
Al_2O_3	TiO_2	CVD	[110]
Glass fiber, Fe_2O_3/GO	TiO_2	Vacuum filtration	[60]
Mixed cellulose ester	Cu_2O/TiO_2/GO	Vacuum filtration	[81]
GO	TiO_2	Vacuum filtration	[57, 111]
P(VDF-TrFE)	TiO_2	Solvent casting	[97, 98]

As discussed earlier, membranes have remained a popular choice for the removal of these types of contaminants from the water. The conventional membranes successfully work in the removal of various impurities present in water. The photocatalytic membranes overcome the major limitation of conventional membrane such as fouling.

Photocatalytic membranes are being applied for the removal of various pollutants like MB [46, 47, 74], Rhodamine blue [40, 58, 114], methyl orange [80, 114], acid orange [115], Congo red [41], direct black 168 [34, 116], reactive black [93], acid red [89], reactive red and reactive orange [97, 117], and oil-water suspension [59, 118]. Also, researchers have designed photocatalytic membranes for degradation of antibiotic-resistant bacteria and genes [119]. Furthermore, photocatalytic membranes are capable of removing microorganisms like e-coli [40] and also effective in the removal of humic acid [60], diphenyl diamine [80], nitrate [120], phenol [71, 121], surfactants [122], benzoic acid, and aniline [81]. The photocatalytic membranes have shown applications in the degradation of pharmaceuticals such as norfluoxetine, lincomycin, sulfamethoxazole, diclofenac, trimethoprim, bisphenol A, fluoxetine, venlafaxin, gemfibrozil, atrazine, carbamazepine, ibuprofen, and atorvastatin [38]. Furthermore, reported studies showed successful photocatalytic degradation of carbamazepine [123], sulfamethoxazole [70], and chlorhexidine digluconate [79] by photocatalytic membrane. Experiments on real industrial wastewater also demonstrate the capability of photocatalytic membranes in degrading organic pollutants [45, 57].

This confirms the successful application of photocatalytic membrane-based systems for the degradation/removal of a wide range of the previously mentioned pollutants, and it can be concluded that the photocatalytic membrane-based systems are effective for various organic contaminants present in the water. Also, in most of the photocatalytic membranes, the problem

This book belongs to Badji Mokhtar Annaba University Central Library Copyright Elsevier 2025

of membrane fouling is taken care of. In addition, the photocatalytic membranes with good mechanical strength are being put into application. Further research is directed in finding up-scalable photocatalytic membranes.

22.5 Types of photocatalytic membrane reactors and their configurations

Coupling membrane technology with photocatalytic degradation is a promising technology for wastewater treatment. There are many configurations reported in the literature, which uses a combination of membrane technology and photocatalysis. Early efforts of combining photocatalysis and membrane separation involved the use of slurry reactors where the photocatalyst was used in powdered form. The photocatalyst was separated after the operation and recycled back. So there were modules where the membrane performed the function of separation and the photocatalyst performed the function of degradation. It is observed that, in the whole configuration of photocatalytic membrane reactor, the important element is the membrane itself. The membrane properties and functioning strongly affects the whole process.

The classification of photocatalytic membranes used in the photocatalytic membrane reactors are depicted in Fig. 22.8. Photocatalytic membranes are generally fabricated with the help of titanium dioxide nanoparticles. The prepared photocatalytic membranes could be broadly divided into two categories such as with TiO_2 as one of the important constituents or without TiO_2. However, TiO_2 is active in UV light. Therefore, the photocatalytic membrane should be modified to make it active in visible light, which makes it active in visible and UV light. Such type of modifications makes it possible to design photocatalytic membrane reactors working in solar light. These design modifications in photocatalytic membranes makes it suitable to work in solar light irradiations. Solar light-based photocatalytic membranes are a good option because of their light harvesting nature, which is a desired choice for many researchers. Other categories of photocatalytic membranes are ceramic-based membranes and polymeric membranes. Polymers are found to be popular in the preparation of membranes as a support.

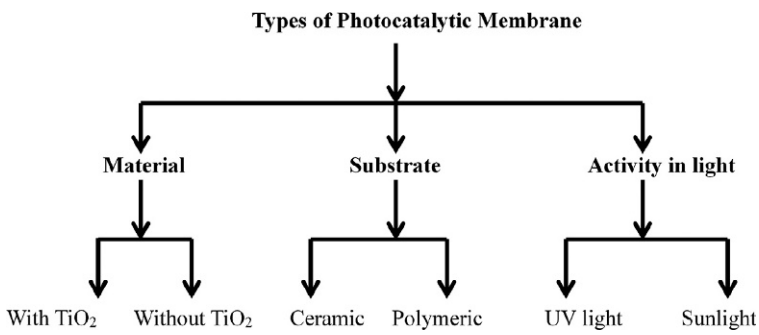

Fig. 22.8
Classification of photocatalytic membranes used in photocatalytic membrane reactors.

This book belongs to Badji Mokhtar Annaba University Central Library Copyright Elsevier 2025

Due to which the behavior of selected polymers in the presence of UV and visible light needs to be considered while selecting it as a support. Furthermore, ceramic membranes with a homogeneous morphology and crack-free design are highly desired.

Photocatalytic membrane reactors are designed with an objective such as feeding solution flow over the membrane coating or through the membrane. When the feed solution flows over the coating applied on the membrane, the molecules close to the membrane surface are in the position to react with the photocatalyst. On the other hand, when the feed solution was forced to flow through the membrane, it resulted in better contact between pollutants and the photocatalyst. The engineering parameters that affect the photocatalytic membrane reactor operation are the resistance to mass transfer and diffusion of the pollutants. A simple dead end filtration configuration, as shown in Fig. 22.9, allows minimum mass transfer resistance [123]. Photocatalytic membranes operating in dead end mode are common due to ease of control and operation [40]. The photocatalytic membranes are active in sunlight, which harvest more sunlight for efficient degradation of pollutants with the use of a suitable nanophotocalyst in the membrane. For the same, a suitable location is essential where these membranes can be exposed

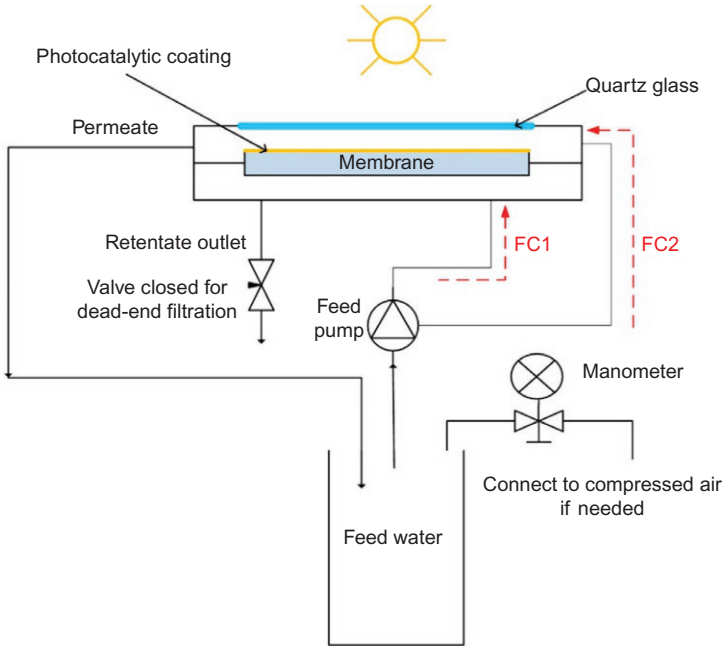

Fig. 22.9

Custom-made photocatalytic membrane reactor for concurrent filtration and solar photocatalytic degradation of micropollutant carbamazepine with dead end filtration system [123]. *Reprinted with permission from I. Horovitz, D. Avisar, M.A. Baker, R. Grilli, L. Lozzi, D. Di Camillo, H. Mamane, Carbamazepine degradation using a N-doped TiO_2 coated photocatalytic membrane reactor: influence of physical parameters, J. Hazard. Mater. 310 (2016) 98–107. Copyright (2016) Elsevier.*

This book belongs to Badji Mokhtar Annaba University Central Library
Copyright Elsevier 2025

to sunlight for 3–4 h, approximately. Membrane support also plays an important role in membrane design that are polymeric or ceramic.

The photocatalytic membrane reactors are classified and depicted in Fig. 22.10. The reactors are classified on the basis of mode of operation like continuous or dead end filtration, handling of photocatalyst slurry present in wastewater, immobilization of photocatalyst, etc. The hybrid system combines photocatalysis and membrane separation within the photocatalytic membrane reactor. In such configuration of photocatalytic membrane reactor, the photocatalytic membrane is submerged in wastewater containing photocatalyst. However, the major limitation of such a reactor system is catalyst loss. Furthermore, slurry system often blocks the radiation and decreases the photocatalytic degradation efficiency of the process. However, this process has advantages such as it offers the process in a single unit.

Fu et al. [124] have reported a submerged membrane reactor (Fig. 22.11) with two different reaction zones, which are UV slurry TiO_2 photocatalyst zone with a movable baffle arrangement that divides the submerged membrane module. These photocatalytic membrane reactors can be classified as irradiation of the membrane module and irradiation of a feed tank containing photocatalyst in the suspension.

The photocatalytic membrane reactors can be operated in continuous manner with slurry-type reactor without any photocatalyst loss with particular residence time of water. This allows the treated water to attain the prescribed level and then it can be then filtered with the hybrid membrane system. In the photocatalytic membrane reactors immobilized with photocatalysts

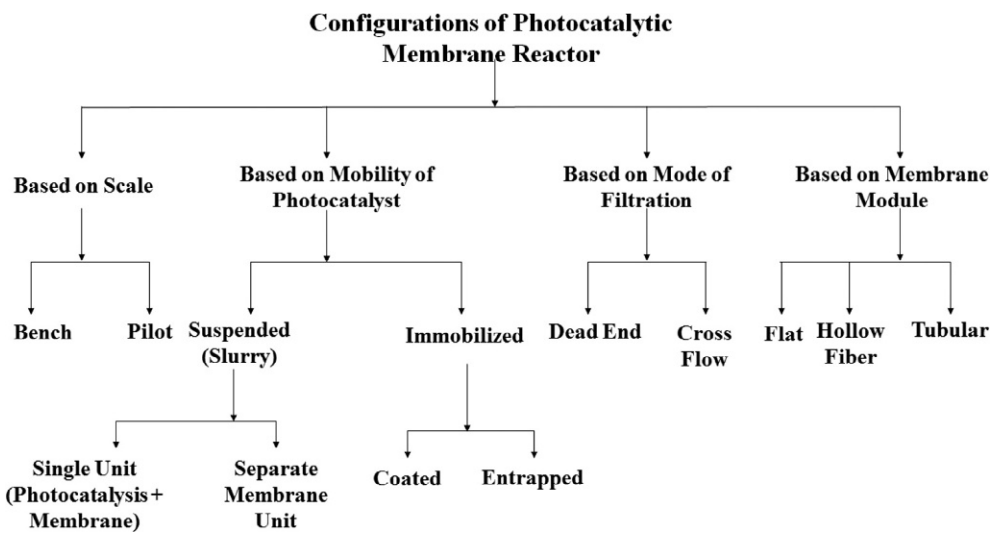

Fig. 22.10
Classification and configuration of photocatalytic membrane reactors based on their applications and the way they work.

This book belongs to Badji Mokhtar Annaba University Central Library Copyright Elsevier 2025

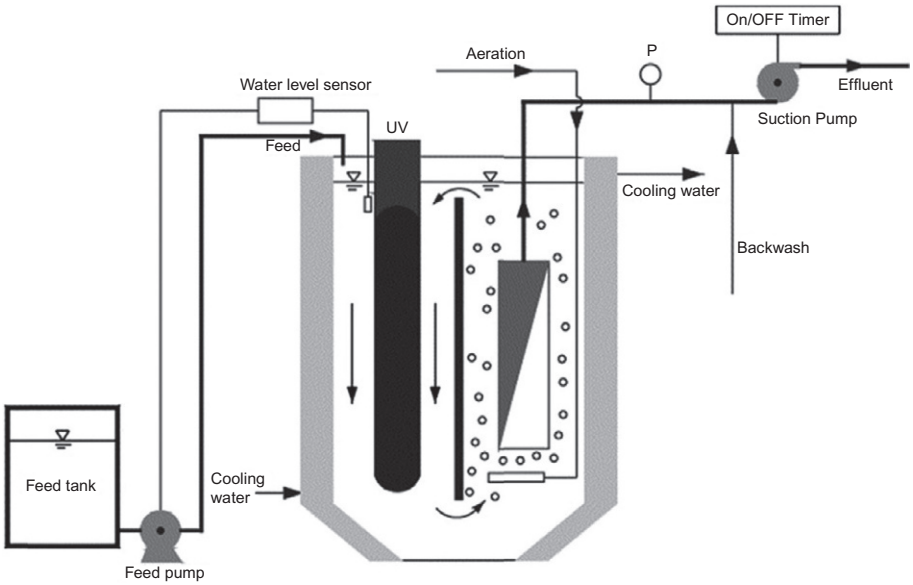

Fig. 22.11
Representation of submerged photocatalytic membrane reactor [124]. *Reprinted with permission from J. Fu, M. Ji, Z. Wang, L. Jin, D. An, A new submerged membrane photocatalysis reactor (SMPR) for fulvic acid removal using a nano-structured photocatalyst, J. Hazard. Mater. 131 (2006) 238–242. Copyright (2006) Elsevier.*

on the membrane surfaces, the membrane acts as a support to photocatalyst nanomaterials and also acts as a barrier for various organic molecules and photocatalyst nanomaterials present in the reaction medium. Furthermore, immobilized photocatalyst on the membranes or in the membrane matrix used in photocatalytic membrane reactors allows photocatalytic degradation reaction on the surface or in the pores of the membranes. Also, membrane pore size will be tailored based on the particle size of photocatalysts as well as the pollutant or product molecule size, and also it depends on the quality of the water for targeted applications like microfiltration (0.1–5 mm), ultrafiltration (smaller particle size), nanofiltration (smaller particle size), etc. Immobilized photocatalyst on membrane or in membrane matrix showed better degradation efficiency compared with suspended photocatalysts in wastewater system. Various operating parameters of photocatalytic membrane reactors like photocatalyst loading, pH, temperature, dissolved oxygen, contaminants and their loadings, light wavelength, light intensity, etc. are important for deciding the configuration and efficiency of the process [125].

For industrial applications, it is believed that a crossflow model could be a good option. The membrane either with a coated or entrapped photocatalyst with crossflow model can lead to better efficiency. Another option is creating cylindrical channels and allowing the polluted water to flow through it. To summarize, the different configurations mentioned in Fig. 22.10 have their own merits and demerits. In a slurry system, the photocatalyst is suspended in the

This book belongs to Badji Mokhtar Annaba University Central Library Copyright Elsevier 2025

reactor. The membrane could be placed in the same tank with a photocatalyst or it could be used externally. So, in some designs of slurry reactors, the membrane was kept in a separate tank. However, due to the problems of recycling the photocatalyst in slurry reactors, these is a need of immobilization of the photocatalyst on a support. This originates the need of preparation/fabrication of membranes with photocatalyst immobilized on its surface or in the matrix of membrane that performs the dual functions (1) to separate the pollutants and (2) to hold the photocatalyst. This photocatalyst immobilized on its surface or in the matrix of membrane is a fair solution to the problem of catalyst recovery. Although the problem of photocatalyst recovery is solved in this case, there are other limitations of the process that include exposure of the membrane to the irradiation. The polymeric membranes are more susceptible to damage than ceramic membranes. Therefore, during the fabrication of the membrane, the probabilities of damage to the membrane due to products of the degradation process should also be taken into consideration. Wang [126] nicely compared the polymeric and ceramic membranes in a photocatalytic membrane reactor. The comparative study is represented in Table 22.2.

Generally, the membrane modules are hollow fibers, flat sheet, or tubular. In the case of photocatalytic membrane reactor, it is a challenge to design a reactor with a configuration where the radiation reaches the photocatalyst present in the membrane. Another disadvantage of photocatalytic membranes with immobilized photocatalyst is that the photocatalyst dose cannot be adjusted according to level of contaminants in the polluted stream. The loading of the photocatalyst nanomaterials depends on the compatibility and loading capacity of nanomaterials in and on the membrane matrix.

Furthermore, the membranes could be operated as a dead end filtration mode or continuous mode. In dead end mode, feed solution is passed on the membrane. In a crossflow mode, the feed solution enters through the membrane and flows along the direction of membrane. Depending on the process parameters and membrane properties, these modes may be selected. A continuous mode is preferably used for large scale treatment options. To operate a photocatalytic membrane in continuous mode, the strength of membrane, its recycling nature, permeability, etc. are the deciding parameters that need to be considered in various applications.

Table 22.2: Comparison of different types of membrane in application [126].

Membrane material	Polymeric membrane		Ceramic membrane
Membrane morphology	**Hollow-fiber membrane**	**Flat-sheet membrane**	**Tubular membrane**
Stability	Medium	Medium	Good
Price	Less expensive	Less expensive	Expensive
Combination mode	Internal, external	Internal, external	Internal, external
Module processing	Very easy	Easy	Hard

Reprinted with permission from L. Wang, Configurations and membranes of photocatalytic membrane reactors for water and wastewater treatment, {IOP} Conf. Ser. Earth Environ. Sci. 208 (2018) 12078. Copyright (2018) IOP Publishing: Open Access: Creative Commons Attribution 3.0 licence.

This book belongs to Badji Mokhtar Annaba University Central Library

Copyright Elsevier 2025

22.6 Treatment of organic pollutants by photocatalytic membrane

Because a POP possesses a serious threat to lives, it becomes important to minimize their release into the environment or treat these pollutants and degrade them into less hazardous components. Various processes like adsorption, biological treatments, oxidation, and photocatalytic degradation are used conventionally to get rid of these pollutants. Adsorption process simply uses an adsorbent to remove a pollutant from a stream of fluid. This method is an extensively accepted method for the removal of organic pollutants because of its simplicity and lower cost compared with other treatment methods. Most commonly used adsorbents are charcoal, zeolites, activated carbon, clay minerals, etc. This method has been utilized for the removal of various chemicals like dyes, phenols, pesticides, herbicides, hydrocarbons, VOCs, etc. [113]. Furthermore, biological treatment methods including aerobic, anaerobic digestion, or activated sludge methods are commonly used at sewage treatment plants. This method is most economical as it employs microorganisms for degradation of organic products into harmless products.

AOP is another efficient process used for treatment of organic pollutants. In this method, highly reactive hydroxyl radicals are generated that react with organic pollutants, which oxidize them to form some less hazardous products. Photocatalysis is an example of AOP. Various semiconductor photocatalysts like TiO_2, ZnO, Fe_2O_3, etc. have been extensively investigated for their applications in pollution remediation [127]. TiO_2 is found to have good photocatalytic activity and reported to have good capabilities in degradation of dyes, pharmaceutical ingredients, insecticides, etc. [128].

In recent years, for efficient wastewater remediation, a combination of photocatalysis with membrane separation technology has been employed. Nanomaterial-based photocatalytic membrane is nothing but membranes incorporated with photocatalyst nanomaterials. Generally, photocatalysts have been used for the degradation of various pollutants present in wastewater. These nanomaterials are dispersed in wastewater in the form of slurry or immobilized in the form of coatings during the degradation process. In these processes, there is a bulk loss of the photocatalysts in the effluents. This can be controlled with incorporation of the photocatalyst on the membrane or in the membrane matrix. These membranes have duel effects, which are photocatalytic degradation of pollutants and then separation of the formed products with the suitable membranes. Therefore, photocatalytic membranes (PMRs) are suitable and interesting for the wastewater treatment. PMRs are the membrane process that combines with photocatalyst nanomaterials [129, 130]. PMR-based processes have various benefits such as enhanced process efficiency, stability, and reusability of photocatalyst with reduced cost [131, 132]. In different types of PMRs, the first case deals with the separate zones in PMR such as photocatalytic degradation and membrane separation [133], and in second case the immobilization of the photocatalyst was done on membranes or in the membrane matrix [134]. In both cases, proper light irradiations were positioned on the active surface. Also

This book belongs to Badji Mokhtar Annaba University Central Library Copyright Elsevier 2025

immobilization of photocatalyst results in lowering the photocatalyst membrane performance. This is attributed to reduction in light harvesting due to lower exposed surface area of the photocatalyst and reduction in mass transfer.

Subramaniam et al. [135] explored the potential of photocatalytic membrane made up of PVDF with titanate nanotubes for removal of color from effluent of palm oil mill. With incorporation of just 0.5 wt% titanate nanotube, they reported almost twofold increase in color removal, i.e., 67.3% as compared to color removal by only membrane, which was only 34.2%. The schematic representation of working of photocatalytic membrane is depicted in Fig. 22.12.

Various researches have been carried out for the treatment of humic acid with photocatalytic membrane. Zhang et al. [106] fabricated a TiO_2 nanofiber incorporated in ceramic hollow-fiber membrane that was reported to be employed for the removal of humic acid from water and reported excellent performance of photocatalytic membrane with 90% as opposed to only 29% in the case of membrane alone. In another study conducted by Alias et al. [136], water containing humic acid was treated using TiO_2 coated ceramic membrane and reported excellent

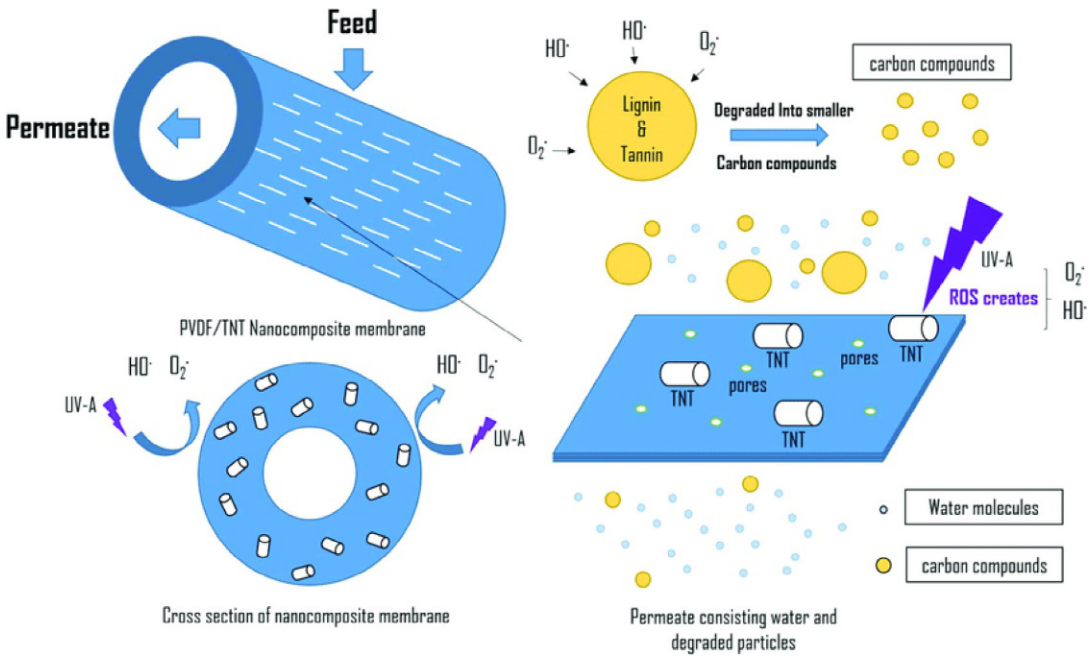

Fig. 22.12
Schematic illustration of working photocatalytic membrane [135]. *Reprinted with permission from M.N. Subramaniam, P.S. Goh, W.J. Lau, B.C. Ng, A.F. Ismail, AT-POME colour removal through photocatalytic submerged filtration using antifouling PVDF-TNT nanocomposite membrane, Sep. Purif. Technol. 191 (2018) 266–275. Copyright (2018) Elsevier.*

This book belongs to Badji Mokhtar Annaba University Central Library Copyright Elsevier 2025

performance of this membrane with 98% rejection rate and TiO_2 imparting self-cleaning property that avoids the fouling of the membrane and enhances the life of the membrane.

Dye is another major pollutant from textile industry that poses a serious threat to marine life. Martins et al. [98] treated MB by use of TiO_2 photocatalyst immobilized on P(VDF-TrFE) membrane with removal efficiency of 85%. It has been also reported that an increase in the amount of photocatalyst in the membrane increases the photocatalytic degradation rate and efficiency. In another study [137], an organic pollutant called Direct Black 168 was treated with TiO_2/Al_2O_3 composite membrane. An increment in the performance has been reported with removal efficiency of 82% when compared with individual method, i.e., 65% by photocatalysis. In another study conducted by Zang et al. [138], a hollow-fiber membrane of TiO_2/PEI was fabricated and used for treatment of Acid Orange 7 present in wastewater. An excellent treatment resulted in 2.2-time higher flux, and organic pollutant removal rate of over 90% was reported. These results showed an enhanced characteristic of PMR due to incorporation of TiO_2 photocatalyst. A comparatively higher flux was indicative of improved fouling resistance of photocatalytic membrane.

In the investigation carried out by Chakraborty et al. [79], 30% removal of MB and 40% removal of pharmaceutical compound, i.e., chlorhexidine digluconate from wastewater occurred by employing a PES membrane with TiO_2 photocatalyst immobilized on it. This is attributed to improved membrane's hydrophilicity due to TiO_2 coating on it. Simone et al. [139] also performed MB treatment present in the wastewater with the use of TiO_2/PES hollow-fiber membrane. TiO_2 nanoparticle concentration varied from 0.3 to 1 wt% in PES hollow membrane, and with addition of 0.3 wt% nanoparticles, they obtained best fiber morphology and properties. Dou et al. [87] synthesized a hybrid membrane of g-C_3N_4 nanosheet and carbon paper for the treatment of MB and reported 60% removal of MB from wastewater. In another study, MB was treated by using N-doped graphene/TiO_2 membrane in the presence of sunlight and UV light [35]. Researchers reported a 77.5% and 80.6% MB removal, respectively. Galiano et al. [140] synthesized a nano-TiO_2 incorporated PVDF hollow-fiber membrane and used it for MB treatment. With 0.5 wt% loading of photocatalyst, they reported superior photocatalytic activity with 97% reduction in MB.

Kamaludin and coworkers [93] synthesized a dual-layer, hollow-fiber membrane with N-doped TiO_2 and utilized it for treatment of water containing Reactive Black 5 and reported a lower energy of excitation of TiO_2 photocatalyst due to nitrogen doping. With this lowered energy of excitation, 75% removal in exposure of visible light was reported and an exceptional performance with 100% removal in exposure to UV light after 360 min of exposure has been reported. Kuvarega et al. [141] synthesized a doped TiO_2 polysulfone membrane by phase inversion method. Two dopant nitrogen and palladium were doped at different concentrations. These prepared photocatalytic membranes were then employed for the degradation of eosin yellow dye and, with incorporation of these nanoparticles of photocatalyst, showed improved

This book belongs to Badji Mokhtar Annaba University Central Library Copyright Elsevier 2025

characteristics of membrane like porosity and wettability. These photocatalytic membranes reported 92% degradation of eosin yellow under visible light exposure for 180 min. Furthermore, Nair et al. [142] prepared a photocatalytic membrane with incorporation of Ag-doped TiO_2 nanosheets and evaluated membrane efficiency for Congo Red dye removal. Investigation was accomplished for photocatalyst concentration varying from 100 to 500 mg and reported an increased in dye removal rate with an increase in photocatalyst concentration in the membrane. Complete removal of dye was noted for 500 mg photocatalyst membrane system. Acid orange is another dye that was treated using carbonaceous char-TiO_2 nanocomposite hollow-fiber membrane that was prepared by Wang et al. [116]. Incorporation of nanoparticle-induced superhydrophilicity reported excellent fouling resistance, which reported over 99% rejection of dye at water flux rate of 7.9 L/m^2 h.

Oil spilled into water must be treated, and this was well addressed by Rusli et al. [143] by employing TiO_2/PVDF photocatalytic membrane for the treatment procedure. They reported a very positive result of incorporating TiO_2 in PVDF membrane with 60% removal of oil as opposed to only 5% removal when only PVDF membrane was employed. Wang et al. [81] employed vacuum filtration method for the synthesis of Cu_2O/TiO_2/rGO nanowire that was incorporated in methyl cellulose ester composite membrane, and the prepared membrane was then utilized for treatment of methyl orange, benzoic acid, and aniline present in wastewater.

In spite of several advantages of PMR-based processes for wastewater treatment, these processes suffer from various challenges like membrane fouling, which affects reduction in permeate flux and, in turn, reduces productivity. This creates a problem in the operation of the process like increased energy consumption, frequent cleaning, lesser life span, and higher replacement cost [132, 144]. Furthermore, agglomeration of photocatalysts on the membrane or in membrane matrix is another challenge during the preparation of the photocatalytic membrane.

22.7 Challenges of photocatalytic membrane-based processes

Every technology with its advantages also has some limitations or challenges, and photocatalytic membranes are no exception. The amount of photocatalyst loading is a major issue in photocatalytic membrane. Although increased catalyst amount increases photocatalytic degradation, it also results in agglomeration of nanoparticles, which has a detrimental effect on the performance of membrane caused due to blocking of pores. Another reason is that it results in blockage of membrane pores by solids in process material [135]. pH of processed feed can also have a significant effect on the flux where membrane have shown higher flux at certain pH. This is more likely because of a change in agglomeration properties of processed feed with respect to the pH of solution [135, 137].

This book belongs to Badji Mokhtar Annaba University Central Library Copyright Elsevier 2025

A comparative study conducted by Martins et al. [98] between use of photocatalyst in suspension and immobilized on membrane surface showed that immobilization of photocatalyst results in relatively lower performance. This is because of a reduction in light harvesting due to lower exposed surface area of photocatalyst and reduction in mass transfer.

22.8 Scale-up of photocatalytic membrane-based processes

Looking at the various studies conducted by researchers, it seems that nanomaterial-based photocatalytic membrane treatment holds the key for organic pollutant treatments. Even though there are several investigations on photocatalytic membrane reactor, scale-up of this process has been rarely studied. This might be because of the number of factors that need to be considered such as light intensity gradient, concentration gradient, interaction of light with the photocatalyst, quantum efficiency, operation mode of a reactor, hybrid system and design, stability and reusability of photocatalyst, and agglomeration of nanoparticles [81, 140, 145–147]. These all affect efforts to develop and scale-up the photocatalytic membrane system for effective organic pollutant treatment and showed positive potential of photocatalytic membrane process. Incorporation of photocatalyst nanoparticles in membrane matrix or on a membrane enhances the performance of the photocatalytic membrane process and holds promising future in wastewater treatment.

There might be a lack of studies on nanomaterial-based photocatalytic reactors, but numerous scale-up studies have been performed for photocatalytic reactors. The interest in photocatalytic membrane reactors is due to advantages over conventional reactors. These reactors offer a safe and effective treatment of wastewater. Photocatalytic membrane reactors could be operated in slurry or immobilized mode.

TiO_2 has proved to be a stable material for the photocatalytic application and is regarded as good material for photocatalytic degradation of organic compounds. Barni and coworkers [148] set up a lab scale module of photocatalytic membrane with TiO_2 for degradation of phenol. For this study, they used PHOTOPERM® CPPI313 membrane with up to 30 wt% TiO_2 immobilized. Another pilot study was conducted by Benotti and coworkers [149] and is depicted in Fig. 22.13. This investigation evaluated the potential of TiO_2-based photocatalytic membrane reactor for treatment of water containing pharmaceutical compounds and endocrine-disrupting compounds. A total of 32 pharmaceuticals were treated, out of which in 29 compounds more than 70% removal was obtained, and the remaining showed only up to 50% removal.

Konstantinos and coworkers [150] developed a pilot scale photocatalytic membrane reactor system as represented in Fig. 22.14. The system had two main components, membrane vessel and UV system with working volume of 10 and 15 L, respectively. The membrane vessel was

This book belongs to Badji Mokhtar Annaba University Central Library Copyright Elsevier 2025

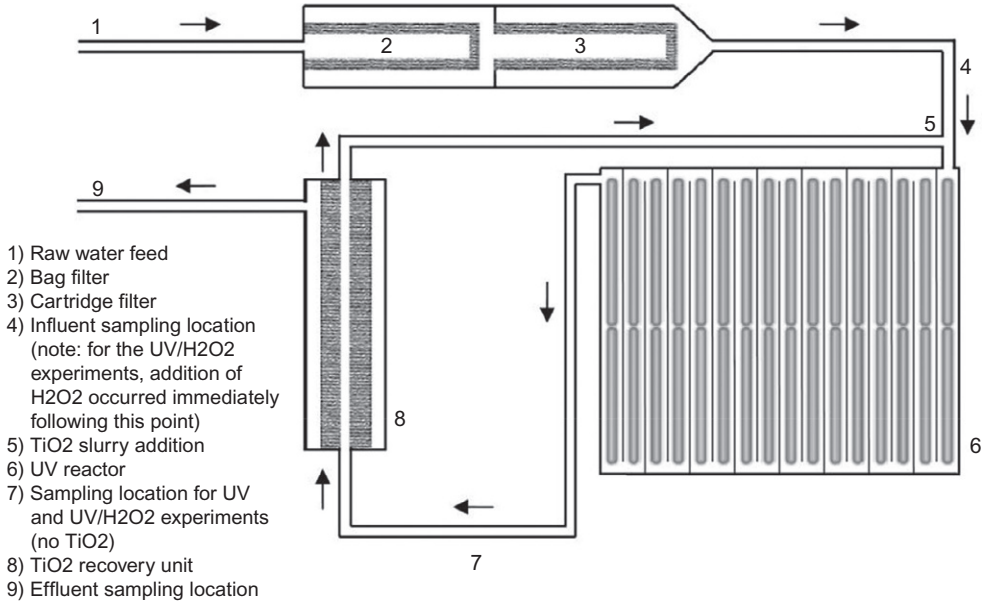

Fig. 22.13
Schematic of pilot scale system for pharmaceutical component removal developed by Benotti and coworkers [149]. *Reprinted with permission from M.J. Benotti, B.D. Stanford, E.C. Wert, S.A. Snyder, Evaluation of a photocatalytic reactor membrane pilot system for the removal of pharmaceuticals and endocrine disrupting compounds from water, Water Res. 43 (2009) 1513–1522. Copyright (2009) Elsevier.*

fitted with a hollow-fiber membrane inside which had a total surface area of 4.19 m^2. The UV system employed four 39 W lamps. This system was developed for continuous operation with automation units like level controller, backwashing, and in situ cleaning unit. This pilot scale unit had treatment capacity of 1.2 m^3/day.

All these attempts to develop and scale-up the photocatalytic membrane system for efficient organic pollutant treatment and positive result shows the potential of the photocatalytic membrane system. With an incorporation of nanoparticles, properties of membranes are reported to improve by several researchers. This can positively augment the performance of a photocatalytic membrane system and holds a promising future in wastewater treatment that should be explored.

22.9 Conclusions and future perspectives

Photocatalytic membranes appear to be a promising alternative compared with conventional water treatment methods for removal of organic pollutants. The development in the field of photocatalysis is bringing new benefits to the world of photocatalytic membranes. The

This book belongs to Badji Mokhtar Annaba University Central Library Copyright Elsevier 2025

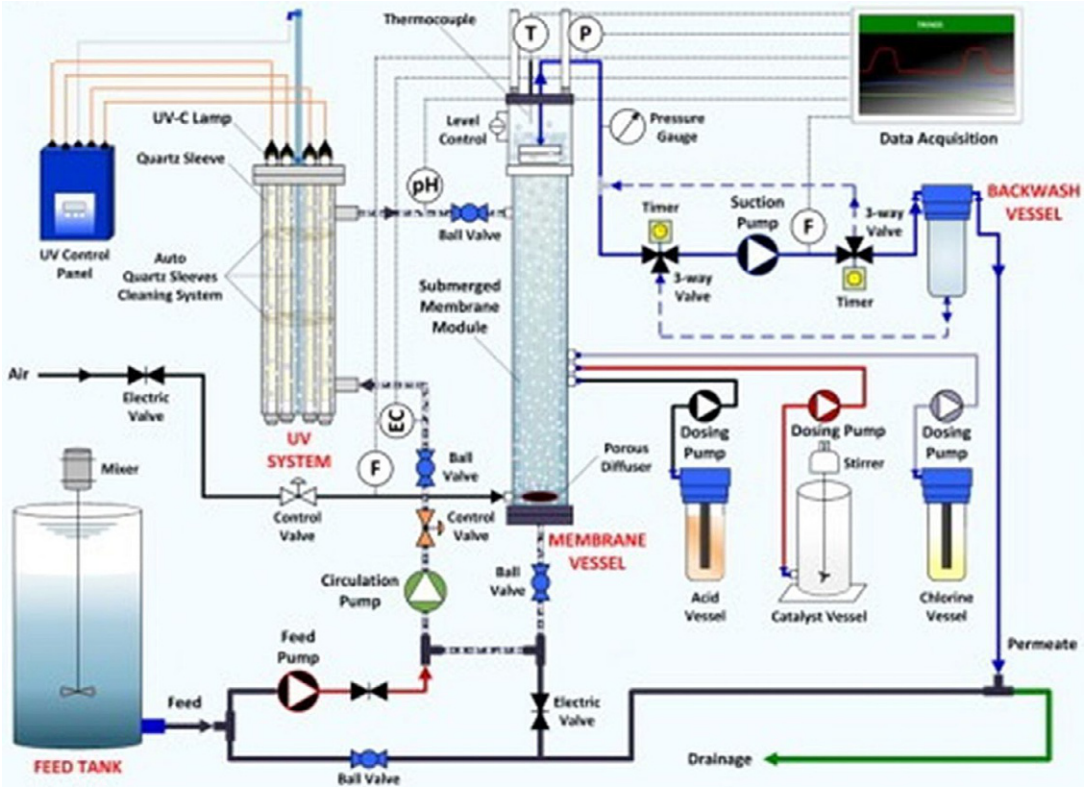

Fig. 22.14
Schematic representation of pilot scale PMR setup developed by Konstantinos and coworkers [150]. *Reprinted with permission from K.V. Plakas, V.C. Sarasidis, S.I. Patsios, D.A. Lambropoulou, A.J. Karabelas, Novel pilot scale continuous photocatalytic membrane reactor for removal of organic micropollutants from water, Chem. Eng. J. 304 (2016) 335–343. Copyright (2016) Elsevier.*

laboratory research carried out by many researchers shows the potential of photocatalytic membrane in treatment of organic pollutants because of improved performance as compared to individual method. For any coupled technology, there is a need to study the merits and demerits of individual technologies. This is true for photocatalytic membranes. For this technology to make its way from laboratory to industry, there is a need to overcome the limitations of up-scaling. The most considered option for up-scaling is a photocatalytic membrane reactor that commonly operates in slurry mode or immobilization of photocatalyst on membrane. However, the removal of a photocatalytic nanomaterial from a slurry reactor system could be costly and time consuming. The scattering and reflection due to slurry may significantly affect light penetration and thus reduce photocatalytic activity. On the other hand, immobilization of a photocatalyst on membranes causes reduced exposed area and mass transfer rate. The reusability of a membrane is also a big challenge in reactors operated in such mode. The ease of

This book belongs to Badji Mokhtar Annaba University Central Library Copyright Elsevier 2025

availability and cost of nanomaterials could solve the major problem of the fabrication of photocatalytic membranes. The synergistic effect between the materials in a composite photocatalytic membrane can play a major role in its performance. Similarly, the pollutant to be degraded and photocatalytic membrane to be used should be paired properly. The photocatalytic membranes have a bright future in water treatment technology if these difficulties are overcome.

References

[1] D. Robert, N. Keller, E. Selli, Environmental photocatalysis and photochemistry for a sustainable world: a big challenge. Environ. Sci. Pollut. Res. 24 (2017) 12503–12505, https://doi.org/10.1007/s11356-017-8935-3.

[2] A. Fujishima, T.N. Rao, D.A. Tryk, Titanium dioxide photocatalysis. J. Photochem. Photobiol. C Photochem. Rev. 1 (2000) 1–21, https://doi.org/10.1016/S1389-5567(00)00002-2.

[3] A. Van, C.M. Rochman, E.M. Flores, K.L. Hill, E. Vargas, S.A. Vargas, E. Hoh, Persistent organic pollutants in plastic marine debris found on beaches in San Diego, California. Chemosphere 86 (2012) 258–263, https://doi.org/10.1016/j.chemosphere.2011.09.039.

[4] F. Akbal, S. Camcı, Comparison of electrocoagulation and chemical coagulation for heavy metal removal. Chem. Eng. Technol. 33 (2010) 1655–1664, https://doi.org/10.1002/ceat.201000091.

[5] E. Yamal-Turbay, E. Jaén, M. Graells, M. Pérez-Moya, Enhanced photo-Fenton process for tetracycline degradation using efficient hydrogen peroxide dosage. J. Photochem. Photobiol. A Chem. 267 (2013) 11–16, https://doi.org/10.1016/j.jphotochem.2013.05.008.

[6] M. Koch, A. Yediler, D. Lienert, G. Insel, A. Kettrup, Ozonation of hydrolyzed azo dye reactive yellow 84 (CI). Chemosphere 46 (2002) 109–113, https://doi.org/10.1016/S0045-6535(01)00102-3.

[7] F. Martínez, M.J. López-Muñoz, J. Aguado, J.A. Melero, J. Arsuaga, A. Sotto, R. Molina, Y. Segura, M.I. Pariente, A. Revilla, L. Cerro, G. Carenas, Coupling membrane separation and photocatalytic oxidation processes for the degradation of pharmaceutical pollutants. Water Res. 47 (2013) 5647–5658, https://doi.org/10.1016/j.watres.2013.06.045.

[8] R. Thiruvenkatachari, S. Vigneswaran, I.S. Moon, A review on UV/TiO_2 photocatalytic oxidation process (Journal Review). Korean J. Chem. Eng. 25 (2008) 64–72, https://doi.org/10.1007/s11814-008-0011-8.

[9] Q. Wei, D. Yang, M. Fan, H.G. Harris, Applications of nanomaterial-based membranes in pollution control. Crit. Rev. Environ. Sci. Technol. 43 (2013) 2389–2438, https://doi.org/10.1080/10643389.2012.672066.

[10] S. Banerjee, S.C. Pillai, P. Falaras, K.E. O'Shea, J.A. Byrne, D.D. Dionysiou, New insights into the mechanism of visible light photocatalysis. J. Phys. Chem. Lett. 5 (2014) 2543–2554, https://doi.org/10.1021/jz501030x.

[11] C. Minero, D. Vione, A quantitative evalution of the photocatalytic performance of TiO_2 slurries. Appl. Catal. B Environ. 67 (2006) 257–269, https://doi.org/10.1016/j.apcatb.2006.05.011.

[12] B.A. Bhanvase, T.P. Shende, S.H. Sonawane, A review on graphene–TiO_2 and doped graphene–TiO_2 nanocomposite photocatalyst for water and wastewater treatment. Environ. Technol. Rev. 6 (2017) 1–14, https://doi.org/10.1080/21622515.2016.1264489.

[13] T.P. Shende, B.A. Bhanvase, A.P. Rathod, D.V. Pinjari, S.H. Sonawane, Sonochemical synthesis of graphene-Ce-TiO_2 and graphene-Fe-TiO_2 ternary hybrid photocatalyst nanocomposite and its application in degradation of crystal violet dye. Ultrason. Sonochem. 41 (2018) 582–589, https://doi.org/10.1016/j.ultsonch.2017.10.024.

[14] S. Weon, F. He, W. Choi, Status and challenges in photocatalytic nanotechnology for cleaning air polluted with volatile organic compounds: visible light utilization and catalyst deactivation. Environ. Sci. Nano 6 (2019) 3185–3214, https://doi.org/10.1039/C9EN00891H.

[15] X. Wang, F. Wang, Y. Sang, H. Liu, Full-spectrum solar-light-activated photocatalysts for light-chemical energy conversion. Adv. Energy Mater. 7 (2017) 1700473, https://doi.org/10.1002/aenm.201700473.

This book belongs to Badji Mokhtar Annaba University Central Library

Copyright Elsevier 2025

[16] G. Wang, B. Huang, X. Ma, Z. Wang, X. Qin, X. Zhang, Y. Dai, M.-H. Whangbo, $Cu_2(OH)PO_4$, a near-infrared-activated photocatalyst. Angew. Chem. Int. Ed. 52 (2013) 4810–4813, https://doi.org/10.1002/anie.201301306.
[17] G. Odling, N. Robertson, Bridging the gap between laboratory and application in photocatalytic water purification. Catal. Sci. Technol. 9 (2019) 533–545, https://doi.org/10.1039/C8CY02438C.
[18] C. Turchi, Photocatalytic degradation of organic water contaminants: mechanisms involving hydroxyl radical attack. J. Catal. 122 (1990) 178–192, https://doi.org/10.1016/0021-9517(90)90269-P.
[19] B. Van Der Bruggen, C. Vandecasteele, T. Van Gestel, W. Doyen, R. Leysen, A review of pressure-driven membrane processes in wastewater treatment and drinking water production. Environ. Prog. 22 (2003) 46–56, https://doi.org/10.1002/ep.670220116.
[20] G. Amy, Fundamental understanding of organic matter fouling of membranes. Desalination 231 (2008) 44–51, https://doi.org/10.1016/j.desal.2007.11.037.
[21] H. Zangeneh, A.A. Zinatizadeh, S. Zinadini, M. Feyzi, D.W. Bahnemann, Preparation and characterization of a novel photocatalytic self-cleaning PES nanofiltration membrane by embedding a visible-driven photocatalyst boron doped-TiO_2–SiO_2/$CoFe_2O_4$ nanoparticles. Sep. Purif. Technol. 209 (2019) 764–775, https://doi.org/10.1016/j.seppur.2018.09.030.
[22] T. Degnan, Photocatalytic water treatment: are we getting closer to large-scale commercialization?. Focus Catal. 2018 (2018) 1, https://doi.org/10.1016/j.focat.2018.09.001.
[23] R. Molinari, C. Lavorato, P. Argurio, K. Szymański, D. Darowna, S. Mozia, Overview of photocatalytic membrane reactors in organic synthesis, energy storage and environmental applications. Catalysts 9 (2019) 239, https://doi.org/10.3390/catal9030239.
[24] X. Zhang, J. Zhou, X. Zou, Z. Wang, Y. Chu, S. Wang, Preparation of nano-SiO_2/Al_2O_3/ZnO-blended PVDF cation-exchange membranes with improved membrane permselectivity and oxidation stability. Materials 11 (2018) 2465, https://doi.org/10.3390/ma11122465.
[25] H.-R. Chae, J. Lee, C.-H. Lee, I.-C. Kim, P.-K. Park, Graphene oxide-embedded thin-film composite reverse osmosis membrane with high flux, anti-biofouling, and chlorine resistance. J. Membr. Sci. 483 (2015) 128–135, https://doi.org/10.1016/j.memsci.2015.02.045.
[26] L.-S. Wan, Z.-M. Liu, Z.-K. Xu, Surface engineering of macroporous polypropylene membranes. Soft Matter 5 (2009) 1775, https://doi.org/10.1039/b813600a.
[27] L. Yao, L. Zhang, R. Wang, S. Chou, Z. Dong, A new integrated approach for dye removal from wastewater by polyoxometalates functionalized membranes. J. Hazard. Mater. 301 (2016) 462–470, https://doi.org/10.1016/j.jhazmat.2015.09.027.
[28] D.A. Athanasiou, G.E. Romanos, P. Falaras, Design and optimization of a photocatalytic reactor for water purification combining optical fiber and membrane technologies. Chem. Eng. J. 305 (2016) 92–103, https://doi.org/10.1016/j.cej.2015.11.080.
[29] R. Molinari, L. Palmisano, E. Drioli, M. Schiavello, Studies on various reactor configurations for coupling photocatalysis and membrane processes in water purification. J. Membr. Sci. 206 (2002) 399–415, https://doi.org/10.1016/S0376-7388(01)00785-2.
[30] G. Plantard, A. Azais, J. Mendret, S. Brosillon, V. Goetz, Coupling of photocatalytic and separation processes as a contribution to mineralization of wastewater. Chem. Eng. Process. Process Intensif. 134 (2018) 115–123, https://doi.org/10.1016/j.cep.2018.10.014.
[31] A. Maciel-Cerda, Membranes. Springer International Publishing, Cham, 2017https://doi.org/10.1007/978-3-319-45315-6.
[32] Y. Liu, Beyond graphene oxides: emerging 2D molecular sieve membranes for efficient separation. Chin. J. Chem. Eng. 27 (2019) 1257–1271, https://doi.org/10.1016/j.cjche.2018.08.019.
[33] J.N. Sahu, R.R. Karri, H.M. Zabed, S. Shams, X. Qi, Current perspectives and future prospects of nano-biotechnology in wastewater treatment. Sep. Purif. Rev. (2019) 1–20, https://doi.org/10.1080/15422119.2019.1630430.
[34] Y. Lin, Y. Cai, E. Drioli, Y. Fan, Enhancing mechanical and photocatalytic performances on TiO_2/Ti composite ultrafiltration membranes via Ag doping method. Sep. Purif. Technol. 145 (2015) 29–38, https://doi.org/10.1016/j.seppur.2015.02.024.

This book belongs to Badji Mokhtar Annaba University Central Library Copyright Elsevier 2025

[35] H. Xu, M. Ding, W. Chen, Y. Li, K. Wang, Nitrogen-doped GO/TiO_2 nanocomposite ultrafiltration membranes for improved photocatalytic performance. Sep. Purif. Technol. 195 (2018) 70–82, https://doi.org/10.1016/j.seppur.2017.12.003.

[36] S. Ahmed, Impact of operating conditions and recent developments in heterogeneous photocatalytic water purification process. Crit. Rev. Environ. Sci. Technol. 42 (2012) 601–675, https://doi.org/10.1080/10643389.2010.526492.

[37] J.M. Ochando-Pulido, J.R. Corpas-Martínez, M. Stoller, A. Martínez-Férez, Organic/TiO_2 nanocomposite membranes: recent developments. in: Organic-Inorganic Composite Polymer Electrolyte Membrane, Springer International Publishing, Cham, 2017, pp. 25–46, https://doi.org/10.1007/978-3-319-52739-0_2.

[38] A. Hu, X. Zhang, K.D. Oakes, P. Peng, Y.N. Zhou, M.R. Servos, Hydrothermal growth of free standing TiO_2 nanowire membranes for photocatalytic degradation of pharmaceuticals. J. Hazard. Mater. 189 (2011) 278–285, https://doi.org/10.1016/j.jhazmat.2011.02.033.

[39] D.M.A. Alrousan, P.S.M. Dunlop, T.A. McMurray, J.A. Byrne, Photocatalytic inactivation of E. coli in surface water using immobilised nanoparticle TiO_2 films. Water Res. 43 (2009) 47–54, https://doi.org/10.1016/j.watres.2008.10.015.

[40] R. Goei, T.-T. Lim, Ag-decorated TiO_2 photocatalytic membrane with hierarchical architecture: photocatalytic and anti-bacterial activities. Water Res. 59 (2014) 207–218, https://doi.org/10.1016/j.watres.2014.04.025.

[41] Ahmad, Kim, Kim, Kim, Diethylene glycol-assisted organized TiO_2 nanostructures for photocatalytic wastewater treatment ceramic membranes. Water 11 (2019) 750, https://doi.org/10.3390/w11040750.

[42] H. Zhang, X. Quan, S. Chen, H. Zhao, Fabrication and characterization of silica/titania nanotubes composite membrane with photocatalytic capability. Environ. Sci. Technol. 40 (2006) 6104–6109, https://doi.org/10.1021/es060092d.

[43] F. Bosc, A. Ayral, C. Guizard, Mesoporous anatase coatings for coupling membrane separation and photocatalyzed reactions. J. Membr. Sci. 265 (2005) 13–19, https://doi.org/10.1016/j.memsci.2005.04.039.

[44] L. Xue, Z. Lü, Y. Cheng, X. Sun, H. Lin, X. Xiao, X. Liu, S. Zhuo, Three-dimensional layered double hydroxide membranes: fabrication technique, growth mechanism, and enhanced photocatalytic activity. Chem. Commun. 54 (2018) 8494–8497, https://doi.org/10.1039/C8CC04162H.

[45] S.F. Zakeritabar, M. Jahanshahi, M. Peyravi, Photocatalytic behavior of induced membrane by ZrO_2–SnO_2 nanocomposite for pharmaceutical wastewater treatment. Catal. Lett. 148 (2018) 882–893, https://doi.org/10.1007/s10562-018-2303-x.

[46] T. Li, Y. Gao, J. Zhou, M. Zhang, X. Fu, F. Liu, A membrane modified with nitrogen-doped TiO_2/graphene oxide for improved photocatalytic performance. Appl. Sci. 9 (2019) 855, https://doi.org/10.3390/app9050855.

[47] R. Zhang, Y. Cai, X. Zhu, Q. Han, T. Zhang, Y. Liu, Y. Li, A. Wang, A novel photocatalytic membrane decorated with PDA/RGO/Ag_3PO_4 for catalytic dye decomposition. Colloids Surf. A Physicochem. Eng. Asp. 563 (2019) 68–76, https://doi.org/10.1016/j.colsurfa.2018.11.069.

[48] Y. Zhang, J. Zhu, Composite photocatalytic membrane prepared by embedding porous SiO_2 shell/void/TiO_2 core particles into polycarbonate for photodegrading and removing pollutant from water. Chem. Eng. Sci. 126 (2015) 390–398, https://doi.org/10.1016/j.ces.2014.12.043.

[49] V.D. Potle, S.R. Shirsath, B.A. Bhanvase, V.K. Saharan, Sonochemical preparation of ternary rGO-ZnO-TiO_2 nanocomposite photocatalyst for efficient degradation of crystal violet dye. Optik 208 (2020) 164555, https://doi.org/10.1016/j.ijleo.2020.164555.

[50] S.P. Deshmukh, D.P. Kale, S. Kar, S.R. Shirsath, B.A. Bhanvase, V.K. Saharan, S.H. Sonawane, Ultrasound assisted preparation of rGO/TiO_2 nanocomposite for effective photocatalytic degradation of methylene blue under sunlight. Nano-Struct. Nano-Objects 21 (2020) 100407, https://doi.org/10.1016/j.nanoso.2019.100407.

[51] D.P. Kale, S.P. Deshmukh, S.R. Shirsath, B.A. Bhanvase, Sonochemical preparation of multifunctional rGO-ZnS-TiO_2 ternary nanocomposite and its application for CV dye removal. Optik 208 (2020) 164532, https://doi.org/10.1016/j.ijleo.2020.164532.

[52] I. Ali, O.M.L. Alharbi, A. Tkachev, E. Galunin, A. Burakov, V.A. Grachev, Water treatment by new-generation graphene materials: hope for bright future. Environ. Sci. Pollut. Res. 25 (2018) 7315–7329, https://doi.org/10.1007/s11356-018-1315-9.

This book belongs to Badji Mokhtar Annaba University Central Library Copyright Elsevier 2025

[53] F. Pendolino, N. Armata, Graphene Oxide in Environmental Remediation Process. Springer International Publishing, Cham, 2017https://doi.org/10.1007/978-3-319-60429-9.
[54] H.M. Hegab, L. Zou, Graphene oxide-assisted membranes: fabrication and potential applications in desalination and water purification. J. Membr. Sci. 484 (2015) 95–106, https://doi.org/10.1016/j.memsci.2015.03.011.
[55] W.-L. Jiang, X. Xia, J.-L. Han, Y.-C. Ding, M.R. Haider, A.-J. Wang, Graphene modified electro-Fenton catalytic membrane for in situ degradation of antibiotic florfenicol. Environ. Sci. Technol. 52 (2018) 9972–9982, https://doi.org/10.1021/acs.est.8b01894.
[56] M. Safarpour, A. Khataee, V. Vatanpour, Preparation of a novel polyvinylidene fluoride (PVDF) ultrafiltration membrane modified with reduced graphene oxide/titanium dioxide (TiO_2) nanocomposite with enhanced hydrophilicity and antifouling properties. Ind. Eng. Chem. Res. 53 (2014) 13370–13382, https://doi.org/10.1021/ie502407g.
[57] C. Zhu, G. Liu, K. Han, H. Ye, S. Wei, Y. Zhou, One-step facile synthesis of graphene oxide/TiO_2 composite as efficient photocatalytic membrane for water treatment: crossflow filtration operation and membrane fouling analysis. Chem. Eng. Process. Process Intensif. 120 (2017) 20–26, https://doi.org/10.1016/j.cep.2017.06.012.
[58] Y. Wei, Y. Zhu, Y. Jiang, Photocatalytic self-cleaning carbon nitride nanotube intercalated reduced graphene oxide membranes for enhanced water purification. Chem. Eng. J. 356 (2019) 915–925, https://doi.org/10.1016/j.cej.2018.09.108.
[59] Z. Yu, X. Min, F. Li, D. Yin, Y. Peng, G. Zeng, A mussel-inspired method to fabricate a novel reduced graphene oxide/$Bi_{12}O_{17}Cl_2$ composites membrane for catalytic degradation and oil/water separation. Polym. Adv. Technol. 30 (2019) 101–109, https://doi.org/10.1002/pat.4448.
[60] G. Rao, Q. Zhang, H. Zhao, J. Chen, Y. Li, Novel titanium dioxide/iron (III) oxide/graphene oxide photocatalytic membrane for enhanced humic acid removal from water. Chem. Eng. J. 302 (2016) 633–640, https://doi.org/10.1016/j.cej.2016.05.095.
[61] W. Wang, E. Eftekhari, G. Zhu, X. Zhang, Z. Yan, Q. Li, Graphene oxide membranes with tunable permeability due to embedded carbon dots. Chem. Commun. 50 (2014) 13089–13092, https://doi.org/10.1039/C4CC05295A.
[62] F. Dong, Y. Li, Z. Wang, W.-K. Ho, Enhanced visible light photocatalytic activity and oxidation ability of porous graphene-like g-C_3N_4 nanosheets via thermal exfoliation. Appl. Surf. Sci. 358 (2015) 393–403, https://doi.org/10.1016/j.apsusc.2015.04.034.
[63] K.-G. Zhou, D. McManus, E. Prestat, X. Zhong, Y. Shin, H.-L. Zhang, S.J. Haigh, C. Casiraghi, Self-catalytic membrane photo-reactor made of carbon nitride nanosheets. J. Mater. Chem. A 4 (2016) 11666–11671, https://doi.org/10.1039/C5TA09152G.
[64] S. Min, G. Lu, Enhanced electron transfer from the excited eosin Y to mpg-C3 N4 for highly efficient hydrogen evolution under 550 nm irradiation. J. Phys. Chem. C 116 (2012) 19644–19652, https://doi.org/10.1021/jp304022f.
[65] E. Bet-Moushoul, Y. Mansourpanah, K. Farhadi, M. Tabatabaei, TiO_2 nanocomposite based polymeric membranes: a review on performance improvement for various applications in chemical engineering processes. Chem. Eng. J. 283 (2016) 29–46, https://doi.org/10.1016/j.cej.2015.06.124.
[66] A.-Y. Zhang, W.-K. Wang, D.-N. Pei, H.-Q. Yu, Degradation of refractory pollutants under solar light irradiation by a robust and self-protected ZnO/CdS/TiO_2 hybrid photocatalyst. Water Res. 92 (2016) 78–86, https://doi.org/10.1016/j.watres.2016.01.045.
[67] H. Bai, Z. Liu, D.D. Sun, Hierarchically multifunctional TiO_2 nano-thorn membrane for water purification. Chem. Commun. 46 (2010) 6542, https://doi.org/10.1039/c0cc01143f.
[68] N.A.M. Nor, J. Jaafar, A.F. Ismail, M.A. Mohamed, M.A. Rahman, M.H.D. Othman, W.J. Lau, N. Yusof, Preparation and performance of PVDF-based nanocomposite membrane consisting of TiO_2 nanofibers for organic pollutant decomposition in wastewater under UV irradiation. Desalination 391 (2016) 89–97, https://doi.org/10.1016/j.desal.2016.01.015.

This book belongs to Badji Mokhtar Annaba University Central Library Copyright Elsevier 2025

[69] Z.A.M. Hir, P. Moradihamedani, A.H. Abdullah, M.A. Mohamed, Immobilization of TiO_2 into polyethersulfone matrix as hybrid film photocatalyst for effective degradation of methyl orange dye. Mater. Sci. Semicond. Process. 57 (2017) 157–165, https://doi.org/10.1016/j.mssp.2016.10.009.

[70] S. Yu, Y. Wang, F. Sun, R. Wang, Y. Zhou, Novel mpg-C_3N_4/TiO_2 nanocomposite photocatalytic membrane reactor for sulfamethoxazole photodegradation. Chem. Eng. J. 337 (2018) 183–192, https://doi.org/10.1016/j.cej.2017.12.093.

[71] N. Salim, N. Nor, J. Jaafar, A. Ismail, T. Matsuura, M. Qtaishat, M. Othman, M. Rahman, F. Aziz, N. Yusof, Performance of PES/LSMM-OGCN photocatalytic membrane for phenol removal: effect of OGCN loading. Membranes 8 (2018) 42, https://doi.org/10.3390/membranes8030042.

[72] B. Lee, Y. Baek, M. Lee, D.H. Jeong, H.H. Lee, J. Yoon, Y.H. Kim, A carbon nanotube wall membrane for water treatment. Nat. Commun. 6 (2015) 7109, https://doi.org/10.1038/ncomms8109.

[73] J.R. Werber, C.O. Osuji, M. Elimelech, Materials for next-generation desalination and water purification membranes. Nat. Rev. Mater. 1 (2016) 16018, https://doi.org/10.1038/natrevmats.2016.18.

[74] G. Liu, K. Han, Y. Zhou, H. Ye, X. Zhang, J. Hu, X. Li, Facile synthesis of highly dispersed ag doped graphene oxide/titanate nanotubes as a visible light photocatalytic membrane for water treatment. ACS Sustain. Chem. Eng. 6 (2018) 6256–6263, https://doi.org/10.1021/acssuschemeng.8b00029.

[75] A. Comite, Preparation of silica membranes by sol-gel method. in: A Basile, K Ghasemzadeh (Eds.), Current Trends and Future Developments on (Bio-)Membranes Silica Membranes: Preparation, Modelling, Application, and Commercialization, Elsevier Inc., 2017, pp. 3–23, https://doi.org/10.1016/B978-0-444-63866-3.00001-7

[76] H. Choi, M.G. Antoniou, A.A. de la Cruz, E. Stathatos, D.D. Dionysiou, Photocatalytic TiO_2 films and membranes for the development of efficient wastewater treatment and reuse systems. Desalination 202 (2007) 199–206, https://doi.org/10.1016/j.desal.2005.12.055.

[77] H. Choi, E. Stathatos, D.D. Dionysiou, Sol-gel preparation of mesoporous photocatalytic TiO_2 films and TiO_2/Al_2O_3 composite membranes for environmental applications. Appl. Catal. B Environ. 63 (2006) 60–67, https://doi.org/10.1016/j.apcatb.2005.09.012.

[78] H. Choi, A.C. Sofranko, D.D. Dionysiou, Nanocrystalline TiO_2 photocatalytic membranes with a hierarchical mesoporous multilayer structure: synthesis, characterization, and multifunction. Adv. Funct. Mater. 16 (2006) 1067–1074, https://doi.org/10.1002/adfm.200500658.

[79] S. Chakraborty, S. Loutatidou, G. Palmisano, J. Kujawa, M.O. Mavukkandy, S. Al-Gharabli, E. Curcio, H.A. Arafat, Photocatalytic hollow fiber membranes for the degradation of pharmaceutical compounds in wastewater. J. Environ. Chem. Eng. 5 (2017) 5014–5024, https://doi.org/10.1016/j.jece.2017.09.038.

[80] L.M. Pastrana-Martínez, S. Morales-Torres, J.L. Figueiredo, J.L. Faria, A.M.T. Silva, Graphene oxide based ultrafiltration membranes for photocatalytic degradation of organic pollutants in salty water. Water Res. 77 (2015) 179–190, https://doi.org/10.1016/j.watres.2015.03.014.

[81] W. Wang, Z. Wu, E. Eftekhari, Z. Huo, X. Li, M.O. Tade, C. Yan, Z. Yan, C. Li, Q. Li, D. Zhao, High performance heterojunction photocatalytic membranes formed by embedding Cu_2O and TiO_2 nanowires in reduced graphene oxide. Catal. Sci. Technol. 8 (2018) 1704–1711, https://doi.org/10.1039/c8cy00082d.

[82] B.A. Bhanvase, D.V. Pinjari, P.R. Gogate, S.H. Sonawane, A.B. Pandit, Process intensification of encapsulation of functionalized $CaCO_3$ nanoparticles using ultrasound assisted emulsion polymerization. Chem. Eng. Process. Process Intensif. 50 (2011) 1160–1168, https://doi.org/10.1016/j.cep.2011.09.002.

[83] B.A. Bhanvase, D.V. Pinjari, P.R. Gogate, S.H. Sonawane, A.B. Pandit, Synthesis of exfoliated poly(styrene-co-methyl methacrylate)/montmorillonite nanocomposite using ultrasound assisted in situ emulsion copolymerization. Chem. Eng. J. 181–182 (2012) 770–778, https://doi.org/10.1016/j.cej.2011.11.084.

[84] M. Sheydaei, M. Fattahi, L. Ghalamchi, V. Vatanpour, Systematic comparison of sono-synthesized Ce-, La- and Ho-doped ZnO nanoparticles and using the optimum catalyst in a visible light assisted continuous sono-photocatalytic membrane reactor. Ultrason. Sonochem. 56 (2019) 361–371, https://doi.org/10.1016/j.ultsonch.2019.04.031.

This book belongs to Badji Mokhtar Annaba University Central Library

Copyright Elsevier 2025

[85] A. Muhulet, C. Tuncel, F. Miculescu, A.M. Pandele, C. Bobirica, C. Orbeci, L. Bobirica, A. Palla-Papavlu, S.I. Voicu, Synthesis and characterization of polysulfone–TiO_2 decorated MWCNT composite membranes by sonochemical method. Appl. Phys. A Mater. Sci. Process. 126 (2020) 233, https://doi.org/10.1007/s00339-020-3408-9.
[86] J.-O. Carlsson, P.M. Martin, Chemical vapor deposition. in: Handbook of Deposition Technologies for Films and Coatings, Elsevier, 2010, pp. 314–363, https://doi.org/10.1016/B978-0-8155-2031-3.00007-7.
[87] T. Dou, L. Zang, Y. Zhang, Z. Sun, L. Sun, C. Wang, Hybrid g-C_3N_4 nanosheet/carbon paper membranes for the photocatalytic degradation of methylene blue. Mater. Lett. 244 (2019) 151–154, https://doi.org/10.1016/j.matlet.2019.02.066.
[88] B.J. Starr, V.V. Tarabara, M. Herrera-Robledo, M. Zhou, S. Roualdès, A. Ayral, Coating porous membranes with a photocatalyst: comparison of LbL self-assembly and plasma-enhanced CVD techniques. J. Membr. Sci. 514 (2016) 340–349, https://doi.org/10.1016/j.memsci.2016.04.050.
[89] W.-Y. Wang, A. Irawan, Y. Ku, Photocatalytic degradation of Acid Red 4 using a titanium dioxide membrane supported on a porous ceramic tube. Water Res. 42 (2008) 4725–4732, https://doi.org/10.1016/j.watres.2008.08.021.
[90] A.K. Hołda, I.F.J. Vankelecom, Understanding and guiding the phase inversion process for synthesis of solvent resistant nanofiltration membranes. J. Appl. Polym. Sci. 132 (2015) 1–17, https://doi.org/10.1002/app.42130.
[91] D.R. Tree, K.T. Delaney, H.D. Ceniceros, T. Iwama, G.H. Fredrickson, A multi-fluid model for microstructure formation in polymer membranes. Soft Matter 13 (2017) 3013–3030, https://doi.org/10.1039/c6sm02839j.
[92] G.R. Xu, J.N. Wang, C.J. Li, Strategies for improving the performance of the polyamide thin film composite (PA-TFC) reverse osmosis (RO) membranes: surface modifications and nanoparticles incorporations. Desalination 328 (2013) 83–100, https://doi.org/10.1016/j.desal.2013.08.022.
[93] R. Kamaludin, A.S. Mohamad Puad, M.H.D. Othman, S.H.S.A. Kadir, Z. Harun, Incorporation of N-doped TiO_2 into dual layer hollow fiber (DLHF) membrane for visible light-driven photocatalytic removal of reactive black 5. Polym. Test. 78 (2019) 105939, https://doi.org/10.1016/j.polymertesting.2019.105939.
[94] S.S. Ray, S.S. Chen, C.W. Li, N.C. Nguyen, H.T. Nguyen, A comprehensive review: electrospinning technique for fabrication and surface modification of membranes for water treatment application. RSC Adv. 6 (2016) 85495–85514, https://doi.org/10.1039/c6ra14952a.
[95] S. An, M.W. Lee, B.N. Joshi, A. Jo, J. Jung, S.S. Yoon, Water purification and toxicity control of chlorophenols by 3D nanofiber membranes decorated with photocatalytic titania nanoparticles. Ceram. Int. 40 (2014) 3305–3313, https://doi.org/10.1016/j.ceramint.2013.09.104.
[96] P. Wan, Z. Zhang, B. Deng, Photocatalytic polysulfone hollow fiber membrane with self-cleaning and antifouling property for water treatment. Ind. Eng. Chem. Res. 58 (2019) 3339–3348, https://doi.org/10.1021/acs.iecr.8b05783.
[97] L. Aoudjit, P.M. Martins, F. Madjene, D.Y. Petrovykh, S. Lanceros-Mendez, Photocatalytic reusable membranes for the effective degradation of tartrazine with a solar photoreactor. J. Hazard. Mater. 344 (2018) 408–416, https://doi.org/10.1016/j.jhazmat.2017.10.053.
[98] P.M. Martins, R. Miranda, J. Marques, C.J. Tavares, G. Botelho, S. Lanceros-Mendez, Comparative efficiency of TiO_2 nanoparticles in suspension vs. immobilization into P(VDF-TrFE) porous membranes. RSC Adv. 6 (2016) 12708–12716, https://doi.org/10.1039/c5ra25385c.
[99] H. Song, J. Shao, Y. He, B. Liu, X. Zhong, Natural organic matter removal and flux decline with PEG-TiO_2-doped PVDF membranes by integration of ultrafiltration with photocatalysis. J. Membr. Sci. 405–406 (2012) 48–56, https://doi.org/10.1016/j.memsci.2012.02.063.
[100] R.A. Damodar, S.J. You, H.H. Chou, Study the self cleaning, antibacterial and photocatalytic properties of TiO_2 entrapped PVDF membranes. J. Hazard. Mater. 172 (2009) 1321–1328, https://doi.org/10.1016/j.jhazmat.2009.07.139.
[101] A. Rahimpour, S.S. Madaeni, A.H. Taheri, Y. Mansourpanah, Coupling TiO_2 nanoparticles with UV irradiation for modification of polyethersulfone ultrafiltration membranes. J. Membr. Sci. 313 (2008) 158–169, https://doi.org/10.1016/j.memsci.2007.12.075.

This book belongs to Badji Mokhtar Annaba University Central Library Copyright Elsevier 2025

[102] Y. Yang, H. Zhang, P. Wang, Q. Zheng, J. Li, The influence of nano-sized TiO_2 fillers on the morphologies and properties of PSF UF membrane. J. Membr. Sci. 288 (2007) 231–238, https://doi.org/10.1016/j.memsci.2006.11.019.

[103] S. Zinadini, S. Rostami, V. Vatanpour, E. Jalilian, Preparation of antibiofouling polyethersulfone mixed matrix NF membrane using photocatalytic activity of ZnO/MWCNTs nanocomposite. J. Membr. Sci. 529 (2017) 133–141, https://doi.org/10.1016/j.memsci.2017.01.047.

[104] K. Fischer, M. Grimm, J. Meyers, C. Dietrich, R. Gläser, A. Schulze, Photoactive microfiltration membranes via directed synthesis of TiO_2 nanoparticles on the polymer surface for removal of drugs from water. J. Membr. Sci. 478 (2015) 49–57, https://doi.org/10.1016/j.memsci.2015.01.009.

[105] L. Djafer, A. Ayral, A. Ouagued, Robust synthesis and performance of a titania-based ultrafiltration membrane with photocatalytic properties. Sep. Purif. Technol. 75 (2010) 198–203, https://doi.org/10.1016/j.seppur.2010.08.001.

[106] Q. Zhang, H. Wang, X. Fan, F. Lv, S. Chen, X. Quan, Fabrication of TiO_2 nanofiber membranes by a simple dip-coating technique for water treatment. Surf. Coat. Technol. 298 (2016) 45–52, https://doi.org/10.1016/j.surfcoat.2016.04.054.

[107] L. Naszályi, F. Bosc, A. El Mansouri, A. van der Lee, D. Cot, Z. Hórvölgyi, A. Ayral, Sol-gel-derived mesoporous SiO_2/ZnO active coating and development of multifunctional ceramic membranes. Sep. Purif. Technol. 59 (2008) 304–309, https://doi.org/10.1016/j.seppur.2007.07.001.

[108] N. Daels, M. Radoicic, M. Radetic, S.W.H. Van Hulle, K. De Clerck, Functionalisation of electrospun polymer nanofibre membranes with TiO_2 nanoparticles in view of dissolved organic matter photodegradation. Sep. Purif. Technol. 133 (2014) 282–290, https://doi.org/10.1016/j.seppur.2014.06.040.

[109] J. Guo, D.Y.S. Yan, F.L.Y. Lam, B.J. Deka, X. Lv, Y.H. Ng, A.K. An, Self-cleaning BiOBr/Ag photocatalytic membrane for membrane regeneration under visible light in membrane distillation. Chem. Eng. J. 378 (2019) 122137, https://doi.org/10.1016/j.cej.2019.122137.

[110] C.P. Athanasekou, G.E. Romanos, F.K. Katsaros, K. Kordatos, V. Likodimos, P. Falaras, Very efficient composite titania membranes in hybrid ultrafiltration/photocatalysis water treatment processes. J. Membr. Sci. 392–393 (2012) 192–203, https://doi.org/10.1016/j.memsci.2011.12.028.

[111] G. Liu, K. Han, H. Ye, C. Zhu, Y. Gao, Y. Liu, Y. Zhou, Graphene oxide/triethanolamine modified titanate nanowires as photocatalytic membrane for water treatment. Chem. Eng. J. 320 (2017) 74–80, https://doi.org/10.1016/j.cej.2017.03.024.

[112] H.W. Vallack, D.J. Bakker, I. Brandt, E. Broström-Lundén, A. Brouwer, K.R. Bull, C. Gough, R. Guardans, I. Holoubek, B. Jansson, R. Koch, J. Kuylenstierna, A. Lecloux, D. Mackay, P. McCutcheon, P. Mocarelli, R.D.F. Taalman, N.G. Weavers, Controlling persistent organic pollutants-what next?. Environ. Toxicol. Pharmacol. 6 (1998) 143–175, https://doi.org/10.1016/s1382-6689(98)00036-2.

[113] A. Machulek Jr., S. C. Oliveira, M. E. Osugi, V. S. Ferreira, F. H. Quina, R. F. Dantas, S. L. Oliveira, G. A. Casagrande, F. J. Anaissi, V. O. Silva, R. P. Cavalcante, F. Gozzi, D. D. Ramos, A. P. P. da Rosa, A. P. F. Santos, D. C. de Castro, J. A. Nogueira, Application of different advanced oxidation processes for the degradation of organic pollutants, in: N. Nogueira Rashed (Ed.), Organic Pollutants—Monitoring, Risk and Treatment, IntechOpen, 2013, DOI 10.5772/53188.

[114] Y. Lv, C. Zhang, A. He, S.J. Yang, G.P. Wu, S.B. Darling, Z.K. Xu, Photocatalytic nanofiltration membranes with self-cleaning property for wastewater treatment. Adv. Funct. Mater. (2017), https://doi.org/10.1002/adfm.201700251.

[115] H. Bai, X. Zan, L. Zhang, D.D. Sun, Multi-functional CNT/ZnO/TiO_2 nanocomposite membrane for concurrent filtration and photocatalytic degradation. Sep. Purif. Technol. 156 (2015) 922–930, https://doi.org/10.1016/j.seppur.2015.10.016.

[116] D.K. Wang, M. Elma, J. Motuzas, W.C. Hou, F. Xie, X. Zhang, Rational design and synthesis of molecular-sieving, photocatalytic, hollow fiber membranes for advanced water treatment applications. J. Membr. Sci. 524 (2017) 163–173, https://doi.org/10.1016/j.memsci.2016.10.052.

[117] A. Rajeswari, S. Vismaiya, A. Pius, Preparation, characterization of nano ZnO-blended cellulose acetate-polyurethane membrane for photocatalytic degradation of dyes from water. Chem. Eng. J. (2017), https://doi.org/10.1016/j.cej.2016.10.124.

This book belongs to Badji Mokhtar Annaba University Central Library Copyright Elsevier 2025

[118] D. Zioui, H. Salazar, L. Aoudjit, P.M. Martins, Photocatalytic polymeric nanocomposite membrane towards oily wastewater. Preprints (2019), https://doi.org/10.20944/preprints201904.0060.v1.
[119] S. Ren, C. Boo, N. Guo, S. Wang, M. Elimelech, Y. Wang, Photocatalytic reactive ultrafiltration membrane for removal of antibiotic resistant bacteria and antibiotic resistance genes from wastewater effluent. Environ. Sci. Technol. (2018), https://doi.org/10.1021/acs.est.8b01888.
[120] H. Xu, Y. Li, M. Ding, W. Chen, K. Wang, C. Lu, Engineered photocatalytic material membrane assemblies for removing nitrate from water. ACS Sustain. Chem. Eng. (2018), https://doi.org/10.1021/acssuschemeng.8b00917.
[121] N.E. Salim, J. Jaafar, A.F. Ismail, M.H.D. Othman, M.A. Rahman, N. Yusof, M. Qtaishat, T. Matsuura, F. Aziz, W.N.W. Salleh, Preparation and characterization of hydrophilic surface modifier macromolecule modified poly (ether sulfone) photocatalytic membrane for phenol removal. Chem. Eng. J. (2018), https://doi.org/10.1016/j.cej.2017.10.147.
[122] H. Rawindran, J.W. Lim, P.S. Goh, M.N. Subramaniam, A.F. Ismail, N.M. Radi bin Nik M Daud, M. Rezaei-Dasht Arzhandi, Simultaneous separation and degradation of surfactants laden in produced water using PVDF/TiO_2 photocatalytic membrane. J. Clean. Prod. (2019), https://doi.org/10.1016/j.jclepro.2019.02.230.
[123] I. Horovitz, D. Avisar, M.A. Baker, R. Grilli, L. Lozzi, D. Di Camillo, H. Mamane, Carbamazepine degradation using a N-doped TiO_2 coated photocatalytic membrane reactor: influence of physical parameters. J. Hazard. Mater. 310 (2016) 98–107, https://doi.org/10.1016/j.jhazmat.2016.02.008.
[124] J. Fu, M. Ji, Z. Wang, L. Jin, D. An, A new submerged membrane photocatalysis reactor (SMPR) for fulvic acid removal using a nano-structured photocatalyst. J. Hazard. Mater. 131 (2006) 238–242, https://doi.org/10.1016/j.jhazmat.2005.09.039.
[125] M.F. Hossain, Water. in: Sustainable Design and Build, Elsevier, 2019, pp. 301–418, https://doi.org/10.1016/B978-0-12-816722-9.00006-9.
[126] L. Wang, Configurations and membranes of photocatalytic membrane reactors for water and wastewater treatment. IOP Conf. Ser. Earth Environ. Sci. 208 (2018) 12078, https://doi.org/10.1088/1755-1315/208/1/012078.
[127] H. Anwer, A. Mahmood, J. Lee, K.-H. Kim, J.-W. Park, A.C.K. Yip, Photocatalysts for degradation of dyes in industrial effluents: opportunities and challenges. Nano Res. 12 (2019) 955–972, https://doi.org/10.1007/s12274-019-2287-0.
[128] N. Bahadur, N. Bhargava, Novel pilot scale photocatalytic treatment of textile & dyeing industry wastewater to achieve process water quality and enabling zero liquid discharge. J. Water Process Eng. 32 (2019) 100934, https://doi.org/10.1016/j.jwpe.2019.100934.
[129] S.O. Ganiyu, E.D. van Hullebusch, M. Cretin, G. Esposito, M.A. Oturan, Coupling of membrane filtration and advanced oxidation processes for removal of pharmaceutical residues: a critical review. Sep. Purif. Technol. 156 (2015) 891–914, https://doi.org/10.1016/j.seppur.2015.09.059.
[130] M.N. Chong, B. Jin, C.W.K. Chow, C. Saint, Recent developments in photocatalytic water treatment technology: a review. Water Res. 44 (2010) 2997–3027, https://doi.org/10.1016/j.watres.2010.02.039.
[131] S. Mozia, Photocatalytic membrane reactors (PMRs) in water and wastewater treatment. A review. Sep. Purif. Technol. 73 (2010) 71–91, https://doi.org/10.1016/j.seppur.2010.03.021.
[132] W. Zhang, L. Ding, J. Luo, M.Y. Jaffrin, B. Tang, Membrane fouling in photocatalytic membrane reactors (PMRs) for water and wastewater treatment: a critical review. Chem. Eng. J. 302 (2016) 446–458, https://doi.org/10.1016/j.cej.2016.05.071.
[133] S. Mozia, D. Darowna, K. Szymański, S. Grondzewska, K. Borchert, R. Wróbel, A. W. Morawski, Performance of two photocatalytic membrane reactors for treatment of primary and secondary effluents. Catal. Today 236 (2014) 135–145, https://doi.org/10.1016/j.cattod.2013.12.049.
[134] S. Leong, A. Razmjou, K. Wang, K. Hapgood, X. Zhang, H. Wang, TiO_2 based photocatalytic membranes: a review. J. Membr. Sci. 472 (2014) 167–184, https://doi.org/10.1016/j.memsci.2014.08.016.
[135] M.N. Subramaniam, P.S. Goh, W.J. Lau, B.C. Ng, A.F. Ismail, AT-POME colour removal through photocatalytic submerged filtration using antifouling PVDF-TNT nanocomposite membrane. Sep. Purif. Technol. 191 (2018) 266–275, https://doi.org/10.1016/j.seppur.2017.09.042.

This book belongs to Badji Mokhtar Annaba University Central Library Copyright Elsevier 2025

[136] S.S. Alias, Z. Harun, I.S.A. Latif, Characterization and performance of porous photocatalytic ceramic membranes coated with TiO_2 via different dip-coating routes. J. Mater. Sci. 53 (2018) 11534–11552, https://doi.org/10.1007/s10853-018-2392-3.

[137] H. Zhang, X. Quan, S. Chen, H. Zhao, Y. Zhao, Fabrication of photocatalytic membrane and evaluation its efficiency in removal of organic pollutants from water. Sep. Purif. Technol. 50 (2006) 147–155, https://doi.org/10.1016/j.seppur.2005.11.018.

[138] X. Zhang, D.K. Wang, D.R.S. Lopez, J.C. Diniz da Costa, Fabrication of nanostructured TiO_2 hollow fiber photocatalytic membrane and application for wastewater treatment. Chem. Eng. J. 236 (2014) 314–322, https://doi.org/10.1016/j.cej.2013.09.059.

[139] S. Simone, F. Galiano, M. Faccini, M. Boerrigter, C. Chaumette, E. Drioli, A. Figoli, Preparation and characterization of polymeric-hybrid PES/TiO_2 hollow fiber membranes for potential applications in water treatment. Fibers 5 (2017) 14, https://doi.org/10.3390/fib5020014.

[140] F. Galiano, X. Song, T. Marino, M. Boerrigter, O. Saoncella, S. Simone, M. Faccini, C. Chaumette, E. Drioli, A. Figoli, Novel photocatalytic PVDF/nano-TiO_2 hollow fibers for environmental remediation. Polymers 10 (2018) 1134, https://doi.org/10.3390/polym10101134.

[141] A.T. Kuvarega, N. Khumalo, D. Dlamini, B.B. Mamba, Polysulfone/N,Pd co-doped TiO_2 composite membranes for photocatalytic dye degradation. Sep. Purif. Technol. 191 (2018) 122–133, https://doi.org/10.1016/j.seppur.2017.07.064.

[142] A.K. Nair, P.E. Jagadeesh Babu, Ag-TiO_2 nanosheet embedded photocatalytic membrane for solar water treatment. J. Environ. Chem. Eng. 5 (2017) 4128–4133, https://doi.org/10.1016/j.jece.2017.07.046.

[143] U.N. Rusli, N.H. Alias, M.Z. Shahruddin, N.H. Othman, Photocatalytic degradation of oil using polyvinylidene fluoride/titanium dioxide composite membrane for oily wastewater treatment. MATEC Web Conf. 69 (2016) 05003, https://doi.org/10.1051/MATECCONF/20166905003.

[144] M. Pidou, S.A. Parsons, G. Raymond, P. Jeffrey, T. Stephenson, B. Jefferson, Fouling control of a membrane coupled photocatalytic process treating greywater. Water Res. 43 (2009) 3932–3939, https://doi.org/10.1016/j.watres.2009.05.030.

[145] R.K. Herz, Intrinsic kinetics of first-order reactions in photocatalytic membranes and layers. Chem. Eng. J. 99 (2004) 237–245, https://doi.org/10.1016/j.cej.2003.11.013.

[146] R. Ahmad, Z. Ahmad, A.U. Khan, N.R. Mastoi, M. Aslam, J. Kim, Photocatalytic systems as an advanced environmental remediation: recent developments, limitations and new avenues for applications. J. Environ. Chem. Eng. 4 (2016) 4143–4164, https://doi.org/10.1016/j.jece.2016.09.009.

[147] M. Zhou, Novel photocatalytic TiO_2-based porous membranes prepared by plasma-enhanced chemical vapor deposition (PECVD) for organic pollutant degradation in water, To cite this version : HAL Id : tel-01693147 To obtain the grade of Doctor PREPARED BY PLASMA-ENHANhttps://tel.archives-ouvertes.fr/tel-01693147, 2018.

[148] B. Barni, A. Cavicchioli, E. Riva, L. Zanoni, F. Bignoli, I.R. Bellobono, F. Gianturco, A. De Giorgi, H. Muntau, L. Montanarella, S. Facchetti, L. Castellano, Laboratory-scale photodegradation of phenol in aqueous solution by photocatalytic membranes immobilizing titanium dioxides. Chemosphere 30 (1995) 1847–1860, https://doi.org/10.1016/0045-6535(95)00066-H.

[149] M.J. Benotti, B.D. Stanford, E.C. Wert, S.A. Snyder, Evaluation of a photocatalytic reactor membrane pilot system for the removal of pharmaceuticals and endocrine disrupting compounds from water. Water Res. 43 (2009) 1513–1522, https://doi.org/10.1016/j.watres.2008.12.049.

[150] K.V. Plakas, V.C. Sarasidis, S.I. Patsios, D.A. Lambropoulou, A.J. Karabelas, Novel pilot scale continuous photocatalytic membrane reactor for removal of organic micropollutants from water. Chem. Eng. J. 304 (2016) 335–343, https://doi.org/10.1016/j.cej.2016.06.075.

This book belongs to Badji Mokhtar Annaba University Central Library Copyright Elsevier 2025

This page intentionally left blank

This book belongs to Badji Mokhtar Annaba University Central Library

Copyright Elsevier 2025

SECTION V

Industrial water remediation processes: Current trends and scale-up challenges

This book belongs to Badji Mokhtar Annaba University Central Library

Copyright Elsevier 2025

This page intentionally left blank

This book belongs to Badji Mokhtar Annaba University Central Library

Copyright Elsevier 2025

CHAPTER 23

Introduction of water remediation processes

Vikesh G. Lade

Chemical Engineering Department, Laxminarayan Institute of Technology, Rashtrasant Tukadoji Maharaj Nagpur University, Nagpur, Maharashtra, India

23.1 Introduction

One of the most essential entities of every living organism for its survival is water; there is no substitute. Water is used to realize various types of essential needs such as drinking, irrigation, cleaning, construction, industrial operations, and in each and every phase of life and nutrient cycle. Out of the total water present, 0.3% of water is useful to human race and other 99.7% is nonuseful water found in oceans, aerosols, icebergs, and soil [1]. This small portion of water is directly accountable for the sustainability of living organisms on Earth, and therefore it needs be protected from pollution.

There is a growing need and increased demand of energy and materials for a rapidly growing population; all industrial sectors are continuously polluting the environment. Due to industrial and technological development, heavy metals are delivered into the environment. The major contribution to emerging organic contaminants (EOC) or pollutants is from chemicals used in medicines, active pharmaceutical ingredients (APIs), pharmaceutical products, agrochemicals, specialty chemicals, and industrial chemicals that have complex molecular structures. Since these contaminants are relatively new, the detection by available methods and equipment becomes critical. At the same time, the available wastewater treatment plants (WWTP) are not capable of removing these contaminants. Therefore, these contaminants may escape from the WWTP and bioaccumulate as they move up the food chain, thereby posing environmental and occupational hazards. Water contains many types of suspended, dissolved, emulsified, or colloidal inorganic and organic pollutants. The presence of these pollutants above critical levels may cause various types of acute and chronic disorders in human health and are toxic to the ecosystem. Several conditions are imposed by different government monitoring agencies for the discharge of effluents into natural water resources. There is a need and necessity to first conserve water and second to find cost-effective and environmentally friendly techniques required for water remediation. Worldwide, scientists are searching for newer and cheaper alternatives to treat wastewater.

Handbook of Nanomaterials for Wastewater Treatment. https://doi.org/10.1016/B978-0-12-821496-1.00033-7
Copyright © 2021 Elsevier Inc. All rights reserved.

This book belongs to Badji Mokhtar Annaba University Central Library Copyright Elsevier 2025

The application of known available technologies to treat wastewater to such an extent where the quality of treated water meets the specification of environmental government regulatory agencies is called "water remediation". Collection of water in designed locations and subjecting this water to various remediation methods are the two major steps of water purification and remediation. Water remediation methods that are already well established are preliminary, primary treatment (viz., mechanical separation, sedimentation, coagulation); secondary treatment (biological treatment); and tertiary treatment (disinfection, chemical purification, aeration, and boiling, etc.) [2]. The block diagram represents the conventional WWTP in Fig. 23.1. The complete water remediation system may comprise of the application of a number of physical, chemical, and biological processes to the wastewater.

The technologies and processes commonly used for water remediation can be classified in five different stages as it moves from impure to pure. These are: (i) preliminary treatment (consisting of screens, comminutor, grit chamber, etc.); (ii) primary treatment (consisting of sedimentation, coagulation, flocculation, etc.); (iii) secondary treatment (involves biological treatment and various biological reactors and filters); (iv) tertiary treatment (disinfection, filtration, etc.); and (v) advanced treatment (viz., adsorption, ion exchange, membrane and advanced oxidation process (AOPs), etc.). The details pertaining to this five-stage wastewater treatment process is shown in Fig. 23.2. This figure also includes examples of each treatment process and their intended applications.

Inorganic species can be removed using ion exchange and reverse osmosis, whereas organic species can be removed using adsorption/activated carbon [3]. Using these technologies, the

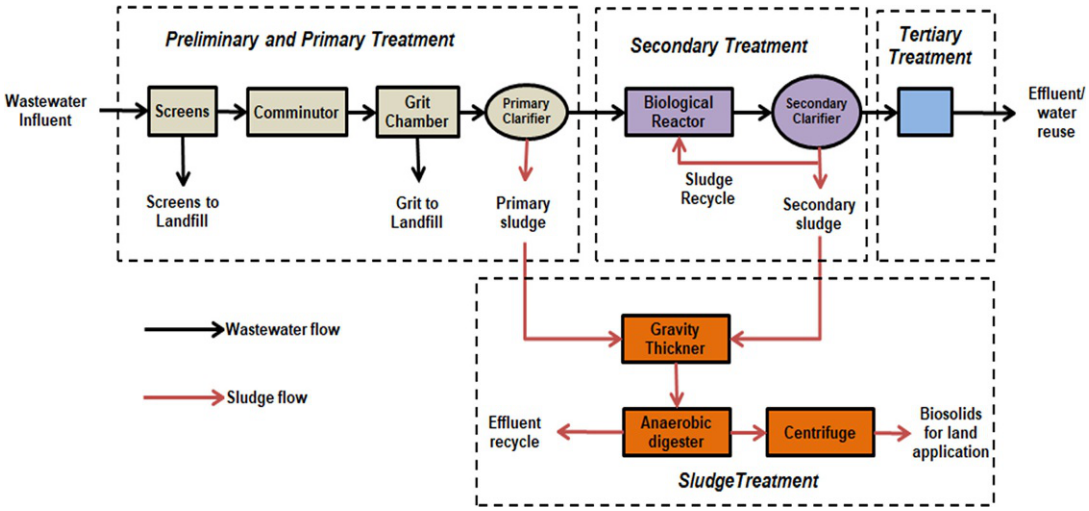

Fig. 23.1
The process flow diagram of a conventional WWTP with sludge digestion [2]. *Redrawn from R. Riffat, Fundamentals of Wastewater Treatment and Engineering, CRC Press, 2012.*

This book belongs to Badji Mokhtar Annaba University Central Library
Copyright Elsevier 2025

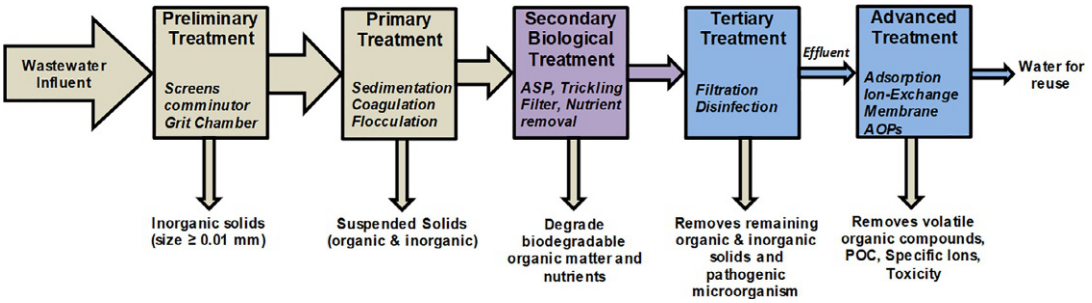

Fig. 23.2
The five-stage block diagram of a wastewater treatment process.

drinking water specification can be met depending on the various contaminants in the wastewater. There are newer technologies such as membrane separation, nanomaterial, photocatalysis, and AOPs that can be used for the remediation of water. It is normal practice for water remediation across the world to use a combination of various remediation methods as no single technology can completely eliminate all contaminants and impurities present in wastewater [4].

Industrial wastewater treatment is aimed at elimination of unwanted contaminants and impurities from wastewater before it is directed to a surface water source. The composition of industrial wastewater should be known well before, so that the prior planning for pretreatment can be made and recovery opportunity (if any) can be identified. The approach for water remediation can be sequential removal of the contaminants present in the wastewater. After detection and removal of the particles of different sizes, the effluent is analyzed for different chemical (chemical oxygen demand (COD), total organic carbon (TOC), heavy metals, etc.) and microbiological (biochemical oxygen demand (BOD), microbial population, etc.) parameters. The analysis will decide the further course of action to the wastewater, i.e., technology requirement is evaluated. The advanced analytical tools and instruments are used for the characterization of organic pollutants by their functional groups and molecular structure.

In a broader sense, water remediation processes can be categorized based on the nature of the operation, viz., physical, chemical, physicochemical, biological, and AOPs. This chapter is meant for the introduction of each water remediation processes/operation.

23.2 Physical methods of wastewater remediation

Water purification starts naturally by amalgamation of natural components, i.e., air, soil, water, sunlight, and other aquatic animals. A natural water purification process has emerged to bring equilibrium in the quality of natural water and water from pollution and stresses in the environment. Both natural and man-made efforts can affect water quality. Natural water

This book belongs to Badji Mokhtar Annaba University Central Library Copyright Elsevier 2025

purification has a direct effect on humans as most of the world's population even today uses direct water. Some of natural methods of purification include aeration, oxidation, and filtration through layers of soil, aquatic animals, evaporation, and flow of water.

The physical methods of water remediation encompass technologies that separate solid contaminants from water, which are only physical phenomena without chemical or microorganism action. These methods include the preliminary and primary treatment methods aimed at the elimination of larger suspended particles and inert matter present in the effluent. These methods help remove larger suspended particles and debris, thereby helping the pumps and other equipment from malfunctioning as well as increasing the efficiency of following biological treatment. The preliminary treatment includes screens for large particle separation, size reduction by grinders, and grit chambers.

The primary treatment is aimed at the separation by sedimentation (settling by gravity) of the suspended solids (which are of organic nature and responsible for BOD) and floating material (oil, grease, and rags) from the wastewater. The floating matter is eliminated as scum from the surface. These are removed as scum from water surface in the tank. These solids are processed in a digester and are disposed of by stabilization method. The primary treatment reduces the load on the secondary treatment. The enhancement in sedimentation can be achieved by the addition of coagulating or flocculation agents.

In this separation method, solid contaminants are transferred to another solid and/or porous media and water is collected as a diluted effluent. The medium of separation requires additional treatment based on the quality and quantity of the wastewater. This further additional treatment may help in complete removal of the contaminant, may concentrate it for recovery and reuse, or may be sent for disposal. The treatment train of other additional treatment is required for complete removal by primary treatment.

The classification of the contaminants of particles present in the industrial/municipal wastewater is as: (i) dissolved (<0.08 μm); (ii) colloidal (0.08–1 μm); (iii) supracolloidal (>1–100 μm); and settleable (>100 μm) [5]. One of most important factors is the size of particles that are in the wastewater, which determines the type of treatment to be selected. The treatment efficiency of the physical treatment is also a function of the size of particles. Various methods of physical water treatment are discussed in detail in the following sections.

23.2.1 Screens

A substantial amount of suspended solids (organic matter, variety of solids, etc.) and floating matter (rags, weeds, twigs, oil, grease, etc.) are present in industrial and municipal wastewater. The solids present in wastewater could make the processes less efficient, thereby contaminating water and perhaps damaging expensive pumps and mechanical equipment. Rotating equipment

This book belongs to Badji Mokhtar Annaba University Central Library Copyright Elsevier 2025

are prevented from solid damage by placing screens ahead of the flow to the inlet, thereby removing the larger solids, called debris (screenings). Disposal of this debris is done in landfills or combusted by incineration.

The classification of screens is based on the size of the screen opening and other mechanical traits. The wastewater treatment screens can be classified in three categories, viz., coarse, fine, and micro.

Coarse screens or bar screens are used to eliminate coarse solids such as rags, large objects, and debris. Course screens have clear openings in the range 25–75 mm and are similar to trash racks. These screens can be mechanically or manually cleaned.

Fine screens have clear openings less than 6 mm and are made of wire cloth, wedge wire, or perforated plates. Fine screens are placed after coarse screens in preliminary treatment, prior to secondary trickling filters in primary treatment, and are used to remove suspended solids that may create operation and maintenance problems [2]. Fine screens are classified into three categories based on mode of operation, viz., (i) static (fixed) wedge wire screen, (ii) rotary drum screen and, (iii) step-type screen.

Microscreens are typically low-speed (up to 4 RPM) rotating drum screens that have openings less than 50 μm. The drums are lined with filtering fabrics with openings of 10–35 μm that are continuously backwashed while operating in gravity flow conditions. Wastewater enters the drum lined with fabric, and the retained solid waste is collected through backwash and disposed of. The fine solids from treated wastewater in tertiary treatment can be removed by the microscreens.

23.2.2 Grit chambers

Wastewater may have sand, gravel, and hard, inert heavy mineral particles with nominal particle size in the range 0.15–0.20 mm or greater, which is called grit [6]. Ash, wood chips, egg shells, and other nonputrescible organic matter may also be considered as grit. Grit chamber facilitates the removal of solids that can settle and form sediment in pipelines, thereby it protects pumps and other mechanical equipment from abrasion. A grit chamber behaves like a sedimentation tank placed before primary clarifiers and after screens. Depending on the plant scale, the grit removal operation can be continuous screw or manual.

23.2.3 Aeration

Aeration is the natural or physical remediation method used for adding oxygen and releasing entrained gases. It improves the physical and chemical quality of water [7]. It is used for the removal of CO_2 before chemical precipitation by soda-lime softening process. Aeration can

This book belongs to Badji Mokhtar Annaba University Central Library Copyright Elsevier 2025

also be used for the oxidation of dissolved iron and manganese available in water to convert it into ferric and manganic that are insoluble. Using settling and filtration, these insoluble salts can be removed.

23.2.4 Sedimentation (clarification)

Eventually the dissolved solids are precipitated in a stage of precipitation and flocculation. Prior to this stage, removal of the floc can be done by solid-liquid separation, which is called sedimentation. This is one of the physical phenomena that relates to the settling of solids by gravity. Therefore, settling velocity of the solid particles is an important factor that needs to be considered for the design of sedimentation tank.

23.2.5 Filtration

Filtration is defined as the separation of suspended solids from water using some media. Industrially it is carried out by passing the solution or suspension through a porous medium or membrane, thereby retaining solids on the medium's surface, called as filtrate. It also removes microbiological organisms and color. Conventionally for wastewater treatment, depending on the application, the filtration can be classified into: (i) sand filtration (slow sand filters, rapid sand filters, or other granular media including multimedia) and (ii) pressure (or vacuum)-type filtration [7]. The novel treatment process of membrane filtration is discussed in Section 23.6.1 whereas the conventional filtration techniques are discussed as follows.

23.2.5.1 Sand filtration

The suspended solids are separated by sand filtration wherein the permeate obtained consists of smaller suspended and dissolved solids that require secondary filtration. There are basically three types of commercial sand filters: (i) slow sand filter; (ii) green sand filter; and (iii) rapid sand filter.

The brief comparisons of the slow sand filter and rapid sand filter is shown in Table 23.1. The slow sand filter gives enhanced quality water in comparison with the rapid sand filtration. But the low output flow rate and high area requirement are the major drawback associated with slow sand filter. The green sand filtration uses filter media, Glauconite (a mineral also called green sand), for the removal of dissolved iron, hydrogen sulfide, and manganese from water.

23.2.5.2 Multimedia filtration

Multimedia filtration (MMF) is a filtration technique that uses more than three layers of filtration media. Normally these media are place in accordance with size and density. The placement of these filter media are anthracite coal (larger and lighter) at the top, sand between, and garnet (smaller and heavier) at the bottom, with gravel at the bottom as support. Due to this

This book belongs to Badji Mokhtar Annaba University Central Library Copyright Elsevier 2025

Table 23.1: A brief comparison of slow sand filter and rapid sand filter.

Criteria	Slow sand filter	Rapid sand filter
Filter media	Fine sand	Layer of activated carbon or anthracite coal above the sand (dual-media filters)
Filter sand quality	Effective size (ES) = 0.15–0.35 mm; uniformity coefficient (UC) = 1.5–3	Effective size (ES) > 0.55 mm; uniformity coefficient (UC) <1.5
Pretreatment	Not required for waters with turbidity <50 NTU	Pretreatment is necessary Coagulation and flocculation, followed by sedimentation
Quality of water	<1 NTU, 95% removal of Pathogens, 75% removal of color, 10% removal of TOC	<1 NTU, 90% Pathogen removal, 10% color removal, 5% removal of TOC
Area requirement	Very large (50–200 m^2)	Small (10–100 m^2)
Flow rate	100–200 LPH/m^2	4800–7200 LPH/m^2

type of arrangement, larger dirt particles are trapped at the top of the filter bed while smaller particles are retained deeper in the media. MMF is used to remove suspended solids (10–25 μm in size), including clay, algae, silt, rust, and other organic matter and turbidity greater than 0.2 NTU.

23.2.6 Distillation

In context to water remediation, distillation is one of the desalination processes that uses difference in volatility of constituent components of the liquid mixture as a driving force. The distillation operation depends on the vapor pressure of the constituents of the liquid mixture, thereby the boiling point of the individual components. The heat energy as input is given to the feed, which raises vapor pressure equal to the surrounding pressure, the liquid mixture boils, and distillation occurs. The separation of inorganic substances and inhibition of microorganisms can also be accomplished by distillation. The problem associated with distillation is the separation of the organics having boiling points lower than 100°C, as these organics become concentrated at the bottom as well as in the product distillate. To make water really safe for drinking, these organics must be removed from the water stream by using a carbon filter system. Because the carbon filter can become a breeding spot for microbial growth, it must be replaced regularly.

The distillation technology is a very slow process and produces distilled water that does not contain nutrient minerals so it is safe but not healthy. Some of the advantages of this technology are: (i) removal of a wide range of pollutants (toxic chemicals, heavy metals, bacteria, viruses, parasites), (ii) can be operated in a continuous mode, (iii) physical barriers (filters) are not required, and (iv) additional disinfection is not required.

This book belongs to Badji Mokhtar Annaba University Central Library Copyright Elsevier 2025

Distillation has drawbacks such as a large energy input is required for both heating and cooling and lower chemical contaminants will be carried with water, but the purity of water can be achieved by careful maintenance and operation.

The emerging newer technology of *membrane distillation (MD)* for desalination and wastewater treatment had been invented by Bodell in 1963 [8]. The driving force for the operation of the MD process is the difference in vapor pressure between the feed and the permeate, which is brought about by the temperature gradient across the hydrophobic semipermeable membrane surface, which only allows water vapor to pass but not liquid water as illustrated in Fig. 23.3 [9].

The operating temperature of the feed water stream is maintained around 50–80°C, and the hydrophobic membrane act as a barrier to liquid phase water and does not allow it to enter the pores, whereas vapor phase passes through the membrane and collects at the permeate side.

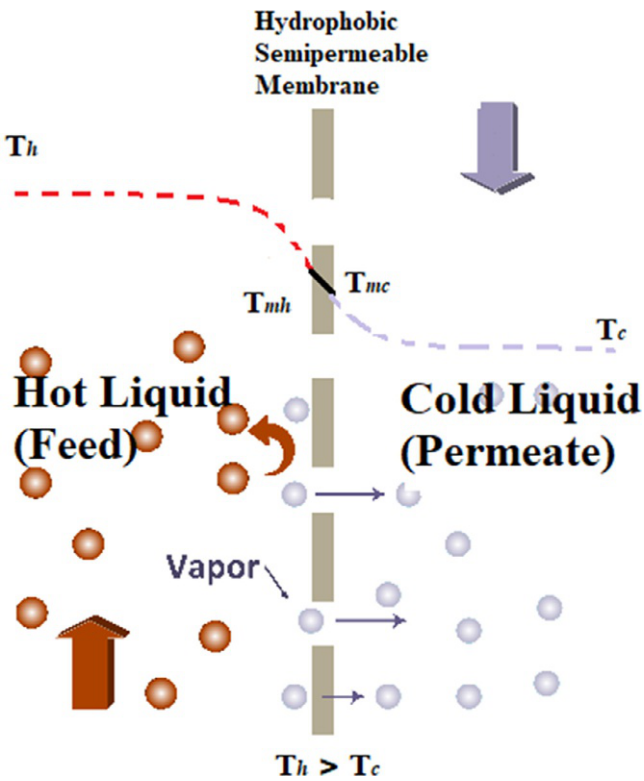

Fig. 23.3
Basic principle of membrane distillation process [9]. *Redrawn from A. Shirazi, M. Mahdi, A. Kargari, A review on applications of membrane distillation (MD) process for wastewater treatment, J. Membr. Sci. Res. 1 (2015) 101–112. Copyright (2015) FIMTEC & MPRL.*

This book belongs to Badji Mokhtar Annaba University Central Library
Copyright Elsevier 2025

The major advantage of MD as separation processes is lower operating temperature that is lower than the boiling point of water, therefore it requires minimum energy, operation, capital, and land cost. It requires no extensive pretreatment in comparison to conventional distillation column and also has a smaller footprint and volume. MD can coupled with the waste heat, alternate energy, or renewable sources (like solar energy, geothermal energy) for economical and energy efficient operation of the plant [10]. Water flux for MD process is low as compared to reverse osmosis, which is one of the drawbacks of MD, and therefore the commercial application at a large scale has been limited. Due to advancement in membrane fabrication technology, the manufacture of highly porous electrospun nanofiber membranes (ENMs) that can provide high water flux has become easier, and therefore the trend is reversed [8]. Hydrophobic polymers such as polyethylene (PE), polyvinyl chloride (PVC), and halogenated PEs can be used for fabrication of MD membranes. But recently, polyvinylidene fluoride (PVDF) was given special attention as a preferred membrane material [9].

23.3 Physicochemical water treatment processes

The primary aim of the physicochemical treatment is the separation of colloidal particles from wastewater. The two major processes that can be classified as physicochemical water treatment processes are: (i) precipitation and coagulation and (ii) adsorption.

23.3.1 Precipitation and coagulation

Microscopic particles (size <1 μm), having a colloidal nature, do not settle readily and have significant stable pollution capability, and therefore must be removed by means other than settling. These particles have electrostatic surface negative charges that prevent them from conglomeration due to their repulsive nature. The suspended particles are responsible for the color and turbidity of water, which essentially consist of inorganic matter (clay and salt, etc.) and organic matter (microorganisms, viz., algae, bacteria, viruses, protozoa, and biomass).

The method of addition of reagents for the removal of one or more insoluble solid substances from a solution is called "*Precipitation*." The driving force for precipitation is "solubility". One of the examples is formation of a precipitate (solubility product) when a solution has ionic concentration solubilized in a reagent.

The chloride and sulfate salts of trivalent metal ions of iron and aluminum can be used as coagulant in water treatment practice. The process of destabilization of the negatively charged particles available in wastewater by the reaction of hydrolysis with its hydrolysis product of "microflocs" during rapid mixing is called "*Coagulation*."

The particles present in water interact with inorganic coagulant salts (aluminum sulfate (or alum) or iron (III) salts), and negatively charged particles are neutralized by positive charge of

This book belongs to Badji Mokhtar Annaba University Central Library Copyright Elsevier 2025

the ionic Fe(III) or Al(II). The reaction product of metal hydroxide of the Fe and Al ions start to appear in the form of precipitate. Flocculation is the formation of the agglomerate into larger particles of the precipitates due to Brownian motion and induced mixing [11]. These large agglomerates of the hydroxides of Al and Fe(III) remain in suspension and can be removed further by sedimentation and filtration. The coagulation is because of the intense mixing whereas the flocculation is because of slow mixing (natural convection). The quantity of the coagulant/flocculent required depends on the quality of the wastewater. The classification of flocculants can be based on nature (mineral or organic); origin (synthetic or natural); or electric charge (anionic, cationic, or nonionic). Organic flocculants have low effectiveness, and they are obtained from natural products like alginates (seaweed extract), starches (plant grain extracts), and cellulose derivatives.

Heavy metals also can be removed from industrial wastewater by *chemical precipitation*. The studies related to removal of arsenic and nickel (about 98%) from synthetic wastewater using granulated lime as coagulant were performed [12]. Because this process uses chemicals for removal of dissolved/particulate solids from wastewater, it is sometimes called as chemically enhanced primary treatment (CEPT).

23.3.2 Adsorption

Adsorption is a surface phenomenon where the dissolved contaminants (adsorbate) are accumulated (adsorbed) onto the surface of the solid particles called adsorbents. Adsorption is one of the most efficient and utilized techniques for removing several organic and inorganic contaminants in wastewater.

The type of bond formation depends on the surrounding nature of the contaminant (adsorbate) and adsorbent. The general classifications of adsorption are physisorption (attributed by weak Van der Waals forces) and chemisorption (originates from covalent forces). The removal of dissolved contaminant with characteristics of color, taste, and odor from water can be accomplished by the adsorbent combining chemical and physical processes. The basic criterion for adsorbent is that it should be highly microporous, thereby have high surface area-to-volume ratio. The adsorption isotherm is the quantitative interrelation between the equilibrium concentration of solute (contaminant) on the adsorbent surface to concentration of solute in bulk solution at constant temperature. Based on the mechanism of adsorption, there are many theories, therefore various isotherms types are available [13]. However, two most well-known adsorption isotherms are Langmuir (theoretical and practical basis and can be derived from first principle) and Freundlich (empirical nature), which are normally used for development and design purposes.

The major limitation of the adsorption process is the high cost of adsorbents as well as operation. The factors that influence the economic and commercial feasibility of adsorption

This book belongs to Badji Mokhtar Annaba University Central Library Copyright Elsevier 2025

processes are type of adsorbent, properties of the contaminant and the bulk, mode of operation, operating conditions, regenerability of adsorbent, and waste disposal [14].

The carbon-based microporous solids, e.g., activated carbon [15], biochar [16], carbon nanotubes [17], and graphene oxides [18] have been used as adsorbents. Also, silica [19], clay minerals [20], aluminas [21], zeolites [22], etc. are used as adsorbents because of lower cost, large surface area due to microporous nature, and nonpolar nature for the elimination of organic and inorganic species and odor, color, and taste from water [23]. To date, many adsorbents have been synthesized and used for the removal of contaminants like radionuclides, heavy metals, pharmaceutical compounds, dyes, and especially emerging pollutants from water. However, in recent times, researchers are inclined toward bioadsorbents (biomass and agricultural waste as raw materials of sorbents) and nanomaterials as adsorbents due to their effective, safe, eco-friendly, low-cost, and low-energy intensive material properties [24].

23.4 Chemical remediation

In chemical remediation, the chemical reactions are used to improve water quality. The best results can be achieved by using a chemical remediation method along with physical water treatment methods. The processes and methods through which the chemical remediation can be achieved are chemical disinfection, halogenation, ozonation, neutralization, ion exchange, and oxidation.

23.4.1 Chemical disinfection

23.4.1.1 Chlorination

Chlorination is the one of the disinfection methods that is normally used before preliminary treatment and in tertiary treatment, as well as used in all stages of wastewater treatment. Most often conventional chlorination is accomplished by use of chloramine or chlorine oxide. Microorganisms like bacteria and protozoa can be disinfected by chlorine [25]. Since handling chlorine gas is hazardous and dangerous, there are two methods by which the chlorination can be done: (i) use of sodium and calcium hypochlorite and (ii) electrolytic method. The first one is more popular where, after dissolution, the free chlorine is released in water. The chlorination is associated with major drawback of formation of hazardous by-products, like trihalomethanes (THM) and haloacetic acids (THAA) due to the reaction between organic compounds in water with chlorine [26]. These hazardous by-products are potential carcinogens and are increased due to operating parameters like temperature, pH, contact time, and the concentration of organics in water. The concentration of THM and THAA can be lowered by reducing the organics from wastewater. Therefore, chlorination should be used after elimination of organics from water.

This book belongs to Badji Mokhtar Annaba University Central Library Copyright Elsevier 2025

The use of chloramine is advantageous as there is no formation of THMs or THAA. However, chloramine releases ammonia, which results in nitrification by bacterial growth.

Another chlorinating agent is bleaching powder. It should be used in a stoichiometric amount because, in excess, it will give off a disagreeable odor and bad taste, whereas if it is a limited reactant, there will not be complete disinfection of water [27].

23.4.1.2 Iodination

Iodine is a cost-effective, simple to use, and efficient chemical disinfectant method. It has good oxidizing properties, similar to chlorine. The major controversy associated with iodine is the dosage and time for use. However, within a short time with small dosage, it can disinfect various types of pathogens such as spores, viruses, and cysts, etc. [28]. The regulated release of iodine is accomplished by use of the following three forms: (i) organic iodide compound; (ii) iodophors: (combination of iodine and nonionic surfactant); and (iii) iodine integrated resins, cross-linked *co*-polymers of styrene, and divinylbenzene.

23.4.1.3 Ozonation

Ozone (O_3) is an unstable allotrope of oxygen that protects organisms from UV radiation, and it has to be generated wherever it is used [29]. O_3 is prepared by passing dry oxygen through silent electrical discharge or UV light. The mechanism of disinfection can be understood by knowing the reaction where organic compounds are converted in aldehydes and ketone by the addition of oxygen due to the high oxidation potential of ozone. The organic material of the bacteria cell membrane is oxidized by ozone, thereby it disinfects water. It also clarifies water by enhancing the coagulation of insoluble Fe(III) and Mn(VII). The mass transfer limitation can be eliminated by use of appropriate gas-liquid contactor so that ozone is contacted efficiently with the target contaminant in water phase.

23.4.1.4 Hydrogen peroxide

The decomposition of hydrogen peroxide (H_2O_2) yields the free oxygen radical, which is the main agent responsible for disinfection and oxidation (eliminating protein). H_2O_2 is not a very powerful disinfectant in comparison to chlorine, iodine, ozone, and other disinfectants. It does not produce residues or gasses, which are major advantages. However, the disadvantages are related to safety issues such as it cause severe skin burns and eye damage, inflammation, and pulmonary edema.

23.4.2 Neutralization

Neutralization is a chemical treatment method normally used in industrial wastewater treatment, wherein acid or base is added to the wastewater so as to adjust pH levels to neutral. One chemical characteristic of wastewater is pH, which needs to be restrained, as both lower

This book belongs to Badji Mokhtar Annaba University Central Library Copyright Elsevier 2025

and higher pH will be dangerous and corrosive. In some industrial operations, the wastewater generated contains a high level of organic material tending to acidic nature, thereby increasing in numerous pathogenic microorganisms that raise concern in environmental and health hazards. In the cement and beverage industry, wastewater has alkaline with high pH ranging from 8.0 to 12. High alkalinity will damage equipment and thereby the overall process. Therefore, pretreatment can be done in the form of neutralization and furthermore it can be sent for treatment process before disposal. Highly alkaline wastewater and by-products can be neutralized by using several chemicals like hydrochloric acid, sulfuric acid, phosphoric acid, carbon dioxide, and some microorganisms [30].

Sodium hydroxide or sodium carbonate can be used to neutralize hexafluorosilicic acid to sodium fluorosilicate in certain operations of the fertilizer and fluorochemical industry. A pH control system plays an important role in a wide range of industrial applications particularly in wastewater treatment management.

23.4.3 Ion exchange

Replacement of impure ions of water with the ions released by immobilized solid particles in a reversible manner is called an ion exchange process, which is used for the demineralization of water. Ion exchange units consist of insoluble substances that have loosely held ions and are capable of ion exchange with the solution. The removal of hardness and nitrates can be accomplished by ion exchange. The cation-exchange resins and anion-exchange resins are two types of resins used for exchange of charged impurities. Positive charge impurity present in water will be exchanged with cations of the cation-exchange resin, whereas negative charge impurity present in water will be exchanged with anions of the anion-exchange resin. In an operation, water flows through two packed columns consisting of both types of ion exchange resins. One consists of cation-exchange resins where hydrogen ions are exchanged with the cation of water, while in the second bed, anions are exchanged with the hydroxyl ions. The periodic regeneration of these beds is necessary to restore the original ionic form once the beds are exhausted.

23.5 Biological remediation/treatment

Biological treatment of industrial wastewater is normally a secondary treatment that uses microorganisms to convert organic matter and colloidal material, unwanted chemicals that are not easily separable into harmless inorganics, simpler molecules (CO_2, H_2O, CH_4), and biomass under aerobic/anaerobic/semi-aerobic conditions. Microorganisms used for the treatment could have four sources such as natural, commercial, specific group, and acclimated sewage sludge [31]. Reduction of the BOD and suspended solids to meet the specifications laid down by the organizations is another goal of the biological secondary treatment. The

This book belongs to Badji Mokhtar Annaba University Central Library Copyright Elsevier 2025

Table 23.2: Various types of Biological water treatment processes. [32].

Process	Suspended growth	Attached growth	Hybrid	Lagoon
Aerobic process	Activated sludge Aerated lagoons Aerobic digestion Sequencing batch reactors Membrane bioreactors	Trickling filters Rotating biological contactor (RBC) Packed bed reactors	Trickling filter/activated sludge	Aerobic lagoons
Anoxic process	Suspended growth denitrification	Attached growth denitrification		
Anaerobic processes	Anaerobic contact processes Anaerobic digester	Anaerobic packed and fluidized bed	Upflow sludge blanket/ attached growth	Anaerobic lagoons
Facultative				Facultative lagoons

Redrawn from L. Metcalf, H.P. Eddy, G. Tchobanoglous, Wastewater Engineering: Treatment, Disposal, and Reuse, McGraw-Hill, New York, 1979.

decomposition rate of aerobic is higher than anaerobic processes. Anaerobic processes release methane and sulfur compounds, and therefore it gives off unpleasant odors and requires higher detention time.

Three major categories of biological treatment processes using different electron acceptors are: (1) suspended growth (activated sludge); (2) fixed/bio film or attached growth (e.g., trickling filters, rotating biological contactors (RBCs)); and (3) hybrid process (combination of biofilm and suspended growth). Table 23.2 represents various processes that fall under different types of biological water treatment.

23.5.1 Suspended growth process

Suspended growth process consists of the aggregates of microorganisms that are in suspension and are growing as flocs in a reactor by the use of appropriate mixing technology. Organic matter in the wastewater is consumed by the microorganisms as food that is converted into energy, new biological cells, and waste matter. Only specific types of microorganisms or mixed culture can help the decomposition of the specific composition of the wastewater, i.e., it is organism-specific. Therefore, the food that is most suitable to metabolism of microorganisms in the mixed culture also varies [33]. Bacteria, protozoa, and metazoan are the most relevant microorganisms, whereas fungi and viruses are of negligible importance in treatment of wastewater. Treatment of wastewaters in suspended growth environments offers many process advantages, which has led to the proliferation of this type of treatment system.

This book belongs to Badji Mokhtar Annaba University Central Library
Copyright Elsevier 2025

Suspended growth processes can be exemplified as (i) aerobic: activated sludge process, the sequencing batch reactor, waste stabilization ponds, aerated lagoons and (ii) anaerobic: conventional high-rate anaerobic digesters. To design an efficient process reactor, an understanding of growth mechanisms of microorganisms using wastewater as a substrate is necessary [34]. In comparison with an activated sludge system, in recent times, the advanced technology of membrane bioreactors (MBRs) have emerged as an important process of interest for research and application.

23.5.1.1 Activated sludge process

The fundamental scientific principle behind activated sludge processes is that the organic contaminants provide carbon and energy required for microbial growth and reproduction thus converting organic contaminants into waste products and cell mass. This process is very effective in removal of carbonaceous matter and nitrification from wastewater.

The activated sludge process is a three-stage operation as shown in Fig. 23.4 and described as follows:

(i) Biological reactor or aeration tank: Pretreated wastewater is mixed with the return activated sludge (RAS) taken from final sedimentation (mixed liquor) containing high concentration of microorganisms and is circulated in a continuous manner into an aeration tank [36]. The mixing of air with microorganisms in wastewater is ensured by passing a large quantity of air, thereby the oxygen demand of microorganisms is met. This also ensures the solids are in suspension to maintain aerobic conditions (mixed liquor suspended solids, MLSS).

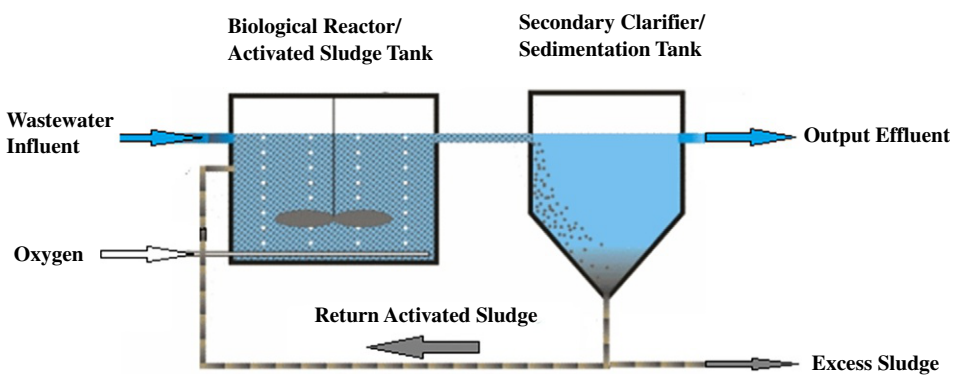

Fig. 23.4

Staged operation of activated sludge process. [35]. *Redrawn from P. Fracz, Nonlinear modeling of activated sludge process using the Hammerstein-Wiener structure, in: E3S Web of Conferences, 2016, This is an open access article distributed under the terms of the Creative Commons Attribution License 4.0, http://creativecommons.org/licenses/by/4.0/.*

This book belongs to Badji Mokhtar Annaba University Central Library Copyright Elsevier 2025

(ii) Sedimentation tank or clarifier: Once the biochemical reaction is complete, mixed liquor consisting of particles and clumps that are able to settle flows to a clarifier (normally a settling tank) so that they can separate with a simple settling process. Flotation tank or membranes can be used to separate microorganisms in some special cases. A part of thickened settled solids sludge is removed as underflow (called waste-activated sludge, WAS). The clarified effluent flows on for further treatment if needed or for disposal.

(iii) Recycle system: Part of the activated sludge (about 20%–50%) from secondary clarifier is recycled back to the first biological reactor, which is called RAS. RAS ensures that the hydraulic retention time is much less than the mean cell residence time. The concentration of activated sludge in the biological reactor is maintained by RAS; this helps in effective and fast oxidation of organic compounds. The sludge from treatments, the primary treatment, and biological secondary treatment is combined; solid separation and further treatment is performed. Due to stringent environmental regulations in relation to excess sludge disposal, the focus has shifted toward the minimization of the sludge production by effective utilization of organic carbon for carbon dioxide production [37].

23.5.2 Attached growth (biofilm) processes

In an attached growth process, bioconversion of organic matter to stable simpler molecules is carried out by microbial cells, which adhere to an inert medium (rock, plastics, synthetic material, etc.) inside the reactor where it grows and forms film [32]. This process is not common compared with suspended growth process. The operation of attached growth process can be aerobic or anaerobic and can be exemplified by well-known commercial processes like trickling filters, biotowers, and rotating biological contactors (RBCs).

23.5.2.1 Rotating bioreactor contactor

The construction of an RBC unit consists of a series of closely spaced flat or corrugated parallel disks of polymeric material that are mounted on a rotating horizontal shaft, which is partially or completely submerged in the wastewater (see single module of RBC in Fig. 23.5) [38]. The microbial media (biological film) passes through effluent and absorbs the organic material, which in turn forms a film and absorbs oxygen as it is carried into air. Aerobic condition is maintained by the complete rotation, as the water film mixes with a pool of wastewater adding oxygen into the tank. Rotation speed of 2 to 5 RPM ensures solids in suspension and the hydraulic shear necessary for the removal of biofilm from media [33].

The amalgamation of both suspended growth process and attached growth biological reactors is called a hybrid process. This can be illustrated by having a trickling filter between the aeration tank and sedimentation tank of activated sludge process. Implication of having a hybrid process is to decrease the cost and time required for removal organic matter in the primary effluent. Based on this requirement, new ways of hybrid arrangements can be done. Integrated fixed-film

This book belongs to Badji Mokhtar Annaba University Central Library Copyright Elsevier 2025

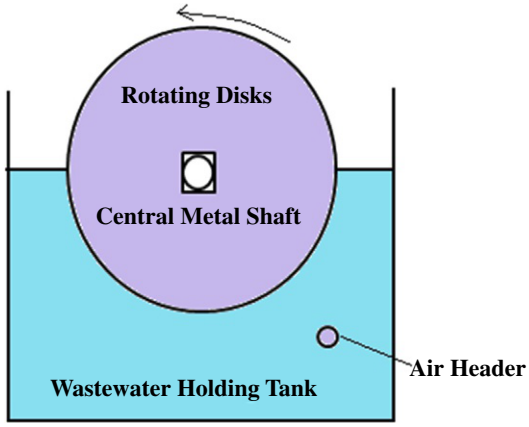

Fig. 23.5
Single module of rotating bioreactor contactor [33]. *Redrawn from H.S. Peavy, D.R. Rowe, G. Tchobanoglous, Environmental Engineering, McGraw-Hill, 1985. Hybrid processes (suspended/attached growth).*

activated sludge reactor (IFAS) [39] [40], moving bed biofilm reactors (MBBR) [41], and fluidized bed biological reactors (FBBR) [42] are some of the examples of hybrid systems [43].

23.5.3 Combined processes

Combined process is the combination of trickling filter and activated sludge process. Due to advantages such as high efficiency, low energy requirement, stability, resistance to shock loads, high quality of effluent, and improved sludge settling characteristics, the combined processes are the most preferred choice as compared to individual processes. The combinations for the combined process can be trickling filter/activated sludge (TF/AS) process or a trickling filter/solids contact (TF/SC) process.

23.6 Advanced/novel water remediation processes

Conventionally, any process followed by primary and biological treatment (secondary) was considered as tertiary or advanced treatment. In recent times, advanced treatment processes are additional specialized processes or steps required for removing specific toxic substances (heavy metal, inorganics, and hazardous waste), nutrients (nitrogen, phosphorus), residual total suspended solids, and emerging contaminants of concern when effluent from secondary treatment do not comply the discharge water standards. Conventional advanced processes hold true in most cases, however in the case of industrial wastewater, it may entirely substitute for all conventional processes. The quality requirement of the reclaimed processed water defines the selection of the technology and their combination [44].

This book belongs to Badji Mokhtar Annaba University Central Library Copyright Elsevier 2025

As industrial growth persists, the emergent environmental pollutants (EEP), i.e., newer organic contaminants have become a major problem for water. EOCs is the broad term used for newly developed and discovered chemicals in the environment. It also includes the wide range of compounds such as pharmaceutical, specialty chemicals, pesticides, additives, etc., and products and by-products of all combined transformations. These EOCs from the wastewater cannot be removed by conventional wastewater chemical, physical, and biological treatment processes.

Conventional water treatment technologies were matured enough and well established to satisfy the requirement throughout the 20th century (to the beginning of third industrial revolution). The conventional treatment methods such as screens, sedimentation, filtration, distillation, coagulation, adsorption, chemical disinfection, ion exchange, biological treatment, aeration, etc., are described in detail in previous sections of this chapter. The effectiveness of removal pathogens and new chemical pollutants (EOCs, EEP, etc.) using conventional water treatment processes is not up to the mark, rather they fail to remove some of the contaminants. Therefore, to satisfy new requirements of stringent specifications across the globe, the need for the development new innovative technologies called advanced/novel water treatment methods are in place. The advanced/novel water treatment techniques like adsorption, membrane separation, and AOPs can effectively remove EOC [45]. Adsorption is already described in Section 23.3.2. We will discuss membrane technology and AOPs in detail in the following sections.

23.6.1 Membrane technology

The membrane is a semipermeable (highly permeable to some ingredient components and less permeable to other ingredients of wastewater) synthetic polymeric material. The classification of the membranes is based on the types of compound rejected, operating pressure, and nominal pore size of the membrane. There are generally two broad categories of membranes based on the (1) separation of suspended particles from water, i.e., *microfiltration* (MF) and *ultrafiltration* (where membranes act as barrier) and (2) separation of ions from water, i.e., *nanofiltration* (NF) and *reverse osmosis* (RO) (semipermeable). A membrane unit can have two types of flow pattern, i.e., crossflow and dead end. Fig. 23.6 shows the separation of product and waste streams using a membrane.

Contaminants such as suspended solids or microorganisms and bacteria from wastewater are normally separated using membranes with nominal pore size ranging from 0.1 μm to 10 μm, which is called *microfiltration (MF)*. The mechanism of separation is based on the fact that the larger particles are rejected whereas the particles size smaller than the pore size flow freely through the pore, which is stereochemical exclusion.

This book belongs to Badji Mokhtar Annaba University Central Library Copyright Elsevier 2025

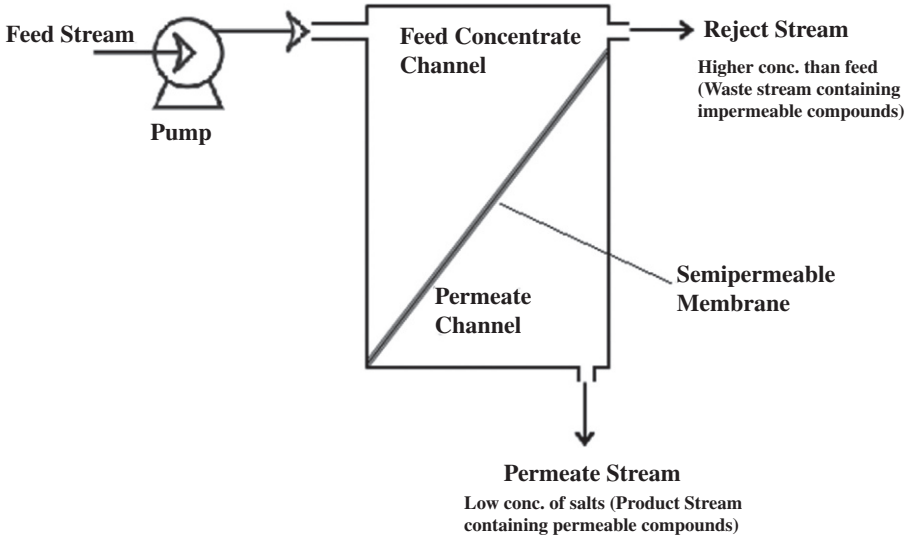

Fig. 23.6
Schematic of separation of product and waste streams using RO/NF membranes [46]. *Redrawn from L. Masson, B.S. Richards, A.I. Schäfer, System design and performance testing of a hybrid membrane—photovltaic desalination system, Desalination 179 (2005) 51–59. Copyright (2005) Elsevier.*

Ultrafiltration (UF) is normally used for the partition and accumulation of macromolecules, utilizing membranes having nominal pore size of 0.01–0.1 μm. The molecular exclusion and diffusion is the basic principle associated with the transport mechanisms that govern separation, and membrane efficiency is evaluated on molecular weight cut-off (MWCO).

MF and UF technologies in some cases are also functions of the nature of the feed stream just as adsorption and clogging are functions of the colloidal particles present in water. Regardless of the wastewater feed concentration variation, MF and UF advanced treatment processes are normally used for treating water with high turbidity (high suspended solids concentration), removal of microorganisms (viruses and bacteria) from potable water, or as a pretreatment in reverse osmosis [47].

Reverse osmosis (RO) operates on the preferred separation mechanism of solution/diffusion where a semipermeable membrane is used to remove salts and small organic species from water and is operated at higher operating pressure.

Water containing high concentration of TDS is subjected to high pressure against the semipermeable membrane, thereby increasing applied pressure greater than osmotic pressure, which makes water molecules move from the higher concentration to the less concentrated

This book belongs to Badji Mokhtar Annaba University Central Library Copyright Elsevier 2025

solution (product). The semipermeable membranes act as a barrier to nearly all of the dissolved solids in water and permit the passage of water molecules. In this way, the TDS concentration is increased on the high-pressure side, which can then be discharged as reject stream from the process. *Nanofiltration (NF)* has a preferred separation mechanism between diffusion (as in RO) and molecular exclusion (as in UF), but in some cases electrostatic interactions are also found. NF is similar to RO that works at a lower pressure. The NF is used for the demineralization of polyvalent salts and also for the removal of organic solutes having low molecular weight (200–1000 Da) [48]. The operating mechanism, pressures, retentate, and permeate conditions of all previously mentioned membrane technologies are shown in Table 23.3.

The design, operation, and cost effectiveness of membranes depend on factors such as membrane material, high flux, high solute rejection, configuration of module, stability (mechanical/chemical/thermal/temporal), and process scale-up ability, etc. The most often used commercial membrane material is polymer, which can be either hydrophilic (polyacrylonitrile, hydrophilized polysulfone, hydrophilized polyethylene (PE), etc.) or hydrophobic [such as polyvinylidene fluoride (PVDF), polytetrafluroethylene (PTFE), polyacrylonitrile, and poly(acrylonitrile)-poly(vinyl chloride) *co*-polymers] [3, 49].

In recent times, the *inorganic membranes* are given importance in research as well as industrial scenario of wastewater treatment applications because it has thermal, chemical, and mechanical robustness in comparison with organic membranes. The most significant advantages of an inorganic membrane are reusability and photocatalytic ability. With macroporous support and few top layers of microporous material, *inorganic membrane* is made up of ceramics or zeolites. In a recent development in the fabrication technologies, the nanocrystalline form of ceramic materials such as alumina (Al_2O_3) [50], silicon dioxide (SiO_2), titanium dioxide (TiO_2), zirconium dioxide (ZrO_2), and composite (containing two or more materials, TiO_2-SiO_2, TiO_2-ZrO_2, and Al_2O_3-SiC) are being synthesized [49].

There are four configurations of membranes: (i) flat sheet and plate and frame, (ii) hollow fiber, (iii) tubular, and (iv) spiral wound. The most commonly used for laboratory separations is flat sheet and plate and frame configuration, whereas NF and RO normally use hollow fiber and spiral wound membrane configurations. Inorganic ceramic membranes are fabricated into tubular configurations that have low packing densities.

The advantages of the membrane technology in comparison to the conventional technologies are: (1) wider industrial range of application; (2) uniform quality of the treated water; (3) no extra chemicals are added; (4) waste streams recycle within a plant; (5) smaller space requirement; (6) simple and easy-to-operate, thereby no requirement of highly skilled operator; (7) low maintenance cost by making it highly automated; and (8) lower energy costs as compared to thermal treatments [51].

This book belongs to Badji Mokhtar Annaba University Central Library
Copyright Elsevier 2025

This book belongs to Badji Mokhtar Annaba University Central Library

Table 23.3: Membrane separation process characteristics [48].

Membrane technology	Microfiltration (MF)	Ultrafiltration (UF)	Nanofiltration (NF)	Reverse osmosis (RO)	Electrodialysis (ED)
Pore size (μm)	≥0.1	≈0.01	≈0.001	≈0.0001 (nonporous)	
Driving force	ΔP	ΔP	ΔP	ΔP	ΔE
Operating pressure (bar)	0.5–2	1–7	5–25	15–80	
Separation mechanism	Sieve	Sieve	Sieve + Solution/ Diffusion + exclusion	Solution/Diffusion + exclusion	Ion exchange
Retentate	Suspended solids, bacteria, algae, and protozoans $MW >$ 500,000 Da (0.01 μm)	Colloids and macromolecules $MW >$ 2000 Da	Molecules 500 Da $< MW <$ 2000 Da bacteria, viruses, divalent and multivalent ions	All soluble and suspended material (ions, bacteria, viruses, and other contaminants)	Macromolecules and nonionic compounds
Permeate	Water and dissolved solids	Water, salts, and compounds of low MW	Water, salts, and compounds of low MW	Water, solvent	Ions

ΔP = Pressure difference, ΔE = Potential difference, MW = Molecular weight.

Redrawn from A. Bernardes, M. Rodrigues, J. Ferreira, Electrodialysis and Water Reuse, Springer, 2016.

Copyright Elsevier 2025

The disadvantages of the membrane processes are linear scale-up that makes a high capital cost for large effluent volumes and fouling and degradation of membrane, which increases operating costs significantly.

23.6.2 Electrodialysis

Electrodialysis (ED) is an electrochemical desalination process in which transfer of ions through semipermeable ion selective membranes occurs under the influence of an applied electric potential [52]. *ED* is used for the removal of charged compounds from a feed solution. Water containing charged ions flows between the multiple cation and anion selective membranes in a row; this facilitates removal of positively and negatively charged ions, respectively. The spacers are provided between membranes to provide a flow path for water, support the membranes, and create turbulent flow [53]. The two types of membranes, cation-selective (sulphonated polystyrene) and anion-exchange (quaternary ammonia polystyrene), are alternated in a membrane stack obtaining repeating unit. The pretreatment of the source water is required most often before ED can be used in wastewater purification.

23.6.3 Electrocoagulation

Contaminants in wastewater are typically dissolved colloidal particles or suspended emulsified; the process of destabilizing these contaminants by the introduction of an electric current is one of the advanced methods of wastewater treatment with combination of chemical coagulation and electrical field known as *electrocoagulation (EC)* [54] [55]. It is an environmental friendly approach as no chemical is used and it requires minimal personnel training and inexpensive equipment. Under the influence of DC voltage, the electrodes, normally made of iron or aluminum, an oxidation (formation of hydroxyl ions and hydrogen gas)/reduction (dissolution of metal) process takes place [56]. Advantages of EC are electrodes are cheap and readily available, and it produces lesser amount of sludge. EC has been used for the treatment of number of wastewaters, phenol, and number of heavy metal pollutants. The various parameters on which EC and its efficiency depends are choice of electrode materials, pH of solution, current density, electrolysis time, concentration, flow rate, temperature, electrode arrangement, and reactor design [55].

23.7 Advanced oxidation processes

AOPs are newer technologies where highly reactive and oxidizing free radical molecules like hydroxyl radical (OH•) are used to treat biologically inert, hazardous, toxic, and persistent organic pollutants (POPs) found in water and wastewater [57]. AOPs are “clean technologies” as hydroxyl radicals react with dissolved constituents, and recalcitrant organic compounds are completely mineralized into CO_2 and H_2O, in turn, thus no environmental loadings of secondary contaminants [58].

This book belongs to Badji Mokhtar Annaba University Central Library Copyright Elsevier 2025

The AOPs can be categorized based on the reactive phase (homogeneous and heterogeneous) and hydroxyl radical generation methods (chemical, electrochemical, sonochemical, and photochemical) [59].

For complete mineralization so that effluent can be sent to natural water bodies, relatively more energy and/or chemicals are consumed. The main purpose of AOP is a decomposition of specific organic recalcitrant compounds, reduction in toxicity, and increased biodegradability of organic compounds; therefore, it is mostly augmented into water treatment train of various other technologies. It is not advised to use this treatment for effluent with COD value greater than 5000 mg/L [60].

The homogeneous processes are the reactions carried out especially only in liquid phase or gas phase, i.e., the reaction/interactions between the chemical reagents used for oxidation and target compounds/contaminants are in same phase. The heterogeneous processes are multiphase (liquid/solid, gas/solid, and gas/liquid/solid) reactions, which occur at the active catalytic sites of the catalyst surface. The surface reactions are the result of intermolecular interactions that occur during adsorption of reactants to the surface and desorption of products from the active site. Therefore, the surface characteristics and the pore structure of the catalyst are the parameters, which need to be considered for the design of the reactor.

The major advantages of AOPs are oxidation of any contaminants present in wastewater (nonselective), possibility of complete mineralization of pollutants, and less solid waste formation. Therefore, the current research trend is around finding new commercial ways for AOPs for different industrial wastewater.

23.7.1 Chemical AOPs

23.7.1.1 Fenton processes

Fenton oxidation process can be defined as an AOP wherein highly reactive hydroxyl radical (•OH) is formed by the catalytic degradation of Fenton's reagent (solution of hydrogen peroxide (H_2O_2) with ferrous iron (typically Fe(II) salt)) [60], as shown in the following equation:

$$Fe^{2+} + H_2O_2 \rightarrow Fe^{3+}OH^- + \bullet OH \tag{23.1}$$

Although the Fenton reaction was discovered about 100 years ago, the direct use of this process in the wastewater treatment started in the 1960s [61, 62]. Fenton process can be used for the removal of numerous hazardous organic contaminants from water by complete decomposition of contaminants into nontoxic compounds, e.g., CO_2, water, and inorganic salts. The Earth's crust has plenty of iron and a is nontoxic element, and H_2O_2 is a green chemical; therefore oxidative degradation by Fenton process is attractive [63].

This book belongs to Badji Mokhtar Annaba University Central Library Copyright Elsevier 2025

The reduction of Fe^{3+} to Fe^{2+} can be accomplished by a variation in proper value of pH (2.7–2.8) (Fenton-like) [64]:

$$Fe^{3+} + H_2O_2 \rightarrow H^+ + FeOOH^{2+} \tag{23.2}$$

$$FeOOH^{2+} \rightarrow HO_2 \bullet + Fe^{2+} \tag{23.3}$$

In this case, the iron can be regarded as a real catalyst.

23.7.1.2 O_3/H_2O_2 treatment (peroxonation)

The principle of O_3/H_2O_2 treatment is based on the fact that the addition of both ozone (O_3) and hydrogen peroxide (H_2O_2) to wastewater results in formation of a large number of very reactive oxidizing radicals •OH because of accelerated decomposition of ozone [65]. The formation of •OH radicals is a very fast reaction; the mechanism can be represented by the reaction:

$$O_3 + HO_2^- \rightarrow O_2 + \bullet OH + O_2^- \tag{23.4}$$

23.7.2 Photochemical advanced oxidation processes

Photochemical AOPs are based on the amalgamation of UV radiations with strong oxidants like O_3 and H_2O_2, also in some cases, Fenton reagent or TiO_2. The decomposition of contaminants/pollutants from wastewater occurs by three possible ways: (i) photodecomposition: UV irradiation or excitation and degradation of contaminants; (ii) oxidation: by direct action of O_3 and H_2O_2; and (iii) oxidation by photocatalysis: generating •OH radicals by Fe^{3+} or TiO_2. This section deals with the details regarding the principles and applications of different AOPs, viz., H_2O_2 photolysis (H_2O_2/UV), O_3 photolysis (O_3/UV), photo-Fenton process (H_2O_2/Fe^{2+}/UV), and heterogeneous photocatalysis (TiO_2/UV).

23.7.2.1 H_2O_2 photolysis (H_2O_2/UV)

In H_2O_2 photolysis, the generation of •OH radicals occurs due to homolytic cleavage of O—O bond of hydrogen peroxide molecule by the use of UV radiations using wavelength of 200–300 nm [66]. The mechanism of H_2O_2 photolysis accompanied by several successive and competitive reaction steps is as follows:

$$\text{Initiation steps: } H_2O_2 + h\nu \rightarrow 2 \bullet OH \tag{23.5}$$

$$\text{Propagation steps: } \bullet OH + H_2O_2 \rightarrow H_2O + HO_2^\bullet \tag{23.6}$$

$$HO_2^\bullet + H_2O_2 \rightarrow \bullet OH + H_2O + O_2 \tag{23.7}$$

$$\bullet OH + HO_2^- \rightarrow HO_2^\bullet + OH^- \tag{23.8}$$

$$\text{Termination steps: } 2HO_2^\bullet \rightarrow H_2O_2 + O_2 \tag{23.9}$$

This book belongs to Badji Mokhtar Annaba University Central Library
Copyright Elsevier 2025

$$\bullet OH + HO_2^{\bullet} \rightarrow H_2O + O_2 \tag{23.10}$$

$$2 \bullet OH \rightarrow H_2O_2 \tag{23.11}$$

Ionization of H_2O_2 results in HO_2^- anions, which generate free radicals (HO_2• and •OH) as a result of absorption of UV radiations; the greater the alkalinity of the medium (at pH > 10), the higher the rate of reaction. The limitation to this process is the requirement of strong concentration of H_2O_2 for the efficient oxidation of organic contaminants, as H_2O_2 has weak molar absorption coefficient in the UV region.

H_2O_2 photolytic oxidation have been used for decomposition of contaminants of emerging concern (CECs) like bisphenol-A, estrone, diclofenac, ibuprofen, and triclosan [67] and various groups of pesticides [68].

23.7.2.2 O_3 photolysis (O_3/UV)

O_3 photolysis process is AOP wherein the aqueous solution saturated with ozone is irradiated with UV radiation (wavelength from 200 to 360 nm and maximum of 253.7 nm having molar absorption coefficient $\varepsilon_{max} = 3600\ Lmol^{-1}\ cm^{-1}$) in an apparatus convenient for such heterogeneous media. Oxidation potential of ozone is 2.07 eV, which rises to 2.8 eV in the presence of UV irradiation. The molar absorption coefficient of H_2O_2 $\varepsilon_{max} = 18.6\ Lmol^{-1}\ cm^{-1}$, which is much smaller than that of the O_3. The generation of •OH radicals as a result of O_3 photolysis in water occurs via different reaction mechanism [69]. The reaction scheme is shown as:

$$\text{Initiation step: } O_3 + H_2O + hv \rightarrow 2 \bullet OH + O_2 \tag{23.12}$$

$$\text{Propagation steps: } O_3 + \bullet OH \rightarrow HO_2^{\bullet} + O_2 \tag{23.13}$$

$$O_3 + HO_2^{\bullet} \rightarrow \bullet OH + 2O_2 \tag{23.14}$$

$$\text{Termination step: } \bullet OH + HO_2^{\bullet} \rightarrow H_2O + 2O_2 \tag{23.15}$$

$$2 \bullet OH \rightarrow H_2O_2 \tag{23.16}$$

O_3 photolysis process has been used to get rid of the numerous volatile chlorinated organic compounds (VCOCs) like chloroform, trichloromethane, trichloroethylene, tetrachloroethylene, etc. [70].

23.7.2.3 Photo-Fenton reaction (H_2O_2/Fe^{2+}/UV)

A photo-Fenton reaction is a supplementary of Fenton process in which, the UV-VIS light irradiation (at wavelength > 300 nm) is used to stimulate the catalytic reduction of Fe^{3+} into Fe^{2+} as shown in following general arrangement scheme:

$$Fe^{3+} + H_2O + hv \rightarrow Fe^{2+} + H^+ + \bullet OH \tag{23.17}$$

This book belongs to Badji Mokhtar Annaba University Central Library
Copyright Elsevier 2025

The best form of Fe^{3+} is the $[Fe(OH)]^{2+}$ ion at pH 2.8–3.5 [71]. The direct decomposition of H_2O_2 molecules into •OH radicals can be assisted by UV irradiation in the H_2O_2/UV.

23.7.2.4 Photocatalysis

Photocatalysis is a type of catalysis where the rate of chemical reaction is accelerated by either direct irradiation or by irradiation of a photocatalyst without being consumed in the reaction as a result of absorption of photons and due to reduction in the activation energy of the reaction [72]. The photocatalytic activity is a function of ability of the photocatalyst to create electron-hole pairs that, in turn, will generate free radicals (e.g., •OH radicals) that are able to undergo secondary reactions. There are numerous solids that can be considered as photocatalysts. However, metal oxide semiconductors are the most appropriate photocatalysts because of their photocorrosion resistance and wide bandgap energies [60, 73]. Similar to catalysts, photocatalysts remain unchanged during and after reaction. But, from a thermodynamic point of view, photocatalysis drives energy-storing reactions ($\Delta G > 0$), and chemical catalysis is limited to thermodynamically possible reactions ($\Delta G < 0$) [74].

There are different noble metal nanoparticles, metal oxides semiconductors (ZnO, Fe_2O_3, WO_3, SiO_2, SnO_2, PtO_2, CeO_2, and $SrTiO_3$, etc.), and nanocomposites and chalcogenides (CdS, ZnS, etc.) that can be used as photocatalysts. However, their application in water treatment processes is limited due to solubility in water and toxicity [75]. Fixed-bed photoreactors and slurry batch photoreactors (mechanically or magnetically stirred) are the two photoreactors normally used in industry based on the reaction.

TiO_2 is a highly chemically and thermally stable, nontoxic, biologically inert, superconductor metal oxide. The generation of active oxygen species on its surface occurs as a result of absorption of ultraviolet light, which can be used for photo-oxidation. The reaction mechanism of the photocatalytic process is shown as:

$$\text{Initiation step: } TiO_2 + hv \rightarrow e^- + h^+ \tag{23.18}$$

$$\text{Propagation steps: } TiO_2(h^+) + H_2O_{ad} \rightarrow TiO_2 + HO^{\bullet}_{ad} + H^+ \tag{23.19}$$

$$TiO_2(h^+) + HO_{ad}{}^- \rightarrow TiO_2 + HO^{\bullet}_{ad} \tag{23.20}$$

$$\text{Termination step: } TiO_2(h^+) + RX_{ad} \rightarrow TiO_2 + RX^{\bullet +}_{ad} \tag{23.21}$$

The first initiation step is the absorption of the radiation, which leads to the formation of electron-hole pairs (Eq. 23.18). Some metals and dissolved oxygen are reduced using electrons and formation of the superoxide radical ion $O^{\bullet 2}$, whereas remaining holes oxidize the adsorbed H_2O or HO^- to reactive •HO radicals (Eqs. 23.20, 23.21). The last termination step is of great significance in photo-oxidation processes where desired adsorbed substrate can be rightly oxidized by electron transfer (Eq. 23.21).

This book belongs to Badji Mokhtar Annaba University Central Library
Copyright Elsevier 2025

TiO_2 is mostly chosen and broadly used in water and wastewater treatment. The main factors that govern the photocatalytic activity of TiO_2 are crystal composition, orientation and surface area, particle size distribution, porosity, and bandgap energy [76]. TiO_2 heterogeneous photocatalyst can be used in two forms: (i) dispersed form and (ii) thin film form layer. The synthesis of TiO_2 films using TiO_2 coatings on different varieties of support materials have been studied [77]. The dispersed TiO_2 catalyst is the suspension of TiO_2 in aqueous media, which is easy to use, has high specific surface, and has high catalyst efficiency. Dispersed TiO_2 can be charged with air that prevents the recombination of electron-hole pairs. The major limitation of TiO_2 dispersed form is reduction in photoreactor performance and efficiency with time as it slowly forms dark catalytic sludge, thereby creating mass transfer resistance. In contrast, for TiO_2 film form, the catalytic layer is very stable and active, so there is no need of separation of particles at the completion of the process. According to the nature of the organic pollutants, pH is to be optimized prior to the reaction, as efficiency of photocatalysis is also a function of pH.

23.7.3 Sonochemical advanced oxidation processes

The process technology that utilizes ultrasound in aqueous medium can act in two distinct types of mechanisms: one physical (direct) and other chemical (indirect). In these processes, the degradation of contaminant is based on cavitation effects that are generated by means of ultrasound irradiation (acoustic cavitation) or employing constrictions to flow by providing valves, orifices, and venturi (hydrodynamic cavitation) [58, 78]. In an indirect mechanism, high-frequency ultrasound waves interact with water and dissolved oxygen molecules and are subjected to homolytic cleavage to produce •OH, HO_2•, and •O radicals [79].

The physical (direct) mechanism (also called as sonication) involves formation of liquid bubbles as a result of the expansion of waves possessing sufficient intensity to surpass the molecular forces. Due to alternating compression and expansion cycles of ultrasound, these bubbles continually absorb energy and the bubbles grow (due to diffusion of vapor or gas from liquid medium) until they come to a critical size and then disintegrate [80–82]. This bubble collapse creates strong breaking intensity with extremely high temperatures ($T = 2000–5000$ K) and pressures (nearly 1000 atm) that act as a localized "hot spot" for short-life. In these conditions, chemical processes (bond cleavage) occur, which generate very reactive hydrogen atom and hydroxyl radicals capable of reacting with organic compounds present in effluent [65, 83].

$$H_2O +))) \rightarrow \bullet OH + \bullet H \tag{23.22}$$

$$\bullet OH + R \rightarrow \text{Products} \tag{23.23}$$

$$R + \Delta H \rightarrow \text{Products} \tag{23.24}$$

where:))) = ultrasound, X = organic compound(s).

This book belongs to Badji Mokhtar Annaba University Central Library Copyright Elsevier 2025

Ultrasound bath and probe (also called horn) are the two common apparatus for the generation of acoustic cavitation in water. In direct sonication, the ultrasonic source is in direct contact with the liquid medium, whereas indirect sonication can be obtained when a vessel containing the solution to treat is immersed. In both cases, the ultrasound waves are produced by a transducer coupled to a vibrating plate for the bath and a tip for the probe. To maintain temperature, an additional thermostat (cooler/heater) can be incorporated in the main setup [84].

There is plenty of recent research that supports the utilization of ultrasound for the oxidation and degradation of organic contaminants in waters and wastewaters [85–90]. The limitation of this process is that the number of •OH radicals generated are not sufficient enough for effective degradation of the contaminants. But if ultrasound is utilized in the presence of additional oxidants, like H_2O_2 and oxygen, UV irradiation, or Fenton's reagent (accompanied by different forms of iron: Fe^0, Fe^{2+}, and Fe^{3+}) (sono-Fenton), these hybrid technologies have better degradation/destruction efficiencies [65, 84, 88].

23.7.4 Electrochemical advanced oxidation processes

When electron transfer between chemical species, where one is reductant (electron donor) while other the oxidant (electron acceptor), a chemical transformation in the chemical species with an odd number of valence electrons takes place. The electrochemical AOPs (EAOPs) are the green processes of decontamination of effluent having various toxic and persistent organic contaminants based on the transfer of electrons, which produce hydroxyl radicals (•OH) responsible for degradation. The electrooxidation process can be categorized in two ways, i.e., direct and mediated oxidation [91, 92]. Direct as well as mediated oxidation processes occur concurrently in the solution [93].

The mechanism of direct oxidation, also called anodic oxidation (AO), consists of production of heterogeneous hydroxyl radicals M(•OH) (Eq. 23.25) upon water electrolysis on a high O_2-overvoltage anode such as a Pt, PbO_2, and boron-doped diamond (BDD) electrode [94, 95] and oxidation of organics (Eq. 23.26):

$$\mathrm{M} + \mathrm{H_2O} \rightarrow \mathrm{M}(\bullet\mathrm{OH}) + \mathrm{H}^+ + e^- \tag{23.25}$$

$$\mathrm{M}(\bullet\mathrm{OH}) + \mathrm{R} \rightarrow \mathrm{M} + m\mathrm{CO_2} + n\mathrm{H_2O} + p\mathrm{X} \tag{23.26}$$

where, M = anode material; •OH = heterogeneous •OH radicals adsorbed on the anode material; R = organic matter and X = inorganic ions.

The removal of various organic pollutants, especially diclofenac [94] and phenol [96, 97] using Pt anode, have been well studied. In comparison to Pt anode, BDD thin film anode is a new, effective, powerful, and promising anode material for electrochemical AOPs [98, 99].

This book belongs to Badji Mokhtar Annaba University Central Library
Copyright Elsevier 2025

Mediated process is based on the generation of reactive species indirectly via electrochemistry coupling with another AOP. An example of mediated process can be electrocatalytically produced Fenton's reagent (electro-Fenton (EF) process) [100], coupled with another photochemical (photoelectro-Fenton (PEF)) [101] or sonochemical (sonoelectro-Fenton) [91, 102, 103]. The mechanism of the Fenton is shown in Eq. (23.1), and two-electron reduction of dissolved O_2 in acidic medium is responsible for in situ electrogeneration of H_2O_2 (Eq. 23.27) using catalytic quantity of ferrous ions [91].

$$O_2 + 2H^+ + 2e^- \rightarrow H_2O_2 \tag{23.27}$$

Previously, mercury pool (Hg) was used as a cathode material, but due to its hazardous nature, graphite, activated carbon fiber, and carbon nanotubes are preferred [65].

23.8 Nanomaterial for wastewater remediation

One of the most important scientific accomplishments of the 20th century is nanotechnology (nanomaterial synthesis and application). Recent advances in the field of nanomaterials shows that it is used in almost all water remediation processes like filtration, membranes (RO, MD), adsorbents, photocatalysts, pervaporation, electrodialysis, bioremediation, desalination, and water disinfection [104, 105]. New generation nanomaterials, viz., carbon nanotubes (CNTs), graphene, and zeolites have been used in water remediation processes [106] [107].

There are a number of reviews related to the use of nanotechnology for water remediation and purification, such as carbon-based nanomaterials [108], nanomaterials-based AOPs [109], cellulose nanomaterials [110], inorganic nanomaterials and organic molecule-based nanomaterials [111], chitosan-based nanomaterials [112], graphene/metal oxide composites [113–115], carbon nanotubes, and graphene [116]. Biogenic metal nanoparticles (MNPs) are one of the more interesting NPs, as explained here.

23.8.1 Biogenic metal nanoparticles

Metal oxides and zero-valent metals can be deposited on cells of microbes, and this can change the oxidation state of metals. Biogenic MNPs have high surface area and high reactivity. Due to presence of bacteria in MNPs, it can be used as a bioadsorbent, catalyst, oxidizing agent, and reducing agent. Advanced water pollutants like EOPs, heavy metals, and pathogenic microorganisms have been treated using biogenic MNPs [117]. There are several papers around the biogenic manganese [118] and iron [119] for denitrification, and precious metal biogenic metals been applied for water remediation technology [117].

This book belongs to Badji Mokhtar Annaba University Central Library Copyright Elsevier 2025

23.9 Path forward

Finding newer technologies and improved materials for water remediation is a never-ending demand for the human race. To obtain clean drinking water in a sustainable manner, we need to revisit existing technologies and materials. This necessitates the application of advanced materials and technologies in the field of wastewater treatment, water purification, conservation, and reuse. The following can lead the way forward in sustainable water remediation technology:

(1) *Nanotechnology*: The application of the nanotechnology to improve water by applying nanomaterial in existing technologies and revisiting its basics. There are also major challenges that should be addressed for judicial use of nanotechnology in water remediation: (i) the environmental impact assessment of nanomaterials; (ii) health effects and life cycle assessment of the nanomaterials; (iii) scale-up issues in nanomaterial synthesis; and (iv) cost-effective processes for commercialization.

(2) *Sustainable development*: As per the Brundtland Commission's report to the United Nations in 1987, sustainable development is defined as "development that meets the needs of the present without the ability of future generations to meet their own needs." The holistic approach to environmental management is the *sustainability*. The practices that are based on preservation and augmentation of economic and natural resources, ecology, human health and safety, and quality of life are called sustainable practices [4].

(3) *Green remediation*: It is the practice of minimizing the environmental footprint of clean-up actions. The strategies for green remediation that are based on sustainable development wherein along with economic development the philosophy of environmental protection is integral, which is ecologically viable today and in the long run. Green and sustainable remediation of water is a rapidly growing field of interest.

(4) *A green economy:* It can be defined as an economy that results in improved human well-being and social equity, while significantly reducing environmental and ecological scarcities. It includes efficient use of raw materials (resource efficient), efficient processes (low carbon emission, water management, low liquid effluent generation, low process cost), stakeholders (socially inclusive, manufacturer, customer), and product (by-products and wastewater management, lower environmental impact, life cycle assessment). Safeguarding freshwater ecosystems, proper water management, and judicial wastewater management and treatments are necessary for facilitating social and economic development by maintaining biodiversity.

(5) *Scale-up*: Existing and new processes and products have to be redesigned based on sustainability and green principles. More attention has to be given to the scale-up of the processes as major processes can fail due to scale-up issues. The manufacture of the nanomaterial at a commercial scale to meet market demand is a major challenge. So, equipment scale-up has to be undertaken by scientists and engineers to come up with sustainable green processes and products at a commercial scale.

This book belongs to Badji Mokhtar Annaba University Central Library Copyright Elsevier 2025

(6) *Policy*: Wastewater management specialists (engineers/chemists/scientists) identify threats to human and ecological health as a result of disposal of wastewater in water bodies. These threats are potential opportunities where appropriate policy and management can create new economic and employment opportunities, thereby public and ecosystem health can be improved in developing and underdeveloped countries. All stakeholders such as government agencies, corporations, academia, environmental consultants, public interest groups, and individuals are benefitted by these opportunities.

(7) *Safety*: Safety remains an integral part of all raw materials, processes, and products. This also signifies the capabilities of organization, and thereby the market value is increased.

(8) *New developments*: Conventional methods for water treatment cannot address all the issues of water and wastewater treatment. Therefore, there is a need to develop the processes that are minimally dependent on *chemicals* and *energy*. The new processes should be easy to operate, and require less capital and operation cost. The operational infrastructure, engineering expertise, and excellence can be incorporated into the organizational goal.

(9) *Research direction*: The research needs to be more focused toward creating lighter and stronger materials for remediation of water and wastewaters. The research should be oriented toward identification of the sources for green materials including inorganic to organic to hybrid, plant biomass to animal biomass, nonporous to porous, microbial to antimicrobial, and solids to liquids.

(10) *Renewable materials*: The replacements for conventional methods can be based on the environmental considerations that demand the development of strong, economically viable, and eco-friendly methods. The renewable materials that are economical and eco-friendly can always be considered when replacing existing processes and products.

23.10 Conclusion

Water remediation methods have been classified based on the physical, chemical, physicochemical, biological, and advanced/novel treatments and AOPses. AOPs have been classified as chemical, photochemical, sonochemical, and electrochemical and are discussed alone and as combined with chemical or photochemical processes, like ozonation/H_2O_2 to develop efficient water treatment technologies. The adsorption and membrane-related processes have also been discussed, which are still useful and effective. Biosorbents and nanomaterials are recent trends in water remediation technologies. The need of the sustainable and green remediation principles for synthesis of new and existing processes and products have been identified with major challenges in scale-up, safety, and policymaking being stressed. Therefore, the need for new technologies and improved materials for water remediation is a never-ending demand for the human race.

This book belongs to Badji Mokhtar Annaba University Central Library Copyright Elsevier 2025

References

[1] S. Bhattacharya, A.B. Gupta, A. Gupta, A. Pandey, Introduction to Water Remediation: Importance and Methods, 2018 https://doi.org/10.1007/978-981-10-7551-3_1.

[2] R. Riffat, Fundamentals of Wastewater Treatment and Engineering, CRC Press, 2012.

[3] A. Hu, A. Apblett, Nanotechnology for Water Treatment and Purification, Springer, 2014, https://doi.org/10.1007/978-3-319-06578-6.

[4] A. Mishra, J.H. Clark, Green Materials for Sustainable Water Remediation and Treatment, Royal Society of Chemistry, 2013.

[5] A.D. Levine, G. Tchobanoglous, T. Asano, Size distributions of particulate contaminants in wastewater and their impact on treatability, Water Res. 25 (1991) 911–922, https://doi.org/10.1016/0043-1354(91)90138-G.

[6] R.L. Droste, R.L. Gehr, Theory and Practice of Water and Wastewater Treatment, John Wiley & Sons, 2018.

[7] N.L. Nemerow, F.J. Agardy, J.A. Salvato, Environmental Engineering: Water, Wastewater, Soil and Groundwater Treatment and Remediation, John Wiley & Sons, 2009.

[8] M. Khayet, T. Matsuura, Membrane Distillation: Principles and Applications, Elsevier, 2011.

[9] A. Shirazi, M. Mahdi, A. Kargari, A review on applications of membrane distillation (MD) process for wastewater treatment, J. Membr. Sci. Res. 1 (2015) 101–112.

[10] K.W. Lawson, D.R. Lloyd, Membrane distillation, J. Membr. Sci. 124 (1997) 1–25.

[11] S. Sharma, A. Bhattacharya, Drinking water contamination and treatment techniques, Appl. Water Sci. 7 (2017) 1043–1067, https://doi.org/10.1007/s13201-016-0455-7.

[12] O. Akpor, M. Muchie, Remediation of heavy metals in drinking water and wastewater treatment systems: processes and applications, Int. J. Phys. Sci. 5 (2010) 1807–1817.

[13] D.C. Panadare, V.G. Lade, V.K. Rathod, Adsorptive removal of copper(II) from aqueous solution onto the waste sweet lime peels (SLP): equilibrium, kinetics and thermodynamics studies, Desalin. Water Treat. 52 (2014) 7822–7837, https://doi.org/10.1080/19443994.2013.831789.

[14] A. Bonilla-Petriciolet, D.I. Mendoza-Castillo, H.E. Reynel-Ávila, Adsorption Processes for Water Treatment and Purification, Springer, 2017.

[15] C. Shen, Y. Zhao, W. Li, Y. Yang, R. Liu, D. Morgen, Global profile of heavy metals and semimetals adsorption using drinking water treatment residual, Chem. Eng. J. 372 (2019) 1019–1027, https://doi.org/10.1016/j.cej.2019.04.219.

[16] A.I. Osman, A. Abdelkader, C. Farrell, D. Rooney, K. Morgan, Reusing, recycling and up-cycling of biomass: a review of practical and kinetic modelling approaches, Fuel Process. Technol. 192 (2019) 179–202, https://doi.org/10.1016/j.fuproc.2019.04.026.

[17] Z. Yin, Duoni, H. Chen, J. Wang, W. Qian, M. Han, F. Wei, Resilient, mesoporous carbon nanotube-based strips as adsorbents of dilute organics in water, Carbon N. Y. 132 (2018) 329–334, https://doi.org/10.1016/j.carbon.2018.02.074.

[18] T.H. Tu, P.T.N. Cam, L.V.T. Huy, M.T. Phong, H.M. Nam, N.H. Hieu, Synthesis and application of graphene oxide aerogel as an adsorbent for removal of dyes from water, Mater. Lett. 238 (2019) 134–137, https://doi.org/10.1016/j.matlet.2018.11.164.

[19] T. Okura, K. Goto, M. Murai, Fundamentals in the use of activated silica in water purification, Mem. Fac. Eng. Hokkaido Univ. 11 (1960) 25–39.

[20] O. Abollino, M. Aceto, M. Malandrino, C. Sarzanini, E. Mentasti, Adsorption of heavy metals on Na-montmorillonite. Effect of pH and organic substances, Water Res. 37 (2003) 1619–1627, https://doi.org/10.1016/S0043-1354(02)00524-9.

[21] B. Kasprzyk-Hordern, Chemistry of alumina, reactions in aqueous solution and its application in water treatment, Adv. Colloid Interface Sci. 110 (2004) 19–48, https://doi.org/10.1016/j.cis.2004.02.002.

[22] N.M. Mahmoodi, M.H. Saffar-Dastgerdi, Zeolite nanoparticle as a superior adsorbent with high capacity: synthesis, surface modification and pollutant adsorption ability from wastewater, Microchem. J. 145 (2019) 74–83, https://doi.org/10.1016/j.microc.2018.10.018.

[23] S. Babel, T.A. Kurniawan, Low-cost adsorbents for heavy metals uptake from contaminated water: a review, J. Hazard. Mater. 97 (2003) 219–243, https://doi.org/10.1016/S0304-3894(02)00263-7.

This book belongs to Badji Mokhtar Annaba University Central Library

Copyright Elsevier 2025

[24] D. Mehta, S. Mazumdar, S.K. Singh, Magnetic adsorbents for the treatment of water/wastewater—a review, J. Water Process Eng. 7 (2015) 244–265, https://doi.org/10.1016/j.jwpe.2015.07.001.
[25] H. Galal-Gorchev, Chlorine in water disinfection, Pure Appl. Chem. 68 (1996) 1731–1735.
[26] S.D. Richardson, A.D. Thruston, T.V. Caughran, P.H. Chen, T.W. Collette, K.M. Schenck, B. W. Lykins, C. Rav-Acha, V. Glezer, Identification of new drinking water disinfection by-products from ozone, chlorine dioxide, chloramine, and chlorine, Water Air Soil Pollut. 123 (2000) 95–102.
[27] M.M. Benjamin, Water Chemistry, Waveland Press, 2014.
[28] S. Punyani, P. Narayana, H. Singh, P. Vasudevan, Iodine based water disinfection: a review, J. Sci. Ind. Res. 65 (2006) 116–120.
[29] C. Gottschalk, J.A. Libra, A. Saupe, Ozonation of Water and Waste Water: A Practical Guide to Understanding Ozone and its Applications, second ed., (2010), https://doi.org/10.1002/9783527628926.
[30] R.A. Kunal, R. Siddique, Bacterial treatment of alkaline cement kiln dust using Bacillus halodurans strain KG1, Braz. J. Microbiol. 47 (2016) 1–9.
[31] A. Fakhru'l-Razi, A. Pendashteh, L.C. Abdullah, D.R.A. Biak, S.S. Madaeni, Z.Z. Abidin, Review of technologies for oil and gas produced water treatment, J. Hazard. Mater. 170 (2009) 530–551, https://doi.org/10.1016/j.jhazmat.2009.05.044.
[32] L. Metcalf, H.P. Eddy, G. Tchobanoglous, Wastewater Engineering: Treatment, Disposal, and Reuse, McGraw-Hill, New York, 1979.
[33] H.S. Peavy, D.R. Rowe, G. Tchobanoglous, Environmental Engineering, McGraw-Hill, 1985.
[34] D. Mara, N. Horan, Handbook of Water and Wastewater Microbiology, 2003, https://doi.org/10.1016/B978-0-12-470100-7.X5000-6.
[35] P. Fracz, Nonlinear modeling of activated sludge process using the Hammerstein-Wiener structure, in: E3S Web of Conferences, 2016, https://doi.org/10.1051/e3sconf/20161000119.
[36] M. Sustarsic, Wastewater treatment: understanding the activated sludge process, in: Safety in Ammonia Plants and Related Facilities Symposium, 2009, pp. 26–29.
[37] Y. Liu, J.-H. Tay, Strategy for minimization of excess sludge production from the activated sludge process, Biotechnol. Adv. 19 (2001) 97–107, https://doi.org/10.1016/S0734-9750(00)00066-5.
[38] S. Cortez, P. Teixeira, R. Oliveira, M. Mota, Bioreactors: rotating biological contactors, Encycl. Ind. Biotechnol. Bioprocess, Biosep. Cell Technol. (2009) 1013–1030.
[39] F. Veuillet, S. Lacroix, A. Bausseron, E. Gonidec, J. Ochoa, M. Christensson, R. Lemaire, Integrated fixed-film activated sludge ANITA™Mox process—a new perspective for advanced nitrogen removal, Water Sci. Technol. 69 (2013) 915–922, https://doi.org/10.2166/wst.2013.786.
[40] A. Malovanyy, J. Trela, E. Plaza, Mainstream wastewater treatment in integrated fixed film activated sludge (IFAS) reactor by partial nitritation/anammox process, Bioresour. Technol. 198 (2015) 478–487, https://doi.org/10.1016/j.biortech.2015.08.123.
[41] D. Di Trapani, M. Christensso, H. Ødegaard, Hybrid activated sludge/biofilm process for the treatment of municipal wastewater in a cold climate region: a case study, Water Sci. Technol. 63 (2011) 1121–1129, https://doi.org/10.2166/wst.2011.350.
[42] W.K. Shieh, J.D. Keenan, Fluidized bed biofilm reactor for wastewater treatment BT—bioproducts, in: Advances in Biochemical Engineering/Biotechnology, Springer Berlin Heidelberg, Berlin, Heidelberg, 1986, pp. 131–169.
[43] M.L. Davis, Water and Wastewater Engineering Design Principles and Practice, Wetpress, 2010, https://doi.org/10.1016/0016-0032(67)90545-5.
[44] T. Nawaz, S. Sengupta, Chapter 4—contaminants of emerging concern: occurrence, fate, and remediation, in: S. Ahuja (Ed.), Advances in Water Purification Techniques, Elsevier, 2019, pp. 67–114, https://doi.org/10.1016/B978-0-12-814790-0.00004-1.
[45] D. Banks, B.-M. Jun, J. Heo, N. Her, C.M. Park, Y. Yoon, Selected advanced water treatment technologies for perfluoroalkyl and polyfluoroalkyl substances: a review, Sep. Purif. Technol. 231 (2020) 115929, https://doi.org/10.1016/j.seppur.2019.115929.
[46] L. Masson, B.S. Richards, A.I. Schäfer, System design and performance testing of a hybrid membrane—photovoltaic desalination system, Desalination 179 (2005) 51–59, https://doi.org/10.1016/j.desal.2004.12.022.

This book belongs to Badji Mokhtar Annaba University Central Library Copyright Elsevier 2025

[47] A.J.M. Gottberg, J.M. von Persechino, A. Yessodi, Integrated Membrane Systems for Water Reuse, GE Water and Process Technologies, TP1027EN 0601, 2005.
[48] A. Bernardes, M. Rodrigues, J. Ferreira, Electrodialysis and Water Reuse, Springer, 2016.
[49] A. Lee, J.W. Elam, S.B. Darling, Membrane materials for water purification: design, development, and application, Environ. Sci. Water Res. Technol. 2 (2016) 17–42, https://doi.org/10.1039/C5EW00159E.
[50] K.A. DeFriend, M.R. Wiesner, A.R. Barron, Alumina and aluminate ultrafiltration membranes derived from alumina nanoparticles, J. Membr. Sci. 224 (2003) 11–28, https://doi.org/10.1016/S0376-7388(03)00344-2.
[51] A. Basile, A. Cassano, N.K. Rastogi, Advances in Membrane Technologies for Water Treatment: Materials, Processes and Applications, Elsevier, 2015.
[52] D.R. Rowe, I.M. Abdel-Magid, Handbook of Wastewater Reclamation and Reuse, CRC Press, 1995.
[53] F. Valero, A. Barceló, R. Arbós, Electrodialysis technology-theory and applications, in: Desalination, Trends and Technologies, InTech, InTech Rijeka, 2011.
[54] M. Vepsäläinen, M. Sillanpää, Chapter 1—electrocoagulation in the treatment of industrial waters and wastewaters, in: M. Sillanpää (Ed.), Advanced Water Treatment Electrochemical Methods, Elsevier, 2020, pp. 1–78, https://doi.org/10.1016/B978-0-12-819227-6.00001-2.
[55] E.H. Ezechi, A.C. Affam, K. Muda, Principles of electrocoagulation and application in wastewater treatment, in: Handbook of Research on Resource Management for Pollution and Waste Treatment, IGI Global, 2020, pp. 404–431.
[56] S.M.D.-U. Islam, Electrocoagulation (EC) technology for wastewater treatment and pollutants removal, Sustain. Water Resour. Manag. 5 (2019) 359–380, https://doi.org/10.1007/s40899-017-0152-1.
[57] A.R. Ribeiro, O.C. Nunes, M.F.R. Pereira, A.M.T. Silva, An overview on the advanced oxidation processes applied for the treatment of water pollutants defined in the recently launched directive 2013/39/EU, Environ. Int. 75 (2015) 33–51, https://doi.org/10.1016/j.envint.2014.10.027.
[58] V.K. Saharan, D.V. Pinjari, P.R. Gogate, A.B. Pandit, Advanced oxidation technologies for wastewater treatment: an overview, in: Industrial Wastewater Treatment, Recycling and Reuse, 2014, https://doi.org/10.1016/B978-0-08-099968-5.00003-9.
[59] A. Babuponnusami, K. Muthukumar, A review on Fenton and improvements to the Fenton process for wastewater treatment, J. Environ. Chem. Eng. 2 (2014) 557–572, https://doi.org/10.1016/j.jece.2013.10.011.
[60] R. Andreozzi, V. Caprio, A. Insola, R. Marotta, Advanced oxidation processes (AOP) for water purification and recovery, Catal. Today 53 (1999) 51–59, https://doi.org/10.1016/S0920-5861(99)00102-9.
[61] C.P. Huang, C. Dong, Z. Tang, Advanced chemical oxidation: its present role and potential future in hazardous waste treatment, Waste Manag. 13 (1993) 361–377, https://doi.org/10.1016/0956-053X(93)90070-D.
[62] E. Neyens, J. Baeyens, A review of classic Fenton's peroxidation as an advanced oxidation technique, J. Hazard. Mater. 98 (2003) 33–50, https://doi.org/10.1016/S0304-3894(02)00282-0.
[63] O. Legrini, E. Oliveros, A.M. Braun, Photochemical processes for water treatment, Chem. Rev. 93 (1993) 671–698, https://doi.org/10.1021/cr00018a003.
[64] J.J. Pignatello, Dark and photoassisted iron (3+)-catalyzed degradation of chlorophenoxy herbicides by hydrogen peroxide, Environ. Sci. Technol. 26 (1992) 944–951, https://doi.org/10.1021/es00029a012.
[65] M.A. Oturan, J.-J. Aaron, Advanced oxidation processes in water/wastewater treatment: principles and applications. A review, Crit. Rev. Environ. Sci. Technol. 44 (2014) 2577–2641, https://doi.org/10.1080/10643389.2013.829765.
[66] R. Hernandez, M. Zappi, J. Colucci, R. Jones, Comparing the performance of various advanced oxidation processes for treatment of acetone contaminated water, J. Hazard. Mater. 92 (2002) 33–50, https://doi.org/10.1016/S0304-3894(01)00371-5.
[67] Y. Huang, M. Kong, S. Coffin, K.H. Cochran, D.C. Westerman, D. Schlenk, S.D. Richardson, L. Lei, D. D. Dionysiou, Degradation of contaminants of emerging concern by UV/H_2O_2 for water reuse: kinetics, mechanisms, and cytotoxicity analysis, Water Res. 174 (2020) 115587, https://doi.org/10.1016/j.watres.2020.115587.
[68] K. Ikehata, M.G. El-Din, Aqueous pesticide degradation by hydrogen peroxide/ultraviolet irradiation and Fenton-type advanced oxidation processes: a review, J. Environ. Eng. Sci. 5 (2006) 81–135, https://doi.org/10.1139/s05-046.

This book belongs to Badji Mokhtar Annaba University Central Library Copyright Elsevier 2025

[69] G.R. Peyton, W.H. Glaze, Destruction of pollutants in water with ozone in combination with ultraviolet radiation. 3. Photolysis of aqueous ozone, Environ. Sci. Technol. 22 (1988) 761–767, https://doi.org/10.1021/es00172a003.
[70] M. Bhowmick, M.J. Semmens, Ultraviolet photooxidation for the destruction of VOCs in air, Water Res. 28 (1994) 2407–2415, https://doi.org/10.1016/0043-1354(94)90057-4.
[71] J.J. Pignatello, E. Oliveros, A. MacKay, Advanced oxidation processes for organic contaminant destruction based on the Fenton reaction and related chemistry, Crit. Rev. Environ. Sci. Technol. 36 (2006) 1–84, https://doi.org/10.1080/10643380500326564.
[72] B. Ohtani, Chapter 10—photocatalysis by inorganic solid materials: revisiting its definition, concepts, and experimental procedures, in: R. van Eldik, G.B. Stochel (Eds.), Inorganic Photochemistry, Academic Press, 2011, pp. 395–430, https://doi.org/10.1016/B978-0-12-385904-4.00001-9.
[73] M.A. Fox, M.T. Dulay, Heterogeneous photocatalysis, Chem. Rev. 93 (1993) 341–357, https://doi.org/10.1021/cr00017a016.
[74] B. Ohtani, Photocatalysis A to Z—what we know and what we do not know in a scientific sense, J. Photochem. Photobiol. C Photchem. Rev. 11 (2010) 157–178, https://doi.org/10.1016/j.jphotochemrev.2011.02.001.
[75] R.V. Prihod'ko, N.M. Soboleva, Photocatalysis: oxidative processes in water treatment, J. Chem. 2013 (2013) 168701, https://doi.org/10.1155/2013/168701.
[76] M. Umar, H.A. Aziz, Photocatalytic degradation of organic pollutants in water, in: Organic Pollutants-Monitoring, Risk and Treatment, Intech Rijeka, 2013, pp. 196–197.
[77] A. Fujishima, T.N. Rao, D.A. Tryk, Titanium dioxide photocatalysis, J. Photochem. Photobiol. C Photchem. Rev. 1 (2000) 1–21, https://doi.org/10.1016/S1389-5567(00)00002-2.
[78] S. Rajoriya, J. Carpenter, V.K. Saharan, A.B. Pandit, Hydrodynamic cavitation: an advanced oxidation process for the degradation of bio-refractory pollutants, Rev. Chem. Eng. 32 (2016) 379–411, https://doi.org/10.1515/revce-2015-0075.
[79] F. Trabelsi, H. Ait-Lyazidi, B. Ratsimba, A.M. Wilhelm, H. Delmas, P.L. Fabre, J. Berlan, Oxidation of phenol in wastewater by sonoelectrochemistry, Chem. Eng. Sci. 51 (1996) 1857–1865, https://doi.org/10.1016/0009-2509(96)00043-7.
[80] K.S. Suslick, Y. Didenko, M.M. Fang, T. Hyeon, K.J. Kolbeck, W.B. McNamara III, M.M. Mdleleni, M. Wong, Acoustic cavitation and its chemical consequences, Philos. Trans. R. Soc. B 357 (1999) 335–353, https://doi.org/10.1098/rsta.1999.0330.
[81] V.S. Sutkar, P.R. Gogate, Design aspects of sonochemical reactors: techniques for understanding cavitational activity distribution and effect of operating parameters, Chem. Eng. J. 155 (2009) 26–36, https://doi.org/10.1016/j.cej.2009.07.021.
[82] R.A. Torres-Palma, E.A. Serna-Galvis, Chapter 7—sonolysis, in: S.C. Ameta, R. Ameta (Eds.), Advanced Oxidation Processes for Waste Water Treatment, Academic Press, 2018, pp. 177–213, https://doi.org/10.1016/B978-0-12-810499-6.00007-3.
[83] P.R. Gogate, Cavitation: an auxiliary technique in wastewater treatment schemes, Adv. Environ. Res. 6 (2002) 335–358, https://doi.org/10.1016/S1093-0191(01)00067-3.
[84] P. Sathishkumar, R.V. Mangalaraja, S. Anandan, Review on the recent improvements in sonochemical and combined sonochemical oxidation processes—a powerful tool for destruction of environmental contaminants, Renew. Sustain. Energy Rev. 55 (2016) 426–454, https://doi.org/10.1016/j.rser.2015.10.139.
[85] M. Badve, P. Gogate, A. Pandit, L. Csoka, Hydrodynamic cavitation as a novel approach for wastewater treatment in wood finishing industry, Sep. Purif. Technol. 106 (2013) 15–21, https://doi.org/10.1016/j.seppur.2012.12.029.
[86] M. Gągol, A. Przyjazny, G. Boczkaj, Wastewater treatment by means of advanced oxidation processes based on cavitation—a review, Chem. Eng. J. 338 (2018) 599–627, https://doi.org/10.1016/j.cej.2018.01.049.
[87] M. Gągol, A. Przyjazny, G. Boczkaj, Effective method of treatment of industrial effluents under basic pH conditions using acoustic cavitation—a comprehensive comparison with hydrodynamic cavitation processes, Chem. Eng. Process. Process Intensif. 128 (2018) 103–113, https://doi.org/10.1016/j.cep.2018.04.010.
[88] Y.-S. Ma, C.-F. Sung, J.-G. Lin, Degradation of carbofuran in aqueous solution by ultrasound and Fenton processes: effect of system parameters and kinetic study, J. Hazard. Mater. 178 (2010) 320–325, https://doi.org/10.1016/j.jhazmat.2010.01.081.

This book belongs to Badji Mokhtar Annaba University Central Library Copyright Elsevier 2025

[89] S. Rajoriya, S. Bargole, V.K. Saharan, Degradation of a cationic dye (Rhodamine 6G) using hydrodynamic cavitation coupled with other oxidative agents: reaction mechanism and pathway, Ultrason. Sonochem. 34 (2017) 183–194, https://doi.org/10.1016/j.ultsonch.2016.05.028.
[90] V.K. Saharan, A.B. Pandit, P.S. Satish Kumar, S. Anandan, Hydrodynamic cavitation as an advanced oxidation technique for the degradation of acid red 88 dye, Ind. Eng. Chem. Res. 51 (2012) 1981–1989, https://doi.org/10.1021/ie200249k.
[91] E. Brillas, I. Sirés, M.A. Oturan, Electro-Fenton process and related electrochemical technologies based on Fenton's reaction chemistry, Chem. Rev. 109 (2009) 6570–6631, https://doi.org/10.1021/cr900136g.
[92] M. Panizza, G. Cerisola, Direct and mediated anodic oxidation of organic pollutants, Chem. Rev. 109 (2009) 6541–6569, https://doi.org/10.1021/cr9001319.
[93] N. Oturan, E. Brillas, M.A. Oturan, Unprecedented total mineralization of atrazine and cyanuric acid by anodic oxidation and electro-Fenton with a boron-doped diamond anode, Environ. Chem. Lett. 10 (2012) 165–170, https://doi.org/10.1007/s10311-011-0337-z.
[94] E. Brillas, S. Garcia-Segura, M. Skoumal, C. Arias, Electrochemical incineration of diclofenac in neutral aqueous medium by anodic oxidation using Pt and boron-doped diamond anodes, Chemosphere 79 (2010) 605–612, https://doi.org/10.1016/j.chemosphere.2010.03.004.
[95] P. Canizares, J. Garcia-Gomez, C. Saez, M.A. Rodrigo, Electrochemical oxidation of several chlorophenols on diamond electrodes. Part I. Reaction mechanism, J. Appl. Electrochem. 33 (2003) 917–927, https://doi.org/10.1023/A:1025888126686.
[96] R.C. Koile, D.C. Johnson, Electrochemical removal of phenolic films from a platinum anode, Anal. Chem. 51 (1979) 741–744, https://doi.org/10.1021/ac50042a037.
[97] M. Li, C. Feng, W. Hu, Z. Zhang, N. Sugiura, Electrochemical degradation of phenol using electrodes of Ti/RuO_2-Pt and Ti/IrO_2-Pt, J. Hazard. Mater. 162 (2009) 455–462, https://doi.org/10.1016/j.jhazmat.2008.05.063.
[98] M.E.H. Bergmann, J. Rollin, T. Iourtchouk, The occurrence of perchlorate during drinking water electrolysis using BDD anodes, Electrochim. Acta 54 (2009) 2102–2107, https://doi.org/10.1016/j.electacta.2008.09.040.
[99] J. Cai, M. Zhou, Y. Pan, X. Lu, Degradation of 2,4-dichlorophenoxyacetic acid by anodic oxidation and electro-Fenton using BDD anode: influencing factors and mechanism, Sep. Purif. Technol. 230 (2020) 115867https://doi.org/10.1016/j.seppur.2019.115867.
[100] N. Klidi, F. Proietto, F. Vicari, A. Galia, S. Ammar, A. Gadri, O. Scialdone, Electrochemical treatment of paper mill wastewater by electro-Fenton process, J. Electroanal. Chem. 841 (2019) 166–171, https://doi.org/10.1016/j.jelechem.2019.04.022.
[101] A. Xu, E. Brillas, W. Han, L. Wang, I. Sirés, On the positive effect of UVC light during the removal of benzothiazoles by photoelectro-Fenton with UVA light, Appl. Catal. Environ. 259 (2019) 118127, https://doi.org/10.1016/j.apcatb.2019.118127.
[102] A. Babuponnusami, K. Muthukumar, Advanced oxidation of phenol: a comparison between Fenton, electro-Fenton, sono-electro-Fenton and photo-electro-Fenton processes, Chem. Eng. J. 183 (2012) 1–9, https://doi.org/10.1016/j.cej.2011.12.010.
[103] M.A. Oturan, An ecologically effective water treatment technique using electrochemically generated hydroxyl radicals for in situ destruction of organic pollutants: application to herbicide 2,4-D, J. Appl. Electrochem. 30 (2000) 475–482, https://doi.org/10.1023/A:1003994428571.
[104] Z. Ali, R. Ahmad, Nanotechnology for water treatment, in: Environmental Nanotechnology, vol. 3, Springer, 2020, pp. 143–163.
[105] G. Pranjali, M. Deepa, A.N.B. Nair, Nanotechnology in waste water treatment: a review, Int. J. ChemTech Res. 5 (2013) 2303–2308.
[106] Y.H. Teow, A.W. Mohammad, New generation nanomaterials for water desalination: a review, Desalination 451 (2019) 2–17, https://doi.org/10.1016/j.desal.2017.11.041.
[107] C. Santhosh, V. Velmurugan, G. Jacob, S.K. Jeong, A.N. Grace, A. Bhatnagar, Role of nanomaterials in water treatment applications: a review, Chem. Eng. J. 306 (2016) 1116–1137, https://doi.org/10.1016/j.cej.2016.08.053.

This book belongs to Badji Mokhtar Annaba University Central Library Copyright Elsevier 2025

[108] S.C. Smith, D.F. Rodrigues, Carbon-based nanomaterials for removal of chemical and biological contaminants from water: a review of mechanisms and applications, Carbon N. Y. 91 (2015) 122–143, https://doi.org/10.1016/j.carbon.2015.04.043.

[109] B. Bethi, S.H. Sonawane, B.A. Bhanvase, S.P. Gumfekar, Nanomaterials-based advanced oxidation processes for wastewater treatment: a review, Chem. Eng. Process. Process Intensif. 109 (2016) 178–189, https://doi.org/10.1016/j.cep.2016.08.016.

[110] J. Carpenter, M. Badve, S. Rajoriya, S. George, V.K. Saharan, Hydrodynamic Cavitation: An Emerging Technology for the Intensification of Various Chemical and Physical Processes in a Chemical Process Industry, (2016), https://doi.org/10.1515/revce-2016-0032.

[111] F. Lu, D. Astruc, Nanocatalysts and other nanomaterials for water remediation from organic pollutants, Coord. Chem. Rev. 408 (2020) 213180, https://doi.org/10.1016/j.ccr.2020.213180.

[112] S.K. Shukla, A.K. Mishra, O.A. Arotiba, B.B. Mamba, Chitosan-based nanomaterials: a state-of-the-art review, Int. J. Biol. Macromol. 59 (2013) 46–58, https://doi.org/10.1016/j.ijbiomac.2013.04.043.

[113] B.A. Bhanvase, T.P. Shende, S.H. Sonawane, A review on graphene–TiO_2 and doped graphene–TiO_2 nanocomposite photocatalyst for water and wastewater treatment, Environ. Technol. Rev. 6 (2017) 1–14, https://doi.org/10.1080/21622515.2016.1264489.

[114] F. Perreault, A.F. De Faria, M. Elimelech, Environmental applications of graphene-based nanomaterials, Chem. Soc. Rev. 44 (2015) 5861–5896, https://doi.org/10.1039/C5CS00021A.

[115] R.K. Upadhyay, N. Soin, S.S. Roy, Role of graphene/metal oxide composites as photocatalysts, adsorbents and disinfectants in water treatment: a review, RSC Adv. 4 (2014) 3823–3851, https://doi.org/10.1039/C3RA45013A.

[116] J. Xu, Z. Cao, Y. Zhang, Z. Yuan, Z. Lou, X. Xu, X. Wang, A review of functionalized carbon nanotubes and graphene for heavy metal adsorption from water: preparation, application, and mechanism, Chemosphere 195 (2018) 351–364, https://doi.org/10.1016/j.chemosphere.2017.12.061.

[117] T. Hennebel, B. De Gusseme, N. Boon, W. Verstraete, Biogenic metals in advanced water treatment, Trends Biotechnol. 27 (2009) 90–98, https://doi.org/10.1016/j.tibtech.2008.11.002.

[118] E.B. Martínez-Ruiz, M. Cooper, J. Fastner, U. Szewzyk, Manganese-oxidizing bacteria isolated from natural and technical systems remove cylindrospermopsin, Chemosphere 238 (2020) 124625, https://doi.org/10.1016/j.chemosphere.2019.124625.

[119] K. Kiskira, S. Papirio, M.C. Mascolo, C. Fourdrin, Y. Pechaud, E.D. van Hullebusch, G. Esposito, Mineral characterization of the biogenic Fe(III)(hydr) oxides produced during Fe(II)-driven denitrification with Cu, Ni and Zn, Sci. Total Environ. 687 (2019) 401–412, https://doi.org/10.1016/j.scitotenv.2019.06.107.

This book belongs to Badji Mokhtar Annaba University Central Library

Copyright Elsevier 2025

This page intentionally left blank

This book belongs to Badji Mokhtar Annaba University Central Library

Copyright Elsevier 2025

CHAPTER 24

Nanocomposite photocatalysts-based wastewater treatment

Ananya Dey[a,b] **and Parag R. Gogate**[a]

[a]*Chemical Engineering Department, Institute of Chemical Technology, Mumbai, India,* [b]*NMIMS Mukesh Patel School of Technology Management & Engineering, Mumbai, India*

24.1 Introduction

Nanotechnology is a field of study that deals with the substances at nanoscale length of around 1–100 nm. Nanoparticles are gaining interest for their size-dependent properties and specific applications. Nanomaterials in general are unique because of their catalytic, mechanical, optical, and magnetic properties and also for their very high surface area per unit mass, especially because of nanosize and the porous structures. It is necessary to understand that the movement of electrons and holes, which is crucial for the application of photocatalysis, is also affected by the size and configuration of the materials [1]. The governing principle of photocatalysis is the excitement of photocatalyst with the irradiation of light energy [mainly ultraviolet (UV) or in some cases, visible range] corresponding to the bandgap of the photocatalysts. Various photocatalysts that are used for wastewater treatment are TiO_2, ZnO, WO_3, CuS, SnO_2, CdS, etc., but most of these photocatalysts are active in UV light only because of a comparatively large bandgap. Unfortunately, in nature, only 3%–5% is UV light, and around 43% is visible light. Therefore development of the catalysts, which show high activity under visible light, is very important [2]. Synthesis of nanocomposites is one of the options to obtain photocatalysts with improved activity under visible light.

Nanocomposites are the multiphase materials that can consist of metals, polymers, and ceramics, and where one of the constituents has dimension less than 100 nm. The presence of other phase maintains the grain size and the thickness of the interphase layer within dimensions comparable with Debye length. The use of oxides at specific loadings helps to restrict the growth of the other oxides, thus avoiding the overall grain growth [3]. Composites typically combine different materials that can be tailored to improve the overall properties and giving effects that might not be obtained using the single materials [4].

Handbook of Nanomaterials for Wastewater Treatment. https://doi.org/10.1016/B978-0-12-821496-1.00022-2
Copyright © 2021 Elsevier Inc. All rights reserved.

This book belongs to Badji Mokhtar Annaba University Central Library Copyright Elsevier 2025

24.2 Types of nanocomposites and their synthesis

Nanocomposites can be typically classified as metal matrix nanocomposites (MMNCs), ceramic matrix nanocomposites (CMNCs), and polymer matrix nanocomposites (PMNCs) [5]. MMNC consists of a metallic matrix with soft reinforcement or hard ceramics [6]. The metal matrix includes materials such as titanium, nickel, iron, aluminum, and copper, and the second phase materials include oxides, carbides, nitrides, borides, and their mixtures. CMNCs contain a ceramic (chemical compound of oxides and nitrides) as the first material and metal as the second material. PNMC has a polymer matrix and an additive, which may be one-dimensional, two-dimensional or three-dimensional. Polymer is mainly used as substrate, and reinforcement fillers nanoparticles can be incorporated in the polymeric substrate [7].

There are five types of methods for synthesis of metal matrix nanocomposites namely, (1) liquid-phase processes, (2) solid-phase processes, (3) two-phase processes, (4) deposition processes, and (5) in situ processes [6]. The synthesis of MMNC mainly involves either solid sintering or liquid processing. Use of ultrasound during the synthesis of MMNC helps in dispersing ceramic particles in liquid metals, giving better morphology of the final product.

CMNCs can be synthesized using mechanical synthesis approaches that involve high-energy milling operation under controlled atmosphere. Ball milling is a classic example of mechanical synthesis of the nanocomposites. Chemical methods such as vapor-phase reaction, high-temperature synthesis, and solution-based techniques can also be used for synthesizing these materials. Vapor-phase techniques involve evaporation of solid to form a supersaturated vapor and subsequent condensation of supersaturated vapor. This process is widely used for commercial synthesis of nanocomposite powders. High-temperature synthesis is also classified into two types as self-propagating synthesis at high temperature and combustion synthesis. Different solution-based approaches are sol-gel method, coprecipitation method, spray decomposition, and solution combustion [6].

Major routes for obtaining PMNC are solution blending, melt processing, and in situ polymerization. Solution blending involves mixing and dispersion of polymers and fillers in the solvents. Melt processing involves direct dispersion of fillers into melt polymers. In situ polymerization involves mixing of monomers and fillers, which are subsequently polymerized by standard polymerization routes [6].

24.3 Advanced oxidation processes for wastewater treatment

The increase in wastewater discharge from several industries coupled with the presence of harmful toxic contaminants causes harmful effects in the environment, also affecting human and aquatic life. Owing to the limitations of conventional wastewater treatment approaches, including the most commonly applied aerobic oxidation, advanced oxidation processes (AOPs) have shown an increasing interest for application in wastewater treatment. AOPs can be

This book belongs to Badji Mokhtar Annaba University Central Library Copyright Elsevier 2025

classified as (1) irradiated processes and (2) nonirradiated processes. Nonirradiated processes include Fenton chemistry, electrochemical oxidation, ozonation, and wet air oxidation, whereas the irradiation processes include photolysis and photocatalysis [8]. Photocatalysis is a type of AOP that relies on hydroxyl radical generation based on the interaction of photocatalyst with the incident light energy. It is understood to be more effective as compared to only photolysis applied for treatment of wastewater. An important advantage of photocatalytic degradation is that pollutants can be completely mineralized to nontoxic end products such as CO_2, H_2O, NO_3^-, or PO_4^{3-} depending upon the constituents of the wastewater. Photocatalytic oxidation comprises a primary initiation reaction that generates electron and hole and a subsequent secondary reaction step that generates reactive oxygen species, including the hydroxyl radicals [9]. Composites of two different materials as catalysts have gained interest because they form heterojunctions. Typically, the energy absorbed by one photocatalyst will be transferred to another photocatalyst if they form a heterojunction. This also causes a charge separation that leads to a higher efficacy in terms of generation of oxidizing species and in turn higher rate of degradation [10]. Photocatalytic oxidation is considered to be an important AOP because of its low cost, ability to yield complete mineralization, and no waste disposal problems. In addition, the process operates under conditions of mild temperature and pressure [11].

24.4 Governing mechanism of photocatalysis

In photocatalysis, photons are bombarded through UV light irradiation. The incident photons excite the electron present in the valence band of the photocatalysts and cause the electrons to go up to the conduction band. The migration of electron results in the formation of a hole in the valance bond. The excited electrons in conduction band react with oxygen to produce the different oxidizing agents as hydroxyl radicals or the superoxide or hydroperoxide radicals. These radicals in turn react with organic compounds giving a chain of intermediates, and finally, continued oxidation can yield water and carbon dioxide [10]. The schematic of the mechanism of photocatalysis is shown in Fig. 24.1. The overall process leading to the formation of the oxidizing agents is given by the following set of reactions:

$$TiO_2 + h\nu \rightarrow h^{vb+} + e^{cb-} \tag{24.1}$$

$$e^{cb-} + O_2 \rightarrow O_{2^-} \tag{24.2}$$

$$h^{vb+} + H_2O \rightarrow {}^{\bullet}OH + H^+ \tag{24.3}$$

The success of photocatalysis depends on the competition between the reaction of the electron with water on the semiconductor surface and the recombination process of electrons and holes. Based on the governing mechanisms in the photocatalytic oxidation, it is necessary to understand that the activity of the photocatalysts can be increased by addressing the following three main points (1) reduction in the extent of electron-hole recombination, (2) increase in the

This book belongs to Badji Mokhtar Annaba University Central Library Copyright Elsevier 2025

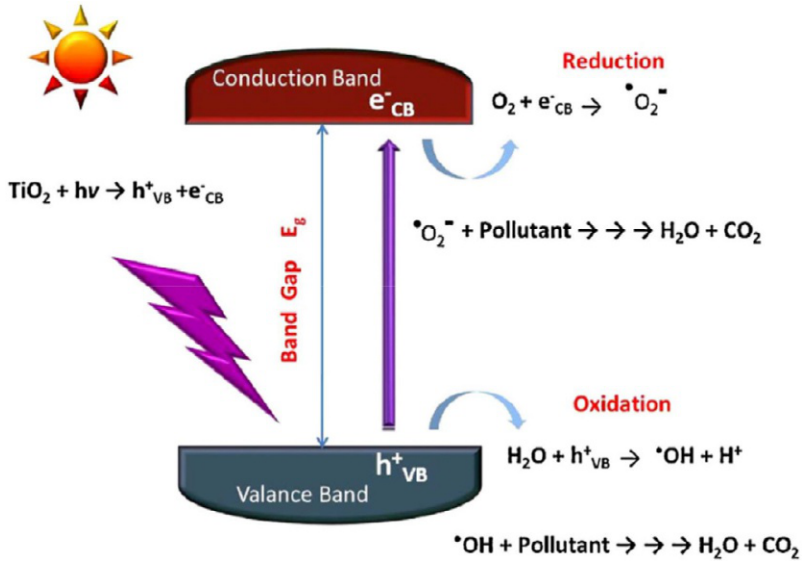

Fig. 24.1
Mechanism of photocatalysis. *Reprinted with permission from C. Byrne, G. Subramaniun, S.C. Pillai, Recent advances in photocatalysis and environmental applications, J. Environ. Chem. Eng. 6 (2018) 3531–3555.*

active sites of the photocatalysts, and (3) extending the excitation wavelength [12] to the visible range.

The overall process of photocatalysis can be considered to be composed of different steps, depending upon the type of pollutants present in wastewater as (1) photodecolorization, (2) photodegradation, (3) photomineralization, and (4) photodecomposition. The photodecolorization process involves simple breakage of the chromophores that impart the color, especially in the case of dyes. Photodegradation implies the degradation of pollutants to some stable products. Photomineralization implies total degradation of the pollutants to final possible products as CO_2, H_2O, and different inorganic ions such as NO_3^- and NO_2^-. Photodecomposition implies direct decomposition of pollutants subsequently leading to either degradation or mineralization [13]. In any treatment process, it will be imperative to maximize the mineralization because decolorization or degradation would only mean initial treatment and not complete elimination of toxicity.

24.5 Different nanocomposites used as photocatalysts for wastewater treatment

Single-component nanocatalysts generally exhibit poor photocatalytic efficacy under visible light because of a large bandgap and higher degree of electron-hole recombination. Use of nanocomposites offers advantages in processing for photodegradation of pollutants in

This book belongs to Badji Mokhtar Annaba University Central Library Copyright Elsevier 2025

wastewater under visible light. We now present an overview of different nanocomposites typically reported in the literature.

24.5.1 Metal-doped nanocomposites

A number of transition metals have been reported as doping agents that can extend the light absorption from UV to visible. For example, doping TiO_2 with Fe^{3+}, Os^{3+}, Mo^{5+}, Re^{5+}, V^{5+}, Rh^{3+}, Ru^{3+}, etc. was demonstrated to enhance the photocatalytic activity [14]. In another study, it was reported that photodegradation ability of TiO_2 catalyst was improved when the catalyst was doped with iron. Fe ion alters the absorption of TiO_2 from UV to visible range and also retards the recombination of electron-holes [15]. Fe-TiO_2 and Ce-TiO_2 nanocomposites synthesized by Shirsath et al. [16] were also shown to be effective for remediation of crystal violet. It was reported that the overall activity of Ce-TiO_2 was more when compared to Fe-TiO_2, and also the photocatalytic oxidation was more effective at low concentration of the contaminants. Moradi et al. [15] synthesized Fe-TiO_2 nanocomposites and used it for degradation of reactive red 198 dye. They observed that Fe doping in TiO_2 increased the photocatalytic activity till an optimum content, beyond which the photocatalytic activity decreased. A ternary nanocomposite Ag/$CeVO_4$/g-C_3N_4 (7% Ag-doped) synthesized using ultrasonic precipitation method by Wang et al. [2] was reported to degrade methylene blue (MB) dye completely within 120 min under the action of visible light. Bhosale et al. [17] reported the effective use of Cr_2O_3/SnO_2 nanocomposite for degradation of rhodamine B, with about 98% of the dye removal in 60 min under visible light. Zr,Ce-TiO_2/SiO_2 nanocomposites thin film was also reported to be an effective photocatalyst for degradation of methyl orange [18]. Fig. 24.2 illustrates a representative SEM image of metal (Mn and Ni)-doped ZnO. From the figure, it is seen that both Mn/ZnO and Ni/ZnO are spherical and discrete particles with broad size distribution (inset figure shows size distribution) [19].

24.5.2 Nonmetal-doped nanocomposites

Doping nanomaterials with nonmetal elements such as B, C, N, F, and S also improves the utilization of solar light for photocatalysis. Boron-doped carbon nitride and nickel ferrite (C_3N_4/$NiFe_2O_4$) were reported as effective photocatalysts for degradation of MB by Kamal et al. [20], with 98% degradation under visible light. Carbon-doped TiO_2/Fe_3O_4 was also used successfully as visible light photocatalysts for methyl orange degradation [21]. Nitrogen doping in substitutional sites in TiO_2 was reported to reduce the bandgap and enhance the photocatalytic activity [22] in the visible range. In another study, it was reported that nonmetal, nitrogen, doping improved the activity of ZnO and also shifted the absorption range from UV to visible range [23]. It was also reported that N-doped ZnO/g-C_3N_4 has good degradation properties for MB and phenol under the influence of visible light. Overall, it can be said that N, C, S, B, and P can be effectively doped in TiO_2 for narrowing band gap, thus enhancing the

This book belongs to Badji Mokhtar Annaba University Central Library Copyright Elsevier 2025

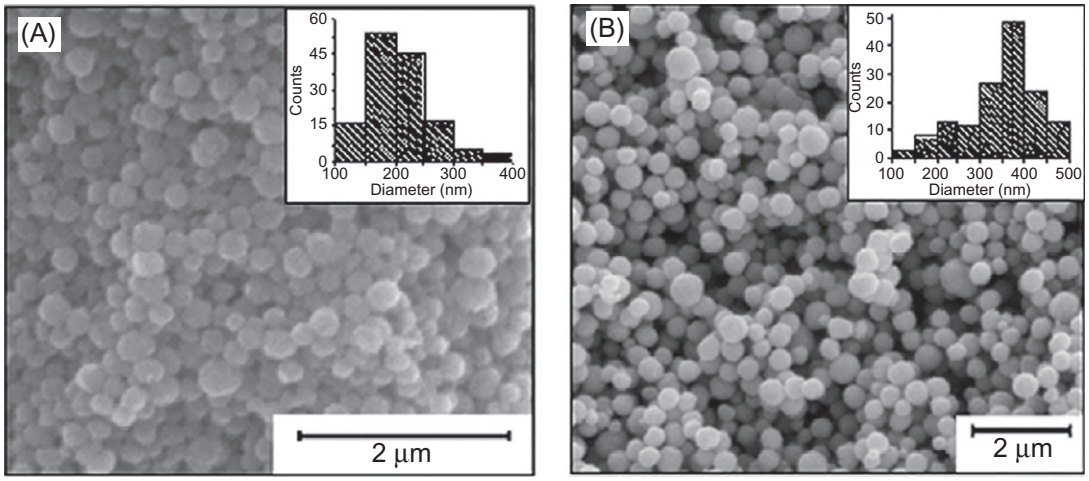

Fig. 24.2
SEM image of (A) Mn-doped ZnO and (B) Ni-doped ZnO. *Reprinted with permission from K.C. Barick, S. Singh, M. Aslam, D. Bahadur, Porosity and photocatalytic studies of transition metal doped ZnO nanoclusters, Microporous Mesoporous Mater. 134 (2010) 195–202.*

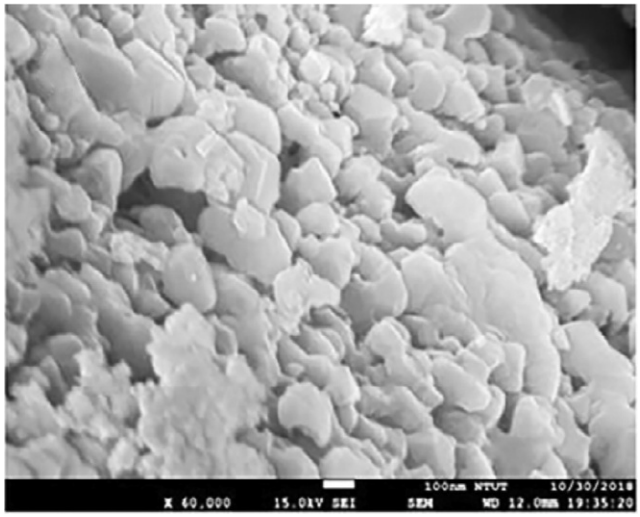

Fig. 24.3
SEM image of boron-doped $C_3N_4/NiFe_2O_4$. *Reprinted with permission from S. Kamal, S. Balu, S. Palanisamy, K. Uma, V. Velusamy, T.C.K. Yang, Synthesis of boron doped C3N4/NiFe2O4 nanocomposite: an enhanced visible light photocatalyst for the degradation of methylene blue, Results Phys. 12 (2019) 1238–1244.*

photodegradation ability of TiO_2 [24]. Fig. 24.3 illustrates a representative SEM image of nonmetal-doped nanocomposites. The image shows boron-doped $C_3N_4/NiFe_2O_4$, where an aggregated structure of Ni Fe_2O_4 is embedded on sheet like boron-doped C_3N_4 [20].

This book belongs to Badji Mokhtar Annaba University Central Library Copyright Elsevier 2025

24.5.3 Binary metal oxides

Binary oxides improve charge separation and increase interfacial charge transfer, resulting in higher photocatalytic activity. For example, cerium oxide/titanium dioxide (CeO_2/TiO_2) binary oxide nanocomposites are considered good photocatalysts. First, both the oxides themselves are active photocatalysts. Second, CeO_2/TiO_2 nanocomposites are effective in many redox photoreactions. Munoz-Batista et al. [25] synthesized CeO_2/TiO_2 nanocomposites and tested them for photocatalytic elimination of toluene. It was reported that the optimum Ce content improved the photocatalytic activity of TiO_2 by almost 3.5 times. In another study, bismuth vanadate and CeO_2 ($BiVO_4/CeO_2$) nanocomposite was synthesized by Wetchakun et al. [26] and subsequently applied for degradation of dyes using the visible light irradiation (>400 nm). It was reported that mole ratio of 0.6:0.4 ($BiVO_4$:CeO_2) gave the best results for photocatalytic activity. Anderson and Bard [27] also reported that TiO_2/SiO_2 nanocomposites are three times more active than the conventional form of Degussa P-25 for degradation of rhodamine-6G. CeO_2/ZnO nanocomposites (core-shell structures) were synthesized by Shah et al. [28], and their effective use was demonstrated for photodegradation of rhodamine B dye. Similarly, Saravana et al. [29] reported that vanadium pentoxide/ZnO (V_2O_5/ZnO) nanocomposites can degrade MB in visible light region. In another study, MgO/TiO_2 was synthesized by Satishkumar et al. [30] using the microemulsion methods and used for degradation of azo dye methyl red. An increase of 11.3% was reported in degradation efficiency when compared with pure TiO_2. Fig. 24.4 shows representative SEM images of binary metal oxides effectively used as photocatalysts. Fig. 24.4A and B shows ZnO and 1 wt% ZnO/CuO, which are nanorods of around 35 nm diameter and 500 nm length. In Fig. 24.4C and D, the lower length of the nanorods is observed as the doping percentage of CuO increased to 3 and 5 wt%. Fig. 24.4E and F represent that the size of materials with 10 and 50 wt% CuO in ZnO is over the range of 50–100 nm. The data clearly show that the doping percentage of CuO influences the size and morphology of ZnO [31].

24.5.4 Metal sulfides

Metal sulfides have relatively smaller bandgaps than metal oxides, and hence metal sulfides are considered as important semiconductor-based photocatalysts. Sulfides are also applied for the synthesis of different nanocomposites. For example, cadmium indium sulfide nanocomposites were synthesized and tested for MB degradation by Tu et al. [32]. The result showed that $CdIn_2S_4$ offered strong degradation efficiency. Photocatalytic activity of TiO_2/Ag_2S was studied in another work [33] for decomposition of *p*-xylene and chlorophenol. According to the researchers, TiO_2/Ag_2S was effective in degradation of both the pollutants. In another study [34], the application of molybdenum disulfide/TiO_2 (MoS_2/TiO_2) nanocomposite for MB degradation established that MoS_2/TiO_2 is an excellent photocatalyst in visible light region. The actual degradation was also influenced by catalyst dosage and initial concentration of

This book belongs to Badji Mokhtar Annaba University Central Library Copyright Elsevier 2025

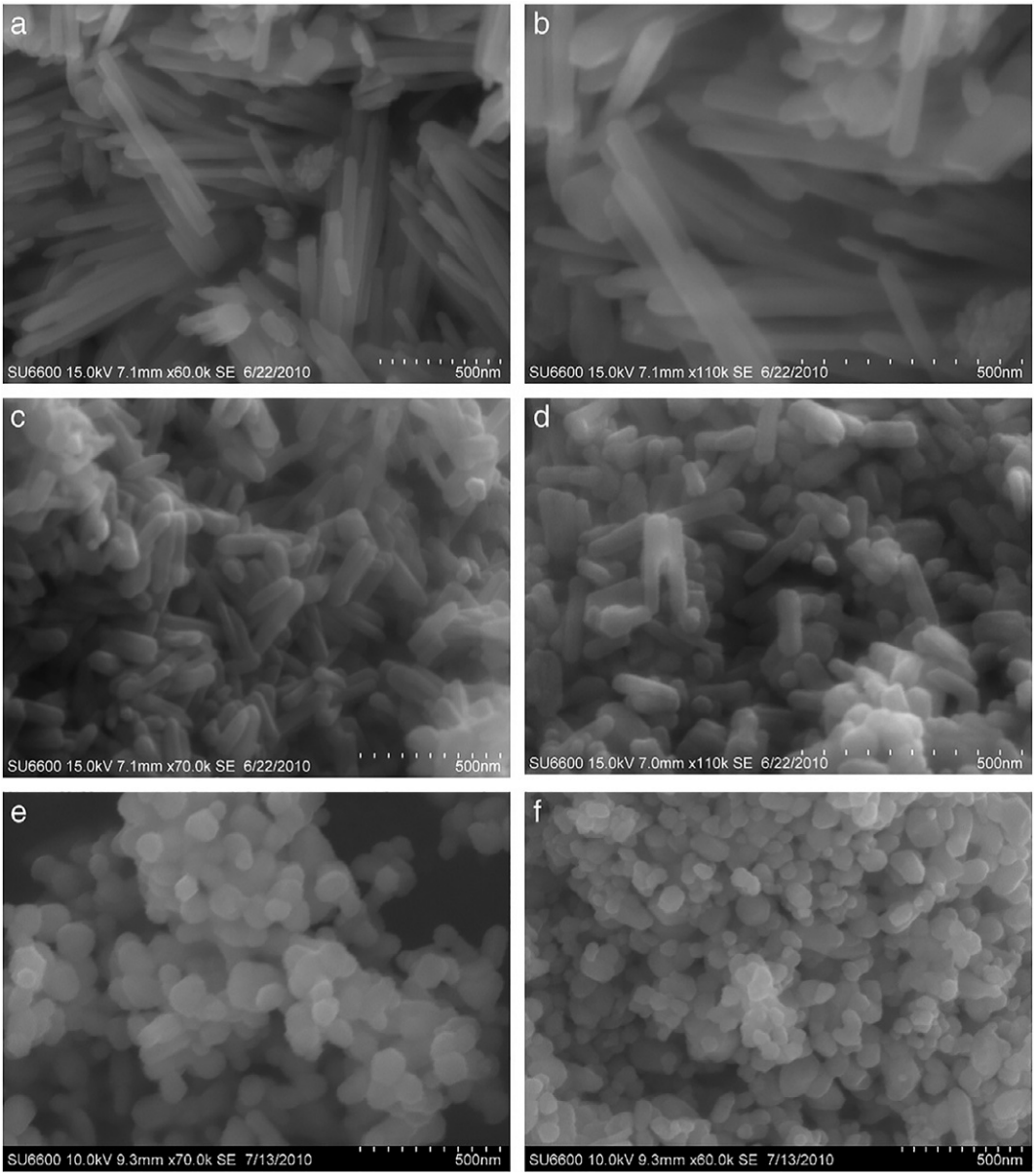

Fig. 24.4

SEM image of (A) ZnO, (B) ZnO/CuO, (99:1) (C) ZnO/CuO (97:3), (D) ZnO/CuO (95:5), (E) ZnO/CuO (90:10), and (F) ZnO/CuO (50:50). *Reprinted with permission from R. Saravanan, S. Karthikeyan, V.K. Gupta, G. Sekaran, V. Narayanan, A. Stephen, Enhanced photocatalytic activity of ZnO/CuO nanocomposite for the degradation of textile dye on visible light illumination, Mater. Sci. Eng. C 33 (2013) 91–98.*

This book belongs to Badji Mokhtar Annaba University Central Library
Copyright Elsevier 2025

pollutant. The catalyst demonstrated a good regeneration property. The associated mechanism for excellent activity was photoexcited electron transfer from conduction band of MoS_2 to TiO_2, which is then taken by oxygen in water. Subsequently, hydroxyl radicals are formed, and these radicals help in the degradation of organic chemicals as per the series of reactions given below.

$$MoS_2/TiO_2 + h\nu \rightarrow MoS_2\,(h^+ + e^-)/TiO_2 \tag{24.4}$$

$$MoS_2\,(h^+ + e^-)/TiO_2 \rightarrow MoS_2\,(h^+)/TiO_2\,(e^-) \tag{24.5}$$

$$TiO_2\,(e^-) + O_2 \rightarrow TiO_2 + O_2{}^- \tag{24.6}$$

$$O_2{}^- + H_2O \rightarrow HO_2{}^\bullet + OH^- \tag{24.7}$$

24.5.5 Polymer-based nanocomposites

Nanocomposites of conducting polymers and other nanoparticles exhibit some properties that are unique and not observed in individual components. Thus these nanocomposites can be more effective for the application of photocatalysis. For example, PANI/TiO_2 was reported to show high potential in photodegradation of organic pollutants [35]. Use of conducting polymers like polyaniline (PANI), poly-*O*-phynylenediamine (PoPD), polythiophene (PTh), and their derivatives in the nanocomposite increases the efficiency of TiO_2-based photocatalysts. Conducting polymers and TiO_2 nanocomposites can act in visible light range because the TiO_2 bandgap is reduced by conducting polymers [9]. Eskizeybek et al. [36] also reported that PANI/ZnO nanocomposites are efficient photocatalysts for degrading dyes from textile industry wastewater. It is evident from the SEM micrograph that the degree of agglomeration decreases as the PANI/TiO_2 mole ratio increases from 20 to 80 [35].

24.5.6 Graphene-based nanocomposites

Graphene has tightly packed carbon atoms with 2D hexagonal honeycomb structures. In recent years, graphene has gained interest because of its potential for a wide range of applications, including as photocatalysts. Graphene combination with semiconductors also yields nanocomposites with potential use as photocatalysts. Graphene-semiconductor nanocomposites offer many advantages such (1) introduction of graphene reduces the recombination of electron and holes, (2) graphene also improves the charge separation, (3) surface area of the photocatalysts is increased because graphene has a two-dimensional structure, and (4) a strong π-π bonding between graphene and organic molecules helps in the adsorption of organic pollutants [37] and subsequent utilization in photocatalytic oxidation. In addition, graphene is a zero-bandgap semiconductor [38]. Different types of graphene-based nanocomposites such as graphene-semiconductor, reduced graphene oxide-semiconductor, and graphene oxide-semiconductor have been reported. Typically as a semiconductor material,

This book belongs to Badji Mokhtar Annaba University Central Library Copyright Elsevier 2025

ZnO, TiO_2, CdS, and CeO_2 are used in combination with graphene oxide. For example, RGO/CeO_2 nanocomposites were prepared by Kumar and Kumar [39, 40], and it was reported that the nanocomposite yielded higher extent of MB degradation under visible light than individual CeO_2 nanoparticles. Graphene sheets with high specific surface area can enhance the activity of $BaCrO_4$. In one of the studies, it was reported that R-GO/$BaCrO_4$ showed enhanced photocatalytic activity than $BaCrO_4$ toward MB dye degradation [41]. Fig. 24.5 illustrates SEM

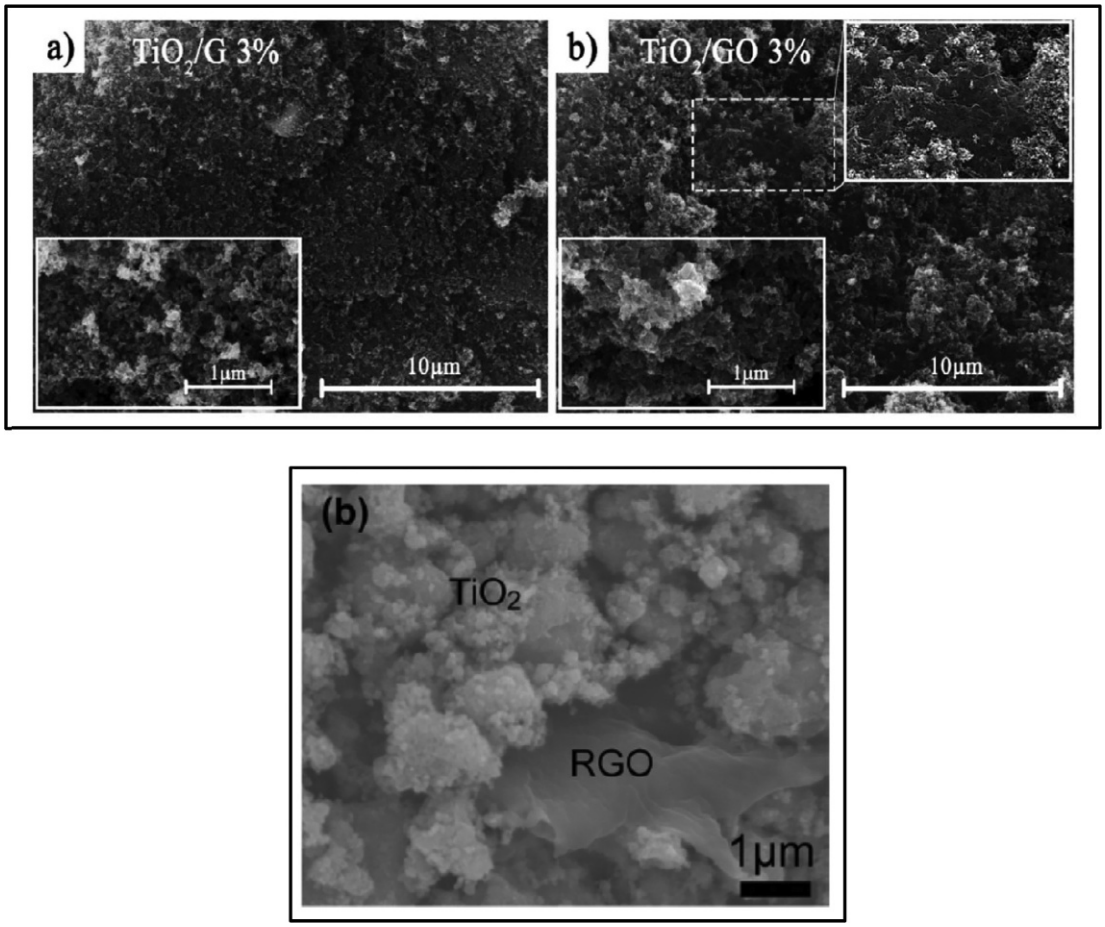

Fig. 24.5
SEM image of (A)TiO_2/graphene, (B) TiO_2/graphene oxide, and (C) TiO_2/reduced graphene.
Reprinted with permission from P.M. Martins, C.G. Ferreira, A.R. Silva, B. Magalhães, M.M. Alves, L. Pereira, P.A.A.P. Marques, M. Melle-Francod, S. Lanceros-Méndez, TiO_2/graphene and TiO_2/graphene oxide nanocomposites for photocatalytic applications: a computer modeling and experimental study, Compos. Part B 145 (2018) 39–46; D. Liang, C. Cui, H. Hub, Y. Wang, S. Xu, B. Ying, P. Li, B. Lu, H. Shen, One-step hydrothermal synthesis of anatase TiO_2/reduced graphene oxide nanocomposites with enhanced photocatalytic activity, J. Alloys Compd. 582 (2014) 236–240.

This book belongs to Badji Mokhtar Annaba University Central Library
Copyright Elsevier 2025

image of graphene-based nanocomposites based on TiO_2 [42, 43] and different forms of graphene (native form, graphene oxide, and reduced graphine oxide). It is evident that proper synthesis approach gives better dispersion of the TiO_2 on graphene sheets.

24.5.7 Clay-based nanocomposites

It is reported in the literature that rate constant for photocatalytic reaction will be much higher for TiO_2/clay nanocomposites than pure TiO_2. The enhanced activity is probably because of small crystallite size, large surface area, and high porosity. TiO_2/clay has been reported as a promising photocatalyst for degradation of dimethachlore [44]. Bentonite clay-based nanocomposites fall under the category of semiconductor/lamellar nanocomposites. Bentonite clay is a cheaper source and has layered structures consisting of two silica tetrahedral sheets fused to one alumina octahedral sheet [45]. There have been reports that TiO_2/bentonite clay is a promising photocatalyst in wastewater treatment. Bentonite layer improves the optical properties of TiO_2 and also enhances the ability separation of charge carriers [46]. Phenol has been reported to be continuously removed from a wastewater stream using photocatalysis based on ZnO-bentonite nanocomposite by using a simple CSTR. The photocatalytic degradation was performed under UV radiation [47]. Photodegradation of MB and chlorobenzene (CB) was also reported using TiO_2/clay as a catalyst under UV light. TiO_2/bentonite showed five to eight times more degradation capacity toward MB and CB than the native form of Degussa P25 [48, 49].

24.6 Factors affecting the wastewater treatment using photocatalysis

Efficiency of photocatalysis is affected by different factors ranging from the conditions for synthesis of the photocatalysts to the actual operating conditions applied for the degradation of the pollutants. We now discuss the studies related to the effect of methods of synthesis and the associated conditions on the efficacy of the synthesized photocatalyst. In addition, the studies related to the effect of important operating parameters during the actual application for degradation are also discussed.

24.6.1 Synthesis of photocatalysts

Sol-gel is the conventional method of preparation of photocatalysts. The advantage of this method is that it gives high purity at a low temperature [50]. Variations in the preparation method of any catalysts results in different catalytic activity; for example, it was observed that doping of photocatalysts is affected by the pH of precursor solution [51]. Polymer-based nanocomposites are mainly synthesized by different processes such as in situ deposition oxidative polymerization, chemical oxidative polymerization, solution evaporation, and

This book belongs to Badji Mokhtar Annaba University Central Library Copyright Elsevier 2025

chemisorption. The processing steps in the synthesis and type of method affect the final catalyst characteristics. Synthesis of same nanocomposites using different precursors and synthesis approaches might result in nanocomposites of different size, shape, and morphology. These obtained catalysts in turn show different photocatalytic activity. For example, comparison of photocatalytic activity of N-doped TiO_2 synthesized from $TiCl_4$ and $TiOSO_4$ as TiO_2 precursor and NH_3 and NH_4Cl as nitrogen sources under UV light demonstrated that samples prepared from $TiCl_4$ were more active, but under visible light, a higher response was found in the samples synthesized from $TiOSO_4$ and calcined at 400°C [52]. Table 24.1 illustrates the different methods of synthesizing nanocomposites, also giving the main properties of the obtained catalysts and the results for the efficacy of the photodegradation process.

24.6.2 Catalyst loading

Catalyst loading is an important parameter that decides the efficacy of photocatalytic degradation. Establishing the optimum dosages of catalyst [56] is important because of the counteracting effects of higher activity and problems in transmission of light energy. Typically, the photodegradation of dyes increases as the loading is increased till an optimum where the generation of electron/hole pair is optimally favored. For example, results from study dealing with the effect of loading shown in Fig. 24.6 clearly demonstrate that degradation of crystal violet dye (initial concentration as 30 mg/L and pH of 6.5) increased dominantly with initial increase in catalyst dose from 0.1 to 0.2 g/L, whereas subsequent increase to 0.3 g/L resulted in marginal changes. The maximum reported degradation as 92% was observed at catalyst loading of 0.3 g/L with 0.8 mol% Ce-TiO_2 catalyst [16], although the optimum recommended catalyst loading was 0.2 g/L. At much higher loadings, catalyst blocks the irradiation of the light, thus reducing the effective energy available and the generation of oxidizing agents, and hence the rate of photodegradation reduces.

Moreover, catalyst loading above an optimum limit might lead to agglomeration of catalyst, which also reduces the available surface for photon absorption, thus reducing the efficacy for photocatalytic degradation [50]. Effect of catalyst loading (TiO_2) on the extent of degradation of reactive black 5 dye was studied by Kritikos et al. [57] over a range of 0.05–1 g/L at constant initial concentration of 60 mg/L. The photocatalytic activity was reported to increase with an increase in TiO_2 loading over the above range. In another work, Li et al. [55] reported that binary oxide (Bi_2O_3-MgO) photocatalysts can effectively degrade rhodamine B dye, with the best catalyst loading as 0.05 g. Lower loading as 0.025 g showed poor results, whereas there was no further improvement in degradation beyond the optimum catalyst loading. Mohamed and Aazam [53] studied the effect of the catalyst (PANI/Cu_2O) loading over the range of 0.4–2 g/L for degradation of 1000 mL of 600 ppm thiophene solution. The photocatalytic activity was reported to increase for a positive change in catalyst loading from 0.4 to 1.2 g/L, beyond which lower photocatalytic activity was reported. C-TiO_2/Fe_2O_4 was used as a catalyst by

This book belongs to Badji Mokhtar Annaba University Central Library Copyright Elsevier 2025

This book belongs to Badji Mokhtar Annaba University Central Library

Table 24.1: Different methods of synthesizing nanocomposite photocatalysts with application.

Name of the method	Name of the photocatalyst	Precursor/ starting materials	Preparation conditions	Properties of the nanocomposites	Results	References
Hydrothermal	Polyaniline/ Cu_2O	$CuCl_2 \cdot 2H_2O$ and polyaniline	CU_2O was separately prepared. PANI-Cu_2O was mixed, sonicated for 30 min, and stirred for 24 h. Precipitates were dried for 24 h at 60°C.	Particle size of 250 nm, surface area 120 m^2/g	100% degradation of thiophene (600 mg/L) within 60 min in visible-light irradiation	[53]
Thermal condensation and sol-gel	Boron-C_3N_4(BCN)/ $NiFe_2O_4$	$FeCl_3$, $NiCl_2 \cdot 6H_2O$, H_3BO_3, $C_2H_4N_4$	BCN $FeCl_3$ and $NiCl_2 \cdot 6H_2O$ were mixed, sonicated for 30 min at pH of 13, stirred for 1 h at 80°C, dried at 90°C, and then calcined at 450°C for 3 h.	Rough sheet-like structure of BCN and aggregated $NiFe_2O_4$ of 100 nm size	It is a low-cost photocatalyst used for degradation of MB and can be used for other organic compounds	[20]
Sol-gel	C-TiO_2/ Fe_3O_4	$TiCl_3$ and $FeCl_3 \cdot 6H_2O$	Fe_2O_3 and C-TiO_2 were mixed and stirred for 30 min. The mixture was aged for 5 h, dried at 60°C, and calcined at 450°C for 3 h.	Tiny C-TiO_2 adhered to Fe_2O_3	Degraded MO (99.68%) in 150 min and was stable for four cycles	[21]
Sol-gel	N-doped ZnO/g-C_3N_4	Melamine, zinc acetate	g-C_3N_4 and N-Doped ZnO prepared separately. N-ZnO, zinc acetate, and urea were dissolved in ethanol, kept in water bath at 80°C for 5 h, and dried at 400°C for 1 h.	Heterostructure nanocomposites with specific surface area of 18.5 m^2/g	Effective for degradation of MB and phenol	[23]
Coprecipitation	ZnO-SnO_2	$ZnCl_2$, $SnCl_4 \cdot 5H_2O$	Precursors were mixed and stirred for 3 h at pH of 7. The precipitate was filtered, dried, and calcined at 600°C for 2 h.	Particle size of the nanocomposites varied from 10 to 120 nm	The nanocomposite could mineralize MB to 40% extent, and 60% of MB was oxidized to smaller molecules	[54]

Continued

Copyright Elsevier 2025

This book belongs to Badji Mokhtar Annaba University Central Library

Table 24.1: Different methods of synthesizing nanocomposite photocatalysts with application—cont'd

Name of the method	Name of the photocatalyst	Precursor/ starting materials	Preparation conditions	Properties of the nanocomposites	Results	References
Solvent-based thermal method	Bi_2O_3-MgO	$Bi(NO_3)_3 \cdot 5H_2O$, $Mg(NO_3)_2 \cdot 6H_2O$	Precursors were mixed with ethylene glycol and sonicated for 10 min. Citric acid was mixed with ethylene glycol and sonicated for 10 min separately. Both the solutions were autoclaved and calcined at 550°C for 3 h.	Particle size varied from 50 to 300 nm	Effective for degradation of RhB in the presence of HCl	[55]
Sol-Gel	TiO_2/SiO_2	Tetraisopropyl orthotitanate	Precursors were added dropwise to anhydrous 2-propanol and conc. HCl at 0°C and heated at 200°C for 12 h.	Crystallite size was 16 ± 9 Å	Effective for rhodamine-6G degradation	[27]
Thermal decomposition method	ZnO/CuO	Zinc acetate, copper acetate	Starting materials were mixed and ground for 1 h and annealed at 350°C for 3 h.	BET surface area of 9.7–15.4 m^2/g	Effective for treatment of real textile industry wastewater under visible light	[31]

Copyright Elsevier 2025

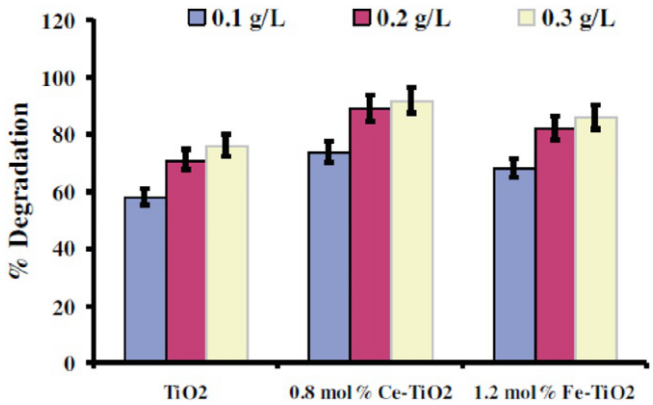

Fig. 24.6

Effect of catalyst loading in photocatalytic degradation [crystal violet dye with initial concentration 30 mg/L and pH 6.5]. *Reprinted with permission from S.R. Shirsath, D.V. Pinjari, P.R. Gogate, S.H. Sonawane, A.B. Pandit, Ultrasound assisted synthesis of doped TiO_2 nanoparticles: characterization and comparison of effectiveness for photocatalytic oxidation of dyestuff effluent, Ultrason. Sonochem. 20 (2013) 277–286.*

Gebrezgiabher et al. [21] for photodegradation of methyl orange, and the catalyst loading was varied over the range of 10–50 mg/L. It was noted that the degradation increased for an initial increase in loading from 10 to 20 mg/L, and after the observed optimum, the photocatalytic activity reduced. Bhosale et al. [17] investigated the effect of catalyst (Cr_2O_3/SnO_2) loading over the range of 0.2–4 g/L for rhodamine B degradation. It was reported that degradation extent increased till 0.5 g/L and then decreased. In another study, decolorization of MB was reported to increase with an increase in dosage of catalyst (MoS_2/TiO_2) from 0.025 g/100 mL to 0.1 g/100 mL [34]. Similarly, brilliant golden yellow degradation [56] was reported to increase for an increase in catalyst ($ZnO\text{-}TiO_2$) loading from 1 to 6 g/L, and beyond this loading, the degradation was constant till 8 g/L of catalyst loading. The experiments were performed using solar radiation for 2 h as the treatment time at pH 7 and initial dye concentration of 20 mg/L [56]. It is important to note that though the trends are similar, the exact value of optimum loading is dependent on the specific system and hence need to be clearly established as also reported by Ahmad et al. [58]. The optimum catalyst loading will reduce the cost and increase the efficiency of the catalysts.

24.6.3 pH of the solution

Heterogeneous photocatalytic processes are dependent on the pH of the solution, and this also depends on the type of the pollutant present. Typically, alkaline pH is favorable for inducing the degradation of cationic pollutants [45]. For example, the pH effect on degradation of rhodamine B was studied using Cr_2O_3/SnO_2 as catalyst, and it was reported that photodegradation

This book belongs to Badji Mokhtar Annaba University Central Library Copyright Elsevier 2025

efficiency reduced in the order of pH as 10 > 7 > 3 [17]. In another study, decolorization rate of brilliant golden yellow dye using catalyst ZnO-TiO_2 was reported to increase with an increase in pH from 6 to 7.5, although further increase in pH decreased the decolorization rate [56]. On the contrary to favorable alkaline conditions, Wang et al. [2] studied methyl orange degradation with Cu_2O/ZnO catalyst and observed that photodegradation increased with the increase in pH till pH of 3.8, and then it decreased. In another study, it was reported that MB exhibits a very good decolorization rate in both acidic and alkaline media [34]. It can be, thus, said that the effect of pH is strongly dependent on the compound characteristics, and the trends need to be established for the specific effluent in question based on pilot-scale studies before the actual application.

24.6.4 Characteristics of the nanocomposite photocatalysts

The morphology and size of nanoparticle catalysts highly influence the catalytic activity because these characteristics contribute to the surface to volume ratio. Scheme 24.1 shows the governing fundamentals between size, shape, surface chemistry, and activity of the catalysts [59].

While there is uniformity about the effects of particle size and the surface area in terms of higher activity at lower size and higher surface area, there are different opinions about the correlations between the efficacy of catalytic processes and crystallite size. There have been reports suggesting that the crystallite size improves catalytic activity, while some reports claimed the opposite observation or no correlation between crystallite size and catalytic activity [60]. We now report different literature illustrations to further explain the role of catalyst characteristics in deciding the efficacy of photocatalysts. Reddy et al. [61] reported that the particle size of $BiFeO_3$ influenced the photocatalytic activity. A reduction in particle size of $BiFeO_3$ from 615 to 190 nm led to an enhanced catalytic activity for rhodamine B degradation under visible light. It was also reported that a further decrease in particle size below 195 nm led to a lower photocatalytic activity. The shape of nanocomposites obtained also has been reported to affect the degradation performance. For example, a study reported that a special rod-like structure of Ce-ZnO nanocomposite gave an enhanced performance for degradation of rhodamine B dye attributed to a higher specific surface area [62]. Kumar and Pandey [63, 64]

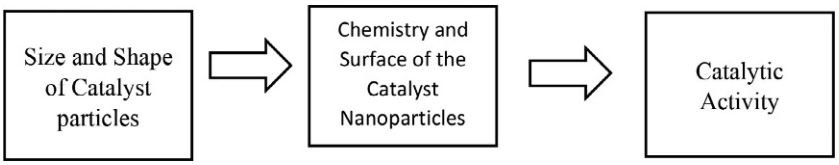

Scheme 24.1
Relations between size, shape, surface chemistry, and activity of the catalysts [59].

This book belongs to Badji Mokhtar Annaba University Central Library Copyright Elsevier 2025

also reported that Cu-TiO_2 showed good photocatalytic activity than pure TiO_2 because Cu-TiO_2 has a rough zig-zag surface, which enhanced the adsorption of organic molecules and hence subsequent degradation performance. It is also reported in the literature that the size and shape of silver nanoparticles influences the photodegradation of organic compounds when used as composites with TiO_2. Under UV-light radiation, spherical Ag/TiO_2 nanocomposites showed an enhanced photocatalytic activity than Ag/TiO_2 nanorods and dendritic structures toward methyl orange degradation [65]. According to Xu et al. [66], photocatalytic activity of zinc ferrite ($ZnFe_2O_4$) was also related to surface area. The researchers studied the degradation of methyl orange using $ZnFe_2O_4$. Photocatalytic activity was observed to be higher if the crystallite size is smaller and surface area is more.

24.6.5 Reaction temperature

The rate of reaction typically is favored with higher temperature, and this is equally applicable for photocatalytic degradation. Fig. 24.7 shows the effect of temperature on photodegradation of rhodamine B based on the use of catalysts as Ag-TiO_2. As shown in the figure, increase in the reaction temperature increases the extent of degradation. The experiments were performed by Barakat et al. [67] by increasing the reaction temperature from 5°C to 55°C, and it was reported that the best temperature was found as 55°C.

The attributing reasons for better effects at higher temperature are (1) enhanced formation of free radicals, (2) lower extent of electron-hole recombination, and (3) increased rate of reaction between the radicals and pollutant molecules [51]. However, it is imperative to note that a reaction temperature greater than 80°C increases charge recombination and is not favorable for photocatalysis. Also, a decrease in temperature below 0°C increases the activation energy. Hence temperature range between 20°C and 80°C is considered to be ideal for photomineralization [63, 64]. Arrhenius equation can be used for calculating the activation energy for photocatalytic reactions, and there are some literature reports that indeed show the temperature dependency of photocatalytic reaction using Arrhenious equation. It is important to note that effects of reaction temperature in photocatalytic system cannot be studied properly at low reaction rates and hence care should be taken to use high light intensity so as to get appreciable rates to study the temperature effects [68].

24.6.6 Concentration of pollutants

Generally, it is observed that the extent of degradation obtained in photocatalytic oxidation decreases with an increase in the pollutant concentration. For example, a study performed at a constant catalyst (C-TiO_2/Fe_2O_4) dose revealed that photocatalytic degradation efficiency decreased for an increase in the methyl orange concentration from 5 to 25 mg/L [21]. Hu et al. [34] reported that the decolorization rate decreased with the use of higher initial concentration

This book belongs to Badji Mokhtar Annaba University Central Library Copyright Elsevier 2025

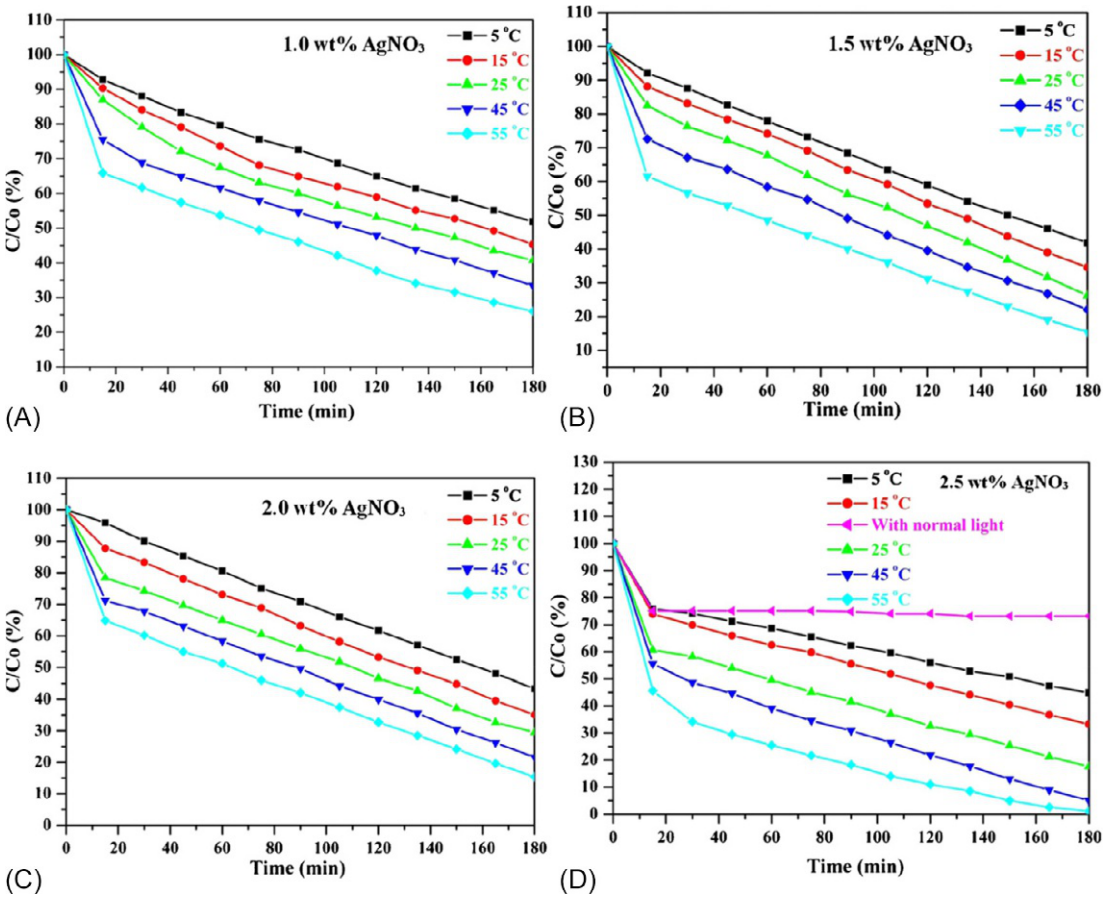

Fig. 24.7

Effect of temperature on degradation of rhodamine B dye with Ag-TiO_2 [1, 1.5, 2, 2.5 wt% $AgNO_3$, respectively]. *Reprinted with permission from N.M.A. Barakat, M.A. Kanjwal, I.S. Chronakis, H.Y. Kim, Influence of temperature on the photodegradation process using Ag-doped TiO_2 nanostructures: negative impact with the nanofibers, J. Mol. Catal. A: Chem. 366 (2013) 333–340.*

of MB beyond an optimum when MoS_2/TiO_2 was used as a catalyst. The initial concentration was varied from 10 to 70 mg/L, and it was observed that more than 50 mg/L of the pollutant concentration was not satisfactory, giving lower rates of degradation. Wang et al. [2] reported that initial concentration of methyl orange had a considerable effect on degradation obtained using photocatalysis based on Cu_2O/ZnO as the photocatalyst. To give a quantitative idea on the effect of initial concentration, Fig. 24.8 illustrates the results for a specific case of crystal violet dye degradation with Ce-TiO_2 and Fe-TiO_2 applied as catalysts [16]. It was observed that higher the initial concentration, lower was the rate of degradation. The experiments were performed at two initial concentrations (30 and 60 mg/L), pH as 6.5, and catalyst loading

This book belongs to Badji Mokhtar Annaba University Central Library
Copyright Elsevier 2025

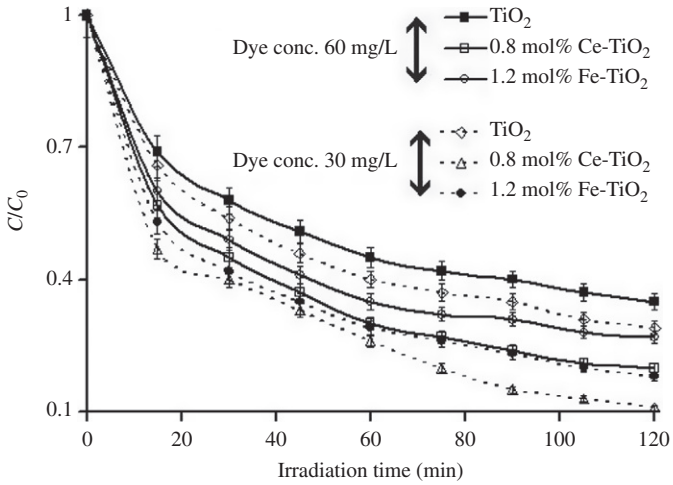

Fig. 24.8

Effect of initial concentration of crystal violet dye on the degradation using catalysts as Ce-TiO_2 and Fe-TiO_2. *Reprinted with permission from S.R. Shirsath, D.V. Pinjari, P.R. Gogate, S.H. Sonawane, A.B. Pandit, Ultrasound assisted synthesis of doped TiO_2 nanoparticles: characterization and comparison of effectiveness for photocatalytic oxidation of dyestuff effluent, Ultrason. Sonochem. 20 (2013) 277–286.*

as 0.2 g/L. According to the authors, the decrease of degradation rate might be based on two reasons (1) higher dye concentration at the surface of the catalyst decreases the path length of the photons and (2) OH• radical formation decreases with an increase in dye concentration.

24.6.7 Effect of type of light and intensity

The efficacy of photodegradation process is strongly dependent on light intensity because electron-hole pair is generated by the incident light energy. Both wavelength and intensity are important for the final effects in photocatalysis. Lakshmi et al. [69] conducted studies with ZnO/MgO nanocomposites applied for degradation of Eosin yellow dye. It was reported that the photodegradation was more under UV light than sunlight. Soltani et al. [70] reported that there is a direct relationship between photodegradation of MB using ZnO/SiO_2 nanocomposites as the catalyst and light intensity. Quantitatively, with an increase in light intensity from 2030 to 3950 $\mu W/cm^2$, the photodegradation was reported to increase from 32% to 92.2%. It is important to state that in countries where intense sunlight is available throughout the year, solar photocatalytic degradation can be effectively used for the treatment of pollutants present in the wastewater. It is important to note that marginally lower effects are obtained based on the use of solar light compared to UV. For example, photocatalytic degradation of spiramycin (a pharmaceutical pollutant) is reported in the literature, with 19% degradation based on the use of

This book belongs to Badji Mokhtar Annaba University Central Library Copyright Elsevier 2025

UV light and 10% degradation using visible light achieved after 7 h of illumination [71]. Thus to overcome the lower degradation using visible range, improved catalysts or the focused use of solar energy based on the application of good concentrators can be thought about.

24.6.8 Irradiation time

Irradiation time has also a great influence on the extent of photocatalytic degradation. It is necessary to decide on the optimum treatment time so as to achieve maximum benefits. Saravanan et al. [31] reported that color disappeared steadily with an increase in the treatment time for the system of methyl orange and MB using ZnO/CuO nanocomposite as the catalyst. In another study, it was reported that degradation of crystal violet using nanocomposites Fe/TiO_2 and Ce/TiO_2 as the catalysts increased with an increase in treatment time [16]. A similar result of increase in degradation with increase in irradiation time was reported by Kamal et al. [20] for photodegradation of MB with boron-doped C_3N_4/$NiFe_2O_4$ as the catalyst. Fig. 24.9A and B represent the reproduced data of the effect of irradiation time on degradation of different dyes. Fig. 24.9A shows that crystal violet degradation increased gradually with increase in irradiation time The comparison of percentage degradation presented for Ce-TiO_2, Fe-TiO_2, and TiO_2 (all synthesized with the assistance of ultrasound) reveals that maximum degradation is obtained for Ce-TiO_2. Fig. 24.9B shows the degradation efficacies of $NiFe_2O_4$, BCN, BCN/$NiFe_2O_4$ with actual extent of degradation of methylene blue dye as 25.6%, 69%, and 98%, respectively. Table 24.2 gives a summary of previous studies of nanocomposite photocatalysts applied for photocatalytic oxidation briefly highlighting the conditions used in the study along with the pollutant investigated.

24.7 Recent trends in types of photocatalytic reactors

Photoreactors can be broadly classified as (1) suspension or slurry photoreactors, (2) photoreactor with immobilized photocatalyst, and (3) multifunctional photoreactors. The important points to be considered for design of photoreactors are (1) source of irradiation, (2) wavelength or lamp selection, and (3) placement of light source and light distribution [76]. The reactor design should be such that at the incident light intensity, there should be uniform irradiations over the entire catalyst surface [77]. We now discuss some of the recent trends in photocatalytic reactors applied with an objective of achieving higher efficacy for degradation.

24.7.1 Photocatalytic membrane reactors

Photocatalytic membrane reactors (PMRs) are mainly of two types (1) slurry reactors and (2) immobilized reactors. The first type can be further divided into three categories according to the position of the irradiation source (1) irradiation at the feed tank, (2) irradiation at the membrane module, and (3) irradiation at an additional reservoir (which is placed between feed tank and

This book belongs to Badji Mokhtar Annaba University Central Library Copyright Elsevier 2025

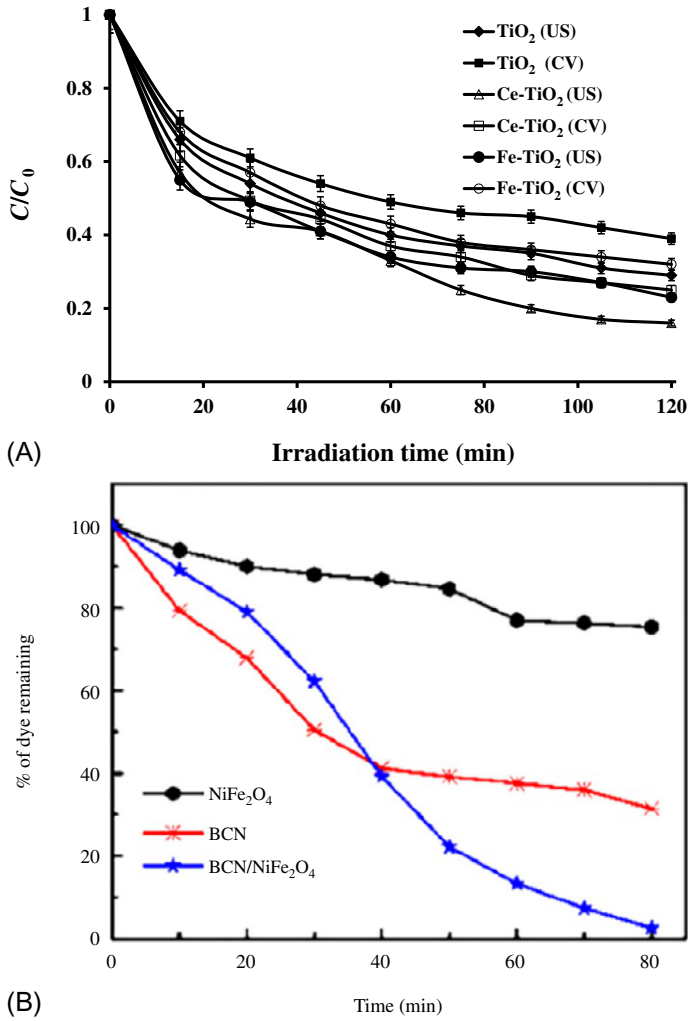

Fig. 24.9

Effect of Irradiation time for degradation of (A) crystal violet dye with Ce-TiO_2 and Fe-TiO_2 and (B) methylene blue with boron-doped $C_3N_4/NiFe_2O_4$. *Reprinted with permission from S.R. Shirsath, D.V. Pinjari, P.R. Gogate, S.H. Sonawane, A.B. Pandit, Ultrasound assisted synthesis of doped TiO_2 nanoparticles: characterization and comparison of effectiveness for photocatalytic oxidation of dyestuff effluent, Ultrason. Sonochem. 20 (2013) 277–286; S. Kamal, S. Balu, S. Palanisamy, K. Uma, V. Velusamy, T.C.K. Yang, Synthesis of boron doped $C_3N_4/NiFe_2O_4$ nanocomposite: an enhanced visible light photocatalyst for the degradation of methylene blue, Results Phys. 12 (2019) 1238–1244.*

membrane module). Fig. 24.10A–C depicts different PMRs where the photocatalysts are in suspension and irradiation sources are at membrane module, at the feed tank and at the additional reservoir, respectively. Fig. 24.10D shows a PMR, in which photocatalyst is in the immobilized form [77]. These reactors have many advantages over conventional reactors such

This book belongs to Badji Mokhtar Annaba University Central Library Copyright Elsevier 2025

Table 24.2: Overview of Studies for application of nanocomposites photocatalysts for wastewater treatment.

Details on nanocomposites	Pollutants degraded	Reaction conditions (pH, reaction temperature, irradiation time, light intensity	References
Ce-TiO_2	Propranolol	Irradiation time = 1.5 h Initial pollutant concentration of 0.14 g/L	[72]
Ce-TiO_2, Bare TiO_2 of 10 nm size and CeO_2 of ~5 nm size	Chlorophenol	pH of 5.8, Initial pollutant concentration of 100 mg/L	[73]
C-doped TiO_2/Fe_2O_4	Methyl orange	Catalyst loading range =5–50 mg. Initial pollutant concentration as 5 mg/L, 100 mL solution	[21]
N-doped ZnO/g-C_3N_4	Methylene blue, phenol	Irradiation time = 120 min	[23]
$BiVO_4/CeO_2$	Methylene blue, methyl orange	Initial pollutant concentration as 7.5 mg/L	[26]
CeO_2/TiO_2 over the size range of 5.3–8.5 nm	Toluene	Temperature = 30°C, Initial pollutant concentration as 300 ppm	[25]
CeO_2/ZnO	Rhodamine B	Irradiation time = 90 min	[28]
MsO_2/TiO_2 Layered structure of 10–40 nm **length** and layered distance of 0.62 nm	Methylene blue	pH range of 3–11, Reaction temperature = 10–40°C Initial pollutant concentration = 10–70 mg/L	[34]
V_2O_5/ZnO V_2O_5 **of** orthorhombic, and ZnO **of** hexagonal structures	Methylene blue	Irradiation time = 30–120 min	[29]
Ag_3Po_4/MoS_2 with size ~5.4 nm Ag_3PO_4 and MoS_2 nanosheets	Methylene blue	Irradiation time = 15 min	[74]
TiO_2/In_2S_3 with size range of 5.8–6.3 nm and anatase TiO_2	Orange II	Irradiation time = 65 min	[75]
PANI/TiO_2	Methylene blue and rhodamine B	Initial pollutant concentration of 1×10^{-5} mol L^{-1} and 50 mL of dye solution used for studies	[35]
PANI/ BiY Ti_2O_7	Azocarmine G	Irradiation time of 330 min, initial pollutant concentration as 20 mg/L	[11]
Chitosan/carbon black nanoparticles	Congo red	Optimum pH of 6 Light intensity over the range of 20–80 W Initial pollutant concentration as 8 mg/L	[7]

This book belongs to Badji Mokhtar Annaba University Central Library
Copyright Elsevier 2025

Table 24.2: Overview of Studies for application of nanocomposites photocatalysts for wastewater treatment—cont'd

Details on nanocomposites	Pollutants degraded	Reaction conditions (pH, reaction temperature, irradiation time, light intensity	References
TiO_2/graphene oxide	Methylene blue	pH as 4 Irradiation time = 60 min 50 mg catalyst in 50 mL of solution	[43]
ZnO/bentonite nanospheres of particle size of 20–30 nm range	Phenol	pH range of 2–12	[47]
TiO_2/bentonite with Surface area range of 69–97 m^2/g	CB	Irradiation time of 10 min for UV and 60 min for visible light Catalyst loading of 2 mg/20 mL Initial pollutant concentration as 400 ppm	[48, 49]

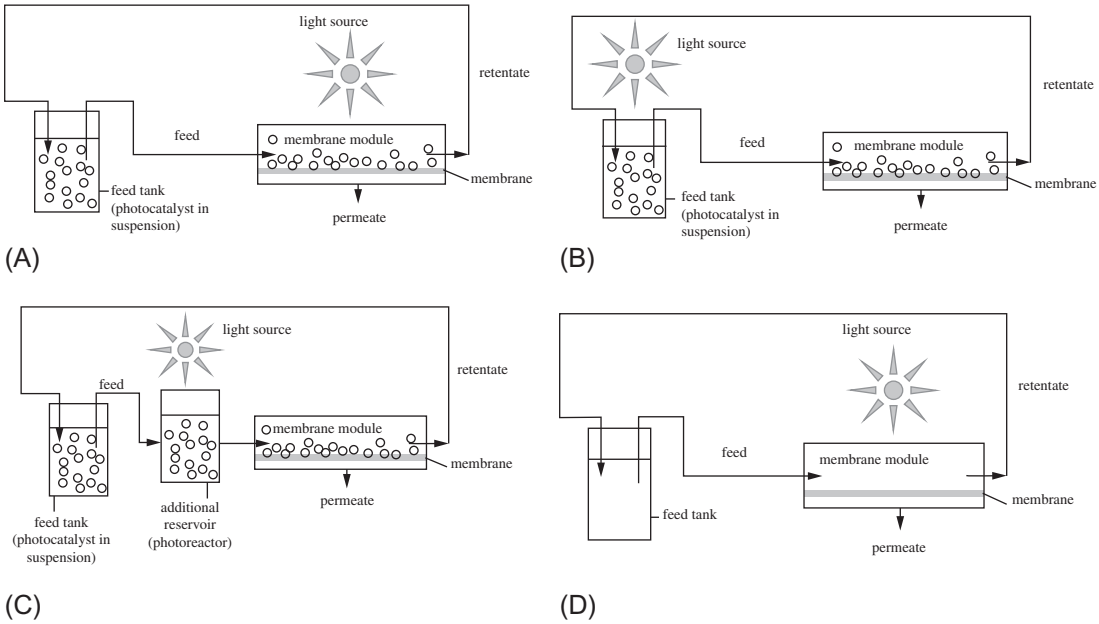

Fig. 24.10

Different PMRs where the photocatalysts are in suspension and irradiation sources are (A) at membrane module (B) at the feed tank and (C) at the additional reservoir (D) photocatalysts are immobilized. *Reprinted with permission from S. Mozia, Photocatalytic membrane reactors (PMRs) in water and wastewater treatment. A review, Sep. Purif. Technol. 73 (2010) 71–91.*

This book belongs to Badji Mokhtar Annaba University Central Library
Copyright Elsevier 2025

as reduced loss of catalysts, control over retention time in the reactor, improved efficiency, and stability. It also reduces the cost of operation by allowing reuse of the catalysts. The main disadvantage of these types of reactors is membrane fouling [78]. Most of the PMRs combine photocatalysis with microfiltration, nanofiltration, or ultrafiltration. Some types of photocatalytic reactors are also coupled with dialysis and pervaporation [77].

There are very few studies involving the use of nanocomposites in PMRs, and most of PMRs used TiO_2 as catalysts. Yu et al. [79], fabricated a PMR for degradation of sulfamethoxazole. A membrane of mesoporous graphitic carbon nitride/titanium dioxide (mpg-C_3N_4/TiO_2) was used, and it was reported from their experiments that this reactor is suitable for degrading sulfamethoxazole (a pharmaceutical component). Regenerated cellulose and N-doped TiO_2 nanocomposites were also used for fabricating a PMR (acrylic membrane of dimension 15 × 15 cm and depth of 16 cm) with application for degradation of phenol by Mohamed et al. [80]. Degradation of phenol under UV and visible light irradiation was reported as 96.6% and 78.8%, respectively. In another study, a PMR was fabricated using TiO_2/poly-vinylidene-flouride-triflouro-ethylene nanocomposites and applied for treating oily wastewater. It was reported that after 7 h of sunlight irradiation, colorless water was obtained, establishing clearly that the nanocomposite membrane is efficient for treating the oily wastewater [81].

24.7.2 Microreactors and microfluidic reactors

Photocatalytic microreactors are further classified as packed-bed, wall-coated, and micromonolithic, although the packed-bed type is the most utilized. In wall-coated system, thin film of photocatalysts is deposited on microchannel walls, and hence these reactors are more complicated than the packed-bed system. Micromonolithic reactors are generated by polymerization of the porous channels with photocatalysts immobilized on the channels [82]. Photocatalytic microreactors yield large surface to volume ratio (>10,000 m^2/m^3) and hence show much higher heat and mass transfer rates due to this high surface to volume ratio. Furthermore, small size enables safe operation and less waste generation. Different microreactors have been developed to improve the efficiency of the micro photoreactor, namely microcapillary reactor, single microchannel reactor, and multimicrochannel reactors [83]. Microreactors have some special features such as short diffusion distance, large specific interfacial surface area, and good heat transfer properties [84]. Very few literature that deal with microreactors and microfluidic reactors using nanocomposite as photocatalysts is available, as far as the knowledge of the authors. In one study [85], ZnO/TiO_2 nanorods were synthesized and applied in the inner wall of the capillary-based photocatalytic microreactors. It was demonstrated that capillary microreactors are efficient in photodegradation. Lamberti [86] fabricated a microfluidic reactor using polydimethylsiloxane/TiO_2 (PDMS/TiO_2) nanocomposites. The microfluidic reactor was reported to be efficient to degrade MB in a very short time. Fig. 24.11 shows a specific design of glass microreactor reported to be beneficial for

This book belongs to Badji Mokhtar Annaba University Central Library Copyright Elsevier 2025

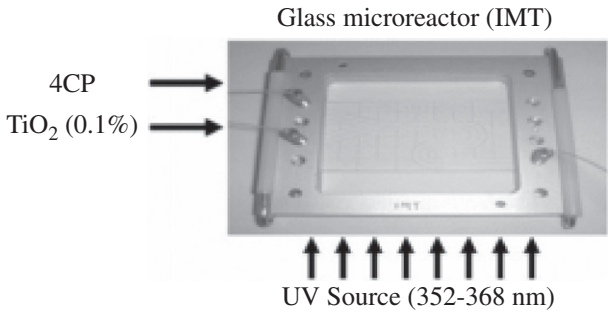

Fig. 24.11
Glass microreactor. *Reprinted with permission from A. Yusuf, C. Garlisi, G. Palmisano, Overview on microfluidic reactors in photocatalysis: applications of graphene derivatives, Catal. Today 315 (2018) 79–92.*

degradation of chlorophenol [82]. One more study on the use of PDMS/TiO_2 nanocomposites in microfluidic reactor for degradation of MB and rhodamine B demonstrated that this reactor is efficient for degradation of both the dyes with a good potential for scale-up [87].

24.7.3 Hybrid photoreactors

There are some studies reporting the use of hybrid systems such as photocatalytic reactor and a membrane permeation cell or a combination of photocatalytic and ultrasonic reactors. A study dealing with combined photocatalytic and membrane reactors for the treatment of petroleum refinery wastewater demonstrated that almost 90% of the organic pollutants was degraded in photocatalytic reactor, and almost 99% separation was possible with hybrid operation of photocatalytic reactor followed by membrane filtration [88]. Another study dealing with sonophotocatalytic reactors demonstrated that trypan blue and vesuvine were degraded effectively based on the use of nanocomposite as Ag_3PO_4/Bi_2S_3-HKUST-1-MOF. It was reported that 98.44% and 99.36% degradation was possible for trypan blue and vesuvine, respectively, at optimum conditions as initial concentration of dye of 25 mg/L, 70 mL/min as the solution flow rate, 25 min as treatment time, pH of 6, and catalyst dose of 0.25 g/L. It was reported that hybrid system is more efficient than individual system. Fig. 24.12 shows the schematic representation of the sonophotocatalytic reactor, which is basically a flow-loop reactor containing reactor vessel, ultrasonic bath, peristaltic pump, blue LED, reservoir tank, magnetic stirrer, aeration pump, and sampling valve [89]. Pan et al. [90] reported another synergistic combination as photoelectrocatalytic oxidation (PECO) where photocatalytic oxidation is combined with electrocatalytic oxidation. TiO_2/CAC (columnar activated carbon) particles were used for the studies of degradation of methyl orange, and it was clearly demonstrated that the PECO process shows synergy, that is, more than the additive effect and has potential applications in wastewater treatment.

This book belongs to Badji Mokhtar Annaba University Central Library Copyright Elsevier 2025

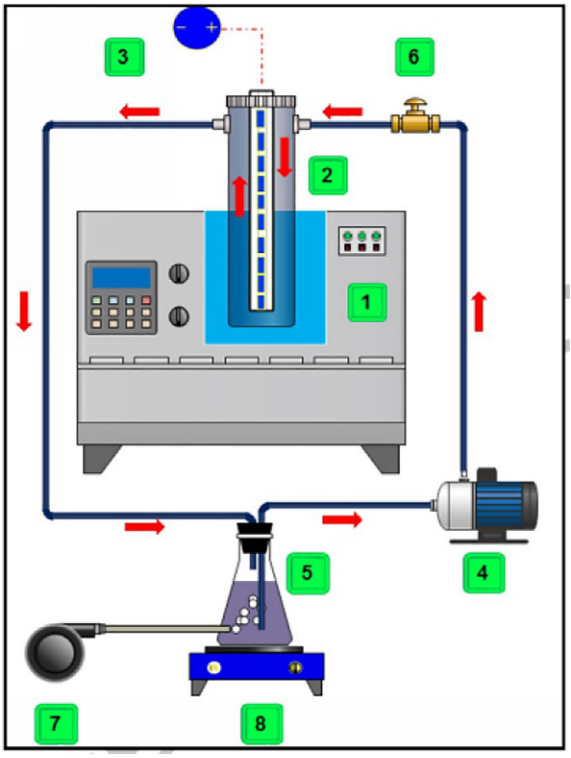

Fig. 24.12
Sonophotocatalytic reactor (1) ultrasonic bath (2) reactor (3) LED source (4) peristaltic pump (5) reservoir (6) sampling valve (7) aeration tank (8) magnetic stirrer. *Reprinted with permission from S. Mosleh, M.R. Rahimi, M. Ghaedi, K. Dashtian, Sonophotocatalytic degradation of trypan blue and vesuvine dyes in the presence of blue light photocatalyst of Ag_3PO_4/Bi_2S_3-HKUST-1-MOF: central composite optimization and synergistic effect study, Ultrason. Sonochem. 32 (2016) 387–397.*

24.8 Challenges

Photocatalytic oxidation reactors are not very prominently considered option for industries. Most of the limitations are associated with the designing and modeling of the photoreactors such as (1) size limitations, (2) construction difficulties, (3) lamp operations and maintenance issues, and (4) reactor wall deposits that reduce the radiation intensity into the reactors. In addition, photocatalytic reactors generally work under nonuniform concentrations, temperatures, and radiations [91]. More limitations are high cost for catalyst and low stability in the long run. In the case of slurry reactor, powdered photocatalysts are used. The recovery of these photocatalysts at the downstream increases the capital costs. Moreover, at the time of scale-up, insufficient light penetration over the larger reactor is also a serious problem [83]. Large land area requirement is another major hurdle for solar heterogeneous photocatalytic

This book belongs to Badji Mokhtar Annaba University Central Library Copyright Elsevier 2025

oxidation process. As a typical example, for treating secondary municipal effluent, the light collecting area required is 70 m^2 for a purification target of 2 mg/L of the desired contaminants. For wastewater from chemical industry, the light collecting area required is 1000 m^2 to treat 1 m^3 within 1 day. Similarly, for treating oily wastewater (pretreated), 19 m^2 land is required. Therefore solar photocatalytic processes are not very attractive to treat large volume of wastewater [92]. Overall, these reactors need to be improved before industrialization at large scale [78].

24.9 Conclusions

Photocatalysis appears to be promising among all the oxidation processes for wastewater treatment. One of the concerns in this field is poor visible light-induced activity for the catalyst, which can be overcome by the use of nanocomposites that are more active in visible light range than a single-component catalyst. Photocatalysts mainly work on photoredox reactions, and the rate of generation of radicals plays a very important role in deciding the efficacy of treatment. It can be said that application of photocatalytic degradation for wastewater treatment is gaining interests, especially in the visible light range. Analysis of literature revealed that most studies deal with dye as a representative organic pollutant instead of real wastewater from the industries. More studies should be performed to improve the feasibility of applying the technology in real industrial wastewater treatment and also at large scale. It has been demonstrated in the chapter that the efficacy is dependent on various operational parameters such as pH, dose and morphology of the catalyst, reaction temperature, initial concentration of the pollutants, and light intensity. Overall, it can be said that optimum considerations during the synthesis and actual application in the photocatalytic oxidation coupled with use of process intensification is the key to successful application in wastewater treatment.

References

[1] X. Chen, S.S. Mao, Titanium oxide nanomaterials: synthesis, properties, modifications, and applications, Chem. Rev. 107 (2007) 2891–2959.
[2] X.S. Wang, Y.D. Zhang, Q.C. Wang, B. Dong, Y.J. Wang, W. Feng, Photocatalytic activity of Cu_2O/ZnO nanocomposite for the decomposition of methyl orange under visible light irradiation, Sci. Eng. Compos. Mater. 26 (2019) 104–113.
[3] E. Cominia, M. Ferroni, V. Guidi, G. Faglia, G. Martinelli, G. Sberveglieri, Nanostructured mixed oxides compounds for gas sensing applications, Sens. Actuators B: Chem. 84 (2002) 26–32.
[4] S.S. Pooyan, Sol-gel process and its application in nanotechnology, J. Polym. Eng. Technol. 13 (2005) 38–41.
[5] K.R. Sachinjith, K.R.S. Krishna, A review on types of nanocomposites and their applications, Ideas Innov. Technol. 4 (2018) 235–236.
[6] K. Ravichandran, P.K. Prasheetha, T. Arun, S. Gobalakrishnan, Synthesis of nanocomposites, in: Synthesis of Inorganic Nanomaterials, Elsevier, 2018, pp. 141–167 (Chapter 6).
[7] M.N. Alshabanat, M.M. Al-Anazy, An experimental study of photocatalytic degradation of congo red using polymer nanocomposite films, J. Chem. 2018 (2018) 1–8.

This book belongs to Badji Mokhtar Annaba University Central Library Copyright Elsevier 2025

[8] V. Camargo, E. Ortiz, H. Solis, C.M. Cortes-Romero, S. Serna, C.Z. Perez, Chemical degradation of indigo potassium tetrasulfonate dye by advanced oxidation processes, J. Environ. Prot. 5 (2014) 1342–1351.
[9] C. Yang, W. Dong, G. Cuid, Y. Zhaod, X. Shid, X. Xiad, B. Tang, W. Wang, Enhanced photocatalytic activity of PANI/TiO_2 due to their photosensitization-synergetic effect, Electrochim. Acta 247 (2017) 486–495.
[10] C. Byrne, G. Subramaniun, S.C. Pillai, Recent advances in photocatalysis and environmental applications, J. Environ. Chem. Eng. 6 (2018) 3531–3555.
[11] J. Luan, Y. Shen, S. Wang, N. Guo, Synthesis, property characterization and photocatalytic activity of the polyaniline/$BiYTi_2O_7$ polymer composite. Polymers 9 (3) (2017) 69https://doi.org/10.3390/polym9030069.
[12] X. An, J.C. Yu, Graphene-based photocatalytic composites, RSC Adv. 1 (2011) 1426–1434.
[13] A. Ajmal, I. Majeed, R.N. Malik, H. Idriss, M.A. Nadeem, Principles and mechanisms of photocatalytic dye degradation on TiO_2 based photocatalysts: a comparative overview, RSC Adv. 4 (2014) 37003–37026.
[14] A.D. Paola, E. Garc´ıa-López, S. Ikeda, G. Marc'ı, G. Ohtani, L. Palmisano, Photocatalytic degradation of organic compounds in aqueous systems by transition metal doped polycrystalline TiO_2, Catal. Today 75 (2002) 87–93.
[15] H. Moradi, A. Eshaghi, S.R. Hosseini, K. Ghani, Fabrication of Fe-doped TiO_2 nanoparticles and investigation of photocatalytic decolourization of reactive red 198 under visible light irradiation, Ultrason. Sonochem. 32 (2016) 314–319.
[16] S.R. Shirsath, D.V. Pinjari, P.R. Gogate, S.H. Sonawane, A.B. Pandit, Ultrasound assisted synthesis of doped TiO_2 nanoparticles: characterization and comparison of effectiveness for photocatalytic oxidation of dyestuff effluent, Ultrason. Sonochem. 20 (2013) 277–286.
[17] R. Bhosale, S. Pujari, G. Muley, G. Pagare, A. Gambhire, Visible-light-activated nanocomposite photocatalyst of Cr_2O_3/SnO_2, J. Nanostruct. Chem. 46 (2013) 2–7.
[18] S. Samadi, R. Ahmadi, M. Kohi, Synthesis, characterization, and application of Zr, Ce-TiO2/SiO2 nanocomposite thin film as visible-light active photocatalyst, Int. J. New Chem. 2 (2015) 8–16.
[19] K.C. Barick, S. Singh, M. Aslam, D. Bahadur, Porosity and photocatalytic studies of transition metal doped ZnO nanoclusters, Microporous Mesoporous Mater. 134 (2010) 195–202.
[20] S. Kamal, S. Balu, S. Palanisamy, K. Uma, V. Velusamy, T.C.K. Yang, Synthesis of boron doped C_3N_4/$NiFe_2O_4$ nanocomposite: an enhanced visible light photocatalyst for the degradation of methylene blue, Results Phys. 12 (2019) 1238–1244.
[21] M. Gebrezgiabher, G. Gebreslassie, T. Gebretsadik, G. Yeabyo, F. Elemo, Y. Bayeh, M. Thomas, W. Linert, A C-doped TiO_2/Fe_3O_4 nanocomposite for photocatalytic dye degradation under natural sunlight irradiation, J. Comput. Sci. 3 (2019) 2–11.
[22] R. Asahi, T. Morikawa, T. Ohwaki, K. Aoki, Visible-light photocatalysis in nitrogen-doped titanium oxides, Science 293 (2001) 269–271.
[23] J. Kong, H. Zhai, W. Zhang, S. Wang, X. Zhao, M. Li, H. Li, A. Li, D. Wu, Visible light-driven photocatalytic performance of N-doped ZnO/g-C_3N_4 nanocomposites, Nanoscale Res. Lett. 12 (2017) 2–10.
[24] Y. Yalcın, M. Kılıc, Z. Cınar, The role of non-metal doping in TiO_2 photocatalysis, J. Adv. Oxid. Technol. 13 (2010) 281–296.
[25] M.J. Munoz-Batista, M.N. Goomez-Cerezo, A. Kubacka, D. Tudela, M. Fernaandez-Garcia, Role of interface contact in CeO_2-TiO_2 photocatalytic composite materials, ACS Catal. 4 (2013) 63–72.
[26] N. Wetchakun, S. Chaiwichain, B. Inceesungvorn, K. Pingmuang, S. Phanichphant, A. I. Minett, J. Chen, $BiVO_4/CeO_2$ nanocomposites with high visible-light-induced, ACS Appl. Mater. Interfaces 4 (7) (2012) 3718–3723.
[27] C. Anderson, A.J. Bard, An improved photocatalyst of TiO_2/SiO_2 prepared by a sol-gel synthesis, J. Phys. Chem. 99 (1995) 9882–9885.
[28] N. Shah, K. Bhangaonkar, D.V. Pinjari, S.T. Mhaske, Ultrasound and conventional synthesis of CeO_2/ZnO nanocomposites and their application in the photocatalytic degradation of rhodamine B dye, J. Adv. Nanomater. 2 (2017) 133–145.
[29] R. Saravanan, V.K. Gupta, E. Mosquera, F. Gracia, Preparation and characterization of V_2O_5/ZnO nanocomposite system for photocatalytic application, J. Mol. Liq. 198 (2014) 409–412.

This book belongs to Badji Mokhtar Annaba University Central Library Copyright Elsevier 2025

[30] K. SatishKumar, K.R.R. Narayanan, S. Siddarth, R.P. Kumar, R.B. Narayan, R. Gautham, V. Swamynaathan, Synthesis of MgO/TiO_2 nanocomposite and its application in photocatalytic dye degradation, Int. J. Chem. React. Eng. 16 (2017).
[31] R. Saravanan, S. Karthikeyan, V.K. Gupta, G. Sekaran, V. Narayanan, A. Stephen, Enhanced photocatalytic activity of ZnO/CuO nanocomposite for the degradation of textile dye on visible light illumination, Mater. Sci. Eng. C 33 (2013) 91–98.
[32] K. Tu, X. Wu, C. Wang, X. Liao, S. Yang, Microwave synthesis and photocatalytic activity of cadmium indium sulfide nanocomposite, Mod. Res. Catal. 6 (2017) 73–79.
[33] H. Mossalayi, A. Moghimi, Fabrication of TiO_2/Ag_2S nano-composites via a new method for photocatalytic degradation of p-xylene & chlorophenol, J. Chem. Pharm. Res. 3 (2011) 718–724.
[34] K. Hu, Y. Cai, S. Li, Photocatalytic degradation of methylene blue on MoS_2/TiO_2 nanocomposite, Adv. Mater. Res. 197–198 (2011) 997–999.
[35] M. Radoicica, G. Ciric-Marjanovi, V. Spasojevica, P. Ahrenkielc, M. Mitrica, T. Novakovic, Z. Saponji, Superior photocatalytic properties of carbonized PANI/TiO_2 nanocomposites, Appl. Catal. B Environ. 213 (2017) 155–166.
[36] V. Eskizeybeka, F. Sarı, H. Gulce, A. Gulce, A. Avcı, Preparation of the new polyaniline/ZnO nanocomposite and its photocatalytic activity for degradation of methylene blue and malachite green dyes under UV and natural sun lights irradiations, Appl. Catal. B: Environ. 119 (2012) 197–206.
[37] K.S. Divya, T.U. Umadevi, S. Mathewa, Graphene-based semiconductor nanocomposites for photocatalytic applications, J. Nanosci. Lett. 4 (2013) 1–34.
[38] Z. Xiong, L.L. Zhang, J. Ma, X.S. Zhao, Photocatalytic degradation of dyes over graphene–gold nanocomposites under visible light irradiation, Chem. Commun. 46 (2010) 6099–6101.
[39] S. Kumar, A. Kumar, Enhanced photocatalytic of r-GO-CeO_2 nanocomposite driven by sunlight, Mater. Sci. Eng. B 223 (2017) 98–108.
[40] S. Kumar, A. Kumar, Enhanced photocatalytic activity of rGO-CeO_2 nanocomposites driven by sunlight, Mater. Sci. Eng. B 223 (2017) 98–108.
[41] S. Gawande, S.R. Thakare, Synthesis of visible light active graphene-modified $BaCrO_4$ nanocomposite photocatalyst, Int. Nano Lett. 3 (2013) 2–8.
[42] D. Liang, C. Cui, H. Hub, Y. Wang, S. Xu, B. Ying, P. Li, B. Lu, H. Shen, One-step hydrothermal synthesis of anatase TiO_2/reduced graphene oxide nanocomposites with enhanced photocatalytic activity, J. Alloys Compd. 582 (2014) 236–240.
[43] P.M. Martins, C.G. Ferreira, A.R. Silva, B. Magalhães, M.M. Alves, L. Pereira, P.A.A.P. Marques, M. Melle-Francod, S. Lanceros-Méndez, TiO_2/graphene and TiO_2/graphene oxide nanocomposites for photocatalytic applications: a computer modeling and experimental study, Compos. Part B 145 (2018) 39–46.
[44] V. Belessi, D. Lambropoulou, I. Konstantinou, A. Katsoulidis, P. Pomonis, D. Petridis, T. Albanis, Structure and photocatalytic performance of TiO_2/clay nanocomposites for the degradation of dimethachlor, Appl. Catal. B: Environ. 73 (2007) 292–299.
[45] Z. Sun, Y. Chen, Q. Ke, Y. Yang, J. Yuan, Photocatalytic degradation of cationic azo dye by TiO_2/bentonite nanocomposite, J. Photochem. Photobiol. A: Chem. 149 (2002) 169–174.
[46] Y.S. Ngoh, M.A. Nawi, Role of bentonite adsorbent sub-layer in the photocatalytic-adsorptive removal of methylene blue by the immobilized TiO_2/Bentonite system, Int. J. Environ. Sci. Technol. 13 (2016) 907–926.
[47] S. Meshram, R. Limaye, S. Ghodke, S. Nigam, S. Sonawane, R. Chikate, Continuous flow photocatalytic reactor using ZnO-bentonite nanocomposite for degradation of phenol, Chem. Eng. J. 172 (2011) 1008–1015.
[48] A. Mishra, A. Mehta, M. Sharma, S. Basu, Enhanced heterogeneous photodegradation of VOC and dye using microwave synthesized TiO_2/clay nanocomposites: a comparison study of different type of clays, J. Alloys Compd. 694 (2017) 574–580.
[49] A. Mishra, A. Mehta, M. Sharma, S. Basu, Impact of Ag nanoparticles on photomineralization of chlorobenzene by TiO_2/bentonite nanocomposite, J. Environ. Chem. Eng. 5 (2017) 644–651.
[50] U.G. Akpan, B.H. Hameed, Parameters affecting the photocatalytic degradation of dyes using TiO_2-based photocatalysts: a review, J. Hazard. Mater. 170 (2009) 520–529.

This book belongs to Badji Mokhtar Annaba University Central Library Copyright Elsevier 2025

[51] A. Gnanaprakasam, V.M. Sivakumar, M. Thirumarimurugan, Influencing parameters in the photocatalytic degradation of organic effluent via nanometal oxide catalyst: a review, Indian J. Mater. Sci. 2015 (2015) 1–16 601827.
[52] M. Bellardita, M. Addamo, A.D. Paola, L. Palmisano, A.M. Venezia, Preparation of N-doped TiO_2: characterization and photocatalytic performance under UV and visible light, Phys. Chem. Chem. Phys. 11 (2009) 4082–4093.
[53] R.M. Mohamed, E.S. Aazam, Preparation and characterization of core–shell polyaniline/mesoporous Cu_2O nanocomposites for the photocatalytic oxidation of thiophene, Appl. Catal. A: Gen. 480 (2014) 100–107.
[54] J. Lin, Z. Luo, J. Liu, P. Li, Photocatalytic degradation of methylene blue in aqueous solution by using ZnO-SnO2 nanocomposites, Mat. Sci. Semicond. Proc. 87 (2018) 24–31.
[55] E.J. Li, K. Xia, S.F. Yina, W.L. Dai, S.L. Luo, C.T. Au, Preparation, characterization and photocatalytic activity of Bi_2O_3–MgO composites, Mater. Chem. Phys. 125 (2011) 236–241.
[56] M.A. Habib, M.T. Shahadat, M.N. Bahadur, I.M. Ismail, A.J. Mahmood, Synthesis and characterization of ZnO-TiO_2 nanocomposites and their application as photocatalysts, Int. Nano Lett. 3 (2013) 2–8.
[57] D.E. Kritikos, N.P. Xekoukoulotakis, E. Psillakis, D. Mantzavinos, Photocatalytic degradation of reactive black 5 in aqueous solutions: effect of operating conditions and coupling with ultrasound irradiation, Water Res. 41 (2007) 2236–2246.
[58] R. Ahmad, Z. Ahmad, A.U. Khan, N.R. Mastoi, M. Aslam, J. Kim, Photocatalytic systems as an advanced environmental remediation: recent developments, limitations and new avenues for applications, J. Environ. Chem. Eng. 4 (2016) 4143–4164.
[59] S. Cao, F. Tao, Y. Tang, Y. Lia, J. Yu, Size- and shape-dependent catalytic performances of oxidation and reduction reactions on nanocatalysts, Chem. Soc. Rev. 45 (2016) 4747–4765.
[60] A.B.D. Nandiyanto, R. Zaen, R. Oktiani, Correlation between crystallite size and photocatalytic performance of micrometer-sized monoclinic WO_3 particles, Arab. J. Chem. 13 (2017) 1283–1296.
[61] B.P. Reddy, V. Rajendar, M.C. Shekar, S.H. Park, Particle size effects on the photocatalytic activity of $BiFeO_3$ particles, Dig. J. Nanomater. Biostruct. 13 (2018) 87–95.
[62] B. Hu, Q. Sun, C. Zuo, Y. Pei, S. Yang, H. Zheng, F. Liu, A highly efficient porous rod-like Ce-doped ZnO photocatalyst for the degradation of dye contaminants in water, Beilstein J. Nanotechnol. 10 (2019) 1157–1165.
[63] A. Kumar, G. Pandey, A review on factors affecting the photocatalytic degradation of hazardous materials, Mater. Sci. Eng. Int. J. 1 (2017) 1–10.
[64] A. Kumar, G. Pandey, A review on the factors affecting the photocatalytic degradation of hazardous materials, Mater. Sci. Eng. Int. J. 1 (2017) 106–114.
[65] P. Nyamukamba, H.H. Mungondori, L. Tichagwa, L. Petrik, O. Okoh, The effect of Ag nanoparticles of varying morphology on the photocatalytic activity of Ag/TiO2 nanocomposites, SF J. Nanochem. Nanotechnol. 1 (2018) 1009.
[66] H.-Y. Xu, B. Li, P. Li, Morphology dependent photocatalytic efficacy of zinc ferrite probed for methyl orange degradation, J. Serb. Chem. Soc. 83 (2018) 1261–1271 https://doi.org/10.2298/JSC180501060X.
[67] N.M.A. Barakat, M.A. Kanjwal, I.S. Chronakis, H.Y. Kim, Influence of temperature on the photodegradation process using Ag-doped TiO_2 nanostructures: negative impact with the nanofibers, J. Mol. Catal. A: Chem. 366 (2013) 333–340.
[68] J.Z. Bloh, A holistic approach to model the kinetics of photocatalytic reactions, Front. Chem. 7 (2019) 1–13.
[69] G.C. Lakshmi, S. Anand, R. Somashekar, C. Ranganathaiah, Synthesis of ZnO/MgO nanocomposites by electrochemical method for photocatalytic degradation kinetics of eosin yellow dye, Int. J. Nanosci. Nanotechnol. 3 (2012) 47–63.
[70] R.D.C. Soltani, G.S. Khoramabadi, H. Godinib, Z. Noorimotlagh, The application of ZnO/SiO_2 nanocomposite for the photocatalytic degradation of a textile dye in aqueous solutions in comparison with pure ZnO nanoparticles, Desalin. Water Treat. 56 (2015) 2551–2558.
[71] V. Vaiano, O. Sarcco, D. Sannino, P. Ciambelli, Photocatalytic removal of spiramycin under visible light with N-doped TiO_2 photocatalysts, Chem. Eng. J. 261 (2014) 3–8.

This book belongs to Badji Mokhtar Annaba University Central Library Copyright Elsevier 2025

[72] J. Santiago-Morales, A. Aguera, M.D.M. Gomez, A.R. Fernandez-Alba, J. Gimenez, S. Esplugas, R. Rosal, Transformation products and reaction kinetics in simulated solar light photocatalytic degradation of propranolol using Ce-doped TiO2, Appl. Catal. B Environ. 129 (2013) 13–29.
[73] A.M.T. Silva, C.G. Silva, G. Drazic, J.L. Faria, Ce-doped TiO2 for photocatalytic degradation of chlorophenol, Cat. Today 144 (2009) 13–18.
[74] M. Sharma, P.K. Mohapatra, D. Bahadur, Improved photocatalytic degradation of organic dye using Ag_3PO_4/MoS_2 nanocomposite, Front. Mater. Sci. 11 (2017) 366–374.
[75] V. Stengl, F. Oplustil, T. Neˇmec, In^{3+}-doped TiO_2 and TiO_2/In_2S_3 nanocomposite for photocatalytic and stoichiometric degradations, Photochem. Photobiol. 88 (2012) 265–276.
[76] E. Kowalska, S. Rau, Photoreactors for wastewater treatment: a review, Recent Pat. Eng. 4 (2010) 1–25.
[77] S. Mozia, Photocatalytic membrane reactors (PMRs) in water and wastewater treatment. A review, Sep. Purif. Technol. 73 (2010) 71–91.
[78] W. Zhanga, L. Ding, J. Luo, M.Y. Jaffrin, B. Tanga, Membrane fouling in photocatalytic membrane reactors (PMRs) for water and wastewater treatment: a critical review, Chem. Eng. J. 302 (2016) 446–458.
[79] S. Yu, Y. Wang, F. Sun, R. Wang, Y. Zhou, Novel mpg-C_3N_4/TiO_2 nanocomposite photocatalytic membrane reactor for sulfamethoxazole photodegradation, Chem. Eng. J. 337 (2017) 183–192.
[80] A.M. Mohamed, W.N.W. Slleha, J. Jaafar, A.F. Ismaila, M. Abd Mutalib, N.A.A. Sani, S.E.A.M. Asri, C. S. Ong, Physicochemical characteristic of regenerated cellulose/N-doped TiO_2 nanocomposite membrane fabricated from recycled newspaper with photocatalytic activity under UV and visible light irradiation, Chem. Eng. J. 284 (2015) 202–215.
[81] D. Zioui, H. Salazar, L. Aoudjit, P.M. Martins, S. Lanceros-Méndez, Photocatalytic polymeric nanocomposite membrane towards oily wastewater, Polymers 12 (2019) 2–11.
[82] A. Yusuf, C. Garlisi, G. Palmisano, Overview on microfluidic reactors in photocatalysis: applications of graphene derivatives, Catal. Today 315 (2018) 79–92.
[83] D. Heggo, S. Ookawara, Multiphase photocatalytic microreactors, Chem. Eng. Sci. 169 (2017) 67–77.
[84] R. Gorges, S. Meyer, G. Kreisel, Photocatalysis in microreactors, J. Photochem. Photobiol. A: Chem. 167 (2004) 95–99.
[85] Z. He, Y. Lib, Q. Zhang, H. Wang, Capillary microchannel-based microreactors with highly durable ZnO/TiO_2 nanorod arrays for rapid, high efficiency and continuous-flow photocatalysis, Appl. Catal. B: Environ. 93 (2010) 376–382.
[86] A. Lamberti, Microfluidic photocatalytic device exploiting PDMS/TiO_2 nanocomposite, Appl. Surf. Sci. 335 (2015) 50–54.
[87] D.S. De Sa, L.E. Vasconcellos, R.J. De Souza, B.A. Marinkovic, T. Del Rosso, D. Fulvio, D. Maza, A. Massi, O. Pandoli, Intensification of photocatalytic degradation of organic dyes and phenol by scale-up and numbering-up of meso- and microfluidic TiO_2 reactors for wastewater treatment, J. Photochem. Photobiol. A: Chem. 364 (2018) 59–75.
[88] A. Moslehyani, A.F. Ismail, M.H.D. Othman, T. Matsuura, Design and performance study of hybrid photocatalytic reactor-PVDF/MWCNT nanocomposite membrane system for treatment of petroleum refinery wastewater, Desalination 363 (2015) 99–111.
[89] S. Mosleh, M.R. Rahimi, M. Ghaedi, K. Dashtian, Sonophotocatalytic degradation of trypan blue and vesuvine dyes in the presence of blue light photocatalyst of Ag_3PO_4/Bi_2S_3-HKUST-1-MOF: central composite optimization and synergistic effect study, Ultrason. Sonochem. 32 (2016) 387–397.
[90] G. Pan, X. Jing, X. Ding, Y. Shen, S. Xu, X. Miao, Synergistic effects of photocatalytic and electrocatalytic oxidation based on a three-dimensional electrode reactor toward degradation of dyes in wastewater, J. Alloys Compd. 809 (2019) 1–8.
[91] A.E. Cassano, C.A. Martin, R.J. Brandi, O.M. Alfano, Photoreactor analysis and design: fundamentals and applications, Ind. Eng. Chem. Res. 34 (1995) 2155–2201.
[92] H. Gulyas, Solar heterogeneous photocatalytic oxidation for water and wastewater treatment: problems and challenges, J. Adv. Chem. Eng. 4 (2014) 2–11.

This book belongs to Badji Mokhtar Annaba University Central Library Copyright Elsevier 2025

This page intentionally left blank

This book belongs to Badji Mokhtar Annaba University Central Library

Copyright Elsevier 2025

CHAPTER 25

Nanomaterial-based advanced oxidation processes for degradation of waste pollutants

Jaykumar B. Bhasarkar[a] and Dharmendra Kumar Bal[b]

[a]*Department of Pulp and Paper Technology, Laxminarayan Institute of Technology, R.T.M. Nagpur University, Nagpur, Maharashtra, India,* [b]*School of Chemical Engineering, Vellore Institute of Technology, Vellore, India*

25.1 Introduction

Water is not only precious but also the most important factor in social service due to increased demand. Clean or drinkable water is a vital source for sustainability and social development in various fields. A supply of clean water is needed for good health, whether human or animal. However, an increase in industrialization and urbanization leads to waste pollutants introduced to the aqueous ecosystem. Thus, wastewater effluents contain toxic chemicals released through a variety of chemical-based industrial processes. The wastewater generated from industries is estimated as ~70% effluent released to the environment without effective treatment. Hence, novel and advanced technology have to be developed for the production of clean water. Many researchers are developing new and alternative methods to treat toxic chemicals economically and effectively. Many convection and existing techniques are available to produce clean and portable water, such as adsorption, filtration, membrane separation technique, and advanced oxidation processes (AOPs). Among all techniques, AOP is well known as a highly effective and efficient process. A few studies have reported the use of nanomaterials as an efficient adsorbent as well as a catalyst for the degradation of waste pollutants [1–3]. The importance and significance of nanoparticles in AOPs for the degradation of toxic pollutants is reported in many articles. AOPs process generates highly reactive radicals (•OH, HO_2, and other radicals) responsible for degrading waste pollutants. These radicals are highly reactive and unstable. Due to its high reactivity, these radicals rapidly oxidized organic molecules present in wastewater. AOPs are sometimes referred to as a highly versatile method for degradation of toxic/recalcitrant pollutants due to radical hydroxyl production through various alternative systems. Compared with conventional techniques, AOPs are highly efficient techniques due to the

Handbook of Nanomaterials for Wastewater Treatment. https://doi.org/10.1016/B978-0-12-821496-1.00003-9
Copyright © 2021 Elsevier Inc. All rights reserved.

This book belongs to Badji Mokhtar Annaba University Central Library Copyright Elsevier 2025

formation of less toxic intermediates in the reaction system. The conventional techniques for degradation of toxic pollutants such as surface adsorption, membrane separation, sedimentation, etc. convert the organic pollutants from one form to another form; however, the convectional AOPs and hybrid-assisted AOPs methods can degrade various types of toxic pollutants including intermediates produced during the oxidation process. In effluent treatment, the functioning of a catalyst can be altered by selective reactor design, performance, and characterization of nanoparticles.

Limited studies have reported that degradation of the organic pollutants can be carried out under sunlight irradiation rather using a stimulated light source (under UV visible). Other AOPs such as ozonation (O_3) combined with H_2O_2 system, H_2O_2/UV, Fenton, photo-Fenton, and ultrasound have been successfully utilized for the degradation of toxic pollutants. In most of the environmental-based applications, nanostructured materials are being used as novel catalysts to improve the kinetics as well as degradation yield. Therefore, many researchers have focused on the field of wastewater treatment using nanomaterials as a catalyst and observed that nanomaterials are the most suitable candidate to efficiently degrade organic pollutants from wastewater. It has also been observed that the activity of catalysts not only depends on the nature of materials but also depends on the geometry (i.e., size and shape) of the nanomaterial used in the wastewater treatment [4]. The physiochemical properties (i.e., optical) of nanocatalysts are strongly influenced by the structure of materials. Nanomaterials have a high surface area, which leads to enhanced adsorption capacity of the sorbent. Recent studies have reported the use of different nanomaterials such as *nanoclays*, nanocatalysts, nanorods, nanocomposites, etc. with AOPs for wastewater treatment on AOP-assisted nanomaterials for wastewater treatment.

This chapter describes the various AOPs and hybrid AOPs processes with the combination of nanoparticles for degradation of toxic pollutants from various industries such as textile, pharmaceutical, and petroleum products. This chapter also has an emphasis to deliver a detailed explanation of various AOPs processes, including photocatalysis, oxidation, and *sonolysis* used for organic pollutant degradation.

25.2 Advanced oxidation processes

AOPs are the generation of oxidizing species through a chemical oxidation reaction. These oxidizing agents can degrade recalcitrant organic pollutants. The efficiency of AOPs can be enhanced with the use of appropriate catalysts and hybrid processes such as UV/photocatalysis, UV/Fenton, and photo-Fenton, as shown in Fig. 25.1. In most of the AOPs, the system follows the generation of hydroxyl or other reactive radicals and species such as sulfate radical anion. These radicals are readily available to react with organic molecules at faster rates. Due to its highly reactive, oxidizing, and selectivity, they attack most of the organic pollutants in aqueous media. Due to their instability in the reaction system, the in situ production of hydroxyl radicals

This book belongs to Badji Mokhtar Annaba University Central Library Copyright Elsevier 2025

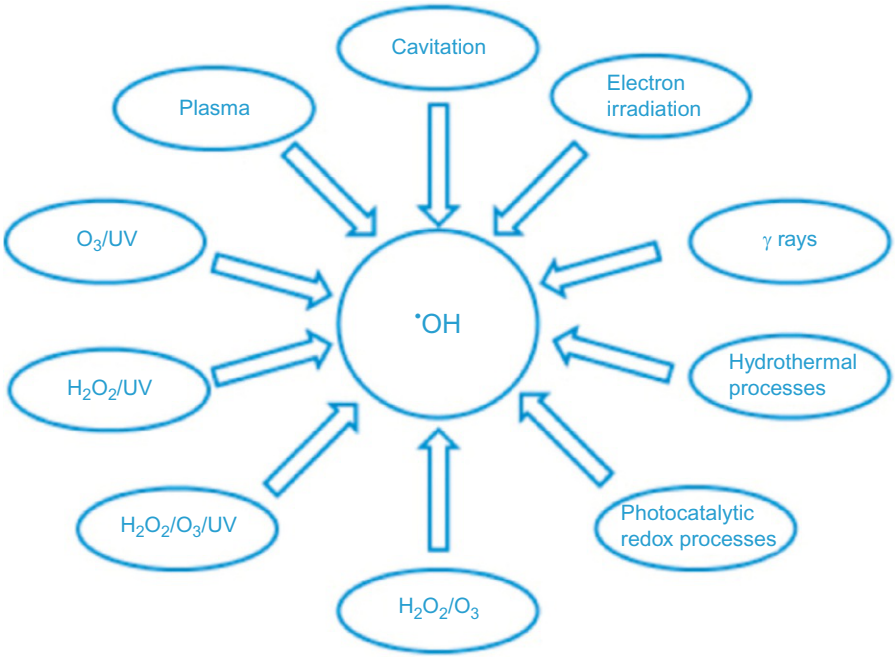

Fig. 25.1
Different advance oxidation processes. *Reprinted with permission from V. Vadillo, J. Sánchez-Oneto, J.R. Portela, E.J. Martínez de la Ossa, Supercritical water oxidation, in: S.C. Ameta, R. Ameta (Eds.), Advanced Oxidation Processes for Waste Water Treatment, Academic Press, 2018, pp. 333–358. Copyright 2018, Elsevier.*

by oxidation of water is more favorable. The main reaction mechanism for the production of hydroxyl radicals is dissociation or decomposition of water molecules into hydroxyl radicals. These reactions produce highly organic radicals as unstable intermediates, which further undergo subsequent reactions, finally resulting in the final oxidized products.

25.2.1 Supercritical water oxidation

Supercritical water oxidation (SCWO) processes are well known for degrading highly recalcitrant organic pollutants without generation of side products. This process is carried out above the critical point of water, i.e., 374°C and 22.1 MPa. In this condition, the water volume is around three-fold higher than at room temperature [5–8]. A homogeneous reaction was carried out in the reaction solution when oxygen molecule and organic pollutants are dispersed in water at the supercritical stage [6–8]. Several studies have reported on SCWO for the degradation of nitrogenated pollutants such as aniline, nitrobenzene, ammonia, and phenolic compounds [7]. However, this process may cause corrosion and fouling problems during the halogenated hydrocarbon's degradation process [9].

This book belongs to Badji Mokhtar Annaba University Central Library Copyright Elsevier 2025

25.2.2 Photocatalysis

In the photocatalysis process, radiation energy is absorbed by the catalyst, and it is raised from a higher energy level state to an excited state. This mechanism of the catalyst leads to production of highly unstable and reactive radicals. The main sources of these radiations are via UV or mercury lamp [10, 11]. In this process, the hydroxyls radicals are formed through the splitting of water, and the reaction scheme is shown as:

$$H_2O \xrightarrow{h\vartheta} H^{\cdot} + OH^{\cdot}$$

These generated radicals react with organic pollutants present in the reaction system to produce more bioavailable compounds. However, the production of radicals with this process is not much more sufficient to degrade all organic pollutants due to slow kinetics and generation of radicals.

25.2.2.1 Mechanism of photocatalysis

The reaction mechanism of photocatalysis process with TiO_2 can be explained in the following steps [12, 13]:

(a) The bandgap is much lower than the excitation state of the photon resulting in the production of electrons and lone pair holes:

$$TiO_2 + hv \rightarrow e^- + h^+ \tag{25.1}$$

(b) The trapping of carrier charge generated through reaction (25.1)

$$h^+ + Ti^{IV}OH \rightarrow \left[Ti^{IV}OH^{\cdot}\right]^+ \tag{25.2}$$

$$e^- + Ti^{IV}OH \rightarrow Ti^{III}OH \tag{25.3}$$

(c) Production of thermal energy through charge carrier

$$h^+ + Ti^{III}OH \rightarrow Ti^{IV}OH + Heat\Delta \tag{25.4}$$

(d) Interfacial charge transfer

$$\left[Ti^{IV}OH^{\cdot}\right]^+ + R \rightarrow Ti^{IV}OH + R^{\cdot +} \tag{25.5}$$

where R is an electron donor(e) Metal ions reduction

This book belongs to Badji Mokhtar Annaba University Central Library
Copyright Elsevier 2025

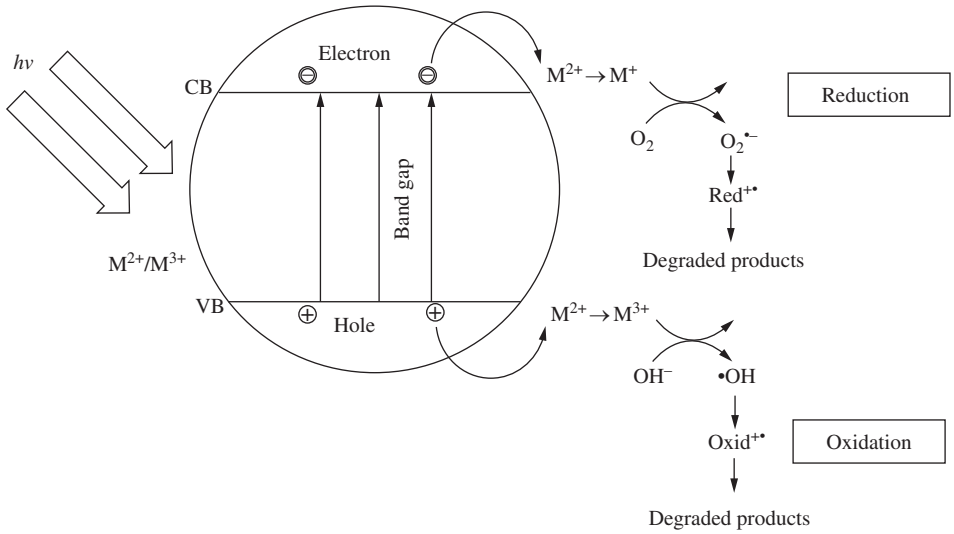

Fig. 25.2
Mechanism of photocatalyst bonding energy of TiO_2 [13, 14]. *Reprinted with permission from M.R. Hoffmann, S.T. Martin, W. Choi, D.W. Bahnemann, Environmental applications of semiconductor photocatalysis, Chem. Rev. 95 (1995) 69–96. Copyright 1995, ACS.*

$$ne^- + M^{n+} \rightarrow M^0 \tag{25.6}$$

This fundamental mechanism of semiconductor photocatalysis is responsible for degrading the organic pollutants in aqueous media with oxidation and reduction of metal ions shown in Fig. 25.2. This process is a very promising treatment for the complete degradation of toxic or organic pollutants.

25.2.2.2 Modification of TiO_2

Reducing the band of TiO_2 is a key factor for the photocatalysis process. The modification of TiO_2 provides a reduction in the bandgap and shift in the optical response in the UV region. This increases its photoreactivity with a reduction in the rate of lone pair electrons [10, 15]. The reduction in bandgap of TiO_2 can be made by introducing a donor. The details of the modification mechanism of TiO_2 is shown in Fig. 25.3. The well-known method for modification of TiO_2 includes doping of anion and/or dye sensitizers without changing the anatase phase of TiO_2. The exciting state TiO_2 can be broken into three parts: low energy (δ bonding of O p), medium energy (π bonding of O pπ and Ti e states), and high energy region (O pπ states), as shown in Fig. 25.4.

This book belongs to Badji Mokhtar Annaba University Central Library Copyright Elsevier 2025

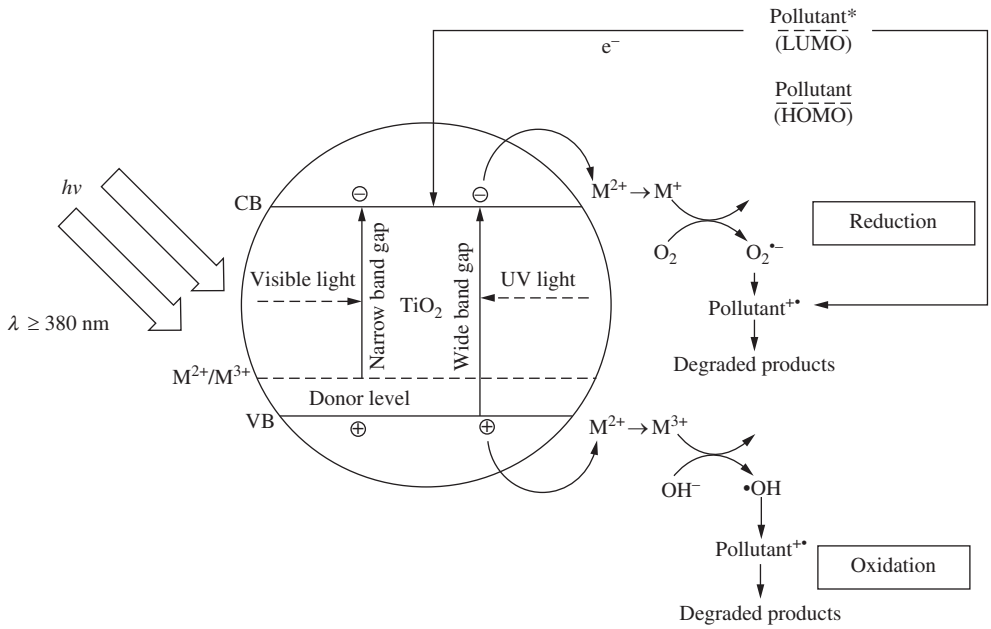

Fig. 25.3
Effect of doping and mechanism of photocatalysis with TiO_2 [13, 14]. *Reprinted with permission from M.R. Hoffmann, S.T. Martin, W. Choi, D.W. Bahnemann, Environmental applications of semiconductor photocatalysis, Chem. Rev. 95 (1995) 69–96. Copyright 1995, ACS.*

25.2.3 Metal oxide-containing nanoparticles

Various metal-containing nanoparticles such as silver, gold, zirconium, and palladium have been used for the treatment of wastewater. The geometry of nanomaterials plays a vital role in various AOPs. Some typical research has been conducted with different nanoparticles, such as silver being ~10 to ~200 nm in size with a high surface area. Another study has reported that silver and silver nanomaterials can be utilized as antimicrobial agents for wastewater treatment [16]. Trichloroethane (TCE) from groundwater has been degraded by using gold nanoparticle-infused palladium. The catalytic activity of gold nanoparticle-impregnated palladium was shown as far better (~2200-fold) than only palladium catalyst alone [17]. Among the various nanomaterials developed, controllable incorporation of different materials such as metal oxides (e.g., TiO_2, ZnO, CeO_2, ZrO_2, etc.) into sole nanostructures has lately become one of the new and advanced topics for research in various fields due to their functionality, synergetic, and collective catalyst properties compared with individual nanomaterials. The degradation of the organic pollutants from an aqueous system with TiO_2, ZnO, and CeO_2 was found to be very prominent with metal oxide nanomaterials. These metal-containing nanomaterials have high surface area and better catalytic activity [18]. Magnesium (Mg) and magnesium oxide (MgO) nanoparticles are capable of absorbing microorganisms such as *Escherichia coli* and *Bacillus*

This book belongs to Badji Mokhtar Annaba University Central Library Copyright Elsevier 2025

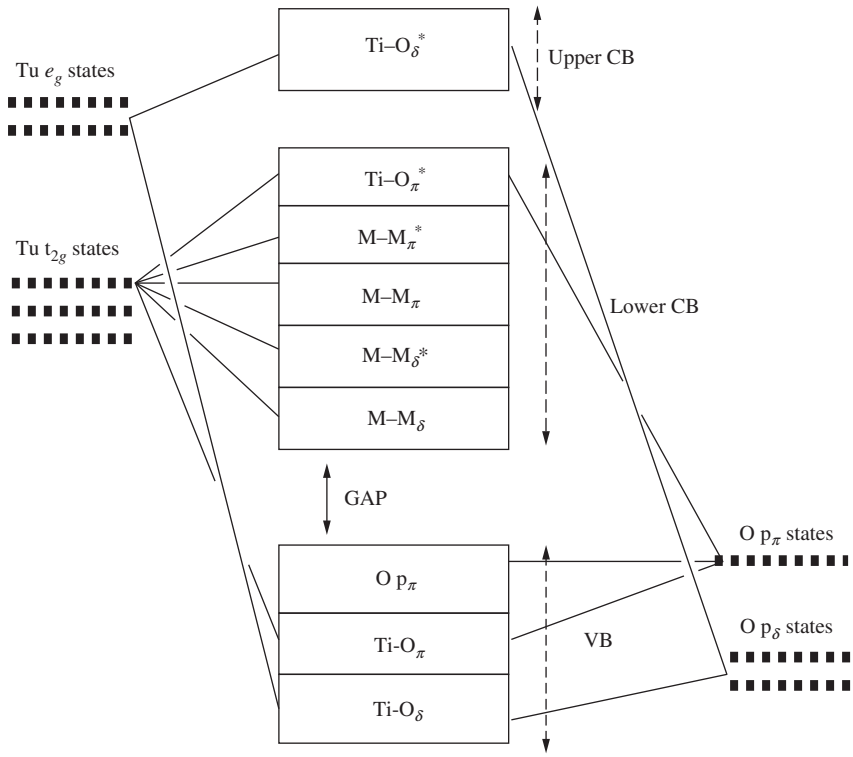

Fig. 25.4
Bonding energy of TiO_2 [13, 14]. *Reprinted with permission from M.R. Hoffmann, S.T. Martin, W. Choi, D.W. Bahnemann, Environmental applications of semiconductor photocatalysis, Chem. Rev. 95 (1995) 69–96. Copyright 1995, ACS.*

subtilis [19]. The use of TiO_2, ZnO, and Cu_2O nanoparticles in electro- and photocatalytic-assisted oxidation processes was reported. The oxidation rate and COD removal rate were found to be efficient with these nanoparticles in the presence of UV irradiation [20]. Iron oxides and titanium also show high adsorption capacity for the removal of heavy metals due to higher surface area.

25.2.4 Carbon-based nanoparticles

Carbon-based nanoparticles were used as some prominent catalysts for the removal of toxic or recalcitrant pollutants. These carbon-based nanoparticles have a higher surface area, sorption capacity, and selectivity toward the solute. Carbon-based nanomaterials show some excellent properties such as high thermal and electrical conductivity, which have high stability with limited reactivity [21]. Graphene, carbon nanostructures such as nanotubes and nanorods, and fullerenes, etc. are the notable nonmetal catalysts that have been used widely for various AOPs. Fullerenes is one of the forms (allotropic) of carbon-based nanomaterials with a hollow

This book belongs to Badji Mokhtar Annaba University Central Library Copyright Elsevier 2025

spherical cage. These materials (fullerenes) are more fascinating due to their beneficial properties such as high thermal strength, electrical conductivity, and flexibility [22]. Another type of nonmetal nanoparticle is a carbon nanotube (CNT). These CNTs are available in various different forms, such as tubular or rod structures [23]. The enhancement in CNT's colloidal stability was attained by the improvement of surface and structure with acid. These modified surface CNTs have been successfully studied for the degradation of hexavalent chromium [24]. Another form of CNTs, i.e., multiwalled CNTs (MWCNTs), have been adapted for the degradation of 2,4,6-trichlorophenol and Cu(II) metal ion using adsorption process [25]. MWCNTs have prominent properties such as unique structures and semiconductors, which lead to improving the surface adsorption capacity and removal rate. Another study has been reported for removal of acid dyes with chitosan nanoparticles as the adsorbent. Chitosan nanoparticles show a higher dye removal rate with enhanced absorption capacities [26].

25.2.5 Ceramics-based nanoparticles

Ceramic nanoparticles composed of inorganic nonmetallic ceramics are made up of carbide and carbonates of metals such as calcium, titanium, and silicon. They are synthesized at various sintering temperatures, followed by a successive cooling method. Ceramic nanoparticles are inorganic solids with porous structures. Ceramic nanomaterials can be easily synthesized with the desired structure, proper size, and porosity. These nanomaterials have shown keen interest in various fields such as drug delivery and wastewater treatment. These nanomaterials are highly stable at a specific pH and temperature of the system [27]. Recently, many researchers have been attracted to these nanomaterials because it's amorphous, polycrystalline, and porous, which leads to application in various fields like catalysis and photocatalysis [28]. These nanomaterials can be modified for different applications. Generally, ceramic nanomaterials are found in different mesostructures, morphologies, and dimensions [29].

25.2.6 Polymer nanoparticles

Polymer nanoparticles (PNPs) are produced from a polymeric material with the colloidal organic compounds in nanosize. In recent times, PNPs have raised more attraction in the polymeric material due to its versatile applications. PNPs are synthesized in nanosphere or nanocapsule shape and structure [30]. The bulk of the matrix particles are generally in solid form, and the targeted molecules (i.e., recalcitrant pollutant) are adsorbed on the outer surface of the bulk of the matrix particles, which is spherical. Later, this solid bulk of the matrix is encapsulated inside the particle [31]. PNPs and nanofluids have been widely used in controlled drug delivery systems due to their biocompatibility and biodegradability [32, 33]. In a recent study, poly lactide-*co*-glycolide (PLGA) NPs have been expended to synthesize peptide-based nanomedicine, and these NPs are used for controlled gene delivery systems intruded by

This book belongs to Badji Mokhtar Annaba University Central Library Copyright Elsevier 2025

ultrasound waves [34]. Another study has reported that PNPs lead the photoacoustic amplification by modification of the chemical structure of semiconducting polymer [35].

25.3 Individual AOPs involving nanomaterials

Over the last two decades, AOPs have provided growing attention to the new development of wastewater treatment technologies. Such methods (e.g., *sonolysis*, photochemical oxidation, Fenton oxidation, ozonation, etc.) have been successfully implemented for the degradation of organic pollutants at a laboratory scale. Table 25.1 provides a detailed summary of various AOPs used for degradation of different recalcitrant pollutants. AOPs were studied at different phases of the system well in advance throughout the field of wastewater treatment. Various oxidants (O_2, H_2O_2, O_3), ultraviolet (UV) or visible light, and catalysts (TiO_2) are required to activate the AOPs. During the activation cycle, AOPs generate active radicals such as •OH and •HO_2, which further attack the organic pollutants present in the aqueous solution. Owing to the use of organic colors during the manufacturing processes of textile and paper are among the main polluting industries. The presence of toxic colored content in aqueous media limits the mechanism of sunlight, such as absorption and reflection, which eventually raises the toxic content. Several experiments have shown the action of different AOPs toward effective dye degradation in the aqueous system. Photocatalytic-assisted advanced oxidation cycle pledges the chain reactions, which can create the pale organic intermediates. However, these unstable intermediates are more complex and toxic than substrate compounds. The primary goal of the AOPs is the complete mineralization of these pollutants. Several types of research have been carried out in the last few decades, which focused on the complete degradation of organic pollutants using microsized catalysts.

25.3.1 Degradation of organic pollutants using different nanomaterials as photocatalysts

The clean quality and quantity of water are more demanded nowadays due to rapid industrialization. Hence it is acceptable that only one possible solution cannot solve all water contamination problems. Therefore, the nanotechnology-assisted process always plays a key role in wastewater treatment.

The advantages of nanomaterials in the form of semiconductor photocatalyst provide a higher efficiency in optimum conditions. Semiconductor nanomaterials have higher surface areas with maximum available surface sites for the adsorption process. In the nanoscale range, the surface energy required per nanomaterial increases extensively. This enhancement in energy leads to an increase in removal rate even at a low concentration of substrate. However, the nanocatalyst also produces less by-product and waste generation during reaction, which increases the efficiency of the process at a low quantity of nanoparticles.

This book belongs to Badji Mokhtar Annaba University Central Library Copyright Elsevier 2025

Table 25.1: Literature summary on various AOPs for degradation of recalcitrant pollutant from wastewater.

References	AOPs	Pollutant	Reaction condition	Conclusion
[36]	US/Fenton	Bisphenol A	$f_{US} = 40$ kHz, initial conc. BPA = 20 mg/L; H_2O_2 = 160 mM; operating pH = 3, 7, and 9; reaction temp = 35°C; reaction time $t = 480$ min	Maximum degradation (~100%) was obtained at pH = 3 with $k = 1.39 \times 10^{-4}\ s^{-1}$
[37]	US/UV/Fenton	Antipyrine (ANP)	$f_{US} = 24$ kHz (probe type), initial conc. ANP = 50 mg/L, H_2O_2 = 1500 mg/L, Fe^{2+} = 12 mg/L, operating pH = 2.7, reaction temp. = ambient, reaction time = 50 min	~92% TOC was removed in US/UV/Fenton
[38]	UV/TiO_2/ Ferrioxilate	Bisphenol A	Initial conc. BPA = 0.01 mM, oxilate = 0.2 mM, H_2O_2 = 0.5 mM, reaction temp. = 27°C, operating pH = 3, time = 90 min, UV = 15 W at 365 nm	~80% reduction was observed in combination of hybrid (UV/TiO_2/ Ferrioxilate) process
[39]	Sonophotolysis	Phthalate acid esters (PAEs)	$f_{US} = 40$ kHz (sonication bath), initial conc. PAEs = 0.01 mM H_2O_2 = in situ production, UV bulb = 6 nos with 254 nm max. Wavelength, operating pH = 6.5, temp. = 28°C, time = 90 min	Maximum degradation: ~82% was observed with $k = 0.0712\ min^{-1}$
[40]	Sonoenzymatic	Cholesterol in egg yolk	Probe type ultra-sonicator, egg yolk = 10–40 g, cholesterol conc. = 0.6 U/g egg yolk, operating pH = 7, temp. = 37°C, reaction time = 15 min	91.68% yolk cholesterol was degraded at optimum conditions
[41]	Sonoenzymatic	Sericin from textile fibers	Savinase conc. = 0.5–1 g/L, pH = 8–9, time = 15 min	Ultrasound increases the removal rate (~21.02%) by improving the properties such as strength and elongation

This book belongs to Badji Mokhtar Annaba University Central Library
Copyright Elsevier 2025

25.4 Hybrid AOPs

Due to the generation of the higher quantity of hydroxyl radicals compared with individual oxidation cycle, hybrid AOPs (a combination of two or more AOPs) were identified as a more effective treatment of wastewater. Many experiments were conducted on the combination of different AOPs such as UV irradiation/O_3/hydrogen peroxide, photo-Fenton-assisted processes with sonochemistry, and other convectional AOPs. Numerous strategies have been researched and published in the wastewater treatment literature [42–45]. To improve the mineralization performance of organic compounds, a combination of specific AOPs may be beneficial for improving the efficiency of the oxidation process.

25.4.1 Ultrasound-assisted photocatalytic degradation of organic pollutants

Over the last few decades, the ultrasound-assisted process has received keen interest in organic pollutant degradation in aqueous phase due to its physical (intense mixing) and chemical effect (cavitation). When the ultrasound waves generated using the transducer is passed through a liquid media, i.e., wastewater or water, the ultrasound creates two basic effects such as physical and chemical effects at extreme conditions, for example, temperature 5000°C and pressure of 2000 atm for few microseconds [46, 47]. The physical effect of ultrasound refers to the micro and intense mixing created in the reaction mixture, whereas the chemical effect refers to the cavitation effects of ultrasound. The cavitation effect during reaction induced by the ultrasonic waves is shown in Fig. 25.5.

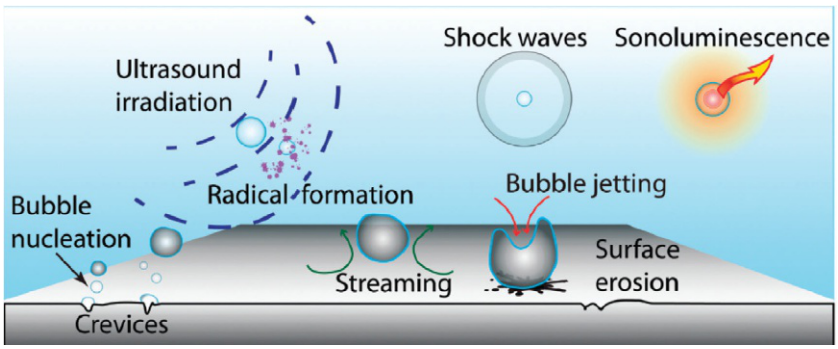

Fig. 25.5
Cavitation effect induced by ultrasonic waves. *Reprinted with permission from D.F. Rivas, P. Cintas, H.J.G.E. Gardeniers, Merging microfluidics and sonochemistry: towards greener and more efficient micro-sono-reactors, Chem. Commun. 48 (2012) 10935–10947. Copyright 2012, Royal Society of Chemistry.*

This book belongs to Badji Mokhtar Annaba University Central Library Copyright Elsevier 2025

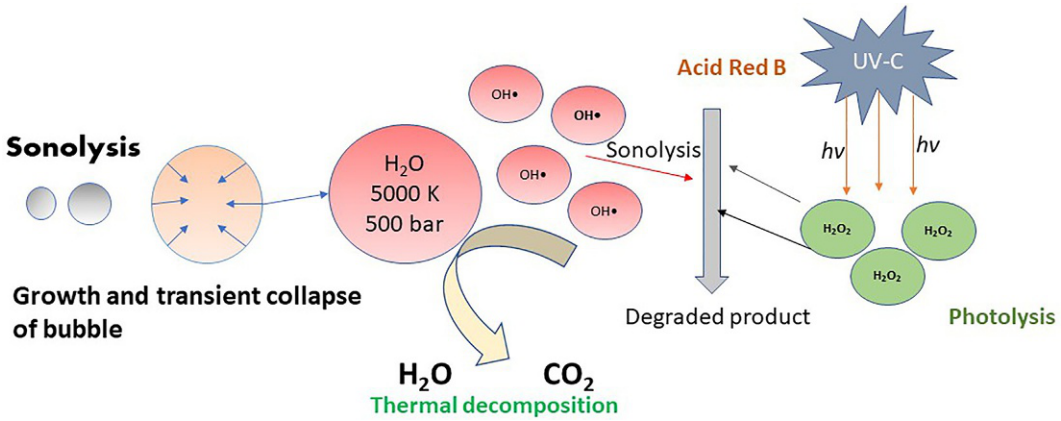

Fig. 25.6
Reaction mechanism of photocatalysis and *sonolysis. Reprinted with permission from S. Chakma, V.S. Moholkar, Mechanistic analysis of sono-photolysis degradation of carmoisine, Ind. Eng. Chem. 33 (2016) 276–287. Copyright 2016, Elsevier.*

Sonolysis is another method to effectively degrade the organic pollutant. Although, sonication is not very efficient in an industrial scale due to its limitations. To enhance the efficiency of ultrasound, it has to be combined with convectional oxidation processes. Among all the oxidation processes, photocatalysis is the critical process to provide maximum degradation rate, but as discussed in the previous section, the kinetic rate is the limitation of this process. To accelerate the kinetics of this process, the metal-containing semiconductor nanoparticles in the presence of UV or visible or UV-visible light and *sonolysis* process has been used in several studies. Nanoparticles used for photolysis act as a catalyst in the given reaction system, whereas a combination of sonolysis process enhances the kinetic and yield of the photolysis process through the generation of more radicals due to cavitation effects. Due to these reasons, this process has gained significant interest in modern days. The actual mechanism of *sonolysis* and photocatalysis is depicted in Fig. 25.6. *Sonolysis* is the process where the more reactive radicals are generated through the sudden collapse (implosive) of the microbubbles at extreme operating conditions.

The convoluted intermediates produced during sonolysis process are highly unstable. Consequently, *sonolysis* or ultrasound alone degradation process takes a long time for complete degradation of organic pollutants. However, due to the combination of sonolysis with photocatalysis, the intermediate degradation rate is faster as compared to the only sonication process. The hybrid process has the following major advantages: (i) addition production of highly reactive free radicals through both the processes such as sonolysis and photocatalysis; (ii) intense mixing, i.e., the physical effect of ultrasound helps to wipe the active catalyst site continuously, so that the activity of this catalyst increased and is maintained for a long period; and (iii) combined process can degrade both organic compounds such as hydrophilic and

This book belongs to Badji Mokhtar Annaba University Central Library Copyright Elsevier 2025

hydrophobic. A quantitative analysis of this hybrid process can be identified by means of the synergistic effect.

The synergy index for both the processes can be calculated as:

$$\text{Synergy index (SI)} = \frac{E_{(\text{US}+\text{UV}+\text{TiO}_2)}}{E_{(\text{US}+\text{TiO}_2)} + E_{(\text{UV}+\text{TiO}_2)}}$$

The SI value was estimated from the degradation efficiency of *sonolysis* with TiO_2 catalyst $E_{(US+TiO2)}$, UV with TiO_2 (photocatalyst) $E_{(UV+TiO2)}$, and combined process, i.e., sonophotocatalysis $E_{(US+UV+TiO2)}$. Chakma and Moholkar [48] studied the mechanistic effects of ultrasound with catalysis and photocatalysis using ZnO and Fe-doped ZnO catalyst. They studied the hybrid system on decolorization of dye in presence of ZnO and Fe-doping of ZnO as a catalyst with ultrasound irradiation and synergetic effect between sonolysis, sonocatalysis, and sonophotocatalysis, as shown in Fig. 25.7. These catalysts help in production of more hydroxyl radicals that could enhance the decolorization rate. However, these generated radicals through sonolysis and photocatalysis process mainly attack the adsorbed dye molecules.

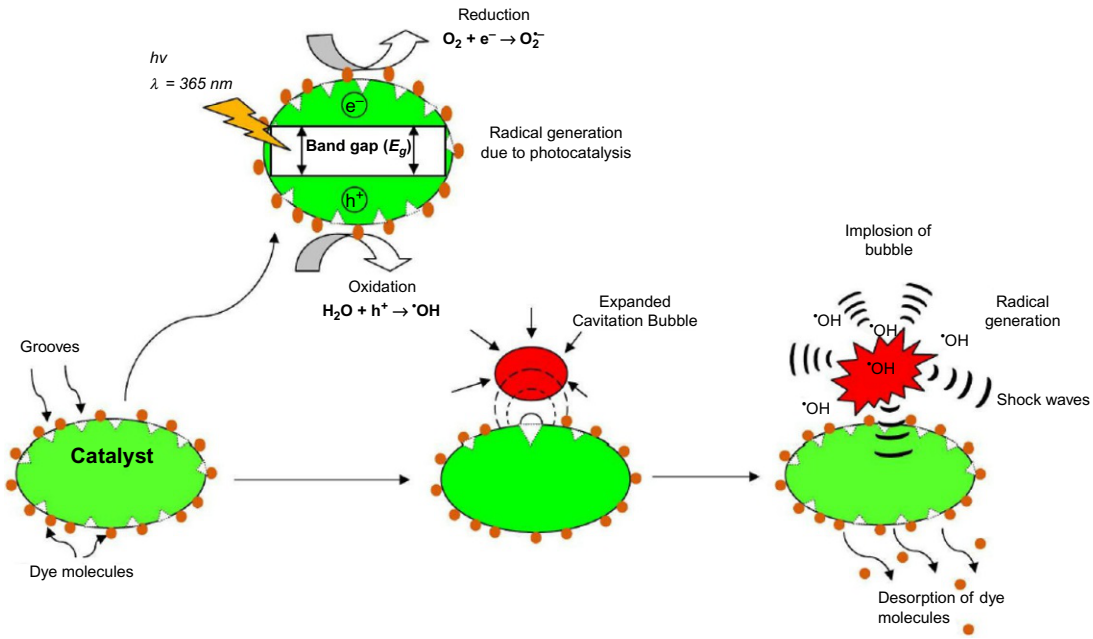

Fig. 25.7

Schematic diagram shows the synergy of between *sonolysis* alone, *sonocatalysis*, and *sonophotocatalysis*. *Reprinted with permission from S. Chakma, V.S. Moholkar, Investigation in mechanistic issues of sonocatalysis and sonophotocatalysis using pure and doped photocatalysts, Ultrason. Sonochem. 22 (2015) 287–299. Copyright 2015, Elsevier.*

This book belongs to Badji Mokhtar Annaba University Central Library Copyright Elsevier 2025

The physical phenomena of ultrasound, i.e., intense mixing to generate shockwaves, leads to desorption of dye molecules from the catalytic surface and a further reduction in decolorization rate.

Finally, they concluded that the negative synergy was observed between the sonolysis alone and photocatalysis. Fe-doped ZnO catalyst enhances the extent of decolorization rate, but the synergetic effects between the individual AOPs such as sonocatalysis and sonophotocatalysis remain unchanged.

25.5 Nonphotochemical AOPs

Nonphotochemical AOP methods are capable of producing more oxidized radicals in the absence of light. These nonphotochemical AOPs have been found to be more efficient in wastewater treatment. The reaction mechanisms of these processes for generating the hydroxyl radical are discussed in this section.

25.5.1 Sonolysis

As mentioned earlier, the ultrasound-assisted process is the key process for the generation of hydroxyl radicals through the transient collapse of cavitation bubbles. The moment of transient collapse of bubbles at extreme conditions is responsible for generating many chemical species, including oxidized radicals. Generally, the *sonolysis* process is carried out in water, which acts as a liquid media. The thermal dissociation of water molecules produces highly oxidizing radicals. The reaction mechanisms of this phenomenon can be discussed as [49]:

$$H_2O_2 \xrightarrow{US} OH^{\bullet} + H^{\bullet}$$

$$OH^{\bullet} + H^{\bullet} \rightarrow H_2O$$

$$2OH^{\bullet} \rightarrow O^{\bullet} + H_2O$$

$$2OH^{\bullet} \rightarrow H_2O_2$$

25.5.2 Ozonation

Ozone is another oxidizing agent for the degradation of the toxic pollutants from wastewater. Ozone gas is comprised of three oxygen atoms, which is a very influential oxidant. Ozonation is a type of AOP involving the generation of highly reactive oxygen species. These oxygen species can degrade the full range of toxic pollutants. The chemical reaction mechanism of the ozonation process can be written as [50]:

$$3O_3 + OH^- + H^+ \rightarrow 2OH^{\bullet} + 4O_2$$

This book belongs to Badji Mokhtar Annaba University Central Library
Copyright Elsevier 2025

25.5.3 Fenton process

Fenton process is one of the efficient processes for the production of hydroxyl radicals without using any cost-effective method. The main advantage of this process is that it does not require any type of specific reactor and operates at ambient reaction conditions. In this process, H_2O_2 is initiated by Fe^{2+} ions (Fenton's reagent) to generate hydroxyl radicals. The reaction mechanism for the generation of hydroxyl radical through Fenton reaction is described as [51]:

$$Fe^{2+} + H_2O_2 \rightarrow Fe^{3+} + OH^- + OH^\bullet$$

$$Fe^{3+} + H_2O_2 \rightarrow Fe^{2+} + HO_2^\bullet + H^+$$

$$Fe^{3+} + HO_2^\bullet \rightarrow Fe^{2+} + O_2 + H^+$$

Another major advantage of this process is that it has no adverse effect on the environment. Over the past few decades, many researchers have improved the fundamental mechanisms of the Fenton-assisted process. The improved Fenton processes is combined with the convection method such as UV-assisted Fenton, ozonation-assisted Fenton, and UV/Fe^{3+}-oxalate/persulfate/H_2O_2 process.

25.5.4 Persulfate oxidation process

Persulfate-assisted AOP systems are generally used for degradation of recalcitrant organic pollutants. Many researchers have explored persulfate-based AOPs. In this process, metal persulfates can be produced by sulfate radicals, which are highly reactive and can quickly degrade a wide range of recalcitrant pollutants. The generation of sulfate radicals in the reaction system can be enhanced by the activation of persulfate. The activation of persulfate has been done by conventional activation methods, i.e., with the assistance of UV at 254 nm. The thermal and UV activation of persulfate anions is described by the following reaction mechanism [52]:

$$S_2O_8^{2-} \xrightarrow{UV} 2SO_4^{\bullet -}$$

$$S_2O_8^{2-} \xrightarrow{\Delta} 2SO_4^{\bullet -}$$

Ultrasound is another method for the activation of Fe^{2+} ions. In ultrasound, the activation of persulfate anion can occur at the interface of the bubbles. During the transient collapse of the bubbles at very extreme conditions, these anions are heated. The generation of various chemical species, including H• and •OH radicals during transient collapse of bubble, can also initiate the activation of the persulfate anion. The detailed reaction mechanism for the activation of persulfate anions by ultrasound method is as follows [52, 53]:

$$S_2O_8^{2-} \xrightarrow{US} 2SO_4^{\bullet -}$$

This book belongs to Badji Mokhtar Annaba University Central Library Copyright Elsevier 2025

$$H_2O \xrightarrow{US} OH^{\bullet} + H^{\bullet}$$

$$S_2O_8^{2-} + H^{\bullet} \rightarrow SO_4^{\bullet -} + H^{+} + SO_4^{2-}$$

$$S_2O_8^{2-} + OH^{\bullet} \rightarrow SO_4^{\bullet -} + HSO_4^{-} + \frac{1}{2}O_2$$

The reaction mechanism of heterogeneous activation of peroxymonosulfate/persulfate by metal oxide nanocatalyst and carbon-based nanomaterials is explained in Fig. 25.8. For the activation of the peroxymonosulfate/persulfate system in a heterogeneous manner, the active site of the catalyst plays a significant role since the heterogeneous catalytic chemical reaction is carried out on the surface of the catalyst. Hence, the activation process requires more surface area. Therefore, the use of nanomaterial is more favorable for the activation of peroxymonosulfate/persulfate. Nanomaterials have provided not only a larger surface area but also higher reactivity.

25.6 Factors affecting on AOP performance

Many factors affect the performance of various AOPs including pH, temperature, oxidant concentration, surface size of catalyst, shape and size of nanoparticles, and reaction time. Some main factors that affect the efficiency of AOPs are described in the following sections.

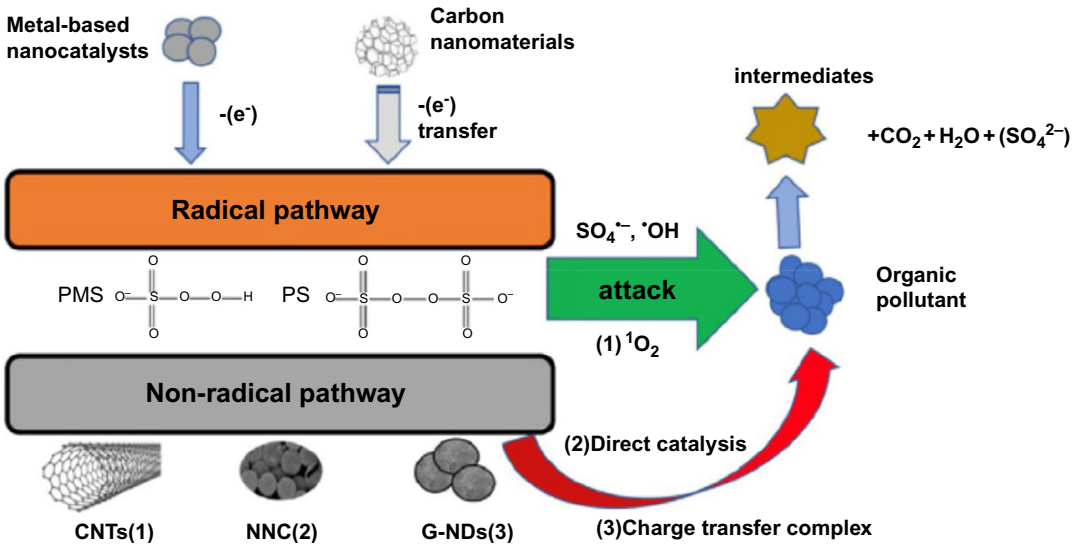

Fig. 25.8
Reaction mechanism of activation of PMS/PS by metal-based nanocatalysts and carbon nanomaterials. *Reprinted with permission from R. Xiao, Z. Luo, Z. Wei, S. Luo, R. Spinney, W. Yang, D. Dionysiou, Activation of peroxymonosulfate/persulfate by nanomaterials for sulfate radical-based advanced oxidation technologies, Curr. Opin. Chem. Eng. 19 (2018) 51–58. Copyright 2018, Elsevier.*

This book belongs to Badji Mokhtar Annaba University Central Library
Copyright Elsevier 2025

pH of the reaction mixture: Generally, the quality of water may exist at any pH. Hence, it is imperative to identify the effect of pH on the degradation of recalcitrant pollutants present in wastewater. Degradation rate is strongly influenced by the pH in catalytic oxidation in the presence of H_2O_2. Fenton-assisted oxidation process is mainly dependent on the pH of the reaction mixture as it controls the generation of hydroxyl radicals and Fe^{3+} ions. The maximum activity of the Fenton process was achieved at acidic medium. The activity of the process reduces with a higher pH range due to generation iron oxohydroxides, which are inactive in nature, and precipitation of ferric hydroxide. In strong acidic medium, the efficiency of the process also reduces due to the formation of an iron complex in the reaction mixture. Another possible reason for reduced efficiency of the process is the presence of H^+ ions in the reaction mixture at very low pH. These H^+ ions form a more stable oxonium ion in the reaction mixture. These oxonium ions make H_2O_2 more stable in the reaction mixture, which reduces the reactivity of H_2O_2 toward ferrous ions [54]. Consequently, it is essential to optimize the pH of the solution, which strongly influences not only the activity of the catalyst but also the type of oxidant used in the various AOPs.

Temperature: Most of the studies have reported that the enhancement in reaction temperature is more beneficial for oxidation efficiency. Many Fenton-based oxidation processes have been carried out at atmospheric conditions to achieve the desired oxidation rate [55]. The decomposition of H_2O_2 in hydroxyl radicals was observed at higher temperatures. These produced radicals at higher temperatures may extend the oxidation kinetics as well as the yield of the process. Salem et al. [56] have studied the effect of reaction temperature on degradation of acid blue 29 dye using Cu heterogeneous catalyst. They have found that the degradation efficiency was doubled by increasing reaction temperature from 20°C to 40°C with the extending of oxidation rate. In the persulfate-assisted oxidation process, the generation of sulfate radical, which acts as an oxidant, was also investigated at ambient reaction temperature [57]. In sonoassisted oxidation process, the inverse effect of temperature on the oxidation rate was observed [58]. This reduction of oxidation rate at higher temperatures is attributed to significant water evaporation and successive entrapment of these solvent vapors in the cavitation bubble. Vapor entrapped in the cavitation bubble leads to reduction of the intensity of the bubble's transient collapse. Therefore, the oxidation rates that are augmented by the chemical effect of ultrasound, i.e., generation of chemical species are also reduced at a higher temperature. Hence, detailed investigation of temperature on oxidation efficiency is highly needed.

Shape and size of nanoparticles: Shape and size of nanoparticles is a critical parameter for degradation of the recalcitrant pollutants from wastewater using nanomaterials. When the size of the nanoparticles decreases to nanoscale, then the melting point of the nanoparticles also reduces to a certain extent [59]. Nanomaterials with various geometries have similar energy levels that quickly transform their shape. Generally, the oxidation or degradation of recalcitrant pollutants mainly depends on the catalytic activity with the proper shape of the

This book belongs to Badji Mokhtar Annaba University Central Library Copyright Elsevier 2025

nanoparticles, i.e., the rod, sphere, hollow, or core shell-spheres. Although the size of the particles is an important parameter, other parameters such as particle shape, geometry, and surface properties can also have a distinct role in the degradation of pollutants using AOPs. Moreover, the primary reaction occurs at the active site of a catalyst via the adsorption process, and the exposure of these active sites mainly depends on the shape of the nanoparticles. The shape of the nanoparticles could offer special reactivities, selectivities, and binding strength and configurations, which indicate the performance of the catalyst or nanoparticles on AOPs.

25.7 Conclusions, challenges, and future directions

Initially, many researchers and scientists focused only on conventional methods for wastewater treatment. Due to some limitations of these conventional methods, researchers have shifted to a new modified version of AOPs such as sonolysis-assisted with photocatalysis, ozonation, UV-assisted oxidation process, etc. Recently, nanomaterials have gained more attention in various fields due to its versatile nature and high surface area. The application of nanomaterials in wastewater treatment with different AOPs has shown a high potential for effective treatment. The combined oxidation processes in the presence of nanomaterials is one of the superior techniques for degradation of wastewater pollutants.

Most of the photocatalysts used for the oxidation or degradation of organic pollutants are UV-based. Rigorous studies are required for utilization of these AOPs with different nanomaterials in a very efficient way and large-scale applications. There are many catalysts available that can be synthesized efficiently by hybrid AOPs, which can be replaced with UV light irradiation photocatalysts. In the future, various novel catalysts should be identified and synthesized for the development of photocatalysis. The combination of ultrasound with convectional AOPs is providing higher kinetics and yield of the degradation process. Reaction parameters such as temperature, pressure, pH, energy, etc. are also important factors that contribute to the degradation of organic pollutants. It is essential to optimize the operating conditions of the reaction system to attain the maximum yield with higher kinetics and also reduce the overall cost of the reaction system. The overall cost of the reaction system mainly depends on the energy required for the process. To achieve this objective, more attention is required to develop novel catalytic materials such as nanomaterials.

Despite the laboratory scale, many researchers have not studied the oxidation efficiencies with nanomaterials for organic content present in wastewater. These studies focus only on the targeted pollutants, but in actuality the concentration of other organic contents is much higher than the norm set by regulatory agencies. The presence of other organic contents in wastewater can reduce the efficiencies of AOPs using scavenging of oxidized radicals, insufficient radiation in UV-driven AOPs, and competing pathways on the adsorbent surface between nanomaterials and other untargeted substances. Another challenge that needs to be considered during the scale-up of nanomaterials-based AOPs is

This book belongs to Badji Mokhtar Annaba University Central Library Copyright Elsevier 2025

the appropriate design of the reactor with a proper engineering system, which affects the development of the process. Separation of nanomaterials from treated wastewater is another issue that can affect the economy of the process. The recovery of nanomaterials from wastewater is enabled by membrane technology, i.e., membrane filtration, which eventually raises the total cost of the process and also increases the complexity of the nanomaterial-based AOPs. The nanomaterial-based AOPs can suggest a significant method for the treatment of wastewater by addressing the challenges and issues discussed in this chapter.

References

[1] UN, World Water Development Report, World Water Assessment Programme, 2016.
[2] Y. Zhang, B. Wu, H. Xu, H. Liu, M. Wang, Y. He, B. Pan, Nanomaterials-enabled water and wastewater treatment, NanoImpact 3–4 (2016) 22–39.
[3] P. Xu, Z.M. Zeng, D.L. Huang, C.L. Feng, S. Hu, M.H. Zhao, C. Lai, Z. Wei, C. Huang, G.X. Xie, Z.F. Liu, Use of iron oxide nanomaterials in wastewater treatment: a review, Sci. Total Environ. 424 (2012) 1–10.
[4] J.N. Tiwari, R.N. Tiwari, K.S. Kim, Zero-dimensional, one-dimensional, two-dimensional and three-dimensional nanostructured materials for advanced electrochemical energy devices, Prog. Mater. Sci. 57 (2012) 724–803.
[5] P.E. Savage, Organic chemical reactions in supercritical water, Chem. Rev. 99 (1999) 603–621.
[6] H.E. Barner, C.Y. Huang, T. Johnson, G. Jacobs, M.A. Martch, W.R. Killilea, Supercritical water oxidation: an emerging technology, J. Hazard. Mater. 31 (1992) 1–17.
[7] V. Marulanda, G. Bolaños, Supercritical water oxidation of a heavily PCB-contaminated mineral transformer oil: laboratory-scale data and economic assessment, J. Supercrit. Fluids 54 (2010) 258–265.
[8] S.H. Son, J.H. Lee, C.H. Lee, Corrosion phenomena of alloys by subcritical and supercritical water oxidation of 2-chlorophenol, J. Supercrit. Fluids 44 (2008) 370–378.
[9] P.A. Marrone, G.T. Hong, Corrosion control methods in supercritical water oxidation and gasification processes, J. Supercrit. Fluids 51 (2009) 83–103.
[10] S. Jiao, S. Zheng, D. Yin, L. Wang, L. Chen, Aqueous photolysis of tetracycline and toxicity of photolytic products to luminescent bacteria, Chemosphere 73 (2008) 377–382.
[11] L. Fang, J. Huang, G. Yu, X. Li, Quantitative structure-property relationship studies for direct photolysis rate constants and quantum yields of poly-brominated di-phenyl ethers in hexane and methanol, Ecotoxicol. Environ. Saf. 72 (2009) 1587–1593.
[12] K. Kabra, R. Chaudhary, R.L. Sawhney, Treatment of hazardous organic and inorganic compounds through aqueous phase photocatalysis: a review, Ind. Eng. Chem. 43 (2004) 7683–7696.
[13] M.R. Hoffmann, S.T. Martin, W. Choi, D.W. Bahnemann, Environmental applications of semiconductor photocatalysis, Chem. Rev. 95 (1995) 69–96.
[14] M.M. Mahlambi, C.J. Ngila, B.B. Mamba, Recent developments in environmental photocatalytic degradation of organic pollutants: the case of titanium dioxide nanoparticles—a review. J. Nanomater. 2015 (2015) 1–29, https://doi.org/10.1155/2015/790173 Special Issue.
[15] V. Vadillo, J. Sánchez-Oneto, J.R. Portela, E.J. Martínez de la Ossa, Supercritical water oxidation, in: S. C. Ameta, R. Ameta (Eds.), Advanced Oxidation Processes for Waste Water Treatment, Academic Press, 2018, pp. 333–358.
[16] P. Jain, T. Pradeep, Potential of silver nanoparticle-coated polyurethane foam as an antibacterial water filter, Biotechnol. Bioeng. 90 (2005) 59–63.
[17] M. Tobiszewski, J. Namieśnik, Abiotic degradation of chlorinated ethanes and ethenes in water, Environ. Sci. Pollut. Res. 19 (2012) 1994–2006.

This book belongs to Badji Mokhtar Annaba University Central Library Copyright Elsevier 2025

[18] B. Bethi, S.H. Sonawane, B.A. Bhanvase, S. Gumfekar, Nanomaterials-based advanced oxidation processes for waste water treatment: a review, Chem. Eng. Process. 109 (2016) 178–189.
[19] P.K. Stoimenov, R.L. Klinger, G.L. Marchin, K.J. Klabunde, Metal oxide nanoparticles as bactericidal agents, Langmuir 18 (2002) 6679–6686.
[20] J.H. Chang, T.J. Yang, C.H. Tung, Performance of nano- and nonnanocatalytic electrodes for decontaminating municipal wastewater, J. Hazard. Mater. 163 (2009) 152–157.
[21] S.N. Schierz, H. Zanker, Aqueous suspensions of carbon nanotubes: surface oxidation, colloidal stability and uranium sorption, Environ. Pollut. 157 (2009) 1088–1094.
[22] A. Astefanei, O. Nunez, M.T. Galceran, Characterisation and determination of fullerenes: a critical review, Anal. Chim. Acta 882 (2015) 1–21.
[23] T. He, X. He, P. Tang, D. Chu, X. Wang, P. Li, The use of cryogenic milling to prepare high performance Al2009 matrix composites with dispersive carbon nanotubes, Mater. Des. 114 (2017) 373–382.
[24] B. Geng, Z. Jin, T. Li, X. Qi, Kinetics of hexavalent chromium removal from water by chitosan-Fe0 nanoparticles, Chemosphere 75 (2009) 825–830.
[25] G.C. Chen, X.Q. Shan, Y.S. Wang, B. Wen, Z.G. Pei, Y.N. Xie, T. Liu, J.J. Pignatello, Adsorption of 2,4,6-trichlorophenol by multi-walled carbon nanotubes as affected by Cu(II), Water Res. 43 (2009) 2409–2418.
[26] W.H. Cheung, Y.S. Szeto, G. McKay, Enhancing the adsorption capacities of acid dyes by chitosan nano particles, Bioresour. Technol. 100 (2009) 1143–1148.
[27] I. Roy, T.Y. Ohulchanskyy, H.E. Pudavar, E.J. Bergey, A.R. Oseroff, J. Morgan, T.J. Dougherty, P. N. Prasad, Ceramic-based nanoparticles entrapping water-insoluble photosensitizing anticancer drugs: a novel drug carrier system for photo-dynamic therapy, J. Am. Chem. Soc. 125 (2003) 7860–7865.
[28] S. Thomas, B.S.P. Harshita, P. Mishra, S. Talegaonkar, Ceramic nanoparticles: fabrication methods and applications in drug delivery, Curr. Pharm. Des. 21 (2015) 6165–6188.
[29] L. Han, C. Gao, X. Wu, Q. Chen, P. Shu, Z. Ding, S. Che, Anionic surfactants templating route for synthesizing silica hollow spheres with different shell porosity, Solid State Sci. 13 (2011) 721–728.
[30] M. Mansha, I. Khan, N. Ullah, A. Qurashi, Synthesis, characterization and visible-light-driven photoelectrochemical hydrogen evolution reaction of car-bazole-containing conjugated polymers, Int. J. Hydrogen Energy 42 (2017) 10952–10961.
[31] J.P. Rao, K.E. Geckeler, Polymer nanoparticles: preparation techniques and size-control parameters, Prog. Polym. Sci. 36 (2011) 887–913.
[32] Y.C. Xiong, Y.C. Yao, X.Y. Zhan, G.Q. Chen, Application of polyhydroxy-alkanoates nanoparticles as intracellular sustained drug-release vectors, J. Biomater. Sci. Polym. Ed. 21 (2010) 127–140.
[33] J.B. Bhasarkar, D. Bal, Kinetic investigation of a controlled drug delivery system based on alginate scaffold with embedded voids, Appl. Biomater. Funct. Mater. 17 (2019) 1–8.
[34] M. Figueiredo, R. Esenaliev, PLGA nanoparticles for ultrasound-mediated gene delivery to solid tumors, J. Drug Deliv. 2012 (2012) 1–20.
[35] C. Xie, P.K. Upputuri, X. Zhen, M. Pramanik, K. Pu, Self-quenched semi-conducting polymer nanoparticles for amplified in vivo photoacoustic imaging, Biomaterials 119 (2017) 1–8.
[36] R. Huang, Z. Fang, X. Yan, W. Cheng, Heterogeneous sono-Fenton catalytic degradation of bisphenol a by Fe_3O_4 magnetic nanoparticles under neutral condition, Chem. Eng. J. 197 (2012) 242–249.
[37] A. Duran, J.M. Monteagudo, I. Sanmartín, A. García-Díaz, Sonophotocatalytic mineralization of antipyrine in aqueous solution, Appl. Catal. Environ. 138–139 (2013) 318–325.
[38] E.M. Rodríguez, G. Fernández, P.M. Álvarez, R. Hernández, F.J. Beltrán, Photocatalytic degradation of organics in water in the presence of iron oxides: effects of pH and light source, Appl. Catal. Environ. 102 (2011) 572–583.
[39] L.J. Xu, W. Chu, N. Graham, Sonophotolytic degradation of phthalate acid esters in water and wastewater: influence of compound properties and degradation mechanisms, J. Hazard. Mater. 288 (2015) 43–50.
[40] Y. Sun, H. Yang, X. Zhong, L. Zhang, W. Wang, Ultrasound-assisted enzymatic degradation of cholesterol in egg yolk, Innov. Food Sci. Emerg. Technol. 12 (2011) 505–508.

This book belongs to Badji Mokhtar Annaba University Central Library Copyright Elsevier 2025

[41] N.M. Mahmoodi, M. Arami, F. Mazaheri, S. Rahimi, Degradation of sericin (degumming) of Persian silk by ultrasound and enzymes as a cleaner and environmentally friendly process, J. Clean. Prod. 18 (2010) 146–151.
[42] K.C. Namkung, A.E. Burgess, D.H. Bremner, H. Staines, Advanced Fenton processing of aqueous phenol solutions: a continuous system study including sonication effects, Ultrason. Sonochem. 15 (2008) 171–176.
[43] I. Ioan, S. Wilson, E. Lundanes, A. Neculai, Comparison of Fenton and sono-Fenton bisphenol A degradation, J. Hazard. Mater. 142 (2007) 559–563.
[44] M. Papadaki, R.J. Emery, M.A.A. Hassan, A.D. Bustos, I.S. Metcalfe, D. Mantzavinos, Sonocatalytic oxidation processes for the removal of contaminants containing aromatic rings from aqueous effluents, Sep. Purif. Technol. 34 (2004) 35–42.
[45] J.H. Sun, S.P. Sun, J.Y. Sun, R.X. Sun, L.P. Qiao, H.Q. Guo, M.H. Fan, Degradation of azo dye acid black 1 using low concentration iron of Fenton process facilitated by ultrasonic irradiation, Ultrason. Sonochem. 14 (2007) 761–766.
[46] J.B. Bhasarkar, S. Chakma, V.S. Moholkar, Mechanistic features of oxidative desulfurization using Sono-Fenton-Peracetic acid (ultrasound/Fe^{2+}–CH_3COOH-H_2O_2) system, Ind. Eng. Chem. 52 (2013) 9038–9047.
[47] V.S. Moholkar, P.S. Kumar, A.B. Pandit, Hydrodynamic cavitation for sonochemical effects, Ultrason. Sonochem. 6 (1999) 53–65.
[48] S. Chakma, V.S. Moholkar, Mechanistic analysis of sono-photolysis degradation of carmoisine, Ind. Eng. Chem. 33 (2016) 276–287.
[49] J.J. Lin, X.S. Zhao, D. Liu, Z.G. Yu, Y. Zhang, H. Xu, The decoloration and mineralization of azo dye C.I. Acid Red 14 by sonochemical process: rate improvement via Fenton's reactions, J. Hazard. Mater. 157 (2008) 541–546.
[50] C. Gottschalk, J.A. Libra, A. Saupe, Ozonation of Water and Waste Water: A Practical Guide to Understanding Ozone and its Applications, second ed., Willey, Weinheim, 2009.
[51] E. Brillas, I. Sires, M.A. Oturan, Electro-Fenton process and related electrochemical technologies based on fenton's reaction chemistry, Chem. Rev. 109 (2009) 6570–6631.
[52] X. Wang, L. Wang, J. Li, J. Qiu, C. Cai, H. Zhang, Degradation of acid Orange 7 by persulfate activated with zero valent iron in the presence of ultrasonic irradiation, Sep. Purif. Technol. 122 (2014) 41–46.
[53] R. Xiao, Z. Luo, Z. Wei, S. Luo, R. Spinney, W. Yang, D. Dionysiou, Activation of peroxymonosulfate/persulfate by nanomaterials for sulfate radical-based advanced oxidation technologies, Curr. Opin. Chem. Eng. 19 (2018) 51–58.
[54] X. Xu, X. Li, X. Li, H. Li, Degradation of melatonin by UV, UV/H_2O_2, Fe^{2+}/H_2O_2 processes, Sep. Purif. Technol. 68 (2009) 261–266.
[55] J.A. Zazo, G. Pliego, S. Blasco, J.A. Casas, J.J. Rodriguez, Intensification of the Fenton process by increasing the temperature, Ind. Eng. Chem. Res. 50 (2011) 866–870.
[56] I.A. Salem, H.A. El-ghamry, M.A.E. Ghobashy, Application of montmorillonite-Cu(II) ethylenediamine catalyst for the decolorization of Chromotrope 2R with H_2O_2 in aqueous solution, Spectrochim. Acta A 139 (2015) 130–137.
[57] P. Hu, M. Long, Cobalt-catalyzed sulfate radical-based advanced oxidation: a review on heterogeneous catalysts and applications, Appl. Catal. Environ. 181 (2016) 103–117.
[58] J.B. Bhasarkar, M. Singh, V.S. Moholkar, Mechanistic insight in phase transfer agent assisted ultrasonic desulfurization, RSC Adv. 5 (2015) 102953–102964.
[59] B. Akbari, M.P. Tavandashti, M. Zandrahimi, Particle size characterization of nanoparticles—a practical approach, Iran. J. Mater. Sci. Eng. 8 (2011) 48–56.

This book belongs to Badji Mokhtar Annaba University Central Library Copyright Elsevier 2025

This page intentionally left blank

This book belongs to Badji Mokhtar Annaba University Central Library

Copyright Elsevier 2025

CHAPTER 26

Electro-photocatalytic degradation processes for dye/colored wastewater treatment

Siddharth D. Parashar, Anjali A. Meshram, and Sharad M. Sontakke

Department of Chemical Engineering, Birla Institute of Technology and Science, K. K. Birla Goa Campus, Goa, India

26.1 Introduction

Dyes are extensively used as a colorant in industries such as textiles, paper, food processing, cosmetics, etc. Considering their wide range of applications, several million tons of dye are manufactured annually worldwide [1]. There are more than 1,00,000 commercially available dyes that are known to be used for various applications; however, the exact number of dyes in existence is yet to be known [1]. Various operations are involved in the applications of these dyes, which result in the generation of large quantities of colored effluent [1,2]. In general, a loss of about 1%–2% during production and 1%–10% during their use is assumed [1]. The dye pollutant not only disturbs the aesthetic beauty of water but also poses a potential threat to aquatic life [3]. In addition, the consumption of dye polluted water by animals and humans can cause health hazards [4]. Therefore, the release of such colored effluent in nearby water resources can cause significant environmental pollution and serious health hazards. Thus, treatment of such harmful pollutants is necessary before their discharge.

In literature, several techniques for the removal of dyes have been reported. These include conventional physicochemical methods (such as adsorption, coagulation, filtration, and ion exchange), advanced oxidation methods (such as ozonation, photocatalysis, and Fenton process), biological processes (such as activated sludge and enzymatic decomposition), and electrochemical methods (such as electrocoagulation, electrochemical reduction, and electro-oxidation) [5]. However, because of their complex chemical structure, thermal stability, and recalcitrant nature, dyes are difficult to treat by most of the conventional methods [6, 7]. In addition to this, the conventional methods also generate large volumes of secondary solid waste

Handbook of Nanomaterials for Wastewater Treatment. https://doi.org/10.1016/B978-0-12-821496-1.00031-3
Copyright © 2021 Elsevier Inc. All rights reserved.

This book belongs to Badji Mokhtar Annaba University Central Library Copyright Elsevier 2025

[2, 7]. Among the reported methods, photocatalysis and electrochemical processes have attracted considerable attention in recent years [2, 5]. The use of moderate operating conditions, a requirement of less contact time, involvement of no mechanical operations, no sludge/secondary solid waste generation, process efficiency, and economy make these processes versatile [2, 5]. Therefore, several studies on application of the abovementioned methods for the removal of various dyes have been reported in the literature [2, 5].

Photocatalysis is an advanced oxidation process that has been shown to remove not only the dyes/colorant effluent but also a wide range of other pollutants such as phenols, polymers, pharmaceuticals, pesticides, and microorganisms [8]. This method has two essential components namely, a photon source and catalyst. When the catalyst is irradiated with light having energy greater than or equal to the bandgap of the energy of catalyst, electrons from valence band get excited to conduction band thereby leaving behind a hole in the valence band [8, 9]. The generation of electron-hole pair on the surface of catalyst and their interaction with water and/or pollutant results in a series of redox reactions that degrade the pollutant [8–10]. Among the reported catalysts, TiO_2 is considered to be the best material, and photocatalytic degradation of various dyes in the presence of UV light as a photon source is reported using this material [8–10]. The fundamental mechanism of photocatalysis, reported catalysts, and their combinations with suitable light source can be found in various review articles [2, 6, 8–10].

Over the past 10 years, electrochemical technology has proved to be a promising alternative for wastewater remediation [5]. In fact, the first research publication by Fujishima and Honda reporting the decomposition of water using a TiO_2 electrode was based on electro-photocatalysis [11]. The major advantages of these techniques are electrons as clean reagents, energy efficiency, ease of automation, versatility, operation under milder conditions, etc. Emerging technologies such as electro-Fenton, electro-photocatalysis, and photo-assisted systems such as photoelectro-Fenton have been gaining significant attention in the past few years [5, 12]. Martínez-Huitle and Brillas have presented a summary of research works on the application of electrochemical methods for the decontamination of wastewaters containing synthetic organic dyes [5, 12]. In their review papers, different electrochemical methods, their advantages and disadvantages along with reported literature have been explained in detail. Among the reported electrochemical methods, photo-assisted methods, mainly electro-photocatalysis (also referred to as photoelectrocatalysis, PEC) is receiving considerable attention. In this method, the major disadvantage of charge pair recombination associated with photocatalysis can be successfully solved by the application of an anodic bias. Thus, the external potential applied in electro-photocatalysis was observed to play a significant role in improving the photocatalytic efficiency.

This chapter presents a summary of literature reported on electro-photocatalysis. The fundamental mechanism, experimental configuration, effect of reaction conditions, and major outcomes are discussed.

This book belongs to Badji Mokhtar Annaba University Central Library Copyright Elsevier 2025

26.2 Mechanisms of electro-photocatalysis

To understand the mechanism of electro-photocatalysis, it is important to understand the fundamental reactions of photocatalysis. These reactions follow a free radical mechanism, and therefore it is very difficult to list all of them [10]. However, as mentioned earlier, the key step involved in photocatalysis is the generation of electron-hole pair. In general, in photocatalysis, the following reactions are involved in the generation of electron-hole pair and the free radicals [13].

$$TiO_2 + h\nu \rightarrow e^-_{CB} + h^+_{VB} \tag{26.1}$$

$$h^+_{VB} + H_2O \rightarrow OH^\bullet + H^+ \tag{26.2}$$

$$e^-_{CB} + O_2 \rightarrow O_2^{-\bullet} \tag{26.3}$$

$$O_2^{-\bullet} + H^+ \rightarrow HO_2^\bullet \tag{26.4}$$

$$2HO_2^\bullet \rightarrow H_2O_2 + O_2 \tag{26.5}$$

$$H_2O_2 + O_2^{-\bullet} \rightarrow OH^\bullet + OH^- + O_2 \tag{26.6}$$

$$e^-_{CB} + OH^\bullet \rightarrow OH^- \tag{26.7}$$

$$e^-_{CB} + h^+_{VB} \rightarrow TiO_2 + \text{heat} \tag{26.8}$$

When TiO_2 photocatalyst is irradiated with an energy equivalent or greater than its bandgap energy, there is an excitation of electrons from the valance band of the material to the conduction band (e^-_{CB}). This also results in the formation of holes in the valence band (h^+_{VB}). The electron-hole (e^-_{CB} - h^+_{VB}) charge carrier generation process, as mentioned in Eq. (26.1), gets completed within a few femtoseconds, making it very rapid [9]. The generated charge carrier pairs can react, get trapped, or recombine [8, 9]. The reaction between surface absorbed water with the holes (Eq. 26.2) results in the formation of hydroxyl radicals. Besides, the reaction between oxygen and electrons (Eq. 26.3) results in the formation of superoxide radicals [8, 9]. The formation of highly reactive oxygen species such as hydroxyl and superoxide radicals is considered to be an important step in light-induced catalytic reactions [8, 9]. Furthermore, the generated reactive oxygen species can undergo a series of reactions as shown in Eqs. (26.4)–(26.7). However, these are just representative reactions, and there are many possible reactions well-documented in the literature [8, 9]. If the electron-hole charge carrier pairs are not quickly utilized in the reaction as discussed earlier, they tend to recombine, and the input energy is dissipated as heat (Eq. 26.8). This proves to be a detrimental reaction, hindering the entire charge transfer process, thereby affecting the quantum efficiency of the process [8, 9]. Although the above mechanism is discussed for TiO_2, it is also applicable to other photocatalyst materials such as ZnO, CdS, ZnS, WO_3, and Fe_2O_3.

This book belongs to Badji Mokhtar Annaba University Central Library
Copyright Elsevier 2025

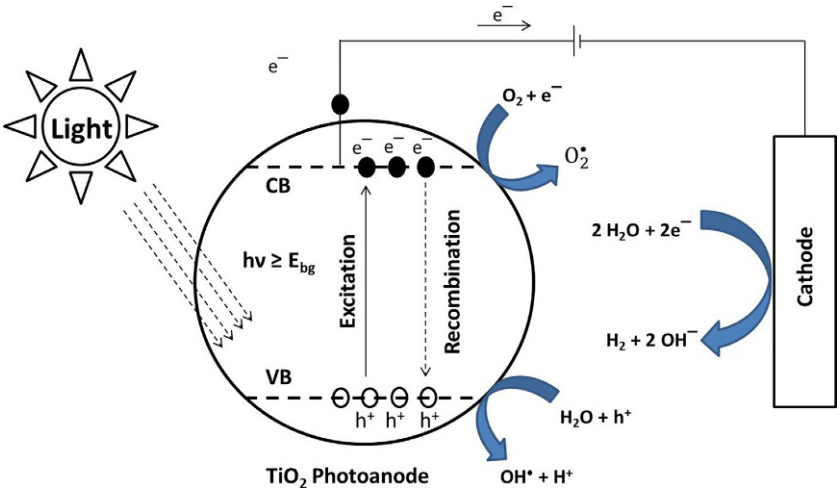

Fig. 26.1
A schematic representation of mechanism of electro-photocatalysis.

Electro-photocatalysis is a combination of photocatalysis and electrochemical process, which imparts greater efficiency to the wastewater treatment when compared to the individual methods. A major drawback of photocatalysis has been its lower process efficiency due to the recombination of electrons and holes. Electro-photocatalysis, on the other hand, overcomes this limitation by continuously withdrawing the photo-induced electron in an external electrical circuit by means of a constant current or a constant bias anodic potential [13]. This allows the continuous generation of a large amount of holes at the semiconductor-based thin film anode of the electrochemical cell. Thus in electro-photocatalysis, reactions mentioned in Eqs. (26.3)–(26.8) are minimized. The increase in the amount of hole subsequently results in the production of a large number of hydroxyl radicals (•OH), which is considered to be the key factor in enhancing the organics oxidation and the process efficiency when compared to photocatalysis [13]. A schematic representation of the mechanism of electro-photocatalysis is presented in Fig. 26.1.

26.3 Experimental assembly in electro-photocatalysis

Research on electro-photocatalytic systems is limited to a laboratory-scale setup. A typical experimental assembly used in electro-photocatalysis consisted of a photo-illuminated electrochemical cell acting as a reactor having a thin-film semiconductor material as an anode and a counter electrode. A schematic representation of a typical assembly is shown in Fig. 26.2.

There are different reactor configurations reported in the literature, which include three-dimensional electrode-slurry reactor, three-dimensional electrode-packed bed reactor, continuous flow reactor, immobilized film reactor, cylindrical reactors with annular electrodes,

This book belongs to Badji Mokhtar Annaba University Central Library Copyright Elsevier 2025

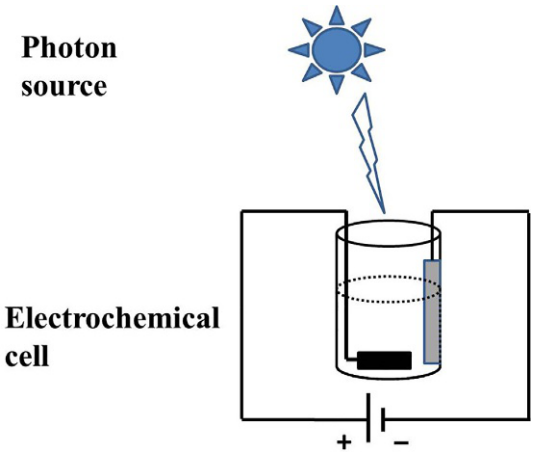

Fig. 26.2
A schematic representation of a typical electro-photocatalytic assembly.

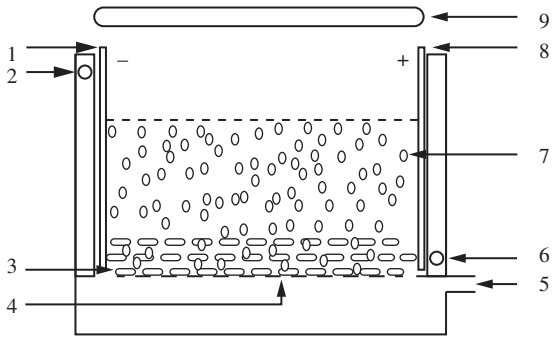

Fig. 26.3
Schematic representation of three-dimensional electrode-slurry electro-photocatalytic reactor; 1: stainless steel cathode, 2: recycled water outlet, 3: granulated activated carbon layer, 4: microporous plate, 5: pressured air inlet, 6: recycled water inlet, 7: TiO_2 particle layer, 8: stainless steel anode, and 9: UV lamp. *Reprinted from X. Meng, Z. Zhang, X. Li, Synergetic photoelectrocatalytic reactors for environmental remediation: a review, J. Photochem. Photobiol. C: Photochem. Rev. 24 (2015) 83–101 with permission from Elsevier.*

and rotating disc reactor [5, 12–18]. An et al. reported the application of a three-dimensional electrode for electro-photochemical degradation of methylene blue [14]. A schematic representation of the experimental assembly reported in their work is shown in Fig. 26.3. They reported an increase in the rate of conversion using a three-dimensional electrode having extensive specific surface area when compared to conventional two-dimensional electrodes. In their work, they used an open double-layered reactor made of PTFE containing methylene blue and TiO_2 suspension. The main electrodes (anode and cathode) were made up of stainless steel,

This book belongs to Badji Mokhtar Annaba University Central Library Copyright Elsevier 2025

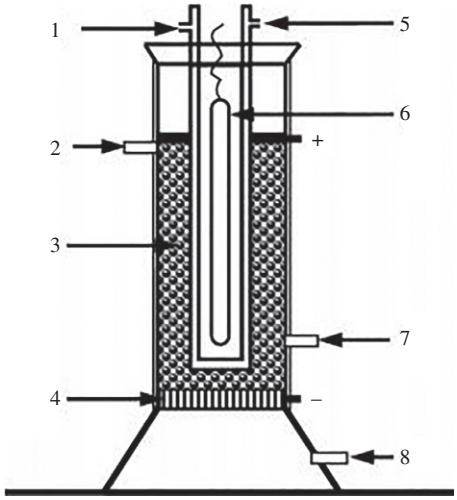

Fig. 26.4
Schematic representation of three-dimensional electrode packed-bed electro-photocatalytic reactor; 1: inlet of recycle water; 2: outlet for the purified solution; 3: packed TiO_2 material; 4: microporous titanium plate anode; 5: outlet of recycle water; 6: high-pressure UV lamp; 7: solution inlet; 8: pressured air inlet. *Reprinted from X. Meng, Z. Zhang, X. Li, Synergetic photoelectrocatalytic reactors for environmental remediation: a review, J. Photochem. Photobiol. C: Photochem. Rev. 24 (2015) 83–101 with permission from Elsevier.*

and the air was sparged from the bottom of the reactor cell. A 500 W high-pressure mercury lamp located above the reactor was used as a UV source. They observed 95% degradation of methylene blue in a reactor containing a three-dimensional electrode when compared to 78% with the electrochemical process and 89% with the photocatalytic process [14].

Zhang and coworkers reported a continuous flow electro-photocatalytic reactor for the degradation of reactive brilliant orange K-R [15]. The reactor assembly was a combination of a packed-bed photocatalytic reactor and a three-dimensional electrode flow through electrochemical reactor (Fig. 26.4). From the bottom of the reactor, compressed air was sparged through a porous titanium plate. The titanium plate was also used as an anode, and the cathode was made up of porous titanium. A potentiostat was used to control external cell voltage. The reaction solution was circulated using a peristaltic pump. UV illumination was provided using a 500 W high-pressure mercury lamp, which was suspended vertically in a double-walled U-tube. Similar to their earlier work, they observed enhanced degradation efficiency using a three-dimensional electrode. Although three-dimensional electrodes have been widely reported, their application in the fixed-bed reactor system is limited by poor heat and mass transfer and the difficulties associated with the process of changing the fixed catalyst [16]. In comparison, a packed-bed reactor configuration is reported to be a promising choice [16]. The drawback of light transmission inside a three-dimensional electrode packed-bed reactor has been addressed

This book belongs to Badji Mokhtar Annaba University Central Library Copyright Elsevier 2025

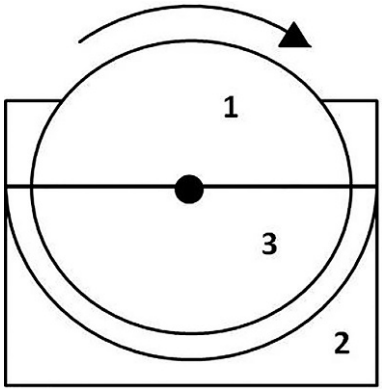

Fig. 26.5
Schematic representation of rotating disc reactors electro-photocatalytic reactor, 1: thin-film rotating disc; 2: target solution; and 3: conventional electro-photocatalytic system. *Adapted from Y. Xu, Y. He, X. Cao, D. Zhong, J. Jia, TiO_2/Ti rotating disk photoelectrocatalytic (PEC) reactor: a combination of highly effective thin-film PEC and conventional PEC processes on a single electrode, Environ. Sci. Technol. 42 (2008) 2612–2617.*

by making use of a quartz tube [17]. In any of the slurry-type reactor configuration, the problems related to the separation of fine catalyst particles; its reuse has remained as a serious disadvantage.

To overcome the issues with the slurry reactor, the application of a thin-film electrode is recommended [16]. Various solid substrates such as conductive glass, stainless steel, titanium foil, and porous metal mesh have been reported for the film deposition. The deposition process has been reported using different methods that include chemical vapor deposition, dip-coating, spin-coating, brush-painting, anodizing, direct-thermal, etc. [16]. The thin-film reactor configuration consisted of a photocatalyst film (generally TiO_2) coated on a conductive substrate as the photoanode and a conductive cathode in a closed circuit. The placement of the two electrodes in a single compartment and in two separate compartments (double compartment) has been reported. It was observed that the degradation of pollutants in a single compartment was superior to a double compartment [16]. Furthermore, in order to make maximum utilization of the irradiating light, a cylindrical reactor with the annular placement of electrodes has been reported [16].

An application of rotating disc reactors (Fig. 26.5) has been reported for the electro-photocatalysis. Those reactors had a distinct advantage of maximum mixing, enhancing the mass transfer in the system. Xu et al. reported a TiO_2/Ti rotating disc electro-photocatalytic reactor for the degradation of Rhodamine B (RB) and other dyes in textile effluents [18].

The reactor was designed as a combination of a conventional electro-photocatalytic reactor with the thin-film electro-photocatalytic reactor on a single electrode. The rotating disc electrode in this type of configuration allowed the formation of a thin-film pollutant on the

This book belongs to Badji Mokhtar Annaba University Central Library Copyright Elsevier 2025

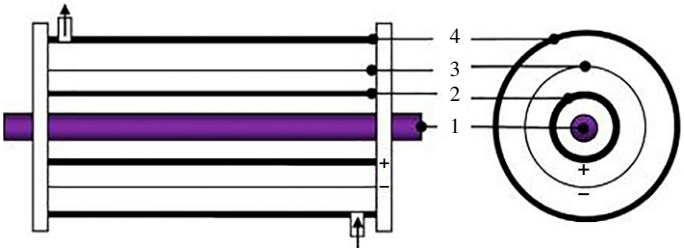

Fig. 26.6
Schematic representation of cylindrical electro-photocatalytic reactor; 1: UV lamp; 2: photoanode; 3: cathode; and 4: outer glass tube. *Reprinted from X. Meng, Z. Zhang, X. Li, Synergetic photoelectrocatalytic reactors for environmental remediation: a review, J. Photochem. Photobiol. C: Photochem. Rev. 24 (2015) 83–101 with permission from Elsevier.*

upper-half surface of the disc, which was exposed to light, and the remaining half of the disc operated as a conventional electro-photocatalytic reactor using the same light [18]. They observed about 84% decolorization efficiency of 20 ppm RB dye using a thin-film rotating disc reactor. The rotating disc electrode was observed to be stable when repeatedly used in multiple cycles [18].

In addition to the mode of operation and use of slurry or immobilized catalyst, the design of electro-photocatalytic reactor is observed to be influenced by several parameters such as the positioning of photon source, distance between the light source and the working electrode, flow rate of recycle stream, and gas sparging. The placement of UV lamp inside the reactor (Fig. 26.6) was observed to be superior compared to placing it outside. It has been reported that a large distance between the light source and the working electrode reduces the efficiency of the process because of the reduced radiation flux. The mass transfer inside the reactor can be enhanced by recycling a part of the treated water using a recycling pump and can also be enhanced further using a spinning disc or gas sparging [19].

To the best of our knowledge, no commercial setup has been reported till date, which has utilized an electro-photocatalytic reactor for large-scale water treatment applications. The slurry reactors largely fail during catalyst separation and reuse, whereas the fixed-bed reactor systems are limited by poor heat and mass transfer. A continuous flow reactor system with the least possible drawbacks is required for practical applications of the process. Thus considering various advantages and disadvantages of the reactor systems reported in the literature, we suggest the use of a thin-film coated wall reactor as a feasible option for pilot plant studies.

26.4 Effect of reaction conditions

Similar to photocatalysis, electro-photocatalytic reactions get influenced by various design and operating parameters.

This book belongs to Badji Mokhtar Annaba University Central Library Copyright Elsevier 2025

26.4.1 Effect of applied cell voltage

This is one of the most important parameters that differentiates electro-photocatalysis from the photocatalytic reactions. As described earlier, the enhanced efficiencies in the electro-photocatalysis process are because of the withdrawal of electrons with the application of an external potential. Zhang et al. [15] studied the effect of applied cell voltage on the degradation of reactive brilliant orange K-R (RBOKR) by the photoelectrochemical process. Fig. 26.7 shows the results obtained in their study. They observed that when the cell voltage was increased from 2 to 30 V, the degradation rate constant increased from 0.0213 to 0.0539 min^{-1}, indicating about 2.5-fold increases in the apparent rate constant. Jia et al. [20] studied the effects of cell voltage in the range of 9–18 V on the photoelectrocatalytic degradation of rhodamine B using $ZnFe_2O_4/TiO_2$/flake graphite composite as a particle electrode. The percentage removal efficiency of the dye increased from 67% to 100%, with an increase in the cell voltage from 9 to 18 V. Wang and coworkers [21] made a similar conclusion for degradation of Reactive Brilliant Red Dye X-3B dye using graphene-titania composite film electrodes on an F-doped tin oxide (FTO) substrate.

The enhanced degradation is attributed to the decrease in the charge pair (electron-hole pair) recombination. Furthermore, the higher applied cell voltage is considered to improve the direct and/or indirect electro-oxidation reactions of anodes.

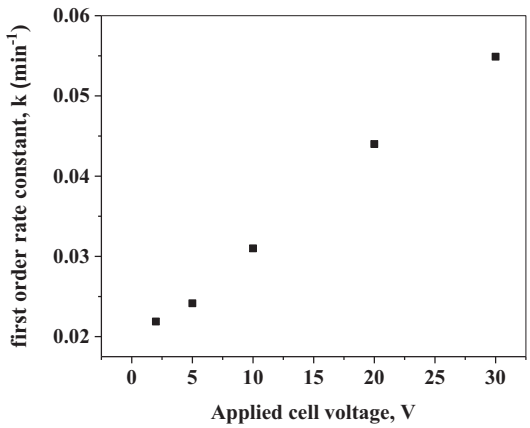

Fig. 26.7
Effect of applied cell voltage on the degradation of RBOKR. *Adapted from W. Zhang, T. An, X. Xiao, J. Fu, G. Sheng, M. Cui, G. Li, Photoelectrocatalytic degradation of reactive brilliant orange K-R in a new continuous flow photoelectrocatalytic reactor, Appl. Catal. A: Gen. 255 (2003) 221–229.*

This book belongs to Badji Mokhtar Annaba University Central Library
Copyright Elsevier 2025

26.4.2 Effect of photoanodic materials

The choice of photoanode is another important parameter of electro-photocatalytic reactions because the collection of electrons highly depends on the electrode. Typically, photoanode made up of TiO_2 in the form of meshes or thin-film coated on a suitable substrate has been extensively reported in the literature [14–22]. In recent works, composite materials have been reported [21, 23–25]. Wang and coworkers [21] reported enhanced photoelectrocatalytic degradation of Reactive Brilliant Red dye X-3B dye using graphene-titania composite film electrodes on an FTO substrate. The concentration of graphene oxide was varied as 2.5%, 5%, and 10%. The maximum percentage dye degradation of 78.7% was observed for 5% graphene-titania composite electrode at an applied potential of 2 V [23]. Fraga and coworkers reported photoelectrocatalytic oxidation of hair dye basic red 51 using a $W/WO_3/TiO_2$ bicomposite photoanode [23]. They observed that the bicomposite electrode not only improved the dye degradation efficiency by improving photoelectrocatalysis-charge separation but also extended the photoexcitation energy to the visible region of the solar spectrum [23]. They also found enhanced dye degradation efficiency using the WO_3-containing TiO_2 electrode when compared to the independent WO_3 and TiO_2 electrodes [23]. The addition of boron to the TiO_2 nanotube anode has been reported as efficient for the degradation of acid dye [24]. Wang and coworkers [25] reported a highly efficient $BiVO_4/TiO_2(N_2)$ nanotube heterojunction photoanode for the photoelectrocatalytic degradation of methylene blue dye. Yang et al. [26] reported ultrafine Si nanowires/Sn_3O_4 nanosheets 3D hierarchical heterostructured array as a photoanode for the degradation of methylene blue dye. They observed that the composite material possessed eight times higher photocurrent density compared to single-phase structures of Si nanowires (SiNWs) [26]. Thus, the application of composite materials for the fabrication of electrode is shown to be superior with TiO_2 alone.

26.4.3 Effect of photon source and light intensity

The photon source and light intensity have been observed to be one of the most important parameters influencing photocatalytic reactions [8–10]. Thus, electro-photochemical reactions are also influenced by these factors. In the electro-photochemical reactions, the photon source is chosen based on the bandgap energy of the irradiating material. Any light source with irradiating energy greater than or equal to the bandgap energy of photoanodic material initiates the generation of electron-hole pair. Because most of the reports indicate the application of TiO_2 as a photoanodic material, UV lamp is used as a photon source [14–18]. An et al. reported the use of a 500 W high-pressure mercury lamp as a photon source, and it was placed 12 cm above the reactor [14]. The intensity spectrum of the lamp was observed in the range 200–800 nm, with the highest peak at 365 nm. The photon flux corresponding to this arrangement was observed to be 6.64 mW/cm^2. Zhang et al. reported similar use of a 500 W high-pressure

This book belongs to Badji Mokhtar Annaba University Central Library Copyright Elsevier 2025

mercury lamp. However, it was suspended vertically in a double-walled quartz U-tube photoelectrochemical reactor [15]. Xu et al. demonstrated the photoelectrochemical degradation of Rhodamine B and other dyes in textile effluent using an 11 W mercury lamp placed 3 cm away from the rotating disc electro-photocatalytic reactor [18]. Thus, a majority of the literature reports the use of UV lamp for the electro-photochemical degradation of dyes, irrespective of the reactor configuration (slurry, packed-bed, rotating disc, etc.) [16]. In recent years, considering the economy of the process, the photoelectrochemical degradation in the presence of visible light or direct solar light has attracted significant attention [27]. Along with the use of visible light, the choice of a suitable photoanode material to absorb the irradiating light has become an area of research in this field [27]. Peleyeju and Arotiba presented an extensive summary of the literature reported on the application of visible light for photoelectrochemical degradation of various pollutants [27]. As indicated in Table 1 of their review paper (please refer to Ref. [27]), photoelectrochemical degradation of various dyes, namely, methylene blue, methyl orange, rhodamine B, reactive red 152, congo red, etc. along with suitable photoanodic materials in the presence of visible light have been reported [27].

Zainal et al. reported electro-photodegradation of methyl orange dye on TiO_2 thin films [28]. The light sources in this study were chosen as halogen (Tungsten type, 50 and 300 W), fluorescent (energy save type, 15 W), and near UV lamp (100 W). The light sources were chosen such that it covered the UV and visible range of the spectrum. Furthermore, a halogen lamp was chosen because of its close resemblance to the natural sunlight, whereas fluorescent lamps were used to provide an economic solution [28]. Fig. 26.8 shows the results obtained in their work for the electro-photodegradation of methyl orange dye.

They observed equivalent photoelectrochemical degradation rate with an apparent rate constant of $0.6 \times 10^{-3}\ \text{min}^{-1}$ for the dye degradation experiments using a 50 W Tungsten halogen lamp and 15 W fluorescent lamp (1 bulb). The photoelectrochemical degradation rate using a 100 W UV lamp was significantly higher than a 50 W Tungsten lamp and a 15 W fluorescent lamp. However, it was equivalent to a 300 W halogen lamp. The apparent rate constant using a 300 W halogen lamp was observed to be $21.9 \times 10^{-3}\ \text{min}^{-1}$. Furthermore, they studied the effect of light intensity using a 300 W halogen lamp at different photon flux. They observed increased dye degradation rates with an increase in light intensity. They attributed this to the enhancement in the electron-hole pairs with an increase in the light intensity. Similar observations and justifications have been reported for the photocatalytic degradation of a large number of dyes [29].

Apart from the abovementioned parameters, the electro-photocatalytic reactions are observed to be influenced by solution pH, thickness of semiconductor film, presence of ions, type of cathode, etc. [22]. However, the effect of these parameters is not as significant as those discussed earlier.

This book belongs to Badji Mokhtar Annaba University Central Library Copyright Elsevier 2025

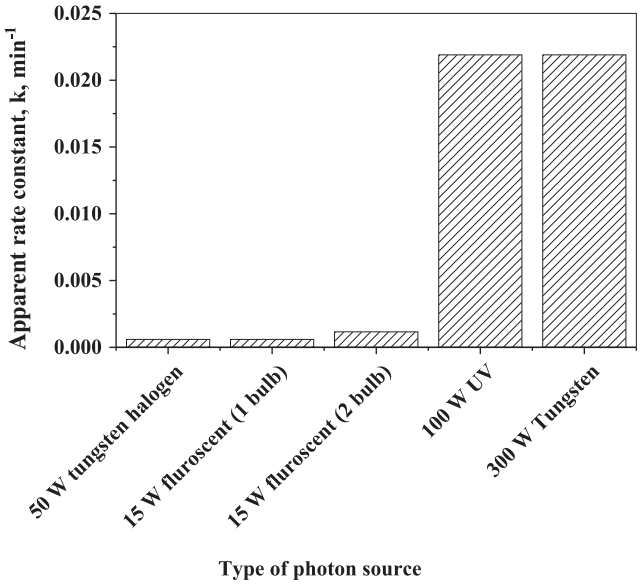

Fig. 26.8

Effect of various photon sources on the electro-photodegradation of methyl orange dye. *Adapted from Z. Zainal, C.Y. Lee, M.Z. Hussein, A.K.N.A. Yusof, Electrochemical-assisted photodegradation of dye on TiO_2 thin films: investigation on the effect of operational parameters, J. Hazard. Mater. B 118 (2005) 197–203.*

26.5 Scope for future work

From a large amount of literature on electro-photocatalytic degradation of dyes, it is evident that the technology has been successfully demonstrated at the research level. However, the large-scale application of this technology or any commercial set-up is not yet demonstrated. High operating costs and a unique set of operating conditions for the treatment of mixed pollutant still remains as a challenge. Furthermore, the large number of materials reported in the literature needs a thorough screening from a theoretical point of view. The effective use of direct sunlight has still remained a challenge in photocatalysis and electro-photocatalysis.

References

[1] E. Forgacs, T. Cserháti, G. Oros, Removal of synthetic dyes from wastewaters: a review, Environ. Int. 30 (2004) 953–971.
[2] I.K. Konstantinou, T.A. Albanis, TiO_2-assisted photocatalytic degradation of azo dyes in aqueous solution: kinetic and mechanistic investigations: a review, Appl. Catal. B: Environ. 49 (2004) 1–14.
[3] S. Gita, A. Hussan, T.G. Choudhury, Impact of textile dyes waste on aquatic environments and its treatment, Environ. Ecol. 35 (2017) 2349–2353.
[4] R. Nilsson, R. Nordlinder, U. Wass, B. Meding, L. Belin, Asthma, rhinitis, and dermatitis in workers exposed to reactive dyes, Occup. Environ. Med. 50 (1993) 65–70.

This book belongs to Badji Mokhtar Annaba University Central Library Copyright Elsevier 2025

[5] C.A. Martínez-Huitle, E. Brilla, Decontamination of wastewaters containing synthetic organic dyes by electrochemical methods: a general review, Appl. Catal. B: Environ. 87 (2009) 105–145.
[6] F. Han, V.S.R. Kambala, M. Srinivasan, D. Rajarathnam, R. Naidu, Tailored titanium dioxide photocatalysts for the degradation of organic dyes in wastewater treatment: a review, Appl. Catal. A: Gen. 359 (2009) 25–40.
[7] K.Y. Foo, B.H. Hameed, An overview of dye removal via activated carbon adsorption process, Desalin. Water Treat. 19 (2010) 255–274.
[8] R. Vinu, G. Madras, Environmental remediation by photocatalysis, J. Indian Inst. Sci. 90 (2010) 189–230.
[9] M.R. Hoffmann, S.T. Martin, W. Choi, D.W. Bahnemann, Environmental applications of semiconductor photocatalysis, Chem. Rev. 95 (1995) 69–96.
[10] A.L. Linsebigler, G. Lu, J.T. Yates Jr., Photocatalysis on TiO_2 surfaces: principles, mechanisms, and selected results, Chem. Rev. 95 (1995) 735–758.
[11] A. Fujishima, K. Honda, Electrochemical photolysis of water at a semiconductor electrode, Nature 238 (1972) 37–39.
[12] E. Brilla, C.A. Martínez-Huitle, Decontamination of wastewaters containing synthetic organic dyes by electrochemical methods. An updated review, Appl. Catal. B: Environ. 166–167 (2015) 603–643.
[13] I. Sirés, E. Brillas, M.A. Oturan, M.A. Rodrigo, M. Panizza, Electrochemical advanced oxidation processes: today and tomorrow. A review, Environ. Sci. Pollut. Res. 21 (2014) 8336–8367.
[14] T. An, X. Zhu, Y. Xiong, Feasibility study of photoelectrochemical degradation of methylene blue with three-dimensional electrode-photocatalytic reactor, Chemosphere 46 (2002) 897–903.
[15] W. Zhang, T. An, X. Xiao, J. Fu, G. Sheng, M. Cui, G. Li, Photoelectrocatalytic degradation of reactive brilliant orange K-R in a new continuous flow photoelectrocatalytic reactor, Appl. Catal. A: Gen. 255 (2003) 221–229.
[16] X. Meng, Z. Zhang, X. Li, Synergetic photoelectrocatalytic reactors for environmental remediation: a review, J. Photochem. Photobiol. C: Photochem. Rev. 24 (2015) 83–101.
[17] T. An, Y. Xiong, G. Li, X. Zhu, G. Sheng, J. Fu, Improving ultraviolet light transmission in a packed-bed photoelectrocatalytic reactor for removal of oxalic acid from wastewater, J. Photochem. Photobiol. A: Chem. 181 (2006) 158–165.
[18] Y. Xu, Y. He, X. Cao, D. Zhong, J. Jia, TiO_2/Ti rotating disk photoelectrocatalytic (PEC) reactor: a combination of highly effective thin-film PEC and conventional PEC processes on a single electrode, Environ. Sci. Technol. 42 (2008) 2612–2617.
[19] R. Daghrir, P. Drogui, D. Robert, Photoelectrocatalytic technologies for environmental applications, J. Photochem. Photobiol. A: Chem. 238 (2012) 41–52.
[20] D. Jia, J. Yu, S.M. Long, H.L. Tang, Novel $ZnFe_2O_4$/TiO_2/flake graphite composite as particle electrodes for efficient photoelectrocatalytic degradation of rhodamine B in water, Water Sci. Technol. 2017 (2018) 752–761.
[21] P. Wang, Y. Ao, C. Wang, J. Hou, J. Qian, Enhanced photoelectrocatalytic activity for dye degradation by graphene–titania composite film electrodes, J. Hazard. Mater. 223–224 (2012) 79–83.
[22] E. Zarei, R. Ojani, Fundamentals and some applications of photoelectrocatalysis and effective factors on its efficiency: a review, J. Solid State Electrochem. 21 (2017) 305–336.
[23] L.E. Fraga, J.H. Franco, M.O. Orlandi, M.V.B. Zanoni, Photoelectrocatalytic oxidation of hair dye basic red 51 at W/WO_3/TiO_2 bicomposite photoanode activated by ultraviolet and visible radiation, J. Environ. Chem. Eng. 1 (2013) 194–199.
[24] G.G. Bessegato, J.C. Cardoso, M.V.B. Zanoni, Enhanced photoelectrocatalytic degradation of an acid dye with boron-doped TiO_2 nanotube anodes, Catal. Today 240 (2015) 100–106.
[25] R. Wang, J. Bai, Y. Li, Q. Zeng, J. Li, B. Zhou, $BiVO_4$/$TiO_2(N_2)$ nanotubes heterojunction photoanode for highly efficient photoelectrocatalytic applications, Nano-Micro Lett. 9 (2017) 1–9.
[26] R. Yang, Y. Ji, Q. Li, Z. Zhao, R. Zhang, L. Liang, F. Liu, Y. Chen, S. Han, X. Yu, H. Liu, Ultrafine Si nanowires/Sn_3O_4 nanosheets 3D hierarchical heterostructured array as a photoanode with high-efficient photoelectrocatalytic performance, Appl. Catal. B: Environ. 256 (2019) 117798 (1–8).
[27] M.G. Peleyeju, O.A. Arotiba, Recent trend in visible-light photoelectrocatalytic systems for degradation of organic contaminants in water/wastewater, Environ. Sci.: Water Res. Technol. 4 (2018) 1389–1411.

This book belongs to Badji Mokhtar Annaba University Central Library Copyright Elsevier 2025

[28] Z. Zainal, C.Y. Lee, M.Z. Hussein, A.K.N.A. Yusof, Electrochemical-assisted photodegradation of dye on TiO_2 thin films: investigation on the effect of operational parameters, J. Hazard. Mater. B 118 (2005) 197–203.
[29] K.M. Reza, A.S.W. Kurny, F. Gulshan, Parameters affecting the photocatalytic degradation of dyes using TiO_2: a review, Appl. Water Sci. 7 (2017) 1569–1578.

This book belongs to Badji Mokhtar Annaba University Central Library
Copyright Elsevier 2025

CHAPTER 27

Fenton with zero-valent iron nanoparticles (nZVI) processes: Role of nanomaterials

Prashant L. Suryawanshi[a], Prachi Upadhyay[a], Bhaskar Bethi[b], Vijayanand S. Moholkar[c], and Sankar Chakma[a]

[a]Department of Chemical Engineering, Indian Institute of Science Education and Research Bhopal, Bhopal, Madhya Pradesh, India, [b]Department of Chemical Engineering, B.V. Raju Institute of Technology, Narsapur, Medak, Telangana, India, [c]Department of Chemical Engineering, Indian Institute of Technology Guwahati, Guwahati, Assam, India

27.1 Introduction

Nanomaterials ("Nano" comes from Greek word "Dwarf") are the critical components in the Earth system's past, present, and future characteristics and behavior. Nanomaterials are substances or materials meaning any organic, inorganic, or mixed (metallics/organometallic) particles that have a size between 1 and 100 nm (nm); roughly 1 million times smaller than the human hair diameter in at least one dimension, or 100 nm or less. It is a predefined superstructure in all three dimensions [1, 2]. It has distinct physical, chemical, electrical, and/or thermal properties due to its ultrasmall size structure or small materials. Nanomaterials can embrace new scenarios in an effort to raise a catalyst's utilization and activity. They show novel characteristics and specific surface property due to increased strength, hardness, chemical reactivity, high catalytic activity, and conductivity [3, 4]. Due to their nanoscale dimension, nanomaterials have shown extraordinary performance, improved functionality, high catalytic activity, and long-term durability because of unique and tailored electrical, optical, and magnetic properties [5, 6]. In addition, nanomaterials can be produced in various shapes and structures such as spherical, hexagonal, rods, wires, fibers, tubes, and sheets depending upon the applications [7, 8].

Nanomaterials are classified according to their dimensional structures: (i) zero dimensions (0D) such as nanoparticles, quantum dots, and fullerene; (ii) one dimension (1D) such as nanotubes, nanobelts, and nanowires; and (iii) two dimensions (2D) such as graphene or reduced graphene oxide, nanofilms, and nanowalls [9]. Therefore, nanomaterials may contain carbon-based

Handbook of Nanomaterials for Wastewater Treatment. https://doi.org/10.1016/B978-0-12-821496-1.00004-0
Copyright © 2021 Elsevier Inc. All rights reserved.

This book belongs to Badji Mokhtar Annaba University Central Library Copyright Elsevier 2025

materials (carbon nanotubes, graphene, fullerenes), metal-based materials (inorganic nanoparticles such as gold, silver, iron, cobalt, nickel, copper, and molybdenum), metal oxides (titanium oxide, zinc oxide, copper oxide, tungsten oxide, tin oxide, and iron oxide), dendrimers, and quantum dots (selenide, cadmium sulfide, CdS/CdSe, CdSe/ZnS, and CdSe/ZnO) [10, 11]. Among these, the metal nanoparticles have attracted much attention due to their unique properties associated with their dimensions [12, 13]. The unique and novel properties of the nanoparticles are not only due to their small size but also their narrow size distribution [14]. The nanostructured form of metal colloids is described to redisperse the metals in solution, in a small aggregate with zero-valent metal (1–50 nm), that can be stabilized by organic-protecting agents such as surfactant, polymer, and ligands [15]. The lipophilic- or hydrophilic-protecting agents are used for stabilizing the metal colloids, which are soluble in organic or aqueous solvents [16]. Nanomaterials have versatile applications in producing novel catalysts with high selectivity and enhanced activity. So, nanostructured materials have synergetic effects, long-term catalytic stability, and sustainability [17, 18].

For the last two decades, zero-valent iron (ZVI) has been the most commonly used zero-valent metal (e.g., Fe and Zn) for environmental remediation. ZVI is used as a reductant (or reducing agent) and is capable of transforming (degrading) or sequestering a variety of contaminants found in surface water (groundwater) and soil [19]. ZVI-based technologies act as a reductant and are involved in many environmental oxidation-reduction (redox) reactions operating at ambient temperature and pressure [20]. Therefore, ZVI is used for treating a wide range of diverse pollutants such as metals and metalloids, chlorinated solvents, nitrates, dyes, arsenic, phenol, halogenated compounds, and nitroaromatic compounds [21–23]. Also, ZVI can work in both in situ and ex situ applications. Due to remediation applications, ZVI can be categorized as granular ZVI, nanoscale ZVI (nZVI), bimetallic nZVI, and combined iron (ZVI and nZVI) products as mentioned in Table 27.1 [24–27].

Table 27.1: Various types of zero-valent iron with their characteristics.

Sl. no.	Types of ZVI	Description
1.	Granular ZVI	Granular ZVI is classically used as construction- or industrial-grade materials. Scrap iron (from automotive parts) or molten iron is a source of granular nZVI
2.	Nanoscale ZVI (nZVI)	It has a diameter in the range of 1–100 nm. Typically, it has larger surface area and higher reactivity than granular nZVI
3.	Bimetallic nZVI	One ZVI is composed with second zero-valent metals (such as Pd, Pt, Ni, Ag, and/or Cu). It has increased catalytic reactivity toward removal of contaminates from water
4.	Combined iron products (ZVI and nZVI)	ZVI and nZVI are combined with other modifications to capitalize on other remediation processes (in situ sorption and biostimulants and in situ bioremediation)

This book belongs to Badji Mokhtar Annaba University Central Library
Copyright Elsevier 2025

ZVI particles come in contact with water and dissolved oxygen or both, become unstable, and corrode spontaneously [28]. ZVI have a tendency to aggregate quickly into micrometer- to millimeter-scale flocs, owing to vast area-to-volume ratio, magnetic attraction between them, reactivity, and high surface energy [20]. In the last 5–10 years, numerous studies have focused on ZVI nanoparticles because of their inherent characteristics than bulk or microscopic materials. The particle size of granular ZVI materials, decreasing from mm to nm (10–100 nm), enhances the surface area and improves the catalytic activity, selectivity, and chemical reactivity; thus the higher the contaminant's removal efficiency, the higher surface-to-diameter ratio and specific surface area [29, 30]. nZVI is the most used nanomaterial for removal of impurities from an environmental system (such as soils, sediments, groundwater, air, drinking, and wastewater) [31]. Hence, nZVI is also called an environmental nanoparticle for in situ remediation. It comprises low toxicity, sufficient reactive longevity, and mobility within porous structures and higher reactivity for removal of pollutants [19]. An nZVI shows a typical core-shell structure and shows higher reactivity with high removal efficiency because of its smaller particle size and large surface area [32, 33].

Recently, many new contaminants found in the surface water (groundwater remediation) and municipal effluents have attracted the attention of the scientific community [34]. Several studies have mainly focused on traditional and conventional available systems such as physical and physicochemical techniques, chemical oxidation, photocatalytic, biological treatment, and electrochemical treatment used for groundwater remediation. So, a number of difficulties has been observed in removing these contaminants from wastewater using these traditional techniques [35]; to overcome such difficulties, advanced oxidation processes (AOPs), one of the tertiary treatment techniques, are found to be significantly effective and efficient for removing the contaminants/pollutants from water and wastewater. The most widely used AOPs include Fenton, ozonation, photocatalytic oxidation, and sonolysis [35, 36]. In AOPs, Fenton reaction is very popular in which radicals are formed in the presence of hydrogen peroxide (H_2O_2) and Fe^{2+} ions [36–38]. Fenton reaction can also be performed in a homogeneous and heterogeneous system. Homogeneous Fenton reaction or Fenton-like reaction consists of a combination of H_2O_2 and metal ion(s)/metal ion-organic ligand complexes, while heterogeneous Fenton reaction is established by replacing Fe^{2+} in the Fenton reagent with a solid catalyst [39].

The use of zero-valent iron nanoparticles (nZVI) in a Fenton reaction has many advantages over conventional methods and some advantages beyond the addition of only Fenton (Fe^{2+}/H_2O_2) because (i) it is operated at ambient condition (at atmospheric pressure and room temperature) for organics oxidation; (ii) nontoxic end product generation; (iii) high performance and environmentally safe (H_2O_2 can break into H_2O and O_2); (iv) decreases the reductant dosage; (v) increases reaction rate of reductive degradation; (vi) minimizes the toxic intermediates released during treatment; and (vii) nZVI is capable of coating or attaching to large particles. Therefore, nZVI is used as absorbed media for filtration system to treat contaminated water by

This book belongs to Badji Mokhtar Annaba University Central Library Copyright Elsevier 2025

passing through the sand filter; and (viii) higher stability and higher reactivity for removal of contaminants [31,37,40]. Therefore, it is also called advanced Fenton process.

ZVI-based Fenton technologies are involved in wide variety of remediation technologies that include both physical processes (co-precipitations or adsorption) and chemical transformations (oxidation and reduction) whose comparative importance not only strongly depend on the operating reaction conditions but also the nature of the targeted pollutant [28,41]. Also, the H_2O_2 dosage, reaction pH, reaction conditions (temperature and others), and amount of catalyst are equally important as they significantly affect the oxidation capacity of the Fenton reagent. Therefore, the systematic introduction and analysis of these parameters is also essential [39].

27.2 Synthesis methods for zero-valent iron nanoparticles

As of now, several techniques have been introduced for synthesis of nZVI. The mode of synthesis of nanoparticles highly affects the efficacy of the nZVI. The most followed methods for the synthesis of nZVI are chemical reduction processes either by employing H_2 at elevated temperature or by using borohydride for the reduction of Fe^{+2} ions or by using plant extracts [42]. One of the limitations encountered while synthesizing nZVI is that it agglomerates easily in the solution due to its high magnetic and electrostatic attractions. Additionally, nZVI oxidize easily when it comes in contact with air and water. The oxide or hydroxide layer that forms on the surface reduces the efficacy of the nanomaterials for water treatment. This problem is usually handled by employing surfactants or doing some necessary surface modification. Supporting agents and the capping agents increase the stability and mobility by preventing any further agglomeration but at the cost of decreased reactivity [43–46]. To now, thermal reduction, top-down, and bottom-up processes are mainly considered for the synthesis of nZVI. The thermal reduction process is quite popular at the industrial scale. In this method, temperature and the source of iron plays an important role in guiding the shape and morphology of the nanoparticles. Top-down process involves the use of either laser ablation or ball milling for reducing the size from bulk to nanoscale. Contrary to top-down, bottom-up method involves precipitation of iron salt sources, agglomeration, or deposition. Bottom-up approach is easy, cost effective, and provides better control over size and shape compared with the other methods, and usually involves borohydride reduction of Fe^{+2} salts [47]. The synthetic methods played a crucial role in controlling the structural properties of nZVI. In the proceeding section, a brief discussion about the different synthesis methods and their effects on morphology and shape is given.

27.2.1 Synthesis of nZVI using chemical methods

Chemical synthesis methods are the mainly preferred techniques because of better control over size and morphology. The chemical reduction process involves a series of steps as follows: (i) preparation of the supersaturated solution, (ii) nucleation phase of the nZVI cluster,

This book belongs to Badji Mokhtar Annaba University Central Library Copyright Elsevier 2025

(iii) growth phase of the nZVI nuclei, (iv) agglomeration phase of nZVI, and (v) washing, separation, and dehydration of nanoparticles. The final steps are mainly responsible for the formation of a thin coating of oxide layer on the outer surface [48].

For example, Bhatti et al. have synthesized nZVI by treating ferrous sulfate with borohydrate in the presence of EDTA as a capping agent. The nZVI obtained were spherical in shape with its diameter within the 100 nm range and the characteristic XRD peak at 44.7°, which is similar to the reported literature [49]. One problem associated with reduction using borohydrate is the occurrence of unwanted side reactions of borohydride hydrolysis. To prevent this from happening, a higher amount of costly and toxic reagents are required. The following reaction equations (Eq. 27.1–27.3) show the mechanism of chemical reduction of Fe^{2+} salts in the presence of borohydride [44,46].

$$2Fe^{+2} + 3OH^- + BH_4^- \rightarrow 2Fe^0 + 2H_2 + H_3BO_3 \tag{27.1}$$

$$4Fe^{+2} + 9OH^- + 3BH_4^- \rightarrow 4Fe^0 + 12H_2 + 3H_3BO_3 \tag{27.2}$$

$$BH_4^- + 4H_2O \rightarrow H_3BO_3 + 4H_2 + OH^- \tag{27.3}$$

Another study reported the effect of different functionalization on nZVI by employing EDTA and dipicolinic acid [50]. In comparison to bare nZVI, EDTA-functionalized particles were smaller in size. Furthermore, after functionalization with EDTA, modification of chain-like morphology was obtained. The variation in concentration of dipicolinic acid with respect to Fe also showed significant changes in the morphology. Due to surface functionalization of nZVI, lengthening of nanoparticles in ellipsoidal forms of reduced size was seen [50]. Since bare nZVI are quite unstable in the environment, once they come in contact with the atmosphere a layer of oxide or hydroxide forms on its surface that reduces the activity of the as-synthesized nanoparticles. Therefore, it becomes important to find better support material or require some necessary surface changes without hampering the activity of the nZVIs and increase its stability in the atmosphere.

27.2.2 Sonochemical synthesis of nZVI

In the sonic spectrum, ultrasound frequency lies in the range of 20 kHz to 10 MHz, and this region can be further classified into three distinct regions: (i) high-power and low-frequency region (20–100 kHz), (ii) medium-power and high-frequency region (100 kHz to 1 MHz), and (iii) low-power and high-frequency region (1–10 MHz). For the synthesis, ultrasound energy plays an important role, and it is a very effective substitute for the traditional energy sources. In sonochemical process, the ultrasound wave moves through the liquid phase in the form of rarefaction-compression cycles that can then be utilized by the reaction in the form of pressure and heat. The cavitation's nuclei formed in the liquid are basically the gas pockets that are captured in the crevices of solid boundaries in the reactor. During rarefaction half-cycle, the bubbles pass through the growth phase, while during compression half-cycle, the bubbles passes

This book belongs to Badji Mokhtar Annaba University Central Library Copyright Elsevier 2025

through the collapse or decay phase. Furthermore, sonochemical synthesis can be either heterogeneous or homogeneous. Heterogeneous sonochemistry deals basically with the cavitation phenomenon due to the mechanical effects. It results in better mass transport, smaller particle sizes, and cleaning of the surfaces. Homogeneous sonochemistry, on the other hand, proceeds through the formation of radical-ion intermediaries. During cavitation, local hot-spots are formed with high temperature and pressure (approx. 5000 K and 500 bar) that play a role in chemical bond breaking and formation. One of the main benefits of employing sonochemical method for the nanoparticle's synthesis process is that the setup is not very expensive and the process is green as it does not use any hazardous chemicals. The ultrasound power, duration of exposure, precursor, and solvent have huge influence on the particle morphology and size [51–53].

Kamali et al. have investigated the role of BH^{4-}/Fe^{3+} ratios, effect of iron precursor concentration, and rate of addition of reducing agent along with irradiation effect of ultrasound. The ratio of BH^4/Fe^{3+} and iron precursor concentration both resulted in an increase in crystallinity with high surface area of the as-synthesized nanoparticles. However, the rate of addition of reductant doesn't produce any significant change. Ultrasound resulted in low particle size with an increase in active surface area [54]. Jamei et al. also studied the effect of different parameters, for example, power, precursor, and reductant amount [51]. With an increase in power, morphology of the as-synthesized nanoparticles switches from spherical morphology to plate and needle morphology. Additionally, when the concentration of precursor-reductant is high and at high ultrasonic power, the size of the nZVI is reduced. The nanoparticles synthesized using ultrasound energy showed enhanced surface area in comparison to other synthesis methods. The greener approach with ultrasound co-precipitation technique has been coupled for the synthesis of zero-valent iron-guar gum nanocomposite (ZGNC) [55]. In this, guar gum, a natural polymer, was used as the capping and reducing agent for the synthesis of nZVIs. Using this method, the average particle size between 60 and 70 nm can be achieved as shown in Fig. 27.1. The TEM analysis revealed that the particles possess spherical morphology with guar gum covering the surface of zero-valent nanoparticles in a core-shell manner. Ultrasound energy enhances the rate of reaction due to turbulent mixing and acoustic streaming. Furthermore, it was observed that the shelf life of the as-synthesized NPs using ultrasound energy improved in comparison to mechanical stirring [55]. Ultrasound-based synthesis methods are better in terms of size controlling, but due to a large amount of heat released during the process, it becomes important to use some surfactant that can control the agglomeration of the nanoparticles. Further, better optimization of ultrasound amplitude along with duration of exposure will also be highly effective for the morphology of the nanoparticles.

27.2.3 Biological synthesis of nZVI

The nZVIs synthesized by chemical process are very expensive and also uses toxic chemical substances (organic solvents, stabilizing agents, and reducing agents such as $NaBH_4$). Therefore, a biological technique has been introduced, which is a green synthesis technique,

This book belongs to Badji Mokhtar Annaba University Central Library Copyright Elsevier 2025

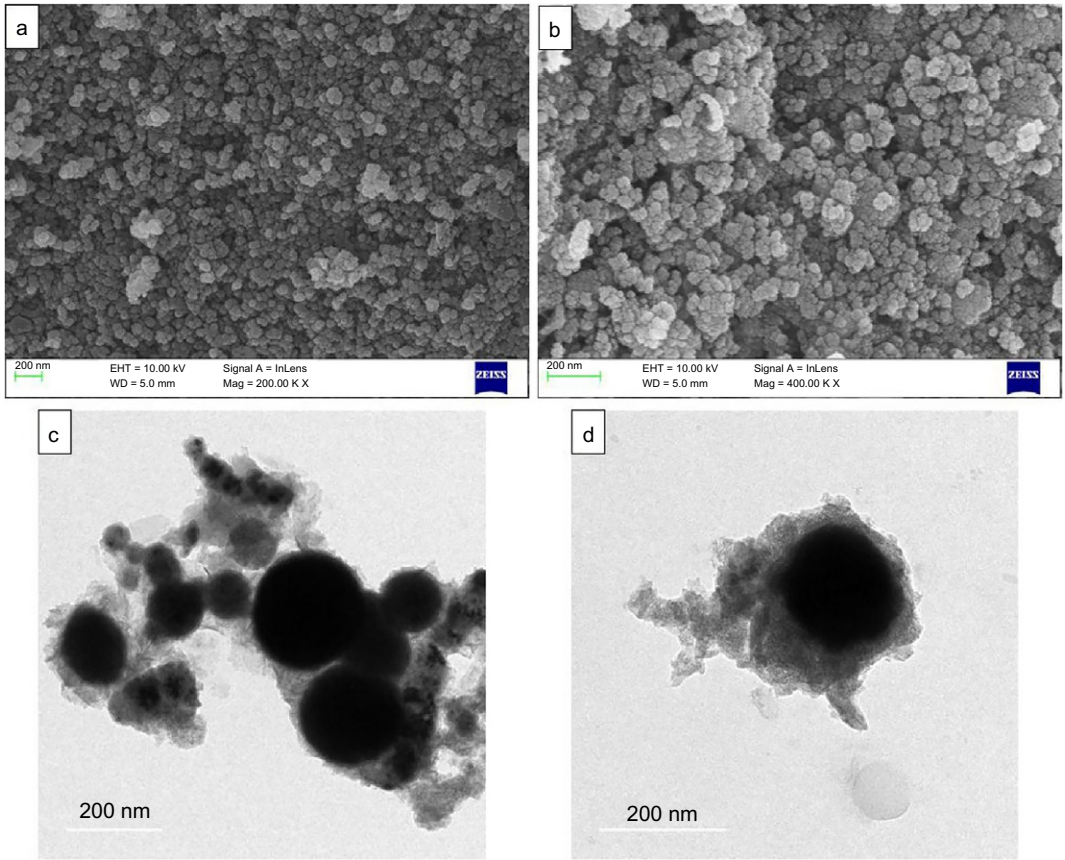

Fig. 27.1
SEM and TEM images. (A) SEM of ZVI particle, (B) SEM of ZGNC, (C) TEM of ZGNC, and (D) TEM images of Single ZGNC with size of ~60–70 nm. *Reprinted with permission of Elsevier from J. Balachandramohan, T. Sivasankar, Ultrasound assisted synthesis of guar gum-zero valent iron nanocomposites as a novel catalyst for the treatment of pollutants, Carbohydr. Polym. 199 (2018) 41.*

eco-friendly, nontoxic, biocompatible, and clean approach for the synthesis of nZVI. In this method, naturally occurring plant extract materials are used as reducing and stabilizing agents. Also, it has some advantages over other synthesis processes such as the method is simple, cost effective, and reproducible [56,57].

In an attempt to minimize the use of toxic chemicals for the synthesis of nanoparticles, biological synthesis methods are gaining momentum. Biological method involves the use of plant or animal extracts for the synthesis of nanoparticles. Several works are being aligned in this area of research by utilizing those plant extracts that are rich in polyphenols. This approach paves the way for a greener or environmental friendly route as only natural extracts are being used at ambient conditions. The main ingredients that act as capping and reducing agents are *flavonoids* and *polyphenols* that are present in wine, tea and coffee, vitamins, and proteins.

This book belongs to Badji Mokhtar Annaba University Central Library Copyright Elsevier 2025

Additionally, the major benefit is low agglomeration and better movement of the as-synthesized nanoparticles, which is very essential for groundwater treatment. Another vital factor of stabilized nZVIs in comparison to unstabilized is that the treatment efficiency improves as the green support provided increases the stability of the nanoparticles and the active surface area available for reaction. Furthermore, biological methods are more favored because, once the application is over, they don't act as a secondary pollutant and mingles easily with the environment without harming it [57–59].

On a similar note, Machado et al. have investigated 26 different tree leaf extracts and effectively synthesized ZVI nanoparticles [60]. In this study, Fe^{+3} was reduced using tree leave extracts in water as a solvent. On the basis of their antioxidant property, the efficiency of the dried and nondried leaves extracts was analyzed. Additionally, it was observed that nondried leaves' antioxidant capacity is low in comparison to dried leaves. The extracts were categorized into three different categories depending on their antioxidant amount in terms of Fe^{+2} concentration: (i) concentration more than 40 mmol/L, (ii) concentration lying between 20 and 40 mmol/L, and (iii) concentration lying between 2 and 10 mmol/L. Also, while extracting from different leaves, volume-mass ratio, temperature, and contact time plays an important role. The extracts of oak tree leaves, green tea leaves, and pomegranate leaves were very effective in producing nZVI. The characterization results of TEM showed sizes lying in the range of 10–20 nm.

Desalegn et al. used mango peel extract for the green synthesis of nZVIs. Herein, Fe (III) chloride hexahydrate was treated with mango peel extract at ambient conditions and the pH was maintained at 2.1 throughout the reaction. A change in color from light brown to dark brown was observed with a slow addition of the mango peel extract into the solution of iron establishing the formation of ZVI nanoparticles. Further UV-visible spectra analysis of all the samples shows UV active spectra in the 200–400 nm wavelength range as shown in Fig. 27.2. The phenolic acid and its derivatives peak in the range of 250–280 nm, which is visible from the surface plasmon resonance effect. An increase in concentration of mango peel extract with respect to iron salt shows an increase in the intensity of the absorption peak. Furthermore, due to the high polyphenol content, agglomeration of the as-synthesized nanoparticles is very low due to steric stabilization and was found to be very stable [57]. Biological methods are gaining momentum since they are environmental friendly and not very costly. Therefore, this domain opens a lot of options for the synthesis of nZVI.

27.3 Influences of process parameters on synthesis of nZVI

27.3.1 Effect of initial Fe^{3+} concentration for the ZVI particle size

Turabik et al. reported that both ferro and ferric iron can be used to produce ZVI nanoparticles [61]. It's often understood that, even for a particular ligand, the stability constant of ferrous iron is below that of ferric iron. Therefore, this Fe(III) compound can provide more stable

This book belongs to Badji Mokhtar Annaba University Central Library Copyright Elsevier 2025

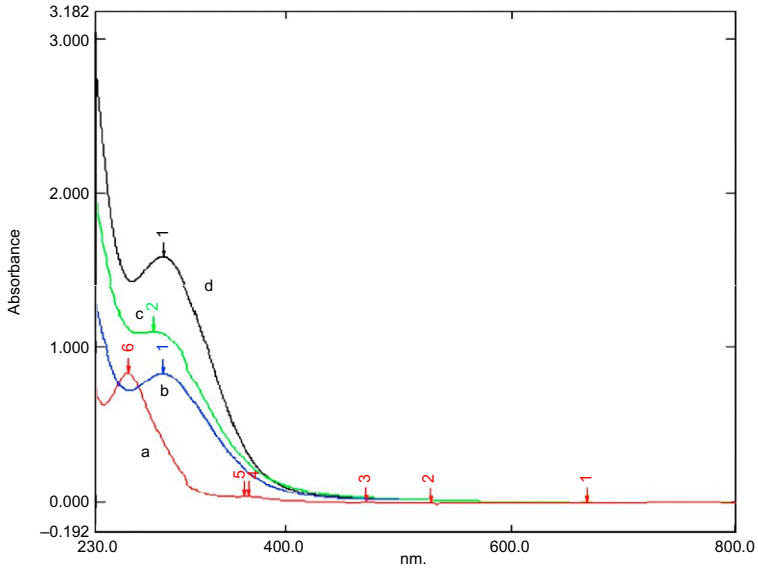

Fig. 27.2

UV-vis spectra of iron nanoparticles synthesized using mango peel extract. (A) Extract alone, (B–D) increasing concentrations of the extracts. *Reprinted with permission of Elsevier from B. Desalegn, M. Megharaj, Z. Chen, R. Naidu, Green synthesis of zero valent iron nanoparticle using mango peel extract and surface characterization using XPS and GC-MS, Heliyon 5 (5) (2019) e01750.*

suspensions of nanoparticles with tiny crystal size; hence, the synthesis of ZVI is preferred. The typical reaction mechanism for formation of nZVI crystals from ferric chloride in the presence of $NaBH_4$ is as follows:

$$2FeCl_3 + 6NaBH_4 + 18H_2O \rightarrow 2Fe^0 + 6NaCl + 6B(OH_3) + 21H_2 \tag{27.4}$$

In compliance with Eq. (27.4), for 0.2 M of $NaBH_4$ (7.56 g/L), stoichiometrically 18.03 g/L of $FeCl_3{\cdot}6H_2O$ is required. The sizes of the synthesized nanoparticles were larger than that of 0.05 M Fe^{3+} (13.52 g/L) owing to the limited amount of Fe(III) ion about 0.01 M Fe^{3+} (2.705 g/L) than even the molar ratio specification. ZVI production with a greater proportion of Fe^{3+} than molar ratio specification for 0.1 M (27.05 g/L) and 0.2 M (54.10 g/L) Fe^{3+} led to an increase in the white precipitation; therefore, no color change was detected even at excess concentration of borohydride. This white precipitate is assumed to be a relatively insoluble cluster of Fe(III)-stabilizer, thus there is zero reaction to producing a ZVI nanoparticle.

27.3.2 Effect of chemical reducing agent on the ZVI particle size

The concentration of $NaBH_4$ is among the most significant factors affecting the particle sizes of nZVI. According to Eq. (27.4), the molar ratio formulation reaction equation demands a quantity of 0.901, 4.508, 18.033, and 45.083 g/L of Fe(III) salts at amounts of 0.01, 0.05, 0.20,

This book belongs to Badji Mokhtar Annaba University Central Library Copyright Elsevier 2025

and 0.50 M $NaBH_4$ (or 0.378, 1.89, 7.56, and 18.9 g/L $NaBH_4$ in reaction mixture). Therefore, 0.01 and 0.05 M of $NaBH_4$ is inadequate for the reaction or excess $NaBH_4$ at 0.2 and 0.5 M concentration levels, the different particles sized have been observed [61].

With the competitive pressure from its reaction mixture, the rise in nanoparticle size with relatively high initial borohydride dose for HTAB-stabilized particles can be viewed. If excessive borohydride is present in the mixture of reaction, the borohydride can interact with water molecules resulting in hydrogen gas generation as given by Eq. (27.5). The intense formation of hydrogen gas during the synthesis stage of nanoparticles stimulates the production of gas bubbles within the reaction mixture resulting in increased mixing, thereby destroying the stabilizer layer on the surface of the nanoparticles [61].

$$BH_4^- + H^+ + 3H_2O \rightarrow H_3BO_3 + 4H_2 \uparrow \tag{27.5}$$

Dithionite is often used as a substitute to borohydride to minimize Fe(III) and produce nZVI at high pH, and even in the oxygen-free environment, the dithionite can help produce better nZVI compared to borohydride-based synthesized nZVI, while eliminating the heavy amount of hydrogen generated by borohydride technique. Also, it was found that the dithionite-based nZVI reactivity with trichloroethane was similar to that seen with borohydride-based nZVI. Recently, methods have been progressively improved toward producing nanoparticles utilizing natural sources ingredients like plant materials. Polyphenols found in tea leaves, wine and winery waste, and red grape pomace was believed to be the key active substances in plant materials [62]. These biomaterials are processed under moderate to high temperatures with a liquid mixture of water and alcohol, and thus the extracted polyphenols behave as moderately environment friendly. Polydispersed nZVI particles have been reported to be produced utilizing polyphenols from tea [63]. As the concentration of these polyphenols increased or decreased, the particle size of the nZVI also varied as discussed in the previous section.

27.3.3 Effect of stabilizer concentration on the ZVI particle size

After the formation of the NPs, it is necessary to stabilize the NPs using a stabilizing agent. During ZVI production through reduction of Fe^{3+}, the formation of metal atoms begins and forms the center of a matured nanoparticle. Those nuclei continue to expand into some kind of cluster before it reaches a certain size. Then stabilizing agents such as HTAB (a cationic quaternary surfactant based on an amine) are used to control the shape of the NPs and stabilize them. When a stabilizer is present in the reaction mixture, it can be grafted to the particle surface and probably delay the crystal growth, then they obstruct some expansion locations on particles resulting in a surface of negative charges [64]. As a result, surface aggregation can be avoided; however, nanomaterials expand until they reach a critical size. HTAB was used in the reaction mixture of 0.05 M $FeCl_3$ and 0.2 M $NaBH_4$ to stabilize the ZVI. Also, different HTAB concentrations (0.0, 0.00001, 0.0001, and 0.01 M) as stabilizing agents for ZVI nanoparticle were

This book belongs to Badji Mokhtar Annaba University Central Library Copyright Elsevier 2025

used to assess the effect of stabilizing agent concentration. At these concentrations, the obtained particle size was 84.46, 66.62, 13.25, and 32.98 nm, respectively [61].

Apart from HTAB, other polymers and surfactants have also been used as stabilizing agents for nZVI. He and Zhao investigated the synthesis of nZIV using Fe^{2+} in the presence carboxymethyl cellulose (CMC) as a stabilizer [65]. In this study, it was shown that, by increasing the molar ratio of CMC/Fe^{2+}, the size of the ZVI was reduced and a similar nanoparticle can also be obtained with only one-fourth of the CMC when the Fe^{2+} concentration was 1 g/L. Also, greater CMC value of more than 0.2% (*w*/w) or higher degree of substitution showed formation of smaller nZVI at lower temperature. CMC compounds with larger molecular mass and magnitude of replacement, i.e., the number of COO groups present within CMC, yield excellently dispersed small nanoparticles with a narrow range of distribution [66]. Cetylpyridinium chloride (CPC), a cationic surfactant combined with something like a dispersing agent polyvinyl pyrrolidine (PVP), has also been found to produce excellently dispersed nZVI with a size of 1–20 nm having specific surface area of about 25.4 m^2/g [67].

27.3.4 Effect of temperature for controlling the particle size of nZVI

Turabik et al. studied the influence of temperature on particle size of nZVI with 0.05 M $FeCl_3$, 0.2 M $NaBH_4$, and 0.0001 M HTAB [61]. The reactions were performed at various temperatures, viz., 9°C, 25°C, 35°C, and 45°C. The study revealed that the sizes of the nanomaterials during reduction reaction are significantly influenced by the reaction temperature. However, the early amount of sodium borohydride and ferric iron were the most significant factors on particle sizes than temperature, as the reaction takes place at almost all temperature conditions. The normal reaction phase of a solution of nanomaterials is somewhere around 9°C, and indeed the smallest particle shape during that temperature was measured as 13.25 nm. When temperature was increased to 45°C, the size of the ZVI particles also increased, and the broader nanoparticles are formed. Particle size had been reported to be 108.2, 118.1, and 130.3 nm at reaction temperatures of 25°C, 3°C, and 45°C, respectively.

27.3.5 Influence of reaction pH on formation of nZVI and particle size

The pH of the reaction solution plays an important role for formation and size controlling of the ZVI nanoparticles. According to Eq. (27.5), BH_4^- ions are consumed by H^+ reduction leading to an increase in the solution pH. It was reported that, at lower pH, the formation of ZVI nanoparticles is comparatively less when the reaction pH is high. In the study reported by Turabik et al., the pH of the reaction mixture increases slowly during the reactions (Eqs. 27.4, 27.5) and finally reached the pH value of 8.12. As the pH value of the reaction mixture increases from 2 to 8, the nZVI particle size also increased from 6.20 to 21.52 nm [61]. Also, Joo et al. studied the nZVI-induced Fenton oxidation for contaminant degradation. In this study, the degradation of herbicide and molinate were investigated in the presence of oxygen or air and

This book belongs to Badji Mokhtar Annaba University Central Library Copyright Elsevier 2025

effect of pH. Therefore, it was shown that the degradation of molinate was 60% at higher pH 8.1 and 65% at lower pH 4 [68].

27.4 Reaction mechanism and catalytic activity of nZVI for treatment of wastewater

Metallic iron effortlessly acts as electron donor. The nZVI is a reactive reagent, which oxidizes to ferrous (Fe^{2+}). The nZVI are easily oxidized to 2^+ and 3^+ oxidation states as shown by Eqs. (27.6), (27.7). In Fenton-like chemistry, the reactions (Eqs. 27.7–27.11) are the rate-limiting steps. The chemical reactions of Fe^{2+} and Fe^{3+} with H_2O_2 (Eqs. 27.7–27.8) generate the OH radicals, while the reactions (Eqs. 27.9–27.11) lead to loss of oxidation potential.

$$Fe^0 \rightarrow Fe^{2+} + 2e^- \tag{27.6}$$

$$Fe^{2+} + H_2O_2 \rightarrow Fe^{3+} + HO^- + {}^{\bullet}OH \tag{27.7}$$

$$Fe^{3+} + H_2O_2 \rightarrow Fe^{2+} + HO_2^{\bullet} + H^+ \tag{27.8}$$

$$Fe^{2+} + {}^{\bullet}OH \rightarrow Fe^{3+} + OH^- \tag{27.9}$$

$$Fe^{3+} + HO_2^{\bullet} \rightarrow Fe^{2+} + H^+ + O_2 \tag{27.10}$$

$$Fe^{2+} + HO_2^{\bullet} \rightarrow Fe^{3+} + HO_2^- \tag{27.11}$$

The reactive radical •OH is produced through the reaction Eq. (27.7), which is also known as the classical Fenton reaction. In the Fenton process, hydrogen peroxide is used as an oxidant and continuously consumed during the reaction, while the Fe^{2+} ion in the reaction solution acts as a catalyst. In the Fenton chemistry, Fe^{2+} helps to produce strong reactive species including •OH radicals capable of transforming environmental recalcitrant contaminants, for example, heavy metals, pesticides, inorganic anions, polychlorinated biphenyls, and chlorinated compounds [31]. During the Fenton reaction, the Fe^{2+} is regenerated from Fe3+ through the reaction Eq. (27.8), thus the process continues until H_2O_2 is available in the solution. However, there is also a diverse effect when the concentration of H_2O_2 is in excess in the solution, which leads to formation of H_2O and O_2 as shown in reaction mechanism Eqs. (27.12)–(27.15). As a result, the rate of oxidation degradation is affected significantly. Therefore, it is essential to monitor the process parameters including the solution pH during the Fenton reaction.

$$H_2O_2 + {}^{\bullet}OH \rightarrow HO_2^{\bullet} + H_2O \tag{27.12}$$

$${}^{\bullet}OH + {}^{\bullet}OH \rightarrow H_2O_2 \tag{27.13}$$

$$HO_2^{\bullet} + HO_2^{\bullet} \rightarrow H_2O_2 + O_2 \tag{27.14}$$

$${}^{\bullet}OH + HO_2^{\bullet} \rightarrow H_2O + O_2 \tag{27.15}$$

This book belongs to Badji Mokhtar Annaba University Central Library
Copyright Elsevier 2025

Besides iron Fe^{2+}, the other transition metal ions (Fe^{3+}, Mn^{2+}, or Cu^{+}) can promote similar processes, which are called Fenton-type or Fenton-like processes. The Fe^{3+} has lower reactivity toward hydrogen peroxide; therefore, the efficiency of Fe^{3+} is lower than Fe^{2+} [29]. Also, Fe^{2+} and Fe^{3+} can oxidize or reduce organic radicals, or the radicals can recombine as shown in Eqs. (27.16)–(27.18):

$$R^{\bullet} + Fe^{3+} \rightarrow R^{+} + Fe^{2+} \tag{27.16}$$

$$R^{\bullet} + Fe^{2+} \rightarrow R^{-} + Fe^{3+} \tag{27.17}$$

$$2R^{\bullet} \rightarrow R - R \tag{27.18}$$

Metallic iron (e.g., Fe^{0}) produces Fe^{2+} and iron corrosion products including nascent oxides, which play a vital role in H_2O_2 activation. The use of iron particles along with H_2O_2 induces iron oxidation. ZVI goes through a number of corrosion reactions in the presence of water. The anodic method has always dissolved Fe^{0}, whereas the cathodic method creates $H_2(g)$ under an anaerobic environment as well as O_2 reduced under oxic conditions [69,70]. Upon immersion, metallic iron (Fe^{0}) produces iron oxides and Fe^{2+} that plays an important role in activating H_2O_2. As shown in Fig. 27.3 during the oxidation reaction, the metallic iron (Fe^{0}) is oxidized in the presence of O_2 and forms Fe^{2+} and H_2O_2. These Fe^{2+} ions react with H_2O_2 present in the solution to generate •OH radicals. Also, Fe^{0} can bring Fe^{3+} down to the Fe^{2+} level. Next, the reaction pathways follow its usual Fenton reaction mechanism for yielding oxidized compounds or the complete decomposition of organic substances [70]. The presence of O_2 in the reaction mixture also plays a crucial role for formation of radicals, which is described here.

In the absence of oxygen (O_2): Oxidation of Fe^{0} by H^{+} in the absence of O_2 yields Fe^{2+} (Eq. 27.19), which is available for reaction with H_2O_2 to promote the Fenton reaction through Eq.

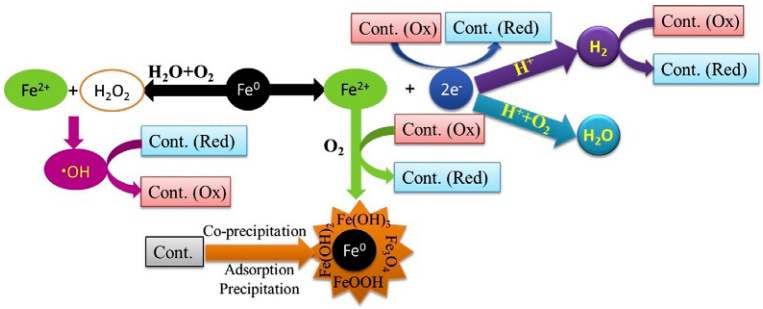

Fig. 27.3

Reaction mechanism of nZVI in Fenton-like reaction. *Reprinted with permission of Elsevier from X. Guan, Y. Sun, H. Qin, J. Li, I. M.C. Lo, D. He, H. Dong, The limitations of applying zero-valent iron technology in contaminants sequestration and the corresponding countermeasures: the development in zero-valent iron technology in the last two decades (1994–2014), Water Res. 75 (2015) 224–248.*

This book belongs to Badji Mokhtar Annaba University Central Library
Copyright Elsevier 2025

(27.7). Another parallel reaction of nZVI with H_2O_2 is given by Eq. (27.20) in which Fe^{2+} and H_2O are generated along with Fe^{2+}.

$$Fe^0 + 2H^+ \rightarrow Fe^{2+} + H_2 \tag{27.19}$$

$$Fe^0 + H_2O_2 + 2H^+ \rightarrow Fe^{2+} + 2H_2O \tag{27.20}$$

In the presence of oxygen (O_2): Fe^0 and Fe species react with oxygen via the following reaction mechanism.

$$Fe^0 + O_2 + 2H^+ \rightarrow Fe^{2+} + H_2O_2 \tag{27.21}$$

$$2\,Fe^0 + O_2 + 4H^+ \rightarrow 2Fe^{2+} + 2H_2O \tag{27.22}$$

$$2Fe^0 + O_2 + 2H_2O \rightarrow 2Fe^{2+} + 4OH^- \tag{27.23}$$

$$6Fe^{2+} + O_2 + 6H_2O \rightarrow 2Fe_3O_4 \downarrow + 12H^+ \tag{27.24}$$

$$4\,Fe^{2+} + O_2 + 10H_2O \rightarrow 4Fe(OH)_3 \downarrow + 8H^+ \tag{27.25}$$

$$4Fe^{2+} + O_2 + 6H_2O \rightarrow 4FeOOH \downarrow + 8H^+ \tag{27.26}$$

In the presence of O_2, the resulting Fe^{2+} readily precipitates, hydrolyzes, and transforms to (hydro) oxides such as Fe_3O_4, $Fe(OH)_3$, and FeOOH (Eqs. 27.24–27.26), forming a thick layer of iron oxides, even more oxidized like maghemite, thereby decreasing the reactivity of ZVI.

In addition, a faster recycling of Fe^{3+} process at the iron surface occurred and regenerates Fe^{2+} as per the following reaction [27] and then produces •OH radicals that react with organic molecules in the bulk medium to produce the products including some intermediates as shown in Eqs. (27.27–27.28).

$$2Fe^{3+} + Fe^0 \rightarrow 3Fe^{2+} \tag{27.27}$$

$$^{\bullet}OH + \text{Organic pollutants} \rightarrow \text{Intermediates} + CO_2 + H_2O \tag{27.28}$$

Therefore, under acidic conditions, the active oxygen substances (ROS) including H_2O_2 and •OH are generated in the $Fe^0/H_2O/O_2$ system through the two-electron oxidation of Fe^0 followed by the Fenton reaction [27, 29]. Also, at natural pH range of waters, Fe^{2+} may hydrolyze to produce $Fe(OH)_2$ through reaction Eq. (27.29). Fe^{2+} is very sensitive with oxygen, and its oxidation by O_2 is quite rapid, increasing the reaction rate with pH.

$$Fe^{2+} + 2H_2O \rightarrow Fe(OH)_2 \downarrow + 2H^+ \tag{27.29}$$

The corrosion kinetics of iron depends on the intrinsic reactivity of the used Fe^0 and other factors like pH and oxygen concentration. With increasing pH up to 4, the corrosion rate decreases; at pH between 4 and 10, it becomes almost stable; and above pH 10, it decreases slightly. In nZVI/O_2 system, the mechanisms of oxidation are pH dependent. Under acidic conditions, oxidation takes place by H_2O_2 to produce •OH [71,72].

This book belongs to Badji Mokhtar Annaba University Central Library
Copyright Elsevier 2025

27.5 Catalytic activity of nZVI for wastewater treatment

The Fenton process has greatly attracted the interest of the scientific community. Many forms of Fenton reaction are being used in homo- and heterogeneous systems including substitution of Fe^{2+} ions, which is one of the main reagents for Fenton reaction. The other widely used nanomaterials are Fe^{3+} [73], Cu^{2+}/Cu^{+} [74], pyrite [75], nZVI [76], etc. and this type of reaction is called a Fenton-like reaction. The other forms of Fenton-like or Hybrid-Fenton reactions are photo-Fenton [77–80], electro-Fenton [81–83], sono-Fenton [84–86], and microwave/Fenton processes [87,88]. The heterogeneous Fenton-like systems could be modified by replacing Fe^{2+} with just a heterogeneous substrate in the Fenton reagent, whereas homogeneous Fenton-like operations seem to be probably a combination of many other metal ion(s)/metal ion-organic ligand complexes and H_2O_2 [89]. The pH, H_2O_2 dosage, catalyst dosage, and reaction temperature were extensively investigated in Fenton-like systems due to their influences on the Fenton-like oxidation reaction.

Various recalcitrant pollutants in wastewater have been degraded using nanomaterial such as nZVI and H_2O_2 catalyzed via Fenton-like technique, which reported efficient total organic carbon (TOC) removal. The nZVI remains in the solution and generates •OH radicals as long as H_2O_2 is present in the solution. Most of the organic contaminants including petroleum hydrocarbon, phenol, and 1-alkyl-3-methylimidazolium bromides can been substantially eliminated within an hour using nZVI.

For example, Weng et al. adapted a Fenton-like system catalyzed by ZVI in the presence of ultrasound to mineralize textile wastewater with overall treatment cost varying from USD 2.12 to 3.58 per m^3 of wastewater [90]. Chakinala et al. integrated hydrodynamic cavitation with Fenton-like reaction with nZVI nanoparticles for textile wastewater treatment. Findings of the study indicated that perhaps the corrosion effect upon this exterior of ZVI that results in the dormant abatement of the wastewater, i.e., the organic wastes in wastewater were gradually deteriorated but with no intervention after the hydrodynamic cavitation-enhanced heterogeneous Fenton-like method lasted 15 min [91]. Dehghani et al. have studied the application of nZVI for the degradation of petroleum hydrocarbon (TPH), and 95.8% of THP removal was seen under the photo-Fenton-like process using 0.02 g/L of nZVI [77,80]. Babuponnusami et al. have studied the phenol degradation using nZVI as catalyst for Fenton-like reaction through photo-electro-Fenton process. The removal rate constant was proportional to the nZVI and H_2O_2 dosage but inversely proportional to the initial phenol concentration and initial pH of the solution. It is reported that 0.5 g/L nZVI dosage can remove 100% phenol [76]. Zhou et al. have investigated the degradation of 4-chlorophenol (4CP) and EDTA with ZVI and ultrasound. The presence of ultrasound increased the degradation efficiency of 4CP and EDTA. In this study, 100% 4CP, 83% EDTA, and 76% of TOC removal were achieved with nZVI dosage of 25.0 g/L [92]. Chand et al. have investigated the degradation of phenol under ZVI and H_2O_2. Complete 100% removal of phenol and 37% removal of TOC have been reported just by 0.6 g/L of ZIV [84].

This book belongs to Badji Mokhtar Annaba University Central Library Copyright Elsevier 2025

27.6 Future perspective and new directions

- The catalyst tends to play a crucial role in the efficiency of a process mechanism similar to Fenton. The ability of the catalyst may be primarily influenced mostly by desorption property. Thereby, the advancement of a certain kind of catalyst with reduced desorption level (high stability) as well as high reactivity is very important for the efficient mineralization of hazardous wastewater.
- Physical forces such as photo, electro, cavitation, and microwave irradiation will show favorable effect over Fenton-like process efficiency during the treatment of wastewater. Even though there have been extensive studies of single physical field-assisted Fenton-like processes, the mixing of two physical fields really couldn't attract adequate attention. Therefore, in forthcoming studies, different pairs of various physical fields, such as photo-electro-Fenton process, microwave-sono-Fenton process, and microwave-electro-Fenton process must be explored in detail.
- Moreover, few studies have suggested and criticized the potentiality of nZVI in terms of cost-effectiveness, and hence prospective investigations are necessary to evaluate the massive, long-term, cost-effective potential as an alternative for environmental abatement.

References

[1] N.L. Rosi, C.A. Mirkin, Nanostructures in biodiagnostics, Chem. Rev. 105 (2005) 1547.
[2] N. Kumar, S. Kumbhat (Eds.), Essentials in Nanoscience and Nanotechnology, Wiley, 2016, p. 149 (Chapter 4).
[3] G. Sharma, A. Kumar, S. Sharma, M. Naushad, R.P. Dwivedi, Z.A. ALOthman, G.T. Mola, Novel development of nanoparticles to bimetallic nanoparticles and their composites: a review. J. King Saud Univ. Sci. 31 (2) (2019) 257–269, https://doi.org/10.1016/j.jksus.2017.06.012.
[4] M. Sahooli, S. Sabbaghi, R. Saboori, Synthesis and characterization of mono sized CuO nanoparticles, Mater. Lett. 81 (2012) 169.
[5] R.V. Kurahatti, A.O. Surendranathan, S.A. Kori, N. Singh, A.V. Kumar, S. Srivastava, Defenceapplications of polymer nanocomposites, Def. Sci. J. 60 (5) (2010) 551.
[6] M.S. Saha, V. Neburchilov, D. Ghosh, J. Zhang, Nanomaterials-supported Pt catalysts for proton exchange membrane fuel cells, WIREs Energy Environ. 2 (1) (2013) 31–51, https://doi.org/10.1002/wene.47.
[7] J. Gangwar, B.K. Gupta, A.K. Srivastava, Prospects of emerging engineered oxide nanomaterials and their applications, Def. Sci. J. 66 (4) (2016) 323.
[8] C.M. Lieber, Nanoscale science and technology: building a big future from small things, MRS Bull. 28 (2003) 486.
[9] G. Cao, Nanostructures & Nanomaterials Synthesis, Properties & Applications, second ed., Imperial College Press, 2004. 2.
[10] Y. Ju-Nam, J.R. Lead, Manufactured nanoparticles: an overview of their chemistry, interactions and potential environmental implications, Sci. Total Environ. 400 (1) (2008) 396.
[11] N.V. Long, C.M. Thi, M. Nogami, M. Ohtaki, Pt and Pd based catalysts with novel alloy and core-shell nanostructures for practical applications in next fuel cells: patents and highlights, Recent Pat. Mater. Sci. 5 (2012) 175.
[12] I. Khan, K. Saeed, I. Khan, Nanoparticles: properties, applications and toxicities, Arab. J. Chem. 12 (2019) 908.

This book belongs to Badji Mokhtar Annaba University Central Library Copyright Elsevier 2025

[13] D. Sundaram, V. Yang, R.A. Yetter, Metal-based nanoenergetic materials: synthesis, properties, and applications, Prog. Energy Combust. Sci. 61 (2017) 293.
[14] N. Toropov, T. Vartanyan, Noble metal nanoparticles: synthesis and optical properties, in: D.L. Andrews, R. H. Lipson, T. Nann (Eds.), Reference Module in Materials Science and Materials Engineering, 1 Elsevier, 2019, pp. 61–88.
[15] H. Bonnemann, R. Richards, W. Hermann, G. Brauer (Eds.), Synthetic Methods of Organometallic and Inorganic Chemistry, ThiemeVerlag, Stuttgart, 2002, p. 209 10.
[16] H. Bonnemann, W. Brijoux, W. Moser (Ed.), Advanced Catalysts and Nanostructured Materials, Academic Press, NY, 1996, p. 165 Ch. 7.
[17] Y. Liu, G. Zhao, D. Wang, Y. Li, Heterogeneous catalysis for green chemistry based on nanocrystals, Natl. Sci. Rev. 2 (1) (2015) 150.
[18] C. Ray, T. Pal, Recent advances of metal–metal oxide nanocomposites and their tailored nanostructures in numerous catalytic applications, J. Mater. Chem. A 5 (2017) 9465.
[19] M.M. Johnson, L.J. Matheson, Permeable reactive barriers of iron and other zero-valent metals, in: M.A. Tarr (Ed.), Chemical Degradation Methods for Wastes and Pollutants: Environmental and Industrial Applications, Marcel Dekker, New York, 2003, p. 371 (Chapter 9).
[20] Y.P. Sun, X.Q. Li, J. Cao, W.X. Zhang, H.P. Wang, Characterization of zero-valent iron nanoparticles, Adv. Colloid Interf. Sci. 120 (2006) 47.
[21] R.C. Martins, L.R. Henriques, R.M. Quinta-Ferreira, Catalytic activity of low-cost materials for pollutants abatement by Fenton's process, Chem. Eng. Sci. 100 (2013) 225.
[22] B. Lai, Y.H. Zhang, R. Li, Y.X. Zhou, J. Wang, Influence of operating temperature on the reduction of highconcentration p-nitrophenol (PNP) by zero valent iron (ZVI), Chem. Eng. J. 249 (2014) 143.
[23] F. Rezaei, D. Vione, Effect of pH on zero valent iron performance in heterogeneous Fenton and Fenton-like processes: a review, Molecules 23 (2018) 3127.
[24] D. O'Carroll, B. Sleep, M. Krol, H. Boparai, C. Kocur, Nanoscale zero valent iron and bimetallic particles for contaminated site remediation, Adv. Water Resour. 51 (2013) 104.
[25] X.Q. Li, D.W. Elliott, W.X. Zhang, Zero-valent iron nanoparticles for abatement of environmental pollutants: materials and engineering aspects, Crit. Rev. Solid State Mater. Sci. 31 (4) (2006) 111.
[26] P.G. Tratnyek, R.L. Johnson, Nanotechnologies for environmental cleanup, Nano Today 1 (2) (2006) 44.
[27] F. Fu, D.D. Dionysiou, H. Liu, The use of zero-valent iron for groundwater remediation and wastewater treatment: a review, J. Hazard. Mater. 267 (2014) 194.
[28] I.A. Katsoyiannis, T. Ruettimann, S.J. Hug, pH dependence of Fenton reagent generation and As (III) oxidation and removal by corrosion of zero valent iron in aerated water, Environ. Sci. Technol. 42 (2008) 7424.
[29] M.I. Litter, M. Slodowicz, An overview on heterogeneous Fenton and Photo-Fenton reactions using zerovalent iron materials, J. Adv. Oxid. Technol. 20160164 (2017) 1–19.
[30] C. Noubactep, S. Care, On nanoscale metallic iron for groundwater remediation, J. Hazard. Mater. 182 (2010) 923.
[31] X. Chen, D. Ji, X. Wang, L. Zang, Review on nanozerovalent iron (nZVI): from modification to environmental applications, IOP Conf. Ser.: Earth Environ. Sci. 51 (2017) 012004.
[32] Y.F. Xi, M. Megharaj, R. Naidu, Dispersion of zero valent ironnanoparticles onto bentonites and use of these catalysts fororange II decolourisation, Appl. Clay Sci. 53 (2011) 716.
[33] R.L. Frost, Y.F. Xi, H.P. He, Synthesis, characterization ofpalygorskite supported zero-valent iron and its application formethylene blue adsorption, J. Colloid Interface Sci. 341 (2010) 153.
[34] A.D. Luca, B.B. Ferrer, Nanomaterials for water remediation: synthesis, application and environmental fate, in: Nanotechnologies for Environmental Remediation: Applications and Implications, Springer Nature, 2020, p. 25 (Chapter 2).
[35] B. Bethi, S.H. Sonawane, B.A. Bhanvase, S.P. Gumfekar, Nanomaterials-based advanced oxidation processes for wastewater treatment: a review, Chem. Eng. Process. Process Intensif. 109 (2016) 178.
[36] S. Chakma, V.S. Moholkar, Investigation in mechanistic issues of sonocatalysis and sonophotocatalysis using pure and doped photocatalysts, Ultrason. Sonochem. 22 (2014) 287.

This book belongs to Badji Mokhtar Annaba University Central Library Copyright Elsevier 2025

[37] T. Bao, J. Jin, M.M. Damtie, K. Wua, Z.M. Yu, L. Wang, J. Chen, Y. Zhang, R.L. Frost, Green synthesis and application of nanoscale zero-valent iron/rectorite composite material for P-chlorophenol degradation via heterogeneous Fenton reaction, J. Saudi Chem. Soc. 23 (2019) 864.
[38] S. Chakma, V.S. Moholkar, Physical mechanism of sono-fenton process, AICHE J 59 (11) (2013) 4303.
[39] N. Wang, T. Zheng, G. Zhang, P. Wang, A review on Fenton-like processes for organic wastewater treatment, J. Environ. Chem. Eng. 4 (2016) 762.
[40] J.A. Bergendahl, T.P. Thies, Fenton's oxidation of MTBE with zero-valent iron, Water Res. 38 (2) (2004) 327.
[41] J.A. Donadelli, L. Carlos, A. Arques-Sanz, F.S.G. Einschlag, Kinetic and mechanistic analysis of azo dyes decolorization by ZVI-assisted Fenton systems: pH-dependent shift in the contributions of reductive and oxidative transformation pathways, Appl. Catal. B Environ. 231 (2018) 51.
[42] Z. Shi, D. Fan, R.L. Johnson, P.G. Tratnyek, J.T. Nurmi, Y. Wu, K.H. Williams, Methods for characterizing the fate and effects of nanozerovalent iron during groundwater remediation, J. Contam. Hydrol. 181 (2015) 17.
[43] P.G. Tratnyek, A.J. Salter-Blanc, J.T. Nurmi, J.E. Amonette, J. Liu, C. Wang, A. Dohnalkova, D. R. Baer, Reactivity of zerovalent metals in aquatic media: effects of organic surface coatings, in: P. G. Tratnyek, T.J. Grundl, S.B. Haderlein (Eds.), Aquatic Redox Chemistry. ACS Symposium Series 1071, ACS Publications, 2011, pp. 381–406.
[44] T. Pasinszki, M. Krebsz, Synthesis and application of zero-valent iron nanoparticles in water treatment, environmental remediation, catalysis, and their biological effects, Nanomaterials 10 (2020) 917.
[45] M.M. Khin, A.S. Nair, V.J. Babu, R. Murugan, S. Ramakrishna, A review on nanomaterials for environmental remediation. Environ. Sci. Rev. 5 (2012) 8075–8109, https://doi.org/10.1039/C2EE21818F.
[46] T. Pasinszki, M. Krebsz, Synthesis and application of zero-valent iron nanoparticles in water treatment, environmental remediation, catalysis, and their biological effects, Nanomaterials 10 (2020) 917.
[47] P. Slovak, O. Malina, J. Kašlík, O. Tomanec, J. Tucek, M. Petr, J. Filip, G. Zoppellaro, R. Zboril, Zero-valent iron nanoparticles with unique spherical 3D architectures encode superior efficiency in copper entrapment, ACS Sustain. Chem. Eng. 4 (5) (2016) 2748.
[48] D. Zhang, W. Gao, G. Chang, L. Shuai, W. Jiao, Y. Liu, Removal of heavy metal lead (II) using nanoscale zero-valent iron with different preservation methods, Adv. Powder Technol. 30 (2019) 581.
[49] H.N. Bhatti, Z. Iram, M. Iqbal, J. Nisar, M.I. Khan, Facile synthesis of zero valent iron and photocatalytic application for the degradation of dyes, Mater. Res. Express 7 (1) (2020) 015802.
[50] S. Roncevic, I. Nemet, T.Z. Ferri, D. Matkovic-Calogovic, Characterization of nZVI nanoparticles functionalized by EDTA and dipicolinic acid: a comparative study of metal ion removal from aqueous solutions, RSC Adv. 9 (53) (2019) 31043.
[51] M.R. Jamei, M.R. Khosravi, B. Anvaripour, A novel ultrasound assisted method in synthesis of NZVI particles, Ultrason. Sonochem. 21 (1) (2014) 226.
[52] S. Chakma, V.S. Moholkar, Intensification of wastewater treatment using sono-hybrid processes: an overview of mechanistic synergism, Indian Chem. Eng. 57 (3–4) (2015) 359.
[53] R.S. Varma, Greener and sustainable trends in synthesis of organics and nanomaterials, ACS Sustain. Chem. Eng. 4 (11) (2016) 5866.
[54] M. Kamali, M.E.V. Costa, G. Otero-Irurueta, I. Capela, Ultrasonic irradiation as a green production route for coupling crystallinity and high specific surface area in iron nanomaterials, J. Clean. Prod. 211 (2019) 185.
[55] J. Balachandramohan, T. Sivasankar, Ultrasound assisted synthesis of guar gum-zero valent iron nanocomposites as a novel catalyst for the treatment of pollutants, Carbohydr. Polym. 199 (2018) 41.
[56] K.S. Navid Saleh, Y. Liu, T. Phenrat, B. Dufour, K. Matyjaszewski, R.D. Tilton, G.V. Lowry, Surface modifications enhance nanoiron transport and NAPL targeting in saturated porous media, Environ. Eng. Sci. 24 (2007) 45.
[57] B. Desalegn, M. Megharaj, Z. Chen, R. Naidu, Green synthesis of zero valent iron nanoparticle using mango peel extract and surface characterization using XPS and GC-MS, Heliyon 5 (5) (2019) e01750.
[58] M.N. Nadagouda, A.B. Castle, R.C. Murdock, S.M. Hussain, R.S. Varma, In vitro biocompatibility of nanoscale zerovalent iron particles (NZVI) synthesized using tea polyphenols, Green Chem. 12 (1) (2010) 114.
[59] G. Kozma, A. Ronavari, Z. Kónya, A. Kukovecz, Environmentally benign synthesis methods of zero-valent iron nanoparticles, ACS Sustain. Chem. Eng. 4 (1) (2016) 291.

This book belongs to Badji Mokhtar Annaba University Central Library Copyright Elsevier 2025

[60] S. Machado, S.L. Pinto, J.P. Grosso, H.P.A. Nouws, J.T. Albergaria, C. Delerue-Matos, Green production of zero-valent iron nanoparticles using tree leaf extracts, Sci. Total Environ. 445–446 (2013) 1–8.
[61] M. Turabik, U. BulutSimsek, Effect of synthesis parameters on the particle size of the zero valent iron particles, Inorg. Nano-Met. Chem. 47 (7) (2017) 1033.
[62] O.V. Kharissova, H.V.R. Dias, B.I. Kharisov, B.O. Perez, V.M.J. Perez, The greener synthesis of nanoparticles, Trends Biotechnol. 31 (4) (2013) 240.
[63] G.E. Hoag, J.B. Collins, J.L. Holcomb, J.R. Hoag, M.N. Nadagouda, R.S. Varma, Degradation of bromothymol blue by 'greener' nano-scale zero-valent iron synthesized using tea polyphenols, J. Mater. Chem. 19 (45) (2009) 8671.
[64] N. Goldstein, F.L. Greenlee, Influence of synthesis parameters on iron nanoparticle size and zeta potential, J. Nanopart. Res. 14 (2012) 760.
[65] F. He, D. Zhao, Manipulating the size and dispersibility of zero-valent iron nanoparticles by use of carboxymethyl cellulose stabilizers, Environ. Sci. Technol. 41 (2007) 6216.
[66] F. He, D. Zhao, J. Liu, C.B. Roberts, Stabilization of Fe-Pd nanoparticles with sodium carboxymethyl cellulose for enhanced transport and dechlorination of trichloroethylene in soil and groundwater, Ind. Eng. Chem. Res. 46 (2007) 29.
[67] S.S. Chen, H.D. Hsu, C.W. Li, A new method to produce nanoscale iron for nitrate removal, J. Nanopart. Res. 6 (2004) 639.
[68] S.H. Joo, A.J. Feitz, T.D. Waite, Oxidative degradation of the carbothioate herbicide, molinate, using nanoscale zero-valent iron, Environ. Sci. Technol. 38 (7) (2004) 2242.
[69] C. Noubactep, A critical review on the process of contaminant removal in Fe^0-H_2O systems, Environ. Technol. 29 (2008) 909.
[70] X. Guan, Y. Sun, H. Qin, J. Li, I.M.C. Lo, D. He, H. Dong, The limitations of applying zero-valent iron technology in contaminants sequestration and the corresponding countermeasures: the development in zero-valent iron technology in the last two decades (1994–2014), Water Res. 75 (2015) 224–248.
[71] C.R. Keenan, D.L. Sedlak, Factors affecting the yield of oxidants from the reaction of nanoparticulate zero-valent iron and oxygen, Environ. Sci. Technol. 42 (2008) 1262–1267.
[72] C.R. Keenan, D.L. Sedlak, Ligand-enhanced reactive oxidant generation by nanoparticulate zero-valent iron and oxygen, Environ. Sci. Technol. 42 (2008) 6936–6941.
[73] X.Q. Fan, H.Y. Hao, Y.C. Wang, F. Chen, J.L. Zhang, Fenton-like degradation of nalidixic acid with Fe^{3+}/H_2O_2, Environ. Sci. Pollut. Res. 20 (2013) 36490.
[74] J. Maekawa, K. Mae, H. Nakagawa, Fenton-Cu^{2+} system for phenol mineralization, J. Environ. Chem. Eng. 2 (2014) 1275.
[75] A. Shinya, L. Bergwall, Pyrite oxidation: review and prevention practices, J. Vertebr. Paleontol. 27 (2007) 145A.
[76] A. Babuponnusami, K. Muthukumar, Removal of phenol by heterogeneous photo electro Fenton-like process using nano-zero valent iron, Sep. Purif. Technol. 98 (2012) 130.
[77] M. Dehghani, E. Shahsavani, M. Farzadkia, M.R. Samaei, Optimizing photo-Fenton like process for the removal of diesel fuel from the aqueous phase, J. Environ. Health Sci. Eng. 12 (2014) 1.
[78] B.L. Fei, Q.L. Yan, J.H. Wang, Q.B. Liu, J.Y. Long, Y.G. Li, K.Z. Shao, Z.M. Su, W.Y. Sun, Green oxidative degradation of methyl orange with copper (II) Schiff base complexes as photo-Fenton-like catalysts, Z. Anorg. Allg. Chem. 640 (2014) 2035.
[79] S.R. Pouran, A.R.A. Aziz, W.M.A.W. Daud, Review on the main advances in photo-Fenton oxidation system for recalcitrant wastewaters, J. Ind. Eng. Chem. 21 (2015) 53.
[80] M. Dehghani, E. Shahsavani, M. Farzadkia, M.R. Samaei, Optimizing photo-Fenton like process for the removal of diesel fuel from the aqueous phase, J. Environ. Health Sci. Eng. 12 (2014) 1.
[81] E. Alfaya, O. Iglesias, M. Pazos, M.A. Sanroman, Environmental application of an industrial waste as catalyst for the electro-Fenton-like treatment of organic pollutants, RSC Adv. 5 (2015) 14416.
[82] B. Balcl, M.A. Oturan, N. Oturan, L. Sires, Decontamination of aqueous glyphosate (aminomethyl). Phosphonic acid, and glufosinate solutions by electro-Fenton-like process with Mn^{2+} as the catalyst, J. Agric. Food Chem. 57 (2009) 4888.

This book belongs to Badji Mokhtar Annaba University Central Library Copyright Elsevier 2025

[83] E. Brillas, I. Sires, M.A. Oturan, Electro-Fenton process and related electrochemical technologies based on Fenton's reaction chemistry, Chem. Rev. 109 (2009) 6570.
[84] R. Chand, N.H. Ince, D.H. Bremner, Phenol degradation using 20, 300 and 520 kHz ultrasonic reactors with hydrogen peroxide or ozone and zero valent metals, Sep. Purif. Technol. 67 (2009) 103.
[85] G.M.S. Elshafei, F.Z. Yehia, O.I.H. Dimitry, A.M. Badawi, G. Eshaq, Ultrasonic assisted-Fenton-like degradation of nitrobenzene at neutral pH using nanosized oxides of Fe and Cu, Ultrason. Sonochem. 21 (2014) 1358.
[86] C.K. Wang, Y.H. Shih, Degradation and detoxification of diazinon by sono-Fenton and sono-Fenton-like processes, Sep. Purif. Technol. 140 (2015) 6.
[87] A.Y. Atta, B.Y. Jibril, T.K. Al-Waheibi, Y.M. Al-Waheibi, Microwave-enhanced catalytic degradation of 2-nitrophenol on alumina-supported copper oxides, Catal. Commun. 26 (2012) 112.
[88] R. Carta, F. Desogus, The enhancing effect of low power microwaves on phenol oxidation by the Fenton process, J. Environ. Chem. Eng. 1 (2013) 1292.
[89] T. Zhou, T.T. Lim, X.H. Wu, Sonophotolytic degradation of azo dye reactive black 5 in an ultrasound/UV/ferric system and the roles of different organic ligands, Water Res. 45 (2011) 2915.
[90] C.H. Weng, Y.T. Lin, C.K. Chang, N. Liu, Decolourization of direct blue 15 by Fenton/ultrasonic process using a zero-valent iron aggregate catalyst, Ultrason. Sonochem. 20 (2013) 970.
[91] A.G. Chakinala, P.R. Gogate, A.E. Burgess, D.H. Bremner, Industrial wastewater treatment using hydrodynamic cavitation and heterogeneous advanced Fenton processing, Chem. Eng. J. 152 (2009) 498.
[92] T. Zhou, T.T. Lim, X.H. Lu, Y.Z. Li, F.S. Wong, Simultaneous degradation of 4-CP and EDTA in a heterogeneous ultrasound/Fenton like system at ambient circumstance, Sep. Purif. Technol. 68 (2009) 367.

This book belongs to Badji Mokhtar Annaba University Central Library
Copyright Elsevier 2025

CHAPTER 28

Nanocomposite adsorbent-based wastewater treatment processes: Special emphasis on surface-engineered iron oxide nanohybrids

Satish P. Mardikar[a], V.R. Doss[b], P.D. Jolhe[c], R.W. Gaikwad[d], and S.S. Barkade[e]

[a]Department of Chemistry, Smt. R S College, SGB Amravati University, Amravati, India, [b]Department of Engineering Sciences, Sinhgad College of Engineering, Pune, India, [c]Department of Biotechnology, Sinhgad College of Engineering, Pune, India, [d]Department of Chemical Engineering, Pravara Rural Engineering College, Loni, India, [e]Department of Chemical Engineering, Sinhgad College of Engineering, Pune, India

28.1 Introduction

Presently, escalating demands for clean drinking water is imposing an alarming challenge, most worst in developing countries [1]. The well-being of humanity is facing qualitative and quantitative water scarcities. Particularly, rapid industrialization and growing population have led to serious concerns toward the quality of drinking water. The waste products discharged from various industries, including textiles, chemicals, metallurgical, and mining industries, are mainly accountable for water contamination [2, 3]. This contaminated water includes effluent of heavy metal ions and carcinogenic organic wastes that are injurious to environment [4]. Consequently, the need for contaminant removal has become essential. For controlling this contamination, significant progress in wastewater treatment has been exercised, which includes various approaches viz., adsorption/partition processing, ion-exchange resins, reverse osmosis, photocatalytic oxidation, and bioremediation [5]. However, the process efficiency, operating methodology, energy requirement, and process economy always restrict their commercial applications.

Recent studies reveal that nanomaterials (NMs) are competent, cost-effective, and biocompatible alternatives to traditional adsorbents (clay, sand, and silica, to name a few), from the standpoint of environmental remediation [6]. Several kinds of NMs, such as metal, metal oxide, polymer, carbon, graphene, and biomaterials, which are used for wastewater treatment

Handbook of Nanomaterials for Wastewater Treatment. https://doi.org/10.1016/B978-0-12-821496-1.00025-8
Copyright © 2021 Elsevier Inc. All rights reserved.

This book belongs to Badji Mokhtar Annaba University Central Library Copyright Elsevier 2025

have been extensively reviewed by several authors. However, iron oxide-based composite NMs are required to be studied in more detail owing to their synergetic potential for effective water/wastewater treatment application. Although the unique characteristics such as easy to operate/design, paramagnetism, reusability, and flexibility associated with iron oxide-based nanosorbents are expected to be advantageous in wastewater treatment, for wider applications, novel methods for synthesis and surface modification are highly solicited. During designing and synthesis of iron oxide nanoparticles (NPs), especially superparamagnetic, the reaction conditions need to be critically controlled to obtain narrow particle size with homogeneous composition/dispersion [7]. The synthesis and modification methods drive the intrinsic properties of iron oxide NMs, which in turn decides their specific application. Biological and sonochemical approaches are emerging methods; however, they still need further progress [8]. As far as the application of iron oxide NPs in water remediation is concerned, their reactivity and selectivity are critical [9]. To overcome these limitations, novel physical/chemical methods need to be designed, which will be able to generate well-dispersed NPs with better compatibility. Exhaustive understanding of the fundamental characteristics of the NPs can be utilized to control their surface properties and to apply those NPs for various applications. Based on the literature survey, modified NPs can be achieved by several methods viz., partial chemical, mechanical external membrane modification precipitation, esterification, and coupling and grafting reactions [10]. Generally, surface modification is a physical adsorption process. The use of UV rays during plasma surface modification of particles is a kind of physical modification. The chemical reactions can also be adopted for alteration of surface configuration and state of NPs. Agglomeration can be greatly reduced by surface chemical modification. With the help of modifier, adsorption or bonding on the particle surface can be reduced by surface modification [11–14].

28.2 Different strategies for synthesis of iron oxide hybrid adsorbents

In order to enhance the applicability of iron oxide NPs, new composite materials by functionalization with a variety of materials have been practiced. Owing to synergy between individual component, development of multicomponent NMs have become the prime focus of recent research. It could also enhance the overall catalytic performance of the composite catalyst. Presently, semiconductor materials with high surface to volume ratio and surface area are being employed to functionalize iron oxide. Low cost iron oxide-based nanomaterial with tranquil modification holds huge potential for environmental remediation. Nanoscale iron oxide materials possess distinct properties, including nontoxic nature, large surface to volume ratio, superparamagnetic properties, biocompatibility, and chemical inertness and thus can be utilized for immobilization for enhanced catalytic activities [15]. Different hierarchical nanomorphs of iron oxide, including nanobelts, nanoovals, and nanorings have been explored recently [16–19]. During tangible application of iron oxide-based adsorbents for target metal, the composites are prone to aggregation. The large aggregates so formed in aqueous solutions

This book belongs to Badji Mokhtar Annaba University Central Library Copyright Elsevier 2025

may change the magnetic assets of the iron oxide-based composites. Such kind of nondispersion ability of iron oxide-based composites can be controlled by manipulating the synthetic architecture, modifying the surface, and minimizing the surface energy [20]. Functionalization with several organic moieties or inorganic supports can prevent the undesirable oxidation of iron NPs [21–24]. A recent report by *De Velasco-Maldonado and coworkers* reveal that functionalization of iron oxide by –COOH and $–NH_2$ groups enhances stability and surface area and consequently, adsorption efficiency of the composite [25]. Yet another report by *Baghani and coworkers*, showed an enhancement in the surface area of Fe_3O_4–NH_2 composites because of grafting of $–NH_2$ over the Fe_3O_4 surface. As a result, the Fe_3O_4–NH_2 composites were able to remove 97% Cr (VI) and 98% Ni (II) with very low concentrations as low as 1 ppm [26].

Iron oxide exhibiting three different structural forms viz., magnetite (Fe_3O_4), hematite (α-Fe_2O_3), and maghemite (γ-Fe_2O_3) have demonstrated their potential for wastewater treatment through adsorption or photocatalysis. Although the high surface energy associated with magnetite (Fe_3O_4) NPs grades them instability; functionalization with several organic-inorganic supports can be deliberately employed to overcome this issue [27]. In this context, anionic and cationic surfactants have been successfully employed for enhancing stability and removal efficiencies [28, 29]. Hematite (α-Fe_2O_3) NPs exhibit the utmost stability when compared to maghemite and magnetite in aqueous solutions. A variety of substrates, including silica, chitosan and alginate, have been employed for the synthesis of hematite NPs for use in water treatment purposes [30–34]. Maghemite (γ-Fe_2O_3) exhibiting ferromagnetic nature possess more stability when compared to that of magnetite.

A wide number of synthesis techniques, including seed-mediated growth method, sol-gel, hydrothermal, chemical precipitation, microemulsion, and chemical vapor deposition method, have been explored for the synthesis of maghemite NPs and their composites [35–39]. Among all these methods, seed-mediated growth method is widely employed. By using this method, high-quality magnetic composites, especially having a core-shell structure, can be synthesized on a large scale. During the growth process, the magnetic iron oxide NPs are employed as seeds and are added to the bulk semiconductor material. Generally, reduction process is performed for obtaining a growth solution. The rate of deposition and crystal growth is monitored by sequential addition of seeds to the growth solution. A variety of wet chemical methods, including coprecipitation, and solvothermal methods can be used to engender iron oxide-semiconductor composite NMs [40–42].

Another widely used approach for synthesizing iron oxide semiconductor hybrid NMs is sequential step deposition technique [43–45]. This method can be preferentially used for fabricating composite materials with multishell structures. Multishell structures with interlayer introduced within them provides well-improved surface characteristics and the protection of iron oxide itself. Usually, silica and carbon are used as materials for interlayer, which can be easily removed by either calcinations or chemical etching [46].

This book belongs to Badji Mokhtar Annaba University Central Library Copyright Elsevier 2025

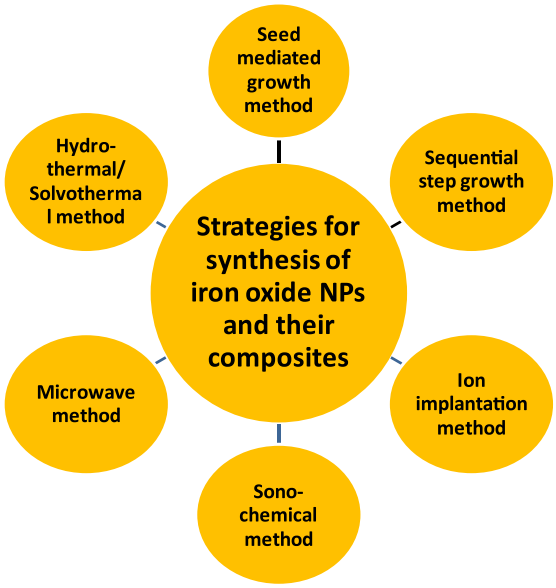

Fig. 28.1
Strategies for synthesis of iron oxide NPs and their composites.

Besides these two approaches, sonochemical method, spray pyrolysis, microwave synthesis, and ion implantation method are also used to produce iron oxide semiconductor hybrid NMs. All these approaches are schematically represented in Fig. 28.1.

28.3 Surface-engineered magnetic nanohybrids

Magnetic nanoparticles (MNPs) such as Fe_3O_4 and α-Fe_2O_3 have been examined for addressing various environmental problems viz., removal of toxic metal ions, seizing of microbial pathogens and organic dyes, stepping up the coagulation of sewage, and remediation of polluted soils [47]. Enhanced adsorption efficiency is achieved by the MNPs that retain a greater surface area with optimal magnetic properties, elevated removal rate of pollutants, and rapid separation of adsorbent. The MNPs can be reused [48, 49]. In order to prevent the process of oxidation, the NPs are stabilized by the attachment of inorganic shell and/or organic molecules. In water treatment process, the heavy metal uptake is greatly enhanced by providing precise functional groups or reaction sites that can be both selective as well as specific for ions uptake [50, 51].

28.3.1 Iron oxide functional groups for heavy metal removal

Yuan et al. reported two-step sol-gel approach for synthesizing Fe_3O_4-SiO_2-meso-SiO_2-R_1-NH_2 particles having 9.9 nm size and spherical morphology for removing Pb (II), Cd (II), and Cu (II) [52]. Zhang et al. through hydrolyzation of Na_2SiO_3-coated SiO_2 shell on Fe_3O_4 and then were

This book belongs to Badji Mokhtar Annaba University Central Library Copyright Elsevier 2025

altered with thiol groups on the Fe_3O_4-SiO_2 through silanization reaction to form Fe_3O_4-SiO_2-SH sorbents. Particles having irregular morphology were formed capable of removing Hg ions [53]. To remove Pb (II), Cd (II), and Cu (II), Fe_3O_4-SiO_2 magnetic nanomaterials functionalized with amino group were developed by Wang et al. [54]. Polyacrylic acid (PAA)-anchored Fe_3O_4 NPs as a magnetic nanoadsorbent were developed by Huang et al., and their amino-functionalization was monitored by means of diethylenetriamine (DETA) through carbodiimide activation, resulting in fine-sized particles, with size ranging from 10 to 14 nm, for removing Cu (II) and Cr (IV) ions [55]. Tan et al. through hydrothermal reduction method synthesized amine-functionalized Fe_3O_4 NPs of 80 nm size for removing Pb (II) ions [56]. The modification of Fe_3O_4 NPs with three different functional groups namely, succinic acid, ethylenediamine, and thiol yielded 10, 40, and 6 nm sized particles, respectively, which could efficiently remove Cr (II), Ni (II), Co (II), Cd (II), Pb (II), and As (II) ions as observed by Singh et al. [57]. Humic acid-functionalized Fe_3O_4 NPs were reported by Liu et al. through coprecipitation method and were employed for the removal of various heavy metals [58]. Xin et al. synthesized amine-functionalized mesoporous Fe_3O_4 NPs for highly efficient water remediation. The removal efficiency was observed to be around 98% [59]. Parham et al. adapted modified-magnetic iron oxide nanoparticles (M-MIONPs) with 2-mercaptobenzothiazole for effective removal of Hg (II) ions [60]. Madrakian et al. using in situ method directly attached reactive blue 19 on the surface of Fe_3O_4 NPs forming 52–54 nm-sized particles, which could remove Pb (II) ions [61]. Feng et al., through an environmental friendly hydrothermal route, successfully synthesized superparamagnetic ascorbic acid-coated Fe_3O_4 NPs that are 10 nm in size, with crystalline nature [62]. Shishebore et al. functionalized salicylic acid on silica-coated magnetite NPs to remove Cd (II), Cu (II), Cr (III), and Ni (II) ions [63]. Faraji et al. reported sodium dodecyl sulfate-coated Fe_3O_4 NPs (SDS-Fe_3O_4NPs) to remove heavy metal ions from water and wastewater samples [28]. Another method for the heavy metal ion removal was the use of thiol-modified superparamagnetic NPs as reported by Yantasee et al. [64]. Rubim et al. functionalized maghemite NPs (α-Fe_2O_3) with glycine for Cu (II) removal. Particle size was reported to be 12 nm [65]. Yaun et al. reported coprecipitation and hydrosol methods for the synthesis of montmorillonite-modified magnetite NPs having particle size around ~15 nm and were found effective in the removal of Cr (VI) ions. It was Mahdavian et al. who successfully modified magnetic iron oxide NPs with 3-aminopropyl triethoxysilane (APTES) and acryloyl chloride (AC) subsequently, resulting in 10–23 nm-sized particles [66,67]. Karatapanis et al. synthesized silica-coated NPs using modified coprecipitation method along with cetylpyridinium bromide having the ability to adsorb trace quantities of Cu (II), Ni (II), Co (II), Cd (II), Pb (II), and Mn (II) from different water samples [68]. Martinez et al. synthesized porous magnetic silica (PMS) spheres using maghemite (α-Fe_2O_3) NPs as fillers and cetyltrimethylammonium bromide (CTAB) as a template [38]. Cao et al. prepared nano-Fe_3O_4/triisopropanolamine-functionalized graphene oxide (GO) composite material for the removal of Pb^{2+} ions [69]. The conceptual scheme for removal of metal ions through iron oxide functionalized with surfactant is shown in Fig. 28.2.

This book belongs to Badji Mokhtar Annaba University Central Library Copyright Elsevier 2025

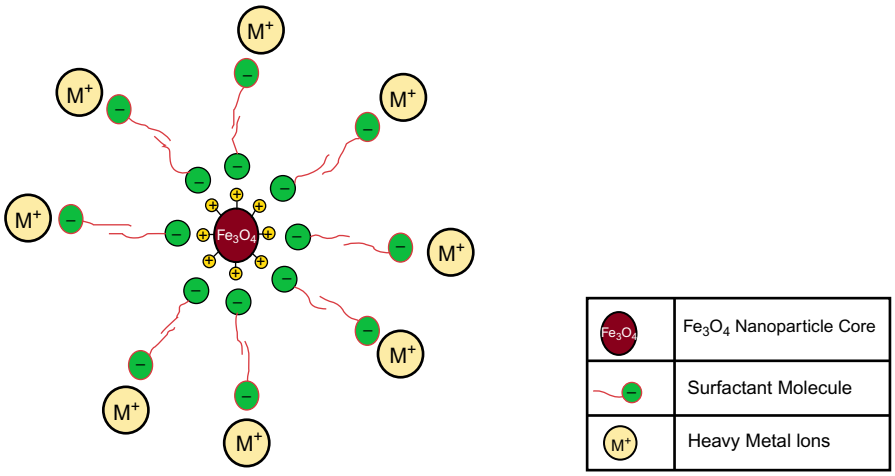

Fig. 28.2
Iron oxide-surfactant functional groups for heavy metal removal.

Table 28.1 summarizes functionalized-iron oxide NPs applied for heavy metal ion removal. From Table 28.1, it reveals that amino-functionalized PAA-coated magnetic nanoadsorbent seems to be most effective compared to bare iron oxide NPs for heavy metal ion removal [55]. Generally, amino-functionalized magnetic NPs have higher adsorption capacity and thereby higher adsorption rates due to lack of internal diffusion rate. The significantly higher capability of amino-functionalized magnetic NPs for adsorbing mono-/polyvalent cations along with metal anions can be explained considering chelation mechanism and electrostatic attraction.

28.3.2 Iron-bimetal oxide NPs for heavy metal removal

In recent years, some researchers have prepared iron-bimetal oxide-based adsorbents for heavy metal adsorption because bimetal doping enhances selectivity and chemical reactivity while still maintaining the magnetic character (Table 28.2). Zhang et al. synthesized bimetal oxide magnetic nanomaterial ($MnFe_2O_4$) and ($CoFe_2O_4$) forming quasi spherical particles sized 30–50 nm, effectively removing As (III) and As (V) ions [70]. Tang et al. reported bimetal oxide magnetic nanomaterial (Mg-α-Fe_2O_3) forming cubic spinel particles sized 3.7 nm to remove arsenic ions [71]. Hu et al. developed an innovative process for simultaneous removal/ recovery of chromium ions from wastewater by combining nanoparticle adsorption with magnetic separation. They used a coprecipitation method to produce 10 nm modified $MnFe_2O_4$ NPs as a new adsorbent. The results showed that surface-modified $MnFe_2O_4$ NPs were effective adsorbents for the fast removal of Cr (VI) from aqueous solutions [72]. Warner et al. reported metal magnetic nanomaterial forming inverse cubic spinel particles sized 25–35 nm to remove Cd ions [73]. Cai et al. used Kaolinite supported Fe/Ni (K-Fe/Ni) bimetallic NPs for simultaneous removal of copper and nitrate ions [74].

This book belongs to Badji Mokhtar Annaba University Central Library Copyright Elsevier 2025

This book belongs to Badji Mokhtar Annaba University Central Library

Table 28.1: Iron oxide functionalized with various functional groups for heavy metal removal.

Name of IONPs	Functional group used	Synthesis method	Morphology	Particle size (nm)	Heavy metal removed	Conditions	Efficiency	References
Fe_3O_4	SiO_2-*meso*-SiO_2-R_2-NH_2	Sol-gel followed by ultrasonication	Spherical	9.9	Pb (II), Cd (II), Cu (II)	pH: 6.2 Temp: 25°C	Pb (II): 99% Cd (II): 91% Cu (II): 95%	[52]
Fe_3O_4	SiO_2-*meso*-SiO_2-R_1-NH_2	Sol-gel followed by ultrasonication	Spherical	2.1	Pb (II), Cd (II), Cu (II)	pH: 6.2 Temp: 25°C	–	[52]
Fe_3O_4	SiO_2-SH	Hydrolyzation followed by silanization reaction	Irregular	10	Pb	pH: 6.5 Temp: 25°C	98%	[53]
Fe_3O_4	Silica-NH_2	Coprecipitation with surface modification	Cubic spinel	18.4	Pb (II), Cd (II), Cu (II)	pH: 6.0–6.4 Temp: 25°C	Cu (II) > Pb (II) > Cd (II)	[54]
Fe_3O_4	Polyacrylic acid-EDTA	Covalent binding followed by carbodiamide activation	Fine	10–14	Cu (II), Cr (IV)	pH: 4.6 Temp: 25°C	100%	[55]
Fe_3O_4	Amine	Hydrothermal reduction	Mesoscopic ordering	80	Pb (II)	pH: 5 Temp: 25°C	98%	[56]
Fe_3O_4	Succinic acid	Coprecipitation	Spherical	10	Cr (II), Ni (II), Co (II), Cd (II), Pb (II), As (II)	pH: 8	91%	[57]

Continued

Copyright Elsevier 2025

This book belongs to Badji Mokhtar Annaba University Central Library

Table 28.1: Iron oxide functionalized with various functional groups for heavy metal removal—cont'd

Name of IONPs	Functional group used	Synthesis method	Morphology	Particle size (nm)	Heavy metal removed	Conditions	Efficiency	References
Fe_3O_4	Ethylene diamine	Thermal decomposition	Discrete/ porous	40	Cr (II), Ni (II), Co (II), Cd (II), Pb (II), As (II)	pH: 8	97%	[57]
Fe_3O_4	2–3 DMSA	Ligand exchange	Spherical	6	Cr (II), Ni (II), Co (II), Cd (II), Pb (II), As (II)	pH: 8	95%	[57]
Fe_3O_4	Humic acid	Coprecipitation	–	10	Hg (II), Pb (II), Cu (II)	pH:5–6	Hg, Pb: 99%, Cu: 95%	[58]
Fe_3O_4	Amine	Hydrothermal	Mesophorous	50	Pb (II), Cu (II), Cd (II)	pH: 7 Temp: 25°C	98%	[59]
Iron oxide	2-Mercaptobenzothiazole	Coprecipitation followed by physical adsorption	Spherical	100	Hg (II)	pH: 9 Temp: 27°C	98.6%	[60]
Fe_3O_4	Reactive blue-19	Coprecipitation followed by in situ method	Cubic spinel	52–54	Pb (II)	pH: 3–5.5 Temp: 27°C	98%	[61]
Fe_3O_4	Ascorbic acid	Hydrothermal	Crystalline	5	As (V), As (III)	pH: 7 Temp: 27°C	45%	[62]

Copyright Elsevier 2025

This book belongs to Badji Mokhtar Annaba University Central Library

Table 28.1: Iron oxide functionalized with various functional groups for heavy metal removal—cont'd

Name of IONPs	Functional group used	Synthesis method	Morphology	Particle size (nm)	Heavy metal removed	Conditions	Efficiency	References
Si-Fe_3O_4	Salicylic acid	Sol-gel	FCC	58–73	Cu (II), Cd (II), Ni (II), Cr (III)	pH: 5–7 Temp: °C	95%	[63]
Fe_3O_4	Sodium dodecyl sulfate	Chemical coprecipitation	–	–	Cu (II), Ni (II), Zn (II)	pH:5–6 Temp: °C	35%–95%	[28]
Fe_3O_4	Dimercapto succinic acid (DMSA)	Chemical coprecipitation	Inverse spinel structure	5.8 ± 0.9	Pb, Ag, Cd, Hg, Ti	pH: 7–8 Temp: 25°C	–	[64]
α-Fe_2O_3	Glycine	Aqueous method of coprecipitation	Spherical	12	Cu (II)	pH: 6.5 Temp: 25°C	89%	[65]
Fe_3O_4	Montmorillonite	Coprecipitation and hydrosol	Spherical	15	Cr (VI)	pH: 2.5 Temp: 25°C	90%	[66]
Fe_3O_4	3-Aminopropyl triethoxy silane (APTES) and acryloyl chloride (AC)	Chemical coprecipitation followed by surface modification	Spinel	10–23	Cu (II), Cd (II), Ni (II), Pb (II)	pH: 8 Temp: 25°C	Pb (II) > Cd (II)	[67]
Fe_3O_4	Cetylpyridinium bromide 8-hydroxyquinoline	Modified coprecipitation	–	–	Cu (II), Ni (II), Co (II), Cd (II), Pb (II) Mn (II)	–	93%	[68]
α-Fe_2O_3	Silica spheres	Stober method combined with hydrothermal treatment	Hollow like	400	Ni (II)	pH: 8 Temp: 25°C	85%	[38]

Copyright Elsevier 2025

This book belongs to Badji Mokhtar Annaba University Central Library

Table 28.2: Iron bimetal oxide nanoparticles for heavy metal removal.

Name of IONPs	Metal used	Synthesis method	Morphology	Particle size (nm)	Heavy metal removed	Conditions	Efficiency	References
Fe_3O_4	Triisopropanolamine	In situ growth method	Spherical	19.03	Pb (II)	pH: 5 Temp: 20°C	–	[69]
Fe_2O_4	Mn	Chemical coprecipitation	Quasi spherical	30–50	As (III), As (V)	pH As (III): 7 As (V): 3 Temp: 25°C	As (III): 80% As (V): 96%	[70]
Fe_2O_4	CO	Chemical coprecipitation	Quasi spherical	30–50	As (III), As (V)	pH As (III): 7 As (V): 3 Temp: 25°C	–	[70]
α-Fe_2O_3	Mg	Solvent thermal process	Cubic spinel	3.7	As (III), As (V)	pH: 7 Temp: 25°C	–	[71]
Fe_2O_4	Mn	Coprecipitation way followed by a surface redox reaction	Crystalline	10	Cr (VI)	pH: 2 Temp: 25°C	95%	[72]
Fe_3O_4	Mn	Chemical coprecipitation	Inverse cubic spinel	25–35	Cd	pH: 7 Temp: 25°C	98%	[73]
Fe	Ni	Liquid-phase chemical reduction	Quasi spherical	1–100	Cu and nitrate	–	96.5%–99.7%	[74]

Copyright Elsevier 2025

As summarized in Table 28.2, the kaolinite (K-Fe/Ni)-supported bimetallic Fe/Ni NPs composite were the found to be the most prospective adsorbents for simultaneous elimination of Cu (II) and nitrate [74]. The significantly increased potential of K-Fe/Ni composite was attributed to the following different factors: First, Cu^{2+} from aqueous solution has adsorption affinity toward both kaolinite and γ-Fe_2O_3/ Fe_3O_4. Second, the formation of trimetalic Fe/Ni/Cu NPs catalyst because of reduction of adsorbed Cu^{2+} to CuO on the K-Fe/Ni surface, which further facilitates the elimination of nitrate through degradation [74].

28.3.3 Iron oxide-metal oxide nanoparticles for heavy metal removal

The ubiquitous presence of Fe (III) oxide as a natural water purifier in various forms is a well-known fact. Apart from being a water purifier, it also shows enhanced heavy metal adsorption capacity over a wide pH range. This has led to the study of a number of impregnated Fe (III) oxide for heavy metal adsorption [75]. However, oxide composites of Fe (III) with other metal ions showed better efficiency in removing heavy metals compared to single metal oxide because of enhanced physical characteristics such as surface area and crystallinity. Thus iron oxide-metal oxide NPs comprises characteristics of both metal oxide (i.e., high affinity) and iron oxide (i.e., low solubility, resistance to acid and bases, and cost-effective) [76]. Singh et al. reported Fe_3O_4-ZnO nanocomposite for 100% removal of heavy metal ions [77]. Kim et al. synthesized Fe_3O_4-MnO_2 nanocomposite through hydrothermal route, effectively removing Cd (II), Cu (II), Pb (II), and Zn (II) ions [78]. Hota et al. synthesized Fe_2O_3-Al_2O_3 nanocomposite by electrospinning method. The removal percentage was in the order of Cu (II) <Pb (II) < Ni (II) < Hg (II) [79]. Basu et al. developed iron-cerium mixed oxide NPs sized 8–10 nm for arsenic removal [80]. Zhang et al. reported a unique nanostructured Fe-Cu binary oxide synthesized through a facile coprecipitation technique forming 50 nm-sized particles for arsenic ion removal [81]. Shan et al. reported the use of modified MNPs with amorphous Fe and Mn oxides (Mag-Fe-Mn) forming quasi spherical particles sized 20–50 nm for the removal of arsenite As (III) from water [82]. Ren et al. used coprecipitation method for the removal of both arsenate and arsenite using an iron-zirconium (Fe-Zr) binary oxide adsorbent and the particles were found to be 200–3000 nm-sized [83]. Wu et al. used magnesium ferrite nano-platelets for the removal of low concentration As (V) in aqueous solution. Vacancy and local defect clusters created because of Mg doping increased surface hydroxyl group concentration and improved its adsorption activity [84]. These iron oxide-metal oxide-based NMs for heavy metal removal are summarized in Table 28.3. From Table 28.3, it can be concluded that amorphous Fe and Mn oxides modified MNPs synthesized by heterogeneous nucleation technique were the most effective for removal of low concentrations of arsenite [As (III)] from water. Additionally, these composites can be regenerated by using NaOH, NaCl, and NaClO solutions. The extraordinary recital of the composite adsorbent material was attributed to synergetic system of the individual constituents as Mn oxides oxidizes As (III) to As (V), which further gets firmly attached to surface of ferric (hydr)oxide.

This book belongs to Badji Mokhtar Annaba University Central Library Copyright Elsevier 2025

This book belongs to Badji Mokhtar Annaba University Central Library

Table 28.3: Iron oxide-metal oxide nanoparticles for heavy metal removal.

Name of IONPs	Metal oxide used	Synthesis method	Morphology	Particle size (nm)	Heavy metal removed	Conditions	Efficiency	References
Fe_3O_4	ZnO	Facile-soft chemical approach	–	–	Ni (II), Cu (II), Pb (II), Hg (II), Cd (II), As (III), Co (II)	–	40%–98%	[77]
Fe_3O_4	MnO_2	Hydrothermal process	Flower-like	–	Cd (II), Cu (II), Pb (II), Zn (II)	pH: 6 Temp: 25°C	80%	[78]
Fe_2O_3	Al_2O_3	Electrospinning sol-gel	Rough/ crystalline	200–500	Ni (II), Cu (II), Pb (II), Hg (II)	pH: 6 Temp: 25°C	Ni (II): 67% Pb (II): 52% Cu (II): 21% Hg (II): 89%	[79]
Iron oxide	Cerium (IV) oxide	Sol-gel	Crystalline	8–10	As (III), As (V)	pH: 7 Temp: 30°C	As (III) > As (V)	[80]
Fe_2O_3	CuO	Coprecipitation	Amorphous	50	As (III), As (V)	pH: 7 Temp: 25°C	As (III): 70% As (V): 80%	[81]
α-Fe_2O_3	Fe-MnO	Coprecipitation followed by heterogeneous nucleation process	Quasi-spherical	20–50	As (III)	pH: 7 Temp: 25°C	98%	[82]
Fe_2O_3	ZrO_2	Coprecipitation	Rough/ porous	200–3000	As (III), As (V)	pH: 7 Temp: 25°C	80%	[83]
Fe_2O_4	Mg	Modified solvent deficient method	Nano spheres	–	As (V)	pH: 7 ± 0.1 Temp: 25°C	–	[84]

Copyright Elsevier 2025

28.3.4 Iron oxide-polymer for heavy metal removal

In the state-of-the-art studies, it has been observed that hybrid polymers are highly favorable for elimination of lethal contaminants from wastewater. In recent years, much focus is on functionalized hybrid magnetic polymeric materials as adsorbents (Table 28.4), as MNP polymers with core-shell nanostructures avert the core part from particle aggregation and enhance the dispersion stability of the core-shell nanostructures. Thus biocompatibility and reduced toxicity of magnetic particles with increased adsorption capacity of polymer provides good solution to water/wastewater treatment [99]. Zhang et al. reported a simplistic path for (EDTA) immobilization on the surface of amine-treated Fe_3O_4 NPs for remediation of heavy metals from aqueous solutions. Fe_3O_4-NH_2/PEI-EDTA magnetic nanoparticles (with an average diameter of 60 nm) effectively removed Pb (II) ions [85]. Shin et al. reported seeded polymerization method for synthesizing Fe_3O_4-poly(3,4-ethylenedioxythiophene) NPs forming spherical particles, 9 nm in size, effectively removing 95% of Ag (II), Hg (II), and Pb (II) ions [86]. Pang et al. developed a steady magnetic α-Fe_2O_3-Fe_3O_4 nanoparticle grafted with polyethylene amine, which demonstrated 95% Cr (VI) ions adsorption [87]. Song et al. synthesized polyrhodanine-coated α-Fe_2O_3 nanoparticles by one-step chemical oxidation polymerization giving 10 nm-sized particles, effectively removing 94.5% Hg (II) ions [88]. Zhang et al. developed Fe_3O_4-SiO_2-poly(1, 2-diaminobenzene) nanoparticles for the exclusion of As (III), Cu (II), and Cr (III) ions from aqueous solution. Particles had core-shell structure with particle size ranging from 23 to 27 nm [89]. Jiang et al. effectively coated Fe_3O_4 onto the outer surface of polystyrene (PS) beads having a diameter of 350–400 nm by the hetero-coacervation method. The particle size was found to be 20 nm, effectively removing As (V) ions [90]. Chang et al. fabricated poly (γ-glutamic acid)-coated Fe_3O_4 magnetic nanoparticles using the coprecipitation method. The γ-PGA/Fe_3O_4 MNPs can remove a little over 99% of Cr (III), Pb (II), and Cu (II) and over 77% of Ni (II) [91]. Zhang et al. synthesized ion-imprinted polymer (Fe_3O_4-SiO_2-IIP) by sol-gel approach for Pb (II) ion removal [92]. Badruddoza et al. synthesized Fe_3O_4 nanoparticles modified by carboxymethyl-β-cyclodextrin (CM-β-CD) polymer for selective adsorption. The particles were spherical in shape and 8–15 nm in size [93]. Ge et al. prepared novel Fe_3O_4 MNPs modified with 3-aminopropyltriethoxysilane (APS) and copolymers of acrylic acid (AA) and crotonic acid (CA). The particles were 15–20 nm in size [94]. Sun et al. prepared polyethylenimine-functionalized poly-(glycidylmethacrylate) superparamagnetic microspheres for Cr (VI) removal. Spherical particles having 227 nm size were formed [95]. Chavez et al., through emulsion polymerization, synthesized polypyrole-γ-Fe_2O_3 nanocomposites for removing Cu, Cd, and Cr ions [96]. Roy et al. synthesized polyvinyl alcohol-iron oxide nanocomposites, with particle size 45 nm having rhombohedral shape and capable of removing As (III) ions with absorption efficiency around 96% [97]. Sarkar et al. investigated application of polyethylene glycol (PEG)-anchored Fe_3O_4 nanoparticles for selective removal of toxic mercury (II) from aqueous solutions by magnetic solid-phase extraction (SPE) [98].

This book belongs to Badji Mokhtar Annaba University Central Library Copyright Elsevier 2025

This book belongs to Badji Mokhtar Annaba University Central Library

Table 28.4: Iron oxide-polymer for heavy metal removal.

Name of IONPs	Polymer used	Synthesis method	Morphology	Particle size (nm)	Heavy metal removed	Conditions	Efficiency	References
Fe_3O_4-NH_2	Polyethylenimine-EDTA	Solvothermal reaction followed by ultrasonication	Spherical	60	Pb (II)	pH: 5.5 Temp: 25°C	98.8%	[85]
Fe_3O_4	Poly (3,4-ethylenedioxythiophene)	Chemical coprecipitation followed by seeded polymerization	Spherical	9	Ag (II), Hg (II), Pb (II)	Contact time: 24 h	95%	[86]
α-Fe_2O_3-Fe_3O_4	Polyethylenimine	Chemical coprecipitation followed by covalent binding	Core-shell	100	Cr (VI)	pH: 2–3 Temp: 35–15°C	95%	[87]
α-Fe_2O_3	Poly-rodanine	One-step chemical oxidation	Core-shell	10	Hg (II)	pH: 4 Temp: 25°C	94.5%	[88]
Fe_3O_4	SiO_2-poly (1,2-diaminobenzene)	Polymerization TEOS Hydrolysis followed by chemical oxidative Polymerization	Spherical/ core-shell	500/23–27	As (III), Cr (II), Cu (III)	pH: 5.3 (Cr), 6.0 (As & Cu) Temp: 25°C	As (III): 97.6% Cr (II): 89.7% Cu (III): 98.1%	[89]
Fe_3O_4	Polystyrene	Hetero-coacervation	Core-shell	20	As (V)	pH: 6 Temp: 25°C	90%	[90]
Fe_3O_4	Poly(γ-glutamic acid)	Coprecipitation	Spherical	52.4	Pb (II), Cr (III), Cu (II), Ni (II)	pH: 6 Temp: 30°C	Pb (II), Cu (II), Cr (III): 99% Ni (II): 77%	[91]

Copyright Elsevier 2025

This book belongs to Badji Mokhtar Annaba University Central Library

Table 28.4: Iron oxide-polymer for heavy metal removal—cont'd

Name of IONPs	Polymer used	Synthesis method	Morphology	Particle size (nm)	Heavy metal removed	Conditions	Efficiency	References
Fe_3O_4	3-(2-Aminoethylamino) propyltrimethoxysilane-TEOS	Sol-gel process	Spherical	200	Pb (II)	pH: 7.5 Temp: 30°C	98%	[92]
Fe_3O_4	Carboxymethyl-β-cyclo dextrin polymer	One-step coprecipitation	Spherical	8–15	Pb (II), Cd (II), Ni (II)	pH: 5.5 Temp: 25°C	Pb (II): 99% Cd (II): 55% Ni (II):24%	[93]
Fe_3O_4	3-Aminopropyltriethoxysilane-acrylic acid (AA) and crotonic acid (CA)	Surface-initiated atom transfer radical polymerization	Spherical	15–20	Pb (II), Cd (II), Cu (II), Zn (II)	pH: 5.5 Temp: 25°C	95%	[94]
Fe_3O_4	Polyethylenimine-functionalized poly(glycidyl methacrylate)	Dispersion polymerization method followed by ring-opening reaction then coprecipitation	Spherical	227	Cr (VI)	pH: 2 Temp: 25°C	47%	[95]
α-Fe_2O_3	Polypyrole	Emulsion polymerization	Irregular	40–60	Cu, Cd, Cr	pH: 2	99%	[96]
Fe_3O_4	Polyvinyl alcohol	Coprecipitation	Rhombohedral	45	As (III)	pH: 4.5–7.5	96%	[97]
Fe_3O_4	Polyethylene glycol	Coprecipitation	Cubic spinel	24	Hg (II)	pH: 6	98%	[98]

Copyright Elsevier 2025

28.3.5 Iron oxide-carbon nanotubes for heavy metal removal

For wastewater treatment and solid-phase extraction, both single-walled carbon nanotubes and multiwalled carbon nanotubes (MWCNTs) have been extensively studied [100, 101]. A variety of carbon nanotube (CNT)-based composite adsorbents have been reported for removal of waterborne pollutants under various conditions [102]. Specifically, the advantage of iron oxide with magnetic characteristics and adsorption properties of CNTs have led to enormous research interest for exploration of their potential. [103]. Yang et al. used low-temperature plasma-induced technique for grafting β-cyclodextrin (β-CD) onto MWCNT/iron oxide cubic particles, which were effective in removing Zn (II) ions [104]. Hasany et al. synthesized maghemite (α-Fe_2O_3)-embedded MWCNTs nanohybrids/nanocomposites and tested them in the removal of Pb (II) [105]. Gupta et al. reported a composite of MWCNT/nanoiron oxide for removing Cr (III) ions with 82%–88% efficiency [106]. Zhou et al. reported polyol method for the synthesis of composite of MWCNTs with amino-modified $CoFe_2O_4$ ($CoFe_2O_4$-NH_2) nanoparticles that effectively removed Pb (II) ions [107]. Zhang et al. successfully grafted 3-mercaptopropyltriethoxysilane (MPTS) on thiol-functionalized multiwall CNT/magnetite nanocomposites forming 20 nm-sized particle, effective in removing Hg (II) and Pb (II) ions [108]. Xiao et al. prepared carboxylated-MWCNT (c-MWCNT)-Fe_3O_4 magnetic composites for removing Cu (II) ions [109]. Xin et al. reported a simple chemical modification of MWCNTs with iron oxide (Fe_3O_4) nanoparticles. The size of the nanoparticles ranged from 30 to 50 nm, which effectively removed Cu (II) ions [110]. Bavio et al. synthesized iron oxide-supported MWCNTs (HNO_3 oxidized MWCNTs-Fe_3O_4), which are basically hybrid-magnetic nanoparticles (HMNPs), for the removal of As (V) [111]. Laoui et al. gave a comparable account of the performance of raw CNTs with iron oxide and aluminum oxide-soaked CNTs for the adsorption of Cr (VI) ions from aqueous solution [112] Table 28.5 summarizes the same.

28.3.6 Iron oxide-graphene for heavy metal removal

Carbon is a multipurpose adsorbent that is widely used for the elimination of various waterborne contaminants [113]. Several types of carbon-based composites have been inspected for their adsorption efficiency [114]. Graphene as one of the carbon family member is assumed to be the most fascinating material. Due to its exclusive two-dimensional assembly and associated band structure, graphene and its composites offer utility in several applications [115]. Most of these composites were anticipated either for catalytic or electronic applications. Single sheets of carbon having large surface area and abundant functional groups offer attractive adsorbent contention for water purification [116]. However, in a large-scale, graphenic materials have their limitations. More avenues were exposed once GO was prepared through chemical methods [117]; furthermore, its consequent reduction to reduced graphene oxide (RGO) opened up the opportunities for the solution phase bulk production of graphene [118, 119]. It was, thus, observed that chemical modifications could enhance the properties of

This book belongs to Badji Mokhtar Annaba University Central Library Copyright Elsevier 2025

This book belongs to Badji Mokhtar Annaba University Central Library

Table 28.5: Iron oxide carbon nanotubes for heavy metal removal.

Name of IONPs	Modifier used	Synthesis method	Morphology	Particle size (nm)	Heavy metal removed	Conditions	Efficiency	References
MWCNT-iron oxide	β-Cyclodextrin	Plasma induced technique	Cubic	–	Zn (II)	pH: 6.5 Temp: 30°C	90%	[104]
Fe_2O_3	MWCNT	Wet chemical	–	–	Pb (II)	pH: 6–7 Temp: 30°C	96%	[105]
Iron oxide	MWCNT	Coprecipitation	Entangled network	30–50	Cr (III)	pH: 5–6 Temp: 30°C	82%–88%	[106]
$CoFe_2O_4$-NH_2	MWCNT	One-pot polyol	Uniform	72.8	Pb (II)	pH: 6 Temp: 30°C	91%	[107]
MWCNT-Fe_3O_4	3-Mercaptopropyltriethoxysilane	Coprecipitation	Spherical network	20	Hg (II), Pb (II)	pH: 6.5 Temp: 30°C	65%	[108]
MWCNT-Fe_3O_4	Caboxyl	Sonication	Entangled network	500	Cu (II)	pH: 6 Temp: 30°C	>90%	[109]
Fe_3O_4	MWCNT	Sonication	Regular and integral	30–50	Cu (II)	pH: 6 Temp: 30°C	57%	[110]
Fe_3O_4	MWCNT-HNO_3	Solvothermal	Short and straight	60	As (V)	pH: 2	95%	[111]
Fe_2O_3	Al_2O_3	Sonication	Tubular	10–20	Cr (VI)	pH: 6	97%	[112]

Copyright Elsevier 2025

GO or RGO. A number of attempts have been made to synthesize GO and RGO composites as they show high adsorption performance for metal ions, but the only drawback is the difficulty to separate from treated water. Thus recent literature indicates that RGO, GO, and their composites with magnetic characteristics are trending into remediation techniques due to high adsorption capacity and ease of separation (Table 28.6). Luo et al. modified Fe_3O_4 and MnO_2 nanoparticles with GO by coprecipitation reaction, giving 10 nm particles having amorphous morphology [120]. Deng et al. synthesized magnetic graphene oxide (MGO) for the removal of Cd (II) ions, which has a particle size of 9–12 nm having absorption efficiency of 65.38% for Cd (II) [121]. Li et al. reported magnetic cyclodextrin-chitosan/GO for removing Cr (VI) ions [122]. Zhou et al. developed cost-effective precursors to prepare RGO-Fe_3O_4 nonnanocomposite using solvothermal strategy [123]. Gollavelli et al. synthesized smart magnetic graphene (SMG). They made use of microwave irradiation of GO and ferrocene precursor having 4.5 nm-sized particles and 99% absorption efficiency [124]. Li et al. fabricated a monolithic Fe_2O_3/graphene hybrid directly by hydrothermal reaction of ferrous oxalate dihydrate and GO without using a reducing agent, with excellent capability for removing As (V) ions from water [125]. Zong et al. synthesized magnetic graphene/iron oxides composite using a chemical reaction approach. The maximum sorption capability of U (VI) was prominent on Fe_3O_4/GO at $T = 293$ K and pH = 5.5. The value was about 69.49 mg/g much higher than that reported in majority of the materials reported [126]. Debnath et al. developed magnetically modified GO-chitosan composite for removal of Cr (VI). The particles were irregular in shape and 10–15 nm in size with 92% absorption efficiency [127]. Zhu et al., using a facile one-pot thermal decomposition method, synthesized magnetic graphene nanoplatelet composites (MGNCs) adorned with core-shell Fe-Fe_2O_3 nanoparticles. Core-shell structured particles are 10–34 nm in size and can effectively and efficiently adsorb As (III) in polluted water [128]. Sun et al. showed a general adsorption ability of heavy metal ions using Fe_3O_4-GO under slightly acidic conditions [129]. The results suggested by Fu et al. showed that the composite exhibits 2D nanosheet structure, in which Fe_3O_4 nanoparticles are sandwiched between the rGO-poly ($C_3N_3S_3$) matrix layers [130]. Priyadarshan et al. reported that WO_3 with Fe_2O_3 nanoparticles grown on graphene sheets resulted in hybrid WO_3-Fe_2O_3-rGO nanocomposites that showed enhanced removal efficiency and antibacterial actions [131].

28.3.7 Iron oxide-biomaterial-based nanoparticles for heavy metal removal

Sorption capacities of biomass and agricultural waste materials have gained a lot of attention, especially in the removal of toxic metal pollutants present in wastewater [132]. Attention has been averted toward the usage of biomaterials, which are offshoots or wastes from large-scale industrial and agricultural production [133]. Bioremediation of heavy metals has been reported using microorganism *Saccharomyces cerevisiae*, which is cheap, easily available, and a safe industrial microorganism [134]. Biological materials such as wheat [135], orange peel [136], hardwood and corn straw [137], loaded with various functional groups such as carboxyl, amide

This book belongs to Badji Mokhtar Annaba University Central Library Copyright Elsevier 2025

This book belongs to Badji Mokhtar Annaba University Central Library

Table 28.6: Iron oxide-graphene for heavy metal removal.

Name of IONPs	Graphene used	Synthesis method	Morphology	Particle size (nm)	Heavy metal removed	Conditions	Efficiency	References
Fe_3O_4	Graphite oxide-MnO_2	Hummers method followed by two-step coprecipitation	Amorphous	10	As (III), As (V)	pH: 7 Temp: 27°C	–	[120]
Iron oxide	Graphene oxide	Hummers method followed by coprecipitation	Cubic spinel	9–12	Cd (II)	pH: 7 Temp: 27°C	65.39%	[121]
Fe_3O_4-β-cyclodextrin	Graphene oxide	Hummers method followed by ultasonication	Cubic-centered	–	Cr (VI)	pH: 3 Temp: 27°C	–	[122]
Fe_3O_4	Reduced graphene oxide	Solvothermal	Spherical	100	Cr (VI)	pH: 7 Temp: 27°C	85%	[123]
Iron oxide	Graphene oxide	Hummers method followed by microwave irradiation	Orthorombic	4.5	Cr (VI), As (V), and Pb (II)	pH: 6.5 Temp: 27°C	99%	[124]
Fe_2O_3	Graphene	Hydrothermal method followed by freeze drying treatment	FCC	10	As (V)	pH: 3 Temp: 30°C	–	[125]
Fe_3O_4	Graphene oxide	Hummers method followed by chemical reaction	FCC	20	U (VI)	pH: 5.5 Temp: 20°C	53%	[126]

Continued

Copyright Elsevier 2025

This book belongs to Badji Mokhtar Annaba University Central Library

Table 28.6: Iron oxide-graphene for heavy metal removal—cont'd

Name of IONPs	Graphene used	Synthesis method	Morphology	Particle size (nm)	Heavy metal removed	Conditions	Efficiency	References
Fe_3O_4	Graphene oxide-chitosan	Hummers method followed by sonication	Irregular	10–15	Cr (VI)	pH: 5.5 Temp: 20°C	92%	[127]
Fe-Fe_2O_3	Graphene-nanoplatelet composites	One-pot thermal decomposition	Core shell	10–34	As (III)	pH: 7 Temp: 20°C	–	[128]
Fe_3O_4	Graphene oxide	Chemical coprecipitation with modification	Cubic crystal	–	Pb (II)	pH: 4 Temp: 20°C	92.63%	[129]
Fe_3O_4	R-GO-poly $C_3N_3S_3$	Hummers method followed by ultrasonic dispersion	FCC	10–20	Pb (II) and Hg (II)	pH: 5 Temp: 25°C	–	[130]
WO_3/Fe_2O_3	Graphene	Modified Hummers method followed by ultrasonication	Polycrystalline	48.14	Pb (II), Cd (II), and Hg (II)	pH: 6 Temp: 25 ± 0.5°C	80%	[131]

Copyright Elsevier 2025

and hydroxylgroup, have a very high affinity for heavy metals and thus have been engaged for heavy metal sorption. MNPs are also broadly applied in various fields such as magnetically assisted biocatalysis, biomedicine, bioseparation, heavy metal removal (Table 28.7), and delivery of small molecule drugs or genes, which is additional to traditional optical, magnetic, and electrical applications [149, 150]. Banerjee et al. developed a nanoadsorbent by considering Fe_3O_4 nanoparticles treated with gum arabic to remove copper ions from aqueous solutions. Particle size was found to be 13–67 nm having spinel morphology, which effectively removed Cu ions [138]. Zhou et al. synthesized chitosan-coated α-Fe_2O_3 magnetic nanoparticles (CCMNPs), improvised with a α-ketoglutaric acid (α-KA) to remove toxic Cu (II) ions having particle size of 30 nm, and the maximum adsorption capacity for Cu (II) ions was projected to be 96.15 mg/g [139]. Chang et al. synthesized chitosan-bound Fe_3O_4 nanoparticles through carbodiimide activation forming 13.5 nm particles, effectively removing Cu (II) with maximum adsorption capacity of 21.5 mg/g [140]. Badruddoza et al. successfully grafted CM-β-CD on the surface of Fe_3O_4 nanoparticles, forming ellipsoidal magnetic nanoparticles with 12 nm size to remove Cu (II) ions [141]. Gong et al. formed shellac-coated magnetic nanoparticles of size 20 nm for effectively removing Cd (II) ions [142]. Sun et al. prepared amino-functionalized Fe_3O_4 magnetic cellulose composite by grafting of glycidyl methacrylate followed by reaction with ethylenediamine forming mesoporous particles of 10 nm size for effectively removing Cr (VI) ions [143]. Xu et al. synthesized baker's yeast biomass and nano Fe_3O_4 with glutaraldehyde as a cross-linking agent. This was then chemically treated with ethylenediaminetetraacetic acid dianhydride (EDTAD). The maximum adsorption capacities of 99.26 mg/g was observed for Pb (II) at pH 5.5, 48.70 mg/g for Cd (II) at pH 6.0, and 33.46 mg/g for Ca (II) at pH 6.0 at a temperature of 30°C [144]. Peng et al. developed Fe_3O_4-silica-xanthan gum composite for the abstraction and retrieval of aqueous Pb (II) heavy metal. A sol-gel process was used for impregnating the xanthan gum (XG) on the surface of the magnetic Fe_3O_4 microspheres. Particles were cubic of 20–50 nm size with 100% removal efficiency [145]. Ren et al. reported magnetic ethylenediaminetetraacetic acid (EDTA)-modified chitosan/SiO_2/Fe_3O_4 adsorbent (EDCMS) as an adsorbent for removal of heavy metal ions [146]. Gong et al. reported pectin-coated iron oxide magnetic nanocomposite as an adsorbent for the effective removal of copper. In order to synthesize a nanocomposite adsorbent, the method adopted was coprecipitation with the iron salt followed by direct encapsulation with pectin coating devoid of cross-linking with calcium ions. Pectin-iron oxide magnetic nanocomposite (PIOMN) adsorbent was found to be spherical in shape having a diameter of 77 ± 5 nm [147]. Jassal et al. used magnetic chitosan nanoparticles in which nanoparticles of magnetic (Fe_3O_4) was coated on chitosan and used this biopolymer for abstraction of heavy metals from aqueous medium [148].

Surface functionality plays a major role in understanding the basic mechanism involved in the removal of heavy metal ions from water/wastewater by surface-engineered magnetic

This book belongs to Badji Mokhtar Annaba University Central Library Copyright Elsevier 2025

This book belongs to Badji Mokhtar Annaba University Central Library

Table 28.7: Iron oxide-biomaterial-based nanoparticles for heavy metal removal.

Name of IONPs	Biomaterial used	Synthesis method	Morphology	Particle size (nm)	Heavy metal removed	Conditions	Efficiency	References
Fe_3O_4	Gum arabic	Sonication	Spinel	13–67	Cu	pH: 5.1 Temp: 27°C	–	[138]
α-Fe_2O_3	Chitosan-γ-ketoglutaric acid	Sonication followed by chemical	Circular	30	Cu (II)	pH: 6 Temp: 27°C	50%	[139]
Fe_3O_4	Chitosan	Carbodiimide activation	Monodisperse	13.5	Cu (II)	pH: 5 Temp: 27°C	–	[140]
Fe_3O_4	Carboxymethyl-β-cyclodextrin	Carbodiimide activation	Ellipsoidal	12	Cu (II)	pH: 5 Temp: 25°C	90%	[141]
Iron oxide	Shellac	Coprecipitation	Core-shell	20	Cd (II)	pH: 8 Temp: 25°C	–	[142]
Fe_3O_4	SiO_2-cellulose-GMA-EDA	Grafting followed by reaction	Mesoporous	10	Cr (VI)	pH: 2 Temp: 25°C	–	[143]
Fe_3O_4	Baker's yeast glutaraldehyde-EDTAD	Ultrasonication	–	–	Pb (II), Cd (II), Ca (II)	pH: 5.5 (Pb), 6.0 (Cd & Ca) Temp: 30°C	85%	[144]
Fe_3O_4	Silica-xanthan gum	Sol-gel process	Cubic	20–50	Pb (II)	pH: 6 Temp: 20°C	100%	[145]
Fe_3O_4	Chitosan/ SiO_2-EDTA	Sol-gel process followed by sonication	Irregular	–	Pb (II), Cd (II), Cu (II)	pH: 5 Temp: 25°C	90%	[146]
Iron oxide	Pectin	Coprecipitation followed by direct encapsulation	Spherical	72–82	Cu (II)	pH: 5 Temp: 25°C	93.7%	[147]
Fe_3O_4	Chitosan	Chemical coprecipitation followed by suspension cross-linking technique	Irregular and spherical	–	Zn (II), Pb (II), Cd (II), Cu (II)	–	–	[148]

Copyright Elsevier 2025

nanohybrids. Magnetic nanoadsorbents utilize different techniques such as chelate complexes, ion exchange process, or electrostatic interactions for the removal of heavy metals.

Although these magnetic nanohybrids have their own advantages, there are still some shortcomings to be overcome, especially relating to their overly complex preparation procedure, use of costly reagents during their preparation, poor shelf life, and reusability. Also, MNPs with a large surface area to volume ratio tend to aggregate; therefore maintaining reaction conditions and suitable chemical modification is essential. Thus it is necessary to develop unique magnetic sorbents for heavy metal ion elimination with simple preparation process, least-cost, high efficacy, good stability, and reusability.

28.4 Current trends and scale-up challenges

The challenges encountered during water and wastewater treatment depends preferentially on menace associated with their utilization, durability, and disposal. The utilization of these bare or hybrid nanoadsorbents seems to be only provisional. Additionally, manufacturing of these hybrid NMs and applying them for targeted wastewater treatment applications is experiencing a declined response because low-cost adsorbents are readily available.

This chapter reviewed the recent developments in functionalized iron oxide-based nanoadsorbents for water/wastewater remediation. The through research investigated into enhanced adsorbing activity of modified iron oxide with different functional groups, metal/metal oxide nanoparticles, organic polymers, and different allotropes of carbon, including CNTs and graphene compared to that of bare iron oxide. Evidently, the significant benefit reinforcing the use of iron oxide-based nanocomposite materials lies in its magnetic nature and tranquil fabrication techniques. Within the scope of knowledge, several parameters viz., structure, morphology, phase of iron oxide along with concentration, pH, and temperature of the aqueous adsorbate solution could influence the process of adsorption by iron oxide-based nanocomposites. Regarding the several advantages associated with surface-engineered iron oxide nanocomposites, the following particulars should be carefully worked so that pilot-scale/commercial developments in this area can advance at a faster lick:

(1) The researchers should focus on designing and fabrication of iron oxide-based nanocomposites with magnetic nature, which helps in magnetic postreaction recovery of the catalyst.
(2) The green routes for synthesis of functionalized magnetic iron oxide nanocomposites must be explored.
(3) The iron oxide-based composites are more prone to photocorrosion. To encounter this issue, iron oxide-based core-shell composites ensuring long-term stability should be developed.

This book belongs to Badji Mokhtar Annaba University Central Library Copyright Elsevier 2025

(4) The adsorbing activity of functionalized iron oxide nanocomposites should be extended for targeted gaseous pollutants.

28.5 Conclusions

Environmental pollution by heavy metal ions and organic contaminants in the water and wastewater is a universal problem that is increasing at an alarming level. However, the latest progression in the field of nanotechnology offers pronounced opportunities for the fabrication of preferred NMs in treating these pollutants armored with large surface-to-volume ratios and distinctive surface functionalities. Ease of separation, less toxic byproducts, chemical inertness, biologically safe, and biocompatibility are unique characteristics of surface-engineered magnetic nanohybrid. Surface-engineered magnetic nanohybrids tend to be the most novel research topic because multifunctional MNPs systems with designed active sites, including functional groups, metals, metal oxide, polymer, biomaterials, and other species, can be formed. These surface functionalities offer sites for the acceptance of specific/selective metal ions and, this in turn is responsible to boost the efficiency of their removal. Also, with the help of high-gradient magnetic (HGM) force field, magnetic nanoadsorbents can be detached and convalesced from treated water after adsorption process. Nonmagnetic impurities can be excluded during recovery of magnetic nanoadsorbents because of HGM, which is significant for practical application. However, a major challenge involved in magnetic nanohybrids design is to carefully control reaction conditions for synthesizing particles with narrow size distribution, homogenous composition, and high magnetic susceptibility. Major aspects such as stability, biodegradability, and surface chemistry need to be considered to predict various types of interactions with target contaminants for successful application of surface-engineered nanohybrids in water and wastewater treatment. In conclusion, surface-engineered magnetic nanohybrids can be widely used for heavy metal removal from water and wastewater.

References

[1] Environmental Protection Agency, US Environmental Protection Agency report DC, PA Washington, 2007 EPA100/B-07/0011-13.
[2] D. Rajkumar, G.K. Jong, Oxidation of various reactive dyes with in situ electro-generated active chlorine for textile dyeing industry wastewater treatment, J. Hazard. Mater. B 136 (2006) 203–212.
[3] A. Gómez-Álvarez, J.L. Valenzuela-García, D. Meza-Figueroa, M. De La O-Villanueva, J. Ramírez-Hernández, J. Almendariz-Tapia, E. Pérez-Segura, Impact of mining activities on sediments in a semi-arid environment: San Pedro River, Sonora, Mexico, Appl. Geochem. 26 (2011) 2101–2112.
[4] S.K. Kansal, M. Singh, D. Sud, Studies on photodegradation of two commercial dyes in aqueous phase using different photocatalysts, J. Hazard. Mater. 141 (2007) 581–590.
[5] S.U.M. Khan, M. Al-Shahry, W.B. Ingler, Efficient photochemical water splitting by a chemically modified n-TiO_2, Science 297 (2002) 22–43.

This book belongs to Badji Mokhtar Annaba University Central Library
Copyright Elsevier 2025

[6] R. Dastjerdi, M. Montazer, A review on the application of inorganic nano-structured materials in the modification of textiles: focus on anti-microbial properties, Colloids Surf. B Biointerfaces 279 (2010) 5–18.
[7] S.H. Sun, H. Zeng, Size-controlled synthesis of magnetite nanoparticles, J. Am. Chem. Soc. 124 (2002) 8204–8205.
[8] Y.F. Shen, J. Tang, Z.H. Nie, Y.D. Wang, Y. Ren, L. Zuo, Preparation and application of magnetic Fe_3O_4 nanoparticles for wastewater purification, Sep. Purif. Technol. 68 (2009) 312–329.
[9] A.B. Cundy, L. Hopkinson, Use of iron-based technologies in contaminated land and groundwater remediation, a review, Sci. Total Environ. 400 (2008) 42–51.
[10] R.D. Ambashta, M. Sillanpaa, Water purification using magnetic assistance: a review, J. Hazard. Mater. 180 (2010) 38–49.
[11] M. Mahmoudi, S. Sant, B. Wang, S. Laurent, T. Sen, Superparamagnetic iron oxide nanoparticles (SPIONs), development, surface modification and applications in chemotherapy, Adv. Drug Deliv. Rev. 63 (2011) 24–46.
[12] L.S. Wang, R.Y. Hong, Synthesis, Surface Modification and Characterisation of Nanoparticles, Intechopen, 2011, pp. 291–322.
[13] J. Siping, C. Miao, H. Liu, L. Feng, Y. Xiangjun, H. Guo, A hydrothermal synthesis of Fe_3O_4@C hybrid nanoparticle and magnetic adsorptive performance to remove heavy metal ions in aqueous solution, Nanoscale Res. Lett. 13 (2018) 178.
[14] J. Lin, M. Sun, B. Su, G. Owens, Z. Chen, Immobilization of Cd in polluted soils by phytogenic iron oxide nanoparticles, Sci. Total Environ. 659 (2019) 491–498.
[15] X. Guo, W. Wang, Y. Yang, Q. Tian, Y. Xiang, Y. Sun, Z. Bai, Magnetic nano capture agent with enhanced anion internal layer diffusion performance for removal of arsenic from human blood, Appl. Surf. Sci. 470 (2019) 296–305.
[16] B. Mukherjee, P.K. Maiti, C. Dasgupta, A. Sood, Single-file diffusion of water inside narrow carbon nanorings, ACS Nano 4 (2010) 985–991.
[17] C.-J. Jia, L.-D. Sun, F. Luo, X.-D. Han, L.J. Heyderman, Z.-G. Yan, C.-H. Yan, K. Zheng, Z. Zhang, M. Takano, Large-scale synthesis of single-crystalline iron oxide magnetic nanorings, J. Am. Chem. Soc. 130 (2008) 16968–16977.
[18] X. Wen, S. Wang, Y. Ding, Z.L. Wang, S. Yang, Controlled growth of large-area, uniform, vertically aligned arrays of α-Fe_2O_3 nanobelts and nanowires, J. Phys. Chem. B 109 (2005) 215–220.
[19] J. Liu, Y. Li, H. Fan, Z. Zhu, J. Jiang, R. Ding, Y. Hu, X. Huang, Iron oxide-based nanotube arrays derived from sacrificial template-accelerated hydrolysis: large area design and reversible lithium storage, Chem. Mater. 22 (2009) 212–217.
[20] M. Palimi, M. Rostami, M. Mahdavian, B. Ramezanzadeh, Surface modification of Fe_2O_3 nanoparticles with 3-aminopropyltrimethoxysilane (APTMS): an attempt to investigate surface treatment on surface chemistry and mechanical properties of polyurethane/Fe_2O_3 nanocomposites, Appl. Surf. Sci. 320 (2014) 60–72.
[21] A. Hasan, L.M. Pandey, Self-assembled monolayers in biomaterials. Nanobiomaterials (2018) 137–178, https://doi.org/10.1016/b978-0-08-100716-7.00007-6.
[22] L.M. Pandey, S.K. Pattanayek, Properties of competitively adsorbed BSA and fibrinogen from their mixture on mixed and hybrid surfaces, Appl. Surf. Sci. 264 (2013) 832–837.
[23] L.M. Pandey, S. Le Denmat, D. Delabouglise, F. Bruckert, S.K. Pattanayek, M. Weidenhaupt, Surface chemistry at the nanometer scale influences insulin aggregation, Colloids Surf. B Biointerfaces 100 (2012) 69–76.
[24] L.M. Pandey, S.K. Pattanayek, D. Delabouglise, Properties of adsorbed bovine serum albumin and fibrinogen on self-assembled monolayers, J. Phys. Chem. C 117 (2013) 6151–6160.
[25] P.S. De Velasco-Maldonado, V. Hernández-Montoya, M.A. Montes-Morán, N.A.-R. Vázquez, M. A. Pérez-Cruz, Surface modification of a natural zeolite by treatment with cold oxygen plasma: characterization and application in water treatment, Appl. Surf. Sci. 434 (2018) 1193–1199.
[26] A.N. Baghani, A.H. Mahvi, M. Gholami, N. Rastkari, M. Delikhoon, One-Pot synthesis, characterization and adsorption studies of amine-functionalized magnetite nanoparticles for removal of Cr (VI) and Ni (II) ions

This book belongs to Badji Mokhtar Annaba University Central Library Copyright Elsevier 2025

from aqueous solution: kinetic, isotherm and thermodynamic studies, J. Environ. Health Sci. Eng. 14 (2016) 11.
[27] Y. Sahoo, A. Goodarzi, M.T. Swihart, T.Y. Ohulchanskyy, N. Kaur, E.P. Furlani, P.N. Prasad, Aqueous ferrofluid of magnetite nanoparticles: fluorescence labeling and magnetophoretic control, J. Phys. Chem. B 109 (2005) 3879–3885.
[28] M. Adeli, Y. Yamini, M. Faraji, Removal of copper, nickel and zinc by sodium dodecyl sulphate coated magnetite nanoparticles from water and wastewater samples, Arab. J. Chem. 10 (2017) S514–S521.
[29] S.A. Elfeky, S.E. Mahmoud, A.F. Youssef, Applications of CTAB modified magnetic nanoparticles for removal of chromium (VI) from contaminated water, J. Adv. Res. 8 (2017) 435–443.
[30] J. Zhang, A. Thurber, C. Hanna, A. Punnoose, Highly shape-selective synthesis, silica coating, self-assembly, and magnetic hydrogen sensing of hematite nanoparticles, Langmuir 26 (2009) 5273–5278.
[31] A. Sánchez-Ferrer, M. Reufer, R. Mezzenga, P. Schurtenberger, H. Dietsch, Inorganic–organic elastomer nanocomposites from integrated ellipsoidal silicacoated hematite nanoparticles as crosslinking agents, Nanotechnology 21 (2010) 185603.
[32] K.L. Chen, S.E. Mylon, M. Elimelech, Enhanced aggregation of alginate-coated iron oxide (hematite) nanoparticles in the presence of calcium, strontium, and barium cations, Langmuir 23 (2007) 5920–5928.
[33] K.L. Chen, S.E. Mylon, M. Elimelech, Aggregation kinetics of alginate-coated hematite nanoparticles in monovalent and divalent electrolytes, Environ. Sci. Technol. 40 (2006) 1516–1523.
[34] V.M. Boddu, K. Abburi, J.L. Talbott, E.D. Smith, R. Haasch, Removal of arsenic (III) and arsenic (V) from aqueous medium using chitosan-coated biosorbent, Water Res. 42 (2008) 633–642.
[35] W. Jiang, M. Pelaez, D.D. Dionysiou, M.H. Entezari, D. Tsoutsou, K. O'Shea, Chromium (VI) removal by maghemite nanoparticles, Chem. Eng. J. 222 (2013) 527–533.
[36] S. Rajput, L.P. Singh, C.U. Pittman Jr., D. Mohan, Lead (Pb^{2+}) and copper (Cu^{2+}) remediation from water using superparamagnetic maghemite (γ-Fe_2O_3) nanoparticles synthesized by flame spray pyrolysis (FSP), J. Colloid Interface Sci. 492 (2017) 176–190.
[37] S. Deka, V. Saxena, A. Hasan, P. Chandra, L.M. Pandey, Synthesis, characterization and in vitro analysis of α-Fe_2O_3-$GdFeO_3$ biphasic materials as therapeutic agent for magnetic hyperthermia applications, Mater. Sci. Eng. C 92 (2018) 932–941.
[38] C. Caparrós, M. Benelmekki, P. Martins, E. Xuriguera, C.J. Silva, L.M. Martinez, S. Lanceros-Méndez, Hydrothermal assisted synthesis of iron oxide-based magnetic silica spheres and their performance in magnetophoretic water purification, Mater. Chem. Phys. 135 (2012) 510–517.
[39] A.S. Teja, P.-Y. Koh, Synthesis, properties, and applications of magnetic iron oxide nanoparticles, Prog. Cryst. Growth Charact. Mater. 55 (2009) 22–45.
[40] J. Zhang, X. Liu, L. Wang, T. Yang, X. Guo, S. Wu, et al., Synthesis and gas sensing properties of α-Fe_2O_3@ZnO core–shell nanospindles. Nanotechnology 22 (18) (2011) 185501, https://doi.org/10.1088/0957-4484/22/18/185501.
[41] W. Yan, H. Fan, C. Yang, Ultra-fast synthesis and enhanced photocatalytic properties of alpha-Fe_2O_3/ZnO core-shell structure. Mater. Lett. 65 (11) (2011) 1595–1597, https://doi.org/10.1016/j.matlet.2011.03.026.
[42] L. Peng, T. Xie, Y. Lu, H. Fan, D. Wang, Synthesis, photoelectric properties and photocatalytic activity of the Fe_2O_3/TiO_2 heterogeneous photocatalysts, Phys. Chem. Chem. Phys. 12 (2010) 8033–8041.
[43] G. Schneider, G. Decher, From functional core/shell nanoparticles prepared via layer-by-layer deposition to empty nanospheres. Nano Lett. 4 (10) (2004) 1833–1839, https://doi.org/10.1021/nl0490826.
[44] Y. Wang, A.S. Angelatos, F. Caruso, Template synthesis of nanostructured materials via layer-by-layer assembly. Chem. Mater. 20 (3) (2008) 848–858, https://doi.org/10.1021/cm7024813.
[45] S. Srivastava, N.A. Kotov, Composite layer-by-layer (LBL) assembly with inorganic nanoparticles and nanowires. Acc. Chem. Res. 41 (12) (2008) 1831–1841, https://doi.org/10.1021/ar8001377.
[46] W. Li, Y. Deng, Z. Wu, X. Qian, J. Yang, Y. Wang, D. Gu, F. Zhang, B. Tu, D. Zhao, Hydrothermal etching assisted crystallization: a facile route to functional yolk-shell titanate microspheres with ultrathin nanosheets-assembled double shells, J. Am. Chem. Soc. 133 (2011) 15830–15833.

This book belongs to Badji Mokhtar Annaba University Central Library Copyright Elsevier 2025

[47] K.C. Barick, M. Aslam, Y.P. Lin, D. Bahadur, P.V. Prasad, V.P. Dravid, Novel and efficient MR active aqueouscolloidal Fe_3O_4 nanoassemblies, J. Mater. Chem. 19 (2009) 7023–7029.
[48] S. Laurent, D. Forge, M. Port, A. Roch, C. Robic, R.N. Muller, Magnetic iron oxide nanoparticles:synthesis, stabilization, vectorization, physicochemical characterizations, and biological applications, Chem. Rev. 108 (2008) 2064–2110.
[49] N. Neyaz, W.A. Siddiqui, K.K. Nair, Application of surface functionalized iron oxide nanomaterials as a nanosorbents in extraction of toxic heavy metals from ground water: a review, Int. J. Environ. Sci. 4 (2013) 472–483.
[50] G. Li, Z. Zhao, J. Liu, G. Jiang, Effective heavy metal removal from aqueous systems by thiol functionalized magnetic mesoporous silica, J. Hazard. Mater. 192 (2011) 277–283.
[51] S. Kumar, R.R. Nair, P.B. Pillai, S.N. Gupta, M.A.R. Iyengar, A.K. Sood, Graphene oxide-Mn Fe_2O_4 magnetic nanohybrides for efficient removal of Lead and Arsenic from water, ACS Appl. Mater. Interfaces 6 (20) (2014) 17426–17436.
[52] Q. Yuan, N. Li, Y. Chi, Effect of large pore size of multifunctional mesoporous microsphere on removal of heavy metal ions, J. Hazard. Mater. 254–255 (2013) 157–165.
[53] S. Zhang, Y. Zhang, J. Liu, Thiol modified Fe_3O_4@SiO_2 as a robust, high effective and recycling magnetic sorbent for mercury removal, Chem. Eng. J. 226 (2013) 30–38.
[54] J. Wang, S. Zheng, Y. Shao, J. Liu, Z. Xu, D. Zhu, Amino-functionalized Fe_3O_4@SiO_2 core-shell magnetic nanomaterial as a novel adsorbent for aqueous heavy metals removal, J. Colloid Interface Sci. 349 (2010) 293–299.
[55] S.H. Huang, D.H. Chen, Rapid removal of heavy metal cations and anions from aqueous solutions by an amino-functionalized magnetic nano-adsorbent, J. Hazard. Mater. 163 (2009) 174–179.
[56] Y. Tan, M. Chen, Y. Hao, High efficient removal of Pb(II) by amino-functionalized Fe_3O_4 magnetic nanoparticles, Chem. Eng. J. 191 (2012) 104–111.
[57] S. Singh, K.C. Barick, D. Bahadur, Surface engineered magnetic nanoparticles for removal of toxic metal ions and bacterial pathogens, J. Hazard. Mater. 192 (2011) 1539–1547.
[58] J.F. Liu, Z.S. Zhao, G.B. Jiang, Coating Fe_3O_4 magnetic nanoparticles with humic acid for high efficient removal of heavy metals in water, Environ. Sci. Technol. 42 (2008) 6949–6954.
[59] X. Xin, Q. Wei, J. Yang, et al., Highly efficient removal of heavy metal ions by amine-functionalized mesoporous Fe_3O_4 nanoparticles, Chem. Eng. J. 184 (2012) 132–140.
[60] H. Parham, B. Zargar, R. Shiralipour, Fast and efficient removal of mercury from water samples using magnetic iron oxide nanoparticles modified with 2-mercaptobenzothiazole, J. Hazard. Mater. 205–206 (2012) 94–100.
[61] T. Madrakian, A. Afkhami, M. Ahmadi, Simple in situ functionalizing magnetite nanoparticles by reactive blue-19 and their application to the effective removal of Pb^{2+} ions from water samples, Chemosphere 90 (2013) 542–547.
[62] L. Feng, M. Cao, X. Ma, Y. Zhu, C. Hu, Superparamagnetic high-surface-area Fe_3O_4 nanoparticles as adsorbents for arsenic removal, J. Hazard. Mater. 217–218 (2012) 439–446.
[63] M.R. Shishehbore, A. Afkhami, H. Bagheri, Salicylic acid functionalized silica-coated magnetite nanoparticles for solid phase extraction and preconcentration of some heavy metal ions from various real samples. Chem. Cent. J. 5 (1) (2011) 41, https://doi.org/10.1186/1752-153x-5-41.
[64] W. Yantasee, C.L. Warner, T. Sangvanich, R.S. Addleman, G.T. Carter, Removal of heavy metals from aqueous systems with thiol functionalized superparamagneticnanoparticles, Environ. Sci. Technol. 41 (2007) 5114–5119.
[65] N.C. Feitoza, M.S. Santos, J.C. Rubim, Fabrication of glycine-functionalized maghemite nanoparticles for magnetic removal of copper from wastewater, J. Hazard. Mater. 264 (2014) 153–160.
[66] P. Yuan, M. Fan, D. Yang, Montmorillonite-supported magnetite nanoparticles for the removal of hexavalent chromium [Cr (VI)] from aqueous solutions, J. Hazard. Mater. 166 (2009) 821–829.
[67] A.R. Mahdavian, M.A.S. Mirrahimi, Efficient separation of heavy metal cations by anchoring polyacrylic acid on superparamagnetic magnetite nanoparticles through surface modification, Chem. Eng. J. 159 (2010) 264–271.

This book belongs to Badji Mokhtar Annaba University Central Library Copyright Elsevier 2025

[68] A.E. Karatapanis, Y. Fiamegos, C.D. Stalikas, Silica-modified magnetic nanoparticles functionalized with cetylpyridinium bromide for the preconcentration of metals after complexation with 8-hydroxyquinoline, Talanta 84 (2011) 834–839.
[69] Z.F. Cao, X. Wen, J. Wang, F. Yang, H. Zhong, S. Wang, Z.K. Wu, In situ nano-Fe_3O_4/triisopropanolamine functionalized graphene oxide composites to enhance Pb^{+2} ions removal, Colloids Surf. A Physicochem. Eng. Asp. 561 (2019) 209–217.
[70] S. Zhang, H. Niu, Y. Cai, Arsenite and arsenate adsorption on coprecipitated bimetal oxide magnetic nanomaterials: $MnFe_2O_4$ and $CoFe_2O_4$, Chem. Eng. J. 158 (2010) 599–607.
[71] W. Tang, Y. Su, Q. Li, S. Gaoa, J.K. Shang, Mg-doping: a facile approach to impart enhanced arsenic adsorption performance and easy magnetic separation capability to α-Fe_2O_3 nanoadsorbents, J. Mater. Chem. A 1 (2013) 830–836.
[72] J. Hu, I.M.C. Lo, G.H. Chen, Fast removal and recovery of Cr (VI) using surface-modified jacobsite ($MnFe_2O_4$) nanoparticles, Langmuir 21 (2005) 11173–11179.
[73] C.L. Warner, L.V. Saraf, R.S. Addleman, Manganese doping of magnetic iron oxide nanoparticles: tailoring surface reactivity for a regenerable heavy metal sorbent, Langmuir 28 (2012) 3931–3937.
[74] X. Cai, Y. Gao, Q. Sun, Z. Chen, M. Megharaj, R. Naidu, Removal of co-contaminants Cu (II) and nitrate from aqueous solution using Kaolin-Fe/Ni nanoparticles, Chem. Eng. J. 244 (2014) 19–26.
[75] B. Saha, R. Bains, F. Greenwood, Physicochemical characterization of granular ferric hydroxide (GFH) for As(V) sorption from water, Sep. Sci. Technol. 40 (2005) 2909–2920.
[76] E.A. Deliyanni, D.N. Bakoyannakis, A.I. Zouboulis, K.A. Matis, Sorption of As(V) ion by akaganeite type nanocrystals, Chemosphere 50 (2003) 155–163.
[77] S. Singh, K.C. Barick, D. Bahadur, Fe_3O_4 embedded ZnO nanocomposites for the removal of toxic metal ions, organic dyes and bacterial pathogens, J. Mater. Chem. A 1 (2013) 3325–3333.
[78] E.J. Kim, C.S. Lee, Y.Y. Chang, Y.S. Chang, Hierarchically structured manganese oxide-coated magnetic nanocomposites for the efficient removal of heavy metal ions from aqueous systems, ACS Appl. Mater. Interface 19 (2013) 9628–9634.
[79] A. Mahapatra, B.G. Mishra, G. Hota, Electrospun Fe_2O_3-Al_2O_3 nanocomposite fibers as efficient adsorbent for removal of heavy metal ions from aqueous solution, J. Hazard. Mater. 258–259 (2013) 116–123.
[80] T. Basu, D. Nandi, P. Sen, U.C. Ghosh, Equilibrium modeling of As(III, V) sorption in the absence/presence of some groundwater occurring ions by iron(III)-cerium(IV) oxide nanoparticle agglomerates: a mechanistic approach of surface interaction, Chem. Eng. J. 228 (2013) 665–678.
[81] G. Zhang, Z. Ren, X. Zhang, J. Chen, Nanostructured iron(III)-copper(II) binary oxide: a novel adsorbent for enhanced arsenic removal from aqueous solutions, Water Res. 47 (2013) 4022–4031.
[82] C. Shan, M. Tong, Efficient removal of trace arsenite through oxidation and adsorption by magnetic nanoparticles modified with Fe-Mn binary oxide, Water Res. 47 (2013) 3411–3421.
[83] G. Zhang, Z. Ren, J. Chen, Adsorptive removal of arsenic from water by an iron-zirconium binary oxide adsorbent, J. Colloid Interface Sci. 358 (2011) 230–237.
[84] C. Wu, J. Tu, C. Tian, J. Geng, Z. Lin, Z. Dang, Defective magnesium ferrite nano-platelets for the adsorption of As (V): the role of surface hydroxyl groups, Environ. Pollut. 235 (2018) 11–19.
[85] F. Zhang, Z. Zhu, Z. Dong, Magnetically recoverable facile nanomaterials: synthesis, characterization and application in remediation of heavy metals, Microchem. J. 98 (2011) 328–333.
[86] S. Shin, J. Jang, Thiol containing polymer encapsulated magnetic nanoparticles as reusable and efficiently separable adsorbent for heavy metal ions, Chem. Commun. 41 (2007) 4230–4232.
[87] Y. Pang, G. Zeng, L. Tang, Preparation and application of stability enhanced magnetic nanoparticles for rapid removal of Cr(VI), Chem. Eng. J. 175 (2011) 222–227.
[88] J. Song, H. Kong, J. Jang, Adsorption of heavy metal ions from aqueous solution by polyrhodanine-encapsulated magnetic nanoparticles, J. Colloid Interface Sci. 359 (2011) 505–511.
[89] F. Zhang, J. Lan, Z. Zhao, Y. Yang, R. Tan, W. Song, Removal of heavy metal ions from aqueous solution using Fe_3O_4-SiO_2-poly-(1,2-diaminobenzene) core-shell sub-micron particles, J. Colloid Interface Sci. 387 (2012) 205–212.
[90] W. Jiang, X. Chen, Y. Niua, B. Pan, Spherical polystyrene-supported nano-Fe_3O_4 of high capacity and low-field separation for arsenate removal from water, J. Hazard. Mater. 243 (2012) 319–325.

This book belongs to Badji Mokhtar Annaba University Central Library Copyright Elsevier 2025

[91] J. Chang, Z. Zhaoxiang, X. Hong, Y. Zhong, C. Rizhi, Fabrication of poly(γ-glutamic acid)-coated Fe_3O_4 magnetic nanoparticles and their application in heavy metal removal, Chin. J. Chem. Eng. 21 (2013) 1244–1250.
[92] M. Zhang, Z. Zhang, Y. Liu, Preparation of core-shell magnetic ion-imprinted polymer for selective extraction of Pb(II) from environmental samples, Chem. Eng. J. 178 (2011) 443–450.
[93] A.Z.M. Badruddoza, Z.B. Shawon, W.J. Tay, K. Hidajat, M.S. Uddin, Fe_3O_4/cyclodextrin polymer nanocomposites for selective heavy metals from industrial wastewater, Carbohydr. Polym. 91 (2013) 322–332.
[94] F. Ge, M.M. Li, H. Ye, B.X. Zhao, Effective removal of heavy metal ions Cd^{2+}, Zn^{2+}, Pb^{2+}, Cu^{2+} from aqueous solution by polymer-modified magnetic nanoparticles, J. Hazard. Mater. 211–212 (2012) 366–372.
[95] X. Sun, L. Yang, H. Xing, Synthesis of polyethylenimine-functionalized poly(glycidyl methacrylate) magnetic microspheres and their excellent Cr (VI) ion removal properties, Chem. Eng. J. 234 (2013) 338–345.
[96] G. Chavez, K. Alves, Use of polypyrrole/γ-Fe_2O_3 magnetic nanocomposites for the removal of heavy metal ions from aqueous solutions, in: XIV SLAP Brazil, 2014.
[97] D. De, S.M. Mandal, S. Ram, S.K. Roy, J. Bhattacharya, Iron oxide nanoparticle-assisted arsenic removal from aqueous system, J. Environ. Sci. Health A Tox. Hazard. Subst. Environ. Eng. 44 (2009) 155–162.
[98] Z. Sarkar Khayyat, K.V. Sarkar, Removal of mercury (II) from wastewater by magnetic solid phase extraction with polyethylene glycol (PEG)-coated Fe_3O_4 nanoparticles, Int. J. Nanosci. Nanotechnol. 14 (1) (2018) 65–70.
[99] B. Samiey, C.H. Cheng, J. Wu, Organic-inorganic hybrid polymers as adsorbents for removal of heavy metal ions from solutions: a review, Materials 7 (2014) 673–726.
[100] M. Trojanowicz, Analytical applications of carbon nanotubes: a review, TrAC Trends Anal. Chem. 25 (2006) 480–489.
[101] K. Yang, L.Z. Zhu, B.S. Xing, Adsorption of polycyclic aromatic hydrocarbons by carbon nanomaterials, Environ. Sci. Technol. 40 (2006) 1855–1861.
[102] N.V. Perez-Aguilar, P.E. Diaz-Flores, J.R. Rangel-Mendez, The adsorption kinetics of cadmium by three different types of carbon nanotubes, J. Colloid Interface Sci. 364 (2011) 279–287.
[103] W.W. Tang, G.M. Zeng, J.L. Gong, Impact of humic/fulvic acid on the removal of heavy metals from aqueous solutions using nanomaterials: a review, Sci. Total Environ. 468–469 (2014) 1014–1027.
[104] S. Yang, Z. Guo, G. Sheng, X. Wang, Application of novel plasma-induced CD/MWCNT/ iron oxide composite in zinc decontamination, Carbohydr. Polym. 90 (2012) 1100–1105.
[105] S.F. Hasany, N.H. Abdurahman, A.R. Sunarti, A. Kumar, Non-covalent assembly of maghemite-multiwalled carbon nanotubes for efficient lead removal from aqueous solution. Aust. J. Chem. 66 (11) (2013) 1440, https://doi.org/10.1071/ch13281.
[106] V.K. Gupta, S. Agarwal, T.A. Saleh, Chromium removal by combining the magnetic properties of iron oxide with adsorption properties of carbon nanotubes, Water Res. 45 (2011) 2207–2212.
[107] L. Zhou, Y. Shao, H. Zhang, Development of carbon nanotubes/$CoFe_2O_4$ magnetic hybrid material for removal of tetrabromobisphenol A and Pb(II), J. Hazard. Mater. 265 (2014) 104–114.
[108] C. Zhang, J. Sui, J. Li, Y. Tang, W. Cai, Efficient removal of heavy metal ions by thiol-functionalized superparamagnetic carbon nanotubes, Chem. Eng. J. 210 (2012) 45–52.
[109] D. Xiao, H. Li, Adsorption performance of carboxylated multi-wall carbon nanotube-Fe_3O_4 magnetic hybrids for Cu(II) in water, New Carbon Mater. 29 (2014) 15–25.
[110] D. Cun-ku, L. Xin, Fe_3O_4 nanoparticles decorated multi-walled carbon nanotubes and their sorption properties, Chem. Res. Chin. Univ. 25 (2009) 936–940.
[111] M.A. Bavio, A.G. Lista, Synthesis and characterization of hybrid-magnetic nanoparticles and their application for removal of arsenic from groundwater, Sci. World J. 2013 (2013) 387458 7 pp.
[112] M.I. Qureshi, F. Patel, N. Al-Baghli, B. Abussaud, S. Tawabini Bassan, L. Tahar, A comparative study of raw and metal oxide impregnated carbon nanotubes for the adsorption of hexavalent chromium from aqueous solution, Bioinorg. Chem. Appl. 2017 (2017) 1624243.
[113] M. Zabihi, A. Ahmadpour, H.A. Asl, Removal of mercury from water by carbonaceous sorbents derived from walnut shell, J. Hazard. Mater. 167 (2009) 230–236.

This book belongs to Badji Mokhtar Annaba University Central Library Copyright Elsevier 2025

[114] S.M. Maliyekkal, K.P. Lisha, T. Pradeep, A novel cellulose-manganese oxide hybrid material by in situ soft chemical synthesis and its application for the removal of Pb(II) from water, J. Hazard. Mater. 181 (2010) 986–995.
[115] J.P. Ruparelia, S.P. Duttagupta, A.K. Chatterjee, S. Mukherji, Potential of carbon nanomaterials for removal of heavy metals from water, Desalination 232 (2008) 145–156.
[116] C.N.R. Rao, A.K. Sood, K.S. Subrahmanyam, A. Govindaraj, Graphene: the new two-dimensional nanomaterial, Angew. Chem. Int. Ed. Engl. 48 (42) (2009) 7752–7777.
[117] W.S. Hummers, R.E. Offeman, Preparation of graphitic oxide, J. Am. Chem. Soc. 80 (1958) 1339.
[118] M.J. McAllister, J.L. Li, D.H. Adamson, H.C. Schniepp, A.A. Abdala, J. Liu, M. Herrera-Alonso, D. L. Milius, R. Car, R.K. Prud'homme, I.A. Aksay, Single sheet functionalized graphene by oxidation and thermal expansion of graphite, Chem. Mater. 19 (2007) 396–4404.
[119] S. Stankovich, D.A. Dikin, G.H.B. Dommett, K.M. Kohlhaas, E.J. Zimney, E.A. Stach, R.D. Piner, S. T. Nguyen, R.S. Ruoff, Graphene-based composite materials, Nature 442 (2006) 282–286.
[120] X. Luo, C. Wang, S. Luo, R. Dong, X. Tu, G. Zeng, Adsorption of As(III) and As(V) from water using magnetite Fe_3O_4-reduced graphite oxide-MnO_2nanocomposites, Chem. Eng. J. 187 (2012) 45–52.
[121] J.H. Deng, X.R. Zhang, G.M. Zeng, Simultaneous removal of Cd(II) and ionic dyes from aqueous solution using magnetic graphene oxide nanocomposite as an adsorbent, Chem. Eng. J. 226 (2013) 189–200.
[122] L. Li, L. Fan, M. Sun, Adsorbent for chromium removal based on graphene oxide functionalized with magnetic cyclodextrin-chitosan, Colloids Surf. B Biointerfaces 107 (2013) 76–83.
[123] L. Zhou, H. Deng, J. Wan, J. Shi, T. Su, A solvothermal method to produce RGO-Fe_3O_4 hybrid composite for fast chromium removal from aqueous solution, Appl. Surf. Sci. 283 (2013) 1024–1031.
[124] G. Gollavelli, C.C. Chang, Y.C. Ling, Facile synthesis of smart magnetic graphene for safe drinking water: heavy metal removal and disinfection control, ACS Sustain. Chem. Eng. 1 (2013) 462–472.
[125] L. Li, G. Zhou, Z. Weng, X.Y. Shan, F. Li, Monolithic Fe_2O_3/graphene hybrid for highly efficiesnt lithium storage and arsenic removal, Carbon 67 (2014) 500–507.
[126] P. Zong, S. Wang, Y. Zhao, Synthesis and application of magnetic graphene/iron oxides composite for the removal of U(VI) from aqueous solutions, Chem. Eng. J. 220 (2013) 45–52.
[127] S. Debnath, A. Maity, K. Pillay, Magnetic chitosan-GO nanocomposite: synthesis, characterization and batch adsorber design for Cr(VI)removal, J. Environ. Chem. Eng. 2 (2014) 963–973.
[128] J. Zhu, R. Sadu, S. Wei, Magnetic graphene nanoplatelet composites toward arsenic removal, ECS J. Solid State Sci. Technol 1 (2012) 1–5.
[129] M. Sun, P. Li, X. Jin, J. Xingrong, W. Yan, J. Yuan, Heavy metal adsorption onto graphene oxide, amino group on magnetic nanoadsorbents and application for detection of Pb(II) by strip sensor, Food Agric. Immunol. 29 (1) (2018) 1053–1073.
[130] W. Fu, X. Wang, Z. Huang, Remarkable reusability of magnetic Fe_3O_4-encapsulated $C_3N_3S_3$ polymer/reduced graphene oxide composite: a highly effective adsorbent for Pb and Hg ions, Sci. Total Environ. 659 (2019) 895–904.
[131] A. Priyadharsan, V. Vasanthakumar, S. Shanavas, S. Karthikeyan, P.M. Ambarasan, Crumpled sheet like graphene based WO_3-Fe_2O_3 nanocomposites for enhanced charge transfer and solar photocatalysts for environmental remediation, Appl. Surf. Sci. 470 (2019) 114–128.
[132] K.K. Krishnani, S. Ayyappan, Heavy metals remediation of water using plants and lignocellulosic agrowastes, Rev. Environ. Contam. Toxicol. 188 (2006) 59–84.
[133] U.K. Garg, M.P. Kaur, V.K. Garg, D. Sud, Removal of hexavalent chromium from aqueous solution by agricultural waste biomass, J. Hazard. Mater. 140 (2007) 60–68.
[134] D.M. Borrok, J.B. Fein, The impact of ionic strength on the adsorption of protons, Pb, Cd, and Sr onto the surfaces of Gram negative bacteria: testing non-electrostatic, diffuse, and triple-layer models, J. Colloid Interface Sci. 286 (2005) 110–126.
[135] U. Farooq, J.A. Kozinski, M.A. Khan, M. Athar, Biosorption of heavy metal ions using wheat based biosorbents: a review of the recent literature, Bioresour. Technol. 101 (2010) 5043–5053.

This book belongs to Badji Mokhtar Annaba University Central Library Copyright Elsevier 2025

[136] S. Liang, X.Y. Guo, N.C. Feng, Q.H. Tian, Isotherms, kinetics and thermodynamic studies of adsorption of Cu^{2+} from aqueous solutions by Mg^{2+}, K^{+} type orange peel adsorbents, J. Hazard. Mater. 174 (2010) 756–762.
[137] X.C. Chen, G.C. Chen, L.G. Chen, Y.X. Chen, J. Lehmann, M.B. McBride, A.G. Hay, Adsorption of copper and zinc by biochars produced from pyrolysis of hardwood and corn straw in aqueous solution, Bioresour. Technol. 102 (2011) 8877–8884.
[138] S.S. Banerjee, D.H. Chen, Fast removal of copper ions by gum arabic modified magneticnano-adsorbent, J. Hazard. Mater. 147 (2007) 792–799.
[139] Y.T. Zhou, H.L. Nie, C. Branford-White, Z.Y. He, L.M. Zhu, Removal of Cu^{2+} from aqueous solution by chitosan-coated magnetic nanoparticles modified with α-ketoglutaric acid, J. Colloid Interface Sci. 330 (2009) 29–37.
[140] Y.C. Chang, D.H. Chen, Preparation and adsorption properties of monodisperse chitosan-bound Fe_3O_4 magnetic nanoparticles for removal of Cu(II) ions, J. Colloid Interface Sci. 283 (2005) 446–451.
[141] A.Z.M. Badruddoza, A.S.H. Tay, P.Y. Tan, K. Hidajat, M.S. Uddin, Carboxymethyl-β-cyclodextrin conjugated magnetic nanoparticles as nano-adsorbents for removal of copper ions: synthesis and adsorption studies, J. Hazard. Mater. 185 (2011) 1177–1186.
[142] J. Gong, L. Chen, G. Zeng, Shell ac-coated iron-oxide nanoparticles for removal of cadmium (II) ions from aqueous solution, J. Environ. Sci. 24 (2012) 1165–1173.
[143] X. Sun, L. Yang, Q. Li, Amino-functionalized magnetic cellulose nanocomposite as adsorbent for removal of Cr(VI): synthesis and adsorption studies, Chem. Eng. J. 241 (2014) 175–183.
[144] M. Xu, Y. Zhang, Z. Zhang, Study on the adsorption of Ca^{2+}, Cd^{2+} and Pb^{2+} by magnetic Fe_3O_4 yeast treated with EDTA dianhydride, Chem. Eng. J. 168 (2011) 737–745.
[145] X. Peng, F. Xu, W. Zhang, Magnetic Fe_3O_4@ silica-xanthan gum composites for aqueous removal and recovery of Pb^{2+}, Colloids Surf. A Physicochem. Eng. Asp. 443 (2014) 27–36.
[146] Y. Ren, H.A. Abbood, F. He, H. Peng, K. Huang, Magnetic EDTA-modified chitosan/SiO_2/Fe_3O_4 adsorbent: preparation, characterization, and application in heavy metal adsorption, Chem. Eng. J. 226 (2013) 300–311.
[147] J.L. Gong, X.Y. Wang, G.M. Zeng, Copper (II) removal by pectin-iron oxide magnetic nanocomposite adsorbent, Chem. Eng. J. 185–186 (2012) 100–107.
[148] P.S. Jassal, N. Chand, G. Sonal, S. Rajendra, Harnessing magnetic chitosan nanocomposites for the adsorption of heavy metal ions from aqueous medium, J. Water Resour. Hydraul. Eng. 4 (2) (2015) 191–197.
[149] D.A. Mbeh, R. Franca, Y. Merhi, X.F. Zhang, T. Veres, E. Sacher, L. Yahia, In vitro biocompatibility assessment of functionalized magnetite nanoparticles: biological and cytotoxicological effects, J. Biomed. Mater. Res. A 100 (2012) 1637–1646.
[150] R.A. Ortega, T.D. Giorgio, A mathematical model of superparamagnetic iron oxide nanoparticle magnetic behavior to guide the design of novel nanomaterials, J. Nanopart. Res. 14 (2012) 1282–1293.

This book belongs to Badji Mokhtar Annaba University Central Library Copyright Elsevier 2025

This page intentionally left blank

This book belongs to Badji Mokhtar Annaba University Central Library

Copyright Elsevier 2025

CHAPTER 29

Preparation of novel adsorbent (marble hydroxyapatite) from waste marble slurry for ground water treatment to remove fluoride

Suja George, Dhiraj Mehta, and Virendra Kumar Saharan

Department of Chemical Engineering, Malaviya National Institute of Technology, Jaipur, India

29.1 Introduction

Fluoride is one of the essential elements for human beings and its optimum concentration (1.5 mg/L) in water is important for the growth of bones and development of dental enamels. Higher concentrations (>1.5 mg/L) of fluoride cause severe health problems such as dental and skeletal fluorosis [1]. Because the surface water supplies are declining, groundwater is now a major water supply source, but problems can occur because of the presence of high concentrations of various minerals of natural occurrence such as arsenic, and fluoride, which cannot be ignored. Numerous technologies used for defluoridation of potable water such as ion exchange [2], electrocoagulation [3], nanofiltration [4], and membrane technology [5] are expensive or may not be considered for long-term usage. Therefore appropriate defluoridation method is needed to be applied for a sustainable solution to the problem [6]. The adsorption process is the most widely adopted defluoridation process because of its advantages over other methods such as effectiveness and involving low-cost easy operational techniques and therefore has been carried out utilizing various adsorbents of naturally occurrence such as calcite, limestone, marble waste powder (MWP), marble apatite, and hydroxyapatite (Hap).

Hap [$Ca_{10}(PO_4)_6(OH)_2$] is the natural form of the mineral calcium apatite that is present in human/animal bone and skeletal tissues. It has also been prepared synthetically by various researchers so that it can be used as an adsorbent for the removal of fluoride from water. Mehta et al. [7] produced Hap nanorods (55.6 nm), using calcium nitrate and potassium phosphate, which had an adsorption capacity of 1.49 mg/g at pH 7. Sundaram et al. [8] synthesized

Handbook of Nanomaterials for Wastewater Treatment. https://doi.org/10.1016/B978-0-12-821496-1.00030-1
Copyright © 2021 Elsevier Inc. All rights reserved.

This book belongs to Badji Mokhtar Annaba University Central Library Copyright Elsevier 2025

nano-Hap (200 nm) using calcium hydroxide slurry and orthophosphoric acid and used as an adsorbent for the removal of fluoride with the adsorption capacity of 1.845 mg/g at a pH of 3.0. Diverse forms of apatites such as synthesized nano-Haps were studied using different raw materials such as bone meal, treated bone meal, and rock phosphate by Gao et al. [9]. However, the quality of Hap material synthesized will depend upon the various process parameters maintained during synthesis such as reaction temperature, reagent addition, method of agitation, time required for aging, and pH. It has been observed that various precursors are required in the synthesis, which leads to severe aggregation, phase impurities, and increase in the cost of the product. An alternative is the synthesis of Hap using natural resources that are rich in calcium such as bone, fish scales, or marble waste.

The growth of marble processing industry has led to an increase in the generation of marble waste. Hence there is a need to look into its potential considering not a waste but as a possible resource that needs to be exploited by developing technically sound and financially viable technologies toward its total resource utilization. Some of the areas of utility of marble waste being explored include its utilization as filler materials for roads and embankments [10], manufacture of cements [11], bricks [12], ceramic tiles [13], sanitaryware products [14], production of concrete [15, 16], etc. However, an economically viable method of effective and complete utilization of marble waste is yet to be found because large amounts of the waste is still being generated everyday with the continuous growth of the marble industries.

The marble waste consists of recrystallized limestone, and its main constituents are calcium carbonate ($CaCO_3$), magnesium carbonate ($MgCO_3$), lime (CaO), and magnesium oxide (MgO), and some impurities in the form of silicates, hematite, and manganese oxide [17]. It has been reported that ground water resources in regions with marble quarries had very low fluoride content, which shows that marble is a natural defluoridating agent. Handa [18] stated that there is a negative correlation between fluoride and calcium concentrations in Indian groundwater. Many researchers report on moderate to good removal of fluoride by using different forms of calcium and magnesium as adsorbents.

Calcium present in MWP can be a good alternative, which can be used as raw material for the synthesis of Hap. Different techniques are used in the synthesis of Hap, which include the precipitation method, sol-gel method, hydrothermal precipitation, ultrasonication method (USM), etc. Among these techniques, the conventional precipitation (CM) technique is found to be the most attractive technique because of its simplicity and low costs involved in the synthesis of Hap. Several reports had published on the use of ultrasonic irradiation as a process intensification tool for various precipitation reactions, which has improved the product yield and decreased the process reaction time in the synthesis of Hap. The basic principle of ultrasonic irradiation is the generation of acoustic cavitations, which causes the sequential formation of millions of microscopic vapor bubbles and their growth and collapse in the liquid

This book belongs to Badji Mokhtar Annaba University Central Library Copyright Elsevier 2025

medium. During the collapse or implosion of these vapor bubbles/cavities, localized hot spots having high temperatures in the range of approx. 5000–10,000 K and high pressure of approx. 1000–2000 atm are created within the cold fluid [19]. These variations between the pressure and temperature stimulate fast chemical reactions and various physical effects, which affect the size, shape, and morphology of the synthesized materials [20]. These methods help to control the particle size and the morphology of Hap synthesized by simply changing the process conditions that regulated the particle nucleation, its aging, and the particle growth kinetics.

This study presents an innovative technique to prepare pure Hap using waste marble slurry powder obtained from the marble industries, which is otherwise a huge problem polluting the environment. A novel method has been developed to synthesize pure marble hydroxyapatite (MA-Hap) utilizing marble waste from CM and in combination with USM for its application in water defluoridation for drinking water treatment. Different characterization techniques were used to compare the MA-Hap synthesized using CM and USM. The study also presents batch and continuous defluoridation column experiments that were conducted for varying process parameters such as dosage, initial fluoride concentrations, pH, and contact time for batch processes and flow rate, particle sizes, and influent fluoride concentrations for column studies. The fluoride adsorption mechanism was studied by fitting various adsorption isotherm models and kinetic models that have been discussed.

29.2 Materials and methods

29.2.1 Materials

The analytical reagent grade chemicals were used for the synthesis of Hap, preparation of fluoride standard solution, and total ionic strength adjustment buffer (TISAB) buffer. All the sample and standard solutions had been prepared using deionized pure water (ultrapure water system, millipore). Potassium dihydrogen phosphate (KH_2PO_4) and ammonia solution (NH_4OH) (LobaChemie) were used for Hap synthesis. Calcium nitrate ($Ca(NO_3)_2$) used was prepared from MWP, which had been obtained as waste from the marble processing industries located in Kishangarh of Rajasthan, India. For defluoridation experiments, sodium fluoride was used in the preparation of the fluoride stock solution of 1000 mg/L, and it was diluted appropriately in the various batch experiments. TISAB added to the fluoride solutions was prepared using sodium chloride, cyclohexanedinitrilo-tetraacetic acid, and glacial acetic acid (AR grade), and the pH of the fluoride solutions was maintained with NaOH (5 M concentration) solution. All defluoridation experiments were specifically conducted in polypropylene labware so as to avoid leaching of any impurities into the fluoride sample solutions.

This book belongs to Badji Mokhtar Annaba University Central Library Copyright Elsevier 2025

29.2.2 Preparation of calcium nitrate using MWP

The MWP that comprises $CaMg(CO_3)_2$ and SiO_2, when subjected to calcination at 650°C and 850°C dissociated thermally and formed calcium carbonate ($CaCO_3$), magnesium oxide (MgO), and calcium oxide (CaO). The marble powder was washed well with deionized water and subjected to calcination at 650°C and 850°C in a muffle furnace for 2 h, while the calcination temperature was increased slowly at the rate of 20°C/min. The reaction that occured during calcination is given in Eqs. (29.1) and (29.2).

$$CaMg(CO_3)_2 \longrightarrow CaCO_3 + MgO + CO_2 \tag{29.1}$$

$$CaMg(CO_3)_2 \longrightarrow CaO + MgO + 2CO_2 \tag{29.2}$$

Weighed amount of calcined MWP was added slowly with regular stirring into the preheated solution of dilute nitric acid (0.64 M) to convert $CaCO_3$ and CaO to calcium nitrate ($Ca(NO_3)_2$), and the reaction that occured is as given in Eqs. (29.3) and (29.4), respectively:

$$CaCO_3 + 2HNO_3 \rightarrow Ca(NO_3)_2 + CO_2 + H_2O \tag{29.3}$$

$$CaO + 2HNO_3 \rightarrow Ca(NO_3)_2 + H_2O \tag{29.4}$$

The MWP was added until the calcium nitrate solution was formed along with the carbon dioxide formation, and further addition was stopped when no more bubbles of carbon dioxide were formed during mixing. The solution was cooled and filtered (using Whatman filter No. 42) to separate the filtrate. The unreacted waste, mostly consisting of unreacted silica obtained by filtration, was separated and characterized by X-ray diffraction (XRD) techniques so as to identify the impurities present in marble waste and to confirm their removal. The two filtrate solutions of $Ca(NO_3)_2$ obtained after the reactions with $CaCO_3$ and CaO was used for the synthesis of Hap separately, which has been named as MA-Hap 650 and MA-Hap 850, respectively, according to the calcination temperature of the marble waste.

29.2.3 Synthesis of MA-Hap

Hap was synthesized from calcium nitrate solution by both methods of CM and combination of precipitation with USM. The detailed methodology for the synthesis of Hap is given in the following sections.

29.2.3.1 Synthesis of MA-Hap using CM

The CM was used for the synthesis of Hap using MWP. The 0.32 M calcium nitrate solution obtained was used as the source of calcium. The solution of 0.19 M KH_2PO_4 was then added dropwise to the $Ca(NO_3)_2$ solution with constant stirring using a magnetic stirrer (Stirrer Model: 5 MLH, Make: Remi, India) with a controlled flow rate of 5 mL/min, as shown in Fig. 29.1. The temperature and solution pH during the reaction was maintained at 80 ± 5°C and 9.0, respectively, using NH_4OH solution during Hap synthesis. After the reaction was completed,

This book belongs to Badji Mokhtar Annaba University Central Library Copyright Elsevier 2025

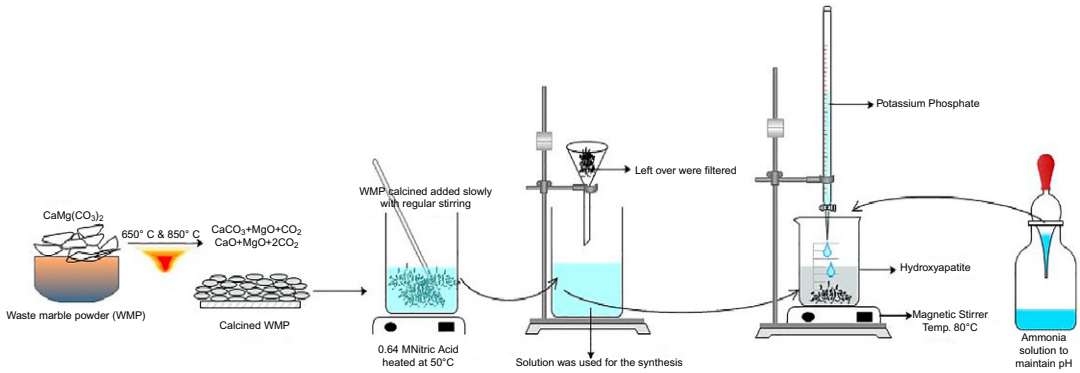

Fig. 29.1
Method of synthesis of marble hydroxyapatite (MA-Hap) by conventional CM method.

white and gelatinous precipitates of Hap was formed, which were aged for 12 h. The solution was centrifuged at an rpm of 2000–2500 rpm for 10 min. The obtained precipitate was washed with ultrapure water and thereafter filtered with Whatman No. 42 filter paper. The filtrate was then dried at 110°C and further crushed using mortar and pestle into fine powder, which was further sieved to obtain uniform particles with size corresponding to 200–250 British Standard Sieve (BSS). This was later used as the adsorbent for water defluoridation and named as MA-Hap 650 CM and MA-Hap 850 CM with respect to the calcination temperature of MWP. The adsorbents were characterized using various techniques such as scanning electron microscope (SEM), XRD, transmission electron microscopy (TEM)/EDS, Fourier transform infrared (FTIR), and thermogravimetric analysis (TGA)/differential thermal analysis (DTA), and a comparative analysis was carried out for all the adsorbents.

29.2.3.2 Synthesis of MA-Hap using USM

In the USM, 40 mL of the 0.32 M solution of $Ca(NO_3)_2$ was subjected to ultrasonication by using an ultrasonic horn (Make: Sonics, United States, operating frequency; 20 kHz and with a rated output power capacity of 750 W) at an amplitude of 40% for 30 min, which had a 30 s pulse and 5 s relaxation cycle along with dropwise addition of 0.19 M of 60 mL KH_2PO_4 solution, as shown in Fig. 29.2. After complete addition of KH_2PO_4, the solution was again ultrasonicated for further 15, 30, and 45 min by keeping the sonication parameters such as the amplitude and pulsation cycles constant (same as those used during mixing) to optimize the time required for the completion of the reaction of calcium nitrate with potassium dihydrogen phosphate to form Hap. After optimization of sonication time, the reaction temperature was maintained at a constant temperature of 80°C using hot plate and the pH at 9 by adding NH_4OH solution during the Hap synthesis in ultrasonication process. The remaining procedure in synthesis was the same as had been described in the earlier section.

This book belongs to Badji Mokhtar Annaba University Central Library Copyright Elsevier 2025

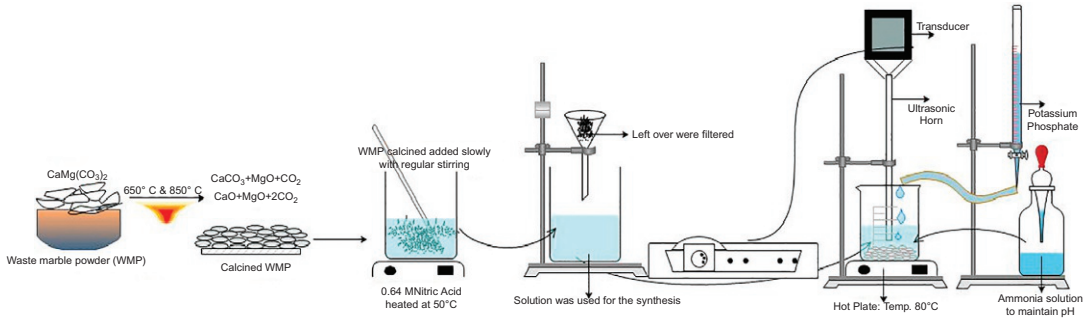

Fig. 29.2
Method of synthesis of marble hydroxyapatite (MA-Hap) using ultrasonication method.

29.2.4 Reaction scheme

The reaction scheme in the synthesis of Hap using calcium nitrate ($Ca(NO_3)_2$) derived from MWP and potassium phosphate (KH_2PO_4) with ammonia solution (NH_4OH) as the basic medium for maintaining the pH is as follows:

$$10Ca(NO_3)_2 + 6KH_2PO_4 + 20NH_4OH \rightarrow Ca_{10}(PO_4)_6(OH)_2 + 6KOH + 20NH_4NO_3 + 12H_2O \tag{29.5}$$

29.2.5 Characterization of MA-Hap

The adsorbents synthesized using CM and USM were characterized using the following techniques:

The FTIR spectra of Hap synthesized using MWP were recorded by using a Perkin Elmer Spectrum FTIR spectrophotometer using KBr powder, and the scanning wavelength range was 4000–400 cm^{-1}. XRD *(X'Pert Powder Panalytical, CuKα radiations)* was used to determine the phase analysis, effect of sonication time, and effect of ultrasonication during the synthesis of Hap. XRD patterns were recorded at 2θ angle between 10 and 80 degrees, with scan step time of 0.600 per s. Crystal size was determined using the Debye-Scherrer equation.

SEM of the conventionally and sonochemically synthesized Hap was carried out on a Nova Nano SEM 450 for evaluation of the surface morphology of the samples. Before SEM analysis, the samples were coated with a thin film of platinum using auto fine coater (JEOL/JFC1600) to increase the conductivity. TEM was performed with a Technai G2T20 coupled with energy-dispersive X-ray spectroscopy (X-flash 6TI30 Bruker). The samples were prepared by dispersing a very small amount in ethanol, which was further treated with ultrasonication (Buehler Ultramet) for obtaining a homogeneous dispersion.

This book belongs to Badji Mokhtar Annaba University Central Library Copyright Elsevier 2025

TGA and DTA were performed in a simultaneous TG-DTA (PerkinElmer STA6000) in the presence of nitrogen atmosphere from room temperature to 900°C, with heating rate of 20°C/min to study the thermal behavior and weight loss. The particle size distribution of the adsorbent was obtained using a Zeta sizer apparatus (JEN 5600, Malvern), with ethanol as the medium of dispersion.

29.2.6 Adsorption experiments

Multi ion analyzer (Thermo scientific Versa star Orion M93) with ion selective fluoride electrode BN 9609 (Orion, United States) was used for the quantitative analysis of fluoride, whereas the pH was measured with Orion Versa star pH meter. 250 mL PVC containers with 100 mL working volume were used in the batch adsorption studies, with known weight of adsorbent added into the fluoridated water of the desired concentrations, and were shaken at a speed of 200 ± 10 rpm and at a temperature of 303 ± 1 K. The effect of various parameters such as the adsorbent dosage, contact and equilibrium time, initial fluoride concentration, solution pH, and the effect of other co-ions on the fluoride removal capacity of MA-Hap 650 CM, MA-Hap 850 CM, and MA-Hap 650 USM were studied. The treated samples were filtrated with Whatman filter paper No. 42 on attainment of equilibrium. TISAB-II buffer solution added in the ratio of 1:1 was also used in the analysis of residual fluoride so as to eliminate any polyvalent cations that may be present and formed complexes with the fluoride ions in solution. The adsorption capacity (mg/g) and percentage fluoride removal were calculated using Eqs. (29.6) and (29.7), respectively:

$$q_e = \frac{C_a - C_b}{W_{ad}} \times V \tag{29.6}$$

$$\text{Fluoride removal}\,(\%) = \frac{C_a - C_b}{W_{ad}} \times 100 \tag{29.7}$$

where C_a and C_b are the initial and final equilibrium fluoride concentrations (mg/L), respectively, W_{ad} is the mass (g) of the adsorbent, V is the volume (L) of fluoride solution, and q_e is the equilibrium adsorption capacity (mg/g). The experiments were repeated twice to confirm for reproducibility of the analytical results obtained. The treated water quality parameters such as total dissolved solids (TDS), electrical conductivity, and dissolved calcium were analyzed using respective ion meters. The turbidity of the treated water was measured with a turbidity meter (NT4000, Spectra Lab). Other parameters such as the total hardness, total alkalinity, and concentration of residual magnesium and phosphorus in treated water were determined using standard APHA procedures. The point of zero charge (pH_{PZC}) of the adsorbent was measured by the solid addition method by adding 150 mg of adsorbent into 0.01 M NaCl, which acted as the background electrolyte, and the pH (2–12) adjustments were carried out either by addition of small quantities of diluted (0.01 M) HCl or NaOH.

This book belongs to Badji Mokhtar Annaba University Central Library Copyright Elsevier 2025

29.3 Results and discussion

29.3.1 Synthesis reaction and yield

The process time required for the synthesis of the conventionally precipitated (by CM) MA-Hap 650 CM and MA-Hap 850 CM was 240 min, whereas the process time required for synthesis of MA-Hap 650 USM using ultrasonication-assisted precipitation (USM) method was only 60 min (Table 29.1). The influence of acoustic cavitation was the apparent reason for the reduction in the synthesis time because of its effects such as rapid micromixing and enhanced mass transfer causing a faster reaction. The percentage yield was estimated on the basis of theoretical and the actual weight of the obtained dried product from the initial weight of the reagents. The product yield of both methods are given in Table 29.1, and it was observed that by using USM, the percentage yield of MA-Hap USM was 89.06%, which is higher when compared to CM with 78.90% yield in the synthesis of MA-Hap CM.

29.3.2 Characterization of MA-Hap

29.3.2.1 XRD analysis of unreacted MWP

During the addition of calcined MWP into preheated nitric acid solution, calcium present in marble waste reacted to form soluble calcium nitrate, but rest of the insoluble impurities settled down, which was filtered out to obtain pure calcium nitrate solution. The unreacted waste was characterized using XRD analysis as shown in Fig. 29.3, which also confirmed the removal of all impurities. The XRD analysis indicated the presence of major peaks of magnesium oxide and calcium magnesium silicate, which indicated that these compounds have remained unreacted as impurities and had been separated out from the solution. Magnesium silicate was also present as an impurity along with the other impurities. These XRD observations make a clear picture that most of the impurities present in the MWP remained unreacted, and a pure solution of calcium nitrate was obtained, which was used for the synthesis of Hap using both CM and USM.

29.3.2.2 FTIR analysis of MA-Hap

FTIR spectra of MA-Hap synthesized by both CM and ultrasonication-assisted precipitated methods are shown in Fig. 29.4. The formation of Hap was denoted by the phosphate band centered from about 1000 to 1100 cm^{-1}. Sharp narrow peaks in the range of 600 and 3500 cm^{-1}

Table 29.1: Reaction time and % yield in the synthesis of the marble hydroxyapatite.

Method	Product material	Reaction time (min)	Yield (%)
Conventional	MA-Hap 650 CM	240	78.90
Ultrasonication	MA-Hap 650 USM	60	89.06

This book belongs to Badji Mokhtar Annaba University Central Library
Copyright Elsevier 2025

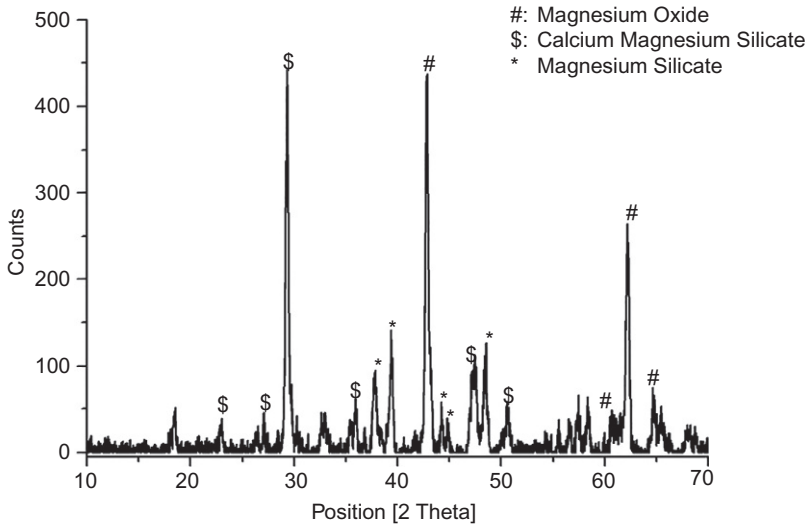

Fig. 29.3
XRD spectra of unreacted marble waste powder.

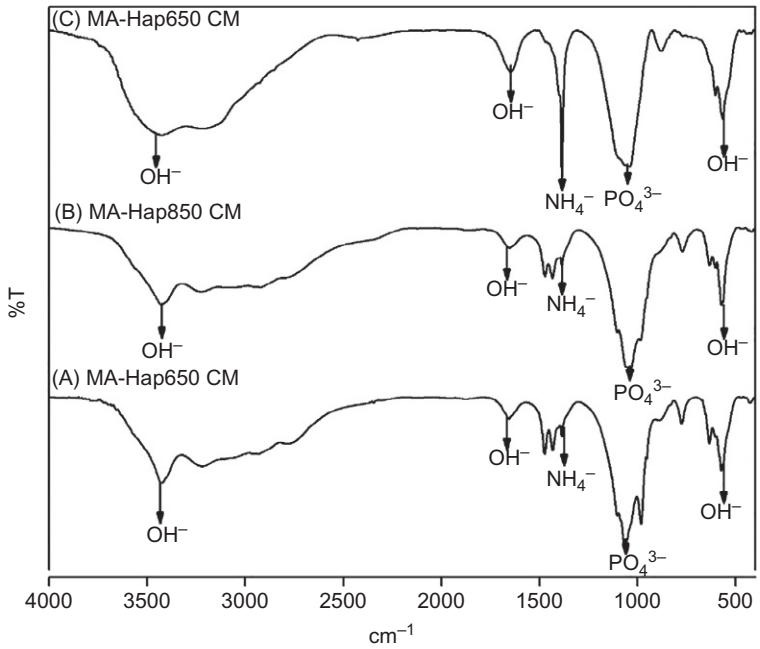

Fig. 29.4
FTIR spectra of marble hydroxyapatite synthesized using (A and B) CM (C) USM.

This book belongs to Badji Mokhtar Annaba University Central Library
Copyright Elsevier 2025

refer to structural OH– groups. Under the influence of thermal treatment, absorption band of physically adsorbed water becomes narrower as seen in Fig. 29.4A and B. In CM, the temperature was maintained at 80°C, and hence the bands are narrower when compared to MA-Hap synthesized using USM. The pH during the synthesis of Hap was maintained using ammonia solution; hence the characteristic peak at 1400 cm^{-1} corresponds to NH_4^- group. Similar characteristics peaks were observed in the FTIR spectra of MA-Hap 650 CM, MA-Hap 850 CM, and MA-Hap 650 USM. The presence of PO_4^{3-} and O—H group in FTIR spectra of MA-Hap synthesized using both CM and USM confirms that Hap was being formed, and further validation was done with XRD analysis.

29.3.2.3 XRD analysis of MA-Hap CM

XRD is primarily used for obtaining the phase identification and analyzing the average bulk composition of a material. The XRD patterns for the synthesis of MA-Hap 650 CM and MA-Hap 850 CM are shown in Fig. 29.5. The purity of Hap synthesized by utilizing calcium nitrate, which was prepared from MWP calcined at 650°C and 850°C was analyzed. It was observed that major peak in both the spectra were of Hap, and the identified phases of synthesized MA-Hap 650 CM and MA-Hap 850 CM exactly matched with the diffraction patterns of Hap with JCPDS card no. 00-001-1008. Fig. 29.5B depicts that MA-Hap 850 CM

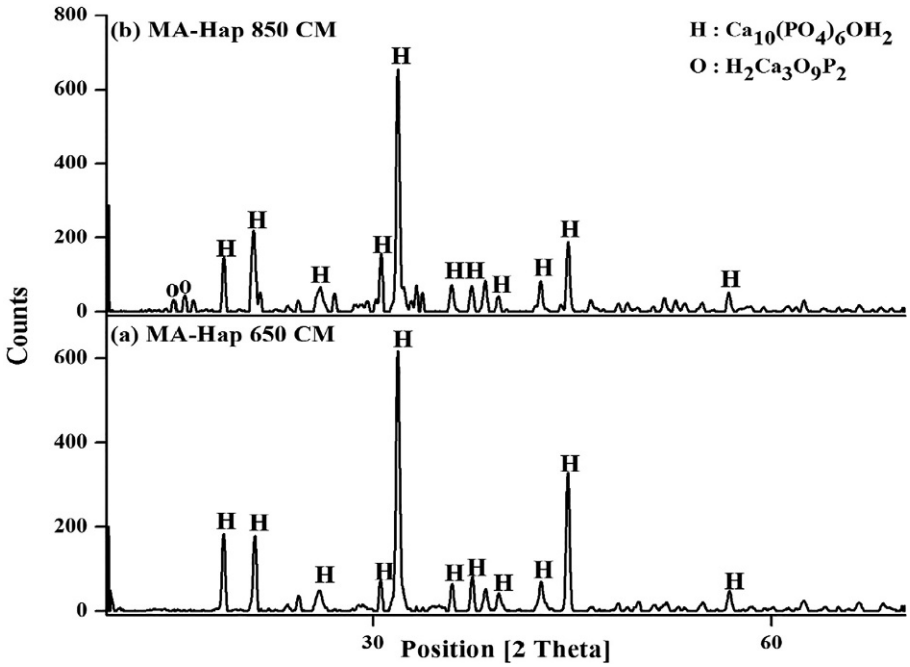

Fig. 29.5
XRD spectra of MA-Hap marble hydroxyapatite using CM when (A) MW calcined at 650°C (B) MW calcined at 850°C.

This book belongs to Badji Mokhtar Annaba University Central Library
Copyright Elsevier 2025

synthesized by CM had fewer intermediate phases of calcium phosphate hydrate (JCPDS card no. 00-015-0204), but the major peaks were of Hap. Whereas in XRD spectra of MA-Hap 650 CM, all the peaks were of Hap with no impurities, and no intermediates were observed, as seen in Fig. 29.5A. It was attributed from the results that calcium nitrate prepared from MWP calcined at 650°C and its utilization will result in pure Hap, and hence there is no further need of calcination. There was no major difference between the two products, that is, MA-Hap 650 CM and MA-Hap 850 CM other than the few intermediates; owing to this, MA-Hap 650 CM was taken into consideration for further studies.

29.3.2.4 XRD analysis of MA-Hap 650 USM

The XRD patterns of MA-Hap samples prepared by USM are shown in Fig. 29.6. USM was used for the synthesis of Hap, and the effect of sonication time on the synthesis of MA-Hap was analyzed. It was observed from the Fig. 29.6A that during the sonication for 45 min, the major peak was of Hap, but few of the intermediates were also formed, which can be attributed to the fact that owing to insufficient sonication time, the reaction was not completed, and hence intermediates were observed. As the sonication time was increased to 60 min, a comprehensive

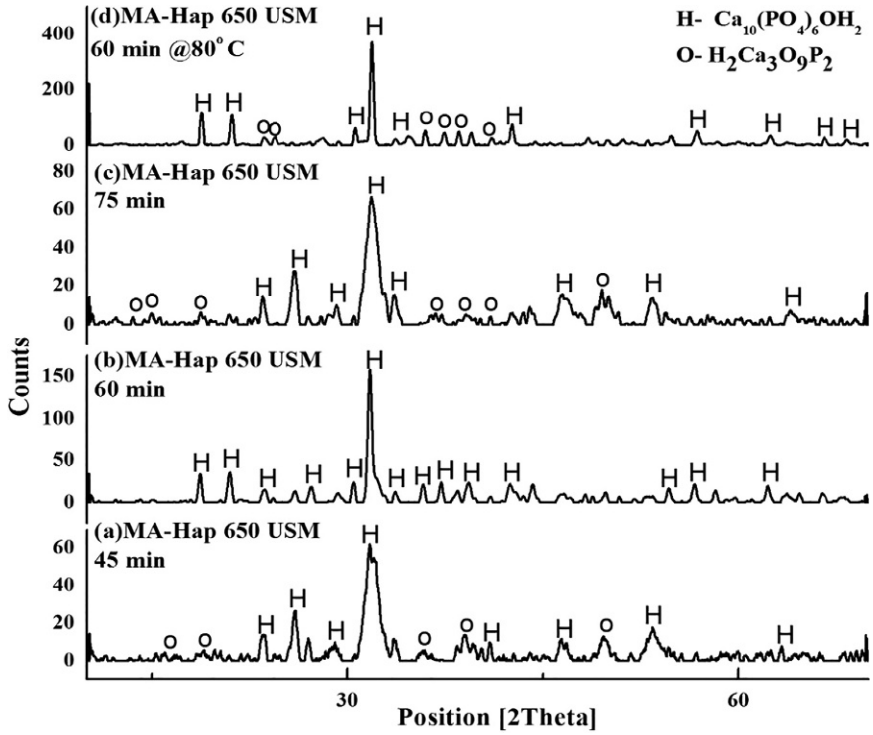

Fig. 29.6
XRD spectra of marble hydroxyapatite synthesized using USM at (A) 45 min (B) 60 min (C) 75 min (D) 60 min @ 80°C.

This book belongs to Badji Mokhtar Annaba University Central Library Copyright Elsevier 2025

phase transformation occurred because all the peaks matched with the diffraction patterns of Hap corresponding to JCPDS card no. 00-001-1008, and pure Hap was obtained as shown in Fig. 29.6B. This indicates the effectiveness of ultrasonication in the process, as with the increase in sonication time, the impact of sonication was efficient micromixing of the reactants, which enhanced the mass transfer and the speed of the reaction system. Acoustic cavitation also caused an increase in the effective surface area of the synthesized product, and resulted in the intensification of the chemical reaction, which primarily occured due to the improved mass transfer at molecular levels. It was observed from Fig. 29.6C that, beyond 60 min of sonication, few peaks of calcium phosphate hydrate were observed, which implies that excess sonication causes the breakdown of the material, and hence intermediates were formed.

In the ultrasonication-based synthesis method, during sonication, the temperature of the reaction material gradually increases. The initial temperature of the calcium nitrate solution used in the Ma-Hap synthesis is 50°C. This solution when sonicated for 40–75 min resulted in a gradual increase of temperature to 72°C. Because the sonication time for a constant reaction mass also decides the quality of Hap produced, initially, the time required for sonication during synthesis was optimized based on the quality of MA-Hap formed, which has been represented by the XRD patterns of MA-Hap for 40, 60, and 75 min of sonication, as given in Fig. 29.6A–C. The MA-Hap synthesis was also carried out by maintaining at a higher temperature of 80°C in the presence of ultrasonication, which was the temperature used for the CM in the preparation of MA-Hap 650 CM. The temperature of the reaction mixture was maintained at 80°C during the synthesis of MA-Hap 650 USM, and the XRD results are presented in Fig. 29.6D, and it was observed that along with the major peak of Hap, few intermediates were formed, which was attributed to the fact that at higher temperature, the magnitude of the cavity collapse would be high, which lead to the breakdown of the material. Therefore comparing the XRD spectra of Fig. 29.6A–D, it can be shown that 60 min of sonication time was only required during the synthesis, when the reaction mixture was initially at 50°C for the synthesis of MA-Hap 650 USM using USM because purer form of Hap was obtained.

29.3.2.5 Comparative XRD analysis of MA-Hap 650 CM and MA-Hap 650 USM

The comparative XRD analysis of MA-Hap 650 synthesized using both CM and USM is shown in Fig. 29.7, and it was observed that the XRD patterns of MA-Hap synthesized for both CM and USM matched with the diffraction pattern of pure Hap. However, there are differences in the crystallinity of the phases in the two products because peaks at different crystal planes match with each other. It was observed that because of ultrasonication, the crystallinity of the product decreased substantially. The CM-synthesized MA-Hap showed better crystallinity than MA-Hap synthesized by USM. This may be because of ultrasonication that facilitated faster reactions and had not allowed the crystal growth to occur fully. The increase in randomness of the Brownian motion of MA-Hap molecules because of high energy dissipation rate caused by

This book belongs to Badji Mokhtar Annaba University Central Library Copyright Elsevier 2025

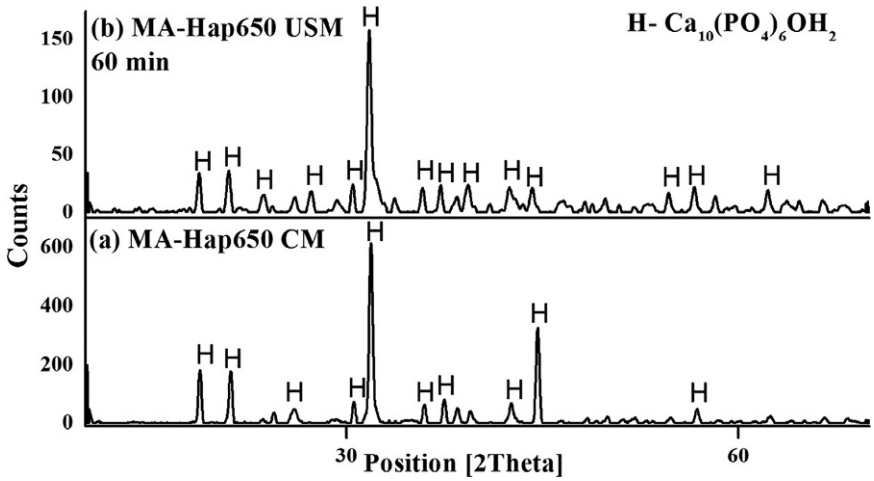

Fig. 29.7
Comparative analysis of marble hydroxyapatite synthesized from MW calcined at 650°C using (A) CM (B) USM.

Table 29.2: Mean crystallite size of MA-Hap synthesized using CM and USM.

Adsorbent	Wavelength (Å)	Peak width (degrees)	Peak position (degrees)	Crystallite size (nm)
MA-Hap 650 CM	1.54056	0.1181	31.8685	73.1
MA-Hap 650 USM	1.54056	0.3936	31.7376	21.93

cavitation did not allow regular crystal formation, which reduced the ability of the molecules to remain stable in its lattice plane, leading to the lowering of crystallinity. Moreover, ultrasonication prevented the particle agglomeration during the synthesis process so as to maintain an effective and uniform-sized distribution of Hap particles. The peak intensity of CM-synthesized MA-Hap is higher than the peak intensity of USM-synthesized MA-Hap as observed from Fig. 29.7A and B, clearly indicating the presence of larger crystals for CM-synthesized MA-Hap. Peak broadening in the case of USM-synthesized MA-Hap clearly indicated that small nanocrystals were present in the USM-synthesized MA-Hap samples.

The Debye-Scherer formula as shown in Eq. (29.8) was used to determine the mean crystallite size of MA-Hap synthesized using different methods, and their respective values are given in Table 29.2.

This book belongs to Badji Mokhtar Annaba University Central Library Copyright Elsevier 2025

$$D_P = \frac{0.94\lambda}{\beta_{1/2} \cos\theta} \tag{29.8}$$

It was found that the average crystallite size of the USM-synthesized MA-Hap was 21.93 nm, which was considerably lower than the MA-Hap (73.1 nm) synthesized conventionally (CM). This may be because of fact that as the crystallinity reduces, its crystallite size is also reduced.

29.3.2.6 SEM analysis

The SEM analysis provided the surface characteristics, morphology, and the crystallographic information of MA-Hap synthesized using CM and USM. The SEM micrographs of conventionally synthesized MA-Hap 650 and MA-Hap 850 at 200,000× magnification are shown in Fig. 29.8A and B, which indicate no major difference in the surface morphology of both products. This observation also supports the results obtained from XRD analysis. In both

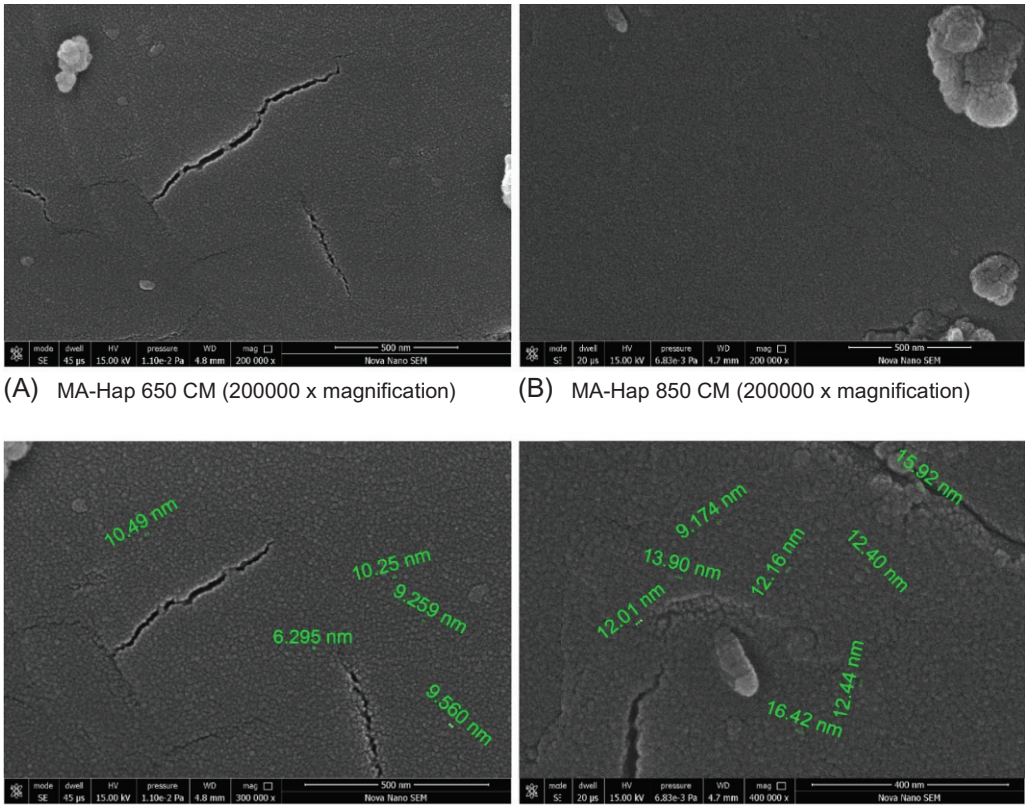

(A) MA-Hap 650 CM (200000 x magnification) (B) MA-Hap 850 CM (200000 x magnification)

(C) MA-Hap 650 CM (300000 x magnification) (D) MA-Hap 850 CM (400000 x magnification)

Fig. 29.8
SEM pictures of MA-Hap 650 CM (A and C) and MA-Hap 850 CM (B and D).

This book belongs to Badji Mokhtar Annaba University Central Library
Copyright Elsevier 2025

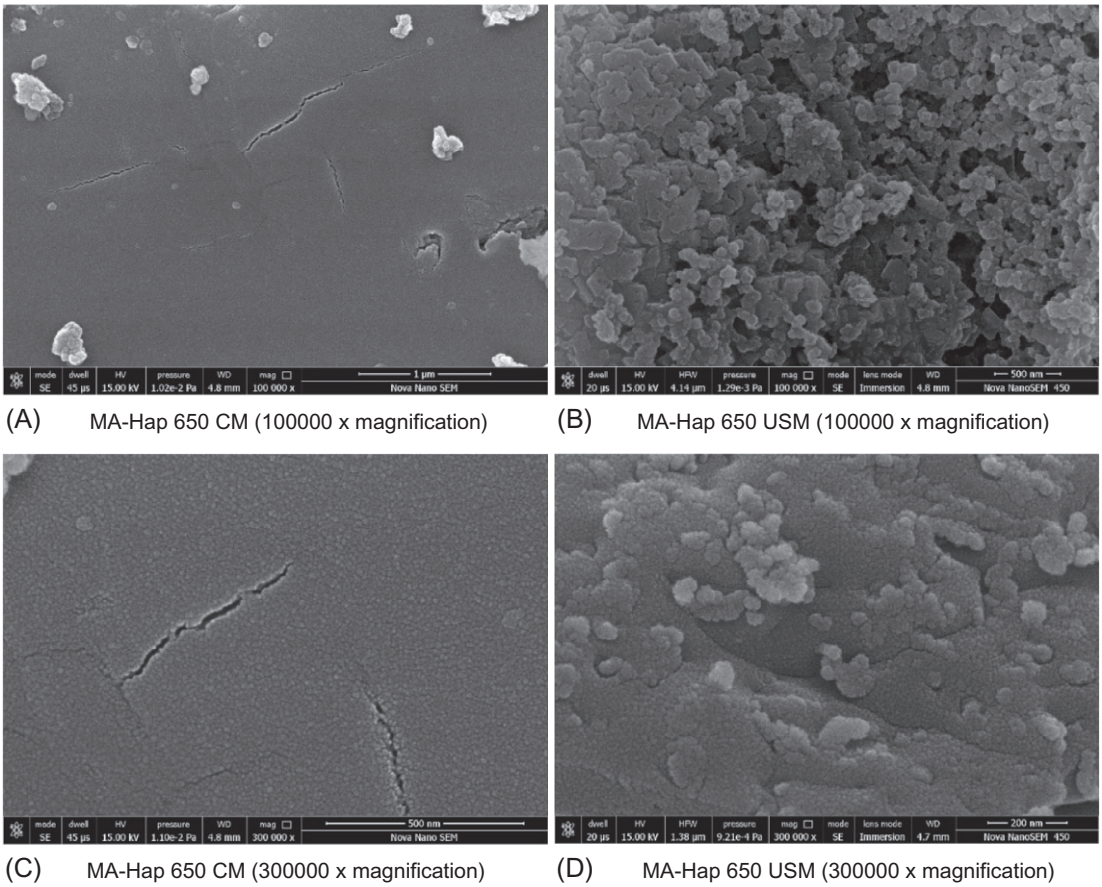

Fig. 29.9
SEM pictures of MA-Hap 650 CM (A and C) and MA-Hap 650 USM (B and D).

MA-Hap 650 CM and MA-Hap 850 CM, the particles were spherical in shape and uniformly distributed throughout the surface. In order to make a more clear observation, samples were analyzed upto their maximum magnification, that is, the spectra for MA-Hap 650 CM was analyzed up to 300,000 ×, whereas MA-Hap 850 CM was analyzed up to 400,000 × magnification, which is depicted in Fig. 29.8C and D, respectively. On higher magnification too, no difference between the surface morphology was observed.

The SEM spectra of MA-Hap synthesized using USM have also been compared with MA-Hap 650 CM synthesized conventionally at the same magnification of 100,000× (Fig. 29.9A and B). The USM-synthesized MA-Hap particles had comparatively smaller particle sizes as per the scale of SEM spectra and also considerably prominent spherical-shaped morphology. Both the low and high magnification SEM images of MA-Hap 650 USM (Fig. 29.9B and D) indicate the presence of uniform nanospherical-shaped and evenly dispersed particles when prepared by

This book belongs to Badji Mokhtar Annaba University Central Library Copyright Elsevier 2025

the ultrasonication approach. The influence of ultrasonication in reducing the particle sizes helped in improving the material properties such as increasing the effective surface area and in the formation of spherical and crystalline products. A more detailed analysis was done using TEM analysis for both the products.

29.3.2.7 TEM/EDS analysis

The TEM images of MA-Hap synthesized by CM and USM are reported in Fig. 29.10. It was observed from the TEM micrographs that needle-like morphology of MA-Hap was obtained when synthesized using CM and USM. The average length of the needles was observed to be around 6 nm (Fig. 29.10). There is significant reduction in size of the particles of MA-Hap 650 USM, as shown in Fig. 29.10B, when USM was used. Moreover, significant reduction in agglomeration was observed, which can be explained on the basis of the effects of ultrasonic irradiation, in which the particle size is controlled by smaller induction period and better control of the growth rate of crystal because of cavitation during chemical precipitation method [21].

The EDS spectra of MA-Hap 650 CM and MA-Hap 650 USM 60 min is shown in Fig. 29.11, respectively, to analyze the elemental composition of the material synthesized. It was observed that other than calcium and phosphorous, which are the primary reagents used for synthesis, no other impurities were present. Other than that, no impurities were present in the case of MA-Hap 650 CM and MA-Hap 650 USM 60 min; hence pure Hap was obtained using MWP from CM and USM.

29.3.2.8 TGA/DTA analysis

The TGA-DTA curves as shown in Fig. 29.12 indicate three occurrences of weight losses in the temperature ranges from 35°C to 102.59°C, 160.50°C to 309.32°C, and 613.59°C to 689.85°C. The DTA curve that corresponds to the endothermic peak at 102.59°C (weight loss 2.66%) is

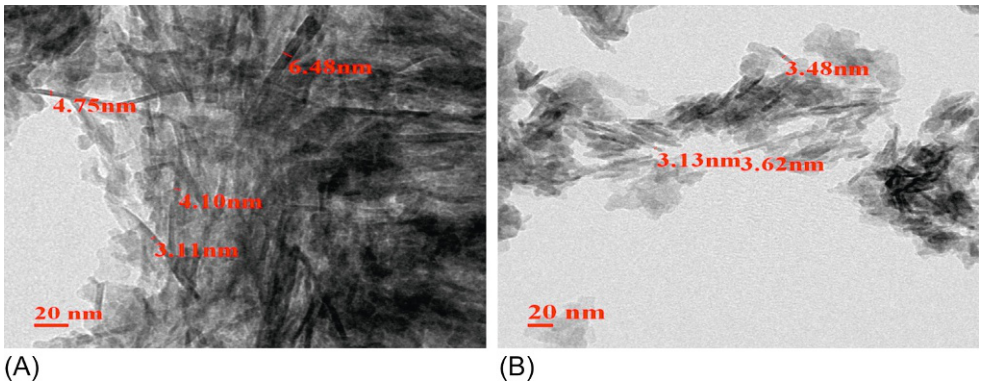

Fig. 29.10
TEM analysis magnification 20 nm (A) MA-Hap 650 CM, (B) MA-Hap 650 USM 60 min.

This book belongs to Badji Mokhtar Annaba University Central Library
Copyright Elsevier 2025

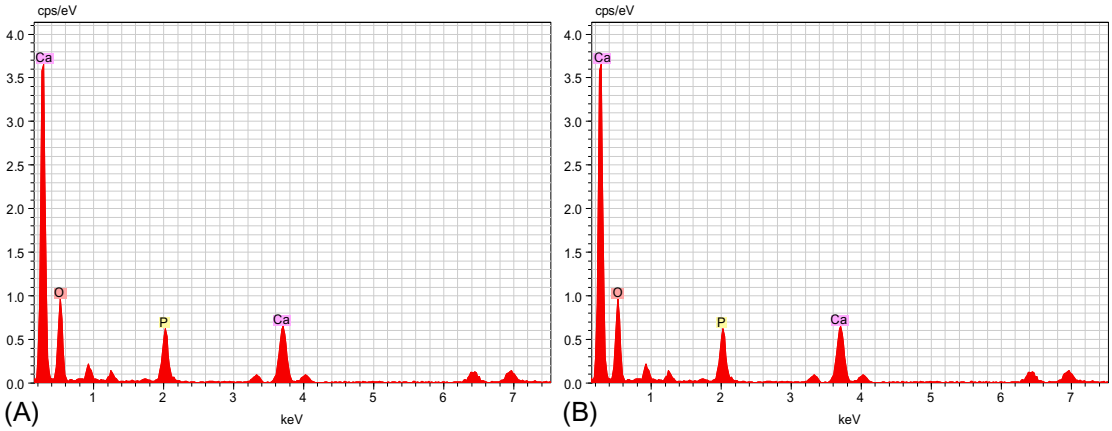

Fig. 29.11
EDS spectra of (A) MA-Hap 650 CM, (B) MA-Hap 650 USM 60.

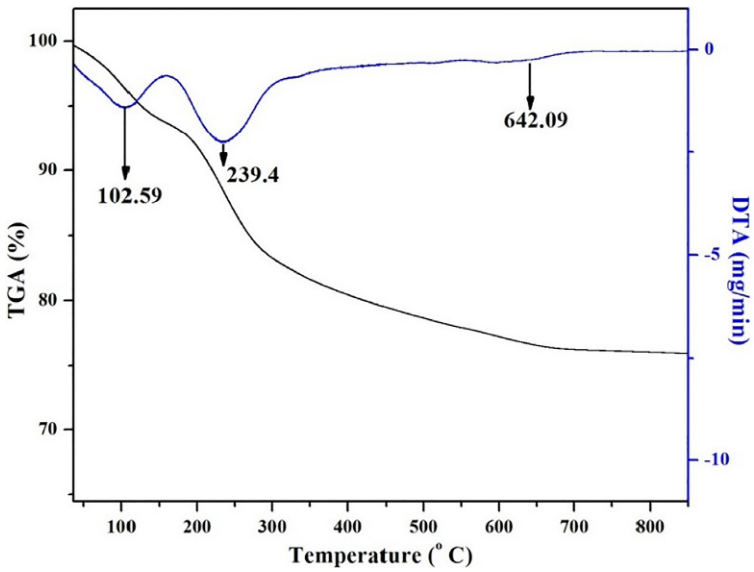

Fig. 29.12
TGA-DTA plot of marble hydroxyapatite.

because of the loss of surface water, and the peak at 239.4°C (weight loss 8.12%) is attributed to the conversion of hydrogen phosphates into pyrophosphates. The peak at 642.09°C (weight loss 7.47%), respectively, in the DTA curve is because at temperatures above 500°C, the structure of Hap had lost OH ions and gets converted to β-tricalcium phosphate. The results of TGA/DTA were comparable to that of pure Hap.

This book belongs to Badji Mokhtar Annaba University Central Library Copyright Elsevier 2025

29.3.2.9 Brunauer-Emmett-Teller surface area analysis

The Brunauer-Emmett-Teller (BET) surface area of MA-Hap 650 CM and MA-Hap 650 USM were 31.19 and 44.92 m^2/g, respectively. The increase in surface area of MA-Hap 650 USM was because of decrease in particle size after USM.

29.3.3 Batch defluoridation studies

The defluoridation experiments were carried out in batch studies using MA-Hap 650 CM, MA-Hap 850 CM, and MA-Hap 650 USM 60 min to check the removal efficiency of fluoride.

29.3.3.1 Effect of adsorbent dosage

To determine the optimum dosage for fluoride removal using MA-Hap, experiments were carried out with varying dosages from 0.5 to 12 g/L for treating an initial fluoride concentration of 10 mg/L for 120 min equilibrium time and are as depicted in Fig. 29.13. It has been observed that with an increase in adsorbent dosage, the percentage removal increased. In the case of MA-Hap 650 CM and MA-Hap 850 CM, dose was optimized to 7 g/L, whereas the dose was optimized to 5 g/L for MA-Hap 650 USM. The fluoride percentage removal was higher in case of MA-Hap 650 USM, that is, 95% of fluoride was removed with the capacity of 1.824 mg/g, whereas adsorption capacity decreased in case of MA-Hap 650 CM and MA-Hap 850 CM to 1.331 mg/g because the adsorbent dosage required to reduce the fluoride concentration within the permissible range (<1 mg/L) was higher. This can be attributed to the effectiveness of

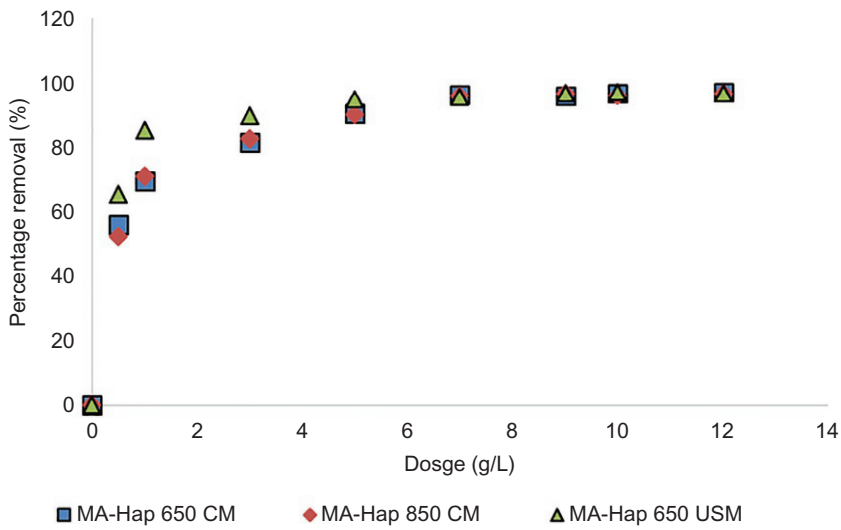

Fig. 29.13
Effect of adsorbent dose on percentage removal (initial F^- concentration: 10 mg/L, adsorbent dosage: 0.5–12 g/L, pH: 7, temperature: 30 ± 0.5°C, equilibrium time −120 min).

This book belongs to Badji Mokhtar Annaba University Central Library
Copyright Elsevier 2025

ultrasonication in particle size reduction of the adsorbent, which eventually increased the surface area, and hence the adsorption capacity was increased.

29.3.3.2 Effect of contact time

Adsorption being an equilibrium-driven process, the time required to approach equilibrium is important for effective defluoridation and proper design of adsorption equipment. The effect of contact time on the defluoridation potential of the adsorbents MA-Hap 650 CM, MA-Hap 850 CM, and MA-Hap 650 USM were determined by treating an initial fluoride concentration of 10 mg/L at 30 ± 0.5°C, pH 7, with agitation at 200 rpm upto 240 min and is as shown in Fig. 29.14. A faster removal rate of fluoride ions from the solution occurred in the initial 20–30 min (approx. 95% removal), indicating rapid adsorption rates during the initial phase, and thereafter, it became slower. It can be attributed to the fact that initially, all the adsorbent sites were vacant, and high solute concentration gradients between the adsorbent surface and the bulk solution concentration favored high mass transfer or adsorption onto the surface of the adsorbent. Adsorption equilibrium was attained around 120 min for the three adsorbents because the fluoride uptake by adsorbents remained unchanged due to exhaustion of adsorption sites and low concentration gradients between adsorbent surface concentration and bulk medium.

29.3.3.3 Effect of varying pH

The effect of pH on fluoride adsorption by MA-Hap synthesized using CM and USM is depicted in Fig. 29.15. The percentage fluoride adsorption was determined at various pH conditions ranging from 3 to 11. Maximum removal was observed at pH 7 for all the three

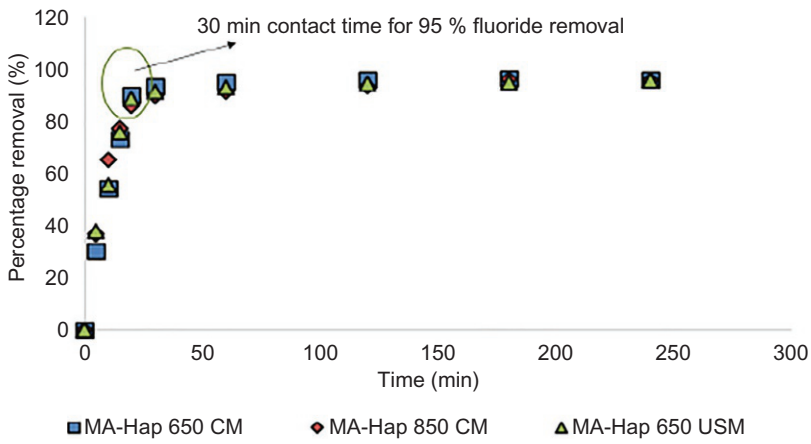

Fig. 29.14
Effect of contact time on percentage fluoride removal (initial F^- concentration: 10 mg/L, contact time: 15–240 min, dosage: 7 g/L (MA-Hap CM) and 5 g/L (MA-Hap USM), pH: 7, temperature: 30 ± 0.5°C).

This book belongs to Badji Mokhtar Annaba University Central Library Copyright Elsevier 2025

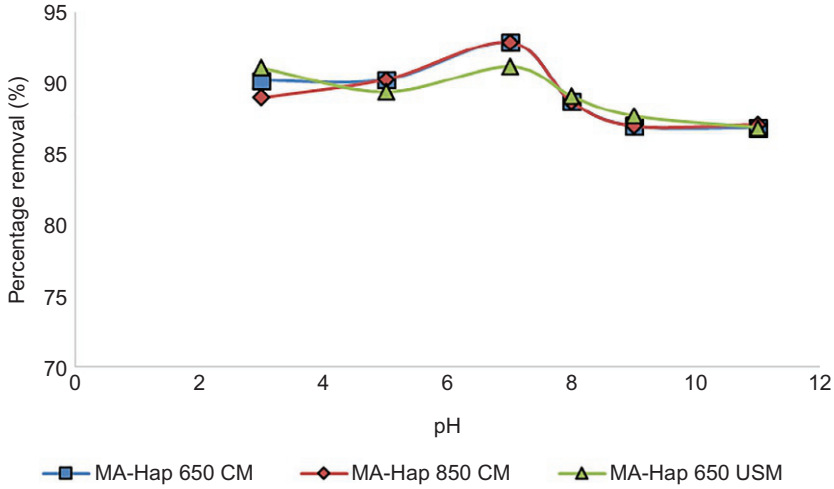

Fig. 29.15
Effect of pH on percentage fluoride removal (initial F^- concentration: 10 mg/L, contact time: 60 min (MA-Hap CM) and 30 min (MA-Hap USM), dose: 7 g/L (MA-Hap CM) and 5 g/L (MA-Hap USM), pH: 4–9, temperature: 30 ± 0.5°C).

adsorbents. In the acidic range (pH < 5), fluoride removal decreased, which may be because of the formation of weakly ionized hydrofluoric acid hindering adsorption. As the pH was increased beyond 7, fluoride removal also decreased, which may be because of the competition between F^- and OH^- ions for the active adsorbent sites. The surface zero charge (pH_{ZPC}) value determined for MA-Hap was found to be at 8, which indicates the pH at which net surface charge is neutral. Therefore for conditions when pH < pH_{ZPC} (8), the MA-Hap surfaces will be positively charged and hence will attract the negative fluoride ions, and therefore the maximum removal was observed at pH 7.

29.3.3.4 Effect of other co-ions

The fluoride removal efficiency of MA-Hap 650, MA-Hap 850 CM, and MA-Hap 650 USM in the presence of other competing ions such as nitrate, chloride, phosphate, sulfate, and bicarbonate were determined experimentally and presented in Fig. 29.16. The concentration of the individual anions studied was 100 mg/L along with the initial fluoride concentration of 10 mg/L. From Fig. 29.16, it can be observed that there was no significant influence on defluoridation capacity in the presence of different anions. Therefore it has been concluded that MA-Hap is an effective adsorbent for fluoride removal because any kind of interference from other anions commonly present in drinking water resources did not affect its adsorption capacity.

This book belongs to Badji Mokhtar Annaba University Central Library Copyright Elsevier 2025

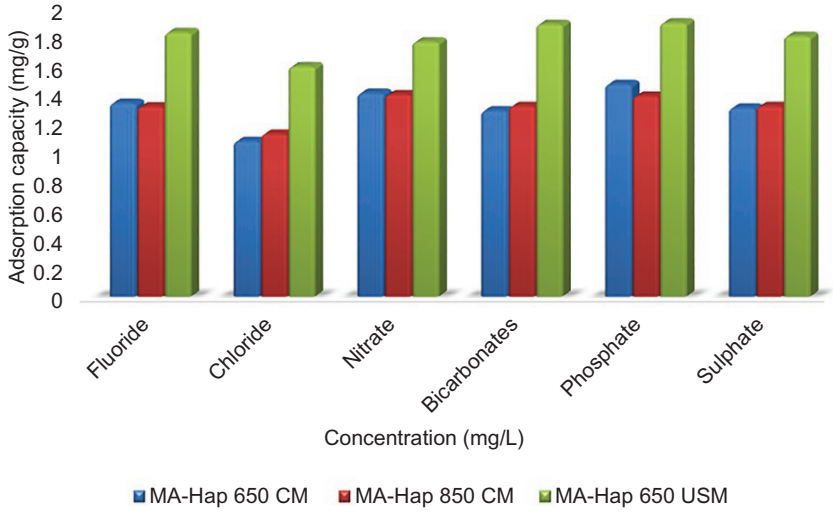

Fig. 29.16
Effect of co-ions on fluoride adsorption capacity (mg/g).

29.3.4 Adsorption equilibrium isotherms

The fluoride adsorption equilibrium was studied by fitting various adsorption isotherm models such as the Langmuir, Freundlich, Dubinin-Raduschkevich, and Temkin equilibrium models so as to obtain the best fit that will describe the relationship between the fluoride adsorption capacity on the adsorbent surface and the equilibrium fluoride concentration in the aqueous medium. The various isotherm constants determined by fitting the various equilibrium models are summarized in Table 29.3. The R^2 and χ^2 values were also determined in fitting these models with respect to both the MA-Hap adsorbents and their values are presented in the table. The experimental data fitted comparatively well with Langmuir isotherm model for both the adsorbents, which is evident from smaller χ^2 value and the R^2 values close to unity, which indicate homogeneous distribution of active sites on the adsorbents surface and monolayer adsorption. The Langmuir fluoride adsorption capacity for MA-Hap 650 CM and MA-Hap 650 USM was obtained at 3.137 and 4.557 mg/g, respectively.

29.3.5 Kinetics of adsorption

The fluoride adsorption kinetics that occur on the surface of MA-Hap 650 CM and MA-Hap 650 USM was studied by fitting various kinetic models such as the pseudo-first order, pseudo-second-order, and intraparticle diffusion models and verifying for their best fit on experimental data. The first- and second-order rate constants (K), R^2, and sum of squared error (SSE) values and adsorption capacity (q_e) values obtained by fitting the pseudo-first-order, pseudo-second-order, and intraparticle diffusion models are presented in Table 29.4.

This book belongs to Badji Mokhtar Annaba University Central Library Copyright Elsevier 2025

Table 29.3: Adsorption isotherm for defluoridation using MA-Hap 650 CM and MA-Hap 650 USM.

Isotherms	Parameters	MA-Hap 650 CM	MA-Hap 650 USM
	q_{exp}	1.331 mg/g	1.824 mg/g
Langmuir	q_{max} (mg/g)	3.137	4.559
	k (L/g)	0.877	1.462
	R^2	0.996	0.9907
	χ^2	0.27	0.025
Freundlich	$1/n$	0.4315	0.4602
	N	2.317	2.172
	k_F (mg/g)	1.28	1.7061
	R^2	0.9014	0.9199
	χ^2	0.011	0.003
Temkin	A_T (L/mg)	4.423	8.019
	B_T	1.5552	1.1109
	R^2	0.9773	0.9773
	χ^2	0.62	0.2
Dubinin-Raduschkevich	q_d (mg/g)	0.6404	0.5908
	B	-7E-08	-6E-08
	R^2	0.9361	0.8663
	χ^2	0.82	0.43

As mentioned earlier, higher correlation coefficient (R^2) values and lower values of SSE depict a better fit of the kinetic model. The R^2 value for the pseudo-second-order kinetic model was the highest for both MA-Hap 650 CM (0.9976) and MA-Hap 650 USM (0.999), with the least corresponding SSE value. Moreover, the theoretically estimated values of equilibrium capacity obtained from the pseudo-second order model fit were closer to the experimental values. Therefore it has been concluded that fluoride adsorption on MA-Hap derived from MWP followed pseudo-second-order adsorption kinetics, which imply that the mechanism of fluoride adsorption followed the chemisorption process.

29.3.6 Water quality parameters and regeneration

The treated water quality using MA-Hap 650 CM, MA-Hap 850 CM and MA-Hap 650 USM for defluoridation was analyzed in order to determine the feasibility of these adsorbents for practical drinking water treatment applications. The values of various drinking water parameters such as alkalinity, total hardness, calcium, TDS, and conductivity, before and after treatment were studied and observed to be within the permissible limit as given in Fig. 29.17. The pH of the water after treating with MA-Hap 650 CM, MA-Hap 850 CM, and MA-Hap 650 USM adsorbents were 7.12, 6.9, and 7.06, respectively. The conductivity of MA-Hap 650 CM, MA-Hap 850 CM, and MA-Hap 650 USM were 785, 935, and 712 μS/cm, respectively, while the permissible limit in drinking water is 2000 μS/cm.

This book belongs to Badji Mokhtar Annaba University Central Library
Copyright Elsevier 2025

This book belongs to Badji Mokhtar Annaba University Central Library

Table 29.4: Kinetic parameters for MA-Hap 650 CM & MA-Hap 650 USM adsorbent.

	Pseudo-first-order kinetics				Pseudo-second-order-kinetics				Intraparticle diffusion		
q_{exp} (mg/g)	K_1	q_e (mg/g)	R^2	SSE	K_2	q_e (mg/g)	R^2	SSE	R^2	K_i	SSE
MA-Hap 650 CM (1.331 mg/g)	0.472	19.63	0.7583	0.54	0.424	1.428	0.9976	2E-3	0.965	3.6193	0.18
MA-Hap 650 USM (1.824 mg/g)	0.167	2.4808	0.9065	0.12	1.949	1.9436	0.9992	1.34E-03	0.9213	2.6156	0.15

Copyright Elsevier 2025

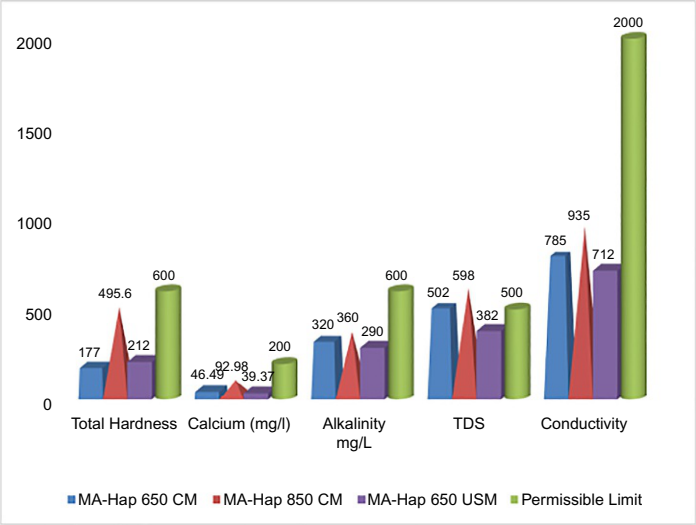

Water Quality Parameters	Before water treatment
pH	7.47
TDS (ppm)	33
Alkalinity (CaCO3) eqv: mg/L)	0
Turbidity (NTU)	<0.3
Total hardness (CaCO3) eqv: mg/L)	0
Calcium (mg/L)	0
Phosphate	0
Fluoride (mg/L)	10

Fig. 29.17
Treated water quality parameter analysis.

It was observed that treated water hardness in the case of MA-Hap 850 CM was 495.6 mg/L, which was higher than the other adsorbents but within the permissible limit (600 mg/L). The above results indicated that all the three synthesized adsorbents were suitable, but MA-Hap USM was the best adsorbent for treating fluoridated water because all the parameters were within permissible limits.

The regeneration and reutilization of used adsorbents is an important aspect of a cost-effective adsorption technology. Both the adsorbents MA-Hap 650 CM and MA-Hap 650 USM can be regenerated by treating with NaOH solution of concentration in the range of 1–1.5 M, where the adsorbed fluoride is removed as NaF. The adsorbent is further washed with deionized water and can be used for next defluoridation experiments. There is a 20% reduction in its adsorption capacity in the second defluoridation cycle and can be used up to three defluoridation cycles.

29.3.7 Energy efficacy of the MA-Hap synthesis methods

The energy efficacy of the two synthesis methods, that is, by CM and USM-assisted precipitation method for obtaining MA-Hap was estimated, and the calculations are described in Appendix. The energy utilized for the synthesis of MA-Hap has been described as the total energy supplied (kJ) per unit weight of the material processed/obtained (g). The process reaction time for the CM was 4 h, whereas for USM, it was 60 min. Therefore the total energy

This book belongs to Badji Mokhtar Annaba University Central Library
Copyright Elsevier 2025

required per unit weight of the MA-Hap material to synthesize MA-Hap CM and MA-Hap USM were obtained at 79.18 kJ/g and 774 J/g, respectively. Therefore among the two methods of synthesis, the USM-assisted approach proved to be the more energy-efficient method when compared to the CM.

29.3.8 Column studies using MA-Hap pellets

The synthesized MA-Hap powder was pelletized to produce pellets using PVA binder through extrusion-spheronization technique, and column studies were conducted for two different pellet sizes viz., 2–2.5 mm and 2.5–3 mm, with other column operational parameters at constant values such as flow rate at 1 LPH, bed height at 25 cm, and inlet fluoride concentration of 10 mg/L. The column performance indicators are the number of bed volumes (BV) treated before the breakthrough point and the adsorbent exhaustion rate (AER). The number of BV is estimated from Eq. (29.9).

$$\mathrm{BV} = \frac{\text{Treated water volume at breakthrough (L)}}{\text{Adsorbent bed volume (L)}} \tag{29.9}$$

The greater the number of BV before the breakthrough point, the better is the performance of the adsorption column system. The mass of adsorbent used per volume of solution treated at breakpoint can be called as AER, which indicates the performance efficiency of the column system. AER is calculated using Eq. (29.10)

$$\mathrm{AER}\ (\mathrm{g/L}) = \frac{\text{Mass of adsorbent (g)}}{\text{Volume of water treated (L)}} \tag{29.10}$$

The breakthrough curves obtained for the two different MA-Hap columns with two different particle sizes 2.0–2.5 mm and 2.5–3 mm are shown in Fig. 29.18. From the breakthrough curves, the column performance parameters were estimated and presented in Table 29.5.

It was observed that with the increase in particle size from 2.0–2.5 mm to 2.5–3 mm, the breakthrough time decreased considerably from 14 to 10 h, and breakthrough adsorption capacity decreased from 1.21 to 0.865 mg/g. This can be attributed that smaller particle sizes have higher interfacial surface area and therefore higher adsorption capacity, whereas large particle sizes have lesser surface area, and some of the interior pores are not accessible for adsorption, resulting in lower capacity and faster breakthrough point. Column 2 had a higher bed performance when used for treating fluoride concentration of 10 mg/L using a bed height of 25 cm with pellets of 2–2.5 mm sizes, at 1 LPH flow rate, and 28.5 BV were processed while the AER was lower at 7.4 g/L and the treated volume of water was 14 L. The AER value represented favorable adsorbent bed performance.

This book belongs to Badji Mokhtar Annaba University Central Library Copyright Elsevier 2025

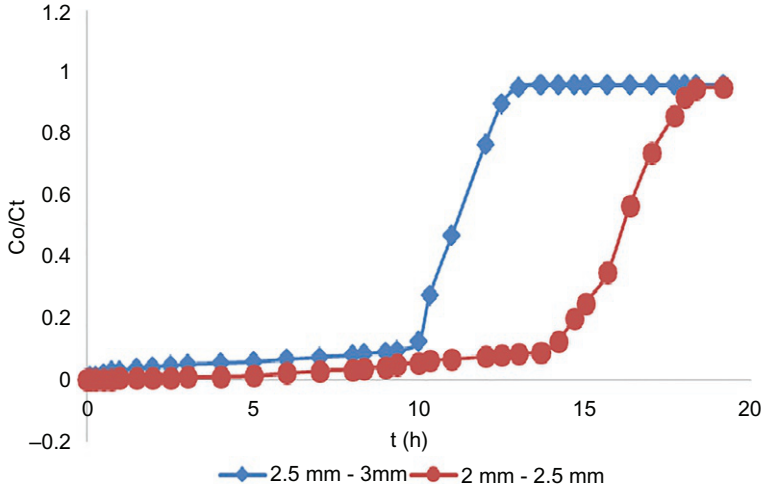

Fig. 29.18
Breakthrough curve for fluoride adsorption onto MA-Hap pellets of different pellet sizes (flow rate = 1 LPH, bed height = 25 cm, and initial fluoride concentration = 10 mg/L).

Table 29.5: Column breakthrough performances for different Ma-Hap pellet sizes.

Column operational parameters	Column 1	Column 2
Bed height (cm)	25	25
Flow rate (L/h)	1	1
Initial fluoride concentration) (mg/L)	10	10
Pellet size (mm)	2–2.5	2.5–3.0
Adsorption capacity at breakthrough (mg/g)	1.21	0.865
Adsorption capacity at exhaustion point (mg/g)	1.55	1.04
Breakthrough time (h)	14	10
Exhaustion time (h)	18	12
BV s processed	28.5	20.4
AER (g/L)	7.4	10.4

29.4 Conclusions

A method was successfully developed to synthesize pure Hap from waste marble slurry powder using the CM and ultrasonication-assisted precipitation method. MWP was calcined at 650°C and treated with preheated nitric acid in the preparation of calcium nitrate, which was used as calcium source for synthesis of MA-Hap. The required 240 min for process synthesis, which reduced to 60 min while using the ultrasonication-assisted approach, and the yield also

This book belongs to Badji Mokhtar Annaba University Central Library Copyright Elsevier 2025

increased from 81.90% to 89.06%. Moreover, XRD studies indicated that when ultrasonication was applied for 60 min, pure MA-Hap 650 USM was obtained with average crystallite size of 21.93 nm, which was much lower than that of MA-Hap 650 CM at 73.1 nm. The SEM morphology of both the adsorbents indicated spherical-shaped particles, whereas the TEM analysis depicted needle-shaped morphology with the average size of 6–10 nm. The BET surface area of MA-Hap 650 USM was 44.92 m^2/g, which was comparatively higher than that of MA-Hap 650 CM at 31.19 m^2/g. The higher surface area resulted in higher defluoridation capacity of MA-Hap 650 USM at 1.824 mg/g than that of MA-Hap 650 CM at 1.331 mg/g. The equilibrium adsorption isotherms and kinetics for both MA-Hap 650 CM and MA-Hap 650 USM followed Langmuir isotherm model and pseudo-second order kinetics. The treated water quality parameters studied were within the permissible drinking water ranges making MA-Hap 650 CM and MA-Hap 650 USM a potential adsorbent for drinking water applications. The adsorption column breakthrough performances of a MA-Hap adsorption bed using pellets of 2–2.5 mm sizes with bed height of 25 cm, and 1 LPH flow rate treating fluoride water of concentration of 10 mg/L indicated favorable bed performances processing 28.5 BV at an AER of 7.4 g/L, and the treated volume of water was 14 L. Hence this research study presents an easier and effective technique in utilizing the waste marble slurry powder from marble industries for the preparation of MA-Hap by the ultrasonication-assisted precipitation technique so as to utilize it as an adsorbent for defluoridation of drinking water. MA-Hap can be a good alternative to other adsorbents for defluoridation because it will lead to effective reuse of tons of marble waste generated and can be cost-effective and reduce the environmental threat of marble waste disposal.

Appendix

Energy calculations for marble hydroxyapatite (MA-Hap):

(i) **Energy delivered in USM**
- Sonication bath efficiency = 3% (estimated by calorimetric study).
- Energy dissipated by Ultrasonication horn = Power of horn × efficiency × process time = 750 (J/s) × (60 × 60) s × 0.03 = 81 kJ.
- Amount of solution processed in sonication horn = 104.57 g.
- Energy per unit mass of MA-Hap material (by ultrasonication) = Actual energy dissipated in sonication bath/weight of solution processed = 81/104.57 = 0.774 kJ/g.

(ii) **Energy delivered by CM**
- Magnetic stirrer voltage (input) (Model Remi, 5MLH) = 230 V.
- Supplied power = 230 V × 2.5 A = 575 W.
- Energy utilized by magnetic stirrer = 575 (J/s) × (4 × 3600) (s) = 8280 kJ.
- Energy per unit mass of MA-Hap material (stirring for 1 h) = 8280/104.57 = 79.18 kJ/g.

This book belongs to Badji Mokhtar Annaba University Central Library Copyright Elsevier 2025

(iii) **Energy saved** saved = (Total energy of CM − Total energy of USM) = (79.18–0.774) kJ/g = 78.406 kJ/g.

References

[1] H.G. Gorchev, G. Ozolins, WHO guidelines for drinking-water quality. WHO Chron. (2011), https://doi.org/10.1016/S1462-0758(00)00006-6.

[2] F. Durmaz, H. Kara, Y. Cengeloglu, M. Ersoz, Fluoride removal by Donnan dialysis with anion exchange membranes. Desalination 177 (2005) 51–57, https://doi.org/10.1016/j.desal.2004.11.016.

[3] Q. Zuo, X. Chen, W. Li, G. Chen, Combined electrocoagulation and electroflotation for removal of fluoride from drinking water. J. Hazard. Mater. 159 (2008) 452–457, https://doi.org/10.1016/j.jhazmat.2008.02.039.

[4] L.A. Richards, M. Vuachère, A.I. Schäfer, Impact of pH on the removal of fluoride, nitrate and boron by nanofiltration/reverse osmosis, Desalination 261 (3) (2010) 331–337.

[5] M. Arora, R.C. Maheshwari, S.K. Jain, A. Gupta, Use of membrane technology for potable water production. Desalination 170 (2004) 105–112, https://doi.org/10.1016/j.desal.2004.02.096.

[6] P. Mondal, S. George, Removal of fluoride from drinking water using novel adsorbent magnesia-hydroxyapatite. Water Air Soil Pollut. 226 (2015) 241, https://doi.org/10.1007/s11270-015-2515-2.

[7] D. Mehta, P. Mondal, V.K. Saharan, S. George, Synthesis of hydroxyapatite nanorods for application in water defluoridation and optimization of process variables: advantage of ultrasonication with precipitation method over conventional method. Ultrason. Sonochem. 37 (2017) 56–70, https://doi.org/10.1016/j.ultsonch.2016.12.035.

[8] C. Sairam Sundaram, N. Viswanathan, S. Meenakshi, Uptake of fluoride by nanohydroxyapatite/chitosan, a bioinorganic composite. Bioresour. Technol. 99 (2008) 8226–8230, https://doi.org/10.1016/j.biortech.2008.03.012.

[9] S. Gao, J. Cui, Z. Wei, Study on the fluoride adsorption of various apatite materials in aqueous solution. J. Fluor. Chem. 130 (2009) 1035–1041, https://doi.org/10.1016/j.jfluchem.2009.09.004.

[10] A.K. Misra, R. Mathur, Y.V. Rao, A.P. Singh, P. Goel, A new technology of marble slurry waste utilisation in roads, J. Sci. Ind. Res. 69 (2010) 67–72.

[11] H.Y. Aruntaş, M. Gürü, M. Dayi, I. Tekin, Utilization of waste marble dust as an additive in cement production. Mater. Des. 31 (2010) 4039–4042, https://doi.org/10.1016/j.matdes.2010.03.036.

[12] R.A. Hamza, S. El-Haggar, S. Khedr, Marble and granite waste: characterization and utilization in concrete bricks. Int. J. Biosci. Biochem. Bioinform. 21 (2011) 115–119, https://doi.org/10.7763/IJBBB.2011.V1.54.

[13] F. Saboya, G.C. Xavier, J. Alexandre, The use of the powder marble by-product to enhance the properties of brick ceramic. Construct. Build Mater. 21 (2007) 1950–1960, https://doi.org/10.1016/j.conbuildmat.2006.05.029.

[14] R. Anwar, H.R. Kamarun, V.V. Vermol, O.H. Hassan, Marble dust incorporate in standard local ceramic body as enhancement in sanitary ware products. in: 2011 IEEE Colloquium on Humanities, Science and Engineering, 2011, pp. 355–357, https://doi.org/10.1109/CHUSER.2011.6163750.

[15] A.A. Aliabdo, A.E.M. Abd Elmoaty, E.M. Auda, Re-use of waste marble dust in the production of cement and concrete. Construct. Build Mater. 50 (2014) 28–41, https://doi.org/10.1016/j.conbuildmat.2013.09.005.

[16] B. Demirel, The effect of the using waste marble dust as fine sand on the mechanical properties of the concrete. Int. J. Phys. Sci. 5 (2010) 1372–1380, https://doi.org/10.1016/j.envint.2006.11.003.

[17] P. Mondal, D. Mehta, S. George, Defluoridation studies with synthesized magnesium incorporated hydroxyapatite and parameter optimization using response surface methodology. Desalin. Water Treat. 3994 (2016) 1–20, https://doi.org/10.1080/19443994.2016.1167628.

[18] B.K. Handa, Geochemistry and genesis of fluoride-containing ground waters in India. Groundwater 13 (3) (1975) 275–281, https://doi.org/10.1111/j.1745-6584.1975.tb03086.x.

[19] W. Lauterborn, C.D. Ohl, Cavitation bubble dynamics, Ultrason. Sonochem. 4 (2) (1997) 65–75.

This book belongs to Badji Mokhtar Annaba University Central Library

Copyright Elsevier 2025

[20] C.A. Correa, J.A. De Sousa, Rubber particle size and cavitation process in high impact polystyrene blends, J. Mater. Sci. 32 (24) (1997) 6539–6547.
[21] W.R. Moser, O.V. Kozyuk, S.C. Emerson, I.M. Krausz, Worcester Polytechnic Institute, Method of Preparing Metal Containing Compounds Using Hydrodynamic Cavitation, (2002) U.S. Patent 6,365,555.

This book belongs to Badji Mokhtar Annaba University Central Library Copyright Elsevier 2025

This page intentionally left blank

This book belongs to Badji Mokhtar Annaba University Central Library

Copyright Elsevier 2025

CHAPTER 30

Nanocomposite/nanoparticle in membrane-based separation for water remediation: Case study

Fatemeh Bagri, Sedigheh Bazgir, and Yagoub Mansourpanah
Membrane Research Laboratory, Lorestan University, Khorramabad, Iran

30.1 Introduction

One of the most abundant natural resources on Earth is water. It is also essential for life of all people around of the world, but only about 1% of these resources are available for human consumption [1]. A significant issue in the water supply chain is ongoing pollution of fresh water resources via contaminants generated by human activities such as chemical waste generated during industrial, agricultural, and domestic activities and also natural contaminants present in water sources [2, 3]. Volatile organic solvents, heavy metals, pesticides, dyes, etc. are the most ordinary types of water contaminants [4]. So, due to the confined quantity of attainable freshwater, the demand to recycle and reuse is obligatory. To entirely remove the emerging pollutant and achieve strict water quality standards, the traditional procedures of treatment are not effective enough. Various technologies including adsorption, chemical precipitation, biological treatment, amalgamation, membrane separation, and ion exchange have been developed and adopted for separating waste materials from contaminated water and mitigating the problem of water pollution [2, 3, 5, 6]. Technology based on membrane is a powerful tool for desalination, wastewater reuse, and supply of potable and agricultural water applications [7, 8]. Compared with conventional process applied for water reclamation and purification, membranes offer economical alternatives that are fast, efficient by high capacity for removal, and also very flexible in terms of how they are used. Separation using membranes consumes lower amounts of energy, it can be done isothermally at lower temperatures, and also does not require additives to be used [9–11].

Membranes are defined as a barrier between two phases that act as a selective partition. The membrane filtration techniques are nanofiltration (NF), which concentrates organics by monovalent ion removal; reverse osmosis (RO), which concentrates solutions by eliminating

Handbook of Nanomaterials for Wastewater Treatment. https://doi.org/10.1016/B978-0-12-821496-1.00029-5
Copyright © 2021 Elsevier Inc. All rights reserved.

This book belongs to Badji Mokhtar Annaba University Central Library Copyright Elsevier 2025

water; microfiltration (MF), which removes bacteria; and ultrafiltration (UF), which concentrates macromolecules [4, 12]. Today, the most ordinary kind of membranes used for filtration are thin film composite (TFC) membranes. In general, TFC membranes are fabricated using a super-thin layer on top of a microporous substrate layer on the nonwoven support. In general, TFC membranes are comparatively inexpensive and show good rejection ratio in conjunction with good mechanical properties and are acceptably permeable. These membrane systems are made in a number of layers, with a support of nonwoven or with a layer formed of nanoscale pore sizes [13–16]. TFC membrane has been used to obtain about 80% improvement in water permeability with high salt rejection.

Among all membranes, polymeric membranes have attracted the most attention owing to its flexibility, chemical stability, and mechanical strength [13]. A useful membrane should be designed to have a stable and higher flux and lower purification pressure. Up to now, numerous studies have been performed to enhance the performance of membranes, including employing inorganic fillers on the surface of the membrane, covalent attachment of anti- (bio) fouling polymers, and physical adsorption/coating of the surface of the membrane. Since the material properties mainly limit the performance of membranes, adding inorganic nanofillers into the structure of polymeric membranes has been considered as an approach to make polymeric membranes more attractive to be commercialized. Membranes containing inorganic nanoparticles (NPs) in a polymer matrix are known as a mixed matrix membrane (MMM) in which both phases are present and have a positive mutual influence [17–20]. This chapter provides a short overview of the extension of MMMs, with a specific focus on the various kinds of most commonly used nanofillers incorporated to membrane materials to construct superior composite membranes for water treatment.

30.2 Nanostructures

30.2.1 Carbon nanomaterials

30.2.1.1 Graphene oxide

Many researchers have been concentrating on addition of graphene into various membranes. Incorporation of a small amount of graphene increases the efficiency of the membranes by some characteristics such as thickness, charge density, surface roughness, hydrophilicity, and pore structure [21]. Including reactive oxygen functional groups like epoxy, carboxylic acid, and hydroxyl moieties on its large surface, graphene oxide (GO) is a desired candidate for use in water treatment applications in comparison to pure graphene [22]. The deprotonation of GO functional groups that aggregate on top of the membrane surface will result in enhancement zeta potential. Therefore, the electrostatic interaction between charged particles and negatively charged membrane surface increases the contamination rejection [23, 24].

This book belongs to Badji Mokhtar Annaba University Central Library Copyright Elsevier 2025

In this part of the chapter, the introduction of GO into different membranes for water treatment is outlined.

Improvement of membrane properties such as hydrophilicity is of huge concern for its practical applications. Incorporation of a small amount of GO powder into polyvinyl chloride (PVC) membrane results in a substantial enhancement in mechanical stability, water flux, and hydrophilicity. The high efficiency of the modified membrane is due to excellent hydrophilicity of the functional group on the GO surface. After increasing the GO content, the water contact angle decreases resulting in further hydrophilicity [25]. As another example, by addition of a layer of GO on polysulfone (PSF) membranes, the surface hydrophilicity and antifouling capabilities of the hybrid membranes increase in comparison to net PSF membrane. The modified membrane is a suitable candidate for antifouling UF [26]. Membrane bioreactor (MBR) has potential for use in wastewater purification, but it suffers from membrane fouling. Adding a small amount of nanoplatelets of GO increases the hydrophilicity of the MBRs and suppresses the fouling problem [27]. Introduction of GO into polyvinylidene fluoride (PVDF) is a technique for increasing the antifouling performances through the improvement of membrane hydrophilicity [28]. The high hydrophilicity property of the GO-based membranes is caused by the presence of hydrophilic functional groups such as –COOH and –OH. These functional groups increase the affinity of the hybrid membranes in comparison to pristine membranes [25].

GO-based membranes are suitable for dye removal from wastewater. GO/polyethersulfone (PES) hybrid membrane had excellent capability to remove cationic dyes from wastewater. The absorption efficiency of GO is because of the large surface area and nature of its electric charge [22]. GO exhibits high removal efficiency of water pollutants, nevertheless the difficult fabrication and hard gathering of GO sheet in the adsorption procedure reduce their application. The hybrid GO/PES membrane not only solves the problem of difficult gathering of GO sheets, it also shows elective removal of cationic dyes from polluted water [29].

GO-based membranes also have high adsorption efficiency toward heavy metals from wastewater as it is not stable in aqueous solution because of electrostatic repulsion between GO nanosheets. This problem can be suppressed by interaction of GO with oxidized carbon nanotubes (CNTs). The hybrid GO/CNTs membranes are used to separate different heavy metals such as Cu(II), Zn(II), Co(II), Ni(II), Pb(II), and Cd(II). The fact the maximum adsorption capacity of the modified membrane decreases due to fabrication of micro- and nanochannels formed from the entangled CNTs increases the efficiency of the removal process [30]. GO is commonly a negatively charged nanosheet due to the existence of carboxyl, hydroxyl, and epoxy functional groups, and it has a zeta potential of −59 mV in neutral aqueous solution. By interpolation of GO into MMM, the modified membrane acquires more charged, hydrophilic, and permeable properties over the pristine MMM. The GO/MMM hybrid membrane has excellent absorption capacity of different heavy metals, namely Pb^{2+}, Cu^{2+}, Cd^{2+}, and Cr^{6+}. As depicted in Fig. 30.1, as concentration of GO is increased, the zeta potential enhanced from

This book belongs to Badji Mokhtar Annaba University Central Library Copyright Elsevier 2025

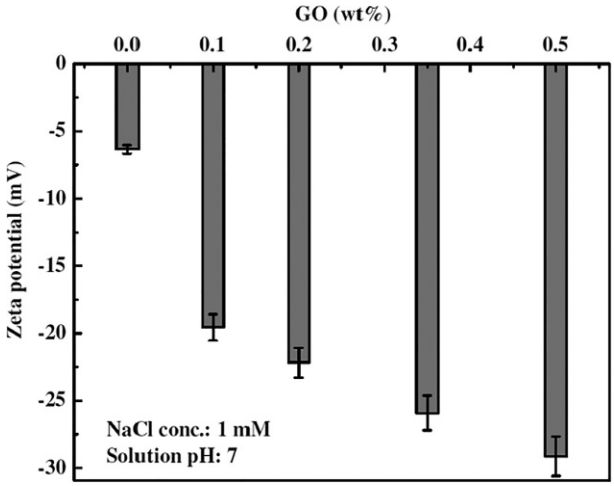

Fig. 30.1
Dependence of membrane zeta potential to GO concentration. *Adapted from R. Mukherjee, P. Bhunia, S. De, Impact of graphene oxide on removal of heavy metals using mixed matrix membrane, Chem. Eng. J. 292 (2016) 284–297.*

almost −6 to −29 mV. This enhancement contributes to the deprotonation of GO functional groups that gather on the top of the membrane surface. The attractive electrostatic force between ions and negatively charged membrane surface causes the ion rejection [23].

The adsorption capabilities in conjunction with durability and reusability of GO/cellulose membranes make them an appropriate candidate to remove heavy metals such as lead, copper, cobalt, cadmium, zinc, and nickel ions. The modified membrane can be employed in separation of heavy metal ions from aqueous solution because of the appropriate negatively charged surface and excellent stability in basic solutions [31].

The GO-base membranes can be used to remove organic materials and heavy metals at the same time. For example, the polydopamine (PDA)/GO membrane exhibits efficient adsorption and UF properties at the same time. Thus, it is used for simultaneous rejection of organic molecules and adsorption of heavy metals [32]. Furthermore, GO-based membranes are also appropriate candidates toward removal of organic materials from wastewater. The PSF membranes are suitable for water treatment due to their high thermal stability and chemical resistance, but this type of membrane has low filtration properties due to low water flux and weak antifouling property. The addition of GO hydrophilic inorganic particles into the structure of these membranes can settle these problems. The modified membranes can be used to efficiently remove methylene blue (MB) from the aqueous flow [33]. As another example, the PES/GO membranes shows higher water flux, enhanced fouling resistance, and more rejection of organic matter in comparison to pristine PES. The efficiency of the hybrid membranes is because of the generation of more hydrophilic and negatively charged PES/GO nanocomposite membranes [34].

This book belongs to Badji Mokhtar Annaba University Central Library Copyright Elsevier 2025

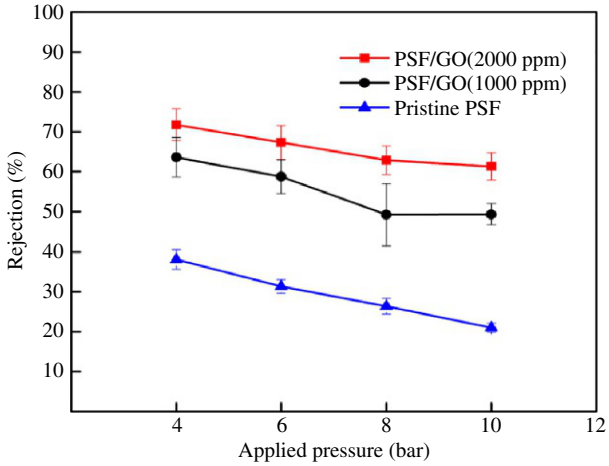

Fig. 30.2

Na_2SO_4 rejection at different operating conditions and GO/PSF combinations. *Adapted from B. Ganesh, A.M. Isloor, A.F. Ismail, Enhanced hydrophilicity and salt rejection study of graphene oxide-polysulfone mixed matrix membrane, Desalination 313 (2013) 199–207.*

Incorporation of GO is also a technique for water desalination. For example, GO/polyamide (PA) membranes can be used for salt rejection from water due to better flux and antifouling resistance in comparison to pure PA [35]. As another example, the GO/PSF membranes with high hydrophilicity and water flux exhibit high salt rejection in comparison to pristine PSF. As illustrated in Fig. 30.2, 2000 ppm GO-doped membrane shows maximum salt rejection of 72% for 1000 ppm Na_2SO_4 solution at 4 bar operating pressure [36]. GO nanosheets can be applied on the membrane surface due to their large aspect ratio and 2D structures. GO/polyethylenimine (PEI) hybrid membranes can be fabricated using layer-by-layer self-assembly method. As shown in Fig. 30.3, the membrane shows high rejection of 93.9% for $MgCl_2$ [37]. The hybrid polypiperazine-amide (PPA)/GO membranes have a water flux 1.4 times than that of the net PPA. These modified membranes can be employed for different salt rejections in the order of $Na_2SO_4 > MgSO_4 > NaCl > MgCl_2$. Furthermore, PPA/GO hybrid membranes exhibit outstanding antifouling resistance because of the enhancement of the hydrophilicity and decrement of the roughness caused by GO nanosheets [38]. Creating a balance between salt rejection and water flux is the most important problem in employing TFC in water softening. Incorporation of GO into PSF membranes has the potential to surpass this problem by increasing water flux and salt rejection. The GO/PSF hybrid membranes show higher water flux, salt solution permeability, and salt rejection. The salt rejection toward Na_2SO_4, $MgSO_4$, $MgCl_2$, and NaCl can be 95.2%, 91.1%, 62.1%, and 59.5%, respectively [39].

Incorporation of GO into different membranes is also a technique for oil/water separation. There are some problems such as wetting behavior and thermal and mechanical stability in

This book belongs to Badji Mokhtar Annaba University Central Library Copyright Elsevier 2025

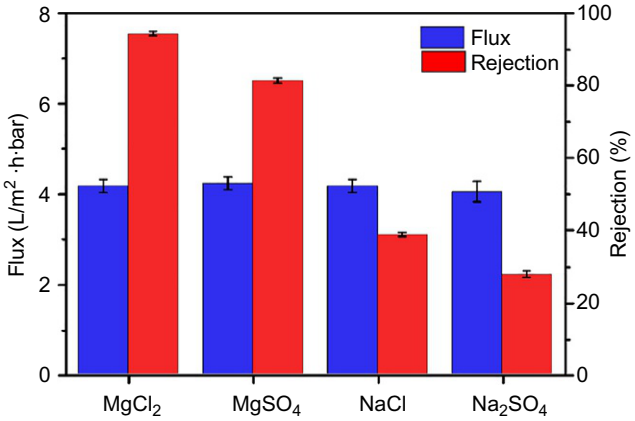

Fig. 30.3

Rejection of different salts for GO/PEI membranes. *Adapted from Q. Nan, P. Li, B. Cao, Fabrication of positively charged nanofiltration membrane via the layer-by-layer assembly of graphene oxide and polyethylenimine for desalination, Appl. Surf. Sci. 387 (2016) 521–528.*

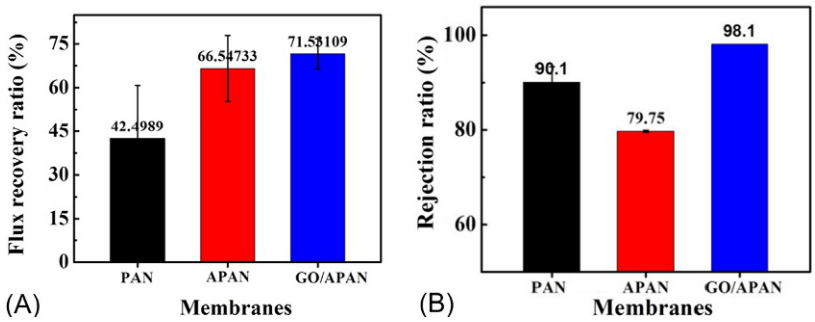

Fig. 30.4

(A) Flux recovery and (B) rejection ratio for different membranes. *Adapted from J. Zhang, Q. Xue, X. Pan, Y. Jin, W. Lu, D. Ding, Q. Guo, Graphene oxide/polyacrylonitrile fiber hierarchical-structured membrane for ultra-fast microfiltration of oil-water emulsion, Chem. Eng. J. 307 (2017) 643–649.*

employing pristine membranes for oil/water separation [9]. For example, addition of GO into aminated polyacrylonitrile (APAN) results in high flux (Fig. 30.4A) and excellent rejection of more than 98% (Fig. 30.4B) in comparison to pristine polyacrylonitrile (PAN) and APAN for oil/water emulsion. The modified membrane also has promising antifouling resistance. The significant water flux is due to great size porosity of GO/APAN membrane, whereas the outstanding rejection ratio and antifouling property are because of the modification of smaller GO sheets on the APAN fibers and connection of larger GO to two or more APAN fibers. As a result, the modified membrane can be employed in practical industrial applications because of its extraordinary stability at a vast ranges of pH [40].

This book belongs to Badji Mokhtar Annaba University Central Library
Copyright Elsevier 2025

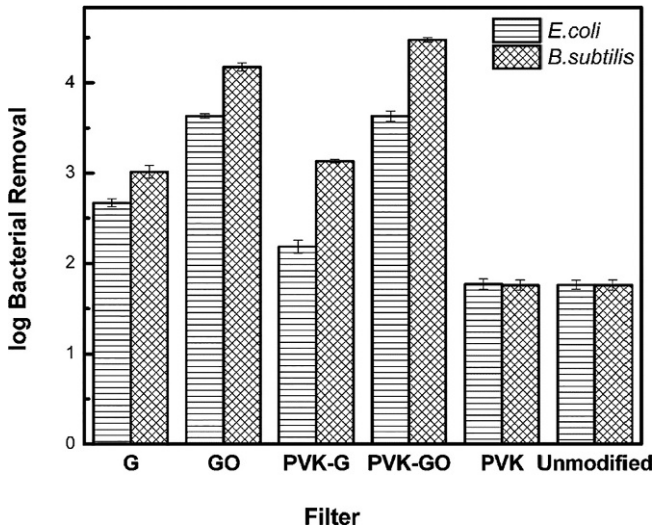

Fig. 30.5
Log bacterial removal after filtration through nanocomposite membrane filter. *Adapted from Y.L.F. Musico, C.M. Santos, M.L.P. Dalida, D.F. Rodrigues, Surface modification of membrane filters using graphene and graphene oxide-based nanomaterials for bacterial inactivation and removal, ACS Sustain. Chem. Eng. 2 (2014) 1559–1565.*

Incorporation of graphene-based nanomaterials into membrane filters can substantially improve the antibacterial capabilities of these filters. In Fig. 30.5, several nanomaterials are compared in terms of their capabilities in removal of *B. subtilis* and *Escherichia coli*. As can be seen in Fig. 30.4, the GO-coated filter has significant removal logs for *B. subtilis* and *E. coli* in comparison to unmodified filter. This efficient antimicrobial is caused by the generation of reactive oxygen species by the nanomaterials [41].

30.2.1.2 Carbon nanotube

Another kind of carbon allotrope that attracted significant attention with attractive features for water purification are CNTs with cylindrical structure. According to the number of cylindrical shells, CNTs are categorized into classifications namely single-wall CNTs (SWCNT) and multiwalled CNT (MWCNT) [3, 42]. The structures of MWCNT and SWCNT are depicted in Fig. 30.6.

CNTs are the superlative sorbents with wonderful features such as unrivaled thermal, chemical, electrical, and textural properties. Also, the characteristics of its pores such as diameter, volume, and large surface determine the adsorption capacity of CNTs.

A major benefit of CNTs is surface modification, which can lead to increasing the flux and overall selectivity. Different functional groups like –COH, –COOH, –NH_2, and –H can be

This book belongs to Badji Mokhtar Annaba University Central Library Copyright Elsevier 2025

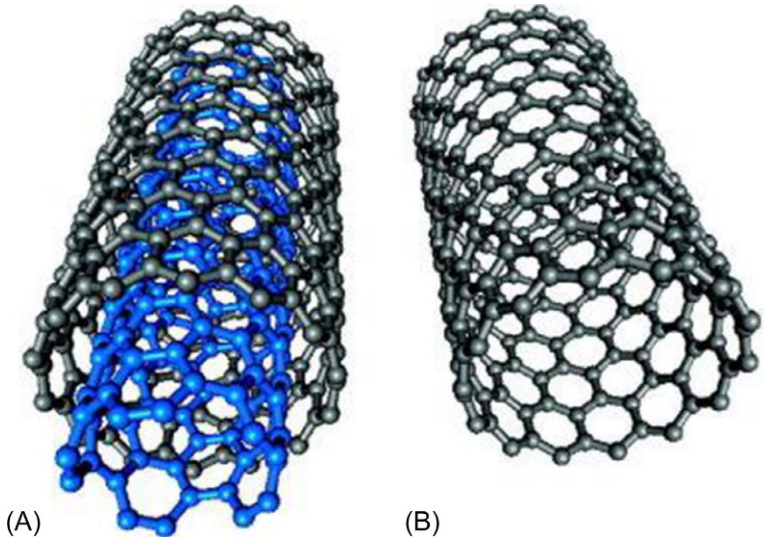

Fig. 30.6
Structure of (A) MWCNT and (B) SWCNT. *Adapted from Ihsanullah, Carbon nanotube membranes for water purification: developments, challenges, and prospects for the future, Sep. Purif. Technol. 209 (2019) 307–337.*

connected to the surface of CNTs by using covalent bonds. Connecting functional groups to CNTs makes them soluble in many organic solvents and changes their hydrophobic nature into hydrophilic [43–46]. Adding CNTs fillers to the membrane structures allows them to act selective toward specific contaminants and also increase the water influx through the nanotube hole. Despite good water permeability and thermal and mechanical stability, CNT-functionalized membranes illustrate resistance to sedimentation and fouling [47].

One of the major water pollutants is ammonia. It is highly soluble in water, and a small amount of ammonia can cause significant damage to water resources, so removing ammonia from water and wastewater is very important. To remove ammonia, CNTs were added to polytetrafluoroethylene (PTFE) membranes, and based on the results, the presence of CNTs significantly improved ammonia flux and mass transfer coefficients compared with uncoated PTFE membranes. This improvement was attributed to the preferential absorption of NH_3 in CNT as well as functionalized-CNT sites, and higher ammonia flux in functionalized CNT immobilized membranes compared with CNT immobilized membranes (CNIM). This can be explained by the existence of a large number of carboxylic functional groups on the F-CNT that provide sites for ammonia preferential adsorption [48]. The schematics for mechanism proposed on CNIM is depicted in Fig. 30.7.

Another dangerous material in industrial effluents discharged from different industries are organic dyes. They act as an important pollutant in water resources. They have high biological toxicity and also decrease the water permeability and oxygen consumption. Thus, their removal

This book belongs to Badji Mokhtar Annaba University Central Library Copyright Elsevier 2025

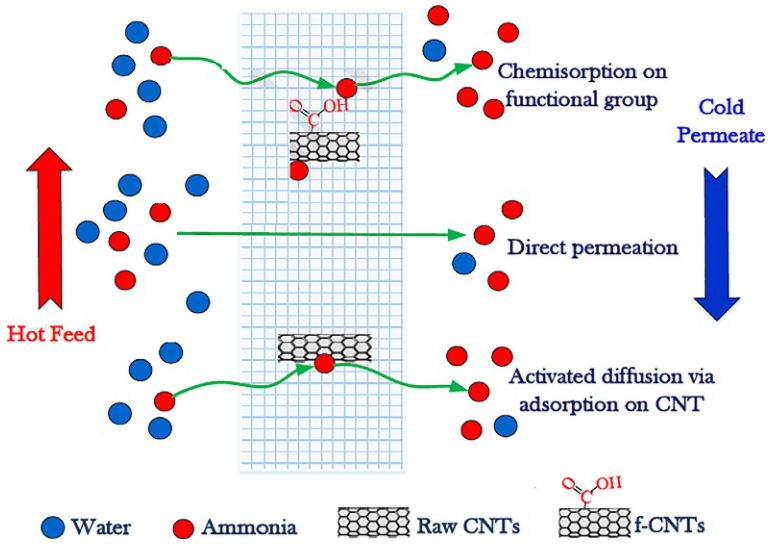

Fig. 30.7
Schematic diagram for mechanism proposed on CNIMs. *Adapted from W. Intrchom, S. Roy, S. Mitra, Functionalized carbon nanotube immobilized membrane for low temperature ammonia removal via membrane distillation, Sep. Purif. Technol. 235 (2020) 116188.*

for reducing water pollution is important. CNTs is a promising absorbent for this purpose due to their high absorption capacity of organic dyes. To now, a large number of researchers use CNT to eliminate dyes from the aqueous solution. Functionalization of CNTs has been undertaken because introducing different functional groups can afford new sites to absorb organic dyes. Among all these modifications, oxidation is a straightforward method to insert carbonyl and hydroxyl groups to sidewalls of the CNT. Oxidized MWCNTs have been shown to be effective in removing MB and methyl red (MR) from aqueous solutions [49].

The volume of water wasted during making of oil/water emulsions causes great harm to both human life and environment. Essentially, owing to the hydrophobicity and sufficient adsorption sites for oil molecules in water of CNTs, assimilation of adsorption into size exclusion separation membrane has been proposed as an effective way to treat oil-in-water emulsion [50].

CNTs, owing to their strong interactions with heavy metal ions or atoms through π-π electronic and hydrophobic interactions, are capable adsorbent materials [51]. The existence of CNTs in membranes reduced pore size to the range of 20–30 nm, thus easing metal ion removal under continuous filtration operation and contributing to an excellent adsorptive nature [50].

As obtained from the results of various studies, adding MWCNT into the structure of PES and PSF membranes resulted in a slightly higher flux, change in rejection rates, and more hydrophilic. By embedding TiO_2-coated MWCNTs into PES membrane, higher flux recovery ratio and smoother membrane surface was achieved [52].

This book belongs to Badji Mokhtar Annaba University Central Library Copyright Elsevier 2025

Polycaprolactone-modified CNTs were added into a sublayer of PES membrane, and sponge-like pores were altered into finger-like ones, thus the porosity of membranes increased. The flux permeation increased, and the fouling tendency of membrane decreased. The separation and removal property of membranes from Cd ions has increased significantly compared with unmodified PES membranes [46].

Amine functions were used for the modification of MWCNTs to improve the hydrophilicity removal performance and fouling resistance of hybrid membrane. As some studies concluded, the NH_2-MWCNT/NF membranes showed better surface characteristics, including smoothness and hydrophilicity. The same improvement results were obtained by adding amine-functionalized MWCNTs into PES membrane [53, 54].

By embedding acid oxidized MWCNTs in PES membrane as a matrix polymer, hydrophilicity sharply increased [47]. Furthermore, CNTs can be used as an absorbent to provide additional pathways for the transfer of solute to CNTs-PVDF membranes, and according to the studies, they are very useful for desalination [44]. Based on the results, incorporating CNTs in membranes have shown improvement in flux and stability.

30.2.2 Metal organic frameworks

Metal organic frameworks (MOFs) are useful for water purification applications with a much smaller structure size due to their excellent surface characteristic functionalities [55]. MOFs can effectively incorporate into several membranes for removal of various pollutions from water including heavy metals, oil, pesticides, and dyes. There are many types of MOFs that have been proposed and used in water purification. In this part of the chapter, the applications of MOFs in water remediation are outlined, all of which include a strong focus on the most known MOFs, namely, ZIFs MIL, and UiO-66. Fig. 30.8 illustrates the structure of ZIF-8, MIL-125, and UiO-66, respectively.

30.2.2.1 ZIFs

ZIFs have a combination of properties of both MOFs and zeolites, such as chemical and thermal stability, great surface area, and microporosity [58]. Addition of these MOFs to various membranes will improve their desirable properties in water purification. For example, a combination of ZIF-8 nanoparticles with a PA matrix made of TFN increased the water permeability of the membrane while reducing its cross-linking [59]. As another example, adding ZIF-8 into PA membrane will improve membrane surface hydrophilicity and decrease the membrane permeability [60].

Development of removing heavy metals efficiently from polluted water has been a serious problem from both environmental and biological viewpoints [61]. The chitosan-*g*-PNVCL/ZIF-8 nanofibers are able to remove As (V), Cr (VI), and phenol from aqueous solutions,

This book belongs to Badji Mokhtar Annaba University Central Library Copyright Elsevier 2025

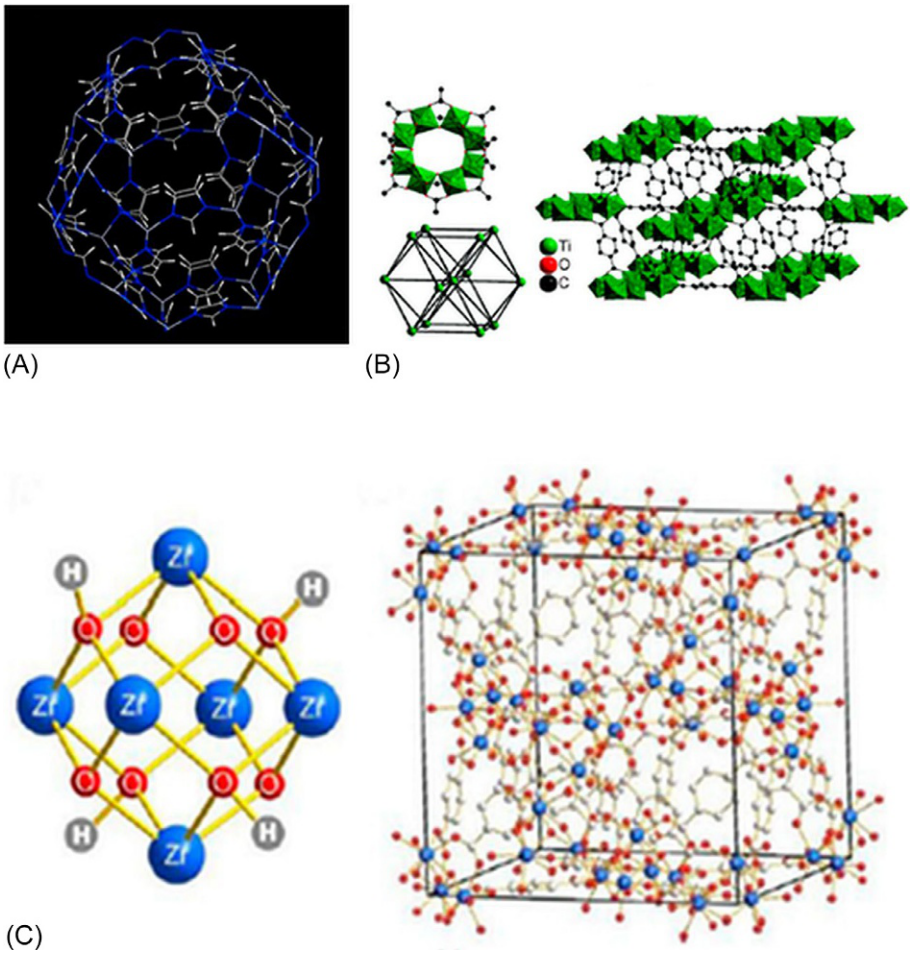

Fig. 30.8
Structure of (A) ZIF-8 [56], (B) MIL-125 [57], and (C) UiO-66. *Adapted from C. Wang, X. Liu, J.P. Chen, K. Li, Superior removal of arsenic from water with zirconium metal-organic framework UiO-66, Sci. Rep. 5 (2015) 16613.*

simultaneously. The Cr (VI) removal efficiency of these nanofibers is more than As (V) and phenol. The ion exchange, π-π stacking, pore filling, and surface adsorption are the phenol removal mechanisms [62].

ZIF-functionalized membranes are also suitable for water desalination. For example, a TFC membrane of PVDF coated with an ultrathin layer of ZIF-8/chitosan is an efficient membrane for this application. The fabricated layer has no substantial effect on water permeability of the TFC membrane while it enhances both antifouling properties and liquid entry pressure of water [56].

This book belongs to Badji Mokhtar Annaba University Central Library Copyright Elsevier 2025

Incorporation of ZIFs into various membranes is a method for dye removals from water. ZIF-67/PAN fiber is an efficient nanofiber to remove dye in industrial applications due to its outstanding adsorption property, easy preparation method, and great reusability [63]. The dye removal rate enhances by increasing the ZIF-8 doping in the (ZIF-8)-polyvinylpyrrolidone (PVP)-PES (ZPP) and the operating time [64]. By incorporation of ZIF-8 particles on a PVDF porous membrane, the rejection enhances are 1.2 and 1.4 times bigger for the Reactive Blue (RB21) and Direct yellow (DY12) dyes, respectively. Molecular size of dyes and surface charges of the ZIF-8-modified membrane are characteristics that contribute to its rejection efficiency [65]. Coating of ZIF-8 and ZIF-67 MOFs on electrospun-silk-nanofiber (ESF) membrane is another technique that can be employed for RB removal with outstanding efficiency of nearly 10% [66]. Incorporation of polystyrene sulfonate polymer (PSS) into ZIF-8 increased its stability in aqueous solutions. The modified membrane has extraordinary rejection of reactive dyes. The further result is that enhancing the ZIF-8 loading will result in increment in the membrane surface roughness and causes an increase in membrane water permeability and flux [67].

Adding ZIFs into the structure of different membranes for oil/water separation is a new technique discovered during recent years. PAN@ZIF-8 composite membrane with unique wettability has excellent capability in separating surfactant-stabilized oil/water emulsions. As shown in Fig. 30.9, PAN@ZIF-8-modified membrane could be fabricated by addition of ZIF-8

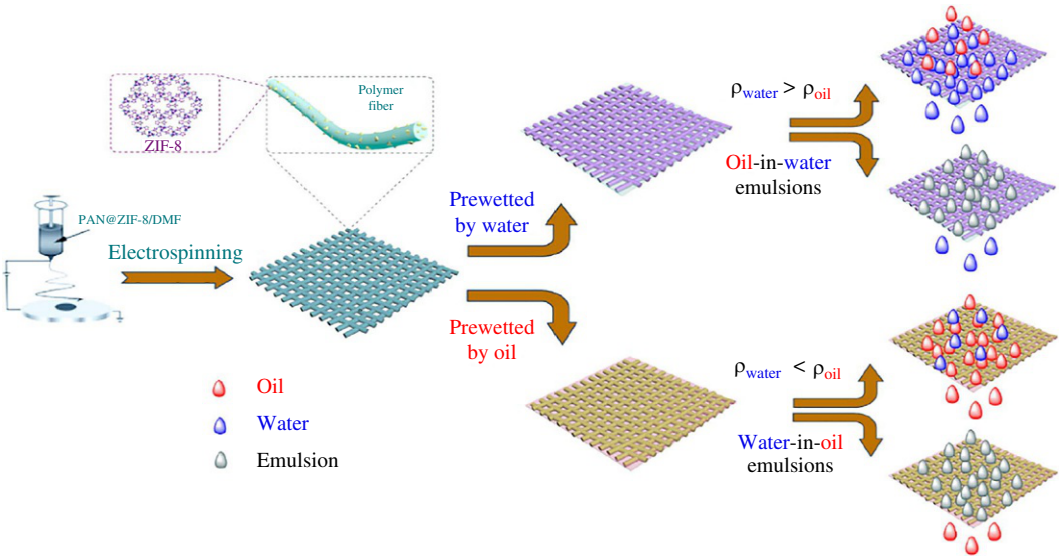

Fig. 30.9

Diagram of generation of the PAN@ZIF-8 composite membrane and separation of oil/water mixtures and emulsions. *Adapted from Y. Cai, D. Chen, N. Li, Q. Xu, H. Li, J. He, J. Lu, Nanofibrous metal–organic framework composite membrane for selective efficient oil/water emulsion separation, J. Membr. Sci. 543 (2017) 10–17.*

This book belongs to Badji Mokhtar Annaba University Central Library
Copyright Elsevier 2025

nanocrystals into PAN nanofibers employing conventional spinning method. Using this membrane, outstanding separation efficiencies (over 99.9%) with suitable recyclability can be achieved for different oil/water mixtures [68].

ZIF-8-coated mesh membrane is used to separate different oil/water mixtures with the help of gravity that increases its separation ability. It shows durability, extensibility of the preparation process, and outstanding stability at high temperature and for different solvents [69]. Electrospun nylon 6, 6 nanofiber membrane (NFM) has a large surface area-to-volume ratio, high porosity, and excellent permeability in comparison to conventional membranes. Low mechanical strength and fouling are the limitations in practical applications of this fiber in oil/water separation. Addition of ZIF-8 to NFM can tackle this problem. Modified NFM shows high oil rejection and high steady-state pure water permeability in comparison to pure NFM fiber [70]. Addition of ZIF-8 to polylactic acid (PLA) nanofiber increases the oil wettability and substantially enhances the mechanical strength in comparison to the reference membrane. In conclusion, ZIF membranes are very efficient in oil/water separation due to its large surface-to-volume ratio of the structures, the fast oil wetting capability, and the promising adsorption effect of the porous ZIF particles [68, 71].

Addition of ZIF-8 into polymeric membrane can be used to remove analgesic acetaminophen from aqueous streams. TFC membranes can be fabricated with several methods such as in situ growth of ZIF-8 on PSF support with PA top layer and ZIF-8 in PA with PSF support. The first method enhances permeance of solvents, but it will result in deteriorating retention of solute in comparison to the pure PA membranes. By employing the second method, the defects of membrane decreases while it can separate acetaminophen more sufficiently [72].

ZIF-8 functionalized MMMs can be used for pervaporation of ethanol from aqueous solution. ZIF-8 has a high water permeability and a good capacity for ethanol adsorption. Addition of this zeolite to the MMMs increase ethanol affinity, hydrophobicity, and thermal stability of the modified membrane in comparison to the reference membrane [73].

ZIF-8/PAN nanofibers can be used to eliminate nuclear pollution. These nanofibers show high adsorption capacity of U (VI). The adsorption is because of surface complexation between U (VI) and 2-methylimidazole (mIM). As shown in Fig. 30.10, the removal rate of U (VI) for in situ grown ZIF-8-PAN nanofibers almost equals that of pure ZIF-8 [74].

30.2.2.2 UiO-66

UiO-66 has outstanding stability in water in comparison to other MOFs [58]. UiO-66-doped membranes show excellent oil/water separation efficiency with improved stability and durability for different oils like diesel, pump oil, vegetable oil, and cyclohexane. The separation mechanism is hydrophilic surface of the modified membrane in comparison to the reference membrane [75].

This book belongs to Badji Mokhtar Annaba University Central Library Copyright Elsevier 2025

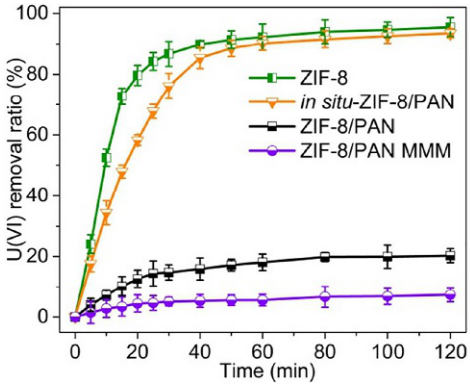

Fig. 30.10

The U (VI) removal rate under different contact times. *Adapted from C. Wang, T. Zheng, R. Luo, C. Liu, M. Zhang, J. Li, X. Sun, J. Shen, W. Han, L. Wang, In situ growth of ZIF-8 on PAN fibrous filters for highly efficient U (VI) removal, ACS Appl. Mater. Interfaces 10 (2018) 24164–24171.*

Addition of ZIFs into different membranes is a method to remove heavy metal from polluted water. UiO-66-NH_2 MOF can be incorporated into PAN/chitosan nanofibers to remove Pb (II), Cd (II), and Cr (VI). The heavy metal ion adsorption is in the order of Pb (II) > Cd (II) > Cr (VI). The outstanding reusability of PAN/chitosan/UiO-66-NH_2 demonstrate that nanofibers are appropriate candidates to exclude heavy metal ions from aqueous solutions. These nanofibers are suitable for membrane filtration process due to their long filtration time while its water flux and metal ions removal is sustained [76].

Incorporation of UiO-66 into various membranes is a technique for water desalination. By increasing the doped UiO-66 into a PA selective layer, the hydrophilicity of the membrane enhances. UiO-66 MOF pore size builds a water pathway with high water permeability and halts hydrated cations passage. Increasing the UiO-66 concentration over 0.1 wt% reduces the water permeability substantially [76].

UiO-modified membranes have also potential for dye removals from water. The UiO-66-NH_2/graphene oxide (UNG) composite membrane (PUF/PDA/UNG), which was doped on polyurethane foam modified with polydopamine (PUF/PDA), has excellent capability in treatment of dye polluted water. The removal mechanisms are electrostatic interaction between dye molecules and the membrane surface, hydrogen bonding, and aggregation of mixed dyes [77].

Addition of UiO-66 into the poly (NVC/DVB) monolith is an appropriate candidate for removal of five fungicides, namely pyrimethanil, tebuconazole, hexaconazole, diniconazole, and flutriafol from pond water. The permeability and mass transfer of modified membrane is more than the reference membrane. Furthermore, adsorption capacity for fungicides increases due to hydrogen bonds, electrostatic forces, and π-π interactions [78].

This book belongs to Badji Mokhtar Annaba University Central Library Copyright Elsevier 2025

30.2.2.3 MIL

MIL-101(Cr) is hydrophilic porous material that has bigger pore size and surface area compared with other water-stable MOFs. Addition of layer of PA on PS support with MIL-101 (Cr) will increase the water permeation of the membrane. The hydrophilic property of this MOF increases the hydrophilicity of the membrane [79].

Incorporation of MIL MOFs into various membranes is a method for efficient water desalination. For example, addition of NH_2-MIL-101(Al) and NH2-MIL-101(Cr) into a chitosan polymer matrix increases the salt rejection of four different salts, namely NaCl, $MgCl_2$, $CaCl_2$, and Na_2SO_4. The highest rejection of 93% can be achieved for $MgCl_2$. The other result is that introduction of NH_2-group into MIL-101(Al) increases the dispersion of the fabricated MOFs [80]. MIL-53(Al), NH_2-UiO-66, and ZIF-8 MOF nanoparticles can be incorporated on TFN for removal of pharmaceuticals. As illustrated in Fig. 30.11, the TFN membranes have high efficiently in removing a set of six pharmaceuticals [81].

30.2.2.4 Other MOFs

Zirconium-based MOF doped on polyurethane foam (Zr-MOFs-PUF) membrane has capability in separating Rhodamine B (RB), Congo red (CR), and MB dyes in both binary and ternary systems. The main removal mechanisms are electrostatic interactions, Lewis acid-base interactions between the membrane and dye molecules, and hydrogen bond interaction [82].

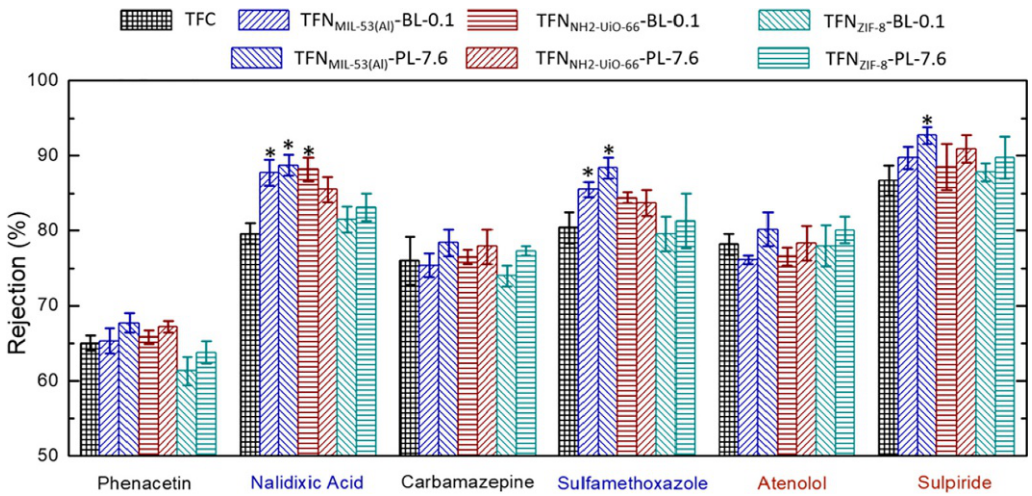

Fig. 30.11

Pharmaceutical rejections by TFC and MOF-polymer composite membranes. *Adapted from Y.-Y. Zhao, Y.-L. Liu, X.-M. Wang, X. Huang, Y.F. Xie, Impacts of metal–organic frameworks on structure and performance of polyamide thin-film nanocomposite membranes, ACS Appl. Mater. Interfaces 11 (2019) 13724–13734.*

This book belongs to Badji Mokhtar Annaba University Central Library
Copyright Elsevier 2025

MOF-polymer nanofibers can be used to separate lead and mercury ions from aqueous water. Fe-MOF/PAN membranes exhibit high water flux of 348 $Lm^{-2}\,h^{-1}$ with a permeance of 870 $Lm^{-1}\,h^{-1}\,bar^{-1}$. The concentration of Pb (II) can be less than 10 ppb in the permeate, which is acceptable for drinking water. Heavy metals adsorption mechanism attributed to the electrostatic interactions with the MOF crystals or polymer, separating heavy metal sufficiently, including competitive ion exchange (CIE) and binding to open metal sites of the MOFs. Because of high removal efficiency in conjunction with outstanding durability, MOF/PAN nanofibers are appropriate for practical water purification applications [83]. The novel PVA/La-TBC, PVA/Sr-TBC, and PVA/La-TBC nanofibers are more efficient than plain PVA nanofibers for heavy metal [Pb (II)] treatment from contaminated water [84].

30.2.3 Zeolites

Zeolite NPs are inorganic environmentally friendly materials with excellent properties like high chemical and mechanical resistance, ion exchange feature, sieving characteristics, and promising adsorption capacity [85–90]. In this part of the chapter, we will outline zeolite-functionalized membrane applications in water remediation. These modified membranes have different applications in water treatment such as desalination, removal of heavy metals, and extraction of acids and organic materials over the past years.

Addition of nanozeolite-Y to PVA-networked cellulose (NC) membranes (PVA-NC-Y) exhibits substantially improved performance with a 34% enhancement in flux in comparison to PVA-NC. This improvement is due to an increment of water permeability by the zeolite-Y 3D nanopore channels. Furthermore, incorporation of this zeolite will result in good stability, higher mechanical strength, and high salt rejection [91]. The research shows that silicalite-1 nanozeolite is an outstanding candidate for practical seawater desalination because of its high permeability and chemical stability. Incorporation of silicalite-1 into PA membrane will result in increased hydrophilic surface, water permeability, and acid stability in comparison to pure PA [92]. The enhancement in permeability is due to zeolite internal pore channels [93]. Solubility and diffusion of water from the bulk feed to the membrane surface are the reasons for high hydrophilicity of the modified membrane [94].

Alumina (Al_2O_3) and Linda type L (LTL) zeolite NPs can be grown on pure PSF UF membrane surface with excellent coverage ratio. Both modified membranes have greater surface hydrophilicity in comparison to pure UF. *E. coli* is a type of bacteria found in natural water and seawater. The studies show that Al_2O_3- and UF-LTL-modified membranes exhibit high antiadhesion efficiency to *E. coli* bacteria [95]. The growth of zeolites 4A on PSF membranes led to a dense, rough, and negatively charged surface with smaller pore size. These modified membranes can be used for bovine serum albumin (BSA) and pepsin rejections

This book belongs to Badji Mokhtar Annaba University Central Library Copyright Elsevier 2025

through Donnan effect and steric exclusion. The mechanical and chemical stability, fouling resistance, and hydrophilicity will also improve for zeolite 4A/PSf membranes in comparison to those of the reference membrane [96].

Addition of zeolite NaA particles to PVA can be used for dehydration of ethylene glycol (EG)-water mixtures. Incorporation of zeolite NaA enhances the separation efficiency and permeation flux through hydrophilicity improvement, molecular sieving action, and selective adsorption of zeolite [97].

Investigation of the use of different zeolites for removing heavy metals from wastewater is profoundly essential. By addition of NaX zeolite, sorption capacity and the water hydraulic permeability of the hybrid NaX/PSf membrane increases in comparison to pure PSf membrane. PSf10-0 is a good candidate for dynamic exclusion of lead and nickel from wastewater at low working pressure and concentrations [98]. Hybrid mordenite zeolite/polymer composite has potential application in heavy metal removal from wastewater. As illustrated in Fig. 30.12, this modified membrane exhibits high adsorption abilities to Pb^{2+} in comparison to Cd^{2+}, Cu^{2+}, and Ni^{2+} [99].

The incorporation of SAPO-5 zeolite into polyurethane membranes is a promising way to remove NaCl from water. The modified membranes show high flux and rejection. The obtained results show that rejection of salt water rises with operating pressure [100]. Doping H-beta zeolite into PVDF led to an increment in the thermal stability and porosity of the membrane. This hybrid membrane can be used to extract lactic acid from aqueous streams. As illustrated in Fig. 30.13, the extraction ratio enhances continuously with enhancing zeolite loading [101].

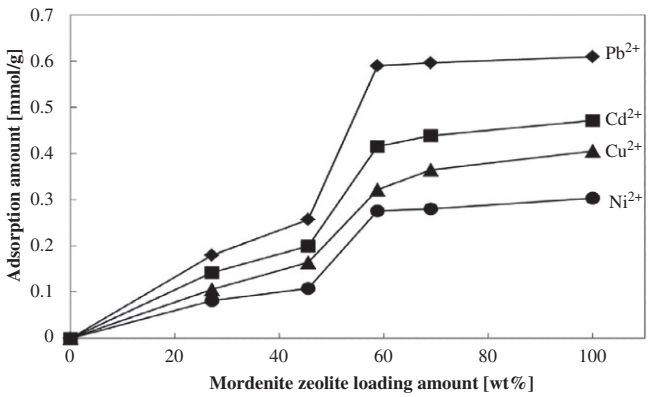

Fig. 30.12

Effect of mordenite zeolite content of composite fibers on adsorption amount of different metals.
Adapted from K. Nakamoto, M. Ohshiro, T. Kobayashi, Mordenite zeolite—polyethersulfone composite fibers developed for decontamination of heavy metal ions, J. Environ. Chem. Eng. 5 (2017) 513–525.

This book belongs to Badji Mokhtar Annaba University Central Library
Copyright Elsevier 2025

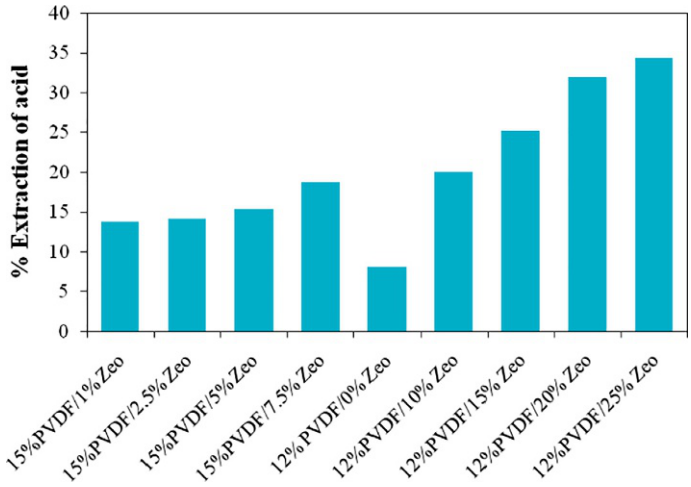

Fig. 30.13
Effect of zeolite content on extraction ratio of lactic acid. *Adapted from M. Madhumala, D. Satyasri, T. Sankarshana, S. Sridhar, Selective extraction of lactic acid from aqueous media through a hydrophobic H-Beta zeolite/PVDF mixed matrix membrane contactor, Indus. Eng. Chem. Res. 53 (2014) 17770–17781.*

30.2.4 Metal oxides nanoparticles

Nanostructured metal oxides represent a significant category of materials that have been extensively used in the manufacture of nanocomposites and water treatment operations. The most widely nanometal oxides—TiO_2, FeO, ZnO, CuO, and SiO_2—are categorized as promising adsorbents for removal of pollutants in water owing to properties such as large surface area, high activity, high adsorption capacity, and superb optical and magnetic properties. They are also presented in various forms such as tubes, particles, and others. Nowadays, metal oxides nanomaterials have been used in electrochemical operations, ion exchange, and membrane filtration. Their incorporation into polymeric membranes improve water diffusion due to their dependence on water. In comparison to purely polymeric membranes, they can improve membrane properties, such as photocatalytic activity, hydrophobicity, permeability, and antifouling property. In the following are examples of metal oxides nanoparticles that researchers incorporate into membranes to investigate their treatments [19].

Among the different groups of nanoparticles used, silica (SiO_2) has received considerable interest due to its convenient operation, mild reactivity, wide range of source, low cost, famed chemical properties, and other excellent characteristics. Therefore, the latest research focuses on the preparation of modified nanosilica membranes for wastewater treatment [102, 103].

Regarding the literature, SiO_2 nanoparticles introduced to PSF membranes improved the antifouling properties and permeability of the manufactured membrane.

This book belongs to Badji Mokhtar Annaba University Central Library Copyright Elsevier 2025

To investigate the effect of adding these NPs, characteristics and permeability tests were performed on all membranes. Results can be mentioned as follows:

1. Owing to the interfacial pressures between the filler (SiO_2) and polymer, the pore size became interconnected.
2. The permeability of membranes was improved by addition of SiO_2 nanoparticles and partial compensation for its NTU reduction.
3. The antifouling properties of fabricated membrane were also improved by addition of SiO_2 nanofillers in the matrix compound [102].

On the other hand, titanium dioxide (TiO_2) has attracted attention due to its photocatalytic and extraordinary hydrophobicity effects. Therefore, TiO_2 nanoparticles are used in the structure of membranes to improve their antifouling and permeability properties. A number of literatures have illustrated the good performance of the presence TiO_2 nanoparticles in membranes [104, 105]. TiO_2 nanoparticles on the surface layer of membranes have resulted in notable hydrophilicity and great antifouling properties [105]. Kim and coworkers, while investigating the antibacterial properties of TiO_2, prepared a hybrid membrane consisting of a PA thin film layer and TiO_2. The modified membranes showed dramatic a photobactericidal effect on *E. coli* under UV light [106]. The surface of PEI nanofiber membranes was modified with TiO_2 by using electrospraying method. The best behavior of membranes was obtained by adding 0.2% TiO_2 by reducing water contact angle and improving water flux of membranes. Also, a significant removal rate of *E. coli* (99%) and humic acid (80%) was achieved along with 85% MB degradation during photocatalytic process [107].

The various types of TiO_2 nanoparticles with different sizes were embedded into PES NF membranes, and the effect of this was investigated. By blending the TiO_2 nanoparticles with PES polymer, the water flux and hydrophilicity of membranes increased. High water flux was obtained owing to low tendency of nanofillers into aggregation that didn't block the membrane pores. Also, due to higher adsorption of water and high surface area, reducing the size of particles led to decreasing the biofouling of membrane [108].

Two methods of modifying membranes include entrapping and coating of PES membranes via TiO_2 were investigated by Rahimpour et al. They reported that surface coating of membranes is an advanced method in comparison to entrapping TiO_2 particles in the membrane matrix [109].

Remarkably, ZnO is another type of metal oxides nanoparticles with significant semiconductor features and superior chemical, optical, mechanical, and electrical properties that could improve the antibacterial functions and antifouling of polymeric membranes. Nano-ZnO is also less expensive than other oxide nanostructures like Al_2O_3 and TiO_2 [13]. ZnO/PVDF membranes were prepared by Hong et al. They used BSA as a model foulant compound, and based on the results, it showed desired hydrophilicity for antifouling [6]. Also, ZnO nanoparticles were added to PVC UF membranes. Significant changes in membrane structure

This book belongs to Badji Mokhtar Annaba University Central Library Copyright Elsevier 2025

and further connection among channels with the addition of ZnO were observed. ZnO led to a surge in water flux of the membranes compared with bare PVC membrane, because of higher surface hydrophilicity of the modified membranes and more porous structure. The results showed best results for BSA rejection, flux recovery, and water flux were obtained by addition of 3 wt% ZnO. However, further loading of ZnO caused a reduction in so-called parameters [110].

It has been reported that FeO nanoparticle is one of the most effective particles for water treatment. The facileness of resource, large surface area, hydrophilic nature, magnetic property, and ease in synthesis rendered nanosized ferric oxides (NFeOs) to be inexpensive adsorbents for water treatment. Meanwhile iron element is eco-friendly, and NFeOs can be pumped directly to contaminated sites with negligible risks of secondary contamination. In an investigation conducted by Lakhotia et al., the FeO nanofillers were added into membranes and their ability of antifouling and separation performance was investigated. The results illustrated that the performance and antifouling properties of FeO nanoparticles-embedded membrane have been increased. The fabricated membranes showed desired properties for the removal of hydrophobic contaminants [7]. By a combination different types of Fe_2O_3 and its derivatives (Fe_3O_4 nanoparticles were coated by metformin, silica, and amine), favorable changes in the structure and morphology of nanocomposites were obtained, and also pure water flux and hydrophilicity of membrane increased. Iron oxide NPs affect the average radius of the pores and the overall porosity of the membranes. The membrane produced with Fe_3O_4 nanoparticles coated with 0.1% metformin modified silica metformin showed the highest amount of copper removal (approximately 92%) because a large number of nitrogen atoms around each particle offered active adsorption sites through their lone electron pairs [111]. In another investigation, Mansourpanah et al. added SiO_2-covered Fe_2O_3 nanoparticles into PA thin layer membranes. They reported that the existence of low amounts of NPs could increase the rejection capability and flux of the membranes, resulting in increased negative charge and decreased thin layer thickness of the modified membranes [112]. Thus, FeO has a large range of applications in water treatment.

CuO is another metal oxide nanoparticle that was also studied. CuO nanoparticles act as a bactericide and, after adding into membranes, increased their antibacterial activity. The studies confirm this, and as an example, PAN NFMs decorated with CuO showed an improvement in purification of drinking water [113].

30.3 Challenges and future prospects

Technology-based membrane is a simple and affordable process that is widespread in the separation industries for various applications, particularly in water treatment processes, and has efficiently replaced conventional water treatment technologies. Ceramic and polymeric membranes were effective before these new demands and current expectations, but due to

This book belongs to Badji Mokhtar Annaba University Central Library Copyright Elsevier 2025

continuous production of new pollutants and finding ways to effectively eliminate them, researchers have to find new ways to deal with the rising crisis. To solve the tradeoff between permeability and selectivity of membranes, the idea of MMMs has surfaced as a promising candidate that provides the combined features of ceramic and polymeric membranes by adding inorganic NPs into organic polymer matrix. It dominates future technology for water purification; however, it is restricted in a wider range of applications because of its own difficulties and complexities [114].

However, fabricating membranes with enhanced permeability and selectivity simultaneously is a remaining issue that needs more effort to be optimized. The most important challenges facing MMMs with targeted separation efficiency are: selection of a compatible NPs/polymer system associated with the ideal performance for a certain morphology; some NPs like MOFs have low water stability; and some are not well dispersed in the matrix of polymer and result in agglomeration at higher concentrations. In addition, improper interfacial interactions of NPs/polymer systems lead to defects in the fabricated MMMs, such as rigidification of the polymer around the filler particles and interfacial voids, filler's pores blocking, and the difficulty of scalability of the MMMs owing to inadequate adhesion among the polymer matrix and the fillers [58].

Owing to the effects of leached nanomaterials into the environment, the stability of nanocomposite and loading concentration of membranes as two main parameters need to be considered. Consequently, the systematic assessment of the release of nanomaterial and its environmental toxicity is so important. There are some NPs like MOFs that are readily commercially available. The reason for their limited applications in the field is the use of hazardous reactants during synthesis and the difficult reaction conditions that limit their synthesis in an industrial scale. However, producing engineered membranes like MMMs is limited due to the high production cost, which makes researchers consider whether the benefits overcome the costs [115].

Future research should focus on developing MMMs. New polymers beside new combinations should also be explored to meet the challenges. Novel materials ought to be considered to reduce fouling phenomena. New additives, agents, and solvents must also be studied to better succeed in the adhesion between inorganic NPs and polymers. As a result, such MMM technology has great potential; nevertheless, it requires persistent effort to succeed in competition with existing purification technologies [116].

References

[1] M. Anjum, R. Miandad, M. Waqas, F. Gehany, M.A. Barakat, Remediation of wastewater using various nanomaterials, Arab. J. Chem. 12 (8) (2019) 4897–4919.
[2] M. Bassyouni, M. Abdel-Aziz, M.S. Zoromba, S. Abdel-Hamid, E. Drioli, A review of polymeric nanocomposite membranes for water purification, J. Ind. Eng. Chem. 73 (2019) 19–46.

This book belongs to Badji Mokhtar Annaba University Central Library Copyright Elsevier 2025

[3] M. Selvaraj, A. Hai, F. Banat, M.A. Haija, Application and prospects of carbon nanostructured materials in water treatment: a review, J. Water Process. Eng. 33 (2020) 100996.
[4] R.S. Dongre, K.K. Sadasivuni, K. Deshmukh, A. Mehta, S. Basu, J.S. Meshram, M.A.A. Al-Maadeed, A. Karim, Natural polymer based composite membranes for water purification: a review, Polym. Plast. Technol. Mater. 58 (2) (2019) 1295–1310.
[5] T. Pradeep, S.M. Maliyekkal, S.T. Sreenivasan, Reduced graphene oxide-based-composites for the purification of water, in: Google Patents, 2018.
[6] M. Sheikh, M. Pazirofteh, M. Dehghani, M. Asghari, M. Rezakazemi, C. Valderrama, J.-L. Cortina, Application of ZnO nanostructures in ceramic and polymeric membranes for water and wastewater technologies: a review, Chem. Eng. J. 391 (2020) 123475.
[7] S.R. Lakhotia, M. Mukhopadhyay, P. Kumari, Iron oxide (FeO) nanoparticles embedded thin-film nanocomposite nanofiltration (NF) membrane for water treatment, Sep. Purif. Technol. 211 (2019) 98–107.
[8] X.-F. Sun, J. Qin, P.-F. Xia, B.-B. Guo, C.-M. Yang, C. Song, S.-G. Wang, Graphene oxide–silver nanoparticle membrane for biofouling control and water purification, Chem. Eng. J. 281 (2015) 53–59.
[9] Y. Mansourpanah, E.M. Habili, Preparation and modification of thin film PA membranes with improved antifouling property using acrylic acid and UV irradiation, J. Membr. Sci. 430 (2013) 158–166.
[10] Y. Mansourpanah, Z. Amiri, Preparation of modified polyethersulfone nanoporous membranes in the presence of sodium tripolyphosphate for color separation; characterization and antifouling properties, Desalination 335 (2014) 33–40.
[11] Y. Mansourpanah, M. Samimi, Preparation and characterization of a low-pressure efficient polyamide multi-layer membrane for water treatment and dye removal, J. Ind. Eng. Chem. 53 (2017) 93–104.
[12] E. Bet-Moushoul, Y. Mansourpanah, K. Farhadi, M. Tabatabaei, TiO_2 nanocomposite based polymeric membranes: a review on performance improvement for various applications in chemical engineering processes, Chem. Eng. J. 283 (2016) 29–46.
[13] H. Saleem, S.J. Zaidi, Nanoparticles in reverse osmosis membranes for desalination: a state of the art review, Desalination 475 (2020) 114171.
[14] A. Rahimpour, M. Jahanshahi, N. Mortazavian, S.S. Madaeni, Y. Mansourpanah, Preparation and characterization of asymmetric polyethersulfone and thin-film composite polyamide nanofiltration membranes for water softening, Appl. Surf. Sci. 256 (2010) 1657–1663.
[15] Y. Mansourpanah, S. Madaeni, A. Rahimpour, Fabrication and development of interfacial polymerized thin-film composite nanofiltration membrane using different surfactants in organic phase; study of morphology and performance, J. Membr. Sci. 343 (2009) 219–228.
[16] Y. Mansourpanah, K. Alizadeh, S. Madaeni, A. Rahimpour, H.S. Afarani, Using different surfactants for changing the properties of poly (piperazineamide) TFC nanofiltration membranes, Desalination 271 (2011) 169–177.
[17] J. Kim, B. Van der Bruggen, The use of nanoparticles in polymeric and ceramic membrane structures: review of manufacturing procedures and performance improvement for water treatment, Environ. Pollut. 158 (2010) 2335–2349.
[18] L.Y. Ng, A.W. Mohammad, C.P. Leo, N. Hilal, Polymeric membranes incorporated with metal/metal oxide nanoparticles: a comprehensive review, Desalination 308 (2013) 15–33.
[19] J. García-Ivars, M.-J. Corbatón-Báguena, M.-I. Iborra-Clar, Development of mixed matrix membranes: incorporation of metal nanoparticles in polymeric membranes, in: Nanoscale Materials in Water Purification, Elsevier, 2019, pp. 153–178.
[20] Y. Mansourpanah, P.M. Rashnou, Influence of sodium tripolyphosphate concentration on characteristics and performance of polyamide thin layer membrane in Cu (II) removal, J. Membr. Sci. Res. 3 (2017) 36–41.
[21] X. Wang, Y. Zhao, E. Tian, J. Li, Y. Ren, Graphene oxide-based polymeric membranes for water treatment, Adv. Mater. Interfaces 5 (2018) 1701427.
[22] J. Zhou, S. Chen, S. Xu, X. Zhang, W. Zhao, C. Zhao, Graphene oxide-based polyethersulfone core–shell particles for dye uptake, RSC Adv. 6 (2016) 102389–102397.

This book belongs to Badji Mokhtar Annaba University Central Library Copyright Elsevier 2025

[23] R. Mukherjee, P. Bhunia, S. De, Impact of graphene oxide on removal of heavy metals using mixed matrix membrane, Chem. Eng. J. 292 (2016) 284–297.
[24] Y. Mansourpanah, H. Shahebrahimi, E. Kolvari, PEG-modified GO nanosheets, a desired additive to increase the rejection and antifouling characteristics of polyamide thin layer membranes, Chem. Eng. Res. Des. 104 (2015) 530–540.
[25] Y. Zhao, J. Lu, X. Liu, Y. Wang, J. Lin, N. Peng, J. Li, F. Zhao, Performance enhancement of polyvinyl chloride ultrafiltration membrane modified with graphene oxide, J. Colloid Interface Sci. 480 (2016) 1–8.
[26] T. Hwang, J.-S. Oh, W. Yim, J.-D. Nam, C. Bae, H.-I. Kim, K.J. Kim, Ultrafiltration using graphene oxide surface-embedded polysulfone membranes, Sep. Purif. Technol. 166 (2016) 41–47.
[27] J. Lee, H.-R. Chae, Y.J. Won, K. Lee, C.-H. Lee, H.H. Lee, I.-C. Kim, J.-M. Lee, Graphene oxide nanoplatelets composite membrane with hydrophilic and antifouling properties for wastewater treatment, J. Membr. Sci. 448 (2013) 223–230.
[28] C. Zhao, X. Xu, J. Chen, F. Yang, Optimization of preparation conditions of poly (vinylidene fluoride)/graphene oxide microfiltration membranes by the Taguchi experimental design, Desalination 334 (2014) 17–22.
[29] X. Zhang, Y. Liu, C. Sun, H. Ji, W. Zhao, S. Sun, C. Zhao, Graphene oxide-based polymeric membranes for broad water pollutant removal, RSC Adv. 5 (2015) 100651–100662.
[30] M. Musielak, A. Gagor, B. Zawisza, E. Talik, R. Sitko, Graphene oxide/carbon nanotube membranes for highly efficient removal of metal ions from water, ACS Appl. Mater. Interfaces 11 (2019) 28582–28590.
[31] R. Sitko, M. Musielak, B. Zawisza, E. Talik, A. Gagor, Graphene oxide/cellulose membranes in adsorption of divalent metal ions, RSC Adv. 6 (2016) 96595–96605.
[32] J. Wang, T. Huang, L. Zhang, Q.J. Yu, L.A. Hou, Dopamine crosslinked graphene oxide membrane for simultaneous removal of organic pollutants and trace heavy metals from aqueous solution, Environ. Technol. 39 (2018) 3055–3065.
[33] H.T.V. Nguyen, T.H.A. Ngo, K.D. Do, M.N. Nguyen, N.T.T. Dang, T.T.H. Nguyen, V. Vien, T. A. Vu, Preparation and characterization of a hydrophilic polysulfone membrane using graphene oxide, J. Chem. (1) (2019) 1–10.
[34] A. Karkooti, A.Z. Yazdi, P. Chen, M. McGregor, N. Nazemifard, M. Sadrzadeh, Development of advanced nanocomposite membranes using graphene nanoribbons and nanosheets for water treatment, J. Membr. Sci. 560 (2018) 97–107.
[35] S. Bano, A. Mahmood, S.-J. Kim, K.-H. Lee, Graphene oxide modified polyamide nanofiltration membrane with improved flux and antifouling properties, J. Mater. Chem. A 3 (2015) 2065–2071.
[36] B. Ganesh, A.M. Isloor, A.F. Ismail, Enhanced hydrophilicity and salt rejection study of graphene oxide-polysulfone mixed matrix membrane, Desalination 313 (2013) 199–207.
[37] Q. Nan, P. Li, B. Cao, Fabrication of positively charged nanofiltration membrane via the layer-by-layer assembly of graphene oxide and polyethylenimine for desalination, Appl. Surf. Sci. 387 (2016) 521–528.
[38] J. Wang, C. Zhao, T. Wang, Z. Wu, X. Li, J. Li, Graphene oxide polypiperazine-amide nanofiltration membrane for improving flux and anti-fouling in water purification, RSC Adv. 6 (2016) 82174–82185.
[39] G. Lai, W. Lau, P. Goh, A. Ismail, N. Yusof, Y. Tan, Graphene oxide incorporated thin film nanocomposite nanofiltration membrane for enhanced salt removal performance, Desalination 387 (2016) 14–24.
[40] J. Zhang, Q. Xue, X. Pan, Y. Jin, W. Lu, D. Ding, Q. Guo, Graphene oxide/polyacrylonitrile fiber hierarchical-structured membrane for ultra-fast microfiltration of oil-water emulsion, Chem. Eng. J. 307 (2017) 643–649.
[41] Y.L.F. Musico, C.M. Santos, M.L.P. Dalida, D.F. Rodrigues, Surface modification of membrane filters using graphene and graphene oxide-based nanomaterials for bacterial inactivation and removal, ACS Sustain. Chem. Eng. 2 (2014) 1559–1565.
[42] M. Bassyouni, A. Mansi, A. Elgabry, B.A. Ibrahim, O.A. Kassem, R. Alhebeshy, Utilization of carbon nanotubes in removal of heavy metals from wastewater: a review of the CNTs' potential and current challenges, Appl. Phys. A 126 (2020) 38.

This book belongs to Badji Mokhtar Annaba University Central Library Copyright Elsevier 2025

[43] Ihsanullah, Carbon nanotube membranes for water purification: developments, challenges, and prospects for the future, Sep. Purif. Technol. 209 (2019) 307–337.
[44] Z.Z. Chowdhury, S. Sagadevan, R.B. Johan, S.T. Shah, A. Adebesi, S.I. Md, R.F. Rafique, A review on electrochemically modified carbon nanotubes (CNTs) membrane for desalination and purification of water, Mater. Res. Express 5 (2018) 102001.
[45] R. Das, M.E. Ali, S.B.A. Hamid, S. Ramakrishna, Z.Z. Chowdhury, Carbon nanotube membranes for water purification: a bright future in water desalination, Desalination 336 (2014) 97–109.
[46] Y. Mansourpanah, S. Madaeni, A. Rahimpour, M. Adeli, M. Hashemi, M. Moradian, Fabrication new PES-based mixed matrix nanocomposite membranes using polycaprolactone modified carbon nanotubes as the additive: property changes and morphological studies, Desalination 277 (2011) 171–177.
[47] V. Vatanpour, S.S. Madaeni, R. Moradian, S. Zinadini, B. Astinchap, Fabrication and characterization of novel antifouling nanofiltration membrane prepared from oxidized multiwalled carbon nanotube/polyethersulfone nanocomposite, J. Membr. Sci. 375 (2011) 284–294.
[48] W. Intrchom, S. Roy, S. Mitra, Functionalized carbon nanotube immobilized membrane for low temperature ammonia removal via membrane distillation, Sep. Purif. Technol. 235 (2020) 116188.
[49] H. Sadegh, G.R. Shahryari, A. Masjedi, Z. Mahmoodi, M. Kazemi, A review on carbon nanotubes adsorbents for the removal of pollutants from aqueous solutions, Int. J. Nano. Dimen. 7 (2) (2016) 109–120.
[50] L. Ma, X. Dong, M. Chen, L. Zhu, C. Wang, F. Yang, Y. Dong, Fabrication and water treatment application of carbon nanotubes (CNTs)-based composite membranes: a review, Membranes 7 (2017) 16.
[51] T.J. Logan, Critical Reviews in Environmental Science and Technology (No. 634.92 C7), (1997).
[52] V. Vatanpour, S.S. Madaeni, R. Moradian, S. Zinadini, B. Astinchap, Novel antibifouling nanofiltration polyethersulfone membrane fabricated from embedding TiO_2 coated multiwalled carbon nanotubes, Sep. Purif. Technol. 90 (2012) 69–82.
[53] H. Zarrabi, M.E. Yekavalangi, V. Vatanpour, A. Shockravi, M. Safarpour, Improvement in desalination performance of thin film nanocomposite nanofiltration membrane using amine-functionalized multiwalled carbon nanotube, Desalination 394 (2016) 83–90.
[54] A. Rahimpour, M. Jahanshahi, S. Khalili, A. Mollahosseini, A. Zirepour, B. Rajaeian, Novel functionalized carbon nanotubes for improving the surface properties and performance of polyethersulfone (PES) membrane, Desalination 286 (2012) 99–107.
[55] Y. Dou, W. Zhang, A. Kaiser, Electrospinning of metal–organic frameworks for energy and environmental applications, Adv. Sci. 7 (3) (2019) 1902590.
[56] M.R.S. Kebria, A. Rahimpour, G. Bakeri, R. Abedini, Experimental and theoretical investigation of thin ZIF-8/chitosan coated layer on air gap membrane distillation performance of PVDF membrane, Desalination 450 (2019) 21–32.
[57] T. Devic, C. Serre, High valence 3p and transition metal based MOFs, Chem. Soc. Rev. 43 (2014) 6097–6115.
[58] A. Elrasheedy, N. Nady, M. Bassyouni, A. El-Shazly, Metal organic framework based polymer mixed matrix membranes: review on applications in water purification, Membranes 9 (2019) 88.
[59] J. Duan, Y. Pan, F. Pacheco, E. Litwiller, Z. Lai, I. Pinnau, High-performance polyamide thin-film-nanocomposite reverse osmosis membranes containing hydrophobic zeolitic imidazolate framework-8, J. Membr. Sci. 476 (2015) 303–310.
[60] I.H. Aljundi, Desalination characteristics of TFN-RO membrane incorporated with ZIF-8 nanoparticles, Desalination 420 (2017) 12–20.
[61] H. Shayegan, G.A.M. Ali, V. Safarifard, Recent progress in the removal of heavy metal ions from water using metal-organic frameworks, ChemistrySelect 5 (2020) 124–146.
[62] E. Bahmani, S. Koushkbaghi, M. Darabi, A. ZabihiSahebi, A. Askari, M. Irani, Fabrication of novel chitosan-g-PNVCL/ZIF-8 composite nanofibers for adsorption of Cr (VI), As (V) and phenol in a single and ternary systems, Carbohydr. Polym. 224 (2019) 115148.
[63] L. Jin, J. Ye, Y. Wang, X. Qian, M. Dong, Electrospinning synthesis of ZIF-67/PAN fibrous membrane with high-capacity adsorption for malachite green, Fibers Polym. 20 (2019) 2070–2077.

This book belongs to Badji Mokhtar Annaba University Central Library Copyright Elsevier 2025

[64] S.M. Maroofi, N.M. Mahmoodi, Zeolitic imidazolate framework-polyvinylpyrrolidone-polyethersulfone composites membranes: from synthesis to the detailed pollutant removal from wastewater using cross flow system, Colloids Surf. A Physicochem. Eng. Asp. 572 (2019) 211–220.
[65] A. Karimi, V. Vatanpour, A. Khataee, M. Safarpour, Contra-diffusion synthesis of ZIF-8 layer on polyvinylidene fluoride ultrafiltration membranes for improved water purification, J. Ind. Eng. Chem. 73 (2019) 95–105.
[66] Z. Li, G. Zhou, H. Dai, M. Yang, Y. Fu, Y. Ying, Y. Li, Biomineralization-mimetic preparation of hybrid membranes with ultra-high loading of pristine metal–organic frameworks grown on silk nanofibers for hazard collection in water, J. Mater. Chem. A 6 (2018) 3402–3413.
[67] J. Zhu, L. Qin, A. Uliana, J. Hou, J. Wang, Y. Zhang, X. Li, S. Yuan, J. Li, M. Tian, Elevated performance of thin film nanocomposite membranes enabled by modified hydrophilic MOFs for nanofiltration, ACS Appl. Mater. Interfaces 9 (2017) 1975–1986.
[68] Y. Cai, D. Chen, N. Li, Q. Xu, H. Li, J. He, J. Lu, Nanofibrous metal–organic framework composite membrane for selective efficient oil/water emulsion separation, J. Membr. Sci. 543 (2017) 10–17.
[69] M. Song, Y. Zhao, S. Mu, C. Jiang, Z. Li, P. Yang, Q. Fang, M. Xue, S. Qiu, A stable ZIF-8-coated mesh membrane with micro-/nano architectures produced by a facile fabrication method for high-efficiency oil-water separation, Sci. China Mater. 62 (2019) 536–544.
[70] A. Halim, N. Syakinah, M.D.H. Wirzal, M.R. Bilad, M. Nordin, N.A. Hadi, Z. Adi Putra, M. Yusoff, A. Rahim, T. Narkkun, Electrospun nylon 6, 6/ZIF-8 nanofiber membrane for produced water filtration, Water 11 (2019) 2111.
[71] X. Dai, Y. Cao, X. Shi, X. Wang, The PLA/ZIF-8 nanocomposite membranes: the diameter and surface roughness adjustment by ZIF-8 nanoparticles, high wettability, improved mechanical property, and efficient oil/water separation, Adv. Mater. Interfaces 3 (2016) 1600725.
[72] S. Basu, M. Balakrishnan, Polyamide thin film composite membranes containing ZIF-8 for the separation of pharmaceutical compounds from aqueous streams, Sep. Purif. Technol. 179 (2017) 118–125.
[73] H. Mao, H.-G. Zhen, A. Ahmad, A.-S. Zhang, Z.-P. Zhao, In situ fabrication of MOF nanoparticles in PDMS membrane via interfacial synthesis for enhanced ethanol permselective pervaporation, J. Membr. Sci. 573 (2019) 344–358.
[74] C. Wang, T. Zheng, R. Luo, C. Liu, M. Zhang, J. Li, X. Sun, J. Shen, W. Han, L. Wang, In situ growth of ZIF-8 on PAN fibrous filters for highly efficient U (VI) removal, ACS Appl. Mater. Interfaces 10 (2018) 24164–24171.
[75] X. Zhang, Y. Zhao, S. Mu, C. Jiang, M. Song, Q. Fang, M. Xue, S. Qiu, B. Chen, UiO-66-coated mesh membrane with underwater superoleophobicity for high-efficiency oil–water separation, ACS Appl. Mater. Interfaces 10 (2018) 17301–17308.
[76] S. Fazlifard, T. Mohammadi, O. Bakhtiari, Chitosan/ZIF-8 mixed-matrix membranes for pervaporation dehydration of isopropanol, Chem. Eng. Technol. 40 (2017) 648–655.
[77] J. Li, J.-L. Gong, G.-M. Zeng, P. Zhang, B. Song, W.-C. Cao, S.-Y. Fang, S.-Y. Huan, J. Ye, The performance of UiO-66-NH_2/graphene oxide (GO) composite membrane for removal of differently charged mixed dyes, Chemosphere 237 (2019) 124517.
[78] W. Yao, Z. Fan, S. Zhang, Preparation of metal-organic framework UiO-66-incorporated polymer monolith for the extraction of trace levels of fungicides in environmental water and soil samples, J. Sep. Sci. 42 (2019) 2679–2686.
[79] Y. Xu, X. Gao, X. Wang, Q. Wang, Z. Ji, X. Wang, T. Wu, C. Gao, Highly and stably water permeable thin film nanocomposite membranes doped with MIL-101 (Cr) nanoparticles for reverse osmosis application, Materials 9 (2016) 870.
[80] X.-H. Ma, Z. Yang, Z.-K. Yao, Z.-L. Xu, C.Y. Tang, A facile preparation of novel positively charged MOF/chitosan nanofiltration membranes, J. Membr. Sci. 525 (2017) 269–276.
[81] Y.-y. Zhao, Y.-l. Liu, X.-m. Wang, X. Huang, Y.F. Xie, Impacts of metal–organic frameworks on structure and performance of polyamide thin-film nanocomposite membranes, ACS Appl. Mater. Interfaces 11 (2019) 13724–13734.

This book belongs to Badji Mokhtar Annaba University Central Library Copyright Elsevier 2025

[82] J. Li, J.-L. Gong, G.-M. Zeng, P. Zhang, B. Song, W.-C. Cao, H.-Y. Liu, S.-Y. Huan, Zirconium-based metal organic frameworks loaded on polyurethane foam membrane for simultaneous removal of dyes with different charges, J. Colloid Interface Sci. 527 (2018) 267–279.
[83] J.E. Efome, D. Rana, T. Matsuura, C.Q. Lan, Metal–organic frameworks supported on nanofibers to remove heavy metals, J. Mater. Chem. A 6 (2018) 4550–4555.
[84] N.D. Shooto, C.W. Dikio, D. Wankasi, L.M. Sikhwivhilu, F.M. Mtunzi, E.D. Dikio, Novel PVA/MOF nanofibres: fabrication, evaluation and adsorption of lead ions from aqueous solution, Nanoscale Res. Lett. 11 (2016) 1–13.
[85] A.K. Goyal, E.S. Johal, G. Rath, Nanotechnology for water treatment, Curr. Nanosci. 7 (2011) 640–654.
[86] G.J. Dahe, R.S. Teotia, J.R. Bellare, The role of zeolite nanoparticles additive on morphology, mechanical properties and performance of polysulfone hollow fiber membranes, Chem. Eng. J. 197 (2012) 398–406.
[87] S.G. Kim, D.H. Hyeon, J.H. Chun, B.-H. Chun, S.H. Kim, Nanocomposite poly (arylene ether sulfone) reverse osmosis membrane containing functional zeolite nanoparticles for seawater desalination, J. Membr. Sci. 443 (2013) 10–18.
[88] M. Rezakazemi, K. Shahidi, T. Mohammadi, Hydrogen separation and purification using crosslinkable PDMS/zeolite A nanoparticles mixed matrix membranes, Int. J. Hydrogen Energy 37 (2012) 14576–14589.
[89] N. Ma, J. Wei, R. Liao, C.Y. Tang, Zeolite-polyamide thin film nanocomposite membranes: towards enhanced performance for forward osmosis, J. Membr. Sci. 405 (2012) 149–157.
[90] M. Fathizadeh, A. Aroujalian, A. Raisi, Effect of added NaX nano-zeolite into polyamide as a top thin layer of membrane on water flux and salt rejection in a reverse osmosis process, J. Membr. Sci. 375 (2011) 88–95.
[91] S.F. Anis, R. Hashaikeh, N. Hilal, Flux and salt rejection enhancement of polyvinyl (alcohol) reverse osmosis membranes using nano-zeolite, Desalination 470 (2019) 114104.
[92] H. Huang, X. Qu, X. Ji, X. Gao, L. Zhang, H. Chen, L. Hou, Acid and multivalent ion resistance of thin film nanocomposite RO membranes loaded with silicalite-1 nanozeolites, J. Mater. Chem. A 1 (2013) 11343–11349.
[93] B.-H. Jeong, E.M. Hoek, Y. Yan, A. Subramani, X. Huang, G. Hurwitz, A.K. Ghosh, A. Jawor, Interfacial polymerization of thin film nanocomposites: a new concept for reverse osmosis membranes, J. Membr. Sci. 294 (2007) 1–7.
[94] J. Yin, E.-S. Kim, J. Yang, B. Deng, Fabrication of a novel thin-film nanocomposite (TFN) membrane containing MCM-41 silica nanoparticles (NPs) for water purification, J. Membr. Sci. 423 (2012) 238–246.
[95] L.-x. Dong, H.-w. Yang, S.-t. Liu, X.-m. Wang, Y.F. Xie, Fabrication and anti-biofouling properties of alumina and zeolite nanoparticle embedded ultrafiltration membranes, Desalination 365 (2015) 70–78.
[96] F. Liu, B.-R. Ma, D. Zhou, Y.-H. Xiang, L.-X. Xue, Breaking through tradeoff of polysulfone ultrafiltration membranes by zeolite 4A, Microporous Mesoporous Mater. 186 (2014) 113–120.
[97] B. Baheri, M. Shahverdi, M. Rezakazemi, E. Motaee, T. Mohammadi, Performance of PVA/NaA mixed matrix membrane for removal of water from ethylene glycol solutions by pervaporation, Chem. Eng. Commun. 202 (2015) 316–321.
[98] Y. Yurekli, Removal of heavy metals in wastewater by using zeolite nano-particles impregnated polysulfone membranes, J. Hazard. Mater. 309 (2016) 53–64.
[99] K. Nakamoto, M. Ohshiro, T. Kobayashi, Mordenite zeolite—polyethersulfone composite fibers developed for decontamination of heavy metal ions, J. Environ. Chem. Eng. 5 (2017) 513–525.
[100] G. Ciobanu, G. Carja, Electrolyte removal by mixed matrix membranes based on polyurethane, Desalination 250 (2010) 698–701.
[101] M. Madhumala, D. Satyasri, T. Sankarshana, S. Sridhar, Selective extraction of lactic acid from aqueous media through a hydrophobic H-Beta zeolite/PVDF mixed matrix membrane contactor, Ind. Eng. Chem. Res. 53 (2014) 17770–17781.
[102] A. Ahmad, M. Majid, B. Ooi, Functionalized PSf/SiO_2 nanocomposite membrane for oil-in-water emulsion separation, Desalination 268 (2011) 266–269.
[103] L. Jin, S. Yu, W. Shi, X. Yi, N. Sun, Y. Ge, C. Ma, Synthesis of a novel composite nanofiltration membrane incorporated SiO_2 nanoparticles for oily wastewater desalination, Polymer 53 (2012) 5295–5303.

This book belongs to Badji Mokhtar Annaba University Central Library Copyright Elsevier 2025

[104] Y. Mansourpanah, S. Madaeni, A. Rahimpour, A. Farhadian, A. Taheri, Formation of appropriate sites on nanofiltration membrane surface for binding TiO_2 photo-catalyst: performance, characterization and fouling-resistant capability, J. Membr. Sci. 330 (2009) 297–306.
[105] Y. Mansourpanah, E. Momeni Habili, Investigation and characterization of TiO_2-TFC nanocomposite membranes; membrane preparation and UV studies, J. Membr. Sci. Res. 1 (2015) 26–33.
[106] S.H. Kim, S.-Y. Kwak, B.-H. Sohn, T.H. Park, Design of TiO_2 nanoparticle self-assembled aromatic polyamide thin-film-composite (TFC) membrane as an approach to solve biofouling problem, J. Membr. Sci. 211 (2003) 157–165.
[107] B. Al-Ghafri, W.-J. Lau, M. Al-Abri, P.-S. Goh, A.F. Ismail, Titanium dioxide-modified polyetherimide nanofiber membrane for water treatment, J. Water Process Eng. 32 (2019) 100970.
[108] V. Vatanpour, S.S. Madaeni, A.R. Khataee, E. Salehi, S. Zinadini, H.A. Monfared, TiO_2 embedded mixed matrix PES nanocomposite membranes: influence of different sizes and types of nanoparticles on antifouling and performance, Desalination 292 (2012) 19–29.
[109] A. Rahimpour, S. Madaeni, A. Taheri, Y. Mansourpanah, Coupling TiO_2 nanoparticles with UV irradiation for modification of polyethersulfone ultrafiltration membranes, J. Membr. Sci. 313 (2008) 158–169.
[110] H. Rabiee, V. Vatanpour, M.H.D.A. Farahani, H. Zarrabi, Improvement in flux and antifouling properties of PVC ultrafiltration membranes by incorporation of zinc oxide (ZnO) nanoparticles, Sep. Purif. Technol. 156 (2015) 299–310.
[111] N. Ghaemi, S.S. Madaeni, P. Daraei, H. Rajabi, S. Zinadini, A. Alizadeh, R. Heydari, M. Beygzadeh, S. Ghouzivand, Polyethersulfone membrane enhanced with iron oxide nanoparticles for copper removal from water: application of new functionalized Fe_3O_4 nanoparticles, Chem. Eng. J. 263 (2015) 101–112.
[112] Y. Mansourpanah, A. Rahimpour, M. Tabatabaei, L. Bennett, Self-antifouling properties of magnetic Fe_2O_3/SiO_2-modified poly (piperazine amide) active layer for desalting of water: characterization and performance, Desalination 419 (2017) 79–87.
[113] T. Shalaby, H. Hamad, E. Ibrahim, O. Mahmoud, A. Al-Oufy, Electrospun nanofibers hybrid composites membranes for highly efficient antibacterial activity, Ecotoxicol. Environ. Saf. 162 (2018) 354–364.
[114] D. Qadir, H. Mukhtar, L.K. Keong, Mixed matrix membranes for water purification applications, Sep. Purif. Rev. 46 (2017) 62–80.
[115] M.R. Esfahani, S.A. Aktij, Z. Dabaghian, M.D. Firouzjaei, A. Rahimpour, J. Eke, I.C. Escobar, M. Abolhassani, L.F. Greenlee, A.R. Esfahani, Nanocomposite membranes for water separation and purification: fabrication, modification, and applications, Sep. Purif. Technol. 213 (2019) 465–499.
[116] A. Kayvani Fard, G. McKay, A. Buekenhoudt, H. Al Sulaiti, F. Motmans, M. Khraisheh, M. Atieh, Inorganic membranes: preparation and application for water treatment and desalination, Materials 11 (2018) 74.

This book belongs to Badji Mokhtar Annaba University Central Library Copyright Elsevier 2025

This page intentionally left blank

This book belongs to Badji Mokhtar Annaba University Central Library

Copyright Elsevier 2025

CHAPTER 31

The process for the removal of micropollutants using nanomaterials

M.V. Bagal[a] and S. Raut-Jadhav[b]

[a]*Department of Chemical Engineering, Bharati Vidyapeeth College of Engineering, Navi Mumbai, India,* [b]*Department of Chemical Engineering, Bharati Vidyapeeth (Deemed to be University) College of Engineering, Pune, India*

31.1 Introduction

Water is a precious resource for human civilization and sustainable life on earth. Potable water demand is increasing because of exponential growth of population. The contamination of water resources has occurred globally because of the rapid pace of industrialization and tremendous increase in the population [1]. The major challenge in the availability of pure water is continuous contamination of water bodies by various organic and inorganic pollutants. Even though most of these compounds called as micropollutants (MPs) are present at low concentrations, it raises considerable toxicological concerns [2] and ecological risk, such as interference with endocrine system, microbiological resistance, and accumulation in soil, plants, and animals [3].

Such MPs are released in water bodies from products of daily use such as pharmaceuticals, personal care products (PCPs), pesticides, endocrine-disrupting compounds (EDCs), dyes, surfactants, and industrial additives. The environmental bioaccumulation of pharmaceuticals and PCPs can affect water quality, intensify the abnormal hormonal control [4], and can stimulate the development of genes that are antibiotic resistant [5]. Pesticides have immune-depressive effects, whereas surfactants can influence the physical stability of human growth hormone compounds [6].

To remove these MPs, various physical, biological, and chemical technologies have already been widely used [7, 8]. However, most of the MPs are nonbiodegradable and hence cannot be removed completely using these biological methods. The conventional chemical treatment technologies such as chlorination, ozonation and Fenton process have limitations of low rate of degradation of MPs, production of byproducts that may be more harmful than the parent

Handbook of Nanomaterials for Wastewater Treatment. https://doi.org/10.1016/B978-0-12-821496-1.00020-9
Copyright © 2021 Elsevier Inc. All rights reserved.

This book belongs to Badji Mokhtar Annaba University Central Library Copyright Elsevier 2025

compound, and high sludge formation. Similarly, many physical processes such as flocculation and sedimentation are not effective for the removal of most of the MPs such as pharmaceuticals and pesticides because they have relatively high water solubility [9, 10]. Also, other conventional physical wastewater treatment processes such as filtration can only transfer the pollutants from one phase to another, producing a very concentrated sludge [11, 12], which is difficult to dispose directly because of its toxicity. As these persistent and nonbiodegradable MPs cannot be completely degraded or removed using conventional treatment methods, alternate methods are imperative for efficient degradation of MPs present in wastewater.

Nanotechnology has attracted the attention of many researchers as it exhibits great potential in wastewater treatment application by enhancing the efficiency and providing a sustainable approach to secure clean water supply. Nanomaterials can be synthesized in various forms such as nanotubes, quantum dots, nanowires, colloids, particles, and films [13]. Nanoparticles (NPs) exhibit high reactivity because of larger number of active sites per unit mass and their smaller particle size and larger specific surface area.

Nanomaterials and nanocomposites have been successfully applied in adsorption, photocatalysis, and membrane separation processes for the removal or degradation of MPs. In conventional adsorption process, the efficiency of adsorption is often limited by selectivity and surface area of adsorbents. However, the use of nanoadsorbents shows significant increase in percentage removal of MPs because of high surface area, tunable pore size, and improved surface chemistry [14]. Theses nanoadsorbents mainly include carbonaceous material, silica and clay materials, and metals and metal oxides. Photocatalytic process using nanophotocatalysts also exhibits higher photocatalytic activity compared with the process utilizing conventional photocatalysts because of the availability of higher surface area and active sites [15]. Most widely applied nanophotocatalysts for the degradation of MPs are TiO_2 and ZnO because they have high reactivity under ultraviolet irradiation, wide band gap, and high stability [16,17]. However, the applications of metal oxide NPs have a serious limitation of requirement of UV light for their activation. This limitation can be eliminated by doping of metal oxides or supporting them on carbon- or clay-based materials.

Membrane processes modified with incorporation of nanomaterials are gaining huge popularity as an effective wastewater treatment method because of their high catalytic reactivity, permeability, and fouling resistance. Highly automated systems, a lesser requirement of chemical and land, and flexibility in design are the major advantages of using membrane processes in wastewater treatment application [14].

In this chapter, advanced wastewater treatment methods such as photocatalysis, adsorption, and membrane processes based on nanomaterials have been discussed in detail with the sole objective of removing the MPs. The effect of operating parameters on the efficiency of these processes has also been discussed for maximizing their performance. Furthermore, various types of reactors applied for the removal of MPs using nanomaterials have also been elaborated.

This book belongs to Badji Mokhtar Annaba University Central Library Copyright Elsevier 2025

Although nanomaterials have received potential applications on the lab scale, their applications at large scale has certain challenges such as aggregation of nanomaterials, difficulty in separation, and adverse effect imposed by nanomaterials on ecosystem and human health. Hence, the scale-up challenges of these processes using nanomaterials have also been exhibited in this chapter for understanding the areas that need to be addressed in near future.

31.2 Types of MPs

The wide applications of chemicals in various industries, agriculture sectors, and household purposes lead to their accumulation in wastewater effluents and pose a growing environmental health concern across the globe. MPs are those substances that are generally present in water bodies in very low concentrations (in the range of ng–μg/L) and cause detrimental effects on humans and environment even at these trace concentration levels. MPs can be classified based on the four major categories [18] namely heavy metals, organic chemicals, hormones, and pharmaceuticals and PCPs.

Heavy metals are composed of group of both metals and metalloids. They have higher density (more than 5 g/cm^3) and are very toxic even at very low concentrations. They include heavy metals such as Zn, Ag, Cu, Pb, As, Hg, Ni, Pd, Cd, Fe, Cr, and Pt. They are nonbiodegradable, carcinogenic in nature, and have the ability to accumulate in living organisms. These heavy metals are discharged into the environment mainly because of mining processes and release of heavy metal containing effluent by various industries and municipal sewage plants [19,20].

Organic chemicals include organic compounds such as pesticides, herbicides, solvents, surfactants, EDCs, PCPs, dyes, and detergents. Various pesticides and herbicides are widely used in the agriculture sector for the sake of increased crop production. Extensive use of these pesticides in the agriculture field and release of pesticides containing effluents leads to their accumulation in various water bodies. These pesticides cause harmful health disorders because most of the pesticides are carcinogenic and may lead to organ damage, reproduction disorders, etc. [21]. Detergents are surfactants that cause critical pollution because of its wide applicability for cleaning purposes. Detergents are of various types such as anionic detergents (linear alkyl benzene sulfonate), cationic detergents (quaternary ammonium cation), and nonionic detergents. Dyes are organic compounds that can be classified as cationic and anionic dyes. Most of the dyes are also very toxic and hazardous in nature. Textile, plastic, and paper industries are the main sources of accumulation of dyes in wastewater. Organic chemicals also include other EDCs such as polychlorinated biphenyls (PCBs) and dioxins, bisphenol A (BPA), phthalates, phenol, and perfluorochemicals.

Hormones mainly include estrogens, androgens, progestin, mineral corticosteroids, and glucocorticosteroids. These hormones are excreted by all animals and human beings and are also found in domestic products such as shampoos, cosmetics, and detergents. Extensive use of

This book belongs to Badji Mokhtar Annaba University Central Library Copyright Elsevier 2025

these products has lead to their accumulation in water bodies. The presence of these hormones in water and wastewater is a major concern to mankind because they are EDCs that pose adverse effects on all living organisms [22].

The pharmaceutical market is growing dynamically because of longer life expectancy, higher income, improved lifestyle, and population growth. The occurrence of these pharmaceuticals in water becomes a matter of concern to health as it causes adverse effects on environment. PCPs are nonbiodegradable because of its highly polar, large, and complex structure. The most widely detected PCPs in water include antibiotics such as sulfamethoxazole, ofloxacin (OFLOX), and ciprofloxacin, antiinflammatory drugs such as ibuprofen, diuretics such as furosemide and hydrochlorothiazide, gastrointestinal drug such as ranitidine, and lipid regulator such as bezafibrate. It has been reported in literature that the occurrence of PCPs in surface water is in concentration range of (ng/L to μg/L), for ground water (ng/L to mg/L), for sewage sludge (μg/kg), and for soil reaching (μg/kg) [23].

31.3 Various methods applied for the treatment of MPs

Conventional wastewater treatment processes primarily include physical, chemical, and biological processes. These conventional methods include processes such as such as filtration, flotation, coagulation, sedimentation, chemical oxidation, and aerobic and anaerobic digestion. Unfortunately, these methods cannot completely remove these MPs or do not convert these MPs into nontoxic elements. Hence, the complete removal of these MPs from wastewater is a challenging task. Major conventional wastewater treatment processes are discussed in the following sections.

31.3.1 Conventional methods

Chemical oxidation process can be used to remove a wide range of organic MPs. Commonly used oxidizing agents are chlorine, hydrogen peroxide, and ozone. Chemical oxidation process usually shows low efficiency for complete removal of MPs because of the insufficient oxidation of MPs leading to the formation of toxic byproducts. The high cost associated with handling and transportation of oxidizing agents and electricity cost for generation of ozone are the other major disadvantages of chemical oxidation processes [24]. Similarly, high energy inputs and problems associated with corrosion in electrochemical oxidation of electrodes limit its application in the removal of organic MPs [25].

Chemical precipitation process is generally used for heavy metal removal. Coagulation and flocculation followed by sedimentation or filtration are used to remove heavy metals and inorganic nonmetals from wastewater [24,26]. Chemical coagulants are also used for effective removal of dyes present in wastewater [27,28]. The major disadvantages associated with these methods are formation of significant amount of sludge, which may be hazardous, and cost of the chemicals used for treatment makes it expensive. Also, removal of specific metal ions from

This book belongs to Badji Mokhtar Annaba University Central Library Copyright Elsevier 2025

multiple metal species makes the treatment difficult as the separation of one metal hinders the removal of another metal because of their amphoteric nature [24].

The widely used biological treatment methods for the removal of various organic pollutants include activated sludge process, aerobic, anaerobic and membrane bioreactors, biosorption, etc. However, these processes are inefficient for the removal of MPs because they are present in much lower concentrations and such processes are very slow [24]. Biological treatment methods combined with other treatment methods such as filtration can be used efficiently to remove various MPs [29]. However, the performance of bioreactors and biofilters decreases because of fouling and filter clogging over the period.

The limitations of conventional methods have created the need of advanced methods for the effective removal of MPs.

31.3.2 Advanced methods using nanomaterials

As the conventional treatment technologies are unable to eliminate the MPs completely, effective treatment methodologies are inevitably required. Many processes have been developed over the years for the effective removal of these pollutants from wastewater.

Nowadays, photocatalysis, adsorption, and membrane-based processes involving nanomaterials have opened up the opportunities to overcome the limitations of conventional treatment technologies [30–32].

The shape and size of the nanomaterials greatly affect the removal efficiency of MPs. NPs exhibit unique properties that depend on the size and shape of the NPs. NPs have larger surface area, which makes them catalytically more active because of more exposure to active sites. Nanomaterials with smaller size possess high surface to volume ratio and high active surface area [33]. The change in size of NPs affects coordination environment, electronic state, and adsorption energy of the pollutant molecules.

NPs exhibit various shapes (zero dimensional (0D), one dimensional (1D), two dimensional (2D), and three dimensional (3D)), which affect the catalytic properties. Spherical, dodecahedral, tetrahedral, octahedral, and cubic shape represent 0D NPs, whereas nanotubes, nanorods, and nano capsules are 1D shape morphologies. Various 2D nanostructured materials (branched structures, nanoprisms, nanoplates, nanosheets, nanowalls, and nanodisks), and 3D nanostructured materials (nanoballs, nanocoils, nanocones, nanopillers and nanoflowers) have been reported in literature [34]. Variations in shape and composition of nanocatalysts lead to different types of catalytic sites that show better selectivity toward a particular application. Branched gold NPs with structures like stars and flowers have been used for catalysis, surface-enhanced Raman scattering, and sensing [35], whereas polyhedral gold NPs exhibit excellent optical and catalytic properties [36]. The details of the advanced methods using nanomaterials have been illustrated in the following sections.

This book belongs to Badji Mokhtar Annaba University Central Library Copyright Elsevier 2025

31.4 Photocatalytic process using nanomaterials

Photocatalysis has emerged as an effective remediation process for the removal of MPs as it can eliminate the persistent organic pollutant from wastewater without further formation of toxic products. It has proved to be an environmentally friendly technique that can completely degrade MPs or convert them into nontoxic forms. Photocatalytic process utilizes a transition metal oxide photocatalyst in the presence of UV light for the generation of hydroxyl radicals. It is capable of degrading chemical pollutants by both oxidative and reductive pathways [37].

When a photocatalyst is irradiated with UV light, it gets activated and generates electron-hole pairs. Valence band electrons (e^-) are promoted to the conduction band leaving a hole (h^+) behind. These electron-hole pairs either recombine to produce heat or interact separately with other molecules generating free radicals. Migration of these photogenerated electrons to the photocatalyst surface initiates simultaneous oxidation and reduction reactions on the surface of photocatalyst. In an aqueous suspension, h^+ reacts with H_2O to give OH• radicals, whereas e^- reacts with adsorbed molecular O_2 to produce superoxide anion radical $\cdot O_2^-$, which also contributes to the production of OH• radicals [38]. Generated OH• radicals subsequently attack on the organic pollutants, which eventually leads to mineralization of these compounds.

31.4.1 Nanomaterials applied as a photocatalyst

Nanotechnology has played a promising role in the effective remediation of wastewater. Nanophotocatalysts are cost effective and lead to the higher active surface area for illumination, which in turn increases their photocatalytic activity. Photocatalysis using NPs of transition metal oxide and their composites has been extensively reported in the literature as they have proved to be an excellent photocatalyst [39]. They have been utilized for the photocatalytic degradation of long-chain organic pollutants into short-chain compounds that are not toxic [40,41]. The most widely used metal oxide nanomaterials are TiO_2, CuO, ZnO, Al_2O_3, CeO_2, SnO_2, Fe_2O_3, ZrO_2, WO_3, and SnO_2. Besides many advantages of metal oxide nanophotocatalysts, their application is seriously limited by the major drawback that they need ultraviolet light for their activation and hence can use only UV range of solar spectrum. To overcome these disadvantages and to improve the photocatalytic efficiency, various types of nanocomposites based on metal oxides have been explored widely, which mainly includes magnetic material–based metal oxides, porous materials–based metal oxides, metal-supported metal oxides, and graphene-supported metal oxides [42]. Furthermore, doping of semiconductor photocatalysts and immobilization techniques are also used for enhancing efficacy of these photocatalysts. Table 31.1 comprises summary of various nanomaterials applied as a photocatalyst along with their target pollutants.

Important nanomaterials and their composites that are applied as a photocatalyst are discussed in detail in the following sections.

This book belongs to Badji Mokhtar Annaba University Central Library Copyright Elsevier 2025

Table 31.1: Summary of nanomaterials applied in photocatalytic applications.

Sr. no.	Nanomaterials applied as a photocatalyst	Target pollutant	Important findings	References
1	$CoFe_2O_4$@TiO_2 decorated rGO nanocomposite	Chlorpyrifos	Photocatalytic activity of nanocomposite was higher compared with bare TiO_2	[41]
2	Reduced graphene oxide—TiO_2 nanocomposite	Antipsychotic drug, risperidone	Photocatalytic activity of nanocomposite was higher as compared with TiO_2—P25	[16]
3	TiO_2-Pt-CeO_2 nanocomposite	Cr (VI) and benzyl alcohol	Photo reduction of Cr (VI) and photo oxidation of benzyl alcohol were the maximum at TiO_2-Pt-CeO_2 nanocomposite compared with bare TiO_2 and CeO_2	[43]
4	Au/TiO_2 nanocomposite	Azo dye, methyl orange	Rate of degradation of methyl orange using nanocomposite was two times higher than the rate obtained in case of bare TiO_2	[44]
5	$ZnSnO_3$/rGO nanocomposite	Metronidazole	Excellent photocatalytic activity of $ZnSnO_3$/rGO nanocomposite under visible light irradiation	[45]
6	Graphene/titanium dioxide nanotubes (GR-TNT) nanocomposite	Acetaminophen, an antipyretic agent	96% degradation of acetaminophen using 0.1 g/L of 5% GR-TNT	[46]
7	TiO_2-rGO nanocomposites immobilized on optical fibers	Pharmaceuticals: carbamazepine, ibuprofen, and sulfamethoxazole	54%, 81%, and 92% degradation of carbamazepine, ibuprofen, and sulfamethoxazole, respectively, after 180 min UV irradiation using TiO_2-rGO nanocomposite with 2.7% rGO	[47]
8	Nitrogen and sulfur co-doped TiO_2/rGO nanocomposites	Congo red, methylene blue, and reactive orange 16 dyes	Nitrogen and sulfur co-doped TiO_2/rGO nanocomposite with 5% rGO showed highest photocatalytic activity under visible light	[15]
9	ZnO/GO nanocomposite	Methylene blue	Under visible light irradiation, ZnO/GO nanocomposite showed higher photocatalytic efficiency than bare GO sheets and ZnO nanoparticles	[48]
10	Manganese-doped ZnO nanoparticles	Methylene blue	Under visible light irradiation, the photo degradation efficiency of manganese-doped ZnO nanoparticles is higher compared with undoped ZnO	[49]

Continued

This book belongs to Badji Mokhtar Annaba University Central Library

Copyright Elsevier 2025

Table 31.1: Summary of nanomaterials applied in photocatalytic applications—cont'd

Sr. no.	Nanomaterials applied as a photocatalyst	Target pollutant	Important findings	References
11	Palladium-doped ZnO nanoparticles	Congo red	Improved photocatalytic activity of Pd-doped ZnO nanoparticles compared with bare ZnO under UV light. 98.2% degradation in 60 min using Pd/ZnO	[50]
12	Er-doped ZnO nanoparticles	Direct red-31	Complete degradation of dye in 60 min using Er-doped ZnO nanoparticles (with 2.5% Er) under UV irradiation	[51]
13	TiO_2-CeO_2-Bi_2O_3 nanocomposite	Rhodamine B	Under visible light irradiation, nanocomposite with the mole ratio of TiO_2:CeO_2:Bi_2O_3 as 2:5:3 degraded 55% of RhB in 2 h of irradiation	[52]
14	Cu_2O/CeO_2	Acid Orange 7	Nanocomposite with Cu_2O/CeO_2 molar ratio of 0.029 exhibited 20% higher photocatalytic activity than that of pure CeO_2	[53]
15	CeO_2-Y_2O_3 nanocomposite	Rhodamine B	Nanocomposite with ratio of CeO_2:Y_2O_3 as 2:1 showed highest photocatalytic activity than the pure CeO_2	[54]

31.4.1.1 Titanium dioxide based nanophotocatalyst

TiO_2 (band gap 3.4 eV) is a widely used photocatalyst in wastewater treatment because of its low cost, high photocatalytic activity, nontoxicity, and photo stability. However, the photocatalytic efficiency of TiO_2 is seriously limited by the higher rate of recombination of photo generated pairs of electrons and holes and low activity in visible light region. To overcome these drawbacks, doping of TiO_2 NPs is gaining large popularity because it is capable of reducing the band gap and enabling its use in the visible light region [16]. The use of dopants can also slow down the recombination rate of electron-hole pairs and thus in turn can increase the photocatalytic activity.

The photocatalytic activity of TiO_2 can be enhanced by coupling it with noble metal [44,55], transition metal ions (or their oxides) [56, 57], and other semiconductors [42,43] or anchoring it on some large-surface-area materials, such as mesoporous materials, zeolites, or carbon-based materials [58]. Gusain et al. [42] have recently reported that nanocomposite of multiwalled carbon nanotubes (MWCNTs) and titanium dioxide (MWCNT-TiO_2) enhances the photocatalytic activity of pristine TiO_2 by preventing the agglomeration of TiO_2 and thus offering larger surface area for photodegradation.

This book belongs to Badji Mokhtar Annaba University Central Library
Copyright Elsevier 2025

31.4.1.2 Graphene-supported nanophotocatalyst

Graphene, graphene oxide (GO), and reduced graphene oxide (rGO) are widely explored nanophotocatalysts having large surface area, excellent electrical and chemical stability, and greater carrier mobility. Graphene-based metal oxide nanocomposites have shown enhanced photocatalytic activity by inhibiting recombination of electron and hole pairs [59]. The metal oxide graphene nanocomposite enhances the photocatalytic activity by lowering the band gap and increasing the surface area of catalyst. The GO-TiO_2 nanocomposite shows better photocatalytic activity compared with pristine TiO_2 as it lowers the band gap and quenches the photoluminescence under visible light [60].

Dong et al. [45] have reported synthesis of $ZnSnO_3$ hollow nanospheres and $ZnSnO_3$/rGO nanocomposites, and its performance was evaluated by the degradation of metronidazole. The photocatalytic degradation efficiencies of the metronidazole wastewater are depicted in Fig. 31.1 under UV (A) and visible light (B) irradiation. It can be seen from Fig. 31.1A that remarkably higher degradation efficiency of metronidazole is obtained using $ZnSnO_3$ hollow nanospheres compared with that in the absence of $ZnSnO_3$ (blank test) applying 60 min UV irradiation, which indicates excellent photocatalytic activity of prepared $ZnSnO_3$ hollow nanospheres. It can be observed from Fig. 31.1B that, under visible light irradiation (duration: 180 min), the degradation efficiencies of metronidazole were 42.1% and 72.5% using the $ZnSnO_3$ hollow nanospheres and $ZnSnO_3$/rGO nanocomposites, respectively, whereas the pure rGO samples and $ZnSnO_3$-rGO physical mixtures showed extremely poor photocatalytic degradation efficiency. Similar results have been reported in the literature for the degradation of various pharmaceutical compounds such as acetaminophen [46], carbamazepine, ibuprofen, and sulfamethoxazole [47], atenolol [61], diclofenac (DCF; [62]), and risperidone [16] using TiO_2-rGO nanocomposites.

Nitrogen and sulfur doping of TiO_2-rGO nanocomposites can enhance the photocatalytic efficiency of TiO_2 by changing its surface properties and enabling its use under solar light irradiation [15]. Many other nanocomposites such as β-tin tungstate-rGO, CuO nanoflower-decorated rGO, GO-Fe_3O_4, and ZnO-GO have also been reported in the literature for the photocatalytic degradation of various organic pollutants [48, 63, 64]. Le et al. [65] have reported the photocatalytic degradation of phenols using novel Fe-Fe_3O_4-GO nanocomposite, whereas Gupta et al. [41] have demonstrated the degradation of chlorpyrifos, an organophosphate insecticide, using $CoFe_2O_4$-TiO_2-rGO nanocomposites. Similarly, other graphene-based nanocomposites have also proved to be efficient for degradation of various organic pollutants. It includes 90.6% degradation of ciprofloxacin using ZnO/$ZnAl_2O_4$/rGO nanocomposite [66] and 88% degradation of tetracycline using GO-TiO_2 nanocomposite with UV light as a source of irradiation [67].

This book belongs to Badji Mokhtar Annaba University Central Library Copyright Elsevier 2025

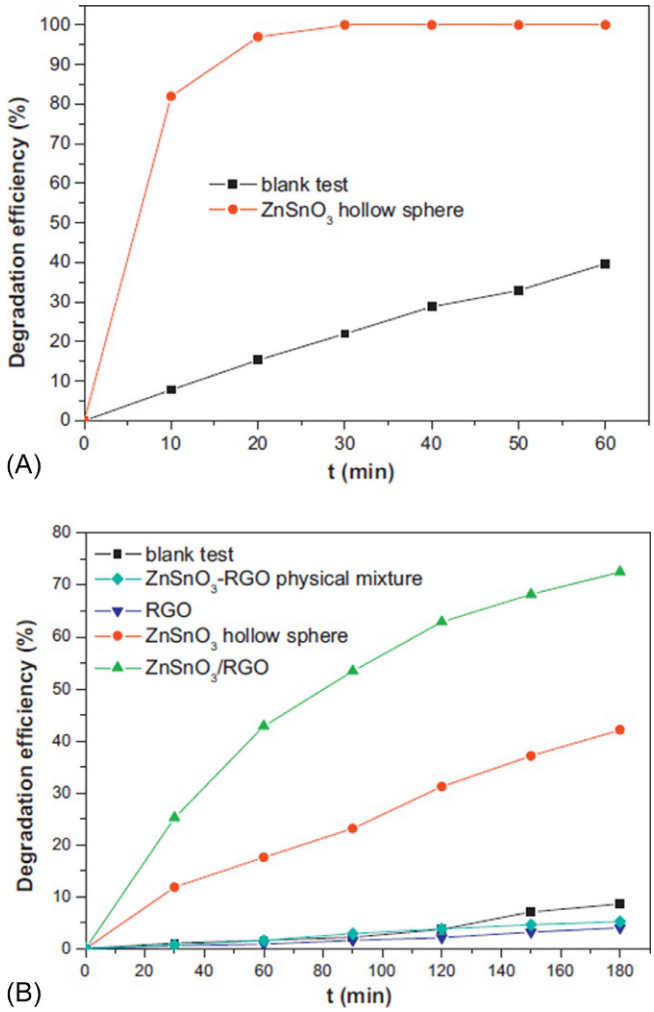

Fig. 31.1

The degradation efficiencies of the metronidazole wastewater by $ZnSnO_3$ hollow nanosphere and $ZnSnO_3$/rGO nanocomposites photocatalysts under UV (A) and visible light (B) irradiation [45].
Reprinted with permission from S. Dong, J. Sun, Y. Li, C. Yu, Y. Li, J. Sun, $ZnSnO_3$ hollow nanospheres/reduced graphene oxide nanocomposites as high-performance photocatalysts for degradation of metronidazole, Appl. Catal. B Environ. 144 (2014) 386–393. Copyright (2014) Elsevier.

31.4.1.3 Zinc oxides–based nanophotocatalyst

The nanocrystalline ZnO (band gap 3.3 eV) also exhibits superior photocatalytic activity for the degradation of various MPs. Many researchers have reported the enhancement in the photocatalytic activity of ZnO by doping it with various metals and nonmetals or supporting it

This book belongs to Badji Mokhtar Annaba University Central Library Copyright Elsevier 2025

on carbon-based materials. Such modifications have resulted in reducing the band gap of ZnO and lowering the rate of recombination of electron and hole pairs. Navarro et al. [68] have reported the photocatalytic degradation of various pesticides in the leaching water using ZnO/$Na_2S_2O_8$ nanocomposite under natural sunlight as a source of irradiation. The authors have reported increased photocatalytic activity of ZnO because of addition of $Na_2S_2O_8$, which in turn has resulted in reduction of photodegradation time. It was also observed that the photocatalytic activity of ZnO strongly depends on the pH of the solution and it decreases at lower pH because of photocorrosion effect [17]. Many studies reported in the literature such as Mn^{2+} doped ZnO for the degradation of methylene blue [49], Pd-doped ZnO for the degradation of Congo red (CR) [50], Cu-doped ZnO nanorods for the degradation of diazinon [69], Er-doped ZnO nanorods for the removal of Direct Red-31 [51] have proved to be effective under visible light irradiation.

31.4.1.4 Cerium oxide–based nanophotocatalyst

The cerium oxide or ceria, which exhibit super photocatalytic activity, can be utilized for photocatalytic degradation of various organic pollutants. It is a nontoxic and thermally stable photocatalyst. The photocatalytic activity of ceria NPs is majorly decided by the calcination temperature. Low calcination temperature facilitates the availability of large number of hydroxyl groups, which facilitate higher rate of adsorption as well as photocatalytic activity when applied for the degradation of organophosphorous pesticides [70].

Certain drawbacks of ceria such as high rate of recombination of photo generated electron-hole pairs and low quantum yield limit its application in visible light region. To overcome these drawbacks, ceria-based hetero structures such as TiO_2-Pt-CeO_2 [43], Au/CeO_2 [71], CdS/CeO_2 [72], Sr-TiO_2/CeO_2 [73], Bi_2O_3/CeO_2 [52], TiO_2/CeO_2 [74,75], and Cu_2O/CeO_2 [53] have been widely used for removal of various MPs. Magdalane et al. [54] have reported 98% degradation of rhodamine B under visible light using CeO_2-Y_2O_3 nanostructures. Mn-doped ceria has shown higher photocatalytic activity compared with ceria.

31.4.1.5 Silver-based nanophotocatalysts

Silver (Ag) NPs are the most popular because of their unique physical, chemical, and biological properties compared with their macro-scaled counterparts [76]. The advantage of the silver NPs includes small loss of the optical frequency during the surface-plasmon propagation [77], chemical stability, nontoxic, stability at ambient conditions, low cost than the other noble metals such as gold and platinum. Advantages also include high electrical and thermal conductivity, wide absorption of visible and surface-enhanced Raman scattering. Silver-based NPs have shown promising application as visible light photocatalysts because of their excellent photocatalytic and photochromic activity [78]. The properties of these nanophotocatalysts such as high surface area, enriching pore structure, design heterojunction, and strong visible light response enhance their photocatalytic activity. However, Ag-based nanophotocatalysts

This book belongs to Badji Mokhtar Annaba University Central Library Copyright Elsevier 2025

show poor stability because of photochemical corrosion. Moreover, silver-based semiconductors when combined with carbon materials such as carbon nanofibers, carbon nanotubes (CNTs), and graphene could produce more efficient nanocomposite photocatalyst [79]. Silver NPs show higher photocatalytic activity by the reduction of electro-hole recombination reaction because of shape-dependent optical properties, its localized surface plasmon resonance, and the collective oscillations of their conduction band electrons [80].

Rostami-Vartooni et al. [81] reported complete mineralization of methyl orange (MO) and CR using highly active and recyclable Ag/TiO_2 nanocomposite as photocatalyst in the presence of irradiation by two 8-W high-pressure mercury lamps at room temperature. In another study, Yola et al. [82] reported high photocatalytic activity for degradation of the reactive dyes from single and binary dye solutions using silver NP-colemanite ore waste (Ag-COW).

31.4.2 Factors influencing the photocatalysis process

The efficiency of photocatalytic process is strongly influenced by various parameters such as loading of photocatalyst, pH of the solution, irradiation source, temperature of the solution, and initial concentration of the pollutant. The details are as follows.

31.4.2.1 Loading of the nanophotocatalyst

The loading of a photocatalyst plays an important role in the photocatalytic degradation of various MPs. Estimation of optimum photocatalyst loading is essential for maximizing the rate of degradation of MPs.

It has been reported that the rate of photocatalytic degradation of MPs increases with an increase in the photocatalyst loading because of increased availability of photo active sites for the degradation of pollutants [83,84]. However, very high catalyst loading may lead to the agglomeration of NPs resulting in to reduced number of active sites available for photodegradation, thereby lowering the photocatalytic efficiency. Highly turbid suspensions at higher loading of photocatalyst may further decrease the net transfer of the incident energy and hinder in the illumination of all the catalyst particles in the reactor. Furthermore, increasing opacity and light scattering effect at increased loading of photocatalyst decrease the photocatalytic activity [85].

Ahmadi et al. [86] have investigated photocatalytic degradation of tetracycline using nanocomposite of TiO_2 and MWCNTs under ultraviolet-C (UVC) as a source of irradiation. To obtain the effect of catalyst loading on the rate of degradation of tetracycline, the loading of MWCNT/TiO_2 nanocomposite was varied over the range of 0.1–0.4 g/L at an optimum pH value of 5. An increase in the photocatalytic degradation of tetracycline was observed with an increase in the catalyst loading till 0.2 g/L. Further increase in the catalyst loading has shown no significant enhancement in the photocatalytic activity because of light scattering effects.

This book belongs to Badji Mokhtar Annaba University Central Library Copyright Elsevier 2025

Naghizadeh et al. [87] have synthesized $ZnO/CoFe_2O_4$ magnetic nanocomposite for photocatalytic degradation of imidacloprid pesticide. It was reported that the photocatalytic degradation of imidacloprid increases by increasing the photocatalyst loading over the selected range of photocatalyst as 0.02–1 g/L.

Similar results have been reported in the literature for photocatalytic degradation of ibuprofen by TiO_2-Fe and TiO_2-rGO coated side-glowing optical fibers [47]. Sayadi et al. [88] have investigated the effect of GO-Fe_3O_4/ZnO/SnO_2 loading on the photocatalytic degradation of azithromycin and reported an increase in the photodegradation efficiency till optimum loading of catalyst. Increase in the catalyst loading above optimum value has shown decrease in the rate of degradation of azithromycin because of higher turbidity of solution resulting into reduced light penetration and dispersion.

31.4.2.2 pH of the solution

The solution pH plays a crucial role in determining the photocatalytic degradation efficiency of MPs using nanomaterials. The operating pH of solution strongly affects adsorption of MPs on the photocatalyst surface, the extent of aggregation of nanomaterial, the surface charge of photocatalyst, and the position of band edge [89]. The catalyst particles are protonated and positively charged at low pH (pH below the point of zero charge), whereas the surface is deprotonated and more negatively charged at higher pH [90]. In photocatalytic degradation process, photo generated holes (h^+) are the dominant oxidizing species at lower pH values, whereas under neutral or alkaline conditions, hydroxyl radicals (OH^-) play an important role [91].

Yuan et al. [92] have investigated photocatalytic degradation of ibuprofen using CNT-TiO_2 and reported highest degradation at acidic pH of 5. This may be because of increased surface affinity between positively charged catalyst surface and negative-charged ibuprofen resulting in higher photocatalytic activity. Another study of photocatalytic degradation of chlortetracycline using GO-TiO_2 showed an increase in the rate of photocatalytic degradation with an increase in the solution pH over the range of 1–4 [93]. Basha et al. [94] have reported highest rate of photocatalytic degradation of amoxicillin (AMX) using activated carbon-TiO_2 at alkaline pH 9. Elmolla and Chaudhuri [95] have reported that the rate of photocatalytic degradation of pharmaceutical drugs (AMX, ciclopirox, and ampicillin) by using TiO_2 is highest at pH of 11, whereas lowest rate was observed at pH of 5. This was attributed to the beneficial changes in the morphology of the photocatalyst and pharmaceutical drug at lower pH. Hu et al. [96] have also reported better removal efficiency of sulfamethoxazole under alkaline pH, which may be because of the higher extent of adsorption of pollutant on the photocatalyst surface or because of changes in the acid-base speciation of sulfamethoxazole.

This book belongs to Badji Mokhtar Annaba University Central Library Copyright Elsevier 2025

Many studies reported in literature have also shown better rate of degradation of organic pollutants at acidic medium compared with alkaline medium [97,98]. Ye et al. [98] have also investigated the effect of solution pH on photocatalytic degradation of metoprolol by using TiO_2 nanotube arrays (TNAs) as photocatalyst and UV-light-emitting diodes (LED) as a source of irradiation. Authors have reported moderate decrease in the rate of photocatalytic degradation of metoprolol under basic operating pH (pH 11). This may be because of electrostatic repulsive effect between deprotonated metoprolol and the catalyst surface. TNA surface that was negatively charged under basic pH conditions [99] make it more repulsive to deprotonated metoprolol. Similar results are also reported in literature for photocatalytic degradation of Reactive Yellow 2 [97]. Authors have reported decrease in the photocatalytic degradation of dye with an increase in the solution pH.

31.4.2.3 Irradiation source

Photocatalytic reactors mostly use solar light, UV lamps, conventional lamps, and LED as a source of irradiation. Conventional lamps are inexpensive compared with UV source but contain toxic mercury and have short life span. LED having longer life time are nontoxic and an energy efficient alternative.

The source of irradiation is important as both the wavelength and light intensity affect the rate and efficiency of degradation reaction. Photocatalyst excitation takes place when photon energy exceeds the band gap. Semiconductor metal oxide NPs need UV light for its activation because they have higher band gap. UV light at wavelengths less than 400 nm is required for pure commercial TiO_2 photocatalyst [100]. Yang et al. [101] have reported high photocatalytic degradation efficiency of formaldehyde using TiO_2 under UV source of irradiation. Similarly, in another study, Hu et al. [96] reported no sulfamethoxazole degradation in TiO_2 suspensions using visible light as a source of irradiation.

However, any modification in the metal oxide by doping or supporting it on carbon-based structures can reduce the band gap and enable their application under visible light. Potential excitation of carbon-based TiO_2 composites (band gap: 2.6–3.0 eV) creates a carbon-oxygen-titanium linkage that can expand the absorption band into visible wavelengths [102,103]. Czech and Buda [104] investigated photocatalytic degradation of DCF using a CNTs-TiO_2-SiO_2 photocatalyst using UV and solar irradiation and reported high degradation efficiency of 70% using UV and >90% using solar light as a source of irradiation. Similarly, Zhang et al. [105] reported higher photodegradation rate of 4-chlorophenol using graphene-nanofiber-TiO_2 composite compared with pristine TiO_2 under visible light irradiation.

31.4.2.4 Reaction temperature

The reaction temperature significantly influences the photodegradation of various MPs. The rate of photocatalytic degradation of MPs increases with an increase in the temperature for majority of the cases. This may be because of modification in kinetic and the activation energies

This book belongs to Badji Mokhtar Annaba University Central Library Copyright Elsevier 2025

of photocatalyst [106]. An increase in the reaction temperature causes formation of bubbles, which may result in higher generation of free radicals and lower electron-hole recombination [107]. Generally, the photocatalytic degradation rate increases with an increase in temperature of solution [83,91]. Barakat et al. [106] have studied the effect of temperature on photocatalytic degradation of rhodamine B dye using Ag-doped TiO_2 NPs using UV light as a source of irradiation. The experiments were conducted by varying temperature over the range of 5–50°C and reported that the maximum degradation efficiency was at 55°C temperature.

Photocatalytic degradation of organic pollutants can occur at ambient temperature and atmospheric pressure [91,108]. The optimum reaction temperature for high photocatalytic activity of TiO_2 is in the range 20–80°C. The photocatalytic activity of TiO_2 decreases at lower temperatures (<0°C) because of the requirement of higher activation energy for excitation of a photocatalyst [100]. The temperature above 80°C may enhance the recombination of charge carriers [40], leading to lesser photocatalytic activity. However, sometimes temperature has negative impact on degradation efficiency in case of the nanofibrous morphology because of the super activity of the surface compared with the NPs [106].

31.4.2.5 Initial concentration of micropollutant

The initial concentration of targeted MP is an important operating parameter that significantly affects the efficiency of photocatalytic process. The photocatalytic degradation efficiency reduces with an increase in the initial concentration of micropollutant. This may be because of the unavailability of the photocatalyst surface because higher number of pollutant molecules get adsorbed on the surface of photocatalyst, thereby lowering the photocatalytic efficiency [109]. Also, the number of photons reaching the photocatalyst surface reduces with an increase in the initial concentration, which leads to reduction in the photo excitation of electrons from valance band to conduction band and further decreases the photocatalytic degradation efficiency [110–112].

Farzadkia et al. [113] have investigated the effect of initial concentration of metronidazole on its photocatalytic degradation using TiO_2 NPs. It was reported that the extent of photocatalytic degradation of metronidazole decreases with an increase in the initial metronidazole concentration. This was attributed to the accumulation of more pollutant and intermediate molecules on the catalyst surface at higher concentration leading to detrimental effect on the degradation efficiency. Ye et al. [98] have also evaluated photocatalytic degradation of metoprolol using TiO_2 nano-arrays (TNAs) over the range of 0.1–1.5 mg/L initial concentration of metoprolol. Decrease in the degradation efficiency as well as rate constants was reported when initial concentration was increased beyond 1 mg/L. This was attributed to lesser availability of reactive species at higher loading of metoprolol under same irradiation conditions.

Sayadi et al. [88] have reported the effect of initial concentration of azithromycin on its photocatalytic degradation efficiency. Reduction in the rate of photocatalytic degradation of

This book belongs to Badji Mokhtar Annaba University Central Library Copyright Elsevier 2025

azithromycin was observed with an increase in its initial concentration because of the availability of limited number of active sites on the catalyst surface. At a low concentration of pollutants, the probability of reaction between reactive radicals and a pollutant species increases, thereby increasing the rate of photocatalytic degradation. Prados-Joya et al. [114] and Palominos et al. [115] have also observed a similar trend.

31.5 Adsorption process using nanomaterials

Adsorption process can effectively be used for removal of various MPs present in wastewater. The high efficiency, sustainable resources of adsorbents, low maintenance cost, faster rate of adsorption, and ease of operation make this process very useful for the removal of many MPs [42]. It is a process wherein a MP molecule adheres on the surface of an adsorbent because of electrostatic and hydrophobic interactions between the targeted MP and the adsorbent [116]. Nanotechnology has found many applications in adsorption operation applied for removal of MPs. Nanomaterials or nanocomposites applied as an adsorbent have the major advantage of higher surface area and active sites compared with conventional adsorbents.

31.5.1 Nanomaterials applied as an adsorbent

Various nanomaterials have been used so far for the effective removal of MPs. It majorly includes metal oxide-based nanoadsorbents, carbon-based nanoadsorbents, and nanocomposites of these metal- and carbon-based NPs. Table 31.2 exhibits the summary of various nanomaterials applied as an adsorbent and the target pollutant.

Various types of nanomaterials and their composites applied as an adsorbent are discussed in detail in the following sections.

31.5.1.1 Metal oxide-based nanoadsorbent

Metal oxide-based nanoadsorbents are widely used for the removal of various MPs. The metal oxides such as titanium dioxide, zinc oxide, alumina, and iron oxide are the low-cost nanoadsorbent for fast and efficient removal of MPs from the wastewater. Titanium dioxide NPs have shown enhanced adsorption efficiency because of ample availability of precursors, higher reactivity, and facile synthesis methods [131]. Similarly, zinc oxide NPs are also extensively used as nanoadsorbent for the wastewater treatment applications because of its inexpensive cost, facile preparation methods, nontoxicity, and tunable surface and textural features. To further enhance the adsorption capacity of ZnO, many researchers have explored doping of ZnO NPs. Moradi Dehaghi et al. [117] have reported increase in the adsorption efficiency of permethrin pesticide using chitosan-ZnO nanocomposites compared with that of chitosan alone. Meng et al. [118] have also reported the high efficiency of Cr-doped ZnO NPs

This book belongs to Badji Mokhtar Annaba University Central Library Copyright Elsevier 2025

Table 31.2: Summary of nanomaterials applied as an adsorbent.

Sr. no.	Nanomaterials applied as an adsorbent	Target pollutant	Important findings	References
1	Chitosan-ZnO nanocomposites	Permethrin pesticide	99% removal of permethrin solution (0.1 mg/L) using 0.5 g of the nanocomposite at room temperature and pH 7	[117]
2	Cr-doped ZnO nanoparticles	Methyl orange	Optimal molar ratio of Cr/Zn is 6%. Maximum adsorption capacity of 310.56 mg of methyl orange per g of adsorbent	[118]
3	Magnetic mesoporous silica, Fe_3O_4-$n$$SiO_2$-$m$$SiO_2$ nanocomposite	DDT (1,1,1-trichloro-2,2-bis(4-chlorophenyl) ethane)	97% removal of DDT from aqueous media in 60 min. Nanocomposite exhibited high specific surface area of 577 m^2/g	[119]
4	Chitosan-modified silver oxide (AgO) nanoparticles	Permethrin pesticide	99% removal of permethrin pesticide using chitosan-modified AgO nanoparticles compared with mere 49% removal using pure chitosan	[120]
5	Zero valent iron-loaded metal oxide nanoparticles	Nitrobenzene	Zero valent iron loaded silica nanoparticles showed maximum adsorption potential (1155 mg/g) for nitrobenzene	[121]
6	Zirconia-carbon (ZrO_2-C) nanocomposite	Trichlorophenol	High level adsorption of chlorophenol by ZrO_2-C nanocomposite because of π–π interactions and hydrogen bonds between chlorophenol and nanocomposite	[122]
7	Hollow spheres of Ceria (CeO_2)	Acid dye, acid black 210	Higher adsorption capacity of 175.75 mg/g because of porous structure and the strong electrostatic interaction	[123]
8	Tungsten dioxide (WO_3) nanosheets	Methylene blue	Maximum adsorption potential of 600 mg/g	[124]
9	Nickel oxide (NiO) microspheres	Congo red	Maximum adsorption capacity of 534.8 mg/g for NiO because of electrostatic interaction between the positively charged microspheres and the anionic dye molecules	[125]

Continued

This book belongs to Badji Mokhtar Annaba University Central Library

Copyright Elsevier 2025

Table 31.2: Summary of nanomaterials applied as an adsorbent—cont'd

Sr. no.	Nanomaterials applied as an adsorbent	Target pollutant	Important findings	References
10	Activated carbon (AC), carbon xerogel (CX), and carbon nanotubes (CNT)	Antibiotic, ciprofloxacin	Maximum adsorption capacity increases as CX < CNT < AC with adsorption capacities from 112 to 230 mg/g	[126]
11	Powdered activated carbon (PAC), single-wall (SWCNTs), and multiwalled carbon nanotubes (MWCNTs)	Antibiotics (lincomycine and sulfamethoxazole) and one contrast medium (iopromide)	The adsorption followed the order SWCNT > PAC > MWCNT	[127]
12	Graphene oxide (GO)	Levofloxacin	GO showed strong adsorption potential of 256.6 mg/g	[128]
13	Reduced graphene oxide (rGO)	Antiinflammatory drug, nimesulide	rGO exhibited the maximum sorption capacity of 82.4 mg/g	[129]
14	Nanocomposite of CNTs and TiO_2	Methyl orange	100% removal of methyl orange in just 30 min of operation	[130]

for the removal of anionic dyes from aqueous solution. This may be attributed to the increased surface defects because of doping, which leads to the formation of hydroxyl groups for the protonation.

Apart from this, iron oxide nanoadsorbents have also been used for adsorption of the MPs. The iron oxide nanomaterials exhibit high surface area to volume ratio and superparamagnetism [132]. The major advantages of using iron oxide-based nanomaterials in wastewater treatment applications are its plentiful availability, easy surface modification, facile synthesis methods, low toxicity, and magnetic segregation [133]. The iron oxide nanocomposites have been extensively used for rapid and effective removal of MPs because of enhanced surface area and availability of higher number of active sites [42]. Liu et al. [119] reported efficient adsorptive removal (97%) of DDT (1,1,1-trichloro-2,2-bis(4-chlorophenyl) ethane) using magnetic mesoporous silica Fe_3O_4-$n$$SiO_2$-$m$$SiO_2$ in 60 min of treatment time. Other metal oxide nanomaterials such as Cu_2O, MoO_2, MoO_3, SnO_2, and CeO_2 have also been extensively used as nanoadsorbents for removal of MPs from wastewater. The MnO_2 nanomaterials because of its negatively charged surface at the higher pH level can be used for the selective adsorption of cationic pollutants [134]. Rahmanifar and Moradi Dehaghi [120] have reported higher percentage removal of permethrin pesticide using chitosan-modified AgO NPs (99% removal) compared with that using pure chitosan (49% removal). Many studies have been reported in the literature using various nanostructures for efficient removal of MPs such as nitrobenzene

This book belongs to Badji Mokhtar Annaba University Central Library Copyright Elsevier 2025

removal using Fe-loaded SiO_2 [121], trichlorophenol removal using ZrO_2-C flower like morphology [122], acid dyes removal using ceria CeO_2 [123], methylene blue removal using tungsten dioxide [124], and Congo red removal using NiO microspheres [125].

31.5.1.2 Carbon-based nanoadsorbents

Nowadays, carbonaceous nanomaterials [135, 136] are gaining attention of many researchers because of its high adsorption capacity owing to its large surface area, physicochemical properties, and availability of functional groups on nanomaterials. CNTs and GOs are the most frequently used carbon-based nanoadsorbents.

CNTs are capable of adsorbing most of the MPs because of the diverse interaction of pollutant and CNT surface, hydrogen bonding, hydrophobic effect, π-π interactions, electrostatic interactions, and covalent bonding [137]. Organic MPs bearing various functional groups can establish hydrogen bond with the graphitic CNT surface that donates electrons [9, 138]. GO has also found extensive applications in adsorption because of its large specific surface area, excellent physical-chemical properties, and availability of large number of surface oxygen-containing groups [139].

Carabineiro et al. [126] reported 67.5% of ciprofloxacin removal using 50 mg of CNTs, whereas Apul and Karanfil [140] reported the effective removal of sulfapyridine, ciprofloxacin, and tetracycline by CNTs. In another study, Kim et al. [127] reported 90% removal of lincomycin and sulfamethoxazole using single-wall carbon nanotubes (SWCNTs) and MWCNTs. It has been reported in the literature that pharmaceutical compounds such as levofloxacin and metformin can be removed effectively using GO as nanoadsorbent [128,139], whereas antiinflammatory nimesulide can be effectively removed using reduced GO [129]. Ahmad et al. [130] have reported that nanocomposite of CNTs and TiO_2 has good affinity for anionic dyes and hence can remove 100% of MO in merely 30 min.

31.5.2 Factors affecting on adsorption

The rate of adsorption of MPs using nanomaterials is governed by many factors such as pH of the solution, ionic strength, agitation time, dosage of adsorbents, initial concentration of MPs, temperature of the solution, and dissolved organic matter. Hence, it is essential to investigate the effect of these parameters on the efficacy of adsorption process. The details of effect of these parameters are discussed in the following sections.

31.5.2.1 pH of solution

The adsorption process for removal of MPs strongly depends on solution pH as it affects protonation or deprotonation of pollutants according to their pK_a values. It is a well-accepted fact that the effect of pH on the extent of adsorption is adsorbate or MP specific [141]. It has also

This book belongs to Badji Mokhtar Annaba University Central Library Copyright Elsevier 2025

been observed that pH of aqueous solution of MP significantly affects the charge and properties of functional groups present on the target MP and absorbent surface [136].

In general, it has been observed that increasing the initial pH of aqueous solution of MP leads to the dissociation of target MP into negatively charged compound with hydrophilic nature and thereby reduces the hydrophobic interactions. Hence, higher pH of the solution leads to increased hydrophobicity of organic pollutants, ionization, and solubility, which further reduces the adsorption of pollutants on carbon-based adsorbents such as CNTs [138, 142]. Further electrostatic interactions between MP molecule and nanoadsorbent may also suppress at higher pH. Reduced hydrophobic and electrostatic interaction at higher pH would further fetch lower rate of adsorption of MPs [141]. Such trend was reported by many researchers in previous studies. Ji et al. [143] reported decrease in the adsorption efficiency of sulfonamide using MWCNTs with increase in the pH. Yu et al. [144] have also reported similar trend while studying the effect of pH over the range of 1–11 on the adsorption of sulfadimethoxine, sulfamethoxazole, and sulfathiazole using MWCNTs.

Zhu et al. [139] have reported increase in the extent of adsorption of metformin with an increase in the pH from 4.0 to 6.0 using GO as an adsorbent. However, further increase in the pH from 6 to 11 has witnessed decrease in the extent of adsorption of metformin. This may be because of the fact that surface charge and zeta potential of GO and speciation of metformin vary with the pH of solution.

31.5.2.2 Ionic strength

Ionic strength of aqueous solution of MPs can also influence the rate of adsorption of MPs because it can affect the interactions between MP molecule and the adsorbent surface. Ionic strength can be adjusted by adding appropriate quantities of NaCl or $CaCl_2$. It has been observed that the rate of adsorption of hydrophobic MPs increases significantly with an increase in the ionic strength. Hydrophobic compound usually shows salting out effect at higher ionic strength, which ultimately increases the tendency of MP molecule to precipitate out from the solution and get adhered to the surface of absorbent [89]. It has also been indicated that when there is electrostatic repulsion between MP molecule and adsorbent, increasing ionic strength would have a positive effect.

Zhou et al. [145] have observed that the amount of adsorption of triclosan on MWCNTs (pH −3) of 136.1 mg/g obtained at the ionic strength of 0.001 M substantially increased to 153.1 mg/g by increasing the ionic strength to 0.01 M. However, this trend is not same for all MPs. Gao et al. [146] have observed that the amount of adsorption of tetracycline on GO decreases by increasing the ionic strength. Higher ionic strength reduces the electrostatic repulsion between GO particles, leading to their aggregation and reduced active surface area, which may thereby reduce the extent of adsorption. Adsorption capacity of GO may reduce at higher ionic strength because both Na^+ and MP molecule will try to get adsorbed [147].

This book belongs to Badji Mokhtar Annaba University Central Library Copyright Elsevier 2025

Zhu et al. [139] have also observed that the amount of adsorption of metformin on surface of GO decreases by enhancing the concentration of NaCl from 0 to 0.1 M. Zhao et al. [136] have also indicated that higher ionic strength reduces the uptake capacity of carbon-based adsorbents like CNTs when applied for the adsorption of sulfamethoxazole, thiamphenicol, and ibuprofen.

31.5.2.3 Agitation time and dosage of adsorbents

Agitation time and dosage of absorbents play a crucial role in maximizing the efficiency of adsorption process. In general, increasing the agitation time and dosage of absorbents provides greater opportunity to the MPs to adhere on the surface on nanoadsorbents [117]. Furthermore, higher dosage of adsorbents can also increase the effective area of adsorption, and higher agitation time can ensure the near equilibrium conditions. However, higher agitation time and dosage of absorbents may also increase the energy requirement and lead to the higher costs of operation [116]. Hence, it is essential to determine the optimum agitation time and optimum dosage of absorbents for making adsorption process a cost-effective one.

Moradi Dehaghi et al. [117] have studied the effect of dosage of adsorbent and agitation time on the percentage removal of permethrin by using nanocomposite of chitosan and ZnO NPs as an adsorbent. It was observed that percentage removal of permethrin increases with an increase in the dosage of nanocomposite because of availability of higher number of total active sites and higher effective surface area of the adsorbent. However, beyond the optimal concentration of adsorbent (0.5 g adsorbent per 25 mL), the availability of active sites would be less because of enhanced sorbent-sorbent interactions compared with sorbate-sorbent interactions. It was also observed that percentage removal of permethrin increases with an increase in the agitation time from 10 to 90 min. However, further increase in the agitation time beyond this optimal value has witnessed no further enhancement because adequate number of active sites is no longer available at the later stage.

Kiran Kumar and Venkata Mohan [135] have also demonstrated that the rate of adsorption of estriol, an endocrine-disrupting estrogen on MWCNTs increases with the agitation time up to 15 min. Adsorption was negligible with further increase in the agitation time. Reduction in the adsorption rate after reaching the equilibrium may be because of less availability of active sites on the surface of the adsorbent. Similar trend was also observed by Rahmanifar and Moradi Dehaghi [120] and Meng et al. [118] for the adsorption of some other MPs.

31.5.2.4 Initial concentration of micropollutant

Initial concentration of MP can also significantly affect its rate of adsorption. Many studies reported in the literature have indicated that percentage removal of MPs generally decreases with an increase in the concentration of MP [118,135]. This may be because of the fact that less number of active sites are available on the adsorbent surface at higher concentration of MPs. Hence, at low MP to adsorbent ratio, the MPs will occupy the higher energy sites. However, at

This book belongs to Badji Mokhtar Annaba University Central Library Copyright Elsevier 2025

higher ratios, low-energy sites will be utilized because higher energy sites are already saturated leading to the decreased rate of adsorption of MPs [117,120].

Meng et al. [118] have illustrated the effect of initial concentration of MO dye on its rate of adsorption using chromium-doped ZnO NPs. It was observed that the rate of adsorption of MO increases with an increase in the initial concentration of MO till the optimal value on 300 mg/L. Increasing the concentration of MO beyond an optimal value has resulted in reduction in the rate of adsorption because saturation of adsorption surface was obtained. Rahmanifar and Moradi Dehaghi [120] have also observed a similar trend when chitosan-based silver oxide NPs were applied for the adsorption of organochlorine pesticide.

31.5.2.5 Temperature of the solution

Temperature has a profound effect on the rate of adsorption of MPs because it has been observed that removal efficiency of the same MP significantly changes in winter and summer period. Increased temperature has shown positive effect on the rate of adsorption of MPs. However, increased rate of adsorption was obtained at the expense of additional cost [116].

Hu et al. [123] have also observed that temperature has a major influence on the rate of adsorption of acid dye using hollow spheres of ceria as an adsorbent. It was reported that higher temperature activates the MP molecules and enhances their dispersing rate. Meng et al. [118] have also observed that the rate of adsorption of MO on Cr-doped zinc oxide NPs increases by increasing the temperature of the solution.

31.5.3 Adsorption kinetics

Kinetic data obtained from the batch adsorption studies of various MPs can be used further to study the kinetic models such as pseudo first-order, pseudo second-order kinetic model and the intra particle diffusion model.

Adsorption rate based on pseudo first-order kinetic model can be obtained by Eq. (31.1) [130]. It indicates that the rate of adsorption of MP is based on the uptake capacity of the adsorbents.

$$\frac{dq_t}{dt} = k_1(q_e - q_t) \tag{31.1}$$

Integrating and solving Eq. (31.1) [130] will provide the necessary mathematical expression Eq. (31.2) [130] for the pseudo first-order kinetic model.

$$\log(q_e - q_t) = \log(q_e) - (k_1/2.303)t \tag{31.2}$$

Where q_e is the amount of MP adsorbed at equilibrium, q_t is the amount of MP adsorbed at any time t, and k_1 is the pseudo first-order rate constant. The plot of $\log(q_e - q_t)$ Vs t will provide the values of k_1 and q_e by the slope and the intercept.

This book belongs to Badji Mokhtar Annaba University Central Library
Copyright Elsevier 2025

Similarly, adsorption rate based on pseudo second-order kinetic model can be obtained by Eq. (31.3) [136]. This model is based on chemisorption controlled adsorption process.

$$\frac{dq_t}{dt} = k_1(q_e - q_t)^2 \tag{31.3}$$

Integrating and solving Eq. (31.3) [136] will provide the necessary expression Eq. (31.4) [136] for the pseudo second-order kinetic model.

$$\frac{t}{q_t} = \frac{1}{k_2 q_e^2} + \frac{1}{q_e} t \tag{31.4}$$

The plot of t/q_t *Vs* t will provide the values of q_e and k_2 by the slope and the intercept. Furthermore, the intraparticle diffusion model based on Fick's second law [135] can be expressed mathematically as Eq. (31.5) [135]

$$q_t = k_p(t)^{0.5} + C \tag{31.5}$$

The plot of q_t *Vs* $t^{0.5}$ can provide the value of k_p, the intraparticle diffusion rate constant. Adsorption studies reported in the literature have observed that batch adsorption data of most of the MPs fit to pseudo first-order, pseudo second-order kinetic models.

Ahmed et al. [9] have performed the batch adsorption studies of MO on functionalized nanotubes and have studied pseudo first-order, pseudo second-order, and the intraparticle diffusion kinetic model. It was observed that kinetic data best fitted to the pseudo second-order kinetic model. Kiran Kumar and Venkata Mohan [135] have evaluated the kinetics of adsorption of endocrine-disrupting estrogens on MWCNTs. It was observed that adsorption data show reasonably good fit to pseudo second-order kinetic model. Zhu et al. [139] have performed the batch adsorption of metformin using GO and obtained adsorption data were processed with pseudo first-order and pseudo second-order kinetic models. The adsorption data of metformin fitted well with the pseudo second-order kinetic model because the correlation coefficient value, i.e., R^2 was better in case of pseudo second-order kinetic model compared with pseudo first-order kinetic model. Meng et al. [118] have also observed that kinetic data for adsorption of MO on chromium-doped ZnO NPs fitted well with pseudo second-order kinetic model.

31.5.4 Adsorption isotherm or adsorption equilibrium

Adsorption isotherms can be used to provide the qualitative information about uptake capacity of adsorbents and to study the equilibrium adsorption data. Freundlich adsorption isotherm, Langmuir adsorption isotherm, and Dubinin-Radushkevich (D-R) adsorption isotherm are frequently applied by many researchers to analyze the adsorption equilibrium data [135].

This book belongs to Badji Mokhtar Annaba University Central Library Copyright Elsevier 2025

The Langmuir adsorption isotherm assumes that adsorption occurs in monolayer only. Hence, when any vacant site is occupied by the MP, further adsorption on the same site is not possible. The mathematical expression for Langmuir adsorption isotherm can be presented by Eq. (31.6) [123].

$$\frac{C_{eq}}{Q_{eq}} = \frac{1}{Q_{max} k_L} + \frac{C_{eq}}{Q_{max}} \tag{31.6}$$

Where C_{eq} represents the equilibrium concentration of MP in the solution, Q_{eq} represents the equilibrium concentration of MP adsorbed, Q_{max} is the maximum adsorption capacity of the MP per unit mass of adsorbent, and k_L is the Langmuir adsorption constant. The values of Q_{max} and k_L can be obtained by plotting the (C_{eq}/Q_{eq}) vs C_{eq}.

The Freundlich adsorption isotherm is not restricted to the monolayer adsorption. It assumes that adsorption occurs in multilayer on the heterogeneous surfaces. The mathematical expression for Freundlich adsorption isotherm can be represented by Eqs. (31.7) and (31.8) [118,123].

$$Q_{eq} = k_F C_{eq}^{1/n} \tag{31.7}$$

$$\log\left(Q_{eq}\right) = \log\left(k_F\right) + \frac{1}{n}\log\left(C_{eq}\right) \tag{31.8}$$

Where k_F and $1/n$ are the Freundlich constants corresponding to adsorption capacity and measure of intensity of adsorption, respectively. These constants can be obtained by plotting $\log(Q_{eq})$ vs $\log(C_{eq})$. Furthermore, Dubinin-Radushkevich (D-R) model has been developed to make a distinction between physical and chemical adsorption by estimating mean free energy of adsorption. The mathematical expression for D-R isotherm model can be represented by Eq. (31.9) [135].

$$\ln Q_{eq} = \ln Q_{max} - \beta\varepsilon^2 \tag{31.9}$$

Where β represents the D-R isotherm constant, which is based on the mean free energy of adsorption and ε represents the Polanyi potential, which can be calculated by using Eq. (31.10) [135].

$$\varepsilon = RT \ln\left(1/C_{eq}\right) \tag{31.10}$$

Kiran Kumar and Venkata Mohan [135] have observed that adsorption of endocrine-disrupting estrogen by using MWCNTs reasonably fits to the Langmuir adsorption isotherm. Meng et al. [118] have also indicated that the adsorption of MO by using chromium-doped ZnO NPs agrees well with Langmuir adsorption isotherm with Q_{max} value of 310.56 mg/g. Hu et al. [123] have applied various adsorption isotherm models to study the equilibrium data obtained by the adsorption of acid dye using ceria hollow spheres. Highest correlation coefficient obtained for Langmuir adsorption isotherm model has confirmed the fact that adsorption data have good

This book belongs to Badji Mokhtar Annaba University Central Library Copyright Elsevier 2025

agreement with that model. Based on Langmuir adsorption isotherm model, the value of Q_{max} was obtained to be 175.75 mg/g. Furthermore, Kim et al. [127] have observed that the data for the adsorption of antibiotics and iopromide on CNTs fitted well with the Freundlich adsorption isotherm model ($R^2 > 0.96$).

31.6 Membrane separation process using nanomaterials

Membrane separation process using nanomaterials has potential application in the removal of MP from wastewater. They have the ability to retain undesired MPs present in water and wastewater streams. The retention of multivalent salts, flexible design with highly automated systems, and a lesser requirement of chemicals and land are some of the advantages of membrane process technology [137]. Membrane selectivity and permeability are the key factors of the membrane technology. Ceramic and polymeric membrane materials have been widely used as conventional membranes in various wastewater treatment applications. Although ceramic membrane possesses chemical inertness and high thermal and mechanical resistance, brittleness and high fabrication cost are the major limitations for its large-scale application [148, 149]. On the other hand, polymeric membranes exhibit better performance and cost effective compared with ceramic membranes. However, poor tolerance to high temperatures, organic solvents, and corrosive environments is the major drawback associated with this membrane [150]. Also, fouling of polymeric and ceramic membranes affects the separation efficiency of these membranes. The high energy consumption, membrane fouling, complexity of operation, and limited life span of membrane are major challenges in the application of membranes in wastewater treatment. To overcome these challenges, nanomembranes have attracted researcher's attention for wastewater effluents of pharmaceutical, dye, and heavy metal industries. Nanomaterials used in nanomembranes improve the membrane permeability, fouling resistance and impart good mechanical and thermal stability. Table 31.3 exhibits the summary of various nanomaterials applied in membrane separation processes for the treatment of water and wastewater.

Following are the details of widely applicable nanomembranes.

31.6.1 Nanofibrous membranes

Nanofibrous membranes developed by electrospinning [160] method exhibits excellent mechanical properties, large surface area, and uniform small pore size with desired functionality [161]. Yüksel et al. [162] reported BPA removal using polyamide nanofiltration (NF) membrane and obtained 98% rejection. In another study, Koyuncu et al. [163] reported the removal of hormones and antibiotics by NF membranes. Authors have reported complete removal of tetracycline because of the larger molecular size. Vergili [164] reported rejection of the model pharmaceuticals carbamazepine, diclofenac, and ibuprofen using nanofibrous

This book belongs to Badji Mokhtar Annaba University Central Library Copyright Elsevier 2025

Table 31.3: Summary of nanomaterials applied in membrane separation processes.

Sr. no.	Type of membrane	Application	Important findings	References
1	Polyethersulfone ultrafiltration membranes modified with alumina (Al_2O_3) nanoparticles	Filtration of activated sludge	Polyethersulfone membranes with 5% weight fraction of showed highest membrane permeability and lowest fouling rate	[151]
2	Polyethersulfone ultrafiltration membranes modified with hybrid nanostructures of multiwalled carbon nanotubes coated with silver nanoparticles	Antimicrobial properties against two bacterial species, *Escherichia coli* and *Staphylococcus aureus*	Antibacterial activity increases by increasing the loading weight of hetero nanostructures	[152]
3	Graphene oxide/Fe(III)-based metal-organic framework membrane	Treatment of synthetic organic pollutants and real textile wastewater	*Organic pollutants*: The rejections were 98.73% for methylene blue, 97.50% for rhodamine B, 93.31% for methyl orange, and 92.66% for bisphenol A by membrane separation *Real textile wastewater*: The removal rates of chemical oxygen demand, total nitrogen, total organic carbon, and suspended matter were about 79.34%, 81.81%, 77.96%, and 93.75%, respectively	[153]
4	TiO_2 nanofiltration membranes	Water purification (removal of salts and dyes)	Rejection of Na_2SO_4 (43%) and $MgSO_4$ (35%) and methylene blue (~96%)	[154]
5	Graphene oxide-doped polysulfone membrane	Removal of organic contaminants from water	Rejection of more than 90% for ofloxacin, benzophenone-3, rhodamine b, diclofenac and triton X-100 after 4 h of treatment time	[155]
6	Polysulfone and graphene oxide nanocomposite membranes	Removal of bisphenol A from water	Nanocomposite membrane with 0.4% of GO exhibited best performance with bisphenol A removal efficiency of 93%	[156]

This book belongs to Badji Mokhtar Annaba University Central Library
Copyright Elsevier 2025

Table 31.3: Summary of nanomaterials applied in membrane separation processes—cont'd

Sr. no.	Type of membrane	Application	Important findings	References
7	Polyvinyl chloride based nanofiltration-membrane modified by cellulose acetate (CA) and iron oxide nanoparticles	Removal of lead from water	Modified membrane with 10 wt% CA and 0.1 wt% Fe_3O_4 nanoparticles exhibited better lead removal efficiency	[157]
8	Polyvinylidene fluoride-based membrane modified by TiO_2 nanoparticles (PVDF/TiO_2)	Antibacterial property against *E. coli* and removal of reactive black 5 under UV light	PVDF/TiO_2 membrane with 1% TiO_2 showed best performance for the removal of reactive black 5 under UV light and membrane with 4% TiO_2 showed highest antibacterial property	[158]
9	Polysulfone (PSF)-based ultrafiltration membrane modified by Fe-doped TiO_2	Removal of bisphenol A	Modified membrane exhibited 90.78% removal efficiency for bisphenol A under visible light	[159]
10	Laccase immobilized electrospun chitosan/poly(vinyl alcohol) composite nanofibrous membranes	Removal of 2,4-dichlorophenol	The removal efficiency of 87.6% for 2,4-dichlorophenol after 6 h of treatment time	[160]

membranes. Xu et al. [160] developed a novel method of immobilization on electrospun chitosan/poly(vinyl alcohol) composite nanofibrous membranes for removal of 2,4-dichlorophenol and reported 87.6% removal efficiency under optimized operating conditions. Electrospun nanofibers can be modified for specific applications by changing diameter, morphology, composition, structure, and spatial alignment. Furthermore, NP-impregnated nanofibers can be fabricated by doping of functional nanomaterials into the spinning solution [165].

31.6.2 Nanocomposite membranes

The inclusion of NPs during synthesis of membranes alters the mechanical, thermal, and magnetic properties of polymer membranes [166, 167]. Nanomaterials are added into polymeric or inorganic membranes for creating synergism or multifunction in wastewater treatment applications. Many researchers have reported that nanocomposite membranes synthesized by the addition of metal oxide NPs such as TiO_2 [168], alumina [151], and zeolite [148] to the polymeric ultrafiltration (UF) membrane reduces fouling and increases water

This book belongs to Badji Mokhtar Annaba University Central Library Copyright Elsevier 2025

permeability and surface hydrophilicity. The addition of inorganic NPs to polymeric membrane enhances thermal and mechanical stability of membranes [148, 169].

Antifungal and antibacterial properties of Ag NPs have made them very popular in water disinfection processes using membranes as they are selective toward specific microorganisms [152, 166]. Furthermore, Fe-based membranes prevent particle aggregation and also permit control regarding particle size [157]. Nanocomposite membranes are broadly classified as metal- and metal oxide-based nanocomposite membranes and carbon-based nanocomposite membrane.

31.6.2.1 Metal- and metal oxide-based nanocomposite membranes

The incorporation of metal and metal oxide NPs in polymeric membranes enhances their selectivity, hydrophilicity, permeability, and strength. However, controlling the aggregation is the major challenge while incorporating such NPs in membrane [166]. Metal and metal oxide NPs applied in membrane separation processes majorly include iron oxide, TiO_2, ZnO, silica, alumina, etc. Few important metal- and metal oxide-based nanocomposite membranes applied for the removal of pollutants are as follows.

Iron-based nanocomposite membranes

Iron metal NPs are unsuitable for application in pure form because of its high reactivity. However, incorporation of iron particles in polymeric membrane enhances the performance of membrane. Iron oxide NPs exhibit enhanced efficiency because of its cost effectiveness, magnetic properties, low toxicity, and hydrophilic nature. Karimnezhad et al. [170] have synthesized nanocomposite membrane by incorporating Fe-based NPs, i.e., goethite (Goe) and maleate ferroxane (Mf) in polyacrylonitrile (PAN) film and its performance was evaluated for AMX removal using NF membrane process combined with Fenton (FT). The authors reported AMX separation efficiency of 92.3% and 86.3% for PAN/Mf and PAN/Goe membranes, respectively. Wang et al. [159] prepared photocatalytic Fe-doped TiO_2/polysulfone (PSF) composite ultrafiltration (UF) membranes and its performance was evaluated for BPA. It has been reported that the high BPA degradation efficiency of 92.30% was obtained within 180 min under visible-light irradiation. In another study, Xie et al. [153] have synthesized a GO/MIL-88A(Fe) membrane and its performance was evaluated for methylene blue and BPA. The nanocomposite membrane showed high photo-Fenton catalytic degradation efficiency for MB (98.81%) within 40 min and for BPA (97.27%) within 80 min.

Titanium-based nanocomposites membrane

Titanium dioxide (TiO_2)-based nanocomposite membranes have attracted researcher's attention because of their photocatalytic and antimicrobial property, which enhances degradation efficiency in wastewater treatment application. TiO_2 NPs have been widely applied in the preparation of antifouling separation membranes [171, 172]. The excellent antifouling

This book belongs to Badji Mokhtar Annaba University Central Library Copyright Elsevier 2025

performance of TiO_2 nanocomposite membrane is attributed to the photocatalytic decomposition of organic foulants and increased hydrophilicity because the layer of water on the surface of membrane prevents the entry of hydrophobic foulants [158, 173, 174]. Song et al. [154] have reported high pure water permeability and rejection of Na_2SO_4-43%, MgSO-35%, methylene blue-96%, and natural organic matter-99% using TiO_2 NF membranes.

Silica-based nanocomposites membrane

Silica NPs incorporated into various polymer membranes such as polyvinylidene fluoride (PVDF) exhibit better temperature resistance and higher selectivity and diffusivity [175], whereas its incorporation in polybenzimidazole membranes resulted in greater selectivity and enhanced permeability [176]. Silica NPs exhibit high surface area and good thermal and chemical stability.

Wu et al. [177] have synthesized nanocomposite membranes by incorporating mesoporous SiO_2 NPs into piperazine aqueous solution. The resultant membranes exhibited a higher water flux (1.5 times higher than that of polyamide membrane without NPs) and relatively higher rejection of Na_2SO_4. Li et al. [178] have also reported synthesis of three types of SiO_2 NPs decorated with the functional groups such as pyridyl, phenyl, and sulfonic groups. Furthermore, the NF membranes were prepared by introducing these SiO_2 NPs into polyethylenimine matrix. It has been reported that the nanocomposite membranes modified with SiO_2 nanospheres exhibit significant increase in the flux of *n*-heptane because such membranes have higher affinity toward the nonpolar organic solvent.

Alumina-based nanocomposites membrane

Alumina NPs can also be incorporated into various polymer membranes to improve their performance. Yan et al. [179] synthesized a PVDF-Al_2O_3 nanocomposite membrane using the phase-inversion process and reported enhanced antifouling performance of the membrane because of improved hydrophilicity. Also increase in permeation flux attributed to increase in the hydrophilicity and surface area because of the addition of hydrophilic Al_2O_3 particles. Aluminum oxide NPs in polyether sulfone membrane [180] showed enhanced performance in wastewater treatment application.

Zinc oxide-based nanocomposites membrane

Zinc oxide (ZnO) can also be used for modifying the polymeric and ceramic membranes by improving the permeability and reducing the fouling. Zinc oxide-based nanocomposite membranes are widely used in water and wastewater treatment for reducing the toxicity [181]. ZnO/polymer nanocomposite membrane is cost effective compared with ZnO/ceramic nanocomposite membrane because of low cost of ZnO and polymer. Hence, ZnO-polymer nanocomposite membrane can be easily scaled up and commercialized [181, 182].

This book belongs to Badji Mokhtar Annaba University Central Library Copyright Elsevier 2025

Leo et al. [183] have synthesized nanocomposite membrane by incorporating ZnO NPs in PSF membranes and studied their transport properties. Increase in the permeate flux was observed compared with that of pristine PSF membrane because incorporation of ZnO NPs has resulted in swelling of the pore size and enhancement in the hydrophilicity of the nanocomposite membrane.

31.6.2.2 Carbon material-based nanocomposite membranes

Carbon-based nanomaterials such as GO, rGO, and CNTs have been widely used in wastewater treatment applications because of its exclusive structures and controllable physicochemical properties that are useful in the membrane separations [184,185]. The details are provided in the following sections.

Graphene-based nanocomposites membrane

Graphene-based membranes can be broadly categorized as single layer or composite membranes and further the composite graphene membranes can be categorized as surface modified, stacked, and mixed matrix membranes based on their methods of synthesis [186]. Cohen-Tanugi and Grossman [187] have reported that a single layer of graphene having pores of sub nanometer scale demonstrates higher water permeability compared with that of conventional reverse osmosis membranes for identical rejection rate of salt. Graphene-based materials can be introduced on the surfaces of membranes in the form of stacked laminates. Similarly, mixed matrix membranes can be synthesized by blending graphene-based material such as GO and rGO with various polymeric compounds such as PVDF, PSF, and polyethersulfone [186]. This integrated approach enhances membrane selectivity and improves antimicrobial, antifouling, mechanical, and thermal properties.

Zambianchi et al. [155] have reported removal of seven emerging contaminants, including pharmaceuticals, PCPs, surfactants using PSF (PS)/GO-based porous membranes (PS-GO). The authors have reported more than 90% removal efficiency of OFLOX, benzophenone-3 (BP-3), rhodamine b (Rh), DCF, and triton X-100 (TRX), which is significantly higher than pristine PS membrane. The removal efficiencies of PS-GO, PS, and GO for all selected MPs have been reported in Fig. 31.2. At any instance, OFLOX is well removed by GO compared with PS and PS-GO, whereas highest BP-3 removal efficiency (90%) was observed using PS-GO. It has been also reported that the compounds DCF and CBZ are removed with higher efficiency compared with only PS and only GO. This may be attributed to hydrophilicity and polarity, which play a crucial role in the adsorption efficiency of GO and of PS-GO. The highly polar molecules such as OFLOX and Rh can be effectively removed using GO, whereas less polar CBZ and DCF showed less removal efficiency.

In another study, Nasseri et al. [156] have synthesized the PSF/GO nanocomposite membranes and evaluated their performance for removal of BPA. BPA removal efficiency of 93% was

This book belongs to Badji Mokhtar Annaba University Central Library Copyright Elsevier 2025

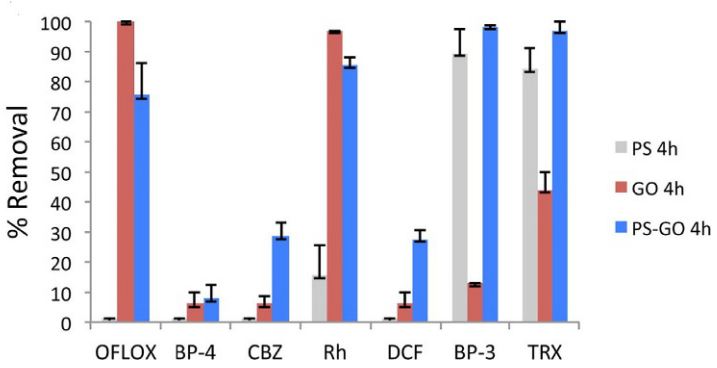

Fig. 31.2

Comparison of removal efficiency using pure PS, GO, and PS-GO membrane after 4 h treatment time [155]. *Reprinted with permission from M. Zambianchi, M. Durso, A. Liscio, E. Treossi, C. Bettini, M.L. Capobianco, A. Aluigi, A. Kovtun, G. Ruani, F. Corticelli, M. Brucale, V. Palermo, M.L. Navacchia, M. Melucci, Graphene oxide doped polysulfone membrane adsorbers for the removal of organic contaminants from water, Chem. Eng. J. 326 (2017) 130–140. Copyright (2017) Elsevier.*

reported under optimized conditions of pressure (1.02 bar), pH (5.5), operating time (10.6 min), and initial concentration of BPA (7.5 mg/L) using PSF/GO 0.4% membrane.

CNT-based nanocomposites membrane

CNTs have received immense attention because of their properties such as high specific surface area, high flexibility, low mass density, and frictionless surface [188]. CNT-based membranes can be classified into vertically and randomly aligned CNT membranes. Randomly aligned CNT membranes are fabricated by surface modification and mixed-matrix approaches [186]. To enhance the performance of CNT membranes for water treatment, these membranes can be modified by addition of NPs, such as TiO_2, Cu, Ag, Au, Pd, Pt [189]. Also, the cost and energy requirement of CNT membranes can be reduced by modifying CNT membranes with other functional agents such as polymers, metal oxides, and biomolecules, which increases the water flux and rejection rate [190]. The membrane biofouling can be reduced by the addition of antimicrobial nanomaterials such as nano-Ag and CNTs. Doping of nano-Ag on polymeric membranes inhibit bacterial attachment and biofilm formation [191, 192] on the membrane surface. Choi et al. [193] reported increase in hydrophilicity and permeability of PSF membranes by addition of oxidized multiwalled nanotubes.

Although CNT membranes have potential application in wastewater treatment, high cost of CNTs limits its application for real wastewater treatment at a large scale. Hence, research must be focused on integration of conventional and CNT-enabled technologies and modification of CNT to develop effective wastewater treatment system.

Overall, it can be said that nanomembranes have potential applications in the field of wastewater treatment.

This book belongs to Badji Mokhtar Annaba University Central Library Copyright Elsevier 2025

31.7 Reactors applied for the treatment of MP using nanomaterials

Design of reactors for wastewater treatment applications is a major challenging task for efficient operation. Throughput, performance, energy efficiency, and cost are some of the important parameters that need to be considered while designing the reactors. Reactors applied for the removal of MPs are generally designed for the multiphase gas solid, liquid solid, and liquid solid gas systems as MPs, photocatalysts, and light photon exist in different phases. Such reactors are majorly based on photocatalysis, membrane separation, and biological operations. Some important reactors successfully applied for the removal of MPs are as follows.

31.7.1 The annular reactor

The classical annular reactor (AR) is a simple tubular type of reactor in which a source of irradiation is located inside the tube, whereas MP is placed in the outer shell [194]. All ARs have advantages of high surface area because of small size of catalyst particles. However, absence of mixing of reaction medium, uneven light illumination, and difficult catalyst recovery are the main drawbacks associated with this AR. Chiou et al. [195] applied this AR for the degradation of phenol using TiO_2 as a photocatalyst and mercury lamps (20, 100, and 400 W) as a source of irradiation. In another study, Chong et al. [99] designed an annular photocatalytic reactor system for photocatalytic degradation of CR using a titania-impregnated kaolinite photocatalyst (TiO_2/K) and reported complete degradation of 40 ppm CR dye in 4 h of treatment time. To ensure mixing and proper illumination of reaction medium, spinning disc reactor (SDR) [196], multilamp reactor [197], and rotating AR [194] can be applied, which illuminate catalyst surface uniformly [198]. The schematic of rotating AR is depicted in Fig. 31.3.

31.7.2 Spinning disc reactor

Yatmaz et al. [196] developed an SDR photoreactor and used it for photocatalytic degradation of 1–4-chlorophenol where the reaction slurry was pumped on the disc to create a thin film, which is illuminated by mercury lamps (40 or 400 W). It is reported that low-pressure lamps are more efficient than medium-pressure lamps as it has significant portion of visible range light emission [196, 199]. Similar studies depicting enhanced photocatalytic degradation efficiency have been reported in literature for the degradation of phenol [200] and MO [201] using spinning disc reactor. The major disadvantages of spinning disc reactors are requirement of a large area for mounting the disc within the reactor and large requirement of electricity [202].

This book belongs to Badji Mokhtar Annaba University Central Library
Copyright Elsevier 2025

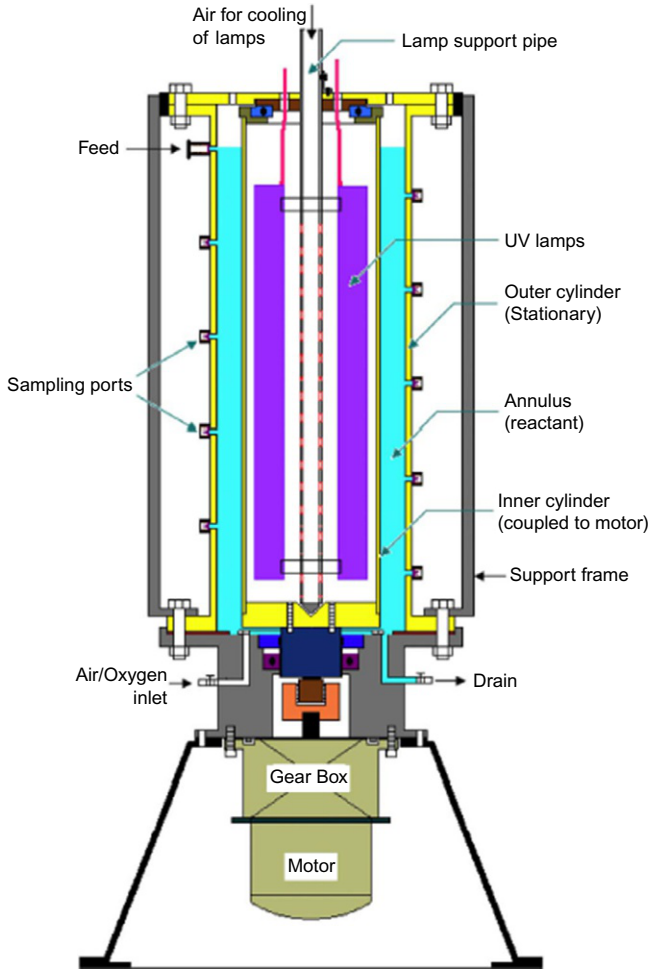

Fig. 31.3
Rotating annular reactor [194]. *Reprinted with permission from M. Subramanian, A. Kannan, Photocatalytic degradation of phenol in a rotating annular reactor, Chem. Eng. Sci. 65 (2010) 2727–2740. Copyright (2010) Elsevier.*

31.7.3 Optical fiber photo reactor

Danion et al. [203] designed the optical fiber photo reactor (OFR) coated with TiO_2 for enhancing the photocatalytic degradation of hydroxy butanedioic acid. The main disadvantage of OFR is illumination of catalyst particle from backside surface-coated optical fiber. Lin and Valsaraj [204] have also designed the OFR for the degradation of dichlorobenzene

This book belongs to Badji Mokhtar Annaba University Central Library Copyright Elsevier 2025

phenanthrene. Ceramic multichannel monolith was used as a support to TiO_2 NPs. Similarly, bare quartz fibers were used as a light-transmitting conductor and as a support for TiO_2. To overcome the light scattering effect, in another study, Zhu et al. [205] designed hybrid fluidized bed–optical fiber reactor using TiO_2/SiO_2 catalyst for the degradation of trichloroethylene.

31.7.4 Ultraviolet light emitting diode–based reactor

The photocatalytic reactors with light-emitting devices are promising alternatives for conventional lamps as these LEDs have high robustness, contain no toxic substances, and also have longer life span, which make it more efficient compared with conventional lamps [202]. Natarajan et al. [206] designed a UV-LED photocatalytic reactor, which was made up of quartz and coated with TiO_2 for the degradation of various dyes. Three catalyst-coated quartz tubes were placed inside the cylindrical vessel and 15 UV-LEDs were placed within the reactor. UV-LED-based photoreactors have been developed by many researchers and their performance was observed to be satisfactory for the degradation of various organic pollutants [206, 207].

31.7.5 Membrane photoreactor/photocatalytic membrane reactors

Nowadays, nano-catalysts are gaining attention in water treatment applications because of their enhanced photocatalytic ability. The reduction in size of catalyst particle leads to enhanced surface area for the photocatalytic degradation of pollutants. Although slurry reactors generally perform better than the immobilized reactors, difficulty in separation of nanocatalyst is a major issue (Sunder and Kanmani, 2020). Integrated photocatalytic membrane reactors (PMRs) can be used to overcome the disadvantage of catalyst separation. The conventional membrane filtration processes need post treatment as it can only concentrate pollutants into a high-concentration retentate. Also, membrane fouling because of formation of cake results in increased treatment cost as well as energy requirement [208]. However, PMR can be used to degrade the MPs by generating hydroxyl radicals using UV or solar as source of irradiation, thereby preventing membrane fouling. Thus, the advantages of PMR include improved process efficiency and stability and reduction in operating cost because of reusability of catalyst [185]. Leong et al. [208] have reported four configurations of PMRs that are widely used for wastewater treatment application such as (a) a slurry photocatalytic reactor followed by a membrane filtration unit, (b) inorganic or polymeric membranes submerged in a slurry photocatalytic reactor, (c) membrane placed inside a photoreactor whose internal walls are coated by a photocatalyst such as TiO_2, and (d) photocatalytic membrane such as pure TiO_2 porous membrane and TiO_2 composite membrane as depicted in Fig. 31.4.

In another study, Mozia [209] has reported two types of PMRs, namely reactors with suspended photocatalyst and reactors with catalyst immobilized on the membrane surface. The design of PMR depends on the mode of operation such as batch or continuous flow, type of membrane

This book belongs to Badji Mokhtar Annaba University Central Library Copyright Elsevier 2025

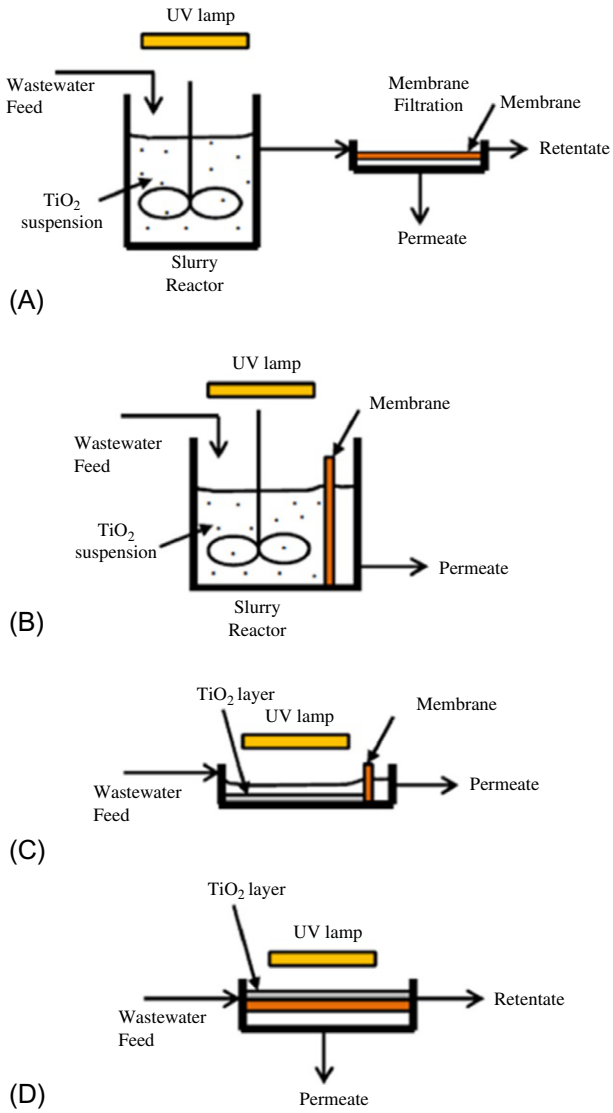

Fig. 31.4

Configurations of photocatalytic membrane reactors (A) slurry reactor followed by a membrane filtration unit; (B) submerged membrane in a slurry reactor; (C) submerged membrane inTiO_2-coated reactor; and (D) photocatalytic membrane [208]. *Reprinted with permission from S. Leong, A. Razmjou, K. Wang, K. Hapgood, X. Zhang, H. Wang, TiO_2 based photocatalytic membranes: a review, J. Membr. Sci. 472 (2014) 167–184. Copyright (2014) Elsevier.*

This book belongs to Badji Mokhtar Annaba University Central Library Copyright Elsevier 2025

technique such as microfiltration (MF), UF, or NF, membrane modules used like flat sheet, hollow fiber, and submerged, and the source of irradiation such as solar and UV. PMR with immobilized photocatalyst (A) on the surface of membrane and (B) within the structure of membrane has been depicted in Fig. 31.5.

Many studies have been reported in the literature for the applications of PMRs for the degradation of MPs [210, 211]. Wang and Lim [211] designed hybrid membrane photoreactor (MPR) combining cross-flow MF membrane module-visible LED photoreactor for simultaneous degradation of penicillin G and visible-light responsive TiO_2 separation. In another study, Damodar and You [210] developed a PMR by combining novel flat plate PTFE membrane module with a slurry photoreactor and its photocatalytic performance was evaluated for the degradation of dye Reactive Black 5. The authors reported 99.99% color removal and 75%–82% total organic carbon (TOC) and chemical oxygen demand (COD) removal by this reactor.

31.7.6 Microreactors

The major drawbacks of immobilized systems are low interfacial surface area. Microreactors foam reactor technologies can be effectively designed to overcome this drawback because of their large surface-to-volume ratios. However, low throughput is the main drawback associated with these microreactors in photodegradation application [212]. Gorges et al. [213] designed a photocatalytic microreactor illuminated by UV-A light emitting diodes and titanium dioxide as immobilized photocatalyst for the successful photocatalytic degradation of 4-chlorophenol.

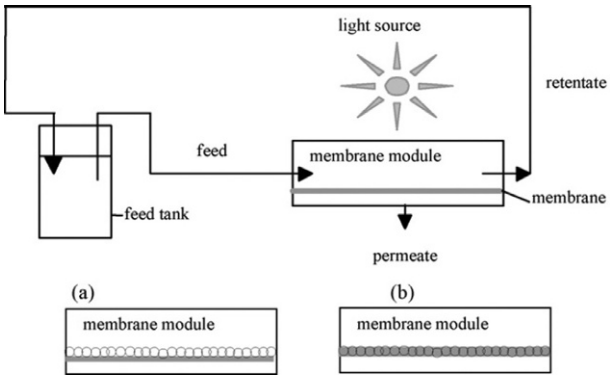

Fig. 31.5
Photocatalytic membrane reactors utilizing catalyst immobilized (A) on the surface of membrane and (B) within the structure of membrane [209]. *Reprinted with permission from S. Mozia, Photocatalytic membrane reactors (PMRs) in water and wastewater treatment. A review, Sep. Purif. Technol. 73 (2010) 71–91. Copyright (2010) Elsevier.*

This book belongs to Badji Mokhtar Annaba University Central Library Copyright Elsevier 2025

31.8 Nanomaterials applied at large-scale operation and associated challenges

The development of effective and affordable nanomaterials that are capable of removing a wide range of MPs is the need of both the developed and developing countries [214]. Although the applications of nanomaterials for the removal of MPs are successful at the laboratory scale, scale up at pilot and industrial scale is a major challenge. Hence, the efficiency and applicability of these nanomaterials must be tested for real industrial wastewater under realistic conditions. The economic feasibility of any large-scale industrial wastewater treatment process involving nanomaterials majorly depends upon the selection of nanomaterials with high removal rates of MPs [215]. The cost of these nanomaterials in turn is dependent on the type of nanomaterial and their desired properties such as level of purity, surface functionalization, and particle size [216].

To investigate the long-term usability of nanomaterials, research on laboratory scale must be extended further for their application to longer operating times [214]. Apart from physical and chemical stability, long lifespan and easy recycling under prolonged operating conditions are the key factors that need to be considered for large-scale operations involving nanomaterials.

Many researchers have reported the application of three dimensional (3D) graphene as a nanoadsorbent and black titania (BT) as a nanophotocatalyst at large scale. Furthermore, the composites of 3D graphene (3DG) and BT are also used for the photocatalytic degradation of pollutants at large scale [217]. In recent years, three-dimensional porous graphene nanostructures such as graphene hydrogels, aerogels, sponges, and foams have been reported to be an upcoming nanoadsorbent for the efficient removal of various MPs such as dyes, toluene, chloroform, and aromatic compounds. The graphene-based 3D nanostructures have received many applications in wastewater treatment because of its huge surface area, high porosity, and excellent electrical conductivity. 3D graphene is majorly synthesized by using hydrothermal route, chemical reduction method, and cross-linking method [218]. Riaz et al. [219] have successfully applied 3D graphene for cleaning of oil spills and for the removal of various dyes at large scale.

Colored TiO_2 has gained enormous attention because of its improved visible light absorption and excellent photocatalytic activity [220]. BT, which is capable of full-spectrum solar photon absorption, has better photocatalytic activity compared with commercially available white TiO_2 [217]. BT can be synthesized using either hydrogenation, aluminum reduction, or chemical reduction methods [221]. The black color of the NPs is because of incorporation of various beneficial defects such as oxygen vacancies or incorporation of OH groups. The exposure of TiO_2 to strong reducing agents such as H_2 may incorporate defects because of removal of oxygen atoms leaving behind Ti^{3+} and oxygen vacancies [222]. Tan et al. [220] have

This book belongs to Badji Mokhtar Annaba University Central Library Copyright Elsevier 2025

demonstrated facile method for massive production of TiO_2, which has the advantages of simple operation, low reaction temperature, short reaction time, and high photocatalytic performance. It was reported that a gel made from a TiO_2 sol and $NaBH_4$ can be converted to BT in 1.5 h of calcination at 500°C in Ar. Wang et al. [223] have also reported a mass production approach to synthesize BT by aluminum reduction.

Zhao et al. [217] have reported application of BT/3DG composite for large-scale operation where BT immobilized on the surface of three-dimensional graphene showed enhanced photocatalytic activity. It also led to facile separation of solid liquid mixture and in turn an easy recovery. A solar active cloth was developed in which composite of BT and 3DG was bonded to a nonwoven cloth by using a polymeric binder and its photocatalytic performance was evaluated for large-scale operation. Significant reduction in TOC, nitrogen, and phosphorus was observed in 2 weeks after the BT/3DG hybrids cloth was deployed at various locations such as rivers, lake, and ponds. It has been reported that polluted water in 600 acres land at four locations in China was treated using solar active BT/3DG cloth made from 8 tons of BT and 100 kg of 3DG. The details of laboratory scale and large-scale applications of solar active cloths are motioned in Fig. 31.6.

The immobilized BT/3DG hybrid nanocomposite utilizes full-spectrum absorption of BT and large surface area of 3DG. However, immobilization of catalyst has lower photocatalytic

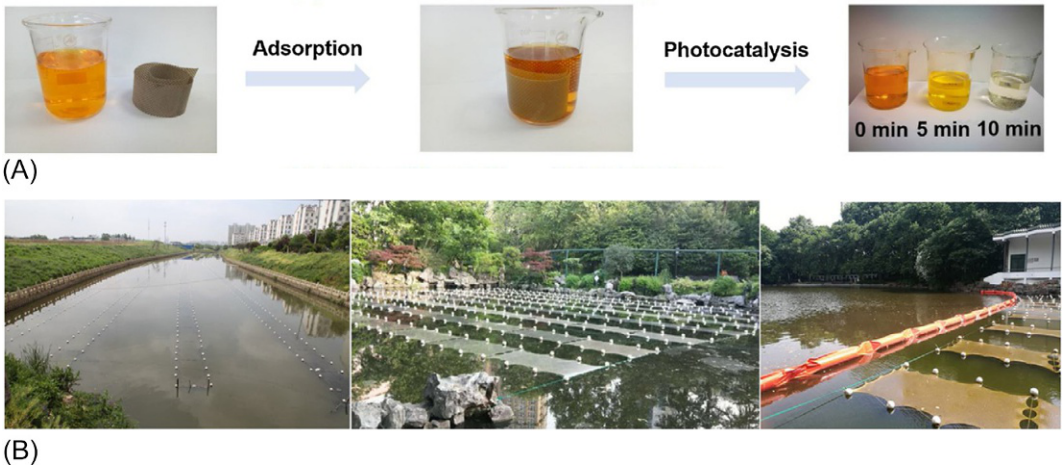

Fig. 31.6
(A) Laboratory scale photocatalytic degradation of MO using a piece of solar active cloth (B) large-scale wastewater treatment using solar active cloths applied at polluted rivers and ponds [217].
Reprinted with permission from W. Zhao, I.W. Chen, F. Huang, Toward large-scale water treatment using nanomaterials, Nano Today 27 (2019) 11–27. Copyright (2019) Elsevier.

This book belongs to Badji Mokhtar Annaba University Central Library Copyright Elsevier 2025

activity compared with powdered suspended photocatalysts. But the latter has disadvantage of separation of photocatalysts. Hence, it is highly essential to develop a photocatalyst that is easily recoverable without hampering the photocatalytic performance.

31.9 Conclusion and a way forward

There is a significant need for novel advanced wastewater treatment technologies, particularly to ensure the high quality of drinking water and complete elimination of hazardous MPs. Majority of MPs can be removed successfully using advanced methods such as photocatalysis, adsorption, and membrane separation using nanomaterials. Nanoengineered materials applied in these processes offer potential applications in the wastewater treatment because it can be tailored as per the customer-specific applications. One of the most important advantages of using nanomaterials-based processes when compared with conventional treatment processes is their ability to integrate various properties, resulting in multifunctional systems such as nanocomposite membranes that enable both particle retention and elimination of contaminants [224]. Furthermore, nanomaterials enable higher process efficiencies because of their unique characteristic of large surface area, which in turn increases the degradation rate of MPs. The major conclusions drawn by studying the application of these processes are as follows:

1. Photocatalysis using nanomaterials has proved to be a promising option for the removal of various types of MPs. Nanomaterials that can be applied as a photocatalyst include various types of metal oxides and their nanocomposites, doped metal and metal oxides, carbon material–supported metal oxides, and magnetic material–based metal oxides. Efforts toward the modification of metal oxides are highly essential for enabling its use in the visible light region, and this can be achieved by using doping or supporting them on carbon-based materials. Hence, development of cost-effective nanophotocatalyst that will remain active in the visible solar light region is highly essential for industrial scale operation. Furthermore, the efficiency of photocatalytic process using nanomaterials can be maximized by optimizing the parameters such as loading of nanophotocatalyst, initial pH of the solution, irradiation source, temperature of solution, and initial concentration of the micropollutant.
2. Metal oxide–based nanoadsorbents, carbon-based nanoadsorbents and nanocomposites of these metal, and carbon-based NPs are the most widely used nanoadsorbents for wastewater treatment because of their microporous structure and high surface area. However, there are certain limitations such as generation of secondary pollution because of smaller size of NPs and difficulties in the separation of these NPs from solution. Also, regeneration and economical reuse are the major challenges in nanomaterial applications [225]. To overcome the challenges associated with nanoadsorbents, they can be further modified by synthesizing organic-inorganic hybrids [226], MWCNTs [227, 228].

This book belongs to Badji Mokhtar Annaba University Central Library Copyright Elsevier 2025

3. Nanomembranes have also witnessed potential applications in wastewater treatment process because of its high removal efficiency, requirement of less space for installing plant [229], and simple inexpensive technology for wastewater treatment application [230, 231]. However, the fouling of membrane because of deposition of particles is a major drawback, which reduces reliability and life of membranes and reduces the efficiency of separation. To overcome the limitation of membrane fouling, membranes can be modified by incorporating nanomaterials in them [232]. However, the life cycle of carbon nanofibers has indicated that it leads to more toxicity, depletion of ozone, and global warming compared with conventional materials [224, 233]. It is the major limitation or environmental concern for the application of nanomembranes in wastewater treatment.
4. Most of the studies reported in the literature are limited to the treatment of model pollutants (single type of pollutant) at laboratory scale. However, real industrial effluents contain various pollutants and other undesirable substances. Therefore, further research must be performed to investigate the simultaneous removal of many coexisting MPs from real industrial waste. The research must be focused on transferring the application of nanotechnology in wastewater treatment from laboratory and pilot scale to real industrial applications.
5. The selection of appropriate nanomaterial is very important for the effective removal of MPs from wastewater. Although nanomaterials have received potential application at laboratory scale, there are certain challenges such as aggregation of nanomaterials, difficulty in separation, and potential adverse effect imposed by nanomaterials on ecosystem and human health. Hence, further research is highly essential to overcome these challenges. Overall, it can be said that the further research in this direction will lead to the development of cost-efficient, economic, and environmentally friendly process for treatment of wastewaters in a sustainable manner.

References

[1] C. Santhosh, V. Velmurugan, G. Jacob, S.K. Jeong, A.N. Grace, A. Bhatnagar, Role of nanomaterials in water treatment applications: a review, Chem. Eng. J. 306 (2016) 1116–1137.
[2] R.P. Schwarzenbach, B.I. Escher, K. Fenner, T.B. Hofstetter, C.A. Johnson, U. Von Gunten, B. Wehrli, The challenge of micropollutants in aquatic systems, Science 313 (2006) 1072–1077.
[3] D. Belhaj, R. Baccar, I. Jaabiri, J. Bouzid, M. Kallel, H. Ayadi, J.L. Zhou, Fate of selected estrogenic hormones in an urban sewage treatment plant in Tunisia (North Africa), Sci. Total Environ. 505 (2015) 154–160.
[4] J.O. Tijani, O.O. Fatoba, L.F. Petrik, A review of pharmaceuticals and endocrine-disrupting compounds: sources, effects, removal, and detections, Water Air Soil Pollut. 224 (2013) 1–29.
[5] M.B. Ahmed, J.L. Zhou, H.H. Ngo, W. Guo, Adsorptive removal of antibiotics from water and wastewater: progress and challenges, Sci. Total Environ. 532 (2015) 112–126.
[6] M. Katakam, L.N. Bell, A.K. Banga, Effect of surfactants on the physical stability of recombinant human growth hormone, J. Pharm. Sci. 84 (1995) 713–716.

This book belongs to Badji Mokhtar Annaba University Central Library Copyright Elsevier 2025

[7] D.P. Grover, J.L. Zhou, P.E. Frickers, J.W. Readman, Improved removal of estrogenic and pharmaceutical compounds in sewage effluent by full scale granular activated carbon: impact on receiving river water, J. Hazard. Mater. 185 (2011) 1005–1011.
[8] Y. Zhang, J.L. Zhou, Occurrence and removal of endocrine disrupting chemicals in wastewater, Chemosphere 73 (2008) 848–853.
[9] M.B. Ahmed, J.L. Zhou, H.H. Ngo, W. Guo, N.S. Thomaidis, J. Xu, Progress in the biological and chemical treatment technologies for emerging contaminant removal from wastewater: a critical review, J. Hazard. Mater. 323 (2017) 274–298.
[10] P.E. Stackelberg, J. Gibs, E.T. Furlong, M.T. Meyer, S.D. Zaugg, R.L. Lippincott, Efficiency of conventional drinking-water-treatment processes in removal of pharmaceuticals and other organic compounds, Sci. Total Environ. 377 (2007) 255–272.
[11] U. Bali, E.Ç. Çatalkaya, F. Şengül, Photochemical degradation and mineralization of phenol: a comparative study, J. Environ. Sci. Health A Tox. Hazard. Subst. Environ. Eng. 38 (2003) 2259–2275.
[12] E.Ç. Çatalkaya, U. Bali, F. Şengül, Photochemical degradation and mineralization of 4-chlorophenol, Environ. Sci. Pollut. Res. 10 (2003) 113–120.
[13] A.S. Edelstein, R.C. Cammaratra, Nanomaterials: Synthesis, Properties and Applications, CRC Press, New York, 1998.
[14] X. Qu, P.J.J. Alvarez, Q. Li, Applications of nanotechnology in water and wastewater treatment, Water Res. 47 (2013) 3931–3946.
[15] A. Brindha, T. Sivakumar, Visible active N, S co-doped TiO_2/graphene photocatalysts for the degradation of hazardous dyes, J. Photochem. Photobiol. A Chem. 340 (2017) 146–156.
[16] P. Calza, C. Hadjicostas, V.A. Sakkas, M. Sarro, C. Minero, C. Medana, T.A. Albanis, Photocatalytic transformation of the antipsychotic drug risperidone in aqueous media on reduced graphene oxide-TiO_2 composites, Appl. Catal. Environ. 183 (2016) 96–106.
[17] N. Daneshvar, D. Salari, A.R. Khataee, Photocatalytic degradation of azo dye acid red 14 in water on ZnO as an alternative catalyst to TiO_2, J. Photochem. Photobiol. A Chem. 162 (2004) 317–322.
[18] M.K. Kim, K.D. Zoh, Occurrence and removals of micropollutants in water environment, Environ. Eng. Res. 21 (2016) 319–332.
[19] N. Verma, G. Kaur, Trends on Biosensing Systems for Heavy Metal Detection, Comprehensive Analytical Chemistry, Elsevier Ltd, 2016.
[20] M. Yadav, R. Gupta, R.K. Sharma, Chapter 14—Green and sustainable pathways for wastewater purification, in: Advances in Water Purification Techniques: Meeting the Needs of Developed and Developing Countries, Elsevier Inc., 2018
[21] M. Arias-Estévez, E. López-Periago, E. Martínez-Carballo, J. Simal-Gándara, J.C. Mejuto, L. García-Río, The mobility and degradation of pesticides in soils and the pollution of groundwater resources, Agric. Ecosyst. Environ. 123 (2008) 247–260.
[22] A.M. Aker, D.J. Watkins, L.E. Johns, K.K. Ferguson, O.P. Soldin, L.V. Anzalota Del Toro, A. N. Alshawabkeh, J.F. Cordero, J.D. Meeker, Phenols and parabens in relation to reproductive and thyroid hormones in pregnant women, Environ. Res. 151 (2016) 30–37.
[23] J. Wang, S. Wang, Removal of pharmaceuticals and personal care products (PPCPs) from wastewater: a review, J. Environ. Manage. 182 (2016) 620–640.
[24] A.S. Adeleye, J.R. Conway, K. Garner, Y. Huang, Y. Su, A.A. Keller, Engineered nanomaterials for water treatment and remediation: costs, benefits, and applicability, Chem. Eng. J. 286 (2016) 640–662.
[25] S. Contreras, M. Rodríguez, F. Al Momani, C. Sans, S. Esplugas, Contribution of the ozonation pre-treatment to the biodegradation of aqueous solutions of 2,4-dichlorophenol, Water Res. 37 (2003) 3164–3171.
[26] F. Fu, Q. Wang, Removal of heavy metal ions from wastewaters: a review, J. Environ. Manage. 92 (2011) 407–418.
[27] A.K. Golder, N. Hridaya, A.N. Samanta, S. Ray, Electrocoagulation of methylene blue and eosin yellowish using mild steel electrodes, J. Hazard. Mater. 127 (2005) 134–140.

This book belongs to Badji Mokhtar Annaba University Central Library Copyright Elsevier 2025

[28] B. Shi, G. Li, D. Wang, C. Feng, H. Tang, Removal of direct dyes by coagulation: the performance of preformed polymeric aluminum species, J. Hazard. Mater. 143 (2007) 567–574.
[29] N.K. Srivastava, C.B. Majumder, Novel biofiltration methods for the treatment of heavy metals from industrial wastewater, J. Hazard. Mater. 151 (2008) 1–8.
[30] P. Drillia, S.N. Dokianakis, M.S. Fountoulakis, M. Kornaros, K. Stamatelatou, G. Lyberatos, On the occasional biodegradation of pharmaceuticals in the activated sludge process: the example of the antibiotic sulfamethoxazole, J. Hazard. Mater. 122 (2005) 259–265.
[31] S. Esplugas, D.M. Bila, L.G.T. Krause, M. Dezotti, Ozonation and advanced oxidation technologies to remove endocrine disrupting chemicals (EDCs) and pharmaceuticals and personal care products (PPCPs) in water effluents, J. Hazard. Mater. 149 (2007) 631–642.
[32] N. Le-Minh, S.J. Khan, J.E. Drewes, R.M. Stuetz, Fate of antibiotics during municipal water recycling treatment processes, Water Res. 44 (2010) 4295–4323.
[33] S. Bhatt, M. Kumar, Effect of size and shape on melting and superheating of free standing and embedded nanoparticles, J. Phys. Chem. Solid 106 (2017) 112–117.
[34] J.N. Tiwari, R.N. Tiwari, K.S. Kim, Zero-dimensional, one-dimensional, two- dimensional and three-dimensional nanostructured materials for advanced electrochemical energy devices, Prog. Mater. Sci. 57 (2012) 724–803.
[35] H. Zhang, N. Toshima, Synthesis of Au/Pt bimetallic nanoparticles with a Pt-rich shell and their high catalytic activities for aerobic glucose oxidation, J. Colloid Interface Sci. 394 (2013) 166–176.
[36] T.T. Tran, X. Lu, Synergistic effect of Ag and Pd ions on shape-selective growth of polyhedral Au nanocrystals with high-index facets, J. Phys. Chem. 115 (9) (2011) 3638–3645.
[37] T.A. McMurray, P.S.M. Dunlop, J.A. Byrne, The photocatalytic degradation of atrazine on nanoparticulate TiO_2 films, J. Photochem. Photobiol. A Chem. 182 (2006) 43–51.
[38] D. Mijin, M. Savić, P. Snežana, A. Smiljanić, O. Glavaški, M. Jovanović, S. Petrović, A study of the photocatalytic degradation of metamitron in ZnO water suspensions, Desalination 249 (2009) 286–292.
[39] S. Ahmed, M.G. Rasul, R. Brown, M.A. Hashib, Influence of parameters on the heterogeneous photocatalytic degradation of pesticides and phenolic contaminants in wastewater: a short review, J. Environ. Manage. 92 (2011) 311–330.
[40] U.I. Gaya, A.H. Abdullah, Heterogeneous photocatalytic degradation of organic contaminants over titanium dioxide: a review of fundamentals, progress and problems, J. Photochem. Photobiol. C Photochem. Rev. 9 (2008) 1–12.
[41] V.K. Gupta, T. Eren, N. Atar, M.L. Yola, C. Parlak, H. Karimi-Maleh, $CoFe_2O_4$@TiO_2 decorated reduced graphene oxide nanocomposite for photocatalytic degradation of chlorpyrifos, J. Mol. Liq. 208 (2015) 122–129.
[42] R. Gusain, K. Gupta, P. Joshi, O.P. Khatri, Adsorptive removal and photocatalytic degradation of organic pollutants using metal oxides and their composites: a comprehensive review, Adv. Colloid Interface Sci. 272 (2019) 102009.
[43] S. Li, J. Cai, X. Wu, B. Liu, Q. Chen, Y. Li, F. Zheng, TiO_2 @Pt@CeO_2 nanocomposite as a bifunctional catalyst for enhancing photo-reduction of Cr (VI) and photo-oxidation of benzyl alcohol, J. Hazard. Mater. 346 (2018) 52–61.
[44] I.M. Arabatzis, T. Stergiopoulos, D. Andreeva, S. Kitova, S.G. Neophytides, P. Falaras, Characterization and photocatalytic activity of Au/TiO_2 thin films for azo-dye degradation, J. Catal. 220 (2003) 127–135.
[45] S. Dong, J. Sun, Y. Li, C. Yu, Y. Li, J. Sun, $ZnSnO_3$ hollow nanospheres/reduced graphene oxide nanocomposites as high-performance photocatalysts for degradation of metronidazole, Appl. Catal. Environ. 144 (2014) 386–393.
[46] H. Tao, X. Liang, Q. Zhang, C.T. Chang, Enhanced photoactivity of graphene/titanium dioxide nanotubes for removal of Acetaminophen, Appl. Surf. Sci. 324 (2015) 258–264.
[47] L. Lin, H. Wang, P. Xu, Immobilized TiO_2-reduced graphene oxide nanocomposites on optical fibers as high performance photocatalysts for degradation of pharmaceuticals, Chem. Eng. J. 310 (2017) 389–398.
[48] B. Li, T. Liu, Y. Wang, Z. Wang, ZnO/graphene-oxide nanocomposite with remarkably enhanced visible-light-driven photocatalytic performance, J. Colloid Interface Sci. 377 (2012) 114–121.

This book belongs to Badji Mokhtar Annaba University Central Library Copyright Elsevier 2025

[49] R. Ullah, J. Dutta, Photocatalytic degradation of organic dyes with manganese-doped ZnO nanoparticles, J. Hazard. Mater. 156 (2008) 194–200.
[50] N. Güy, S. Çakar, M. Özacar, Comparison of palladium/zinc oxide photocatalysts prepared by different palladium doping methods for congo red degradation, J. Colloid Interface Sci. 466 (2016) 128–137.
[51] S. Bhatia, N. Verma, R.K. Bedi, Optical application of Er-doped ZnO nanoparticles for photodegradation of direct red—31 dye, Opt. Mater. 62 (2016) 392–398.
[52] Z. Zou, C. Xie, S. Zhang, X. Yu, T. Zou, J. Li, Preparation and photocatalytic activity of $TiO_2/CeO_2/Bi_2O_3$ composite for Rhodamine B degradation under visible light irradiation, J. Alloys Compd. 581 (2013) 385–391.
[53] S. Hu, F. Zhou, L. Wang, J. Zhang, Preparation of Cu_2O/CeO_2 heterojunction photocatalyst for the degradation of Acid orange 7 under visible light irradiation, Cat. Com. 12 (2011) 794–797.
[54] C.M. Magdalane, K. Kaviyarasu, J.J. Vijaya, B. Siddhardha, B. Jeyaraj, J. Kennedy, M. Maaza, Evaluation on the heterostructured CeO_2/Y_2O_3 binary metal oxide nanocomposites for UV/Vis light induced photocatalytic degradation of rhodamine—B dye for textile engineering application, J. Alloys Compd. 727 (2017) 1324–1337.
[55] J.G. Yu, J.F. Xiong, B. Cheng, S.W. Liu, Fabrication and characterization of Ag-TiO_2multiphase nanocomposite thin films with enhanced photocatalytic activity, Appl. Catal. Environ. 6 (2005) 211–221.
[56] H. Yu, H. Irie, K. Hashimoto, Conduction band energy level control of titanium dioxide: toward an efficient visible-light-sensitive photocatalyst, J. Am. Chem. Soc. 132 (2010) 6898–6899.
[57] H. Yu, H. Irie, Y. Shimodaira, Y. Hosogi, Y. Kuroda, M. Miyauchi, K. Hashimoto, An efficient visible-light-sensitive Fe (III)-grafted TiO_2 photocatalyst, J. Phys. Chem. C 114 (2010) 16481–16487.
[58] R.M. Mohamed, UV-assisted photocatalytic synthesis of TiO_2-reduced graphene oxide with enhanced photocatalytic activity in decomposition of sarin in gas phase, Desalin. Water Treat. 50 (1–3) (2012) 147–156.
[59] R. Gusain, P. Kumar, O.P. Sharma, S.L. Jain, O.P. Khatri, Reduced graphene oxide-CuO nanocomposites for photocatalytic conversion of CO_2 into methanol under visible light irradiation, Appl. Catal. Environ. 181 (2016) 352–362.
[60] M. Cruz, C. Gomez, C.J. Duran-Valle, L.M. Pastrana-Martínez, J.L. Faria, A.M.T. Silva, M. Faraldos, A. Bahamonde, Bare TiO_2 and graphene oxide TiO_2 photocatalysts on the degradation of selected pesticides and influence of the water matrix, Appl. Surf. Sci. 416 (2017) 1013–1021.
[61] V. Bhatia, G. Malekshoar, A. Dhir, A.K. Ray, Enhanced photocatalytic degradation of atenolol using graphene TiO_2 composite, J. Photochem. Photobiol. A Chem. 332 (2017) 182–187.
[62] X. Cheng, X. Deng, P. Wang, H. Liu, Coupling TiO_2 nanotubes photoelectrode with Pd nano-particles and reduced graphene oxide for enhanced photocatalytic decomposition of diclofenac and mechanism insights, Sep. Purif. Technol. 154 (2015) 51–59.
[63] S. Thangavel, G. Venugopal, S.J. Kim, Enhanced photocatalytic efficacy of organic dyes using β-tin tungstate-reduced graphene oxide nanocomposites, Mater. Chem. Phys. 145 (2014) 108–115.
[64] N.A. Zubir, C. Yacou, J. Motuzas, X. Zhang, J.C. Diniz Da Costa, Structural and functional investigation of graphene oxide-Fe_3O_4 nanocomposites for the heterogeneous Fenton-like reaction, Sci. Rep. 4 (2014) 1–9.
[65] G.H. Le, Q.T. Ngo, T.T. Nguyen, Q.K. Nguyen, T.T.T. Quan, L.D. Vu, G.D. Lee, T.A. Vu, High catalytic activity of phenol photodegradation from aqueous solution with novel Fe-Fe_3O_4-GO nanocomposite, J. Mater. Eng. Perform. 27 (2018) 4225–4234.
[66] J. Ni, J. Xue, J. Shen, G. He, H. Chen, Fabrication of ZnAl mixed metal-oxides/RGO nanohybrid composites with enhanced photocatalytic activity under visible light, Appl. Surf. Sci. 441 (2018) 599–606.
[67] J. Wang, R. Liu, X. Yin, Adsorptive removal of tetracycline on graphene oxide loaded with titanium dioxide composites and photocatalytic regeneration of the adsorbents, J. Chem. Eng. Data 63 (2018) 409–416.
[68] S. Navarro, J. Fenoll, N. Vela, E. Ruiz, G. Navarro, Photocatalytic degradation of eight pesticides in leaching water by use of ZnO under natural sunlight, J. Hazard. Mater. 172 (2009) 1303–1310.
[69] M. Shirzad-Siboni, A. Jonidi-Jafari, M. Farzadkia, A. Esrafili, M. Gholami, Enhancement of photocatalytic activity of Cu-doped ZnO nanorods for the degradation of an insecticide: kinetics and reaction pathways, J. Environ. Manage. 186 (2017) 1–11.
[70] P. Janos, P. Kuran, M. Kormunda, V. Stengl, T.M. Grygar, M. Dosek, M. Stastny, J. Ederer, V. Pilarova, L. Vrtoch, Cerium dioxide as a new reactive sorbent for fast degradation of parathion methyl and some other organophosphates, J. Rare Earths 32 (2014) 360–370.

This book belongs to Badji Mokhtar Annaba University Central Library Copyright Elsevier 2025

[71] B. Li, B. Zhang, S. Nie, L. Shao, L. Hu, Optimization of plasmon-induced photocatalysis in electrospun Au/CeO_2 hybrid nanofibers for selective oxidation of benzyl alcohol, J. Catal. 348 (2017) 256–264.
[72] L. Zhang, Q. Zhang, H. Xie, J. Guo, H. Lyu, Y. Li, Z. Sun, H. Wang, Z. Guo, Electrospun titania nanofibers segregated by graphene oxide for improved visible light photocatalysis, Appl. Catal. Environ. 201 (2017) 470–478.
[73] S. Song, L. Xu, Z. He, H. Ying, J. Chen, X. Xiao, B. Yan, Photocatalytic degradation of C.I. Direct Red 23 in aqueous solutions under UV irradiation using $SrTiO_3/CeO_2$ composite as the catalyst, J. Hazard. Mater. 152 (2008) 1301–1308.
[74] X. Lu, X. Li, J. Qian, N. Miao, C. Yao, Z. Chen, Synthesis and characterization of CeO_2/TiO_2 nanotube arrays and enhanced photocatalytic oxidative desulfurization performance, J. Alloys Compd. 661 (2016) 363–371.
[75] S. Pavasupree, Y. Suzuki, S. Pivsa-Art, S. Yoshikawa, Preparation and characterization of mesoporous TiO_2-CeO_2 nanopowders respond to visible wavelength, J. Solid State Chem. 178 (2005) 128–134.
[76] V.K. Sharma, R.A. Yngard, Y. Lin, Silver nanoparticles: green synthesis and their antimicrobial activities, Adv. Colloid Interface Sci. 145 (2009) 83–96.
[77] H.M. Gong, L. Zhou, X.R. Su, S. Xiao, S.D. Liu, Q.Q. Wang, Illuminating dark plasmons of silver nanoantenna rings to enhance exciton–plasmon interactions, Adv. Funct. Mater. 19 (2) (2009) 298–303.
[78] G. Wu, W. Xing, Facile preparation of semiconductor silver phosphate loaded on multi-walled carbon nanotube surface and its enhanced catalytic performance, J. Inorg. Organomet. Polym. 29 (2019) 617–627.
[79] J. Li, W. Fang, C. Yu, W. Zhou, L. Zhu, Y. Xie, Ag-based semiconductor photocatalysts in environmental purification, Appl. Surf. Sci. 358 (2015) 46–56.
[80] J.-F. Guo, B. Ma, A. Yin, K. Fan, W.-L. Dai, Photodegradation of rhodamine B and 4-chlorophenol using plasmonic photocatalyst of Ag–AgI/Fe_3O_4@SiO_2 magnetic nanoparticle under visible light irradiation, Appl. Catal. B 101 (2011) 580–586.
[81] A. Rostami-Vartooni, M. Nasrollahzadeh, M. Salavati-Niasari, M. Atarod, Photocatalytic degradation of azo dyes by titanium dioxide supported silver nanoparticles prepared by a green method using Carpobrotusacinaciformis extract, J. Alloys Compd. 689 (2016) 15–20.
[82] M.L. Yola, T. Eren, N. Atar, W. Shaobin, Adsorptive and photocatalytic removal of reactive dyes by silver nanoparticle-colemanite ore waste, Chem. Eng. J. 242 (2014) 333–340.
[83] L. Karimi, S. Zohoori, M.E. Yazdanshenas, Photocatalytic degradation of azo dyes in aqueous solutions under UV irradiation using nano-strontium titanate as the nanophotocatalyst, J. Saudi Chem. Soc. 18 (2014) 581–588.
[84] B. Neppolian, S.R. Kanel, H.C. Choi, M.V. Shankar, B. Arabindoo, V. Murugesan, Photocatalytic degradation of reactive yellow 17 dye in aqueous solution in the presence of TiO_2 with cement binder, Int. J. Photoenergy 5 (2003) 45–49.
[85] E. Evgenidou, K. Fytianos, I. Poulios, Photocatalytic oxidation of dimethoate in aqueous solutions, J. Photochem. Photobiol. A Chem. 175 (2005) 29–38.
[86] M. Ahmadi, H. Ramezani Motlagh, N. Jaafarzadeh, A. Mostoufi, R. Saeedi, G. Barzegar, S. Jorfi, Enhanced photocatalytic degradation of tetracycline and real pharmaceutical wastewater using MWCNT/TiO_2 nano-composite, J. Environ. Manage. 186 (2017) 55–63.
[87] M. Naghizadeh, D. Snyder, S. Cheraghi, S. Foster, S. Cilensek, E. Floreani, J. Mackie, Acquisition and processing of wider bandwidth seismic data in crystalline crust: progress with the metal earth project, Fortschr. Mineral. 9 (2019) 145.
[88] M.H. Sayadi, S. Sobhani, H. Shekari, Photocatalytic degradation of azithromycin using GO@Fe_3O_4/ZnO/SnO_2 nanocomposites, J. Clean. Prod. 232 (2019) 127–136.
[89] L. Zhao, J. Deng, P. Sun, J. Liu, Y. Ji, N. Nakada, Z. Qiao, H. Tanaka, Y. Yang, Nanomaterials for treating emerging contaminants in water by adsorption and photocatalysis: systematic review and bibliometric analysis, Sci. Total Environ. 627 (2018) 1253–1263.
[90] J. Choina, H. Kosslick, C. Fischer, G.U. Flechsig, L. Frunza, A. Schulz, Photocatalytic decomposition of pharmaceutical ibuprofen pollutions in water over titania catalyst, Appl. Catal. Environ. 129 (2013) 589–598.
[91] K.M. Lee, C.W. Lai, K.S. Ngai, J.C. Juan, Recent developments of zinc oxide based photocatalyst in water treatment technology: a review, Water Res. 88 (2016) 428–448.

This book belongs to Badji Mokhtar Annaba University Central Library Copyright Elsevier 2025

[92] C. Yuan, C.H. Hung, H.W. Li, W.H. Chang, Photodegradation of ibuprofen by TiO_2 co-doping with urea and functionalized CNT irradiated with visible light—effect of doping content and pH, Chemosphere 155 (2016) 471–478.
[93] Z. Li, M. Qi, C. Tu, W. Wang, J. Chen, A.J. Wang, Highly efficient removal of chlorotetracycline from aqueous solution using graphene oxide/TiO_2 composite: properties and mechanism, Appl. Surf. Sci. 425 (2017) 765–775.
[94] S. Basha, C. Barr, D. Keane, K. Nolan, A. Morrissey, M. Oelgemöller, J.M. Tobin, On the adsorption/photodegradation of amoxicillin in aqueous solutions by an integrated photocatalytic adsorbent (IPCA): experimental studies and kinetics analysis, Photochem. Photobiol. Sci. 10 (2011) 1014–1022.
[95] E.S. Elmolla, M. Chaudhuri, Photocatalytic degradation of amoxicillin, ampicillin and cloxacillin antibiotics in aqueous solution using UV/TiO_2 and UV/H_2O_2/TiO_2 photocatalysis, Desalination 252 (2010) 46–52.
[96] L. Hu, P.M. Flanders, P.L. Miller, T.J. Strathmann, Oxidation of sulfamethoxazole and related antimicrobial agents by TiO_2 photocatalysis, Water Res. 41 (2007) 2612–2626.
[97] M.H. Habibi, A. Hassanzadeh, S. Mahdavi, The effect of operational parameters on the photocatalytic degradation of three textile azo dyes in aqueous TiO_2 suspensions, J. Photochem. Photobiol. A Chem. 172 (2005) 89–96.
[98] Y. Ye, Y. Feng, H. Bruning, D. Yntema, H.H.M. Rijnaarts, Photocatalytic degradation of metoprolol by TiO_2 nanotube arrays and UV-LED: effects of catalyst properties, operational parameters, commonly present water constituents, and photo-induced reactive species, Appl. Catal. Environ. 220 (2018) 171–181.
[99] M.N. Chong, B. Jin, C.W.K. Chow, C. Saint, Recent developments in photocatalytic water treatment technology: a review, Water Res. 44 (2010) 2997–3027.
[100] J.M. Herrmann, Heterogeneous photocatalysis: fundamentals and applications to the removal of various types of aqueous pollutants, Catal. Today 53 (1999) 115–129.
[101] L. Yang, Z. Liu, J. Shi, Y. Zhang, H. Hu, W. Shangguan, Degradation of indoor gaseous formaldehyde by hybrid VUV and TiO_2/UV processes, Sep. Purif. Technol. 54 (2007) 204–211.
[102] S. Mallakpour, E. Khadem, Carbon nanotube–metal oxide nanocomposites: fabrication, properties and applications, Chem. Eng. J. 302 (2016) 344–367.
[103] F. Taleshi, Study of morphology and band gap energy of TiO_2-carbon nanotube nanocomposite, J. Mater. Sci. Mater. Electron. 26 (2015) 3262–3267.
[104] B. Czech, W. Buda, Multicomponent nanocomposites for elimination of diclofenac in water based on an amorphous TiO_2 active in various light sources, J. Photochem. Photobiol. A Chem. 330 (2016) 64–70.
[105] P. Zhang, Y. Liu, B. Tian, Y. Luo, J. Zhang, Synthesis of core-shell structured CdS@CeO_2 and CdS@TiO_2 composites and comparison of their photocatalytic activities for the selective oxidation of benzyl alcohol to benzaldehyde, Catal. Today 281 (2017) 181–188.
[106] N.A.M. Barakat, M.A. Kanjwal, I.S. Chronakis, H.Y. Kim, Influence of temperature on the photodegradation process using Ag-doped TiO_2 nanostructures: negative impact with the nanofibers, J. Mol. Catal. A Chem. 366 (2013) 333–340.
[107] A. Gnanaprakasam, V.M. Sivakumar, M. Thirumarimurugan, Influencing parameters in the photocatalytic degradation of organic effluent via nanometal oxide catalyst: a review, Indian J. Mater. Sci. 2015 (2015) 1–16.
[108] D. Awfa, M. Ateia, M. Fujii, M.S. Johnson, C. Yoshimura, Photodegradation of pharmaceuticals and personal care products in water treatment using carbonaceous-TiO_2 composites: a critical review of recent literature, Water Res. 142 (2018) 26–45.
[109] F.D. Mai, C.S. Lu, C.W. Wu, C.H. Huang, J.Y. Chen, C.C. Chen, Mechanisms of photocatalytic degradation of Victoria Blue R using nano-TiO_2, Sep. Purif. Technol. 62 (2008) 423–436.
[110] H.R. Pouretedal, A. Norozi, M.H. Keshavarz, A. Semnani, Nanoparticles of zinc sulfide doped with manganese, nickel and copper as nanophotocatalyst in the degradation of organic dyes, J. Hazard. Mater. 162 (2009) 674–681.
[111] N. Sobana, K. Selvam, M. Swaminathan, Optimization of photocatalytic degradation conditions of Direct Red 23 using nano-Ag doped TiO_2, Sep. Purif. Technol. 62 (2008) 648–653.
[112] N. Sobana, M. Swaminathan, The effect of operational parameters on the photocatalytic degradation of acid red 18 by ZnO, Sep. Purif. Technol. 56 (2007) 101–107.

This book belongs to Badji Mokhtar Annaba University Central Library Copyright Elsevier 2025

[113] M. Farzadkia, E. Bazrafshan, A. Esrafili, J.K. Yang, M. Shirzad-Siboni, Photocatalytic degradation of metronidazole with illuminated TiO_2 nanoparticles, J. Environ. Health Sci. Eng. 13 (2015) 35.
[114] G. Prados-Joya, M. Sánchez-Polo, J. Rivera-Utrilla, M. Ferro-garcía, Photodegradation of the antibiotics nitroimidazoles in aqueous solution by ultraviolet radiation, Water Res. 45 (2011) 393–403.
[115] R.A. Palominos, M.A. Mondaca, A. Giraldo, G. Peñuela, M. Pérez-Moya, H.D. Mansilla, Photocatalytic oxidation of the antibiotic tetracycline on TiO_2 and ZnO suspensions, Catal. Today 144 (2009) 100–105.
[116] S.W. Nam, D.J. Choi, S.K. Kim, N. Her, K.D. Zoh, Adsorption characteristics of selected hydrophilic and hydrophobic micropollutants in water using activated carbon, J. Hazard. Mater. 270 (2014) 144–152.
[117] S. Moradi Dehaghi, B. Rahmanifar, A.M. Moradi, P.A. Azar, Removal of permethrin pesticide from water by chitosan-zinc oxide nanoparticles composite as an adsorbent, J. Saudi Chem. Soc. 18 (2014) 348–355.
[118] A. Meng, J. Xing, Z. Li, Q. Li, Cr-doped ZnO nanoparticles: synthesis, characterization, adsorption property, and recyclability, ACS Appl. Mater. Interfaces 7 (2015) 27449–27457.
[119] F. Liu, H. Tian, J. He, Adsorptive performance and catalytic activity of superparamagnetic Fe_3O_4@$nSiO_2$@$mSiO_2$ core–shell microspheres towards DDT, J. Colloid Interface Sci. 419 (2014) 68–72.
[120] B. Rahmanifar, S. Moradi Dehaghi, Removal of organochlorine pesticides by chitosan loaded with silver oxide nanoparticles from water, Clean Techn. Environ. Policy 16 (2014) 1781–1786.
[121] H. Mangal, A. Saxena, A.S. Rawat, V. Kumar, P.K. Rai, M. Datta, Adsorption of nitrobenzene on zero valent iron loaded metal oxide nanoparticles under static conditions, Microporous Mesoporous Mater. 168 (2013) 247–256.
[122] Y. Tan, L. Zhu, H. Niu, Y. Cai, F. Wu, X. Zhao, Synthesis of flower-shaped ZrO_2-C composites for adsorptive removal of trichlorophenol from aqueous solution, RSC Adv. 5 (2015) 77175–77183.
[123] J. Hu, W. Deng, D. Chen, Ceria hollow spheres as an adsorbent for efficient removal of acid dye, ACS Sustain. Chem. Eng. 5 (2017) 3570–3582.
[124] J.Y. Luo, Z. Cao, F. Chen, L. Li, Y.R. Lin, B.W. Liang, Q.G. Zeng, M. Zhang, X. He, C. Li, Strong aggregation adsorption of methylene blue from water using amorphous WO_3 nanosheets, Appl. Surf. Sci. 287 (2013) 270–275.
[125] Y. Zheng, B. Zhu, H. Chen, W. You, C. Jiang, J. Yu, Hierarchical flower-like nickel(II) oxide microspheres with high adsorption capacity of Congo red in water, J. Colloid Interface Sci. 504 (2017) 688–696.
[126] S.A.C. Carabineiro, T. Thavorn-Amornsri, M.F.R. Pereira, P. Serp, J.L. Figueiredo, Comparison between activated carbon, carbon xerogel and carbon nanotubes for the adsorption of the antibiotic ciprofloxacin, Catal. Today 186 (2012) 29–34.
[127] H. Kim, Y.S. Hwang, V.K. Sharma, Adsorption of antibiotics and iopromide onto single-walled and multi-walled carbon nanotubes, Chem. Eng. J. 255 (2014) 23–27.
[128] S. Dong, Y. Sun, J. Wu, B. Wu, A.E. Creamer, B. Gao, Graphene oxide as filter media to remove levofloxacin and lead from aqueous solution, Chemosphere 150 (2016) 759–764.
[129] I.M. Jauris, C.F. Matos, A.J.G. Zarbin, C.S. Umpierres, C. Saucier, E.C. Lima, S.B. Fagan, I. Zanella, F. M. Machado, Adsorption of anti-inflammatory nimesulide by graphene materials: a combined theoretical and experimental study, Phys. Chem. Chem. Phys. 19 (2017) 22099–22110.
[130] A. Ahmad, M.H. Razali, M. Mamat, F.S.B. Mehamod, K. Anuar Mat Amin, Adsorption of methyl orange by synthesized and functionalized-CNTs with 3-amino propyltriethoxy silane loaded TiO_2 nanocomposites, Chemosphere 168 (2017) 474–482.
[131] I.K. Konstantinou, T.A. Albanis, TiO_2-assisted photocatalytic degradation of azo dyes in aqueous solution: kinetic and mechanistic investigations: a review, Appl. Catal. Environ. 49 (2004) 1–14.
[132] M.E. McHenry, D.E. Laughlin, Nano-scale materials development for future magnetic applications, Acta Mater. 48 (2000) 223–238.
[133] S.T. Selvan, T.T. Yang Tan, D. Kee Yi, N.R. Jana, Functional and multifunctional nanoparticles for bioimaging and biosensing, Langmuir 26 (2010) 11631–11641.
[134] J.W. Murray, The surface chemistry of hydrous manganese dioxide, J. Colloid Interface Sci. 46 (1974) 357–371.
[135] A. Kiran Kumar, S. Venkata Mohan, Removal of natural and synthetic endocrine disrupting estrogens by multi-walled carbon nanotubes (MWCNT) as adsorbent: kinetic and mechanistic evaluation, Sep. Purif. Technol. 87 (2012) 22–30.

This book belongs to Badji Mokhtar Annaba University Central Library Copyright Elsevier 2025

[136] H. Zhao, X. Liu, Z. Cao, Y. Zhan, X. Shi, Y. Yang, J. Zhou, J. Xu, Adsorption behavior and mechanism of chloramphenicols, sulfonamides, and non-antibiotic pharmaceuticals on multi-walled carbon nanotubes, J. Hazard. Mater. 310 (2016) 235–245.
[137] X. Qu, J. Brame, Q. Li, P.J.J. Alvarez, Nanotechnology for a safe and sustainable water supply: enabling integrated water treatment and reuse, Acc. Chem. Res. 46 (2013) 834–843.
[138] K. Yang, W. Wu, Q. Jing, L. Zhu, Aqueous adsorption of aniline, phenol, and their substitutes by multi-walled carbon nanotubes, Environ. Sci. Technol. 42 (2008) 7931–7936.
[139] S. Zhu, Y.G. Liu, S.B. Liu, G.M. Zeng, L.H. Jiang, X.F. Tan, L. Zhou, W. Zeng, T.T. Li, C. P. Yang, Adsorption of emerging contaminant metformin using graphene oxide, Chemosphere 179 (2017) 20–28.
[140] O.G. Apul, T. Karanfil, Adsorption of synthetic organic contaminants by carbon nanotubes: a critical review, Water Res. 68 (2015) 34–55.
[141] F.F. Liu, J. Zhao, S. Wang, P. Du, B. Xing, Effects of solution chemistry on adsorption of selected pharmaceuticals and personal care products (PPCPs) by graphenes and carbon nanotubes, Environ. Sci. Technol. 48 (2014) 13197–13206.
[142] Q. Liao, J. Sun, L. Gao, The adsorption of resorcinol from water using multi-walled carbon nanotubes, Colloids Surf. A Physicochem. Eng. Asp. 312 (2008) 160–165.
[143] L. Ji, W. Chen, S. Zheng, Z. Xu, D. Zhu, Adsorption of sulfonamide antibiotics to multiwalled carbon nanotubes, Langmuir 25 (2009) 11608–11613.
[144] X. Yu, L. Zhang, M. Liang, W. Sun, pH-dependent sulfonamides adsorption by carbon nanotubes with different surface oxygen contents, Chem. Eng. J. 279 (2015) 363–371.
[145] S. Zhou, Y. Shao, N. Gao, J. Deng, C. Tan, Equilibrium, kinetic, and thermodynamic studies on the adsorption of triclosan onto multi-walled carbon nanotubes, Clean Soil, Air, Water 41 (2013) 539–547.
[146] Y. Gao, Y. Li, L. Zhang, H. Huang, J. Hu, S.M. Shah, X. Su, Adsorption and removal of tetracycline antibiotics from aqueous solution by graphene oxide, J. Colloid Interface Sci. 368 (2012) 540–546.
[147] L. Jiang, Y. Liu, S. Liu, X. Hu, G. Zeng, X. Hu, S. Liu, S. Liu, B. Huang, M. Li, Fabrication of β-cyclodextrin/poly (L-glutamic acid) supported magnetic graphene oxide and its adsorption behavior for 17β-estradiol, Chem. Eng. J. 308 (2017) 597–605.
[148] M.T.M. Pendergast, J.M. Nygaard, A.K. Ghosh, E.M.V. Hoek, Using nanocomposite materials technology to understand and control reverse osmosis membrane compaction, Desalination 261 (2010) 255–263.
[149] P. Wu, Y. Xu, Z. Huang, J. Zhang, A review of preparation techniques of porous ceramic membranes, J. Ceram. Process. Res. 16 (2015) 102–106.
[150] Y. Ying, W. Ying, Q. Li, D. Meng, G. Ren, R. Yan, X. Peng, Recent advances of nanomaterial-based membrane for water purification, Appl. Mater. Today 7 (2017) 144–158.
[151] N. Maximous, G. Nakhla, K. Wong, W. Wan, Optimization of Al_2O_3/PES membranes for wastewater filtration, Sep. Purif. Technol. 73 (2010) 294–301.
[152] S. Al Aani, V. Gomez, C.J. Wright, N. Hilal, Fabrication of antibacterial mixed matrix nanocomposite membranes using hybrid nanostructure of silver coated multi-walled carbon nanotubes, Chem. Eng. J. 326 (2017) 721–736.
[153] A. Xie, J. Cui, J. Yang, Y. Chen, J. Lang, C. Li, Y. Yan, J. Dai, Graphene oxide/Fe(III)-based metal-organic framework membrane for enhanced water purification based on synergistic separation and photo-Fenton processes, Appl. Catal. Environ. 264 (2020) 118548.
[154] Z. Song, M. Fathizadeh, Y. Huang, K.H. Chu, Y. Yoon, L. Wang, W.L. Xu, M. Yu, TiO_2 nanofiltration membranes prepared by molecular layer deposition for water purification, J. Membr. Sci. 510 (2016) 72–78.
[155] M. Zambianchi, M. Durso, A. Liscio, E. Treossi, C. Bettini, M. L. Capobianco, A. Aluigi, A. Kovtun, G. Ruani, F. Corticelli, M. Brucale, V. Palermo, M.L. Navacchia, M. Melucci, Graphene oxide doped polysulfone membrane adsorbers for the removal of organic contaminants from water, Chem. Eng. J. 326 (2017) 130–140.
[156] S. Nasseri, S. Ebrahimi, M. Abtahi, R. Saeedi, Synthesis and characterization of polysulfone/graphene oxide nano-composite membranes for removal of bisphenol A from water, J. Environ. Manage. 205 (2018) 174–182.

This book belongs to Badji Mokhtar Annaba University Central Library Copyright Elsevier 2025

[157] A. Gholami, A.R. Moghadassi, S.M. Hosseini, S. Shabani, F. Gholami, Preparation and characterization of polyvinyl chloride based nanocomposite nanofiltration-membrane modified by iron oxide nanoparticles for lead removal from water, J. Ind. Eng. Chem. 20 (2014) 1517–1522.
[158] R.A. Damodar, S.J. You, H.H. Chou, Study the self cleaning, antibacterial and photocatalytic properties of TiO_2 entrapped PVDF membranes, J. Hazard. Mater. 172 (2009) 1321–1328.
[159] Q. Wang, C. Yang, G. Zhang, L. Hu, P. Wang, Photocatalytic Fe-doped TiO_2/PSF composite UF membranes: characterization and performance on BPA removal under visible-light irradiation, Chem. Eng. J. 319 (2017) 39–47.
[160] R. Xu, Q. Zhou, F. Li, B. Zhang, Laccase immobilization on chitosan/poly(vinyl alcohol) composite nanofibrous membranes for 2,4-dichlorophenol removal, Chem. Eng. J. 222 (2013) 321–329.
[161] P. Xu, G.M. Zeng, D.L. Huang, C.L. Feng, S. Hu, M.H. Zhao, C. Lai, Z. Wei, C. Huang, G.X. Xie, Z. F. Liu, Use of iron oxide nanomaterials in wastewater treatment: a review, Sci. Total Environ. 424 (2012) 1–10.
[162] S. Yüksel, N. Kabay, M. Yüksel, Removal of bisphenol A (BPA) from water by various nanofiltration (NF) and reverse osmosis (RO) membranes, J. Hazard. Mater. 263 (2013) 307–310.
[163] I. Koyuncu, O.A. Arikan, M.R. Wiesner, C. Rice, Removal of hormones and antibiotics by nanofiltration membranes, J. Membr. Sci. 309 (2008) 94–101.
[164] I. Vergili, Application of nanofiltration for the removal of carbamazepine, diclofenac and ibuprofen from drinking water sources, J. Environ. Manage. 127 (2013) 177–187.
[165] D. Li, Y. Xia, Direct fabrication of composite and ceramic hollow nanofibers by electrospinning, Nano Lett. 4 (2004) 933–938.
[166] M. Bassyouni, M.H. Abdel-Aziz, M.S. Zoromba, S.M.S. Abdel-Hamid, E. Drioli, A review of polymeric nanocomposite membranes for water purification, J. Ind. Eng. Chem. 73 (2019) 19–46.
[167] X. Chen, X. Gao, K. Fu, M. Qiu, F. Xiong, D. Ding, Z. Cui, Z. Wang, Y. Fan, E. Drioli, Tubular hydrophobic ceramic membrane with asymmetric structure for water desalination via vacuum membrane distillation process, Desalination 443 (2018) 212–220.
[168] T.H. Bae, T.M. Tak, Effect of TiO_2 nanoparticles on fouling mitigation of ultrafiltration membranes for activated sludge filtration, J. Membr. Sci. 249 (2005) 1–8.
[169] K. Ebert, D. Fritsch, J. Koll, C. Tjahjawiguna, Influence of inorganic fillers on the compaction behaviour of porous polymer based membranes, J. Membr. Sci. 233 (2004) 71–78.
[170] H. Karimnezhad, A.H. Navarchian, T. Tavakoli Gheinani, S. Zinadini, Amoxicillin removal by Fe-based nanoparticles immobilized on polyacrylonitrile membrane: individual nanofiltration or Fenton reaction, vs. engineered combined process, Chem. Eng. Res. Des. 153 (2020) 187–200.
[171] S.H. Kim, S.Y. Kwak, B.H. Sohn, T.H. Park, Design of TiO_2 nanoparticle self-assembled aromatic polyamide thin-film-composite (TFC) membrane as an approach to solve biofouling problem, J. Membr. Sci. 211 (2003) 157–165.
[172] K. Sunada, Y. Kikuchi, K. Hashimoto, A. Fujishima, Bactericidal and detoxification effects of TiO_2 thin film photocatalysts, Environ. Sci. Technol. 32 (1998) 726–728.
[173] Y. Ji, W. Qian, Y. Yu, Q. An, L. Liu, Y. Zhou, C. Gao, Recent developments in nanofiltration membranes based on nanomaterials, Chin. J. Chem. Eng. 25 (2017) 1639–1652.
[174] S.S. Madaeni, N. Ghaemi, Characterization of self-cleaning RO membranes coated with TiO_2 particles under UV irradiation, J. Membr. Sci. 303 (2007) 221–233.
[175] S. Yu, X. Zuo, R. Bao, X. Xu, J. Wang, J. Xu, Effect of SiO_2 nanoparticle addition on the characteristics of a new organic-inorganic hybrid membrane, Polymer 50 (2009) 553–559.
[176] Q. Hu, E. Marand, S. Dhingra, D. Fritsch, J. Wen, G. Wilkes, Poly(amide-imide)/TiO_2 nano-composite gas separation membranes: fabrication and characterization, J. Membr. Sci. 135 (1997) 65–79.
[177] H. Wu, B. Tang, P. Wu, Optimizing polyamide thin film composite membrane covalently bonded with modified mesoporous silica nanoparticles, J. Membr. Sci. 428 (2013) 341–348.
[178] Y. Li, H. Mao, H. Zhang, G. Yang, R. Ding, J. Wang, Tuning the microstructure and permeation property of thin film nanocomposite membrane by functionalized inorganic nanospheres for solvent resistant nanofiltration, Sep. Purif. Technol. 165 (2016) 60–70.

This book belongs to Badji Mokhtar Annaba University Central Library Copyright Elsevier 2025

[179] L. Yan, Y.S. Li, C.B. Xiang, S. Xianda, Effect of nano-sized Al_2O_3-particle addition on PVDF ultrafiltration membrane performance, J. Membr. Sci. 276 (2006) 162–167.
[180] M. Sadeghi, M.A. Semsarzadeh, H. Moadel, Enhancement of the gas separation properties of polybenzimidazole (PBI) membrane by incorporation of silica nano particles, J. Membr. Sci. 331 (2009) 21–30.
[181] M. Sheikh, M. Pazirofteh, M. Dehghani, M. Asghari, M. Rezakazemi, C. Valderrama, J.L. Cortina, Application of ZnO nanostructures in ceramic and polymeric membranes for water and wastewater technologies: a review, Chem. Eng. J. 391 (2019) 123475.
[182] D. Qadir, H. Mukhtar, L.K. Keong, Mixed matrix membranes for water purification applications, Sep. Purif. Rev. 46 (2017) 62–80.
[183] C.P. Leo, W.P. Cathie Lee, A.L. Ahmad, A.W. Mohammad, Polysulfone membranes blended with ZnO nanoparticles for reducing fouling by oleic acid, Sep. Purif. Technol. 89 (2012) 51–56.
[184] J. Zhang, M. Terrones, C.R. Park, R. Mukherjee, M. Monthioux, N. Koratkar, Y. S. Kim, R. Hurt, E. Frackowiak, T. Enoki, Y. Chen, Y. Chen, A. Bianco, Carbon science in 2016: status, challenges and perspectives, Carbon 98 (2016) 708–732.
[185] W. Zhang, L. Ding, J. Luo, M.Y. Jaffrin, B. Tang, Membrane fouling in photocatalytic membrane reactors (PMRs) for water and wastewater treatment: a critical review, Chem. Eng. J. 302 (2016) 446–458.
[186] K. Goh, H.E. Karahan, L. Wei, T.H. Bae, A.G. Fane, R. Wang, Y. Chen, Carbon nanomaterials for advancing separation membranes: a strategic perspective, Carbon 109 (2016) 694–710.
[187] D. Cohen-Tanugi, J.C. Grossman, Water desalination across nanoporous graphene, Nano Lett. 12 (2012) 3602–3608.
[188] S. Ali, S.A.U. Rehman, H.Y. Luan, M.U. Farid, H. Huang, Challenges and opportunities in functional carbon nanotubes for membrane-based water treatment and desalination, Sci. Total Environ. 646 (2019) 1126–1139.
[189] E. Van Hooijdonk, C. Bittencourt, R. Snyders, J.F. Colomer, Functionalization of vertically aligned carbon nanotubes, Beilstein J. Nanotechnol. 4 (2013) 129–152.
[190] R. Das, M.E. Ali, S.B.A. Hamid, S. Ramakrishna, Z.Z. Chowdhury, Carbon nanotube membranes for water purification: a bright future in water desalination, Desalination 336 (2014) 97–109.
[191] M.S. Mauter, Y. Wang, K.C. Okemgbo, C.O. Osuji, E.P. Giannelis, M. Elimelech, Antifouling ultrafiltration membranes via post-fabrication grafting of biocidal nanomaterials, ACS Appl. Mater. Interfaces 3 (2011) 2861–2868.
[192] K. Zodrow, L. Brunet, S. Mahendra, D. Li, A. Zhang, Q. Li, P.J.J. Alvarez, Polysulfone ultrafiltration membranes impregnated with silver nanoparticles show improved biofouling resistance and virus removal, Water Res. 43 (2009) 715–723.
[193] J.H. Choi, J. Jegal, W.N. Kim, Fabrication and characterization of multi-walled carbon nanotubes/polymer blend membranes, J. Membr. Sci. 284 (2006) 406–415.
[194] M. Subramanian, A. Kannan, Photocatalytic degradation of phenol in a rotating annular reactor, Chem. Eng. Sci. 65 (2010) 2727–2740.
[195] C.H. Chiou, C.Y. Wu, R.S. Juang, Influence of operating parameters on photocatalytic degradation of phenol in UV/TiO_2 process, Chem. Eng. J. 139 (2008) 322–329.
[196] H.C. Yatmaz, C. Wallis, C.R. Howarth, The spinning disc reactor—studies on a novel TiO_2 photocatalytic reactor, Chemosphere 42 (2001) 397–403.
[197] Y. Boyjoo, M. Ang, V. Pareek, CFD simulation of a pilot scale slurry photocatalytic reactor and design of multiple-lamp reactors, Chem. Eng. Sci. 111 (2014) 266–277.
[198] M.E. Leblebici, G.D. Stefanidis, T. Van Gerven, Comparison of photocatalytic space-time yields of 12 reactor designs for wastewater treatment, Chem. Eng. Process. Process Intensif. 97 (2015) 106–111.
[199] N. Doss, P. Bernhardt, T. Romero, R. Masson, V. Keller, N. Keller, Photocatalytic degradation of butanone (methylethylketone) in a small-size TiO_2/β-SiC alveolar foam LED reactor, Appl. Catal. Environ. 154–155 (2014) 301–308.
[200] M. Mirzaei, M. Jafarikojour, B. Dabir, M. Dadvar, Evaluation and modeling of a spinning disc photoreactor for degradation of phenol: impact of geometry modification, J. Photochem. Photobiol. A Chem. 346 (2017) 206–214.

This book belongs to Badji Mokhtar Annaba University Central Library Copyright Elsevier 2025

[201] C.Y. Chang, N.L. Wu, Process analysis on photocatalyzed dye decomposition for water treatment with TiO_2-coated rotating disk reactor, Ind. Eng. Chem. Res. 49 (2010) 12173–12179.
[202] K.P. Sundar, S. Kanmani, Progression of photocatalytic reactors and it's comparison: a review, Chem. Eng. Res. Des. 4 (2019) 135–150.
[203] A. Danion, J. Disdier, C. Guillard, F. Abdelmalek, N. Jaffrezic-Renault, Characterization and study of a single-TiO_2-coated optical fiber reactor, Appl. Catal. Environ. 52 (2004) 213–223.
[204] H. Lin, K.T. Valsaraj, An optical fiber monolith reactor for photocatalytic wastewater treatment, AICHE J. 52 (2006) 2271–2280.
[205] R. Zhu, S. Che, X. Liu, S. Lin, G. Xu, F. Ouyang, A novel fluidized-bed-optical-fibers photocatalytic reactor (FBOFPR) and its performance, Appl. Catal. A. Gen. 471 (2014) 136–141.
[206] K. Natarajan, T.S. Natarajan, H.C. Bajaj, R.J. Tayade, Photocatalytic reactor based on UV-LED/TiO_2 coated quartz tube for degradation of dyes, Chem. Eng. J. 178 (2011) 40–49.
[207] R.J. Tayade, T.S. Natarajan, H.C. Bajaj, Photocatalytic degradation of methylene blue dye using ultraviolet light emitting diodes, Ind. Eng. Chem. Res. 48 (2009) 10262–10267.
[208] S. Leong, A. Razmjou, K. Wang, K. Hapgood, X. Zhang, H. Wang, TiO_2 based photocatalytic membranes: a review, J. Membr. Sci. 472 (2014) 167–184.
[209] S. Mozia, Photocatalytic membrane reactors (PMRs) in water and wastewater treatment. A review, Sep. Purif. Technol. 73 (2010) 71–91.
[210] R.A. Damodar, S.J. You, Performance of an integrated membrane photocatalytic reactor for the removal of Reactive Black 5, Sep. Purif. Technol. 71 (2010) 44–49.
[211] P. Wang, T.T. Lim, Membrane vis-LED photoreactor for simultaneous penicillin G degradation and TiO_2 separation, Water Res. 46 (2012) 1825–1837.
[212] A. Visan, D. Rafieian, W. Ogieglo, R.G.H. Lammertink, Modeling intrinsic kinetics in immobilized photocatalytic microreactors, Appl. Catal. Environ. 150–151 (2014) 93–100.
[213] R. Gorges, S. Meyer, G. Kreisel, Photocatalysis in microreactors, J. Photochem. Photobiol. A Chem. 167 (2004) 95–99.
[214] R.K. Thines, N.M. Mubarak, S. Nizamuddin, J.N. Sahu, E.C. Abdullah, P. Ganesan, Application potential of carbon nanomaterials in water and wastewater treatment: a review, J. Taiwan Inst. Chem. Eng. 72 (2017) 116–133.
[215] S. Chowdhury, R. Balasubramanian, Recent advances in the use of graphene-family nanoadsorbents for removal of toxic pollutants from wastewater, Adv. Colloid Interface Sci. 204 (2014) 35–56.
[216] M. Kamali, K.M. Persson, M.E. Costa, I. Capela, Sustainability criteria for assessing nanotechnology applicability in industrial wastewater treatment: current status and future outlook, Environ. Int. 125 (2019) 261–276.
[217] W. Zhao, I.W. Chen, F. Huang, Toward large-scale water treatment using nanomaterials, Nano Today 27 (2019) 11–27.
[218] M. Rethinasabapathy, S.M. Kang, S.C. Jang, Y.S. Huh, Three-dimensional porous graphene materials for environmental applications, Carbon Lett. 22 (2017) 1–13.
[219] M.A. Riaz, G. McKay, J. Saleem, 3D graphene-based nanostructured materials as sorbents for cleaning oil spills and for the removal of dyes and miscellaneous pollutants present in water, Environ. Sci. Pollut. Res. 24 (2017) 27731–27745.
[220] H. Tan, Z. Zhao, M. Niu, C. Mao, D. Cao, D. Cheng, P. Feng, Z. Sun, A facile and versatile method for preparation of colored TiO_2 with enhanced solar-driven photocatalytic activity, Nanoscale 6 (2014) 10216–10223.
[221] X. Yan, Y. Li, T. Xia, Black titanium dioxide nanomaterials in photocatalysis, Int. J. Photoenergy 2017 (2017) 1–16.
[222] V.A. Glezakou, R. Rousseau, Shedding light on black titania, Nat. Mater. 17 (2018) 856–857.
[223] Z. Wang, C. Yang, T. Lin, H. Yin, P. Chen, D. Wan, F. Xu, F. Huang, J. Lin, X. Xie, M. Jiang, Visible-light photocatalytic, solar thermal and photoelectrochemical properties of aluminium-reduced black titania, Energy Environ. Sci. 6 (2013) 3007–3014.

This book belongs to Badji Mokhtar Annaba University Central Library Copyright Elsevier 2025

[224] M. Anjum, R. Miandad, M. Waqas, F. Gehany, M.A. Barakat, Remediation of wastewater using various nano-materials, Arab. J. Chem. 12 (2019) 4897–4919.
[225] B. Pan, B. Pan, W. Zhang, L. Lv, Q. Zhang, S. Zheng, Development of polymeric and polymer-based hybrid adsorbents for pollutants removal from waters, Chem. Eng. J. 151 (2009) 19–29.
[226] P.Z. Ray, H.J. Shipley, Inorganic nano-adsorbents for the removal of heavy metals and arsenic: a review, RSC Adv. 5 (2015) 29885–29907.
[227] G. Daneshvar Tarigh, F. Shemirani, Magnetic multi-wall carbon nanotube nanocomposite as an adsorbent for preconcentration and determination of lead (II) and manganese (II) in various matrices, Talanta 115 (2013) 744–750.
[228] W.W. Tang, G.M. Zeng, J.L. Gong, Y. Liu, X.Y. Wang, Y.Y. Liu, Z.F. Liu, L. Chen, X.R. Zhang, D. Z. Tu, Simultaneous adsorption of atrazine and Cu (II) from wastewater by magnetic multi-walled carbon nanotube, Chem. Eng. J. 211–212 (2012) 470–478.
[229] J.H. Jang, J. Lee, S.Y. Jung, D.C. Choi, Y.J. Won, K.H. Ahn, P.K. Park, C.H. Lee, Correlation between particle deposition and the size ratio of particles to patterns in nano- and micro-patterned membrane filtration systems, Sep. Purif. Technol. 156 (2015) 608–616.
[230] J. Guo, Q. Zhang, Z. Cai, K. Zhao, Preparation and dye filtration property of electrospun polyhydroxybutyrate–calcium alginate/carbon nanotubes composite nanofibrous filtration membrane, Sep. Purif. Technol. 161 (2016) 69–79.
[231] C. Zhou, Y. Shi, C. Sun, S. Yu, M. Liu, C. Gao, Thin-film composite membranes formed by interfacial polymerization with natural material sericin and trimesoyl chloride for nanofiltration, J. Membr. Sci. 471 (2014) 381–391.
[232] W. Hu, J. Yin, B. Deng, Z. Hu, Application of nano TiO_2 modified hollow fiber membranes in algal membrane bioreactors for high-density algae cultivation and wastewater polishing, Bioresour. Technol. 193 (2015) 135–141.
[233] V. Khanna, B.R. Bakshi, L.J. Lee, Carbon nanofiber production, J. Ind. Ecol. 12 (2008) 394–410.

This book belongs to Badji Mokhtar Annaba University Central Library
Copyright Elsevier 2025

This page intentionally left blank

This book belongs to Badji Mokhtar Annaba University Central Library

Copyright Elsevier 2025

CHAPTER 32

Antimicrobial activities of nanomaterials in wastewater treatment: A case study of graphene-based nanomaterials

Svetlana Jovanović

"Vinča" Institute of Nuclear Sciences – National Institute of the Republic of Serbia, University of Belgrade, Belgrade, Serbia

32.1 The structure and properties of graphene-based nanomaterials

In the last three decades, graphene-based nanomaterials have been the focus of scientific research in many different fields. An era of graphene and related nanomaterials started with the discovery of fullerene in 1985 [1], followed by carbon nanotubes (CNTs) in 1991 [2], isolation of graphene (G) in 2004 [3], production of graphene oxide (GO) in 2006 [4], and graphene quantum dots (GQDs) in 2008 [5].

Before 1985, only three allotropes of carbon were known: graphite, diamond, and amorphous carbon. But earlier, Benjamin Collins Brodie in 1859 [6] suggested the existence of the lamellar structure of graphite oxide reduced by thermal treatment. Also, the approach for the synthesis of graphite oxide appeared in 1958 [7]. Nevertheless, the progress in graphene-based nanomaterials had to wait for the development of microscopic and other techniques for structural analysis sensitive enough for these new materials. Fullerenes are the first discovered and first synthesized graphene-based nanomaterials. Fullerenes were also found in nature; they have been detected in some rocks from sites around the world as well as in certain meteorites [8, 9]. But they were found only in very low amounts, such as ppb to ppm levels. Thus, they are usually produced artificially using many different procedures such as vaporization of graphite by laser irradiation [1], the vaporization of graphite rods by resistive heating in a helium (He) atmosphere [10], arc and radiofrequency discharge or a hollow cathode arc [11, 12], intramolecular cyclodehydrogenation of planar polycyclic aromatic hydrocarbon precursor molecules or direct synthesis [13], or flash vacuum pyrolysis of fluorine-containing polycyclic aromatic hydrocarbons [14].

Fullerenes consist of carbon atoms and are considered an allotrope of carbon. Here, carbon atoms are sp^2-hybridized. In these molecules, C atoms are connected to each other with single

Handbook of Nanomaterials for Wastewater Treatment. https://doi.org/10.1016/B978-0-12-821496-1.00002-7
Copyright © 2021 Elsevier Inc. All rights reserved.

This book belongs to Badji Mokhtar Annaba University Central Library Copyright Elsevier 2025

or double bonds forming closed, spherical structures. In the case of C_{60}, 12 pentagonal and 20 hexagonal rings form fullerene's closed-cage, soccer-ball shape. Fullerene C_{60} is also called Buckminsterfullerene. The number of C atoms varies from 20 to 2200 [15]. Due to this structure, fullerenes are nonpolar, insoluble in water, and soluble in toluene, 1-chlorobenzene, 1,2,3-thrichloropropane, carbon disulfide, 1-chloronaphthalene, and other organic solvents [16]. To modify polarity, electrical properties, and other structural changes, numerous chemical approaches to modify their structure were proposed [17–22]. Apart from chemical modifications that induced changes in fullerene structure and polarity, water dispersions of fullerenes can be obtained in the form of colloidal aggregate or so-called nano-C_{60} [23, 24]. For C_{60} molecules, Van der Waals diameter is 1.1 nm [25], while the nano-C_{60} nanoparticles are usually larger, up to 90 nm [26].

For the investigation of structural properties, the most often applied techniques are nuclear magnetic resonance (NMR) spectroscopy [27], ultrahigh performance liquid chromatography [28], mass spectroscopy [29], infrared spectroscopy [30, 31], thermogravimetric analysis [32], etc. Morphology of fullerenes and their derivatives was investigated with transmission electron microscopy [33, 34], dynamic light scattering [34], atomic force microscopy [26], etc.

The next discovered nanomaterial was CNTs [2]. They are graphene sheets rolled up into a cylinder. Depending on the number of graphene sheets, two types of CNTs are detected: single-wall and multiwall (SWCNTs and MWCNTs, respectively). In the case of SWCNTs, due to differences in the electrical conductivity, metallic and semiconducting nanotubes have been produced [35]. Considering that their walls are built from only sp^2-hybridized carbon atoms, they are highly hydrophobic. Additional physical properties, such as small radius, from 1 nm [36], and a length in microns, increase the free surface of CNTs [37], as well as adding possibilities for their interaction between each other. These nanomaterials are highly flexible as well [38]. Due to these chemical and physical properties, CNTs attempt to form bundles, i.e., packages of CNTs in which tubes are strongly attached. Bundles are a result of weak but numerous Van der Waals interactions. Thus, they often interfere with the electrical, chemical, and other characteristics of CNTs. Consequently, the bundles reduce the ability to organize NTs into a continual thin film with homogeneous NTs distribution. To overcome this problem, two approaches have been used:

- Covalent
- Noncovalent functionalization

Covalent modification can be achieved using organic reactions such as:

- addition of 1,3-dipolar cycloaddition of azomethine ylides to olefins [39, 40]
- radical addition reactions with aryl diazonium salts [41], nucleophilic [42]
- electrophilic addition [43]
- oxidation using strong organic acids [44]

This book belongs to Badji Mokhtar Annaba University Central Library Copyright Elsevier 2025

Apart from classical organic approaches, innovative ways with low chemical consumption have been proposed such as oxidation by gamma irradiation [45, 46] or laser ablation [47].

Although covalent modification significantly changes the CNTs' structure and therefore increases their solubility in water or other solvents, these approaches induce the disrupting of sp^2 hybridization due to the formation of new δ bonds.

The approach to increase the dispersibility of CNTs in water and polar organic solvents and to avoid rupturing the π-cloud is a noncovalent functionalization [48–50]. It is based on noncovalent CNT functionalization with surfactants. To achieve the stabilization of CNTs in solvents, the molecule of the surfactant has to possess both polar and nonpolar parts of a molecule; the nonpolar part will interact with CNTs and create Van der Waals interaction while the polar part provides electrostatic or another way of stabilization in polar solvents.

Graphene is another nanomaterial that is going to be discussed in this chapter. Its structure is the base, and it is present in all other nanomaterials analyzed in this chapter. Graphene consists of sp^2-hybridized C atoms. These atoms are organized in a honeycomb crystalline layer structure. Inside of each layer, each C atom forms three, strong δ-bonds with three C neighbors making six members, i.e., aromatic rings also known as benzene rings. Considering that these rings are next to each other, the delocalization of π-electrons is not only located around one ring, but these electrons are delocalized over the whole sheet and form a unique π-cloud. Due to this situation, the electron mobility is extraordinarily high, above 200,000 cm^2/Vs [51]. Furthermore, thermal conductivity (theoretically calculated to be 5300 W/mK and experimentally measured in the range 3000–5000 W/mK at 20°C [52] makes graphene the best known thermal conductive material.

While there are very strong δ-bonds connecting the C atoms inside the layers, weak Van der Waals interactions act between layers in the bilayer and multilayer graphenes [53].

Due to the electronic structure, graphene is a semimetal or zero bandgap semiconductor [53]. Namely, the size of the bandgap is zero so conducive and valence bands are touching at six Dirac points in the Brillouin zone [54].

GO is produced by the oxidation of graphene. It is usually synthesized using Hummer's method, where graphite is oxidized with a strong oxidizing agent in harsh conditions (with $KMnO_4$ as an oxidant in the presence of $NaNO_3$ and in the mixture of H_2SO_4 and H_3PO_4). Also, new improved $NaNO_3$-free Hummer's method where $KMnO_4$ was partly replaced with K_2FeO_4 was reported [55]. Similarly, Marcano et al. established that, if the $NaNO_3$ was eliminated from the reaction mixture, and a higher concentration of $KMnO_4$ was added while a medium for the reaction is a mixture of H_2SO_4 and H_3PO_4, highly oxidized graphene sheets can be produced [56]. All these approaches lead to the bonding of functional groups with oxygen in the graphene structure; while keto and carboxyl groups are usually formed at the edges, the basal plane contains both epoxy and hydroxyl groups.

This book belongs to Badji Mokhtar Annaba University Central Library Copyright Elsevier 2025

As a consequence of the functional groups attaching to graphene, changes in both the chemical and physical characteristics occur. While they increase the dispersibility of GO in polar organic solvents including water, these functional groups induce the disruption of π-cloud and changes of the electrical, thermal, structural, morphological, and optical properties, which are characteristic for nonoxidized material (graphene) [57]. These groups induce a complete loss of electrical conductivity. It was observed that, with oxygen coverage of 5%, thermal conductivity of graphene reduces for ~90% and, with a coverage of 20%, lowers it to ~8.8 W/mK [58].

The structure of GQDs can be simply explained if they are observed as very small fragments of GO. GQDs have graphene in the core of the structure and oxygen-containing functional groups [59]. Considering the large amount of O-groups, GQDs are polar and can be dispersed in water and polar solvents. The electronic structure of GQDs is significantly different from G or GO due to their small size and functional groups, which results in the opening of the bandgap. Hence, GQDs have a nonzero bandgap. They are a semiconducting material with one more interesting property: they are photoluminescent [59]. Due to photoluminescence, GQDs are largely investigated for their application in bioimaging, in sensing and, as therapy for carcinoma [60–62]. Certain properties of graphene-based nanomaterials are listed in Table 32.1.

32.2 Mechanisms of antibacterial action of graphene nanomaterials

Graphene and related nanomaterials are extensively studied in the material sciences, physics, chemistry, as well as engineering. Large scientific attention is given to graphene and similar materials due to their unique and exquisite properties, as discussed earlier. Some properties such as biocompatibility, adaptable and multipurpose surface functionalization, extremely high surface area, photoreactivity, and photoluminescence make these materials highly attractive and interesting for biomedicine, particularly sensing/imaging, photodynamic and photothermal therapy, and drug delivery [61, 71–73].

The interest in antibacterial activity of graphene-based nanomaterials started quite recently. While the antibacterial effects of fullerene derivates were widely studied [17, 74], in the case of CNTs discovered in 1991, the antibacterial effects were discovered much later, in 2007 [75]. For G and GO, the discovery of antibacterial effects was in 2010 [76, 77]. As for GQDs, the ability to induce bacterial cell death was detected in 2014 by Ristic et al. [78]. Thus the antibacterial activity of graphene-based nanomaterials has been particularly intensively studied in the last decade [79].

Although this subject has been attracting great scientific attention, the actual mechanism of how these materials induce bacterial cell death is still unclear. Numerous studies proved that different mechanisms are involved. In the next part of the chapter, the possible mechanisms of antibacterial action of different graphene-based nanomaterials will be discussed.

This book belongs to Badji Mokhtar Annaba University Central Library Copyright Elsevier 2025

This book belongs to Badji Mokhtar Annaba University Central Library

Table 32.1: Properties of graphene-based nanomaterials.

Nanomaterial	Dimensionality	Size	Polarity	Conductivity	Specific surface area
Fullerene	0	C_{60} 1.1 nm [25] C_{84} 1.5 nm [63]	Hydrophobic, or hydrophilic derivates	Insulator, 6–10 S/cm [64]	Partially truncated fullerene, 85 m^2/g [65]
CNTs	1	MWCNTs outer diameter from 3 to 30 nm and SWCNTs for 1–2 nm [66]	Hydrophobic	Semiconductor or metallic	Theoretical 1315 m^2/g for SWCNTs [67]; measured for SWCNTs are much lower than theoretical, often 600 m^2/g or less For MWCNTs estimated to be a few 100 m^2/g [67]
G	2	Few μm to cm	Hydrophobic	Semimetal	Theoretically 2630 m^2/g for single-layer graphene [68]
GO	2	Few μm to cm	Hydrophilic	Insulator	Experimental value 736.6 m^2/g, theoretical 890 m^2/g [69, 70]
GQDs	0	2–100 nm	Hydrophilic	Semiconductor	Depending on the supports, they usually increase the surface area of support

Copyright Elsevier 2025

32.2.1 Physical/mechanical destruction

One of the suggested mechanisms is **physical/mechanical destruction**. The purpose of the outer membrane or cell wall of bacteria is the regulation of osmotic pressure, protection against mechanical stress, as well as combating infection. Physical/mechanical destruction of the outer membrane can lead to disrupting of the membrane and leaking of cytoplasmatic components. These events cause the death of bacterial cells. This mechanism was observed for 0D graphene-based nanomaterials, such as fullerenes [80]. Due to the very high surface hydrophobicity of the fullerene particles, they were able to interact easily with membrane lipids and induced the disruption of the cell membrane and/or DNA cleavage. Antimicrobial activity of fullerenes was detected for *Bacillus subtilis* (*B. subtilis*), *Candida albicans*, and *Escherichia coli* (*E. coli*); carboxyfullerens are efficient against *Streptococcus pyogens*, and fullerene with free amino groups are active against *Streptococcus aureus* (*S. aureus*) and *E. coli* [19, 81, 82]. Apart from 0D materials, antibacterial action through physical/mechanical destruction was also observed for 1D graphene-based nanomaterials such as MWCNTs and later SWCNTs [83, 84]. For MWCNTs, bacterial cell death was determined by using the fluorescence staining method with a second test that was selective for cell membrane damage. These experiments showed that short, debundled, well dispersed, uncapped MWCNTs caused the death of *E. coli* cells [83]. In the case of SWCNTs, it was found that the physical puncturing of the cell membrane or wall is the main cause of bacterial death [84]. Here again, well-dispersed SWCNTs showed stronger antibacterial activity. The authors suggested the higher cell death rate is related to higher SWCNT concentration and incubation time. Another study showed that short SWCNTs, both short and long MWCNTs, and hydroxyl and carboxyl MWCNTs induce the antibacterial effects by rupturing the cell wall with a so-called "needle action" [85]. Nanotubes could induce lyse of the walls and the membranes of human gut microbes, causing the piercing of the bacterial walls and covering on the lysis of microbial walls. Due to these events, the intracellular components will release to the extracellular space, promoting damage of the membrane potential and destruction of the bacterial cell. All these studies imply that "sharp" edges of the graphene nanotubes behave as an atomically sharp blade that cuts the cell membrane. Considering the previously discussed studies, it can be concluded that well dispersed, short SWCNTs with a lower diameter at high shaking speed can be more efficient antibacterial agents than MWCNTs, CNTs in bundles, or long nanotubes due to higher edge concentration and "needle action" toward bacterial membrane.

The same mechanism of bacterial cell destruction was also observed for 2D graphene-based nanomaterials, graphene, and GO [86]. Another important factor for antibacterial efficiency is the level of lipophilicity of GO and graphene. This parameter plays a highly significant role in the degree of damage to the bacterial wall [86]. Due to the graphene hydrophobicity, the layer interacts with nonpolar tails of phospholipids in the membrane. To form this interaction, the

This book belongs to Badji Mokhtar Annaba University Central Library Copyright Elsevier 2025

affinity of the graphene surface to nonpolar tails must be higher than lipid-lipid attraction. When this occurs, the physical disruption of the cell membrane is possible. It was observed that graphene sheets interact with hydrophobic tails of membrane phospholipids in bacterial cells that were then induced during insertion of graphene sheets across membrane that can then induce extraction of phospholipids and formation of a pore in the membrane [87, 88]. These pores are responsible for irreversible cell damages such as a subsequent osmotic imbalance, which results in cell death. Molecular dynamics simulation proved that sheets of graphene can be encapsulated with phospholipids and inserted across the membrane through interaction and formation of a bottle-neck vesicle that attracts graphene into the center of the membrane bilayer [89]. Another suggested mechanism is that graphene nanosheets, before approaching the membrane, undergoes fluctuations due to Brownian motion and wrapping with a monolayer of phospholipids; after they establish contact with the bacterial membrane, insertion and rotation are followed by spontaneous entry into the membrane [90]. The factors that have very important effects on the antibacterial activity of graphene nanosheets as well as GO are:

- In solution, it is concentration-dependent, and the higher concentration induces higher cell death [91].
- In solution, the dispersibility of graphene sheets and more stable dispersion leads to higher antibacterial efficiency [92].
- The size of graphene sheets including surface area, layer number, and lateral dimensions [93, 94]; for large GO sheets, antibacterial action is based on the wrapping of sheets around bacterial cells [93], while smaller ones tend to accumulate outside of the cell.
- The level of oxidation and lateral size; relocation of graphene sheets across lipid bilayer is dependent on both of these parameters. While small GO sheets, below 8 nm, with low oxidation level induce little membrane perturbation and directly interact with lipid tails, large GO can form the pores in the bacterial membrane [95]. When the level of oxidation is higher, GO sheets interact with hydrophilic lipid heads [90]. But heavily oxidized GO sheets seem to face the higher energy barrier for insertion, considering they have to be located onto the membrane surface before vibration allows unoxidized part of GO sheets to come in contact with hydrophobic tails of the membrane [95].
- The geometric properties of graphene: sheet density, sharpness, and orientation [96]. These parameters can affect the level of graphene insertion into the bacterial membrane. It was proven that graphene nanomaterials enter the bacterial cell at the place where straight interaction cells and the sharp edges of graphene occurs. Also, if the alignment of GO changes from a horizontal to a vertical orientation, the membrane distraction is more efficient due to the higher density of edges [97].

Graphene-based nanomaterials with different dimensionality show antibacterial activity by inducing mechanical injury of the bacterial wall or outer membrane. The level of membrane disrupting depends highly on dimensionality and determines the nature of membrane/nanomaterial contact.

This book belongs to Badji Mokhtar Annaba University Central Library Copyright Elsevier 2025

32.2.2 Oxidative stress

Oxidative stress is the second pathway by which graphene-based nanomaterials achieved bactericidal activity. Depending if this behavior is triggered by light, it can be reactive oxygen species (ROS)-dependent or ROS-independent. As for ROS-dependent action, graphene-based nanomaterials were excited by light irradiation when the excited nanomaterials are created (photosensitizer-PS) due to transitions of electrons from the highest occupied molecular orbital (HOMO) to the lowest unoccupied molecular orbital (LUMO) [72]. The excited PS undergoes intersystem crossing through which the higher energy excited state (S1) form long/lived triplet excited state (T1). Then one of two outcomes are possible:

1. T1 transfers the access of energy to molecular oxygen and formation of superoxide anion in the nonradiative process. This pathway is named a type I mechanism of photodynamic therapy.
2. T1 transfers the access of energy to molecular oxygen and forms singlet oxygen. The pathway is named a type II mechanism of photodynamic therapy.

No matter the way ROS are generated, they cause inhibition or death of bacterial cells through protein inactivation, lipid peroxidation, or DNA/RNA damage.

The ROS-independent oxidative stress is achieved by electron allocation from a biological donor such as NADH via graphene-based nanomaterial to molecular oxygen [98–100]. In this case, graphene-based nanomaterials without O-groups are the electron transporting agents that stimulate oxidation while graphene-based nanomaterials with O-containing functional groups can directly oxidize lipids or proteins in bacterial cells.

In the case of ROS-depended oxidative stress, graphene-based nanomaterials are capable of producing ROS with or without light excitation and inducing ROS-dependent antibacterial action.

We discovered that GQDs, graphene, and carbon quantum dots, after exposure to blue light, produce a significant amount of single oxygen ($^1O_2$) [61, 78, 101–103, 104]. The efficiency of ROS production has increased by introducing the electron-donating groups such as amino acids into GQDs, due to lowering the gap between HOMO and LUMO [105]. Ge et al. obtained extremely high $^1O_2$ production upon photoexcitation of N, S co-doped GQDs and suggested different mechanism of ROS production named multistate sensitization (MSS); instead of the allocation of energy to O_2 from excited triplet state PS, $^1O_2$ might be produced in two possible pathways: by transfer of energy from the single excited state of PS and by energy transfer from triplet excited state of PS [106].

SWCNTs are also able to produce ROS upon photoexcitation [107]. The amine-functionalized porphyrin (classical PS agent) conjugated it to the oxidized SWCNTs, obtaining an efficient antibacterial agent [108].

This book belongs to Badji Mokhtar Annaba University Central Library Copyright Elsevier 2025

Fullerenes also showed photoinduced antibacterial activity. It was observed that fullerol (hydroxylated C_{60}) produced $^1O_2$ and superoxide (O^{2-}•), while hydroxyl radicals (OH•) were not generated in either water or in medium [109]. On the opposite side, colloidal dispersions of fullerenes produced using tetrahydrofuran as a transition solvent did not show any ROS production. Also, fullerene encapsulated with polymer poly(*N*-vinylpyrrolidone) was an even more efficient producer of $^1O_2$ and O^{2-}• than fullerol. Colloidal water dispersion of fullerene C_{70} showed a higher ability to produces ROS, probably due to the longer lifetime of triplet excited state and smaller HOMO-LUMO gap [110].

ROS-independent oxidative stress is another possible way of antibacterial action of graphene-based nanomaterials. The mechanism of this action is direct interaction of graphene-based nanomaterials with cell components such as membrane or proteins in the respiratory chain [111, 112]. Antibacterial activity of four types of graphene-based materials, namely graphite, graphite oxide, GO, and reduced GO, against *E. coli* was analyzed [113]. Lui et al. proposed a mechanism based on the following three steps:

1. Deposition of the bacterial cells on the graphene surface
2. Sharp nanosheets directly interact with the membrane or cell wall and induce membrane stress
3. Subsequent oxidation independent of the superoxide anion

This study showed the correlation between glutathione (GSH) oxidation capacities of different graphene-based nanomaterials and their antibacterial activity. GSH is a tripeptide included in antioxidative action in cells, and its role is to stop cellular components' damage produced by oxidative stress. It was observed that conductive or metallic graphite oxidizes GSH more than graphite oxide, which is nonconductive. Similarly, reduced GO also caused higher GSH oxidation compared with GO, but smaller GO flakes showed higher antibacterial activity. They concluded that dispersibility, size, and GSH oxidization capacity have an essential role in antibacterial action.

For metallic SWCNTs, antibacterial activity was observed when they acted as a conducive bridge across a phospholipid bilayer, which was the insulator [114]. This conductive bridge induces a transfer of electrons from bacterial intracellular components to extracellular environments.

Similar effects based on electrical conductivity and electron transfer from the bacterial respiratory chain was also observed when graphene was deposited onto conductive, semiconductive, and insulation support, such as Cu, Ge, and SiO_2 [115]. In the case of conducting support, graphene showed significant antibacterial activity against both *E. coli* and *Staphylococcus aureus* (*S. aureus*) as a result of the ability to move the electrons away from graphene.

This book belongs to Badji Mokhtar Annaba University Central Library Copyright Elsevier 2025

Because of the presence of O-functional groups, GO can be involved in an oxidation reaction [77, 116]. Thus, a higher antibacterial activity of GO compared with reduced GO was observed.

32.2.3 Photothermal effect

Another pathway in which graphene-based nanomaterials can induce the death of bacterial cells is a photothermal effect. This effect is based on the excitation of a nanomaterial with a certain light, after which photoexcited material decays to the ground state through nonradiative relaxation pathways inducing an increase in the temperature [117]. Particularly attractive are the materials that can absorb light in the near-infrared (NIR, 700–1000 nm) region owing to the ability of NIR light to enter into deeper tissue. Materials with higher absorption efficiency and lower photoluminescence quantum yield are able to more efficiently convert light into heat. To achieve thermal ablation of microbes, temperature above 55°C must be achieved [118, 119]. Both CNTs and graphene are promising agents in photothermal therapy [116, 119–121]. First, CNTs were studied as photothermal agents and their effects on bacterial cells [121]. Due to high absorption in the NIR region, the affinity to bacterial cells, and the capability of clustering, CNTs were able to produce enough heat to induce bacterial cell death [121]. Comparing GO and rGO, rGO shows better antibacterial photothermal properties due to higher NIR absorption and better conductivity [123].

Recently, Budimir et al. constructed a flexible nanoheater made of a Kapton/Au nanohole substrate and coated with a layer of reduced GO-polyethyleneimine (K/Au NH/rGO-PEI) [120]. While Au nanoholes possess high-intensity absorption in the NIR region, selected polymer strongly binded with bacterial cells. After only 10 min of NIR irradiation, both *S. aureus* and *E. coli* were eliminated.

In Table 32.2, selected nanomaterials that showed efficient photothermal effect are summarized.

32.2.4 Other antibacterial effects

The term **photocatalysis** actually means that, if the catalyst (usually semiconductor) is present, the light-mediated reaction is accelerated [133]. In the case of photocatalytic antibacterial action of graphene-based nanomaterial, the reaction starts with photon absorption. The energy of the photon must be higher than the bandgap. Then, the electron is moved from valent to the conductive zone leaving the hole in the valent zone. Produced hole and excited electron diffuse separately to the surface of the semiconductor and participate in reactions such as:

(a) $O_2 + e \rightarrow O_2^{\bullet -}$
(b) $H_2O + h^+ \rightarrow OH\bullet + H^+$

This book belongs to Badji Mokhtar Annaba University Central Library Copyright Elsevier 2025

Table 32.2: Selected graphene-based nanomaterials, irradiation conditions, the concentration of nanomaterials (c).

Nanomaterial	Irradiation conditions	Bacteria	Thermal effect and conditions	Efficiency
Shortened, oxidized SWCNTs and MWCNTs [121]	1064 and 532 nm 12-ns pulse	*E. coli*, K12 strain	–	50 pulses, duration of 12 ns, nearly 100% killing effect
Graphene-polyvinylpyrrolidone (G-PVP), SWCNTs-ssDNA, or SDBS [124]	808 nm, 2 W/cm^2	U251 human glioma cell line	G-PVP, 65° C for 5 min, 0.01 mg/mL	100% killing effect
MWCNTs with Ig [125]	808 nm, 2 W/cm^2	Multidrug-resistant *S. aureus* (MRSA)	1 min, 0.02 mg/mL	85.75% killing effect
MWCNTs-antibodies [126]	800 nm 1.3 W/cm^2	*Streptococcus pyogenes* MGAS5005, a clinical M1T1 serotype strain, planktonic and biofilm cultures	77°C, light exposure for 10–120 s, 0.1 mg/mL	100% killing after at 30 s
GO coated with glycol chitosan [127]	808 nm, 0.75 W/cm^2	*S. aureus*, ATCC 25923, *E. coli*, ATCC 25922, multidrug-resistant *S. aureus* (MRSA)	66 from 29° C for 10 min irradiation, 0.2 mg/mL	Nearly 100% killing effect
Amino-functionalized GO [128]	White light (0.159 W/cm^2)	*S. aureus* and *E. coli*	81.4°C in10 min of irradiation	Minimal inhibitory concentrations 32 and 16 μg/mL against *S. aureus* and *E. coli*
Ag nanoparticles/GO [129]	NIR irradiation, 0.5–2 W/cm^2	*S. aureus*	58.4°C, 2 min	80% killing effect
Au nanorods (Au NRs) coated with rGO-PEG (rGO-PEG-Au NRs) [130]	700 nm, 8 W/cm^2		69 ± 2°C, 10 min, 0.04 mg/mL	100%
rGO on the Au nanostar [131]	808 nm, 3 W/cm^2	MRSA	70°C for 6 min	93% killing effect
Phosphorus irregular pyramids film covered by GO [132]	>410 nm, 808 nm, and LED light, 0.2 or 0.6 W/cm^2	*S. aureus* and *E. coli*	20 min	99.9%

This book belongs to Badji Mokhtar Annaba University Central Library
Copyright Elsevier 2025

For reaction (a) to occur, the lowest energy of the conductive zone must be located at more negative potential than $O_2/O_2^{\bullet-}$ energy, while reaction (b) demands that the maximum of the valent zone is more positive than $H_2O/OH\bullet$ [134]. This process is similar to photodynamic action with differences such that molecular oxygen is not necessary as in PDT, and radial production can be achieved in anaerobic conditions. However, due to low electrical conductivity, fast recombination of electron-hole pairs, and low conversion upon ambient light, graphene-based nanomaterials were combined with semiconducting nanoparticles [134–136]. It was observed that GO increases the photocatalytic activity of TiO_2 nanoparticles due to an ability to inhibit the electron-hole recombination [136].

One more way to induce bacterial cell death is **lipid extraction**. This approach is different from the previously described nano-knife/dart/needle action because lipids are pulled out of the membrane or extracted [88]. Here, Van der Waals interactions are dominant at the beginning step while hydrophobic interactions are responsible for the second step.

Inhibition of bacterial metabolism is also a possible way of antibacterial action. Derivates of fullerene can induce a bacteriostatic effect by accepting the electrons from the respiratory chain [138] or by blocking the biosynthesis of building blocks like peptidoglycans [139].

Similar to membrane destruction, isolation by wrapping of the bacterial cell from the surrounding environment induced death as a result of the inhibition of the access to nutrients [140]. This mechanism was observed for graphene nanosheets, GO, and long SWCNTs [93, 140, 141].

As presented, graphene-based nanomaterial shows promising antibacterial activity. The mechanisms that induced bacterial cell death are various and influenced by different geometrical, structural, and electrical properties of these nanomaterials. How this knowledge can be exploited in water treatment will be discussed in the following section of this chapter.

32.3 Water treatment with graphene-based nanomaterials

Recently, the possibilities of application of graphene-based nanomaterials in ecology have been explored [142, 143]. Studies showed that these materials can be used for removing different pollutants from water, such as ion, organic compounds, antibiotics, and bacteria [144, 145]. In this section, the approaches for water cleaning will be discussed, as presented in Scheme 32.1.

This book belongs to Badji Mokhtar Annaba University Central Library
Copyright Elsevier 2025

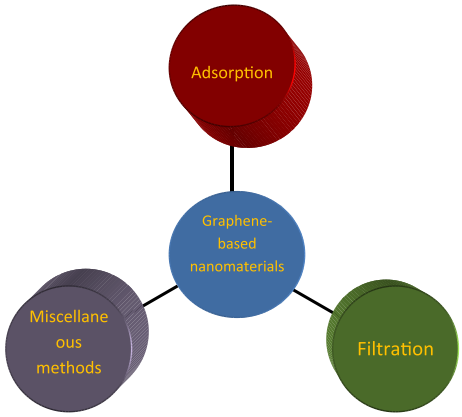

Scheme 32.1
Approaches for water treatment with graphene-based nanomaterials.

32.3.1 Filtration

Graphene-based nanomaterials can be used in water cleaning as a membrane filter. The advantages of graphene over polymeric membranes are very high mechanical strength and ability to work under pressure. Due to hydrophobicity and impermeability to water, graphene cannot be used as a membrane in water cleaning, but GO is hydrophilic and can be used as a nanomembrane in water desalination for removal of contaminates and bacteria [146].

The processes of membrane filtration are micro-, ultra-, and nanofiltration (MF, UF, and NF, respectively); reverse and forward osmosis (RO and FO, respectively); membrane distillation (MD); and membranes for ion exchanging [146]. The driving force in MF, UF, NF, and RO is hydraulic pressure, and for FO, osmotic pressure (hydrostatic pressure on one side of the semipermeable membrane is necessary to block the flow of water). In the case of RO, the cleaned water is collected after high pressure, then osmotic is applied on the salted, unclean water located on one side of a semipermeable membrane [146]. Both MF and UF membranes are porous, as they separate contaminations by sieving or by size exclusion mechanisms; the first one removes microbes and suspended particles, whereas the second removes macromolecules, such as small pathogens and biotoxins [146]. As for NF, the removal of ions such as calcium is possible so they can lower water salinity due to molecular cutoffs in the range of 100–300 Da. The mechanism is based on the diffusion in solution and sieving. Both RO and FO osmotic membranes are nonporous, and they remove all ions thanks to the solution diffusion mechanism.

Graphene-based nanomaterials have been investigated for application in NF, FO, and RO [147], due to the possibility of preparing very thin membranes, controllable hole size, and distance between holes. The mass transfer through these membranes is achieved by the hydrodynamic or

This book belongs to Badji Mokhtar Annaba University Central Library Copyright Elsevier 2025

solution-diffusion model. The membrane based on GO has 0.3 nm pores size, which is extended to 0.9 nm upon hydration [148], which allowed molecules with a diameter below 0.45 nm to pass through the membrane while the larger are eliminated. For the preparation of GO membranes, large numbers of approaches are possible such as layer-by-layer deposition, vacuum filtration, drop-casting, and spin coating. All these methods are affordable while the necessary equipment is inexpensive. The pores of these GO membranes can be functionalized with hydrophobic (H-groups) or hydrophilic (OH-groups) functional groups [149], where larger water flux was measured for OH-functionalized pores due to larger cross-section area for passing water.

Because GO has built-in polymeric structures, improvement of mechanical strength, permeability, as well as antibacterial activity was observed [150, 151]. Using GO membranes:

- Methyl orange was removed by photolytic degradation and adsorption [152]
- Na^{1+}, As^{3+}, and As^{5+} were removed from seawater [153]
- Flocculating agent for removing of micrometer-sized ground calcium carbonate [154]

32.3.2 Adsorption

Due to the wide range of adsorbents and simplicity of the process, adsorption seems attractive for water treatments. Although it is possible to remove different pollutants such as biological contamination and organic and inorganic substances, this method is not widely used in industry possibly due to a shortage of suitable adsorbents with large adsorption capacity.

Thanks to the extraordinary free surface area, the possibilities of changing chemical structure and consequently polarity and magnetic properties, graphene is evaluated as a potential adsorbent in water cleaning procedures based on adsorption. Although CNTs possess similar adsorption properties, the price of this material is too high so their application in industrial water cleaning is less probable.

The mechanism of adsorption varies, from dipole-dipole interactions, H-bond, as well as π-π stacking. Graphene and GO have been examined for application in the production of adsorbents and as presented in Table 32.3, very high efficiencies, above 90%, for removing water contaminations have been reported. Presented results indicate that graphene and similar materials have great potential for application in water cleaning.

32.3.3 Photocatalysis and electrode deposition/degradation

In the process of water cleaning, the application of graphene-like materials in photodegradation (or photocatalysis) and electrode deposition/degradation was also studied. Graphene-based nanocomposites containing cupric oxide and graphene nanoplatelets were synthesized and

This book belongs to Badji Mokhtar Annaba University Central Library Copyright Elsevier 2025

Table 32.3: Absorption properties graphene-based nanomaterial with removal capacity.

Material	Pollutant	Properties	Removal efficiency
GO nanoplatelets [155]	Azo dyes from wastewater	Particles size 60–120 nm, surface roughness of 0.190 nm	97.78%, adsorption capacity (487.80 mg/g)
GO nanoplatelets embedded in the chitosan matrix [156]	A mix of azo dyes (acid yellow 36 and acid blue 74) from their aqueous solutions	The surface roughness of 0.343 nm	98.18% and 98.80% removal in 6.48 min of ultrasonic irradiation
GO and G nanoplatelets [157]	Direct red 81 and Indosol SFGL direct blue, wastewater from the textile industry		Blue: 129.55 mg/g for GO and 97.65 mg/g for G Red dye: 173.7 mg/g for GO and 77.85 mg/g for G
GO nanoplatelets [158]	Ibuprofen drug residues	Particles size 50–100 nm	Highly efficient for IBP removal (98.17%) in extremely low dosage (1.00 g/L)
GO from biosource [159]	Crystal violet from water	Particles size 60–100 nm, surface roughness 0.226–0.167 nm after CV adsorption	99.87%
Rhamnolipid-functionalized GO hybrid [160]	Methylene blue from water		529.10 mg/g
Graphene nanoplatelet/MIL-101 (Cr) nanocomposite [161]	Naphthalene	45–50 nm	93%
Sulfonated graphene nanosheets [162]	Phenanthrene, methylene blue and for Cd^{2+}	Sheets, 1 nm	400 mg/g for phenanthrene, 906 mg/g for methylene blue, and 58 mg/g for Cd^{2+}
Sulphonated graphenes [163]	Naphthalene and 1-naphthol from water		–
Nonpolar and nonporous graphite [164]	Naphthalene, anthracene, and pyrene from water		–
Exfoliated graphite nanoplatelets [165]	Bisphenol A	Specific surface (720 m^2/g), BET surface (771 m^2/g)	550 mg/g
Graphene nanoplatelet composites with iron oxide nanoparticles	Arsenic(III) from water		–
Aluminum metal-organic framework/ reduced graphene oxide composite	Nitrophenol from water		300 mg/g

This book belongs to Badji Mokhtar Annaba University Central Library
Copyright Elsevier 2025

investigated for the photolytic decomposition of methylene blue color exposed to solar light [166]. This study showed that, after 80 min of light exposure, the largest part of the dye was degraded (99.44%). Also, a large number of pharmaceutical residuals can be removed from water by photocatalysis [167]. For example, TiO_2-rGO nanocomposites were deposited on optical fibers, and the structural stability of various medications was investigated (ibuprofen, sulfamethoxazole, and carbamazepine) during UV illumination [168]. Also, composites based on MWCNTs and TiO_2 were able to remove tetracycline in a photocatalytic reaction [169].

Wastewater from textile industry was exposed to electrochemical treatments using graphite electrodes, and it was observed that azo bonds of the dyes were totally fragmented, including the aromatic rings [170].

Described methods show the principle of water cleaning using graphene-based nanomaterials. In the following part of the chapter, the approaches for removing the bacterial cells from water will be presented as well as the synthetic procedure, possible transfer on an industrial level, and the economical and practical aspects.

32.4 Antimicrobial action of graphene-based nanomaterials in wastewater treatment, synthesis, efficiency, and perspective in an industrial application

Due to increasing bacterial pollution in water, the necessity of finding new efficient antibacterial materials and treatment nowadays seems higher than ever. As discussed previously, graphene-based nanomaterials possess significant antibacterial activity. This behavior depends on the shape, size, level of oxidation, orientation, presence of impurities, the dispersibility of graphene sheets, as well as surface area, layer number, and lateral dimensions (Section 32.2).

On the other side, treatments of water with different graphene-based nanomaterials, presented in Section 32.3, show that these materials can remove dyes, residual from the pharmaceutic industry wastewater, polycyclic aromatic compounds, and others with different approaches and mechanisms.

Here, in this part of the chapter, only treatments of wastewater with graphene-based nanomaterials that lead to removing bacterial cells will be discussed.

Photocatalytic antibacterial action was observed for ZnO/GO nanocomposites [171]. Antibacterial activity was accomplished by ROS generation [172]. Minimum inhibitory

This book belongs to Badji Mokhtar Annaba University Central Library Copyright Elsevier 2025

concentrations were obtained: 6.25 g/mL for *E. coli* and *S. typhimurium*, 12.5 g/mL for *B. subtilis*, and 25 g/mL for *Enterococcus faecalis*.

The production of composites based on chitosan chloride-GO (CSCl@GO) was successfully achieved via the solution blending method [173]. Produced composites were used for the modification of quartz sand filter. This modified sand was used as a filler in columns with different sizes. The treatment of *E. coli* and *S. aureus* for 15 min completely deactivated bacterial cells due to the protein leakage. The concentration of CSCl@GO composites was 100 mg/L. By investigating the application of this composite in bacteria removal from the circulating cooling water system, the antibacterial rate was 95.74%. After washing, antibacterial efficiency was above 90%. The synthetic procedure is very simple: CSCl was stirred in water, while GO was separately sonicated, and this dispersion was mixed in the appropriate mass ratio and heated at 60°C for 8 h. Then the precipitate was collected and cleaned with water. A vacuum was used for drying. The impregnation technique was used for sand modification: the sand was soaked in 5% solution of HCl for 6 h, washed with water, and dried. In the next step, the material was sifted and mixed under ultrasonication with dispersed composite. Then, sand was cleaned with water, dried, and named as a CSCl@GO/QS filter. This filter was tested for antibacterial cleaning of domestic sewage. The efficiency of the composite was investigated by filling the column with CSCl@GO/QS. Dimensions of the column were 20 mm in diameter and the length of 20 cm. Antibacterial activity above 99% is achieved with a particle size in the range of 0.4–0.8 mm. As a reference, pure quartz sand was used, and only 20% of the antibacterial rate was observed. It was concluded that the bonding of CSCl@GO to QS induced antibacterial action of GO and increased the ability of the filter to adsorb bacterial cells. The issue here is the possibility to run off the fine media of the filter in the process of backwashing. In the case of larger particle size, 0.8–2 mm, the antibacterial rate is lowered to just 7.5%, which makes these particles the best choice for practical application in wastewater treatment. With 15 cm of the bed height, the antibacterial activity is lower, around 96%. Presented research shows great potential considering the price and reusability in the removal of bacteria in secondary household waste sewage.

Incorporation of GO in the polymeric network or between polymer chains can improve membrane filters, increase their strength, durability, permeability, and antibacterial properties [150, 151]. Since the GO antibacterial effects are higher if direct contact of bacterial cell and GO sheet is possible, it is a better synthetic approach to the functionalized membrane with GO sheets after synthesis. In this way, GO sheets are directly available for contact with bacterial cells. Herein also, the amount of needed nanomaterial is lowered [151]. In this study, thin film composite is produced by polymerization polyamide onto sulfonated hard source. Then, using the reaction of carbodiimide coupling, –COOH groups of polymer were converted into

This book belongs to Badji Mokhtar Annaba University Central Library Copyright Elsevier 2025

amine-reactive esters, then ethylenediamine was attached to the membrane active layer. In the next step, *N*-hydroxysuccinimide-activated GO will react with the membrane surface in a condensation reaction. Produced membrane induced the death of 64.5% bacterial cells (*E. coli*) in direct contact after 1 h due to cell damage. Similar surfaces, such as stainless steel and indium-tin-oxide-coated polymer GO nanocomposites, induced lower bacterial cell death (59% and 42%, respectively) [76, 174]. With an increase in contact time, the antibacterial effect also increases. These results suggest that membranes with GO sheets are highly efficient in the inactivation of bacterial cells and seem like promising material for water treatment due to the simplicity of the procedure, the low price of GO, as well as low amount of GO necessary for preparation. Here a drawback is complicated synthetic procedure increases the price over the fabrication process.

One more membrane for treatment of water and wastewater is prepared from GO and polyethersufone (PES) mixture, where GO was added in a concentration of 0.25, 05, and 1.0 wt% [175]. The synthetic approach is immersion precipitation, where polymer was completely dissolved in *N*-methyl pyrrolidone (NMP) by overnight stirring with magnetic stirrer and then the solution was cast to produce the membrane. GO-incorporated PES membrane was produced by adding GO in different concentrations in the solution. Polyester (PS) was used as a support for PES membranes. First, PS was wetted with solvent then polymer was cast. In the following step, a coagulation bath was used to soak membranes. Then membranes were dried and stored until use. This membrane showed a 69.4% antibacterial activity toward *Salmonella typhi* (*S. typhi*). This bacteria is a cause of typhoid, and it can be found in water. By adding GO in PES membranes, the improvement of flux, water-retaining capacities, and wettability was observed in comparison with pure PES membranes. The authors suggested the use of this composite membrane in water cleaning and removing bacterial cells [175].

Hydrogels based on GO and redox-active ruthenium complexes absorbed bacterial cells and inactivated them in the next step [176]. The process of synthesis is the following:

1. Sonication GO powder in water to obtain stabile dispersion
2. Ru complex was added to GO dispersion
3. Centrifugation at 13,800 relative centrifugal force for 5 min to induce gelation
4. Ru^{2+} to Ru^{3+} was produced in the electrochemical cell, at the anode, using 0.4 mM H_2SO_4 electrolyte, potential 2 V for 0.5 h

Herein, ruthenium complexes induced noncovalent cross-linking by establishing π-π and hydrophobic interactions of GO with the ruthenium ligands. Due to these interactions, immediate gel formation was observed, just after the complex was added to GO dispersion. Bacterial cells were suspended in PBS buffer, and GO-Ru hydrogels were added. The concentration of bacterial cells was counted using a cell-counting chamber. It was observed that bacterial cells were absorbed into hydrogels. Only 1 cm^3 of the hydrogel is able to bind 1×10^8

This book belongs to Badji Mokhtar Annaba University Central Library Copyright Elsevier 2025

E. coli and 3×10^8 *S. aureus*. By applying a high-voltage electric pulse, bacterial cells were deactivated [176]. In the catching and releasing experiment, the bacteria-adsorbed hydrogel was positioned as an anode, and deactivation was accomplished with a voltage of +15 V in a duration of 15 min followed by 15 min of current at a voltage of −15 V. Owing to the acceptable price of production, reusability, and bacterial removal rate, the authors claimed that these hydrogels are the promising choice for purification of water of medical products. Although these facts bring hope and manufacturing potential, other aspects such as the price of the Ru-complex must be considered. According to the Sigma Aldrich website, 1 g of tris (2,2′-bipyridyl)dichlororuthenium(II) hexahydrate is around 90 €, while the price of 250 mL GO water dispersion with the concentration of 2 mg/mL is 244 €. In this paper, 400 μL hydrogel consists of 0.75 mg GO and 0.1 mg Ru(II) was used to clean 400 μL of the bacteria solution. We can calculate the price here: for 400 μL, the price of the product is 0.5 € for GO and 0.01 € for Ru complex, which is in total 0.51 € per 400 μL. This price may be reasonable but there is a question of how many times one hydrogel can be used? To achieve industrial level application, it is important to further investigate reusability.

32.4.1 Cost analysis

Considering that, in the earlier section, the approaches and possible products for water treatment based on graphene nanomaterials are presented, herein the prices of materials, including starting components, synthesis, and necessary time will be discussed. The technological aspects, advantages, and issues of application graphene nanomaterials in water disinfection are discussed in the earlier section. Apart from the technological aspect, the economic aspects play a very important role whether some of the products based on graphene nanomaterials can be expected on the market and how soon.

First, ZnO/GO nanocomposites [171] for photocatalytic removal of bacteria are mentioned. The production of ZnO/GO nanocomposites can be accomplished using in situ ZnO synthesis on the GO, hydrothermal/solvothermal method, or sol-gel methods [171]. The necessary chemicals for the synthesis of composites are Zn salt such as $ZnNO_3$ or $Zn(Ac)_2$, then reducing agents such as $NaBH_4$ or NaOH, and GO are often used. Apart from standard laboratory equipment, a furnace for temperatures of 300–400°C is necessary or autoclaves.

In Table 32.4, the three selected composites based on GO, as discussed in Section 32.4 are analyzed based on the prices of chemicals and the duration of the synthetic process. For proposed GO composites for water disinfection, only standard laboratory pieces of equipment were used, thus this aspect was not considered here. All prices of chemicals were found on the Sigma Aldrich website for the Serbian mark. The research hours necessary for synthesis are also listed, and the price is estimated to cost at 10 €, considering the average wage in Serbia and the European Union.

This book belongs to Badji Mokhtar Annaba University Central Library Copyright Elsevier 2025

Table 32.4: The chemicals, prices, and time for synthesis.

Composites	Chemicals	Price of chemicals used	Time for synthesis	Estimated full price	Cleaning mechanism
ZnO/graphene oxide [177]	ZnAC2 × $2H_2O$ (24.5 € per 250 g), NH_2NH_2 hydrate (250 mL 17.5 €), for GO 200 mL, 4 mg/mL 876 €	1095 € for 1 g GO 300 mg of ZnAc2 0.3 € 30 uL hydrazine, 0.001 €	9 h (90 €)	Obtained around 1185.301 €	Photocatalysis
Chitosan chloride-graphene oxide (CSCl@GO) [173]	Chitosan chloride-2 g price 2 € Graphene oxide 12 mg, 13.2 € 60 g quartz sand, price 4.8 €	10 €/g	Around 30 h (300 €)	31 0 €	Column cleaning, with quartz sand functionalized with GO
GO and polyethersufone (PES) mixture [151]	Polyethersufone 200 g, 245 € Go in 0.25% mass PS, 1 kg 45 €	For 1 g, 1 €, to deposit as a membrane GO 23 PS 1 €	Not found in the paper, estimation around 20 h (200 €)	225 €	Membrane filtration

Based on the short overview of the costs of chemicals and time necessary for synthesis, it seems that the prices of starting chemicals, especially GO, increases the price of overall composites. To estimate the price of water cleaning, the capacity of composites to clean the water must be investigated first. Although composite for photocatalytic water cleaning is the most expensive, the question is which amount of water 1 g of this composite can clean? Another very important aspect is the reusability of composites.

32.5 Conclusions

In this chapter, the physical, chemical, optical, and morphological properties of graphene nanomaterials in their structures are discussed. The mechanisms of antibacterial action of graphene, GO, GQDs, fullerenes, and CNTs are listed and explained in detail. Water cleaning approaches using different graphene-based nanomaterials as well as composites are described. The process of synthesis and methods of water purification from bacterial cells with graphene-based nanomaterials are closely analyzed. The simplicity of the synthetic procedure and technique of water cleaning were analyzed, as well as the price of starting components and reusability. Based on these parameters, in the future, it can be expected that there will be a

This book belongs to Badji Mokhtar Annaba University Central Library Copyright Elsevier 2025

transfer to industrial- or domestic-level graphene-polymer-based nanomaterials for cleaning of wastewater. Both graphene and GO, although the price of fullerenes and CNTs is still too high, their industrial application in the treatment of wastewater may be less probable in the near future. As for GQDs, research on their possible application in this field is still beginning, but due to the low price of their synthesis and high antibacterial activity, it seems that they will have a very important role in the future.

Acknowledgment

This work was financially supported by the Ministry of Education, Science and Technological Development of the Republic of Serbia (Grant No. 451-03-9/2021-14/200017).

Dedication

To little princess Lenka and her grandmother Nada.

References

[1] H.W. Kroto, J.R. Heath, S.C. O'Brien, R.F. Curl, R.E. Smalley, C60: buckminsterfullerene, Nature 318 (1985) 162–163.
[2] S. Iijima, Helical microtubules of graphitic carbon, Nature 354 (1991) 56–58.
[3] K.S. Novoselov, A.K. Geim, S.V. Morozov, D. Jiang, Y. Zhang, S.V. Dubonos, I.V. Grigorieva, A. A. Firsov, Electric field effect in atomically thin carbon films, Science 306 (2004) 666–669.
[4] S. Stankovich, R.D. Piner, S.T. Nguyen, R.S. Ruoff, Synthesis and exfoliation of isocyanate-treated graphene oxide nanoplatelets, Carbon 44 (2006) 3342–3347.
[5] L.A. Ponomarenko, F. Schedin, M.I. Katsnelson, R. Yang, E.W. Hill, K.S. Novoselov, A.K. Geim, Chaotic Dirac billiard in graphene quantum dots, Science 320 (2008) 356–358.
[6] B.C. Brodie, XXIII—Researches on the atomic weight of graphite, Q. J. Chem. Soc. 12 (1860) 261–268.
[7] W.S. Hummers, R.E. Offeman, Preparation of graphitic oxide, J. Am. Chem. Soc. 80 (1958) 1339.
[8] J. Jehlicka, O. Frank, V. Hamplova, Z. Pokorna, L. Juha, Z. Bohacek, Z. Weishauptova, Low extraction recovery of fullerene from carbonaceous geological materials spiked with C(60), Carbon 43 (2005) 1909–1917.
[9] G. Parthasarathy, R. Srinivasan, M. Vairamani, K. Ravikumar, A.C. Kunwar, Occurrence of natural fullerenes in low grade metamorphosed Proterozoic shungite from Karelia, Russia, Geochim. Cosmochim. Acta 62 (1998) 3541–3544.
[10] W. Kratschmer, L.D. Lamb, K. Fostiropoulos, D.R. Huffman, Solid C60: a new form of carbon, Nature 347 (1990) 354–358.
[11] Z. Markovic, B. Todorovic-Markovic, I. Mohai, Z. Farkas, E. Kovats, J. Szepvolgyi, D. Otasevic, P. Scheier, S. Feil, N. Romcevic, Comparative process analysis of fullerene production by the arc and the radio-frequency discharge methods, J. Nanosci. Nanotechnol. 7 (2007) 1357–1369.
[12] Z. Marković, B. Todorović-Marković, T. Nenadović, Synthesis of fullerenes by hollow cathode arc, Fullerenes, Nanotubes, Carbon Nanostruct. 10 (2002) 81–87.
[13] K.Y. Amsharov, M. Jansen, A C(78) fullerene precursor: toward the direct synthesis of higher fullerenes, J. Org. Chem. 73 (2008) 2931–2934.
[14] M.A. Kabdulov, K.Y. Amsharov, M. Jansen, A step toward direct fullerene synthesis: C60 fullerene precursors with fluorine in key positions, Tetrahedron 66 (2010) 8587–8593.

This book belongs to Badji Mokhtar Annaba University Central Library Copyright Elsevier 2025

[15] N. Malik, T. Arfin, A.U. Khan, Chapter 13—Graphene nanomaterials: chemistry and pharmaceutical perspectives, in: A.M. Grumezescu (Ed.), Nanomaterials for Drug Delivery and Therapy, William Andrew Publishing, 2019.
[16] R.S. Ruoff, D.S. Tse, R. Malhotra, D.C. Lorents, Solubility of fullerene (C60) in a variety of solvents, J. Phys. Chem. 97 (1993) 3379–3383.
[17] S. Bosi, T. Da Ros, G. Spalluto, M. Prato, Fullerene derivatives: an attractive tool for biological applications, Eur. J. Med. Chem. 38 (2003) 913–923.
[18] T. Da Ros, Twenty years of promises: fullerene in medicinal chemistry, in: F. Cataldo, T. Da Ros (Eds.), Medicinal Chemistry and Pharmacological Potential of Fullerenes and Carbon Nanotubes, Springer Netherlands, Dordrecht, 2008.
[19] T. Da Ros, M. Prato, F. Novello, M. Maggini, E. Banfi, Easy access to water-soluble fullerene derivatives via 1,3-dipolar cycloadditions of azomethine ylides to C60, J. Org. Chem. 61 (1996) 9070–9072.
[20] K. Kordatos, M. Prato, E. Menna, G. Scorrano, M. Maggini, Synthesis of fullerene derivatives for incorporation in sol-gel glasses, J. Sol-Gel Sci. Technol. 22 (2001) 237–244.
[21] M. Maggini, G. Scorrano, M. Prato, Addition of azomethine ylides to C60: synthesis, characterization, and functionalization of fullerene pyrrolidines, J. Am. Chem. Soc. 115 (1993) 9798–9799.
[22] M. Prato, M. Maggini, Fulleropyrrolidines: a family of full-fledged fullerene derivatives, Acc. Chem. Res. 31 (1998) 519–526.
[23] S.P. Jovanović, Z.M. Marković, D.N. Kleut, V.D. Trajković, B.S. Babić-Stojić, M.D. Dramićanin, T.B. M. Marković, Singlet oxygen generation by higher fullerene-based colloids, J. Serb. Chem. Soc. 75 (2010) 965–973.
[24] A. Trpkovic, B. Todorovic-Markovic, D. Kleut, M. Misirkic, K. Janjetovic, L. Vucicevic, A. Pantovic, S. Jovanovic, M. Dramicanin, Z. Markovic, V. Trajkovic, Oxidative stress-mediated hemolytic activity of solvent exchange-prepared fullerene (C60) nanoparticles. Nanotechnology 21 (2010) 375102, https://doi.org/10.1088/0957-4484/21/37/375102.
[25] R. Qiao, A.P. Roberts, A.S. Mount, S.J. Klaine, P.C. Ke, Translocation of C60 and its derivatives across a lipid bilayer, Nano Lett. 7 (2007) 614–619.
[26] B. Todorović-Marković, S. Jovanović, V. Jokanović, Z. Nedić, M. Dramićanin, Z. Marković, Atomic force microscopy study of fullerene-based colloids, Appl. Surf. Sci. 255 (2008) 3283–3288.
[27] F. Langa, P. De La Cruz, J.L. Delgado, E. Espíldora, M.J. GÓmez-Escalonilla, A. De La Hoz, Relation between charge transfer and solvent polarity in fullerene derivatives: NMR studies, J. Mater. Chem. 12 (2002) 2130–2136.
[28] A. Astefanei, O. Nunez, M.T. Galceran, Analysis of C60-fullerene derivatives and pristine fullerenes in environmental samples by ultrahigh performance liquid chromatography-atmospheric pressure photoionization-mass spectrometry, J. Chromatogr. A 1365 (2014) 61–71.
[29] S.W. Mcelvany, M.M. Ross, Mass spectrometry and fullerenes, J. Am. Soc. Mass Spectrom. 3 (1992) 268–280.
[30] V. Korepanov, A. Popov, V. Senyavin, M. Reynov, M. Yurovskaya, Infrared spectra and structure of C60 heterocyclic derivatives, Fullerenes, Nanotubes, Carbon Nanostruct. 12 (2006) 209–213.
[31] E. Zemanová, K. Klouda, E. Kostakova, Fullerene derivatives, preparation, identification and use, J. Mater. Sci. Eng. B 3 (6) (2013) 331–345.
[32] T. Yu, T. Zhang, X. Wang, Y. Zhao, C. Wei, Y. Li, H. Zhang, Synthesis and photophysical properties of fullerene derivatives containing a C60-fluorene core, New J. Chem. 43 (2019) 4356–4363.
[33] Z. Liu, M. Koshino, K. Suenaga, A. Mrzel, H. Kataura, S. Iijima, Transmission electron microscopy imaging of individual functional groups of fullerene derivatives, Phys. Rev. Lett. 96 (2006) 088304.
[34] R. Partha, M. Lackey, A. Hirsch, S.W. Casscells, J.L. Conyers, Self assembly of amphiphilic C60 fullerene derivatives into nanoscale supramolecular structures, J. Nanobiotechnol. 5 (2007) 6.
[35] M.S.Y. Tang, E.-P. Ng, J.C. Juan, C.W. Ooi, T.C. Ling, K.L. Woon, P.L. Show, Metallic and semiconducting carbon nanotubes separation using an aqueous two-phase separation technique: a review, Nanotechnology 27 (2016) 332002.

This book belongs to Badji Mokhtar Annaba University Central Library
Copyright Elsevier 2025

[36] S. Iijima, T. Ichihashi, Single-shell carbon nanotubes of 1-nm diameter, Nature 363 (1993) 603–605.
[37] S.-G. Cho, K.-C. Ko, Surface free energy and super-hydrophobic coating of multi-walled carbon nanotubes by 3:1 Tmcs/toluene glow discharge plasma under low pressure, Thin Solid Films 518 (2010) 6619–6623.
[38] S. Iijima, C. Brabec, A. Maiti, J. Bernholc, Structural flexibility of carbon nanotubes, J. Chem. Phys. 104 (1996) 2089–2092.
[39] V. Georgakilas, K. Kordatos, M. Prato, D.M. Guldi, M. Holzinger, A. Hirsch, Organic functionalization of carbon nanotubes, J. Am. Chem. Soc. 124 (2002) 760–761.
[40] N. Tagmatarchis, M. Prato, Functionalization of carbon nanotubes via 1,3-dipolar cycloadditions, J. Mater. Chem. 14 (2004) 437–439.
[41] H. Hayden, Y.K. Gun'ko, T.S. Perova, Chemical modification of multi-walled carbon nanotubes using a tetrazine derivative, Chem. Phys. Lett. 435 (2007) 84–89.
[42] R. Graupner, J. Abraham, D. Wunderlich, A. Vencelová, P. Lauffer, J. Röhrl, M. Hundhausen, L. Ley, A. Hirsch, Nucleophilic–alkylation–reoxidation: a functionalization sequence for single-wall carbon nanotubes, J. Am. Chem. Soc. 128 (2006) 6683–6689.
[43] F. Liang, A.K. Sadana, A. Peera, J. Chattopadhyay, Z. Gu, R.H. Hauge, W.E. Billups, A convenient route to functionalized carbon nanotubes, Nano Lett. 4 (2004) 1257–1260.
[44] I.D. Rosca, F. Watari, M. Uo, T. Akasaka, Oxidation of multiwalled carbon nanotubes by nitric acid, Carbon 43 (2005) 3124–3131.
[45] S.P. Jovanovic, Z.M. Markovic, D.N. Kleut, M.D. Dramicanin, I.D. Holclajtner-Antunovic, M. S. Milosavljevic, V. La Parola, Z. Syrgiannis, B.M.T. Markovic, Structural analysis of single wall carbon nanotubes exposed to oxidation and reduction conditions in the course of gamma irradiation, J. Phys. Chem. C 118 (2014) 16147–16155.
[46] D. Kleut, S. Jovanović, Z. Marković, D. Kepić, D. Tošić, N. Romčević, M. Marinović-Cincović, M. Dramićanin, I. Holclajtner-Antunović, V. Pavlović, G. Dražić, M. Milosavljević, B. Todorović Marković, Comparison of structural properties of pristine and gamma irradiated single-wall carbon nanotubes: effects of medium and irradiation dose, Mater. Charact. 72 (2012) 37–45.
[47] M. Spellauge, F.-C. Loghin, J. Sotrop, M. Domke, M. Bobinger, A. Abdellah, M. Becherer, P. Lugli, H. P. Huber, Ultra-short-pulse laser ablation and modification of fully sprayed single walled carbon nanotube networks, Carbon 138 (2018) 234–242.
[48] S.P. Jovanović, Z.M. Marković, D.N. Kleut, N.Z. Romčević, V.S. Trajković, M.D. Dramićanin, B.M. T. Marković, A novel method for the functionalization of γ-irradiated single wall carbon nanotubes with DNA, Nanotechnology 20 (2009) 445602.
[49] D. Kepić, Z. Marković, S. Jovanović, I. Holclajtner Antunović, D. Kleut, B. Todorović Marković, Novel method for graphene functionalization, Phys. Scr. T162 (2014) 4 014024.
[50] Z. Markovic, S. Jovanovic, D. Kleut, N. Romcevic, V. Jokanovic, V. Trajkovic, B. Todorovic-Markovic, Comparative study on modification of single wall carbon nanotubes by sodium dodecylbenzene sulfonate and melamine sulfonate superplasticiser, Appl. Surf. Sci. 255 (2009) 6359–6366.
[51] K.I. Bolotin, K.J. Sikes, Z. Jiang, M. Klima, G. Fudenberg, J. Hone, P. Kim, H.L. Stormer, Ultrahigh electron mobility in suspended graphene, Solid State Commun. 146 (2008) 351–355.
[52] A.A. Balandin, S. Ghosh, W. Bao, I. Calizo, D. Teweldebrhan, F. Miao, C.N. Lau, Superior thermal conductivity of single-layer graphene, Nano Lett. 8 (2008) 902–907.
[53] G. Yang, L. Li, W.B. Lee, M.C. Ng, Structure of graphene and its disorders: a review, Sci. Technol. Adv. Mater. 19 (2018) 613–648.
[54] P.R. Wallace, The band theory of graphite, Phys. Rev. 71 (1947) 622–634.
[55] H. Yu, B. Zhang, C. Bulin, R. Li, R. Xing, High-efficient synthesis of graphene oxide based on improved hummers method, Sci. Rep. 6 (2016) 36143.
[56] D.C. Marcano, D.V. Kosynkin, J.M. Berlin, A. Sinitskii, Z. Sun, A. Slesarev, L.B. Alemany, W. Lu, J. M. Tour, Improved synthesis of graphene oxide, ACS Nano 4 (2010) 4806–4814.

This book belongs to Badji Mokhtar Annaba University Central Library Copyright Elsevier 2025

[57] N.K. Mahanta, A.R. Abramson, Thermal conductivity of graphene and graphene oxide nanoplatelets, in: 13th InterSociety Conference on Thermal and Thermomechanical Phenomena in Electronic Systems, 30 May–1 June 2012, 2012, pp. 1–6.
[58] X. Mu, X. Wu, T. Zhang, D.B. Go, T. Luo, Thermal transport in graphene oxide—from ballistic extreme to amorphous limit, Sci. Rep. 4 (2014) 3909.
[59] P. Tian, L. Tang, K.S. Teng, S.P. Lau, Graphene quantum dots from chemistry to applications, Mater. Today Chem. 10 (2018) 221–258.
[60] S. Jovanovic, Z.M. Markovic, B. Todorović Marković, Carbon based nanomaterials as agents for photodynamic therapy, in: F. Fitzgerald (Ed.), Photodynamic Therapy (Pdt): Principles, Mechanisms and Applications, Nova Science Publishers, Inc., New York, 2017
[61] S.P. Jovanović, Z. Syrgiannis, M.D. Budimir, D.D. Milivojević, D.J. Jovanovic, V.B. Pavlović, J. M. Papan, M. Bartenwerfer, M.M. Mojsin, M.J. Stevanović, B.M. Todorović Marković, Graphene quantum dots as singlet oxygen producer or radical quencher—the matter of functionalization with urea/thiourea, Mater. Sci. Eng. C 109 (2020) 110539.
[62] S.P. Jovanovic, Z. Syrgiannis, Z.M. Markovic, A. Bonasera, D.P. Kepic, M.D. Budimir, D.D. Milivojevic, V. D. Spasojevic, M.D. Dramicanin, V.B. Pavlovic, B.M. Todorovic Markovic, Modification of structural and luminescence properties of graphene quantum dots by gamma irradiation and their application in a photodynamic therapy, ACS Appl. Mater. Interfaces 7 (2015) 25865–25874.
[63] S. Margadonna, C.M. Brown, T.J.S. Dennis, A. Lappas, P. Pattison, K. Prassides, H. Shinohara, Crystal structure of the higher fullerene C84, Chem. Mater. 10 (1998) 1742–1744.
[64] S. Bronnikov, A. Podshivalov, S. Kostromin, M. Asandulesa, V. Cozan, Electrical conductivity of polyazomethine/fullerene C60 nanocomposites, Phys. Lett. A 381 (2017) 796–800.
[65] D. Saha, S. Deng, Hydrogen adsorption on partially truncated and open cage C60 fullerene, Carbon 48 (2010) 3471–3476.
[66] A. Aqel, K.M.M.A. El-Nour, R.A.A. Ammar, A. Al-Warthan, Carbon nanotubes, science and technology part (I) structure, synthesis and characterisation, Arab. J. Chem. 5 (2012) 1–23.
[67] A. Peigney, C. Laurent, E. Flahaut, R. Bacsa, A. Rousset, Specific surface area of carbon nanotubes and bundles of carbon nanotubes, Carbon 39 (2001) 507–514.
[68] M.D. Stoller, S. Park, Y. Zhu, J. An, R.S. Ruoff, Graphene-based ultracapacitors, Nano Lett. 8 (2008) 3498–3502.
[69] P. Montes-Navajas, N.G. Asenjo, R. Santamaría, R. Menéndez, A. Corma, H. García, Surface area measurement of graphene oxide in aqueous solutions, Langmuir 29 (2013) 13443–13448.
[70] P. Bradder, S.K. Ling, S. Wang, S. Liu, Dye adsorption on layered graphite oxide, J. Chem. Eng. Data 56 (2011) 138–141.
[71] T.P. Dasari Shareena, D. Mcshan, A.K. Dasmahapatra, P.B. Tchounwou, A review on graphene-based nanomaterials in biomedical applications and risks in environment and health, Nanomicro Lett. 10 (2018) 53.
[72] S. Jovanović, Z. Marković, B.T. Marković, Carbon based nanomaterials as agents for photodynamic therapy, in: F. Fitzgerald (Ed.), Photodynamic Therapy (PDT): Principles, Mechanisms and Applications, Nova Science Publishers, Inc., Suite N Hauppauge, NY, USA, 2017, pp. 167–196
[73] J. Lin, X. Chen, P. Huang, Graphene-based nanomaterials for bioimaging, Adv. Drug Deliv. Rev. 105 (2016) 242–254.
[74] T. Da Ros, M. Prato, Medicinal chemistry with fullerenes and fullerene derivatives, Chem. Commun. 8 (1999) 663–669.
[75] S. Kang, M. Pinault, L.D. Pfefferle, M. Elimelech, Single-walled carbon nanotubes exhibit strong antimicrobial activity, Langmuir 23 (2007) 8670–8673.
[76] O. Akhavan, E. Ghaderi, Toxicity of graphene and graphene oxide nanowalls against bacteria, ACS Nano 4 (2010) 5731–5736.
[77] W.B. Hu, C. Peng, W.J. Luo, M. Lv, X.M. Li, D. Li, Q. Huang, C.H. Fan, Graphene-based antibacterial paper, ACS Nano 4 (2010) 4317–4323.

This book belongs to Badji Mokhtar Annaba University Central Library Copyright Elsevier 2025

[78] B.Z. Ristic, M.M. Milenkovic, I.R. Dakic, B.M. Todorovic-Markovic, M.S. Milosavljevic, M.D. Budimir, V. G. Paunovic, M.D. Dramicanin, Z.M. Markovic, V.S. Trajkovic, Photodynamic antibacterial effect of graphene quantum dots, Biomaterials 35 (2014) 4428–4435.
[79] S. Szunerits, R. Boukherroub, Antibacterial activity of graphene-based materials, J. Mater. Chem. B 4 (2016) 6892–6912.
[80] A. Al-Jumaili, S. Alancherry, K. Bazaka, M.V. Jacob, Review on the antimicrobial properties of carbon nanostructures, Materials (Basel, Switzerland) 10 (2017) 1066.
[81] T. Mashino, K. Okuda, T. Hirota, M. Hirobe, T. Nagano, M. Mochizuki, Inhibition of E. coli growth by fullerene derivatives and inhibition mechanism, Bioorg. Med. Chem. Lett. 9 (1999) 2959–2962.
[82] N. Tsao, T.Y. Luh, C.K. Chou, J.J. Wu, Y.S. Lin, H.Y. Lei, Inhibition of group A streptococcus infection by carboxyfullerene, Antimicrob. Agents Chemother. 45 (2001) 1788–1793.
[83] S. Kang, M.S. Mauter, M. Elimelech, Physicochemical determinants of multiwalled carbon nanotube bacterial cytotoxicity, Environ. Sci. Technol. 42 (2008) 7528–7534.
[84] S. Liu, L. Wei, L. Hao, N. Fang, M.W. Chang, R. Xu, Y. Yang, Y. Chen, Sharper and faster "nano darts" kill more bacteria: a study of antibacterial activity of individually dispersed pristine single-walled carbon nanotube, ACS Nano 3 (2009) 3891–3902.
[85] H. Chen, B. Wang, D. Gao, M. Guan, L. Zheng, H. Ouyang, Z. Chai, Y. Zhao, W. Feng, Broad-spectrum antibacterial activity of carbon nanotubes to human gut bacteria, Small 9 (2013) 2735–2746.
[86] D.P. Linklater, V.A. Baulin, S. Juodkazis, E.P. Ivanova, Mechano-bactericidal mechanism of graphene nanomaterials, Interface Focus 8 (2018) 20170060.
[87] V.T.H. Pham, V.K. Truong, M.D.J. Quinn, S.M. Notley, Y. Guo, V.A. Baulin, M. Al Kobaisi, R. J. Crawford, E.P. Ivanova, Graphene induces formation of pores that kill spherical and rod-shaped bacteria, ACS Nano 9 (2015) 8458–8467.
[88] Y. Tu, M. Lv, P. Xiu, T. Huynh, M. Zhang, M. Castelli, Z. Liu, Q. Huang, C. Fan, H. Fang, R. Zhou, Destructive extraction of phospholipids from Escherichia coli membranes by graphene nanosheets, Nat. Nanotechnol. 8 (2013) 594–601.
[89] A.V. Titov, P. Král, R. Pearson, Sandwiched graphene–membrane superstructures, ACS Nano 4 (2010) 229–234.
[90] J. Wang, Y. Wei, X. Shi, H. Gao, Cellular entry of graphene nanosheets: the role of thickness, oxidation and surface adsorption, RSC Adv. 3 (2013) 15776–15782.
[91] C.M. Santos, J. Mangadlao, F. Ahmed, A. Leon, R.C. Advincula, D.F. Rodrigues, Graphene nanocomposite for biomedical applications: fabrication, antimicrobial and cytotoxic investigations, Nanotechnology 23 (2012) 395101.
[92] J. He, X. Zhu, Z. Qi, C. Wang, X. Mao, C. Zhu, Z. He, M. Li, Z. Tang, Killing dental pathogens using antibacterial graphene oxide, ACS Appl. Mater. Interfaces 7 (2015) 5605–5611.
[93] S. Liu, M. Hu, T.H. Zeng, R. Wu, R. Jiang, J. Wei, L. Wang, J. Kong, Y. Chen, Lateral dimension-dependent antibacterial activity of graphene oxide sheets, Langmuir 28 (2012) 12364–12372.
[94] V.C. Sanchez, A. Jachak, R.H. Hurt, A.B. Kane, Biological interactions of graphene-family nanomaterials: an interdisciplinary review, Chem. Res. Toxicol. 25 (2012) 15–34.
[95] J. Mao, R. Guo, L.-T. Yan, Simulation and analysis of cellular internalization pathways and membrane perturbation for graphene nanosheets, Biomaterials 35 (2014) 6069–6077.
[96] H.M. Hegab, A. Elmekawy, L. Zou, D. Mulcahy, C.P. Saint, M. Ginic-Markovic, The controversial antibacterial activity of graphene-based materials, Carbon 105 (2016) 362–376.
[97] X. Lu, X. Feng, J.R. Werber, C. Chu, I. Zucker, J.H. Kim, C.O. Osuji, M. Elimelech, Enhanced antibacterial activity through the controlled alignment of graphene oxide nanosheets, Proc. Natl. Acad. Sci. U. S. A. 114 (2017) E9793–E9801.
[98] H.-S. Hsieh, R. Wu, C.T. Jafvert, Light-independent reactive oxygen species (ROS) formation through electron transfer from carboxylated single-walled carbon nanotubes in water, Environ. Sci. Technol. 48 (2014) 11330–11336.

This book belongs to Badji Mokhtar Annaba University Central Library Copyright Elsevier 2025

[99] M. Pelin, L. Fusco, C. Martin, S. Sosa, J. Frontinan-Rubio, J.M. Gonzalez-Dominguez, M. Duran-Prado, E. Vazquez, M. Prato, A. Tubaro, Graphene and graphene oxide induce ROS production in human HaCaT skin keratinocytes: the role of xanthine oxidase and NADH dehydrogenase, Nanoscale 10 (2018) 11820–11830.
[100] Y. Zhao, H.-S. Hsieh, M. Wang, C.T. Jafvert, Light-independent redox reactions of graphene oxide in water: electron transfer from NADH through graphene oxide to molecular oxygen, producing reactive oxygen species, Carbon 123 (2017) 216–222.
[101] Z.M. Marković, S.P. Jovanović, P.Z. Mašković, M.M. Mojsin, M.J. Stevanović, M. Danko, M. Mičušík, D. J. Jovanović, A. Kleinová, Z. Špitalský, V.B. Pavlović, B.M. Todorović Marković, Graphene oxide size and structure pro-oxidant and antioxidant activity and photoinduced cytotoxicity relation on three cancer cell lines, J. Photochem. Photobiol. B Biol. 200 (2019) 111647.
[102] Z.M. Marković, D.M. Matijašević, V.B. Pavlović, S.P. Jovanović, I.D. Holclajtner-Antunović, Z. Špitalský, M. Mičušik, M.D. Dramićanin, D.D. Milivojević, M.P. Nikšić, B.M. Todorović Marković, Antibacterial potential of electrochemically exfoliated graphene sheets, J. Colloid Interface Sci. 500 (2017) 30–43.
[103] Z.M. Markovic, B.Z. Ristic, K.M. Arsikin, D.G. Klisic, L.M. Harhaji-Trajkovic, B.M. Todorovic-Markovic, D.P. Kepic, T.K. Kravic-Stevovic, S.P. Jovanovic, M.M. Milenkovic, D.D. Milivojevic, V.Z. Bumbasirevic, M.D. Dramicanin, V.S. Trajkovic, Graphene quantum dots as autophagy-inducing photodynamic agents, Biomaterials 33 (2012) 7084–7092.
[104] S. Jovanović, Graphene quantum dots—a new member of the graphene family: structure, properties, and biomedical applications, in: Sulaiman Wadi Harun (Ed.), Handbook of Graphene, Volume 7: Biomaterials, Wiley, Hoboken, New Jersey, USA, 2019, pp. 267–301.
[105] W.S. Kuo, H.H. Chen, S.Y. Chen, C.Y. Chang, P.C. Chen, Y.I. Hou, Y.T. Shao, H.F. Kao, C.L. Lilian Hsu, Y. C. Chen, S.J. Chen, S.R. Wu, J.Y. Wang, Graphene quantum dots with nitrogen-doped content dependence for highly efficient dual-modality photodynamic antimicrobial therapy and bioimaging, Biomaterials 120 (2017) 185–194.
[106] J. Ge, M. Lan, B. Zhou, W. Liu, L. Guo, H. Wang, Q. Jia, G. Niu, X. Huang, H. Zhou, X. Meng, P. Wang, C. S. Lee, W. Zhang, X. Han, A graphene quantum dot photodynamic therapy agent with high singlet oxygen generation, Nat. Commun. 5 (2014) 4596.
[107] L. Wang, J. Shi, R. Liu, Y. Liu, J. Zhang, X. Yu, J. Gao, C. Zhang, Z. Zhang, Photodynamic effect of functionalized single-walled carbon nanotubes: a potential sensitizer for photodynamic therapy, Nanoscale 6 (2014) 4642–4651.
[108] U. Sah, K. Sharma, N. Chaudhri, M. Sankar, P. Gopinath, Antimicrobial photodynamic therapy: single-walled carbon nanotube (SWCNT)-porphyrin conjugate for visible light mediated inactivation of Staphylococcus aureus, Colloids Surf. B: Biointerfaces 162 (2018) 108–117.
[109] L. Brunet, D.Y. Lyon, E.M. Hotze, P.J.J. Alvarez, M.R. Wiesner, Comparative photoactivity and antibacterial properties of C60 fullerenes and titanium dioxide nanoparticles, Environ. Sci. Technol. 43 (2009) 4355–4360.
[110] K.J. Moor, S.D. Snow, J.-H. Kim, Differential photoactivity of aqueous [C60] and [C70] fullerene aggregates, Environ. Sci. Technol. 49 (2015) 5990–5998.
[111] D.Y. Lyon, P.J. Alvarez, Fullerene water suspension (nC60) exerts antibacterial effects via ROS-independent protein oxidation, Environ. Sci. Technol. 42 (2008) 8127–8132.
[112] Y. Zhang, S.F. Ali, E. Dervishi, Y. Xu, Z. Li, D. Casciano, A.S. Biris, Cytotoxicity effects of graphene and single-wall carbon nanotubes in neural phaeochromocytoma-derived PC12 cells, ACS Nano 4 (2010) 3181–3186.
[113] S. Liu, T.H. Zeng, M. Hofmann, E. Burcombe, J. Wei, R. Jiang, J. Kong, Y. Chen, Antibacterial activity of graphite, graphite oxide, graphene oxide, and reduced graphene oxide: membrane and oxidative stress, ACS Nano 5 (2011) 6971–6980.
[114] C.D. Vecitis, K.R. Zodrow, S. Kang, M. Elimelech, Electronic-structure-dependent bacterial cytotoxicity of single-walled carbon nanotubes, ACS Nano 4 (2010) 5471–5479.
[115] J. Li, G. Wang, H. Zhu, M. Zhang, X. Zheng, Z. Di, X. Liu, X. Wang, Antibacterial activity of large-area monolayer graphene film manipulated by charge transfer, Sci. Rep. 4 (2014) 4359.

This book belongs to Badji Mokhtar Annaba University Central Library Copyright Elsevier 2025

[116] F. Perreault, A.F. De Faria, S. Nejati, M. Elimelech, Antimicrobial properties of graphene oxide nanosheets: why size matters, ACS Nano 9 (2015) 7226–7236.
[117] M.-C. Wu, A.R. Deokar, J.-H. Liao, P.-Y. Shih, Y.-C. Ling, Graphene-based photothermal agent for rapid and effective killing of bacteria, ACS Nano 7 (2013) 1281–1290.
[118] D. Hu, H. Li, B. Wang, Z. Ye, W. Lei, F. Jia, Q. Jin, K.-F. Ren, J. Ji, Surface-adaptive gold nanoparticles with effective adherence and enhanced photothermal ablation of methicillin-resistant Staphylococcus aureus biofilm, ACS Nano 11 (2017) 9330–9339.
[119] C. Korupalli, C.-C. Huang, W.-C. Lin, W.-Y. Pan, P.-Y. Lin, W.-L. Wan, M.-J. Li, Y. Chang, H.-W. Sung, Acidity-triggered charge-convertible nanoparticles that can cause bacterium-specific aggregation in situ to enhance photothermal ablation of focal infection, Biomaterials 116 (2017) 1–9.
[120] M. Budimir, R. Jijie, R. Ye, A. Barras, S. Melinte, A. Silhanek, Z. Markovic, S. Szunerits, R. Boukherroub, Efficient capture and photothermal ablation of planktonic bacteria and biofilms using reduced graphene oxide–polyethyleneimine flexible nanoheaters, J. Mater. Chem. B 7 (2019) 2771–2781.
[121] J.W. Kim, E.V. Shashkov, E.I. Galanzha, N. Kotagiri, V.P. Zharov, Photothermal antimicrobial nanotherapy and nanodiagnostics with self-assembling carbon nanotube clusters, Lasers Surg. Med. 39 (2007) 622–634.
[122] B. Oruc, H. Unal, Fluorophore-decorated carbon nanotubes with enhanced photothermal activity as antimicrobial nanomaterials, ACS Omega 4 (2019) 5556–5564.
[123] M. Hashemi, M. Omidi, B. Muralidharan, H. Smyth, M.A. Mohagheghi, J. Mohammadi, T. E. Milner, Correction to "evaluation of the photothermal properties of a reduced graphene oxide/arginine nanostructure for near-infrared absorption" ACS Appl. Mater. Interfaces 9 (2017) 39872.
[124] Z.M. Markovic, L.M. Harhaji-Trajkovic, B.M. Todorovic-Markovic, D.P. Kepic, K.M. Arsikin, S. P. Jovanovic, A.C. Pantovic, M.D. Dramicanin, V.S. Trajkovic, In vitro comparison of the photothermal anticancer activity of graphene nanoparticles and carbon nanotubes, Biomaterials 32 (2011) 1121–1129.
[125] L. Mocan, I. Ilie, F. A. Tabaran, C. Iancu, O. Mosteanu, T. Pop, C. Zdrehus, D. Bartos, T. Mocan, C. Matea, Selective laser ablation of methicillin-resistant Staphylococcus aureus with IgG functionalized multi-walled carbon nanotubes, J. Biomed. Nanotechnol. 12 (2016) 781–788.
[126] N. Levi-Polyachenko, C. Young, C. Macneill, A. Braden, L. Argenta, S. Reid, Eradicating group A streptococcus bacteria and biofilms using functionalised multi-wall carbon nanotubes, Int. J. Hyperth. 30 (2014) 490–501.
[127] W. Qian, C. Yan, D. He, X. Yu, L. Yuan, M. Liu, G. Luo, J. Deng, pH-triggered charge-reversible of glycol chitosan conjugated carboxyl graphene for enhancing photothermal ablation of focal infection, Acta Biomater. 69 (2018) 256–264.
[128] L. Mei, C. Lin, F. Cao, D. Yang, X. Jia, S. Hu, X. Miao, P. Wu, Amino-functionalized graphene oxide for the capture and photothermal inhibition of bacteria, ACS Appl. Nano Mater. 2 (2019) 2902–2908.
[129] X. Ran, Y. Du, Z. Wang, H. Wang, F. Pu, J. Ren, X. Qu, Hyaluronic acid-templated Ag nanoparticles/graphene oxide composites for synergistic therapy of bacteria infection, ACS Appl. Mater. Interfaces 9 (2017) 19717–19724.
[130] K. Turcheniuk, C.-H. Hage, J. Spadavecchia, A.Y. Serrano, I. Larroulet, A. Pesquera, A. Zurutuza, M. G. Pisfil, L. HÉliot, J. Boukaert, R. Boukherroub, S. Szunerits, Plasmonic photothermal destruction of uropathogenic E. coli with reduced graphene oxide and core/shell nanocomposites of gold nanorods/reduced graphene oxide, J. Mater. Chem. B 3 (2015) 375–386.
[131] Y. Feng, Q. Chen, Q. Yin, G. Pan, Z. Tu, L. Liu, Reduced graphene oxide functionalized with gold nanostar nanocomposites for synergistically killing bacteria through intrinsic antimicrobial activity and photothermal ablation, ACS Appl. Bio Mater. 2 (2019) 747–756.
[132] Q. Zhang, X. Liu, L. Tan, Z. Cui, Z. Li, Y. Liang, S. Zhu, K.W.K. Yeung, Y. Zheng, S. Wu, An UV to NIR-driven platform based on red phosphorus/graphene oxide film for rapid microbial inactivation, Chem. Eng. J. 383 (2020) 123088.

This book belongs to Badji Mokhtar Annaba University Central Library Copyright Elsevier 2025

[133] P. Suppan, Chemistry and Light, Royal Society of Chemistry, 1994.
[134] R. Yin, T. Agrawal, U. Khan, G.K. Gupta, V. Rai, Y.-Y. Huang, M.R. Hamblin, Antimicrobial photodynamic inactivation in nanomedicine: small light strides against bad bugs, Nanomedicine (Lond.) 10 (2015) 2379–2404.
[135] S. Baek, S.H. Joo, C. Su, M. Toborek, Antibacterial effects of graphene- and carbon-nanotube-based nanohybrids on Escherichia coli: implications for treating multidrug-resistant bacteria, J. Environ. Manage. 247 (2019) 214–223.
[136] R. Fagan, D.E. McCormack, D.D. Dionysiou, S.C. Pillai, A review of solar and visible light active TiO_2 photocatalysis for treating bacteria, cyanotoxins and contaminants of emerging concern, Mater. Sci. Semicond. Process. 42 (2016) 2–14.
[137] Q. Liu, J. Cao, Y. Ji, X. Li, W. Li, Y. Zhu, X. Liu, J. Li, J. Yang, Y. Yang, Construction of a direct Z-scheme ZnS quantum dot (QD)-Fe_2O_3 QD heterojunction/reduced graphene oxide nanocomposite with enhanced photocatalytic activity, Appl. Surf. Sci. 506 (2020) 144922.
[138] T. Mashino, N. Usui, K. Okuda, T. Hirota, M. Mochizuki, Respiratory chain inhibition by fullerene derivatives: hydrogen peroxide production caused by fullerene derivatives and a respiratory chain system, Bioorg. Med. Chem. 11 (2003) 1433–1438.
[139] Q. Xin, Q. Liu, L. Geng, Q. Fang, J.R. Gong, Chiral nanoparticle as a new efficient antimicrobial nanoagent, Adv. Healthc. Mater. 6 (2017) 1601011.
[140] O. Akhavan, E. Ghaderi, A. Esfandiar, Wrapping bacteria by graphene nanosheets for isolation from environment, reactivation by sonication, and inactivation by near-infrared irradiation, J. Phys. Chem. B 115 (2011) 6279–6288.
[141] N. Yadav, A. Dubey, S. Shukla, C.P. Saini, G. Gupta, R. Priyadarshini, B. Lochab, Graphene oxide-coated surface: inhibition of bacterial biofilm formation due to specific surface-interface interactions, ACS Omega 2 (2017) 3070–3082.
[142] I. Ali, O.M.L. Alharbi, A. Tkachev, E. Galunin, A. Burakov, V.A. Grachev, Water treatment by new-generation graphene materials: hope for bright future, Environ. Sci. Pollut. Res. Int. 25 (2018) 7315–7329.
[143] Y. Zhang, B. Wu, H. Xu, H. Liu, M. Wang, Y. He, B. Pan, Nanomaterials-enabled water and wastewater treatment, NanoImpact 3–4 (2016) 22–39.
[144] M.-F. Li, Y.-G. Liu, G.-M. Zeng, N. Liu, S.-B. Liu, Graphene and graphene-based nanocomposites used for antibiotics removal in water treatment: a review, Chemosphere 226 (2019) 360–380.
[145] G. Mamba, L. Moss, G. Gangashe, S. Thakur, V. Muthuraj, S. Vadivel, G.D. Vilakati, T.T.I. Nkambule, 10—Graphene quantum dot-based nanostructures for water treatment, in: K.A. Abd-Elsalam (Ed.), Carbon Nanomaterials for Agri-Food and Environmental Applications, Elsevier, 2020.
[146] A. Boretti, S. Al-Zubaidy, M. Vaclavikova, M. Al-Abri, S. Castelletto, S. Mikhalovsky, Outlook for graphene-based desalination membranes, npj Clean Water 1 (2018) 5.
[147] D. Cohen-Tanugi, J.C. Grossman, Water desalination across nanoporous graphene, Nano Lett. 12 (2012) 3602–3608.
[148] B. Mi, Graphene oxide membranes for ionic and molecular sieving, Science 343 (2014) 740–742.
[149] D.-E. Jiang, V.R. Cooper, S. Dai, Porous graphene as the ultimate membrane for gas separation, Nano Lett. 9 (2009) 4019–4024.
[150] J. Lee, H.-R. Chae, Y.J. Won, K. Lee, C.-H. Lee, H.H. Lee, I.-C. Kim, J.-M. Lee, Graphene oxide nanoplatelets composite membrane with hydrophilic and antifouling properties for wastewater treatment, J. Membr. Sci. 448 (2013) 223–230.
[151] F. Perreault, M.E. Tousley, M. Elimelech, Thin-film composite polyamide membranes functionalized with biocidal graphene oxide nanosheets, Environ. Sci. Technol. Lett. 1 (2014) 71–76.
[152] S. Filice, D. D'Angelo, S. Libertino, I. Nicotera, V. Kosma, V. Privitera, S. Scalese, Graphene oxide and titania hybrid Nafion membranes for efficient removal of methyl orange dye from water, Carbon 82 (2015) 489–499.

This book belongs to Badji Mokhtar Annaba University Central Library
Copyright Elsevier 2025

[153] A.K. Mishra, S. Ramaprabhu, Functionalized graphene sheets for arsenic removal and desalination of sea water, Desalination 282 (2011) 39–45.
[154] M.R. Manafi, P. Manafi, S. Agarwal, A.K. Bharti, M. Asif, V.K. Gupta, Synthesis of nanocomposites from polyacrylamide and graphene oxide: application as flocculants for water purification, J. Colloid Interface Sci. 490 (2017) 505–510.
[155] P. Banerjee, S. Sau, P. Das, A. Mukhopadhayay, Optimization and modelling of synthetic azo dye wastewater treatment using graphene oxide nanoplatelets: characterization toxicity evaluation and optimization using Artificial Neural Network, Ecotoxicol. Environ. Saf. 119 (2015) 47–57.
[156] P. Banerjee, S.R. Barman, A. Mukhopadhayay, P. Das, Ultrasound assisted mixed azo dye adsorption by chitosan–graphene oxide nanocomposite, Chem. Eng. Res. Des. 117 (2017) 43–56.
[157] L.K. De Assis, B.S. Damasceno, M.N. Carvalho, E.H.C. Oliveira, M.G. Ghislandi, Adsorption capacity comparison between graphene oxide and graphene nanoplatelets for the removal of coloured textile dyes from wastewater, Environ. Technol. 41 (2019) 1–12.
[158] P. Banerjee, P. Das, A. Zaman, P. Das, Application of graphene oxide nanoplatelets for adsorption of Ibuprofen from aqueous solutions: evaluation of process kinetics and thermodynamics, Process Saf. Environ. Prot. 101 (2016) 45–53.
[159] S. Goswami, P. Banerjee, S. Datta, A. Mukhopadhayay, P. Das, Graphene oxide nanoplatelets synthesized with carbonized agro-waste biomass as green precursor and its application for the treatment of dye rich wastewater, Process Saf. Environ. Prot. 106 (2017) 163–172.
[160] Z. Wu, H. Zhong, X. Yuan, H. Wang, L. Wang, X. Chen, G. Zeng, Y. Wu, Adsorptive removal of methylene blue by rhamnolipid-functionalized graphene oxide from wastewater, Water Res. 67 (2014) 330–344.
[161] Ş.S. Bayazit, M. Yildiz, Y.S. Aşçi, M. Şahin, M. Bener, S. Eğlence, M. Abdel Salam, Rapid adsorptive removal of naphthalene from water using graphene nanoplatelet/MIL-101 (Cr) nanocomposite, J. Alloys Compd. 701 (2017) 740–749.
[162] Y. Shen, B. Chen, Sulfonated graphene nanosheets as a superb adsorbent for various environmental pollutants in water, Environ. Sci. Technol. 49 (2015) 7364–7372.
[163] M.M. Ali, K.Y. Sandhya, Reduced graphene oxide as a highly efficient adsorbent for 1-naphthol and the mechanism thereof, RSC Adv. 4 (2014) 51624–51631.
[164] Y. Sun, D. Shao, C. Chen, S. Yang, X. Wang, Highly efficient enrichment of radionuclides on graphene oxide-supported polyaniline, Environ. Sci. Technol. 47 (2013) 9904–9910.
[165] E. Radu, A. Catrinel Ion, F. Sirbu, A. Ion, Adsorption of endocrine disruptors on exfoliated graphene nanoplatelets, Environ. Eng. Manage. J. 14 (2015) 551–558.
[166] A. Arshad, J. Iqbal, M. Siddiq, M.U. Ali, A. Ali, H. Shabbir, U.B. Nazeer, M.S. Saleem, Solar light triggered catalytic performance of graphene-CuO nanocomposite for waste water treatment, Ceram. Int. 43 (2017) 10654–10660.
[167] S.K. Fanourakis, J. Peña-Bahamonde, P.C. Bandara, D.F. Rodrigues, Nano-based adsorbent and photocatalyst use for pharmaceutical contaminant removal during indirect potable water reuse, npj Clean Water 3 (2020) 1.
[168] L. Lin, H. Wang, P. Xu, Immobilized TiO_2-reduced graphene oxide nanocomposites on optical fibers as high performance photocatalysts for degradation of pharmaceuticals, Chem. Eng. J. 310 (2017) 389–398.
[169] M. Ahmadi, H.R. Motlagh, N. Jaafarzadeh, A. Mostoufi, R. Saeedi, G. Barzegar, S. Jorfi, Enhanced photocatalytic degradation of tetracycline and real pharmaceutical wastewater using MWCNT/TiO_2 nano-composite, J. Environ. Manage. 186 (2017) 55–63.
[170] R. Bhatnagar, H. Joshi, I.D. Mall, V.C. Srivastava, Electrochemical oxidation of textile industry wastewater by graphite electrodes, J. Environ. Sci. Health A 49 (2014) 955–966.
[171] P. Raizada, A. Sudhaik, P. Singh, Photocatalytic water decontamination using graphene and ZnO coupled photocatalysts: a review, Mater. Sci. Energy Technol. 2 (2019) 509–525.
[172] L. Zhong, K. Yun, Graphene oxide-modified ZnO particles: synthesis, characterization, and antibacterial properties, Int. J. Nanomedicine 10 (2015) 79.

This book belongs to Badji Mokhtar Annaba University Central Library Copyright Elsevier 2025

[173] X. Li, J. Sun, Y. Che, Y. Lv, F. Liu, Antibacterial properties of chitosan chloride-graphene oxide composites modified quartz sand filter media in water treatment, Int. J. Biol. Macromol. 121 (2019) 760–773.
[174] I.E. Mejias Carpio, C.M. Santos, X. Wei, D.F. Rodrigues, Toxicity of a polymer-graphene oxide composite against bacterial planktonic cells, biofilms, and mammalian cells, Nanoscale 4 (2012) 4746–4756.
[175] H.T. Bhatti, N.M. Ahmad, M.B. Khan Niazi, U.R. Alvi, M. Azeem, N. Ahmad, M. N. Anwar, W. Cheema, S. Tariq, M. Batool, Graphene oxide-PES-based mixed matrix membranes for controllable antibacterial activity against salmonella typhi and water treatment. Int. J. Polym. Sci. 2018 (2018) 12, https://doi.org/10.1155/2018/7842148 7842148.
[176] B. Xue, M. Qin, J. Wu, D. Luo, Q. Jiang, Y. Li, Y. Cao, W. Wang, Electroresponsive supramolecular graphene oxide hydrogels for active bacteria adsorption and removal, ACS Appl. Mater. Interfaces 8 (2016) 15120–15127.
[177] G. Shunmugiah, P. Jayabal, K. Samy, V. Ramakrishnan, Synthesis of ZnO decorated graphene nanocomposite for enhanced photocatalytic properties, J. Appl. Phys. 115 (2014) 173504.

This book belongs to Badji Mokhtar Annaba University Central Library
Copyright Elsevier 2025

CHAPTER 33

Potential of nano biosurfactants as an ecofriendly green technology for bioremediation

Mousumi Debnath[a], Neha Chauhan[b], Priyanka Sharma[a], and Indu Tomar[a]

[a]Department of Biosciences, Manipal University Jaipur, Jaipur, Rajasthan, India, [b]Department of Biosciences and Biotechnology, Banasthali Vidyapith, Vanasthali, Rajasthan, India

33.1 Introduction

Remediation of environmental pollution is a big challenge for the world. Microorganisms can provide an ecofriendly solution to resolve this problem. These minute organisms can survive in all environmental conditions because of their unique metabolic activities. They can also sustain in extremophilic environments. Bioremediation is a mechanism for converting wastes from one form to another form and recycle them again and again with the help of some organisms. This process can be accomplished by an array of events including biodegradation, removal/ altering, immobilization, detoxification of a variety of hazardous physical and chemical waste materials [1]. Because of varied nutritional capacity of microorganisms, they can be used as potential bioremediators of environmental pollutants. These microorganisms can induce the process of bioremediation either by adding the microbes from outside (bioaugmentation) or by using the indigenous microorganisms growing in the same polluted environment [2]. The process of bioremediation is reported by using the whole organisms or their enzymes or other metabolites from diverse biological organisms like fungi, bacteria, protists. Many environmental toxic pollutants like heavy metals and metalloids [3], dyes [4], crude oil [2], pesticides [5], antibiotics [6], hydrocarbon, and polyaromatic hydrocarbons (PAHs) [7] are degraded by biosurfactants. Enzymatic breakdown helps in metabolizing the toxic pollutants like organophosphate compounds [8]. Bioremediation by biosurfactants is also reported [9]. In this chapter, an initiative on the use of these surface-active biosurfactant molecules as potential bioremediators with special emphasis on their use as nano biosurfactant is presented.

Handbook of Nanomaterials for Wastewater Treatment. https://doi.org/10.1016/B978-0-12-821496-1.00013-1
Copyright © 2021 Elsevier Inc. All rights reserved.

This book belongs to Badji Mokhtar Annaba University Central Library Copyright Elsevier 2025

33.2 Use of biosurfactants as potential bioremediators

Microbial surfactants, also called as biosurfactants, are surface-active compounds with hydrophilic as well as lipophilic activities. These molecules are synthesized on the living spaces or excreted extracellularly by the microorganisms. They accumulate between fluid phases and reduce the surface and interfacial tension [9]. The microbial surfactants are complex molecules consisting of a large variety of chemical types, including peptides, fatty acids, phospholipids, glycolipids, glycoproteins, lipopeptides, and particulate and polymeric biosurfactants. Because of the exceptional properties of biosurfactants like low toxicity, structural diversity, aptness to function over a wide range of temperature, pH, greater biodegradability, specific activity at extreme salinity, lower critical micelle concentration, and bioavailability, these molecules have drawn the attention of various industries [10].

33.2.1 Biosurfactants as the molecule for present and future applications

Biosurfactants play a dual role in bioremediation by increasing the surface area and the bioavailability of hydrophobic and water-insoluble substrates. Potential applications of biosurfactants gained importance in the field of soil and marine bioremediation, including PAHs, polychlorinated biphenyls (PCBs), pesticide bioremediation, bioreclamation of soil, metal-contaminated soils bioremediation, oil storage tank cleaning, and microbial enhanced oil recovery [11]. Environmental industries use biosurfactants for biodegradation and solubilization of even the least soluble compounds [12]. Now-a-days, many biosurfactants are used in pharmaceutical industries as antimicrobial agents. Biosurfactants have a potential to be used as major immunomodulatory molecules, adhesive agents, and even in vaccines and gene therapy [13]. Once the production economics for biosurfactants improves in future, they will find increased use in various other applications also.

33.2.2 Microorganisms producing biosurfactants

Biosurfactants have been reported from many organisms [Table 33.1; 9, 14–33]. Among these organisms, *Bacillus* sp. [9, 14–16, 21, 22, 30, 33–37] are predominant producers of lipopolypeptide (surfactin) type of biosurfactants. Among the glycolipid (rhamnolipid) producer, *Pseudomonas aeruginosa* [18, 21, 24, 25, 32, 38–40] is the most popular bacteria capable of bioremediation. Most of the bacteria were able to grow on oil-contaminated soil or water. They were reported to utilize different types of carbon sources on which they showed optimum growth and high production of biosurfactants [14, 27, 34–36, 38–48]. The different carbon sources were mostly hydrocarbon sources, alcohol, carbohydrate sources, or organic acids (Table 33.2). The bacteria mentioned in Tables 33.1 and 33.2 show that most of the recently published biosurfactants are either lipopolypeptide or glycolipid producer type of

This book belongs to Badji Mokhtar Annaba University Central Library Copyright Elsevier 2025

Table 33.1: Potential microorganisms producing different types of biosurfactants for bioremediation of heavy metal, crude oil, and organic hydrocarbon.

S. no.	Potential microorganisms	Types of biosurfactant	Applications	References
1	*Bacillus licheniformis* strain W16	Lipopeptide	Microbial oil recovery	[14]
2	*Bacillus subtilis* M495086	Lipopeptide	Microbial oil recovery	[15]
3	*B. subtilis* RSL2	Lipopeptide	Microbial oil degradation	[16]
4	*Paenibacillus dendritiformis* CN5	Lipopeptide	Bioremediation of polycyclic aromatic hydrocarbons	[17]
5	*Pseudomonas aeruginosa*	Rhamnolipid	Bioremediation of crude oil contamination	[18]
6	*Rhodococcus ruber*	Trehalolipid	In situ remediation of oil-contaminated soil	[19]
7	*P. aeruginosa* UCP 0992	Rhamnolipid	Decontamination processes of sea contaminated by petroleum products	[20]
8	*P. aeruginosa* J4, *B. subtilis* ATCC 2132	Rhamnolipid, lipopeptide	Biodegradation of diesel from contaminated soil and water	[21]
9	*Bacillus cereus, Bacillus sphaericus, Bacillus fusiformis, Pseudomonas* sp., and *Bacillus pumilus*	Rhamnolipids	Soil remediation contaminated with diesel oil	[22]
10	*Staphylococcus* sp. Strain 1E	Lipopeptide	Bioremediation of hydrocarbons	[23]
11	*P. aeruginosa* NCIM 5514	Rhamnolipids	Enhanced oil recovery	[24]
12	*P. aeruginosa* ZS1	Rhamnolipids	Bioremediation of petroleum pollutants	[25]
13	*Ochrobactrum intermedium* CN3	Lipopeptide	Biodegradation of the long-chain hydrophobic aliphatic hydrocarbons and polycyclic aromatic hydrocarbons	[26]
14	*Achromobacter* sp. HZ01	Lipopeptide	Degradation of marine hydrocarbon	[27]
15	*Paenibacillus popilliae*	Lipopeptide	Bioremediation of polycyclic aromatic hydrocarbons	[28]
16	*Achromobacter* sp. A-8	Lipopeptide	Bioremediation of crude oil contamination and microbial enhanced oil recovery	[29]
17	*Bacillus cereus*	Lipopeptide	Marine oil-spill bioremediation	[30]
18	*Paenibacillus* sp. D9	Lipopeptide	Bioremediation of contaminated diesel and motor oil	[31]
19	*P. aeruginosa* 9027	Rhamnolipids	Bioremediation of heavy metal	[32]
20	*Bacillus* MS154	Lipopeptide	Bioremediation of heavy metal	[9]
21	*B. subtilis*	Lipopeptide	Bioremediation of heavy metal	[33]

This book belongs to Badji Mokhtar Annaba University Central Library
Copyright Elsevier 2025

Table 33.2: Biosurfactant: sources, carbon sources, and types.

S. no.	Potential microorganisms	Biosurfactant types	Carbon sources	References
1	*Arthrobacter* sp. N3	Lipopeptide	Sunflower oil	[41]
2	*Pseudomonas aeruginosa* strain NY3	Glycolipid (rhamnolipids)	Diesel oil, hexane and octane	[38]
3	*Rhodococcus erythropolis* ATCC 4277	Glycolipids	Glycerol	[42]
4	*Bacillus lichenformis* W16	Lipopeptide	Glucose	[14]
5	*Paenibacillus* sp. D9	Lipopeptide	Diesel fuel	[31]
6	*P. aeruginosa* A41	Glycolipid (rhamnolipid)	Palm oil	[34]
7	*Marinobacter* sp. MCTG107b	Glycolipid (rhamnolipids)	Glucose	[43]
8	*Pseudoxanthomonas* sp. G3	Glycolipid	Heavy oil	[39]
9	*Achromobacter* sp. HZ01	Glycolipid (rhamnolipid)	Citric acid	[27]
10	*P. aeruginosa* strain CR1	Glycolipid (rhamnolipid)	Glycerol	[44]
11	*Shewanella chilikensis, Halomonas hamiltonii, Bacillus firmus*	Lipoprotein	Oil sludge (petroleum hydrocarbon)	[45]
12	*Bacillus atrophaeus* 5-2a	Lipopeptides	Brown sugar	[40]
13	*Bacillus mojavensis* I4	Lipopeptides	Glucose and glutamic acid	[46]
14	*Planococcus maritimus* strain SAMP MCC 3013	Glycolipid (di-rhamnolipids)	Glucose	[35]
15	*Lactobacillus casei* MRTL3	Glycolipid	Paraffin	[36]
16	*Bacillus methylotrophicus* DCS1 strain	Lipopeptide	Starch and glutamic acid	[47]
17	*Alcaligenes faecalis*, *Cellulosimicrobium* sp., and *Rhodococcus ruber*	Lipopeptide	Crude petroleum oil	[48]

microorganisms. These microbes are also adapted to life at extreme pH, salt, and temperature conditions. Biosurfactants are used for bioremediation of the hydrocarbons and removal of heavy metals (Table 33.1). Hence, the transfer of the hydrocarbons to the aqueous phase in bulk is an important process for its bioavailability [49]. They can also disinfect water because of their antimicrobial activity.

33.2.3 Diverse habitats of biosurfactants

Biosurfactant-producing bacteria are omnipresent in the world. These microorganisms produce various types of biosurfactants that are chemically different in nature. They have been reported from different environmental conditions. Some of these biosurfactant-producing bacteria have

This book belongs to Badji Mokhtar Annaba University Central Library
Copyright Elsevier 2025

been recovered from oil-polluted soil and help in microbial oil recovery. A notable few are *Bacillus licheniformis* W16 from Omani oil wells [14], *Bacillus subtilis* M495086 from Assam reservoir fields in India [15], *B. subtilis* RSL2 from contaminated sludge from Assam, India [16], *Serratia marcescens* from the rhizosphere of legumes planted on the crude oil-contaminated soil from Escravos light crude oil in Nigeria [17]. Vijayakumar et al. [50] isolated a biosurfactant producer *P. aeruginosa* PB3A from oil-contaminated soil from India that exhibit antibacterial and anticancer activity. *Bacillus cereus, Bacillus sphaericus, Bacillus fusiformis, Pseudomonas* sp., *Acinetobacter junii*, and *Bacillus pumilus* are a microbial population group producing biosurfactant from long beach soil, California (USA) and Hong Kong soil (China) contaminated with diesel oil [22]. Mesbaiah et al. [28], isolated a biosurfactant producer *Paenibacillus popilliae* from Algerian contaminated soil that restores its property to survive at a wide range of pH, salinity, and high temperature values and could use PAH as carbon and energy source.

Halophilic microorganisms (salt-loving organisms) are also capable of producing biosurfactants. These organisms are found over a broad range of extreme conditions (pH, salinity, temperature, light intensity, pressure, oxygen, and nutrient conditions) [37]. The genomic as well as functional features of the biosurfactant *Bacillus* sp. AM13 isolated from Indian soil was utilized to characterize the antibacterial lipopeptide [51]. Biosurfactant producer like *Staphylococcus* sp. Strain 1E is reported with potent application on bioremediation hydrocarbons [23]. A unique biosurfactant was isolated and characterized from halophilic *Bacillus* sp. BS3 and was screened for antimicrobial and anticancer activity [52]. Deng et al. [53] has characterized a biosurfactant synthesized by marine hydrocarbon-degrading bacterium *Achromobacter* sp. HZ01. *Halomonas* sp. BS4 was isolated from the solar salt works in India that could effectively control human pathogenic bacteria and fungi [13]. A marine *B. subtilis* C19 isolated from Indonesia, Central Java, Indonesia, also showed specific inhibition against pathogenic bacteria and fungus [54]. Biosurfactants with antimicrobial activity are fascinating tools for bioremediation of the different types of pollutants.

33.2.4 Mechanism of action of the biosurfactant

Biosurfactants are molecules that are amphiphilic in nature with both hydrophobic as well as hydrophilic moieties. These halophilic biosurfactants show a significant mechanism of promoting bioremediation by enhancing the surface area and increased use of hydrophobic and water-insoluble substrates. So, they have the ability to reduce surface tension of medium where they are applied. These surfactants are popular as they are biodegradable and low in toxicity. The biosurfactants are usually produced from low- cost substrates like agro-industrial wastes or contaminated soil, which reduce the cost of production. They are produced as extracellular

This book belongs to Badji Mokhtar Annaba University Central Library Copyright Elsevier 2025

particles or a part of the cell membrane by bacteria [55]. These surfactants help to remove the heavy metals from the soil. The biosurfactants are attached to one another and closely associated with the soil surface on which the metal forms a complex. These surfactants adhere at the junction of the soil and metal ion and try to remove the metal ions by precipitating out of the complex. The strong bonds between the anionic biosurfactants and the complexes are broken because of the reduction of the interfacial tension (Fig. 33.1). But in case of cationic surfactants, ion exchange for the negatively charged surfaces helps to remove the metal ions from the soil surfaces.

Biosurfactants are capable of biodegradation of crude oil and polyaromatic compounds present in soil and water. Tripathi et al. [43] reported a bacterial consortium identified as rhamnolipid from *Ochrobactrum anthropi* IITR07, *Pseudomonas mendocina* IITR46, *P. aeruginosa* IITR48, and *Stenotrophomonas maltophilia* IITR87 and glycolipid from *Microbacterium esteraromaticum* IITR47 for enhanced biodegradation of PAHs present in crude oil. Low water solubility of PAHs affected the biodegradation efficiency [28]. *Pseudomonas* was reported to degrade around 80% of a component of PAH, phenanthrene. This organism helped in

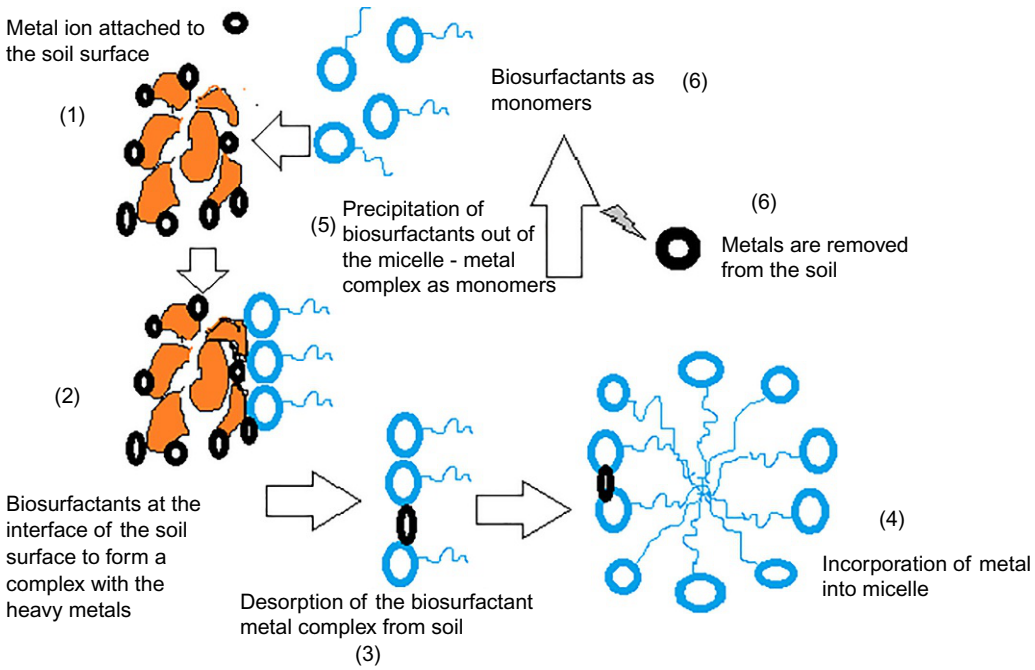

Fig. 33.1
Mechanisms of biosurfactant action to remove heavy metal present in the soil.

This book belongs to Badji Mokhtar Annaba University Central Library
Copyright Elsevier 2025

remediation of hydrocarbons by increasing their bioavailability or mobility and remove the contaminants by pseudo-solubilization and emulsification in a treatment process [11]. The mechanisms of action is briefly elucidated in Fig. 33.2. The biosurfactants can help in the biological degradation of hydrocarbons derived from oil. The first mechanism ensures high availability of the substrate to biosurfactant-synthesizing microbes. They act by reducing the surface tension as well as interfacial tension. The next mechanism allows the biosurfactant to interact with the cell surface and change the membrane allowing more increased

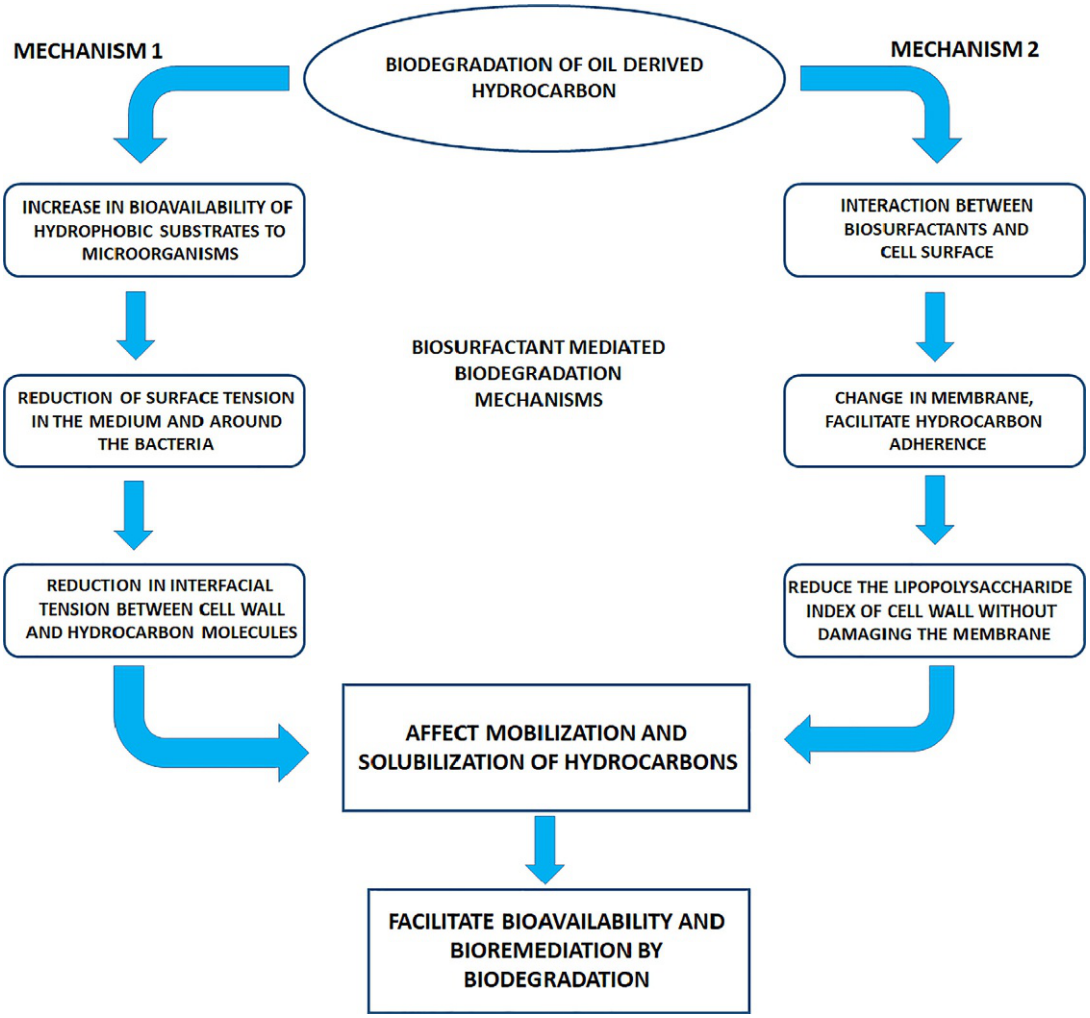

Fig. 33.2
Mechanism of biosurfactant action for biodegradation of oil-derived hydrocarbon.

This book belongs to Badji Mokhtar Annaba University Central Library Copyright Elsevier 2025

hydrophobicity and reduction of the lipopolysaccharide present in the cell wall (Fig. 33.2). These changes promote the biosurfactant mobility, permit hydrophobic-hydrophilic interactions but at the same time restrict the new formation of the hydrogen bridges. Thereby new formation of molecular structures helps to reduce the surface tension of the liquid. There is now increased surface area and this helps in better bioavailability and more biodegradability [56].

33.3 Recent trends for using nanoscale material as agents for bioremediation

Nanomaterials are considered to have a size from 1 to 100 nm. These synthesized materials show a large surface area and have a unique increase in the surface area to unit volume of the material [57]. They have spatial confinement, allowing large amount of material to come in contact. They have potential optical, magnetic, catalytic, and electronic properties. Because of these properties, they have good adsorbing characteristics. Nanoparticles (NPs) can be organic or inorganic in nature. The organic ones are usually made up of carbon also called fullerenes. The inorganic NPs are usually composed of silver, gold, or palladium, broadly classified as noble metals possessing magnetic properties. They can also be made up of zinc oxide or titanium oxide that are semiconductors in nature [58]. The surrounding material affect the reactivity. The NPs have different shapes, less activation energy, quantum effect and possess interaction active sites with chemicals [59]. The method for synthesis of these NPs can be by photochemical/electrochemical/biochemical/thermochemical/chemical vapor deposition/laser ablation/reverse micelles method/electrochemical deposition/solvothermal/electrochemical polymerization/chemical vapor deposition and many more innovative methods [60].

Using naturally occurring or modified microorganisms to remove or biodegrade pollutants from environment is termed as bioremediation. But certain NPs, as mentioned earlier in this chapter, can act as a potential agent to clean up pollutants (bioremediation) present in the environment. These NPs are also clubbed with a single bacterial strain or a group of bacterial culture for increasing the pace of bioremediation [61]. The nanomaterials used for preparation of NPs for nanobioremediation are usually microorganisms or their products of metabolism. They are highly reactive with the pollutants, can act as carriers for immobilization of the bacterial cell or enzymes [62] and thus capable of degrading toxic compounds into nontoxic form in less time and ecofriendly manner by ex situ or in situ methods of bioremediation. Different shapes and sizes of NPs are used for nanoremediation. Most often during the process of nano bioremediation, microorganisms are used to form nano powders, NPs, nanomembranes, or nanomaterials. They are used to degrade/detect/convert/remove toxic metals and various organic compounds from the environment [59]. This is achieved by different methods like photocatalysis, transformation, catalytic reduction, or adsorption. These bio NPs show potential

This book belongs to Badji Mokhtar Annaba University Central Library Copyright Elsevier 2025

for in situ remediation of heavy metal, solid waste, uranium, ground and wastewater, hydrocarbon and many more.

Nanomaterials are of different chemical nature and can be categorized according to their forms and shapes. Recently, Weijie et al. [63] suggested the use of *Pseudocohnilembus persalinus* to monitor the toxic effect of TiO_2 NPs as well as use for it as a model to study its bioremediation. The onsite treatment and removal of pollutants from the contaminated soil, in situ methods are discussed below. In another report, it was found that silica-based nanomaterials show greater ability to remove heavy metals for air pollution treatment and water remediation. The different forms used are self-assembled monolayers on mesoporous silica, nanoporous silica-based molecular baskets, and many more. Nanoiron synthesis using the polyphenols from different plants was reported [64]. It was effective in removal of hexavalent chromium. PCBs belong to the group of endocrine disruptors causing different types of cancer to human as well as to other mammals. The use of nZVI was reported [61] to remove PCB. The process of using nZVI as a physiochemical approach was found to remove the PCB to certain extent. But when a consortium of microorganisms isolated from the PCB-contaminated site was used, the effect of PCB removal was faster. So an integrated approach was taken up. It was found that the efficiency of removal can be enhanced only if, after treatment with nZVI, a consortium of bacterial strains was also used along with a nonionic surfactant Triton X-100. All these three equally contributed and that enhanced the process of degradation. The seven different bacterial species isolated from the PCB-contaminated site had a definite role to play as the biological system. This gave a new direction to the bio nanoremediation. PCB degradation was high by the integration of bioaugmentation. The whole process also needed a periodic treatment of both nZVI and the consortium of microbial inoculants. From the above discussion, it is evident that metallic nanomaterials have profound effect on the nanobioremediation of heavy metals. Moreover, the use of bacterial cultures and surfactant paved a path toward the probable use of a surfactant derived from microorganisms. Yang et al. [65] categorized the metallic nanomaterials as carbon-based nanomaterials (carbon nanotubes and graphene nanomaterial), silica-based nanomaterials, metal oxide-based nanomaterials, zero-valent metal-based nanomaterials, and nanocomposite nanomaterials. The zero-valent metal-based nanomaterials were further classified as nanozerovalent iron (nZVI), silver NPs, and gold NPs. The metal oxide-based nanomaterials were categorized as oxides-based nanomaterials for iron, manganese, zinc, titanium, aluminum, magnesium, cerium, and zirconium. Inorganic-supported nanocomposites, organic polymer-supported nanocomposites, and magnetic nanocomposites are the various forms of nanocomposite nanomaterials. All these forms are actively used for detection and for the removal of toxic metals and organic compounds from the environment. Graphene oxide NPs show the ability to reduce arsenic and metals available in polluted soils [65]. It was suggested that in future these graphene NPs can be a part of the hybrid technologies where phytoremediation can also be introduced to mobilize or reduce the heavy metals.

This book belongs to Badji Mokhtar Annaba University Central Library Copyright Elsevier 2025

33.4 Nano biosurfactants as source of bioremediation

Biosurfactant is a promising material for NP synthesis in green chemistry. Biosurfactants synthesized from microorganisms are often used for removal of heavy metals, specifically copper, nickel, and zinc. Thus, they are suitable for ecofriendly mode of bioremediation. Zeolite and clay also serve as potential adsorbent material for removal of heavy material for water remediation. Zeolites have high ion exchange and molecular sieving property. They have a strong affinity for metal cations. To increase the efficiency of the bioremediation potential for heavy metals, zeolite is often modified with the addition of surfactants. Similarly, surfactant-modified clay offers better adsorption properties at a low cost and shows anion exchange capacity. Nanoclay forms a composite with biodegradable biomass from living resources like vegetable oil, fungi, bacteria, seeds, and leaves. These biotic components function as a sorbent. It is favored because of its zero toxicity and least cost. Recently Biswas and his coworkers [66] showed the importance of the combinatorial use of biosurfactant-producing bacteria to form a biocompatible conjugate with nanoclay. This synergistic interaction helps in bioremediation of organic and inorganic pollutants where the substrate molecule is the clay. As a substrate, the minerals present in the clay allows coupling to biosurfactant by binding to the functional groups and the cations, improving the rate of biodegradation and biotransformation of the PAHs. The innovative idea for using biologically derived surfactant allowed better adsorption and removal of PAH components specifically naphthalene [66].

Hence, clubbing with biosurfactant can be a possibility for a low toxic biocompatible and ecofriendly modified nanoclay. Such approaches using a biosurfactant isolated from bacteria conjugated with nanoclay or nano zeolite or nano zirconia can be a biocompatible approach for in situ bioremediation [66, 67]. Biswas and Raichur studied the interactions of nano zirconia with a biosurfactant. Chemically with the increase in the concentration of the rhamnolipid, a glycolipid type of the biosurfactant, there was a strong interaction because of high electronegativity on the surface of nano zirconia with the rhamnolipid. This biosurfactant acted like a dispersant, foaming agent, increased flocculation, and is favorable because of its least toxicity and ability to remove heavy metals.

Biosurfactants are now in regular use for the synthesis of nano biosurfactants. Biosurfactants are usually used with the metallic NPs in many ways during the synthesis of a NP. They act as a green source during the NP synthesis and help in aggregation and in the stabilization of the metallic NP. Initially, they are adsorbed onto the metallic NP and help in stabilization and aggregation. They are also widely used as capping agents during NP synthesis. The resulting NPs are synthesized in much simpler process. Thus, biosurfactants act as a nontoxic, biodegradable stabilizing agent and an ecofriendly green partner in the synthesis of metallic NPs [68–73].

This book belongs to Badji Mokhtar Annaba University Central Library
Copyright Elsevier 2025

To understand their use in bioremediation, it is worth to know about their classification and categorization according to their functional properties. Biosurfactants are classified into various groups according to their chemical nature. Some group the biosurfactants as the surface-active agents according to low and high molecular weights. Glycolipids, phospholipids, and lipopeptides are the low-molecular-weight surface-active biosurfactants, whereas particulate and polymeric ones are high-molecular-weight surface-active biosurfactants [74]. Most of these biosurfactants used for bioremediation are anionic or neutral in nature.

Rhamnolipid is the common type of biosurfactant belonging to the group, glycolipid, widely known for their bioremediation activity [75]. The rhamnolipid is composed of rhamnose molecule(s) linked to β-hydroxydecanoic acid molecule(s). *Pseudomonas aeruginosa* is the most researched rhamnolipid producer. Using rhamnolipid, many researchers have successfully synthesized silver and good nano biosurfactant. Kiran et al. [76] synthesized silver NPs using the enhancer glycolipid biosurfactant produced from marine *Brevibacterium casei* MSA19 by water in oil microemulsion method. Saeedi et al. [68] produced a rhamnolipid nano biosurfactant with a diameter of 631.4 nm from *P. aeruginosa* MM1011. Fariasa et al. [69] also synthesized a silver NP of the size of 1.13 nm using biosurfactant from *P. aeruginosa* acting as a stabilizing agent. This biosurfactant (rhamnolipid) was developed using vegetable oil refinery residue and 2.5% corn steep liquor and showed no toxicity and was biodegradable.

Water-in-oil microemulsion technique using biosurfactant was used to produce nickel nanorod [77]. The use of biosurfactant had profound role in maintaining the particle size. It was also noted that pH played a significant role in reducing the size of the nickel oxide NPs. The resultant nano biosurfactants showed uniformity in distribution and appeared crystalline and spherical in shape [78]. In another experiment, Xei et al. [79] used reverse micelle method and added specific amount of biosurfactant during the synthesis of silver NP. This addition reduced the aggregation of the particles and helped in stabilizing the NP. Hazra et al. [80] found that this nano biosurfactant produced by reverse micelle method if mixed with poly (methyl methacrylate) will form the core and the biosurfactant will form the shell of the newly formed NPs. They can be utilized for different applications whereby sustained drug release can also be done. The rhamnolipid biosurfactants have exhibited their role as stabilizers during the nano biosurfactant formation. Basnet et al. [81], while working with the zerovalent iron NPs noticed that biosurfactant can help in stabilizing the aggregation and movement of palladium during doping for the formation of the NP. In another similar instance, it was found that the rhamnolipid biosurfactant had a positive effect on the behavior of the nanozirconia was like zircornia in flocculating and dispersing the solid particles [67]. Saikia et al. [70] successfully synthesized silver nano biosurfactants by using rhamnolipid from *P. aeruginosa* and could keep them stable for more than a month. Kiran et al. [71, 72] also used surfactants as a green stabilizer and the resultant nano biosurfactants were used to bioleach the heavy metals from the soil and water. These biosurfactants act as nano reactors that control the size of the crystal NP.

This book belongs to Badji Mokhtar Annaba University Central Library Copyright Elsevier 2025

Lipopeptides are also low-molecular-weight surface-active biosurfactants produced mostly by *Bacillus* sp. [73]. Borohydrate reduction method was used to synthesize gold NPs using anionic lipopeptide biosurfactant *Surfactin* isolated from *B. subtilis* as a renewable stabilizing agent. Surfactin has also been used to form silver NP [73]. Surfactin from *Bacillus amyloliquifaciens* strain KSU-109 was successfully used to synthesize cadmium sulfide NPs [82]. Lipopeptide biosurfactant produced from *Acinetobacter* sp. D3-2 showed their ability to biodegrade crude oil [83]. Zhang et al. [40] also reported the use of lipopeptide biosurfactants by *Bacillus atrophaeus* 5-2a in microbial enhanced oil recovery. Heavy metal removal from metal- and hydrocarbon-contaminated soil was effectively found using surfactant (lipopeptide) from *B. subtilis* [84]. The activity of surfactin as a nano biosurfactant is a promising future.

Sophorolipids are also a type of glycolipids, usually found in nonpathogenic yeast. Metallic NPs using sophorolipid have been successfully synthesized from different species of nonpathogenic yeast. The cobalt NP capped by sophorolipid from *Starmerella bombicola* and was reported around 50 nm [85]. They were targeted for many applications. The capping activity of rhamnolipid (produced by *P. aeruginosa*) to zinc sulfide NPs resulted in NPs of size 4.5 nm [86]. Capping can help in stabilizing the NP and bioremediation of heavy metals. Hazra et al. [87] synthesized zinc sulfide NPs using rhamnolipids from *P. aeruginosa* BS01. They used it as capping and stabilizing agent. They advocated the use of these ZnS NPs to function as a nano photocatalyst. According to their research, it was clear that the biosurfactant rhamnolipid when capped with ZnS NPs could increase the efficiency of textile dye decolorization and degradation.

33.5 Conclusions and future perspective

Metallic nano biosurfactants promise to focus on the remediation process. They are the biomolecules of the next generation with multitudes of multifunctional attributes [88]. Future research should focus on the stabilization of the NPs by biosurfactants before addition during remediation processes. Among the various roles of these nano biosurfactant as stabilizers and capping agents, literature survey showed that they can minimize environmental pollution like remediation of heavy metal, removal of organic contaminants, oil spill bioremediation, and recovery of petroleum. In future, researches can be focused to develop more robust and reliable methods to stabilize these nano biosurfactants and can be the start to create biorepositories for nano particles for remediation with better flocculation and dispersion ability. A NP designed to develop from biosurfactants of different chemical nature will open the possibility of remediation of soil and water polluted with different composition of micropollutants and micropollutants from food, textile, pharmaceutical, paper, herbal, petroleum, and many more types of industries, including domestic waste. These synthesized ecofriendly metallic nano biosurfactants can be a sustainable biomaterial for remediation because of their nontoxic and biodegradable nature with antimicrobial activities. Studies to elucidate the mechanism of action of a metallic nano biosurfactant and different pollutants can be an interesting future interest.

This book belongs to Badji Mokhtar Annaba University Central Library Copyright Elsevier 2025

References

[1] E. Abatenh, B. Gizaw, Z. Tsegaye, M. Wassie, The role of microorganisms in bioremediation—a review, Open J. Environ. Biol. 2 (1) (2017) 038–046.

[2] N. Ali, N. Dashti, M. Khanafer, H. Al-Awadhi, S. Radwan, Bioremediation of soils saturated with spilled crude oil, Sci. Rep. 10 (1) (2020) 1–9.

[3] K.A. Mosa, I. Saadoun, K. Kumar, M. Helmy, O.P. Dhankher, Potential biotechnological strategies for the clean-up of heavy metals and metalloids, Front. Plant Sci. 7 (2016) 303, https://doi.org/10.3389/fpls.2016.00303.

[4] R.K. Sonwani, G. Swain, B.S. Giri, R.S. Singh, B.N. Rai, Biodegradation of Congo red dye in a moving bed biofilm reactor: performance evaluation and kinetic modeling, Bioresour. Technol. 302 (2020) 122811, https://doi.org/10.1016/j.biortech.2020.122811.

[5] J. Nie, Y. Sun, Y. Zhou, M. Kumar, M. Usman, J. Li, J. Shao, L. Wang, D.C. Tsang, Bioremediation of water containing pesticides by microalgae: mechanisms, methods, and prospects for future research, Sci. Total Environ. 707 (2020) 136080, https://doi.org/10.1016/j.scitotenv.2019.136080.

[6] M. Kumar, S. Jaiswal, K.K. Sodhi, P. Shree, D.K. Singh, P.K. Agrawal, P. Shukla, Antibiotics bioremediation: perspectives on its ecotoxicity and resistance, Environ. Int. 124 (2019) 448–461.

[7] Ł. Ławniczak, M. Woźniak-Karczewska, A.P. Loibner, H.J. Heipieper, L. Chrzanowski, Microbial degradation of hydrocarbons—basic principles for bioremediation: a review, Molecules 25 (4) (2020) 856, https://doi.org/10.3390/molecules25040856.

[8] M. Thakur, I.L. Medintz, S.A. Walper, Enzymatic bioremediation of organophosphate compounds-progress and remaining challenges, Front. Bioeng. Biotechnol. 7 (2019) 289, https://doi.org/10.3389/fbioe.2019.00289.

[9] A. Ravindran, A. Sajayan, G.B. Priyadharshini, J. Selvin, G.S. Kiran, Revealing the efficacy of thermostable biosurfactant in heavy metal bioremediation and surface treatment in vegetables, Front. Microbiol. 11 (2020) 222, https://doi.org/10.3389/fmicb.2020.00222.

[10] A. Dadrasnia, S. Ismail, Biosurfactant production by *Bacillus salmalaya* for lubricating oil solubilization and biodegradation, Int. J. Environ. Res. Public Health 12 (8) (2015) 9848–9863.

[11] I.M. Banat, R.S. Makkar, S.S. Cameotra, Potential commercial applications of microbial surfactants, Appl. Microbiol. Biotechnol. 53 (2000) 495–508.

[12] S. Akbari, N.H. Abdurahman, R.M. Yunus, F. Fayaz, O.R. Alara, Biosurfactants—a new frontier for social and environmental safety: a mini review, Biotechnol. Res. Innov. 2 (1) (2018) 81–90.

[13] M.B.S. Donio, F.A. Ronica, V.T. Viji, S. Velmurugan, J.S.C.A. Jenifer, M. Michaelbabu, P. Dhar, T. Citarasu, *Halomonas* sp. BS4, a biosurfactant producing halophilic bacterium isolated from solar salt works in India and their biomedical importance, SpringerPlus 2 (1) (2013) 149, https://doi.org/10.1186/2193-1801-2-149.

[14] S.J. Joshi, Y.M. Al-Wahaibi, S.N. Al-Bahry, A.E. Elshafie, A.S. Al-Bemani, A. Al-Bahri, M.S. Al-Mandhari, Production, characterization, and application of *Bacillus licheniformis* W16 biosurfactant in enhancing oil recovery, Front. Microbiol. 7 (2016) 1853, https://doi.org/10.3389/fmicb.2016.01853.

[15] P. Datta, P. Tiwari, L.M. Pandey, Isolation and characterization of biosurfactant producing and oil degrading *Bacillus subtilis* MG495086 from formation water of Assam oil reservoir and its suitability for enhanced oil recovery, Bioresour. Technol. 270 (2018) 439–448.

[16] S. Sharma, L.M. Pandey, Production of biosurfactant by *Bacillus subtilis* RSL-2 isolated from sludge and biosurfactant mediated degradation of oil, Bioresour. Technol. 307 (2020) 123261, https://doi.org/10.1016/j.biortech.2020.123261.

[17] F.A. Bezza, E.M.N. Chirwa, Pyrene biodegradation enhancement potential of lipopeptide biosurfactant produced by *Paenibacillus dendritiformis* CN5 strain, J. Hazard. Mater. 321 (2017) 218–227.

[18] T.A.A. Moussa, M.S. Mohamed, N. Samak, Production and characterization of di-rhamnolipid produced by *Pseudomonas aeruginosa* TMN, Braz. J. Chem. Eng. 31 (4) (2014) 867–880.

[19] A. Krivoruchko, M. Kuyukina, I. Ivshina, Advanced Rhodococcus biocatalysts for environmental biotechnologies, Catalysts 9 (3) (2019) 236.

This book belongs to Badji Mokhtar Annaba University Central Library

Copyright Elsevier 2025

[20] E.J. Silva, P.F. Correa, D.G. Almeida, J.M. Luna, R.D. Rufino, L.A. Sarubbo, Recovery of contaminated marine environments by biosurfactant-enhanced bioremediation, Colloids Surf. B: Biointerfaces 172 (2018) 127–135.
[21] L.M. Whang, P.W.G. Liu, C.C. Ma, S.S. Cheng, Application of biosurfactants, rhamnolipid, and surfactin, for enhanced biodegradation of diesel-contaminated water and soil, J. Hazard. Mater. 151 (1) (2008) 155–163.
[22] F.M. Bento, F.A. de Oliveira Camargo, B.C. Okeke, W.T. Frankenberger Jr., Diversity of biosurfactant producing microorganisms isolated from soils contaminated with diesel oil, Microbiol. Res. 160 (3) (2005) 249–255.
[23] K. Eddouaouda, S. Mnif, A. Badis, S.B. Younes, S. Cherif, S. Ferhat, N. Mhiri, M. Chamkha, S. Sayadi, Characterization of a novel biosurfactant produced by *Staphylococcus* sp. strain 1E with potential application on hydrocarbon bioremediation, J. Basic Microbiol. 52 (4) (2012) 408–418.
[24] S. Varjani, V.N. Upasani, Evaluation of rhamnolipid production by a halotolerant novel strain of *Pseudomonas aeruginosa*, Bioresour. Technol. 288 (2019) 121577.
[25] T. Cheng, J. Liang, J. He, X. Hu, Z. Ge, J. Liu, A novel rhamnolipid-producing *Pseudomonas aeruginosa* ZS1 isolate derived from petroleum sludge suitable for bioremediation, AMB Express 7 (1) (2017) 120.
[26] F.A. Bezza, M. Beukes, E.M.N. Chirwa, Application of biosurfactant produced by *Ochrobactrum intermedium* CN3 for enhancing petroleum sludge bioremediation, Process Biochem. 50 (11) (2015) 1911–1922.
[27] Y.H. Hong, M.C. Deng, X.M. Xu, C.F. Wu, X. Xiao, Q. Zhu, X.X. Sun, Q.Z. Zhou, J. Peng, J.P. Yuan, J.H. Wang, Characterization of the transcriptome of *Achromobacter* sp. HZ01 with the outstanding hydrocarbon-degrading ability, Gene 584 (2) (2016) 185–194.
[28] F.Z. Mesbaiah, K. Eddouaouda, A. Badis, A. Chebbi, D. Hentati, S. Sayadi, M. Chamkha, Preliminary characterization of biosurfactant produced by a PAH-degrading *Paenibacillus* sp. under thermophilic conditions, Environ. Sci. Pollut. Res. 23 (14) (2016) 14221–14230.
[29] Z. Deng, Y. Jiang, K. Chen, J. Li, C. Zheng, F. Gao, X. Liu, One biosurfactant-producing bacteria *Achromobacter* sp. A-8 and its potential use in microbial enhanced oil recovery and bioremediation, Front. Microbiol. 11 (2020) 247.
[30] I.J.B. Durval, A.H.M. Resende, M.A. Figueiredo, J.M. Luna, R.D. Rufino, L.A. Sarubbo, Studies on biosurfactants produced using *Bacillus cereus* isolated from seawater with biotechnological potential for marine oil-spill bioremediation, J. Surfactant Deterg. 22 (2) (2019) 349–363.
[31] A.A. Jimoh, J. Lin, Biotechnological applications of *Paenibacillus* sp. D9 lipopeptide biosurfactant produced in low-cost substrates, Appl. Biochem. Biotechnol. 191 (2020) 921–941.
[32] M.L. Ibrahim, U.J.J. Ijah, S.B. Manga, L.S. Bilbis, S. Umar, Production and partial characterization of biosurfactant produced by crude oil degrading bacteria, Int. Biodeter. Biodegr. 81 (2013) 28–34.
[33] C.N. Mulligan, R.N. Yong, B.F. Gibbs, S. James, H.P.J. Bennett, Metal removal from contaminated soil and sediments by the biosurfactant surfactin, Environ. Sci. Technol. 33 (21) (1999) 3812–3820.
[34] J. Thaniyavarn, A. Chongchin, N. Wanitsuksombut, S. Thaniyavarn, P. Pinphanichakarn, N. Leepipatpiboon, M. Morikawa, S. Kanaya, Biosurfactant production by *Pseudomonas aeruginosa* A41 using palm oil as carbon source, J. Gen. Appl. Microbiol. 52 (4) (2006) 215–222.
[35] M.V. Suryavanshi, L. Dama, S. Kansara, V.C. Ghattargi, P. Das, A.G. Banpurkar, D. Satpute, K. Surekha, Genomic insights of halophilic *Planococcus maritimus* SAMP MCC 3013 and detail investigation of its biosurfactant production, Front. Microbiol. 10 (2019) 235.
[36] D. Sharma, B. Singh Saharan, Simultaneous production of biosurfactants and bacteriocins by probiotic *Lactobacillus casei* MRTL3, Int. J. Microbiol. (2014) 698713 7 pages, https://doi.org/10.1155/2014/698713.
[37] N. Merino, H.S. Aronson, D.S. Bojanova, J. Feyhl-Buska, M.L. Wong, S. Zhang, D. Giovannelli, Living at the extremes: extremophiles and the limits of life in a planetary context, Front. Microbiol. 10 (2019) 780, https://doi.org/10.3389/fmicb.2019.00780.
[38] M. Nie, X. Yin, C. Ren, Y. Wang, F. Xu, Q. Shen, Novel rhamnolipid biosurfactants produced by a polycyclic aromatic hydrocarbon-degrading bacterium *Pseudomonas aeruginosa* strain NY3, Biotechnol. Adv. 28 (5) (2010) 635–643.
[39] D.I. Astuti, I.A. Purwasena, R.E. Putri, M. Amaniyah, Y. Sugai, Screening and characterization of biosurfactant produced by *Pseudoxanthomonas* sp. G3 and its applicability for enhanced oil recovery, J. Pet. Explor. Prod. Technol. 9 (3) (2019) 2279–2289.

This book belongs to Badji Mokhtar Annaba University Central Library Copyright Elsevier 2025

[40] J. Zhang, Q. Xue, H. Gao, H. Lai, P. Wang, Production of lipopeptide biosurfactants by *Bacillus atrophaeus* 5-2a and their potential use in microbial enhanced oil recovery, Microb. Cell Fact. 15 (1) (2016) 168.
[41] V. Čipinytė, S. Grigiškis, D. Šapokaitė, E. Baškys, Production of biosurfactants by *Arthrobacter* sp. N3, a hydrocarbon degrading bacterium, Environ. Technol. Res. 1 (2011) 68.
[42] E.M. Ciapina, W.C. Melo, L.M. Santa Anna, A.S. Santos, D.M. Freire, N. Pereira, Biosurfactant production by *Rhodococcus erythropolis* grown on glycerol as sole carbon source, Appl. Biochem. Biotechnol. 131 (1–3) (2006) 880–886.
[43] L. Tripathi, M.S. Twigg, A. Zompra, K. Salek, V.U. Irorere, T. Gutierrez, G.A. Spyroulias, R. Marchant, I. M. Banat, Biosynthesis of rhamnolipid by a *Marinobacter s*pecies expands the paradigm of biosurfactant synthesis to a new genus of the marine microflora, Microb. Cell Fact. 18 (1) (2019) 164.
[44] U. Sood, D.N. Singh, P. Hira, J.K. Lee, V.C. Kalia, R. Lal, M. Shakarad, Rapid and solitary production of mono-rhamnolipid biosurfactant and biofilm inhibiting pyocyanin by a taxonomic outlier *Pseudomonas aeruginosa* strain CR1, J. Biotechnol. 307 (2020) 98–106.
[45] S.H. Suganthi, S. Murshid, S. Sriram, K. Ramani, Enhanced biodegradation of hydrocarbons in petroleum tank bottom oil sludge and characterization of biocatalysts and biosurfactants, J. Environ. Manage. 220 (2018) (2018) 87–95.
[46] I. Ghazala, A. Bouallegue, A. Haddar, S. Ellouz-Chaabouni, Characterization and production optimization of biosurfactants by *Bacillus mojavensis* I4 with biotechnological potential for microbial enhanced oil recovery, Biodegradation 30 (4) (2019) 235–245.
[47] N. Hmidet, N. Jemil, M. Nasri, Simultaneous production of alkaline amylase and biosurfactant by *Bacillus methylotrophicus* DCS1: application as detergent additive, Biodegradation 30 (4) (2019) 247–258.
[48] K. Madani, Biodegradation potential of crude petroleum by hydrocarbonoclastic bacteria isolated from Soummam wadi sediment and chemical-biological proprieties of their biosurfactants, J. Petrol. Sci. Eng. 184 (2020) 106554, https://doi.org/10.1016/j.petrol.2019.106554.
[49] A.C. Adrion, D.R. Singleton, J. Nakamura, D. Shea, M.D. Aitken, Improving polycyclic aromatic hydrocarbon biodegradation in contaminated soil through low-level surfactant addition after conventional bioremediation, Environ. Eng. Sci. 33 (9) (2016) 659–670.
[50] S. Vijayakumar, V. Saravanan, In vitro cytotoxicity and antimicrobial activity of biosurfactant produced by *Pseudomonas aeruginosa* strain PB3A, Asian J. Sci. Res. 8 (4) (2015) 510.
[51] S. Shaligram, S.V. Kumbhare, D.P. Dhotre, M.G. Muddeshwar, A. Kapley, N. Joseph, H.P. Purohit, Y. S. Shouche, S.P. Pawar, Genomic and functional features of the biosurfactant producing *Bacillus* sp. AM13, Funct. Integr. Genomics 16 (5) (2016) 557–566.
[52] M.B.S. Donio, S.F.A. Ronica, V.T. Viji, S. Velmurugan, J.A. Jenifer, M. Michaelbabu, T. Citarasu, Isolation and characterization of halophilic *Bacillus* sp. BS3 able to produce pharmacologically important biosurfactants, Asian Pac. J. Trop. Med. 6 (11) (2013) 876–883.
[53] M.C. Deng, J. Li, Y.H. Hong, X.M. Xu, W.X. Chen, J.P. Yuan, J. Peng, M. Yi, J.H. Wang, Characterization of a novel biosurfactant produced by marine hydrocarbon-degrading bacterium *Achromobacter* sp. HZ 01, J. Appl. Microbiol. 120 (4) (2016) 889–899.
[54] H. Yuliani, M.S. Perdani, I. Savitri, M. Manurung, M. Sahlan, A. Wijanarko, H. Hermansyah, Antimicrobial activity of biosurfactant derived from *Bacillus subtilis* C19, Energy Procedia 153 (2018) 274–278.
[55] A.P. Karlapudi, T.C. Venkateswarulu, J. Tammineedi, L. Kanumuri, B.K. Ravuru, V. ramu Dirisala, V. P. Kodali, Role of biosurfactants in bioremediation of oil pollution—a review, Petroleum 4 (3) (2018) 241–249.
[56] A. Franzetti, P. Caredda, P. La Colla, M. Pintus, E. Tamburini, M. Papacchini, G. Bestetti, Cultural factors affecting biosurfactant production by *Gordonia* sp. BS29, Int. Biodeter. Biodegr. 63 (7) (2009) 943–947.
[57] J. Jeevanandam, A. Barhoum, Y.S. Chan, A. Dufresne, M.K. Danquah, Review on nanoparticles and nanostructured materials: history, sources, toxicity and regulations, Beilstein J. Nanotechnol. 9 (2018) 1050–1074.
[58] H. Al-Zahrani, A. El-Waseif, D. El-Ghwas, Biosynthesis and evaluation of TiO_2 and ZnO nanoparticles from *in vitro* stimulation of *Lactobacillus johnsonii*, J. Innov. Pharm. Biol. Sci. 5 (2018) 16–20.
[59] S. Das, J. Chakraborty, S. Chatterjee, H. Kumar, Prospects of biosynthesized nanomaterials for the remediation of organic and inorganic environmental contaminants, Environ. Sci. Nano 5 (12) (2018) 2784–2808.

This book belongs to Badji Mokhtar Annaba University Central Library Copyright Elsevier 2025

[60] M. Rizwan, M. Singh, C.K. Mitra, R.K. Morve, Ecofriendly application of nanomaterials: nanobioremediation, J. Nanopart. 2014 (2014) 431787 7 pages, https://doi.org/10.1155/2014/431787.
[61] H. Horváthová, K. Lászlová, K. Dercová, Bioremediation vs. nanoremediation: degradation of polychlorinated biphenyls (PCBS) using integrated remediation approaches, Water Air Soil Pollut. 230 (2019) 204, https://doi.org/10.1007/s11270-019-4259-x.
[62] K.N. Yogalakshmi, A. Das, G. Rani, V. Jaswal, J.S. Randhawa, Nano-bioremediation: a new age technology for the treatment of dyes in textile effluents, in: G. Saxena, R. Bharagava (Eds.), Bioremediation of Industrial Waste for Environmental Safety, Springer, Singapore, 2020, https://doi.org/10.1007/978-981-13-1891-7_15.
[63] M. Weijie, W. Chongnv, P. Xuming, J. Weixin, W. Yuhang, S. Benhui, TiO_2 nanoparticles and multi-walled carbon nanotubes monitoring and bioremediation potential using ciliates *Pseudocohnilembus persalinus*, Ecotoxicol. Environ. Saf. 187 (2020) 109825.
[64] C. Mystrioti, T.D. Xanthopoulou, P. Tsakiridis, N. Papassiopi, A. Xenidis, Comparative evaluation of five plant extracts and juices for nanoiron synthesis and application for hexavalent chromium reduction, Sci. Total Environ. 539 (2016) 105–113.
[65] J. Yang, H. Baohong, Q. Jingkang, T. Beiqian, J. Bi, N. Wang, X. Li, X. Huang, Nanomaterials for the removal of heavy metals from wastewater, Nanomaterials 9 (3) (2019) 424.
[66] B. Biswas, L.N. Warr, E.F. Hilder, N. Goswami, M.M. Rahman, J.G. Churchman, K. Vasilev, G. Pan, R. Naidu, Biocompatible functionalisation of nanoclays for improved environmental remediation, Chem. Soc. Rev. 48 (14) (2019) 3740–3770.
[67] M. Biswas, A.M. Raichur, Electrokinetic and rheological properties of nano zirconia in the presence of rhamnolipid biosurfactant, J. Am. Ceram. Soc. 91 (2008) 3197–3201.
[68] L.H. Saeedi, M.M. Assadi, S.M. Heydarian, M. Jahangiri, The production and evaluation of a nano-biosurfactant, Pet. Sci. Technol. 32 (2014) 125–132.
[69] C.B. Farias, A.F. Silva, R.D. Rufino, J.M. Luna, J.E.M. Souza, L.A. Sarubbo, Synthesis of silver nanoparticles using a biosurfactant produced in low-cost medium as stabilizing agent, Electron. J. Biotechnol. 17 (2014) 122–125.
[70] J.P. Saikia, P. Bharali, B.K. Konwar, Possible protection of silver nanoparticles against alt by using rhamnolipid, Colloids Surf. B: Biointerfaces 104 (2013) 330–332.
[71] G.S. Kiran, J. Selvin, A. Manilal, S. Sujith, Biosurfactants as green stabilizer for the biological synthesis of nanoparticles, Crit. Rev. Biotechnol. 31 (2011) 354–364.
[72] G.S. Kiran, A. Sabu, J. Selvin, Synthesis of silver nanoparticles by glycolipid biosurfactant produced from marine *Brevibacterium casei* MSA19, J. Biotechnol. 148 (2010) 221–225.
[73] A.S. Reddy, C.Y. Chen, C.C. Chen, J.S. Jean, C.W. Fan, H.R. Chen, J.C. Wang, V.R. Nimie, Synthesis of gold nanoparticles via an environmentally benign route using a biosurfactant, J. Nanosci. Nanotechnol. 9 (2009) 6693–6699.
[74] E. Rosenberg, E.Z. Ron, High- and low-molecular mass microbial surfactants, Appl. Microbiol. Biotechnol. 52 (1999) 154–162.
[75] G. Liu, H. Zhong, X. Yang, Y. Liu, B. Shao, Z. Liu, Advances in applications of rhamnolipids biosurfactant in environmental remediation: a review, Biotechnol. Bioeng. 115 (2018) 796–814.
[76] G.S. Kiran, A.S. Ninawe, A.N. Lipton, V. Pandian, J. Selvin, Rhamnolipid biosurfactants: evolutionary implications, applications and future prospects from untapped marine resource, Crit. Rev. Biotechnol. 36 (3) (2016) 399–415.
[77] P. Palanisamy, Biosurfactant mediated synthesis of NiO nanorods, Mater. Lett. 62 (4–5) (2008) 743–746.
[78] M. Ohadi, A. Shahravan, N. Dehghannoudeh, T. Eslaminejad, I.M. Banat, G. Dehghannoudeh, Potential use of microbial surfactant in microemulsion drug delivery system: a systematic review, Drug Des. Devel. Ther. 14 (2020) 541.
[79] Y. Xie, R. Ye, H. Liu, Synthesis of silver nanoparticles in reverse micelles stabilized by natural biosurfactant, Colloids Surf. A: Physicochem. Eng. Asp. 279 (1–3) (2006) 175–178.
[80] C. Hazra, D. Kundu, A. Chatterjee, A. Chaudhari, S. Mishra, Poly(methyl methacrylate)(core)–biosurfactant (shell) nanoparticles: size controlled sub-100 nm synthesis, characterization, antibacterial activity, cytotoxicity

This book belongs to Badji Mokhtar Annaba University Central Library Copyright Elsevier 2025

and sustained drug release behaviour, Colloids Surf. A: Physicochem. Eng. Asp. 449 (2014) 96–113, https://doi.org/10.1016/j.colsurfa.2014.02.051.

[81] M. Basnet, S. Ghoshal, N. Tufenkji, Rhamnolipid biosurfactant and soy protein act as effective stabilizers in the aggregation and transport of palladium-doped zerovalent iron nanoparticles in saturated porous media, Environ. Sci. Technol. 47 (2013) 13355–13364.

[82] B.R. Singh, S. Dwivedi, A.A. Al-Khedhairy, J. Musarrat, Synthesis of stable cadmium sulfide nanoparticles using surfactin produced by *Bacillus amyloliquifaciens* strain KSU-109, Colloids Surf. B: Biointerfaces 85 (2011) 207–213.

[83] M. Bao, Y. Pi, L. Wang, P. Sun, Y. Li, L. Cao, Lipopeptide biosurfactant production bacteria *Acinetobacter* sp. D3-2 and its biodegradation of crude oil, Environ. Sci.: Processes Impacts 16 (4) (2014) 897–903.

[84] A.K. Singh, S.S. Cameotra, Efficiency of lipopeptide biosurfactants in removal of petroleum hydrocarbons and heavy metals from contaminated soil, Environ. Sci. Pollut. Res. 20 (2013) 7367–7376.

[85] M.B. Kasture, P. Patel, A.A. Prabhune, C.V. Ramana, A.A. Kulkarni, B.L.V. Prasad, Synthesis of silver nanoparticles by sophorolipids: effect of temperature and sophorolipid structure on the size of particles, J. Chem. Sci. 120 (2008) 515–520.

[86] J. Narayanan, R. Ramji, H. Sahu, P. Gautam, Synthesis, stabilisation and characterisation of rhamnolipid-capped ZnS nanoparticles in aqueous medium, IET Nanobiotechnol. 4 (2) (2010) 29–34.

[87] C. Hazra, D. Kundu, A. Chaudhari, T. Jana, Biogenic synthesis, characterization, toxicity and photocatalysis of zinc sulphide nanoparticles using rhamnolipids from *Pseudomonas aeruginosa* BS01 as capping and stabilizing agent, J. Chem. Technol. Biotechnol. 88 (2013) 1039–1048.

[88] E.O. Fenibo, G.N. Ijoma, R. Selvarajan, C.B. Chikere, Microbial surfactants: the next generation multifunctional biomolecules for applications in the petroleum industry and its associated environmental remediation, Microorganisms 7 (11) (2019) 581.

This book belongs to Badji Mokhtar Annaba University Central Library

Copyright Elsevier 2025

This page intentionally left blank

This book belongs to Badji Mokhtar Annaba University Central Library

Copyright Elsevier 2025

CHAPTER 34

Potential risk and safety concerns of industrial nanomaterials in environmental management

Saurabh Joglekar and Renuka Gajaralwar

Chemical Engineering Department, Laxminarayan Institute of Technology, Rashtrasant Tukadoji Maharaj Nagpur University, Nagpur, Maharashtra, India

34.1 Introduction

The rapid development in nanotechnology and material development have increased the industries demand for more specific tailor-made products. Indeed, nanotechnology is one of the most fast-growing technology with a wide range of applications. The applications include display technology, electronic, advanced material for property enhancement, biomedical, construction, etc. Fig. 34.1 shows the various application of INMs developed in the recent past.

The advancements in properties of a variety of nanomaterials have increased their commercial applications to a greater extent. Nanomaterials have found a wide variety of applications in all the branches of science as the research in this field has geared up speed [1]. This has led the researchers to assess the toxicological and environmental impacts of nanomaterial synthesis and usage. Although nanomaterials have been prevailing on earth in the form of naturally occurring nanomaterials like silver, cellulose, and carbon, commercially made industrial nanomaterials (INMs) have a specific usage and so they can poses a health risk for humans and environmental destructive impacts at high concentrations [2]. The entire life cycle of an INM can be divided into various stages like raw material acquisition, research, manufacturing, efficacy evaluation, use phase, and end of life phases [3]. Many of the manufactured nanomaterials are considered as "emerging pollutants" as their environmental release during the various life cycle stages (either accidentally or incidentally) is not regulated despite the health risk involved [4]. The direct and indirect emission can be evaluated using the conventional life cycle assessment wherein a cumulative of entire emissions is made along the various life cycle stages [5]. Fig. 34.2 explains the various hazards of INMs during its life cycle.

Handbook of Nanomaterials for Wastewater Treatment. https://doi.org/10.1016/B978-0-12-821496-1.00019-2
Copyright © 2021 Elsevier Inc. All rights reserved.

This book belongs to Badji Mokhtar Annaba University Central Library

Copyright Elsevier 2025

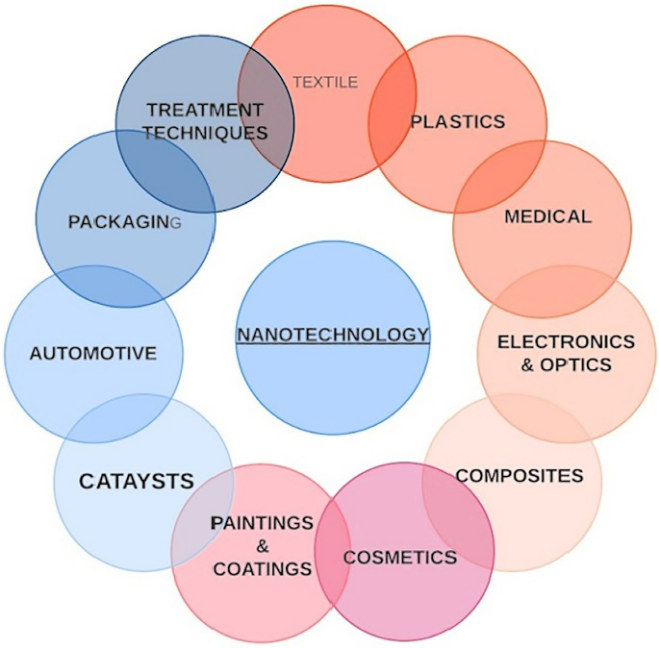

Fig. 34.1
Different applications of INMs.

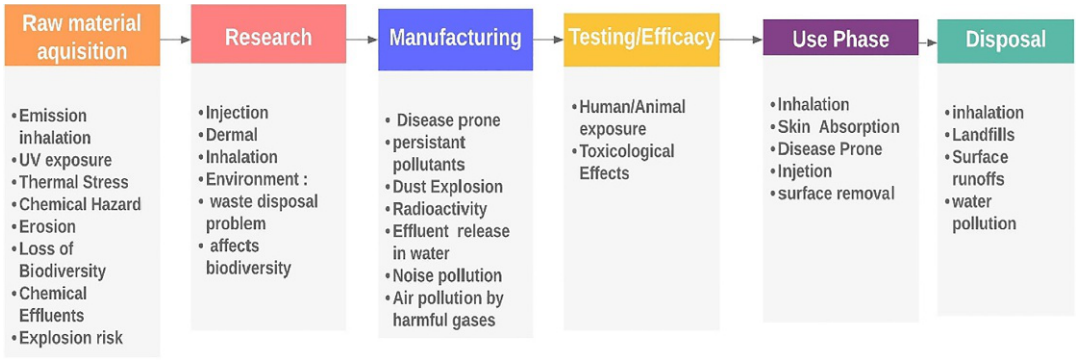

Fig. 34.2
Life cycle stages of INMs and its potential exposure.

Along with the emission, it has become necessary to evaluate the human health and ecosystem hazard over the entire stages [4].

INMs have emerged as a promising material in addressing various modern-day challenges; however, inadequate estimation of exposure of INMs has led to several regulatory and risk assessment challenges in adopting them. Also because of the poor risk assessment framework

This book belongs to Badji Mokhtar Annaba University Central Library Copyright Elsevier 2025

available for INMs, a significant uncertainty is observed around use of INMs. To be specific, evaluation of INMs toxicity has become necessary because of its physiochemical and biological interactions at the nano level; however, it is difficult to predict INMs toxicity from the source material.

Three primary reasons are identified for lack of development of a risk assessment framework: (1) Insufficient data generation during development of nanomaterial for risk assessment. (2) Inadequate availability of number of data points for a robust risk assessment. (3) Lack of research funds for estimation of health and safety assessment of INMs compared to development of new materials [2]. The chapter aims at reviewing the health, toxicological, and environmental risks of INMs to enable future research in the field.

34.2 Health risk

INMs have a vast application; however, safety aspects and health risk from INMs have become a global concern. The focus is currently on exposure of emission to researchers, workers, and consumers by direct or indirect way. INMs are potential risks to humans because of prolonged exposure through various routes. The studies regarding toxicology have been mostly animal based and hence accurate data about human toxicology is unavailable. The major routes of exposure are inhalation, dermal penetration, and ingestion.

34.2.1 Ingestion

Particles of INMs that move down the respiratory tract sometimes get swallowed, causing direct exposure to gastrointestinal tract [6]. Along with this ingestion can take place from hand-to-mouth contact [7]. The increasing exposure through this route is because of usage of nanomaterials in water treatment process, food and drug industry [8]. In these industries, INMs are used for increasing efficiency of fertilizers, manipulation of nanostructure of plants, food processing to form nutritional supplements, and even in food packaging. Through the food, the nanoparticles enter the blood streams and settle on various tissues, causing harmful effects. It may also enter brain tissue and hamper the immune system, making us prone to various diseases. Majority of studies in this field are required to have consistent data about hazards on mankind [9].

34.2.2 Dermal

The dermal route of entry of INMs has gained significance in recent years because of increased use of INMs in cosmetics. The exposure route through absorption in skin occurs through the increased use of nanoparticles in sunscreens containing TiO_2 and zinc oxide as UV ray–repellent agent [6]. Moreover, nano-level liposome is being used as transport medium in cosmetics and skincare products. Some studies have even stated that atoms at the nano level

This book belongs to Badji Mokhtar Annaba University Central Library Copyright Elsevier 2025

combine with sunlight and poses increased reactivity, allowing deeper penetration in skin [10]. Through the mechanism of absorption, the nanomaterials penetrate through the protective layers of skin and reach the dermal or epidermal layer, and from there, it diffuses in the blood stream, causing significant impact on the body [11]. But studies have also shown that a healthy and intact skin can restrict the penetration of INMs inside the body [12]. On the other hand, the hair follicles present on skin could act as a depository for nano-sized particles. A study by Ryman-Rasmussen on outer layers of pig skin showed penetration of quantum dots into the dermis or epidermis within 24 h [13]. Thus, penetration of INMs through skin occurs by various mechanisms and this can lead to several health issues. Researchers suggest that these INMs could be transferred to lymphatic system in the body and may affect the immune system [9]. Dermal penetration can also occur during handling of INMs [7]. This has ill effects on the immune system and can also lead to oxidative damage to skin.

34.2.3 Inhalation

Inhalation of nanoparticles through air is one of the significant exposure routes. Exposure by this route not only affects the individual in contact with the INMs but also individuals who are present in its vicinity. Aerosol penetration and persisting in respiratory systems is a fact of major concern and many studies are done for this exposure route [6]. The inhalation route poses a greater threat because of mainly two factors: one is smaller size of the particle and the other is respirable fraction concentration of INMs. Nanoparticles have size less than 100 nm, and all particles less than 5 μm are inhaled and considered a part of respirable fraction [7]. As these INMs enter the respiratory tract, the nanoparticles get accumulated in different parts depending upon its size, shape, and density. Fig. 34.3 depicts the deposition

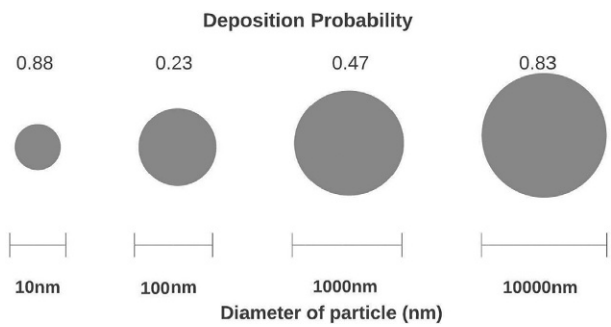

Fig. 34.3
Deposition probability of aerosol particle in the respiratory tract for an adult breathing at 25 L/min and having exposure to spherical particle with density 1000 kg/m^3 [6]. *Drawn based on the data reported in A.D. Maynard, Nanotechnology: assessing the risks, Nano Today 1 (2006) 22–33. Copyright (2013) Springer.*

This book belongs to Badji Mokhtar Annaba University Central Library
Copyright Elsevier 2025

probability of INMs depending on the particle diameter in the respiratory tract of human body. These particles move through the respiratory system and get deposited on the alveoli and also diffuse in blood. The transfer of INMs from the respiratory tract to circulatory system is a significant issue. At higher doses, it may also affect the functioning of kidney, which fails to remove nanoparticles via filtration from blood streams [7]. A study on rats showed that when exposed to 60 μg/m^3 of 26 nm diameter polytetrafluoroethylene (PTFE) particles, the rats were killed because of hemorrhagic pulmonary inflammation in less than 30 min [14]. INMs penetration into cells has been observed and also evidences are present showing deposition of ultrafine particles in mitochondria, causing significant structural damages [15]. Several studies demonstrate inhaled INMs entering the nervous system through olfactory nerves and or blood-brain barrier [16]. Thus, major exposure occurs through inhalation and hence majority of the scientific world is focusing on studying the effects and hazards of this exposure.

34.3 Toxicological impact

Toxicological impacts are nowadays becoming more prevalent with the increased use of INMs in day-to-day life. A high degree of uncertainty prevails around the use of INMs because of the limited knowledge about the factors considered for evaluation of toxicological impacts. The ability of INMs to penetrate the human cell poses a great toxicological threat [17]. Although a lot of research has been performed with regards to the toxicological and environmental impact of nano material synthesis, very less information is available pertaining to effective quantity of nano material in circulation [18]. Early toxicological data generated did not consider the behavior of the INMs in biological environment that prevented the researchers to evaluate the toxicological impact of individual INM [19]. The physicochemical properties such as surface area and reactivity, dosage, coatings particle size, and tendency to agglomerate of INMs play a significant role in determining its toxicity [20]. The principle factors that define the toxicity of INMs can be outlined as follows.

34.3.1 Chemical composition

Particle chemistry and surface orientation play a significant role is defining the toxic effects of the INM. PTFE upon heating up to 480°C releases fumes containing nano-size particles of count mean diameter of 18 nm. Such fumes on exposure to humans are reported to cause acute lung injury [21, 22]. Severe lung damage with high mortality within 4 h is observed for rats exposed to PTFE fumes (50 micrograms per cubic meters) for 15 min [14]. Presence of metallic materials or transition elements in INMs increases it toxicity because of its ability to generate free radicals [23].

This book belongs to Badji Mokhtar Annaba University Central Library Copyright Elsevier 2025

34.3.2 Particle size

Particle size plays a vital role in measuring the toxicity of the INMs. Several studies supported the concept of "Smaller size equals greater hazard" wherein the data shows an increased toxicity with decrease in particle size. Primary research is on development of models for effect of particle size on deposition in three regions of respiratory tract (nasopharyngeal, tracheobronchial, and alveolar). It was observed that of the total 1 nm particle size inhaled, 90% got deposited in the nasopharyngeal region and the rest in the tracheobronchial region of the respiratory tract. Also, of the total 5-nm particle size, INMs inhaled equal amounts of 30% got deposited in all three regions of the respiratory tract. It is reported that the different rate of depositions and size of INMs in regions has a different resultant toxicological effect on the pulmonary organs [9]. Jani observed an increase in absorption rate with decrease in particle size [24, 25]. A study on toxicological effects on rats was reported by Renwick, which measured toxicological effects on rats that were (lung) administered with different sizes of TiO_2 and carbon black [26]. Along with the particle size of the INMs, the medium also plays a vital role in uptake of nanomaterial in biological systems [27]. Murdock studied the toxicity of silver and copper nanoparticles and observed increased cytotoxicity upon its suspension in serum compared with suspension without serum [28]. Ahmad observed a wide distribution of coated silver nanomaterials, whereas the agglomerated uncoated silver nanomaterials appeared to be excluded from organelles such as the nucleus [29].

34.3.3 Surface area and reactivity

The surface area and reactivity play a vital role in utilization of INMs in medicines [30]. Stoeger on studying the effect of different particle sizes of carbon particles suggested a threshold for particle surface area (20 cm^2) below which no significant response is observed in mice [31]. For the same dose amount, a higher pulmonary inflammatory neutrophil response was observed for ultrafine anatase TiO_2 (20 nm), instilled intratracheally into rats and mice compared to fine anatase TiO_2 [32]. Previous research repeatedly mentions about expressing the toxicological impact per dose calculated in terms of surface area of an INM [26, 33–35]. However, there is very little understanding regarding the relationship between the size of INM and its biological effect. In one study done to evaluate the cytotoxicity of silver nanomaterial normalized by the specific surface area, it was found that the 30 and 15 nm silver nanoparticles showed more toxicity compared with 55 nm silver nanoparticles [36]. There are other contradicting research findings that suggest no effect of size on toxicity normalized by surface area or by weight [37, 38].

This book belongs to Badji Mokhtar Annaba University Central Library
Copyright Elsevier 2025

34.3.4 Surface treatments on particles, particularly for engineered nanoparticulates

Surface coatings or surface type of INMs are of particular importance during toxicological evaluation of INMs specifically to humans. INMs are often coated to reduce its uptake in the human body, thereby decreasing its toxicological effect. Researchers have observed that cadmium selenides (CDSe) quantum dots are cytotoxic under specific conditions attributed to release of Cd^{2+} ions because of collapse of its structure. However, the coated CDSe quantum dots were observed to be nontoxic in nature and are used to track cell migration and reorganization in vitro [39]. Jani et al. have shown that 59-nm uncoated polystyrene beads were absorbed from the intestinal tract but surfactant-coated beads were not absorbed; and carboxylate-coated polystyrene beads were not absorbed, but nonionic beads were absorbed [25]. By using a pulmonary bridging methodology in rats, acute lung toxicity of hydrophobic surface-coated (triethoxyoctylsilane) titanium oxide nanoparticles were compared with hydrophilic-coated titanium oxide. It was observed that a high dose of pigment grade titanium oxide produced a transient pulmonary inflammatory response compared with hydrophobic-coated titanium oxide nanoparticles [40].

34.3.5 Degree of agglomeration

Agglomeration of INMs plays a significant role in determining its deposition and thereby its toxicity. Wang et al. showed that the zinc nanoparticles introduced in animals orally caused death; however, the microsized zinc particles did not show any such effect [41]. INMs of larger diameter are more probable to deposit in the upper respiratory track, whereas the INMs of smaller diameter are able to penetrate deeper and more sensitive areas of the respiratory systems [9]. Thus, along with the size of INMs, it is necessary to evaluate the toxicological effects of the INMs in all its individual and agglomerated forms [27]. The agglomeration of the nanoparticle is majorly affected by the surface characteristics. A small change in the surface charge can alter the hydrodynamic size of the nanomaterial [42]. Hydrodynamic size and its surface charge for nanomaterials of Ag, TiO_2, and carbon nanotubes (CNTs) in biologically relevant solutions were characterized by Murdock et al. [28]. Several studies show the inaccuracy of toxicity measurement because of unstable and agglomerated nanoparticles used in in vitro or in vivo experiments [43, 44]. The inhalation study of 2–5 nm TiO_2 nanoparticles found that INMs aggregated together to form aerosol particles with a mean mobility diameter between 120 and 130 nm [45].

34.3.6 Particle shape and/or electrostatic attraction potential

Based on the properties desired and applications, INMs are synthesized in various shapes such as spherical, fibrous, tubular, and rings. Studies find that prolonged exposure of spherical- and

This book belongs to Badji Mokhtar Annaba University Central Library Copyright Elsevier 2025

fibrous-shaped INMs is associated with increased risk of fibrosis and cancer [46]. Particle shape also plays a significant role in evaluation of the toxicological impacts of INMs. It is observed in literature that titanium oxide in fibrous form is observed to be more cytotoxic compared with its spherical form. Upon equal exposure of 1–2 μm of fibrous and spherical TiO_2 to rats alveolar macrophages showed an increased vaculor and cell surface damage in fibrous TiO_2 with no significant damage noted for spherical TiO_2 [46, 47]. Gold nanomaterials can be found in many different shapes, especially as spherical clusters and nanorods. Chitrani et al. observed the effect of shape of INM on the uptake. They concluded that uptake in HeLa cells was relatively slower for nanorods compared with spherical-shaped gold nanoparticles [48]. Wang et al. [37] observed the nanorod-shaped gold nanoparticle to be more cytotoxic to human HeCaT keratinocytes compared with spherical-shaped gold nanoparticle. The effect of shape of ZnO nanoparticle on cytotoxicity was investigated by Hsiao and Huang [20]. It was found that nanorods and nanospheres showed similar cytotoxicity for an exposure time of 12 and 24 h; however, the nanorod ZnO nanoparticle was considered more toxic than the nanosphere ZnO nanoparticle owing to values of EC50 to be 8.5 and 12.1 μg mL^{-1}, respectively [20].

34.4 Environmental impact

It is known that the manufacturing, use, and disposal of INMs has a significant environmental impact. Along with the indirect emissions occurring, a major environmental impact is observed because of uncontrolled release of synthesized nanomaterial during the process and use. Some of the latest articles discuss the effect of such synthesized nanomaterial on health and environment [49–51].

34.4.1 Release during manufacturing

Gottschalk and Nowack estimated INM discharges from 0.1% to 2% of the absolute production rate, with a conveyance to air, water, and landfill [50]. These discharge gauges are collective for all INMs, given the absence of INM-explicit fabricating data. Despite the fact that there are a few control gadgets for various procedures identified with the combination and treatment of INMs, there is significant doubt with regards to the nature and quantity of INMs that might be expelled by such control gadgets. It can be expected that distinctions may emerge depending on the technique for INM production and products in which INMs are used. However, in the current stage, because of the lack of proper monitoring of emissions of INMs and very little information available about the production of these products, it is difficult to account for this difference. The process should be enhanced in such a way that emissions of INMs should be reduced and its toxicity level must also be decreased.

This book belongs to Badji Mokhtar Annaba University Central Library
Copyright Elsevier 2025

34.4.2 Release in use

Because of the set number of concentrates that have been done on emissions from explicit applications, a few evaluations depend on data from comparable applications on other nanomaterials. The gauges fluctuate relying on the field of use and afterward its estimated release to soil, water bodies, and air. Fig. 34.4 shows the percentage release of INMs in air, water, and soil through various applications. INMs that do not get filtered through the treatment forms are at last discharged into the land as effluent [49]. Numerous of these estimates will require top to bottom investigations of producer and customer practices to improve and refine the determined emissions.

34.4.3 Release in disposal

Information regarding the evaluations of INM release during disposal [52–54], waste generated, and removal [55] was studied from literature. The information about waste

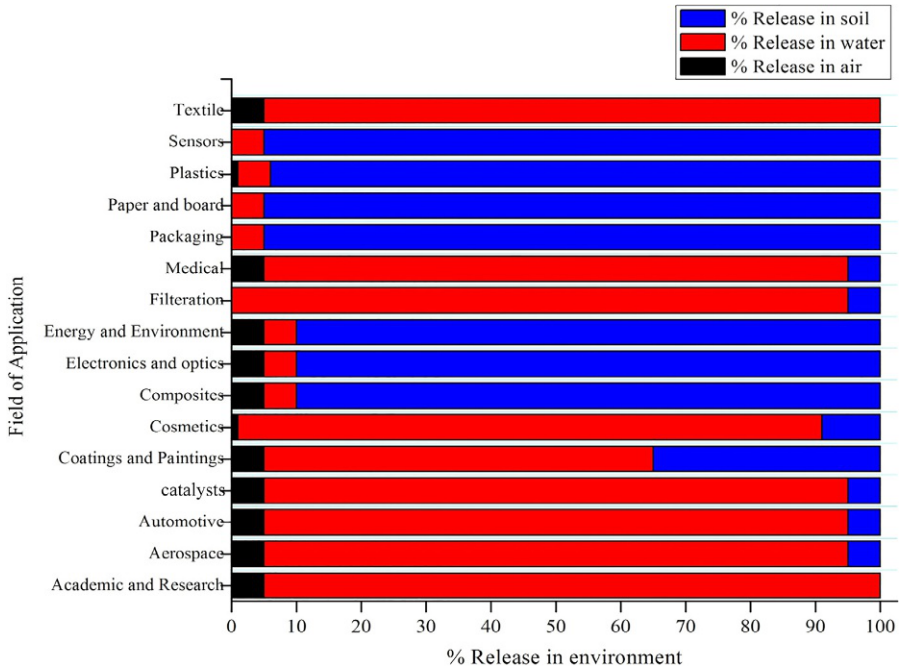

Fig. 34.4

Release of INMs into environment through air, water, and soil [49]. *Drawn based on the data reported in A.A. Keller, S. McFerran, A. Lazareva, S. Suh, Global life cycle releases of engineered nanomaterials, J. Nanoparticle Res. 15 (2013) 1692. Copyright (2013) Springer.*

This book belongs to Badji Mokhtar Annaba University Central Library
Copyright Elsevier 2025

formation was accessible for 71 nations and waste incineration information was accessible for 61 nations. By partitioning the world into eight districts and extrapolating the accessible per capita waste production and incineration rates to the whole region, the average world municipal waste cremation pace was estimated at 19%. A comparison between different disposal methods like landfills, incineration, and waste water treatment plant (WWTP) was done by utilizing consistent multipliers for all INMs and applications considered, missing INM-explicit information. With an assumption that the waste slag and filters from waste incineration are ultimately disposed into landfill, the rate of discharge of INM is estimated at 0.05%–1%—air, 1%–50%—slag, and 50%–98% captured by filters [53]. WWTPs are assessed to expel 75%–97% of INMs from the inflow waters [54] and move them to biosolids, which are disposed by incineration, agricultural land, and landfill. Although there are different methods for disposal of biosolids, a range for release can be narrowed based on the common practices for each method [56, 57]. INMs that are not filtered through water by the treatment are at last discharged into the land as effluent. Thus, an efficient waste management should be done of the INMs considering their harmful effects.

34.5 Risk and safety associated for using INMs

Utilization of nanotechnology offers a great advantage in decreasing the dependence of large infrastructure for waste water treatment. Development of INMs for water and waste water treatment also provides new methods for economic utilization of other water resources. The methods developed takes advantage of specific properties of INMs such as fast dissolution, high reactivity, and strong sorption, superparamagnetism, localized surface plasmon resonance, and quantum confinement effect. INMs find their application in several waste water treatment processes such as adsorption, photocatalysis, disinfection, microbial control, and sensing and monitoring. Although many of the applications are still in laboratory scale, the technologies hold great promise for upscaled commissioning. Following are certain applications of INMs in water/waste water treatment. Waste waters contain a major part of nanomaterials that have been released in the environment. The major issue lies in the removal of INMs because of its lower concentrations in waste waters. Various WWTPs make use of biological treatment, which is hindered by the properties of INMs present in it. The studies are being conducted based on the commonly used INMs basically silver, TiO_2, ZnO, and carbon-based nanomaterials [58]. The INMs released during manufacturing, use, and disposal find its way into water bodies, WWTP, or waste incineration plants or landfill [59–61]. Hence, various WWTPs are affected by the concentration of INMs present in them. As per a study, TiO_2 has been detected in surface runoffs in urban areas [54, 62]. The solubility of oxides of INMs (TiO_2, ZnO) exits cytotoxicity to the cells in in vitro studies [63]. Whereas metallic INMs like silver nanoparticles having antibacterial properties are toxic to several bacteria [64], which reduces the bacterial degradation of waste in WWTPs.

This book belongs to Badji Mokhtar Annaba University Central Library Copyright Elsevier 2025

Carbon-based nano-adsorbents: Owing to its high surface area and associated adsorption sites, CNTs show high affinity to organic chemicals. The surface functional groups of CNTs are responsible for removal of metal ions. Aggregation of ultrafine carbon particles affected the functioning of alveolar macrophages in rats and humans that can be linked to increased risk of infections and affecting sensitive lung cells [65, 66]. Carbon-based INMs are observed to be more toxic than metal oxide-based INMs [67].

Metal-based nano-adsorbents: Metal-based nano-adsorbents (titanium oxide, alumina, etc.) have proved to be efficient in removal of varied heavy metals that include arsenic, mercury, copper, cadmium, etc. Another advantage of use of metal oxide-based adsorbent is easy regeneration.

Nano fiber membrane: Synthesis of ultra-fine nano fibers using electrospinning offers increased surface area and porosity. The nano fiber membrane has been observed to remove micro-sized contaminants in aqueous phase at a high rejection rate without fouling. The addition of metal oxide nanoparticle of alumina, zeolite, and silica in the ultrafiltration membrane increases the surface hydrophobicity and fouling resistance. Doping of active layer or surface alteration of membrane using INMs such as silver and zeolites has shown to increase permeability.

Photocatalyst: Semiconductor photocatalyst like TiO_2 is commonly used because of its lower chemical toxicity, stability, low cost, and abundance. However, challenges in the application of photocatalyst include (1) utilization of visible light; (2) efficient reactor design and catalyst recovery/immobilization techniques; (3) better reaction selectivity.

34.5.1 Associated risks

For INMs used in waste water treatment that pose a risk, it is very important to understand the extent of exposure and the associated hazard such as toxicity. The extent of exposure is determined based on the material handling, source of exposure, and positioning of INM in different phases (like aqueous and air). Most of the risks evaluated for worker exposure in manufacturing facility are for air borne pathway. Specific associated risks for certain INMs in waste water treatment are as follows.

CNTs: Several studies show the pulmonary effect of exposure of CNTs [68]. A study presented a transient independent of dose inflammation and granulomas in mice lung upon exposure of single-walled CNTs [69]. A study conducted by National Institute for Occupational Safety and Health (NIOSH) showed a stronger inflammation, granulomas, oxidative stress, and fibrosis upon exposure to carbon nanotubes compared with carbon black and silica [70]. Another study presented that exposure of multiwalled carbon nanotubes stimulates the proinflammatory cytokine production related to pathogenesis of particle-induced lung diseases and pneumonia [71].

This book belongs to Badji Mokhtar Annaba University Central Library Copyright Elsevier 2025

Quantum dots: Quantum dots have a core of cadmium or lead or any other noble metal. The core is covered with a coating of variety of material like zinc sulfide and polyethylene glycol that degrade upon oxidative environment or UV radiation exposing it. Cadmium and lead are proven toxins for the vertebrate systems at lower concentrations. Although no cytotoxicity of quantum dots has been reported, they affect the cell growth and viability [68]. Some in vivo studies show the accumulation in various organs such as kidney, spleen, and bone marrow [72].

Carbon fullerenes: Carbon fullerenes are an ultrafine combustion particulate product and hollow spheres of carbon arranged in hexagonal and pentagonal panels. Some studies showed a cytotoxic effect of fullerenes when exposed to light. It also affected embryo development and distributed itself to various tissues of the body where it is retained for a long time. Fullerenes toxicity levels change with its form. A pure form of fullerenes is observed to be more toxic compared with its derivatized form [68].

Inorganic INMs: The inorganic INMs such as silica (SiO_2 TiO_2 [anatase] and ZnO) have shown a pulmonary effect on rodents and humans [73–77]. A study shows in vitro uptake of CeO_2 nanoparticles in humans [78]. The metal oxide nanoparticles magnetite and nano iron produce an oxidative stress response and are taken up into cells. The toxicity of TiO_2 nanoparticles has even reached seawaters through its release in water bodies from industries, and the studies on embryo toxicity of D shell larvae stage of *Mytilus galloprovincialis* (Lmk) by Libralato et al. showed that nTiO$_2$ causes formation of deformed larvae in both light and dark scenario [79].

A comparative risk assessment was performed by Robichaud et al. [80] for fabrication of INMs. The list of feedstock, products and synthesis pathways, and waste streams is compiled and the physicochemical properties and mass balance were used to assess risks related to factors such as volatility, carcinogenicity, flammability, toxicity, and persistence. The analysis provided an overall environmental risk of the INMs that can be compared to products manufactured by conventional manufacturing processes.

It is evident from the above discussion that INMs pose a great toxicological threat to humans and other living organisms. Also, it is observed that with increased production volumes of INMs, majority of INMs waste is likely to be deposited in WWTPs or water bodies, soil, and air [81]. A pathway suggested shows the stages of INMs leading to nano-waste that are nanotechnologies (nanoparticles, quantum dots, nanotubes, etc.), nanoproduct, used products, and nano-waste. It also suggested the need of recycling of INMs and various methods for it [82]. Hence, it has become necessary to explore the various separation techniques and include in the environmental management plan for INMs. The conventional WWTPs may not be reliable in removal of INMs because of its small size and other chemical specifications. A detail discussion of various removal techniques is presented by Liu et al. [67] Fig. 34.5 illustrates certain processes for removal of INMs from waste water.

This book belongs to Badji Mokhtar Annaba University Central Library Copyright Elsevier 2025

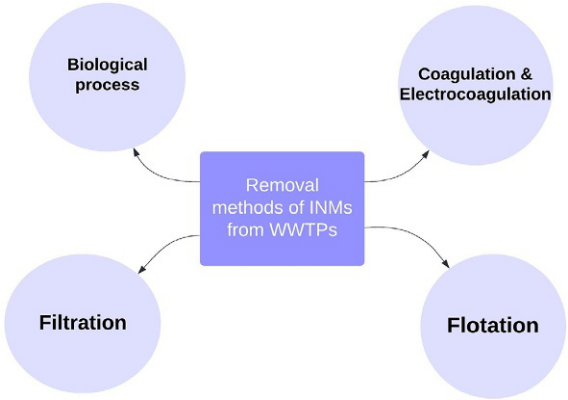

Fig. 34.5
Methods of removal of INMs from wastewaters.

Coagulation and electrocoagulation: Chuang et al. [83] studied removal of colloidal silica removal from waste water using coagulation technique. Similar silica nanoparticle removal was observed for two coagulants such as PACl and $Al_2(OH)_nCl_{6-n}$. Electrocoagulation technique was studied by Lai and Lin [84] for removal of copper CMP (chemical mechanical polishing) waste water. A high copper ion removal and turbidity removal were observed for Al/Fe electrode pair used for electrocoagulation. The method is very efficient and is able to achieve 99% copper ion and 96.5% turbidity removal in less than 30 min.

Flotation: A good removal of particles (turbidity removal of more than 98%) was achieved for CMP effluent treatment using dissolved air floatation and cetyl trimethylammonium bromide (CTAB) as collector [85]. Tsai et al. [86] found a combination of PACl/sodium oleate (NaOl) for nano bubble floatation using coagulation as a cost-effective treatment for CMP waste water.

Filtration: Zhong et al. utilized ceramic membrane for complete removal of nickel catalyst from slurry [87]. Polyamide nanofiltration membrane is observed to remove 98% of fullerol [88].

Biological process: The INMs associated with biomass in the waste water sludge can be removed upon removal of biomass. More than 96% TiO_2 nanoparticles attached with the biomass are removed by secondary sedimentation. However, it is pertinent to note that nanoparticles entrapped within the sludge materials may re-enter the environment as most of wastewater sludge are used in fields or incineration or landfills [89].

Even though many methods have been explored for removal of nanoparticles from wastewaters to avoid the hazardous effects, still there is scope for improving the efficiency of various

This book belongs to Badji Mokhtar Annaba University Central Library Copyright Elsevier 2025

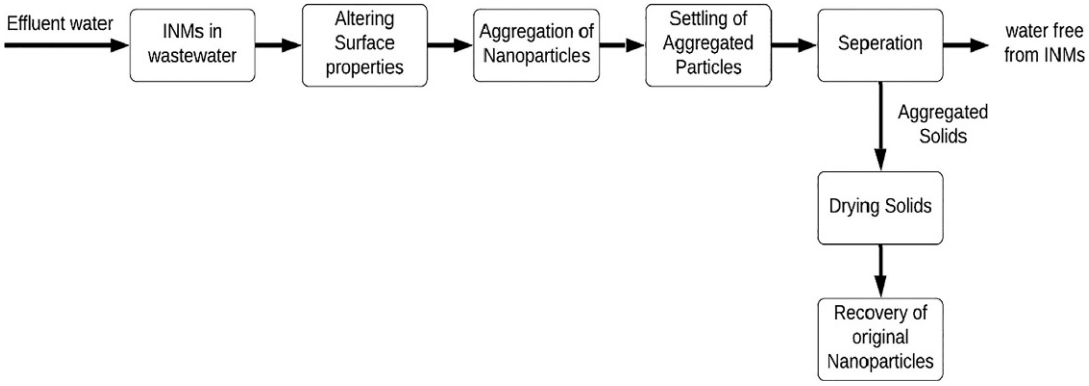

Fig. 34.6
The pathway/framework for technologies leading to removal of INMs from wastewater.

processes. A Monte Carlo simulation by Ogilvie et al. [90] found that the external coating used to stabilize the silver nanoparticles during synthesis plays a significant role in its removal. Leung et al. [91] suggested a framework for possible emerging technologies in the field of treatment of wastewater containing INMs, which would also lead to recovery of original nanoparticles. This framework is well depicted in Fig. 34.6.

34.5.2 Food industry

Nanotechnology is being used in food science for increasing its functionality and applicability [92]. For protection from bacterial deterioration, the usage of nano antimicrobials has been a successful attempt in increasing the shell-life of food stuff. Metal and metal oxides are used as antimicrobials whose properties lead to reactive oxygen species, leading to cell damage of bacteria [93, 94]. Silver nanoparticles providing Ag+ ions and nanocomposites made up of polymers combined with metal and metal oxides, for Ag/LDPE, ZnO/LDPE etc., are used as antimicrobials [95, 96]. Another functionality includes increased bioavailability with the help of nano-delivery vehicles for compounds being used as nutritional supplements like vitamins, calcium, and bioactives. Some polymeric nanoparticles like SiO_2-gallic acid are used as nano-antioxidants. Studies have shown that silver nanoparticle can have allergic immune responses in vivo. The nanoparticles that enter the body through food can affect tissues, causing inflammation and oxidative stress [97]. Nano ZnO coating is used for improving the shell-life of cut fruits like “Fuji apples” and avoid its early browning. Flavor release and retention in food products make use of nano-encapsulation technology [98]. Even though not many studies are available regarding toxicity of INMs in this industry, the health risk from use of them cannot be neglected.

This book belongs to Badji Mokhtar Annaba University Central Library Copyright Elsevier 2025

34.5.3 Agri-food industry

An important field in which INMs can pose a major hazard to mankind is the agri-food industry. The application of nanoparticles for agriculture has gained significance recently with new researches being done. Nanotechnology is used for developing genetically modified seeds, pesticides, nanosensors, and also in novel farming techniques. These INMs then reach the body through the route of ingestion, and studies have shown that exposure to nanoparticles can cause oxidation and inflammatory reaction, leading to the damage of gastrointestinal tract. Studies [99–101] suggest that longer exposure to INMs causes harm to liver, kidney, and even poses serious threats of cancer. Thus, several studies, as stated above, on risk assessment suggest that incorporation of INMs in food can lead to severe health issues.

34.5.4 Automobile industry

The automobile industry has been revolutionized with the usage of nanotechnology. INMs, particularly nanotubes, nanoparticles, nanofibers, nanocomposites, and other advanced materials, find their use in development of various features of automobile industry [102]. Nanotechnology has its applications in the fields of coating and lubrication, nanostructured automobile parts, nano-based energy generation, storage data processing technology, and in sensors [102]. The additives used in automobile industry have nanoparticles that are retained in the body and cause various illness related to the respiratory system, cardiovascular diseases, variety of cancers, and some major illness like Parkinson's diseases, Crohn's disease, and Alzheimer's disease [103, 104]. The protection of automobile parts against environmental deterioration is provided by dispersion of various INMs like TiO_2, carbon black, graphene, CNTs, SiO_2, ZnO, nano-clay in coatings, and primers [105–107]. A study conducted on human skin cells showed that CNTs, both single-walled CNTs (SWCNTs) and multiwalled CNTs (MWCNTs), have the potential of penetration and cause oxidative stress, cytokines, and reduced cell viability [108]. Studies have shown that ZnO nanoparticles pose higher toxicity on cells of mammals than TiO_2 nanoparticles [36, 109]. The most important purpose lies in manufacturing of vehicle parts using nanocomposites. Nanofluids are being used as lubricants majorly containing tungsten nanospheres, copper nanoparticles, graphene, etc.

34.5.5 Aerospace industry

Although the use of INMs has not gained so much pace, these find application in manufacturing of composite panels, spray coatings, lubricants, air filters, and for reduction of emissions. Mainly CNTs, fullerene, graphene, and carbon nanofibers are being used to make nanocomposites used to make aircraft parts and increase its strength, resistance, and durability [110]. Types of CNTs such as MWCNTs at higher dosage show cytotoxicity in alveolar macrophage, whereas SWCNTs show cytotoxicity even at lower dosage in the body.

This book belongs to Badji Mokhtar Annaba University Central Library Copyright Elsevier 2025

The nanocomposites are used to make parts of aircrafts. Some INMs can cause nano corrosion on aircraft equipment materials used for manufacturing when it comes in contact with its surfaces. The instability of nanoparticles can lead to oxidation or reduction of its parts also [111].

34.6 Design of an ideal nanomaterial

From the discussions, it is evident that although nanotechnology helps in altering the overall properties and achieving desired results, yet increasing use of synthesized nanomaterials has a major environmental and health risk.

Following are certain principles that need to be followed while designing any new nanomaterial for commercial purpose (Fig. 34.7).

1. Use of nonhazardous material: Use of nonhazardous material for synthesis of nanomaterial can eliminate the risk of accidental discharge to the environment or exposure. Prior toxicological tests of all the raw materials at nanoscale would enhance the risk cover.
2. Life cycle considerations: While designing any new nanomaterial, environmental emissions and health and ecological risks pertaining to the entire life cycle of nanomaterial (i.e., from raw material acquisition to end-of-life phase) should be evaluated.

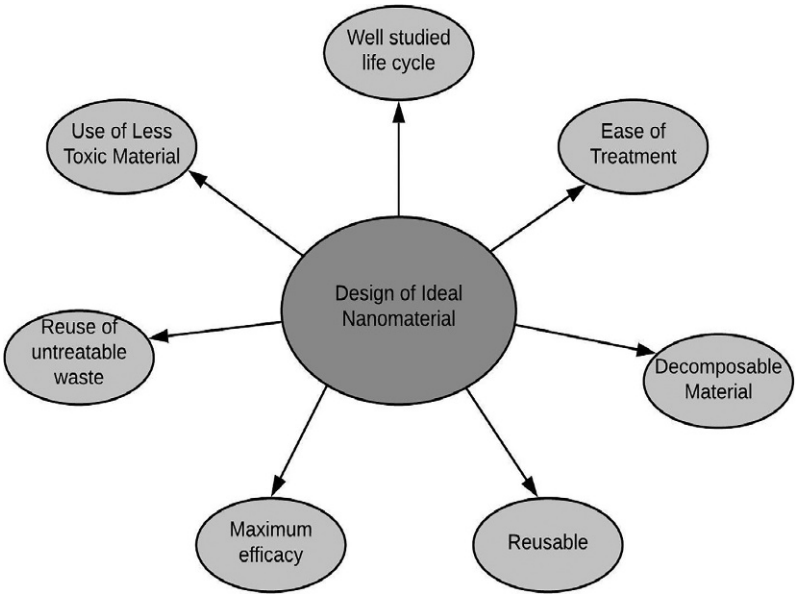

Fig. 34.7
Guiding principles of designing of an ideal INMs.

This book belongs to Badji Mokhtar Annaba University Central Library
Copyright Elsevier 2025

3. Ease of removal and treatment of waste: The wastes generated during the synthesis and use phase of synthesized nanomaterial should be easily removed (using basic process like coagulation) and treated to nullify the toxic effects of ecology and mankind.
4. Use of energy-efficient pathways for synthesis of nanomaterials: Optimum use of energy and materials for maximum output. Increasing selectivity and conversion by removing the products instead of using excess of raw material. Finding different sources of energy transfer (like ultrasound sonication and microwave) to facilitate increased selectivity.
5. Manufacturing of tailor-made nanomaterials that decompose or disintegrate to its inert form after their intended application.
6. Maximizing the efficacy of the nanomaterial, enabling lower dosage for intended applications.
7. Designing of the processes to reuse the "untreatable" waste: Along with the reduction of waste generated during the synthesis and use phase of nanomaterials, development of process pathways to reuse the untreatable waste without getting exposed.

34.7 Conclusion

The chapter aims at reviewing the various health, toxicological, and environmental risks associated with INMs. Several areas of applications for INMs are discussed along with toxicity studies. It is realized that with increase in the production of INMs, it has become necessary in identifying the health, environmental, and toxicological impacts. The chapter also addresses various risks and removal methods for INMs from waste waters. Major challenges in achieving a more sustainable nanotechnology or sustainable INMs include framework development for evaluation of the exposure of INMs in air and water, toxicity evaluation of INMs, and evaluation of health and environmental impacts of INMs over the entire life cycle. Other aspects that should be considered during designing of INMs is based on the associated impacts of production and use of INMs.

References

[1] V.L. Colvin, The potential environmental impact of engineered nanomaterials, Nat. Biotechnol. 21 (2003) 1166–1170.
[2] S.J. Klaine, A.A. Koelmans, N. Horne, S. Carley, R.D. Handy, L. Kapustka, Paradigms to assess the environmental impact of manufactured nanomaterials, Environ. Toxicol. Chem. 31 (2012) 3–14, https://doi.org/10.1002/etc.733.
[3] M.J. Gallagher, C. Allen, J.T. Buchman, T.A. Qiu, P.L. Clement, M.O.P. Krause, L.M. Gilbertson, Research highlights: applications of life-cycle assessment as a tool for characterizing environmental impacts of engineered nanomaterials, Environ. Sci. Nano 4 (2017) 276–281, https://doi.org/10.1039/C7EN90005H.
[4] J. Lee, S. Mahendra, P.J.J. Alvarez, Nanomaterials in the construction industry : a review of their applications, Am. Chem. Soc. 4 (2010) 3580–3590.
[5] S.N. Joglekar, A.P. Tandulje, S.A. Mandavgane, B.D. Kulkarni, Environmental impact study of bagasse valorization routes, Waste Biomass Valoriz. 10 (2019) 2067–2078.

This book belongs to Badji Mokhtar Annaba University Central Library Copyright Elsevier 2025

[6] A.D. Maynard, Nanotechnology: assessing the risks, Nano Today 1 (2006) 22–33, https://doi.org/10.1016/S1748-0132(06)70045-7.
[7] V.W. Hoyt, E. Mason, Nanotechnology: emerging health issues, J. Chem. Health Safety 15 (2008) 10–15.
[8] S.M. Amini, M. Gilaki, Safety of nanotechnology in food industries, Electron. Physician 6 (2014) 962–968.
[9] G. Oberdörster, E. Oberdörster, J. Oberdörster, Review nanotoxicology : an emerging discipline evolving from studies of ultrafine particles, Environ. Health Perspect. 113 (2005) 823–839, https://doi.org/10.1289/ehp.7339.
[10] M. Willander, O. Nur, Y.E. Lozovik, S.M. Al-hilli, Z. Chiragwandi, Q. Hu, Solid and soft nanostructured materials : fundamentals and applications, Microelectron. J. 36 (2005) 940–949, https://doi.org/10.1016/j.mejo.2005.04.020.
[11] S.S. Tinkle, J.M. Antonini, B.A. Rich, J.R. Roberts, R. Salmen, K. Depree, E.J. Adkins, Skin as a route of exposure and sensitization in chronic beryllium disease, Environ. Health Perspect. 111 (2003) 1202–1208, https://doi.org/10.1289/ehp.5999.
[12] J.S. Tsuji, A.D. Maynard, P.C. Howard, J.T. James, C. Lam, D.B. Warheit, A.B. Santamaria, Research strategies for safety evaluation of nanomaterials, part IV: risk assessment of nanoparticles, Toxicol. Sci. 89 (2006) 42–50.
[13] J.P. Ryman-Rasmussen, J.E. Riviere, N.A. Monteiro-Riviere, Penetration of intact skin by quantum dots with diverse physicochemical properties, Toxicol. Sci. 91 (2006) 159–165.
[14] G. Oberdörster, R.M. Celein, J. Ferin, B. Weiss, Association of particulate air pollution and acute mortality: involvement of ultrafine particles? Inhal. Toxicol. 7 (1995) 111–124.
[15] N. Li, C. Sioutas, A. Cho, D. Schmitz, C. Misra, J. Sempf, Ultrafine particulate pollutants induce oxidative stress and mitochondrial title damage, Environ. Health Perspect. 111 (2003) 455–460, https://doi.org/10.1289/ehp.6000.
[16] C. Buzea, Nanomaterials and nanoparticles: sources and toxicity, Biointerphases 2 (2007) 17–71, https://doi.org/10.1116/1.2815690.
[17] H.F. Krug, P. Wick, Nanotoxicology: an interdisciplinary challenge, Angew. Chem. Int. Ed. 50 (2011) 1260–1278.
[18] F. Piccinno, F. Gottschalk, Industrial production quantities and uses of ten engineered nanomaterials in Europe and the world, J. Nanopart. Res. 14 (2012), https://doi.org/10.1007/s11051-012-1109-9.
[19] D.R. Boverhof, R.M. David, Nanomaterial characterization : considerations and needs for hazard assessment and safety evaluation, Anal. Bioanal. Chem. (2010) 953–961, https://doi.org/10.1007/s00216-009-3103-3.
[20] I. Hsiao, Y. Huang, Science of the total environment effects of various physicochemical characteristics on the toxicities of ZnO and TiO_2 nanoparticles toward human lung epithelial cells, Sci. Total Environ. 409 (2011) 1219–1228, https://doi.org/10.1016/j.scitotenv.2010.12.033.
[21] F. Auclair, P. Baudot, D. Beiler, J. Limasset, Minor and fatal complications due to treating polytetrafluoroethylene in an industrial environment: clinical observations and physicochemical measurement of the polluted atmosphere, Toxicol. Eur. Res. 5 (1983) 43–48.
[22] M. Goldstein, H. Weiss, K. Wade, J. Penek, L. Andrews, P. Brandt-Rauf, An outbreak of fume fever in an electronics instrument testing laboratory, J. Occup. Med. 29 (1987) 746–749.
[23] W. MacNee, K. Donaldson, Mechanism of lung injury caused by PM10 and ultrafine particles with special reference to COPD, Eur. Respir. J. 40 (2003) 47–51.
[24] P. Jani, G.W. Halbert, J. Langridge, A.T. Florence, Nanoparticle uptake by the rat gastrointestinal mucosa: quantitation and particle size dependency, J. Pharm. Pharmacol. 42 (1990) 821–826.
[25] P. Jani, A. Florence, T. Nomura, F. Yamashita, Y. Takakura, M. Hashida, Biliary excretion of polystyrene microspheres with covalently linked FITC fluorescence after oral and parenteral administration to male Wistar rats, J. Drug Target. 4 (1996) 87–93.
[26] L. Renwick, D. Brown, A. Clouter, K. Donaldson, Increased inflammation and altered macrophage chemotactic responses caused by two ultrafine particle types, Occup. Eniron. Med. (2004) 442–448, https://doi.org/10.1136/oem.2003.008227.

This book belongs to Badji Mokhtar Annaba University Central Library Copyright Elsevier 2025

[27] D.R. Boverhof, R.M. David, Nanomaterial characterization: considerations and needs for hazard assessment and safety evaluation, Anal. Bioanal. Chem. (2015), https://doi.org/10.1007/s00216-009-3103-3.
[28] R.C. Murdock, L. Braydich-Stolle, A.M. Schrand, J.J. Schlager, S.M. Hussain, M.E.T. Al, Characterization of nanomaterial dispersion in solution prior to in vitro exposure using dynamic light scattering technique, Toxicol. Sci. 101 (2008) 239–253, https://doi.org/10.1093/toxsci/kfm240.
[29] M. Ahamed, M. Karns, M. Goodson, J. Rowe, S.M. Hussain, J.J. Schlager, Y. Hong, DNA damage response to different surface chemistry of silver nanoparticles in mammalian cells, Toxicol. Appl. Pharmacol. 233 (2008) 404–410, https://doi.org/10.1016/j.taap.2008.09.015.
[30] S. Lanone, J. Boczkowski, Biomedical applications and potential health risks of nanomaterials : molecular mechanisms, Curr. Mol. Med. 6 (2006) 651–663.
[31] T. Stoeger, C. Reinhard, S. Takenaka, A. Schroeppel, E. Karg, B. Ritter, J. Heyder, H. Schulz, Instillation of six different ultrafine carbon particles indicates a surface area threshold dose for acute lung inflammation in mice, Environ. Health Perspect. (2006) 328–334, https://doi.org/10.1289/ehp.8266.
[32] G. Oberdörster, J. Finkelstein, C. Johnston, R. Gelein, C. Cox, R. Baggs, A. Elder, Acute pulmonary effects of ultrafine particles in rats and mice, Res. Rep. Health Eff. Inst. 96 (2000) 5–74.
[33] D.M. Brown, M.R. Wilson, W. Macnee, V. Stone, K. Donaldson, Size-dependent proinflammatory effects of ultrafine polystyrene particles: a role for surface area and oxidative stress in the enhanced activity of ultrafines, Toxicol. Appl. Pharmacol. 175 (2001) 191–199, https://doi.org/10.1006/taap.2001.9240.
[34] K. Driscoll, J. Carter, B. Howard, D. Hassesnbein, D. Pepelko, R. Baggs, G. Oberdörster, Pulmonary inflammatory, chemokine, and mutagenic responses in rats after subchronic inhalation of carbon black, Toxicol. Appl. Pharmacol. 136 (1996) 372–380.
[35] C.L. Tran, D. Buchanan, R.T. Cullen, A. Searl, A.D. Jones, Inhalation of poorly soluble particles. II. Influence of particle surface area on inflammation and clearance, Inhal. Toxicol. 12 (2000) 1113–1126.
[36] M. Auffan, J. Rose, J. Bottero, G.V. Lowry, J. Jolivet, M.R. Wiesner, Towards a definition of inorganic nanoparticles from an environmental, health and safety perspective, Nat. Nanotechnol. 4 (2009) 634–641, https://doi.org/10.1038/nnano.2009.242.
[37] S. Wang, W. Lu, O. Tovmachenko, U.S. Rai, H. Yu, P.C. Ray, Challenge in understanding size and shape dependent toxicity of gold nanomaterials in human skin keratinocytes, Chem. Phys. Lett. 463 (2008) 145–149, https://doi.org/10.1016/j.cplett.2008.08.039.
[38] E. Park, J. Choi, Y. Park, K. Park, Oxidative stress induced by cerium oxide nanoparticles in cultured BEAS-2B cells, Toxicology 245 (2008) 90–100, https://doi.org/10.1016/j.tox.2007.12.022.
[39] A.M. Defus, W.C.W. Chan, S.N. Bhatia, Probing the cytotoxicity of semiconductor quantum dots, Am. Chem. Soc. 4 (2004) 11–18.
[40] D.B. Warheit, K.L. Reed, T.R. Webb, Pulmonary toxicity studies in rats with triethoxyoctylsilane (otes)-coated, pigment-grade titanium dioxide particles: bridging studies to predict inhalation hazard, Exp. Lung Res. (2003) 593–606, https://doi.org/10.1080/01902140390240104.
[41] B. Wang, W. Feng, M. Wang, T. Wang, Y. Gu, M. Zhu, H. Ouyang, J. Shi, F. Zhang, Y. Zhao, Z. Chai, Acute toxicological impact of nano- and submicro-scaled zinc oxide powder on healthy adult mice, J. Nanopart. Res. 10 (2008) 263–276, https://doi.org/10.1007/s11051-007-9245-3.
[42] J. Jiang, G. Oberdörster, P. Biswas, Characterization of size, surface charge, and agglomeration state of nanoparticle dispersions for toxicological studies, J. Nanopart. Res. 11 (2009) 77–89, https://doi.org/10.1007/s11051-008-9446-4.
[43] T.M. Sager, D.W. Porter, V.A. Robinson, G. William, D.E. Schwegler-Berry, V. Castranova, Improved method to disperse nanoparticles for in vitro and in vivo investigation of toxicity, Nanotoxicology 1 (2015) 118–129, https://doi.org/10.1080/17435390701381596.
[44] M.C. Buford, R.F. Hamilton, A. Holian, A comparison of dispersing media for various engineered carbon, Part. Fibre Toxicol. 4 (2007) 1–9, https://doi.org/10.1186/1743-8977-4-6.
[45] V.H. Grassian, P.T.O. Shaughnessy, A. Adamcakova-Dodd, J.M. Pettibone, P.S. Thorne, Inhalation exposure study of titanium dioxide nanoparticles with a primary particle size of 2 to 5 nm, Environ. Health Perspect. 115 (2007) 397–402, https://doi.org/10.1289/ehp.9469.

This book belongs to Badji Mokhtar Annaba University Central Library Copyright Elsevier 2025

[46] H. Greim, P. Borm, R. Schins, K. Donaldson, K. Driscoll, A. Hartwig, G. Oberdörster, G. Speit, P. Borm, R. Schins, K. Donaldson, K. Driscoll, A. Hartwig, Toxicity of fibers and particles? Report of the workshop held in Munich, Germany, 26–27 October 2000, Inhal. Toxicol. 13 (2008), https://doi.org/10.1080/08958370118273.
[47] M. Watanabe, M. Okada, Differences in the effects of fibrous and particulate titanium dioxide on alveolar macrophages of of Fischer 344 rats, J. Toxicol. Environ. Health A (2014) 1047–1060, https://doi.org/10.1080/152873902760125219.
[48] B.D. Chithrani, W.C.W. Chan, Elucidating the mechanism of cellular uptake and removal of protein-coated gold nanoparticles of different sizes and shapes, Nano Lett. 7 (2007) 1542–1550, https://doi.org/10.1021/nl070363y.
[49] A.A. Keller, S. McFerran, A. Lazareva, S. Suh, Global life cycle releases of engineered nanomaterials, J. Nanopart. Res. (2013), https://doi.org/10.1007/s11051-013-1692-4.
[50] F. Gottschalk, B. Nowack, The release of engineered nanomaterials to the environment, J. Environ. Monit. (2011) 1145–1155, https://doi.org/10.1039/c0em00547a.
[51] B. Viswanath, S. Kim, Influence of nanotoxicity on human health and environment: the alternative strategies, Rev. Environ. Contam. Toxicol. 242 (2016) 61–104.
[52] M.M. Shafer, J.T. Overdier, D.E. Armstong, Removal, partitioning, and fate of silver and other metals in wastewater treatment plants and effluent-receiving streams, Environ. Toxicol. Chem. 17 (2009) 630–641.
[53] N. Muller, B. Nowack, Exposure modeling of engineered nanoparticles in the environment, Environ. Sci. Technol. 41 (2008) 4447–4453.
[54] D.H.M.A. Kiser, P. Westerhoff, Y. Wang, J. Prerez-Rivera, Titanium nanomaterial removal and release from wastewater treatment plants, Environ. Sci. Technol. 43 (2009) 6757–6763.
[55] United Nations, Municipal Waste Treatment, United Nations Statistics Division, 2011.
[56] DEFRA, Sewage Treatment in the UK, Department for Environment, Food and Rural Affairs, London, UK, 2002.
[57] J.M. Peckenham, The use of biosolids in Maine: a review, Biosolids White Paper(2005).
[58] D. Rejeski, Project on Emerging Nanotechnologies, Woodrow Wilson International Center for Scholars, 2006, pp. 1–26.
[59] F. Gottschalk, T. Sun, B. Nowack, Environmental concentrations of engineered nanomaterials: review of modeling and analytical studies, Environ. Pollut. 181 (2013) 287–300, https://doi.org/10.1016/j.envpol.2013.06.003.
[60] A.A. Keller, A. Lazareva, Predicted releases of engineered nanomaterials: from global to regional to local, Environ. Sci. Technol. Lett. 1 (2014) 65–70.
[61] T.Y. Sun, F. Gottschalk, K. Hungerbühler, B. Nowack, Comprehensive probabilistic modelling of environmental emissions of engineered nanomaterials, Environ. Pollut. 185 (2014) 69–76, https://doi.org/10.1016/j.envpol.2013.10.004.
[62] R. Kaegi, A. Ulrich, B. Sinnet, R. Vonbank, A. Wichser, S. Zuleeg, H. Simmler, S. Brunner, H. Vonmont, M. Burkhardt, M. Boller, Synthetic TiO_2 nanoparticle emission from exterior facades into the aquatic environment, Environ. Pollut. 156 (2008) 233–239, https://doi.org/10.1016/j.envpol.2008.08.004.
[63] T.J. Brunner, P. Wick, A. Bruinink, In vitro cytotoxicity of oxide nanoparticles: comparison to asbestos, silica, and the effect of particle solubility, Environ. Sci. Technol. 40 (2006) 4374–4381.
[64] B.H. Normark, S. Normark, Evolution and spread of antibiotic resistance, J. Intern. Med. 252 (2002) 91–106.
[65] M. Lundborg, A. Johansson, L. La, Ingested aggregates of ultrafine carbon particles and interferon-impair rat alveolar macrophage function, Environ. Res. 81 (1999) 309–315.
[66] M. Lundborg, U. Johard, L. La, Human alveolar macrophage phagocytic function is impaired by aggregates of ultrafine carbon particles, Environ. Res. 253 (2001) 244–253, https://doi.org/10.1006/enrs.2001.4269.
[67] Y. Liu, M. Tourbin, S. Lachaize, P. Guiraud, Nanoparticles in wastewaters: hazards, fate and remediation, Powder Technol. 255 (2014) 149–156, https://doi.org/10.1016/j.powtec.2013.08.025.
[68] M.C. Powell, M.S. Kanarek, Nanomaterial health effects—part 2 : uncertainties and recommendations for the future, Wis. Med. J. 105 (2006) 18–23.

This book belongs to Badji Mokhtar Annaba University Central Library
Copyright Elsevier 2025

[69] D.B. Warheit, B.R. Laurence, K.L. Reed, D.H. Roach, G.A.M. Reynolds, T.R. Webb, Comparative pulmonary toxicity assessment of single-wall carbon nanotubes in rats, Toxicol. Sci. 77 (2004) 117–125, https://doi.org/10.1093/toxsci/kfg228.

[70] C. Lam, J.T. James, R. Mccluskey, R.L. Hunter, Pulmonary toxicity of single-wall carbon nanotubes in mice 7 and 90 days after intratracheal instillation, Toxicol. Sci. 77 (2003) 126–134, https://doi.org/10.1093/toxsci/kfg243.

[71] J. Muller, N. Moreau, P. Misson, M. Delos, M. Arras, A. Fonseca, J.B. Nagy, D. Lison, Respiratory toxicity of multi-wall carbon nanotubes, Toxicol. Appl. Pharmacol. 207 (2005) 221–231, https://doi.org/10.1016/j.taap.2005.01.008.

[72] R. Hardman, Review: A toxicologic review of quantum dots: toxicity depends on physicochemical and environmental factors, Environ. Health Perspect. 114 (2006) 165–172, https://doi.org/10.1289/ehp.8284.

[73] Y. Chen, J. Chen, J. Dong, Y. Jin, Comparing study of the effect of nanosized silicon dioxide and microsized silicon dioxide on fibrogenesis in rats, Toxicol. Ind. Health 20 (2004) 20–27, https://doi.org/10.1191/0748233704th190oa.

[74] B. Rehn, F. Seiler, S. Rehn, J. Bruch, M. Maier, Investigations on the inflammatory and genotoxic lung effects of two types of titanium dioxide: untreated and surface treated, Toxicol. Appl. Pharmacol. 189 (189) (2003) 84–95, https://doi.org/10.1016/S0041-008X(03)00092-9.

[75] C. Wei, W. Lin, Z. Zaina, N.E. Williams, K. Zhu, A.P. Krurlc, R.L. Smith, K. Rajeshwar, Bactericidal activity of TiO_2 photocatalyst in aqueous media: toward a solar-assisted water disinfection system, Environ. Sci. Technol. 28 (1994) 934–938.

[76] T. Gordon, L.C. Chen, J.M. Fine, R.B. Schlesinger, W.Y. Su, T.A. Kimmel, M.O. Amdur, T. Gordon, L.C. Chen, J.M. Fine, R.B. Schlesinger, Pulmonary effects of inhaled zinc oxide in human subjects, guinea pigs, rats, and rabbits, Am. Ind. Hyg. Assoc. J. 8894 (1992) 503–509, https://doi.org/10.1080/15298669291360030.

[77] J. Sawai, A. Hashimoto, K. Takao, H. Igarashi, M. Shimizu, Effect of ceramic powder slurry on spores of Bacillus subtils, J. Chem. Eng. Japan 28 (1995) 556–561.

[78] L.K. Limbach, Y. Li, M.A. Hintermann, M. Muller, D. Gunther, Oxide nanoparticle uptake in human lung fibroblasts: effects of particle size, agglomeration, and diffusion at low concentrations, Environ. Health Perspect. 39 (2005) 9370–9376.

[79] G. Libralato, D. Minetto, S. Totaro, I. Mi, E. Sabbioni, A. Marcomini, A. Volpi, Embryotoxicity of TiO_2 nanoparticles to *Mytilus galloprovincialis* (Lmk), Mar. Environ. Res. 92 (2013) 71–78.

[80] C.O. Robichaud, Relative risk analysis of several manufactured nanomaterials: an insurance industry context, Environ. Sci. Technol. 39 (2005) 8985–8994.

[81] B. Nowack, T.D. Bucheli, Occurrence, behavior and effects of nanoparticles in the environment, Environ. Pollut. 150 (2007) 5–22, https://doi.org/10.1016/j.envpol.2007.06.006.

[82] G. Bystrzejewska-piotrowska, J. Golimowski, P.L. Urban, Nanoparticles: their potential toxicity, waste and environmental management, Waste Manage. 29 (2009) 2587–2595, https://doi.org/10.1016/j.wasman.2009.04.001.

[83] S.H. Chuang, T.C. Chang, C.F. Ouyang, J.M. Leu, Colloidal silica removal in coagulation processes for wastewater reuse in a high-tech industrial park, Water Sci. Technol. (2007), https://doi.org/10.2166/wst.2007.054.

[84] C.L. Lai, S.H. Lin, Electrocoagulation of chemical mechanical polishing (CMP) wastewater from semiconductor fabrication, Chem. Eng. J. 95 (2003) 205–211, https://doi.org/10.1016/S1385-8947(03)00106-2.

[85] C.Y. Lien, J.C. Liu, Treatment of polishing wastewater from semiconductor manufacturer by dispersed air flotation, J. Environ. Eng. 132 (2006) 51–57.

[86] J. Tsai, M. Kumar, S. Chen, J. Lin, Nano-bubble flotation technology with coagulation process for the cost-effective treatment of chemical mechanical polishing wastewater, Sep. Purif. Technol. 58 (2007) 61–67, https://doi.org/10.1016/j.seppur.2007.07.022.

This book belongs to Badji Mokhtar Annaba University Central Library

Copyright Elsevier 2025

[87] Z. Zhong, W. Li, W. Xing, N. Xu, Crossflow filtration of nanosized catalysts suspension using ceramic membranes, Sep. Purif. Technol. 76 (2011) 223–230, https://doi.org/10.1016/j.seppur.2010.08.005.
[88] K.D. Pickering, Photochemistry and Environmental Applications of Water-Soluble Fullerene Compounds, PhD Dissertation, Rice University, 2005.
[89] N. Wu, Y. Wyart, Y. Liu, J. Rose, An overview of solid/liquid separation methods and size fractionation techniques for engineered nanomaterials in aquatic environment, Environ. Technol. (2013) 37–41, https://doi.org/10.1080/09593330.2013.788073.
[90] C. Ogilvie, A.R. Badireddy, E. Casman, M.R. Wiesner, Modeling nanomaterial fate in wastewater treatment: Monte Carlo simulation of silver nanoparticles (nano-Ag), Sci. Total Environ. 449 (2013) 418–425, https://doi.org/10.1016/j.scitotenv.2013.01.078.
[91] S.W. Leung, B. Williams, K. De Jesus, J.C.K. Lai, Critical review of removal of nano materials in waste streams, in: 3rd International Conference on Advances in Environment Research, vol. 68, 2017, 012019.
[92] X. He, H. Hwang, Nanotechnology in food science : functionality, applicability, and safety assessment, J. Food Drug Anal. (2016) 1–11, https://doi.org/10.1016/j.jfda.2016.06.001.
[93] H. Wu, J. Yin, W.G. Wamer, M. Zeng, Y.M. Lo, Reactive oxygen species-related activities of nano-iron metal and nano-iron oxides 5, J. Food Drug Anal. 22 (2014) 86–94, https://doi.org/10.1016/j.jfda.2014.01.007.
[94] P.P. Fu, Q. Xia, H. Hwang, P.C. Ray, Mechanisms of nanotoxicity: generation of reactive oxygen species, J. Food Drug Anal. 22 (2014) 64–75, https://doi.org/10.1016/j.jfda.2014.01.005.
[95] A. Properties, A.A. Becaro, F.C. Puti, D.S. Correa, E.C. Paris, J.M. Marconcini, M.D. Ferreira, Polyethylene films containing silver nanoparticles for applications in food packaging: characterization of physico-chemical and anti-microbial properties, J. Nanosci. Nanotechnol. 15 (2015) 2148–2156, https://doi.org/10.1166/jnn.2015.9721.
[96] F. Beigmohammadi, S.H. Peighambardoust, J. Hesari, S. Azadmard-damirchi, S.J. Peighambardoust, N. K. Khosrowshahi, Antibacterial properties of LDPE nanocomposite films in packaging of UF cheese, LWT – Food Sci. Technol. (2015), https://doi.org/10.1016/j.lwt.2015.07.059.
[97] C. Carlson, S.M. Hussain, A.M. Schrand, K.L. Hess, R.L. Jones, J.J. Schlager, Unique cellular interaction of silver nanoparticles: size-dependent generation of reactive oxygen species, J. Phys. Chem. 112 (2008) 13608–13619.
[98] H.-S. Kwak, Overview of nano- and microencapsulation for foods, in: Nano- and Microencapsulation for Foods, John Wiley & Sons, Hoboken, NJ, 2014, pp. 1–14.
[99] P.J.A. Borm, D. Robbins, S. Haubold, T. Kuhlbusch, H. Fissan, K. Donaldson, R. Schins, V. Stone, W. Kreyling, J. Lademann, J. Krutmann, D. Warheit, E. Oberdorster, The potential risks of nanomaterials: a review carried out for ECETOC, Part. Fibre Toxicol. 3 (2006) 1–35, https://doi.org/10.1186/1743-8977-3-11.
[100] J.K. Momin, C. Jayakumar, J.B. Prajapati, Potential of nanotechnology in functional foods, Emir. J. Food Agric. 25 (2013) 10–19, https://doi.org/10.9755/ejfa.v25i1.9368.
[101] C. Silvestre, D. Duraccio, S. Cimmino, Progress in polymer science food packaging based on polymer nanomaterials, Prog. Polym. Sci. 36 (2011) 1766–1782, https://doi.org/10.1016/j.progpolymsci.2011.02.003.
[102] R. Asmatulu, P. Nguyen, E. Asmatulu, Nanotechnology safety in the automotive industry, in: Nanotechnology Safety, first ed., Elsevier B.V., 2013, pp. 57–72, https://doi.org/10.1016/B978-0-444-59438-9.00005-9
[103] R. Asmatulu, E. Asmatulu, A. Yourdkhani, Toxicity of nanomaterials and recent developments in the protection, in: SAMPE Fall Technical Conference, Wichita, KS, 2009.
[104] R. Asmatulu, E. Asmatulu, A. Yourdkhani, Importance of nanosafety in engineering education, in: ASEE Midwest Conference, Lincoln, NB, 2009.
[105] R. Asmatulu, G.A. Mahmud, C. Hille, H.E. Misak, Progress in organic coatings effects of UV degradation on surface hydrophobicity, crack, and thickness of MWCNT-based nanocomposite coatings, Prog. Org. Coat. 72 (2011) 553–561, https://doi.org/10.1016/j.porgcoat.2011.06.015.
[106] R. Asmatulu, R.O. Claus, J.B. Mecham, S.G. Corcoran, Nanotechnology-associated coatings for aircrafts, Mater. Sci. 43 (2007) 103–108.

This book belongs to Badji Mokhtar Annaba University Central Library Copyright Elsevier 2025

[107] D. Zaarei, A.A. Sarabi, F. Sharif, S.M. Kassiriha, Structure, properties and corrosion resistivity of polymeric nanocomposite coatings based on layered silicates, J. Coat. Technol. Res. 5 (2008) 241–249, https://doi.org/10.1007/s11998-007-9065-5.

[108] L. Ding, J. Stilwell, T. Zhang, O. Elboudwarej, H. Jiang, J.P. Selegue, P.A. Cooke, J.W. Gray, F.F. Chen, Molecular characterization of the cytotoxic mechanism of multiwall carbon nanotubes and nano-onions on human skin fibroblast, Nano Lett. 5 (2005) 2448–2464.

[109] L. Wang, D.K. Nagesha, S. Selvarasah, M.R. Dokmeci, R.L. Carrier, Toxicity of CdSe nanoparticles in Caco-2 cell cultures, J. Nanobiotechnol. 15 (2012) 1–15, https://doi.org/10.1186/1477-3155-6-11.

[110] J. Suhr, P.M. Ajayan, G.P. Mathur, Nanotechnology enabled multifunctional damping for aerospace composite structures, in: International Congress on Sound and Vibration, 2008, pp. 438–439.

[111] H. Haynes, R. Asmatulu, Nanotechnology safety in the aerospace industry, in: Nanotechnology Safety, Elsevier, 2013, pp. 85–97.

This book belongs to Badji Mokhtar Annaba University Central Library

Copyright Elsevier 2025

This page intentionally left blank

This book belongs to Badji Mokhtar Annaba University Central Library

Copyright Elsevier 2025

CHAPTER 35

A novel SnO_2/polypyrrole/SnO_2 nanocomposite modified anode with improved performance in benthic microbial fuel cell

Mohammad Imran[a], Alka Mungray[a], Suresh Kumar Kailasa[b], and Arvind Kumar Mungray[a]

[a]*Department of Chemical Engineering, Sardar Vallabhbhai National Institute of Technology, Surat, India,* [b]*Department of Applied Chemistry, Sardar Vallabhbhai National Institute of Technology, Surat, India*

35.1 Introduction

Microbial fuel cell (MFC) may be considered to be a remarkable technology for the production of energy from organic compounds like domestic or industrial wastewater, marine sediment, and human excreta [1]. MFC has a tendency of simultaneous electricity production and wastewater treatment, resulting in a wide variety of favorable applications [2]. MFC works on the principle of transformation of chemical energy of the organic wastes directly into electrical energy through the action of electroactive bacteria and hence can be considered as an ecofriendly source of energy [3]. Benthic microbial fuel cell (BMFC) can be regarded as a specific kind of MFC operating exactly on the same principle as that of MFC. However, the only difference between the two is that in the later one, the marine sediment itself acts as a source of organic substance [4]. The performance of BMFC depends on many factors such as nature of organic substrate, microbial consortia, electrode materials, external and internal resistances, and design of the reactor. The material of anode has a vital part in the generation of electricity because it governs the effectiveness of the extracellular transfer of electron and thus the formation of the biofilm on its surface [5]. Therefore, it is important to enhance the biocompatibility of the anode by modifying its surface with a suitable material for improving electricity generation.

Handbook of Nanomaterials for Wastewater Treatment. https://doi.org/10.1016/B978-0-12-821496-1.00010-6
Copyright © 2021 Elsevier Inc. All rights reserved.

This book belongs to Badji Mokhtar Annaba University Central Library Copyright Elsevier 2025

Several metal oxides are being extensively used for improving the efficiency of MFC anodes. They are usually nontoxic and possess biocompatibility. Moreover, they have high surface area and chemical stability [6]. Tin oxide (SnO_2) is of huge interest to researchers because of its distinctive chemical and physical properties besides several advantages like electrical conductivity, abundance, low cost, and chemical stability [2]. Consequently, SnO_2 has been used in various research areas like solar cells, batteries, photocatalyst, oxidation catalyst, lithium-ion batteries, capacitors, and gas sensor material [7, 8]. In addition, it has been used in the form of a catalyst to enhance oxygen reduction reaction in MFC [9]. Hashem et al. [10] observed that the composite of MnO_2 along with SnO_2 is compatible to act as a supercapacitor and results in the enhancement of electrochemical performance of Li/MnO_2 cells. The hybrid electrodes of SnO_2 with various other metal oxides such as Fe_2O_3 [11], CuO [12], and NiO [13] have been fabricated and found to give better results for the lithium-ion batteries. It has also been established that SnO_2 has higher conductivity than TiO_2 [6]. These characteristics of SnO_2 make it a suitable alternative for improving the performance of BMFC anode.

Some conducting polymers like polypyrrole (PPy) and polyaniline (PANI) are utilized as a supercapacitor electrode material for their higher capacitive behavior [14]. PPy is a conducting polymer that is used in the form of an electrode material owing to its high specific capacitance, greater electrical conductivity, low charge transfer resistance, biocompatibility, redox properties, chemical stability, easy synthesis, environmental friendliness, and nontoxicity [15, 16]. However, the poor mechanical properties make it inaccessible to be widely used for specific applications. It was acknowledged that the combination of PPy with some metal oxide changes the morphology and size of particles. This, in turn, leads to the improved physical and electrochemical performance for the composite material [4].

Consequently, various composites such as reduced graphene oxide/polypyrrole (rGO/PPy) [15], PPy/rGO/Fe_2O_3 [16], MnO_2/PPy [4], multiwalled carbon nanotube (MWCNT)/SnO_2 [5], microwave-assisted synthesized rGO/SnO_2 [6], TiO_2/PANI [17], carbon nanotubes/PANI (CNT/PANI) [18] electrochemically reduced graphene oxide/PANI (ERGNO/PANI) [19], carbon nanotube/polypyrrole (CNT/PPy) [20], Co/Al_2O_3-rGO [21], Fe_3O_4/CNT [22], MnO_2/rGO [23], CNT/MnO_2 [24], manganese cobaltite ($MnCo_2O_4$)/polypyrrole (PPy) [25], carbon nanotube blended with gold-titania (CNT/Au/TiO_2) [26], and nickel oxide/carbon nanotube/PANI (NiO/CNT/PANI) [27] have been extensively used for the modification of electrodes of MFC. Moreover, SnO_2@ PPy nanowire composite [28], SnO_2/PPy hollow spheres [29], core-shell–structured hollow SnO_2-PPy nanocomposites [30], and three-dimensional hollow SnO_2@ PPy nanotube arrays [31] have been proved to be excellent alternatives for the enhancement of performance of anodes for lithium-ion batteries. Duan et al. [2] modified the MFC anode with three-dimensional macroporous CNT-SnO_2. The modified anode was found to possess higher electrical conductivity and biocompatibility. Mehdinia et al. [6] observed that the rGO/SnO_2-modified electrode has greater specific surface area, increased conductivity, and power density. It was concluded by the work of Mehdinia et al. [5] that the glassy carbon

This book belongs to Badji Mokhtar Annaba University Central Library Copyright Elsevier 2025

electrode (GCE) modified with MWCNT/SnO_2 exhibited higher surface area, enhanced conductivity, improved biocompatibility, and excellent electrochemical performance in comparison with MWCNT/GCE and unmodified anodes. As stated in the above literatures, SnO_2 has been used along with CNT, MWCNT, and rGO for the modification of MFC anodes. However, the literature lacks the incorporation of a conducting polymer with SnO_2, which has already been used with other metal oxides as mentioned in the literatures [15–17]. Moreover, the implementation of SnO_2 in BMFC is still unavailable, which has totally different microbial consortia and environment.

In this work, different reactors were installed to incorporate the effect of SnO_2 and PPy for the modification of BMFC anode. A sandwiched coating of SnO_2/PPy/SnO_2 was applied on anode surface and compared with SnO_2/PPy and SnO_2-modified anodes. All the reactors were operated in duplicate for better accuracy of the results. The base material used for the construction of cathode and anode was carbon felt. All the modified anodes were characterized by performing scanning electron microscopy (SEM), contact angle experiment, and Fourier-transform infrared spectroscopy (FTIR). Electrochemical impedance spectroscopy (EIS), cyclic voltammogram (CV), and Tafel plots were implemented to study the electrochemical performance of the coated anodes. The power generation of the reactors containing modified anodes was matched with the reactor having unmodified cathode and anode. The objective of the modification of the anodes was to improve the power generation of BMFC.

35.2 Experimental work

35.2.1 Acid-treatment of the electrode surface

The anode was fabricated from carbon felt having a dimension of 4 cm × 4 cm, whereas the cathode was made up of the same material with a dimension of 8 cm × 8 cm. The fabricated anodes and cathodes were immersed in 35% HCl solution followed by heating at 50°C for about half an hour. The pretreatment was performed for removing the impurities from the surface of the anodes and cathodes. It was followed by washing of the electrodes with deionized (DI) water multiple times for removing the leftover acid from the surface of the electrodes. The electrodes were then kept for drying in an oven at around 50°C for 6 h before using in the reactor.

35.2.2 SnO_2 nanoparticles synthesis

The synthesis of tin oxide (SnO_2) nanoparticles was performed by using the sol-gel method as defined previously [32]. In a typical process, 100 mL high performance liquid chromatography–grade water was taken in a three-neck round bottom flask followed by addition of 5.88 g tin (IV) chloride to it. This mixture was exposed to magnetic stirring for 20

This book belongs to Badji Mokhtar Annaba University Central Library Copyright Elsevier 2025

min. To this mixture, 24 mL 3.20 M ammonia solution (25%) was added. This solution was added at a feed rate of 0.2 mL/min accompanied by continuous stirring for 2 h. Then, the obtained sol was kept for aging at ambient temperature for 24 h. The aged sol was filtered and the gel formed was then rinsed repeatedly with ethanol till the solution became neutral (having a pH value 7). Then, the gel was dried in an oven at 80°C for 24 h and the particles obtained were crushed using mortar and pestle. The powdered SnO_2 was finally calcined at 450°C for about 2 h.

35.2.3 Preparation of nanocomposites of SnO_2/PPy

The synthesis of SnO_2/PPy nanocomposites was achieved using an in situ chemical polymerization method [30]. The synthesis process consists of addition of 8 mg of sodium lauryl sulfate (SDS) to 80 mL of distilled water. Then, 0.2 g SnO_2 nanoparticles were added to this solution. Further, the solution was sonicated for 30 min followed by magnetic stirring for 3 h. A total of 51.6 μL of pyrrole monomer was added to this solution and stirred for another 1 h. Then, 22.4 mL of 0.1 M ammonium persulfate aqueous solution was added drop-wise at a flow rate of 0.1 mL/min. It resulted in the transformation of color of the suspended solution from light gray to black, which indicates the formation of PPy. The resulting black solution was then centrifuged and rinsed with ethanol and DI water multiple times. The black composites were finally vacuum dried at 90°C overnight.

35.2.4 Preparation of modified anodes

The prepared SnO_2 nanoparticles and SnO_2/PPy nanocomposites were mixed with a mixture of Nafion, isopropanol, and DI water in a ratio 0.05/1/4 (volume basis), which results in the formation of a catalyst ink. The nanocomposites were dispersed into the ink solution and sonicated for about 30 min. The catalyst loading rate for preparation of the dispersed solution to be coated on the surface of the anode was 1.25 mg/mL [33]. The extent of loading of the nanocomposites was 0.5 mg/cm^2 electrode surface [34]. The separately synthesized SnO_2 and SnO_2/PPy catalyst ink were coated on the surface of the anodes to obtain a constant film. The coating of SnO_2/PPy/SnO_2 was achieved by depositing the layers of SnO_2/PPy and SnO_2. Table 35.1 depicts the established BMFC reactors and the corresponding anode modifications.

Table 35.1: BMFC reactors and corresponding anode modifications.

Reactor	Cathode	Anode
1	Unmodified	Unmodified
2	Unmodified	Modified with SnO_2
3	Unmodified	Modified with SnO_2/PPy
4	Unmodified	Modified with SnO_2/PPy/SnO_2

This book belongs to Badji Mokhtar Annaba University Central Library
Copyright Elsevier 2025

The marine grade Ancor wire was used for all the electrical connections, and silver epoxy, which has considerably higher electrical conductivity, was used as an adhesive material.

35.2.5 Construction of BMFC reactors

The sediment and seawater collection was achieved at Dumas seashore, Surat, India, having coordinates 72° 42′ 55″ E and 21° 4′ 45″ N, respectively. The homogenization of collected fresh sediment was performed, which was followed by its use as a substrate material in the BMFC reactors. The reactors were set up in previously labeled and marked plastic containers with an equivalent volume of 1.5 L. All the reactors were 2/3rd filled with the sediment followed by placing the anodes at 1/3rd level of the sediment layer measured from the bottom. Then, the reactors were filled gradually with the seawater to fill the container completely and the plastic clamps were used to fix the cathodes into it. All the plastic containers were then kept uninterrupted in an 80 cm × 55 cm × 40 cm crate and supervised regularly. A power management system was established for the measurement of voltage and current. The open circuit potential (OCP) was allowed to attain a constant value followed by connecting the identical resistors for measuring the current values thereafter. The graph showing the polarization behavior was plotted on the 8th day after the reactors were installed. The voltage and current were measured manually with the help of a digital multimeter. The seawater in the crate was replaced at an interval of 10 days from establishing of the reactors. For the maintenance of suitable conditions in the reactors, various parameters such as temperature, pH, dissolved oxygen (DO) concentration, and oxidation-reduction potential (ORP) were monitored by their corresponding probes.

35.2.6 Physical and electrochemical characterization

A SEM was obtained at 15.0 kV resolution for analyzing the surface morphology of the modified anodes. For studying the chemical bonds present in the modified anodes, FTIR was performed. The sessile drop technique was performed on a contact angle meter for the measurement of water wettability. CV was performed within a potential range of −0.8 to 0.8 V at a scan rate and sample interval of 0.05 V/s and 0.001 V, respectively. Tafel graphs were plotted at a scan rate and potential range of 0.01 V/s and −0.8 to 0.8 V, respectively. The EIS was performed at an amplitude of 0.05 V and frequency range of $1–10^4$ Hz. All the electrochemical studies were accomplished in a three-electrode system on CHI760 electrochemical analyzer. The modified anode, KCl-saturated Ag/AgCl, and the unmodified electrode were taken as working, reference, and counter electrodes, respectively, in 50 mM phosphate buffer at neutral pH value.

This book belongs to Badji Mokhtar Annaba University Central Library Copyright Elsevier 2025

35.3 Results and discussion

35.3.1 Surface characterization of modified anode

35.3.1.1 Scanning electron microscopy

The surface structure and the morphology of the anodes were analyzed by performing SEM. Fig. 35.1A–D shows the SEM pictures of the unmodified, SnO_2, SnO_2/PPy, and SnO_2/PPy/SnO_2-modified anodes, respectively. It can be observed from Fig. 35.1A that the unmodified anode surface is very smooth. In addition, it shows a cluster of soft and thin threads. Fig. 35.1B represents the surface of SnO_2-modified anodes showing that the surface is fully covered with the tin oxide nanoparticles having an average particle size of around 100 nm. Moreover, it depicts that the surface is fully covered with the nanoparticles with nearly whole carbon felt unexposed to the surface. It can also be visualized that the surface of SnO_2-modified anode is more rough than the unmodified. As seen in Fig. 35.1C, the particle size of SnO_2/PPy-modified

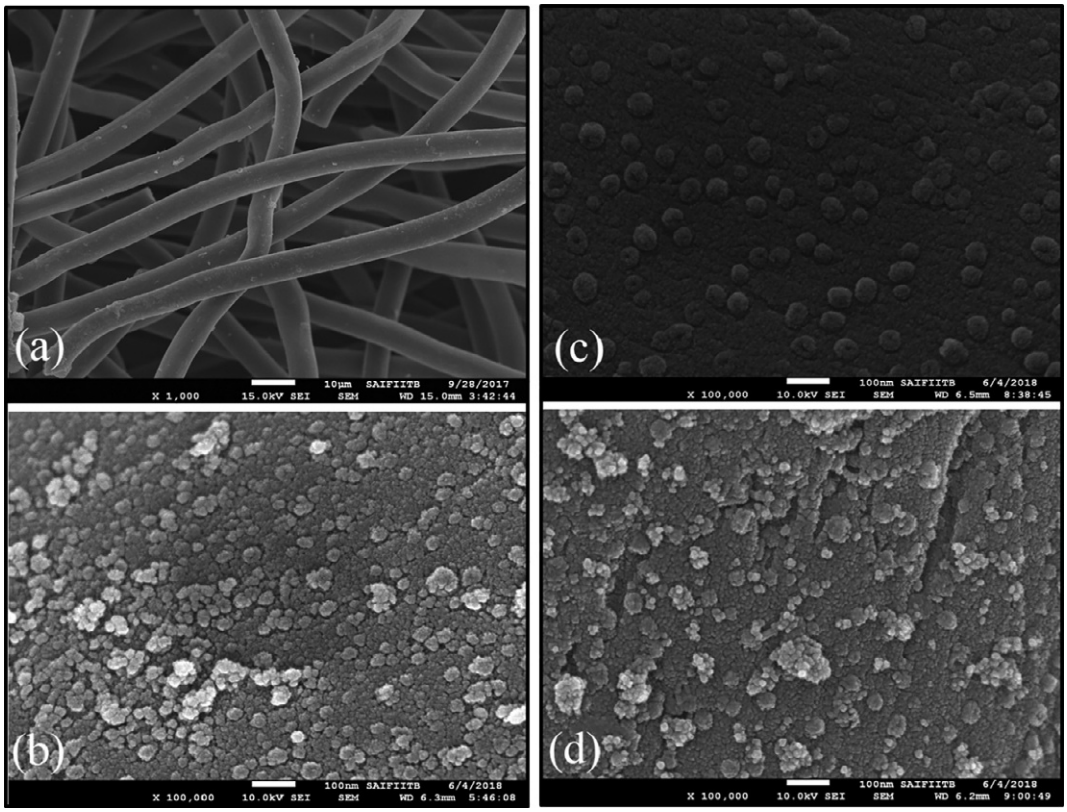

Fig. 35.1
SEM images of (A) unmodified, (B) SnO_2 coated, (C) SnO_2/PPy coated, and (D) SnO_2/PPy/SnO_2 coated anodes.

This book belongs to Badji Mokhtar Annaba University Central Library
Copyright Elsevier 2025

anode is a little bit larger due to the polymerization of pyrrole monomer. It can be visualized that the SnO_2 nanoparticles are entrapped in the PPy aggregation. The surface of the SnO_2/PPy/SnO_2-sandwiched modified anode is much similar to the SnO_2-modified anode because the external layer in the SnO_2/PPy/SnO_2 coating is of SnO_2 nanoparticles.

35.3.1.2 Fourier-transform infrared spectroscopy

Fig. 35.2A–C displays the attenuated total reflection-FTIR spectra of the unmodified, SnO_2-coated, and SnO_2/PPy-coated anodes, respectively. A characteristic peak at 1648 cm^{-1} was detected in the spectrum of the unmodified anode as shown in Fig. 35.2A. This peak can be assigned to the OH stretching vibrations of the water molecule present on the surface of the anode [35]. The peak detected at 1628 cm^{-1} in the SnO_2-coated anode is exhibited by the bending vibration of water molecules [35]. A supplementary peak was detected at 621 cm^{-1} in the SnO_2-coated anode owing to the stretching vibrations of the Sn—O—Sn bond [36]. The stretching vibrations of the terminal Sn—OH bond lead to a peak at 492 cm^{-1} as supported by the previous literatures [36–38]. In the sample containing SnO_2/PPy coating, the peak at 614 cm^{-1} confirms the presence of SnO_2 nanoparticles in the sample [11, 39]. The characteristic bands at 1699 and 1552 cm^{-1} are exhibited by the typical C═C in the plane vibration [30]. This sample, in addition, shows a peak at 1208 cm^{-1} for the C—H and C—C ring stretching corresponding to polypyrrole [30]. The sharp peak exhibited at 1042 cm^{-1} represents the plane vibrations of C—H bond [30]. The stretching vibrations of the terminal Sn—OH bond indicate a peak at 501 cm^{-1} [36–38]. The characteristic peak at 926 cm^{-1} can be associated with the plane vibrations of N—H bond [40, 41].

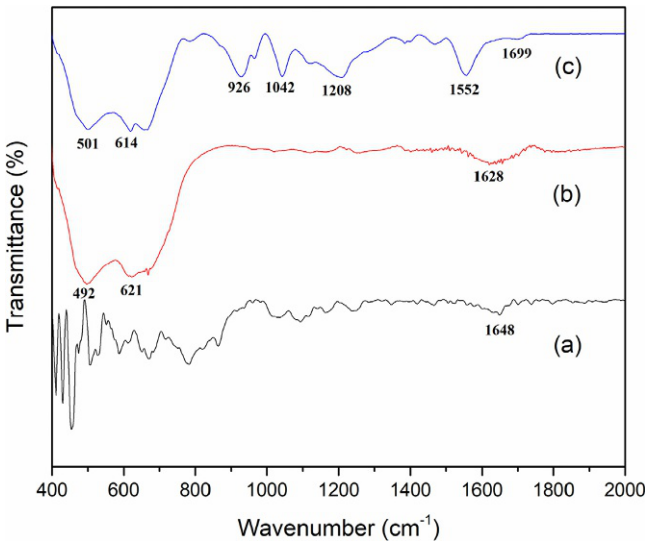

Fig. 35.2
FTIR of (A) unmodified, (B) SnO_2-coated, and (C) SnO_2/PPy-coated anodes.

This book belongs to Badji Mokhtar Annaba University Central Library Copyright Elsevier 2025

35.3.1.3 Wettability of modified anode

The wettability of the modified anode surface was studied by performing contact angle experiment by sessile drop technique [42]. The images depicting the contact angle of different types of anodes are shown in Fig. 35.3. The contact angles of SnO_2/PPy-modified and SnO_2-modified anodes were 105.95 and 124.65 degrees, respectively, which were relatively much lesser than 140.9 degrees for the unmodified anode. From the obtained results, it can be established that the modification of the anode surface through SnO_2 and SnO_2/PPy enhanced its hydrophilicity, which ensures the formation of more stable biofilm [43].

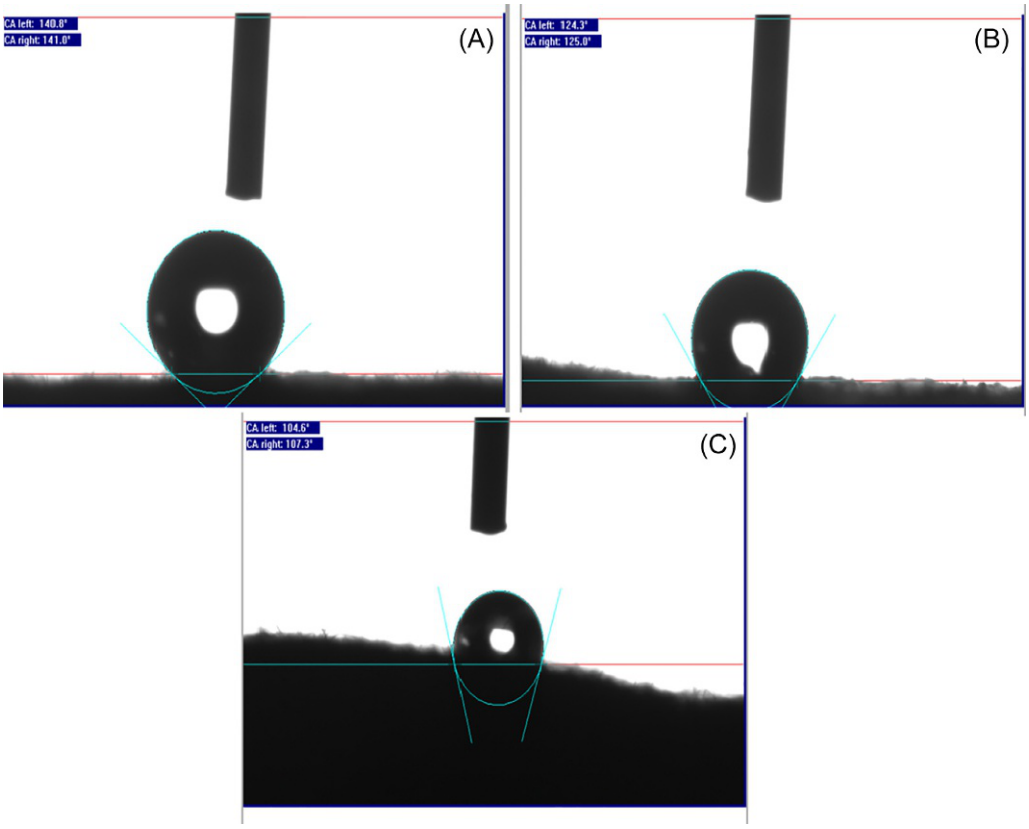

Fig. 35.3
Surface wettability of (A) unmodified, (B) SnO_2-coated, and (C) SnO_2/PPy-coated anodes.

This book belongs to Badji Mokhtar Annaba University Central Library
Copyright Elsevier 2025

35.3.2 Electrochemical analyses of the composite anode

35.3.2.1 Cyclic voltammogram

The capacitive behavior and the electron transfer process of both the unmodified and modified anodes were observed by using CV tests. The CV curves of different anodes are represented in Fig. 35.4. It is evident from Fig. 35.4 that the SnO_2/PPy composite–modified anode had the highest current, which concludes that the active surface area required for the attachment of the microbes was improved due to the implementation of the SnO_2/PPy complex [44]. The aforementioned fact was also confirmed by the contact angle experiment as previously discussed in Section 35.3.1.3. It can also be observed from Fig. 35.4 that both the SnO_2/PPy- and SnO_2-modified anodes had a higher response current compared with the unmodified one. The capacitive behavior was witnessed by calculating the charge storage capacity of the modified and unmodified anodes from the formula [45] $C = S/(2VU)$. The terms C, S, U, and V denote the capacitance of the anode, the enclosed area of the CV curve, sweeping potential range (in V), and the scan rate (in V/s), respectively. The values of the capacitance for various anodes are stated in Table 35.2. The obtained results suggest that the SnO_2/PPy composite

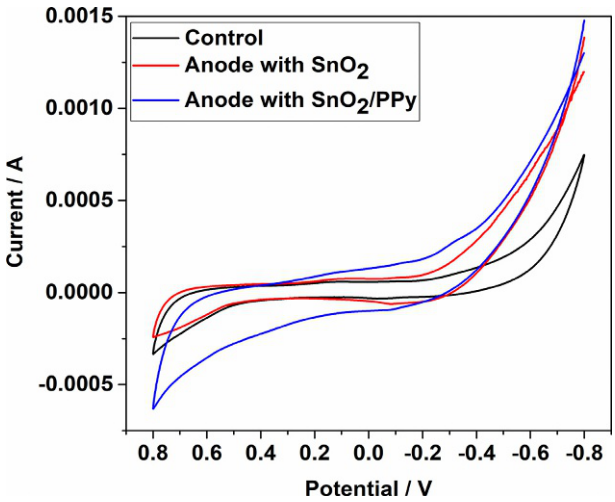

Fig. 35.4
Cyclic voltammograms of various anodes in phosphate buffer solution.

Table 35.2: Capacitance values of different anodes.

Anodes	Capacitance (F)
Unmodified	0.002305
SnO_2 modified	0.004253
SnO_2/PPy modified	0.005841

This book belongs to Badji Mokhtar Annaba University Central Library
Copyright Elsevier 2025

anode possesses the maximum capacitance, almost 2.5 times the unmodified anode. However, the capacitance value of the SnO_2-modified anode was 1.8 times higher in comparison with the unmodified anode. These results suggest that the SnO_2/PPy composite anode exhibited the best capacitive behavior among all the anodes [4].

35.3.2.2 Kinetics of the composite anode

The kinetic activity of different composite anodes in terms of direct electron transfer was studied by plotting Tafel equation. Tafel plot of different anodes was drawn by plotting logarithm of current density (log i) versus overpotential (η) as shown in Fig. 35.5 as given by the Tafel equation, $\eta = a + b^{*}\log i$. All the curves showed an augmentation of the initial steep current followed by linearization as depicted in Fig. 35.5. It is also evident from Fig. 35.5 that the initial current of SnO_2/PPy-modified anode was much higher in comparison with the SnO_2-coated and unmodified anodes. The values of exchange current density (i_0) and corresponding kinetic activity of various anodes are presented in Table 35.3. The i_0 value of SnO_2/PPy-modified anode was maximum accompanied by highest kinetic activity, almost 57 times the unmodified anode. The significance of the exchange current density (i_0) value is

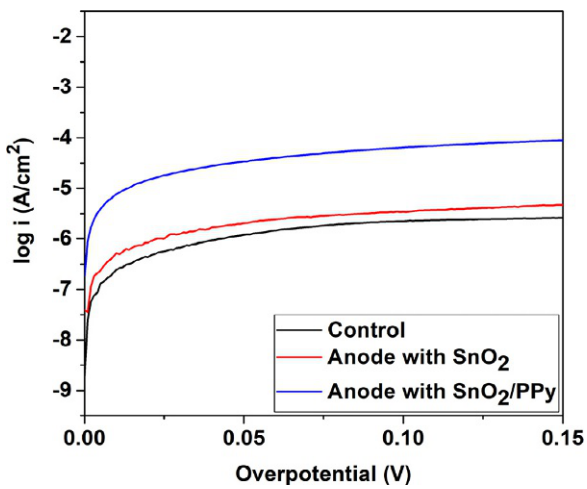

Fig. 35.5
Tafel plot of different anodes.

Table 35.3: Exchange current density of different anodes.

Anodes	Exchange current density (A/cm^2)	Kinetic activity
Unmodified	6.902×10^{-7}	1.00
SnO_2 modified	2.512×10^{-6}	3.640
SnO_2/PPy modified	3.981×10^{-5}	57.68

This book belongs to Badji Mokhtar Annaba University Central Library
Copyright Elsevier 2025

Table 35.4: Exchange current density of different nanocomposites.

Anodes	Exchange current density (A/cm^2)	Kinetic activity	References
PPy-modified anode	2.7×10^{-4}	1.588	[4]
MnO_2/PPy modified	3.6×10^{-4}	2.118	[4]
MWCNTs	3.1×10^{-5}	2.385	[42]
MnO_2 (25%)/MWCNTs	7.9×10^{-5}	6.077	[42]
MnO_2 (50%)/MWCNTs	3.2×10^{-3}	246.15	[42]
MnO_2 (75%)/MWCNTs	2.5×10^{-5}	1.923	[42]
PANI	1.84×10^{-5}	2.137	[45]
MWCNTs/PANI	3.62×10^{-5}	4.204	[45]
PANI/CC	3.68×10^{-4}	375.89	[46]
PANI/GP	2.25×10^{-6}	1.832	[46]
Fe_2O_3/PPy	4.5×10^{-4}	409.09	[47]
MnO_2/PPy	1.53×10^{-4}	139.09	[47]
MnO_2/Fe_2O_3/PPy	3×10^{-4}	272.73	[47]
Graphite powder (GP)/polyvinylidene fluoride (PVDF)	2.88×10^{-4}	1.846	[48]
GP/PVDF/CeO_2	3.34×10^{-4}	2.141	[48]

that the anode having greater value of i_0 requires less activation energy for the transfer of the electron, which results in an increased rate of electron transfer through the surface of anode to the surface of cathode. Furthermore, the increased kinetic activity can be accredited to the higher density of the biofilm formed on the surface of anode and greater conductivity of SnO_2/PPy nanocomposite. It can be inferred that the SnO_2/PPy anode has the lowest internal resistance and requires least value of the activation energy for the surface reaction having biochemical nature [4]. It has been found from the literature that various nanocomposites show enhanced kinetic activity when used for the modification of the surface anode of BMFC. The kinetic activity and exchange current density obtained for different nanocomposites are reported in Table 35.4. The variation in the results in terms of exchange current densities and kinetic activities for different nanocomposites may be attributed to the nature of the bacterial community of the sediment, material of the electrode surface, and synthesis method of the nanocomposite.

35.3.2.3 Electrochemical impedance spectroscopy

For gaining a detailed comprehension about the impact of modification of the anode surface on the electron transfer characteristics, the EIS analyses were performed. The study provides an insight about different types of resistances that are being introduced as a result of the redox reactions of the system [46]. Nyquist plot is used to represent the EIS data, which comprise of a half circle representing a high-frequency region followed by a linear portion demonstrating a low-frequency region. The coordinate at the starting point of the half circle is named as solution

This book belongs to Badji Mokhtar Annaba University Central Library Copyright Elsevier 2025

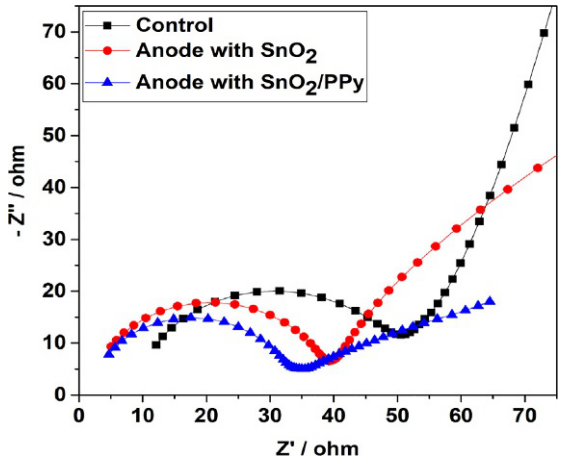

Fig. 35.6
Nyquist plots of different anodes.

Table 35.5: Rs and Rct values of modified and unmodified anodes.

Anodes	Rs (Ω)	Rct (Ω)
Unmodified	8.88	34.86
SnO_2 modified	1.37	30.79
SnO_2/PPy modified	1.24	29.26

or ohmic resistance (Rs). The charge transfer resistance (Rct) is represented by the length of the half circle [49]. Fig. 35.6 represents the impedance values of modified and the unmodified anodes. Table 35.5 lists the values of resistance for different anodes. It is evident from Table 35.5 that the SnO_2/PPy composite–modified anode had the lowest value of both Rs and Rct in comparison with the SnO_2-modified and unmodified anode. The lower values of Rct for the modified anodes infer a faster rate of oxidation of the organic matter on their surfaces [5]. It has been previously established that the attachment of bacteria on the surface of the anode can significantly decrease its overpotential [50]. Hence, the reduced Rct values are not due to the improved conductivity alone but also because of the enhanced biocompatibility [51].

35.3.3 Working of reactors containing different anodes

35.3.3.1 Physicochemical properties

The physicochemical parameters of seawater such as pH, temperature, DO, and ORP are represented in Fig. 35.7A and B. It is mandatory to monitor these parameters on a regular basis because the microbial colonies and their performance are affected largely with a very minor deflection in these values. Furthermore, the continuous assessment of these parameters helps in

This book belongs to Badji Mokhtar Annaba University Central Library Copyright Elsevier 2025

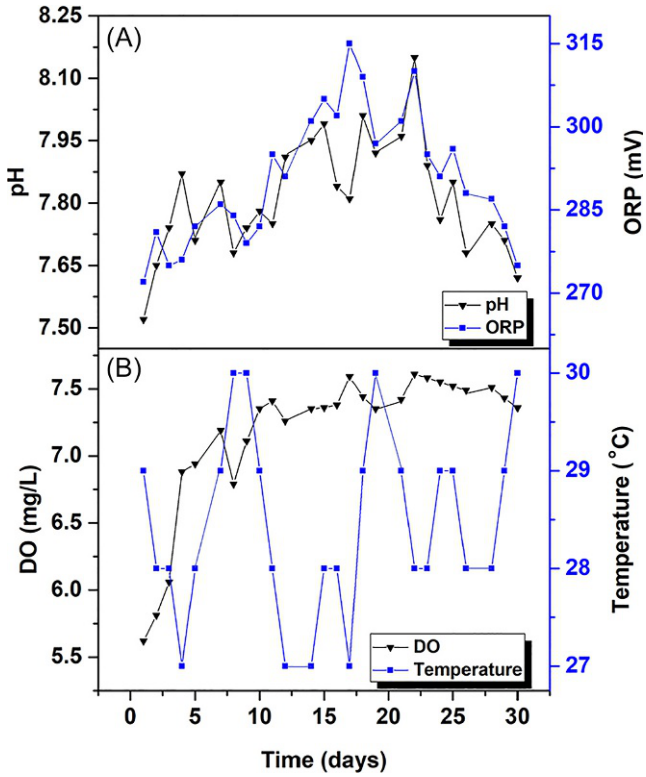

Fig. 35.7
Physicochemical properties of seawater: variation of (A) pH and ORP, and (B) DO and temperature with time.

completely replicating the marine environment. The pH value of the seawater was found to vary from 7.5 to 8.2, which was well within the range of seawater (7.5–8.4). It is apparent from Fig. 35.7B that an increment in temperature lowers the DO concentration because the tendency of water to hold the oxygen reduces with an increase in the temperature. It can also be noticed from Fig. 35.7A and B that the DO concentration and ORP are directly proportional to each other. The seawater was aerated externally by an air pump for maintaining the DO concentration.

35.3.3.2 Open circuit potential

The reactors were started in the month of May during the summer season. For an initial period, the reactors were operated in open circuit for developing an OCP. The OCP values were monitored three times daily for getting more accurate results. Fig. 35.8 shows the variation of the OCP values of all the reactors with the progress of time. Among all the reactors, anode coated with SnO_2/PPy/SnO_2-sandwiched layer attained the maximum OCP value. It was followed by the reactors having anode coated with SnO_2/PPy, anode coated with SnO_2, and the

This book belongs to Badji Mokhtar Annaba University Central Library Copyright Elsevier 2025

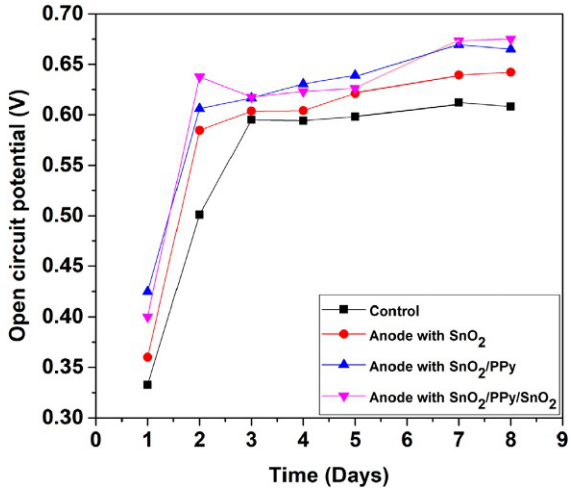

Fig. 35.8
OCP values of the reactors containing unmodified and modified anodes.

reactor with unmodified anode and cathode. After all the reactors acquired the stabilized OCP values, an identical resistance of 100 Ω was connected across them and the current values were recorded.

35.3.3.3 Power density and polarization curves

The polarization curve is plotted by observing the constant voltages generated at various external resistances, altered from 10 Ω to 47 kΩ. The calculation for generated power density was done based on the generated potentials at each resistance. The polarization and power density curves represent the graph of potentials and the power densities versus corresponding values of current densities, respectively. Fig. 35.9A and B represents the graph of generated power and voltage with respect to current density, respectively. From Fig. 35.9A, it can be observed that the reactor containing SnO_2/PPy/SnO_2 composite modified anode yielded a maximum power density of 130 mW/m^2 followed by the reactors containing SnO_2/PPy-modified anode, SnO_2-modified anode, and unmodified anode. The maximum power densities attained for these reactors were 73.09, 37.21, and 20.70 mW/m^2, respectively. The polarization curves, shown in Fig. 35.9B, follow the same order like power density curve. It can be observed that unmodified anode yielded least value of maximum power density compared with all the reactors with modified anode.

These results are consistent with the physical and electrochemical analyses discussed previously. The composite-modified anode possessed the least value of contact angle leading to the provision of the most hydrophilic surface. As the microbial adhesion increases with the hydrophilicity of the anodic surface, SnO_2/PPy/SnO_2 composite–modified anode might have achieved the maximum biocompatibility among all the reactors. The electrochemical results

This book belongs to Badji Mokhtar Annaba University Central Library Copyright Elsevier 2025

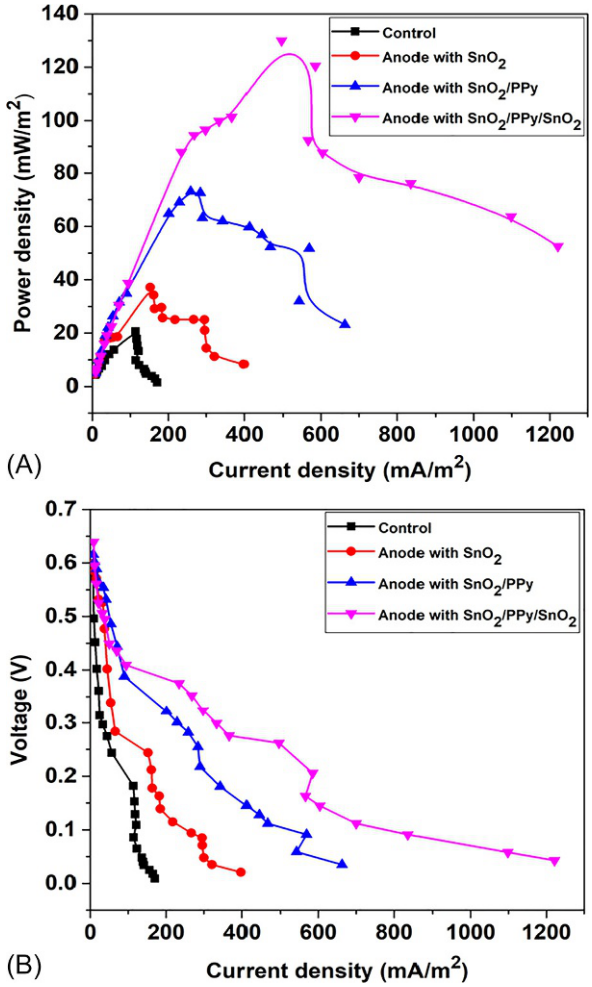

Fig. 35.9
(A) Power generation and (B) polarization behavior of the reactors containing unmodified and modified anodes.

also suggest that the SnO_2/PPy/SnO_2 composite–modified anode had the maximum kinetic activity, lower values of resistances, and better capacitive properties. The modification of the anode with SnO_2 nanoparticles increased the surface area, facilitating the enhanced bacterial adhesion on the inner side of the pores. Moreover, it helps to transport the organic substrate toward the attached microbes and efficiently transfer the electrons from the microbes to the anode surface [2]. The improved performance might be credited to the binding of SnO_2 nanoparticles and the cytochrome via Coulombic and electrostatic attractions [52]. The SnO_2/PPy modification showed a superior performance over SnO_2-modified anode on account of the capacitive behavior of polypyrrole having a property to hold the charge and release when required [16]. The composite-modified anode exhibited the excellent superior performance

This book belongs to Badji Mokhtar Annaba University Central Library Copyright Elsevier 2025

because the interlayer can reduce the resistances and enhance the electron transfer rate from microbes to the anode surface [53]. In addition, the incorporation of the PPy interlayer can assist the bacterial colonization and electron transfer. Moreover, the PPy layer improves the contact between the inner and outer layers of SnO_2 coatings, leading to the enhanced power production [53].

35.4 Conclusion

In this work, different anodes modified with SnO_2, SnO_2/PPy, and SnO_2/PPy/SnO_2 were used for the power enhancement of BMFC and the results were compared with the unmodified anode. The contact angle experiment revealed that the nanocomposite-modified anode has the maximum hydrophilicity, which increases the biocompatibility of the surface. It was then followed by the anode modified with SnO_2 and the unmodified anode. The CV results established that the nanocomposite-modified anode has the highest capacitance among all the reactors. It was also found to exhibit the maximum kinetic activity as depicted by Tafel plot. The EIS results revealed that this anode has the lowest values of the solution and charge transfer resistances. The power and polarization curves depicted that the reactor containing SnO_2/PPy/SnO_2 composite anode harvested a maximum power density of 130 mW/m^2. It was followed by SnO_2/PPy-modified anode, SnO_2-modified anode, and unmodified anode. The maximum power densities attained for these reactors were 73.09, 37.21, and 20.70 mW/m^2, respectively. The enhanced performance can be credited to the binding of SnO_2 nanoparticles and the cytochrome via Coulombic and electrostatic attractions and the capacitive behavior of polypyrrole. Furthermore, the interlayer can reduce the resistances and increase the electron transfer rate from the microbes to the surface of the anode. This further proves the feasibility and viability of SnO_2/PPy/SnO_2 nanocomposite as an anode of BMFC.

Acknowledgments

The financial assistance provided by DRDO-NRB (Research Grant No. NRB/4003/PG/324), New Delhi, for conducting this research work is highly acknowledged by the authors. Moreover, we are grateful to Sophisticated Analytical Instrument Facility (SAIF), IIT Bombay for the analytical characterization facilities.

Declarations of interest

None.

References

[1] S. Khilari, S. Pandit, J.L. Varanasi, D. Das, D. Pradhan, Bifunctional manganese ferrite/polyaniline hybrid as electrode material for enhanced energy recovery in microbial fuel cell, ACS Appl. Mater. Interfaces 7 (37) (2015) 20657–20666.

This book belongs to Badji Mokhtar Annaba University Central Library Copyright Elsevier 2025

[2] T. Duan, Y. Chen, Q. Wen, J. Yin, Y. Wang, Three-dimensional macroporous CNT-SnO_2 composite monolith for electricity generation and energy storage in microbial fuel cells, RSC Adv. 6 (64) (2016) 59610–59618.
[3] H. Yuan, L. Deng, Y. Chen, Y. Yuan, MnO_2/polypyrrole/MnO_2 multi-walled-nanotube-modified anode for high-performance microbial fuel cells, Electrochim. Acta 196 (2016) 280–285.
[4] W. Chen, Z. Liu, G. Su, Y. Fu, X. Zai, C. Zhou, J. Wang, Composite-modified anode by MnO_2/polypyrrole in marine benthic microbial fuel cells and its electrochemical performance, Int. J. Energy Res. 41 (6) (2017) 845–853.
[5] A. Mehdinia, E. Ziaei, A. Jabbari, Multi-walled carbon nanotube/SnO_2 nanocomposite: a novel anode material for microbial fuel cells, Electrochim. Acta 130 (2014) 512–518.
[6] A. Mehdinia, E. Ziaei, A. Jabbari, Facile microwave-assisted synthesized reduced graphene oxide/tin oxide nanocomposite and using as anode material of microbial fuel cell to improve power generation, Int. J. Hydrogen Energy 39 (20) (2014) 10724–10730.
[7] Z. Chen, D. Pan, Z. Li, Z. Jiao, M. Wu, C.H. Shek, C.L. Wu, J.K. Lai, Recent advances in tin dioxide materials: some developments in thin films, nanowires, and nanorods, Chem. Rev. 114 (15) (2014) 7442–7486.
[8] M. Batzill, U. Diebold, The surface and materials science of tin oxide, Prog. Surf. Sci. 79 (2–4) (2005) 47–154.
[9] N. Garino, A. Sacco, M. Castellino, J. A. Muñoz-Tabares, A. Chiodoni, V. Agostino, V. Margaria, M. Gerosa, G. Massaglia, M. Quaglio, Microwave-assisted synthesis of reduced graphene oxide/SnO_2 nanocomposite for oxygen reduction reaction in microbial fuel cells, ACS Appl. Mater. Interfaces 8 (7) (2016) 4633–4643.
[10] A.M. Hashem, H.M. Abuzeid, A.E. Abdel-Ghany, A. Mauger, K. Zaghib, C.M. Julien, SnO_2-MnO_2 composite powders and their electrochemical properties, J. Power Sources 202 (2012) 291–298.
[11] G. Xia, N. Li, D. Li, R. Liu, C. Wang, Q. Li, X. Lü, J.S. Spendelow, J. Zhang, G. Wu, Graphene/Fe_2O_3/SnO_2 ternary nanocomposites as a high-performance anode for lithium ion batteries, ACS Appl. Mater. Interfaces 5 (17) (2013) 8607–8614.
[12] S.H. Choi, Y.C. Kang, One-pot facile synthesis of Janus-structured SnO_2-CuO composite nanorods and their application as anode materials in Li-ion batteries, Nanoscale 5 (11) (2013) 4662–4668.
[13] M.F. Hassan, M.M. Rahman, Z. Guo, Z. Chen, H. Liu, SnO_2-NiO-C nanocomposite as a high capacity anode material for lithium-ion batteries, J. Mater. Chem. 20 (43) (2010) 9707–9712.
[14] E. Antolini, Composite materials for polymer electrolyte membrane microbial fuel cells, Biosens. Bioelectron. 69 (2015) 54–70.
[15] G. Gnana Kumar, C.J. Kirubaharan, S. Udhayakumar, K. Ramachandran, C. Karthikeyan, R. Renganathan, K. S. Nahm, Synthesis, structural, and morphological characterizations of reduced graphene oxide-supported polypyrrole anode catalysts for improved microbial fuel cell performances, ACS Sustain. Chem. Eng. 2 (10) (2014) 2283–2290.
[16] Y.C. Eeu, H.N. Lim, Y.S. Lim, S.A. Zakarya, N.M. Huang, Electrodeposition of polypyrrole/reduced graphene oxide/iron oxide nanocomposite as supercapacitor electrode material, J. Nanomater. 2013 (2013) 157.
[17] Y. Qiao, S.J. Bao, C.M. Li, X.Q. Cui, Z.S. Lu, J. Guo, Nanostructured polyaniline/titanium dioxide composite anode for microbial fuel cells, ACS Nano 2 (1) (2007) 113–119.
[18] Y. Qiao, C.M. Li, S.J. Bao, Q.L. Bao, Carbon nanotube/polyaniline composite as anode material for microbial fuel cells, J. Power Sources 170 (1) (2007) 79–84.
[19] J. Hou, Z. Liu, P. Zhang, A new method for fabrication of graphene/polyaniline nanocomplex modified microbial fuel cell anodes, J. Power Sources 224 (2013) 139–144.
[20] M. Ghasemi, W.R.W. Daud, S.H. Hassan, T. Jafary, M. Rahimnejad, A. Ahmad, M.H. Yazdi, Carbon nanotube/polypyrrole nanocomposite as a novel cathode catalyst and proper alternative for Pt in microbial fuel cell, Int. J. Hydrogen Energy 41 (8) (2016) 4872–4878.
[21] F. Papiya, A. Nandy, S. Mondal, P.P. Kundu, Co/Al_2O_3-rGO nanocomposite as cathode electrocatalyst for superior oxygen reduction in microbial fuel cell applications: the effect of nanocomposite composition, Electrochim. Acta 254 (2017) 1–13.
[22] I.H. Park, M. Christy, P. Kim, K.S. Nahm, Enhanced electrical contact of microbes using Fe_3O_4/CNT nanocomposite anode in mediator-less microbial fuel cell, Biosens. Bioelectron. 58 (2014) 75–80.

This book belongs to Badji Mokhtar Annaba University Central Library Copyright Elsevier 2025

[23] S. Rout, A.K. Nayak, J.L. Varanasi, D. Pradhan, D. Das, Enhanced energy recovery by manganese oxide/reduced graphene oxide nanocomposite as an air-cathode electrode in the single-chambered microbial fuel cell, J. Electroanal. Chem. 815 (2018) 1–7.
[24] S. Kalathil, V.H. Nguyen, J.J. Shim, M.M. Khan, J. Lee, M.H. Cho, Enhanced performance of a microbial fuel cell using CNT/MnO_2 nanocomposite as a bioanode material, J. Nanosci. Nanotechnol. 13 (11) (2013) 7712–7716.
[25] S. Khilari, S. Pandit, D. Das, D. Pradhan, Manganese cobaltite/polypyrrole nanocomposite-based air-cathode for sustainable power generation in the single-chambered microbial fuel cells, Biosens. Bioelectron. 54 (2014) 534–540.
[26] Y. Wu, X. Zhang, S. Li, X. Lv, Y. Cheng, X. Wang, Microbial biofuel cell operating effectively through carbon nanotube blended with gold–titania nanocomposites modified electrode, Electrochim. Acta 109 (2013) 328–332.
[27] F. Nourbakhsh, M. Mohsennia, M. Pazouki, Nickel oxide/carbon nanotube/polyaniline nanocomposite as bifunctional anode catalyst for high-performance Shewanella-based dual-chamber microbial fuel cell, Bioprocess Biosyst. Eng. 40 (11) (2017) 1669–1677.
[28] L. Cui, J. Shen, F. Cheng, Z. Tao, J. Chen, SnO_2 nanoparticles@ polypyrrole nanowires composite as anode materials for rechargeable lithium-ion batteries, J. Power Sources 196 (4) (2011) 2195–2201.
[29] J. Yuan, C. Chen, Y. Hao, X. Zhang, B. Zou, R. Agrawal, C. Wang, H. Yu, X. Zhu, Y. Yu, Z. Xiong, SnO_2/polypyrrole hollow spheres with improved cycle stability as lithium-ion battery anodes, J. Alloys Compd. 691 (2017) 34–39.
[30] R. Liu, D. Li, C. Wang, N. Li, Q. Li, X. Lü, J.S. Spendelow, G. Wu, Core-shell structured hollow SnO_2-polypyrrole nanocomposite anodes with enhanced cyclic performance for lithium-ion batteries, Nano Energy 6 (2014) 73–81.
[31] Z. Cao, H. Yang, P. Dou, C. Wang, J. Zheng, X. Xu, Synthesis of three-dimensional hollow SnO_2@ PPy nanotube arrays via template-assisted method and chemical vapor-phase polymerization as high performance anodes for lithium-ion batteries, Electrochim. Acta 209 (2016) 700–708.
[32] R. Adnan, N.A. Razana, I.A. Rahman, M.A. Farrukh, Synthesis and characterization of high surface area tin oxide nanoparticles via the sol-gel method as a catalyst for the hydrogenation of styrene, J. Chin. Chem. Soc. 57 (2) (2010) 222–229.
[33] L.X. Zuo, L.P. Jiang, J.J. Zhu, A facile sonochemical route for the synthesis of MoS_2/Pd composites for highly efficient oxygen reduction reaction, Ultrason. Sonochem. 35 (2017) 681–688.
[34] X. Li, B. Hu, S. Suib, Y. Lei, B. Li, Manganese dioxide as a new cathode catalyst in microbial fuel cells, J. Power Sources 195 (9) (2010) 2586–2591.
[35] Ö. Acarbaş, E. Suvacı, A. Doğan, Preparation of nanosized tin oxide (SnO_2) powder by homogeneous precipitation, Ceram. Int. 33 (4) (2007) 537–542.
[36] J. Zhang, L. Gao, Synthesis and characterization of nanocrystalline tin oxide by sol–gel method, J. Solid State Chem. 177 (4–5) (2004) 1425–1430.
[37] K.C. Song, Y. Kang, Preparation of high surface area tin oxide powders by a homogeneous precipitation method, Mater. Lett. 42 (5) (2000) 283–289.
[38] C.A. Ibarguen, A. Mosquera, R. Parra, M.S. Castro, J.E. Rodríguez-Páez, Synthesis of SnO_2 nanoparticles through the controlled precipitation route, Mater. Chem. Phys. 101 (2–3) (2007) 433–440.
[39] S. Fujihara, T. Maeda, H. Ohgi, E. Hosono, H. Imai, S.H. Kim, Hydrothermal routes to prepare nanocrystalline mesoporous SnO_2 having high thermal stability, Langmuir 20 (15) (2004) 6476–6481.
[40] L. Jiwei, Q. Jingxia, Y. Miao, J. Chen, Preparation and characterization of Pt-polypyrrole nanocomposite for electrochemical reduction of oxygen, J. Mater. Sci. 43 (18) (2008) 6285.
[41] G. Cho, B.M. Fung, D.T. Glatzhofer, J.S. Lee, Y.G. Shul, Preparation and characterization of polypyrrole-coated nanosized novel ceramics, Langmuir 17 (2) (2001) 456–461.
[42] Y. Fu, J. Yu, Y. Zhang, Y. Meng, Graphite coated with manganese oxide/multiwall carbon nanotubes composites as anodes in marine benthic microbial fuel cells, Appl. Surf. Sci. 317 (2014) 84–89.

This book belongs to Badji Mokhtar Annaba University Central Library Copyright Elsevier 2025

[43] S. Roy, C.Y. Yue, Y.C. Lam, Z.Y. Wang, H. Hu, Surface analysis, hydrophilic enhancement, ageing behavior and flow in plasma modified cyclic olefin copolymer (COC)-based microfluidic devices, Sens. Actuators B 150 (2) (2010) 537–549.
[44] J. Liu, Y. Liu, C. Feng, Z. Wang, T. Jia, L. Gong, L. Xu, Enhanced performance of microbial fuel cell using carbon microspheres modified graphite anode, Energy Sci. Eng. 5 (4) (2017) 217–225.
[45] Y.B. Fu, Z.H. Liu, G. Su, X.R. Zai, M. Ying, J. Yu, Modified carbon anode by MWCNTs/PANI used in marine sediment microbial fuel cell and its electrochemical performance, Fuel Cells 16 (3) (2016) 377–383.
[46] O. Prakash, A. Mungray, S.K. Kailasa, S. Chongdar, A.K. Mungray, Comparison of different electrode materials and modification for power enhancement in benthic microbial fuel cells (BMFCs), Process Saf. Environ. Prot. 117 (2018) 11–21.
[47] O. Prakash, A. Mungray, S. Chongdar, S.K. Kailasa, A.K. Mungray, Performance of polypyrrole coated metal oxide composite electrodes for benthic microbial fuel cell (BMFC), J. Environ. Chem. Eng. 8 (2) (2020) 102757.
[48] P. Pushkar, O. Prakash, M. Imran, A.A. Mungray, S.K. Kailasa, A.K. Mungray, Effect of cerium oxide nanoparticles coating on the electrodes of benthic microbial fuel cell, Sep. Sci. Technol. 54 (2) (2019) 213–223.
[49] Z. He, F. Mansfeld, Exploring the use of electrochemical impedance spectroscopy (EIS) in microbial fuel cell studies, Energy Environ. Sci. 2 (2) (2009) 215–219.
[50] A.K. Manohar, O. Bretschger, K.H. Nealson, F. Mansfeld, The polarization behavior of the anode in a microbial fuel cell, Electrochim. Acta 53 (9) (2008) 3508–3513.
[51] A. Dumitru, A. Morozan, M. Ghiurea, K. Scott, S. Vulpe, Biofilm growth from wastewater on MWNTs and carbon aerogels, Phys. Status Solidi A 205 (6) (2008) 1484–1487.
[52] J.L. Willit, E.F. Bowden, Adsorption and redox thermodynamics of strongly adsorbed cytochrome c on tin oxide electrodes, J. Phys. Chem. 94 (21) (1990) 8241–8246.
[53] Y. Wang, Q. Wen, Y. Chen, L. Qi, A novel polyaniline interlayer manganese dioxide composite anode for high-performance microbial fuel cell, J. Taiwan Inst. Chem. Eng. 75 (2017) 112–118.

This book belongs to Badji Mokhtar Annaba University Central Library
Copyright Elsevier 2025

This page intentionally left blank

This book belongs to Badji Mokhtar Annaba University Central Library

Copyright Elsevier 2025

CHAPTER 36

Visible light photocatalysis: Case study (process)

Sandeep Kumar Lakhera[a] and Bernaurdshaw Neppolian[b]

[a]*Department of Physics and Nanotechnology, SRM Institute of Science and Technology, Kattankulathur, Chennai, Tamil Nadu, India,* [b]*SRM Research Institute, SRM Institute of Science and Technology, Kattankulathur, Chennai, Tamil Nadu, India*

36.1 Introduction

Life on the Earth depends on the availability of water, and three-fourths of the Earth's surface is covered with water. Of this, ~97.5% of the water is saline and hence unusable for human consumption [1]. Only 2.7% of the water on the Earth is fresh and potable. Most of it is in the form of ice and groundwater, and the remaining fresh water is accumulated in the lakes and rivers [1]. With industrial revolution and rapid population growth over the past century, these surface and ground water bodies are continuously getting contaminated. The dumping of untreated sewage water from the cities, agricultural waste, and industrial solid and liquid waste directly into the surface and ground water resulted in severe contamination of the fresh water bodies. The consumption of water containing toxic pollutants such as heavy metals, industrial dyes, fertilizers, pesticides, hospital waste, animal waste, microorganisms, and chemicals causes various diseases such as cancer, arsenicosis, polio, trachoma, typhoid, schistosomiasis, cholera, diarrhea, and malaria [2]. Treatment of the wastewater from organic and inorganic toxic pollutants is the foremost requirement for the betterment of humanity and flora, fauna on the Earth.

Conventional wastewater treatment techniques such as adsorption on activated carbon, ultrafiltration, reverse osmosis, coagulation by chemical agents, and ion exchange methods are not very efficient and unable to remove the toxic contaminations from wastewater completely. To overcome the shortcoming of the existing energy-intensive methods, new methods and technologies are required. Advanced oxidation processes (AOPs) can be classified as photo-driven such as light/H_2O_2, photo-Fenton, and heterogeneous photocatalysis and nonphoto-driven such as ozone (O_3), Fenton, and O_3/H_2O_2. Among the AOPs, solar light-driven photocatalytic processes-based wastewater treatment methods are considered as

Handbook of Nanomaterials for Wastewater Treatment. https://doi.org/10.1016/B978-0-12-821496-1.00001-5
Copyright © 2021 Elsevier Inc. All rights reserved.

This book belongs to Badji Mokhtar Annaba University Central Library Copyright Elsevier 2025

one of the most promising and pollution free ways to clean water for human consumption. In photocatalytic process, semiconducting materials are used, which absorb the sun light and produce electrons and holes. These photogenerated charge carriers can directly or indirectly breakdown the toxic pollutants. The photocatalytic degradation of pollutants into environment friendly and nontoxic byproducts offers a cost-effective and an efficient method for wastewater treatment [3].

36.2 Visible light photocatalytic processes for wastewater treatment

The semiconducting materials absorb UV or visible light because of their unique electronic structure. The presence of bandgap between the filled valance band and empty conduction band results in the absorption of a photon with energy equal to or larger than the bandgap. As shown in Fig. 36.1, after absorbing a photon, electron-hole pairs are generated in the semiconductor. In the absence of a reactant, these charge pairs recombine quickly within a few nanoseconds. However, in the presence of suitable reactants, the electrons and holes can directly react or produce radicals such as superoxide, peroxide, and hydroxyl, which in turn act on the pollutant molecules and break them down [4]. Several semiconducting materials such as TiO_2, ZnO, and NiO have been utilized for photocatalytic degradation of toxic pollutants [5, 6] However, these materials suffer from low efficiency because the bandgap of these materials are in the UV region of light, and the solar spectrum consists of ~45% visible and only ~3%–5% of UV light

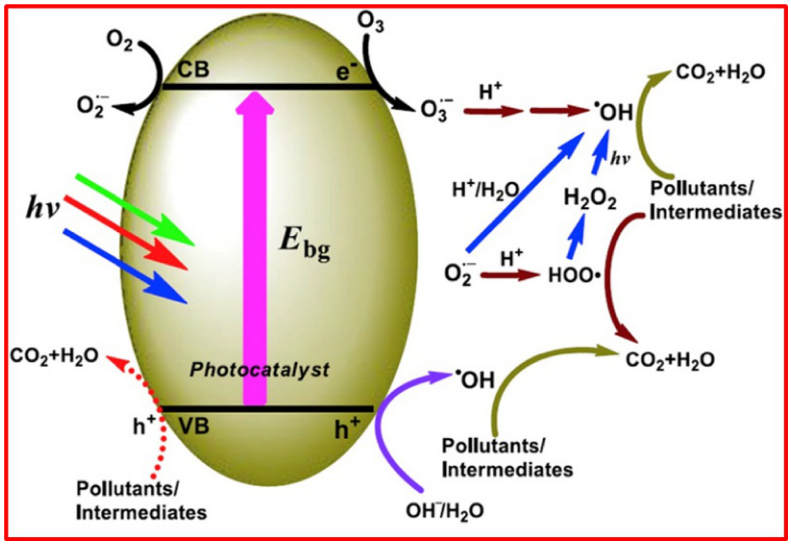

Fig. 36.1
The photocatalytic wastewater treatment mechanism. *Reproduced with permission from N. Serpone, Y.M. Artemev, V.K. Ryabchuk, A.V. Emeline, S. Horikoshi, Curr. Opin. Green Sustain. Chem. 6 (2017) 18–33, Copyright (2017), Elsevier.*

This book belongs to Badji Mokhtar Annaba University Central Library
Copyright Elsevier 2025

[7, 8]. For commercial applications, it is necessary that the photocatalytic materials absorb the visible light.

Photocatalytic processes such as homogenous or heterogeneous have been utilized extensively for wastewater treatment [9]. Moreover, a combination of photocatalytic processes with other processes such as Fenton, sonolysis, membrane filtration, ozonation, and hybrid processes have been shown to be more efficient. The photocatalytic pollutants degradation reaction mechanism can be described by the following reactions [3].

$$\text{Semiconductor} + \text{light} \rightarrow \text{Semiconductor}\left(e_{cb}^{-} + h_{vb}^{+}\right) \tag{36.1}$$

$$\text{Dye} + \text{Semiconductor}\left(h_{vb}^{+}\right) \rightarrow \text{Oxidation Process} \tag{36.2}$$

$$\text{Semiconductor}\left(h_{vb}^{+}\right) + H_2O \rightarrow \text{Semiconductor} + H^{+} + OH^{-} \tag{36.3}$$

$$\text{Semiconductor}\left(h_{vb}^{+}\right) + OH^{-} \rightarrow \text{Semiconductor} + {}^{\bullet}OH \tag{36.4}$$

$$\text{Dye} + \text{Semiconductor}\left(e_{cb}^{-}\right) \rightarrow \text{Reduction process} \tag{36.5}$$

$$\text{Semiconductor}\left(e_{cb}^{-}\right) + O_2 \rightarrow \text{Semiconductor} + O_2^{\bullet -} \tag{36.6}$$

$$O_2^{\bullet -} + H^{+} \rightarrow HO^{\bullet}{}_2 \tag{36.7}$$

$$HO^{\bullet}{}_2 + HO^{\bullet}{}_2 \rightarrow H_2O_2 + O_2 \tag{36.8}$$

$$H_2O_2 + O_2^{\bullet -} \rightarrow {}^{\bullet}OH + OH^{-} + O_2 \tag{36.9}$$

$$\text{Dye} + {}^{\bullet}OH \rightarrow \text{Degradation Products} \tag{36.10}$$

36.2.1 Heterogeneous photocatalysis

Wastewater treatment by using a heterogeneous photocatalyst is a promising technique because of the availability of abundant solar light, simplicity, and cost-effectiveness of the method. For a semiconducting material to be photocatalytically active, its valence and conduction band edges should be sufficiently positive and negative on the normalized hydrogen electrode (NHE), respectively. Without an appropriate band structure, a photocatalyst will not be able to produce the reactive oxygen species (ROS) required to degrade the pollutants. Eqs. (36.11) (36.16) present the redox potential required to generate the ROS such as superoxide radical ($O_2^{\bullet -}$), hydroxyl ions (OH^{-}), and hydroxyl radical ($^{\bullet}OH$) [10]. These ROS have a very short lifetime of micro to nanoseconds (Table 36.1).

$$O_2 \xrightarrow{\text{energy transfer}} {}^{1}O_2 \tag{36.11}$$

$$O_2 \xrightarrow{e^{-}(-0.16\ \text{V})} O_2^{\bullet -} \tag{36.12}$$

This book belongs to Badji Mokhtar Annaba University Central Library

Copyright Elsevier 2025

Table 36.1: The lifetime of photocatalytically generated reactive oxygen species [11, 12].

Name	Formula	Oxidation potential (V)	Lifetime	No. of e^-
Superoxide anion radical	$O_2^{\bullet -}$	−0.16	10^{-6} s	17
Hydroxyl radical	$^{\bullet}OH$	2.8	10^{-9} s	9
Singlet oxygen	$^1O_2$	2.42	$2 * 10^{-6}$ s	16
Hydroperoxy radical	$HO_2^{\bullet}$	1.7	10^{-9} s	17
Hydroxyl ions	OH^-	1.30	$70 * 10^{-6}$ s	10
Ozone	O_3	2.07		24

$$O_2^{\bullet -} \xrightarrow{H^+} HO_2^{\bullet} \tag{36.13}$$

$$O_2^{\bullet -} \xrightarrow{e^- + 2H^+ (+0.94\ V)} H_2O_2 \tag{36.14}$$

$$H_2O_2 \xrightarrow{e^- + H^+ (+0.38\ V)} {}^{\bullet}OH \tag{36.15}$$

$${}^{\bullet}OH \xrightarrow{e^- + H^+ (+2.33\ V)} H_2O \tag{36.16}$$

Over the years, several visible light active photocatalysts have been discovered for photocatalytic pollutants degradation activity, such as g-C_3N_4, $BiVO_4$, MFe_2O_4 (M = Zn, Cu), Bi_2O_3, BiOX (X =Cl, Br, I), MOS_2, Fe_3O_4, Bi_2WO_6, AgI, WO_3, CdS, and ZnS [7, 13–20]. However, the photocatalytic activity of these photocatalysts is limited because of unsuitable redox potential or fast recombination rate of the charge carriers. Modifications of these photocatalysts with suitable cocatalysts have shown superior activity for wastewater treatment (Table 36.2). For long-term usage and commercial feasibility, the photocatalysts should be nontoxic, low-cost, and stable in the aqueous environment. Besides visible light absorption, quick separation and transfer of generated electrons from the conduction band of the semiconductor is necessary for improving the efficiency of the photocatalytic process. Water dissolved oxygen can accept the electrons from the conduction band of the semiconductor and form a superoxide radical, hydroperoxide radicals, and hydrogen peroxide, represented by Eqs. (36.12), (36.14), and (36.15). The photogenerated valence band holes migrate to the surface and oxidize the surface-adsorbed pollutants directly or produce hydroxyl ion and radicals. The superoxide anion and hydroxyl radicals are highly reactive species because of the presence of an unpaired electron [28].

The photocatalytic activity of a photocatalyst largely depends on the band structure, surface area, crystallinity, and charge separation efficiency. As depicted in Fig. 36.2, the photocatalytic efficiency of a heterogeneous photocatalyst can be increased by introducing defect states, doping with metals (Ni, Cu, Co, W, Mn, Fe, Ce, etc.), plasmonic metals (Au, Pt, Ag), using a sensitizer such as dyes, formation of a heterojunction (binary, ternary) with other semiconductors, and incorporating a carbon support (graphene, carbon nanotubes, activated carbon) for providing a large surface area and an efficient charge transfer [29–31].

This book belongs to Badji Mokhtar Annaba University Central Library
Copyright Elsevier 2025

Table 36.2: Wastewater pollutants degradation efficiency of visible light absorbing photocatalysts.

S. no.	Photocatalyst	Bandgap (in eV)	Pollutant	Degradation efficiency (%)	Stability (cycles)	Ref.
1	Titania/black volcanic ashes	2.8	Methylene blue	95	–	[21]
2	Graphene/ Ag_3PO_4/Ag/ $BiVO_4$	–	Tetracycline	94.96	3	[22]
3	Bi_2S_3/Bi_2O_3/ $Bi_2O_2CO_3$	1.32	HCHO	99	5	[13]
4	Bi_2MoO_6/SnO_2	2.66	Nitrobenzene, Rhodamine B	90, 97	3	[23]
5	g-C_3N_4/ $NaNbO_3$	–	Rhodamine B	95.6	5	[24]
6	RGO-WO_3	2.15	Sulfamethoxazole	98	–	[25]
7	$CoFe_2O_4$/MoS_2	2	Congo Red	94.9	3	[14]
8	WO_3	2.48	Oxalic acid	98.6	–	[15]
9	AgI/$BiVO_4$	2.29	Methylene blue	99	5	[16]
10	$CoFe_2O_4$-RGO	–	Methylene blue	93.1	3	[17]
11	α-Fe_2O_3/Cu_2O	1.75	Methyl Orange	95	4	[7]
12	AgI/rGO/$BiVO_4$	2.24	Tetracycline, RhB	84, 99	4	[8]
13	g-C_3N_4/$NiFe_2O_4$	2.7/2.19	Oxytetracycline	94	10	[18]
14	Mesoporous g-C_3N_4	2.75	Tetracycline	90.8	5	[26]
15	SnO_2/BiOI	3.48/1.70	Oxytetracycline hydrochloride	94	4	[27]

Besides the structural, optical, and electronic properties of the heterogeneous photocatalysts, several other factors also affect the overall wastewater treatment process, such as pollutants concentration, pH of the solution, catalyst amount, particle size of the photocatalyst, temperature, nature of pollutants, and presence of inorganic ions, light intensity, and dissolved oxygen [32]. With the increasing pollutants concentration, the degradation efficiency first increases, as more number of molecules adsorbs on the surface of the photocatalysts, and then the activity decreases because the high concentration of the pollutants causes light blocking effect. Similarly, the degradation efficiency decreases when the catalysts amount in the solution is increased beyond a threshold value because the catalysts particles tend to agglomerate and block the light irradiation. The variation in the pH of solution can alter the surface charges (protonation or deprotonation) and shift the redox potential of the photocatalysts, which affects the rate of the reaction. Higher reaction temperature (>80°C) and light intensity make the charge separation and recombination rate to compete with each other, thus lowering the reaction rate. The nature of the pollutants (cationic, anionic) and surface charge of the photocatalysts also affect the adsorption and overall degradation reaction. The presence of

This book belongs to Badji Mokhtar Annaba University Central Library
Copyright Elsevier 2025

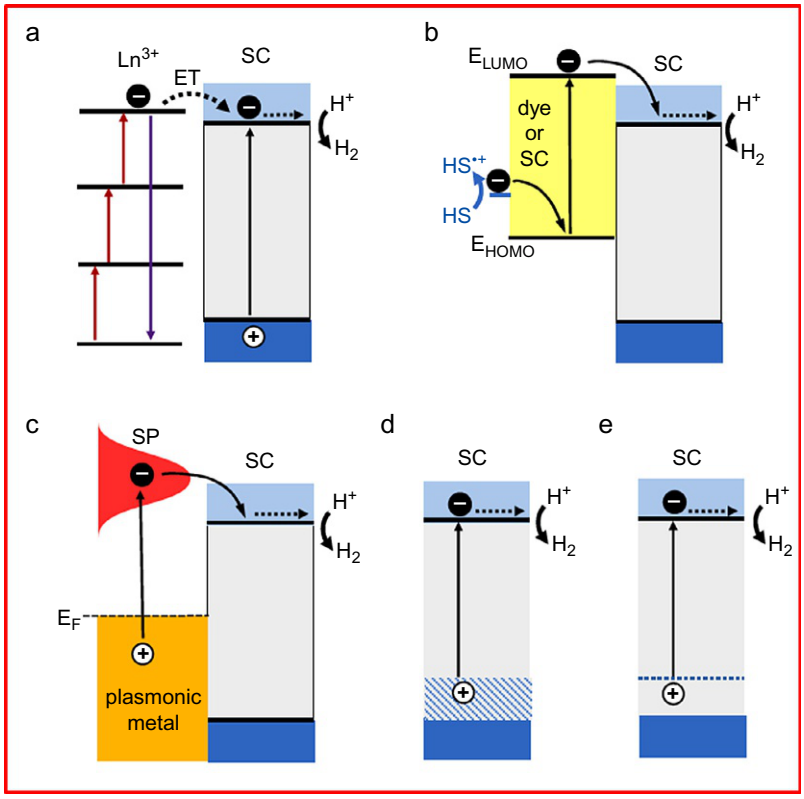

Fig. 36.2
Techniques to improve visible light absorption (A) upconversion process (B) sensitizers, (C) hot electron injection by surface plasmon resonance, (D) hybridization of energy level, and (E) defect states generation. *Reproduced with permission from J.K. Stolarczyk, S. Bhattacharyya, L. Polavarapu, J. Feldmann, ACS Catal. 8(4) (2018) 3602–3635, Copyright (2018), ACS publications.*

inorganic ions such as phosphate, zinc, nitrate, and sulfate can slow down the reaction and deactivate the photocatalysts by adsorbing on its surface [32].

36.2.2 Homogenous photocatalysis

In homogeneous photocatalysis, the catalysts and the reactants are in the same phase and uniformly distributed. The homogenous catalysts contribute ~20% in the chemical industry such as polymer, pharmaceuticals, and wastewater treatment [33]. Homogeneous solar-driven AOPs include H_2O_2/sunlight, solar photo-Fenton (Fe^{+2}/H_2O_2/sunlight), solar photo-Fenton with ethylenediamine-*N*,*N*′-disuccinic acid (EDDS) complex (Fe^{+2}/H_2O_2/EDDS/sunlight), O_3/H_2O_2, ultrasonic, and light/O_3 or light/O_3/H_2O_2 [34, 35]. In case of O_3/H_2O_2 process, hydroxyl radicals are produced, as shown further [36].

This book belongs to Badji Mokhtar Annaba University Central Library
Copyright Elsevier 2025

$$H_2O_2 + 2O_3 \rightarrow 2^{\bullet}OH + 3O_2 \tag{36.17}$$

Under sunlight/H_2O_2, hydroxyl radicals are produced by photolysis of hydrogen peroxide [37]. Homogenous catalysts are highly selective for the decomposition of pollutants, and because of uniform distribution, they have a high catalytic activity. However, it is difficult to separate after completion of the reaction, and they have temperature limitations. To overcome the shortcoming of homogenous catalysts, hybrid processes have been developed by integrating heterogeneous and homogenous photocatalysts. In Section 36.2.3, these processes have been discussed in detail.

36.2.3 Hybrid processes

The heterogeneous and homogeneous processes have their advantages in cleaning the toxic wastewater. However, the photocatalysis, Fenton, membrane filtration, and ozonation processes have some disadvantages, which hinder their efficiency in complete mineralization of the toxic pollutants. For example, photocatalytic process is slow because of low oxidation rate, and ozonation process suffers from incomplete mineralization. Because of the shortcomings, these technologies have low economical and practical feasibility. One method to overcome the individual shortcomings and efficiency of the AOP techniques is to combine the processes such as photocatalysis and ozonation together. The hybrid processes containing visible light photocatalysis and other AOP techniques for wastewater remediation are given in the case studies further.

36.2.3.1 Case-1: Photo-Fenton process

Photo-Fenton technique combines the Fenton process with photocatalysis. In Fenton process, Fe^{2+} or Cu^{2+} and H_2O_2 react in acidic medium to produce hydroxyl radicals ($^{\bullet}OH$). These $^{\bullet}OH$ are highly reactive and transform the pollutants into carbon dioxide and mineral acids. When the visible light photocatalysts are combined with Fe^{2+} and H_2O_2, the pollutants degradation rate increases [38]. The Fenton reaction process is shown further [39–42]. The reaction between Fe^{3+} and H_2O_2 is called Fenton-like reaction, and it produces less oxidative species, hydroperoxyl ($HO^{\bullet}{}_2$).

$$H_2O_2 + Fe^{2+} \rightarrow Fe^{3+} + {}^{\bullet}OH + OH^- \tag{36.18}$$

$$Fe^{3+} + H_2O_2 \rightarrow Fe^{2+} + HO^{\bullet}{}_2 + H^+ \tag{36.19}$$

$${}^{\bullet}OH + H_2O_2 \rightarrow HO^{\bullet}{}_2 + H_2O \tag{36.20}$$

$${}^{\bullet}OH + Fe^{2+} \rightarrow Fe^{3+} + OH^- \tag{36.21}$$

$$Fe^{3+} + HO^{\bullet}{}_2 \rightarrow Fe^{2+} + O_2 + H^+ \tag{36.22}$$

$$Fe^{2+} + HO^{\bullet}{}_2 + H^+ \rightarrow Fe^{3+} + H_2O_2 \tag{36.23}$$

This book belongs to Badji Mokhtar Annaba University Central Library
Copyright Elsevier 2025

$$HO^{\bullet}{}_2 + HO^{\bullet}{}_2 \rightarrow H_2O_2 + O_2 \tag{36.24}$$

$$HO^{\bullet}{}_2 + H_2O_2 \rightarrow {}^{\bullet}OH + H_2O + O_2 \tag{36.25}$$

The Fe^{3+}/Fe^{2+} catalyzes H_2O_2 and produces the $^{\bullet}OH$ radical [43]. This homogeneous Fenton catalytic process can also be presented by the following equations [39, 40]:

$$Fe^{3+} + H_2O_2 \leftrightarrow Fe\left(HO_2\right)^{2+} + H^+ \tag{36.26}$$

$$Fe\left(HO_2\right)^{2+} \leftrightarrow Fe^{2+} + {}^{\bullet}OH \tag{36.27}$$

Incorporation of light in Fenton reaction leads to photoreduction of $Fe(OH)^{2+}$, which produces more amount of $^{\bullet}OH$ radicals by Fe^{2+} regeneration [40].

$$Fe^{3+} + H_2O \rightarrow Fe\left(OH\right)^{2+} + H^+ \tag{36.28}$$

$$Fe(OH)^{2+} + h\nu\ (\lambda < 400\,\text{nm}) \rightarrow Fe^{2+} + {}^{\bullet}OH \tag{36.29}$$

Thus in photo-Fenton process, the intermediate species utilize the light to produce more $^{\bullet}OH$ radicals and regenerate Fe^{2+}. The improvement in $^{\bullet}OH$ radical production occurs because of the photolysis and photochemical reaction of Fe^{3+} hydroxide complex and $Fe^{3+/}Fe^{2+}$/organic acids complexes, respectively [43]. These complexes are not only stable but also photoactive [44, 45].

The Fenton reaction is pH-dependent, and in the presence of homogeneous catalysts, the pH may vary from ~2.5 to 4. The optimized pH is 3, and any variation in the pH below 2.5 or above 4 results in the reduction in degradation activity by scavenging of H^+, or precipitation of ferric oxyhydroxides may occur. In the case of basic pH, the redox potential of $^{\bullet}OH$ radical changes and affects the reaction rate. When Fenton is combined with a photocatalyst, the acidic pH (~3) of the solution affects the stability and reactivity of the photocatalyst. It is important to develop and use a photocatalyst with a wider pH operating range to protect it from leaching. When using the direct sunlight, the temperature of the photo-Fenton reaction should be controlled, as H_2O_2 above 40°C breaks down into H_2O and O_2 [46]. The table below presents the visible light active photo-Fenton catalysts and their wastewater degradation efficiency (Table 36.3).

36.2.3.2 Case-2: Sonophotocatalysis

The generation of ultrasound (US) waves by ship propellers was observed by the British nautical engineer (1894), and the process was termed as hydrodynamic cavitation [59]. Today, the use of US for the treatment of wastewater is a powerful advanced oxidation technology. US is produced by a transducer in a liquid medium by transmitting the mechanical vibrations. The mechanical vibrations create pressure waves in the liquid, which lead to compression and rarefaction of liquid. The rarefaction (negative pressure) waves tear the liquid apart, cavitation occurs, and microbubbles form in the liquid. These microbubbles sinusoidally shrink and grow with the pressure waves. Upon reaching a critical size within microseconds,

This book belongs to Badji Mokhtar Annaba University Central Library Copyright Elsevier 2025

Table 36.3: Photo-Fenton catalysts and their wastewater degradation activity.

S. no.	Catalyst	Light source	Pollutant	Reaction time (min)	Efficiency (%)	Ref
1	Fe-Z4A/H_2O_2	UV-vis	Safranin	120	88.34	[47]
2	ZnO/$ZnFe_2O_4$/ H_2O_2	NIR	Methyl Orange	3600	97.3	[48]
3	ZnO-Fe_3O_4/rGO/ H_2O_2	Visible	Methylene Blue	150	97	[49]
4	Millimetric zero-valent iron (mmZVI)/RhB/ H_2O_2	Visible	Tetrabromobisphenol A	60	96.6	[50]
5	CS/$CoFe_2O_4$/ GONCs/H_2O_2	Visible	Maxilon dye	120	99	[51]
6	CuFeO/H_2O_2	Visible	Sulfamethazine	30	100	[52]
7	Fe_3O_4@GO@MIL-100(Fe)/H_2O_2	Visible	2,4-Dichlorophenol	40	100	[53]
8	Fe^{3+}-doped BiOBr/H_2O_2	Solar	Methylene Blue	50	97	[54]
9	rGS/FexOy/NCL/ H_2O_2	Visible	Rhodamine B	90	100	[55]
10	Fe_3O_4-MWCNT/ H_2O_2	Solar	Methylene Blue	70	94	[56]
11	α-Fe_2O_3@g-C_3N_4/ H_2O_2	Visible	Tetracycline	60	92	[57]
12	NiFe-based nanocubes/H_2O_2	Visible	MB	10	98.9	[58]

these microbubbles explode violently and produce extremely high temperature and pressure locally [60]. Any toxic pollutant molecules present in the vicinity of the microbubbles gets pyrolyzed into CO_2 and H_2O. Owing to the extremely high temperature and pressure, the vaporized water molecules in the bubble form $^{\bullet}OH$ and H radicals. The production of these radicals in the liquid by US is termed as sonochemical activity. Once the temperature of exploded bubble subsidized to the bulk liquid temperature, the short-lived $^{\bullet}OH$ and H radicals combine to form H_2O_2. The $^{\bullet}OH$, H, and H_2O_2 breakdown the pollutants from wastewater and produce no sludge [61, 62]. The bubble formation by cavitation process is shown in Fig. 36.3.

The US frequencies of 20 kHz–2 MHz have been utilized for environmental remediation applications. The physical effects of US dominate at low frequencies and chemical effects at higher frequencies range (200–600 kHz) [62, 63]. The sonochemical technique provides safe and clean method for wastewater remediation without causing toxic byproducts. However, sonolysis process is energy-intensive and has limitations. The $^{\bullet}OH$ radical formation slows down when the concentration of the pollutant is high in the solution because a high

This book belongs to Badji Mokhtar Annaba University Central Library Copyright Elsevier 2025

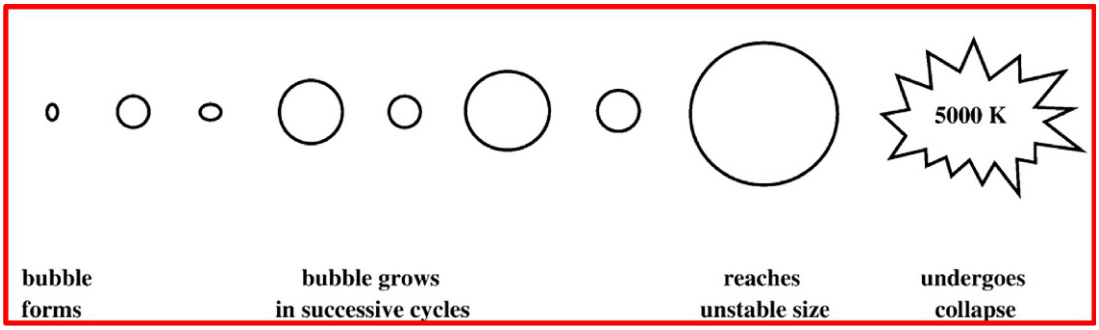

Fig. 36.3
The formation and collapse process of cavitation bubbles. *Reproduced with permission from P. Chowdhury, T. Viraraghavan, Sci. Total Environ. 407(8) (2009) 2474–2492, Copyright (2009), Elsevier.*

concentration of pollutants makes the liquid viscous, which hinders the nucleation of bubble formation. Also, if the wastewater contains several pollutants, the degradation of the most volatile takes precedent over the least volatile [60]. Also, sonolysis process exhibits a low efficiency toward hydrophobic compounds; on the other hand, photocatalytic process shows higher efficiency with hydrophilic compounds because they tend to adsorb on the surface of the catalysts. Hence combining the visible light photocatalytic process with the sonolysis method offers some advantages because both processes produce ROS and complement each other. The sonophotocatalytic process can degrade a wide range of pollutants, as shown in Table 36.4. The semiconductor-mediated photo-US method can synergistically enhance the overall degradation efficiency of pollutants. Moreover, the surface of the photocatalysts continuously gets cleaned, and the surface area is increased by the acoustic cavitation process, which provides more active sites for wastewater treatment [46].

36.2.3.3 Case-3: Photocatalytic membrane filtration

Separation of size-dependent particles by membrane filtration is a very useful technique for filtration of bacteria, biomolecules, viruses, and inorganic salts. Various types of membranes such as polymeric, inorganic, or hybrid membranes are used for purification of wastewater. However, because of fouling and operation cost, the membrane filtration system suffers from low efficiency, which hinders its large-scale applications. Integration of membrane filtration and photocatalytic techniques in a photocatalytic membrane reactor (PMR) brings the benefits of both the processes for efficient wastewater treatment. A PMR system provides better fouling and antibacterial resistance. Graphene, carbon nanotubes, and semiconducting nanoparticles have been successfully incorporated in the PMR system [79]. The PMR system is relatively of low cost, nontoxic, and can run continuously with a membrane and reusable photocatalyst. In the hybrid system, on one hand, the photocatalyst degrades and mineralizes the organic pollutants into CO_2, H_2O, and salts; on the other hand, the membrane filters the salts from the wastewater and provides clean fresh water. The PMR system has a photocatalytic

This book belongs to Badji Mokhtar Annaba University Central Library Copyright Elsevier 2025

This book belongs to Badji Mokhtar Annaba University Central Library

Table 36.4: Sonophotocatalytic wastewater pollutants degradation efficiency.

S. no.	Photocatalyst	Bandgap (eV)	Pollutant	Experimental parameters	Catalyst dosage (g/L)	Reaction time (min)	Degradation efficiency (%)	Stability (cycles)	Ref.
1	CuO-TiO_2/rGO	3.08	Methyl Orange	40 kHz, UV light	1	90	98	5	[64]
2	WO_3/CNT	2.36	Tetracycline	24 kHz, 40 W	0.06	60	100	6	[65]
3	N-Cu/ TiO_2/FCNT	2.62	Sulfamethoxazole	50 W Xe lamp	0.08	60	100	6	[66]
4	ZnO/CuO	3.2	Parathion	80 kHz, 60 W	0.02	60	100	–	[67]
5	Fe_3O_4/TiO_2-N-GO	2.7	Humic acid	40 kHz, 60 W	1.0	90	94	5	[68]
6	ZnO/GO	2.63	Methylene Blue	40 kHz, 400 W	0.1	180	98	5	[69]
7	Ag/g-C_3N_4	2.64	Tetracycline	40 kHz, 60 W	1	180	90.2	4	[70]
8	MgO@zeolite	–	TOC	100–400 W	2	210	97.2	4	[71]
9	MgO/CNT	3.3	Sulfadiazine	24 kHz, 150 W	1.2	80	100	6	[72]
10	Pyrite	–	Sulfasalazine	40–60 kHz, 100 W	0.5	30	97	4	[73]
11	(Au/BTiO_2/ rGO)	3.02	Tetracycline	40 kHz, 600 W	–	60	100	–	[74]
12	Ti^{3+}/TiO_2	2.9	Methyl Orange	40 kHz, 600 W	1	120	95	3	[75]
13	Copper phthalocyanine	2.49	Rhodamine B	40 kHz, 400 W	0.083	60	81	–	[76]
14	NiFe-LDH/rGO	2.46	Moxifloxacin	36 kHz, 150 W	1	60	90.40	5	[77]
15	N/Ti^{3+} co-doping biphasic TiO_2/ Bi_2WO_6	2.20	Rhodamine B	36 kHz, 180 W	1	100	98	4	[78]

Copyright Elsevier 2025

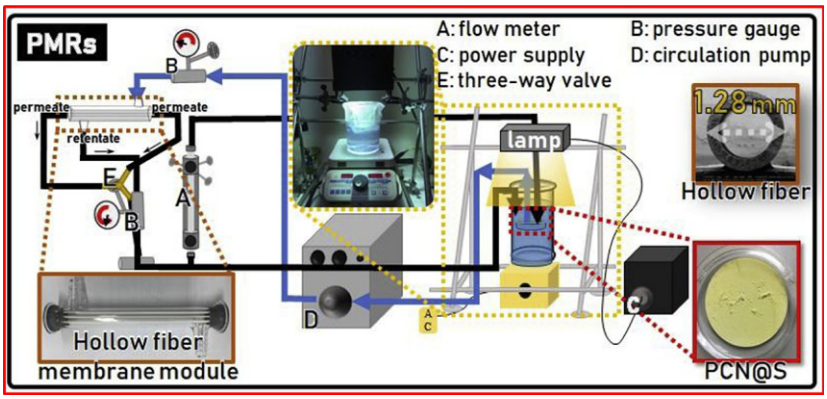

Fig. 36.4
Al_2O_3 hollow fiber and P-doped g-C_3N_4-based photocatalytic membrane separation and purification system. *Reproduced with permission from C. Hu, M.-S. Wang, C.-H. Chen, Y.-R. Chen, P.-H. Huang, K.-L. Tung, J. Membr. Sci. 580 (2019) 1–11, Copyright (2019), Elsevier.*

reactor and photocatalytic membrane filtration zone. On the surface of the membrane substrate, a photocatalyst is immobilized to reduce the fouling. As depicted in Fig. 36.4, Hu et al. used a visible light active P-doped g-C_3N_4 (PCN) photocatalyst in combination with an Al_2O_3 hollow fiber membrane for methyl blue and phenol degradation and achieved 90% and 92% mineralization efficiency, respectively [80]. Table 36.5 presents organic/inorganic photocatalytic membrane system for the decomposition of various pollutants present in the wastewater.

36.2.3.4 Case-4: Photocatalytic ozonation process

O_3 is a strong oxidizing species and known to react directly with the organic pollutants. Upon reaction with water, it produces highly oxidizing hydroxyl radicals. O_3 decomposes water into the ROS by following the reaction path given below [46].

$$\text{Initiation}: \quad O_3 + H_2O = 2^{\bullet}OH + O_2 \tag{36.30}$$

$$O_3 + OH^- = O_2^{\bullet -} + HO_2^{\bullet} \tag{36.31}$$

$$\text{Propagation}: \quad O_3 + {}^{\bullet}OH = O_2 + HO_2^{\bullet} \tag{36.32}$$

$$O_2 + HO_2^{\bullet} = 2O_2^{\bullet -} + H^+ \tag{36.33}$$

$$O_3 + HO_2^{\bullet} = 2O_2 + {}^{\bullet}OH \tag{36.34}$$

$$\text{Termination}: \quad 2\,HO_2^{\bullet} = O_2 + H_2O_2 \tag{36.35}$$

Ozonation is a pH-dependent reaction, and at higher pH, O_3 reacts nonselectively with all the compounds. The oxidation power of the hydroxyl radicals also decreases with the increase in the pH of the solution [46]. The pollutants degradation efficiency of O_3 depends on its

This book belongs to Badji Mokhtar Annaba University Central Library Copyright Elsevier 2025

This book belongs to Badji Mokhtar Annaba University Central Library

Table 36.5: The pollutants removal efficiency of photocatalytic membranes.

S. no.	Photocatalyst	Light source	Membrane	Pollutant	Reaction time (min)	Efficiency (%)	Ref.
1	P-g-C_3N_4	Visible	Al_2O_3 hollow fiber membrane	Methylene Blue	120	>90	[80]
2	N-TiO_2	Visible	Regenerated cellulose membrane matrix	Phenol	120	78.8	[81]
3	Ce-ZnO	Visible	Polypropylene hollow fiber membrane	Methyl Orange	50	97.84	[82]
4	mpg-C_3N_4/ TiO_2	Solar	Membrane PSf-3	Sulfamethoxazole	1800	69	[83]
5	MWCNTs/ Ag_3PO_4/PAN	Visible	TCFM	Rhodamine B	80	100	[84]
6	Fe-TiO_2	Visible	Fe-TiO_2-PSF	Bisphenol A	180	92.30	[85]
7	GO-TiO_2	Visible	GO-TiO_2-MCE	Diphenhydramine and Methyl Orange	300–400	61–65	[86]
8	Novel-TiO_2-ceramic	Visible	Novel-TiO_2-ceramic	Methylene Blue and Methyl Orange	–	25.2 and 13.3	[87]
9	N-GO/TiO_2	Solar	N-GO/TiO_2-PSF	Methylene Blue	300	75	[88]
10	Cu_2O	250 W lamp with (390–800 nm)	Cu_2O-PSF	Ibuprofen	60	86	[89]
11	Modified TiO_2-γ-alumina	Six visible SMD LEDs	Modified TiO_2-γ-alumina	Methylene Blue	300	60	[90]
12	Fe^{3+} @ ZnO	Solar simulator	Fe^{3+} @ ZnO PMR	Reactive Black 5	180	98.34	[91]

Copyright Elsevier 2025

selectivity for the organic compounds, and the O_3 reaction byproducts such as aldehydes and carboxylic acids do not react with O_3; these limitations reduce the mineralization efficiency of the ozonation process. However, integrating the ozonation process with photocatalysis gives a new process of photocatalytic ozonation. In this process, the organic pollutants can be decomposed simultaneously by the O_3 and the hydroxyl radicals produced by the photocatalysts. In addition, the O_3 can produce more reactive radicals (H^+, $^{\bullet}OH$, and $^{\bullet}O_2^-$) by capturing the conduction band electrons of the semiconducting photocatalyst. By capturing the CB electrons, O_3 also reduces the photogenerated charge recombination rate, thus increasing the overall hydroxyl radical production and hence the pollutants degradation efficiency. These $^{\bullet}OH$ radicals can break C—C, C—H, C—O, C—N, and N—H bonds in organic pollutants [92, 93]. The photocatalytic ozonation process provides the synergistic high pollutants removal efficiency without any secondary pollutants, as displayed in Table 36.6 [104].

36.3 Current trends and scale-up challenges

Semiconductor photocatalysis integrated with one or more AOPs have the potential to efficiently decompose the pollutants from wastewater. This hybrid process can be used for various organic pollutants such as pesticides, herbicides, industrial dyes, metal ions, and detergents. One of the challenges is to find a suitable bandgap and visible light absorbing photocatalyst with high charge carrier separation efficiency. Selecting a nontoxic, stable semiconductor with control of the morphology to increase the surface area and designing an appropriate band structure is the need of the hour. Optimization of the solution pH, reaction temperature, pressure, catalysts amount, oxygen, O_3 and pollutants concentration, ionic force, turbidity, light intensity, cost, and design of the reactor system will dictate the overall wastewater degradation efficiency of the hybrid process. The solution parameters of the pollutants in river and lakes water may differ from region to region; therefore designing a catalytic system that can work with a wide range of solution parameters is a challenge for commercial implementation. Immobilization of the catalysts on the substrate for recovery and prevention of agglomeration is another technological problem yet to be addressed. The large-scale wastewater treatment reactors will be feasible with the reusable and visible light-driven hybrid catalysts. Several attempts were made to scale-up the wastewater treatment process with varied levels of success.

Recently, Zhao et al. bonded black titania and three-dimensional graphene (BT/3DG) photocatalysts on a cloth by a polymeric binder and used the cloth for large-scale field trial for wastewater treatment in rivers, lakes, and ponds, as depicted in Fig. 36.5 [105]. The photoactive and buoyant cloth was used under direct sunlight for wastewater degradation activity without primary and secondary treatments. After deploying for 2 weeks, the water color changed from turbid to clear, and the nitrogen, phosphorous, and total organic carbon (TOC) content was found to reduce significantly. By using BT (8 tons) and 3DG (100 kg), 600 acres of wastewater was remediated.

This book belongs to Badji Mokhtar Annaba University Central Library Copyright Elsevier 2025

This book belongs to Badji Mokhtar Annaba University Central Library

Table 36.6: Pollutants degradation efficiency of various visible light active photocatalytic ozonation catalysts.

S. no.	Ozone	Photocatalyst	Pollutant	Degradation efficiency (in %)	Stability (cycles)	Ref.
1	O_3-oxygen (10 mg/L ozone concentration)	WO_3	Ibuprofen sodium salt	87	–	[94]
2	O_3, 45 mg/L	L-$BiVO_4$	Oxalic acid	97.5	5	[95]
3	O_3, 50 mg/L	Composite of TiO_2 and MWCNT	Aniline	90	–	[96]
4	O_3, 80 mg/L	TiO_2-rGO	Bisphenol A	98.4	5	[97]
5	O_3, 3 mg/L	TiO_2/carbon paper composite	MB	98.3	–	[98]
6	O_3, 50 mg/L	Ag-g-C_3N_4/SBA-15	Oxalic acid	100	4	[99]
7	O_3	ZnO nanoparticles immobilized on montmorillonite	Metronidazole	97	5	[100]
8	O_3	TiO_2/carbon dots	Ciprofloxacin	99.7	–	[101]
9	O_3	$Co_{0.6}Zn_{0.4}Fe_2O_4$	RhB	99.9	–	[102]
10	O_3	O_3/olive stone activated carbon	Clopyralid	90	–	[103]

Copyright Elsevier 2025

Fig. 36.5
Field trials of photoactive cloths deployed on polluted rivers for wastewater remediation. *Reproduced with permission from W. Zhao, I.-W. Chen, F. Huang, Nano Today 27 (2019) 11–27, Copyright (2019), Springer.*

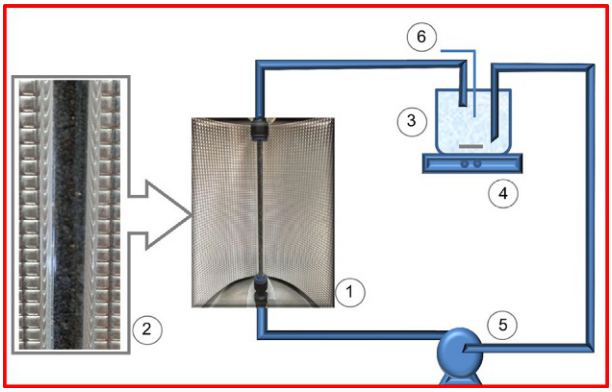

Fig. 36.6
Photocatalytic packed-bed reactor system for methylene blue dye degradation. *Reproduced with permission from M.E. Borges, M. Sierra, P. Esparza, Clean Technol. Environ. Policy 19(4) (2017) 1239–1245, Copyright (2017), Springer.*

Borges et al. used volcanic ash (VA) as a photocatalyst under direct solar light for wastewater treatment in a packed-bed photocatalytic reactor [106]. The reactor assembly consisted of a cylindrical parabolic solar concentrator (1), photocatalytic reactor (2), 150 mL feed storage (3), agitation (4), peristaltic pump (5), and inlet air (6) in a packed-bed reactor, as shown in Fig. 36.6. The VA photocatalyst degrades more than 90% of MB dye (20 mg/L) in a 5 h reaction time by continuous-flow photocatalytic treatment [106].

This book belongs to Badji Mokhtar Annaba University Central Library
Copyright Elsevier 2025

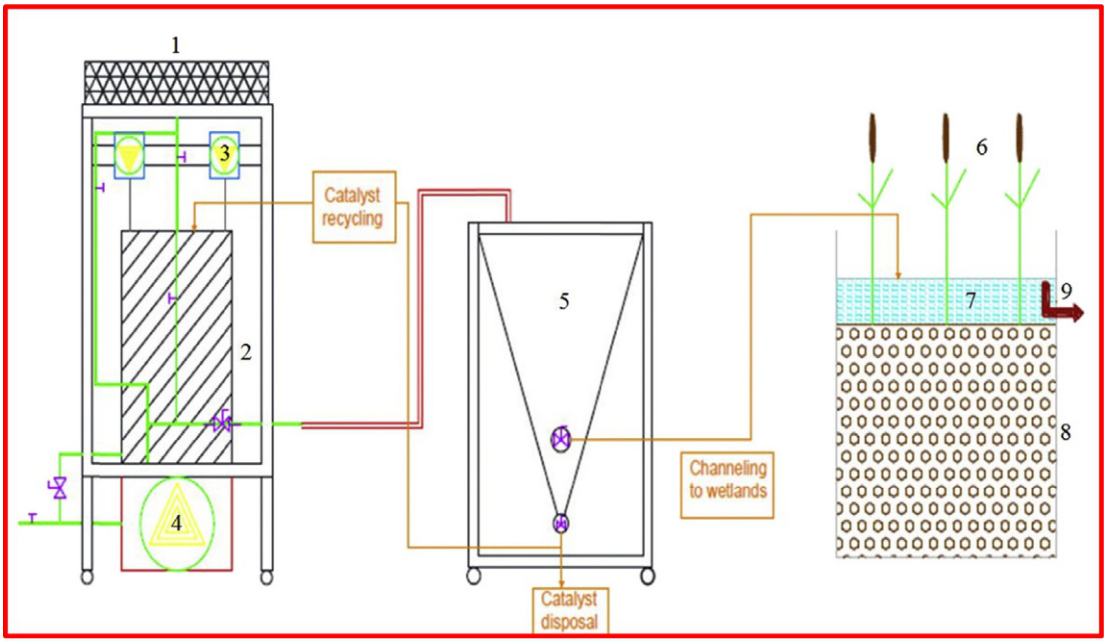

Fig. 36.7
Integrated photocatalytic system constructed with a wetland for pesticides removal from simulated wastewater. *Reproduced with permission from C. Berberidou, V. Kitsiou, D.A. Lambropoulou, A. Antoniadis, E. Ntonou, G.C. Zalidis, I. Poulios, J. Environ. Manage. 195 (2017) 133–139, Copyright (2016), Elsevier.*

Similarly, Berberidou investigated the degradation of herbicide clopyralid in a simulated horizontal flow designed wastewater wetland under solar light irradiation [107]. The investigation involved three different photocatalytic processes, that is, photo-Fenton, ferrioxalate reagent, and combining the photo-Fenton with TiO_2. As displayed in Fig. 36.7, the pilot-scale test system used a fountain-type photocatalytic reactor, a wastewater reservoir, and an Imhoff-type tank for catalysts separation. The assembly consists of a photoreactor (1), storage tank (2), dosimetric pump (3), pump (4), Imhoff tank (5), Typha spp. plants (6), wastewater (7), soil (8), and wetland outlet (9). The plant was able to treat 20 L of wastewater, and only trace level of intermediates was detected in the outflow line of the reactor system [107].

Sacco et al. prepared visible light active nitrogen-doped TiO_2 photocatalysts immobilized on polystyrene spheres by solvent casting method for the treatment of MB-containing municipal wastewater [108]. As shown in Fig. 36.8, by using a packed-bed photocatalytic reactor combined with a solar compound triangular collector (CTC), a complete MB degradation was achieved after 3 h reaction time. The photocatalyst was also used to clean *Escherichia coli* from real wastewater.

This book belongs to Badji Mokhtar Annaba University Central Library Copyright Elsevier 2025

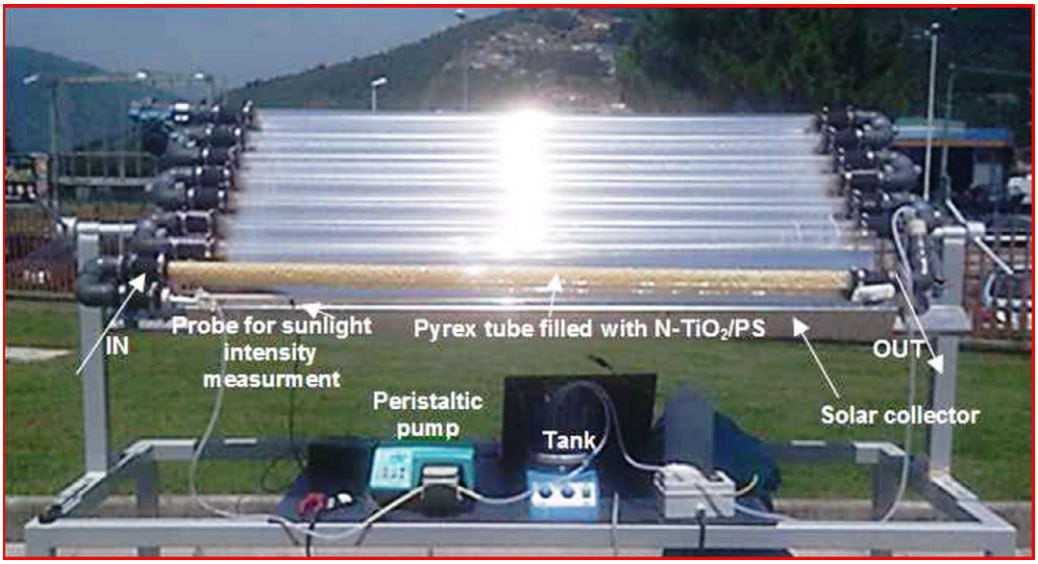

Fig. 36.8
Pilot-scale solar photoreactor for cleaning wastewater from *Escherichia coli* and MB dye. *Reproduced with permission from O. Sacco, V. Vaiano, L. Rizzo, D. Sannino, J. Clean. Prod. 175 (2018) 38–49, Copyright (2018), Elsevier.*

Fig. 36.9
Design of the solar photoreactor for the degradation of textile dyes present in the wastewater. *Reproduced with permission from P. Dhatshanamurthi, M. Shanthi, M. Swaminathan, J. Water Process Eng. 16 (2017) 28–34, Copyright (2017), Elsevier.*

This book belongs to Badji Mokhtar Annaba University Central Library Copyright Elsevier 2025

Fig. 36.10
The Solar Falling Film Reactor for the degradation of polychlorinated biphenyls mixed in seawater.
Reproduced with permission from Y.A. Shaban, M.A. El Sayed, A.E. Maradny, R.K.A. Farawati, M.I.A. Zobidi, S.U.M. Khan, Int. J. Photoenergy (2016) 8471960, https://doi.org/10.1155/2016/8471960, Copyright (2016), Hindawi.

Dhatshanamurthi et al. investigated solar photocatalytic degradation of industry dyes effluent by using nano ZnO catalysts in a solar photoreactor (Fig. 36.9) [109]. The ZnO sample was mixed with fevicol (adhesive) and coated on the acrylic sheet by brush coating. The photocatalysts exhibited ~86% mineralization efficiency for the wastewater collected from textile dying industry in 4 h with the optimized thin film coating. Similarly, Shaban et al. used carbon-modified titanium oxide for the solar photocatalytic degradation of polychlorinated biphenyls from seawater in a pilot-scale Solar Falling Film Reactor (SFFR) [110]. As shown in Fig. 36.10, the SFFR was made of stainless steel batch tank, flat tray, and a pump. Using the SFFR, the polychlorinated biphenyls mixed in seawater was completely degraded in 75 min.

36.4 Conclusions

All the AOPs have some advantages and disadvantages; selecting one AOP process over the other necessitates careful consideration of the solution parameters. Although various AOPs have been reported for wastewater treatment, herein, we have presented the integrated visible light photocatalysis with other AOP techniques such as photocatalysis, sonolysis, Fenton, ozonoation, and membrane filtration. Recent progresses made in this hybrid technology have

This book belongs to Badji Mokhtar Annaba University Central Library Copyright Elsevier 2025

been presented with the possibility of scalability. Several parameters limiting the large-scale applications of the hybrid process have been discussed.

Acknowledgments

The authors are grateful for funding from MNRE, New Delhi, India (103/239/2015-NT) and SERB-DST, New Delhi, India [File No: EMR/2014/000645]. The authors also thank Ms. Rugma T.P., Mr. Rishi Krishna B.S., Mr. Vijayarajan V.S., and Ms. Deepika Venugopal for their help in editing the chapter.

References

[1] A.K. Mishra, C.M. Hussain (Eds.), Nanotechnology for Sustainable Water Resources, Scrivener Publishing, 2018.
[2] Y. Li, F. Chen, R. He, Y. Wang, N. Tang, Nanoscale Materials in Water Purification, Elsevier Inc., 2019, pp. 689–705
[3] M.M. Khan, D. Pradhan, Y. Sohn (Eds.), Nanocomposites for Visible Light-Induced Photocatalysis, Springer, 2017, https://doi.org/10.1007/978-3-319-62446-4.
[4] D. Bahnemann, Sol. Energy 77 (5) (2004) 445–459.
[5] B. Neppolian, Q. Wang, H. Jung, H. Choi, Ultrason. Sonochem. 15 (4) (2008) 649–658.
[6] B. Neppolian, S. Sakthivel, B. Arabindoo, M. Palanichamy, V. Murugesan, J. Environ. Sci. Health A 34 (9) (1999) 1829–1838.
[7] S.K. Lakhera, A. Watts, H.Y. Hafeez, B. Neppolian, Catal. Today 300 (2018) 58–70.
[8] S.K. Lakhera, H.Y. Hafeez, R. Venkataramana, P. Veluswamy, H. Choi, B. Neppolian, Appl. Surf. Sci. 487 (2019) 1289–1300.
[9] G. Maniakova, K. Kowalska, S. Murgolo, G. Mascolo, G. Libralato, G. Lofrano, O. Sacco, M. Guida, L. Rizzo, Sep. Purif. Technol. 236 (2020) 116249.
[10] G. Cosa, S. Nonell, J.M. Aubry, F. Anquez, J. Kanofsky, D. Fresnadillo, P. Ogilby, E. San Román, C. Frochot, C. Geddes, W. Bäumler, Singlet Oxygen: Applications in Biosciences and Nanosciences, vol. 1, Royal Society of Chemistry, 2016.
[11] S. Horikoshi, N. Serpone, Catal. Today 340 (2020) 334–346.
[12] Y. Einaga, Analyst 144 (2019) 4499–4504.
[13] Y. Huang, W. Fan, B. Long, H. Li, F. Zhao, Z. Liu, Y. Tong, H. Ji, Appl. Catal. B: Environ. 185 (2016) 68–76.
[14] B. Ren, W. Shen, L. Li, S. Wu, W. Wang, Appl. Surf. Sci. 447 (2018) 711–723.
[15] J. Yang, J. Xiao, H. Cao, Z. Guo, J. Rabeah, A. Brückner, Y. Xie, J. Hazard. Mater. 360 (2018) 481–489.
[16] S.K. Lakhera, R. Venkataramana, G. Mathew, H.Y. Hafeez, B. Neppolian, Mater. Sci. Semicond. Process. 106 (2020) 104756.
[17] G. He, J. Ding, J. Zhang, Q. Hao, H. Chen, Ind. Eng. Chem. Res. 54 (11) (2015) 2862–2867.
[18] A. Sudhaik, P. Raizada, P. Shandilya, P. Singh, J. Environ. Chem. Eng. 6 (4) (2018) 3874–3883.
[19] S.K. Lakhera, T.P. Rugma, H.Y. Hafeez, B. Neppolian, ChemSusChem 12 (18) (2019) 4293–4303.
[20] S.K. Lakhera, V.S. VIjayrajan, B.S. Rishi Krishna, P. Veluswamy, B. Neppolian, Int. J. Hydrogen Energy 45 (13) (2020) 7562–7573.
[21] M.E. Borges, M. Sierra, E. Cuevas, R.D. García, P. Esparza, Sol. Energy 135 (2016) 527–535.
[22] F. Chen, Q. Yang, X. Li, G. Zeng, D. Wang, C. Niu, J. Zhao, H. An, T. Xie, Y. Deng, Appl. Catal. B: Environ. 200 (2017) 330–342.
[23] B. Liu, X. Liu, M. Ni, C. Feng, X. Lei, C. Li, Y. Gong, L. Niu, J. Li, L. Pan, Appl. Surf. Sci. 453 (2018) 280–287.
[24] S. Chengjie, F. Mingshan, H. Bo, C. Tianjun, W. Liping, S. Weidong, CrystEngComm 17 (24) (2015) 4575–4583.
[25] W. Zhu, F. Sun, R. Goei, Y. Zhou, Appl. Catal. B: Environ. 207 (2017) 93–102.

This book belongs to Badji Mokhtar Annaba University Central Library
Copyright Elsevier 2025

[26] Z. Zhu, W. Fan, Z. Liu, H. Dong, Y. Yan, P. Huo, J. Photochem. Photobiol. A: Chem. 359 (2018) 102–110.
[27] X.-J. Wen, C.-G. Niu, L. Zhang, G.-M. Zeng, ACS Sustain. Chem. Eng. 5 (6) (2017) 5134–5147.
[28] L.M.T. Martínez, O.V. Kharissova, B.I. Kharisov, Handbook of Ecomaterials, Springer, 2019.
[29] R.V. Prihod'ko, N.M. Soboleva, J. Chem. (2013) 2013.
[30] S.K. Lakhera, B. Neppolian, Int. J. Hydrogen Energy 45 (13) (2020) 7627–7640.
[31] H.Y. Hafeez, S.K. Lakhera, M.V. Shankar, B. Neppolian, Int. J. Hydrogen Energy 45 (13) (2020) 7530–7540.
[32] A. Kumar, G. Pandey, Mater. Sci. Eng. Int. J. 1 (3) (2017) 106–114.
[33] P.W.N.M. van Leeuwen, Homogeneous Catalysis, first ed., Springer Science, 2004.
[34] S. Kim, H. Park, W. Choi, J. Phys. Chem. B 108 (2004) 20. 6402–6411.
[35] C.D. Stan, I. Cretescu, C. Pastravanu, I. Poulios, M. Drăgan, Int. J. Photoenergy (2012) 194823.
[36] S. Lemeune, J.M. Barbe, A. Trichet, R. Guilard, Ozone Sci. Eng. (2008) 129–144.
[37] C.W. Jones, J.H. Clark, Applications of Hydrogen Peroxide and Derivatives, first ed., Royal Society of Chemistry, 1999.
[38] M.R. Hoffmann, S.T. Martin, W. Choi, D.W. Bahnemann, Chem. Rev. 95 (1) (1995) 69–96.
[39] F. Haber, J. Weiss, Proc. R. Soc. Lond. A: Math. Phys. Sci. 147 (861) (1934) 332–351.
[40] J.J. Pignatello, E. Oliveros, A. MacKay, Crit. Rev. Environ. Sci. Technol. 36 (1) (2006) 1–84.
[41] G.G. Jayson, J.P. Keene, D.A. Stirling, A.J. Swallow, Trans. Faraday Soc. 65 (1969) 2453–2464.
[42] Z. Stuglik, Z. Paweł Zagórski, Radiat. Phys. Chem. (1977) 17 (4) (1981) 229–233.
[43] Y.H. Huang, Y.J. Huang, H.C. Tsai, H.T. Chen, J. Taiwan Inst. Chem. Eng. 41 (6) (2010) 699–704.
[44] D.R. Manenti, P.A. Soares, A.N. Módenes, F.R. Espinoza-Quiñones, R.A. Boaventura, R. Bergamasco, V.J. Vilar, Chem. Eng. J. 266 (2015) 203–212.
[45] A.G. Gutierrez-Mata, S. Velazquez-Martínez, A. Álvarez-Gallegos, M. Ahmadi, J.A. Hernández-Pérez, F. Ghanbari, S. Silva-Martínez, Int. J. Photoenergy 2017 (2017).
[46] C. Descorme, Catal. Today 297 (2017) 324–334.
[47] A. Ikhlaq, F. Javed, M.S. Munir, S. Hussain, K.S. Joya, A.M. Zafar, Desalin. Water Treat. 148 (2019) 152–161.
[48] H. Chen, W. Liu, Z. Qin, Catal. Sci. Technol. 7 (11) (2017) 2236–2244.
[49] D.P. Ojha, M.K. Joshi, H.J. Kim, Ceram. Int. 43 (1) (2017) 1290–1297.
[50] Y. Ju, Y. Yu, X. Wang, M. Xiang, L. Li, D. Deng, D.D. Dionysiou, J. Hazard. Mater. 323 (2017) 611–620.
[51] A.A. Al-Kahtani, M.F. Taleb, J. Hazard. Mater. 309 (2016) 10–19.
[52] M. Cheng, Y. Liu, D. Huang, C. Lai, G. Zeng, J. Huang, Z. Liu, C. Zhang, C. Zhou, L. Qin, W. Xiong, Chem. Eng. J. 362 (2019) 865–876.
[53] Q. Gong, Y. Liu, Z. Dang, J. Hazard. Mater. 371 (2019) 677–686.
[54] Y. Liu, J. Li, J. Li, X. Yan, F. Wang, W. Yang, D.H. Ng, J. Yang, J. Clean. Prod. 252 (2020) 119573.
[55] T. Yao, W. Jia, Y. Feng, J. Zhang, Y. Lian, J. Wu, X. Zhang, J. Hazard. Mater. 362 (2019) 62–71.
[56] A. Tolba, M.G. Alalm, M. Elsamadony, A. Mostafa, H. Afify, D.D. Dionysiou, Process Saf. Environ. Prot. 128 (2019) 273–283.
[57] T. Guo, K. Wang, G. Zhang, X. Wu, Appl. Surf. Sci. 469 (2019) 331–339.
[58] D. Wang, X. Guo, F. Zha, X. Tang, H. Tian, J. Taiwan Inst. Chem. Eng. 102 (2019) 202–211.
[59] C.G. Joseph, G. Li Puma, A. Bono, D. Krishnaiah, Ultrason. Sonochem. 16 (2009) 583–589.
[60] D. Chen, S.K. Sharma, A. Mudhoo, Handbook on Applications of Ultrasound Sonochemistry for Sustainability. first ed., Taylor and Francis Group, 2011, https://doi.org/10.1201/b11012.
[61] Y.G. Adewuyi, Ind. Eng. Chem. Res. 40 (2001) 4681–4715.
[62] L.H. Thompson, L.K. Doraiswamy, Ind. Eng. Chem. Res. 38 (1999) 1215–1249.
[63] K. Thangavadivel, M. Megharaj, R.S.C. Smart, P.J. Lesniewski, R. Naidu, J. Hazard. Mater. 168 (2009) 1380–1386.
[64] S.G. Babu, P. Karthik, M.C. John, S.K. Lakhera, M. Ashokkumar, J. Khim, B. Neppolian, Ultrason. Sonochem. 50 (2019) 218–223.
[65] A.A. Isari, M. Mehregan, S. Mehregan, F. Hayati, R.R. Kalantary, B. Kakavandi, J. Hazard. Mater. (2020) 122050.

This book belongs to Badji Mokhtar Annaba University Central Library Copyright Elsevier 2025

[66] A.A. Isari, F. Hayati, B. Kakavandi, M. Rostami, M. Motevassel, E. Dehghanifard, Chem. Eng. J. (2019) 123685.
[67] M. Aghaei, S. Sajjadi, A.H. Keihan, Environ. Sci. Pollut. Res. (2020) 1–13.
[68] N. Geng, W. Chen, H. Xu, M. Ding, Z. Liu, Z. Shen, Ultrason. Sonochem. 57 (2019) 242–252.
[69] M. Zarrabi, M. Haghighi, R. Alizadeh, S. Mahboob, Sep. Purif. Technol. 211 (2019) 738–752.
[70] M. Jodeyri, M. Haghighi, M. Shabani, J. Mater. Sci. Mater. Electron. 30 (15) (2019) 13877–13894.
[71] S. Jorfi, S. Pourfadakari, B. Kakavandi, Chem. Eng. J. 343 (2018) 95–107.
[72] F. Hayati, A.A. Isari, B. Anvaripour, M. Fattahi, B. Kakavandi, Chem. Eng. J. 381 (2020) 122636.
[73] A. Khataee, S. Fathinia, M. Fathinia, Ultrason. Sonochem. 34 (2017) 904–915.
[74] V. Vinesh, A.R. Shaheer, B. Neppolian, Ultrason. Sonochem. 50 (2019) 302–310.
[75] P. Karthik, V. Vinesh, A.M. Shaheer, B. Neppolian, Appl. Catal. A: Gen. 585 (2019) 117208.
[76] M. Samanta, M. Mukherjee, U.K. Ghorai, C. Bose, K.K. Chattopadhyay, Mater. Res. Bull. 123 (2020) 110725.
[77] A. Khataee, T.S. Rad, S. Nikzat, A. Hassani, M.H. Aslan, M. Kobya, E. Demirbaş, Chem. Eng. J. 375 (2019) 122102.
[78] M. Sun, Y. Yao, W. Ding, S. Anandan, J. Alloys Compd. 820 (2020) 153172.
[79] S.N. Ahmed, W. Haider, Nanotechnology 29 (34) (2018) 342001.
[80] C. Hu, M.-S. Wang, C.-H. Chen, Y.-R. Chen, P.-H. Huang, K.-L. Tung, J. Membr. Sci. 580 (2019) 1–11.
[81] M.A. Mohamed, W.N. Salleh, J. Jaafar, A.F. Ismail, M.A. Mutalib, N.A. Sani, S.E. Asri, C.S. Ong, Chem. Eng. J. 284 (2016) 202–215.
[82] M. Sheydaei, M. Fattahi, L. Ghalamchi, V. Vatanpour, Ultrason. Sonochem. 56 (2019) 361–371.
[83] S. Yu, Y. Wang, F. Sun, R. Wang, Y. Zhou, Chem. Eng. J. 337 (2018) 183–192.
[84] X.Q. Wu, J.S. Shen, F. Zhao, Z.D. Shao, L.B. Zhong, Y.M. Zheng, J. Mater. Sci. 53 (14) (2018) 10147–10159.
[85] Q. Wang, C. Yang, G. Zhang, L. Hu, P. Wang, Chem. Eng. J. 319 (2017) 39–47.
[86] L.M. Pastrana-Martinez, S. Morales-Torres, J.L. Figueiredo, J.L. Faria, A.M. Silva, Water Res. 77 (2015) 179–190.
[87] C.P. Athanasekou, N.G. Moustakas, S. Morales-Torres, L.M. Pastrana-Martínez, J.L. Figueiredo, J.L. Faria, A.M. Silva, J.M. Dona-Rodriguez, G.E. Romanos, P. Falaras, Appl. Catal. B: Environ. 178 (2015) 12–19.
[88] W. Chen, T. Ye, H. Xu, T. Chen, N. Geng, X. Gao, RSC Adv. 7 (16) (2017) 9880–9887.
[89] R. Singh, V.S.K. Yadav, M.K. Purkait, Sep. Purif. Technol. 212 (2019) 191–204.
[90] N.G. Moustakas, F.K. Katsaros, A.G. Kontos, G.E. Romanos, D.D. Dionysiou, P. Falaras, Catal. Today 224 (2014) 56–69.
[91] A. Ashar, I.A. Bhatti, M. Ashraf, A.A. Tahir, H. Aziz, M. Yousuf, M. Ahmad, M. Mohsin, Z.A. Bhutta, J. Clean. Prod. 246 (2020) 119010.
[92] J.C. Cardoso, G.G. Bessegato, M.V.B. Zanoni, Water Res. 98 (2016) 39–46.
[93] A.C. Mecha, M.S. Onyango, A. Ochieng, M.N.B. Momba, Chemosphere 186 (2017) 669–676.
[94] A. Rey, E. Mena, A.M. Chávez, F.J. Beltrán, F. Medina, Chem. Eng. Sci. 126 (2015) 80–90.
[95] X. Liu, Z. Guo, L. Zhou, J. Yang, H. Cao, M. Xiong, Y. Xie, G. Jia, Chemosphere 222 (2019) 38–45.
[96] C.A. Orge, J.L. Faria, M.F.R. Pereira, J. Environ. Manage. 195 (2017) 208–215.
[97] G. Liao, D. Zhu, J. Zheng, J. Yin, B. Lan, L. Li, J. Taiwan Inst. Chem. Eng. 67 (2016) 300–305.
[98] X. He, R. Chen, X. Zhu, Q. Liao, L. An, X. Cheng, L. Li, Ind. Eng. Chem. Res. 55 (31) (2016) 8627–8635.
[99] Y. Ling, G. Liao, W. Feng, Y. Liu, L. Li, J. Photochem. Photobiol. A: Chem. 349 (2017) 108–114.
[100] A. Khataee, M. Kıranşan, S. Karaca, M. Sheydaei, J. Taiwan Inst. Chem. Eng. 74 (2017) 196–204.
[101] Y. Zeng, D. Chen, T. Chen, M. Cai, Q. Zhang, Z. Xie, R. Li, Z. Xiao, G. Liu, W. Lv, Chemosphere 227 (2019) 198–206.
[102] M. Sundararajan, V. Sailaja, L. John Kennedy, J. Judith Vijaya, Ceram. Int. 43 (1) (2017) 540–548.
[103] Z. Rajah, M. Guiza, R.R. Solís, N. Becheikh, F.J. Rivas, A. Ouederni, J. Environ. Chem. Eng. (2019) 102900.
[104] J. Wu, J. Ren, W. Pan, P. Lu, Y. Qi, The photocatalytic technology for wastewater treatment, in: Photo-Catalytic Control Technologies of Flue Gas Pollutants. Energy and Environment Research in China, Springer, Singapore, 2019.

This book belongs to Badji Mokhtar Annaba University Central Library
Copyright Elsevier 2025

[105] W. Zhao, I.-W. Chen, F. Huang, Nano Today 27 (2019) 11–27.
[106] M.E. Borges, M. Sierra, P. Esparza, Clean Technol. Environ. Policy 19 (4) (2017) 1239–1245.
[107] C. Berberidou, V. Kitsiou, D.A. Lambropoulou, A. Antoniadis, E. Ntonou, G.C. Zalidis, I. Poulios, J. Environ. Manage. 195 (2017) 133–139.
[108] O. Sacco, V. Vaiano, L. Rizzo, D. Sannino, J. Clean. Prod. 175 (2018) 38–49.
[109] P. Dhatshanamurthi, M. Shanthi, M. Swaminathan, J. Water Process Eng. 16 (2017) 28–34.
[110] Y.A. Shaban, M.A. El Sayed, A.E. Maradny, R.K.A. Farawati, M.I.A. Zobidi, S.U.M. Khan, Int. J. Photoenergy (2016) 8471960, https://doi.org/10.1155/2016/8471960.

This book belongs to Badji Mokhtar Annaba University Central Library

Copyright Elsevier 2025

This page intentionally left blank

This book belongs to Badji Mokhtar Annaba University Central Library

Copyright Elsevier 2025

CHAPTER 37

Nanomaterials for wastewater treatment: Concluding remarks

Bharat A. Bhanvase[a], V.B. Pawade[b], Shirish H. Sonawane[c], and A.B. Pandit[d]

[a]Chemical Engineering Department, Laxminarayan Institute of Technology, Rashtrasant Tukadoji Maharaj Nagpur University, Nagpur, Maharashtra, India, [b]Department of Applied Physics, Laxminarayan Institute of Technology, Rashtrasant Tukadoji Maharaj Nagpur University, Nagpur, MS, India, [c]Department of Chemical Engineering, National Institute of Technology, Warangal, Telangana, India, [d]Department of Chemical Engineering, Institute of Chemical Technology, Mumbai, India

37.1 Introduction

Adequate clean fresh water is necessary for the survival of life. However, its acquisition has become the biggest challenge due to the release of various pollutants in the water bodies [1]. Clean water is, in fact, a basic requirement for all living beings. In recent years, quick growth in the industrial sector and economy have adversely affected the global environment, i.e., the addition of industrial pollution and overexploitation of natural resources around the globe [2]. Thus, globalization and industrialization produces large amounts of industrial effluents, and it has significantly affected the sustainability of the existing natural resources (water, air, etc.) [3–6] and has become a major concern worldwide [7]. This increases the toxic substance level in the water bodies, which has a direct effect on aquatic life due to the release of harmful industrial waste effluents without any operative treatment [8,9]. The treatment of industrial effluents is very much essential and is an effective approach for controlling the resultant pollution, which then offers the possibility to reuse water [10].

The common techniques used are physical and chemical methods. The physical techniques used are boiling, sedimentation, desalination, reverse osmosis (RO), filtration, etc. for purification/treatment of wastewater. The physicochemical techniques used are coagulation, flocculation, and chlorination for the treatment of wastewater [1]. However, there is a dire need to develop efficient and effective industrial effluent treatment technologies to handle the problem of wastewater that is not properly tackled with conventional methods, which is on the frontier among other research fields within the scientific communities. Recent revolution in the field of nanotechnology has shown the possibility of novel nanostructured materials having

Handbook of Nanomaterials for Wastewater Treatment. https://doi.org/10.1016/B978-0-12-821496-1.00034-9
Copyright © 2021 Elsevier Inc. All rights reserved.

This book belongs to Badji Mokhtar Annaba University Central Library Copyright Elsevier 2025

unique and advantageous properties in the treatment of wastewater [11]. These nanomaterials have excellent adsorption properties due to their exceptional physicochemical properties like a higher surface area-to-volume ratio [12]. Furthermore, several types of nanomaterials like metal nanoparticles, polymer nanocomposites, zeolites, photocatalytic membrane (PMR), carbon nanostructures, and semiconductor photocatalysts have been reported to be useful for photocatalytic degradation of pollutants [13–20]. Thus, researchers have proposed photocatalysis techniques as an effective way to treat the presence of toxic dyes in wastewater. The preparation of tailored photocatalysts (which is of two types, e.g., homogeneous and heterogeneous photocatalysts) with narrow bandgap is essential that can absorb the incident radiation, generate a charge carrier, and help photochemical reaction for the degradation of harmful dyes in the presence of ultraviolet (UV) or visible light. However, the development of photocatalytic nanomaterials that will harness available natural sunlight in a greater amount for large-scale process for the treatment of wastewater is a challenge.

Furthermore, various nanotechnology-based processes have been developed for the wastewater treatment and are depicted in Fig. 37.1. Those are adsorption, photocatalytic processes, membrane-based processes, antimicrobial nanomaterial-based processes, etc. Various novel developed nanomaterials are being used in these processes that are used for wastewater treatment processes. However, these processes are facing certain challenges when planned at

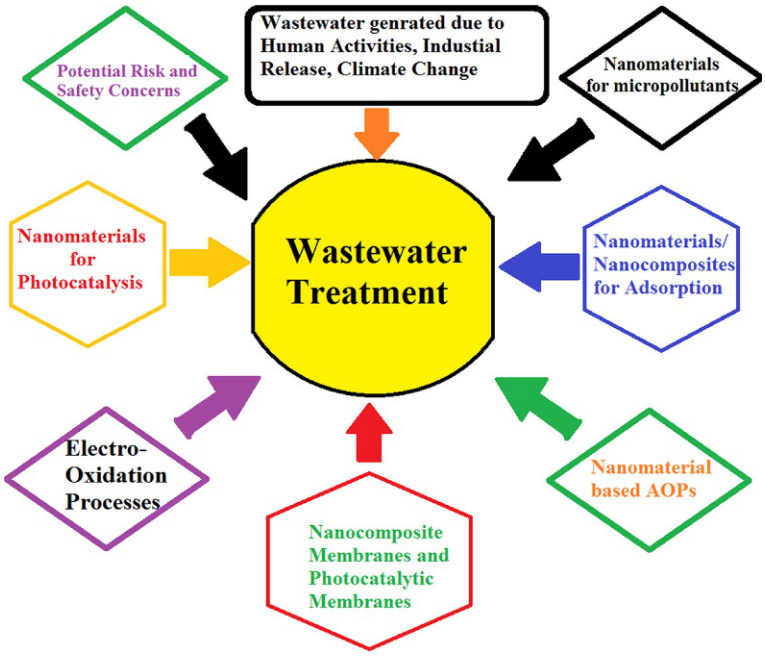

Fig. 37.1
Engineering nanomaterials/nanocomposites for various wastewater treatment processes.

This book belongs to Badji Mokhtar Annaba University Central Library
Copyright Elsevier 2025

pilot or industrial scale. In view of this, this chapter discusses the various aspects of these processes for wastewater treatment. Also, brief discussion on the current issues and challenges on the actual application of these nanomaterials-based processes for wastewater treatment are reported.

37.2 Nanomaterials and their properties for wastewater treatment

Various nanomaterials have been extensively used for wastewater treatments, reporting several developments in existing processes for wastewater treatment. Nanomaterials have been widely used for addressing wastewater problems due to exceptional properties of the nanomaterials (having one dimension less than 100 nm) such as smaller particle size, larger surface area, high reactivity, fast dissolution, and strong sorption [21]. Furthermore, several researchers have proposed various novel nanomaterials for the removal of heavy metals, organics, pharmaceuticals, textile dyes, etc. [21–25]. Due to the excellent properties of novel nanostructured materials, these are applied in the development of various processes/technologies for water remediation, purification, and separation of the pollutants. In the current chapter, various types of nanomaterials and their scope in water treatment processes have been discussed. Also, representative nanostructured materials are discussed in the following section with their properties.

37.2.1 Zero-valent nanomaterials

Various zero-valent nanoparticles like Ag, Fe, Zn, etc. have great applicability in the treatment of wastewater. Disinfection/degradation of pollutants/microorganisms present in wastewater was carried out by zero-valent metal nanoparticles. The nanomaterials used were Ag, Zn, and iron nanoparticles. Out of these nanomaterials, Ag nanoparticles are known for their excellent antimicrobial properties against various microorganisms like viruses, bacteria, and fungi [25–27]. In view of these antimicrobial properties, Ag nanoparticles are being used in various processes for the disinfection of water. The reduction in the particle size of Ag nanoparticles was reported to have a better effect in disinfection [28,29]. Direct application of Ag nanoparticles will be difficult for the disinfection of wastewater due to its aggregation tendency that reduces its antimicrobicidal properties and also reduces efficiency in long-term usage [30,31]. This problem is being resolved with the loading of Ag nanoparticles (immobilizing) on various supports or incorporation in a membrane forming nanocomposites for various wastewater treatments [32,33]. Incorporation of Ag nanoparticles during membrane formation itself substantially reduces the activity of microorganisms on the membrane surface and enhances the activity of the formed membrane in wastewater treatment [34,35].

Furthermore, Fe and Zn have great reduction potentials that act as reducing agents in wastewater treatment. Also, Fe showed great advantages over Zn due to its lower cost, excellent

This book belongs to Badji Mokhtar Annaba University Central Library Copyright Elsevier 2025

adsorption capacity, and precipitation and oxidation in the presence of oxygen present in the wastewater [36,37]. Zero-valent iron is present in abundant quantiles and is nontoxic, easy to prepare, and requires less maintenance in the process of wastewater treatment [36]. Zero-valent iron has negative redox potential equal to −0.44 V. In a wastewater treatment process, direct electron transfer mechanism from zero-valent iron to pollutants occurs in the presence of dissolved oxygen leading to degradation of pollutants present in the wastewater as per the reaction scheme given here in presence of H_2O_2 and O_2 [36].

$$Fe^0 + O_2 + 2H^+ \rightarrow Fe^{2+} + H_2O_2 \tag{37.1}$$

$$Fe^0 + H_2O_2 + 2H^+ \rightarrow Fe^{2+} + 2H_2O \tag{37.2}$$

$$Fe^{2+} + H_2O_2 \rightarrow Fe^{3+} + OH + OH^- \tag{37.3}$$

These zero-valent nanomaterials have been reported to be successfully used for the treatment of various organic compounds [38,39], heavy metals [40–42], and dyes [43]. Presently, zero-valent iron-based processes have been successfully applied at pilot-scale and full-scale applications for wastewater treatment remediation.

Zn nanoparticles have more negative potential and therefore are a stronger reductant compared with others that have been applied for the degradation of various pollutants present in wastewater. Zero-valent zinc is mainly exploited for the degradation of halogenated organic pollutants and therefore shows limited applicability [44].

However, zero-valent nanoparticles faces several disadvantages like aggregation, oxidation, and difficulty in the separation and recycling in the process. These challenges are being addressed with the modification of zero-valent nanoparticles that, in turn, enhances the performance in wastewater treatment. It is being modified by doping with other metals/metal oxides, deposition on various supports, incorporation in matrix, and emulsification. Application of these modification processes enhances the reactivity, prevents aggregation, enhances dispersibility, and facilitates the separation of zero-valent nanoparticles/nanocomposites from the wastewater degradation process.

37.2.2 Metal oxide nanomaterials

Metal oxides like TiO_2 and ZnO with suitable doping are well-known heterogeneous photocatalysts used in effective water and air purification processes [45,46]. Anatase phase of TiO_2 is highly photoactive out of three existing phases like anatase, rutile, and brookite, and has been investigated intensively [14,15,45,47]. Various TiO_2 preparation methods have been reported in the literature like simple sol-gel method, ultrasound assisted method, etc., which are helpful to control the particle size, specific surface area, crystallite size, and bandgap energy [15,47]. Several researchers have reported the use of TiO_2 nanoparticles for the degradation of chloroform [48], phenol [49], and trichloroethylene [50]. It has been further observed that the

This book belongs to Badji Mokhtar Annaba University Central Library Copyright Elsevier 2025

optimal particle size of anatase phase of TiO_2 depend on the nature of the test molecule. Hence, the optimum particle size and photoactivity of titania can also be enhanced by an increase in the number and strength of surface acidic sites, and the photoactivity can be tailored by doping with various metallic and nonmetallic elements. Furthermore, TiO_2 photocatalysts suffer from larger bandgap energy (3.2 eV) and has UV excitation to induce charge separation within the particles. These can be overcome with suitable metal and metal oxide doping in TiO_2 or forming its nanocomposite with carbon nanostructured materials, which enhances the charge separation and then photocatalytic degradation of pollutants in visible light.

ZnO nanoparticles act as another efficient photocatalyst nanomaterial. Due to the unique shape and size-dependent properties of ZnO, it has gained more interest for a technological wastewater solution. It has wide bandgap near the UV region and strong oxidation capability, so it is a good candidate for photocatalysis [51]. Photocatalytic properties of ZnO are similar to TiO_2, which showed higher recombination rate of electrons and holes and has lower cost compared with TiO_2. ZnO also can absorb a wider range of solar spectra and more light quanta compared with other metal oxides semiconductors. Similar to TiO_2, doping in ZnO can enhance the photocatalytic activity in the visible region.

37.2.3 Luminescent and Ln^{3+}-doped oxide nanomaterials

Semiconductor nanophosphors have served as ultimate and effective photocatalysts for three decades [52]. These nanophosphors have excellent photocatalytic properties like stability, cost effectiveness, nontoxic, and highly photoactive, which makes them an ideal candidate for photocatalysis. The semiconductors with larger bandgap energies are capable of catalyzing various chemical reactions. Semiconductor nanophosphors such as TiO_2, WO_3, $SrTiO_3$, α-Fe_2O_3, ZnO, and ZnS are being widely used in photocatalysis [53,54]. Size quantization in semiconductor particles encourages radical changes in numerous significant properties of the material. This affects the electronic properties like sustaining discrete highest occupied molecular orbitals (HOMOs) and lowest unoccupied molecular orbitals (LUMOs) of the semiconductor particle. Furthermore, it also influences the charge-carrier dynamics. Photocatalytic degradation of pollutants released from various industries requires efficient photocatalysts.

Luminescent phosphors can emit high energy photons by absorbing two or more low energy photons, and these phosphors are called upconverting luminescent phosphors. These phosphor materials contain luminescent dopants like Eu, Tb, Tm, Er, etc., which cause quick transition that permits an electron to absorb a low energy photon and jump to the valance band. Furthermore, these electrons jump back to the conduction band by emitting combined energy, which is obviously greater than the incident low energy photons [55–58]. The luminescent materials generally have host and dopant materials. The host materials like $BiWO_6$, $SrTiO_3$, CdS, etc. can absorb the high energy photons, which are obtained from the upconverting

This book belongs to Badji Mokhtar Annaba University Central Library Copyright Elsevier 2025

luminescent dopant or activators under excitation of low energy photons that could not be harvested by the host materials themselves due to wide bandgap energy, which enables band-to-band transition in the host materials. In this process, the host materials uphold their photocatalytic activity like redox reaction of charge carriers in the valance band and the conduction band. Furthermore, long persistent phosphors are more effective materials for photocatalytic activities. In these nanomaterials, the mobility of electrons is higher, which traps the electrons from the valance band and acts as an electron storage level; this, in turn, enhances the photocatalytic properties [59,60].

Furthermore, trivalent lanthanide (Ln^{3+}) ion-doped oxide nanomaterials are technologically important due to their potential applications in optoelectronics and display devices. Along with this, these nanomaterials act as an effective photocatalyst because of their narrow bandgap and high absorption in UV and visible range and has higher light conversion ability [61]. One suitable example is Ce^{3+}-doped ZnO photocatalyst, which works effectively for the oxidation of cyanide and cyanate under UV light illumination [62,63]. Furthermore, Ln-doped ZnO (Ln = La, Nd, and Sm) showed better photocatalytic activity for the degradation of 4-nitrophenol [64]. The separation of the nanomaterials from treated water is the challenge of a large-scale treatment. In this case, the reactor configuration is very important to resolve this issue to have better efficiency of degradation of pollutants present in the wastewater.

37.2.4 Nanozeolites

It is well known that zeolites are widely used in petroleum and chemical industries due to their exceptional catalytic and selective adsorption properties, as well as thermal and chemical stability for environmental friendliness. Currently, several research articles reveal the possible applications of extremely active zeolites and their selective way of synthesis [65–67]. Due to the intrinsic microporosity, even pore shapes, and narrow size distributions, these nanomaterials exhibit outstanding properties as molecular sieves and as shape-selective catalysts. However, zeolites suffer from a bulky nature, which cannot access the internal active sites. Therefore, several researchers are working to overcome these limitations to enhance the properties [68]. Furthermore, the decrease in the crystal size to the nanometer scale is an effective strategy to enhance the external surface area and the ratio of external/internal active sites, which enhances their accessibility to bulky molecules. According to some modifications in size and shape of zeolite, their catalytic applications can be expanded to those reactions involving large molecules. Among the different crystal sizes obtainable within the category of nanozeolites, there is special interest on reaching values of crystallite below 100 nm due to the unique properties and the potential applications in a variety of fields such as heterogeneous catalysis, molecular separation, ion exchange, chemical sensors, medicine, etc. [69].

The zeolites are being produced with various available processes such as pulsed laser on the zeolite LTA microparticles, hydrothermal activation of fly ash, etc. The laser-induced breakup

This book belongs to Badji Mokhtar Annaba University Central Library Copyright Elsevier 2025

of zeolite LTA microparticles leads to generation of zeolite nanoparticles. Furthermore, an ultrasound-assisted method also finds great application for the preparation of zeolites. These formed zeolite nanoparticles have great ion exchange properties and are being extensively applied in an ion exchange media for wastewater remediation. These zeolites have excellent sorption properties and therefore are being used in the removal of various pollutants like dyes, organic pollutants, and heavy metals like Cr(III), Ni(II), Zn(II), Cu(II), and Cd(II) from wastewater [70]. Furthermore, it has been reported that silver- and lead-loaded zeolites were applied for the treatment of pathogenic microbes and removal of heavy metals by forming insoluble complexes [19]. Also, chemically synthesized zeolites have more specificity, thermal stability, structural rigidity, and adsorption efficiency compared with natural zeolites, which is attributed to their tailored channel networks and controlled pore shape and size with higher modified surfaces [1].

37.2.5 Carbon/graphene-supported nanocomposites

Carbon nanoparticles, due to their low cost, nontoxicity, and excellent properties, have great applications in wastewater treatment. These nanomaterials are being used in wastewater treatment due to higher adsorption capacity for a wide range of pollutants, fast degradation and adsorption kinetics, very high surface area, and excellent selectivity toward aromatics [71]. These are attributed to the presence of a functional group on the carbon nanomaterials [72]. Physical and chemical functionalization of carbon nanomaterial is accomplished with targeted wastewater treatment application [72]. Hydrophilic functionalization of carbon nanomaterials like carbon nanotubes (CNTs) and graphene allows for better dispersion in aqueous systems, thus enhancing microbial and chemical pollutant's access toward its surface and thereby enhancing treatment [73]. Furthermore, depending on the target pollutants, carbon nanomaterials are being functionalized to enhance adsorption, photocatalytic degradation, etc. [72,74,75]. The activated carbon has more microscale pores and contains more mesopores, which is better compared with conventional carbon-based materials and are better for adsorption of various pollutants present in the wastewater [76].

Recently, graphene and their derivatives have shown to act as an emerging nanomaterial and established great attention in researchers due to the excellent properties for diverse applications [16,18,77]. To date, several researchers have worked on the preparation of graphene-based nanocomposite materials for photocatalysis and adsorption applications. Graphene with 2D and 3D structure is highly promising in energy and environment applications. Graphene is a single-atom layered aromatic carbon material that has 2D and 3D nanostructure with bandgap equal to zero. Graphene has been proven to have very high charge carrier mobility at room temperature, higher surface area, optical transparency, higher mechanical stiffness, higher thermal conductivity, and higher electrical conductivity [14,15]. The higher surface area enhances interfacial contact with other inorganic/organic compounds, which prevents the agglomeration

This book belongs to Badji Mokhtar Annaba University Central Library Copyright Elsevier 2025

of the nanoparticles deposited on the graphene or graphene derivative surfaces. These deposited nanomaterials act as spacers between graphene nanosheets, and this phenomena is responsible for the minimization of agglomeration of graphene in nanocomposites [17,18,78–80]. Therefore, graphene-based and carbon nanocomposites find diverse applications in various wastewater treatment processes like adsorption, membrane nanocomposites, photocatalytic degradation, etc.

37.2.6 Metal organic frameworks nanocomposites

In recent years, metal-organic frameworks (MOFs) have been developed, which is a class of solids that contain metal ions linked by molecular species. MOFs are porous coordination polymers (PCPs), i.e., hybrid organic-inorganic materials that emerged as a class of promising crystalline microporous materials [81,82]. MOFs have distinctive properties among several classes of microporous and mesoporous materials for a wide range of applications [83]. These materials offer higher thermal stability, which ensures wide temperature range applicability [84]. MOFs are composed of metal-oxide units connected by organic linkers through strong covalent bonds leading to formation of one-, two-, or three-dimensional structures, which are a combination of coordination bonds formed between metal cations such as Zn^{2+} and electron donors such as carboxylates or amines. The self-assembly of these constituents generates stiff pores that do not collapse upon removal of the solvent or other "guest" molecules occupying the pores following synthesis [83]. The formed MOFs are robust due to strong bonding with geometrically well-defined structure compared with a widely used adsorbent like activated carbon, which has a disordered structure.

MOFs act as molecular sieves for the selective adsorption of dyes and other pollutants due to their pore size, shape, and dimensionality. To achieve this, the structure of MOFs can be certainly tailored with a suitable choice of building blocks that are metal and organic linkers [85]. Modification of MOF's pore size and shape from a microporous to a mesoporous scale can be accomplished with alteration in the connectivity of the inorganic moiety and the nature of the organic linkers that increases the range of their potential applications in wastewater treatment [86]. MOFs have ultrahigh porosity, up to 90% free volume, due to its prominent structure and considerably high internal surface areas, extending beyond a Langmuir surface area of 10,000 m^2/g [81]. Furthermore, higher surface areas and porosity of MOFs facilitate the mass transfer process, and the unsaturated metal atoms, metal-hydroxyl, and other functional groups in the structure provides numerous adsorption sites for inorganic oxyanions [87]. Due to the distinctive feature and their outstanding network flexibility that are closely linked with the coordination bonds, noncovalent bonds, and weak interactions, MOFs are exceptional compared with porous materials like zeolites, activated carbons, and metal oxides [88–90].

This book belongs to Badji Mokhtar Annaba University Central Library Copyright Elsevier 2025

37.2.7 Nanocomposite membranes/nanocomposite photocatalytic membranes

Membranes are a physical barrier made of various constituent materials having specific pore size, which permit the transport of the selective ions, molecules, or small particles. In the current decade, membranes are considered to be key materials that are being used in wastewater as well as water treatment. Membranes are flexible in design with the use of various constituent species in its preparation for targeted separation of pollutants from wastewater [21,91]. The membrane performance is mainly controlled by the selection of the membrane material. During the preparation of membranes, dispersion of functionalized nanomaterials into membrane matrix enhances the formed membrane properties like membrane permeability, resistance to fouling, mechanical and thermal stability, etc. Furthermore, incorporation of targeted nanoparticles in membrane enhances degradation of pollutants and also promotes self-cleaning [21].

Nanofibers with higher surface area, porosity, etc. prepared with various methods like electrospinning are incorporated in the membrane materials forming a complex pore structure. Various properties of the formed membrane like diameter, composition, morphological and structural properties, and orientation of prepared nanofibers can be monitored for specific targeted wastewater treatment applications [92]. These type of membranes find applications in waster pretreatment plants, air filtration, etc. [93] due to exceptional features and tunable properties of the electrospun nanofibers-based multifunctional media/membrane filters.

Furthermore, nanocomposite membranes are being prepared with the incorporation of both organic and inorganic nanomaterials in the membrane's matrix, which is a new class of membranes that claimed to have improved the performance of the membrane in terms of permeability, thermal and chemical stability, hydrophilicity, mechanical strength, and porosity in comparison with conventional membranes [94,95]. Nanocomposite materials are extremely specific and selective in nature, and because of their exclusive properties, they have varied applications in several fields [96,97]. This is attributed to technological developments that achieve controlled synthesis and fabrication of these materials. The nanocomposite membranes have exceptional properties like excellent durability, mechanical strength, and good hydraulic properties with its reusability over several cycles of operation [98]. The nanocomposite membranes are reported to be prepared with polyamide, polysulfone, polyvinyl alcohol, chitosan, polymethyl methacrylate, polyetherimide, and cellulose acetate-based membrane and comprise micro- to nanofiltration [99–102]. Nanocomposite membrane acquires the properties of both inorganic and organic materials leading to improved separation properties like selectivity, thermal stability, mechanical strength, chemical resistance, and permeability [103]. Furthermore, incorporation of Ag nanoparticles and CNTs can reduce membrane biofouling, which attributes to the antimicrobial properties of these nanomaterials [104–106].

This book belongs to Badji Mokhtar Annaba University Central Library
Copyright Elsevier 2025

37.3 Current status and challenges of use of nanomaterial-based processes

Water pollution due to rapid globalization, industrialization, and climate change leads to water scarcity. In view of treatment of wastewater, several conventional and advanced water treatment methods have been proposed and are being used. However, conventional processes for wastewater treatment are often chemical and energy intensive and require large investment and engineering practices that limit the application of these processes. Nanotechnology application in wastewater treatment processes seems to be interesting. Various nanomaterials/nanostructured materials have been applied in various nanotechnology-based processes for efficient wastewater treatment. This is attributed to excellent properties of nanomaterials, as discussed in the earlier section, which are used in wastewater treatment processes like adsorption, photocatalysis, membrane-based processes, advanced oxidation processes (AOPs), electro-oxidation processes, micropollutants removal, etc. and attracts more interest in the research and development sectors. However, these processes have some limitation and challenges when applied at a pilot/industrial scale. These are discussed in the following sections.

37.3.1 Photocatalytic nanomaterials-based processes

Preparation of photocatalytic nanomaterials for wastewater treatment application should be accomplished with various aspects like suitable bandgap, structural and electronic properties that control electron-hole pair formation and recombination, high degree of crystallinity that favors photocatalysis, doping of nanomaterials, surface area, etc. [1,21]. The photocatalytic reactions are carried out in the presence of light, which generates photogenerated electron-hole pairs, and those control the degradation rates of pollutants. Therefore, the electron mobility and life/reusability of the photocatalysts are the very essential parameters that control the efficiency of photocatalytic degradation process. Separation of photogenerated electrons and holes are very essential in this process, and the use of materials having excellent electron mobility like graphene favors the photocatalytic degradation process. Apart from positive aspects of the photocatalysis processes such as low-cost, eco-friendly, and viable water treatment process, there are various practical challenges for its large-scale implementation such as photocatalyst optimization that improves the utilization of light, effective design of photocatalytic reactor, recovery of photocatalyst and its reusability, photocatalyst immobilization practices, and better reaction selectivity. Various photocatalysts like metals, metal oxides, semiconductors, carbon nanomaterials, quantum dots (QDs), MOFs, magnetic cored dendrimer, and other materials have been broadly investigated for degradation of pollutants present in wastewater. The photocatalysts are classified in three generations, which is depicted in Fig. 37.2.

Various process parameters, such as intensity of light radiation used, reaction temperature, humidity, oxygen concentration in the reaction medium, and photocatalyst loading, have

This book belongs to Badji Mokhtar Annaba University Central Library Copyright Elsevier 2025

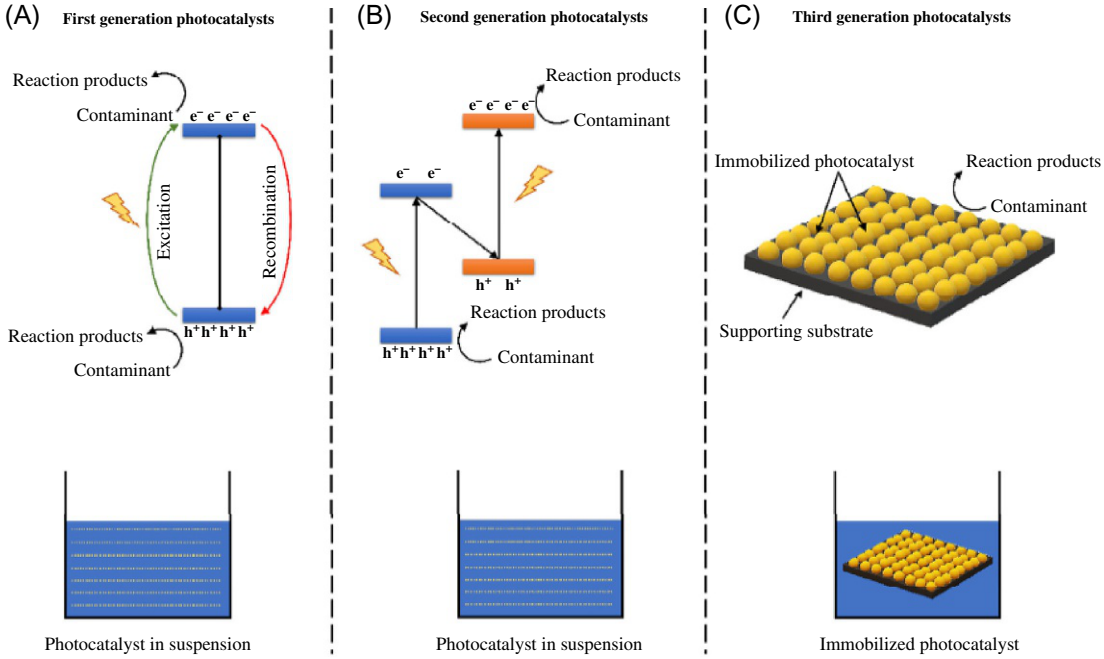

Fig. 37.2

Generations of photocatalyst's uses in photocatalytic degradation of pollutants present in wastewater [107]. *Reprinted with permission from H. Anwer, A. Mahmood, J. Lee, K.H. Kim, J.W. Park, A.C. Yip, Photocatalysts for degradation of dyes in industrial effluents: opportunities and challenges, Nano Res. 12 (2019) 955–972. Copyright (2019) Springer.*

substantial effects on the rate efficiency of photocatalytic degradation of the pollutants [1]. Furthermore, other key factors that affect the photocatalytic degradation of the pollutants are pH, pollutant adsorption on the photocatalyst, light intensity, photocatalyst loading, and dye concentration in reaction medium [107]. Further various uncertainties/doubts remain about photocatalytic dye degradation. These are degradation mechanism, knowledge about intermediate species formed during photocatalytic degradation process, electron-hole recombination processes, bandgap, etc.

Various types of reactor systems have been used for the degradation of pollutants in the photocatalytic degradation processes. The degradation rate of pollutants decides the amount of catalyst and volume of the reactor. These reactor systems are continuous mixed flow reactor, slurry reactor, and fixed-bed reactor for the degradation of pollutants. Several engineering factors that affect the design of the photocatalytic reactor are reactant catalyst contacting, catalyst exposure to light irradiations, flow patterns, mixing, mass transfer, reaction kinetics, catalyst installation, temperature control, etc. [108]. Exposure of a photocatalyst to light and its uniform distribution that covers a larger surface area are the main issues in a photocatalytic

This book belongs to Badji Mokhtar Annaba University Central Library Copyright Elsevier 2025

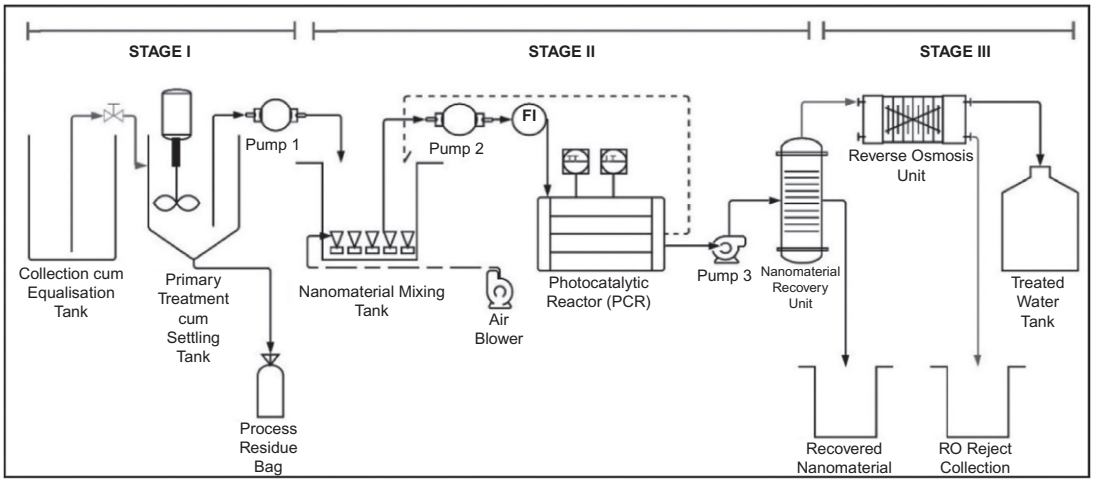

Fig. 37.3
Innovative three-stage pilot scale photocatalytic treatment process for the treatment of real textile and dyeing industry [109]. *Reprinted with permission from N. Bahadur, N. Bhargava, Novel pilot scale photocatalytic treatment of textile & dyeing industry wastewater to achieve process water quality and enabling zero liquid discharge, J. Water Process Eng. 32 (2019) 100934. Copyright (2019) Elsevier.*

reactor. This decides photocatalytic reactor geometry when designing a wastewater treatment process in a large scale.

Recently, Bahadur and Bhargava [109] have designed and operated an innovative three-stage pilot scale photocatalytic treatment process for the treatment of real textile and dyeing industry effluent (Fig. 37.3). These three stages are primary treatment, aeration in presence of TiO_2 photocatalyst, and photocatalytic degradation of pollutant in the presence of TiO2 nanoparticles under UV irradiations in a photocatalytic reactor. It was reported that the time taken for the degradation was 5 h with an estimated cost of 1.55 USD/m^3.

Furthermore, the major problem of photocatalytic degradation process is its slowest degradation kinetics, which leads to the requirement of large volume reactors, which needs a large land area for solar irradiations and for space of the reaction system. Also, an increase in the mass transfer is essential in the degradation process. Therefore, design of photocatalyst that harvests a wide range of photons (wavelength) from irradiated light and having excellent stability is a challenge.

37.3.2 Adsorbent nanomaterials-based processes

Adsorption is a surface phenomenon that binds ions, atoms, or molecules of gases, liquid, or dissolved solid on a solid material surface. On the surface of materials, potential sites are available that are responsible for the binding of various species. Conventional adsorbents suffer

This book belongs to Badji Mokhtar Annaba University Central Library Copyright Elsevier 2025

from various limitations like lesser surface area with less number of active sites, lack of selectivity, and kinetics of adsorption process. These problems are resolved with the use of nanosized materials with outstanding surface area and higher number of active sites, lesser intraparticle length, and tunable pore size [21]. Various adsorbents like activated carbon, zeolites, porous silica nanoparticles, surface functionalized nanoparticles, etc. were reported to be applied for the removal of various ions and organic pollutants from wastewater [1]. Surface modification is very much suitable for nanomaterials, which enhances the adsorption process. Various surface-modified nanomaterials like CNTs, graphene oxide (GO), graphene-Fe_3O_4 nanocomposites, core-shell nanoparticles, functionalized silica gel, etc. have been reported for effective adsorption of pollutants [110–114].

A variety of adsorbent materials ranging from biological waste, biomaterials, low-cost materials, nanoparticles, CNTs, etc. have been used for wastewater treatment. Although detailed research is being carried out for removal of pollutant using various adsorbents, a number of limitations still restricts the use of adsorption as an effective removal technique in the industry. The main limitation is the effectiveness and cost of the nanomaterials. Therefore, researchers are facing problems to develop a cost-effective wastewater treatment process. Therefore, the development of low-cost nanomaterials as an adsorbent for the treatment of wastewater is a challenge that, in turn, can reduce the cost of the process [115–117]. Furthermore, the adsorbents with effective pollutant removal capacity are costlier. This can be addressed with the regeneration of the saturated adsorbent in the adsorption process, which takes an hour. Several researchers have reported the regeneration of adsorbents with the use of suitable chemicals. Also, the storage and recovery of the metal/pollutant from the adsorbent is critical [118,119].

Furthermore, in the wastewater treatment process with the use of nanoadsorbents, generally, slurry reactors or columns packed with adsorbent called adsorbers are used. In a slurry reactor, nanoadsorbents used in the powder form are highly effective. This is attributed to effective utilization of all the surfaces of the nanoadsorbents and also the effective mixing significantly expedites the mass transfer. However, the separation of such some smaller-sized nanoparticles from large volume wastewater, i.e., from a slurry reactor is critical and is a challenge that limits its use at an industrial scale. Another separation unit is implemented in the process to recover the nanoparticles [21]. This issue is further resolved with the use of a fixed- or fluidized-bed adsorption system in which nanoadsorbents can be fixed/immobilized in a fixed-bed adsorber or can be used in the form of pellets/beads or porous granules loaded with nanoadsorbents in fluidized-bed adsorbers. Immobilization of nanoadsorbents or formation of beads leads to a loss of surface area, which limits separation efficiency. Also, the fixed-bed adsorbers suffer from lower mass transfer of the pollutants in the process. However, in these types of processes, installation of a separation unit is not required [21]. Various processes are commercialized for the removal of heavy metals like arsenic and pollutants with the use of nanoadsorbents [120,121] and reported efficient removal of pollutants [122–124].

This book belongs to Badji Mokhtar Annaba University Central Library Copyright Elsevier 2025

37.3.3 Nanocomposite membranes-based processes

Nanocomposite membrane-based processes are proven to be promising for wastewater treatment in bench-scale studies. Preparation of nanocomposite membrane has several issues like agglomeration of nanoparticles during preparation of membrane, fouling and regeneration of membrane, etc. Production of nanocomposite membrane also has various challenges during its fabrication, application, and disposal. This nanocomposite membrane process faces many challenges at an industrial level during its implementation. The performance of the industrial-scale process is largely affected compared with bench-scale studies. Furthermore, the toxicity of nanomaterials used in the membrane that is getting exposed to the environment is a very important issue [125]. The nanoparticles incorporated in the nanocomposite membrane are leached out during its use due to poor interaction between nanoparticles and membrane matrix. This creates toxicity in the environment and reduces surface area and pore size during the long run of filtration process. Compatibility and interaction of nanomaterials with membrane matrices also controls the performance of the membrane and nanomaterial's stability inside the polymer matrix [126,127].

Cost of the nanomaterials incorporated in the membrane matrix is another important issue which limits its use as large-scale treatment [128]. Also these nanocomposite membrane processes are pressure driven that requires extensive energy in the separation [125]. At large-scale treatment of industrial wastewater containing diverse pollutants like heavy metals, organic and inorganic pollutants resist the selective separation of the pollutants, which block the membrane pores leading to fouling of the membranes; this is a major issue in membrane technology [125]. Membrane fouling occurs due to the accumulation of various impurities, which block the pores and create a barrier for permeation of water. This largely affects the lifespan and performance of the membrane, which requires a high maintenance cost. To clean the membranes, a large amount of cleaning agents is used for regeneration, which makes this technology more expensive. This also results in an increase in the transmembrane pressure requirement for the same flux [94]. Important aspects that need to be considered during the commercialization of nanocomposite membrane is the durability of nanomaterials under various operating conditions and degradability of nanomaterials at the end of useful service life [129,130]. Therefore, it is important to develop simple, cost-effective, and reliable techniques for the production of nanocomposite membranes that must sustain and be resistant toward all types of pollutants and fouling in actual waste conditions [125].

Ceramic membranes have very high resistance to various operating conditions like pH, temperature, flux, backwash, oxidizing agents, UV light exposure, etc. This is because these membranes are made up of zirconium, aluminum, silica, titanium, etc., due to which the cost of these membranes is more, which limits its use at a higher scale. However, polymeric membranes cannot be applied for high-temperature operation, heavily loaded feeds, and feed

This book belongs to Badji Mokhtar Annaba University Central Library Copyright Elsevier 2025

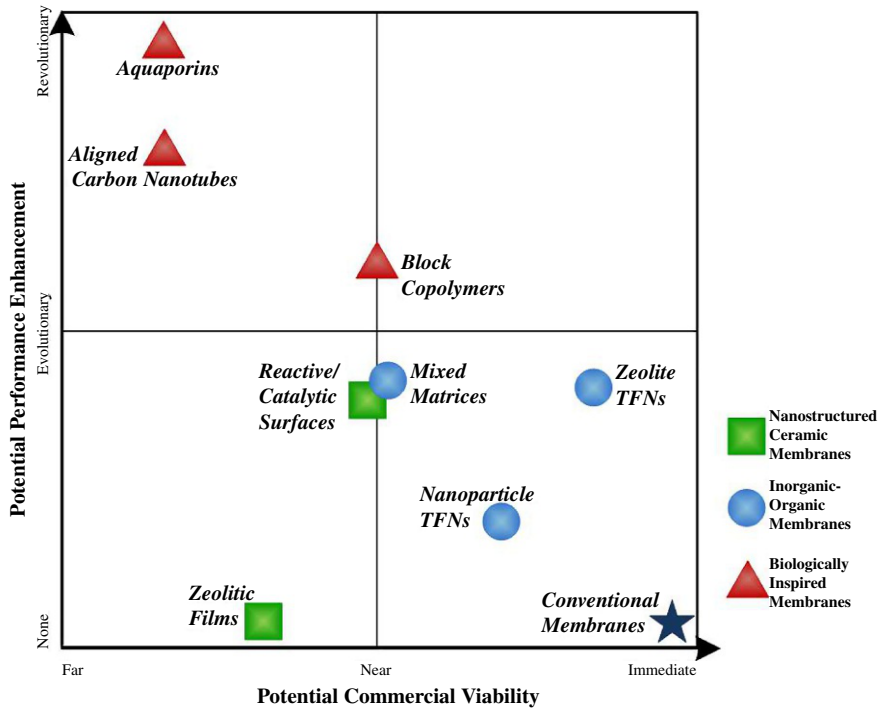

Fig. 37.4

Comparative investigation on the commercial viability of the nanotechnology-enabled membrane advances and its potential performance [132]. *Reprinted with permission from M.M. Pendergast, E.M.V. Hoek, A review of water treatment membrane nanotechnologies, Energy Environ. Sci. 4 (2011) 1946–1971. Copyright (2012) Royal Society of Chemistry.*

containing radioactive materials. To reduce biofouling and increase disinfection, silver- and titanium-based nanocomposite membranes are used. However, the cost is again an issue. Zeolite- and CNT-based nanocomposite membranes provide higher permeability, which has application in RO systems [131]. But these membranes face problems like interaction between the organic and inorganic materials in their production. Fig. 37.4 depicts the comparative potential performance and commercial feasibility of nanotechnology-enabled membrane advances. The performance enrichment of nanotechnology-enabled membrane is related to permeability, selectivity, and robustness, and for commercial feasibility, parameters like material cost, scalability, and compatibility with current manufacturing infrastructure was considered. It has been further reported that none of the available membrane nanotechnologies attends the upper-right quadrant on the chart, which can be considered optimal; however, in the time to come, biologically inspired membrane technology may mature [132].

This book belongs to Badji Mokhtar Annaba University Central Library Copyright Elsevier 2025

37.3.4 Nanomaterial-based photocatalytic membrane-based processes

Nanomaterial-based PMR is a membrane incorporated with nanosized photocatalyst materials. Generally, a photocatalyst used for the degradation of the pollutants present in the wastewater are dispersed in the wastewater in the form of slurry or immobilized in the form of a coating. Both methods have their pros and cons. Furthermore, to avoid the loss of the photocatalyst in bulk, to control the molecule's retention in the rector, and to have a continuous process that separates the products and catalyst, PMRs were found suitable and interesting. PMRs are the membrane process coupled with nanosized photocatalysts [133,134]. PMR-based process has various advantages such as improved process efficiency, stability, and reusability of the photocatalyst with reduced operating cost [135,136]. In different types of PMRs, the first case deals with the separate zones in the PMR like photocatalytic degradation and membrane separation [137], and in second case, the immobilization of the photocatalyst was done on membranes or in the membrane matrix [138]. In both cases, proper light irradiations were positioned on the active surface. Also immobilization of photocatalyst results in lowering the photocatalyst membrane performance. This is attributed to reduction in light harvesting arising due to lower exposed surface area of the photocatalyst and reduction in mass transfer.

In spite of several advantages of PMR-based processes for wastewater treatment, these processes suffer from various challenges like membrane fouling, which affects the reduction in permeate flux and, in turn, reduces productivity. This creates a problem in the operation of the process like increased energy consumption, frequent cleaning, lesser lifespan, and higher replacement cost [136,139]. Further agglomeration of photocatalysts on the membrane or in the membrane matrix is yet another challenge during the preparation of the PMR.

Even though there are several investigations on PMR reactors, scale-up of this process has been hardly studied. This might be due to a number of factors that need to be taken care of, like light intensity gradient, concentration gradient, interaction of light with the photocatalyst, quantum efficiency, operation mode of a reactor, hybrid system and design, stability and reusability of the photocatalyst, and agglomeration of nanoparticles [140–143]. All these efforts to develop and scale up the PMR system for effective organic pollutant treatment and showed positive potential of the PMR process. Incorporation of photocatalyst nanoparticles in membrane matrix or on the membrane enhances the performance of the PMR process and holds promising future in wastewater treatment.

37.3.5 Nanomaterials-based advanced oxidation processes

Nanomaterials are effective catalysts/photocatalysts compared with conventional catalysts due to their smaller particle size with very high surface area-to-volume ratio. These nanomaterials have very high reactivity at lower particle size and higher surface area. Design and preparation of a catalyst with most effective size and structure is of prime

This book belongs to Badji Mokhtar Annaba University Central Library Copyright Elsevier 2025

importance. Nanosized catalysts are being effectively used in AOPs for chemical oxidation of various organic and inorganic pollutant species present in wastewater. In this process, formation of highly reactive radicals rapidly react with the pollutant species or oxygen that leads to the formation of hydroxyl radicals and other oxygenated reactive species. Therefore, AOPs are able to degrade nonbiodegradable, recalcitrant, and toxic organic pollutants under ambient conditions [144]. To achieve complete mineralization of organic pollutants, AOPs are being used in combination with mineralization and partial oxidation to inert compounds, which will be cost effective [145]. In homogeneous AOPs, various combinations have been reported such as H_2O_2/Fe^{2+}, O_3/H_2O_2, O_3/UV, and H_2O_2/UV processes responsible for the production of OH• radicals in the presence of added O_3 or H_2O_2. Furthermore, other reactive oxidants are $SO_4^{\bullet-}$ and Cl•. These AOPs usually required considerable chemicals and energy in full-scale processes for wastewater treatment that are better than conventional processes. Engineered nanomaterials, due to their excellent physicochemical, optical, and electrical properties, can solve these practical challenges, which make AOPs more effective for water treatment. These nanomaterials are integrated in AOPs more suitable [21,146]. The nanomaterials have specific properties like higher electron mobility due to the 2D structure of graphene, optimal charge diffusion and path length for light in 1D materials, and higher specific surface areas in the case of 0D nanoparticles, which favors their catalytic properties for the degradation of pollutants. This leads to heterogeneous AOPs for the degradation of pollutants.

In spite of excellent performance of heterogeneous AOPs, this process faces some unusual problems like leaching of nanomaterials in the system [147]. Also, some of the nanomaterials changes their oxidation state in the degradation process, and those need to be regenerated after use [148]. Furthermore, engineered nanomaterial-based AOPs have been applied for the degradation of pollutants, which are (1) peroxy-based AOPs that use Fenton, ozone, and persulfates used in the presence of a photocatalyst, (2) photocatalytic AOPs that are used in a light-driven process in the presence of a photocatalyst, and (3) electrochemical AOPs driven by electricity in the presence of engineered nanomaterials [149].

For the implementation of nanomaterial-based AOPs in industrial and domestic wastewater treatment, several problems need to be effectively handled in the previously mentioned AOPs. Fig. 37.5 defines the challenges and future prospects for nanomaterials-based heterogeneous AOPs in water treatment. Some problems with these methods are: (1) engineered nanomaterials are functional in a precise range of conditions, (2) problems created by the presence of nanomaterials in the reaction medium, which are inherent challenges of AOPs, and (3) unconventional difficulties in the process design of nanomaterial-based AOPs [149]. Fig. 37.5 elaborates a high demand of energy and chemicals due to the presence of radical scavenging materials like natural organic matter and various bicarbonates. Also, a reduction in radiation and turbidity for photocatalyst-based AOPs and probable formation of highly toxic by-products comprised of halogenated compounds are possible problems [149].

This book belongs to Badji Mokhtar Annaba University Central Library Copyright Elsevier 2025

This book belongs to Badji Mokhtar Annaba University Central Library

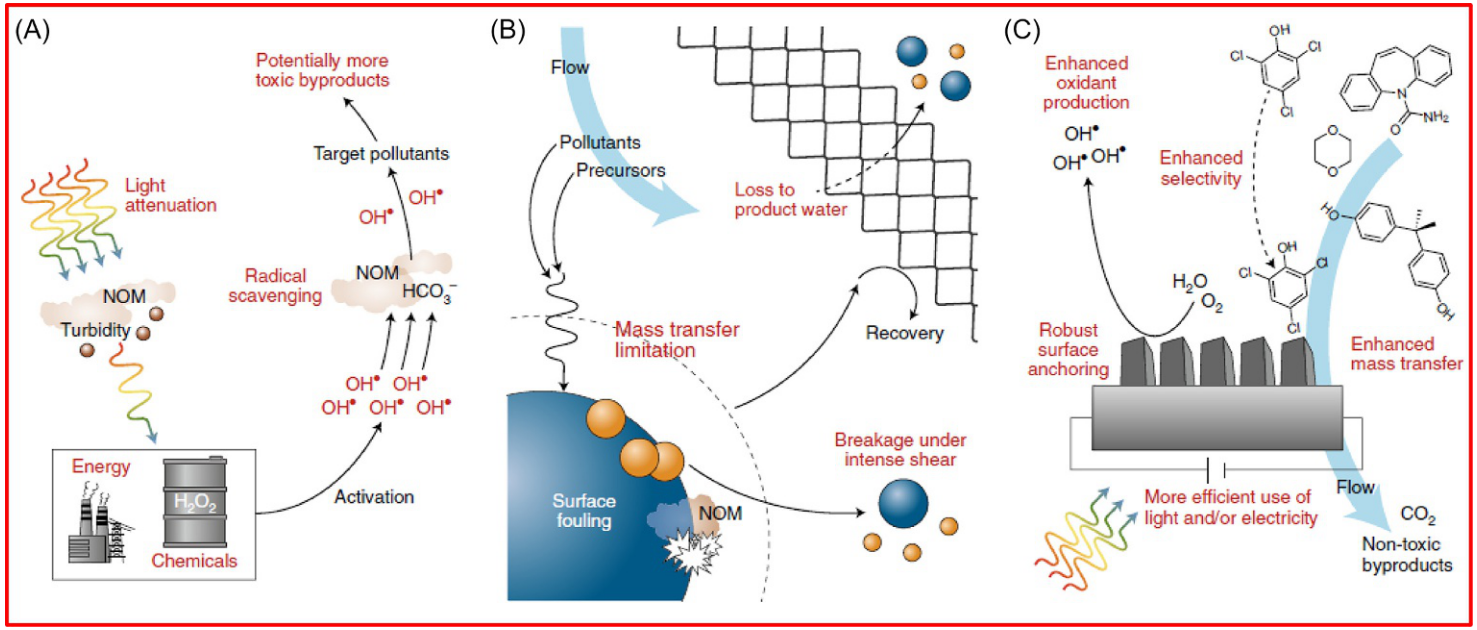

Fig. 37.5

Challenges and prospects for nanomaterials-based heterogeneous advanced oxidation processes in water treatment [149]. *Reprinted with permission from B.C. Hodges, E.L. Cates, J.-H. Kim, Challenges and prospects of advanced oxidation water treatment processes using catalytic nanomaterials, Nat. Nanotechnol. 13 (2018) 642–650. Copyright (2018) Springer Nature.*

Copyright Elsevier 2025

Furthermore, nanomaterial-based heterogeneous AOPs faces challenges like (1) brittleness of nanomaterial structure leading to breaking, which contributes to the probable loss to the discharge stream, (2) offers mass transfer resistance in the presence of nanomaterials, and (3) irreversible adsorption of the reactants and products on the catalyst surface leading to its fouling [149]. These challenges can be overcome, which are nothing but opportunities, by designing robust immobilization of effective nanomaterials that have enormous surface areas and selectivity, which will take care of the polluting organic matter [149]. This also enables the design of innovative reactors for nanomaterial-based AOPs that overcome mass transfer resistances offered by the presence of nanomaterials and enhances the unitization of light and electricity, which are nothing but process-specific difficulties [149].

37.3.6 Nanomaterial-based electro-oxidation processes

Wastewaters released by various industries are in the form of complex organic and inorganic compounds mixtures, which are sometimes toxic in nature and challenging to degrade [150]. Conventional methods are not able to degrade some of these complex toxic pollutants; however, some more advanced processes like membrane [151], photocatalysis [54,77], adsorption [74,118], AOPs [70], and ozonation [152] are being applied, but these processes have several individual shortcomings. Therefore, electrochemical processes like electro-oxidation, electrochemical coagulation, and electrochemical flotation are important for the degradation of toxic compounds [153,154] due to their simple operation and possibly complete degradation of harmful pollutants. Therefore, these are green processes because of little or no chemical requirements during wastewater treatment process. In these processes, development of high performance electrode materials is essential and has great potential in enhanced wastewater treatment.

In an electro-oxidation processes, oxidation of various pollutants is carried out with hydroxyl radicals generated on the surface of the anode or oxidants like chlorine, hypochlorous acid, and hypochlorite or hydrogen peroxide/ozone generated at the electrodes [155–159]. Numerous electrodes like lead oxide, graphite, boron-doped diamond, etc. have been used for water treatment by electrochemical oxidation. Design of novel electrodes are essential that can be done with the use of nanomaterials, which have lower particle size with higher surface area and more regular and compact morphology that enhances the mass transfer of pollutants toward electrodes, hence reaction rates [160]. Also, electrochemical catalytic oxidation process in the presence of ultrasonication with the use of nanocoated electrodes show enhanced degradation of the pollutants [161]. The use of nanocoated electrodes generates more quantum of hydroxyl radicals compared with conventional electrodes. Application of ultrasonic irradiations in the process also enhances the mass transfer on the nanocoated electrode surface, which leads to rapid diffusion of formed hydroxyl radicals in the reaction medium. The electro-oxidation process is able to effectively mineralize the nonbiodegradable organic matter. However, in

This book belongs to Badji Mokhtar Annaba University Central Library Copyright Elsevier 2025

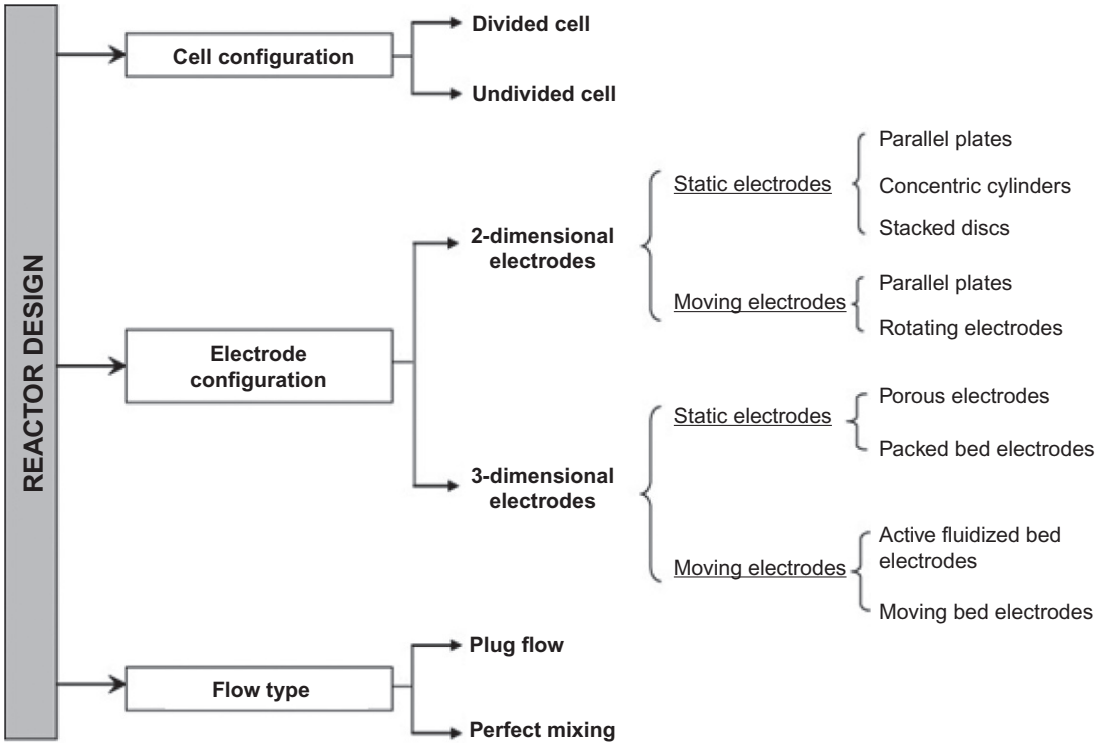

Fig. 37.6
Classification of electrochemical reactors in view of cell configuration, electrode geometry, and flow type [162]. *Reprinted with permission from A. Anglada, A. Urtiaga, I. Ortiz, Contributions of electrochemical oxidation to waste-water treatment: fundamentals and review of applications, J. Chem. Technol. Biotechnol. 84 (2009) 1747–1755. Copyright (2009) Wiley Interscience.*

these processes, formation of toxic by-products is a main problem and needs to be investigated thoroughly before its application at the pilot or industrial scale. Also, the service life of the electrodes in this process is a challenge and requires investigation on the same fundamental aspects. Finally, the economics of the electro-oxidation process for the treatment of real wastewaters is mainly dependent on the type of reactor system used in the process and can be resolved with the optimization of electrolytic reactors [154]. Fig. 37.6 represents the summary of different aspects that are considered in the electrochemical reactor design [162].

37.3.7 Nanomaterials-based processes for removal for micropollutants

The micropollutants released in water bodies from the products used on daily basis are pharmaceuticals, personal care products (PCPs), pesticides, endocrine disrupting compounds (EDCs), dyes, surfactants, and industrial additives, etc. The details are nicely explained in Chapter 31 by one of the contributors to this book. There is a requirement of advanced

This book belongs to Badji Mokhtar Annaba University Central Library Copyright Elsevier 2025

technologies for the complete removal of hazardous micropollutants. These are reported to be generally treated with various well-known advanced processes like photocatalysis, adsorption, and membrane separation using suitable nanomaterials. The advantages of using novel nanomaterials-based processes in comparison with the conventional processes are the former's capability to incorporate numerous properties, resulting in multifunctional systems such as nanocomposite membranes that permit both particle retention and the removal of contaminants [163]. Also, nanomaterials-based processes have higher efficiencies due to their exceptional characteristics like large surface area, which enhances the degradation of micropollutants.

Photocatalysis using tailored nanomaterials, like metal oxides and their nanocomposites, doped metal and metal oxides, carbon material-supported metal oxides, and magnetic material-based metal oxides, has proven to be a promising option for the removal of various types of micropollutants. Development of cost-effective nanophotocatalysts suitable in degradation process of micropollutants in visible solar light is highly desirable for industrial-scale operation. Furthermore, the efficacy of photocatalytic process using tailored nanomaterials can be maximized with suitable process parameters at pilot/large-scale degradation of micropollutants. Furthermore, various nanoadsorbents are the most widely used for wastewater treatment due to their microporous structure and high surface area. However, these processes face certain limitations in terms of the generation of secondary pollution due to the smaller size of particles and difficulties in the separation from the solution. Also, regeneration and economical reuse are major challenges in nanomaterial applications [164]. This can be resolved with nanoadsorbent modifications such as organic-inorganic hybrids [165], multiwall CNTs [166,167], or hydrous manganese oxide [168], which is very essential. Furthermore, as discussed in earlier sections, nanomaterial-based membranes have great applications in wastewater treatment process due to excellent removal efficiency, low space requirement for the plant [169], and highly economical and simple design for removal of micropollutants [170–172]. However, as mentioned earlier, membrane fouling due to the deposition of pollutants/particles is a major shortcoming that reduces the consistency and lifespan of the membranes and reduces the efficacy of separation. These can be resolved with the incorporation of nanomaterials on the membrane or in its matrix [173]. Leaching of the immobilized nanomaterials and its secondary toxicity is a major limitation or environmental concern for the application of nanomaterial-based membranes in wastewater treatment.

In the literature to date, most of the investigation reported is limited to the treatment of model pollutants (one type of pollutant molecule) at a laboratory scale. However, real industrial effluents contain various micropollutants and other undesirable substances. Therefore, there is a need to investigate the simultaneous removal of several co-existing micropollutants from real industrial wastewater. This type of investigation must be focused on transferring the application of nanotechnology in wastewater treatment from a laboratory or pilot scale to real industrial applications. In these processes, proper selection of suitable nanomaterial is essential for the effective removal of micropollutants from wastewater. Although nanomaterials have received

This book belongs to Badji Mokhtar Annaba University Central Library Copyright Elsevier 2025

potential application at the laboratory scale, there are certain challenges such as aggregation of the presence of nanomaterials, difficulty in the separation, and also potential adverse effects imposed by nanomaterials on the ecosystem and human health. Overall, it can be said that the further investigation in this direction will lead to the development of cost-efficient, economic, and environmentally friendly and safe processes for the treatment of wastewater in a sustainable manner. The economic feasibility of any large-scale industrial wastewater treatment process involving nanomaterials largely depends upon the selection of nanomaterials with high removal rates of micropollutants. The cost of these nanomaterials, in turn, depend on the type of nanomaterial and their desired properties such as level of purity, surface functionalization, and particle size [174].

37.4 Challenges for nanomaterial-based processes, potential risk, and safety concerns

Engineered nanomaterial-based processes for the degradation/separation/adsorption of various pollutants are promising at the laboratory scale. Very few of these nanomaterial-based processes are commercialized and in the market. However, these processes need substantial advancement and research for pilot/industrial-scale applications. The cost, technological competency, and risk to the environment and humans are the major hurdles in their pilot/industrial-scale applications. Furthermore, the functional lifespan of these nanomaterials in these processes is also an important issue that enables these processes for long-term application for wastewater treatment. The performance of the nanomaterial-based processes is superior to conventional processes; however, it depends on the cost effectiveness and potential risk of nanomaterials and the nanomaterial-based processes. The cost issues can be resolved with the application of low-cost nanomaterials with slightly lower performance and low purity nanomaterials. Separation and reusing the nanomaterials for wastewater treatment processes can also reduce the cost substantially.

Nanomaterials are very small particles that can be released into treated waste due to leaching, and ineffective separation is the challenge for the application of nanomaterials. The risk assessment and management of these very small nanoparticles is essential, and risk assessment framework and related protocols need to be put in place. The risk of secondary pollution due to nanomaterials is again one of the major hurdles in the application of nanomaterial-based processes for wastewater treatment.

37.5 Concluding remarks

In summary, this concluding chapter highlights the numerous features of nanomaterial-based processes for wastewater treatment applications. In this chapter, properties of various types of nanomaterials have been discussed that has confirmed and validated their suitability for

This book belongs to Badji Mokhtar Annaba University Central Library Copyright Elsevier 2025

application in wastewater treatment processes, at least as a proof of concept. Current status and challenges of various nanomaterial-based processes like photocatalysis, adsorption, nanocomposite membrane, nanomaterial-based PMR, nanomaterials-based AOPs, nanomaterial-based electro-oxidation processes, and nanomaterials-based processes for the removal of micropollutants have been discussed in depth. The particle size, shape, and the surface area of the nanomaterials are very important properties that are essential in wastewater treatment processes. These properties enhance the efficiency of the processes by many folds. Nanocomposite membrane-based processes for treating wastewater are exceptionally effective and most commonly use technology on a domestic scale and partly on an industrial scale. However, there are several nanomaterials-based processes that are expensive, and this is the main challenge for its ready adaption. The performance of the nanomaterial-based processes is superior to conventional processes; however, it depends on the cost effectiveness and potential secondary risk of nanomaterials and these nanomaterials-based processes. Nanomaterials are very small particles that could be released in the treated waste due to leaching and ineffective separation, which is a challenge for its application. The risk assessment and management of these very small nanoparticles is very essential.

References

[1] A. Baruah, V. Chaudhary, R. Malik, V.K. Tomer, Nanotechnology based solutions for wastewater treatment. in: Nanotechnology in Waste Water Treatment, Elsevier, 2019, pp. 337–368, https://doi.org/10.1016/B978-0-12-813902-8.00017-4.

[2] S.R. Mudakkar, K. Zaman, M.M. Khan, M. Ahmad, Energy for economic growth, industrialization, environment and natural resources: living with just enough. Renew. Sust. Energ. Rev. 25 (2013) 580–595, https://doi.org/10.1016/j.rser.2013.05.024.

[3] R.C. Olvera, S.L. Silva, E. Robles-Belmont, E.Z. Lau, Review of nanotechnology value chain for water treatment applications in Mexico. Resour. Technol. 3 (2017) 1–11, https://doi.org/10.1016/j.reffit.2017.01.008.

[4] L. Zhang, L. Cheng, F. Chiew, B. Fu, Understanding the impacts of climate and landuse change on water yield. Curr. Opin. Environ. Sustain. 33 (2018) 167–174, https://doi.org/10.1016/j.cosust.2018.04.017.

[5] F. Xiaoming, L. Qinglong, Y. Lichang, B. Fu, C. Yongzhe, Linking water research with the sustainability of the human-natural system. Curr. Opin. Environ. Sustain. 33 (2018) 99–103, https://doi.org/10.1016/j.cosust.2018.05.012.

[6] C. Tortajada, A.K. Biswas, Achieving universal access to clean water and sanitation in an era of water scarcity: strengthening contributions from academia. Curr. Opin. Environ. Sustain. 34 (2018) 21–25, https://doi.org/10.1016/j.cosust.2018.08.001.

[7] A.V.B. Reddy, M. Moniruzzaman, T.M. Aminabhavi, Polychlorinated biphenyls (PCBs) in the environment: recent updates on sampling, pretreatment, cleanup technologies and their analysis. Chem. Eng. J. 358 (2019) 1186–1207, https://doi.org/10.1016/j.cej.2018.09.205.

[8] D.S. Fraser, K. O'Halloran, M.R. van den Heuvel, Toxicity of pulp and paper solid organic waste constituents to soil organisms. Chemosphere 74 (2009) 660–668, https://doi.org/10.1016/j.chemosphere.2008.10.065.

[9] M. Ali, T. Sreekrishnan, Aquatic toxicity from pulp and paper mill effluents: a review. Adv. Environ. Res. 5 (2001) 175–196, https://doi.org/10.1016/S1093-0191(00)00055-1.

[10] P.S. Goh, A.F. Ismail, A review on inorganic membranes for desalination and wastewater treatment. Desalination 434 (2018) 60–80, https://doi.org/10.1016/j.desal.2017.07.023.

This book belongs to Badji Mokhtar Annaba University Central Library Copyright Elsevier 2025

[11] H. Lu, J. Wang, M. Stoller, T. Wang, Y. Bao, H. Hao, An overview of nanomaterials for water and wastewater treatment. Adv. Mater. Sci. Eng. 2016 (2016) 1–10, https://doi.org/10.1155/2016/4964828.
[12] N. Gupta, P. Pant, C. Gupta, P. Goel, A. Jain, S. Anand, A. Pundir, Engineered magnetic nanoparticles as efficient sorbents for wastewater treatment: a review. Mater. Res. Innov. (2017) 1–17, https://doi.org/10.1080/14328917.2017.1334846.
[13] A. Baruah, M. Jha, S. Kumar, A.K. Ganguli, Enhancement of photocatalytic efficiency using heterostructured SiO_2-Ta_2O_5 thin films. Mater. Res. Express 2 (2015) 056404https://doi.org/10.1088/2053-1591/2/5/056404.
[14] B.A. Bhanvase, T.P. Shende, S.H. Sonawane, A review on graphene-TiO_2 and doped graphene-TiO_2 nanocomposite photocatalyst for water and wastewater treatment. Environ. Technol. Rev. 6 (2017) 1–14, https://doi.org/10.1080/21622515.2016.1264489.
[15] T.P. Shende, B.A. Bhanvase, A.P. Rathod, D.V. Pinjari, S.H. Sonawane, Sonochemical synthesis of Graphene-Ce-TiO_2 and Graphene-Fe-TiO_2 ternary hybrid photocatalyst nanocomposite and its application in degradation of crystal violet dye. Ultrason. Sonochem. 41 (2018) 582–589, https://doi.org/10.1016/j.ultsonch.2017.10.024.
[16] D.P. Kale, S.P. Deshmukh, S.R. Shirsath, B.A. Bhanvase, Sonochemical preparation of multifunctional rGO-ZnS-TiO_2 ternary nanocomposite and its application for CV dye removal. Optik (Stuttg.) 208 (2020) 164532, https://doi.org/10.1016/j.ijleo.2020.164532.
[17] S.P. Deshmukh, D.P. Kale, S. Kar, S.R. Shirsath, B.A. Bhanvase, V.K. Saharan, S.H. Sonawane, Ultrasound assisted preparation of rGO/TiO_2 nanocomposite for effective photocatalytic degradation of methylene blue under sunlight. Nano-Struct. Nano-Objects 21 (2020) 100407, https://doi.org/10.1016/j.nanoso.2019.100407.
[18] V.D. Potle, S.R. Shirsath, B.A. Bhanvase, V.K. Saharan, Sonochemical preparation of ternary rGO-ZnO-TiO_2 nanocomposite photocatalyst for efficient degradation of crystal violet dye. Optik (Stuttg.) 208 (2020) 164555, https://doi.org/10.1016/j.ijleo.2020.164555.
[19] B. Kwakye-Awuah, C. Williams, M.A. Kenward, I. Radecka, Antimicrobial action and efficiency of silver-loaded zeolite X. J. Appl. Microbiol. 104 (2008) 1516–1524, https://doi.org/10.1111/j.1365-2672.2007.03673.x.
[20] G. Lofrano, M. Carotenuto, G. Libralato, R.F. Domingos, A. Markus, L. Dini, R. K. Gautam, D. Baldantoni, M. Rossi, S.K. Sharma, M.C. Chattopadhyaya, M. Giugni, S. Meric, Polymer functionalized nanocomposites for metals removal from water and wastewater: an overview. Water Res. 92 (2016) 22–37, https://doi.org/10.1016/j.watres.2016.01.033.
[21] X. Qu, P.J.J. Alvarez, Q. Li, Applications of nanotechnology in water and wastewater treatment. Water Res. 47 (2013) 3931–3946, https://doi.org/10.1016/j.watres.2012.09.058.
[22] W.-W. Tang, G.-M. Zeng, J.-L. Gong, J. Liang, P. Xu, C. Zhang, B.-B. Huang, Impact of humic/fulvic acid on the removal of heavy metals from aqueous solutions using nanomaterials: a review. Sci. Total Environ. 468–469 (2014) 1014–1027, https://doi.org/10.1016/j.scitotenv.2013.09.044.
[23] A. Shan, U. Farooq, S. Lyu, W. Q. Zaman, Z. Abbas, M. Ali, A. Idrees, P. Tang, M. Li, Y. Sun, Q. Sui, Efficient removal of trichloroethylene in surfactant amended solution by nano Fe0-Nickel bimetallic composite activated sodium persulfate process. Chem. Eng. J. 386 (2020) 123995, https://doi.org/10.1016/j.cej.2019.123995.
[24] F. Liu, J. Yang, J. Zuo, D. Ma, L. Gan, B. Xie, P. Wang, B. Yang, Graphene-supported nanoscale zero-valent iron: removal of phosphorus from aqueous solution and mechanistic study. J. Environ. Sci. 26 (2014) 1751–1762, https://doi.org/10.1016/j.jes.2014.06.016.
[25] R.S. Kalhapure, S.J. Sonawane, D.R. Sikwal, M. Jadhav, S. Rambharose, C. Mocktar, T. Govender, Solid lipid nanoparticles of clotrimazole silver complex: an efficient nano antibacterial against Staphylococcus aureus and MRSA. Colloids Surf. B: Biointerfaces 136 (2015) 651–658, https://doi.org/10.1016/j.colsurfb.2015.10.003.
[26] B. Borrego, G. Lorenzo, J.D. Mota-Morales, H. Almanza-Reyes, F. Mateos, E. López-Gil, N. de la Losa, V. A. Burmistrov, A.N. Pestryakov, A. Brun, N. Bogdanchikova, Potential application of silver nanoparticles to control the infectivity of Rift Valley fever virus in vitro and in vivo. Nanomed. Nanotechnol. Biol. Med. 12 (2016) 1185–1192, https://doi.org/10.1016/j.nano.2016.01.021.

This book belongs to Badji Mokhtar Annaba University Central Library Copyright Elsevier 2025

[27] C. Krishnaraj, R. Ramachandran, K. Mohan, P.T. Kalaichelvan, Optimization for rapid synthesis of silver nanoparticles and its effect on phytopathogenic fungi. Spectrochim. Acta A Mol. Biomol. Spectrosc. 93 (2012) 95–99, https://doi.org/10.1016/j.saa.2012.03.002.

[28] J.S. Kim, E. Kuk, K.N. Yu, J.-H. Kim, S.J. Park, H.J. Lee, S.H. Kim, Y.K. Park, Y.H. Park, C.-Y. Hwang, Y.-K. Kim, Y.-S. Lee, D.H. Jeong, M.-H. Cho, Antimicrobial effects of silver nanoparticles. Nanomed. Nanotechnol. Biol. Med. 3 (2007) 95–101, https://doi.org/10.1016/j.nano.2006.12.001.

[29] M. Gao, L. Sun, Z. Wang, Y. Zhao, Controlled synthesis of Ag nanoparticles with different morphologies and their antibacterial properties. Mater. Sci. Eng. C 33 (2013) 397–404, https://doi.org/10.1016/j.msec.2012.09.005.

[30] X. Li, J.J. Lenhart, H.W. Walker, Aggregation kinetics and dissolution of coated silver nanoparticles. Langmuir 28 (2012) 1095–1104, https://doi.org/10.1021/la202328n.

[31] L.-J.A. Ellis, M. Baalousha, E. Valsami-Jones, J.R. Lead, Seasonal variability of natural water chemistry affects the fate and behaviour of silver nanoparticles. Chemosphere 191 (2018) 616–625, https://doi.org/10.1016/j.chemosphere.2017.10.006.

[32] D. Qian, D. Chen, N. Li, Q. Xu, H. Li, J. He, J. Lu, TiO_2/sulfonated graphene oxide/Ag nanoparticle membrane: in situ separation and photodegradation of oil/water emulsions. J. Membr. Sci. 554 (2018) 16–25, https://doi.org/10.1016/j.memsci.2017.12.084.

[33] J.H. Jhaveri, Z.V.P. Murthy, A comprehensive review on anti-fouling nanocomposite membranes for pressure driven membrane separation processes. Desalination 379 (2016) 137–154, https://doi.org/10.1016/j.desal.2015.11.009.

[34] A.M. Ferreira, É.B. Roque, F.V. da Fonseca, C.P. Borges, High flux microfiltration membranes with silver nanoparticles for water disinfection. Desalin. Water Treat. 56 (2015) 3590–3598, https://doi.org/10.1080/19443994.2014.1000977.

[35] M. Sharma, N. Padmavathy, S. Remanan, G. Madras, S. Bose, Facile one-pot scalable strategy to engineer biocidal silver nanocluster assembly on thiolated PVDF membranes for water purification. RSC Adv. 6 (2016) 38972–38983, https://doi.org/10.1039/C6RA03143A.

[36] F. Fu, D.D. Dionysiou, H. Liu, The use of zero-valent iron for groundwater remediation and wastewater treatment: a review. J. Hazard. Mater. 267 (2014) 194–205, https://doi.org/10.1016/j.jhazmat.2013.12.062.

[37] R. Mukherjee, R. Kumar, A. Sinha, Y. Lama, A.K. Saha, A review on synthesis, characterization, and applications of nano zero-valent iron (nZVI) for environmental remediation. Crit. Rev. Environ. Sci. Technol. 46 (2016) 443–466, https://doi.org/10.1080/10643389.2015.1103832.

[38] K. Choi, W. Lee, Enhanced degradation of trichloroethylene in nano-scale zero-valent iron Fenton system with Cu(II). J. Hazard. Mater. 211–212 (2012) 146–153, https://doi.org/10.1016/j.jhazmat.2011.10.056.

[39] W. Yin, J. Wu, P. Li, X. Wang, N. Zhu, P. Wu, B. Yang, Experimental study of zero-valent iron induced nitrobenzene reduction in groundwater: the effects of pH, iron dosage, oxygen and common dissolved anions. Chem. Eng. J. 184 (2012) 198–204, https://doi.org/10.1016/j.cej.2012.01.030.

[40] V. Tanboonchuy, N. Grisdanurak, C.-H. Liao, Background species effect on aqueous arsenic removal by nano zero-valent iron using fractional factorial design. J. Hazard. Mater. 205–206 (2012) 40–46, https://doi.org/10.1016/j.jhazmat.2011.11.090.

[41] X. Lv, J. Xu, G. Jiang, J. Tang, X. Xu, Highly active nanoscale zero-valent iron (nZVI)–Fe_3O_4 nanocomposites for the removal of chromium(VI) from aqueous solutions. J. Colloid Interface Sci. 369 (2012) 460–469, https://doi.org/10.1016/j.jcis.2011.11.049.

[42] N. Arancibia-Miranda, S.E. Baltazar, A. García, D. Muñoz-Lira, P. Sepúlveda, M.A. Rubio, D. Altbir, Nanoscale zero-valent supported by Zeolite and Montmorillonite: template effect of the removal of lead ion from an aqueous solution. J. Hazard. Mater. 301 (2016) 371–380, https://doi.org/10.1016/j.jhazmat.2015.09.007.

[43] S. Luo, P. Qin, J. Shao, L. Peng, Q. Zeng, J.-D. Gu, Synthesis of reactive nanoscale zero-valent iron using rectorite supports and its application for Orange II removal. Chem. Eng. J. 223 (2013) 1–7, https://doi.org/10.1016/j.cej.2012.10.088.

This book belongs to Badji Mokhtar Annaba University Central Library Copyright Elsevier 2025

[44] P.G. Tratnyek, A.J. Salter, J.T. Nurmi, V. Sarathy, Environmental applications of zerovalent metals: iron vs. zinc. ACS Symp. Ser. (2010) 165–178, https://doi.org/10.1021/bk-2010-1045.ch009.
[45] S.R. Shirsath, D.V. Pinjari, P.R. Gogate, S.H. Sonawane, A.B. Pandit, Ultrasound assisted synthesis of doped TiO_2 nano-particles: characterization and comparison of effectiveness for photocatalytic oxidation of dyestuff effluent. Ultrason. Sonochem. 20 (2013) 277–286, https://doi.org/10.1016/j.ultsonch.2012.05.015.
[46] A.B.V. Kiran Kumar, S. Billa, E.G. Shankar, M.C.S. Subha, C, N dual-doped ZnO nanofoams: a potential antimicrobial agent, an efficient visible light photocatalyst and SXAS studies. J. Synchrotron Radiat. 27 (2020) 90–99, https://doi.org/10.1107/S160057751901364X.
[47] B. Bethi, S.H. Sonawane, G.S. Rohit, C.R. Holkar, D.V. Pinjari, B.A. Bhanvase, A.B. Pandit, Investigation of TiO_2 photocatalyst performance for decolorization in the presence of hydrodynamic cavitation as hybrid AOP. Ultrason. Sonochem. 28 (2016) 150–160, https://doi.org/10.1016/j.ultsonch.2015.07.008.
[48] C.-C. Wang, Z. Zhang, J.Y. Ying, Photocatalytic decomposition of halogenated organics over nanocrystalline titania. Nanostruct. Mater. 9 (1997) 583–586, https://doi.org/10.1016/S0965-9773(97)00130-X.
[49] C.B. Almquist, P. Biswas, Role of synthesis method and particle size of nanostructured TiO_2 on its photoactivity. J. Catal. 212 (2002) 145–156, https://doi.org/10.1006/jcat.2002.3783.
[50] A.J. Maira, K.L. Yeung, C.Y. Lee, P.L. Yue, C.K. Chan, Size effects in gas-phase photo-oxidation of trichloroethylene using nanometer-sized TiO2 catalysts. J. Catal. 192 (2000) 185–196, https://doi.org/10.1006/jcat.2000.2838.
[51] A. Janotti, C.G. Van de Walle, Fundamentals of zinc oxide as a semiconductor. Rep. Prog. Phys. 72 (2009) 126501, https://doi.org/10.1088/0034-4885/72/12/126501.
[52] T. Matsuzawa, A new long phosphorescent phosphor with high brightness, SrAl[sub 2]O[sub 4]:Eu[sup 2+], Dy[sup 3+]. J. Electrochem. Soc. 143 (1996) 2670, https://doi.org/10.1149/1.1837067.
[53] S. Weon, F. He, W. Choi, Status and challenges in photocatalytic nanotechnology for cleaning air polluted with volatile organic compounds: visible light utilization and catalyst deactivation. Environ. Sci. Nano 6 (2019) 3185–3214, https://doi.org/10.1039/C9EN00891H.
[54] T. Su, Z. Qin, H. Ji, Z. Wu, An overview of photocatalysis facilitated by 2D heterojunctions. Nanotechnology 30 (2019) 502002, https://doi.org/10.1088/1361-6528/ab3f15.
[55] J. Silver, M.I. Martinez-Rubio, T.G. Ireland, G.R. Fern, R. Withnall, Yttrium oxide upconverting phosphors. 3. Upconversion luminescent emission from europium-doped yttrium oxide under 632.8 nm light excitation. J. Phys. Chem. B 105 (2001) 9107–9112, https://doi.org/10.1021/jp011143q.
[56] J. Silver, E. Barrett, P.J. Marsh, R. Withnall, Yttrium oxide upconverting phosphors. 5. Upconversion luminescent emission from holmium-doped yttrium oxide under 632.8 nm light excitation. J. Phys. Chem. B 107 (2003) 9236–9242, https://doi.org/10.1021/jp034160j.
[57] H. Yang, Z. Dai, Z. Sun, Upconversion luminescence and kinetics in Er^{3+}:$YAlO_3$ under 652.2 nm excitation. J. Lumin. 124 (2007) 207–212, https://doi.org/10.1016/j.jlumin.2006.02.021.
[58] W. Qin, D. Zhang, D. Zhao, L. Wang, K. Zheng, Near-infrared photocatalysis based on $YF^3 : Yb^{3+}$,Tm^{3+}/TiO_2 core/shell nanoparticles. Chem. Commun. 46 (2010) 2304, https://doi.org/10.1039/b924052g.
[59] T. Peng, L. Huajun, H. Yang, C. Yan, Synthesis of $SrAl_2O_4$:Eu, Dy phosphor nanometer powders by sol-gel processes and its optical properties. Mater. Chem. Phys. 85 (2004) 68–72, https://doi.org/10.1016/j.matchemphys.2003.12.001.
[60] C.R. García, L.A. Diaz-Torres, J. Oliva, M.T. Romero, P. Salas, Photocatalytic activity and optical properties of blue persistent phosphors under UV and solar irradiation. Int. J. Photoenergy 2016 (2016) 1–8, https://doi.org/10.1155/2016/1303247.
[61] Y. Liu, R. Li, W. Luo, H. Zhu, X. Chen, Optical spectroscopy of Sm^{3+} and Dy^{3+} doped ZnO nanocrystals. Spectrosc. Lett. 43 (2010) 343–349, https://doi.org/10.1080/00387010.2010.486717.
[62] X. Liu, H. Chu, J. Li, L. Niu, C. Li, H. Li, L. Pan, C.Q. Sun, Light converting phosphor-based photocatalytic composites. Cat. Sci. Technol. 5 (2015) 4727–4740, https://doi.org/10.1039/C5CY00622H.
[63] C. Karunakaran, P. Gomathisankar, G. Manikandan, Preparation and characterization of antimicrobial Ce-doped ZnO nanoparticles for photocatalytic detoxification of cyanide. Mater. Chem. Phys. 123 (2010) 585–594, https://doi.org/10.1016/j.matchemphys.2010.05.019.

This book belongs to Badji Mokhtar Annaba University Central Library Copyright Elsevier 2025

[64] M. Khatamian, A.A. Khandar, B. Divband, M. Haghighi, S. Ebrahimiasl, Heterogeneous photocatalytic degradation of 4-nitrophenol in aqueous suspension by Ln (La^{3+}, Nd^{3+} or Sm^{3+}) doped ZnO nanoparticles. J. Mol. Catal. A Chem. 365 (2012) 120–127, https://doi.org/10.1016/j.molcata.2012.08.018.

[65] V. Valtchev, L. Tosheva, Porous nanosized particles: preparation, properties, and applications. Chem. Rev. 113 (2013) 6734–6760, https://doi.org/10.1021/cr300439k.

[66] T. Tago, H. Konno, Y. Nakasaka, T. Masuda, Size-controlled synthesis of nano-zeolites and their application to light olefin synthesis. Catal. Surv. Asia 16 (2012) 148–163, https://doi.org/10.1007/s10563-012-9141-4.

[67] Y. Yan, X. Guo, Y. Zhang, Y. Tang, Future of nano-/hierarchical zeolites in catalysis: gaseous phase or liquid phase system. Cat. Sci. Technol. 5 (2015) 772–785, https://doi.org/10.1039/C4CY01114G.

[68] E. Koohsaryan, M. Anbia, Nanosized and hierarchical zeolites: a short review. Chin. J. Catal. 37 (2016) 447–467, https://doi.org/10.1016/S1872-2067(15)61038-5.

[69] L. Tosheva, V.P. Valtchev, Nanozeolites: synthesis, crystallization mechanism, and applications. Chem. Mater. 17 (2005) 2494–2513, https://doi.org/10.1021/cm047908z.

[70] B. Bethi, S.H. Sonawane, B.A. Bhanvase, S.P. Gumfekar, Nanomaterials-based advanced oxidation processes for wastewater treatment: a review. Chem. Eng. Process. Process Intensif. 109 (2016) 178–189, https://doi.org/10.1016/j.cep.2016.08.016.

[71] M.M. Khin, A.S. Nair, V.J. Babu, R. Murugan, S. Ramakrishna, A review on nanomaterials for environmental remediation. Energy Environ. Sci. 5 (2012) 8075, https://doi.org/10.1039/c2ee21818f.

[72] S.C. Smith, D.F. Rodrigues, Carbon-based nanomaterials for removal of chemical and biological contaminants from water: a review of mechanisms and applications. Carbon N. Y. 91 (2015) 122–143, https://doi.org/10.1016/j.carbon.2015.04.043.

[73] F. Ahmed, C.M. Santos, R.A.M.V. Vergara, M.C.R. Tria, R. Advincula, D.F. Rodrigues, Antimicrobial applications of electroactive PVK-SWNT nanocomposites. Environ. Sci. Technol. 46 (2012) 1804–1810, https://doi.org/10.1021/es202374e.

[74] H. Wang, X. Yuan, Y. Wu, H. Huang, G. Zeng, Y. Liu, X. Wang, N. Lin, Y. Qi, Adsorption characteristics and behaviors of graphene oxide for Zn(II) removal from aqueous solution. Appl. Surf. Sci. 279 (2013) 432–440, https://doi.org/10.1016/j.apsusc.2013.04.133.

[75] G.D. Vuković, A.D. Marinković, M. Čolić, M.Đ. Ristić, R. Aleksić, A.A. Perić-Grujić, P. S. Uskoković, Removal of cadmium from aqueous solutions by oxidized and ethylenediamine-functionalized multi-walled carbon nanotubes. Chem. Eng. J. 157 (2010) 238–248, https://doi.org/10.1016/j.cej.2009.11.026.

[76] V.K.K. Upadhyayula, S. Deng, G.B. Smith, M.C. Mitchell, Adsorption of Bacillus subtilis on single-walled carbon nanotube aggregates, activated carbon and NanoCeram^{TM}. Water Res. 43 (2009) 148–156, https://doi.org/10.1016/j.watres.2008.09.023.

[77] S. Sakthivel, H. Kisch, Daylight photocatalysis by carbon-modified titanium dioxide. Angew. Chem. Int. Ed. 42 (2003) 4908–4911, https://doi.org/10.1002/anie.200351577.

[78] D.P. Barai, B.A. Bhanvase, V.K. Saharan, Reduced graphene oxide-Fe_3O_4 nanocomposite based nanofluids: study on ultrasonic assisted synthesis, thermal conductivity, rheology, and convective heat transfer. Ind. Eng. Chem. Res. 58 (2019) 8349–8369, https://doi.org/10.1021/acs.iecr.8b05733.

[79] M.P. Deosarkar, S.M. Pawar, S.H. Sonawane, B.A. Bhanvase, Process intensification of uniform loading of SnO2 nanoparticles on graphene oxide nanosheets using a novel ultrasound assisted in situ chemical precipitation method. Chem. Eng. Process. Process Intensif. 70 (2013) 48–54, https://doi.org/10.1016/j.cep.2013.05.008.

[80] M.P. Deosarkar, S.M. Pawar, B.A. Bhanvase, In situ sonochemical synthesis of Fe_3O_4-graphene nanocomposite for lithium rechargeable batteries. Chem. Eng. Process. Process Intensif. 83 (2014) 49–55, https://doi.org/10.1016/j.cep.2014.07.004.

[81] Q.L. Zhu, Q. Xu, Metal-organic framework composites. Chem. Soc. Rev. 43 (2014) 5468–5512, https://doi.org/10.1039/c3cs60472a.

[82] J.L.C. Rowsell, O.M. Yaghi, Metal-organic frameworks: a new class of porous materials. Microporous Mesoporous Mater. 73 (2004) 3–14, https://doi.org/10.1016/j.micromeso.2004.03.034.

This book belongs to Badji Mokhtar Annaba University Central Library Copyright Elsevier 2025

[83] S.T. Meek, J.A. Greathouse, M.D. Allendorf, Metal-organic frameworks: a rapidly growing class of versatile nanoporous materials. Adv. Mater. 23 (2011) 249–267, https://doi.org/10.1002/adma.201002854.
[84] J. He, J. Li, W. Du, Q. Han, Z. Wang, M. Li, A mesoporous metal-organic framework: potential advances in selective dye adsorption. J. Alloys Compd. 750 (2018) 360–367, https://doi.org/10.1016/j.jallcom.2018.03.393.
[85] I. Ahmed, S.H. Jhung, Composites of metal-organic frameworks: preparation and application in adsorption. Mater. Today 17 (2014) 136–146, https://doi.org/10.1016/j.mattod.2014.03.002.
[86] G. Zhao, N. Qin, A. Pan, X. Wu, C. Peng, F. Ke, M. Iqbal, K. Ramachandraiah, J. Zhu, Magnetic nanoparticles@metal-organic framework composites as sustainable environment adsorbents. J. Nanomater. 2019 (2019) 1–11, https://doi.org/10.1155/2019/1454358.
[87] R. Wang, H. Xu, K. Zhang, S. Wei, W. Deyong, High-quality Al@Fe-MOF prepared using Fe-MOF as a micro-reactor to improve adsorption performance for selenite. J. Hazard. Mater. 364 (2019) 272–280, https://doi.org/10.1016/j.jhazmat.2018.10.030.
[88] W.G. Shim, K.J. Hwang, J.T. Chung, Y.S. Baek, S.J. Yoo, S.C. Kim, H. Moon, J.W. Lee, Adsorption and thermodesorption characteristics of benzene in nanoporous metal organic framework MOF-5. Adv. Powder Technol. 23 (2012) 615–619, https://doi.org/10.1016/j.apt.2011.07.002.
[89] R. Ricco, L. Malfatti, M. Takahashi, A.J. Hill, P. Falcaro, Applications of magnetic metal-organic framework composites. J. Mater. Chem. A 1 (2013) 13033–13045, https://doi.org/10.1039/c3ta13140h.
[90] H.R. Moon, D.W. Lim, M.P. Suh, Fabrication of metal nanoparticles in metal-organic frameworks. Chem. Soc. Rev. 42 (2013) 1807–1824, https://doi.org/10.1039/c2cs35320b.
[91] X. Qu, J. Brame, Q. Li, P.J.J. Alvarez, Nanotechnology for a safe and sustainable water supply: enabling integrated water treatment and reuse. Acc. Chem. Res. 46 (2013) 834–843, https://doi.org/10.1021/ar300029v.
[92] D. Li, Y. Xia, Electrospinning of nanofibers: reinventing the wheel?. Adv. Mater. 16 (2004) 1151–1170, https://doi.org/10.1002/adma.200400719.
[93] S. Ramakrishna, K. Fujihara, W.-E. Teo, T. Yong, Z. Ma, R. Ramaseshan, Electrospun nanofibers: solving global issues. Mater. Today 9 (2006) 40–50, https://doi.org/10.1016/S1369-7021(06)71389-X.
[94] S. Al Aani, C.J. Wright, M.A. Atieh, N. Hilal, Engineering nanocomposite membranes: addressing current challenges and future opportunities. Desalination 401 (2017) 1–15, https://doi.org/10.1016/j.desal.2016.08.001.
[95] M.G. Kochameshki, A. Marjani, M. Mahmoudian, K. Farhadi, Grafting of diallyldimethylammonium chloride on graphene oxide by RAFT polymerization for modification of nanocomposite polysulfone membranes using in water treatment. Chem. Eng. J. 309 (2017) 206–221, https://doi.org/10.1016/j.cej.2016.10.008.
[96] G. Sharma, D. Pathania, M. Naushad, N.C. Kothiyal, Fabrication, characterization and antimicrobial activity of polyaniline Th(IV) tungstomolybdophosphate nanocomposite material: efficient removal of toxic metal ions from water. Chem. Eng. J. 251 (2014) 413–421, https://doi.org/10.1016/j.cej.2014.04.074.
[97] O.M. Vatutsina, V.S. Soldatov, V.I. Sokolova, J. Johann, M. Bissen, A. Weissenbacher, A new hybrid (polymer/inorganic) fibrous sorbent for arsenic removal from drinking water. React. Funct. Polym. 67 (2007) 184–201, https://doi.org/10.1016/j.reactfunctpolym.2006.10.009.
[98] Y.-M. Zheng, S.-W. Zou, K.G.N. Nanayakkara, T. Matsuura, J.P. Chen, Adsorptive removal of arsenic from aqueous solution by a PVDF/zirconia blend flat sheet membrane. J. Membr. Sci. 374 (2011) 1–11, https://doi.org/10.1016/j.memsci.2011.02.034.
[99] A. Hafiane, D. Lemordant, M. Dhahbi, Removal of hexavalent chromium by nanofiltration. Desalination 130 (2000) 305–312, https://doi.org/10.1016/S0011-9164(00)00094-1.
[100] S.-S. Chen, B.-C. Hsu, C.-H. Ko, P.-C. Chuang, Recovery of chromate from spent plating solutions by two-stage nanofiltration processes. Desalination 229 (2008) 147–155, https://doi.org/10.1016/j.desal.2007.08.015.
[101] C. Neelakandan, G. Pugazhenthi, A. Kumar, Preparation of NOx modified PMMA-EGDM composite membrane for the recovery of chromium (VI). Eur. Polym. J. 39 (2003) 2383–2391, https://doi.org/10.1016/S0014-3057(03)00183-6.

This book belongs to Badji Mokhtar Annaba University Central Library Copyright Elsevier 2025

[102] M. Mukhopadhyay, S.R. Lakhotia, A.K. Ghosh, R.C. Bindal, Removal of arsenic from aqueous media using zeolite/chitosan nanocomposite membrane. Sep. Sci. Technol. 54 (2019) 282–288, https://doi.org/10.1080/01496395.2018.1459704.

[103] M. Zanetti, S. Lomakin, G. Camino, Polymer layered silicate nanocomposites. Macromol. Mater. Eng. 279 (2000) 1–9, https://doi.org/10.1002/1439-2054(20000601)279:1<1::AID-MAME1>3.0.CO;2-Q.

[104] M.S. Mauter, Y. Wang, K.C. Okemgbo, C.O. Osuji, E.P. Giannelis, M. Elimelech, Antifouling ultrafiltration membranes via post-fabrication grafting of biocidal nanomaterials. ACS Appl. Mater. Interfaces 3 (2011) 2861–2868, https://doi.org/10.1021/am200522v.

[105] K. Zodrow, L. Brunet, S. Mahendra, D. Li, A. Zhang, Q. Li, P.J.J. Alvarez, Polysulfone ultrafiltration membranes impregnated with silver nanoparticles show improved biofouling resistance and virus removal. Water Res. 43 (2009) 715–723, https://doi.org/10.1016/j.watres.2008.11.014.

[106] B. De Gusseme, T. Hennebel, E. Christiaens, H. Saveyn, K. Verbeken, J. P. Fitts, N. Boon, W. Verstraete, Virus disinfection in water by biogenic silver immobilized in polyvinylidene fluoride membranes. Water Res. 45 (2011) 1856–1864, https://doi.org/10.1016/j.watres.2010.11.046.

[107] H. Anwer, A. Mahmood, J. Lee, K.-H. Kim, J.-W. Park, A.C.K. Yip, Photocatalysts for degradation of dyes in industrial effluents: opportunities and challenges. Nano Res. 12 (2019) 955–972, https://doi.org/10.1007/s12274-019-2287-0.

[108] P.S. Mukherjee, A.K. Ray, Major challenges in the design of a large-scale photocatalytic reactor for water treatment. Chem. Eng. Technol. 22 (1999) 253–260, https://doi.org/10.1002/(SICI)1521-4125(199903)22:3<253::AID-CEAT253>3.0.CO;2-X.

[109] N. Bahadur, N. Bhargava, Novel pilot scale photocatalytic treatment of textile & dyeing industry wastewater to achieve process water quality and enabling zero liquid discharge. J. Water Process Eng. 32 (2019) 100934, https://doi.org/10.1016/j.jwpe.2019.100934.

[110] J. Zhang, S. Zhai, S. Li, Z. Xiao, Y. Song, Q. An, G. Tian, Pb(II) removal of Fe_3O_4@SiO_2-NH_2 core-shell nanomaterials prepared via a controllable sol-gel process. Chem. Eng. J. 215–216 (2013) 461–471, https://doi.org/10.1016/j.cej.2012.11.043.

[111] H. Vojoudi, A. Badiei, S. Bahar, G. Mohammadi Ziarani, F. Faridbod, M.R. Ganjali, A new nano-sorbent for fast and efficient removal of heavy metals from aqueous solutions based on modification of magnetic mesoporous silica nanospheres. J. Magn. Magn. Mater. 441 (2017) 193–203, https://doi.org/10.1016/j.jmmm.2017.05.065.

[112] S. Wang, H. Sun, H.M. Ang, M.O. Tadé, Adsorptive remediation of environmental pollutants using novel graphene-based nanomaterials. Chem. Eng. J. 226 (2013) 336–347, https://doi.org/10.1016/j.cej.2013.04.070.

[113] G. Zhao, J. Li, X. Ren, C. Chen, X. Wang, Few-layered graphene oxide nanosheets as superior sorbents for heavy metal ion pollution management. Environ. Sci. Technol. 45 (2011) 10454–10462, https://doi.org/10.1021/es203439v.

[114] G. Zhao, X. Ren, X. Gao, X. Tan, J. Li, C. Chen, Y. Huang, X. Wang, Removal of Pb(ii) ions from aqueous solutions on few-layered graphene oxide nanosheets. Dalton Trans. 40 (2011) 10945, https://doi.org/10.1039/c1dt11005e.

[115] A.E. Burakov, E.V. Galunin, I.V. Burakova, A.E. Kucherova, S. Agarwal, A.G. Tkachev, V.K. Gupta, Adsorption of heavy metals on conventional and nanostructured materials for wastewater treatment purposes: a review. Ecotoxicol. Environ. Saf. 148 (2018) 702–712, https://doi.org/10.1016/j.ecoenv.2017.11.034.

[116] M. Ghorbani, O. Seyedin, M. Aghamohammadhassan, Adsorptive removal of lead (II) ion from water and wastewater media using carbon-based nanomaterials as unique sorbents: a review. J. Environ. Manag. 254 (2020) 109814, https://doi.org/10.1016/j.jenvman.2019.109814.

[117] R. Gusain, N. Kumar, S.S. Ray, Recent advances in carbon nanomaterial-based adsorbents for water purification. Coord. Chem. Rev. 405 (2020) 213111, https://doi.org/10.1016/j.ccr.2019.213111.

[118] A.M. Awad, R. Jalab, A. Benamor, M.S. Nasser, M.M. Ba-Abbad, M. El-Naas, A.W. Mohammad, Adsorption of organic pollutants by nanomaterial-based adsorbents: an overview. J. Mol. Liq. 301 (2020) 112335, https://doi.org/10.1016/j.molliq.2019.112335.

This book belongs to Badji Mokhtar Annaba University Central Library

Copyright Elsevier 2025

[119] S. Wadhawan, A. Jain, J. Nayyar, S.K. Mehta, Role of nanomaterials as adsorbents in heavy metal ion removal from wastewater: a review. J. Water Process Eng. 33 (2020) 101038, https://doi.org/10.1016/j.jwpe.2019.101038.

[120] M. Siegel, A. Aragon, H. Zhao, S. Deng, M. Nocon, M. Aragon, Prediction of arsenic removal by adsorptive media: comparison of field and laboratory studies. in: Arsenic Contamination of Groundwater, John Wiley & Sons, Inc., Hoboken, NJ, USA, 2008, pp. 227–268, https://doi.org/10.1002/9780470371046.ch10

[121] P. Sylvester, P. Westerhoff, T. Möller, M. Badruzzaman, O. Boyd, A hybrid sorbent utilizing nanoparticles of hydrous iron oxide for arsenic removal from drinking water. Environ. Eng. Sci. 24 (2007) 104–112, https://doi.org/10.1089/ees.2007.24.104.

[122] K.E. Greenstein, J. Lew, E.R.V. Dickenson, E.C. Wert, Investigation of biotransformation, sorption, and desorption of multiple chemical contaminants in pilot-scale drinking water biofilters. Chemosphere 200 (2018) 248–256, https://doi.org/10.1016/j.chemosphere.2018.02.107.

[123] A. Pandiarajan, R. Kamaraj, S. Vasudevan, Enhanced removal of cephalosporin based antibiotics (CBA) from water by one-pot electrosynthesized $Mg(OH)_2$: a combined theoretical and experimental study to pilot scale. New J. Chem. 41 (2017) 4518–4530, https://doi.org/10.1039/C6NJ04075F.

[124] H. Wang, F. Qu, A. Ding, H. Liang, R. Jia, K. Li, L. Bai, H. Chang, G. Li, Combined effects of PAC adsorption and in situ chlorination on membrane fouling in a pilot-scale coagulation and ultrafiltration process. Chem. Eng. J. 283 (2016) 1374–1383, https://doi.org/10.1016/j.cej.2015.08.093.

[125] A.M. Nasir, P.S. Goh, M.S. Abdullah, B.C. Ng, A.F. Ismail, Adsorptive nanocomposite membranes for heavy metal remediation: recent progresses and challenges. Chemosphere 232 (2019) 96–112, https://doi.org/10.1016/j.chemosphere.2019.05.174.

[126] S. Kar, R.C. Bindal, P.K. Tewari, Carbon nanotube membranes for desalination and water purification: challenges and opportunities. Nano Today 7 (2012) 385–389, https://doi.org/10.1016/j.nantod.2012.09.002.

[127] F. Paquin, J. Rivnay, A. Salleo, N. Stingelin, C. Silva-Acuña, Multi-phase microstructures drive exciton dissociation in neat semicrystalline polymeric semiconductors. J. Mater. Chem. C 3 (2015) 10715–10722, https://doi.org/10.1039/C5TC02043C.

[128] J. Brame, Q. Li, P.J.J. Alvarez, Nanotechnology-enabled water treatment and reuse: emerging opportunities and challenges for developing countries. Trends Food Sci. Technol. 22 (2011) 618–624, https://doi.org/10.1016/j.tifs.2011.01.004.

[129] J. Kim, B. Van der Bruggen, The use of nanoparticles in polymeric and ceramic membrane structures: review of manufacturing procedures and performance improvement for water treatment. Environ. Pollut. 158 (2010) 2335–2349, https://doi.org/10.1016/j.envpol.2010.03.024.

[130] A.P. Kumar, D. Depan, N. Singh Tomer, R.P. Singh, Nanoscale particles for polymer degradation and stabilization—trends and future perspectives. Prog. Polym. Sci. 34 (2009) 479–515, https://doi.org/10.1016/j.progpolymsci.2009.01.002.

[131] K.P. Lee, T.C. Arnot, D. Mattia, A review of reverse osmosis membrane materials for desalination—development to date and future potential. J. Membr. Sci. 370 (2011) 1–22, https://doi.org/10.1016/j.memsci.2010.12.036.

[132] M.M. Pendergast, E.M.V. Hoek, A review of water treatment membrane nanotechnologies. Energy Environ. Sci. 4 (2011) 1946, https://doi.org/10.1039/c0ee00541j.

[133] S.O. Ganiyu, E.D. van Hullebusch, M. Cretin, G. Esposito, M.A. Oturan, Coupling of membrane filtration and advanced oxidation processes for removal of pharmaceutical residues: a critical review. Sep. Purif. Technol. 156 (2015) 891–914, https://doi.org/10.1016/j.seppur.2015.09.059.

[134] M.N. Chong, B. Jin, C.W.K. Chow, C. Saint, Recent developments in photocatalytic water treatment technology: a review. Water Res. 44 (2010) 2997–3027, https://doi.org/10.1016/j.watres.2010.02.039.

[135] S. Mozia, Photocatalytic membrane reactors (PMRs) in water and wastewater treatment. A review. Sep. Purif. Technol. 73 (2010) 71–91, https://doi.org/10.1016/j.seppur.2010.03.021.

[136] W. Zhang, L. Ding, J. Luo, M.Y. Jaffrin, B. Tang, Membrane fouling in photocatalytic membrane reactors (PMRs) for water and wastewater treatment: a critical review. Chem. Eng. J. 302 (2016) 446–458, https://doi.org/10.1016/j.cej.2016.05.071.

This book belongs to Badji Mokhtar Annaba University Central Library

Copyright Elsevier 2025

[137] S. Mozia, D. Darowna, K. Szymański, S. Grondzewska, K. Borchert, R. Wróbel, A. W. Morawski, Performance of two photocatalytic membrane reactors for treatment of primary and secondary effluents. Catal. Today 236 (2014) 135–145, https://doi.org/10.1016/j.cattod.2013.12.049.
[138] S. Leong, A. Razmjou, K. Wang, K. Hapgood, X. Zhang, H. Wang, TiO_2 based photocatalytic membranes: a review. J. Membr. Sci. 472 (2014) 167–184, https://doi.org/10.1016/j.memsci.2014.08.016.
[139] M. Pidou, S.A. Parsons, G. Raymond, P. Jeffrey, T. Stephenson, B. Jefferson, Fouling control of a membrane coupled photocatalytic process treating greywater. Water Res. 43 (2009) 3932–3939, https://doi.org/10.1016/j.watres.2009.05.030.
[140] W. Wang, Z. Wu, E. Eftekhari, Z. Huo, X. Li, M.O. Tade, C. Yan, Z. Yan, C. Li, Q. Li, D. Zhao, High performance heterojunction photocatalytic membranes formed by embedding Cu_2O and TiO_2 nanowires in reduced graphene oxide. Cat. Sci. Technol. 8 (2018) 1704–1711, https://doi.org/10.1039/C8CY00082D.
[141] F. Galiano, X. Song, T. Marino, M. Boerrigter, O. Saoncella, S. Simone, M. Faccini, C. Chaumette, E. Drioli, A. Figoli, Novel photocatalytic PVDF/Nano-TiO_2 hollow fibers for environmental remediation. Polymers (Basel) 10 (2018) 1134, https://doi.org/10.3390/polym10101134.
[142] R.K. Herz, Intrinsic kinetics of first-order reactions in photocatalytic membranes and layers. Chem. Eng. J. 99 (2004) 237–245, https://doi.org/10.1016/j.cej.2003.11.013.
[143] R. Ahmad, Z. Ahmad, A.U. Khan, N.R. Mastoi, M. Aslam, J. Kim, Photocatalytic systems as an advanced environmental remediation: recent developments, limitations and new avenues for applications. J. Environ. Chem. Eng. 4 (2016) 4143–4164, https://doi.org/10.1016/j.jece.2016.09.009.
[144] W.H. Glaze, J.-W. Kang, D.H. Chapin, The chemistry of water treatment processes involving ozone, hydrogen peroxide and ultraviolet radiation. Ozone Sci. Eng. 9 (1987) 335–352, https://doi.org/10.1080/01919518708552148.
[145] L.W. Gassie, J.D. Englehardt, Advanced oxidation and disinfection processes for onsite net-zero greywater reuse: a review. Water Res. 125 (2017) 384–399, https://doi.org/10.1016/j.watres.2017.08.062.
[146] M.S. Mauter, I. Zucker, F. Perreault, J.R. Werber, J.-H. Kim, M. Elimelech, The role of nanotechnology in tackling global water challenges. Nat. Sustain. 1 (2018) 166–175, https://doi.org/10.1038/s41893-018-0046-8.
[147] C.-C. Kuan, S.-Y. Chang, S.L.M. Schroeder, Fenton-like oxidation of 4-chlorophenol: homogeneous or heterogeneous?. Ind. Eng. Chem. Res. 54 (2015) 8122–8129, https://doi.org/10.1021/acs.iecr.5b02378.
[148] Z. Weng, J. Li, Y. Weng, M. Feng, Z. Zhuang, Y. Yu, Surfactant-free porous nano-Mn_3O_4 as a recyclable Fenton-like reagent that can rapidly scavenge phenolics without H_2O_2. J. Mater. Chem. A 5 (2017) 15650–15660, https://doi.org/10.1039/C7TA04042C.
[149] B.C. Hodges, E.L. Cates, J.-H. Kim, Challenges and prospects of advanced oxidation water treatment processes using catalytic nanomaterials. Nat. Nanotechnol. 13 (2018) 642–650, https://doi.org/10.1038/s41565-018-0216-x.
[150] G. Thompson, J. Swain, M. Kay, C. Forster, The treatment of pulp and paper mill effluent: a review. Bioresour. Technol. 77 (2001) 275–286, https://doi.org/10.1016/S0960-8524(00)00060-2.
[151] Z. Beril Gönder, S. Arayici, H. Barlas, Advanced treatment of pulp and paper mill wastewater by nanofiltration process: effects of operating conditions on membrane fouling. Sep. Purif. Technol. 76 (2011) 292–302, https://doi.org/10.1016/j.seppur.2010.10.018.
[152] M. Mänttäri, M. Kuosa, J. Kallas, M. Nyström, Membrane filtration and ozone treatment of biologically treated effluents from the pulp and paper industry. J. Membr. Sci. 309 (2008) 112–119, https://doi.org/10.1016/j.memsci.2007.10.019.
[153] G. Chen, Electrochemical technologies in wastewater treatment. Sep. Purif. Technol. 38 (2004) 11–41, https://doi.org/10.1016/j.seppur.2003.10.006.
[154] H. Särkkä, A. Bhatnagar, M. Sillanpää, Recent developments of electro-oxidation in water treatment—a review. J. Electroanal. Chem. 754 (2015) 46–56, https://doi.org/10.1016/j.jelechem.2015.06.016.
[155] A. Kapałka, G. Fóti, C. Comninellis, Kinetic modelling of the electrochemical mineralization of organic pollutants for wastewater treatment. J. Appl. Electrochem. 38 (2007) 7–16, https://doi.org/10.1007/s10800-007-9365-6.

This book belongs to Badji Mokhtar Annaba University Central Library Copyright Elsevier 2025

[156] D. Rajkumar, J. Kim, Oxidation of various reactive dyes with in situ electro-generated active chlorine for textile dyeing industry wastewater treatment. J. Hazard. Mater. 136 (2006) 203–212, https://doi.org/10.1016/j.jhazmat.2005.11.096.
[157] M.E.H. Bergmann, A.S. Koparal, Studies on electrochemical disinfectant production using anodes containing RuO2. J. Appl. Electrochem. 35 (2005) 1321–1329, https://doi.org/10.1007/s10800-005-9064-0.
[158] A. Sakalis, K. Fytianos, U. Nickel, A. Voulgaropoulos, A comparative study of platinised titanium and niobe/synthetic diamond as anodes in the electrochemical treatment of textile wastewater. Chem. Eng. J. 119 (2006) 127–133, https://doi.org/10.1016/j.cej.2006.02.009.
[159] Y.Y. Chu, Y. Qian, W.J. Wang, X.L. Deng, A dual-cathode electro-Fenton oxidation coupled with anodic oxidation system used for 4-nitrophenol degradation. J. Hazard. Mater. 199–200 (2012) 179–185, https://doi.org/10.1016/j.jhazmat.2011.10.079.
[160] W. Wu, Z.-H. Huang, T.-T. Lim, Recent development of mixed metal oxide anodes for electrochemical oxidation of organic pollutants in water. Appl. Catal. A Gen. 480 (2014) 58–78, https://doi.org/10.1016/j.apcata.2014.04.035.
[161] B. Yang, J. Zuo, X. Tang, F. Liu, X. Yu, X. Tang, H. Jiang, L. Gan, Effective ultrasound electrochemical degradation of methylene blue wastewater using a nanocoated electrode. Ultrason. Sonochem. 21 (2014) 1310–1317, https://doi.org/10.1016/j.ultsonch.2014.01.008.
[162] A. Anglada, A. Urtiaga, I. Ortiz, Contributions of electrochemical oxidation to waste-water treatment: fundamentals and review of applications. J. Chem. Technol. Biotechnol. 84 (2009) 1747–1755, https://doi.org/10.1002/jctb.2214.
[163] M. Anjum, R. Miandad, M. Waqas, F. Gehany, M.A. Barakat, Remediation of wastewater using various nano-materials. Arab. J. Chem. 12 (2019) 4897–4919, https://doi.org/10.1016/j.arabjc.2016.10.004.
[164] B. Pan, B. Pan, W. Zhang, L. Lv, Q. Zhang, S. Zheng, Development of polymeric and polymer-based hybrid adsorbents for pollutants removal from waters. Chem. Eng. J. 151 (2009) 19–29, https://doi.org/10.1016/j.cej.2009.02.036.
[165] P.Z. Ray, H.J. Shipley, Inorganic nanoadsorbents for the removal of heavy metals and arsenic: a review. RSC Adv. 5 (2015) 29885–29907, https://doi.org/10.1039/C5RA02714D.
[166] W.-W. Tang, G.-M. Zeng, J.-L. Gong, Y. Liu, X.-Y. Wang, Y.-Y. Liu, Z.-F. Liu, L. Chen, X.-R. Zhang, D.-Z. Tu, Simultaneous adsorption of atrazine and Cu(II) from wastewater by magnetic multi-walled carbon nanotube. Chem. Eng. J. 211–212 (2012) 470–478, https://doi.org/10.1016/j.cej.2012.09.102.
[167] G. Daneshvar Tarigh, F. Shemirani, Magnetic multi-wall carbon nanotube nanocomposite as an adsorbent for preconcentration and determination of lead (II) and manganese (II) in various matrices. Talanta 115 (2013) 744–750, https://doi.org/10.1016/j.talanta.2013.06.018.
[168] V.K. Gupta, I. Tyagi, H. Sadegh, R.S. Ghoshekand, A.S.H. Makhlouf, B. Maazinejad, Nanoparticles as adsorbent; a positive approach for removal of noxious metal ions: a review. Sci. Technol. Dev. 34 (2015) 195–214, https://doi.org/10.3923/std.2015.195.214.
[169] J.H. Jang, J. Lee, S.-Y. Jung, D.-C. Choi, Y.-J. Won, K.H. Ahn, P.-K. Park, C.-H. Lee, Correlation between particle deposition and the size ratio of particles to patterns in nano- and micro-patterned membrane filtration systems. Sep. Purif. Technol. 156 (2015) 608–616, https://doi.org/10.1016/j.seppur.2015.10.056.
[170] C. Zhou, Y. Shi, C. Sun, S. Yu, M. Liu, C. Gao, Thin-film composite membranes formed by interfacial polymerization with natural material sericin and trimesoyl chloride for nanofiltration. J. Membr. Sci. 471 (2014) 381–391, https://doi.org/10.1016/j.memsci.2014.08.033.
[171] X. Zhang, B. Lin, K. Zhao, J. Wei, J. Guo, W. Cui, S. Jiang, D. Liu, J. Li, A free-standing calcium alginate/polyacrylamide hydrogel nanofiltration membrane with high anti-fouling performance: preparation and characterization. Desalination 365 (2015) 234–241, https://doi.org/10.1016/j.desal.2015.03.015.
[172] J. Guo, Q. Zhang, Z. Cai, K. Zhao, Preparation and dye filtration property of electrospun polyhydroxybutyrate-calcium alginate/carbon nanotubes composite nanofibrous filtration membrane. Sep. Purif. Technol. 161 (2016) 69–79, https://doi.org/10.1016/j.seppur.2016.01.036.

This book belongs to Badji Mokhtar Annaba University Central Library Copyright Elsevier 2025

[173] W. Hu, J. Yin, B. Deng, Z. Hu, Application of nano TiO_2 modified hollow fiber membranes in algal membrane bioreactors for high-density algae cultivation and wastewater polishing. Bioresour. Technol. 193 (2015) 135–141, https://doi.org/10.1016/j.biortech.2015.06.070.

[174] M. Kamali, K.M. Persson, M.E. Costa, I. Capela, Sustainability criteria for assessing nanotechnology applicability in industrial wastewater treatment: current status and future outlook. Environ. Int. 125 (2019) 261–276, https://doi.org/10.1016/j.envint.2019.01.055.

This book belongs to Badji Mokhtar Annaba University Central Library

Copyright Elsevier 2025

This page intentionally left blank

This book belongs to Badji Mokhtar Annaba University Central Library

Copyright Elsevier 2025

Index

Note: Page numbers followed by *f* indicate figures *t* indicate tables, and *s* indicate schemes.

A

Absorption
graphene-based nanomaterials, removal capacity, 1023*t*
spectra, 42–44, 43*f*
visible light photocatalysis, 1104, 1105*t*, 1106*f*
Acid treatment
of electrode surface, 1083
natural zeolites, 436, 437*f*
Acoustic cavitation, 88–92, 91*f*, 92–93*t*, 253–254
Activated carbon (AC), 12, 14, 14*f*
Activated carbon nanofiber (ACNF), 330–331
Activated charcoal (AC), 251
Activated sludge process, 755–756
Adsorbent dosage, 346–347
Adsorbent exhaustion rate (AER), 923
Adsorption, 593–594, 750–751
air pollution treatment, 315–316
carbon-based nanoparticles, 817–818
challenges, 1136–1137
of chemicals to TiO_2 photocatalysis, 159–161
of dyes, 496–501, 496*f*, 498*f*
equilibrium, 979–981
isotherms, marble hydroxyapatite, 919, 920*t*
graphene-based nanomaterials, 1022
isotherm, 428, 430*t*, 979–981
marble hydroxyapatite, 905
of methane, 493, 495*f*
micropollutants removal, 972–975, 973–974*t*
agitation time, 977
carbon, 975
dosage, 977
factors affecting, 975–978
initial concentration, 977–978
ionic strength, 976–977
isotherm/equilibrium, 979–981
kinetic models, 978–979
metal oxide, 972–975
solution pH, 975–976
temperature, 978
of solar spectra, 173
wastewater treatment, 251–252
Adsorption of pollutant and heavy metals
challenges in, 357
characterization, 349–354
Brunauer-Emmett-Teller (BET) surface area, 352–353
energy dispersive X-ray spectroscopy (EDS), 351, 351*f*
Fourier-transform infrared spectroscopy, 352, 352*f*
scanning electron microscopy, 350, 350*f*
thermogravimetric analysis, 353–354, 354*f*
transmission electron microscopy, 351
X-ray powder diffraction, 353, 353*f*
mechanism, 354–357, 355*f*
electrostatic interactions, 355–356
hydrogen bonding, 356–357
hydrophobic interactions, 356
π-π interactions, 355
parameters affecting, 345–349
contact time, 346
dissolved organic matters, 349
dosage, 346–347
initial concentration, 347
ionic strength, 348–349
pH, 347–348
temperature, 348
Advanced Fenton process, 849–850
Advanced/novel water remediation processes, 757–762
Advanced oxidation processes (AOPs), 85–101, 142, 157, 252–260, 722, 762–769, 811–813, 813*f*, 849
challenges, 828–829, 1140–1143
classification, 1101–1102
electrochemical advanced oxidation processes, 768–769
factors affecting, 826–828
Fenton process, 99–101, 100*f*, 102*t*, 763–764
heterogeneous photocatalytic technique, 255
magnetic materials in water treatment, 256

This book belongs to Badji Mokhtar Annaba University Central Library
Copyright Elsevier 2025

Advanced oxidation processes (AOPs) *(Continued)*
magnetic materials used for water treatment, 258
homogeneous photocatalysis process, 253
Fenton reaction, 254
ozonation and catalytic ozonation, 255
sonochemical methods, 253
hybrid, 821–824
hydrodynamic cavitation, 87–88, 89–90*t*, 124–125*t*
industrial/domestic wastewater treatment, 1141
nanomaterials, 819–820
nonphotochemical, 824
Fenton process, 825
ozonation, 824
persulfate oxidation process, 825–826, 826*f*
sonolysis, 824
O_3/H_2O_2 treatment (peroxonation), 764
photocatalysis, 93–99, 94*f*, 95–98*t*
photochemical advanced oxidation processes, 764
H_2O_2 photolysis (H_2O_2/UV), 764–765
O_3 photolysis (O_3/UV), 765
photocatalysis, 766–767
photo-Fenton reaction (H_2O_2/Fe^{2+}/UV), 765–766
sonochemical advanced oxidation processes, 767–768
sonolysis/acoustic cavitation, 88–92, 91*f*, 92–93*t*
supercritical water oxidation, 813
for wastewater treatment, 780–781
Aeration, 745–746
Aerobic process, wastewater treatment, 248
Aerospace industry, 1071–1072
Agglomeration, 595–596, 1063
Aggregation, 62
Agitation time, 977
Agricultural waste, 243
Agri-food industry, 1071
Air pollutants, 315, 316*t*
treatment of
CO_2, 318–324
NO_x, 324–326, 332*f*
sulfur monoxide (SO_x), 326–327
volatile organic compounds, 328–331, 328*f*
Air pollution, 313–314
treatment
adsorption, 315–316
nanofiltration, 318
nanotechnology, 315–331
photocatalysis, 317–318
pilot-scale studies, 331–332
role of nanotechnology in, 314–315
usage of nanomaterials for, 333–334
Al@Fe-MOF composite, 503
Alginate, 391–392
Allotropes of carbon, 1009
α-cages, 420
Alumina, 8–9, 985
Aluminum oxide (Al_2O_3), 31
Aminated polyacrylonitrile (APAN), 933–934
Amino-functionalized magnetic NPs, 872
Amorphous carbon, 639
Amphiphilic polymer, 619–631
Anaerobic process, wastewater treatment, 248
Analcime, 422, 423*t*
Anatase, 162, 282
Anchoring dyes on TiO_2, 165
Animal manure, 243
Annular photoreactor (APR), 171
Annular reactor, micropollutants, 988, 989*f*
Anodes
anodic oxidation (AO), 768
capacitance values, 1089–1090, 1089*t*
modifications, BMFC, 1084–1085, 1084*t*
capacitance values, 1089–1090, 1089*t*
cyclic voltammogram, 1089–1090, 1089*f*
electrochemical characterization, 1085
electrochemical impedance spectroscopy, 1091–1092
exchange current density, 1090–1091, 1090–1091*t*
Fourier-transform infrared spectroscopy, 1087, 1087*f*
kinetics, 1090–1091
Nyquist plot, 1091–1092, 1092*f*
open circuit potential, 1085, 1093–1094, 1094*f*
physical characterization, 1085
power density and polarization curves, 1094–1096, 1095*f*
scanning electron microscopy, 1086–1087, 1086*f*
surface characterization, 1086–1088
surface wettability, 1088, 1088*f*
Tafel plot, 1090–1091, 1090*f*
Antibacterial activity, graphene-based nanomaterials, 1012–1020
inhibition of bacterial metabolism, 1020
lipid extraction, 1020
oxidative stress, 1016–1018
photocatalysis, 1018–1020
photothermal effect, 1018, 1019*t*
physical/mechanical destruction, 1014–1015
Antibacterial challenges, wastewater treatment, 546–548
carbon-based nanoparticles, 548
copper nanoparticles, 547
metal oxide-based nanoparticles, 548
silver nanoparticles, 547
titanium dioxide nanoparticles, 547
Antiferromagnetic materials, 256–257

This book belongs to Badji Mokhtar Annaba University Central Library
Copyright Elsevier 2025

Antifouling, challenges for wastewater treatment, 546, 547*f*
Antimicrobial action, 1024–1028
Antimicrobial agents, 243
AOPs. *See* Advanced oxidation processes (AOPs)
Applied cell voltage, electro-photocatalytic reactions, 841, 841*f*
APR. *See* Annular photoreactor (APR)
Aquaporins (AQPs), 642–643
Arsenic, 261–262, 593
Artificial photosynthesis, 138–139, 139*f*
Asymmetric (anisotropic) membranes, 676–677
Atom transfer radical polymerization (ATRP), 682–683, 693
Attached growth processes, 756
Automobile industry, 1071

B

Bacillus amyloliquifaciens, 1050
Bacillus atrophaeus, 1050
Bacterial metabolism, inhibition of, 1020
Ball milling method, 231
Bandgap, 4–5
Bed volumes (BV), 923
Benthic microbial fuel cell (BMFC), 1081–1083
  anode modifications, 1084–1085, 1084*t*
    capacitance values, 1089–1090, 1089*t*
    cyclic voltammogram, 1089–1090, 1089*f*
    electrochemical characterization, 1085
    electrochemical impedance spectroscopy, 1091–1092
    exchange current density, 1090–1091, 1090–1091*t*
    Fourier-transform infrared spectroscopy, 1087, 1087*f*
    kinetics, 1090–1091
    Nyquist plot, 1091–1092, 1092*f*
    open circuit potential, 1085, 1093–1094, 1094*f*
    physical characterization, 1085
    power density and polarization curves, 1094–1096, 1095*f*
    scanning electron microscopy, 1086–1087, 1086*f*
    surface characterization, 1086–1088
    surface wettability, 1088, 1088*f*
    Tafel plot, 1090–1091, 1090*f*
  construction, 1085
Bentonite clay, 789
Benzene rings, 1011
Benzothiophene, 501, 502*f*
β-cages, 420
Bimetallic nanoscale zero-valent iron (nZVI), 848*t*
Binary metal oxides, 785, 786*f*
Biodegradation
  oil-derived hydrocarbon, 1044–1046, 1045*f*
  polyaromatic hydrocarbons, 1044–1046, 1048
Biogenic metal nanoparticles, 769
Bioinspired materials (BIMs), 642–643
Biological oxygen demand (BOD), 610–611
Biological process, industrial nanomaterials, 1069
Biological reactor/aeration tank, 755
Biological synthesis, nanoscale zero-valent iron, 852–854
Biological water remediation, 753–757
Bionanocomposites, 11–12
Bioremediation, 1039
  of heavy metals, 884–887
  nano biosurfactants as source of, 1048–1050
  nanoscale material as agents for, 1046–1047
Biosurfactants, 1040
  carbon sources, 1042*t*
  diverse habitats, 1042–1043
  mechanism of action, 1043–1046, 1044*f*
  microorganisms producing, 1040–1042, 1041*t*
  types, 1042*t*
Bismuth molybdate (Bi_2MoO_6), 223–224
Bismuth oxybromide (BiOBr), 325–326
Black titania (BT), 993–995
Blending, 518, 519*f*
Bottom-up method, MOFs, 486
Brevibacterium casei, 1049
Brønsted acid sites, zeolites, 437*f*, 438
Brunauer-Emmett-Teller (BET)
  assays, 424
  surface area, 352–353
    marble hydroxyapatite, 916
Buckminsterfullerene, 1009–1010

C

Cadmium, 344–345, 589–591
Cadmium selenides (CDSe) quantum dots, 1063
Cadmium sulfide (CdS)-based nanomaterials for water splitting, 291–292
Calcium alginate (CA), 391
Calcium nitrate ($Ca(NO_3)_2$), 901–902
Candle soot (CS) nanoparticles, 640
Capacitive deionization (CDI), 528–529
Carbon
  atoms, 368
  dots, 39–40
  fullerenes, 1068
  nanoparticles, 1131–1132
Carbon-based magnetic nanoparticles, 260
Carbon-based membranes, 541
Carbon-based nano-adsorbents, 1067
Carbon-based nanocomposite materials (CNCMs), 557–558
  applications, 556*f*, 565–568
    organic/inorganic pollutants removal, 565–568

This book belongs to Badji Mokhtar Annaba University Central Library
Copyright Elsevier 2025

Carbon-based nanocomposite materials (CNCMs) *(Continued)*
development and synthesis
chemical vapor deposition (CVD), 559–560
phase inversion, 562–563
polymer grafting, 560–561
in situ colloidal precipitation, 560
in situ polymerization, 561
solution mixing, 558
spray-assisted layer-by-layer, 563
fabrications techniques and types, 563–564
carbon nanotube (CNT) membranes, 564
CNT-polymer composite, 564–565
Carbon-based nanomaterials, 31, 74
toxicity potential, 549
for water splitting
graphene-based nanomaterials, 295
graphitic carbon nitride (g-C_3N_4)-based nanomaterials, 296
Carbon-based nanoparticles, 74, 548, 817–818
Carbon dioxide (CO_2), 191, 318–324, 390–391
Carbonized bamboo (CB), 329–330
Carbon nanomaterials (CNs), 632–640
amorphous carbon, 639
carbon nanotube, 638–639, 935–938, 936–937*f*
fullerenes, 639
GO-incorporated mixed-matrix membrane, 634–638
graphene oxide, 930–935, 932–934*f*
graphene oxide-based membranes, 633–634
in mixed-matrix membrane, 632–640
thin-film composite membrane, 644–647
Carbon nanotube (CNT), 6–7, 516, 538, 549, 557–558, 632–633, 638–639, 935–938, 936–937*f*, 1067
colloidal stability, 817–818
covalent modification, 1010–1011
membrane, 568, 569*f*
membranes, 564
polymer composite, 564–565
micropollutants
adsorption process, 975
nanocomposite membranes, 987
nanocomposite, 1131–1132
membranes, micropollutants, 987
noncovalent functionalization, 1011
photothermal effect, 1018
potential safety concerns, 74
properties, 1013*t*
synthesis of, 66–68, 69–70*t*
types, 1010
Carbon nanotube-based photocatalytic membrane, 705–706
Carbon nanotube immobilized membranes (CNIM), 936, 937*f*
Carbon quantum dots (CQDs), 186, 187*f*
Carboxymethyl cellulose (CMC), 857
Carrier traps, 158–159
Catalyst
catalytic activity, nanoscale zero-valent iron, 858–861
loading, 790–793
for organic component degradation, 4
oxidation, 4
Cation exchange capacity (CEC), zeolites, 420
Cationic substrates, 164–165
Cavitation
bubbles, 1108–1109, 1110*f*
effect, 821–822, 821*f*
process, 87
Cellulose, 11, 262, 394–395
Cellulose acetate (CA), 576–577
Cellulose nanofibrils (CNF), 395
Centrifugal separation, wastewater treatment, 247
Ceramic
based nanoparticles, 818
membranes, 538–539, 1138–1139
ZnS nanocomposites, 226
Ceramic matrix nanocomposites (CMNCs), 780
Cerium oxide, 785, 967
Cetylpyridine bromide (CPB), 445
Cetylpyridinium chloride (CPC), 857
Chabazite, 422, 423*t*
Charge carrier
species, generation of, 157–159
traps, 158–159
Charge transfer resistance (Rct), 1091–1092, 1092*f*
Chemical precipitation, 417, 750
Chemical reducing agent, 855–856
Chemical synthesis, nanoscale zero-valent iron, 850–851
Chemical vapor deposition (CVD), 66–68, 182–183, 559–560, 710
Chemisorption controlled adsorption process, 979
Chitosan (CS), 12, 262, 392, 393*f*
nanocomposites, 392–394
nanoparticles, 817–818
polymer, 576–577
Chitosan chloride-GO (CSCl@GO), 1025, 1028*t*
Chlorination, 751–752
Chlorine stability, 648–649
4-Chlorophenol (4CP), 861
Chromium, 261, 591
Ciprofloxacin (CPX), 391
Classical Mie theory, 44–45
Clay-based nanocomposites, 789
Clay-based polymeric nanocomposites (CPNs), 13–14
Clinoptilolite, 422, 423*t*, 436, 449*t*
CMNCs. *See* Ceramic matrix nanocomposites (CMNCs)

This book belongs to Badji Mokhtar Annaba University Central Library
Copyright Elsevier 2025

CNCMs. *See* Carbon-based nanocomposite materials (CNCMs)
CNT. *See* Carbon nanotube (CNT)
Coagulation, 247, 749, 1069
Coarse screens, 745
Coextrusion method, 712
Combustion method, 230
Composite anode
  electrochemical analyses, 1089–1092
  kinetics, 1090–1091
Concentration polarization (CP), 615–616
Conduction band (CB), 139, 209–211
Contact time
  adsorption, 346
  effect, 917, 917–918*f*
Continuous flow electro-photocatalytic reactor, 838–839
Continuous MOFs, 488
Controlled precipitation, method of, 34–35
Conventional biological treatment, 85–86
Conventional cleaning technique, 674
Conventional membranes, 538–540, 539*f*
  ceramic membranes, 539
  polymeric membranes, 539–540
Conventional precipitation (CM) technique, MA-Hap, 900–901, 903, 904*f*
  adsorbent dosage, 916–917, 916*f*
  adsorption equilibrium isotherms, 919, 920*t*
  co-ions effect, 918, 919*f*
  column breakthrough, 923, 924*t*, 924*f*
  contact time effect, 917, 917–918*f*
  energy efficacy, 922–923
  FTIR analysis, 906–908, 907*f*
  kinetics of adsorption, 919–920, 921*t*
  pH effect, 917–918
  SEM analysis, 912–914, 912–913*f*
  TEM/EDS analysis, 914, 914–915*f*
  TGA/DTA analysis, 914–915, 915*f*
  water quality parameters and regeneration, 920–922, 922*f*
  XRD analysis, 908–912, 908*f*, 911*f*
Conventional wastewater treatment plants (WWTP), 742, 742*f*, 1101–1102
Copper, 591–592
  nanoparticles, 62, 547, 549, 652–653
Copper-based MOF-505-GO composite, 490–492, 492*f*
Copper sulfide nanocomposites, 225–226
Co-precipitation method, 38, 231, 872
Cosmetic industries, 245
Cosmetic products, 245
Coupling
  membrane technology, 717
  TiO2 photocatalysis, 171–172
Covalent interaction, 375–376
Covalent modification, carbon nanotube, 1010–1011
Covalent organic frameworks (COF), 653
CPNs. *See* Clay-based polymeric nanocomposites (CPNs)
Crbon-based nanomaterials synthesis, 39–40
Crystallization, wastewater treatment, 249
Cu-based MOF, 505
Cu/CNT polymer composite membrane, 567
Cupric oxide (CuO), 948
CVD. *See* Chemical vapor deposition (CVD)
Cyclic voltammogram, 1089–1090, 1089*f*
Cylindrical reactor, 840, 840*f*
Cytotoxicity, 548

D

Dealumination, of zeolites, 440, 440*f*
Debye-Scherer formula, 911–912
Defluoridation process, MA-Hap, 899, 901, 916
  adsorbent dosage, 916–917, 916*f*
  co-ions effect, 918, 919*f*
  contact time effect, 917, 917–918*f*
  materials, 901
  pH effect, 917–918
Degradation effect, 700
Degree of sorption, 432
Deposition process, 839
Derivatives-based binary nanocomposites, graphene, 184–186, 192–193
Derivatives-based ternary nanocomposites, graphene, 186–188, 193–194
Dermal penetration, 1059–1060
Differential thermal analysis (DTA), 905, 914–915, 915*f*
Dimethyl dibenzothiophene (DMDBT), 501
Direct Black, 724
Discontinuous MOFs, 488
Disinfection using nanomaterials, 5–6
Dissolved organic matters, 349
Distillation, 249, 747–749
Donnan equilibrium, 432–433
Downconversion phosphors, 213–216, 214–215*f*
3D quantum confinement, II-VI and III-V nanoparticles, 44–45
Dubinin-Radushkevich (D-R) isotherm, 430*t*, 919, 920*t*, 980
Dye, 724
  anchoring, 165
  degradation, electro-photocatalysis, 833–834
    applied cell voltage, 841, 841*f*
    cylindrical reactor, 840, 840*f*
    effect of reaction conditions, 840

This book belongs to Badji Mokhtar Annaba University Central Library
Copyright Elsevier 2025

Dye *(Continued)*
experimental assembly in, 836–840, 837*f*
large-scale application, 844
light intensity, 842–843
mechanisms, 835–836, 836*f*
photoanodic materials, 842
photon source, 842–843, 844*f*
rotating disc reactors, 839–840, 839*f*
three-dimensional electrode packed-bed reactor, 838–839, 838*f*
three-dimensional electrode-slurry reactor, 837*f*
Dye-sensitized catalyst, 10–11

E

EDTA. *See*. *See* Ethylenediaminetetraacetic acid (EDTA)
EDXS. *See* Energy dispersive X-ray spectroscopy (EDXS)
Electrochemical advanced oxidation processes (EAOPs), 768–769
Electrochemical analyses, 1089–1092
Electrochemical impedance spectroscopy (EIS), 1091–1092
Electrochemical technology, 39–40, 834
Electrocoagulation (EC), 762, 1069
Electrode deposition/degradation, 1022–1024
Electrode surface, acid-treatment of, 1083
Electrodialysis (ED), 762
Electrolysis, 419, 455
Electrolyte, 688–689
Electron-hole recombination, 158–159
Electro-oxidation process, 1143–1144, 1144*f*
Electro-photocatalysis, 833–834
cylindrical reactor, 840, 840*f*
effect of reaction conditions, 840
applied cell voltage, 841, 841*f*
light intensity, 842–843
photoanodic materials, 842
photon source, 842–843, 844*f*
experimental assembly in, 836–840, 837*f*
large-scale application, 844
mechanisms, 835–836, 836*f*
rotating disc reactors, 839–840, 839*f*
three-dimensional electrode packed-bed reactor, 838–839, 838*f*
three-dimensional electrode-slurry reactor, 836–838, 837*f*
Electroplating method, 15–17
Electroresponsive membranes, 689–691
Electrospinning, 545
Electrospun nanofibers, 981–983
Electrospun-silk-nanofiber (ESF) membrane, 940
Electrostatic attraction potential, 1063–1064
Electrostatic interactions, adsorption, 355–356
Elovich model, 460
Emerging organic contaminants (EOC), 741, 758
Emerging pollutants, definition of, 608–610
Energy dispersive X-ray spectroscopy (EDXS), 299, 351, 351*f*
analysis, marble hydroxyapatite, 914, 914–915*f*
zeolite, 424
Energy gap, 29
Erionite, 422, 423*t*
Ethylenediaminetetraacetic acid (EDTA), 395–396
Evaporation, wastewater treatment, 249
Exchange current density, anodes, 1090–1091, 1090–1091*t*
Exciton radius, 29

F

Faujasite, 423*t*
F-doped tin oxide (FTO) substrate, 841–842
Fenton process, 99–101, 100*f*, 102*t*, 763–764
nanoscale zero-valent iron, 847–850, 848*t*, 859*f*, 862
biological synthesis, 852–854
catalytic activity, 858–861
chemical reducing agent effects, 855–856
chemical synthesis methods, 850–851
initial Fe^{3+} concentration effect, 854–855
mango peel extract for green synthesis, 854, 855*f*
pH reaction effect, 857–858
reaction mechanism, 858–860
SEM and TEM, 852, 853*f*
sonochemical synthesis, 851–852
stabilizer concentration effects, 856–857
temperature for controlling, 857
top-down *vs*. bottom-up process, 850
nonphotochemical advanced oxidation processes, 825
Fenton reaction, 254
visible light photocatalysis, 1107–1108
zero-valent iron nanoparticles, 849–850
Fe_3O_4@AMCA-MIL-53 (Al) nanocomposite
adsorption-desorption mechanism, 498, 500*f*
pH effect on MB and MG adsorption, 498, 499*f*
Fe_3O_4@MIL-68 (Al), 504
Fe_3O_4/MIL-101(Cr), 498–499
Fe_3O_4/MIL-88A composite, 497–498, 498*f*
Ferric oxide (FeO) nanoparticle, 948
Ferrierite, 423*t*
Ferromagnetic materials, 256–257

This book belongs to Badji Mokhtar Annaba University Central Library
Copyright Elsevier 2025

Fe-zeolites, 446
FeZSM-5, 447, 447*f*
FHA. *See* Fluorinated hybrid aerogel (FHA)
Fick's second law, 979
Field emission spectrometers, 350
Filtration, 746–747
  graphene-based nanomaterials, 1021–1022
  industrial nanomaterials, 1069
  wastewater treatment, 247
Fine screens, 745
Fixed-bed system, 452–453, 454*f*, 838–840
Flocculants, 612
Flocculation, 247, 749–750
Flotation, 1069
Fluidized bed systems, 452–453
Fluorescent lamp, 843
Fluoride, 899
Fluorinated hybrid aerogel (FHA), 395
Flux rejection trade-off, 615
Food industry, industrial nanomaterials, 1070
Forward osmosis (FO), 1021–1022
Fouling, 546, 615–616, 674
Fourier-transform infrared (FTIR)
  analysis, marble hydroxyapatite, 904, 906–908, 907*f*
  spectroscopy, 188–189, 352, 352*f*, 520, 1087, 1087*f*
    H-Y zeolite, 438, 439*f*
    zeolite, 425
Freundlich isotherm, 251–252, 430*t*, 919, 920*t*, 980
Fullerene, 639, 817–818, 1009–1010, 1046
  inhibition of bacterial metabolism, 1020
  properties, 1013*t*
  reactive oxygen species, 1017
Functionalization of GO, 374, 375*f*
  covalent interaction, 375–376
  noncovalent interaction, 376–377
Functionalized graphene oxide (fGO), 635–636
Functionalized-iron oxide NPs, 872
Functionalized multiwalled CNTs (f-MWCNTs), 563

G

Gallium oxide, 320
Gas-phase adsorption, nanocomposite-based MOFs, 489–495, 491*f*
Gibbs free energy, 430–431
Glassy carbon electrode (GCE), 1082–1083
Glutathione (GSH), 1017
GO. *See* Graphene oxide (GO)
GO-CNTs/ZIF-8 nanocomposite, 496–497, 497*f*
GQDs. *See* Graphene quantum dots (GQDs)
Graft copolymerization/crosslinking, 517–518
Grafting-from method, 682–683
Grafting-to methodology, 682
Granular zero-valent iron (ZVI), 848, 848*t*
Graphene, 7–8, 8*f*, 181–182, 183*f*, 368–370, 391–392, 516, 538, 557*f*, 1011
  antibacterial activity, 1014–1015
  characterization of, 188–190
  and derivative-based photocatalyst, 184–188
  derivative-based ternary nanocomposites, 186–188
  derivatives based binary nanocomposites, 184–186
  geometric properties, 1015
  mechanism of photocatalytic degradation, 194–197
  nanocomposite, 1131–1132
  nanocomposite membranes, micropollutants, 986–987, 987*f*
  nanomaterials, 7–8
  photocatalytic applications, 190–194, 199*t*
  preparation methods, 182–184, 199*t*
  properties, 1013*t*
  properties and derivatives, 182
Graphene-based adsorbents, 368
Graphene-based inorganic nanocomposites
  magnetic graphene-based nanocomposites, 382–388
  metal and metal-oxides graphene-based nanocomposites, 378–382
Graphene-based materials, 367
  functionalization, 374–377
  graphene, 368–370
  graphene oxide, 371–373, 372*f*
  kinetic of adsorption, 377–378
  reduced graphene oxide, 373–374, 373*f*
Graphene-based nanocomposites, 380–383*t*, 382, 387–389*t*, 395–397, 787–789, 793*f*
  for adsorption
    of heavy metal contaminants, 379, 380–382*t*
    of organic contaminants, 386, 387–389*t*
  for adsorptive removal of gas pollutants, 382, 383*t*
  with multidentate organic chelating ligands, 395–397
Graphene-based nanomaterials
  antibacterial activity, 1012–1020
    inhibition of bacterial metabolism, 1020
    lipid extraction, 1020
    oxidative stress, 1016–1018
    photocatalysis, 1018–1020
    photothermal effect, 1018, 1019*t*
    physical/mechanical destruction, 1014–1015
  antimicrobial action, industrial application, 1024–1028
  bacterial cell destruction, 1014–1015
  cost analysis, 1027–1028, 1028*t*
  properties, 1009–1012, 1013*t*
  structure, 1009–1012
  for water splitting, 295
  water treatment with, 1020, 1021*s*
    absorption properties, with removal capacity, 1023*t*
    adsorption, 1022

This book belongs to Badji Mokhtar Annaba University Central Library
Copyright Elsevier 2025

Graphene-based nanomaterials *(Continued)*
electrode deposition/degradation, 1022–1024
filtration, 1021–1022
photocatalysis, 1022–1024
Graphene-based organic nanocomposites, 379
graphene-based nanocomposites, 395–397
graphene-based organic polymer nanocomposites, 389–395
polymer, 389–395
alginate nanocomposites, 391–392
cellulose nanocomposites, 394–395
chitosan nanocomposites, 392–394
Graphene-based photocatalytic membrane, 703–704
Graphene-MOF adsorbents, 490
Graphene oxide (GO), 7–8, 8*f*, 68–72, 182, 183*f*, 371–373, 371–372*f*, 522, 522*f*, 541, 548, 644–645, 704, 930–935, 932–934*f*
chemical modification of, 374
functionalization of, 374, 375*f*
nanocomposite membranes, micropollutants, 986–987, 987*f*
nanoparticles, 1047
nanosheets, 646
SEM images of, 189–190, 190*f*
surface-located membrane, 650–652
TEM images of, 189–190, 190*f*
Graphene oxide-based membranes, 633–634
Graphene oxide/polyamide (GO-PA) membrane, 568
Graphene quantum dots (GQDs), 646–647
antibacterial activity, 1012
properties, 1013*t*
structure, 1012
Graphene-supported nanocomposites, 1131–1132
Graphene-titania composite film electrodes, 841–842
Graphite, 367, 369*f*
Graphite nanoplatelets (GNPs), 320
Graphite oxide (GO), 1009, 1011
antibacterial activity, 1014–1015
in polar organic solvents, 1012
in polyethersufone membranes, 1026, 1028*t*
properties, 1013*t*
Graphitic carbon nitride ($g\text{-}C_3N_4$)-based nanomaterials, 296
Graphitic carbon nitride-based photocatalytic membrane, 704–705
Gravity separation, 247
Green economy, 770
Green remediation, 770
Green synthesis, 68, 76
Grit chambers, 745
Groundwater, 242–243

H

Halogenated hydrocarbon's degradation process, 813
Halogen lamp, 843
Hard water, 451
HC. *See* Hydrodynamic cavitation (HC)
H-clinoptilolite, thermal treatment, 442, 442*f*
Heavy metal-based product, 245–246
Heavy metals, 3–4, 344
removal, 575–577, 589*f*
arsenic, 593
biosurfactants, mechanism of action, 1043–1046, 1044*f*
cadmium, 589–591
chromium, 591
copper, 591–592
iron-bimetal oxide NPs for, 872–877, 876*t*
iron oxide-biomaterial-based nanoparticles, 884–889, 888*t*
iron oxide-carbon nanotubes, 882, 883*t*
iron oxide functional groups, 870–872, 872*f*, 873–875*t*
iron oxide-graphene, 882–884, 885–886*t*
iron oxide-metal oxide nanoparticles, 877–878, 878*t*
iron oxide-polymer, 879–881, 880–881*t*
lead, 588–589, 590*f*
nanocomposite membranes with conventional processes, 593–594
nanomaterials, 583–585
need of, 577–578
nickel, 593
Hematite
catalysts, 259
nanoparticles, 259, 869
Heterogeneous Fenton process, 103–104, 103*f*, 105–107*t*
Heterogeneous photocatalysis, 225, 255, 1103–1106
magnetic materials
used for water treatment, 258
in water treatment, 256
Heterogeneous photo-Fenton process, 104–111, 108*f*, 109–110*t*
Heterogeneous sonochemistry, 851–852
Heulandite, 422, 423*t*
Hexadecyltrimethylammonium (HDTMA)-modified zeolite, 465
Hollow-fiber membrane, 713, 714*f*
Homogeneous photocatalysis, 1106–1107
Fenton reaction, 254
ozonation and catalytic ozonation, 255
sonochemical methods, 253
Homogeneous precipitation, 521–522
Homogeneous sonochemistry, 851–852
H_2O_2 photolysis (H_2O_2/UV), 764–765
H-shaped zeolites, 437
Humic acid SMZ (HA-SMZ), 460

This book belongs to Badji Mokhtar Annaba University Central Library
Copyright Elsevier 2025

Hummer's method, 1011
Hybrid advanced oxidation processes (AOPs), 821–824
involving nanocatalyst, 101–123
heterogeneous Fenton process, 103–104, 103*f*, 105–107*t*
heterogeneous photo-Fenton process, 104–111, 109–110*t*
photocatalytic oxidation with hydrodynamic cavitation, 123
sono-Fenton process, 116–118, 116*f*, 117–118*t*
sono-photocatalytic process, 111–115, 111*f*, 113–115*t*
sono-photo-Fenton process, 119–123, 119*f*, 120–122*t*
Hybrid-magnetic nanoparticles (HMNPs), 882
Hybrid photocatalytic membrane, 701–702
Hybrid photoreactors, 803
Hydrodynamic cavitation (HC), 87–88, 89–90*t*, 124–125*t*, 172, 1108–1109
Hydrogels, 14
Hydrogen bonding, adsorption, 356–357
Hydrogen peroxide, 752
Hydrolyzed polyacrylonitrile (HPAN) membrane, 588
Hydrophilic polymer (HP), 619–631
Hydrophobic compounds, 171–172
Hydrophobic interactions, adsorption, 356
Hydrothermal technique, 38, 230, 521–522
Hydroxyl radicals, 139–140, 161
H-Y zeolite, 438, 439*f*

I

Immersion
method, 711–712
precipitation, 1026
well photoreactors, 170
Immobilized catalyst reactors, 168–170
Immobilized photocatalytic systems, 174
Industrialization, 242–243
Industrial nanomaterials (INMs), 1057–1059
aerospace industry, 1071–1072
agri-food industry, 1071
applications, 1058*f*
associated risks, 1067–1070
automobile industry, 1071
environmental impact, 1064
during disposal, 1065–1066, 1065*f*
during manufacturing, 1064
release in use, 1065
food industry, 1070
health risk, 1059
dermal penetration, 1059–1060
ingestion, 1059
inhalation, 1060–1061, 1060*f*
ideal designs, 1072–1073, 1072*f*
life cycle stages, 1058*f*
removal from waste water, 1068–1070, 1069–1070*f*
risk and safety associated using, 1066–1072
toxicological impact, 1061
chemical composition, 1061
degree of agglomeration, 1063
electrostatic attraction potential, 1063–1064
particle shape, 1063–1064
particle size, 1062
surface area and reactivity, 1062
surface coatings/type, 1063
Industry
dyes, 1118*f*, 1119
effluents, 344–345
industrial application, 1024–1028
revolution, 313
waste, 244–245
wastewater treatment, 743
Ingestion, 1059
Inhalation, 1060–1061, 1060*f*
Inorganic contaminants in wastewater, 261
Inorganic industrial nanomaterials (INMs), 1068
Inorganic luminescent materials, 227, 228–229*t*
Inorganic membranes, 612–613, 760
Inorganic nanomaterials (iNPs), 631–632
in mixed-matrix membrane, 631–632
surface-located membranes, 652–653
thin-film composite membrane, 641–642
Inorganic nanoparticle-based membranes, 540–541
Inorganic phosphors, 211–213
Inorganic pollutants, 343
Inorganic pollutants removal, 565–568
Insecticides, 243
In situ colloidal precipitation, 560
In situ polymerization, 518, 561
Interfacial polymerization (IP), 543–544, 588
International Zeolite Association (IZA-SC), 422
Interpenetrating polymer networks (IPNs), 679
Iodination, 752
Ion exchange, 753
definition, 432
of zeolite, 433*f*
Ion exchange capacity (IEC), 515
Ionic strength, 348–349, 688–689, 976–977
Iron-based magnetic nanoparticles, 258–259
Iron-based oxide, 258
Iron-bimetal oxide nanoparticles, 872–877, 876*t*
Iron(III)-chloride-modified zeolite, 466
Iron(III)-modified zeolite, 447–448, 465–466
Iron oxide, 8–9
biomaterial-based nanoparticles, 884–889, 888*t*
carbon nanotubes, 882, 883*t*
functional groups, 870–872, 872*f*, 873–875*t*
graphene, 882–884, 885–886*t*
metal oxide nanoparticles, 877–878, 878*t*

This book belongs to Badji Mokhtar Annaba University Central Library
Copyright Elsevier 2025

Iron oxide *(Continued)*
nanoadsorbents, 974–975
nanoparticles (NPs), 867–868, 948
potential safety concerns, 74–75
synthesis of, 68, 70*t*
polymer, 879–881, 880–881*t*
Irradiation time, 798, 800–801*t*, 801*f*
Isotropic (symmetric) membranes, 676, 677*f*

K

Kinetic of adsorption, 377–378

L

Langmuir adsorption isotherm, 251–252, 980–981
Langmuir-Hinshelwood rate equation, 255–256
Langmuir isotherms, 391, 430*t*, 919, 920*t*
Lanthanum-doped TiO_2 (La-TiO_2), 324–325, 328–329
Laumontite, 422, 423*t*
Layer-by-layer (LBL)
assembly, 545
technique, 649, 652
Layered perovskite-based nanomaterials for water splitting, 290–291
Lead removal, 588–589, 590*f*
Lewis acid sites, zeolites, 438, 438*f*
Light-emitting diodes (LED), 970
Light intensity, 842–843
Lipid extraction, 1020
Lipopeptides, 1050
Liquid combustion method, 230
Lithium-ion batteries, 1082–1083
Ln^{3+}-doped oxide nanomaterials, 1129–1130
Long-lasting phosphors, 219–221, 219–220*f*
Long persistent phosphors (LPP), 210–211
Low-dimensional nanomaterials
optical properties
of 1D and 2D nanomaterials, 46–47
of 0D of II–VI and III–V nanomaterials, 42–45
synthesis of, 32–41, 32*f*
carbon-based nanomaterials, 39–40
1D and 2D nanomaterials, 37–39
0D nanomaterials, 33–37
II–VI and III–V semiconductor nanomaterials, 40–41
in wastewater treatment, 48
Luminescence materials in photocatalysis
future perspectives of, 233
mechanism and challenges, 211–213
rare-earth-doped inorganic phosphor materials, 213–221
downconversion phosphors, 213–216
long-lasting phosphors, 219–221
upconversion phosphors, 216–218
Luminescent phosphors, 210–211, 1129–1130

M

Maghemite, 869
Magnetic adsorbents, 261–263
inorganic contaminants in wastewater, 261
mineralization of organic pollutants, 262–263
Magnetic chitosan, 394
Magnetic graphene-based nanocomposites, 382–388
Magnetic graphene nanoplatelet composites (MGNCs), 882–884
Magnetic graphene oxide (MGO), 882–884
Magnetic materials
advantages in water treatment, 256
used for water treatment, 258
carbon-based magnetic nanoparticles, 260
iron-based magnetic nanoparticles, 258–259
zeolite based magnetic nanoparticles, 260
Magnetic metal-organic frameworks (MOFs), 504
Magnetic nanohybrids, 870–889
Magnetic nanoparticles (MNPs), 9, 257–258, 262–263, 870, 884–887
limitations of, 267
photocatalysis decontamination of water using, 263–266
potential safety concerns, 74–75
Magnetic solid-phase extraction (SPE), 879
Magnetism, 256–257
Magnetite, 259, 869
Magnetoresponsive membranes, 691–692
Malachite green (MG), 496–497, 497*f*
Mango peel extract, 854, 855*f*
Marble hydroxyapatite (MA-Hap), 901. *See also* Marble waste powder (MWP)
adsorption
equilibrium isotherms, 919, 920*t*
experiments, 905
batch defluoridation studies, 916
adsorbent dosage, 916–917, 916*f*
co-ions effect, 918, 919*f*
contact time effect, 917, 917–918*f*
pH effect, 917–918
Brownian motion, 910–911
characterization, 904–905
Brunauer-Emmett-Teller surface area, 916
FTIR analysis, 906–908, 907*f*
SEM analysis, 912–914, 912–913*f*
TEM/EDS analysis, 914, 914–915*f*
TGA/DTA analysis, 914–915, 915*f*
XRD analysis, 906, 907–909*f*, 908–912, 911*f*

This book belongs to Badji Mokhtar Annaba University Central Library
Copyright Elsevier 2025

column breakthrough, 923, 924*t*, 924*f*
energy calculations, 925–926
energy efficacy, 922–923
kinetics of adsorption, 919–920, 921*t*
point of zero charge, 905
surface zero charge, 917–918
synthesis, 902
conventional precipitation (CM) technique, 902–903, 903*f*
mean crystallite size, 911–912, 911*t*
reaction time and yield, 906, 906*t*
ultrasonication method, 903, 904*f*
water quality parameters and regeneration, 920–922, 922*f*
Marble waste powder (MWP), 900–901. *See also* Marble hydroxyapatite (MA-Hap)
calcium nitrate, 902
FTIR spectra of Hap synthesized using, 904
XRD analysis of unreacted, 906, 907*f*
Mechanical exfoliation techniques, 182–183
Mechanochemical synthesis, MOFs, 487
Membrane
application of, 167–168
filtration, 249–251, 674, 929–930
graphene-based nanomaterials, 1021–1022
nanofiltration, 250
reverse osmosis, 250–251
ultrafiltration, 250
visible light photocatalysis, 1110–1112, 1112*f*, 1113*t*
fouling, 595–596, 1138, 1140, 1145
materials, 677–678
separation, 612, 655, 981, 982–983*t*
nanocomposite membranes, 983–987
nanofibrous membranes, 981–983
technology, 538, 674
advanced/novel water remediation processes, 758–762
advantages of, 760
configurations of, 760
separation process characteristics, 759–760, 761*t*
types of, 675–677
asymmetric (anisotropic) membranes, 676–677
isotropic (symmetric) membranes, 676, 677*f*
vessel, 726–727
Membrane-based technology, 15–18
Membrane bioreactor (MBR), 631, 931
Membrane distillation (MD), 748–749, 748*f*
Membrane photoreactor (MPR), 990–992
Mesopores, 488
Metal and metal oxides, 8–9, 378–382
Metal-based nano-adsorbents, 1067
Metal-containing nanoparticles, 9
Metal deposition, 162–163
Metal-doped nanocomposites, 783, 784*f*
Metal matrix nanocomposites (MMNCs), 780
Metal nanoparticles, 847–848
Metal-organic frameworks (MOFs), 382, 483, 653, 938, 943–944
challenges, 505–507
for wastewater treatment, 506–507
graphite oxide (GO) composites, 490
MIL, 939*f*, 943
mixed-matrix membrane, 632
nanocomposite-based, 488–489
in adsorption, 489–504
dyes adsorption, 496–501, 496*f*, 498*f*
gas-phase adsorption, 489–495, 491*f*, 495*f*
general adsorption, 501–504
industrial applications, 505
nanocomposites, 1132
properties, 484–485
synthesis methods, 486–488
thin-film composite membrane, 643–644
types, 485
UiO-66, 939*f*, 941–942, 942*f*
for water splitting, 293–295
zeolitic imidazolate frameworks, 938–941, 939–940*f*
Metal oxide-based nanoparticles, 548
Metal oxide-containing nanoparticles, 816–817
Metal oxides, 516–517, 1082
micropollutants
adsorption process, 972–975
nanocomposite membranes, 984–986
nanomaterials, 30–31, 1128–1129
nanoparticles, 946–948
as photocatalyst, 9–11
for water splitting
layered perovskite-based nanomaterials, 290–291
titanium oxide (TiO_2)-based nanomaterials, 282–285
zinc oxide (ZnO)-based nanomaterials, 285–290
Metal sulfide (MS), 34, 785–787
for water splitting, 291–293
cadmium sulfide (CdS)-based nanomaterials, 291–292
molybdenum sulfide (MoS_2) based nanomaterials, 293
tungsten sulfide (WS_2)-based nanomaterials, 293
zinc sulfide (ZnS) based nanomaterials, 291–292
Metal sulfide-based photocatalysts for H2 production, 293, 294*t*
Methane, adsorption of, 493, 495*f*
Method-activated zeolite plasma, 443

This book belongs to Badji Mokhtar Annaba University Central Library
Copyright Elsevier 2025

Methylene blue (MB) dye, 702–704, 724, 1116, 1116*f*
Methyl orange (MO), 46
$MgFe_2O_4$/MOF composite, 498–499
Micellar-enhanced ultrafiltration (MEUF), 250
Microbial fuel cell (MFC), 1081–1082
Microbial surfactants. *See* Biosurfactants
Microfiltration (MF), 758–759
  graphene-based nanomaterials, 1021
  micropollutants, 992
Microfluidic reactors, 802–803, 804*f*
Microplastics, 245–246
Micropollutants (MPs), 957–959
  adsorption process, 972–975, 973–974*t*
    agitation time, 977
    carbon, 975
    dosage, 977
    factors affecting, 975–978
    initial concentration, 977–978
    ionic strength, 976–977
    isotherm/equilibrium, 979–981
    kinetic models, 978–979
    metal oxide, 972–975
    solution pH, 975–976
    temperature, 978
  advanced methods, 961
  annular reactor, 988, 989*f*
  conventional methods, 960–961
  large-scale operation, 993–995, 994*f*
  membrane photoreactor, 990–992
  membrane separation process, 981, 982–983*t*
    nanocomposite membranes, 983–987
    nanofibrous membranes, 981–983
  microreactors, 992
  nanomaterials-based process, 1144–1146
  optical fiber photo reactor, 989–990
  photocatalysis process, 962–968, 963–964*t*
    cerium oxide, 967
    factors influencing, 968–972
    graphene-supported nanophotocatalyst, 965
    initial concentration, 971–972
    irradiation source, 970
    loading of, 968–969
    metronidazole wastewater, degradation efficiencies, 965, 966*f*
    reaction temperature, 970–971
    silver (Ag) NPs, 967–968
    solution pH, 969–970
    titanium dioxide, 964
    zinc oxides, 966–967
  photocatalytic membrane reactors, 990–992, 991–992*f*
  spinning disc reactor, 988
  types of, 959–960
  ultraviolet light emitting diode–based reactor, 990
Microreactors, 802–803, 992
Microscreens, 745
MIL, 939*f*, 943
MIL-100(Fe)@Fe_3O_4@AC, 498–499
Mineralization of organic pollutants contaminated wastewater, 262–263
Minocycline (MC), 504
Mixed matrix membrane (MMM), 576–577, 617, 618*f*, 930. *See also* Polymer nanocomposite, mixed-matrix membranes
  challenges, 949
  GO-based membranes into, 931–932
  ZIF-8 functionalized, 941
MMNCs. *See* Metal matrix nanocomposites (MMNCs)
Modified-magnetic iron oxide nanoparticles (M-MIONPs), 870–871
Modified zeolites
  sorption
    of ammonium, 466–468
    of metal cations, 463–466
MOF Fe_3O_4@AMCA-MIL-53 (Al) nanocomposite, 498, 499*f*
MOFs. *See* Metal-organic frameworks (MOFs)
Molecular dynamics simulation, 1014–1015
Molybdenum sulfide (MoS_2) based nanomaterials, 293
Montmorillonite (MMT), 321
Mordenite, 422, 423*t*, 459–460
MPs. *See* Micropollutants (MPs)
Multilamp photoreactor, 171
Multimedia filtration (MMF), 746–747
Multistate sensitization (MSS), 1016
Multiwalled carbon nanotube (MWCNT), 6, 7*f*, 265, 492, 494*f*, 518, 520, 527–528, 560–562, 638–639, 817–818, 935–938
  aerospace industry, 1071–1072
  automobile industry, 1071
  for heavy metal removal, 882
  Langmuir adsorption isotherm, 980–981
  physical/mechanical destruction, 1014
  structure, 936*f*

N

Nanocatalyst, 4
Nanocellulose, 394–395
Nanoclay, 1048
Nanocomposite, 779
  classification of, 514–515, 514*f*
  hydrogels, 14–15
  inorganic supports, 12–14
  photocatalysts (*see* Photocatalysts)
  and synthesis, 780
  types of, 780
  for wastewater treatment
    bionanocomposites, 11–12
    nanocomposite hydrogels, 14–15
    nanocomposite inorganic supports, 12–14

This book belongs to Badji Mokhtar Annaba University Central Library
Copyright Elsevier 2025

Nanocomposite ion exchange (IEX) materials, 513–514
application, 524–529
background, 515
characterization, 520
fourier transform infrared spectroscopy, 520
scanning electron microscope (SEM), 522–523
thermogravimetric analysis (TGA), 522
X-ray diffraction (XRD), 521–522
nanomaterials, 515–517
low-dimension carbon, 516
metal oxide, 516–517
silica, 517
processing methods
blending, 518, 519*f*
graft copolymerization/crosslinking, 517–518
in situ polymerization, 518
sol-gel technique, 519, 519*f*
suspension polymerization, 518
resins, 524, 525*t*
scale-up conundrum, 530
types of, 514–515
Nanocomposite membranes, 17–18, 617–619, 618*f*, 620–630*t*, 983–984
carbon material, micropollutants, 986
carbon nanotube, 987
graphene, 986–987, 987*f*
metal and metal oxide, micropollutants, 984
alumina, 985
silica, 985
titanium dioxide, 984–985
zinc oxide, 985–986
nanocomposite membranes-based processes, 1138–1139, 1139*f*
nanomaterials, 1133
role of, 579–583, 584–585*f*
synthesis, 585–588
interfacial polymerization method, 588
phase inversion method, 586–588
Nanofibers, 541, 1067, 1133
Nanofibrous membranes, 981–983
Nanofiltration (NF), 17, 250, 759–760
air pollution treatment, 318
graphene-based nanomaterials, 1021–1022
Nanoiron synthesis, 1047
Nanomaterial-based membranes, 540
carbon-based membranes, 541
inorganic nanoparticle-based membranes, 540–541
nanofiber-based membranes, 541
synthesis techniques, 541–546
interfacial polymerization (IP), 543–544
phase inversion method, 542–543
Nanomaterial-based photocatalytic membrane (PMR), 1140
Nanomaterial-enabled products, 61–62
Nanomaterials (NMs)., 27–28, 60, 62, 641, 654, 847, 867–868
See also specific nanomaterials
as adsorbents for wastewater treatment
carbon nanotubes, 6–7
graphene nanomaterials, 7–8
magnetic nanoparticles, 9
metal and metal oxides, 8–9
advanced oxidation processes, 819–820
as agents for bioremediation, 1046–1047
biosurfactants as source of, 1048–1050
carbon nanoparticles, 1131–1132
challenges, 1134–1146, 1142*f*
classification, 28–31, 847–848
carbon-based nanomaterials, 31
metal oxide nanomaterials, 30–31
semiconducting nanomaterials, 28–30
disinfection using, 5–6
engineering, 1126–1127, 1126*f*
graphene-supported nanocomposites, 1131–1132
life cycle of, 60, 61*f*
Ln^{3+}-doped oxide nanomaterials, 1129–1130
luminescent phosphors, 1129–1130
metal organic frameworks, 1132
metal oxide nanomaterials, 1128–1129
micropollutants removal (*see* Micropollutants (MPs))
nanocomposite membranes/photocatalytic membranes, 1133
nanozeolites, 1130–1131
overview of, 555–557
properties, 1127–1133
risk and safety concerns, 1146
for sensing, 6
for wastewater remediation, 769
biogenic metal nanoparticles, 769
for water splitting, 280–296
carbon-based nanomaterials, 295–296
metal organic frameworks, 293–295
metal oxides, 282–291
metal sulfides, 291–293
in water treatment by photocatalysis, 142–144
zero-valent (*see* Zero-valent nanomaterials)
1D and 2D nanomaterials, synthesis of, 37–39
0D nanomaterials, synthesis of, 33–37
method of controlled precipitation, 34–35
organometallic synthesis of II–VI and III–V nanoparticles, 35–37, 37*t*
Nanoparticles (NPs), 27–28, 60, 1046
bioremediation

This book belongs to Badji Mokhtar Annaba University Central Library
Copyright Elsevier 2025

Nanoparticles (NPs) *(Continued)*
nano biosurfactants as source of, 1048–1050
nanoscale material as agents for, 1046–1047
biorepositories for, 1050
energy band gap, 317–318, 319*t*
potential safety concerns
carbon-based nanomaterials/nanoparticles, 74
carbon nanotubes, 74
iron oxide and magnetic nanoparticles, 74–75
silver nanoparticles, 73
titanium dioxide (TiO2) nanoparticles, 75–76
zinc oxide (ZnO) nanoparticles, 72–73
synthesis of, 63–72
carbon nanotube, 66–68, 69–70*t*
extracted from plants, 65–66, 66*t*
iron oxide nanoparticle, 68, 70*t*
silver nanoparticles, 65–66, 67–68*t*
TiO2 nanoparticles, 68, 71*t*
zinc oxide nanoparticles, 63–65, 64–65*t*
II–VI and III–V nanoparticles
optical properties, 42–45
absorption spectra, 42–44, 43*f*
3D quantum confinement, 44–45
photoluminescent spectra, 44
organometallic synthesis of, 35–37, 37*t*
structure and morphology of, 40–41
Nanophosphors
for photocatalysis, 221–227
oxide-based nanophosphors, 222–225
plasmonic-metal nanoparticles, 226–227
sulfide-based phosphors, 225–226
synthesis of, 227–231
ball milling method, 231
combustion method, 230
co-precipitation method, 231
hydrothermal method, 230
sol-gel method, 230
solid-sate reaction methods, 227–229
Nanoporous graphene sheets, 650
Nanoremediation, 1046–1047. *See also* Bioremediation
Nanoscale zero-valent iron (nZVI), 8, 266, 848*t*, 862, 1047
biological synthesis, 852–854
catalytic activity, 858–861
chemical reducing agent effects, 855–856
chemical synthesis methods, 850–851
initial Fe^{3+} concentration effect, 854–855
mango peel extract for green synthesis, 854, 855*f*
pH reaction effect, 857–858
reaction mechanism, 858–860
SEM and TEM, 852, 853*f*
sonochemical synthesis, 851–852
stabilizer concentration effects, 856–857
temperature for controlling, 857
top-down *vs*. bottom-up process, 850
Nanosized ferric oxides (NFeOs), 948
Nanosized magnetite, 9
Nanostructures
carbon nanomaterials, 930–938
metal organic frameworks, 938–944
metal oxides nanoparticles, 946–948
zeolites, 944–945, 945–946*f*
Nanotechnology, 538, 770, 1057
agri-food industry, 1071
automobile industry, 1071
enabled membrane, 1138–1139, 1139*f*
in food science, 1070
in treatment of air pollution, 315–331
Nanotubes, 1014
Nanozeolites, 1130–1131
Nano-zirconium vanadate ion exchanger, 521–522, 521*f*
National Institute for Occupational Safety and Health (NIOSH), 1067
Natrolite, 422, 423*t*
Natural photosynthesis, 138–139, 139*f*
Natural zeolites, 422, 423*t*
acid treatment, 436, 437*f*
NaCl treated, 440–441
regeneration of, 456
sorption of, 457–462
ammonium, 466–468
metal cations, 463–466
Neutralization, 752–753
Ni-based MOF/GO nanocomposite, 490
Nickel, 593
N-methyl pyrrolidone (NMP), 1026
Noncovalent CNT functionalization, 1011
Noncovalent interaction, 376–377
Nonlinear Langmuir isotherm, 391
Nonmetal-doped nanocomposites, 783–784
Nonphotochemical advanced oxidation processes (AOPs), 824
Fenton process, 825
ozonation, 824
persulfate oxidation process, 825–826, 826*f*
sonolysis, 824
Nonradiative transition, 212, 212*f*
Nonsolvent-induced phase separation technique (NIPS), 543
Normalized hydrogen electrode (NHE), 1103–1104
NO_x, 324–326, 332*f*
Nyquist plot, 1091–1092, 1092*f*
nZVI. *See* Nanoscale zero-valent iron (nZVI)

O

OFR. *See* Optical fiber photo reactor (OFR)

This book belongs to Badji Mokhtar Annaba University Central Library
Copyright Elsevier 2025

O_3/H_2O_2 treatment (peroxonation), 764
OH• radical, 160
Oil-derived hydrocarbon, 1044–1046, 1045*f*
Open circuit potential (OCP), 1085, 1093–1094, 1094*f*
O_3 photolysis (O_3/UV), 765
Optical fiber photo reactor (OFR), 989–990
Optical properties
  of 1D and 2D nanomaterials, 46–47
  of II–VI and III–V nanoparticles, 42–45
    absorption spectra, 42–44, 43*f*
    3D quantum confinement, 44–45
    photoluminescent spectra, 44
  of metal sulfide, 226
Organic cation sorption, zeolites, 433–434
Organic functional groups, 485
Organic matter, 248
Organic pollutants, 343
  degradation, using nanomaterials as photocatalysts, 819–820
  removal, 565–568, 715–717
  treatment by photocatalytic membrane, 722–725
  ultrasound-assisted photocatalytic degradation, 821–824, 821*f*
Organometallic synthesis of II–VI and III–V nanoparticles, 35–37, 37*t*
Oxidative stress, 1016–1018
Oxide-based nanophosphors, 222–225
  bismuth molybdate, 223–224
  TiO_2 nanophosphors, 222–223
  zinc oxide, 224–225
Ozonation, 752
  and catalytic ozonation, 255
  nonphotochemical advanced oxidation processes, 824
  visible light photocatalysis, 1112–1114, 1115*t*

P

PAN@ZIF-8-modified membrane, 940–941, 940*f*
Particle shape, toxicological impact of INMs, 1063–1064
Particle size, toxicological impact of INMs, 1062
Peanut-shaped carbon nanotubes (PSNTs), 323–324
Pectin-iron oxide magnetic nanocomposite (PIOMN), 884–887
Peristaltic pump, 838–839
Persistent organic pollutants (POPs), 699, 715
Persulfate-based AOPs systems, 825–826
Pesticides, 243
Pharmaceutical component removal, 727*f*
Pharmaceutical waste, 244
Phase inversion, 542–543, 710–711
  multiwalled nanomembrane (MNMs) fabrication, 562–563
  nanocomposite membranes synthesis, 586–588
pH/chemical-responsive membranes, 685–688
pH effect
  advanced oxidation processes, 827
  marble hydroxyapatite, 917–918
  nanoscale zero-valent iron, 857–858
Phenolic compounds, 345
Phillipsite, 422, 423*t*
Phosphate sequestration, 526
Photoactive cloths, 1114, 1116*f*
Photoactivity of TiO_2 polymorphs, 162
Photoanode, 842
Photocatalysis, 4, 48, 93–99, 94*f*, 95–98*t*, 137, 699, 766–767, 814, 822*f*
  air pollution treatment, 317–318
  antibacterial activity, graphene-based nanomaterials, 1018–1020
  applications of, 138
  basic principal of phosphor for, 209–211
  decontamination of water, 263–266
  drawback, 836
  fundamental mechanism, 834
  governing mechanism of, 781–782
  graphene-based nanomaterials, 1022–1024
  lifetime, reactive oxygen species, 1104*t*
  mechanism of, 138–140
  micropollutants
    cerium oxide, 967
    factors influencing, 968–972
    graphene-supported nanophotocatalyst, 965
    initial concentration, 971–972
    irradiation source, 970
    loading of, 968–969
    metronidazole wastewater, degradation efficiencies, 965, 966*f*
    nanomaterials as, 962–968, 963–964*t*
    reaction temperature, 970–971
    silver (Ag) NPs, 967–968
    solution pH, 969–970
    titanium dioxide, 964
    zinc oxides, 966–967
  nanomaterials in water treatment by, 142–144
  photocatalytic materials and factors affecting, 144–147
  pollutants degradation reaction mechanism, 1103
  principles of, 138–140, 779
  reactions, 138
  schematic diagram, 210*f*
  synthesis of, 789–790, 791–792*t*
  titanium dioxide (TiO_2)
    mechanism, 814–815, 815*f*
    modification, 815, 816–817*f*
  in wastewater treatment, 147–149
  in water purification, 231–233
  with wetland for pesticides removal, 1117, 1117*f*
Photocatalysts, 782–789
  affecting factors, 789

This book belongs to Badji Mokhtar Annaba University Central Library
Copyright Elsevier 2025

Photocatalysts *(Continued)*
catalyst loading, 790–793
irradiation time, 798, 800–801*t*, 801*f*
light and intensity, effect of, 797–798
nanocomposite photocatalysts, characteristics of, 794–795
pH of solution, 793–794
photocatalysts synthesis, 789–790, 791–792*t*
pollutants, concentration of, 795–797
reaction temperature, 795, 797*f*
applications, 190–194, 199*t*
derivatives-based binary nanocomposites, 192–193
derivatives-based ternary nanocomposites, 193–194
binary metal oxides, 785, 786*f*
challenges, 804–805
clay-based nanocomposites, 789
degradation, 46, 1134–1136
mechanism, graphene, 194–197, 194–197*f*
effect due to nanoscale, 4–5
graphene-based nanocomposites, 787–789, 793*f*
industrial nanomaterials, 1067
materials, 144–145
metal-doped nanocomposites, 783, 784*f*
metal sulfides, 785–787
modification and doping, 165–166
nonmetal-doped nanocomposites, 783–784
polymer-based nanocomposites, 787
Photocatalytic membrane, 166–167, 169*f*, 175, 722–723
challenges, 725–726, 1140
fabrication, 706–715, 707*f*
chemical vapor deposition (CVD), 710
immersion method, 711–712
phase inversion method, 710–711
plasma-enhanced chemical vapor deposition, 710
sol-gel dip-coating, 706–708
solvent casting method, 714–715, 716*t*
spinning/electrospinning method, 712–713
ultrasonication, 709–710
vacuum filtration, 708–709
materials, 700–706
CNT-based photocatalytic membrane, 705–706
graphene-based photocatalytic membrane, 703–704
graphitic carbon nitride-based photocatalytic membrane, 704–705
hybrid photocatalytic membrane, 701–702
polymer-based photocatalytic membrane, 702–703
porous photocatalytic membranes, 702
for organic pollutant removal, 715–717
organic pollutants, treatment of, 722–725
properties, 1133
pure TiO_2 membranes, 167
reactors and their configurations, 717–721
scale-up of, 726–727
schematic illustration of working, 723*f*
TiO_2 ceramic membranes, 167
TiO_2 polymer membranes, 166–167
Photocatalytic membrane reactor (PMR), 798–802, 803*f*, 990–992, 991–992*f*, 1110–1112
Photocatalytic nanomaterials, 1134–1136, 1135–1136*f*
Photocatalytic oxidation with hydrodynamic cavitation, 123
Photocatalytic packed-bed reactor system, 1116, 1116*f*
Photocatalytic reactors, 798–803
hybrid photoreactors, 803
microfluidic reactors, 802–803, 804*f*
microreactors, 802–803
photocatalytic membrane reactors (PMRs), 798–802
photocatalytic reaction of TiO2, 139–140, 140*f*
Photocatalytic research, 156–157
Photochemical advanced oxidation processes, 764–767
Photochemical reactors, 168–171
annular, 171
immersion well, 170
multilamp, 171
thin film, 170
Photochemical water splitting, 278–279, 279*f*
Photocorrosion, 278
Photodynamic therapy, 1016
Photoelectrocatalysis (PEC). *See* Electro-photocatalysis
Photoelectrochemical water splitting, 278, 279*f*
Photoexcited CB electrons, 160
Photo-Fenton reaction (H_2O_2/Fe^{2+}/UV), 765–766
Photo-Fenton technique, 1107–1108, 1109*t*
Photoluminescence, graphene quantum dots, 1012
Photoluminescent spectra, II-VI and III-V nanoparticles, 44
Photolytic degradation of pollutants, 253
Photon, 212
efficiency, 157–158
source, 842–843, 844*f*
Photoresponsive membranes, 692
Photothermal effect, 1018, 1019*t*
pH value of adsorption, 347–348
Physicochemical properties, seawater, 1092–1093, 1093*f*
Physicochemical techniques, 1125–1126
Pilot scale system, 727*f*
Piperazine (PIP), 543–544
Plasma-activated zeolite, 443, 444*f*
Plasma-enhanced chemical vapor deposition (PECVD), 710
Plasmonic-metal nanoparticles (PNPs), 226–227
Plasmonic photocatalysis, 226–227

This book belongs to Badji Mokhtar Annaba University Central Library
Copyright Elsevier 2025

Plastic pollution, 245–246
Plastic waste, 245–246
PMNCs. *See* Polymer matrix nanocomposites (PMNCs)
PMR. *See* Photocatalytic membrane reactor (PMR)
PNPs. *See* Plasmonic-metal nanoparticles (PNPs)
Polarization curves, unmodified/modified anodes, 1094–1096, 1095*f*
Pollutants, 172, 173*t*, 315
Poly(methacrylic acid) (PMAA), 680–681
Poly(N-isopropylacrylamide) (PNIPAAm), 685
Polyacrylonitrile (PAN), 330–331, 562
Polyamide-thin-film composite (PA-TFC), 645
Polyamide thin-film nanocomposite membrane, 648–649
Polyaniline, 390, 1082
Polyaromatic hydrocarbons (PAHs), 1044–1046, 1048
Polychlorinated biphenyls (PCBs), 1047
Polydispersed nZVI particles, 856
Polyelectrolytes (PELs), 686, 688
Polyester (PS), 1026
Polyethersulfone (PES), 586–588, 613, 1026, 1028*t*
Polyethersulfone mixed-matrix membranes (PSF MMMs), 636–637
Polyethylenimine (PEI), 933, 934*f*
Poly lactide-*co*-glycolide (PLGA) NPs, 818–819
Polymer, 11
  chain density, 682–683
  grafting, 560–561
  nanoparticles, 818–819
  polymeric membranes, 538–540, 613–619, 614*f*, 930, 946–948, 1138–1139
Polymer-based nanocomposites, 787
Polymer-based photocatalytic membrane, 702–703
Polymer matrix nanocomposites (PMNCs), 780
Polymer nanocomposite, 12, 13*f*, 613–619
  issue
    flux rejection trade-off, 615
    fouling, 615–616
    nanocomposite membranes as solution, 617–619
  for membrane synthesis, 613–615
  mixed-matrix membranes, 619–640
    carbon nanomaterials (CNs) (*see* Carbon nanomaterials (CNs))
    hydrophilic and amphiphilic polymer (HP)-incorporated in, 619–631
    inorganic nanomaterials (iNPs)-incorporated in, 631–632
    metal-organic frameworks (MOFs), 632
  perspective of, 654–655
  thin-film nanocomposite membrane, 640–649
    bioinspired materials (BIMs), 642–643
    carbon nanomaterials, 644–647
    chlorine stability of polyamide TFN, 648–649
    inorganic nanomaterials (iNPs), 641–642
    metal-organic frameworks (MOFs), 643–644
    with nanoparticles in substrate, 647–648
Polyoxometallate (POM)-loaded porous HKUST-1, 501
Polypyrrole (PPy), 1082. *See also* SnO_2/PPy nanocomposites, anode modifications
Polystyrene (PS), 186
Polysulfone (PSF), 613, 931–932
Polytetrafluoroethylene (PTFE), 1061
Polyvinylidene fluoride (PVDF), 528–529, 560, 985
Porosity, of zeolites, 431
Porous coordination polymers (PCPs), 1132. *See also* Metal-organic frameworks (MOFs)
Porous inorganic graphene-based nanocomposites, 382
Porous photocatalytic membranes, 702
Potassium permanganate ($KMnO_4$), 184
Power density, unmodified/modified anodes, 1094–1096, 1095*f*
π-π interactions, adsorption, 355
Precipitation, 749–750
Pressure-driven membrane filtration processes, 613, 614*f*
Primary pollutants, 315
Primary treatment, wastewater, 246–247
  coagulation and flocculation, 247
  gravity separation and sedimentation, 247
  screening, centrifugal separation, and filtration, 247
Proton exchange membranes, 541
Pseudocohnilembus persalinus, 1047
Pseudomonas aeruginosa, 1049
Pseudo second-order kinetic model, 979
Pulsed laser deposition (PLD) method, 282
Pure TiO_2 membranes, 167

Q

Quantum confinement, 29–30, 45
Quantum dots, 1068
Quantum-mechanical phenomena, 44–45
Quantum size effect, 4–5

R

Radiative transition, 212, 212*f*
Radical attack on organics, 161–162
Raman scattering, 189
Raman spectroscopy, 189

This book belongs to Badji Mokhtar Annaba University Central Library
Copyright Elsevier 2025

Rare-earth-doped inorganic phosphor, 213–221
downconversion phosphors, 213–216, 214–215*f*
long-lasting phosphors, 219–221, 219–220*f*
upconversion phosphors, 216–218, 216*f*, 218*f*
Rarefaction-compression cycles, 851–852
Reaction mechanism, nanoscale zero-valent iron, 858–860
Reaction temperature, 795, 797*f*, 970–971
Reactive brilliant orange K-R (RBOKR), 841–842, 841*f*
Reactive oxygen species (ROS), 73, 317–318
photocatalysis lifetime, 1104*t*
SWCNTs, 1016
Recalcitrant pollutant
advanced oxidation processes, 819, 820*t*
carbon-based nanoparticles, 817–818
nanoscale zero-valent iron, 861
pH effect, 827
Recycled lanthanum, 328–329
Recycle system, 756
Reduced graphene oxide (rGO), 7–8, 182, 183*f*, 373–374, 373*f*, 965
membrane, 568, 569*f*
Removing-transferring method, 648–649
Responsive membranes, 674
Reverse micelle method, 38
Reverse osmosis (RO), 250–251, 759, 1021–1022
rGO. *See* Reduced graphene oxide (rGO)
Rhamnolipid, 1049
Rotating bioreactor contactor (RBC), 756–757
Rotating disc reactors, 839–840, 839*f*
Rutile, 162

S

Saccharomyces cerevisiae, 884–887
Salt responsiveness, 688–689
Sand filtration, 746
Scale-up conundrum, 530
Scanning electron microscopy (SEM), 522–523
adsorption, 350, 350*f*
BMFC, modified anode, 1086–1087, 1086*f*
marble hydroxyapatite, 904, 912–914, 912–913*f*
nanoscale zero-valent iron, 852, 853*f*
Scarcity of water, 59
Screens/screening, 247, 744–745
Seawater, physicochemical properties, 1092–1093, 1093*f*
Secondary treatment, wastewater, 248
aerobic process, 248
anaerobic process, 248
Sedimentation, 247, 744, 746
tank/clarifier, 756
Self-assembled and nonsolvent-induced phase separation (SNIPS), 543
Semiconductor, 1104, 1114
nanophosphors, 221
photocatalysis, 174
semiconducting nanomaterials, 28–30
TiO_2, 158
Semiconductor-mediated photo-US method, 1109–1110
Sessile drop technique, 1088
Sigma Aldrich, 1026–1027
Silica, 517
nanoparticle-based membranes, 541
nanoparticles, 946
nanocomposite membranes, micropollutants, 985
toxicity potential, 548
Silicon, 28–29
Silicon dioxide, 68–72
Silver (Ag)
nanoparticles, 641
antibacterial agent, 547
photocatalysis process, micropollutants, 967–968
potential safety concerns, 73
synthesis of, 65–66, 67–68*t*
toxicity potential, 548
nanotubes, 73
Single-step synthesis methods, 284
Single-walled carbon nanotubes (SWCNT), 6, 7*f*, 548, 935–938
aerospace industry, 1071–1072
automobile industry, 1071
for heavy metal removal, 882
physical/mechanical destruction, 1014
reactive oxygen species, 1016
structure, 936*f*
Sintering, 545
SLN. *See* Surface-located nanocomposite (SLN) membranes
Smart magnetic graphene (SMG), 882–884
SnO_2/PPy nanocomposites, anode modifications
BMFC (*see* Benthic microbial fuel cell (BMFC))
capacitance values, 1089*t*
cyclic voltammogram, 1089–1090, 1089*f*
electrochemical impedance spectroscopy, 1091–1092
exchange current density, 1090–1091, 1090–1091*t*
Fourier-transform infrared spectroscopy, 1087, 1087*f*
kinetics, 1090–1091
open circuit potential, 1085, 1093–1094, 1094*f*
power density and polarization curves, 1094–1096, 1095*f*
preparation, 1084
scanning electron microscopy, 1086–1087, 1086*f*
surface wettability, 1088, 1088*f*
Sn_3O_4-ZnO nanoflowers
energy dispersive X-ray spectroscopy, 299, 301*f*
for hydrogen generation, 296–302

This book belongs to Badji Mokhtar Annaba University Central Library
Copyright Elsevier 2025

preparation, characterization, and photoactivity, 297
results and discussion, 298–302
Raman spectrum of, 298–299, 299*f*
UV-visible diffuse reflectance spectra of, 299–300, 300–301*f*
XRD spectrum of, 298, 298*f*
Sodalite, 420
Sodium dodecyl sulfate (SDS), 250
Sodium nitrate ($NaNO_3$), 184
Sodium-rich zeolites, 441
Solar energy, 156–157
Solar Falling Film Reactor (SFFR), 1119, 1119*f*
Solar light-based photocatalytic membranes, 717–718
Solar photocatalytic degradation, 1118*f*, 1119
Solar photoreactor, 1117, 1118*f*
Sol-gel technique, 38, 185, 230, 789–790
dip-coating, 706–708
nanocomposite ion exchange (IEX) materials, 519, 519*f*
zirconium vanadate ion exchangers synthesis, 521–522
Solid-sate reaction methods, 227–229
Solution mixing, 558
Solution pH
micropollutants
adsorption process, 975–976
photocatalysis process, 969–970
Solution (ohmic) resistance (Rs), 1091–1092, 1092*f*
Solvent casting method, 714–715, 716*t*, 1117
Sonication, 706
Sonoassisted oxidation process, 827
Sonocatalysis, 823–824, 823*f*
Sonochemical activity, 1108–1109
Sonochemical advanced oxidation processes, 767–768
Sonochemical methods, 253, 487
Sonochemistry, 851–852
Sono-Fenton process, 116–118, 116*f*, 117–118*t*
Sonolysis, 88–92, 91*f*, 92–93*t*, 822–823, 822–823*f*
nonphotochemical advanced oxidation process, 824
process, 1109–1110
Sonophotocatalysis, 823–824, 823*f*, 1108–1110, 1111*t*
process, 111–115, 111*f*, 113–115*t*
reactor, 803
Sono-photo-Fenton process, 119–123, 119*f*, 120–122*t*
Sophorolipids, 1050
Sorption, 417, 431–432, 457–462, 462*t*
Spinel ferrites, 259–260
Spinning disc reactor (SDR), 988
Spinning/electrospinning method, 712–713, 714*f*
Spray-assisted layer-by-layer, 563
Spray coating, 708
Stabilization method, 744
Stabilizers, 33
Stainless steel CNT (SS-CNT) membrane, 567
Starmerella bombicola, 1050
Stimuli-responsive membrane (SRM), 676
characteristics of, 692
flexibility, 692–693
surface modification, 693
design and fabrication of, 678–683
functionalization
by incubation in liquid, 679
by responsive groups incorporation, in base membrane, 679–681
by surface modification, 681–683
industrial applications, 693–694
preparation and processing, 678–683
Stormwater, 242–243
Stretching, 545
Submerged photocatalytic membrane reactor, 719, 720*f*
Sulfadiazine (SDZ), 104
Sulfide-based phosphors, 225–226
Sulfonated polyethersulfone (SPES), 522, 522*f*, 529
Sulfur monoxide (SO_x), 326–327
Supercritical water oxidation (SCWO), 813
carbon-based nanoparticles, 817–818
ceramics-based nanoparticles, 818
metal oxide-containing nanoparticles, 816–817
photocatalysis, 814
mechanism, 814–815, 815*f*
TiO_2 modification, 815, 816–817*f*
polymer nanoparticles, 818–819
Superparamagnetic materials, 256–257
Surface adsorbates, 163–164
Surface areas, of MOFs, 485
Surface charge modification, 164–165
Surface-engineered iron oxide nanohybrids, 867–868
adsorbents strategies, 868–870
challenges, 890
heavy metal removal
iron-bimetal oxide NPs for, 872–877, 876*t*
iron oxide-biomaterial-based nanoparticles, 884–889, 888*t*
iron oxide-carbon nanotubes, 882, 883*t*
iron oxide functional groups, 870–872, 872*f*, 873–875*t*
iron oxide-graphene, 882–884, 885–886*t*
iron oxide-metal oxide nanoparticles, 877–878, 878*t*
iron oxide-polymer, 879–881, 880–881*t*
strategies, 870*f*
Surface-engineered magnetic nanohybrids, 870–889
Surface fluorination of metal oxides, 163–164
Surface-located nanocomposite (SLN) membranes, 617, 619

This book belongs to Badji Mokhtar Annaba University Central Library
Copyright Elsevier 2025

Surface-located nanoparticle membranes, 649–653
covalent organic frameworks, 653
graphene oxide surface-located membrane, 650–652
inorganic nanomaterials (iNPs), 652–653
metal-organic frameworks, 653
nanoporous graphene sheets, 650
Surface modification
functionalization by, 681–683
grafting-from method, 682–683
grafting-to methodology, 682
stimuli-responsive membrane, 693
of TiO_2
dye anchoring, 165
metal deposition, 162–163
surface adsorbates, 163–164
surface charge modification, 164–165
Surface-modified zeolite (SMZ), 443, 464–465
Surface water, 242–243
Surface wettability, 1088, 1088*f*
Surface zero charge, 917–918
Suspended growth process, 754–756
Suspension bed reactors, 168–170
Suspension polymerization, 518
Sustainable development, 770
SWCNT. *See* Single-walled carbon nanotubes (SWCNT)
Synergistic coefficient, of sono-photocatalysis, 112
Synergistic effect, 727–729
Synergy index (SI), 823
Synthetic zeolites, 422, 423*t*
regeneration of, 456
sorption of, 457–462

T

Tafel equation, 1090–1091, 1090*f*
TC. *See* Tetracycline (TC)
Temkin isotherm, 430*t*, 919, 920*t*
Temperature
adsorption, 348
for controlling nanoscale zero-valent iron, 857
effect, advanced oxidation processes, 827
Tertiary treatment, wastewater
adsorption, 251–252
advance oxidation method (*see* Advanced oxidation processes (AOPs))
evaporation, crystallization, and distillation, 249
membrane processing, 249–251
Tetracycline (TC), 146–147
Tetrapropylammonium bromide (TPABr)-modified zeolite, 465
TFN. *See* Thin-film nanocomposite (TFN) membranes
Thermal activation, zeolites, 441–443, 442*f*
Thermal conductivity, 1011
Thermally induced phase separation (TIPS), 543
Thermogravimetric analysis (TGA), 353–354, 354*f*, 522, 522*f*
marble hydroxyapatite, 905, 914–915, 915*f*
Thermoresponsive membrane, 684–685
Thin-film composite (TFC), 633, 640–642
membranes, 929–930, 933, 943*f*
Thin-film nanocomposite (TFN) membranes, 617. *See also* Polymer nanocomposite, thin-film nanocomposite membrane
Thin-film reactors, 170
Three-dimensional electrode packed-bed reactor, 838–839, 838*f*
Three-dimensional electrode-slurry reactor, 836–838, 837*f*
Three dimensional graphene (3DG), 993–995
Three-dimensional (3D) graphite, 368
Three-dimensional printing (3D printing), 546
Tin oxide (SnO_2) nanoparticles, anode modifications, 1082
BMFC (*see* Benthic microbial fuel cell (BMFC))
capacitance values, 1089*t*
cyclic voltammogram, 1089–1090, 1089*f*
electrochemical impedance spectroscopy, 1091–1092
exchange current density, 1090–1091, 1090–1091*t*
Fourier-transform infrared spectroscopy, 1087, 1087*f*
kinetics, 1090–1091
open circuit potential, 1085, 1093–1094, 1094*f*
power density and polarization curves, 1094–1096, 1095*f*
scanning electron microscopy, 1086–1087, 1086*f*
surface wettability, 1088, 1088*f*
synthesis, 1083–1084
TiO_2-coated nano $CaCO_3$, 322–323, 322*f*
Titanate-based perovskites ($MTiO_3$), 290
Titanate nanotubes (TNTs), 586–588
Titanium dioxide (TiO_2), 30–31, 46, 704–705, 717–718, 766–767, 785, 947
bandgap, 158
bonding energy, 817*f*
ceramic membranes, 167
micropollutants
nanocomposite membranes, 984–985
photocatalysis process, 964
micropollutants removal, 964
nanoparticles, 547
potential safety concerns, 75–76
synthesis of, 68, 71*t*
nanophosphors, 222–223
photocatalysis process, 814–815, 815–816*f*
polymer membranes, 166–167
semiconductor nanoparticles, 256
types of, 947

This book belongs to Badji Mokhtar Annaba University Central Library
Copyright Elsevier 2025

Titanium dioxide (TiO_2) photocatalysis, 157
advancements in
application of membranes, 167–168
photocatalyst modification and doping, 165–166
photocatalytic membranes, 166–167
surface modifications, 162–165
challenges and issues, 172–174
combination/coupling with other treatment methods, 171–172
mechanism of, 157–162
adsorption of chemicals, 159–161
generation of charge carrier species, 157–159
radical attack on organics, 161–162
photoactivity of, 162
photochemical reactors, 168–171
Titanium oxide, 10–11
Titanium oxide-based nanomaterials, 282–285
Total ionic strength adjustment buffer (TISAB), 901
Total organic carbon (TOC) removal, 861
Toxicity, 594–595
Toxicological impact, industrial nanomaterials, 1061
chemical composition, 1061
degree of agglomeration, 1063
electrostatic attraction potential, 1063–1064
particle shape, 1063–1064
particle size, 1062
surface area and reactivity, 1062
surface coatings/type, 1063
Track etching, 545
Transition metal dichalcogenides (TMDCs), 293
Transition metal ions, 485
Transmembrane pressure (TMP), 686
Transmission electron microscopy (TEM), 351
marble hydroxyapatite, 914, 914–915*f*
nanoscale zero-valent iron, 852, 853*f*
Trimesoyl chloride (TMC), 543–544
Trioctylphosphine (TOP), 36
Trioctylphosphine oxide (TOPO), 36
Tungsten sulfide (WS_2)-based nanomaterials, 293

U

UiO-66, 939*f*, 941–942, 942*f*
Ultrafiltration (UF), 250, 758–759, 1021
Ultrasonication method (USM), 709–710
marble hydroxyapatite, 901, 903, 904*f*
adsorbent dosage, 916–917, 916*f*
adsorption equilibrium isotherms, 919, 920*t*
co-ions effect, 918, 919*f*
column breakthrough, 923, 924*t*, 924*f*
contact time effect, 917, 917–918*f*
energy efficacy, 922–923
FTIR analysis, 906–908, 907*f*
kinetics of adsorption, 919–920, 921*t*
pH effect, 917–918
SEM analysis, 912–914, 912–913*f*
TEM/EDS analysis, 914, 914–915*f*
TGA/DTA analysis, 914–915, 915*f*
water quality parameters and regeneration, 920–922, 922*f*
XRD analysis, 909–912, 909*f*, 911*f*
Ultrasonic spray pyrolysis, 38
Ultrasound
co-precipitation technique, 852
persulfate-based AOPs systems, 825–826
Ultrasound-assisted photocatalytic degradation, 821–824, 821*f*
Ultraviolet light emitting diode–based (UV-LED) reactor, 990
Ultraviolet (UV) system, 726–727
Ultraviolet-visible diffuse reflectance spectra (UVDRS)
Ultraviolet-visible spectroscopy, 189
Untreated wastewater, 241–242
Upconversion phosphors, 216–218, 216*f*, 218*f*
Upconverting luminescent phosphors, 1129–1130
Upwnconverting phosphors, 213
Urbanization, 242–243
US-Y zeolite, 422, 423*f*

V

Vacuum coating, 708
Vacuum filtration, 708–709
Valance band (VB), 139, 209
Vapor-phase techniques, 780
Vertically aligned carbon nanotube (VA-CNT) membranes, 639
Viscoelastic response, 685–686
Visible light photocatalysis, 1101–1103, 1102*f*
absorption, 1104, 1105*t*, 1106*f*
challenges, 1114–1119
heterogeneous photocatalyst, 1103–1106
homogenous photocatalysis, 1106–1107
hybrid processes, 1107
membrane filtration, 1110–1112, 1112*f*, 1113*t*
ozonation process, 1112–1114, 1115*t*
Photo-Fenton technique, 1107–1108, 1109*t*
sonophotocatalysis, 1108–1110, 1111*t*
solar photoreactor, 1117, 1118*f*
Volatile organic compounds (VOCs), 328–331, 328*f*, 490, 503

This book belongs to Badji Mokhtar Annaba University Central Library
Copyright Elsevier 2025

W

Wairakite, 423*t*
Wastewater
classification, 241–242
treatment of inorganic contaminants in, 261
Wastewater treatment, 608
advanced oxidation processes, 780–781 (*see also* Advanced oxidation processes (AOPs))
challenges, 546–549
antibacterial challenges (*see* Antibacterial challenges, wastewater treatment)
antifouling challenges, 546, 547*f*
toxicity potential, 548–549
hybrid AOP's involving nanocatalyst, 101–123
heterogeneous Fenton process, 103–104
heterogeneous photo-Fenton process, 104–111
photocatalytic oxidation with hydrodynamic cavitation, 123
sono-Fenton process, 116–118
sonophotocatalytic process, 111–115
sono-photo-Fenton process, 119–123
and its contaminants, 608–612, 610*t*
low-dimensional nanomaterials in, 48
membrane-based technology, 15–18
nanocomposite membranes, 17–18
membranes in, 612–613
methods, 142
nanocomposites for
bionanocomposites, 11–12
nanocomposite hydrogels, 14–15
nanocomposite inorganic supports, 12–14
nanomaterials (*see also* Nanomaterials)
role of, 578–579
nanomaterials as adsorbents for
carbon nanotubes, 6–7
graphene nanomaterials, 7–8
magnetic nanoparticles, 9
metal and metal oxides, 8–9
nZVI (*see* Nanoscale zero-valent iron (nZVI))
photocatalysis, challenges of, 147–149
polymer nanocomposite membranes (*see* Polymer nanocomposite)
primary treatment, 246–247
coagulation and flocculation, 247
gravity separation and sedimentation, 247
screening, centrifugal separation, and filtration, 247
role of nanomaterials by photocatalysis, 142–144
secondary treatment, 248
aerobic process, 248
anaerobic process, 248
sources of water pollution, 141–142
tertiary treatment
adsorption, 251–252
advance oxidation method, 252–260
evaporation, crystallization, and distillation, 249
membrane processing, 249–251
using different nanomaterials, 42, 43*t*
water scarcity, 608, 609*f*
Wastewater treatment plants (WWTP), 741, 743*f*
Water, 3–4, 85
consumption, 241
hardening system, 452, 454*f*
pollutants, types, 242–246
agricultural waste, 243
industrial waste, 244–245
pharmaceutical waste, 244
plastic waste, 245–246
pollution, source of, 141–142, 242–246
purification, 743
carbon-based nanocomposite membranes (CNCMs) (*see* Carbon-based nanocomposite materials (CNCMs))
photocatalysis in, 231–233
Water-in-oil microemulsion technique, 1049
Water remediation processes, 741–743
advanced/novel water remediation processes, 757–762
electrocoagulation, 762
electrodialysis (ED), 762
membrane technology, 758–762
advanced oxidation processes (AOPs) (*see* Advanced oxidation processes (AOPs))
biological treatment, 753–757
activated sludge process, 755–756
attached growth (biofilm) processes, 756–757
combined processes, 757
suspended growth process, 754–756
chemical disinfection
chlorination, 751–752
hydrogen peroxide, 752
iodination, 752
ozonation, 752
classification, 742
ion exchange, 753
nanomaterial, 769
biogenic metal nanoparticles, 769
neutralization, 752–753
physical methods, 743–749
aeration, 745–746
distillation, 747–749
filtration, 746
grit chambers, 745
screens, 744–745
sedimentation, 746
physicochemical treatment, 749

This book belongs to Badji Mokhtar Annaba University Central Library
Copyright Elsevier 2025

adsorption, 750–751
precipitation and coagulation, 749–750
Water splitting
developing photocatalysts for, 280
nanomaterials for, 280–296
carbon-based nanomaterials, 295–296
metal organic frameworks, 293–295
metal oxides, 282–291
metal sulfides, 291–293
photochemical water splitting, 278–279, 279*f*
photoelectrochemical water splitting, 278, 279*f*
Water-stable MOFs, 506–507
Water treatment
with graphene-based nanomaterials, 1020, 1021*s*
absorption properties, with removal capacity, 1023*t*
adsorption, 1022
electrode deposition/degradation, 1022–1024
filtration, 1021–1022
photocatalysis, 1022–1024
magnetic materials advantages in, 256
magnetic materials used for, 258
magnetic adsorbents, 261–263
photocatalysis decontamination, 263–266
stimulation approach and application, classification of, 683–692
electroresponsive membranes, 689–691
ionic strength/electrolyte/salt responsiveness, 688–689
magnetoresponsive membranes, 691–692
pH/chemical-responsive membranes, 685–688
photoresponsive membranes, 692
thermoresponsive membrane, 684–685
Wet chemical methods, 869
WWTP. *See* Wastewater treatment plants (WWTP)

X

X-ray diffraction (XRD), 188
marble hydroxyapatite, 902
conventional precipitation technique, 908–912, 908*f*, 911*f*
ultrasonication method, 909–912, 909*f*, 911*f*
nanocomposite ion exchange (IEX) materials, 521–522
unreacted MWP, 906, 907*f*
X-ray powder diffraction (XRD), 353, 353*f*

Z

Zeolites, 417–418, 584–585, 944–945, 945–946*f*, 1048
adsorption
kinetics, 429–430
thermodynamics of, 430–431
types of, 428
based magnetic nanoparticles, 260
characterization, 422–425
chemical formulas, 422, 423*t*
composition, 419–422
cost of, 422, 424*t*
dealumination of, 440, 440*f*
ion-exchange properties, 418
modification
chemical activation, 436–441, 437*f*
by iron oxides, 446–448, 446*f*
processes, 436–448
of surface-active substances, 443–445, 445*f*
thermal activation, 441–443, 442*f*
organic cation sorption, 433–434
physicochemical properties, 434–435
regeneration of, 454–457, 455–456*f*
in softening drinking water, 451–453, 454*f*
sorption and ion-exchange, 457–462
factors affecting, 431–432
mechanisms, 425–431
principles of, 432–433
structures, 420, 421*f*
in water treatment
ammonium ion removal, 448–450, 450*t*
metal ion removal, 448, 449*t*
radioactive elements removal, 450–451, 451*t*
Zeolitic imidazolate framework (ZIF-8), 496–497
Zeolitic imidazolate frameworks (ZIFs), 938–941, 939–940*f*
Zero charge point, 431
Zero liquid discharge (ZLD), 242
Zero-valent iron (ZVI), 848
nanoparticles, 8–9, 258–259
nanoscale (*see* Nanoscale zero-valent iron (nZVI))
types, 848, 848*t*
Zero-valent iron-guar gum nanocomposite (ZGNC), 852, 853*f*
Zero-valent iron nanoparticles (ZVIN), 265
Zero-valent nanomaterials, 1127–1128
Zinc oxide (ZnO), 31, 224–225
nanocomposite membranes, micropollutants, 985–986
nanoparticles, 72–73, 187–188
potential safety concerns, 72–73
synthesis of, 63–65, 64–65*t*
photocatalysis process, micropollutants, 966–967
Zinc oxide (ZnO)-based nanomaterials for water splitting, 285–290
Zinc sulfide (ZnS) based nanomaterials for water splitting, 291–292
Zirconium-based MOF doped on polyurethane foam (Zr-MOFs-PUF) membrane, 943

This book belongs to Badji Mokhtar Annaba University Central Library
Copyright Elsevier 2025

Zirconium (IV) benzene-tricarboxylate Zr(BTC), 501, 502*f*
ZLD. *See* Zero liquid discharge (ZLD)
ZnO/C-MOF-5 nanocomposite, 496, 496*f*
ZnO/GO nanocomposites, 1027, 1028*t*
Z-scheme photocatalyst, 280
ZVIN. *See* Zero-valent iron nanoparticles (ZVIN)
Zwitterionic polyelectrolyte nanoparticles (ZPNPs), 642–643

This book belongs to Badji Mokhtar Annaba University Central Library
Copyright Elsevier 2025

HANDBOOK OF NANOMATERIALS FOR WASTEWATER TREATMENT

Edited by Bharat A. Bhanvase, Shirish H. Sonawane, Vijay B. Pawade and Aniruddha B. Pandit

Nanotechnology has the potential to substantially improve current water and wastewater treatment processes in terms of efficacy and cost. The synthesis methods and physicochemical properties of nanomaterials and noble metal nanoparticles improve the efficiency of the performance and mechanisms in the treatment of various pollutants. The treatment methods are presented in this book. The processing of nanomaterials is subject to technical bottlenecks such as aggregation, difficulty in subsequent separation, leakage into contact water, and their potentially adverse effects on ecosystems and human health. The book covers the fundamentals of nanomaterials, photocatalytic nanocomposite materials, nanomaterials used as adsorbents and in water remediation processes, their current status, and challenges in their mass production and application.

Handbook of Nanomaterials for Wastewater Treatment covers the nanomaterials used for wastewater treatment. It explores the major applications of nanomaterials for effective catalysis and adsorption. The book also provides in-depth information about the properties and application of newly synthesized advanced nanomaterials for wastewater treatment processes. This is an important reference source for researchers, aimed at solving some basic and advanced problems related to the use of nanomaterials in the development of wastewater treatment processes and technologies.

Key Features

- Explains the properties of the most commonly used nanomaterials in wastewater treatment
- Describes the major nanoscale materials synthesis and their processing techniques for wastewater treatment
- Assesses the major technological challenges of using nanomaterials on a mass scale in wastewater treatment

Bharat A. Bhanvase is Professor of Chemical Engineering at Laxminarayan Institute of Technology, Rashtrasant Tukadoji Maharaj Nagpur University, Nagpur, Maharashtra, India. His research focuses on wastewater treatment, solid waste processing, cavitation-based processes for nanomaterials and nanocomposites preparation, process intensification, microfluidics, and nanofluids.

Shirish H. Sonawane is Professor of Chemical Engineering at the National Institute of Technology, Warangal, Telangana, India. His research focuses on the synthesis of hybrid nanomaterials, process intensification, and wastewater treatment.

Vijay B. Pawade is Assistant Professor of Applied Physics at Laxminarayan Institute of Technology, Rashtrasant Tukadoji Maharaj Nagpur University, Nagpur, Maharashtra, India, India. His research focuses on optical properties of rare earth-doped oxide materials and their applications in LEDs, display, and Si solar cell applications.

Aniruddha B. Pandit is Professor of Chemical Engineering at the Institute of Chemical Technology Mumbai, India. His research focuses on the area of cavitation, sonochemistry, wastewater treatment, design of multiphase reactors, and nanomaterial synthesis and applications.

ELSEVIER elsevier.com/books-and-journals

Technology and Engineering/
Material Science

ISBN 978-0-12-821496-1

9 780128 214961

This book belongs to Badji Mokhtar Annaba University Central Library

Copyright Elsevier 2025